Acta Chemica Scandinavica A 28 (1974) 1—7

An Electron Diffraction Investigation of the Molecular Structure of *cis*-2-Methyl-1,3,5-hexatriene in the Vapour Phase

M. TRÆTTEBERG and G. PAULEN

Department of Chemistry, University of Trondheim, NLHT, N-7000 Trondheim, Norway

The molecular structure of *cis*-2-methyl-1,3,5-hexatriene has been studied by the gas electron diffraction method. The $C_3=C_4$ and $C_5=C_6$ double bonds were found to be coplanar corresponding to *s-anti* conformation at the intervening CC single bond. The $C_1=C_2$ double bond was found to be out of the plane of the other CC double bonds. It was not possible definitely to distinguish between a *syn*-clinal and *anti*-clinal conformation at the C_2-C_3 single bond, but the results indicate that *syn*-clinal (*s-gauche*) is the correct one.

The following bond distances and mean vibrational amplitudes were observed:

$R(C=C)_{Av.}$: 1.345 Å, $u(C=C)_{Av.}$: 0.0391 Å, $R(C_{sp^2}-C_{sp^2})_{Av.}$: 1.462 Å, $u(C_{sp^2}-C_{sp^2})_{Av.}$: 0.0460 Å, $R(C_{sp^2}-C_{sp^3})$: 1.515 Å, $u(C_{sp^2}-C_{sp^3})$: 0.0461 Å, $R(C_{sp^2}-H)$: 1.094 Å, $R(C_{sp^3}-H)$: 1.104 Å, $u(C-H)_{Av.}$: 0.0775 Å. The distances are given as R_a values.

Nearly all experimentally determined noncyclic organic molecules with conjugated double bonds are found to have an essentially planar *anti* arrangement of two consecutive double bonds, *i.e.* an *s-anti* conformation at the intervening single carbon bond. The torsional potential energy connected with rotation about a $C_{sp^2}-C_{sp^2}$ single bond obviously has its lowest minimum at a dihedral angle equal to 180°. At this conformation the conjugation between the two neighbouring π-bonds is at its maximum while the repulsions between the bonds at the two carbon atoms constituting the single bond are minimal. However, very little is known about the general shape of the potential energy function in relation to the torsional angle around a single bond between two sp^2-hybridized carbon atoms. In order to elucidate this problem it is of interest to gather experimental information about molecular structures where other conformations than those corresponding to *s-anti* at the single bonds in conjugated systems might be observed. In *cis*-2-methyl-1,3,5-hexatriene there will be serious steric interaction between the methyl group and the methine group at C_5 if an all planar conformation of the carbon skeleton is assumed. It will be of special interest to find out how the steric inhibition is overcome in this case. A study of *trans*-2-methyl-1,3,5-hexatriene was carried out simultaneously.[13]

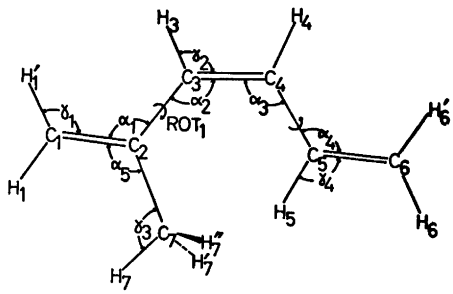

Fig. 1. cis-2-Methyl-1,3,5-hexatriene. Molecular model which shows the numbering of the atoms.

EXPERIMENTAL

The sample of *cis*-2-methyl-1,3,5-hexatriene used in the present study was kindly provided by the late professor R. Turner, Rice University, Houston, Texas. The electron diffraction pattern from the gas was recorded on the Oslo electron diffraction unit [1] at a temperature of about 30°C. Exposures were made at nozzle to photographic plate distances of about 48 cm and 20 cm. Four apparently faultless plates for each nozzle-to-plate distance were photometered and the data processed in the usual way.[2] The resulting molecular intensity function extended

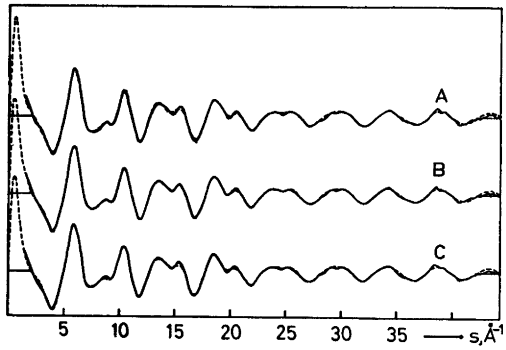

Fig. 2. cis-2-Methyl-1,3,5-hexatriene. Experimental (—) and theoretical (---) molecular intensity functions. The theoretical data correspond to A: Model I, B: Model II and C: Model III.

from $s = 1.375$ Å^{-1} to $s = 44.25$ Å^{-1}. $s = (4\pi/\lambda) \sin(\theta/2)$ where λ is the electron wavelength (determined by diffraction from gaseous CO_2) and θ is the diffraction angle. The modified experimental molecular $[sM(s)]$ function is shown in Fig. 2.

Theoretical intensity functions were calculated from eqn. (1)

$$sM(s) = \sum_{i \neq j} \frac{|f_i(s)||f_j(s)|}{|f_C(s)|^2} \cos\left[\eta_i(s) - \eta_j(s)\right] \times \frac{\sin(sR_{ij})}{R_{ij}} \exp(-\tfrac{1}{2}u_{ij}^2 s^2) \quad (1)$$

The sum extends over all atom pairs i, j in the molecule. R_{ij} represents an internuclear distance and u_{ij} the corresponding root-mean-square amplitude of vibration. $f_j(s) = |f_j(s)|\exp[i\eta_j(s)]$ is the complex atomic scattering factor of atom j.

Radial distribution (RD) functions were calculated by Fourier inversion of experimental and theoretical intensity functions after multiplication with the artificial damping function $\exp(-ks^2)$.

STRUCTURE ANALYSES

The interpretation of the peaks in the radial distribution curve for $R < 2.7$ Å is independent of the conformational arrangement. The peak at 1.1 Å represents the carbon hydrogen bond distances, while the peak at 1.4 Å contains contributions from the various carbon carbon bond distances. Non-bonded carbon hydrogen and carbon carbon distances over one valence angle is found at 2.14 Å and 2.5 Å, respectively.

Starting parameters for the bond distances were assigned by comparing experimental and theoretical autocorrelation power spectra.[3] In the electron diffraction studies of *cis* and *trans* isomers of 1,3,5-hexatriene [4,5] it was possible to show that the length of the central carbon carbon double bond was slightly different from the terminal ones. In the present case it is more complicated to determine the bond distances accurately as introduction of the methyl group destroys the symmetry in the molecule and adds two new types of bond distances. From the study of autocorrelation power spectra it was not possible to distinguish the central CC double bond from the terminal ones. In the following the lengths of the three CC double bonds were therefore assumed to be equal.

The outer part of the RD curve contains information about the overall conformation of the molecule. Calculation of a theoretical RD function corresponding to a planar carbon skeleton for *cis*-2-methyl-1,3,5-hexatriene was not in agreement with the experimental RD function, and this model was therefore rejected.

The conformation problem was attacked by making graphs of the nonbonded carbon carbon interatomic distances as functions of the C_2-C_3 and C_4-C_5 torsional angles. As the RD function showed no peak beyond the complex at about 4.5 Å that could clearly be attributed to a distance between carbon atoms, it was first assumed that torsional angles at both $C_{sp^2}-C_{sp^2}$ single bonds were different from 180° (*s-anti*). It was possible to find a model that fitted this description and that converged in the least squares refinement process. The implied torsional angles did refine in the least squares analysis and gave values of about 133° and 93° for the C_2-C_3 and C_4-C_5 torsional angles, respectively. The corresponding radial distribution curve is shown in Fig. 3, A. It is seen that the area of the peaks in the 3.0—4.0 Å region is considerably larger on the theoretical RD curve. The discrepancy might be somewhat diminished by altering the envelope [2] of the experimental RD curve, but is still significant. Besides it was not possible to get good correspondence between experimental and theoretical data in the region around 4.5 Å. Other models were therefore also tested.

If one of the torsional angles around C_2-C_3 or C_4-C_5 corresponds to *s-anti* conformation, the longest carbon carbon distance will appear

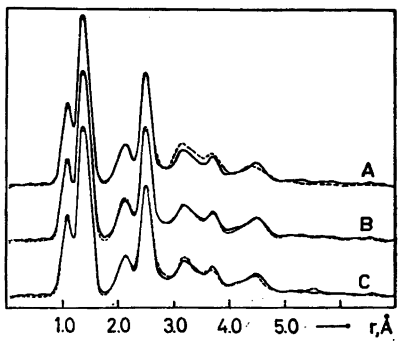

Fig. 3. cis-2-Methyl-1,3,5-hexatriene. Experimental (—) and theoretical (---) radial distribution functions. Artificial damping constant $k = 0.0015$ Å^2. The theoretical data correspond to A: Model I, B: Model II and C: Model III.

beyond the peak at 4.5 Å on the RD curve, probably around 5.6 Å. Even if no peak is clearly recognizable on the experimental RD curve, it is fully possible that a long carbon carbon non-bonded distance with large vibrational amplitude might give contribution in this region.

Models with *s-anti* conformation at the C_4-C_5 bond were clearly superior to those with *s-anti* conformation at the C_2-C_3 bond. This observation is in agreement with what would be expected, as more strain will be relieved by rotation around the C_2-C_3 bond than by a similar effect at the C_4-C_5 bond.

Inspection of a chart showing the distribution of CC nonbonded distances as functions of the C_2-C_3 dihedral angle indicated that a dihedral angle corresponding to *s-gauche* conformation at the C_2-C_3 bond should give fairly good correspondence with peaks on the experimental RD curve. A molecular model corresponding to this conformation (Model B) converged in the least squares analyses, and it was possible to refine the C_2-C_3 as well as the C_4-C_5 dihedral angles. However, it is not surprising that it was also possible to get good correspondence between theoretical and experimental data for a model that differed from the one described above in that the C_2-C_3 dihedral angle is about 120°, corresponding to *anti*-clinal conformation (Model C). The main difference in electron-diffraction data from molecules corresponding to Model B and Model C is in the relative scattering power of a methyl and a methylene group as these are interchanged in the two models. The prospect of distinguishing these two models was therefore not very promising.

The two molecular models discussed above were treated independently. During the structure refinements the following assumptions were made in addition to those discussed above for the CC bond distances: all $C=C-H$ angles involving the terminal methylene groups were set equal, $\angle C_3=C_4-H_4$ was supposed to be equal to $\angle C_4=C_3-H_3$, the three-fold axes of the methyl group was supposed to coincide with the C_7-C_2 bond and one of the hydrogens in the methyl group was supposed to be eclipsed with the $C_1=C_2$ double bond.

When these assumptions were made the geometry of the molecular structure is given by the following 16 parameters:

Five bond distances:
$C=C$, C_2-C_3, C_2-C_7, C_1-H_1 and C_7-H_7

Five CCC bond angles:
$\angle C_1=C_2-C_3(\alpha_1)$, $\angle C_2-C_3=C_4(\alpha_2)$,
$\angle C_3=C_4-C_5(\alpha_3)$, $\angle C_4-C_5=C_6(\alpha_4)$,
$\angle C_1=C_2-C_7(\alpha_5)$

Four CCH bond angles:
$\angle C_2=C_1-H_1(\gamma_1)$, $\angle C_3=C_4-H_4(\gamma_2)$,
$\angle C_2-C_7-H_7(\gamma_3)$, $\angle C_6=C_5-H_5(\gamma_4)$

Two dihedral angles:
$\angle C_1=C_2-C_3=C_4(\mathrm{ROT}_1)$ and
$\angle C_3=C_4-C_5=C_6(\mathrm{ROT}_2)$

It was not possible to vary all the bond angles simultaneously in the least squares refinements. This problem was solved by picking out some of the bond angles and keeping these constant within a least squares run. These bond angles were studied by running several least squares programs simultaneously. In each run all starting parameters were identical except for the bond angle that was being studied and that was systematically varied within the expected range. The squared error sums and the standard deviations of the parameters that were refined in the least square process were studied in order to find the best value for each of the bond angles in question. This process was repeated until selfconsistency. The results were practically independent of which of the bond angles that were picked out and treated as described above.

Table 1. cis-2-Methyl-1,3,5-hexatriene. Results obtained by least squares refinements of the molecular intensity data. The two models correspond to *syn*-clinal (II) and *anti*-clinal (III) conformations at the C_2-C_3 bond. The numbers in brackets are standard deviation values.

Distance	II R_a, Å	II u, Å	III R_a, Å	III u, Å
C=C	1.3445(5)	0.0391(9)	1.3445(6)	0.039
C_2-C_3	1.4616(10)	0.0462(33)	1.4653(23)	
C_2-C_7	1.5148(20)	0.0459(44)	1.5080(41)	
$C_{sp}-H$	1.0914(13)	0.0775	1.0915(18)	
$C_1\cdots C_7$	2.4461			
$C_1\cdots C_3$	2.4619			
$C_4\cdots C_6$	2.4840			
$C_3\cdots C_5$	2.5172	0.0600		
$C_2\cdots C_4$	2.5305			
$C_3\cdots C_7$	2.5766			
$C_2\cdots C_5$	3.1490	0.1300[a]		
$C_1\cdots C_4$	3.2071	0.1000[a]		
$C_1\cdots C_5$	3.4040	0.1800[a]		
$C_4\cdots C_7$	3.6932	0.0800[a]		
$C_3\cdots C_6$	3.7304	0.0800[a]		
$C_5\cdots C_7$	4.3136	0.1300[a]		
$C_2\cdots C_6$	4.4750	0.0850[a]		
$C_1\cdots C_6$	4.6104	0.0900[a]		
$C_6\cdots C_7$	5.6558	0.2000[a]		
	II		III	
$\angle\alpha_1$	122.6 (0.3)°		128.3 (1.2)°	
$\angle\alpha_2$	128.7 (0.3)°		128.4 (0.5)°	
$\angle\alpha_3$	127.5°		126.5°	
$\angle\alpha_4$	124.5°		123°	
$\angle\alpha_5$	117.5°		118.5°	
$\angle\gamma_1$	119.1 (0.7)°		116°	
$\angle\gamma_2$	114°		115°	
$\angle\gamma_3$	110.5°		110.5°	
$\angle\gamma_4$	116°		115°	
$\angle ROT_1$	58.0 (0.8)°		115.6 (1.8)°	
$\angle ROT_2$	193.1 (4.6)°		197.4 (6.7)°	

[a] Assumed value.

Table 1 shows results obtained for the two models under consideration. Theoretical RD curves corresponding to the parameters listed in Table 1 for Models B and C are presented in Fig. 3. The correspondence between experimental and theoretical RD curves is clearly best for Model B. Only in the region around 4.0 – 4.2 Å do the theoretical data for Model C give a better fit.

There is no doubt that it will be possible to improve the fit between the theoretical RD curve for Model C and the experimental RD curve by adjusting some of the u values for non-bonded CC distances. Most of the u values used so far were estimated by analogy from similar molecules, and it is of course possible that the estimates have been better for Model B than for Model C. In order to increase the objectivity when comparing the three models it was decided to calculate the mean vibrational amplitudes for the three models that have been discussed for *cis*-2-methyl-1,3,5-hexatriene, using Gwinn's method.[7,8] The calculations were based on force field parameters published by Allinger *et al.*[9] Even if the resulting u values for the long distances might be inaccurate, the distribution between small and large vibrational amplitudes within one model should be correct. The quality of the calculated u values for the three models should also be the same. If the three models were compared using least squares refinements and the calculated mean vibrational amplitudes, they should therefore be judged on an objective scale.

Table 2. cis-2-Methyl-1,3,5-hexatriene. Calculated mean vibrational amplitudes for the carbon carbon interatomic distances that vary with torsion around the C_2-C_3 and C_4-C_5 bonds. The calculations are carried out for three different conformations.

Distance	A R_a, Å	u, Å	B R_a, Å	u, Å	C R_a, Å	u, Å
$C_2\cdots C_5$	3.08	0.1534	3.13	0.1535	3.15	0.1535
$C_1\cdots C_4$	3.11	0.1292	3.20	0.1218	3.63	0.0882
$C_1\cdots C_5$	3.20	0.2218	3.40	0.2091	4.20	0.1629
$C_4\cdots C_7$	3.71	0.0882	3.67	0.0933	3.15	0.1290
$C_3\cdots C_6$	3.41	0.1079	3.75	0.0769	3.75	0.0769
$C_5\cdots C_7$	4.36	0.1578	4.26	0.1636	3.33	0.2148
$C_2\cdots C_6$	3.73	0.1865	4.47	0.1520	4.50	0.1520
$C_1\cdots C_6$	3.86	0.2370	4.68	0.2304	5.52	0.1666
$C_6\cdots C_7$	4.71	0.2167	5.56	0.1677	4.59	0.2396

A: ROT_1, 50°; ROT_2, 90°.
B: ROT_1, 60°; ROT_2, 180°.
C: ROT_1, 120°; ROT_2, 180°.

Table 3. cis-2-Methyl-1,3,5-hexatriene. Parameters determined from least squares intensity refinements for three different conformations, when theoretically calculated mean vibrational amplitudes were applied.

Parameter	I	II	III
C=C	1.3450(9) Å	1.3446(7)	1.3439(7)
C_2-C_3	1.4631(15) Å	1.4631(15)	1.4615(15)
C_2-C_7	1.5327(36) Å	1.5158(32)	1.5149(31)
C_1-H_1	1.0903(22) Å	1.0893(18)	1.0889(18)
$\angle C_2-C_3=C_4$	124.5(0.6)°	126.7(0.5)°	128.2(0.6)°
$\angle C_1=C_2-C_3$	124.3(0.6)°	123.4(0.5)°	128.9(0.7)°
$\angle C_2=C_1-H_1$	118.1(1.7)°	119.6(1.3)°	119.9(1.3)°
$\sum_i w_i \Delta_i^2$	0.471×10^5	0.320×10^5	0.321×10^5
ROT_1	50°	60°	120°
ROT_2	90°	180°	180°

The number in brackets are standard deviations as resulting from the least squares refinements.

Table 4. Comparison of bond distances in structurally similar molecules. The distances are given in Å as R_a values.

	C=C	$C_{sp^2}-C_{sp^2}$	$C_{sp^2}-C_{sp^3}$	$C_{sp^2}-H$	$C_{sp^3}-H$
cis-2-Methyl-1,3,5-hexatriene[b]	1.345	1.462	1.515	1.091	1.101
trans-2-Methyl-1,3,5-hexatriene [13]	1.348	1.456	1.510	1.094	1.104
cis-1,3,5-Hexatriene [5]	1.345[a]	1.462		1.090	
trans-1,3,5-Hexatriene [4]	1.347[a]	1.458		1.104	
1,3-Butadiene [12]	1.344	1.467			
trans-trans-3,4-Dimethyl-2,4-hexadiene [6]	1.349	1.479	1.521		1.119
cis-cis-3,4-Dimethyl-2,4-hexadiene [6]	1.350	1.473	1.521		1.117

[a] Average value.
[b] Present study.

The calculated mean vibrational amplitudes for the carbon carbon non-bonded distances of the three models are listed in Table 2. As might be expected the u values calculated for Model A are on average somewhat larger than those for the other models.

The results of the least squares refinements of the three models, when calculated mean vibrational amplitudes were applied, are presented in Table 3. In accordance with earlier obtained results Model A is clearly inferior to the other models. The squared error sums and standard deviations for the varied parameters were essentially the same for Model B and Model C. The results will be discussed below.

The outer, conformation-dependent part of the RD curves with calculated mean vibrational amplitudes and based on the parameters listed in Table 3, are shown in Fig. 4.

DISCUSSION

The bond distances obtained for *cis*-2-methyl-1,3,5-hexatriene are compared with structurally similar molecules in Table 4. The bond distances for this molecule are in especially good agreement with results obtained for bond distances in *cis* and *trans* isomers of 1,3,5-hexatriene,[4,5] both of which are found to have planar conformation. This lend support to the view that conjugation effects are of minor importance for the length of a single bond between two sp^2-hybridized carbon atoms.[10]

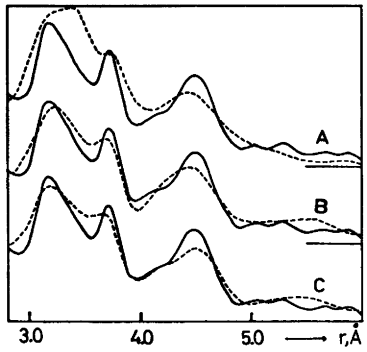

Fig. 4. cis-2-Methyl-1,3,5-hexatriene. The outer, conformation dependent part of the radial distribution functions for Model A, Model B, and Model C. The theoretical RD functions are based on the parameters listed in Table 3 and on calculated mean vibrational amplitudes.

The distribution of C=C–C bond angles may be seen from Table 1 (Model B). The fairly large values for $\angle C_2-C_3=C_4$ and $\angle C_3=C_4-C_5$ should be noted. These angles appear to be somewhat larger than corresponding angles in *cis*-2-butene and *cis*-1,3,5-hexatriene. In both the latter cases the relevant angles were about 126°. The differences can, however, not be claimed to be significant.

When the results obtained for Models B and C (Tables 1 and 3) are compared, one should notice the large difference in the $C_1=C_2-C_3$ bond angle which is found for both approaches. For Model B this bond angle is found to be about 123° while for Model C the angle is about 128°. C=C–C bond angles in comparable structural environments are usually observed to be in the 122° – 124° range. The result obtained for this bond angle in Model C is therefore unreasonable. If, however, one should try to fit a false molecular model with a C_2-C_3 dihedral angle of about 120° to data corresponding to a molecule where the dihedral angle actually is about 60°, one would expect to observe an increased $C_1=C_2-C_3$ angle to account for the difference in magnitude between the $C_1=C_2$ and C_2-C_7 bonds. Even if the observations made above cannot be considered as decisive evidence, they indicate that Model B is slightly preferred over Model C.

Acknowledgement. The sample of *cis*-2-methyl-1,3,5-hexatriene used in the present study was kindly provided by the late professor Richard B. Turner, Rice University, Houston, Texas, who also originally suggested this research project, and took deep interest in the investigation. The authors want to thank cand.real. A. Almenningen for making all the electron-diffraction diagrams. Financial support from *Norges almenvitenskapelige forskningsråd* is gratefully acknowledged.

REFERENCES

1. Bastiansen, O., Hassel, O. and Risberg, E. *Acta Chem. Scand. 9* (1955) 232.
2. Andersen, B., Seip, H. M., Strand, T. G. and Stølevik, R. *Acta Chem. Scand. 23* (1969) 3224.
3. Trætteberg, M. and Bonham, R. A. *J. Chem. Phys. 42* (1965) 587.
4. Trætteberg, M. *Acta Chem. Scand. 22* (1968) 628.
5. Trætteberg, M. *Acta Chem. Scand. 22* (1968) 2294.

6. Trætteberg, M. *Acta Chem. Scand. 24* (1970) 2295.
7. Gwinn, W. D. *J. Chem. Phys. 55* (1971) 477.
8. Stølevik, R., Seip, H. M. and Cyvin, S. J. *Chem. Phys. Letters 15* (1972) 263.
9. Allinger, H. L. and Sprague, J. T. *J. Amer. Chem. Soc. 94* (1972) 5734.
10. Trætteberg, M. *Doctoral Thesis*, University of Trondheim 1969.
11. Almenningen, A., Anfinsen, I. M. and Haaland, A. *Acta Chem. Scand. 24* (1970) 43.
12. Haugen, W. and Trætteberg, M. *Selected Topics in Structure Chemistry*, Universitetsforlaget, Oslo 1967.
13. Trætteberg, M. and Paulen, G. *Acta Chem. Scand. A 28* (1974). *In press.*

Received July 25, 1973.

Acta Chemica Scandinavica A 28 (1974) 8—12

Absorption of Circularly Polarized Light by the $^4A_2 \rightarrow {}^2E$ and $^4A_2 \rightarrow {}^2T_2$ Transitions of Ruby in Strong Magnetic Fields

I. TRABJERG and H. U. GÜDEL

Chemical Laboratory IV, Universitetsparken 5, DK-2100 Copenhagen Ø, Denmark

The longitudinal Zeeman effects exhibited by the R and B lines of ruby have been measured at 80 K using circularly polarized light and magnetic fields up to 200 k gauss. By employing as a standard the EPR-determined value for $g\|(^4A_2)$ of 1.984 and a method that is independent of the absolute magnitude of the magnetic field, analysis of the R lines gives $g\|(\bar{E}(^2E)) = 2.49 \pm 0.02$, $g\|(2\bar{A}(^2E)) = 1.41 \pm 0.02$ and $\Delta = 0.37 \pm 0.03$ cm^{-1}. Corresponding results derived from the B lines are: $g\|(2\bar{A}(^2T_2)) = 0.58 \pm 0.02$ and $g\|(\bar{E}_a(^2T_2)) = 2.90 \pm 0.05$, consistent with values published previously.

1. INTRODUCTION

The observation of magnetic circular dichroism (MCD) is increasingly being used as a supplementary method to absorption spectroscopy in the study of transition metal complexes.[1] In the usual MCD experiments the magnetic field is constant, the polarization of the light beam is modulated between left-handed (LH) and right-handed (RH), and the difference in the absorption for the two polarizations is recorded. It is, of course, possible to measure the magnetic circular dichroism simply by performing a longitudinal Zeeman experiment with circularly polarized radiation in which Zeeman absorption spectra are recorded separately for the two polarizations LH and RH using a procedure analogous to that normally employed in crystal spectroscopy to measure linear dichroism. In theory, the difference between these two spectra is the MCD spectrum, while their sum gives the linear polarized axial Zeeman absorption spectrum. The method has the advantage that Zeeman components with $\Delta M = +1$ appear only in LH spectra while those with $\Delta M = -1$ appear only in RH spectra. Estimates of the positions of such components can be made more easily than can the splittings of incompletely separated lines. In addition, measurement of line intensity is facilitated by the removal of light of opposite polarization from the background.

The Zeeman absorption spectrum due to the $^4A_2 \rightarrow {}^2E$ transition of Cr^{3+} in $2[Cr(en)_3Cl_3].KCl.6H_2O$ has recently been investigated using circularly polarized light,[2] and accurate g values for the excited states were derived. It seemed worthwhile to extend this study to other crystals containing Cr^{3+} in trigonal coordination, and also to other transitions found in these systems. The present paper describes some high magnetic field spectra of the spin-forbidden $^4A_2 \rightarrow {}^2E$ and $^4A_2 \rightarrow {}^2T_2$ transitions of Cr^{3+} in the host lattice Al_2O_3 (ruby). Since both these transitions have been examined both theoretically [3-6] and by other experimental techniques [7-11] the project appeared to be a good test of our method as well as existing theoretical models.

2. THEORY

The combined action of a trigonal crystal field component and the spin-orbit coupling split the ^2E state of Cr^{3+} in ruby into two Kramers doublets, $\bar{E}$ and $2\bar{A}$. The $\bar{E}$ sub-level lies at a lower energy than does the $2\bar{A}$ level.[3,8] Similarly the $^2T_2$ state is split into three components $2\bar{A}$, $\bar{E}_a$ and $\bar{E}_b$, while the $^4A_2$ ground state is split into two Kramers doublets separated by 0.38 cm^{-1}.[7] $g\|$ values (H parallel to the threefold axis) for all these levels except

$E_b(^2T_2)$ have been estimated from the results of Zeeman experiments using linearly polarized light.[7,9,10] The published experimental values vary over a broad range. Of these only $g\|(\bar{E}(^2E))$ has been determined very accurately by a paramagnetic resonance technique.[8] The $^4A_2 \rightarrow {}^2T_2$ system of transitions has been studied in a low field MCD experiment conducted at room temperature and at low resolution.[11]

The crystal field theory for this chromophore, first treated by Sugano and Tanabe,[3] has been continuously extended with the concurrent introduction of more and more adjustable parameters. Sugano and Peter,[4] for example, included parameters for covalency and for mixing between the t_2^3 and t_2^2e configurations. The earlier work has recently been criticized and new g values have been computed using a numerical method based on the use of a set of functions of the complete d^3 configuration.[6] The relatively large errors in some of the experimental data have made comparisons of these theories quite difficult.

3. EXPERIMENTAL

Two crystals containing 0.15 mol % and 0.41 mol % of Cr^{3+}, respectively, were cut into plates with faces perpendicular to the c axis. They were oriented using X-ray diffraction methods. The spectroscopic technique was as described previously;[2] that is, the sample temperature was 77 K. The R lines ($^4A_2 \rightarrow {}^2E$) were recorded on 35 mm Kodak High Speed Infrared Film and on Kodak 103F plates. For the B lines ($^4A_2 \rightarrow {}^2T_2$) Ilford HP3 plates and Polaroid 4 × 5 Land Film, Type 57, were used. The magnetic field was calibrated using the ground state $g\|$ value of ruby determined by EPR.[12]

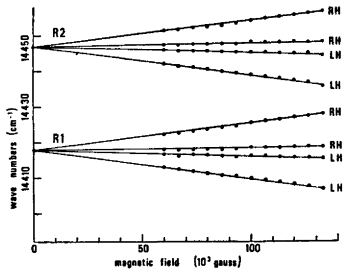

Fig. 1. Splitting patterns observed for the R lines. R1 = $^4A_2 \rightarrow \bar{E}$ (^2E); R2 = $^4A_2 \rightarrow \bar{2}A(^2E)$.

4. RESULTS FROM THE R-LINES

Figs 1 and 2 show the experimentally observed splitting pattern of the R lines and the corresponding transition diagram, respectively. From the order of the components with decreasing energy, namely RH, RH, LH, LH for both R1 and R2, it follows that $g\|(2\bar{A}(^2E)) < g\|(^4A_2) < g\|(\bar{E}(^2E))$. Each pair of LH − RH exposures permits field-independent determinations of the ratios $g\|(\bar{E}(^2E))/g\|(^4A_2)$ and $g\|(2\bar{A}(^2E))/g\|(^4A_2)$ and of the zero-field splitting. By using $g\|(^4A_2) = 1.984$ [12] and the averages from 13 pairs of exposures, the $g\|$ values shown in Table 1 were derived. The $g\|(\bar{E}(^2E))$ result presented here is within two estimated standard deviations of the low field value determined by EPR (2.445 [8]). The agreement of the zero field splitting Δ with corresponding values determined from EPR and a low field Zeeman experiment is also good.[7] However, the present g factors do not agree particularly well with values previously obtained from high field Zeeman experiments with linearly polarized light.[9]

The present results do not show any evidence of non-linearity of the splitting with the magnetic field for fields between zero and 170 k gauss.

A LH-RH pair of microdensitometer tracings is shown in Fig. 3. The relative intensities do not resemble those calculated,[3] even with the Boltzmann distribution accounted for.

Figs 2 and 3 clearly demonstrate that in this case more information can be gained using circularly polarized rather than linearly polarized light. The two heavily overlapping

Table 1. Δ values and numerical values for $g\|$.

	Ours	Ref. 9	Ref. 6	Ref. 4
$g\|(\bar{E}(^2E))$	2.49 ± 0.02	2.56 ± 0.16	2.67	2.59
$g\|(2\bar{A}(^2E))$	1.41 ± 0.01	1.63 ± 0.13	1.21	1.23
$g\|(2\bar{A}(^2T_2))$	0.58 ± 0.02	0.69 ± 0.09	0.65	0.96
$g\|(\bar{E}_a(^2T_2))$	2.90 ± 0.05	2.97 ± 0.15	3.39	2.97
Δ in cm^{-1}	0.37 ± 0.03		0.31	0.16

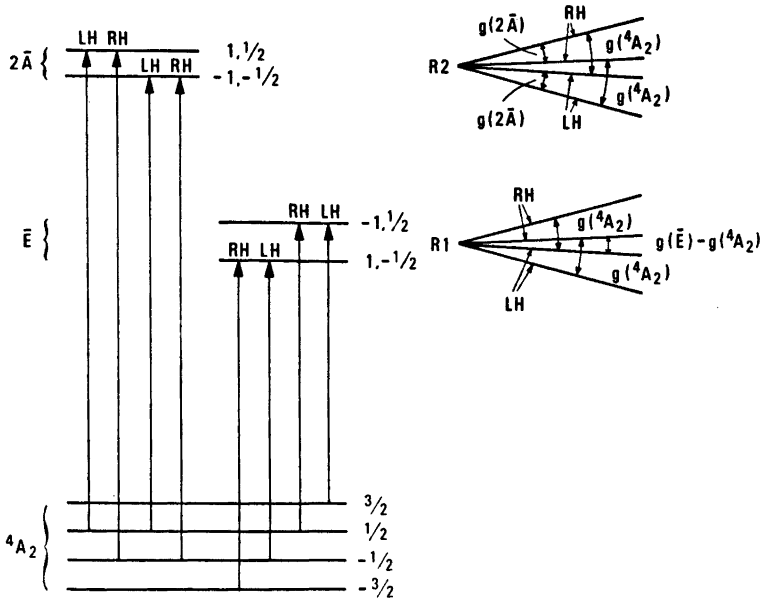

Fig. 2. Transition diagram for the R lines.

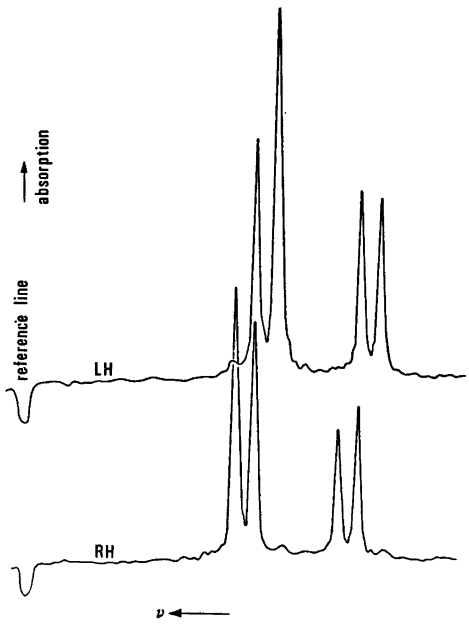

Fig. 3. Microdensitometer tracing of the R lines at H = 97 k gauss.

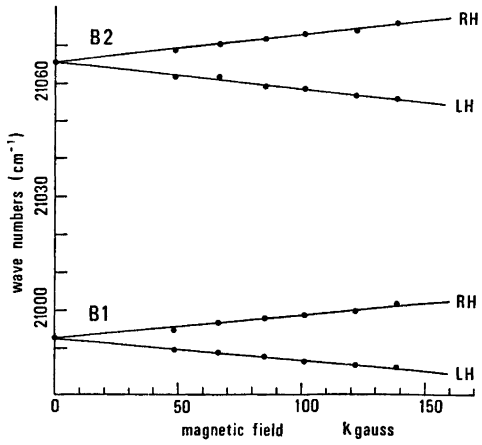

Fig. 4. Splitting patterns observed for the B lines.

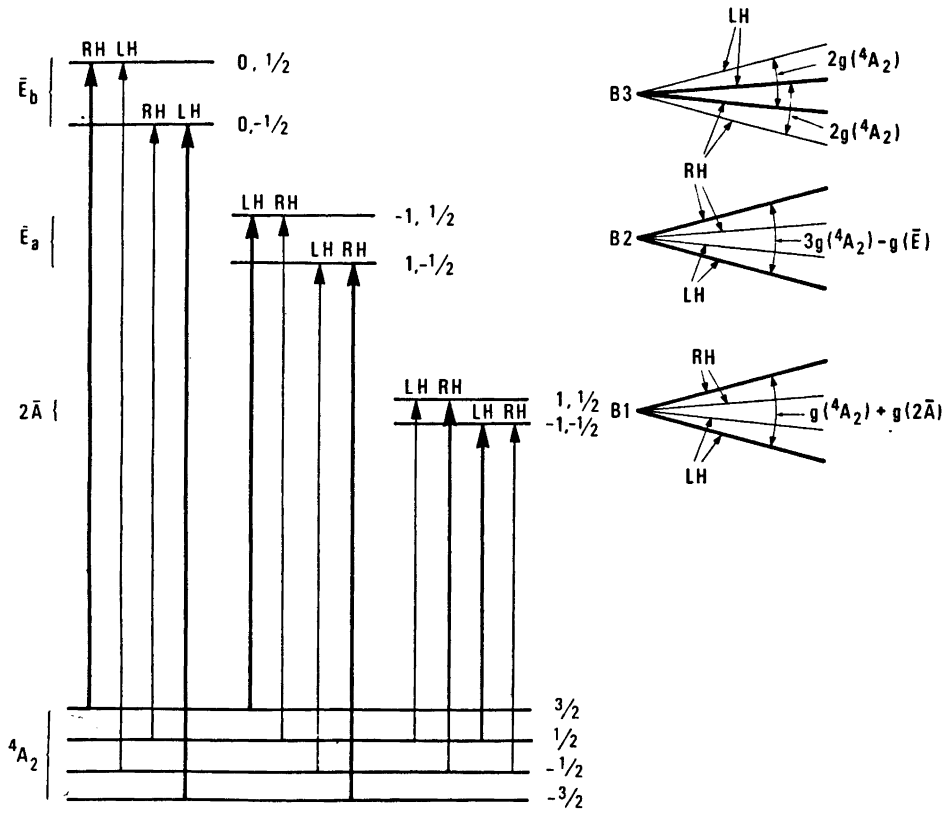

Fig. 5. Transition diagram for the B lines.

inner components in both R1 and R2 Zeeman patterns are of opposite polarization and can thus be resolved. This has led to $g\|\|$ values which are more accurate than those resulting from corresponding Zeeman experiments using linearly polarized light.[9] The separation also enables reliable estimates of the relative intensities of the components to be made.

5. RESULTS FROM THE B-LINES

The splitting pattern of the B1 and B2 lines is shown in Fig. 4 and the corresponding transition diagram for all three B lines is given in Fig. 5. As expected for both B1 and B2 the high energy component has RH polarization. The splitting pattern of B3 could not be fully resolved but it was possible to establish beyond doubt that a LH component is on the high energy side, in accordance with Fig. 5 and an earlier low field MCD experiment. A straight line plotted through the experimental points obtained for magnetic fields up to 140 k gauss leads to the g values shown in Table 1. These are in agreement with those obtained previously.[9] To determine $g\|\|(\bar{E}_b(^2T_2))$ either a very strong magnetic field or a careful analysis of the line shape is necessary. Neither could be achieved under the conditions of the present study.

From Figs 4 and 5 it is clear that for B1 and B2 no overlapping lines can be resolved using circularly polarized light. Only the sign of ΔM has not already been determined earlier.[9]

6. DISCUSSION

Our experimental results are seen to be in better overall agreement with the crystal field theoretical predictions of Sugano and Peter [4] than with those made by Macfarlane.[6] Since

the number of adjustable parameters was six in both these calculations, the present experimental ruby values do not appear to substantiate Macfarlane's claim that his perturbation treatment gives accurate results. However, as Macfarlane points out, comparison with other systems is necessary before a definite assessment can be made; there does, in fact, seem to be better agreement between his values and experimental results obtained from other Cr^{3+}-doped lattices.

7. CONCLUSION

Measurements of the longitudinal Zeeman effect of the R and B lines of ruby using circularly polarized light have given information which previously had been obtained only from two independent experiments. The polarizations of all the observed transitions are in accordance with the theoretical predictions. There is no reason to believe that the $g_{\|}$ values are more accurate than those previously determined from "conventional" Zeeman experiments.

Acknowledgement. The authors wish to thank Professor C. J. Ballhausen for helpful discussions and Dr. K. J. Watson for revising the text of this paper.

REFERENCES

1. *E.g.* Schatz, P. N. and McCaffery, A. J. *Quart. Rev. 23* (1969) 552; *Errata, Ibid. 24* (1970) 329.
2. Güdel, H. U., Trabjerg, I., Vala, M. and Ballhausen, C. J. *Mol. Phys. 24* (1972) 1227.
3. Sugano, S. and Tanabe, Y. *J. Phys. Soc. Jap. 13* (1958) 880.
4. Sugano, S. and Peter, M. *Phys. Rev. 122* (1961) 381.
5. Macfarlane, R. M. *J. Chem. Phys. 39* (1963) 3118.
6. Macfarlane, R. M. *Phys. Rev. B 1* (1970) 989.
7. Sugano, S. and Tsujikawa, I. *J. Phys. Soc. Jap. 13* (1958) 899.
8. Geschwind, S., Collins, R. J. and Schawlow, A. L. *Phys. Rev. Lett. 3* (1959) 545.
9. Aoyagi, K., Misu, A. and Sugano, S. *J. Phys. Soc. Jap. 18* (1963) 1448.
10. Zakhardhenya, B. P., Sibilev, A. I., Kanskaya, L. M. and Ryskin, A. Ya. *Sov. Phys. – Solid State 3* (1962) 2563.
11. Aoyagi, K., Kajiura, M. and Uesugi, M. *J. Phys. Soc. Jap. 25* (1968) 1387.
12. Ref. 27 in Ref. 6.

Received August 13, 1973.

Acta Chemica Scandinavica A 28 (1974) 13—19

A Stopped-flow Kinetic Study of the Copper(II) Cyanide Reaction in Water and in Aqueous Methanol

GWYNETH NORD and HANS MATTHES

Department I, Inorganic Chemistry, H. C. Ørsted Institute,
University of Copenhagen, Universitetsparken 5, DK-2100 Copenhagen Ø, Denmark

The copper(II) cyanide reaction is second order in copper(II) and inversely proportional to the uncomplexed cyanide. This is attributed to reaction between $Cu(CN)_3^-$ and $Cu(CN)_4^{2-}$. $k_1 = k/[CN^-]$, where k, the observed second order rate constant at 25°C, decreases from 470 $M^{-1}s^{-1}$ in water to 5.6 $M^{-1}s^{-1}$ in 50 % and to 1.23 $M^{-1}s^{-1}$ in 80 %, by weight, methanol. The measurements were made at 25°C, 15°C, and 0°C and at an ionic strength of 0.1 M. The energy of activation in water is 6 ± 1 kcal M^{-1}. The results are correlated with those of earlier workers for water, aqueous methanol, and also aqueous ammonia.

The rate of the reaction

$$2\ Cu(CN)_4^{2-} \rightarrow C_2N_2 + 2\ Cu(CN)_3^{2-} \qquad (1)$$

has previously been measured at low temperatures in aqueous methanol.[1,2] In water the reaction is fast and has hitherto been followed in the presence of a competing ligand [3,4] and in a buffered solution of HCN.[5] The reaction is second order in copper(II).*

The determination of the stoicheiometry and rate, of reactions of labile complexes, usually only enables the composition of the transition state (or reactive intermediate) to be established. However, if alternative pathways lead to impossibly high rate constants, or involve species with improbably large coordination numbers, then it should be possible to identify the reactants. We have studied the copper(II)-cyanide reaction using concentrations which, at about 25°C, gave rates suitable for measurement by the stopped-flow technique. We combine our results with those of earlier workers and attempt to assess the validity of the mechanism we have used in order to correlate all the available experimental data.

EXPERIMENTAL

The chemicals were the same and the solutions were standardised in the same way as in previous papers from this laboratory.[1,2] Ionic strengths were adjusted with sodium *p*-toluene sulphonate.

Kinetic measurements were made with the apparatus described in Ref. 6. The optical absorbance at 535 nm was measured for solutions produced by mixing equal volumes of copper(II) *p*-toluene sulphonate and of sodium cyanide. For any one solution, at constant flow rate, the initial plateau absorption (before stopping the flow) was reproducible, as also was the rate of decay of this absorption (see Figs. 1a and 1b). Second order plots were linear and were constructed as illustrated in Fig. 2. In all cases, some of the copper reacted during mixing and before measurement. This amount of copper was particularly large for the aqueous solutions which were therefore investigated over a series of flow rates. Fig. 3 illustrates that the rate of the homogeneous reaction was independent of flow rate and of stopping time. It is the plateau optical density divided by $\varepsilon = 213$ for minimum initial reduction which is reported in the tables.

RESULTS AND DISCUSSION

The copper(II) in our solutions is almost entirely present as $Cu(CN)_4^{2-}$ (Ref. 1) and the absorbance at 535 nm can be entirely attributed to this species (Refs. 2, 7). Tables 1 and 2 give the total copper concentration in the mixed

* The data from Ref. 4, which were interpreted by the authors in the terms of a first order rate law is recalculated and discussed later in this paper.

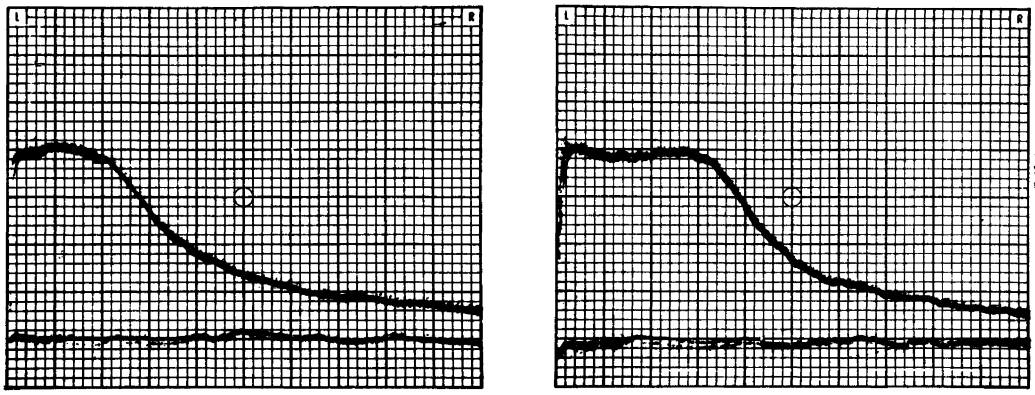

Fig. 1(a) and *Fig. 1(b)*. Oscilloscope traces for Series 24, Table 2, see text.

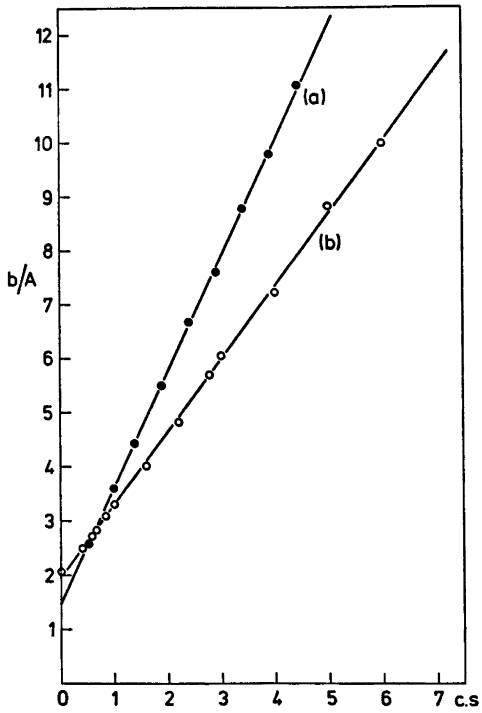

Fig. 2. Second order plots. Ordinate b/A where A is absorbance, abscissa cs where s is seconds. (a) Series 15, Table 1; c = 0.05, b = 0.464. (b) Series 19, Table 1; c = 0.10, b = 0.716.

solutions (C_{Cu}); the uncomplexed cyanide concentration $[CN^-] = (C_{CN^-} - 4C_{Cu})$; together with $\Delta(1/A)/\Delta t = S$, where A is the absorbance per cm cell length (calculated from the measured absorbance and a calibration curve constructed using ferroin solutions), t is seconds. S is therefore equal to k/ε where ε is the molar absorbance of $Cu(CN)_4^{2-}$ and $k(M^{-1}s^{-1})$ the rate constant with respect to the reduction of this species.

The rate constants have an inverse dependence on $[CN^-]$ (see Tables 1 and 3) but S is constant during each run (see Figs. 1 – 3). This means that $[CN^-]$ is constant during any one run in accord with the stoicheiometry given in eqn. 1. Changes due to the equilibrium

$$Cu(CN)_3^{2-} + CN^- \rightleftharpoons Cu(CN)_4^{3-};\ K_4(Cu(I)) \qquad (2)$$

are small.

The value taken for the molar extinction coefficient ε for $Cu(CN)_4^{2-}$, used to calculate $[Cu(CN)_4^{2-}]_0$ given in the tables, was 213 and was obtained in the following way.

It was observed that the plateau absorbance (ΔA_0) decreased, at constant flow rate, with increasing S. For the methanolic solutions (series 1 to 7 in Tables 1 and 3) the amount of this reduction was small enough to allow extrapolation to zero reduction. A plot of $(C_{Cu}/\Delta A_0)^2$ *versus* S is linear and from this ε was calculated to be 213 (intercept $= (1/\varepsilon)^2$; $S \rightarrow 0$). Thus for series 1 to 7, $k = 213\ S\ M^{-1}s^{-1}$. The large amount of initial reduction in aqueous solution precluded accurate extrapolation so that we have used $\varepsilon = 213$ to calculate k throughout. It may be noted that the general trend is the same for all media. This value of 213 is in fair agreement with the results of earlier workers who describe a broad band at 560 nm with ε about 220 at $-30°C$ [7] and λ_{max} 535 nm, ε_{max} 172 at $-70°C$.[2]

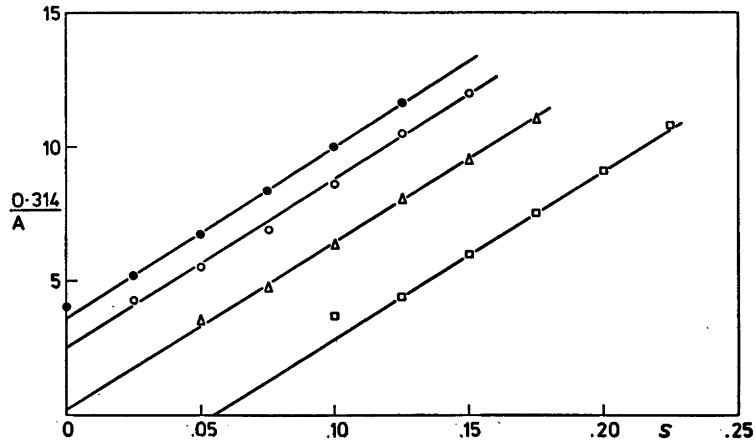

Fig. 3. Series 12, Table 1; see text.

Table 1.

Number of series	Temperature °C	C_{Cu} mM	[CN⁻] mM	S	$[Cu(CN)_4^{2-}]_0$ mM	$10^{-4}k_{obs}$ $M^{-1}s^{-1}$	$10^{-4}k_{calc}$ $M^{-1}s^{-1}$
Solvent is 50 % by weight methanol-water							
1	25	5.020	13.67	1.99 ± 0.02	1.70	0.0425	0.0410
2	25	5.020	9.22	2.76 ± 0.12	1.51	0.0588	0.0608
3	25	5.020	7.02	3.73 ± 0.24	1.32	0.0795	0.0798
Solvent is 80 % by weight methanol-water							
4	25	3.575	15.10	0.406	2.56	0.0087	0.0088
5	25	3.255	9.48	0.784 ± 0.01	1.63	0.0167	0.0145
6	25	3.575	1.85	4.85 ± 0.01	0.85	0.1032	0.1048
7	25	3.575	1.40	7.32	0.94	0.1560	0.1543
Solvent is water							
8	25	2.085	35.4	53.0	1.10	1.130	1.310
9	25	3.150	25.9	60.6	0.70	1.292	1.815
10	25	3.700	22.0	125.5	0.47	2.680	2.140
11	25	4.175	20.8	112.5	0.48	2.400	2.260
12	25	4.175	10.7	204	0.67	4.350	4.400
13	25	4.080	8.58	282	0.38	6.010	5.470
14	15	2.085	35.4	37.1	0.745	0.790	1.004
15	15	4.175	20.8	94.2	0.833	2.020	1.710
16	15	4.170	19.0	97.8	1.03	2.083	1.870
17	15	4.820	11.2	154.0	1.06	3.280	3.170
18	15	4.175	10.7	137.2	1.25	2.925	3.320
19	0	2.085	35.4	20.1	1.58	0.428	0.510
20	0	4.175	20.8	48.8	1.14	1.255	0.868
21	0	4.175	10.7	78.0	0.98	1.660	1.690
22	0	2.085	8.35	96.2	0.80	2.050	2.110

Ionic strength = 0.10 M

Table 2.

Number of series	Number of runs	Ionic strength	C_{Cu} M	[CN⁻] M	S	$Cu(CN)_4]_0$	$k_{obs} \times [CN^-]$
23	1	0.21	0.0118	0.0428	73.2	1.03	667
24	3	0.25	0.1045	0.0517	55 ± 1	3.44	605
25	4	0.50	0.1045	0.0830	33 ± 3	1.54	583
26	1	0.62	0.0047	0.5540	4.44	3.93	523

Solvent water; 15°C.

The rapid reaction during mixing was also observed at low temperatures [1,2] and was attributed [8] to the more rapid reaction of $[Cu(CN)_n]^{(n-2)-}$ with $n < 4$ formed in the inhomogeneous solutions. Since the bulk species is $Cu(CN)_4^{2-}$ and the rate is inversely proportional to $[CN^-]$, then the composition of the transition state in water must be $[Cu_2(CN)_7]^{3-}$ (see Tables 1 to 3). The simplest interpretation of this is that it represents reaction of the bulk copper(II) species, *viz.*: $Cu(CN)_4^{2-}$, with $Cu(CN)_3^-$ formed according to eqn. 3;

$$Cu(CN)_4^{2-} \rightleftharpoons Cu(CN)_3^- + CN^-; K_4^{-1}\,(Cu(II)) \quad (3)$$

Thus

$$k_1 = k_t/K_4(Cu(II)) \text{ (see Table 3)} \quad (4)$$

where k_t is the true rate constant for the reaction between $Cu(CN)_3^-$ and $Cu(CN)_4^{2-}$. The small change in k_1, with change of ionic strength from 0.2 to 0.6 M, parallels that found for the stability constants of other cyanide complexes.*

Using k_1 from series (8 – 13), (14 – 18), and (19 – 22) in Table 1, then the energy of activation, E_A, is 6 ± 1 kcal M^{-1}. Using reaction rate theory, then $E_A = \Delta H^* + RT$, and from the above treatment, $\Delta H^* = \Delta H_4 - \Delta H_t^*$ where

* *E.g.*, K_4(Cu(I)) (eqn. 2) is 200 ($\Delta H_4^\circ = 6.7$ kcal) at 15°C and is, within the experimental error, constant between ionic strengths of 0.2 and 1.0.[9] K_4(Cu(I)) is about 300 at 15°C and an ionic strength of 0.1.[10] K_4(Cu(II)) is of course much larger than this (see text).

Table 3.

Series	Range of [CN⁻] M	Solvent	Rate law: $k = k_1/[CN^-] + k_2/[CN^-]^2$
1 to 3	0.01367 to 0.00702	50 % wt. Methanol – water (25°C)	$k_{calc} = 5.6/[CN^-]$
4 to 7	0.01510 to 0.00140	80 % wt. Methanol – water (25°C)	$k_{calc} = 1.23/[CN^-] + 0.0013/[CN^-]^2$
8 to 13	0.0354 to 0.00858	Water (25°C)	$k_{calc} = 470/[CN^-]$
14 to 18	0.0354 to 0.0107	Water (15°C)	$k_{calc} = 355/[CN^-]$
19 to 22	0.0354 to 0.00835	Water (0°C)	$k_{calc} = 181/[CN^-]$

Table 4. $C_{Cu} = 1.25 \times 10^{-3}$ M; $C_{NH_3} = 12.5$ M. 0°C. Ionic strength 1.0 M with $NaNO_3$. Data from Fig. 1, Ref. 4. For calculation of k see text. $k_{average} = 2.2 \times 10^8$ $M^{-1}s^{-1}$.

	C_{CN^-}/C_{Cu}	C_{CN^-}/C_{NH_3}	k $M^{-1}s^{-1}$	$10^8 k/[CN^-]^4$
a	12	1.2×10^{-3}	11.3	2.48
b	8	8×10^{-4}	2.28	2.28
c	6	6.25×10^{-4}	0.93	2.94
d	5	5×10^{-4}	0.3	1.97

ΔH_t^* is the true activation enthalpy. Similarly, the abnormally low value for the frequency factor corresponding to k_1 results from the composite form of this rate constant.

The only stability constant for Cu(II) – CN^- equilibria which has been reported, is that of Bjerrum and Paterson, who found the decadic logarithm of the overall stability constant (β_4) to be 26.7 in 60 % methanol-water at −45°C. We use this value, later in the discussion, to check the plausibility of the values we now estimate for β_4 in water at 0°C and at 25°C.

For the Cu(II) – CN^- – H_2O system, Baxendale gave graphically recorded results (Figs. 4 and 5, Ref. 5) for 25°C with $[CN^-] \sim 10^{-7}$ and at pH 5.05 and 4.75. He showed that the reaction was second order in copper(II) and that the composition of the transition state, under his conditions, was $[Cu_2(CN)_6]^{2-}$. From his figures we find that $\log k - 6 \log [CN^-] = 43.4$ for both pH. k is the second order rate constant, $M^{-1}\,s^{-1}$, and $[CN^-]$ has been calculated from C_{CN^-} using $pK_{HCN} = 9.21$. Following our interpretation, the reactants either (a) are both $Cu(CN)_3^-$, so that

$$k[Cu(CN)_3^-]^2 = k_t\beta_3^2[CN^-]/(C_{Cu} - ([Cu(CN)_3^-])^2$$

and since $[Cu(CN)_3^-] \ll C_{Cu}$,

then $\log k_t + 2 \log \beta_3 = 43.4$,

or (b) are $Cu(CN)_4^{2-}$ and $Cu(CN)_2$, resulting in the substitution of $\log \beta_4 + \log \beta_2$ for $2 \log \beta_3$. Considering first (a), then since the limiting value of $k_t \approx 10^{10}$, $\beta_3 < 10^{16.7}$. Using the β_4/β_3 ratio of the Cu(II) – NH_3 system [11] we find $\beta_4 \geq 10^{20}$ and $K_4 \approx 10^4$. Considering (b), then an analogous treatment gives $\beta_4 \geq 10^{21}$. In both (a) and (b) $\log \beta_n \times 1/n \approx 5$ and we use this approximated value below. That $\log \beta_4 \approx 20$ is reasonable as it would not be expected to be very different from the $\log \beta_4$ values for Zn(II) and Cd(II), which are 17 and 18, respectively.[12] Also, combining $\log \beta_4 = 20$ at 25°C with $\log \beta_4 = 26.7$ at −45°C gives $\Delta H_{1-4} = -30$ kcal M^{-1} which is about the same as that for Cd(II) (29 kcal M^{-1}). We do not know the solvent effect on β_4 but believe that it cannot be large.

Using K_4 at 24°C = 10^4 then k_t, defined by eqn. 4, for the reaction between $Cu(CN)_4^{2-}$ and $Cu(CN)_3^{2-} \approx 10^7\ M^{-1}s^{-1}$. The decrease in reaction rate with increase in coordination number is also found for other redox reactions involving coordinated CN^- and also Cl^- and has been attributed to stabilisation of the reactive intermediate by bridging.

The data in Refs. 3 and 4 can also be satisfactorily accounted for using $\log \beta_n \times 1/n = 5$. Thus, Tanaka *et al.*[3] measured the rate of cyanide oxidation by copper(II) in the presence of excess ethylenediamine tetraacetate anion (Y^{4-}) and at 25°C with an ionic strength of 0.5 found that

$$-d[CuY^{2-}]/dt = 6.8 \times 10^7 \frac{[CN^-]^4[CuY^{2-}]^2}{[Y^{4-}]} \quad (5)$$

Here the bulk species is CuY^{4-} but with $[CN^-]$ large enough to ensure that $n = 4$ for the very small concentration of $Cu(CN)_n^{(n-2-)}$. We rewrite eqn. 5 as

$$-dC_{Cu}/dt = k_t[Cu(CN)_4^{2-}][CuY^{2-}]$$
$$= k\frac{[CN^-]^4}{[Y^{4-}]} \times C_{Cu}^2 \quad (6)$$

where $\log_{10} k = \log_{10} k_t + \log \beta_4 - \log \beta_{Y^{4-}}$. $\log \beta_{Y^{4-}}$ a is 18.5 [12] so that using $\log \beta_4 \approx 20$ gives $k_t \approx 10^6\ M^{-1}s^{-1}$.

We would expect analogous behaviour for the Cu(II) – CN^- – NH_3 system studied by Duke and Courtney,[4] and therefore reexamined their experimental data as recorded in Fig. 1 of Ref. 4. The results of our calculations are given in Table 4 of the present paper. We find that for solution *a* then a plot of $1/C_{Cu}$ *vs.* t (sec) is linear for all of the 97 % of the reaction measured. Solution *b* gives a similar second order plot for about the first half life, while the other second order rate constants were obtained from initial slopes. We agree with the authors that the transition state contains four cyanide ions but find that it should be formulated as $[Cu_2(CN)_4(NH_3)_n]^{2-}$. Here n is presumably 4 or 5. Substitution of 4 for the coordination number of the bulk species (5) does not affect the following conclusions. From Table 4 and following our treatment,

$$\log \beta_4(CN^-) - \log \beta_5(NH_3) + \log k_t = 8.34 + 5 \log a_{NH_3}.$$

Since $\log \beta_5 + 5 \log_{10} a_{NH_3} = 20.4$ [11] then using $\log \beta_4 \approx 21$ at 0°C gives $k \approx 10^8\ M^{-1-s^1}$ which is again less than the diffusion controlled limiting value. For this NH_3 – CN^- system the rate decreases enormously when the ratio of coor-

dinated cyanide:copper becomes less than two. We therefore believe that the first formed products of the second order reaction are the mixed Cu(I) cyanoammonia complexes $CuCN(NH_3)_n$ and that the probable reactants are both the mixed Cu(II) complex $Cu(CN)_2(NH_3)_2$. Any extra stability (over the statistical values) associated with these mixed complexes would lower the calculated k.

Data in aqueous methanol. In aqueous methanol at 25°C, except at the very lowest [CN⁻], the rate is again dominated by the k_1 term corresponding to reaction of $Cu(CN)_3^-$ with $Cu(CN)_4^{2-}$ (see Table 3). Increasing the concentration of methanol decreases the rate as also was found by Mønsted and Bjerrum.[2] These latter authors observed that, except for very high methanol content, then the linear log k *vs.* D^{-1} relation, theoretically expected, was not strictly obeyed. This behaviour is usual for systems where "specific solvation" can be postulated. Throughout this paper we have adopted the usual convention of omitting solvent molecules and written $Cu(CN)_3^-$ and $Cu(CN)_4^{2-}$ for the reacting species. The maximum coordination number for copper(II) in solution is, however, probably five [13] so that both inner and outer coordinated solvent may play an important role in the transition state. Change in reactivity accompanying change of composition of coordinated solvent would mean that the dependence of rate on methanol content of the solvent would no longer be expected to reflect only macroscopic properties of the solvent, but would also follow the dependence known for activity coefficients of inner solvated ions. This would lead to a decrease of log k proportional to decreasing x where x is the mol fraction of the more strongly coordinated solvent,[14,15] in this case water. The extensive data in Ref. 2 do show this trend. Specific solvation can also explain changes in E_A, which increases from 6 kcal M^{-1} in water to 11.9 kcal M^{-1} in 50 % methanol [2] and to 14 kcal M^{-1} in 80 % methanol.[2]

In neither of the mixtures at −20°C and −28°C was the rate found to be strictly proportional to 1/[CN⁻]. This may reflect the presence of a k_0 term corresponding to reaction between two $Cu(CN)_4^{2-}$ complexes.† Since, however, the low temperature work was made with free cyanide 0.027 to 0.074 M, so that a large fraction of the sodium *p*-toluene sulphonate used to adjust the ionic strength to 0.1 was replaced by cyanide, it may well, as pointed out by the authors, reflect an opposing medium effect.

For 50 % methanol at −28°C then k_1 (as defined in Table 3 and calculated from $k_1 = 5.6$ at 25°C together with $E_A = 11.9$ kcal M^{-1}) is 0.073 $M^{-1}s^{-1}$. The product of the observed rate constant and the free cyanide (k[CN⁻]) is 0.043, 0.073, and 0.105 for [CN⁻] = 0.028, 0.0508, and 0.0736, respectively. For 80 % methanol E_A is 14.0 kcal M^{-1} and using $k_1 = 1.23$ at 25°C gives $k_1 = 0.0178$ at −20.5°C. At this temperature k[CN⁻] is 0.0185, 0.0230, and 0.0279 for [CN⁻] = 0.0273, 0.0501, and 0.0729, respectively. It is therefore possible that only the k_1 term appears at low temperatures also and that the deviation with increasing [CN⁻] represents a kinetic salt effect. If this is so then the large changes in E_A can be attributed, as above, to change in $\Delta H^* = \Delta H_4 - \Delta H_t^*$.

Acknowledgement. The authors thank Professor Jannik Bjerrum for invaluable discussions both during the course of the work and during the preparation of the manuscript.

REFERENCES

1. Paterson, R. and Bjerrum, J. *Acta Chem. Scand. 19* (1965) 729.
2. Mønsted, O. and Bjerrum, J. *Acta Chem. Scand. 21* (1967) 1116.
3. Tanaka, N., Kamada, M. and Murayama, T. *Bull. Chem. Soc. Jap. 31* (1959) 895.
4. Duke, F. R. and Courtney, W. G. *J. Phys. Chem. 56* (1952) 19.
5. Baxendale, J. H. and Westcott, D. T. *J. Chem. Soc.* (1959) 2347.
6. Nord, G. and Wernberg, O. *J. Chem. Soc. Dalton Trans.* (1972) 866.
7. Long, A. and Busch, T. *Inorg. Chem. 6* (1967) 556.
8. Mønsted, O. *Private communication* to G. Nord.

† If this is so, then it is difficult to understand the disappearance of the k_1 term (see later discussion). However, the data can be reproduced using a $[CN^-]^{-\frac{1}{2}}$ dependence, possibly reflecting the protonation of the transition state in methanol-rich solvents at low temperatures.

9. Rothbaum, H. P. *J. Electrochem. Soc. 104* (1957) 682.
10. Simpson, E. A. *Ph. D. Thesis*, London 1959.
11. Bjerrum, J. *Metal Ammine Formation in Aqueous Solution*, Copenhagen 1941.
12. *Stability Constants, Special Publication 17*, The Chemical Society, London 1964.
13. Bjerrum, J. and Romano, V. *Acta Chem. Scand. 24* (1970) 155.
14. Rossotti, H. *Proc. VII, I.C.C.C.* 1962, p. 197, and references therein.
15. Baltisberger, R. J. and King, E. L. *J. Amer. Chem. Soc. 86* (1964) 795, and references therein.

Received August 13, 1973.

Acta Chemica Scandinavica A 28 (1974) 20—22

Equilibrium Studies of Polyanions. 20. A Recalculation of emf Data on the Reactions of H^+ and WO_4^{2-} in 3 M $Na(ClO_4)$ at 25°C

ROBERT ARNEK and YUKIYOSHI SASAKI*

Department of Inorganic Chemistry, The Royal Institute of Technology, S-100 44 Stockholm 70, Sweden

In 1961 one of us (Y.S.) published emf data on the reactions between H^+ and WO_4^{2-} in 3 M $Na(ClO_4)$ at 25°C.[1] Recently we have performed a new analysis of the data by means of the generalized least-squares computer program LETAGROP.[2,3] A large number of combinations of species $(H)_p(WO_4)_q^{(2q-p)-}$ have been tried in order to get the best fit with the data. We find that the emf data can best be explained by assuming the species H_2WO_4, $W_6O_{21}^{6-}$, and $W_{12}O_{41}^{10-}$ in addition to $HW_6O_{21}^{5-}$ with the equilibrium constants (deviations correspond to 3σ):

$$2H^+ + WO_4^{2-} \rightleftharpoons H_2WO_4$$
$$6H^+ + 6WO_4^{2-} \rightleftharpoons W_6O_{21}^{6-} + 3H_2O$$
$$7H^+ + 6WO_4^{2-} \rightleftharpoons HW_6O_{21}^{5-} + 3H_2O$$
$$14H^+ + 12WO_4^{2-} \rightleftharpoons W_{12}O_{41}^{10-} + 7H_2O$$

$$\log \beta_{2,1} = 11.30 \pm 0.10$$
$$\log \beta_{6,6} = 52.46 \pm 0.10$$
$$\log \beta_{7,6} = 60.76 \pm 0.03$$
$$\log \beta_{14,12} = 123.24 \pm 0.15$$

At this Institute in 1961 Sasaki[1] studied the reactions between H^+ and the wolframate ion WO_4^{2-} in 3 M $Na(ClO_4)$ medium at 25°C using a glass electrode. The main reaction was found to be

$$7H^+ + 6WO_4^{2-} \rightleftharpoons HW_6O_{21}^{5-} + 3H_2O$$

with the equilibrium constant $\log \beta_{7,6} = 60.68 \pm 0.03$

In connexion with a calorimetric study of the $H^+ - WO_4^{2-}$ system[4] it was found to be desirable to recalculate the emf data with the modern computer methods now available, and so we have used a recent version of the generalized least-squares computer program LETAGROP.

Various authors have proposed species $H_p(WO_4)_q^{(2q-p)-}$, with many different (p,q) values, in acidified wolframate solutions; for reviews see Refs.[5,6]

THE LETAGROP TREATMENT

The calculations were performed on the sets of data, $Z(\log h)_B$, given by Sasaki. The aim was to find a mechanism which gives a minimum to the error square sum defined

$$U = \sum (Z_{calc} - Z_{exp})^2$$

By means of LETAGROP it is possible to select, out of a number of suggested complexes, that set of complexes $(p,q,\beta_{p,q})$, which gives the lowest error square sum. Species which diminish the U-value and for which the condition $\beta_{pq} > F_\sigma \, \sigma(\beta_{pq})$ is fulfilled are accepted, others are rejected ("species selector").[7]

Many species, $H_p(WO_4)_q^{(2p-q)-}$, besides $HW_6O_{21}^{5-}$, have been suggested in literature,[5,6] among others the following: (p,q); (1,1), (2,1), (6,6), (8,6), (9,6), (12,12), (13,12), (14,12), (15,12), (16,12), (17,12), and (18,12).

We have now systematically tested these species with the "species selector" (the F_σ value used was 3). In this work we found rather soon that the combination of species (7,6), (6,6), and (14,12) gave a considerably lower U-value than the species (7,6) alone (Table 1, calc. I—III).

To the set (7,6) (6,6), and (14,12) we tried to add the other complexes suggested above, but all these complexes were ultimately rejected

* Present address: Department of Chemistry, Faculty of Science, The University of Tokyo, Japan.

Table 1. log $\beta_{p,q}$, U and $\sigma(Z)$. $\delta Z = 0$.

(p,q)	I	II	III	IV	V
2,1	–	–	–	–	10.79 ± 0.08
6,6	–	–	52.46 ± 0.04	52.47 ± 0.04	52.48 ± 0.04
7,6	60.68 n.v.[a]	60.75 ± 0.01	60.71 ± 0.01	60.71 ± 0.01	60.70 ± 0.01
9,6	–	–	–	70.47 ± 0.07	–
14,12	–	123.17 ± 0.05	123.22 ± 0.05	123.23 ± 0.05	123.25 ± 0.05
U	0.157	0.050	0.031	0.027	0.028
$\sigma(Z)$	0.018	0.014	0.011	0.010	0.010

[a] Not varied

Table 2. log $\beta_{p,q}$, U and $\sigma(Z)$; adjusting for δZ.

(p,q)	I	II	III
2,1	11.30 ± 0.03	–	–
6,6	52.46 ± 0.03	52.56 ± 0.03	52.62 ± 0.03
7,6	60.76 ± 0.01	60.70 ± 0.01	60.64 ± 0.01
9,6	–	70.61 ± 0.05	–
14,12	123.24 ± 0.05	123.44 ± 0.04	123.52 ± 0.04
U	0.0082	0.0130	0.018
$\sigma(Z)$	0.0056	0.0071	0.0083

except (9,6). Initially the (2,1) species was accepted but it was subsequently rejected in favour of (9,6). However, σ_Z has the same value when (2,1) or (9,6) is accepted (Table 1, calc. IV and V).

In the above treatment, we have assumed no analytical errors, hence all $\delta Z = 0$. In a more complete treatment we assume a constant error in Z, δZ, for each "titration". These systematic errors are treated as unknown parameters to be adjusted together with the equilibrium constants.[8] This leads to the results given in Table 2 and Table 3. Starting with the (6,6), (7,6), (14,12), (9,6), and (2,1) set of species and adjusting the δZ, $\beta_{9,6}$ is found to be negative. If the (9,6) species is then left out (Table 2, calc. I), the value for $\sigma(Z)$ drops from 0.010 to 0.0056 with the δZ adjustment. Other sets of species give higher $\sigma(Z)$ with the δZ adjustment (Table 2, calc. II and III).

If the set of species (6,6), (7,6), (14,12), and (2,1) is assumed and taking the δZ in calc. I in Table 3, there remains no systematic deviation in the $(Z_{calc} - Z_{exp})$ values.

Table 3. Analytical errors $100 \times \delta Z$, calculated for various titrations by LETAGROP adjustment to best fit.

$W(VI)_{total}$,M	I	II	III
0.00125	−3.0 ± 0.4	−0.7 ± 0.5	0.4 ± 0.7
0.0025	−1.9 ± 0.3	−0.7 ± 0.3	0.4 ± 0.4
0.0050	−1.1 ± 0.2	−0.4 ± 0.2	0.2 ± 0.3
0.0100	0.3 ± 0.4	0.8 ± 0.6	1.4 ± 0.7
0.0200	0.2 ± 0.3	0.4 ± 0.4	0.7 ± 0.4
0.0399	−0.2 ± 0.2	−0.2 ± 0.2	−0.01 ± 0.2
0.0797	−0.3 ± 0.3	−0.5 ± 0.2	−0.5 ± 0.2
0.1604	−1.4 ± 0.3	−1.9 ± 0.4	−2.0 ± 0.4

In Fig. 1 are given the species fraction curves for $B = 0.1604$ M, calculated using the scheme with $HW_6O_{21}^{5-}$, $W_6O_{21}^{6-}$, $W_{12}O_{41}^{10-}$, and H_2WO_4. The fraction of the species H_2WO_4 for $[W(VI)]_{total} = 0.1604$ M is almost negligible, but amounts to about 10 % for $[W(VI)]_{total} = 0.00125$ M.

Slow formation of $W_{12}O_{41}^{10-}$ from $HW_6O_{21}^{5-}$ (ordinarily called parawolframate B and A, respectively) has been repeatedly reported.[9–12]

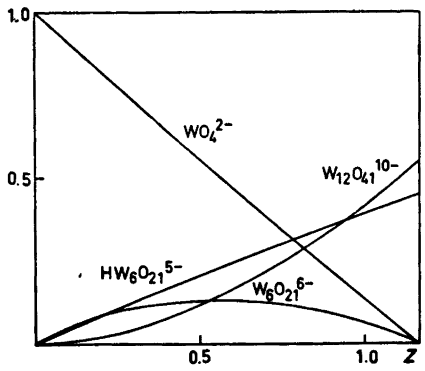

Fig. 1. Fractions of total W(VI) as WO_4^{2-}, $HW_6O_{21}^{5-}$, $W_6O_{21}^{6-}$ and $W_{12}O_{41}^{10-}$ in 3 M $Na(ClO_4)$ at 25° for 0.1604 M W(VI). Z = average number of H^+ bound per WO_4^{2-}. The fraction of H_2WO_4 is too small (< 0.004) as to appear in the figure.

In the present investigation, however, the establishment of equilibrium is found to be practically instantaneous, so the relationship between the anion $W_{12}O_{41}^{10-}$ found in the present study and "parawolframate B" is not yet clear.

Acknowledgements. We thank Dr. Erik Högfeldt for valuable comments on the manuscript. This work has been supported by *Statens Naturvetenskapliga Forskningsråd (Swedish Natural Science Research Council)*. Dr. Derek Lewis was kind enough to correct the English of the text.

REFERENCES

1. Sasaki, Y. *Acta Chem. Scand. 15* (1961) 175.
2. Sillén, L. G. *Acta Chem. Scand. 18* (1964) 1085.
3. Ingri, N. and Sillén, L. G. *Ark. Kemi 23* (1964) 97, and following publications.
4. Arnek, R. *Acta Chem. Scand. 23* (1969) 1986.
5. Sillén, L. G. and Martell, A. E. *Stability Constants (Inorganic ligands)* 2nd Edition, Chem. Soc., Spec. Publ. No. 17, London 1964; Supplement: Chem. Soc. Spec. Publ. No. 25, London 1970.
6. Souchay, P., Boyer, M. and Chauveau, F. *Trans. Roy. Inst. Technol. Stockholm* (1972) No. 259.
7. Sillén, L. G. and Warnqvist, B. *Ark. Kemi 31* (1969) 341.
8. Sillén, L. G. and Warnqvist, B. *Ark. Kemi 31* (1969) 315.
9. Souchay, P. *Ann. Chim. (Paris) 18* (1943) 61, 169.
10. Kepert, D. L. *Progr. Inorg. Chem. 4* (1962) 199.
11. Glemser, O., Holznagel, W., Höltje, W. and Schwarzmann, E. *Z. Naturforsch. 20b* (1965) 725.
12. Boyer, M. *Thesis*, Paris 1972.

Received July 25, 1973.

Acta Chemica Scandinavica A 28 (1974) 23—28

Reaction Rate Studies of the Acid Hydrolysis of Some Chromium(III) Complexes. II. The Acid Hydrolysis of Facial and of Meridional Triamminetriaquachromium(III) and of *cis*- and of *trans*-Tetraamminediaquachromium(III) Ions in Aqueous Perchloric Acid

L. MØNSTED and O. MØNSTED

Chemistry Department I, Inorganic Chemistry, The H. C. Ørsted Institute, University of Copenhagen, DK-2100 Copenhagen, Denmark

The acid hydrolysis of facial and of meridional triamminetriaquachromium(III) and of *cis*- and of *trans*-tetraamminediaquachromium(III) cations has been investigated in 0.5 to 1.0 M perchloric acid at an ionic strength of 1.0, adjusted by the addition of sodium perchlorate, in the temperature range 60 – 80°C.

In the reaction scheme (a = ammonia, aq = = water):

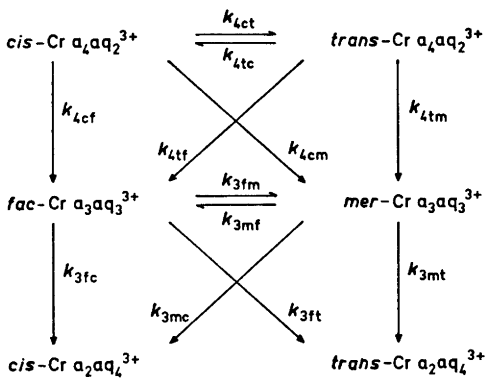

most reaction pathways were found to be kinetically significant. Rate constants at 70°C and activation energies were found to be:

k_{3mf}: $(1.1 \pm 0.4) \times 10^{-6}$ sec^{-1}, 26 ± 9 kcal/mol, and k_{4tc}: $(4.2 \pm 0.8) \times 10^{-6}$ sec^{-1}, 26 ± 5 kcal/mol for the well defined isomerization reactions and k_{3fc}: $(7.6 \pm 0.3) \times 10^{-6}$ sec^{-1}, 27.6 ± 0.9 kcal/mol, k_{3mc}: $(23.5 \pm 0.5) \times 10^{-6}$ sec^{-1}, 26.1 ± 0.5 kcal/mol, k_{4cf}: $(25.3 \pm 1.0) \times 10^{-6}$ sec^{-1}, 24.5 ± 0.9 kcal/mol, k_{4cm}: $(3.7 \pm 0.9) \times 10^{-6}$ sec^{-1}, 24 ± 4 kcal/mol, and k_{4tm}: $(44.2 \pm 1.0) \times 10^{-6}$ sec^{-1}, 26.4 ± 0.6 kcal/mol for the well defined hydrolysis reactions.

The remaining paths were not kinetically well defined, but upper limits for the rate constants at 70°C (taken as the mean value plus twice the standard deviation) were found to be: k_{3ft}: 0.5×10^{-6} sec^{-1}, k_{3fm}: 0.8×10^{-6} sec^{-1}, k_{3mt}: 1.5×10^{-6} sec^{-1}, k_{4ct}: 1.6×10^{-6} sec^{-1} and k_{4tf}: 3×10^{-6} sec^{-1}.

In the acidity range studied no dependence of the rate constants upon the hydrogen ion concentration was observed.

As part of a continued research on the acid hydrolysis of chromium(III) ammine complexes, of which results for the monoamminepentaaqua- and the isomeric diamminetetraaquachromium(III) ions have been given earlier,[1] we here present data for the reactions of the isomeric triamminetriaqua- and the isomeric tetraamminediaquachromium(III) complexes.

In spite of numerous investigations of halide hydrolysis in both *cis*- and *trans*-tetraamminedihalogenido- and aquahalogenidochromium(III) systems, no quantitative investigations of the further reactions of the *cis*- and *trans*-tetraamminediaquachromium(III) ions produced by these reactions seem to have been carried out. Qualitative observations indicate the non-significance of chromium nitrogen bond breaking in the time necessary for the study of

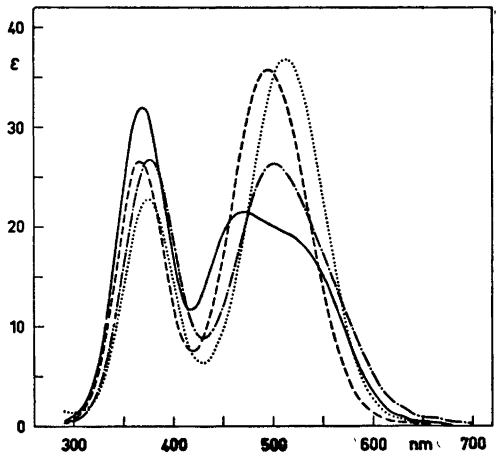

Fig. 1. Visible absorption spectra of ammineaquachromium(III) complexes prepared and purified as described in the text.
···, facial $[Cr(NH_3)_3(OH_2)_3]^{3+}$; – . – , meridional $[Cr(NH_3)_3(OH_2)_3]^{3+}$; – – – , *cis*-$[Cr(NH_3)_4(OH_2)_2]^{3+}$ and ———, *trans*-$[Cr(NH_3)_4(OH_2)_2]^{3+}$.
No hydrogen ion dependence of these spectra was observed in the acidity range 0.5 to 1.0 in 1 M $(Na^+ + H^+)ClO_4$ solution.

the chromium halogen bond breaking. The hydrolysis of the *cis*-tetraamminediaquachromium(III) ion has been investigated by Jørgensen and Bjerrum.[2] Since their study, however, was made in a medium containing nitrate ions and in some cases sulphate or dithionate ions also, and since all these ions are now known to excert specific influence upon the hydrolysis of chromium(III) ammine complexes, a reinvestigation of the reactions of this cation in perchloric acid solution was undertaken together with the investigation of the reactions of the *trans*-tetraamminediaquachromium(III) ion and the isomeric triamminetriaquachromium(III) ions. For these latter ions no quantitative data seem to have been produced previously.

EXPERIMENTAL

Preparation of solutions. The *cis*-tetraamminediaquachromium(III) ion and the isomeric triamminetriaquachromium(III) ions were purified by the ion exchange method described in detail in Ref. 1, after being formed in solution as described below. By this method chromium complexes with different numbers of coordinated ammonia molecules were easily separated. The greater the number of coordinated water molecules the easier the elution from the resin column with 2 M sulphuric acid took place. Contrary to what was observed for the isomeric diammines, both the isomeric triammines and tetraammines were rather easily separated from each other. The meridional triamminetriaquachromium(III) ion was eluted before the corresponding facial isomer and the *trans*-tetraamminediaquachromium(III) ion was

Table 1. Comparison of spectral characteristics of compounds, prepared and purified as described in the text, with literature values.

Complex ion	Medium	λ_1 max (nm)	ε_1 max [l/(mol cm)]	λ_2 max (nm)	ε_2 max [l/(mol cm)]	ε_1 max/ ε_2 max	Ref.
facial							
$[Cr(NH_3)_3(OH_2)_3]^{3+}$	0.5 M $HClO_4$ + 0.5 M $NaClO_4$	513	36.6	374	22.6	1.62	[a]
	2 M $HClO_4$	513[b]	34.5	374	22.2	1.55	8
meridional							
$[Cr(NH_3)_3(OH_2)_3]^{3+}$	0.5 M $HClO_4$ + 0.5 M $NaClO_4$	502	26.3	376	26.8	0.98	[a]
	3 M $HClO_4$	503	25.6	373	25.6	1.00	9
	0.6–2 M $HClO_4$	504	26.3	376	26.0	1.01	6
cis-							
$[Cr(NH_3)_4(OH_2)_2]^{3+}$	0.5 M $HClO_4$ + 0.5 M $NaClO_4$	495	35.8	366	26.8	1.34	[a]
	1 M $HClO_4$	495	36.1	366	26.6	1.36	10
	0.5 M HNO_3	495	36	365	26.5	1.36	2[c]
trans-							
$[Cr(NH_3)_4(OH_2)_2]^{3+}$	0.5 M $HClO_4$ + 0.5 M $NaClO_4$	470	21.5	369	32.1	0.67	[a]
	1 M $HClO_4$	476	20.6	368	29.7	0.69	10

[a] This work. [b] Frequently misquoted as 518 in the literature. [c] Estimated from the graph is this reference.

eluted before the corresponding *cis*-isomer. Both these observations are in agreement with numerous observations in other closely related systems, in which such behaviour has been rationalized qualitatively in terms of the dipole moments of the ions in question. In connection with this purification technique the exclusion of light is especially important, except for the *cis*-tetraamminediaquachromium(III) ions, as light greatly accelerated the isomerization reactions, and to a lesser extent also the hydrolysis reactions.

trans-*Tetraamminediaquachromium(III)*. Since the decomposition of this ion was greatly accelerated not only by Dowex 50 W resins as noted earlier [3] but also by the Sephadex resin employed, solutions of the *trans*-tetraamminediaquachromium(III) ion were prepared by dissolving *trans*-tetraammineaquahydroxochromium(III) perchlorate [4] directly in perchloric acid.

cis-*Tetraamminediaquachromium(III)*. A stock solution of this ion in perchloric acid was prepared as follows: 5 g of *cis*-tetraammineaquachloridochromium(III) chloride [5] was treated with 10 ml of 2 M sodium hydroxide solution at room temperature for about 2 min. *cis*-Tetraamminediaquachromium(III) perchlorate was precipitated from this solution, cooled to 0°C, by the dropwise addition of 150 ml of 70 % perchloric acid. The perchlorate thus prepared was filtered off, washed with a little ice cold 70 % perchloric acid, dissolved in about 100 ml of water, and reprecipitated with 100 ml 70 % perchloric acid as described above. Finally the precipitate was dissolved in 50 ml 1 M perchloric acid. This solution could be kept almost unchanged in the dark at 0°C for several months. The small amounts of triamminetriaquachromium(III) complexes initially present and formed during the storage were readily removed in the final steps of the purification procedure.

Facial triamminetriaquachromium(III). 10 ml of the stock solution of the *cis*-tetraamminediaquachromium(III) ion was diluted five times with 1 M perchloric acid, and the resulting solution was aged in the dark at 50°C for 75 h. The triammines were separated as described above from the complex mixture of chromium(III) ammine complexes thus formed. This mixture of triammines, with the facial isomer as main constituent, was used directly for the kinetic experiments. A solution of the pure facial triamminetriaquachromium(III) ion, needed in order to obtain the visible absorption spectrum of this ion, which was necessary for the chosen calculation procedure, was prepared in the following way: The mixture of triammines was rechromatographed at 0°C on a 2 × 25 cm column packed with Dowex 50W X8 200/400 mesh resin; 2 M sulphuric acid was employed as the eluent. Spectrophotometric control of the effluent showed that small amounts of the meridional isomer was eluted first mixed with the facial isomer. After the first few fractions the chromium species in the eluent had a constant absorption spectrum, judged both by the ratio of the absorbance of the first spin allowed band to the absorbance of the second spin allowed band, and by the constant position of these two bands. The indistinguishable fractions were assumed to contain the pure facial triamminetriaquachromium(III) ion.

Meridional triamminetriaquachromium(III). This ion was generated in solution by mercury(II) accelerated hydrolysis of the chloride ligands in the meridional triammineaquadichloridochromium(III) ion dissolved as the chloride [6,7] in dilute perchloric acid. No facial triamminetriaquachromium(III) ions could be detected in solutions thus prepared. For some kinetic experiments the triammine mixture, with the meridional triamminetriaquachromium(III) ion as main constituent, from solutions of the *trans*-tetraamminediaquachromium(III) ion aged in 1 M perchloric acid at 50°C for 75 h was employed.

Chemicals, kinetic measurements and the *method of analysis* were essentially as described earlier,[1] and for the *method of calculation* the discussion given for the hydrolysis of the isomeric diamminetetraaqua- and the monoamminepentaaquachromium(III) ions applies also to the present work. In connection with the calculation procedure it should also be mentioned that experiments with a mixture of complex ions as initial reactants, as was always the case in experiments with predominantly the facial triamminetriaquachromium(III) ion, gave reaction rate constants of comparable accuracy to those experiments where only one complex ion was initially present. This was investigated by comparing the experiments started with the pure meridional triamminetriaquachromium(III) ion with those started with the mixture of the isomeric triammines obtained by the hydrolysis of the *trans*-tetraamminediaquachromium(III) ion. For this reason no great effort was made to further purify the solutions of the facial triamminetriaquachromium(III) ion used for kinetic runs.

RESULTS AND DISCUSSION

When an acid solution of the *trans*-tetraamminediaquachromium(III) ion is left to hydrolyse small amounts of the facial triamminetriaquachromium(III) ion appear. If the uptake of ammonia by the chromium(III) complexes is not taken into consideration, then the formation of this cation may occur in the following four different ways (see Fig. 2):

(i) Directly by hydrolysis of the *trans*-tetraamminediaquachromium(III) ion (4tf-path).

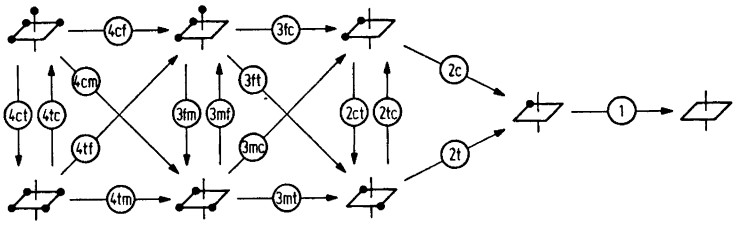

Fig. 2. Isomerization and hydrolysis reactions of $[Cr(NH_3)_n(OH_2)_{6-n}]^{3+}$ ions ($n = 4, 3, 2, 1$). Filled circles depict coordinated ammonia whereas the coordinated water is shown only by the absence of such circles. Reaction pathways are indicated by the subindices of the symbols used for the reaction rate constants.

Table 2. Initial composition of reaction kinetic experiments in 1.0 M perchlorate medium, started with triamminetriaquachromium(III) ions.

Exp. No.	Chromium concentration		Hydrogen ion concentration[a] (mol/l)	Temp. (°C)	Max. reaction time (h.)
	facial (mmol/l)	meridional (mmol/l)			
1	0.723 ± 0.006	0.169 ± 0.007	1.0	60.18	410
2	0.150 ± 0.006	0.932 ± 0.007	1.0	60.18	96
3	1.207 ± 0.010	0.252 ± 0.012	1.0	69.70	263
4	0.042 ± 0.008	0.924 ± 0.009	1.0	69.70	48
5	–	1.102 ± 0.003	1.0	80.15	24
6	–	1.060 ± 0.005	1.0	80.02	12
7	1.513 ± 0.010	0.232 ± 0.012	1.0	80.15	72

[a] The hydrogen ion concentration was only varied in experiments started with the tetraamminediaquachromium(III) ions (Table 3). This was done since tetraamminediaquachromium(III) solutions were easier to prepare than triamminetriaquachromium(III) solutions. As the *trans*-tetraamminediaquachromium(III) ion reacts to give mainly the meridional triamminetriaquachromium(III) ion and the *cis*-tetraamminediaquachromium(III) ion gives mainly the facial triamminetriaquachromium(III) ion no effects from this restriction should be observed.

(ii) By hydrolysis of the *cis*-tetraamminediaquachromium(III) ion formed by isomerization of the *trans*-isomer (4tc + 4cf paths).

(iii) By isomerization of the meridional triamminetriaquachromium(III) ion formed by hydrolysis of the initial *trans*-compound (4tm + 3mf paths), or

(iv) by a combination of the two above isomerization reactions with the hydrolysis reaction of the *cis*-tetraamminediaquachromium(III) ion to yield the meridional triamminetriaquachromium(III) ion (4tc + 4cm + + 3mf paths).

Similar uncertainties exist for the origin of most other reaction products. Therefore, in order to deal with this ambiguity of the origin of the reaction products in a rigorous fashion, the reaction scheme of Fig. 2 in which all isomerization- and hydrolysis reactions are included was employed for the interpretation of the kinetic data. No experimental evidence for the uptake of ammonia by the ammineaquachromium(III) complexes investigated, in solutions as acid as those employed in this research ($[H^+] \geq 0.5$ mol/l), have been found. These reactions have consequently not been included in the reaction scheme used to explain the kinetic data.

Tables 2 and 3 show the reaction kinetic experiments with triamminetriaqua- and tetraamminediaquachromium(III) ions as reactants, respectively. In Table 4, rate constants at 60, 70, and 80°C and activation energies calculated from those experiments and those of Ref. 1 are tabulated. As seen from this table there are no significant differences between the rate con-

Table 3. Initial composition of reaction kinetic experiments in 1.0 M perchlorate medium, started with tetraamminediaquachromium(III) ions.

Exp. No.	Chromium concentration *cis* (mmol/l)	Chromium concentration *trans* (mmol/l)	Hydrogen ion concentration (mol/l)	Temp. (°C)	Max. reaction time (h.)
8[a]	2.044±0.014	–	1.0	60.18	264
9[a,b]	0.137±0.010	2.120±0.013	1.0	60.18	216
10[a]	2.052±0.014	–	1.0	69.70	144
11[a,b]	0.119±0.009	2.138±0.011	1.0	69.70	216
12	2.633±0.004	–	1.0	80.15	24
13	1.197±0.006	–	0.5	80.02	24
14	–	1.969±0.006	1.0	80.15	12
15	–	1.468±0.005	0.5	80.02	12

[a] These four solutions were pairwise prepared from the same stock solutions. [b] Unfortunately the stock solution used for these experiments was exposed to light for some time. This accounts for the *cis*-isomer present. Since the rate constants, however, were almost as equally well defined in these experiments as in those started with the pure isomer the experiments were not repeated.

Table 4. Rate constants at 60, 70, and 80°C and activation energies [a]calculated from the experiments of tables 2 and 3 and Ref. 1.

($\times 10^6$)	All experiments 60°C (sec^{-1})	70°C (sec^{-1})	80°C (sec^{-1})	E_A (kcal/mol)	Experiments in 1 M acid. 80°C (sec^{-1})	E_A (kcal/mol)
k_1	0.314±0.006	1.109±0.012	3.64±0.05	28.6±0.3	3.56±0.07	28.3±0.3
k_{2c}	1.03±0.04	3.38±0.12	10.4±0.4	27.0±0.4	10.5±0.4	27.2±0.5
k_{2ct}	0.00±0.06	0.00±0.18	0.0±0.6	–	0.0±0.6	–
k_{2t}	5.50±0.17	17.5±0.3	52.4±1.1	26.3±0.5	53.6±1.3	26.7±0.5
k_{2tc}	1.56±0.13	5.3±0.2	16.5±0.9	27.6±1.2	17.0±1.1	28.0±1.3
k_{3fc}	2.25±0.15	7.6±0.3	23.8±1.2	27.6±0.9	23.7±1.2	27.4±0.9
k_{3ft}	0.03±0.11	0.1±0.2	0.3±0.8	–	0.2±0.9	–
k_{3fm}	0.06±0.15	0.2±0.3	0.6±1.1	–	0.6±1.1	–
k_{3mc}	7.5±0.3	23.5±0.5	69±2	26.1±0.5	69±2	26.0±0.6
k_{3mt}	0.1±0.2	0.5±0.5	1.3±1.9	–	1±2	–
k_{3mf}	0.3±0.2	1.1±0.4	3.2±1.4	26±9	2.9±1.5	26±10
k_{4cf}	8.6±0.6	25.3±1.0	69.9±1.6	24.5±0.9	70.4±1.7	24.5±0.9
k_{4cm}	1.3±0.4	3.7±0.9	10±2	24±4	10±2	24±4
k_{4ct}	0.0±0.3	0.0±0.8	0±2	–	0±2	–
k_{4tf}	0.2±0.4	0.6±0.8	2±3	–	1±3	–
k_{4tm}	13.8±0.6	44.2±1.0	132±4	26.4±0.6	137±4	26.7±0.6
k_{4tc}	1.3±0.5	4.2±0.8	13±2	26±5	14±3	27±4

[a] It should be noted that the standard deviations upon the tabulated parameters are correlated, that is, the quoted standard deviations cannot be used as realistic error estimates independently of each other. The full table of correlation coefficients will be given later in connection with additional data for the reactions of the hexaammine- and the pentaammineaquachromium(III) ions.

stants and activation energies calculated from all the experiments and those calculated from the experiments in 1 M acid only. This means that the reactions of deprotonated ammineaquachromium(III) complexes plays no important role at hydrogen ion concentrations greater than 0.5 mol/l.

It is noteworthy that the standard deviations associated with the parameters k_{2c} and k_{2ct} are somewhat smaller than the values reported in Ref. 1. This is due to the fact that many of the experiments of Tables 2 and 3 have been followed for such an extended period of time as to contain an appreciable amount of information about the reactions of the *cis*-diamminetetraaquachromium(III) ion. Both the isomeric triammines form this ion almost exclusively by their hydrolysis reactions. The results obtained for the standard deviations of the parameters k_{2t} and k_{2tc}, which are seen to be almost unchanged from those of the earlier research, also illustrate this fact. That the standard deviation upon the parameter k_1 is also unchanged simply reflects that only few of the additional experiments have been followed for so long a time as to produce significant amounts of the hexaaquachromium(III) ion.

The inclusion of the data from Ref. 1 in the calculation of the parameters of Table 4 should also be noted. These data are needed in order to have information about the reactions of the *trans*-diamminetetraaquachromium(III) ion, as this ion, as already mentioned, is not formed in significant quantities by the hydrolysis reactions of the isomeric triamminetriaquachromium(III) ions. Consequently, problems analogous to those discussed at length in Ref. 1, in connection with those kinetic experiments started with the pure *cis*-diamminetetraaquachromium(III) ion, where also no *trans*-diamminetetraaquachromium(III) ions are formed, would have been encountered, had these data not been used.

A further discussion of the results given here will be presented in connection with data for the acid hydrolysis of the hexaammine- and the pentaammineaquachromium(III) ions, when the investigations into the reactions of these ions have been concluded.

REFERENCES

1. Mønsted, L. and Mønsted, O. *Acta Chem. Scand. 27* (1973) 2121.
2. Jørgensen, E. and Bjerrum, J. *Acta Chem. Scand. 12* (1958) 1047.
3. Hoppenjans, D. W., Hunt, J. B. and Gregoire, C. R. *Inorg. Chem. 7* (1968) 2506.
4. Glerup, J. *Acta Chem. Scand. To be published.*
5. Mori, M. *J. Inst. Polytechn. Osaka City Univ. Ser. C. 3* (1952) 41.
6. Caldwell, S. H. and House, D. A. *Inorg. Chem. 8* (1969) 151.
7. Schlessinger, G. G. *Inorganic Laboratory Preparations*, New York 1962 p. 249.
8. Schäffer, C. E. and Andersen, P. *Proc. Wroclaw Symposium*, London 1964, p. 571.
9. Hughes, R. G., Ebsworth, E. A. V. and Garner, C. S. *Inorg. Chem. 7* (1968) 882.
10. Hoppenjans, D. W. and Hunt, J. B. *Inorg. Chem. 8* (1969) 505.

Received August 28, 1973.

Acta Chemica Scandinavica A 28 (1974) 29—36

On the Application of the Intermediate Neglect of Differential Overlap Method to Inorganic Complexes

T. ZIEGLER

Department of Chemistry, The University of Calgary, Calgary, Alberta, Canada

A new semiquantitative SCF LCAO MO calculation scheme has been applied to: $Ni(CO)_4$, $Ni(CN)_4^{2-}$, $Cr(CO)_6$, and $Fe(C_5H_5)_2$. Comparison is made to current *ab initio* calculations.[1-3]

1. INTRODUCTION

The advent of *ab initio* calculations on inorganic complexes [4-5] has since been followed up by calculations with more extended basis sets [6] leading to a recent Hartree-Fock limit calculation.[7]

The great advantage of such examinations compared with semiempirical and semiquantitative theories is of course an elimination of all empirical parameters such as atomic ionization energies and scaling factors, which are often introduced in a somewhat arbitrary way, in order to fit the electronic spectrum.

The disadvantage of *ab initio* calculations is the great number of integrals, especially when any arbitrariness in the choice of atomic orbitals (minimal basis set) has to be avoided by the use of a rather flexible set of functions (extended basis set).

The possible manner in which to reduce the number of integrals by a suitable set of numerical approximations, and then calculating the remaining exact, has been discussed by Dahl and Ballhausen [8] inside the CNDO (complete neglect of differential overlap) scheme. Due to the lack of photoelectron spectra and *ab initio* calculations, they could only check their approximation scheme rather crudely by comparison between electronic spectra and transition energies determined from ground state calculations.

Now a much more safe test can be made by direct comparison with *ab initio* calculations. The present work suggests an INDO (intermediate neglect of differential overlap [9]) scheme, which is discussed in connection with *ab initio* calculations and photoelectron spectra.

2. DESCRIPTION OF METHOD

2a. Core and valence orbitals. Consider an inorganic complex for which the ground state is a totally symmetric singlet state. In the Hartree-Fock model we represent it by a single Slater determinant:

$$\Xi = |\mu^+_1\mu^-_1 \ldots \mu^+_i\mu^-_i \ldots \mu^+_q\mu^-_q| \qquad (1)$$

where μ_i depends only on the three space coordinates. The + and − refer to alpha and beta spin functions in the usual way. The molecular orbitals (MO's) μ_i are divided into core orbitals, denoted ψ^{core}, and valence orbitals, denoted ψ.

The core orbitals include the ligand 1*s* orbitals and the 1*s*, 2*s*, and 2*p* orbitals of the central metal ion; these orbitals are all assumed to be the same as in the free ions.

The valence MO's are constructed as linear combinations of atomic orbitals, LCAO's:

$$\psi_i = \sum_{r=1}^{m} A_{ri}\chi_r \qquad (2)$$

assuming m atomic orbitals (AO's), denoted χ_r or just r, s, t....

The problem is now to determine A_{ri} of eqn. (2) together with the molecular orbital energy, denoted ε_i, by the aid of Roothaan's method.[8]

2b. Roothaan's method. The core orbitals, as defined in Section 2a, come close to being orthogonal to each other, and also the "strong orthogonality condition":

$$\int \psi_i^{\text{core}}(1)\ \varphi_j(1)\ d\tau_1 = 0 \tag{3}$$

for all pairs $(\varphi_j, \psi_i^{\text{core}})$ is reasonably fulfilled. It is then expedient to introduce the one electron core operator:

$$H^{\text{core}}(1) = T(1) + \sum_g V_g(1) \tag{4a}$$

$$V_g(1) = -\frac{Z_g\, e^2}{r_{1g}} + \sum_{j\ \text{on}\ g} [2J_j^{\text{core}}(1) - K_j^{\text{core}}(1)] \tag{4b}$$

where g numbers the various nuclei, with charges $Z_g\, e$. $T(1)$ is the kinetic energy operator, and J_j^{core} (1) and K_j^{core} (1) are the usual Coulomb and exchange operators:

$$J_j^{\text{core}}(1)\ \psi_i(1) = \int \psi_j^{\text{core}}(2)\psi_j^{\text{core}}(2)\ \frac{e^2}{r_{12}}\, d\tau_2 \times \psi_i(1) \tag{5a}$$

$$K_j^{\text{core}}(1)\ \psi_j(1) = \int \psi_j^{\text{core}}(2)\psi_i(2)\ \frac{e^2}{r_{12}}\, d\tau_2 \times \psi_j^{\text{core}}(1) \tag{5b}$$

Application of Roothaan's method then leads to the following set of equations:[8]

$$\sum_{s=1}^{m} \{(r|H^{\text{core}}(1)|s) + \sum_{t,u}^{m} P'_{tu}\{[rs|tu] - \tfrac{1}{2}ru|ts]\}A_{si} = \varepsilon_i \sum_{s=1}^{m} (\delta_{rs} + S_{rs})\, A_{si} \tag{6}$$

with r = 1, 2,...,m, and:

$$(r|H^{\text{core}}(1)|s) = \int \chi_r(1)\ H^{\text{core}}(1)\ \chi_s(1)\ d\tau_1 \tag{7a}$$

$$[rs|tu] = \int\int \chi_r(1)\chi_s(1)\ \frac{e^2}{r_{12}}\ \chi_t(2)\chi_u(2)\ d\tau_1\, d\tau_2 \tag{7b}$$

$$P'_{tu} = 2 \sum_{j}^{n} A_{tj}A_{uj} \tag{7c}$$

$$S_{rs} = \int (\chi_s(1)\chi_r(1) - \delta_{rs})\ d\tau_1. \tag{7d}$$

Here n is the number of occupied MO's and δ_{rs} the well known Kronecker symbol.

2c. Symmetrical orthogonalization. As suggested in an article by Löwdin,[10] the AO's χ_r: are replaced by a set of orbitals λ_r:

$$\lambda_r = \chi_r - \sum_{v \neq r} \tfrac{1}{2} S_{rv}\ \chi_v \tag{8}$$

orthonormal to first order in S_{rv}. In the λ-basis the Roothaan equations have the form:

$$\sum_{s}^{m} \left\{ (\lambda_r|H^{\text{core}}(1)|\lambda_s) + \sum_{t,u} P_{tu}\{[\lambda_r\lambda_s|\lambda_t\lambda_u] - \tfrac{1}{2}[\lambda_r\lambda_u|\lambda_t\lambda_s]\} \right\} C_{si} = \varepsilon_i C_{ri} \tag{9}$$

with

$$\psi = \sum_{r=1} C_{ri}\lambda_r \tag{10}$$

and

$$P_{tu} = \sum_{j}^{n} C_{tj}C_{uj} \tag{11}$$

2d. Integral approximations. A number of semiquantitative features are now introduced to facilitate the evaluation of integrals in eqn. (9).

In the case of a two center charge distribution we have adopted either the general Löwdin approximation:[11]

$$\chi_r(1)\chi_s(1) \simeq \alpha\widetilde{\chi}_r(1)\widetilde{\chi}_s(1) + \beta\widetilde{\chi}_s(1)\widetilde{\chi}_s(1) \tag{12}$$

$$\alpha + \beta = S_{rs} \tag{13}$$

or the special Mulliken approximation:[12]

$$\chi_r(1)\chi_s(1) \simeq \tfrac{1}{2}S_{rs}\left(\widetilde{\chi}_r(1)\widetilde{\chi}_r(1) + \widetilde{\chi}_s(1)\widetilde{\chi}_s(1)\right) \tag{14}$$

In order to keep the approximations rotationally invariant, all one center charge distributions to the right in (12) and (14) have been replaced by their spherical averages, indicated by a [~]. Table 1 gives a detailed description of the approximations. Here column one and two show the integrals and number of centers, whereas column three contains expressions for the charge distributions $\lambda_r\lambda_s$ in terms of χ_r and χ_s.

Additionally we have adopted the point charge approximation:

$$V_g(1) \simeq -Z_g^{(ef)}/r_{1g} \tag{15}$$

when more than one center is involved. Here $Z_g^{(ef)}$ denotes the number of valence electrons from center g.

2e. Relation to other methods. The method described in the previous sections can be considered as the INDO counterpart to the CNDO scheme suggested by Dahl and Ballhausen.[8] As a deviation, however, we have chosen only to retain terms to first order in the overlap.

Table 1. Integral approximations.

Integral	Orbitals	$\lambda_r\lambda_s$
$(\lambda_r\|T\|\lambda_s)$	[r,s] arbitrary	$\chi_r\chi_s - S_{rs}(\chi_r\chi_r - \chi_s\chi_s)/2$ [exact to first order in S_{rs}]
$(\lambda_r\|V_a\|\lambda_s)$	[r,s] on the same a	$\chi_r\chi_s$ [exact to first order in S_{rs}]
	[r,s] on the same center b, different from a	$\widetilde{\chi_r\chi_r}\delta_{rs}$ [including a spherical average exact to first order in S_{rs}]
	[r,s] on two centers (a,b)	$\chi_r\chi_s - S_{rs}\cdot(\widetilde{\chi_r\chi_r} + \widetilde{\chi_s\chi_s})/2$ [including a spherical average exact to first order in S_{rs}]
	[r,s] on two centers (b,c)	$(\alpha - S_{rs}/2)\widetilde{\chi_r\chi_r} + (\beta - S_{rs}/2)\widetilde{\chi_s\chi_s}$ [with the Löwdin-approximation exact to first order in S_{rs}]
$[\lambda_r\lambda_s\|\lambda_t\lambda_u]$	[r,s] and [t,u] all on the same center	$\chi_r\chi_s$, $\chi_t\chi_u$ [exact to first order in S_{rs}]
	[r,s] and [t,u] on more than one center	$\widetilde{\chi_r\chi_r}\cdot\delta_{rs}$, $\widetilde{\chi_t\chi_t}\cdot\delta_{tu}$ [with the Mulliken-approximation exact to first order in S_{rs}]

Table 2. STO basis B1 and B2.

	1*s*	2*s*	3*s*	4*s*	2*p*	3*p*	4*p*	3*d*	3*d*
Ni [B1]	27.4	10.6	4.9	1.5	11.5	4.6	1.2	4.2	2.6
	1*s*	2*s*	3*s*	3*s*	2*p*	3*p*	3*p*	3*d*	3*d*
Ni [B2]	27.4	10.6	4.9	2.8	11.5	4.6	2.7	4.2	2.6
Fe [B2]	25.4	9.3	4.6	2.7	11.1	4.3	2.5	3.7	2.2
Cr [B2]	23.4	8.5	4.1	2.5	10.0	3.8	2.3	3.3	2.0
C	5.7	1.6	—	—	1.6	—	—	—	—
O	7.7	2.2	—	—	2.2	—	—	—	—
H	1.2	—	—	—	—	—	—	—	—

3. RESULTS AND DISCUSSIONS

3a. Radial functions. Two STO (Slater Type Orbitals) basis sets have been used (see Table 2). In the first [B1] 1*s*, 2*s*, and 2*p* on the metal and 1*s* on the ligands were taken as core with 3*s*, 3*p*, 3*d*, 4*s*, 4*p* from the central atom and 2*s*, 2*p* on the ligands in the valence shell. The exponents for B1 were taken from Clementi *et al.*,[13] but in order to simulate the basis of Demuynck *et al.*[2] a 3*d* polarization component was added.

In B2 polarization functions were added to 3*s*, 3*p* on the metal, whereas the 4*s*, 4*p* orbitals were omitted. Each STO component was Schmidt orthogonalized to the inner shells.

The geometries of $Ni(CO)_4$, $Ni(CN)^{42-}$ and $Fe(C_5H_5)_2$ were taken as in Ref. 2 and that of $Cr(CO)_6$ from Ref. 14.

3b. Comparison with ab initio *calculations.* In Table 3 we have the eigenvalues and atomic composition from a B1 INDO calculation on $Ni(CN)_4^{2-}$, together with the calculated eigen-

Table 3. INDO Calculation on $Ni(CN)_4^{2-}$ using [B1].

Orbital energies (a.u.)			Symmetry	Atomic composition (%)						
				Ni orbital			C orbital		N orbital	
				3d	4s	4p	2s	2p	2s	2p
.0157[a]	−.185[b]	.033[c]	$9a_{1g}$	94.0	5.2		.3	1.0	0.2	0.2
− .0013	−.267	−.013	$2e_g$	83.2				1.6		15.2
− .0609	−.335	−.026	$2b_{2g}$	72.9				3.7		23.4
− .1277	−.123	−.116	$1a_{2g}$					34.3		65.7
− .1319	−.136		$1b_{2u}$					46.0		54.0
− .1445	−.121	−.113	$8e_u$			0.7	0.1	19.7	0.1	79.4
− .1617	−.132		$1e_g$	13.8				46.0		40.2
− .2141	−.160		$3a_{2u}$			17.6		46.9		35.5
− .2392	−.156		$1b_{2g}$	22.9				44.4		32.7
− .2670	−.182		$5b_{1g}$	13.0			10.4	36.3	23.9	36.4
− .3562	−.195		$7e_u$			1.7	6.1	5.98	45.4	40.8
− .3578	−.231		$8a_{1g}$	1.7	0.1		5.8	4.9	49.0	38.5
− .4540	−.263		$4b_{1g}$	7.			50.0	6.4	23.3	13.3
− .8702			$6e_u$			37.1	20.7	37.6	4.3	0.4
− .9898			$7a_{1g}$		36.0		43.4	16.0	0.9	3.7
−1.2578			$3b_{1g}$				18.8	22.8	43.7	14.7
−1.2655			$6a_{1g}$		2.2		10.3	31.0	42.4	14.1
−1.2858			$5e_u$			3.9	27.3	13.3	41.1	14.4

[a] This work. [b] Ref. 2. [c] Calculated ionization potentials from Ref. 2.

Table 4. INDO on $Ni(CO)_4$ using [B1].

Orbital energies (a.u.)				Symmetry	Atomic composition (%)						
					Ni orbital			C orbital		O orbital	
					3d	4s	4p	2s	2p	2s	2p
.2024[a]				$11t_2$	3.3		36.3	35.0	4.1	2.9	18.2
− .1891				$9a_1$		34.3		40.8	.3	1.3	23.3
.0125				$10t_2$	11.2				56.4		21.2
.0442				$3e$	10.8				60.1		29.1
− .0102				$2t_1$					63.6		36.4
− .3847	−.35[b]	− .395[c]	−.3234[d]	$9t_2$	64.4		7.1	.5	6.3		21.7
− .4371	−.39	− .471	−.3564	$2e$	80.1				1.6		18.3
− .6384	−.43	− .653		$1t_1$					29.4		70.6
− .6642	−.45	− .644	−.5439	$8t_2$	5.8		.3	.8	31.7	.1	61.3
− .6713	−.46	− .665		$1e$	6.4				31.5		62.1
− .8571	−.50	− .662		$7t_2$	.1		2.4	7.1	9.1	31.1	48.2
− .8648	−.53	− .693	−.6688	$8a_1$		1.2		9.3	6.1	35.6	47.8
−1.2315	−.56	− .793		$6t_2$	1.0		32.6	35.4	24.5	1.5	5.0
−1.3983	−.58	− .809		$7a_1$		42.3		39.4	12.7	1.5	4.1
−1.9184	−.95	−1.530		$5t_2,6a_1$				14.5	20.0	55.2	10.6

[a] This work. [b] Eigenvalues extrapolated from Fig. 5 in Ref. 3. [c] Eigenvalues from Ref. 2. [d] Photoelectron spectrum as assigned by Ref. 2.

values and ionization potentials from Demuynck *et al.*[2] The agreement is good for the highest 4 levels, between our eigenvalues and the calculated ionization potentials in Ref. 2.

Koopmans' theorem is thus reasonably well fulfilled in our case. This is in contrast to the claim by Demuynck *et al.*, that this theorem is invalid for $Ni(CN)_4^{2-}$. A possible explanation of

Table 5. INDO calculation on $Ni(CO)_4$ using [B2].

Orbital energies (a.u.)		Symmetry	Atomic composition (%) Ni Orbital 3d	3p	3s	C orbital 2s	2p	O orbital 2s	2p
− .2335	−.3234[a]	$9t_2$	62.4			5.7	8.0	1.0	22.9
− .2977	−.3564	$2e$	74.9				3.7		21.4
− .5526	−.5439	$1t_1$					30.6		69.4
− .5694	−	$8t_2$	1.5				34.6		63.8
− .5742	−	$1e$	4.4				33.9		61.7
− .6090	−	$8a_1$			12.3	31.4	27.0	4.9	24.4
− .7032	−.6688	$7t_2$	10.1	2.6		12.5	24.9	16.0	33.9
− .8198		$7a_1$			1.5	36.0	1.2	29.2	32.1
− .8436		$6t_2$	3.7	1.0		51.9	2.6	20.1	20.7
−1.8205		$6a_1$				14.4	21.1	54.1	10.4
−1.8344		$5t_2$				13.9	22.0	53.8	10.3

[a] Photoelectron spectrum (Ref. 2).

Table 6. INDO calculation on $Fe(C_5H_5)_2$ using [B2].

Orbital energies (a.u.)				Symmetry	Atomic composition (%) Fe orbital 3d	3s	3p	C orbital 2s	2p	H orbital 1s
− .3491	−.530[b]	−.3050[c]	−.2499[a]	$3e_{2g}$	70.0				28.8	1.2
− .4165	−.429	−.4079	−.2646	$4e_{1u}$	71.2				27.9	.9
− .4360	−.609	−.3711	−.3234	$4a_{1g}$	86.4				11.5	2.1
− .4972	−.437	−.4116	−.3417	$4e_{1g}$	12.4				84.6	3.0
− .6242	−.589	−.5567		$3a_{2u}$			9.3		89.8	.9
− .6621	−.585			$3e_{2u}$				1.2	79.4	19.4
− .6782				$4a_{1g}$	7.5	10.4			80.5	1.6
− .6819				$3e_{1g}$				9.3	62.3	28.4
− .6892	−.594			$2e_{2g}$				7.8	60.4	31.8
− .6901				$3e_{1g}$	5.1			1.9	58.0	35.0
− .8304				$2a_{2u}$			1.5	14.4	48.0	36.1
− .8584				$3a_{1g}$	4.2	.5		14.4	44.6	36.3
− .9836				$2e_{1g}$				26.9	54.7	18.4
− .9957				$1e_{2g}$			2.2	25.0	54.5	18.3
−1.2396				$2e_{1u}$			2.0	62.4	28.1	7.4
−1.2737				$1e_{1g}$	2.9			64.4	27.8	4.9
−1.6413				$2a_{2u}$	11.6			57.6	29.9	.9
−1.6631				$2a_{1g}$	2.4	8.5		57.9	39.8	.5
−2.9892				$1e_{1u}$			100			
−3.1376				$1a_{2u}$			100			
−4.5993				$1a_{1g}$	100					

[a] Photoelectron spectrum (Ref. 2). [b] Orbital energies from Ref. 1. [c] Calculated ionization potentials from Ref. 1.

the improved agreement with experimental ionization potentials may lie in our use of a Slater orbital as a 3d polarization function, where Demuynck *et al.* use a single Gaussian orbital.

For the two non-bonding π-orbitals ($1a_{2g}$, $1b_{2u}$), the four bonding π-orbitals ($8e_u$, $1e_g$, $3a_{2u}$, $1b_{2g}$) and the remaining σ-orbitals, no comparison can be made, as Demuynck *et al.* have not directly calculated the ionization po-

Table 7. INDO calculation on $Ni(CN)_4^{2-}$ using [B2].

Orbital energies (a.u.)	Symmetry	Atomic composition						
		Ni orbital			C orbital		N orbital	
		3s	3p	3d	2s	2p	2s	2p
.1532	$9a_{1g}$	1.7		85.8	5.8	2.7	.4	3.6
.1073	$2e_g$			89.0		.3		10.7
.0429	$2b_{2g}$			77.0		3.3		19.7
− .0406	$1b_{2u}$					41.0		59.0
− .0556	$8e_u$		0.5		5.8	41.2	0.8	52.7
− .0671	$1a_{2g}$					48.3		51.7
− .0873	$3a_{2u}$					48.3		51.7
− .0880	$1e_g$			7.6		48.3		44.1
− .1441	$1b_{2g}$			18.1		50.1		31.8
− .1707	$7e_u$		4.5		15.7	31.6	16.3	31.6
− .1903	$8a_{1g}$	5.7		10.2	10.0	22.1	21.2	30.8
− .2042	$5b_{1g}$			7.4	10.3	25.0	25.6	31.7
− .3459	$6e_u$		2.3		46.1	4.5	15.1	32.0
− .3599	$7a_{1g}$	4.5		3.2	46.9	4.5	26.3	14.6
− .3620	$4b_{1g}$			5.9	52.4	6.4	21.5	13.8
−1.1788	$6a_{1g}$				23.1	21.2	41.0	14.7
−1.1860	$5e_u$				21.4	21.6	42.2	14.9
−1.1948	$3b_{1g}$				18.6	23.1	41.0	17.3

Table 8. INDO calculation on $Cr(CO)_6$ using [B2].

Orbital energies (a.u.)		Symmetry	Atomic composition (%)						
			Cr Orbital			C Orbital		O Orbital	
			3d	4s	4p	2s	2p	2s	2p
− .2684	−.3087[a]	$2t_{2g}$	63.3				12.7		24.0
− .5660	−.4895	$1t_{1g}$					31.1		68.9
− .5747	−.5189	$5t_{1u}$			.7	4.0	28.1	.1	67.7
− .5842	−.5325	$1t_{2u}$					37.3		62.7
− .6268	−.5586	$1t_{2g}$	3.6				41.9		54.5
− .6928	−.5733	$4t_{1u}$			9.4	16.0	28.1	5.2	43.0
− .7281	−.6424	$4a_{1g}$		12.3		8.1	24.0	17.3	38.3
− .7799	−.6872	$3e_g$	5.1				15.1	30.1	49.7
− .8591	−.7092	$3t_{1u}$			2.2	43.6	1.2	23.9	29.1
− .8887		$3a_{1g}$		8.8		54.0	3.8	17.3	16.1
− .9570		$2e_{1g}$	18.0			60.3	11.6	3.0	7.1
−1.8573		$2a_{1g}$				17.3	19.4	54.0	9.3
−1.8650		$2t_{1u}$			1.7	11.6	18.0	54.3	14.4
−1.8826		$1e_{1g}$				12.3	17.1	53.2	17.4

[a] Photoelectron spectrum (Ref. 14).

tentials for all of those orbitals as their basis seems to require.

In Table 4 we compare eigenvalues from an INDO calculation on $Ni(CO)_4$ with those of Ref. 2 and a recent Xα calculation by Johnson *et al.*[3] Our ordering of the occupied levels is in agreement with that of Ref. 3, and differ only for closely spaced orbitals from the ordering in Ref. 2. In addition, the magnitude of the eigenvalues is the same for INDO and *ab initio*. However, as the eigenvalues of Ref. 3 are defined differently they cannot be brought directly into this comparison.

As for the lower lying levels there is a qualitative as well as a quantitative difference between the INDO and the *ab initio* calculation, in as

much as our calculations give a significant $4s$ and $4p$ population. We will discuss this point in the next section.

3c. Limitations of the method. Consider the overlap charge distribution between two orbitals on the centres (a,b):

$$\varrho_{a,b}=\chi_a(1)\chi_b(1) \qquad (16)$$

In case the gravity point of $\varrho_{a,b}$ is placed close to one of the centres (a,b), say a, then the Mulliken approximation is quite inadequate for the hybrid type integral:

$$\int\chi_b(1)\chi_a(1)\chi_a(2)\chi_a(2)\frac{1}{r_{12}}d\tau_1 d\tau_2$$

and it would be unbalanced to calculate the analogous one electron nucleus split integral:

$$\int\chi_b(1)\chi_a(1)\frac{1}{r_a}d\tau_1$$

exactly as suggested in Section 2.

Investigations show that errors will enter into the Fock-matrix element between χ_a and χ_b, increasing it numerically up to 200 %.

In calculations on inorganic complexes this situation is important if $4s$ and $4p$ atomic orbitals are used, as the charge distribution of those orbitals usually has a maximum close to the ligand nucleus. The results in Section 3b are representative for a vast number of INDO calculations using $4s$ and $4p$ atomic orbitals. Due to the overestimation of the Fock-matrix elements between $2s_L$ and $4s_M$, and between $2s_L$ and $4p_M$ the calculations usually predicted considerably $4s$ and $4p$ populations.

Fortunately, it is only calculations relying on spectroscopic data that has to use $4s$ and $4p$ atomic orbitals for the sake of consistency.

In methods where all matrix elements are calculated over the basis set it is hard to see how $4s$ and $4p$ atomic orbitals with group overlaps up to 0.7 can add much new to the basis. For the calculations in the next section we have therefore replaced the $4s$ and $4p$ by more contracted $3s$ and $3p$ polarization functions [B2].

A number of calculations on small molecules show that the method estimates too small bond distances. In the case of CO our INDO method calculated an equilibrium bond distance of 0.83 Å compared to the experimental of 1.13 Å.

This trend can be accounted for by the sperical average used in Section 2. Such an approximation does not treat the repulsion between two orbitals pointing towards each other correctly.

In the CNDO/2 scheme [9] this deficiency is corrected by replacing:

$$\int\chi_a(1)\chi_a(1)\frac{1}{r_b} \text{ with } \int\chi_a(1)\chi_a(1)\chi_b(2)\chi_b(2)\frac{1}{r_{12}}d\tau_1 d\tau_2,$$

and this possibility might be investigated in a later work.

3d. Use of the basis [B2]. The nature of the bonding in $Ni(CO)_4$ has been a matter of dispute between an *ab initio* calculation by Demuynck *et al.*[2] and an Xα scattered-wave calculation by Johnson *et al.*[3]

Whereas Johnson *et al.* do not find any significant metal to ligand π-back bonding, Demuynck calculates an increase in the $2p\pi_C$ population when going from CO to the $Ni(CO)_4$. This trend is taken as an indication of π-back bonding. In our calculations on $Ni(CO_4)$, $Ni(CN)_4^{2-}$, and $Cr(CO)_6$, Tables 9, 11, and 12, a similar increase in the $2p\pi_C$ was found, greatest in the case of $Cr(CO)_6$ and smallest in $Ni(CN)_4^{2-}$ As for the ordering of the levels, the reader is referred to Tables 5, 7, and 8.

We will close this section by presenting a calculation on $Fe(C_5H_5)_2$. Although it is a different system, the situation is the same as for our previous comparison with the *ab initio* calculation on $Ni(CN)_4^{2-}$. Our assignment, Table 6, only agrees with that of Ref. 2 after Demuynck *et al.* have performed calculations on the ionization potentials.

In Table 10 we give the population analysis of $Fe(C_5H_5)_2$ compared to $C_5H_5^-$. The trend is the same as in the *ab initio* calculation: an increase in the population on $1s_H$ and a decrease in the population of $2p\pi_C$, when going from $Fe(C_5H_5)_2$ to $C_5H_5^-$.

Table 9. Gross atomic and orbital populations from an INDO calculation on $Ni(CO)_4$ using [B2].

	$Ni(CO)_4$			CO	
	Ni	C	O	C	O
$3s/2s$	0.18	1.74	1.79	1.85	1.79
$3p_x/2p_\sigma$	0.08	1.04	1.33	1.02	1.33
$3p_y/2p_\pi$	0.08	0.77	1.41	0.57	1.42
$3p_z/2p_\pi$	0.08	0.77	1.41	0.57	1.42
$3d_{t2}$	1.62				
$3d_e$	1.58				

Table 10. Gross atomic and orbital populations from an INDO calculation on $Fe(C_5H_5)_2$ using [B2].

	Fe	C	H
S	6.30	3.19(3.15)[a]	.86(.98)
p_x+p_y	8.24	1.96(1.92)	
p_z	4.25	1.17(1.19)	
d_{xz},d_{yz}	.43		
$d_{xy},d_{x^2-y^2}$	1.45		
d_{z^2}	2.03		

Table 11. Gross atomic and orbital populations from an INDO calculation on $Cr(CO)_6$.

	$Cr(CO)_6$			CO	
	Cr	C	O	C	O
$3s/2s$	0.29	1.60	1.79	1.85	1.79
$3p_x/2p_\sigma$	0.20	1.04	1.46	1.02	1.33
$3p_y/2p_\pi$	0.20	0.82	1.22	0.57	1.42
$3p_z/2p_\pi$	0.20	0.82	1.22	0.57	1.42
$3d_{t_2}$	4.01	–	–	–	–
$3d_e$	0.92	–	–	–	–

Table 12. Gross atomic and orbital populations from an $Ni(CN)_4^{2-}$ using [B2].

	$Ni(CN)_4^{2-}$			CN^-	
	Ni	C	N	C	N
$3s/2s$	0.13	1.7	1.81	1.85	1.81
$3p_x/2p_\sigma$	0.1	1.09	1.19	1.09	1.24
$3p_y/2p_\pi$	0.1	0.95	1.07	0.86	1.13
$3p_z/2p_\pi$	0.0	0.96	1.06	0.86	1.13
$3d_{xy}$	1.92				
$3d_{xz},3d_{yz}$	1.93				
$3d_{z^2}$	2.0				
$3d_{x^2-y^2}$	0.28				

4. CONCLUSION

A new semiquantitative SCF LCAO MO calculation scheme has been applied to $Ni(CO)_4$, $Cr(CO)_6$, $Fe(C_5H_5)_2$, and $Ni(CN)_4^{2-}$. Comparison to recent *ab initio* calculations seems promising, and calculations on tetrahedral tetrahalid complexes [15] and tetrahedral oxo complexes [16] are now in preparation.

Acknowledgement. A large part of the work described in this paper was carried out at the Department of Physical Chemistry, University of Copenhagen, and the author would like to thank Dr. J. P. Dahl for valuable discussions.

A general program (ODIN) based on our method has been developed by J. A. Geer and D. R. Truax of the Department of Chemistry, University of Calgary.

REFERENCES

1. Coutiere, M. M., Demuynck, J. and Veillard, A. *Theor. Chim. Acta 27* (1972) 281.
2. Demuynck, J. and Veillard, A. *Theor. Chim. Acta 28* (1973) 241.
3. Johnson, K. H. and Walgren, U. *Int. J. Quantum Chem. 6S* (1971) 250.
4. Demuynck, J. and Veillard, A. *Chem. Phys. Lett. 6* (1970) 204.
5. Hilliers, I. H. and Saunders, V. R. *Chem. Commun.* (1969) 1275.
6. Hilliers, I. H. and Saunders, V. R. *Chem. Phys. Lett. 9* (1971) 219.
7. Johansen, H. *Chem. Phys. Lett. 17* (1972) 569.
8. Dahl, J. P. and Ballhausen, C. J. *Advan. Quantum Chem. 4* (1968) 170.
9. Pople, J. A., Santry, D. P. and Segal, G. A. *J. Chem. Phys. 43* (1965) S129.
10. Löwdin, P. O. *Phil. Mag. Suppl.* Vol. *5* (1956) No. 17.
11. Löwdin, P. O. *J. Chem. Phys. 21* (1953) 374.
12. Mulliken, R. S. *J. Chim. Phys. Physicochim. Biol. 46* (1949) 675.
13. Clementi, E. and Raimolni, D. L. *J. Chem. Phys. 38* (1968) 2686.
14. Caulton, K. G. and Fenske, R. F. *Inorg. Chem. 7* (1968) 1273.
15. Geer, J. A., Truax, D. R. and Ziegler, T. *To be published.*
16. Ziegler, T. *To be published.*

Received July 2, 1973.

Acta Chemica Scandinavica A 28 (1974) 37—44

The Vacuum Ultraviolet Spectrum of Tetramethyl-1,3-cyclobutanedione

MARTIN VALA,[a,*] IB TRABJERG [b] and E. N. SVENDSEN [b,**]

[a] Department of Chemistry, University of Florida, Gainesville, Florida 32601 and [b] Department of Chemistry, H. C. Ørsted Institute, University of Copenhagen, DK-2100 Copenhagen Ø, Denmark

An experimental and theoretical investigation of the higher-lying electronic states of the cyclic diketone, tetramethyl-1,3-cyclobutanedione, has been performed. Vapor phase vacuum ultraviolet spectra have been recorded to 65 000 cm^{-1}. Single crystal polarized spectral results are presented for a band at 43 500 cm^{-1}. Vibrational analyses have been carried out and band assignments made. Transitions to $\sigma\pi^*$, $n\sigma^*$, and mixed $n\sigma^*$, $\pi\pi^*$ states have been observed. Molecular orbital calculations including configuration interaction have been done on the parent molecule, cyclobutanedione, in the CNDO/S, CNDO/2, and INDO approximations. The results from the CNDO/S computation are shown to fit the experimental results reasonably well.

I. INTRODUCTION

Although the electronic structure and spectra of nonconjugated monocarbonyl compounds such as formaldehyde have been much studied and are now well characterized, a similar situation does not exist for dicarbonyl compounds. The primary interest in these systems and also their major complication is the magnitude and mechanism of the electronic interaction between the two carbonyl moieties. Because of this current interest we have initiated a spectroscopic and photochemical investigation of one particular diketone, tetramethyl-1,3-cyclobutanedione, Fig. 1. This molecule has a number of desirable characteristics which should, in principle, be helpful in understanding the mechanism and magnitude of its transannular interaction. Its chromophoric groups are spatially close enough to expect a readily observable interaction, its molecular framework is planar and symmetrical in its ground electronic state, its crystal structure is known and simple, and its vapor pressure at room temperature is sufficient for vapor studies. In the present paper, we report on our experimental and theoretical study of the higher-lying excited electronic states of tetramethyl-1,3-cyclobutanedione (TMCBD). Discussion of the low-lying energy region (*i.e.*, including $n\pi^*$ transitions) will be presented in another paper.

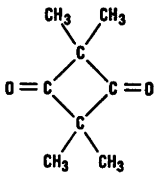

Fig. 1. Tetramethylcyclobutane-1,3-dione.

In order to elucidate the nature of the higher-lying electronic states of TMCBD we have investigated its vacuum ultraviolet spectrum to 65 000 cm^{-1} in the vapor phase and have also studied the polarized single crystal absorption spectrum for the band at 43 500 cm^{-1}. Additionally we have calculated the transition energies of the parent molecule, cyclobutanedione, in the CNDO/S, and CNDO/2, and INDO approximations. The experimental details are presented in Section II and the computational

* Senior Fulbright Fellow, Laboratoire d'Optique Physique, ESPCI, Paris, France, 1973—1974.

** Present address: Department of Chemistry, Odense University, Niels Bohrs Allé, DK-5000 Odense, Denmark.

procedures in Section III; the results are given in Section IV, discussed in Section V, and compared to the theoretical molecular orbital predictions in Section VI.

II. EXPERIMENTAL

The TMCBD was obtained from Aldrich Chemical Company as a white solid with a vapor pressure of about 0.5 torr at room temperature[1]; recrystallization was carried out from benzene or toluene solvent. The vacuum UV spectra were obtained from the gas phase on a McPherson Model 240 Two Meter UV spectrograph and scanning monochromator equipped with a modified Model 630 Hinteregger type discharge lamp filled with either hydrogen or xenon gas. Each spectrum was recorded at least twice photographically to check for sharp lines and twice photoelectrically, using a double beam technique, to detect broad bands and to insure that photoproducts, if produced, were not responsible for the observed bands. Except for small changes, possibly due to temperature fluctuations or deposits on the cell windows, the spectra were reproducible. The temperature of the cell was 297 K.

The single crystal spectrum was run on a Cary 14 spectrophotometer, at room temperature. The crystal was mounted over a hole in a copper square which was in turn held in the beam by a sample holder.

III. COMPUTATIONAL PROCEDURES

In our calculations, it has been assumed that the neglect of the methyl groups will play no major role, other than possibly shifting the energy levels slightly. The geometry of the parent molecule, cyclobutanedione, was assumed to coincide with that of TMCBD, as given by an X-ray crystallographic study.[2] The C – C bond distances were taken as 1.56 Å, the C – O distances 1.20 Å, the C – H distances 1.10 Å, the C – C – C ring angles as 90°, and the HCH angles [3] as 116°. The CNDO/2, CNDO/S, and INDO calculations were performed with a

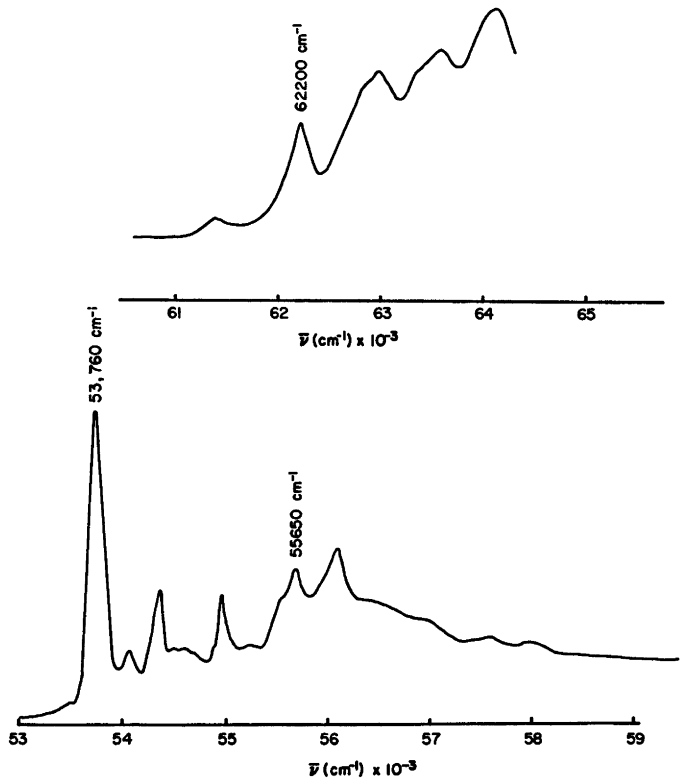

Fig. 2. Vapor phase vacuum ultraviolet spectrum of tetramethyl-1,3-cyclobutanedione.

revised version of QCPE program 141. Further details on the computation procedures employed are provided elsewhere.[4-6]

IV. RESULTS

The vapor vacuum UV spectrum is shown in Fig. 2 and the band positions given in Table 1.

In addition, we have measured the room temperature polarized absorption spectrum of the 43 500 cm^{-1} band on a single crystal. TMCBD belongs to the monoclinic space group $C2/m(C_{2h}^3)$. In the primative unit cell, there is only one molecule which is aligned such that the planar molecular skeleton (excluding the methyls) is perpendicular to the b crystallographic axis.[2] Transitions polarized parallel-to-b are therefore out-of-plane with respect to the molecular framework and transitions polarized perpendicular-to-b are in-plane. The band at 43 500 cm^{-1} is broad and structureless with a predominant out-of-plane polarization, although some intensity in the in-plane polarization was observed. Crystals thin enough to observe the band maximum of the former polarization could not be successfully grown.

Table 2 gives the results of our molecular orbital computations. The symmetry of the upper state and the nature of the transition are also given. The $n\pi^*$ transition energies have been included for comparison, although a complete study of them, utilizing low temperature (4.2 K) single crystal polarized absorption techniques, will be the subject of a separate report.[7]

V. DISCUSSION OF SPECTRAL RESULTS

a. The 43 500 cm^{-1} transition

Ballard and Park [8] have reported the solution spectrum of the 43 500 cm^{-1} region (as well as the lower energy $n\pi^*$ region) in TMCBD and assigned the broad band observed there to the $n\sigma^*$ transition, in analogy with the 53 000 cm^{-1} band in acetone. Whitlock and Duncan [9] in their study of cyclobutanone observed a transi-

Table 1. Observed electronic transitions in tetramethyl-1,3-cyclobutanedione.

State Symmetry	Energy (cm^{-1})	Interval (cm^{-1})	Vibrational assignment (cm^{-1})	Ground state vibration
$^1B_{1u}$	43500	–	–	–
$^1B_{3u}$	53500	−260	−260	270(R)
	53560	−200	−200	217(R)
	53760	0	0−0	–
	54050	+290	+290	298(R)
	54350	+590	+590	584(R)
	54500	+740	+740	760(IR)
	54560	+800	+800	820(IR)
	54650?	+890	+290+590	–
	54880	+1120	?	?
	54950	+1190	+2×590	–
	55250	+1490	+2×590+290	–
	55560	+1800	+3×590	–
$^1B_{2u}$,$^1B_{1g}$	55650	0	0−0	–
	56030	+380	+380	?
	56120	+470	+470	?
	56500	+850	+470+380	–
	56880	+1230	+470+2×380	–
	57410	+1760	+2×470+2×380?	–
	57970	+2320	?	?
^1A_g	61385	0	0−0	–
	62200	+815	+815	820(IR)
	62800	+1415	+815+600	632 or 584(R)
	62900	+1515	+815+700	?
	63350	+1965	+815+1150	1851(R)
	63600	+2215	+815+600+700	–
	64100	+2715	+815+1150+700	–

Table 2. Energies of electronic states in tetramethyl-1,3-cyclobutanedione.

Observed energies (eV)		Calculated energies (eV) CNDO/S		CNDO/2		INDO	
		$^1B_{3g}(n\pi^*)$	3.16	$^1B_{3g}(n\pi^*)$	4.27	$^1B_{3g}(n\pi^*)$	4.24
		$^1A_u(n\pi^*)$	3.16	$^1A_u(n\pi^*)$	4.44	$^1A_u(n\pi^*)$	4.39
$^1B_{1u}$	5.46	$^1B_{1u}(\sigma\pi^*)$	6.00	$^1B_{2g}(\sigma\pi^*)$	9.04	$^1B_{2g}(\sigma\pi^*)$	8.69
		$^1B_{2g}(\sigma\pi^*)$	6.04	$^1B_{1g}(n\sigma^*)$	9.24	$^1B_{1g}(n\sigma^*)$	8.96
				$^1B_{1u}(\sigma\pi^*)$	9.35	$^1B_{1u}(\sigma\pi^*)$	9.04
		$^1B_{3g}(n\pi^*)$	6.20				
		$^1A_u(n\pi^*)$	6.22				
$^1B_{3u}$	6.67	$^1B_{3u}(n\sigma^*)$	7.08	$^1B_{3g}(n\pi^*)$	9.81	$^1B_{3g}(n\pi^*)$	9.44
$^1B_{2u}$	6.90	$^1B_{2u}(n\sigma^*)$	7.23	$^1B_{2u}(n\sigma^*)$	10.34	$^1B_{2u}(n\sigma^*)$	9.66
$^1B_{1g}$		$^1B_{1g}(n\sigma^*)$	7.26	$^1A_u(n\pi^*)$	10.38	$^1A_u(n\pi^*)$	9.96
^1Ag	7.71	$^1A_g(n\sigma^*,\pi\pi^*)$	7.63	$^1A_g(n\sigma^*)$	10.55	$^1B_{3u}(n\sigma^*)$	10.32
				$^1B_{3u}(n\sigma^*)$	10.88	$^1A_g(\pi\pi^*)$	10.59

tion at 49 281 cm^{-1} which they assigned to an $n'\pi^*$ transition, the n' orbital being essentially a $2p$ orbital extending along the carbonyl axis.[10]

In theory, an unambiguous assignment of this electronic band to either a $n\sigma^*$ or $\sigma\pi^*$ (*i.e.*, $n'\pi^*$-like) transition should be possible by investigation of the polarized crystal spectrum. Because of the presence of the two carbonyl groups, each of these transitions could be split into a maximum of four separate transitions, the exact number depending upon the magnitude of the splittings of the MO's involved in the transition. From our MO computations, it can be seen (in Table 2) that four $n\sigma^*$ transitions with symmetries $^1B_{2u}$, $^1B_{3u}$, $^1B_{1g}$, and ^1A_g and two $\sigma\pi^*$ transitions (for the energy range under consideration) with symmetries $^1B_{1u}$ and $^1B_{2g}$ are predicted. Optical transitions to the $^1B_{3u}$ and $^1B_{2u}$ $n\sigma^*$ states are allowed with x and y (in-plane) polarizations, respectively, while the transition to the $^1B_{1u}$ $\sigma\pi^*$ state is allowed only in a z (out-of-plane) polarization.

The observed absorption spectrum shows a band whose polarization is predominantly out-of-plane, thus lending very strong support to its characterization as a $\sigma\pi^*$ transition. The observed in-plane component could possibly be the $^1B_{2g}$ transition whose appearance is made allowed by vibronic coupling *via* a b_{1u} vibration (such as the out-of-plane ring puckering mode [1]). Alternatively, the in-plane component could be ascribed to a transition between n and π^* or σ^* orbitals, both of which should be in-plane polarized. This possibility exists because of the strong mixing between n and σ type orbitals in this molecule (*vide infra*). However, in the absence of vibrational structure on the band both these explanations must be regarded as speculative at present.

The interpretation of the 43 500 cm^{-1} band as a $\sigma\pi^*$ transition is consistent with the $n'\pi^*$ assignment of Whitlock and Duncan,[9] since the n' orbital is mixed strongly with a number of different σ orbitals. It is also consistent with previous assignments of a similarly-positioned transition in other cyclic ketones,[4] *e.g.* cyclopentanone and cyclohexanone.

b. The 54 000 and 55 600 cm^{-1} transitions

In the region between 53 500 cm^{-1} and 58 000 cm^{-1}, the spectrum of TMCBD shows some vibrational structure. Due to the irregularity of the absorption envelope (see Fig. 2), the presence of two electronic transitions in this region is indicated. If we assign the band at 53 760 cm^{-1} to the 0 – 0 band of the first electronic transition, a reasonable and consistent vibrational analysis is possible. Table 1 gives the analysis of the band structure.

A progression of at least three members in a 590 cm^{-1} mode built on the 0 – 0 transition is prominent in the region from 53 500 cm^{-1} to

55 560 cm^{-1}. Built upon each of these modes is one quantum of a 290 cm^{-1} vibration. The ground state counterparts of these two vibrations have been observed in the single crystal Raman spectrum:[1] one at 584 cm^{-1} has been identified as the totally symmetric ring breathing mode and the other at 298 cm^{-1} as one of the carbonyl wagging modes. The bands at 53 500 cm^{-1} (0 – 0 minus 260 cm^{-1}) and 53 560 cm^{-1} (0 – 0 minus 200 cm^{-1}) can be assigned to vibrational hot bands. An attempt was made to substantiate the latter tentative assignment by varying the temperature of the cell, but the results was inconclusive due to the overlapping tail of the intense 0 – 0 absorption band. However, two vibrational modes, one at 270 cm^{-1} and the other at 217 cm^{-1}, have been observed [1] in the Raman spectrum of a polycrystalline TMCBD sample and are likely the vibrations involved.

Two factors point toward the symmetry-allowed nature of this transition: (1) the shape of the Franck-Condon envelope with the 0 – 0 band most intense, and (2) the proximity in energy of the ground and excited state vibrational frequencies. One expects that for an allowed transition with little or no geometry change in the excited state that the 0 – 0 band will be most intense and, furthermore, that the excited state vibrational force constants (and therefore frequencies) will be similar to those in the ground state. The appearance of a progression in the ring breathing mode plus the carbonyl wagging activity is indicative of the presence of an electronic transition originating from either a σ and/or an n type orbital. Since the σ and n orbitals are substantially mixed in TMCBD and since the 43 500 cm^{-1} transition has previously been characterized as a predominantly $\sigma\pi^*$ transition, we interpret this band as an allowed $n\sigma^*$ transition. Using a symmetry argument it is possible to choose between the two allowed orbital designations for the excited state, $^1B_{2u}$ or $^1B_{3u}$. With two types of carbonyl wagging vibrations in TMCBD, an in-phase b_{1u} mode and an out-of-phase b_{2g} mode, the most probable vibronic symmetry of the 54 050 cm^{-1} band can be determined from the direct product of the electronic symmetries, B_{2u} and B_{3u}, with the possible vibrational ones, b_{1u} and b_{2g}. Only in the case of a b_{2g} vibration built on a B_{3u} electronic origin is a state of allowed vibronic symmetry generated (B_{1u}). Thus it can be concluded that the 53 760 cm^{-1} band is an allowed $n\sigma^*$ transition of $^1B_{3u}$ symmetry.

An alternate analysis of the vibrational structure in this region is possible, though much less preferable. With the one dominant vibrational mode frequency half the other, to whithin experimental error (590 cm^{-1} *vs.* 290 cm^{-1}) the observed structure could be due to a *single* multimembered progression in a 290 cm^{-1} mode. Since there are two carbonyl wags in TMCBD, neither of which is totally symmetric, the observation of an every-member progression dictates that the geometry of the excited state must be distorted, such that either or both of these modes become totally symmetric. In such a case the intensity alternation could then be the result of inversion doubling. However, the shape of the Franck-Condon envelope with the 0 – 0 band most intense mitigates against this interpretation, since this is an observation one does not expect in a transition to a distorted excited state.

A second electronic transition is indicated in the region from 55 650 cm^{-1} to 58 000 cm^{-1} with its origin most probably at 55 650 cm^{-1}. Because of the diffuseness of the bands a precise vibrational analysis in this region is difficult, although a tentative one is given in Table 1. Average vibrational intervals of 380 cm^{-1} and 470 cm^{-1} are apparent in this region. Identification of these vibrations has not been possible, other than to conclude that they most likely involve skeletal bending modes. Thus, with the present data, the assignment of this electronic transition is very difficult; however, taken together with our MO computations the data lead to its assignment as one (or more) of the remaining $n\sigma^*$ transitions (*i.e.*, ^1A_g, $^1B_{1g}$, or $^1B_{2u}$) (*vide infra*).

c. The 63 000 cm^{-1} transition

The absorption in this region is characterized by several broad vibrational bands built on a rising background (see Fig. 1). With the 61 385 cm^{-1} band assigned as the 0 – 0 transition the vibrational analysis for this electronic transition is straightforward (see Table 1). The 62 200 cm^{-1} band is assigned to the 815 cm^{-1} non-totally symmetric carbon-carbon stretching

mode, correlating well with the solution 820 cm^{-1} mode (of b_{1u} or b_{3u} symmetry [1]) in the ground state. This assignment is consistent with the fact that the shape of the spectral envelope indicates the transition is a symmetry forbidden one; it is vibronically induced *via* the 815 cm^{-1} non-totally symmetric vibration. The 62 800 cm^{-1} band is assigned to a combination of the 815 cm^{-1} mode and a 600 cm^{-1} mode. The latter vibration is probably a totally symmetric mode involving skeletal bending. Two such vibrations are found in this frequency range in the solution Raman spectrum (632 and 584 cm^{-1}). The 63 350 cm^{-1} band is assigned to a combination of the 815 cm^{-1} mode and an 1150 cm^{-1} vibration, the latter of which is believed to be the in-phase totally symmetric carbonyl stretching mode, which in the ground state occurs at 1851 cm^{-1}. In the corresponding electronic transition in cyclobutanone the carbonyl stretching frequency appears at 1040 cm^{-1} in the $\pi\pi^*$ state and at 1816 cm^{-1} in the electronic ground state.[9]

The nature of this electronic transition and its symmetry assigment cannot conclusively be made with the present data. Interestingly however, neither the 54 000 cm^{-1} band nor the 56 000 cm^{-1} band(s) show any carbonyl stretching frequencies, whereas the present band appears to do so, in addition to displaying several skeletal frequencies. This vibrational activity indicates an electronic transition to a state of mixed origin, probably involving σ (and/or n) orbitals and π orbitals. By analogy with cyclobutanone [9] and other alkyl ketones,[4] it could be argued that this transition should be characterized as a $\pi\pi^*$ transition. However, a complicating factor with this assignment in the present dione is the possibility of a finite transannular interaction between the two chromophoric carbonyl groups. Such an interaction would result in a splitting of the π and π^* orbitals as well as any n, σ, or σ^* orbitals involved in the transition. Mixing between such electronic states with similar symmetries is possible (*e.g.* between $\pi\pi^*$ and $n\sigma^*$ ^1A_g states) provided the energy separation of the zeroth order states is not too great. Given the symmetry-forbidden nature of this band, its unique vibrational activity, and the molecular orbital calculational results (*vide infra*), the most probable assignment for this state is ^1A_g. The major *calculated* contributions to this state are from $n\sigma^*$ and $\pi\pi^*$ transitions, a result consistent with the experimental observations.

Finally, it is of interest to determine whether any of the bands thus far discussed could be assigned to a Rydberg transition. The first ionization potential of TMCBD, as determined by photoelectron spectroscopy, is 8.80 eV.[11] Assuming a Rydberg defect of 1.05 (the cyclobutanone value [9]), Rydberg transitions, if present, should appear at approximately 59 200 cm^{-1} ($n=4$), 64 300 cm^{-1} ($n=5$), and 66 700 cm^{-1} ($n=6$). The first transition falls in a transparent region and the latter two to higher energies than our last observed band, beyond which a continuum appears to be setting in. Thus, it seems unlikely that any of the bands discussed above are Rydberg transitions.

VI. DISCUSSION OF MOLECULAR ORBITAL CALCULATIONS

Three different MO approximations [5,8] were used in calculating the transition energies of cyclobutanedione. Table 2 outlines the overall findings of the three calculations and compares them to the experimental data. As determined in our previous work [4] on the cycloalkanones, the CNDO/2 and INDO approximations give energies which are too high by 3 to 4 eV, whereas the CNDO/S scheme more closely fits the observed energy pattern. In the following discussion we thus concentrate exclusively on the CNDO/S results.

Table 3 gives the CNDO/S results again but in somewhat greater detail: the specific MO's involved in the transitions and the contribution of each to the particular band are described explicitly. Because of the inclusion of configuration interaction, many of the transitions are composite ones made up of several electronic transitions of the same symmetry. The shapes of the most important molecular orbitals as determined by this calculation are sketched in Fig. 3.

The first calculated transition to higher energy of the $n\pi^*$ transitions is to the allowed $^1B_{1u}$ ($\sigma\pi_-^*$) state with the forbidden $^1B_{2g}$ ($\sigma\pi_+^*$) to slightly higher energy. This is in excellent agreement with the polarized single crystal results (see Sec. VA). That the $^1B_{1u}$ state lies lower than the $^1B_{2g}$ one (*i.e.*, the π_-^* orbital

Table 3. Calculational results on cyclobutanedione using the CNDO/S method.

Symmetry	Energy(eV)	Orbitals [a]
$^1B_{3g}$	3.16	$n_+ \rightarrow \pi_+^*(.71)$ $n_- \rightarrow \pi_-^*(.68)$
^1A_u	3.16	$n_+ \rightarrow \pi_-^*(.72)$ $n_- \rightarrow \pi_+^*(.67)$
$^1B_{1u}$	6.00	$\sigma_1(n') \rightarrow \pi_-^*(.90)$ $\sigma_2(n') \rightarrow \pi_+^*(.42)$
$^1B_{2g}$	6.04	$\sigma_2(n') \rightarrow \pi_+^*(.90)$ $\sigma_1(n') \rightarrow \pi_-^*(.43)$
$^1B_{3g}$	6.20	$n_+ \rightarrow \pi_+^*(.70)$ $n_- \rightarrow \pi_-^*(.68)$ $\sigma_3 \rightarrow \pi_+^*(.21)$
^1A_u	6.22	$n_+ \rightarrow \pi_-^*(.69)$ $n_- \rightarrow \pi_+^*(.69)$ $\sigma_3 \rightarrow \pi_-^*(.21)$
$^1B_{3u}$	7.08	$n_+ \rightarrow \sigma_1^*(.96)$
$^1B_{2u}$	7.23	$n_+ \rightarrow \sigma_2^*(.81)$ $n_- \rightarrow \sigma_3^*(.53)$
$^1B_{1g}$	7.26	$n_+ \rightarrow \sigma_3^*(.84)$ $n_- \rightarrow \sigma_2^*(.49)$
^1A_g	7.63	$n_- \rightarrow \sigma_1^*(.91)$ $\pi_+ \rightarrow \pi_+^*(.30)$ $\pi_- \rightarrow \pi_-^*(.20)$

[a] The orbital designations are shown pictorially in Fig. 3. The numbers in parenthesis after the orbital descriptions denote the percentage of configuration mixing. Only the major contributors are listed.

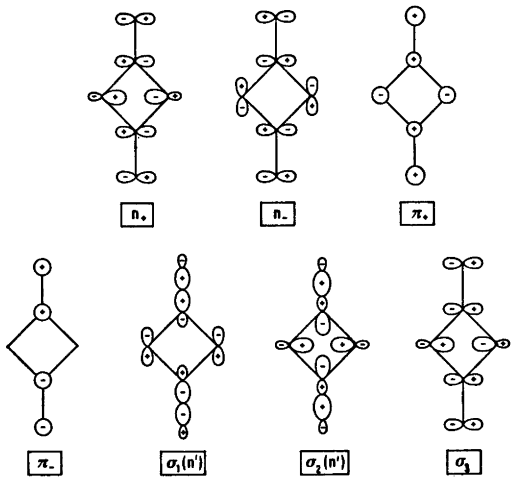

Fig. 3. Several molecular orbitals of cyclobutanedione as determined by a CNDO/S-CI calculation. The orbitals involving the ring hydrogens are omitted for the sake of clarity.

lying lower than the π_+^* orbital (see Table 3)) is also in agreement with the results deduced from the bands in the $n\pi^*$ region.[7] It is also of interest to note here that the σ orbitals from which the electronic transition originates are clearly n'-like, (see Fig. 3) as first proposed by Barnes and Simpson,[10] although they are substantially mixed with the σ framework of the cyclobutane ring.

Transitions to two symmetry-forbidden $n\pi^*$ states are predicted to occur next, at an energy slightly higher than the $\sigma\pi^*$ transitions. Because of their intrinsically lower intensity it is expected that such transitions would be difficult, if not impossible, to identify if they were to occur in a region close to a symmetry-allowed band, such as the $^1B_{1u}$ $\sigma\pi^*$ transition. Indeed, we have been unable to uncover any evidence for or against their appearance in this region and therefore comment no further on them here.

The next group of calculated transitions are to several $n\sigma^*$ states, the lowest of which is a $^1B_{3u}$ state. Again, this prediction is in excellent agreement with the observations (see Sec. VB). From the spectrum it is obvious that the band at 54 000 cm^{-1} is an allowed transition and our analysis shows it to be of $^1B_{3u}$ symmetry. Moreover, the fact that the $^1B_{3u}$ band, whose electron transition originates from the n_+ orbital, lies at lower energy than any of the bands of n_- origin is in accordance with our results in the $n\pi^*$ region.[7] As has been noted, the observed bands in the 55 600 cm^{-1} region are difficult to assign. From their overall shape one would expect them to be symmetry forbidden, however, if two electronic origins are present within the spectral envelope and are close-lying, the relative heights of the sharper 55 560 cm^{-1} and 56 120 cm^{-1} bands could be the result of an under-lying broad band. If this were true, then one could assign the sharper bands to the $^1B_{2u}$ transition and the under-lying broader ones to the $^1B_{1g}$ transition. We note, but put no particular stress on, the fact that the observed energy interval between the origin of the 54 000 cm^{-1} band and the origin of 55 600 cm^{-1} band is 0.23 eV, a value not very different from the calculated splitting between the $^1B_{3u}$ and $^1B_{2u}$ states of 0.15 eV. With the present data, the assignment of the 55 560 cm^{-1} and 56 120 cm^{-1} bands to the $^1B_{2u}$ transition and the higher energy,

broader ones to the $^1B_{1g}$ transition is regarded as tentative at present.

The final calculated transition before the observed onset of the continuum is to a mixed $n\sigma^*$, $\pi\pi^*$ state of ^1A_g symmetry. Although the data are not conclusive enough for an unambiguous identification, this assignment is consistent with both experiment and theory.

Acknowledgements. This work was supported in part by the *National Science Foundation* (Grant GP 12740). MV wishes to thank the *Scandinavian-American Foundation* through the *Denmark-America Fund* for the *George Marshall Memorial Fund Fellowship* for partial support during the summer of 1971 at the H.C. Ørsted Institute. Acknowledgement is also gratefully made to the *Northern Europe University Computing Center* (NEUCC) at Lundtofte, Denmark, for free computer time on their IBM 7094. Finally, we thank Dr. Aage E. Hansen for many helpful discussions. The UV spectrograph was put at our disposal by *Statens Naturvidenskabelige Forskningsråd.*

REFERENCES

1. Nicolaisen, F. O., Nielsen, O. F. and Vala, M. *J. Mol. Struct. 13* (1972) 349.
2. Friedlander, P. H. and Robertson, J. M. *J. Chem. Soc.* (1956) 3083.
3. *Tables of Interatomic Distances and Configuration in Molecules and Ions*, Sutton, L. E., Ed., Chem. Soc., London 1958.
4. Svendsen, E. N. and Vala, M. *Acta Chem. Scand. 26* (1972) 3475.
5. Bené, J. Dél and Jaffe, H. H. *J. Chem. Phys. 48* (1968) 1807, 4050.
6. Pople, J. A., Santry, D. F. and Segal, G. A. *J. Chem. Phys. 43* (1965) s129; Pople, J. A. and Segal, G. A. *J. Chem. Phys. 43* (1965) s136; *44* (1966) 3289.
7. Vala, M., Wrobel, J. and Spafford, R. *To be published.*
8. Ballard, R. E. and Park, C. H. *Spectrochim. Acta A 26* (1970) 43.
9. Whitlock, R. F. and Duncan, A. B. F. *J. Chem. Phys. 55* (1971) 218.
10. Barnes, E. and Simpson, W. *J. Chem. Phys. 39* (1963) 670.
11. Cowan, D. O., Gleiter, R., Hashmall, J. A., Heilbronner, E. and Hornung, V. *Angew. Chem. 10* (1971) 401.

Received August 30, 1973.

Acta Chemica Scandinavica A 28 (1974) 45—47

The Molecular Structure of Dimethylaluminium Chloride Dimer, $[(CH_3)_2AlCl]_2$, Redetermined by Gas Phase Electron Diffraction

KRISTEN BRENDHAUGEN, ARNE HAALAND and DAVID P. NOVAK

Department of Chemistry, University of Oslo, Blindern, Oslo 3, Norway

$[(CH_3)_2AlCl]_2$ has been studied by gas phase electron diffraction. The scattering pattern is consistent with a molecular model of D_{2h} symmetry with bridging Cl atoms. The main molecular parameters are Al—C = 1.935(4) Å, Al—Cl = 2.303(3) Å, ∠C—Al—C = 126.9(0.8)° and ∠Cl—Al—Cl = 89.4(0.5)°. The Al—C bond is significantly *shorter* than the Al—C (terminal) bond in $[(CH_3)_3Al]_2$, the Al—Cl bond significantly *longer* than the Al—Cl (bridge) bond in $[AlCl_3]_2$.

As part of our study of associated organoaluminium compounds we have carried out a reinvestigation of dimeric $(CH_3)_2AlCl$ which was first investigated by means of gas phase electron diffraction more than 30 years ago.[1]

EXPERIMENTAL AND CALCULATION PROCEDURE [2,3]

$[(CH_3)_2AlCl]_2$ was prepared from $[(CH_3)_3Al]_2$ and $[AlCl_3]_2$ and was distilled twice before use. The electron scattering pattern was recorded on Balzers Eldiograph KD-G2. The sample reservoir was maintained at about 25°C, corresponding to a vapor pressure of about 15 mmHg.[4] Exposures were made with nozzle to photographic plate distances of 50 cm and 25 cm. The optical densities of four plates from the first set were recorded at $\Delta s = 0.125$ Å^{-1} intervals, the optical densities of five plates from the last set were recorded at $\Delta s = 0.250$ Å^{-1} intervals. The optical densities were converted into intensities and the data processed in the usual way.[2]

Every other modified molecular intensity point obtained from the 50 cm plates is shown in Fig. 1A, the modified molecular intensity points obtained from the 25 cm plates are shown in Fig. 2A.

Theoretical intensity curves were calculated from:

$$I^{AlC}(s) = \sum_{i \neq j} \frac{|f_i(s)|\,|f_j(s)|}{|f_{Al}(s)|\,|f_C(s)|} \cos[\eta_i(s) - \eta_j(s)] \frac{\sin(R_{ij}s)}{R_{ij}} \exp(-\tfrac{1}{2}l^2_{ij}s^2)$$

The sum extends over all atom pairs i,j in the molecule. R_{ij} is the internuclear distance, l_{ij} the root mean square amplitude of vibration. $f_j(s) = |f_j(s)| \exp[i\eta_j(s)]$ is the complex atomic scattering factor of atom j.

The molecular structure was refined by least-squares calculations on the intensity data with a non-diagonal weight matrix and a separately refined scale factor for the intensity data obtained for each nozzle-to-plate distance.[3] The

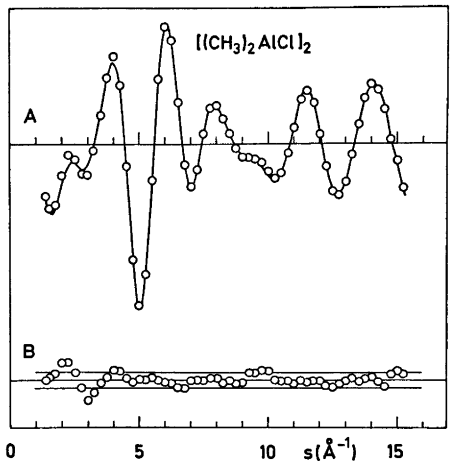

Fig. 1. A, O: Experimental modified molecular intensity points from $s = 1.50$ to 15.26 Å^{-1}. Only every other experimental point is shown. Full line: Theoretical intensity curve calculated for best model. B: Difference points. *Note:* The scale of B is twice that of A.

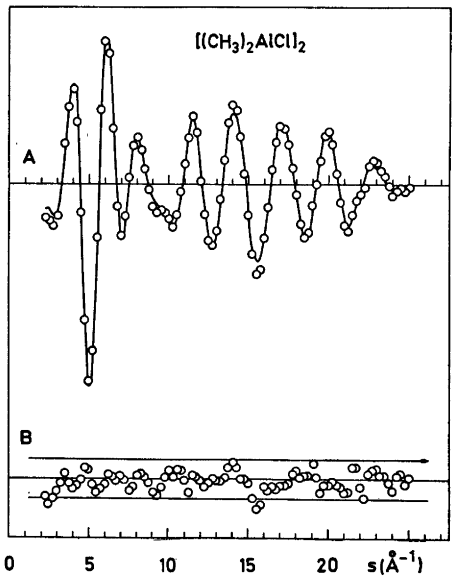

Fig. 2. A, O: Experimental modified molecular intensity points from $s = 2.25$ to 25.00 Å^{-1}. Full line: Theoretical intensity curve calculated for best model. B: Difference points. *Note*: The scale of B is twice that of A.

standard deviations obtained were expanded to take into account an estimated uncertainty of 0.1 % in the electron wavelength.

Radial distribution functions were calculated by Fourier inversion of experimental and theoretical intensity curves after multiplication with the artificial damping function $\exp(-ks^2)$. The experimental intensity functions were then spliced to each other and to the theoretical curve calculated for the best model below $s =$ 1.50 Å^{-1}.

STRUCTURE ANALYSIS

A molecular model of $[(CH_3)_2AlCl]_2$ is shown in Fig. 3. It was assumed that:

(i) The molecular symmetry is D_{2h};

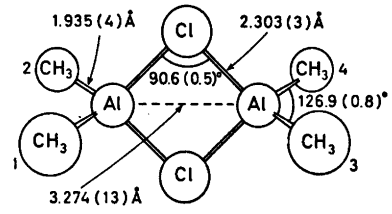

Fig. 3. Molecular model of $[(CH_3)_2AlCl]_2$.

(ii) The methyl groups have C_{3v} symmetry with the threefold axes coinciding with the Al – C bonds;

(iii) The angle of rotation of the methyl groups about the Al – C bonds is such that the H atoms are staggered with respect to the bonds radiating from the Al atom.

The molecular structure is then determined by six independent parameters, *e.g.* the three bond distances Al – Cl, Al – C, and C – H and the three valence angles ∠Cl – Al – Cl ∠C – Al – C, and ∠Al – C – H. Vibrational effects ("shrinkage") were neglected.

Least squares refinement of the six structure parameters and eleven vibrational amplitudes converged to the values listed in Table 1.

The vibrational amplitude of the $C_1 \cdots C_2$

Table 1. Bond distances, valence angles, and root mean square vibrational amplitudes (l) of $[(CH_3)_2AlCl]_2$. (Estimated standard deviations in parentheses). For numbering of the atoms consult Fig. 3. The distances are given as r_a. The angles have not been corrected for shrinkage.

	R(Å)	l(Å)
Bond distances		
C – H	1.104(8)	0.081(9)
Al – C	1.935(4)	0.054(4)
Al – Cl	2.303(3)	0.069(2)
Nonbonded distances		
Al···Al	3.274(13)	0.106(38)
Al···C	4.487(13)	0.182(16)
Al···H	2.528(14)	0.095(11)
Cl···Cl	3.241(13)	0.077(11)
Cl···C	3.447(5)	0.124(5)
Cl···H	3.467(17)	0.74(11)[a]
Cl···H	3.697(14)	0.74(11)[a]
Cl···H	4.417(9)	0.45(11)
$C_1 \cdots C_2$	3.462(15)	0.133[b]
$C_1 \cdots C_3$	5.004(24)	0.43(14)
$C_1 \cdots C_4$	6.085(14)	0.160(33)
Valence angles (deg.)		
∠Al – C – H	109.5(1.1)	
∠C – Al – C	126.9(0.8)	
∠Cl – Al – Cl	89.4(0.5)	
∠Al – Cl – Al	90.6(0.5)	

[a] These amplitudes were assumed equal. [b] Assumed value, see text.

distance was fixed at the value found in monomeric $(CH_3)_3Al$,[5] $l(C_1\cdots C_2)=0.133(5)$ Å, because refinement did not converge when it was allowed to vary.

Modified molecular intensity curves calculated for the best model are shown in Fig. 1A and Fig. 2A. The difference between experimental and calculated intensities is shown in Fig. 1B and Fig. 2B. The agreement is satisfactory except in the region below $s=5$ Å^{-1}. It is possible that the disagreement in this region is due to the neglect of shrinkage. The data in this range were given a very low weight during the least squares refinement.

An experimental radial distribution function is shown in Fig. 4A, the difference between this curve and a theoretical curve calculated for the best model is shown in Fig. 4B.

DISCUSSION

The molecular structure of $[(CH_3)_2AlCl]_2$ may be compared with the molecular structure of the related molecules $[(CH_3)_3Al]_2$,[5] $[(CH_3)AlCl_2]_2$,[6] and $[AlCl_3]_2$.[7]

The Al – C bond in $[(CH_3)_2AlCl]_2$ is significantly *shorter* than the terminal Al – C bonds in $[(CH_3)_3Al]_2$ or monomeric $(CH_3)_3Al$, in either compound $Al-C_t=1.957(3)$ Å. Similarly the $\angle C-Al-C$ angle in $[(CH_3)_2AlCl]_2$ is significantly larger than in $[(CH_3)_3Al]_2$. Both differences indicate that the atomic orbitals on Al used for bonding to C_t have more *s*-character in $[(CH_3)_2AlCl]_2$ than in $[(CH_3)_3Al]_2$.

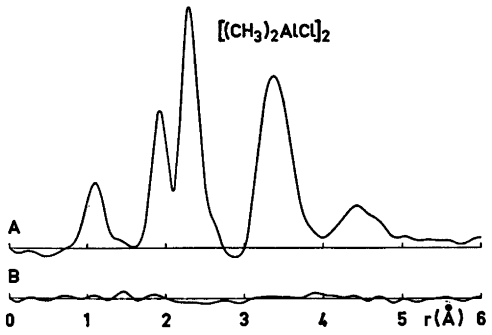

Fig. 4. A: Experimental radial distribution curve. Artificial damping constant $k=0.0025$ Å^2. B: Difference between the experimental curve and a theoretical curve calculated for the best model.

The Al – Cl bond in $[(CH_3)_2AlCl]_2$ is significantly longer than the bridging Al – Cl bond in $[AlCl_3]_2$, 2.252(4) Å, or in $[(CH_3)AlCl_2]_2$ where the two crystallographically nonequivalent $Al-Cl_b$ bonds are 2.25(1) and 2.26(1) Å, respectively. The reason is probably that exchange of the terminal CH_3 groups in $[(CH_3)_2AlCl]_2$ with more electronegative Cl atoms increases the acceptor strength of the Al atom. Since there is no detectable difference between the $Al-Cl_b$ distances in $[(CH_3)AlCl_2]_2$ and $[AlCl_3]_2$, it would appear that the effect of the introduction of a second terminal Cl atom on each Al atom is considerably less than the effect of the first.

Despite the difference in bond distances the angles in the central Al_2Cl_2 rings are very similar in the three compounds; all angles are very close to 90°.

The large amplitudes obtained for the Cl···H distances in $[(CH_3)_2-AlCl]_2$ suggest that the barrier to internal rotation of the methyl groups is of the order of or less than the thermal energy available.

Acknowledgements. We are grateful to the *Norwegian Research Council for Science and the Humanities* and the *Norwegian Research Council for Science and Technology* for financial support, and to professor Ken Hedberg and coworkers for informing us of their results on $[AlCl_3]_2$ before publication.

REFERENCES

1. Brockway, L. O. and Davidson, N. R. *J. Amer. Chem. Soc. 63* (1941) 328.
2. Andersen, B., Seip, H. M., Strand, T. G. and Stølevik, R. *Acta Chem. Scand. 23* (1969) 3224.
3. Seip, H. M., Strand, T. G. and Stølevik, R. *Chem. Phys. Lett. 3* (1969) 617.
4. Davidson, N. R. and Brown, H. C. *J. Amer. Chem. Soc. 64* (1942) 316.
5. Almenningen, A., Halvorsen, S. and Haaland, A. *Acta Chem. Scand. 25* (1971) 1937.
6. Allegra, G., Perego, G. and Immirzi, A. *Makromol. Chem. 61* (1963) 69.
7. Shen, M., Hagen, K. and Hedberg, K. *Personal communication.*

Received August 22, 1973.

Acta Chemica Scandinavica A 28 (1974) 48—54

Thermodynamic Properties of Binary Liquid Aluminium Chloride—Alkali Chloride Mixtures

HARUHIKO IKEUCHI and CONRAD KROHN

Universitetet i Trondheim, Norges tekniske högskole, Institutt for uorganisk kjemi, N-7034 Trondheim—NTH, Norway

The EMF of the formation cells

$Al(s) \mid AlCl_3 - MCl(l) \mid Cl_2(g)(graphite)$

has been measured in the temperature range from 200 to 600°C. M denotes Na, K, Rb, and Cs, respectively, in the present investigation.

For the systems investigated, a model characterized by the two equilibria

$Al_2Cl_6 + Cl^- = Al_2Cl_7^-$

$Al_2Cl_7^- + Cl^- = 2AlCl_4^-$

seems to be adaptable to the liquid mixture in a narrow concentration region around 50 mol % of aluminium chloride.

Molten mixtures of aluminium chloride and alkali chlorides are of interest both for industrial and for more fundamental research purposes. For some years these mixtures have been considered as potential electrolytes for aluminium deposition,[1-5] and as solvent electrolyte for the deposition of heavier metals.[7,8] Recently also a new electrolysis process for the commerical production of aluminium, employing a molten alkali chloride-aluminium chloride electrolyte, has been developed. But no details have as yet been published.

As to the more fundamental aspect of the interest in these liquids they represent an extension of the field of more or less purely ionic molten salts into that of the covalent liquids.

We have for some years studied alkali and light metal reference electrodes and their application in formation cells for the study of properties of molten salt mixtures.[9,10] The present work adds to the previous ones in its general aim.

Aluminium chloride is mainly a molecular substance in the liquid state. By melting the solid ionic layer structure is expanded by 83 %[11] and the liquid is constituted of Al_2Cl_6 species, corresponding to a very low specific conductance of 0.56×10^{-6} Ohm^{-1} cm^{-1} at 190°C [12] and a very high vapour pressure.

By adding chloride ion to liquid aluminium chloride ionic species are formed. There is evidence that the process can be characterized by the two equilibria:

$$Al_2Cl_6 + Cl^- = Al_2Cl_7^- \qquad \text{I}$$

$$Al_2Cl_7^- + Cl^- = 2AlCl_4^- \qquad \text{II}$$

The existence of $AlCl_4^-$ is firmly established, and the ion has been isolated in the solid state as such crystals as $NaAlCl_4$ [13] and $Co(AlCl_4)_2$.[14] The $Al_2Cl_7^-$ ion has been detected in liquid $KCl - AlCl_3$ mixtures, employing Raman spectroscopy, by Cyvin, Klæboe, Rytter and Øye.[15] They have also studied the relative stability of chloroaluminate complex ions in a varying alkali cation environment.[16] EMF-studies by Tremillon and Létisse [17] also give indication of the presence of $Al_2Cl_7^-$.

In the present investigation a reversible aluminium electrode was developed, and thermodynamic data for aluminium chloride-alkali chloride mixtures evaluated from EMF measurements of formation cells of the following type:

$Al(s) \mid AlCl_3 - MCl(l) \mid Cl_2(g)(graphite)$

M being Na, K, Rb, and Cs in the present investigation.

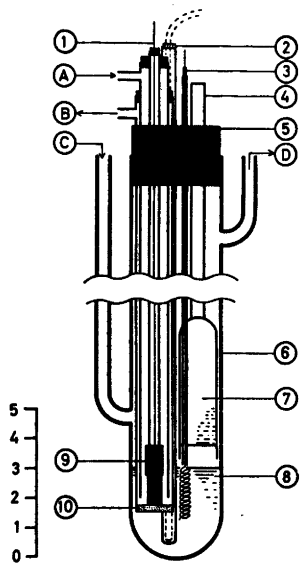

Fig. 1. Galvanic cell assembly. (A) Cl_2 inlet. (B) Cl_2 outlet. (C) Ar inlet. (D) Ar outlet. (1) Pt lead for Cl_2 electrode. (2) Chromel-Alumel thermocouple. (3) Al electrode. (4) Ampoule containing the salt mixture. (5) Rubber stopper. (6) Silica glass vessel. (7) Salt mixture. (8) Salt mixture transferred from (7). (9) Cl_2 graphite electrode. (10) Fritted silica glass diaphragm.

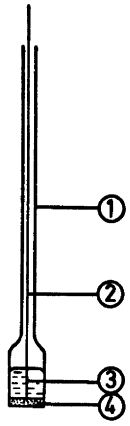

Fig. 2. Liquid 20 mol % Al–Ga electrode. (1) Silica glass tube. (2) Ta lead for Al-Ga electrode. (3) Alloy. (4) Fritted silica glass filter (No. 3).

EXPERIMENTAL

The arrangement of the cell is shown in Fig. 1. A pyrex crucible was used at low temperatures and a crucible of silica glass at the high temperature measurements.

The chlorine electrode consisted of a spectrographic graphite rod suspended in a concentric silica glass tube with a 0.8 mm ⌀ Pt wire lead.

The aluminium electrode employed was a coiled piece of Al wire (1.0 mm ⌀, 99.9 %, Johnson & Matthew) supported in silica glass tubes. For some of the measurements also a liquid Al–Ga electrode, shown in Fig. 2, was used, 99.99 % Ga (Koch-Light Laboratories) was employed.

$AlCl_3$ was prepared by passing dry HCl over Al metal at 400°C, and the salt mixtures were prepared on a vacuum line and filtered into ampoules, which were sealed off. The sealed ampoule was placed in the cell assembly and opened in an Ar atmosphere. By heating the cell above the melting point the mixture is transferred to the cell, as shown in Fig. 1.

Prior to the EMF measurements the mixture was electrolyzed by Al and graphite electrodes (not shown) for some minutes at lower voltages (1.6–1.8V) than the Al decomposition potential, to remove impurities. This procedure gave a clean transparent melt, and the small amounts of black substance sometimes observed, was easily coagulated around aluminium pieces at the bottom of the cell (not shown in Fig. 1). The black substance either may be finely dispersed metallic aluminium, or possibly elemental silicon that may form in the system.

After pre-electrolysis a new solid Al electrode was introduced into the melt, and the surface oxide was removed by electrolysis. This procedure was found essential to ensure the functioning of the Al electrode.

An ordinary pot furnace with Kanthal resistors was used for heating.

The measurements were carried out both at continuously decreasing and increasing temperatures in the actual temperature range, or at a few constant temperatures. The EMF of the cell and T was recorded simultaneously on a Varian G-2000 potentiometric recorder with suppressed zero point. Temperature was measured by a Chromel-Alumel thermocouple calibrated against $AgNO_3$ and $NaNO_3$. The EMF values recorded were corrected for the thermoelectric EMF which arises in the measuring circuit due to the application of Pt and Al leads to the electrode.

RESULTS

The observed values of EMF *versus* temperature for the systems $AlCl_3$–NaCl, $AlCl_3$–KCl, $AlCl_3$–RbCl, and $AlCl_3$–CsCl are shown in Figs. 3, 4, 5, and 6, respectively. The reproduc-

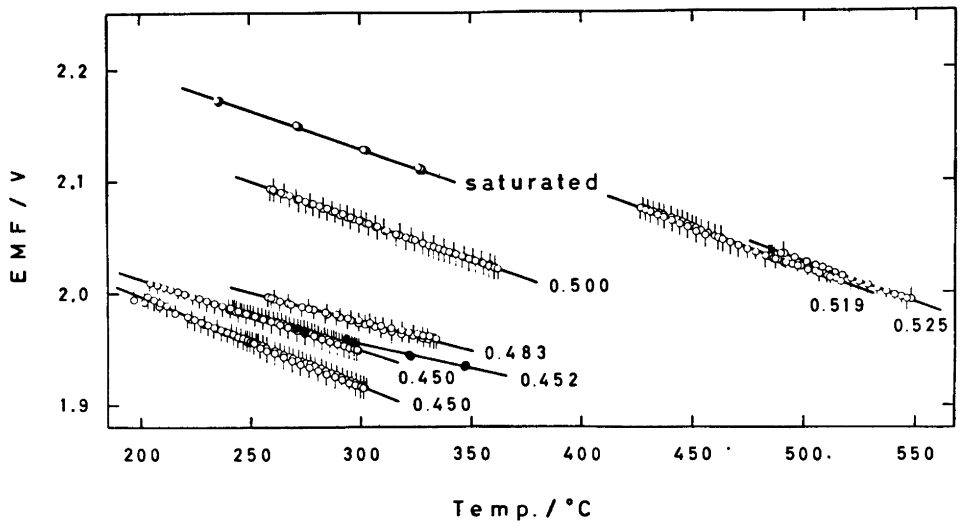

Fig. 3. EMF *versus* T for the system $AlCl_3-NaCl$. Lines are at different N_{NaCl}.

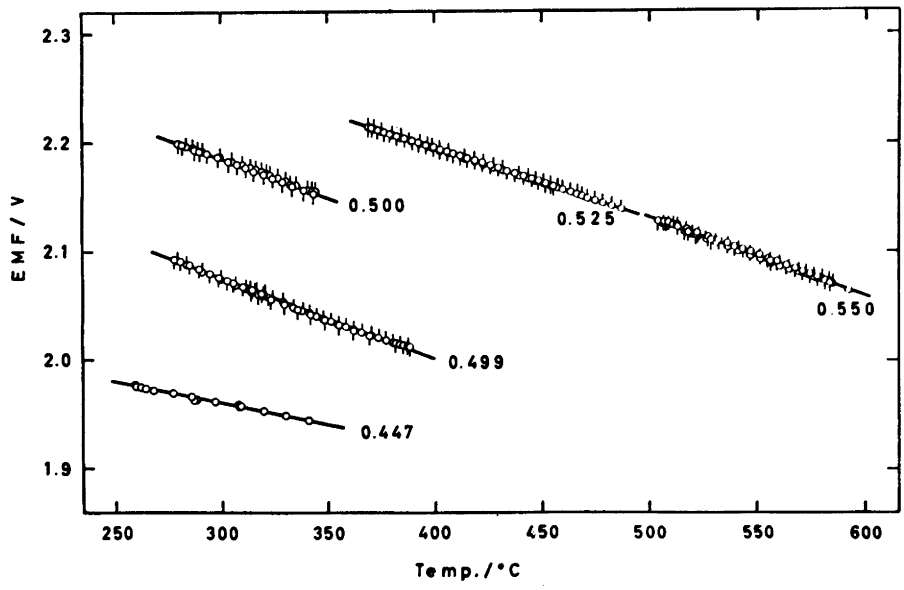

Fig. 4. EMF *versus* T for the system $AlCl_3-KCl$. Lines are at different N_{KCl}.

ibility is better than 5 mV in all experiments. Reversibility is demonstrated by the agreement of the EMF values at increasing temperature with those at decreasing temperature, and the linearity of EMF *versus* T. The reversibility has also been checked by the application of an external potential over the cell, the EMF of which was re-established after cutting the potential.

The cell reaction in the present case may be written as:

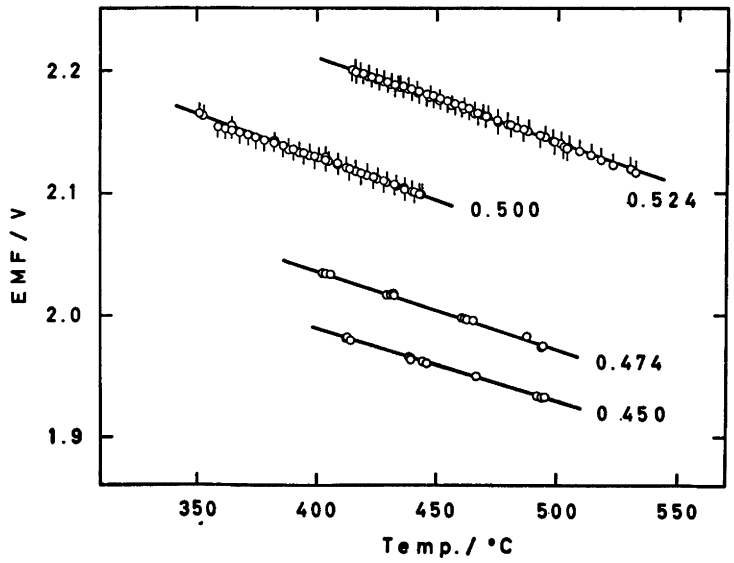

Fig. 5. EMF *versus* T for the system $AlCl_3$ – RbCl. Lines are at different N_{RbCl}.

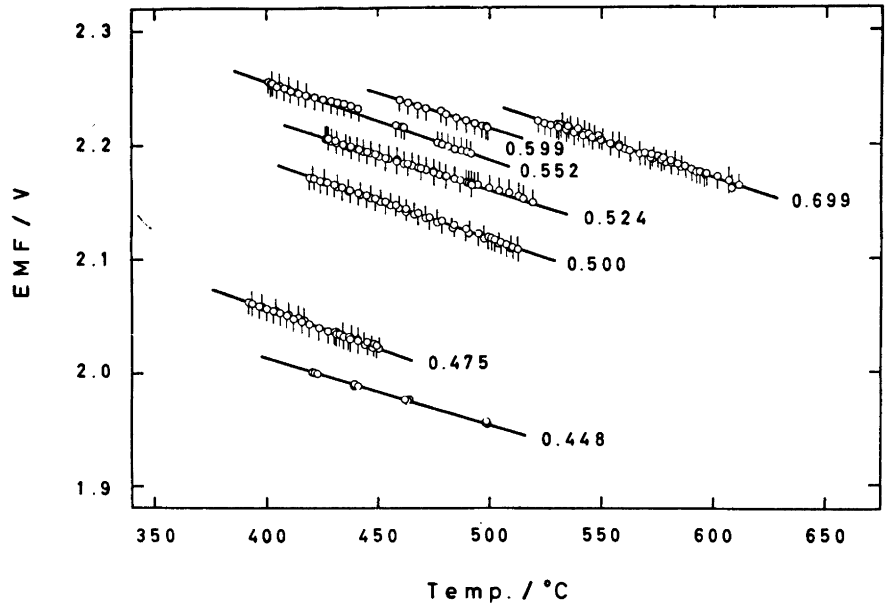

Fig. 6. EMF *versus* T for the system $AlCl_3$ – CsCl. Lines are at different N_{CsCl}.

$2Al(s) + 3Cl_2(g, 1\ atm) = Al_2Cl_6(l)$ (in mixture) III

with a solid Al electrode, or

$2Al(l)(in\ mixture) + 3Cl_2(g, 1\ atm) = Al_2Cl_6(l)(in\ mixture)$ IV

with a liquid Al-Ga alloy electrode.

The corresponding change in Gibbs' free energy is given by:

$$\Delta G = \Delta G^\circ + RT \ln \frac{a_{Al_2Cl_6}}{a^2_{Al}\, p^3_{Cl_2}} \quad (1)$$

Then, in a reversible electrochemical cell with the cell reaction (III), choosing as the standard states pure, liquid aluminium chloride, pure solid aluminium metal and gaseous chlorine at 1 atm:

$$E = E^\circ - \frac{RT}{6F} \ln a_{Al_2Cl_6} \quad (2)$$

where E is the observed EMF of the cell.

An experimental determination of E° by the present formation cell method is impossible, due to the high vapour pressure of $AlCl_3$. The value has been calculated from the JANAF data [18] to 1.973 V at 300°C.

The partial molar Gibbs' free energy of formation of Al_2Cl_6 has been calculated from the relation:

$$\Delta \bar{G}_{Al_2Cl_6} = -6F(E - E^\circ) \quad (3)$$

Some results are given in Table 1.

At the $AlCl_3$-rich side of some of the $AlCl_3$–NaCl and $AlCl_3$–KCl mixtures, the observed EMF appeared to be slightly lower than the E° value. This seemed to be caused by a breaking of the graphite electrode by swelling, giving rise to depolarization effects. The phenomenon was only apparent at higher $AlCl_3$-concentration in the remaining binary mixtures. This phenomenon is not readily explainable. A hypothesis, however, is the formation of a lamellar graphite–$AlCl_3$ intercalation compound. In the literature such compounds have been reported to form when graphite is exposed to liquid $AlCl_3$ in the presence of Cl_2 gas,[19] in the temperature range between 180 and 470°C. Tremillon and Létisse [17] recommend the use of a very hard glassy carbon instead of graphite for such electrodes.

Table 1. Experimental EMF and partial molar Gibbs' free energy values.
E° (300°C) = 1.973 V and E° (450°C) = 1.890 V, calculated from JANAF data.[18] The precision in the Gibbs' free energy values (kcal/mol) has been evaluated to ±0.25 kcal/mol from the experimental data.

N_{AlCl_3}	E	$E - E^\circ$	$\Delta G_{Al_2Cl_6}$
$AlCl_3$–NaCl at 300°C or 450°C			
0.475	2.064*	0.174	−24.1
0.488	2.058*	0.168	−23.2
sat.	2.129	0.156	−21.6
0.500	2.065	0.092	−12.7
$AlCl_3$–KCl at 300°C or 450°C			
0.450	2.167*	0.277	−38.3
0.476	2.163*	0.273	−37.8
0.500	2.185	0.212	−29.3
0.501	2.075	0.102	−14.1
$AlCl_3$–RbCl at 450°C			
0.476	2.176	0.286	−39.5
0.500	2.094	0.204	−28.2
0.526	2.004	0.104	−14.4
0.550	1.959	0.069	− 9.55
$AlCl_3$–CsCl at 450°C			
0.301	2.270	0.380	−52.6
0.401	2.246	0.356	−49.3
0.448	2.221	0.331	−45.8
0.476	2.191	0.301	−41.7
0.500	2.152	0.262	−36.3
0.525	2.022	0.132	−18.3
0.552	1.983	0.093	−12.9

* at 450°C.

DISCUSSION

The results obtained at the saturation point of NaCl in NaCl–$AlCl_3$ is in good agreement with results by Tremillon and Létisse.[17] Other EMF data from formation cell studies of the present system do not seem to have entered chemical literature.

The vapour pressure of liquid mixtures containing aluminium chloride has been measured by several investigators. Thus Dewing [20] and Rao [21] have studied the $AlCl_3$–NaCl and $AlCl_3$–RbCl systems, respectively. It is generally recognized that the vapour on the $AlCl_3$-rich side probably only consists of Al_2Cl_6 molecules, and the activity of Al_2Cl_6 in the melt, therefore,

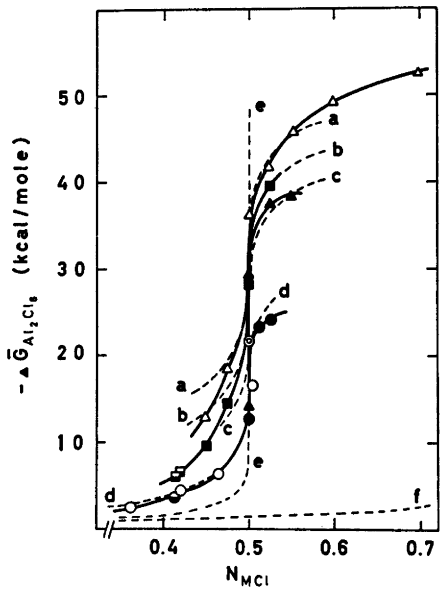

Fig. 7. Partial molar Gibbs' free energy of Al_2Cl_6. Full drawn curves: This investigation; filled circles, $AlCl_3-NaCl$ at 300°C or 450°C; double open circles, $AlCl_3$-saturated NaCl at 300°C; filled triangles, $AlCl_3-KCl$ at 300°C or 450°C; filled squares, $AlCl_3-RbCl$ at 450°C; open triangles, $AlCl_3-CsCl$ at 450°C. Open circles: From vapour pressure measurement by Dewing [20] $AlCl_3-NaCl$, Half filled circle: From vapour pressure measurement by Rao [21] $AlCl_3-NaCl$ at 300°C. Half filled squares, from vapor pressure measurement by Rao $AlCl_3-RbCl$ at 450°C; Dotted curves, calculated from complex molecular model; (a) $K_1=3\times10^9$, $K_2=3\times10^5$, (b) $K_1=3\times10^8$, $K_2=3\times10^5$, (c) $K_1=3\times10^7$, $K_2=3\times10^5$, (d) $K_1=3\times10^6$, $K_2=3\times10^5$, (e) Ideal mixture of $Al_2Cl_6-MAlCl_4$, (f) Ideal mixture of Al_2Cl_6-MCl.

may be calculated from the ratio of the total vapour pressure of the mixture to that of pure aluminium chloride. The values calculated from the cited vapour pressure data connect smoothly to those of the present investigation, as shown in Fig. 7.

In the $AlCl_3-NaCl$ and $AlCl_3-KCl$ phase diagrams, the liquidus rises steeply around the composition $N_{AlCl_3}=0.5$. Consequently, a study of thermodynamic properties at the same temperature for both sides of the equimolar composition is difficult. The calculation was, therefore, carried out at 300°C and 450°C, in the aluminium chloride rich region and on the alkali chloride side, respectively. For the mixture $AlCl_3-RbCl$ and $AlCl_3-CsCl$, however, values are presented at 450°C for the whole concentration range.

Adding chloride ions to aluminium chloride may be considered as a stepwise titration, involving the two previously mentioned equilibria I and II.

Considerable amounts of $Al_2Cl_7^-$ are formed in the concentration range $0.33 < N_{AlCl_3} < 0.50$. When N_{AlCl_3} exceeds 0.5, $AlCl_4^-$ will tend to be the dominating complex anion species. The corresponding equilibrium quotients are:

$$K_1 = N_{Al_2Cl_7^-}/N_{Cl^-}N_{Al_2Cl_6} \quad (4)$$

$$K_2 = N^2_{AlCl_4^-}/N_{Cl^-}N_{Al_2Cl_7^-} \quad (5)$$

The quotients K_1 and K_2 are probably not true constants, as shown previously for the corresponding $MgCl_2-$Alk. Cl systems.[10]

Øye and Gruen [22] introduced the mol fraction of each species as the activity and compared the activity of Al_2Cl_6 with that obtained from the vapour pressure data of Dewing [20] on the assumption that the mol fraction of chloride ion is negligibly small at higher aluminium chloride concentrations. This assumption definitely is valid at $N_{AlCl_3} > 0.5$. The applicability of this model will be tested in the following.

Consider a mixture of $2N$ mol of aluminium chloride corresponding to N mol of Al_2Cl_6, and $1-N$ mol of alkali chloride. Then:

$$1-N = n_{Cl^-} + n_{Al_2Cl_7^-} + n_{AlCl_4^-} \quad (6)$$

$$N = 2n_{Al_2Cl_6} + 2n_{Al_2Cl_7^-} + n_{AlCl_4^-} \quad (7)$$

n denotes the molar amounts of the constituent species. By combining (4), (5), (6), and (7) the following relation between the weighed – in mol fraction N and the activity x (taken as the mol fraction of Al_2Cl_6) is obtained:

$$N = \frac{4Ax + (1-x)(A - 1/K_1x)}{A(1+3x) + (1-x)(A-1+K_1x)} \quad (8)$$

$$\text{Here } A = 1 + K_1x + (K_1K_2x)^{\frac{1}{2}} \quad (9)$$

Some solutions of this equation are shown in Fig. 7 for a few combinations of the equilibrium quotients K_1 and K_2. This model seems to fit the observed values rather well around $N_{AlCl_3} = 0.5$.

The equilibrium quotient, K_2, for the reaction:

$$Al_2Cl_7^- + Cl^- = 2\ AlCl_4^-$$

has been taken as constant, $K_2 = 3 \times 10^5$, which can be taken as true over a narrow concentration range. This value, combined with $K_1 = 3 \times 10^9$ seems to fit the $AlCl_3 - CsCl$ data rather well. The corresponding value given by Tremillon *et al.* amounts to $K_2 = 2.9 \times 10^5$.

It is seen from Fig. 7 that this model demands the value of K_1 to decrease when going from the $CsCl - AlCl_3$ to the $NaCl - AlCl_3$. The system $KCl - AlCl_3$ seems to be rationalized fairly well with the combination $K_1 = 3 \times 10^7$, $K_2 = 3 \times 10^5$.

Øye *et al.*[23] have evaluated the dissociation equilibrium constant for the reaction

$$2Al_2Cl_7^- = Al_2Cl_6 + 2AlCl_4^-$$

from spectroscopic data on molten $KCl - AlCl_3$ mixtures, and arrived at value $K_V = (4 \pm 2) \times 10^{-3}$ in the temperature range 170 – 240°C. In the present work $K_V = K_2/K_1$, which for the same system at 300°C should amount to $K_V = 3 \times 10^5/3 \times 10^7 = 10^{-2}$. This seems to be in fair agreement with the value given by Øye *et al.*

The precision of the present data, and the tabulated JANAF data on the standard Gibbs' free energy of formation as well, does not permit sufficiently precise entropy values to be calculated from the slope of the EMF *versus T* curve.

An estimate from the present data gives values around −20 e.u., being somewhat lower for the $NaCl - AlCl_3$ than for the $CsCl - AlCl_3$ system.

REFERENCES

1. Fink, C. G. and Solanki, C. N. *Trans Electrochem. Soc. 91* (1947) 203.
2. Collins, F. R. *Iron Age 169* (1952) 100.
3. Good, P. C., Butler, M. O. and Jerkes, L. A. *U. S. Bur. Mines Rept. Invest.* No. 6785 (1966).
4. Plotnikow, W. A., Fortunatow, N. S. and Maskovits, W. P. *Z. Elektrochem. 37* (1931) 83.
5. Singleton, E. L., Kriby, D. E. and Sullivan, T. A. *U. S. Bur. Mines Rept. Invest.* No. 7212 (1969).
6. Midorikawa, R. *Denki Kagaku 23* (1955) 72, 127.
7. Wade, W. H., Twillmeyer, G. O. and Yntema, L. F. *Trans. Electrochem. Soc. 78* (1940) 77.
8. Verdick, R. G. and Yntema, L. F. *J. Phys. Chem. 48* (1944) 268.
9. Krohn, C. and Moser, Z. *Kgl. Norske Videnskab. Selskabs Skrifter* (1967) No. 8.
10. Ikeuchi, H. and Krohn, C. *Acta Chem. Scand. 23* (1969) 2230.
11. Schinke, H. and Sauerwald, F. *Z. Anorg. Allg. Chem. 287* (1956) 313.
12. Schulze, K. and Engell, H. J. *Erzmetall 22* (1969) 87.
13. Baenziger, N. C. *Acta Crystallogr. 4* (1951) 216.
14. Ibers, J. A. *Acta Crystallogr. 15* (1962) 967.
15. Cyvin, S. J., Klæboe, P., Rytter, E. and Øye, H. A. *J. Chem. Phys. 52* (1970) 2776.
16. Rytter, E., Øye, H. A., Cyvin, S. J., Cyvin. B. N., Klæboe, P. *Acta Chem. Scand. 27* (1973). *In press.*
17. Tremillon, B. and Létisse, G. *J. Electroanal. Chem. 17* (1968) 371.
18. *JANAF Thermochemical Data*, The Dow Chemical Co., Midland Mich. 1960.
19. Rüdorff, W. and Zeller, R. *Z. Anorg. Allg. Chem. 279* (1955) 182.
20. Dewing, E. W. *J. Amer. Chem. Soc. 77* (1955) 2639.
21. Rao, D. B. *Private communication.*
22. Øye, H. A. and Gruen, D. M. *Inorg. Chem. 3* (1964) 836.
23. Øye, H. A., Rytter, E., Klæboe, P. and Cyvin, S. J. *Acta Chem. Scand. 25* (1971) 559.

Received July 21, 1973.

Acta Chemica Scandinavica A 28 (1974) 55—60

The Structures of Yttrium and Bismuth Trifluorides by Neutron Diffraction

A. K. CHEETHAM[a] and N. NORMAN[b,*]

[a]Inorganic Chemistry Department, University of Oxford, England and [b]Department of Physics, University of Oslo, Oslo 3, Norway

The crystal structures of YF_3 and BiF_3 have been re-examined by powder neutron diffraction. The positional and thermal parameters were refined by a least-squares method based on profile intensities. The cell constants from Guinier X-ray diagrams are
YF_3: $a = 6.3537(7)$, $b = 6.8545(7)$, $c = 4.3953(5)$ Å.
BiF_3: $a = 6.5605(4)$, $b = 7.0155(4)$, $c = 4.8416(2)$ Å.
Space group *Pnma*
In YF_3, yttrium has eight nearest neighbours at distances between 2.281 Å and 2.310 Å and a ninth at 2.538 Å. In BiF_3, the eight corresponding distances vary between 2.217 Å and 2.502 Å but the ninth fluorine is at 3.100 Å. The possibility that the lone pair of electrons on bismuth is stereochemically active is considered.

1. INTRODUCTION

The trifluorides of the rare-earth elements from samarium to lutetium adopt the orthorhombic YF_3-type structure at room temperature.[1] A single crystal X-ray study of YF_3 by Zalkin and Templeton [2] suggests that yttrium has eight nearest neighbour fluoride ions at distances between 2.25 and 2.32 Å with a further neighbour at 2.60 Å. However, the exact details of this structure are still uncertain since in the mentioned work the fluoride ions were located on the basis of geometrical considerations alone. We have therefore undertaken a detailed neutron diffraction study of YF_3

Bismuth trifluoride is reported to be isostructural with YF_3 but the positions of the fluoride ions have not been established.[3] This compound is particularly interesting since it is well known that in the oxides and oxyfluorides of tin(II), lead(II), antimony(III), and bismuth(III), the lone pair of electrons on the metal ion is stereochemically active.[4] In order to examine the possibility of such behaviour in BiF_3 we have also carried out a precise structure determination of this compound.

2. EXPERIMENTAL

2.1 *Sample preparation.* The YF_3 was obtained as a specpure material from Koch-Light Ltd. BiF_3 was prepared from Bi_2O_3 and 40 % HF solution in the manner described by Aurivillius.[3]

2.2 *X-Ray data.* The compounds crystallize in space group Pnma.

The unit cell dimensions of the compounds were determined from Guinier patterns taken with Cu$K\alpha_1$ radiation and with KCl as internal standard. The values and standard deviations obtained from least-squares refinements were

YF_3: $a = 6.3537(7)$, $b = 6.8545(7)$, $c = 4.3953(5)$ Å

BiF_3: $a = 6.5605(4)$, $b = 7.0155(4)$, $c = 4.8416(2)$ Å

2.3 *Neutron diffraction experiments.* Powder neutron diffraction experiments were carried out on YF_3 and BiF_3 at room temperature using the PANDA diffractometer at A.E.R.E. Harwell. Data were collected over a range of 2θ from 20 to 100 degrees in steps of 1/50 degree. A monitor was used to register the intensity of the direct beam and integrated counts were printed out every 1/10 degree. The recording rate was approximately 1.5 degrees per hour. A neutron wavelength of 1.504 Å was obtained by reflection from the (331) planes of a germanium monochromator at a take-off angle of 72 degrees. The measurements comprised 105 reflections for YF_3 and 131 reflections for BiF_3. The maximum counts observed were 5000 for YF_3 and 7000 for BiF_3, the background for each compound being

* Visisting scientist to A.E.R.E., Harwell.

almost constant at 500 and 600 counts, respectively. Absorption effects were negligible and no corrections were necessary.

3. REFINEMENTS

The structural parameters were refined by a full-matrix least-squares analysis of the powder diffraction profile.[5-6] In this method, each Bragg reflection is assumed to be gaussian in shape and the profile is calculated from the sum of gaussian peaks corresponding to the set of reflections. Thus, each intensity observation is the sum of the contributions from the reflections which overlap at that point, and the weighted difference between the observed and calculated profiles is minimized by least-squares. The unit cell dimensions, diffractometer zero-point error and three instrumental half-width parameters [6] are refined simultaneously with the atomic positional and thermal parameters.

The starting values for the analysis were taken from the work by Zalkin and Templeton [2] with the space group *Pnma*. Independent isotropic Debye-Waller factors for all atoms were included as variables. Scattering lengths of 0.79, 0.86, and 0.574 ($\times 10^{-14}$ m) were used for yttrium bismuth, and fluorine, respectively.[7] Final structural parameters for YF_3 and BiF_3 are given in Tables 1 and 2. The reliability factors based upon the profile ($R_{pr}=100\sum(y_i^o-y_i^c)/\sum y_i^o$) are 8.39 % and 8.65 % for YF_3 and BiF_3, respectively. Estimates of the more conventional reliability factors based upon the intensities of the Bragg reflections ($100\sum|F_o^2-F_c^2|/\sum F_o^2$) are 3.99 % for YF_3 (105 reflections) and 4.68 % for BiF_3 (131 reflections). The final observed and calculated diffraction profiles for YF_3 and BiF_3 are shown in Figs. 1 and 2.

4. SPACE GROUP AMBIGUITY

The measurements showed that $(0kl)$-reflections were observed only for $k+l=2n$ and $(hk0)$-reflections only for $h=2n$. Thus the centric space group *Pnma* and the non-centric $Pn2_1a$ are both possible. Nyburg *et al.*[8] conclude that molecular $BiCl_3$ crystallizes in the latter space group and recommend that the structures of other group V trihalides be re-examined.

Refinements based on space group $Pn2_1a$ were carried out for both YF_3 and BiF_3. For starting values the parameters were removed from their centric positions in order to reduce correlation effects. The refinements converged towards a model very close to the centric one, the shifts in atomic positions being less than 0.1 Å and in the same directions for corresponding atoms in the two compounds. The apparent deviations from centric symmetry were similar to those reported for $BiCl_3$. With 5 more parameters to refine the R(profile) factors dropped

Table 1. Atomic coordinates and thermal parameters (B) for YF_3. Standard deviations in parentheses.

Atom	x	y	z	B(Å²)
Yttrium	0.3673(4)	0.25	0.0591(5)	0.37(5)
Fluorine(1)	0.5227(5)	0.25	0.5910(8)	0.89(7)
Fluorine(2)	0.1652(4)	0.0643(3)	0.3755(5)	0.57(5)

Table 2. Atomic coordinates and thermal parameters (B) for BiF_3. Standard deviations in parentheses.

Atom	x	y	z	B(Å²)
Bismuth	0.3554(4)	0.25	0.0359(4)	0.46(4)
Fluorine(1)	0.5392(6)	0.25	0.6257(8)	1.49(8)
Fluorine(2)	0.1662(4)	0.0581(4)	0.3532(6)	1.20(5)

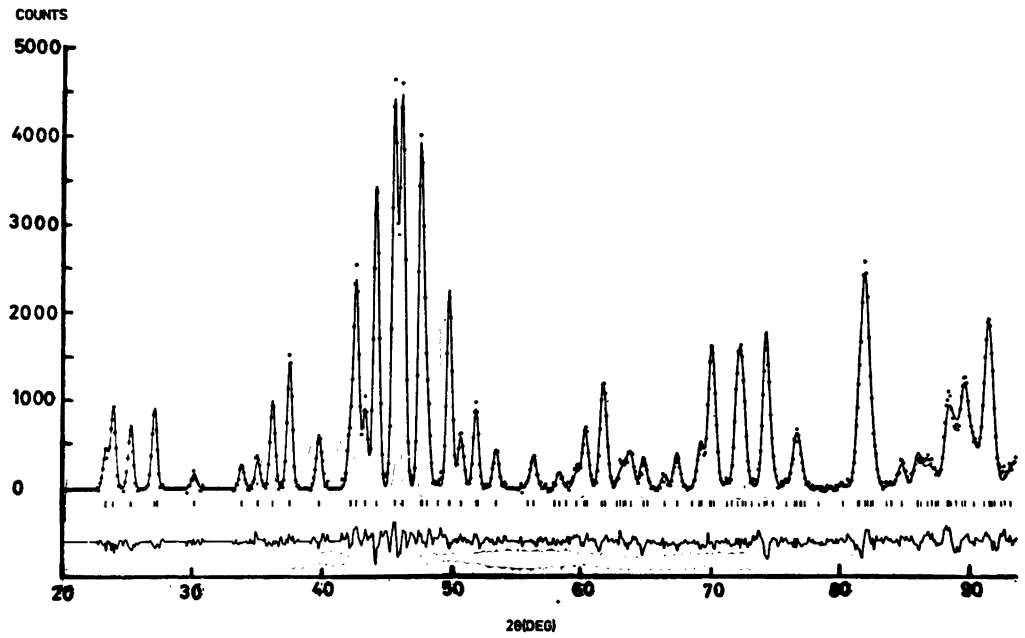

Fig. 1. The observed and calculated diffraction profiles for YF_3 (observed profile-dots; calculated profile-smooth curves). The difference profile and reflection positions are also shown.

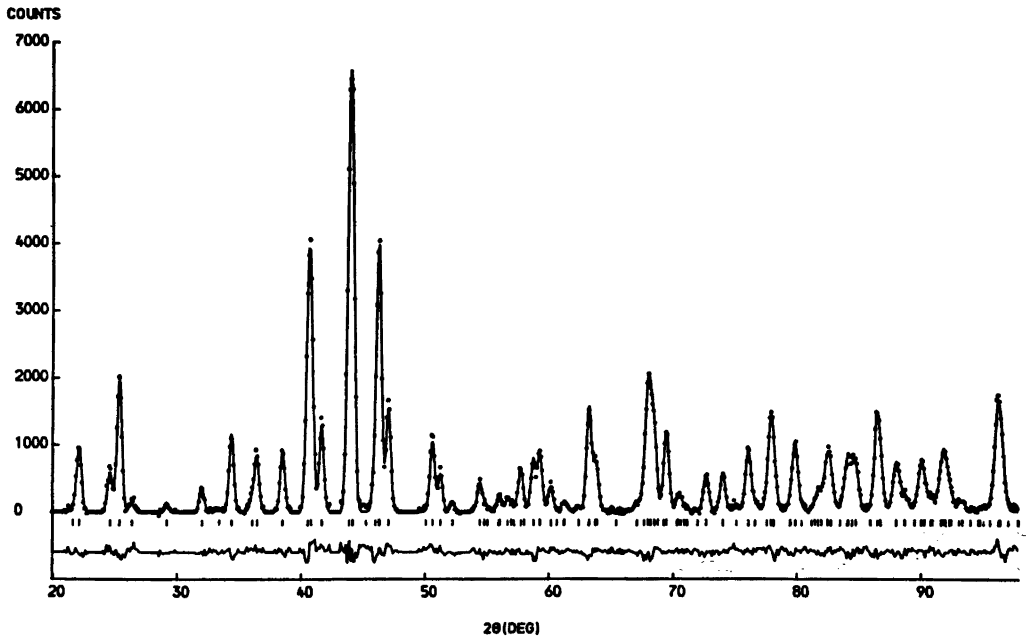

Fig. 2. The observed and calculated diffraction profiles for BiF_3 (observed profile-dots; calculated profile-smooth curve). The difference profile and reflection positions are also shown.

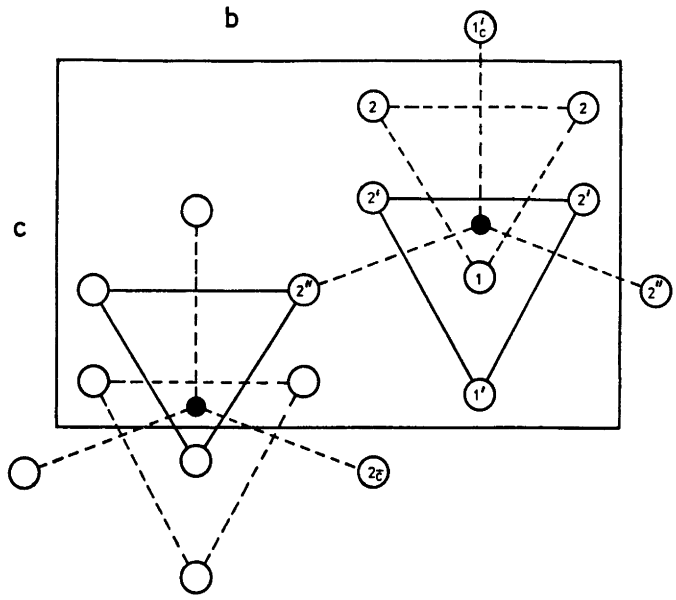

Fig. 3. Projection of the YF_3 structure down the *a*-axis.

from 8.39 and 8.65 to 8.27 and 8.53 % for YF_3 and BiF_3, respectively. Due to strong positional correlations between the previously mirror-related fluoride ions, the standard deviations increased by as much as a factor of 8 and a larger spread of calculated metal-fluorine distances was also found. Even though both models are chemically reasonable, considering the very small shifts and the large standard deviations, we found insufficient evidence for preferring the non-centric space group. All our later discussions of the structures are thus based on space group *Pnma*.

5. DISCUSSION OF THE STRUCTURES

5.1 *Yttrium trifluoride.* The arrangement of the atoms is demonstrated by the projection along the *a*-axis shown in Fig. 3. The yttrium ion has nine nearest-neighbour fluoride ions comprising a slightly deformed trigonal prism with atoms opposite each of the lateral faces as reported by Zalkin and Templeton.[2] In Table 3 the computed interatomic distances show that eight of the nearest neighbours lie at distances between 2.281 Å [Y – F(2)] and 2.310 Å [Y – F(2'')]. The ninth distance [Y – F($1_c'$)] of 2.538 Å as compared to 2.60 Å in the previous work can hardly be said to be exceptionally long, so that the yttrium ion in YF_3 can be considered to have genuine 9 coordination. From the same table is seen that the next shortest fluorine distance is 3.507 Å [Y – F($2_{\bar{c}}$)]. The triangular

Table 3. Interatomic distances (in Å) with standard deviations.

Distance [a]	YF_3	BiF_3
Metal – F(1)	2.287(4)	2.217(5)
Metal – F(2)	2.281(3)	2.390(3)
Metal – F(1')	2.282(4)	2.323(5)
Metal – F($1'_c$)	2.538(4)	3.100(5)
Metal – F(2')	2.299(3)	2.502(3)
Metal – F(2'')	2.310(2)	2.340(3)
Metal – F($2_{\bar{c}}$)	3.507(3)	3.779(3)
F(1) – F(2)	2.578(4)	2.808(4)
F(1) – F(2'')	2.932(3)	2.901(4)
F(2) – F(2)	2.546(3)	2.693(3)
F(2) – F($1'_c$)	2.771(4)	3.089(5)
F(2) – F(2')	3.363(4)	3.429(4)
F(2) – F(2'')	2.601(3)	2.781(4)
F(1') – F(2')	2.818(4)	2.979(5)
F(1') – F(2'')	2.762(3)	2.775(4)
F(2') – F(2'')	2.526(3)	2.728(4)

[a] A subscript refers to an axial translation of an atom.

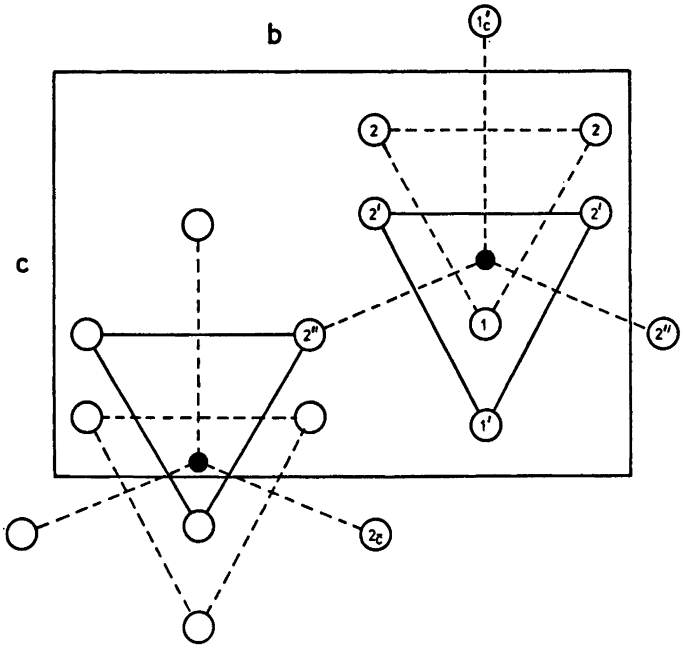

Fig. 4. Projection of the BiF_3 structure down the *a*-axis.

bases of the trigonal prism are almost parallel (2.60°), but there are small deviations from threefold symmetry. The distance between nearest neighbour fluoride ions varies between 2.526 Å [F(2′)–F(2″)] and 2.932 Å [F(1)–F(2″)].

5.2 *Bismuth trifluoride.* A projection of the BiF_3 structure on to the *bc* plane is shown in Fig. 4 and the interatomic distances are given in Table 3. In contrast to the metal coordination in YF_3, bismuth has eight nearest neighbour fluoride ions at distances between 2.217 Å [Bi–F(1)] and 2.502 [Bi–F(2′)] with the ninth ion now at 3.100 Å. Bismuth can therefore be described as 8-coordinated. It is attractive to postulate that the distortion of the coordination sphere compared with that in YF_3 stems from the stereochemical activity of the lone pair of electrons on bismuth. This type of behaviour is normally associated with an anomalously high unit cell volume [4] and a comparison of the cell volumes of BiF_3 (222.8 Å^3) and EuF_3 (204.3 Å^3) reveals such an anomaly in the bismuth compound (Eu^{3+} has approximately the same ionic radius as bismuth [9]). It would therefore appear that the lone pair protrudes along the Bi–F(1′$_c$) direction giving rise to the exceptionally long Bi–F(1′$_c$) distance and the elongation of the *c*-axis. It should also be noted that the Bi–F(2) and Bi–F(2′) distances are rather longer than expected. The shortest F–F distances vary between 2.693 Å [F(2)–F(2)] and 3.089 Å [F(2)–F(1′$_c$)]. The larger spacings between nearest-neighbour fluoride ions in BiF_3 are reflected in the larger Debye-Waller factors for fluorine (Table 2).

Acknowledgements. The authors are indebted to the S.R.C. for the provision of neutron diffraction facilities at A.E.R.E. Harwell. Our thanks are also due to Dr. B.T.M. Willis for valuable discussions and to Dr. A. W. Hewat for providing his version of the Rietveld program. The work was carried out while one of us (N.N.) was engaged as a Vacation Associate at A.E.R.E., for which he wishes to express his gratitude. A.K.C. wishes to thank the E.P.A. Cephalosporin Fund for financial support.

REFERENCES

1. Thoma, R. E. and Brunton, G. D. *Inorg. Chem. 5* (1966) 1937.
2. Zalkin, A. and Templeton, D. H. *J. Amer. Chem. Soc. 75* (1953) 2453.
3. Aurivillius, B. *Acta Chem. Scand. 9* (1955) 1206.
4. Andersson, S. and Åström, A. *NBS Special Publication 364*, Solid State Chemistry 1972.
5. Rietveld, H. M. *Acta Crystallogr. 22* (1967) 151.
6. Rietveld, H. M. *J. Appl. Cryst. 2* (1969) 65.
7. Neutron Diffraction Commission, *Acta Crystallogr. A 25* (1969) 391.
8. Nyburg, S. C., Ozin, G. A. and Szymański, J. T. *Acta Crystallogr. B 27* (1971) 2298.
9. Shannon, R. D. and Prewitt, C. T. *Acta Crystallogr. B 25* (1969) 925.

Received July 28, 1973.

Acta Chemica Scandinavica A 28 (1974) 61—70

Magnetic Structures and Properties of $Mn_{1-t}Fe_tAs$ Phases

KARI SELTE, [a] ARNE KJEKSHUS [a] and ARNE F. ANDRESEN [b]

[a] Kjemisk Institutt, Universitetet i Oslo, Blindern, Oslo 3, Norway and [b] Institutt for Atomenergi, Kjeller, Norway

The pseudo-binary MnAs-FeAs system has been investigated by X-ray and neutron diffraction, density, magnetic susceptibility, and magnetization measurements. $Mn_{1-t}Fe_tAs$ exhibits temperature dependent regions of limited solid solubility with a virtually constant 1:1 ratio between the metal and non-metal components. The crystal structure is of the MnP type at room temperature, except for a very small range near the composition MnAs where the NiAs type structure prevails.

In the range $0.00 \leqq t < \sim 0.12$, high temperature X-ray and neutron diffraction and magnetic susceptibility measurements demonstrate a transition from MnP to NiAs type structure at temperatures between 385 and 575 K, depending on composition. The temperature dependence of the magnetic susceptibility obeys the Curie-Weiss Law in the region of the NiAs type structure (*viz.* the high temperature phase for $t \approx 0$) with an essentially constant (paramagnetic) spin quantum number of $2S_T = 3.7 \pm 0.2$ ("spin only" approximation) per metal atom. The low temperature phase with NiAs type structure is found to exhibit ferromagnetism in agreement with previous studies. In the region of the MnP type crystal structure, a helimagnetic ordering of the spins is adopted at low temperatures ($T_N = 206 \pm 1$ K for $t = 0.10$) with spiral propagation along the a axis ($0.133 \times 2\pi\mathbf{a}^*$ for $t = 0.10$ at 90 K; the setting of the MnP type unit cell is in accordance with space group *Pnma*). The magnetic structure is of the double spiral type previously found for compounds with the MnP type structure, but differs by propagating along the a axis and by having a different phase relation between the spirals. The spiral periodicity is rather temperature dependent.

No crystallographic transformations have been observed between 4.2 and 1300 K within the interval $\sim 0.65 < t \leqq 1.00$, where the reciprocal magnetic susceptibility cannot be expressed as a simple linear function over an appreciable temperature range, implying that the Curie-Weiss Law is not satisfied. An antiferromagnetic structure with doubling of the crystallographic a and c axes is found in the composition range $0.65 \leqq t < \sim 0.90$ at lower temperatures ($T_N = 54 \pm 1$ K for $t = 0.85$ where, moreover, $\mu_T (= 2S_T) = 0.71 \pm 0.04$ μ_B at 13.5 K). A double helix magnetic spin arrangement along the c axis is adopted in a narrow region close to FeAs.

The endeavour within many research fields has a tendency to oscillate, for various reasons, between periods of low and high activity. This is rather characteristic of the historical development of the investigations on phases with the MnP type crystal structure. An initial diligent period primarily devoted to syntheses, phase analyses, and approximate structure determinations was followed by one of less attention, which in turn was relieved in 1966 by a more intense period with the emphasis centered mainly on magnetic properties. It is clearly impossible, at this stage, to estimate the significance of the achievements in the latter, hitherto incomplete, period. However, the binary MnP phases have apparently been fully explored by the experimental methods available at present without providing a credible clue as to their strange magnetic behaviour. Faced with this unsatisfactory situation it is natural to turn to the ternary MnP phases. The MnAs-FeAs system was selected as the first target for the extension of our research programme.

EXPERIMENTAL

Samples of MnAs and FeAs were made by heating weighed quantities of the elements [99.9+ % Mn (The British Drug Houses; crushed powder from the commercial, electrolytic grade material), 99.99+ % Fe (Johnson, Matthey & Co.; turnings from rods), and 99.9999 % As (Koch-Light Laboratories)] in

evacuated, sealed quartz tubes. FeAs was prepared as described in Ref. 1. During the syntheses of MnAs the temperature was slowly increased to 900°C, the sample was kept at this temperature for 3 days, and then quenched in ice water. After careful grinding, the sample was reheated at 700°C for 10 days and cooled to room temperature over 3 days. The binary arsenides produced in this way were mixed in proportions appropriate to the desired ternary compositions and subjected to a first annealing at 850°C for 8 days. All samples were crushed and subjected to three further annealings at 850°C with intermediate crushings, and finally cooled to room temperature over a period of 3 days or quenched in ice water.

The experimental details concerning the X-ray and neutron diffraction, density, magnetic susceptibility, and magnetization measurements have been presented in previous communications.[1,2]

RESULTS

(i) *Homogeneity ranges and atomic arrangements.* Since the main purpose of the present work is to examine the variation in the magnetic properties of $Mn_{1-t}Fe_tAs$ as a function of t, the necessary phase analysis was minimized to surveying the situation at a single annealing temperature. As a compromise between various competing factors, 850°C was chosen, and in the initial experiments all samples were quenched from this temperature. However, the results unfortunately showed that the quenching technique did not give entirely homogeneous samples, and a slow cooling procedure was accordingly adopted for the subsequent, larger scale syntheses.

The extents of the homogeneity ranges have been determined from the variation of the unit cell dimensions with the composition parameter t (Fig. 1), the overall solubility limits being also confirmed by application of the disappearing phase principle on the X-ray powder data. As evident from Fig. 1, MnAs and FeAs are only partially soluble in each other at temperatures below 850°C. The extent of the Mn rich phase is strongly temperature dependent ($0.00 \leqq t < \sim 0.35$ and $0.00 \leqq t \leqq 0.12 \pm 0.02$ for quenched and slowly cooled samples, respectively) whereas the homogeneity range of the Fe rich phase is essentially temperature independent ($0.65 \pm 0.02 \leqq t \leqq 1.00$).

Apart from $t \approx 0$ all single phase samples exhibit the MnP type crystal structure at room

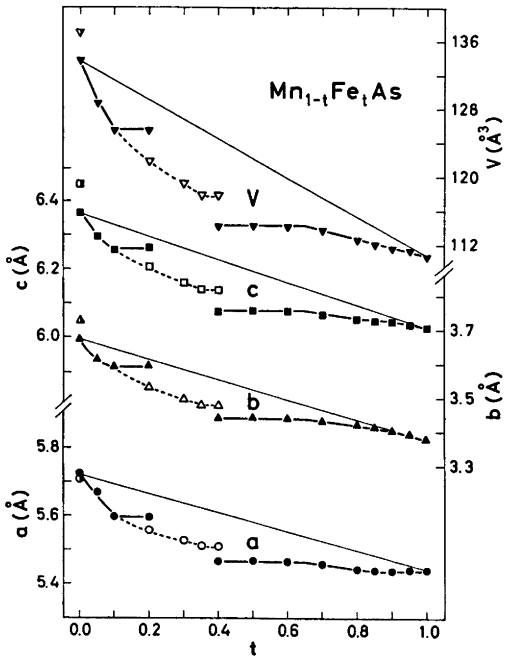

Fig. 1. Unit cell dimensions of the ternary solid solution series MnAs-FeAs as a function of composition. Filled and open symbols represent slowly cooled and quenched samples from 850°C, respectively. Half filled symbols give the corresponding data for the room temperature modification of MnAs with NiAs type structure.

temperature. The pycnometrically determined densities show that the solid solubility is of the strictly substitutional type with a virtually constant 1:1 ratio between the metal and non-metal components. The lack of additional superstructure reflections in the X-ray and neutron diffraction diagrams confirms that the substituted atoms are arranged at random in the metal sublattice.

The positional parameters for the MnP type atomic arrangement vary very little (Table 1) with composition and temperature ($T < 300$ K). (Corresponding data for MnAs and FeAs are given in Refs. 1, 3–5.) This constancy is somewhat remarkable in view of the exceptional position of the MnAs coordinates (at 55°C) in this respect, implying that there must be rather rapid changes in the variables near $t = 0$.

A tentative phase diagram for the pseudo-binary MnAs-FeAs system is presented in Fig. 2. The diagram shows *inter alia* that the Mn rich samples follow the trend from MnAs in that a

Table 1. Unit cell dimensions and positional parameters with standard deviations for some $Mn_{1-t}Fe_tAs$ phases; space group *Pnma*, positions 4(*c*).

t	0.10			0.85			0.95		
T(K)	21	90	293	13.5	81	293	16	81	293
a (Å)	5.537(3)	5.526(3)	5.615(3)	5.442(2)	5.429(2)	5.435(2)	5.450(1)	5.448(1)	5.434(1)
b (Å)	3.483(3)	3.477(3)	3.589(3)	3.372(1)	3.375(1)	3.404(1)	3.344(1)	3.349(1)	3.385(1)
c (Å)	6.151(3)	6.137(3)	6.252(3)	6.034(1)	6.028(1)	6.041(1)	6.031(1)	6.028(1)	6.030(1)
x_T	0.0091(19)	0.0084(21)	0.0126(20)		0.0042(7)	0.0036(7)	0.0041(7)	0.0051(6)	0.0044(5)
z_T	0.2053(25)	0.2101(28)	0.2138(25)	as for	0.1989(5)	0.1997(5)	0.1978(5)	0.1976(4)	0.1988(4)
x_X	0.1967(6)	0.1962(7)	0.2073(6)	81 K	0.1992(7)	0.2006(6)	0.2010(7)	0.2007(6)	0.2007(5)
z_X	0.5805(9)	0.5830(10)	0.5811(11)		0.5766(8)	0.5780(8)	0.5740(10)	0.5753(8)	0.5787(7)

second-order phase transformation from the MnP to the NiAs type structure takes place above room temperature, the transformation temperature *versus* concentration relationship being approximately linear. For the purpose of comparison, Fig. 2 includes data for the CrAs-MnAs system,[6] where a similar phase relationship is observed.

(ii) *Magnetic susceptibility and magnetization.* The gradual change in the temperature dependence of the magnetic susceptibility with progressively increasing concentration of Fe is shown in Fig. 3.

In the Fe rich phase all characteristics show a consistent change from being convex towards the temperature axis at the lowest temperature to concave at higher temperatures. For FeAs the $\chi^{-1}(T)$ curve has a linear range between ~ 300 and ~ 650 K, which permits a deduction of a tentative value for its paramagnetic moment.[1] Already in the $\chi^{-1}(T)$ curve for $t = 0.95$, this linear dependence is completely destroyed and, in fact, none of the samples within the composition range $0.65 \leqq t < 1.00$ satisfied the Curie-Weiss Law. Hence, information concerning the number of unpaired electrons in the paramagnetic state of the Fe rich phase is inaccessible. The magnetic susceptibility of the samples with $0.65 \leqq t < 1.00$ has not been examined below 80 K, and for this reason the

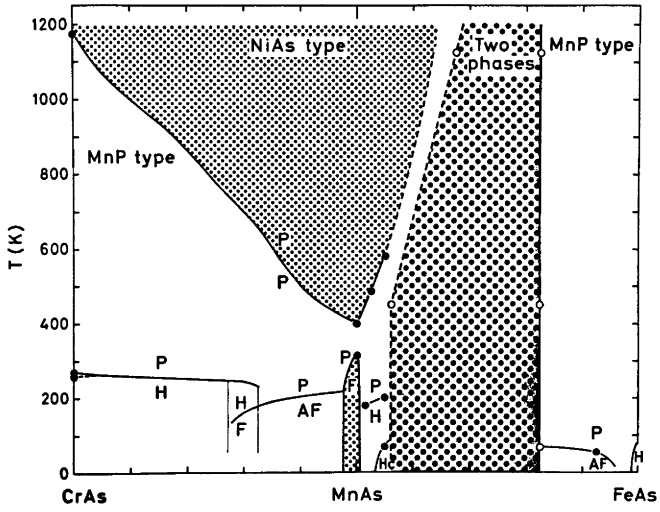

Fig. 2. Diagram of phase relations in the pseudo-binary CrAs-MnAs and MnAs-FeAs systems. Data for the CrAs-MnAs system are quoted from Kazama and Watanabe.[6] Phase boundaries indicated by broken lines are uncertain. The location of the open circles along the temperature axis should be regarded as somewhat undetermined. Magnetic state is indicated by: AF antiferro., F ferro., H helical, P para., c conical.

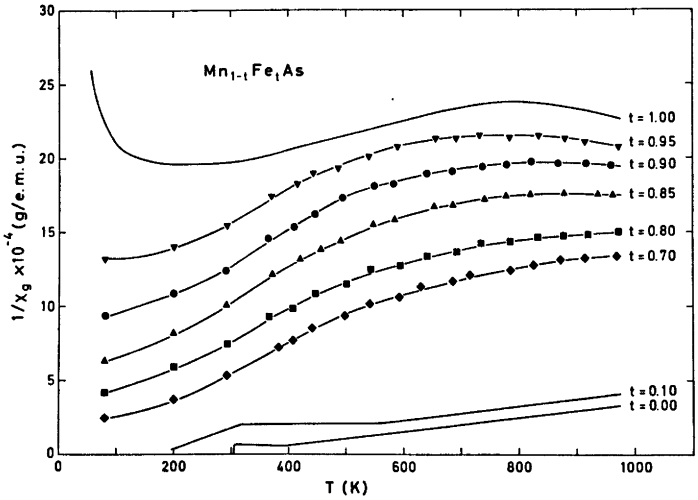

Fig. 3. Reciprocal magnetic susceptibility *versus* temperature for typical $Mn_{1-t}Fe_tAs$ samples.

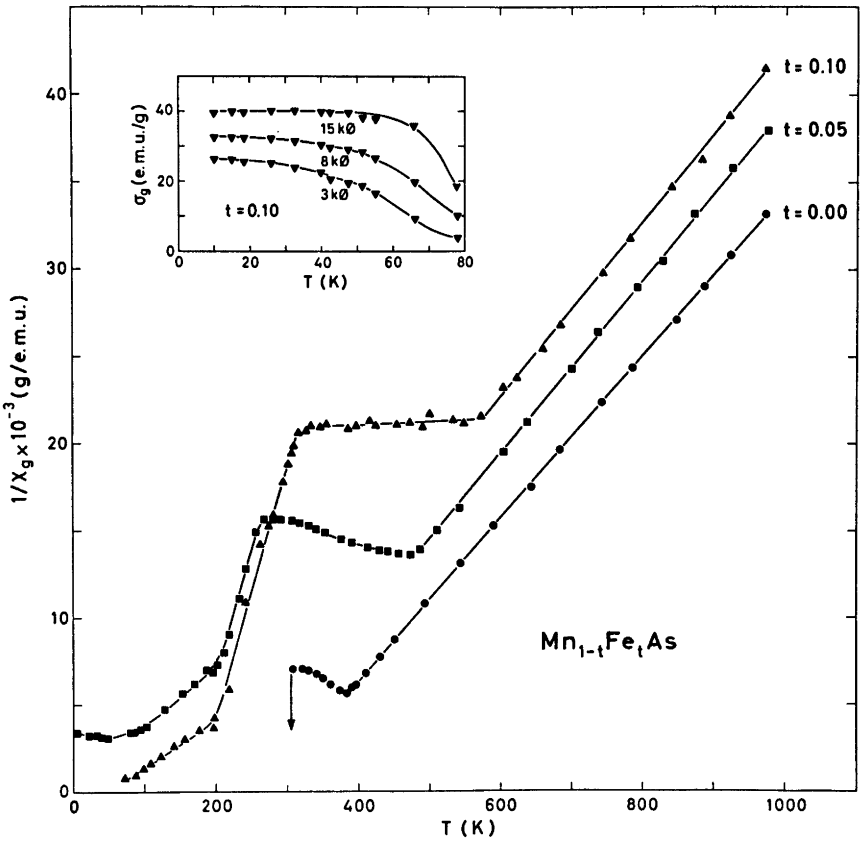

Fig. 4. Thermomagnetic data for Mn-rich $Mn_{1-t}Fe_tAs$ samples.

possible completion of a convex portion of the $\chi^{-1}(T)$ curves towards a rapid increase at lower temperatures could not be verified (*cf.* Fig. 3).

The physical origin of the anomalous $\chi^{-1}(T)$ curves for the Fe rich phase is essentially unknown. Variation in the electronic band structure with temperature may, in principle, account for the observations, but such an explanation must be subject to a future experimental and/or theoretical verification.

The magnetic behaviour of the Mn rich phase is shown in more detail in Fig. 4. These data are more in line with the requirements of conventional theories of magnetism. The present data for MnAs (Fig. 4), which are in excellent agreement with those reported earlier (*cf.*, *e.g.*, surveys in Refs. 7, 8), concur with those for the samples $t=0.05$ and $t=0.10$.

As shown in Fig. 4, the three samples obey almost perfectly the Curie-Weiss Law at high temperatures. The linear $\chi^{-1}(T)$ curves are interrupted at temperatures which correspond very closely to the values obtained, by other means, for the transformation from the NiAs to the MnP type structure. The paramagnetic moment derived according to the "spin only" formula from the high temperature paramagnetic portions of the $\chi^{-1}(T)$ curves, corresponds to an essentially constant spin quantum number of $2S_T=3.7\pm0.2$ per metal atom.

The virtually horizontal, intermediate portions of the $\chi^{-1}(T)$ curves are, according to the neutron diffraction data, to be associated with the paramagnetic state of the MnP type structure of the phase. The temperature dependence of $\chi^{-1}(T)$ within these intervals can again, in principle, be accounted for by assuming gradual changes in the electronic band structures. In this case, there is also experimental evidence available which favours this interpretation (*vide infra*).

On the low temperature side the three curves in Fig. 4 have in common a rapid fall in χ^{-1}. The differences between the three curves at the lower temperatures, which are also clearly demonstrated in the magnetization data (see inset), are due to distinctions in magnetic structure. In accordance with previous findings and the magnetic structure, the magnetization of MnAs is very strong. No detectable zero field magnetization has been observed for the sample with $t=0.05$, whereas the sample with $t=0.10$ exhibits magnetization of intermediate strength (*vide infra*).

The information derived from the magnetic susceptibility data is incorporated in the phase diagram in Fig. 2.

(iii) *Magnetic structures.* The helimagnetic arrangement in pure FeAs extends slightly into the ternary range. According to the results obtained for the sample with $t=0.95$ a tentative boundary is indicated in the phase diagram (Fig. 2) as $t=\sim0.98$. The parameters specifying the spirals are $T_N=77\pm1$ K, $\mu_T=0.5\pm0.1$ μ_B, $\tau=0.375\times2\pi c^*$ for FeAs at 12 K.[1] The helimagnetic structure of FeAs is illustrated in Fig. 5A.

In the range $0.65\leqq t<\sim0.90$ an antiferromagnetic spin structure with doubled a and c axes relative to the chemical unit cell prevails. The Néel temperature varies comparatively little with composition, and is 54 ± 1 K for $t=0.85$. The normalized intensity of the magnetic reflection 101 *versus* reduced temperature for $t=0.85$ follows closely the Brillouin function for $2S=1$. The antiferromagnetic structure is maintained down to liquid helium temperature.

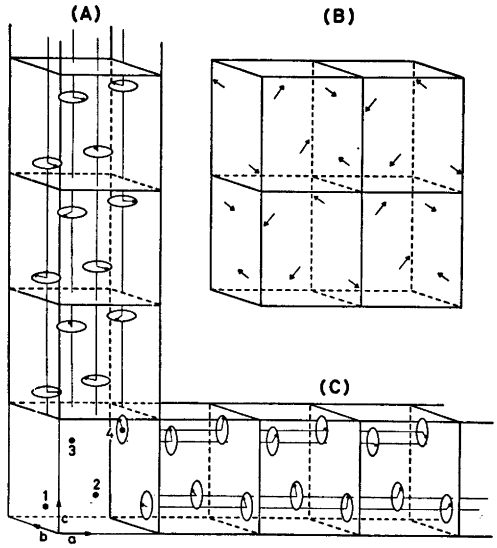

Fig. 5. Spin arrangements in $Mn_{1-t}Fe_tAs$ phases: (A) helical arrangement in FeAs (12 K), (B) antiferromagnetic arrangement in $Mn_{0.15}Fe_{0.85}As$ (13.5 K), and (C) helical arrangement in $Mn_{0.90}Fe_{0.10}As$ (90 K).

Unfortunately the neutron diffraction diagrams contain only a few, rather weak magnetic reflections. Hence, it is impossible to establish the magnetic arrangement unambiguously, and the proposed magnetic structure for $Mn_{0.15}Fe_{0.85}As$ shown in Fig. 5B should only be regarded as a chemically and physically reasonable model which can be adjusted to the observed neutron diffraction pattern at 13.5 K. The model depicted in Fig. 5B consists of two interpenetrating, mutually perpendicular spin systems within (100), the spin of (say) metal atom No. 1 making an angle of $\sim 30°$ with the b axis. (To facilitate comparison between the spin arrangements in Fig. 5B and C, the former may also be regarded as consisting of spirals propagating along the a axis with a periodicity equal to two unit cell lengths.) The value of $\mu_T = 0.71 \pm 0.04$ μ_B derived through the least squares refinement process is consistent with the temperature dependence of the 101 reflection (*vide supra*). On going from $t = 0.85$ to $t = 0.65$ only minor variations are observed in the intensities of the magnetic reflections. This demonstrates that the cooperative magnetic parameters are essentially invariable over the composition interval.

Apart from a narrow region near $t = 0$, where the NiAs type atomic arrangement gives rise to a ferromagnetic state, the Mn rich phase ($\sim 0.01 < t < \sim 0.12$) obtains a helimagnetic ordering below a Néel temperature which varies between 180 ± 3 K for $t = 0.03$ and 206 ± 1 K for $t = 0.10$. The helical arrangement is in this case directed along the a axis (contrary to what has been found hitherto for compounds with MnP type structure; *cf.* Ref. 1) with an overall propagation vector of $0.133 \times 2\pi\mathbf{a}^*$ for $t = 0.10$ at 90 K. The propagation vector is rather temperature dependent between 90 K and T_N, as illustrated in the upper part of Fig. 6 where the spiral turn angle (α) is plotted against temperature. Further parameters specifying the spiral structure are obtained from the abcences ($hk0$ with $h = 2n+1$ extinguished) governing the satellite reflections, and the intensities of those present. In terms of the labelling of the four equivalent metal positions in the unit cell shown on Fig. 5 (*cf.* Refs. 1, 2) these extinctions imply that the spins on atoms 1 and 2 (and equivalently on 3 and 4) are in phase. (It should be noted that for the double c axis spirals previously found atoms 1 and 3, and 2 and 4 are in phase; *cf.* Fig. 5A for the case of FeAs.[1]) By assuming that the magnetic moments μ_T are at right angle to the spiral axis (*vide infra*), and of equal magnitude for the independent spirals, there are accordingly two parameters to be determined, *viz.* μ_T and $\phi(=\phi_{1,4})$. A step-wise refinement procedure like that used in earlier work,[1,2] gave $\mu_T = 1.6 \pm 0.1$ μ_B and $\phi = 60 \pm 10°$ for $Mn_{0.90}Fe_{0.10}As$ at 90 K. The spiral arrangement is illustrated in Fig. 5C. It should be emphasized also in this connection that the deductions are based on reflections with, in general, low intensities.

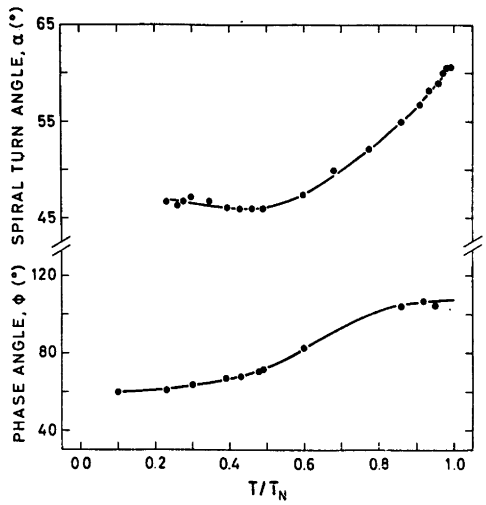

Fig. 6. Phase and turn angles for the spirals in $Mn_{0.90}Fe_{0.10}As$ as functions of reduced temperature.

The attempts to establish the integrated intensity *versus* reduced temperature relationship for the strongest satellites $000^{\pm}$ and $001^{\pm}$ of $Mn_{0.90}Fe_{0.10}As$ resulted in the somewhat strange looking data shown in Fig. 7. Characteristic features are the drop in intensity at low temperature and the difference in temperature behaviour closer to the Néel temperature. The anomalies in the integrated intensities at low temperatures (< 90 K) correspond rather closely to the onset of field strength dependent magnetic susceptibility in Fig. 4. Comparison of observed and calculated intensities for the whole diagram (21 K; nuclear as well as magnetic reflections) shows that this behaviour can be attributed to a conical deformation of the

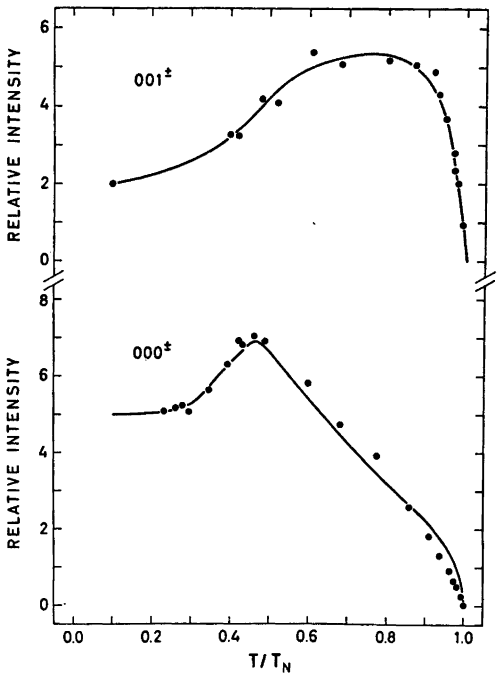

Fig. 7. Temperature dependence of relative integrated intensities of 000± and 001± for $Mn_{0.90}Fe_{0.10}As$.

spiral, the angle between the moments and the spiral axis (β) being estimated to $\sim 60°$. Apart from a slight increase due to the reduction in temperature the total moment remains virtually unaltered. The ferromagnetic component (along the a axis) is 1.0 ± 0.1 μ_B (at 21 K) according to the least squares profile analyses.

Moreover, the marked difference in the temperature variation of the integrated intensities of 000± and 001± (Fig. 7) must be accounted for. The only reasonable explanation of the distinction between the two sets of data for $T/T_N \geqq 0.46$ must be that there is a change in ϕ with temperature. The temperature variation for $T/T_N < 0.46$ is mostly associated with the decreasing cone angle from 90° at $T/T_N = 0.46$ to $\sim 60°$ in the interval $\sim 0.1 < T/T_N < \sim 0.3$. (This effect, which produces the ferromagnetic component in the spiral structure, can be corrected for rather accurately.) Assuming that the apparent reduction in magnetic moment with increasing temperature follows that of FeAs,[1] it is possible to deduce a temperature dependence for ϕ (bottom part of Fig. 6, where it is seen that ϕ increases from 60° at 21 K to 107° at T_N) from the observed intensities of 000± and 001±. As a check of the mutual consistency of the data, the smooth curves in Fig. 7 have been calculated on the basis of the deduced spiral parameters ϕ, β, and μ_T. It is seen that the calculated curves match the experimental points remarkably well. It is worth while to note that the latter agreement also provides additional evidence for the overall correctness of the spiral arrangements in $Mn_{0.90}Fe_{0.10}As$.

In order to observe the position and intensity of 000±, great care had to be taken in improving the collimation and in subtracting the background, which had to be obtained above T_N. The detailed drawing of the peak at the different temperatures revealed the interesting phenomenon shown in Fig. 8. The peak is seen to consist of two partly or completely overlapping reflections, one being considerably stronger than the other. The weaker 000± falls at the high angle side of the stronger at the lowest temperatures ($< \sim 70$ K), whereas the opposite situation prevails at higher temperatures ($> \sim 90$ K). At temperatures where the 000± doublet is partly separated, the intensity of the weaker component has been estimated to 5 – 10 % of that of the main satellite. While the main satellite is shifted only relatively little towards higher angles with increasing temperature, the weaker is shifted more rapidly in the opposite direction.

A similar exploration of the shape of 001± as a function of temperature is more difficult since this reflection is considerably weaker than 000±, but the results indicate a similar behaviour.

The establishment of the doubled 000± and (probably) 001± satellites clearly implies that some of the spiral parameters for $Mn_{0.90}Fe_{0.10}As$ given above should be corrected. The only reasonable explanation we can find for this doubling of the satellites is that the sample is not quite homogeneous. It is conceivable that the substituted Fe atoms are not uniformly distributed over the metal sublattice and that there are domains of different concentration giving rise to spirals of different periodicities. The amount of the minor component is so small that we cannot detect the other satellites and we are therefore unable to say whether this spiral structure deviates significantly from that

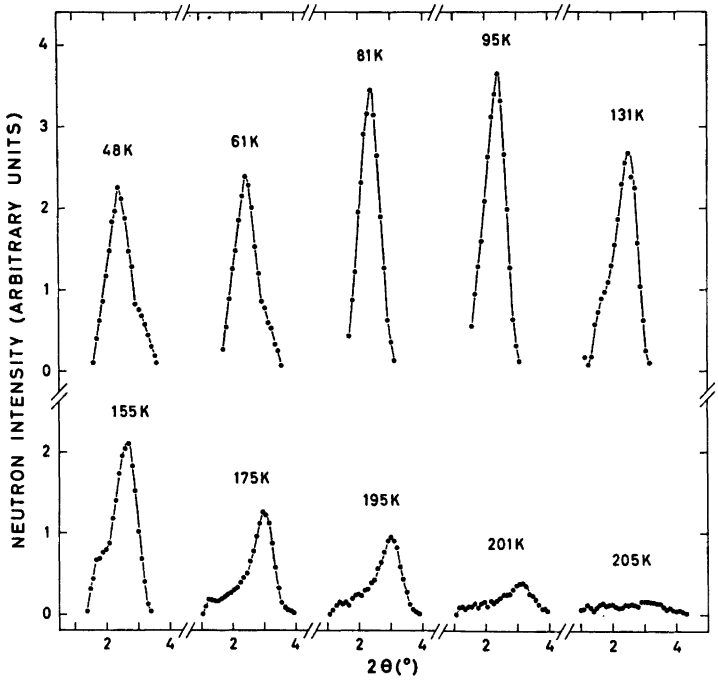

Fig. 8. Profiles of 000± for $Mn_{0.90}Fe_{0.10}As$ at different temperatures; background subtracted.

of the major component. However, since its contribution to the 000± reflection is only 5 – 10 % it can be assumed that very small errors are made by neglecting the inferred correction. It should be emphasized in this connection that in deriving the spiral period and its temperature variation (Fig. 6) for $Mn_{0.90}Fe_{0.10}As$ the peak position of the main 000± satellite has been used, whereas its total intensity has been utilized in obtaining the other spiral parameters (see also Fig. 7).

It should also be remarked that the careful study of the temperature variation of the 000± satellite revealed that this peak does not completely vanish at the Néel point. A small remanent peak is observed several degrees above T_N and moves with increasing temperature to even larger scattering angles. This can be ascribed to a short range spiral order existing above T_N with a periodicity which increases with increasing temperature.

DISCUSSION

The incomplete randomization of Mn and Fe over the metal sublattice may be between the various spiral chains (see Fig. 5C) and/or correspond to local regions of variable t within the chains. Since the spiral period (τ) clearly varies with composition, the occurrence of "concentration domains" would provide a natural explanation, although this raises a number of closely connected questions:

(1) To what degree can an individual, crystallographic character be attributed to the Mn and Fe atoms in a solid solution of this type? Is there a corresponding individuality in their magnetic moments?

(2) Compared with the reflections on X-ray diagrams obtained for a number of other ternary solid solution series of transition metal chalcogenides and pnictides, those of the present Mn rich samples are relatively broad. The corresponding neutron diffraction diagrams are, on the other hand, composed of relatively sharp, nuclear peaks. An explanation of this unexpected result must be sought in the difference in the scattering process, *viz.* in nucleus *versus* electron cloud.

(3) A fundamental problem in connection with (2) is why a substitutionally disordered phase leads to sharp X-ray and/or neutron dif-

fraction diagrams in the general case. An immediate inference of the latter observation is that there is a "constant" average chemical unit cell for each composition which is translated through the crystals. (The metal atoms may well have a degree of individual magnetic character without a corresponding crystallographic identity.)

Closely connected with "concentration domains" is in the present case the occurrence of an insolubility region (Fig. 2). The limited solubility cannot be attributed to a size effect, since the difference in the radius of the metal atom in MnAs [3] and FeAs[1,4,5] is only some 10 %. On the other hand, the distinction in electronic band structure between MnAs and FeAs can, in principle, easily account for the observations. This distinction may either involve the location of the Fermi surface in relation to the Brillouin zone boundaries or be associated with the *d* electron configurations. In connection with the latter suggestion it is of interest to recapitulate that the Mn atoms in the NiAs type structures of MnAs are in "high spin" states, as compared with the "low spin" states generally attributed to the metal atoms in phases with the MnP type structure. No reliable information is unfortunately available for the spin situation in the MnP type modification of MnAs,[9] but this view is supported by the results of magnetic studies of MnAs [10-12] with up to 10 % P substituted for As. The large deviation of the experimental points in Fig. 1 from the linear relationship predicted by Vegard's Law suggests a relatively rapid shrinkage in the size of the Mn atoms near $t=0$. As pointed out in, *e.g.*, Ref. 9 there is a close correlation between atomic size and spin state.

Within the MnAs-FeAs system a wide variety of different types of cooperative magnetism have been found, depending on composition and temperature. Despite distinct difference in formal classification the antiferromagnetic structure within the range $0.65 \leqq t < \sim 0.90$ and the helimagnetic arrangement within $\sim 0.01 < t < \sim 0.12$ are closely related. In both cases the spins are perpendicular to the *a* axis and the crystallographically equivalent metal atoms obtain a corresponding equivalence in the magnetic sense. Similar relations are found when comparisons are made with the cooperative magnetism in $Cr_{1-t}Mn_tAs$ [6] (see also Fig. 2). At the present stage it is impossible to give a more or less complete account for the findings. It is nevertheless tempting to point out some features which appear to be of special interest:

(1) Apart from the region near $t=0$ all the magnetic structures require not less than three exchange parameters to describe their magnetic behaviour.

(2) In the case of MnP, Takeuchi and Motizuki [13] take into account 7 different isotropic (direct and indirect) exchange interactions. Their deductions were based on a number of simplifying assumptions (of which the most important appears to be the assumption $a=b=c$, *i.e.* making the unit cell cubic). Even with the increased translational and internal symmetry of the unit cell, these authors do not provide a complete solution of the exchange interaction problem. Their treatment is limited to prove that the experimental results are consistent with theory. It is feasible that a similar analysis can be performed for the cooperative states of other phases with MnP type structure, but in the lack of a general treatment of the problem such an analysis seems to be of rather limited value.

(3) Similar objections can be raised in connection with Bertaut's [14] treatment of the same problem in terms of two isotropic and one antisymmetric exchange coupling. In fact, the results for FeP,[15] FeAs,[1] $Cr_{1-t}Mn_tAs$,[6] and $Mn_{1-t}Fe_tAs$ suggest very strongly that the number of isotropic and/or antisymmetric exchange couplings must be increased. With such a high number of variables it seems, in principle, possible to account for the observations.

(4) Immediately before this communication was submitted for publication, we received a preprint of a paper by Kallel *et al.*[16] which gives a comprehensive treatment of the exchange interactions in compounds with the MnP type structure. However, as was the case for the treatments by Takeuchi and Motizuki [13] and by Bertaut,[14] the considerations by Kallel *et al.* appear to suffer from a number of weaknesses. In the first place only one of four solutions of the four by four matrix equations is presented in the paper. A more serious objection concerns the fact that only the stability relationship between the ferromagnetic and *c* axis helimagnetic modes are taken into account. Thus, the three antiferromagnetic modes theoretically predicted by Kallel *et al.*, as well as, *e.g.*, the experi-

mentally verified antiferromagnetic and *a* axis helimagnetic modes for $Mn_{1-t}Fe_tAs$ are not considered.

(5) Considering all data for $Mn_{1-t}Fe_tAs$ the magnetic arrangements seem to be determined by details in crystallographic parameters (interatomic distances and angles), electronic band structure (Fermi surface in relation to Brillouin zone boundaries), and the number of unpaired electrons. At present it is tempting to suggest that the behaviour of the itinerant electrons plays an important role in determining the atomic arrangement, and, in particular, the spin orientations.

REFERENCES

1. Selte, K., Kjekshus, A. and Andresen, A. F. *Acta Chem. Scand. 26* (1972) 3101.
2. Selte, K., Kjekshus, A., Jamison, W. E., Andresen, A. F. and Engebretsen, J. E. *Acta Chem. Scand. 25* (1971) 1703.
3. Wilson, R. H. and Kasper, J. S. *Acta Crystallogr. 17* (1964) 95.
4. Selte, K. and Kjekshus, A. *Acta Chem. Scand. 23* (1969) 2047.
5. Selte, K. and Kjekshus, A. *Acta Chem. Scand. 27* (1973) 1448.
6. Kazama, N. and Watanabe, H. *J. Phys. Soc. Japan 30* (1971) 1319.
7. Kjekshus, A. and Pearson, W. B. *Progr. Solid State Chem. 1* (1964) 83.
8. Hulliger, F. *Struct. Bonding (Berlin) 4* (1968) 83.
9. Selte, K. and Kjekshus, A. *Acta Chem. Scand. 25* (1971) 3277.
10. Ido, H. *J. Phys. Soc. Japan 25* (1968) 1543.
11. Hall, E. L., Schwartz, L. H., Felcher, G. P. and Ridgley, D. H. *J. Appl. Phys. 41* (1970) 939.
12. Schwartz, L. H., Hall, E. L. and Felcher, G. P. *J. Appl. Phys. 42* (1971) 1621.
13. Takeuchi, S. and Motizuki, K. *J. Phys. Soc. Japan 24* (1967) 742.
14. Bertaut, E. F. *J. Appl. Phys. 40* (1969) 1592.
15. Felcher, G. P., Smith, F. A., Bellavance, D. and Wold, A. *Phys. Rev. B 3* (1971) 3046.
16. Kallel, A., Boller, H. and Bertaut, E. F. *J. Phys. Chem. Solids. In press.*

Received July 6, 1973.

Acta Chemica Scandinavica A 28 (1974) 71—76

Iodine Oxides. Part V. The Crystal Structure of $(IO)_2SO_4$

SIGRID FURUSETH, KARI SELTE, HÅKON HOPE,* ARNE KJEKSHUS and BERNT KLEWE

Kjemisk Institutt, Universitetet i Oslo, Blindern, Oslo 3, Norway

The crystal structure of $(IO)_2SO_4$ at 100 ± 5 K has been determined from three-dimensional X-ray data. The structure is monoclinic, space group $C2/c$. The elementary cell contains four formula units and has the dimensions: $a = 15.177(3)$ Å, $b = 4.6854(8)$ Å, $c = 9.810(2)$ Å, $\beta = 125.17(2)°$. The following values were found for the positional parameters: $x = 0.16348(7)$, $y = 0.7066(2)$, $z = 0.2519(1)$ for I in 8(f); $y = 0.1773(11)$ for S in 4(e); $x = 0.2835(8)$, $y = 0.9861(24)$, $z = 0.3576(13)$ for O(1) in 8(f); $x = 0.0960(8)$, $y = -0.0032(26)$, $z = 0.3677(14)$ for O(2) in 8(f); $x = 0.0212(8)$, $y = 0.3550(25)$, $z = 0.1471(13)$ for O(3) in 8(f).

The structure comprises distinct, sandwich-like layers arranged parallel to (001). Within the layers infinite $(IO)_n$ spiral chains along [010] are linked together by SO_4 tetrahedra. A tentative discussion of the chemical bonding in $(IO)_2SO_4$ is presented.

Iodine dioxide (I_2O_4) decomposes irreversibly in I_2O_5 and I_2 at a temperature of about 125°C. However, on introducing H_2SO_4 (or H_2SeO_4) as a reaction medium for I_2O_5 and I_2, the process can be reversed through a two-stage reaction. The first stage terminates by the isolation of an intermediate product with the composition I_2SO_6 (or I_2SeO_6).

Although I_2SO_6 was first isolated as early as 1844 [1] and subjected to regular studies [2–22] thereafter, very little decisive information concerning its properties is available. In fact, most of the research effort on the compound has been concentrated on establishing its correct composition. (The controversy, which seems now unequivocally resolved, concerned the question of whether one,[9,14,15] one half,[4,5,7,11] or no [11–13,16–22] molecule of water is to be included in the formula.) Another subject open to discussion is whether I_2SO_6 is to be regarded as essentially ionic,[12,13,16,18] *i.e.* $(IO^+)_2(SO_4)^{2-}$ (iodosyl sulphate), as a covalent inorganic polymer [17] containing $(IO)_n$ groups linked to SO_4 tetrahedra, or as an addition compound[11–13] of the type $I_2O_3.SO_3$. The latter problem can only be resolved by means of a complete structure determination, and the results of such a study are presented here.

EXPERIMENTAL

Several batches of I_2SO_6 were prepared by shaking the theoretical quantities of finely powdered I_2O_5 and I_2 in conc. H_2SO_4, *cf.*, *e.g.*, Ref. 20. The products were thoroughly washed with conc. H_2SO_4. Well shaped single crystals were obtained by recrystallization from a hot solution of I_2SO_6 in conc. H_2SO_4.

Crystals were removed from the mother liquor by pipetting, quickly dried on a porous plate, and immediately picked up with a goniometer head readied with a glass fibre and adhesive. The crystal was then placed in a cold gas stream on a Syntex $P\bar{1}$ diffractometer fitted with a modified Enraf-Nonius cooling device. The time elapsed from a crystal had been dried until it was positioned in the cold gas stream was ~ 10 s. This quick manipulation is necessary because a ~ 30 s exposure to laboratory atmosphere will cause serious decomposition. The temperature at the crystal site (constant to ± 0.2 K) was 100 ± 5 K. Under these conditions no crystal decay was observed.

The crystals showed a marked tendency towards twinning, and 5 – 10 specimens were examined before one which gave a reasonably good ω scan for several reflections was found. As became apparent later (see section on structure determination and refinement) the crystal used for data collection was not entirely free of twinning symptoms.

Three-dimensional intensity data were obtained by diffractometer measurements using graphite crystal monochromatized Mo$K\alpha$-radiation. Reflections with $2\theta < 55°$ were

*Present address: Department of Chemistry, University of California, Davis, California 95616, U.S.A.

measured with the ω-2θ scan technique in a variable scan rate mode (2° min^{-1} for the majority of the reflections, but up to 6° min^{-1} for the strongest reflection), very weak reflections (*viz.* those with intensities below a threshold value) being automatically omitted. The scan range was $2\theta(\alpha_1) - 1.4$ to $2\theta(\alpha_2) + 1.1°$, and the background was measured (for 70 % of the scan time) at each of the scan range limits. Measurement of check reflections was repeated every 50th reflection, no systematic variation being detected. A total of 648 unique reflections were recorded as "observed" [$I_{net.} > 3\sigma(I)$]. Unobserved reflections were not included in the calculations.

The crystal was sufficiently large to warrant absorption corrections to be made. However, the amount of adhesive needed to pick up the crystal quickly was large enough to impede subsequent measurement of crystal dimensions, and absorption correction was accordingly not performed.

The calculations were performed on CD 3300 and CD 7600 computers using programmes by Dahl *et al.*[23] and Hope.[24] The atomic scattering factors used in the final refinements were taken from Doyle and Turner [25] and the values for the real and imaginary parts of the dispersion (for iodine only) from Cromer and Liberman.[26]

Throughout this paper estimated standard deviations (e.s.d.) applying to the least significant digits are given in parentheses following the corresponding parameter values.

CRYSTAL DATA

I_2SO_6, $M = 381.85$.
Transparent, approximately prismatically shaped crystals of yellow colour.
Monoclinic.
$a = 15.177(3)$ Å, $b = 4.6854(8)$ Å,
$c = 9.810(2)$ Å, $\beta = 125.17(2)°$.
Unit cell volume: 570.2(4) Å^3.
Unit cell content: 4 I_2SO_6 groups.
Calculated density: 4.447 g cm^{-3}.
Systematic extinctions:
hkl absent when $h + k = 2n + 1$
$h0l$ absent when $l = 2n + 1 (h = 2n + 1)$
Space group: $C2/c$
(The preliminary crystallographic data reported in the preceding paper of this series [22] refer to a pseudo cell defined by: $\mathbf{a}' = \mathbf{a}$, $\mathbf{b}' = \mathbf{b}$, $\mathbf{c}' = 1/3\mathbf{a} + \mathbf{c}$, which give $\beta' \approx 90°$.)

STRUCTURE DETERMINATION AND REFINEMENT

Space group extinct reflections with l odd were recorded for the $h0l$ zone. A number of these reflections with $h = \pm 4, \pm 12$ were found to have significant intensities. The dimensions of the reciprocal lattice are such that a 180° rotation about the vector $\mathbf{b}^* \times \mathbf{c}^*$ places even l lattice points of the original lattice with $h = \pm 4, \pm 12$ at odd l points in the rotated lattice, whereas for $h = 0, \pm 8, \pm 16$ the coincidence is even-even. The relative magnitudes of the individual parts of a crystal assumed to be twinned as described were established from the $h0l$ intensities to be near 10:1. Based on this model the intensities of all $4n,k,l$ reflections were adjusted to correspond to those of the major crystal.

The approximate positions of the crystallographic equivalent iodine atoms were easily deduced from a three-dimensional Patterson synthesis. A set of structure factors calculated on the basis of these iodine parameters gave $R = 0.32$, and the corresponding Fourier map produced the location of the sulphur atoms in addition to shifts of the iodine atoms. After a preliminary refinement of the atomic coordinates of iodine and sulphur (giving $R = 0.18$), the positions of the three non-equivalent oxygen atoms were deduced from a second Fourier map. Subsequent full matrix least squares refinement with isotropic temperature factors converged to $R = 0.092$. A refinement with anisotropic temperature factors for all atoms lowered R to 0.057, but it is clear that the indicated anisotropy is, at least partly, a result of lacking absorption correction rather than of anisotropic motion. The β_{22} values for I and S are nearly zero. We therefore decided to base the description of the structure on the results from the isotropic refinement. Because the low-order reflections normally are most seriously affected by experimental errors, we excluded observations with $\sin\theta/\lambda < 0.25$ from the refinement. Although e.s.d. for F_{obs} based on counting statistics was available, the model errors indicated above led us to use the weighting scheme of Hughes,[27] with $4I_{min.} = 67$.

The final R factor is higher than normally seen for good diffractometer data. We therefore have used additional criteria to establish the essential correctness of the structure. A difference Fourier synthesis showed that all atoms had been accounted for, and that no atom had been grossly misplaced. A listing of F_{obs}/F_{calc} ratios in groups with constant h,k and varying l shows a uniform variation of the ratio as a function of l. Individual ratios within each

Table 1. Final positional and thermal parameters for the crystal structure of $(IO)_2SO_4$. [I, O(1), O(2), and O(3) in position 8(*f*) and S in position 4(*e*) of space group $C2/c$.]

Atom	*x*	*y*	*z*	B(Å^2)
I	0.16348(7)	0.7066(2)	0.2519(1)	0.48(4)
S	0	0.1773(11)	1/4	0.56(9)
O(1)	0.2835(8)	0.9861(24)	0.3576(13)	0.71(15)
O(2)	0.0960(8)	−0.0032(26)	0.3677(14)	1.03(17)
O(3)	0.0212(8)	0.3550(25)	0.1471(13)	0.83(16)

group rarely deviate by as much as 5 % from values estimated from a smooth curve fitted for the group. This is a strong indication that the positional parameters are reliable in spite of a poor determination of the thermal parameters.

The final positional and thermal parameters are listed in Table 1. The observed and calculated structure factor data are available from the authors upon request.

DESCRIPTION AND DISCUSSION OF THE STRUCTURE

Important interatomic distances and angles calculated from the unit cell dimensions and the positional parameters in Table 1 are given in Table 2.

As shown in Fig. 1, the crystal structure of I_2SO_6 comprises distinct, sandwich-like layers arranged parallel to (001). The layers are in turn built up of infinite $(IO)_n$ spiral chains along [010] linked together by SO_4 tetrahedra. Hence, the complete structure may to a reasonable approximation be illustrated by a schematic, two-dimensional diagram of the type postulated by Dasent and Waddington.[17] The overall structural inferences of the latter authors are, in fact, remarkably correct when it is borne in mind that they were based on somewhat poorly resolved infra-red spectroscopic data.

The immediate coordination of each I is most usefully regarded as an almost planar arrangement, comprising two O(1), one O(2), and one O(3). However, the corresponding iodine-oxygen distances separate in two categories [I−O(1) *versus* I−O(2) and I−O(3)], which differ considerably. (The difference between the two I−O(1) distances is not significant, whereas that between I−O(2) and I−O(3) is to be classified as highly signifi-

Table 2. Important interatomic distances and angles in the crystal structure of $(IO)_2SO_4$. (The standard deviations correspond to those in the positional parameters.)

Interatomic distances (Å)			
I−O(1′)	1.966(8)	I−O(3)	2.424(9)
I−O(1)	1.983(9)	2S−O(2)	1.494(11)
I−O(2′)	2.351(9)	2S−O(3)	1.480(10)

Interatomic angles (°)			
O(1) −I−O(1′)	95.2(.3)	O(2)−S−O(2′)	111.1(.7)
O(1) −I−O(2′)	83.7(.3)	2O(2)−S−O(3)	106.8(.6)
O(1′)−I−O(3)	87.5(.3)	2O(2)−S−O(3′)	110.3(.4)
O(2′)−I−O(3)	93.9(.3)	O(3)−S−O(3′)	111.5(.7)
O(1′)−I−O(2′)	175.7(.4)	I−O(1)−I	127.1(.6)
O(1) −I−O(3)	175.0(.4)	I−O(2′)−S	117.1(.6)
		I−O(3)−S	125.7(.6)

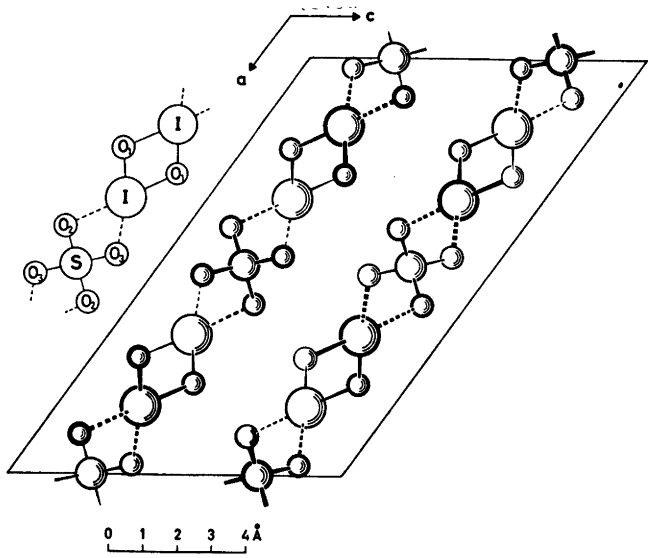

Fig. 1. The crystal structure of $(IO)_2SO_4$ projected along [010]. The numbering of the crystallographically non-equivalent atoms is shown on the left hand side of the diagram. Broken lines indicate contacts between $(IO)_n$ chains and SO_4 tetrahedra.

cant according to the significance test of Cruickshank.[28,29]) This distinction gives rise to the characteristic $(IO)_n$ spiral chains of the structure, the short I–O(1) distances being located within these chains. The longer I–O(2) and I–O(3) contacts join the $(IO)_n$ and SO_4 units of the structure, and as a consequence the already commonly used formula $(IO)_2SO_4$ is appropriate whatever conclusion one may arrive at regarding the nature of the bonding.

The SO_4 units, which are easily recognized in Fig. 1, are of almost perfect tetrahedral symmetry (*viz.* T_d rather than C_2 symmetry imposed by the space group). The bonding S–O(2) and S–O(3) distances are virtually identical and the mutual differences between the O–S–O bond angles as well as their deviations from the ideal tetrahedral value of 109.47° are unimportant (Table 2).

The almost conjectural formulation of $(IO)_2SO_4$ as a simple salt between IO^+ and SO_4^{2-} must immediately be rejected as incompatible with the actual structure. The fact that the S–O bond length in $(IO)_2SO_4$ coincides with the corresponding distances in the ionic sulphates is to be regarded as an accidental circumstance in view of the relatively strong I–O(2) and I–O(3) bonds (*vide infra*).

It has been suggested [17,21] that effective IO^+ cations are present as

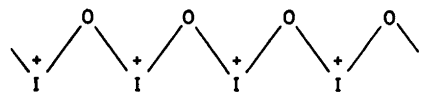

This extreme distribution of positive unit-charges located on iodine and, hence, approximately neutral oxygen atoms within the $(IO)_n$ chains seems intuitively improbable. On the contrary, the fact that the intra-chain I–O(1) bond lengths very nearly match the expected value for the I–O single-bond, and the close correspondence in the values for the angles I–O(1)–I, I–O(2)–S, and I–O(3)–S (Table 2 and *vide infra*) strongly suggest that only comparatively small effective charges are located on the different atoms in $(IO)_2SO_4$. However, although the bonding is predominantly covalent, there is a degree of uneven charge distribution on iodine, sulphur, and oxygen, due to their different electronegativities. These partial charge separations may *inter alia* be responsible for the yellow colour of $(IO)_2SO_4$, as suggested by Dasent and Waddington.[17] The following simplified discussion, nevertheless, neglects the polarity of the bonds, and considers $(IO)_2SO_4$ as an idealized covalent macromolecule.

A comprehensive discussion of the bonding characteristics of iodine is difficult due to the many atomic orbitals potentially available for bonding, and the relatively large size and easy polarizability of this atom. In general, a considerable number of possible hybridization schemes for iodine are open for consideration. However, the situation for I in $(IO)_2SO_4$ appears fortunately to be relatively simple and clearcut. The simplest bonding scheme for I involves that two of its p-orbitals are engaged in regular σ-bonds to two O(1) and the (originally empty) $d_{x^2-y^2}$ and d_{z^2} orbitals are used in dative σ-bonding with O(2) and O(3). [The three remaining d-orbitals (d_{xy}, d_{yz}, and d_{xz}) on each iodine are of appropriate symmetry for π-contribution to the I–O(1) bonds (*vide infra*).] This interpretation is consistent with the almost coplanar arrangement of I, two O(1), O(2), and O(3), and the approximately 90° O–I–O bond angles. The differences between the I–O(1) bond lengths on the one hand and I–O(2) and I–O(3) on the other suggest that it is justified to neglect hybridization of the iodine orbitals in this case. The fact that the I–O(2) and I–O(3) bond distances exceed the regular single bond length (*vide infra*) is attributed to the use of d- rather than p- (or s-) orbitals on iodine.

Alternatively, the electron arrangement at I can be compared with that at Xe in, *e.g.*, XeF_4.[30] A twelve-electron system at the central I atom would be arranged in six pairs in a quadrangular bipyramid with the electrons in its basal plane involved in ligand bonding and the apical ones left as unshared pairs. In the present structure we observe a distorted planar arrangement around I, but otherwise the analogy may be reasonable. This picture corresponds well with the assumption of only a small degree of charge separation in $(IO)_2SO_4$.

Because of the non-availability of atomic d-orbitals, the bonding situation associated with oxygen is simpler than for sulphur and iodine. Each oxygen is bonded to either two iodine or one iodine and one sulphur atom. In common with the vast majority of compounds containing two-coordinate oxygen, the arrangements I–O(1)–I, I–O(2)–S, and I–O(3)–S are non-linear. The situation with respect to these bond angles is analogous to that discussed[31] for the intra- and intermolecular I–O–I bond angles in I_2O_5. Following the arguments advocated for the latter case, the two bonding orbitals on each oxygen may be either:

(i) essentially pure p-orbitals for which the theoretical 90° bond angle has been enlarged due to iodine-iodine or iodine-sulphur repulsion* (including charge as well as size effects), or

(ii) result from incomplete sp-hybridization.

Although the average I–O(1) bond distance of 1.97(2) Å is only insignificantly shorter than the currently accepted I–O single-bond length of 1.99 Å (*cf.*, *e.g.*, Ref. 31) we suggest that the I–O(1) bonds possess a slight, but finite degree of π-character (*viz.* p_π–d_π back-bonding from O(1) to I) in addition to a normal single σ-bond. In the S–O(2) and S–O(3) bonds the contribution of π-bonding is unquestionable, since the average S–O bond distance of 1.48(2) Å is 0.21 Å shorter than the presumed S–O single-bond length (derived from the Schomaker-Stevenson[32,33] rule). The theoretically best founded scheme for deriving π-bond order for the type of compounds under consideration appears to be due to Cruickshank.[34] Following Cruickshank the observed S–O bond distances in $(IO)_2SO_4$ amount to an average π-bond order of 0.52(4), which is a quite reasonable value from the point of view of the I–O skeleton of the structure. The implied large degree of freedom for the SO_4 tetrahedra to arrange themselves in favourable positions relative to the $(IO)_n$ chains is also reflected in their almost perfect T_d symmetry. Hence, the sulphur employs four virtually ideally sp^3-hybridized orbitals for the σ-bonds and the originally empty atomic $d_{x^2-y^2}$ and d_{z^2} orbitals for the π-bonding system.

The crystal structure of $(IO)_2SO_4$ is consistent with its instability towards moisture. The H_2O molecules clearly attack the crystals at the SO_4 units. This reaction produces H_2SO_4 and, at least in principle, asymmetric I_2O_3 fragments as may be imagined from Fig. 1. The further separation of I_2 and the rearrangement of the residual unit to form the crystal structure of I_2O_4 is another problem, however.

REFERENCES

1. Millon, M. E. *Ann. Chim. Phys. 12* (1844) 345, 353; *J. Prakt. Chem. 34* (1845) 321, 337.
2. Kaemmerer, H. *J. Prakt. Chem. 83* (1861) 65.
3. Weber, R. *Ber. Deut. Chem. Ges. 20* (1887) 8.
4. Chrétien, P. *C. R. Acad., Sci. Ser. C 123* (1896) 814.
5. Chrétien, P. *Ann. Chim. Phys. 15* (1898) 358.
6. Muir, M. M. P. *J. Chem. Soc. 95* (1909) 656.
7. Kappeler, H. *Ber. Deut. Chem. Ges. 44* (1911) 3496.
8. Fichter, F. and Kappeler, H. *Z. Anorg. Chem. 91* (1915) 134.
9. Bahl, R. K. and Partington, J. R. *J. Chem. Soc.* (1935) 1258.

*The interatomic I–I ($\geqq$3.53 Å), I–S ($\geqq$3.32 Å), and O–O ($\geqq$2.38 Å) distances in $(IO)_2SO_4$ appear to be consequences of the crystal structure and are therefore regarded as virtually non-bonding, even when they are shorter than the corresponding van der Waals distances of 4.3, 4.0, and 2.8 Å, respectively.

10. Fichter, F. and Dinger, A. *Helv. Chim. Acta 19* (1936) 607.
11. Masson, I. *Nature (London) 139* (1937) 150.
12. Masson, I. and Argument, C. *J. Chem. Soc.* (1938) 1702.
13. Masson, I. *J. Chem. Soc.* (1938) 1708.
14. Kikindai, T. *C. R. Acad. Sci. Ser. C 240* (1955) 873.
15. Semin'ko, V. A. *Trudy Kar'kov Farm. Inst. 1* (1957) 160.
16. Symons, M. C. R. *J. Chem. Soc.* (1957) 2186.
17. Dasent, W. E. and Waddington, T. C. *J. Chem. Soc.* (1960) 3350.
18. Arotsky, J., Mishra, H. C. and Symons, M. C. R. *J. Chem. Soc.* (1962) 2582.
19. Dasent, W. E. and Waddington, T. C. *J. Inorg. Nucl. Chem. 25* (1963) 132.
20. Dæhlie, G. and Kjekshus, A. *Acta Chem. Scand. 18* (1964) 144.
21. Gillespie, R. J. and Senior, J. B. *Inorg. Chem. 3* (1964) 972.
22. Selte, K. and Kjekshus, A. *Acta Chem. Scand. 25* (1971) 751.
23. Dahl, T., Gram, F., Groth, P., Klewe, B. and Rømming, C. *Acta Chem. Scand. 24* (1970) 2232.
24. Hope, H. *Unpublished results.*
25. Doyle, P. A. and Turner, P. S. *Acta Crystallogr. A 24* (1968) 392.
26. Cromer, D. T. and Liberman, D. *J. Chem. Phys. 53* (1970) 1891.
27. Hughes, E. W. *J. Amer. Chem. Soc. 63* (1941) 1737.
28. Cruickshank, D. W. J. *Acta Crystallogr. 2* (1949) 65.
29. Cruickshank, D. W. J. and Robertson, A. P. *Acta Crystallogr. 6* (1953) 698.
30. Burns, J. H., Argon, P. A. and Levy, H. A. In Hyman, H. H., Ed., *Noble-Gas Compounds*, University of Chicago Press, Chicago 1963, p. 211.
31. Selte, K. and Kjekshus, A. *Acta Chem. Scand. 24* (1970) 1912.
32. Schomaker, V. and Stevenson, D. P. *J. Amer. Chem. Soc. 63* (1941) 37.
33. Pauling, L. *The Nature of the Chemical Bond*, Cornell University Press, Ithaca 1960.
34. Cruickshank, D. W. J. *J. Chem. Soc.* (1961) 5486.

Received July 6, 1973.

Acta Chemica Scandinavica A 28 (1974) 77—82

Interpretation of Kinetic Data for Reactions Involving Ions and Ion-Pairs using an Extended Conductance Equation

PER BERONIUS

Division of Physical Chemistry, University of Umeå, S-901 87 Umeå, Sweden

Electrolytic conductance parameters according to the Fuoss-Hsia equation in the form of Fernandez-Prini and the less complete equation of Fuoss and Onsager have been used in analyzing, by means of the Acree equation, kinetic data for the exchange of halogen between alkyl halides and ionic 1:1-halides in methanol, aqueous ethanol, and acetone at 25°C. The results suggest that the rate constant for the exchange reaction between alkyl halide and paired halide ions is underestimated if conductance parameters according to the Fuoss-Onsager relation are used. This effect is especially pronounced when association to ion-pairs is only slight. The choice between the two different conductance equations in evaluating the rate constant for the corresponding reaction involving unpaired halide ions is, however, immaterial.

The parameters derived from the more complete conductance equation are discussed in terms of Bjerrum's theory for ion association.

One problem encountered in interpreting kinetic data for ion-molecule reactions in solvent media where the ionic reactant associates to ion-pairs is to determine with sufficient accuracy, *e.g.* from electrical conductance data, the extent of ion-pair formation. The purpose of the present article is to discuss kinetic data for a few reactions of this kind in the light of recent progress in the theory of electrolytic conductance; *cf.* Refs. 1 – 9.

The halogen exchange reactions [10–12] to be discussed, see Table 3, were selected to cover a range of association constants for the ionic reactant. The association constants vary from $K_A \simeq 10$ to 500 M^{-1}.

CONDUCTANCE EQUATIONS

For an 1:1-electrolyte which is subject to ion-pair formation the degree of dissociation, α, may be iteratively calculated from the set of equations,

$$\alpha = \Lambda/\Lambda_c \quad (1)$$

$$K_A = (1-\alpha)/c\gamma^2\alpha^2 \quad (2)$$

$$\log \gamma \simeq -A(c\alpha)^{\frac{1}{2}}/[1+BR(c\alpha)^{\frac{1}{2}}] \quad (3)$$

where Λ = molar conductivity at the stoichiometric concentration, c; Λ_c = molar conductivity of the hypothetical completely dissociated electrolyte; γ = mean molar activity coefficient of the dissociated electrolyte; A and B are functions [13] of the permittivity, ε, of the solvent and the absolute temperature, T. The parameter R, the so-called association distance, is defined [5–9] as the closest distance of approach of free ions (equivalent to the furthest distance of separation of the ions in the ion-pair).

For approximately the past 15 years the Fuoss-Onsager conductance equation,[14–15] (FO equation),

$$\Lambda_c = \Lambda_\infty - S(c\alpha)^{\frac{1}{2}} + E\,c\alpha \log (c\alpha) + J\,c\alpha \quad (4)$$

has been one of the more frequently employed reference functions to represent the conductance of the hypothetical completely dissociated electrolyte. Within the last few years the use of a more complete conductance equation according to Fuoss and Hsia [1,2] in the form of Fernandez-Prini [4] (FHFP equation),

$$\Lambda_c = \Lambda_\infty - S(c\alpha)^{\frac{1}{2}} + Ec\alpha \log (c\alpha) + J_1 c\alpha - J_2(c\alpha)^{3/2} \quad (5)$$

has been discussed in a number of publications, *e.g.* in Refs. 5 – 9. The parameters of this equation are explained below.

It has been shown by DeRossi *et al.*[8] among others, that omission of the $J_2(c\alpha)^{3/2}$ term introduces errors in K_A and R which are not negligible. In fact, electrolytes classified [16] as completely dissociated according to eqn. (4) appear to be weak when treated [5] by means of eqn. (5).

A further recent development [17] of the conductance theory, which takes into account the influence of the relaxation field on the electrophoretic effect ("Chen effect"), should be mentioned. Consideration of this effect changes the coefficients, E, J_1, and J_2 in eqn. (5) according to Ref. 9. However, the discrepancy between values of K_A and R derived from the FHFP equation and the conductance equation modified with respect to the Chen effect does not exceed the experimental error for several electrolytic systems examined by DeRossi *et al.*[8] and by Barthel *et al.*,[9] see Tables III and IV in Ref. 8 and Table 2 in Ref. 9. Hence, the Chen effect is not considered in the present study.

Evaluation of conductance parameters. The coefficients J_1 and J_2 in the FHFP equation are defined [4] by the following equations:

$$J_1 = \sigma_1 \Lambda_\infty + \sigma_2 \tag{6}$$

$$J_2 = \sigma_3 \Lambda_\infty + \sigma_4 \tag{7}$$

$$\sigma_1 = \frac{\varkappa^2 R^2 b^2}{24c\alpha}\left(1.8147 + 2\ln\frac{\varkappa R}{(c\alpha)^{\frac{1}{2}}} + \frac{2(2b^2+2b-1)}{b^3}\right) \tag{8a}$$

$$\sigma_2 = B_1 B_2 + \frac{B_2\varkappa R}{(c\alpha)^{\frac{1}{2}}} - \frac{B_2\varkappa R b}{16(c\alpha)^{\frac{1}{2}}}\left(1.5337 + \frac{4}{3b} + 2\ln\frac{\varkappa R}{(c\alpha)^{\frac{1}{2}}}\right) \tag{8b}$$

$$\sigma_3 = \frac{b^2\varkappa^3 R^3}{24(c\alpha)^{3/2}}\left(0.6094 + \frac{4.4748}{b} + \frac{3.8284}{b^2}\right) \tag{8c}$$

$$\sigma_4 = \frac{B_2\varkappa^2 R^2 b^2}{24c\alpha}\left(\frac{2(2b^2+2b-1)}{b^3} - 1.9384\right) + \frac{B_1 B_2 \varkappa R}{(c\alpha)^{\frac{1}{2}}} + \frac{B_2\varkappa^2 R^2}{c\alpha} - \frac{B_2 b\varkappa^2 R^2}{16c\alpha}\left(1.5405 + \frac{2.2761}{b}\right) - \frac{B_2^2\varkappa R b}{16\Lambda_\infty (c\alpha)^{\frac{1}{2}}}\left(\frac{4}{3b} - 2.2194\right) \tag{8d}$$

The coefficients B_1 and B_2, the electrophoretic and relaxation coefficients of the limiting law, and $\varkappa$, the Debye parameter, are defined in a monograph;[15] $b = |z_+ z_-| e^2/\varepsilon \mathbf{k} T R$ where z_+ and z_- are the valencies of the ions, e = elementary charge, and $\mathbf{k}$ = Boltzmann's constant.

Combination of eqns. (1), (2), and (5) yields the following expression,

$$\Lambda = \Lambda_\infty - S(c\alpha)^{\frac{1}{2}} + Ec\alpha\log(c\alpha) + J_1 c\alpha - J_2(c\alpha)^{3/2} - K_A c\alpha\gamma^2\Lambda \tag{9}$$

Starting with preliminary values for Λ_∞ and K_A obtained from the FO equation by means of the computer program described in Ref. 18, the corresponding parameters according to the FHFP equation were calculated by numerical compensation.

Using a pre-selected value for R and the preliminary figure for Λ_∞, α-values were iteratively calculated from eqns. (1) and (5) for all the experimental points, c_i/Λ_i, *cf.* Ref. 12. The differences, $\Delta\Lambda_i$, between the experimental molar conductivities and the corresponding quantities obtained from eqn. (9) were then established. Successive improvements of Λ_∞ and K_A were obtained by additions of $\Delta\Lambda_\infty$'s and ΔK_A's obtained from the equations,

$$\Delta\Lambda_\infty \sum_{i=1}^{N}\left(\frac{\partial\Lambda}{\partial\Lambda_\infty}\right)_i^2 + \Delta K_A \sum_i \left(\frac{\partial\Lambda}{\partial\Lambda_\infty}\right)_i\left(\frac{\partial\Lambda}{\partial K_A}\right)_i = \sum_i \left(\frac{\partial\Lambda}{\partial\Lambda_\infty}\right)_i \Delta\Lambda_i \tag{10a}$$

$$\Delta\Lambda_\infty \sum_{i=1}^{N}\left(\frac{\partial\Lambda}{\partial K_A}\right)_i\left(\frac{\partial\Lambda}{\partial\Lambda_\infty}\right)_i + \Delta K_A \sum_i \left(\frac{\partial\Lambda}{\partial K_A}\right)_i^2 = \sum_i \left(\frac{\partial\Lambda}{\partial K_A}\right)_i \Delta\Lambda_i \tag{10b}$$

The calculations were discontinued when $\Delta\Lambda_\infty < 1 \times 10^{-7}$. Finally the standard deviation in the single Λ-value was calculated from the N values of the set using the expression,

$$\sigma(\Lambda) = \left(\frac{\sum(\Delta\Lambda_i)^2}{N-3}\right)^{\frac{1}{2}} \tag{11}$$

The calculations were repeated for a series of association distances between 1 and 25 Å using 0.2 Å increments in R to investigate the dependence of $\sigma(\Lambda)$ on R. The reason for not adjusting simultaneously all three parameters, Λ_∞, K_A, and R, which yields one set of values corresponding to $\sigma(\Lambda)$ = minimum, *cf.* Ref. 19, is that different combinations of values for Λ_∞, K_A, and R may provide almost equally good

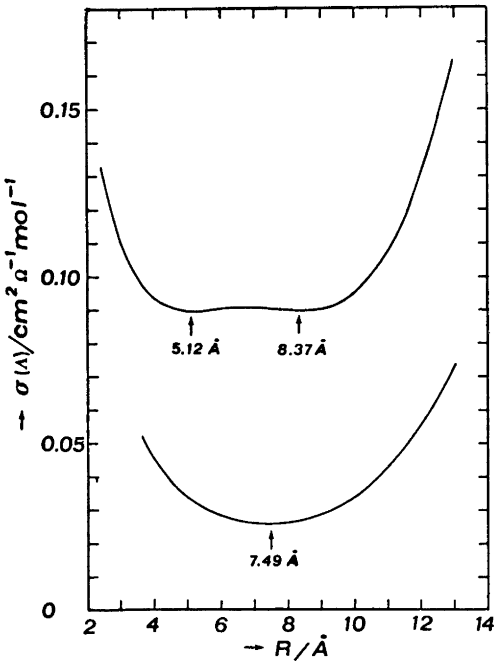

Fig. 1. Standard deviation of single Λ-value as a function of association distance. Upper curve derived from electrical conductance data in Ref. 18 for CsI in CH_3OH. Bottom curve calculated from data in Ref. 11 for NaI in C_2H_5OH, 6.26 wt-% H_2O at 25°C.

fits of the conductance equation to the experimental values as pointed out in Ref. 5.

To illustrate this statement, $\sigma(\Lambda)$ for cesium iodide in methanol at 25°C, calculated from the conductance data in Ref. 18, has been plotted *vs.* R in Fig. 1 (upper curve). As can be seen two minima corresponding to nearly identical standard deviations appear. The minimum at $R=$ 5.12 Å ($\Lambda_\infty = 124.13$; $K_A = 14.0$) corresponds to $\sigma(\Lambda) = 0.0897$ while the minimum at $R = 8.37$ Å ($\Lambda_\infty = 124.15$; $K_A = 23.7$) corresponds to the insignificantly larger value, $\sigma(\Lambda) = 0.0900$.

For comparison the bottom curve in Fig. 1 derived from conductance data in Ref. 11 for sodium iodide in aqueous ethanol at 25°C shows only one minimum.

After the main shape of the $\sigma(\Lambda)$ *vs.* R curve (*cf.* Fig. 1) had been established, further calculations with successively decreasing increments in R were performed near the minimum (or minima) to obtain the R-value for the latter to within 5×10^{-3} Å.

Of the ten electrolytic systems examined, three systems, *viz.* cesium iodide in methanol, potassium iodide in aqueous ethanol, and tetrabutylammonium chloride in acetone yielded error curves with two minima (*cf.* upper curve in Fig. 1) while the remaining systems yielded curves with a single minimum.

Conductance parameters according to the FO equation were calculated using the computer program outlined in Ref. 18. This program, which operates essentially according to the method of Kay,[19] involves iterative determinations of Λ_∞, K_A, and R from the three normal equations derived from the expression,

$$\Delta\Lambda = \frac{\partial\Lambda}{\partial\Lambda_\infty}\Delta\Lambda_\infty + \frac{\partial\Lambda}{\partial K_A}\Delta K_A + \frac{\partial\Lambda}{\partial R}\Delta R \qquad (12)$$

Accordingly, only one set of values for the quantities sought are obtained in this case.

RESULTS AND DISCUSSION

Conductance data. Conductance parameters derived from the FHFP equation for sodium, potassium, rubidium, and cesium iodides in methanol[18] and aqueous ethanol,[11] and for tetrabutylammonium chloride and bromide in acetone,[12] are compared in Table 1 with the corresponding data obtained from the FO equation. This table also includes the permittivities [11,20,21] and viscosities [11,21,22] used in the calculations and Bjerrum's critical distance,[23]

$$q = |z_+ z_-| e^2/2\varepsilon kT \qquad (13)$$

Two sets of values according to the FHFP equation are given for those three systems for which two minima appeared in the $\sigma(\Lambda)$ *vs.* R curve (*cf.* Fig. 1). The values corresponding to the minimum with the larger $\sigma(\Lambda)$ are given in brackets.

Comparison of the data listed in Table 1 for the FHFP and FO equations reveals a better fit of the FHFP equation to the experimental conductance data; see the $\sigma(\Lambda)$'s given in the last column. The FHFP equation yields larger association constants and association distances than the FO equation. The discrepancy between the values of K_A for the two conductance equations concerned is especially pronounced when association to ion-pairs is only slight, see the data for sodium, potassium, and rubidium iodides in methanol.

Table 1. Electrical conductance parameters according to the FHFP and FO equations at 25°C.

Electrolyte	Eqn.	Λ_∞ $cm^2\Omega^{-1}mol^{-1}$	K_A M^{-1}	R Å	$\sigma(\Lambda)$ $cm^2\Omega^{-1}mol^{-1}$
	CH_3OH; $\varepsilon=32.63$; $\eta=0.5445$ cP; $q=8.59$ Å; c,Λ-values according to Table 1, Ref. 18.				
NaI	FHFP	108.37	9.2	6.6	0.083
	FO	108.38	2.2	4.3	0.084
KI	FHFP	115.45	13.0	7.4	0.046
	FO	115.43	2.3	4.0	0.053
RbI	FHFP	119.62	17.1	7.4	0.067
	FO	119.60	6.0	4.0	0.072
CsI	FHFP	124.13	14.0	5.1	0.0897
		(124.15)	(23.7)	(8.4)	(0.0900)
	FO	124.12	9.4	3.8	0.0934
	C_2H_5OH, 6.26 wt-% H_2O; $\varepsilon=27.1$; $\eta=1.329$ cP; $q=10.34$ Å; c,Λ-values according to Table 2, Ref. 11.				
NaI	FHFP	46.81	26.7	7.5	0.026
	FO	46.81	13.2	4.7	0.028
KI	FHFP	49.80	25.7	5.2	0.020
		(49.84)	(44.9)	(9.0)	(0.024)
	FO	49.79	18.9	4.0	0.020
RbI	FHFP	50.68	51.3	7.6	0.012
	FO	50.65	34.4	4.4	0.015
CsI	FHFP	51.33	61.7	5.9	0.029
	FO	51.31	52.2	4.3	0.031
	$(CH_3)_2CO$; $\varepsilon=20.7$; $\eta=0.304$ cP; $q=13.54$ Å; c,Λ-values according to Table 1, Ref. 12.				
$(C_4H_9)_4NBr$	FHFP	187.09	363	11.6	0.237
	FO	186.82	297	5.0	0.341
$(C_4H_9)_4NCl$	FHFP	187.88	466	6.2	0.167
		(188.03)	(528)	(13.6)	(0.178)
	FO	187.85	453	5.1	0.192

Table 2. Comparisons of the association distance, R, according to the FHFP equation at 25°C with Bjerrum's critical distance, q, and of the closest distance of approach of the ions, $a_K{}^B$, according to Bjerrum's equation with the crystal radii sum, $r_+ + r_-$.

Electrolyte	K_A M^{-1}	R Å	q Å	$a_K{}^B$ Å	$r_+ + r_-$ Å
	CH_3OH				
NaI	9.2	6.6	8.6	6.4	3.1
KI	13.0	7.4	8.6	5.6	3.5
RbI	17.1	7.4	8.6	4.9	3.6
CsI	14.0	5.1	8.6	5.4	3.9
	(23.7)	(8.4)	8.6	(4.0)	3.9
	C_2H_5OH, 6.26 wt-% H_2O				
NaI	26.7	7.5	10.3	6.2	3.1
KI	25.7	5.2	10.3	6.4	3.5
	(44.9)	(9.0)	10.3	(4.5)	3.5
RbI	51.3	7.6	10.3	4.2	3.6
CsI	61.7	5.9	10.3	3.7	3.9
	$(CH_3)_2CO$				
$(C_4H_9)_4NBr$	363	11.6	13.5	3.2	6.9
$(C_4H_9)_4NCl$	466	6.2	13.5	3.0	6.8
	(528)	(13.6)	13.5	(2.9)	6.8

Table 3. Acree equation rate constants obtained on the basis of electrical conductance parameters according to the FHFP and FO equations at 25°C.

Reactants	Cond. eqn.	$k_i \times 10^3$ M^{-1} s^{-1}	$k_m \times 10^3$ M^{-1} s^{-1}
	CH_3OH		
$Na^{131}I + CH_3I$	FHFP	3.319 ± 0.018	0.58 ± 0.90
	FO	3.320 ± 0.018	−8.2 ± 3.9
$K^{131}I + CH_3I$	FHFP	3.332 ± 0.031	0.35 ± 1.11
	FO	3.332 ± 0.031	−13.7 ± 6.5
$Rb^{131}I + CH_3I$	FHFP	3.309 ± 0.016	1.61 ± 0.44
	FO	3.309 ± 0.016	−1.54 ± 1.27
$Cs^{131}I + CH_3I$	FHFP	3.301 ± 0.020	1.11 ± 0.71
		(3.301 ± 0.020)	(2.02 ± 0.41)
	FO	3.301 ± 0.020	0.03 ± 1.07
	C_2H_5OH, 6.26 wt-% H_2O		
$Na^{131}I + CH_3I$	FHFP	10.72 ± 0.029	3.92 ± 0.60
	FO	10.72 ± 0.029	−3.07 ± 1.26
$K^{131}I + CH_3I$	FHFP	10.70 ± 0.032	−2.95 ± 0.72
		(10.70 ± 0.032)	(2.81 ± 0.40)
	FO	10.70 ± 0.031	−7.90 ± 0.97
$Rb^{131}I + CH_3I$	FHFP	10.69 ± 0.028	2.42 ± 0.32
	FO	10.69 ± 0.028	−1.58 ± 0.50
$Cs^{131}I + CH_3I$	FHFP	10.75 ± 0.030	2.58 ± 0.44
	FO	10.75 ± 0.030	1.14 ± 0.52
	$(CH_3)_2CO$		
$(C_4H_9)_4N^{82}Br +$ C_4H_9Br	FHFP	7.041 ± 0.041	1.92 ± 0.08
	FO	7.043 ± 0.041	0.86 ± 0.11
$(C_4H_9)_4N^{36}Cl +$ $p\text{-}NO_2C_6H_4CH_2Cl$	FHFP	34.20 ± 0.15	2.68 ± 0.37
		(34.22 ± 0.15)	(6.10 ± 0.31)
	FO	34.21 ± 0.15	1.82 ± 0.39

Justice [7] has suggested that the association distance, R, should be identified with Bjerrum's critical distance, q. Values for these parameters are compared in Table 2 from which it may be seen that the association distances derived from the FHFP equation are generally a little less than Bjerrum's critical distance.

In Table 2 comparison is also made between the crystal radii [24] sum, $r_+ + r_-$, and the distance of closest approach, $a_K{}^B$, of the ions as derived from Bjerrum's equation,[23]

$$K_A = \frac{4\pi N}{1000} \int_{a_K{}^B}^{q} r^2 \exp\left(\frac{|z_+ z_-| e^2}{\varepsilon k T r}\right) dr \qquad (14)$$

For the alcoholic solvents the distance of closest approach derived from eqn. (14) shows a tendency to increase with decreasing size of the cation, which may be attributed to solvation phenomena. For acetone as solvent the unsatisfactory result, $a_K{}^B < r_+ + r_-$, is obtained.

Kinetic data. The exchange reactions examined, which may be symbolized by the general formula,

$$RY + AY^* \underset{}{\overset{k}{\rightleftharpoons}} RY^* + AY \qquad (15)$$

where RY is an alkyl halide, AY an ionic halide, and where the asterisks indicate radioactive atoms (^{36}Cl, ^{82}Br, or ^{131}I), are listed in Table 3.

The primary kinetic data, *viz.* overall second-order rate constants, k, at several different concentrations of the ionic reactant, were taken from Table I in Ref. 10, Table 1 in Ref. 11, and from Tables 2 and 3 in Ref. 12.

The separated rate constants, k_i and k_m, for the two exchange reactions,

$$RY + Y^{*-} \underset{}{\overset{k_i}{\rightleftharpoons}} RY^* + Y^- \quad (15a)$$

$$RY + A^+Y^{*-} \underset{}{\overset{k_m}{\rightleftharpoons}} RY^* + A^+Y^- \quad (15b)$$

involving unpaired and paired halide ions, Y^- and A^+Y^-, respectively, were evaluated from the Acree equation,

$$k/\alpha = k_i + k_m(1-\alpha)/\alpha \quad (16)$$

using the method of least squares.

The results of these calculations are listed in columns 3 and 4 of Table 3. The errors quoted are standard deviations. Values given in brackets are rate constants corresponding to the bracketed association constants and association distances in Table 1.

Table 3 reveals that the rate constant, k_i, calculated on the basis of K_A- and R-values derived from the two different conductance equations discussed, are almost identical. This is not so for the corresponding rate constants, k_m, for the reaction between alkyl halide and paired halide ions. Values of k_m derived using conductance parameters from the FHFP equation are significantly larger than the k_m's based on the FO equation.

For six of the systems listed in Table 3 the rate constant, k_m, based on the FO equation exhibits physically impossible negative values. It may be noted as an encouraging fact that the k_m's derived using association constants and association distances from the FHFP equation are no longer negative, disregarding one of the values for the reaction between potassium iodide and methyl iodide in aqueous ethanol.

From Table 3 it may also be concluded that the choice between the two conductance equations concerned, with respect to the evaluation of the rate constant, k_m, becomes less important with increasing K_A-value. For example the large discrepancy between the k_m-values 0.6×10^{-3} and -8.2×10^{-3} M^{-1} s^{-1} according to the FHFP and FO equations for the reaction involving sodium iodide and methyl iodide in methanol ($K_A = 9.2$ and 2.2 M^{-1}, respectively) may be compared with the considerably smaller deviation between the corresponding k_m-values 1.9×10^{-3} and 0.9×10^{-3} M^{-1} s^{-1} for the reaction between tetrabutylammonium bromide and butyl bromide in acetone ($K_A = 363$ and 297 M^{-1}, respectively).

Acknowledgement. The financial support from the *Swedish Natural Science Research Council* is gratefully acknowledged.

REFERENCES

1. Fuoss, R. M. and Hsia, K.-L. *Proc. Nat. Acad. Sci. U.S. 57* (1967) 1550.
2. Fuoss, R. M. and Hsia, K.-L. *Proc. Nat. Acad. Sci. U.S. 58* (1968) 1818.
3. Fernandez-Prini, R. *Trans. Faraday Soc. 64* (1968) 2146.
4. Fernandez-Prini, R. *Trans. Faraday Soc. 65* (1969) 3311.
5. Hanna, E. M., Pethybridge, A. D. and Prue, J. E. *J. Phys. Chem. 75* (1971) 291.
6. Hanna, E. M., Pethybridge, A. D. and Prue, J. E. *Electrochim. Acta 16* (1971) 677.
7. Justice, J.-C. *Electrochim. Acta 16* (1971) 701.
8. DeRossi, C., Sesta, B., Battistini, M. and Petrucci, S. *J. Amer. Chem. Soc. 94* (1972) 2961.
9. Barthel, J., Justice, J.-C. and Wachter, R. *Z. Physik. Chem. (Frankfurt am Main) 84* (1973) 100.
10. Beronius, P. and Pataki, L. *J. Amer. Chem. Soc. 92* (1970) 4518.
11. Beronius, P. and Pataki, L. *Acta Chem. Scand. 25* (1971) 3705.
12. Beronius, P., Nilsson, A.-M. and Wikander, G. *Acta Chem. Scand. 24* (1970) 2826.
13. Robinson, R. A. and Stokes, R. H. *Electrolyte Solutions*, Butterworths, London 1965, p. 230.
14. Fuoss, R. M. and Onsager, L. *J. Phys. Chem. 61* (1957) 668.
15. Fuoss, R. M. and Accascina, F. *Electrolytic Conductance*, Interscience, New York 1959.
16. Atkinson, G. and Petrucci, S. *J. Phys. Chem. 67* (1963) 1880.
17. Chen, M. S. *Thesis*, Yale University 1969.
18. Beronius, P., Wikander, G. and Nilsson, A.-M. *Z. Physik. Chem. (Frankfurt am Main) 70* (1970) 52.
19. Kay, R. L. *J. Amer. Chem. Soc. 82* (1960) 2099.
20. Weast, R. C., Ed., *Handbook of Chemistry and Physics, 52nd Ed.*, The Chemical Rubber Co., Cleveland, Ohio, 1971 – 1972, E44.
21. Nilsson, A.-M. and Beronius, P. *Z. Physik. Chem. (Frankfurt am Main) 79* (1972) 83.
22. Weissberger, A., Ed., *Technique of Organic Chemistry*, 2nd Ed., Interscience, New York 1955, Vol. VII, p. 90.
23. Bjerrum, N. *Kgl. Dan. Vidensk. Selsk. 7* (1926) No. 9.
24. Robinson, R. A. and Stokes, R. H. *Electrolyte Solutions*, Butterworths, London 1965, pp. 125 and 461.

Received July 17, 1973.

Acta Chemica Scandinavica A 28 (1974) 83—85

The Vapour Pressure of *O*-Ethyl,*S*-2-(*N*,*N*-diisopropylamino)-ethylmethylphosphonothioate

HARALD FROSTLING*

Research Institute of National Defence, Dept. 1, S-172 04 Sundbyberg 4, Sweden

The vapour pressure of the super toxic compound *O*-ethyl,*S*-2-(*N*,*N*-diisopropylamino)-ethylmethylphosponothioate has been determined in the temperature range 7.5 – 42.4°C. The substance was sprayed into a specially designed rotating aerosol chamber and the analysis was carried out with the aid of a combined flame photometric – flame ionization method. The volatility of the compound at 25°C was found to be 3.0 ± 0.5 mg m^{-3} and $\Delta H_{vap} = 100.0$ kJ mol^{-1}.

The vapour pressure of the super toxic compound *O*-Ethyl,*S*-2-(*N*,*N*-diisopropylamino)-ethylmethylphosphonothioate

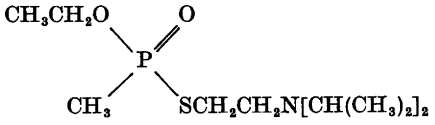

with $LCt_{50} = 5$ mg m^{-3} min^{-1} has earlier been determined at room temperature. The results have been expressed in the form of volatility and reported to vary between 3 and 30 mg m^{-3} at 25°C.[1-4] Between the volatility V_t and the vapour pressure the following relation is valid:

$$V_t = m/V = Mp/RT \quad (1)$$

where m is the mass of the vapourized substance in the volume V and p is the vapour pressure at the temperature T. The variations in volatility found in earlier determinations may be due to the different measurement methods used.

The dynamic or air-flow method can be used and the amount of condensed vapour can be detected by using a ^{32}P-labelled compound and subsequent measurement with the aid of a Geiger-Müller counter.[5] With this method it is, however, impossible to decide if the measured value obtained originates from the actual compound or some of its ^{32}P-containing decomposition products.

METHOD

To avoid such disadvantages a special analysis method was utilized which employed a combined flame ionization – flame photometric detector (FID–FPD). With this method it is possible to achieve a reliable control process of the condition of the compound used during the measurements. An approximate calculation could be made of the ratio of the carbon response (FID) to the phosphorus response (FPD). The responses of the two different detectors are known from earlier experiments.[6,7] For the FID the response is almost linear to the number of C-atoms in the molecule. Divergences of the recorded values compared with the precalculated ratios and arising from decomposition of the substance could in this way be observed during the measurements.

By using a technique to disperse the substance in aerosol form into the rotating aerosol chamber, a rapid equilibrium was obtained between the individual particles and the vapour phase.[8] A small continuous sampling from the drum – 1 ‰ min^{-1} of the total volume – did not influence the equilibrium.

* Also affiliated to Institute of Analytical Chemistry, University of Stockholm, Sweden.

EXPERIMENTAL

The *O*-Ethyl,*S*-2-(*N*,*N*-diisopropylamino)-ethylmethylphosphonothioate was synthesized according to the description of Fagerlind *et al.*[9] The small amount, 1 – 2 %, of one of the initial substances (2-isopropylaminoethyl chloride) present did not influence the FPD-response. Depending on the high toxicity of the compound a special routine was worked out for a safe handling of the equipment in connection with the dispersion of the compound.

The spray generator was sealed against the atmosphere and the outlet of the rotating drum was connected to the atmosphere *via* a collective filter with a capacity of 1.2 m^3 min^{-1} made up of activated carbon and an aerosol filter. The sealing rings were replaced when a leakage was observed at a testing with an overpressure of ≤ 100 N m^{-2}.

The sample outlet in the drum was equipped with two aerosol filter papers in series, each of them with a reported filtration efficiency of 99.99 % for particles with a MMD of 0.3 μm.[10] To avoid condensation of the gaseous sample in the connection between the drum and the analysis apparatus the connection was heated to a temperature somewhat higher than that of the temperature within the drum.

The vapour pressure determinations were done in the temperature region 7.5 – 42.4°C. For the measurements above room temperature the heat regulation system of the drum was utilized, while measurements below this temperature were done with the whole equipment placed in an air-conditioned room. The temperature variations for the heat regulation system of the drum were ±0.2°C and at about ±0.5°C in the air-conditioned room. Between the three first recordings at every temperature, a new spray generation was carried out in order to be certain that a saturation equilibrium between the walls of the drum and its sample volume was established.

The decontamination of the drum and the analysis apparatus was done with a commercial detergent with a high content of sodium perborate (20 %).[11]

RESULT

The FPD-responses at the different temperatures are listed in Table 1. The conversions of the FPD-responses (μA) to the concentration values (10^{-4} g mol P m^{-3}) are done with the aid of a calibration diagram. The concentrations are also expressed in mg m^{-3}, the simple relationship that 0.0374×10^{-4} g mol P m^{-3} of the compound is equivalent to 1 mg m^{-3} being valid. No values for the ratio FPD/FID response are listed in the table for the three lowest temperatures as the FID-amplifier did not function at these temperatures. The decreasing values for the ratios at higher concentrations depend on the different character of the two detectors, *i.e.* the response is linear to the concentration for the FID and nonlinear for the FPD and decreases with the concentration. The vapour phase can be considered to be an ideal gas and the molar volume of the aerosol particles is negligible compared with that of the vapour. The concentration of the vapour phase found at the analysis can therefore be converted to vapour pressure by the aid of the familiar gas laws. The Clausius-Clapeyron equation may be integrated on the assumption that ΔH_{vap} is constant within the temperature interval (~35°C) and gives

$$\log p = -A/T + B \qquad (2)$$

Table 1.

Temp (°C)	(K)	FPD-response (mean value) (μA)	Concentration (10^{-4} g atom P m^{-3})	(mg^{-3})	Vapour pressure (Torr)	Ratio FPD/FID ($\times 10^2$)
7.5	280.7	0.010	0.012	0.32	2.1×10^{-5}	–
11.0	284.2	0.011	0.014	0.36	2.4×10^{-5}	–
15.2	288.4	0.023	0.035	0.94	6.4×10^{-5}	–
19.1	292.3	0.031	0.048	1.28	8.9×10^{-5}	4.4
22.0	295.2	0.044	0.074	1.98	13.8×10^{-5}	4.2
28.2	301.4	0.11	0.23	6.15	43.7×10^{-5}	2.2
33.1	306.3	0.13	0.28	7.48	54.1×10^{-5}	1.8
37.0	310.2	0.24	0.60	16.1	118×10^{-5}	1.3
42.4	315.6	0.37	1.00	26.7	199×10^{-5}	1.1

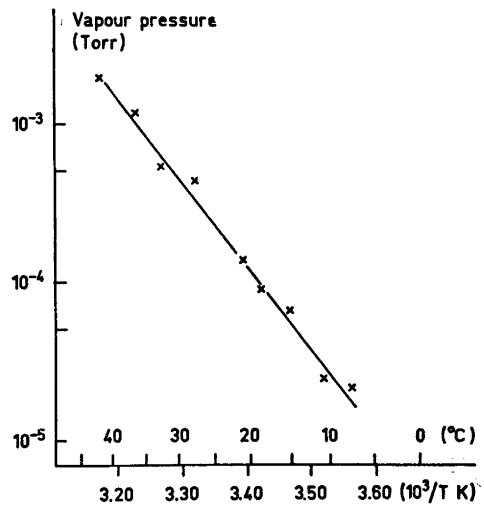

Fig. 1. The vapour pressure as a function of temperature.

where $A = \Delta H_{vap}/2.303R$ (3)

The constants in eqn. (2) were determined with the least squares method in a PDP-8 computer and were found to be $A = 5235$ $B = 13.90$ and the residual mean square = 0.0058. The relationship (3) gives ΔH_{vap} = 100.0 kJ mol^{-1}.

The volatility of the title compound in 25°C was 3.0 ± 0.5 mg m^{-3}. The vapour pressure as a function of the temperature is shown in Fig. 1.

Acknowledgement. I thank Mr. N. Ekman and Mr. L. Pettersson for valuable laboratory assistance.

REFERENCES

1. *FOA Om, BC Warfare Agents*, FOA Info, Stockholm 1969, p. 36.
2. *Chemical and Bacteriological (Biological) Weapons and the Effects of their Possible Use*, United Nations Publication A/7575, New York 1969, p. 90.
3. *The Problem of Chemical and Biological Warfare*, Sipri, Stockholm 1971, Vol. 1, p. 86.
4. *Bescherming Tegen Toxische Stoffen*, Chemisch Laboratorium TNO, den Haag 1973.
5. Kensington Adam, N. *Physical Chemistry*, Clarendon Press, Oxford 1962, p. 237.
6. Frostling, H. and Brantte, A. *J. Sci. Instrum. 5* (1972) 251.
7. Frostling, H. *J. Sci. Instrum. 6* (1973) 863.
8. Frostling, H. *Aerosol Sci.*, Academic 1973, Vol IV, pp. 5,411.
9. Fagerlind, L., Lindgren, I., Santesson, J., J., Stensiö, K.-E., Wallerberg, G. and Östman, B. *FOA 1 report A* 1541 – C2(C4), 1971.
10. Ringquist, G. *VVS-Tidskrift 4* (1965) 195.
11. Kowalska, M., Lindgren, I. and Santesson, J. *FOA 1 report A* 1573 – C2(C5), 1973.

Received September 6, 1973.

Acta Chemica Scandinavica A 28 (1974) 86—92

Kinetics and Overvoltage of the Electrodeposition of Zinc from Sulfate Solutions in the Presence of Na, Ca, and Mg Ions at a Rotating Disk Electrode

MIGUEL SALOMA* and HANS HOLTAN JR.

The University of Trondheim, NTH, Laboratories of Industrial Electrochemistry, N-7034 Trondheim-NTH, Norway

A study of the effect of temperature on the velocity of electrodeposition and polarization of zinc in the presence of Na, Ca, and Mg ion impurities has been undertaken by the method of polarization curves using a rotating disk electrode.

In the presence of Na, Ca, and Mg ion impurities, crystallization overvoltage occurs; probably caused by difficulties in penetration of metal atoms to the growing crystal faces. The influence of metal ion impurities is probably of adsorptive character.

The results are consistent with the suggestion that metal ion impurities act to eliminate the retarding action of hydrogen. The metal ion impurities do not directly promote discharge of zinc but suppress the inhibiting action of hydrogen.

Commercial electrolytes always contain additives in the form of salts of electronegative metals: sodium, magnesium, calcium, aluminium, and manganese. The latter of these is usually introduced into the electrolyte in dioxide form for the purpose of oxidizing the ions of divalent iron to the trivalent state to effect deposition of iron as hydrate.

Most investigators consider that the ions of alkali and alkali earth metals do not exert any influence on the electrolysis of zinc.[1,2] Izgaryshev and Maiorova [3] found that the cations of the alkali and alkali earth metals serve to reduce polarization of the zinc cathode and explain this phenomenon by formation of complex ions.

Studies of hydrogen overvoltage, by Iofa *et al.*[4] have shown that addition of neutral salts to acid solutions usually causes a rise in hydrogen overvoltage; however, this effect occurs only in dilute solutions.

Pecherskaya and Stender [5] noted that the admixtures of alkali and alkali earth metals salts cause a considerable rise in the specific resistence of zinc sulfate and they noted that the ions of electronegative metals are carried to the cathode where they do not discharge. The ions accumulate in the layers of the electrolyte adjacent to the cathode blocking access of zinc to the cathode. This phenomenon is capable of causing reduction in the current efficiency. In further work, Turomshina and Stender [6] studied the effect of admixtures of the ions of electronegative metals upon the current efficiency and cathode potential. They concluded that the sodium, calcium, magnesium, and manganese ions present in a zinc electrolyte are capable of discharging jointly with the zinc ions forming intermetallic compounds with the zinc which serve as microanodes in short-circuited elements on the cathode surface. However, Kletenik,[7] in a study on the effect of manganese in the electrodeposition of zinc, reported that attempts to detect manganese in electrodeposited layers of zinc, obtained at very different current densities and concentrations of manganese in the electrolyte, were unsuccessful.

Published data do not permit an unambiguous conclusion to be reached on the influence of ions of electronegative metals on the cathodic deposition of zinc in zinc sulfate solutions or on

* Present address: Facultad de Quimica, Universidad Nal. Aut. de Mexico, Mexico 20, D.F.

the nature of the polarization accompanying this process. Because of the complexity of these effects, it would be highly desirable to study the electrodeposition process under conditions where the number of uncontrolled variables were minimal.

The present work is concerned with a study of the influence of temperature on the rate of deposition of zinc at a rotating disk electrode in the presence of Na, Ca, and Mg.

To determine the rate-limiting stage in the cathodic processes and to elucidate the type of cathodic polarization in the electrodeposition of zinc in the presence of electronegative metal ion impurities, Gorbachev's temperature-kinetic method [8] was used.

An important stage in the development of the temperature-kinetic method is its application under conditions of forced convection. The use of forced convection – rotating disk electrode – in the study of electrochemical reactions makes it possible to control the stage involving the transport of the reactants to the electrode surface and to eliminate experimental errors due to natural convection.

EXPERIMENTAL

The experiments involved the measurement of polarization curves using a rotating disk electrode recently described.[9] The polarization measurements were made by a galvanostatic method. The electrolytic cell consisted of a glass cylinder 340 ml vessel. The large volume of the catholyte combined with a small surface area of the cathode ensured the constancy of the composition of the solution during the measurements of the polarization curve. The electrolytic cell was fitted in a jacket through which water from a precision thermostat circulated. The auxilary electrode consisted of a 2.26 cm diam. platinum plate. A saturated calomel half-cell served as the reference electrode.

The electrode was prepared as described recently.[9] Its surface area was 0.196 cm^2. The electrode was rotated by a synchronous motor, the rate of rotation being 771 rev. min^{-1}. In the determination of the polarization curves the potential was measured at 2 min after the attainment of a specific current density. This time was sufficient for a virtually steady value of the potential to be established. To ensure reproducible results, each polarization curve was measured for a fresh deposit. The potential of the zinc electrode in absence of current was determined immediately after completion of the polarization curve. Measurements were made with current densities of 0.5 – 60 mA cm^{-2} at intervals.

The polarization potential of the zinc cathode was measured in solutions of 1 M zinc sulfate, reagent grade, with additions of Na, Ca, and Mg, introduced into the zinc electrolyte as sulfate. Sodium and magnesium effects were studied at three different concentrations: 0.1, 0.5, and 1.0 g/l. Because calcium sulfate is relatively insoluble in solutions of zinc sulfate only one concentration, 0.1 g/l, was studied; all concentrations were studied at four different temperatures: 20, 30, 40, and 50°C. The solutions were treated with activated carbon to remove all surface-active material from the electrolyte.

RESULTS

Sodium. The effect of the concentration of the sodium ion on the polarization potential of the zinc cathode at 20°C is shown in Fig. 1. The

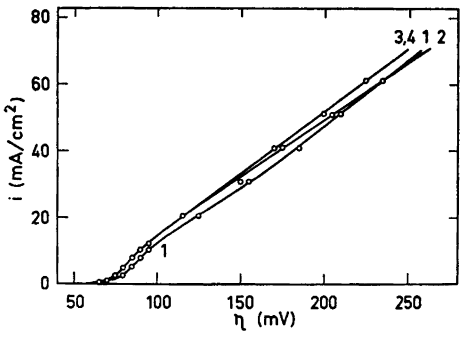

Fig. 1. Effect of sodium ion concentration on the cathode potential-current density relation in 1 M $ZnSO_4$ solution at 20°C; concentration of sodium (g/l): 1, 0; 2, 0.1; 3, 0.5; 4, 1.0.

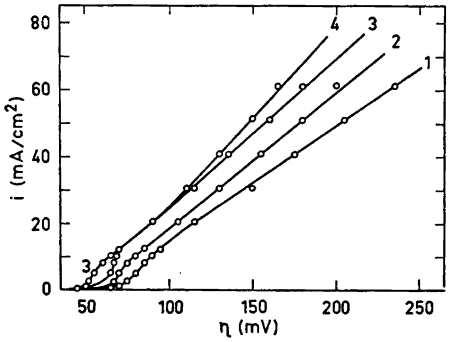

Fig. 2. Effect of the temperature on the cathode potential-current density curve in 1 M $ZnSO_4$ containing 0.1 g/l Na; temperature (°C): 1, 20; 2, 30; 3, 40; 4, 50.

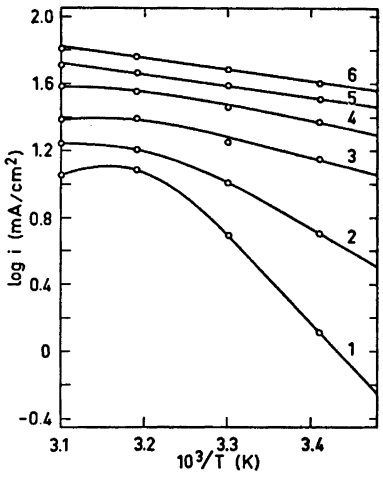

Fig. 3. Dependence of log i on $1/T$ in 1 M $ZnSO_4$ containing 0.1 g/l Na at constant polarization potential (mV): 1, 70; 2, 80; 3, 100; 4, 125; 5, 150; 6, 175.

addition of sodium ions to 1 M zinc sulfate shifts the electrode potential in the positive direction. This depolarizing effect is less noticeable at increasing temperatures.

Fig. 2 shows that the polarization potential of the zinc cathode in 1 M zinc sulfate solution containing 0.1 g/l Na decreases with increasing temperature. However, at 50°C an increase is observed, relative to 40°C, at low cathode potential. Similar effects were observed at other concentrations of sodium.

To ascertain the nature of the cathodic polarization accompanying the deposition of zinc in the above solutions, plots for the different concentrations of sodium were made of the logarithm of current density against the reciprocal of the absolute temperature at a constant polarization potential (Fig. 3).

The characteristic of the curves representing log i as a function of $1/T$ is that it passes through a maximum at high temperatures in the region of low cathode potentials. With increase in the polarization potential the first nonlinear portion of the curve becomes linear and the shape of the equipotential curves is characterised by a linear section of definite slope.

The deviation of the equipotential curves from linearity which passes through a maximum is characteristic of crystallization overvoltage.[8]

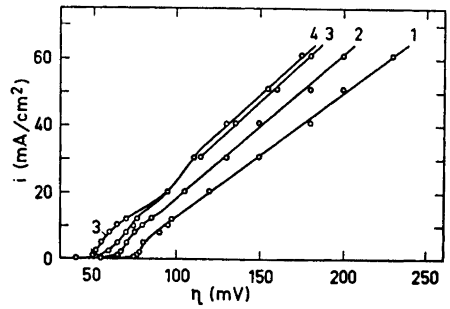

Fig. 4. Effect of the temperature on the cathode potential-current density curve in 1 M $ZnSO_4$ containing 0.1 g/l Ca; temperature (°C): 1, 20; 2, 30; 3, 40; 4, 50.

More generally, divergence from linearity is due to the cumulative effect of some additional, secondary factor, which distorts the normal temperature variation of the electrode process.[10]

The deposits of zinc on the cathode were more porous and darker with increasing concentrations of sodium in the electrolyte.

Calcium. Calcium showed a depolarizing effect at all temperatures except at 50°C in which an opposite effect is observed.

Fig. 4 exhibits the degree to which the presence of 0.1 g/l Ca affects the cathode potential-current density curve with temperature. The polarization potential of the zinc cathode decreases with increase in temperature up to 40°C.

The equipotential plots based on the polarization measurements show deviation from linearity in the variation of the logarithm of the current density with reciprocal of the absolute temperature (Fig. 5). The equipotential plots show a maximum in the region of high temperatures, characteristic of crystallization overpotential; at higher potentials the curve approaches linearity.

The deposit of zinc in the presence of 0.1 g/l Ca in the electrolyte did not differ from that obtained with pure solutions.

Magnesium. The presence of magnesium in the electrolyte caused a depolarization in the cathode potential at all temperatures studied except at 50°C where a polarization was obtained in the low cathode potential region. This was observed at all concentrations investigated. The effect of the concentration of magnesium

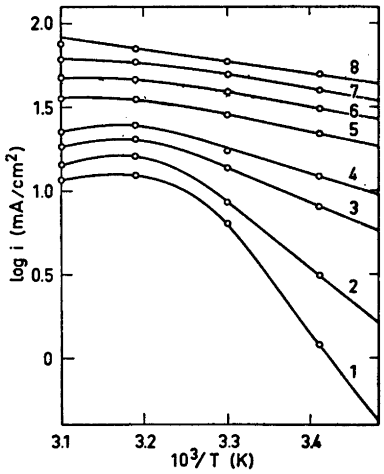

Fig. 5. Dependence of log i on $1/T$ in 1 M $ZnSO_4$ containing 0.1 g/l Ca at constant polarization potential (mV): 1, 75; 2, 80; 3, 90; 4, 100; 5, 125; 6, 150; 7, 175; 8, 200.

on the polarization potential of the zinc cathode at 20°C is shown in Fig. 6.

Fig. 7 depicts the effect of the temperature on the cathode potential-current density curve in the zinc sulfate solution containing 0.5 g/l of magnesium. The polarization potential of the cathode decreases with rise in temperature except at 50°C. This was observed at all the concentrations investigated.

The characteristic of the equipotential plots (Fig. 8) in the variation of the logarithm of the current with the reciprocal of the absolute temperature, at the different concentrations, is the

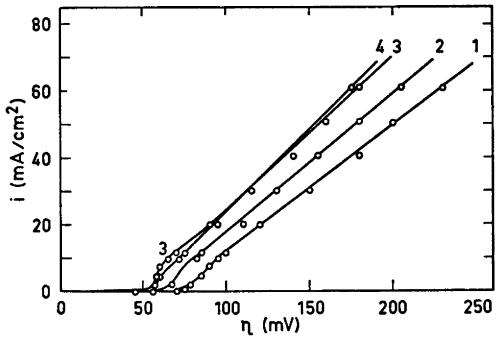

Fig. 7. Effect of the temperature on the cathode potential-current density curve in 1 M $ZnSO_4$ containing 0.5 g/l magnesium; temperature (°C): 1, 20; 2, 30; 3, 40; 4, 50.

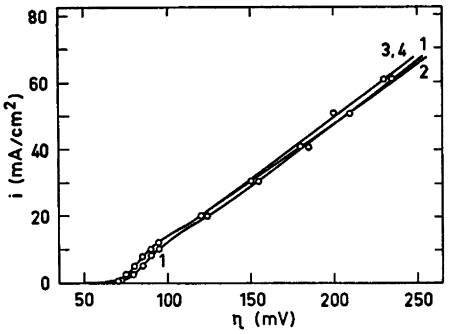

Fig. 6. Effect of magnesium ion concentration on the cathode potential-current density relation in 1 M $ZnSO_4$ solution at 20°C; concentration of magnesium (g/l): 1, 0; 2, 0.1; 3, 0.5; 4, 1.0.

deviation from linearity with passage through a maximum at high temperatures in the region of low cathode potentials. This is depicted in Fig. 8 for a solution containing 0.5 g/l of magnesium.

The deposition of zinc in the presence of small quantities of magnesium, 0.1 g/l, did not differ in appearance or color from that obtained with pure solutions. As the concentration of magnesium increased the cathode deposits of zinc became somewhat darker and more porous.

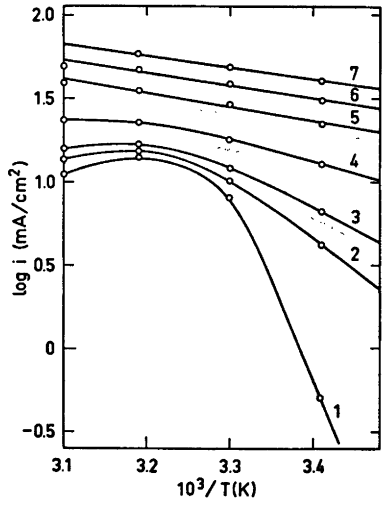

Fig. 8. Dependence of log i on $1/T$ in 1 M $ZnSO_4$ containing 0.5 g/l magnesium at constant polarization potential (mV): 1, 75; 2, 80; 3, 85; 4, 100; 5, 125; 6, 150; 7, 175.

DISCUSSION

The results obtained from the treatment of experimental data applying the temperature-kinetic method showed that admixtures of ions of electronegative metals affect the deposition of zinc, hindering the process by which atoms are incorporated into crystal lattice, namely the appearance of crystallization overpotential as a rate controlling step.

The impurities of electronegative metals appear to affect the crystal growth of zinc electrodeposits by a mechanism involving the adsorption of impurities at growth sites. This supposition is confirmed by the following experimental facts:

(i) The zinc deposits in presence of admixtures of ions of electronegative metals are irregular and loose. At a low adsorption rate the electrodeposition is less uniform, because the electrode surface is unequally covered by the species of the added impurities.[11]

(ii) A general feature of the cathodic deposition of zinc in presence of admixtures of ions of electronegative metals is that zinc deposition is strongly affected in the region of low cathode potential – kinetically-controlled range – and slightly affected at higher potentials – diffusion-controlled range. The action of impurities, which act as surface-active agents, would be expected to be more pronounced as the current density is lowered. At high current densities on fast growing crystallite facets, the surface-active agents do not accumulate sufficiently to stop growth.[11]

(iii) Zinc is deposited at potentials on the negative side of the zero-charge potential of zinc [$\phi_N = -0.63$ V (NHE)].[12] Therefore surface-active cations can be adsorbed on the cathode.

(iv) There is a very slight deviation between the stationary potential with and without impurities.

In the absence of effective surface inhibitors and at low overvoltage, metal crystals will grow without the formation of nuclei.

In this case, the ad-atoms will preferentially enter existing dislocations. But with increasing coverage of the electrode surface by adsorbed species, the mean free path for lateral diffusion of the ad-ions will be shortened. This is equivalent to a decrease in the diffusion coefficient of ad-ions which can result in an increase in surface diffusion control or an increase in ad-ion concentration at steady state to a point such that the rate of two-dimensional nucleation becomes appreciable. Hence, a decrease in surface diffusion control due to the reduction in the distance between growth steps. Therefore, with high inhibition the diminished surface diffusion may be the rate-controlling step or with very high inhibition, nucleus formation or diminished surface diffusion both may become the rate-controlling steps. If two-dimensional nucleation is rate-determing, the logarithm of the current density should be a linear function of the reciprocal overvoltage.[13] Figs. 9 – 11 show that linear relationships are obtained in $1/\eta$ *vs.* log i coordinates for the different solutions con-

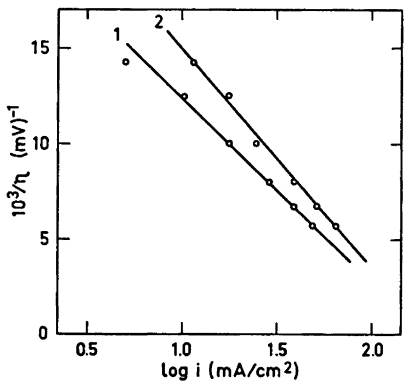

Fig. 9. Variation of log i on $1/\eta$ in 1 M $ZnSO_4$ containing 0.1 g/l sodium; temperature (°C): 1, 30; 2, 50.

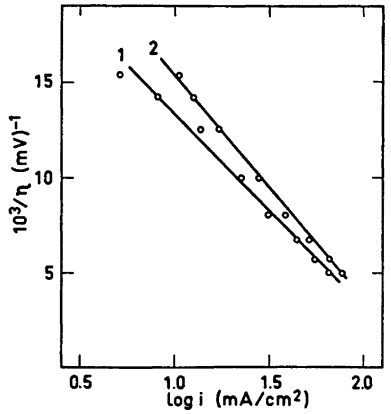

Fig. 10. Variation of log i on $1/\eta$ in $ZnSO_4$ containing 0.1 g/l calcium; temperature (°C): 1, 30; 2, 50.

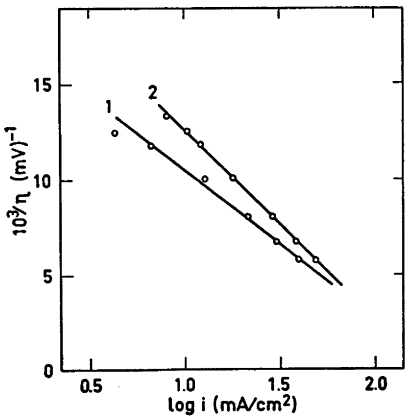

Fig. 11. Relationship between $1/\eta$ and log i in 1 M $ZnSO_4$ containing 0.5 g/l magnesium; temperature (°C): 1, 20; 2, 30.

taining metal ion impurities. Thus, the conclusion which follows from the analysis of Figs. 9 – 11 is consistent with the conclusion derived by the temperature-kinetic method.[8]

The depolarizing effect of impurities. As a rule, changes in the structure of the electrolytic deposit are due to adsorption of surface-active substances which block the active sites and cause increased electrode polarization.[14] From the above data it can be seen that in the electrodeposition of zinc electronegative metal ion impurities reduce the electrode polarization. The absence of a direct relation between the polarization and the structure of the electrolytic deposits indicates that surface-active substances added to the electrolyte act on various stages of the electrode process.

Studies of the effect of the concentration of hydrogen ion on the kinetics of the electrolytic deposition of zinc from sulfuric acid solutions,[15,16] have shown that increase in the pH of the solution causes a reduction in the polarization of the zinc electrode. With increase in temperature, the retarding effect of the hydrogen on the discharge of zinc is removed. Thus, the polarization and structural investigations have shown that the effect of hydrogen on the electrolytic deposition of zinc is associated, not with a change in the condition of the ion undergoing discharge from the solution, but with the adsorption of hydrogen at the electrode surface, which retards the electrode process.

Therefore, in all probability, the influence of metal ion impurities on the reduction potential of metal ions from electrolyte arises because, in the presence of ions of impurities on the electrode, the metal-hydrogen bond becomes weaker,[17] which promotes adsorption of metal ions, and consequently their reduction. Such a weakening of the bond between hydrogen and the electrode and promotion of discharge is observed in the reduction not only of metal ions, but also hydrogen. Measurements of the overvoltage of hydrogen on zinc in solutions of acids[18] have revealed that hydrogen overvoltage decreases with the nature of the acids in the following sequence: $ClO_4^- < SO_4^{2-} < Cl^-$.

Since the depolarization of the cathode potential is associated with the inhibiting action of surface-active species on the electrode, it might be expected that the depolarization effect would decrease with increasing temperature.[19] In actual fact, experimental results show that depolarization increases until some limit and then falls with rising temperature.

It can be concluded that in the presence of electronegative metal ion impurities the reduction in electrode polarization is associated with elimination of the retarding action of hydrogen. The metal ion impurities do not directly promote the discharge of zinc but suppress the inhibiting action of hydrogen.

Acknowledgement. One of the authors (M.S.) wants to thank the NORAD for the fellowship which made this investigation possible.

REFERENCES

1. Weimer, F. S., Wever, G. T. and Lapee, R. J. In Mathewson, C. H., Ed., *Zinc. The Science and Technology of the Metal, Its Alloys and Compounds*, Reinhold, New York 1964, p. 218.
2. Wever, G. T. *J. Metals 130* (1959).
3. Izgaryshev, N. A. and Maiorova, E. Ya. *J. Gen. Chem. USSR 6* (1936) 1298.
4. Iofa, Z. A. *et al. Dokl. Akad Nauk SSSR 84* (1952) 543.
5. Pecherskaya, A. G. and Stender, V. V. *J. Appl. Chem. USSR 23* (1950) 920.
6. Turomshina, U. F. and Stender, V. V. *J. Appl. Chem. USSR 28* (1955) 151.
7. Klenetik, Iu. B. *J. Appl. Chem. USSR 30* (1957) 1320.
8. Gorbachev, S. V. *Soviet Electrochem., Proc. 4th Conf. Electrochem.*, Consultant Bureau, New York 1961, Vol. 1, p. 63.

9. Saloma, M. and Holtan, Jr., H. *Acta Chem. Scand. A 28* (1974) 93.
10. Gorbachev, S. V. and Kondratev, V. P. *Russ. J. Phys. Chem. 38* (1964) 842.
11. Bockris, J. O'M. and Despic, A. R. In Eyring, H., Ed., *Physical Chemistry. An Advanced Treatise*, Academic, New York 1970, Vol. IXB/Electrochem., p. 669.
12. Levin, A. I. *et al. J. Appl. Chem. USSR 31* (1958) 569.
13. Erdey-Grüz, T. and Volmer, M. *Z. Phys. Chem. Abt. A 157* (1931) 165.
14. Erdey-Grüz, T. *Kinetics of Electrode Processes*, Adan Hilger, London 1972, p. 291.
15. Titova, V. N. and Vagramyan, A. T. *Soviet Electrochemistry 2* (1966) 1052.
16. Schwabe, K. *Z. Electrochem. 59* (1955) 663.
17. Frumkin, A. N., Petry, O. A., Schigorev, I. G. and Safonow, W. A. *Z. Phys. Chem. (Frankfurt am Main) 243* (1970) 261.
18. Vagramyan, A. T. and Titova, V. N. *Zashchita Metal 3* (1967) 102.
19. Vagramyan, A. T. and Uvarov, L. A. *Izv. Akad. Nauk SSSR. Otd. Khim. Nauk* (1962) 1250.

Received July 7, 1973.

Acta Chemica Scandinavica A 28 (1974) 93—98

The Effect of Manganese Ion Impurity on the Kinetics and Overvoltage of Zinc Electrodeposition from a Sulfate Solution

MIGUEL SALOMA* and HANS HOLTAN JR.

The University of Trondheim, NTH, Laboratories of Industrial Electrochemistry, N-7034 Trondheim-NTH, Norway

The kinetics of the electrochemical deposition of zinc from pure sulfate solutions and in the presence of manganese ion impurity have been investigated by the method of polarization curves using a rotating disk electrode. Analysis of the data by Gorbachev's temperature-kinetic method demonstrated that deposition of zinc from pure sulfate solution is accompanied by charge-transfer overvoltage; in the presence of manganese ion impurity crystallization overvoltage occurs. The influence of manganese ion impurity is probably of adsorptive character.

The nature of the influence of manganese on the electrodeposition of zinc from sulfate electrolytes, occupies an intermediate position between metal cations more active and less active than zinc. The influence of manganese has been considered by several investigators:

Fedotieff and Stender [1] showed that current efficiency for zinc depends on the manganese concentration in the electrolyte. Marshall [2] found that the current efficiency for zinc was lower in presence of manganese. Weimer *et al.*[3] consider that manganese is a harmless impurity in the electrodeposition of zinc. Stender *et al.*[4] showed that permanganate ions formed at the anode migrate to the cathode and depolarize it. According to the data of a number of investigators,[5–7] manganese is harmless up to a definite concentration in solution (2 – 3 g/l); on further increase of the manganese content the current efficiency drops appreciably.

Most research has been aimed at the effect of manganese on current efficiency and on the effects of manganese with other impurities but the mechanistic details are still obscure.

A study of deposition of zinc in the presence of manganese ion impurity under conditions of known rate of transport of this impurity to the cathode is valuable in furthering the understanding of the mechanism of impurity action. A rotating disk electrode is particularly suitable for such study. Levich [8] has shown that the rate of a transport-controlled reaction is uniform over such a disk and has derived an expression for the limiting rate of reaction. His theoretical results have been verified experimentally by Gregory and Riddiford [9] and by Newson and Riddiford.[10]

In the present study the effect of temperature on the rate of deposition of zinc at a rotating disk electrode in the presence of manganese was investigated. The results were treated in accordance with Gorbachev's temperature-kinetic method.[11]

In the temperature-kinetic method the nature of polarization is assessed by studying the temperature variation of current density under conditions of constant polarization potential. The determination of the effective activation energy makes it possible to distinguish between concentration and charge transfer overvoltage. This allows the individual stages of electrochemical reactions, including those involving a combination of charge transfer and concentration overvoltage, to be studied.

In order to understand how impurities work, it is desirable first to have some concept of how metal ions are discharged and built into a crystal lattice in the absence of impurities. Thus, the determination of polarization curves of zinc

* Present address: Facultad de Quimica, Universidad Nal. Aut. de Mexico, Mexico 20, D.F.

deposition were made at four different concentrations: 0.05 M, 0.1 M, 0.5 M, and 1 M $ZnSO_4$, and the concentrations studied at four different temperatures: 20, 30, 40, and 50°C.

The effect of admixtures of manganese at four different concentrations and at 20, 30, 40, and 50°C was studied with 1 M $ZnSO_4$ as standard.

EXPERIMENTAL

The rotating disk electrode (RDE) used in this work was a modification of that described by Khomutov and Skornyakova [12]. The 0.5 cm diam. aluminium disk (99.998 % Vigeland Metal Refinery A/S) was attached to a 1.6 cm diam. brass extension shaft, precision ground (Fig. 1). The disk and extension shaft pressure fitted into a polyvinyl chloride (PVC) insulating sleeve. The aluminium disk and subsequently the PVC sleeve were accurately machined by using the ground extension shaft to fix the axis of rotation. The electrode face was polished, before each experiment, to a mirror finish on a metallurgical polisher by using AB Microcloth and AB Polishing alumina No. 1 (Buehler Ltd. Evanston Ill., levigated alumina 5.0 μ). The electrode was driven by a 885 r.p.m. synchronous motor, obtaining other rotation speeds with a belt and pulleys of different diameters. The speeds were measured with a stroboscope. The current was fed to the RDE through graphite contacts sliding on a carefully centered shaft mounted in a pair of bearings fitted in a heavy brass cylinder.

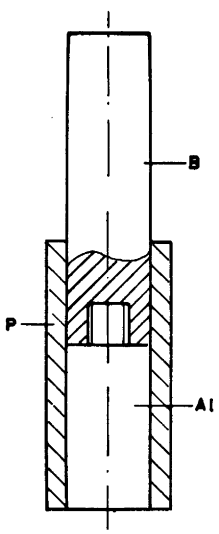

Fig. 1. Interchangeable rotating disk electrode: B, brass extension; P, PVC shield; Al, Aluminium disk electrode, pressure fitted in PVC shield.

The electrolysis cell was a glass cylinder, 7.8 cm diam. by 9.4 cm deep, and was filled with *ca.* 340 ml solution. The dimensions of the cell and cathode were chosen to meet the hydrodynamics requirements of the Levich theory.[9,13,14] The temperature was maintained constant by circulating water from a thermostat set through a water jacket around the cell.

The three-electrode cell consisted of the RDE as the working electrode, a large platinum disk as auxillary electrode and a saturated calomel electrode (SCE) as reference. The platinum auxiliary electrode had a diameter of 2.26 cm and was positioned about 6.5 cm below and parallel to the face of the RDE. The capillary connection to the test solution (Luggin capillary) was made at a point in the solution slightly to the rear and to one side of the disk where the ohmic drop is negligible.[10] The capillary was filled with the electrolyte by drawing solution into the capillary until it made contact with the porous plug of the salt bridge of the SCE.

The electrolyte used in this study consisted of zinc sulfate reagent grade. The cathode potential-current density curves obtained in highly purified solution, zinc sulfate recrystallized 3 times, were not significantly different from the results obtained without improving reagent purity. However, it was important to remove all surface-active material from the electrolyte. This was done by treatment with activated carbon.

The polarization measurements were made by a galvanostatic method. Measurements were made of steady values of the potential attained 1 – 2 min after passage of a given current. Direct measurements gave the cathode potential with respect to the saturated calomel electrode. The overvoltage was calculated by substracting the potential value of the zinc electrode in absence of current from the determined potential values at constant current. The potential of the zinc electrode in absence of current was determined immediately after completion of the polarization curve.

It was shown by Frumkin [15] that when metals dissolve (with evolution of hydrogen) in acidic electrolytes the potential obtained can be either practically equilibrium values or differ substantially from the equilibrium values, depending on the relative rates of the electrode processes occurring on the surface of the metal while dissolving. Kravtsov and Ermolova,[16] in a study of the steady-state potentials of zinc and zinc amalgam in sulfate solutions, have shown that the reduction in the acid concentration and increase in the zinc ion concentration make it possible to bring a shift from non-equilibrium to practically equilibrium values of the zinc potential.

The polarization potential of the zinc cathode was measured in solutions containing 0.05 M,

0.1 M, 0.5 M, and 1 M zinc sulfate; and 1 M zinc sulfate with additions of manganese, introduced into the zinc electrolyte as sulfate. Manganese effects were studied at four concentrations: 0.1, 0.5, 1.0, and 3.0 g/l. Measurements were made with current densities of 0.5 – 60 mA cm^{-2} at intervals in the range 20 – 50°C. The electrode was rotated at 771 r.p.m.

RESULTS AND DISCUSSION

Electrodeposition of zinc from pure sulfate solutions. Fig. 2 presents the data for the electrolyte solutions containing 1 M zinc sulfate. The polarization curves show that the cathodic polarization varies with temperature and current density. With increase of temperature, the polarization potential of the cathode falls. Similar behavior was observed with various concentrations of zinc sulfate. The cathodic polarization increases with increasing current density.

Fig. 3 demonstrates the effect of the concentration of zinc sulfate on the polarization potential at 20°C. With increasing zinc sulfate concentration, the zinc polarization potential decreases. Similar relations were observed at other temperatures.

To elucidate the type of polarization in the deposition of zinc in the solutions studied, the logarithm of current density was plotted against the reciprocal of the absolute temperature (log $i - 1/T$) at a constant polarization potential (η = const.) (Fig. 4). In the range of temperatures and polarization potentials investigated, the log $i - 1/T$ plot is linear for all the solutions.

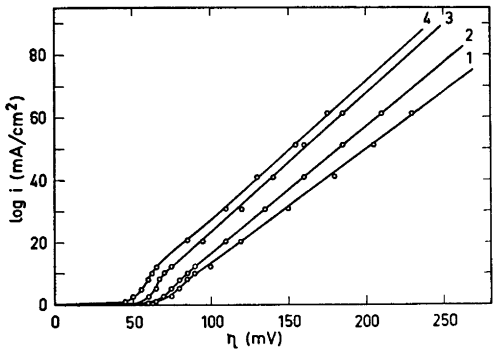

Fig. 2. Effect of temperature on the cathodic polarization curves in solution 1 M $ZnSO_4$; temperature (°C): 1, 20; 2, 30; 3, 40; 4, 50.

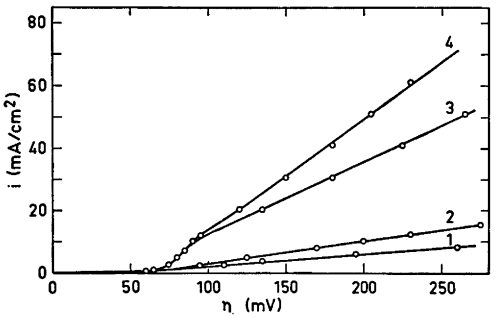

Fig. 3. Effect of zinc sulfate concentration on the cathodic polarization at 20°C: 1, 0.05 M; 2, 0.1 M; 3, 0.5 M; 4, 1.0 M.

The apparent activation energy for the electrode process can be found from the slopes of the log $i - 1/T$ plots, with the aid of the relation:

$$2.3 \log i = -\Delta E^{\neq}/RT + \text{constant}$$

It is very interesting to follow the variation of the apparent activation energy with polarization potential. The $\Delta E^{\neq} - \eta$ plot in Fig. 5 shows that the apparent activation energy for solutions containing 1 M and 0.5 M zinc sulfate depends on the polarization potential. With increase in polarization potential from 65 to 150 mV, the apparent activation energy falls from 86.02×10^3 to 13.47×10^3 J/mol and from 44.35×10^3 to 13.39×10^3 J/mol in 1 M and 0.5 M zinc sulfate solutions, respectively.

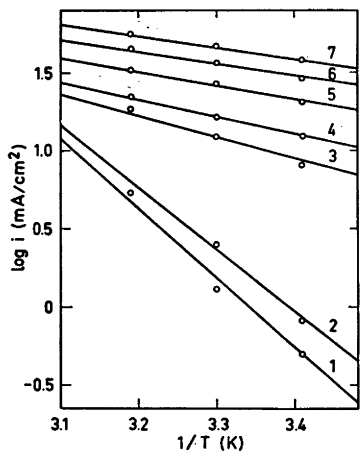

Fig. 4. Variation of log i with $1/T$ at constant polarization potential in solution of 1 M $ZnSO_4$; polarization potential η(mV): 1, 65; 2, 70; 3, 90; 4, 100; 5, 125; 6, 150; 7, 175.

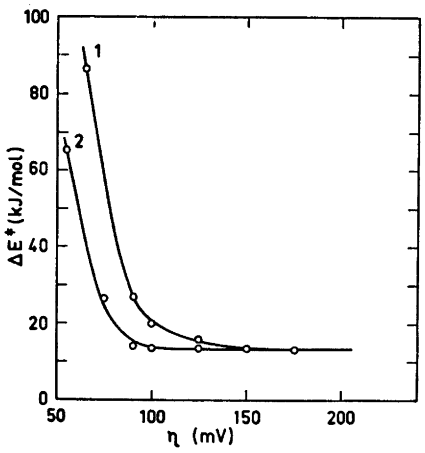

Fig. 5. Variation of the activation energy $\Delta E^{\neq}$ with polarization potential η in $ZnSO_4$ solutions: 1, 1 M; 2, 0.5 M.

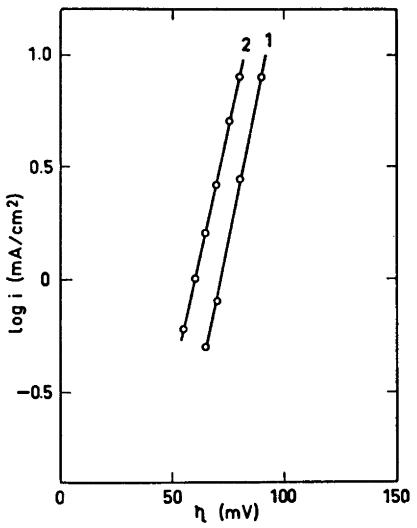

Fig. 6. Dependence of η on log i at 20°C for $ZnSO_4$ solutions: 1, 0.5 M; 2, 1.0 M.

Some decrease of the apparent activation energy with polarization potential was observed in solutions containing 0.1 M and 0.05 M zinc sulfate. As polarization is raised from 50 to 150 mV, the apparent activation energy decreases from 55.44×10^3 to 17.32×10^3 J/mol and from 37.53×10^3 to 13.47×10^3 J/mol in 0.1 M and 0.05 M zinc sulfate solutions, respectively.

The absolute values of the apparent activation energy (Fig. 5) and the nature of its variation with polarization potential indicate that the rate of deposition of zinc is limited by the electrode reaction itself, *i.e.* activation overpotential or charge-transfer overvoltage.

With increase in the zinc sulfate concentration the polarization potential of the zinc cathode decreases, while the rate of cathodic deposition of zinc and the effective activation energy both increase. At the same time the relative proportion of charge-transfer overpotential compared with concentration polarization also increases, *i.e.* material transport ceases to be the rate-determining stage, the cathodic deposition of zinc being limited by one of the stages in the electrode reaction.

Fig. 6 depicts the polarization curves plotted in terms of Tafel coordinates and shows that these relations are linear. $\eta - \log i$ plots are known to be linear if the charge-transfer at the electrode is rate controlling.[17] Thus the conclusion which follows from the analysis of Fig. 6 is consistent with the conclusion derived by the temperature-kinetic method.

Effect of manganese. At 0.1 and 0.5 g/l manganese reduced polarization of the zinc cathode at all the temperatures investigated except at 50°C. At a concentration of 1.0 g/l the depolarizing effect ceased at 40°C. At 3.0 g/l a polarization was observed at 20° and 50°C; with small depolarization, in the low cathode potential region, at 30° and 40°C. Fig. 7 shows the effect of manganese ion on the cathode potential-current density relation at 20°C.

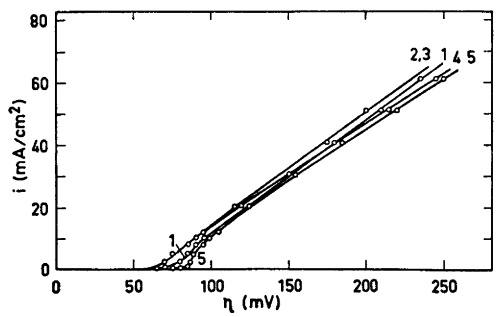

Fig. 7. Effect of manganese ion concentration on the cathode potential-current density relation in 1 M $ZnSO_4$ solution at 20°C; concentration of manganese (g/l): 1, 0; 2, 0.1; 3, 0.5; 4, 1.0; 5, 3.0.

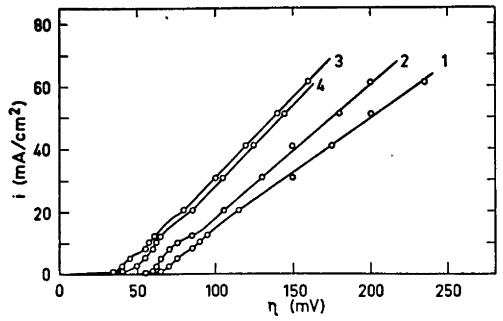

Fig. 8. Effect of the temperature on the cathode potential-current density curve in 1 M $ZnSO_4$ containing 0.1 g/l manganese; temperature (°C): 1, 20; 2, 30; 3, 40; 4, 50.

A typical behavior of the cathode potential with temperature in solutions containing manganese was a decrease with increase in temperature except at 50°C. Fig. 8 shows the effect of temperature for a solution containing 0.1 g/l manganese.

The deviation of the equipotential curves from linearity with passage through a maximum in the plots of log i against $1/T$ is observed at all concentrations studied. At 0.1 g/l the deviation of the equipotential curves from linearity persist at higher overpotentials (Fig. 9) than in the rest of the concentrations investigated.

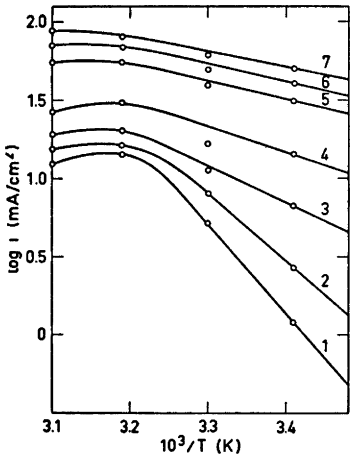

Fig. 9. Dependence of log i on $1/T$ in 1 M $ZnSO_4$ containing 0.1 g/l manganese at constant polarization potential (mV): 1, 65; 2, 70; 3, 80; 4, 100; 5, 150; 6, 175; 7, 200.

The deviation of the equipotential curves from linearity with passage through a maximum is characteristic of crystallization overvoltage.[11]

When the quantity of manganese present in the electrolyte was higher than 0.1 g/l, dark flakes of manganese hydrates were observed to move from the anode into the electrolyte. With increase in manganese content and elevation of temperature, the cathode deposits of zinc become darker.

A characteristic of the cathodic deposition of zinc in presence of admixtures of manganese ion is that zinc is strongly affected in the region of low cathode potential – kinetically-controlled range – and a slight dependence at higher potentials – diffusion-controlled range; this may possibly indicate adsorption of manganese on the electrode. The action of impurities, which act as surface active agents, would be expected to be more pronounced as the current density is lowered. At high current densities on fast growing crystallite facets the surface-active agents do not accumulate sufficiently to stop growth.[18] This idea of absorption is also confirmed by the very slight deviation between the stationary potentials in the solution studied with and without manganese.

The absorption of manganese may be supposed to alter either the effective metal charge and, hence, the electrochemical free energy change across the double layer or the number of effective growth sites.[19] If the number of effective growth sites is reduced by adsorbed species, the mean free path for lateral diffusion

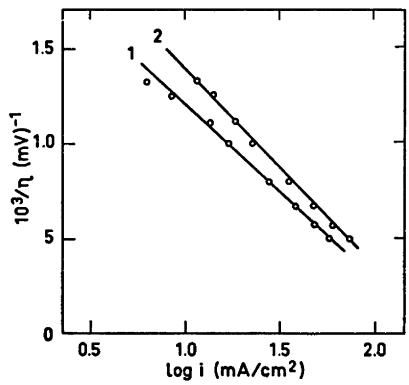

Fig. 10. Relationship between $1/\eta$ and log i in 1 M $ZnSO_4$ containing 0.5 g/l manganese; temperature (°C): 1, 30; 2, 50.

of the adions will be shortened. This is equivalent to a decrease in diffusion coefficient of adions which can result in an increase in surface control or an increase in adion concentration at steady state to a point such that the rate of two-dimensional nucleation becomes appreciable. If two-dimensional nucleation is rate determining, the logarithm of current density should be a linear function of the reciprocal overvoltage.[20] Fig. 10 shows that linear relationships are obtained in $1/\eta$ *vs.* log i coordinates for the solution containing manganese ion impurity. Thus, the conclusion which follows from the analysis of Fig. 10 is consistent with the conclusion derived by the temperature-kinetic method.

Acknowledgement. One of the authors (M.S.) wants to thank the NORAD for the fellowship which made this investigation possible.

REFERENCES

1. Fedotieff, P. P. and Stender, W. W. *Z. Anorg. Allg. Chem. 130* (1923) 51.
2. Marshall, A. L. *Trans. Faraday Soc. 21* (1925–1926) 297.
3. Weimer, F. S., Wever, G. T. and Lapee, R. J. In Mathewson, C. H., Ed., *Zinc. The Science and Technology of the Metal, Its Alloys and Compounds*, Reinhold, New York 1964, p. 218.
4. Zaidler, V. Yu., Ponomarev, V. D. and Stender, V. V. *Zhur. Priklad. Khim. 17* (1944) 282.
5. Turomshina, U. F. and Stender, V. V. *J. Appl. Chem. 28* (1955) 151.
6. Salin, A. A. *et al. Tsvetnye Metally 35* (1962) 13.
7. Pecherskaya, A. G. and Stender, V. V. *J. Appl. Chem. USSR 23* (1950) 975.
8. Levich, V. G. *Acta Physicochim. USSR 17* (1942) 257.
9. Gregory, D. P. and Riddiford, A. C. *J. Chem. Soc.* (1956) 3756.
10. Newson, J. D. and Riddiford, A. C. *J. Electrochem. Soc. 108* (1961) 695.
11. Gorbachev, S. V. *Soviet Electrochem., Proc. 4th Conf. Electrochem.*, Consultant Bureau, New York 1961, Vol. 1 p. 63.
12. Khomutov, N. E. and Skornyakova, T. N. *Russ. J. Phys. Chem. 39* (1965) 101.
13. Levich, V. G. *Physicochemical Hydrodynamics*, Prentice-Hall, Englewood Cliff, N. J. 1962.
14. Fujishima, A., Iketani, H. and Honda, K. *Bull. Chem. Soc. Jap. 43* (1970) 3949.
15. Frumkin, A. N. *Z. Physik. Chem. Abt. A 160* (1932) 116.
16. Kravtsov, V. I. and Ermolova, A. F. *Doklady Phys. Chem. 136* (1961) 171.
17. Vetter, K. J. *Electrochemical Kinetics*, Academic, London 1967. p. 143.
18. Bockris, J. and Despic, A. R. In Eyring. H., Ed., *Physical Chemistry. An Advanced Treat ise*, Academic, New York 1970, Vol. IXB/ Electrochem., p. 669.
19. West, J. M. *Electrodeposition and Corrosion Processes*, Van Nostrand-Reinhold, London 1970, p. 17.
20. Erdey-Grüz, T. and Volmer, M. *Z. Physik. Chem. Abt. A 157* (1931) 165.

Received July 7, 1973.

Acta Chemica Scandinavica A 28 (1974) 99—103

Compounds with the Skutterudite Type Crystal Structure. III. Structural Data for Arsenides and Antimonides

ARNE KJEKSHUS and TROND RAKKE

Kjemisk Institutt, Universitetet i Oslo, Blindern, Oslo 3, Norway

The crystal structures of $CoAs_3$, $CoSb_3$, $Fe_{0.5}Ni_{0.5}Sb_3$, $RhAs_3$, $RhSb_3$, $IrAs_3$, and $IrSb_3$ with the $CoAs_3$ (skutterudite) type structure have been (re)determined by X-ray powder diffraction methods. The results are discussed in relation to those for the isostructural phosphides and the mineral itself.

Following the structure determination [1] of the cubic mineral skutterudite, mineralogical studies [2–6] (by chemical analyses and syntheses, optical microscopy, and X-ray diffraction) have revealed that this is a triarsenide with a general formula (Fe,Co,Ni)As_3. Since $CoAs_3$ is the only binary arsenide with 1:3 composition in this system, this compound is commonly associated with the mineralogical name skutterudite and constitutes the prototype for the structure type.

Over the years, a number of isostructural phases have been synthesized and studied by various methods.[7–35]

Considering the structural properties in particular, among the binary compounds, only the phosphides CoP_3, NiP_3, RhP_3, and IrP_3 have been subjected to structure determinations [31] of sufficient accuracy for bonding considerations. In addition, there has also been a recent accurate redetermination of the mineral itself.[33] The accurate structure determinations have unequivocally demonstrated that the non-metal (X) atoms of the $CoAs_3$ type structure form a planar, rectangular rather than square arrangement. The latter aspect is a consequence of the failure of the variable positional parameters y and z for X to satisfy the so-called [24] Oftedal's relation $y+z=\frac{1}{2}$. Based on these sparse experimental evidences, we previously took the liberty of proposing a model [34] which accounts for these observations. On this background we have felt a provocation to undertake correspondingly accurate (re)determinations of the other binary compounds. In addition, we conveniently included the ternary compound $Fe_{0.5}Ni_{0.5}Sb_3$ which was prepared for ^{121}Sb Mössbauer studies.[35]

EXPERIMENTAL

Samples of $CoSb_3$, $Fe_{0.5}Ni_{0.5}Sb_3$, $RhSb_3$, and $IrSb_3$ were prepared earlier.[35] The triarsenides were prepared similarly by heating stoichiometric quantities of the elements (Co, Rh, and Ir from the same batches as before,[35] and 99.9999 % As from Koch-Light Laboratories) in pure alumina crucibles placed inside evacuated, sealed quartz tubes. The samples were heated at 800 ($CoAs_3$) or 900°C ($RhAs_3$ and $IrAs_3$) for a period of three weeks. After intermediate crushing the samples were reannealed for a further week at the same temperatures, and finally cooled to room temperature over a period of two weeks.

The purities of the samples were ascertained from X-ray powder photographs taken in a Guinier type camera with monochromatized Cu$K\alpha_1$-radiation using KCl as internal standard. The unit cell dimensions were refined by applying the method of least squares.

Integrated X-ray intensities were obtained from 2θ counting scans by subtracting appropriate background counts. Three or more scans were taken of each compound. A General Electric wide angle powder diffractometer (calibrated with Si as standard) was employed using Ni-filtered Cu$K\alpha$-radiation and 1° slits.

The intensity data were corrected for the combined Lorentz and polarization factors. The determinations of the positional parameters followed the method described in Refs. 24 and 31. To perform the calculations, a special computer programme was written for the CD 3300 com-

puter. Atomic scattering factors used were taken from tables by Hanson *et al.*[36]

RESULTS AND DISCUSSION

The unit cell dimensions of the various compounds subject to this study are listed in Table 1.

Table 1. Unit cell dimension (with standard deviation) and positional parameters for arsenides and antimonides with $CoAs_3$ type structure. Probable errors in y and z range from 0.0005 to 0.001.

Compound	a (Å)	y	z
$CoAs_3$	8.2055(3)	0.344_2	0.151_4
$RhAs_3$	8.4507(3)	0.348_3	0.145_9
$IrAs_3$	8.4673(8)	0.347_7	0.145_4
$CoSb_3$	9.0347(6)	0.335_1	0.160_2
$Fe_{0.5}Ni_{0.5}Sb_3$	9.0904(5)	0.335	0.159
$RhSb_3$	9.2322(6)	0.342_0	0.151_7
$IrSb_3$	9.2533(5)	0.340_7	0.153_8

The space group, $Im3$, attributed to skutterudite was very carefully determined in the original work of Oftedal,[1] and was recently confirmed by Mandel and Donohue.[33] All the structural evidences which have been accumulated [11-15,20-24,29,31,32] hitherto, strongly suggest that this space group also applies to the isostructural compounds. Since the space group cannot be explicitly determined on the basis of powder diffraction data, $Im3$ was postulated also for the present investigation.

In terms of $Im3$, the $CoAs_3$ type structure places 8 T (metal atoms) in position (c) and 24 X in (g). The atomic arrangement is accordingly specified by the lattice constant a and two positional parameters y and z. In addition, there are two thermal parameters open to determination on the basis of powder diffraction data which permit only isotropic temperature factors.

The cubic $Im3$ symmetry of the unit cell provides for the overlap of reflections with different structure factors $F(hkl)$. For this reason, the refinement procedure used in Refs. 24 and 31 was adopted. In brief outline, this method aims at minimizing the function $R(y_X,z_X,B_T,B_X) = \sum|jF_o^2 - jF_c^2|/\sum jF_o^2$. In order to simplify the calculations and to facilitate the graphical representation of the results, the simplifying assumption of $B_T = B_X = 0.5$ Å^2 was introduced. The assumption of constant B values is not a serious limitation, however, since R generally is known to be a slowly varying function of the thermal parameters.

In accordance with considerations presented in Ref. 34, the variables y and z were varied in steps of 0.01 over the ranges $1/4 \leqq y < \frac{1}{2}$ and $0 < z \leqq 1/4$. The resulting R maps revealed in all cases only one well defined minimum. The areas around these minima were explored in detail in order to determine them with the best possible accuracy. The positional parameters as defined by the location of these minima are given in Table 1, R factors between 0.056 and 0.113 being obtained. Judging from the curvatures of the $R(y,z)$ surfaces, the probable uncertainties in y and z are likely to be 0.0005 to 0.001. Since secondary minima previously were recorded [24] in corresponding R maps for $IrAs_3$ and $IrSb_3$, recalculations on the basis of these data were also performed as a part of this study. Contrary to the earlier findings, no secondary minima could be found this time. (The non-computerized work reported in Ref. 24 consumed about one man-year and the computational mistakes should be estimated on this background.) The location of the minima were found to be 0.349, 0.145 for $IrAs_3$ and 0.341, 0.154 for $IrSb_3$ in satisfactory agreement with the values given in Table 1.

The results of the present study together with those of Rundqvist and Ersson,[31] and Mandel and Donohue,[33] are illustrated in Fig. 1. The diagram clearly shows that none of the compounds satisfy Oftedal's relation $y + z = \frac{1}{2}$, the confirmation of this fact being the main object of the study. It is interesting to note that with the exception of NiP_3 which occupies a special position among these compounds (*vide infra*), the points define an approximately parallel line with that given by Oftedal's relation. A least squares fitted line on this basis would follow the equation $\frac{1}{2} - (y + z) = 0.006$.

The bonding interatomic distances and angles are listed in Table 2. As a consequence mainly of the empirical relationship inferred above, the difference $d_2 - d_1$ between the 2 $X-X$ bond distances is constant to within 0.10 ± 0.02 Å for all compounds except NiP_3.

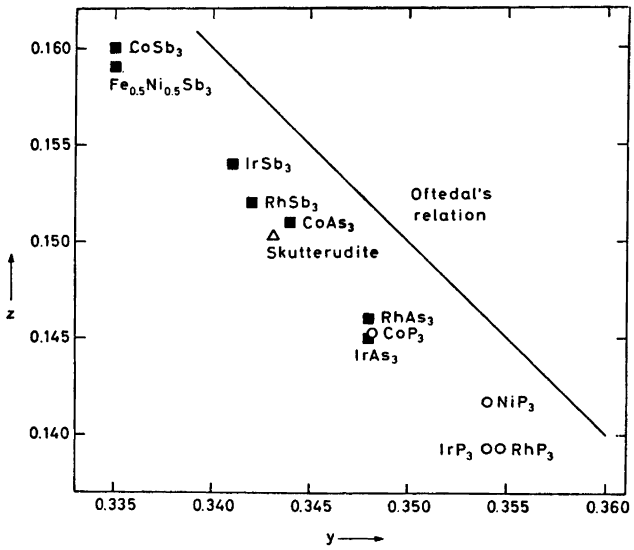

Fig. 1. Positional parameters for compounds with $CoAs_3$ type structure, Oftedal's relation being included for comparison. Points marked O quoted from Rundqvist and Ersson,[31] △ from Mandel and Donohue.[33]

Table 2. Interatomic distances (Å) and angles (°) in compounds with $CoAs_3$ type structure. (Angle $X-X-X$ (1) is fixed at 90°.)

Compound	$T-X(6)$ (d)	$X-X(1)$ (d_1)	$X-X(1)$ (d_2)	$X-T-X$ (6)	$X-T-X$ (6)	$T-X-T$ (1)	$X-X-T$ (2)	$X-X-T$ (2)
CoP_3[a]	2.222	2.240	2.340	84.0	96.0	120.3	109.9	111.3
NiP_3[a]	2.280	2.216	2.283	83.1	96.9	118.0	110.9	111.8
RhP_3[a]	2.341	2.227	2.323	83.2	96.8	117.3	111.0	112.2
IrP_3[a]	2.345	2.233	2.340	83.4	96.6	117.4	110.8	112.2
Skutterudite[b]	2.334	2.464	2.572	84.6	95.4	122.8	109.1	110.5
$CoAs_3$	2.337	2.478	2.560	84.3	95.7	122.7	109.3	110.3
$RhAs_3$	2.434	2.468	2.569	84.0	96.0	120.5	109.9	111.2
$IrAs_3$	2.441	2.456	2.574	84.1	95.9	120.2	109.9	111.4
$CoSb_3$	2.520	2.891	2.982	85.3	94.7	127.3	107.7	108.8
$Fe_{0.5}Ni_{0.5}Sb_3$	2.539	2.891	3.000	85.4	94.6	127.1	107.7	109.0
$RhSb_3$	2.621	2.807	2.917	84.6	95.4	123.5	108.9	110.2
$IrSb_3$	2.617	2.850	2.943	84.6	95.4	124.2	108.8	109.8

[a] Calculated from data in Ref. 31. [b] Calculated from data in Ref. 33.

We have previously attributed[34] the rectangular distortion of the X_4 groups to anisotropic interactions arising from charges on the X sublattice. Thus, at first sight the approximate constancy of the distortion seemed somewhat surprising. However, d_2-d_1 is determined by a difference in force (acting in mutually perpendicular directions) which in turn is proportional to square of charge and inversely proportional to square of distance, and a constant value for d_2-d_1, may therefore simply imply that two effects are counterbalanced. The smaller value for d_2-d_1 in NiP_3 is consistent with the assumption[26] of delocali-

zation of one surplus electron over the lattice which thus would provide a shielding effect.

In accordance with the anisotropic interaction model,[34] d_2-d_1 does not show any simple systematic correlation with bonding interatomic distances or angles. If, on the other hand, the rectangular distortion had been a consequence of competition between the X_4 group and the TX_6 octahedron,[31] the $X-T-X$ angle is expected to show some relation to d_2-d_1.

Important features of the bonding situation in these compounds are unquestionably reflected in the value of d_2-d_1. Another parameter which reflects the inequality of the two $X-X$ bonds is the nuclear quadrupole interaction. Hence it seems natural that d_2-d_1 *versus* $|eQV_{zz}|$[35] shows (Fig. 2) an approximately linear relationship for the antimonides. It is not surprising that the electron imbalance reflected in the different bond lengths of d_1 and d_2 by far outweighs the minor variations in the average bond angle around X as opposed to the situation prevailing in compounds with pyrite, marcasite, and arsenopyrite type structures.[37]

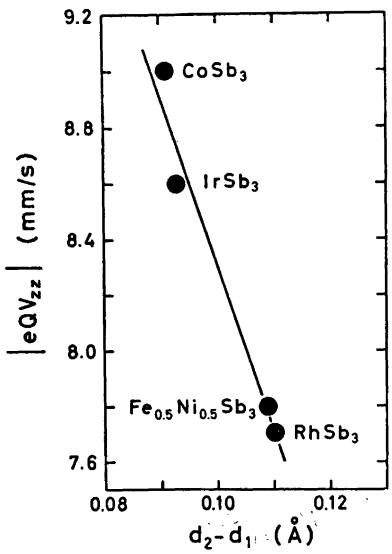

Fig. 2. ^{121}Sb Mössbauer quadrupole interaction as a function of d_2-d_1 for $CoSb_3$, $Fe_{0.5}Ni_{0.5}Sb_3$, $RhSb_3$, and $IrSb_3$.

As expected (*cf.*, *e.g.*, Ref. 38) d_1, d_2, or their average shows approximately linear and mutually parallel dependences when plottet against the $T-X$ bond distance d for the sequences $CoP_3-CoAs_3-CoSb_3$, $RhP_3-RhAs_3-RhSb_3$, and $IrP_3-IrAs_3-IrSb_3$.

A few comments concerning the work of Mandel and Donohue [33] seem appropriate. Their analytical composition indicating a 10 % metal excess (or arsenic deficiency) as often found [2] by chemical analysis of natural skutterudites. The work of Roseboom [6] on the arsenic content of synthetic $CoAs_3$ and X-ray investigations on mixtures of the minerals skutterudite and rammelsbergite (β-$NiAs_2$) indicate * that the formula given by Mandel and Donohue is not representative for the crystal used in the structure determination. Moreover, 10 % deviation from stoichiometry is also expected to be reflected in y_X and z_X. Since skutterudite nicely follows the same trend as the other isostructural compounds (Fig. 1), a 1:3 ratio between metal and non-metal appears most probable. The only reasonable explanation of the analytical deficiency is therefore that the apparent metal-excess arises from impurities. The thermal parameters given by these authors are fully consistent with the anisotropic interaction model,[34] in that the relative difference between the root mean square vibration amplitudes equals the relative difference between the corresponding $X-X$ distances.

REFERENCES

1. Oftedal, I. *Z. Kristallogr. 66* (1928) 517.
2. Holmes, R. J. *Geol. Soc. Amer. Bull. 58* (1947) 299.
3. Jouravsky, G. *Bull. Soc. Fr. Minér. Crist. 74* (1948) 316.
4. Ventriglia, U. *Periodico Mineral. (Rome) 26* (1957) 345.
5. Godovikov, A. A. *Trudy Mineral. Museya, Akad. Nauk SSSR 10* (1960) 57.
6. Roseboom, E. H. *Amer. Mineralogist 47* (1962) 310.
7. Jolibois, P. *C. R. Acad. Sci. 150* (1910) 106.
8. Biltz, W. and Heimbrecht, M. *Z. Anorg. Allg. Chem. 237* (1938) 132.
9. Biltz, W. and Heimbrecht, M. *Z. Anorg. Allg. Chem. 241* (1939) 349.
10. Faller, F.-E., Strotzer, E. F. and Biltz, W. *Z. Anorg. Allg. Chem. 244* (1940) 317.

* Roseboom observed no significant differences in the lattice constant on either side of the stoichiometric 1:3 ratio and he added as much as 7 % by weight of rammelsbergite without being able to detect it by powder X-ray methods.

11. Belov, N. V. and Mokeeva, V. I. *Trudy Inst. Kristallografiya 5* (1949) 13.
12. Rosenqvist, T. *Acta Met. 1* (1953) 761; *N. T. H.-Trykk*, Trondheim 1953.
13. Zhuravlev, N. N. and Zhdanov, G. S. *Kristallografiya 1* (1956) 509.
14. Dudkin, L. D. and Abrikosov, N. Kh. *Zh. Neorg. Khim. 1* (1956) 2096.
15. Kuz'min, R. N., Zhdanov, G. S. and Zhuravlev, N. N. *Kristallografiya 2* (1957) 48.
16. Dudkin, L. D. and Abrikosov, N. Kh. *Zh. Neorg. Khim. 2* (1957) 212.
17. Dudkin, L. D. *Soviet Phys.-Techn. Phys. 3* (1958) 216.
18. Dudkin, L. D. and Abrikosov, N. Kh. *Soviet Phys. Solid State 1* (1959) 126.
19. Zobnina, V. I. and Dudkin, L. D. *Fiz. Tv. Tela. 1* (1959) 1821.
20. Rundqvist, S. and Larsson, E. *Acta Chem. Scand. 13* (1959) 551.
21. Rundqvist, S. *Nature (London) 185* (1960) 31.
22. Rundqvist, S. and Hede, A. *Acta Chem. Scand. 14* (1960) 893.
23. Heyding, R. D. and Calvert, L. D. *Can. J. Chem. 39* (1961) 955.
24. Kjekshus, A. and Pedersen, G. *Acta Crystallogr. 14* (1961) 1065.
25. Kjekshus, A. *Acta Chem. Scand. 15* (1961) 678.
26. Hulliger, F. *Helv. Phys. Acta 34* (1961) 782.
27. Pleass, C. M. and Heyding, R. D. *Can. J. Chem. 40* (1962) 590.
28. Bennett, S. L. and Heyding, R. D. *Can. J. Chem. 44* (1966) 3017.
29. Kuz'min, R. N. and Snovidov, V. M. In Sirota, N. N., Ed., *Chemical Bonds in Semiconductors and Solids*, Consultants Bureau, New York 1967, p. 257.
30. Kuz'min, R. N. In Sirota, N. N., Ed., *Chemical Bonds in Semiconductors and Solids*, Consultants Bureau, New York 1967, p. 265.
31. Rundqvist, S. and Ersson, N. O. *Ark. Kemi 30* (1968) 103.
32. Bjerkelund, E. and Kjekshus, A. *Acta Chem. Scand. 24* (1970) 3317.
33. Mandel, N. and Donohue, J. *Acta Crystallogr. B 27* (1971) 2288.
34. Kjekshus, A., Nicholson, D. G. and Rakke, T. *Acta Chem. Scand. 27* (1973) 1307.
35. Kjekshus, A., Nicholson, D. G. and Rakke, T. *Acta Chem. Scand. 27* (1973) 1315.
36. Hanson, H. P., Herman, F., Lea, J. D. and Skillmann, S. *Acta Crystallogr. 17* (1964) 1040.
37. Donaldson, J. D., Kjekshus, A., Nicholson, D. G. and Tricker, M. J. *Acta Chem. Scand. 26* (1972) 3215.
38. Kjekshus, A. and Nicholson, D. G. *Acta Chem. Scand. 25* (1971) 866.

Received July 6, 1973.

Acta Chemica Scandinavica A 28 (1974) 104—112

The Crystal and Molecular Structure of a *trans* Square-Planar Complex of Tellurium Dibenzenethiosulphonate with Tetramethylthiourea

KJELL ÅSE and INGVALD ROTI

Chemical Institute, University of Bergen, N-5000 Bergen, Norway

The crystal and molecular structure of *trans*-dibenzenethiosulphonatobis(tetramethylthiourea)tellurium(II), $Te(SC[N(CH_3)_2]_2)_2(S_2O_2C_6H_5)_2$, has been determined by three-dimensional X-ray diffraction methods. The space group is $P2_1/c$ (No. 14) with $Z=2$, and with cell dimensions (standard deviations in parentheses), $a=10.254(5)$ Å, $b=10.029(8)$ Å, $c=15.929(7)$ Å, and $\beta=110.35(5)°$. Based on the intensities of 1251 independent, non-zero reflections, collected by integrating Weissenberg techniques, least squares refinement procedures resulted in a conventional R value of 0.075.

The tellurium atom is bonded to two tetramethylthiourea sulphur atoms and to two benzenethiosulphonate sulphur atoms in a *trans* square-planar arrangement. Bond lengths are: Te – S(tetramethylthiourea) = 2.724(6) Å, Te – S (benzenethiosulphonate) = 2.657(4) Å, and benzenethiosulphonate S – S = 2.025(6) Å. The value of the S – Te – S angle, 79.51(15)°, implies a marked deviation from a strictly square TeS_4 coordination group.

A remarkable feature of *trans*-dibenzenethiosulphonatobis(tetramethylthiourea)tellurium(II), $Te(SC[N(CH_3)_2]_2)_2(S_2O_2C_6H_5)_2$, as compared with other complexes of divalent tellurium thiosulphonates with thioureas, is its red colour.[1] All other complexes of this type have been found to be yellow. The structures of three yellow complexes have been reported;[2–4] they all display a *trans* square-planar coordination, with four sulphur atoms bonded to the central tellurium atom. The benzenethiosulphonate group as well as the tetramethylthiourea group occur separately as ligands in such complexes without inducing red colour, the former in $Te(trtu)_2(S_2O_2C_6H_5)_2$,[3] (trtu = trimethylenethiourea), and $Te(etu)_2(S_2O_2C_6H_5)_2$,[4] (etu = ethylenethiourea), and the latter in $Te(tmtu)_2(S_2O_2CH_3)_2$,[1] (tmtu = tetramethylthiourea). The "abnormal" colour of $Te(tmtu)_2(S_2O_2C_6H_5)_2$ would be expected to be associated with the tellurium-ligand bonding. A crystal structure study of this compound has therefore been carried out. It was also thought of interest to record the visible spectrum of the complex, together with the spectra of some of the related, yellow compounds.

EXPERIMENTAL

The crystals of $Te(tmtu)_2(S_2O_2C_6H_5)_2$ were prepared, and unit cell and space group determined by Foss and Johannessen.[1]

For redetermination of unit cell dimensions, 2θ-values of 51 reflections were measured from zero-layer Weissenberg photographs around the a and b axes, using Cu$K\alpha_1$ radiation ($\lambda=1.5405$ Å). Sodium chloride powder lines ($a=5.6394$ Å at 18°C)[5] were superimposed on the films for reference.

Intensity data were collected for the $h0l$–$h3l$, $0kl$, and $1kl$ reflections, using multiple-film, integrating, equi-inclination Weissenberg techniques with (Ni-filtered) Cu$K\alpha$ radiation. The crystal rotating about the a axis had the dimensions, given as distances from a common origin to faces: Distance to $(10\bar{1})$, $(\bar{1}0\bar{1})$, $(1\underline{0}\bar{1})$, and $(\bar{1}01) = 0.045$ mm; to $(0\bar{1}1)$ and $(0\bar{1}\bar{1}) = 0.062$ mm; to $(010) = 0.073$ mm. The dimensions of the crystal rotating about the b axis were: Distances to (001) and $(00\bar{1}) = 0.056$ mm; to (101) and $(\bar{1}0\bar{1}) = 0.048$ mm; to $(1\underline{0}\bar{1})$ and $(\bar{1}01) = 0.049$ mm; to $(0\bar{1}1)$ and $(0\bar{1}\bar{1}) = 0.069$ mm; to $(010) = 0.082$ mm.

Out of 1681 accessible, independent reflections, 1251 had intensities strong enough to be

estimated visually by comparison with a scale of timed exposures. The remaining 430 reflections were assigned an intensity equal to the observable limit, and labelled as unobserved reflections.

Estimated corrections for the splitting of α_1 and α_2 at high angles, and absorption, Lorentz, and polarization corrections were applied ($\mu = 120$ cm^{-1}). The absorption correction was based on a modified version of the method described by Busing and Levy,[6] using an $8 \times 8 \times 8$ grid for each of the crystals.

The calculated structure factors were based on the scattering factor curves listed in *International Tables* (Ref. 5, p. 202). Using the $\Delta f'$ and $\Delta f''$ values given by Cromer,[7] the tellurium and sulphur scattering factor curves were corrected for anomalous dispersion, by taking the amplitude of f as the corrected value.

The structure was refined by a least squares, full-matrix program minimizing the function

$$r = \sum W(|F_o| - K|F_c|)^2$$

where K is a scale factor. The weight, W, is defined by $W = 1/[(Ka_1)^2 + \sigma^2(F_o)]$, where a_1 is a constant and $\sigma(F_o)$ is the estimated standard deviation of F_o. Non-observed reflections for which $K|F_c|$ exceeds the observable limit, are included in the refinement with $|F_o|$ equal to the observable limit.

The calculations were carried out on an IBM 360/50 H computer. Most computer programs were made available by the Weizmann Institute of Science, Rehovoth, Israel, and modified for the IBM computer by Dr. D. Rabinovich. A program calculating weighted least squares planes was written by Mr. Knut Maartmann-Moe, of this Institute; and two other programs, one for Fourier summations and another for extinction corrections, were written by Kjell Åse.

Measurement of reflectance spectra in the

Table 1. Atomic coordinates in fractions of monoclinic cell edges. Isotropic thermal parameters (Å^2) in the form $\exp[-8\pi^2 U(\sin^2\theta/\lambda^2)]$. Standard deviations from the least squares refinement in parentheses.

	x	y	z	U
Te	0	0	0	
S(1)	−0.0190(4)	0.2646(6)	0.0326(3)	
S(2)	0.2636(4)	0.0735(6)	0.0401(3)	
S(3)	0.3617(4)	0.0024(7)	0.1653(3)	
O(1)	0.3346(15)	−0.1367(17)	0.1704(8)	0.084(5)
O(2)	0.5043(13)	0.0442(15)	0.1917(7)	0.072(4)
N(1)	−0.2606(13)	0.2544(18)	0.0575(8)	0.060(4)
N(2)	−0.2492(12)	0.3977(17)	−0.0532(7)	0.047(3)
C(1)	−0.1889(14)	0.3049(21)	0.0075(9)	0.050(4)
C(2)	−0.4136(20)	0.2348(25)	0.0237(11)	0.083(6)
C(3)	−0.1936(17)	0.1834(23)	0.1440(11)	0.072(5)
C(4)	−0.1979(17)	0.4208(22)	−0.1273(10)	0.061(5)
C(5)	−0.3522(20)	0.4936(24)	−0.0453(12)	0.078(6)
C(6)	0.2869(15)	0.0889(21)	0.2346(9)	0.047(4)
C(7)	0.1826(19)	0.0179(22)	0.2588(11)	0.073(5)
C(8)	0.1256(21)	0.0883(27)	0.3162(12)	0.081(6)
C(9)	0.1661(19)	0.2167(25)	0.3400(12)	0.072(6)
C(10)	0.2660(19)	0.2831(26)	0.3145(12)	0.083(6)
C(11)	0.3289(17)	0.2196(23)	0.2615(11)	0.065(5)

Table 2. Anisotropic thermal parameters (Å^2) in the form $\exp[-2\pi^2(h^2a^{-2}U_{11} + \cdots + 2hka^{-1}b^{-1}U_{12} + \cdots)]$. All values have been multiplied by 10^4. Standard deviations from the least squares refinement in parentheses.

	U_{11}	U_{22}	U_{33}	U_{12}	U_{23}	U_{13}
Te	387(7)	378(9)	455(6)	55(15)	−5(11)	140(5)
S(1)	445(19)	452(35)	1049(30)	66(40)	−114(31)	207(20)
S(2)	528(20)	693(39)	588(20)	28(39)	−2(28)	201(17)
S(3)	475(19)	546(31)	715(21)	0(53)	50(36)	124(17)

Table 3. Observed and calculated structure factors (× 10). Unobserved reflections are indicated by a minus sign on $F(O)$ and included at the threshold values.

H	K	L	F(O)	F(C)	H	K	L	F(O)	F(C)	H	K	L	F(O)	F(C)	H	K	L	F(O)	F(C)	H	K	L	F(O)	F(C)
0	0	2	1262	1303	0	5	14	-107	28	1	0	10	443	429	1	3	-4	602	-587	1	6	14	208	180
0	0	4	1455	1609	0	5	15	293	243	1	0	12	258	267	1	3	-5	492	488	1	6	15	-89	2
0	0	6	1491	1587	0	5	16	-85	47	1	0	-2	2013	2134	1	3	-6	316	-291	1	6	-1	286	-269
0	0	8	186	165	0	5	17	179	161	1	0	-4	1342	1473	1	3	-7	728	710	1	6	-2	513	517
0	0	10	148	-117	0	6	0	148	121	1	0	-6	827	850	1	3	-8	92	-72	1	6	-3	96	-84
0	0	12	340	315	0	6	1	305	-261	1	0	-8	1182	1293	1	3	-9	633	628	1	6	-4	259	278
0	0	14	-100	20	0	6	2	79	39	1	0	-10	519	521	1	3	-10	-104	6	1	6	-5	203	-205
0	0	16	185	167	0	6	3	134	124	1	0	-12	217	227	1	3	-11	275	255	1	6	-6	212	200
0	0	18	208	192	0	6	4	132	130	1	0	-14	303	289	1	3	-12	-111	48	1	6	-7	254	-232
0	1	1	1150	1347	0	6	5	170	146	1	0	-16	92	56	1	3	-13	293	292	1	6	-8	587	559
0	1	2	-38	-47	0	6	6	644	652	1	0	-18	-97	50	1	3	-14	-117	100	1	6	-9	-115	-12
0	1	3	248	210	0	6	7	-95	12	1	1	0	256	198	1	3	-15	289	254	1	6	-10	167	179
0	1	4	1050	-1109	0	6	8	439	451	1	1	1	280	-344	1	3	-16	-118	74	1	6	-11	136	-133
0	1	5	1222	1297	0	6	9	-104	-15	1	1	2	708	665	1	3	-17	139	125	1	6	-12	319	302
0	1	6	536	-535	0	6	10	417	423	1	1	3	2188	1935	1	3	-18	-86	11	1	6	-13	-126	3
0	1	7	718	761	0	6	11	121	75	1	1	4	473	-453	1	3	-19	110	119	1	6	-14	369	328
0	1	8	332	-344	0	6	12	532	513	1	1	5	188	237	1	4	0	672	692	1	6	-15	-109	-4
0	1	9	188	190	0	6	13	-109	-3	1	1	-6	63	-74	1	4	1	349	-348	1	6	-16	218	205
0	1	10	334	-335	0	6	14	349	282	1	1	7	202	199	1	4	2	1195	1209	1	6	-17	-67	-4
0	1	11	428	455	0	6	15	-88	13	1	1	8	175	-157	1	4	3	-75	-86	1	7	0	98	-71
0	1	12	-95	-58	0	6	16	161	148	1	1	9	478	491	1	4	4	1030	1112	1	7	1	428	515
0	1	13	312	303	0	7	1	576	589	1	1	10	99	-96	1	4	5	120	-103	1	7	2	-100	-26
0	1	14	-101	-8	0	7	2	-87	-57	1	1	11	412	403	1	4	6	704	711	1	7	3	747	740
0	1	15	75	74	0	7	3	172	159	1	1	12	74	-27	1	4	7	-98	37	1	7	4	-105	51
0	1	16	-103	-20	0	7	4	242	253	1	1	13	135	126	1	4	8	503	511	1	7	5	776	794
0	1	17	182	154	0	7	5	487	493	1	1	-1	1412	1396	1	4	9	-108	53	1	7	6	176	178
0	1	18	-76	33	0	7	6	188	157	1	1	-2	937	948	1	4	10	453	474	1	7	7	315	354
0	1	19	126	138	0	7	7	534	572	1	1	-3	1172	1284	1	4	11	222	217	1	7	8	169	143
0	2	0	927	950	0	7	8	-103	47	1	1	-4	90	103	1	4	12	176	150	1	7	9	488	444
0	2	1	658	-741	0	7	9	242	238	1	1	-5	447	396	1	4	13	-121	36	1	7	10	-126	84
0	2	2	172	93	0	7	10	119	102	1	1	-6	393	355	1	4	14	201	158	1	7	11	333	264
0	2	3	291	-238	0	7	11	404	370	1	1	-7	931	989	1	4	15	112	74	1	7	12	-120	51
0	2	4	455	436	0	7	12	-110	8	1	1	-8	204	193	1	4	-1	583	-590	1	7	13	107	95
0	2	5	380	-432	0	7	13	343	299	1	1	-9	847	899	1	4	-2	779	830	1	7	14	-90	2
0	2	6	665	699	0	7	14	-89	24	1	1	-10	158	139	1	4	-3	72	59	1	7	15	153	137
0	2	7	137	-129	0	7	15	147	144	1	1	-11	209	195	1	4	-4	600	608	1	7	-1	684	714
0	2	8	367	350	0	8	0	611	599	1	1	-12	-106	25	1	4	-5	233	238	1	7	-2	194	-198
0	2	9	238	-223	0	8	1	-94	67	1	1	-13	542	537	1	4	-6	200	171	1	7	-3	648	617
0	2	10	379	352	0	8	2	386	387	1	1	-14	161	144	1	4	-7	-92	-33	1	7	-4	-103	-43
0	2	11	-93	4	0	8	3	-95	0	1	1	-15	331	291	1	4	-8	574	606	1	7	-5	105	102
0	2	12	411	392	0	8	4	312	342	1	1	-16	-119	45	1	4	-9	264	273	1	7	-6	-109	-79
0	2	13	108	97	0	8	5	-99	29	1	1	-17	100	78	1	4	-10	280	247	1	7	-7	335	324
0	2	14	232	181	0	8	6	425	398	1	1	-18	66	24	1	4	-11	355	354	1	7	-8	-116	9
0	2	15	109	55	0	8	7	-104	-41	1	1	-19	124	125	1	4	-12	280	296	1	7	-9	275	263
0	2	16	203	181	0	8	8	144	174	1	2	0	129	-85	1	4	-13	117	106	1	7	-10	-123	30
0	2	17	-90	49	0	8	9	-113	25	1	2	1	718	-707	1	4	-14	312	296	1	7	-11	128	139
0	2	18	204	185	0	8	10	165	144	1	2	2	660	-568	1	4	-15	135	106	1	7	-12	-126	1
0	3	1	1028	1190	0	8	11	-108	-48	1	2	3	714	-707	1	4	-16	241	206	1	7	-13	209	172
0	3	2	326	285	0	8	12	314	257	1	2	4	665	609	1	4	-17	-98	33	1	7	-14	-108	7
0	3	3	739	704	0	8	13	-86	-24	1	2	5	272	246	1	4	-18	111	99	1	7	-15	207	200
0	3	4	404	481	0	8	14	111	121	1	2	6	223	-184	1	5	0	356	-351	1	7	-16	-70	-5
0	3	5	526	984	0	9	1	175	160	1	2	7	187	169	1	5	1	324	302	1	8	0	322	373
0	3	6	76	17	0	9	2	-100	-63	1	2	8	269	259	1	5	2	268	265	1	8	1	131	150
0	3	7	675	702	0	9	3	-101	78	1	2	9	74	61	1	5	3	587	614	1	8	2	410	417
0	3	8	177	188	0	9	4	-103	-29	1	2	10	542	521	1	5	4	382	-399	1	8	3	-109	21
0	3	9	339	333	0	9	5	276	255	1	2	11	245	264	1	5	5	512	547	1	8	4	667	696
0	3	10	-93	17	0	9	6	-108	-13	1	2	12	368	393	1	5	6	210	-187	1	8	5	-113	-120
0	3	11	450	474	0	9	7	344	321	1	2	13	124	112	1	5	7	359	377	1	8	6	298	324
0	3	12	-99	33	0	9	8	-113	-25	1	2	14	300	288	1	5	8	-110	-54	1	8	7	-121	-78
0	3	13	367	336	0	9	9	217	210	1	2	-1	489	-526	1	5	9	444	450	1	8	8	240	224
0	3	14	-105	-35	0	9	10	-104	30	1	2	-2	1953	1802	1	5	10	-116	-5	1	8	9	142	-110
0	3	15	176	162	0	9	11	296	276	1	2	-3	713	-744	1	5	11	395	370	1	8	10	350	331
0	3	16	99	66	0	9	12	-80	-7	1	2	-4	974	964	1	5	12	-123	-10	1	8	11	-118	-93
0	3	17	210	187	0	9	13	220	206	1	2	-5	332	-308	1	5	13	195	163	1	8	12	128	104
0	3	18	-66	43	0	10	0	340	340	1	2	-6	653	703	1	5	14	-118	54	1	8	13	-98	-58
0	4	0	1524	1704	0	10	1	-108	42	1	2	-7	157	153	1	5	15	221	196	1	8	-1	130	125
0	4	1	480	-458	0	10	2	167	149	1	2	-8	1353	1386	1	5	-1	539	551	1	8	-2	565	574
0	4	2	870	875	0	10	3	115	112	1	2	-9	-94	-26	1	5	-2	111	57	1	8	-3	-108	109
0	4	3	224	-221	0	10	4	209	196	1	2	-10	582	609	1	5	-3	588	592	1	8	-4	247	259
0	4	4	873	905	0	10	5	-110	89	1	2	-11	176	175	1	5	-4	267	242	1	8	-5	177	178
0	4	5	404	-416	0	10	6	303	286	1	2	-12	328	328	1	5	-5	237	202	1	8	-6	162	128
0	4	6	784	842	0	10	7	126	113	1	2	-13	112	116	1	5	-6	-94	-24	1	8	-7	-118	-24
0	4	7	429	-430	0	10	8	232	217	1	2	-14	418	395	1	5	-7	299	275	1	8	-8	329	324
0	4	8	395	410	0	10	9	-94	69	1	2	-15	-119	27	1	5	-8	117	97	1	8	-9	-125	81
0	4	9	107	-112	0	10	10	151	140	1	2	-16	222	183	1	5	-9	502	487	1	8	-10	156	133
0	4	10	264	260	0	10	11	69	59	1	2	-17	-110	-20	1	5	-10	223	209	1	8	-11	-126	-35
0	4	11	163	-134	0	10	12	168	206	1	2	-18	114	117	1	5	-11	100	135	1	8	-12	132	120
0	4	12	446	408	0	11	1	313	299	1	2	-19	168	-4	1	5	-12	-118	-7	1	8	-13	-105	-11
0	4	13	-104	-8	0	11	2	-105	59	1	3	-4	387	-416	1	5	-13	314	278	1	8	-14	202	195
0	4	14	207	177	0	11	3	214	200	1	3	1	625	624	1	5	-14	123	81	1	8	-15	-67	-1
0	4	15	111	92	0	11	4	129	108	1	3	2	237	-228	1	5	-15	327	280	1	9	0	113	100
0	4	16	171	136	0	11	5	249	238	1	3	3	1243	1228	1	5	-16	-105	28	1	9	1	-113	53
0	4	17	-78	27	0	11	6	162	128	1	3	4	446	-430	1	5	-17	176	167	1	9	2	-114	-9
0	4	18	164	147	0	11	7	214	207	1	3	5	753	767	1	6	0	177	188	1	9	3	348	374
0	5	1	469	511	0	11	8	78	57	1	3	6	377	350	1	6	1	-89	18	1	9	4	-119	0
0	5	2	331	-323	0	11	9	112	109	1	3	7	453	455	1	6	2	333	352	1	9	5	330	337
0	5	3	96	-58	0	12	0	311	305	1	3	8	191	151	1	6	3	-93	-20	1	9	6	-124	-92
0	5	4	343	-359	0	12	1	-85	-36	1	3	9	495	492	1	6	4	731	783	1	9	7	228	194
0	5	5	417	442	0	12	2	211	203	1	3	10	233	226	1	6	5	-102	-7	1	9	8	172	-136
0	5	6	491	-525	0	12	3	-81	-27	1	3	11	431	413	1	6	6	308	297	1	9	9	249	247
0	5	7	556	588	0	12	4	151	159	1	3	12	193	157	1	6	7	117	105	1	9	10	-110	-75
0	5	8	327	-308	0	12	5	-72	-27	1	3	13	225	211	1	6	8	393	429	1	9	11	237	228
0	5	9	223	210	0	12	6	155	160	1	3	14	-121	61	1	6	9	118	66	1	9	12	-80	-45
0	5	10	102	-82	1	0	2	1047	1129	1	3	15	300	244	1	6	10	608	582	1	9	13	79	83
0	5	11	490	478	1	0	4	520	661	1	3	-1	1232	1239	1	6	11	-125	13	1	9	-1	256	294
0	5	12	-105	-63	1	0	6	324	314	1	3	-2	848	-894	1	6	12	242	205	1	9	-2	-114	83
0	5	13	333	287	1	0	8	460	420	1	3	-3	1252	1307	1	6	13	135	75	1	9	-3	199	207

visible and ultraviolet region were performed on a Zeiss spectrophotometer PMQ II equipped with an integrating sphere. The finely powdered compound was kept in a 0.05 cm quartz cell, and the absorption of light in the cell window was ignored. A sample of MgO, built into the instrument, was used as a white standard of 100 % reflectance. In addition to the tetramethylthiourea complex, the spectra of the corresponding trimethylenethiourea complex and ethylenethiourea complex were measured.

CRYSTAL DATA

The crystals of $Te(tmtu)_2(S_2O_2C_6H_5)_2$ are monoclinic. Most of them were prisms elongated

Table 3. Continued.

H	K	L	F(O)	F(C)	H	K	L	F(O)	F(C)	H	K	L	F(O)	F(C)	H	K	L	F(O)	F(C)	H	K	L	F(O)	F(C)
1	9	-4	175	145	3	0-14	231	207	10	0	6	215	235	4	1	0	252	-171	7	1	4	114	-102
1	9	-5	-119	63	3	0-16	184	185	10	0	-2	123	123	4	1	1	616	539	7	1	5	266	248
1	9	-6	-122	43	3	0-18	321	285	10	0	-4	279	231	4	1	2	339	-257	7	1	6	-72	-14
1	9	-7	154	145	3	0-20	159	183	10	0	-6	89	39	4	1	3	789	824	7	1	7	306	281
1	9	-8	-127	-46	4	0	0	1278	1302	10	0	-8	241	258	4	1	4	363	-305	7	1	8	95	-61
1	9	-9	310	285	4	0	2	1105	1126	10	0-10		320	287	4	1	5	784	744	7	1	9	375	346
1	9-10		-122	-32	4	0	4	1237	1263	10	0-12		184	195	4	1	6	251	-246	7	1	10	-65	-60
1	9-11		136	117	4	0	6	195	186	10	0-14		220	232	4	1	7	157	150	7	1	11	99	104
1	9-12		-98	-36	4	0	8	176	160	10	0-16		275	283	4	1	8	331	-321	7	1	12	-41	-35
1	9-13		196	192	4	0	10	275	277	11	0	0	452	432	4	1	9	429	388	7	1	-1	479	443
1	9-14		-57	-67	4	0	12	-91	0	11	0	2	316	295	4	1	10	140	-110	7	1	-2	248	250
1	10	0	156	171	4	0	14	-79	70	11	0	4	215	247	4	1	11	194	189	7	1	-3	791	758
1	10	1	-123	53	4	0	16	138	169	11	0	-2	221	206	4	1	12	-75	-23	7	1	-4	362	330
1	10	2	144	133	4	0	-2	1877	2003	11	0	-4	154	127	4	1	13	81	85	7	1	-5	334	340
1	10	3	-124	86	4	0	-4	1052	1086	11	0	-6	138	163	4	1	14	-65	-29	7	1	-6	426	454
1	10	4	228	212	4	0	-6	428	430	11	0	-8	-89	8	4	1	15	176	171	7	1	-7	163	170
1	10	5	132	70	4	0	-8	593	659	11	0-10		-87	19	4	1	-1	1239	1163	7	1	-8	167	139
1	10	6	168	151	4	0-10		268	279	11	0-12		135	128	4	1	-2	350	406	7	1	-9	487	512
1	10	7	-118	48	4	0-12		140	-125	11	0-14		116	135	4	1	-3	1232	1206	7	1	-10	210	193
1	10	8	189	170	4	0-14		330	341	11	0-16		93	124	4	1	-4	-43	75	7	1	-11	-68	36
1	10	9	-98	55	4	0-16		215	213	12	0	0	214	204	4	1	-5	646	681	7	1	-12	78	-78
1	10	10	222	234	4	0-18		100	104	12	0	-2	328	313	4	1	-6	467	496	7	1	-13	256	242
1	10	11	-65	-11	4	0-20		140	177	12	0	-4	191	188	4	1	-7	432	477	7	1	-14	-74	-63
1	10	-1	-122	28	5	0	0	810	876	12	0	-6	166	146	4	1	-8	-52	30	7	1	-15	314	280
1	10	-2	293	256	5	0	2	1192	1145	12	0	-8	192	168	4	1	-9	735	729	7	1	-16	93	-98
1	10	-3	-123	-18	5	0	4	246	230	12	0-10		89	89	4	1-10		101	80	7	1-17		262	233
1	10	-4	261	261	5	0	6	492	531	12	0-12		73	73	4	1-11		287	267	7	1-18		-62	-50
1	10	-5	-125	-32	5	0	8	610	595	12	0-14		85	108	4	1-12		-65	8	7	1-19		160	166
1	10	-6	242	248	5	0	10	100	105	1	1	14	83	73	4	1-13		124	126	8	1	0	-68	54
1	10	-7	-123	-65	5	0	12	303	274	1	1	15	335	301	4	1-14		-70	-28	8	1	1	515	533
1	10	-8	296	267	5	0	14	246	235	1	1	16	-71	49	4	1-15		285	256	8	1	2	-70	73
1	10	-9	-111	-51	5	0	-2	830	843	1	1	17	219	224	4	1-16		94	-106	8	1	3	182	186
1	10-10		187	206	5	0	-4	946	939	1	1	18	-46	28	4	1-17		154	125	8	1	4	-73	-3
1	10-11		85	-90	5	0	-6	868	943	2	1	0	48	54	4	1-18		-70	-17	8	1	5	201	187
1	10-12		100	109	5	0	-8	702	698	2	1	1	1184	1130	4	1-19		118	110	8	1	6	84	-87
1	11	0	-119	10	5	0-10		655	646	2	1	2	296	-195	5	1	0	258	208	8	1	7	307	286
1	11	1	252	235	5	0-12		373	332	2	1	3	708	641	5	1	1	754	749	8	1	8	-67	-45
1	11	2	-117	92	5	0-14		274	285	2	1	4	383	329	5	1	2	61	29	8	1	9	80	77
1	11	3	330	331	5	0-16		180	162	2	1	5	191	160	5	1	3	344	302	8	1	10	-47	-35
1	11	4	-112	59	5	0-18		152	145	2	1	6	339	-331	5	1	4	-60	4	8	1	11	-23	100
1	11	5	237	231	5	0-20		-53	52	2	1	7	704	676	5	1	5	70	24	8	1	-1	586	529
1	11	6	-101	30	6	0	0	882	858	2	1	8	-58	37	5	1	6	171	-175	8	1	-2	272	250
1	11	7	121	132	6	0	2	82	34	2	1	9	614	619	5	1	7	515	493	8	1	-3	375	375
1	11	8	-79	9	6	0	4	681	697	2	1	10	-65	-45	5	1	8	128	-140	8	1	-4	254	276
1	11	9	137	152	6	0	6	680	721	2	1	11	344	336	5	1	9	178	158	8	1	-5	780	805
1	11	-1	313	317	6	0	8	349	382	2	1	12	123	-124	5	1	10	108	-111	8	1	-6	133	103
1	11	-2	-119	43	6	0	10	487	440	2	1	13	401	380	5	1	11	187	171	8	1	-7	459	461
1	11	-3	277	266	6	0	12	299	295	2	1	14	-75	-4	5	1	12	-72	-52	8	1	-8	136	130
1	11	-4	-116	15	6	0	-2	323	353	2	1	15	380	328	5	1	13	306	283	8	1	-9	371	396
1	11	-5	195	202	6	0	-4	70	37	2	1	16	-64	6	5	1	14	-51	-22	8	1-10		-69	56
1	11	-6	-108	-27	6	0	-6	563	648	2	1	17	105	130	5	1	-1	108	76	8	1-11		393	401
1	11	-7	203	201	6	0	-8	583	640	2	1	-1	333	290	5	1	-2	356	317	8	1-12		-72	-52
1	11	-8	-93	-54	6	0-10		136	139	2	1	-2	309	408	5	1	-3	834	802	8	1-13		194	166
1	11	-9	151	158	6	0-12		588	627	2	1	-3	521	537	5	1	-4	226	213	8	1-14		-76	-28
1	11-10		-62	-14	6	0-14		294	288	2	1	-4	-33	40	5	1	-5	965	1034	8	1-15		89	91
1	12	1	-94	-15	6	0-16		214	217	2	1	-5	1246	1285	5	1	-6	65	69	8	1-16		81	-65
1	12	2	134	132	6	0-18		205	202	2	1	-6	68	8	5	1	-7	583	614	8	1-17		174	158
1	12	3	-88	-23	6	0-20		139	164	2	1	-7	431	408	5	1	-8	167	218	8	1-18		-56	-51
1	12	4	191	201	7	0	0	465	460	2	1	-8	302	406	5	1	-9	553	601	8	1-19		87	88
1	12	5	-73	-63	7	0	2	850	860	2	1	-9	594	642	5	1-10		-61	-11	9	1	0	-72	60
1	12	6	72	98	7	0	4	780	801	2	1-10		-56	-1	5	1-11		741	784	9	1	1	90	75
1	12	-1	-95	8	7	0	6	360	363	2	1-11		702	769	5	1-12		146	95	9	1	2	-75	71
1	12	-2	236	246	7	0	8	446	420	2	1-12		85	89	5	1-13		273	300	9	1	3	198	168
1	12	-3	-92	27	7	0	10	266	261	2	1-13		343	326	5	1-14		94	89	9	1	4	-75	47
1	12	-4	150	155	7	0	12	60	57	2	1-14		78	46	5	1-15		268	249	9	1	5	292	278
1	12	-5	-82	45	7	0	-2	719	679	2	1-15		409	410	5	1-16		98	50	9	1	6	-66	-23
1	12	-6	128	137	7	0	-4	560	578	2	1-16		-76	19	5	1-17		201	173	9	1	7	117	103
1	12	-7	-60	30	7	0	-6	87	-65	2	1-17		371	316	5	1-18		-69	24	9	1	8	-48	-45
1	0	0	817	779	7	0	-8	169	157	2	1-18		-66	4	5	1-19		109	103	9	1	9	-32	137
1	0	14	306	311	7	0-10		160	107	2	1-19		114	126	6	1	0	388	406	9	1	-1	332	348
1	0	16	368	338	7	0-12		145	156	3	1	0	245	202	6	1	1	337	350	9	1	-2	-70	66
1	0	18	150	176	7	0-14		142	144	3	1	1	973	908	6	1	2	175	164	9	1	-3	398	387
2	0	0	714	-588	7	0-16		282	251	3	1	2	-62	-56	6	1	3	217	231	9	1	-4	-69	92
2	0	2	1954	1844	7	0-18		182	195	3	1	3	357	314	6	1	4	65	75	9	1	-5	138	128
2	0	4	238	221	8	0	0	786	756	3	1	4	116	-97	6	1	5	606	618	9	1	-6	142	-107
2	0	6	917	537	8	0	2	641	685	3	1	5	1214	1186	6	1	6	-68	45	9	1	-7	563	594
2	0	8	1001	585	8	0	4	292	290	3	1	6	102	-105	6	1	7	301	298	9	1	-8	70	-31
2	0	10	567	556	8	0	6	405	369	3	1	7	649	685	6	1	8	-73	2	9	1	-9	444	433
2	0	12	331	333	8	0	8	156	143	3	1	8	150	-146	6	1	9	292	263	9	1-10		89	-91
2	0	14	426	387	8	0	10	-58	39	3	1	9	424	414	6	1	10	-74	-53	9	1-11		360	341
2	0	16	113	89	8	0	-2	373	411	3	1	10	123	-107	6	1	11	420	368	9	1-12		-76	-5
2	0	18	-30	70	8	0	-4	482	546	3	1	11	439	434	6	1	12	70	-63	9	1-13		454	390
2	0	-2	135	-81	8	0	-6	521	524	3	1	12	-73	-73	6	1	13	126	149	9	1-14		-76	-27
2	0	-4	1433	1514	8	0	-8	290	-277	3	1	13	323	298	6	1	-1	520	514	9	1-15		276	245
2	0	-6	605	684	8	0-10		254	275	3	1	14	97	-73	6	1	-2	104	104	9	1-16		-66	22
2	0	-8	148	125	8	0-12		97	80	3	1	15	69	90	6	1	-3	89	44	9	1-17		106	113
2	0-10		1211	1249	8	0-14		-92	28	3	1	16	-53	-27	6	1	-4	234	221	9	1-18		-47	-5
2	0-12		462	460	8	0-16		140	130	3	1	-1	1267	1282	6	1	-5	309	319	10	1	0	173	141
2	0-14		233	230	8	0-18		166	173	3	1	-2	251	167	6	1	-6	177	192	10	1	1	279	245
2	0-16		346	315	9	0	0	229	236	3	1	-3	240	268	6	1	-7	590	616	10	1	2	-72	71
2	0-18		165	139	9	0	2	216	182	3	1	-4	843	846	6	1	-8	88	61	10	1	3	272	275
3	0	0	1367	1484	9	0	4	305	290	3	1	-5	213	261	6	1	-9	278	260	10	1	4	-62	59
3	0	2	1209	1187	9	0	6	207	204	3	1	-6	370	398	6	1-10		-63	-20	10	1	5	166	166
3	0	4	1395	1452	9	0	8	110	107	3	1	-7	922	914	6	1-11		451	476	10	1	6	-46	7
3	0	6	1005	1044	9	0	-2	475	476	3	1	-8	252	271	6	1-12		-68	25	10	1	-1	119	93
3	0	8	414	431	9	0	-4	254	249	3	1	-9	171	174	6	1-13		521	548	10	1	-2	188	157
3	0	10	351	376	9	0	-6	364	379	3	1-10		153	159	6	1-14		88	-97	10	1	-3	289	297
3	0	12	357	330	9	0	-8	557	547	3	1-11		382	335	6	1-15		409	392	10	1	-4	-74	57
3	0	14	-89	33	9	0-10		305	269	3	1-12		-64	-34	6	1-16		-76	40	10	1	-5	212	204
3	0	16	-65	36	9	0-12		261	245	3	1-13		467	498	6	1-17		237	232	10	1	-6	141	107
3	0	-2	1109	1165	9	0-14		353	303	3	1-14		126	-154	6	1-18		-66	-19	10	1	-7	123	105
3	0	-4	541	469	9	0-16		132	120	3	1-15		191	185	6	1-19		225	226	10	1	-8	-74	-7
3	0	-6	274	251	9	0-18		74	89	3	1-16		126	-115	7	1	0	198	207	10	1	-9	249	249
3	0	-8	104	120	10	0	0	202	164	3	1-17		322	310	7	1	1	460	467	10	1-10		-75	-59
3	0-10		220	-249	10	0	2	350	330	3	1-18		-49	-85	7	1	2	107	88	10	1-11		339	295
3	0-12		350	355	10	0	4	326	295	3	1-19		221	230	7	1	3	804	785	10	1-12		-75	-63

in the b axis direction, bounded by {001}, {101}, and {10$\bar{1}$}, and terminated by {011}. Based on 51 measured 2θ-values, a least squares procedure gave the following unit cell dimensions: $a = 10.254(5)$ Å; $b = 10.029(8)$ Å; $c = 15.929(7)$ Å; $\beta = 110.35(5)°$. Other pertinent data are:

Table 3. Continued.

H	K	L	F(o)	F(c)	H	K	L	F(o)	F(c)	H	K	L	F(o)	F(c)	H	K	L	F(o)	F(c)	H	K	L	F(o)	F(c)
10	1-13		210	157	3	2 -1		160	177	6	2 13		-56	-13	9	2-14		349	311	3	3 6		184	30
10	1-14		-69	-51	3	2 -2		668	630	6	2 -1		-72	-15	9	2-15		98	61	3	3 7		517	546
10	1-15		266	265	3	2 -3		115	134	6	2 -2		499	522	9	2-16		98	103	3	3 8		-205	120
10	1-16		-55	-59	3	2 -4		116	30	6	2 -3		237	-199	9	2-17		69	65	3	3 9		311	313
10	1-17		191	218	3	2 -5		688	671	6	2 -4		276	226	9	2-18		100	117	3	3 10		-221	-143
11	1 0		109	108	3	2 -6		808	862	6	2 -5		334	-291	10	2 0		-93	105	3	3 11		294	304
11	1 1		296	290	3	2 -7		406	-407	6	2 -6		561	553	10	2 1		-91	29	3	3 12		-241	10
11	1 2		-56	46	3	2 -8		492	502	6	2 -7		388	-373	10	2 2		207	213	3	3 13		270	227
11	1 3		144	148	3	2 -9		109	-91	6	2 -8		640	642	10	2 3		83	63	3	3 -1		708	740
11	1 4		-39	3	3	2-10		326	354	6	2 -9		202	-199	10	2 4		125	105	3	3 -2		-121	-8
11	1 -1		296	289	3	2-11		189	-178	6	2-10		460	490	10	2 5		93	77	3	3 -3		435	476
11	1 -2		133	128	3	2-12		593	638	6	2-11		191	-161	10	2 6		-54	63	3	3 -4		-127	47
11	1 -3		182	148	3	2-13		172	-159	6	2-12		552	523	10	2 -1		119	75	3	3 -5		338	372
11	1 -4		171	127	3	2-14		502	525	6	2-13		-88	-9	10	2 -2		105	92	3	3 -6		441	-446
11	1 -5		333	319	3	2-15		-93	-56	6	2-14		427	407	10	2 -3		-93	-75	3	3 -7		676	693
11	1 -6		160	129	3	2-16		220	205	6	2-15		-95	-24	10	2 -4		367	376	3	3 -8		275	-268
11	1 -7		253	229	3	2-17		-94	-2	6	2-16		362	306	10	2 -5		-93	-80	3	3 -9		399	415
11	1 -8		94	78	3	2-18		279	274	6	2-17		-91	56	10	2 -6		197	215	3	3-10		-190	-108
11	1 -9		73	76	3	2-19		-68	-6	6	2-18		213	190	10	2 -7		152	-138	3	3-11		284	262
11	1-10		0	5	3	2-20		101	171	6	2-19		-66	12	10	2 -8		267	267	3	3-12		224	-193
11	1-11		172	158	4	2 0		283	240	6	2-20		92	152	10	2 -9		129	-92	3	3-13		443	483
11	1-12		84	-70	4	2 1		209	-195	7	2 0		50	50	10	2-10		500	460	3	3-14		-231	-55
11	1-13		179	175	4	2 2		425	448	7	2 1		126	99	10	2-11		-94	-67	3	3-15		243	205
11	1-14		60	-44	4	2 3		250	-243	7	2 2		441	414	10	2-12		302	271	3	3-16		-247	-78
11	1-15		74	79	4	2 4		596	573	7	2 3		-85	16	10	2-13		-89	-32	3	3-17		236	181
11	1-16		74	-67	4	2 5		249	-239	7	2 4		380	402	10	2-14		273	241	3	3-18		-203	34
12	1 0		75	69	4	2 6		-76	25	7	2 5		-88	-69	10	2-15		-76	-28	3	3-19		179	172
12	1 1		67	93	4	2 7		90	-79	7	2 6		155	149	10	2-16		264	258	4	3 0		248	-214
12	1 -1		264	249	4	2 8		435	440	7	2 7		-94	-86	10	2-17		-53	49	4	3 1		848	838
12	1 -2		86	72	4	2 9		110	-49	7	2 8		336	313	11	2 0		292	294	4	3 2		237	-194
12	1 -3		228	250	4	2 10		366	366	7	2 9		143	-109	11	2 1		-73	-3	4	3 3		916	882
12	1 -4		97	83	4	2 11		-92	57	7	2 10		203	191	11	2 2		137	142	4	3 4		286	238
12	1 -5		232	211	4	2 12		170	163	7	2 11		-66	-55	11	2 3		-57	-8	4	3 5		605	583
12	1 -6		-61	54	4	2 13		-90	46	7	2 12		-46	93	11	2 4		72	108	4	3 6		-200	-54
12	1 -7		297	292	4	2 14		177	179	7	2 -1		205	176	11	2 -1		-83	38	4	3 7		209	210
12	1 -8		-20	44	4	2 15		-63	73	7	2 -2		434	430	11	2 -2		178	171	4	3 9		459	456
12	1 -9		256	252	4	2 16		-30	196	7	2 -3		-77	-9	11	2 -3		-89	58	4	3 10		-232	73
12	1-10		-57	1	4	2 -1		170	127	7	2 -4		498	516	11	2 -4		282	254	4	3 11		241	184
12	1-11		140	146	4	2 -2		644	659	7	2 -5		167	139	11	2 -5		-91	21	4	3 12		-239	19
12	1-12		-50	18	4	2 -3		135	129	7	2 -6		113	103	11	2 -6		307	287	4	3 -1		680	653
12	1-13		119	135	4	2 -4		815	895	7	2 -7		-78	-28	11	2 -7		-91	-22	4	3 -2		197	-164
13	1 -1		134	187	4	2 -5		293	280	7	2 -8		558	612	11	2 -8		276	246	4	3 -3		1205	1171
13	1 -2		-36	-14	4	2 -6		702	731	7	2 -9		170	-167	11	2 -9		-90	-16	4	3 -4		324	-358
13	1 -3		105	141	4	2 -7		270	291	7	2-10		547	553	11	2-10		203	191	4	3 -5		441	475
13	1 -4		-37	-53	4	2 -8		773	736	7	2-11		210	-174	11	2-11		-84	-53	4	3 -6		165	131
13	1 -5		208	230	4	2 -9		170	160	7	2-12		287	303	11	2-12		293	259	4	3 -7		445	464
0	2 15		-37	47	4	2-10		580	627	7	2-13		-90	-40	11	2-13		118	-79	4	3 -8		-174	-6
1	2 15		-94	40	4	2-11		121	117	7	2-14		399	395	11	2-14		140	135	4	3 -9		458	462
1	2 16		346	327	4	2-12		219	226	7	2-15		131	-106	11	2-15		-58	-25	4	3-10		-195	93
1	2 17		-73	-13	4	2-13		-85	-65	7	2-16		357	300	11	2-16		80	127	4	3-11		316	318
1	2 18		103	145	4	2-14		359	344	7	2-17		-87	-58	12	2 0		106	115	4	3-12		251	262
2	2 0		446	475	4	2-15		-93	-36	7	2-18		163	165	12	2 1		-35	-58	4	3-13		222	195
2	2 1		209	202	4	2-16		186	156	7	2-19		-60	6	12	2 -1		71	-85	4	3-14		-232	24
2	2 2		446	448	4	2-17		-96	-41	8	2 0		568	538	12	2 -2		287	336	4	3-15		356	333
2	2 3		317	313	4	2-18		135	119	8	2 1		177	-131	12	2 -3		-68	-27	4	3-16		-248	-18
2	2 4		148	144	4	2-19		-70	-36	8	2 2		265	246	12	2 -4		235	253	4	3-17		236	156
2	2 5		449	445	4	2-20		71	119	8	2 3		127	-111	12	2 -5		-72	-3	4	3-18		-207	-26
2	2 6		837	836	5	2 0		273	264	8	2 4		135	68	12	2 -6		278	277	4	3-19		165	154
2	2 7		-69	26	5	2 1		322	-330	8	2 5		145	-136	12	2 -7		-74	29	5	3 0		486	-455
2	2 8		532	540	5	2 2		295	253	8	2 6		275	236	12	2 -8		327	354	5	3 1		741	737
2	2 9		249	236	5	2 3		121	-97	8	2 7		103	-75	12	2 -9		-71	15	5	3 2		-183	-91
2	2 10		451	486	5	2 4		159	-133	8	2 8		132	120	12	2-10		211	231	5	3 3		463	465
2	2 11		-85	-42	5	2 5		79	79	8	2 9		-70	7	12	2-11		-65	36	5	3 4		-198	-52
2	2 12		365	416	5	2 6		104	51	8	2 10		-55	64	12	2-12		117	139	5	3 5		281	310
2	2 13		-93	-66	5	2 7		155	131	8	2 -1		-85	-94	1	3 16		-214	40	5	3 6		213	198
2	2 14		412	418	5	2 8		363	346	8	2 -2		331	337	1	3 17		185	175	5	3 7		440	461
2	2 15		-90	-71	5	2 9		131	131	8	2 -3		-83	32	2	3 0		101	-114	5	3 8		-225	120
2	2 16		157	171	5	2 10		136	117	8	2 -4		582	551	2	3 1		880	858	5	3 9		263	248
2	2 17		-60	-59	5	2 11		136	107	8	2 -5		-83	16	2	3 2		261	194	5	3 10		270	256
2	2 -1		327	-318	5	2 12		242	246	8	2 -6		822	839	2	3 3		534	521	5	3 11		237	202
2	2 -2		316	-288	5	2 13		-76	70	8	2 -7		271	235	2	3 4		182	166	5	3 12		265	84
2	2 -3		509	-532	5	2 14		184	242	8	2 -8		391	408	2	3 5		429	391	5	3 -1		647	592
2	2 -4		502	540	5	2 15		-12	25	8	2 -9		-85	23	2	3 6		299	338	5	3 -2		653	-596
2	2 -5		531	-583	5	2 -1		473	-454	8	2-10		458	431	2	3 7		698	696	5	3 -3		756	720
2	2 -6		481	491	5	2 -2		159	143	8	2-11		89	78	2	3 8		305	304	5	3 -4		551	-472
2	2 -7		194	-202	5	2 -3		95	58	8	2-12		449	435	2	3 9		398	410	5	3 -5		863	889
2	2 -8		336	318	5	2 -4		789	874	8	2-13		-94	20	2	3 10		-213	179	5	3 -6		366	-358
2	2 -9		473	-450	5	2 -5		493	-516	8	2-14		216	185	2	3 11		313	277	5	3 -7		641	657
2	2-10		858	865	5	2 -6		718	745	8	2-15		-94	3	2	3 12		-231	34	5	3 -8		195	-181
2	2-11		-77	-58	5	2 -7		-67	-36	8	2-16		181	160	2	3 13		342	308	5	3 -9		373	395
2	2-12		584	613	5	2 -8		541	588	8	2-17		-80	-56	2	3 14		-241	76	5	3-10		-201	-69
2	2-13		-85	69	5	2 -9		243	234	8	2-18		158	161	2	3 15		247	227	5	3-11		539	565
2	2-14		368	379	5	2-10		588	628	8	2-19		-49	-14	2	3 -1		792	736	5	3-12		-218	66
2	2-15		-93	46	5	2-11		98	71	9	2 0		206	183	2	3 -2		208	165	5	3-13		263	280
2	2-16		461	448	5	2-12		601	578	9	2 1		-92	-51	2	3 -3		305	353	5	3-14		-234	110
2	2-17		-92	57	5	2-13		-86	53	9	2 2		99	65	2	3 -4		437	-436	5	3-15		245	170
2	2-18		187	189	5	2-14		185	193	9	2 3		-94	-49	2	3 -5		1048	1183	5	3-16		-246	115
2	2-19		-63	41	5	2-15		128	120	9	2 4		151	122	2	3 -6		489	-529	5	3-17		273	223
3	2 0		639	640	5	2-16		321	281	9	2 5		-88	37	2	3 -7		300	325	5	3-18		-204	5
3	2 1		929	902	5	2-17		-93	-5	9	2 6		120	96	2	3 -8		236	-272	5	3-19		164	141
3	2 2		846	809	5	2-18		211	197	9	2 7		-70	56	2	3 -9		518	555	6	3 0		-192	17
3	2 3		246	216	5	2-19		-70	9	9	2 8		-57	32	2	3-10		349	-372	6	3 1		334	322
3	2 4		443	409	5	2-20		53	69	9	2 9		-29	71	2	3-11		450	496	6	3 2		-202	-32
3	2 5		180	-165	6	2 0		516	443	9	2 -1		219	-184	2	3-12		-212	-170	6	3 3		396	386
3	2 6		923	933	6	2 1		-75	18	9	2 -2		513	501	2	3-13		221	189	6	3 4		-213	82
3	2 7		-74	11	6	2 2		102	-43	9	2 -3		152	-149	2	3-14		-231	-84	6	3 5		621	635
3	2 8		373	344	6	2 3		220	196	9	2 -4		287	291	2	3-15		272	216	6	3 6		-223	42
3	2 9		154	-157	6	2 4		355	348	9	2 -5		119	-111	2	3-16		-246	47	6	3 7		327	316
3	2 10		333	319	6	2 5		165	176	9	2 -6		546	592	2	3-17		256	212	6	3 8		-239	105
3	2 11		108	-121	6	2 6		376	363	9	2 -7		88	-81	2	3-18		-195	64	6	3 9		269	236
3	2 12		368	367	6	2 7		94	93	9	2 -8		567	570	3	3 0		-126	32	6	3 10		-231	55
3	2 13		106	-82	6	2 8		-92	61	9	2 -9		90	31	3	3 1		720	699	6	3 11		318	325
3	2 14		156	155	6	2 9		94	41	9	2-10		314	324	3	3 2		232	190	6	3 -1		820	776
3	2 15		-79	-45	6	2 10		323	305	9	2-11		132	87	3	3 3		577	537	6	3 -2		186	-189
3	2 16		77	103	6	2 11		-84	-36	9	2-12		318	314	3	3 4		235	211	6	3 -3		312	343
3	2 17		-21	26	6	2 12		194	215	9	2-13		-95	43	3	3 5		706	682	6	3 -4		224	-250

$V = 1535.9(17)$ Å^3; $M = 738.52$; $F(000) = 748$; $Z = 2$. Systematic absences are $h0l$ when l is odd, $0k0$ when k is odd. The uniquely determined space group is $P2_1/c$ (No. 14).

STRUCTURE DETERMINATION

The structure was solved through Fourier synthesis. The tellurium atom, which is located

Table 3. Continued.

H	K	L	F(O)	F(C)	H	K	L	F(O)	F(C)	H	K	L	F(O)	F(C)	H	K	L	F(O)	F(C)	H	K	L	F(O)	F(C)
6	3	-5	451	417	7	3	-2	-204	-75	8	3	-3	256	205	9	3	-6	241	-223	10	3	-15	233	218
6	3	-6	305	-285	7	3	-3	634	616	8	3	-4	352	-303	9	3	-7	437	397	10	3	-14	-203	-26
6	3	-7	582	596	7	3	-4	-201	-108	8	3	-5	636	567	9	3	-8	-232	-114	10	3	-13	-219	109
6	3	-8	333	-279	7	3	-5	310	312	8	3	-6	-216	-50	9	3	-9	311	314	11	3	0	-191	-93
6	3	-9	445	445	7	3	-6	-203	-115	8	3	-7	383	351	9	3	-10	-239	29	11	3	1	207	251
6	3	-10	305	-264	7	3	-7	205	174	8	3	-8	-220	21	9	3	-11	243	159	11	3	-1	248	268
6	3	-11	314	315	7	3	-8	-208	-98	8	3	-9	222	160	9	3	-12	-244	66	11	3	-2	-212	-19
6	3	-12	235	-177	7	3	-9	418	419	8	3	-10	-226	174	9	3	-13	296	287	11	3	-3	219	153
6	3	-13	397	390	7	3	-10	-217	-67	8	3	-11	318	316	9	3	-14	-233	88	11	3	-4	-224	-63
6	3	-14	-239	-47	7	3	-11	222	193	8	3	-12	-239	170	9	3	-15	216	179	11	3	-5	265	239
6	3	-15	275	240	7	3	-12	-228	-132	8	3	-13	244	212	10	3	0	-235	-25	11	3	-6	-227	9
6	3	-16	-243	51	7	3	-13	237	162	8	3	-14	-244	83	10	3	1	302	289	11	3	-7	278	251
6	3	-17	225	156	7	3	-14	-244	-67	8	3	-15	-237	103	10	3	2	-217	-15	11	3	-8	-225	30
6	3	-18	-196	55	7	3	-15	300	243	8	3	-16	-219	37	10	3	3	294	281	11	3	-9	-221	120
6	3	-19	153	154	7	3	-16	-235	-80	8	3	-17	216	180	10	3	4	-181	29	11	3	-10	-215	21
7	3	0	-210	54	7	3	-17	213	168	9	3	0	237	-187	10	3	-1	-239	130	11	3	-11	230	197
7	3	1	442	457	8	3	0	352	-333	9	3	1	-241	174	10	3	-2	-241	-104	11	3	-12	-195	-31
7	3	2	-217	-74	8	3	1	508	504	9	3	2	-242	-63	10	3	-3	410	367	11	3	-13	190	186
7	3	3	597	594	8	3	2	-230	-195	9	3	3	268	265	10	3	-4	-241	-71	12	3	-1	167	225
7	3	4	-225	-36	8	3	3	-236	190	9	3	4	-232	-22	10	3	-5	352	305	12	3	-2	-148	-118
7	3	5	231	247	8	3	4	-241	-128	9	3	5	315	282	10	3	-6	242	-137	12	3	-3	179	203
7	3	6	-239	11	8	3	5	242	228	9	3	6	-194	51	10	3	-7	242	151	12	3	-4	168	-133
7	3	7	307	297	8	3	6	-236	20	9	3	-1	405	377	10	3	-8	242	-117	12	3	-5	-173	102
7	3	8	-236	-14	8	3	7	304	278	9	3	-2	337	-311	10	3	-9	353	285	12	3	-6	-176	-39
7	3	9	278	277	8	3	8	-198	-18	9	3	-3	396	362	10	3	-10	256	-171	12	3	-7	177	178
7	3	10	-191	-55	8	3	-1	456	440	9	3	-4	-228	-122	10	3	-11	336	295	12	3	-8	-175	31
7	3	-1	320	326	8	3	-2	218	-204	9	3	-5	227	189	10	3	-12	-231	-64	12	3	-9	190	186
																				12	3	-10	-162	76

in a centre of symmetry, does not contribute to reflections with $k+l$ odd. With phases based on the tellurium contributions alone, the first three-dimensional Fourier map was calculated for reflections with $k+l$ even. The map had extra symmetry because of the omission of the $k+l$ odd reflections. A set of coordinates for one sulphur atom was picked out arbitrarily among six peaks. On inclusion of some $k+l$ odd reflections, subsequent maps permitted the coordinates of the two remaining sulphur atoms to be determined. It turned out to be difficult to locate the light atoms from three-dimensional Fourier maps, probably because of an insufficient amount of data. It was, however, possible to determine the light atom coordinates from two-dimensional Fourier maps along the a and b axes.

Three-dimensional least squares refinement on scale factors, positional parameters and individual isotropic thermal parameters resulted in an R value of 0.096. Further refinement, where scale factors were not varied, and anisotropic thermal parameters for the tellurium and sulphur atoms were introduced, lowered the R value to 0.083.

Extinction corrections were then carried out, using the expression given by Zachariasen.[8] The absorption term in this expression was set equal to one. With observed intensities on an absolute scale, the value of the extinction parameter, C, was found to be 3.12×10^{-6} for the crystal rotating about the a axis, and 0.76×10^{-6} for the crystal rotating about the b axis.

After introduction of an overall scale factor, the refinement was continued until to parameter shift was greater than 0.18 times the standard deviation. The value of the constant a_1 in the weighting scheme was kept equal to one during the last refinement cycles. The final value of R, including non-observed reflections when $K|F_c|$ exceeded the observable limit, was 0.075. A three-dimensional difference Fourier summation after the last cycle showed no peaks higher than 0.8 e/Å^3.

The final atomic coordinates and isotropic thermal parameters are listed in Table 1, and the final anisotropic thermal parameters for the tellurium and sulphur atoms are listed in Table 2. Observed and calculated structure factors are listed in Table 3.

RESULTS

The reflectance spectrum of the complex of tellurium dibenzenethiosulphonate with tetramethylthiourea, $Te(tmtu)_2(S_2O_2C_6H_5)_2$, is shown in Fig. 1. The spectra of the corresponding trimethylenethiourea complex, $Te(trtu)_2(S_2O_2C_6H_5)_2$, and the ethylenethiourea complex, $Te(etu)_2(S_2O_2C_6H_5)_2$, have been included in Fig. 1 for comparison.

Bond lengths and angles are listed in Table 4. The standard deviations are calculated from those of Table 2, without regard to coordinate covariances and standard deviations in unit cell dimensions. Fig. 2 is a drawing of the molecule, with selected bond lengths and angles.

The tellurium atom is bonded to two tetramethylthiourea sulphur atoms and two benzenethiosulphonate sulphur atoms. With the tellu-

Table 4. Bond lengths (Å) and angles (°). Standard deviations in parentheses.

TeS_4 coordination group			
Te – S(1)	= 2.724(6)	∠S(1) – Te – S(2)	= 79.51(15)
Te – S(2)	= 2.657(4)		
Benzenethiosulphonate group			
S(2) – S(3)	= 2.025(6)	∠Te – S(2) – S(3)	= 104.7(3)
S(3) – O(1)	= 1.430(18)	∠S(2) – S(3) – O(1)	= 111.1(6)
S(3) – O(2)	= 1.436(13)	∠S(2) – S(3) – O(2)	= 107.0(6)
S(3) – C(6)	= 1.776(19)	∠S(2) – S(3) – C(6)	= 105.5(6)
C(6) – C(7)	= 1.444(28)	∠O(1) – S(3) – O(2)	= 117.8(9)
C(7) – C(8)	= 1.430(32)	∠O(1) – S(3) – C(6)	= 107.8(10)
C(8) – C(9)	= 1.366(35)	∠O(2) – S(3) – C(6)	= 106.9(8)
C(9) – C(10)	= 1.395(32)	∠S(3) – C(6) – C(7)	= 116.4(15)
C(10) – C(11)	= 1.383(31)	∠S(3) – C(6) – C(11)	= 119.6(14)
C(11) – C(6)	= 1.399(30)	∠C(11) – C(6) – C(7)	= 124.0(17)
		∠C(6) – C(7) – C(8)	= 115.6(19)
		∠C(7) – C(8) – C(9)	= 119.4(22)
		∠C(8) – C(9) – C(10)	= 123.5(22)
		∠C(9) – C(10) – C(11)	= 120.2(22)
		∠C(10) – C(11) – C(6)	= 117.3(19)
Tetramethylthiourea group			
S(1) – C(1)	= 1.696(16)	∠Te – S(1) – C(1)	= 108.8(8)
C(1) – N(1)	= 1.356(23)	∠S(1) – C(1) – N(1)	= 119.7(12)
C(1) – N(2)	= 1.329(22)	∠S(1) – C(1) – N(2)	= 121.2(13)
N(1) – C(2)	= 1.485(23)	∠C(1) – N(1) – C(2)	= 123.8(12)
N(1) – C(3)	= 1.489(22)	∠C(1) – N(1) – C(3)	= 123.5(13)
N(2) – C(4)	= 1.468(22)	∠C(1) – N(2) – C(4)	= 119.3(15)
N(2) – C(5)	= 1.466(27)	∠C(1) – N(2) – C(5)	= 124.3(14)
		∠C(2) – N(1) – C(3)	= 111.2(15)
		∠C(4) – N(2) – C(5)	= 115.8(15)
		∠N(1) – C(1) – N(2)	= 118.6(14)

rium atom in a centre of symmetry, the TeS_4 coordination is *trans* square-planar. There is a marked difference between the Te – S (benzenethiosulphonate) bond length and the Te – S-(tetramethylthiourea) bond length, the latter being the longer. As is seen in Table 5, a similar tendency has been observed for the corresponding trimethylenethiourea complex and the ethylenethiourea complex. The Te – S bond lengths do not differ much from the average values, 2.68 Å, found for Te – S bond lengths in *trans* square-planar complex of divalent tellurium.[9] There is, however, a striking difference between the present complex and the other complexes of Table 5, inasmuch as the S – Te – S angle in the former differs with about 10° from the corresponding values in the others. As the present complex is the only red one among the otherwise yellow complexes of Table 5, one is tempted to conclude that the "abnormal" colour of the former is associated with the large deviation from 90° of the bond angles at tellurium. A simple explanation of the tellurium-ligand bonds in square-planar complexes of divalent tellurium is provided by the three-centre, two-electron-

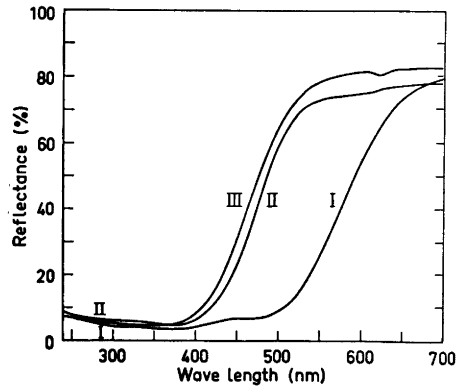

Fig. 1. Visible and ultraviolet reflectance spectra of solid $Te(tmtu)_2(S_2O_2C_6H_5)_2$ (I), $Te(trtu)_2(S_2O_2C_6H_5)_2$ (II), and $Te(etu)_2(S_2O_2C_6H_5)_2$ (III), with MgO as a white standard of 100 % reflectance.

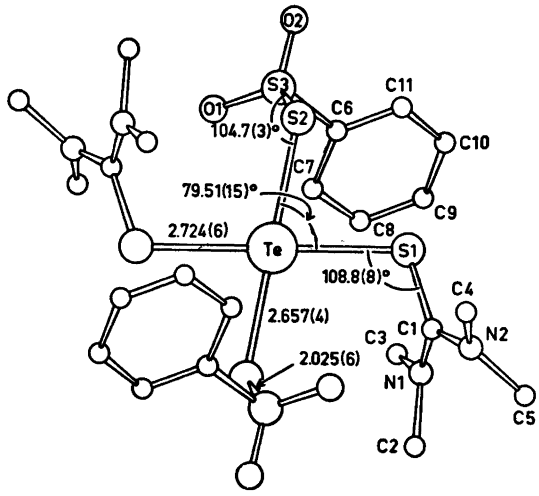

Fig. 2. trans-Dibenzenethiosulphonatobis(tetramethylthiourea)tellurium(II) as seen normal to the plane of the TeS_4 coordination group.

pair bonding scheme, based on tellurium 5*p* orbitals. This would imply a S – Te – S angle of 90°. The observed value, 79.51(15)°, which probably is the result of the steric requirements of the rather bulky ligands, does not fit as well into this picture as is normally the case. Nevertheless, the tellurium-sulphur bond lengths indicate that these bonds are essentially of the same kind as in other square-planar complexes of divalent tellurium.

The benzenethiosulphonate S – S bond length is in good agreement with the corresponding bond lengths in the other complexes of Table 5. Bond lengths and angles between light atoms are in the normal range. With the sulphur coordinates given three times the weight of the carbon and nitrogen coordinates, the atoms of a least squares plane through S(3) and the benzene ring deviate 0.000 – 0.017 Å from the plane. The atoms of a least squares plane through the thiourea part of the tetramethylthiourea group deviate 0.004 – 0.047 Å from the plane. The angle between the latter plane and a plane through the TeS_4 coordination group is 61.0°. The methyl carbon atoms, C(2), C(3), C(4), and C(5) are −0.554, 0.364, −0.492, and 0.742 Å, respectively, distant from the plane through the thiourea part of the tetramethylthiourea group. This plane makes an angle of 22.1° with a least squares plane through N(1) and the carbon atoms bonded to N(1), and an angle of 30.1° with a least squares plane through N(2) and the carbon atoms bonded to N(2).

The steric requirements of the ligands lead to short non-bonding, intramolecular distances. (A prime denotes an atom generated by the centre of symmetry). The distances S(2) – C(2′) = 3.747 Å, S(2) – C(3′) = 3.779 Å, O(1) – C(1′) = 3.189 Å, and O(1) – C(4′) = 3.145 Å imply that the S(1′) – Te – S(2) angle, which is 100.49°, can hardly be decreased without a reorientation of the ligands. As will be seen from Fig. 2, the

Table 5. Principal bond lengths (Å) and angles (°) in complexes of tellurium dibenzenethiosulphonate with thioureas. Standard deviations in parentheses.

Complex	Reference	Te – S (thiosulphonate)	Te – S (thioureas)	∠S – Te – S	S – S
$Te(tmtu)_2(S_2O_2C_6H_5)_2$	Present	2.657(4)	2.724(6)	79.51(15)	2.025(6)
$Te(trtu)_2(S_2O_2C_6H_5)_2$	3	2.668(3)	2.691(4)	88.85(9)	2.018(4)
$Te(etu)_2(S_2O_2C_6H_5)_2$	4	2.686(4)	2.713(5)	90.80(13)	2.016(5)

area around the tellurium atom is rather crowded. In addition to the distances just mentioned, some other, short distances within the molecule are: Te – C(3) = 3.968 Å, Te – C(6) = 3.971 Å, Te – C(7) = 3.894 Å, S(2) – C(11) = 3.659 Å, O(1) – C(7) = 2.888 Å, O(2) = C(11) – 2.992 Å, C(3) – C(8) = 3.592 Å. No intermolecular distances are essentially shorter than the sum of the appropriate van der Waals radii.[10] It may therefore be concluded that the deviation of the S – Te – S angle from 90° is caused mainly by strain within the molecule, and not by crystal packing effects.

Acknowledgement. We thank Professor Olav Foss for supplying the crystals. One of us (K. Å.) is indebted to *Norges Almenvitenskapelige Forskningsråd* for financial support.

REFERENCES

1. Foss, O. and Johannessen, I.-J. *Acta Chem. Scand. 15* (1961) 1943.
2. Foss, O., Marøy, K. and Husebye, S. *Acta Chem. Scand. 19* (1965) 2361.
3. Åse, K. *Acta Chem. Scand. 23* (1969) 3206.
4. Åse, K., Maartmann-Moe, K. and Solheim, J. O. *Acta Chem. Scand. 25* (1971) 2467.
5. *International Tables for X-Ray Crystallography*, Kynoch Press, Birmingham 1962, Vol. III, p. 122.
6. Busing, W. R. and Levy, A. H. *Acta Crystallogr. 10* (1957) 180.
7. Cromer, D. T. *Acta Crystallogr. 18* (1965) 17.
8. Zachariasen, W. H. *Acta Crystallogr. 16* (1963) 1139.
9. Foss, O. In Andersen, P., Bastiansen, O. and Furberg, S., Eds., *Selected Topics in Structure Chemistry*, Universitetsforlaget, Oslo 1967, p. 145.
10. Pauling, L. *The Nature of the Chemical Bond*, 3rd Ed., Cornell University Press, Ithaca, New York 1960.

Received July 13, 1973.

Acta Chemica Scandinavica A 28 (1974) 113—124

Short Communications

Force Field of Ethylthiocyanate*

ALF BJØRSETH**

Department of Chemistry and Center for Structural Studies, The University of Texas at Austin, Austin, Texas 78712, U.S.A.

The vibrational spectra and conformation of ethylthiocyanate have been of interest to several research groups during the last years. A thorough analysis of the vibrational spectrum was done by Hirschman *et al.*,[1] who interpreted the spectrum on the basis of two rotational isomers, *anti* (with C_s symmetry) and *gauche* (C_1 symmetry). The *anti*-form was found to be the more stable. Crowder [2] calculated a force field which reproduces most of the observed frequencies, based on the *anti*-conformation. From a recent microwave investigation [3] of ethylthiocyanate, however, it was concluded that the *gauche* form was the more stable, and no lines originating from the *anti* conformer were assigned. This led to a reinvestigation [4] of the IR-spectrum in the solid (crystalline and amorphous), liquid, and vapour phase and the liquid Raman spectrum. This work concludes that all bands in all states can be ascribed to one isomer only, and that the polarization data and vapor phase contours indicate that this rotamer is the *gauche* isomer. In the present communication the determination of the force field based on the *gauche* conformation is reported.

Method of calculation. The normal coordinate program used in this work is described by Gwinn.[5] In this program mass weighted cartesian coordinates are used and rotation and translation are not separated until the matrix diagonalization is performed. The **V** matrix is generated numerically and only one transformation, from cartesian to normal coordinates, is involved.

In the initial calculations a valence force field

$$\mathbf{V} = \tfrac{1}{2}\sum K_{ij}(\Delta r_{ij})^2 + \tfrac{1}{2}\sum H_{ijk}(\Delta\phi_{ijk})^2 + \tfrac{1}{2}\sum Y_{ijkl}(\Delta t_{ijkl})^2$$

was used, where the diagonal force constants K, H, and Y represent stretching, bending, and torsion, respectively. In many cases, redundant internal coordinates are used, *i.e.* the three H_{CCH} and three H_{HCH} of the methyl group. During the transformation to the basis of cartesian displacement coordinates these redundancies are removed automatically. Likewise, the torsional force constant is read for all H C C H combinations in the ethyl group, *i.e.* $9Y_{HCCH}$ force constants (with the same value). To improve the agreement between observed and calculated frequencies it was found necessary to introduce interaction constants, defined as F^1 for interaction between two stretching force constants, F^2 between stretching and bending, and F^3 between two bending force constants. The structure of the molecule was taken from the microwave work.[3]

Table 1. Force constants of CH_3CH_2SCN.

Force constant	Value[a]
$K_{C\equiv N}$	16.73
$K_{S-C\equiv}$	3.72
K_{CS}	2.65
K_{CH}	4.73
K_{CC}	4.70
H_{SCN}	0.392
H'_{SCN}	0.369
H_{CSC}	0.68
H_{SCC}	1.16
H_{SCH}	0.66
$H_{CCH}(CH_2)$	0.56
$H_{CCH}(CH_3)$	0.66
$H_{HCH}(CH_2)$	0.50
$H_{HCH}(CH_3)$	0.54
Y_{SC}[b]	0.02
Y_{CC}	0.0114
$F^1{}_{CH,CH}(CH_2)$	0.10
$F^1{}_{CS,SC}$	0.30
$F^2{}_{CC,CCH}(CH_3)$	0.51
$F^2{}_{SC,SCH}$	0.35
$F^3{}_{SCH,SCH}$	−0.125
$F^3{}_{HCH,HCH}(CH_3)$	0.015
$F^3{}_{SCH,CCH}(CH_2)$	−0.015

[a]Units are mdyn/Å for K and F^1, mdyn for F^2 and mdynÅ for H, Y, F^3. [b]Transferred from Ref. 8.

*This research has been supported by a grant from the Robert A. Welch Foundation.

**Permanent address: Department of Chemistry, University of Oslo, Oslo 3, Norway.

Results and discussion. The force field defined above is very convenient from a practical point of view since force constants can be transferred between similar molecules.[6] For simplicity the force field of methylthiocyanate was calculated first. The results are in good agreement with those previously published by Crowder [2] and Lett and Flygare.[7] The force field of ethylthiocyanate is listed in Table 1. The force constants are quite similar to those of methylthiocyanate and of thioalkanes.[8] The calculated and observed frequencies are listed in Table 2 together with an approximate description of the vibrations. With a few exceptions, the assignments are the same as reported in Ref. (4). The bands at 453 and 394 cm^{-1} were assigned to C–C–S bend and the bands at 326 and 308 cm^{-1} as S–C≡N bend. The calculations clearly indicate that the S–C≡N bending vibrations are the ones previously assigned as C–C–S bend (453 and 394 cm^{-1}) and that the C–C–S bend is at 326 cm^{-1}. This is more in accordance with the assignment of the corresponding vibrations in methylthiocyanate, where the two S–C≡N bending vibrations are 460 and 389 cm^{-1}.[9,10] In $CH_3CH_2SCH_3$ [11] the CCS vibration is observed at 335 cm^{-1}, which also is in agreement with the reassignment of these vibrations. Using the force constants found for the C–S torsion reported for several thioalkanes,[6] this vibration was calculated to be 72 cm^{-1}, in accordance with the value calculated by Ohsaku *et al.*[11] for the C–S torsion in $CH_3CH_2-SCH_3$. Only one vibration was observed below 200 cm^{-1}, the CSC bend at 149 cm^{-1}. Although it is not very likely, it is possible that there is an overlap of the C–S torsion and the CSC bending at this frequency. The possibility also exists that, despite the thorough studies both in infrafred and Raman, the lowest fundamental vibration is still not observed.

Table 2. Observed and calculated frequencies and approximate description of vibratons in CH_3CH_2SCN.

Observed[a] (cm^{-1})	Calculated (cm^{-1})	Approximate description
2999	2999.1	CH_3 asym. str.
2984	2988.7	CH_3 asym. str.
2948	2961.2	CH_2 asym. str.
2946[b]	2949.5	CH_2 sym. str.
2888	2880.3	CH_3 sym. str.
2170	2170.1	CN str.
1456	1463.1	CH_3 scissor
1456	1451.4	CH_3 scissor
1434	1436.9	CH_2 scissor
1389	1386.2	CH_3 sym. def.
1283	1272.6	CH_2 wag
1244[b]	1248.1	CH_2 twist
1066	1058.2	CH_3 rock
1049[b]	1046.2	CH_3 rock
971	971.8	CC str.
774	793.6	CH_2 rock
675	685.4	CS str.
640	640.8	SC≡ str.
453[c]	453.0	SCN bend
394	393.8	SCN bend
326	323.6	CCS bend
249[b]	249.8	CH_3 torsion
149	149.9	CSC bend
–	72.2[d]	C–S torsion

[a]Observed frequencies taken from Ref. 4. Unless marked, IR vapour phase values. [b]Liquid IR value. [c]Liquid Raman value. [d]This calculated frequency depends mainly on the transferred force constant value for Y_{SC}.

Acknowledgement. Professor J. E. Boggs and his coworkers at The Center for Structural Studies are thanked for several helpful discussions during the course of this work. Stan McNeme is thanked for doing some of the calculations in this work.

1. Hirschmann, R. P., Knisley, R. N. and Fassel, V. A. *Spectrochim. Acta. 20* (1964) 809.
2. Crowder, G. A. *J. Mol. Struct. 7* (1971) 147.
3. Bjørseth, A. and Marstokk, K.-M. *J. Mol. Struct. 11* (1972) 15.
4. Ellestad, O. H. and Torgrimsen, T. *J. Mol. Struct. 12* (1972) 79.
5. Gwinn, W. D. *J. Chem. Phys. 55* (1971) 477.
6. Shimanouchi, T. In Henderson, D., Ed., *Physical Chemistry, An Advanced Treatise*, Academic, New York 1970, Vol. IV, Chapter 6.
7. Lett, R. G. and Flygare, W. H. *J. Chem. Phys. 47* (1967) 4730.
8. Scott, D. W. and El-Sabban, M. Z. *J. Mol. Spectrosc. 30* (1969) 317.
9. Moritz, A. G. *Spectrochim. Acta. 22* (1966) 1021.
10. Crowder, G. A. *J. Mol. Spectrosc. 23* (1967) 108.
11. Ohsaku, M., Shiro, Y. and Murata, H. *Bull. Chem. Soc. Jap. 46* (1973) 1399.

Received November 15, 1973.

A Study of the Reaction between Germanium Dioxide and Concentrated Sulfuric Acid. A New Spectrophotometric Method for the Determination of the Stability Complexes of the Form AB_n and AD_p in Mixture

GUNNAR NORHEIM*

Chemical Institute A, University of Oslo, Blindern, Oslo 3, Norway

The reaction in concentrated sulfuric acid between germanium(IV) and 1,1'-dianthrimide has been described in two earlier papers.[1,2] The conditional constant of the 1:1 complex found present was determined. In these previous studies the solvation reaction of germanium dioxide was not considered since the concentration of the sulfuric acid and the hydrogen sulfate ion were maintained constant.

In the present paper the reaction between germanium(IV) and hydrogen sulfate is studied. The hydrogen sulfate ion concentration in concentrated sulfuric acid can be varied by varying the water content, and this possibility was utilized to determine the stability constants of the two germanium(IV) complexes with 1,1'-dianthrimide or hydrogen sulfate. A new spectrophotometric method for the simultaneous determination of the two stability constants is described.

Experimental. Standard solutions of germanium dioxide and 1,1'-dianthrimide in concentrated sulfuric acid were prepared as described in a previous paper.[2] The reaction mixtures were heated for 16 h at 70°C before the extinctions were measured in a Zeiss PMQII spectrophotometer at 660 nm. The conditional constant for the germanium(IV)-1,1-dianthrimide complex was determined from the spectrophotometric data for five different concentrations of the hydrogen sulfate ion. The Lang method [3,4] was used and optimum conditions [5] were chosen.

Theory. When a central atom A forms complexes with two different ligands B and D, the reactions are

$$A + nB = AB_n \quad (1)$$

$$A + pD = AD_p \quad (2)$$

and the stability constants are

$$K_1 = c_1/(a - c_1 - c_2)(b - nc_1)^n \quad (3)$$

$$K_2 = c_2/(a - c_1 - c_2)(d - pc_2)^p \quad (4)$$

where a, b, and d are the initial concentrations of A, B, and D, and c_1 and c_2 are the actual concentrations of the complexes AB_n and AD_p, respectively. The conditional constant for the AB_n complex is calculated from the following formula

$$K_{cal} = c_1/(a - c_1)(b - nc_1)^n \quad (5)$$

When D represents the solvent, D is in great excess. By introducing $(d - pc_2)^p \approx d^p$ in eqn. (4), the following relation can be set up

$$1/K_{cal} = K_2 d^p/K_1 + 1/K_1 \quad (6)$$

By determining K_{cal} for different concentrations of D, eqn. (6) gives a basis for the determination of K_1 and K_2. Eqn. (6) can be represented graphically with $1/K_{cal}$ as ordinate and d^p as abscissa, this giving a straight line.

The composition of the complex AB_n can be determined independent of the complex AD_p, if the latter is not too stable and c_1/a not too small. The composition of the complex AD_p can be determined from eqn. (6), because the curve representing this equation will be a straight line only for the correct value of p.

To demonstrate that the new method, represented by eqn. (6), gives correct values for K_1, K_2, and p it was tested with values for a, b, d, c_1, and c_2 calculated from eqns. (3) and (4) for given values of K_1 and K_2. These data were obtained in the following way.

Eqns. (7) and (8) can be rearranged to:

$$\left(1 - \frac{c_1}{a} - \frac{c_2}{a}\right)\left(\frac{b}{a} - n\frac{c_1}{a}\right)^n - \frac{c_1/a}{K_1 a^n} = 0 \quad (7)$$

$$\left(1 - \frac{c_1}{a} - \frac{c_2}{a}\right)\left(\frac{d}{a} - p\frac{c_2}{a}\right)^p - \frac{c_2/a}{K_2 a^p} = 0 \quad (8)$$

For $y_1 = c_1/a$, $y_2 = c_2/a$, $x_1 = b/a$, $x_2 = d/a$, $W_1 = 1/K_1 a^n$ and $W_2 = 1/K_2 a^p$ the eqns. (7) and (8) become

$$(1 - y_1 - y_2)(x_1 - ny_1)^n - y_1 W_1 = 0 \quad (9)$$

$$(1 - y_1 - y_2)(x_2 - py_2)^p - y_2 W_2 = 0 \quad (10)$$

For any given value of W_1, W_2, x_1 and x_2, y_1 and y_2 can be calculated.

These data were then used to calculate K_{cal}. In the calculations a was kept constant. Using eqn. (6) and the calculated values for K_{cal}, K_1 and K_2 were determined. The new method was tested on a series of combinations between K_1, K_2, n and p. These calculations gave a satisfactory result and the curves drawn were straight lines only for the correct value of p.

Results and discussion. When arsenic trioxide and selenium dioxide are dissolved in sulfuric acid, the ions AsO^+ and SeO_2H^+ are formed, respectively. These ions are in equilibria with hydrogen sulfate.[6,7]

$$AsO^+ + HSO_4^- \rightleftharpoons AsOHSO_4 \qquad K_{As} = 8.3 \quad (11)$$

$$SeO_2H^+ + HSO_4^- \rightleftharpoons SeO(OH)HSO_4 \qquad K_{Se} = 23 \quad (12)$$

At concentrations similar to those used for germanium dioxide in the present study, arsenic trioxide and selenium dioxide form very little polymeric ions.

In Table 1 the results of the determinations of the conditional constants for the germanium-

* Present address: Institute of Forensic Medicine, University of Oslo, Rikshospitalet, Oslo 1, Norway.

Table 1. The conditional constant for the germanium(IV)-1,1′-dianthrimide complex calculated for different mol concentrations of the hydrogen sulfate ion in concentrated sulfuric acid.

% H_2SO_4	86.4	89.8	93.2	95.8	97.2
C_{HSO_4}	11.4	9.4	6.8	4.3	2.8
K_{cal}	144	174	221	336	432

(IV)-1,1′-dianthrimide complex are presented. Curves were drawn from the data in Table 1 with $(C_{HSO_4^-})^p$ as ordinate and $1/K_{cal}$ as abscissa for $p=1$ and $p=2$. For $p=1$ the curve is a straight line, for $p=2$ the line is curved. This shows that one mol of hydrogen sulfate reacts with one mol of germanium dioxide. Using linear least squares analysis the two stability constants were calculated from the intercept on the ordinate axis and the slope of the line. The following reaction may be suggested:

$$GeO_2^+ + HSO_4^- \rightleftharpoons GeO(OH)HSO_4 \qquad K_1 = 0.7 \qquad (13)$$

As may be expected the stability constant for the reaction between germanium dioxide and hydrogen sulfate is less than the corresponding constants for arsenic trioxide and selenium dioxide. The 1:1 complex between selenium dioxide and 1,1′-dianthrimide has been studied both in concentrated sulfuric acid and in solid form.[8] This complex did not contain sulfur. The present study indicates a similar reaction for the germanium(IV) complex:

$$GeO_2H^+ + Di \rightleftharpoons GeO_2HDi^+ \qquad K_2 = 1.3 \times 10^3 \qquad (14)$$

Attempts to isolate the solid germanium(IV)-1,1′-dianthrimide complex failed.

1. Skaar, O. B. and Langmyhr, F. J. *Anal. Chim. Acta 21* (1959) 370.
2. Langmyhr, F. J. and Norheim, G. *Anal. Chim. Acta 41* (1968) 341.
3. Lang, R. P. *J. Amer. Chem. Soc. 84* (1962) 1185.
4. Norheim, G. *Acta Chem. Scand. 25* (1971) 987.
5. Norheim, G. *Acta Chem. Scand. 23* (1969) 2808.
6. Gillespie, R. J. and Robinson, E. A. *Can. J. Chem. 41* (1963) 450.
7. Flowers, R. H., Gillespie, R. J. and Robinson, E. A. *J. Inorg. Nucl. Chem. 9* (1959) 155.
8. Langmyhr, F. J. and Myhrstad, J. A. *Anal. Chim. Acta 35* (1966) 212.

Received October 12, 1973.

Über Kupferselenocyanate

ERIK SÖDERBÄCK

Chemisches Institut der Universität Uppsala, Box 531, S-751 21 Uppsala 1, Schweden

CuSeCN. Das CuSeCN ist von V. F. Toropova[1] dargestellt worden und zwar durch Einwirkung von KSeCN in Wasser auf Cu_2SO_4 oder $Cu_2S_2O_3$. Bevor diese Untersuchung mir bekannt war, hatte ich CuSeCN durch Reaktion von KSeCN mit einer Mischung von $CuSO_4$ und $Na_2S_2O_3$ dargestellt. Es bildet sich der Komplex $NaCuS_2O_3$, welcher dann anschliessend mit KSeCN reagiert. Um gute Ausbeuten zu erhalten, ist es notwendig, dass bei Reaktionsende kein Thiosulfat übrig ist. Es wurde deshalb das $CuSO_4$ mit nur *einem* Mol $Na_2S_2O_3$ versetzt. Die Bruttoreaktion ist:

$$Cu^{2+} + S_2O_3^{2-} + SeCN^- \rightarrow CuSeCN + 1/2\ S_4O_6^{2-}$$

Das CuSeCN wurde in etwa quantitativer Ausbeute erhalten und war von gräulich weisser Farbe. Es ist dem CuSCN äusserlich sehr ähnlich und wie dieses sehr schwerlöslich in Wasser. Es kann mit diesem ohne Selenabscheidung zum Kochen erhizt werden. Wie von Toropova beobachtet, löst sich CuSeCN in konzentrierten wässrigen Lösungen von KSeCN. Die Lösungen sind nicht stabil, sondern scheiden bald rotes Selen aus. Die Lösungen in KSCN sind jedoch, wie ich gefunden habe, stabiler.

$Cu(SeCN)_2$. Eine sehr alte Untersuchung über $Cu(SeCN)_2$ geht auf Sir William Crookes [2] zurück.* Mischt man eine Cu^{2+}-Lösung mit einer Lösung von KSeCN, entsteht nach diesem Autor zunächst ein brauner Niederschlag von $Cu(SeCN)_2$, der bald in schwarzes CuSe übergeht. Analytische Belege fehlen. Bei Wiederholen des Versuches von Crookes wurde eine Lösung von Cu^{2+}-Nitrat in Wasser zu einer solchen von KSeCN in äquivalenter Mengen getropft. Jeder Tropfen erzeugte einen hellbraunen Niederschlag, der sich beim Umschütteln mit der Mutterlange in einen ziegelroten verwandelte. Allmählich wurde die Farbe dunkler und war bei Reaktionsende dunkelbraun. Beim Stehen unter gelegentlichem Umschütteln wurde die Farbe schwarz. Nach etwa 12 Stunden Stehens in der Kälte wurde der feinkristalline Niederschlag abfiltriert, mehrmals mit Wasser gewaschen und im Vakuum über H_2SO_4 getrocknet. Sowohl qualitative wie quantitative Analysen zeigten, dass das schwarze Produkt nicht aus CuSe, sondern aus $Cu(SeCN)_2$ bestand. Das Salz ist in Wasser schwerlöslich und geht bei der Behandlung mit wässrigem Chlor oder Brom glatt in Lösung,

* Später ausgeführte Versuche von Bergstrom [3] und von Watkins und Schütt [4] führten zu nicht einheitlichen Produkten.

Table 1. The conditional constant for the germanium(IV)-1,1′-dianthrimide complex calculated for different mol concentrations of the hydrogen sulfate ion in concentrated sulfuric acid.

% H_2SO_4	86.4	89.8	93.2	95.8	97.2
C_{HSO_4}	11.4	9.4	6.8	4.3	2.8
K_{cal}	144	174	221	336	432

(IV)-1,1′-dianthrimide complex are presented. Curves were drawn from the data in Table 1 with $(C_{HSO_4^-})^p$ as ordinate and $1/K_{cal}$ as abscissa for $p=1$ and $p=2$. For $p=1$ the curve is a straight line, for $p=2$ the line is curved. This shows that one mol of hydrogen sulfate reacts with one mol of germanium dioxide. Using linear least squares analysis the two stability constants were calculated from the intercept on the ordinate axis and the slope of the line. The following reaction may be suggested:

$$GeO_2^+ + HSO_4^- \rightleftharpoons GeO(OH)HSO_4 \qquad K_1 = 0.7 \qquad (13)$$

As may be expected the stability constant for the reaction between germanium dioxide and hydrogen sulfate is less than the corresponding constants for arsenic trioxide and selenium dioxide. The 1:1 complex between selenium dioxide and 1,1′-dianthrimide has been studied both in concentrated sulfuric acid and in solid form.[8] This complex did not contain sulfur. The present study indicates a similar reaction for the germanium(IV) complex:

$$GeO_2H^+ + Di \rightleftharpoons GeO_2HDi^+ \qquad K_2 = 1.3 \times 10^3 \qquad (14)$$

Attempts to isolate the solid germanium(IV)-1,1′-dianthrimide complex failed.

1. Skaar, O. B. and Langmyhr, F. J. *Anal. Chim. Acta 21* (1959) 370.
2. Langmyhr, F. J. and Norheim, G. *Anal. Chim. Acta 41* (1968) 341.
3. Lang, R. P. *J. Amer. Chem. Soc. 84* (1962) 1185.
4. Norheim, G. *Acta Chem. Scand. 25* (1971) 987.
5. Norheim, G. *Acta Chem. Scand. 23* (1969) 2808.
6. Gillespie, R. J. and Robinson, E. A. *Can. J. Chem. 41* (1963) 450.
7. Flowers, R. H., Gillespie, R. J. and Robinson, E. A. *J. Inorg. Nucl. Chem. 9* (1959) 155.
8. Langmyhr, F. J. and Myhrstad, J. A. *Anal. Chim. Acta 35* (1966) 212.

Received October 12, 1973.

Über Kupferselenocyanate

ERIK SÖDERBÄCK

Chemisches Institut der Universität Uppsala, Box 531, S-751 21 Uppsala 1, Schweden

CuSeCN. Das CuSeCN ist von V. F. Toropova[1] dargestellt worden und zwar durch Einwirkung von KSeCN in Wasser auf Cu_2SO_4 oder $Cu_2S_2O_3$. Bevor diese Untersuchung mir bekannt war, hatte ich CuSeCN durch Reaktion von KSeCN mit einer Mischung von $CuSO_4$ und $Na_2S_2O_3$ dargestellt. Es bildet sich der Komplex $NaCuS_2O_3$, welcher dann anschliessend mit KSeCN reagiert. Um gute Ausbeuten zu erhalten, ist es notwendig, dass bei Reaktionsende kein Thiosulfat übrig ist. Es wurde deshalb das $CuSO_4$ mit nur *einem* Mol $Na_2S_2O_3$ versetzt. Die Bruttoreaktion ist:

$$Cu^{2+} + S_2O_3^{2-} + SeCN^- \rightarrow CuSeCN + 1/2\ S_4O_6^{2-}$$

Das CuSeCN wurde in etwa quantitativer Ausbeute erhalten und war von gräulich weisser Farbe. Es ist dem CuSCN äusserlich sehr ähnlich und wie dieses sehr schwerlöslich in Wasser. Es kann mit diesem ohne Selenabscheidung zum Kochen erhizt werden. Wie von Toropova beobachtet, löst sich CuSeCN in konzentrierten wässrigen Lösungen von KSeCN. Die Lösungen sind nicht stabil, sondern scheiden bald rotes Selen aus. Die Lösungen in KSCN sind jedoch, wie ich gefunden habe, stabiler.

$Cu(SeCN)_2$. Eine sehr alte Untersuchung über $Cu(SeCN)_2$ geht auf Sir William Crookes [2] zurück.* Mischt man eine Cu^{2+}-Lösung mit einer Lösung von KSeCN, entsteht nach diesem Autor zunächst ein brauner Niederschlag von $Cu(SeCN)_2$, der bald in schwarzes CuSe übergeht. Analytische Belege fehlen. Bei Wiederholen des Versuches von Crookes wurde eine Lösung von Cu^{2+}-Nitrat in Wasser zu einer solchen von KSeCN in äquivalenter Mengen getropft. Jeder Tropfen erzeugte einen hellbraunen Niederschlag, der sich beim Umschütteln mit der Mutterlange in einen ziegelroten verwandelte. Allmählich wurde die Farbe dunkler und war bei Reaktionsende dunkelbraun. Beim Stehen unter gelegentlichem Umschütteln wurde die Farbe schwarz. Nach etwa 12 Stunden Stehens in der Kälte wurde der feinkristalline Niederschlag abfiltriert, mehrmals mit Wasser gewaschen und im Vakuum über H_2SO_4 getrocknet. Sowohl qualitative wie quantitative Analysen zeigten, dass das schwarze Produkt nicht aus CuSe, sondern aus $Cu(SeCN)_2$ bestand. Das Salz ist in Wasser schwerlöslich und geht bei der Behandlung mit wässrigem Chlor oder Brom glatt in Lösung,

* Später ausgeführte Versuche von Bergstrom [3] und von Watkins und Schütt [4] führten zu nicht einheitlichen Produkten.

wobei sich reichlich Halogencyan entwickelt und das Selen in H_2SeO_3 oder H_2SeO_4 überführt wird. Diese Reaktion wurde zur quantitativen Bestimmung von Cu und Se verwendet. Wenn man beim obigen Versuch KSeCN in grösserem Überschuss, etwa dem Doppelten der äquivalenten Menge verwendet, bleibt die rote Farbe des Niederschlags bis zum Reaktionsende bestehen. Die rote Substanz wurde isoliert, mit Wasser gewaschen und im Vakuum getrocknet. Analysen zeigten, dass hier ein Komplexsalz $KCu(SeCN)_3$ vorlag. Mit Cu^{2+}-Salzen in Wasser behandelt, geht es in $Cu(SeCN)_2$ über. Bei Verwendung von $CuSO_4$ in etwa 5 %-igem Überschuss wurde eine praktisch quantitative Ausbeute an $Cu(SeCN)_2$ erhalten, und die durch H_2S vom Cu-Überschuss befreite Mutterlauge gab beim Einengen einen Rückstand, der als K_2SO_4 identifiziert wurde. Die Reaktion von $KCu(SeCN)_3$ mit Cu^{2+}-Salzen erklärt den Farbwechsel des Niederschlags bei Zutropfen von $Cu(NO_3)_2$ zu KSeCN. In ähnlicher Weise konnte aus RbSeCN und $Cu(NO_3)_2$ das analoge Rubidiumsalz dargestellt werden. Wenn bei der Reaktion von Cu^{2+}-Salz mit $SeCN^-$ im Überschuss statt KSeCN NaSeCN verwendet wird, ist auch dann der zunächst gebildete Niederschlag rot, allmählich wird aber die Farbe dunkler und ist bei Reaktionsende schwarz. Die Stabilität des Na-Komplexes ist offenbar geringer als die des K-Salzes.

Experimentelles. Das für die Synthesen gebrauchte KSeCN wurde nach der üblichen Methode aus Selenpulver und KCN dargestellt, die Wasserlösung auf dem Wasserbade eingetrocknet, der Rückstand in absolutem Äthanol aufgenommen und daraus umkristallisiert. Das NaSeCN wurde aus reinstem NaCN und Se in abs. Äthanol bereitet und aus der Lösung isoliert. Das Präparat reagierte alkalisch und löste sich nicht klar in Aceton und wurde deshalb aus diesem Lösungsmittel umgelöst.

Darstellung von CuSeCN. 5.0 g $CuSO_4.5H_2O$ wurden in 100 ml H_2O gelöst und mit 5,0 g $Na_2S_2O_3.5H_2O$ versetzt. Die grüne Lösung wurde mit Eis gekühlt und mit einer Lösung von 1,94 g KSeCN in H_2O in kleinen Portionen gemischt. Es entstand zunächst ein blauschwarzer Niederschlag, der beim Rühren weiss wurde. Das Gemisch blieb unter Eiskühlung etwa 20 Minuten stehen, wonach auf einem Glasfilter abfiltriert, mit Wasser, Alkohol und Äther gewaschen und im Vakuum getrocknet wurde. Ausbeute 2,43 g, gleich der theoretischen. Zur Analyse wurde mit Na_2S in Wasser umgesetzt, der Niederschlag von Cu_2S nach zweitägigem Stehen abfiltriert, mit Wasser, Alkohol und Äther gewaschen und in Vakuum getrocknet. Gef. Cu 37,67 %. Ber. für CuSeCN 37,66 %.

Darstellung von $Cu(SeCN)_2$. Zu einer Lösung von 4,32 g KSeCN in 25 ml H_2O wurde eine Lösung von 3,72 (theor. 3,62) g $Cu(NO_3)_2 3H_2O$ in 50 ml H_2O getropft. Nach etwa 12-stündigem Stehen in der Kälte wurde der Niederschlag abfiltriert, mit Wasser gewaschen und in Vakuum über H_2SO_4 getrocknet. Ausbeute 3,70 g (theoretisch 4,10) Zur Analyse wurde mit Brom in Wasser behandelt, die Lösung im schwachen Vakuum über konz. Natronlange bis zum Verschwinden von Br_2 und BrCN aufbewahrt. Aus der verdünnten grünen Lösung wurde Cu als CuO ausgefällt und als solches gewogen. Gef. Cu 23,82 %. Ber. für $Cu(SeCN)_2$ 23,24 %. Die Mutterlauge des CuO wurde mit konz. HCl angesäuert, mit SO_2-Wasser versetzt und nach tagelangem Stehen bei Zimmertemperatur auf dem Wasserbade erhitzt. Das schwarze Selen wurde isoliert, gewaschen, getrocknet und gewogen. Gef. Se 58,01 %. Ber. für $Cu(SeCN)_2$ 57,73 %. Das Salz wurde auch aus $Cu(NO_3)_2$. $3H_2O$ und NaSeCN in entsprechenden Proportionen und Konzentrationen dargestellt. Gef. Cu 23,74 %, Se 57,62 %.

Darstellung von $KCu(SeCN)_3$. 3,62 g $Cu(NO_3)_2$. $3H_2O$ in 50 ml H_2O wurden unter Eiskühlung zu einer ebenfalls gekühlten Lösung von 8,64 g KSeCN in 25 ml H_2O getropft. Das Reaktionsgemisch blieb unter Eiskühlung etwa 30 Minuten stehen, worauf der Niederschlag abfiltriert, mit eiskaltem Wasser gewaschen und in Vakuum über H_2SO_4 getrocknet wurde. Ausbeute 5,03 g (theoretisch 6,26 g). Das Präparat färbt sich beim Trocknen oberflächlich gräulich, die rote Farbe kommt beim Anfeuchten mit Wasser zurück, namentlich, wenn dieses eine Spur von Br_2 oder Cl_2 enthält. Die Cu- und Se-Analysen wurden wie beim $Cu(SeCN)_2$ ausgeführt. Gef. Cu 15,36; 14,82; Se 57,63. Ber. für $KCu(SeCN)_3$: Cu 15,22; Se 56,72.

1. Toropova, V. F. *Zh. Neorgan. Khim. 1* (1956) 243.
2. Crookes, W. *J. Chem. Soc. 4* (1852) 12.
3. Bergstrom, F. W. *J. Amer. Chem. Soc. 48* (1926) 2319.
4. Watkins, G. und Schütt, R. *Inorg. Syn. 2* (1941) 188.

Eingegangen am 28. November 1973.

Comment on Broadband Microwave Investigations on Monobromostyrenes

LISE NYGAARD

Chemical Laboratory V, University of Copenhagen, The H. C. Ørsted Institute, DK-2100 Copenhagen, Denmark

The recent paper [1] on the possible molecular structure of monobromostyrenes based on broadband microwave spectra can be read as a serious overinterpretation of the experimental data. As stated in eqn. (1) of Ref. 1, one piece of evidence is found in a broadband spectrum of each molecular species, *i.e.* the sum of the two rotational constants B and C. It is therefore not to be expected, that more than one structural parameter can be extracted from the experiments, or maybe a set of two or three strongly correlated parameters, assuming values for all other parameters.

Since bromobenzene and a few of its isotopic species have been investigated by high resolution microwave spectroscopy [2] (a tentative molecular structure of bromobenzene was only proposed), an improved data treatment would be to use the *moments of inertia* of bromobenzene as a starting point for the *m*- and *p*-bromostyrenes *without discussing the structure of the C_6H_4Br fragment* and try to extract some values for the vinyl group with structural assumptions for that part only. It should be remembered, however, that this rather qualitative procedure will result in a partial r_0-structure based on an insufficient amount of I_0-values, and that nothing can be said about a possible deformation of the benzene ring here (or in bromobenzene) without data from the spectra of the ^{13}C-species.

The structure of the vinyl group in styrene can be described by the following parameters, two CC bond lengths, three CH bond lengths, two CCC angles, and three CCH angles. The dihedral angle between the vinyl group and the benzene ring will be ignored, since the present experimental results can give no information of this detail. High resolution experiments are needed to determine the three rotational constants separately and find the inertial defect, as *e.g.* in the microwave spectrum of benzaldehyde,[3] which was shown to be planar.

Assuming vinyl parameters in accordance with the structure of the planar *trans*-form of 1,3-butadiene [4] (CH 1.09 Å, C=C 1.34 Å, and C=C−H 122°), trial values of the three parameters marked in Fig. 1 in the range $r = 1.49 \pm 0.03$ Å, $\alpha = 123° \pm 3°$, and $\beta = 122° \pm 2°$ all give a satisfactory fit within ±20 MHz of the measured (B+C)-value for *p*-^{79}Br-styrene. The (B+C)-difference for the two Br-species is reproduced exactly, but is only slightly dependent on the model.

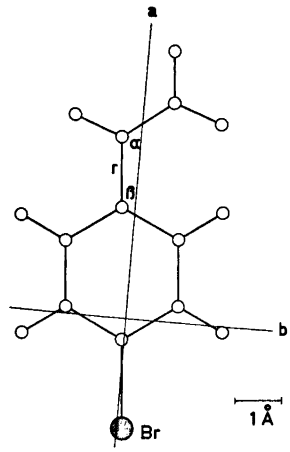

Fig. 1. Model of *p*-bromostyrene.

For *m*-^{79}Br-styrene a similar treatment shows that the assigned broadband spectrum is probably that of the *cis*-form, since the calculated (B+C)-value for the *trans*-form is about 150 MHz smaller, and the model variations are less than 30 MHz from the experimental B+C. The (B+C)-difference for the two Br-species is calculated to be 11.2 and 9.7 MHz for the *cis*- and the *trans*-form, respectively. A high resolution experiment is needed to decide the possible presence of the spectrum of the *trans*-form or a non-planar form.

For *trans*-*β*-bromostyrene model calculations with benzene as a starting point, assuming distances and angles for the vinyl part as shown above and using model values from *p*- and *m*-bromostyrene, agree with a C(vinyl)−Br distance of 1.87 ± 0.02 Å. This compares favourably with the electron diffraction result for this molecule [5] and for *cis*-1,2-dibromoethylene,[6] and with the microwave substitution structure of vinyl bromide.[7]

1. Ralowski, W., Wettermark, G. and Ljunggren, S. *Acta Chem. Scand. 27* (1973) 1565.
2. Rosenthal, E. and Dailey, B. P. *J. Chem. Phys. 43* (1965) 2093.
3. Kakar, R. K., Rinehart, E. A., Quade, C. R. and Kojima, T. *J. Chem. Phys. 52* (1970) 3803.
4. Kuchitsu, K., Fukuyama, T. and Morino, Y. *J. Mol. Struct. 1* (1967−68) 463.
5. Igarashi, M., Cho, S. and Someno, K. *Nippon Kagaka Zasshi 81* (1960) 23; *Chem. Abstr. 54* (1960) 12021 i.
6. Davis, M. I., Kappler, H. A. and Cowan, D. J. *J. Phys. Chem. 68* (1964) 2005.
7. De Kerckhove, V. D. *Ann. Soc. Sci. Bruxelles, Ser. 1 84* (1971) 277.

Received November 22, 1973.

On the Structures of Three Different Forms of Solid Cadmium Oxydiacetate Hydrate

CARL-ERIK BOMAN

Inorganic Chemistry 1, Chemical Center, University of Lund, P.O.B. 740, S-220 07 Lund, Sweden

Two monoclinic phases of cadmium oxydiacetate hydrate, in the following called CDOXY I and CDOXY II, are formed simultaneously when aqueous solutions of equimolar amounts of cadmium nitrate and disodium oxydiacetate are evaporated slowly at room temperature. From solutions of the same composition an orthorhombic phase, called CDOXY III, precipitates at slightly elevated temperatures. Table 1 shows some relevant data for the three structures.

Three-dimensional X-ray intensity data were collected for CDOXY I and CDOXY II using non-integrated Weissenberg photographs, and for CDOXY III by means of an automatic linear single crystal diffractometer of type PAILRED. In all three cases Cu$K\alpha$ radiation was used. The structure of CDOXY II is being reinvestigated by means of an automatic four-circle diffractometer of type CAD-4.

The positions of the cadmium atoms in the three structures were obtained from Patterson syntheses and the positions of the oxygen and carbon atoms could then be determined in the difference electron density maps. The structures were refined by least-squares methods to the R-values given in Table 1.

In the three cadmium oxydiacetate structures each cadmium atom is coordinated by seven oxygen atoms and the coordination polyhedra are somewhat distorted pentagonal bipyramids. The Cd – O distances, given in Tables 2 and 3, agree well with those published. A compilation of Cd – O distances in various cadmium compounds is given by Harrison and Trotter.[1]

In the unit cell of CDOXY I two cadmium atoms, denoted Cd(1) and Cd(2), two ligands and seven water molecules are independent. Each Cd(1) atom is joined by two ligands to two other Cd(1) atoms and in this way infinite zigzag chains parallel to the b-axis are formed. Each Cd(1) atom is also bound to a Cd(2) atom by an oxygen bridge, which means that the pentagonal bipyramids have one vertex in common. The structure thus consists of broad chains which are held together by hydrogen bonds *via* the water molecules. A part of the structure is shown in Fig. 1. Two ligands are bound to each cadmium atom; those coordinated by Cd(1) are tridentate and monodentate and those by Cd(2) are tridentate and bidentate. The bidentate ligand forms a carboxylate chelate with a bite of 2.20(3) Å.

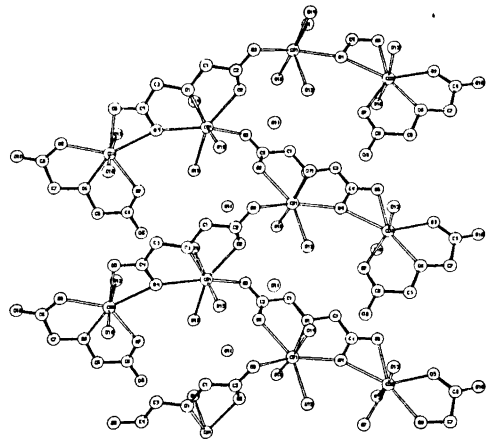

Fig. 1. Part of the structure of CDOXY I showing one of the broad chains parallel to the b-axis.

The structure of CDOXY II is composed of discrete units containing two cadmium atoms,

Table 1. Data for the three phases of cadmium oxydiacetate hydrate. (Oxy = $O(CH_2COO)_2^{2-}$)

Phase	CDOXY I	CDOXY II	CDOXY III
Formula	CdOxy.3½H_2O	CdOxy.3H_2O	CdOxy.3H_2O
Space group	$P2_1/c$	$P2_1/c$	$P2_12_12_1$
a/Å	7.3215(11)	6.3848(7)	7.3934(7)
b/Å	7.3012(8)	10.2093(9)	8.8955(10)
c/Å	37.1411(38)	14.0470(16)	13.3536(15)
β/°	90.673(11)	101.753(10)	–
Z	8	4	4
V/Å^3	1985.3	896.4	878.2
R-value	0.11	0.13	0.065
Number of independent reflexions	1800	800	550

Table 2. Coordination distances (Å) in CDOXY I with their estimated standard deviations. The oxygen atoms in one of the independent ligands are numbered 1 – 5 and in the other 6 – 10. The water oxygens are numbered 11 – 17. Oxygen atoms belonging to symmetry-related ligands are distinguished by the sign ′.

Cd(1) – O(15)	2.27(2)
Cd(1) – O(3)′	2.30(2)
Cd(1) – O(14)	2.30(2)
Cd(1) – O(12)	2.32(3)
Cd(1) – O(1)	2.38(2)
Cd(1) – O(2)	2.41(2)
Cd(1) – O(4)	2.41(2)
Cd(2) – O(9)	2.30(2)
Cd(2) – O(5)	2.31(2)
Cd(2) – O(6)	2.31(2)
Cd(2) – O(13)	2.31(2)
Cd(2) – O(7)	2.33(2)
Cd(2) – O(16)	2.35(2)
Cd(2) – O(4)	2.49(2)

Table 3. Coordination distances (Å) in CDOXY II and CDOXY III with their estimated standard deviations. The oxygen atoms in the ligand are numbered 1 – 5 and the water oxygens are numbered 6 – 8. Oxygen atoms belonging to different ligands are distinguished by the signs ′ and ″.

CDOXY II

Cd – O(6)	2.26(2)
Cd – O(1)	2.33(2)
Cd – O(8)	2.33(2)
Cd – O(2)	2.34(2)
Cd – O(4)′	2.34(2)
Cd – O(7)	2.36(2)
Cd – O(4)	2.45(2)

CDOXY III

Cd – O(5)	2.26(1)
Cd – O(2)′	2.30(1)
Cd – O(6)	2.31(1)
Cd – O(3)″	2.36(1)
Cd – O(7)	2.36(1)
Cd – O(1)′	2.47(1)
Cd – O(4)	2.63(1)

two ligands and six water molecules. In these units, which are almost planar, except for the four oxygen atoms at the apices of the pentagonal bipyramids, the two cadmium atoms are held together by two oxygen bridges. In this structure the pentagonal bipyramids share an edge in the pentagonal base. The structure is shown in Fig. 2. The separate units are

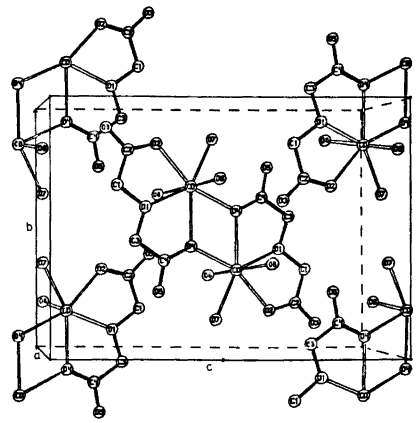

Fig. 2. The crystal structure of CDOXY II.

joined by hydrogen bonds *via* water molecules to a three-dimensional network. Two ligands are coordinated by each cadmium atom, one being tridentate and the other monodentate.

CDOXY III has a layer structure, which is shown in Fig. 3. The layers are held together

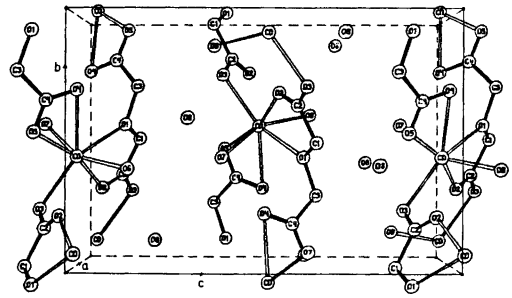

Fig. 3. The crystal structure of CDOXY III.

by an extensive hydrogen bond system in which the water molecules are involved. In this structure there are no oxygen bridges between cadmium atoms, the pentagonal bipyramids being linked up by the ligand. Three ligands are bound to each cadmium atom, two of which are bidentate and the third monodentate. One of the bidentate ligands forms a carboxylate chelate with a bite of 2.15(2) Å.

The oxydiacetate ion is planar in CDOXY II and almost planar in CDOXY I. In CDOXY III the two ligand halves about the ether oxygen are planar but form an angle of 85.5°. This was the first structure to be determined in which the oxydiacetate ion is not planar. It has later been found that this is also the case in the monoclinic phase of oxydiacetic acid.[2]

The three cadmium oxydiacetate hydrate structures can be compared with the structure of cadmium diacetate dihydrate, which has recently been determined.[1] In this compound the coordination about cadmium is also sevenfold although the coordination polyhedron is a square base-trigonal cap. Both acetate groups are bidentate forming carboxylate chelates and one oxygen is also in a bridging position in such a way that infinite cadmium-oxygen spirals are formed.

The cadmium oxydiacetate hydrate structures will be described in detail in forthcoming publications.

1. Harrison, W. and Trotter, J. *J. Chem. Soc. D* (1972) 956.
2. Herbertsson, H. and Boman, C.-E. *Acta Chem. Scand. 27* (1973) 2234.

Received October 29, 1973.

Titrimetric Determination of Acidity and pK Values of Humic Acid

OLE K. BORGGAARD

Royal Veterinary and Agricultural University, Department of Soils and Agricultural Chemistry, DK-1871 Copenhagen, Denmark

COOH and phenolic OH groups in humic acid are responsible for the cation exchange capacity and complexing ability of soil humic acid. Therefore, several methods have been proposed for the determination of the amounts (expressed as mequiv./g humic acid) of each of these groups.[1,2] The COOH content is normally estimated by the calcium acetate method or by decarboxylation and the phenolic OH is estimated as the difference between total acidity (determined by the $Ba(OH)_2$ method) and the COOH content.[1,2] As humic acid is a polyelectrolyte the individual carboxylic acids and phenols have different acid dissociation constants. These dissociation constants fall, however, in groups each associated with an average dissociation constant (denoted $p\bar{K}$).[3,4]

This note presents a titrimetric method for the estimation of the amounts of COOH and phenolic OH and the p$\bar{K}$ values of these groups in humic acid.

It has been shown that the titration of humic acid ought to be carried out as fast as a normal acid-base titration.[5] Therefore, it seems possible to determine the amounts of COOH and phenolic OH and the p$\bar{K}$ values from a simple titration. The inflection points of the titration curve are, however, blurred. This problem is overcome by differentiation of the titration curve.

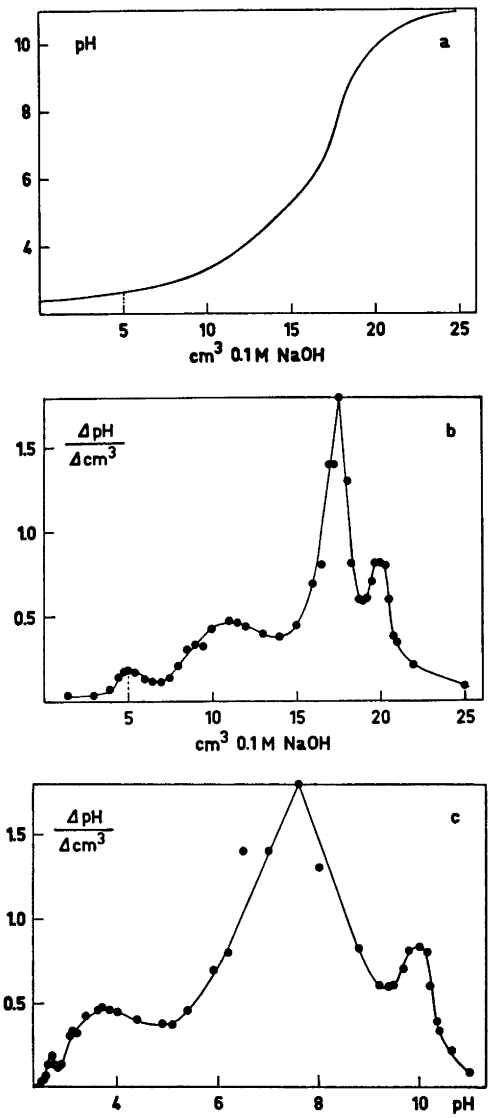

Fig. 1. The titration of 0.2 g Skarild A_1 humic acid. *a.* The original titration curve. *b.* ΔpH/Δcm³ plotted against cm³ 0.1 M NaOH. *c.* ΔpH/Δcm³ plotted against pH.

Humic acid from four soil samples were tested. The soils are described elsewhere [5] as is the extraction procedure. The titrations were

The three cadmium oxydiacetate hydrate structures can be compared with the structure of cadmium diacetate dihydrate, which has recently been determined.[1] In this compound the coordination about cadmium is also sevenfold although the coordination polyhedron is a square base-trigonal cap. Both acetate groups are bidentate forming carboxylate chelates and one oxygen is also in a bridging position in such a way that infinite cadmium-oxygen spirals are formed.

The cadmium oxydiacetate hydrate structures will be described in detail in forthcoming publications.

1. Harrison, W. and Trotter, J. *J. Chem. Soc. D* (1972) 956.
2. Herbertsson, H. and Boman, C.-E. *Acta Chem. Scand. 27* (1973) 2234.

Received October 29, 1973.

Titrimetric Determination of Acidity and pK Values of Humic Acid

OLE K. BORGGAARD

Royal Veterinary and Agricultural University, Department of Soils and Agricultural Chemistry, DK-1871 Copenhagen, Denmark

COOH and phenolic OH groups in humic acid are responsible for the cation exchange capacity and complexing ability of soil humic acid. Therefore, several methods have been proposed for the determination of the amounts (expressed as mequiv./g humic acid) of each of these groups.[1,2] The COOH content is normally estimated by the calcium acetate method or by decarboxylation and the phenolic OH is estimated as the difference between total acidity (determined by the $Ba(OH)_2$ method) and the COOH content.[1,2] As humic acid is a polyelectrolyte the individual carboxylic acids and phenols have different acid dissociation constants. These dissociation constants fall, however, in groups each associated with an average dissociation constant (denoted $p\bar{K}$).[3,4]

This note presents a titrimetric method for the estimation of the amounts of COOH and phenolic OH and the p$\bar{K}$ values of these groups in humic acid.

It has been shown that the titration of humic acid ought to be carried out as fast as a normal acid-base titration.[5] Therefore, it seems possible to determine the amounts of COOH and phenolic OH and the p$\bar{K}$ values from a simple titration. The inflection points of the titration curve are, however, blurred. This problem is overcome by differentiation of the titration curve.

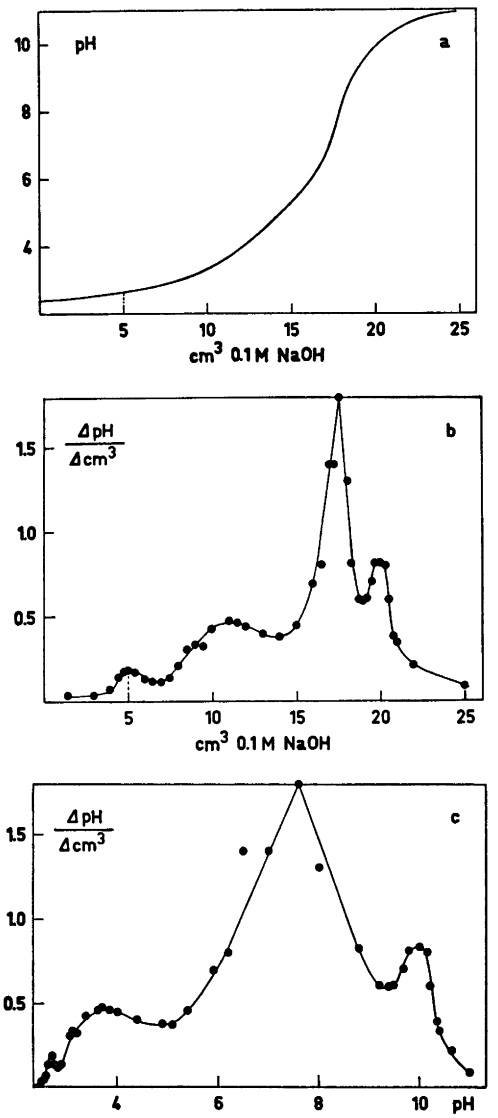

Fig. 1. The titration of 0.2 g Skarild A_1 humic acid. *a.* The original titration curve. *b.* ΔpH/Δcm³ plotted against cm³ 0.1 M NaOH. *c.* ΔpH/Δcm³ plotted against pH.

Humic acid from four soil samples were tested. The soils are described elsewhere [5] as is the extraction procedure. The titrations were

Table 1. The amounts of COOH and phenolic OH expressed as mequiv./g humic acid and the $p\bar{K}$ values for the four humic acids. Ionic strength 0.1 (NaCl). Values in brackets determined by the calcium acetate and $Ba(OH)_2$ methods.

Humic acid	mequiv. per g humic acid				$p\bar{K}$ values		
	COOH Type I	COOH Type II	Total COOH Type 1 + Type II	Phenolic OH	$p\bar{K}_1$	$p\bar{K}_2$	$p\bar{K}_3$
Skarild A_1	2.8 ± 0.1[a]	3.6 ± 0.1	6.4 (6.2)	1.2 ± 0.2 (1.4)	2.8 ± 0.2	5.1 ± 0.2	9.4 ± 0.3
Skarild B_h	2.6 ± 0.1	3.9 ± 0.1	6.5 (6.6)	1.4 ± 0.1 (1.3)	3.0 ± 0.3	5.1 ± 0.2	9.5 ± 0.3
Sdr. Vissing	3.0 ± 0.1	4.2 ± 0.1	7.2	1.7 ± 0.1	2.8 ± 0.2	5.0 ± 0.3	9.7 ± 0.4
Stavning	1.5 ± 0.1	2.7 ± 0.1	4.2 (4.4)	1.1 ± 0.1 1.2)	3.4 ± 0.2	4.9 ± 0.1	9.6 ± 0.2

[a] The figures are the mean values and the standard deviations calculated from at least five titrations.

carried out in the following way: Dried humic acid was dissolved in NaOH solution under CO_2- and O_2-free N_2. This solution was either titrated with 0.1 M HCl or it was mixed with HCl in excess and titrated with 0.1 M NaOH. No hysteresis occurred between the titration curves. The titrations were carried out by means of an automatic titration equipment (Radiometer SBR 2, TTT 11, ABU 11, and PHM 26). From the titration curves the $\Delta pH/\Delta cm^3$ values were calculated. In order to check the accuracy of the method EDTA and a mixture of acetic acid and NH_4Cl were titrated. The number of milliequivalents calculated from the titration curves agreed within ± 0.5 % with the theoretical values and the pK_A values obtained agreed within ± 0.05 with the literature.[6]

Fig. 1 a shows the original titration curve of Skarild A_1 humic acid; part of the acidity (indicated by the dotted line) was due to free hydrochloric acid. In Fig. 1b $\Delta pH/\Delta cm^3$ is plotted against cm^3 0.1 M NaOH. In Fig. 1c $\Delta pH/\Delta cm^3$ is plotted against pH. The maxima correspond to equivalence points while the minima correspond to $p\bar{K}$ values. As seen from Fig. 1 there are three equivalence points and three $p\bar{K}$ values. The first two correspond to two types of carboxyl groups: Type I is probably COOH on aromatic rings *ortho* to phenolic OH groups and Type II more weakly acidic carboxyl.[4] The third equivalence point corresponds to phenolic OH. Table 1 gives the number of mequiv./g humic acid and the $p\bar{K}$ values of the three groups in the four humic acids. The figures in brackets are determined by the calcium acetate and the $Ba(OH)_2$ methods and they are in good agreement with the values found by the titration procedure proposed here.

The carboxyl content (mequiv. Type I + mequiv. Type II) is greater than normally found [1,7] but this is certainly due to the extraction procedure which gives more oxidized humic acid than the NaOH extraction procedure.[5] On the other hand the content of phenolic OH is less than the phenolic OH content in humic acid extracted by NaOH [1,7] but in good agreement with that found in pyrophosphate extracted humic acid.[8]

The $p\bar{K}$ values given in Table 1 agree with those presented in the literature.[4,8,9] In spite of the fact, that the $p\bar{K}$ values depend on the degree of dissociation,[4] they are important in the characterization of humic acids extracted from different soils and by different methods.

From the data presented it is concluded, that the proposed titration procedure is a simple and rapid method for the determination of the COOH and phenolic OH content and the average dissociation constants of humic acid. These data are valuable in the characterization of soil humic acid.

1. Schnitzer, M. and Gupta, U. C. *Soil Sci. Soc. Amer. Proc. 29* (1965) 274.
2. Wright, J. R. and Schnitzer, M. *7. Int. Congr. Soil Sci., Trans. II* (1960) 120.
3. Posner, A. M. *8. Int. Congr. Soil Sci., Comm. II* (1964) 161.
4. Gamble, D. S. *Can. J. Chem. 48* (1970) 2662.
5. Borggaard, O. K. *To be published.*
6. Sillén, L. G. and Martell, A. E. *Stability Constants*, 2nd Ed., Special Publication No. 17, The Chemical Society, London 1964.
7. Dormaar, J. F. *Can. J. Soil Sci. 52* (1972) 67.
8. Stevenson, F. J., Krastanov, S. A. and Ardakani, M. S. *Geoderma 9* (1973) 129.
9. Khanna, S. S. and Stevenson, F. J. *Soil Sci. 93* (1962) 298.

Received October 5, 1973.

Unit Cell Dimensions of CeP_2 and PrP_2

EIVIND HASSLER, TORSTEN JOHNSSON and STIG RUNDQVIST

Institute of Chemistry, University of Uppsala, Box 531, S-751 21 Uppsala 1, Sweden

An X-ray crystallographic investigation of rare earth metal phosphides has been started at this institute. In the present paper, X-ray powder diffraction data are given for CeP_2 and PrP_2. These compounds are found to be isostructural, and belong to the $NdAs_2$ structure type,[1] which also includes $LaAs_2$ (below 750°C), $CeAs_2$ and $PrAs_2$. The existence of these diphosphides has earlier been discussed in the literature. By X-ray investigations Olcese [2] has shown the occurrence of CeP_2. Schmid and Hahn,[3] who have studied the system Ce-P report a phase, which probably is CeP_2. The occurrence of PrP_2 has been suggested by Franceschi and Olcese,[4] but unsuccessful attempts to prepare PrP_2 have also been reported.[5]

The starting materials for the preparations were a cerium metal ingot (Koch-Light Laboratories, Ltd., claimed purity 99.95 %), a praseodymium metal ingot (Rare Earth Products, Ltd., claimed purity 99.9 %) and red phosphorus of purity higher than 99 %. Powders of the metals were prepared by filing, fragments of the file being removed from the powders by a magnet. Appropriate amounts of the metals and phosphorus were thoroughly mixed and transferred to silica ampoules. All the above mentioned operations were performed in an argon-filled glove box. The silica ampoules were evacuated, sealed off and heated for various periods of time at temperatures below 1000°C.

Praseodymium diphosphide was obtained by heating a mixture of the elements for a week at 750°C. Cerium diphosphide has also been obtained by direct reaction between the elements. The sample used for the cell dimension determination was, however, prepared by heating arc-melted monophosphide and red phosphorus

Table 1. Powder diffraction data for CeP_2 and PrP_2. Hägg-Guinier camera (Philips XDC 700) with $CrK\alpha_1$ radiation.

h k l	CeP_2 $\sin^2\theta \times 10^5$ obs	CeP_2 $\sin^2\theta \times 10^5$ calc	CeP_2 d calc	CeP_2 I obs	PrP_2 $\sin^2\theta \times 10^5$ obs	PrP_2 $\sin^2\theta \times 10^5$ calc	PrP_2 d calc	PrP_2 I obs
0 0 1		1370	9.7808		1316	1385	9.7277	w-
0 1 0		3025	6.5826			3050	6.5553	
0 1 1	4383	4395	5.4610	w+	4433	4435	5.4362	w+
0 0 2	5462	5480	4.8904	w-	5533	5540	4.8638	w-
-1 0 1		8079	4.0277			8207	3.9961	
0 1 2	8494	8505	3.9256	s-	8590	8590	3.9061	s-
1 0 0	8550	8561	3.9128	w+	8703	8701	3.8811	m
-1 0 2	10326	10337	3.5607	m+	10482	10484	3.5357	m+
-1 1 1	11104[a]	11103	3.4356	w	11256[a]	11257	3.4121	w-
1 1 0	11576	11585	3.3634	w+	11750	11751	3.3397	w
1 0 1		11782	3.3352			11964	3.3097	
0 2 0	12095	12099	3.2913	m	12197	12200	3.2776	m
0 0 3		12330	3.2603			12465	3.2426	
-1 1 2	b	13362	3.1319		13533	13534	3.1119	s
0 2 1	13461	13469	3.1194	w+		13585	3.1061	
1 1 1	14818[a]	14807	2.9751	w+	15017[a]	15014	2.9545	w+
-1 0 3	15346	15335	2.9234	s-	15516	15530	2.9050	m+
0 1 3		15355	2.9216			15515	2.9064	
0 2 2	17570	17579	2.7305	w-	17734	17740	2.7181	w-
1 0 2	17734	17744	2.7177	w	17997	17998	2.6985	w
-1 1 3		18360	2.6718		18596	18580	2.6559	w-
-1 2 1	20175	20177	2.5486	s	20410	20407	2.5342	s
1 2 0		20659	2.5187		20899	20900	2.5041	w
1 1 2	20767	20769	2.5121	s-	21050	21047	2.4954	s
0 0 4	21917	21920	2.4452	m-	22167	22160	2.4319	w+
-1 2 2	22440	22436	2.4169	w-	22679	22683	2.4037	w
-1 0 4	23068	23073	2.3833	w	23343	23347	2.3693	w+
1 2 1	23867	23881	2.3427	w-	24154	24164	2.3289	w-
0 2 3	24427	24429	2.3162	w+	24669	24664	2.3051	w+
0 1 4	24944	24944	2.2922	w-	25213	25210	2.2801	w
-1 1 4	26098	26098	2.2409	m	26401	26397	2.2282	m+
1 0 3		26446	2.2262			26801	2.2114	
0 3 0	27215	27222	2.1942	w-		27449	2.1851	
-1 2 3		27434	2.1857			27730	2.1740	
0 3 1	28599[a]	28592	2.1410	w+	28833	28834	2.1320	w+
1 1 3	29460[a]	29470	2.1088	w-	29856	29851	2.0953	w-
1 2 2	29834	29843	2.0956	w-	30172[a]	30197	2.0833	w-
-2 0 1		31909	2.0266			32431	2.0103	
-2 0 2	32315	32315	2.0139	m-	32829	32829	1.9980	w+
0 3 2	32694	32702	2.0019	w-	32988	32989	1.9932	w-
-1 0 5		33552	1.9764			33933	1.9653	
0 2 4	34022	34018	1.9628	w	34361	34359	1.9530	w+
2 0 0	34230	34242	1.9564	w-	34803	34803	1.9406	w-
0 0 5		34250	1.9562			34625	1.9455	
-2 2 1		34933	1.9369		b	35481	1.9219	w-
-1 2 4	35172	35172	1.9303	w-		35546	1.9202	
-1 3 1	35296	35301	1.9268	w-		35656	1.9172	
-2 1 2		35340	1.9258		35872	35879	1.9112	w-
-2 0 3	b	35462	1.9224			35997	1.9081	
1 3 0	35750	35782	1.9138	w-	36150	36150	1.9041	w-
-1 1 5		36576	1.8929			36983	1.8825	
2 1 0	37274	37267	1.8753	w+	37867	37853	1.8607	m-
0 1 5		37274	1.8751			37675	1.8651	
-1 3 2	37564	37559	1.8680	w-		37933	1.8588	
1 0 4	37888	37887	1.8599	w-	38381	38374	1.8480	w
-2 1 3	38514	38486	1.8454	w	39043	39047	1.8321	w+
1 2 3		38544	1.8440			39001	1.8332	
1 3 1	39020	39004	1.8331	w	39408	39413	1.8235	w+
2 0 1		39316	1.8258		39921	39945	1.8114	m
0 3 3	39562	39552	1.8203	m-		39914	1.8121	
1 1 4		40912	1.7898			41424	1.7787	
-2 0 4		41348	1.7804			41935	1.7679	
2 1 1	42351	42340	1.7594	w	43002	42994	1.7459	
-1 3 3	42569	42557	1.7549	w-		42979	1.7462	w+
-2 2 1		44007	1.7257		44627	44630	1.7136	w-
-2 1 4	44406[a]	44373	1.7186	w+	45015	44985	1.7069	w+
-2 2 2		44414	1.7178			45028	1.7060	
1 3 2		44966	1.7072			45446	1.6982	
-1 2 5	45653	45650	1.6944	m-	46145	46133	1.6855	m-
2 2 0	46335	46341	1.6817	w-	47007	47002	1.6698	w-
0 2 5		46348	1.6816			46824	1.6730	
-1 0 6		46770	1.6740			47290	1.6648	
2 0 2	47117	47129	1.6676	w-	47875	47856	1.6549	w-
-2 2 3	47561	47560	1.6600	w-	48200	48196	1.6490	w-
0 4 0	48400	48394	1.6456	w-	b	48798	1.6388	w-
0 3 4	49119	49142	1.6331	w-		49609	1.6254	
0 0 6	49318	49320	1.6301	w-	49843	49860	1.6213	w-
0 4 1	49778	49764	1.6228	w-				
-1 1 6		49794	1.6223					
-2 0 5	49973	49975	1.6194	w-				
1 2 4		49986	1.6192					

[a] Overlapped by a monophosphide line. [b] Overlapped by a silicon line.

at 700°C for a week.

X-Ray powder diffraction data were recorded in a Hägg-Guinier-type camera (Philips XDC 700) using $CrK\alpha_1$ radiation and silicon (a= 5.43054 Å) as internal calibration standard.

Comparison of the diffraction data for the diphosphides with those reported for $CeAs_2$ ($NdAs_2$-type) by Ono *et al.*[1] indicated that all these compounds are isostructural. The symmetry is monoclinic, but a determination of the crystal structure has not yet been reported. The unit cell dimensions were refined by the least squares method using the local program CELNE [6] on an IBM 1800 computer.

The following values were obtained (numbers in parenthesis are the calculated standard deviations referring to the last significant digits):
CeP_2: a=4.0641(2) Å; b=6.5826(3) Å; c= 10.1591(6) Å; β=105.686(5)°.
PrP_2: a=4.0315(2) Å; b=6.5553(3) Å; c= 10.1046(5) Å; β=105.698(5)°.
For identification purposes, powder diffraction data are presented in Table 1.

Acknowledgement. The work has been financially supported by the Swedish Natural Science Research Council.

1. Ono, S., Despault, J. G., Calvert, L. D. and Taylor, J. B. *J. Less-Common Metals 22* (1970) 51.
2. Olcese, G. L. *Atti Accad. naz. Lincei, Rend., Cl. Sci. Fis., Mat. e Nat. 40* (1966) 629.
3. Schmid, R. and Hahn, H. *Z. Anorg. Allg. Chem. 372* (1970) 106.
4. Franceschi, E. and Olcese, G. L. *J. Phys. Chem. Solids 30* (1969) 903.
5. Mironov, K. E., Vasil'eva, I. G. and Pritchina, T. G. *Revue de Chimie Minérale 10* (1973) 383.
6. Ersson, N.-O. Institute of Chemistry, Uppsala 1972. *Unpublished.*

Received December 4, 1973.

Acta Chemica Scandinavica A 28 (1974) 125—136

Thermodynamic Properties of Rare Earth Complexes. XX. Free Energy, Enthalpy and Entropy Changes for the Formation of Rare Earth(III) Complexes with Dicarboxylates, $^{-}OCOCH_2RCH_2CH_2RCH_2COO^{-}$, R=S, O, or NH

INGMAR GRENTHE and GÖRAN GÅRDHAMMAR

Division of Physical Chemistry I, Chemical Center, University of Lund, P.O.B. 740, S-220 07 Lund 7, Sweden

The changes in free energy, enthalpy and entropy for the formation of lanthanoid(III) complexes with anions, A^{2-}, of dicarboxylic acids of the type $(-CH_2RCH_2COOH)_2$, R=S, O, or NH, have been determined at 25°C in 1 M $NaClO_4$. For 1,2-bis(carboxymethylthio)-ethane (R=S), complexes of the stoichiometry MA^+, MA_2^- and MHA^{2+} were formed. For 1,2-bis(carboxymethyloxy)ethane (R=O) the dominating species were MA^+ and MA_2^-. Small amounts of a ternary complex MHA_2 were formed in the solutions with low pH. At high ligand concentrations the presence of a weak complex MA_3^{3-} was indicated. In the 1,2-bis-(carboxymethylamino)ethane system complexes of the compositions MA^+, MA_2^- and MH_2A^{3+} were formed. MH_2A is present in significant amount only in solutions of pH around 3.

The ligand containing sulphur donors gives only weak complexes, in keeping with the poor donor ability of sulphur to hard acceptors such as the lanthanoids. There is a large difference in the magnitude of the variation of β_2 within the rare earth series for the two other ligands. When R=NH, this variation is equal to 2×10^5, while it is only a factor of 9 when R=O. From calorimetric determinations of the enthalpy changes for the complexation reactions it was shown that this difference is nearly entirely an enthalpy effect. We suggest that these differences between the two ligands are related to differences in geometry between the two series of complexes.

In a previous part of this series [1] we discussed the changes in thermodynamic functions such as ΔG_j°, ΔH_j° and ΔS_j° for the formation of lanthanoid(III) complexes in a series of tridentate dicarboxylate ligands *viz.*, thiodiacetate, oxydiacetate, iminodiacetate, and 2,6-pyridine-dicarboxylate (dipicolinate). These ligands form complexes of quite different stability and have β_1 values ranging from 2×10^2 for thiodiacetate to 10^9 in dipicolinate. This large difference in stability is nearly entirely an enthalpy effect, *i.e.* the ΔS° for the formation of a complex with a given lanthanoid ion is almost the same for all four ligands. The differences in ΔH_{101}° between the sulphur containing ligand and the other three are approximately -15.0 kJ/mol, -15.6 kJ/mol, and -29 kJ/mol, respectively. In spite of these large differences one finds that the *variation* in ΔH° through the rare earth series is very nearly the same for all four ligands (*cf.* Fig. 1). It is tempting to relate the differences in ΔH° between the various ligands to differences in affinity of the various donor atoms, R, to the lanthanoid ions. However, variations in ΔH° (or β_j) between different ligands depend on many factors. One is the relative affinity of the various donor atoms, others are the coordination geometry of the ligand and the basicity of its donor groups. It is difficult to estimate the relative importance of these factors in ligands which contain more than one donor atom and no quantitative values of the differences in affinity between the various donors can thus be obtained.

The rare earth oxydiacetates and dipicolinates have approximately the same coordination

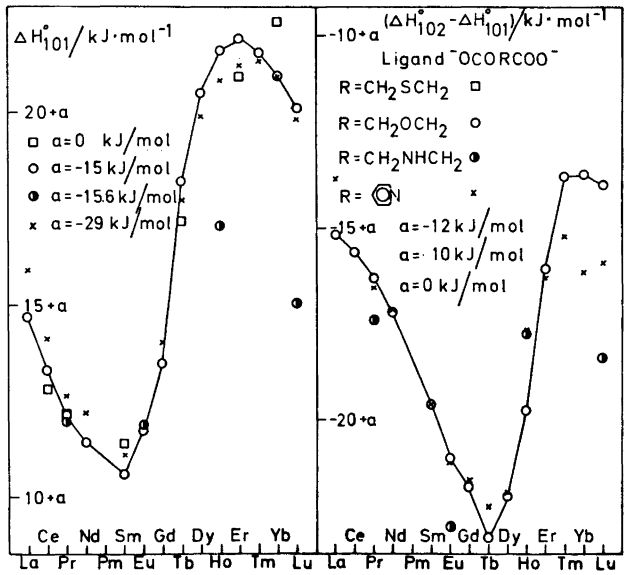

Fig. 1. ΔH°_{101} and $(\Delta H^\circ_{102} - \Delta H^\circ_{101})$ for the formation of rare earth complexes with thiodiacetate, oxydiacetate, iminodiacetate, and 2,6-pyridinedicarboxylate. The enthalpy changes for the various systems have been displaced by the quantity a given in the figure, in order to illustrate the very similar pattern of variation through the lanthanoid series.

geometry in the solid state,[16,17] and presumably also in solution. However, the difference in ΔH° is due not only to differences in affinity between O and N, but also to some extent to the different basicities of the carboxylate groups in the two ligands due to different inductive effects from the groups R. Oxydiacetate and thiodiacetate have, on the other hand, about the same basicity towards protons, hence the observed difference in ΔH° may be a rather good estimate of the difference in affinity of O and S to the lanthanoid ion.

In this investigation we have extended the previous study to include potentially tetradentate dicarboxylate ligands of the type $^-OCOCH_2RCH_2CH_2RCH_2COO^-$, where R equals S, O, or NH.

The points of main interest to us were

a. To investigate how a change from a tridentate to a tetradentate ligand affects the variation of thermodynamic quantities through the rare earth series.

b. To try to get an estimate of how a change in geometry of the ligand affects the relative affinities of the various donor atoms in R, as measured by differences in ΔH° or β_j.

c. To study the possible formation of ternary complexes MH_pA_q.

Point *a* is of interest for the problem of separating the various rare earth elements from one another. The efficiency of a separation process depends, among other things on differences in stability constants between the various elements. These are approximately the same for most of the tridentate ligands, *i.e.* they have all about the same *size specificity* and thus the same efficiency in a separation process. It seems reasonable to assume that the size specificity of a ligand increases with the number of donor atoms, until all of them no longer are coordinated to the central ion. One also expects size specific effects to be more important in the higher complexes formed with a given ligand. We intend to illustrate these points by a comparison of the tri- and tetradentate ligands.

No previous measurements of stability constants have been reported between rare earths and 1,2-bis(carboxymethylthio)ethane or 1,2-bis(carboxymethyloxy)ethane. Stability constants for the rare earth complexes MA^+ and MA_2^- with A equal to 1,2-bis(carboxymethylamino)ethane have been published.[2,3] This in-

vestigation will extend the previous studies to include measurements of the corresponding enthalpy changes. We have also made determinations of the stability constants of the La, Nd, Sm, Tb, Er, and Yb systems at the ionic strength $I = 1.00$ M as the data previously published refer to a medium with an ionic strength of 0.1 M.

All symbols used are defined in Refs. 4, 5, and 6. The calculation procedure is the same as used before.[4-6]

EXPERIMENTAL

All measurements have been performed at 25.0°C in a medium with the ionic strength 1.0 M using sodium perchlorate as the neutral salt. The stability constants were determined by the potentiometric standard method of emf-measurements of the hydrogen ion concentration. The enthalpy changes were obtained from calorimetric titrations.

Potentiometric measurements. The emf E of galvanic elements of the following type was measured:

(1)

Ag, AgCl(s)	0.02500 M NaCl 0.975 M $NaClO_4$	C_M $M(ClO_4)_3$ C_{HClO_4} $HClO_4$ C_{H_2A} H_2A C_{Na_2A} Na_2A 1.00 M $Na(ClO_4)$	glass electrode

The experimental details have been described before.[4] The system was calibrated before and after each titration by measuring the emf, E_R, when the right half-cell of (1) contained a solution with known hydrogen ion concentration, h_R. The unknown hydrogen ion concentration, h, was then calculated from eqn. 2.

$$-(RT/F)\log h/h_R = (E_R - E_j') - (E - E_j'') \qquad (2)$$

where E_j' and E_j'' are liquid junction potentials which depend both on the hydrogen ion concentration and on the perchlorate ion concentration, *i.e.* $E_j = E_{h,j} + E_{a,j}$. These two terms were measured as described in Ref. 4, p. 1393. The glass electrode used was of type Jena "Thalamide" and the potentiometer of type Orion 801 or Radiometer pHM4d. The reproducibility of the emf was usually within 0.1 mV. The temperature was controlled at 25.0 ± 0.1°C by using a water thermostat. The various proton-ligand systems were examined by using a cell of type (1) with $C_M = 0$.

Calorimetric measurements. The titration calorimeter described by Ots [7] was used in all the calorimetric titrations. The experimental procedure is the same as described before.[6] The inner vessel was initially filled with a volume V_0, of a solution S. Titrant T was then added successively, in portions varying between 1.00 and 3.00 ml. The system was calibrated electrically, usually at ten different values of the total volume.

The $(-CH_2SCH_2COO^-)_2$ system. The ligand acid was obtained by the courtesy of Dr. A. Sandell. Its purity was checked by an alkalimetric determination of the formula weight; found 210.3 ± 0.5, calc. 210.2. The samarium system was investigated potentiometrically at three different values of C_M (10, 20 and 30 mM) using two different buffers with the ratio C_{H_2A}/C_{Na_2A} equal to 1:1 and 1:3. Some experimental data are given in Table 1. The dysprosium and erbium systems were investigated at only one metal ion concentration equal to 20 mM. The correction for the diffusion potential was

$$E_j/\text{mV} = -0.065h/\text{mM} + 0.042C_{Na_2A}/\text{mM}$$

The lighter rare earths were not investigated due to the formation of a sparingly soluble solid $M_2A_3.xH_2O$.

The calorimetric titrations were made at $C_M = 20$ mM using a buffer with $C_{H_2A}/C_{Na_2A} = 1:4$. Only very small amounts of the ternary complexes are formed in these titrations, hence ΔH°_{111} cannot be calculated. Experimental data for the samarium system are given in Table 2. The protonation enthalpies of the ligand were determined by titration of a Na_2A solution with perchloric acid.

The $(-CH_2OCH_2COO^-)_2$ system. The ligand was prepared by oxidation of triethyleneglycol with nitric acid using ammonium vanadate as catalyst.[8] It was difficult to purify the product. Several different methods were tried and recrystallization from a mixture of acetone and water seemed to work best. The purity was checked by NMR, elemental analyses and alkalimetric determinations of the formula weight. Several different batches of the acid were used throughout this study. The purity, as judged from the alkalimetric formula weight determinations, varied somewhat. Some samples had a formula weight of 178.0, others had values as low as 176.2, calc. 178.1. Repeated recrystallizations of the latter product did not improve its purity. We have not been able to determine the nature of the impurity.

The cerium and erbium systems were investigated potentiometrically at three different values of C_M (10 mM, 20 mM, and 30 mM) using four different buffers with C_{H_2A}/C_{Na_2A} ratios equal to 3:1, 1:1, 1:3, and 1:5, respectively. The other systems were studied at $C_M = 20$ mM using the 3:1, 1:1, and 1:3 buffers. The correction for the diffusion potential was

$$E_j/\text{mV} = -0.065h/\text{mM} + 0.024C_{Na_2A}/\text{mM}$$

This correction was checked by measuring the protonation constants of the ligand using a diffusion free cell as described in Ref. 4, p. 1393.

Table 1. Corresponding values of v/ml, $-\log(h/\mathrm{M})$ and $[(C_{H,calc}-C_{H,obs})/C_A]\times 10^3$ for some potentiometric measurements in the $(-CH_2R-CH_2COO^-)_2$ systems. Half the experimental material in each titration series has been included.

The $Sm^{3+}-(-CH_2SCH_2COO^-)_2$ system

Series 1: $C_{H(S)}=0.00008$ M, $C_{A(S)}=0$ M, $C_{M(S)}=0.02000$ M, $C_{H(T)}=0.07500$ M, $C_{A(T)}=0.1500$ M, $C_{M(T)}=0.02000$ M, $V_0=19.97$ ml.

0.00, 4.084, 0.00; 0.20, 3.717, −4.1; 0.60, 3.680, −4.7; 1.20, 3.685, −5.9; 2.10, 3.704, −4.7; 3.40, 3.733, −3.6; 5.10, 3.763, −1.5; 7.00, 3.790, −0.9; 9.00, 3.810, −0.2; 12.00, 3.832, −0.8; 16.00, 3.853, −0.4; 20.00, 3.868, −0.1; 30.00, 3.885, −1.0.

Series 2: $C_{H(S)}=0.00008$ M, $C_{A(S)}=0$ M, $C_{M(S)}=0.02000$ M, $C_{H(T)}=0.1500$ M, $C_{A(T)}=0.1500$ M, $C_{M(T)}=0.02000$ M, $V_0=19.97$ ml.

0.20, 3.383, 4.8; 0.60, 3.298, −1.0; 1.20, 3.276, 1.6; 1.60, 3.274, 2.4; 2.70, 3.281, 4.6; 4.20, 3.296, 6.5; 6.00, 3.310, 12.8; 8.00, 3.323, 16.8; 10.00, 3.339, 14.7; 14.00, 3.357, 15.9; 18.00, 3.369, 17.5; 25.00, 3.384, 17.2.

Series 3: $C_{H(S)}=0.00004$ M, $C_{A(S)}=0$ M, $C_{M(S)}=0.01000$ M, $C_{H(T)}=0.0750$ M, $C_{A(T)}=0.1500$ M, $C_{M(T)}=0.01000$ M, $V_0=19.97$ ml.

0.20, 3.841, −8.4; 0.60, 3.809, −7.4; 1.20, 3.819, −6.8; 2.10, 3.842, −5.9; 3.40, −3.866, −0.8; 5.10, 3.890, 0.0; 7.00, 3.910, 0.1; 9.00, 3.924, 0.0; 12.00, 3.934, 0.2; 16.00, 3.944, 0.2; 20.00, 3.951, 0.3; 30.00, 3.959, 0.5.

Series 4: $C_{H(S)}=0.00012$ M, $C_{A(S)}=0$ M, $C_{M(S)}=0.03000$ M, $C_{H(T)}=0.0750$ M, $C_{A(T)}=0.1500$ M, $C_{M(T)}=0.03000$ M, $V_0=19.97$ ml.

0.20, 3.628, 12.1; 0.40, 3.604, 3.7; 0.80, 3.597, −1.7; 1.60, 3.606, −3.2; 2.70, 3.626, −4.1; 4.20, 3.655, −5.5; 6.00, 3.684, −5.3; 8.00, 3.711, −6.0; 10.00, 3.731, −5.4; 14.00, 3.765, −8.3; 18.00, 3.785, −8.1; 20.00, 3.793, −8.5; 30.00, 3.817, −6.3.

The $Ce^{3+}-(-CH_2OCH_2COO^-)_2$ system

Series 1: $C_{H(S)}=0.00086$ M, $C_{A(S)}=0$ M, $C_{M(S)}=0.02000$ M, $C_{H(T)}=0.2303$ M, $C_{A(T)}=0.1526$ M, $C_{M(T)}=0.02000$ M, $V_0=19.97$ ml.

0.00, 3.067, 0; 0.60, 2.235, 24.4; 0.80, 2.174, 12.9; 1.20, 2.101, −0.5; 2.10, 2.023, −1.3; 3.40, 1.983, −4.4; 5.10, 1.964, 1.9; 7.00, 1.966, −0.9; 9.00, 1.973, 1.9; 12.00, 1.990, 3.4; 16.00, 2.015, 3.8; 20.00, 2.040, 2.3; 30.00, 2.084, 5.1.

Series 2: $C_{H(S)}=0.00086$ M, $C_{A(S)}=0$ M, $C_{M(S)}=0.02000$ M, $C_{H(T)}=0.1565$ M, $C_{A(T)}=0.1532$ M, $C_{M(T)}=0.02000$ M, $V_0=19.97$ ml.

0.60, 2.372, −3.0; 0.80, 2.313, −4.2; 1.20, 2.248, −12.8; 1.60, 2.215, −12.5; 2.70, 2.187, −11.3; 4.20, 2.204, −5.3; 6.00, 2.253, −1.8; 8.00, 2.319, −2.8; 10.00, 2.378, 0.0; 14.00, 2.483, −1.7, 18.00, 2.561, 1.0; 20.00, 2.593, 2.5; 30.00, 2.713, 5.6.

Series 3: $C_{H(S)}=0.00086$ M, $C_{A(S)}=0$ M, $C_{M(S)}=0.02000$ M, $C_{H(T)}=0.08005$ M, $C_{A(T)}=0.1523$ M, $C_{M(T)}=0.02000$ M, $V_0=19.97$ ml.

0.60, 2.571, 9.1; 0.80, 2.519, 5.3; 1.20, 2.461, 1.3; 2.10, 2.433, −1.5; 3.40, 2.480, 0.4; 5.10, 2.598, −2.2; 7.00, 2.730, −2.0; 9.00, 2.859, −4.0; 12.00, 3.024, −1.3; 16.00, 3.187, 1.0; 20.00, 3.286, 1.3; 30.00, 3.410, −1.4.

Series 4: $C_{H(S)}$ 0.00086 M, $C_{A(S)}=0$ M, $C_{M(S)}=0.02000$ M, $C_{H(T)}=0.05408$ M, $C_{A(T)}=0.1516$ M, $C_{M(T)}=0.02000$ M, $V_0=19.97$ ml.

0.60, 2.684, −2.3; 0.80, 2.635, −3.0; 2.10, 2.563, −8.6; 3.40, 2.629, −3.6; 5.10, 2.776, −3.4; 7.00, 2.938, −4.2; 10.00, 3.175, −1.6; 14.00, 3.408, −2.0; 18.00, 3.531, −3.5; 25.00, 3.638, −6.1.

Series 5: $C_{H(S)}=0.00038$ M, $C_{A(S)}=0$ M, $C_{M(S)}=0.01000$ M, $C_{H(T)}=0.08005$ M, $C_{A(T)}=0.1523$ M, $C_{M(T)}=0.01000$ M, $V_0=19.95$ ml.

0.60, 2.706, −2.3; 0.80, 2.668, −3.1; 1.20, 2.652, −2.4; 2.10, 2.747, 0.7; 3.40, 2.950, −1.7; 5.10, 3.175, 4.5; 7.00, 3.747, 4.3; 9.00, 3.447, 3.3; 12.00, 3.526, 1.8; 16.00, 3.579, 2.0; 20.00, 3.609, 1.4; 30.00, 3.648, 0.3.

Series 6: $C_{H(S)}=0.00130$ M, $C_{A(S)}=0$ M, $C_{M(S)}=0.03000$ M, $C_{H(T)}=0.08005$ M, $C_{A(T)}=0.1523$ M, $C_{M(T)}=0.03000$ M, $V_0=19.97$ ml.

0.60, 2.483, 18.3; 0.80, 2.433, 14.5; 1.20, 2.370, 8.8; 2.10, 2.314, 4.0; 3.40, 2.309, 4.0; 5.10, 2.350, 6.1; 7.00, 2.419, 8.2; 9.00, 2.502, 4.8; 12.00, 2.612, 3.6; 16.00, 2.737, 0.9; 20.00, 2.842, 1.4; 30.00, 3.036, 4.4.

The $Sm^{3+}-(-CH_2NHCH_2COO^-)_2$ system
The error is $[(C_{H,calc}-C_{H,obs})/C_A]\times 10^4$

Series 1: $C_{H(S)}=0.0622$ M, $C_{A(S)}=0.03078$ M, $C_{M(S)}=0.00950$ M, $C_{OH(T)}=0.1485$ M, $C_{A(T)}=0$ M, $C_{M(T)}=0$ M, $V_0=20.00$ ml.

0.20, 4.319, −14; 0.45, 4.549, −23; 0.95, 4.796, −38; 1.67, 5.053, −58; 2.40, 5.327, −28; 3.00, 5.595, 4; 3.65, 5.861, −14; 4.50, 6.155, −21; 5.28, 6.458, −25; 5.80, 6.730, −11; 6.20, 7.041, −19.

Series 2: $C_{H(S)}=0.1007$ M, $C_{A(S)}=0.0497$ M, $C_{M(S)}=0.01900$ M, $C_{OH(T)}=0.1490$ M, $C_{A(T)}=0$ M, $C_{M(T)}=0$ M, $V_0=20.00$ ml.

0.00, 3.797, 2; 0.20, 4.066, −2; 0.49, 4.301, 9; 1.05, 4.530, 25; 2.06, 4.767, 32; 3.40, 5.011, 22; 4.70, 5.266, 37; 5.80, 5.533, 31; 7.00, 5.808, 1; 8.30, 6.069, 4; 9.60, 6.356, 15; 10.55, 6.650, 19; 11.10, 6.917, 16.

Table 1. Continued.

Series 3: $C_{H(S)} = 0.0798$ M, $C_{A(S)} = 0.0399$ M, $C_{M(S)} = 0.01900$ M, $C_{H(T)} = 0.2328$ M, $C_{A(T)} = 0$ M, $C_{M(T)} = 0$ M, $V_0 = 20.00$ ml.

0.00, 4.001, 14; 0.20, 3.521, 18; 0.40, 3.236, 24; 0.67, 3.006, 25; 1.08, 2.779, 31; 1.70, 2.553, 11; 2.60, 2.321, −13; 3.90, 2.074, −17; 5.70, 1.819, −17.

Series 4: $C_{H(S)} = 0.03147$ M, $C_{A(S)} = 0.01530$ M, $C_{M(S)} = 0.01330$ M, $C_{H(T)} = 0.2328$ M, $C_{A(T)} = 0$ M, $C_{M(T)} = 0$ M, $V_0 = 20.00$ ml.

0.00, 3.628, 2; 0.10, 3.276, 5; 0.20, 3.070, 20; 0.40, 2.815, 30; 0.69, 2.583, 18.

Series 5: $C_{H(S)} = 0.04200$ M, $C_{A(S)} = 0.02036$ M, $C_{M(S)} = 0.01900$ M, $C_{H(T)} = 0.2328$ M, $C_{A(T)} = 0$ M, $C_{M(T)} = 0$ M, $V_0 = 20.00$ ml.

0.00, 3.555, −4; 0.10, 3.286, −15; 0.24, 3.051, −7; 0.46, 2.821, −7.

Series 6: $C_{H(S)} = 0.04160$ M, $C_{A(S)} = 0.02049$ M, $C_{M(S)} = 0.00950$ M, $C_{H(T)} = 0.2328$ M, $C_{A(T)} = 0$ M, $C_{M(H)} = 0$, $V_0 = 20.00$ ml.

0.00, 3.834, 4; 0.10, 3.442, 17; 0.20, 3.220, 28; 0.40, 2.955, 30; 0.67, 2.732, 18; 1.10, 2.493, 7; 1.70, 2.265, −54; 2.60, 2.015, −11.

Table 2. Corresponding values of v/ml, $(Q_{corr} \times 100)$/J and $(Q_{corr,calc} - Q_{corr,obs}) \times 100$ J^{-1} from selected calorimetric titrations.

The $Sm^{3+} - (-CH_2SCH_2COO^-)_2$ system

Series 1: $C_{H(S)} = 0.00053$ M, $C_{A(S)} = 0.00038$ M, $C_{M(S)} = 0.01928$ M, $C_{H(T)} = 0.1200$ M, $C_{A(T)} = 0.3000$ M, $C_{M(T)} = 0$ M, $V_0 = 80.07$ ml.

2.00, 375.6, −4.1; 4.00, 321.1, 0.3; 6.00, 257.2, 5.9; 9.00, 294.3, 4.5; 12.00, 212.8, 1.7; 15.00, 158.2, 1.6.

Series 2: The various concentrations are the same as in series 1.

1.00, 181.0, 9.0; 3.00, 353.7, −4.2; 5.00, 289.9, 2.2; 8.00, 339.7, −5.0; 11.00, 243.4, −4.6; 14.00, 176.7, −1.3.

The $Ce^{3+} - (-CH_2OCH_2COO^-)_2$ system

Series 1: $C_{H(S)} = 0.00081$ M, $C_{A(S)} = 0.00038$ M, $C_{M(S)} = 0.01956$ M, $C_{H(T)} = 0.1510$ M, $C_{A(T)} = 0.3000$ M, $C_{M(T)} = 0$ M, $V_0 = 80.07$ ml.

2.00, 245.0, −1.0; 4.00, 170.4, −1.3; 6.00, 58.5, −1.7; 9.00, −192.8, 2.4; 12.00, −347.3, −0.1; 15.00, −275.9, 2.9.

Series 2: The various concentrations are the same as in series 1.

1.00, 132.9, 4.0; 3.00, 211.1, 0.8; 5.00, 120.4, −1.3; 8.00, −84.3, 0.4; 11.00, −326.1, −0.7; 14.00, −311.5, −3.0; 17.00, −175.0, −0.4.

The $H^+ - (-CH_2NHCH_2COO^-)$ system

Series 1: $C_{H(S)} = 0.00680$ M, $C_{A(S)} = 0.01613$ M, $C_{H(T)} = 0.05980$ M, $C_{A(T)} = 0$ M, $V_0 = 86.00$ ml.

2.00, 454, −3; 4.00, 452, −2; 6.00, 448, 1; 8.00, 449, −1; 10.00, 448, 0; 12.00, 444, 3; 14.00, 442, 4.

Series 2: $C_{H(S)} = 0.02346$ M, $C_{A(S)} = 0.02019$ M, $C_{H(T)} = 0.05980$ M, $C_{A(T)} = 0$ M, $V_0 = 80.00$ ml.

2.00, 442, 3; 4.00, 449, −4; 6.00, 450, −5; 8.00, 446, −1; 10.00, 448, −3; 12.00, 446, −1; 14.00, 442, 3; 16.00, 441, 4.

The $Sm^{3+} - (-CH_2NHCH_2COO^-)_2$ system

Series 1: $C_{H(S)} = 0.00072$ M, $C_{A(S)} = 0.001284$ M, $C_{M(S)} = 0.00938$ M, $C_{H(T)} = 0.00860$ M, $C_{A(T)} = 0.1040$ M, $C_{M(T)} = 0$ M, $V_0 = 81.00$ ml.

2.00, 250, −4; 4.00, 248, −3; 6.00, 245, 0; 8.00, 241, 5; 10.00, 248, 0; 12.00, 246, −1; 14.00, 242, −9.

Series 2: $C_{H(S)} = 0.00081$ M, $C_{A(S)} = 0.002537$ M, $C_{M(S)} = 0.00927$ M, $C_{H(T)} = 0.00860$ M, $C_{A(T)} = 0.1040$ M, $C_{M(T)} = 0$ M, $V_0 = 82.00$ ml.

2.00, 248, −2; 4.00, 243, 2; 6.00, 242, 3; 8.00, 239, 9; 10.00, 244, 3; 12.00, 245, −4.

Experimental data for the cerium system are given in Table 1.

As our main interest was to determine the enthalpy changes for the formation of the first two complexes the calorimetric titrations were designed with this object in mind. Only one buffer with C_{H_2A}/C_{Na_2A} ratio equal to 1:3 was used. The titrations were made at one value of C_M equal to 20 mM and extended to a C_A/C_M ratio equal to 3:1. Hence, no accurate information can be obtained about $\Delta H°_{103}$, *cf.* Fig. 3. The enthalpy change for the formation of MHA_2 was also rather uncertain. Within the estimated error limits $\Delta H°_{103}$ seemed to have approximately constant values equal to −10 kJ/mol throughout the rare earth series. In the final least-squares calculation we refined only the constants $\Delta H°_{101}$, $\Delta H°_{102}$ and $\Delta H°_{112}$ while keeping $\Delta H°_{103}$ constant at −10 kJ/mol. Refinements where the enthalpy changes for the formation of MA^+ and MA_2^- were varied while keeping both $\Delta H°_{103}$ and $\Delta H°_{112}$ at given constant values always resulted in *sig y* values three or four times larger than in the method we used.

The experimental data for the cerium system are shown in Table 2.

The $(-CH_2NHCH_2COO^-)_2$ systems. 1,2-Bis-(carboxymethylamino)ethane (La Mont Laboratories) was purified by repeated recrystallizations from water. The purity was determined by a complexometric titration with copper(II) using murexide as indicator. Formula weight: found 176.3, calc. 176.2.

The experimental procedure used in the potentiometric titrations differed slightly from that described previously. The S solution contained the metal ion and a buffer of Na_2A and H_2A. This solution was then titrated with a solution T containing either sodium hydroxide or perchloric acid. The compositions of the S and T solutions are shown in Table 1, where some of the experimental findings for the samarium system are given. The change in the perchlorate ion concentration was so small that only the hydrogen ion dependent term was included in E_j.

The calorimetric titrations were made in solutions of such a low hydrogen ion concentration that the complex MH_2A^{3+} was negligible. Hence the values of ΔH°_{101} and ΔH°_{102} are not influenced by an error in β_{121} (*cf.* Fig. 3). Both the potentiometric and the calorimetric titrations were made in fairly alkaline solutions. Hence the possible formation of hydroxocomplexes, and in the calorimetric titrations also the enthalpy change for the process $H^+ + OH^- \rightarrow H_2O$, had to be taken into account. This was done as described in Ref. 6, pp. 3212–3213.

Experimental data from the calorimetric titrations of the samarium system are given in Table 2.

It has been possible to include only a small part of the experimental material in this communication. However, these data are representative of all the systems studied with a given ligand. An estimate of the precision of the experiments is obtained from the standard deviations of the experimental quantities C_H/C_A, and Q_{corr} given in Tables 3–8. The complete experimental material may be obtained from the authors.

Calculations. Stability constants and molar enthalpy changes were calculated by using a least-squares procedure with equal weight to all the experimental points. Two programmes in the "Letagrop" series were used: ETITER [9] for the potentiometric data, with C_H/C_A as the error carrying variable, and LETAGROP KALLE [10] with Q_{corr} as the error carrying variable for the calorimetric data.

RESULTS

The equilibrium models used for the description of the various metal-ligand systems were deduced from measurements where the various total concentrations of metal, ligand and protons were varied over a fairly large concentration range. Only data for one or two elements were used to deduce the model. This was then applied to all other rare earth systems investigated with a given ligand. By this procedure the total number of experimental determinations decreased considerably with only a small loss of accuracy in the stability constants.

The potentiometric data showed that ternary complexes were present only in small amounts. Hence the calorimetric titrations were designed to give their main information about the binary complexes, *cf.* Figs. 2 and 3 which show the distribution of the various species in the terbium 1,2-bis(carboxymethyloxy)ethane system for the potentiometric and calorimetric titrations, respectively.

The 1,2-bis(carboxymethylthio)ethane systems. The protonation constants of the ligand were

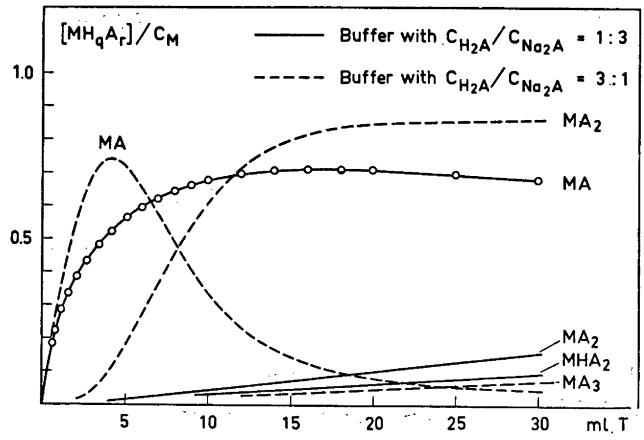

Fig. 2. The relative concentrations of the various complexes formed in the terbium 1,2-bis(carboxymethyloxy)ethane system in the potentiometric investigations. The circles indicates the total volumes of titrant added in the various titrations.

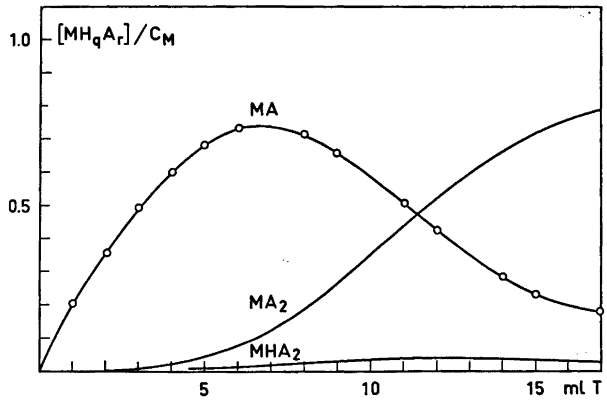

Fig. 3. The relative amounts of the various complexes formed in the calorimetric study of the terbium 1,2-bis(carboxymethyloxy)ethane system. The circles denote the total volume of titrant added.

Table 3. Stability constants for complexes formed in the rare earth-1,2 bis(carboxymethylthio)-ethane system at 25°C, $I = 1.00$ M. All errors are given as 3σ, where σ is the estimated standard deviation in the constant, referring to the least significant digit. *Sig y* is the standard deviation in the error carrying variable C_H/C_A and N denotes the number of experimental points. The protonation constants are $\beta_{011} = 7.41(5) \times 10^3$ M^{-1} and $\beta_{021} = 1.361(74) \times 10^7$ M^{-2}. *Sig* $y = 3.9 \times 10^{-3}$ and $N = 154$.

Metal	$\beta_{101} \times 10^{-2} \times M$	$\beta_{102} \times 10^{-3} \times M^2$	$\beta_{111} \times 10^{-5} \times M^2$	*sig* $y \times 10^3$	N
Sm	2.09(5)	3.1(2)	2.3(1)	7.2	96
Dy	1.22(7)	3.0(2)	1.9(7)	12.0	48
Er	1.02(5)	1.4(4)	1.4(4)	7.4	46

$\beta_{011} = 7.41(5) \times 10^3$ M^{-1} and $\beta_{021} = 1.36(7) \times 10^7$ M^{-2}. The numbers in parantheses are here and in the following equal to 3σ, where σ is the estimated standard deviation in the constant referring to the least significant digit. The constants were determined in solutions where the total ligand concentration, C_A, was constant in each titration series. C_A-values of 25, 50, 100, and 150 mM were used. The data could be well described (*sig* $y = 3.9 \times 10^{-3}$) by the above two constants in spite of the fairly large correction for the diffusion potential (at most 6.3 mV).

The potentiometric data for the samarium system were described by using a model with the metal complexes MA^+, MA^-_2 and MHA^{2+}. This model gives a satisfactory description of the measurements as judged by the value of *sig* $y = 7.2 \times 10^{-3}$. The same model also gives a fairly good description of the experimental data for the other two systems. The stability constants are given in Table 3. $\Delta H°$ and $\Delta S°$ values are given in Table 4.

The 1,2-bis(carboxymethyloxy)ethane systems. The protonation constants of the ligand were $\beta_{011} = 4.75(3) \times 10^3$ M^{-1} and $\beta_{021} = 5.38(3) \times 10^6$ M^{-2}. These data are based on 263 experimental points collected from ten different titration series at $C_A/mM = 10$, 25, 50, 100, and 150. The protonation constants fit these data well as judged by the value of *sig* $y = 4.2 \times 10^{-3}$.

The metal ligand systems were described by a model with the species MA^+, MA_2^-, MA_3^{3-}, and MHA_2. We have tested other possible models which include complexes of the type MHA^{2+} and M_2A^{4+} on the cerium and erbium systems. In the least-squares refinement we found that the corresponding stability constants β_{111} and β_{201} were negative or zero. Hence these models were discarded.

The dominating species are MA^+ and MA_2^-

Table 4. Over-all enthalpy and entropy changes for the formation of some rare earth 1,2-bis-(carboxymethylthio)ethane complexes at 25.00°C and $I = 1.00$ M. The enthalpy changes for the formation of MHA complexes have not been determined. All errors are equal to 3σ, referring to the least significant digit. The units for the enthalpy and entropy changes are kJ/mol and kJ/(K mol), respectively.

Metal	ΔH°_{101}	ΔH°_{102}	ΔS°_{101}	ΔS°_{102}	*sig* Q/J
Sm	12.3(17)	21.2(26)	86	138	0.050
Dy	20.4(29)	24.3(22)	108	148	0.048
Er	19.6(25)	33.0(28)	104	171	0.037

Table 5. Stability constants for complexes formed in the rare earth 1,2-bis(carboxymethyloxy)-ethane system at 25°C, $I = 1.00$ M. The error carrying variable and the method used to estimate the errors are defined in Table 3. The protonation constants are $\beta_{011} = 4.748(27) \times 10^3 M^{-1}$ and $\beta_{021} = 5.384(26) \times 10^6 M^{-2}$. *Sig* $y = 4.2 \times 10^{-3}$ and $N = 263$.

Metal	$\beta_{101} \times 10^{-4} \times M$	$\beta_{102} \times 10^{-7} \times M^2$	$\beta_{103} \times 10^{-9} \times M^3$	$\beta_{112} \times 10^{-10} \times M^3$	*sig* $y \times 10^3$	N
La	2.26(1)	5.18(9)	0.40(11)	0.266(2)	4.2	66
Ce	4.41(3)	7.71(12)	0.67(14)	0.315(5)	5.3	132
Pr	6.40(15)	7.79(65)	0.39(2)	0.35(4)	8.7	71
Nd	8.32(26)	9.02(79)	0.43(1)	0.73(3)	9.5	66
Sm	11.87(14)	9.61(30)	0.89(8)	2.16(17)	6.6	66
Gd	7.83(13)	7.45(31)	0.68(1)	1.61(17)	7.2	66
Tb	5.66(12)	7.91(48)	0.49(3)	0.55(2)	10.1	70
Dy	4.66(5)	8.44(34)	0.60(1)	0.89(1)	7.6	66
Er	4.04(9)	10.91(40)	0.88(3)	0.26(15)	9.7	130
Tm	4.34(8)	17.13(49)	0.29(3)	0.32(6)	6.4	70
Yb	7.03(15)	47.4(15)	0.33(8)	0.59(24)	9.3	66

Table 6. Over-all enthalpy and entropy changes for the formation of rare earth complexes with 1,2-bis(carboxymethyloxy)ethane at 25.00°C and $I = 1.00$ M. MA^- and MA_2^- are the dominating species. The enthalpy value ΔH°_{103} has been assumed to be constant -10.0 kJ/mol throughout the rare earth series. The protonation enthalpies of the ligand are $\Delta H^\circ_{011} = 1.10(6)$ kJ/mol and $\Delta H^\circ_{021} = 2.10(6)$ kJ/mol, respectively.

Metal	ΔH°_{101}	ΔH°_{102}	ΔH°_{112}	ΔS°_{101}	ΔS°_{102}	*sig* Q/J
La	6.75(12)	−4.04(15)	−16.5(23)	106	153	0.025
Ce	5.52(11)	−3.27(17)	−17.8(35)	107	159	0.040
Pr	4.31(21)	−2.12(35)	−44(66)	106	144	0.061
Nd	3.30(13)	0.58(22)	3.9(31)	105	154	0.038
Sm	1.58(7)	7.94(15)	−0.8(9)	102	178	0.023
Gd	3.56(9)	12.23(18)	−1.0(9)	106	192	0.027
Tb	7.30(17)	14.06(30)	−1.8(41)	115	198	0.049
Dy	10.84(15)	17.77(23)	9.5(15)	126	211	0.043
Ho	12.97(30)	19.43(59)	7(9)	132	216	0.077
Er	15.61(17)	29.04(26)	11(8)	141	251	0.047
Tm	16.74(26)	31.78(31)	38(11)	145	264	0.065
Yb	15.95(28)	31.53(31)	48(11)	146	272	0.077
Lu	15.22(21)	29.43(24)	21.0(6)	143	268	0.049

(*cf.* Fig. 2). The $\bar{n}$-curves have a plateau at $\bar{n}=2$ but with a slight increase at high ligand concentrations indicating the possible formation of a third complex MA_3^{3-}. The value of the third stepwise stability constant is rather small, varying between 1 M^{-1} and 10 M^{-1}. The magnitude of the constant is very sensitive towards systematic errors in the diffusion potential correction and/or in the various total concentrations. An impurity in the acid may cause an error in the total concentration of ligand. We have investigated how this may effect the magnitude of the stability constants by repeating the potentiometric titrations for the neodymium system by using two different batches of ligand acid with formula weights differing by one percent. The stability constants agreed within 3σ. Furthermore both $\bar{n}$-curves show a pronounced inflexion at $\bar{n}=2$ and this would not have been the case if the ratio C_A/C_M had been in error. In view of this we judge the third complex to be real and not an artefact brought about by impure chemicals. The various stability constants are given in Table 5, $\Delta H°$ and $\Delta S°$ values in Table 6.

The 1,2-bis(carboxymethylamino)ethane systems. The samarium system is used as a model for all the other systems. The equilibrium model suggested from these data includes the complexes MA^+, MA_2^- and MH_2A^{3+}. The possible existence of a complex MHA^{2+} was also tested. A stability constant $\beta_{111}=7.1(3)\times10^{11}$ M^{-2}, corresponding to an equilibrium constant of 1.4×10^2 M^{-1} for the reaction $M^{3+}+HA^-\rightleftharpoons MHA^{2+}$, was obtained. A calculation of the concentrations of the various species in the solutions studied showed that at most 2 % of the metal ion was present as MHA^{2+}. Hence, the existence of the complex cannot be unequivocally decided, *e.g.* a very slight change in the total concentrations C_H and/or C_A gave a negative value of β_{111}. For this reason the complex has not been included in the equilibrium model used.

The magnitude of the stability constants and their estimated errors are to some extent influenced by the number of titration series used. This difference is illustrated for the samarium system in Table 7, where the second set of stability constants refers to titration series of similar stoichiometric compositions as those used in the other lanthanoid systems investigated.

The variation within the rare earth series of the stability constants obtained in this study agrees well with earlier results.[2,3] The ratio between our stability constants and those of Thompson is equal to 0.6 and 0.8 for β_1 and β_2, respectively. This difference is presumably due to the different ionic media used. In view of the constant ratio between the two sets of stability constants the magnitude of the constants for the seven elements which were not investigated potentiometrically at $I=1.0$ M, *viz.* Ce, Pr, Gd, Dy, and Tm may be estimated from the constants given by Thompson.[2]

The stability constants are given in Table 7, $\Delta H°$ and $\Delta S°$ values in Table 8.

Comparison between models and experimental data. The models suggested for the various metal-ligand systems give estimates of the standard-deviations in the quantity C_H/C_A

Table 7. Stability constants for complexes formed in the rare earth 1,2-bis(carboxymethylamino)-ethane system at 25°C and $I=1.00$ M. The error carrying variable and the method used to estimate the errors are defined in Table 3. The protonation constants are $\beta_{011}=4.95(7)\times10^9M^{-1}$, $\beta_{021}=2.574(41)\times10^{16}M^{-2}$, $\beta_{031}=6.02(12)\times10^{18}M^{-3}$ and $\beta_{041}=2.775(54)\times10^{20}M^{-4}$. *Sig* $y=3.6\times10^{-3}$ and $N=140$.

Metal	$\beta_{101}\times10^{-6}\times M$	$\beta_{102}\times10^{-11}\times M^2$	$\beta_{121}\times10^{-17}\times M^3$	*sig* $y\times10^3$	N
La	9.02(28)	3.57(18)	4.53(39)	3.8	36
Nd	94.7(17)	$3.88(10)\times10^2$	3.98(23)	2.7	39
Sm	181.7(19)	$2.75(4)\times10^3$	3.98(10)	2.2	97
Sm	175.8(44)	$2.62(8)\times10^3$	4.01(27)	1.7	37
Tb	183.4(59)	$1.12(4)\times10^4$	4.50(35)	2.3	38
Er	322(7)	$8.68(23)\times10^4$	3.69(60)	2.1	39
Yb	672(24)	$8.65(28)\times10^5$	2.83(24)	2.1	38

Table 8. Over-all enthalpy and entropy changes for the formation of proton and rare earth 1,2-bis-(carboxymethylamino)ethane complexes at 25.00°C and $I = 1.00$ M.

Proto-nation	$-\Delta H^\circ_{011}$	$-\Delta H^\circ_{021}$	ΔS°_{011}	ΔS°_{021}	*sig Q*/J
	37.3(11)	74.5(14)	61	64	0.035
Metal	$-\Delta H^\circ_{101}$	$-\Delta H^\circ_{102}$	ΔS°_{101}	ΔS°_{102}	*sig Q*/J
La	4.69(50)	13.22(66)	117	177	0.076
Ce	7.22(20)	12.94(29)	117	191	0.031
Pr	8.76(39)	15.90(54)	119	194	0.061
Nd	10.50(18)	19.21(24)	117	196	0.029
Sm	12.20(36)	25.17(47)	117	192	0.055
Gd	8.89(68)	24.95(87)	127	194	0.101
Tb	4.76(58)	22.12(70)	142	214	0.082
Dy	3.54(85)	19.82(97)	148	229	0.114
Ho	2.02(67)	13.99(82)	153	260	0.092
Er	1.40(47)	14.39(49)	158	257	0.059
Tm	1.63(42)	15.69(39)	160	264	0.044
Yb	3.24(35)	19.15(33)	158	260	0.041

which are in the range $3 \times 10^{-3} - 10 \times 10^{-3}$. In order to decide whether a model gives a fair description of the experimental data or not, one has to decide whether this range of *sig y* values corresponds to reasonably small errors in the various system variables or not. These variables are, *e.g.*, the various total concentrations and the measured E and E_R values.

Dellien [11] has given an account of one possible method for checking this: the measured emf-values are adjusted until an exact fit is obtained with the final set of constants. Reasonable "random errors" are then added to the various total concentrations and emf values and a new set of stability constants is then calculated. In this way one can for each estimate of the random errors obtain an estimate both of *sig y* and the errors in the various constants. The mean errors expected from our experimental procedure are 0.1 mV in E and 0.15 % in the various total concentrations. These errors give *sig y* values in the range $3 \times 10^{-3} - 7 \times 10^{-3}$. The equilibrium models we have used, all have *sig y* values in this range and we can thus conclude that the models do give a satisfactory description of the experimental data.

It is obvious from the data presented in Table 1 that systematic errors are present in some of the titration series. However, these errors are small and we did not feel it justified to decrease them by variations of the system variables.

Sillén [12] has given an account of how the errors in the constants are estimated in the "Letagrop" procedure. However, the magnitude of the error estimate is strongly dependent on the weighting of the experimental data. It is at best very difficult to assign weights to the various experimental data in measurements of the kind discussed here. For this reason one must not take the error estimates of the various constants literally. A better estimate may be obtained by the previously outlined procedure of assigning random errors to the system variables. This procedure indicates that mean errors of the magnitude mentioned above for the system variables give errors in the stability constants which are approximately 3σ for the dominating complexes, while the errors in the species present in small amounts might be 10 – 20 times their estimated standard deviations.

DISCUSSION

1,2-Bis(carboxymethylthio)ethane gives complexes of such low stability, $\beta_1 = 10^2$ M^{-1}, that one might assume that no chelate is formed and that the metal is bonded to only one carboxylate group. This is in keeping with the poor donor ability of sulphur noted already in thio-

diacetate. The complexes formed by 1,2-bis-(carboxymethyloxy)ethane and 1,2-bis(carboxymethylamino)ethane are much more stable, $\beta_1 = 10^5$ and 10^8 M^{-1}, respectively, suggesting the formation of chelates. The characteristic coordination number for both the latter ligands is two, indicating a coordination number of at least eight for the lanthanoid ions in the various MA_2^- complexes.

The second consecutive stability constant K_2 varies with a factor of 8 through the rare earth series for 1,2-bis(carboxymethyloxy)ethane. In the 1,2-bis(carboxymethylamino)ethane system the variation is much larger, a factor of 3.3×10^3. In this system K_2 turns out to be an approximately linear function of the atomic number Z. The data in Tables 6 and 8 show that a large part of the observed difference between the two ligands is a ligand specific enthalpy effect (*cf.* Fig. 4). The variation of ΔH°_{101} for the elements La through Tb is very similar to the type of variation previously found for a number of other ligands, *e.g.* those depicted in Fig. 1. Noticeable differences in ΔH°_{101} between the two ligands appear for the smallest lanthanoid ions. These differences are more pronounced in the enthalpy change for the second consecutive complex formation reactions.

The variations in ΔS°_{101} through the rare earth series are for both ligands very nearly the same as those found previously for a number of other ligands.[1,13] This similarity also extends to the entropy changes for the reactions $MA + A \rightarrow MA_2$, except for the heaviest lanthanoid elements (Er – Lu) in the 1,2-bis(carboxymethyloxy)ethane system where there is an additional increase in ΔS°.

From the study of the tridentate dicarboxylate ligands, we infer that the observed differences in the thermodynamic quantities between 1,2-bis(carboxymethyloxy)ethane and 1,2-bis-(carboxymethylamino)ethane cannot be due to the nature of the donor atoms. The fact that the differences between the two ligands are largest (*i.*) for the smallest central ions and (*i.i.*) in the second complexes, indicates that the differences are due to geometric factors. Even the presumably small differences in geometry between these tetradentate ligands give rise to large variations in the thermodynamic parameters with the size of the central ion. 1,2-Bis-(carboxymethylamino)ethane has obviously a much better size specificity than 1,2-bis-(carboxymethyloxy)ethane and the tridentate dicarboxylates and is the ligand to be preferred if one wants to separate the various rare earths

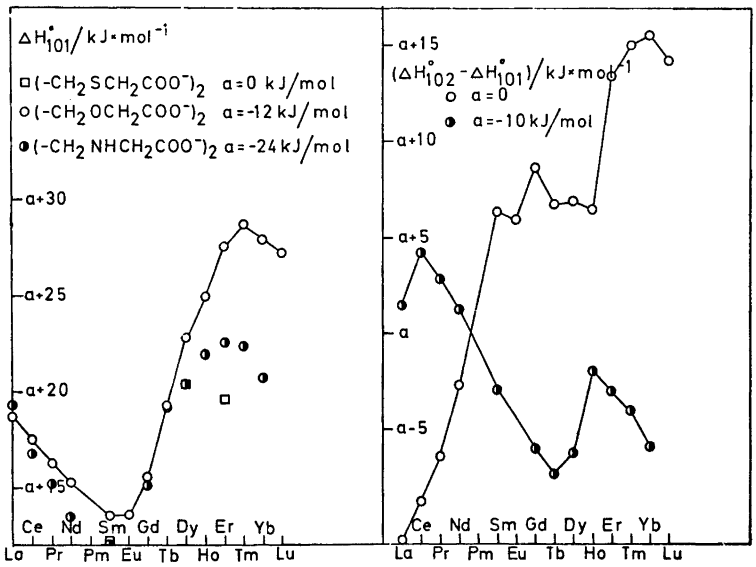

Fig. 4. ΔH°_{101} and $(\Delta H^\circ_{102} - \Delta H^\circ_{101})$ for the formation of rare earth complexes with 1,2-bis-(carboxymethylthio)ethane, 1,2-bis(carboxymethyloxy)ethane, and 1,2-bis(carboxymethylamino)-ethane. The various enthalpy values have been displaced by the quantity a given in the figure.

from one another.

From our data it seems as if the coordination geometry is more important for the size of the enthalpy term than for the corresponding entropy term. A similar finding has been noted for the formation of the third oxydiacetate and dipicolinate complexes where the relative decrease in the third consecutive stability constant observed for the rare earth elements with smallest ionic radius, was found to be predominantly an enthalpy effect.

The non-monotonic variation of ΔH°_{102} for the 1,2-bis(carboxymethylamino)ethane system may be due to a solvation equilibrium of the type discussed in previous communications,[14,15] *e.g.* a change in coordination number from nine to eight according to the following equilibrium

$$MA_2(H_2O)^- \rightleftharpoons MA_2^-$$

where K is near unity for Ho. Work is in progress to obtain more quantitative information about the possible occurrence of such equilibria in this system.

The difficulty of getting a quantitative estimate of differences in affinity between various donors is illustrated in Fig. 4. The difference in the quantity $(\Delta H^\circ_{102} - \Delta H^\circ_{101})$ between 1,2-bis(carboxymethyloxy)ethane and 1,2-bis(carboxymethylamino)ethane varies through the lanthanoid series from -3 kJ/mol to $+31.5$ kJ/mol. This variation does not depend on differences in the affinity of ether oxygen and NH or on the basicity of the carboxylate groups, but only on variations in the geometry of the complexes. The differences in ΔH°_{101} between ligands containing ether oxygen, ether sulphur, and iminogroups are quite different for the tri- and the tetradentate ligands. Hence, it seems as if estimates of relative affinities for one series of ligands cannot be used for quantitative prediction of the corresponding values for other ligands.

Ternary complexes are formed for all the three ligands investigated. The magnitude of the stability constants indicates that the ligands HA^- and H_2A are bonded to one carboxylate group only, *i.e.* that no chelates are formed. The amounts of the ternary complexes formed depend on the basicity of the ligand, the pH of the solution and on the relative magnitude of the stability constants for the ternary and binary complexes. Fairly high concentrations of MHA may be obtained in the 1,2-bis(carboxymethylthio)ethane system because of the low stability of the binary complexes. In the 1,2-bis(carboxymethyloxy)ethane system the binary complexes are much more stable and the concentration of MHA is thus too small to be detectable in the concentration range available.

No ternary complexes were detected in the earlier investigation of the rare earth 1,2-bis-(carboxymethylamino)ethane system. This is not especially surprising since the previous investigators did not study the complexation reactions at high hydrogen ion concentrations. The stability constants for the reaction

$$M^{3+} + H_2A \rightleftharpoons MH_2A^{3+}$$

are in the range $11 - 18$ M^{-1} in keeping with a unidentate coordination of the H_2A ligand. The acid H_2A exists mainly in the zwitter-ion form, a fact supported both by the magnitude of the protonation constants and the protonation enthalpies; *cf.* Table 8.

Acknowledgements. This work has been supported by a grant from the Swedish Natural Science Research Council. We also thank Mr. Sten Willstrand for his help with part of the experimental work.

REFERENCES

1. Dellien, I., Grenthe, I. and Hessler, G. *Acta Chem. Scand. 27* (1973) 2431.
2. Thompson, L. C. *J. Inorg. Nucl. Chem. 24* (1962) 1083.
3. Sevost'yanova, N. J., Martynenko, L. J., and Spitsyn, V. J. *Russ. J. Inorg. Chem. 15* (1970) 633.
4. Dellien, I. and Grenthe, I. *Acta Chem. Scand. 25* (1971) 1387.
5. Grenthe, I. and Gårdhammar, G. *Acta Chem. Scand. 25* (1971) 1401.
6. Grenthe, I. and Gårdhammar, G. *Acta Chem. Scand. 26* (1972) 3207.
7. Ots, H. *Acta Chem. Scand. 26* (1972) 3810.
8. Harrison, E. and May, R. *Pat. Brit. 639, 491, C.A. 44*, 10733*h*.
9. Ingri, N. and Sillén, L. G. *Ark. Kemi 23* (1968) 97.
10. Arnek, R. *Ark. Kemi 32* (1970) 55.
11. Dellien, I. *Thesis*, Lund 1973.
12. Sillén, L. G. *Acta Chem. Scand. 16* (1962) 159.
13. Grenthe, I. *Acta Chem. Scand. 18* (1964) 293.
14. Grenthe, I. and Ots, H. *Acta Chem. Scand. 26* (1972) 1229.
15. Ots, H. *Acta Chem. Scand. 27* (1973) 2351.
16. Albertsson, J. *Acta Chem. Scand. 24* (1970) 3527.
17. Albertsson, J. *Acta Chem. Scand. 24* (1970) 1213.

Received September 12, 1973.

Acta Chemica Scandinavica A 28 (1974) 137—144

The Crystal Structure of Tetramethylammonium Diisocyanatoargentate(I)

KJELL AARFLOT and KJELL ÅSE

Chemical Institute, University of Bergen, N-5000 Bergen, Norway

The crystal structure of tetramethylammonium diisocyanatoargentate(I), $(CH_3)_4NAg(NCO)_2$, has been determined by three-dimensional X-ray diffraction methods. The crystals are orthorhombic, space group *Pnma* (No. 62), with cell dimensions $a = 10.867(6)$ Å, $b = 6.614(5)$ Å, and $c = 13.852(7)$ Å. Intensity data were collected with an automatic single-crystal diffractometer, using Nb-filtered Mo$K\alpha$ radiation. Least squares refinement, based on 640 independent, non-zero reflections, resulted in a conventional R value of 0.048.

The crystals contain diisocyanatoargentate(I) ions and tetramethylammonium ions. The approximately linear $[OCNAgNCO]^-$ ions are located in mirror planes. The Ag—N bond lengths are 2.015(13) and 2.068(12) Å, and the N—Ag—N bond angle is 177.2(5)°. The tetramethylammonium ions also possess mirror plane symmetry. They are subject to disorder or extreme thermal motion, with rotation about one of the N—C bonds.

The synthesis of tetramethylammonium diisocyanatoargentate(I), $(CH_3)_4NAg(NCO)_2$, has been reported earlier.[1] From vibrational spectra it has been deduced that the crystals contain complex anions $Ag(NCO)_2^-$ with a symmetry centre, and with the silver atom bonded to the nitrogen atoms of the pseudohalide groups.[2] In conformance with the vibrational spectra, a ^{14}N NMR study has shown that the NCO groups are nitrogen-bonded in this compound.[3] The crystal structure has now been determined by X-ray diffraction methods, and is reported here.

EXPERIMENTAL

Collection of X-ray data was done by means of a Siemens automatic, off-line, single-crystal diffractometer (AED), using Mo$K\alpha$ radiation (Nb-filtered). The diffractometer was operated as a three-circle instrument.

The measurements were performed on a crystal with the following dimensions, given as distances from a common origin to faces: Distances to (001) and $(00\bar{1}) = 0.25$ mm; to (101) and $(\bar{1}0\bar{1}) = 0.22$ mm; to $(10\bar{1})$ and $(\bar{1}01) = 0.21$ mm; and to (011), $(0\bar{1}\bar{1})$, $(01\bar{1})$, and $(0\bar{1}1) = 0.24$ mm. The crystal was mounted with the c axis approximately along the ϕ axis of the diffractometer, and its orientation and cell dimensions were determined by measuring the θ, χ, and ϕ angles for five non-coplanar reciprocal vectors. Intensity data were collected with a scintillation counter, using the $\theta - 2\theta$ scan technique. The scan-speed was set to 5-degrees per minute in the θ angle, with automatic setting of twice this speed for strong reflections. The rather high scan speed was chosen because of rapid blackening of the crystal when exposed to air and X-rays. Counting losses were avoided by means of attenuation filters, which were automatically inserted into the primary beam when needed. Each reflection was scanned between $\theta_1 = \theta - 0.40°$ and $\theta_2 = \theta + 0.40° + 0.35° \operatorname{tg} \theta$, where θ is the Bragg angle for the α_1 peak. The scan was carried out by going from θ to θ_1, then from θ_1 to θ_2, and finally from θ_2 to θ. The intensities over each scanning range were recorded at the end of each step. The background was measured for one half of the total scan time at θ_1 and one half at θ_2. The intensities of all independent reflections with $\theta \leqq 25°$ were measured.

Using the intensity variations of two reference reflections, measured at intervals of 50 reflections, the net intensities were brought to a common scale. The lower limit for an observed reflection was set equal to two times the standard deviation in net intensity. The standard deviation in net intensity is $(I_t + I_b)^{\frac{1}{2}}$, where I_t is the total intensity, and I_b is the background intensity. Out of 966 measured reflections, 640 had intensities above the lower limit. The remaining 326 reflections were assigned an intensity equal to the observable limit, and la-

belled as unobserved reflections.

The intensities were corrected for absorption ($\mu = 19.4$ cm^{-1}), using a modified version of the correction method originally described by Busing and Levy.[4] A $10 \times 10 \times 8$ grid was applied in the calculations. Lorentz and polarization corrections were carried out, and the corrected intensities were reduced to relative observed structure factors.

The calculated structure factors were based on the atomic scattering factor curves listed in *International Tables*.[5] Using the $\Delta f'$ and $\Delta f''$ values given by Cromer,[6] the silver scattering curve was corrected for anomalous dispersion, by taking the amplitude of f as the corrected value.

Least squares refinement was carried out with a full-matrix program minimizing the function

$$r = \sum W(|F_o| - K|F_c|)^2$$

where K is a scale factor, and the weight, W, is the inverse of the variance in F_o. The variance in F_o is

$$\sigma^2(F_o) = F_o^2[I_t + I_b + k^2(I_t - I_b)^2]/4(I_t - I_b)^2$$

where k may be interpreted as the relative standard deviation in the scaling curve. The value of k was estimated to be 0.02. Non-observed reflections for which $K|F_c|$ is greater than the observable limit, are included in the refinement with $|F_o|$ equal to the observable limit.

The calculations were carried out on an IBM 360/50 H computer. Most programs used have been listed in an earlier paper.[7] Rigid-body motion analysis was carried out with the program RBM, written by Schomaker and Trueblood,[8] and adapted for the IBM computer by L. Milje, of this Institute. A drawing was performed with the program OR TEP, written by C. K. Johnson.[9]

CRYSTAL DATA

The crystals of tetramethylammonium diisocyanatoargentate(I) occurred as colourless, orthorhombic prisms bounded by {001}, {101}, and {011}. Calculations of unit cell dimensions by a least squares procedure were based on 10 high-angle θ-values measured on the diffractometer. The numbers in parentheses are standard deviations in last digits:

$a = 10.867(6)$ Å; $b = 6.614(5)$ Å; $c = 13.852(7)$ Å; $V = 995.6(11)$ Å^3; $M = 266.05$; $F(000) = 528$; $Z = 4$;

ϱ_o(flotation) $= 1.775$ g/cm^3; $\varrho_c = 1.774$ g/cm^3.

Systematic absences are $0kl$ when $k + l = 2n + 1$, and $hk0$ when $h = 2n + 1$. The space group is either $Pna2_1$ (No. 33) or $Pnma$ (No. 62). (Most data quoted here were reported in the earlier paper.[1])

STRUCTURE DETERMINATION

A test for centrosymmetry was made by applying the method of Foster and Hargreaves [10] to the intensities, but no definite conclusion could be reached. No further attempts were made to distinguish between the two possible space groups at this stage.

As both space groups have centrosymmetric $h0l$ projections (indexing according to space group $Pnma$), this projection was first examined. A Patterson synthesis readily gave the x and z coordinates of the silver atom. Most of the lighter non-hydrogen atoms were located through subsequent Fourier syntheses. Only the nitrogen atom [N(3)] and one methyl carbon atom [C(3)] of the tetramethylammonium ion showed up as distinct peaks in the maps. This was thought to be due to disorder of the remaining methyl carbon atoms.

From the positions of the atoms in the $h0l$ projection, and assumed bond lengths, the centrosymmetric space group $Pnma$ appeared to be the most probable one, and the three-dimensional structure analysis was therefore based on this space group. The determination of the y coordinates offered no problem, since most of the atoms, including the silver atom, has to be situated in mirror planes normal to the b axis. The disorder of the methyl carbon atoms showed up in the three-dimensional Fourier maps as well, no matter whether these atoms had been included in the preceding structure factor calculations or not. The disorder might be described as a 60° rotation of the tetramethylammonium ion about one of the nitrogen-carbon bonds, N(3)–C(3), transferring the three other methyl carbon atoms of the ion from one set of positions to another. Two requirements have to be imposed on the occupancy factors when this model is applied. The occupancy factors have to be equal within each set of positions (leaving out of account the factor of 0.5 for atoms situated in mirror planes). Also, the sum of occupancy factors have to make up one tetramethylammonium ion. The least squares program used for refinement of

Table 1. Atomic coordinates in fractions of orthorhombic cell edges, and occupancy factors. Standard deviations from the least squares refinement in parentheses.

	x	y	z	Occupancy
Ag	0.03938(8)	0.25	0.07657(6)	0.5
N(1)	−0.1152(12)	0.25	−0.0039(9)	0.5
C(1)	−0.2059(14)	0.25	−0.0351(10)	0.5
O(1)	−0.3058(9)	0.25	−0.0723(7)	0.5
N(2)	0.2029(10)	0.25	0.1530(9)	0.5
C(2)	0.2972(13)	0.25	0.1843(10)	0.5
O(2)	0.3932(11)	0.25	0.2157(9)	0.5
N(3)	0.1458(7)	0.75	0.3517(5)	0.5
C(3)	0.2778(11)	0.75	0.3333(11)	0.5
C(4)	0.0811(21)	0.75	0.2539(14)	0.278(9)
C(5)	0.1197(21)	0.9289(29)	0.4061(17)	0.556(15)
C(6)	0.1189(28)	0.75	0.4635(18)	0.222(9)
C(7)	0.0838(23)	0.9336(38)	0.3163(25)	0.444(16)

structural parameters did not contain options for these requirements, and the occupancy factors therefore had to be adjusted after each cycle in which they had been subject to refinement. The initial values of the occupancy factors were estimated from the relative hights of the corresponding peaks in the electron density map.

The three-dimensional least squares refinement was started with individual isotropic thermal parameters. After a series of cycles, including one refinement cycle on the occupancy factors of the disordered carbon atoms, the conventional R value was 0.119. Anisotropic thermal parameters were introduced for the atoms of the diisocyanatoargentate ion, and the refinement was continued to an R value of 0.087. At this stage the observed structure factors were corrected for extinction, using the expression given by Zachariasen.[11] With the absorption term set equal to unity, and with observed intensities on an absolute scale, the value of the extinction parameter, C, was found to be 6.40×10^{-6}. Additional refinement on the parameters mentioned above lowered the R value to 0.059. Introduction of anisotropic thermal parameters for the atoms of the tetramethylammonium ion resulted in an R value of

Table 2. Anisotropic thermal parameters (Å²) in the form $\exp[-2\pi^2(h^2a^{-2}U_{11}+\cdots+2hka^{-1}b^{-1}U_{12}+\cdots)]$. All values have been multiplied by 10^3. Standard deviations from the least squares refinement in parentheses.

	U_{11}	U_{22}	U_{33}	U_{12}	U_{23}	U_{13}
Ag	82(1)	105(1)	105(1)	0	0	−7(1)
N(1)	114(9)	175(11)	160(12)	0	0	−72(10)
C(1)	90(9)	93(8)	93(8)	0	0	−17(8)
O(1)	112(7)	114(7)	155(8)	0	0	−21(7)
N(2)	91(7)	113(8)	160(10)	0	0	−20(8)
C(2)	78(8)	85(8)	118(10)	0	0	−2(8)
O(2)	94(7)	209(11)	209(12)	0	0	−52(8)
N(3)	62(5)	67(5)	62(5)	0	0	6(4)
C(3)	53(7)	256(18)	157(12)	0	0	22(8)
C(4)	113(19)	146(21)	68(13)	0	0	−30(12)
C(5)	179(18)	97(13)	162(20)	29(13)	−67(15)	−7(16)
C(6)	127(23)	113(22)	58(14)	0	0	8(16)
C(7)	147(22)	116(19)	212(31)	26(16)	94(22)	−15(20)

0.048. Another refinement cycle on the occupancy factors of the disordered atoms was carried out, no other parameters being refined in this cycle. In a final cycle, all positional and anisotropic thermal parameters were allowed to vary. No shift was greater than 0.012 times the standard deviation. The final R value, including non-observed reflections with $K|F_c|$ exceeding the observable limit, was 0.048. The final atomic coordinates and occupancy factors are listed in Table 1, the thermal parameters in Table 2, and the structure factors in Table 3.

Table 3. Observed and calculated structure factors (× 10). Unobserved reflections are indicated by a minus sign on $F(O)$ and included at the threshold values.

H	K	L	F(O)	F(C)	H	K	L	F(O)	F(C)	H	K	L	F(O)	F(C)	H	K	L	F(O)	F(C)	H	K	L	F(O)	F(C)
0	0	2	807	858	6	0	9	207	206	2	1	4	511	460	8	1	10	54	-44	4	2	4	260	279
0	0	4	520	-495	6	0	10	60	-5	2	1	5	689	-691	8	1	11	-44	-44	4	2	5	483	480
0	0	6	719	-704	6	0	11	106	107	2	1	6	515	495	8	1	12	51	-53	4	2	6	321	316
0	0	8	504	-525	6	0	12	-45	11	2	1	7	125	114	9	1	1	248	-247	4	2	7	96	-101
0	0	10	-43	-44	6	0	13	-44	6	2	1	8	286	279	9	1	2	199	195	4	2	8	198	197
0	0	12	209	210	6	0	14	51	16	2	1	9	341	355	9	1	3	41	-53	4	2	9	270	-269
0	0	14	90	93	7	0	1	173	-163	2	1	10	49	-35	9	1	4	111	109	4	2	10	65	-60
0	0	16	-45	-4	7	0	2	550	-546	2	1	11	185	185	9	1	5	178	178	4	2	11	132	-133
1	0	1	1063	1265	7	0	3	-38	34	2	1	12	88	-77	9	1	6	88	77	4	2	12	61	-65
1	0	2	364	-450	7	0	4	498	-486	2	1	13	-41	9	9	1	7	132	129	4	2	13	-42	7
1	0	3	671	652	7	0	5	42	51	2	1	14	55	-49	9	1	8	50	-32	4	2	14	-44	-19
1	0	4	443	-428	7	0	6	80	-96	2	1	15	66	-59	9	1	9	-44	38	4	2	15	-46	21
1	0	5	805	-794	7	0	7	-38	-30	2	1	16	-46	-15	9	1	10	53	-50	5	2	1	194	-192
1	0	6	301	-301	7	0	8	152	145	3	1	1	886	-859	9	1	11	-45	-21	5	2	2	626	615
1	0	7	612	-604	7	0	9	73	71	3	1	2	559	-514	10	1	0	109	-135	5	2	3	69	60
1	0	8	141	131	7	0	10	194	195	3	1	3	186	-168	10	1	1	-40	30	5	2	4	505	512
1	0	9	151	-153	7	0	11	-44	41	3	1	4	558	-574	10	1	2	-41	-44	5	2	5	95	100
1	0	10	100	101	7	0	12	-45	39	3	1	5	507	491	10	1	3	188	191	5	2	6	91	84
1	0	11	163	174	7	0	13	-46	-18	3	1	6	253	-246	10	1	4	69	80	5	2	7	89	86
1	0	12	-41	6	8	0	0	203	-194	3	1	7	559	550	10	1	5	154	155	5	2	8	111	-113
1	0	13	136	139	8	0	1	277	-279	3	1	8	313	307	10	1	6	100	91	5	2	9	-38	32
1	0	14	-43	2	8	0	2	104	-112	3	1	9	105	108	10	1	7	-44	-18	5	2	10	163	-169
1	0	15	49	49	8	0	3	341	-346	3	1	10	207	211	10	1	8	-45	51	5	2	11	-41	3
1	0	16	-46	-7	8	0	4	67	68	3	1	11	-39	-35	10	1	9	69	-53	5	2	12	80	-66
2	0	0	641	703	8	0	5	112	-110	3	1	12	-40	19	10	1	10	-46	-9	5	2	13	-45	-23
2	0	1	605	-532	8	0	6	118	118	3	1	13	83	-84	11	1	1	60	-46	5	2	14	-46	28
2	0	2	660	662	8	0	7	51	52	3	1	14	-43	-25	11	1	2	110	120	6	2	0	92	-82
2	0	3	915	-939	8	0	8	118	116	3	1	15	-45	-19	11	1	3	-43	32	6	2	1	239	246
2	0	4	162	-164	8	0	9	164	171	4	1	0	625	-662	11	1	4	108	117	6	2	2	47	-47
2	0	5	230	-218	8	0	10	-43	24	4	1	1	288	-303	11	1	5	45	37	6	2	3	494	486
2	0	6	908	-857	8	0	11	81	91	4	1	2	589	-571	11	1	6	-45	28	6	2	4	117	119
2	0	7	38	32	8	0	12	47	-15	4	1	3	642	-656	11	1	7	60	42	6	2	5	345	347
2	0	8	321	-312	9	0	1	140	-134	4	1	4	210	210	11	1	8	-46	-35	6	2	6	40	13
2	0	9	66	58	9	0	2	115	-104	4	1	5	155	-159	12	1	0	56	-13	6	2	7	95	-96
2	0	10	73	74	9	0	3	-38	-38	4	1	6	447	449	12	1	1	-46	59	6	2	8	-38	15
2	0	11	136	135	9	0	4	217	-213	4	1	7	82	79	12	1	2	-44	-15	6	2	9	175	-174
2	0	12	150	155	9	0	5	115	113	4	1	8	286	279	12	1	3	89	86	6	2	10	-41	2
2	0	13	-42	0	9	0	6	-41	-3	4	1	9	140	135	12	1	4	-46	28	6	2	11	87	-83
2	0	14	89	81	9	0	7	150	166	4	1	10	-38	-12	12	1	5	72	57	6	2	12	-44	-11
2	0	15	-45	-35	9	0	8	111	128	4	1	11	109	114	0	2	0	2318	-2584	6	2	13	-45	-2
2	0	16	-46	12	9	0	9	-44	36	4	1	12	80	-85	0	2	2	721	-694	6	2	14	-46	-12
3	0	1	977	1037	9	0	10	82	76	4	1	13	-42	-3	0	2	4	221	235	7	2	1	119	122
3	0	2	393	-380	9	0	11	-45	-18	4	1	14	58	-63	0	2	6	541	537	7	2	2	387	394
3	0	3	-31	-57	10	0	0	113	-114	4	1	15	47	-35	0	2	8	389	389	7	2	3	-37	-33
3	0	4	548	-562	10	0	1	48	-39	5	1	1	763	-757	0	2	10	43	63	7	2	4	373	381
3	0	5	654	-659	10	0	2	102	-109	5	1	2	279	-274	0	2	12	157	-157	7	2	5	-37	-20
3	0	6	186	-180	10	0	3	177	-166	5	1	3	153	-148	0	2	14	92	-80	7	2	6	80	81
3	0	7	549	-568	10	0	4	53	68	5	1	4	236	-241	1	2	1	1185	-1134	7	2	7	-38	27
3	0	8	285	275	10	0	5	76	-66	5	1	5	389	388	1	2	2	612	552	7	2	8	112	-112
3	0	9	131	-127	10	0	6	118	118	5	1	6	-33	5	1	2	3	250	-267	7	2	9	52	-62
3	0	10	199	212	10	0	7	-43	32	5	1	7	471	463	1	2	4	316	311	7	2	10	157	-152
3	0	11	106	102	10	0	8	-45	57	5	1	8	168	159	1	2	5	641	626	7	2	11	-44	-34
3	0	12	79	65	10	0	9	63	55	5	1	9	90	96	1	2	6	195	196	7	2	12	-45	-34
3	0	13	104	112	10	0	10	-46	11	5	1	10	75	71	1	2	7	505	504	7	2	13	-46	15
3	0	14	-43	-18	11	0	1	152	-149	5	1	11	124	-115	1	2	8	118	-121	8	2	0	168	169
3	0	15	-45	33	11	0	2	97	-97	5	1	12	-41	26	1	2	9	121	113	8	2	1	222	228
3	0	16	-46	-33	11	0	3	-43	-15	5	1	13	77	-86	1	2	10	84	-91	8	2	2	94	94
4	0	0	287	280	11	0	4	51	-24	5	1	14	-44	-21	1	2	11	157	-153	8	2	3	269	276
4	0	1	613	-570	11	0	5	87	66	5	1	15	59	-31	1	2	12	-39	7	8	2	4	45	-53
4	0	2	334	341	11	0	6	-45	-15	6	1	0	998	-1035	1	2	13	97	-109	8	2	5	89	86
4	0	3	887	-883	11	0	7	98	96	6	1	1	-33	-22	1	2	14	-42	0	8	2	6	99	-105
4	0	4	334	-326	11	0	8	-46	25	6	1	2	380	-379	1	2	15	-44	-37	8	2	7	43	-38
4	0	5	611	-593	12	0	0	145	-155	6	1	3	-32	-11	2	2	0	529	-499	8	2	8	84	-90
4	0	6	373	-366	12	0	1	-46	-3	6	1	4	256	257	2	2	1	142	148	8	2	9	137	-134
4	0	7	113	100	12	0	2	66	-67	6	1	5	-35	-44	2	2	2	547	-525	8	2	10	-43	-14
4	0	8	252	-255	12	0	3	-44	-20	6	1	6	387	395	2	2	3	547	532	8	2	11	78	-73
4	0	9	353	342	12	0	4	-45	35	6	1	7	-36	26	2	2	4	129	133	8	2	12	-45	12
4	0	10	46	49	12	0	5	-46	-8	6	1	8	190	193	2	2	5	199	202	9	2	1	107	104
4	0	11	169	172	12	0	6	58	60	6	1	9	-39	22	2	2	6	697	693	9	2	2	80	80
4	0	12	34	77	0	1	1	533	-624	6	1	10	-40	7	2	2	7	-33	-3	9	2	3	-39	31
4	0	13	-43	-12	0	1	3	876	-837	6	1	11	-41	-9	2	2	8	231	237	9	2	4	187	182
4	0	14	-44	28	0	1	5	470	-491	6	1	12	117	-119	2	2	9	-35	-17	9	2	5	71	-85
4	0	15	-45	-26	0	1	7	213	216	6	1	13	-44	-37	2	2	10	44	-56	9	2	6	-41	2
5	0	1	351	358	0	1	9	545	546	6	1	14	75	-73	2	2	11	117	-114	9	2	7	118	-126
5	0	2	818	-819	0	1	11	188	186	7	1	1	456	-465	2	2	12	123	-123	9	2	8	103	-107
5	0	3	231	-211	0	1	13	-40	10	7	1	2	43	-30	2	2	13	-41	-10	9	2	9	-44	-32
5	0	4	731	-732	0	1	15	59	-49	7	1	3	69	-66	2	2	14	78	-66	9	2	10	-45	-60
5	0	5	126	-125	1	1	1	418	-347	7	1	4	128	131	2	2	15	-45	30	9	2	11	-45	15
5	0	6	77	-89	1	1	2	1366	-1400	7	1	5	276	282	3	2	1	694	-696	10	2	0	115	103
5	0	7	131	-127	1	1	3	888	872	7	1	6	-37	7	3	2	2	495	479	10	2	1	-41	39
5	0	8	173	167	1	1	4	1237	-1216	7	1	7	204	210	3	2	3	-29	42	10	2	2	85	83
5	0	9	42	-41	1	1	5	-27	23	7	1	8	76	-86	3	2	4	435	426	10	2	3	135	126
5	0	10	202	207	1	1	6	122	-113	7	1	9	54	54	3	2	5	449	438	10	2	4	63	-56
5	0	11	-44	7	1	1	7	65	62	7	1	10	-42	43	3	2	6	125	121	10	2	5	73	69
5	0	12	-72	74	1	1	8	323	322	7	1	11	-38	-81	3	2	7	400	407	10	2	6	98	-93
5	0	13	-44	26	1	1	9	104	106	7	1	12	-44	-26	3	2	8	234	-232	10	2	7	-44	-20
5	0	14	-45	-35	1	1	10	355	351	7	1	13	71	-77	3	2	9	118	117	10	2	8	-45	-46
5	0	15	50	-10	1	1	11	-38	-19	8	1	0	402	-387	3	2	10	177	-180	10	2	9	-45	-43
6	0	0	-33	6	1	1	12	121	122	8	1	1	95	91	3	2	11	76	-75	11	2	1	123	116
6	0	1	272	-278	1	1	13	49	-53	8	1	2	219	-223	3	2	12	-41	-44	11	2	2	83	80
6	0	2	109	111	1	1	14	62	-54	8	1	3	140	143	3	2	13	91	-93	11	2	3	-44	20
6	0	3	570	-564	1	1	15	-44	-12	8	1	4	-37	5	3	2	14	-44	16	11	2	4	-44	29
6	0	4	134	-145	1	1	16	-46	-51	8	1	5	-37	6	3	2	15	-45	-28	11	2	5	55	-59
6	0	5	449	-449	2	1	0	88	70	8	1	6	262	270	4	2	0	419	-418	11	2	6	-44	9
6	0	6	-37	-45	2	1	1	611	-581	8	1	7	-41	32	4	2	1	347	333	11	2	7	76	-79
6	0	7	94	107	2	1	2	493	-480	8	1	8	150	140	4	2	2	266	-264	12	2	0	125	125
6	0	8	-37	-5	2	1	3	1284	-1352	8	1	9	-43	-53	4	2	3	687	667	12	2	1	-45	-1

Table 3. Continued.

H	K	L	F(O)	F(C)
12	2	2	-46	53
12	2	3	-45	15
12	2	4	-45	-27
0	3	1	548	515
0	3	3	624	607
0	3	5	306	310
0	3	7	130	-127
0	3	9	373	-379
0	3	11	111	-118
0	3	13	-42	4
0	3	15	-45	31
1	3	1	99	97
1	3	2	648	648
1	3	3	348	-321
1	3	4	680	670
1	3	5	-31	-15
1	3	6	60	63
1	3	7	-34	-4
1	3	8	177	-170
1	3	9	71	-66
1	3	10	193	-203
1	3	11	-39	1
1	3	12	91	-87
1	3	13	-42	35
1	3	14	45	34
1	3	15	-45	10
2	3	0	272	259
2	3	1	360	349
2	3	2	257	257
2	3	3	744	747
2	3	4	230	-235
2	3	5	400	403
2	3	6	330	-330
2	3	7	74	-69
2	3	8	183	-184
2	3	9	217	-221
2	3	10	50	50
2	3	11	115	-115
2	3	12	-42	56
2	3	13	-43	-5
2	3	14	-44	29
2	3	15	-46	39
3	3	1	437	419
3	3	2	321	336
3	3	3	138	152
3	3	4	401	397
3	3	5	281	-282
3	3	6	151	142
3	3	7	276	-276
3	3	8	199	-207
3	3	9	69	-76
3	3	10	133	-139
3	3	11	-40	11
3	3	12	-42	-7
3	3	13	55	56
3	3	14	-44	16
4	3	0	510	515
4	3	1	166	160
4	3	2	230	286
4	3	3	327	322
4	3	4	141	-136
4	3	5	65	78
4	3	6	262	-256
4	3	7	-37	-31
4	3	8	187	-191
4	3	9	71	-67
4	3	10	-40	11
4	3	11	86	-77
4	3	12	70	57
4	3	13	-43	-2
4	3	14	50	40
5	3	1	430	445
5	3	2	206	210
5	3	3	118	116
5	3	4	156	146
5	3	5	266	-273
5	3	6	-36	-8
5	3	7	308	-303
5	3	8	109	-110
5	3	9	-40	-53
5	3	10	65	-55
5	3	11	79	74
5	3	12	-43	-13
5	3	13	62	55
6	3	0	541	548
6	3	1	37	-20
6	3	2	225	227
6	3	3	-36	7
6	3	4	156	-156
6	3	5	40	32
6	3	6	235	-235
6	3	7	49	-26
6	3	8	111	-121
6	3	9	-41	-12
6	3	10	-41	-12
6	3	11	-43	6
6	3	12	71	74
6	3	13	-45	22
7	3	1	300	305
7	3	2	-37	16
7	3	3	-37	19
7	3	4	94	-94
7	3	5	182	-178
7	3	6	-38	-1
7	3	7	146	-151
7	3	8	44	55
7	3	9	-42	-33
7	3	10	-43	23
7	3	11	59	55
7	3	12	-45	16
8	3	0	234	230
8	3	1	69	-64
8	3	2	147	147
8	3	3	74	-77
8	3	4	41	-11
8	3	5	-40	-2
8	3	6	170	-169
8	3	7	-42	-25
8	3	8	93	-90
8	3	9	-44	31
8	3	10	-44	25
8	3	11	-46	30
9	3	1	160	161
9	3	2	116	-121
9	3	3	-41	24
9	3	4	74	-83
9	3	5	109	-106
9	3	6	-44	-45
9	3	7	75	-81
9	3	8	-44	25
9	3	9	-45	-25
9	3	10	-46	33
10	3	0	72	81
10	3	1	-42	-17
10	3	2	-42	37
10	3	3	113	-119
10	3	4	52	-47
10	3	5	104	-102
10	3	6	88	-67
10	3	7	46	12
10	3	8	-46	-29
11	3	1	-45	28
11	3	2	77	-83
11	3	3	-46	-18
11	3	4	73	-71
11	3	5	-46	-22
11	3	6	-47	-18
0	4	0	1010	995
0	4	2	311	310
0	4	4	199	-195
0	4	6	247	-243
0	4	8	186	-173
0	4	10	-40	-34
0	4	12	87	78
0	4	14	-46	39
1	4	1	461	458
1	4	2	184	-183
1	4	3	138	137
1	4	4	144	-145
1	4	5	279	-277
1	4	6	95	-109
1	4	7	275	-288
1	4	8	62	56
1	4	9	44	-55
1	4	10	44	52
1	4	11	67	76
1	4	12	-43	-3
1	4	13	56	58
1	4	14	-46	0
2	4	0	274	274
2	4	1	142	-137
2	4	2	233	235
2	4	3	256	-252
2	4	4	92	-91
2	4	5	60	-52
2	4	6	307	-309
2	4	7	-38	7
2	4	8	107	-118
2	4	9	-39	2
2	4	10	42	22
2	4	11	58	56
2	4	12	56	67
2	4	13	-44	4
2	4	14	-46	35
3	4	1	343	344
3	4	2	173	-173
3	4	3	61	-42
3	4	4	241	-244
3	4	5	206	-206
3	4	6	57	-70
3	4	7	179	-177
3	4	8	124	130
3	4	9	44	-54
3	4	10	99	94
3	4	11	53	41
3	4	12	-44	26
3	4	13	55	48
4	4	0	184	184
4	4	1	153	-152
4	4	2	125	135
4	4	3	297	-304
4	4	4	71	-74
4	4	5	204	-207
4	4	6	163	-170
4	4	7	47	44
4	4	8	98	-101
4	4	9	139	136
4	4	10	-42	33
4	4	11	68	70
4	4	12	-44	34
4	4	13	-45	-4
5	4	1	111	101
5	4	2	307	-312
5	4	3	39	-16
5	4	4	234	-237
5	4	5	54	-59
5	4	6	46	-38
5	4	7	-39	-25
5	4	8	44	63
5	4	9	-41	-16
5	4	10	84	85
5	4	11	-44	0
5	4	12	-45	33
6	4	0	61	59
6	4	1	106	-102
6	4	2	-38	15
6	4	3	252	-248
6	4	4	53	-49
6	4	5	181	-178
6	4	6	-40	-12
6	4	7	-41	44
6	4	8	-41	-8
6	4	9	94	90
6	4	10	-43	2
6	4	11	-46	47
6	4	12	47	5
7	4	1	66	-64
7	4	2	201	-203
7	4	3	-39	9
7	4	4	183	-180
7	4	5	-40	13
7	4	6	-41	-44
7	4	7	-41	-10
7	4	8	74	57
7	4	9	-44	25
7	4	10	85	77
7	4	11	46	19
8	4	0	87	-86
8	4	1	109	-106
8	4	2	42	-48
8	4	3	148	-145
8	4	4	-41	17
8	4	5	-42	-52
8	4	6	46	53
8	4	7	-43	26
8	4	8	-46	47
8	4	9	63	70
9	4	1	56	-58
9	4	2	45	-41
9	4	3	50	-11
9	4	4	88	-94
9	4	5	-44	40
9	4	6	50	-5
9	4	7	58	62
9	4	8	56	55
10	4	0	66	-60
10	4	1	-44	-28
10	4	2	-45	-43
10	4	3	65	-64
10	4	4	-45	31
10	4	5	47	-25
10	4	6	51	50
11	4	1	55	-58
11	4	2	65	-44
0	5	1	102	-109
0	5	3	202	-202
0	5	5	135	-142
0	5	7	-40	41
0	5	9	141	137
0	5	11	68	55
1	5	1	82	-82
1	5	2	301	-302
1	5	3	119	116
1	5	4	223	-232
1	5	5	-38	27
1	5	6	-39	-22
1	5	7	-39	8
1	5	8	88	77
1	5	9	-42	21
1	5	10	94	91
1	5	11	-44	-11
1	5	12	-45	29
2	5	0	38	-35
2	5	1	114	-105
2	5	2	95	-97
2	5	3	276	-276
2	5	4	-38	26
2	5	5	154	-167
2	5	6	117	123
2	5	7	-40	38
2	5	8	60	63
2	5	9	93	82
2	5	10	-43	-9
2	5	11	54	47
2	5	12	-45	-19
3	5	1	196	-201
3	5	2	106	-104
3	5	3	-38	-24
3	5	4	149	-149
3	5	5	119	112
3	5	6	46	-64
3	5	7	108	102
3	5	8	79	70
3	5	9	-43	32
3	5	10	63	58
3	5	11	-44	-16
3	5	12	-45	4
4	5	0	200	-203
4	5	1	107	-109
4	5	2	116	-116
4	5	3	137	-139
4	5	4	42	47
4	5	5	53	-24
4	5	6	115	111
4	5	7	-42	19
4	5	8	75	74
4	5	9	-44	40
4	5	10	-44	-1
4	5	11	-45	30
5	5	1	156	-156
5	5	2	47	-45
5	5	3	-40	-45
5	5	4	63	-66
5	5	5	96	98
5	5	6	-41	9
5	5	7	122	122
5	5	8	-43	38
5	5	9	-44	28
5	5	10	-45	21
5	5	11	-46	-31
6	5	0	213	-215
6	5	1	-40	-4
6	5	2	107	-95
6	5	3	-40	2
6	5	4	69	77
6	5	5	-41	-6
6	5	6	106	109
6	5	7	-43	5
6	5	8	53	50
6	5	9	-45	13
6	5	10	-46	0
7	5	1	121	-116
7	5	2	-41	-8
7	5	3	-42	-8
7	5	4	-42	27
7	5	5	72	71
7	5	6	-43	6
7	5	7	62	64
7	5	8	-44	-17
7	5	9	-45	17
8	5	0	108	-100
8	5	1	-43	33
8	5	2	64	-57
8	5	3	-44	36
8	5	4	-43	8
8	5	5	-44	5
8	5	6	66	67
8	5	7	-45	4
9	5	1	87	-70
9	5	2	-45	46
9	5	3	-44	-12
9	5	4	-45	37
9	5	5	-47	50
10	5	0	-46	-32
0	6	0	300	-307
0	6	2	95	-97
0	6	4	72	66
0	6	6	85	92
0	6	8	77	75
0	6	10	-45	2
1	6	1	118	-123
1	6	2	45	41
1	6	3	44	-44
1	6	4	50	37
1	6	5	88	89
1	6	6	57	28
1	6	7	84	81
1	6	8	-43	-7
1	6	9	-44	19
1	6	10	-45	-12
2	6	0	85	-98
2	6	1	63	63
2	6	2	67	-70
2	6	3	83	87
2	6	4	-41	33
2	6	5	-41	31
2	6	6	106	101
2	6	7	-43	-3
2	6	8	63	44
2	6	9	-44	-16
2	6	10	-45	-13
3	6	1	118	-115
3	6	2	-41	37
3	6	3	-41	13
3	6	4	75	81
3	6	5	78	69
3	6	6	-42	8
3	6	7	65	61
3	6	8	45	-32
3	6	9	-45	19
3	6	10	-46	-24
4	6	0	57	-50
4	6	1	50	57
4	6	2	42	-40
4	6	3	81	91
4	6	4	-42	16
4	6	5	69	66
4	6	6	-44	45
4	6	7	-44	-13
4	6	8	-45	27
4	6	9	-47	-57
5	6	1	48	-43
5	6	2	108	106
5	6	3	-42	-3
5	6	4	95	83
5	6	5	-43	24
5	6	6	-44	10
5	6	7	-44	19
5	6	8	-45	-21
6	6	0	-44	-16
6	6	1	-44	24
6	6	2	-43	-5
6	6	3	85	80
6	6	4	-45	18
6	6	5	53	55
6	6	6	-45	-1
6	6	7	-46	-11
7	6	1	-45	24
7	6	2	74	71
7	6	3	-45	2
7	6	4	71	64
7	6	5	-46	-9
8	6	0	-46	30
8	6	1	56	34
8	6	2	-46	13
8	6	3	-47	51
0	7	1	-43	35
0	7	3	57	60
0	7	5	59	26
0	7	7	-46	-15
1	7	1	-43	19
1	7	2	86	72
1	7	3	-44	-24
1	7	4	59	65
1	7	5	-44	-3
1	7	6	-45	14
1	7	7	-45	-5
2	7	0	-43	17
2	7	1	53	27
2	7	2	-44	23
2	7	3	67	73
2	7	4	-44	-14
2	7	5	52	40
2	7	6	-46	-30
2	7	7	-45	-9
3	7	1	62	51
3	7	2	-44	33
3	7	3	51	17
3	7	4	-45	42
3	7	5	-45	-29
3	7	6	-46	17
4	7	0	-46	62
4	7	1	51	27
4	7	2	-45	28
4	7	3	-46	35
4	7	4	-46	-17
4	7	5	-46	11
5	7	1	-46	42
5	7	2	-45	14
5	7	3	-46	13
5	7	4	-46	13

An electron density map, with phases based on the final parameters, was calculated. The electron densities (e/Å^3) in the atomic positions had the values, 51.6 for Ag; 4.1 for N(1); 4.9 for C(1); 5.7 for O(1); 4.7 for N(2); 4.7 for C(2); 4.5 for O(2); 7.6 for N(3); 4.3 for C(3); 2.6 for C(4); 2.3 for C(5); 2.3 for C(6); and 1.9 for C(7). The last four atoms are the disordered methyl carbon atoms. It was not possible, on the basis of the electron density map, to distinguish between the atoms of the isocyanate groups. The areas of highest electron density in a final dif-

Table 4. Bond lengths (Å) and angles (°). Standard deviations, in parentheses, have been calculated from those of Table 1, without regard to coordinate covariances and errors in unit cell dimensions. A prime denotes an atom generated by a mirror plane.

Ag–N(1) = 2.015(13)	∠N(1)–Ag–N(2) = 177.2(5)
Ag–N(2) = 2.068(12)	∠Ag–N(1)–C(1) = 170.0(13)
N(1)–C(1) = 1.076(19)	∠Ag–N(2)–C(2) = 172.1(12)
N(2)–C(2) = 1.111(18)	∠N(1)–C(1)–O(1) = 178.2(16)
C(1)–O(1) = 1.200(17)	∠N(2)–C(2)–O(2) = 179.8(17)
C(2)–O(2) = 1.129(18)	∠C(3)–N(3)–C(4) = 107.2(11)
N(3)–C(3) = 1.456(14)	∠C(3)–N(3)–C(5) = 106.7(10)
N(3)–C(4) = 1.53(3)	∠C(4)–N(3)–C(5) = 112.2(10)
N(3)–C(5) = 1.43(3)	∠C(5)–N(3)–C(5′) = 111.4(14)
N(3)–C(6) = 1.58(3)	∠C(3)–N(3)–C(6) = 110.8(13)
N(3)–C(7) = 1.47(3)	∠C(3)–N(3)–C(7) = 104.2(15)
	∠C(6)–N(3)–C(7) = 111.0(16)
	∠C(7)–N(3)–C(7′) = 113.0(11)

ference Fourier summation were located near the disordered methyl carbon atoms. The maximum peak height in this map was 0.38 e/Å³. No attempts were made to locate the hydrogen atoms. On the basis of the successful refinement, it was concluded that the correct space group is *Pnma*.

RESULTS

Thermal motion. The thermal parameters of all atoms except the nitrogen atom of the tetramethylammonium ion [N(3)] have unusually high and strongly anisotropic values (Table 2). It was thought reasonable to analyze the thermal motions of the diisocyanatoargentate(I) ion in terms of the rigid-body tensors of translation (**T**), libration (**L**), and screw motion (**S**), according to Schomaker and Trueblood.[8] The results of the analysis, however, indicated that the rigid-body assumption was not applicable. The root mean square discrepancy between the observed U_{ij} values and the values calculated from the rigid-body model was 0.020 Å², indicating a considerable internal motion. Moreover, the eigenvalue of one of the libration axes was negative. Further results of the analysis are therefore not reported.

Due to the disorder of the methyl carbon atoms of the tetramethylammonium ion, and hence the large standard deviations of the corresponding thermal parameters, a similar rigid-body thermal analysis of this ion was not attempted.

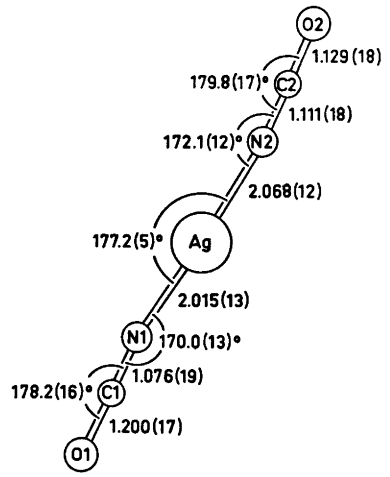

Fig. 1. The diisocyanatoargentate ion as seen along the normal to the mirror plane.

The diisocyanatoargentate(I) ion. The bond lengths and angles are given in Table 4. The structure analysis did not provide a determination of whether the silver atom is nitrogen-bonded or oxygen-bonded. From the earlier studies [2,3] it can be concluded that both ligands are bonded to the silver atom through the nitrogen atoms, and this has been presupposed throughout the present crystal structure determination.

All the atoms of the ion are located in a crystallographic mirror plane. A drawing of the diisocyanatoargentate(I) ion, as seen along the

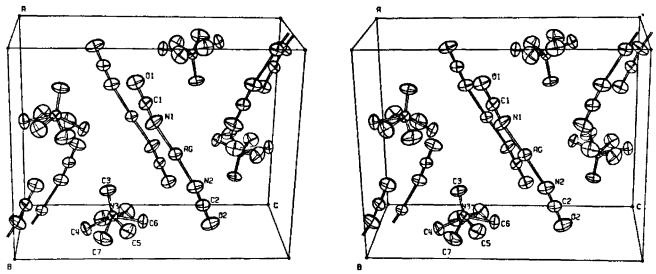

Fig. 2. A stereoscopic pair of drawings, with 20 % probability ellipsoids, showing the content of one unit cell. The labelled atoms of the diisocyanatoargentate ion are at $\frac{1}{2}-x$, $\frac{1}{2}+y$, $\frac{1}{2}+z$ relative to Table 1. Both sets of positions for the disordered methyl carbon atoms of the tetramethylammonium ions have been included.

normal to this plane, is shown in Fig. 1. The ion is approximately linear, with the largest deviations from linearity occurring in the Ag – N – C angles. The isocyanate groups do not deviate significantly from linearity, and the deviation of the N – Ag – N angle from 180° is rather small.

The standard deviations in bond lengths, as calculated from the least squares values, are probably too small. An adequate thermal analysis would most likely imply rather large corrections in bond lengths. If corresponding bond lengths from opposite sides of the silver atom are compared, they are seen to differ to some extent. The sum of bond lengths within the Ag – N(1) – C(1) – O(1) part of the ion is 4.291 Å, while the sum for the Ag – N(2) – C(2) – O(2) part is 4.308 Å. The average values for the bond lengths are: Ag – N = 2.042 Å, N – C = 1.094 Å, and C – O = 1.165 Å. The Ag – N bond lengths may be compared with the corresponding bond length, 2.115(18) Å, in silver isocyanate, AgNCO.[12] In the crystals of the latter compound there are zigzag chains, with alternating silver and nitrogen atoms, the nitrogen atoms being sp^2 hybridized ($\angle$Ag – N – C = 128.2°), rather than *sp* hybridized as in the diisocyanatoargentate(I) ion. In silver thiocyanate, AgSCN, the nitrogen atom seems to be *sp* hybridized, with an Ag – N bond length of 2.223(28) Å.[13] In this compound, a sulphur atom is bonded to the silver atom approximately opposite to the nitrogen atom.

The tetramethylammonium ion. The space group *Pnma* requires that the tetramethylammonium ion possesses mirror plane symmetry, with the nitrogen atom and two methyl carbon atoms located in the mirror plane. The bond lengths and angles are listed in Table 4, and the shape of the ion appears from Fig. 2. Three methyl carbon atoms of the tetramethylammonium ion are disordered. With a prime denoting an atom generated by the mirror plane, they are labelled C(4), C(5), and C(5′) in one set of positions. From these positions, the other ones are generated by rotating the entire ion approximately 60° about the N(3) – C(3) bond. The atoms in the other set are then C(6), C(7), and C(7′). In Fig. 2 both sets of positions have been included. The large thermal parameters might indicate that the disorder is due to extreme thermal motion, with the ion rotating more or less freely about the N(3) – C(3) bond. It appears more plausible, however, that there is a statistical distribution of ions in two different orientations, and that transition from one orientation to the other is not possible.

The tetramethylammonium ion is approximately tetrahedral. Due to the disorder, the derived bond lengths and angles are rather inaccurate, but the values are within the normal range.

Crystal packing. A stereoscopic drawing of the cell content is shown in Fig. 2. There are no particularly short non-bonding distances. The shortest distances from the silver atom to atoms of different ions involve isocyanate nitrogen and oxygen atoms. One silver-oxygen distance is 3.29(2) Å, with the oxygen atom [O(2)] located in the same mirror plane as the silver atom. Two equivalent silver-nitrogen distances are 3.552(5) Å, with the nitrogen atoms [N(1)] located in mirror planes $\pm b/2$ from the mirror plane con-

taining the silver atom. The silver atom and its three non-bonded neighbours just mentioned are positioned approximately in a plane normal to the silver-nitrogen bond directions.

REFERENCES

1. Austad, T., Songstad, J. and Åse, K. *Acta Chem. Scand. 25* (1971) 1136.
2. Ellestad, O. H., Klæboe, P., Tucker, E. E. and Songstad, J. *Acta Chem. Scand. 26* (1972) 3579.
3. Chew, K. F., Derbyshire, W., Logan, N., Norbury, A. H. and Sinha, A. I. P. *Chem. Commun.* (1970) 1708.
4. Busing, W. R. and Levy, A. H. *Acta Crystallogr. 10* (1957) 180.
5. *International Tables for X-Ray Crystallography,* Kynoch Press, Birmingham 1962, Vol. III, p. 202.
6. Cromer, D. T. *Acta Crystallogr. 18* (1965) 17.
7. Åse, K. *Acta Chem. Scand. 25* (1971) 838.
8. Schomaker, V. and Trueblood, K. N. *Acta Crystallogr. B 24* (1968) 63.
9. Johnson, C. K. *OR TEP, A Fortran Thermal-Ellipsoid Plot Program for Crystal Structure Illustrations.* Report ORNL-3794 (Second Revision), Oak Ridge National Laboratory, Tennessee 1965.
10. Foster, F. and Hargreaves, A. *Acta Crystallogr. 16* (1963) 1124.
11. Zachariasen, W. H. *Acta Crystallogr. 16* (1963) 1139.
12. Britton, D. and Dunitz, J. D. *Acta Crystallogr. 18* (1965) 424.
13. Lindqvist, I. *Acta Crystallogr. 10* (1957) 29.

Received July 13, 1973.

Acta Chemica Scandinavica A 28 (1974) 145—149

The Crystal Structure of $NaGa_{11}O_{16}(OH)_2$

A. NØRLUND CHRISTENSEN

Department of Inorganic Chemistry, Aarhus University, DK-8000 Aarhus C, Denmark

The compound $NaGa_{11}O_{16}(OH)_2$ was prepared using hydrothermal techniques. X-Ray diffraction shows the compound to be monoclinic, the space group is $P2_1/m$ with $a=8.602(5)$ Å, $b=8.906(5)$ Å, $c=9.571(4)$ Å, $\beta=117.1(2)°$; there are 2 formula units per cell.

Least squares refinement with 801 reflections gave a final R-value of 7.5 % for 73 parameters. The intensity data were collected on an automatic diffractometer using monochromatized Cu$K\alpha$-radiation.

The structure contains GaO_6 octahedra and GaO_4 tetrahedra. The mean gallium-ogygen distance within the octahedra is 2.00 Å, $\sigma=0.01$ Å, while the mean gallium-oxygen distance within the tetrahedra is 1.85 Å, $\sigma=0.01$ Å.

A high pressure high temperature hydrothermal investigation of metal oxides has resulted in preparation of dense metal oxide hydroxides with crystal structures of the indium oxide hydroxide type or of the tetragonal type of the ytterbium oxide hydroxide structure.[1-4]

The hydrothermal investigation of the Ga_2O_3-H_2O-Na_2O system yielded a monoclinic compound of unknown composition.[1] A three-dimensional X-ray analysis has shown that this compound, which in Ref. 1 was called a gallium hydroxide phase, [Ga(I)], has the formula $NaGa_{11}O_{16}(OH)_2$.

EXPERIMENTAL

The preparation of $NaGa_{11}O_{16}(OH)_2$, together with its X-ray powder pattern, is given in Ref. 1. The crystal used was 0.012 cm in length and 0.004 by 0.004 cm in cross section. It was mounted with its [010] axis as rotation axis, and was investigated using Weissenberg and precession methods. Only the reflections $0k0$ with $k=2n+1$ were absent, indicating the space group $P2_1$ or $P2_1/m$. A total of 801 independent hkl reflections with $I>2\sigma(I)$ were measured with a Picker diffractometer, using Cu$K\alpha$ radiation monochromatised by reflection from a graphite crystal and a scintillation counter in conjunction with a pulse height analyzer. Lorentz-polarization corrections were applied and a correction was made for absorption using Well's method.[5]

STRUCTURE DETERMINATION

The space group $P2_1/m$ (No. 11) has been used in the structure determination. The structure was solved using direct methods. The program SYMBAD [6] was used to normalize the structure factors and the program MULTAN [7] to determine four sets of phases for 152 reflections. Using the program JIMDAP,[8] three-dimensional Fourier maps were calculated, and those showing positions of heavy atoms at (0.35, 0.60, 0.05), (0.35, 0.25, 0.05), (0.35, 0.10, 0.35), (0.35, 0.75, 0.35), (0.95, 0.60, 0.25), and (0.70, 0.10, 0.35) were used. After a series of refinement cycles and Fourier calculations all the atoms required by the formula $NaGa_{11}O_{16}(OH)_2$, except the hydrogen atoms, were located. Refinement was carried out with the Fortran crystallographic least squares program LINUS,[9] using isotropic temperature coefficients and the refinement converged at a conventional R-value of 7.5 %. Parameters refined were atomic coordinates, thermal parameters, and two scale factors.

CRYSTAL DATA

The formula of the compound is $NaGa_{11}O_{16}(OH)_2$, and the unit cell contains two formula units. The crystal system is monoclinic, and the space group is $P2_1/m$ (No. 11). The unit

Table 1. Atomic coordinates and temperature factors for $NaGa_{11}O_{16}(OH)_2$, with their standard deviations.

Atom	x/a	y/b	z/c	B (Å²)
Na_1	0.041(1)	0.25	0.057(1)	1.7(2)
Ga_1	0.3679(3)	0.5771(3)	0.0490(2)	0.77(6)
Ga_2	0.3727(4)	0.25	0.0465(3)	0.74(7)
Ga_3	0.3471(3)	0.0848(3)	0.3597(2)	0.76(6)
Ga_4	0.3600(4)	0.75	0.3615(4)	0.86(7)
Ga_5	0.9698(3)	0.5786(3)	0.2579(2)	0.79(6)
Ga_6	0.7133(3)	0.0760(3)	0.3469(2)	0.77(6)
Ga_7	0.8877(4)	0.75	0.5404(4)	0.74(7)
O_1	0.612(1)	0.083(1)	0.478(1)	0.2(2)
O_2	0.368(2)	0.25	0.509(2)	0.7(3)
O_3	0.341(2)	0.582(1)	0.231(1)	0.4(2)
O_4	0.338(2)	0.25	0.230(2)	0.5(3)
O_5	0.554(1)	0.081(1)	0.130(1)	0.0(2)
O_6	0.546(2)	0.75	0.120(2)	0.1(3)
O_7	0.098(1)	0.091(1)	0.305(1)	0.0(2)
O_8	0.847(2)	0.25	0.368(2)	0.6(3)
O_9	0.794(1)	0.584(1)	0.050(1)	0.1(3)
O_{10}	0.849(1)	0.593(1)	0.376(1)	0.2(2)
O_{11}	0.097(2)	0.75	0.282(2)	0.4(3)
O_{12}	0.784(2)	0.25	0.052(2)	0.8(4)

Table 2. Interatomic distances (Å) and bond angles (degrees). Standard deviations in parentheses.

Na_1-O_{12}''	2.19(3)	$O_7'-Na_1-O_7$	65.6(5)
Na_1-O_7	2.61(2)	$O_7-Na_1-O_9'''$	140.0(5)
Na_1-O_7'	2.61(2)	$O_9'''-Na_1-O_9''$	70.3(6)
Na_1-O_4	2.33(2)	$O_9''-Na_1-O_7$	140.0(5)
Na_1-O_9''	2.57(2)	$O_{12}''-Na_1-O_4$	141.9(9)
Na_1-O_9'''	2.57(2)		
Ga_1-O_3	1.86(2)	$O_3-Ga_1-O_5'$	93.2(5)
Ga_1-O_5'	2.01(1)	$O_5'-Ga_1-O_9''$	86.5(5)
Ga_1-O_6	2.06(1)	$O_9''-Ga_1-O_{12}'$	99.2(5)
Ga_1-O_5''	2.10(2)	$O_{12}'-Ga_1-O_6$	78.6(5)
Ga_1-O_9''	1.92(1)	$O_3-Ga_1-O_5''$	169.7(5)
Ga_1-O_{12}'	1.96(1)		
Ga_2-O_4	1.91(2)	$O_5'-Ga_2-O_5$	94.3(5)
Ga_2-O_5	2.05(1)	$O_5-Ga_2-O_9'''$	84.1(5)
Ga_2-O_5'	2.05(1)	$O_9'''-Ga_2-O_9''$	97.0(5)
Ga_2-O_6'	2.01(2)	$O_9''-Ga_2-O_5'$	84.1(5)
Ga_2-O_9'''	1.97(1)	$O_4-Ga_2-O_6'$	169.9(6)
Ga_2-O_9''	1.97(1)		
Ga_3-O_7	1.96(1)	$O_2-Ga_3-O_1''''$	93.8(5)
Ga_3-O_1''''	2.06(1)	$O_1''''-Ga_3-O_3''$	82.3(5)
Ga_3-O_2	2.00(1)	$O_3''-Ga_3-O_4$	101.5(6)
Ga_3-O_1	2.03(1)	$O_4-Ga_3-O_2$	82.1(6)
Ga_3-O_3''	1.91(1)	$O_7-Ga_3-O_1$	163.7(5)
Ga_3-O_4	1.90(1)		
Ga_4-O_{11}	2.03(2)	$O_1'''-Ga_4-O_1''$	92.1(5)
Ga_4-O_1''	2.07(1)	$O_1''-Ga_4-O_3$	82.2(5)
Ga_4-O_1'''	2.07(1)	$O_3-Ga_4-O_3'$	103.4(6)
Ga_4-O_2'	2.09(2)	$O_3'-Ga_4-O_1'''$	82.2(5)
Ga_4-O_3	1.91(1)	$O_{11}-Ga_4-O_2'$	167.6(8)
Ga_4-O_3'	1.91(1)		
Ga_5-O_{10}	1.86(2)	$O_9-Ga_5-O_{10}$	103.9(6)
Ga_5-O_7''	1.80(1)	$O_9-Ga_5-O_7''$	113.2(5)
Ga_5-O_{11}'	1.83(1)	$O_9-Ga_5-O_{11}'$	105.0(5)
Ga_5-O_9	1.87(1)	$O_{10}-Ga_5-O_7''$	110.7(6)
		$O_{10}-Ga_5-O_{11}'$	109.5(7)
		$O_7''-Ga_5-O_{11}'$	114.0(6)
Ga_6-O_1	1.83(2)	$O_5-Ga_6-O_1$	114.9(5)
Ga_6-O_{10}''	1.84(1)	$O_5-Ga_6-O_{10}''$	106.1(5)
Ga_6-O_8	1.89(1)	$O_5-Ga_6-O_8$	101.4(6)
Ga_6-O_5	1.90(1)	$O_1-Ga_6-O_{10}''$	112.7(6)
		$O_1-Ga_6-O_8$	110.9(7)
		$O_{10}''-Ga_6-O_8$	110.0(6)
Ga_7-O_2'	2.03(2)	$O_7''''-Ga_7-O_7'''$	89.5(5)
Ga_7-O_7'''	2.01(1)	$O_7'''-Ga_7-O_{10}$	91.0(5)
Ga_7-O_7''''	2.01(1)	$O_{10}-Ga_7-O_{10}'$	88.0(5)
Ga_7-O_8'	2.04(2)	$O_{10}'-Ga_7-O_7''''$	91.0(5)
Ga_7-O_{10}	2.01(1)	$O_2'-Ga_7-O_8'$	169.5(8)
Ga_7-O_{10}'	2.01(1)		

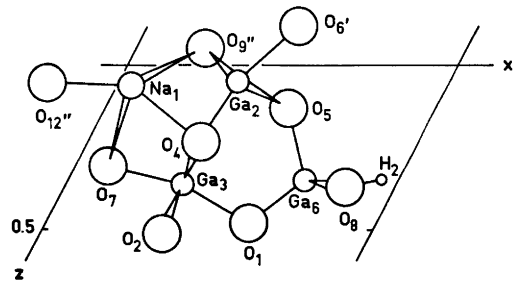

Fig. 1. Projection of metal-oxygen coordination polyhedra on (010). The y coordinates of the metal atoms are: Na_1 (0.25), Ga_2 (0.25), Ga_3 (0.0848), and Ga_6 (0.0760). O_3' is covered by O_4, O_1'''' by O_2, and O_{10}'' by O_8. O_5' is over O_5, and O_9''' is over O_9''. (The atoms with primes after the suffix numbers are symmetry related to the atoms with the same suffix number of which atom the coordinates are listed in Table 1).

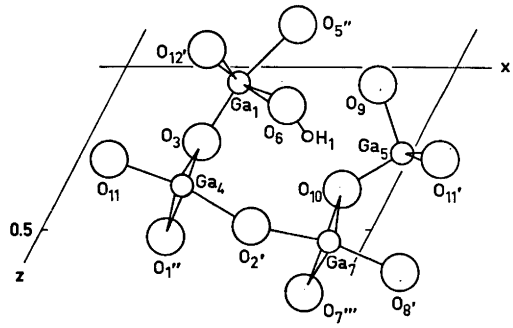

Fig. 2. Projection of metal oxygen coordination polyhedra on (010). The y coordinates of the metal atoms are: Ga_4 (0.75), Ga_7 (0.75), Ga_1 (0.5771), and Ga_5 (0.5786). O_9'' is covered by O_{12}', O_5' by O_6, and O_7'' by O_{11}'. O_3' is over O_3, O_1'' is over O_1''', O_{10}' is over O_{10}, and O_7'''' is over O_7'''.

Table 3. Observed and calculated structure factors. Reading from left to right, the columns are h, k, l, F_{obs}, F_{calc}.

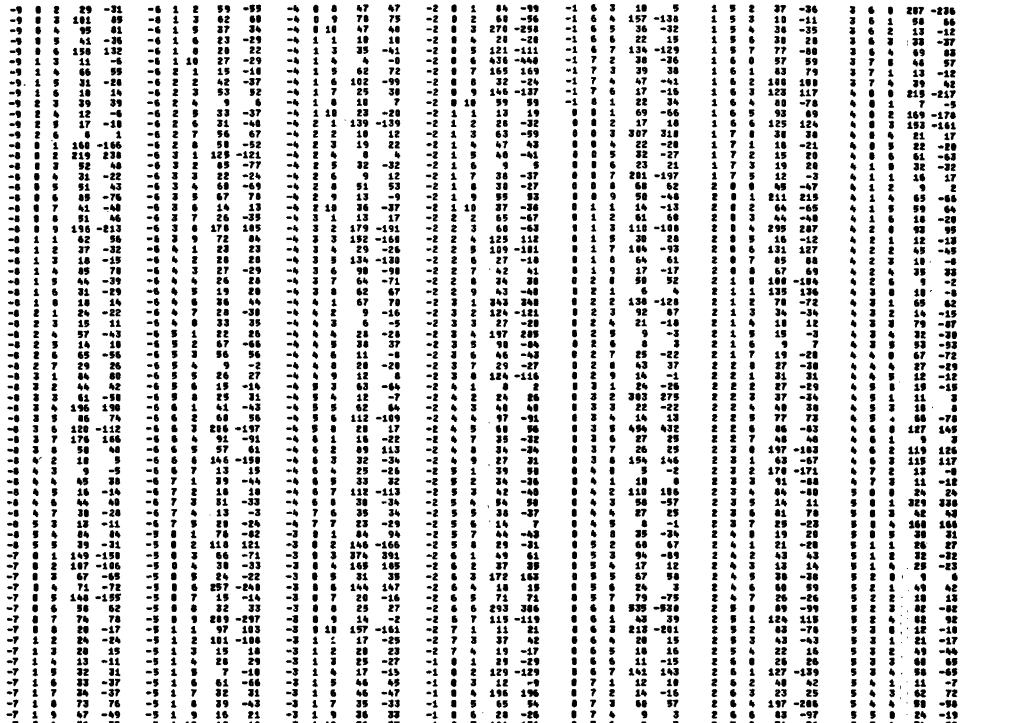

cell parameters are $a = 8.602(5)$ Å, $b = 8.906(5)$ Å, $c = 9.571(4)$ Å, and $\beta = 117.1(2)°$. The calculated density is 5.52 g/cm³, and the absorption coefficient for *Cu*-radiation is 287 cm⁻¹. The structure factors for the atoms were calculated from atomic scattering factors reported by Cromer and Mann.[10] Atomic coordinates and temperature factors are listed in Table 1, interatomic distances and bond angles in Table 2, and observed and calculated

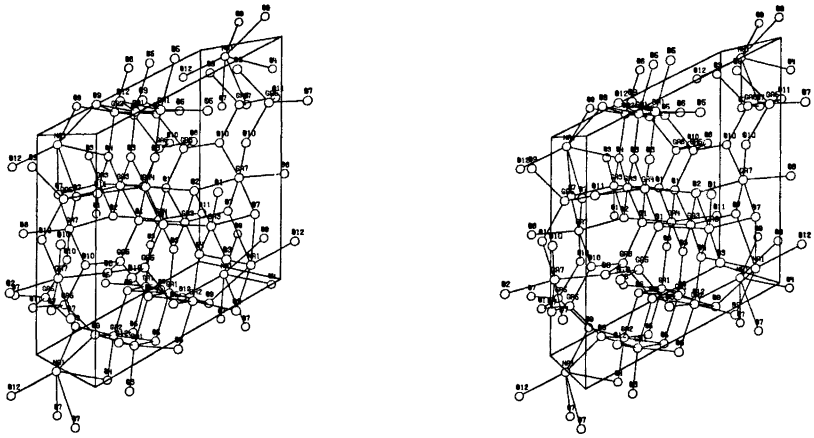

Fig. 3. Three-dimensional model of the crystal structure of $NaGa_{11}O_{16}(OH)_2$.

structure factors in Table 3. Fig. 1 is a projection on (010) showing the metal-oxygen coodination polyhedra for the metal atoms Na_1, Ga_2, Ga_3, and Ga_6, and Fig. 2 is a projection on (010) showing the coordination polyhedra for the metal atoms Ga_1, Ga_4, Ga_5, and Ga_7. Fig. 3 shows a three-dimensional model of the structure.

DISCUSSION

The crystal structure of $NaGa_{11}O_{16}(OH)_2$ contains GaO_6 octahedra and GaO_4 tetrahedra The Ga_1, Ga_2, Ga_3, Ga_4, and Ga_7 atoms are coordinated by six oxygen atoms, while the Ga_5 and Ga_6 atoms are coordinated by four oxygen atoms. The GaO_6 octahedra are distorted and resemble the octahedra found in the diaspore modification of GaOOH [11] and of AlOOH.[12] The distances from gallium to oxygen within the octahedra have a mean of 2.00 Å, $\sigma = 0.01$ Å, in good agreement with the Ga–O distances of 2.00 Å found in the GaO_6 octahedra of the β-Ga_2O_3 structure.[13] The GaO_4 tetrahedra are fairly regular and the gallium oxygen distances have a mean of 1.85 Å, $\sigma = 0.01$ Å, also in good agreement with the Ga–O distance of 1.834 Å found in the GaO_4 tetrahedra of the β-Ga_2O_3 structure.[13] The sodium atom is coordinated by six oxygen atoms in a rather distorted octahedron, the Na–O distances having a mean of 2.48 Å, $\sigma = 0.02$ Å.

The oxygen atoms O_1, O_2, O_4, O_5, O_7, and O_9 are tetrahedrally coordinated by metal atoms, and the oxygen atoms O_3, O_6, O_8, O_{10}, O_{11}, and O_{12} are each coordinated by three metal atoms giving coordination polyhedra with geometries close to that of an ammonia molecule. It was not possible to determine the positions of the two hydrogen atoms from the last difference Fourier. It is, however, likely that the hydrogen atoms are bonded to two of the four oxygen atoms: O_6, O_8, O_{11}, and O_{12} which are all situated on mirror planes. From packing considerations it is suggested that one hydrogen atom at (0.66, 0.75, 0.21) is bonded to O_6, and the other hydrogen atom at (0.94, 0.25, 0.34) is bonded to O_8.

The temperature factor coefficients for the oxygen atoms are within three standard deviations similar to the temperature factor coefficients of the gallium atoms. It is normally found in oxide structures where the metal oxygen coordination polyhedra have a dense packing, that the temperature factor coefficients of the metal atoms and of the oxygen atoms are of the same order of magnitude.[14,15]

The compound was not a pure gallium hydroxide phase as assumed in Ref. 1, but was a sodium gallium oxide hydroxide. It has a rather dense packing of atoms in the structure and the density of the compound is comparable with that of β-Ga_2O_3. The stacking of the GaO_6 coordination octahedra found in this structure is similar to the stacking of the octahedra in the β-Ga_2O_3 structure.[13] Although the formula of the compound $NaGa_{11}O_{16}(OH)_2$ resembles that of β-alumina,

$NaAl_{11}O_{17}$, and that of the isomorphous gallium compound, $NaGa_{11}O_{17}$, the crystal structures of these two compounds [16,17] are different from that of $NaGa_{11}O_{16}(OH)_2$.

REFERENCES

1. Christensen, A. N. *Mater. Res. Bull. 6* (1971) 691.
2. Christensen, A. N. *Acta Chem. Scand. 24* (1970) 3074.
3. Gondrand, M. and Christensen, A. N. *Mater. Res. Bull. 6* (1971) 239.
4. Christensen, A. N. and Hazell, R. G. *Acta Chem. Scand. 26* (1972) 1171.
5. Wells, M. J. *Acta Crystallogr. 13* (1960) 722.
6. Danielsen, J. *SYMBAD, A program for direct methods in crystalloghraphy*, 1972, Department of Chemistry, Aarhus University, DK-8000 Aarhus C.
7. Germain, G., Université de Louvain, Louvain, Belgique, Woolfson, M. M. and Main, P., University of York, York, England, *Computer program MULTAN, 1971.*
8. Zalkin, A., University of California, Berkeley, California, *JIMDAP* is a Brookhaven version of the Zalkin *FORDAP program*, 1971.
9. Busing, W. R., Martin, K. O. and Levy, H. A. (1962), *ORFLS, A Fortran Crystallographic Least Squares Program*, Oak Ridge National Laboratory Report, ORNL-TM-305. *LINUS* is a 1971 version of *ORFLS.*
10. Cromer, D. T. and Mann, J. B. *Acta Crystallogr. A 24* (1968) 321.
11. Roy, R., Hill, V. G. and Osborn, E. F. *J. Amer. Chem. Soc. 74* (1952) 719.
12. Busing, W. R. and Levy, H. A. *Acta Crystallogr. 11* (1958) 798.
13. Geller, S. *J. Chem. Phys. 33* (1960) 676.
14. Lehmann, M. S., Larsen, F. K., Poulsen, F. R., Christensen, A. N. and Rasmussen, S. E. *Acta Chem. Scand. 24* (1970) 1662.
15. Christensen, A. N. *Acta Chem. Scand. 26* (1972) 1955.
16. Beevers, C. A. and Ross, M. A. S. *Z. Kristallogr. 97* (1937) 59.
17. Foster, L. M. and Stumpf, H. C. *J. Amer. Chem. Soc. 73* (1951) 1590.

Received September 11, 1973.

Acta Chemica Scandinavica A 28 (1974) 150—152

Note on the Crystal Structure of $Co_3(PO_4)_2$

ANDERS G. NORD

Department of Structural Chemistry, Arrhenius Laboratory, University of Stockholm, S-104 05 Stockholm 50, Sweden

$Co_3(PO_4)_2$ crystallizes in the monoclinic space group $P2_1/n$ with $Z=2$ and the cell constants $a=7.5557\pm0.0007$ Å, $b=8.3736\pm0.0006$ Å, $c=5.0615\pm0.0006$ Å, $\beta=94.03\pm0.02°$. The isomorphism between $Co_3(PO_4)_2$ and γ-$Zn_3(PO_4)_2$ has been verified through a rigid group least-squares refinement based on X-ray powder data.

A comparison of the X-ray powder data for the orthophosphates of zinc (γ-phase),[1] magnesium,[2] and cobalt [3] indicates isomorphism between these three phases, a fact which has been reported earlier in the literature.[1,2] However, in γ-$Zn_3(PO_4)_2$ the zinc atoms may be regarded as 4- and 6-coordinated, whereas in $Mg_3(PO_4)_2$ the magnesium atoms would rather be described as 5- and 6-coordinated.[2] In order to find out which of these two orthophosphates $Co_3(PO_4)_2$ resembles a structure investigation of cobalt orthophosphate was carried out.

EXPERIMENTAL

Cobalt orthophosphate was prepared according to the method of Sarver,[4] *i.e.* mixing $CoCO_3$ and $(NH_4)H_2PO_4$ under ethyl alcohol, whereupon drying and slow heating to 900°C yields deep purple crystals of $Co_3(PO_4)_2$. However, all attempts to produce crystals big enough for single crystal work proved fruitless and powder data, therefore, had to be used. Powder photographs were taken with strictly monochromatized Fe$K\alpha_1$ radiation ($\lambda=1.9360$ Å) in a Guinier-Hägg focusing camera using different exposure times (6, 12, 15, 24 h). Potassium chloride ($a=6.29288$ Å) [5] was used as an internal standard. The intensities and positions of the reflections on the photographs were determined with a SAAB film scanner and the programs by Malmros and Werner.[6] Corrections for multiplicity and the Lorentz-polarization effects were applied to the intensities, and the $|F_{obs}|$ values thus arrived at are listed in Table 1.

COMPUTING METHODS AND RESULTS

The lattice parameters were refined from the $\sin^2\theta$ values of 34 distinct reflections measured on the 12*h* powder photograph.[7] Twentyone other reflections could thereafter be unambiguously indexed, *cf.* Table 1. The cell constants are: $a=7.5557\pm0.0007$ Å, $b=8.3736\pm0.0006$ Å, $c=5.0615\pm0.0006$ Å, and $\beta=94.03\pm0.02°$. The space group is $P2_1/n$ with two formula units per unit cell. In a conventional least-squares refinement of this structure with isotropic temperature factors there would be 26 parameters to refine. However, with the rigid group least-squares program system developed by Scheringer,[8] the number of parameters can be reduced to ten by assuming the phosphate group to be a rigid regular tetrahedron with P – O distances of 1.53 Å, and by keeping the isotropic temperature factors fixed. The average value of the isotropic temperature factors from the structure of magnesium orthophosphate,[2] $B=0.41$ Å^2, was used. The weights applied by the refinement program were $w=1/(\Delta^2+4)$. Twelve cycles of refinement reduced the conventional reliability index R to 14 %. The structure factors for all non-extinct reflections with $\sin^2\theta<0.4$ were then calculated with the final atomic parameters, *cf.* Table 1.

To test the reliability of this method, powder data of $Mg_3(PO_4)_2$ were treated in the same way. 59 reflections were refined to $R=15$ % and the final parameters arrived at were close to those obtained from Weissenberg data.[2]

The values of I_{obs}, d_{obs}, d_{calc}, $|F_{obs}|$, and

Table 1. X-Ray powder data for $Co_3(PO_4)_2$. Fe$K\alpha_1$ radiation. The 34 reflections marked with an asterisk were used to refine the cell constants. All $|F_{obs}|$ values listed below were used in the final refinement of the crystal structure of $Co_3(PO_4)_2$.

h	k	l	I_{obs}	d_{obs}	d_{calc}	$\|F_o\|$	F_c
1	1	0	9	5.5758	5.6021	22	23
1	0	-1	94*	4.3381	4.3382	111	-113
0	1	1	9	4.3204	4.3238	25	36
0	2	0	6*	4.1901	4.1869	28	-27
1	0	1	42*	4.0663	4.0648	78	-91
1	1	-1	42*	3.8532	3.8520	59	-60
2	0	0	–		3.7686		4
1	2	0	3	~3.6579	3.6601		15
1	1	1			3.6567		-6
2	1	0	100*	3.4381	3.4366	105	-127
0	2	1	35*	3.2242	3.2229	67	-64
1	2	-1	70	3.0137	3.0127	98	-55
2	1	-1	1	2.9309	2.9297	12	-13
1	2	1	8*	2.9173	2.9164	36	-35
2	2	0	28*	2.8017	2.8011	69	70
2	1	1	21*	2.7603	2.7599	61	-52
1	3	0	14*	2.6180	2.6175	53	53
0	0	2	36*	2.5241	2.5245	123	125
2	2	-1	41*	2.5056	2.5055	95	-93
0	3	1	62*	2.4432	2.4428	120	-122
0	1	2	8*	2.4171	2.4170	43	-47
3	1	0	28*	2.4064	2.4064	83	78
2	2	1	9*	2.3971	2.3968	47	-46
1	1	-2	6	~2.3477	2.3480		-4
1	3	-1			2.3474		-39
3	0	-1	6*	2.3155	2.3152	57	-35
1	3	1	11*	2.3014	2.3010	53	49
1	1	2	2	2.2589	2.2578	24	25
2	3	0	–		2.2430		-1
3	1	-1	19*	2.2313	2.2315	74	69
3	0	1	3*	2.1889	2.1888	42	27
2	0	-2	1	2.1695	2.1691	19	26
0	2	2	2	2.1627	2.1619	19	23
3	2	0	5*	2.1534	2.1543	36	18
3	1	1	26*	2.1174	2.1176	89	75
1	2	-2	27*	2.1126	2.1121	90	-64
2	1	-2	3	2.0994	2.0998	30	-33
0	4	0	11*	2.0938	2.0935	82	-68
2	3	-1	35*	2.0826	2.0824	104	-89
1	2	2	31*	2.0459	2.0457	97	91
2	0	2	8*	2.0324	2.0324	70	-55
3	2	-1	4*	2.0263	2.0261	34	-17
2	3	1	1	~2.0184	2.0188		11
1	4	0			2.0171		8
2	1	2			1.9750		-4
3	2	1	1	1.9400	1.9397	17	-16
0	4	1	5	1.9333	1.9338	40	39
2	2	-2	7*	1.9255	1.9260	50	40
1	4	-1	6	~1.8847	1.8854		37
4	0	0			1.8843		-41
0	3	2	3	1.8719	1.8723	30	-26
3	3	0	3	1.8676	1.8674	32	33
1	4	1	2*	1.8611	1.8611	29	-38
1	3	-2	22	~1.8396	1.8397		82
4	1	0			1.8383		3
2	4	0	21	~1.8287	1.8301		31
2	2	2			1.8284		75
3	1	-2	–		1.8036		-6
1	3	2	2	1.7949	1.7953	30	31
3	3	-1	1	1.7821	1.7820	23	24
4	1	-1	30*	1.7668	1.7668	108	-92
2	4	-1	16*	1.7397	1.7397	80	56
3	3	1	1	1.7227	1.7224	16	-17
4	2	0	2	1.7187	1.7183	31	43
2	3	-2	–		1.7127		8
2	4	1	5	1.7019	1.7020	46	47
4	1	1	23	~1.6902	1.6905		-79
3	2	-2			1.6898		58
3	1	2	28*	1.6858	1.6861	108	90
1	0	-3	3	1.6674	1.6677	50	-49
4	2	-1	4*	1.6591	1.6595	36	-46
0	1	3	3	1.6498	1.6500	39	-41
2	3	2	–		1.6430		2
1	1	-3	28	~1.6353	1.6356		-84
1	5	0			1.6349		67
1	0	3	–		1.6185		1
0	4	2	–		1.6115		-2
3	4	0	3	1.6078	1.6083	36	-28
4	2	1	3	1.5962	1.5958	38	43
3	2	2			1.5920		-6
1	4	-2			1.5905		14
0	5	1	4	~1.5897	1.5896		-35
1	1	3			1.5891		-6
4	0	-2			1.5637		9
1	5	-1			1.5624		15
4	3	0	23	~1.5617	1.5618		-36
0	2	3			1.5616		-95
1	4	2			1.5616		-11
3	4	-1			1.5528		-35
2	1	-3	13	~1.5500	1.5513		-12
1	2	-3			1.5493		-47
1	5	1			1.5485		-45
3	3	-2	30	~1.5392	1.5403		112
4	1	-2			1.5371		-15

Table 2. Fractional atomic coordinates for $Co_3(PO_4)_2$. The estimated standard deviations given in parentheses refer to the last digit of the respective values.

Atom	x	y	z
Co_1	0.617(1)	0.141(1)	0.093(1)
Co_2	0	0	$\frac{1}{2}$
P	0.197(2)	0.191(2)	0.042(1)
O_1	0.058(4)	0.124(4)	−0.162(3)
O_2	0.119(4)	0.201(4)	0.312(3)
O_3	0.253(4)	0.357(4)	−0.043(3)
O_4	0.359(4)	0.080(4)	0.062(3)

F_{calc} from the present study of $Co_3(PO_4)_2$ are listed in Table 1. The final atomic parameters are given in Table 2. Table 3 contains some interatomic metal-oxygen distances in the isomorphous orthophosphates of cobalt, zinc (γ-phase [9]), and magnesium.[2] The data for γ-$Zn_3(PO_4)_2$ refer to a later structure refinement of γ-$(Zn_{0.97}Mn_{0.03})_3(PO_4)_2$ by Calvo.[9] It follows from the metal-oxygen bond distances in Table 3 that $Co_3(PO_4)_2$ resembles γ-$Zn_3(PO_4)_2$ more than it resembles $Mg_3(PO_4)_2$. This is probably due to the fact that the Co^{2+} and Zn^{2+} ions have similar ionic radii and electron configurations.

Table 3. Some metal-oxygen bond distances (Å) in three isomorphous orthophosphates. The atoms are numbered as in Table 2 (this work). The standard deviations of the distances in $Co_3(PO_4)_2$ are probably ± 0.05 Å.

Compound:	$Co_3(PO_4)_2$[a]	γ-$Zn_3(PO_4)_2$[b]	$Mg_3(PO_4)_2$[c]
6-coordinated metal atoms			
$M_2-2\,O_1$	2.02	2.010	2.034
$2\,O_2$	2.16	2.201	2.179
$2\,O_3$	2.21	2.227	2.150
Average:	2.13	2.146	2.121
4- and 5-coordinated metal atoms			
M_1-O_1	(2.38)	(2.396)	2.142
O_2	1.94	1.934	1.965
O_3	2.05	1.984	2.063
O_4	2.01	1.955	1.961
O_4'	2.02	2.007	2.012

[a] This work. [b] *Cf.* Ref. 9. [c] *Cf.* Ref. 2.

Acknowledgements. The author sincerely thanks Professor Peder Kierkegaard for his encouraging and stimulating interest in this work. This investigation has been performed with financial support from the *Swedish Natural Science Research Council* and from the *Tri-Centennial Fund of the Bank of Sweden.*

REFERENCES

1. Calvo, C. *J. Phys. Chem. Solids 24* (1963) 141.
2. Nord, A. G. and Kierkegaard, P. *Acta Chem. Scand. 22* (1968) 1466.
3. de Wolff, P. *ASTM X-Ray Powder Data File*, Card 13–503.
4. Sarver, J. F. *Trans. Brit. Ceram. Soc. 65* (1966) 191.
5. Hambling, P. G. *Acta Crystallogr. 6* (1953) 98.
6. Malmros, G. and Werner, P. E. *Acta Chem. Scand. 27* (1973) 493.
7. Werner, P. E. *Ark. Kemi 31* (1969) 513.
8. Scheringer, C. *Acta Crystallogr. 16* (1963) 546.
9. Calvo, C. (1973) *Private communication.*

Received September 24, 1973.

Acta Chemica Scandinavica A 28 (1974) 153—156

The Molecular Structures of Cyclopentadienylberyllium Bromide, $(C_5H_5)BeBr$, and Cyclopentadienylberyllium Acetylide, $(C_5H_5)BeCCH$, Determined by Gas Phase Electron Diffraction

ARNE HAALAND and DAVID P. NOVAK

Department of Chemistry, University of Oslo, Blindern, Oslo 3, Norway

$(C_5H_5)BeBr$ and $(C_5H_5)BeCCH$ have been studied by gas phase electron diffraction. Both compounds contain symmetrically π-bonded (C_5H_5) rings. The bond distances and estimated standard deviations are: $(C_5H_5)BeBr$: C–C = 1.424(2) Å, Be–C = 1.950(12) Å, Be–Br = 1.943(15) Å. $(C_5H_5)BeCCH$: C–C = 1.428(2) Å, Be–C(Cp) = 1.919(5) Å, Be–C≡ = 1.634(8) Å, C≡C = 1.231(10) Å.

The investigations of CpBeBr (Cp = cyclopentadienyl) and CpBeCCH by means of gas phase electron diffraction reported here are part of a series of investigations of compounds of the type CpBeX. Similar studies of Cp_2Be,[1] $CpBeCH_3$,[2] CpBeCl,[3] and $CpBeBH_4$ [4] have already been published.

EXPERIMENTAL AND CALCULATION PROCEDURE

CpBeBr was supplied by Drew and Morgan,[5] CpBeCCH by Starowieyski and Morgan.[6] Both were used without further purification. The electron scattering pattern was recorded on Balzers Eldiograph KD-G2. The experimental conditions are summarized in Table 1. The data were processed and the molecular structure refined using the program packages described by Andersen *et al.*[7] and Seip *et al.*[8]

Theoretical intensity curves were calculated from:

$$I^{AC}(s) = \sum_{i \neq j} \frac{|f_i(s)||f_j(s)|}{|f_A(s)||f_C(s)|} \cos[\eta_i(s) - \eta_j(s)] \frac{\sin(R_{ij}s)}{R_{ij}} \exp(-\tfrac{1}{2}l^2_{ij}s^2)$$

The sum extends over all atom pairs i, j in the molecule. R_{ij} is the internuclear distance, l_{ij} the root mean square amplitude of vibration. $f_j(s) = |f_j(s)|\exp[i\eta_j(s)]$ is the complex atomic scattering factor of atom j.

The molecular structure was refined by least-squares calculations on the intensity data with a non-diagonal weight matrix and a separately refined scale factor for the intensity data obtained for each nozzle-to-plate distance. The

Table 1. Information about the intensity data.

Compound	$(C_5H_5)BeBr$		$(C_5H_5)BeCCH$	
Nozzle to plate distance (mm)	498.86	249.04	498.58	248.80
Nozzle temperature	50 – 55°	50 – 55°	80 – 85°	80 – 85°
Number of plates used	5	4	3	4
Atom A eqn. (1)	Br	Br	C	C
s-Range (Å^{-1})	1.500 – 14.750	3.500 – 30.000	1.500 – 15.250	2.500 – 28.500
Increment (Å^{-1})	0.125	0.250	0.125	0.250

standard deviations obtained were expanded to take into account an estimated uncertainty of 0.1 % in the electron wavelength.

Radial distribution functions were calculated by Fourier inversion of experimental and theoretical intensity curves after multiplication with the artificial damping function $\exp(-ks^2)$. The experimental intensity functions were then first spliced to each other and then to the theoretical curve calculated for the best model below $s = 1.50$ Å^{-1}.

STRUCTURE REFINEMENT

It was assumed that both compounds contain symmetrically π-bonded Cp rings, as do CpBeCl and CpBeMe. Molecular models are shown in Fig. 1. It was further assumed that both molecules have C_{5v} symmetry. Since H-atoms could not be located with great precision it was assumed that the Cp rings are completely planar. Bastiansen-Morino shrinkage effects were neglected for both molecules.

CpBeBr. The molecular structure is determined by four independent parameters, *e.g.* by the C–H, C–C, Be–C, and Be–Br bond distances. These were refined along with the

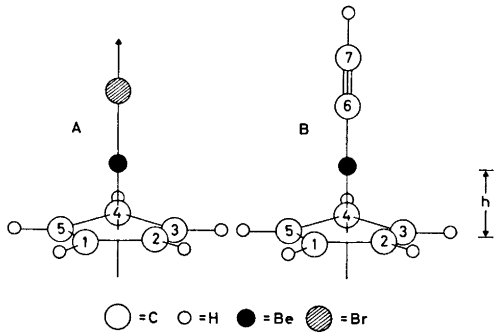

Fig. 1. Molecular models of $(C_5H_5)BeBr$ (A) and $(C_5H_5)BeCCH$ (B).

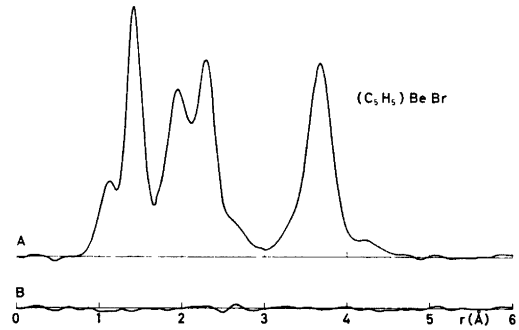

Fig. 2. A: Experimental radial distribution curve for $(C_5H_5)BeBr$. Artificial damping constant $k = 0.0025$ Å^2. B: Difference between the experimental curve and a theoretical curve calculated for best model.

Table 2. Interatomic distances (r_a) and root mean square vibrational amplitudes (l) of $(C_5H_5)BeBr$ and $(C_5H_5)BeCCH$. (Estimated standard deviations in parentheses). For numbering of the C atoms consult Fig. 1. The H atoms are numbered as the C atoms to which they are bonded.

	$(C_5H_5)BeBr$ r_a (Å)	l (Å)	$(C_5H_5)BeCCH$ r_a (Å)	l (Å)
Bond distances				
C_1-H_1	1.087(7)	0.044(12)	1.127(8)	0.060(12)
C_1-C_2	1.424(2)	0.034(4)	1.428(2)	0.038(3)
$Be-C_1$	1.950(12)	0.110(23)	1.919(5)	0.085(4)
$Be-Br$	1.943(15)	0.02(6)		
$Be-C_6$			1.634(8)	0.091(23)
C_6-C_7			1.231(10)	0.058(12)
C_7-H_7			1.060[a]	0.060(12)[b]
h	1.528(16)		1.487(5)	
Non-bonded distances				
$C_1\cdots C_3$	2.303(3)	0.053(4)	2.310(3)	0.062(6)
$C_1\cdots H_2$	2.242(6)	0.096(25)	2.280(7)	0.050(16)
$C_1\cdots H_3$	3.353(7)	0.088(14)	3.400(7)	0.096(23)
$Br\cdots C_1$	3.676(4)	0.097(3)		
$Br\cdots H_1$	4.162(5)	0.255(30)		
$C_1\cdots C_6$			3.349(7)	0.103(9)
$C_1\cdots C_7$			4.518(7)	0.146(7)
$Be\cdots C_7$			2.865(8)	0.041(19)

[a] Assumed value. [b] $l(C_1-H_1)$ and $l(C_7-H_7)$ were assumed equal.

nine most important vibrational amplitudes. The resulting values and their estimated standard deviations are listed in Table 2. The generalized R-factor [8]

$$R_3 = 100(\sum_k \sum_l P_{kl} V_k V_l / \sum_k \sum_l P_{kl} I_k I_l)$$

was equal to 14.8. The two amplitudes l (Be – C) and l(Be – Br) are strongly correlated, the correlation coefficient being $\varrho = -0.91$. As a consequence these amplitudes are poorly determined. The $C_1 - C_2$ vibrational amplitude obtained in this compound as well as in CpBeCCH is very low. This is probably due to an error in the blackness correction that was employed. However, parallel refinement on benzene data strongly indicates that the effect of the error is confined to the values obtained for the smallest vibrational amplitudes, *i.e.* $l(C_1 - C_2)$ and $l(C_1 - H_1)$.

CpBeCCH. The molecular structure is determined by six parameters, *e.g.* by the bond distances $C_1 - H_1$, $C_1 - C_2$, $Be - C_1$, $Be - C_6$, $C_6 - C_7$, and $C_7 - H_7$. The latter was fixed at 1.06 Å and not refined. The remaining five bond distances were refined along with the twelve most important vibrational amplitudes. The resulting values and their estimated standard deviations are listed in Table 2. The generalized R-factor was $R_3 = 14.4$.

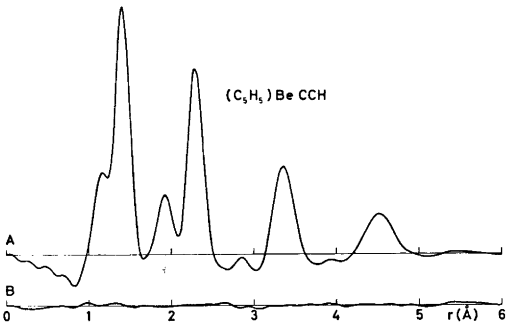

Fig. 3. A: Experimental radial distribution curve for (C_5H_5)BeCCH. Artificial damping constant $k = 0.0025$ Å^2. B: Difference between the experimental curve and a theoretical curve calculated for the best model.

DISCUSSION

No significant differences are found between the CpBe fragments in the two molecules studied here or those previously described.[1–4]

While the Be-C(methyl) bond distance in $CpBeCH_3$ is equal to the Be-C bond distance in free monomeric $(CH_3)_2Be$ [9] the Be – Cl bond distance in CpBeCl was found to be about 0.08 Å longer than in free monomeric $BeCl_2$.[10] It was suggested that the bonds in $BeCl_2$ are shortened by dative π-bonding and that such π-bonding is absent – or at least reduced – in CpBeCl because the pertinent Be $2p$ atomic orbitals are used for bonding to the Cp ring *via* the $e_1\pi$-orbitals of the latter. This view receives some support from recent MO-calculations on Cp_2Be,[11] which show that bonding between Be and the nearest Cp ring is effected primarily through molecular orbitals formed from the ring $e_1\pi$-orbitals and the $2p_x$ and $2p_y$ atomic orbitals on Be.

The Be – Br distance found in CpBeBr is greater than in free monomeric $BeBr_2$,[10] 1.92 ± 0.02 Å, but not significantly so. Because of greater disparity in the size of the pertinent p orbitals in $BeBr_2$ than in $BeCl_2$ one would perhaps expect less dative π-bonding in the former compound.

The Be – C≡ bond distance in CpBeCCH is considerably shorter than the terminal Be – C≡ bond distance in dimeric methylpropynylberyllium-trimethylamine,[12] 1.75 Å. The latter bond length must, however, have been increased considerably through formation of the dative N→Be bond, as can be seen from the fact that the Be – C bond distance in $(CH_3)_2Be$,[5] 1.70 Å is increased to 1.83 Å in dimethylbis(quinuclidine)beryllium.[13]

The $Be - C_6$ bond in CpBeCCH is also considerably shorter than the Be – C(methyl) bond in $CpBeCH_3$, but the difference is of the order expected on going from sp^3- to sp-hybridized C. The $C_6 - C_7$ triple bond distance is not significantly different from the triple bonds in $H_3C{=}C{\equiv}CH_3$ [14] or $HC{\equiv}C - C{\equiv}CH$.[15]

Acknowledgements. We are grateful to Professor G. L. Morgan and coworkers for samples of (C_5H_5)BeBr and (C_5H_5)BeCCH, to Mr. Kristen Brendhaugen for help in recording the electron diffraction data and to the *Norwegian Research Council for Science and the Humanities* and the *Norwegian Research Council for Science and Technology* for financial support.

REFERENCES

1. Haaland, A. *Acta Chem. Scand. 22* (1968) 3030.
2. Drew, D. A. and Haaland, A. *Acta Chem. Scand. 26* (1972) 3079.
3. Drew, D. A. and Haaland, A. *Acta Chem. Scand. 26* (1972) 3351.
4. Drew, D. A., Gundersen, G. and Haaland, A. *Acta Chem. Scand. 26* (1972) 2147.
5. Drew, D. A. and Morgan, G. L. *Unpublished results*, and Drew, D. A. *Ph. D. Thesis*, The University of Wyoming 1971.
6. Starowieyski, K. G. and Morgan, G. L. *Unpublished results.*
7. Andersen, B., Seip, H. M., Strand, T. G. and Stölevik, R. *Acta Chem. Scand. 23* (1969) 3224.
8. Seip, H. M., Strand, T. G. and Stölevik, R. *Chem. Phys. Lett. 3* (1969) 617.
9. Almenningen, A., Haaland, A. and Morgan, G. L. *Acta Chem. Scand. 23* (1969) 2921.
10. Akishin, P. A. and Spiridinov, V. P. *Kristallografiya 2* (1957) 475.
11. Lopatko, O. Y., Klimenko, N. M. and Dyatkina, M. E. *J. Struct. Chem. USSR 13* (1972) 1044.
12. Morosin, B. and Howatson, J. *J. Organometal. Chem. 29* (1971) 7.
13. Whitt, C. D. and Atwood, J. L. *J. Organometal. Chem. 32* (1971) 17.
14. Tanimoto, M., Kuchitsu, K. and Morino, Y. *Bull. Chem. Soc. Jap. 42* (1969) 2519.
15. Tanimoto, M., Kuchitsu, K. and Morino, Y. *Bull. Chem. Soc. Jap. 44* (1971) 386.

Received September 18, 1973.

Acta Chemica Scandinavica A 28 (1974) 157—161

Mössbauer Investigation of Dinitrosyl Iron Compounds

H. MOSBÆK and K. G. POULSEN

Chemistry Department A, The Technical University of Denmark, DK-2800 Lyngby, Denmark

In continuation of earlier work with mononitrosyl iron compounds,[1] we have investigated several dinitrosyl compounds $Fe(NO)_2LL'$, which can all be derived from $Fe(NO)_2(CO)_2$. It is found that the quadrupole splitting increases as the N – O stretch constant decreases. This dependence can be explained qualitatively by the strong π-bonding in the complexes, but in order to arrive at a quantitative conformity it is apparently necessary to suppose that in the compounds $Fe(NO)_2LL'$ the (ON) – Fe – (NO) bond angle depends on the ligands present.

All the investigated compounds (symbolized: $Fe(NO)_2LL'$ where L(L') is a Lewis base) can be theoretically derived and conveniently made from $Fe(NO)_2(CO)_2$. For this latter compound there exists an early determination of the molecular structure [2] (by means of electron diffraction in the gas phase) which shows that the iron atom is surrounded by the 4 ligands in an approximately tetrahedral way, making the overall symmetry of the compound C_{2v}. This structure will be assumed to be valid also for the substituted complexes.

The scope of this work was to investigate the bonding in such dinitrosyl complexes by using the Mössbauer effect, a technique which has already given valuable results with nitrosyl complexes.[1,3,4] As with the mononitrosyl iron compounds, there have been discussions regarding the bonding in the dinitrosyl complexes, but in one respect these discussions have differed from those regarding the mononitrosyl complexes. It has never really been challenged that for these complexes the only reasonable structures involve coordination of the nitrosyl group as NO^+; more or less connected with this view is the fact that the linearity of Fe – N – O has never been questioned.

The only application of a formal oxidation number will be to lead to a d^{10} electronic configuration as the starting point of the discussion.

The assumption of a d^{10} configuration agrees with the diamagnetic properties [5] of the complexes and their inclusion in the isoelectronic series: $Fe(CO)_4^{2-}$, $Fe(CO)_3NO^-$, $Fe(CO)_2(NO)_2$, $Co(CO)_4^-$, $Co(CO)_3NO$, $Ni(CO)_4$.

EXPERIMENTAL

The Mössbauer spectra were obtained with the instrument previously described.[6] ^{57}Co in Pd-matrix was used as a source of approximately 2 mCi strength. Except in the case of $Fe(NO)_2(CO)_2$ for which the spectrum was taken in frozen benzene, the spectra were taken on the solids wafered between aluminium foils and polyethylene. The temperature of the absorbers was *ca.* 100 K (metallic contact with liquid N_2). All the parameters mentioned are given relative to sodium nitroprusside and were obtained by a least squares fitting with Lorentzian curves. The force constants used in this paper were obtained using the Cotton-Kraihanzel method [7] except those in Table 2, where literature values are used.

Preparations and identifications of the compounds were as follows: $Fe(NO)_2(CO)_2$,[28] m.p. 18°C,[28] found: 15°C; νNO 1808, 1760 cm^{-1}, νCO 2084, 2037 cm^{-1};[29] found: νNO 1810, 1760 cm^{-1}, νCO 2084, 2038 cm^{-1}. $Fe(NO)_2(P(OC_6H_5)_3)_2$,[30] Fe: calc. 7.6 %, found 7.5 %; νNO: 1770, 1719 cm^{-1},[29] found 1775, 1715 cm^{-1}. $Fe(NO)_2(CO)P(C_6H_5)_3$,[30] Fe: calc: 13.8 %, found 14.2 %; m.p. 138 – 140°C,[30] found 138°C; νNO 1766, 1721 cm^{-1}, νCO 2010 cm^{-1},[30] found νNO 1763, 1722 cm^{-1}, νCO 2010 cm^{-1}. $[Fe(NO)_2CO]_2P(C_6H_5)_2C_2H_4P(C_6H_5)_2$,[31] Fe: calc. 16.3 %, found 16.2 %, N: calc. 8.1 % found 8.2 %; νNO 1760, 1713 cm^{-1}, νCO 2010 cm^{-1},[31] found νNO 1715, 1753 cm^{-1}, νCO 2013 cm^{-1}. $Fe(NO)_2(P(C_6H_5)_3)_2$,[14] Fe: calc. 8.8 %, found 8.6 %, N: calc. 4.4 %, found 4.3 %, m.p. 194°C,[30]

found 190°C; νNO 1723, 1679 cm^{-1},[29] found νNO 1722, 1680 cm^{-1}. $Fe(NO)_2(C_6H_5NC)_2$,[32] Fe: calc. 17.4 %, found 16.6 %. N: calc. 17.4 %, found 17.6 %; m.p. 143°C,[32] found 143°C. $Fe(NO)_2(C_2H_5NC)_2$,[33] Fe: calc. 24.6 %, found 23.6 %; m.p. 97°C,[33] found 95°C. $Fe(NO)_2$ phenanthroline,[34] Fe: calc. 28.1 %, found 27.2 %, N: calc. 28.1 %, found 27.2 %.

DISCUSSION

When considering the electronic structure of d^{10} complexes it is a great simplification that there is no need to take the σ-bonds into consideration; this is possible because the bonding and antibinding σ-orbitals are both filled (using the electronic structure of tetrahedral complexes as a guide). Consequently, these σ-orbitals will have an approximately spherical appearance and will only give minor contributions to the changes observed in the Mössbauer parameters. These minor changes will be due only to differences in overlaps which are considered small. This lack of σ-contribution should be especially pronounced since MO calculations for isoelectronic and isostructural nitrosyl cyanide compounds of first row transition metals indicate that there is a constancy in the strength of σ-(NO) bonds.[8]

In what follows the charge transferred to NO and CO will frequently be considered. It is calculated here as charge transferred to the π^* (NO, CO) orbitals only, a procedure which we find justified by the above mentioned constancy of σ-(NO) bond strength and the smoothing effect of the completely filled bonding and antibonding σ-orbitals on any differences. However, we are aware of the fact that the antibonding character of the σ-(NO, CO) orbital with regard to the NO (CO) bond makes calculations sensitive to large variations in σ-bonding to the central atom.

The isomer shift. All the Mössbauer parameters of the investigated compounds appear in Table 1 together with IR-data. It is obvious that within reasonable limits there is a constancy in the isomer shift and consequently also in the s-electron density at the iron nucleus, disregarding in the first instance the compounds with nitrogen bonded L-ligands.

There has been much controversy regarding the most important influence on the total s-electron density in iron-compounds but up till now it has apparently not been possible to produce any general theory concerning this phenomenon.[9] In this paper it will be assumed that only changes in $3d$-electron density have an influence on the s-electron density at the iron nucleus in the investigated series. This rather coarse approximation can be partly justified by the following 2 points:

1. The above mentioned constancy of the σ(NO)-bonding in isoelectronic compounds.

2. It is possible to account for the changes in isomer shift (Table 2) qualitatively and also semi-quantitatively (considering the accumulated correlations between electron configurations and isomer shifts [9]) simply by considering the changes in charge transferred from the iron $3d$ orbitals to the π^* (XO) orbitals (X=N,C); These changes are calculated from the X−O stretch constants and the magnitude of $\Delta k_{XO}/\Delta N$ (N = bond order).

The constancy of the isomer shift in Table 1 must imply the same $3d$ electron density in the listed compounds. As it can be inferred from k_{NO} that the charge transferred to the π^*-orbitals of NO is a variable it follows that the charge transferred by π-bonding to the other ligands must change in the opposite way. Using IR-data it is found that the sequence

Table 1. Mössbauer and infrared data of dinitrosyl iron compounds. σ, (isomershift) and ΔE_Q, (quadrupole splitting) are in mm/s and are given relative to sodium nitroprusside. The temperature of the absorbers was approximately 100 K.

2 L	σ	ΔE_Q	k_{NO} mdyn/Å
2 CO	0.34	0.34	14.1
2 $P(OC_6H_5)_3$	0.28	0.48	13.4
$P(C_6H_5)_3$,CO	0.29	0.53	13.2
CO,½$[(C_6H_5)_2PC_2H_4]_2$	0.30	0.54	13.2
2$P(C_6H_5)_3$	0.33	0.67	12.7
2 C_6H_5NC	0.31	0.76	12.6
2 C_2H_5NC	0.34	0.80	12.6
2$[(CH_3)_2N]_3P$ [a]	0.31	0.87	12.4
o-phenanthroline	0.54	0.71	12.3
o-phenanthroline[b]	0.56	0.74	12.3
α,α′-bipyridine[b]	0.52	0.72	12.5
2 CO [c]	0.29	0.32	14.1
2 $P(C_6H_5)_3$ [c]	0.33	0.69	12.7
CO, $P(C_6H_5)_3$ [c]	0.29	0.55	13.2

[a] From Ref. 5. [b] From Ref. 12. [c] From Ref. 14.

Table 2. Force constants for d^{10} iron compounds.

$\Delta k_{NO}/\Delta N_{NO} = 9.1$ mdyn/Å [25]
$\Delta k_{NO}/\Delta N_{CO} = 7.8$ mdyn/Å [25]
ΔN = change in bond order
Δe_M = electrons transferred to π-orbitals of M

Compound	k_{NO}	k_{CO}	Δe_{NO} (electrons)	Δe_{CO} (electrons)	$\sum \Delta e$ (electrons)	σ^a mm/S	Ref.
$Fe(CO)_4^{2-}$	–	11.4	–	1.90	7.6	0.08	23, 26
$Fe(CO)_3NO^-$	10.0	13.8	2.9	1.25	6.65	0.20	25, 14
$Fe(CO)_2(NO)_2$	13.02	16.92	2.2	0.40	5.20	0.33	24,

[a] σ relative to sodium nitroprusside.

of the π-bond strengths is very close to "the spectrochemical row for π-bonding ligands" as found by Horrocks and Taylor.[10] Only the isocyanide compounds are a little out of place. Returning to the complexes with N-bonded ligands it is obvious that the above mentioned explanations cannot be applicable because the constancy of the isomer shift is not extended to such compounds. It is now well known that such ligands in contrast to the other ligands in Table 1 are quite good σ-donors and rather poor π-acceptors.[11] Even though one should expect a gradual transition from good acceptors to poor acceptors, it may be that these complexes have a quite different electronic structure (*i.e*, not d^{10}) and they will therefore not be included in the following discussion. One of the reasons for proposing a different structure for the complexes with N-bonded ligands is their anomalous behaviour after oxidation, when the compounds display an increase in isomer shift corresponding to either an increase in $3d$ electron density or decrease in $4s$ electron density.[12] None of these explanations seems to be in accordance with bonding to a rather good σ-donor. The reason for rejecting the latter interpretation of the change in isomer shift is that the half-filled orbital in the oxidized species is supposed to be of a symmetry corresponding to d_{xz}, d_{xy} or d_{yz}. In the case of C_{2v} symmetry, these orbitals cannot mix with the $4s$ orbital of iron.

Only unsymmetric π-bonding can give rise to quadrupole splitting in these d^{10} complexes and all d-orbitals participate in the π-bonding due to the low symmetry (C_{2v} and C_s). Hence, the magnitude of the π-overlap (S_π) was selected as the measure of the π-bond strength between ligands and central-ion d-orbitals. S_π^2, which is then proportional to the charge transferred *via* relevant molecular orbitals (Table 3), was calculated by wellknown methods.[18,19]

Table 3. Group overlap of molecular orbitals. The group overlap is given relative to the atomic overlap integral, $S(d_{\pi M}, p_{\pi L})$. Only the angular dependence is considered.

Representation	Metal orbital	Ligand combination	Group overlap (S_π)
a_1	d_{z^2}	$(1/\sqrt{2})(\pi_{y_1} + \pi_{y_2})_{NO}$	$\frac{1}{2}\sqrt{6} \sin 2\theta$
a_1	$d_{x^2-y^2}$	$(1/\sqrt{2})(\pi_{y_1} + \pi_{y_2})_{NO}$	$\frac{1}{2}\sqrt{2} \sin 2\theta$
a_2	d_{xy}	$(1/\sqrt{2})(\pi_{x_1} + \pi_{x_2})_{NO}$	$\sqrt{2} \sin \theta$
b_1	d_{xz}	$(1/\sqrt{2})(\pi_{y_1} - \pi_{y_2})_{NO}$	$\sqrt{2} \cos 2\theta$
b_2	d_{yz}	$(1/\sqrt{2})(\pi_{x_1} - \pi_{x_2})_{NO}$	$\sqrt{2} \cos \theta$
a_1	d_{z^2}	$(1/\sqrt{2})(\pi_{y_1} + \pi_{y_2})_L$	$\frac{1}{2}\sqrt{6} \sin 2\theta$
a_1	$d_{x^2-y^2}$	$(1/\sqrt{2})(\pi_{y_1} + \pi_{y_2})_L$	$\frac{1}{2}\sqrt{2} \sin 2\theta$
a_2	d_{xy}	$(1/\sqrt{2})(\pi_{x_1} + \pi_{x_2})_L$	$\sqrt{2} \sin\theta$
b_1	d_{xz}	$(1/\sqrt{2})(\pi_{x_1} - \pi_{x_2})_L$	$\sqrt{2} \cos \theta$
b_2	d_{yz}	$(1/\sqrt{2})(\pi_{y_1} - \pi_{y_2})_L$	$\sqrt{2} \cos 2\theta$

Table 4. EFG elements of ON–Fe–NO molecule.

θ	V_{xx}	V_{yy}	ΔV_{zz}	ΔE_Q	η
50	−1.39	0.90	0.71	−1.41	0.31
52	−1.10	0.82	0.28	−1.14	0.50
54	−0.67	0.67	0.00	±0.77	1.00
56	−0.45	0.57	−0.12	−0.61	0.57
58	−0.11	0.42	−0.31	+0.44	0.49
59	0.06	0.34	−0.40	−0.47	0.58
60	0.25	0.25	−0.50	−0.50	0.0
61	0.43	0.16	−0.59	−0.61	0.46
62	0.62	0.06	−0.68	−0.75	0.81
63	0.80	−0.02	−0.76	+0.91	0.91
64	0.98	−0.14	−0.84	+1.06	0.72
65	1.17	−0.24	−0.93	+1.23	0.59

Values for the elements of the EFG tensor calculated in this way are shown in Table 4. It is seen that for fixed θ [$2\theta = \angle(\mathrm{ON})-\mathrm{Fe}-(\mathrm{NO})$ and $\theta < 60°$] and in agreement with our experimental data, ΔE_Q increases with increasing difference in the transferred charge. On the other hand, IR-data and the nearly constant isomer shift point to other causes for the sizeable ΔE_Q-differences rather than the relatively small transferred charges. Table 4 indicates that variation in θ could be responsible.

To obtain a reasonable conformity between calculated and experimental values the (ON)–Fe–(NO)-bond angle in $Fe(NO)_2(CO)_2$ should be *ca.* 58°. The angle should be larger in the complexes with ligands of smaller π-bond strength than CO. Table 5 gives the results of a detailed calculation of the quadrupole splitting. The magnitude of θ used in the table differs significantly from earlier estimates, but is in reasonable agreement with the value indicated by the X-ray structure of $(NO)_2Fe P\phi_2C_5F_6P\phi_2$ and with the structures of Co(NO)-$(CO)_2P\phi_3$ and $Co(NO(CO)(P\phi_3)_2$.

The authors are indebted to John Reeve for valuable linguistic advice.

REFERENCES

1. Mosbæk, H. and Poulsen, K. G. *Acta Chem. Scand. 25* (1971) 2421.
2. Brockway, L. O. and Anderson, J. S. *Trans. Faraday Soc. 33* (1937) 1233.
3. Oosterhuis, W. T. and Lang, C. *J. Chem. Phys. 50* (1969) 4381.
4. Johnson, C. E., Richards, R. and Hill, H. A. O. *J. Chem. Phys. 50* (1969) 2594.

Table 5. Calculation of quadrupole splitting for 2 $Fe(NO)_2L_2$ compounds.

	$Fe(NO)_2(CO)_2$	$Fe(NO)_2[P(C_6H_5)_3]_2$
θ_N	60°	62°
θ_L	52°	54°
$\sum \Delta e(L)$ [a]	0.8 elec.	0.2 elec.
$\sum \Delta e(NO)$ [a]	4.0 elec.	4.6 elec.
$\sum S_\pi^2$	4.0	4.0
$V_{xx}(L)\frac{\sum \Delta e(L)}{\sum S_\pi^2} + V_{xx}(NO)\frac{\sum \Delta e(NO)}{\sum S_\pi^2}$	0.41	0.74
$V_{yy}(L)\frac{\sum \Delta e(L)}{\sum S_\pi^2} + V_{yy}(NO)\frac{\sum \Delta e(NO)}{\sum S_\pi^2}$	0.03	0.04
$V_{zz}(L)\frac{\sum \Delta e(L)}{\sum S_\pi^2} + V_{zz}(NO)\frac{\sum \Delta e(NO)}{\sum S_\pi^2}$	−0.44	−0.78
η	0.84	0.74
ΔE_Q, calc.	−0.48	−0.85
ΔE_Q for 1 electron	4.0	4.0
Quadrupole splitting for 1 elec.	3.60 mm/S	3.60 mm/S
ΔE_Q	−0.43 mm/S	−0.77 mm/S
ΔE_Q experimental [b]	−0.34 mm/S	−0.67 mm/S
η experimental [b]	0.85	0.76

[a] See Table 3. [b] Ref. 14.

5. Herber, R. H., King, R. B. and Wertheim, G. K. *Inorg. Chem. 3* (1964) 101.
6. Mosbæk, H. and Poulsen, K. G. *Chem. Commun.* (1969) 479.
7. Cotton, F. A. and Kraihanzel, C. S. *J. Amer. Chem. Soc. 84* (1962) 4432.
8. Fenske, R. F. and DeKock, R. L. *Inorg. Chem. 11* (1972) 437.
9. Erickson, N. E. *The Mössbauer Effect and Its Applications in Chemistry, Advan. Chem. Ser. 68* (1967) 86.
10. Horrocks, W. D. and Taylor, R. C. *Inorg. Chem. 2* (1963) 723.
11. Orgel, L. *Introduction to Transition-Metal Chemistry*, Wiley, New York 1960, p. 134.
12. Dessy, R. E., Charkoudian, J. C. and Rheingold, A. L. *J. Amer. Chem. Soc. 94* (1972) 738.
13. Clark, M. G., Maddock, A. G. and Platt, R. H. *J. Chem. Soc. Dalton Trans.* (1972) 281.
14. Mazak, R. A. and Collins, R. L. *J. Chem. Phys. 51* (1969) 3220.
15. Bancroft, G. M., Mays, M. J. and Prater, B. E. *Chem. Commun.* (1968) 1374.
16. Bancroft, G. M., Garrod, R. E. B., Maddock, A. G., Mays, M. J. and Prater, B. E. *Chem. Commun.* (1970) 200.
17. Bancroft, G. M., Mays, M. J. and Prater B. E. *J. Chem. Soc. A* (1970) 956.
18. Ballhausen, C. J. and Gray, H. B. *Molecular Orbital Theory*, Benjamin, New York 1964, p. 111.
19. Kettle, S. F. A. *Inorg. Chem. 4* (1965) 1821.
20. Harrison, W. and Trotter, J. J. *J. Chem. Soc. A* (1971) 1542.
21. Albano, V. G., Bellon, P. L. and Ciano, O. *J. Organomet. Chem. 38* (1972) 155.
22. Beck, W., Melnikoff, A. and Stahl, R. *Chem. Ber. 99* (1966) 3721.
23. Santucci, A., Poletti, A. and Foffani, A. *J. Mol. Struct. 5* (1970) 49.
24. Poletti, A., Santucci, A. and Foffani, A. *J. Mol. Struct. 3* (1969) 311.
25. Siebert, H. *Z. Anorg. Allg. Chem. 275* (1954) 210.
26. Farmery, K., Kilner, M., Greatex, R. and Greenwood, N. N. *J. Chem. Soc. A* (1969) 2339.
27. Bancroft, G. M., Garrod, R. and Maddock, A. G. *J. Chem. Soc. A* (1971) 3165.
28. Hieber, W. and Beutner, H. *Z. Anorg. Allg. Chem. 320* (1963) 101.
29. Beck, W. and Lottes, K. *Chem. Ber. 98* (1965) 2657.
30. Malatesta, L. and Araneo, A. *J. Chem. Soc.* (1957) 3803.
31. Mawby, R. J., Morris, D., Thorsteinsson, E. M. and Basolo, F. *Inorg. Chem. 5* (1966) 27.
32. Malatesta, L. and Sacco, A. *Z. Anorg. Allg. Chem. 274* (1953) 341.
33. Hieber, W. and Pigenot, P. *Chem. Ber. 89* (1956) 610.
34. Hieber, W. and Anderson, J. S. *Z. Anorg. Allg. Chem. 211* (1933) 132.

Received October 31, 1973.

Acta Chemica Scandinavica A 28 (1974) 162—168

Kinetics and Equilibria for the Reversible Hydration of the Aldehyde Group in Glyoxylic Acid

P. E. SØRENSEN, K. BRUHN and F. LINDELØV

Chemistry Laboratory A, The Technical University of Denmark, Building 207, DK-2800 Lyngby, Denmark

The kinetics of the dehydration of the hydrated aldehyde group in glyoxylic acid in aqueous solution have been studied at 298 K by means of a scavenger technique. In the pH-ranges 1 – 5.5 and 7 – 8.5 semicarbazide, followed by spectrophotometry, and sulphite, followed by pH-stat, were used as scavengers, respectively, and for a single experiment at pH = 6 hydroxylamine, followed by spectrophotometry, was found most suitable. The dependence of the first-order dehydration rate constant on pH and scavenger concentration indicated general acid-base catalysis and also showed that the rates of dehydration of hydrated glyoxylic acid and glyoxylate ion are different. The various spontaneous and catalytic rate constants are reported.

The equilibrium constants for the hydration of the two protolytic forms of glyoxylic acid were determined by combination of the present kinetic data with polarographic literature values. Thus, $K_h = [R_1R_2C(OH)_2]/[R_1R_2CO]$ for glyoxylic acid and glyoxylate ion are found to be 3.0×10^2 and 15.1, respectively.

The mechanism of the hydration process is discussed. The apparent existence of intramolecular catalysis by the carboxyl group may be attributed to activation entropy effects, caused by additional water molecules attached to this group, rather than to intramolecular general acid catalysis.

The study of intramolecular catalysis in simple molecules as models for more complicated catalytic phenomena such as enzyme activity has developed in recent years and has become an important discipline within chemical kinetics.[1] Thus, a very simple model for the function of the biological enzyme carbonic anhydrase – catalysing carbonyl group hydrations – might be a carbonyl compound possessing some catalytically active group, such as a carboxyl or an amino group. Suitable amino carbonyl compounds are not particularly well known and will not be treated further in the present paper, but several well defined carboxylic carbonyl compounds are commercially available and a few have already been studied with respect to hydration of the carbonyl group, for example, pyruvic acid [2–7,30] ($CH_3COCOOH$) and glyoxylic acid [4,8,9] (CHOCOOH). Both of these compounds participate in metabolic processes in living organisms and the degree and rate of their hydration occupy a central position in this respect as pointed out by Davis.[10] The kinetics and equilibria for the hydration of pyruvic acid have now been extensively investigated, but this is not the case for glyoxylic acid. In the polarographic work by Kůta,[8] where the limiting current at the dropping mercury cathode in certain pH-ranges is mainly determined by the rate of dehydration of the irreducible hydrated carbonyl group to the reducible free form only the quantity $k_d/K_h = k_d^2/k_h$ [for definition see eqn. (1)] could be determined.

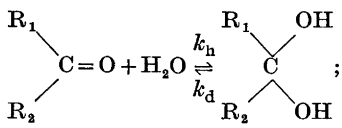

;

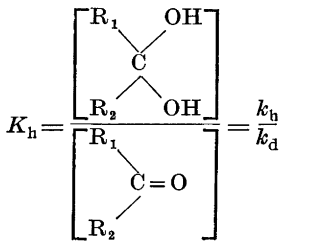

(1)

(R_1: COOH or COO^-, R_2: H)

More recently Ahrens [9] has obtained data for the rate of dehydration of hydrated glyoxylic acid using a *t*-jump technique and for the degree of hydration using UV spectrophotometry, but the reliability of the rate constants seems to be rather limited, probably because of the many assumptions involved in explaining the experimental behaviour of the system.

The present paper reports the results of a more detailed study of the dehydration of hydrated glyoxylic acid using a scavenger technique. The same method was employed for the investigation of glycolaldehyde [11] ($CHOCH_2OH$), but in the case of glyoxylic acid the situation is somewhat more complicated by the dependence of the rate and equilibrium constants on the dissociation of the carboxylic group.

EXPERIMENTAL

Glyoxylic acid, monohydrate, cryst. (Fluka, *purum*) M = 92.054 was kept over P_2O_5 in a desiccator. The mean of three determinations of the molecular weight by titration with standard alkali (phenolphthalein as indicator) was M = 92.6. The compound was used without further purification. BDH Analar $Na_2SO_3.7H_2O$, $Na_2S_2O_5$, semicarbazide hydrochloride, and hydroxylamine hydrochloride were used for preparation of scavenger solutions. Analar NaCl for adjusting the ionic strength and doubly distilled water were used throughout.

In the pH-range 7 – 8.5 sulphite (pK_A^{II} = = 7.20) was used as a scavenger by a pH-stat technique (Radiometer, Copenhagen), which has been described in detail earlier.[11,12] The scavenger solutions had total sulphite concentrations in the range $1 \times 10^{-2} - 5 \times 10^{-2}$ mol dm^{-3} and ionic strengths (NaCl) 0.10 – 0.15. A 0.2 M solution of bisulphite was used as titrant and the initial concentration of glyoxylic acid in the reaction solution was about 5×10^{-3} mol dm^{-3} established by dilution of a 0.5 mol dm^{-3}, neutral, aqueous stock solution of glyoxylic acid (glyoxylate ion).

Semicarbazide ($pK_A = 3.65$) was used as a scavenger in the pH-range 1 – 5.5, where a UV spectrophotometer (Beckman DB GT) recorded the appearance of the semicarbazone at its maximum absorbance, 255 nm. No other species present in the solution absorbed to an appreciable extent at this wavelength. At the higher pH-values (> *ca.* 2.6) a scavenger solution of known pH and total scavenger concentration ($10^{-2} - 10^{-1}$ mol dm^{-3}, $I = 0.1$) was thermostated in a 1 cm silica cell and the reaction was initiated by adding 1 – 5 nm^3 of a 0.1 mol dm^{-3} aqueous stock solution of glyoxylic acid. The same procedure was applied at the lower pH-values (< *ca.* 2.6) but because of the risk of reduced scavenger capacity (discussed later) higher total scavenger concentrations were used ($5 \times 10^{-2} - 2.5 \times 10^{-1}$ mol dm^{-3}, I = = 0.25).

A single series of similar experiments with hydroxylamine ($pK_A = 5.97$) as a scavenger was carried out at pH = 6.0 (concentration range $1 \times 10^{-2} - 6 \times 10^{-2}$ mol dm^{-3}, $I = 0.1$). The maximum of absorbance of the reaction product in this case was at 220 nm and there was no appreciably interference from other species in the solution at this wavelength.

All experiments in the present paper were carried out at 298.2 ± 0.2 K.

RESULTS AND DISCUSSIONS

The application of the scavenger principle, illustrated by the consecutive reaction scheme A ⇌ B (I) and B + C → D (II), where the process (I) is to be studied and C is the scavenger, requires that B reacts with C much faster than it is converted to A. If this is so, the conversion of A to B will be the rate determining step and the velocity will be independent of the concentration of C (if this is not too small) apart from possible catalytic effects.

The kinetic curves for the dehydration of hydrated glyoxylic acid (A) were found to be of first order and there was no sign of incomplete scavenging in the concentration ranges used, but at the lower pH-values it was necessary to increase the total concentration of semicarbazide because of "deactivation" of this species due to conversion into the protonated form.[12] The observed rate constants (k_{obs}) could be obtained as $-$slope/0.4343 from plots of $\log |a_t - a_\infty|$ *versus* time, where a represents an arbitrary scale. The main results of the kinetic measurements are collected in Table 1. Table 2 contains results which can be used for calculation of catalytic constants of the scavengers in question except for hydroxylamine, which was not examined in detail. The values for the two protolytic forms of semicarbazide can easily be determined to a good approximation as the slopes of k_{obs} *versus* total scavenger concentration, which showed good linearity. This is so because semicarbazide at the extreme pH-values (2.00 and 5.20) exists mainly in its acidic and basic forms, respectively. The catalytic constants are given in Table 3 and it is worth noticing that $k_{RNH_3^+}$ and k_{RNH_2} apply to the catalysis of dehydration of the acidic and

basic forms of glyoxylic acid, respectively ($pK_A \approx 3.3$, see later).

For sulphite, the situation is less simple, but it can easily be shown [11] that the slope of the line k_{obs} *versus* total sulphite concentrations is

$$\text{slope} = \frac{f_{SO_3} f_H [H^+] k_{HSO_3} + f_{HSO_3} K_A k_{SO_3}}{f_{SO_3} f_H [H^+] + K_A f_{HSO_3}} \quad (2)^*$$

where f denotes activity coefficients (f_{HSO_3} and f_{SO_3} taken as 0.78 and 0.37, respectively [14]) and K_A is the thermodynamic dissociation constant for the bisulphite ion, $10^{-7.20}$ mol dm^{-3} at 298.2 K.[15] Thus, k_{HSO_3} and k_{SO_3} can be determined by combining the slopes at two different pH-values. From the combinations at pH 7.20/7.40, 7.20/7.60, and 7.40/7.60, respectively, the following values were found for k_{HSO_3}/k_{SO_3}: $-0.050/0.187$, $-0.007/0.167$, and $0.061/0.154$. Therefore, k_{HSO_3} and k_{SO_3} can be taken as ≈ 0 and 0.17 dm^3 mol^{-1} s^{-1}, respectively. These can be compared with the values of ≈ 0 and 0.30 and ≈ 0 and 0.22 dm^3 mol^{-1} s^{-1} for glycol-and formaldehyde, respectively.[11,12]

After correction for catalysis by the scavenger, *i.e.* after extrapolation to zero scavenger concentration, the rate of dehydration can be expressed in the following way for glyoxylic acid:**

$$\text{Rate} = (k_0' + k_H'[H^+] + k_{OH'}[OH^-])[HA] + (k_0 + k_H[H^+] + k_{OH}[OH^-])[A^-] \quad (3)$$

where HA and A^- represent the acidic and the basic forms of hydrated glyoxylic acid, respectively, k_0 and k_0' are the "spontaneous" rate constants, *i.e.* the rate constants for catalysis by the solvent (H_2O), and k_H, k_H', k_{OH}, $k_{OH'}$ are catalytic constants for catalysis by H^+ and OH^-.

Using the relation $[H^+][A^-]/[HA] = K_A$, where K_A now denotes the concentration acid dissociation constant for hydrated glyoxylic acid, eqn. (3) can be rearranged to

$$\text{Rate} = (k_0' + k_H K_A + k_H'[H^+])[HA] + (k_0 + k'_{OH} K_{H_2O}/K_A + k_{OH}[OH^-])[A^-] \quad (4)$$

* As a simplification the ion charges of H^+, OH^-, HSO_3^-, SO_3^{2-} and A^- are omitted when these ions are used as indices.

** Intermolecular catalysis by glyoxylic acid and glyoxylate ion is neglected which was shown experimentally to be reasonable because of the low concentrations ($< 5 \times 10^{-3}$ mol dm^{-3}).

By applying the relations $[HA] = [H^+] \times ([HA] + [A^-])/(K_A + [H^+])$ and $[A^-] = K_A \times ([HA] + [A^-])/(K_A + [H^+])$ to eqn. (4) and taking into account that the rate constants k_0' and $k_H K_A$ cannot be separated experimentally ($k_0' + k_H K_A = k_{HA}^0$) – the same applies to k_0 and $k'_{OH} K_{H_2O}/K_A$ ($k_0 + k_{OH'} K_{H_2O}/K_A = k_A^0$) – eqn. (4) becomes:

$$\text{Rate} = k_{obs}([HA] + [A^-]) \quad (5)$$

where

$$k_{obs} = \frac{k_{HA}^0 + k_H'[H^+]}{1 + K_A/[H^+]} + \frac{k_A^0 + k_{OH}[OH^-]}{1 + [H^+]/K_A} \quad (6)$$

which can also be written as

$$k_{obs} = \frac{k_{HA}^0}{1 + K_A f_H/10^{-pH}} + \frac{k_H' 10^{-pH}}{f_H + K_A f_H^2/10^{-pH}} + \frac{k_A^0}{1 + 10^{-pH}/K_A f_H} + \frac{k_{OH} 10^{pH - pK_{H_2O}}}{f_{OH} + 10^{-pH} f_{OH}/K_A f_H} \quad (7)$$

or

$$k_{obs} = \frac{k_{HA}^0}{1 + 10^{pH - 3.38}} + \frac{k_H'}{10^{pH - 0.10} + 10^{2pH - 3.50}} + \frac{k_A^0}{1 + 10^{3.38 - pH}} + \frac{k_{OH}}{10^{13.88 - pH} + 10^{17.26 - 2pH}} \quad (8)$$

where f_H is taken as 0.83 and 0.79 at $I = 0.1$ and 0.25, respectively, and f_{OH} as 0.76.[14] The value of K_A was determined by Kůta [8] to be $10^{-3.30}$ (0.1 M citrate, 298 K).

The four rate constants in eqn. (8) were chosen so that the resulting values of k_{obs} – as a function of pH – fitted the experimental data in Table 1. This is shown graphically in Fig. 1, where the solid curve was calculated from the rate constants given in Table 3. The good agreement implies that the four rate constants are determined with fair accuracy and that the value 3.30 used for pK_A of hydrated glyoxylic acid is reasonable.

These values can now be compared with the results obtained by Kůta [8] and Ahrens.[9] For the dehydration Kůta found $k_{HA}^0/K_h^{HA} = 8.3 \times 10^{-5}$ s^{-1}, $k_A^0/K_h^A = 3.65 \times 10^{-4}$ s^{-1}, and $k_{OH}/k_h^A = 2.8 \times 10^2$ dm^3 mol^{-1} s^{-1}, K_h^{HA} and K_h^A being the hydration equilibrium constants of glyoxylic acid and its anion, respectively, which combined with the results of the present paper give $K_h^{HA} = 3.0 \times 10^2$, $K_h^A = 15.1$, and

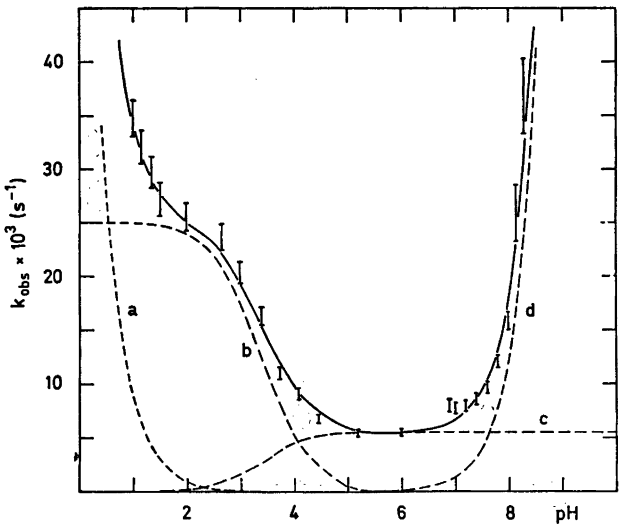

Fig. 1. Dependence of k_{obs} on pH. Experimental points are indicated with standard deviations. ——— calculated curve. — — — single terms of eqn. (8): a = k_H'-term, b = k_{HA}^0-term, c = k_A^0-term, d = k_{OH}-term.

$K_h^A = 32.2$. These values are again comparable with $K_h^{HA} \approx 10^3$ and $K_h^A = 16.5$ given by Ahrens, who used a spectrophotometric technique for this purpose. It would seem that the most acceptable of these four values are $K_h^{HA} = 3.0 \times 10^2$ and $K_h^A = 15.1$ (16.5). The acid dissociation constant for dehydrated glyoxylic acid can now be determined as $K_A \times K_h^{HA}/K_h^A = 1 \times 10^{-2}$ mol dm^{-3} which is in fair agreement with the value 1.3×10^{-2} mol dm^{-3} reported by Turjan.[16]

The agreement of equilibrium constants is within reasonable limits. However, this is not the case for the dehydration rate constants obtained by Ahrens and the present authors. Ahrens [9] found $k_A^0 \leq 6 \times 10^{-4}$ s^{-1} [$(5.5 \pm 0.2) \times 10^{-3}$], $k_{HA}^0 = (125 \pm 75) \times 10^{-3}$ s^{-1} [$(25 \pm 1) \times 10^{-3}$], and $k_{OH} = (2.6 \pm 2) \times 10^5$ dm^3 mol^{-1}s^{-1}[$(9 \pm 1) \times 10^3$], where the figures in square brackets are results from the present paper. It is clear that the many assumptions and approximations involved in reducing the experimental "*t*-jump"-results by Ahrens to single rate constants tend to increase the uncertainty of these. We therefore believe that our results, which have been obtained in a much more direct way, are the more reliable.

Intramolecular catalysis of carbonyl hydration and keto-enol tautomerism by the carboxyl group of α-keto acids has often been discussed. Thus, the considerably higher rates of spontaneous hydration and dehydration of pyruvic acid than, *e.g.*, acetaldehyde (see Table 4), although the extent of hydration is approximately the same, has been attributed to intramolecular general acid catalysis by the carboxyl-group.[2,17] Similarly, the higher rates of iodination of α-keto-acids compared with these for "normal" carbonyl compounds have been explained by such an effect.[19-21] As can be seen from Table 4 pyruvic acid is not unique in this respect; glyoxylic acid can be conveniently compared with formaldehyde and shows higher rates of spontaneous reaction if the difference in the degree of hydration of the two substances is taken into account.

However, in a recent paper by Pocker *et al.*[22] strong arguments against this theory are put forward. Investigation of the hydration kinetics of the methyl and ethyl esters of pyruvic acid, where no intramolecular acid catalysis is possible, showed that the rate constants for spontaneous hydration (273 K) were similar to that for the acid itself. Similarly, it was shown by Bell and Ridgewell,[26] Meany,[23] and by Fischer and Schellenberger [24] that the rates of keto-enol tautomerism of the methyl and ethyl esters of pyruvic acid were close to that of the free acid.

Table 1. Collected dehydration rate constants (s^{-1}) corrected for scavenger catalysis. The maximum standard deviation is ± 0.02 for pH and ± 5 % for k_{obs} apart from the last two values, where it is estimated to ± 10 % for k_{obs}.

pH	$k_{obs} \times 10^3$	Scavenger
1.00	34.7	
1.15	32.0	
1.35	29.7	
1.50	27.0	semicarb-
2.00	25.5	azide
2.65	23.6	
3.00	20.3	
3.40	16.3	
3.75	10.9	
4.10	9.0	
4.46	6.7	
5.20	5.4	
6.00	5.4	hydroxyl- amine
6.90	8.0	
7.00	7.7	
7.20	7.9	
7.40	8.5	sulphite
7.60	9.6	
7.80	12.0	
8.00	15.8	
8.15	25.9	
8.30	36.7	

Table 2. Catalysis by scavenger substances.

$C_{tot} \times 10^2$ (mol dm^{-3})	$k_{obs} \times 10^3$ (s^{-1})	$k_{calc} \times 10^3$ (s^{-1})
Semicarbazide; pH 2.00		
5	26.2	–
10	28.5	–
15	29.2	–
20	31.0	–
25	32.8	
Semicarbazide; pH 5.20		
5	5.9	–
10	6.0	–
15	6.2	–
20	6.7	–
25	7.1	–
Sulphite; pH 7.20		
10	9.1	9.1
20	10.1	10.0
30	10.9	10.9
40	11.5	11.8
50	13.6	12.9
Sulphite; pH 7.40		
10	10.4	10.1
20	10.7	11.0
30	12.6	12.2
40	12.7	13.0
50	14.3	14.2
Sulphite; pH 7.60		
10	10.6	11.5
20	12.2	12.6
30	13.4	13.6
40	13.8	14.8
50	15.6	15.9

We therefore believe that the pronounced catalytic effect of the carboxylic group in the hydration of α-keto-acids may be attributed to additional water molecules attached to the carboxylic group in the hydrated compound. It has been postulated and shown by various authors [5,25,30,31] that the hydration equilibrium constant for pyruvic acid shows a third-power dependence on water concentration, which means that two molecules of water, in excess of the one used for hydration, are attached to the hydrated substance. A similar behaviour has been shown by Jen and Knoche [29] for the hydration of α-keto-glutaric acid and it may be reasonable to believe that it also applies to glyoxylic acid.

Bell and coworkers [33–35] have clearly demonstrated that the transition state for the spontaneous hydration of simple carbonyl compounds undoubtly consists of the carbonyl compound and at least three water molecules probably in a ring structure such as (*9*).

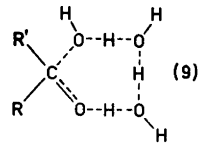
(9)

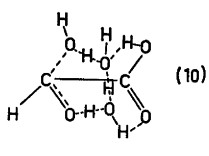
(10)

As a conclusion a plausible transition state for the hydration of α-keto-acids may be illustrated as (*10*), where the process proceeds *via* a transition state of ring structure as (*9*), but where this transition state is stabilized by hydrogen bondings to the carboxyl group as shown. As can be seen this mechanism does not necessarily imply acid-base activity of the carboxyl group and the catalytic effect would seem to be an entropy effect. This is shown experimentally by a comparison of activation entropy values for the hydration of pyruvic acid and acetaldehyde (Table 4). That for pyru-

Table 3. Collected catalytic constants, k_A and k_B, for the dehydration reaction. k_A and k_B are catalytic constants for the acidic and basic catalytic species, respectively. Temperature 298.0 K.

Compound	Catalyst(acidic species)	K_A (mol dm^{-3})	$k_A \times 10^3$ (mol^{-1} dm^3 s^{-1})	$k_B \times 10^3$ (mol^{-1} dm^3 s^{-1})
Glyoxylic acid	H_3O^+	55.5	$76 \pm 5 (k_H')$	$(25 \pm 1)/55.5$
	HSO_3^-	6.2×10^{-8}	–	–
	$N^+H_3NHCONH_2$	2.24×10^{-4}	30 ± 5	–
	H_2O	1.8×10^{-16}	$(25 \pm 1)/55.5)$ $(k_{HA}^0/55.5)$	–
Glyoxylate ion	H_3O^+	55.5	–	$(5.5 \pm 0.2)/55.5$
	HSO_3^-	6.2×10^{-8}	≈ 0	170 ± 10
	$N^+H_3NHCONH_2$	2.24×10^{-4}	–	6 ± 1
	H_2O	1.8×10^{-16}	$(5.5 \pm 0.2)/55.5$ $(k_A^0/55.5)$	$(9 \pm 1) \times 10^6$ (k_{OH})

Table 4. Kinetic values and activation parameters for the hydration of various carbonyl compounds in aqueous solution of 298.2 K.

Carbonyl compound	Spontaneous rate constants $k_{hydr.}^0$ (s^{-1})	$k_{dehydr.}^0$ (s^{-1})	Hydration equil.const.	$\Delta H^{\ddagger}_{hydr.}$ (kJ)	$\Delta S^{\ddagger}_{hydr.}$ (J K^{-1} mol^{-1})	Ref.
Acetaldehyde	9.0×10^{-3}	6.1×10^{-3}	1.49	37.2	−159	27, 28
Formaldehyde	10.2	5.1×10^{-3}	2×10^3	–	–	32
Glycolaldehyde	8.6×10^{-2}	9.6×10^{-3}	9	–	–	11
Pyruvic acid	1.56×10^{-1}[a]	9.6×10^{-2}	1.63	39.3	−100	7, 25
Ethyl pyruvate	9.0×10^{-2}	3.9×10^{-2}	2.33	31.8	− 89.5	22
Methyl pyruvate	1.15×10^{-1}	4.0×10^{-2}	2.85	31.4	− 89.0	22
Glyoxylic acid	7.5	2.5×10^{-2}	3.0×10^2	–	–	[b]
Glyoxylate ion	8.3×10^{-2}	5.5×10^{-3}	15.1	–	–	[b]
α-Keto-glutaric acid	1.75×10^{-1}	1.3×10^{-1}	1.35	–	–	29

[a] Extrapolation from 273 K. [b] This paper.

vic acid is considerably less negative than that for acetaldehyde while the enthalpy of activation is actually slightly higher for pyruvic acid.

Furthermore, the apparent intramolecular catalysis in the methyl and ethyl esters of pyruvic acid may be explained in a similar way. Pocker *et al.*[22] have reported that the hydration of the two esters shows a second-power dependence on water concentration so that at least one water molecule is attached to the ester group in the hydrated compound. The transition state for this reaction may be very similar to that for the pure acid [(*10*)] but less hydrogen bonded due to the replacement of −OH with −OR. Activation enthalpy and entropy considerations for the two esters (Table 4) also support this explanation as they do for the free acid, although it is difficult to see why the esters should have less negative activation entropy values than pyruvic acid.

This explanation of intramolecular catalysis in α-keto-acids may also explain the lower degrees of hydration of the basic forms of these acids, *e.g.* glyoxylic acid/glyoxylate ion in Table 4, the carboxylate group having reduced hydrogen bonding capability and so is unlikely to bind the extra water molecules needed to facilitate the hydration of the carbonyl group. This also implies that the carboxylate ions do not show intramolecular catalysis and indeed the rate constants of hydration and dehydration of the glyoxylate ion are very similar to those of glycolaldehyde which shows no sign of intramolecular catalysis (Table 4).

Intramolecular catalysis of carbonyl hydration by carboxyl groups is not yet clear. The homologous series $CO_2H-(CH_2)_n-CO-CH_3$ studied by Bell and Fluendy [18] with respect to iodination does not hydrate sufficiently for easy study. The only member of the series $CO_2H-(CH_2)_n-CO-CO_2H$, where carbonyl hydration is "activated" by the neighbouring carboxyl group in the manner already described, that has been studied, is α-keto-glutaric acid ($n=2$).[29] This compound shows higher rates of hydration and dehydration (Table 4) than pyruvic acid though not as high as might be expected if intramolecular catalysis also by the remote carboxyl group was important.

Acknowledgements. We thank Dr. R. L. Tranter and Professor R. P. Bell for valuable discussions.

REFERENCES

1. Bender, M. L. *Mechanisms of Homogeneous Catalysis from Protons to Proteins*, Wiley, New York 1971, Chapter 9.
2. Eigen, M., Kustin, K. and Strehlow, H. *Z. Phys. Chem. (Frankfurt am Main) 31* (1962) 140.
3. Strehlow, H. *Z. Elektrochem. 66* (1962) 392.
4. Becker, M. and Strehlow, H. *Z. Elektrochem. 64* (1960) 813.
5. Becker, M. *Ber. Bunsenges. Phys. Chem. 68* (1964) 669.
6. Griffiths, V. S. and Socrates, G. *Trans. Faraday Soc. 63* (1967) 673.
7. Pocker, Y. and Meany, J. E. *J. Phys. Chem. 74* (1970) 1486.
8. Kˇta, J. *Collect. Czech. Chem. Commun. 24* (1959) 2532.
9. Ahrens, M.-L. *Ber. Bunsenges. Phys. Chem. 72* (1968) 691.
10. Davis, R. P. *Enzymes 5* (1961) 545.
11. Sørensen, P. E. *Acta Chem. Scand. 26* (1972) 3357.
12. Bell, R. P. and Evans, P. G. *Proc. Roy. Soc. (London) Ser. A 291* (1966) 297.
13. Bell, R. P. and Jensen, M. B. *Proc. Roy. Soc. (London) Ser. A 261* (1961) 38.
14. Kieland, J. *J. Amer. Chem. Soc. 59* (1937) 1675.
15. Tartar, H. V. and Garretson, H. H. *J. Amer. Chem. Soc. 63* (1941) 808.
16. Turjan, Ja. I. *Z. Phys. Chem. (Leipzig) 229* (1965) 305.
17. Strehlow, H. *Z. Elektrochem. 66* (1962) 3921.
18. Bell, R. P. and Fluendy, M. A. D. *Trans. Faraday Soc. 59* (1963) 1623.
19. Albery, W. J., Bell, R. P. and Powell, A. L. *Trans. Faraday Soc. 61* (1965) 1194.
20. Schellenberger, A. and Hübner, G. *Chem. Ber. 98* (1965) 1938.
21. Schellenberger, A., Oehme, G. and Hübner, G. *Chem. Ber. 98* (1965) 3578.
22. Pocker, Y., Meany, J. E. and Zadorojny, C. *J. Phys. Chem. 75* (1971) 792.
23. Meany, J. E. *J. Phys. Chem. 75* (1971) 150.
24. Fischer, G. and Schellenberger, A. *Tetrahedron 28* (1972) 4113.
25. Patting, H. and Strehlow, H. *Ber. Bunsenges. Phys. Chem. 73* (1969) 534.
26. Bell, R. P. and Ridgewell, H. F. F. *Proc. Roy. Soc. (London) Ser. A 298* (1967) 178.
27. Bell, R. P. and Clunie, J. C. *Trans. Faraday Soc. 48* (1952) 440.
28. Kurtz, J. L. and Coburn, J. I. *J. Amer. Chem. Soc. 89* (1967) 3528.
29. Jen, J. and Knoche, W. *Ber. Bunsenges. Phys. Chem. 73* (1969) 539.
30. Pocker, Y., Meany, J. E., Nist, B. J. and Zadorojny, C. *J. Phys. Chem. 73* (1969) 2879.
31. Gold, V., Socrates, G. and Crampton, M. R. *J. Chem. Soc.* (1964) 5888.
32. Bell, R. P. *Advan. Phys. Org. Chem. 4* (1966) 1.
33. Bell, R. P., Millington, J. P. and Pink, J. M. *Proc. Roy. Soc. (London) Ser. A 303* (1968) 1.
34. Bell, R. P. and Critchlow, J. E. *Proc. Roy. Soc. (London) Ser. A 325* (1971) 35.
35. Bell, R. P. and Sørensen, P. E. *J. Chem. Soc. Perkin Trans. 2* (1972) 380.

Received September 7, 1973.

Acta Chemica Scandinavica A 28 (1974) 169—174

The Crystal Structure of $Hg(OH)_2.2HgSO_4.H_2O$

GERT BJÖRNLUND

Inorganic Chemistry 1, Chemical Center, University of Lund, P. O. B. 740, S-220 07 Lund 7, Sweden

The crystal structure of $Hg(OH)_2.2HgSO_4.H_2O$ has been determined from X-ray intensity data collected with a four-circle single crystal diffractometer. The crystals are monoclinic, space group $C2/c$, with $a=7.152$, $b=8.919$, $c=14.488$ Å and $\beta=98.94°$. The unit cell contains four formula units.

The structure is built up by finite zig-zag chains $O1-Hg-(OH)-Hg-(OH)-Hg-O1$, where O1 is an oxygen atom in a sulphate group. The chains run approximately parallel to the bc-plane in the b-direction. There probably exist hydrogen bonds directly between the finite chains as well as between the chains *via* water molecules. In this way the structure constitutes a three-dimensional network.

According to Hoitsema there exist four solid phases in the system $HgO-SO_3-H_2O$.[1] One of these was described by the formula $3HgO.2SO_3.2H_2O$. The crystal structure of this phase was later studied by Bonefačić, who presented the formula $2HgSO_4.HgO.2H_2O$.[2] However, only the locations of the mercury and the sulphur atoms were reported. The purpose of the present investigation was to study the coordination of the mercury atoms and thus a complete structure determination was performed. In a manner consistent with this examination the formula of the compound should be written $Hg(OH)_2.2HgSO_4.H_2O$.

EXPERIMENTAL

Crystals of $Hg(OH)_2.2HgSO_4.H_2O$ were formed when diluted sulphuric acid was allowed to be in contact with solid, freshly precipitated, yellow mercury(II) oxide. Transparent crystals grew out of the solid HgO. The homogeneity of the crystals was checked by X-ray Guinier-Hägg photographs.

X-Ray powder diffraction photographs were recorded in a Guinier-Hägg focusing camera using $CuK\alpha_1$ radiation and potassium chloride as an internal standard. The powder pattern could be interpreted by means of a monoclinic unit cell with the following lattice parameters, with standard deviations in brackets: $a=7.152(1)$, $b=8.919(2)$, $c=14.488(2)$ Å and $\beta=98.94(2)°$.

The density of the crystals, 6.18 g cm^{-3}, was determined from the apparent loss of weight in benzene. Assuming a unit cell content of four formula units, the calculated density is 6.17 g cm^{-3}.

A single crystal, elongated along b, of the approximate dimensions $0.03\times0.09\times0.01$ mm^3, mounted along the b-axis, was used for recording the layers $h0l-h7l$ with a Weissenberg camera using Ni-filtered $CuK\alpha$ radiation. The multifilm technique was used. The intensities were estimated visually by comparing with a calibrated scale and corrected for Lorentz and polarization effects in the usual way. As the linear absorption coefficient [3] was 1002 cm^{-1}, an absorption correction was carried out, the crystal being described by means of six planes. These film data were used for the preliminary determination of the structure.

The computer controlled four-circle diffractometer CAD-4 (manufactured by Enraf-Nonius, Delft, Holland) was employed for the refinement of the structure. The diffractometer was equipped with a graphite monochromator. $MoK\alpha$ radiation and the same crystal as above were used.

The intensities were recorded at a take off angle of 5°. The $\omega-2\theta$ scan technique was employed with the scan interval $\Delta\omega=0.9+0.5\tan\theta$. A fast pre-scan was used in order to determine the speed at which a predetermined minimum number of counts (2000) were received. The background intensity was measured for one fourth of the scan time at both ends of the interval. The intensities of 867 independent reflections were recorded in the range $3°<\theta<25°$. The intensities of 658 reflections were considered significantly different from the background as they had $I>3\sigma_0(I)$. The values of $\sigma_0(I)$ were based on counting statistics.

The stability of the crystal and of the electronics was checked by measuring two control reflections, 224 and 353, every 90 min. The

values of I and $\sigma_o(I)$ were corrected for Lorentz, polarization and absorption effects. The expression $p=(1+\cos^2 2\theta_M \cos^2 2\theta)/(1+\cos^2 2\theta_M)$ with $\theta_M=6.08°$ was used for the polarization factor. The linear absorption coefficient [3] was calculated to be 518 cm^{-1} and the transmission factor, evaluated by numerical integration, varied in the interval 0.26 – 0.57.

The computer UNIVAC 1108 in Lund was used for the calculations. The programmes employed were CELSIUS, DATAPC, DRF, LINUS, WAL, ORTEP, LALS, DISTAN and SACTA. Information about the programmes is given elsewhere.[4,5]

DETERMINATION AND REFINEMENT OF THE STRUCTURE

The systematic extinctions of the reflections hkl for $h+k$ odd and $h0l$ for h,l odd suggest one of the space groups Cc (No. 9) or $C2/c$ (No. 15) in both cases b as unique axis.[6]

Film data. A three-dimensional Patterson function was used to find preliminary positions of the mercury atoms. The space group was assumed to be $C2/c$. Least-squares refinements followed by three-dimensional difference Fourier-sections revealed the positions of the sulphur and oxygen atoms. The positional parameters of all the atoms, the anisotropic temperature factors for the mercury atoms, the isotropic factors for the other atoms and the inter-layer scale factors were then refined using a full matrix least-squares programme. The resulting discrepancy factor $R=\sum||F_o|-|F_c||/\sum|F_o|$ was 0.114. The parameters of the mercury and sulphur atoms were in good agreement with those earlier given by Bonefačić.[2]

Diffractometer data. For the refinement of the crystal structure there were 658 non-zero, independent reflections available. Employing the preliminary parameters as input for the diffractometer data the least-squares calculations performed in the same way as above resulted in $R=0.037$. The quantity minimized was $w(|F_o|-|F_c|)^2$ with weighting according to $w=1/(\sigma_o^2+a|F_o|^2+b)$, where a and b were chosen to make the quantity minimized equal in the different $|F_o|$ and sin θ intervals. The convergence of the least-squares refinements was checked

by $R_w=[\sum w(|F_o|-|F_c|)^2/\sum w|F_o|^2]^{\frac{1}{2}}$

as well as by the R-factor.

Table 1. Final positional and thermal parameters with standard deviations (in brackets). The temperature factor expression used is exp $-[(\beta_{11}h^2+\beta_{22}k^2+\beta_{33}l^2+2\beta_{12}hk+2\beta_{13}hl+2\beta_{23}kl)]$.

Atom	Point position	x	y	z
Hg1	4(*c*)	1/4	1/4	0
Hg2	8(*f*)	0.25210(10)	0.93488(7)	0.14825(5)
S	8(*f*)	0.2167(5)	0.5923(4)	0.1050(3)
O1	8(*f*)	0.1579(16)	0.2109(12)	0.3381(9)
O2	8(*f*)	0.3764(18)	0.0037(14)	0.3311(8)
O3	8(*f*)	0.3490(18)	0.5019(15)	0.0611(9)
O4	8(*f*)	0.0809(18)	0.6684(15)	0.0361(10)
O5	8(*f*)	0.2190(16)	0.1639(12)	0.1353(8)
O6	4(*e*)	0	0.8354(17)	1/4

	$\beta_{11}\times10^3$	$\beta_{22}\times10^3$	$\beta_{33}\times10^3$	$\beta_{12}\times10^3$	$\beta_{13}\times10^3$	$\beta_{23}\times10^3$
Hg1	9.1(2)	4.1(1)	1.29(5)	0.0(1)	−0.45(7)	0.23(6)
Hg2	8.8(2)	3.4(1)	1.85(4)	−0.15(9)	−0.10(6)	0.03(5)
S	3.7(7)	3.5(6)	1.2(2)	−0.4(5)	−0.1(3)	0.0(3)
O1	6(2)	1(1)	2.5(6)	−0(1)	−1(1)	0.0(7)
O2	11(3)	5(1)	1.2(6)	2(2)	0(1)	0.4(8)
O3	10(3)	8(2)	2.5(7)	−1(2)	3(1)	−2.6(9)
O4	9(3)	8(2)	3.7(8)	−2(2)	−3(1)	3(1)
O5	8(3)	2(1)	1.9(6)	−3(1)	−1(1)	0.3(7)
O6	6(3)	2(2)	4(1)	0	−3(2)	0

Table 2. Observed and calculated structure factors for $Hg(OH)_2.2HgSO_4.H_2O$. The columns are l, $|F_o|$ and $|F_c|$.

H= 0 K= 0			6 333 335			5 581 594			13 112 119			4 288 281			4 143 139			-6 131 132			5 239 249		
-14 312 327			8 289 283			4 148 152			15 156 162			5 235 227			6 342 326			-5 207 203			7 73 74		
-12 283 287			9 164 155			5 258 262						6 198 187			8 291 283			-4 139 133			8 102 89		
-10 203 194			11 99 89			7 148 136			H= 2 K= 6			7 109 98			10 78 66			-3 266 263			9 141 149		
-8 432 404			12 147 141			8 234 225			-15 279 288			8 586 587			12 206 201			-2 309 306					
-6 404 432			14 210 226			9 317 317			-14 124 116			9 249 244						-1 83 85			H= 6 K= 6		
-4 353 320						11 319 313			-13 150 149			11 170 166			H= 4 K= 2			1 90 87			-12 123 119		
4 347 320			H= 0 K= 8			12 157 156			-12 149 144			12 252 257						2 317 320			-11 148 147		
6 479 432			-10 343 345						-11 273 272						-16 181 177			3 275 268			-10 126 123		
8 413 404			-6 385 395			H= 1 K= 7			-10 154 155			H= 5 K= 3			-15 157 156			4 219 228			-9 176 171		
10 195 194			-2 234 249			-13 191 170			-9 292 307			-15 123 128			-12 136 137			5 174 163			-8 92 91		
12 236 237			0 168 165			-12 231 222			-8 116 126			-13 290 282			-11 178 179			6 182 184			-7 67 55		
14 310 327			2 244 242			-11 86 73			-7 79 92			-12 90 87			-10 307 315			7 109 105			-6 74 77		
			4 394 395			-9 75 49			-6 189 198			-8 92 80			-9 142 165			8 275 276			-5 197 193		
H= 0 K= 2			6 76 74			-8 256 254			-5 387 417			-7 512 535			-7 90 89			9 191 194			-4 153 150		
-16 207 218			9 81 60			-7 204 208			-4 339 354			-6 156 157			-5 172 179			11 166 166			-3 102 97		
-15 182 181			10 352 345			-6 103 116			-3 140 151			-5 136 138			-4 406 415			12 202 217			-2 152 153		
-13 94 109						-5 181 182			-2 262 257			-3 212 224			-3 98 97						-1 177 176		
-12 174 114			H= 0 K= 10			-4 176 176			-1 363 363			-2 167 164			-2 270 274			H= 5 K= 3			0 81 78		
-11 225 222			-5 191 188			-3 110 120			0 166 162			-1 442 475			-1 100 109			-13 239 252			1 222 227		
-10 401 399			-1 157 154			-2 269 272			1 373 376			1 531 539			0 54 52			-8 73 66			2 81 81		
-9 234 228			0 206 215			-1 185 188			2 181 182			2 104 101			1 251 248			-7 434 450			3 66 59		
-8 152 148			1 152 154			1 196 196			4 241 238			3 153 147			2 249 255			-5 95 103			4 155 151		
-7 94 99			5 188 188			2 295 285			5 440 435			4 138 140			4 397 403			-3 184 188			5 242 238		
-5 313 311						3 92 99			6 204 188			5 106 115			5 287 285			-2 102 112			6 125 128		
-4 587 591			H= 1 K= 1			4 171 170			7 111 115			7 473 465			7 104 114			-1 361 356			8 114 123		
-2 358 360			-17 189 182			5 225 224			8 156 147			8 75 81			9 231 236			1 376 384					
-1 221 231			-16 196 200			6 183 182			9 304 302			13 325 330			10 300 304			2 117 113			H= 6 K= 6		
0 126 144			-15 140 147			7 234 228			10 128 130						11 153 153			3 108 109			-9 120 125		
1 229 231			-14 124 113			8 278 270			11 225 223			H= 5 K= 5			12 90 82			5 127 125			-8 181 189		
2 352 360			-13 79 76			12 249 237			12 149 147			-12 140 123						7 342 345			-6 215 213		
4 434 391			-12 332 322						13 115 117			-11 290 300			H= 4 K= 6			8 103 98			-5 168 160		
5 352 311			-11 262 253			H= 1 K= 9			14 125 133			-9 246 260			-14 103 104						-1 127 133		
7 94 99			-9 304 291			-9 191 198						-8 138 136			-13 120 118			H= 5 K= 5			0 295 297		
8 151 140			-8 378 376			-7 251 245			H= 2 K= 6			-7 151 155			-12 111 111			-11 193 190			-12 87 91		
9 247 228			-7 68 59			-6 170 164			-14 202 212			-6 200 216			-11 193 190			-10 139 150			-11 256 246		
10 404 399			-6 323 332			-5 83 71			-13 81 54			-5 480 485			-10 139 150			-9 225 241			-9 203 198		
11 217 222			-5 355 364			-4 123 131			-12 140 151			-3 73 62			-9 225 241			-8 124 124			-8 71 83		
12 113 114			-4 295 299			-2 260 262			-11 100 93			0 77 76			-8 124 124			-7 73 81			H= 7 K= 1		
13 109 109			-3 479 508			-1 254 252			-9 149 151			1 65 62			-7 73 81			-7 109 103			-11 150 152		
15 171 181			-2 362 371			1 240 243			-8 295 307			2 110 106			-6 120 125			-6 67 56			-9 106 111		
16 211 218			-1 99 97			2 300 299			-6 312 321			3 475 482			-5 318 325			-5 166 167			-8 159 156		
			1 96 82			4 117 127			-5 206 207			4 157 155			-4 245 246			-3 405 407			-6 101 99		
H= 0 K= 4			2 383 366			5 96 90			-4 99 105			5 199 183			-3 122 123			-2 67 72			-5 125 125		
-15 226 228			3 506 489			6 149 152			-3 92 81			6 83 82			-2 240 240			0 85 85			-4 77 75		
-14 136 140			4 340 345			7 228 227			-2 109 115			7 86 94			-1 208 208			2 66 73			-3 227 219		
-13 138 148			5 204 201			8 165 174			-1 206 210			8 136 144			0 61 69			3 355 357			-2 195 187		
-12 181 176			6 241 236						0 500 512			9 256 256			1 302 303			4 123 113			-1 70 67		
-11 259 252			7 83 79			H= 2 K= 0			1 181 180			11 279 279			2 144 143			5 149 153			0 86 68		
-10 131 142			8 390 371			-14 343 332			2 90 93			12 136 128			3 69 81			6 65 63			2 208 215		
-9 334 332			9 274 263			-12 150 153			3 112 108						4 212 216			7 74 85			3 159 163		
-8 102 101			10 72 65			-10 154 154			5 211 209			H= 3 K= 7			5 353 348			8 125 122			4 142 143		
-7 164 169			11 212 221			-8 396 412			6 305 306			-12 193 191			6 172 171			9 185 203			5 112 111		
-6 241 242			12 304 308			-6 577 588			8 214 207			-11 90 79			7 102 93						6 149 146		
-5 459 466			13 74 59			-4 324 323			9 167 151			-9 87 74			8 147 153			H= 5 K= 7					
-4 258 268			15 149 169			-2 104 106			11 108 102			-8 219 217			9 235 230			-8 166 174			H= 7 K= 3		
-3 162 161			16 151 165			0 923 950			12 175 171			-7 166 171			10 160 151			-7 139 138			-8 75 55		
-2 218 228						2 179 165						-6 127 128			11 177 172			-6 141 136			-7 329 331		
-1 381 396			H= 1 K= 3			4 328 305			H= 2 K= 8			-5 159 158			12 93 93			-5 109 108			-5 79 73		
0 202 203			-15 123 131			6 562 541			-10 317 332			-4 152 150			H= 4 K= 6			-4 113 112			-3 126 127		
1 382 396			-13 324 319			7 393 382			-8 68 70			-3 105 104			-12 113 101			-3 117 110			-1 244 242		
2 226 228			-12 97 96			10 96 85			-6 421 421			-2 210 211			-11 85 89			-2 207 205			1 244 247		
3 169 161			-9 84 87			12 243 249			-2 213 220			-1 183 186			-9 131 137			-1 168 170			2 67 68		
4 270 268			-8 87 89			14 320 340			0 155 155			1 127 124			-8 219 217			1 115 119			3 68 60		
5 479 486			-7 588 582						2 241 238			2 241 242			-6 273 276			2 206 199			5 94 112		
6 257 242			-6 115 115			H= 2 K= 2			4 356 349			3 41 63			-5 195 202			4 170 169					
7 182 169			-5 144 147			-16 195 192			6 93 91			4 185 183			-4 114 118			5 137 140			H= 7 K= 5		
8 114 101			-4 202 211			-15 189 188			8 76 79			5 170 167			-2 94 86			6 124 125			-7 93 89		
9 353 332			-2 217 217			-13 102 91						6 183 179			-1 189 192			H= 6 K= 0			-5 105 111		
10 147 142			-1 546 583			-12 154 150			H= 2 K= 10			7 220 216			0 427 427			-14 240 232			-3 278 271		
11 254 252			1 597 629			-11 194 186			-7 93 71			8 228 231			1 157 161			-12 87 82			-2 84 86		
12 183 176			3 189 182			-10 360 365									2 120 122			-10 103 103			2 82 86		
13 146 148			4 111 108			-8 194 204			-1 123 115			H= 3 K= 9			3 95 87			-8 296 294			3 261 269		
14 135 140			5 127 119			-6 111 110			0 219 214			-7 236 237			5 126 132			-6 362 361					
15 228 228			7 589 557			-4 151 149			1 162 155			-6 136 137			6 286 294			-4 140 161			H= 8 K= 0		
			8 139 128			-2 263 266						-4 112 109			8 144 154			0 447 441			-8 178 172		
H= 0 K= 6			9 94 76			-4 382 404			H= 3 K= 1			-2 230 228			9 124 131			2 131 129			-6 247 242		
-14 217 226			13 347 345			-3 66 63			-16 175 168			-1 218 217						4 294 293			-4 91 97		
-12 162 161			15 127 128			-2 350 356			-15 108 109			1 221 216			H= 4 K= 8			8 174 174			0 300 297		
-9 159 155						-1 142 144			-14 128 125			2 211 214			-4 341 329								
-8 278 283			H= 1 K= 5			1 137 131			-12 308 305			5 88 92			-2 197 184						H= 8 K= 2		
-6 335 335			-15 82 84			1 270 269			-11 241 241						0 151 150			H= 6 K= 2			-5 96 91		
-5 208 212			-13 84 66			2 293 296			-9 176 180			H= 4 K= 0			2 199 200			-12 91 79			-4 223 228		
-4 100 97			-12 162 162			3 78 72			-8 341 340			-14 296 292			4 313 306			-11 124 123			-3 79 85		
-3 93 99			-11 329 326			4 597 581			-6 209 214			-12 105 106			5 81 72			-10 255 250			-2 129 124		
-2 98 112			-9 271 279			5 328 315			-5 294 293			-10 117 119			6 76 60			-9 112 108			-1 76 67		
-1 182 188			-8 204 203			6 63 73			-4 221 223			-8 434 451						-5 160 161			1 176 172		
0 434 452			-7 161 165			7 164 159			-3 430 437			-6 473 471			H= 5 K= 1			-4 346 349			2 134 134		
1 188 188			-5 210 215			8 91 83			-2 445 460			-4 172 176			-15 75 75			-3 106 100					
2 114 112			-4 127 120			9 245 239			-1 93 97			-2 74 71			-12 223 230			-2 207 207					
3 96 99			-3 525 510			11 416 404			1 208 204			0 615 623			-11 196 197			-1 89 95					
4 87 97			-2 169 176			11 191 190			2 378 373			2 80 83			-9 135 143			1 262 204					
5 209 212			2 165 170			12 106 98			3 381 384						-8 249 246			2 222 233					
																			4 254 260					

A refinement using anisotropic thermal parameters for all the atoms resulted in $R = 0.034$ and $R_w = 0.043$. Correction for isotropic secondary extinction and the use of anomalous scattering factors [7] for the mercury and sulphur atoms affected the refinement little. The extinction parameter [8] $g = 2.1(2) \times 10^3$ corresponds to a mosaic spread of 28.2 seconds or a domain size of 1.47×10^{-5} cm. The finally obtained agreement factors were $R = 0.032$ and $R_w = 0.041$. The average value of the quantity minimized in different $|F_o|$ and sin θ intervals was fairly

constant. The values $a = 0.0018$ and $b = 0$ were used for the weighting. The atomic scattering factors used for the neutral mercury were those given by Cromer and Waber,[9] and those for sulphur and oxygen by Hanson *et al.*[10]

As the peaks in the Fourier sections were distinct, the least-squares refinements converged in a normal way and the interatomic distances and angles were reasonable it was concluded that space group $C2/c$ was the correct one.

A three-dimensional difference Fourier calculation based on the final least-squares refinement showed no peaks of importance. Thus, it was not possible to locate the hydrogen atoms.

The positional and anisotropic thermal parameters of all the atoms with estimated standard deviations are listed in Table 1 and the observed and calculated structure factors in Table 2.

DESCRIPTION AND DISCUSSION OF THE STRUCTURE

A fundamental building element of the structure of $Hg(OH)_2.2HgSO_4.H_2O$ is finite zig-zag chains O1 – Hg – (OH) – Hg – (OH) – Hg – O1, where O1 is an oxygen atom in a sulphate group. This is to the authors knowledge the first example of a mercury compound with finite chains as a structural element. The distances and angles in the chains show good agreement with the values found in other chains containing mercury and oxygen.[1]

Selected interatomic distances and angles in $Hg(OH)_2.2HgSO_4.H_2O$ are given in Table 3 and a stereoscopic pair of drawings of the structure is shown in Fig. 1 (notations of the atoms, *cf.* Table 1). As seen from Table 1 the atoms Hg1 occupy the point position 4(*c*) with point symmetry $\bar{1}$ and the atoms Hg2 the general point position 8(*f*). Each mercury atom Hg1 is bonded to two oxygen atoms O5 with distances Hg1 – O5 2.14(1) Å. The mercury atoms Hg1 are also surrounded by two other pairs of oxygen atoms, at distances of 2.48(1) and 2.45(1) Å, belonging to sulphate groups. The six oxygen atoms form a deformed octahedron. The mercury atoms Hg2 are each bonded to two oxygen atoms, *viz.* the atoms O1 and O5, with distances 2.10(1) and 2.06(1) Å, and the angle O1 – Hg2 – O5 168.8(4)°. Around Hg2 there are further oxygen atoms at distances ≥ 2.65 Å.

The sulphate groups are slightly distorted,

Table 3. Distances (Å) and angles (°) with standard deviations in brackets.

Distanes mercury to oxygen

Hg1 – 2 O5	2.14(1)	Hg2 – O1	2.10(1)
Hg1 – 2 O3	2.48(1)	Hg2 – O5	2.06(1)
Hg1 – 2 O4	2.45(1)		

Angles in the chains

∠O5 – Hg1 – O5	180	∠Hg2 – O1 – S	117.3(7)
∠O1 – Hg2 – O5	168.8(4)		
∠Hg1 – O5 – Hg2	114.2(5)		

Distances and angles within the sulphate tetrahedron

S – O1	1.54(1)	S – O3	1.46(1)
S – O2	1.46(1)	S – O4	1.45(1)
∠O1 – S – O2	108.5(7)	∠O2 – S – O3	111.6(8)
∠O1 – S – O3	104.4(7)	∠O2 – S – O4	111.7(8)
∠O1 – S – O4	108.6(7)	∠O3 – S – O4	111.7(8)

Distances and angles indicating hydrogen bonding

O1 – O5	2.81(1)	O5 – O6	2.85(1)
∠Hg2 – O1 – O5	114.5(5)	∠Hg2 – O5 – O1	103.5(5)
∠S – O1 – O5	108.3(6)	∠Hg2 – O5 – O6	114.7(5)
∠Hg1 – O5 – O1	108.0(5)	∠O1 – O5 – O6	116.4(5)
∠Hg1 – O5 – O6	100.2(4)	∠O5 – O6 – O5	115.0(7)

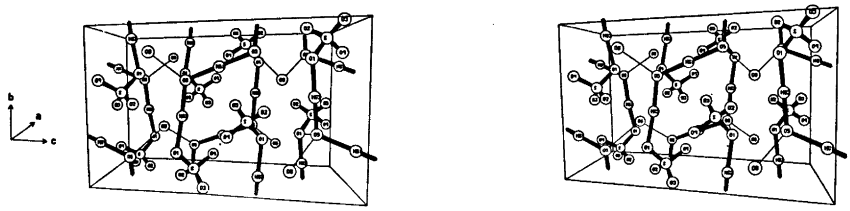

Fig. 1. A stereoscopic pair of drawings showing the structure of $Hg(OH)_2.2HgSO_4.H_2O$. The hydrogen bonds in the cell are drawn with thin lines.

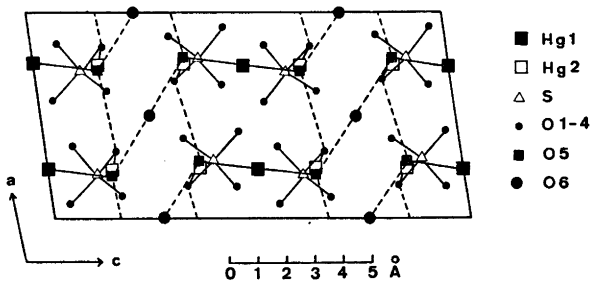

Fig. 2. A projection of a unit cell of the structure on the *ac*-plane. The hydrogen bonds are dotted and other bonds full lined.

giving an extra long bond, 1.54(1) Å, between S and O1, probably caused by the bonding O1 to Hg2. The same effect is found in the chromate group in the structure of $HgCrO_4 \cdot \frac{1}{2}H_2O$.[12]

The oxygen atoms O5 may form hydrogen bonds to the sulphate oxygen atoms O1 outside their own finite groups since the closest distance O1–O5 is 2.81(1) Å, which is a possible hydrogen bond distance.[13] The angles involved are a further support for hydrogen bonding. For chemical reasons the hydrogen atom is closer to O5 than to O1, which means that the hydrogen bonding should be described O5–H···O1. The chains therefore resemble those found in $Hg(OH)BrO_3$ [5] and in Hg(OH)F.[14] In this way two-dimensional networks are built up parallel to each other, which is shown in a projection, Fig. 2.

Between the networks there are water molecules. The two-dimensional networks are probably knitted together by hydrogen bonds *via* the water molecules. The closest distance O5–O6, where O6 is the water oxygen atom, is 2.85(1) Å. The angles involved indicate that this is a hydrogen bond as well.

Acknowledgements. The author thanks Dr. Karin Aurivillius for valuable discussions and comments on this work. The author is also indebted to Professor Sture Fronæus for his kind interest in this work. This investigation is part of a research project, supported by the Swedish Natural Science Research Council.

REFERENCES

1. Hoitsema, C. *Z. Phys. Chem. 17* (1895) 651.
2. Bonefačić, A. *Croat. Chem. Acta 34* (1962) 119.
3. *International Tables for X-Ray Crystallography*, 2nd Ed., Kynoch Press, Birmingham 1968, Vol III, p. 162.
4. Oscarsson, Å. *Acta Crystallogr. B 29* (1973) 1747.
5. Björnlund, G. *Acta Chem. Scand. 25* (1971) 1645.
6. *International Tables for X-Ray Crystallography*, 3rd Ed., Kynoch Press, Birmingham 1969, Vol I.
7. *Ibid.* Vol III, p. 213.
8. Zachariasen, W. H. *Acta Crystallogr. 23* (1967) 558–564.
9. Cromer, D. T. and Waber, I. T. *Acta Crystallogr. 18* (1965) 104.
10. Hanson, H. P., Herman, F., Lea, I. D. and Skillman, S. *Acta Crystallogr. 17* (1964) 1040.
11. Aurivillius, K. *Ark. Kemi 24* (1965) 151.

12. Aurivillius, K. *Acta Chem. Scand. 26* (1972) 2113.
13. Hamilton, W. C. and Ibers, J. A. *Hydrogen Bonding in Solids*, Benjamin, New York 1968, p. 259.
14. Grdenic, D. and Sikirica, M. *Inorg. Chem. 12* (1973) 544.

Received October 20, 1973.

Acta Chemica Scandinavica A 28 (1974) 175—184

The Crystal Structure of the Addition Compound *N*-Methylthiocaprolactam-Iodine (1:1)

E. L. AHLSEN and K. O. STRØMME

Department of Chemistry, University of Oslo, Blindern, Oslo 3, Norway

The crystal structure of the molecular complex formed by *N*-methylthiocaprolactam (MTCL) and iodine in the mol ratio 1:1 has been determined at 18°C, using X-ray diffraction techniques. The donor molecule is a cyclic thioamide. The crystalline adduct as crystallized from a benzene solution, is monoclinic, the space group being $P2_1/c$ with four molecules per unit cell. The I—S separation [2.688 Å(2)] is significantly shorter than the corresponding I—S distances observed in iodine complexes with thioethers, and the I—I bond length [2.880 Å(1)] somewhat larger. The I—I—S group is nearly linear. The C_1-S and C_1-N bond lengths [1.716(5) Å and 1.302(7) Å, respectively] are close to the corresponding distances observed in pure thioamides. The thioamide group and the methyl carbon atom form an approximately planar grouping with the iodine molecule. Inter-molecular contact distances are of the van der Waals type.

However, crystals grown from solutions containing carbon tetrachloride were found to contain equimolecular amounts of the present adduct and carbon tetrachloride. Crystal data for this compound are given.

The crystal structures of molecular complexes formed by iodine and thioethers have previously been reported.[1a-1d] The structures of related adducts such as thiourea-, merocyanine-, and triphenylphosphine sulfide-iodine are also known.[1a-1d] On the other hand, complexes formed by halogen and thioamides are probably usually too unstable to yield crystals suitable for single crystal work. However, previous studies had shown [2,3] that a relatively stable complex was formed between iodine and *N*-methylthiocaprolactam (MTCL) in the mole ratio 1:1, the acceptor molecule being most likely joined to sulphur. The nitrogen atom in thioamides is expected to be a relatively poor electron donor since the lone electron pair is probably considerably delocalized.

Attempts at obtaining single crystals of MTCL and iodine chloride or bromine, respectively, did not succeed. The latter compound was formed as an unstable, yellow precipitate in pentane.

EXPERIMENTAL

The solid complex was precipitated from a solution of MTCL in pentane by adding an equimolecular portion of iodine (reagent grade) dissolved in pentane.[2] The sample of MTCL was kindly supplied by mag.scient. E. Augdahl. The orange-coloured precipitate was subsequently filtered, washed and dried.

Reddish single crystals (m.p. 97 ± 1°C) in the form of somewhat elongated prisms were found to crystallize from solutions of the adduct in benzene.

When crystallized from solutions containing carbontetrachloride, needle-shaped, orange-coloured crystals of a different molecular complex containing equimolecular amounts of CCl_4 and the former components are formed. Exposed to air, the compound loses rapidly carbon tetrachloride, leaving the MTCL-I_2 adduct as a powder. The latter dissolves easily in polar solvents.

The crystals of MTCL-I_2 were sealed in thin-walled boron-lithium glass-capillaries before exposure to X-ray radiation. A single crystal of about $0.15 \times 0.20 \times 0.25$ mm³ was used in the intensity recording made on an automatic Picker four-circle diffractometer, using graphite monochromated Mo*K*-radiation. 2711 reflections with intensity $> 2.5\sigma(I)$ were used in the structure determination, while 555 reflections with intensity $< 2.5\sigma(I)$ were excluded from the calculations. Further experimental details are: Range: $2° < 2\theta < 60°$; scan: $[2\theta(\alpha_1) - 0.7°] - [2\theta(\alpha_2) + 0.7°]$; scan speed: 1°/min, background counts in 20 sec on either side of scan region; *b*-axis along ϕ-axis; experimental temperature

Table 1. Observed and calculated structure factors.

l	Fo	Fc
	h=0,k=0	
2	45.9	40.40
4	54.9	47.63
6	7.0	5.93
8	119.1	119.72
12	61.5	62.64
	h=0,k=1	
0	60.2	58.77
1	122.5	120.25
2	57.8	59.09
3	15.9	17.10
4	134.6	132.60
5	134.0	135.78
6	44.4	47.78
1	127.4	173.47
	h=0,k=2	
0	46.6	51.05
4	133.9	132.43
5	83.7	81.70
6	108.3	100.61
7	192.5	186.66
8	66.0	66.98
9	4.0	3.94
10	46.2	44.26
11	60.5	57.73
12	40.2	38.53
13	21.6	21.57
14	7.7	7.48
15	64.4	64.95
	h=0,k=3	
14	82.6	80.03
13	17.1	17.40
12	20.3	18.90
11	5.5	3.71
9	20.4	20.37
8	80.9	78.06
7	17.0	17.12
6	101.4	98.45
5	31.7	30.82
4	200.3	226.40
3	38.2	40.14
2	35.8	40.71
1	10.9	11.08
	h=0,k=4	
0	103.3	117.82
1	9.3	6.43
2	68.0	75.36
3	117.3	135.81
4	48.5	50.35
5	77.6	78.85
6	3.8	1.28
7	79.4	77.40
8	64.0	62.64
9	41.0	39.96
10	45.3	44.16
11	17.3	17.70
12	14.8	14.64
13	38.7	37.06
14	9.4	10.04
	h=0,k=5	
12	9.3	10.78
11	73.5	69.24
10	36.8	36.90
9	14.2	14.51
8	55.0	52.68
7	74.2	74.35
6	20.1	22.13
5	19.9	20.20
4	49.5	54.28
3	73.6	81.91
2	61.8	67.87
1	71.2	80.34
	h=0,k=6	
0	112.5	136.86
1	43.1	47.19
2	9.1	8.69
4	32.8	34.71
5	14.8	15.00
6	32.7	34.56
7	5.5	7.49
8	48.7	48.69
9	43.2	42.10
10	53.6	50.65
12	37.0	37.01
	h=0,k=7	
10	5.9	6.07
9	8.9	9.85
7	36.7	38.06
6	19.8	19.96
5	28.5	29.61
4	41.6	45.04
3	5.5	3.43
2	27.2	29.06
1	61.6	67.66
	h=0,k=8	
0	25.1	27.72
1	12.9	13.48
2	21.7	22.51
3	30.4	33.62
4	23.4	24.76
5	19.5	20.15
6	36.8	37.94
7	30.3	30.83
	h=0,k=9	
2	18.0	19.22
	h=1,k=9	
-2	11.0	11.38
0	26.5	28.53
1	25.2	25.65
3	29.5	29.83
	h=1,k=8	
6	19.5	19.61
5	18.8	20.18
4	8.3	9.42
3	29.9	31.60
2	45.2	49.08
1	40.0	44.64
0	15.5	15.33
-1	13.6	15.23
-2	11.3	11.05
-3	10.4	11.20
-4	23.8	24.38
-5	8.5	7.60
-6	19.6	20.86
-7	34.2	35.40
	h=1,k=6	
9	40.6	40.09
8	77.8	79.83
7	12.3	11.76
6	30.7	31.68
5	22.6	23.94
4	37.0	40.58
3	19.6	21.02
2	11.2	13.33
1	19.0	21.23
0	60.7	66.13
-1	53.7	59.26
-2	61.4	67.60
-3	28.7	30.84
-4	100.8	107.25
-5	6.5	5.12
-7	23.2	23.63
-8	12.7	12.81
-9	5.4	6.21
-10	59.5	58.59
-11	18.7	17.89
-12	20.6	19.38
	h=1,k=5	
-13	28.5	27.57
-12	45.9	45.02
-9	5.7	4.65
-8	31.7	31.98
-7	24.5	23.22
-6	56.4	55.04
-5	4.8	1.22
-3	116.0	127.96
-2	71.3	80.29
-1	70.6	81.83
0	68.9	79.56
1	49.6	56.79
3	22.5	24.45
4	39.3	43.22
5	64.2	70.27
6	30.9	31.84
7	83.5	83.73
8	16.5	16.97
9	15.7	15.69
10	44.5	42.87
11	24.9	24.53
12	16.5	15.00
	h=1,k=4	
	6.5	6.51
11	82.3	78.66
10	37.3	35.89
9	8.9	8.03
7	5.1	3.99
6	21.7	22.11
5	104.2	109.90
4	97.2	107.04
3	120.1	137.02
2	17.8	18.68
1	88.2	106.64
0	101.9	121.24
-1	54.3	60.66
-2	15.8	16.79
-3	14.2	15.81
-4	63.5	63.82
-5	63.2	62.56
-6	74.8	71.92
-7	154.7	150.34
-8	33.5	32.64
-10	33.5	33.22
-12	23.4	23.07
-13	22.8	22.78
-14	42.6	42.90
	h=1,k=3	
-15	13.9	13.12
-14	31.1	29.86
-13	10.9	11.10
-12	10.8	11.05
-11	21.6	21.22
-10	68.0	65.43
-9	33.4	33.45
-8	146.2	140.49
-7	30.1	28.44
-6	147.7	140.96
-5	36.7	36.75
-4	91.0	87.20
-3	17.7	18.23
-2	7.7	9.42
-1	13.8	13.78
0	6.2	7.64
3	67.7	73.42
5	55.0	52.86
6	14.7	13.99
7	8.5	9.42
12	81.2	79.49
13	26.7	26.69
14	37.4	36.13
	h=1,k=2	
15	42.0	42.47
14	31.1	30.31
12	24.4	23.53
11	113.9	112.39
10	31.2	31.30
9	14.7	14.82
8	55.5	54.56
7	5.2	4.46
6	16.5	15.10
5	80.9	79.19
4	105.0	101.95
3	147.5	157.06
2	91.0	97.43
1	219.0	286.59
0	143.2	178.10
-1	94.7	103.17
-2	38.8	39.99
-3	10.7	13.24
-4	99.3	90.68
-5	69.3	62.35
-6	10.8	9.23
-7	206.0	193.44
-8	30.5	28.70
-9	36.0	33.98
-10	68.4	65.00
-11	73.6	71.44
-12	5.3	4.79
-13	16.5	15.99
-14	44.9	44.82
-15	46.9	47.11
-16	19.5	18.85
	h=1,k=1	
-16	7.1	8.28
-15	42.2	43.87
-14	44.0	44.27
-13	39.6	39.74
-12	22.2	21.23
-11	115.9	113.83
-10	65.1	64.65
-9	26.4	26.17
-8	58.4	54.72
-7	23.7	25.19
-6	71.9	63.49
-5	67.1	65.35
-4	126.1	109.44
-2	67.8	62.68
-1	84.1	79.19
0	63.4	66.03
1	113.8	120.64
2	39.3	38.85
3	37.8	41.68
4	164.7	170.39
5	103.7	104.09
6	25.7	25.42
8	39.1	36.87
9	47.9	47.96
10	14.7	14.67
11	56.7	57.17
12	48.3	48.45
13	9.0	9.07
14	46.4	46.41
15	46.1	45.22
	h=1,k=0	
14	44.6	44.62
12	4.4	5.51
10	13.7	13.71
8	216.8	231.04
6	118.9	119.26
4	128.9	127.92
2	68.9	75.42
0	138.5	144.24
-2	155.5	138.39
-4	315.4	317.74
-6	85.8	76.73
-8	11.2	11.95
-10	130.5	130.52
-12	62.8	62.44
	h=2,k=0	
-12	32.4	33.11
-10	37.3	37.41
-8	60.6	61.39
-6	240.0	226.20
-4	186.1	187.61
-2	250.5	289.08
0	45.9	44.21
2	78.9	83.57
4	60.0	60.58
6	49.1	50.58
	h=2,k=1	
13	14.9	9.45
12	34.5	34.68
10	29.6	30.08
9	9.7	10.06
8	87.9	90.47
7	98.2	99.15
6	15.2	15.65
5	157.4	162.86
4	57.3	58.43
3	137.4	142.48
2	27.0	23.20
1	50.3	54.03
0	155.3	150.92
-1	35.8	30.52
-2	135.1	133.81
-3	262.7	255.44
-4	69.9	71.45
-5	18.9	19.01
-6	61.4	55.20
-7	207.5	190.91
-8	74.1	69.16
-10	86.5	82.16
-11	15.3	13.90
-12	4.4	3.22
-13	72.9	74.08
-14	24.2	25.09
-15	47.2	47.36
	h=2,k=2	
-16	16.2	13.50
-15	19.5	19.52
-14	32.4	31.93
-13	54.4	55.50
-12	28.4	23.53
-11	103.1	102.17
-10	23.7	23.43
-9	72.2	68.43
-8	65.4	61.58
-7	114.7	107.30
-6	107.5	99.19
-5	25.8	24.07
-4	66.8	64.85
-3	188.8	188.36
-2	70.2	68.91
-1	59.6	59.85
0	75.9	71.41
1	198.2	215.31
2	23.4	21.96
3	81.7	82.71
4	104.6	108.50
5	14.2	14.81
6	6.6	7.23
7	79.1	79.24
8	60.2	62.41
9	87.9	88.81
10	40.4	40.66
11	74.9	76.18
12	27.9	26.74
13	10.1	10.57
14	22.5	22.31
	h=2,k=3	
13	10.1	9.87
12	66.4	66.76
11	10.7	9.70
10	42.1	42.04
9	50.7	50.13
8	122.7	121.98
7	5.3	3.88
5	31.8	31.50
4	38.5	36.38
3	10.5	8.65
2	89.1	91.08
-8	58.4	54.72
-1	93.6	99.38
-2	108.8	113.68
-3	16.6	15.74
-4	43.0	41.98
-5	5.1	4.74
-6	45.9	43.66
-7	6.3	6.39
-8	39.8	37.91
-9	43.0	42.04
-10	161.2	153.92
-11	15.5	15.25
-12	38.0	36.96
-13	5.6	4.06
-14	15.1	14.11
-15	8.0	6.69
	h=2,k=4	
-14	27.9	28.22
-13	7.0	5.55
-12	31.0	31.05
-11	97.4	93.73
-10	6.9	4.80
-9	81.8	78.25
-8	19.3	18.14
-7	90.5	48.95
-6	95.3	93.39
-5	33.9	33.06
-4	81.6	82.32
-3	92.7	99.97
-2	10.4	9.27
-1	59.5	64.91
0	19.7	19.56
1	144.8	170.19
2	79.1	86.05
3	4.6	3.74
4	70.8	73.13
5	4.6	3.53
6	23.3	22.07
7	71.0	71.28
8	37.5	37.69
9	30.8	30.41
10	7.8	6.25
11	62.5	61.97
12	45.7	44.92
13	21.2	20.90
	h=2,k=5	
12	25.6	24.08
11	31.1	29.75
10	7.8	5.86
9	15.5	15.27
8	42.6	41.67
7	77.0	76.22
6	70.3	70.74
5	71.3	74.08
4	8.5	9.35
3	28.4	28.46
2	47.6	52.24
1	66.5	72.09
0	37.7	41.09
-1	8.9	6.08
-2	14.1	13.68
-3	113.1	121.64
-4	68.5	71.03
-5	9.4	8.32
-6	46.2	46.36
-7	95.8	92.29
-9	5.4	2.67
-10	28.1	26.05
-11	28.2	28.60
-12	13.2	12.40
-13	29.2	29.02
	h=2,k=6	
-12	15.8	15.69
-11	9.3	9.97
-10	1.7	1.80
-9	8.6	8.46
-8	29.7	27.92
-7	4.5	1.14
-6	76.1	77.99
-5	68.6	71.33
-4	52.2	54.94
-3	4.9	2.47
-2	34.6	34.52
0	12.2	12.86
1	8.6	9.65
2	5.4	.96
3	22.0	23.14
4	112.3	124.19
5	46.8	48.05
6	27.2	28.59
7	17.8	18.05
8	28.3	27.89
9	13.1	13.40
10	11.3	11.15
	h=2,k=7	
9	21.5	20.91
8	39.2	38.99
6	16.6	16.08
5	48.8	51.32
4	14.1	15.84
3	55.4	59.31
2	10.8	8.89
0	35.8	36.37
-1	36.2	36.81
-2	39.8	41.32
-3	48.1	50.34
-4	8.0	7.60
-5	8.8	8.81
-6	5.4	2.76
-7	54.6	54.01
-8	36.2	35.68
-9	18.0	17.89
-10	16.9	15.52
	h=2,k=8	
-8	32.6	30.53
-7	28.0	29.81
-6	14.4	14.39
-4	6.2	6.88
-3	39.2	40.69
-2	44.5	46.01
0	26.2	27.17
1	35.3	38.25
2	21.4	20.55
3	14.3	14.55
4	15.2	15.23
5	6.4	7.18
	h=2,k=9	
0	30.9	31.59
-1	31.0	30.56
-2	12.9	13.21
	h=3,k=0	
4	17.7	18.84
3	7.0	6.62
2	5.1	5.75
1	14.6	14.82
0	33.3	33.97
-1	5.5	4.91
-2	24.8	24.20
-3	39.5	40.31
-4	29.8	29.43
-5	18.9	19.15
-6	28.6	28.37
-7	12.3	12.12
	h=3,k=1	
-2	26.2	28.28
-1	34.6	35.37
0	33.3	35.04
1	53.8	55.86
2	26.9	27.35
3	12.2	12.51
-1	12.9	10.43
-2	35.3	33.30
-3	201.3	204.52
-4	3.7	1.19
-5	94.0	87.54
-6	70.9	66.52
-7	53.0	50.81
-8	22.0	21.43
-9	37.8	35.75
-10	102.8	97.07
-11	75.9	72.36
-12	56.8	56.49
-13	79.1	77.63
-14	25.4	25.78
-15	34.5	34.49
-16	9.6	10.80
	h=3,k=2	
-16	5.4	5.70
-15	11.6	10.35
-14	38.5	36.82
-13	27.1	26.89
-12	9.4	6.41
-11	65.8	63.88
-10	76.6	74.80
-9	91.0	86.63
-8	11.2	9.50
-7	182.2	173.68
-6	97.1	92.18
-5	65.7	61.92
-4	44.9	43.08
-3	11.7	9.57
-2	112.6	109.09
-1	5.8	4.68
0	119.3	116.45
1	236.7	243.41
2	43.3	40.74
3	57.9	57.59
4	102.4	103.71
5	105.5	107.35
6	55.3	55.80
8	60.7	57.44
9	36.5	36.97
10	24.5	25.06
11	81.0	83.53
12	31.8	34.52
13	33.8	34.74
	h=3,k=3	
12	93.7	97.38
10	102.5	104.90
8	38.3	40.01
6	4.2	3.25
4	172.4	182.05
2	175.8	180.46
0	194.5	201.15
-2	96.4	93.22
-4	12.2	11.04
-6	240.3	246.85
-8	78.7	77.45
-10	103.1	101.02
-12	26.4	25.90
-14	6.0	4.59
-16	53.1	54.57
	h=4,k=0	
-16	19.9	20.53
-14	41.7	41.52
-12	5.4	4.98
-10	199.0	196.08
-8	64.0	60.73
-6	4.5	4.16
-4	20.5	17.95
-2	146.2	150.62
0	139.3	142.40
2	116.1	118.11
4	34.8	33.87
6	36.8	37.57
8	125.0	130.60
10	37.4	38.56
12	43.0	46.25
	h=4,k=1	
12	48.5	50.03
11	43.0	45.30
10	8.1	9.42
9	86.7	88.85
8	47.8	50.15
7	42.6	42.73
6	13.4	13.50
5	25.3	23.96
4	61.3	62.64
3	11.7	10.96
2	103.4	101.93
1	192.8	197.71
0	13.2	13.62
-1	54.4	49.28
-2	73.7	70.84
-3	164.1	165.11
-4	84.4	82.33
-5	6.2	5.04
-6	103.7	100.90
-7	45.7	43.88
-8	22.5	21.63
-9	133.2	129.94
-10	26.9	26.85
-11	12.6	11.39
-12	32.0	31.66
-13	62.0	61.46
-14	50.9	52.28
-15	22.2	22.76
-16	29.2	30.70
	h=4,k=2	
-14	38.3	37.57
-13	57.7	56.97
-12	30.8	29.09
-11	7.6	9.27
-10	46.2	44.62
-9	37.1	35.62
-8	5.4	5.34
-7	119.1	112.55
-6	65.8	62.21
-5	122.0	118.45
-4	80.9	77.21
-3	133.9	129.36
-2	122.5	120.39
-1	91.4	90.83
0	91.4	90.83
1	64.4	62.22
2	15.6	13.47
3	6.6	6.46
5	143.8	145.71
6	7.2	6.34
7	35.6	34.93
8	61.4	61.87
10	4.5	3.23
11	15.0	15.53
12	30.5	31.20
	h=4,k=3	
10	8.2	7.21
9	14.4	14.48
8	26.6	27.48
7	20.9	22.25
6	78.7	77.13
5	26.8	25.75
4	141.8	142.96
3	37.5	35.79
2	71.9	72.83
1	15.3	11.99
0	23.8	24.04
-1	7.0	7.53
-2	8.4	7.90
-3	8.3	8.21
-4	31.3	29.92
-5	49.5	48.28
-6	194.3	192.63
-7	30.3	28.66
-8	36.2	34.65
-9	6.3	5.21
-10	17.1	15.09
-12	40.4	39.74
-14	66.1	65.37
-15	21.4	21.29
	h=4,k=4	
-14	19.0	16.43
-13	63.7	62.63
-12	34.5	33.59
-11	32.6	31.38
-10	41.8	40.44
-9	32.8	32.28
-8	36.0	34.40
-7	83.9	79.93
-6	36.0	35.12
-5	89.9	88.28
-4	12.9	14.26
-3	75.4	72.48
-2	106.3	105.24
-1	53.7	51.49
0	41.0	37.50
1	63.4	61.31
2	20.2	18.20
4	28.8	27.65
5	111.3	108.31
6	56.5	55.84
7	11.6	8.99
8	36.0	37.47
9	19.5	19.18
10	7.8	9.31
	h=4,k=5	
9	52.7	52.28
8	15.2	15.62
7	16.2	14.69
6	23.5	23.43
5	20.5	18.58
4	37.7	36.37
3	5.1	4.16
2	5.1	2.09
1	101.2	99.89
0	51.6	50.67
-1	45.5	44.77
-2	55.9	55.69
-3	94.9	94.32
-4	9.7	9.99
-6	49.2	47.99
	h=5,k=3	
-14	6.9	6.85
-13	8.6	8.12
-12	9.9	9.49
-11	27.0	25.27
-10	40.7	38.90
-9	73.6	69.07
-8	48.8	47.65
-7	36.5	35.57
-6	124.2	120.23
-5	4.2	5.35
-4	24.3	22.99
-3	29.8	28.57
-2	59.9	57.51
0	56.7	55.15
2	154.3	155.11
3	37.2	35.80
4	52.0	50.79
6	19.6	21.56
8	25.6	24.76
10	18.6	17.78
	h=5,k=2	
8	57.4	57.70
7	25.0	25.51
6	5.6	5.91
5	12.9	11.07
4	6.5	6.51
3	13.8	13.87
2	76.1	74.74
1	54.7	55.71
0	17.5	16.23
-1	24.0	22.29
-2	151.7	150.35
0	7.9	9.25
-1	62.6	62.01
-2	59.9	57.14
-3	15.7	14.11
-4	7.2	5.54
-5	74.4	71.47
-6	81.6	77.55
-7	72.6	71.66
-8	50.0	48.94
-9	129.0	125.80
-10	36.4	36.31
-11	26.0	24.93
-12	28.1	26.60
-13	6.7	5.28
-14	34.1	34.26
-15	39.7	41.70
	h=5,k=1	
-13	13.0	12.47
-14	14.1	14.23
-15	25.6	25.60
-12	5.2	4.82
-10	71.0	69.55
-9	43.2	41.53
-8	20.3	21.67
-7	53.7	52.71
-6	79.1	76.02
-7	87.9	86.27
-4	17.7	17.73
-3	159.5	157.94
-2	64.9	63.66
-1	94.2	90.84
0	94.2	94.75
1	37.1	35.03
2	78.0	77.16
4	53.0	53.28
5	107.2	107.7
6	15.6	16.43
7	12.6	13.20
8	24.2	24.43
9	63.0	63.38
10	26.5	25.96
	h=5,k=0	
8	88.8	92.79
6	15.5	15.40
4	5.4	5.23
2	18.9	21.07
0	23.8	25.00
-2	24.3	25.53
-4	12.5	13.81
-6	105.4	104.72
-10	57.5	58.67
-12	15.7	14.72
-14	63.1	63.86
	h=6,k=0	
4	37.1	38.02
-12	45.5	46.56
-10	26.4	25.70
-8	32.5	32.26
-6	180.0	190.08
-4	50.4	46.71
-2	50.1	48.97
0	7.8	7.75
2	107.1	108.61
4	70.4	72.29
6	81.5	84.02
8	19.3	19.75
	h=6,k=1	

Table 1. Continued.

l	Fo	Fc
8	20.3	21.27
7	14.7	14.90
6	36.6	36.36
5	101.5	104.21
4	7.1	6.61
3	51.5	50.73
2	48.7	48.40
1	60.4	61.63
0	15.2	13.96
-1	12.8	11.60
-2	98.0	97.23
-3	33.2	31.62
-4	4.7	2.87
-5	136.5	136.71
-6	28.1	27.05
-7	47.9	47.53
-8	13.6	12.44
-9	51.8	51.78
-10	24.0	23.57
-11	29.3	28.81
-12	49.7	50.96
-13	52.6	53.78
-14	37.0	36.64
	h=6,k=2	
-13	60.8	59.67
-12	38.1	37.57
-11	8.6	9.16
-10	40.8	40.45
-9	99.4	99.71
-8	18.6	17.45
-7	17.1	18.41
-6	54.4	52.82
-5	42.2	41.39
-4	15.9	14.98
-3	61.3	59.91
-2	61.4	59.87
-1	100.3	97.83
0	46.5	44.76
1	95.8	94.05
2	48.1	46.72
3	11.6	11.38
4	16.7	15.96
5	32.1	31.00
6	32.6	32.51
7	14.0	13.89
8	8.7	8.64
9	63.2	64.23
	h=6,k=3	
8	50.4	49.62
7	6.6	5.20
6	42.1	42.99
5	11.9	12.18
3	18.5	18.19
2	84.7	83.61
1	25.7	25.06
0	17.7	17.04
-1	46.9	45.32
-2	134.5	130.27
-3	10.2	3.81
-4	5.4	5.48
-5	13.2	12.72
-6	13.1	12.56
-7	8.3	7.49
-8	78.3	76.20
-10	88.5	86.29
-11	20.0	20.68
-12	52.2	52.08
-12	5.94	7.22
	h=6,k=4	
-10	9.08	5.39
-9	75.0	72.04
-8	45.2	44.10
-7	26.2	24.79
-6	44.4	41.64
-5	7.4	7.48
-4	17.9	16.13
-3	69.4	65.72
-2	41.9	39.08
-1	70.8	68.11
0	11.9	11.02
1	56.2	53.59
2	68.2	65.86
3	34.5	34.08
4	8.5	5.63
5	17.7	13.51
6	20.9	20.17
7	10.6	8.26
	h=6,k=5	
6	9.7	8.91
5	50.1	47.98
4	23.1	22.58
3	49.0	48.32
2	33.1	31.16
1	50.2	48.39
-1	9.0	3.69
-2	43.1	41.25
-3	46.3	43.01
-4	43.2	40.94
-5	65.8	63.24
-6	10.2	7.98
-7	12.7	10.89
-8	45.3	44.06
-9	48.5	46.49
-10	24.8	23.63
-11	9.6	8.88
	h=6,k=6	
-8	6.7	5.74
-7	25.3	23.88
-6	80.8	76.12
-5	23.6	21.74
-4	41.6	40.82
-3	18.9	18.35
-2	18.8	17.30
-1	9.6	8.74
0	9.5	7.90
1	6.5	5.68
2	36.9	33.89
3	32.5	30.40
	h=6,k=7	
-1	19.1	17.26
-2	32.3	29.47
-3	10.6	10.04
-4	24.2	23.90
	h=7,k=6	
-1	10.4	9.22
-2	28.8	25.98
-4	18.6	17.75
-5	6.7	5.24
	h=7,k=5	
-9	59.3	56.88

l	Fo	Fc
-8	31.2	28.99
-6	38.8	37.21
-5	28.7	27.05
-4	7.7	6.50
-3	9.8	10.19
-2	24.3	23.13
-1	54.5	51.84
0	30.2	29.03
1	33.5	31.96
3	32.7	31.96
	h=7,k=4	
4	22.7	21.18
2	38.2	35.53
1	5.1	3.26
0	30.5	30.35
-1	64.7	63.79
-2	33.8	32.29
-3	30.8	28.93
-4	6.4	5.50
-5	69.0	66.68
-6	41.2	39.90
-7	26.9	25.19
-8	29.9	29.92
-9	10.4	9.44
-10	24.4	22.13
-11	39.0	38.98
	h=7,k=3	
-12	80.6	79.72
-11	21.8	23.08
-7	8.7	9.53
-6	56.9	54.87
-4	43.3	42.29
-3	30.7	29.23
-2	107.3	103.94
-1	21.9	22.16
0	30.2	29.26
2	24.3	24.35
4	5.2	5.04
6	65.7	64.76
	h=7,k=2	
6	19.1	20.48
5	53.9	53.18
4	10.6	10.40
3	30.7	30.89
2	41.0	41.30
1	11.8	11.02
0	16.3	15.16
-1	76.7	75.06
-2	51.4	50.98
-3	51.8	52.34
-4	44.0	43.18
-5	101.2	99.69
-6	44.5	44.21
-7	25.9	25.40
-8	35.9	34.49
-9	18.8	18.43
-10	33.7	33.48
-11	22.3	22.34
-12	5.4	4.43
-13	59.7	60.91
	h=7,k=1	
-13	19.5	20.24
-12	32.4	32.99
-10	27.8	27.38
-9	102.7	103.28
-8	13.0	12.37
-7	6.2	6.68
-6	54.7	54.54
-5	71.4	70.86
-4	56.8	56.37
-3	21.5	22.04
-2	51.0	49.20
-1	65.3	64.90
0	23.6	24.56
1	74.4	76.26
3	61.0	59.98
4	6.4	5.49
5	31.3	32.00
6	52.4	53.85
7	7.0	5.26
	h=7,k=0	
6	7.5	8.30
2	132.9	136.51
0	12.1	13.16
-2	31.3	31.60
-4	8.9	8.40
-6	61.2	62.55
-8	94.4	96.15
-10	77.5	80.86
-12	26.2	26.60
	h=8,k=0	
-8	69.8	70.16
-6	18.3	18.86
-4	31.8	31.90
-2	106.6	111.02
0	63.6	64.54
2	44.0	45.57
4	12.2	11.15
	h=8,k=1	
4	9.4	9.25
3	21.0	21.06
2	47.9	49.07
1	28.4	29.27
0	5.0	3.47
-1	85.8	87.22
-2	16.0	15.08
-3	17.5	18.47
-4	24.1	23.60
-5	30.3	31.30
-6	23.3	24.63
-7	23.4	23.58
-8	49.6	51.03
-9	62.4	64.26
-10	19.1	16.76
-11	32.5	33.17
	h=8,k=2	
-11	19.6	19.63
-9	51.2	50.95
-8	30.3	29.88
-7	18.3	18.25
-6	17.3	18.10
-5	82.6	80.34
-3	9.1	6.99
-2	34.7	34.65
-1	5.7	7.06
0	6.1	6.45
1	24.9	25.22
2	32.8	33.66
3	62.1	62.65
	h=8,k=3	

l	Fo	Fc
2	58.6	58.29
1	9.4	9.44
0	13.1	12.51
-1	6.9	6.07
-2	10.1	8.90
-3	18.8	18.37
-4	68.6	67.35
-5	15.2	15.16
-6	64.7	63.11
-7	20.9	20.93
-8	48.8	49.21
-10	18.2	17.34
	h=8,k=4	
-8	7.9	8.64
-7	13.7	13.67
-5	75.6	73.08
-4	31.5	30.18
-3	19.6	18.65
-2	28.7	26.85
-1	6.8	1.07
0	12.5	13.11
	h=9,k=2	
-2	18.0	18.57
-4	35.5	35.63
-5	29.8	29.61
-6	32.6	33.90
	h=9,k=1	
-6	18.9	18.96
-5	64.8	65.51
-4	9.7	9.16
-3	10.8	9.99
-2	16.2	16.50
-1	45.1	45.02
	h=9,k=0	
0	23.8	23.81
-2	52.8	55.73
-4	64.1	64.63
-6	30.6	31.76
-8	15.2	15.63
18	49.3	47.61
	h=0,k=1	
20	8.1	7.84
19	25.8	25.08
18	21.8	22.62
17	23.7	23.67
	h=0,k=2	
16	10.4	12.29
17	18.2	18.30
18	15.5	16.05
19	7.6	9.12
	h=0,k=3	
19	8.1	9.88
18	11.4	11.88
17	11.5	9.70
16	26.4	26.30
	h=0,k=4	
15	56.1	52.11
16	12.4	12.32
17	7.9	6.67
18	16.4	15.35
19	14.1	14.33
	h=0,k=5	
19	11.8	11.64
18	14.5	12.20
17	10.4	7.76
15	8.6	7.91
14	25.6	23.80
	h=0,k=6	
13	11.3	10.23
14	5.6	4.27
15	6.7	7.00
16	7.8	7.69
18	23.3	21.57
	h=0,k=7	
17	20.2	19.08
15	6.6	8.02
14	11.3	9.32
13	13.3	13.46
12	25.3	23.46
11	41.7	38.27
	h=0,k=8	
9	6.8	7.00
10	16.3	14.12
11	19.2	18.78
12	16.8	15.44
14	6.0	4.38
15	16.7	15.03
	h=0,k=9	
14	16.0	14.57
13	6.5	7.91
12	6.4	2.33
10	9.4	10.98
9	9.1	7.74
8	22.4	20.20
7	8.8	8.33
6	11.6	12.52
5	36.5	36.08
4	30.0	31.72
	h=0,k=10	
0	7.8	10.06
1	11.4	12.69
2	9.4	7.97
3	21.2	22.03
5	8.7	7.61
6	8.7	7.27
7	11.6	9.54
8	12.1	10.96
9	16.4	14.82
	h=0,k=11	
8	10.8	10.46
7	10.5	9.86
4	9.8	8.85
3	9.5	9.58
2	20.5	19.03
	h=0,k=12	
0	11.2	10.69
1	7.0	6.82
2	7.0	6.25
-1	9.9	9.04
	h=1,k=11	
-8	8.3	7.15
-6	13.4	13.18
-3	8.2	8.34
-2	17.7	16.17
-1	6.4	6.58
0	9.0	9.40
3	8.2	7.91
4	6.3	7.56
5	9.9	10.00
6	11.4	11.49

l	Fo	Fc
8	7.4	5.79
	h=1,k=10	
11	15.1	13.67
9	14.1	12.65
8	7.2	7.04
6	6.7	5.94
5	20.1	19.99
4	9.5	9.73
3	10.2	10.14
2	10.6	9.84
1	11.9	12.26
0	9.3	9.54
-1	23.3	23.30
-3	8.9	8.55
-5	16.5	15.06
-6	9.5	7.50
-7	20.7	19.85
-8	9.9	8.71
-9	5.6	6.84
	h=1,k=9	
-14	8.9	8.37
-12	9.9	9.82
-10	9.1	8.50
-9	21.6	20.91
-8	21.4	22.98
-6	24.9	25.76
-5	15.3	16.14
4	31.7	34.36
5	10.1	10.14
6	15.9	16.55
8	7.6	7.98
9	5.3	4.15
10	13.1	13.20
12	10.9	11.76
13	16.7	16.07
	h=1,k=8	
15	10.6	8.70
14	12.3	12.31
12	17.4	17.33
11	23.3	23.03
10	7.3	8.47
9	10.3	10.04
8	17.4	17.83
-9	9.7	8.71
-10	24.2	23.18
-11	18.6	17.26
-13	7.9	9.14
-14	13.9	13.12
-15	14.3	13.40
-16	14.3	14.49
	h=1,k=7	
-16	13.6	14.22
-15	17.6	16.63
-14	12.3	13.47
-13	13.3	12.61
-12	11.4	10.40
-11	32.3	32.29
11	8.0	8.07
12	20.5	20.56
13	18.6	18.75
14	8.4	5.98
15	14.7	12.93
	h=1,k=6	
17	12.4	10.19
16	14.8	13.38
14	24.6	23.15
13	7.2	5.78
12	5.8	6.13
-13	28.2	28.25
-14	35.1	33.15
-15	8.8	7.66
-16	10.0	9.84
	h=1,k=5	
-19	11.7	12.31
-18	11.3	9.48
-17	7.5	7.20
-16	7.4	7.31
-15	29.8	29.71
-14	23.4	23.61
14	12.1	11.41
15	30.0	29.60
16	21.2	21.21
17	6.5	5.24
18	11.5	10.01
	h=1,k=4	
19	9.1	6.70
18	13.5	14.18
17	8.0	9.02
16	19.4	20.46
15	29.2	28.40
14	15.5	15.01
-15	11.1	10.49
-17	34.2	34.15
-18	11.2	9.97
-19	21.5	21.54
	h=1,k=3	
-18	48.8	49.28
-17	8.5	9.55
-16	11.2	10.76
15	8.4	7.52
16	12.3	12.11
18	6.6	4.73
	h=1,k=2	
20	6.5	6.45
19	12.2	12.82
18	21.4	20.69
17	8.2	6.96
16	12.7	11.91
-17	37.7	38.34
-18	5.6	5.42
-19	18.7	19.49
-20	9.2	9.65
-21	12.1	11.32
	h=1,k=1	
-21	21.9	23.31
-18	18.2	19.54
16	12.4	11.68
17	17.9	17.80
18	11.1	11.94
19	24.1	24.07
20	11.2	10.33
	h=1,k=0	
20	11.0	10.75
18	36.3	38.41
16	24.9	24.60
-20	17.0	17.96
-18	24.4	26.48
16	46.6	47.80
18	10.6	12.24
	h=1,k=1	

l	Fo	Fc
19	6.4	6.18
18	10.9	11.28
16	13.7	14.04
15	58.2	58.25
-17	35.6	37.07
-18	22.7	24.59
-19	13.4	14.83
-20	6.9	7.66
-21	9.7	10.46
	h=2,k=2	
-21	21.9	22.81
-20	13.7	14.44
-19	10.2	10.61
-18	29.0	30.48
-17	27.4	28.33
15	10.7	10.34
16	12.7	12.05
19	25.3	26.88
	h=2,k=3	
18	28.8	26.99
16	7.3	7.21
15	5.9	4.47
14	7.1	6.88
-16	16.2	16.07
-18	28.6	29.65
-19	8.4	9.78
-20	15.8	17.15
	h=2,k=4	
-18	15.2	16.32
-17	25.4	25.40
-16	10.7	11.07
-15	16.6	16.55
14	7.8	6.09
15	7.7	6.61
16	12.0	12.60
17	12.7	12.43
	h=2,k=5	
17	6.5	1.95
16	10.5	10.37
15	31.4	30.16
14	10.6	10.52
13	20.8	20.38
-14	22.7	23.23
-15	25.5	26.32
-16	29.1	29.85
-17	22.1	22.31
-18	13.9	13.27
-19	10.4	9.09
	h=2,k=6	
-18	17.4	16.44
-17	8.3	9.12
-15	20.7	20.27
-14	49.3	48.53
-13	6.5	7.37
12	23.3	21.97
13	15.5	14.40
14	26.4	24.32
16	19.3	18.71
17	9.7	9.36
	h=2,k=7	
15	23.0	21.14
14	10.9	9.57
13	9.6	9.29
11	16.2	16.32
-11	15.1	14.83
-12	8.3	6.94
-13	34.7	34.05
-14	8.9	7.51
-15	19.8	19.73
-17	8.2	7.99
	h=2,k=8	
-15	5.5	2.75
-14	11.7	11.30
-13	10.2	7.87
-12	19.2	20.34
-11	18.6	18.58
-10	9.0	9.65
-9	10.1	10.69
7	19.8	20.21
8	21.7	20.99
9	21.5	22.74
10	26.9	26.49
11	18.0	17.50
14	10.2	9.86
	h=2,k=9	
12	17.3	16.00
11	5.8	6.15
10	6.2	6.32
9	19.5	18.56
8	18.5	18.83
6	9.5	9.68
3	10.8	10.99
2	20.4	22.34
1	11.4	11.35
-3	6.3	5.33
-4	20.1	22.05
-5	6.2	4.93
-6	14.0	13.82
-7	8.7	8.04
-9	20.0	20.10
-10	25.9	26.28
-11	10.4	9.62
-12	11.0	12.15
-13	7.6	6.36
	h=2,k=10	
-12	6.3	5.90
-11	15.6	15.62
-9	15.4	15.74
-6	8.8	8.88
-5	20.6	20.79
-4	8.8	9.03
-3	8.7	9.15
-1	14.6	14.77
1	22.7	23.64
2	17.3	17.42
3	10.9	10.49
5	10.3	10.04
7	13.7	15.09
	h=2,k=11	
6	16.6	15.30
2	13.7	13.88
0	9.8	8.88
-3	8.2	8.59
-4	12.6	13.11
-6	11.5	10.37
-7	8.7	9.42
-8	8.9	7.13
	h=3,k=11	
-8	15.1	14.01
-4	10.8	10.86

l	Fo	Fc
-3	5.3	.36
-2	13.1	11.99
0	6.9	5.19
1	10.2	11.00
2	14.2	13.58
4	8.9	9.00
	h=3,k=10	
9	15.8	15.17
7	13.0	12.79
6	8.3	6.98
4	5.6	5.93
3	15.8	16.68
2	7.4	7.51
1	8.0	5.35
-1	16.4	17.24
-2	13.4	13.22
-3	21.3	22.44
-4	10.6	9.81
-5	8.5	8.89
-7	10.1	9.79
-9	15.6	15.00
-10	5.6	4.15
-12	8.3	5.87
	h=3,k=9	
-14	18.6	17.11
-13	12.6	11.53
-12	7.4	7.04
-11	15.9	15.91
-10	14.4	14.28
-8	14.0	14.94
-7	7.9	8.38
-6	12.0	10.91
-5	15.0	14.24
-4	19.9	19.23
-3	6.0	3.16
-2	27.8	29.83
-1	22.9	24.12
0	7.1	6.17
2	15.3	16.48
4	21.7	21.67
5	12.3	12.29
7	17.7	17.35
8	21.0	20.57
9	11.6	12.03
10	10.6	9.39
	h=3,k=8	
12	7.0	5.90
10	15.3	15.25
9	10.0	11.38
7	9.9	8.96
6	34.0	34.19
5	37.8	40.43
-8	4.8	4.11
-9	10.9	12.28
-10	16.3	15.64
-11	20.4	20.10
-12	23.7	23.17
-13	19.2	18.89
-16	15.8	14.50
	h=3,k=7	
-17	24.4	23.43
-16	6.6	6.64
-15	14.9	13.91
-14	10.1	11.30
-13	12.5	13.00
-12	7.1	6.46
-11	28.5	27.10
8	21.7	21.76
9	5.8	4.97
10	11.6	9.70
11	31.5	29.50
12	6.4	5.58
13	8.6	18.09
	h=3,k=6	
13	20.5	19.67
12	45.2	44.24
11	8.5	6.87
10	15.8	13.75
-13	6.3	3.30
-14	9.3	8.73
-15	11.3	12.04
-16	22.9	23.12
-18	21.3	20.75
	h=3,k=5	
-18	11.6	12.87
-17	32.1	32.15
-16	6.9	8.31
-15	13.2	14.74
-14	24.4	23.12
12	12.3	13.02
13	13.0	13.76
14	20.1	20.84
15	19.8	19.50
16	8.5	8.75
	h=3,k=4	
15	30.9	29.48
14	12.6	11.28
13	9.2	10.36
-15	30.0	29.90
-17	10.0	8.96
-18	12.1	10.92
-19	19.6	19.95
	h=3,k=3	
-20	22.7	23.96
14	16.7	15.12
16	30.1	29.71
17	12.6	12.12
18	17.8	17.24
	h=3,k=2	
18	7.4	7.26
17	6.7	7.13
16	13.3	13.83
15	35.9	36.28
14	6.4	6.59
-17	6.3	5.54
-18	9.6	8.98
-19	5.4	4.47
-20	10.8	10.42
-21	19.4	20.21
	h=3,k=1	
-21	14.7	15.76
-20	12.1	12.95
-19	11.8	11.43
-17	57.8	60.37
14	9.3	8.22
15	24.9	26.80
16	20.5	21.51
18	10.4	9.43
	h=3,k=0	
18	9.7	8.64

l	Fo	Fc
16	6.3	9.27
14	17.4	18.46
-18	56.7	59.78
-20	8.6	9.58
	h=4,k=0	
-20	31.0	34.58
-18	7.2	9.23
16	14.6	15.37
18	12.6	12.51
	h=4,k=1	
16	1.3	12.56
15	7.7	8.33
14	5.8	5.54
13	18.5	20.40
-17	25.9	27.52
-18	18.6	20.15
-19	13.1	14.16
-21	27.1	29.49
	h=4,k=2	
-20	17.4	18.24
-19	11.4	10.83
-18	9.9	8.42
-17	47.0	48.77
-16	27.7	28.63
13	34.3	36.17
14	11.0	10.93
15	32.6	33.25
16	8.5	8.89
17	7.1	8.83
	h=4,k=3	
16	32.1	33.26
15	6.0	3.62
14	13.1	12.37
13	9.9	8.81
12	40.6	40.10
-16	35.3	35.89
-18	31.2	32.81
	h=4,k=4	
-19	8.6	8.01
-18	13.1	14.61
-17	26.2	26.71
-16	6.9	7.77
-15	12.9	11.78
11	26.1	25.45
12	18.7	19.91
13	18.2	19.01
15	21.8	20.74
16	16.5	15.55
	h=4,k=5	
16	10.1	8.33
15	7.0	8.19
13	8.2	9.58
12	16.0	15.74
11	25.4	24.30
10	28.7	28.94
-14	13.1	12.26
-15	14.0	14.24
-16	13.5	13.61
-17	20.6	21.81
-18	18.5	18.76
	h=4,k=6	
-17	7.6	8.21
-16	11.5	12.42
-15	9.8	9.08
-14	19.5	17.58
9	25.4	24.05
10	9.6	11.63
11	16.4	16.21
12	21.4	19.81
13	11.8	12.99
	h=4,k=7	
13	9.8	10.76
12	16.0	14.88
11	7.4	7.55
10	14.7	13.81
9	27.9	28.15
8	10.6	9.62
7	31.4	29.89
-11	24.8	25.01
-12	8.2	7.39
-13	10.9	8.12
-14	14.4	14.95
-15	14.5	15.31
-16	5.8	5.55
-17	9.5	8.57
	h=4,k=8	
-16	15.7	15.17
-14	19.3	19.18
-13	13.2	13.39
-12	5.6	2.51
-10	18.4	17.13
-9	15.3	14.15
-8	20.3	20.00
-7	21.3	20.84
4	13.5	15.62
5	27.2	27.02
6	23.1	22.29
7	7.3	6.39
8	17.6	16.79
11	7.6	8.30
12	8.9	8.13
	h=4,k=9	
9	8.7	6.02
7	9.8	10.98
6	15.4	16.89
5	9.0	7.50
4	18.5	18.58
3	18.6	18.40
2	13.2	14.78
0	17.1	16.78
-1	6.2	4.97
-2	19.6	21.14
-3	11.7	11.78
-5	28.9	27.53
-6	27.9	27.45
-8	10.2	9.24
-10	5.2	3.59
-12	14.8	14.89
-14	9.8	10.08
	h=4,k=10	
-11	12.1	10.57
-8	7.5	6.46
-7	20.1	19.86
-5	16.3	16.43
-4	8.1	6.62
-3	6.1	4.31
-2	11.7	12.27
-1	18.5	18.39
1	7.3	8.40
3	12.5	11.48

l	Fo	Fc
5	18.3	18.26
6	11.8	11.29
7	8.1	8.90
	h=4,k=11	
2	6.6	5.95
0	11.5	10.95
-1	6.1	7.17
-2	7.9	8.01
-3	10.2	9.23
-6	8.9	7.61
	h=5,k=11	
-4	15.6	13.77
0	10.3	11.52
	h=5,k=10	
6	8.7	9.47
5	8.0	4.97
3	6.4	9.22
2	9.8	7.53
1	17.0	17.78
0	7.5	6.52
-1	9.5	9.08
-3	10.4	11.35
-4	6.4	7.59
-5	18.5	18.18
-6	5.6	6.07
-8	7.7	5.42
-9	13.0	11.91
	h=5,k=9	
-12	5.7	6.32
-11	5.8	6.33
-10	19.6	19.53
-9	12.9	11.71
-8	9.9	10.71
-7	19.6	19.91
-6	18.9	19.11
-5	6.9	6.40
-4	15.6	15.82
-2	12.8	12.47
-1	8.4	6.99
0	10.6	10.89
2	23.9	22.90
3	24.8	23.47
4	6.5	4.29
6	6.7	8.93
8	11.1	11.19
	h=5,k=8	
10	13.2	13.07
9	20.1	19.27
8	6.4	6.89
5	13.0	12.08
4	27.8	26.71
3	9.1	8.79
2	24.5	23.02
1	27.4	25.86
0	18.5	17.58
-1	17.8	18.34
-2	18.3	18.06
-3	5.1	4.21
-4	5.5	2.95
-5	14.4	14.93
-6	25.0	23.99
-7	14.6	12.97
-8	37.5	36.95
-9	27.6	26.49
-11	10.4	9.74
-12	11.9	11.25
-14	8.4	8.72
	h=5,k=7	
-17	8.8	8.71
-16	6.0	6.20
-15	10.4	11.77
-14	5.6	6.70
-13	39.3	37.43
-12	10.9	9.31
-11	15.6	15.08
-10	14.3	13.13
-9	19.6	19.47
4	12.1	11.72
5	29.7	29.26
6	10.4	9.02
7	6.5	4.38
8	8.3	7.75
9	21.0	20.23
10	19.3	19.52
11	9.7	10.11
12	7.9	8.14
	h=5,k=6	
10	16.5	17.02
9	7.5	8.55
8	36.2	33.96
7	33.0	31.79
-11	27.7	27.59
-12	41.8	39.84
-13	6.9	7.26
-14	40.1	38.88
-15	12.8	12.80
-16	6.7	4.67
-18	10.7	10.36
	h=5,k=5	
-19	10.3	10.81
-17	16.3	14.18
-16	22.7	22.28
-14	6.3	8.35
-13	50.2	49.23
9	35.9	36.06
12	12.6	11.71
13	14.9	13.36
	h=5,k=4	
14	12.2	11.54
13	29.1	28.78
12	5.7	3.91
11	28.0	27.59
-14	14.6	14.25
-15	31.9	31.73
-16	14.2	14.44
-17	40.7	40.75
-18	6.0	4.31
	h=5,k=3	
-20	16.0	15.99
-19	9.7	10.98
-18	27.5	27.64
-16	56.0	56.42
11	6.9	8.77
12	59.2	59.94
13	11.3	11.82
14	7.6	10.20
	h=5,k=2	
16	10.0	8.88
15	13.6	13.21
13	29.1	30.80

l	Fo	Fc
12	9.4	6.24
11	26.6	17.62
-16	10.3	9.51
-17	39.8	41.57
-18	12.2	13.81
-19	11.5	11.99
-20	10.3	10.73
-21	14.7	15.98
	h=5,k=1	
-21	14.5	15.55
-20	21.3	22.87
-19	17.8	19.81
-18	7.7	7.27
-17	24.0	25.36
-16	9.8	10.03
12	22.6	23.74
13	13.8	13.76
15	19.3	20.28
16	7.6	6.73
	h=5,k=0	
16	36.7	36.74
-16	18.1	19.62
-18	13.3	13.98
-20	29.3	32.02
	h=6,k=0	
-20	12.8	12.44
-18	14.1	14.70
-16	61.4	64.05
10	13.4	14.43
12	34.6	35.42
14	8.4	9.77
	h=6,k=1	
15	11.2	12.41
13	33.5	34.22
12	19.0	20.21
11	7.8	7.88
10	21.3	22.61
-15	24.3	23.83
-16	20.0	20.66
-17	44.2	46.27
-20	7.2	7.99
	h=6,k=2	
-19	21.8	23.50
-18	17.2	18.55
-17	19.5	21.07
-16	29.4	30.42
-15	14.3	13.18
10	6.3	5.74
11	14.0	13.73
12	17.2	16.57
13	12.4	12.85
15	6.7	4.27
	h=6,k=3	
12	16.4	16.96
11	12.5	12.02
10	37.5	39.31
-14	28.0	27.73
-15	5.8	6.27
-18	14.9	16.77
-20	35.1	37.70
	h=6,k=4	
-19	22.1	22.86
-18	7.2	6.16
-16	22.2	23.27
-15	18.9	19.50
-14	17.6	17.69
-13	40.4	38.82
8	17.1	16.95
9	49.2	49.00
10	17.0	16.94
12	11.8	11.23
13	7.5	8.76
14	7.8	8.28
	h=6,k=5	
13	23.1	23.37
12	6.9	6.80
10	6.9	6.51
8	19.5	19.15
-12	22.0	21.03
-13	29.9	29.98
-14	29.1	29.65
-15	15.9	15.27
-16	13.4	15.01
-17	26.6	26.52
	h=6,k=6	
-16	26.8	25.06
-15	18.6	19.46
-13	6.6	7.59
-12	25.8	25.86
-10	24.2	23.14
4	29.4	26.93
6	37.7	38.15
7	18.8	18.51
10	7.4	3.14
12	18.7	17.19
	h=6,k=7	
11	11.1	10.69
10	7.5	8.69
7	15.8	17.57
6	23.7	22.66
5	34.2	32.28
4	12.2	12.82
2	6.7	6.09
1	25.9	25.02
-5	49.8	48.93
-7	30.2	29.26
-9	10.3	9.06
-10	15.9	15.30
-11	23.1	23.08
-12	15.2	16.55
-13	19.0	17.79
-15	13.0	11.38
	h=6,k=8	
-13	18.5	17.40
-12	21.5	20.29
-11	6.6	4.99
-10	20.3	19.52
-9	16.8	17.09
-8	6.5	6.11
-6	15.9	14.50
-4	14.5	12.63
-3	17.1	15.72
-2	16.0	14.86
-1	26.5	27.13
0	35.7	34.84
1	16.6	15.96
2	8.9	9.02
4	8.8	7.77
5	12.0	11.03
6	15.5	13.22

Table 1. Continued.

l	Fo	Fc
7	6.9	8.44
8	6.5	5.72
9	14.0	14.38
h=6,k=9		
6	6.5	6.89
4	10.6	10.69
3	8.5	8.15
2	15.6	15.28
1	9.7	9.97
0	6.0	3.20
-1	20.8	19.96
-2	29.5	25.05
-4	8.4	8.80
-8	15.1	14.90
-10	12.3	10.86
-11	14.1	14.42
-12	12.1	11.73
h=6,k=10		
-8	9.7	8.27
-7	15.3	13.94
-3	12.5	12.11
-1	10.3	9.30
0	9.0	6.26
2	10.2	10.33
3	16.3	14.47
h=7,k=9		
-8	6.5	7.58
-6	19.0	17.62
-5	14.8	12.66
-4	10.5	10.44
-3	19.3	17.81
-2	14.9	13.74
-1	8.8	7.96
0	10.8	10.82
4	7.6	5.20
h=7,k=8		
7	8.0	9.88
6	11.5	9.29
5	18.4	15.55
4	12.1	8.78
3	10.8	9.52
2	12.7	11.11
0	10.0	10.99
-1	11.9	13.40
-2	10.1	10.29
-4	26.5	24.87
-5	30.4	28.53
-7	6.1	4.93
-8	14.9	13.17
-10	18.4	17.76
-12	6.4	5.29
-13	11.0	10.23
h=7,k=7		
-15	21.0	21.60
-13	13.5	13.33
-12	6.6	6.66
-11	8.2	9.85
-10	8.9	9.17
-9	36.1	34.65
-8	15.3	14.47
-7	9.9	11.31
-6	8.7	6.88
-5	23.5	21.87
-4	20.2	19.26
-3	24.7	23.59
-2	16.2	14.98
-1	6.2	5.58
0	9.5	6.51
1	31.5	30.59
2	13.2	11.77
3	27.8	27.13
4	11.7	10.27
6	19.6	19.25
7	12.3	11.15
9	13.1	11.94
h=7,k=6		
10	16.2	16.14
8	12.2	10.75
5	5.7	.78
4	6.8	7.95
3	25.8	24.65
2	58.0	57.01
1	14.5	14.73
-6	26.9	25.00
-7	31.9	32.35
-8	39.5	38.89
-9	6.6	6.40
-10	28.8	26.73
-11	10.6	11.29
-12	7.1	5.57
-14	15.7	16.21
-16	27.7	27.66
h=7,k=5		
-18	20.8	21.01
-17	11.7	-11.21
-16	16.5	15.59
-15	9.3	-10.67
-14	9.6	-10.50
-12	21.5	-20.79
	4	30.1	28.52
	9	24.0	24.05
	7	18.0	-17.89
	5	53.7	-52.91
-12	12.0	12.67
-13	51.5	50.30
-14	6.1	-9.46
-15	5.8	-5.53
-16	10.8	10.54
-17	19.3	-19.33
-18	6.5	-3.60
h=7,k=3		
-18	13.1	13.88
-16	21.2	21.48
-14	34.3	-34.39
	7	26.2	25.40
	8	22.5	-21.98
	10	14.8	-17.03
	13	15.5	13.69
h=7,k=2		
	12	13.3	12.99
	10	14.2	-15.66
	9	35.4	36.42
	8	18.7	-19.33
	7	22.1	-21.40
-14	7.0	-7.72
-15	20.9	-21.35
-16	19.2	-19.60
-17	24.3	-23.85
-18	9.8	10.29
-19	9.0	-10.08
-20	21.1	22.88
h=7,k=1		
-20	13.6	14.87
-19	21.1	-23.01
-18	16.0	16.39
-17	21.7	23.11
-16	30.5	31.76
-15	35.1	36.02
	8	13.2	-14.05
	9	35.6	36.05
13	24.6	-25.53
14	11.2	-11.52
h=7,k=0		
14	12.4	14.85
12	26.4	30.60
10	35.4	-35.62
8	7.3	-9.01
-14	31.0	-32.06
-16	54.4	-58.82
-18	9.5	-9.39
-20	24.1	26.25
h=8,k=0		
-18	27.0	27.98
-16	6.9	6.84
-14	11.0	-10.89
-12	54.4	-57.33
	6	29.5	29.26
	8	20.6	-20.97
	10	40.7	-41.69
	12	8.9	9.9
h=8,k=1		
	10	6.5	6.3
	9	35.4	35.3
	8	8.1	8.9
	7	22.8	23.8
	6	20.1	19.9
	5	17.0	17.9
-12	19.2	19.1
-13	45.3	46.8
-14	11.0	10.0
-16	16.6	17.4
-17	9.5	9.7
-19	29.3	31.4
h=8,k=2		
-19	7.2	7.8
-18	5.9	6.8
-17	25.3	27.2
-16	7.3	7.0
-15	34.6	36.0
-14	26.8	27.4
-13	19.4	20.1
-12	41.1	43.9
	4	24.5	24.8
	5	41.2	41.6
	6	22.1	22.3
	7	14.2	15.6
	10	14.3	11.7
	11	8.3	9.4
h=8,k=3		
	10	14.1	13.2
	7	9.8	11.0
	6	47.9	49.0
	3	11.8	11.2
-12	16.9	16.6
-13	11.7	13.5
-14	17.2	17.8
-15	13.2	16.4
-16	45.9	47.6
h=8,k=4		
-17	20.8	21.8
-15	34.3	35.3
-14	10.3	8.5
-13	10.3	9.7
-12	31.0	32.2
-11	25.7	26.6
-10	5.6	3.1
-9	34.4	34.5
1	23.5	23.4
2	22.8	24.5
3	29.5	30.0
4	9.1	6.9
5	27.4	26.6
6	24.1	24.0
7	18.4	18.6
10	12.9	12.9
h=8,k=5		
9	21.0	20.1
8	9.0	8.3
7	22.5	23.4
6	13.2	13.0
5	5.9	8.3
2	23.3	22.5
1	16.3	14.0
0	33.4	32.7
-1	52.5	52.3
-4	25.9	24.8
-5	18.0	17.2
-6	16.7	15.4
-8	10.7	10.7
-9	31.8	31.3
-10	34.6	35.1
-11	29.1	28.9
-12	19.2	18.72
-13	33.0	32.52
-14	8.4	8.85
-15	7.6	4.92
-16	15.0	13.89
h=8,k=6		
-15	5.9	3.80
-14	7.4	7.70
-12	29.6	29.65
-11	20.5	20.12
-10	13.0	11.90
-8	34.2	34.19
-7	5.6	4.77
-6	16.4	15.06
-5	7.5	3.97
-4	11.5	11.81
-3	9.0	8.08
-2	44.1	41.80
-1	19.7	19.32
0	21.4	21.73
1	19.2	18.71
2	18.8	18.10
3	8.4	7.55
4	8.1	7.77
6	21.0	19.84
7	6.4	6.46
8	6.3	5.76
h=8,k=7		
5	11.2	10.97
4	11.0	11.56
3	14.9	13.30
2	17.9	15.91
0	16.3	15.13
-1	29.0	28.18
-2	6.4	7.43
-3	20.3	19.22
-5	7.5	7.06
-7	27.8	26.97
-8	19.2	18.30
-9	23.5	21.94
-11	8.4	6.97
-13	19.3	18.37
h=8,k=8		
-9	17.5	15.30
-8	16.5	14.66
-6	14.7	13.88
-5	18.8	17.89
-4	12.4	10.27
-2	17.0	15.43
0	12.0	9.13
1	7.6	6.52
2	6.8	6.28
3	19.1	19.29
4	16.1	14.87
h=8,k=9		
-17	9.1	9.42
-16	17.5	19.32
-14	15.4	13.21
-13	7.9	8.69
-12	25.9	26.13
-10	20.0	20.32
-8	87.1	69.67
-7	18.1	16.51
-6	7.2	6.63
h=9,k=7		
-5	6.0	2.68
-4	9.5	9.76
-11	25.0	25.49
-2	25.7	26.49
-1	8.2	8.01
0	26.9	26.65
1	18.3	17.09
2	52.9	53.27
3	9.8	9.49
4	15.3	15.51
h=9,k=2		
9	19.1	19.00
7	8.4	6.81
6	17.1	17.70
5	13.3	13.85
3	36.6	40.00
2	9.0	8.21
0	21.8	22.01
-1	55.1	50.91
-7	26.1	28.33
-8	12.5	12.34
-9	56.4	51.89
-10	6.9	6.90
-11	20.2	21.26
-12	16.8	17.01
-13	19.2	19.28
-14	12.7	12.97
-15	24.7	26.44
-16	23.5	25.46
h=9,k=1		
-18	12.9	14.46
-17	19.0	19.07
-16	7.7	10.57
-15	24.2	25.65
-14	11.9	10.10
-13	31.4	33.89
-12	18.3	18.21
-11	39.1	40.57
-10	5.8	5.38
-8	31.9	32.92
-7	29.7	29.66
-6	24.2	25.25
-5	22.8	23.64
-4	23.1	23.80
-3	6.5	3.51
-2	29.2	28.95
-1	14.3	14.98
0	14.7	16.46
h=9,k=0		
10	8.1	9.06
6	53.2	55.83
4	10.7	12.26
2	13.8	14.83
-10	29.0	29.93
-12	71.0	76.23
-14	30.6	32.12
-16	35.0	38.77
-17	37.2	39.90
-9	41.5	42.30
-12	6.0	6.65
-8	41.1	44.56
-6	18.8	20.65
-4	59.5	61.98
-2	6.9	6.13
0	16.9	18.42
2	30.7	32.54
4	23.4	23.23
6	25.4	27.07
h=10,k=1		
7	12.1	11.70
6	14.9	14.69
5	7.9	8.68
3	37.9	39.87
2	16.1	16.82
1	6.2	5.95
0	16.1	16.08
-2	12.0	12.99
-3	20.3	21.17
-4	23.1	23.88
-5	45.1	47.88
-7	27.2	29.03
-8	12.9	13.61
-9	32.2	34.26
-10	8.9	9.21
-11	6.5	6.60
-12	26.9	28.73
-13	8.0	7.05
-15	30.2	32.78
h=10,k=2		
-16	9.9	10.18
-15	7.4	11.41
-13	15.5	16.61
-12	16.2	16.91
-11	38.1	41.07
-10	24.0	26.24
-9	17.2	18.76
-8	32.8	33.24
-7	18.3	19.26
-5	25.4	26.70
-4	16.8	16.98
-3	15.5	15.32
-1	49.4	51.39
0	20.7	20.83
1	10.4	9.69
0	39.0	39.98
-2	26.9	27.07
-3	9.6	7.28
-4	27.9	28.75
-6	14.2	14.32
-8	27.6	28.25
-10	10.7	10.40
-11	13.5	13.07
-12	37.6	39.20
h=10,k=4		
-14	7.0	.98
-13	21.9	22.84
-12	6.8	8.18
-11	30.4	32.13
-9	10.7	9.79
-8	30.6	31.90
-7	20.4	20.49
-5	18.7	18.51
-4	10.4	9.57
-2	8.8	8.25
-1	37.7	38.00
0	15.8	16.17
1	10.7	9.61
2	12.0	11.09
3	6.6	7.17
4	12.0	11.67
h=10,k=5		
3	24.8	23.92
0	14.2	14.01
-1	6.2	5.93
-2	14.3	13.59
-3	6.0	6.63
-5	19.2	19.25
-6	17.0	17.71
-7	23.9	24.65
-8	15.4	15.28
-9	21.0	20.38
-12	15.4	15.78
h=10,k=6		
-10	6.4	7.19
-8	20.2	19.23
-7	16.0	15.95
-6	7.3	5.93
-4	25.7	25.17
-3	11.6	11.87
-2	8.3	8.25
0	7.5	6.02
h=11,k=5		
-15	15.5	17.47
-6	12.9	13.13
-4	15.7	15.11
h=11,k=4		
1	9.3	8.96
0	20.4	21.11
-1	12.5	11.05
-3	18.4	18.15
-5	23.6	25.20
-6	6.7	5.16
-8	7.5	8.24
-9	15.7	17.19
-10	12.4	14.09
h=11,k=3		
-12	21.1	22.25
-10	16.7	20.03
-8	14.7	15.37
-7	6.0	4.47
-6	5.8	4.52
-4	39.6	40.89
-3	11.7	12.53
-2	6.0	4.90
0	13.8	13.42
2	6.0	7.13
h=11,k=2		
3	18.7	18.95
2	6.0	6.80
0	15.4	15.93
-1	16.9	17.69
-2	17.1	18.15
-3	22.1	23.06
-4	12.5	13.51
-5	25.4	27.16
-7	16.0	16.18
-8	10.8	11.93
-10	9.5	10.71
-11	20.2	20.73
-12	20.8	22.98
h=11,k=1		
8	61.0	60.86
-11	39.6	37.76
h=11,k=3		
0	133.7	176.08
1	120.0	149.02
4	175.7	197.10
8	30.3	31.16
9	5.3	4.56
10	59.9	58.61
11	8.1	7.65
h=11,k=2		
-3	314.2	287.37
-1	168.7	191.62
h=11,k=0		
-14	6.4	7.09
h=12,k=4		
-8	5.6	6.79
-6	5.7	3.85
-4	18.9	15.73
-2	7.1	8.39
h=12,k=1		
-3	16.7	17.06
-4	12.9	12.99
-5	17.9	18.25
-6	6.3	6.98
-7	11.2	10.24
-8	14.9	16.52
-9	8.0	4.07
h=12,k=2		
-7	26.4	30.02
-6	12.5	13.57
-5	8.5	8.76
-4	14.6	16.05
h=0,k=2		
10	165.4	163.95
14	16.6	19.14
h=0,k=1		
14	18.6	17.02
12	40.4	40.81
11	120.0	119.43
9	15.4	12.78
h=0,k=2		
1	62.1	98.84
2	52.6	55.34
3	197.7	218.89
h=1,k=9		
-1	11.6	10.77
h=1,k=8		
-8	25.9	25.14
h=1,k=7		
-10	24.2	24.07
-9	36.3	36.14
-8	16.1	19.04
-7	12.6	12.55
-6	5.9	7.42
-5	37.0	37.95
-4	38.8	40.15
-3	71.4	76.52
-2	26.0	27.95
0	35.3	38.18
1	36.8	40.74
2	16.1	18.00
3	31.8	34.79
4	21.8	23.63
5	8.2	7.64
6	35.6	36.14
7	61.6	62.96
8	13.6	13.38
9	30.1	29.53
h=1,k=1		
11	7.8	8.03
10	8.1	7.00
-5	29.8	30.17
h=1,k=5		
-11	62.8	60.49
-10	30.8	31.30
h=1,k=4		
8	61.0	60.86
-11	39.6	37.76
h=1,k=3		
0	133.7	176.08
1	120.0	149.02
4	175.7	197.10
8	30.3	31.16
9	5.3	4.56
10	59.9	58.61
11	8.1	7.65
h=1,k=2		
-3	314.2	287.37
-1	168.7	191.62
h=1,k=0		
-14	6.4	7.09
h=2,k=9		
-16	11.6	12.30
h=2,k=8		
-16	6.1	1.92
-14	113.1	116.63
-2	127.1	126.26
0	34.7	36.06
2	65.4	63.72
11	38.9	38.51

18°C. Three test-reflections were measured for every 100 reflections. Two test-reflections varied less than 10 %, while the third one varied up to 25 %, probably due to a slight change in crystal position in the capillary. The crystal position was readjusted once during experiment. Precision unit cell data were determined by least squares methods,[4] using 48 reflections measured with a manual diffractometer and Cu$K\alpha$-radiation. The intensities were corrected for effects due to absorption [4-6] and secondary extinction.[4,7]

Oscillation and Weissenberg photographs were taken of the molecular complex formed by equimolecular amounts of carbon tetrachloride and the present addition compound, sealed off in glass-capillaries containing a trace of free carbon tetrachloride.

CRYSTAL DATA

The crystals of MTCL:I_2 (1:1) are monoclinic. The unit cell dimensions are (estimated standard deviations in parenthesis)

$a = 8.777$ (4) Å, $b = 8.724$ (4) Å
$c = 15.595$ (3) Å and $\beta = 104.64$ (1)°.

The space group is $P2_1/c$. The unit cell contains four molecules of the addition compound (formula $C_7H_{13}NSI_2$). The experimental density is 2.27 ± 0.02 g/cm³, the calculated value is 2.283 g/cm³.

Crystalline MTCL:I_2:CCl_4 (1:1:1) is also monoclinic. The space group is $P2_1/c$ and the unit cell dimensions are $a = 13.6$ Å, $b = 8.0$ Å, $c = 16.4$ Å and $\beta = 104°$. The figures are probably correct to about 0.5 %. There are four molecules of the adduct per unit cell. Experimental density was obtained as *ca.* 2.2 g/cm³. The theoretical value is 2.11 g/cm³.

Table 2. Atomic parameters. E.s.d. in parenthesis. The β_{ij}-values are computed according to the formula exp $[-(\beta_{11}h^2+\beta_{22}k^2+\beta_{33}l^2+\beta_{12}hk+\beta_{13}hl+\beta_{23}kl)]$. The left-hand index on H denotes the attached carbon atom.

Atom	x	y	z	β_{11}	β_{22}	β_{33}	β_{12}	β_{13}	β_{23}
I_1	−0.09216(5)	−0.10107(6)	0.31189(3)	0.01293(7)	0.02133(9)	0.00487(2)	0.0005(1)	0.00193(6)	−0.00081(7)
I_2	0.17056(4)	0.07421(4)	0.41263(2)	0.01111(6)	0.01458(6)	0.00369(2)	0.0055(1)	0.00573(5)	0.00228(5)
S	0.4154(2)	0.2262(2)	0.5159(1)	0.0135(2)	0.0180(3)	0.00392(7)	−0.0026(4)	0.0081(2)	−0.0034(2)
N	0.6930(5)	0.3141(6)	0.5016(3)	0.0115(7)	0.0136(7)	0.0030(2)	0.000(1)	0.0042(5)	−0.0003(6)
C_1	0.5645(6)	0.2411(6)	0.4633(3)	0.0117(8)	0.0113(7)	0.0032(2)	0.001(1)	0.0051(7)	−0.0011(7)
C_2	0.5490(7)	0.1729(9)	0.3737(4)	0.0134(9)	0.021(1)	0.0044(3)	−0.008(2)	0.0086(9)	−0.0084(9)
C_3	0.5458(9)	0.292(1)	0.3020(4)	0.015(1)	0.031(2)	0.0033(3)	0.010(2)	0.0031(9)	−0.003(1)
C_4	0.7042(9)	0.3513(9)	0.2966(4)	0.019(1)	0.021(1)	0.0042(3)	0.004(2)	0.010(1)	0.004(1)
C_5	0.7985(9)	0.4274(8)	0.3811(5)	0.020(1)	0.017(1)	0.0057(4)	−0.003(2)	0.013(1)	0.000(1)
C_6	0.8284(7)	0.3231(8)	0.4607(4)	0.0102(8)	0.020(1)	0.0043(3)	−0.003(2)	0.0047(8)	−0.0001(9)
C_7	0.7182(8)	0.3877(8)	0.5893(4)	0.018(1)	0.018(1)	0.0031(3)	−0.000(2)	0.0043(8)	−0.0035(8)
H_{21}	0.649	0.096	0.377						
H_{22}	0.439	0.107	0.356						
H_{31}	0.489	0.240	0.238						
H_{32}	0.476	0.390	0.314						
H_{41}	0.773	0.255	0.282						
H_{42}	0.686	0.435	0.243						
H_{51}	0.912	0.464	0.371						
H_{52}	0.733	0.528	0.394						
H_{61}	0.853	0.208	0.440						
H_{62}	0.931	0.366	0.510						
H_{71}	0.711	0.301	0.639						
H_{72}	0.628	0.475	0.587						
H_{73}	0.835	0.441	0.607						

DETERMINATION OF THE STRUCTURE OF MTCL:I_2 (1:1).

Approximate coordinates of the two crystallographically nonequivalent iodine atoms were derived from the three-dimensional Patterson map. The electron density map showed peaks of reasonable peak heights and positions for all atoms, except hydrogen, corresponding to an ordered structure. The R-value, computed on the basis of these positions and an overall isotropic B-value of 4 Å^2, was obtained as 0.195. The structure was refined further, using least squares techniques and anisotropic temperature factors, yielding an R-value of 5.84 % and a weighted R-value of 6.43 %.

The experimental intensity data were then corrected for effects of absorption [4-6] and extinction.[4,7] As a result the atomic parameter values changed, however, only insignificantly.

The positions of the hydrogen atoms of the ring system were now calculated on the basis of a C–H bond length of 1.09 Å [8] and tetrahedral bond angles. The positional parameters thus derived were then included as fixed parameters together with an overall isotropic temperature factor of 4 Å^2 in a least squares refinement of the previous parameters. While most of the intermolecular parameters remained practically unchanged, two of the C–C bond lengths changed by as much as 0.02–0.03 Å by this procedure. The final R-value is 4.87 % and the weighted R-value 5.34 %. Observed and calculated structure factors are given in Table 1 and atomic parameters in Table 2. However, neither the positions of the hydrogen atoms of the cyclic group nor those of the methyl hydrogen atoms showed up distinctly in the three-dimensional electron density difference map.

The matrices of the β_{ij}-values given in Table 2 are all positive definite. The corresponding root-mean square amplitudes of vibration are presented in Table 3. These values served as basis of a least squares analysis of the librational motion of the organic molecule taken as a rigid body.[9,10] The result is given in Table 4.[4]

DISCUSSION OF THE STRUCTURE

Values of intramolecular parameters are given in Table 5 and Fig. 1. The C_1–N and C_1–S bond lengths are not significantly different from

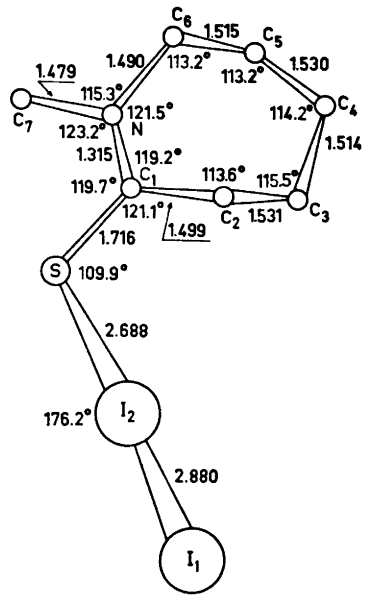

Fig. 1. The molecular complex as view along the [010]-direction of the unit cell.

the corresponding values reported for other thioamides [11] and related compounds.[12-14] The results are consistent with the assumption that the lone electron pair on nitrogen is considerably delocalized over the N, C_1 (and S) centres in the compound.

The bond angles centred at C_1 are close to 120°. The methyl group seems to be somewhat bent away from the sulfur atom, probably for sterical reasons.

The positions of C_1, C_2, C_6, C_7, N, and S deviate slightly, although probably significantly, from a planar arrangement, while C_1, C_2, C_6 and N are found to be co-planar within experimental error.

The cyclic group has the chair conformation, with C_1 and N at the basis and C_4 at the top. The observed C–C bond lengths are near to the corresponding covalent single bond distances.[8] The angles between single bond directions within the ring are found to be somewhat larger than tetrahedral, possibly because of sterical repulsions between non-bonded next-neighbour carbon atoms. The N–C_6 and N–C_7 bond lengths are found to be significantly larger than 1.44 Å observed in 1,3-dimethyl-2(3H)-imidazolethione [13] and quoted for amides.[15] A

Table 3. R.m.s. amplitudes of vibration along principal axes of vibration defined by the components of the unit vector in fractional coordinates.

	R.m.s. ampl.(Å)	Components of unit vectors of principal axes		
S	.276	.0421	−.0983	.0297
	.231	.0924	.0583	.0374
	.164	−.0597	.0178	.0459
C_1	.214	.0911	−.0451	.0448
	.213	.0580	.0993	.0031
	.170	−.0470	.0352	.0487
C_2	.318	.0439	−.0933	.0348
	.210	.0967	.0538	.0299
	.163	−.0510	.0312	.0478
C_3	.359	.0298	.1090	−.0071
	.227	.1137	−.0297	.0156
	.190	.0065	.0192	.0640
C_4	.302	.0627	.0893	.0302
	.258	.0926	−.0688	.0227
	.181	.0380	.0208	−.0545
C_5	.299	.0985	−.0191	.0475
	.261	.0046	.1110	.0164
	.191	.0644	.0212	−.0432
C_6	.280	.0153	−.1137	.0016
	.223	.0493	.0054	.0652
	.183	.1058	.0139	−.0120
N	.229	.0145	.1136	−.0017
	.207	.1123	−.0117	.0342
	.177	−.0325	.0104	.0567
C_7	.275	.0000	−.1101	.0178
	.250	.1173	−.0027	.0114
	.176	.0101	.0317	.0628
I_2	.253	.0560	.0939	.0285
	.201	.0601	−.0634	.0508
	.174	−.0844	.0172	.0316
I_1	.288	.0063	.1132	−.0085
	.248	−.0428	.0178	.0528
	.212	.1095	.0005	.0391

simple, non-trivial explanation of this has not been found.

The I_1-I_2-S group is almost linear, the deviation from linearity is believed to be due to intermolecular interactions in the lattice. The observed iodine-iodine bond length of nearly 2.88 Å is about 0.22 Å longer than in the free molecule and also significantly greater than

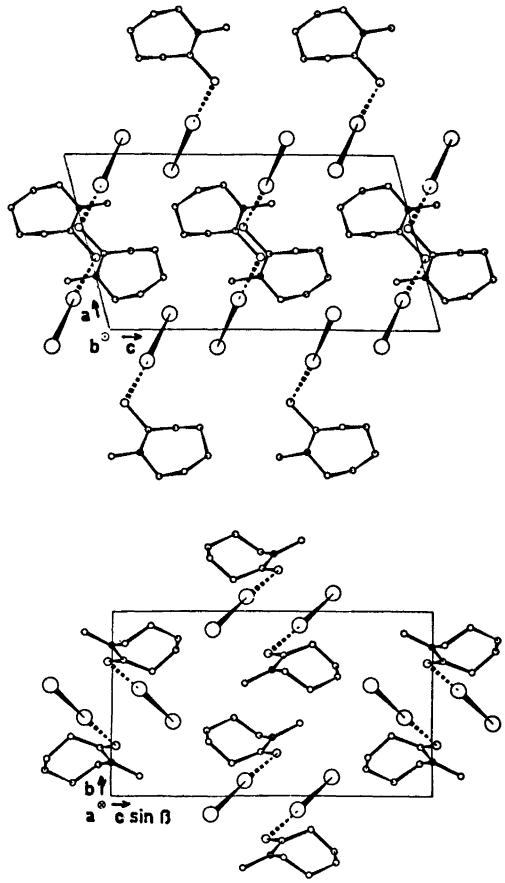

Fig. 2. The [010]- and [100]-projection of the unit cell, respectively.

observed in iodine complexes with thioethers, ethers, and amines.[1] On the other hand, the iodine-sulfur distance of 2.69 Å is significantly shorter than observed in iodine complexes with thioethers. These findings are consistent with the view that the present charge-transfer bond is somewhat stronger than that observed in complexes between iodine and thioethers.[1a–1d] The sulfur atom, no doubt, acts as an electron donor towards the electrophilic iodine molecule. The delocalization of the lone electron pair on nitrogen leads to an accumulation of negative charge on the thioamide sulfur atom in excess of that existing in thioethers. Hence the former sulfur should be able to donate electrons more strongly to the acceptor than the sulfur atom in thioethers, giving rise to a stronger charge-transfer bond.[2]

Table 4. The results of the rigid body analysis. Mass centre of MTCL in (0.612, 0.292, 0.446). $\Delta u_{rms} = 0.0032$ Å.[10]

$$\widetilde{T} = \begin{Bmatrix} 37(2) & 5(2) & 4(1) \\ & 47(3) & -2(2) \\ & & 33(2) \end{Bmatrix} \times 10^{-4} \text{ Å}^2$$

Principal axes of $\widetilde{T}$:

Eigenvalue (Å²)	R.M.S.(Å)	Direction cosines I_1	I_2	I_3
0.0496	0.223	0.3861	0.9223	0.0165
0.0385	0.196	0.6914	−0.3010	0.6567
0.0286	0.169	0.6106	−0.2421	−0.7540

$$\widetilde{L} = \begin{Bmatrix} 9(1) & -2(1) & -8(1) \\ & 3(1) & 1(1) \\ & & 11(1) \end{Bmatrix} \times 10^{-4} \text{rad.}^2$$

Principal axes of $\widetilde{L}$:

Eigenvalue (rad²)	R.M.S. (rad.)	Direction cosines I_1	I_2	I_3
0.0190	0.138	−0.6571	0.1219	0.7439
0.0036	0.060	−0.2684	0.8843	−0.3821
0.0014	0.038	−0.7044	−0.4507	−0.5484

$$\widetilde{S} = \begin{Bmatrix} -7(13) & 67(6) & -23(8) \\ 1(5) & -11(11) & -12(5) \\ -29(8) & -38(6) & 18(40) \end{Bmatrix} \times 10^{-4} \text{ rad. Å}$$

Trace of S has been set = 0

Principal axes of $\widetilde{S}$.

Eigenvalue (rad.Å)	Direction cosines I_1	I_2	I_3
0.0038	−0.5097	−0.4140	0.7542
0.0002	0.2043	0.7933	0.5735
0.0040	−0.8358	0.4464	−0.3197

Displacement of libration axes (Å) ($^{j}\varrho_i$ = displ. of L_j along L_i) $^{1}\varrho_2 = -0.159$, $^{2}\varrho_1 = 0.068$, $^{3}\varrho_1 = 2.038$, $^{1}\varrho_3 = -0.373$, $^{2}\varrho_3 = 0.531$, and $^{3}\varrho_2 = -0.508$. Effective cross translation parallel with the L_1, L_2, and L_3-axes (Å): 0.016, −0.019, and −0.029, respectively.

The C_1-S-I_2 bond angle is close to 110° and the iodine molecule is nearly co-planar with the $S-C_1-C_2$ group. Because of the double bond character of the C_1-S bond, a strong electron density due to one of the lone pairs on the sulfur atom should be set up in directions close to the $S-I_2$ direction. This orbital is therefore believed to be the main source of charge-transfer on complex formation. If sp^2-hybridized orbitals are not formed on sulfur, as has been claimed,[16] the lone pair orbitals are pure p-orbitals, the deviation of $\angle C_1-S-I_2$ from 90° originating in sterical interactions.

A reasonable description of bond and symmetry properties of the $S-I_2-I_1$ group in the ground state is provided by a model, wherein the four σ-electrons of the $S-I_2-I_1$ group are assumed axially delocalized in the complex giving rise to three-centre bonds, centred at the S, I_2 and I_1 sites. This principle is frequently used to describe related molecular complex structures.[17]

Table 5. Intramolecular parameters.

a. Bond lengths (Å) and angles (°).

	Observed	Corrected		Observed
I_1-I_2	2.880(1)		I_1-I_2-S	176.21(04)
I_2-S	2.688(2)		I_2-S-C_1	109.9 (2)
$S-C_1$	1.716(5)	1.721	$S-C_1-C_2$	121.1 (4)
C_1-C_2	1.493(7)	1.499	$C_1-C_2-C_3$	113.3 (6)
C_2-C_3	1.523(10)	1.531	$C_2-C_3-C_4$	115.5 (6)
C_3-C_4	1.506(11)	1.514	$C_3-C_4-C_5$	114.2 (5)
C_4-C_5	1.520(10)	1.530	$C_4-C_5-C_6$	113.2 (6)
C_5-C_6	1.508(9)	1.515	C_5-C_6-N	113.2 (5)
C_6-N	1.487(7)	1.490	C_6-N-C_7	115.3 (5)
$N-C_7$	1.476(7)	1.479	C_6-N-C_1	121.5 (4)
$N-C_1$	1.302(7)	1.315	$N-C_1-C_2$	119.2 (4)
			C_1-N-C_7	123.2 (5)
			$N-C_1-S$	119.7 (4)

b. Atomic deviations (Å) from least squares plane through C_1, C_2, C_6, C_7, N, and S.

C_1	C_2	C_6	C_7	N	S	I_1	I_2
−0.07	−0.024	0.039	−0.023	−0.015	0.012	0.051	−0.039

The atoms execute pronounced vibrational motion in the solid. The outer halogen atom vibrates more strongly than the central one, as is to be expected (Table 3).

Results of the rigid body motion analysis for the organic molecule are shown in Table 4. The root mean square deviation of the Δu(ij)'s[10] is relatively close to the values reported for other cyclic systems.[18] The magnitude of the figure indicates that the rigid-body motion approximation is acceptable, although not a good one,[10] as to be expected. It appears that the rotational oscillation is quite marked, especially about one of the principal axes. This gave rise to bond length corrections [4,10] ranging from 0.004 Å to 0.013 Å (Table 5).

The methyl group is likely to reorientate about the $N-C_7$ bond. The shortest S−H separation is 2.38 Å, assuming a C−H bond length of 1.09 Å and tetrahedral H−C−C bond angles. This is considerably shorter than expected for a normal S−H van der Waals contact distance.[14] The region of minimum potential energy corresponds most likely to the maximum S−H separation of 2.89 Å, which occurs when each of two hydrogen atoms are equally distant from the sulfur atom. None of the H−H separations or other types of separation involving the methyl group in this position, are less than the corresponding normal contact distance. These interactions can therefore hardly displace the methyl group appreciably from the predicted equilibrium orientation.

Other short intramolecular distances between "non-bonded" atoms of particular interest are $S-C_2=2.80$ Å, $S-N=2.62$ Å, $S-C_7=2.97$ Å, $I_2-C_1=3.65$ Å, and $I_2-C_2=3.63$ Å.

The structure viewed along the [010]- and [100]-directions of the unit cell is shown in Fig. 2. Intermolecular distances are of the van der Waals type.

The crystallographic computer program used is quoted in Ref. 4.

Acknowledgement. Thanks are due to mag. scient. E. Augdahl for helpful discussions and the gift of a sample of MTCL.

REFERENCES

1. a. Bent, H. A. *Chem. Rev. 68* (1968) 587; b. Lin, G. H.-Y. and Hope, H. *Acta Crystallogr. B 28* (1972) 643; c. Bois

D'Enghien-Peteau, M., Meunier-Piret, J. and Van Meerssche, M. *J. Chim. Phys. Physicochim. Biol. 65* (1968) 1221; d. Schweekert, W. W. and Meyers, E. A. *J. Phys. Chem. 72* (1968) 1561.
2. Rogstad, A. and Augdahl, E. *Acta Chem. Scand. 25* (1971) 225.
3. Møllendal, H., Grundnes, J. and Augdahl, E. *Acta Chem. Scand. 23* (1969) 3525.
4. Dahl, T., Gram, F., Groth, P., Klewe, B. and Rømming, C. *Acta Chem. Scand. 24* (1970) 2232.
5. Busing, W. R. and Levy, H. A. *Acta Crystallogr. 10* (1957) 180.
6. *Int. Tab. of X-Ray Cryst. 3* (1962) 157 and 166.
7. Åsbrink, S. and Werner, P.-L. *Acta Crystallogr. 20* (1966) 407.
8. Dewar, M. J. S. *An Epistologue on Carbon Bonds, Tetrahedron 17* (1962) 125.
9. Cruickshank, D. W. J. *Acta Crystallogr. 9* (1956) 679.
10. Shomaker, V. and Trueblood, K. N. *Acta Crystallogr. B 24* (1968) 63.
11. Truter, M. R. *J. Chem. Soc.* (1960) 997.
12. Piazzesi, A. M., Bardi, R., Mammi, M. and Walter, W. *Ric. Sci. A 6* (1964) 173.
13. Ansell, G. B., Forhey, D. M. and Moore, D. W. *Chem. Commun.* (1970) 56.
14. Heilbronner, E. and Bock, H. *Das HMO-Modell und seine Anwendung*, Verlag Chemie 1970, p. 249.
15. Zabicky, J. and Patai, S. *The Chemistry of Amides*, Wiley, New York 1970, p. 2.
16. Lin, G. H.-Y. *Thesis*, Univ. California, Davis 1969.
17. Marstokk, K.-M. and Strømme, K. O. *Acta Crystallogr. B 24* (1968) 713.
18. Groth, P. *Acta Chem. Scand. 23* (1969) 1311 and 2277.

Received September 17, 1973.

Acta Chemica Scandinavica A 28 (1974) 185—193

Nonplanar Electron Transfer Complexes. I. The Chemistry of Five $Ni-N_2S_2^z$ Complexes derived from Nickel-bis-*N*,*N*-diethylphenylazothioformamide

KLAUS BECHGAARD

Department of General and Organic Chemistry, University of Copenhagen, The H. C. Ørsted Institute, DK-2100 Copenhagen, Denmark

The existence of a series of five electron transfer complexes, of which the nonplanar nickel-bis-*N*,*N*-diethylphenylazothioformamide is the prototype, has been demonstrated by cyclic voltammetry and coulometric techniques. The nature of four members of the series has been elucidated by a combination of electrochemical, ESR, and electronic spectral studies and measurements of magnetic susceptibilities of solid samples. The properties of three members of the $Ni-N_2S_2^z$ series ($z = 1+$, 0, and $1-$) have been rationalized in a simple bonding model for nonplanar electron transfer complexes, in which the highest occupied orbitals seem to be mainly ligand-based.

In recent years several reports have appeared concerning electron transfer complexes of the general type $M-N_2S_2^z$ (Refs. 1–6). Among the ligands used, arylazothioformamides are especially interesting in view of their ability to form planar electron transfer complexes with platinum,[5] as well as nonplanar complexes with nickel [6] and copper described in this and a following paper, respectively.

Additionally, *N*,*N*-diethylphenylazothioformamide (L) has been found to form a very unusual bis complex with zinc, $Zn(L)_2^0$, having a vanishingly small energy difference between a ^1B and a ^3B ground state.[6]

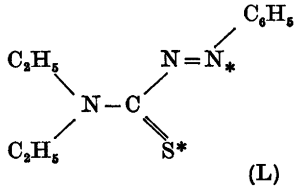

(L)

The pseudotetrahedral structure [6,7] of nickel-bis-*N*,*N*-diethylphenylazothioformamide (*3*) makes a detailed study of this compound attractive since, to our knowledge, it represents the first serious distortion from planarity ever reported for bis-chelate electron transfer complexes. The stability of planar electron transfer series is frequently ascribed to favorable out-of-plane π type interactions which create MO's extensively delocalized over both metal and ligands.[8,9] These interactions tend to be somewhat reduced in tetrahedral species [10] and thus do not contribute to the stability of tetrahedral $M-N_2S_2^z$ species.

It is the purpose of the present work to document the existence of the series of electron transfer complexes in question, to present results obtained for individual species, and to try to rationalize some of these in a simple model of the bonding.

In our first paper [6] we reported electrochemical results obtained in acetonitrile solutions which indicated that nickel-bis-*N*,*N*-diethylphenylazothioformamide [$Ni(L)_2^0$,(*3*)] was the neutral representative of a three-membered series of electron transfer complexes.

The present work describes results mainly obtained in the less coordinating solvent methylene chloride, in which five discrete members have been identified:

$$\underset{(1)}{Ni(L)_2^{2+}} \overset{e^-}{\rightleftharpoons} \underset{(2)}{Ni(L)_2^{+}} \overset{e^-}{\rightleftharpoons} \underset{(3)}{Ni(L)_2^{0}} \overset{e^-}{\rightleftharpoons} \underset{(4)}{Ni(L)_2^{-}} \overset{e^-}{\rightleftharpoons} \underset{(5)}{Ni(L)_2^{2-}}$$

RESULTS

Preparation. The preparation of (*3*) follows the general procedure for neutral $M(L)_2^0$ compounds, oxidation of the corresponding bisthiosemicarbazidates. It has been reported in detail elsewhere.[6] The most oxidized member (*1*) of the series was prepared by treatment of 1 mol of $Ni(ClO_4)_2.6H_2O$ dissolved in dry acetone with two mol of L (eqn. 1).

$$Ni^{2+} + 2L \rightarrow \underset{(1)}{Ni(L)_2^{2+}} \qquad (1)$$

This procedure, although simple-looking, deserves further comment. By cyclic voltammetry (see below) is has been shown that (*1*) is generated at a fairly positive potential ($E_{\frac{1}{2}} = +0.7$ V *vs.* SCE). This means that the solvent in which (*1*) is formed has to be stable towards oxidants of this strength. As shown below (*1*) is also unstable towards acetonitrile, the reason being that this solvent is too good a ligand compared to L. This illustrates two important features, solvent oxidation and solvent coordination which have to be controlled in the preparation of individual members of electron transfer series.

$Ni(L)_2^{2+}$ (*1*) can be isolated as a perchlorate containing 1 mol of water. The water, which cannot be removed without destruction of the complex (*ca.* 180°C), seems to accompany the perchlorate ion, since an anhydrous tetrafluoroborate can be prepared, exhibiting the same properties as the perchlorate as solid as well as in solution. The perchlorate was used in the investigation of (*1*) because the tetrafluoroborate turned out to be unstable on storage.

$Ni(L)_2^{+}$ (*2*) can be prepared electrolytically by one-electron oxidation of (*3*) or by mol to mol mixing of (*1*) and (*3*) in dry CH_2Cl_2 (eqn. 2):

$$(1) + (3) \rightleftharpoons 2(2) \qquad (2)$$

The identity of (*2*) generated by the different procedures was checked by means of its electronic spectrum.

$Ni(L)_2^{-}$ (*4*) was generated electrolytically by one-electron reduction of (*3*) and was stable when protected from oxygen and moisture.

Attempts to prepare stable solutions of (*5*) by either electrolytic or Na-Hg reduction of (*3*) were, however, unsuccesful.

Electrochemical evidence for the electron transfer series

CH_2Cl_2. The solution equilibria set up as a consequence of reduction or oxidation of (*3*) are illustrated by the cyclic voltammogram given in Fig. 1. In the cathodic scan starting at S (*3*) is reduced to (*4*) at R_3 in a reversible

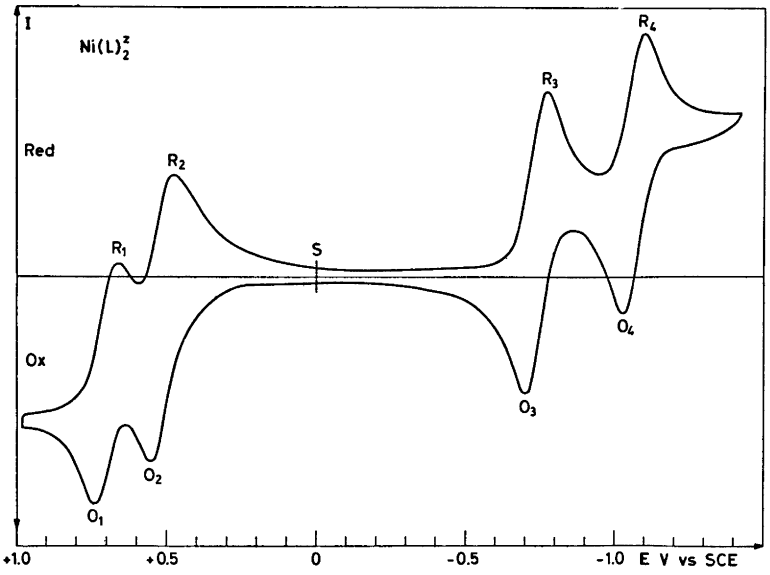

Fig. 1. Cyclic voltammogram of $Ni(L)_2^z$ in CH_2Cl_2.

process. Coulometric reduction [11] uses precisely 1 F/mol and (*4*) can be reoxidized to (*3*) in 95 – 100 % yield. The peak separation $R_3 - O_3$ is 60 mV at 298 K, and the peak current ratio 1:1. Thus there is no doubt that (*4*) is formed by one-electron reduction of (*3*). At the more negative potential, R_4, (*4*) is reduced to (*5*). Again the criteria for a reversible one-electron reduction are fulfilled, but (*5*) is not stable under the conditions employed, since the voltammograms taken after one-electron coulometric reduction of (*4*) change rapidly with time.

Starting at S and scanning anodically it has been shown, by the technique outlined above, that (*3*) undergoes two reversible one-electron oxidations to (*2*) and (*1*) at O_2 and O_1, respectively. (*2*) and (*1*) are both stable under the conditions employed.

CH_3CN. In CH_3CN the two reversible couples $R_3 - O_3$ and $R_4 - O_4$ are recognized from the investigation in CH_2Cl_2. In the anodic scan, however, (*3*) is oxidized irreversibly at O_2. Coulometric oxidation of (*3*) uses precisely 2F/mol. Electronic spectra show that the resulting solution consists of L and $[Ni(CH_3CN)_6]^{2+}$ according to:

$$Ni(L)_2^0 + 6CH_3CN \xrightarrow{-2e^-} 2L + [Ni(CH_3CN)_6]^{2+} \quad (3)$$

(*3*)

The results obtained in CH_2Cl_2 clearly demonstrate the existence of an electron transfer series consisting of five discrete members (*1*) – (*5*). In CH_3CN only three members, (*3*) – (*5*), can be demonstrated owing to the higher affinity of the solvent for nickel which promotes destruction of the cationic complexes.

The voltammetric results are summarized in Table 1.

ESR and magnetic susceptibilities. Results are set out in Tables 2 and 3 and Fig. 2. ESR spectra of (*2*) and (*4*) were recorded in frozen CH_2Cl_2 at liquid nitrogen temperature. Magnetic susceptibilities of powdered samples of $Ni(L)_2(ClO_4)_2.H_2O$ and $Ni(L)_2^0$ (*3*) were determined in the temperature range 80 – 278 K.

Electronic spectra of (*1*), (*2*), (*3*), and (*4*) were recorded in dry CH_2Cl_2. The solution spectra are shown in Fig. 3 and the results summarized in Table 4. The diffuse reflectance spectrum of $Ni(L)_2(ClO_4)_2.H_2O$ in $BaSO_4$ is shown in Fig. 4 together with the solution spectrum in CH_2Cl_2.

DISCUSSION

$Ni(L)_2^{2-}$ (5). This species is produced at potentials more negative than −1.0 V (*vs.* SCE). The one-electron relationship to (*4*) has been

Table 1. Voltammetry of $Ni(L)_2^z$ in CH_3CN and CH_2Cl_2.

Complex	Solvent	Peak Potentials [a] O_1	R_1	O_2	R_2	O_3	R_3	O_4	R_4
$Ni(L)_2^z$	CH_2Cl_2 [b]	0.74	0.67	0.55	0.48	−0.70	−0.76	−1.03	−1.09
$Ni(L)_2^z$	CH_3CN [b]		0.52 [c]			−0.76	−0.82	−1.09	−1.15

[a] Volts *vs.* SCE, scan rate 200 mV/s, $T = 298$ K. [b] Supporting electrolyte, n-Bu_4NBF_4 (0.2 M). [c] 2e Oxidation.

Table 2. ESR spectral data.

Complex	Medium	sol. [a] $\langle g \rangle$	frozen sol. [b] g_1	g_2	g_3
$Ni(L)_2^+$	CH_2Cl_2 [c]	2.000	–	2.000	–
$Ni(L)_2^-$	CH_2Cl_2 [d]	2.022	1.999	2.017	2.063

[a] $T = 298$ K. [b] Microcrystalline solid matrix at 77 K. [c] Gegenion ClO_4^-. [d] Containing n-Bu_4NBF_4 (0.2 M).

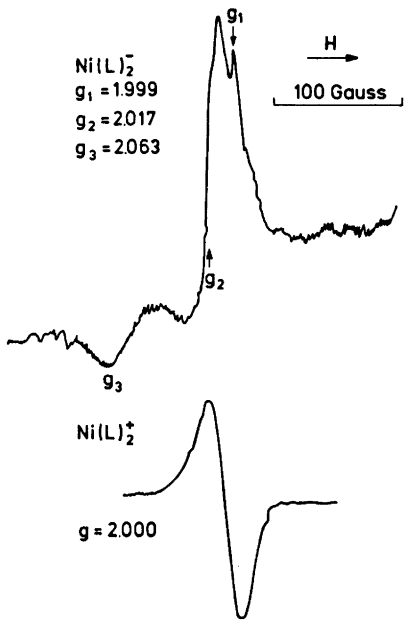

Fig. 2. X-band ESR spectra of (*4*) and (*2*) in frozen CH_2Cl_2 at 77 K.

demonstrated by coulometry. The instability of (*5*) has however, to date prevented further investigation. The cyclic voltammetry and coulometry results, which are the sole experimental evidence for the existence of (*5*) are uninformative with respect to structural changes on going from (*4*) to (*5*) since structural inter-

Table 3. Magnetic susceptibility results.

Complex	T, K	χ^a cgs/mol	μ_{eff} BM
	80	156.2×10^{-4}	3.16
$Ni(L)_2(ClO_4)_2$	150	866.4×10^{-5}	3.22
H_2O	278	482.1×10^{-5}	3.27
$Ni(L)_2^0$	...	...	dia.

[a] Dia. correction -200×10^{-6} cgs/mol.

Table 4. Electronic spectral data for $Ni(L)_2^z$ in CH_2Cl_2.

Complex	λ_{max} nm	ε [a]
$Ni(L)_2^{2+}$	375	24 520
	840	2 000
	570	5 570
$Ni(L)_2^+$	375 sh	15 000
	322	18 900
	290	20 000
	840	2 340
	572	11 700
$Ni(L)_2^0$	510 sh	7 950
	425	12 000
	320	27 000
	295 sh	22 100
	860	2 100
	580	2 200
$Ni(L)_2^-$	480 sh	2 400
	320	14 300

[a] Uncorrected for underlying absorptions.

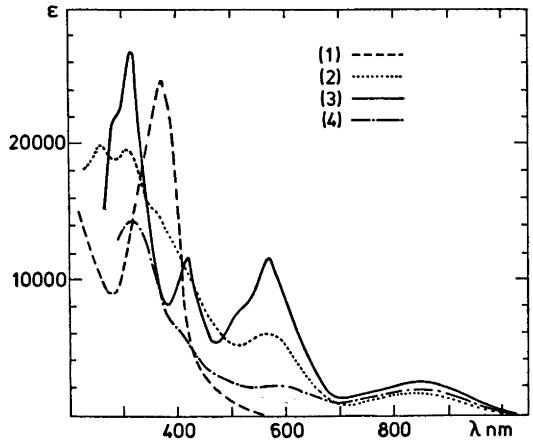

Fig. 3. Electronic spectra of $Ni(L)_2^z$ in CH_2Cl_2.

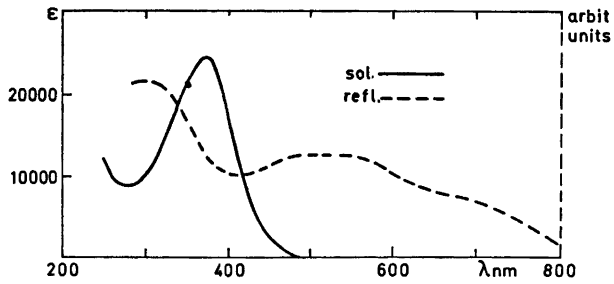

Fig. 4. Diffuse reflectance and solution spectra of $Ni(L)_2(ClO_4)_2H_2O$.

conversions (planar-tetrahedral) are not necessarily detected by the rather slow technique employed.

Species corresponding to (*5*) are in planar $M-S_4^{2-}$ and $M-N_2S_2^{2-}$ series normally described as Me^{2+} coordinated by two dianion ligands,[5,9] and it seems reasonable in view of the results discussed below to accept the same formalism when describing (*5*).

$Ni(L)_2^-$ (*4*). This species is readily produced by electrochemical reduction of (*3*) and is stable when protected from oxygen and moisture. The electronic spectrum of (*4*) in CH_2Cl_2 is shown in Fig. 3. It is characteristic that the shifts to longer wavelengths always found [12] on going from neutral (*3*) to monoanionic nickel group members of planar electron transfer series are lacking. In fact, the electronic spectrum of (*4*) exhibits nearly the same transitions as the spectrum of (*3*), although the extinction coefficients are smaller. This strongly indicates that the electronic and geometric (tetrahedral) structures are similar, and the additional electron on going from (*3*) to (*4*) is placed in a nonbonding orbital (probably an orbital of predominantly ligand π^* character).

The ESR spectrum of (*4*) in frozen CH_2Cl_2 (Fig. 2) supports this conclusion. A predominant feature is a rather small g-tensor anisotropy, which is significantly smaller than the rhombic anisotropy normally found in planar $Ni\text{-}N_2S_2^-$ species.[1,*]

Provided the odd electron is located in an orbital of predominant ligand π^* character, a slight or unresolvable g-tensor anisotropy is to be expected.[1] If, on the other hand the odd electron resides in an orbital or primarily 3*d* character fairly large g-tensor anisotropies are expected in tetrahedral system both of high and of low symmetry.[13,14]

The experimental spectrum of $Ni(L)_2^-$ favours the first description ($\Delta g = 0.06$), although it must be stated that the use of g-tensor anisotropies as criteria of metal orbital involvement in the odd-electron orbital can be misleading.[1,2]

$Ni(L)_2^0$ (*3*). All previously investigated bis complexes showing electron transfer properties have either been found [15] or are assumed to be planar,[12] exhibiting only small tetragonal distortions. However, the structure of $Ni(L)_2^0$, as described in detail elsewhere,[6,7] is pseudo-tetrahedral, with a dihedral angle of 70° between the average planes of the chelate rings. Another important feature is that the chelate rings and the phenyl groups are not strictly coplanar (the dihedral angle is 30°).

The nonplanarity of $Ni(L)_2^0$ is indeed surprising since L would be expected to exhibit the same coordinative properties as the ligands giving rise to planar electron transfer species. Furthermore L can form planar electron transfer complexes with platinum [5] and palladium.[16]

The phenyl group, which singles L from other ligands evidently introduces both steric and electronic chances.

Steric effects are not easily elucidated. Ni-bis-dithizonate (*6*), which has a coordination sphere similar to that of $Ni(L)_2^0$, has been shown to be planar.[17,18] In (*6*) the chelate ring and the phenyl group attached to it are perpendicular.

Furthermore a group of Ni and $Co-N_2S_2$ complexes in which the metal is part of a six-membered ring have been shown to vary be-

* $[Ni(o\text{-}C_6H_4(NH)S)_2]^-$ has $g_1 = 2.005$, $g_2 = 2.028$, and $g_3 = 2.128$, and $[Ni(C_6H_5CSNNH)_2]^-$ has $g_1 = 2.006$, $g_2 = 2.028$, and $g_3 = 2.126$.[1]

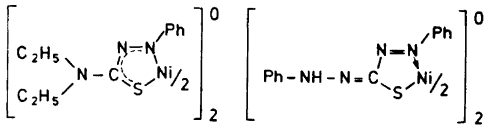

(3) (6)

Fig. 5.

tween planar and tetrahedral depending on the bulk of the ring substituents. Phenyl groups have a moderate effect, and typical energy differences are as low as 0 – 3 kcal/mol in $CDCl_3$ at 40°C.[19]

Likewise the electronic effects are not easily explained. The nonplanarity of $Ni(L)_2^0$ allows the ligand to be nearly planar and it is probably not a bad approximation to take in account interactions between the π orbitals of the chelate ring and the phenyl group attached to it. The intense long wavelength transitions found in the electronic spectrum of $Ni(L)_2^0$ are probably M→L, L→L, or L→M transitions rather than ligand field transitions since their positions and relative intensities are very dependent of the substituent pattern of L. It might be mentioned that an analogue of $Ni(L)_2^0$ derived from *N*-isopropyl-*tert*-butylazothioformamide [6] exhibits the first detectable electronic transitions at 570 nm ($\varepsilon_{app} = 1500$) and 479 nm ($\varepsilon_{app} =$ 16 600) in accordance with the hypsochromic shifts expected on going from phenyl to *tert*-butyl substituents.

It seems reasonable to conclude from the data mentioned above that the major effect of the phenyl (and *tert*-butyl) groups is sterical hindrance of the planar geometry, but it has further been demonstrated that other azothioformamides carrying less bulky substituents form planar nickel complexes which are unstable.[6]

The electronic structure of diamagnetic $Ni(L)_2^0$ is interesting. Characteristic are the very small, but significant, temperature independent contact shifts found in the ^1H NMR spectra of $Ni(L)_2^0$ and analogous compounds.[6] The paramagnetism found is not arising from second order Zeeman terms, since direct unpaired spin densities are observed in the ^1H NMR spectra, but probably arises from thermal population of low lying exited states.[20] The electronic spectrum of $Ni(L)_2^0$ given in Fig. 3 is complicated and has not been interpreted.

$Ni(L)_2^+$ (*2*). An important property of this monocation is found in the ESR spectrum given in Fig. 2. The spectrum of (*2*) in frozen CH_2Cl_2 is centered around $g = 2.000$ and exhibits a complete lack of g-tensor anisotropy. If the arguments given above are valid, this means that the odd electron resides in an orbital of primarily ligand character.

The electronic spectrum of (*2*) is remarkable, since it, except for the 290 nm transition, appears to be a superposition of the spectra of (*1*) and (*3*). This raises the question whether (*2*) has a real existence or the solution is an equilibrium mixture consisting mainly of (*1*) and (*3*) (note also that (*2*) was generated by mol to mol mixing of (*1*) and (*3*), as well as electrochemically).

Against this the well-defined ESR spectrum may be emphasized, and also the cyclic voltammetry results. Analysis of these, in terms of the Nernst equation (differences in peak-potentials are taken to be representative of differences in redox potentials), tells us that a solution of (*2*) in CH_2Cl_2 will disproportionate after eqn. 4:

$$2(2) \rightleftharpoons (1) + (3) \qquad (4)$$

in such a way that less than 1 % is found as (*1*) + (*3*). The influence of these in the spectrum of (*2*) may thus be regarded as vanishingly small.

Obviously the spectral similarities between (*3*) and (*2*) means the removal of an electron on going from (*3*) to (*2*) are unimportant for the relative ordering of the orbitals in the two species. This strongly indicates that the highest filled orbital of $Ni(L)_2^0$ is essentially a nonbonding ligand based orbital, since spectral similarities of this type are frequently found when comparing spectra of organic cation radicals (n electrons) with the spectra of the corresponding dications ($n-1$ electrons), where only the intensities of the long wave length bands [as in comparing (*3*) and (*2*)] are different.

$Ni(L)_2^{2+}$ (*1*). The results obtained for this species are somewhat confusing. It is thus important to note the difference between solid state and solution properties.

The solid state magnetic moment is 3.27 BM

per nickel atom at 278 K (falling to 3.12 BM at 77 K). These values were determined for the hydrated perchlorate, $Ni(L)_2(ClO_4)_2.H_2O$. These values are uninformative with regard to structure [21] due to the low symmetry (C_2) of (*1*) in a possible tetrahedral geometry.

As demonstrated by Fig. 4, the diffuse reflectance spectrum of $Ni(ClO_4)_2.H_2O$ is very different from the solution spectrum. This strongly indicates that (*1*) has a different structure in the solid state than in solution.

The electronic spectral similarities of (*1*) and (*2*) in solution, as well as the nature of the ^1H NMR spectrum of (*1*) in $(CD_3)_2CO$, indicate however that (*1*) is tetrahedral in solution. An X-ray structure determination of $Ni(L)_2(ClO_4)_2.H_2O$ is in progress, but has not yet been completed. Only a few tetrahedral cationic nickel complexes have been described previously; characteristic of these are bulky groups in the ligands [22,23] as in (*1*).

Simplified bonding model for tetrahedral $Ni-N_2S_2^x$ complexes

A very important feature of the $Ni(L)_2^x$ series is the electronic spectra similarities of (*2*), (*3*) and (*4*). This strongly indicates that addition of one or two electrons to (*2*) has only a minor effect, and thus that the orbitals in question are essentially nonbonding.

We can utilize this in treating at least (*2*), (*3*), and (*4*) in the same simple model of the bonding. Examination of the X-ray data [6] of $Ni(L)_2^0$ suggests that it is not a bad approximation to treat the chelate as a butadiene-like system carrying σ binding lone pairs directed towards the metal. From arguments given above it seems also to be a reasonable approximation to treat the phenyl group of the ligand as having an inductive effect on the π system of the chelate, rather than influencing the σ type bonding to the metal.

Tetrahedral $Ni(L)_2^x$ posses a structure (*7*) of C_2 symmetry. The important orbitals in the ground state description are assumed to be the *d* metal orbitals transforming as *a*; (d_{z^2}, $d_{x^2-y^2}$, and d_{xy}) and *b*; (d_{xz} and d_{yz}) together with the ligand π^* orbitals (see Fig. 8). The eigenvector properties of the ligand orbitals were determined from a simple Hückel (or a CNDO/2) calculation. These calculations suggest that the energy of the third π orbital of the N–N–C–S chelate is of the same order as the *d* orbitals of nickel. Addition of one electron to the neutral chelate corresponds to formation of the radical anion of the ligand and half fills the π orbital in question, this π orbital is therefore in the following denoted as a π^* orbital.

The π^* orbitals of the two ligands in the complex are mixed during the C_2 operation to form a degenerate set of *a* and *b* symmetry, respectively.

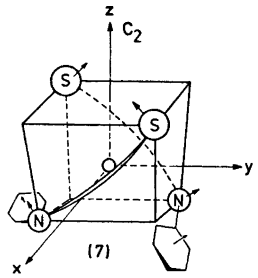

Fig. 6.

To a first approximation let us assume a complete removal of degeneracy of the *d*-orbitals in the distorted low symmetry structure, as well as the ordering of *d*-orbitals given in Fig. 7. It is important that the d_{xy} orbital is expected to rise continuously in energy as the tetrahedron flattens. The relative ordering of *d*-orbitals in systems of low symmetry is uncertain, but the suggestion made has some support from MO calculations and single crystal spectra.[24]

We may then consider the effect of a set of π^* ligand orbitals energetically situated slightly higher than the *d*-orbitals. Inspection of the π^* eigenvectors show that π^* (*b*) and d_{xz} (*b*) are

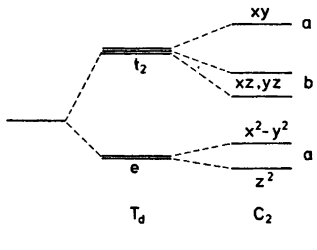

Fig. 7. Schematic *d*-orbital splitting in T_d and C_2 symmetry.

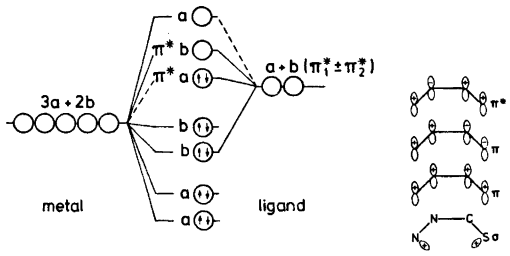

Fig. 8. Qualitative molecular orbital diagram for tetrahedral $Ni-N_2S_2^0$.

expected to mix more heavily than π^* (*b*) and d_{yz} (*b*).

This may, if other effects are neglected, lead to the restricted, qualitative MO diagram of Fig. 8, which has strong support in the experimental results summarized below.

The neutral complex contains 10 electrons in these orbitals (Fig. 8), and the highest occupied orbital is predicted to be the ligand π^* (*a*) orbital.

The present model predicts the first two transitions of $Ni(L)_2^0$ to be L→L and L→M in accordance with the large intensities found.

One-electron oxidation of $Ni(L)_2^0$ would give $Ni(L)_2^+$, a ^2A ground state. The model predicts that the odd electron will be in a π^* (*a*) "ligand" orbital, in accordance with the lack of *g*-tensor anisotropy found in the ESR spectrum.

One-electron reduction half fills the π^* (*b*) orbital. The model predicts this orbital to have some d_{xz} character, in accordance with the slight, but resolvable, rhombic *g*-tensor anisotropy of $Ni(L)_2^-$.

The bonding model outlined above seems useless in interpreting the results obtained for $Ni(L)_2^{2+}$. However, there might be unaccounted structural changes on going from (*2*) to (*1*).

The possibility of a reversal of the ordering of the two π^* orbitals and d_{xy} is recognized. However, this description has no support in the experimental results, since greater changes in electronic spectra on going from (*3*) to (*2*) or (*4*) would then be expected, as well as some *g*-tensor anisotropy of (*2*).

EXPERIMENTAL

N,N Diethylphenylazothioformamide and $Ni(L)_2^0$ were prepared as described in Ref. 6.

$Ni(L)_2(ClO_4)_2.H_2O$. $Ni(ClO_4)_2.6H_2O$ (2 mmol) dissolved in 10 ml of dry acetone was mixed with L (4 mmol) in 5 ml of dry acetone. After standing for 30 min 40 ml of dry diethyl ether was added, and the precipitate was filtered off. Soxhlet extraction with 80 ml of CH_2Cl_2-diethyl ether (1:3) yielded 0.7 g (50 %) of shining black-brown crystals, m.p. 183°C (d). (Found: C 36.75; H 4.50; N 11.64. Calc. for $C_{22}H_{32}Cl_2N_6NiO_9S_2$: C 36.80; H 4.46; N 11.70).

Analytical grade CH_3CN and CH_2Cl_2 were purified by passage through basic alumina (Woelm W 200), deoxygenated by purging with argon and stored in sealed siphon bottles until use. Equipment and techniques used for voltammetry and coulometry have been described elsewhere.[11,25] The reference electrode was a saturated aqueous calomel electrode. The working electrode for voltammetry was a Beckman platinum button and for coulometry a platinum gauze.

ESR spectra were recorded on a JES-ME-IX spectrometer, and *g*-values standardized by use of DPPH and Mn^{2+} in MgO. Susceptibilities were obtained by the Faraday method using $Hg[Co(NCS)_4]$ as a calibrant.

Electronic (and ESR) spectra of (*2*) and (*4*) were recorded in sealed cuvettes filled directly from the electrolysis chamber, which was placed in an argon-filled glove box.

REFERENCES

1. Holm, R. H., Balch, A. L., Davidson, A., Maki, A. H. and Berry, T. E. *J. Amer. Chem. Soc. 89* (1967) 2866.
2. Dori, Z., Eisenberg, R., Stiefel, E. I. and Gray, H. B. *J. Amer. Chem. Soc. 92* (1970) 1506.
3. Jones, C. J. and McCleverty, J. A. *J. Chem. Soc. A* (1970) 2829.
4. Warren, L. E., Horner, S. M. and Hatfield, W. E. *J. Amer. Chem. Soc. 94* (1972) 6392.
5. Forbes, C. E., Gold, A. and Holm, R. H. *Inorg. Chem. 10* (1971) 2479.
6. Jensen, K. A., Bechgaard, K. and Pedersen, C. T. *Acta Chem. Scand. 26* (1972) 2913.
7. Hazell, R. G. *Acta Chem. Scand. To be published.*
8. Schmitt, R. D. and Maki, A. H. *J. Amer. Chem. Soc. 90* (1968) 2288.
9. Schrauzer, G. N. and Mayweg, V. P. *J. Amer. Chem. Soc. 87* (1965) 3585.
10. Eaton, D. R. and Philips, W. D. *J. Chem. Phys. 43* (1965) 392.
11. Parker, V. D. *Acta Chem. Scand. 24* (1970) 2768.
12. McCleverty, J. A. *Progr. Inorg. Chem. 10* (1968) 49.
13. Watts, R. K. *Phys. Rev. 188* (1969) 568.
14. Fritz, H. P., Golla, B. M. and Keller, H. J. *Z. Naturforsch. B 21* (1966) 1015.
15. Eisenberg, R. *Progr. Inorg. Chem. 12* (1970) 295.

16. Bechgaard, K. *Thesis*, University of Copenhagen, 1973.
17. Laing, M. and Alsop, P. A. *Talanta 17* (1970) 242.
18. Mawby, A. and Irving, N. M. N. H. *J. Inorg. Nucl. Chem. 34* (1972) 109.
19. Holm, R. H. and O'Connor, M. J. *Progr. Inorg. Chem. 14* (1971) 241.
20. Bechgaard, K. *Unpublished results.*
21. Figgis, B. N. and Lewis, J. *Progr. Inorg. Chem. 6* (1964) 37.
22. Donoghue, J. T. and Drago, R. S. *Inorg. Chem. 1* (1962) 866.
23. Drago, R. S., Donoghue, J. T. and Herlocker, D. W. *Inorg. Chem. 4* (1965) 836.
24. Hush, N. S. and Hobbs, R. J. M. *Progr. Inorg. Chem. 10* (1968) 259.
25. Hammerich, O. and Parker, V. D. *J. Chem. Soc. Perkin Trans. 1* (1972) 1718.

Received October 1, 1973.

Acta Chemica Scandinavica A 28 (1974) 194—200

The Crystal Structure of Anilinium Tetrachlorocuprate(II)

KARL PEDER LARSEN

Department of Inorganic Chemistry, Aarhus University, DK-8000 Aarhus C, Denmark

Anilinium tetrachlorocuprate(II), $(C_6H_5NH_3)_2CuCl_4$, is monoclinic, space group $P2_1/c$ with $a=15.050$ Å, $b=7.443$ Å, $c=7.180$ Å, $\beta=100.7°$ and $Z=2$. The structure has been determined from three-dimensional X-ray data and refined by the method of least squares to a conventional R-value of 0.033. The coordination around the copper atom consists of an approximately square planar arrangement of chlorine atoms, with an average Cu-Cl distance of 2.29 Å. These units are linked together through longer chlorine bonds from neighbouring complexes, thus constituting the typical 4+2 coordination around the copper atom.

Complexes of the type $CuCl_n^{(n-2)-}$, $n=3$, 4, 5 are known to exist in various geometries, more or less dependent on the cation employed. Reviews have been given by Hathaway and Billing[1] and Hatfield and Whyman.[2] Some of these complexes exist in the crystal as isolated units; this is the case in Cs_2CuCl_4 where $CuCl_4^{2-}$ shows approximately D_{2d} symmetry.[3] In $[Cr(NH_3)_6][CuCl_5]$ the $CuCl_5^{3-}$ ion, which has regular D_{3h} symmetry,[4] also forms discrete species. Complexes containing isolated $CuCl_6^{4-}$ ions do not, however, seem to have been reported in the literature. The compound investigated, $(C_6H_5NH_3)_2CuCl_4$, is the product obtained from a synthesis described by Dubský and Wagenhofer [5] who claimed to have prepared the complex $(CuCl_6).H_4.aniline_4.2H_2O$.

EXPERIMENTAL

Chemistry. 1.70 g $CuCl_2.2H_2O$ and 7.77 g $C_6H_5NH_3Cl$ corresponding to a 1:6 molar ratio was dissolved in 200 ml conc. HCl. The mixture was boiled and depending on the cooling rate, crystals of different shapes were formed:
(a) thin yellow-brownish quadratic plates (predominant),
(b) yellow-brownish quadratic prisms.

The crystals of type (a) were shown to be twins of the (b)-form. The density was measured by the flotation technique in a mixture of $CHBr_3$ and CCl_4.

X-Ray technique. Lattice type and space group were determined from Weissenberg and precession photographs using Cu and Mo radiation ($\lambda_{Cu}=1.5418$ Å, $\lambda_{Mo}=0.7109$ Å). Lattice parameters were obtained from a least squares refinement of setting angles for 18 reflections with $20° \leq 2\theta \leq 45°$. Three dimensional intensity data were collected with an automatic Picker four-circle instrument using graphite monochromatized Mo$K\alpha$ radiation. The crystal employed which had the linear dimensions $0.30 \times 0.40 \times 0.25$ mm³ and was bounded by {100} and {011}, was mounted along [011]. Data were collected up to $\sin\theta/\lambda=0.7$, yielding 2469 independent reflections of which 1993 had $F_{obs}^2 \geq 2\sigma(F_{obs}^2)$. The linear absorption coefficient for Mo$K\alpha$ radiation was 20.9 cm^{-1}. Data processing was performed with the program DATAPP [6] and included absorption correction using a $6 \times 4 \times 4$ grid. The transmission factor varied between 0.5348 and 0.6299.

CRYSTAL DATA

Crystal system: monoclinic (b-axis unique).
Unit cell: $a=15.050(2)$ Å, $b=7.443(1)$ Å, $c=7.180(1)$ Å, $\beta=100.71(1)°$, $Z=2$, $d_{calc}=1.654$ g/cm³, $d_{obs}=1.650$ g/cm³.
Systematic absences: $h0l$: $l=2n+1$.
$0k0$:$k=2n+1$.
Space group: $P2_1/c$.

STRUCTURE DETERMINATION

With two molecules per unit cell the Cu atom had to be in a special position. This was confirmed by the three-dimensional Patterson function from which the chlorine positions were also determined. A Fourier map calculated with the signs determined from copper and the two

Table 1. Atomic coordinates and their standard deviations $\times 10^5$. For hydrogen standard deviations $\times 10^4$ and isotropic B values (Å^2) with standard deviations $\times 10$ are given.

Atom	x	$\sigma(x)$	y	$\sigma(y)$	z	$\sigma(z)$	B	$\sigma(B)$
Cu	0.00000	(0)	0.00000	(0)	0.00000	(0)		
Cl_1	0.02237	(4)	0.29064	(7)	0.27751	(7)		
Cl_2	0.15241	(4)	−0.04141	(7)	0.88166	(8)		
N	0.14957	(14)	−0.02748	(31)	0.54458	(33)		
C_1	0.24762	(14)	−0.00803	(28)	0.60750	(29)		
C_2	0.27999	(18)	0.11263	(34)	0.74825	(37)		
C_3	0.37231	(19)	0.12543	(42)	0.81044	(42)		
C_4	0.43052	(19)	0.01868	(40)	0.73438	(43)		
C_5	0.39680	(17)	−0.10016	(38)	0.59154	(42)		
C_6	0.30473	(16)	−0.11462	(33)	0.52837	(36)		
H_1	0.2395	(18)	0.1759	(36)	0.7945	(36)	4.6	(6)
H_2	0.3945	(21)	0.2122	(44)	0.9084	(41)	6.5	(8)
H_3	0.4951	(18)	0.0207	(34)	0.7741	(38)	4.5	(6)
H_4	0.4391	(17)	−0.1727	(35)	0.5449	(38)	4.6	(6)
H_5	0.2787	(17)	−0.1880	(36)	0.4445	(37)	4.6	(7)
H_6	0.1192	(21)	0.0424	(40)	0.6144	(44)	5.8	(8)
H_7	0.1313	(21)	−0.1316	(46)	0.5630	(44)	7.1	(9)
H_8	0.1444	(26)	−0.0125	(49)	0.4038	(64)	10.2	(2)

Table 2. Mean square vibration amplitudes, u_{ij}, with standard deviations (both in Å$^2 \times 10^4$).

Atom	u_{11}	$\sigma(u_{11})$	u_{22}	$\sigma(u_{22})$	u_{33}	$\sigma(u_{33})$	u_{12}	$\sigma(u_{12})$	u_{13}	$\sigma(u_{13})$	u_{23}	$\sigma(u_{23})$
Cu	250	(2)	233	(2)	228	(2)	12	(1)	43	(1)	62	(1)
Cl_1	406	(3)	270	(3)	271	(3)	26	(2)	68	(2)	−74	(2)
Cl_2	254	(3)	378	(3)	394	(3)	36	(2)	42	(2)	33	(2)
N	298	(10)	369	(11)	407	(12)	−8	(9)	38	(9)	11	(9)
C_1	269	(10)	305	(10)	290	(10)	7	(9)	27	(8)	56	(9)
C_2	429	(14)	427	(14)	447	(14)	−48	(11)	111	(12)	−95	(12)
C_3	500	(17)	699	(20)	512	(17)	−177	(15)	10	(14)	−178	(15)
C_4	304	(13)	728	(20)	581	(17)	−60	(14)	−27	(12)	44	(16)
C_5	336	(13)	543	(16)	612	(17)	98	(12)	123	(13)	20	(14)
C_6	372	(13)	394	(13)	414	(14)	5	(10)	56	(11)	−65	(11)

chlorine atoms showed clearly all the atoms in the aniline molecule. The scattering factors used were those given by Cromer and Mann [7] for the heavy atoms and by Stewart, Davidson and Simpson [8] for hydrogen. The structure was refined isotropically with the full matrix least squares program LINUS [9] to an R-value of 0.102. Further refinement with anisotropic temperature factor coefficients and reflections weighted by $w = 1/[\mu(F)]^2$, where $\mu(F) = \{\sigma(F^2)_{count} + 1.01F_{obs}^2\}^{\frac{1}{2}} - |F_{obs}|$ lowered R to 0.042. The approximate positions of the hydrogen atoms belonging to the benzene ring were calculated and included with isotropic temperature factor coefficients. A difference Fourier synthesis showed the remaining hydrogen atoms (N−H) and no further features. Including isotropic extinction a final conventional R-value of 0.033 was obtained. The extinction parameter was 0.0120(7), and the correction factor varied from 1.00 down to 0.71 for a few low order reflections. Coordinates and isotropic temperature factor parameters are given in Table 1, anisotropic temperature factor parameters for heavy atoms in Table 2, and a list of observed and calculated structure factors is given in Table 3.

Table 3. Observed and calculated structure factors, 10 × absolute values.

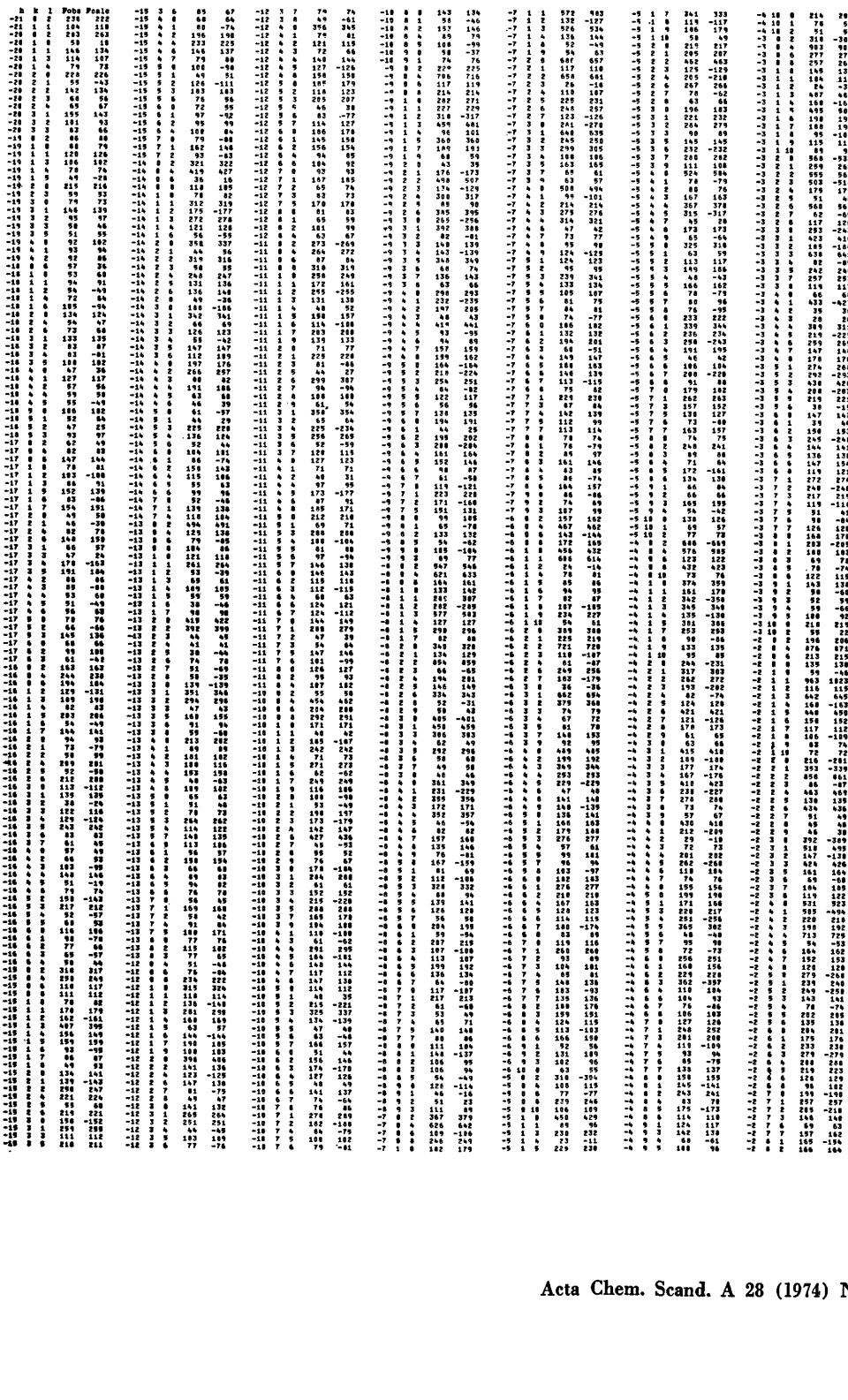

Table 3. Continued.

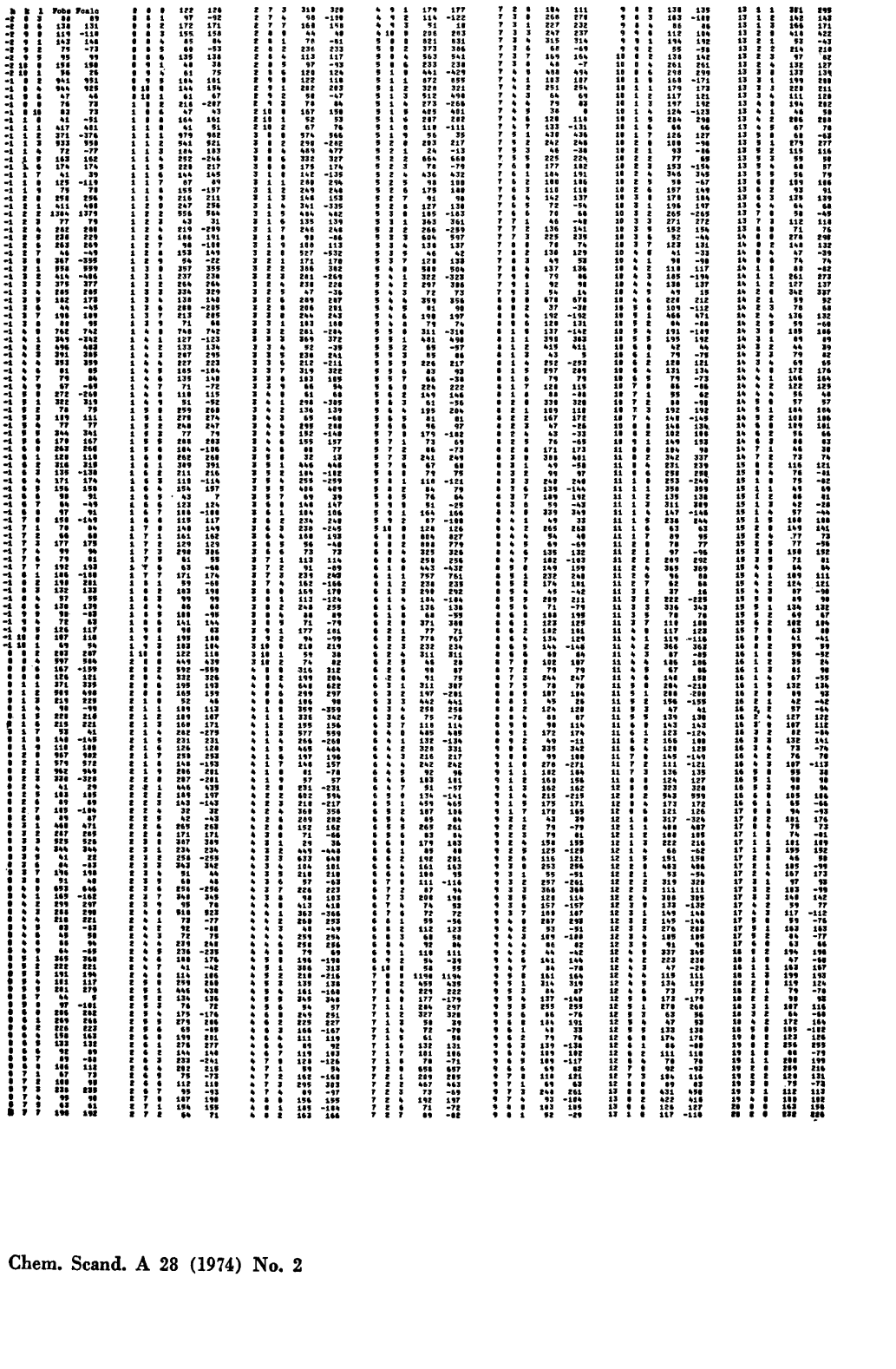

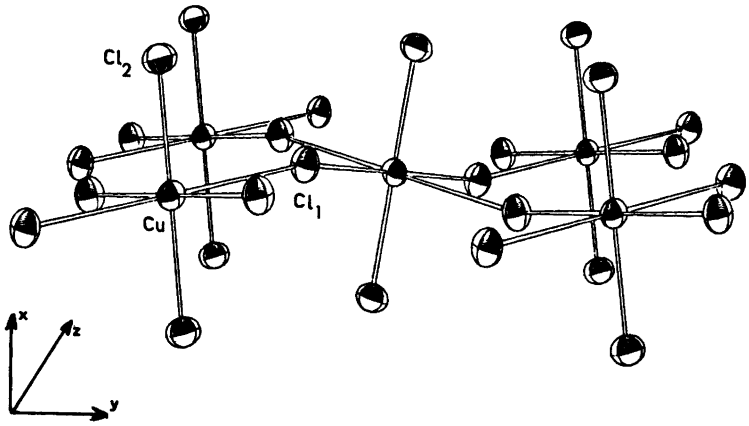

Fig. 1. Coordination around Cu in $(C_6H_5NH_3)_2CuCl_4$. Thermal ellipsoids enclose 50 % probability. (ORTEP II).[10]

DESCRIPTION OF THE STRUCTURE

The coordination around the Cu^{2+} ion which is located on a centre of symmetry, is the normal tetragonally distorted octahedron or 4+2 coordination often found in Cu-complexes. In this compound this is established through a two dimensional network in the $b-c$ plane consisting of $CuCl_4^{2-}$ units linked together through chlorine bonds as shown in Fig. 1.

This gives the three unique Cu – Cl distances shown in Table 4 which also includes the corresponding angles.

The observed bond lengths are in agreement with previously obtained Cu – Cl distances mentioned in the discussion. Apart from the

Table 4. Interatomic distances and angles with standard deviations in parentheses, calculated with the program ORFFE [11] including variance-covariance matrix and cell parameter errors.

Distance	Å
$Cu-Cl_1$	2.9178(5)
$Cu-Cl_2^{(i)}$	2.3007(5)
$Cu-Cl_2$	2.2804(6)
Angle	**Degrees**
$Cu-Cl_1-Cu^{(ii)}$	164.38(2)
$Cl_2-Cu-Cl_2$	86.66(2)
$Cl_1^{(i)}-Cu-Cl_2$	90.01(2)
$Cl_1^{(i)}-Cu-Cl_1$	92.36(1)

(i) Symmetry operation $\bar{x}\ y-\frac{1}{2}\ \frac{1}{2}-z$
(ii) Symmetry operation $x\ \frac{1}{2}-y\ \frac{1}{2}+z$

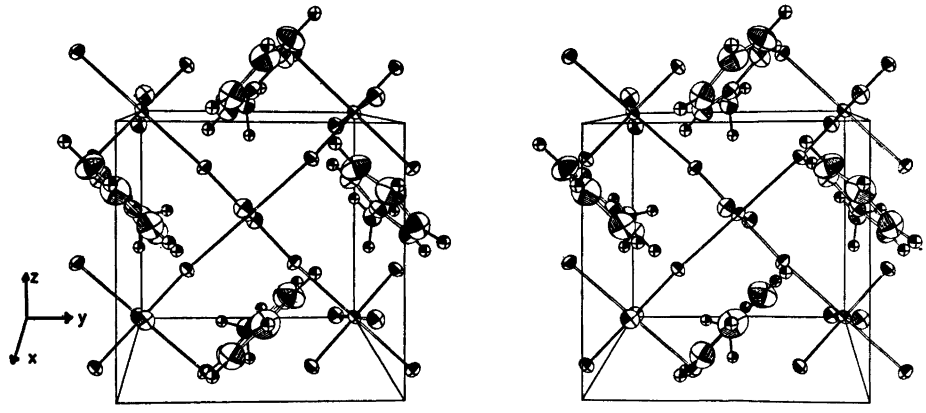

Fig. 2. Stereoscopic drawing of the packing in $(C_6H_5NH_3)_2CuCl_4$. Only half the unit cell is shown for clarity. Thermal ellipsoids enclose 50 % probability. All hydrogen atoms have been given the same temperature parameter. (ORTEP II).[10]

Table 5. Interatomic distances and angles with standard deviations in parentheses.

Distance	Å	Distance	Å
$N-C_1$	1.468(3)	H_1-C_2	0.88(3)
C_1-C_2	1.372(3)	H_2-C_3	0.97(3)
C_2-C_3	1.381(4)	H_3-C_4	0.96(3)
C_3-C_4	1.369(4)	H_4-C_5	0.94(3)
C_4-C_5	1.378(4)	H_5-C_6	0.85(3)
C_5-C_6	1.380(3)	H_6-N	0.90(3)
C_6-C_1	1.368(3)	H_7-N	0.84(3)
		H_8-N	1.00(5)

Angle	Degrees	Angle	Degrees
$N-C_1-C_2$	119.4(2)	$C_2-C_3-C_4$	120.7(3)
$N-C_1-C_6$	119.2(2)	$C_3-C_4-C_5$	119.7(3)
$C_2-C_1-C_6$	121.4(2)	$C_4-C_5-C_6$	120.2(3)
$C_1-C_2-C_3$	118.8(2)	$C_5-C_6-C_1$	119.2(2)

small deviations from right angles in the $CuCl_4^{2-}$ unit, the bond lengths also violate the regular D_{4h} symmetry. The angle $Cu-Cl_1-Cu^{(ii)}$ also indicates that the packing which is shown in Fig. 2 is determined not only by the Cu – Cl network, but also by interaction between the chlorine ions and the anilinium ion. The following short Cl···H distances were found (standard deviations in parentheses):

$Cl_1^{(ii)}\cdots H_6$	2.38(3) Å
$Cl_2^{(ii)}\cdots H_7$	2.46(3) Å
$Cl_2\cdots H_8$	2.35(5) Å.

The bond lengths and angles in the anilinium molecule, listed in Table 5, are in agreement with the geometry of the benzene ring.

DISCUSSION

$CuCl_n^{(n-2)-}$ complexes containing ammonium or substituted ammonium ions as cations are known in several different geometries. NH_4CuCl_3 contains planar $Cu_2Cl_6^{2-}$ dimers [12] with Cu – Cl distances ranging from 2.25 Å to 2.32 Å. The stacking of these dimers completes the 4 + 2 coordination with two Cu – Cl bonds of 2.99 Å and 3.19 Å. A square pyramidal coordination is found in $(CH_3)_2NH_2CuCl_3$ (Ref. 13). The Cu – Cl distances in the base are 2.25 Å – 2.33 Å, the fifth 2.73 Å, while the sixth position is empty out to 3.78 Å. In $[(C_2H_5)_3NH]_2CuCl_4$ the coordination figure is a distorted tetrahedron [14] with four nearly equal distances of 2.24 Å. The 4 + 2 coordination is also adopted in $(C_2H_5NH_3)_2CuCl_4$ (Ref. 15) which resembles the structure of $(C_6H_5NH_3)_2CuCl_4$ very much although the former crystallises in space group *Pbca*. The observed Cu – Cl distances [15] were 2.28 Å and 2.98 Å, but a close resemblance is also to be expected due to the cations.

In all these compounds, hydrogen bonding seems to be of importance in affecting the geometries adopted by the $CuCl_n$ units. This might explain the small deviations from the regular geometries (T_d, O_h, D_{4h}, C_{4v}, *etc.*), which are found in bond lengths and angles. An explanation of the non-regularity is also offered by the Jahn-Teller effect, which should be operative in the $3d^9$ system, Cu^{2+}. But it is difficult to determine which of these is the governing factor.

REFERENCES

1. Hathaway, B. J. and Billing, D. E. *Coord. Chem. Rev. 5* (1970) 143.
2. Hatfield, W. E. and Whyman, R. *Transition Metal Chem. 5* (1969) 123.
3. Helmholz, L. and Kruh, R. F. *J. Amer. Chem. Soc. 74* (1952) 1176.
4. Raymond, K. N., Meek, D. W. and Ibers, J. A. *Inorg. Chem. 7* (1968) 1111.
5. Dubský, J. V. and Wagenhofer, E. *Z. Anorg. Allg. Chem. 230* (1936) 112.
6. Coppens, P., Leiserowitz, L. and Rabinovich, D. *Acta Crystallogr. 18* (1965) 1035.
7. Cromer, D. T. and Mann, J. B. *Acta Crystallogr. A 24* (1968) 321.
8. Stewart, R. F., Davidson, E. R. and Simpson, W. T. *J. Chem. Phys. 42* (1965) 3175.

9. Busing, W. R., Martin, K. O. and Levy, H. A. (1962). *ORFLS Report ORNL-TM 305*, Oak Ridge National Laboratory, Oak Ridge, Tennessee. LINUS, modification of ORFLS by Hamilton, W. C., Ibers, J. A. and Edmonds, J.
10. Johnson, C. K. (1965). *ORTEP Report ORNL-3794*, Oak Ridge National Laboratory, Oak Ridge, Tennessee. Revised 1971, ORTEP II.
11. Busing, W. R., Martin, K. O. and Levy, H. A. (1964). *ORFFE Report ORNL-TM 306*, Oak Ridge National Laboratory, Oak Ridge, Tennessee.
12. Willett, R. D., Dwiggins, C., Kruh, R. F. and Rundle, R. E. *J. Chem. Phys. 38* (1963) 2429.
13. Willett, R. D. *J. Chem. Phys. 44* (1966) 39.
14. Lamotte-Brasseur, J., Dupont, L. and Dideberg, O. *Acta Crystallogr. B 29* (1973) 241.
15. Steadman, J. P. and Willett, R. D. *Inorg. Chim. Acta 4* (1970) 367.

Received November 19, 1973.

Acta Chemica Scandinavica A 28 (1974) 201—205

Measured and Calculated Vibration-rotation Constants in the Microwave Spectrum of Chlorobutatriene

FRED KARLSSON, MATS GRANBERG and RAGNAR VESTIN

Department of Physical Chemistry, Arrhenius Laboratory, University of Stockholm, S-104 05 Stockholm 50, Sweden

The inertial defects for the ground state and three excited vibrational states have been measured with microwave spectroscopy and calculated from an estimated diagonal valence force field for chlorobutatriene, $CH_2CCCH^{35}Cl$, in order to test the significance of a transformation of inertial moments from the effective structure to the average structure. The measured inertial moments are $I_b^0 = 325.82$ and $I_c^0 = 346.20$ au Å^2. The calculated r_z-parameters are $I_b^z = 326.01$ and $I_c^z = 346.20$ au Å^2.

The excited vibrational states correspond to a single excited out-of-plane vibration at 220 ± 50 cm^{-1} and to a single excited in-plane vibration at 100 ± 50 cm^{-1}. The vibration-rotation constants, α_b and α_c, are -0.12 ± 0.02 and -1.58 ± 0.02 MHz and -5.72 ± 0.02 and 3.25 ± 0.02 MHz, respectively.

The inertial moments of a molecule in the ground vibrational state, obtained by microwave spectroscopy, are related to the effective structure r_0. This is a different structure than that observed in electron diffraction experiments,[1] because of the internal vibrations. However, both these methods are comparable in the average structure, r_z, which can be calculated if the harmonic potentials are known.[2,3] In contrast to the r_0 structure, the r_z structure has a physically well-defined meaning.

Since we have used both electron diffraction and microwave spectroscopy to obtain structural information from three isomeric chlorobutenynes; *cis*-1-chlorobuten-3-yne, *trans*-1-chlorobuten-3-yne,[4] and 2-chlorobuten-3-yne, and chlorobutatriene,[5] we are interested to see if it is possible to carry out this kind of corrections for these molecules with a rather simple estimated force field.

In the microwave spectrum of chlorobutatriene it is possible to observe satellite spectra of two low-lying vibrational states. We have used this information to test the validity of the method on this kind of molecule. The result is probably of significant value even for the chlorobutenynes, since they have the same atoms, C_4H_3Cl, and symmetry.

MICROWAVE SPECTRUM

The microwave spectrum of chlorobutatriene, $CH_2CCCH^{35}Cl$, is that of a near prolate symmetric rotor and has been described previously.[5] These measurements have been improved and the standard deviations of the rotational constants have been given more realistic values.

The strong $K_{-1} = 1 \rightarrow 1$ transitions and the strongest and best resolved band, $J = 12 \rightarrow 13$, have been used for the assignment of the vibrational satellites; see Table 1. Three vibrational states have been examined; the first excited state of a vibrational mode ν_2 and the first and second excited state of a vibrational mode ν_1. The rotational constants are listed in Table 2. Only a-type R-lines have been observed so far which accounts for the low precision in the A constants which have to be obtained from the deviation of the observed lines from the symmetric top pattern.

The vibration-rotation coupling constants are listed in Table 3. It is not possible to calculate these constants from the force field due to the large contribution from the anharmonicity.

Due to the near degeneracy to a symmetric rotor with $\varkappa = -0.992$, the observable quad-

Table 1. Observed rotational transitions and nuclear quadrupole hyperfine splitting in MHz for the ground state and low-lying vibrational states of chlorobutatriene $CH_2CCCH^{35}Cl$.

Transition						G.S.		ν_2		ν_1		$2\nu_1$	
J	K_{-1}	K_{+1}	J	K_{-1}	K_{+1}	ν_{obs}	$\Delta\nu_{Qobs}$	ν_{obs}	$\Delta\nu_{Qobs}$	ν_{obs}	$\Delta\nu_{Qobs}$	ν_{obs}	$\Delta\nu_{Qobs}$
9	1	9	8	1	8	26679.46							
9	0	9	8	0	8	27065.57							
9	2	8	8	2	7	27095.61							
9	1	8	8	1	7	27501.15							
10	1	10	9	1	9	29641.60		29666.35		29718.50		29795.08	
10	0	10	9	0	9	30064.10							
10	2	9	9	2	8	30104.60							
10	1	9	9	1	8	30554.35		30564.45		30655.80		30756.96	
11	1	11	10	1	10	32603.02		32630.37		32687.50		32771.57	
11	0	11	10	0	10	33060.13							
11	2	10	10	2	9	33113.09							
11	1	10	10	1	9	33606.81		33617.97		33718.30		33829.38	
12	1	12	11	1	11	35563.72		35593.55		35655.71		35747.30	
12	0	12	11	0	11	36053.23							
12	2	11	11	2	10	36120.94							
12	1	11	11	1	10	36658.35		36670.63		36779.82		36900.83	
13	1	13	12	1	12	38523.50		38555.75		38623.05		38772.16	
13	0	13	12	0	12	39043.19				39155.12		39266.71	
13	2	12	12	2	11	39128.15		39151.05				39359.30	
13	3	11	12	3	10	39161.27		39183.57				39394.82	
13	3	10	12	3	9	39162.69		39184.95		39279.85		39396.42	
13	4	10	12	4	9	39164.65		39187.37		39281.30		39397.33	
13	5	9	12	5	8	39172.89	0.35	39196.05	0.39	39289.24	0.45	39405.00	0.40
13	6	8	12	6	7	39184.62	0.60	39208.28	0.77	39300.70	0.61	39416.10	0.61
13	7	7	12	7	6	39199.17	0.90			39314.99	0.84	39430.00	0.80
13	8	6	12	8	5	39216.25	1.13	39240.93	1.15	39331.76	1.12	39446.44	1.00
13	2	11	12	2	10	39223.60		39243.95		39344.15		39464.04	
13	9	5	12	9	4	39235.80	1.42			39350.95	1.45		
13	10	4	12	10	3	39257.58	1.72			39372.40	1.80		
13	1	12	12	1	11	39708.90		39722.32		39840.35		39971.25	

Table 2. Observed rotational constants in MHz for the ground state and low-lying vibrational states of chlorobutatriene $CH_2CCCH^{35}Cl$.

	G.S.		ν_2		ν_1		$2\nu_1$	
A	25181	±50	25200	±50	25304	±50	25475	±50
B	1551.10	±0.02	1551.22	±0.02	1556.82	±0.02	1562.52	±0.02
C	1459.80	±0.02	1461.38	±0.02	1463.05	±0.02	1466.30	±0.02
D_J	0.00034	±0.00005	0.00035	±0.00005	0.00034	±0.00005	0.00035	±0.00005
D_{JK}	−0.0454	±0.0001	−0.0474	±0.0001	−0.0447	±0.0001	−0.0437	±0.0001

Table 3. Vibration-rotation coupling constants for the ν_1 and ν_2 states (in MHz).

	ν_1	ν_2
α^a	−130 ±50	−20 ±50
α^b	−5.72±0.02	−0.12±0.02
α^c	−3.25±0.02	−1.58±0.02

rupole hyperfine splitting is only dependent on the constant χ_{aa}, which is, for the ^{35}Cl nucleus, $\chi_{aa} = -25.8 \pm 0.5$ MHz.[4]

FORCE FIELD

The main difficulty with vibrational problems arises in the determination of an appropriate

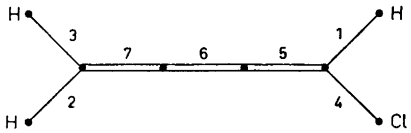

Fig. 1. Estimated diagonal force constants for chlorobutatriene in md/Å and md Å; $K_1 = 5.6$, $K_2 = K_3 = 5.5$, $K_4 = 3.8$, $K_5 = K_7 = 9.4$, $K_6 = 10.1$, $K_{15} = 0.50$, $K_{27} = K_{37} = 0.56$, $K_{45} = 0.85$, $K_{56} = K_{67} = 0.35$ $\varrho_5^{14} = 0.312$, $\varrho_7^{23} = 0.250$, $\chi_{23}^{14} = 0.35$.

force field. We have used a simple diagonal valence force field with force constants estimated from similar bonds in simpler molecules such as butatriene [6] and vinyl chloride;[7] see Fig. 1. We have used the same symbols as Gribov.[7] K_i is the force constant for stretching the bond i, K_{ij} is the force constant for bending the angle between the bonds i and j, ϱ_k^{ij} is the bending of the bond k out of the plane spanned by the bonds i and j, and χ_{kl}^{ij} finally, is the torsion between the planes spanned by the bonds i and j, and k and l, respectively. We have assumed the same force constants for bending in plane and out of plane for the linear C=C=C groups. The calculated fundamental frequencies were compared with the observed IR-spectrum in the region 4000 – 400 cm^{-1}. We have not been able to make a complete assignment of this spectrum yet but some of the eighteen fundamentals are readily observed. The most characteristic transition is the strong line at 2070 cm^{-1} which is identified as a C=C stretch ν_{15}. This characteristic frequency is also observed for the simple butatriene at 2079 cm^{-1} but, due to the butatriene symmetry, this C=C stretch is only Raman active there.[8] Another C=C stretch, ν_{14}, for chlorobutatriene is probably observed at 1610 cm^{-1}.

The low-lying fundamental vibrations make an important contribution to the transformation of r_0 to r_z parameters but the corresponding transitions are not observable with an ordinary IR-spectrometer. However, we have obtained the frequency of the two lowest fundamentals, $\nu_1 = 100 \pm 50$ cm^{-1} and $\nu_2 = 200 \pm 50$ cm^{-1} by intensity measurements on the corresponding vibrational satellites observed with microwave spectroscopy.[9] These fundamentals are characterized as skeletal bending modes, ν_1 in plane and ν_2 out of plane; see Fig 2. The calculated frequencies were $\nu_1 = 113$ cm^{-1} and $\nu_2 = 198$ cm^{-1}.

VIBRATION – ROTATION

The moments of inertia from the average structure are given by

$$I_\alpha^z = I_\alpha^v - \sum_s \left(v_s + \frac{d_s}{2} \right) \varepsilon_s^\alpha(\text{har}) + \delta I_\alpha(\text{cent}) \qquad (1)$$

α = a, b or c

where I_α^v is one of the three principal moments of inertia for the effective structure in the

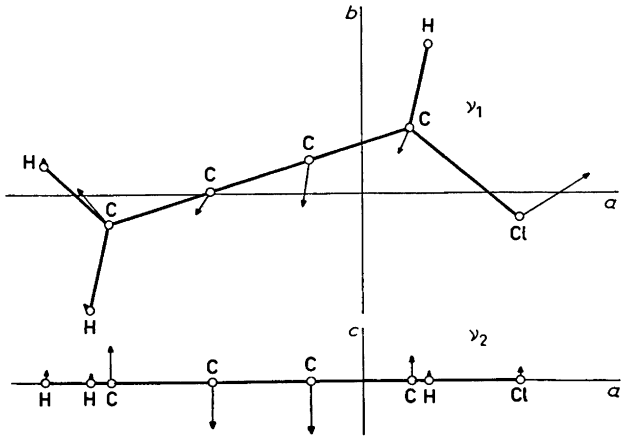

Fig. 2. The two lowest fundamental vibrations of chlorobutatriene $CH_2CCCH^{35}Cl$ with principal axes of inertia. The vectors are obtained from the matrix of transformation from Cartesian to normal coordinates. Each component of a vector has been divided by the mass of the atom for appropriate scaling.

Table 4. Vibration-rotation correction for the moments of inertia in the ground vibrational state (in au Å²) for chlorobutatriene $CH_2CCCH^{35}Cl$. Conversion factor 505376 au Å² MHz.

	r_0-parameters	vibration correction	centrifugal distortion correction	r_z-parameters
I_b	325.818	0.1908	0.0004	326.009
I_c	346.196	−0.0002	−0.0006	346.195

ground state or some excited vibrational state.[10] The sum includes all vibrations with degeneracy d_s.

The vibration-rotation correction term ε_s^α (har) is only dependent on the harmonic potentials and can be obtained from the transformation matrix from the Cartesian displacements to the normal coordinates and the fundamental frequencies.[11] So it is possible to calculate the parameters ε_s^α(har) when the geometry and force field of the molecule are known.

The term δI_α(cent) is the correction for the centrifugal distortion, and can also be calculated if the force field and geometry are known;[11] see Table 4. The effect of the centrifugal distortion is negligible in this case. It is also interesting to note that the I_c^0 constant is very little affected by these corrections as compared to I_b^0. The inertial defect is defined as

$$\Delta = I_c - I_a - I_b \qquad (2)$$

For the moments of inertia corresponding to an average planar structure, Δ vanishes as it would for a hypothetical rigid planar rotor. This implies that the inertial defect for the effective structure in the ground state or some vibrationally excited state can be calculated from the harmonic terms, ε_s^α(har), and the centrifugal distortion terms $\delta I\alpha$.[12,13] Thus the combination of (1) and (2) gives

$$\Delta^v = \sum \left(v_s + \frac{d_s}{2}\right)[\varepsilon_s^c(\text{har}) - \varepsilon_s^a(\text{har}) - {}_s^b(\text{har})] - \delta I_c(\text{cent}) + \delta I_a(\text{cent}) + \delta I_b(\text{cent})$$

Since Δ^v can be obtained from the measured rotational constants, it is possible to control the vibration-rotation parameters used in the transformation from r_0 to r_z parameters; see Table 5.

It is interesting to see that the inertial defect decreases for out of plane vibrations and increases for in plane vibrations compared with the ground state.[14]

Table 5. Inertial defect for the ground state and low-lying vibrational states of chlorobutatriene $CH_2CCCH^{35}Cl$ in au Å².

	From observed microwave spectra	From normal coordinate analysis
G.S.	0.31 ± 0.05	0.35
ν_2	−0.03 ± 0.05	0.02
ν_1	0.83 ± 0.05	0.85
$2\nu_1$	1.39 ± 0.05	1.35

CENTRIFUGAL DISTORTION

If the force field and geometry are known it is possible to calculate the centrifugal distortion constants.[6] A planar asymmetric rotor has four independent centrifugal distortion constants τ_{aaaa}, τ_{bbbb}, τ_{aabb} and τ_{abab}.[10] Due to the near degeneracy to a symmetric rotor it is not possible to fit these four constants to the observed spectra.[15] The spectrum is only dependent on two centrifugal distortion constants and we have used D_J and D_{JK} according to Kivelson and Wilson.[16] However, if the constants τ_{aaaa}, τ_{bbbb}, τ_{aabb}, and τ_{abab} are obtained from theoretical calculations, it is possible to calculate D_J and D_{JK};[10,16] see Table 6.

It is interesting to see that the unusually large and negative value of the D_{JK} term arises quite naturally from the theoretical calculations. This kind of D_{JK} value has been observed for some other molecules of about the same size and form.[17] We have observed the same effect for *trans*-1-chlorobuten-3-yne.[4]

It has been pointed out that the centrifugal distortion constants are mostly dependent on the diagonal force constants.[18] This might be

Table 6. Calculated and measured centrifugal distortion constants for chlorobutatriene $CH_2CCCH^{35}Cl$ (in MHz).

Calculated constants from estimated force field		Measured constants	
$\tau_{aaaa} = -7.730$	$D_J = 0.00033$	$D_J = 0.00034$	± 0.00005
$\tau_{bbbb} = -0.001804$	$D_{JK} = -0.0405$	$D_{JK} = -0.0454$	± 0.0001
$\tau_{aabb} = 0.1028$			
$\tau_{abab} = -0.003531$			

the reason for the good agreement between calculated and measured constants despite the fact that a very simple diagonal force field was used.

DISCUSSION

The critical point in the measured inertial defect is of course the contribution from the I_a moment since that is obtained from the rather uncertain rotational constant, A. However, the significance is enough to show that the corrections from r_0 to r_z parameters are meaningful although a very simple force field is used. Great care must be taken if these r_z parameters are to be used in the evaluation of the average structure, but they are valuable in showing the expected magnitude of the corrections and how the different inertial moments are affected.

As for calculation of the contribution from centrifugal distortion, it is immediately clear that they do not affect the corrections significantly for this molecule.

Acknowledgements. We wish to thank all those who have contributed to this paper and especially Dr. Allan Rupprecht for valuable discussions.

REFERENCES

1. Morino, Y., Kuchitsu, K. and Oka, T. *J. Chem. Phys. 36* (1962) 1108.
2. Herschbach, D. R. and Laurie, V. W. *J. Chem. Phys. 37* (1962) 1668.
3. Oka, T. *J. Phys. Soc. Jap. 15* (1960) 2274.
4. Karlsson, F. and Vestin, R. *Acta Chem. Scand. 27* (1973) 3033.
5. Karlsson, F. and Vestin, R. *Acta Chem. Scand. 26* (1972) 3394.
6. Ramaswamy, K. and Srinivasan, K. *J. Mol. Struct. 3* (1969) 473.
7. Gribov, L. A. *Vvedenie v teoriyu i rachet kolebatel'nŷkh spektrov mnogoatomnŷkh molekul*, Izdatel'stvo Leningradskogo Universiteta, 1965.
8. Miller, F. A. and Matsubara, I. *Spectrochim. Acta 22* (1966) 173.
9. Bodenseh, H.-K., Gegenheimer, R., Mennicke, J. and Zeil, W. *Z. Naturforsch. 22* (1967) 523.
10. Gordy, W. and Cook, R. L. *Microwave Molecular Spectra*, Interscience, New York 1970.
11. Oka, T. and Morino, Y. *J. Mol. Spectrosc. 8* (1962) 300.
12. Darling, B. T. and Dennison, D. M. *Phys. Rev. 57* (1940) 128.
13. Oka, T. and Morino, Y. *J. Mol. Spectrosc. 6* (1961) 472.
14. Herschbach, D. R. and Laurie, V. W. *J. Chem. Phys. 40* (1964) 3142.
15. Marstokk, K.-M. and Möllendal, H. *J. Mol. Struct. 8* (1971) 234.
16. Kivelson, D. and Wilson, E. B. *J. Chem. Phys. 20* (1952) 1575.
17. Laurie, V. W. and Lide, D. R. *J. Chem. Phys. 31* (1959) 939.
18. Gerry, M. C. L. *Can. J. Chem. 49* (1971) 255.

Received November 2, 1973.

Acta Chemica Scandinavica A 28 (1974) 206—212

Microwave Spectrum, Nuclear Quadrupole Coupling, and Structure Dependent Parameters of 2-Chlorobuten-3-yne

FRED KARLSSON, MATS GRANBERG and RAGNAR VESTIN

Department of Physical Chemistry, Arrhenius Laboratory, University of Stockholm, S-104 05 Stockholm 50, Sweden

The microwave spectra of the two natural species of 2-chlorobuten-3-yne, $CH_2C^{35}ClCCH$ and $CH_2C^{37}ClCCH$, have been measured in the region 27 000 – 40 000 MHz. The rotational constants A, B and C for the ground state as well as the centrifugal distortion constants Δ_J, Δ_{JK}, Δ_K, δ_J, and δ_K were determined. From the hyperfine splittings of the rotational lines, the nuclear quadrupole coupling constants χ_{aa} and χ_{bb} were calculated for the $CH_2C^{35}ClCCH$ and $CH_2C^{37}ClCCH$ species, in the principal-axis system of the molecules.

In order to supply complementary data for electron diffraction measurements, the inertial moments corresponding to the average structure were calculated from an estimated force field. The obtained values are $I_a^z = 73.634$, $I_b^z = 163.405$ and $I_c^z = 237.054$ au Å² for $CH_2C^{35}ClCCH$ and $I_a^z = 74.393$, $I_b^z = 166.740$ and $I_c^z = 241.149$ au Å² for $CH_2C^{37}ClCCH$.

For some time we have been concerned with the study of the structure of the three isomeric chlorobutenynes, *trans*-1-chlorobuten-3-yne, *cis*-1-chlorobuten-3-yne, and 2-chlorobuten-3-yne, by electron diffraction in the gas phase (in cooperation with the electron diffraction group at Oslo University).

In order to supply additional structural information we have started to investigate the three chlorobutenynes by microwave spectroscopy.[1]

The primary structure dependent parameters obtained by microwave spectroscopy are the principal moments of inertia. These are related to the spectroscopic effective structure r_0 which is a different structure to that obtained by electron diffraction in gases due to the internal vibrations.[2] However, it is possible in both methods to obtain the average structure if the harmonic potentials are known.[3,4] These corrections of the microwave spectroscopic parameters have been made for a simple estimated diagonal force field.

The centrifugal distortion parameters have also been calculated and compared with those obtained from the measured microwave spectrum to test the validity of the estimated force field. The value of these corrections is, of course, very limited due to the uncertainty in the estimated force field and the approximations used. However, the magnitudes of the corrections form the r_0- to r_s-parameters are interesting in themselves and may be used to see how the inertial moments are affected.

EXPERIMENTAL

According to the method of Nieuwland *et al.*[5] acetylene is dimerized in a liquid Cu(I) catalyst in a continuous process:

$$2\ HC{\equiv}CH \rightarrow CH_2{=}CH{-}C{\equiv}CH$$

If a small flow of O_2 and HCl is introduced with the entering gas a small amount of chlorohydrocarbon forms:[6,7]

$$2\ C_2H_2 + \tfrac{1}{2}O_2 + HCl \rightarrow C_4H_3Cl + H_2O$$

We used a sample from this reaction and the substance was isolated and purified with gas liquid chromatography at a temperature of 50°C. The column was packed with diethylhexyl-sebacate (15 %) absorbed on Chromosorb.

The product was originally identified as 2-chlorobuten-3-yne with IR, NMR, and mass spectroscopy.[7] The microwave spectroscopic investigation confirms this result.

The microwave spectra were recorded on a Hewlett-Packard model 8460A R-band

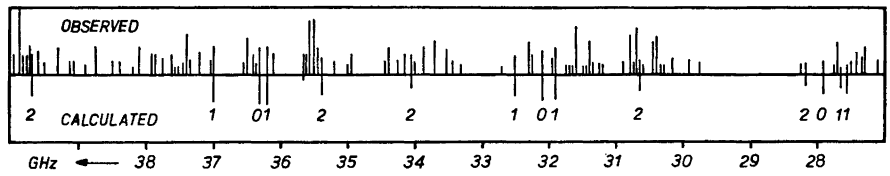

Fig. 1. The observed microwave transitions from a fast sweep (1 MHz/sec) in the region 27 – 40 GHz together with the expected strongest R_a-transitions $K_{-1}=0\rightarrow0$, $K_{-1}=1\rightarrow1$ and $K_{-1}=2\rightarrow2$ with their relative intensities.

microwave spectrometer with a phase stabilized source oscillator. The recordings were made at room temperature, with the pressure ranging from 5 – 20 mTorr. The frequency region was 27 000 – 40 000 MHz. The precision of the measured transitions was estimated to be 0.05 MHz.

MICROWAVE SPECTRUM

In order to assign the spectrum the region 27 000 – 40 000 MHz was swept at a rate of 1 MHz/s. The observed transitions were plotted on a 50 MHz/mm scale; see Fig. 1.

Rotational constants obtained from an estimated planar structure and dipole moments obtained from CNDO calculations suggested a spectrum mainly composed of R-branch transitions active through the μ_a dipole moment; see Fig. 2.

We expected to find three nearly equidistant a-type R-lines with $K_{-1}=0\rightarrow0$. Once these were found it was easy to determine the positions of the corresponding transitions $K_{-1}=1\rightarrow1$ and $K_{-1}=2\rightarrow2$; see Fig. 1.

However, it is evident from comparison with the observed spectrum that the R_a-transitions only form a part of this spectrum. The remaining spectral lines were indentified as Q- and R-type transitions active through the μ_b dipole moment. From this it is apparent that the μ_a and μ_b components of the dipole moment are of nearly equal magnitude, contrary to what was expected from the CNDO calculations.

The spectra of the two isotopic species $CH_2C^{35}ClCCH$ and $CH_2C^{37}ClCCH$ were distinguished and the strongest transitions were measured with high resolution; see Tables 1 and 2.

The rotational constants and five centrifugal distortion parameters were fitted to the observed spectrum by the least squares method; see Tables 3 and 4.

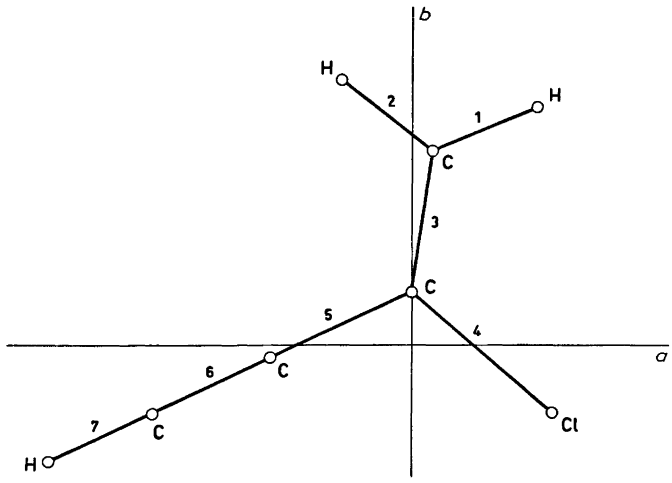

Fig. 2. Assumed structure of 2-chlorobuten-3-yne with principal axes of inertia.

Table 1. The observed rotational transitions for 2-chlorobuten-3-yne, $CH_2C^{35}ClCCH$, are given as $\nu_{obs} = \nu_{center} + \Delta\nu_i$(MHz) where ν_{center} is the center of the hypothetical unsplit line and $\Delta\nu_1$, $\Delta\nu_2$, $\Delta\nu_3$, and $\Delta\nu_4$ are the observed nuclear quadrupole hyperfine splitting of the rotational transition.

$CH_2CH^{35}ClCCH$ J'	K_{-1}'	K_{+1}'	J	K_{-1}	K_{+1}	μ	ν_{center} $J'K_{-1}'K_{+1}' \leftarrow JK_{-1}K_{+1}$	$\Delta\nu_1$ $F=J+\frac{3}{2}$	$\Delta\nu_2$ $F=J+\frac{1}{2}$	$\Delta\nu_3$ $F=J-\frac{1}{2}$	$\Delta\nu_4$ $F=J-\frac{3}{2}$
6	1	6	5	1	5	a	27571.78	0.45	−0.06	−0.52	−0.06
5	1	4	4	1	3	a	27655.80	0.60	−0.60	−0.60	0.60
6	0	6	5	0	5	a	27908.99	0.55	−0.33	−0.55	0.22
5	2	3	4	2	2	a	28170.07	0.28	−0.28	−0.28	0.28
6	2	5	5	2	4	a	30653.63	0.62	−0.63	−0.63	0.62
6	3	4	5	3	3	a	31863.50	0.67	−0.99	−0.65	1.06
6	4	3	5	4	2	a	31904.40	1.05	−1.81	−0.95	1.91
7	1	7	6	1	6	a	31911.89	0.35	−0.03	−0.41	−0.03
6	4	2	5	4	1	a	31957.64	1.01	−1.75	−0.88	1.83
7	0	7	6	0	6	a	32093.08	0.40	−0.18	−0.45	0.15
6	1	5	5	1	4	a	32515.04	0.64	−0.65	−0.65	0.64
6	3	3	5	3	2	a	32704.69	0.36	−0.55	−0.36	0.64
6	2	4	5	2	3	a	34060.29	0.21	−0.21	−0.21	0.21
7	2	6	6	2	5	a	35393.24	0.48	−0.49	−0.49	0.48
8	1	8	7	1	7	a	36216.51	0.28	−0.03	−0.29	−0.03
8	0	8	7	0	7	a	36307.46				
7	1	6	6	1	5	a	37005.51	0.67	−0.67	−0.67	0.67
7	3	5	6	3	4	a	37118.84	0.57	−0.57	−0.57	0.57
7	4	4	6	4	3	a	37341.30	0.70	−1.13	−0.65	0.95
7	4	3	6	4	2	a	37512.02	0.61	−0.99	−0.48	0.71
7	3	4	6	3	3	a	38768.29	0.09	−0.10	−0.10	0.09
7	2	5	6	2	4	a	39725.92	0.27	−0.27	−0.27	0.27
6	1	6	5	0	5	b	28260.99	0.63	−0.46	−0.68	0.41
7	0	7	6	1	6	b	31741.10	0.31	−0.04	−0.34	−0.04
7	1	7	6	0	6	b	32263.90	0.44	−0.32	−0.51	0.18
8	0	8	7	1	7	b	36136.59				
8	1	8	7	0	7	b	36387.33				
16	5	11	16	4	12	b	27367.92	−0.73	0.72	0.72	−0.73
13	5	8	13	4	9	b	27690.70	0.19	−0.20	−0.20	0.19
12	5	7	12	4	8	b	29903.39	0.30	−0.30	−0.30	0.30
17	5	12	17	4	13	b	30384.34	−1.09	1.09	1.09	−1.09
18	6	12	18	5	13	b	30684.75	−0.15	0.15	0.15	−0.15
19	6	13	19	5	14	b	31375.11	−0.49	0.49	0.49	−0.49
17	6	11	17	5	12	b	31609.18	0.09	−0.09	−0.09	0.09
11	5	6	11	4	7	b	32293.77	0.19	−0.19	−0.19	0.19
16	6	10	16	5	11	b	33741.40	0.31	−0.32	−0.32	0.31
20	6	14	20	5	15	b	33864.55	−0.80	0.79	0.79	−0.80
10	5	5	10	4	6	b	34379.12				
18	5	13	18	4	14	b	34934.45	−1.33	1.32	1.32	−1.33
22	7	15	22	6	16	b	35522.62	−0.31	0.30	0.30	−0.31
21	7	14	21	6	15	b	35564.87				
15	6	9	15	5	10	b	36504.02	0.36	−0.36	−0.36	0.36
20	7	13	20	6	14	b	37227.33	0.23	−0.22	−0.22	0.23
23	7	16	23	7	17	b	37377.10	−0.62	0.61	0.61	0.62
21	6	15	21	5	16	b	38088.53	−1.08	1.07	1.07	−1.08
12	5	8	12	4	9	b	38443.08	−0.88	0.87	0.87	−0.88
14	6	8	14	5	9	b	39290.12	0.27	−0.28	−0.28	0.27
13	5	9	13	4	10	b	39601.23	−0.93	0.92	0.92	−0.93
25	8	17	25	7	18	b	39875.31	−0.12	0.12	0.12	−0.12

Table 2. The observed rotational transitions for 2-chlorobuten-3-yne, $CH_2C^{37}ClCCH$, given as in Table 1.

$CH_2CH^{37}ClCCH$ J'	K_{-1}'	K_{+1}'	J	K_{-1}	K_{+1}	μ	ν_{center} $J'_{K_{-1}'K_{+1}'} \leftarrow J_{K_{-1}K_{+1}}$	$\Delta\nu_1$ $F=J+\frac{3}{2}$	$\Delta\nu_2$ $F=J+\frac{1}{2}$	$\Delta\nu_3$ $F=J-\frac{1}{2}$	$\Delta\nu_4$ $F=J-\frac{3}{2}$
6	1	6	5	1	5	a	27097.12	0.36	−0.06	−0.36	−0.06
6	0	6	5	0	5	a	27441.68	0.45	−0.23	−0.48	0.15
6	2	5	5	2	4	a	30098.45	0.48	−0.48	−0.48	0.48
7	1	7	6	1	6	a	31365.91	0.26	−0.02	−0.32	−0.02
6	1	5	5	1	4	a	31938.57	0.44	−0.44	−0.44	0.44
6	2	4	5	2	3	a	33388.35	0.18	−0.19	−0.19	0.18
7	2	6	6	2	5	a	34761.56	0.39	−0.39	−0.39	0.39
8	0	8	7	0	7	a	35694.64	0.10	−0.10	−0.10	0.10
7	1	6	6	1	5	a	36373.95	0.50	−0.51	−0.51	0.50
8	2	7	7	2	6	a	39300.53	0.32	−0.33	−0.33	0.32
9	1	9	8	1	8	a	39811.86				
9	0	9	8	0	8	a	39858.00				
7	0	7	6	1	6	b	31185.01	0.22	−0.02	−0.03	−0.02
7	1	7	6	0	6	b	31734.44	0.38	−0.38	−0.38	0.38
8	0	8	7	1	7	b	35513.67				
8	1	8	7	0	7	b	35780.23	0.20	−0.20	−0.20	0.20
9	0	9	8	1	8	b	39772.35				
9	1	9	8	0	8	b	39897.53				
13	5	8	13	4	9	b	27850.47	0.07	−0.08	−0.08	0.07
17	5	12	17	4	13	b	29563.19	−0.75	0.74	0.74	−0.75
18	6	12	18	5	13	b	30615.62				
19	6	13	19	5	14	b	30950.69	−0.34	0.34	0.34	−0.34
17	6	11	17	5	12	b	31790.55	0.06	−0.07	−0.07	0.06
20	6	14	20	5	15	b	33018.42	−0.59	0.58	0.58	−0.59
18	5	13	18	4	14	b	33772.03	−0.95	0.94	0.94	−0.95
16	6	10	16	5	11	b	34045.91	0.22	−0.22	−0.22	0.22
22	7	15	22	6	16	b	35213.51	−0.17	0.17	0.17	−0.17
23	7	16	23	6	17	b	36567.66	−0.41	0.40	0.40	−0.41
15	6	9	15	5	10	b	36807.87	0.21	−0.22	−0.22	0.21
21	6	15	21	5	16	b	36810.64	−0.76	0.76	0.76	−0.76
20	7	13	20	6	14	b	37594.53	0.16	−0.16	−0.16	0.16
14	6	8	14	5	9	b	39505.29	0.11	−0.11	−0.11	0.11
25	8	17	25	7	18	b	39747.82				

Table 3. Observed rotational constants in MHz and asymmetry parameters for the two isotopic species of 2-chlorobuten-3-yne.

	$CH_2C^{35}ClCCH$	$CH_2C^{37}ClCCH$
A	6875.239 ± 0.004	6804.974 ± 0.006
B	3096.353 ± 0.002	3034.415 ± 0.003
C	2131.950 ± 0.002	2095.763 ± 0.003
$\varkappa$	−0.593	−0.601

QUADRUPOLE COUPLING

Because of the nuclear quadrupole coupling each rotational transition is split into four observable peaks with $\Delta F = +1$ for R-transitions and $\Delta F = 0$ for Q-transitions.[8] However, in many cases the components overlap partially or completely so that only a doublet or a single line can be distinguished.

We have used the splitting into quartets and doublets to obtain a least squares fitting of the two quadrupole coupling constants χ_{aa} and χ_{bb}. For a doublet with line positions ν_1 and ν_2 the observed splitting used in the least squares fitting was $\Delta\nu_Q\text{obs} = \nu_2 - \nu_1$, and for a quartet ν_1, ν_2, ν_3, and ν_4 the observed splittings used were $\Delta\nu_Q\text{obs} = (\nu_4 + \nu_3 - \nu_2 - \nu_1)/2$ and $\Delta\nu_Q\text{obs} = (\nu_4 - \nu_3 + \nu_2 - \nu_1)/2$.

If two lines are lying too close they may disturb each others line shape. Therefore in order to avoid systematic errors we only accepted splitting values $\Delta\nu_Q\text{obs} > 0.70$ MHz. The error square sum is

$$U = \sum(\Delta\nu_Q\text{obs} - \Delta\nu_Q\text{calc})^2 \quad (1)$$

Table 4. Measured and calculated centrifugal distortion constants in kHz for the two isotopic species of 2-chlorobuten-3-yne.

	$CH_2C^{35}ClCCH$ obs		calc	$CH_2C^{37}ClCCH$ obs		calc
Δ_J	1.05	±0.02	0.89	1.00	±0.02	0.87
Δ_{JK}	−3.08	±0.05	−1.60	−3.46	±0.10	−1.91
Δ_K	16.0	±0.2	12.0	16.6	±0.3	12.4
δ_J	0.427	±0.003	0.349	0.425	±0.006	0.344
δ_K	2.39	±0.05	2.19	2.17	±0.10	2.05

It is possible to get rather good estimated values of χ_{aa}' and χ_{bb}' by comparing 2-chlorobuten-3-yne with vinylchloride.[9] The difference between the true values and the estimated values are

$$\Delta\chi_{aa} = \chi_{aa} - \chi_{aa}' \quad (2a)$$

$$\Delta\nu_{bb} = \chi_{bb} - \chi_{bb}' \quad (2b)$$

If $\Delta\chi_{aa}$ and $\Delta\chi_{bb}$ are assumed to be small it is possible to use the LETAGROP method to make the nonlinear least square fitting.[10] According to this method, U is regarded as a function of $\Delta\chi_{aa}$ and $\Delta\chi_{bb}$.

$$U = U(\Delta\chi_{aa}, \Delta\chi_{bb}) \quad (3)$$

The function U is approximated by a second degree surface in the vicinity of χ_{aa}' and χ_{bb}'.

$$U = U' + C_1\Delta\chi_{aa}^2 + C_2\Delta\chi_{bb}^2 + C_3\Delta\chi_{aa}\Delta\chi_{bb} + C_4\Delta\chi_{aa} + C_5\Delta\chi_{bb} \quad (4)$$

where C_1, C_2, C_3, C_4, and C_5 are constants and U' is the calculated error square sum for the estimated values

χ_{aa}' and χ_{bb}'.

The improvements sought, $\Delta\chi_{aa}$ and $\Delta\chi_{bb}$, will give a minimum value for U. That is

$$\partial U/\partial\Delta\chi_{aa} = 2C_1\Delta\chi_{aa} + C_3\Delta\chi_{bb} + C_4 = 0 \quad (5a)$$

$$\partial U/\partial\Delta\chi_{bb} = 2C_2\Delta\chi_{bb} + C_3\Delta\chi_{aa} + C_5 = 0 \quad (5b)$$

These are the well known normal equations according to Gauss. The improvements $\Delta\chi_{aa}$ and $\Delta\chi_{bb}$ are obtained as solutions to these equations.

However, to be able to solve the normal equations the constants C_1, C_2, C_3, C_4, and C_5 have to be known. These constants could be determined if a sufficient set of trial values $\Delta\chi_{aa}$ and $\Delta\chi_{bb}$ is chosen and inserted in the expression 4.

The method could be iterated and the convergence tested in the same way as the Gauss least square method.[11] The LETAGROP method converges as rapid as the Gauss method. The great advantage is the simple way of obtaining the normal equations, but the number of computational operations increases rapidly with the number of constants sought.[11]

The values obtained are for ^{35}Cl in $CH_2C^{35}ClCCH$: $\chi_{aa} = -27.1 \pm 0.1$ and $\chi_{bb} = -6.4 \pm 0.1$ MHz and for ^{37}Cl in $CH_2C^{37}ClCCH$: $\chi_{aa} = -21.8 \pm 0.3$ and $\chi_{bb} = -4.0 \pm 0.3$ MHz.

It is presently not possible to transform the quadrupole coupling constants from the inertial system to the principal axis system of the quadrupole tensor, since the angle between the C−Cl bond and the principal axis a is not accurately known; see Fig. 2.

CENTRIFUGAL DISTORTION

It was necessary to include the centrifugal distortion in the least square fitting process of the rotational constants. We used the five distortion parameters Δ_J, Δ_{JK}, Δ_K, δ_J and δ_K according to Watson.[12] The 2-chlorobuten-3-yne molecule is planar but as it was possible to obtain a good fit with all five distortion constants we did not invoke the planarity constraints for these constants;[13] see Table 4.

If the force field and geometry of a molecule is known it is possible to calculate the centrifugal distortion constants.[8,14] We have used a simple diagonal valence force field with force constants estimated from similar bonds in simpler molecules.[15]

The following symbols are used for the force constants according to Gribov.[15] K_i is the force

constant for the stretching of the bond i, K_{ij} is the bending of the angle between the bonds i and j, l_{kl}^{ij} is the interaction between the bending K_{ij} and K_{kl}, ϱ_k^{ij} is the bending of the bond k out of the plane spanned by the bonds i and j, χ_{kl}^{ij} finally is the torsion between the planes spanned by the bonds i and j, and k and l, respectively.

The values of the constants are, with the bond numbers of Fig. 2:
$K_1 = K_2 = 5.53$, $K_3 = 8{,}44$ $K_4 = 3.85$, $K_5 = 3.77$, $K_6 = 13.33$, $K_7 = 5.99$, $K_{12} - 2\,l_{13}^{12} + l_{23}^{13} = 0.42$, $K_{13} - l_{23}^{13} = 0.59$, $K_{34} - l_{34}^{35} - l_{34}^{45} + l_{35}^{45} = 0.84$, $K_{35} - l_{34}^{35} + l_{34}^{45} - l_{35}^{45} = 0.84$, $K_{45} + l_{34}^{35} - l_{34}^{45} - l_{35}^{45} = 1.03$, $K_{56} = 0.32$, $K_{67} = 0.23$, $\varrho_3^{12} = 0.224$, $\varrho_3^{45} = 0.406$ and $\chi_{45}^{12} = 0.512$ in md/Å and md Å for stretching and bending constants, respectively.

We have assumed the same force constants for bending in plane and out of plane for the linear acetylenic group.

The calculated fundamental frequencies were compared with the observed IR-spectrum but we have not been able to make a complete assignment yet. However, some of the eighteen fundamentals are readily observed. For a planar asymmetric rotor theoretical calculations give four independent distortion constants τ_{aaaa}, τ_{bbbb}, τ_{aabb} and τ_{abab}.[8]

The centrifugal distortion parameters according to Watson could be obtained from these constants if the rotational constants are known;[12] see Table 4. The agreement between measured and calculated values is rather good for all constants but Δ_{JK}. However, the constant Δ_{JK} seems to be extremely sensitive to the bending force constants K_{34}, K_{35} and K_{45}, and it has been rather difficult to obtain a good estimation of it.

MOLECULAR STRUCTURE

The rotational constants A, B, and C are accurately obtained from the measured spectrum since both R- and Q-type transitions have been observed. Therefore we could expect the derived principal moments of inertia I_a^0, I_b^0 and I_c^0 to be accurate. These are structure dependent parameters and could eventually be used as additional constraints in other structure determining methods, *e.g.* electron diffraction in gases.[16] However, it is then necessary to transform the observed moments of inertia I_a^0, I_b^0 and I_c^0 for rotational spectroscopy to the moments of inertia I_a^z, I_b^z and I_c^z for the average structure.[2,17] This correction is given by

$$I_\alpha^z = I_\alpha^0 - \tfrac{1}{2}\sum \varepsilon_s^\alpha(\text{har}) + \delta I_\alpha(\text{cent})\ \alpha = \text{a, b or c} \quad (6)$$

for an asymmetric rotor, where I_α^0 is one of the three principal moments of inertia for the effective structure in the ground state, and I_α^z is one of the three principal moments of inertia for the average structure.[8] The sum is over all fundamental vibrations.

The vibration-rotation term $\varepsilon_s^\alpha(\text{har})$ depends on the harmonic potentials and is obtained from a normal coordinate analysis.

The centrifugal distortion term $I_\alpha(\text{cent})$ is also obtainable from the force field and geometry.[17] The effects of the corrections according to (6) is given in Table 5. Evidently the centrif-

Table 5. Vibration-rotation correction for the moments of inertia and inertial defect for the ground vibrational state (in au Å²). Conversion factor 505376 au Å² MHz.

		r_0-parameters	vibration correction	centrifugal distortion correction	r_z-parameters
$C_4H_3{}^{35}Cl$	I_a	73.5066	0.1270	0.0000	73.6336
	I_b	163.2165	0.1884	0.0002	163.4051
	I_c	237.0487	0.0063	−0.0007	237.0543
	Δ	0.3256	–	–	0.0156
$C_4H_3{}^{37}Cl$	I_a	74.2657	0.1271	0.0000	74.3928
	I_b	166.5481	0.1919	0.0002	166.7402
	I_c	241.1418	0.0078	−0.0007	241.1489
	Δ	0.3280	–	–	0.0159

ugal distortion contribution can be neglected in this case.

It is also interesting to see that the I_c^0 constant is little affected by these corrections compared with I_a^0 and I_b^0.

The inertial defect

$$\Delta = I_c - I_a - I_b \quad (7)$$

vanishes for an average planar structure as it would for a hypothetical stiff planar rotor. Thus the combination of (6) and (7) gives

$$\Delta^z = \Delta^0 - \tfrac{1}{2}\sum_s(\varepsilon_s^c - \varepsilon_s^a - \varepsilon_s^b) + \delta I_c(\text{cent}) - \delta I_a(\text{cent}) - \delta I_b(\text{cent}) = 0$$

where Δ^z and Δ^0 are the inertial defect for the average and effective structure respectively.[18,19] Therefore it is possible to calculate the inertial defect and to control the validity of the correction terms to some extent by comparing the measured and calculated inertial defects. See Table 5. The obtained deviation of Δ^z from zero is the difference between the measured and calculated inertial defects and this is found to be 0.016 for both isotopic species. This is quite satisfactory considering the simple estimated force field used.

Acknowledgements. We thank all those who have contributed to this paper and especially Mr. Hasse Karlsson. Dr. Stig Ljunggren, and Professor Gunnar Erlandsson for their generous cooperation.

REFERENCES

1. Karlsson, F. and Vestin, R. *Acta Chem. Scand. 27* (1973) 3033.
2. Morino, Y., Kuchitsu, K. and Oka, T. *J. Chem. Phys. 36* (1962) 1108.
3. Herschbach, D. R. and Laurie, V. W. *J. Chem. Phys. 37* (1962) 1668.
4. Oka, T. *J. Phys. Soc. Jap. 15* (1960) 2274.
5. Nieuwland, J. A. and Vogt, R. *The Chemistry of Acetylene*, New York 1945, p. 160.
6. Finlay, J. B. (du Pont) U. S. 2.999.887, 1961.
7. Vestin, R., Borg, A. and Lindblom, T. *Acta Chem. Scand. 22* (1968) 687.
8. Gordy, W. and Cook, R. L. *Microwave Molecular Spectra*, Interscience, New York 1970.
9. Gerry, M. C. L. *Can. J. Chem. 49* (1971) 255.
10. Sillén, L. G. *Acta Chem. Scand. 16* (1962) 159.
11. Karlsson, F. and Vestin, R. *Chem. Scr. 2* (1972) 207.
12. Watson, J. K. G. *J. Chem. Phys. 46* (1967) 1935.
13. Kirchhoff, W. H. *J. Mol. Spectrosc. 41* (1972) 333.
14. Ramaswamy, K. and Srinivasan, K. *J. Mol. Struct. 3* (1969) 473.
15. Gribov, L. A. *Vvedenie v teoriyu i raschët kolebatel' nŷkh spektrov mnogoatomnŷkh molekul*, Istadel'stvo Leningradskogo Universita, 1965.
16. Kuchitsu, K., Fukuyama, T. and Morino, Y. *J. Mol. Struct. 1* (1968) 463.
17. Oka, T. and Morino, Y. *J. Mol. Spectrosc. 8* (1962) 300.
18. Darling, B. T. and Dennison, D. M. *Phys. Rev. 57* (1940) 128.
19. Oka, T. and Morino, Y. *J. Mol. Spectrosc. 6* (1961) 472.

Received November 2, 1973.

Acta Chemica Scandinavica A 28 (1974) 213—216

Activation Parameters for Inversion of 1-(1-Naphthyl)-isoquinoline. II.* Determination of the Enthalpy and Entropy of Activation for the Free Base

JÖRGEN R. PEDERSEN

Department of Organic Chemistry, University of Göteborg and Chalmers University of Technology, Fack, S-402 20 Göteborg 5, Sweden

The activation parameters for inversion of 1-(1-naphthyl)-isoquinoline in methanol solution have been determined from the temperature dependence of the rate of racemization of the levorotatory enantiomer in the temperature interval -36.2 to -5.9°C. The results obtained from 113 runs correspond to a $\Delta H^{\ddagger}$ for inversion of 80.4 ± 1.7 kJ mol^{-1} and a $\Delta S^{\ddagger}$ for inversion of 7.1 ± 6.7 J mol^{-1} K^{-1}.

The concept of "size" of the lone electron pair on nitrogen is a subject of some controversy.[1,2] This is partly due to the fact that it is difficult to design an experiment which will measure only this factor, resulting in different "operational" definitions of the van der Waals volume of the lone pair. Another reason is that the concept of "size" of the lone pair is classical in nature and lacks precise theoretical definition.

It has recently been shown [3] that the "size" of an electron pair (*i.e.* a localized two-electron group) can be related to the expectation values of two quantum mechanical operators corresponding to the first and second moments of the electronic charge distribution of localized molecular orbitals. This hopefully brings the discussion of "size" of the lone pair on a sounder foundation.

In Part I of this series [4] it was suggested that the optical stability of 1-(1-naphthyl)-isoquinoline *1* relative to that of 1,1′-binaphthyl *2* can be used to gauge the van der Waals volume of the lone pair in comparison to that of hydrogen. The basis for this rationale is the

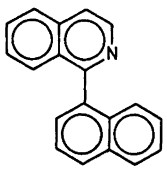

1

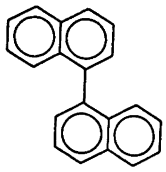

2

success of the classical model for calculating the barriers to inversion as introduced by Westheimer *et al.*[5–7] and later used by Howlett.[8] In their model the major part of the barrier to inversion comes from the van der Waals interaction between interfering atoms and the bending of the bonds of these atoms. In addition, Hill has suggested that the barriers to inversion of biphenyls can be used to obtain information on the van der Waals volumes of substituents in the interfering positions.[9] The two molecules *1* and *2* are so similar that one may hope that they are inverted through similar transition states and that comparison of their respective $\Delta H^{\ddagger}$ values for inversion will yield an estimate of the difference in "size" between

* For Part I of this series, see Ref. 4.

the lone pair and hydrogen. The activation parameters for inversion of *2* in dimethylformamide solution are already known with high precision.[10,11] It is not appropriate to compare the free energies of activation for inversion of *1* and *2*, as the entropies of activation for inversion of biphenyls and biphenyl-like compounds are known to range between +42 and −63 J mol^{-1} K^{-1}.[12] In addition, due to differences in solubility of *1* and *2*, and the method used to obtain optically active *1*, the rates of racemization of *1* and *2* must necessarily be determined in different solvents.

EXPERIMENTAL

Kinetic runs were made on a Perkin-Elmer 141 polarimeter placed in a "dry box" filled with nitrogen. The polarimeter cells were standard Perkin-Elmer 1 ml and 5 ml "micro cells", and the cell windows were kept free of frost by a stream of dry nitrogen. The nitrogen was pre-dried by passing through a column of Drierite, and the residual water was then frozen out in a trap cooled by liquid nitrogen. The error in each reading, determined by measurements on pure methanol, was ±0.003°.

The temperature in the cells was measured using a calibrated thermistor and a Fluke 8300A digital voltmeter. The thermistor was calibrated against a Hewlett Packard 2801 A quartz thermometer to a precision of ±0.1 K.

The cooling liquid was supplied by a Hetofrig cooling bath, type CB 6, together with a Heto thermostat, type 01 PT 623, capable of keeping the preset temperature at ±0.05 − ±0.001 K depending on the temperature chosen. Due to the non-optimal design of the polarimeter cells and the cell compartment, the temperature in the cell fluctuated somewhat, at most ±0.1 K during any run. The temperature range was from 237.0 K to 267.3 K. The measurements were distributed fairly evenly throughout the interval with the largest density of measurements at higher temperatures. The largest temperature difference between two runs occurred at low temperatures and was slightly less than one degree.

The solvent used was Merck "Methanol zur Analyse" which was used without further purification.

The individual rate constants were calculated using the least squares method. The activation parameters for inversion were then calculated from an Eyring-plot using a weighted least squares method to find the best line through the points. The calculations were done on an IBM 365/65 computer using standard linear regression analysis routines.

(−)-1-(1-Naphthyl)-isoquinoline. A solution of (−)-1-(1-naphthyl)-isoquinolinium α-bromocamphor-π-sulfonate [4] (5 mg ml^{-1} in methanol) was added to Amberlite IRA 400 ion exchange resin in the OH-form (0.5 g per ml of the salt solution) in a test tube inserted in a cooling medium kept at −20 ± 1°C. After stirring for 2 min, the solution was filtered into the cooled polarimeter cell. The initial rotation was measured 5 min after contact with the ion exchange resin. In each run the rotation was followed to zero and remained there, within experimental error. After completion of the first 10 runs the solutions were evaporated to dryness. The IR-spectra (in KBr) of these residues were identical to the spectrum of racemic 1-(1-naphthyl)-isoquinoline.

RESULTS AND DISCUSSION

The initial rotations obtained for the different (−)-1-(1-naphthyl)-isoquinoline solutions seemed to vary at random. It was found very difficult to get rotations higher than 1°, even with higher initial concentrations of optically active salt, apparently because the free base *1* is adsorbed or trapped to some extent in the polymer matrix of the ion exchange resin at the low temperatures used. Out of the 113 runs 79 had an initial rotation between 0.5 and 1° and the other 34 had rotations between 0.1 and 0.5°.

The standard errors in the rate constants did not show any correlation with the magnitude of the rotations obtained. Although the relative errors tend to be larger at higher temperatures, this trend is not constant. The range of the standard errors was from 0.2 to 3.5 % with the majority of the errors less than 1 %. Table 1 shows results obtained in a few typical runs taken from the whole temperature range.

Table 1. Rate constants for racemization of (−)-1-(1-naphthyl)-isoquinoline obtained in some typical runs.

Temp. K	$k \times 10^4$ sec^{-1}	Standard deviation × 10^6 sec^{-1}
242.8	1.35	0.48
246.6	2.80	0.49
253.2	7.18	2.5
258.2	11.8	6.3
262.7	41.0	80.0
266.4	57.0	100.0

Table 2. Enthalpy and entropy of activation for inversion of 1-(1-naphthyl)-isoquinoline (*1*) and 1,1′-binaphthyl (*2*).

Compound	Solvent	Temp. range K	$\Delta K^{\ddagger}$ kJ mol^{-1}	$\Delta S^{\ddagger}$ J mol^{-1} K^{-1}
1	methanol	237.0 – 267.3	80.4 ± 1.7	7.1 ± 6.7
2[a]	DMF	295.3 – 337.2	89.9 ± 0.8	−33.4 ± 2.4
2[b]	DMF	–	91.6	−21.8

[a] Calculated from the values given in Ref. 11 in kcal mol^{-1} and corresponding e.u. [b] Calculated from the values given in Ref. 10 in kcal mol^{-1} and corresponding e.u., no error limits are available from this work.

All runs were included in an Eyring-plot and were weighted statistically by the inverse of the variance (σ^2) resulting from the least-squares calculation of the rate constant. A least-squares treatment of the rate data, plotted as ln (k/T) *vs.* $1/T$ and weighted by $1/\sigma^2$, yielded a $\Delta H^{\ddagger}$ for inversion of 80.4 ± 1.7 kJ mol^{-1} and a $\Delta S^{\ddagger}$ for inversion of 7.1 ± 6.7 J mol^{-1} K^{-1}. The errors are given here as twice the standard error derived from the weighted least-squares treatment. Table 2 contains $\Delta H^{\ddagger}$ and $\Delta S^{\ddagger}$ for *1* and the corresponding data available for *2*.[10,11]

The results show that the large difference in optical stability between *1* and *2*, $\Delta\Delta G^{\ddagger} = -20$ kJ mol^{-1} at −20°C,[4] is to a large extent due to the difference in $\Delta S^{\ddagger}$.

No information exists, of course, about the exact path of racemization of *1* and *2*, *i.e.* whether they undergo inversion through the transoid or the cisoid transition state. Cooke and Harris assumed that *2* and similar compounds undergo inversion through two transoid transition states (with the interfering atoms passing each other one pair at a time) but point out that this choice is arbitrary.[10]

If one makes the reasonable but perhaps erroneous assumption that both compounds undergo inversion through similar transition states, then the conclusion is that the steric volume of the free electron pair on nitrogen, while less than that for hydrogen, is still of the same order of magnitude. This is supported by crystallographic work on SbOF.[13] The configuration around antimony in the crystal structure is typical for an element having a stereochemically active lone pair and similar to the structures of Sb_2O_4, $SbNbO_4$ and $SbPO_4$.[14,15] In these structures the stereochemically active lone pair is more extended than a bonding pair and requires more room on the surface of the atom.

Finally, even if *1* and *2* undergo inversion through different transition states, the non-bonded interaction between hydrogen and the lone pair must be appreciable. If the barrier consisted only of H...H non-bonded interaction and no contribution from interactions involving the lone pair, then the former interaction would probably be almost completely relieved in the transition state by bending of the pivot bond, and the rate of racemization would be too fast for observation.

Acknowledgement. The author thanks Professor Lars Melander for reading the manuscript. A grant from Bengt Lundquists Minne is gratefully acknowledged.

REFERENCES

1. Allinger, N. L., Hirsch, J. A. and Miller, M. A. *Tetrahedron Lett.* (1967) 3729.
2. Aroney, M. and LeFèvre, R. J. W. *J. Chem. Soc.* (1958) 3002.
3. Robb, M. A., Haines, W. J. and Csizmadia, J. G. *J. Amer. Chem. Soc. 95* (1973) 42.
4. Pedersen, J. R. *Acta Chem. Scand. 26* (1972) 929.
5. Westheimer, F. H. and Mayer, J. E. *J. Chem. Phys. 14* (1946) 733.
6. Westheimer, F. H. *J. Chem. Phys. 15* (1947) 252.
7. Rieger, M. and Westheimer, F. H. *J. Amer. Chem. Soc. 72* (1950) 19.
8. Howlett, K. E. *J. Chem. Soc.* (1960) 1055.
9. Hill, T. L. *J. Chem. Phys. 16* (1948) 399.
10. Cooke, A. S. and Harris, M. M. *J. Chem. Soc. C* (1967) 988.
11. Carter, R. E. and Dahlgren, L. *Acta Chem. Scand. 23* (1969) 504.

12. Hall, M. and Harris, M. M. *J. Chem. Soc.* (1960) 490.
13. Åström, A. and Andersson, S. *Acta Chem. Scand. 25* (1971) 1519.
14. Skapski, A. C. and Rogers, D. *Chem. Commun. 23* (1965) 611.
15. Kinberger, B. *Acta Chem. Scand. 24* (1970) 320.

Received November 15, 1973.

Acta Chemica Scandinavica A 28 (1974) 217—225

Multicomponent Polyanions. VIII. On the Crystal Structure of $Na_3H_6Mo_9PO_{34}(H_2O)_x$, a Compound Containing Protonized Enneamolybdomonophosphate Anions

ROLF STRANDBERG

Department of Inorganic Chemistry, University of Umeå, S-901 87 Umeå, Sweden

In $Na_3H_6Mo_9PO_{34}(H_2O)_x$ the Mo, Na, P, and O positions have been determined from three dimensional X-ray diffraction data collected with a PAILRED diffractometer using Mo$K\alpha$-radiation. Chemical analysis indicated an x-value of around 12 – 13. However, none of these water molecules could be detected with certainty in the X-ray analysis. There are two formula units in the hexagonal unit cell and the cell dimensions of the crystal used are $a = 14.248$ Å and $c = 10.83$ Å. Different crystals seem to give slightly different cell dimensions. The space group is $P6_3$. It was found that the structure is built up of $H_6Mo_9PO_{34}^{3-}$ anions coupled together through O – Na – O bonds forming a three-dimensional network. Possible positions for the water molecules are discussed. Refinement by least squares methods using anisotropic vibrational parameters resulted in an R-value of 0.037, based on 1930 independent reflexions.

An equilibrium analysis in the aqueous system $H^+ - MoO_4^{2-} - HPO_4^{2-}$ has indicated that at excess of molybdate ions a series of protonized enneamolybdomonophosphates are formed and the complexes $(H^+)_{14}(MoO_4^{2-})_9(HPO_4^{2-})^{6-}$, $(H^+)_{15}(MoO_4^{2-})_9(HPO_4^{2-})^{5-}$, $(H^+)_{16}(MoO_4^{2-})_9(HPO_4^{2-})^{4-}$ and $(H^+)_{17}(MoO_4^{2-})_9(HPO_4^{2-})^{3-}$ have been proposed.[1] By crystallisation of aqueous solutions with compositions lying between the complexes $(H^+)_{16}(MoO_4^{2-})_9(HPO_4^{2-})^{4-}$ and $(H^+)_{17}(MoO_4^{2-})_9(HPO_4^{2-})^{3-}$ a crystalline phase of the formula $Na_3H_6Mo_9PO_{34}(H_2O)_x$ was obtained. In the present work the crystal structure of this compound will be presented and discussed especially with reference to $H_6Mo_9PO_{34}^{3-}$, a polyanion group which forms the buildning units in the structure. The mentioned anion corresponds to the complex $(H^+)_{17}(MoO_4^{2-})_9(HPO_4^{2-})^{3-}$ found in the equilibrium analysis. Also the Na^+ coordination to the group is of particular interest.

EXPERIMENTAL

In a typical preparation of the crystals, $Na_2MoO_4.2H_2O$ and $NaH_2PO_4.2H_2O$ were dissolved in concentrated $HClO_4$ and then kept for crystallization at room temperature. The concentrations used were $[MoO_4^{2-}]_{tot} = 1.0$ M, $[HPO_4^{2-}]_{tot} = 0.11$ M and $[HClO_4]_{tot} = 1.78$ M. After a few days (sometimes weeks) of evaporation, yellowish crystals, grown as regular hexagonal prisms, were obtained. They are not stable in air and during the X-ray exposures they were enclosed together with part of the mother liquid in a sealed capillary of Lindemann glass. The contents of Na, Mo, and P were determined by elemental analysis (carried out at the Department of Analytical Chemistry, University of Umeå). (Found weight-%: Na 4.3; P 1.8; Mo 49.8. Calc. for $Na_3H_6Mo_9PO_{34}(H_2O)_{12}$: Na 4.0; P 1.8; Mo 49.9). In some experiments we measured the loss of water in thermobalance analysis. The results found here were 12 – 13 H_2O per formula unit. From rotation photographs around [001] and [100] and the corresponding Weissenberg photographs (zero, first and second layer lines) taken with Cu$K\alpha$-radiation it was concluded that the crystals are hexagonal. The dimension of the c-axis was determined from rotation photographs and the a-axis was calculated from omega measurements on the diffractometer. The parameters of the crystals used in the collection of the intensity material had the values $a = 14.248$ Å and $c = 10.83$ Å. When the cell dimensions were calculated and refined from powder photographs the following parameters were obtained: $a = 14.182$ Å and $c = 10.758$ Å. The differences between the two determinations are too large to

arise from experimental errors; they are most probably due to variable water contents in the crystals. Systematic extinctions were found only for $00l$-reflexions with l odd. This is characteristic for the three space groups $P6_322$, $P6_3/m$, and $P6_3$. From the diffraction symmetry $P6_322$ could be rejected. Precession photographs were taken as a check on the space-group determination.

The density of the crystals was determined by flotation in a bromoform diiodomethane solution and the result was $d = 3.04 \pm 0.03$ g/cm^3 ($d_{calc} = 3.02$ with 12 H_2O; 3.05 with 13 H_2O). Three-dimensional intensity data were collected with a Philips PAILRED linear diffractometer using Mo$K\alpha$-radiation. The crystal was mounted along the c-axis. Reflexions with a relative statistical error of $\Delta I_o/I_o$ greater than 0.5 were omitted leaving a total of 5159 reflexions from the layers $hk0 - hk11$. The intensities were corrected for Lorentz and polarization effects and absorption correction was applied. In each level the reflexions h, k; $-k$, $(h+k)$ and $-(h+k)$, h were equivalent within experimental errors. For equivalent reflexions an arithmetic mean value was calculated which gave a set of 1930 independent reflexions. In connection with this calculation the quotient between the strongest and weakest reflexions in every triplet was computed. This test showed very good agreement between equivalent F_o-values. In about 90 % of the triplets the quotient varied from 0.9 to 1.1 and for the remaining triplets, which all included weak reflexions, the range was 0.8 – 1.2. The computer programs used were the same as those given in Ref. 2.

Crystal data

$Na_3H_6Mo_9PO_{34}(H_2O)_x$
Hexagonal, $P6_3$
$Z = 2$
$a = 14.248(1)$ Å
$c = 10.83(1)$ Å
$d_{calc} = 3.02$ ($x = 12$); 3.05 ($x = 13$) g/cm^3
$d_{exp} = 3.04 \pm 0.03$ g/cm^3
$V = 1903.9$ Å^3
$\mu = 30.2$ cm^{-1} (Mo$K\alpha$)

STRUCTURE DETERMINATION AND REFINEMENT

The structure determination was initiated assuming the space group $P6_3/m$ but this failed and the space group $P6_3$ was tried. In a Patterson synthesis the symmetry vectors should be found in Harker planes such as $(2x, 2y, \frac{1}{2})$ and $(2y, 2y-2x, \frac{1}{2})$. From the calculations of the highest of these peaks the three molybdenum atoms were located. A refinement at this stage gave an R-value of 0.17. Using the known Mo-atoms a three-dimensional Fourier synthesis was performed. This gave the positions of Na, P and the oxygens bound to P and Mo. The R-value decreased to 0.05 using isotropic temperature factors and to 0.04 when anisotropic temperature factors were used. A second Fourier synthesis using the known atoms gave no distinct water oxygen peaks neither did a difference Fourier map. The highest peaks in the latter were equivalent to an electron density of about 4e$^-$/Å^3. The reason for the failure to find the water oxygens is most likely that the water in the structure is not structural. The highest peaks in the difference Fourier map are probably only partly occupied positions. In the description and discussion of the structure the water content will be treated further.

The positional parameters and anisotropic temperature factors for the atoms were refined by full-matrix least squares methods and the final R-value was 0.037. $R = \sum||F_o| - |F_c||/\sum|F_o|$. The atomic scattering factors used for Mo^{3+} were those given by Cromer and Waber,[3] for P those given by Hanson, Herman, Lea and Skillman [4] and for Na^+ and O^- the values in International Tables.[5] Account was taken of the real part of the dispersion correction.[5] A weight-

Table 1. The fractional atomic coordinates and in parentheses their estimated standard deviations (referring to the last decimal place given). For the oxygen atoms indexed O(ij) or OP(ij) the (ij) means that the atom is bonded to the molybdenum atoms i and j.

	X	Y	Z
Mo1	0.75741(6)	0.49246(6)	0.0001(1)
Mo2	0.71956(7)	0.59972(7)	0.3201(1)
Mo3	0.46374(6)	0.40204(7)	0.2643(1)
P	0.6667(0)	0.3333(0)	0.2745(5)
O(1)	0.8272(7)	0.5903(6)	−0.1090(8)
O(11′)	0.7909(6)	0.3771(5)	−0.0702(7)
OP(11′1″)	0.6667(0)	0.3333(0)	0.130 (1)
O(13)	0.8870(5)	0.5133(5)	0.1074(7)
O(12)	0.7303(5)	0.5607(5)	0.1206(7)
O1(2)	0.7742(7)	0.7330(6)	0.279 (1)
O2(2)	0.7051(8)	0.5979(8)	0.476 (1)
O1(23)	0.8522(5)	0.5884(6)	0.3191(9)
O2(23)	0.5693(6)	0.5491(6)	0.2717(9)
OP(23)	0.6298(6)	0.4123(6)	0.3182(9)
O1(3)	0.3516(7)	0.4137(8)	0.245 (1)
O2(3)	0.4636(7)	0.4274(7)	0.4660(9)
Na	0.167 (1)	0.339 (1)	0.172 (2)
Aq1	0.18	0.51	0.14
Aq2	0.03	0.25	0.01

Table 2. Final anisotropic thermal parameters ($\times 10^4$) and their estimated standard deviations ($\times 10^4$) in parentheses. The parameters are calculated according to the formula $\exp[-(h^2\beta_{11}+k^2\beta_{22}+l^2\beta_{33}+hk\beta_{12}+hl\beta_{13}+kl\beta_{23})]$

	β_{11}	β_{22}	β_{33}	β_{12}	β_{13}	β_{23}
Mo1	19 (0)	17 (0)	23 (1)	18 (1)	2 (1)	4 (1)
Mo2	26 (0)	23 (0)	36 (1)	26 (1)	−2 (1)	−15 (1)
Mo3	22 (0)	26 (0)	28 (1)	29 (1)	4 (1)	−3 (1)
P	18 (1)	18 (1)	17 (4)	18 (1)	0 (0)	0 (0)
O(1)	40 (5)	24 (4)	39 (8)	26 (7)	18 (9)	23 (8)
O(11′)	24 (4)	30 (4)	14 (6)	32 (6)	1 (6)	0 (6)
OP(11′1″)	15 (4)	15 (4)	30(13)	15 (4)	0 (0)	0 (0)
O(13)	24 (4)	23 (4)	30 (7)	21 (6)	−3 (7)	5 (7)
O(12)	22 (4)	23 (4)	26 (6)	22 (6)	0 (7)	−7 (7)
O1(2)	40 (5)	31 (5)	71(10)	38 (8)	−5(11)	−10(11)
O2(2)	36 (5)	54 (7)	44(11)	39(10)	3(10)	−24(11)
O1(23)	23 (4)	30 (4)	44 (7)	29 (6)	−15 (8)	−25 (9)
O2(23)	28 (4)	25 (4)	48 (7)	32 (7)	−3(10)	−11 (9)
OP(23)	26 (4)	23 (4)	32 (7)	31 (6)	−1 (8)	−16 (8)
O1(3)	36 (5)	48 (6)	51(10)	63 (9)	10(10)	1(11)
O2(3)	46 (5)	40 (5)	34 (9)	44 (9)	21 (9)	−10 (9)
Na	166(13)	311(20)	184(19)	233(27)	−5(28)	−46(35)

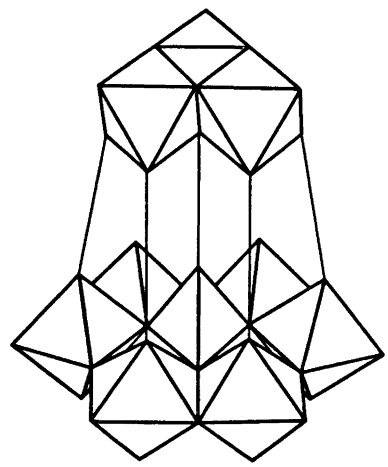

Fig. 1. The coupling of the nine MoO_6-octahedra and the PO_4-tetrahedron in the Mo_9PO_{34}-group. For clarity the figure is idealised.

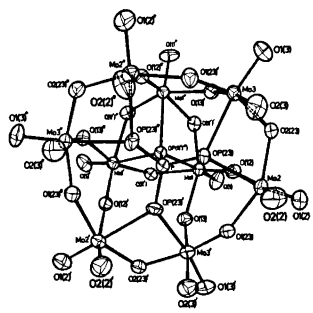

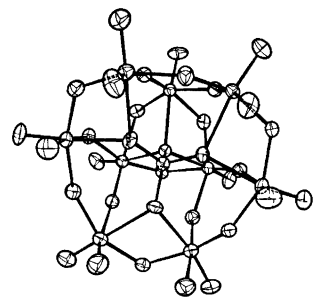

Fig. 2. Stereoscopic view of the Mo_9PO_{34}-group.

Table 3. Observed and calculated structure factors (× 10).

K	H		
L=	0		
1	2	1479	1847
1	3	105	13
1	4	1107	1310
1	5	1610	1538
1	6	527	512
1	7	121	87
1	8	239	159
1	9	407	375
1	10	1604	1559
1	11	493	460
1	12	716	726
1	13	165	147
1	14	743	739
1	15	146	83
1	16	408	394
2	16	127	132
2	15	257	274
2	14	200	196
2	13	670	665
2	12	96	109
2	11	100	43
2	10	1494	1557
2	9	160	147
2	8	538	434
2	7	437	486
2	6	2154	2146
2	5	2395	2279
2	4	170	20
2	3	314	590
2	2	122	400
2	1	861	800
2	0	278	89
3	0	442	384
3	1	2838	2777
3	2	159	165
3	3	1193	1018
3	4	930	897
3	5	2074	2115
3	6	3120	3084
3	7	125	42
3	8	257	296
3	9	236	285
3	10	1440	1413
3	12	499	479
3	13	243	255
3	14	907	875
4	14	415	421
4	13	669	667
4	12	296	310
4	11	254	268
4	10	580	565
4	8	733	708
4	7	98	48
4	6	1254	1302
4	5	486	564
4	4	1222	1385
4	3	621	721
4	1	2704	2492
4	0	918	521
5	0	277	102
5	1	465	442
5	2	997	970
5	3	274	301
5	4	175	252
5	5	502	524
5	6	153	161
5	7	446	416
5	8	120	91
5	9	148	155
5	10	391	379
5	11	1592	1606
5	12	509	512
5	13	677	703
6	13	412	416
6	12	262	270
6	11	633	639
6	10	573	573
6	9	137	148
6	8	161	195
6	7	1017	993
6	6	1546	1517
6	5	809	808
6	4	298	337
6	3	1314	1389
6	2	1550	1473
6	1	1668	1681
6	0	2089	2161
7	0	491	523
7	1	523	414
7	2	597	532
7	3	599	553
7	4	968	1024
7	5	1007	1031
7	6	452	437
7	7	91	31
7	8	325	343
7	9	239	250
7	10	456	448
7	11	557	574
7	12	611	632
8	11	134	132
8	10	179	188
8	9	470	490
8	8	717	717
8	7	463	459
8	6	195	202
8	5	791	842
8	4	1271	1253
8	3	587	610
8	2	514	534
8	1	888	905
8	0	1208	1124
9	0	1364	1376
9	1	925	923
9	2	205	132
9	3	210	193
9	4	695	688
9	5	929	944
9	6	712	679
9	8	788	799
9	9	369	375
9	10	471	493
10	9	362	376
10	7	764	782
10	6	233	217
10	5	106	78
10	4	823	836
10	3	525	493
10	2	321	350
10	1	569	549
10	0	112	37
11	0	611	612
11	1	130	88
11	2	1483	1518
11	3	861	829
11	4	438	441
11	5	754	773
11	6	452	430
11	7	512	517
11	8	554	533
12	7	567	574
12	6	265	272
12	5	351	352
12	4	1082	1084
12	3	113	124
12	2	181	174
12	1	500	523
12	0	352	347
13	0	499	493
13	1	343	329
13	2	112	99
13	3	314	301
13	4	347	315
13	5	107	87
14	5	473	482
14	4	382	373
14	3	396	401
14	2	133	110
14	1	295	306
14	0	437	391
15	0	859	863
15	1	258	253
15	2	685	687
15	3	241	258
16	2	346	351
16	1	679	689
16	0	108	86
17	0	397	415
L=	1		
1	2	1705	1886
1	3	1422	1205
1	4	1184	1189
1	5	844	786
1	6	324	274
1	7	537	499
1	8	967	975
1	9	516	488
1	10	323	272
1	11	700	674
1	12	332	367
1	13	588	594
1	14	967	958
1	15	475	473
2	16	326	321
2	15	354	345
2	14	620	626
2	12	547	537
2	11	301	277
2	10	1441	1449
2	9	908	888
2	8	902	896
2	7	772	828
2	6	2442	2502
2	5	290	203
2	4	621	539
2	3	918	792
2	2	426	481
2	1	616	339
2	0	1231	1133
3	0	1118	1209
3	1	3821	3767
3	2	1533	1561
3	3	230	206
3	4	1153	1063
3	5	2373	2282
3	6	208	201
3	7	939	896
3	8	408	421
3	9	1030	978
3	10	241	250
3	11	450	449
3	12	710	695
3	13	557	561
3	14	491	486
3	15	342	346
4	14	356	356
4	13	467	464
4	12	652	649
4	11	750	728
4	10	538	532
4	9	928	919
4	8	196	186
4	7	300	311
4	6	1629	1550
4	5	1293	1242
4	4	253	262
4	3	1909	1935
4	2	1032	1113
4	1	1301	1281
4	0	1985	2174
5	0	1011	1000
5	1	283	212
5	2	985	954
5	3	879	817
5	4	1023	1035
5	5	289	312
5	6	321	302
5	7	1070	1050
5	8	779	805
5	9	771	756
5	10	443	439
5	11	144	173
5	12	294	298
6	13	143	142
6	12	212	201
6	11	274	275
6	10	504	523
6	9	367	364
6	8	243	264
6	7	1428	1444
6	6	600	598
6	5	125	121
6	4	891	793
6	3	408	489
6	2	1202	1179
6	1	587	498
6	0	400	428
7	0	1242	1186
7	1	1170	1138
7	2	2549	2536
7	3	1148	1116
7	4	570	568
7	5	1054	1024
7	6	777	796
7	7	767	765
7	8	561	542
7	9	774	768
7	10	227	201
7	11	471	461
7	12	261	220
8	11	141	123
8	10	502	493
8	9	622	631
8	8	259	248
8	7	644	616
8	6	407	383
8	5	735	749
8	4	658	626
8	3	492	487
8	2	504	478
8	1	1535	1552
8	0	883	827
9	0	896	877
9	1	384	413
9	2	888	865
9	3	714	718
9	4	508	499
9	5	252	239
9	6	278	237
9	7	549	543
9	8	893	889
9	9	288	302
9	10	352	344
10	9	290	303
10	8	501	484
10	7	406	415
10	6	619	628
10	5	449	459
10	4	286	271
10	3	1253	1247
10	2	442	458
10	1	587	555
10	0	670	670
11	0	418	384
11	1	636	631
11	2	265	273
11	3	946	937
11	5	409	408
11	6	119	96
11	7	425	424
11	8	542	559
12	7	280	291
12	6	634	636
12	5	457	455
12	4	112	128
12	3	445	434
12	2	506	499
12	1	886	880
12	0	317	303
13	0	917	894
13	1	493	498
13	2	763	752
13	3	524	519
13	4	266	255
13	5	457	456
13	6	129	171
14	5	162	155
14	4	967	975
14	3	434	439
14	2	147	108
14	1	375	377
14	0	627	611
15	0	147	132
15	1	333	337
15	3	369	403
16	2	525	525
16	1	661	666
16	0	166	153
17	0	211	212
L=	2		
1	1	1687	1833
1	2	1381	1083
1	3	619	584
1	4	437	302
1	5	410	300
1	6	648	673
1	7	509	381
1	8	1005	1000
1	9	531	545
1	10	1789	1753
1	11	628	647
1	12	857	828
1	13	200	190
1	14	441	447
1	15	519	540
1	16	249	227
2	16	159	129
2	15	593	594
2	14	357	381
2	13	460	441
2	12	354	329
2	11	278	253
2	10	547	509
2	9	1346	1336
2	8	371	389
2	7	419	371
2	6	578	599
2	5	857	839
2	4	916	925
2	3	416	540
2	2	1264	1284
2	1	839	858
2	0	1574	1430
3	0	1047	994
3	1	816	649
3	2	1595	1573
3	3	1086	1202
3	4	435	468
3	5	605	547
3	6	787	725
3	7	461	438
3	8	1012	995
3	9	662	688
3	10	385	354
3	11	110	76
3	12	361	357
3	13	607	614
3	14	645	619
3	15	239	223
4	14	554	551
4	13	236	251
4	12	820	818
4	11	234	238
4	10	228	235
4	9	565	601
4	8	943	922
4	7	321	330
4	6	401	318
4	5	839	844
4	4	1450	1329
4	3	1060	1102
4	2	1383	1441
4	1	2353	2608
4	0	2490	2322
5	0	799	893
5	1	1478	1383
5	2	887	879
5	3	629	642
5	4	993	993
5	5	1591	1609
5	6	533	541
5	7	605	611
5	8	690	672
5	9	308	314
5	10	127	111
5	11	1192	1178
5	12	123	129
5	13	384	375
6	13	416	403
6	12	466	471
6	11	210	184
6	10	178	163
6	9	882	890
6	8	202	194
6	7	689	709
6	6	1943	1969
6	5	571	548
6	4	485	439
6	3	1031	982
6	2	766	723
6	1	415	356
6	0	1535	1437
7	0	938	908
7	1	1432	1469
7	2	1991	1991
7	3	425	434
7	4	550	515
7	5	181	179
7	6	1096	1100
7	7	228	202
7	8	886	905
7	9	721	742
7	10	878	873
7	11	711	700
7	12	155	171
8	10	470	463
8	9	158	157
8	8	365	359
8	7	445	441
8	6	787	780
8	5	160	76
8	4	275	242
8	3	690	661
8	2	1107	1147
8	1	538	574
8	0	1454	1435
9	0	389	324
9	1	545	493
9	2	696	706
9	3	366	387
9	4	282	258
9	5	755	732
9	6	326	296
9	7	326	319
9	8	402	371
9	9	119	61
10	9	128	118
10	8	164	149
10	7	961	950
10	6	667	669
10	5	426	382
10	4	968	930
10	3	777	770
10	2	492	487
10	1	907	896
10	0	502	514
11	0	403	369
11	1	673	691
11	2	594	590
11	3	419	410
11	4	151	173
11	5	328	317
11	6	912	912
11	7	116	84
11	8	214	207
12	7	172	164
12	6	249	247
12	5	429	437
12	4	479	471
12	3	386	377
12	2	569	572
12	1	258	274
12	0	902	913
13	0	465	465
13	1	909	886
13	2	538	519
13	3	252	234
13	4	606	598
13	5	759	766
13	6	375	375
14	5	343	352
14	4	497	511
14	3	236	239
14	2	134	110
14	1	335	339
14	0	190	198
15	0	1092	1075
15	1	125	122
15	2	247	240
15	3	533	536
16	2	180	165
16	1	238	217
16	0	630	647
17	0	699	722
L=	3		
1	1	1078	929
1	2	1145	1029
1	3	808	850
1	4	556	647
1	5	418	438
1	6	316	338
1	7	892	885
1	8	1338	1324
1	9	194	173
1	10	382	388
1	11	815	826
1	13	717	727
1	14	417	417
1	15	332	341
1	16	306	311
2	16	238	245
2	15	358	381
2	14	671	691
2	12	932	928
2	11	540	556
2	10	627	637
2	9	617	640
2	8	665	642
2	7	685	674
2	6	2081	2066
2	5	192	224
2	4	511	480
2	3	1027	1055
2	2	307	186
2	1	496	448
2	0	736	936
3	0	1524	1481
3	1	1051	1067
3	2	270	404
3	3	371	297
3	4	1036	1066
3	5	2702	2814
3	6	109	101
3	7	655	650
3	8	866	866
3	9	764	765
3	11	853	852
3	12	212	224
3	13	857	862
3	14	420	410
3	15	215	200
4	14	549	552
4	13	754	767
4	12	571	571
4	11	398	391
4	10	421	423
4	9	852	847
4	8	251	250
4	7	1052	1064
4	6	577	535
4	5	1210	1236
4	4	705	695
4	3	826	664
4	2	522	587
4	1	1162	1157
4	0	450	440
5	0	1193	1190
5	1	841	802
5	2	899	780
5	3	824	833
5	4	653	738
5	5	947	957
5	6	462	454
5	7	798	792
5	8	137	82
5	9	303	309
5	10	530	517
5	11	149	177
5	12	218	234
5	13	320	325
6	13	237	246
6	12	298	292
6	11	660	666
6	10	771	777
6	9	510	509
6	8	241	211
6	7	871	853
6	6	519	542
6	5	341	334
6	4	532	617
6	3	401	352
6	2	636	682
6	1	728	710
6	0	1439	1415
7	0	985	996
7	1	1111	1057
7	2	1962	2051
7	3	549	531
7	4	614	608
7	5	615	631
7	6	799	791
7	7	259	258
7	8	556	547
7	9	211	206
7	10	280	280
7	11	164	165
7	12	420	430
8	10	414	405
8	9	485	474
8	8	415	403
8	7	559	561
8	6	852	848
8	5	1050	1054
8	4	775	791
8	3	1054	1027
8	2	498	494
8	1	750	768
8	0	628	676
9	0	1245	1211
9	1	603	571
9	2	989	986
9	3	103	93
9	4	631	648
9	5	206	206
9	6	525	532
9	7	542	550
9	8	812	806
9	9	178	173
9	10	290	284
10	9	284	287
10	8	516	535
10	7	353	354
10	6	292	279
10	5	496	522
10	4	267	264
10	3	1246	1262
10	2	286	287
10	1	445	449
10	0	449	449
11	0	328	313
11	1	559	558
11	2	174	178
11	3	1176	1181
11	4	327	307
11	5	897	898
11	6	272	271
11	7	280	266
11	8	383	396
12	7	354	345
12	6	252	229
12	5	807	811
12	4	165	162
12	3	477	464
12	2	794	809
12	1	883	877
12	0	475	451
13	0	100	96
13	1	440	437
13	2	326	342
13	3	490	503
13	4	414	437
13	5	485	484
14	4	716	721
14	3	213	189
14	2	531	551
14	1	491	470
14	0	639	635
15	1	413	413
15	2	152	150
15	3	388	391
16	1	231	212
16	0	208	201
17	0	345	326
L=	4		
1	1	672	491
1	2	1244	1242
1	3	485	444
1	4	847	827
1	5	1041	996
1	6	389	383
1	7	383	415
1	8	752	767
1	9	314	289
1	10	1104	1137
1	11	308	271
1	12	463	459
1	14	577	582
1	15	307	335
1	16	288	308
2	15	265	282
2	14	452	449
2	13	650	673
2	12	489	495
2	11	306	299
2	10	832	822
2	9	491	498
2	8	780	792
2	7	240	270
2	6	1264	1279
2	5	1812	1839
2	4	1423	1426
2	3	1402	1369
2	2	260	381
2	1	259	324
2	0	1120	1085
3	0	303	269
3	1	1615	1732
3	2	888	954
3	3	593	564
3	4	881	935
3	5	1140	1215
3	6	1443	1396
3	7	541	529
3	8	475	491
3	9	583	611
3	10	1218	1216
3	11	292	300
3	12	227	236
3	14	415	410
3	15	130	104
4	14	174	199
4	13	330	341
4	12	111	120
4	10	414	425
4	9	980	1037
4	8	582	576
4	7	485	492
4	6	447	390
4	5	346	352
4	4	1368	1266
4	3	1108	1157
4	2	1129	1110
4	1	1762	1712
4	0	1869	1833
5	0	584	680
5	1	388	347
5	2	414	371
5	3	1037	1008
5	4	987	1045
5	5	705	672
5	6	291	306
5	7	423	394
5	8	121	129
5	9	609	624
5	10	264	239
5	11	1148	1160
5	12	412	411
5	13	578	603

Table 3. Continued.

K	H		
L=	4		
6	13	295	297
6	12	271	271
6	11	385	385
6	10	467	465
6	9	193	194
6	8	208	189
6	7	589	579
6	6	1034	1048
6	5	438	439
6	4	237	203
6	3	1101	1131
6	2	797	796
6	1	1427	1462
6	0	1467	1462
7	0	892	956
7	1	712	750
7	2	899	906
7	3	392	378
7	4	626	587
7	5	994	1055
7	6	803	791
7	7	278	288
7	8	814	819
7	9	206	179
7	10	528	529
7	11	435	424
8	11	142	132
8	10	614	625
8	9	382	403
8	8	739	747
8	7	190	188
8	6	414	402
8	5	717	730
8	4	1592	1612
8	3	509	503
8	2	701	711
8	1	609	620
8	0	703	687
9	0	764	766
9	1	1345	1342
9	2	679	645
9	3	200	180
9	4	549	583
9	5	559	558
9	6	360	351
9	7	185	193
9	8	681	658
9	9	506	506
9	10	355	352
10	9	472	472
10	8	191	210
10	7	673	670
10	6	278	264
10	5	160	155
10	4	692	682
10	3	584	577
10	2	250	252
10	1	361	375
10	0	648	645
11	0	456	416
11	1	161	137
11	2	1114	1097
11	3	571	566
11	4	323	320
11	5	581	599
11	6	369	372
11	7	357	366
11	8	434	432
12	7	566	584
12	6	215	229
12	5	118	105
12	4	780	787
12	3	118	117
12	2	254	265
12	1	940	969
12	0	581	577
13	0	216	207
13	1	679	691
13	2	280	289
13	3	300	301
13	4	293	301
13	5	326	323
14	4	265	254
14	3	174	181
14	2	225	238
14	1	422	432
14	0	276	278
15	0	702	699
15	1	442	449
15	2	956	981
15	3	376	397
16	1	490	500
16	0	264	280
17	0	288	286
L=	5		
1	1	1316	1325
1	2	1420	1385
1	3	695	742
1	4	1915	2021
1	5	716	721
1	6	982	886
1	7	578	618
1	8	446	422
1	9	369	379
1	10	115	87
1	11	269	283
1	12	158	95
1	13	189	205
1	14	770	767
1	15	378	369
1	16	375	385
2	15	325	339
2	14	699	726
2	13	122	48
2	12	439	450
2	11	395	403
2	10	1174	1177
2	9	699	706
2	8	750	762
2	7	341	320
2	6	901	882
2	5	289	282
2	4	761	866
2	3	908	956
2	2	572	468
2	1	772	708
2	0	1181	1223
3	0	1201	1205
3	1	2778	2794
3	2	1107	1101
3	3	287	173
3	4	995	964
3	5	414	439
3	6	99	92
3	7	921	885
3	8	618	630
3	9	656	691
3	10	140	158
3	11	205	208
3	12	537	557
3	13	408	404
3	14	355	353
3	15	333	335
4	13	304	315
4	12	427	439
4	11	516	504
4	10	686	678
4	9	696	705
4	8	121	131
4	7	710	724
4	6	949	944
4	5	527	579
4	4	703	760
4	3	1625	1671
4	2	1044	964
4	1	1580	1597
4	0	953	902
5	0	1276	1277
5	1	296	265
5	2	1155	1248
5	3	951	995
5	4	953	941
5	5	1126	1123
5	6	456	430
5	7	970	997
5	8	847	864
5	9	514	508
5	10	250	254
5	11	154	154
5	12	231	233
6	13	217	213
6	12	298	298
6	11	326	339
6	10	242	260
6	9	646	661
6	8	215	232
6	7	971	987
6	6	344	367
6	5	133	127
6	4	769	731
6	3	532	545
6	2	865	872
6	1	521	487
6	0	1375	1435
7	0	464	440
7	1	973	978
7	2	1493	1493
7	3	844	855
7	4	884	839
7	5	1010	1029
7	6	600	621
7	7	694	707
7	8	460	471
7	9	769	782
7	10	348	345
7	11	425	436
8	11	119	119
8	10	528	532
8	9	722	736
8	8	440	456
8	7	517	512
8	6	393	408
8	5	579	558
8	4	519	540
8	3	398	383
8	2	682	693
8	1	1505	1529
8	0	875	886
9	0	1146	1144
9	1	522	526
9	2	607	606
9	3	405	412
9	4	608	607
9	5	108	55
9	6	507	514
9	7	267	261
9	8	425	418
9	9	202	202
10	9	301	287
10	8	256	262
10	7	309	334
10	6	500	507
10	5	220	219
10	4	139	146
10	3	546	548
10	2	422	426
10	1	1184	1191
10	0	517	529
11	0	533	517
11	1	676	669
11	2	175	165
11	3	255	264
11	4	208	216
11	5	771	797
11	6	319	330
11	7	458	463
12	7	187	171
12	6	593	605
12	5	534	538
12	4	200	202
12	3	459	464
12	2	448	442
12	1	951	965
12	0	687	704
13	0	887	908
13	1	310	323
13	2	604	619
13	3	411	426
13	4	130	147
13	5	370	384
14	4	680	684
14	3	662	668
14	2	324	332
14	1	219	225
14	0	198	182
15	0	117	42
15	1	431	434
15	3	311	315
16	1	851	867
L=	6		
1	1	617	597
1	2	2037	2129
1	3	347	335
1	4	546	590
1	5	408	436
1	6	506	475
1	7	533	551
1	8	1339	1358
1	9	791	808
1	10	812	824
1	11	307	312
1	12	373	385
1	13	200	202
1	14	411	420
1	15	228	268
2	15	355	364
2	13	220	209
2	12	621	639
2	11	184	188
2	10	594	623
2	9	666	664
2	8	103	26
2	7	330	318
2	6	841	841
2	5	980	951
2	4	1079	1020
2	3	987	975
2	2	673	579
2	1	262	342
2	0	1811	1858
3	0	518	542
3	1	966	875
3	2	1136	1176
3	3	490	462
3	4	373	401
3	5	893	886
3	6	1151	1172
3	7	1033	1071
3	8	1227	1249
3	9	168	206
3	10	376	360
3	11	455	454
3	12	509	485
3	13	563	578
3	14	963	982
3	15	293	298
4	14	179	178
4	13	414	423
4	12	618	636
4	11	368	370
4	10	199	209
4	9	534	512
4	8	904	901
4	7	477	451
4	6	477	498
4	5	1112	1152
4	4	1279	1307
4	3	1507	1526
4	2	412	392
4	1	1557	1665
4	0	1066	967
5	0	916	925
5	1	1455	1488
5	2	387	366
5	3	978	945
5	4	374	385
5	5	565	586
5	6	213	199
5	7	187	198
5	8	684	691
5	9	160	171
5	10	237	230
5	11	573	562
5	12	233	251
5	13	282	278
6	12	128	114
6	11	195	204
6	10	303	308
6	9	517	520
6	8	170	159
6	7	321	333
6	6	814	822
6	5	795	804
6	4	840	862
6	3	646	616
6	2	760	754
6	1	636	603
6	0	679	687
7	0	708	730
7	1	340	344
7	2	993	995
7	3	225	246
7	4	482	459
7	5	311	293
7	6	642	636
7	7	102	87
7	8	569	567
7	9	782	792
7	10	726	742
7	11	597	607
8	10	362	349
8	9	310	306
8	8	173	174
8	7	411	409
8	6	1093	1108
8	5	266	265
8	4	254	266
8	3	804	822
8	2	463	475
8	1	899	934
8	0	1706	1683
9	0	492	499
9	1	100	63
9	2	406	399
9	3	351	334
9	4	220	240
9	5	1323	1328
9	6	293	290
9	7	109	118
9	8	192	197
10	9	172	165
10	7	396	413
10	6	529	540
10	5	266	265
10	4	568	564
10	3	214	215
10	2	673	667
10	1	231	209
10	0	411	402
11	0	149	145
11	1	494	495
11	2	1112	1145
11	3	356	374
11	4	391	382
11	5	217	212
11	6	720	731
11	7	126	113
12	7	287	279
12	6	366	374
12	5	523	550
12	4	722	770
12	3	164	164
12	2	397	403
12	1	197	170
12	0	472	468
13	0	743	758
13	1	401	393
13	2	749	759
13	3	428	443
14	4	433	439
13	5	468	471
14	4	163	141
14	3	190	184
14	2	252	250
14	1	603	608
14	0	225	210
15	0	524	518
15	1	152	126
15	2	119	31
15	3	214	212
16	1	315	303
16	0	278	282
L=	7		
1	2	896	903
1	3	692	708
1	4	1880	1836
1	5	192	201
1	6	928	948
1	7	502	497
1	8	958	952
1	9	225	235
1	10	195	178
1	11	561	564
1	12	319	314
1	13	373	363
1	14	171	177
1	15	296	276
1	16	342	325
2	15	219	220
2	14	503	476
2	12	381	374
2	11	384	400
2	10	466	457
2	9	376	368
2	8	94	75
2	7	443	451
2	6	1091	1110
2	5	250	248
2	4	750	766
2	3	928	970
2	2	353	466
2	1	608	620
2	0	760	685
3	0	1161	1133
3	1	337	363
3	2	573	539
3	3	444	385
3	4	723	653
3	5	1448	1424
3	6	92	68
3	7	440	415
3	8	555	544
3	9	861	846
3	10	101	68
3	11	495	494
3	12	591	600
3	13	575	574
3	14	325	325
4	14	215	227
4	13	503	505
4	12	481	477
4	11	208	193
4	10	766	782
4	9	949	955
4	8	90	86
4	7	1014	999
4	6	104	90
4	5	958	947
4	4	539	510
4	3	1171	1151
4	2	105	145
4	1	1263	1262
4	0	646	662
5	0	833	808
5	1	511	513
5	2	1274	1246
5	3	465	461
5	4	447	423
5	5	1179	1171
5	6	136	155
5	7	302	306
5	8	615	604
5	9	395	424
5	10	355	345
5	11	166	130
5	12	137	150
5	13	234	234
6	12	337	328
6	11	398	411
6	10	621	620
6	9	620	599
6	8	385	376
6	7	108	75
6	6	534	531
6	5	184	187
6	4	735	745
6	3	357	370
6	2	156	129
6	1	490	489
6	0	1609	1573
7	0	782	747
7	1	716	712
7	2	693	704
7	3	439	423
7	4	829	801
7	5	951	926
7	6	460	475
7	7	271	264
7	8	257	271
7	9	736	723
7	10	486	475
7	11	358	359
8	11	190	198
8	10	297	308
8	9	751	737
8	8	459	473
8	7	215	233
8	6	505	484
8	5	771	774
8	4	523	537
8	3	292	306
8	2	675	646
8	1	723	706
8	0	748	732
9	0	906	879
9	1	575	558
9	2	411	416
9	3	367	379
9	4	263	276
9	5	238	233
9	6	653	664
9	7	348	353
9	8	552	550
9	9	133	142
10	9	293	285
10	8	198	209
10	7	245	246
10	6	247	253
10	5	272	274
10	4	125	86
10	3	738	735
10	2	568	542
10	1	1431	1405
10	0	120	95
11	0	656	659
11	1	459	453
11	2	218	209
11	3	590	600
11	4	401	418
11	5	671	657
11	6	337	348
11	7	473	464
12	7	279	249
12	6	562	557
12	5	468	464
12	4	96	80
12	3	432	412
12	2	550	542
12	1	640	628
12	0	760	748
13	0	736	743
13	1	202	209
13	2	553	543
13	3	379	366
13	4	225	239
13	5	413	398
14	4	121	133
14	3	275	279
14	2	440	449
14	1	332	337
14	0	494	497
15	1	230	229
16	1	739	744
L=	8		
1	1	377	373
1	2	1310	1277
1	3	464	479
1	4	262	255
1	5	431	428
1	6	320	365
1	7	433	429
1	8	892	894
1	9	276	298
1	10	374	379
1	11	113	113
1	12	339	339
1	13	109	126
1	14	132	93
1	15	175	183
2	15	142	160
2	14	453	451
2	13	561	568
2	12	716	713
2	10	262	269
2	9	626	628
2	8	342	333
2	7	270	284
2	6	446	409
2	5	625	599
2	4	1469	1474
2	3	1094	1132
2	2	438	471
2	1	906	868
2	0	589	595
3	0	375	370
3	1	813	787
3	2	633	602
3	3	476	514
3	4	534	530
3	5	352	357
3	6	621	616
3	7	800	779
3	8	704	679
3	9	731	764
3	10	1104	1099
3	11	388	379
3	12	104	82
3	13	158	148
3	14	336	328
4	13	160	142
4	12	206	213
4	11	346	361
4	10	186	162
4	9	1214	1221
4	8	592	584
4	7	149	157
4	6	216	212
4	5	318	265
4	4	731	713
4	3	1209	1216
4	2	1403	1396
4	1	230	215
4	0	1523	1509
5	0	469	469
5	1	326	314
5	2	362	391
5	3	1062	1094
5	4	994	968
5	5	380	391
5	6	111	89
5	7	138	98
5	8	331	331
5	9	604	614
5	10	148	141
5	11	330	329
5	12	162	181
5	13	399	371
6	11	254	238
6	10	260	279
6	9	327	342
6	8	157	146
6	7	175	171
6	6	631	611
6	5	304	299
6	4	476	478
6	3	502	512
6	2	122	101
6	1	926	928
6	0	151	149
7	0	942	924
7	1	612	622
7	2	618	616
7	3	265	250
7	4	96	80
7	5	701	676
7	6	797	803
7	8	1063	1049
7	9	340	328
7	10	488	492
7	11	363	350
8	10	650	643
8	9	296	285
8	8	756	754
8	7	168	154
8	6	546	544
8	5	409	429
8	4	1265	1254
8	3	608	588
8	2	242	241
8	1	217	217
8	0	449	441
9	0	313	345
9	1	1181	1179
9	2	829	801
9	3	250	265
9	4	479	485
9	5	624	627
9	8	332	337
9	9	459	466
10	9	524	519
10	8	121	51
10	7	313	303
10	6	235	224
10	5	141	120
10	4	553	568
10	3	210	205
10	2	387	382
10	1	331	343
10	0	804	798
11	0	138	116
11	1	221	223
11	2	260	229
11	3	178	174
11	5	277	273
11	6	400	414
11	7	282	297
12	6	123	110
12	5	200	191
12	4	145	133
12	3	193	194
12	2	301	305
12	1	827	836
12	0	760	752
13	0	300	298
13	1	618	611
13	2	505	504
13	3	436	429
13	4	217	240
13	5	331	335
14	4	164	160
14	2	145	124
14	1	469	469
14	0	233	232
15	0	283	277
15	1	505	480
15	2	886	863
16	1	187	194
16	0	337	338
L=	9		
1	2	660	668
1	3	721	725
1	4	945	925
1	6	677	698
1	7	762	757
1	8	994	988
1	9	130	131
1	10	232	229
1	11	145	128
1	12	137	164
1	13	131	126
1	14	174	162
1	15	120	110
2	15	234	236
2	14	710	699
2	12	336	328
2	11	579	576
2	10	429	432
2	9	185	182

Table 3. Continued.

K	H		
L=	9		
2	8	383	360
2	7	238	234
2	6	308	315
2	5	83	54
2	4	536	533
2	3	845	813
2	1	365	355
2	0	602	638
3	0	1485	1500
3	1	898	885
3	2	292	283
3	3	283	286
3	4	666	656
3	5	621	633
3	6	117	114
3	7	818	806
3	8	789	793
3	9	658	659
3	11	455	447
3	12	325	319
3	13	713	697
3	14	258	261
4	14	269	266
4	13	596	610
4	12	335	316
4	11	237	222
4	10	302	305
4	9	440	439
4	8	299	294
4	7	969	972
4	6	534	536
4	5	610	596
4	4	470	469
4	3	446	424
4	2	221	208
4	1	617	617
4	0	92	81
5	0	625	607
5	1	153	151
5	2	627	639
5	3	523	538
5	4	581	571
5	5	1138	1167
5	6	247	238
5	7	625	636
5	8	306	312
5	9	180	193
5	10	171	166
5	11	129	82
5	12	198	222
5	13	211	218
6	12	289	282
6	11	412	416
6	10	642	649
6	9	658	641
6	8	263	263
6	7	465	477
6	6	357	343
6	5	119	101
6	4	570	562
6	3	197	197
6	2	444	438
6	1	556	571
6	0	1536	1580
7	0	394	354
7	1	507	495
7	2	148	124
7	3	537	528
7	4	592	573
7	5	452	441
7	6	322	305
7	7	301	300
7	8	536	533
7	9	324	330
7	10	435	414
7	11	116	138
8	10	418	412
8	9	316	316
8	8	305	321
8	7	120	120
8	6	615	613
8	5	566	551
8	4	522	526
8	3	138	148
8	2	375	372
8	1	622	622
8	0	629	603
9	0	1286	1315
9	1	274	261
9	2	345	339
9	3	131	136
9	4	577	563
9	5	138	108
9	6	648	654
9	8	122	151
9	9	214	214
10	7	298	303
10	6	311	313
10	5	303	309
10	4	262	272
10	3	171	158
10	2	121	100
10	1	840	840
10	0	478	481
11	0	262	275
11	1	478	494
11	2	220	219
11	3	181	172
11	4	405	404
11	5	973	974
11	6	284	291
11	7	193	197
12	6	301	300
12	5	649	652
12	4	123	125
12	3	290	279
12	2	461	470
12	1	958	964
12	0	680	658
13	0	263	270
13	1	124	118
13	2	318	325
13	3	289	283
13	4	221	224
13	5	381	379
14	4	170	148
14	3	187	198
14	2	484	505
14	1	131	138
14	0	141	124
15	0	137	128
15	1	440	432
15	2	145	172
16	0	157	156
L=	10		
1	1	440	494
1	2	1322	1361
1	3	179	146
1	4	81	87
1	5	286	261
1	6	179	166
1	7	314	305
1	8	998	999
1	9	470	477
1	10	450	449
1	11	197	199
1	12	219	212
1	13	182	185
1	14	148	173
1	15	202	191
2	15	133	154
2	14	144	175
2	13	306	308
2	12	488	496
2	10	239	235
2	9	546	547
2	8	167	185
2	6	90	95
2	5	283	303
2	4	924	938
2	3	797	765
2	2	564	583
2	1	382	429
2	0	1102	1125
3	0	341	345
3	1	305	316
3	2	554	599
3	3	268	258
3	4	262	257
3	5	379	364
3	6	668	652
3	7	627	634
3	8	979	987
3	9	295	304
3	10	508	517
3	11	246	240
3	12	373	358
3	13	512	491
3	14	708	703
4	13	270	276
4	12	562	563
4	11	196	206
4	10	115	83
4	9	647	670
4	8	544	540
4	7	106	100
4	6	316	322
4	5	888	886
4	4	802	785
4	3	1219	1251
4	2	668	667
4	1	595	601
4	0	899	897
5	0	489	484
5	1	745	749
5	2	218	217
5	3	776	782
5	4	376	369
5	5	517	515
5	6	221	208
5	7	265	261
5	8	482	483
5	9	288	294
5	10	223	226
5	11	117	74
6	12	134	79
6	10	189	182
6	9	507	496
6	8	237	215
6	6	352	344
6	5	328	346
6	4	399	401
6	3	402	407
6	2	199	199
6	1	505	499
7	0	241	226
7	0	498	507
7	1	272	257
7	2	653	657
7	3	138	150
7	4	195	194
7	5	278	284
7	6	613	600
7	7	128	96
7	8	626	623
7	9	564	561
7	10	522	510
7	11	318	335
8	10	387	384
8	9	276	275
8	8	321	327
8	7	133	122
8	6	728	736
8	5	215	212
8	4	533	548
8	3	367	358
8	2	281	293
8	1	598	591
8	0	1275	1251
9	0	257	277
9	1	412	405
9	2	501	495
9	3	154	142
9	4	309	312
9	5	876	883
9	6	127	98
9	7	110	96
9	8	109	145
9	9	216	249
10	7	121	145
10	6	478	463
10	5	273	260
10	4	507	515
10	3	195	204
10	2	536	542
10	1	273	274
10	0	434	446
11	1	519	503
11	2	594	590
11	4	181	187
11	5	130	119
11	6	569	564
12	6	288	280
12	5	385	395
12	4	344	348
12	3	190	194
12	2	247	234
12	1	438	433
12	0	458	462
13	0	523	548
13	1	363	363
13	2	584	582
13	3	249	263
13	4	178	171
13	5	285	307
14	3	113	102
14	2	128	121
14	1	448	443
14	0	151	175
15	0	325	321
15	1	207	221
15	3	252	262
16	0	240	246
L=	11		
1	2	657	658
1	3	457	461
1	4	1476	1495
1	5	294	273
1	6	611	602
1	7	246	234
1	8	211	206
1	9	284	284
1	10	120	127
1	11	429	434
1	12	226	226
1	13	236	234
1	14	292	290
1	15	227	181
2	14	149	152
2	13	137	117
2	12	406	410
2	11	116	77
2	10	553	550
2	9	335	314
2	8	231	227
2	7	209	224
2	6	633	635
2	5	269	292
2	4	353	371
2	3	508	516
2	2	435	405
2	1	361	358
2	0	482	491
3	0	129	128
3	1	660	599
3	2	250	254
3	3	125	111
3	4	355	353
3	5	559	583
3	6	102	74
3	7	369	379
3	8	177	161
3	9	687	678
3	11	115	113
3	12	541	535
3	13	174	167
3	14	204	200
4	13	120	85
4	12	286	301
4	11	157	150
4	10	574	581
4	9	771	772
4	8	134	132
4	7	414	404
4	6	296	295
4	5	685	709
4	4	451	466
4	3	934	962
4	2	364	365
4	1	799	786
4	0	124	142
5	0	563	582
5	1	209	197
5	2	681	698
5	3	218	222
5	4	330	335
5	5	768	764
5	6	137	138
5	7	147	153
5	8	559	552
5	9	338	333
5	12	126	135
6	12	120	147
6	9	440	428
6	8	252	234
6	7	271	280
6	6	341	338
6	5	133	119
6	4	508	492
6	3	316	301
6	2	165	173
6	1	232	221
6	0	951	952
7	0	545	553
7	1	616	615
7	2	421	431
7	3	147	140
7	4	713	709
7	5	871	877
7	6	303	309
7	7	270	274
7	8	250	239
7	9	621	619
7	10	287	264
7	11	347	336
8	10	154	170
8	9	614	628
8	8	252	270
8	7	278	258
8	6	129	90
8	5	432	437
8	4	434	421
8	3	362	352
8	2	514	538
8	1	690	703
8	0	429	414
9	0	145	138
9	1	338	340
9	2	473	461
9	3	383	391
9	4	150	159
9	5	132	126
9	6	373	380
9	7	115	128
9	8	318	334
9	9	117	62
10	8	162	172
10	7	247	232
10	6	313	309
10	5	134	107
10	3	332	352
10	2	288	301
10	1	915	918
11	0	509	517
11	1	304	298
11	2	125	112
11	3	346	353
11	4	154	162
11	5	288	295
11	6	245	269
11	7	384	385
12	6	552	535
12	5	164	183
12	4	167	175
12	3	355	366
12	2	243	242
12	1	254	219
12	0	556	550
13	0	596	597
13	2	508	517
13	3	338	328
13	4	144	128
14	3	347	345
14	1	289	290
14	0	247	263

ing scheme according to Cruickshank was applied:

$\omega = 1/(a + |F_o| + c|F_o|^2 + d|F_o|^3)$ where the values of the constants were $a = 50$, $c = 0.0004$ and $d = 0.00009$.

Final atomic coordinates, vibrational parameters and corresponding standard deviations are given in Tables 1 and 2, and a comparison between the observed and calculated structure factors is reported in Table 3.

DESCRIPTION AND DISCUSSION OF THE STRUCTURE

The structure is built up of $H_6Mo_9PO_{34}^{3-}$-groups coordinated by sodium ions. Each Na^+-ion connects four adjacent groups by forming O–Na–O-bridges and in this way a three-dimensional network is formed.

The $H_6Mo_9PO_{34}^{3-}$-group. This group consists of a central PO_4 tetrahedron surrounded by nine MoO_6 octahedra. Three of the octahedra form a compact group in which each octahedron is linked to its neighbour on either side by a shared edge. The corner common to the three octahedra is then shared with the PO_4 tetrahedron. The structure of the compact group is shown in the upper part of Fig. 1.

The remaining six MoO_6 octahedra are then coupled together in a zigzag arrangement forming a ring. The ring may be considered as built up of three Mo_2O_{10}-groups linked together by sharing corners. The two MoO_6 octahedra in the Mo_2O_{10}-group share two oxygens in a common edge and one of these oxygens is shared with the PO_4 tetrahedron. The arrangement of the ring and the PO_4-group is illustrated in the lower part of Fig. 1. The ring is then linked to

Table 4. Distances (Å) and angles (degrees) within the $H_6Mo_9PO_{34}^{3-}$-group. The numbering of the atoms is in accordance with that shown in Table 1, with primes indicating atoms in symmetry related positions. The standard deviations given in parentheses refer to the last decimal place given.

Mo, P			
Mo1 – Mo1′	3.411(1)	P – Mo1	3.564(11)
Mo1 – Mo2	3.933(3)	P – Mo2	3.516 (2)
Mo1 – Mo3	3.690(3)	P – Mo3	3.486 (1)
Mo2 – Mo3	3.364(1)	Mo3 – Mo2 – Mo3′	117.23(4)
Mo2 – Mo3′	3.703(1)	Mo2 – Mo3 – Mo2′	117.04(4)
MoO_6-octahedra			
Mo1 – O(1)	1.713(9)	OP(11′1″) – Mo1 – O(13)	80.3(3)
Mo1 – O(11′)	2.080(7)	OP(11′1″) – Mo1 – O(12)	85.8(4)
Mo1 – O(11′)′	1.826(8)	OP(11′1″) – Mo1 – O(11′)	72.3(3)
Mo1 – O(12)	1.778(8)	OP(11′1″) – Mo1 – O(11′)′	76.4(3)
Mo1 – O(13)	2.075(8)	O(1) – Mo1 – O(13)	99.1(4)
Mo1 – OP(11′1″)	2.419(9)	O(1) – Mo1 – O(12)	104.9(4)
OP(11′1″) – O(13)	2.908(7)	O(1) – Mo1 – O(11′)	97.1(4)
OP(11′1″) – O(12)	2.894(7)	O(1) – Mo1 – O(11′)′	102.0(4)
OP(11′1″) – O(11′)	2.67 (1)	O(13) – Mo1 – O(12)	85.9(3)
O(1) – O(13)	2.89 (1)	O(12) – Mo1 – O(11′)′	101.2(3)
O(1) – O(12)	2.77 (1)	O(11′) – Mo1 – O(11′)′	87.0(4)
O(1) – O(11′)	2.85 (1)	O(11′) – Mo1 – O(13)	77.2(3)
O(1) – O(11′)′	2.75 (1)		
O(13) – O(12)	2.63 (1)		
O(12) – O(11′)′	2.79 (1)		
O(11′) – O(11′)′	2.70 (1)		
O(11′) – O(13)	2.59 (1)		
Mo2 – O1(2)	1.708(9)	O2(2) – Mo2 – O1(23)	97.2(5)
Mo2 – O2(2)	1.70 (1)	O2(2) – Mo2 – OP(23)	90.3(4)
Mo2 – O(12)	2.258(9)	O2(2) – Mo2 – O2(23)	98.8(5)
Mo2 – O1(23)	1.971(7)	O2(2) – Mo2 – O1(2)	104.9(5)
Mo2 – O2(23)	1.942(8)	O(12) – Mo2 – O1(23)	77.7(4)
Mo2 – OP(23)	2.312(7)	O(12) – Mo2 – OP(23)	76.8(3)
O2(2) – O1(23)	2.76 (1)	O(12) – Mo2 – O2(23)	81.5(3)
O2(2) – OP(23)	2.87 (1)	O(12) – Mo2 – O1(2)	88.4(5)
O2(2) – O2(23)	2.77 (1)	O1(23) – Mo2 – OP(23)	84.2(3)
O2(2) – O1(2)	2.70 (2)	OP(23) – Mo2 – O2(23)	72.9(3)
O(12) – O1(23)	2.66 (1)	O2(23) – Mo2 – O1(2)	97.8(4)
O(12) – OP(23)	2.84 (1)	O1(2) – Mo2 – O1(23)	100.1(4)
O(12) – O2(23)	2.75 (1)		
O(12) – O1(2)	2.79 (1)		
O1(23) – OP(23)	2.88 (1)		
OP(23) – O2(23)	2.55 (1)		
O2(23) – O1(2)	2.76 (1)		
O1(2) – O1(23)	2.83 (1)		
Mo3 – O1(3)	1.697(9)	O2(3) – Mo3 – O1(23)′	79.4(4)
Mo3 – O2(3)	2.21 (1)	O2(3) – Mo3 – OP(23)	80.4(3)
Mo3 – O(13)′	1.813(9)	O2(3) – Mo3 – O2(23)	81.2(4)
Mo3 – O1(23)′	1.825(8)	O2(3) – Mo3 – O1(3)	91.3(4)
Mo3 – O2(23)	1.886(7)	O(13)′ – Mo3 – O1(23)′	94.9(4)
Mo3 – OP(23)	2.375(7)	O(13)′ – Mo3 – OP(23)	87.7(3)
O2(3) – O1(23)′	2.60 (1)	O(13)′ – Mo3 – O2(23)	99.0(4)
O2(3) – OP(23)	2.96 (1)	O(13)′ – Mo3 – O1(3)	101.0(4)
O2(3) – O2(23)	2.68 (1)	O1(23)′ – Mo3 – OP(23)	80.8(3)
O2(3) – O1(3)	2.82 (1)	OP(23) – Mo3 – O2(23)	72.3(3)
O(13)′ – O1(23)′	2.68 (1)	O2(23) – Mo3 – O1(3)	99.9(4)
O(13)′ – OP(23)	2.93 (1)	O1(3) – Mo3 – O1(23)′	104.5(4)

Table 4. Continued.

O(13)′ – O2(23)	2.81 (1)		
O(13)′ – O1(3)	2.71 (1)		
O1(23)′ – OP(23)	2.75 (1)		
OP(23) – O2(23)	2.55 (1)		
O2(23) – O1(3)	2.74 (1)		
O1(3) – O1(23)′	2.79 (1)		
PO_4-tetrahedron			
P – OP(11′1″)	1.57 (2)	OP(11′1″) – P – OP(23)	108.0(6)
P – OP(23)	1.532(8)	OP(23) – P – OP(23)′	110.9(5)
OP(11′1″) – OP(23)	2.51 (1)		
OP(23) – OP(23)′	2.52 (1)		

the compact group by sharing of corners as outlined in the same figure. Fifteen of the oxygen atoms in the group are unshared, two per octahedron in the ring and one per octahedron in the compact group. The symmetry in the group is a three-fold rotation axis (parallel to the *c*-axis).

Distances and angles between the Mo-atoms are collected in Table 4. It can be seen that when the MoO_6 octahedra share edges the Mo – Mo distances are 3.41 Å (Mo1 – Mo1′) and 3.36 Å (Mo2 – Mo3).

When the octahedra share only a corner the distances increase to 3.70 Å (Mo2 – Mo3′), 3.69 Å (Mo1 – Mo3) and 3.93 Å (Mo1 – Mo2). All these Mo – Mo distances are quite normal [2] but the distance Mo1 – Mo2 = 3.93 Å is comparatively long. This is a result of the zigzag MoO_6 arrangement in the ring which in turn surely, is caused by the attached protons. However, the positions of these protons could not be determined in the present investigation.

The coordination of Na^+-ions around the $H_6Mo_9PO_{34}^{3-}$-groups. As mentioned above the $H_6Mo_9PO_{34}^{3-}$-group has fifteen unshared oxygens. To twelve of these Na^+-ions are coordinated. There is only one crystallographic sodium atom in the structure and this is attached to four Mo-oxygens, one in each of four different groups. In this way a three-dimensional network of $H_6Mo_9PO_{34}^{3-}$-groups connected by O – Na – O bridges is formed. In all there are twelve Na^+-ions around the group and since every ion is shared between four groups this implies that the charge of the group has been neutralized by the coordinated Na^+-ions.

The MoO_6-octahedra. Distances and angles are collected in Table 4. The MoO_6-octahedra are somewhat distorted from an ideal octahedron and the Mo – O distances can be divided into three groups according to the number of atoms that the oxygen atom is coordinated to:

(i) coordinated to one Mo atom, the distances are 1.71; 1.70; 1.71; 1.70; 2.21 (Å)

(ii) coordinated to two Mo atoms, the distances vary between 1.78 and 2.26 Å

(iii) coordinated to P and to two or three Mo atoms the distances vary between 2.31 and 2.42 Å.

The trend of increasing distances with increasing coordination numbers seems to be well documented. The same trend is found also in other structures.[2] An exception in the present study is the distance 2.21 Å occurring between Mo3 and O2(3). The explanation for this long distance must be that the oxygen is protonized.

The PO_4-tetrahedron. Distances and angles within the group are collected in Table 4. The distances P – O are 1.53 and 1.57 Å and the O – O distances are 2.51 and 2.52 Å. These distances and the angles O – P – O agree well with values found in other compounds containing phosphate groups and the group is almost regular.

The water molecules. The elemental analysis, calculation of formula weight from density and cell-volume as well as thermobalance analysis showed that the crystals contain 12 – 13 water molecules per formula unit. The positions of these water oxygens could, however, not be definitely determined in the structure analysis. One explanation for this could be that the water oxygen atoms are not structural. The positions of the oxygen atoms in relation to the Mo-atoms can also be so special that their contributions to the F_o-values are "drowned" in the contributions from the Mo-atoms. The small *R*-value (0.17), based on the Mo-atoms only,

shows how the contributions from these atoms dominate the intensity-material.

In earlier determinations of similar structures the Na^+-ions have always coordinated six oxygen atoms. The Na^+-ion in this structure coordinates four group-oxygens, therefore a reasonable assumption is that two water molecules should be found at a suitable distance from the sodium atom. Two of the highest peaks in the final difference Fourier map are also in such positions. (As these are general six-fold positions the two peaks correspond to six water molecules per formula unit). When these atoms were included in the refinement their temperature factors became very large and they were excluded in the final refinement. The positions of these presumed water oxygen atoms are, however, given in Table 1. It has not been possible to locate the remaining water molecules, perhaps they may be in the channels that can be found in the structure. In order to determine these remaining water oxygen positions, the intensity material must be completed with reflexions in a higher $\sin \theta/\lambda$ range perhaps also collected at lower temperatures. Work in this direction is in progress.

Acknowledgements. I thank Professor Nils Ingri for much valuable advice, for his great interest, and for all the facilities placed at my disposal. Thanks are also due to Dr. Lage Pettersson and Lab. ing. Ewa Lundström for much valuable help. The English of the present paper has been corrected by Dr. Michael Sharp. The work forms part of a program supported by the Swedish Natural Science Research Council.

REFERENCES

1. Pettersson, L. *Acta Chem. Scand. Submitted for publication.*
2. Hedman, B. *Acta Chem. Scand. 27* (1973) 3335.
3. Cromer, D. T. and Waber, J. T. *Acta Crystallogr. 18* (1965) 104.
4. Hanson, H. P., Herman, F., Lea, J. D. and Skillman, S. *Acta Crystallogr. 17* (1964) 1040.
5. *International Tables for X-Ray Crystallography,* Kynoch Press, Birmingham 1962, Vol. III.

Received October 25, 1973.

Acta Chemica Scandinavica A 28 (1974) 226—228

Measurements of Phase Equilibria in the Aluminium–Aluminium Sulfide System

TORMOD FØRLAND,[a] JAIRO GOMEZ,[a,*] SIGNE KJELSTRUP RATKJE[a] and TERJE ØSTVOLD[b]

[a] The University of Trondheim, Norwegian Institute of Technology, Division of Physical Chemistry, Trondheim, Norway and [b] The University of Trondheim, College of Arts and Science, Chemistry Department, Trondheim, Norway

Measurements of phase equilibria in the system $Al - Al_2S_3$ in the region 0.5 – 1.0 mol fraction Al_2S_3 were performed by using differential thermal analysis, quenching and X-ray techniques. The $Al - Al_2S_3$ system shows an intermediate compound, the subsulfide AlS, which seems to be stable only at high temperatures (between 1010 and 1060°C). A eutectic point exists in the Al_2S_3 rich end of the phase diagram and a peritectic point close to the AlS composition. The phase diagram proposed is different from those previously reported.

The system $Al - Al_2S_3$, aluminium – aluminium sulfide, is of interest both from a theoretical and from an industrial point of view. Aluminium sulfide may be an important reagent in the production of aluminium using a non-electrolytic method.[1,2] It is fundamental for such processes to know the phase equilibria of the system $Al - Al_2S_3$. Moreover, the study of this system is important in the field of metal-metal salt equilibria.

There has been little experimental data reported for the system aluminium – aluminium sulfide and the phase diagrams proposed differ widely.[3,4] The first investigators to study the change in the melting point of aluminium sulfide after the addition of aluminium were Biltz and Caspari.[5] Murakami and Shibata [3] first proposed a complete phase diagram based on chemical and X-ray studies. These authors reported two compounds in the system, AlS with a very high melting point, 2100°C, and Al_2S_3, formed by a peritectic reaction between AlS and a liquid. These results have not been confirmed neither by other investigators [4,5] nor by the present work. The melting point reported by these authors for the compound AlS is particularly high and this is probably due to some contamination from aluminium oxide in the samples.

The phase diagram proposed by Kohlmeyer and Retzlaff [4] is in better agreement with our experimental data. The melting points for the compounds Al_2S_3 and AlS are given as 1100 and 1200°C, respectively. There is a liquid miscibility in this system which starts at 1070°C. The diagram is, however, only ment to be hypothetical. Some sections of the diagram violate the phase rule and the continuous liquid – Al_2S_3 region starting from pure Al_2S_3 and increasing in temperature was not observed by Biltz and Caspari [5] and the present authors.

The subsulfide Al_2S is observed in the gas phase.[6,7] Different modifications of Al_2S_3 are also reported.[8]

EXPERIMENTAL

Al_2S_3 was prepared by direct synthesis between sulfur(g) and aluminium(l) [2] employing a method similar to the one proposed by Kohlmeyer and Retzlaff.[4] Chemical analysis showed an excess of 10 ± 2 mol % Al in the sulfide compared with stoichiometric Al_2S_3. Emission spectrographic analysis indicated impurities of Fe, Mg, and Si in the 0.5 weight % range. The excess aluminium in the sulfide was essentially metallic aluminium dissolved in the salt. Alloys of aluminium and aluminium(III) sulfide, were prepared at 1200°C

* Present address: Facultad De Minas, Universidad Nacional de Colombia, Medellin, Colombia.

in an ordinary laboratory furnace, which had an argon tight water cooled quenching device connected at the bottom. After quenching, the samples were examined by chemical, X-ray, and DTA studies.

DTA was carried out in a platinum furnace. The sample and reference material (Al_2O_3) were mounted in graphite and platinum crucibles, respectively, in an alsint block. A graphite crucible was necessary because the sulfide samples attack platinum. The temperature and differential temperature were measured by Pt/Pt 10 % Rh thermo-couples calibrated against the melting point of silver. The DTA curves were recorded by a Varian G 2022 Dual Channel Recorder and the signal was amplified by use of DC Microvolt Amplifier, (Leeds & Northrup, USA). Sample size varied from 0.5 to 1.5 g. The heating rate was 9 – 10°C/min and the cooling rate 5 – 6°C/min.

The room temperature X-ray experiments of quenched samples were performed using a Debye-Scherrer camera. The samples were ground to a very fine particle size and filled in 0.5 mm O.D. low absorption glass capillary tubes in a dry box. Qualitative high temperature X-ray diffraction studies were carried out in a metal ribbon furnace, similar to the one described by Smith.[9] The heating element was a platinum – 10 % rhodium sheet which also served as sample holder. The temperature was recorded with a Pt/Pt 10 % Rh thermocouple welded to the strip.

The DTA and X-ray equipment has been described in detail elsewhere.[2] All high temperature work was carried out in an atmosphere of purified argon (99.99 %, Norsk Hydro, Norway).

RESULTS

The phase diagram of the system Al – Al_2S_3 is presented in Fig. 1. This diagram is drawn mainly from DTA results. Both heating and cooling curves were recorded during DTA-runs, and the lower temperatures obtained for phase changes observed during cooling indicate some supercooling of the liquid in these melts. Some preliminary high temperature X-ray powder patterns obtained were in qualitative agreement with the phase change indicated at 1010°C. The phase diagram must be considered only as preliminary since precise high-temperature X-ray data are lacking. Moreover, the melting point of the pure sulfide was not obtained experimentally because of difficulties in obtaining pure Al_2S_3. The indicated melting point of Al_2S_3, $T_f = 1100$°C, is reported elsewhere.[3,4,10]

The solubility of aluminium in aluminium sulfide, Al_2S_3, was determined by quenching experiments and confirmed by X-ray and chemical analysis. Aluminium dissolves very slowly in aluminium(III) sulfide, especially after the composition has exceeded 30 mol % aluminium. With alloys of more than 20 mol % aluminium stirring in periods of 48 h or more, was necessary to dissolve the metal. The maximum solubility obtained, after 10 days at 1200°C and continuous stirring, was 51.0 mol %

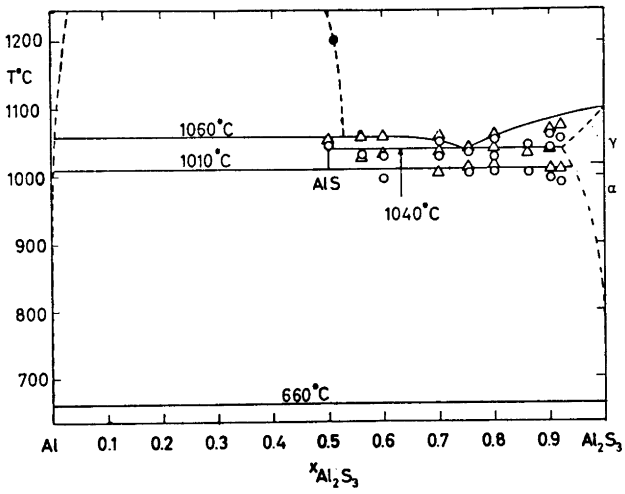

Fig. 1. Preliminary phase diagram for the system Al – Al_2S_3. ○: DTA cooling curves. △: DTA heating curves. ●: Solubility.

aluminium. The same results were obtained, with similar conditions, after one week.

After quenching of samples of different compositions, powder patterns at room temperature were obtained using a Debye-Scherrer camera. The X-ray results for the aluminium(III) sulfide rich phases showed essentially the lines given in the ASTM table 1-0726 for pure Al_2S_3. Samples with a composition higher than 25 mol % aluminium showed some additional lines. At the composition AlS, the quenched samples showed different lines than the ones given in the ASTM tables either for pure Al_2S_3 or for aluminium (ASTM table 4-0787). It was assumed this was the X-ray pattern of the compound AlS. Also, powder X-ray diagrams were obtained for the Al_2S_3 compound which contained some Al metal ($\approx$10 mol %). The lattice parameters were calculated for the α modification of Al_2S_3 (10 mol % Al in excess). These values were slightly higher than the ones determined by Flahaut.[8]

The phase diagram for the system aluminium-aluminium sulfide presented in this work, shows some new features when compared with the diagrams proposed previously.[3,4] A eutectic point was observed in the system at composition 25 mol % aluminium and 1040°C. At the eutectic point a liquid AlS, and a mixture of Al_2S_3 and AlS should coexist in equilibrium. This finding has not previously been reported.

The system shows as intermediate compound, the subsulfide AlS, which is stable at temperatures higher than 1010°C. At 1010°C there is a peritectic transformation at which AlS decomposes to Al_2S_3(s) and Al (l) according to the following equation:

$$3\,AlS(s) \rightleftharpoons Al_2S_3(s) + Al(l)$$

This result agrees with a previous finding,[4] eventhough the temperature is a little higher.

It was found that AlS melts at 1060°C. Its solubility in aluminium is probably very small. The melting point found for AlS is lower than that reported previously.[3,4]

No other compounds were found in this system in the condensed state. This confirms the results of Klemm [6] and Margrave *et al.*[7] who reported that the compound Al_2S only exists in the gas phase.

There is a miscibility gap in the liquid state reaching from somewhere around 50 mol % Al to the Al rich side of the phase diagram. It can be observed from the $Al - Al_2S_3$ phase diagram presented in Fig. 1 that at a temperature above 1010°C a mixture of Al_2S_3 and AlS coexist at equilibrium. Below 1010°C such a mixture decomposes to liquid aluminium metal and solid Al_2S_3. It was found that the addition of about 10 mol % BaS to the $Al - Al_2S_3$ mixtures in the concentration range 50 to 10 mol % Al reduced the liquidus temperature to about 960°C, that is below the decomposition temperature of AlS. From these observations one may conclude that the barium sulfide containing $Al - Al_2S_3$ melts may be used in a preparation of aluminium metal from aluminium – silicon alloys.

Acknowledgement. The authors want to express their gratitude to Elkem A/S Norway for financial support and also for many stimulating discussions with Elkem's experts on aluminium production.

REFERENCES

1. Vereinigte Aluminium-Werke. *A-G-Brit.* 763, 709 (1955).
2. Gomez, J. Thesis, *An Investigation on the Solubility of Metallic Aluminum in Sulfides*, The University of Trondheim 1973.
3. Murakami, T. and Shibata, N. *Nippon Kinzoku Gakkaishi. 4* (1940) 228.
4. Kohlmeyer, E. J. and Retzlaff, H. W. *Z. Anorg. Allg. Chem. 261* (1950) 248.
5. Biltz, W. and Caspari, F. *Z. Anorg. Allg. Chem. 71* (1911) 182.
6. Klemm, W. *Z. Anorg. Allg. Chem. 255* (1948) 287.
7. Margrave, J. L., Ficalora, P. J. and Hastie, J. W. *J. Phys. Chem. 72* (1968) 1660.
8. Flahaut, J. *Ann. Chim. (Paris) 7* (1952) 632.
9. Smith, D. K. *Norelco Rep. 10* (1963) 19.
10. Klemm, W., Geierberger, K., Schaeler, B. and Mindt, M. *Z. Anorg. Allg. Chem. 255* (1948) 287.

Received September 26, 1973.

Acta Chemica Scandinavica A 28 (1974) 229—232

Application of the Grain-counting Technique to Electron Diffraction Experiments

B. TURMAN and PER ANDERSEN

Department of Chemistry, University of Oslo, Oslo 3, Norway

The grain-counting technique has been applied to determine the scattered electron intensity recorded on photographic plates from gas electron diffraction experiments. Photographic plates were made with 1 μ emulsion thickness from an Ilford K-5 nuclear research emulsion. A microscope focused the grain image into a television camera and signals from the camera were analyzed by a special logic circuit.

The scattering pictures from CCl_4 and CO_2 were studied using this technique and the results compared with calculated theoretical curves based on the well known structures of these molecules.

In the normal electron diffraction experiment a photographic plate is used to record scattered electron intensity. The photographic density of the exposed plate is measured with a photometer and converted to electron exposure. A new technique was developed at Uppsala University for obtaining intensity information from plates.[1-3] In this method, the number of developed grains per unit area in the emulsion is observed and related to exposure. Rundgren pointed out that this method would be useful for intensity measurements in the electron diffraction experiment.[4] Use of the grain-counting method in electron diffraction work has been studied in this laboratory, and the results are reported in this paper.

EXPERIMENTAL ARRANGEMENT

The principle of operation of the grain counting equipment is described in Ref. 2. A 100-power microscope focused the grain image into a television camera, the observation area on the plate being 0.01 mm^2. Signals from the camera were detected and analyzed by a special logic circuit and data output was printed on paper tape. Dark field illumination, with a tungsten lamp source, was used in the microscope. With dark-field illumination, light was projected downward onto the silver grains, so that grains were viewed as bright objects against a dark background. The image contrast was higher than that observed with bright-field illumination, and dust particles on the optical components would not be mistaken for grains. Since oil immersion was required on both sides of the glass plate, the use of dark-field illumination presented a special problem. The light intensity was found to be dependent on the oil film thickness, so that care was required to maintain this film at a constant thickness during a scan across the plate. The rectangular stage movement provided on the microscope was used to scan through the diffraction pattern. The radial distance from the pattern center was determined by a dial indicator to an accuracy of 0.01 mm. The microscope and television camera were mounted on an isolated table to protect them from mechanical vibration.

The depth-of-focus of the microscope objective lens was quite small, of the order of 1 μ. The thinnest emulsion available commercially was about 5 μ, so that a subjective error could be made in focusing the microscope. To eliminate this problem, plates with 1 μ emulsion thickness were made in this laboratory. Ilford K-5 nuclear research emulsion in gel form was used. After the emulsion was melted at 50°C, it was poured over a treated glass plate. A stainless steel blade was pulled across the plate, spreading the emulsion uniformly and setting the desired emulsion thickness. The emulsion was then allowed to cool slowly.

The electronic equipment was manufactured by Securitas Corporation of Sweden. The television camera and power supply were of standard design. The output signal from the camera was led into a detector-discriminator circuit. The discriminator level was adjusted so that noise was eliminated and only pulses

arising from the grain image were analyzed in the logic circuit. The logic circuit could be operated in one of three modes, called "project", "count", and "area". In the first mode, all pulses coming from a grain image were counted. Since the grain image dimensions in our apparatus were typically about 7 times as large as the television scan width, approximately 7 pulses were produced from one grain. In effect, the number of pulses in this mode gave the length of the grain projection on an axis perpendicular to the television scan direction. In the second mode, only one pulse was produced per grain. To accomplish this feat, a delay line and anti-coincidence circuit were provided. The pulse from a grain image was divided into two parts: one part went directly to the anti-coincidence circuit, while the second pulse traveled through the delay line. The time delay was adjusted so that this delayed signal arrived at the anti-coincidence circuit simultaneously with the next direct pulse. The direct pulse was blocked under these conditions. Thus only the first direct pulse was passed, and the counting unit counted total number of grains. In the area mode, both the total number of pulses and the time duration of each pulse were measured, so that the output from the counter was related to the area of the grains. A series of reproducibility measurements were made with the count and project modes. The project mode was better in this respect than the count mode; approximately 1 % deviation in the project data and 5 % deviation in the count data were observed. Averaging 10 measurements with the count mode improved the reproducibility to a figure similar to that of the project mode.

Irregularities in grain shape could upset the operation of the grain counting system. For instance, a crescent-shaped grain was often counted twice in the count mode, while a long, narrow grain could give a misleading projection value in the project mode. The error due to this effect, however, was small. One solution to this problem might be the use of physical development [6] for the plates, since grain shape and size could be regulated in this process.

DATA ANALYSIS AND RESULTS

Two molecules were studied in this experiment: CCl_4 and CO_2. The molecular structures and vibrational data of these two compounds are of course well documented, so that theoretical scattering functions can be assumed to represent ideal experimental results. The data for CCl_4 were taken with the count mode, while the project mode was used for CO_2 data. Each plate was scanned at least three times. At each measurement point along the scan line the number of grains within at least three different areas was averaged. The three scans were then averaged together with the statistical averaging program of Stølevik.[5] A total number of about 1000 counts was taken at each measurement point. Next, the sector correction was applied and the theoretical background removed. Finally, a smooth background function through the experimental points was determined by a least squares program written by Strand.[5] Only the molecular scattering function remained after subtraction of the background function.

It was found that the measured intensity required a blackness correction. The one-hit blackness correction,[6] responsible for the exposure characteristics of emulsions at higher densities, showed practically no effect at the low photographic density used in this experiment. The main effect appeared to be due to the formation of grain clusters which were counted as single grains. Since all of the grains were observed to lie essentially in a plane, a two-dimensional theory should be sufficient to describe the clustering. Considering only two and three-grain clusters, the corrected intensity would have the form $(1+\alpha N)(1+\beta N)N$, where N was the number of grains counted. A least squares procedure was used to find the values of α and β which gave the best agreement between corrected experimental molecular intensity and theoretical molecular intensity. These parameters were: $\alpha = 0.04$, $\beta = 0.0018$. A calculation of the effect of four-grain clustering showed less than 1 % change in the correction. Reasonable agreement with these values for the parameters was obtained from a theoretical calculation based on the observed grain

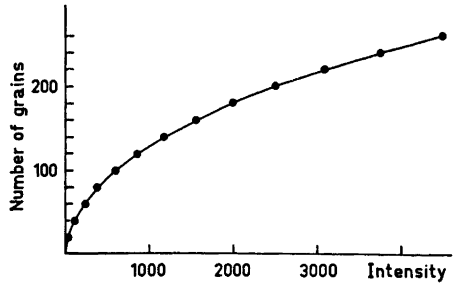

Fig. 1. Corrected intensity of the form $(1+0.04N)(1+0.0018N)N$ where N is the number of grains counted.

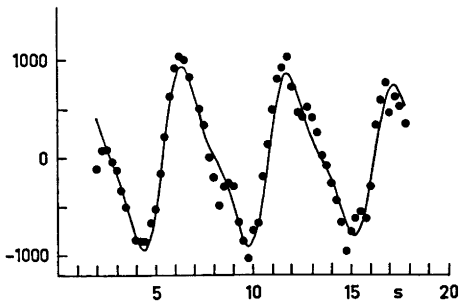

Fig. 2. Theoretical intensity curve for CO_2(—) and corresponding experimental points (●) from the grain-counting experiment.

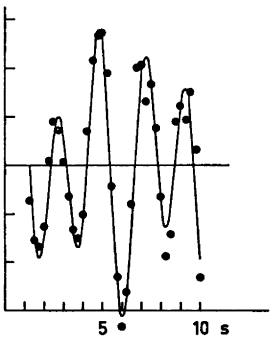

Fig. 3. Theoretical intensity curve for CCl_4(—) and the corresponding experimental points (●) from the grain-counting experiment.

size. Fig. 1 shows the form of this correction curve.

The project mode data were divided by the mean projection per grain to obtain the number of grains counted. This ratio was determined by counting with both the project and count modes at a large number of points on the photographic plate, and then treating the data with the least squares method. The value of the ratio was 7.43. This number is of course dependent on the magnification of the microscope and the grain size of the emulsion.

Experimental results from CO_2 and CCl_4 scattering patterns are compared with theoretical curves in Figs. 2 and 3. As stated earlier, these molecules have been so thoroughly studied that any discrepancies between theory and experiment here must be interpreted as experimental errors. There are several bad points which deviate considerably from the theoretical curve for CO_2. The least squares calculation of blackness correction will be influenced by these points, since the criterion is to minimize the sum of the squared deviations. Therefore the calculated blackness correction may be a bit conservative, so that the experimental data at low s-value may agree with theory slightly better than shown here. The CCl_4 data have been multiplied by the blackness correction determined from the CO_2 curves. Again there is considerable deviation from the theoretical curve, and a small increase in blackness correction for small s-values would be helpful. Random deviations in the number of grains developed per unit area in the emulsion are probably the major source of error in these measurements. Since a total of about 1000 grains were counted at each s-value, the statistical error is approximately 3 % on the total scattering intensity, or roughly 20 % on the molecular scattering. This error can be reduced by collecting a larger number of counts. For example, the plate could be scanned in concentric circles, thereby assuring a very large number of counts. Another advantage in the circular scan would be that any emulsion imperfections could be easily detected and discarded. The collection of large numbers of counts demands the use of an automated system, but the problem of automatically focusing the microscope has yet to be solved.

The main advantage in using the grain counting technique rather than the photometer is that a much smaller electron exposure is required when the individual grains are counted. In the present experiment, only one-tenth the normal exposure was used. The maximum number of grains counted was around 200 grains per 0.01 mm², and from Fig. 1 it appears that an even lower exposure would be better. This lower exposure could be of great benefit when analyzing highly reactive compounds, or small quantities of a compound. In addition, the grain-counting method should be useful in those problems in X-ray crystallography where a reduction of exposure time is important.

Acknowledgement. One of us (B. T.) gratefully acknowledges financial support from the *Royal Norwegian Council for Scientific and Industrial Research.*

REFERENCES

1. Carlsson, R., Fahlman, A., Hallin, R. and Siegbahn, K. *Ark. Fys. 32* (1966) 99.
2. Carlsson, R., Fahlman, A. and Siegbahn, K. *Uppsala University Institute of Physics Report* (1966) 485.
3. Fahlman, A. and Siegbahn, K. *Ark. Fys. 32* (1966) 111.
4. Rundgren, J. *Ark. Fys. 35* (1967) 31.
5. Andersen, B., Seip, H. M., Strand, T. G. and Stølevik, R. *Acta Chem. Scand. 23* (1969) 3224.
6. Mees, C. and James, T. *The Theory of the Photographic Process*, McMillan, New York 1966.

Received October 12, 1973.

Acta Chemica Scandinavica A 28 (1974) 233—238

The Crystal Structure of $[Pb_4(OH)_4](ClO_4)_4.2H_2O$

SAM-HYO HONG and ÅKE OLIN

Institute of Chemistry, University of Uppsala, S-751 21 Uppsala, Sweden

The crystal structure of $[Pb_4(OH)_4](ClO_4)_4.2H_2O$ has been determined from three-dimensional X-ray data. The crystals are monoclinic and the space group is $P2_1/c$. The dimensions of the unit cell are $a = 16.665 \pm 0.009$ Å, $b = 9.168 \pm 0.006$ Å, $c = 14.227 \pm 0.006$ Å, $\beta = 112.09 \pm 0.03°$ and it holds 4 formula units. The uncertainties given are three times the estimated standard deviations.

The structure contains discrete $[Pb_4(OH)_4^{4+}]$-units in which the lead atoms occupy the corners of a slightly distorted tetrahedron and the hydroxide groups are located outside the faces of this tetrahedron. The same unit has previously been found in $[Pb_4(OH)_4]_3(CO_3)(ClO_4)_{10}.6H_2O$ as well as in the solution from which the title compound crystallizes.

From solutions containing more than one mol but less than two mol of $HClO_4$ per mol of PbO crystalline lead(II) hydroxide perchlorates can be prepared. According to Ref. 1 Marignac apparently was the first to report on these compounds. He obtained two solids to which he ascribed the same formula, $Pb_2O(ClO_4)_2.2H_2O$. Only one of them was stable in contact with air. These findings were later confirmed by Weinland and Stroh,[2] but the formula was changed to $Pb_2(OH)_2(ClO_4)_2 \cdot 1.5H_2O$ which agreed better with their analysis. The solutions from which these solids crystallize contain $[Pb_4(OH)_4^{4+}]$ as a main species. X-Ray scattering studies [3,4] on solutions containing the complex have been interpreted in terms of a Pb_4-tetrahedron with one hydroxide group outside each of the four faces of the tetrahedron. This interpretation is corroborated by the crystal structure determination of $[Pb_4(OH)_4]_3(CO_3)(ClO_4)_{10}.6H_2O$.[5] This compound was, however, obtained from solutions which has been exposed to the carbon dioxide of the air. Since the compound written above as $Pb_2(OH)_2(ClO_4)_2 \cdot 1.5H_2O$ is normally formed a crystal structure determination of this solid was considered appropriate.

EXPERIMENTAL

Preparation and analysis of the crystals. The crystals were obtained from a hydrolysed lead(II) perchlorate solution prepared by dissolving lead(II) oxide in perchloric acid to give a ratio OH:Pb = 0.8 (mol-mol) in the resulting solution. This ratio should be well below 1 since otherwise α-$[Pb_6O(OH)_6](ClO_4)_4.H_2O$ may be formed together with the desired compound. This observation may explain why Willard and Kassner,[6] who worked with solutions with OH:Pb = 1, could not confirm the earlier works by Marignac, and Weinland and Stroh.

After dissolution in water the crystals were analysed as follows. The lead content was determined gravimetrically as $PbSO_4$ and the number of basic groups was found from a titration with standard perchloric acid using a Gran plot to obtain the equivalence point. No analysis of the water content was made. The ratio OH:Pb was found to be 0.98 and the lead content 62.18 %. Calculated lead content for $Pb_2(OH)_2ClO_4)_2.H_2O = 62.28$ % and for $Pb_2(OH)_2(ClO_4)_2 \cdot 1.5H_2O = 61.45$ %.

X-Ray diffraction measurements. The space group was determined from oscillation and equi-inclination Weissenberg photographs. The unit cell dimensions were calculated from 42 indexed lines on a powder photograph taken with a Guinier-Hägg focussing camera using Cr$K\alpha_1$ ($\lambda = 2.28962$ Å) with silicon ($a = 5.4305$ Å) as internal standard. The intensity data were collected with a Stoe Weissenberg diffractometer using Ni-filtered Cu$K\alpha$ radiation under essentially the same experimental conditions as described previously.[7] The data were corrected for background and converted to the standard scan rate 1°/min. The expressions in Ref. 7 were used in the calculations of the corrected intensities, I, and their standard deviations, $\sigma(I)$. The crystal was rotated about the b-axis and 2047 independent reflections

were measured from 8 layers. The crystals decompose in the X-ray beam. Therefore a new crystal was mounted for each layer. The scale factors between the different crystals were obtained from three standard reflections in the zero layer, which were measured before the crystal was used to collect the data for a layer. An approximate correction for the decomposition was obtained as follows. Three reflections were remeasured at regular intervals during the recording of a layer. The mean of the relative values of the intensities of these reflections at the beginning and at the end of an interval were used by linear interpolation to correct the data collected during the interval. The correction so introduced was 30 % or more in I for the last reflections measured in a layer.

$|F|$- and $\sigma(F)$-values were calculated from I- and $\sigma(I)$-values by applying absorption, Lorentz and polarization corrections. The atomic scattering factors were taken from Hanson *et al.*[8] and the real part of the dispersion correction was introduced.

CRYSTAL DATA

Formula unit:	$[Pb_4(OH)_4](ClO_4)_4.2H_2O$
Lattice parameters (σ):*	$a = 16.665(3)$ Å; $b = 9.168(2)$ Å; $c = 14.227(2)$ Å; $\beta = 112.09(1)°$; $V = 2014$ Å^3
Density (measured):	4.39 g cm^{-3}
Number of formula units per unit cell:	4
Density calculated:	4.389 g cm^{-3}
Linear absorption coefficient:	698 cm^{-1} (Cu$K\alpha$)
Systematic absences:	$0k0$ for $k = 2n+1$ $h0l$ for $l = 2n+1$
Space group:	$P2_1/c$

STRUCTURE SOLUTION

The $|F|$-values were converted to $|E|$-values and 216 of these with $|E| > 1.70$ were used to solve the structure by means of the sign-determining program written by Long.[9] This program uses Sayre's relation $s(E_{hkl}) \approx s(E_{h'k'l'})s(E_{h-h',k-k',l-l'})$ to predict the signs. The starting set consisted of seven $|E|$-values. Three of these (h,k,l,E $-7,3,5,3.72$; $-11,4,3,3.35$; $-6,2,7,2.77$) were given plus signs in order to fix the origin of the unit cell. The signs of the remaining four (h,k,l,E; $-9,4,9,3.38$; $4,3,5,3.11$; $8,0,2,2.57$; $4,1,2,2.50$) were varied systematically. Of the 16 starting sets of signs so obtained, two had a consistency index[9] greater than 0.99 and converged in 7 cycles. E maps were calculated for these sets. Only the set with the highest consistency index (0.999) showed the required four large peaks from the four lead atoms in the asymmetric unit. The positions of these atoms were checked against a three-dimensional Patterson synthesis. All the expected maxima corresponding to Pb–Pb vectors were found. The predicted signs were later found to all agree with those in the final list of calculated structure factors.

The chlorine atoms, the oxygen atoms bound to the lead atoms, and the water oxygens were found without difficulty from consecutive Fourier synthesis of ΔF alternating with least squares refinements. Most of the perchlorate oxygens were found in the same way but a few of them were quite poorly resolved. These were allocated to maxima consistent with the known geometry of the perchlorate ion.

The final refinement of the structure was carried out with anisotropic temperature factors for the lead atoms. Reflections with $|F| < 3\sigma(F)$ were excluded and no correction for extinction was applied. $\Sigma w(|F_o| - |F_c|)^2$ was minimized and the weighting function $w^{-1} = \sigma^2(F) + (kF)^2$ was used. The value of k in the final cycles was 0.05. The refinement was continued until the shifts were less than 0.2σ except for some of the perchlorate oxygen coordinates. It was found necessary to fix the coordinates from the ΔF map of one of the perchlorate oxygens, O(44), since the refinement shifted this atom to a position with an improbable Cl–O distance. The conventional R-value for the last cycle was 0.074 for 1840 reflections. The atomic parameters from this cycle are listed in Table 1.

DESCRIPTION AND DISCUSSION OF THE STRUCTURE

The lead atoms and the hydroxide groups form units of composition $Pb_4(OH)_4^{4+}$. The

* Estimated standard deviations here and elsewhere in the paper refer to the least significant digits.

Table 1. Final positional and thermal parameters with standard deviations (σ) within parentheses. O(1) – O(4) are hydroxide and O(5) – O(6) water oxygens.

Atom	x	y	z	B(Å^2)
Pb(A)	0.2296(1)	0.3346(2)	0.0963(1)	
Pb(B)	0.3252(1)	0.6829(2)	0.2463(1)	see below
Pb(C)	0.1623(1)	0.4597(2)	0.3044(1)	
Pb(D)	0.3985(1)	0.3105(2)	0.3652(1)	
O(1)	0.315(2)	0.529(3)	0.373(2)	4.3(5)
O(2)	0.365(1)	0.436(2)	0.210(2)	3.4(4)
O(3)	0.251(2)	0.257(3)	0.269(2)	4.7(5)
O(4)	0.195(1)	0.549(2)	0.168(2)	3.0(4)
O(5)	0.073(2)	0.302(4)	0.114(3)	5.1(7)
O(6)	0.187(2)	0.757(4)	0.325(3)	5.3(8)
Cl(1)	0.3704(6)	0.569(1)	−0.0145(7)	2.1(2)
O(11)	0.401(3)	0.708(4)	−0.038(3)	6.0(9)
O(12)	0.444(3)	0.497(4)	0.064(3)	6.5(9)
O(13)	0.347(3)	0.470(4)	−0.103(3)	8(1)
O(14)	0.298(3)	0.596(4)	0.012(3)	6.2(8)
Cl(2)	0.4282(7)	0.091(1)	0.1393(8)	3.0(2)
O(21)	0.358(3)	0.161(4)	0.059(3)	5.9(8)
O(22)	0.491(4)	0.058(6)	0.092(5)	12(2)
O(23)	0.479(4)	0.190(6)	0.223(5)	11(2)
O(24)	0.420(7)	−0.060(9)	0.143(8)	18(3)
Cl(3)	0.0604(6)	0.071(1)	0.3518(7)	2.3(2)
O(31)	0.087(2)	−0.013(3)	0.440(2)	4.9(7)
O(32)	0.053(2)	−0.005(5)	0.268(4)	9(1)
O(33)	−0.018(3)	0.144(4)	0.328(3)	7(1)
O(34)	0.128(2)	0.177(4)	0.364(3)	5.3(7)
Cl(4)	0.1512(8)	−0.069(1)	0.0522(8)	3.5(2)
O(41)	0.198(6)	−0.028(8)	0.158(7)	17(3)
O(42)	0.103(4)	−0.179(7)	0.066(5)	12(2)
O(43)	0.219(6)	−0.113(9)	0.027(7)	18(3)
O(44)	0.117(−)	0.018(−)	−0.024(−)	15(−)

Coefficients ($\times 10^5$) in the expression $\exp -(B_{11}hh + \cdots + 2.B_{12}hk + \cdots)$ for the anisotropic temperature factors for lead.

Atom	B_{11}	B_{22}	B_{33}	B_{12}	B_{13}	B_{23}
Pb(A)	295(8)	922(30)	328(10)	102(12)	44(7)	−230(13)
Pb(B)	298(8)	439(28)	554(12)	−72(11)	132(8)	95(13)
Pb(C)	265(8)	1040(30)	477(11)	77(12)	217(7)	147(14)
Pb(D)	210(7)	619(26)	315(10)	65(11)	65(6)	113(12)

arrangement of these units, the perchlorate ions, and the water molecules is shown in Fig. 1. The metal atoms, Pb(A) – Pb(D), are at the corners of a slightly distorted tetrahedron and the hydroxide oxygens, O(1) – O(4), are situated outside the faces of this tetrahedron. The metal atoms are thus joined by double hydroxide bridges. The oxygen atoms form another, slightly distorted, tetrahedron. The two tetrahedra are positioned with respect to each other so, that the lead and oxygen atoms are at the alternate corners of a distorted cube; See Fig. 1.

The Pb – Pb and Pb – O distances in the $[Pb_4(OH)_4^{4+}]$-group are presented in Table 2. The metal-metal distances range between 3.72 and 3.95 Å with a mean value of 3.81 Å. The mean deviation of an Pb – Pb – Pb angle from 60° is 1.5° and the largest difference 3.1°. An hydroxide oxygen coordinates three lead atoms and the Pb – O distances range between 2.34 and 2.54 Å with a mean value of 2.41 Å.

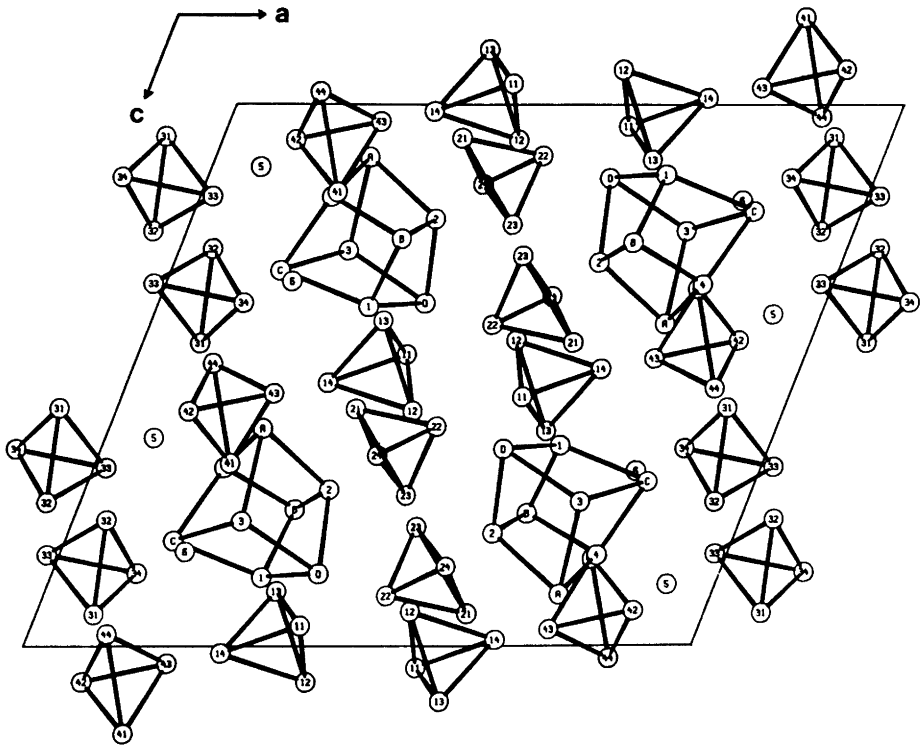

Fig. 1. Projection of the structure of $[Pb_4(OH)_4]$ $(ClO_4)_4.2H_2O$ along the *b*-axis. A – D lead atoms, 1 – 4 hydroxide, 5 – 6 water, and 11 – 44 perchlorate oxygen atoms.

The hydroxide oxygens are apparently in van der Waals contact since the O – O distances range between 2.84 and 3.00 Å with a mean value of 2.89 Å. The mean deviation of an O – O – O angle from 60° is 1.4° and the largest difference 3.6°.

Of the four perchlorate groups, $ClO_4(1)$ – $ClO_4(4)$, two, $ClO_4(1)$ and $ClO_4(3)$, are better resolved than the others as can be seen from the *B*-values. The chlorine-oxygen distances [excluding Cl(4) – O(44)] are within $2\sigma(\lesssim 0.1$ Å) equal to the expected value of 1.45 Å[10] and range between 1.35 and 1.48 Å with a mean value of 1.42 Å.

The electron density map showed only two molecules of water per $[Pb_4(OH)_4^{4+}]$-group. This is in agreement with Marignac's analytical data and our lead analysis of the compound. Since, however, the presence of three molecules of water has also been suggested [2] the structure was searched for cavities. The largest spherical hole found had a radius of 2.3 Å. The shortest distance between a water oxygen and another atom in the lead hydroxide perchlorates so far investigated exceeds 2.7 Å.[5,7,11] We may therefore conclude that there is not room for another water molecule.

The $[Pb_4(OH)_4^{4+}]$-units definitely occur as discrete groups since the shortest distance between a metal atom and an hydroxide oxygen in an adjacent unit is 4.88 Å. The shortest inter-unit metal-metal vector is 4.72 Å. The closest perchlorate oxygen is situated 2.80 Å ($\sigma \approx 0.05$ Å) from a lead atom. From this value on there is a "continuous" range of distances and no definite statements can be made about the coordination of the metal atoms by the perchlorate groups. If, for instance, perchlorate oxygens less distant than approximately 3.1 Å are considered coordinated the $[Pb_4(OH)_4^{4+}]$-units may be considered linked through O(34). The link is between a Pb(A) and a Pb(C) atom. The distances are Pb(A) – O(34) 3.10 Å and Pb(C) – O(34) 2.85 Å. The angle Pb(A) –

Table 2. Some distances (Å) in the $[Pb_4(OH)_4^{4+}]$-unit. Standard deviations (σ) within parentheses.

Atoms		Distance	Atoms		Distance
Pb(A)	– Pb(B)	3.838(2)	Pb(B)	– Pb(C)	3.732(2)
	– Pb(C)	3.721(2)		– Pb(D)	3.802(2)
	– Pb(D)	3.810(2)		– O(1)	2.34(3)
	– O(2)	2.41(2)		– O(2)	2.47(2)
	– O(3)	2.45(3)		– O(4)	2.37(2)
	– O(4)	2.38(2)			
Pb(C)	– Pb(D)	3.945(2)	Pb(D)	– O(1)	2.47(2)
	– O(1)	2.44(3)		– O(2)	2.37(2)
	– O(3)	2.54(3)		– O(3)	2.37(3)
	– O(4)	2.35(2)			

O(34) – Pb(C) is 105°. The metal – metal distance is the smallest inter-unit distance, 4.72 Å, mentioned above.

Each hydroxide oxygen has one or two perchlorate or water oxygens at distances between 2.83 and 2.95 Å ($\sigma \approx 0.05$ Å) to which hydrogen bonds may be formed. One might expect the O – H vector to be essentially perpendicular to and directed away from the plane formed by the three lead atoms bound to the hydroxide group (with one exception the Pb – OH – Pb angles are quite close to the tetrahedral value). In no case, however, is the presumed acceptor oxygen close to this direction. This circumstance and the uncertainty in the bond lengths do not allow any assignment of hydrogen bonds to be made.

The water molecules, O(5) and O(6), are coordinated to one lead atom each at 2.74 and 2.75 Å, respectively. The next lead atom is 2.93, and 3.00 Å away, respectively. The closest oxygen atom is approximately 2.9 Å from a water molecule. This fairly long O – O distance and the Pb – O(H_2O) – O angle (50°) suggests the absence of hydrogen bonds.

The $[Pb_4(OH)_4^{4+}]$-unit present in $[Pb_4(OH)_4](ClO_4)_4.2H_2O$, I, is the same as previously found in $[Pb_4(OH)_4]_3(CO_3)(ClO_4)_{10}.6H_2O$, II.[5] The interatomic distances are, however, more varied in I than in II. In I the Pb – Pb distances range between 3.72 and 3.95 Å, and in II between 3.76 and 3.85 Å. The mean values are almost the same 3.81 and 3.78 Å, respectively. The value for I is thus closer to the mean Pb – Pb distance, 3.85 Å, observed for this group in solution.

In II the $[Pb_4(OH)_4^{4+}]$-group possesses a plane of symmetry. This plane is very nearly retained by the Pb_4-tetrahedron in I but is lost when the hydroxide oxygens are added. The Pb – O distances vary between 2.34 and 2.54 Å in I, and 2.29 and 2.49 Å in II. The mean values are 2.41 and 2.38 Å. If the two groups are compared so as to minimize the differences between the Pb – Pb distances (mean difference 0.05 Å, max. difference 0.10 Å), the greatest difference in a Pb – O link becomes 0.18 Å and the mean difference 0.07 Å. Differences of this magnitude were also observed between the $[Pb_6O(OH)_6^{4+}]$-units in α- and β-$[Pb_6O(OH)_6]$ $(ClO_4)_4.H_2O$.[7] The cause of these differences and the reason why these clusters do not possess the higher symmetry permitted by their topology is not understood.

Acknowledgements. We thank Professor Ivar Olovsson and his group for generous help, Dr. Georg Johansson for valuable discussions, and Dr. Marcus Richardson for correcting the English of this paper.

This work has been financially supported by grants from the Swedish Natural Science Research Council.

REFERENCES

1. Groth, P. *Chemische Krystallographie 2. Teil*, Engelmann, Leipzig 1908, p. 186.
2. Weinland, R. and Stroh, R. *Ber. 55* (1922) 2706.
3. Esval, O. E. *Diss. Abstracts 24* (1964) 3091.
4. Johansson, G. and Olin, Å. *Acta Chem. Scand. 22* (1968) 3197.
5. Hong, S.-H. and Olin, Å. *Acta Chem. Scand. 27* (1973) 2309.
6. Willard, H. H. and Kassner J. L. *J. Amer. Chem. Soc. 52* (1930) 2391.
7. Olin, Å. and Söderquist, R. *Acta Chem. Scand. 26* (1972) 3505.

8. Hansson, H. P., Herman, F., Lea, J. D. and Skillman, S. *Acta Crystallogr. 17* (1964) 1040.
9. Long, R. E. *Diss. Abstracts 26* (1966) 3651.
10. Olovsson, I. *J. Chem. Phys. 49* (1968) 1063.
11. Spiro, T. G., Templeton, D. H. and Zalkin, A. *Inorg. Chem. 8* (1969) 856.

Received October 29, 1973.

Acta Chemica Scandinavica A 28 (1974) 239—242

An Electron Diffraction Investigation of Hexachloroacetone

PER ANDERSEN, E. E. ASTRUP and A. BORGAN

Department of Chemistry, University of Oslo, Oslo 3, Norway

The molecular structure of hexachloroacetone has been determined by the gas electron diffraction method at 65°C and 300°C. The following bond distances and angles have been found at 65°C: C–O: 1.184(13) Å; C–C: 1.574(9) Å; C–Cl: 1.764(4); ∠OCC: 118.9°(0.7°); ∠OCCCl: 16.2°(1.4°) and 36.1°(1.8°); the angle between the three-fold axes of the CCl_3 group and C–Cl: 70.5°(0.3°). The three-fold axis is tilted 3.7° towards the carbonyl group. A structure having a C_2 symmetry could be determined by assuming a small amount of another conformer to be present. To see if this was probable, the structure determination was repeated at 300°C but no change in the ratio of the possible two conformers could be seen.

In an attempt to verify the structure of the CCl_3 free radical [1-3] hexachloroacetone was used as a source of the radicals through thermal decomposition. The decomposition took place within a quartz nozzle which could be heated to about 1000°C over a region of a few mm of the nozzle 1–2 mm from the point of scattering.[3] In the earlier experiment [1,2] the decomposition took place in front of the nozzle about 12 mm from the point of scattering. In both cases the reaction products were studied in a mass spectrometer by letting the gas in through the same nozzle as is used in the electron diffraction unit. The analysis of the radial distribution (RD) curve made it necessary to determine the structure of the parent molecule, $(CCl_3)_2C=O$. This structure has not been determined earlier although acetone itself and hexafluoroacetone have been studied [2,4-6] in the gas phase by many groups using the microwave or the electron diffraction methods. From the most recent electron diffraction investigation by Bauer and coworkers [4] it is concluded that both molecules have a C_2 symmetry and that the dihedral angles are (OCCH) = 32° and (OCCF) = 36.6°. In hexachloroacetone where both the non-bonded Cl···Cl and Cl···O distances could be expected to be fairly short, one should probably expect a similar staggering of the two CCl_3 groups as in the fluoro compound.

EXPERIMENTAL

The hexachloroacetone was obtained from Fluka AG, Switzerland, and was further purified in a gas chromatograph. The electron diffraction photographs were taken in the usual way. One set of data was obtained from the Balzers apparatus at two nozzle-plate distances of 250 mm and 500 mm, and 60 kV electrons; the nozzle temperature was 65°C. The second set was obtained from the Oslo apparatus at 200 mm and 480 mm nozzle-plate distances, 35 kV electrons, and a nozzle temperature of 300°C. The first set covers an s range of 1.25–18.625 $Å^{-1}$ and 2.75–35.25 $Å^{-1}$, and the second set an s range of 1.375–18.625 $Å^{-1}$ and 7.25–42.75 $Å^{-1}$.

The resulting modified molecular intensity values over the range from 1.25 $Å^{-1}$ to 30.0 $Å^{-1}$ for the first set and from 1.375 $Å^{-1}$ to 38.0 $Å^{-1}$ for the second set are shown in Fig. 1.

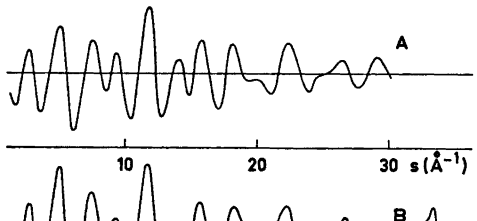

Fig. 1. Hexachloroacetone. Experimental molecular intensity curves. A: nozzle temperature 65°C. B: nozzle temperature 300°C.

The data were analysed in the usual way using the radial distribution curve to determine an approximate structure and then refining the molecular parameters by a least-squares fitting of the intensity data. The computer programs available in Oslo [6] were used throughout this investigation.

STRUCTURE ANALYSIS

The radial distribution curve obtained by Fourier transformation of the experimental molecular intensity curve of the low temperature experiment is shown in Fig. 2. The structure

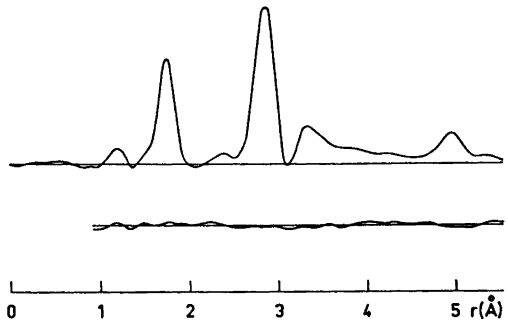

Fig. 2. Hexachloroacetone. Experimental radial distribution curve. The lower curve shows the difference between the experimental and the calculated values. Nozzle temperature 65°C. Artificial damping constant $k = 0.0023$ Å.

was initially analysed assuming the molecule to possess a C_2 symmetry. Approximate values for the C=O, C–C, and C–Cl bond lengths could be determined from the two first peaks on the RD curve at about 2.9 Å and 1.75 Å. The CCC angle, the ClCCl angle, and the twist angle of the CCl_3 groups could be estimated from the maxima at about 2.9 Å, 3.3 Å, and 5.0 Å. Attempts to reproduce the experimental RD curve in the region of 2–5 Å assuming the approximate values of bond lengths and angles was unsuccessful and so were least-squares refinements. Two possibilities were taken into account at this stage, one which assumed that the molecule did not have a C_2 symmetry and one which assumed that two conformations were present both having a C_2 symmetry. Refinements assuming that the molecule did not have a two-fold axis gave a fairly good agreement in the 3–5 Å region with approximately 36° and 16° twist angles of the two CCl_3 groups. In order to improve the agreement between the calculated and the experimental RD curve a new parameter, the angle between the three-fold axis of the CCl_3 group and the C–C bond direction (Fig. 3),

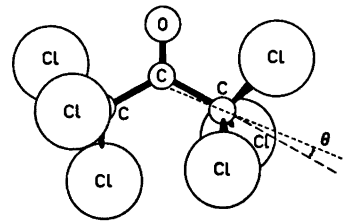

Fig. 3. Hexachloroacetone. θ is the angle between the three-fold axis of the CCl_3 group (···) and the continuation of the C–C bond (– – –).

was introduced. Further refinements showed that the best agreement was obtained when the CCl_3 groups were tilted 3.7° towards the carbonyl group.

The result of these refinements was unexpected since one could not see why the two sides of the molecule should behave differently as far as the twist angles of the CCl_3 groups were concerned. The possibility of two conformations being present was then taken into account. The two conformations were assumed to have a C_2 symmetry and the two determined twist angles were used as starting parameters for a least-squares refinement. A good agreement was obtained for a predominant contribution of a conformation having approximately 35° twist angle and a small contribution of a conformation having a small twist angle. In order to decide whether one or two conformations could be present the experiment was repeated with a nozzle temperature of 300°C where the contribution of the higher energy conformation could be expected to increase.

The analysis of the RD and molecular intensity curves from the high temperature experiment was carried out in the same way as on the 65° curves. The RD and the difference curve between the high and low temperature curves are reproduced in Fig. 4. The analysis of the high temperature structure did not result in any significant changes in the molecular parameters except for the thermal vibrations as can be seen from Table 1. If the presence of a small contribution of another conformation

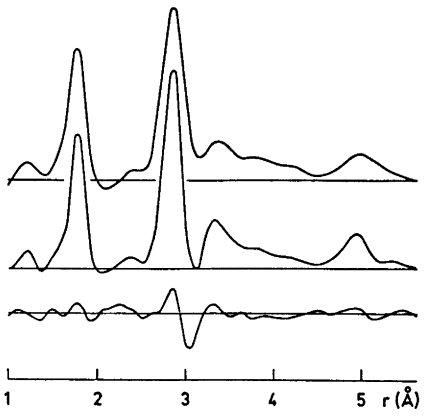

Fig. 4. Hexachloroacetone. Experimental radial distribution curves. A: nozzle temperature 300°C. B: nozzle temperature 65°C. C: the difference between the high and low temperature curves. Artificial damping constant $k = 0.0023$ Å.

was assumed, this ratio between the two conformations was not changed by increasing the temperature from 65°C to 300°C. This indicates that only one conformation is present.

Attempts to calculate the energy difference between the conformations did not give results which could justify the conclusion that the molecule should have a C_1 symmetry. Harmonic shrinkage corrections [8,9] on the best conformation having a C_2 symmetry were calculated. But the value of these calculations is doubtful since the force constants for hexachloroacetone were not known and had to be estimated from the values known for similar molecules.[10,11] The shrinkage corrections improved somewhat the agreement with the experimental curve, but did not indicate in a conclusive way that the molecule could have a C_2 symmetry.

DISCUSSION

The C–O bond length (Table 1) of 1.184 Å differs somewhat from the values determined for acetone and hexafluoroacetone [4] which are 1.210 Å and 1.246 Å, respectively. The resolved peak corresponding to this distance on the RD curve is probably well determined for this molecule. The increase in the C–C bond length from 1.507 Å in acetone to 1.549 Å in hexafluoroacetone and 1.574 Å in this work could be expected. Some of the non-bonded Cl···Cl and Cl···O distances (Table 2) are much shorter than should be expected from the size of the van der Waals radii. No change in bond angles or twist angles would increase all these distances appreciably and the lengthening is not unexpected. The C–Cl bond length of 1.764 Å is reasonable and so are the CCC angle of 122.2° and the ClCCl angle of 109.4°. The shortest Cl···Cl distance between the two CCl_3 groups are about 3.24 Å and 3.31 Å and the shortest Cl···O distances on the other side of the molecule are 2.73 Å and 2.84 Å. These four distances are all shorter than could be assumed from the van der Waals radii of the chlorine and oxygen atoms. It is obviously preferred to tilt the three-fold axis of the CCl_3 groups towards the oxygen atom instead of increasing the CCC angle to approximately 130° which is the angle between the two three-fold axes.

The dihedral angle Cl(5)–C(3)···C(4)–Cl(8) (Fig. 3) is 66° so that the two CCl_3 groups are staggered. This is in good agreement with what was found for hexafluoroacetone. However,

Table 1. Structure parameters for hexachloroacetone obtained by least squares refinement on the intensity data. Distances (r_a-values) and mean amplitudes of vibration (u-values) are given in Å, angles in degrees. The standard deviations given in parentheses have been corrected to take into account data correlation. The uncertainty arising from error in the electron wave length is included. (For numbering system of the atoms see Fig. 5.).

	Low temperature (65°C)		High temperature (300°)	
Distances	r	u	r	u
C=O	1.184(13)	0.037	1.200(14)	0.038
C–C	1.574(9)	0.050	1.595(9)	0.054
C–Cl	1.764(4)	0.043(4)	1.766(4)	0.052(4)
Angles		deg.		deg.
∠OCC		118.9(0.7)		118.3(0.9)
α^a		70.5(0.3)		70.8(0.3)
θ^b		3.7(0.8)		2.7(1.0)
$\tau_1{}^c$		16.2(1.4)		16.9(1.4)
$\tau_2{}^c$		36.1(1.8)		39.5(1.8)

[a] α is the angle between the C–Cl bond and the three-fold axis of the CCl_3 group. [b] θ is the angle between the three-fold axis of the CCl_3 group and the continuation of the C–C bond. [c] τ_1 and τ_2 are the twist angles of the CCl_3 groups about the C–C bonds.

Table 2. Hexachloroacetone. Non-bonded Cl···O and Cl···Cl distances in Å. Nozzle temperature 65°C. (For numbering system of the atoms see Fig. 5.)

Distances	*r*
Cl(5)···O(1)	2.727
Cl(6)···O(1)	3.749
Cl(7)···O(1)	3.488
Cl(8)···O(1)	2.843
Cl(9)···O(1)	3.290
Cl(10)···O(1)	3.847
Cl(5)···Cl(8)	5.280
Cl(5)···Cl(9)	4.900
Cl(5)···Cl(10)	4.910
Cl(6)···Cl(8)	4.991
Cl(6)···Cl(9)	3.643
Cl(6)···Cl(10)	3.241
Cl(7)···Cl(8)	4.553
Cl(7)···Cl(9)	4.985
Cl(7)···Cl(10)	3.309

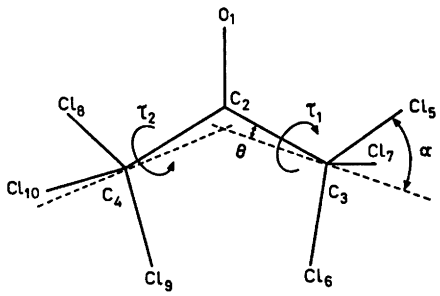

Fig. 5. Hexachloroacetone. The symbols and numbering system.

we have no good explanation for why the two twist angles Cl(5) – C(3) – C(2) – O and Cl(8) – C(4) – C(2) – O of the CCl_3 groups should be 16.2° and 36.1° and not equal.

Acknowledgements. The authors are grateful to Dr. Arne Almenningen and Mr. K. Brendhaugen for valuable help during the electron diffraction and mass spectrometer work.

REFERENCES

1. Andersen, P. *Selected Topics in Structural Chemistry*, Universitetsforlaget, Oslo 1967, p. 141.
2. Prater, B. G. L. *Diss. Abstr. Int. B 30* (1970) 5454.
3. Andersen, P. and Astrup, E. E. 5th Hungarian Conference on X-Rays, Electron and Neutron Diffraction, 1970.
4. Hilderbrandt, R. L., Andreassen, A. L. and Bauer, S. H. *J. Phys. Chem. 74* (1970) 1586.
5. Swalen, J. D. and Costain, C. C. *J. Chem. Phys. 31* (1959) 1562.
6. Nelson, R. and Piers, L. *J. Mol. Spectrosc. 18* (1965) 344.
7. Andersen, B., Seip, H. M., Strand, T. G. and Stølevik, R. *Acta Chem. Scand. 23* (1969) 3224.
8. Gwinn, W. D. *J. Chem. Phys. 55* (1971) 477.
9. Stølevik, R., Seip, H. M. and Cyvin, S. J. *Chem. Phys. Lett. 15* (1972) 263.
10. Cosse, P. and Schachtschneider, J. H. *J. Chem. Phys. 44* (1966) 97.
11. Schachtschneider, J. H. and Snyder, R. G. *Vibrational Analysis of Polyatomic Molecules*, IV. Project No 31450, Technical Report No. 122 – 63 of Shell Development Company.

Received October 17, 1973.

Acta Chemica Scandinavica A 28 (1974) 243—247

Aqueous Chemistry of Protactinium(IV). I. Stability Constants for Pa(IV) – Acetylacetone Complexes

ROBERT LUNDQVIST

Department of Nuclear Chemistry, Chalmers University of Technology, Fack, S-402 20 Göteborg 5, Sweden

Stability and distribution constants for the tetravalent protactinium acetylacetone complexes MAA^{+} and $M(AA)_3$ ($M^{4+} = Pa(OH)_2^{2+}$ or PaO^{2+}, HAA = acetylacetone) were obtained from the liquid-liquid distribution of Pa(IV) between HAA in C_6H_6 and in 1 M $(Na,H)ClO_4$. The constants for 25°C were calculated as $\log \beta_1 = 6.1$, $\log \beta_2 = 13.15 \pm 0.13$ and $\log \lambda_2$ ($[M(AA)_3]org/[M(AA)_3]$) $= 2.07 \pm 0.10$. For the extraction reaction ($M^{4+} + 2HAA(org) \rightleftharpoons M(AA)_3(org) + 2H^+$) $\log K_D = -4.13 \pm 0.05$, $\Delta H^\circ = 30 \pm 2$ kJ mol^{-1} and $\Delta S^\circ = 22 \pm 8$ J mol^{-1} K^{-1} were calculated.

In making a systematic study of acetylacetone complexes of tetravalent actinides,[1,2] information on the Pa(IV)-acetylacetonate system was needed. Only a few stability constants for chelate complexes with Pa(IV) have been determined;[3,4] liquid-liquid distribution of Pa(IV) has been used as a tool to study complex formation [5,6] of non-extractable complexes, especially hydrolysis reactions. In this work the distribution of Pa(IV) between a benzene phase and water was investigated as a function of the concentrations of Pa(IV), acetylacetone, and hydrogen ion, as well as of the temperature.

Trace concentrations of ^{234m}Pa and ^{233}Pa were used to avoid polynuclear complexes. A constant ionic strength of 1 M $(Na,H)ClO_4$ was maintained in the aqueous phase.

EXPERIMENTAL

Chemicals. (a) ^{233}Pa was obtained by neutron irradiation for 48 h of 1 g samples of $^{232}Th(NO_3)_4.5H_2O$, sealed in quarts ampules, in the R2-reactor (thermal flux 10^{12} n s^{-1} cm^{-2}) of Aktiebolaget Atomenergi in Nyköping. Two different stock solutions were prepared by solvent extraction. One stock solution consisted of pure acetylacetone and another of 7 M $HClO_4$.

Neither the method of preparing the stock solutions nor their age affected the distribution of Pa(IV), in contrast to what has been found for Pa(V).[7] This is probably due to the much smaller tendency of Pa(IV) to hydrolyse and polymerize. The radiochemical purity was controlled using high resolution gamma-spectroscopy.

(b) Stock solutions of ^{234m}Pa ($t_{1/2}$ 6.7 h) in 0.1 M HCl were prepared by isolation of ^{234m}Pa from its parent ^{234}Th ($t_{1/2}$ 24 d) which was itself recovered, by solvent extraction, from 20 kg of old $UO_2(NO_3)_2.6H_2O$.

(c) The sodium perchlorate solutions were made by neutralization of recrystallized Na_2CO_3 (Merck) with concentrated $HClO_4$ (Merck).

(d) Acetylacetone was purified as recommended by Rydberg.[8] Chromium perchlorate was prepared by dissolving chromium metal (Koch Light) in concentrated $HClO_4$ until neutralization.

Fluid amalgamated zinc, 2 % by weight of Zn in Hg (Merck), was prepared according to Ref. 9. The amalgam was shaken with water three times before use. Doubly-distilled water and reagents of *p.a.* quality were used throughout.

Analysis. (a) A Ge(Li)-detector (Canberra Ind.) was used for the gamma-spectroscopy: It had an efficiency of 13 % and a resolution of 3.7 keV (full width at half maximum) at 1.332 MeV. The detector was connected to a 1024-channel analyzer (Hewlett Packard). The distribution measurements, however, were made with an ordinary NaI(Tl)-detector. About 2000 disintegrations were measured from the least active phase, which was twice as active as the background. As the total measured activity from both phases was around 200 000 counts the radiometric accuracy of the logarithm of the distribution ratio was ± 0.01 or better.

(b) Hydrogen ion concentration measurements were made with a modified glass calomel

combination electrode GK 2303 C (Radiometer) with 1 M $NaClO_4$ replacing the saturated KCl.[10]

(c) The acetylacetone concentration was checked by spectrophotometric determination of the absorbance at 490 nm [11] of the red Fe(III)-acetylacetonate and was found to agree, within the accuracy (± 2 %) of the method, with the calculated.

All experiments were carried out in 1 M $(Na,H)ClO_4$ with a hydrogen ion concentration in the range 10^{-1} to 10^{-3}M. The electrode combination was calibrated by measurements in 1 M $(Na,H)ClO_4$ solutions of well known $ph = -\log [H^+]$. Calibration was carried out before and after each experiment, and the hydrogen ion concentration estimated using the relation

$$E = E^\circ + RTF^{-1} \ln 10 \log [H^+] + \psi[H^+]$$

The constants E^0 and ψ were found to be unaffected by contact of the aqueous phase with the benzene phase. The accuracy of the ph-measurements was ± 0.01 ph-units, or better.

Reduction by Cr(II). Exactly 15 ml of 1 M $(Na,H)ClO_4$, ph 1 – 2, was brought into contact with about 4 ml Zn(Hg) in an atmosphere of nitrogen in a small closed glass titration vessel equipped with a magnetic stirrer. About 10 – 70 μl of 1.92 M $Cr(ClO_4)_3$ was added to make the solution $10^{-2} - 10^{-3}$ M in Cr^{3+}. Complete reduction to blue Cr^{2+} took place in about 30 min, which agrees with other investigations.[12] The ph was increased with 1 M NaOH when required. About 10 μl of the stock solution of ^{233}Pa in acetylacetone and 15 ml of the benzene acetylacetone phase was then added. The nitrogen contained less than 10 ppm of oxygen, which did not affect the system.

The extraction system was equilibrated by stirring vigorously for 5 to 10 min and then allowing some minutes for settling. The EMF and the temperature were then measured. Equal samples of about 1.3 ml were taken from both phases with disposable glass pipettes with the aid of a reproducible syringe (± 0.005 ml). The pipettes containing the samples were crushed in 20 ml glass tubes for gamma counting. A check was made to see that the sum of the activities of the two phases was the same for all the points of a particular experiment. It proved to be better to successively increase the hydrogen ion concentration through an experimental run, rather than lower it, since the addition of NaOH produces stable chromium(III)-acetylacetone complexes,[13] which are extracted from the aqueous phase. Stable chromium(III)-acetylacetonate was always formed at ph-values higher than 3, making it impossible to reduce protactinium.

All extraction experiments were carried out in a water bath, thermostatically controlled to ± 0.1°C. The distribution equilibria of Pa(IV) were established within 5 min and the concentrations of ^{233}Pa were calculated from the gamma intensities relative to a ^{237}Np-^{233}Pa standard.

Electrolytic reduction. Equal volumes (15 ml) of (0.1 $HClO_4$, 0.9 $NaClO_4$) and a solution of acetylacetone in benzene, plus 1 – 3 drops of ^{233}Pa stock solution in 7 M $HClO_4$, were electrolyzed in the glass vessel. The anode compartment consisted of a glass tube, with an almost tight glass fritt separating the platinum anode from the bulk solution. The anode compartment was filled with 1 M $NaClO_4$ and the current was held constant around 20 mA, giving a voltage of 10 – 25 V. The electrolysis continued until all hydrogen ions were removed as hydrogen gas, and until all protactinium had been reduced at the mercury cathode, which reduction was complete at $ph \geq 7$. The continued reduction of protactinium was followed by changes in the distribution factor D_{Pa}, a constant value being reached after 1 – 10 h depending on the composition of the two phase system. When the initial concentration of acetylacetone in the organic phase was lowered from 2.5 M to 0.5 M, the time required to reach the maximum distribution λ_2 increases from about 1 to 10 h of electrolysis; this indicates a competition between hydrolyzation and complex formation with acetylacetone.

After completing the reduction, the ph was lowered with 1 M $HClO_4$ and new equilibria were established within 40 min. As to the rest, the experimental procedures were similar to those described for reduction with chromous ions.

EXTRACTION WITH ACETYLACETONE

The distribution ($D = [Pa(IV)]_{org}/[Pa(IV)]_{aq}$) of tetravalent protactinium as a function of the hydrogen ion concentration is shown in Fig. 1. The initial concentration of acetylacetone in the benzene phase was 0.1 – 2.5 M, and the hydrogen ion concentration in the aqueous phase 1 M $(Na,H)ClO_4$ was varied between 10^{-1} and 10^{-3} M. The uncertainties in the plotted values are indicated by the size of the dots in the figures. The extracted protactinium complex was deduced to be mononuclear, as the distribution of protactinium was the same in the concentration range 0.3×10^{-14} to 1.3×10^{-10} M. The distribution experiments with the lowest protactinium concentrations were investigated using the isotope ^{234m}Pa in aqueous phases 0.14 – 0.5 M (Na,H)Cl. The distribution of Pa(IV) was very little affected by the substitution of a chloride medium for the perchlorate media (see also Fig. 1 for ^{233}Pa – 1 M (Na,H)Cl) or by the addition of less than 10^{-3} M sulphate.

In order to evaluate the extraction mechanism, the logarithm of the distribution of Pa(IV) was plotted as a function of the aqueous acetylacetone anion concentration $[AA^-]$ in the aqueous phase; see Fig. 2. The values

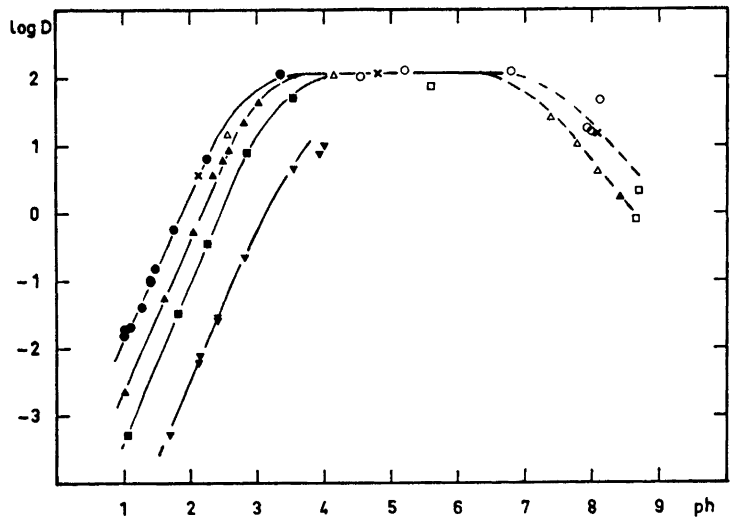

Fig. 1. Distribution of Pa(IV) between benzene and 1 M $(Na,H)ClO_4$, at 25°C, as a function of ph and at different initial acetylacetone concentrations in the organic phase, $[HAA]_{org}^{init}$. Unfilled symbols denote electrolytic reduction and filled symbols denote reduction with Cr^{2+}.
●, ○, ×, 2.5 M HAA (× denote electrolysis in 1 M NaCl); ▲, △, 1.0 M HAA; ■, □, 0.5 M HAA; ▼, 0.1 M HAA.

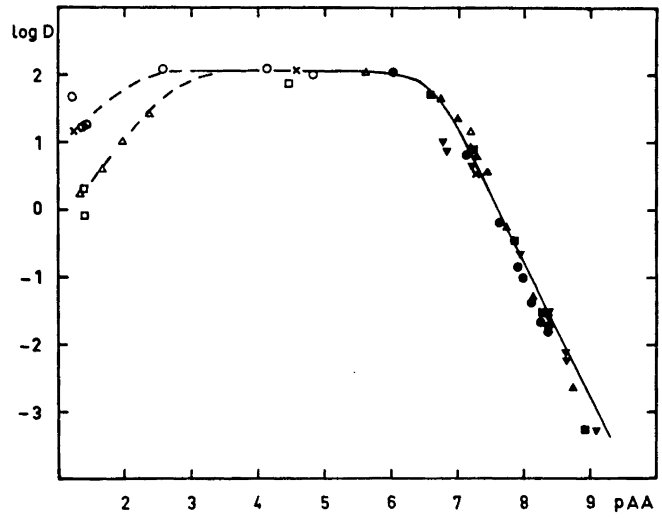

Fig. 2. Distribution of Pa(IV) between benzene and 1 M $(Na,H)ClO_4$, at 25°C, as a function of pAA and for different initial concentrations of acetylacetone in the organic phase. The same symbols as in Fig. 1 are used. The solid curve is calculated from estimated stability constants.

$pAA = -\log [AA^-]$ were calculated for equal phase volumes:

$$pAA = pK_a - ph + \log (K_d + 1 + K_a[H^+]^{-1}) - \log [HAA]_{org}^{init}$$

The following constants were used: $pK_a = 0.3027 - 0.01228T$°C [14] and $K_d = 4.80 \pm 0.02$ (20 − 40°C),[15] $ph \leq 2$. The values, K_d, for the distribution constant for acetylacetone for ph-values less than 2 were estimated from

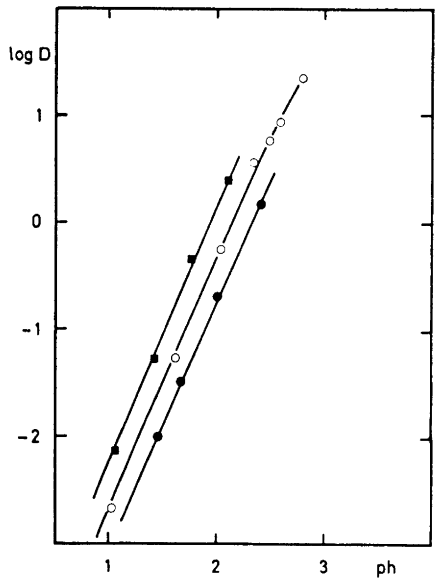

Fig. 3. Distribution of Pa(IV) between benzene and 1 M (Na,H)ClO_4, as a function of ph at different temperatures, for a 1 M initial concentration of acetylacetone in the organic phase. ■, 48.7 ± 0.1°C; ○, 25.0 ± 0.1°C; ●, 3.1 ± 0.1°C.

a figure in Ref. 15 – the corrections were small.

The temperature dependence was investigated at various ph-values but at constant acetylacetone concentration ($[HAA_{org}^{init} = 1$ M) in the temperature interval 3 – 48°C, see Fig. 3.

RESULTS AND DISCUSSION

According to the general theory [16] for evaluating the composition of the composite metal complex $M_mA_n(OH)_p(HA)_r(org)_s(H_2O)_t\cdots$ in a liquid-liquid distribution system one concludes, from the relationship between the functions log $D = f$(ph) and log $D = f$(pAA), that the appropriate type of Pa(IV) acetylacetone complex is MA_n. The limiting slope δ log D/δ log pAA as pAA is increased is equal to -2, implying $n = 2$ for the extracted species. The species of Pa(IV) formed in the aqueous phase are then M^{4+}, MAA^+ and uncharged $M(AA)_2$, the latter being distributed between the benzene phase and the perchlorate media, $\lambda_2 = [M(AA)_2]_{org}/[M(AA)_2]$.

The decrease from the plateau value λ_2 at higher ph may be explained by the formation of hydrolyzed species, and possibly also negatively charged complexes like $M(AA)_3^-$.

From the linearity of the extraction of Pa(IV) for p$h \leq 3$ one can write the extraction mechanism as $M^{4+} + 2HAA(org) \rightleftharpoons M(AA)_2(org) + 2H^+$. The equilibrium constant has been calculated to be log $K_D = -4.13 \pm 0.05$. The enthalpy and entropy changes have been calculated from the temperature dependence shown in Fig. 3.

$\Delta H^\circ_{K_D}(25°C) = 30 \pm 2$ kJ mol^{-1}

$\Delta S^\circ_{K_D} = 22 \pm 8$ J mol^{-1} K^{-1}

The constants $\beta_1([MAA][M^{4+}]^{-1}[AA^-]^{-1})$, $\beta_2([M(AA)_2][M^{4+}]^{-1}[AA^-]^{-2})$ and λ_2 have been calculated by treating the data with an especially designed [17] least squares program for solvent extraction data (arithmetically distributed errors). However, due to the great statistical uncertainty in β_1 new calculations were performed whith only the two parameters β_2 and λ_2. Thus neglecting the formation of MAA^+ the values log $\lambda_2 = 2.07 \pm 0.10$ and log $\beta_2 = 13.16 \pm 0.13$ were obtained. The elimination of the MAA^+ complex from the calculations changed the S_{min}/K value [17] only slightly (from 0.195 to 0.214) which indicates that the MAA^+ complex was statistically insignificant. The calculated distribution function is given by the solid line in Fig. 2. By slope analysis [18] of the function log $D = f$(pA) the following values were obtained: log $\lambda_2 = 2.06$, log $\beta_1 = 6.1$ and log $\beta_2 = 13.0$. (The errors in the logarithm of these values was estimated graphically to be ± 0.1.) The determination of ΔH° and ΔS° for β_1, β_2 and λ_2 needs rather accurate temperature data for the whole distribution curves which could not be obtained because of the experimental difficulties (*e.g.*, two different reduction methods were needed to cover the whole ph range).

Pa(IV) is here shown to coordinate only two acetylacetone molecules, thus differing from the behaviour of the tetravalent actinides Th, U, Np, and Pu which form MA_4 extraction systems.[18,19] Solid $Zr(AA)_4$ and $Hf(AA)_4$ [but not $Pa(AA)_4$] have been prepared,[20,21] and as a consequence the liquid-liquid distribution systems of Zr(IV) [22,23] and Hf(IV) [23–25] with benzoylacetone and acetylacetone have been considered to be MA_4 systems. However, the distribution data reported do not exclude the hydrolyzed MA_2 system.

The doubly charged positive aqueous Pa(IV) ion has hitherto been denoted M^{2+} as its formula is not evident. Neglecting the coordination of water molecules, one may propose the formula PaO^{2+} or $Pa(OH)_2^{2+}$. The formula $Pa(OH)_2^{2+}$ is preferred by some authors.[3,6] However, the rather large stability range of M^{2+} (over more than two p*h*-units) favours the species PaO^{2+} rather than $Pa(OH)_2^{2+}$; the latter may be regarded as an intermediary between $Pa(OH)^{3+}$ and $Pa(OH)_3^{+}$, neither of which was indicated to exist in this investigation. However, a species like PaO^{2+} has not been observed for Zr(IV) [26-28] Hf(IV) or the actinides.

Acknowledgement. The author is grateful to Professor Jan Rydberg and Dr. Jan-Olof Liljenzin for valuable suggestions and criticism, and to Ph. D. Christopher Coombes for linguistic corrections.

REFERENCES

1. Rydberg, J. *Sv. Kem. Tidskr. 67* (1955) 499.
2. Liljenzin, J. O. and Stary, J. *J. Inorg. Nucl. Chem. 32* (1970) 1357.
3. Guillaumont, R. *Actinides Rev. 1* (1968) 135.
4. Sillén, L. G. and Martell, A. E. *Stability Constants of Metal Ion Complexes*, Special publications Nos. 17 and 25, The Chemical Society, Burlington House, London 1964 and 1971.
5. Guillaumont, R. *Physico-chimie du Protactinium*, Editions du C. N. R. S., No. 154, Paris 1966, p. 165.
6. Mitsuji, T. *Bull. Chem. Soc. Jap. 41* (1968) 115.
7. Suzuki, S. and Inoue, Y. *Bull. Chem. Soc. Jap. 42* (1969) 1916.
8. Rydberg, J. *Sv. Kem. Tidskr. 62* (1950) 179.
9. Bauer, G. *Präparativen Anorganischen Chemie*, Ferdinand Enke, Stuttgart 1954, p. 1395.
10. Andersson, C., Andersson, S. O., Liljenzin, J. O., Reinhardt, H. and Rydberg, J. *Acta Chem. Scand. 23* (1969) 2781.
11. Stary, J. *The Solvent Extraction of Metal Chelates*, Pergamon, New York 1964, p. 56.
12. Mitsuji, T. *Bull. Chem. Soc. Jap. 40* (1967) 2822.
13. Hellwege, H. E. and Schweitzer, G. K. *Anal. Chim. Acta 29* (1963) 46.
14. Liljenzin, J. O. *Acta Chem. Scand. 23* (1969) 3592.
15. Johansson, H. and Rydberg, J. *Acta Chem. Scand. 23* (1969) 2797.
16. Rydberg, J. *Rec. Trav. Chim. Pays-Bas 75* (1956) 737.
17. Sullivan, J. C., Rydberg, J. and Miller, W. F. *Acta Chem. Scand. 13* (1959) 2023; rewritten into Fortran by Zielen, A., Argonne National Laboratory (U.S.A.), private communication.
18. Rydberg, J. *Acta Chem. Scand. 4* (1950) 1503.
19. Liljenzin, J. O. and Stary, J. *J. Inorg. Nucl. Chem. 32* (1970) 1357.
20. Larsen, E. M., Terry, G. and Leddy, J. *J. Amer. Chem. Soc. 75* (1953) 5107.
21. Brown, D. *Advan. Inorg. Chem. Radiochem. 12* (1969) 1.
22. Peshkova, V. M., Metchakova, N. V. and Zhemchuzhin, S. G. *Zh. Neorg. Khim. 6* (1961) 1233.
23. Krishen, A. and Freiser, H. *Anal. Chem. 31* (1959) 923.
24. Peshkova, V. M. and Pêng Ang *Russ. J. Inorg. Chem. 7* (1962) 1091.
25. Peshkova, V. M. and Pêng Ang *Russ. J. Inorg. Chem. 6* (1961) 1064.
26. Solovkin, A. S. and Tsvetkova, S. V. *Uspekhi Khim. 31* (1962) 1394.
27. Larsen, E. M. *Advan. Inorg. Chem. Radiochem. 13* (1970) 1.
28. Norén, B. *Acta Chem. Scand. 27* (1973) 1369.

Received November 5, 1973.

Acta Chemica Scandinavica A 28 (1974) 248—253

Short Communications

Corrigenda and Addenda to "Conformational Analysis of Coordination Compounds. I. Tris-diamine Cobalt(III) Complexes with Three Six-membered Chelate Rings"[1]

S.R. NIKETIĆ and F. WOLDBYE

Chemistry Department A, The Technical University of Denmark, DTH-207, DK-2800 Lyngby, Denmark

Due to our misinterpretation of Jurnak and Raymond's nomenclature,[2] as put forward in their manuscript made available to us prior to publication, two pairs of conformers were interchanged in the last column of Table 1 (Ref. 1, p. 625). Entries 8 to 11 should read as follows:

8	*anti*-chair$_2$lel	C_2	paδ
9	*syn*-chair$_2$lel	C_2	apδ
10	*anti*-chair$_2$ob	C_2	paλ
11	*syn*-chair$_2$ob	C_2	apλ

For the same reason the conformer mentioned in the fifth line of the *Note added in proof* (Ref. 1, p. 624) should read *syn*-chair$_2$lel instead of *anti*-chair$_2$lel, and consequently, the statement in the conclusion of the same sentence, namely that the conformation of Cr tn$_3$ found by Jurnak and Raymond in [Cr tn$_3$][Ni(CN)$_5$].2H$_2$O corresponds to one of those shown by our conformational calculations to have a low potential energy, is incorrect. In fact, the conformation found (a highly twisted form of the *syn*-chair$_2$lel conformation) is one of the three theoretically possible conformations which we omitted from our calculations partly because molecular models indicated that in their *idealized* forms they would be highly unstable.

Prompted by this apparent disagreement we have submitted also the *syn*-chair$_2$lel conformer to minimization in force field FF-1, starting from two different initial conformations: the experimental (of which the coordinates were kindly supplied by Jurnak and Raymond prior to publication), and the idealized in itself highly unlikely conformation. Although the energy of the former proved very high it minimized with rather small changes in geometry to a value slightly above the energy of the chair$_3$(C_3) conformer, and well below some of the other "mixed" M(tn)$_3$ conformations.[1]

In the idealized *syn*-chair$_2$lel conformation two hydrogen atoms were too close to permit its direct treatment by FF-1. However, omitting the interaction of these two hydrogen atoms from the first few cycles of minimization and subsequently including it (when their distance had grown to make the interaction amenable to the usual treatment) we succeeded in minimizing also the energy of this initial conformation by the method of steepest descent. The convergence of this method, in this case associated with the considerable modification of the initial geometry, was extremely time consuming and in order to obtain a coalescence of the two minimized conformations we resorted to the use of Davidon-Fletcher-Powell and modified Newton minimization methods.*

These findings further support our main conclusion (Ref. 1, p. 640), namely that several conformations (now including a rather twisted *syn*-chair$_2$lel conformation) possess comparable low potential energy so that they could be represented in an equilibrium solution of M(tn)$_3$ species.

We take this opportunity to correct also the following misprints. The value for bending force constants in the second part of Table 2 (Ref. 1, p. 628) are given as $\frac{1}{2}K^\theta$ and not as K^θ as erroneously indicated in the head of the table. Further, in the first four columns of the entries 2 to 5 of Table 3 (p. 629) some numbers have been interchanged. The entries concerned should read as follows:

H···C	3.14	4.20	121.1
H···N	2.81	4.32	99.2
C···C	23.70	4.32	297.8
C···N	21.21	4.44	244.0

These trivial misprints were without consequence to the results and conclusions of Ref. 1.

1. Niketić, S. R. and Woldbye, F. *Acta Chem. Scand. 27* (1973) 621.
2. Jurnak, F. A. and Raymond, K. N. *Inorg. Chem. 11* (1972) 3149.
3. Niketić, S. R. *Force Field Calculations on Coordination Compounds*, Thesis, The Technical University of Denmark, 1974.

Received January 31, 1974.

* Details of the continuation of our studies of the conformations of the M(tn)$_3$ system by more powerful computational methods leading to the refinements of the minimized conformations will be made available[3] shortly.

Complete Analysis of the 100 MHz ^{1}H NMR Spectrum of Triphenylphosphine

S. SØRENSEN and H. J. JAKOBSEN

Department of Chemistry, University of Aarhus, DK-8000 Aarhus C, Denmark

The high-resolution ^{1}H NMR spectrum of triphenylphosphine (I) has long been a puzzling problem to the spectroscopist. Since the first report of its appearance as a singlet at 25 MHz [1] it has been shown that both 60 and 100 MHz spectra of solutions of (I) in most common organic solvents appear as a doublet with no further details.[2,3] Using ^{1}H-{^{31}P} spin decoupling Shaw *et al.*[2] concluded that the ^{1}H-^{31}P spin coupling constants are all of almost similar magnitude with an average value of 3.5 Hz. From the benzene-d_6 ASIS (aromatic solvent induced shift) spectrum Keat [3] obtained a value $^3J_{P-H_2}$ = 7.1 Hz applying ^{1}H-{^{1}H} spin decoupling to the more widely spaced multiplets for the *ortho* and *meta*, *para* protons in this solvent; other spectral parameters remained undetermined.

In this note we wish to report that it is possible to resolve a sufficient number of transitions in the 100 MHz benzene-d_6 ASIS spectrum of (I) for a complete analysis to be performed. The ^{1}H NMR spectrum (Fig. 1) may be analysed as the AA'BB'C part of an AA'BB'CX (X = ^{31}P) spin system since long-range couplings between protons on different rings are negligible in aromatic phosphines.[4] The analysis was performed using a modified version of the iterative computer program LAOCN3.[5] Assignments of experimental frequencies were obtained after a series of trial-and-error calculations in which only the chemical shift difference between the *meta* and *para* protons was slightly changed. Values used for the J_{H-H}'s and J_{H-P}'s in these initial calculations were estimated from our results on corresponding couplings in heteroaromatic phosphines,[4] *i.e.* J_{HH}'s as for benzene [6] and $^nJ_{H-P} = K \times {}^nJ_{H-H}$ ($^nJ_{H-H}$ for benzene) using conversion factors $K = 0.9$, 1.0, and 1.1 for $n = 3$, 4, and 5, respectively. After a few sets of iterative calculations in which all parameters affecting the ^{1}H spectrum were varied, an assignment of a total of 106 theoretical transitions was reached. The r.m.s. error between observed and calculated frequencies was 0.013 Hz and the final NMR parameters (all in Hz; $\nu_0 = 100.1$ MHz; chemical shifts referred to internal TMS) are listed in Table 1; the corresponding simulated spectrum is presented in Fig. 1. Further iterative calculations showed that the J_{H-P}'s all have the same sign, *i.e.* positive as determined for $^3J_{H-P}$ in some *para*-substituted triphenylphosphines.[7]

The magnitudes of the $^nJ_{H-P}$'s in (I) are very similar to the corresponding $^nJ_{H-H}$ values in benzene [6] in agreement with results for other phosphines.[4] Also the ^{31}P(III) substituent effect

Table 1. Proton chemical shifts, ^{1}H-^{31}P and ^{1}H-^{1}H spin-spin coupling constants in triphenylphosphine.[a]

$\nu_{H_2} = \nu_{H_6}$	737.18	$^3J_{H_2-H_3} = {}^3J_{H_5-H_6}$	7.66
$\nu_{H_3} = \nu_{H_5}$	705.10	$^4J_{H_2-H_4} = {}^4J_{H_4-H_6}$	1.28
ν_{H_4}	704.19	$^5J_{H_2-H_5} = {}^5J_{H_3-H_6}$	0.64
$^3J_{P-H_2} = {}^3J_{P-H_6}$	7.58	$^4J_{H_2-H_6}$	1.71
$^4J_{P-H_3} = {}^4J_{P-H_5}$	1.49	$^3J_{H_3-H_4} = {}^3J_{H_4-H_5}$	7.47
$^5J_{P-H_4}$	0.69	$^4J_{H_3-H_5}$	1.40

[a] As a 55 % w/w solution in benzene-d_6. All values are in Hz. Chemical shifts are downfield from internal TMS (3 % w/w). The errors of both chemical shifts and coupling constants are estimated from the probable errors to be within ± 0.03 Hz.

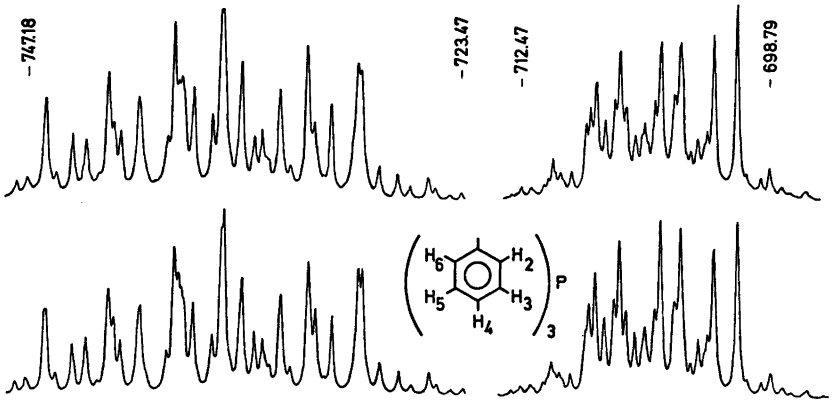

Fig. 1. Experimental (upper) and simulated (lower) 100.1 MHz ^{1}H NMR spectrum of triphenylphosphine in benzene-d_6. The frequency scale (Hz) is downfield from internal TMS.

on the $^nJ_{H-H}$'s is negligible as expected.[4] The magnitudes (and signs) of $^nJ_{H-P}$ in (I) are of interest in connection with studies of effects of ring substituents on these parameters. *Ortho* substituents have been found to have a large influence on both J_{H-P} and J_{C-P} in aromatic phosphines through a twisting of the ring planes with respect to the orientation of the phosphorus lone pair of electrons.[8] CNDO/2 calculations of $^nJ_{H-P}$ in phenylphosphine for different conformations of the $-PH_2$ substituent with respect to the ring plane [9] support these experimental results. Calculations for a dihedral angle (between the ring plane and the C – P – X plane, X = lone pair) of 70°, *i.e.* in the region of the most stable conformation expected for triphenylphosphine,[10] gives values ($^3J_{H_2-P} = 6.69$ Hz, $^4J_{H_3-P} = 1.71$ Hz and $^5J_{H_4-P} = 0.97$ Hz) in good agreement with the experimental results reported here for triphenylphosphine.

Experimental. ^1H NMR spectra were recorded at 100.1 MHz in the continuous wave mode on a Varian XL-100-15 spectrometer and at a temperature of 31°. Spectra were recorded using internal ^1H lock (TMS), a sweep width of 0.5 Hz/cm and a sweep rate of 0.01 Hz/sec. Relative line positions are the average of values for the two sweep directions and are believed to be correct to within ±0.03 Hz. Solutions were prepared in 5 mm o.d. tubes using benzene-d_6 as solvent and TMS as internal standard and lock signal source. The solutions were carefully degassed by the freeze-pump-thaw technique and sealed under vacuum.

Calculations were performed on the CDC 6400 computer system at R.E.C.A.U., University of Aarhus.

1. Mavel, G. *C. R. Acad. Sci. Ser. C 248* (1959) 3699.
2. Shaw, G., Becconsall, J. K., Canadine, R. M. and Murray, R. *Chem. Commun.* (1966) 425, and references therein.
3. Keat, R. *Chem. Ind. (London)* (1968) 1362.
4. Jakobsen, H. J. *J. Mol. Spectrosc. 38* (1971) 243.
5. Castellano, S. and Bothner-By, A. A. *J. Chem. Phys. 41* (1964) 3863.
6. Read, Jr., J. M., Mayo, R. E. and Goldstein, J. H. *J. Mol. Spectrosc. 21* (1966) 235.
7. McFarlane, W. *Org. Magn. Resonance 1* (1969) 3.
8. Sørensen, S., Hansen, R. S. and Jakobsen, H. J. *J. Amer. Chem. Soc. 94* (1972) 5900.
9. Rahn, P. *Thesis*, University of Aarhus 1971.
10. Daly, J. J. *J. Chem. Soc.* (1964) 3799.

Received January 21, 1974.

On the Structure of Deuterated Iminodiacetic Acid Hydrochloride, $C_4H_4D_3NO_4.DCl$

ÅKE OSKARSSON

Inorganic Chemistry 1, Chemical Center, University of Lund, P.O.B. 740, S-220 07 Lund 7, Sweden

The crystal structure of iminodiacetic acid hydrochloride, $C_4H_7NO_4.HCl$ (denoted IDAC), has been reported previously.[1] These crystals decompose within two months at room temperature after being removed from the mother liquor. However, a more stable compound is obtained when the acid hydrogen atoms are replaced by deuterium. This compound (denoted DIDAC) is prepared by repeated recrystallizations of IDAC from $D_2O + DCl$ (containing more than 99.5 % D). The crystal structure of DIDAC has been determined in order to study if the observed difference in the stabilities of the two compounds can be correlated with any structural differences.

Powder photographs of DIDAC were taken as described in Ref. 1. The spectra could be indexed using the lattice parameters of IDAC. The unit cell dimensions were then improved by least-squares refinement. The orthorhombic unit cell dimensions are $a = 12.380$ (1),* $b = 5.718$ (1), and $c = 5.111$ (1) Å.

A single crystal with the dimensions $0.25 \times 0.20 \times 0.17$ mm was mounted in a thin-walled glass capillary and used for the collection of X-ray intensity data on a four-circle diffractometer of type CAD-4. Experimental conditions and data reduction are described in Ref. 1. The systematically absent reflexions indicated the same space groups as for IDAC, *Pmmn* or $Pm2_1n$.

The atomic parameters of the non-hydrogen atoms from IDAC were used as starting parameters in a least-squares refinement assuming the space group to be *Pmmn*. After including an isotropic extinction parameter in the refinement,[2] a difference map, calculated from data with $\sin\theta/\lambda < 0.5$ Å^{-1}, revealed the remaining atoms. In the further calculations, the H and D atoms were given a fixed isotropic temperature factor (3.0 Å^2). The refined value of the extinction parameter, 2.5×10^4, corresponds to a mosaic spread of 2.4″ or a domain size of 3.8×10^{-4} cm. Weights used in the last cycle of refinement, $w = 1/(\sigma_c^2 + 0.0001|F_o|^2 + 4.0)$, gave $R = 0.074$, $R_w = 0.096$ and a smooth weighting scheme. The resulting positional and thermal parameters are given in Table 1. Tables with $|F_o|$, $|F_c|$, $\sin^2\theta_o$, and $\sin^2\theta_c$ can be obtained from the author.

* Figures within parentheses represent e.s.d.'s in the least significant digits.

on the $^nJ_{H-H}$'s is negligible as expected.[4] The magnitudes (and signs) of $^nJ_{H-P}$ in (I) are of interest in connection with studies of effects of ring substituents on these parameters. *Ortho* substituents have been found to have a large influence on both J_{H-P} and J_{C-P} in aromatic phosphines through a twisting of the ring planes with respect to the orientation of the phosphorus lone pair of electrons.[8] CNDO/2 calculations of $^nJ_{H-P}$ in phenylphosphine for different conformations of the $-PH_2$ substituent with respect to the ring plane [9] support these experimental results. Calculations for a dihedral angle (between the ring plane and the C – P – X plane, X = lone pair) of 70°, *i.e.* in the region of the most stable conformation expected for triphenylphosphine,[10] gives values ($^3J_{H_2-P} = 6.69$ Hz, $^4J_{H_3-P} = 1.71$ Hz and $^5J_{H_4-P} = 0.97$ Hz) in good agreement with the experimental results reported here for triphenylphosphine.

Experimental. ^1H NMR spectra were recorded at 100.1 MHz in the continuous wave mode on a Varian XL-100-15 spectrometer and at a temperature of 31°. Spectra were recorded using internal ^1H lock (TMS), a sweep width of 0.5 Hz/cm and a sweep rate of 0.01 Hz/sec. Relative line positions are the average of values for the two sweep directions and are believed to be correct to within ±0.03 Hz. Solutions were prepared in 5 mm o.d. tubes using benzene-d_6 as solvent and TMS as internal standard and lock signal source. The solutions were carefully degassed by the freeze-pump-thaw technique and sealed under vacuum.

Calculations were performed on the CDC 6400 computer system at R.E.C.A.U., University of Aarhus.

1. Mavel, G. *C. R. Acad. Sci. Ser. C 248* (1959) 3699.
2. Shaw, G., Becconsall, J. K., Canadine, R. M. and Murray, R. *Chem. Commun.* (1966) 425, and references therein.
3. Keat, R. *Chem. Ind. (London)* (1968) 1362.
4. Jakobsen, H. J. *J. Mol. Spectrosc. 38* (1971) 243.
5. Castellano, S. and Bothner-By, A. A. *J. Chem. Phys. 41* (1964) 3863.
6. Read, Jr., J. M., Mayo, R. E. and Goldstein, J. H. *J. Mol. Spectrosc. 21* (1966) 235.
7. McFarlane, W. *Org. Magn. Resonance 1* (1969) 3.
8. Sørensen, S., Hansen, R. S. and Jakobsen, H. J. *J. Amer. Chem. Soc. 94* (1972) 5900.
9. Rahn, P. *Thesis*, University of Aarhus 1971.
10. Daly, J. J. *J. Chem. Soc.* (1964) 3799.

Received January 21, 1974.

On the Structure of Deuterated Iminodiacetic Acid Hydrochloride, $C_4H_4D_3NO_4.DCl$

ÅKE OSKARSSON

Inorganic Chemistry 1, Chemical Center, University of Lund, P.O.B. 740, S-220 07 Lund 7, Sweden

The crystal structure of iminodiacetic acid hydrochloride, $C_4H_7NO_4.HCl$ (denoted IDAC), has been reported previously.[1] These crystals decompose within two months at room temperature after being removed from the mother liquor. However, a more stable compound is obtained when the acid hydrogen atoms are replaced by deuterium. This compound (denoted DIDAC) is prepared by repeated recrystallizations of IDAC from $D_2O + DCl$ (containing more than 99.5 % D). The crystal structure of DIDAC has been determined in order to study if the observed difference in the stabilities of the two compounds can be correlated with any structural differences.

Powder photographs of DIDAC were taken as described in Ref. 1. The spectra could be indexed using the lattice parameters of IDAC. The unit cell dimensions were then improved by least-squares refinement. The orthorhombic unit cell dimensions are $a = 12.380$ (1),* $b = 5.718$ (1), and $c = 5.111$ (1) Å.

A single crystal with the dimensions $0.25 \times 0.20 \times 0.17$ mm was mounted in a thin-walled glass capillary and used for the collection of X-ray intensity data on a four-circle diffractometer of type CAD-4. Experimental conditions and data reduction are described in Ref. 1. The systematically absent reflexions indicated the same space groups as for IDAC, *Pmmn* or $Pm2_1n$.

The atomic parameters of the non-hydrogen atoms from IDAC were used as starting parameters in a least-squares refinement assuming the space group to be *Pmmn*. After including an isotropic extinction parameter in the refinement,[2] a difference map, calculated from data with $\sin\theta/\lambda < 0.5$ Å^{-1}, revealed the remaining atoms. In the further calculations, the H and D atoms were given a fixed isotropic temperature factor (3.0 Å^2). The refined value of the extinction parameter, 2.5×10^4, corresponds to a mosaic spread of 2.4″ or a domain size of 3.8×10^{-4} cm. Weights used in the last cycle of refinement, $w = 1/(\sigma_c^2 + 0.0001|F_o|^2 + 4.0)$, gave $R = 0.074$, $R_w = 0.096$ and a smooth weighting scheme. The resulting positional and thermal parameters are given in Table 1. Tables with $|F_o|$, $|F_c|$, $\sin^2\theta_o$, and $\sin^2\theta_c$ can be obtained from the author.

* Figures within parentheses represent e.s.d.'s in the least significant digits.

Table 1. Positional and thermal parameters $\beta_{ij} \times 10^4$ with e.s.d.'s. The expression used is $\exp[-(\beta_{11}h^2+\cdots+2\beta_{12}hk+\cdots)]$. The atoms are denoted in accordance with Ref. 1.

Atom	x	y	z	β_{11}	β_{22}	β_{33}	β_{12}	β_{13}	β_{23}
Cl	1/4	3/4	0.5304(7)	34(2)	253(12)	563(27)	0	0	0
N	1/4	1/4	0.274(2)	42(6)	306(39)	242(38)	0	0	0
O(1)	0.4356(5)	1/4	0.532(1)	53(4)	383(26)	291(31)	0	4(7)	0
O(2)	0.5369(4)	1/4	0.170(1)	39(4)	386(26)	380(31)	0	16(8)	0
C(1)	0.4442(6)	1/4	0.300(2)	45(5)	222(29)	349(36)	0	9(9)	0
C(2)	0.3501(6)	1/4	0.117(2)	44(5)	384(38)	324(38)	0	13(10)	0
D(1)	1/4	0.15(1)	0.39(2)						
H(2)	0.349(4)	0.10(1)	0.03(1)						
D(3)	0.599(7)	1/4	0.26(2)						

Table 2. Hydrogen bond distances (Å) and angles (°) with e.s.d.'s in DIDAC.

N···Cl	3.146(4)	$O(2^{ii})\cdots Cl$	3.052(6)	$\angle D(1^{iv})\cdots Cl\cdots D(1^{v})$	144(4)
$N-D(1^{iv})$ [a]	0.84(8)	$O(2^{ii})-D(3^{ii})$	0.90(8)	$\angle D(3^{ii})\cdots Cl\cdots D(3^{ii})$	120(5)
$Cl\cdots D(1^{iv})$	2.37(8)	$Cl\cdots D(3^{ii})$	2.15(8)	$\angle D(1^{iv})\cdots Cl\cdots D(3^{ii})$	99(1)
$\angle N-D(1^{iv})\cdots Cl$	154(7)	$\angle O(2^{ii})-D(3^{ii})\cdots Cl$	179(8)		

[a] The superscripts are in accordance with Ref. 1.

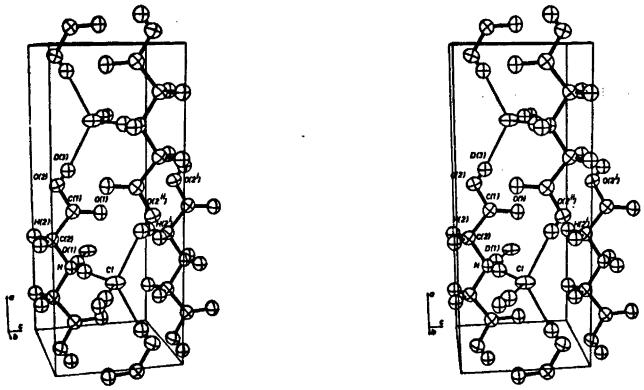

Fig. 1. A stereoscopic pair of drawings showing the structure of DIDAC.

Five cycles of refinement in the space group $Pm2_1n$ did not improve R, R_w or the e.s.d.'s, and it was concluded that a centrosymmetric model well describes the structure of DIDAC.

IDAC and DIDAC are closely isostructural. Positively charged iminodiacetic acid ions, $[C_4H_4D_4NO_4]^+$, with the symmetry *mm* are connected by hydrogen bonds N–D···Cl and O–D···Cl forming zigzag shaped layers. These layers are stacked in the **c**-direction and the forces between the layers are of van der Waals type. The structure is shown in Fig. 1. The dimensions of the positively charged iminodiacetic acid ion are not significantly different in DIDAC and IDAC.

Isotope effects on the hydrogen bond lengths in solids are well-known.[3] By comparing Table 4c in Ref. 1 with Table 2 in this paper, there are no such effects observed within the limits of error. However, the unit cell dimensions in DIDAC are 0.030 (2), 0.017 (2), and 0.017 (2) Å smaller for the **a**, **b**, and **c** parameters, respectively, as compared to IDAC. It is reasonable to assume that these discrepancies are due

to differences in the hydrogen bond systems. Since the N···Cl bond is situated in the mirror plane at $x = 1/4$ (and $x = 3/4$) it cannot influence the **a** parameter. For similar reasons the O···Cl bond cannot influence the **b** parameter. Therefore both types of hydrogen bonds might be shortened on deuteration and this could explain the difference in the stabilities of IDAC and DIDAC.

This work is part of a research project supported by the Swedish Natural Science Research Council.

1. Oskarsson, Å. *Acta Crystallogr. B 29* (1973) 1747.
2. Zachariasen, W. H. *Acta Crystallogr. 23* (1967) 558.
3. Hamilton, W. C. and Ibers, J. A. *Hydrogen Bonding in Solids: Methods of Molecular Structure Determination*, Benjamin, Amsterdam 1968, p. 104.

Received November 27, 1973.

Note on the Crystal Structure of a Mixed Nb-Zr-Oxide

BERTIL NOLANDER and ROLF NORIN

Department of Inorganic Chemistry, Chalmers University of Technology and University of Göteborg, P. O. Box, S-402 20 Göteborg, Sweden

In our studies on the ZrO_2-Nb_2O_5 system [1] we have observed a phase with the approximate composition $(Nb,Zr)O_{2.46}$. Powder data (Table 1) show that this is identical with that first found by Trunov *et al.*,[2] who suggested the formula $ZrO_2.(5-7)Nb_2O_5$. The same phase has later been studied by Allpress and Roth [3] who thought it to be a polymorph of $Nb_{24}ZrO_{62}$ which they called β-$Nb_{24}ZrO_{62}$. Stephenson *et al.*[4] have also investigated the phase, formulating it as $ZrO_2.16Nb_2O_5$ and proposing a structure.

Since we failed to prepare the phase "$(Nb,Zr)O_{2.46}$" in a pure form, we are unable to give accurate data on its composition. Weissenberg photographs $h0l - h3l$ have been taken from single crystals of the oxide and the relative intensities of the reflections measured visually. The Patterson projection $P(u,p,w)$ as well as the Harker sections $(u,0,w)$ and $(u,\frac{1}{2},w)$ have been calculated and these clearly show "$(Nb,Zr)O_{2.46}$" to be closely related to other monoclinic niobium-rich oxides with $b = 3.82$ Å (*cf.* H-Nb_2O_5[5]), but with a more complicated crystal structure. The Patterson projection indicates that the structure is built up of blocks with ReO_3-structure extending infinitely in the y-direction and 3 or 4 MeO_6-octahedra in each of two directions in the xz plane. The best explanation of the Patterson distributions is that each unit cell contains two 4×4, two 4×3, two 3×4, and two 3×3 blocks. The blocks are fitted together in a way analogous to that in H-Nb_2O_5 and leave space for some tetrahedrally surrounded metal atoms (probably two). We have calculated structure factors for several proposed structures built up from the blocks mentioned above, using the metal positions derived from known structures. For the best of these models the agreement between observed and calculated structure amplitudes was satisfactory except for some of the weaker reflexions. We have also made similar calculations based on the crystal structure proposed by Stephenson *et al.* These give approximately the same agreement as that for the best of our models.

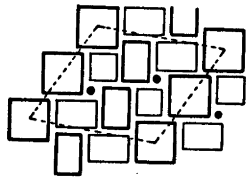

Fig. 1. Idealized projection of the most favoured of our proposed structures for "$(Nb,Zr)O_{2.46}$". The full circles represent metal atoms in tetrahedral positions.

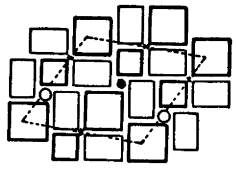

Fig. 2. Idealized projection of the structure of $ZrO_2.16Nb_2O_5$ proposed by Stephenson *et al.* The filled circle represents a metal atom in a tetrahedral position, the open circles are empty positions and intersecting shear planes are marked with a cross.

The main difference between our (Fig. 1) and Stephenson's (Fig. 2) proposals is that the latter introduces two new forms of block junctions and that the former employs only known block junctions. In Stephenson's model, corners of

to differences in the hydrogen bond systems. Since the N···Cl bond is situated in the mirror plane at $x = 1/4$ (and $x = 3/4$) it cannot influence the **a** parameter. For similar reasons the O···Cl bond cannot influence the **b** parameter. Therefore both types of hydrogen bonds might be shortened on deuteration and this could explain the difference in the stabilities of IDAC and DIDAC.

This work is part of a research project supported by the Swedish Natural Science Research Council.

1. Oskarsson, Å. *Acta Crystallogr. B 29* (1973) 1747.
2. Zachariasen, W. H. *Acta Crystallogr. 23* (1967) 558.
3. Hamilton, W. C. and Ibers, J. A. *Hydrogen Bonding in Solids: Methods of Molecular Structure Determination*, Benjamin, Amsterdam 1968, p. 104.

Received November 27, 1973.

Note on the Crystal Structure of a Mixed Nb-Zr-Oxide

BERTIL NOLANDER and ROLF NORIN

Department of Inorganic Chemistry, Chalmers University of Technology and University of Göteborg, P. O. Box, S-402 20 Göteborg, Sweden

In our studies on the ZrO_2-Nb_2O_5 system [1] we have observed a phase with the approximate composition $(Nb,Zr)O_{2.46}$. Powder data (Table 1) show that this is identical with that first found by Trunov *et al.*,[2] who suggested the formula $ZrO_2.(5-7)Nb_2O_5$. The same phase has later been studied by Allpress and Roth [3] who thought it to be a polymorph of $Nb_{24}ZrO_{62}$ which they called β-$Nb_{24}ZrO_{62}$. Stephenson *et al.*[4] have also investigated the phase, formulating it as $ZrO_2.16Nb_2O_5$ and proposing a structure.

Since we failed to prepare the phase "$(Nb,Zr)O_{2.46}$" in a pure form, we are unable to give accurate data on its composition. Weissenberg photographs $h0l - h3l$ have been taken from single crystals of the oxide and the relative intensities of the reflections measured visually. The Patterson projection $P(u,p,w)$ as well as the Harker sections $(u,0,w)$ and $(u,\frac{1}{2},w)$ have been calculated and these clearly show "$(Nb,Zr)O_{2.46}$" to be closely related to other monoclinic niobium-rich oxides with $b = 3.82$ Å (*cf.* H-Nb_2O_5[5]), but with a more complicated crystal structure. The Patterson projection indicates that the structure is built up of blocks with ReO_3-structure extending infinitely in the y-direction and 3 or 4 MeO_6-octahedra in each of two directions in the xz plane. The best explanation of the Patterson distributions is that each unit cell contains two 4×4, two 4×3, two 3×4, and two 3×3 blocks. The blocks are fitted together in a way analogous to that in H-Nb_2O_5 and leave space for some tetrahedrally surrounded metal atoms (probably two). We have calculated structure factors for several proposed structures built up from the blocks mentioned above, using the metal positions derived from known structures. For the best of these models the agreement between observed and calculated structure amplitudes was satisfactory except for some of the weaker reflexions. We have also made similar calculations based on the crystal structure proposed by Stephenson *et al.* These give approximately the same agreement as that for the best of our models.

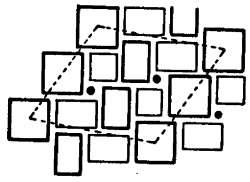

Fig. 1. Idealized projection of the most favoured of our proposed structures for "$(Nb,Zr)O_{2.46}$". The full circles represent metal atoms in tetrahedral positions.

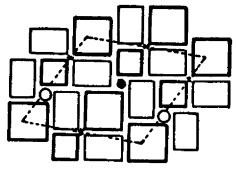

Fig. 2. Idealized projection of the structure of $ZrO_2.16Nb_2O_5$ proposed by Stephenson *et al.* The filled circle represents a metal atom in a tetrahedral position, the open circles are empty positions and intersecting shear planes are marked with a cross.

The main difference between our (Fig. 1) and Stephenson's (Fig. 2) proposals is that the latter introduces two new forms of block junctions and that the former employs only known block junctions. In Stephenson's model, corners of

Table 1. Crystallographic data for "$(Zr,Nb)O_{2.46}$".
Unit cell dimensions: $a = 39.82 \pm 0.02$ Å; $b = 3.829 \pm 0.002$ Å; $c = 35.34 \pm 0.02$ Å, and $\beta = 116.46 \pm 0.05°$.
Systematically absent reflexions: None.
Possible space group: $P2$.
Powder data. $CuK\alpha_1$ radiation. $a(CuK\alpha_1) = 1.54051$ Å.

I obs	$\sin^2\theta \times 10^5$ obs	d obs	$h\ k\ l$	$\sin^2\theta \times 10^5$ calc	d calc
m	374	12.60	3 0 $\bar{2}$	376	12.56
			1 0 2	378	12.53
vvw	435	11.71	2 0 $\bar{3}$	439	11.63
			1 0 $\bar{3}$	439	11.63
vvw	528	10.60	3 0 $\bar{3}$	532	10.56
			0 0 3	533	10.55
vvw	619	9.790	2 0 2	611	9.854
			4 0 $\bar{1}$	619	9.790
			3 0 $\bar{1}$	620	9.782
vvw	717	9.097	4 0 $\bar{3}$	718	9.090
			1 0 3	721	9.071
vvw	941	7.940	3 0 2	939	7.949
			4 0 $\bar{4}$	945	7.924
vvw	997	7.414	5 0 $\bar{3}$	997	7.714
			2 0 3	1001	7.699
vvw	1167	7.130	5 0 0	1167	7.130
vw	1359	6.607	4 0 2	1359	6.607
vvw	1840	5.678	4 0 3	1843	5.874
vvw	1920	5.559	7 0 $\bar{4}$	1924	5.553
vw	2119	5.291	6 0 $\bar{6}$	2127	5.281
			7 0 $\bar{5}$	2129	5.279
vs	2438	4.933	8 0 $\bar{4}$	2436	4.935
			4 0 4	2446	4.925
			7 0 $\bar{6}$	2450	4.921
vvw	2873	4.544	8 0 $\bar{6}$	2871	4.546
vvw	3053	4.408	9 0 $\bar{3}$	3050	4.410
vw	3990	3.856	10 0 $\bar{6}$	3990	3.856
			4 0 6	4006	3.848
w	4099	3.805	1 1 0	4093	3.807
			1 1 $\bar{1}$	4105	3.802
			0 1 1	4106	3.801
vs	4239	3.741	2 1 0	4233	3.744
			1 1 $\bar{2}$	4236	3.742
s	4274	3.726	9 0 $\bar{1}$	4264	3.730
			2 1 $\bar{2}$	4283	3.722
m	4568	3.604	6 0 5	4569	3.604
vs	4705	3.551	5 0 6	4707	3.550
			10 0 $\bar{8}$	4711	3.549
w	4758	3.531	4 1 $\bar{3}$	4764	3.529
w	4941	3.465	11 0 $\bar{7}$	4944	3.464

some of the adjacent blocks are characterized either by an empty tetrahedral position or by the sharing of an octahedral edge, thereby leading to intersecting shear planes.

The authors wish to thank Professor Georg Lundgren for valuable discussions.

1. Nolander, B. and Norin, R. *In press.*
2. Trunov, V. K. *et al. Izv. Akad. Nauk. Neorg. Mat. 7* (1965) 1152.
3. Allpress, J. G. and Roth, R. S. *J. Solid State Chem. 2* (1970) 366.
4. Stephenson, N. C., Beale, J. P. and Craig, D. C. *Nat. Bur. Stand. Spec. Publ. 364*, Sol. State Chem., Proc. of 5th Material Res. Symp. July 1972.
5. Wadsley, A. D. *Acta Crystallogr. 17* (1964) 1545.

Received December 10, 1973.

Acta Chemica Scandinavica A 28 (1974) 255—266

Isocyanides from Alkyl Halides and Onium Dicyanoargentates. Scope and Mechanism

LARS B. ENGEMYR, ARVE MARTINSEN and JON SONGSTAD

Chemical Institute, University of Bergen, N-5000 Bergen, Norway

Alkyl halides and tetramethylammonium dicyanoargentate give, when a reaction takes place, exclusively the corresponding alkyl isocyanide in nearly quantitative yield. The reactivity sequence of the alkyl halides is shown to be very dependent upon the alkyl group: tertiary > secondary > primary, and the displaced halide ion: $I^- > Br^- > Cl^-$. Acyl halides and activated aromatic iodides are found to be unreactive toward the dicyanoargentate ion.

From a kinetic study in acetonitrile employing some substituted benzhydryl halides, the reactions have been found to be second order, first order in each reactant. The Br/Cl ratio of the rates was found to be highly dependent upon the substrate, being 100 for 4,4'-dimethylbenzhydryl halides but $>10^5$ for unsubstituted benzhydryl halides.

Various possible reaction mechanisms are evaluated and discussed.

A large number of reactions are known where metal compounds, either ionic or neutral ones, are employed as catalysts in replacement reactions. Generally, the HSAB principle [1] may be applied as a useful guide when selecting the appropriate metallic catalyst.[2,3]

The catalytic properties of silver compounds in various reactions and the application of silver salts in synthesis has been examined for more than a century. The driving force in reactions where silver salts are employed is the ability of silver ions to complex with polarizable atoms; the stability constants of the various complexes formed is in accordance with Pearson's classification;[1] I > Br > Cl > F [4,5] and Se > S > O.[6,7] Silver cations are thus valuable as catalysts whenever a polarizable atom is to be displaced, for example in the oxidation of aldehydes [8] (H-Ag interaction) and in the aminolysis of *S*-alkyl thiobenzoates [9] (S-Ag interaction). Copper(II) ions, on the other hand, are known to catalyze the hydrolysis of esters and amides.[10] The rather recently observed catalysis of strained σ-bond rearrangements by silver ions [11] has initiated further studies of the chemistry of the silver ion.

The most extensively studied reactions where silver compounds are employed as reagents are the replacement reactions on alkyl halides:

$$RX + AgY \rightarrow RY + AgX \qquad (1)$$

where soluble or slightly soluble silver compounds are employed and where the driving force in the reactions is the formation of less soluble silver compounds, AgX, or in some cases, the formation of silver complexes of high stability.

With regard to the mechanism of these reactions, several kinetic studies have appeared,[12–17] but the mechanism appears far from settled. In numerous reactions, the anion of the applied silver salt may assist nucleophilically, and the order of the reaction may thus be dependent upon the anion attached to the silver cation. The majority of the reactions following eqn. 1 are thus not strictly second order, but, being first order in the applied alkyl halide, the order in the silver compound varies, usually from 1.5 to 2, depending upon the alkyl halide, the solvent, the concentration and, especially, the applied silver compound. Furthermore, the pronounced dependence of the rate of reaction upon the alkyl halide and the leaving group: *tert*-RX ≫ *sec*-RX ≫ *prim*-RX and RI ≫ RBr ≫ RCl, has made the interpretation of kinetic results difficult.

Generally, the reactions following eqn. 1 are believed to go via a quadruple ion intermediate, $Y^{\delta-}-R^{\delta+}-X^{\delta-}-Ag^{\delta+}$,[12] to a varying extent prior to product formation.[14] Kornblum [18,19] has argued convincingly in favour of this electrophilic pull-nucleophilic push mechanism, and has suggested that the rather erratic stereochemical results obtained in his studies on the reaction between 2-bromooctane and silver nitrite and silver nitrate in various solvents is due to the relative importance of the electrophilic pull of silver and the nucleophilic push of the anion.

Recently,[20] it was shown that by applying onium dicyanoargentates instead of silver cyanide, alkyl isocyanides could be obtained in high yields in homogeneous reactions in aprotic solvents:

$$RX + Ag(CN)_2^- \rightarrow RNC + AgX_2^- \qquad (2)$$

No trace of alkyl cyanides was found in the products of these reactions even after repeated analyses directed towards this end. When concentrated solutions of the reactants were applied, the reactions became heterogeneous due to the limited solubility of the onium dihalo-argentates. Tetramethylammonium dichloroargentate and dibromoargentate in acetonitrile started to precipitate at concentrations above 5×10^{-3} M.

We now wish to report an extended study of this reaction to explore the possible generality of this route to organic isocyanides. In Table 1 are collected a number of successful and unsuccessful reactions employing different organic halides, together with obtained yields of isocyanides and semi-quantitative rates of reactions at 25°C in acetonitrile.

For the reactions where no yields of isocyanide could be detected after work-up of the reaction mixture, no precipitation of slightly soluble salts of dihaloargentate ions could be observed, and the applied organic halides were recovered in quantitative yields except for mechanical losses. The yields of 4,4'-dimethylbenzhydryl isocyanide and benzhydryl isocyanide were probably higher than reported in Table 1, as these two isocyanides were quite difficult to purify due to their rather low melting points, their high solubilities in all organic solvents and, especially, to their tendency to polymerize at elevated temperatures which prevented these compounds from being crystallized from warm solution. For this latter reason, the reaction between tetramethylammonium dicyanoargentate and benzhydryl chloride was not examined at elevated temperature to see whether increased

Table 1. Survey of examined reactions with tetramethylammonium dicyanoargentate in acetonitrile in accordance with eqn. 2, with yields of isocyanides and apparent rates of reactions. Concentration of reagents in the $1 \times 10^{-2} - 5 \times 10^{-2}$ M range.

RX	Reaction condition		Yield of RNC in %	Apparent rate of reaction at 25°C
Ph_3CCl	Room temp.,	90 min	97	Very rapid [a]
$(4\text{-}MePh)_2CHBr$	"	4 h	84	Rapid
$(4\text{-}MePh)_2CHCl$	"	20 h	77	Slow
Ph_2CHBr	"	15 h	92	Slow
Ph_2CHCl	"	48 h	0	No reaction
$(4\text{-}NO_2Ph)_2CHBr$	"	48 h	0	"
$(4\text{-}NO_2Ph)_3CBr$	"	6 h	0	No reaction
"	81.5°C (reflux)	2 h	84	Very slow
MeI	80°C	30 min	> 80	Very slow [b]
MeBr	Room temp.,	14 d	trace	Very slow [c]
$4\text{-}NO_2PhCH_2Br$	"	48 h	0	No reaction
$4\text{-}NO_2PhI$	81.5°C (reflux)	24 h	0	"
				"
PhI	"	"	0	"
PhCOCl	"	"	0	"
$4\text{-}NO_2PhCOBr$	"	"	0	"

[a] Reaction appeared instantaneous; Ref. 21. [b] Nitrobenzene as solvent; Ref. 20. [c] Reaction just observable.

temperature would give a measurable quantity of benzhydryl isocyanide. In contrast to trityl isocyanide,[22] 4,4'-dimethylbenzhydryl isocyanide and benzhydryl isocyanide were found to be perfectly stable in acetonitrile at room temperature (see experimental part).

As can be deduced from Table 1, the usual reactivity sequences for Ag(I) assisted reactions are followed for these reactions: *tert*-RX > *sec*-RX > *prim*-RX and RI > RBr > RCl. Acyl halides and aryl halides were found to be completely unreactive. This suggests that the present method for the synthesis of organic isocyanides is only useful for alkyl halides as substrates, and preferably S_N1 type alkyl halides and S_N2 type alkyl iodides.

For the successful reactions, with one exception, no colour was observed during the course of the reactions and the isocyanides isolated were nearly colourless, with a slightly yellowish taint. The reaction between tetramethylammonium dicyanoargentate and tris(4-nitrophenyl)methyl bromide at acetonitrile reflux temperature, however, was completely different. The reaction mixture went through a series of various intensive colours before becoming yellow. (See later discussion for a probable explanation).

In order to gain some insight into the mechanism of this silver-assisted reaction, which appears to be a rare case of a homogeneous one, a kinetic study in acetonitrile was attempted. As it turned out, only a few substrates were found to be useful, because the rates of the reactions were very dependent upon the substrates. Triphenylmethyl chloride was found to react too rapidly for standard analytical methods, while methyl iodide and other very unreactive substrates reacted too slowly, since concentrated solutions of the reactants had to be avoided due to the very limited solubility of the tetramethylammonium dihaloargentates. Some substituted and unsubstituted benzhydryl halides, however, were found to react with rate constants within an acceptable range. 4,4'-Dimethylbenzhydryl bromide and chloride, and benzhydryl bromide, were chosen as substrates.

The UV method, measuring the decrease in alkyl halide concentration, was used for the determination of rate constants. Since the extinction coefficients of the alkyl halides in the 230 – 260 nm region were considerably greater than that of tetramethylammonium dicyanoargentate, rate constants could be determined from runs with greatly varying concentrations of tetramethylammonium dicyanoargentate. The UV method appeared to be the only method by which the rates of reaction could be determined. The IR method could not be applied because the dicyanoargentate ion and the formed isocyanides absorbed at nearly the same wavelength, ≈ 2130 cm^{-1}, with rather similar extinction coefficients. The very limited solubility of the tetramethylammonium dihaloargentates prevented the use of the NMR technique for the determination of accurate rate constants.

EXPERIMENTAL

Acetonitrile, "Baker Analyzed" reagent, was distilled from P_2O_5 and finally from CaH_2 prior to use. A midfraction from the final distillation was used both as solvent for the kinetic studies and for the various syntheses. During the kinetic studies, the distillation from CaH_2 was repeated every two weeks.

Benzene, cyclohexane, diethyl ether, and various fractions of light petroleum were dried with sodium.

Tetraphenylarsonium dicyanoargentate and perchlorate were purified as reported.[20,22]

Tetramethylammonium chloride and bromide, both Fluka *purum*, were washed with acetonitrile and ether and dried in vacuum prior to use.

Tetramethylammonium dicyanoargentate, $Me_4NAg(CN)_2$. To 40 g of purified tetramethylammonium chloride in 250 ml acetonitrile was added 80 g freshly prepared and dried silver cyanide, and the reaction mixture was refluxed for 5 h. After filtration, diethyl ether was added to precipitate the product. The product was repeatedly dissolved in dry acetonitrile, filtered and precipitated with diethyl ether to remove traces of the sparingly soluble products from the reaction. Finally, the salt was crystallized from acetonitrile; the first crop of crystals was discarded and the midfraction was used for the kinetic studies. This purification was continued until the observed rate constants were reproducible to within 3 % for a given concentration of benzhydryl bromide and tetramethylammonium dicyanoargentate. M.p. 194 – 195°C. (Found: C 31.1; H 5.3; N 17.6; Ag 46.0. Calc. for $C_6H_{12}AgN_3$: C 30.8; H 5.2; N 17.9; Ag 46.0).

Tetramethylammonium dibromoargentate was made from equivalent amounts of tetramethylammonium bromide and silver bromide in acetonitrile. M.p. 328 – 330°C. (Found: C 14.6; H 3.5; N 4.0. Calc. for $C_4H_{12}AgBr_2N$: C 14.4; H 3.5; N 4.1). Tetramethylammonium dichloroargentate was made likewise, m.p. 312 – 315°C.

These two salts were only sparingly soluble in acetonitrile.

Benzhydryl isocyanide. To 5.0 g benzhydryl bromide, 0.02 mol, crystallized from acetonitrile, in 150 ml acetonitrile was added 7.0 g, 0.03 mol, tetramethylammonium dicyanoargentate. A white precipitate slowly formed. The reaction mixture was stirred at room temperature for 15 h. After filtration, the mother liquor was evaporated to dryness in vacuum and the product extracted with diethyl ether. Crystallization from this solvent alone or by addition of light petroleum (40 – 60°C) proved unsuccessful. Two crystallizations from luke-warm light petroleum (40 – 60°C) gave a pure, slightly yellowish product. Yield 3.9 g, 92 %, m.p. 48 – 49°C (47°C [20]). (Found: C 86.9; H 5.9; N 7.2. Calc. for $C_{14}H_{11}N$: C 87.0; H 5.7; N 7.3). The white precipitate from the reaction was found to be tetramethylammonium dibromoargentate.

4,4'-Dimethylbenzhydryl isocyanide. To 5.0 g 4,4'-dimethylbenzhydryl bromide, 0.018 mol, m.p. 49 – 50°C (47.5 – 48.5°C [23]), in 100 ml acetonitrile was added 7.0 g, 0.03 mol, tetramethylammonium dicyanoargentate. Tetramethylammonium dibromoargentate started to precipitate immediately. The reaction mixture was stirred for 4 h at room temperature, and the product was then isolated and purified as above. Yield 3.4 g, 84 %, m.p. 57 – 58°C. (Found: C 87.0; H 6.9; N 6.1. Calc. for $C_{16}H_{15}N$: C 86.9; H 6.8; N 6.3). Upon reaction with HCl in acetone, this isocyanide gave the corresponding Passerini product,[20] *N*-(4,4'-dimethylbenzhydryl)-2-hydroxy-2-methylpropionamide, m.p. 146 – 147°C, in nearly quantitative yield.

From 4,4'-dimethylbenzhydryl chloride, m.p. 45°C (45 – 46°C [24]), the isocyanide was obtained in 77 % yield. As this reaction was considerably slower than when the bromide was used, the reaction mixture was stirred for 20 h at room temperature. The white precipitate from the reaction was crystallized from acetonitrile and shown to be tetramethylammonium dichloroargentate.

The reactions between 4,4'-dimethylbenzhydryl bromide, 4,4'-dimethylbenzhydryl chloride and benzhydryl bromide and tetramethylammonium dicyanoargentate were repeated in unpurified acetonitrile and in acetonitrile containing 1 % water by volume. The isocyanides were isolated in yields which were not significantly different from the reactions when performed in dry and purified acetonitrile. The IR spectrum in carbon tetrachloride revealed that the formation of the corresponding benzhydrols from reactions performed in moist acetonitrile was negligible.

Tris(4-nitrophenyl)methyl isocyanide. Method A. To 0.5 g tetramethylammonium dicyanoargentate, 0.0027 mol, in 25 ml acetonitrile was added 0.5 g tris(4-nitrophenyl)methyl bromide, m.p. 195 – 195°C (190 – 191°C [25]). No precipitate was formed when the reaction mixture was stirred at room temperature. The reaction mixture was then refluxed for 2 h and tetramethylammonium dibromoargentate slowly started to precipitate. After the usual treatment of the reaction mixture, the product was extracted with benzene and precipitated with light petroleum. Yield 0.37 g, 84 %, m.p. 167 – 169°C. IR_{NC} 2130 cm^{-1}. Elemental analysis of this compound gave too low values for nitrogen, even after repeated crystallizations from benzene – light petroleum (40 – 60°C) which did not alter the melting point.

To 0.060 g of tris(4-nitrophenyl)methyl isocyanide in 25 ml warm carbon tetrachloride was added 0.5 ml bromine and the mixture was kept at approximately 50°C for 30 min. After evaporation of the solvent and excess bromine in vacuum, the residue was crystallized from carbon tetrachloride – light petroleum (40 – 60°). The product showed no absorbance in the 2100 – 2300 cm^{-1} range, but a new, very strong band at 1660 cm^{-1}, due to C=N, suggested the product to be 2,2-dibromo-1-[tris(4-nitrophenyl)methyl]formimine. Yield 0.050 g, 63 %, m.p. 162 – 163°C. (Found: C 43.1; H 2.6; N 9.2. Calc. for $C_{20}H_{12}Br_2N_4O_6$: C 42.5; H 2.2; N 9.9).

Method B. To 0.3 g tris(4-nitrophenyl)methyl bromide in 25 ml acetonitrile was added a fivefold excess of silver cyanide, and the mixture was stirred at room temperature for 18 h. After the usual work-up, 0.25 g of the product, 93 % was isolated. M.p. and mixed m.p. 164 – 166°C. With excess bromine in carbon tetrachloride a product was obtained which was shown to be identical with that formed from the isocyanide synthesized according to method A using excess bromine.

Attempted isomerization studies of benzhydryl isocyanide, 4,4'-dimethylbenzhydryl isocyanide, and tris(4-nitrophenyl)methyl isocyanide were performed by measuring the peak in the 2130 cm^{-1} region of 2.0×10^{-3} M solution using 0.1 cm liquid cells at approximately 25°C.[22] One solution of each isocyanide was kept in a dark-painted bottle, the other in daylight. No reduction in the intensities of the isocyanide peaks could be observed after 40 to 50 days. A Unicam SP 200 G Infrared Spectrometer was used for the experiments.

Attempted synthesis of methyl isocyanide from methyl bromide and tetramethylammonium dicyanoargentate. To 2.0 g methyl bromide, Fluka *purum*, 0.021 mol, in 25 ml acetonitrile was added 7.0 g, 0.03 mol, tetramethyl dicyanoargentate. After 14 days at room temperature no precipitate of tetramethylammonium dibromoargentate or change in the UV spectrum of the solution could be observed. The slightly obnoxious odour of the reaction mixture suggested that a minute amount of methyl isocyanide had been formed.

The unreacted methyl bromide was then slowly distilled into a concentrated solution of 10 g triphenyl phosphine in acetone. After 3 days at room temperature, 7.0 g methyl tri-

phenylphosphonium bromide, 93 %, precipitated upon addition of diethyl ether.

Benzhydryl chloride and 4,4′-dinitrobenzhydryl bromide, m.p. 93 – 94°C (92 – 93°C [26]) did not give any precipitate with tetramethylammonium dicyanoargentate and no isocyanide could be isolated after stirring at room temperature for 48 h; neither was 4-phenylbenzoyl bromide found to be reactive. Solutions of 4-nitrobenzyl bromide, phenyl iodide, and 4-nitrophenyl iodide were refluxed with tetramethylammonium dicyanoargentate for 24 h without yielding any isocyanides or precipitates of dihaloargentates. From all these unsuccessful synthesis the alkyl halides, acyl halides and aryl halides were recovered in quantitative yields.

All melting points are corrected.

Chemical shifts of methine protons in benzhydryl compounds. The spectra were measured in carbon tetrachloride on a Jeol NMR C-60 H spectrometer and a Spin-decoupler Frequency Counter JNM-SD 30 was used to determine the resonance positions. The measurements were performed on 0.2 M solutions except for 4,4′-dimethylbenzhydrol where the shift at infinite dilution was obtained by extrapolation. The observed shifts in ppm, relative to TMS were: Ph_2CHBr 6.17; Ph_2CHNC 5.79; $(4\text{-MePh})_2CHBr$ 6.12; $(4\text{-MePh})_2CHCl$ 5.95; $(4\text{-MePh})_2CHOH$ 5.64; $(4\text{-MePh})_2CHNC$ 5.69.

Kinetic studies. Between an alkyl halide, RX, and an onium dicyanoargentate, the following reaction take place:

$$RX + Ag(CN)_2^- \xrightarrow{k_2} RNC + NCAgX^- \quad (3)$$

$$NCAgX^- \xrightarrow{k_3} \tfrac{1}{2}Ag(CN)_2^- + \tfrac{1}{2}AgX_2^- \quad (4)$$

As no mixed complex silver anions of type $NCAgX^-$ are known and as no salts of these anions could be isolated, k_3 is assumed to be far greater than k_2. The net reaction will thus be:

$$RX + \tfrac{1}{2}Ag(CN)_2^- \xrightarrow{k_2} RNC + \tfrac{1}{2}AgBr_2^- \quad (5)$$

or simplified for the further calculations:

$$A + \tfrac{1}{2}B \xrightarrow{k_2} C + \tfrac{1}{2}D \quad (6)$$

For a second-order reaction, first order in each of the reactants, the following rate equation is obtained:

$$\left(b - \frac{a}{2}\right)^{-1} \ln \frac{a(2b - x)}{2b(a - x)} = k_2 t \quad (7)$$

where a and b are the concentrations of species A and B, respectively, at $t = 0$.

When ε_A, ε_B, ε_C, and ε_D are the extinction coefficients of species A, B, C, and D, respectively, at a given wavelength, and x is the amount of A reacted at time t, the absorption at this wavelength is given by

$$A_t = \varepsilon_A (a - x) + \varepsilon_B(b - \tfrac{1}{2}x) + \varepsilon_C x + \tfrac{1}{2}\varepsilon_D x \quad (8)$$

With an expression for x, calculated from eqn. 8, one obtains the following rate equation:

$$\left(b - \frac{a}{2}\right)^{-1} \ln \frac{a}{b} \frac{At + 2b\varepsilon_A - a\varepsilon_A - b\varepsilon_D - 2b\varepsilon_C}{2A_t + a\varepsilon_B - 2b\varepsilon_B - a\varepsilon_D - 2a\varepsilon_C} = k_2 t \quad (9)$$

As the calculations according to eqn. 9 were quite timeconsuming, a Fortran N program [27] for Watfor compiler was made whereby plots of the left side of eqn. 9 *versus* time were rapidly obtained.

In some of the runs there was a downward trend in the rate plots after one or two half-lives, in other runs the plots were completely linear up to five half-lives. No relation, however, between concentrations of reactants, substrates or leaving groups and the observed curvature could be found. Several calculations were performed to adjust the kinetics to rate equations using order of the reactants different from one, but in no case was this procedure found to be successful.

For the reaction between benzhydryl bromide and tetramethylammonium dicyanoargentate with equal concentrations of the reactants, 10^{-3} M, an isosbestic point at 225 nm was obtained, and the rate constants were calculated from the change in absorbance at 238 nm. With 4,4′-dimethylbenzhydryl chloride as substrate, an isosbiestic point at 228 nm was observed; the rate constants were calculated from absorbances at 240 nm. Due to the lower extinction coefficient of this substrate in the 230 – 250 nm range, rate constants could not be accurately determined from runs where the initial concentration of the alkyl halide was lower than 5×10^{-4} M. The rate of reaction between 4,4′-dimethylbenzhydryl bromide and tetramethylammonium dicyanoargentate was calculated from the change of absorbance at 250 nm. In this latter reaction, no isosbestic point > 220 nm could be observed.

The extinction coefficients of the compounds at the various wavelengths were determined from different batches and the purification of the compounds was continued until the extinction coefficients were reproducible to within the experimental error, ± 2 %. Beer's law was found to be valid for all compounds at the concentrations used for determination of the kinetic data. For all the reactions studied, the reduction in absorbance in the 230 – 300 nm range during the course of the reactions was due almost entirely to the disappearance of the benzhydryl halides. The neglect of the other species present in the reactions, however, was not found to be justified. The extinction coefficients were determined in 0.1 cm thermostated cells, except for the tetramethylammonium dihaloargentates

where, due to the limited solubility of these salts in acetonitrile, 1 cm cells were used.

The rate studies were performed on a Beckman DB Spectrophotometer using 0.1 cm cells. The thermostated compartments were kept at ±0.05°C.

RESULTS

In Tables 2, 3, and 4 are listed the calculated rate constants in acetonitrile at 25.0°C for the various substrates.

In Table 5 are listed the rates of reaction of two of the three substrates at various temperatures together with calculated activation enthalpies and activation entropies. 4,4'-Dimethylbenzhydryl bromide reacted too rapidly at temperatures above 25°C to allow sufficiently accurate activation parameters to be determined.

Due to the dependence of the rates of reaction upon concentration, the rate constants in Table 5 are determined solely from one set of concentrations of the reactants, 5.00×10^{-4} M in

Table 2. Calculated second order rate constants for the reaction between benzhydryl bromide and tetramethylammonium dicyanoargentate in acetonitrile at 25.0°C.

$[Ph_2CHBr]_0 \times 10^4$ M	$[Me_4NAg(CN)_2]_0 \times 10^4$ M	Number of runs	$k_2 \times 10^2$ M^{-1} s^{-1}
2.30	2.50	2	6.0 ± 0.1
4.60	5.00	2	5.1 ± 0.1
4.80	5.00	3	5.1 ± 0.2
5.00	100	2	5.3 ± 0.2
9.60	10.0	3	3.6 ± 0.2
11.0	100	3	3.8 ± 0.1
10.0	201	2	3.6 ± 0.1
10.2	200	2	3.6 ± 0.1
10.2	200 (0.5 vol % H_2O)	3	4.7 ± 0.2
10.1	200 (1.0 vol % H_2O)	2	6.5 ± 0.2

Table 3. Calculated second order rate constants for the reaction between 4,4'-dimethylbenzhydryl bromide and tetramethylammonium dicyanoargentate in acetonitrile at 25.0°C.

$[(4\text{-MePh})_2CHBr]_0 \times 10^4$ M	$[Me_4NAg(CN)_2]_0 \times 10^4$	Number of runs	k_2 M^{-1} s^{-1}
5.03	5.03	3	5.0 ± 0.2
5.00	5.00	2	4.8 ± 0.2
4.90	5.00	2	5.0 ± 0.2
10.1	10.1	4	3.5 ± 0.2
10.0	10.0	2	3.8 ± 0.2
10.2	10.0	3	3.6 ± 0.2
9.9	10.1	2	3.4 ± 0.2
10.0	10.0	2	3.6 ± 0.2

Table 4. Calculated second order rate constants for the reaction between 4,4'-dimethylbenzhydryl chloride and tetramethylammonium dicyanoargentate in acetonitrile at 25.0°C.

$[(4\text{-MePh})_2CHCl]_0 \times 10^4$ M	$[Me_4NAg(CN)_2]_0 \times 10^4$ M	Number of runs	$k_2 \times 10^2$ M^{-1} s^{-1}
4.80	5.00	2	3.7 ± 0.3
5.00	5.00	4	3.6 ± 0.3
5.05	5.00	2	3.9 ± 0.1
4.95	100	2	3.7 ± 0.2
5.05	5.00 (0.1 vol % H_2O)	2	14.0 ± 0.5

Table 5. Effect of temperature on the rates of reaction together with calculated $\Delta H^{\ddagger}$ and $\Delta S^{\ddagger}$. Concentrations of benzhydryl halides and tetramethylammonium dicyanoargentate 5.00×10^{-4} M and 1.00×10^{-2} M, respectively.

RX	$k_2 \times 10^2$ $M^{-1}s^{-1}$ 25.0°C	35.0°C	45.0°C	$\Delta H^{\ddagger}$ kcal mol^{-1}	$\Delta S^{\ddagger}$ cal $mol^{-1}K^{-1}$
Ph_2CHBr	5.3 ± 0.1	11.7 ± 0.3	23.2 ± 0.5	13.4	−19
$(4\text{-MePh})_2CHCl$	3.7 ± 0.2	8.8 ± 0.1	20.7 ± 0.5	15.4	−13

Table 6. Rate constants for 4,4′-dimethylbenzhydryl bromide reacting with tetraphenylarsonium dicyanoargentate in acetonitrile at 25.0°C in the presence of tetraphenylarsonium perchlorate at a constant ionic strength of 1.00×10^{-3} M.

$[(4\text{-MePh})_2CHBr]_0 \times 10^3$M	$[Ag(CN)_2^-]_0 \times 10^4$M	$[ClO_4^-]_0 \times 10^4$M	k_2 M^{-1} s^{-1}
1.02	10.0	0	3.3 ± 0.2
1.02	5.0	5.00	8.8 ± 0.5
1.02	1.00	9.00	21.5 ± 1

alkyl halide and 1.00×10^{-2} M in ionic dicyanoargentate.

In Table 6 are listed the rates of reaction of 4,4′-dimethylbenzhydryl bromide in the presence of an ionic perchlorate at a constant ionic strength. Due to the dependence of the rates of reaction upon water, Tables 2 and 4, and since tetramethylammonium perchlorate was found to be most difficult to obtain completely dry, tetraphenylarsonium perchlorate and tetraphenylarsonium dicyanoargentate were used for these rate studies. The higher background absorption in the 220 – 260 nm region caused by the tetraphenylarsonium ions necessarily reduced the accuracy by which the rate constants could be determined, but the accuracy was clearly sufficient to show the catalytic effect of the perchlorate ions.

DISCUSSION

The very high rate of reaction of trityl chloride, moderate rates of benzhydryl halides and very low reactivity of typical S_N2 substrates (Table 1), suggest that the rates of these silver(I) assisted reactions are highly dependent upon the ability of the substrates to react by what is usually termed the S_N1 mechanism. The term S_N1Ag^+ for this and related reactions thus appears to be well founded.

In accordance with the idea that the first and rate-determining step in this S_N1Ag^+ reaction, as for other reactions of similar type, is the partly or completely heterolytic fission of the carbon-halogen bond, as for usual S_N1 reactions, any factors affecting the rates of S_N1 reactions are expected to influence in a somewhat similar manner the rate of formation of isocyanides in the present reaction.

However, as has been recently pointed out,[22,28] the mechanisms of S_N1 reactions are very complicated, and the factors determining the rates of these reactions are known to be a function of the substrate, the nucleophile, the leaving group, the ionic strength, the solvent, *etc.*, and depending on which species in the Winstein dissociation scheme is the kinetically most important one. Sneen and co-workers [27] have argued that even in classical S_N2 reactions, electrophilic species other than the alkyl halides in their ground state have to be considered. Koskikallio [30] has recently presented evidence for the "unified mechanism" or the "ion-pair mechanism" in the reaction between some charged nucleophiles and methyl benzenesulphonate, although this mechanism appears most unlikely for primary and secondary alkyl halides as substrates.[31] In any event, factors increasing the amount of ion pairs or charged species from uncharged alkyl substrates will necessarily increase the rates of S_N1 reactions.

As water or protic solvents in dipolar aprotic

or non-polar solvent are known to catalyze S_N1 reactions by assisting the carbon-halogen bond fission by hydrogen bonding to the departing halide,[24,32-34] the catalysis by water in the present reaction is readily understood. The more pronounced catalysis in the case of 4,4′-dimethylbenzhydryl chloride as substrate is thus as expected (Table 4). However, the last two entries in Table 2 indicate that the concentration of water should not be included in the rate equations. Furthermore, the quality of the kinetic runs in moist acetonitrile was not significantly lower than in dry acetonitrile, and more importantly, no yield of benzhydrols or reduction in the yield of the desired isocyanides could be detected when moist acetonitrile was used as solvent for the reactions.

The results listed in Tables 2 and 3 clearly indicate that the calculated second order rate constants are significantly dependent upon the concentration of the alkyl halides, the rates increasing slightly for decreasing concentrations of the alkyl halides. It appears conceivable that for low concentrations of the applied alkyl halides, $< 5 \times 10^{-4}$ M, where the increased rates are observed, the amount of water in the applied purified acetonitrile is of sufficient magnitude to exert a measurable catalytic effect. The second order rate constants were found to be independent, within experimental error, of the concentration of ionic dicyanoargentate for constant concentrations of the alkyl halides, suggesting the order of one for the dicyanoargentate ion in the rate equation to be a valid choice.

The observed catalysis by perchlorate ions (Table 6) is further evidence for the fundamental similarity between the S_N1 and the S_N1Ag^+ mechanism. Although salt effects on S_N1 reactions in aprotic solvents are not very well investigated,[32] there appears presently to be no exception to the rule that salts of perchlorate ions and other indifferent ions exert a positive salt effect on S_N1 reactions in this class of solvents.[35]

Although rates of reactions of only two alkyl bromides, 4,4′-dimethylbenzhydryl bromide and unsubstituted benzhydryl bromide, have been determined, a ϱ^+ of -3.1 and a ϱ of -5.9 may be calculated from σ^+_{Me} and σ_{Me}, respectively. (Accurate values of ϱ^+ and ϱ can hardly be determined due to the lack of additivity of σ^+_{Me} and σ_{Me} in benzhydryl substrates.[36]) The mere magnitudes of these ϱ values, however, suggest that the rates of these reactions are highly dependent upon the formation of positive charge on the reacting carbon atom of the reacting alkyl halides.[37] As benzhydryl chloride was found not to react, an upper value of ϱ^+ of -6 for the benzhydryl chlorides may be estimated.

The rate sequence RI > RBr > RCl, the extreme dependence of the ϱ^+-value upon the halogen atom, and likewise, the dependence of the ratio of the rates for corresponding bromo and chloro compounds upon the substrate, being ~ 100 for 4,4′-dimethylbenzhydryl halides and $> 10^5$ for benzhydryl halides, Tables 1 to 4, clearly indicate that the silver atom is playing an important role in the rate determining step. As the examined reactions are clearly second order, first order in the dicyanoargentate ion, a preformed quadruple intermediate[13] reacting with a second dicyanoargentate ion is excluded as a mechanistic possibility on kinetic grounds. Thus, the formation of isocyanides in the present reactions must take place through an intramolecular collapse of a 1:1 transition state or intermediate of the reacting species. The lack of detectable amounts of benzhydrols when the reactions are performed in moist acetonitrile is further evidence for an intramolecular rearrangement without the formation of solvent-separated ion pairs or free ions.

The activation parameters determined in this work, Table 5, are in the range expected for typical S_N2 reactions, but this mechanism can be ruled out as the typical S_N2 substrates, methyl iodide, methyl bromide, and 4-nitrobenzyl bromide, are the least reactive ones. The dicyanoargentate ion must therefore necessarily be a very poor nucleophile. As there appears to be some similarities between the factors governing the halophilicity and the carbon nucleophilicity of a nucleophile, it is natural to assume that the dicyanoargentate ion is a poor nucleophile toward positive halogen as well. The very negative ϱ-values observed substantiate the conclusion that the dicyanoargentate ion cannot possibly act as a nucleophile in the present reaction.[37]

Due to the electrophilic nature of the silver atom and the low nucleophilicity of the dicyanoargentate ion, the reaction between an alkyl halide and the dicyanoargentate ion may basi-

cally be considered a typical silver(I) assisted reaction, the interaction between the silver atom and the halogen atom promoting ionization of the carbon halogen bond. The isocyanide may then be formed directly or preferably *via* a tight ion pair by expulsion of the unsymmetrical halocyanoargentate ion (Scheme A).

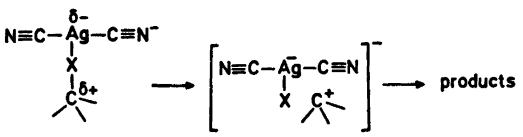

Scheme A.

The observed increase in reactivity from unsubstituted benzhydryl halides to 4,4′-dimethylbenzhydryl halides is compatible with the mechanism suggested above and this mechanism readily explains the rate sequences observed: *tert*-RX > *sec*-RX > *prim*-RX and RI > RBr > RCl. It does not, however, satisfactorily explain the variations in the Br/Cl rate ratios upon the substituents in the benzhydryl halides. As pointed out by Kevill and Horwath [16] in their study on 1-adamantyl halides, any reasonable mechanism for the so-called S_N1Ag^+ reactions must account for the extremely large rate differences between bromides and chlorides. The negative entropies of activation observed in the present reaction, Table 5, may point to a mechanism which is different from the simple Ag^+-catalyzed S_N1 mechanism depicted in Scheme A. In view of these difficulties a closer look at the reactivity pattern of silver(I) species appears necessary.

Silver(I) species, known to be powerful electrophiles, interact strongly with unsaturated organic molecules through a σ coordinate bond to the metal and the metal in turn donates a pair of *d* electrons to the organic molecule through a π bond.[38] The remarkable capability of silver(I) ions to promote σ-bond rearrangements,[11] however, suggest that these species are capable of interacting with saturated organic substrates containing only σ-bonds.

In silver(I) species, the 5*sp* orbitals are unoccupied and it is therefore suggested that these orbitals interact with carbon-carbon or carbon-halogen σ-bonds. This interaction is facilitated by σ-bonds endowed with substantial *p* character,[11] since high levels of *p* character in the σ-bond are necessary to bring the substrate into the metal coordination sphere. The 4*d*-orbitals of silver(I) are filled and in the present reaction these interact with the halogen atoms and transmit electron density to them.

Applying the arguments outlined above, the first step in the reaction between alkyl halides and the dicyanoargentate ion is the ionization of the carbon-halogen bond through transfer of electrons from the carbon-halogen bond to the halogen atom *via* the *sp* and the *d*-orbitals of the silver atom as depicted in Scheme B.

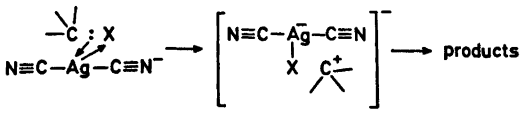

Scheme B.

A reaction mechanism as suggested in Scheme B would imply that the silver atom must act both as an electrophile and as a nucleophile to be able to assist in the breaking of the carbon-halogen bond. The suggestion that the silver atom in the dicyanoargentate ion acts biphilically in the present reaction, a reaction which may be considered as a partly metal insertion reaction, requires some further comments. As this class of reactions of d^{10} metal complexes are not very well investigated,[39] the possible similarity with oxidative addition reactions of other species, notably d^8 elements, [39,40] may allow a comparison. Chock and Halpern [41] noted the following reactivity sequence for Ir(I) complexes reacting with methyl iodide in benzene: $(Ph_3P)_2IrCOCl > (Ph_3P)_2IrCOBr > (Ph_3P)_2IrCOI$. Although better donors than triphenyl phosphine as ligands increase the reactivity of Ir(I) complexes,[41] this reactivity sequence is compatible with the suggestion that the biphilic nature of the reacting metal complex plays an important role in determining the reactivity of this class of compounds toward certain substrates. Furthermore, Chock and Halpern [38] found that the activation energy for the reaction in benzene between methyl iodide and $(Ph_3P)_2IrCOCl$, the presumably most electrophilic Ir(I) complex, was only 5.6 kcal mol^{-1}, which is significantly lower than for any known nucleophilic displacement reaction toward methyl iodide in this solvent.[42] This may be additional evidence for the initial weakening of the carbon-halogen bond

through interaction between the σ-bond orbitals of the carbon-halogen bond and the unoccupied orbitals of the transition metal.

The negative entropies of activation calculated from the rate data in this work, Table 5, accord with a highly constrained or ordered transition state in the rate determining step. The low k_H/k_D ratio, 1.22, found by Chatt and Davidson [48] for the hydrogenation reaction of $(Ph_3P)_2IrCOCl$, suggests little H–H bond breaking in the transition state, in conformity with the first step depicted in Scheme B.

The biphilic mechanism as suggested above may give a reasonable explanation for the variation in the Br/Cl rate ratios observed in this work. Apart from the fact that the bond energy of the C–X bonds decrease with increasing size of the halogen atom, which may be of rather equal importance to the mechanisms in Scheme A and Scheme B, the effect of a heavy halogen atom in S_N2 type alkyl halides appears to be two-fold when the mechanism in Scheme B is considered: to make the electron density of the carbon-halogen σ bond more available for interaction with the unoccupied $5sp$ orbitals of the silver atom and, simultaneously, to provide a better acceptor for the $4d$ electron density of the silver atom. $(Ph_3P)_2IrCOCl$ is known to react easily with methyl iodide while being quite unreactive toward methyl bromide.[41] There appears to be only a very poor relationship between the bond energies of molecules into which a transition metal is to be inserted and the activation energy of the insertion reaction.[41]

For S_N1 alkyl halides, the interaction between the carbon-halogen bond electrons and the unoccupied orbitals of the transition metal may be of limited significance, and a simple electrophilic pull mechanism as indicated in Scheme A may appear satisfactory.

Recently, Halpern and co-workers [44] have proposed that the silver(I)-catalyzed rearrangement of cubane to cunean goes *via* adducts of silver(III) prior to the reductive elimination of the observed products. The formation of a silver(III) adduct would necessarily imply that the silver atom becomes completely inserted into the carbon-carbon bond through an oxidative addition reaction prior to the consecutive steps. If a silver(III) species is formed in the present reaction between the dicyanoargentate ion and S_N2 type alkyl halides, the mechanism would in principle be similar to the one depicted in Scheme B, except that the ion pair is formed *via* a silver(III) species. The strongly oxidizing character of silver(III)[44] would be expected to promote heterolysis to the carbonium ion in the tight ion pair, and the extra step of forming the silver(III) species would thus be kinetically insignificant.

Due to the high ionization potential of silver(I) to give silver(III) species,[45] one has so far hesitated to include species formally of silver(III) as conceivable intermediates or transition states in reactions where silver(I) compounds are used as reagents. In recent years, however, several stable silver(III) compounds have been synthesized.[46–50] They are all diamagnetic in conformity with their dsp^2 electronic structure.[51] It appears that compounds containing silver(III) ions fall into two groups: those with highly electronegative donors as ligands, and those containing biguanide frameworks, in which case the high charge of the Ag(III) ion is accomodated by extensive delocalization over the whole biguanide structure.[52] Whether the two cyano groups in the present case satisfy these demands so as to allow the silver atom in the dicyanoargentate ion to attain a high oxidation state remains unknown. Since the reaction mechanism depicted in Scheme B seems reasonable, at the present stage, the introduction of silver(III) species appears to be an unnecessary complication.

A comparison with reactions of the dicyanoaurate(I) ion [53] is not valid due to the large difference in stability between gold(III) and silver(III) species, relative to gold(I) and silver(I).

Finally the following two cyclic transition states have to be considered (Scheme C).

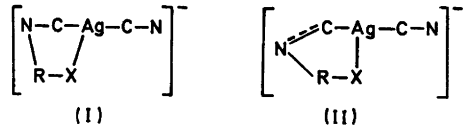

(I) (II)

Scheme C.

In (I), the isocyanide would have to be formed *via* a five-membered ring. As the Ag–C and Ag–N distances in the dicyanoargentate ion are 2.13 Å and 3.28 Å, respectively,[54] and the R–X distances lie in the 1.7 Å – 2.1 Å range,[55] depending upon which halide is employed, it is hard to imagine how a five-membered ring of this type, with linear N–C–Ag, should be completely favoured over a four-membered ring, in which case the alkyl cyanide would be the expected product. It appears safe to conclude that a cyclic transition state like (I) in Scheme C is a most improbable one.

Another possible reaction mechanism would be an interaction between the N–C triple bond and the alkyl moiety, and an interaction between the silver atom and the halogen atom *via* a cyclic alkylcyanonium ion with sp^2 hybridized

carbon and a non-linear N – C – Ag bond (transition state II in Scheme C). Through a transition state of this type, the formation of isocyanides could readily be understood, but this transition state does not appear to be able to explain the large Br/Cl rate ratios observed and its dependence upon the substituents on the phenyl groups in the benzhydryl substrates. Neither are the very negative ϱ values in accordance with this mechanism.

It has become increasingly evident in recent years that the classical S_N2 mechanism does not satisfactorily explain certain displacement reactions, particularly reactions of potentially biphilic nucleophiles with alkyl halides. In Scheme B outlined above, a biphilic reagent, through its valence orbitals is acting as an agent for the transfer of electron density from the bond to be broken to the leaving group, giving rise to exceptional high leaving group ratios.

When an oxidative addition product is stable, the reaction may conveniently be described as an insertion of the attacking biphilic nucleophile into the carbon-halogen bond. The exceptional ability of silver(I) species like the silver(I) ion to react by this mechanism appears to be connected with the silver(I) ion itself being a low-valent transition metal ion without the presence of bulky ligands, allowing it to interact with a minimum of steric hindrance with suitable σ-bonds.

The extreme dependence of rate upon the departing halide in substitution reactions of S_N2 type alkyl halides may be a valuable criterion for this mechanism. Furthermore, for reactions which can not possibly be of the S_N2 type, exceptionally low ΔH^+ values and unfavourable entropies may be an additional criterion for this mechanism, in contrast to the typical S_N1 mechanism where the opposite is the case.

As mentioned earlier, the reaction between tris(4-nitrophenyl)methyl bromide and the dicyanoargentate ion appeared to be of a special nature as a series of intensive colours appeared during the reaction. The intensive colour observed may suggest that this reaction follows a radical mechanism as the tris(4-nitrophenyl)-methyl radical is known to be stable.[56] The radical mechanism for reactions between metal complexes and alkyl halides is well substantiated.[57] Bilevitch and co-workers [58] have shown that potassium *tert*-butoxide and unsubstituted trityl halides react *via* radicals. The reaction between trityl chloride and the dicyanoargentate ion, however, gave a near quantitative yield of trityl isocyanide. No yield of "hexaphenylethane", 1-diphenylmethylene-4-trityl-2,5-cyclohexadiene,[59] could be detected.

Acknowledgement. The authors are indebted to Professors O. Foss and J. Halpern for valuable suggestions.

REFERENCES

1. Pearson, R. G. *J. Amer. Chem. Soc. 85* (1963) 3533.
2. Saville, B. *Angew. Chem. 79* (1967) 966.
3. Jones, M. M. and Clark, H. R. *J. Inorg. Nucl. Chem. 33* (1971) 413.
4. Benoit, R. L., Beauchamp, A. L. and Deneux, M. *J. Phys. Chem. 73* (1969) 3268.
5. Le Demezet, M., Madec, C. and L'Her, M. *Bull. Soc. Chim. Fr.* (1970) 365.
6. Barnes, D., Laye, P. G. and Pettit, L. D. *J. Chem. Soc. A* (1969) 2073.
7. Ford, G. J., Pettit, L. D. and Sherrington, C. *J. Inorg. Nucl. Chem. 33* (1971) 4119.
8. Pearl, I. A. *U. S. Patent* 2419158 (1947).
9. Boopsingh, B. and Satchell, D. P. N. *J. Chem. Soc. Perkin Trans. 2* (1972) 1288.
10. Ågren, A., Ekenved, G., Nilsson, S. O. and Svensjø, E. *Acta Pharm. Suecica 2* (1965) 421.
11. Paquette, L. A. *Accounts Chem. Res. 4* (1971) 280.
12. Hammond, G. S., Hawthorne, M. F., Waters, J. H. and Graybill, B. M. *J. Amer. Chem. Soc. 82* (1960) 704.
13. Hammond, G. S., Emmons, W. D., Parker, C. O., Graybill, B. M., Waters, J. H. and Hawthorne, M. F. *Tetrahedron 19 Suppl. 1* (1963) 177.
14. Pocker, Y. and Kevill, D. N. *J. Amer. Chem. Soc. 87* (1965) 4761, 4771, 4778 and 5060.
15. Kevill, D. N., Johnson, G. H. and Likhite, V. V. *Chem. Ind. (London)* (1969) 1555.
16. Kevill, D. N. and Horvath, V. M. *Tetrahedron Lett.* (1971) 711.
17. Pasto, D. J. and Serve, M. P. *J. Amer. Chem. Soc. 87* (1965) 1236.
18. Kornblum, N., Jones, W. J. and Hardies, D. E. *J. Amer. Chem. Soc. 88* (1966) 1704.
19. Kornblum, N. and Hardies, D. E. *J. Amer. Chem. Soc. 88* (1966) 1707.
20. Songstad, J., Stangeland, L. J. and Austad, T. *Acta Chem. Scand. 24* (1970) 355.
21. Austad, T., Songstad, J. and Stangeland, L. J. *Acta Chem. Scand. 25* (1971) 2327.
22. Austad, T. and Songstad, J. *Acta Chem. Scand. 26* (1972) 3141.
23. Iliceto, A., Fava, A., Mazzucato, U. and Radici, P. *Gazz. Chim. Ital. 90* (1960) 919.

24. Winstein, S., Kleindienst, P. E., Jr. and Robinson, G. C. *J. Amer. Chem. Soc. 83* (1961) 885.
25. Lewis, G. N., Lipkin, D. and Magel, T. T. *J. Amer. Chem. Soc. 66* (1944) 1579.
26. Ceccon, A., Papa, I. and Fava, A. *J. Amer. Chem. Soc. 88* (1966) 4643.
27. Cress, P., Dirksen, P. and Graham, J. W. *Fortran IV with Watfor*, Prentice-Hall, New Jersey 1968, p. 1.
28. Ritchie, C. D. In Coetzee, J. F. and Ritchie, C. D., Eds., *Solute-Solvent Interactions*, Dekker, New York and London 1969, p. 272.
29. Sneen, R. A. and Robbins, H. M. *J. Amer. Chem. Soc. 94* (1972) 7868.
30. Koskikallio, J. *Acta Chem. Scand. 26* (1972) 1201.
31. Abraham, M. H. *Chem. Commun.* (1973) 51.
32. Swain, C. G. Pergues, E. H. *J. Amer. Chem. Soc. 80* (1958) 812.
33. Bartlett, P. D. and Dauben, H. J., Jr. *J. Amer. Chem. Soc. 62* (1940) 1339.
34. Brown, H. C. and Bell, H. M. *J. Org. Chem. 27* (1962) 1928.
35. Martinsen, A., Austad, T. and Songstad, J. *To be published.*
36. Nishida, S. *J. Org. Chem. 32* (1967) 2692 and 2695.
37. Leffler, J. E. and Grunwald, E. *Rates and Equilibria of Organic Reactions*, Wiley, New York and London 1963, p. 206.
38. Chatt, J. *Nature 177* (1956) 852.
39. Halpern, J. *Accounts Chem. Res. 3* (1971) 386.
40. Collmann, J. P. and Roper, W. R. *Advan. Organometal. Chem. 7* (1968) 54.
41. Chock, P. B. and Halpern, J. *J. Amer. Chem. Soc. 88* (1966) 3511.
42. Okamoto, K., Fukui, S., Nitta, J. and Shingu, H. *Bull. Chem. Soc. Jap. 40* (1967) 2350.
43. Chatt, J. and Davidson, J. M. *J. Chem. Soc.* (1965) 843.
44. Byrd, J. E., Cassar, L., Eaton, P. E. and Halpern, J. *Chem. Commun.* (1971) 40.
45. Gilbert, W. P. *Phys. Rev. 48* (1935) 338.
46. McMillan, J. A. *Chem. Rev. 62* (1962) 65.
47. Poddar, S. N. and Podder, N. G. *Indian J. Chem. 47* (1970) 39.
48. Chatterjee, B. and Syamal, A. *Indian J. Chem. 47* (1970) 1021.
49. Siebert, H., Siebert, C. and Wieghardt, K. *Z. Anorg. Allg. Chem. 380* (1971) 30.
50. Kukuskin, Y. N., Rabinovich, V. A. and Goloseva, R. A. *Zh. Neorg. Khim. 14* (1969) 1863.
51. Sen, D. *J. Chem. Soc. A* (1969) 1304.
52. Simms, M. L., Atwood, J. L. and Zatko, D. A. *Chem. Commun.* (1973) 46.
53. Ford-Smith, M. H., Habeeb, J. J. and Rawsthorne, J. H. *J. Chem. Soc. Dalton Trans.* (1972) 2116.
54. Hoard, J. L. *Z. Kristallogr. 84* (1933) 231.
55. Rajput, A. S. and Chandra, S. *Bull. Chem. Soc. Jap. 39* (1966) 1854.
56. Andersen, P. and Klewe, B. *Acta Chem. Scand. 21* (1967) 2549.
57. Halpern, J. and Phelan, P. F. *J. Amer. Chem. Soc. 94* (1972) 1881.
58. Bilevitch, K. A., Bubnov, N. N. and Okhlobystin, O. Y. *Tetrahedron Lett.* (1968) 3465.
59. Lankamp, H., Nauta, W. T. and MacLean, C. *Tetrahedron Lett.* (1968) 249.

Received August 19, 1973.

Acta Chemica Scandinavica A 28 (1974) 267—274

The Crystal Structure of $Sb_4O_4(OH)_2(NO_3)_2$

JAN-OLOV BOVIN

Division of Inorganic Chemistry 2, Chemical Center, The Lund Institute of Technology, Box 740, S-220 07 Lund 7, Sweden

The crystal structure of the compound $Sb_4O_4(OH)_2(NO_3)_2$ has been determined by conventional methods from three-dimensional X-ray intensity data measured on an automatic diffractometer. The crystals are monoclinic (space group $P2_1/c$). The unit cell contains two formula units and has the dimensions $a = 11.020(2)$ Å, $b = 5.5355(5)$ Å, $c = 10.270(1)$ Å and $\beta = 123.71(1)°$. The structure was refined by a full matrix-least-squares technique, using 1084 observed reflections, to an R value of 0.046. It contains distorted trigonal bipyramidal SbO_4- and tetrahedral SbO_3-polyhedra, with the lone pair of electrons at one of the equatorial corners of the bipyramids and at one corner of each tetrahedron, respectively. Each SbO_4-polyhedron shares two edges with other SbO_4-units and two corners with SbO_3-polyhedra. Since each SbO_3-unit shares oxygens with two SbO_4-units infinite layers parallel to the bc-plane are formed. The nitrate ions are situated between these layers. The Sb—O distances in SbO_3 are 1.942(7), 2.052(6), and 2.067(6) Å and in SbO_4 2.019(6), 2.020(6), 2.236(6), and 2.265(6) Å, respectively.

The investigation of the crystal structure of $Sb_4O_4(OH)_2(NO_3)_2$ is a part of several studies on the chemistry of antimony(III) in solid state as well as in solution. The crystal structures of the following compounds have already been determined or are worked upon in this laboratory, *viz.* Sb_2O_3 (*orth.*).[1] SbOF,[2,3] $Sb_4O_5Cl_2$,[4,5] $SbPO_4$,[6] $SbO(H_2PO_4).H_2O$,[7] $Sb_4O_5(OH)ClO_4.\frac{1}{2}H_2O$,[8] and $Sb(OH)_2ClO_4.H_2O$. The hydroxo complexes of antimony(III) existing in solutions of perchloric and nitric acid has been investigated by Ahrland and Bovin,[9] applying solubility measurements. It was essential during that work to know the structure and composition of this solid phase, which has previously been described as $Sb_4O_5(NO_3)_2.H_2O$ in Gmelins Handbuch[10] and by Jander and Hartmann.[11] The formula is written $Sb_4O_4(OH)_2(NO_3)_2$ instead of $Sb_2O_2OHNO_3$.

EXPERIMENTAL

Crystal preparation and analysis. Crystals of $Sb_4O_4(OH)_2(NO_3)_2$ were prepared in perchloric acid according to the method described by Jander and Hartmann.[11] Since these were too small for a single crystal study the following method was evolved: 6 M nitric acid was heated to 110°C in an Erlenmeyer flask and orthorhombic Sb_2O_3 was added until a saturated solution was obtained. A little more Sb_2O_3 was then added so that some of the solid phase persisted. The flask was stoppered and its temperature was decreased by 5—10°C per day to roomtemperature. $Sb_4O_4(OH)_2(NO_3)_2$ crystallized as thin, colourless transparent plates. The homogeneity of the sample was confirmed by Guinier-Hägg X-ray powder photographs.

The material thus prepared was analysed for antimony(III) by the methods of Belcher[12] and Elkind *et al.*[13] Nitrogen analysis was made according to Dumas[14] and for the water analysis a modification of the method of Fischer[15,16] was employed. The results were 68.8 % antimony(III), 3.8 % nitrogen and 2.2 % water. Calc. for $Sb_4O_4(OH)_2(NO_3)_2$: 68.69, 3.95, and 2.5 %.

Crystal data. Preliminary Weissenberg photographs showed the crystals to be monoclinic with systematic absences $h0l$ with $l = 2n+1$ and $0k0$ with $k = 2n+1$. These are characteristic of the space group $P2_1/c$ (No. 14).

The unit cell dimensions were determined by least-squares refinement using as data the diffraction angles of 28 lines on the Cu$K\alpha_1$ ($\lambda = 1.5405$ Å) powder pattern made at room temperature in a Guinier-Hägg focusing camera equipped with a quartz monochromator and using KCl (cubic, $a = 6.2929$ Å) as internal standard, *cf.* Table 1. The density determined by measuring the loss of weight in benzene was in good agreement with the calculated value for two formula units of $Sb_4O_4(OH)_2(NO_3)_2$ per unit cell. Some crystal data are presented in Table 2.

Table 1. Guinier powder pattern of $Sb_4O_4(OH)_2(NO_3)_2$ using Cu$K\alpha$ radiation.

$h\,k\,l$	$10^5\sin^2\theta$ obs	$10^5\sin^2\theta$ calc	I obs
1 0 0	708	706	vs
1 1 0	2 647	2 642	v
0 1 1	2 751	2 749	vw
$\bar{2}$ 1 2	4 647	4 648	w
2 1 0	4 766	4 760	vw
0 1 2	5 196	5 187	m
$\bar{3}$ 0 0	6 360	6 353	w
$\bar{3}$ 1 2	6 498	6 496	s
1 1 2	7 577	7 575	w
0 2 0	7 750	7 745	vs
3 1 0	8 290	8 289	vw
$\bar{1}$ 2 0	8 446	8 451	w
$\bar{2}$ 0 4	9 105	9 103	vs
$\bar{3}$ 0 4	9 264	9 270	w
4 1 0	13 233	13 231	m
$\bar{3}$ 2 0	14 105	14 098	w
$\bar{2}$ 2 4	16 847	16 848	s
$\bar{3}$ 2 4	17 006	17 014	m
4 2 0	19 052	19 039	vw
5 2 2	20 230	20 237	vw
$\bar{0}$ 2 4	20 745	20 749	vw
$\bar{5}$ 2 1	21 987	21 999	vw
$\bar{3}$ 3 2		21 986	vw
3 2 2	22 387	22 393	vw
$\bar{1}$ 3 2	23 059	23 064	vw
$\bar{5}$ 1 6	23 625	23 624	w
$\bar{6}$ 1 6	26 351	26 345	vw
$\bar{0}$ 4 0	30 972	30 979	vw
$\bar{1}$ 4 2	33 257	33 255	vw
7 1 0	36 508	36 525	vw

Table 2. Crystallographic data for $Sb_4O_4(OH)_2(NO_3)_2$.

Unit cell:	$a = 11.020(2)$ Å
	$b = 5.5355(5)$ Å
	$c = 10.270(1)$ Å
	$\beta = 123.71(1)°$
	$V = 521.2$ Å^3
	$Z = 2$
Formula weight:	$M = 709.12$
Density, 20 °C.	$D_m = 4.45$ g cm^{-3}
	$D_x = 4.52$ g cm^{-3}

Collection of intensity data. Three-dimensional intensity data from a single crystal (*cf.* Table 3) were collected on an Enraf-Nonius computer controlled four-circle diffractometer, CAD4, using graphite monochromatized Mo$K\alpha$ radiation ($\lambda = 0.71069$ Å). The intensities were recorded at a take-off angle of 5°. The $\omega - 2\theta$ scan technique was used with an ω range of $(0.9 + 0.5 \text{ tg } \theta)°$. A minimum net count of 3000 for each reflection was attained within the maximum measuring time of 5 min. The scan speed thus required was calculated from the net intensity after a fast pre-scan. Two octants of the reciprocal space out to $(\sin\theta)/\lambda = 0.65$ Å^{-1} were examined. Of the 1265 reflections measured, 14 were considered to be below background since they gave counts of less than 10 in the fast (9 s) pre-scan, and 167 were rejected as being unobserved since their intensities were less than $3\sigma(I)$, where $\sigma(I)$ is the standard deviation of the intensity estimated from counting statistics. The remaining 1084 reflections were corrected for Lorentz, polarisation and absorption (*cf.* Table 3) effects using the program DATAPC [17] as modified by Christer Svensson of this Institute.

Table 3. Crystal dimensions. Boundary planes and their distances from an internal origin.

Plane	d (cm)
(1$\bar{0}$0)	0.00245
($\bar{1}$00)	0.00245
(0$\bar{1}$0)	0.01220
(010)	0.01220
(10$\bar{2}$)	0.00070
($\bar{1}$02)	0.00070

Crystal volume: 0.17×10^{-3} mm^3.

The linear absorption coefficient [18] for Mo$K\alpha$ radiation is 105 cm^{-1}. The transmission factors were in the range 0.60 – 0.86. Two standard reflections, 132 and 402, were measured with 90 min intervals to check for crystal decomposition and radiation stability. A mean decrease of 10 % in their intensities was found during the course of data collection. All intensities were therefore scaled with a first-order polynomial determined by least-squares.

STRUCTURE DETERMINATION AND REFINEMENT

From a three-dimensional Patterson synthesis the eight antimony atoms were found to occupy two sets of fourfold positions 4(*e*) in $P2_1/c$. A least-squares refinement of these positions was performed. A subsequent three-dimensional difference electron density synthesis revealed the positions of all other non-hydrogen atoms, which also were in the general equivalent positions 4(*e*). A preliminary full matrix least-squares refinement was now performed refining the atomic coordinates and isotropic temperature factors for all atoms, and a scale factor.

The refinement converged to an R-value ($R = \sum||F_o| - |F_c||/\sum|F_o|$) of 0.086.

Anisotropic temperature factors were then introduced for all atoms and again the positional and thermal parameters were refined together with an overall scale factor. The R-value was now reduced to 0.056. When the anisotropic refinement was repeated with data corrected for absorption effects the R-value was 0.048. Corrections were then made for isotropic secondary extinction with the full matrix least-squares program LINUS.[19] The function minimized was $\sum w_i(|F_o| - |F_c|)^2$, where the weights, w_i, were calculated from the expression $w_i^{-1} = \sigma^2(F_o^2)/4F_o^2 + cF_o^2$. The value of the constant c was chosen so as to give the most constant averages of $w_i(|F_o| - |F_c|)^2$ over ranges of F and sin θ. A value of $c = 0.001$ was used in the last refinement. The R-value converged to 0.046 and the R_w-value to 0.058 where $R_w = [\sum w(|F_o| - |F_c|)^2/\sum w|F_o|^2]^{1/2}$. The final value of S defined by $S = [\sum w(|F_o| - |F_c|)^2/(m-n)]^{1/2}$ where m and n are the number of observations and parameters varied, respectively, was 1.52. The atomic scattering factors used were those given by Hanson *et al.*[20]

The final value of the isotropic extinction parameter g was $0.07(4) \times 10^4$. In the last cycle of refinement the shifts for all parameters were less than 0.01 times their corresponding standard deviations. The final positional and thermal parameters are given in Table 4, and observed and calculated structure amplitudes are compared in Table 5. Interatomic distances and bond angles presented in Table 6 were calculated with the program DISTAN, written by A. Zalkin. The drawings (Figs. 1 and 2) were obtained with the program ORTEP.[21]

DESCRIPTION AND DISCUSSION OF THE STRUCTURE

The fundamental structural elements of the structure of $Sb_4O_4(OH)_2(NO_3)_2$ are distorted SbO_4- and SbO_3-polyhedra. The SbO_4-polyhedron is trigonal pyramidal with the lone electron pair in one of the equatorial corners (Fig. 1). The SbO_3-polyhedron is tetrahedral with the lone pair in one of the corners (Fig. 1). The SbO_4-polyhedra each share two edges and thus build up infinite chains parallel to b. These chains are linked by two corners of each SbO_3-polyhedron to form infinite layers parallel to the bc-plane (*cf.* Fig. 1).

Table 4. Final positional and thermal parameters in $Sb_4O_4(OH)_2(NO_3)_2$. The form of the anisotropic temperature factor is exp $[-(h^2\beta_{11} + k^2\beta_{22} + l^2\beta_{33} + 2\,hk\beta_{12} + 2\,hl\beta_{13} + 2\,kl\beta_{23})]$. Standard deviations are given within parentheses.

Atom	x	y	z	Atom	x	y	z
Sb(1)	0.17601(6)	0.20160(11)	0.35476(7)	O(4)	0.2845(11)	0.2689(17)	0.1680(11)
Sb(2)	0.11237(7)	0.74852(11)	0.06549(7)	O(5)	0.4655(9)	0.2371(15)	0.4074(10)
O(1)	0.0326(6)	0.0720(12)	0.1328(6)	O(6)	0.5050(11)	0.2725(16)	0.2223(11)
O(2)	0.0307(6)	0.0705(12)	0.4049(6)	N	0.4228(10)	0.2641(16)	0.2676(12)
O(3)	0.7557(7)	0.1305(13)	0.6048(7)				

Atom	β_{11}	β_{22}	β_{33}	β_{12}	β_{13}	β_{23}
Sb(1)	0.00469(9)	0.01077(23)	0.00315(9)	−0.00074(8)	0.00267(7)	−0.00062(8)
Sb(2)	0.00409(9)	0.01283(24)	0.00343(10)	0.00010(8)	0.00228(7)	0.00176(9)
O(1)	0.0049(7)	0.0094(19)	0.0020(7)	0.0006(9)	0.0023(6)	0.0004(9)
O(2)	0.0042(7)	0.0102(19)	0.0025(7)	−0.0001(9)	0.0026(6)	−0.0005(9)
O(3)	0.0060(8)	0.0115(21)	0.0052(9)	0.0009(11)	0.0030(7)	0.0004(11)
O(4)	0.0068(10)	0.0367(40)	0.0064(11)	0.0030(15)	0.0020(9)	−0.0012(15)
O(5)	0.0061(10)	0.0283(34)	0.0054(11)	0.0032(13)	0.0022(9)	0.0005(13)
O(6)	0.0109(12)	0.0237(32)	0.0111(14)	0.0013(14)	0.0084(11)	0.0024(15)
N	0.0038(9)	0.0186(30)	0.0078(13)	0.0002(12)	0.0031(10)	0.0005(14)

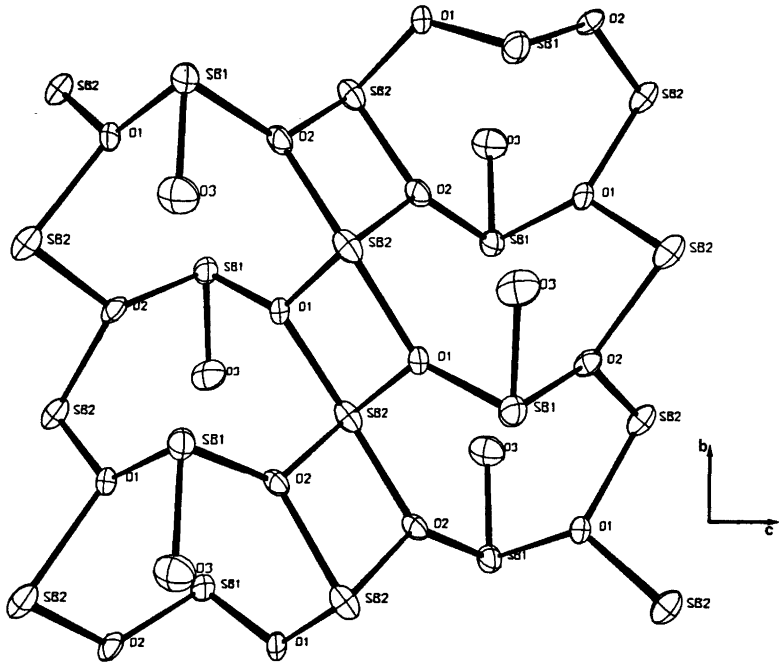

Fig. 1. The antimony-oxygen coordination within a layer. Projection along the *a*-axis.

The three oxygen atoms O(4), O(5), O(6) (*cf.* Table 4) and the nitrogen atoms form the planar NO_3^--ion. The distances N–O and the angles O–N–O (*cf.* Table 5) are normal (*cf. International Tables*,[18] Luzzati,[22] Taylor *et al.*[23]). The nitrate ions are situated between the layers described above (*cf.* Fig. 2). For the interpretation of the solubility function of Sb(III) in nitric acid with $Sb_4O_4(OH)_2(NO_3)_2$ as solid phase it was necessary to verify the existence of the OH^--ion in the structure. Since the hydrogen atoms could not be located from the available X-ray data it was difficult to distinguish O^{2-} and OH^--ions from each other. In order to establish the nature of the oxygen atoms O(1), O(2), O(3), a procedure due to Donnay *et al.*[24] was used. It is based on the principle of local neutralization of charge and makes it possible to recognize O^{2-}, OH^-, and H_2O in crystal structures derived by X-ray

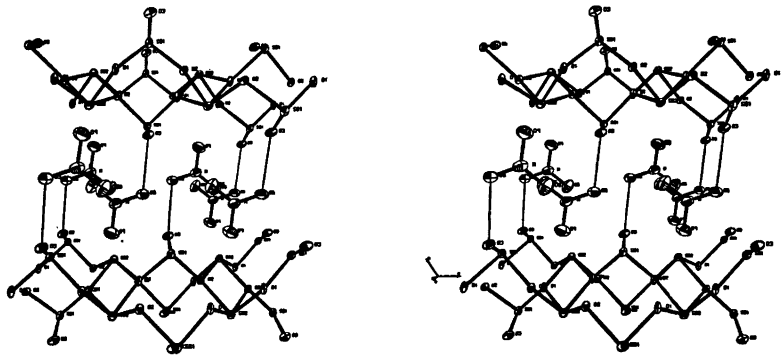

Fig. 2. Stereoview down the *b*-axis. Possible hydrogen bonds are marked with thin lines.

Table 5. Observed and calculated structureamplitudes. The columns list l, $|F_o|$ and $|F_c|$.

H=	0 K=	0	-5	58	54	-5	72	68	-6	33	30	3	52	56	-5	97	90	-10	89	90	-6	124	123
-10	97	97	-3	42	40	-4	55	51	-5	48	42	4	56	59	-3	54	56	-9	32	31	-5	25	26
-8	30	28	-2	42	42	-3	59	55	-4	139	128	5	17	18	-2	107	107	-7	69	68	-4	77	77
-6	37	36	-1	58	54	-1	52	50	-3	112	107	6	32	30	-1	62	67	-6	150	147	-3	81	81
-4	199	184	0	65	66	0	31	34	-2	62	62	7	45	46	0	114	125	-5	77	77	-2	71	71
-2	47	41	1	50	54	1	74	77	-1	20	19	8	65	63	1	73	77	-4	99	101	-1	18	16
2	47	41	2	43	42	2	84	81	1	93	99				2	74	75	-3	44	44	0	69	71
4	198	186	3	41	40	4	60	56	2	28	30	H=	3 K=	4	3	26	25	-2	16	16	1	49	51
6	36	36	5	57	54	5	64	61	3	43	42	-9	53	54	4	107	111	-1	71	76	2	28	29
8	28	28	6	56	52	7	34	33	4	82	81	-8	26	23	5	54	53	2	46	48	3	40	42
10	97	97							5	55	54	-7	13	12	6	37	37	3	54	56	4	45	45
			H=	0 K=	7	H=	1 K=	6	6	88	86	-6	69	66	7	14	16	4	119	123	5	17	18
H=	0 K=	1	-1	32	30	-6	24	25	7	46	44	-5	93	89				5	25	25			
-10	40	38	1	28	30	-5	16	16	8	15	17	-4	114	111	H=	4 K=	4	6	13	11	H=	6 K=	6
-8	49	48				-4	25	23				-3	46	46	-10	24	24				-11	66	68
-7	18	16	H=	1 K=	0	-3	48	47	H=	2 K=	5	-2	24	25	-8	75	73	H=	5 K=	6	-10	47	46
-5	21	21	-10	127	129	-2	89	86	-8	47	51	-1	97	97	-7	74	69	-10	34	34	-9	45	43
-4	115	107	-8	111	108	-1	73	70	-7	37	38	0	89	97	-6	64	60	-9	51	52	-8	40	39
-3	40	39	-6	127	115	0	43	43	-6	69	68	1	61	65	-5	41	41	-8	104	99	-7	41	41
-2	288	265	-4	123	115	3	70	67	-5	75	70	2	61	64	-4	36	35	-7	40	39	-5	75	73
-1	70	59	-4	16	19	4	37	36	-4	16	15	3	50	53	-3	56	53	-6	37	36	-4	89	91
1	42	59	-2	43	39				-3	24	24	4	39	37	-1	86	88	-5	57	53	-2	84	89
2	244	265	2	180	185	H=	1 K=	7	-2	45	44	5	69	70	0	90	98	-4	52	51	-1	63	69
3	41	39	4	224	224	-5	22	25	-1	82	80	6	19	19	1	19	22	-3	65	66	1	31	34
4	112	107	6	142	140	-1	18	15	0	71	77				2	99	106	-2	55	60	2	22	26
5	21	21	8	20	19	0	56	57	1	22	25	H=	3 K=	5	3	69	72	0	65	68	3	34	35
7	16	16				1	42	44	2	54	55	-9	37	38	6	39	39	1	68	72	4	21	23
8	48	48	H=	1 K=	1	2	32	30	3	55	55	-8	47	49				2	51	52			
10	39	38	-10	79	78				4	19	17	-7	54	52	H=	4 K=	5	3	26	27	H=	6 K=	7
			-9	24	23	H=	2 K=	0	5	51	50	-6	27	26	-9	46	47	4	28	28	-9	39	38
H=	0 K=	2	-8	128	125	-10	32	33	6	39	39	-4	26	29	-8	19	19	5	48	48	-8	33	35
-10	89	87	-6	188	175	-8	130	128				-3	77	75	-6	25	27				-7	44	45
-9	46	45	-5	33	31	-6	58	53	H=	2 K=	6	-2	87	86	-5	69	68	H=	5 K=	5	-6	68	70
-8	51	50	-4	59	56	-4	362	304	-9	39	41	-1	60	60	-4	40	40	-9	27	26	-4	62	61
-7	27	26	-3	53	44	-2	28	27	-8	18	14	0	56	60	-3	51	52	-7	53	52	-3	71	71
-6	73	69	-2	17	17	0	14	16	-7	26	22	1	57	61	-2	63	66	-6	44	45	-2	20	20
-4	90	93	-1	38	34	2	32	34	-6	37	35	3	53	54	-1	63	66	-5	69	69	-1	26	25
-3	51	49	0	54	65	4	109	109	-5	62	62	4	32	33	0	24	23	-4	83	83	0	55	57
-2	39	33	1	70	69	6	188	191	-4	66	63	6	44	43	1	73	77	-3	26	26	1	47	48
-1	86	70	2	254	271	8	60	58	-3	35	34				2	34	34	-2	23	24	2	56	53
0	276	345	3	30	28				-2	57	50	H=	3 K=	6	3	20	20	-1	70	73	3	45	45
1	70	70	4	154	151	H=	2 K=	1	2	50	52	-7	25	25	4	41	40	0	38	41			
2	34	33	5	42	42	-11	27	27	3	38	36	-6	63	61	5	55	56	1	21	17	H=	6 K=	8
3	50	49	6	101	99	-10	47	49	4	61	61	-5	57	57				2	51	56	-7	19	18
4	86	83	8	61	59	-9	16	14				-4	29	31	H=	4 K=	6	3	58	60	-6	24	27
5	72	69				-8	98	98	H=	2 K=	7	-3	58	59	-7	69	70	4	44	43	-5	55	55
6	25	24	H=	1 K=	7	-7	31	30	-1	43	43	1	30	31	-6	45	42				-4	41	43
8	51	50	-11	29	31	-6	243	220	0	70	71	2	45	48	-5	19	19	H=	5 K=	6	-2	37	37
9	45	45	-10	114	115	-5	54	48	1	22	20	3	28	30	-4	17	14	-7	43	44	-1	49	51
10	58	57	-8	120	114	-4	12	11				4	59	58	-3	51	53	-6	21	21	0	33	34
			-7	51	48	-3	22	19	H=	3 K=	0				-2	37	37	-5	47	48			
H=	0 K=	3	-6	98	88	-2	144	158	-12	64	60	H=	3 K=	7	-1	48	48	-4	53	55	H=	7 K=	0
-10	31	30	-5	38	34	-1	78	78	-10	54	57	-2	23	22	0	41	42	-3	53	56	-12	134	144
-9	20	19	-4	98	83	0	60	68	-8	12	11	-1	27	27	1	21	24	-1	18	18	-10	30	31
-8	29	28	-3	40	36	1	15	17	-6	11	14				2	36	35	0	58	58	-8	30	27
-7	68	68	-2	64	58	2	91	91	-4	256	234	H=	4 K=	0	3	43	43	1	49	50	-6	93	93
-6	17	16	-1	98	96	3	58	57	-2	125	126	-12	99	107							-4	184	184
-4	91	85	0	80	92	4	141	142	0	187	242	-10	88	92	H=	5 K=	0	H=	6 K=	0	0	44	44
-3	108	94	1	28	26	5	24	25	2	107	112	-8	186	183	-12	51	54	-12	61	65	2	146	146
-2	212	178	2	105	107	6	87	86	4	14	13	-6	24	20	-10	29	32	-8	83	81	4	39	39
-1	94	82	3	90	86	7	29	29	6	38	40	-4	51	43	-8	275	266	-6	86	83			
1	86	82	4	151	152	8	145	146				-2	119	127	-6	98	95	-4	189	195	H=	7 K=	1
2	185	178	5	29	28	9	15	17	H=	3 K=	1	0	95	101	-4	234	231	-2	195	199	-13	15	19
3	101	94	6	109	107				-12	75	81	2	246	244	-2	74	74	0	51	52	-12	13	14
4	87	85	7	45	47	H=	2 K=	2	-11	24	29	4	32	33	0	28	32	2	46	45	-11	15	17
5	16	16	9	35	35	-10	39	40	-10	73	77	6	78	76	2	99	110	6	82	83	-10	116	114
7	47	48				-9	18	17	-9	13	15				4	25	24				-9	34	35
8	28	29	H=	1 K=	3	-8	121	117	-7	45	43	H=	4 K=	1	6	127	128	H=	6 K=	1	-8	58	58
9	21	19	-10	58	57	-7	25	24	-6	104	100	-12	73	81				-13	20	24	-5	38	37
10	31	30	-9	58	57	-6	40	56	-5	52	50	-10	135	140	H=	5 K=	1	-12	16	19	-4	114	116
			-8	100	95	-5	19	17	-2	299	321	-9	37	38	-12	18	18	-11	14	14	-3	24	27
H=	0 K=	4	-7	42	41	-4	319	277	-1	27	29	-8	35	31	-11	17	19	-10	27	28	-2	86	90
-9	56	55	-6	122	113	-3	33	33	0	105	123	-6	94	87	-10	121	124	-9	25	24	-1	31	32
-8	59	54	-5	82	76	-2	37	36	1	23	27	-5	53	48	-9	17	14	-8	31	28	0	195	210
-7	24	22	-3	94	80	-1	29	26	2	117	119	-4	15	13	-7	44	40	-7	36	35	1	28	30
-6	63	60	-2	20	18	0	67	67	3	38	39	-2	158	165	-6	226	214	-6	195	192	2	18	22
-5	79	71	-1	52	49	1	44	47	4	25	26	-1	23	26	-5	34	32	-5	24	24	3	15	14
-4	21	21	0	10	11	3	47	48	7	31	31	0	149	174	-4	138	134	-4	135	136	4	85	89
-3	33	31	1	98	101	4	85	85	8	109	109	1	13	15	-3	49	44	-3	55	56	5	15	18
-2	50	42	2	175	173	5	35	34				2	125	133	-2	65	62	-2	137	145			
-1	80	56	4	99	94	6	151	154	H=	3 K=	2	4	134	137	-1	15	17	-1	14	12	H=	7 K=	2
0	152	158	5	73	72	7	46	46	-11	42	45	5	13	15	1	16	16	0	115	124	-12	123	130
1	57	56	6	57	55	8	29	29	-10	25	28	6	13	13	2	37	38	1	33	35	-11	26	28
2	44	42	7	26	25	9	14	16	-9	35	34	7	18	18	3	13	7	4	36	37	-10	17	17
3	31	31	8	38	40				-7	43	39				4	147	164	6	30	32	-8	75	73
4	22	21	9	27	26	H=	2 K=	3	-6	54	52	H=	4 K=	2	6	15	14				-7	46	41
5	72	71				-11	38	41	-5	50	47	-12	75	78				H=	6 K=	2	-5	26	26
6	41	40	H=	1 K=	4	-9	34	32	-4	247	231	-11	65	68	H=	5 K=	2	-12	66	71	-4	72	73
7	22	22	-8	77	75	-8	83	82	-3	49	71	-10	53	55	-12	27	27	-11	26	28	-3	44	44
8	47	46	-7	91	95	-7	45	44	-1	40	42	-8	126	123	-10	20	20	-10	13	10	-2	144	139
9	43	55	-6	19	16	-6	141	149	0	190	228	-7	80	75	-9	40	39	-9	36	34	-1	49	51
			-5	41	38	-5	107	92	1	41	45	-6	31	29	-8	100	103	-8	50	48	0	38	36
H=	0 K=	5	-4	64	58	-3	96	84	2	89	93	-5	20	21	-7	61	54	-6	65	64	1	31	34
-8	15	16	-3	100	91	-2	121	117	3	24	26	-4	35	35	-6	42	59	-5	72	70	2	121	126
-7	65	65	-2	97	89	-1	115	113	5	55	58	-3	66	64	-5	46	45	-4	136	139	3	38	38
-6	37	36	-1	87	82	0	92	90	6	34	34	-2	64	67	-4	130	127	-3	32	31	4	33	32
-4	89	82	0	64	69	1	18	19				-1	59	63	-3	83	84	-2	153	162			
-3	85	74	1	24	25	2	66	66	H=	3 K=	3	0	126	141	-2	64	69	-1	63	69	H=	7 K=	3
-2	74	69	2	26	27	3	76	73	-11	39	42	1	22	23	-1	15	16	0	26	26	-11	28	30
-1	40	56	3	80	76	4	56	55	-10	66	67	2	180	198	0	61	65	1	35	36	-10	80	87
1	54	56	4	89	88	5	48	47	-9	35	34	3	55	56	1	70	75	2	37	38	-9	72	74
2	73	69	5	12	11	6	68	69	-8	33	32	4	33	34	2	91	97	3	31	33	-8	71	68
3	79	74	6	68	66	7	35	34	-7	75	70	6	65	66	3	20	20	5	32	34	-5	66	65
4	87	82	7	46	45	8	85	85	-6	73	69	7	35	35	4	28	28	6	67	70	-4	32	32
6	37	36	8	19	19				-3	106	101				5	41	42				-3	27	28
7	47	45				H=	2 K=	4	-2	205	204	H=	4 K=	3	6	107	110	H=	6 K=	3	-2	66	67
8	20	16	H=	1 K=	5	-10	33	34	-1	40	42	-10	102	105	7	26	23	-11	30	32	-1	43	46
			-8	29	29	-9	46	47	0	115	129	-9	77	76				-10	20	21	0	109	113
H=	0 K=	6	-7	29	31	-7	50	49	1	72	78	-7	15	15	H=	5 K=	3	-9	49	47	1	45	46
-6	55	52	-6	71	69	-7	74	71	2	47	48	-6	66	63	-11	47	50	-7	57	56	2	29	27

Table 5. Continued.

diffraction methods. A calculation of cation to anion distances and associated bond valences leads to valence sums for the oxygen atoms. The valence sum $\sum v$ is approximately equal to 2 for an O^{2-}-ion, 1 for an OH^--ion and 0 for a water molecule. $\sum v$ for O(1), O(2), and O(3) were calculated to 2.2, 2.2, and 1.1. In the present case the oxygen atom O(3) should thus be a hydroxide ion. This is also supported by the distance O(3)–O(5) of 2.74(1) Å (*cf.* Table 6), which is in good agreement with hydrogen bond distances in inorganic solids given in the *International Tables*.[18] The angle O(3)···O(5)–N of 114.°7(7) also agrees well with that found by Luzzati [22] in $HNO_3.3H_2O$. It has been shown by Andersson, Åström, Galy and Meunier [25] that for many solid oxides, or oxide fluorides of Sb(III), Pb(II), Bi(III), and Te(IV), the volume of the lone pair and its cation is about the same as that of an anion. If the volume of the unit cell is divided by the number of anions and lone pairs of antimony in $Sb_4O_4(OH)_2(NO_3)_2$, the result is 16.3 Å^3. This value compared with data from Andersson and Åström [26] indicated that the total struc-

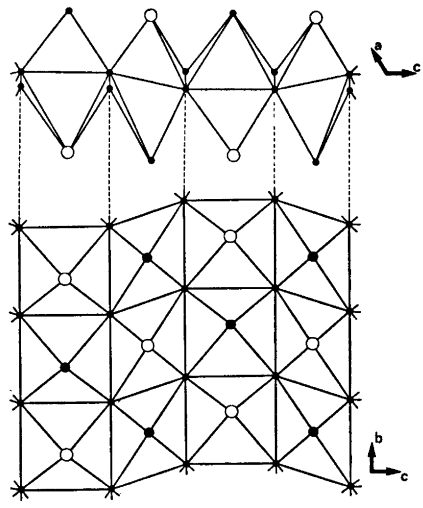

Fig. 3. The distorted cubic close packing of oxygen and lone pairs of electrons of antimony in the layer parallel to the *bc*-plane. The upper view is along the *b*-axis and the lower is perpendicular to the *bc*-plane.

Table 6. Coordination distances (Å) and angles (°) with standard deviations (in brackets) in $Sb_4O_4(OH)_2(NO_3)_2$. Notation of the atoms, *cf.* Table 4.

The SbO_3-polyhedron			
Sb(1) – O(3)	1.942(7)	∠O(1) – Sb(1) – O(2)	85.90(22)
Sb(1) – O(1)	2.052(6)	∠O(1) – Sb(1) – O(3)	82.79(26)
Sb(1) – O(2)	2.067(6)	∠O(2) – Sb(1) – O(3)	82.91(26)
O(1) – O(3)	2.642(9)		
O(2) – O(3)	2.656(9)		
O(1) – O(2)	2.807(8)		
The SbO_4-polyhedron			
Sb(2) – O(1)	2.019(6)	∠O(1′) – Sb(2) – O(1)	72.23(23)
Sb(2) – O(2)	2.020(6)	∠O(1′) – Sb(2) – O(2′)	141.60(20)
Sb(2) – O(2′)	2.236(6)	∠O(1′) – Sb(2) – O(2)	82.67(23)
Sb(2) – O(1′)	2.265(6)	∠O(1) – Sb(2) – O(2′)	82.84(23)
O(1′) – O(2′)	3.056(8)	∠O(1) – Sb(2) – O(2)	98.34(23)
O(1′) – O(2)	2.820(9)	∠O(2′) – Sb(2) – O(2)	72.39(24)
O(1′) – O(1)	2.533(11)		
O(2′) – O(2)	2.519(11)		
O(1) – O(2)	2.836(9)		
The nitrate ion			
N – O(6)	1.227(14)	∠O(4) – N – O(5)	116.3(9)
N – O(5)	1.247(13)	∠O(4) – N – O(6)	120(1)
N – O(4)	1.281(13)	∠O(5) – N – O(6)	124(1)
O(4) – O(5)	2.148(12)		
O(4) – O(6)	2.170(14)		
O(5) – O(6)	2.181(13)		
Possible hydrogen bond distance			
O(3)···O(5)	2.737(11)	∠O(3)···O(5) – N	114.7(7)

ture has an approximately close-packed arrangement of oxygens and lone pairs of electrons. If only the Sb – O layers and one oxygen atom, O(4), from the nitrate ion are considered the result is 15.6 Å³. The arrangement of these oxygen atoms and the electron pairs is approximately cubic close packed; (*cf.* Fig. 3).

Acknowledgements. The author thanks Professor Bengt Aurivillius for his introduction to the techniques of structure determination, his valuable discussions during this work and his stimulating and helpful interest. The author is also indebted to Professor Sten Ahrland, Dr. Karin Aurivillius and Dr. Sten Andersson for their kind interest in this work. Christer Svensson and Kerstin Renhult Aspelin are thanked for their assistance with the data collection.

This work received financial support from the Swedish Natural Science Research Council.

REFERENCES

1. Svensson, C. *Acta Crystallogr. B 30* (1974) 458.
2. Åström, A. and Andersson, S. *J. Solid State Chem. 6* (1973) 191.
3. Åström, A. *Acta Chem. Scand. 26* (1972) 3849.
4. Edstrand, M. *Acta Chem. Scand. 1* (1947) 178.
5. Särnstrand, C. *To be published.*
6. Kinberg, B. *Acta Chem. Scand. 24* (1970) 320.
7. Särnstrand, C. *Acta Chem. Scand. A 28* (1974) 275.
8. Bovin, J.-O. *To be published.*
9. Ahrland, S. and Bovin, J.-O. *To be published.*
10. *Gmelins Handbuch der anorganischen Chemie*, Gmelin-Verlag, Clausthal-Zellerfeld 1949, p. 18.
11. Jander, G. and Hartmann, H.-J. *Z. Anorg. Allg. Chem. 339* (1965) 239.
12. Belcher, R. *Anal. Chem. Acta 3* (1949) 578.

13. Elkind, A., Gayer, K. H. and Boltz, D. F. *Anal. Chem. 11* (1953) 1744.
14. Welcher, F. J. *Standard Methods of Chemical Analysis*, 6th Ed., Van Nostrand, London 1963, Vol II, Part A, p. 337.
15. Vogel, A. T. *A Textbook of Quantitative Inorganic Analysis*, 3rd Ed., Longmans, London 1961, p. 944.
16. Karlsson, R. *Talanta 19* (1972) 1639.
17. Coppens, P., Leiserowitz, L. and Rabinovich, D. *Acta Crystallogr. 18* (1965) 1035.
18. *International Tables for X-Ray Crystallography*, Kynoch Press, Birmingham 1962, Vol III.
19. Coppens, P. and Hamilton, W. *Acta Crystallogr. A 26* (1970) 71.
20. Hansen, H. P., Herman, F., Lea, I. D. and Skillman, S. *Acta Crystallogr. 17* (1964) 1040.
21. Johnson, C. K. *A Fortran Thermal-Ellipsoid Plot Program for Crystal Structure Illustration*, Oak Ridge National Laboratory, Chemistry Division, Oak Ridge, Tennessee 1965.
22. Luzzati, V. *Acta Crystallogr. 6* (1953) 157.
23. Taylor, J. C., Mueller, M. H. and Hitterman, R. L. *Acta Crystallogr. 20* (1966) 842.
24. Donnay, G. and Allman, R. *Amer. Mineral. 55* (1970) 1003.
25. Andersson, S., Åström, A., Galy, J. and Meunier, G. *J. Solid State Chem. 6* (1973) 187.
26. Andersson, S. and Åström, A. *NBS Special Publication 364, Solid State Chemistry*, Proceedings of 5th Materials Research Symposium, issued July 1972.

Received January 2, 1974.

Acta Chemica Scandinavica A 28 (1974) 275—283

The Crystal Structure of the Antimony Phosphate, $SbO(H_2PO_4).H_2O$

CHRISTER SÄRNSTRAND

Division of Inorganic Chemistry 2, Chemical Center, The Lund Institute of Technology, P.O.B. 740, S-220 07 Lund 7, Sweden

The crystal structure of the antimony phosphate $SbO(H_2PO_4).H_2O$ has been determined from X-ray single crystal film data and refined to a final R-value of 0.056 (1380 independent reflections). The crystals are monoclinic (space group $P2_1/c$). The unit cell contains four formula units and has the dimensions $a = 9.120$ Å, $b = 10.730$ Å, $c = 5.790$ Å, and $\beta = 95.5°$.

The antimony atom has the usual one-sided coordination to four oxygen atoms and the SbO_4 polyhedron can be described as a distorted trigonal bipyramid with a lone pair of electrons in one of the equatorial corners.

The fundamental structural element of the crystal structure is an infinite layer of the composition $SbO(H_2PO_4)$ parallel to the bc plane. Each layer is built up of SbO_4 polyhedra and PO_4 tetrahedra that share corners only. The water molecules are situated between the layers.

Several studies on the crystal chemistry of antimony(III) compounds, *e.g.* Sb_2O_3 (*orth.*),[1] SbOF,[2,3] $Sb_4O_5Cl_2$,[4,5] $SbPO_4$,[6] $Sb_4O_4(OH)_2(NO_3)_2$[7] have been completed or are in progress in this laboratory. In connection with these it was of interest to investigate the coordination of the metal atom in the salt described as $SbPO_4.2H_2O$ in *Gmelins Handbuch*.[8]

The results of this study show that the formula of the salt should be written as $SbO(H_2PO_4).H_2O$ instead of $SbPO_4.2H_2O$.

EXPERIMENTAL

Crystal preparation. An excess of $(NH_4)_2HPO_4$ solution was added to an acid water solution of $SbCl_3$ and the mixture was filtered. Tabular (100) colourless crystals separated in the filtrate within a day.

Crystal data and space group. Preliminary Weissenberg exposures of the layers $hk0$ and $hk1$ showed the crystals to be monoclinic. The only systematic absences found were: $h0l$ with $l = 2n+1$ and $0k0$ with $k = 2n+1$ which are characteristic of the space group $P2_1/c$ (No. 14). The dimensions of the unit cell were determined from powder photographs taken in a Guinier-Hägg focusing camera with Cu$K\alpha_1$ radiation ($\lambda = 1.54051$ Å) and potassium chloride (cubic, $a = 6.2929$ Å) as an internal standard. Refinement of the cell parameters was performed with a least-squares program.

The density observed by measuring the loss of weight in benzene was in fair agreement with the calculated value for four formula units $SbO(H_2PO_4).H_2O$ per unit cell. Some crystal data are presented in Table 1.

Table 1. Crystal data for $SbO(H_2PO_4).H_2O$. The estimated standard deviations are given within brackets.

Space group $P2_1/c$ (No. 14)

Unit cell dimensions:

$a = 9.1199(10)$ Å	$D_m = 2.86$ g cm^{-3}
$b = 10.7301(8)$ Å	$Z = 4$
$c = 5.7899(5)$ Å	Formula weight =
$\beta = 95.49(1)°$	252.75 g mol^{-1}
$V = 564.0$ Å^3	$D_x = 2.82$ g cm^{-3}

Collection and reduction of intensity data. A crystal with the dimensions $0.01 \times 0.07 \times 0.12$ mm^3 was chosen for the single crystal work. The rotation axis [001] chosen coincides with the dimension 0.12 mm of the crystal. Intensity data were collected for the reflections $hk0$ to $hk7$ (1380 independent reflections) with an integrating Weissenberg camera using Zr-filtered Mo$K\alpha$ radiation. The multiple film technique (3 films) with thin (0.05 mm) steelfoils between the films was used. The relative intensities of the reflections were measured by means of a microdensitometer (Enraf-Nonius). Corrections for Lorentz and polarization effects were performed and an absorption correction was applied. The linear absorption coefficient was 44.2 cm^{-1}.

Table 2. Analysis of the weights used in the last cycle of the least-squares refinement. The averages $\overline{w\Delta^2}$ are normalized. w = weighting factor. $\Delta = |F_o| - |F_c|$.

F_o-interval	Number of independent reflections	$\overline{w\Delta^2}$	sin θ-interval	Number of independent reflections	$\overline{w\Delta^2}$
0.0 – 28.2	138	1.06	0.000 – 0.302	255	0.99
28.2 – 32.7	138	1.49	0.302 – 0.380	245	0.64
32.7 – 36.6	138	0.93	0.380 – 0.435	214	0.80
36.6 – 40.3	138	0.99	0.435 – 0.479	188	0.71
40.3 – 44.8	138	0.76	0.479 – 0.516	141	0.85
44.8 – 49.6	138	0.98	0.516 – 0.548	115	1.35
49.6 – 55.7	138	0.81	0.548 – 0.577	83	1.12
55.7 – 66.0	138	0.91	0.577 – 0.603	50	1.49
66.0 – 80.7	138	0.92	0.603 – 0.628	30	0.85
80.7 – 168.1	138	1.16	0.628 – 0.650	36	1.21

Table 3a. Positional and thermal parameters obtained in the least-squares refinement. Estimated standard deviations are given within brackets. The anisotropic thermal parameters for the antimony atom are based on the expression exp $[-(h^2\beta_{11} + k^2\beta_{22} + l^2\beta_{33} + 2\ hk\beta_{12} + 2\ hl\beta_{13} + 2\ kl\beta_{23})]$.

Atom	x	y	z	B (Å^2)
Sb	0.46144(7)	0.16360(6)	0.24294(11)	[0.72]
P	0.74434(30)	0.40469(26)	0.28149(47)	0.81(3)
O(1)	0.5917(9)	0.3464(9)	0.2586(15)	1.69(12)
O(2)	0.8376(10)	0.3608(9)	0.0921(16)	1.77(14)
O(3)	0.8268(11)	0.3722(10)	0.5257(18)	2.08(15)
O(4)	0.7316(9)	0.5484(8)	0.2823(15)	1.39(12)
O(5)	0.3547(8)	0.2507(7)	0.4753(13)	0.91(9)
O(6)	0.1384(13)	0.4079(11)	0.1916(20)	2.53(18)

Atom	β_{11}	β_{22}	β_{33}	β_{12}	β_{13}	β_{23}
Sb	0.00247(5)	0.00152(3)	0.00569(14)	0.00067(7)	0.00047(5)	0.00009(9)

Table 3b. The r.m.s. components (Å) of the thermal displacement along the principal axes of the ellipsoid of thermal vibration for Sb.

$R(1) = 0.114(2)$	$R(2) = 0.079(2)$	$R(3) = 0.098(1)$

Computer programs. The following crystallographic computer programs were used in this work:

1. PIRUM: Indexing of powder photographs and refinement of unit cell parameters, written by P. E. Werner, Stockholm, Sweden.
2. DRF: Data reduction and Fourier calculations, written by A. Zalkin, Berkeley, USA. Modified by R. Liminga and J.-O. Lundgren, Uppsala, Sweden.
3. DATAP2: Absorption correction, written by P. Coppens, L. Leiserowitz and D. Rabinowich, Rehovoth, Israel. Modified by O. Olofsson and M. Elfström, Uppsala, Sweden.
4. LALS: Full matrix least-squares refinement of atomic parameters, written by P. K. Gantzel, R. A. Sparks and K. N. Trueblood, Los Angeles, USA. Modified by A. Zalkin, J.-O. Lundgren, R. Liminga and C.-I. Brändén, Uppsala, Sweden.
5. DISTAN: Calculation of interatomic distances and bond angles, written by A. Zalkin.
6. ORFFE: Crystallographic function and error program, written by W. R. Busing, K. O. Martin and H. A. Levy, Oak Ridge, USA.

All programs are modified and adopted for the UNIVAC 1108 computer in Lund by G. Malmros, C. Svensson and C. Särnstrand, Lund, Sweden.

Table 4. Observed and calculated structure factors for $SbO(H_2PO_4).H_2O$. The columns are h, $|F_o|$, and $|F_c|$, respectively. Each group is headed by k and l common to the group.

K=-10 L= 0

0	53	51
1	46	40

K=-9 L= 0

0	36	26

K=-8 L= 0

3	57	54
4	45	45
7	64	60
8	65	63

K=-7 L= 0

0	81	91
1	77	84
2	58	64
3	44	47
4	37	42

K=-6 L= 0

1	34	33
2	34	41
3	42	44
4	56	58
5	64	67
6	65	67
7	63	63
8	58	60
9	54	54

K=-5 L= 0

0	63	67
1	71	73
2	66	67
3	58	57
8	40	34

K=-4 L= 0

2	36	36
5	42	40

K=-3 L= 0

0	98	100
0	26	18
1	44	42
2	43	43
4	47	44
5	30	29

K=-2 L= 0

1	52	48
2	30	32
4	73	71
5	116	114
6	86	87
7	51	54
8	48	48
9	57	60
10	46	49

K=-1 L= 0

0	98	97
1	129	137
2	159	158
3	111	109
4	45	49
6	37	24
8	58	58
9	42	43
11	45	45
12	63	60
13	59	58

K=0 L= 0

1	39	36
2	55	54
3	72	71
4	81	80
5	121	124
6	100	102
7	86	86
8	84	89
9	56	56
10	36	33

K=1 L= 0

0	168	168
1	61	59
2	49	45
3	122	119
4	51	45
7	40	39
10	45	42

K=2 L= 0

1	111	111
2	112	107
3	41	41
6	31	33
8	31	26
9	33	30

K=-1 L= 0

2	107	99
3	105	111
4	65	65
5	92	88
6	102	104
7	101	102
8	103	103
9	67	67
10	38	39
11	39	38

K= 0 L= 0

2	56	57
3	144	155
4	76	76
5	35	35
7	42	41
10	88	90
11	74	75
12	43	39
13	48	45
14	53	55
15	46	44

K= 1 L= 0

1	73	77
2	66	67
3	38	37
4	40	34

K= 2 L= 0

0	26	18
1	44	42
2	43	43
4	47	44
5	30	29

K= 3 L= 0

1	52	48
2	30	32
4	73	71
5	116	114
6	86	87
7	51	54
8	48	48
9	57	60
10	46	49

K= 4 L= 0

0	98	97
1	129	137
2	159	158
3	111	109
4	45	49
6	37	24
8	58	58
9	42	43
11	45	45
12	63	60
13	59	58

K= 5 L= 0

1	39	36
2	55	54
3	72	71
4	81	80
5	121	124
6	100	102
7	86	86
8	84	89
9	56	56
10	36	33

K= 6 L= 0

0	168	168
1	61	59
2	49	45
3	122	119
4	51	45
7	40	39
10	45	42

K= 7 L= 0

1	57	53
2	27	20
3	30	28

K=-10 L= 1

10	46	46

K=-9 L= 1

11	35	34
12	35	33
13	28	41

K=-8 L= 1

-9	53	49
1	17	16
2	50	51
3	60	61
4	53	53
5	59	62
6	68	63
7	52	49
8	30	33
9	24	25
10	29	25

K=-7 L= 1

-8	36	33
2	50	51
3	60	61
4	53	53
5	59	62
6	68	63
7	52	49
8	30	33
9	24	25
10	29	25

K=-6 L= 1

-7	22	23
1	72	69
2	50	47
5	19	16
6	19	17
8	31	27
10	24	19
11	24	24

K=-5 L= 1

-6	50	50
2	20	21
-3	19	22
0	20	27
1	30	33
4	49	53
5	32	34

K=-4 L= 1

-5	56	55
-4	74	77
-3	96	94
-2	161	171
-1	129	137
1	155	166
2	139	145
3	77	75
4	81	78
5	52	46
6	26	28
8	59	56
9	55	53
10	40	37
11	59	59
12	68	69
13	55	47

K=-3 L= 1

-4	48	48
-3	20	19
1	17	16
2	50	51
3	60	61
4	53	53
5	59	62
6	68	63
7	52	49
8	30	33
9	24	25
10	29	25
11	24	24

K=-2 L= 1

-3	43	42
-2	66	66
-1	91	101
0	73	91
1	100	109
2	112	109
3	74	72
4	28	29
5	42	38
6	27	30
7	36	34
8	53	50
9	38	35
10	46	46
11	52	55
12	55	55

K=-1 L= 1

-2	36	36
-1	46	55
0	99	105
1	96	101
2	57	56
3	42	42
4	33	31
5	45	48
6	36	30
7	60	53
8	49	45

K= 2 L= 6

-9	24	18
-5	20	16
-4	35	32
-3	47	50
-2	36	39
-1	19	20
0	30	33
1	43	48
2	40	38
3	19	18
4	30	18
11	26	21

K= 2 L= 7

-13	37	39
-12	42	36
-10	30	22
-9	37	29
-7	26	27
-6	23	22
-5	31	28
-4	50	51
-3	58	64
-2	53	62
-1	43	50
0	43	49
1	58	62
2	46	49
3	25	16
7	27	30

K= 3 L= 1

-11	36	32
-10	53	49
-9	66	71
-8	77	86
-7	88	97
-6	110	111
-5	117	124
-4	127	129
-3	118	118
-2	80	82
-1	47	43
0	65	62
1	92	93
3	125	123
4	132	138
5	108	116
6	105	107
7	97	99
8	80	76
9	64	63
10	46	46

K= 3 L= 2

-7	36	35
-5	40	39
-3	21	19
-1	34	30
0	31	24
3	50	46
5	42	38
7	30	25

K= 3 L= 3

-11	36	35
-10	49	50
-9	67	70
-8	78	81
-7	79	84
-6	99	103
-5	101	107
-4	89	91
-3	91	93
-2	56	56
1	56	56
2	98	99
3	89	92
4	110	109
5	106	111
6	81	82
7	77	79
8	71	72
9	44	46
10	36	32

K= 3 L= 4

-13	40	40
-12	37	37
-11	52	49
-10	50	49
-9	26	20
-8	29	26
-7	29	26
-6	50	48
-5	50	48
-4	77	76
-3	89	91
-2	76	74
-1	106	104
0	105	112
1	74	74
2	79	80
3	76	75
4	48	47
5	28	24
9	50	45
10	53	52
11	43	41
12	37	38
13	40	41
14	35	36

K= 3 L= 5

-11	39	36
-10	53	49
-9	52	57
-8	69	70
-7	75	73
-6	69	73
-5	84	84
-4	69	70
-3	46	44
-2	38	37
0	33	33
1	41	43
2	63	63
3	82	87
4	72	78
5	74	76
6	72	75
7	58	57
8	47	49
9	41	41

K= 3 L= 6

-4	22	21
2	21	20
6	16	16

K= 3 L= 7

-11	33	28
-10	41	43
-9	48	51
-8	47	48
-7	57	57
-6	60	61
-5	48	49
-4	44	46
-3	35	34
0	18	20
1	45	45
2	46	47
3	53	55
4	64	66
5	54	55
6	48	49
7	47	48
8	34	35

K= 4 L= 1

-13	38	39
-12	55	47
-11	36	34
-10	36	36
-9	48	38
-8	36	30
-7	22	23
-6	99	111
-5	106	111
-4	69	70
-3	43	45
-2	28	26
-1	19	16
0	22	18
1	29	26

K= 4 L= 2

-10	41	47
-9	38	39
-8	38	41
-7	79	84
-6	78	81
-5	38	39
-4	36	31
-3	29	30
-2	89	82
-1	109	103
0	123	117
1	108	101
2	45	42
3	23	23
4	50	44
6	30	25
9	40	41
10	40	42
11	37	32

K= 4 L= 3

-15	34	35
-14	40	42
-13	40	40
-12	37	37
-11	52	49
-10	50	49
-9	26	20
-8	29	26
-7	99	101
-6	69	70
-5	76	75
-4	96	96
-3	60	58
-2	43	40
-1	37	32
1	42	41
2	50	48
3	97	90
4	86	83
5	70	66
6	94	91
7	93	94
8	76	75
9	57	61
10	36	34

K= 4 L= 4

-15	32	29
-14	32	32
-11	34	34
-10	27	22
-8	24	19
-7	21	14
-5	30	26
-4	70	67
-3	50	49
-2	37	31
-1	89	86
0	76	74
1	36	35
2	57	58
3	56	50
4	27	22
6	29	28
9	28	28
10	31	32

K= 4 L= 5

-1	83	83
0	76	76
1	57	59
2	53	54
3	53	49
4	40	35

K= 4 L= 6

-14	26	19
-11	40	32
-10	30	23
-5	28	26
2	42	41
3	37	39

K= 5 L= 1

-8	42	40
-7	64	63
-6	40	41
-4	60	58
-3	72	73
2	32	24
3	75	74
4	43	41
6	47	47
7	63	59
8	36	37

K= 5 L= 2

-10	53	55
-9	64	67
-8	83	90
-7	99	101
-6	69	70
-5	76	75
-4	96	96
-3	60	58
-2	43	40
-1	37	32
1	42	41
2	50	48
3	97	90
4	86	83
5	70	66
6	94	91
7	93	94
8	76	75
9	57	61
10	36	34

K= 5 L= 3

-12	32	24
-8	43	46
-7	58	56
-6	22	18
-4	62	61
-3	42	37
2	35	32
3	71	72
4	24	20
6	57	53
7	50	47

K= 5 L= 4

-12	31	24
-11	29	27
-10	41	38
-9	60	63
-8	68	69
-7	74	75
-6	89	90
-5	74	73
-4	59	56
-3	47	46
1	28	25
2	53	50
3	67	61
4	84	84
5	82	82
6	69	70
7	64	64
8	52	52
9	33	34
10	31	27

K= 5 L= 5

-8	37	39
-7	42	39
-5	27	16
-4	49	46
-3	26	27
2	42	41
3	37	39

Table 4. Continued.

6	38	38	-15	33	25	-4	52	53	2	27	24	3	59	60	5	38	36	-4	45	46	1	47	51
7	43	37	-14	33	35	-3	29	25	3	28	27	4	54	56				-3	42	42	2	47	44
			-13	44	45	2	42	45	4	26	25	5	58	58	K= 11 L=		2	-2	44	45			
K=	5 L=	6	-12	41	38	3	60	60				6	54	60	-9	43	48	-1	57	56	K= 14 L=		7
-11	33	31	-11	30	26	4	32	30	K=	8 L=	5	7	46	52	-8	49	53	0	48	50	-3	43	46
-10	42	43	-10	32	28	5	40	33	-11	48	49	8	47	37	-7	57	61	1	39	41	-2	41	39
-9	55	56	-9	28	27	6	52	49	-10	43	35				-6	72	76	2	42	41	-1	32	28
-8	61	62	-7	25	22	7	28	33	-5	60	57	K=	9 L=	6	-5	72	74	3	39	33	0	39	37
-7	50	53	-5	19	19				-4	59	59	-6	33	26	-4	53	50	4	24	17	1	40	41
-6	51	50	-4	43	41	K=	7 L=	6	-3	39	42	4	26	24	-2	32	25						
-5	53	53	-3	82	83	-11	29	30	-2	54	56	5	23	18	2	33	32	K=	13 L=	1	K=	15 L=	1
-4	43	43	-2	80	85	-10	45	48	-1	83	88				3	45	44	-7	38	38	-8	42	39
-3	35	31	-1	63	64	-9	47	46	0	77	77	K=	9 L=	7	4	63	64	-6	44	43	-7	33	38
-2	20	17	0	72	76	-8	32	33	1	44	44	-11	37	28	5	78	78	-5	46	42	-6	47	53
0	31	28	1	78	80	-7	40	42	2	38	39	-10	33	30	6	67	68	-4	44	43	-5	62	60
1	35	34	2	51	52	-6	59	60	3	53	53	-9	43	39	7	53	53	-3	43	41	-4	34	39
2	46	47	3	26	21	-5	40	39	4	45	42	-8	47	49	8	48	49	3	38	37	4	42	45
3	50	50	7	30	31	-3	26	27	9	47	45	-7	47	47	9	39	42	4	52	47	5	57	62
4	50	50	8	40	38	-2	29	31	10	41	47	-6	44	40				5	48	44	6	48	48
5	51	54	9	28	29	0	33	32				-5	39	42	K=	11 L=	3	6	41	38	9	43	41
6	55	57	10	39	35	1	40	40	K=	8 L=	6	-4	37	38	-9	30	25	7	40	39			
7	52	55	11	43	42	2	24	21	-1	35	34	-3	28	24	-6	27	24				K=	15 L=	3
8	42	45	12	39	38	3	27	28				1	28	27	-5	30	28	K=	13 L=	2	-10	38	36
9	28	28				4	55	56	K=	8 L=	7	2	47	45	4	27	25	-8	45	45	-9	40	40
			K=	7 L=	1	5	52	52	-6	29	22	3	45	47	5	29	25	-7	47	49	-8	35	36
K=	5 L=	7	-8	43	45	6	33	34	-5	45	46	4	41	42				-6	37	39	-7	33	39
-8	38	38	-7	64	62	7	36	36	-4	46	46	5	50	47	K=	11 L=	4	-4	41	42	-6	51	51
-5	24	23	-6	55	53	8	40	45	-3	27	31	6	43	47	-10	42	43	-3	42	43	-5	48	51
-4	27	29	-5	43	41	9	30	34	-2	48	49	7	38	37	-9	50	51	2	35	29	-4	33	31
2	36	36	-4	71	75				-1	69	71	8	29	27	-8	50	51	3	52	49	1	35	30
3	29	27	-3	73	77	K=	7 L=	7	0	44	48				-7	51	55	6	40	44	2	29	23
6	36	35	-2	31	27	-8	37	32	1	32	29	K=	10 L=	1	-6	54	57	7	45	50	3	31	30
			2	45	39	-7	40	32	2	37	35	-5	29	26	-5	49	51				4	50	49
K=	6 L=	1	3	82	84	-6	35	25	3	39	37	-4	37	40	-4	42	41	K=	13 L=	3	5	48	53
-2	46	41	4	71	70	-5	27	27	9	33	39	-3	55	55	-3	31	32	-8	38	35	6	39	42
0	30	29	5	37	37	-4	36	37	10	39	36	-2	68	70	-2	26	26	-7	36	35	7	33	34
1	26	23	6	59	57	-3	20	20				-1	68	70	0	26	19	-6	39	37	8	33	36
2	37	36	7	64	62	1	29	24	K=	9 L=	1	0	64	62	1	39	37	-5	45	42	9	32	37
			8	39	36	2	36	36	-11	38	33	1	66	68	2	35	35	-4	34	36			
K=	6 L=	2				3	33	33	-10	42	39	2	73	69	3	46	42	-3	33	30	K=	15 L=	5
-13	45	54	K=	7 L=	2	4	32	30	-9	46	49	3	50	51	4	55	54	2	38	33	-6	43	48
-12	57	61	-10	51	54	5	35	28	-8	62	63	4	31	30	5	54	56	3	40	40	-5	38	36
-9	47	52	-9	66	71	6	34	31	-7	80	82				6	50	53	4	39	40	4	53	47
-8	27	28	-8	52	57				-6	79	84	K=	10 L=	2	7	52	51	5	38	39	5	47	45
-5	32	28	-7	45	46	K=	8 L=	1	-5	64	69	-3	47	48	8	40	46	6	39	37			
-4	36	34	-6	82	83	-12	43	41	-4	77	80	-2	76	79	9	39	37	7	34	32	K=	16 L=	1
-3	84	87	-5	92	89	-11	60	60	-3	82	79	-1	50	50				-1	37	36			
-2	167	162	-4	30	29	-10	63	62	-2	45	41	0	38	39	K=	11 L=	6	0	48	40			
-1	133	129	-3	34	32	-9	48	51	1	34	29	1	78	73	-10	32	32	-8	43	48	1	39	37
0	113	110	-2	69	66	-8	91	89	2	58	57	2	60	61	-9	39	39	-7	44	43			
1	167	159	-1	33	34	-7	71	72	3	77	78	3	33	33	-8	42	42	-5	26	24	K=	16 L=	2
2	120	117	1	73	64	-6	48	51	4	82	81	8	38	38	-7	53	49	-4	48	44	-1	43	49
3	56	52	2	58	56	-1	101	106	5	72	75				-6	55	54	-3	27	29	0	57	59
4	27	27	4	67	63	0	127	136	6	81	80	K=	10 L=	3	-5	39	43	2	36	36			
8	59	56	5	102	96	1	77	79	7	76	79	-12	34	33	-4	27	25	3	51	46	K=	16 L=	3
9	46	44	6	60	60	2	60	59	8	60	60	-5	32	30	1	28	22	6	44	44	-4	29	24
11	49	50	7	44	47	3	78	75	9	45	41	-4	37	35	2	35	30	7	40	44	-3	31	26
12	55	58	8	68	64	4	81	76	10	37	37	-3	56	54	3	40	40	8	30	29	-2	39	33
			9	63	64	5	42	41	11	39	31	-2	72	71	4	47	52				-1	39	36
K=	6 L=	3				9	43	41				-1	53	54	5	50	52	K=	13 L=	6	0	32	34
-3	32	26	K=	7 L=	3	10	69	66	K=	9 L=	2	0	56	55	6	40	41	-9	23	26	1	34	34
-2	20	19	-9	29	30	11	56	52	-5	36	37	1	69	68	7	36	34	-8	32	37	2	32	28
2	35	31	-8	51	48	12	45	40	-1	28	22	2	54	51	8	34	32	-7	37	34			
4	22	20	-7	53	52	13	50	39	5	34	33	3	39	37	9	22	24	-6	29	22	K=	16 L=	4
			-6	45	44	14	47	42				4	33	30				-5	24	25	-4	34	29
K=	6 L=	4	-5	47	43				K=	9 L=	3				K=	12 L=	1	-4	35	32	-2	26	27
-16	28	30	-4	61	62	K=	8 L=	2	-10	36	38	K=	10 L=	4	0	37	31	2	34	31	-1	37	41
-15	32	33	-3	62	60	-3	29	31	-9	43	46	-3	43	44				3	36	34	0	41	39
-14	47	44	2	60	58	-1	52	52	-8	63	66	-2	63	62	K=	12 L=	2	4	30	23	1	30	27
-13	47	52	3	66	65	0	67	64	-7	72	76	-1	54	53	-4	51	55	5	28	27	2	31	23
-12	41	47	4	50	47	3	28	27	-6	70	67	0	49	48	-3	66	67	6	39	37			
-11	28	27	5	43	47				-5	68	66	1	60	58	-2	51	55	7	35	30	K=	16 L=	6
-10	29	24	6	50	48	K=	8 L=	3	-4	71	71	2	42	43	-1	71	74				-2	35	28
-9	45	45	7	52	48	-14	34	41	-3	60	56				0	80	84	K=	14 L=	1	-1	30	42
-8	25	27	8	34	35	-13	37	35	-2	35	33	K=	10 L=	5	1	55	60	-3	51	51	0	40	34
-7	18	15				-12	36	40	1	27	26	-4	39	39	2	55	60	-2	68	71			
-6	22	24	K=	7 L=	4	-11	60	59	2	60	57	-3	48	47	3	59	61	-1	58	59	K=	17 L=	4
-5	33	31	-11	29	28	-10	50	51	3	78	78	-2	51	50				0	41	43	-7	45	43
-4	62	60	-10	40	50	-9	57	55	4	64	65	-1	49	50	K=	12 L=	3	1	63	61	-6	36	36
-3	101	101	-9	46	47	-8	81	77	5	66	67	0	44	46	0	29	30	2	74	70	-5	36	35
-2	119	115	-8	38	40	-7	67	63	6	78	77	1	50	47				3	46	42	-4	31	33
-1	75	79	-7	53	55	-6	48	50	7	61	65	2	50	45	K=	12 L=	4				3	37	37
0	80	78	-6	85	84	-1	103	105	8	46	48				-13	39	32	K=	14 L=	3	4	34	35
1	117	114	-5	75	73	0	111	116	9	39	37	K=	10 L=	6	-12	36	33	-9	37	31	5	34	37
2	98	99	-4	28	24	1	54	54				-4	31	25	-11	39	36	-4	30	27	6	40	41
3	48	49	-3	18	13	2	53	50	K=	9 L=	4	-3	50	47	-10	33	33	-3	57	55	7	31	34
4	23	19	-2	33	31	3	76	72	-6	32	27	-2	40	41	-5	30	32	-2	66	68			
5	23	17	-1	20	19	4	60	57	-2	24	19	-1	28	27	-4	40	40	-1	43	44	K=	18 L=	4
7	34	35	0	27	25	9	44	44	1	32	30	0	37	37	-3	46	47	0	39	43	-3	25	34
8	46	46	1	47	41	10	59	62	4	20	20	1	46	44	-2	59	61	1	64	64	-2	30	37
9	29	29	3	33	32	11	40	45	5	26	21	2	36	33	-1	72	74	2	65	55	-1	28	33
10	28	30	4	79	80	12	34	33							0	68	72	3	30	30	0	37	35
11	42	46	5	82	81	13	42	38	K=	9 L=	5	K=	10 L=	7	1	56	57	8	38	34	1	32	36
12	46	53	6	50	51	14	41	38	-10	42	36	-4	34	28	2	41	42				2	28	30
13	37	41	7	38	37				-9	43	45	-3	46	43	3	35	35	K=	14 L=	4	3	31	26
14	32	28	8	44	43	K=	8 L=	4	-8	50	57	-2	41	40	4	30	27	0	26	22			
			9	43	46	-5	34	31	-7	60	64	-1	34	32	9	36	36						
K=	6 L=	5	10	26	24	-4	25	25	-6	49	54	0	44	40	10	30	37	K=	14 L=	5			
-2	24	21				-3	25	27	-5	44	50	1	40	37	11	29	33	-4	39	33			
1	24	26	K=	7 L=	5	-2	37	32	-4	57	56	2	27	25	12	32	30	-3	49	52			
			-8	47	46	-1	27	22	-3	40	41							-2	54	52			
K=	6 L=	6	-7	46	45	0	26	26	1	28	31	K=	11 L=	1	K=	12 L=	6	-1	39	39			
-16	35	25	-5	40	42	1	35	32	2	60	53	-5	43	36	-5	30	33	0	43	39			

STRUCTURE DETERMINATION

From a two-dimensional Pattersson projection $P(uv)$ and a Harker section $P(u\frac{1}{2}w)$ the antimony atoms were found to occupy the four-fold point position 4(*e*) in $P2_1/c$. A least-squares refinement based solely on the deduced antimony atom position was performed. Subsequent three-dimensional electron density difference syntheses revealed the positions of all other non-hydrogen atoms, *viz.* one phosphorus and six oxygen atoms. All atoms occupy the general point position 4(*e*).

A full matrix least-squares refinement was now performed with eight inter-layer scale factors and isotropic temperature factors for all atoms. The refinement converged to an *R*-value of 0.064 ($R=\sum||F_o|-|F_c||/\sum|F_o|$). After the absorption correction was applied the *R*-value was reduced to 0.058. An anisotropic temperature factor was introduced for the antimony atom and the positional and thermal parameters were refined together with an overall scale factor. The final *R*-value was 0.056 (1380 reflections). Only observed reflections were included in the calculations. The contributions of the antimony and phosphorus atoms were corrected for anomalous dispersion in a least-squares refinement. This gave no significant decrease in the *R*-factor or in the standard deviations as compared with the calculations based on the uncorrected values. No correction was applied for extinction as nothing in the intensity data indicates the presence of such effects. The atomic scattering factors used were those given by Cromer and Waber [9] for neutral antimony, and those by Hanson *et al.*[10] for neutral phosphorus and oxygen. Several weighting schemes were tried. That recommended by Hughes,[11] which gave the best result from the weight analysis (*cf.* Table 2), was used in the last refinement. The final atomic fractional coordinates and thermal parameters are given in Table 3. Observed and calculated structure factors are listed in Table 4.

Table 5. Interatomic distances (Å) and bond angles (°) in the structure of $SbO(H_2PO_4).H_2O$ (*cf.* Table 3 and Fig. 2).
The superscripts (*i*) – (*iii*) are used to indicate the following equivalent sites in the structure:

	x,*y*,*z*	(*ii*)	$\bar{x}\bar{y}\bar{z}$
(*i*)	$x,\frac{1}{2}-y,\frac{1}{2}+z$	(*iii*)	$x-1,y,z$

where *x*,*y*,*z*, are the atomic coordinates given in Table 3.

The phosphate tetrahedron			
P – O(1)	1.520(9)	∠O(1) – P – O(2)	112.3(5)
P – O(2)	1.525(10)	∠O(1) – P – O(3)	110.0(5)
P – O(3)	1.576(11)	∠O(1) – P – O(4)	110.0(5)
P – O(4)	1.546(9)	∠O(2) – P – O(3)	109.0(5)
		∠O(2) – P – O(4)	110.9(5)
		∠O(3) – P – O(4)	104.3(5)
The SbO_4 polyhedron			
Sb – O(1)	2.291(10)	∠O(1) – Sb – O(4)	156.3(3)
Sb – O(4)	2.145(9)	∠O(1) – Sb – O(5)	81.7(3)
Sb – O(5)	1.970(8)	∠O(1) – Sb – O(5^i)	81.2(3)
Sb – O(5^i)	1.977(8)	∠O(4) – Sb – O(5)	82.2(3)
		∠O(4) – Sb – O(5^i)	82.8(3)
		∠O(5) – Sb – O(5^i)	94.4(3)
The water oxygen atom			
O(6) – O(2^{iii})	2.794(15)	∠O(2^{iii}) – O(6) – O(3^{ii})	108.7(5)
O(6) – O(3^{ii})	2.872(16)		
O(6) – O(5)	2.969(14)		
O(6) – O(5^i)	2.971(14)		
O(6) – O(2^{ii})	2.996(15)		

DESCRIPTION AND DISCUSSION OF THE STRUCTURE

Six oxygen positions were found. Four of them [O(1) – O(4)], grouped around the phosphorus atom, form the phosphate tetrahedron (*cf.* Tables 3 and 5 for the atom notations). The distances P – O and the angles O – P – O (Table 5) are normal (*cf. International Tables* [12]).

One of the other two oxygen atoms, O(5), is directly bound to two antimony atoms. Thus it cannot belong to a water molecule, but it could be an ion O^{2-} or OH^-. The last oxygen atom, O(6), is situated at hydrogen bond distance from the nearest oxygen atom, $O(2^{iii})$, and is certainly a water oxygen. The temperature factors of the atoms O(5) and O(6) (*cf.* Table 3) also reflect their different situations.

That atom O(5) is an oxygen ion is supported by the following considerations. Since the X-ray data did not show the positions of the hydrogen atoms, it was difficult to distinguish O^{2-} and OH^-. To establish the nature of the oxygen atom, a calculation was made based on the principle of local neutralization of charge. This procedure makes it possible to recognize O^{2-}, OH^- and H_2O in crystal structures determined by X-ray diffraction methods. The valence sum $\sum v$ of possible bonds to O(5) was calculated according to Donnay and Allman.[13] Values of 2.0, 1.0, and 0.0 for $\sum v$ indicate, respectively, the presence of O^{2-}, OH^-, and H_2O. In the present case $\sum v$ for O(5) was found to be 1.9. It should thus be O^{2-}.

If O(5) is an oxide ion it follows that the phosphate tetrahedron must be an $H_2PO_4^-$ group and thus the structural formula should be written $SbO(H_2PO_4).H_2O$ instead of $SbPO_4.2H_2O$.

The antimony atom is coordinated to four oxygen atoms, O(1), O(4), O(5), and $O(5^i)$. The coordination polyhedron can be described as a distorted trigonal bipyramid with the unshared electron pair of the antimony atom occupying one of the equatorial corners. This type of coordination polyhedron has been found in several structures containing Sb^{3+}, Te^{4+}, or Pb^{2+}.[14] The distances and angles within the SbO_4 polyhedron are similar to those in related structures and to the calculated values given by Andersson *et al.*[14] A comparison of some distances and angles in the SbO_4 polyhedra in structures containing trivalent antimony is given in Table 6.

Table 6. Distances (Å) and angles (°) within the SbO_4 polyhedra (*cf.* Fig. 3) in some compounds containing antimony(III).
d_1 is the average of the axial distances Sb – O(1) and Sb – O(4), d_2 is the average of the equatorial distances Sb – O(5) and $Sb - O(5^i)$, α is the angle O(1) – Sb – O(4), and β is the angle $O(5) - Sb - O(5^i)$.

	$SbO(H_2PO_4).H_2O$	$SbPO_4$[5]	$\beta - Sb_2O_4$[14]	$SbNbO_4$[15]	L – SbOF[2,a]	M – SbOF[3,a]
d_1	1.97	2.01	2.02	2.02	1.97	2.00
d_2	2.22	2.18	2.22	2.23	2.16	2.19
α	156.3	164.8	148.1	150.7	142.9	145.0
β	94.4	87.9	87.9	92.1	95.9	93.7

[a] SbO_3F polyhedra instead of SbO_4 polyhedra.

The fundamental structural element in $SbO.(H_2PO_4).H_2O$ is an infinite layer of the composition $SbO(H_2PO_4)$ parallel to the *bc* plane. The water molecules are situated between the $SbO.(H_2PO_4)$ layers. Each layer consists of SbO_4 polyhedra and PO_4 tetrahedra sharing corners only. The interrelationships of the polyhedra are shown in Figs. 1a, 1b, and 1c. As can be seen in the figures, every SbO_4 polyhedron shares two oxygen atoms [O(5) and $O(5^i)$] with two

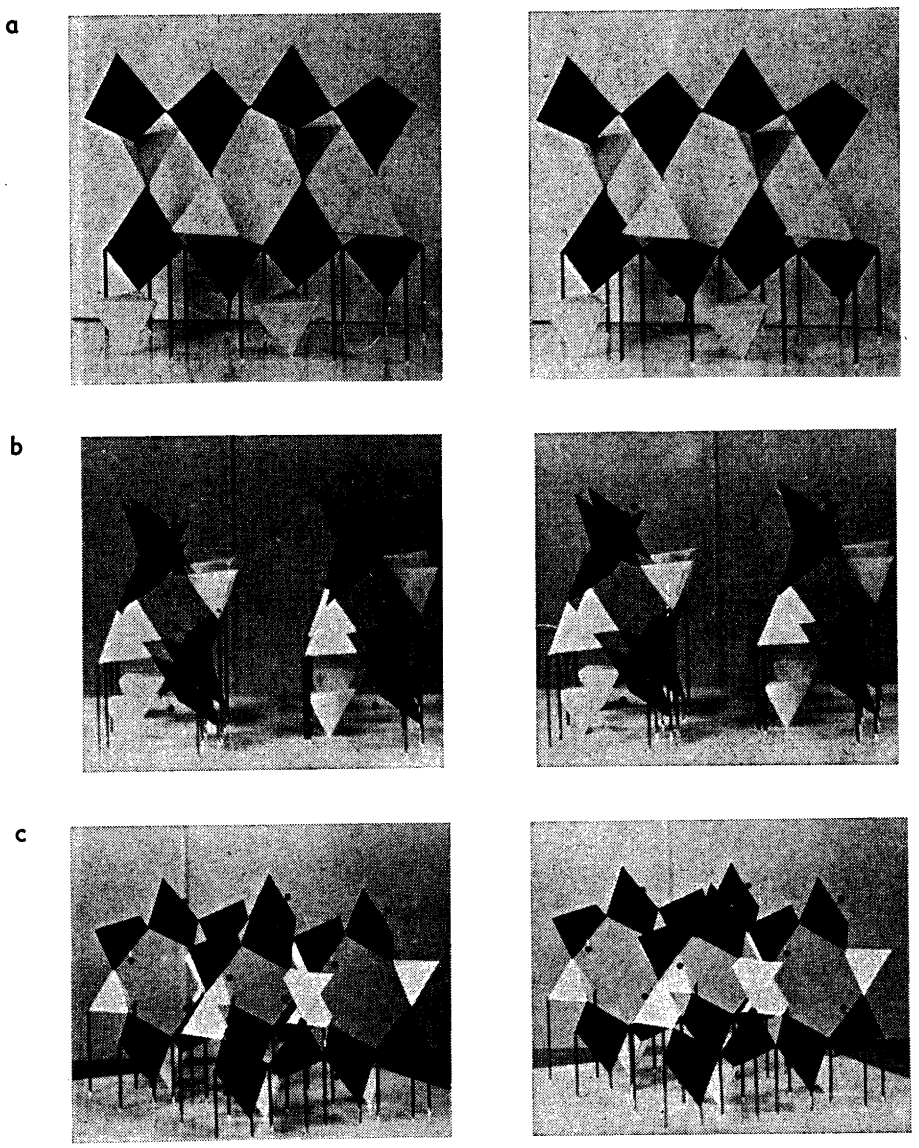

Fig. 1. Stereo views of the structure of $SbO(H_2PO_4).H_2O$. (Black polyhedra = SbO_4, white polyhedra = PO_4). a. The structure viewed along the x-axis. Only one layer is shown. b. The structure viewed along the z-axis. c. The structure viewed along [101].

other SbO_4 polyhedra and two oxygen atoms [O(1) and O(4)] with two PO_4 tetrahedra. The PO_4 tetrahedron shares two oxygen atoms [O(1) and O(4)] with two SbO_4 polyhedra. The other two oxygen atoms [O(2) and O(3)] are OH-groups. These two corners of the tetrahedron are directed out from the layer.

The layers are probably held together by weak hydrogen bonds involving the water molecules. Some possible hydrogen bonds are indicated by dashed-dotted lines in Fig. 2.

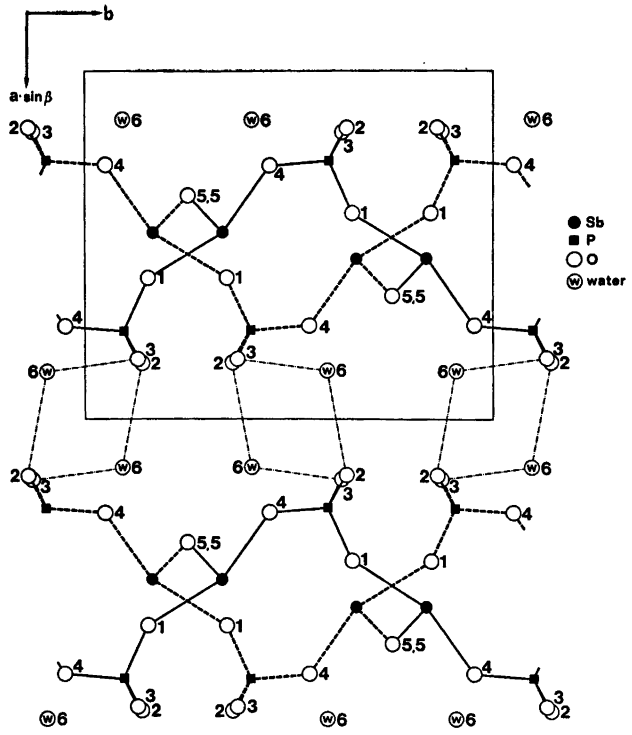

Fig. 2. Projection of the structure of $SbO(H_2PO_4).H_2O$ along [001]. The numbering of the oxygen atoms is given in the figure (*cf.* Table 3).

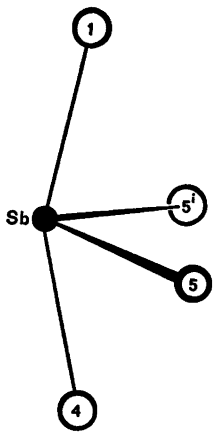

Fig. 3. The SbO_4 polyhedra. The notations of the oxygen atoms are given in the figure (*cf.* Tables 3 and 6).

Acknowledgements. The author is grateful to Professor Bengt Aurivillius for his kind and encouraging interest and to Dr. Karin Aurivillius and Dr. Sten Andersson for many valuable discussions and comments. Thanks are also due to Dr. Brian Thomas for correcting the English of the manuscript. This investigation is a part of a research project supported by the Swedish Natural Science Research Council.

REFERENCES

1. Svensson, C. *Acta Crystallogr. B 30* (1974) 458.
2. Åström, A. and Andersson, S. *J. Solid State Chem. 6* (1973) 191.
3. Åström, A. *Acta Chem. Scand. 26* (1972) 3849.
4. Edstrand, M. *Acta Chem. Scand. 1* (1947) 178.
5. Särnstrand, C. *To be published.*
6. Kinberger, B. *Acta Chem. Scand. 24* (1970) 320.
7. Bovin, J.-O. *Acta Chem. Scand. A 28* (1974) 267.
8. *Gmelins Handbuch der Anorganischen Chemie*, Gmelin-Verlag, Clausthal-Zellerfeld 1949, Vol. 18.
9. Cromer, D. T. and Waber, J. T. *Acta Crystallogr. 18* (1965) 104.

10. Hanson, H. P., Herman, F., Lea, J. D. and Skillman, S. *Acta Crystallogr. 17* (1964) 1040.
11. Hughes, E. W. *J. Amer. Chem. Soc. 63* (1941) 1737.
12. *International Tables for X-Ray Crystallography*, Kynoch Press, Birmingham 1962, Vol III.
13. Donnay, G. and Allman, R. *Amer. Mineral. 55* (1970) 1003.
14. Andersson, S., Åström, A., Galy, J. and Meunier, G. *J. Solid State Chem. 6* (1973) 187.
15. Rodgers, D. and Skapski, A. C. *Proc. Chem. Soc. London* (1964) 400.
16. Skapski, A. C. and Rodgers, D. *Chem. Commun.* (1965) 611.

Received October 4, 1973.

Acta Chemica Scandinavica A 28 (1974) 284—288

Is the Nernst Equation Applicable to Silver(I) Concentration Cells in Fused Nitrate Medium?

BERTIL HOLMBERG

Division of Physical Chemistry, Lund University, Chemical Center, P.O.B. 740, S-220 07 Lund 7, Sweden

Further improvements of a previously described high-temperature thermostat for potentiometric measurements in molten salt media are described. From measurements of the emf of cells

$$\mathrm{Ag} \;\left|\; \begin{matrix} C\ \mathrm{AgNO_3} \\ (\mathrm{K,Na})\mathrm{NO_3} \end{matrix} \;\right|\; \left|\; \begin{matrix} C^0\ \mathrm{AgNO_3} \\ (\mathrm{K,Na})\mathrm{NO_3} \end{matrix} \;\right|\; \mathrm{Ag}$$

at 280°C it is safely concluded that the activity factor for silver ion remains constant in the range 10^{-4} mol kg^{-1} $\leq C \leq$ 1 mol kg^{-1}. The deviations from Nernst's equation at very high and very low C are discussed. For $C < 10^{-4}$ mol kg^{-1} the deviations may be attributed to an increment in the silver ion content of the melt, mainly by corrosion.

Concentrations, in mol fractions or in molality units, of solute species, have frequently been used for activities in studies on, *e.g.*, silver(I) complexation in nitrate melts. This is often justified by an experimental verification of the approximate applicability of the Nernst equation in the form

$$E = E_0 - RTF^{-1} \ln 10 \log C \qquad (1)$$

for the emf, E, of concentration cells of the general type

$$\mathrm{Ag} \;\left|\; \begin{matrix} C\ \mathrm{AgNO_3} \\ \mathrm{MNO_3(l)} \end{matrix} \;\right|\; \left|\; \begin{matrix} C^0\ \mathrm{AgNO_3} \\ \mathrm{MNO_3(l)} \end{matrix} \;\right|\; \mathrm{Ag}$$

(*cf.* Ref. 1 and references quoted therein). M stands for an alkali metal or an alkaline earth metal or a mixture of two or more of them.

The measurements are often said to be described by Nernst's equation *e.g.* to within 1 mV. In cases when the experimental value of RTF^{-1} ln 10 has been given explicitly by an author, this value is, however, as a rule somewhat smaller than the theoretical one. For instance, in (K,Na)NO_3(l) Flengas and Rideal [2] found 102.8 mV at 250°C (theoretical: 103.4 mV), Duke and Garfinkel [3] found 124 mV at 366°C (theoretical: 126 mV), Cigén and Mannerstrand [4] found 108.1 mV at 280°C (theoretical: 109.7 mV) and Holmberg [1] later found (109.2 ± 0.2) mV at the same temperature with a different design of the thermostat. Actually, there seem to be no accurate measurements on this cell in equimolar (K,Na)NO_3(l), which have confirmed that Nernst's equation in the simple form (1) can perfectly describe the results over a very wide concentration range.

Deviations of about 1 % are often considered to be of minor importance in studies on complex formation in melts, but they are, from a general thermodynamic point of view, very unsatisfactory. This is so because the deviations from the theoretical values are of a systematic nature and are as a rule outside the limits of uncertainty as predicted from the estimated random errors in the measurements. A linear relationship between E and log C is generally taken as a proof for constancy of the activity factor for silver ions. The linearity in itself does not prove, however, that the activity factor is constant. It may change in a way that can be expressed by the equation

$$\ln \gamma = \left(\frac{kF}{RT \ln 10} - 1 \right) \ln C + \mathit{constant} \qquad (2)$$

within the range of linearity. (γ stands for the activity factor and k is the experimentally obtained slope for E *vs.* log C.)

Hence, if the linearity persists when C is varied over four powers of ten, a deviation of 1 % from the theoretical value of the slope

might have its origin in a change of γ by about 10 % over this concentration range, provided the liquid junction potentials are negligible. If eqn. (2) is used to explain the non-theoretical value of k, it means that the melts are significantly non-ideal. This conclusion is most disturbing for the calculation of complexity constants – and even so for deciding which complex species exist in the melts – since these calculations presuppose ideal solutions.

From previous studies [1,4,5] at this laboratory it has become evident that heat leakage through the electrode wires will give rise to systematic errors in the Nernst slope, simply caused by too low a temperature at the electrode surface. The high precision and reproducibility in the measurements, which is necessary if one wishes to make confident statements on the constancy of activity factors over a very wide concentration range, requires a very careful control of the temperature. In this paper further improvements of a new furnace construction are described, and measurements of the emf of the concentration cell mentioned above are reported. From these measurements more definite conclusions about the ideal behaviour of the liquid system $AgNO_3$ – (K,Na)NO_3 may be drawn.

EXPERIMENTAL

Chemicals used. Potassium nitrate and sodium nitrate (Merck, *p.a.*) were powdered, ground together and dried at 120°C. Selected crystals of silver nitrate (Merck, *p.a.*) were used.

Apparatus. The same kind of electrodes, reference half-cells, and thermostating system as previously described [1] were used, except for two important modifications.

Firstly, the temperature was controlled by a fast cycling, overshoot-free creep controller, type CR/DHS/PID/SCR, from EUROTHERM, Worthing, England. The temperature calibration was carried out by the use of a standard platinum resistance thermometer, immersed in the test melt under operating conditions. During the experiments the test melt temperature was 280.08°C (IPTS – 68) with maximum over-all short-time variations of ±0.01°C in the bulk melt.

Secondly, the electrode compartment of the asbestos lid was furnished with cylindrical aluminium blocks, embedding the upper part of the electrodes. The blocks were electrically heated to the same temperature as the test melt by means of a separate variable transformer. These electrical heating circuits were temporarily switched off at the very moment of the emf reading, in order to avoid induction in the electrode wires from the closely situated windings of the heating elements.

The emf was read to 0.1 mV by means of a digital instrument, PHM 52, from Radiometer, Copenhagen.

Procedure. The measurements were performed as titrations. The cell was set up with 250.00 g equimolar (K,Na)NO_3 and kept at 280°C without $AgNO_3$ in the test melt for at least 24 h (sometimes 70 h) before the measurements were started. Weighed amounts of $AgNO_3$ or solidified stock melts of $AgNO_3$ in equimolar (K,Na)NO_3 were successively added to the test melt. After stabilization of the temperature a stable emf could as a rule be read within 1 min. Repeated series were made with $C^0 = 1$, 0.1, 0.01 or 0.001 mol kg^{-1} in the approximate range 4×10^{-5} mol kg^{-1} $\leq C \leq 3$ mol kg^{-1}.

Analyses. The silver content of the $AgNO_3$ preparations, stock melts, reference melts and the test melt at the end of a series were checked by electroanalytical precipitation of silver on a rotating platinum cathode from hot cyanide solutions.

RESULTS AND DISCUSSION

The electrodes. It is generally recognized [6] that silver wires in electrodes become very brittle even after a rather short exposure to a salt melt at elevated temperature. Sometimes, in rather primitive experimental arrangements, migration of silver on the wire can be observed. These phenomena are obviously due to a recrystallization process, which is probably enhanced by temperature differences in the electrodes and in a melt layer close to the electrode metal surface.

With the experimental arrangement described

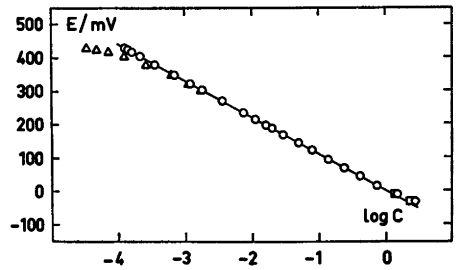

Fig. 1. E versus log C. Data from a series with a large $\bar{d}$-value. Symbols: uncorrected concentrations, $C_{i,\mathrm{add}}$ (△); corrected values according to eqn. (5) (○); concentrations C' according to eqn. (6) (□).

in this paper, temperature differences in the silver electrodes seem to be eliminated. The same electrodes were used throughout all the experiments, and they were exposed to the melt at 280°C for more than seven weeks with occasional periods of *ca* 4 h at room temperature between the measurement series. No change in the mechanical properties of the silver wires could be detected.

The measurements. Fig. 1 gives an example of a plot of E *vs.* log C in a series with $C^0 = 1$ mol kg^{-1}. In the range 10^{-4} mol kg^{-1} $\leq C \leq$ 1 mol kg^{-1} the data of all series fit to linear relationships

$$E = E_0 - k \log C$$

At very low silver(I) concentrations, as calculated from the added amounts of $AgNO_3$, a pronounced deviation from linearity always occurs. In series when the cell was allowed to stand for only about 24 h before the measurements were started, a decrease in the emf with time was observed at the very smallest C-values (*viz.* in the first two or three experimental points). In other cases, when the cell was allowed to stand for *ca.* 70 h before the measurements started, a time-independent, stable emf could be read, even when no addition of $AgNO_3$ to the test melt had been made. (The further calculations and the data of Fig. 1 and Table 1 refer only to stable emf readings.)

The deviation from linearity at low silver(I) concentrations might be due either to the presence of additional redox systems in minor concentrations, causing a mixed electrode potential, or to the fact that the true C is larger than that calculated from the added amount of $AgNO_3$. The above mentioned time-dependence of the emf could of course mean that the oxidant of the additional redox system corrodes the silver wires, so that an extra amount of silver(I) is introduced into the test melt. Such a small increase in C might also be brought about in other ways, *e.g.* by leakage of reference melt into the test melt through the asbestos fibre connecting the half-cells or by "back exchange" of silver ions for sodium ions between the Pyrex glass equipment and the melt, if the glass had been exposed to melts concentrated in silver(I) in previous experiments. The last explanation is ruled out, however, by the observation that results from experiments performed with fresh Pyrex glass apparatus, do not differ from those where the same glass equipment was used in repeated experimental series.

The magnitude of the deviation seems to be somewhat dependent on C^0 (*cf.* Table 1), which may suggest some contribution by diffusion from the melt in the reference compartment, but probably some type of corrosion of the silver wires [7-9] makes the main contribution to the extra amount of silver(I) present in the test melt.

The silver(I) concentration may be written as

$$C_i = C_{i,\mathrm{add}} + d_i \qquad (3)$$

where i refers to a cell with the emf E_i. $C_{i,\mathrm{add}}$ stands for the concentration, calculated from the added amount of $AgNO_3$, and d_i stands for the extra contribution to the silver(I) concentration. After E_0 and k were determined from the linear part of E_i *vs.* log $C_{i,\mathrm{add}}$, it was assumed that d_i could be calculated from the relation

Table 1. Results from some typical runs.

C^0/(mol kg^{-1})	n_d	$\bar{d} \times 10^5$ / mol kg^{-1}	$\overline{\Delta d} \times 10^5$ / mol kg^{-1}	n	E_0/mV	$\sigma(E_0)$/mV	k/mV	$\sigma(k)$/mV	$k \log C^0$/mV
1.021	4	8.59	0.07	19	−0.33	0.09	109.80	0.04	0.99
1.021	4	8.12	0.04	20	−0.80	0.11	109.69	0.04	0.99
1.021	6	9.02	0.03	20	−0.19	0.12	109.69	0.05	0.99
0.0994	6	5.17	0.06	20	−110.04	0.12	109.80	0.05	−110.08
0.0994	7	6.04	0.09	20	−109.79	0.10	109.58	0.04	−109.86
0.01000	5	4.31	0.03	20	−218.54	0.09	109.52	0.04	−219.04
0.01000	7	4.56	0.09	19	−219.03	0.08	109.77	0.03	−219.54
0.001001	5	4.22	0.02	20	−329.22	0.14	109.98	0.05	−329.90
						Average:	109.73	0.04	

$$E_i = E_0 - k \log (C_{i,\mathrm{add}} + d_i) \quad (4)$$

in the range where an appreciable deviation from linearity is found.

It appeared that the d-values were remarkably constant within a series, but differed significantly between different series. This behaviour suggests that once the emf is stabilized, the melt has got an additional contribution of silver ions, which is not changed when further additions of $AgNO_3$ are made. Therefore, the average value

$$\bar{d} = \frac{1}{n_d} \sum_i d_i$$

was calculated for each series. n_d stands for the number of experimental points used in the calculation of the d_i-values. The total amount of data within each series was then corrected according to

$$C_{\mathrm{corr}} = C_{\mathrm{add}} + \bar{d} \quad (5)$$

This correction brings about a small change in the values of E_0 and k. The calculations were therefore iterated until the parameters remained constant within the limits of experimental uncertainty.

Fig. 1 shows E *vs.* log C for the series with the largest $\bar{d}$ found (9×10^{-5} mol kg^{-1}). The results from some representative series are collected in Table 1. The parameters E_0 and k and the standard deviations $\sigma(E_0)$ and $\sigma(k)$ are computed from least-squares treatments of n experimental points according to $E = E_0 - k \times \log C_{\mathrm{corr}}$ in the concentration range $-4 \leq \log C_{\mathrm{corr}} \leq 0$. The constancy of the d_i-values may be judged from $\overline{\Delta d}$, calculated as

$$\overline{\Delta d} = \frac{1}{n_d} \sum_i \left| \bar{d} - d_i \right|$$

The view that the extra amount of silver ions in the melt remains constant once the emf is stabilized, is supported by the fact that $\sigma(E_0)$, $\sigma(k)$ and $\overline{\Delta d}$ as a rule took their minimum values simultaneously, *i.e.* when the final corrections of Table 1 were applied, yielding values of k very close to RTF^{-1} ln 10.

The following features of Table 1 should be noticed:

1. The d-value cannot be well reproduced in different series. d ranged between 4×10^{-5} mol kg^{-1} and 9×10^{-5} mol kg^{-1}. An increment in C of this order of magnitude will generally not influence the results obtained in complex formation studies.

2. There is some decrease in $\bar{d}$ with decreasing C^0, suggesting some influence of the reference half-cell melt on $\bar{d}$.

3. In some experiments, when the cell was allowed to stand for more than 70 h before any $AgNO_3$ had been added to the test melt, a stable emf could be read, corresponding to a small silver(I) concentration in the test melt. This concentration was found to coincide very well with the value of $\bar{d}$ for the actual series.

4. Series with the same value of C^0 give somewhat different E_0-values. The maximum differences amount to about 0.6 mV, whereas $3\sigma(E_0)$ amounts to about 0.3 mV as a rule. These numbers reflect the difficulty in reproducing the properties of the junction between the half-cells.

5. The differences between k log C^0 and E_0 are of the same order of magnitude as those between the E_0-values referring to the same C^0, except for $C^0 = 1$ mol kg^{-1}, where the experimental E_0 is about 1.2 to 1.8 mV smaller than k log C^0. This is expected, since a small deviation from linearity at high values of C starts just around $C = 1$ mol kg^{-1} (*vide* Fig. 1).

6. The variations in k between different series are small (≈ 0.2 mV). The experimental values are closely gathered around the theoretical RTF^{-1} ln 10 = 109.75 mV.

7. The standard deviations $\sigma(E_0)$ and $\sigma(k)$ are remarkably small, indicating very small random errors in the measurements. This, as well as the coincidence between the experimental and the theoretical value of k, is evidently a consequence of the work on improving the temperature uniformity in the system.

From the results discussed above, it is obvious that concentrations on the molality scale can be used for activities for silver(I) in the range $-4 \leq \log C \leq 0$ in the $AgNO_3 - (K,Na)NO_3$(l) system. In this range the simple Nernst equation (1) describes the results from emf measurements, provided that the thermostating of the system is good enough.

In more concentrated solutions a weak deviation from the ideal curve occurs. These deviations may be reduced if another concentration unit is used, *viz.*

$$C' = C \times 10.747/(C + 10.747) \quad (6)$$

where C is expressed in molality units. C′ is proportional to mol fractions and coincides with C at small values of C. Still, however, a weak deviation remains (*cf.* Fig. 1). This behaviour might be due to a change in the activity factor, γ for silver ions, and to increased liquid junction potentials. The junction potentials may be roughly estimated and corrected for as done by Boxall and Johnsson,[9] according to Klemm's [10] method, leaving a remaining deviation from the straight line of 1 to 5 mV at $C = 2$ mol kg^{-1}. If this effect is thought to be caused exclusively by a change in γ on increasing C from 1 mol kg^{-1}, this change would amount to some five percent. (At concentrations below 1 mol kg^{-1} the junction potentials, as estimated in this way, are on the whole negligible.)

Obviously no safer conclusion about the thermodynamics of these more concentrated melts can be drawn from measurements of this kind, but the deviations from ideality that may occur at values of C around 2 mol kg^{-1} are certainly not very large.

Acknowledgements. I thank Professor Ido Leden for helpful discussions and support during this work. Miss Bodil Jönsson and Mrs. Siv Olsson have skilfully assisted in the experimental work. Thanks are also due to Dr. Peter Sellers for his correction of the English of this paper.

REFERENCES

1. Holmberg, B. *Acta Chem. Scand. 27* (1973) 875.
2. Flengas, S. N. and Rideal, E. *Proc. Roy. Soc. (London) A 233* (1956) 433.
3. Duke, F. R. and Garfinkel, H. M. *J. Phys. Chem. 65* (1961) 461.
4. Cigén, R. and Mannerstrand, N. *Acta Chem. Scand. 18* (1964) 1755.
5. Elding, I. and Leden, I. *Acta Chem. Scand. 23* (1969) 2430.
6. Morand, G. and Hladik, J. *Electrochimie des sels fondus, Tome II*, Masson et C^{ie}, Paris 1969.
7. Manning, D. L. and Blander, M. *Inorg. Chem. 1* (1962) 594.
8. Conte, A. and Ingram, M. D. *Electrochim. Acta 13* (1968) 1551.
9. Boxall, L. G. and Johnson, K. E. *Trans. Faraday Soc. 67* (1971) 1433.
10. Klemm, A. In Blander, M., Ed., *Molten Salt Chemistry*, Interscience, New York 1964, p. 535.

Received October 11, 1973.

Acta Chemica Scandinavica A 28 (1974) 289–293

Induced Optical Activity in $Co(NH_3)_6^{3+}$ by Outer-sphere Association with Chiral Anions

IVAN JONÁŠ and BENGT NORDÉN

Division of Inorganic Chemistry, University of Lund, Box 740, S-220 07 Lund 7, Sweden

The formation of outer-sphere 1:1 complexes $[Co(NH_3)_6^{3+}]L$ has been studied with the optically active divalent anions, L = (*R*)-tartrate (I), (*S*)-glutamate (II), (+)camphorate (III) and the monovalent anions, L = (+)10-camphorsulphonate (IV), (*S*)-leucinate (V), (*S*)-alaninate (VI), (*S*)-prolinate (VII), (*S*)-lactate (VIII), (*S*)-mandelate (IX). The stability constants for the complexes were determined at 25.0°C in 0.1 M $NaClO_4$ by UV spectrophotometry:[1]

$\beta_1(M^{-1}) =$			
20.3 ± 1.5	(I)	4.0 ± 0.3	(V)
16.1 ± 1.6	(II)	5.4 ± 0.4	(VI)
11.9 ± 1.3	(III)	4.5 ± 0.3	(VII)
[14.6	(IV)]	5.2 ± 0.6	(VIII)
		6.1 ± 0.7	(IX)

In all these complexes optical activity is induced in the magnetic dipole allowed $d-d$-transition $^1A_{1g} \rightarrow {}^1T_{1g}$. Only one circular dichroism band was observed but as it appears at a wavelength (480 – 484 nm) slightly shifted from that of the absorption maximum (476 nm) an oppositely directed weak component at shorter wavelength is presumably present. The molar circular dichroism peak values for the complexes were calculated using the above stability constants:

$\Delta\varepsilon_{ML}(M^{-1}\,cm^{-1}) \times 10^2 =$			
−1.57	(I)	−0.47	(V)
−0.30	(II)	−0.23	(VI)
−0.09	(III)	−0.41	(VII)
−0.61	(IV)	−0.39	(VIII)
		+0.62	(IX)

For the $^1A_{1g} \rightarrow {}^1T_{2g}$ transition, without magnetic moment, no significant circular dichroism was observed ($|\Delta\varepsilon| < 10^{-4}\ M^{-1}\ cm^{-1}$).

The circular dichroism is explained by a chelatic fixation of the outer-sphere ligand to two adjacent ammonia molecules by hydrogen bonding.

In previous papers,[1] it was concluded that a negative circular dichroism (CD) band could be associated with the formation of a 1:1 outer-sphere complex $[Co(NH_3)_6]$ (*R*)-tartrate$^+$, at the wavelength of the $d-d$ transition $^1A_{1g} \rightarrow {}^1T_{1g}$. Attempts to use other chiral ligands were also made but it was not then possible either to detect any definite effects or to relate them to any defined complex. Later, a more sensitive CD spectrophotometer has become available and the interference of strong competitive complex formation became obvious, when using perchlorate as an ionic medium, so it was considered worthwhile to make a new attempt, *e.g.* by using the sensitive CD instrument to study the very weak resulting CD at a high constant ionic strength.

The present expansion of the earlier study has been made to examine the validity of the earlier suggestion that the CD was conformationally induced by a type of chelate ring (adjacent ammonia molecules joined by hydrogen bonding *via* the bidentate anion). It should also be very pertinent to try to find a correlation, in a series of such outer-sphere complexes, between the chirality and structure of the ligand and the sign and the magnitude of the induced CD.

The chosen ligands have been mono- and divalent anions derived from amino and hydroxy acids with different complexing capabilities, and with similar chirality with respect to an asymmetric carbon atom (*cf.* footnote of Table 1). Further, two derivatives of camphor with more rigid structures have been studied.

METHOD

Stability constants were obtained by the spectrophotometric method described in earlier

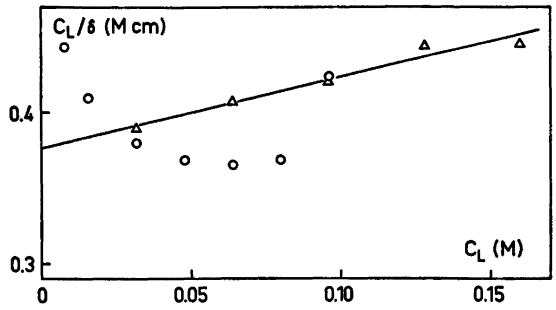

Fig. 1. Typical result indicating interference with perchlorate. L(+)lactate⁻, ○ $I = 0.14$ M, $\beta_1 = \pm 0$ M^{-1}; △ $I = 0.20$ M, $\beta_1 = 1.2$ M^{-1}. The result can be interpreted by a serious perchlorate ion complexation. The stability constant for the complex $[Co(NH_3)_6]ClO_4^{2+}$ should be 1 – 10 M^{-1}, with a β_1 of about 5 M^{-1} for the lactate complex.

papers[1] and the notation from there will be used also here.

At a first attempt to keep a constant "ionic strength",

$$I = 6C_M + 0.5(|z|^2 + |z|)[L^z] + [NaClO_4],$$

deviations were obtained, which could be explained by a competitive outer-sphere complex formation with perchlorate ions.* Fig. 1 thus indicates the unreliability of using a low formal ionic strength; *e.g.* with $I = 0.14$ M no reasonable result was obtained. The use of much higher ionic strengths was not possible due to precipitation of $Co(NH_3)_6(ClO_4)_3$ and to a lower accuracy in the absorbance differences as a result of the quenched complexation.

By compromising, using a low constant perchlorate concentration, we have obtained stability constants which fulfil our demands. Thus, though the absolute accuracy can be discussed of a stability constant obtained with 0.1 M $NaClO_4$ as a medium buffer, due to considerable activity coefficient variations, the reexamination in this medium of the complex formation with tartrate gave a result which was in acceptable agreement with the earlier values.[1]

On the basis of an assumed analogy between the case of tartrate, where only the 1:1 complex is of any importance, the investigation was made with a fixed C_M, $C_M \ll C_L$. This restriction was moreover necessary as with $C_M > C_L$ the δ values obtained were of a questionably low precision and the variations of the activity coefficients more serious.

From the determined β_1 values and measured CD, on a few solutions with different concentrations of ML, molar circular dichroism coefficients were calculated.

EXPERIMENTAL

Chemicals. Analytical grade chemicals were used, when available. (The lactic acid and the 10-camphor sulphonic acid were of *puriss.* quality.) The ligand stock-solutions were prepared by adding one or two equivalents of sodium hydroxide to the commercial acids. The $Co(NH_3)_6Cl_3$ (preparation in Ref. 3) was not transformed into the perchlorate salt. This was found unsuitable due to a low solubility of the perchlorate leading to difficulties with the stock-solutions. It was also considered unnecessary, in the light of the discussion on the perchlorate ion as a potent ligand,[2] especially as the complex salt was used in a low and constant concentration in all solutions.

Absorbance measurements. (Notation, see Ref. 1). Solutions with the composition $C_M = 6.00$ mM $Co(NH_3)_6Cl_3$, C_L ligand and 0.100 M $NaClO_4$ were prepared and measured within 0.5 h after mixing in a Zeiss PMQII spectrophotometer at 260 nm (273 nm with mandelate), using (when possible) 1, 0.5, and 0.2 cm pathlengths. Mean absorbances, A (normalized to cm^{-1}) were calculated and the difference formed:

$\delta = A(C_M, C_L, 0.1\text{ M } NaClO_4) - A(C_M, C_L = 0, 0.1\text{ M } NaClO_4) - A(C_M = 0, C_L)$

The function C_L/δ was plotted *versus* C_L and from the straight line obtained the stability constant was computed, using a least-squares programme, as

$\beta_1 = (\text{slope})/[\text{intercept} - 1/(\varepsilon_{ML} - \varepsilon_M)]$ and

$$(\varepsilon_{ML} - \varepsilon_M) = 1/C_M \times (\text{slope}) \qquad (2)$$

The solutions were tested for Co(II),[3] and it

* A recent report has focussed interest on the possibilities in different connections for the perchlorate ion to act as a ligand.[2]

was checked that the absorbance maximum at 476 nm had neither shifted nor decreased the day after the measurements. Absorption spectra were recorded on a Hitachi EPS 3T spectrophotometer.

CD measurements. The instrument used was the JASCO model of 1973 ("J – 40"). A slit programme for 8 nm spectral band width was used, 5 cm cells, time-constant: 4 s, and a recording speed of 0.17 nm/s. A few solutions, with $C_M = 6.00$ mM and C_L between 80 and 200 mM, were recorded in the range 300 – 600 nm. The spectrum obtained for water was used as a baseline, but it was also checked that no important "absoption artefact" was obtained with a solution, $C_L = 0$, $C_M = 6$ mM. The molar circular dichroism was calculated from the observed CD (cm^{-1}) by

$$\Delta\varepsilon = \mathrm{CD}(1 + \beta_1 C_L)/C_L C_M \beta_1 \qquad (3)$$

RESULTS

The experimental results of the stability study are represented by the C_L/δ values in Figs. 2 – 4; the computed constants are found in Table 1. With respect to the low ionic strength and in comparison with other outer-sphere complexes,[1-2] the majority of the complexes must be considered weak.

Tests with varying $C_M > C_L$ which were performed with prolinate indicated that the 1:2

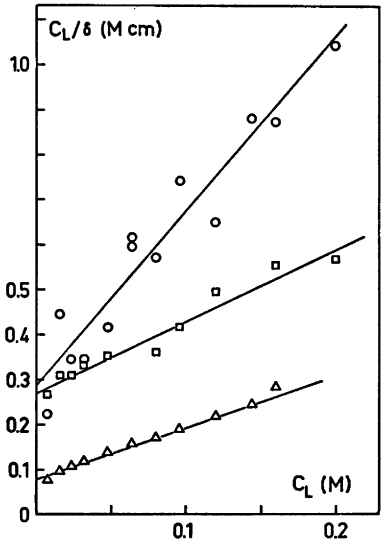

Fig. 2. C_L/δ plotted *versus* C_L for solutions M, L, for determination of β_1 (ML). L = ○ (+)-10-camphorsulphonate, □ (*S*)-mandelate, △ (*S*)-glutaminate.

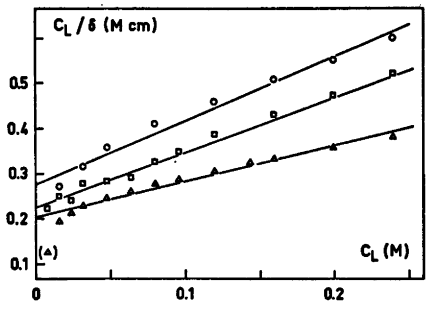

Fig. 3. L = ○ (*S*)-lactate, □ (*S*)-alaninate, △ (*S*)-leucinate.

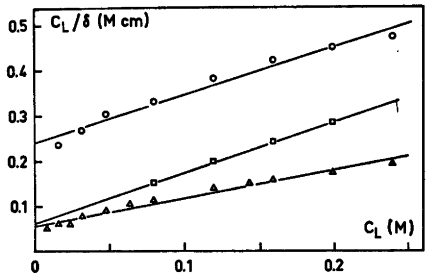

Fig. 4. L = ○ (*S*)-prolinate, □(*R*)-tartrate, △ camphorate.

outer-sphere complexes were most probably not formed to any significant extent. This was as expected at the present low ionic strength.[1] Also the good agreement between the $\Delta\varepsilon$ values shown in Table 2, obtained from opposite limits of the ligand concentration interval, strongly supports the assumption of the absence of higher complexes.

After having ruled out other more trivial effects, such as CD due to complexation with contaminating species [Co(II), $Co(NH_3)_5L$ by quantitative analysis and from careful inspection of the absorption spectrum in the ligand field range [1]] the calculated molar circular dichroisms could thus be connected with a series of 1:1 outer-sphere complexes. The recorded CD spectra did not at any wavelength show deviation from a linear dependence on the concentration of the outer-sphere complex. Furthermore, the lineshapes $|\Delta\varepsilon(\lambda)|$ appeared very similar and were almost symmetric (Fig. 5) with peaks at about 480 nm. The small shift compared with the position of the absorption

Table 1. Determined stability constants, β_1, for the outer-sphere complexes $[Co(NH_3)_6]L^{+ \text{ or } 2+}$ in 0.1 M $NaClO_4$ at 25.0°C. For comparison, literature values on stability constants ($\beta_{1,i}$) for certain inner-sphere complexes (aqueous solution) [7] have been tabulated. *=at 273 nm.

	H_nL	L[a]	$\varepsilon_{ML}-\varepsilon_M$ at 260 nm (M^{-1} cm^{-1})	β_1 (M^{-1})	M, log $\beta_{1,i}$
I	HOOC–CH(OH)–CH(OH)COOH	(*R*)-tartrate^{2-}	149± 2	20.3± 1.5	Co^{2+}, 3
II	HOOC–CH(NH_2)(CH_2)$_2$COOH	(*S*)-glutamate^{2-}	146± 4	16.1± 1.6	Ni^{2+}, 5.2; Co^{2+}, 5
III	HOOC–(C_8H_{14})COOH	(+)-camphorate^{2-}	269± 12	11.9± 1.3	–
IV	O=(C_9H_{13})CH_2SO_3H	(+)-10-camphor-sulphonate$^-$	43± 4	14.6± 1.5	–
V	$(CH_3)_2CHCH_2CH(NH_2)COOH$	(*S*)-leucinate$^-$	211± 11	4.0± 0.3	Ni^{2+}, 5.6; Co^{2+}, 5
VI	$CH_3CH(NH_2)COOH$	(*S*)-alaninate$^-$	141± 7	5.4± 0.4	Ni^{2+}, 6.0; Co^{2+}, 5
VII	$C_4H_7NHCOOH$	(*S*)-prolinate$^-$	158± 11	4.5± 0.3	Cu^{2+}, 9
VIII	$CH_3CH(OH)COOH$	(*S*)-lactate$^-$	119± 7	5.2± 0.6	Co^{2+}, 3
IX	$C_6H_5CH(OH)COOH$	(*S*)-mandelate$^-$	618± 27*	6.1± 0.7	Co^{2+}, 3

[a] For the α-amino acids and α-hydroxy acids the absolute configuration *S* corresponds to L; for tartaric acid, *R* corresponds to L, according to the notation of Cahn, Ingold and Prelog.[9]

Table 2. Molar circular dichroism peak values for the outer-sphere complexes $[Co(NH_3)_6]L=ML$ (C_M=6.00 mM). [ML] calculated by means of eqn. (3).

L	C_L (mM)	−CD × 10^4 (cm^{-1})	CD peak (nm)	$-\Delta\varepsilon_{ML} \times 10^2$ ($M^{-1}cm^{-1}$)	mean
I	80.0	0.575	480	1.55	1.57
	200.0	0.758		1.58	
II	80.0	0.102	482	0.30	0.30
	200.0	0.137		0.30	
III	80.0	0.023	482	0.08	0.09
	200.0	0.039		0.09	
IV	80.0	0.167	483	0.52	0.61
	200.0	0.312		0.70	
V	80.0	0.068	483	0.47	0.47
	200.0	0.126		0.47	
VI	80.0	0.039	480	0.21	0.23
	200.0	0.078		0.25	
VII	80.0	0.065	484	0.41	0.41
	200.0	0.114		0.40	
VIII	80.0	0.061	482	0.35	0.39
	200.0	0.133		0.43	
IX	80.0	−0.116		−0.59	
	160.0	−0.191	480	−0.64	−0.62
	200.0	−0.212		−0.64	

maximum can indicate (though not prove) [4] the existence of a band with opposite sign at shorter wavelength.

It can be observed that the magnitude of the molar circular dichroisms are of about the same order as those of $[Co(NH_3)_5$L-amino acid$]^{3+}$ complexes for which also negative signs have been reported, except for the complex with prolinate.[5]

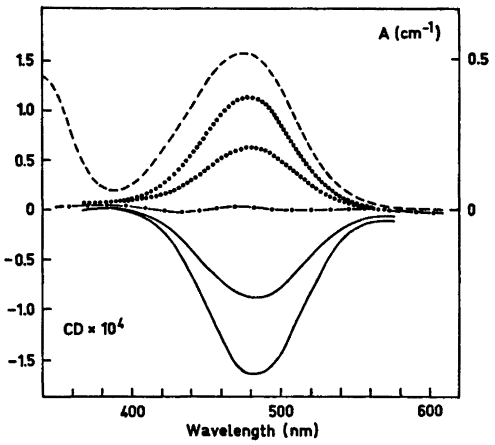

Fig. 5. Some typical recorded spectra (C_M= 0.006 M), – – – absorption (1 cm cell, C_L= 0.080 M), circular dichroism (5 cm cell, C_L= 0.080 and 0.200 M) ··· L=(*S*)-mandelate, ——L=(+)-10-camphorsulphonate.

After a correction for the CD of the ligand no significant CD (less than 10^{-4} M^{-1} cm^{-1}) remained to be associated with the magnetic-dipole forbidden $A_{1g} \rightarrow T_{2g}$ at 340 nm.

DISCUSSION

As expected the strongest complexes are obtained with the divalent anions. The somewhat lower β_1 value for camphorate compared with

glutamate is expected, due to a steric hindrance leading to difficulty of coordination with both carboxylate groups. For tartrate the considerably higher value might be referred to a possibility of using the $-OH$ groups as well, but can also be explained by this anion being more strongly hydrated.[6]

The high stability constant obtained for the 10-camphorsulphonate complex may probably be considerably in error due to the small difference between ε_M and ε_{ML}. This is also suggested by the large difference between the two estimated molar circular dichroisms (Table 2). From a comparison with the stabilities of the other complexes a β_1 even as low as 5 M^{-1} may be expected, which would also yield more consistent molar circular dichroisms (-0.97×10^{-2} and -1.04×10^{-2} M^{-1} cm^{-1} instead of -0.52×10^{-2} and -0.70×10^{-2} M^{-1} cm^{-1}).

Literature values for some inner-sphere complexes have been included in Table 1. It can be seen that the larger β_1 for glutamate is not due to a coordinating amino group but to the second carboxylate group and the larger negative charge, as leucinate, alaninate and prolinate give much lower constants. The latter are even lower than those for the lactate and mandelate complexes, which, by comparison with corresponding inner-sphere constants, gives evidence for the prevalence of hydrogen bonding or electrostatic bonding in the outer sphere.

With tartrate a lower β_1 should be expected than that from an earlier determination (30 ± 1 M^{-1}) [1] as in average a higher ionic strength range has been used in the present study. Actually a reduction with almost 50 % could be estimated from the dependence on the ionic strength ($NaClO_4$).[1] In view of a certain increase in the yielded β_1, due to the perchlorate ion concentration constancy, the obtained value therefore seems quite reasonable.

In general it is very difficult to correlate a CD effect with a certain molecular structure or even with one of two enantiomeric alternatives, on a purely theoretical basis. Even semi-empirical predictions often hold only within a series of strongly related homologues. As no quantitative data of circularly dichroic outer-sphere complexes have been reported before, the material seems too limited to provide any empirical rules. In other words, as we do not know for certain how the ligands coordinate or how the optical activity is transmitted into the centre of the metal complex, we are in principle incapable of presenting even a qualitative discussion on the sign of the CD. We therefore establish only the "correlation" here * that, with the exception of mandelate, the studied α-amino and α-hydroxy acids (tartrate not included), with the same absolute configurations (*S*) with respect to the moieties $CH(NH_2)COO$ and $CH(OH)COO$, display negative virtually single CD bands positioned in very close connection to the $d-d$ transition $^1A_{1g} \rightarrow {}^1T_{1g}$.

The present investigation extends the earlier study of the $[Co(NH_3)_6](R)$-tartrate$^+$ complex, and gives evidence for the existence of 1:1 outer-sphere complexes with a series of other chiral ligands. It further supports the theory of a chelatic bonding correlated to a large stability constant and a strong induced optical activity in the Co(III) magnetic-dipole $d-d$ transition.

Acknowledgement. The CD instrument has been purchased through donations from Knut och Alice Wallenbergs Stiftelse, Carl Tryggers Stiftelse, Magnus Bergvalls Stiftelse, Hierta Retzius Stiftelse and by support from the Departments of Inorganic and Organic Chemistry at the University of Lund. Professors Sture Fronæus and Ragnar Larsson and Dr. Lennart Johansson are acknowledged for interest and discussions.

REFERENCES

1. Nordén, B. *Acta Chem. Scand. 25* (1971) 2156; *26* (1972) 111.
2. Johansson, L. *Coord. Chem. Rev. In press.*
3. Bjerrum, J. and McReynolds, J. P. *Inorg. Syn. 2* (1964) 217.
4. Hawkins, C. J. *Absolute Configuration of Metal Complexes*, Wiley, New York 1971.
5. Moffitt, W. and Moscowitz, A. *J. Chem. Phys. 30* (1959) 648.
6. Yoneda, H., Muto, M., Baba, T. and Miura, T. *Bull. Chem. Soc. Jap. 44* (1971) 689.
7. Martell, A. E., Ed., *Stability Constants of Metal-ion Complexes*, Supplement No.1, The Chemical Society, London 1971.
8. Nordén, B. *Chem. Scr. 4* (1974). *In press.*
9. Cahn, R. S., Ingold, C. K. and Prelog, V. *Angew. Chem. Int. Ed. Engl. 5* (1966) 385.

Received October 13, 1973.

* By assuming that the outer-sphere complexes are well-defined chelates, however, we have found evidence for a tentative correlation between the CD and the positions of the coordinating groups, by means of a regional rule.[8]

Acta Chemica Scandinavica A 28 (1974) 294—298

Crystal Structure of Cycloundecanone at —165°C

P. GROTH

Department of Chemistry, University of Oslo, Oslo 3, Norway

The crystals are monoclinic with space group $P2_1/c$, cell dimensions $a = 7.305(2)$ Å, $b = 5.600(2)$ Å, $c = 24.566(7)$ Å, $\beta = 91.29(2)°$, and four molecules in the unit cell. The structure was solved by direct methods and refined by full-matrix least squares technique to an R-value of 4.8 % (R_w = 5.7 %) for 1416 reflections recorded on an automatic four circle diffractometer. The conformation may be described as "triangular" with the carbonyl group in an asymmetric position.

Very little structural information for the eleven- and higher odd-membered saturated rings is available. To the best of the authors' knowledge, an X-ray analysis of cyclodecylamine hydrobromide [1] has not led to a clear picture of the conformation. Strain-minimization calculations of medium and large cycloalkanes have been carried out for a period of more than ten years,[2-5] and it seems to be need for detailed structure information.

Cycloundecanone was synthesized (by T. Ledaal at this university) from *cis* 2,12-dibromocyclododecanone according to the procedure of Garbisch and Wohllebe,[6] and redistilled under reduced pressure (b.p. 111 – 113° (9 mm), m.p. 15°C). Identification was performed by the aid of high resolution NMR and IR-spectra.

The crystals are monoclinic with space group $P2_1/c$, cell dimensions $a = 7.305(2)$ Å, $b = 5.600(2)$ Å, $c = 24.566(7)$ Å, $\beta = 91.29(2)°$, and four molecules in the unit cell. The intensities were measured (at −165°C) on a Syntex $P\bar{1}$ diffractometer with Enraf-Nonius liquid nitrogen cooling device (modified by H. Hope). With an

Table 1. Final fractional coordinates and anisotropic thermal vibration parameters with estimated standard deviations (multiplied by 10^5 for oxygen and carbon atoms, and 10^4 for hydrogens). Hn1 are Hn2 bonded to Cn.

ATOM	X	Y	Z	B	B11	B22	B33	B12	B13	B23
O	79863(25)	18887(38)	28445(7)		1989(44)	1343(59)	107(3)	-298(82)	215(18)	88(22)
C1	83867(32)	31136(41)	19583(8)		1212(50)	1382(62)	47(4)	-172(104)	-53(21)	-8(30)
C2	102386(33)	36682(43)	17114(10)		1073(50)	1463(62)	74(4)	-177(106)	-198(23)	-62(32)
C3	110263(34)	15812(46)	13971(10)		1861(54)	1658(67)	88(4)	488(111)	-78(24)	-48(33)
C4	98142(34)	6645(43)	9192(9)		969(50)	1458(61)	79(4)	95(111)	51(23)	-58(32)
C5	94533(33)	25325(45)	4714(9)		1816(48)	1652(66)	63(4)	-103(106)	63(22)	-16(29)
C6	74731(33)	25232(46)	2425(10)		1284(51)	1756(69)	63(4)	-122(114)	-33(22)	11(32)
C7	68256(34)	31995(43)	6598(10)		988(50)	1637(65)	73(4)	-169(107)	-65(22)	39(33)
C8	62853(34)	57488(43)	8753(10)		982(50)	1584(61)	66(4)	-57(104)	-37(22)	130(32)
C9	49258(34)	63929(45)	13348(10)		995(51)	1485(66)	106(4)	121(106)	18(23)	-88(31)
C10	52165(34)	58364(48)	18665(10)		1894(51)	1847(91)	87(4)	26(113)	121(24)	-171(33)
C11	71782(34)	51912(47)	21185(10)		1357(54)	1388(86)	78(4)	-631(110)	9(24)	-126(31)
H21	18996(32)	3955(42)	2816(10)	1,9(,5)						
H22	10169(30)	4958(46)	1478(10)	2,8(,6)						
H31	11231(31)	212(45)	1652(10)	2,8(,6)						
H32	12256(33)	2698(42)	1251(9)	2,8(,6)						
H41	8628(32)	223(46)	1869(9)	1,6(,6)						
H42	10428(28)	-797(40)	757(8)	1,1(,4)						
H51	10293(29)	2266(48)	181(9)	1,2(,6)						
H52	9718(29)	4191(43)	618(9)	1,8(,5)						
H61	7139(32)	845(46)	186(10)	2,3(,6)						
H62	7379(30)	3596(43)	-92(10)	2,1(,5)						
H71	6151(29)	2889(42)	966(9)	1,6(,5)						
H72	4778(34)	3218(43)	485(10)	2,3(,6)						
H81	5957(31)	6989(44)	558(10)	2,1(,6)						
H82	7468(31)	6802(38)	1803(9)	1,3(,5)						
H91	3616(34)	6188(42)	1285(9)	2,2(,5)						
H92	5141(31)	8179(46)	1415(10)	2,2(,5)						
H101	4937(29)	3285(42)	1814(9)	1,3(,5)						
H102	4341(35)	5635(47)	2137(11)	2,9(,6)						
H111	7115(30)	5031(44)	2498(10)	2,2(,5)						
H112	7785(31)	6655(47)	2928(9)	1,8(,5)						

Table 2. Observed and calculated structure factors on 10 times absolute scale.

Hk	0,Kk	0	16	51	36	19	76	77	16	24	26	-26	113	111	3	181	146	-13	27	14	8	65	70
2	173	173	18	26	29	20	155	154	17	106	113	-24	50	50	4	47	46	-12	38	37	6	126	131
4	281	296	19	69	63	21	151	150	18	69	66	-22	257	257	5	157	153	- 8	117	123	8	314	323
6	154	155	21	49	37	22	120	122	20	90	90	-20	53	52	6	79	69	- 7	35	34	9	59	54
8	628	630	Hk	0,Kk	5	23	30	36	21	34	22	-18	167	157	7	134	134	- 6	62	60	10	67	70
10	379	375	1	71	74	24	164	161	22	34	31	-16	215	223	8	33	35	- 5	82	88	11	143	139
12	280	286	2	51	43	25	51	64	23	86	81	-14	41	44	9	199	201	- 4	38	43	12	74	71
14	171	172	3	108	109	26	96	91	25	43	41	-12	79	80	10	168	165	- 3	87	95	13	57	57
16	277	278	4	171	165	28	40	40	Hk	1,Kk	4	-10	579	566	12	39	43	- 2	104	100	14	83	84
20	95	95	5	207	202	Hk	1,Kk	2	-22	50	50	- 8	97	93	14	89	83	- 1	80	87	16	222	227
22	46	42	6	27	27	-27	98	87	-20	47	42	- 6	231	232	17	29	28	0	148	152	17	83	86
24	48	46	7	203	205	-26	97	79	-19	56	58	- 4	478	462	18	83	81	1	51	54	18	69	67
26	177	170	8	67	72	-25	25	14	-17	114	121	- 2	692	525	19	156	161	2	21	1	19	61	65
28	60	54	10	121	125	-24	95	91	-15	74	76	0	353	361	21	38	37	3	45	40	20	43	43
Hk	0,Kk	1	12	48	48	-23	101	95	-13	43	46	2	102	98	23	130	131	4	97	100	21	132	135
1	281	289	13	97	94	-21	40	38	-12	76	87	4	912	893	24	134	125	5	133	135	22	95	91
2	655	655	15	147	136	-20	54	59	-11	117	125	6	201	207	26	43	44	6	25	24	23	64	66
3	324	335	16	47	41	-19	38	39	-10	187	191	8	182	173	Hk	2,Kk	3	7	41	44	24	76	80
5	270	277	17	44	51	-18	120	120	- 7	136	139	10	211	213	-25	31	15	8	86	88	25	29	20
6	699	705	19	41	36	-17	119	123	- 6	118	125	12	456	454	-24	39	25	9	129	125	26	63	66
7	195	199	Hk	0,Kk	6	-16	91	86	- 4	64	60	14	330	328	-23	58	53	10	88	84	Hk	3,Kk	2
9	203	214	1	42	39	-15	31	34	- 3	152	154	16	42	49	-22	41	43	11	119	121	-24	59	60
9	153	161	2	142	140	-14	97	98	- 2	133	137	18	44	49	-21	76	80	12	58	60	-23	104	103
10	54	51	4	48	50	-13	99	102	- 1	164	169	20	49	45	-19	201	204	13	56	47	-21	24	26
11	71	72	6	98	94	-12	163	172	0	53	45	22	356	355	-17	76	74	14	124	128	-20	128	131
12	126	127	7	32	18	-11	95	99	1	126	131	24	78	79	-16	69	66	15	30	37	-19	124	129
13	55	55	8	30	21	- 9	151	151	2	208	211	26	79	72	-14	239	243	16	51	45	-18	146	150
14	110	111	9	38	43	- 8	396	396	3	39	49	28	48	52	-13	63	69	17	72	67	-16	140	141
15	62	59	10	31	33	- 7	331	329	4	34	45	Hk	2,Kk	1	-12	201	201	Hk	2,Kk	6	-15	162	164
16	52	52	11	45	47	- 6	62	62	5	104	108	-28	38	37	-11	205	208	-11	27	24	-14	65	60
17	110	112	12	36	31	- 5	271	275	6	93	95	-26	91	87	-10	103	113	- 9	106	104	-13	168	173
18	37	36	Hk	1,Kk	0	- 4	16	18	7	125	124	-25	59	56	- 8	224	218	- 8	50	53	-11	197	203
19	76	76	-28	31	26	- 3	43	39	8	215	213	-24	173	170	- 6	117	110	- 7	92	93	-10	77	78
20	33	37	-26	97	86	- 2	104	100	9	69	70	-23	78	68	- 4	40	36	- 6	136	131	- 9	160	164
21	47	49	-24	171	164	- 1	104	103	11	46	45	-20	132	135	- 3	40	48	- 5	62	56	- 7	61	65
22	73	73	-20	61	59	0	158	167	12	77	84	-19	90	98	- 2	34	39	- 1	33	26	- 6	25	25
23	44	42	-18	224	222	1	158	151	13	93	86	-18	76	78	- 1	52	38	0	83	46	- 5	34	42
24	43	44	-16	426	427	2	166	159	14	64	72	-17	86	91	0	108	68	1	42	45	- 4	79	82
28	72	69	-12	244	244	3	146	146	15	142	137	-16	285	287	1	224	221	2	66	63	- 3	177	176
Hk	0,Kk	2	-10	80	85	4	349	338	17	55	48	-15	164	169	2	45	21	3	65	66	- 2	23	19
0	45	47	- 8	379	375	6	318	317	18	32	29	-14	47	48	3	133	129	5	68	72	- 1	191	188
1	358	340	- 6	757	742	7	155	166	19	58	51	-13	71	73	4	110	106	6	69	71	0	75	74
2	485	461	- 4	84	80	8	101	99	20	32	33	-12	182	188	5	146	144	8	48	36	1	57	55
3	178	171	- 2	585	572	9	130	131	21	38	25	- 9	485	484	6	73	79	9	57	60	2	69	75
4	128	127	0	178	178	10	28	26	23	33	33	- 8	172	162	7	83	85	10	33	34	3	74	71
5	118	123	2	564	563	11	123	124	Hk	1,Kk	5	- 7	62	60	8	39	44	Hk	3,Kk	0	4	61	63
6	172	171	4	18	12	12	41	44	-19	34	30	- 5	491	482	9	52	57	-26	121	122	5	247	250
7	371	359	6	967	1071	13	39	39	-18	102	87	- 4	384	366	10	168	169	-24	75	63	6	239	230
8	37	37	8	513	510	14	101	103	-17	138	138	- 3	219	207	11	48	45	-22	38	40	7	133	128
10	279	351	10	22	13	15	114	111	-16	57	59	- 2	60	50	12	29	26	-20	33	33	8	157	151
11	276	291	12	286	274	16	22	28	-15	25	19	- 1	261	262	13	34	26	-18	119	119	9	112	111
12	163	163	14	209	205	17	114	111	-13	127	127	0	35	36	14	131	135	-16	24	26	10	110	108
13	142	144	16	55	62	18	45	47	-11	106	109	1	104	101	15	25	19	-14	39	42	11	105	108
14	53	57	18	90	95	19	133	137	-10	138	144	2	103	103	16	73	73	-12	397	399	12	158	166
15	240	242	20	206	204	20	22	22	- 9	180	177	3	347	335	17	36	38	-10	248	244	13	98	101
16	99	103	22	37	41	21	118	111	- 8	32	35	4	21	23	18	72	69	- 8	78	73	14	248	254
17	37	40	28	106	110	22	136	140	- 7	98	97	5	73	72	19	74	71	- 6	278	280	15	219	226
19	213	223	Hk	1,Kk	1	23	28	21	- 6	170	176	6	65	61	20	23	19	- 4	543	537	16	27	23
20	34	31	-28	66	64	24	62	57	- 5	96	95	7	136	136	21	136	135	- 2	474	474	17	57	60
21	56	52	-27	34	36	25	118	108	- 4	178	183	8	221	221	23	161	148	0	17	15	19	76	82
22	56	56	-26	116	115	27	30	27	- 3	93	97	9	81	83	24	35	28	2	371	377	20	63	60
23	33	45	-25	45	45	Hk	1,Kk	3	- 2	63	63	10	450	454	Hk	2,Kk	4	4	556	554	23	45	41
24	74	77	-24	74	74	-26	31	21	- 1	153	155	11	22	12	-21	26	20	6	421	414	24	37	33
25	139	135	-23	67	70	-25	129	129	1	170	175	13	168	173	-20	183	176	8	117	117	25	69	64
27	25	16	-22	153	147	-24	97	95	2	99	94	14	160	158	-19	25	24	10	428	422	Hk	3,Kk	3
Hk	0,Kk	3	-21	68	71	-23	59	49	3	109	112	15	32	26	-17	90	93	12	249	249	-24	45	41
1	139	135	-20	111	112	-22	64	65	4	171	177	16	180	182	-16	99	100	14	87	92	-22	47	53
2	88	78	-19	118	118	-19	38	38	5	29	32	17	150	157	-15	31	32	16	92	102	-21	66	70
3	88	86	-18	155	163	-18	52	48	6	43	46	19	74	76	-14	39	50	18	226	233	-20	126	134
4	303	290	-17	112	112	-17	77	74	7	98	95	20	94	99	-11	111	121	20	132	134	-18	37	35
5	132	132	-16	58	52	-16	151	158	8	178	175	22	34	37	-10	80	95	22	82	90	-17	49	44
6	73	73	-15	147	149	-15	79	84	10	34	19	23	21	20	- 9	26	25	24	128	118	-16	76	73
8	76	130	-14	84	84	-14	186	189	11	104	102	25	53	53	- 8	213	218	26	43	51	-15	144	154
9	171	166	-12	141	133	-13	89	94	12	43	35	26	30	29	- 5	111	117	Hk	3,Kk	1	-13	185	190
10	104	101	-10	278	277	-12	21	19	13	110	105	Hk	2,Kk	2	- 4	28	24	-27	62	58	-12	63	59
11	72	77	- 9	95	89	-11	353	359	14	97	91	-26	109	109	- 2	75	77	-26	44	39	-11	78	79
15	36	31	- 8	64	66	- 8	145	164	16	23	16	-25	25	16	- 1	63	65	-25	73	71	- 8	155	162
16	25	3	- 7	281	275	- 7	147	139	17	62	59	-24	119	119	0	64	63	-24	116	118	- 6	89	90
17	145	146	- 6	63	64	- 6	151	105	18	62	51	-23	65	73	3	190	191	-21	134	134	- 5	64	66
18	38	49	- 5	158	157	- 5	260	256	Hk	1,Kk	6	-21	209	217	4	164	164	-20	58	63	- 4	32	21
19	27	32	- 4	177	177	- 4	67	42	-12	78	75	-20	136	133	5	95	90	-19	167	170	- 3	44	38
20	53	52	- 3	186	179	- 3	286	283	-11	63	55	-19	26	29	6	93	97	-18	187	195	- 2	72	68
21	31	29	- 2	754	743	- 2	69	78	-10	51	41	-18	219	228	7	95	99	-17	150	151	- 1	89	84
23	27	37	- 1	699	706	- 1	23	12	- 9	34	30	-17	148	154	8	47	53	-14	73	73	0	120	120
Hk	0,Kk	4	0	463	467	0	126	122	- 8	103	108	-15	35	34	9	74	74	-13	107	112	1	125	127
0	86	71	1	363	311	1	113	103	- 7	27	29	-14	169	162	10	54	50	-12	106	111	2	34	40
1	227	228	2	489	497	2	427	430	- 5	81	87	-12	221	226	11	57	56	-11	40	36	3	22	15
2	131	128	3	389	377	3	42	40	- 4	34	30	-10	127	128	12	85	93	-10	113	113	4	62	75
3	90	60	4	583	578	4	85	51	- 3	78	75	- 9	145	150	13	210	213	- 9	63	68	5	82	88
4	219	217	5	291	296	5	190	175	0	80	82	- 8	24	23	15	44	41	- 7	137	139	6	146	150
5	125	124	6	92	117	6	152	146	1	35	30	- 7	361	364	16	29	33	- 6	392	389	8	75	69
7	52	53	7	147	150	7	125	120	2	78	73	- 6	248	248	19	25	17	- 5	57	55	9	109	105
8	72	62	8	371	376	8	163	161	3	35	30	- 5	16	4	20	85	83	- 4	148	143	10	53	57
9	295	300	9	180	184	9	23	19	4	76	68	- 4	163	166	21	122	119	- 3	172	184	11	92	92
10	24	9	10	39	40	10	140	134	5	31	26	- 3	257	251	22	53	48	- 2	157	156	13	130	132
11	41	38	11	191	187	11	202	195	6	95	98	- 2	112	112	Hk	2,Kk	5	- 1	47	55	14	77	79
12	44	43	12	163	166	12	90	91	7	52	51	- 1	203	197	-18	109	107	0	105	107	17	98	104
13	57	59	14	53	57	13	110	110	10	25	26	0	23	34	-17	65	65	1	45	46	18	79	76
14	130	134	15	43	45	14	47	56	Hk	2,Kk	0	1	115	112	-15	78	82	3	108	104	19	25	24
15	51	47	17	144	142	15	225	216	-28	52	52	2	17	14	-14	45	44	4	241	244	20	60	45

Table 2. Continued.

21	68	44	= 8	29	33	3	24	27	= 4	84	76	=14	29	44	14	52	54	= 2	135	139	= 7	97	103
22	67	71	= 6	303	302	4	102	101	= 3	56	66	=13	49	44	15	64	67	= 1	47	47	= 6	84	85
Hs	3,Ks	4	= 4	168	165	5	98	103	= 2	146	147	=11	157	157	Hs	5,Ks	5	0	92	98	= 5	107	108
=21	40	33	= 2	55	57	6	52	52	= 1	81	82	=10	68	54	=10	30	21	1	116	121	= 4	77	79
=20	107	110	0	344	339	8	235	235	0	114	119	= 9	178	183	= 8	67	67	2	68	69	= 3	73	80
=19	46	43	2	283	289	10	78	77	1	39	37	= 8	205	210	= 5	26	24	3	196	196	= 1	30	19
=17	30	45	4	382	385	11	37	41	2	77	80	= 7	106	98	= 2	32	33	4	31	31	1	94	93
=15	89	94	6	189	183	12	29	31	4	151	150	= 6	82	38	0	108	108	5	48	50	2	93	95
=14	236	239	8	38	32	13	132	136	5	24	28	= 5	208	205	1	56	51	6	96	97	3	116	122
=13	109	111	10	216	220	14	106	103	6	51	51	= 4	111	101	2	88	87	7	70	72	4	41	39
=12	132	129	12	143	141	16	168	170	7	98	104	= 3	140	148	3	26	14	8	55	48	5	110	111
=11	44	43	14	49	54	17	25	19	8	46	45	= 2	87	86	7	30	27	10	69	65	8	27	28
= 9	33	34	16	176	174	20	125	127	9	114	116	0	40	44	8	26	27	11	70	67	10	30	42
= 8	59	52	18	84	85	21	88	92	10	104	102	1	77	76	Hs	6,Ks	0	12	75	68	12	91	87
= 7	138	140	20	70	64	24	38	43	13	28	26	2	108	104	=20	81	78	13	40	44	15	43	38
= 5	106	112	22	49	44	Hs	4,Ks	3	Hs	5,Ks	0	3	42	45	=18	45	46	14	60	62	16	33	31
= 4	102	104	24	134	126	=21	65	68	=22	106	90	4	254	262	=14	39	48	17	81	82	Hs	7,Ks	2
= 3	149	153	Hs	4,Ks	1	=20	73	75	=18	89	95	5	37	41	=12	121	125	Hs	6,Ks	3	=14	44	16
= 2	101	101	=25	116	109	=16	90	93	=16	53	51	6	49	51	=10	102	106	=17	84	68	=13	108	90
= 1	109	111	=24	29	37	=17	28	27	=12	139	125	8	23	17	= 8	28	29	=16	35	33	=12	96	97
0	66	61	=23	76	77	=15	67	76	=10	35	35	9	124	127	= 6	57	61	=15	37	38	=11	34	36
1	70	74	=22	26	24	=13	57	58	= 8	250	262	10	102	102	= 4	281	300	=14	121	112	=10	37	17
2	88	94	=21	68	69	=12	159	167	= 6	356	340	11	46	43	= 2	265	274	=11	49	43	= 9	47	42
3	132	130	=20	46	38	=11	51	63	= 4	74	69	12	60	71	4	93	88	=10	78	70	= 8	67	69
4	59	55	=19	27	23	=10	127	128	= 2	64	68	13	129	134	6	55	53	= 9	80	82	= 6	31	45
5	127	136	=17	122	124	= 8	166	133	0	83	81	14	56	60	8	105	98	= 8	22	13	= 3	34	31
6	80	83	=16	117	123	= 7	227	236	2	106	110	15	45	43	10	83	89	= 7	86	86	= 1	45	44
7	72	70	=15	46	44	= 6	58	44	4	105	104	16	36	41	12	44	41	= 6	82	77	1	142	134
8	108	106	=14	61	65	= 5	75	80	6	69	67	17	79	82	14	90	82	= 5	49	45	2	36	39
9	52	48	=12	201	190	= 4	56	44	8	170	166	18	40	35	16	123	118	= 4	116	116	3	28	28
10	68	74	=11	200	206	= 3	48	44	10	242	243	19	93	97	18	91	90	= 3	104	106	5	57	53
11	79	81	=10	131	133	= 2	134	136	12	191	191	20	34	21	20	56	52	= 2	50	45	7	50	51
12	205	208	= 9	108	112	= 1	46	51	14	40	48	Hs	5,Ks	3	Hs	6,Ks	1	1	53	49	8	48	47
15	49	44	= 8	71	76	0	112	114	16	62	65	=20	57	45	=21	67	55	2	121	115	9	63	60
16	68	61	= 7	233	234	1	24	19	22	62	63	=18	102	96	=20	67	66	3	114	109	10	52	45
17	24	21	= 6	55	55	2	34	29	Hs	5,Ks	1	=17	64	63	=19	92	91	4	69	65	14	73	57
18	58	63	= 5	150	146	4	61	59	=22	27	19	=12	65	68	=15	52	49	5	78	76	Hs	7,Ks	3
19	82	87	= 4	107	100	5	164	163	=21	33	30	=11	77	85	=14	79	66	6	35	27	= 8	49	47
Hs	3,Ks	5	= 3	86	84	6	43	48	=20	56	54	=10	128	135	=13	82	82	7	61	57	= 6	93	84
=15	33	34	= 2	173	174	7	162	166	=19	64	67	= 9	135	138	=11	63	57	10	65	81	= 4	68	60
=13	62	61	= 1	86	83	8	230	229	=17	61	59	= 8	29	32	=10	143	156	12	89	90	= 3	24	21
=12	31	28	0	130	127	9	65	71	=16	30	41	= 5	25	10	= 9	103	107	13	55	56	= 2	96	102
= 8	32	33	1	39	38	10	205	213	=13	150	154	= 4	150	150	= 8	160	160	14	43	42	= 1	85	78
= 7	30	38	2	243	254	11	37	40	=12	45	42	= 3	138	141	= 7	174	173	Hs	6,Ks	4	0	82	76
= 6	58	66	3	209	296	12	90	91	=11	43	41	= 1	195	203	= 6	28	25	=12	44	48	1	44	43
= 5	110	111	4	29	33	13	79	71	=10	105	112	1	39	49	= 5	33	17	=11	104	91	3	63	62
= 4	21	15	5	215	221	14	55	59	= 9	146	147	2	114	114	= 4	95	92	=10	72	63	4	113	111
= 3	33	29	6	236	236	15	67	67	= 8	27	24	5	100	97	= 3	219	226	= 9	38	40	5	70	66
= 2	91	94	7	163	163	16	24	24	= 7	77	83	6	115	125	= 1	145	144	= 8	112	101	7	72	68
= 1	25	28	8	20	21	19	106	102	= 6	28	19	7	162	162	0	80	87	= 7	70	64	9	75	69
0	44	46	10	94	95	Hs	4,Ks	4	= 5	141	147	10	75	77	1	124	132	= 5	109	106	10	79	76
1	51	56	11	42	37	=18	37	33	= 4	43	21	12	29	33	2	96	88	= 4	103	95	Hs	8,Ks	0
2	44	41	12	172	172	=17	82	83	= 3	164	168	13	44	38	4	123	125	= 1	96	97	=12	126	127
3	140	138	13	207	214	=16	33	36	= 2	278	289	14	86	89	5	134	135	0	56	57	= 8	74	80
4	81	84	14	260	265	=15	42	39	= 1	35	36	15	70	67	6	86	86	2	99	86	= 4	178	178
5	121	121	15	109	109	=14	31	32	0	79	79	16	24	15	7	27	19	3	61	60	= 2	54	53
7	80	80	16	39	42	=13	61	69	1	27	34	17	24	19	8	55	55	4	58	55	0	138	138
9	46	39	17	64	66	=12	23	19	2	65	67	Hs	5,Ks	4	10	61	62	5	28	38	2	123	116
10	36	42	18	102	101	=10	32	25	3	31	29	=16	56	52	11	94	98	6	37	40	10	76	67
11	164	159	19	25	35	= 9	75	73	4	106	105	=14	32	36	12	174	175	7	85	87	Hs	8,Ks	1
12	82	87	22	146	153	= 7	40	37	5	110	106	=13	22	12	13	27	28	8	55	57	= 6	52	54
13	95	99	23	34	24	= 6	105	106	6	112	118	=12	37	40	14	48	40	9	38	39	= 2	29	22
14	30	26	25	26	26	= 5	101	102	7	107	114	=11	53	48	15	45	51	Hs	7,Ks	0	= 1	35	38
15	94	89	Hs	4,Ks	2	= 4	84	94	8	97	94	=10	120	120	16	79	72	=16	39	47	0	60	60
Hs	3,Ks	6	=23	26	16	= 2	30	41	9	83	90	= 9	47	49	17	50	53	=14	104	93	1	42	38
= 7	37	31	=22	30	32	0	42	46	11	21	27	= 8	73	77	18	51	44	=12	47	54	2	65	51
= 6	39	29	=21	59	52	1	28	12	12	50	49	= 6	83	85	19	42	42	=10	28	33	3	66	61
= 5	63	60	=19	68	55	2	135	137	13	44	47	= 4	97	95	20	58	56	= 4	142	142	5	68	58
= 4	69	55	=17	124	123	3	71	77	14	39	38	= 3	142	143	Hs	6,Ks	2	= 2	28	23	6	37	41
= 3	23	26	=15	36	34	4	36	44	15	85	87	= 1	85	84	=17	72	79	0	41	38	7	27	20
= 1	130	132	=13	93	92	6	96	93	16	82	88	0	94	86	=16	44	42	4	47	52	8	46	47
0	99	94	=11	188	192	7	46	41	17	58	61	1	114	105	=14	142	142	6	31	23	Hs	8,Ks	2
1	114	104	=10	76	82	10	46	44	18	74	70	2	149	151	=13	32	14	8	39	43	= 8	28	6
2	67	66	= 9	120	124	11	56	56	19	26	6	3	59	59	=12	34	31	10	92	89	= 5	66	76
4	56	55	= 8	26	31	12	67	70	20	69	71	4	75	75	=11	34	33	12	56	55	= 4	36	34
6	66	58	= 6	24	27	14	29	36	22	53	47	5	42	43	=10	28	8	14	110	113	= 2	37	28
Hs	4,Ks	0	= 5	37	40	15	68	59	Hs	9,Ks	2	6	82	88	= 9	44	48	16	39	31	= 1	64	60
=26	144	134	= 4	44	33	16	31	27	=22	31	33	7	54	58	= 8	34	21	Hs	7,Ks	1	0	34	24
=24	63	58	= 3	36	30	17	34	33	=21	33	31	8	223	221	= 7	92	86	=16	71	35	2	36	30
=22	88	86	= 2	183	185	18	134	127	=19	62	65	9	85	85	= 6	86	82	=15	117	116	3	113	108
=20	44	52	= 1	91	90	Hs	4,Ks	5	=18	57	62	10	89	89	= 5	59	48	=14	51	53	4	30	14
=18	68	62	0	86	90	=13	56	57	=17	82	81	12	26	10	= 4	29	13	=12	45	35	5	25	23
=16	74	81	1	20	19	=11	84	86	=16	111	115	13	26	21	= 3	45	50	=11	90	93	6	75	71

observed-unobserved cutoff at 2.5 $\sigma(I)$, 1416 reflections were recorded as observed. The radiation was Mo$K\alpha$ and $2\theta_{max} = 50°$. No corrections for absorption or secondary extinction effects have been carried out.

The structure was solved by direct methods [7]* and refined by full-matrix least squares technique. Anisotropic temperature factors were introduced for oxygen and carbon atoms. The weights in least squares were obtained from the standard deviations in intensities, $\sigma(I)$, taken as

$$\sigma(I) = [C_T + (0.02C_N)^2]^{\frac{1}{2}}$$

where C_T is the total number of counts, and C_N the net count (peak minus background). The atomic form factors were those of Hanson *et al.*[8] except for hydrogen.[9] The R-value arrived at was 4.8 % (weighted value $R_w = 5.7$ %) for 1416 observed reflections.

Final fractional coordinates and thermal

* All programs used are included in this reference.

Table 3. Interatomic distances, bond angles and dihedral angles with estimated standard deviations.

DISTANCE	(Å)	DISTANCE	(Å)	DISTANCE	(Å)
O - C1	1,213(3)	C1 - C2	1,515(3)	C2 - C3	1,532(3)
C3 - C4	1,528(3)	C4 - C5	1,536(3)	C5 - C6	1,548(3)
C6 - C7	1,537(3)	C7 - C8	1,523(3)	C8 - C9	1,527(3)
C9 - C10	1,522(3)	C10 - C11	1,536(3)	C11 - C1	1,516(3)

ANGLE	(°)	ANGLE	(°)
O - C1 - C2	120,5(2)	O - C1 - C11	120,1(2)
C11 - C1 - C2	119,3(2)	C1 - C2 - C3	114,3(2)
C2 - C3 - C4	113,8(2)	C3 - C4 - C5	115,4(2)
C4 - C5 - C6	113,8(2)	C5 - C6 - C7	114,2(2)
C6 - C7 - C8	114,0(2)	C7 - C8 - C9	115,6(2)
C8 - C9 - C10	116,0(2)	C9 - C10 - C11	114,6(2)
C10 - C11 - C1	113,9(2)		

DIHEDRAL ANGLE	(°)	DIHEDRAL ANGLE	(°)
C1 - C2 - C3 - C4	-59,8(3)	C2 - C3 - C4 - C5	-61,3(3)
C3 - C4 - C5 - C6	139,8(2)	C4 - C5 - C6 - C7	-64,8(3)
C5 - C6 - C7 - C8	-63,6(3)	C6 - C7 - C8 - C9	173,7(2)
C7 - C8 - C9 - C10	-64,6(3)	C8 - C9 - C10 - C11	-55,7(3)
C9 - C10 - C11 - C1	95,1(3)	C10 - C11 - C1 - C2	-127,2(2)
C11 - C1 - C2 - C3	159,7(2)		

parameters with estimated standard deviations are given in Table 1. The expression for anisotropic vibration is:

$$\exp[-(B11h^2 + B22k^2 + B33l^2 + B12hk + B13hl + B23kl)]$$

A comparison between observed and calculated structure factors is presented in Table 2.

The principal axes of the thermal vibration ellipsoids for oxygen and carbon atoms were calculated from the temperature parameters of Table 1. Maximum root mean squares amplitudes range from 0.17 Å to 0.20 Å for carbon atoms, while that of oxygen is 0.24 Å. Due to the size of the molecule, no rigid-body analysis of translational, librational, and screw motion has been carried out.

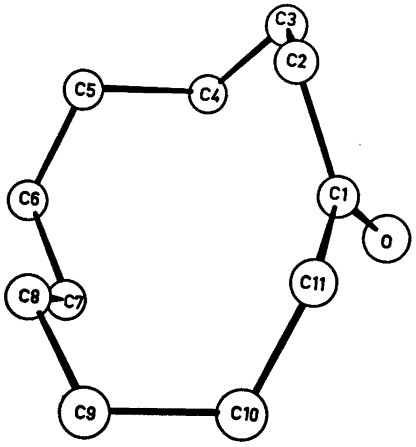

Fig. 1. Schematical drawing of the molecule.

Interatomic distances, bond angles, and dihedral angles are given in Table 3. The standard deviations, in parentheses, are estimated from the correlation matrix of the last least squares refinement cycle. Fig. 1 is a schematical drawing of the molecule.

Temperature dependency of the NMR-spectra of cycloundecanone in the range $-80°$ to $-170°$ indicates a single asymmetric conformation.[10] Strain minimization calculations for cycloundecane [4] give four conformations with about equally low enthalpies, one of which corresponds roughly to the "triangular" ring skeleton of cycloundecanone.

Except for *gauche* bonds, the agreement of calculated dihedral angles of cycloundecane [4] and those of Table 3 is rather poor. The asymmetric position of the carbonyl group confirms the NMR-indication mentioned above. The C=O

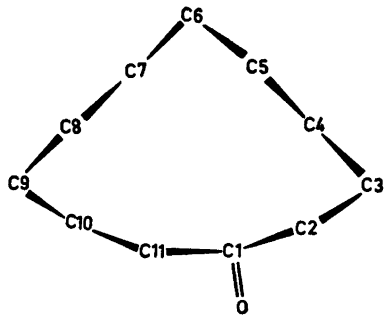

bond direction is approximately normal to the plane defined by C1,. . .,C11. H41 – H71 [2.10(4) Å] is the only H – H distance being significantly shorter than the van der Waals contact of 2.4 Å.

As may be seen from Table 3, bond distances and angles are normal. The mean value of C – C bonds (excluding C1 – C2 and C1 – C11 of 1.515 Å and 1.516 Å, respectively) is 1.532 Å. A corresponding average for C – C – C bond angles is 114.6°. C – H bond lengths range from 0.93 Å to 1.03 Å with estimated standard deviations of about 0.04 Å. C – C – H and C – H – C angles are found between 104° and 114° (e.s.d. ~2°).

The (C11 – C1 – C2)-group is planar (to within 0.008 Å) and the C – O bond distance of 1.213(3) Å agrees within error limits with corresponding distances in cyclohexane-1,4-dione [11] [1.220(6) Å; 1.223(8) Å].

No short *inter* molecular contacts are observed.

Acknowledgement. The author would like to thank A. Aasen for technical assistance during data collection, and Cand. real. T. Ledaal for supplying the compound.

REFERENCES

1. Dunitz, J. D. and Ibers, J. A. *Perspect. Struc. Chem. 2* (1968) 43.
2. Hendrickson, J. B. *J. Amer. Chem. Soc. 83* (1961) 4537; *86* (1964) 4854; *89* (1967) 7036.
3. Bixon, M. and Lifson, S. *Tetrahedron 23* (1967) 769.
4. Dale, J. *Acta Chem. Scand. 27* (1973) 1115.
5. Wiberg, K. B. J. *J. Amer. Chem. Soc. 97* (1965) 1070.
6. Garbisch, E. W. and Wohllebe, J. *J. Org. Chem. 33* (1968) 2157.
7. Groth, P. *Acta Chem. Scand. 27* (1973) 3131.
8. Hanson, H. P., Herman, F., Lea, J. D. and Skillman, S. *Acta Crystallogr. 17* (1964) 1040.
9. Stewart, R. F., Davidson, E. R. and Simpson, W. T. *J. Chem. Phys. 42* (1965) 3175.
10. Anet, F. A. L., Cheng, A. K. and Krane, J. *J. Amer. Chem. Soc. In press.*
11. Groth, P. and Hassel, O. *Acta Chem. Scand. 18* (1964) 923.

Received November 6, 1973.

Acta Chemica Scandinavica A 28 (1974) 299—314

Conformational Analysis. I. The Molecular Structure, Torsional Oscillations, and Conformational Equilibria of Gaseous 1,2,3-Tribromopropane as Determined by Electron Diffraction and Compared with Semiempirical Calculations

REIDAR STØLEVIK

Department of Chemistry, University of Oslo, Blindern, Oslo 3, Norway

Gaseous 1,2,3-tribromopropane has been studied by electron diffraction at a (nozzle) temperature of 88°C. Three different pairs of enantiomeric conformations were detected: 82 %(2) of GG(ag)+GG(ga), 8 %(4) of GA(gg)+AG(gg), and 10 %(4) of AG(ga)+GA(ag); see Fig. 1. The following values for distances (r_a) and angles ($\angle_\alpha$) are appropriate for the structure of the most abundant conformer:
C−H = 1.132(18) Å, C−C = 1.534(12) Å, C−Br = 1.948(6) Å, ∠CCC = 117.4°(1.4), ∠C_2CX = 110.4°(0.8), ∠CC_2X = 110.5°(0.6), ∠C_2CH = 110.8°(2.0), ∠CC_2H = 109.1°(2.0).

Results are presented with error limits (2σ). Non-bonded distances were computed as dependent quantities, restricted under the constraints of geometrically consistent r_α parameters.

The torsional angles of the conformers have been determined and their values are significantly different from exact staggered values, in aggreement with semiempirical calculations.

Torsional force constants and frequencies, 45 cm^{-1}(10) and 86 cm^{-1}(10), corresponding to torsional modes in the most abundant conformer, were determined by combining information from electron diffraction and vibrational spectroscopy. The observed spectroscopic frequencies (97 cm^{-1} and 107 cm^{-1}) do not agree with the "electron-diffraction" values. Torsional force constants compatible with the spectroscopic frequencies lead to mean amplitudes of vibration significantly smaller than those observed.

Semiempirical calculations of conformational energies, geometries, barriers, and torsional force constants have been carried out, and some shortcomings of the present semiempirical force field are pointed out.

I. INTRODUCTION

The present work is one of several in a series of electron-diffraction studies. The investigations are concerned with substituted propanes and related molecules in an attempt to understand and quantitatively describe the conformational equilibria in these molecules in the gas phase.

1,2,3-Trisubstituted propanes represent an interesting and complex problem of structural chemistry. Simultaneous rotation about the two C−C bonds can occur, therefore the number of staggered conformers is nine. The numbering and system of naming for conformers of 1,2,3-tribromopropane (TBP) adopted here are presented in Fig. 1. Unfortunately there is no general agreement about the nomenclature in this type of compounds.

The system of naming uses four letters: Capital letters, A or G, indicate whether the X atom of a $-CH_2X$ group is *anti* or *gauche* to the $C_1C_2C_3$ framework. Small letters, a or g, indicate whether the X atom of a $-CH_2X$ group is *anti* or *gauche* to the central halogen atom (X_2). The four letters are then combined in the following way: GA(ag), for example, means that X_1 is *gauche*, while X_3 is *anti* to the $C_1C_2C_3$ framework, further X_1 is *anti* and X_3 is *gauche* to the central halogen atom.

GG(ag) and GG(ga) are non-superimposable mirror images of each other (enantiomers), and the present system of naming can distinguish

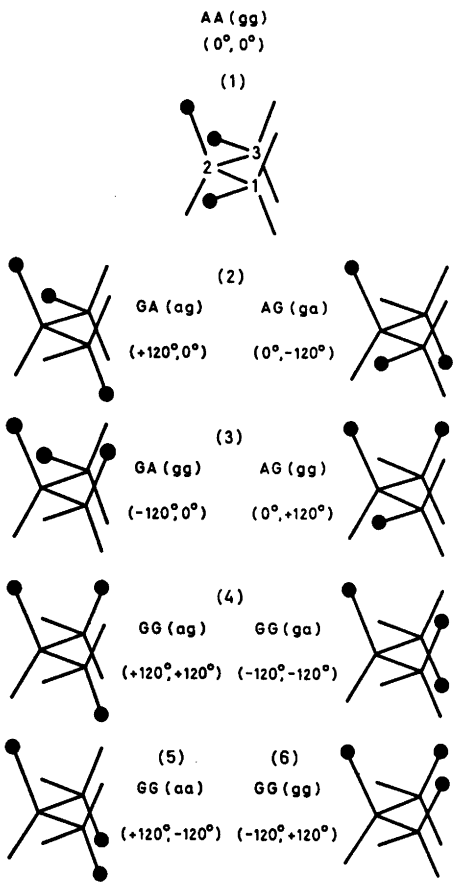

Fig. 1. The numbering and names of staggered conformers in 1,2,3-tribromopropane.

between them. If the numbering $C_1-C_2-C_3$ is changed to $C_3-C_2-C_1$, the enantiomers will have their names exchanged.

Enantiomers cannot be distinguished by electron diffraction, therefore whenever possible, such pairs will be mentioned by a number only, as indicated in Fig. 1. For example, the conformers GG(ag) and GG(ga) may be referred to as conformer (4) (Fig. 2).

II. CALCULATION OF CONFORMATIONAL ENERGIES, GEOMETRIES, BARRIERS, AND TORSIONAL FORCE CONSTANTS

The method of classical mechanics was used. The method is basically that introduced by Westheimer, as subsequently modified by

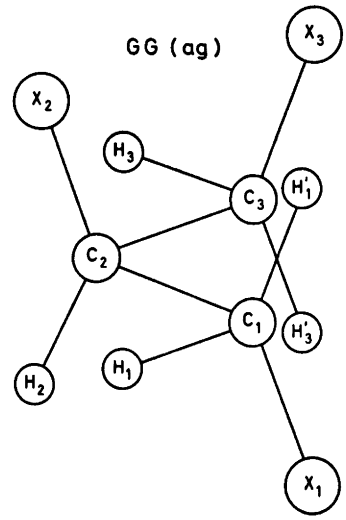

Fig. 2. Numbering of atoms in the conformer GG(ag).

Hendrickson and Wiberg, and widely used by others. Energy parameters were taken from the paper [1] by Abraham and Parry, and references to the original works are found therein.

The energy of a given conformer was calculated from eqn. 1 adjusting the geometry for minimum energy. The computer program that performs all the calculations was written by S. Rustad in FORTRAN.[2]

The energy minimum was in most cases found by a combination of different methods. The method of *steepest descent* was first used, and then close to the minimum *Newton-Raphsons* method was applied. In some cases, only one of the methods was used.

Details about the program will be presented in a forthcoming paper, based upon the thesis of S. Rustad.[2]

$$E = E_r + E_\theta + E_\phi + E_R \qquad (1)$$

$E_r = \frac{1}{2}\sum F_r(r-r_0)^2$; strain in bond distances.
r represents a bond distance and r_0 the "normal" value of r.[3]
F_r is the force constant of that bond.
$E_\theta = \frac{1}{2}\sum F_\theta(\theta-\theta_0)^2$; strain in bond angles.
θ represents a bond angle and θ_0 the "normal" value of θ.
F_θ is the force constant of that angle.
$E_\phi = \frac{1}{2}V_0\sum\{1+\cos[3(\phi-\phi_0)]\}$, torsional strain.
ϕ represents a torsional angle and V_0 is the

Table 1. Calculated conformational energy and geometry of staggered conformers in 1,2,3-tribromopropane.

Parameter (normal value)	GG(ag)	AG(gg)	AG(ga)	AA(gg)	GG(aa)	GG(gg)
C–H(1.094Å)	1.094	1.095	1.094	1.095	1.094	1.095
C–C(1.513Å)	1.528	1.526	1.525	1.525	1.529	1.533
C–X(1.935Å)	1.945	1.945	1.943	1.946	1.941	1.947
∠CCC(110.0°)	113.6	111.9	111.4	109.7	114.0	115.1
$\angle C_3C_1X$(109.47°)	111.9	111.6	111.0	111.1	112.7	115.0
$\angle C_1C_2X$(109.47°)	110.5	110.8	109.3	109.7	108.9	112.1
$\angle C_3C_1H$(109.47°)	109.8	109.8	110.0	109.9	109.7	109.0
$\angle C_1C_2H$(109.47°)	107.8	109.2	109.3	108.4	105.5	106.6
$\angle\phi_{1-2}(\phi_0)^a$	+117.3	+18.1	+13.0	+11.5	+101.0	−107.1
$\angle\phi_{2-3}(\phi_0)^a$	+122.8	+125.2	−111.2	−11.5	−101.0	+107.1
Energy (kcal/mol)						
E(bonded)	1.16	1.32	0.80	0.85	2.44	4.21
E(van der Waals)	1.09	0.96	0.75	1.17	1.10	2.20
E(polar, X···H)	−6.59	−6.04	−6.29	−5.79	−6.31	−5.68
E(polar, X···X)	4.84	4.93	4.61	4.84	4.77	5.67
E(total)	0.50	1.17	−0.12	1.07	2.01	6.39
E(total) − E[AG(ga)]	0.62	1.29	0	1.19	2.13	6.51

[a] $\phi_0 = 60°$, see E_ϕ in eqn. (1), sect. II.

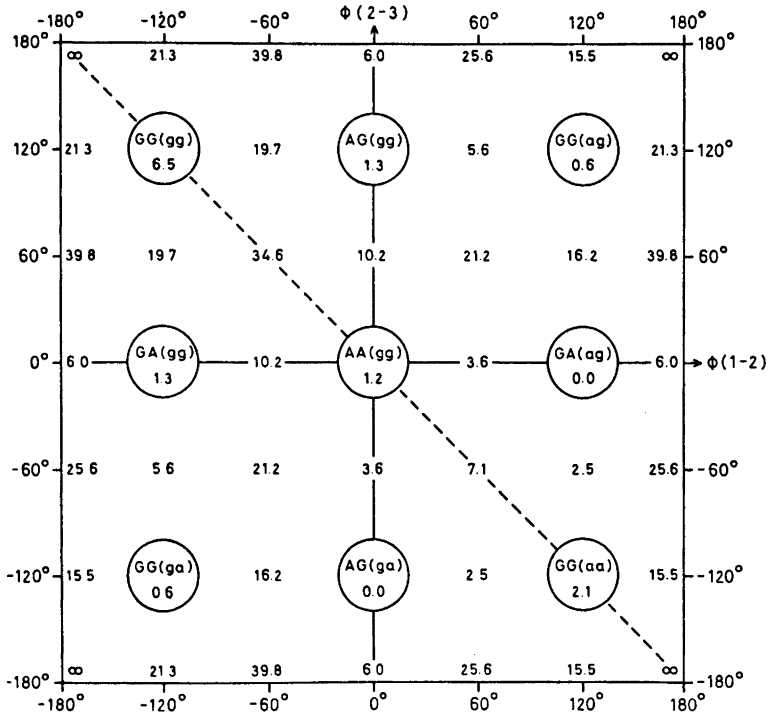

Fig. 3. Potential energy map for 1,2,3-tribromopropane. The numbers within the square are energy values corresponding to a conformation having most structural parameters minimized; see also text. The lowest energy value, for AG(ga) or GA(ag), is arbitrarily set equal to zero. ϕ_{1-2} and ϕ_{2-3} are torsion angles; see Fig. 1.

intrinsic torsional barrier,[1] $\phi_0 = 60°$.
$E_R = \sum(a \exp(-bR) - c/R^6 + d/R)$
R represents a distance between two atoms *not bonded to the same carbon atom:* The first two terms in the summation of E_R represents repulsive and attractive van der Waals interactions, respectively, and the third term gives the electrostatic interaction of the polar substituents.

The choice of force constants and "normal" values [3] is subject to a certain arbitrariness. The force constants actually used are those given in Table 2, and values for r_0 and θ_0 are shown in Table 1. The parameter $V_0 = 2.65$ kcal/mol and values for a, b, c, and d were taken from the work of Abraham and Parry.[1]

The zero-point vibrational energy is not included in the energy expression.

In minimizing the energy, the geometry was constrained in the same way as described in sect. V–A in order to keep the number of variables small.

The results of calculations for staggered conformations are given in Table 1, but the values demand a few comments. Firstly, the experimental finding (Table 9) that the conformer GG(ag) is more stable than AG(ga), does not follow from the energy values in Table 1. Secondly, the difference in energy between AG(gg) and AG(ga) is probably not as large as calculated (see sect. VII).

The force field allows the CCC angle to open up, but not as much as demanded by the experimental value of 117.4°.

A map of energies, including staggered and eclipsed conformations, is presented in Fig. 3. Whenever a ϕ-value is close to 0° or ±120°, that parameter has been refined. The energy values for some of the conformers are thus shown in positions which are not exactly corresponding to the ϕ angles obtained. Torsional barriers between conformers might be estimated from this map.

Each value on the potential energy surface corresponds to a conformation having all structural parameters minimized, except for one or two torsion angles being kept at constant values.

If torsional angles alone are used as variables, then the calculated quantities are different from those given here.

Valence torsional force constants were calculated according to their definitions:

$F_\phi(1-2) = \partial^2 E/\partial\phi^2_{1-2}$, $F_\phi(2-3) = \partial^2 E/\partial\phi^2_{2-3}$,
$F_\phi(1-2;\ 2-3) = \partial^2 E/\partial\phi_{1-2}\partial\phi_{2-3}$.

The derivatives were numerically computed at the minimum of potential energy, and results are given in mdyn Å $(\text{rad})^{-2}$:

Conformer:	GG(ag)	GA(gg)	AG(ga)	AA(gg)
$F_\phi(1-2)$:	0.165	0.204	0.140	0.154
$F_\phi(2-3)$:	0.233	0.144	0.183	0.154
$F_\phi(1-2;2-3)$:	−0.041	−0.016	−0.022	−0.011

The agreement with torsional force constants determined from the electron diffraction data is quite good for $F_\phi(1-2)$, and moderate for $F_\phi(2-3)$; the interaction constant being too small for experimental determination.

Interaction force constants between a torsional angle and other internal coordinates are not included in the valence force field applied in the present work. However, such interaction constants were also calculated with the energy program. All such quantities turned out to be very small.

Anharmonicity is expected in the torsional part of the force field, and will certainly lead to errors in the determination of torsional force constants, obtained from the electron diffraction data, since the vibrational quantities have been calculated using an harmonic force field. No attempt was made to establish anharmonic corrections from the experimental data. But it is possible to get some ideas about the degree of anharmonicity from the energy curves in Fig. 4.

Let us consider the energy minimum corresponding to the conformer GG(ag). The deviations from parabolic behaviour are negligible, near minimum, when ϕ_{2-3} is varied, while variation of ϕ_{1-2} leads to an asymmetric change in the energy. The barrier between GG(ag) and GA(ag) is seen to be much higher than the one between GG(ag) and AG(gg), and this leads to asymmetry in the ϕ_{1-2} direction. At higher temperatures the effects of anharmonicity on the observed intensities will be stronger. Anharmonic corrections for the torsional part of the force field must then be considered.

The energy curves in Fig. 4 have been computed by varying ϕ_{1-2} or ϕ_{2-3} while the

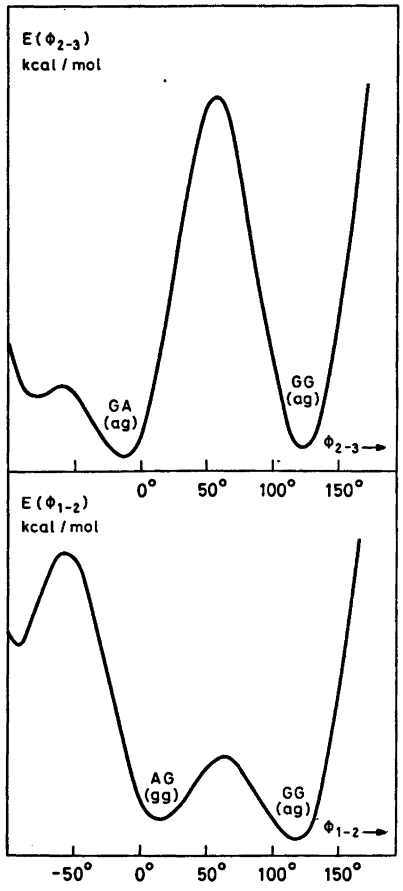

Fig. 4. Energy curves, $E(\phi_{1-2})$ and $E(\phi_{2-3})$, computed by varying the torsional angles ϕ_{2-3} ϕ_{1-2} separately; the remaining structural parameters were kept at constant values corresponding to GG(ag).

remaining structural parameters were kept at constant values corresponding to GG(ag). The minima, and barriers between them, are therefore better represented by the values in Fig. 3.

The destabilizing effect of parallel (1:3) Br···Br interactions in conformers like GG(aa) and GG(gg) is reproduced by the calculations. However, the minima of these conformers lie at (101°, −101°) and (−107°, 107°), considerably displaced from staggered dihedral angles. Moreover, the CCC angles have been opened up to 114° and 115°, also considerably lowering the conformational energies. Therefore, the conformer GG(aa) is not much higher in energy than the conformers found to be present in the vapour. Between the conformers GG(aa) and AG(ga), or GA(ag), is a very low barrier [0.4 kcal/mol higher in energy than the minimum of GG(aa)].

The amount of GG(aa) would probably be increased by increases in the temperature, but the very shallow and asymmetrical energy minimum of GG(aa) indicates, that this conformer will be very difficult to detect and determine by electron diffraction, even at a very high temperature.

All the other conformers correspond to well defined minima on the potential surface.

The intention of the author is to use the present force field, without essential changes in parameters, for a series of related compounds. After comparing calculated and experimental results for several molecules, changes in energy parameters are going to be considered.

Some obvious shortcomings of the present force field have already been mentioned. Nevertheless, the results from these calculations are very useful in many ways, despite of the discrepancies pointed out. In particular, the results were valuable in planning the structural analysis. Moreover, the time and efforts demanded are negligible, provided a suitable computer program is at hand. Finally, it must be admitted that some of the experimental findings probably would not have been looked for without the aid of such calculations.

III. CALCULATION OF VIBRATIONAL QUANTITIES

Valence force constants, except for the torsional part, were taken from the extensive work of Schachtschneider and Snyder on haloparaffins,[4] and partly from a second work, also by Snyder.[5] It was decided that the degree of transferability was high enough to use their force constants in calculating mean amplitudes and related quantities for TBP. The results of the present investigation strengthen this conclusion.

Certain compromises between force constant values had to be made, and the final values selected for TBP are given in Table 2.

The normal coodinate program described by Gwinn [6] was used in computing vibrational

Table 2. Valence force constants for 1,2,3-tribromopropane. The torsional force constants have been defined in the following way: Each fragment of type $A'-C_1-C_2-A''$ (A = H,C,X, see Fig. 2) has been assigned an equal torsional force constant. Each fragment of type $A'-C_2-C_3-A''$ has been assigned an equal force constant but different from those of fragments $A'-C_1-C_2-A''$. The total force constant for the torsional coordinate ϕ_{1-2} (i = 1,3) is thus the sum of *nine* equal contributions. The input to Gwinn's normal coordinate program demands a separate specification for each torsional fragment. Moreover, all interaction force constants have to be multiplied by two if Gwinn's program is used.

Type of force constant	Value in $C-CH_2X$	Value in $C-CHX-C$
Stretch (mdyn Å^{-1})		
C–C	(4.73)	(4.40)
C–H	4.85	4.59
C–X	2.63	2.31
Bend (mdyn Å (rad)$^{-2}$)		
CCC	(0.90)	(0.94)
CCH	0.67	0.66
HCH	0.50	–
CCX	0.91	1.05
HCX	0.69	0.74
Stretch/Stretch (mdyn Å)$^{-1}$)		
C–X/C–C (C common)	0.350	0.347
C–H/C–H (C common)	−0.007	–
C–C/C–C (C common)	–	0.64
Stretch/Bend (mdyn (rad)$^{-1}$)		
C–X/CCX (C–X common)	0.49	0.42
C–X/HCX (C–X common)	0.26	0.226
C–C/CCX (C–C common)	0.30	0.121
C–C/CCC (C–C common)	(0.35)	(0.225)
C–C/CCH (C–C common)	0.26	0.265
Bend/Bend (mdyn Å (rad)$^{-2}$)		
HCC/CCC (C–C common)	−0.124	−0.136
HCX/HCX (C–X common)	0.050	–
HCC/HCC (C–C common)	−0.026	–
HCC/HCC (C–H common)	–	0.012
HCC/HCX (C–H common)	0.074	0.088
HCC/HCX (C common)	0.029	–
HCC/CCX (C–C common)	–	−0.030
HCX/CCX (C–X common)	–	−0.031
CCX/CCX (C–X common)	–	−0.041
CCC/CCX (C–C common)	–	−0.041
Bend/Bend (C–C common and dihedral angle *anti* or *gauche*)	*anti*	*gauche*
HCC/CCX	0.022	−0.030
CCC/CCX	0.093	−0.024
HCC/CCC	0.072	−0.058
HCC/HCC	0.106	−0.024
CCX/CCX	−0.001	+0.011
Torsional force constants (mdyn Å (rad)$^{-2}$)		
$F_\phi(1-2)^a = 0.20 \pm 0.05$, $F_\phi(2-3)^a = 0.41 \pm 0.10$		

Table 3. Vibrational frequencies (cm^{-1}) in 1,2,3-tribromopropane.

Approximate mode	Spectroscopic values Ref. 7	Calculated values for conformers (4)	(3)	(2)	(1)
Torsion [a]	97	46	62	55	58
Torsion [a]	107	87	77	98	75
CCX bend	(?) [b]	160	87	117	84
CCX bend	186	167	167	181	198
CCX bend	195	199	292	216	213
CCX bend	308	325	342	342	368
CCC bend	458	471	453	371	413
C−X stretch	562	570	514	571	506
C−X stretch	622	619	590	658	593
C−X stretch	672	696	701	668	722
C−C stretch	954	837	880	849	856
CH_2 rock	849	893	930	940	969
CH_2 rock	867	999	983	999	1001
CH_2 twist	1110	1129	1106	1113	1118
C−C stretch	1071	1142	1145	1141	1126
CH_2 twist	1159	1201	1179	1175	1152
CH def.	1189	1206	1224	1232	1238
CH_2 wag.	1233	1255	1287	1270	1270
CH_2 wag.	1252	1291	1296	1317	1360
CH def.	1329	1362	1371	1377	1368
CH_2 scissor	1414	1421	1430	1430	1416
CH_2 scissor	1429	1425	1435	1434	1421
C−H stretch	2902	2903	2903	2904	2904
C−H stretch	2948	2945	2943	2943	2945
C−H stretch	2970	2946	2944	2944	2946
C−H stretch	3012	3018	3021	3021	3019
C−H stretch	3027	3021	3022	3022	3022

[a] An average torsional force constant $\overline{F}_\phi = 0.304$ mdyn Å $(rad)^{-2}$ $F_\phi(1-2) = F_\phi(2-3) = \overline{F}_\phi$, was used, and the remaining force field is found in Table 2. For definition of F_ϕ values see text to Table 2.
[b] See Ref. 7.

frequencies. Results for some staggered conformers are presented in Table 3, together with the spectroscopic frequencies observed by Thorbjørnsrud *et al.*[7]

Mean amplitudes of vibration were calculated as described in Ref. 8. In Table 4 are given the u and K values of the conformer GG(ag).

Since observed frequencies are available, it is possible to adjust the force constants of Table 2 to fit TBP even better. However, this was not done for several reasons. The aim was to calculate mean amplitudes of vibration to be used in the structure analysis. The force field required for this purpose may be rather approximate. The u and K values are quite insensitive to moderate errors in the force field, except for the torsional part of it, which has been adjusted (see sect. V−B).

Moreover, it is important to make use of *typical* force constants as much as possible to test the degree of transferability and usefulness in various situations. The works by Snyder [5] and Schachtschneider [4] are in this respect extremely valuable. Their information, combined with electron-diffraction data, made it possible to determine the torsional force constants for the most abundant conformer of TBP. Several vibrational quantities in a molecule like TBP varies with the torsional force constants. To illustrate this point some of the quantities have been calculated using three different values of the average ($F_\phi(1-2) = F_\phi(2-3) = \overline{F}_\phi$) torsional force constant, and the results are found in Table 5.

Table 4. Mean amplitudes (u) and K values for the conformer GG(ag) of 1,2,3-tribromopropane at 88°C. The conformation was staggered, ($\phi_{1-2} = \phi_{2-3} = 120°$) and the valence force field has been given in Table 2. The numbering of atoms is shown in Fig. 2.

Type of distance	Dist. (Å)	$F_\phi(1-2)=0.203$ u (Å)	$F_\phi(2-3)=0.406$ K (Å)	$F_\phi(1-2)=F_\phi(2-3)=0.304$ u (Å)	K (Å)
C_2-H_2	(1.13)	.0791	.0157	.0791	.0156
C_1-H_1'	(1.13)	.0780	.0252	.0780	.0222
C_1-H_1	(1.13)	.0780	.0249	.0780	.0218
C_3-H_3'	(1.13)	.0780	.0213	.0780	.0229
C_3-H_3	(1.13)	.0780	.0202	.0780	.0217
C_1-C_2	(1.53)	.0512	.0055	.0513	.0053
C_2-C_3	(1.53)	.0513	.0051	.0513	.0050
C_2-X_2	(1.95)	.0587	.0064	.0587	.0060
C_1-X_1	(1.95)	.0554	.0173	.0554	.0134
C_3-X_3	(1.95)	.0554	.0135	.0555	.0154
$C_2\cdots X$	(2.83)	.0795	.0094	.0794	.0080
$C_2\cdots H$	(2.23)	.1086	.0177	.1085	.0157
$C\cdots C$	(2.64)	.0712	.0057	.0712	.0056
$C\cdots X_2$	(2.88)	.0768	.0065	.0769	.0059
$C\cdots H_2$	(2.11)	.1097	.0112	.1099	.0111
$H\cdots X_1$	(2.53)	.1138	.0290	.1134	.0224
$H_1\cdots H_2'$	(1.79)	.1290	.0349	.1286	.0298
$H_2\cdots X_2$	(2.43)	.1163	.0113	.1163	.0109
$X_1\cdots X_2$(a)	(4.61)	.0819	.0034	.0810	.0035
$X_2\cdots X_3$(g)	(3.57)	.1678	.0057	.1771	.0051
$X_1\cdots H_2$(g)	(2.95)	.1803	.0120	.1727	.0110
$X_2\cdots H_1'$(g)	(3.18)	.1701	.0140	.1621	.0121
$X_2\cdots H_2$(g)	(2.98)	.1692	.0166	.1632	.0139
$X_3\cdots H_2$(a)	(3.84)	.1067	.0114	.1066	.0108
$X_2\cdots H_3'$(a)	(3.89)	.1061	.0114	.1063	.0115
$X_2\cdots H_3$(g)	(2.98)	.1615	.0099	.1647	.0107
$X_1\cdots C_3$(g)	(3.35)	.1648	.0063	.1542	.0057
$X_3\cdots C_1$(g)	(3.35)	.1486	.0074	.1542	.0071
$X_1\cdots X_3$	(4.23)	.2788	.0014	.2676	.0014
$X_1\cdots H_3'$	(2.94)	.2575	.0155	.2494	.0155
$X_1\cdots H_3$	(4.35)	.1783	.0081	.1756	.0082
$X_3\cdots H_1'$	(2.94)	.2461	.0186	.2479	.0164
$X_3\cdots H_1$	(4.35)	.1767	.0105	.1755	.0096

IV. EXPERIMENTAL AND DATA REDUCTION

TBP was obtained from Fluka, and the purity of the actual sample used was better than 98 %. Electron-diffraction photographs were made at a nozzle temperature of 88°C in the Oslo apparatus,[9] under conditions summarized below.

Nozzle-to-plate distance, (mm):	480.76	200.76
Electron wavelength (Å):	0.064616	0.064616
Number of plates:	5	5
Range of data, in s (Å^{-1}):	1.375 – 19.875	7.0 – 44.25
Data interval, Δs (Å^{-1}):	0.125	0.250
Uncertainty in s-scale:	0.14 %	0.14 %

The electron wavelength was determined by calibration against gold. The data were reduced in the usual way [10] to yield an intensity curve for each plate.

Average curves for each set of distances were formed. A composite curve was then made by connecting the two average curves after scaling. Unfortunately the quality of the 20 cm data were poor, while the 48 cm data were excellent. The 20 cm data were used, with low weight, in some least-squares refinements. However, in the final adjustments the 20 cm data were not included for $s > 19.875$ Å^{-1}, and all intensities were given equal weight.

The final experimental intensity curve is shown in Fig. 5.

Table 5. Vibrational quantities in 1,2,3-tribromopropane at 88°C. The valence force field has been given in Table 2, and the numbering of atoms is shown in Fig. 2.

Torsional force constants			
$F_\phi(1-2)=F_\phi(2-3)=\overline{F}_\phi$ in mdyn Å (rad)$^{-2}$	0.180	0.304	0.405
Torsional frequencies for	37	46	51
conformer (4), in cm^{-1}	77	87	91
Ratios between vibrational partition functions (Q). (1), (2), (3), and (4) refer to Fig. 1			
$Q_{(4)}(0.304)/Q_{(3)}(\overline{F}_\phi)$	0.41	1.02	1.86
$Q_{(4)}(0.304)/Q_{(2)}(\overline{F}_\phi)$	0.48	1.20	2.19
$Q_{(3)}(0.304)/Q_{(1)}(\overline{F}_\phi)$	0.32	0.80	1.45
u Values for the distance $X_1\cdots X_3$, in Å			
In conformer (4)	0.325	0.268	0.243
In conformer (3)	0.158	0.149	0.145
In conformer (2)	0.218	0.195	0.186
In conformer (1)	0.144	0.143	0.143
u Values for $X_2\cdots X_3$ in GG(ag)	0.202	0.177	0.167

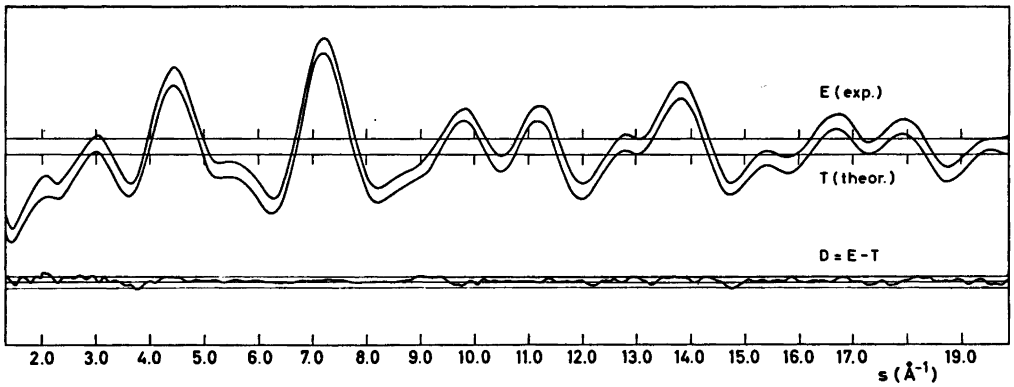

Fig. 5. Curve E shows the experimental intensity, and curve T the theoretical intensity corresponding to the final least-squares parameters. Curve D is the experimental minus the theoretical. The straight lines give the experimental uncertainty (± 3 × experimental standard deviation).

The intensities have been modified by $s/|f_{Br}|^2$. The scattering amplitudes were calculated by the partial wave method [11] using Hartree-Fock atomic potentials.[12]

Contributions to the theoretical intensities from H···H distances, the H atoms bonded to different carbon atoms, were not included.

V. STRUCTURE ANALYSIS AND REFINEMENTS

The calculated conformational energies for staggered conformers suggest that the amount of conformer (6) is negligible. Conformers (2) and (4) must be expected to be present in detectable amounts. The fact that conformer (4) is the most abundant one, and not conformer (2) as suggested by the calculated energies,

is obvious from the radial distribution (RD) curves in Fig. 6. From the RD curves it also follows that conformer (1) can hardly be present in detectable amounts. Conformer (3) is present, but in small amounts, as also suggested by the results of energy calculations. From the energy calculations, it was concluded that conformer (5) might be present. The contribution to the experimental RD curve would thus be very small.

The conclusion is that conformers (4), (3), and (2) have to be considered in calculating theoretical intensities. Since conformer (4) contributes more than 80 % to the intensities at 88°C, exact structural information about that conformer can be obtained from diffraction data. A limited amount of information can be obtained for the conformers (2) and (3) at 88°C, but the amount of information may be increased by increases in temperature.

A. Least-squares refinements. The least-squares program was written by H. M. Seip, and it is a modified version of the one explained in Ref. 10. Several conformers might be included in the refinements with the present version of the program.

The models for the conformers were constructed with the following geometrical assumptions: (1) the plane of the $H_2C_2X_2$ group is perpendicular to the plane of C atoms and bisect the CCC angle; (2) the two $C-CH_2X$ groups are equal; (3) $\angle C_2C_1H_1 = \angle C_2C_1H_1'$ and $\angle X_1C_1H_1 = \angle X_1C_1H_1'$, the projection of $\angle H_1C_1H_1$ on the plane perpendicular to the C_1-C_2 axis is 120°; (4) all C–H bond lengths are equal; (5) all C–X bond lengths are equal; (6) the conformers have identical structures, except for the C–C torsion angles.

The last assumption is probably the most questionable, and can only be tested if the experiment is carried out at a much higher temperature. The assumptions are partly justified by the results of Table 1, remembering that the conformers AA(gg), GG(aa), and GG(gg) are not present in detectable amounts.

Models were defined in terms of the following average parameters: C–H, C–C, C–X, CCC, C_2CX, CC_2X, C_2CH, and CC_2H. The torsion angles of the conformers were refined, but not all of them independently. Also adjusted were the composition parameters, the relative amounts of the conformers. Non-bonded distances were computed as dependent parameters, restricted under the constraints of geometrically consistent r_α parameters.[13,14]

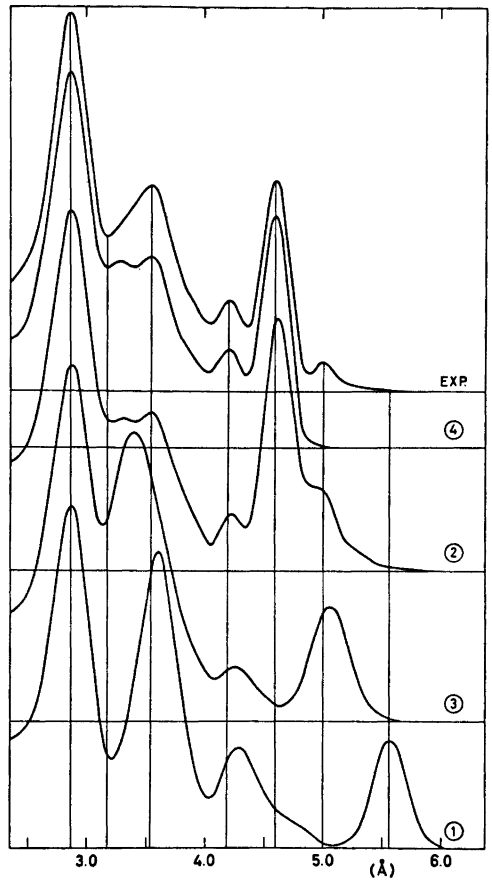

Fig. 6. Theoretical RD curves of four conformers and the final experimental one are shown. The theoretical curves have been labelled in the same way as the conformers in Fig. 1. The artificial damping constant was equal to 0.0020 Å^2.

Only a limited part of the total experience gained by the investigator himself can reasonably be presented here. In the first part of the structural analysis a large number of refinements were carried out, in which selected combinations of parameters were allowed to vary, while others were held constant at plausible values. It seems practically impossible to report on all these intermediate refinements. At some stages the background had to be corrected,

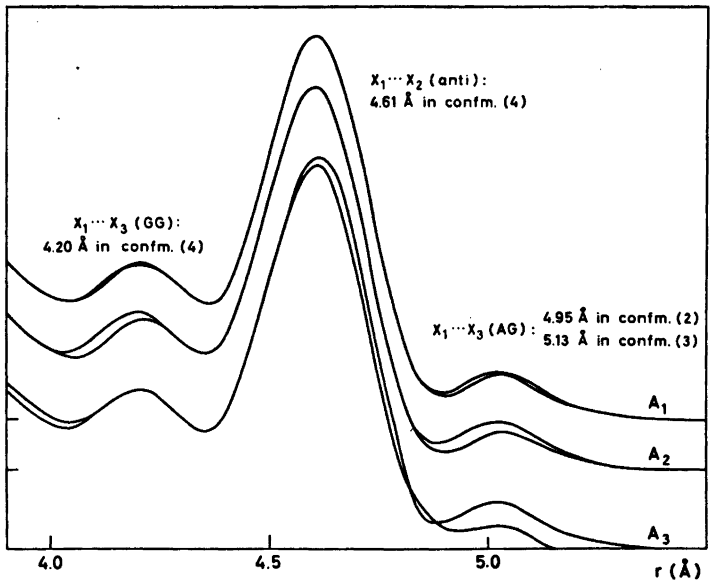

Fig. 7. Three theoretical radial distribution curves are shown together with the final experimental RD curve. The theoretical curves were calculated under conditions, as follows:

A_1: $\alpha_2 = 10$ %, $\alpha_3 = 8$ %, $\alpha_4 = 82$ %
A_2: $\alpha_2 = 0$ %, $\alpha_3 = 12$ %, $\alpha_4 = 88$ %
A_3: $\alpha_2 = 13$ %, $\alpha_3 = 0$ %, $\alpha_4 = 87$ %

An artificial damping constant 0.0020 Å^2 was used.

and finally the 20 cm data for $s > 19.875$ Å^{-1} were excluded because of low quality. However, none of the important conclusions about the structure and composition were changed thereby.

Not all possible parameters could be simultaneously refined. Nevertheless, the combination of all (except for CCH angles) geometry variables, the important u values for X···X distances, composition parameter, and a scale factor refined to give convergence and reasonable parameter values. Other combinations, with a reduced number of geometry parameters and a larger number of u values, also gave convergence.

Least-squares refinements, with the amount of conformer (2) or (3) set equal to zero, were carried out. Radial distribution curves corresponding to these refinements are shown in Fig. 7. It is obvious that a mixture of the conformers (4) and (2) alone does not fit the experimental data very well. Much better fit is obtained with a mixture of (4) and (3), but still the agreement is not quite satisfactory. The agreement, when all three conformers are included, is seen to be very good.

B. Determination of torsional force constants. Mean amplitudes of vibration (u values) and perpendicular amplitude correction coefficients (K values) are easily calculated if a reasonable force field is known for the molecule.[8] Torsional force constants were not known for TBP, however, some of the u values get a considerable contribution from the torsional modes. Therefore, since a reasonable force field is known, except for the torsional force constants, the latter can be adjusted to fit the experimental data. This procedure worked out very well, because some of the u values, that get large contributions from torsional oscillations, are well determined from the diffraction data. Such u values are $u(X_1 \cdots X_3)$ and $u(X_2 \cdots X_3)$ in conformer GG(ag). Torsional modes alone contribute more than 70 % to $u(X_1 \cdots X_3)$. Torsional modes also contribute substantially to the K values.

The following procedure was adopted: First an average torsional force constant ($\overline{F}_\phi$),

$\overline{F}_\phi(1-2)=\overline{F}_\phi(2-3)=\overline{F}_\phi$, was determined. Parallel and perpendicular amplitudes for several values of $\overline{F}_\phi$ were calculated and included in the least-squares refinements. The value of $\overline{F}_\phi$ which lead to minimum in the error sum (**V'PV**) was obtained for $\overline{F}_\phi=0.304$ mdyn Å (rad)$^{-2}$.

If the conformer GG(ag) is considered, the force constant $F_\phi(1-2)$ ought to be less than $F_\phi(2-3)$.

Keeping the average value of $F_\phi(1-2)$ and $F_\phi(2-3)$ at 0.304 mdyn Å (rad)$^{-2}$, a deeper minimum of **V'PV** was obtained with $F_\phi(1-2)=0.203$ and $F_\phi(2-3)=0.406$ mdyn Å (rad)$^{-2}$.

The interaction constant $F_\phi(1-2,\ 2-3)$ could not be experimentally determined. However, the interaction constant has been calculated (sect. III) and the value was -0.041 mdyn Å (rad)$^{-2}$. This value was included in some computations of vibrational quantities. The influence on the vibrational frequencies was small. The effects on u and K values were negligible, even with interaction constants given much larger absolute values than 0.041.

It is difficult to estimate uncertainties in the F_ϕ values, but a *minimum* uncertainty might be estimated. The u values vary approximately as $u^2 \propto 1/F_\phi$. Therefore the relative uncertainty in F_ϕ values must be approximately twice the relative uncertainty in the u values. Only those u values corresponding to well determined internuclear distances, and having a large derivative with respect to F_ϕ, should be considered.

The final, and most probable, torsional force constants and their estimated error limits are:
Conformer GG(ag):

$F_\phi(1-2)=0.20\pm0.05$ mdyn Å (rad)$^{-2}$

Conformer GG(ag):

$F_\phi(2-3)=0.41\pm0.10$ mdyn Å (rad)$^{-2}$

The error limits need a few comments: Not all combinations of $F_\phi(1-2)$ and $F_\phi(2-3)$ values are equally probable. Certain combinations of the extremes of the permissible ranges are very much less likely than others. Combinations being highly probable are found within a radius of approximately 0.03 Å (rad)$^{-2}$ from the most probable values. The error limits do not allow for systematic errors within the remaining force field. However, the force constants F(CCX) and F(CCC) seem to be the only critical ones in this respect, but their values are probably close to the correct ones for TBP (See Table 3).

VI. FINAL RESULTS

Results from least-squares refinements, and standard deviations (σ), corrected for correlation in the experimental data,[15] are given. Refinements of intensities from five 48 cm plates separately were also carried out, and the standard deviations (σ_5) calculated from these individual results are shown too. Usually σ_5 is much smaller than σ.

Non-bonded distances were restricted under the geometrical constraint of r_α parameters,[13,14]

Table 6. Bond lengths for 1,2,3-tribromopropane. 0.14 % uncertainty in the wavelength has been included in the σ-values. An experiment with CO_2 gave a correction of +0.1 % in the s-scale, therefore the bond lengths given are 0.1 % longer than those obtained directly by refinements. Parameter correlation involving bond distances was always less than 0.5 in absolute value.

Bond	r_a(Å)	σ	σ_5
C–H	1.132	0.009	(0.008)
C–C	1.534	0.006	(0.002)
C–Br	1.948	0.003	(0.001)

Table 7. Bond angles for 1,2,3-tribromopropane. The CCH angles could not be refined simultaneously along with the other parameters, and their values were finally determined by trial and error. Parameter correlation: $\varrho(CCC/\phi_G)=0.91$, $\varrho(CCC/\phi_A)=-0.75$, $\varrho(C_2CX/\phi_G)=-0.58$, $\varrho(C_2CX/\phi_A)=0.59$, $\varrho(CC_2X/\phi_G)=0.64$, $\varrho(CC_2X/\phi_A)=-0.91$, $\varrho(CCC/C_2CX)=-0.62$, $\varrho(CCC/CC_2X)=0.53$, $\varrho(C_2CX/CC_2X)=-0.63$.

Bonds	$\angle_\alpha$°	σ	σ_5
CCC	117.4	0.7	(0.2)
C_2CX	110.4	0.4	(0.1)
CC_2X	110.5	0.3	(0.1)
C_2CH	(110.8)	(1.0)	(–)
CC_2H	(109.1)	(1.0)	(–)

by including correction terms $D=r_\alpha-r_a$ ($D=u^2/r-K$) for all distances. Calculated u and K values, corresponding to final torsional force constants, are shown in Table 4. Bond lengths, r_a values,[10] are given in Table 6 and bond angles in Table 7.

Several refinements were carried out in order to determine the torsional angles, not all of them being successful. Finally the angles were restricted under constraints which are shown together with their values. Two parameters, ϕ_A and ϕ_G were adjusted, and their meaning is understood when comparing Fig. 1 with the relations in Table 8. Although only two

Table 8. Torsion angles (°) for the conformers of 1,2,3-tribromopropane. Parameter correlation: $\varrho(\phi_G/\phi_A)=-0.84$.

Conformer	ϕ_{1-2}	ϕ_{2-3}
GG(ag)	$120°-\phi_G=114.7$	$120+\phi_G=125.3$
AG(gg)	$\phi_A=12.2$	$120+\phi_G=125.3$
AG(ga)	$\phi_A=12.2$	$\phi_G-120=-114.7$

$\phi_G=5.3$ ($\sigma=1.0$) and $\phi_A=12.2$ ($\sigma=3.0$)

torsional parameters were adjusted, their values are significantly different from 0°, which implies that the conformers most probably have torsion angles different from exact staggered values. If conformers AG(gg) and AG(ga) were assigned torsion angles with the values of Table 1, then the two angles ϕ_{1-2} and ϕ_{2-3} in GG(ag) could be refined independently, giving values not significantly different from 114.7° and 125.3°. The calculated torsion angles of Table 1 are different from the experimental ones, however, the general agreement is quite good, and in both cases the value of ϕ_A is seen to be larger than ϕ_G.

Table 9. Relative amounts of conformers of 1,2,3-tribromopropane at 88°C. Parameter correlation: $\varrho(\alpha_4/\alpha_2)=-0.84$, α_4 and α_2 are the composition parameters refined and $\alpha_3=100-\alpha_2-\alpha_4$; $\varrho(\alpha_3/u_a)=-0.78$, $\varrho(\alpha_2/u_a)=0.79$, and $u_a=u$[C···X(*anti*)].

Conformer	α(%)	σ	σ_5
(4); GG(ag)+GG(ga)	82	1	(0.5)
(3); GA(gg)+AG(gg)	8	2	(1.0)
(2); AG(ga)+GA(ag)	10	2	(1.0)

The final composition parameters are presented in Table 9. The fact that conformers (4), (3), and (2) are present in detectable amounts, is well established. Moreover, it has also been demonstrated that conformers (1), (5), and (6) are not present in detectable amounts at 88°C.

Refined mean amplitudes of the most important internuclear distances are compared with calculated ones as summarized in Table 10.

Table 10. Mean amplitudes of vibration at 88°C for 1,2,3-tribromopropane. If a value is in parentheses it has been refined together with the preceding u value as *one* parameter.

Dist.	Least-squares u value (Å)	Calculated u value (Å)	σ	σ_5
C−H	0.074	0.078	0.009	(0.013)
C−C	0.051	0.051	0.006	(0.006)
C_1-X_1	0.051	0.055	0.005	(0.003)
C_2-X_2	(0.055)	0.059	−	(−)
$C_3\cdots X_1$	0.078	0.080	0.006	(0.002)
$C_1\cdots X_2$	(0.075)	0.077	−	(−)
in GG(ag)				
$C_1\cdots X_3$(g)	0.181	0.149	0.025	(0.008)
$C_3\cdots X_1$(g)	(0.197)	0.165	−	(−)
$X_1\cdots X_2$(a)	0.070	0.081	0.004	(0.002)
$X_2\cdots X_3$(g)	0.161	0.168	0.004	(0.003)
$X_1\cdots X_3$	0.281	0.279	0.008	(0.008)

The u values independently refined are in good agreement with those calculated using final torsional force constants. Several, less important, amplitude values could not be refined. These values have been adjusted along with the torsional force constants (Sect. V−B).

Probably the conformers (2) and (3) have torsional force fields not too different from the most abundant conformer, therefore, the average torsional force constant of conformer (4) was used in calculating u and K values for the conformers (2) and (3).

Correlation coefficients from least-squares refinements are summarized in Tables 6−9.

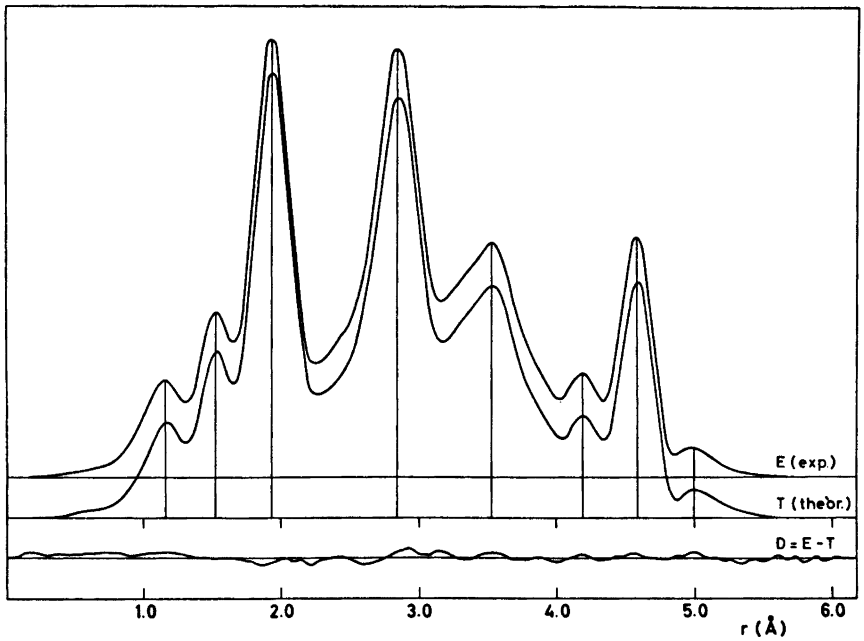

Fig. 8. Experimental (E) and theoretical (T) radial distribution curves and difference curve (D). The RD curves were calculated from the intensity curves of Fig. 5 with an artificial damping constant 0.0020 Å^2.

It seemed out of place to report on all coefficients; only those with absolute values larger than 0.5 have been shown.

The theoretical intensity, corresponding to the final least-squares parameters, is shown in Fig. 5, and the RD curve in Fig. 8. The agreement between theoretical and experimental curves is very good, and only slightly better than the fit obtained with all u and K values calculated using the final force constants.

Cartesian coordinates for the GG(ag) conformer are given in Table 11. The principal axes' moments of inertia for the conformers (1), (2), (3), and (4) are also found in Table 11.

VII. DISCUSSION

Recently, the NMR spectra of dilute solutions of TBP have been examined by Ernst and Schaefer.[16] From the three- and four-bond spin-spin coupling constants and from a comparison between observed and calculated dipole moments they concluded that in non-polar solvents TBP exists preferably in the enantiomeric conformations GG(ag) and GG(ga). In polar solvents other conformers contribute to the equilibrium but still seem to play a minor role. The authors[16] emphasize that their conclusions can only be of a qualitative nature, nevertheless, their results are in good agreement with the present work.

An extensive study of the vibrational spectra of 1,2,3-trihalopropanes (X = Br,Cl) have been carried out by Thorbjørnsrud, Ellestad, Klæboe, and Torgrimsen.[7] From the IR, far-IR, and Raman spectra alone it could not be concluded that (4) is the abundant conformer of the vapour phase. However, it was possible for Thorbjørnsrud *et al.*[7] to conclude that the most abundant conformer of the vapour phase also predominates in the liquids and is the preferred conformer in the crystals.

The torsional frequencies calculated, using the force field in Table 2 and torsional force constants determined from the diffraction data, are $\omega_1 = 45 \pm 10$ cm^{-1} and $\omega_2 = 86 \pm 10$ cm^{-1}.

The results reported by Thorbjørnsrud *et al.*[7] ($\omega_1 = 97$ cm^{-1} and $\omega_2 = 107$ cm^{-1}) would lead to u-values very much smaller than those obtained by electron diffraction (Table 5).

Table 11. Cartesian coordinates for the GG(ag) conformer of 1,2,3-tribromopropane (see Fig. 2). The coordinates have been computed using the final structure parameters in Tables 6–8 and the numbering of atoms is shown in Fig. 2. The principal axes' moments of inertia (amu Å^2) are:

Conformer (4): $I_a = 569.12$, $I_b = 948.75$, and $I_c = 1441.07$

Conformer (3): $I_a = 387.13$, $I_b = 1151.41$, and $I_c = 1446.09$

Conformer (2): $I_a = 520.90$, $I_b = 1140.77$, and $I_c = 1627.72$

Conformer (1): $I_a = 297.64$, $I_b = 1360.28$, and $I_c = 1573.24$

Torsion angles for AA(gg) were $\phi_{1-2} = 12.2°$ and $\phi_{3-2} = -12.2°$

Atom	*X*-Coor. (Å)	*Y*-Coor. (Å)	*Z*-Coor. (Å)
C_2	0.0000	0.0000	0.0000
C_1	1.3106	0.7972	0.0000
X_1	1.4939	1.8011	−1.6593
H_1'	1.3357	1.5287	0.8635
H_1	2.2014	0.1056	0.0978
C_3	−1.3106	0.7972	0.0000
X_3	−1.3421	2.0508	1.4907
H_3'	−1.4237	1.3841	−0.9613
H_3	−2.2014	0.1056	0.0978
X_2	0.0000	−1.3113	1.4405
H_2	0.0000	−0.7120	−0.8800

Perhaps part of the discrepancy is due to the fact that the electron diffraction data are from the vapour phase, while the spectroscopic data are from the liquid phase. Moreover, the spectroscopic determination of frequencies below 100 cm^{-1} is very difficult. An error in assignment of low frequencies is not ruled out (see Table 3). The lowest frequency (45 cm^{-1}) could have escaped detection.

It is strongly felt that electron-diffraction data together with low frequencies from vibrational spectra, preferably from the gas phase, is really the combination needed for determining the torsional force constants in TBP and related molecules.

Following standard statistical thermodynamics,[17] the percentages α and α' for two conformers (C⇌C′) in equilibrium in the gas phase, are related to the theoretical expression for the equilibrium constant, as given in eqn. (2):

$$\alpha'/\alpha = (Q_{rot}'/Q_{rot})(\sigma'/\sigma)^{-1}(Q_{vib}'/Q_{vib}) \exp(-\Delta E/RT) \quad (2)$$

If a pair of enantiomeric conformations are treated as *one* conformer, when computing equilibrium constants, that conformer must be assigned a statistical weight of two. If each of the *distinguishable* conformers are given a statistical weight equal to *one*, no problem should occur when the symmetry number σ is included in eqn. (2).

Q_{rot} is the *classical* rotational partition function,[18] $Q_{rot} \propto (I_a I_b I_c)^{\frac{1}{2}}$, and the factor Q'_{rot}/Q_{rot} is very near to 1.0 for all combinations in TBP and similar molecules.

Q_{vib} is the vibrational partition function,[18] referred to the *minimum* of potential energy, for a conformer.

$\Delta E = E' - E$ is the difference in potential energy between two conformers, and the difference is measured between energy *minima*.

R and T have their usual thermodynamic meaning.

A considerable simplification of eqn. (2) is possible if the vibrational partition functions for the conformers are equal, or nearly equal. Eqn. (3) is the simplified form of eqn. (2).

$$\alpha'/\alpha = (\sigma'/\sigma)^{-1} \exp(-\Delta E/RT) \quad (3)$$

The approximation that $Q'_{vib} = Q_{vib}$, is not obvious for molecules like TBP. A moderate difference in torsional force constants alone will lead to values of Q'_{vib}/Q_{vib} quite different from 1.0, as shown in Table 5.

Experimental torsional force constants for conformer (4) are known, while the corresponding quantities for the remaining conformers are unknown. However, the energy calculations indicated that the average torsional force constants for the conformers (4), (3), and (2) are not very different.

If the approximation $Q'_{vib} = Q_{vib}$ is assumed to be valid, the experimental differences in conformational energies might be calculated from eqn. (3). These calculations lead to the conclusions that the conformers (2) and (3) are nearly *equal* in energy and about 1.5 ± 0.4 kcal/mol *less* stable than conformer (4).

The theoretical energy calculations (Table 1) gave the answer that conformer (4) was *less* stable, about 0.6 kcal/mol, than conformer (2). The two values −1.5 and +0.6 for $\Delta E = E_4 - E_2$

do not agree. Could the disagreement be explained by a difference in vibrational partition functions between the two conformers? If that was the explanation, the ratio between the functions had to be about 18, but no *reasonable* values of torsional force constants, or other force constants, could lead to such a large ratio.

Moreover, similar disagreements were encountered in 1,3-dibromopropane [21] as well as in 1,2,3-trichloropropane.[21]

The discrepancy can not easily be explained in terms of simple adjustments in the applied force field. In the vapour phase, it seems that the GG conformer of low energy is always more stable than any other conformer in this type of molecules, also including 3-chloro-1-propanol investigated by Bastiansen *et al.*[19]

Additional information [20] about the thermodynamic equilibrium quantities, and the geometry of the conformers (2) and (3), may be obtained by studying TBP at higher temperatures. The expected composition at 200°C is approximately $\alpha_4 = 50$ % and $\alpha_2 = \alpha_3 = 25$ %.

Acknowledgements. I am grateful to Cand.real. A. Almenningen for recording the diffraction photographs, and to Professor O. Bastiansen, Professor S. J. Cyvin, Professor J. Dale, Cand.real. O. Ellestad, Dr. A. Haaland, Dr. P. Klæboe, and Dr. H. M. Seip for helpful discussions. Computer programs made available by Dr. H. M. Seip, Cand.real. S. Rustad, and Professor W. D. Gwinn have been extensively used in this work. Financial support from Norges almenvitenskapelige forskningsråd is gratefully acknowledged.

REFERENCES

1. Abraham, R. J. and Parry, K. J. *J. Chem. Soc. B* (1970) 539.
2. Rustad, S. *Thesis, at Oslo University*, Oslo 1973.
3. Allinger, N. L., Hirsch, J. A., Miller, M. N., Tyminski, I. J. and Van-Catledge, F. A. *J. Amer. Chem. Soc. 90* (1968) 1199.
4. Schachtschneider, J. H. and Snyder, R. G. *Vibrational Analysis of Polyatomic Molecules. IV* (force constants for the haloparaffins) Project No. 31450, Technical Report No. 122-63 of Shell Development Company.
5. Snyder, R. G. *J. Mol. Spectrosc. 28* (1960) 273.
6. Gwinn, W. D. *J. Chem. Phys. 55* (1971) 477.
7. Thorbjørnsrud, J., Ellestad, O. H., Klæboe, P. and Torgrimsen, T. *J. Mol. Struct. 17* (1973) 5.
8. Stølevik, R., Seip, H. M. and Cyvin, S. J. *Chem. Phys. Lett. 15* (1972) 263.
9. Bastiansen, O., Hassel, O. and Risberg, E. *Acta Chem. Scand. 9* (1955) 232.
10. Andersen, B., Seip, H. M., Strand, T. G. and Stølevik, R. *Acta Chem. Scand. 23* (1969) 3224.
11. Peacher, J. and Willis, J. C. *J. Chem. Phys. 46* (1967) 4809.
12. Strand, T. G. and Bonham, R. A. *J. Chem. Phys. 40* (1964) 1686.
13. Morino, Y., Kuchitsu, K. and Oka, T. *J. Chem. Phys. 36* (1962) 1108.
14. Kuchitsu, K. *J. Chem. Phys. 49* (1968) 4456.
15. Seip, H. M. and Stølevik, R. In Cyvin, S. J., Ed., *Molecular Structure and Vibrations*, Elsevier, Amsterdam 1972.
16. Ernst, L. and Schaefer, T. *Can. J. Chem. 51* (1973) 565.
17. Seip, H. M. In Sim, G. A. and Sutton, L. E., Eds., *Molecular Structure by Diffraction Methods* (Specialist Periodical Reports), The Chemical Society, London 1973, Vol 1, Part 1, Chapter 1.
18. Herzberg, G. *Infrared and Raman Spectra of Polyatomic Molecules*, Van Nostrand, Princeton.
19. Bastiansen, O., Brunvoll, J. and Hargittai, I. In Cyvin, S. J., Ed., *Molecular Structure and Vibrations*, Elsevier, Amsterdam 1972.
20. Almenningen, A., Bastiansen, O., Fernholt, L. and Hedberg, K. *Acta Chem. Scand. 25* (1971) 1946.
21. Færup, P. E. and Stølevik, R. *Acta Chem. Scand. To be published.*

Received October 15, 1973.

Acta Chemica Scandinavica A 28 (1974) 315—326

On the Charge Corrections of the Semi-empirical Parameters in the Pariser-Parr-Pople Method. II. Molecules Containing Oxygen and Nitrogen

BARBRO GRABE

Institute of Theoretical Physics, University of Stockholm, S-113 46 Stockholm, Sweden

In an extension of the modified Pariser-Parr-Pople approximation, the numerical values of the parameters W and γ have been varied with charge. Calculations have been made on phenol, furan, benzaldehyde, aniline, pyrrole, pyridine, *sym*-triazine, imidazole, and the pyridinium cation. For comparison CNDO calculations have also been made.

The necessity of varying some parameters with charge in the Pariser-Parr-Pople method (PPP) is discussed in an earlier paper [1] where calculations on formaldehyde, acrolein, formic acid, and formate ion are made with W_μ and $\gamma_{\mu\mu}$ values dependent on the charge on the atom. The present paper is a continuation of this study and includes calculations on oxygen containing molecules, *viz.* phenol, furan, and benzaldehyde, and on nitrogen containing molecules, *viz.* aniline, pyrrole, pyridine, *sym*-triazine, imidazole, and the pyridinium cation.

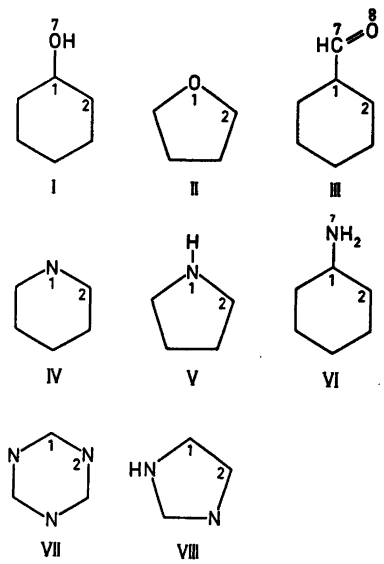

Fig. 1. I: Phenol, II: furan, III: benzaldehyde, IV: pyridine, V: pyrrole, VI: aniline, VII: *sym*-triazine, VIII: imidazole.

METHOD

As in the earlier paper,[1] two different alternatives for determining the parameters have been used. In Alt. 1 the parameters determined in Refs. 2—5 are assumed to be valid for formally neutral atoms. In Alt. 2 the uncorrected values in Refs. 2—5 are assumed to be valid for the net atomic charge predicted by their use on the chosen reference molecules. In both alternatives two different functions giving the variation of W with charge are used, *viz.* $F_1(\varrho)$ and $F_2(Z_{\text{eff}})$.

In $F_1(\varrho)$ the difference between the valence state ionization potentials (IP) of the anion, the neutral atom, and the cation have been used to estimate the variation of W with ϱ, the charge on the atom. These ionization potentials are given in Table 1 and Ref. 1.

In $F_2(Z_{\text{eff}})$ the variation of the valence state IP is considered a function of Z_{eff}, calculated according to Slater's rules. The IP's of three isoelectronic atoms have been taken as fixed points. These values are found in Table 2 and Ref. 1.

Table 1. Valence state ionization potentials for atoms and atomic ions, obtained from tables in Refs. 6 – 8 directly or by combination of values in these tables. All values in eV. It has been possible to get values only for the uncharged atom and for either the negatively or positively charged atom. To get the third value in the series the IP value of an isoelectronic atom with different charge of the core has been transformed according to Brown and Hefferman.[9] These transformed values are given in parentheses. A corresponding table for carbon and oxygen has been given in Ref 1.

C^-	N (pyrrole)	N^+
$t_1t_2t_3z^2 \rightarrow t_1t_2t_3z$	$t_1t_2t_3z^2 \rightarrow t_1t_2t_3z$	$t_1t_2t_3z \rightarrow t_1t_2t_3$
0.62[a] (N^- 0.78)	12.25[a]	28.72[b,c]
N^-	N (pyridine)	O^+
$t_1^2t_2t_3z^2 \rightarrow t_1^2t_2t_3z$	$t_1^2t_2t_3z \rightarrow t_1^2t_2t_3$	$t_1^2t_2t_3z \rightarrow t_1^2t_2t_3$
1.20[a]	14.51[a]	34.50[a,b,c] (N^+ 28.75)

[a] Ref. 6; [b] Ref. 7; [c] Ref. 8.

Table 2. The left hand side of the table gives valence state ionization potentials for isoelectronic series obtained from tables in Refs. 6 – 8 directly or by combination of values in these tables. Values are given in eV. The atoms in one series differ both in Z_{eff} and in core charge. Ionization potentials obtained after correcting for the difference in core charge according to Brown and Heffernan [9] are given in the right hand side of the table. A corresponding table for carbon and oxygen has been given in Ref. 1.

	C^-	N	O^+		N, core charge 5		
Core charge	4	5	6	Z_{eff}	2.90	3.90	4.90
Pyrrole nitrogen $t_1t_2t_3z^2 \rightarrow t_1t_2t_3z$ IP., eV	0.62[a]	12.25[a]	31.1[b,c]		0.78	12.25	25.90
Pyridine nitrogen $t_1^2t_2t_3z \rightarrow t_1^2t_2t_3$ IP, eV	2.14[a,c]	14.51[a]	34.5[a,b,c]		2.67	14.51	28.75

[a] Ref. 6; [b] Ref. 7; [c] Ref. 8.

The numerical values of the one-center two-electron integrals for different charges on the atom have been determined by linear interpolation. The data for the anion, the neutral atom, and the cation used for C and O are given in Ref. 1. The values used for nitrogen in eV are N^- 13.58, N 15.44, and N^+ 17.31.

A more detailed description of Alt. 1 and Alt. 2 and the two F-functions is given in the earlier paper.[1]

In determining the parameters for uncharged atoms according to Alt. 2, one or two reference molecules must be chosen for which the parameters are assumed to be valid for the predicted charge.

In the earlier paper [1] formaldehyde was chosen as the reference molecule for determining the parameters for the keto oxygen. In that paper both carbon and oxygen parameters were corrected according to Alt. 2. In the present paper, for the ether bond in phenol, where oxygen is bound only to one carbon, only Alt. 1 has been used since the charges are small. In the ether bond in furan, where oxygen is bound to two carbon atoms, the charge on the oxygen atom with uncorrected parameters has been calculated to 0.26 and the charge on the neighbour carbon to −0.08. On this molecule both alternatives have been used for oxygen, but only Alt. 1 for the carbon atom.

For pyridine nitrogen, where the charges are small, only Alt. 1 has been used. In pyrrole the charges are large on nitrogen and both alternatives have been used for this atom. Aniline, with

Table 3. The semi-empirical W values used for uncharged atoms and standard distances ($R_{C=O} = 1.22$ Å, $R_{C-OH} = 1.35$ Å and $R_{CN} = 1.338$ Å).
The values in Alt. 2 have been calculated as described in text, the other values are taken from Refs. 2–5, where also the dependence on bond length is given. Values given in eV.

W_C°		−9.84				
$\Delta W_C(N)$		0.03				
	Ether oxygen				Keto oxygen	
	Alt. 1	Alt. 2			Alt. 1	Alt. 2
		$F_1(\varrho)$	$F_2(Z_{eff})$			$F_1(\varrho)$ $F_2(Z_{eff})$
$\Delta W_C(O)$	−0.09	−0.09	−0.09	$\Delta W_C(O)$	−0.71	4.56 0.90
W_O°	−11.18	−15.74	−12.62	$W_O^\circ + \Delta W_O(C)$	−19.60	−26.17 −21.50
$\Delta W_O(C)$	1.52	6.08	2.96			
	Pyridine nitrogen				Pyrrole nitrogen	
	Alt. 1				Alt. 1	Alt. 2
						$F_1(\varrho)$ $F_2(Z_{eff})$
W_N°	−12.57				−8.52	−10.22 −9.05
$\Delta W_N(C)$	0.14				0.14	3.60 1.23

one carbon bound to nitrogen, and pyrrole, with two carbons bound, have been used as reference molecules. The choice of parameters of the pyridinium cation merits a special description. It has been assumed that the charge contributed to the system by adding H^+ becomes equally distributed on the N and the H atoms. The net charge on the N atom is therefore assumed to be $+0.5+\pi$-electron charge, *cf.* Table 4. This net value has been employed in the determination of W and γ. The possible distribution of charge within this ion and different types of calculations are discussed in great detail by Mataga and Mataga [39] and will not be repeated here. For the lowest transitions these authors obtained the values 38.3 and 49.5 kK.

The semi-empirical W_μ values used with zero atomic charges are given in Table 3.

It seems to be valuable to compare the results obtained with the method described above with results obtained with a method that takes σ-electrons in consideration explicitly. Therefore calculations have been made with the CNDO method (complete neglect of differential overlap) with parameters given by Höjer and Meza.[10]

The SCF-MO's in the PPP-method have been evaluated using a program written by B. Roos and M. Sundbom. This program also calculates the energy levels of the excited states by mixing all on the configurations obtained from single excitations (max. 140 configurations). Oscillator strengths for the dipole transitions, according to formula by Mulliken and Rieke,[11] and eigenvectors for the multi-configurational problem are also given in computer output. The program used for the CNDO calculations has been written by G. Höjer and S. Meza. The computer IBM 360/75 at Stockholm's data central has been used for the calculations.

For C–C and C–O bonds, bond lengths have been calculated from the bond orders between nearest neighbours using eqns. 6–8 in Ref. 1; and for C–N, the relation

$$R_{\mu\nu}(CN) = 1.458 - 0.18\, p_{\mu\nu} \qquad (1)$$

has been used according to Ref. 3.

The charges on the atoms, but not the bond lengths, have been varied to self-consistency. The structure of the molecules are taken from experimental data.

RESULTS

The ground state properties, *i.e.* net charges on the atoms, bond orders, bond lengths, and dipole moments, together with ionization potentials calculated with Koopmans' theorem, are given in Table 4. Calculated values of singlet π-π^* transition energies and of oscillator strengths are given in Table 5. In both tables some typical experimental values obtained by different workers are given. Most of the experimental values on IP's are adiabatic. All the experimental values of transition energies are determined in the vapour phase except the values for *sym*-triazine given by Favini *et al.*,[35] for imidazole,[37,38] and for the pyridinium ion.

Comparing the results of calculations made

Table 4. π-Electron net charges, bond orders, bond distances (in Å), dipole moments (in Debye) and ionization potentials (in eV), predicted by use of different sets of charge-corrected parameters for the PPP method. For the CNDO method both π-electron and total net charges and total dipole moments are given. For the description of the methods, see text. IP's calculated according to Koopmans' theorem.

		PPP-method Uncorr.	Alternative 1 $F_1(\varrho)$	F_2 (Z_{eff})	CNDO method π	total	Exp. values
Phenol							
Net charge	C_1	0.01	0.00	0.01	0.08	0.16	
	C_2	−0.03	−0.02	−0.03	−0.09	−0.14	
	C_3	0.00	−0.01	0.00	0.04	−0.03	
	C_4	−0.02	−0.01	−0.01	−0.06	−0.10	
	O_7	0.06	0.05	0.06	0.07	−0.22	
Bond order C_1-C_2		0.645	0.649	0.647			
Bond dist.		1.401	1.400	1.401			1.395[a]
Bond order C_2-C_3		0.670	0.669	0.669			
Bond dist.		1.396	1.397	1.397			1.395[a]
Bond order C_3-C_4		0.665	0.665	0.665			
Bond dist.		1.397	1.397	1.397			1.395[a]
Bond order C_1-O_7		0.251	0.228	0.240			
Bond dist.		1.366	1.370	1.368			1.379[a] 1.364−69[b]
Dipole moment		0.74	0.65	0.72		1.68	1.40[c]
IP		8.45	8.58	8.50	8.29		8.46[d] ad. 8.75[e] vert.
		9.14	9.11	9.11	9.64		9.34[d] ad. 9.45[e] vert.
		10.75	11.08	10.89			11.30[d] ad.
		12.55	12.64	12.57	14.19		

		PPP-method Uncorr.*	Alternative 1 $F_1(\varrho)$	$F_2(Z_{eff})$	Alternative 2 $F_1(\varrho)$	$F_2(Z_{eff})$	CNDO-method π	total	ab initio[f] π	total	Exp. values
Furan											
Net charge	O_1	0.26	0.15	0.20	0.24	0.25	0.28	−0.07	0.23	−0.41	
	C_2	−0.08	−0.04	−0.06	−0.06	−0.07	−0.06	−0.02	−0.03	0.12	
	C_3	−0.05	−0.03	−0.04	−0.06	−0.05	−0.08	−0.11	−0.08	−0.14	
Bond order O_1-C_2		0.408	0.316	0.367	0.397	0.404					
Bond dist.		1.334	1.353	1.343	1.337	1.335					1.362[g]
Bond order C_2-C_3		0.831	0.865	0.847	0.837	0.833					
Bond dist.		1.367	1.361	1.365	1.366	1.367					1.361[g]
Bond order C_3-C_4		0.494	0.460	0.478	0.487	0.492					
Bond dist.		1.428	1.434	1.431	1.429	1.428					1.431[g]
Dipole moment		1.66	0.95	1.34	1.71	1.66		0.42		1.29	0.66[c] 0.72[c]
IP		8.72	8.50	8.63	8.20	8.58	8.19		9.06		8.89[h] ad. 8.9[q] vert.
		9.33	9.96	9.65	9.00	9.25	10.43		11.03		10.25[h] ad. 10.3[q] vert.
		12.16	12.99	12.41	11.76	12.06	18.99		17.28		14.4[q] vert.

* The same values are obtained with Alt. 2 when only O_1 is corrected for the charge

Table 4. Continued.

		PPP-method					CNDO-method		Exp. values
		Uncorr.	Alt. 1 for all atoms		Alt. 2 for C_7 and O_8, Alt. 1 for the other				
			$F_1(\varrho)$	$F_2(Z_{eff})$	$F_1(\varrho)$	$F_2(Z_{eff})$	π	total	
Benzaldehyde									
Net charge	C_1	0.08	0.03	0.06	0.04	0.05	−0.01	0.01	
	C_2	0.01	0.01	0.01	0.01	0.01	0.01	−0.06	
	C_3	0.01	0.00	0.01	0.02	0.01	0.00	−0.07	
	C_4	0.01	0.01	0.01	0.01	0.01	0.01	−0.06	
	C_5	0.01	0.00	0.00	0.00	0.00	0.00	−0.06	
	C_6	−0.05	−0.01	−0.02	−0.02	−0.03	0.01	−0.07	
	C_7	0.49	0.15	0.31	0.47	0.48	0.11	0.06	
	O_8	−0.56	−0.20	−0.37	−0.53	−0.54	−0.14	−0.14	
Bond order C_1-C_2		0.639	0.639	0.638	0.641	0.639			
Bond dist.		1.402	1.402	1.402	1.402	1.402			
Bond order C_2-C_3		0.669	0.669	0.669	0.669	0.669			
Bond dist.		1.397	1.397	1.397	1.397	1.397			
Bond order C_3-C_4		0.665	0.666	0.666	0.666	0.666			
Bond dist.		1.397	1.397	1.397	1.397	1.397			
Bond order C_4-C_5		0.663	0.661	0.662	0.662	0.662			
Bond dist.		1.398	1.398	1.398	1.398	1.398			
Bond order C_5-C_6		0.672	0.674	0.674	0.673	0.673			
Bond dist.		1.396	1.396	1.396	1.396	1.396			
Bond order C_6-C_1		0.636	0.635	0.635	0.638	0.637			
Bond dist.		1.403	1.403	1.403	1.402	1.402			
Bond order C_1-C_7		0.280	0.286	0.288	0.277	0.281			
Bond dist.		1.467	1.466	1.465	1.467	1.466			
Bond order C_7-O_8		0.800	0.939	0.890	0.817	0.809			
Bond dist.		1.221	1.196	1.205	1.218	1.219			
Dipole moment		3.39	1.45	2.38	3.37	3.36		2.14	ca. 2.7[c] liq.
IP		9.51	9.26	9.35	9.55	9.53	9.04		9.46[d] ad. 9.80[e] vert.
		9.78	9.49	9.62	9.74	9.75	9.71		11.48[d] ad.
		12.56	12.21	12.35	12.45	12.52			
		13.66	13.59	13.57	13.45	13.59	13.98		

Table 4. Continued.

	PPP-method Uncorr.	Alternative 1 $F_1(\varrho)$	F_2 (Z_{eff})	CNDO-method π	total	ab initio[r] π	total	Exp. values
Pyridine								
Net charge N_1	−0.07	−0.03	−0.05	−0.04	−0.06	−0.11	−0.63	
C_2	0.03	0.00	0.02	0.02	−0.02	0.05	0.25	ca. 0.08[i]
C_3	0.00	0.01	0.00	−0.03	−0.09	−0.04	−0.18	" 0.00[i]
C_4	0.01	0.00	0.01	0.04	−0.04	0.07	−0.04	" 0.04[i]
Bond order N_1-C_2	0.670	0.671	0.671					
Bond dist.	1.337	1.337	1.337					1.3394[k]
Bond order C_2-C_3	0.657	0.657	0.657					
Bond dist.	1.399	1.399	1.399					1.3958[k]
Bond order C_3-C_4	0.671	0.671	0.671					
Bond dist.	1.396	1.396	1.396					1.3936[k]
Dipole moment	0.30	0.22	0.27		2.04		2.49	2.15[c] 2.25[c]
IP	9.33	9.37	9.35	9.43		9.52		9.28[d]
	9.74	9.66	9.70	10.02		10.38		10.54[d]**
	12.81	12.78	12.80	17.68		14.74		12.22[d]
Pyridinium ion								
Net charge N_1*		−0.26	−0.15	−0.35	0.02			
C_2		0.09	0.06	0.10	0.05			
C_3		0.02	0.01	−0.02	−0.08			
C_4		0.03	0.02	0.19	0.04			
Bond order N_1-C_2		0.647	0.663					
Bond dist.		1.342	1.339					
Bond order C_2-C_3		0.661	0.658					
Bond dist.		1.398	1.399					
Bond order C_3-C_4		0.669	0.671					
Bond dist.		1.397	1.396					
IP		9.87	9.42	16.26				
		10.78	10.07	17.78				
		13.88	13.12					

* Assuming half of the charge on the ion to be located on N and half on the H, W and γ are determined for the charge 0.50 − 0.26 = 0.24.
** Interpreted as σ lone pair.

Table 4. Continued.

		PPP-method Uncorr.*	Alternative 1		Alternative 2		CNDO-method		Exp. values	
			$F_1(\varrho)$	F_2 (Z_{eff})	$F_1(\varrho)$	F_2 (Z_{eff})	π	total		
Pyrrole										
Net charge	N_1	0.34	0.19	0.27	0.32	0.33	0.43	−0.07		
	C_2	−0.07	−0.04	−0.05	−0.08	−0.07	−0.10	−0.06		
	C_3	−0.10	−0.06	−0.08	−0.08	−0.09	−0.11	−0.11		
Bond order N_1-C_2		0.472	0.364	0.427	0.455	0.465				
Bond dist.		1.373	1.392	1.381	1.376	1.374			1.374[l]	
Bond order C_2-C_3		0.790	0.836	0.811	0.797	0.793				
Bond dist.		1.375	1.366	1.371	1.374	1.374			1.381[l]	
Bond order C_3-C_4		0.541	0.501	0.523	0.538	0.539				
Bond dist.		1.420	1.427	1.423	1.420	1.420			1.417[l]	
Dipole moment		2.55	1.45	2.08	2.22	2.46		2.23	1.55−1.84[c]	
IP		8.23	7.92	8.12	7.58	8.03	7.74		8.22[d]	
		9.08	9.48	9.32	8.50	8.94	9.00		9.03[d]	
		12.27	13.32	12.61	11.74	12.13	18.19		12.38[d]	
Aniline										
Net charge	C_1	0.05	0.01	0.03	0.00	0.03	0.08	0.13		
	C_2	−0.08	−0.03	−0.05	−0.03	−0.05	−0.09	−0.13		
	C_3	0.01	0.00	0.00	−0.02	0.00	0.04	−0.03		
	C_4	−0.03	−0.02	−0.02	−0.02	−0.03	−0.06	−0.10		
	N_7	0.12	0.09	0.11	0.12	0.12	0.31	−0.28		
Bond order C_1-C_2		0.623	0.637	0.630	0.628	0.626				
Bond dist.		1.405	1.402	1.404	1.404	1.404			1.392[m]	
Bond order C_2-C_3		0.673	0.671	0.672	0.673	0.673				
Bond dist.		1.396	1.396	1.396	1.396	1.396			1.392[m]	
Bond order C_3-C_4		0.663	0.664	0.663	0.663	0.663				
Bond dist.		1.398	1.397	1.398	1.398	1.398			1.392[m]	
Bond order C_1-N_7		0.355	0.297	0.329	0.338	0.346				
Bond dist.		1.394	1.405	1.399	1.397	1.396			1.431[m]	
dipole moment		1.60	1.18	1.44	1.65	1.58		1.68	1.49[c]	
IP		7.66	8.03	7.82	7.54	7.63	7.83**		7.71[d]ad	8.04[e]vert.
		9.03	8.91	8.99	8.84	8.95	9.13**		8.95[d]ad	9.11[e]vert.
		10.17	10.60	10.34	10.12	10.17	9.50		10.49[d]ad	10.70[e]vert.

* The same values are obtained with Alt. 2, when only N is corrected for the charge.
** 7.83 not pure π; 9.13 σ mixed up with π.

Table 4. Continued.

		PPP-method Uncorr.*	Alternative 1 $F_1(\varrho)$	Alternative 1 $F_2(Z_{eff})$	Alternative 2 $F_1(\varrho)$	Alternative 2 $F_2(Z_{eff})$	CNDO-method π	CNDO-method total	ab initio[r] π	ab initio[r] total	Exp. values
sym-Triazine											
Net charge	C	0.07	0.02	0.04			0.10	0.05	0.17	0.49	
	N	−0.07	−0.02	−0.04			−0.10	−0.11	−0.17	−0.62	
Bond order C−N		0.665	0.667	0.666							
Bond dist.		1.338	1.338	1.338							1.338[n]
IP		10.08	10.09	10.09			10.52		12.08		10.01[o]** ad. 10.4[o]vert.
							10.58				11.69[o] ad. 12.0[o]vert.
		13.48	13.50	13.49			18.48		16.85		13.26[o] ad. 13.3[o]vert.
Imidazole											
Net charge	C_1	−0.07	−0.03	−0.05	−0.07	−0.07	−0.11	−0.08			
	C_2	−0.09	−0.06	−0.08	−0.08	−0.09	−0.11	−0.10			
	N_3	−0.14	−0.07	−0.11	−0.10	−0.12	−0.19	−0.10			
	C_4	−0.04	−0.03	−0.03	−0.07	−0.05	−0.04	−0.01			
	N_5	0.34	0.20	0.27	0.32	0.33	0.45	−0.08			
Bond order C_1-C_2		0.781	0.824	0.802	0.784	0.782					
Bond dist.		1.376	1.369	1.373	1.376	1.376					1.358[p]
Bond order C_2-N_3		0.552	0.521	0.538	0.554	0.554					
Bond dist.		1.359	1.364	1.361	1.358	1.358					1.378[p]
Bond order N_3-C_4		0.779	0.825	0.802	0.788	0.783					
Bond dist.		1.318	1.309	1.314	1.316	1.317					1.326[p]
Bond order C_4-N_5		0.479	0.367	0.428	0.456	0.469					
Bond dist.		1.372	1.392	1.381	1.376	1.374					1.349[p]
Bond order N_5-C_1		0.477	0.372	0.430	0.466	0.473					
Bond dist.		1.372	1.391	1.381	1.374	1.373					1.369[p]
dipole moment		2.87	1.62	2.27	2.42	2.67		4.13			3.9−6.2[c] benzene
											4.0−4.9[c] dioxane
IP		8.36	8.11	8.29	7.62	8.21	8.11				
		9.49	10.00	9.80	8.73	9.33	9.40				
		12.57	13.46	12.87	11.86	12.43	18.62				

* The same values are obtained for imidazole with Alt. 2 when only N_5 is corrected for the charge.
** Interpreted as σ lone pair.

[a] Ref, 12; [b] Ref. 13; [c] Ref. 14; [d] Ref. 15; [e] Ref. 16; [f] Ref. 17; [g] Ref. 18; [h] Ref. 19; [i] Ref. 20; [k] Ref. 21; [l] Ref. 22; [m] Ref. 23; [n] Ref. 24; [o] Ref. 25; [p] Ref. 26; [q] Ref. 27; [r] Ref. 28.

with the PPP method with different parameter sets, it is seen that the values of charge densities and the connected dipole moments have the largest percent differences from set to set of the other calculated quantities.

Unfortunately there are no experimental data on the charge densities. Furthermore the values calculated with the PPP method give only π-electron densities, not total densities. Thus the comparison between calculated and experimental values on dipole moments lacks significance.

As mentioned above, calculations with the CNDO method have been made for comparison; *cf.* Table 4. In this method both σ- and π-densities are calculated and, therefore, comparison between calculated and experimental dipole moments is relevant.

For some of the molecules, *ab initio* calculations have been made by other investigators and their values on electron densities, dipole moments, and ionization potentials are given in Table 4. The values of total $(\sigma+\pi)$ densities differ very much from the values obtained by CNDO calculations, while the dipole moments do not differ at all so much. This depends on the definitions of the densities, where the *ab initio* calculations give gross atomic densities. Since the purpose of the study is to determine the dependence on charge of the semi-empirical W values, it seems to be more significant to compare the charges on the atoms obtained with the PPP method with those obtained with CNDO method, and not with the *ab initio* calculations. The reason for this is that both CNDO and PPP are ZDO (zero differential overlap) methods and thus the charge densities obtained with these methods are comparable. In the *ab initio* calculations, on the other hand, a non-orthogonal basis is employed together with Mulliken population analysis.

It seems reasonable, with guidance from Table 4 and 5, to vary W and γ with charge only when the absolute value of the charge on the atom is > 0.2.

Molecules where no charge is > 0.2 are phenol, aniline, pyridine, and *sym*-triazine. In phenol and aniline the hetero-atom (O resp. N) is not a ring atom and it gives two electrons to the π-system. In pyridine and *sym*-triazine the hetero-atom is a ring nitrogen which gives one electron to the π-system.

Molecules where W and γ ought to be corrected, charges on some atoms being large, are benzaldehyde, furan, pyrrole, and imidazole. In benzaldehyde, oxygen, being outside the ring, gives one electron to the π-system. The parameters for both oxygen and the carbon next to it should be corrected. In furan, pyrrole, and imidazole, the hetero-atom for which the parameters should be corrected is a ring oxygen or a ring nitrogen, giving two electrons to the π-system.

Alt. 2 as opposed to Alt. 1 seems to give the best results for all the molecules except in determining the charge densities for benzaldehyde. This conclusion is drawn from comparing PPP results both with experimental data for bond lengths, ionization potentials, and spectra and with CNDO calculated charge densities as discussed above.

When Alt. 2 is used, in most cases there are no large differences in results between calculations with $F_1(\varrho)$ and $F_2(Z_{\text{eff}})$. $F_2(Z_{\text{eff}})$ seems, however, to give better results, and furthermore it seems theoretically to be correct to use $F_2(Z_{\text{eff}})$ when the electrons contributing to the charge are explicitly taken into consideration in the calculation, *i.e.* π-electrons.

To get charge densities in benzaldehyde which are in best accordance with the CNDO calculations, in Alt. 1, $F_1(\varrho)$ has to be used.

To complete the investigation we have made CNDO calculations on the molecules treated by Grabe and Skancke.[1] Just as in the case of benzaldehyde, Alt. 1 $F_1(\varrho)$ gives charge densities in best accordance with the CNDO calculations for formaldehyde and acrolein. For the formate ion, Alt. 2 is best, as was also the conclusion in Ref. 1 drawn from calculations of bond lengths.

CONCLUSIONS

In making calculations on other molecules with oxygen and nitrogen the intention is to use the W° and ΔW values for uncharged atoms in Table 3; Alt. 2 $F_2(Z_{\text{eff}})$ for ether oxygen, keto oxygen, and pyrrole nitrogen; and Alt. 1 for pyridine nitrogen. The corrections are to be made according to $F_2(Z_{\text{eff}})$. To get densities for keto bonds, however, the values for uncharged atoms for Alt. 1 are to be used and the corrections are to be made according to $F_1(\varrho)$ for both

Table 5. Transition energies and oscillator strengths predicted by use of different sets of charge-corrected parameters. For description of methods, see text.

Molecule	Uncorrected		Alternative 1				Alternative 2				Exp. values (vapour)	
			$F_1(\varrho)$		$F_2(Z_{eff.})$		$F_1(\varrho)$		$F_2(Z_{eff.})$			
	Energy kK	Osc. strength f	Energy kK	Osc. strength f	Energy kK	Osc. strength f	Energy kK	Osc. strength f	Energy kK	Osc. strength f	ν_{max} kK	Osc. strength f
Phenol	37.9	0.01	38.2	0.01	38.0	0.01					37.0[a]	0.02
	47.1	0.16	48.0	0.11	47.5	0.13					46.9[a]	0.13
	53.7	0.83	54.5	0.99	54.1	0.91					54.0[a]	0.64
	54.7	1.04	55.0	1.11	54.8	1.08					55.9[a]	0.47
	62.5	0.30	64.7	0.14	63.5	0.22						
	63.2	0.08	64.8	0.03	64.0	0.05						
												log ε
Furan	45.5	0.29	44.2	0.31	44.8	0.30	45.1	0.29	45.2	0.29	46[b]	2.9 shoulder
	48.4	0.12	49.7	0.05	49.0	0.08	48.9	0.09	48.7	0.11	48.9[b]	3.6
											52.2[b]	4.1
	59.5	0.81	61.3	0.93	60.1	0.86	59.4	0.85	59.4	0.83	59.6[b]	3.8
	62.0	0.22	69.1	0.13	65.2	0.18	62.9	0.21	62.3	0.21	62.8[b]	
												f
Benz-	37.4	0.01	37.1	0.01	37.2	0.01	37.6	0.004	37.5	0.01	36.4[c]	0.02
aldehyde	44.3	0.39	43.2	0.45	43.2	0.44	45.2	0.39	44.6	0.40	43.1[c]	0.26
	51.6	0.56	50.4	0.38	50.6	0.44	52.1	0.57	51.7	0.54	51.3[c]	
	53.5	0.90	52.9	0.67	53.1	0.75	53.8	0.99	53.6	0.92	(53.8)[c]	1.7
	60.7	0.31	58.9	0.46	59.5	0.40	60.9	0.30	60.6	0.32	56.2[c]	
	62.2	0.04	59.6	0.31	60.5	0.18	62.9	0.06	62.2	0.08	60.6[c]	
	63.8	0.51	63.3	0.44	63.1	0.53	63.9	0.41	63.8	0.45		

Table 5. Continued.

Pyrrole	47.3	0.32	45.4	0.36	46.3	0.35	46.8	0.33	46.9	0.33	47.4[d] >0.12
	49.1	0.06	49.4	0.03	49.3	0.04	49.0	0.06	49.2	0.05	
											54.7[d] >0.08
	59.0	0.90	60.9	0.96	59.6	0.93	59.2	0.90	59.0	0.91	58.5[d] >0.60
	62.9	0.31	68.8	0.16	65.5	0.23	63.7	0.28	63.1	0.30	
											f
Aniline	36.1	0.05	37.4	0.02	36.6	0.04	36.2	0.04	36.1	0 05	35.5[a] 0.03
	44.1	0.29	46.1	0.21	44.9	0.26	43.8	0.29	44.0	0.28	43.5[a] 0.14
	51.3	0.38	53.2	0.79	52.1	0.55	51.0	0.45	51.2	0.43	51.6[a] 0.51
	54.3	0.92	54.6	1.03	54.4	0.97	54.3	0.91	54.3	0.92	55.5[a] 0.57
	60.0	0.69	62.9	0.31	61.0	0.54	60.5	0.64	60.2	0.66	
	61.7	0.11	63.5	0.06	62.4	0.08	61.7	0.11	61.7	0.10	(63.5)[a] (0.68)
											log ε
											(in ethanol)
Imidazole	47.6	0.33	45.9	0.37	46.7	0.36	47.2	0.35	47.4	0.34	48.2[i] 3.70
	52.5	0.03	52.4	0.02	52.4	0.03	52.0	0.05	52.3	0.04	48.4[j] 3.32
	61.4	0.83	64.2	0.89	62.6	0.87	61.9	0.82	61.6	0.83	
	69.7	0.39	78.1	0.26	73.6	0.32	71.0	0.36	70.2	0.38	
											kK log ε
											(in hexane)
sym-Tri-	44.0	0	43.8	0	43.9	0					~46[e] 45.1[g] 2.23[g]
azine	59.7	0	59.6	0	59.6	0					55.8[f] 54.3s 4.12[g]
	62.3	1.17	62.3	1.18	62.3	1.18					
											f
Pyridine	40.7	0.01	40.7	0.001	40.7	0.003					40.1[d] 0.04
	52.1	0.15	52.1	0.15	52.1	0.15					51.4[d] 0.10
	57.5	1.16	57.5	1.17	57.5	1.16					57.5[d] 1.3
	59.3	1.00	59.3	1.00	59.3	1.00					
											(in ethanol-ether)
Pyridini-			40.0	0.09	40.4	0.03					38.0[h]
um ion			52.0	0.10	52.2	0.14					43.5[h]
			58.4	1.01	57.9	1.11					
			58.5	1.02	59.2	0.99					

s=shoulder. [a] Ref. 29; [b] Ref. 30; [c] Ref. 31; [d] Ref. 32; [e] Ref. 33; [f] Ref. 34; [g] Ref. 35; [h] Ref. 36; [i] Ref. 37; [j] Ref. 38; Some experimental values are given in eV in the reference papers. The conversion factor 1 eV = 8.06573 kK is used here.

carbon and oxygen. Only charges > 0.2 are to be corrected.

Calculations on lumiflavin after these lines have been completed and the results will be given in a following paper.

Acknowledgements. The author wishes to thank Professor Inga Fischer-Hjalmars for valuable discussions and Fil.kand. Lars Norén for skilful assistance in the numerical computations. The investigation has been supported by grants from the Swedish Natural Science Research Council.

REFERENCES

1. Grabe, B. and Skancke, P. N. *Acta Chem. Scand. 26* (1972) 468.
2. Roos, B. *Acta Chem. Scand. 21* (1967) 2318.
3. Fischer-Hjalmars, I. and Sundbom, M. *Acta Chem. Scand. 22* (1968) 607.
4. Jensen, H. and Skancke, P. N. *Acta Chem. Scand. 22* (1968) 2899.
5. Höjer, G. *Acta Chem. Scand. 23* (1969) 2589.
6. Pilcher, G. and Skinner, H. A. *J. Inorg. Nucl. Chem. 24* (1962) 937.
7. Moore, C. E. *Atomic Energy Levels, Nat. Bur. Stand. Circ. 467* (1949).
8. Hinze, J. and Jaffé, H. H. *J. Amer. Chem. Soc. 84* (1962) 540.
9. Brown, R. D. and Heffernan, M. L. *Aust. J. Chem. 12* (1959) 319.
10. Höjer, G. and Meza, S. *Acta Chem. Scand. 26* (1972) 3723.
11. Mulliken, R. S. and Rieke, C. A. *Rep. Progr. Phys. 8* (1941) 231.
12. Forest, H. and Dailey, B. P. *J. Chem. Phys. 45* (1966) 1736.
13. Quade, C. R. *J. Chem. Phys. 48* (1968) 5490.
14. McClellan, A. L. *Tables of experimental dipole moments*, Freeman, San Francisco and London 1963.
15. Turner, D. W. *Advan. Phys. Org. Chem. 4* (1966) 31.
16. Baker, A. D., May, D. P. and Turner, D. W. *J. Chem. Soc. B* (1968) 22.
17. Siegbahn, P. *Chem. Phys. Lett. 8* (1971) 245.
18. Bak, B., Christensen, D., Dixon, W. B., Hansen-Nygaard, L., Rastrup-Andersen, J. and Schottländer, M. *J. Mol. Spectrosc. 9* (1962) 124.
19. Turner, D. W., Baker, C., Baker, A. D. and Brundle, C. R. *Molecular Photoelectron Spectroscopy*, Wiley, New York 1970.
20. Bak, B. *Mol. Phys. 6* (1963) 373.
21. Bak, B., Hansen-Nygaard, L. and Rastrup-Andersen, J. *J. Mol. Spectrosc. 2* (1958) 361; Bak, B., Mahler, J. L., Nygaard, L. and Sörensen, G. O. *Private communication.*
22. Bak, B., Christensen, D., Hansen, L. and Rastrup-Andersen, J. *J. Chem. Phys. 24* (1956) 720; Bak, B. Report at Nordisk Strukturkjemikermøte, Oslo 1964.
23. Lister, D. G. and Tyler, J. K. *Chem. Commun.* (1966) 152.
24. Lancaster, J. E. and Stoicheff, B. P. *Can. J. Phys. 34* (1956) 1016.
25. Fridh, C., Åsbrink, L., Jonsson, B. Ö. and Lindholm, E. *Int. J. Mass Spectrom. Ion Phys. 8* (1972) 85.
26. Martinez-Carrera, S. *Acta Crystallogr. 20* (1966) 783.
27. Derrick, P. J., Åsbrink, L., Edqvist, O., Jonsson, B.-Ö. and Lindholm, E. *Int. J. Mass Spectrom. Ion Phys. 6* (1971) 161.
28. Almlöf, J., Roos, B., Wahlgren, U. and Johansen, H. *J. Electron Spectrosc. 2* (1973) 51.
29. Kimura, K. and Nagakura, S. *Mol. Phys. 9* (1965) 117.
30. Pickett, L. W. *J. Chem. Phys. 8* (1940) 293; Pickett, L. W., Hoeflich, N. J. and Liu, T. *J. Amer. Chem. Soc. 73* (1951) 4865.
31. Kimura, K. and Nagakura, S. *Theor. Chim. Acta 3* (1965) 164.
32. Pickett, L. W., Corning, M. E., Wieder, G. M., Semenow, D. A. and Buckley, J. M. *J. Amer. Chem. Soc. 75* (1953) 1618.
33. Hirt, R. C., Halverson, F. and Schmitt, R. G. *J. Chem. Phys. 22* (1954) 1148.
34. Brinen, J. S., Hirt, R. C. and Schmitt, R. G. *Spectrochim. Acta 18* (1962) 863.
35. Favini, G. and Bellobono, I. R. *Rend. Ist. Sci. Lett. A 99* (1965) 380.
36. Zanker, V. *Z. Phys. Chem. (Frankfurt am Main) 2* (1954) 52.
37. Leandri, G., Mangini, A., Montanari, F. and Passerini, R. *Gazz. Chim. Ital. 85* (1955) 769.
38. Gelus, M. and Bonnier, J.-M. *J. Chim. Phys. 64* (1967) 1602.
39. Mataga, S. and Mataga, N. *Bull. Chem. Soc. Jap. 32* (1959) 521.

Received October 18, 1973.

Acta Chemica Scandinavica A 28 (1974) 327—339

Conformational Analysis. II. The Molecular Structure, Torsional Oscillations, and Conformational Equilibria of Gaseous Tetrakis-(chloromethyl)methane, $C(CH_2Cl)_4$, as Determined by Electron Diffraction and Compared with Semiempirical Calculations

REIDAR STØLEVIK

Department of Chemistry, University of Oslo, Blindern, Oslo 3, Norway

Gaseous $C(CH_2Cl)_4$ has been studied by electron diffraction at a temperature of 105°C. Only two conformers named **D** (with D_{2d} symmetry) and **S** (with S_4 symmetry) were detected, see Fig. 1. The two conformers are present in equal amounts. Results are presented with error limits (2σ). The following values for distances (r_a) and angles ($\angle_\alpha$) are appropriate for the structure of both conformers: C–H = 1.127(18) Å, C–C = 1.539(8) Å, C–Cl = 1.792(6) Å, $\angle$CCX = 113.5°(0.8), $\angle$CCH = 108.°(2.0).

Non-bonded distances were computed as dependent quantities restricted under the constraints of geometrically consistent r_α parameters.

The carbon-atom framework of both conformers shows small, but significant, deviations from a tetrahedral arrangement, in agreement with semiempirical calculations. The torsion angles of conformer **S** are significantly different from exact staggered values; also predicted by the semiempirical calculations.

Torsional force constants and frequencies for both conformers have been determined by combining information from electron diffraction and vibrational spectroscopy.

The conformational energies have been estimated. Conformer **D** has a higher minimum energy than **S**, but the probability of **D** is considerably increased by a lower vibrational energy and a larger vibrational entropy than **S** (see Table 15). Conformers of low symmetry (C_1, C_2, and C_s) are not present in detectable amounts, as predicted by the semiempirical calculations, too.

INTRODUCTION

$C(CH_2X)_4$(X = F,Cl,Br,I) compounds will be referred to in general as TMX and $C(CH_2Cl)_4$ as TMCL. The number of possible staggered conformers in TMX is 81, but only six are spectroscopically distinguishable, as indicated in Table 1. All conformers, except two, have one or more parallel (1:3) X···X interactions. The two exceptions are shown in Fig. 1, and these conformers will be referred to as **D** (possessing D_{2d} symmetry) and **S** (possessing S_4 symmetry), respectively.

The problem of molecular structure and conformational equilibria of $C(CH_2X)_4$ have engaged several chemists since the first investigation appeared in 1932. The idea about conformational equilibria was not available to the first investigators, and the methods of structural chemistry have been further developed since then.[1,2]

In 1932 Wagner *et al.*[3] carried out the first X-ray investigation on TMX (X = Cl, Br,I) and concluded that the molecules possessed C_{2h} symmetry. De Laszlo [4] in 1934 carried out the first electron-diffraction study on TMX (X = Br,I) and found the X atoms to be in one plane, a finding which is quite close to the arrangement in one of the conformers, the one with D_{2d} symmetry. Hassel *et al.*,[5] in 1937, using both X-ray and electron-diffraction methods proved that their data were not consistent with C_{2h} symmetry for the molecules (X = Cl,Br,I). Hassel also concluded that no simple arrangement of atoms agreed with their electron-diffraction data, and further, that large internal motion is present in these molecules.

Table 1. Characterisation of the six spectroscopically distinguishable staggered conformers of $C(CH_2X)_4$. The symbols A(*anti*) and G(*gauche*) have been used to characterize C–X bonds (*anti* or *gauche* to the CCC framework) of a X–CCC–X′ fragment, while small letters a(*anti*) or g(*gauche*) have been used for C–X bonds (*anti* or *gauche* to the CCC framework) of a C–C–C–X fragment. The type of X···X distance corresponding to a (1:3) X···X *parallel interaction* has been specified as GG(1:3). All staggered conformers possess four C···X(a) and eight C···X(g) distances.

Classical statistical weight	Point group and (symmetry number)	Type of X···X distances			
		GG	AG	AA	GG(1:3)
3	$D_{2d}(4)$	4	0	2	0
24	$C_1(1)$	2	2	1	1
12	$C_2(2)$	1	2	1	2
12	$C_s(1)$	0	2	1	3
24	$C_1(1)$	1	4	0	1
6	$S_4(2)$	2	4	0	0

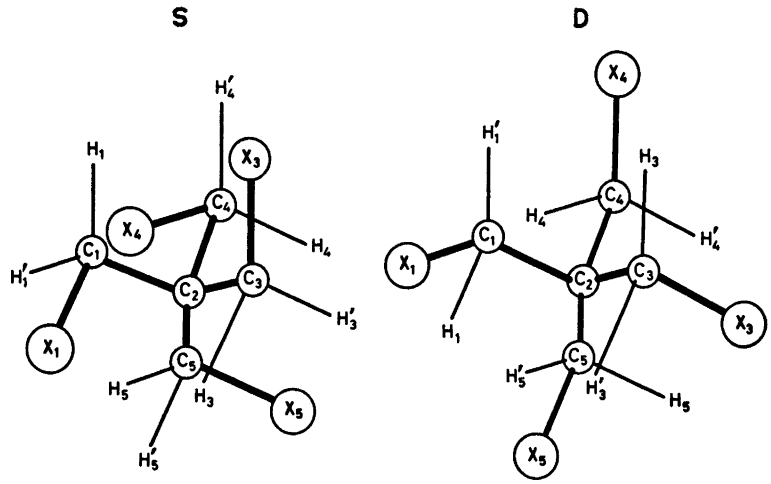

Fig. 1. Numbering of atoms in the two conformers **D** and **S** of $C(CH_2X)_4$. The conformer **D** has D_{2d} symmetry: three C_2 (mutually perpendicular), one S_4 (coincident with one C_2), two σ_d (through S_4). The **S** conformer has S_4 symmetry: one S_4 coincident with one C_2.

In the period 1939–1966 several investigations took place, including spectroscopic studies [6,8,10] and measurements of dipole moments,[7,8,9] however, the conformational equilibrium was not quantitatively described before the present work.

II. CALCULATION OF CONFORMATIONAL ENERGIES, GEOMETRIES, BARRIERS, AND TORSIONAL FORCE CONSTANTS

The method of classical mechanics was used. The semiempirical calculations were carried out as described in Ref. 11. Energy parameters were taken from the work of Abraham and Parry,[12] and the valence force constants in Table 5 were used. The "normal" values of the geometry parameters are given in Table 2. In minimizing the energy, the geometry was constrained in the same way as described in sect. V–A, except that all torsion angles were adjusted as independent variables.

The conformational geometries derived from the semiempirical energy model are presented in Table 2. Calculated structure parameters are in reasonable agreement with the corresponding

Table 2. Calculated geometries for conformers of $C(CH_2Cl)_4$.

Type of parameter	"Normal" value	Conformer D	Conformer S
C–H(Å)	1.094	1.093	1.093
C–C (Å)	1.513	1.544	1.543
C–X (Å)	1.780	1.790	1.790
$C_1C_2C_3$[a](°)	109.47	106.8	111.7
CCX (°)	109.47	113.7	113.7
CCH (°)	109.47	110.2	110.1
ϕ_{1-2} (°)	(60)[b]	0.0	126.3
ϕ_{3-2} (°)	(60)[b]	0.0	126.3
ϕ_{4-2} (°)	(60)[b]	0.0	−126.3
ϕ_{5-2} (°)	(60)[b]	0.0	−126.3

[a] In imimizing the energy, the geometry was constrained in the same way as described in sect. V-A.

[b] $\phi_0 = 60°$, and $V_\phi = \frac{V_0}{2}\sum_k \{1+\cos[3(\phi_{k-2}-\phi_0)]\}$ with $k = 1,3,4,5$.

Table 3. Calculated conformational energies in $C(CH_2Cl)_4$. In minimizing the energy, the geometry was constrained in the same way as described in sect. V-A.

Type of energy (in kcal/mol)	Conformer D	Conformer S	Difference (D–S)
E (bonded)	4.26	4.06	+0.20
E (van der Waals)	4.90	4.68	+0.22
E (polar: X···H)	−17.20	−17.36	+0.16
E (polar: X···X)	10.75	10.58	+0.17
E (total)	2.71	1.96	+0.75

experimental values of Tables 9–11. The value of ϕ_s, 126.3°−120° = +6.3°, for the conformer **S** has the right sign and magnitude, the experimental value being +4.1°. It is also noteworthy that there are no deviations from staggered geometry in the conformer **D**. Moreover, the deviations from a tetrahedral carbon framework seem significant. The deviation parameters (θ_C) are −2.7° (106.8−109.47°) and +2.2° (111.7−109.47°) for the conformers **D** and **S**, respectively. These values are in excellent agreement with the experimental values −2.4° and +2.4°, respectively, (sect. VI).

In Table 3 are the results for conformational energies. According to the present energy model, conformer **S** is 0.75 kcal/mol more stable than conformer **D**.

The conformers with *one* parallel (1:3) X···X interaction, corresponding to C_1 symmetry in Table 1, have their torsion angles displaced from staggered values. The energy of these conformers is thereby considerably lowered. However, the lowest energy obtained was still more than 5 kcal/mol higher than the value for the conformer **D**. The calculations also lead to the conclusion that the *eclipsed* conformer of lowest energy is about 5 kcal/mol less stable than conformer **D**.

Some of the torsional barriers have to be very high, and probably all of them are too high to be detected by electron diffraction. Nevertheless, NMR studies might lead to some information. Therefore, it is of interest to estimate the value of the *lowest* barrier height when a conformation **S** is changed into **D** by rotations of $-CH_2X$ groups around the C–C bonds. If high barriers are to be avoided, then conformational minima, corresponding to conformers of low

symmetry (C_1), are always reached before **S** is changed into **D** by rotations around C–C bonds. The conformers **S** and **D** are thus separated by double-maxima as indicated below:

(max) (max)
S→M→C_1→M′→D
(min) (min) (min)
E: ≃2 <20=8 <20≃3 (kcal/mol)

Valence force constants may be *numerically* computed from the semiempirical energy model.[11] The general expression for a quadratic force constant is:

$F_q = \partial^2 E/\partial q^2$ or $F_{qq'} = \partial^2 E/\partial q \partial q'$

(q: internal coordinate). Torsional force constants (F_ϕ and $F_{\phi\phi'}$) are given in Table 4, together with second order derivatives of the energy under the constraints corresponding approximately to the torsional modes of vibrations.

Table 4. Calculated torsional force constants for conformers of $C(CH_2Cl)_4$.

(mdyn Å (rad)$^{-2}$)	Conformer **D**	Conformer **S**
F_ϕ(diagonal)[a]	0.28	0.30
$F_{\phi\phi'}$ (AA)[b]	−0.012	–
$F_{\phi\phi'}$ (AG)[b]	–	−0.050
$F_{\phi\phi'}$(GG)[b]	−0.087	−0.043
$F(++++)$[c]	0.40	1.43
$F(++--)$[c]	1.77	0.71
$F(+-00)$[c]	0.58[d]	–
$F(+-+-)$[c]	–	0.73[d]

[a] $F_\phi(1-2)=F_\phi(3-2)=F_\phi(4-2)=F_\phi(5-2)=F_\phi$.
[b] in the conformer **D** are two different kinds of $F_{\phi\phi}$, interaction constants (AA and GG) corresponding to XCCCX fragments having their X···X distances AA or GG, respectively; in the **S** conformer are constants of type AG as well as GG. [c] $F(++++)$, $F(++--)$, $F(+-00)$, and $F(+-+-)$ are second order derivatives of the energy with respect to ϕ, under the constraints of the torsional modes (approximately), as follows:
$(++++)$; $\Delta\phi_{1-2}=\Delta\phi_{3-2}=\Delta\phi_{4-2}=\Delta\phi_{5-2}=\Delta\phi$
$(++--)$; $\Delta\phi_{1-2}=\Delta\phi_{3-2}=\Delta\phi$ and $=\Delta\phi_{4-2}=\Delta\phi_{5-2}=-\Delta\phi$
$(+-00)$; $\Delta\phi_{1-2}=\Delta\phi_{3-2}=\Delta\phi$ and $\Delta\phi_{4-2}=\Delta\phi_{5-2}=0$
$(+-+-)$; $\Delta\phi_{1-2}=\Delta\phi_{4-2}=\Delta\phi$ and $\Delta\phi_{3-2}=\Delta\phi_{5-2}=-\Delta\phi$
[d] Degenerate mode belonging to species E.

III. CALCULATION OF VIBRATIONAL QUANTITIES

Valence force constants, except for the torsional part, were taken from the extensive work of Schachtschneider[13] and Snyder.[14] The final force constant values used are shown in Table 5.

The normal coordinate program described by Gwinn[15] was used in computing vibrational frequencies.

Mean amplitudes of vibration corresponding to three different values of the torsional force constants were calculated as described in Ref.[16] In Table 6 are given u and K values[16] for internuclear distances. Some of these quantities are quite sensitive to the values of torsional force constants,[11] which have been adjusted to fit the experimental intensities, as described in sect. V–B.

Several other vibrational quantities in a molecule like TMCL also vary with the torsional force constants. To illustrate this point, some of these quantities have been calculated using different values of the torsional force constants, and the results are found in Table 7 and Table 8.

IV. EXPERIMENTAL AND DATA REDUCTION

The compound was made following the synthesis of Mooradian *et al.*[17] After it was recrystallized from CH_3OH and sublimation of the crystals had been carried out, the compound melted at 96–97°C.

Electron-diffraction photographs were made at a nozzle temperature of 105°C in the Oslo apparatus,[18] under conditions summarized below.

Nozzle-to-plate distance (mm)	480.68	200.63
Electron wavelength (Å)	0.06458	0.06458
Number of plates:	5	5
Range of data, in s(Å^{-1})	1.375–19.875	7.50–35.25
Data interval, Δs (Å^{-1})	0.125	0.250
Estimated uncertainty in the s-scale (%)	0.14	0.14

The electron wavelength was determined by calibration against gold, and corrected by an experiment with CO_2 giving a correction of

Table 5. Valence force constants for $C(CH_2Cl)_4$.
The torsional force constants have been defined in the following way: each fragment A−C−C−C (A = H, X see Fig. 1) has been assigned an equal torsional force constant. The total force constant for the torsional coordinate ϕ_{i-2} ($i = 1,3,4,5$) is thus the sum of *nine* equal contributions, one from each fragment $A-C_i-C_2-C$. The input to Gwinn's normal coordinate program [15] demands a separate specification for each torsional fragment.

Stretch (mdyn/Å)

C−C = 4.534
C−H = 4.850
C−X = 3.140

Bend (mdyn Å (rad)$^{-2}$)

HCH = 0.460
HCX = 0.860
CCH = 0.677
CCX = 0.980
CCC = 1.086

Stretch/Stretch (mdyn Å^{-1})
(C common): C−C/C−X = 0.730, C−C/C−C = 0.101, C−H/C−H = 0.059

Stretch/Bend (mdyn (rad)$^{-1}$)
(C−C common): C−C/CCC = 0.417, C−C/CCX = 0.075, C−C/CCH = 0.260
(C−X common) C−X/HCX = 0.330, C−X/CCX = 0.550

Bend/Bend (combination of two angles with the central C atom common, −mdyn Å (rad)$^{-2}$)
(C−X common): HCX/HCX = 0.161, (C−H common): HCC/HCX = 0.089
(C−C common): HCC/HCC = −0.014, (C common): HCC/HCX = 0.030

Bend/Bend (combination of two angles with C−C common and dihedral angle *anti* or *gauche*)
anti: CCC/CCX = 0.046, HCC/CCC = 0.072
gauche: CCC/CCX = −0.024, HCC/CCC = −0.058

Torsion (mdyn Å (rad)$^{-2}$), see also sect. V-B
F_ϕ(S) = 0.88; for conformer **S**
F_ϕ(D) = 0.36; for conformer **D**

Table 6. Calculated u and (K) values (Å) for internuclear distances in $C(CH_2Cl)_4$ at 105°C. The valence force field given in Table 5 was used, and staggered conformers with tetrahedral C-atom arrangement were assumed. The torsional force constant (F_ϕ) is defined in Table 5.

Distance type	R (Å)	$F_\phi = 0.36$	$F_\phi = 0.62$	$F_\phi = 0.88$
C−H	(1.127)	0.078 (0.0217)	0.078 (0.0185)	0.078 (0.0171)
C−C	(1.539)	0.053 (0.0045)	0.052 (0.0040)	0.052 (0.0037)
C−X	(1.792)	0.055 (0.0152)	0.055 (0.0114)	0.055 (0.0097)
$C_1\cdots C_3$	(2.51)	0.075 (0.0041)	0.074 (0.0035)	0.073 (0.0033)
$C_1\cdots C_4$	(2.51)	0.075 (0.0045)	0.074 (0.0039)	0.073 (0.0036)
C···X	(2.78)	0.076 (0.0108)	0.076 (0.0084)	0.076 (0.0073)
C···H	(2.16)	0.110 (0.0145)	0.109 (0.0120)	0.109(0.0109)
X···H	(2.39)	0.109 (0.0243)	0.109 (0.0182)	0.109 (0.0156)
H···H	(1.85)	0.127 (0.0291)	0.126 (0.0237)	0.125 (0.0213)
X···X(GG)	(3.90)	0.247 (0.0073)	0.209 (0.0064)	0.189 (0.0060)
X···X(AG)	(4.83)	0.165 (0.0069)	0.154 (0.0052)	0.148 (0.0044)
X···X(AA)	(5.56)	0.103 (0.0052)	0.103 (0.0037)	0.103 (0.0030)
C···X(g)	(3.16)	0.150 (0.0087)	0.139 (0.0066)	0.133 (0.0059)
C···X(a)	(4.11)	0.075 (0.0068)	0.075 (0.0052)	0.075 (0.0045)
X···H(GG)	(2.69)	0.239 (0.0167)	0.224 (0.0130)	0.216 (0.0115)
X···H(AG)	(4.19)	0.170 (0.0111)	0.162 (0.0092)	0.157 (0.0083)
X···H(AG)	(4.42)	0.162 (0.0106)	0.157 (0.0082)	0.153 (0.0071)
X···H(GG)	(3.53)	0.225 (0.0122)	0.200 (0.0102)	0.185 (0.0093)
X···H(AA)	(4.95)	0.124 (0.0100)	0.124 (0.0078)	0.124 (0.0068)
C···H(g)	(2.74)	0.157 (0.0109)	0.151 (0.0089)	0.147 (0.0080)
C···H(a)	(3.48)	0.105 (0.0107)	0.105 (0.0092)	0.105 (0.0084)

Table 7. Calculated frequencies in the range 60 – 325 cm^{-1} for conformers of $C(CH_2Cl)_4$. The torsional force constant (F_ϕ) is defined in Table 5. Frequencies corresponding to torsional oscillations are indicated by (ϕ), and degenerate frequencies (belonging to species E) by *d*.

$F_\phi = 0.36$		$F_\phi = 0.62$		$F_\phi = 0.88$	
D	**S**	**D**	**S**	**D**	**S**
66 (ϕ)	67 (ϕ)	79 (ϕ)	82 (ϕ)	88 (ϕ)	91 (ϕ)
82 (ϕ)[d]	80 (ϕ)	89	89	90	91
88	90	100 (ϕ)[d]	90 (ϕ)	112 (ϕ)[d]	110 (ϕ)
151	110 (ϕ)[d]	155	122 (ϕ)[d]	158	129 (ϕ)[d]
217[d]	195	229[d]	197	240[d]	199
236 (ϕ)	220[d]	302 (ϕ)	254[d]	323 (ϕ)	280[d]

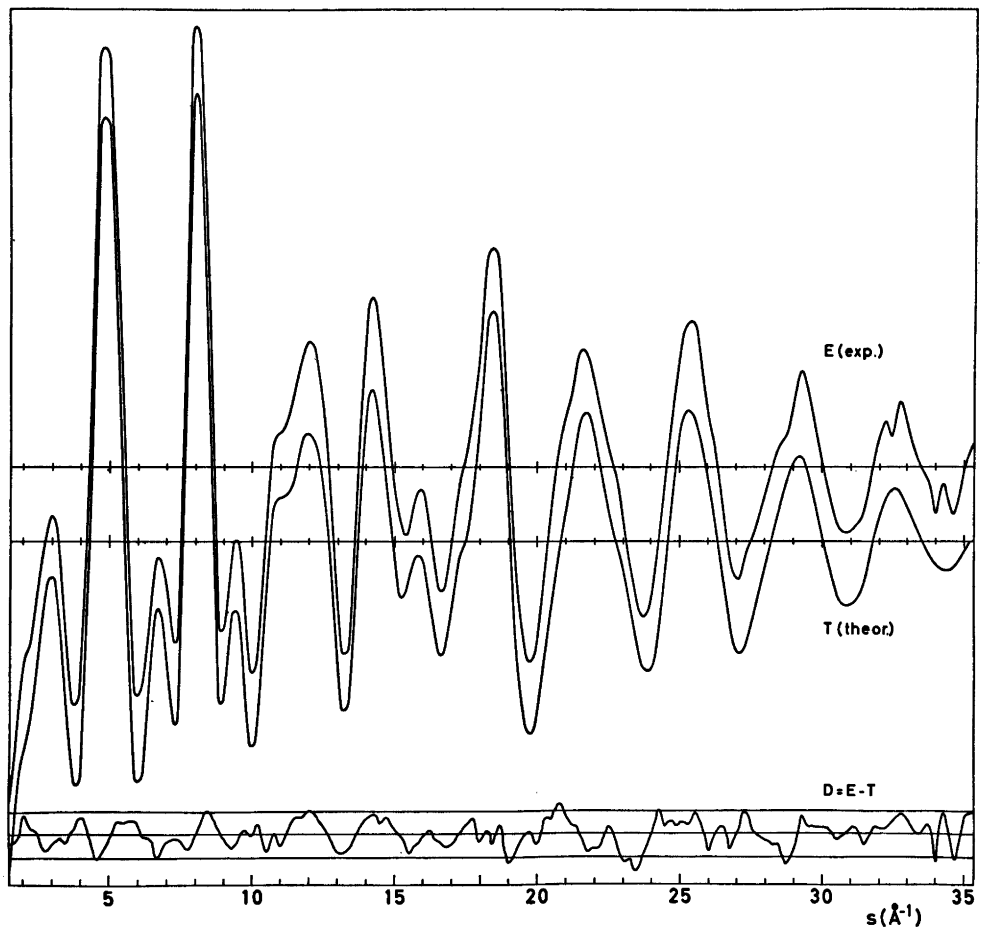

Fig. 2. Curve E shows the experimental intensity, and curve T the theoretical intensity corresponding to the final least-squares parameters. Curve D is the experimental minus theoretical, and the straight lines give the experimental uncertainty (±3× experimental standard deviation).

Table 3. Ratios between vibrational partition functions for conformers of $C(CH_2Cl)_4$ at 105°C. The ratio is defined as $(Q_D/Q_S)^{vib}$, and Q^{vib} is the vibrational partition function, referred to energy *minimum* for the conformer. The difference in vibrational energy is thus included in these ratios. F_ϕ is the torsional force constant as defined in Table 5. $(Q_D/Q_S)^{vib}$ is also a function of temperature, and the values at 205°C and 305°C are 37.5 and 29.8, respectively, with $F_\phi(S) = 0.88$ and $F_\phi(D) = 0.36$ mdyn Å (rad)$^{-2}$. If $F_\phi(S) = F_\phi(D)$ the ratio does *not* vary with temperature.

$F_\phi(S)$	$F_\phi(D)$	(0.36)	(0.62)	(0.88)
(0.36)		1.046	0.114	0.019
(0.62)		9.55	1.046	0.177
(0.88)		56.5	6.17	1.046

+ 0.10 % in the s-scale. The data were reduced in the usual way [19] to yield an intensity curve for each plate.

Average curves for each set of distances were formed. A composite curve was then made by connecting the two average curves after scaling. The final experimental intensity curve is shown in Fig. 2. The intensities have been modified by $s/|f'_{Cl}|^2$. The scattering amplitudes were calculated by the partial wave method [20] using Hartree-Fock atomic potentials.[21]

Contributions to the theoretical intensities from H···H distances, the H atoms bonded to different carbon atoms, were not included.

The radial distribution curve obtained by Fourier transformation of the final experimental intensity is presented in Fig. 3.

V. STRUCTURE ANALYSIS AND REFINEMENTS

The calculated conformational energies suggest that only two spectroscopically distinguishable conformers, **D** and **S**, are present in detectable amounts at 105°C. From the areas under the two peaks (see Fig. 3) corresponding to the distances X···X(AG) and X···X(AA) it was

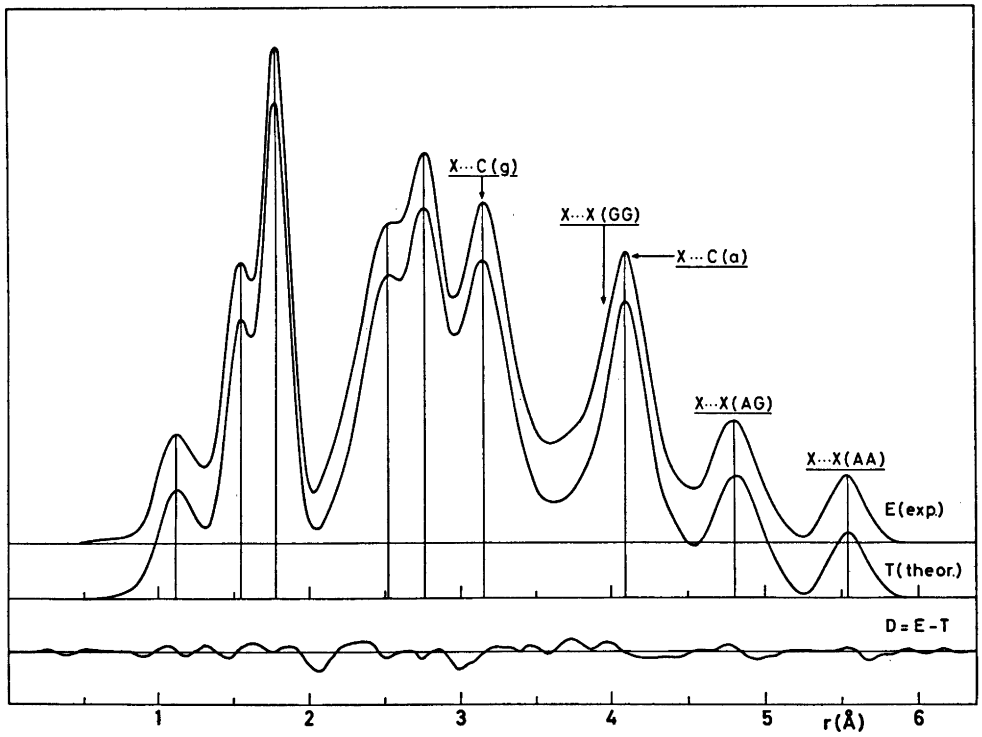

Fig. 3. Experimental (E) and theoretical (T) radial distribution curves and difference curve (D). The RD curves were calculated from the intensity curves of Fig. 2 with an artificial damping constant 0.0020 Å^2.

easily concluded, that **D** and **S** have to be present in nearly equal amounts.

A. Least-squares refinements. The least-squares program was written by H. M. Seip, and it is a modified version of the program explained in Ref. 19. Several conformers may be included in the refinements with the present version of the program.

Models for the conformers were constructed with the following geometrical assumptions: (1) the C-atom framework possess D_{2d}, symmetry, with $\angle C_1C_2C_3 = \angle C_4C_2C_5 = 109.47° - \theta_c$ for the **D** conformer and $\angle C_1C_2C_3 = \angle C_4C_2C_5 = 109.47° + \theta_c$ for the **S** conformer; (2) all four $C-CH_2X$ groups are equal; (3) each of the $C-CH_2X$ groups possess C_s symmetry, and the projection of the angle HCH′ on a plane perpendicular to the C–C axis is 120°; (4) the conformers **D** and **S** have identical structures except for the C–C torsion angles and the CCC angles.

Models were defined in terms of the following average parameters: C–H, C–C, C–X, ∠CCX, ∠CCH and θ_c. The torsion angles of the **S** conformer were defined as follows:

$\phi_{1-2} = \phi_{3-2} = 120° + \phi_s$ and
$\phi_{4-2} = \phi_{5-2} = -120° - \phi_s$.

The deviation angle ϕ_s was refined. All torsion angles for the **D** conformer are equal to 0°. The exact staggered conformers thus have torsional angles: 120, 120, −120, −120° for **S**, and 0, 0, 0, 0° for **D**.

Also adjusted was the composition parameter, the relative amount of conformer **S**. Non-bonded distances were computed as dependent parameters, restricted under the constraints of geometrically consistent r_α parameters.[22,23]

In the first part of the structure analysis a number of refinements were carried out, in which selected combinations of parameters were allowed to vary, while others were held constant at plausible values. At some stages the background had to be corrected, however, none of the important conclusions about the structure and composition were changed thereby.

All important parameters could be simultaneously refined. The combination of all geometry variables, the u values for bond distances and for non-bonded distances of the kinds C···C, X···X, and X···C, the composition parameter, and a scale factor refined to give convergence and reasonable parameter values.

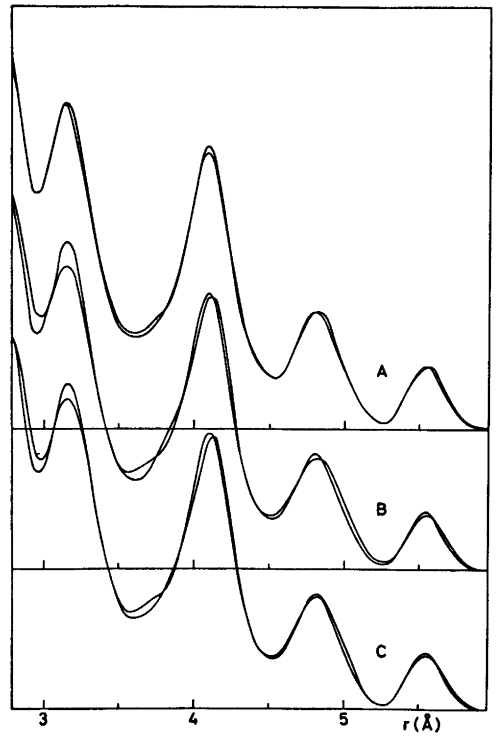

Fig. 4. Three different theoretical RD curves are shown together with the experimental curve. (A) corresponds to final parameters, and several u values have been refined. (B) corresponds to $F\phi(D) = F\phi(S) = 0.53$ mdyn Å (rad)$^{-2}$, and computed u values. (C) corresponds to $F\phi(D) = 0.36$ mdyn Å (rad)$^{-2}$ and $F\phi(S) = 0.88$ mdyn Å (rad)$^{-2}$, and computed u values. A damping constant of 0.0020 Å^2 was used.

B. Determination of torsional force constants. The torsional modes of vibration contribute substantially to the mean amlpitudes of several distances in a molecule like TMCL. Therefore, since a reasonable force field is known, except for the torsional part, the torsional force constants can be adjusted to fit the electron-diffraction data.[11] The following procedure was used: First an average torsional force constant ($\bar{F}\phi$), common to both conformers **D** and **S**, was determined. Parallel and perpendicular amplitudes for several values of $\bar{F}\phi$ were computed and included in the least-squares refinements. The value of $\bar{F}\phi$ which lead to minimum in the error sum (**V′PV** = 862) was obtained for $\bar{F}\phi =$ 0.53 mdyn Å (rad)$^{-2}$. The best fit obtained in this

way was good, but not quite satisfactory. The discrepancies between theoretical and experimental RD curves indicated that the torsional force constant of conformer **D** ought to be smaller than the one for conformer **S**, see Fig. 4. The two conformers were then assigned different values, F_ϕ(D) and F_ϕ(S). The combination of force constants that lead to minimum in the error sum was determined by a systematic iteration procedure, and the best fit was obtained with $F_\phi(D) = 0.36$ and $F_\phi(S) = 0.88$ mdyn Å(rad)$^{-2}$. The new value of **V'PV** [19] is only 5 % less than the value obtained with $F_\phi(D) = F_\phi(S) = \bar{F}$, however the theoretical RD curve [19] corresponding to u values computed with the new set of torsional force constants, was clearly improved compared to the one with $F_\phi(D) = F_\phi(S) = 0.53$ mdyn Å (rad)$^{-2}$; see Fig. 4.

Interaction constants of the type $F_{\phi\phi'}$ have not been determined, but values computed from the energy model are shown in Table 4. Although the absolute values of these interaction constants are small, the effect on torsional frequencies are not negligible. The influence on u and K values are, however, very small.

As already pointed out in a previous paper,[11] it is difficult to estimate uncertainties in the F_ϕ values. However, the most probable torsional force constants and their estimated *minimum* error limits are:
For conformer **D**:

$$F_\phi(D) = 0.36^{+0.17}_{-0.06} \text{ mdyn Å (rad)}^{-2}$$

For conformer **S**:

$$F_\phi(S) = 0.88^{+0.10}_{-0.25} \text{ mdyn Å (rad)}^{-2}$$

Not all combinations of F_ϕ values are equally probable. Certain combinations of the extreme of the permissible ranges are less likely than others. All combinations of values for F_ϕ(D) and F_ϕ(S) within a triangle having corners (0.30, 0.92), (0.44, 0.94), and (0.53, 0.53) are very probable.

The adjustement of F_ϕ values is not a simple and straightforward matter. One has to refine all relevant geometry parameters simultaneously in each least-squares run. If that is not done, the F_ϕ values obtained may be quite biased. Moreover, the adjustments ought to be carried out after a reasonable background has been established. Finally, one should keep in mind that the error limits do not allow for systematic errors in the remainder of the force field.

VI. FINAL RESULTS

Results from the least-squares refinements, and standard deviations (σ) corrected for correlation in the experimental data,[24] are given. All intensities were given equal weights in the final refinements.

Non-bonded distances were restricted under the geometrical constraint of r_α parameters, by including correction terms $D = r_\alpha - r_a$ ($D = u^2/r - K$) for all distances. Calculated u and K

Table 9. Bond lengths (Å) for $C(CH_2Cl)_4$. 0.14 % uncertainty in the wavelength has been included in the σ values. An experiment with CO_2 gave a correction of +0.1 % in the s-scale, therefore the bond lengths given are 0.1 % longer than those obtained directly by refinements. Parameter correlation: $\varrho(C-X,CCX) = -0.51$.

Bond	r_a	σ
C–H	1.127	0.009
C–C	1.539	0.004
C–Cl	1.792	0.003

Table 10. Bond angles for $C(CH_2Cl)_4$.

Angle	$\angle_\alpha$(°)	σ
∠CCX	113.5	0.4
∠CCH	108.0	1.0
$\angle C_1C_2C_3$(D)	106.1	0.9[a]
$\angle C_1C_2C_3$(S)	111.9	0.9[a]
∠XCH	108.2[b]	1.0
∠HCH	110.9[b]	1.0
$\angle C_1C_2C_4$(D)	111.2[b]	0.9
$\angle C_1C_2C_4$(S)	108.3[b]	0.9

[a] It was assumed that the carbon-atom framework in both conformers possessed D_{2d} symmetry. For the conformer **D** $\angle C_1C_2C_3 = \angle C_4C_2C_5 = 109.47° - \theta_c$, and for the conformer **S** $\angle C_1C_2C_3 = \angle C_4C_2C_5 = 109.47° + \theta_c$. The parameter θ_c was refined, and the value obtained was + 2.4° with a standard deviation of 0.9°. Parameter correlation: $\varrho(u_g(C\cdots X), CCX) = 0.58$, $\varrho(u_a(C\cdots X), CCX) = -0.52$. [b] These angles were computed as dependent quantities.

Table 11. Torsion angles [$\angle_\alpha$ values (°)] for the conformers **S** and **D** in $C(CH_2Cl)_4$. The torsion angles of the **S** conformer were confined as follows: $\phi_{1-2}=\phi_{3-2}=120°+\phi_S$ and $\phi_{4-5}=\phi_{5-2}=-120°-\phi_S$, and the deviation angle ϕ_S was refined. (The torsion angles of the **D** conformer are equal to zero by definition.) The value obtained for ϕ_S was +4.1° with a standard deviation of 0.8°. Parameter correlation: $\varrho(\phi_S, \theta_C)=0.80$.

Conformer	ϕ_{1-2}	ϕ_{3-2}	ϕ_{4-2}	ϕ_{5-2}
S	+124.1(0.8)	+124.1(0.8)	−124.(0.8)	−124.1(0.8)
D	(0)	(0)	(0)	(0)

Table 12. Cartesian coordinates (Å) for conformers of $C(CH_2Cl)_4$ (see Fig. 1). The coordinates have been calculated using the final structure parameters, and the numbering of atoms is found in Fig. 1. The principal axes' moments of inertia are (amu Å²): $I_A=I_B=$ 657.94 and $I_C=1193.77$ for conformer **D**, $I_A=$ 629.03 and $I_B=I_C=940.31$ for conformer **S**.

	(*x*)	(*y*)	(*z*)
	Conformer **D** (D_{2d})		
C_2	0	0	0
C_1	1.2299	0.9251	0
X_1	2.7888	0.0413	0
H_1'	1.1860	1.5627	0.9283
H_1	1.1860	1.5627	−0.9283
C_3	−1.2299	0.9251	0
X_3	−2.7888	0.0413	0
H_3'	−1.1860	1.5627	−0.9283
H_3	−1.1860	1.5627	0.9283
C_4	0	−0.9251	1.2299
X_4	0	−0.0413	2.7888
H_4	0.9283	−1.5627	1.1860
H_4'	−0.9283	−1.5627	1.1860
C_5	0	−0.9251	−1.2299
X_5	0	−0.0413	−2.7888
H_5	0.9283	−1.5627	−1.1860
H_5'	0.9283	−1.5627	−1.1860
	Conformer **S** (S_4)		
C_2	0	0	0
C_1	1.2751	0.8617	0
X_1	1.3512	2.0252	−1.3608
H_1'	2.1623	0.1709	−0.0767
H_1	1.3015	1.4446	0.9642
C_3	−1.2751	0.8617	0
X_3	−1.3512	2.0252	1.3608
H_3'	−2.1623	0.1709	0.0767
H_3	−1.3015	1.4446	−0.9642
C_4	0	−0.8617	1.2751
X_4	1.3608	−2.0252	1.3512
H_4	−0.9642	−1.4446	1.3015
H_4'	0.0767	−0.1709	2.1623
C_5	0	−0.8617	−1.2751
X_5	−1.3608	−2.0252	−1.3512
H_5	0.9642	−1.4446	−1.3015
H_5'	−0.0767	−0.1709	−2.1623

values, corresponding to final torsional force constants, are shown in Table 6.

Parameter correlation coefficients with absolute values larger than 0.50 are included in Tables 9 – 13.

Bond lengths corresponding to r_a values [19] are given in Table 9, and bond angles in Table 10. The torsion angles of the conformer **S** have been adjusted and the values are found in Table 11. The torsion angles of conformer **D** have been kept constant at values also shown in Table 11.

Cartesian coordinate for the conformers are found in Table 12.

Several *u* values have been refined and compared to those computed using the final torsional force constants (see Table 13). Both sets of *u* values are experimental, but the calculated values combine information from spectroscopy as well as from electron diffraction. Some *u* values get very small contributions from the torsional modes of vibration. Such *u* values are those corresponding to bond distances, distances over *one* bond angle, distances X···X(AA), and the distance X···C(a). The fact that these *u* values are generally in good agreement with those refined directly, is important. The valence force field used for TMCL thus seems reasonable. The value of *u*(C−X), determined directly by leastsquares refinements, is significantly different from the spectroscopic value, probably due to an error in blackness correction. It is, however, unlikely that other *u* values are significantly disturbed by this type of error. The average deviation between the two sets of *u* values is less than 8 %, while the average, $\langle\sigma/u\rangle$, relative uncertainty of the refined *u* values is 8.5 %.

The relative amounts of the conformers **D** and **S** were easily determined. The composition parameter $\alpha_S(\alpha_D=100-\alpha_S)$ was introduced, and

Table 13. Mean amplitudes (u) of vibration for $C(CH_2Cl)_4$ at 105°C.

Type of distance	Distance (Å)	Calculated u value[a] (Å)	Refined u value[b] (Å)	σ (Å)
C–H	(1.127)	0.078	0.077	0.010
C–C	(1.539)	0.052	0.053	0.005
C–X	(1.792)	0.055	0.045	0.003
C···C	(2.51)	0.074	0.094	0.015
X···C_2	(2.78)	0.076	0.076	0.006
X_1···H_1	(2.40)	0.109	0.105	0.018
X···C(g) in **D**	(3.16)	0.150	0.137	0.017
X···C(g) in **S**	(3.1 – 3.2)	0.133	0.120[c]	(–)[c]
X···C(a)	(4.11)	0.075	0.079	0.006
X···X(AG) in **S**	(4.83)	0.148	0.136	0.006
X···X(GG) in **D**	(3.98)	0.247	0.305	0.030
X···X(GG) in **S**	(3.81)	0.189	0.247[c]	(–)[c]
X···X(AA) in **D**	(5.56)	0.103	0.100	0.009

[a] The u values correspond to the valence force field of Table 5 with torsional force constants $F_\phi(D) = 0.36$ and $F_\phi(S) = 0.88$ mdyn Å (rad)$^{-2}$. [b] Values obtained by least-squares refinements. [c] Refined together with the previous u value as *one* parameter. Parameter correlation: $\varrho[u(C\cdots C), \alpha_s] = 0.59$, $\varrho[u(C\cdots C), u(C-X)] = -0.63$, $\varrho[u_g(C\cdots X), u_a(C\cdots X)] = -0.64$, $\varrho[u_{GG}(X\cdots X), \alpha_s] = -0.54$.

Table 14. Calculations of ΔE^m using three different sets of torsional force constants. F_ϕ: torsional force constant, see Table 5 for definition of F_ϕ. The energy differences were calculated from eqn. (1) using the experimental equilibrium constant of 1.0, and the symmetry numbers $4(D_{2d})$ and $2(S_4)$.

	I	II	III
$F_\phi(D)$, mdyn Å (rad)$^{-2}$	0.36	0.51	0.62
$F_\phi(S)$, mdyn Å (rad)$^{-2}$	0.88	0.74	0.62
$(Q_D/Q_S)^{vib}_{T=378\ K}$	56.5	5.53	1.05
$\Delta E^m = E_D^m - E_S^m$, kcal/mol	+2.50	+0.75	−0.52

Table 15. Values of thermodynamic quantities relevant to the equilibrium between conformers (**S D**) of $C(CH_2Cl)_4$. Differences are always **D** minus **S**. Quantities being dependent on temperature have been marked by the suffix T. ($\Delta H_T = \Delta E_T$ for the gas equilibrium **S** ⇌ **D**).

($T = 378$ K) $\Delta G_T = \Delta E_T - T\Delta S_T = -RT \ln K_p$ ($K_p = 1.0$, $\Delta G_T = 0$)

$\Delta E^m = +2.5$ kcal/mol	$\Delta S_\sigma = -R \ln(\sigma_D/\sigma_S) = -R \ln 2$
$\Delta E_T^{vib} = -1.5^a$ kcal/mol	$\Delta S_T^{vib} = +4.0^b$ cal/(deg mol)
$\Delta E_T = \Delta E^m + \Delta E_T^{vib} = +1.0$ kcal/mol	$\Delta S_T = \Delta S_\sigma + \Delta S_T^{vib} = +2.6$ cal/(deg mol)

[a] The difference in zero-point vibrational energy, $\Delta E_0^{vib} = \frac{1}{2}Nhc(\sum\omega_D - \sum\omega_S)$, is −2.0 kcal/mol. $\Delta E_T^{vib} = RT^2 d \ln q^{vib}/dT$ with $q^{vib} = (Q_D/Q_S)_T^{vib}$ and the vibrational partition function Q^{vib} referred to the *minimum* of potential energy for the conformer; see also Table 14. [b] Calculated according to the standard expression for the contribution of entropy associated with vibrational degrees of freedom: $\Delta S_T^{vib} = R \ln q^{vib} + RTd(\ln q^{vib})/dT$. [m] Difference between potential energy *minima* for the conformers.

the value obtained from least-squares refinements was $\alpha_S = 50$ % ($\sigma = 1$ %).

VII. DISCUSSION

Following standard statistical thermodynamics,[25,26] the relative amounts α_D and α_S for the two conformers (S⇌D) in equilibrium in the gas phase, are related to the theoretical expression for the equilibrium constant, as given in eqn. 1:

$$\alpha_D/\alpha_S = (\sigma_D/\sigma_S)^{-1}(Q_D/Q_S)^{vib}\exp(-\Delta E^m/RT) \quad (1)$$

(The *classical* rotational partition functions for the two conformers are very nearly equal.) Q^{vib} is the vibrational partition function, referred to the *minimum* of potential energy, for a conformer. $\Delta E^m = E_D{}^m - E_S{}^m$ is the difference in potential energy between the two conformers, and the difference is measured between energy *minima*. The difference in zero-point vibrational energy is thus included in the ratio between the vibrational energy partition functions. σ is the symmetry number of a conformer.[26] R and T have their usual thermodynamic meanings.

The difference in free energy (ΔG) between the two conformers is zero at 105°C. If the vibrational partition functions for the conformers are known, then ΔE^m may be estimated from eqn. (1). The *ratio* between the partition functions depends on the *difference* in torsional force constants as demonstrated in Table 8. Calculations of ΔE^m using three different sets of torsional force constants are summarized in Table 14. The combination I (0.36, 0.88) corresponds to the torsional force constants determined from the electron diffraction data. The combination II (0.51, 0.74) lead to the value of ΔE^m (0.75 kcal/mol) predicted by the semi-empirical energy model. Both experiment and semiempirical calculations thus indicate that conformer **D** is *less* stable than conformer **S**, but the ΔE^m values do not agree. The possibility III ($F_\phi(D) = F_\phi(S)$) seems to be unlikely.

The fact that the two conformers are present in equal amounts is thereby given a reasonable explanation: the lower minimum energy of conformer **S** is compensated by the lower *vibrational* energy and larger vibrational entropy of conformer **D**. (The relative amount of **D** ought to be increased by an increase in temperature.)

Values of thermodynamic functions, relevant to the equilibrium between the conformers, S⇌D, have been summarized in Table 15.

Although T, ΔE_T, and ΔS_T are rather uncertain quantities, the values of Table 15 may serve as a warning. Because of lack of spectroscopic information it has been quite common practice to assume equal vibrational partition functions for different conformers. For conformers with torsional oscillations of low frequencies that approximation has to be questioned. If the thermodynamic quantities are computed assuming *equal* torsional force constants, quite different values for ΔE_T and ΔS_T are obtained. However, more important is the consequence that the temperature dependency of ΔE_T and ΔS_T is lost. The study of conformational equilibria at several temperatures [27] is a promising approach. The usual practice has been to obtain ΔS and ΔE from the effect of temperature on composition by use of the relation $\Delta G_T = \Delta E - T\Delta S$ assuming ΔE and ΔS temperature *independent* quantities. The formula may still be used, if the temperature dependency of ΔE and ΔS is taken into consideration. Nevertheless, the most direct relation between composition, temperature, and fundamental thermodynamic quantities is eqn. (1). All information about $\Delta E_T{}^{vib}$ and $\Delta S_T{}^{vib}$ may be derived from the function $(Q_D/Q_S)_T{}^{vib}$, which is directly related to the difference in force fields of the conformers.

The thermodynamic quantities relevant to the equilibrium between the abundant conformers of TMCL have been estimated. However, electron diffraction data at increased temperatures, together with observed vibrational frequencies in the range 50 – 300 cm^{-1} are needed to determine more accurately the thermodynamic quantities. P. Klæboe and coworkers at this university are investigating TMCL by IR and Raman, and electron-diffraction data in the range 150 – 200°C have been recorded. B. Pedersen and coworkers, also at this university, have started on a NMR investigation of TMCL and related compounds.

The conformers **D** and **S** ought to have zero electric dipole moments as suggested by their geometry. The observed moment, however, is

0.43 Debye for TMCL.[9] In their paper [9] Thompson and Sweeney discuss the origin for this non-zero moment. At least two possible explanations exist: (1) the moment is induced by the torsional oscillations, or (2) conformers of low symmetry (C_1 in Table 1) are present in detectable amounts. The second possibility seems to be ruled out by the values of conformational energies obtained from the semiempirical calculations. The electron-diffraction data at 105°C exclude relative amounts of C_1 conformers larger than 5 – 6 %.

Finally, have the results (structure parameters, conformational energy, and torsional force constants) predicted by the semiempirical energy model been confirmed by the experimental findings? Considering the experimental uncertainties, the calculated structure parameters (Table 2) agree with the experimental (Tables 9 – 11) values. The calculated torsional force constants (Table 4) do not agree with those determined from the electron-diffraction data. (sect. V – B) Both experimental and calculated values for $\Delta E^m = E_D{}^m - E_S{}^m$, 2.5 and 0.75 kcal/mol, respectively, indicate that conformer **D** is less stable than conformer **S**. Considering the large uncertainty involved, the two values are not significantly different.

Acknowledgements. I am grateful to Cand. real. A. Almenningen for recording the diffraction photographs, and to Prof. O. Bastiansen, Prof. S. J. Cyvin, Dr. A. Haaland, Dr. P. Rademacher, and Dr. H. M. Seip for helpful discussions. Computer programs made available by Dr. H. M. Seip, Cand. real. S. Rustad, and Prof. W. D. Gwinn have been extensively used in this work. Financial support from Norges almenvitenskapelige forskningsråd is gratefully acknowledged.

REFERENCES

1. Bastiansen, O., Seip, H. M. and Boggs, J. E. In Dunitz, J. D. and Ibers, J. A., Eds., *Perspectives in Structural Chemistry*, Wiley, New York 1971, Vol. IV.
2. Seip, H. M. In Sim, G. A. and Sutton, L. E. Eds., *Molecular Structure by Diffraction Methods* Specialist Periodical Reports, The Chemical Society, London 1973, Vol. 1, Part 1, Chapter 1.
3. Wagner, G. and Dengel, G. *Z. Phys. Chem. B 16* (1932) 382.
4. De Laszlo, H. *C. R. Acad. Sci. 198* (1934) 2235.
5. Hassel, O. and Strømme, L. C. *Z. Phys. Chem. B 38* (1937) 349.
6. Ballaus, O. and Wagner, J. *Z. Phys. Chem. B 45* (1939) 165.
7. Mortimer, C. T., Speeding, H. and Springale, *J. Chem. Soc.* (1957) 188.
8. Lumbroso, H. and Lauranson, D. *Bull. Soc. Chim. Fr.* (1959) 513.
9. Thompson, H. B. and Sweeney, C. C. *J. Phys. Chem. 64* (1960) 221.
10. Geiseler, G. and Ratz, L. *Z. Naturforsch. 21* (1966) 1889.
11. Stølevik, R. *Acta Chem. Scand. A 28* (1974) 299.
12. Abraham, R. J. and Parry, K. J. *J. Chem. Soc. B* (1970) 539.
13. Schachtschneider, J. H. and Snyder, R. G. *Vibrational Analysis of Polyatomic Molecules. IV* (Force constants for the haloparaffins). Project No. 31450, Technical Report No. 122 – 63 of Shell Development Company.
14. Snyder, R. G. and Schachtschneider, J. H. *Spectrochim. Acta 21* (1965) 169.
15. Gwinn, W. D. *J. Chem. Phys. 55* (1971) 477.
16. Stølevik, R., Seip, H. M. and Cyvin, S. J. *Chem. Phys. Letters 15* (1972) 263.
17. Mooradian, A. and Cloke, J. B. *J. Amer. Chem. Soc. 39* (1945) 942.
18. Bastiansen, O., Hassel, O. and Risberg, E. *Acta Chem. Scand. 9* (1955) 232.
19. Andersen, B., Seip, H. M., Strand, T. G. and Stølevik, R. *Acta Chem. Scand. 23* (1969) 3224.
20. Peacher, J. and Willis, J. C. *J. Chem. Phys. 46* (1967) 4809.
21. Strand, T. G. and Bonham, R. A. *J. Chem. Phys. 40* (1964) 1686.
22. Morino, Y., Kuchitsu, K., and Oka, T. *J. Chem. Phys. 36* (1962) 1108.
23. Kuchitsu, K. *J. Chem. Phys. 49* (1968) 4456.
24. Seip, H. M. and Stølevik, R. In Cyvin, S. J., Ed., *Molecular Structures and Vibrations*, Elsevier, Amsterdam 1972.
25. Glasstone, S. *Theoretical Chemistry*, Van Nostrand, London.
26. Herzberg, G. *Infrared and Raman Spectra of Polyatomic Molecules*, Van Nostrand, Princeton.
27. Almenningen, A., Bastiansen, O., Fernholt, L. and Hedberg, K. *Acta Chem. Scand. 25* (1971) 1946.

Received November 27, 1973.

Acta Chemica Scandinavica A 28 (1974) 340—346

The Crystal Structure of Disodium Pentacyanoammineferrate(III) Dihydrate, $Na_2[Fe(CN)_5NH_3].2H_2O$

AINA TULLBERG and NILS-GÖSTA VANNERBERG

Department of Inorganic Chemistry, Chalmers University of Technology and University of Göteborg, P.O. Box, S-402 20 Göteborg 5, Sweden

The crystal structure of disodium pentacyanoammineferrate(III) dihydrate, $Na_2[Fe(CN)_5NH_3].2H_2O$, has been determined by single crystal X-ray diffraction methods. The crystals are orthorhombic space group *Pnnm* with $a = 6.111 \pm 1$ Å, $b = 11.899 \pm 2$ Å, $c = 15.623 \pm 3$ Å, and $Z = 4$. An R-value of 0.091 has been obtained

The structure consists of double chains of distorted sodium ion coordination octahedra, held together in three dimensions by octahedral $[Fe(CN)_5NH_3]^{2-}$ ions. Each sodium ion is thus surrounded by four nitrogen atoms of cyanide groups and two water oxygen atoms all at distances of approximately 2.5 Å.

Each $[Fe(CN)_5NH_3]^{2-}$ ion is octahedral with almost linear Fe − C − N groups. The C − N bond distances are 1.17, 1.14, and 1.14 Å, the Fe − NH_3 distance is 2.01 Å and the Fe − C distances are 1.89, 1.93, and 1.94 Å.

There seems to be no hydrogen bonding between the complex ions and the water molecules.

In a systematic investigation of pentacyanidomonoligandferrates the crystal structure of $Na_2[Fe(CN)_5NH_3]\cdot 2H_2O$ has been determined since the NH_3 ligand can be regarded as only σ-bonded in contrast to the strongly π-bonded NO^+ ligand.

EXPERIMENTAL

Preparation of $Na_2[Fe(CN)_5NH_3].2H_2O$. Crystals of $Na_2[Fe(CN)_5NH_3]\cdot 2H_2O$ were prepared according to a method described by Brauer.[1] $Na_3[Fe(CN)_5NH_3]$ was first prepared by passing ammonia through an aqueous solution of $Na_2[Fe(CN)_5NO]$ at 10 °C. $Na_3[Fe(CN)_5NH_3]$ was then treated at 0 °C with a solution of sodium nitrate and acetic acid. From this solution it is easy to get a pure but microcrystalline precipitate of $Na_2[Fe(CN)_5NH_3]\cdot 2H_2O$ by adding ethanol and ether. To obtain crystals suitable for X-ray diffraction work, however, the original mother liquid was allowed to stand. Single crystals of $Na_2[Fe(CN)_5NH_3].2H_2O$ form in the solution after some time. They are needle-shaped, yellow in colour and decompose slightly in air. The infra-red absorption spectrum from a selection of crystals was recorded. It showed bands characteristic of both $Na_2[Fe(CN)_5NH_3]$ [2] and $Na_2[Fe(CN)_5NO]$.[2] Crystals of the latter may have formed in the solution. They are redder than those of the ammine compound. To prove that the crystals prepared were not of the hypothetical compound, $Na_2[Fe(CN)_4NH_3NO]$, a crystal sample (several mg) was analysed for

Table 1. X-Ray powder diffraction data for $Na_2Fe(CN)_5NH_3\cdot 2H_2O$. Guinier camera. Cu$K\alpha_1$ radiation ($\lambda = 1.54050$ Å).

h	k	l	$10^5\sin^2\theta$ obs	$10^5\sin^2\theta$ calc	d (calc) Å	I_{calc}	I_{obs}
0	0	2	974	972	7.811	385	s
0	2	0	1679	1676	5.950	31	vvw
1	0	1	1830	1832	5.691	427	s
1	1	0	2005	2008	5.436	38	vvw
0	1	3	2607	2607	4.771	45	vw
0	2	2	2641	2648	4.733	632	vs
1	1	2	2978	2980	4.462	148	m
1	2	1	3508	3508	4.113	666	vs
1	0	3	3778	3776	3.964	118	m
0	0	4	3888	3889	3.906	47	w
1	3	0	5358	5360	3.327	27	vvw
1	2	3	5449	5452	3.299	76	w
0	2	4	5565	5565	3.265	99	w
0	3	3	5960	5959	3.155	22	vvw
2	1	0	6776	6774	2.960	34	vvw
2	1	1	7015	7017	2.908	23	vvw
1	2	4	7152	7154	2.880	470	vs
2	0	2	7325	7327	2.846	30	vvw
2	2	1	8270	8274	2.678	112	m
2	2	2	9004	9003	2.567	128	m
1	3	4	9250	9249	2.533	346	s

Table 2. Observed and calculated structure factors for $Na_2[Fe(CN)_5NH_3].2H_2O$.

0 K 0			11 43 -43			0 K 24			1 K 6			20 12 -11			2 K 0		
2	42	-40	13	23	27	2	15	-16	1	27	30				2	19	-19
4	64	-51				4	17	17	2	9	-9		1 K 12		3	35	-36
6	28	25		0 K 10					3	8	-9	1	20	-17	4	166	182
8	87	87					1 K 0		4	38	34	2	11	-8	5	31	30
10	42	43	0	56	56	2	22	32	5	96	90	3	57	-54	6	23	22
12	15	-18	2	97	-94	3	50	-47	6	10	-9	4	11	-12	8	22	23
14	27	26	4	28	27	4	15	14	7	48	-48	5	7	-6	10	26	26
18	13	13	6	12	-9	5	20	25	8	15	-16	7	49	-49	14	31	29
20	13	-18	8	13	-11	7	42	-42	9	46	46	14	12	-2	16	17	-17
22	11	17	12	22	-21	9	51	59	10	7	8	16	10	4	18	16	23
			14	11	11	10	12	-12	11	11	-10	20	10	-3			
0 K 1			16	14	-11	11	48	-54	13	24	24					2 K 1	
3	34	-30	20	14	-14	13	22	23	15	9	-12		1 K 13		2	90	83
5	6	1				15	10	-8	17	8	8	0	62	58	3	51	-55
7	74	-75		0 K 11		16	15	8				1	8	10	4	26	-24
9	45	48	1	26	26	18	12	-3		1 K 7		2	41	-38	5	61	61
11	55	-58	3	34	-35	20	12	-5	0	51	50	3	8	7	6	23	-24
13	30	34	5	17	15	21	9	-7	1	15	-12	4	42	41	7	64	-66
15	9	-9	9	56	56	22	9	1	2	76	-71	6	9	-8	9	29	29
17	9	-11	11	53	-60				3	22	-21	7	9	-6	10	11	13
			13	17	18		1 K 1		4	43	39	8	7	5	11	34	-36
0 K 2						2	117	-132	5	38	35	10	8	7	13	13	14
4	35	34		0 K 12		3	17	21	6	47	-43	12	9	-9	14	11	-10
6	38	-36	0	94	91	4	34	33	7	22	23	14	17	16	15	15	-16
8	24	-25	2	66	-62	5	8	6	8	8	8	16	13	-12	16	17	1
10	8	-4	4	16	16	6	37	-35	9	37	-39	18	11	11	18	15	7
12	26	-23	8	14	13	7	6	-5	11	8	-10	20	10	-10			
14	12	9	12	19	-19	8	11	-10	12	19	-19					2 K 2	
16	16	-18	14	15	13	12	21	-22	13	20	22		1 K 15		2	95	-94
18	12	13	16	11	11	14	15	17	14	19	19	0	31	33	3	26	20
20	14	-16	18	13	-14	16	16	-17	15	10	1	2	30	-34	4	17	17
						18	14	12	16	21	-21	4	26	28	5	14	-16
0 K 4				0 K 15		20	13	-14	18	15	16	5	11	12	6	57	-62
0	90	73	3	29	-28				20	10	-10	6	19	-22	7	18	-19
2	96	-91	5	15	15		1 K 2					7	13	11	9	11	16
4	53	54	7	41	-42	5	79	77		1 K 8		8	9	7	10	10	-3
6	17	-17	9	25	26	6	8	-8	1	16	15	9	16	-18	12	25	-28
8	25	28	11	22	-20	7	28	-32	2	21	-17	13	10	11	13	17	-11
12	24	-26	13	14	12	9	62	67	3	41	-39	14	10	13	14	19	17
14	17	16				11	27	-29	4	25	21	16	15	-14	16	23	-24
16	13	-13		0 K 16		13	26	32	5	44	41	18	12	14	17	18	2
18	20	23	18	18	18				6	12	11				18	14	13
20	12	-14					1 K 3		7	47	-46		1 K 16				
				0 K 17		2	61	-56	8	14	-14	2	20	-19		2 K 3	
0 K 5			3	18	-19	3	37	-33	9	37	38	3	25	-23	1	31	31
1	8	7	5	31	32	4	103	101	11	29	-31	4	13	13	2	16	-17
3	7	7	7	32	-33	5	16	-14	13	17	17	5	30	29	5	74	74
5	104	106	9	16	17	6	17	-17	14	11	9	7	32	-33	6	9	11
7	53	-56	11	17	-16	7	15	16	15	9	-12	8	8	-8	7	66	-68
9	50	50	13	9	9	8	10	11	18	12	-7	9	21	21	8	9	-7
11	16	-14				10	15	15				11	17	-15	9	40	40
13	24	22		0 K 18		14	23	24		1 K 9		15	9	-10	11	11	-8
15	12	-14	0	12	12	15	16	-9	0	28	27				13	24	29
17	12	7	2	37	-36	16	14	-20	1	25	22		1 K 17		15	14	-16
			4	26	25	18	15	17	2	88	-84	2	36	-36	18	14	-2
0 K 6			6	14	-15				3	13	11	4	26	28			
0	50	46	12	14	-12		1 K 4		4	42	40	6	24	-27		2 K 4	
2	94	-89	14	10	9	1	18	-17	5	13	-14	16	16	-19	22	5	7
4	18	18	16	13	-14	2	154	-160	6	38	-35	18	11	12			
6	73	-74				3	134	-134	8	16	-16					2 K 5	
8	8	-8		0 K 19		5	12	-11	12	15	-15		1 K 18		1	53	49
12	24	-20	3	14	-15	6	58	58	14	13	14	1	19	19	3	27	-26
14	14	10	5	19	20	7	86	-86	16	20	-20	2	29	-29	4	20	20
16	25	-27	7	20	-20	9	26	28	18	12	11	3	7	-9	5	71	71
18	16	17	9	21	23	10	12	-11	20	11	-10	5	32	32	6	11	-11
20	13	-13	11	17	-19	11	50	-50				6	12	14	7	40	-37
			13	9	10	12	7	-8		1 K 10		7	17	-18	8	11	-12
0 K 7						14	11	10	1	47	43	9	28	27	9	42	43
3	49	-49		0 K 20		15	17	-19	2	25	-22	11	9	-9	11	16	-19
5	27	25	0	40	41	17	8	3	3	8	-8	13	12	13	13	27	26
7	84	-80	2	26	-27	18	16	-9	4	10	-13				15	13	-8
9	34	33	4	15	14	22	9	2	5	48	45		1 K 19				
11	24	-24	14	10	10				6	13	12	0	30	29		2 K 6	
13	20	21					1 K 5		7	15	-14	2	22	-21	0	16	17
15	18	-17		0 K 21		0	38	38	9	56	55	4	27	27	2	95	-91
21	9	-5	1	12	11	1	24	22	11	29	-30	6	10	-10	3	21	-21
			5	15	15	2	41	-40	13	25	26	7	11	8	4	29	28
0 K 8			7	14	-13	3	23	-17	21	11	-4				5	11	9
0	194	202	9	22	23	4	111	108					1 K 20		6	49	-47
2	7	-6	11	13	-18	5	8	-8		1 K 11		1	8	-7	7	13	16
4	41	41	13	15	20	6	29	-28	0	86	83	3	19	-21	9	18	-19
8	52	49				7	15	14	1	8	-6	5	8	9	10	10	-11
10	36	35		0 K 22		8	12	9	2	48	-46	7	29	-28	12	27	-30
12	10	-7	0	40	44	9	11	-12	3	13	-12	9	14	13	16	22	-22
14	25	22	2	31	-32	10	14	13	4	48	44	11	18	-20	18	12	11
16	9	-9	6	12	-10	12	7	-5	5	8	-7	13	10	10			
18	18	18	12	10	-12	13	9	10	6	7	-2					2 K 7	
						14	24	24	8	8	8		1 K 24		1	28	-26
0 K 9				0 K 23		15	11	-12	9	11	13	3	11	-11	2	9	-8
1	20	-19	3	12	-14	16	24	-25	10	10	10	5	11	9	3	51	-50
3	28	-27	7	12	-11	18	20	19	13	8	-7	7	14	-14	4	12	13
5	29	30	9	16	20	19	8	5	14	16	18	9	15	17	5	57	57
7	53	-52	11	21	-26	22	10	4	16	9	-11	11	13	-17	7	52	-49
9	32	30	13	11	12				18	11	11				8	21	-9

Table 2. Continued.

9 23 22	2 K 17	4 12 -10
10 11 7	3 23 -23	5 61 58
11 34 -35	5 17 20	7 36 -34
13 18 13	7 31 -29	9 36 37
14 14 3	9 18 18	13 22 18
15 14 -12	11 14 -14	15 14 -9
16 16 -3	18 12 -4	
18 15 -3		3 K 11
	3 K 0	0 43 37
2 K 8	5 62 60	2 28 -26
0 64 62		3 20 20
1 17 -16	3 K 2	4 52 50
2 15 -16	3 22 -20	6 17 -20
3 27 -27	4 13 -16	7 25 -25
4 106 106	5 60 61	10 12 12
5 15 14	6 10 12	14 13 13
6 11 11	7 28 -26	16 12 -17
7 15 18	9 54 57	
8 28 28	11 17 -21	3 K 12
10 17 17	12 10 4	1 26 -26
13 12 4	13 19 21	2 18 19
14 27 29		3 43 -39
16 13 -15	3 K 3	4 11 -11
18 20 18	2 48 -46	5 22 22
	3 31 28	7 54 -54
2 K 10	4 46 46	9 11 9
0 50 48	6 14 -13	11 24 -24
1 12 9	7 20 -24	15 18 -15
2 57 -56	8 24 24	17 12 1
3 14 13	10 12 12	
4 17 18	12 14 -15	3 K 13
5 10 -9	14 15 20	0 45 43
6 46 -47	16 11 -14	2 30 -28
7 15 -17		4 35 34
9 12 16	3 K 4	6 15 -16
12 17 -17	1 72 -65	7 11 -12
13 19 -11	2 25 23	8 11 9
14 13 13	3 55 -53	13 15 -10
16 20 -21	4 8 8	14 15 12
20 12 -10	5 21 23	16 15 -15
	7 79 -79	17 13 -1
2 K 11	11 44 -46	18 11 15
2 13 10	13 12 19	
4 15 -16	15 15 -15	3 K 24
5 45 45		4 16 -4
7 54 -56	3 K 5	7 19 -19
9 26 26	0 140 129	
11 12 -6	1 24 23	4 K 1
12 11 0	2 55 -51	3 49 -50
13 23 22	3 10 8	5 15 16
	4 23 23	6 16 19
2 K 12	8 25 29	7 50 -53
0 45 43	12 15 -21	9 34 36
2 35 -35	14 19 21	11 26 -24
4 42 41		13 11 11
6 27 -27	3 K 6	15 16 -12
7 12 -11	1 63 58	
9 11 12	2 19 -16	4 K 2
13 12 -9	3 35 -35	2 68 -74
14 13 17	4 10 -4	3 27 -28
15 11 7	5 30 29	4 20 20
16 16 -17	6 10 9	5 23 25
18 16 14	7 9 -4	6 35 -33
	9 53 59	7 8 9
2 K 13	11 36 -40	8 10 -4
2 32 31	13 19 22	9 10 -13
3 10 -11		12 20 -19
5 46 47	3 K 7	16 17 -18
7 22 -22	0 43 41	18 13 13
9 33 32	1 10 11	20 14 -12
11 15 -17	2 70 -66	
13 18 17	3 10 -8	4 K 3
	4 45 43	1 12 12
2 K 14	5 10 -11	2 22 22
2 53 -54	6 23 -25	3 12 -12
4 30 29	12 11 -11	4 7 -6
5 12 8	14 14 16	5 44 44
6 25 -25	16 17 -17	6 10 -10
10 11 -6		7 21 -22
14 14 12	3 K 8	9 43 44
16 16 -18	1 11 11	10 12 11
	2 11 -6	11 33 -35
2 K 15	3 32 -30	13 18 19
2 11 -7	4 16 -17	14 11 -3
3 25 -25	5 32 30	19 12 5
4 14 6	7 38 -39	
5 31 32	9 38 35	4 K 4
7 32 -31	11 32 -30	0 67 66
9 16 16	13 15 15	1 7 8
11 20 -22		2 67 -66
16 15 -3	3 K 9	3 8 -8
	0 56 51	4 37 38
2 K 16	2 66 -60	12 15 -15
0 48 48	4 10 6	14 18 13
2 16 -14	6 35 -36	18 12 12
4 39 39	7 11 -15	
7 12 9	11 10 6	4 K 5
8 21 21	12 19 -22	1 28 29
14 21 21		3 10 -10
16 13 -12	3 K 10	5 24 23
18 16 11	1 21 20	7 11 -11
	2 23 24	9 52 55
11 39 -42	12 19 -4	12 11 -10
13 21 22	13 14 15	18 11 9
19 13 5		
	5 K 5	5 K 16
4 K 6	0 58 58	1 11 -4
0 68 67	2 36 -36	4 12 -4
1 9 8	3 10 -11	5 16 15
2 78 -77	4 38 40	7 19 -21
3 9 -10	16 13 -10	9 16 18
6 23 -23	20 11 -10	11 19 -19
8 11 -12		13 12 12
12 19 -17	5 K 6	16 12 3
14 11 7	3 13 13	
16 12 -11	5 40 41	5 K 17
	7 31 -31	0 15 18
4 K 7	9 29 32	2 27 -30
1 14 15	11 15 -17	3 12 -6
2 9 7	13 23 24	4 15 16
3 35 -34		6 11 -11
7 36 -36	5 K 7	
9 41 42	0 54 53	5 K 18
11 40 -38	1 22 23	5 16 16
13 17 17	2 46 -46	7 14 -13
	3 13 12	9 20 23
4 K 8	4 14 14	11 14 -13
0 92 91	6 13 -15	13 14 12
1 14 14	7 12 -9	
2 16 -17	12 12 -15	5 K 19
4 52 53	18 17 11	0 20 27
8 14 14	20 11 -11	
10 15 18		5 K 20
14 22 19	5 K 8	3 11 -13
18 12 12	3 14 -13	7 23 -23
	4 8 4	
4 K 9	5 28 29	5 K 19
2 9 -5	7 33 -32	2 13 -17
3 31 -32	8 12 -11	4 14 15
5 18 16	9 21 21	
7 34 -35	11 22 -23	5 K 20
9 29 32	13 15 15	9 13 9
11 28 -28	15 11 -8	
15 12 -7		5 K 21
16 12 -1	5 K 9	0 18 17
	0 18 20	2 13 -14
4 K 10	2 40 -42	3 13 -3
0 18 20	3 13 -14	4 13 13
1 14 -14	4 22 21	6 12 -9
2 50 -49	5 9 9	
3 17 -18	6 23 -24	5 K 22
4 24 24	7 11 10	5 18 19
5 18 18	9 16 -9	6 11 5
6 22 -23	12 12 -12	
12 17 -16	16 14 -15	5 K 23
14 13 10		2 14 -12
16 16 -15	5 K 10	3 14 -6
18 16 14	1 18 19	4 12 13
	2 13 -16	8 12 6
4 K 12	3 11 -11	
0 27 26	5 38 41	5 K 24
1 11 -7	7 18 -18	3 12 -10
2 32 -31	9 22 25	5 12 12
3 11 -11	10 10 7	
4 34 34	13 14 17	6 K 0
5 11 12		2 11 -12
6 11 -14	5 K 11	3 9 -10
14 13 12	0 36 36	4 34 36
16 15 -14	2 18 -20	8 33 34
	3 18 -20	10 11 6
4 K 14	4 26 26	12 12 -15
0 30 30	6 13 -15	14 22 25
2 41 -41	8 14 15	18 12 11
4 14 11	10 10 4	
6 23 -22	14 15 17	6 K 2
16 14 -15	15 12 -4	4 28 28
18 10 7	16 13 -14	6 26 -28
		8 9 -5
4 K 22	5 K 12	12 11 -11
2 20 -18	1 10 -8	14 11 15
5 12 5	2 14 -15	16 20 -19
6 16 -17	3 34 -34	
	5 13 14	6 K 3
4 K 23	7 36 -37	1 25 25
5 15 13	8 12 -8	3 22 -22
6 13 4	11 17 -18	4 6 -5
7 16 -19	13 11 7	5 22 22
11 12 -8	14 12 5	7 22 -23
	15 11 -11	9 28 30
4 K 24		11 11 -14
0 15 17	5 K 13	13 15 11
2 13 -11	0 29 30	
4 13 18	2 21 -21	6 K 4
	4 23 25	0 30 28
5 K 0	6 14 -13	1 6 8
2 14 -14	13 11 5	2 27 -26
3 27 -29	14 16 14	4 34 34
4 16 16	16 12 -12	6 21 -22
5 40 44		7 10 -9
6 8 9	5 K 15	10 10 10
7 36 -37	0 31 32	14 11 13
8 16 -20	2 28 -27	16 15 -16
9 17 18	4 16 16	20 10 -6
11 15 -20	5 10 -1	

Table 2. Continued.

6 K 5			6 K 11			4 17 17			7 K 5			2 21 -20			8 K 3		
1 8 10			1 23 23			6 11 -14			0 25 25			4 12 13			5 20 19		
2 12 13			2 10 -7						2 21 -20			6 10 -4			7 15 -15		
4 11 -11			3 27 -29			6 K 19			4 25 26			14 15 12			9 18 18		
5 32 32			5 14 14			7 18 -17			6 9 -10						11 14 -16		
7 28 -30			7 15 -14			9 14 13			7 12 -12			7 K 12			13 12 11		
9 24 26			8 11 -7						14 13 11			3 19 -21					
13 13 13			9 23 22			6 K 20						7 17 -18			8 K 4		
			11 16 -15			0 15 15			7 K 6			9 12 13			0 23 23		
6 K 6						2 15 -14			1 9 8			11 23 -21			2 21 -20		
2 42 -41			6 K 12			4 14 15			2 16 16						4 16 16		
4 29 29			0 25 25						4 12 -13			7 K 13					
6 21 -23			1 11 11			7 K 0			5 28 29			0 27 27			8 K 5		
7 12 -13			2 19 -19			3 17 -19			7 20 -21			2 20 -18			3 10 -10		
8 13 -11			3 10 -3			4 7 -6			9 21 21			4 14 12			5 19 21		
12 12 -9			4 20 20			5 12 12			11 12 -7						9 14 17		
14 14 7			6 14 -14			6 7 -5			13 13 12			7 K 14					
16 17 -16			12 12 -9			7 16 -18			16 12 -5			3 10 -8			8 K 6		
18 13 12			14 16 18			9 22 22						5 15 16			0 19 18		
			16 12 -12			10 12 10			7 K 7			7 14 -13			2 24 -23		
6 K 7			18 10 6			11 22 -22			0 24 24			9 18 18			6 17 -15		
1 8 -9									1 12 -11			11 14 -10					
2 8 8			6 K 13			7 K 1			2 25 -24			15 11 -3			8 K 8		
3 17 -17			1 14 8			2 30 -33			3 10 -13						0 34 31		
4 9 -9			3 10 -9			3 8 -10			4 15 15			7 K 15			2 11 -11		
5 27 27			5 29 29			4 7 7			5 12 13			0 19 19			4 21 21		
7 31 -30			7 16 -16			6 11 -14			6 14 -15			1 11 -5			14 14 9		
9 17 17			9 14 16			12 14 -14			12 11 -8			2 17 -16					
11 18 -17			11 13 -10			13 11 -4						5 10 7			8 K 10		
15 11 -10									7 K 8			6 14 -11			0 25 24		
			6 K 14			7 K 2			2 9 7						2 27 -26		
6 K 8			0 11 10			2 13 15			3 13 -14			7 K 16					
0 40 39			2 28 -28			3 8 -8			4 9 -10			5 13 13			8 K 11		
2 14 -13			4 13 13			5 22 24			5 15 16			7 16 -19			5 12 11		
4 39 40			6 14 -16			7 11 -14			7 23 -22			9 11 13			9 16 17		
8 15 16			12 13 -14			9 25 26			9 17 18			15 10 -6					
10 11 11						10 10 9			11 15 -14						8 K 12		
14 15 15			6 K 15			11 15 -15			13 12 9			7 K 18			0 28 26		
16 12 -10			1 10 -3			13 15 14						5 14 16			2 18 -19		
18 12 13			3 13 -13						7 K 9			9 15 14					
			5 18 18			7 K 3			0 23 25						8 K 13		
6 K 9			7 17 -20			2 21 -22			1 9 8			7 K 19			9 17 18		
3 23 -23			9 12 14			4 21 23			2 28 -28			0 16 15					
5 23 22			11 15 -13			8 10 8			4 10 10			2 12 -13			8 K 16		
7 24 -25						12 11 -8			6 13 -13			4 13 13			0 21 20		
9 14 15			6 K 16			14 14 13			12 12 -10						4 13 13		
10 10 7			0 21 18			16 13 -9			16 13 -10			8 K 0					
11 13 -16			2 14 -11									2 14 -15			9 K 8		
13 14 11			4 29 31			7 K 4			7 K 10			4 25 25			3 10 -10		
16 15 -1			16 10 -9			1 7 -9			1 13 14			10 17 14			7 14 -13		
						2 6 7			5 18 18								
6 K 10			6 K 17			3 24 -26			7 12 -9			8 K 1			9 K 0		
0 13 14			2 10 8			4 7 -7			9 22 23			3 10 -9			5 10 9		
1 10 13			5 12 13			5 9 10			11 15 -15			7 17 -18			7 17 -17		
2 28 -28			7 19 -22			6 10 12			13 14 13			9 18 21					
4 21 19			9 15 15			7 32 -34			14 11 3			11 17 -21					
6 23 -22						9 12 13											
14 13 15			6 K 18			11 18 -19			7 K 11			8 K 2					
16 20 -17			0 11 11			12 10 4			0 33 33			2 29 -30					
			2 19 -18			15 12 -10			1 10 11			6 10 -10					

Table 3. Atomic coordinates, expressed as fractions of the cell edges, and their standard deviations.

Atom	x	y	z
Fe	0.4952(3)	0.2780(1)	0.5
Na(1)	0.5	0	0.2472(3)
Na(2)	0	0	0.3785(4)
C(1)	0.2519(19)	0.1794(8)	0.5
C(2)	0.6140(14)	0.1830(6)	0.5897(5)
C(3)	0.3448(14)	0.3641(6)	0.4113(5)
N(1)	0.0997(23)	0.1200(12)	0.5
N(2)	0.6725(18)	0.1247(8)	0.6433(6)
N(3)	0.2439(17)	0.4118(8)	0.3610(6)
N(4)	0.7683(21)	0.3733(11)	0.5
O	0.1750(17)	0.1249(7)	0.2690(5)

carbon. The result was 20.4 % carbon; calculated for $[Na_2Fe(CN_5NH_3].2H_2O$ is 21.1 %. This shows beyond reasonable doubt that the complex ions contain five carbon atoms. Further confirmation has subsequently been obtained from the results of the X-ray investigation.

Crystallographic investigation. X-Ray diffraction patterns of crystals of disodium pentacyanoammineferrate(III) dihydrate show the following systematic absences:

$0\,k\,l$ $\quad k+l=2n+1$

$h\,0\,l$ $\quad h+l=2n+1$

These are constant with space groups No. 34, *Pnn*2 and No. 58, *Pnnm*.[3]

The unit cell dimensions were determined from Guinier powder photographs (Cu$K\alpha_1$ radiation, $\lambda = 1.54050$ Å), lead nitrate ($a = 7.8404$ Å, 21 °C)[4] being used as an internal standard. Refinement of the cell dimensions based on the measured Bragg angles of 21 indexed reflexions was made with the program POWDER,[5] and yielded the following values:

$a = 6.110 \pm 0.0006$ Å, $b = 11.8990 \pm 0.0023$ Å,

$c = 15.6228 \pm 0.0028$ Å and $V = 1136$ Å^3.

Table 4. Anisotropic thermal parameters and their standard deviations. The temperature coefficient is expressed as exp $[-(h^2\beta_{11}+k^2\beta_{22}+l^2\beta_{33}+2hk\beta_{12}+2hl\beta_{13}+2kl\beta_{23})]$.

Atom	β_{11}	β_{22}	β_{33}	β_{12}	β_{13}	β_{23}
Fe	0.076(3)	0.0023(1)	0.0009(0)	0.0002(4)	0.0000	0.0000
Na(1)	0.0122(11)	0.0043(3)	0.0015(2)	−0.0029(14)	0.0000	0.0000
Na(2)	0.0162(15)	0.0059(4)	0.0023(2)	0.0033(18)	0.0000	0.0000
C(1)	0.0084(22)	0.0016(4)	0.0020(4)	0.0014(18)	0.0000	0.0000
C(2)	0.0105(17)	0.0028(4)	0.0012(2)	0.0023(14)	0.0012(10)	0.0008(5)
C(3)	0.0116(19)	0.0025(3)	0.0009(2)	0.0032(14)	0.0010(10)	0.0016(5)
N(1)	0.0132(34)	0.0052(8)	0.0034(6)	−0.0058(28)	0.0000	0.0000
N(2)	0.0199(26)	0.0058(6)	0.0026(4)	0.0030(24)	−0.0004(16)	0.0030(8)
N(3)	0.0227(26)	0.0046(5)	0.0021(3)	0.0030(23)	−0.0038(15)	0.0015(7)
N(4)	0.0141(29)	0.0051(8)	0.0017(4)	0.0013(27)	0.0000	0.0000
O	0.0246(25)	0.0050(5)	0.0035(4)	0.0027(21)	−0.0001(16)	0.0017(7)

Table 5. Geometry of the $Fe(CN)_5NH_3^{3-}$ octahedron. Interatomic distances (in Å) and angles, with their standard deviations in parentheses.

Distance		Angle	
Fe−C(1)	1.891(11)	Fe−C(1)−N(1)	179.0(11)
Fe−C(2)	1.932(8)	Fe−C(2)−N(2)	176.1(9)
Fe−C(3)	1.945(8)	Fe−C(3)−N(3)	175.6(8)
Fe−N(4) (NH_3)	2.015(13)	C(1)−Fe−C(2)	86.1(3)
C(1)−N(1)	1.168(18)	C(1)−Fe−C(3)	87.5(3)
C(2)−N(2)	1.141(12)	C(1)−Fe−N(4)	175.9(5)
C(3)−N(3)	1.144(12)	C(2)−Fe−C(3)	88.7(3)
		C(2)−Fe−N(4)	91.1(4)
		C(2)−Fe−C(2)	92.0(5)
		C(3)−Fe−C(3)	90.0(5)
		C(3)−Fe−N(4)	95.4(4)

Table 6. Geometry of the sodium ion coordination octahedra. Interatomic distances (Å) and angles, their standard deviations in parenthesis.

Coordination of Na (1)

Atom	x	y	z
Na(1)	0.5	0	0.2472
N(2)	0.3275	−0.1247	0.3567
N(2)′	0.6725	0.1247	0.3567
N(3)	0.7439	0.0882	0.1390
N(3)′	0.2561	−0.0882	0.1390
O	0.1750	0.1249	0.2690
O′	0.8250	−0.1249	0.2690

Distance

Na(1)−N(2)	2.488(10)
Na(1)−N(3)	2.475(10)
Na(1)−O	2.501(10)
Mean	2.488

Angle

N(2)−Na(1)−N(3)	165.8(3)
N(2)−Na(1)−N(3)′	87.4(3)
N(2)−Na(1)−O	85.8(3)
N(2)−Na(1)−O′	83.6(3)
N(3)−Na(1)−N(3)′	94.7(5)
N(3)−Na(1)−O	108.4(3)
N(3)−Na(1)−O′	82.4(3)
O−Na(1)−O′	164.4(4)

Coordination of Na (2)

Atom	x	y	z
Na(2)	0	0	0.3785
N(1)	0.0997	0.1200	0.5
N(1)′	−0.0997	−0.1200	0.5
N(2)	0.3275	−0.1247	0.3567
N(2)″	−0.3275	0.1247	0.3567
O	0.1750	0.1249	0.2690
O″	−0.1750	−0.1249	0.2690

Distance

Na(2)−N(1)	2.441(10)
Na(2)−N(2)	2.511(11)
Na(2)−O	2.495(10)
Mean	2.482

Angle

N(1)−Na(2)−N(1)′	79.0(5)
N(1)−Na(2)−N(2)	104.5(4)
N(1)−Na(2)−N(2)″	87.5(4)
N(1)−Na(2)−O	94.0(3)
N(1)−Na(2)−O″	168.4(4)
N(2)−Na(2)−N(2)″	164.6(5)
N(2)−Na(2)−O	85.4(3)
N(2)−Na(2)−O″	84.1(3)

Observed and calculated $\sin^2\theta$ values are listed in Table 1. The cell dimensions and the experimental density (1.69 g cm^{-3} as determined by the flotation method) indicate that the unit cell contains four formula units. The corresponding calculated density is 1.66 g cm^{-3}.

STRUCTURE DETERMINATION

The crystal structure was solved and determined using standard methods.

Observed and calculated structure amplitudes are listed in Table 2. Final atomic parameters are given in Tables 3 and 4. Interatomic distances and angles were calculated with the program DISTAN.[6] The results are listed in Tables 5 and 6.

DESCRIPTION AND DISCUSSION OF THE STRUCTURE

The complex ion $[Fe(CN)_5NH_3]^{2-}$ (Fig. 1) lies in a mirror plane and has approximately C_{4v} symmetry if the three hydrogen atoms are not taken into consideration. The distances and angles within it are listed in Table 5. The Fe – C – N groups are almost linear. The cyanide ligand *trans* to the ammonia molecule appears to be more firmly bonded than the other ligands, presumably due to additional π-bonding.

Comparison of the $Fe-N(NH_3)$ distance of 2.02 Å with the short Fe – N(NO) distance of 1.63 Å in $Na_2[Fe(CN)_5NO].2H_2O$ [7] illustrates the importance of the π-bond contribution to the latter bond. The Fe – C distances in the plane perpendicular to the $Fe-N(NH_3)$ bond are

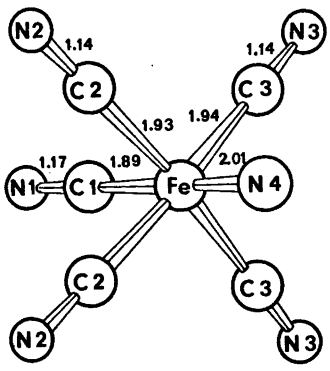

Fig. 1. The complex ion $[Fe(CN)_5NH_3]^{2-}$.

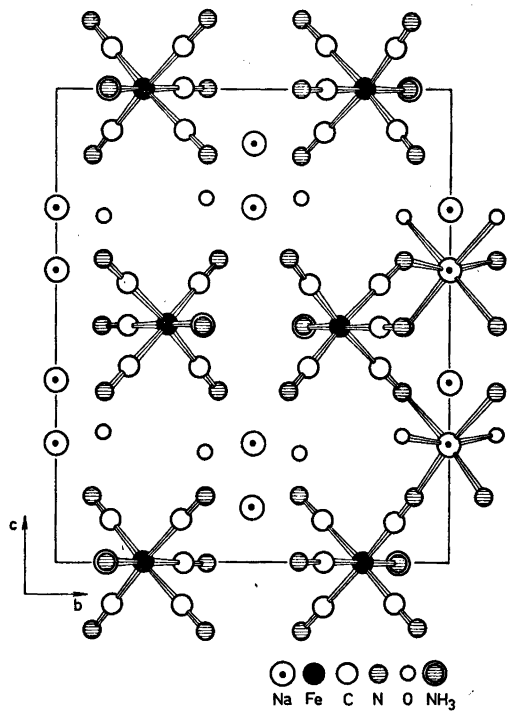

Fig. 2. Projection of the structure of $Na_2[Fe(CN)_5NH_3].2H_2O$ along the *a*-axis. Full lines indicate one unit cell. Two nitrogen atoms in the unit cell below the plane of paper are shown.

1.94 ± 1 Å (mean value), very close to the corresponding distance (1.95 ± 1 Å, mean value) in $K_3[FeCN_6]$,[11] but longer than that (1.91 ± 1 Å, mean value) in $Na_4[Fe(CN)_6].10H_2O$.[12]

The sodium coordination is octahedral, each sodium ion being surrounded by four nitrogen atoms of cyanide groups and two oxygen atoms of water molecules. Although the octahedron is irregular, the Na – L distances are rather similar (2.5 Å). Bond distances and angles for the sodium ion coordination octahedra are listed in Table 6.

The sodium ion coordination octahedra are linked edgewise to form double chains parallel to the *a*-direction of the unit cell, the octahedral $[Fe(CN)_5NH_3]^{2-}$ ion linking these double chains together. Fig. 2 shows a projection of the structure along the *a*-axis. The $[Fe(CN)_5NH_3]^{2-}$-octahedra and two different sodium coordination octahedra are shown in perspective.

Fig. 3 is a perspective view along the *b*-axis, showing how the sodium ion coordination octa-

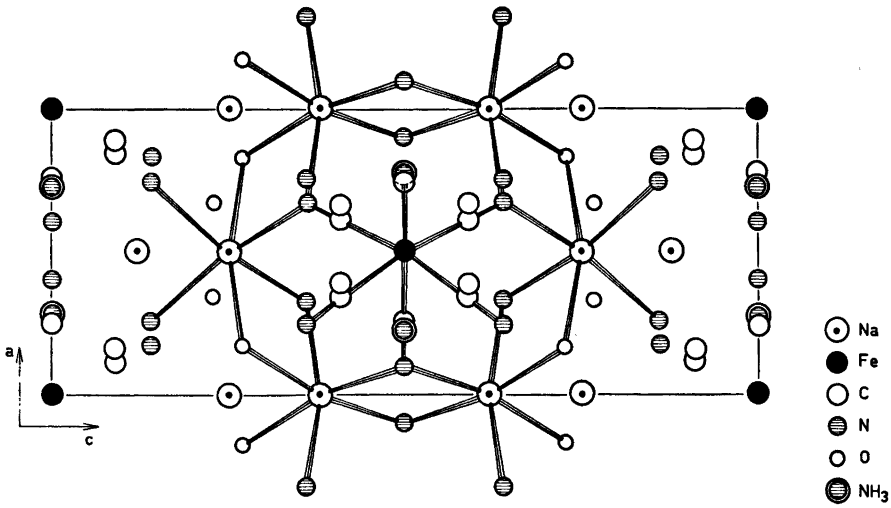

Fig. 3. Projection of the structure of $Na_3[Fe(CN)_5NH_3].2H_2O$ along the *b*-axis showing the arrangement of sodium ion coordination octahedra. Full lines indicate one unit cell. Some of the atoms belonging to the coordination octahedra lie in the unit cell below the plane of the paper.

hedra are linked to form double chains running along the *a*-direction of the unit cell.

Acknowledgements. The authors would like to thank Dr. Susan Jagner for revising the English text and Mrs. Margareta Biéth for skilful technical assistance. This work has been supported by a grant given by the Swedish Natural Science Research Council (Contract No. 2286–19).

REFERENCES

1. Brauer, G. *Handbuch der präparativen anorganischen Chemie 2* (1962) 1318.
2. Herington, E. F. G. and Kynaston, W. *J. Chem. Soc.* (1955) 3555.
3. *International Tables for X-Ray Crystallography*, 2nd Ed., Kynoch Press, Birmingham 1965, Vol. I.
4. *International Tables for X-Ray Crystallography*, Kynoch Press, Birmingham 1962, Vol. III, p. 122.
5. Lindqvist, O. and Wengelin, F. *Ark. Kemi 28* (1967) 179.
6. The program library of the Dept. of Inorg. Chem. Göteborg. DATAP1 and BLOCK have been written locally by O. Lindgren, DATAP2 was originally written by Coppens, Leiserowitz and Rabinowich (1965), DRF and DISTAN by A. Zalkin, Berkeley, California and LALS by P. Gantzel, R. Sparks and K. Trueblood.
7. Manoharan, P. T. and Hamilton, W. C. *Inorg. Chem. 2* (1963) 1043.
8. Cruickshank, D. N. J. *The Equations of Structure Refinements*, Glasgow 1964.
9. Cromer, D. T. and Waber, J. T. *Acta Crystallogr. 18* (1965) 104.
10. Cromer, D. T. *Acta Crystallogr. 18* (1965) 17.
11. Vannerberg, N. G. *Acta Chem. Scand. 26* (1972) 7.
12. Tullberg, A. and Vannerberg, N. G. *To be published.*

Received January 21, 1974.

Acta Chemica Scandinavica A 28 (1974) 347—355

Structural Studies on the Rare Earth Carboxylates. 23. The Crystal Structure of Tetra-aquobis(hydrogeniminodiacetato)-iminodiacetatodipraseodymium(3+) Dichloride Trihydrate at —50 °C

JÖRGEN ALBERTSSON and ÅKE OSKARSSON

Inorganic Chemistry 1, Chemical Center, University of Lund, P.O.B. 740, S-220 07 Lund 7, Sweden

In a systematic study of various lanthanoid dicarboxylate compounds, the crystal structure of $[Pr_2(H_2O)_4(C_4H_6NO_4)_2\ (C_4H_5NO_4)]Cl_2.3H_2O$ has been determined using X-ray intensity data collected at −50°C with a four-circle single crystal diffractometer. The structure of an isotypic neodymium analogue has been reported previously. The space group is $P2_1/m$, and there are two formula units in the cell. The lattice parameters are $a = 8.7198(9)$, $b = 18.4218(27)$, $c = 9.2725(6)$ Å and $\beta = 108.248(6)°$. The structure has been refined to $R = 0.087$. Each of the hydrogeniminodiacetate and iminodiacetate ions is coordinated to four praseodymium ions forming a three-dimensional network. The coordination polyhedron around each metal ion is a distorted monocapped square antiprism formed by seven carboxylate oxygens and two water oxygens. The Pr − O distances are in the range 2.34 − 2.75 Å. The chloride ions are connected by hydrogen bonds *via* two water molecules and two nitrogen atoms, forming chains running in the *a*-direction.

The lanthanoid elements Ce − Gd form an isotypic series of iminodiacetate compounds with the composition $[M_2(H_2O)_4(C_4H_6NO_4)_2(C_4H_5NO_4)]Cl_2.3H_2O$. The crystal structure of the neodymium compound has previously been determined [1] from three-dimensional intensity data recorded with the Weissenberg multiple film technique. Although the main features of the structure were obtained, the accuracy needed for a more quantitative description of it was not achieved. Such a description is desirable for a discussion of the shape of the coordination polyhedron around the metal ion and the geometry of the iminodiacetate ligand in various solid complexes as will be given in a following publication.[2]

The crystal quality is poor for all compounds in the series. Since the crystals of the praseodymium compound were judged to be the most suitable in the series, this compound, referred to as PRIMIN below, was chosen to be investigated with an automatic single crystal diffractometer. To facilitate location of the water molecule not found in the previous analysis, the intensity data were collected at −50 °C.

EXPERIMENTAL

Preparation and analysis. The compounds $[M_2(H_2O)_4(C_4H_6NO_4)_2\ (C_4H_5NO_4)]Cl_2.3H_2O$, M = Ce − Gd, were prepared from an aqueous solution of $M_2(C_4H_5NO_4)_3$ by adjusting the pH to 2.5 with HCl. Crystals were then obtained by slow evaporation of the solution at room temperature. The neodymium compound was analyzed for neodymium, carbon, nitrogen, hydrogen, and water. The results were 32.2(32.6)% Nd, 16.3(16.3) % C, 4.7(4.8) % N, 3.8(3.5) % H and 14.0(14.3) % H_2O, were the number in parentheses are the calculated values for $[Nd_2(H_2O)_4(C_4H_5NO_4)_2(C_4H_5NO_4)]Cl_2.3H_2O$. The praseodymium compound was analyzed only for the metal, the result being 32.0(32.2) % Pr. Powder photographs of all preparations were nearly identical.

The weight loss was determined as a function of the temperature in the range 25 − 200 °C using a Mettler thermogravimetric analyser equipped with a DTA unit. The heating rate used was 2K/min.

Single crystal work. A single crystal with the dimensions $0.13 \times 0.06 \times 0.13$ mm was used for collecting data at -50 ± 2 °C on a Nonius computer-controlled four-circle diffractometer of type CAD-4, equipped with a commercial low temperature device modified as will be described in a forthcoming communication.[3] Intensity data were measured at a take-off angle of 5° using Cu$K\alpha$ radiation. A graphite monochromator was used. The $\omega - 2\theta$ scan technique was employed, with a scan range $\Delta\omega = 0.80 + 0.50 \tan\theta$. A fast pre-scan was used to determine the scan speed at which a predetermined minimum number of counts (3000) was received by the detector. However, the recording time for a reflexion was limited to 3 min. The scan range, $\Delta\omega$, was extended 25 % at both ends for the background measurement. Of the 2443 independent reflexions in the interval $5° < \theta < 70°$ and with $h \leq 6$, 2392 were measured. All the reflexions with $h > 6$ and 51 of those with $h \leq 6$ were not attainable due to obscuration by the low temperature device. Another 620 reflexions with $I < 3\sigma_c(I)$ were considered not to be significantly different from the background and were excluded from the following calculations. The values of $\sigma_c(I)$ were based only on counting statistics. The reflexions 045, 191, and $0\bar{4}5$ were selected as standards, and their intensities were recorded after every 50 reflexion measurements. The intensities of the standard reflexions decreased 20 % during the experiment. The variations could be described with a linearly decreasing function of the recording time and this function was used for scaling the data set. The values of I and $\sigma_c(I)$ were corrected for Lorentz, polarization and absorption effects. The expression $p = (1 + \cos^2 2\theta_M \cos^2 2\theta)/(1 + \cos^2 2\theta_M)$ with $\theta_M = 13.3°$ was used in the correction of the polarization effects. The transmission factors evaluated by numerical integration varied from 0.034 to 0.297.

UNIT CELL AND SPACE GROUP

PRIMIN crystallizes in the monoclinic system. The systematically absent reflexions are $0k0$ with $k \neq 2n$, indicating the space group to be $P2_1$ (No. 4) or $P2_1/m$ (No. 11).[4]

Accurate unit cell dimensions were determined by measuring θ-values for 60 reflexions on the diffractometer. The technique will be described later.[3] The measured θ-values were used for a least-squares refinement of the unit cell dimensions. The density, D_m, was determined from the loss of weight in benzene. The following crystal data were obtained:

$a = 8.7198(9)$ Å* $\quad D_m = 2.07$ g cm^{-3}
$b = 18.4218(27)$ Å $\quad D_x = 2.05$ g cm^{-3}
$c = 9.2725(6)$ Å $\quad Z = 4$
$\beta = 108.248(6)°$ $\quad \mu(\text{Cu}K\alpha) = 270.7$ cm^{-1}
$V = 1414.6$ Å^3

* Numbers within parentheses represent e.s.d.'s in the last significant digits.

REFINEMENT OF THE STRUCTURE

Preliminary atomic parameters were taken from Ref. 1 for all non-hydrogen atoms except the water oxygen atoms O(9) and O(10). Assuming the centrosymmetric space group $P2_1/m$, these parameters, together with a scale factor, were improved by a full matrix least-squares refinement. The quantity minimized was $\sum w(|F_o| - |F_c|)^2$, with weights $w = 1/[\sigma_c^2(F) + a|F_o|^2 + b]$. The constants a and b were chosen so that the average values of $w(|F_o| - |F_c|)^2$ were fairly constant between different $|F_o|$ and sin θ intervals. After the last cycle of the refinement the variations of $w(|F_o| - |F_c|)^2$ were in the ranges $0.9 - 1.5$ and $0.9 - 1.4$ for the various $|F_o|$ and sin θ intervals, respectively. In the last cycles of refinement $a = 0.003$ and $b = 7.0$ were used. A difference electron density map calculated using data with $\sin\theta/\lambda \gtrsim 0.4$ Å^{-1} revealed the positions of remaining water oxygen atoms O(9) and O(10). As the maximum electron density for O(10) was 3 eÅ^{-3} compared to 6 eÅ^{-3} for O(9), the occupancy for O(10) was included as a variable in the further refinements. The final occupancy was 0.81(3). This small number was considered to be caused by a dynamic disorder of this molecule, as will be discussed later. The occupancy number was at a fixed value of 1.0 in the following calculations. The final structural model included anisotropic thermal parameters for the praseodymium ion and an isotropic extinction parameter $g = 0.03 \times 10^4$.[5] The value of g corresponds to a mosaic spread of 171″ or a domain size of 0.05×10^{-4} cm. In the last cycle of refinement, the shifts in all parameters were less than 5 % of their corresponding e.s.d.'s. The agreement index was 0.087. A final difference electron density map was featureless.

The atomic scattering factors used were taken from the International Tables [6] (Cl, O, N, and C) and from Cromer *et al.*[7] (Pr). The atomic scattering factor for Pr was corrected for anomalous dispersion. The final positional and thermal parameters are given in Table 1. Observed and calculated structure amplitudes

Table 1. Atomic parameters with e.s.d.'s in parentheses. B denotes the isotropic temperature factor.

Atom	$x/a(\times 10^4)$	$y/b(\times 10^4)$	$z/c(\times 10^4)$	B(Å^2)
Pr	−89(2)	240(1)	2179(1)	*a*
Cl(1)	3601(17)	2500	4129(13)	3.7(2)
Cl(2)	8058(15)	2500	3986(11)	2.9(2)
O(1)	7701(25)	108(10)	5759(19)	2.6(3)
O(2)	8162(24)	524(9)	3642(18)	2.4(3)
O(3)	2556(22)	320(9)	−521(17)	1.9(3)
O(4)	2323(24)	790(9)	1633(18)	2.2(3)
O(5)	−805(24)	646(9)	−812(18)	2.3(3)
O(6)	−1785(26)	1322(10)	776(19)	2.6(3)
O(7)	700(26)	1414(10)	3751(19)	2.7(3)
O(8)	−737(25)	−950(9)	3245(19)	2.7(3)
O(9)	4485(31)	2500	9780(23)	1.5(4)
O(10)	6113(57)	−1367(22)	2863(43)	10.2(11)
N(1)	5327(30)	1281(11)	2668(22)	2.4(4)
N(2)	−2196(59)	2500	−844(46)	4.7 (9)
C(1)	7279(34)	455(12)	4493(25)	1.9(4)
C(2)	5644(37)	820(13)	4085(27)	2.4 (5)
C(3)	4859(40)	854(15)	1208(30)	3.1(6)
C(4)	3049(34)	647(13)	740(25)	2.1(4)
C(5)	−1928(45)	1821(17)	−1649(33)	3.7(6)
C(6)	−1499(36)	1216(13)	−495(27)	2.3(4)

[a] The anisotropic thermal parameters for praseodymium, calculated from the expression $\exp[-(h^2\beta_{11}+2hk\beta_{12}+\ldots)]$, are $\beta_{11}=0.0099(3)$, $\beta_{22}=0.0010(1)$, $\beta_{33}=0.0031(2)$, $\beta_{12}=0.0002(1)$, $\beta_{13}=0.0017(1)$ and $\beta_{23}=0.0000(1)$.

are compared in Table 2, and selected interatomic distances and angles are shown in Table 3.

All computations were made on the UNIVAC 1108 computer in Lund, Sweden and a list of the programmes used is given in Ref. 8.

DESCRIPTION OF THE STRUCTURE

There are two crystallographically different ligands in the structure. Their atoms are designated in Figs. 1 and 2 and they are referred to below as ligand 1 or 2, depending upon whether

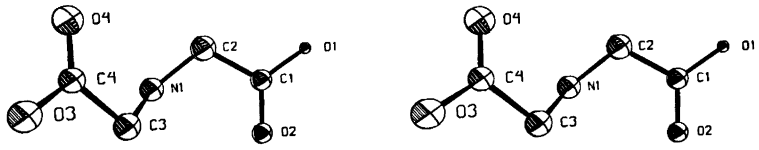

Fig. 1. A stereoscopic pair of drawings showing the hydrogeniminodiacetate ion. The view is perpendicular to a least-squares plane through N(1), C(2), C(1), O(1) and O(2). The Figs. 1–4 have been drawn by the programme ORTEP.

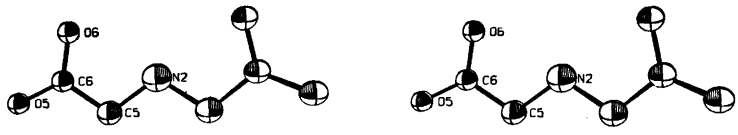

Fig. 2. A stereoscopic pair of drawings showing the iminodiacetate ion. The view is perpendicular to a least-squares plane through N(2), C(5), C(6), O(5), and O(6).

Table 2. Observed and calculated structure factors. The columns are k, $|F_o|$ and $|F_c|$.

L=-11 H= 1
0 68 66

L=-11 H= 2
0 73 63
2 73 66
3 41 39
4 55 50

L=-11 H= 3
0 69 62
2 65 60
4 41 56
6 19 18

L=-11 H= 4
0 72 67
2 84 73
3 14 9
4 50 50

L=-11 H= 5
0 68 67
2 66 58
4 70 62
6 51 52
7 21 23
8 24 22
12 16 17

L=-10 H= 0
0 27 31
2 14 19
3 9 21

L=-10 H= 1
0 27 28
2 33 30
3 22 26
4 32 32
5 56 58
6 30 28
7 45 42
8 18 22
9 59 67

L=-10 H= 2
0 41 33
1 15 15
2 48 47
3 44 37
4 28 24
5 70 69
6 18 17
7 68 63
9 77 72

L=-10 H= 4
0 17 14
1 60 61
4 25 20
5 65 59
7 75 71
9 71 61

L=-10 H= 5
1 17 19
3 36 36
4 20 19
5 59 69
7 41 56
9 70 69

L=-10 H= 6
1 14 18
2 11 7
3 28 26
4 25 26
5 47 44
7 51 45

L=-9 H= 0
0 63 67
2 66 80
4 29 24
6 13 18

L=-9 H= 1
0 83 80
2 83 82
4 55 57
6 16 14
8 55 56
9 37 36
11 15 24
12 14 19

L=-9 H= 2
0 123 120
2 80 74
4 74 80
6 20 21
8 43 39
9 42 46

13 15 17

L=-9 H= 3
0 127 111
2 105 96
3 35 30
4 69 67
5 40 31
6 63 60
8 37 34
12 23 22

L=-9 H= 4
0 95 83
2 92 82
4 83 73
6 67 66
8 43 36
12 22 21

L=-9 H= 5
0 71 69
2 82 80
4 70 62
6 51 52
7 21 23
8 24 22
12 16 17

L=-9 H= 6
0 70 73
2 70 73
4 55 53
6 45 44
8 22 20

L=-8 H= 0
0 27 25
2 64 50
4 52 54
7 93 104

L=-8 H= 1
0 19 17
2 64 66
4 60 65
7 75 83
9 82 96
11 65 96
13 45 65
15 34 55

L=-8 H= 2
0 59 66
1 26 26
2 31 32
3 30 26
4 62 66
6 18 20
7 66 67
9 98 98
11 70 73
13 68 74
15 49 53

L=-8 H= 3
1 20 17
3 59 52
5 87 78
7 88 84
9 80 87
11 49 70
13 63 66
15 60 57

L=-8 H= 4
0 20 18
2 41 36
4 91 81
7 102 90
9 93 95
11 72 70
13 63 63
15 44 44

L=-8 H= 5
2 35 37
4 42 43
6 27 26
8 56 52
7 88 83
9 76 73
11 74 64
13 53 51

L=-8 H= 6
0 47 54
2 43 46
4 45 58
6 27 27
8 44 37
7 70 67
9 60 51
11 65 63
13 48 41

L=-7 H= 0
0 113 117
1 38 42
2 117 122
3 16 7
4 63 75
9 17 34

L=-7 H= 1
0 162 152
2 127 124
3 18 13
4 88 90
6 60 61
8 41 43
9 22 22
12 26 28
14 33 40
16 48 55

L=-7 H= 2
0 107 99
2 130 127
3 73 69
4 88 82
5 32 22
6 81 80
8 28 25
10 26 26
11 20 23
14 29 25
15 24 25
16 41 44

L=-7 H= 3
0 133 123
2 104 94
4 89 82
5 45 45
6 50 44
7 44 47
8 30 30
9 36 34
10 19 14
11 30 30
13 20 30
14 32 32
15 22 22
16 48 47
17 11 10

L=-7 H= 4
0 135 133
2 98 81
4 83 80
5 30 26
6 50 42
7 40 37
8 30 37
9 25 26
11 39 38
13 43 40
14 40 48
15 27 27
16 44 45
17 16 16

L=-7 H= 5
0 84 97
2 83 90
4 69 67
5 38 42
6 58 59
7 35 34
8 38 35
9 29 23
11 22 17
13 40 38
14 28 28
15 24 18
16 26 18
17 12 11

L=-6 H= 0
0 97 96
1 30 26
2 47 45
3 44 44
5 66 72
7 80 88
9 91 101
11 41 77

L=-6 H= 1
0 54 49
1 25 19
2 61 56
3 41 42
4 88 83
5 81 78
6 34 35
7 101 109
8 17 17
9 93 104
11 73 88
13 63 75
14 17 21
15 35 51
16 15 19
17 25 30
18 25 27

L=-6 H= 2
0 53 48
1 17 19
2 75 66
3 56 57
4 32 34
5 54 50
6 35 28
7 130 132
8 22 21
9 90 89
11 114 116
13 65 69
15 62 66
16 24 25
17 13 19
18 23 24

L=-6 H= 3
0 29 32
1 20 21
2 64 54
3 34 29
4 82 77
5 59 55
6 23 21
7 69 67
8 28 24
9 101 101
11 89 88
13 77 78
14 27 25
15 56 59
16 30 26
17 43 43
18 20 20

L=-6 H= 4
0 24 29
1 23 25
2 78 74
3 22 18
4 59 49
5 47 40
6 80 75
7 54 46
8 31 28
9 98 99
10 31 33
11 68 67
12 29 27
13 65 66
14 21 22
15 42 45
16 39 37
17 49 50
18 21 22

L=-6 H= 5
0 57 69
2 60 65
4 33 32
6 68 72
8 48 48
9 36 32
11 82 80
13 58 69
14 37 36
15 45 46
19 25 22

L=-5 H= 0
0 139 140
2 92 88
4 145 150
5 24 25
6 49 64
7 44 48
9 51 52
11 48 60
13 20 47
14 41 56

L=-5 H= 1
0 113 103
2 120 114
3 24 26
4 103 96
5 78 68
6 86 85
7 70 72
8 47 48
9 48 49
11 63 71
12 23 24
13 73 82
14 27 31
15 38 44
16 37 41
17 17 19
18 41 41
20 51 48

L=-5 H= 2
0 125 106
1 18 22
2 129 120
3 21 17
4 95 76
5 102 101
6 56 60
7 57 53
8 34 41
9 87 88
11 80 80
12 34 39
13 91 94
14 36 38
15 30 35
16 48 53
17 27 29
18 45 46
20 50 51

L=-5 H= 3
0 119 115
1 9 6
2 117 113
3 81 72
4 76 65
5 96 84
6 47 45
7 46 59
8 29 22
9 44 44
11 70 69
12 28 31
13 65 66
14 42 43
15 51 51
16 54 58
18 54 54

L=-5 H= 4
0 111 113
2 92 94
3 47 45
4 54 50
5 22 20
6 42 42
7 75 63
9 72 70
11 89 87
13 33 36
14 21 22
15 35 34
16 37 36
18 45 46
19 25 22

L=-5 H= 5
0 57 76
1 15 11
2 63 72
3 22 22
4 65 79
5 38 40
6 29 25
7 40 57
9 73 66
11 75 73
13 75 70
14 25 26
15 50 51
16 32 28
17 33 31
18 37 32

L=-5 H= 6
0 54 72
1 18 24
2 41 53
3 24 23
4 61 82
5 43 48
6 18 17
7 65 67
8 25 21
9 90 84
11 70 62
13 58 57
14 47 45
15 43 39
16 27 26
17 38 37

L=-4 H= 0
0 44 35
1 66 69
2 87 97
3 79 69
4 81 81
5 140 143
6 96 105
7 49 54
8 38 46
9 92 98
11 54 62
13 44 93
14 26 43
15 29 44
17 15 32

L=-4 H= 1
0 33 35
1 24 30
2 114 106
3 80 71
4 124 113
5 105 101
6 29 30
7 92 89
8 81 85
10 13 15
11 79 79
13 42 66
14 38 39
15 38 40
16 51 51
17 28 30
18 37 39
19 21 18
20 50 49

L=-4 H= 2
0 182 159
1 31 28
2 62 63
3 50 45
4 142 148
5 89 83
6 36 44
7 87 82
8 91 83
9 70 67
10 42 35
11 44 61
13 59 58
14 62 57
15 34 36
16 15 21
17 38 38
18 61 56
19 25 24
20 40 46

L=-4 H= 3
0 165 168
1 11 9
2 178 182
3 48 52
4 126 110
5 62 58
6 82 77
7 86 85
9 61 56
11 68 66
13 53 51
14 23 24
15 45 42
16 53 52
17 19 22
18 55 56
19 9 11
20 65 62

L=-4 H= 4
0 113 142
1 28 44
2 104 124
3 37 48
4 90 90
5 45 45
6 88 87
7 90 87
8 25 23
9 42 35
11 80 76
12 38 43
13 39 38
14 23 26

15 49 46
16 32 31
18 44 44
19 15 12

L=-4 H= 5
0 48 71
2 65 83
4 49 62
5 54 70
6 62 59
7 27 25
8 23 16
9 60 53
11 32 28
12 22 17
13 62 57
14 21 21
15 23 23
16 53 48
17 27 25
18 48 44

L=-4 H= 6
0 39 56
2 52 75
4 47 62
5 18 17
6 64 62
7 32 30
8 39 38
9 60 55
11 48 44
12 23 17
13 40 31
14 25 23
16 54 46
17 16 15

L=-3 H= 0
0 35 42
1 53 44
2 112 101
3 41 60
4 90 93
5 81 81
6 68 68
7 142 146
8 21 18
9 100 105
10 21 33
11 142 146
13 69 86
14 16 21
15 69 71
17 23 36
19 25 39

L=-3 H= 1
0 55 54
1 31 37
2 75 68
3 89 75
4 110 105
5 133 126
6 72 65
7 141 135
9 94 99
11 106 104
12 34 35
13 103 107
14 52 52
15 67 69
16 43 40
17 37 37
18 48 48
19 16 19
20 38 38

L=-3 H= 2
0 56 69
1 41 43
2 63 45
3 61 64
4 109 107
5 84 82
6 53 61
7 105 98
8 46 53
9 110 106
10 32 32
11 96 90
12 29 26
13 78 74
14 45 46
15 52 50
16 21 23
17 43 44
18 40 37
19 17 17
20 22 27

L=-3 H= 3
0 12 17
1 45 45
2 56 68
3 87 87
4 88 92
5 104 93
6 49 38

7 81 78
8 27 26
9 105 92
11 90 81
13 94 92
14 18 19
15 79 78
16 30 24
17 43 44
18 19 19
20 27 26

L=-3 H= 4
0 22 28
1 44 66
2 68 71
3 62 90
4 15 21
5 97 100
6 59 53
7 87 84
9 155 142
10 42 41
11 100 100
12 19 18
13 93 86
14 16 17
15 61 65
16 39 38
17 52 46
20 33 29

L=-3 H= 5
0 27 40
1 38 58
2 35 38
4 35 38
5 60 76
7 110 106
9 116 100
11 114 104
13 78 77
14 33 32
15 65 60
16 25 28
17 22 23
18 29 27
19 14 14

L=-3 H= 6
3 30 44
7 79 72
9 79 65
11 114 98
13 84 59
15 66 59
16 16 15
17 22 23
18 15 18

L=-2 H= 0
0 110 115
1 74 68
2 155 149
3 99 96
4 58 59
5 21 25
6 131 122
7 43 44
8 19 35
10 35 44
11 93 87
12 22 30
13 36 43
14 30 40
15 80 76
16 33 39
19 24 23
20 27 22
21 13 20
22 29 49

L=-2 H= 1
0 101 95
1 19 19
2 170 157
3 49 41
4 211 205
5 39 33
6 158 151
7 19 14
8 102 97
9 46 45
10 33 30
11 62 59
12 22 17
13 51 52
14 64 61
15 32 33
16 93 89
18 82 81
20 64 65
22 61 57

L=-2 H= 2
0 163 206
1 51 67
2 222 230
4 87 82
5 107 104
6 194 177

Table 2. Continued.

R 97 94	22 16 15	5 71 67	12 41 40	R 21 35	1R 48 41	7 49 67	3 46 39
9 79 68		6 95 89	13 109 106	10 52 44		8 24 17	4 58 58
10 19 14	L= -1 K= 2	8 66 60	14 21 22	11 97 87	L= 2 K= 6	9 93 89	5 44 45
11 25 32	0 10 25	9 60 63	15 83 81	12 35 30	2 69 65	11 71 68	6 21 17
12 80 71	2 11 19	10 42 35	16 16 15	13 38 45	3 35 35	13 71 67	7 85 83
13 58 57	3 160 153	11 21 17	17 38 40	14 36 40	4 61 56	14 20 1R	R 1R 22
14 26 31	4 48 40	12 34 24	1R 17 15	15 R4 74	5 28 29	15 36 36	9 110 114
15 25 18	5 32 41	14 34 37	20 19 20	16 85 79	6 38 38	16 23 25	11 91 90
16 85 80	6 37 37	15 30 29	22 17 15	1R 62 66	7 61 63	17 34 33	13 66 66
17 19 10	7 172 149	16 86 82		19 29 23	9 43 45	18 54 49	14 37 38
18 66 73	9 151 142	17 35 28	L= 1 K= 2	20 80 72	11 49 48		15 45 45
19 12 11	11 167 158	18 70 75	0 2R 33	21 17 10	13 30 27	L= 3 K= 5	16 31 31
20 79 78	13 78 84	20 77 72	1 8 8	22 47 49	14 35 35	0 93 82	17 35 33
21 10 4	15 96 92	21 21 15	2 51 46		15 41 35	2 81 76	18 3R 32
	17 51 55		3 32 27	L= 2 K= 1	1A 39 33	3 2R 29	
L= -2 K= 3	19 38 32	L= 0 K= 3	4 146 149	0 226 225		4 63 56	L= 4 K= 4
0 95 167	21 27 17	2 155 155	5 102 91	1 13 28	L= 3 K= 0	5 33 31	0 45 41
2 56 R5		3 72 67	7 143 138	2 170 158	0 35 42	6 60 61	1 34 33
3 49 54	L= -1 K= 3	4 160 151	R 31 25	3 37 29	1 55 44	7 58 60	2 37 31
4 128 136	2 14 27	5 34 36	9 170 157	4 157 159	2 114 101	8 33 27	3 40 39
5 61 59	3 74 R9	6 120 101	10 10 9	5 79 70	3 63 60	9 32 26	4 52 51
6 93 79	4 70 74	7 50 49	11 132 135	6 28 29	4 95 93	10 22 21	5 R5 R3
7 63 58	5 156 150	8 31 28	12 22 20	7 54 60	5 R4 81	11 55 51	6 2R 21
8 R8 R0	6 22 18	9 29 30	13 127 120	8 29 33	6 75 68	13 41 40	7 79 79
10 32 26	7 179 169	11 24 22	14 43 40	9 59 55	7 147 146	14 11 10	R 36 37
11 26 26	R 34 32	12 26 24	15 64 71	11 67 69	R 23 18	15 50 46	9 91 90
12 21 19	9 155 147	14 48 48	17 46 44	12 20 18	9 102 105	16 36 31	11 5R 5R
14 57 55	10 33 37	15 30 26	1R 17 14	13 R0 74	10 40 33	17 15 15	12 1A R
16 49 52	11 11R 11R	16 86 R0	20 11 11	14 70 65	11 142 146		13 65 66
18 R0 77	12 16 15	18 60 62		15 30 32	13 R4 R6	L= 3 K= 6	14 36 37
20 54 56	13 101 103	19 27 23	L= 1 K= 3	16 58 60	14 22 21	0 70 68	15 41 40
	15 69 70	20 61 61	1 35 31	1R 71 67	15 77 71	2 65 61	16 33 33
L= -2 K= 4	17 50 46	21 14 12	2 109 97	20 52 53	16 45 44	3 1R 19	17 2R 27
0 77 170	19 19 23		3 40 38		17 30 34	4 52 61	
2 38 79	21 9 P	L= 0 K= 4	4 82 49	L= 2 K= 2	1R 37 39	5 29 27	L= 4 K= 5
3 16 28		3 15 15	5 58 52	0 246 242	19 46 39	6 44 45	0 45 37
4 74 9R	L= -1 K= 4	4 144 136	6 34 24	2 162 148	20 53 49	7 34 36	1 22 16
5 34 38	2 12 27	5 24 2R	7 104 102	3 17 13		R 25 25	2 5R 5R
6 49 52	3 59 107	6 95 82	R 12 12	4 182 166	L= 3 K= 1	9 16 35	3 40 36
7 17 9	5 130 12R	7 50 46	9 90 87	5 80 66	0 96 96	11 49 37	4 24 19
R 48 56	6 40 40	R 32 27	10 60 36	6 42 46	2 R6 75	13 29 2R	5 45 45
10 1R 13	7 87 76	9 15 11	11 114 109	7 R9 94	3 106 R9	14 24 27	6 33 36
13 21 21	9 10R 9R	10 21 15	13 106 100	R 65 65	4 106 102	15 26 23	7 4R 52
14 54 50	10 51 54	11 2R 24	15 63 64	9 63 61	5 149 144		R 15 13
15 13 12	11 R0 75	12 24 20	16 34 28	10 16 15	6 69 69	L= 4 K= 0	9 47 45
1A 39 43	13 9R 9A	13 1R 1R	17 33 36	11 46 48	7 R6 R2	0 43 35	10 20 22
1R R3 76	15 73 72	14 51 44	1R 15 17	12 21 25	R 47 46	1 47 69	11 5R 54
20 57 61	16 16 9	15 32 25	19 22 21	13 69 67	9 55 63	2 93 97	12 13 10
	17 54 52	1A 69 67	20 30 25	14 R1 79	10 13 15	3 79 69	13 51 47
L= -2 K= 5	1R 24 19	17 12 7		15 R5 61	11 69 65	4 R5 R1	14 9 10
0 57 112		1R 44 4R	L= 1 K= 4	1A 38 45	13 77 77	5 145 143	15 45 49
2 70 110	L= -1 K= 5	19 15 12	2 54 43	1R R5 62	15 44 63	6 106 105	
3 21 30	1 47 50	20 46 43	3 98 91	20 47 50	16 23 23	7 52 54	L= 4 K= A
4 R8 10R	3 39 40		4 56 59		17 44 43	R 55 46	0 4P 4P
6 100 116	5 101 97	L= 0 K= 5	5 45 35	L= 2 K= 3	1R 40 37	9 06 9R	2 39 44
7 31 32	6 30 26	4 129 118	A 26 1R	0 151 128	19 25 26	10 26 23	3 33 33
R 24 21	7 105 89	5 36 32	7 122 101	1 24 25	20 50 4R	11 40 42	6 16 19
11 1A 13	9 R2 74	A 73 6R	9 85 79	2 143 158	12 50 4R	12 50 43	7 43 45
12 45 46	11 85 74	R 61 5R	10 36 32	4 98 R2	13 90 93	13 51 47	9 56 A0
14 3A 39	13 76 AR	9 2R 24	11 121 112	5 R3 74	14 61 43	11 52 55	
15 30 27	14 20 16	11 22 17	12 18 17	6 7R R0	15 43 44	13 5R 5A	L= 5 K= 0
1A 5R 54	15 65 57	13 51 53	13 51 53	7 55 55	16 46 53		0 136 140
1R 49 45	17 29 27	14 35 35	9 79 74	R 57 53	17 36 32	L= 5 K= 0	2 95 RR
	19 19 16	15 63 5R	10 3R 42	9 79 74	1R 35 39	0 136 140	4 152 150
L= -2 K= 6		16 47 46	11 44 44	10 3R 42	20 57 54	2 95 RR	6 24 2R
2 44 125	L= -1 K= A	17 25 2R	12 20 23	11 44 44		4 152 150	A 44 44
3 19 29	4 4R 47	1R 35 35	13 51 50	12 20 23	L= 4 K= 1	6 24 2R	7 45 4P
4 7A 9A	5 95 90	19 32 26	14 36 36	13 51 50	0 107 101	A 44 44	R 51 5R
6 70 7R	7 R3 69	20 26 26	1A A3 A2	14 36 36	2 131 116	7 45 4P	9 5A 52
R 33 31	9 103 94		17 30 2R	1A A3 A2	3 94 87	R 51 5R	10 10 11
12 30 27	10 1R 1R	L= 1 K= 5	1R 52 52	17 30 2R	4 100 93	9 5A 52	11 57 A0
13 13 13	11 R3 A7	3 5R 55	19 11 12	1R 52 52	5 64 5R	10 10 11	13 47 47
14 32 2R	13 R2 AR	4 73 19	20 62 59	19 11 12	6 7A 7A	11 57 A0	14 60 5A
15 17 13	14 19 17	R 44 42		20 62 59	7 7A 75	13 47 47	15 24 2R
16 55 49	15 46 41	9 32 30	L= 2 K= 4		R 25 29	14 60 5A	16 43 44
	17 3R 33	11 22 1R	0 R4 69	L= 3 K= 2	9 56 A2	15 24 2R	17 20 19
L= -1 K= 0		12 21 24	1 26 22	0 67 59	10 39 41	16 43 44	1R 72 6R
0 73 51	L= 0 K= 0	13 35 30	2 107 105	1 38 42	11 91 91	17 20 19	19 R 9
1 73 76	4 160 135	14 47 40	3 52 40	2 145 139	13 5R 62	1R 72 6R	
2 3A A3	6 34 27	16 34 2R	4 66 50	3 47 42	14 34 36	19 R 9	
3 121 116	R 126 107		5 63 57	4 95 R6	15 A5 64		
4 9 26	10 73 44	L= 1 K= 0	6 57 54	5 102 107	16 A0 59	L= 5 K= 1	
5 149 143	14 77 62	0 73 51	7 44 39	6 70 74	17 26 29	0 133 124	
7 116 114	16 22 39	1 75 76	R 2R 26	7 78 74	1R 54 54	2 120 114	
9 172 165	1R 78 110	2 37 63	9 55 54	9 108 115	19 26 22	4 69 72	
11 99 9R	20 54 70	3 125 116	10 21 25	10 17 19	20 54 50	5 35 31	
13 91 R0	22 70 65	5 15R 163	11 48 42	11 55 55		6 90 101	
15 75 75		A 11 12	12 25 25	12 33 31	L= 4 K= 2	7 37 37	
17 67 66	L= 0 K= 1	7 11R 114	13 52 51	13 47 44	0 113 106	R 30 35	
20 27 39	1 17 36	9 179 165	14 22 20	14 23 25	2 95 90	9 45 46	
22 14 20	2 234 226	11 101 9R	15 48 47	15 21 20	3 64 66	11 44 51	
	3 17 10	13 93 R9	16 43 39	16 57 53	4 64 63	12 43 39	
L= -1 K= 1	4 149 139	15 76 75	17 42 41	17 41 40	5 53 2R	13 47 49	
0 27 41	6 132 130	17 69 66	1R 36 37	1R 29 34	6 49 49	14 36 39	
1 19 29	7 37 22	20 44 39	19 17 18	19 15 17	7 R3 R2	15 37 37	
2 26 25	R 47 39	22 19 20		20 53 4R	R 20 20	16 47 45	
3 23 19	9 30 35		L= 2 K= 5		9 62 65	17 1R 16	
4 24 14	11 17 15	L= 1 K= 1	0 105 94	L= 3 K= 3	11 R8 91	1R 69 67	
5 35 33	12 41 43	0 61 61	2 91 84	0 158 144	13 64 65		
7 132 114	14 51 49	1 11 14	3 45 39	1 47 45	14 30 26	L= 5 K= 2	
8 19 1R	15 26 24	2 62 60	4 58 57	2 90 89	15 73 73	0 82 77	
9 177 178	16 76 73	3 65 R4	6 21 17	3 36 34	16 31 31	2 90 82	
10 17 19	1R 73 69	4 27 17	7 63 60	4 A3 A2	17 33 35	4 79 73	
11 134 132	20 76 70	5 201 190	9 79 R1	5 145 141	18 39 3R	6 84 R0	
12 16 13	22 62 60	6 16 22	11 R0 77	6 106 105	19 24 24	8 25 24	
13 R3 R2		7 210 216	13 26 25	7 52 54		A R3 R4	
15 R0 75	L= 0 K= 2	R 2R 23	14 30 25	R 55 46	L= 4 K= 3	7 52 56	
17 55 51	2 144 140	9 1R0 173	15 45 39	9 06 9R	0 77 73	R 34 36	
19 22 23	3 20 17	10 20 17	16 43 3R	10 26 23	1 36 3R	9 34 36	
20 30 2R	4 52 55	11 121 122	17 26 25	11 A0 A2	2 54 43	11 54 56	

Table 2. Continued.

they contain N(1) or N(2), respectively. Each ligand is coordinated to four different praseodymium ions. Together with the praseodymium ions ligand 1 forms a two-dimensional network in the *ac*-plane. Ligand 2 connects these layers in the *b*-direction. The resulting three-dimensional arrangement is shown in Fig. 3.

The coordination polyhedron. It was suggested previously [1] that the lanthanoid ion was eight-coordinated, with metal-oxygen distances in the range 2.3 – 2.6 Å. The coordination polyhedron was described as a square antiprism. By including O(5) in the coordination sphere [the Pr – O(5) distance is 2.75(2) Å] each lanthanoid ion is surrounded by nine oxygen atoms forming a distorted monocapped square antiprism (Fig. 4). The atom O(5) is situated at a corner of the square antiprism in one polyhedron (the distance Pr – O(5^{iii}) is 2.34(2) Å] but caps the antiprism of the neighbouring polyhedron. A similar situation is found in the iminodiacetate compound $Nd(C_4H_5NO_4)(H_2O)_3Cl$ [9] where the nine-coordinated neodymium ion is surrounded by a tricapped trigonal prism of one nitrogen and eight oxygen atoms. One of the oxygen atoms is situated at a corner of the trigonal prism in one polyhedron but in the equatorial ("capping") plane of the neighbouring polyhedron. The corresponding metal-oxygen distances are 2.52(2) and 2.78(2) Å, respectively. Bond distances in the coordination polyhedron are given in Table 3a. There are 12 oxygen-

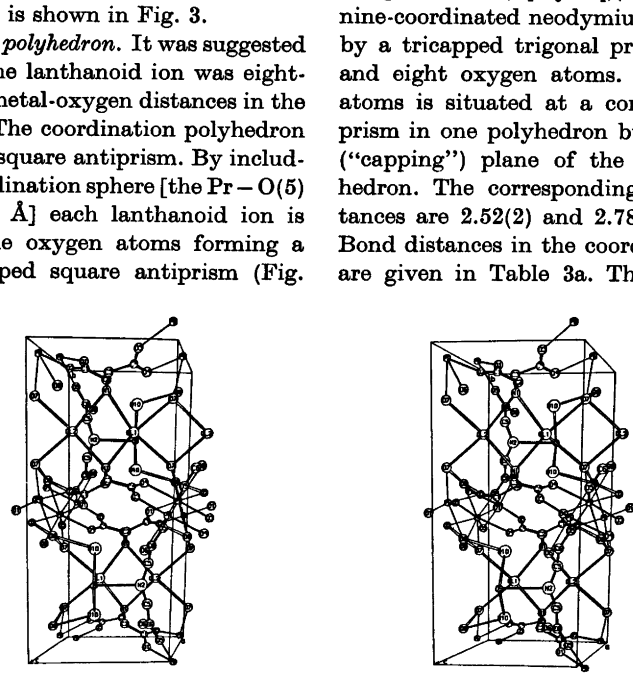

Fig. 3. A stereoscopic pair of drawings showing the structure of PRIMIN.

Table 3. Selected interatomic distances (Å) and angles (°) with estimated standard deviations.

a. The coordination polyhedron

Distance		Distance	
Pr–O(1^{i})[a]	2.43(2)	O(2^{ii})–O(3^{iii})	3.17(2)
Pr–O(2^{ii})	2.40(2)	O(2^{ii})–O(6)	3.05(2)
Pr–O(3^{iii})	2.45(2)	O(2^{ii})–O(7)	2.73(3)
Pr–O(4)	2.53(2)	O(2^{ii})–O(8)	2.94(2)
Pr–O(5)	2.75(2)	O(3^{iii})–O(5)	2.92(3)
Pr–O(5^{iii})	2.34(2)	O(3^{iii})–O(5^{iii})	2.87(2)
Pr–O(6)	2.58(2)	O(3^{iii})–O(6)	3.09(3)
Pr–O(7)	2.58(2)	O(3^{iii})–O(8)	2.78(2)
Pr–O(8)	2.54(2)	O(4)–O(5)	2.95(2)
O(1^{i})–O(4)	2.94(2)	O(4)–O(5^{iii})	2.96(3)
O(1^{i})–O(5^{iii})	3.19(2)	O(4)–O(7)	2.99(3)
O(1^{i})–O(7)	3.10(3)	O(5)–O(5)^{iii}	2.93(3)
O(1^{i})–O(8)	2.96(3)	O(5^{iii})–O(8)	3.02(3)
		O(6)–O(7)	2.93(3)

[a] The superscripts (i)–(vii) indicate the following equivalent sites in the structure

(i)	$1-x$, $-y$, $1-z$	(v)	$-x$, $-y$, $1-z$
(ii)	$-1+x$, y, z	(vi)	$-1+x$, y, $-1+z$
(iii)	$-x$, $-y$, z	(vii)	$-1-x$, $-y$, $-z$
(iv)	x, $\frac{1}{2}-y$, z		

b. Ligand 1

Distance		Angle	
C(1)–O(1)	1.29(3)	O(1)–C(1)–O(2)	124(2)
C(1)–O(2)	1.27(3)	O(1)–C(1)–C(2)	115(2)
C(4)–O(3)	1.27(3)	O(2)–C(1)–C(2)	120(2)
C(4)–O(4)	1.22(3)	O(3)–C(4)–O(4)	129(3)
C(1)–C(2)	1.51(4)	C(3)–C(4)–O(3)	113(2)
C(3)–C(4)	1.55(4)	C(3)–C(4)–O(4)	117(2)
N(1)–C(2)	1.52(3)	C(1)–C(2)–N(1)	112(2)
N(1)–C(3)	1.51(3)	C(2)–N(1)–C(3)	114(2)
		N(1)–C(3)–C(4)	110(2)

c. Ligand 2

Distance		Angle	
C(6)–O(5)	1.29(3)	O(5)–C(6)–O(6)	125(2)
C(6)–O(6)	1.29(3)	O(5)–C(6)–C(5)	117(2)
C(5)–C(6)	1.54(4)	O(6)–C(6)–C(5)	119(2)
N(2)–C(5)	1.54(4)	N(2)–C(5)–C(6)	105(2)
		C(5)–N(2)–C(5iv)	109(3)

d. Possible hydrogen bonds

Distance		Distance	
O(7)–Cl(2^{ii})	3.11(2)	O(8)–O(2^{i})	2.94(2)
O(7)–Cl(1)	3.16(2)	O(8)–O(7^{v})	2.90(2)
N(1)–Cl(1)	3.23(2)	N(2)–O(9^{vi})	3.12(6)
N(1)–Cl(2)	3.22(2)	O(9^{vi})–O(10^{iii})	3.14(4)
		O(10^{iii})–O(8^{vii})	2.77(5)

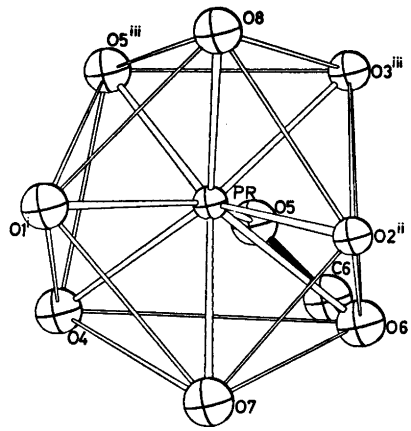

Fig. 4. The coordination polyhedron around the praseodymium ion.

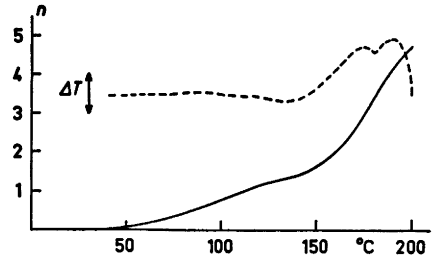

Fig. 5. TGA (solid line) and DTA (dashed line) curves for PRIMIN. n is the number of moles of water lost per two moles of praseodymium. In the DTA curve ΔT is on an arbitrary scale.

oxygen distances within the coordination polyhedron, which are less than 3.0 Å, thus indicating van der Waals contacts.

The ligands. The atoms in ligand 1 are crystallographically independent, while ligand 2 has the symmetry m. From the stoichiometry of the compound, there must be two protons balancing the charge of the chloride ions. These protons are most probably bonded to the nitrogen atoms N(1). Thus, the structure should contain both $-NH_2^+$ (ligand 1) and $-NH-$ groups (ligand 2). In contrast to the situation in $Nd(C_4H_3NO_4)(H_2O)_3Cl$,[9] the $-NH-$ group in ligand 2 is not coordinated to the metal ion. Bond distances and angles for the ligands are given in Tables 3b and 3c. They are compatible with those found for the iminodiacetic acid group in other structures.[8-11]

Possible hydrogen bonds. Judging from the chloride-oxygen and chloride-nitrogen distances (Table 3d), each chloride ion might accept four hydrogen bonds. The arrangement of the hydrogen bonded atoms around the chloride ions may be described as distorted rectangles. These rectangles are connected by sharing the edges N(1)–N(1) and O(7)–O(7), and infinite chains running in the a-direction are formed (Fig. 3). The water oxygen O(8) may donate hydrogen bonds to O(7) and O(2) in the neighbouring coordination polyhedron. It is also possible that there is a hydrogen bonded chain N(2)–O(9)–O(10)–O(8) in the structure. Since N(2) and O(9) are located in a mirror plane, there would be two O(9)–O(10)–O(8) branches.

The water oxygen O(10) could not be located by using the data collected at room temperature.[1] In this analysis it was found to be situated at interstices of the structure. It will probably have a high mobility in these interstices at room temperature. This dynamic disorder will decrease at low temperature to form the above mentioned hydrogen bonded chain. At −50 °C there might still be some disorder since the occupancy number refines to 0.81 for O(10). The large value of the temperature factor supports this view. In Fig. 5 the TGA and DTA curves for PRIMIN are shown. The compound starts losing weight at about 40 °C. A weight loss equivalent to 1.5 mol of water is achieved at about 145 °C, and up to this temperature no change in the DTA curve is observed. There is one maximum in the DTA curve at 175 °C, and the weight loss at this temperature is equivalent to the loss of 3 mol of water. Thus, the DTA curve indicates that half of the hydrated water is very loosely bonded, and can therefore be expected to have a high thermal mobility at room temperature. Similar dynamic disorder of water molecules is found in $Nd_2(C_2O_4)_3 10{\cdot}5\ H_2O$,[12,13] where at room temperature one third of the water molecules are disordered.

We thank the referees for some valuable suggestions and comments. This work is part of a research project supported by the Swedish Natural Science Research Council.

REFERENCES

1. Albertsson, J. and Oskarsson, Å. *Acta Chem. Scand. 22* (1968) 1700.
2. Oskarsson, Å. *To be published.*
3. Danielsson, S., Grenthe, I. and Oskarsson, Å. *To be published.*
4. *International Tables for X-Ray Crystallography*, Kynoch Press, Birmingham 1952, Vol. I.
5. Zacharisen, W. H. *Acta Cryst. 23* (1967) 558.
6. *International Tables for X-Ray Crystallography*, Kynoch Press, Birmingham 1962, Vol. III.
7. Cromer, D. T., Larsson, A. C. and Weber, J. T. *Acta Crystallogr. 17* (1964) 1044.
8. Oskarsson, Å. *Acta Crystallogr. B 29* (1973) 1747.
9. Oskarsson, Å. *Acta Chem. Scand. 25* (1971) 1206.
10. Boman, C.-E., Herbertsson, H. and Oskarsson, Å. *Acta Crystallogr. B 30* (1974) 378.
11. Oskarsson, Å. *Acta Crystallogr. B 30* (1974) 780.
12. Hansson, E. *Acta Chem. Scand. 24* (1970) 2969.
13. Hansson, E. *Acta Chem. Scand. 27* (1973) 2852.

Received December 21, 1973.

Acta Chemica Scandinavica A 28 (1974) 356—362

Short Communications

Normal Coordinate Analysis and Molecular Constants of Tetrolyl Chloride

ASTRI ROGSTAD

Kjemisk Institutt, Universitetet i Oslo, Blindern, Oslo 3, Norway

Recently we made a complete infrared and Raman spectral study [1] of propiolyl chloride (propiolic acid chloride) HC≡CCOCl and tetrolyl chloride (tetrolic acid chloride) $CH_3C{\equiv}CCOCl$ and discussed the assignment of the fundamental vibrational modes. Our attention was particularly drawn to the low frequency vibrations of the COCl group and the relatively free internal rotation of the methyl group of tetrolyl chloride, which was evident from the IR spectrum.

Harmonic force fields [2] were recently developed for the four structurally related molecules HC≡CCOCl, ClC≡CCHO, BrC≡CCHO, and IC≡CCHO. Mean amplitudes of vibration and related quantities were calculated.[3] The molecules display very similar magnitudes of mean amplitudes for corresponding distance types. The present normal coordinate analysis of tetrolyl chloride (TC) has been used to evaluate the following molecular constants:[4] (i) mean amplitudes of vibration, (ii) perpendicular amplitude correction coefficients, and (iii) Bastiansen-Morino linear shrinkage effects.

Symmetry coordinates. The molecular model is shown in Fig. 1. The applied values of interatomic distances are estimated from data of structurally related molecules.[5-7] Tetrahedral angles were assumed.

The symmetry of TC is discussed elsewhere.[1] There are in all $3N-7=20$ fundamentals since one internal rotational degree of freedom replaces the torsional motion of the methyl group. The calculations are based on a rigid molecular model having C_s symmetry in its equilibrium position. The additional vibrational degree of freedom is associated with the torsional motion. In order to test numerically the influences of the almost free internal rotation of the CH_3-group the calculations were performed for torsional frequencies of 20 and 50 cm^{-1}.

The vibrational modes are distributed among the irreducible representations of the C_s point group according to:

$$\Gamma_{vib} = 14\ a' + 7\ a''$$

A suitable set of symmetry coordinates is obtained by combining those for the pyramidal XY_3Z-model [8] and the halopropynal model.[3] In the latter case the valence coordinates are already symmetry coordinates, constituting $S_1(a')$ to $S_9(a')$ and $S_{15}(a'')$ to $S_{17}(a'')$. The remaining nine coordinates are transferred from the C_{3v}-model XY_3Z by correlating the $S(a_1)$ and $S_a(e)$ coordinates to those of the a' type and the $S_b(e)$ coordinates to those of a''. There is one redundant zero-coordinate in species a'. The

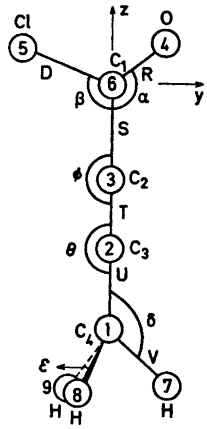

Fig. 1. The $CH_3CCCOCl$ model. The structural parameters are given (capital letters). Stretching valence coordinates are identified by the corresponding small letters. The symbols used for the different types of bending coordinates are indicated. Symmetry coordinates, a'-species: $S_1=r$, $S_2=d$, $S_3=s$, $S_4=t$, $S_5=u$, $S_6=(RS)^{\frac{1}{2}}\alpha$, $S_7=(DS)^{\frac{1}{2}}\beta$, $S_8=(ST)^{\frac{1}{2}}\phi_y$, $S_9=(TU)^{\frac{1}{2}}\theta_y$, $S_{10}=3^{-\frac{1}{2}}(v_1+v_2+v_3)$, $S_{11}=6^{-\frac{1}{2}}(2v_1-v_2-v_3)$, $S_{12}=\left\{\frac{V}{3[V(4-\sec^2E)+U]}\right\}^{\frac{1}{2}}[(4-\sec^2E)^{\frac{1}{2}}V(\varepsilon_1+\varepsilon_2+\varepsilon_3) - U(\delta_1+\delta_2+\delta_3)]$, $S_{13}=6^{-\frac{1}{2}}V(2\varepsilon_1-\varepsilon_2-\varepsilon_3)$, $S_{14}=6^{-\frac{1}{2}}(VU)^{\frac{1}{2}}(2\delta_1-\delta_2-\delta_3)$; a''-species: $S_{15}=(ST)^{\frac{1}{2}}\phi_x$, $S_{16}=(TU)^{\frac{1}{2}}\theta_x$, $S_{17}=[(RD)^{\frac{1}{2}}S]^{\frac{1}{2}}\gamma_{5463}$, $S_{18}=2^{-\frac{1}{2}}(v_2-v_3)$, $S_{19}=2^{-\frac{1}{2}}R(\varepsilon_2-\varepsilon_3)$, $S_{20}=2^{-\frac{1}{2}}(RD)^{\frac{1}{2}}(\delta_2-\delta_3)$, $S_{21}=(VD)^{\frac{1}{2}}\tau_{7165}$. Redundant zero coordinate in species a′:

$$V\left\{\frac{U}{3[V(4-\sec^2E)+U]}\right\}^{\frac{1}{2}}[\varepsilon_1+\varepsilon_2+\varepsilon_3+(4-\sec^2E)^{\frac{1}{2}}(\delta_1+\delta_2+\delta_3)]=0.$$

torsional coordinate is $S_{21}(a'') = \sqrt{VD}\tau_{7165}$, (see Fig. 1).

Force constants. The standard Wilson *GF* matrix method [9] in terms of symmetry coordinates was applied. The initial force constants were taken from Devarajan and Cyvin [10] and Rogstad and Cyvin.[3] Also nonvanishing off-diagonal elements from the *F*-matrix [3] of HC≡COCl were included in the initial force field (F_o). A final force field was produced by iterative calculations in order to fit exactly the observed vibrational frequencies. The diagonal elements of the initial and refined force constant matrices are given in Table 1. Table 2 shows that the frequencies calculated from the initial set of force constants give good agreement with the observed frequencies. This indicates that most of the force constants are transferable among related molecules.

Table 1. Force constants (mdyn/Å) for tetrolyl chloride, $CH_3CCCOCl$.

	Initial	Final
Species *a'*		
$F_{11}(C_1=O)$	10.38	10.19
$F_{22}(C_1-Cl)$	3.97	4.11
$F_{33}(C_1-C_2)$	4.20	4.55
$F_{44}(C_2\equiv C_3)$	15.57	15.22
$F_{55}(C_3-C_4)$	3.95	3.92
$F_{66}(C_1C_2O)$	1.21	1.20
$F_{77}(C_1C_2Cl)$	0.660	0.646
$F_{88}(C_1C_2C_3)$	0.197	0.214
$F_{99}(C_2C_3C_4)$	0.133	0.160
$F_{10\ 10}(C_4-H)$	4.90	4.91
$F_{11\ 11}(C_4-H)$	4.70	4.66
$F_{12\ 12}(HC_4H)$	0.415	0.381
$F_{13\ 13}(HC_4H)$	0.450	0.433
$F_{14\ 14}(HC_3C_4)$	0.430	0.414
Species *a''*		
$F_{11}(C_1C_2C_3)$	0.126	0.136
$F_{22}(C_2C_3C_4)$	0.181	0.164
$F_{33}(OC_1Cl)$	0.241	0.221
$F_{44}(C_4H)$	4.70	4.66
$F_{55}(HC_4H)$	0.450	0.432
$F_{66}(HC_3C_4)$	0.430	0.407
F_{77}(torsion)	0.0008	0.0004

Potential energy distribution. Calculated potential energy distribution terms,[11,12] $100\,F_{ij}L_{ik}/\lambda_k$, are listed in Table 2. The approximate descriptions of normal modes according to these calculations are fairly well compatible with the assignments [1] of frequencies done *a priori*.

Mean amplitudes of vibration and related quantities. The harmonic force field developed was used to calculate the mean amplitudes of vibration (u), perpendicular amplitude correction coefficients (K) and Bastiansen-Morino shrinkages (δ) for the linear chain. The u- and δ-values are given in Table 3. The interatomic separations (R) are included in the table. Only for two distance types of the totality of twenty-four we may expect the mean amplitudes to depend significantly on the barrier of internal rotation. They are the O···H and Cl···H types. The corresponding mean amplitudes are not quoted. As expected the linear shrinkage effects are unaffected by variations in the torsional frequency, whereas the perpendicular correction coefficients (except those for the linear chain) increase considerably on diminishing the barrier of internal rotation. These values are therefore not reported.

The calculated mean amplitudes of vibration were compared with those of propiolyl chloride,[3] propiolaldehyde,[3] and methylated acetylenes.[5,10] Reported values [3,5,10] for various bonded and nonbonded distances were found to be very well consistent with those listed in Table 3. Also the listed values of shrinkage effects (Table 3) were found to be compatible with characteristic

Table 2. Vibrational frequencies (cm^{-1}) and distribution of potential energy for tetrolyl chloride, $CH_3CCCOCl$.

	Obs.	Calc.	PED
Species *a'*			
ν_1	2961	2974	99 v
ν_2	2921	2918	99 v
ν_3	2225	2259	85 t
ν_4	1758	1772	76 r
ν_5	1431	1459	91 ε
ν_6	1378	1451	90 ε
ν_7	1161	1063	41 s + 28 α + 21 d
ν_8	1016	1041	87 δ
ν_9	842	865	42 u + 27 α
ν_{10}	600	639	23 d
ν_{11}	472	542	47 β + 36 ϕ_y + 30 d + 20 s
ν_{12}	395	406	35 α
ν_{13}	293	271	48 θ_y + 31 β
ν_{14}	104	84	51 ϕ_y + 27 θ_y + 22 β
Species *a''*			
ν_{15}	2961	2974	99 v
ν_{16}	1431	1459	92 ε
ν_{17}	1016	1043	89 δ
ν_{18}	652	679	83 γ
ν_{19}	365	412	75 θ_x + 32 ϕ_x
ν_{20}	135	123	57 ϕ_x + 23 θ_x
ν_{21}	20[a]	29	100 τ

[a] Unobserved; calc. are also performed for $\nu_{21} = 50$ cm^{-1}, giving the following numerical variations in the PED terms: $\nu_{18} - 84\gamma$, $\nu_{20} - 58\phi_x + 24\theta_x$, $\nu_{21} - 99\tau$.

Table 3. Mean amplitudes of vibration (u in Å) and linear shrinkage effects (δ in Å) for tetrolyl chloride, $CH_3CCCOCl$.

Distance	(R, Å)	0 K	298 K
$u(C_1=O)$	(1.192)	0.039	0.039
$u(C_1-Cl)$	(1.789)	0.045	0.047
$u(C_1-C_2)$	(1.426)	0.048	0.049
$u(C_2\equiv C_3)$	(1.207)	0.036	0.036
$u(C_3-C_4)$	(1.458)	0.049	0.051
$u(C_4-H)$	(1.110)	0.078	0.078
$u(C_1\cdots C_3)$	(2.633)	0.051	0.053
$u(C_1\cdots C_4)$	(4.091)	0.062	0.066
$u(C_1\cdots H)$	(4.582)	0.135 0.134	0.154 0.151
$u(C_2\cdots C_4)$	(2.665)	0.053	0.055
$u(C_2\cdots O)$	(2.346)	0.055	0.059
$u(C_2\cdots Cl)$	(2.683)	0.058	0.069
$u(C_2\cdots H)$	(3.210)	0.125 0.123	0.132 0.129
$u(C_3\cdots O)$	(3.484)	0.059	0.067
$u(C_3\cdots Cl)$	(3.710)	0.068	0.101
$u(C_3\cdots H)$	(2.106)	0.109	0.110
$u(C_4\cdots O)$	(4.903)	0.071	0.092
$u(C_4\cdots Cl)$	(5.057)	0.081	0.143
$u(O\cdots Cl)$	(2.602)	0.053	0.060
$u(O\cdots H)$	(5.181)	0.156	0.207
$u(O\cdots H)$	(5.461)	0.143	–
$u(Cl\cdots H)$	(5.349)	0.181	–
$u(Cl\cdots H)$	(5.814)	0.122	0.143
$u(H\cdots H)$	(1.813)	0.128	0.128
$\delta(C_1\cdots C_3)$	(2.633)	0.007	0.012
$\delta(C_1\cdots C_4)$	(4.091)	0.015	0.030
$\delta(C_2\cdots C_4)$	(2.665)	0.008	0.012

values deduced from structurally related molecules.[3,5,10]

Acknowledgements. I thank Professor S. J. Cyvin for help in carrying out the calculations and for many stimulating discussions.

1. Augdahl, E., Kloster-Jensen, E. and Rogstad, A. *Spectrochim. Acta 30 A* (1974) 399.
2. Lagset, E., Klaboe, P., Kloster-Jensen, E., Cyvin, S. J. and Nicolaisen, F. M. *Spectrochim. Acta 29 A* (1973) 17.
3. Rogstad, A. and Cyvin, S. J. *Acta Chem. Scand. 27* (1973) 2304.
4. Cyvin, S. J. *Molecular Vibrations and Mean Square Amplitudes*, Universitetsforlaget, Oslo and Elsevier, Amsterdam 1968.
5. Rogstad, A., Benestad, L. and Cyvin, S. J. *J. Mol. Struct. Submitted for publication.*
6. Brand, J. C. D. and Powell, R. A. *J. Mol. Spectrosc. 43* (1972) 342.
7. Sinnott, K. M. *J. Chem. Phys. 34* (1961) 851.
8. Cyvin, S. J., Cyvin, B. N., Elvebredd, I., Hagen, G. and Brunvoll, J. *Kgl. Nor. Vidensk. Selsk. Skr.* (1972) No. 22.
9. Wilson, E. B., Jr., Decius, J. C. and Cross, P. C. *Molecular Vibrations*, McGraw, New York 1955.
10. Devarajan, V. and Cyvin, S. J. *Aust. J. Chem. 25* (1972) 1387.
11. Morino, Y. and Kuchitsu, K. *J. Chem. Phys. 20* (1952) 1809.
12. Nakamoto, K. *Infrared Spectra of Inorganic and Coordination Compounds*, 2nd Ed., Wiley-Interscience, New York 1970.

Received January 16, 1974.

Aqueous Chemistry of Protactinium(IV). 3. Solvent Extraction of Pa(IV) Perchlorate by Trioctyl Phosphine Oxide

ROBERT LUNDQVIST

Department of Nuclear Chemistry, Chalmers University of Technology, Fack, S-402 20 Göteborg 5, Sweden

In studying the aqueous chemistry of Pa(IV)[1,2] it was found that a pH independent extraction method would be of value. An investigation of the extraction of Pa(IV) from perchlorate solutions by neutral adduct forming agents was therefore undertaken. The neutral organophosphorus compounds, which are among the strongest adduct forming molecules,[3] were selected for this investigation. Because the commonly used TBP (tributylphosphate) showed unsatisfactory extraction power, the more basic TOPO (trioctyl phosphine oxide) was chosen for a more detailed study.

Chemicals. Stock solutions of ^{233}Pa (in 7 M $HClO_4$), $(Na,H)ClO_4$, Zn(Hg) and 1.92 M $Cr(ClO_4)_3$ were prepared as described earlier.[1] The isotopes ^{51}Cr and ^{65}Zn were supplied from AB Atomenergi, Studsvik, Sweden, and Institutt for Atomenergi, Kjeller, Norway, respectively. The ^{24}Na was obtained by 1.8 h neutron irradiation (AB Atomenergi, Studsvik, Sweden) of 30 mg Na_2CO_3 at a neutron flux of 2.5×10^{12} n s^{-1} cm^{-2}. Stock solutions of ^{51}Cr (9 mCi/ml) in 0.1 $HClO_4$, ^{65}Zn (0.2 mCi/ml) in 1 M $HClO_4$, and ^{24}Na (0.4 mCi/ml)

Table 3. Mean amplitudes of vibration (u in Å) and linear shrinkage effects (δ in Å) for tetrolyl chloride, $CH_3CCCOCl$.

Distance	(R, Å)	0 K	298 K
$u(C_1=O)$	(1.192)	0.039	0.039
$u(C_1-Cl)$	(1.789)	0.045	0.047
$u(C_1-C_2)$	(1.426)	0.048	0.049
$u(C_2\equiv C_3)$	(1.207)	0.036	0.036
$u(C_3-C_4)$	(1.458)	0.049	0.051
$u(C_4-H)$	(1.110)	0.078	0.078
$u(C_1\cdots C_3)$	(2.633)	0.051	0.053
$u(C_1\cdots C_4)$	(4.091)	0.062	0.066
$u(C_1\cdots H)$	(4.582)	0.135 0.134	0.154 0.151
$u(C_2\cdots C_4)$	(2.665)	0.053	0.055
$u(C_2\cdots O)$	(2.346)	0.055	0.059
$u(C_2\cdots Cl)$	(2.683)	0.058	0.069
$u(C_2\cdots H)$	(3.210)	0.125 0.123	0.132 0.129
$u(C_3\cdots O)$	(3.484)	0.059	0.067
$u(C_3\cdots Cl)$	(3.710)	0.068	0.101
$u(C_3\cdots H)$	(2.106)	0.109	0.110
$u(C_4\cdots O)$	(4.903)	0.071	0.092
$u(C_4\cdots Cl)$	(5.057)	0.081	0.143
$u(O\cdots Cl)$	(2.602)	0.053	0.060
$u(O\cdots H)$	(5.181)	0.156	0.207
$u(O\cdots H)$	(5.461)	0.143	–
$u(Cl\cdots H)$	(5.349)	0.181	–
$u(Cl\cdots H)$	(5.814)	0.122	0.143
$u(H\cdots H)$	(1.813)	0.128	0.128
$\delta(C_1\cdots C_3)$	(2.633)	0.007	0.012
$\delta(C_1\cdots C_4)$	(4.091)	0.015	0.030
$\delta(C_2\cdots C_4)$	(2.665)	0.008	0.012

values deduced from structurally related molecules.[3,5,10]

Acknowledgements. I thank Professor S. J. Cyvin for help in carrying out the calculations and for many stimulating discussions.

1. Augdahl, E., Kloster-Jensen, E. and Rogstad, A. *Spectrochim. Acta 30 A* (1974) 399.
2. Lagset, E., Klaboe, P., Kloster-Jensen, E., Cyvin, S. J. and Nicolaisen, F. M. *Spectrochim. Acta 29 A* (1973) 17.
3. Rogstad, A. and Cyvin, S. J. *Acta Chem. Scand. 27* (1973) 2304.
4. Cyvin, S. J. *Molecular Vibrations and Mean Square Amplitudes*, Universitetsforlaget, Oslo and Elsevier, Amsterdam 1968.
5. Rogstad, A., Benestad, L. and Cyvin, S. J. *J. Mol. Struct. Submitted for publication.*
6. Brand, J. C. D. and Powell, R. A. *J. Mol. Spectrosc. 43* (1972) 342.
7. Sinnott, K. M. *J. Chem. Phys. 34* (1961) 851.
8. Cyvin, S. J., Cyvin, B. N., Elvebredd, I., Hagen, G. and Brunvoll, J. *Kgl. Nor. Vidensk. Selsk. Skr.* (1972) No. 22.
9. Wilson, E. B., Jr., Decius, J. C. and Cross, P. C. *Molecular Vibrations*, McGraw, New York 1955.
10. Devarajan, V. and Cyvin, S. J. *Aust. J. Chem. 25* (1972) 1387.
11. Morino, Y. and Kuchitsu, K. *J. Chem. Phys. 20* (1952) 1809.
12. Nakamoto, K. *Infrared Spectra of Inorganic and Coordination Compounds*, 2nd Ed., Wiley-Interscience, New York 1970.

Received January 16, 1974.

Aqueous Chemistry of Protactinium(IV). 3. Solvent Extraction of Pa(IV) Perchlorate by Trioctyl Phosphine Oxide

ROBERT LUNDQVIST

Department of Nuclear Chemistry, Chalmers University of Technology, Fack, S-402 20 Göteborg 5, Sweden

In studying the aqueous chemistry of Pa(IV)[1,2] it was found that a pH independent extraction method would be of value. An investigation of the extraction of Pa(IV) from perchlorate solutions by neutral adduct forming agents was therefore undertaken. The neutral organophosphorus compounds, which are among the strongest adduct forming molecules,[3] were selected for this investigation. Because the commonly used TBP (tributylphosphate) showed unsatisfactory extraction power, the more basic TOPO (trioctyl phosphine oxide) was chosen for a more detailed study.

Chemicals. Stock solutions of ^{233}Pa (in 7 M $HClO_4$), $(Na,H)ClO_4$, Zn(Hg) and 1.92 M $Cr(ClO_4)_3$ were prepared as described earlier.[1] The isotopes ^{51}Cr and ^{65}Zn were supplied from AB Atomenergi, Studsvik, Sweden, and Institutt for Atomenergi, Kjeller, Norway, respectively. The ^{24}Na was obtained by 1.8 h neutron irradiation (AB Atomenergi, Studsvik, Sweden) of 30 mg Na_2CO_3 at a neutron flux of 2.5×10^{12} n s^{-1} cm^{-2}. Stock solutions of ^{51}Cr (9 mCi/ml) in 0.1 $HClO_4$, ^{65}Zn (0.2 mCi/ml) in 1 M $HClO_4$, and ^{24}Na (0.4 mCi/ml)

in 1 M $HClO_4$ were prepared. The radiochemical purity of the gamma spectra was checked using a high resolution Ge(Li)-detector equipped with a multichannel analyzer. Commercial TBP solution (99 %) was purified [4] by distillation together with 0.1 M NaOH, washing with water and drying under vacuum. Later, TBP from another source (British Drug House, *p.a.*) was used without purification. The IR-spectra of the two TBP batches were measured with a Perkin-Elmer 337 grating IR spectrophotometer in the range 2.5 to 25.0 μ, and were found to be identical. A stock stolution of TOPO was made by successively washing a 1 M TOPO (Eastman Kodak) solution in benzene with equal volumes of first 0.1 NaOH + 0.9 $NaClO_4$ and then (0.1 H, 0.9 Na)ClO_4. The purified TOPO solution was slightly yellow. The chemicals used were of *p.a.* quality, if not otherwise stated.

Extraction technique. The extraction runs were made in an oxygen-free nitrogen atmosphere in a small glass vessel thermostated to ± 0.05 °C. Mixtures composed of 15 ml (Na, H)ClO_4 (of various molarities) + 0.1 ml 1.92 M $Cr(ClO_4)_3$ + 15 ml benzene were reduced either with 3 – 6 ml Zn(Hg) or electrolytically between a mercury cathode and a platinum anode. After complete reduction one drop of the ^{233}Pa stock solution (or ^{51}Cr or ^{65}Zn) and 0.005 – 1.6 ml 1 M TOPO in benzene was added. Separate electrolytic reduction experiments using ^{51}Cr as a tracer showed that chromium could be completely removed from the solution by amalgamation (or deposition) at the cathode, but the process was rather slow under the conditions used (~20 mA, 20 V).

The p*h* (= $-\log[H^+]$) was adjusted if necessary with 1 M NaOH or 1 M $HClO_4$ and the distribution system was stirred for 10 min, which was sufficient to establish equilibrium. In the beginning of some experiments, the organic phase was somewhat opaque after the addition of TOPO but this was found to have no effect on the distribution of Pa. The gamma activities, from equal samples of each phase (80 – 100 keV for ^{233}Pa and ^{51}Cr, above 1 MeV for ^{65}Zn and ^{24}Na), were measured with a NaI(Tl) crystal. The total number of disintegrations registered of each couple of phases was about 200 000. The number of disintegrations registered of the least active phase examined (which was at least twice as active as the background) was more than 2000, giving a radiometric accuracy in the logarithm of the distribution factor D_{Pa} of ± 0.01.

Results. The extraction using TOPO in benzene of $^{233}Pa(IV)$ from aqueous solutions of (Na, H, 0.01 M Cr^{2+})Cl_4O was studied at different concentrations of perchlorate (Figs. 1 and 2), of TOPO (Fig. 2) and of hydrogen ions (Fig. 3). Because the reduction procedure introduced Cr^{2+} and in some cases Zn^{2+} (less than 0.01 M), it was necessary to investigate whether these species affected the extraction of Pa(IV). The distributions of ^{65}Zn and ^{51}Cr

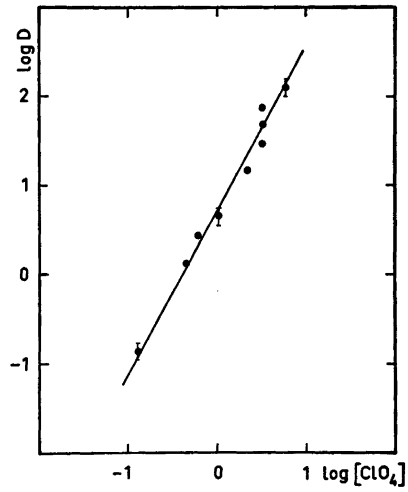

Fig. 1. The distribution of $^{233}Pa(IV)$ between $10^{-1.93}$ M TOPO in benzene and perchlorate media of various concentrations at p*h* 1 and 25 °C. The points marked with error limits are average values from at least 5 experiments.

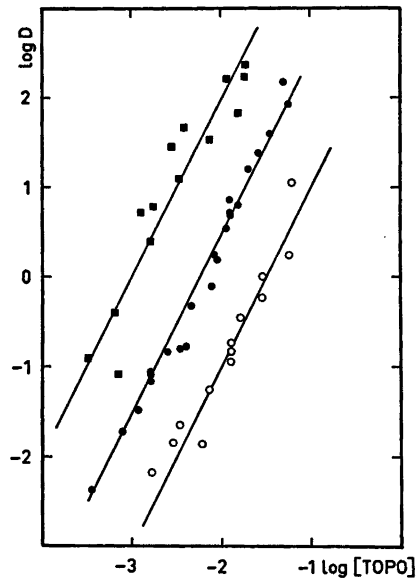

Fig. 2. The influence, at 25 °C, of the TOPO concentration on the distribution of $^{233}Pa(IV)$ between benzene and perchlorate media for different perchlorate concentrations at p*h* 1. ■ $[ClO_4^-] = 5.93$ M; ● $[ClO_4^-] = 1.03$ M; ○ $[ClO_4^-] = 0.13$ M.

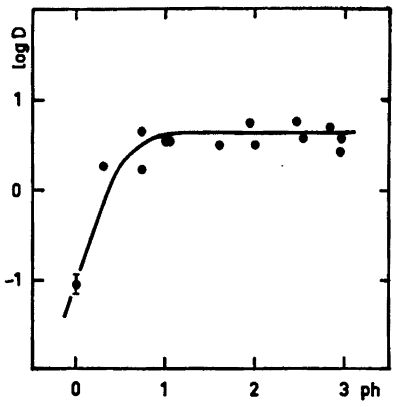

Fig. 3. The p*h* dependence of the distribution of ^{233}Pa(IV) between $10^{-1.93}$ M TOPO in benzene and 1.03 M perchlorate solution at 25 °C.

were found to be very low; about $10^{4.9}$ and $10^{3.7}$ times lower distribution values than for Pa(IV), respectively. The amount of TOPO complexed with Zn and Cr could thus be neglected. As extraction of perchloric acid reduces the free TOPO concentration, the ratio $[TOPO]_o/[HClO_4]_o$ (index o refers to the organic phase) was determined (in separate experiments) by titration of the aqueous and organic phases with 0.01 M NaOH. The extraction of $HClO_4$ (at p*h* 1) was investigated at high concentrations of TOPO (0.01 – 0.07 M) and perchlorate (1 and 6 M) and was found to be proportional to the perchlorate concentration and to the square of the TOPO concentration (if $[TOPO]_o/[HClO_4]_o > 2$). This is in agreement with the known extraction behaviour; $HClO_4$ is extracted [5] as an ion pair with the proton solvated with two TOPO molecules (if $[TOPO]_o/[HClO_4]_o < 2$). The ratio $[TOPO]_o/[HClO_4]_o$ (which is proportional to $[ClO_4]^{-1}$ and $[TOPO]^{-1}$) was found to be about 5 for 0.01 M TOPO ($[ClO_4] = 6$ M) and 10 for 0.072 M TOPO ($[ClO_4] = 1$ M).

The extraction of $NaClO_4$ was studied using the isotope ^{24}Na. The highest distribution ($D = 10^{-2.69}$) of $NaClO_4$ was found at the highest investigated concentrations of TOPO (0.072 M) and perchlorate (6 M). The ratio $[TOPO]_o/[NaClO_4]_o$ was thus ≥ 100 for all the distribution experiments of Pa(IV) and hence the extraction of $NaClO_4$ was neglected. Neither the concentration of ^{233}Pa ($10^{-11} - 10^{-10}$ M) nor the presence of less than 10^{-3} M sulphate or less than 10^{-2} M chloride affected the distribution. The sizes of the dots in the figures correspond approximately to the uncertainties.

The *perchlorate dependence* of the distribution of Pa(IV) was studied in the range from 0.13 to 5.93 M ClO_4. The ionic strength could not be kept constant but varied with the perchlorate concentration, because no weaker complexing anion to Pa(IV) than ClO_4 could be added. The influence of the perchlorate concentration was, however, much stronger than could be expected from the change in ionic strength. The function $\log D = f(\log [ClO_4])$ had a slope of 2; see Fig. 1. The *TOPO dependence* was studied at p*h* 1 (see Fig. 2) and 0 at different perchlorate concentrations. The slopes $\partial \log D/\partial \log [TOPO]$ were constant and equal to +2 over the perchlorate concentration range investigated both at p*h* 1 (0.13 – 5.93 ClO_4) and at p*h* 0 (1 M $HClO_4$). The TOPO dependence of the distributions of Zn(II) and Cr(II) at p*h* 1 (1.03 M ClO_4) was found to be similar to that for Pa(IV), but the distributions were much lower. The *ph dependence* was investigated at 1.03 M perchlorate and $10^{-1.93}$ M TOPO concentrations, see Fig. 3. The distribution of protactinium ($D = [Pa]_o/[Pa]$) at 25 °C was found to be constant from p*h* 1 up to at least 3. The useful p*h* range for extraction was limited by the rapid decrease in D at lower p*h* than 1 and the formation of Cr(II) hydroxides at higher p*h* than about 4 – 5. The *temperature dependence* was rather strong and showed a decreasing distribution of Pa(IV) with increasing temperature; $\log D = 1.22 \pm 0.15$ (10 °C), $\log D = 0.68 \pm 0.07$ (25 °C), $\log D = -0.25 \pm 0.07$ (45 °C). The temperature dependence was studied at p*h* 1 and at constant perchlorate (1.03 M) and TOPO ($10^{-1.93}$ M) concentrations.

Discussion. In evaluating the distribution data for Pa(IV) it is important to bear in mind that the free TOPO concentration in the organic phase may be lowered due to complexation with Na^+, H^+, Pa(IV), Zn(II), Cr(II) and H_2O. TOPO is known to be complexed with water both due to the solubility of water in benzene and as a result of the extraction of water, which occurs with one TOPO molecule solvating each water aggregate.[5] The complexation with water is here assumed to be constant (at least for constant ionic strength). Of the remaining species only H^+ was found to have any influence on the free TOPO concentration, and this only when the ClO_4 concentration was high. For 0.1 M $HClO_4$, the influence of the H^+ concentration was negligible. For 1 M ClO_4 and $[TOPO] \leq 10^{-1.93}$ M, the influence of H^+ was negligible at $ph \geq 1$ which is reflected by the constant distribution of Pa(IV) and further confirmed by the value of the ratio $[TOPO]_o/[HClO_4]_o = 10$ determined for $[TOPO] = 10^{-1.72}$. A small correction of the log D (6 M ClO_4) values may be relevant for the highest TOPO concentrations used, but as the correction is of the same magnitude as the error in log D it does not change the stoichiometric conclusions drawn below. Uncorrected log D values are shown in the figures.

From the zero protactinium concentration dependence ($\partial \log D/\partial \log [Pa] = 0$) and from the strong perchlorate dependence ($\partial \log D/\partial \log [ClO_4] = 2$) of the distribution of Pa(IV), it

is likely that Pa(IV) is distributed in the form of monomeric aggregates of ion pairs. If the degree of complexation between TOPO and water is constant (or nearly constant), and the influence of the ionic strength on the distribution of Pa(IV) is small for the investigated perchlorate concentration range, then the ion pair must consist of two perchlorate and one Pa(IV) ion, which latter from the electroneutrality criterium must be a doubly charged cation. Two cations, PaO^{2+} or $Pa(OH)_2^{2+}$, are possible, which conclusion is in agreement with observations from other perchlorate media extraction systems.[1,2]

From the TOPO dependence of the distribution ($\partial \log D/\partial \log [TOPO] = 2$) one concludes that the ion pair of Pa(IV) is solvated with two TOPO molecules. The extraction of Pa(IV) may then be formulated as $M^{4+} + 2ClO_4^- + 2TOPO(org) \rightleftharpoons [M^{4+}(TOPO)_2][ClO_4^-]_2(org)$. The possible participation of water in the extraction mechanism has not been studied due to experimental difficulties in determining the water content in the extracted complex when working at trace concentrations of Pa, and in evaluating the influence of the water activity on the extraction (one of the difficulties arises from the fact that TOPO itself extracts water). One notes that the number of TOPO solvates is still two at low acidities (1 M $HClO_4$), which indicates that the extraction mechanism is uncharged although dehydrolyzation of Pa(IV) is expected.[6]

The distribution of Cr(II) and Zn(II) was found, from a preliminary investigation, like Pa(IV), to be dependent on the second power of the TOPO concentration. The extraction of the divalent ions with TOPO seems therefore to be similar to their extraction with TBP;[7]

$$M^{2+} + 2ClO_4^- + mH_2O + 2TBP(org) \rightleftharpoons [M^{2+}(H_2O)_m(TBP)_2][ClO_4^-]_2(org).$$

The extraction constant for Pa(IV) has been calculated to be $\log K_D = 4.41 \pm 0.10$ (the total TOPO concentration is used in the calculations, not free TOPO concentration). The thermodynamic constants corresponding to K_D, obtained from the temperature data, were $\Delta H^\circ = -72 \pm 9$ kJ mol^{-1} and $\Delta S^\circ = -157 \pm 31$ J K^{-1} mol^{-1}.

Acknowledgement. The author is grateful to Professor Jan Rydberg and civ.ing. Stig Wingefors for valuable discussions and criticism and to ing. Martin Ohlson for experimental aid. Ph.D. Christopher Coombes kindly made the linguistic correction.

1. Lundqvist, R. *Acta Chem. Scand. A 28* (1974) 243.
2. Lundqvist, R. and Rydberg, J. *Acta Chem. Scand. A 28* (1974). *In press.*
3. Markl, P. *Extraktion und Extraktions-Chromatographie in der anorganischen Analytik*, Vol. 13 of *Metoden der Analyse in der Chemie*, Akademische Verlagsgesellschaft, Frankfurt a.M. 1972.
4. Alcock, K., Grimley, S. S., Healy, T. V., Kennedy, J. and McKay, H. A. *Trans. Faraday Soc. 52* (1956) 39.
5. Bucher, J. J., Zirin, M., Laugen, R. C. and Diamond, R. M. *J. Inorg. Nucl. Chem. 33* (1971) 3869.
6. Guillaumont, R. *Rev. Chim. Minér. 3* (1966) 339.
7. Agett, J., Clark, T. E. and Richardson, R. A. *J. Inorg. Nucl. Chem. 31* (1969) 2919.

Received January 28, 1974.

A High Temperature Iron Telluride with Rhombohedral Structure

ERLING RØST and STEINAR WEBJØRNSEN

Kjemisk institutt, Universitetet i Oslo, Oslo 3, Norway

A high temperature iron-tellurium phase has been found by DTA and X-ray high temperature investigations. This phase melts incongruently at about 920 °C, and transforms eutectoidally at 805 °C into the $Fe_2As-PbO$ type phase with tetragonal structure and the phase with the hexagonal NiAs-$Cd(OH)_2$ type structure. The high temperature phase exists in a rather broad range of homogeneity from about $FeTe_{0.80}$ to $FeTe_{0.93}$ at 845 °C. This temperature corresponds to the peritectoid decomposition of the $Fe_2As-PbO$ type phase. The corresponding composition of this phase is between $FeTe_{0.75}$ and $FeTe_{0.80}$. By the peritectoid decomposition metallic iron and the high temperature phase are formed.

The X-ray high temperature patterns could be indexed according to a rhombohedral unit cell and the data are given in Table 1.

The lattice constants of $FeTe_{0.90}$ were calculated for the temperatures 835 and 870° C, and of a metal rich sample, $FeTe_{0.75}$ at 850 °C. The latter is a two phase sample in which metallic iron exists in equilibrium with the high temperature phase of approximate composition $FeTe_{0.80}$. The following lattice constants refer to hexagonal setting:

$FeTe_{0.90}$, 835 °C:
$a = 4.013 \pm 0.003$ Å, $c = 20.96 \pm 0.02$ Å
$FeTe_{0.90}$, 870 °C:

is likely that Pa(IV) is distributed in the form of monomeric aggregates of ion pairs. If the degree of complexation between TOPO and water is constant (or nearly constant), and the influence of the ionic strength on the distribution of Pa(IV) is small for the investigated perchlorate concentration range, then the ion pair must consist of two perchlorate and one Pa(IV) ion, which latter from the electroneutrality criterium must be a doubly charged cation. Two cations, PaO^{2+} or $Pa(OH)_2^{2+}$, are possible, which conclusion is in agreement with observations from other perchlorate media extraction systems.[1,2]

From the TOPO dependence of the distribution ($\partial \log D/\partial \log [TOPO] = 2$) one concludes that the ion pair of Pa(IV) is solvated with two TOPO molecules. The extraction of Pa(IV) may then be formulated as $M^{4+} + 2ClO_4^- + 2TOPO(org) \rightleftharpoons [M^{4+}(TOPO)_2][ClO_4^-]_2(org)$. The possible participation of water in the extraction mechanism has not been studied due to experimental difficulties in determining the water content in the extracted complex when working at trace concentrations of Pa, and in evaluating the influence of the water activity on the extraction (one of the difficulties arises from the fact that TOPO itself extracts water). One notes that the number of TOPO solvates is still two at low acidities (1 M $HClO_4$), which indicates that the extraction mechanism is uncharged although dehydrolyzation of Pa(IV) is expected.[6]

The distribution of Cr(II) and Zn(II) was found, from a preliminary investigation, like Pa(IV), to be dependent on the second power of the TOPO concentration. The extraction of the divalent ions with TOPO seems therefore to be similar to their extraction with TBP;[7]

$$M^{2+} + 2ClO_4^- + mH_2O + 2TBP(org) \rightleftharpoons [M^{2+}(H_2O)_m(TBP)_2][ClO_4^-]_2(org).$$

The extraction constant for Pa(IV) has been calculated to be $\log K_D = 4.41 \pm 0.10$ (the total TOPO concentration is used in the calculations, not free TOPO concentration). The thermodynamic constants corresponding to K_D, obtained from the temperature data, were $\Delta H^\circ = -72 \pm 9$ kJ mol^{-1} and $\Delta S^\circ = -157 \pm 31$ J K^{-1} mol^{-1}.

Acknowledgement. The author is grateful to Professor Jan Rydberg and civ.ing. Stig Wingefors for valuable discussions and criticism and to ing. Martin Ohlson for experimental aid. Ph.D. Christopher Coombes kindly made the linguistic correction.

1. Lundqvist, R. *Acta Chem. Scand. A 28* (1974) 243.
2. Lundqvist, R. and Rydberg, J. *Acta Chem. Scand. A 28* (1974). *In press.*
3. Markl, P. *Extraktion und Extraktions-Chromatographie in der anorganischen Analytik*, Vol. 13 of *Metoden der Analyse in der Chemie*, Akademische Verlagsgesellschaft, Frankfurt a.M. 1972.
4. Alcock, K., Grimley, S. S., Healy, T. V., Kennedy, J. and McKay, H. A. *Trans. Faraday Soc. 52* (1956) 39.
5. Bucher, J. J., Zirin, M., Laugen, R. C. and Diamond, R. M. *J. Inorg. Nucl. Chem. 33* (1971) 3869.
6. Guillaumont, R. *Rev. Chim. Minér. 3* (1966) 339.
7. Agett, J., Clark, T. E. and Richardson, R. A. *J. Inorg. Nucl. Chem. 31* (1969) 2919.

Received January 28, 1974.

A High Temperature Iron Telluride with Rhombohedral Structure

ERLING RØST and STEINAR WEBJØRNSEN

Kjemisk institutt, Universitetet i Oslo, Oslo 3, Norway

A high temperature iron-tellurium phase has been found by DTA and X-ray high temperature investigations. This phase melts incongruently at about 920 °C, and transforms eutectoidally at 805 °C into the $Fe_2As-PbO$ type phase with tetragonal structure and the phase with the hexagonal NiAs-$Cd(OH)_2$ type structure. The high temperature phase exists in a rather broad range of homogeneity from about $FeTe_{0.80}$ to $FeTe_{0.93}$ at 845 °C. This temperature corresponds to the peritectoid decomposition of the $Fe_2As-PbO$ type phase. The corresponding composition of this phase is between $FeTe_{0.75}$ and $FeTe_{0.80}$. By the peritectoid decomposition metallic iron and the high temperature phase are formed.

The X-ray high temperature patterns could be indexed according to a rhombohedral unit cell and the data are given in Table 1.

The lattice constants of $FeTe_{0.90}$ were calculated for the temperatures 835 and 870° C, and of a metal rich sample, $FeTe_{0.75}$ at 850 °C. The latter is a two phase sample in which metallic iron exists in equilibrium with the high temperature phase of approximate composition $FeTe_{0.80}$. The following lattice constants refer to hexagonal setting:

$FeTe_{0.90}$, 835 °C:
$a = 4.013 \pm 0.003$ Å, $c = 20.96 \pm 0.02$ Å
$FeTe_{0.90}$, 870 °C:

$a = 4.030 \pm 0.003$ Å, $c = 21.09 \pm 0.02$ Å
$FeTe_{0.80}$, 850 °C:
$a = 4.031 \pm 0.003$ Å, $c = 21.13 \pm 0.02$ Å

Table 1. High temperature powder data of $FeTe_{0.90}$ at 835 °C. Cu$K\alpha$ radiation. Hexagonal indexing.

I_{obs}	h k l	d_{obs}	d_{calc}
w	0 0 6	3.50	3.48
m	0 1 2	3.30	3.30
m	1 0 4	2.90	2.90
w	0 1 5	2.671	2.677
St	0 1 8	2.092	2.093
St	1 1 0	2.005	2.006
m	1 0 10	1.795	1.796
w	1 1 6	1.742	1.741
	0 2 1		1.739
w	2 0 2	1.716	1.715
w	2 0 8	1.450	1.449

The crystal structure appears to be similar to that of the ternary phase $Ni_{1.5}Fe_{1.5}Te_2$ found by Stevels.[1] According to Røst and Åkesson [2] the phase exists over a broad homogeneity range at 600 °C, and it seems therefore probable that the ternary phase exists within a range of homogeneity above 805 °C up to the binary composition $FeTe_{0.9}$.

The crystal structure of a sample of the ternary phase having the composition $Fe_{.28}Ni_{.28}Te_{.44}$ has been previously presented by Åkesson and Røst.[3] According to this determination there are partly occupied metal sites in the structure. Therefore, it seems reasonable that an increase of the metal/tellurium ratio will involve expansion of the lattice, as observed for the lattice constants referred above.

Further investigations of the iron-tellurium phases are in progress.

1. Stevels, A. L. N. *Philips Res. Reports Suppl.* No. 9 (1969).
2. Røst, E. and Åkesson, G. *Acta Chem. Scand.* *26* (1972) 3662.
3. Åkesson, G. and Røst, E. *Acta Chem. Scand.* *27* (1973) 79.

Received February 19, 1974.

Acta Chemica Scandinavica A 28 (1974) 363—374

Semi-empirical Calculations on Lumiflavin Regarding Electronic Structure and Spectra

BARBRO GRABE

Institute of Theoretical Physics, University of Stockholm, S-113 46 Stockholm, Sweden

Calculations are made on the lumiflavin molecule in the oxidized and reduced states and on the half-reduced radical in three different dissociation states. A semi-empirical restricted Hartree-Fock SCF-MO-LCAO-CI method in the Pariser-Parr-Pople approximation is used. The numerical values of the parameters W and γ have been varied with charge. To get spin densities with different signs, an unrestricted Hartree-Fock method including annihilation has also been used. For comparison, calculations with a CNDO method have been made on iso-alloxazine.

In an earlier paper [1] calculations on lumiflavin in different oxidation and dissociation states with a semi-empirical restricted Hartree-Fock method (RHF) in the Pariser-Parr-Pople approximation have been reported. In the discussion in that paper it was indicated that further calculations were planned. The announced calculations are now given here.

In the actual calculations some parameter values have been varied with the charge on the atoms according to methods given in Refs. 2 and 3. In other respects the method is the same as in Ref. 1. To get spin densities with different signs, calculations have also been made with an unrestricted Hartree-Fock method (UHF) including annihilation, due to Amos and Snyder.[4] The same parameters as in the restricted method have been used.

For comparison of electron densities, calculations have also been made with the CNDO method given by Höjer and Meza.[5] The lumiflavin molecule was, however, too large, so the CNDO calculations have been made on isoalloxazine; *i.e.*, the three methyl groups on C(7), C(8), and N(10) in lumiflavin are replaced by hydrogen atoms.

The data machine programmes used have been written: restricted HF by B. Roos and M. Sundbom, unrestricted HF by T. Alm and modified by A. Fjelstad and H. H. Jensen and CNDO by G. Höjer and S. Meza.

NOTATIONS, NUMBERING AND STRUCTURE OF THE MOLECULES

The following notations of the molecules treated are used in accordance with Ref. 1.

$$Lf_{ox}H \xrightarrow{+1e} \dot{L}fH^- \xrightarrow{+H^+} \dot{L}fH_2 \xrightarrow{+H^+} \dot{L}fH_3^+ \xrightarrow{+1e} Lf_{red}H_3$$

As in Ref. 1 a hydrogen atom is bound to N(3) in all the molecules, and in $\dot{L}fH_2$ the second H is bound to N(5). (For the numbering of the atoms see Fig. 1.) In $\dot{L}fH_3^+$ and $Lf_{red}H_3$ a further H is bound to N(1), *i.e.*, they correspond to $\dot{L}fH_3^+$ (1,5) and $Lf_{red}H_3$ (1,5) in Ref. 1. The corresponding notations on isoalloxazine are obtained by substituting Ia for Lf.

In the PPP calculations all the molecules are assumed to be plane as in Ref. 1. In the CNDO calculations the coordinates used are obtained

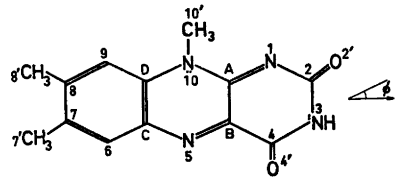

Fig. 1. Lumiflavin in the oxidized state to show the numbering of the atoms and the polarization angle ϕ.

Table 1. Bond distances calculated with restricted Hartree-Fock, in A. Corrections of W and γ due to charges. For notations "Calc. A" and "Calc. B", see the text.

Bond	Exp.	Calculated										Exp.
	Oxidized [a]	$Lf_{ox}H$ Calc. A	Calc. B	$\dot{L}fH^-$ Calc. A	Calc. B	$\dot{L}fH_2$ Calc. A	Calc. B	$\dot{L}fH_3^+$ Calc. A	Calc. B	$Lf_{red}H_3$ Calc. A	Calc. B	Reduced [b]
A1	1.303	1.318	1.315	1.338	1.332	1.322	1.319	1.382	1.379	1.398	1.399	1.391
12	1.368	1.383	1.390	1.362	1.377	1.382	1.389	1.390	1.402	1.377	1.393	1.367
22′	1.207	1.242	1.213	1.258	1.222	1.243	1.215	1.235	1.209	1.245	1.212	1.193
23	1.410	1.381	1.395	1.379	1.394	1.381	1.392	1.380	1.392	1.377	1.393	1.391
34	1.362	1.368	1.385	1.375	1.391	1.371	1.386	1.372	1.388	1.378	1.391	1.380
44′	1.219	1.240	1.211	1.253	1.220	1.246	1.222	1.236	1.210	1.241	1.213	1.223
4B	1.483	1.467	1.467	1.437	1.446	1.448	1.444	1.461	1.463	1.450	1.456	1.432
AB	1.446	1.454	1.456	1.418	1.425	1.439	1.441	1.392	1.397	1.379	1.375	1.350
B5	1.300	1.312	1.310	1.372	1.362	1.380	1.386	1.384	1.381	1.405	1.408	1.385
5C	1.372	1.378	1.382	1.376	1.368	1.405	1.404	1.391	1.396	1.401	1.398	1.394
DC	1.405	1.411	1.410	1.420	1.423	1.407	1.408	1.412	1.409	1.411	1.413	1.404
C6	1.406	1.416	1.413	1.407	1.412	1.404	1.403	1.413	1.412	1.399	1.399	1.370
67	1.371	1.387	1.389	1.401	1.401	1.396	1.397	1.388	1.389	1.403	1.404	1.386
78	1.421	1.411	1.409	1.397	1.396	1.403	1.402	1.418	1.415	1.396	1.395	1.401
89	1.376	1.391	1.392	1.404	1.408	1.396	1.397	1.389	1.390	1.404	1.405	1.402
9D	1.397	1.411	1.410	1.402	1.399	1.406	1.404	1.411	1.411	1.397	1.397	1.380
10D	1.380	1.387	1.389	1.389	1.390	1.398	1.398	1.394	1.397	1.410	1.406	1.438
10A	1.360	1.383	1.387	1.396	1.397	1.389	1.393	1.379	1.377	1.395	1.397	1.386

[a] Norrestam—Stensland [6] 3,7,8,10-tetramethylisoalloxazine. [b] Norrestam—v. Glehn [7] 9-bromo-1,3,7,8,10-pentamethyl-1,5-dihydroisoalloxazine.

Table 2. Charges on the atoms calculated with restricted Hartree-Fock (RHF). In most cases values obtained with unrestricted Hartree-Fock (UHF) are in agreement with those obtained with RHF. If they differ >0.03, they are given in parenthesis.

Atom	Corrections of W and γ due to charges according to Calc. A					Calc. B				
	$Lf_{ox}H$	$\dot{L}fH^-$	$\dot{L}fH_2$	$\dot{L}fH_3^+$	$Lf_{red}H_3$	$Lf_{ox}H$	$\dot{L}fH^-$	$\dot{L}fH_2$	$\dot{L}fH_3^+$	$Lf_{red}H_3$
A	0.04	0.00	−0.01	−0.02	−0.10	0.05	0.02 (−0.02)	0.01 (−0.05)	0.02	−0.08
N1	−0.20	−0.26	−0.17 (−0.12)	0.29	0.27	−0.19	−0.26 (−0.19)	−0.16 (−0.07)	0.28	0.24
2	0.35	0.31	0.35	0.36	0.35	0.06	0.03 (−0.11)	0.07 (−0.02)	0.09 (0.03)	0.05
O2′	−0.64	−0.72	−0.64	−0.62	−0.67	−0.28	−0.35 (−0.23)	−0.30 (−0.17)	−0.29 (−0.25)	−0.31
N3	0.34	0.32	0.34	0.34	0.32	0.28	0.26	0.29	0.28	0.26
4	0.39	0.35	0.34	0.35	0.36	0.10	0.06 (−0.07)	0.05 (−0.06)	0.04 (−0.04)	0.07
O4′	−0.64	−0.71	−0.66	−0.60	−0.64	−0.28	−0.35 (−0.26)	−0.31 (−0.20)	−0.22 (−0.14)	−0.30
B	0.05	−0.18	−0.04	−0.06	−0.14	0.09	−0.15 (−0.09)	−0.01 (0.03)	−0.04	−0.14
N5	−0.04	−0.14	0.33	0.43	0.21	−0.09	−0.19	0.28 (0.23)	0.40 (0.34)	0.21
C	−0.04	0.03	−0.03	0.00	0.00	−0.03	0.03	−0.03	−0.01	0.00
6	−0.01	−0.08	−0.09	−0.08	−0.11	−0.02	−0.11	−0.10	−0.08	−0.12
7	0.02	−0.04	0.03	0.12	0.02	0.01	−0.05	0.02	0.11	0.01
8	0.07	−0.03	0.04	0.13	0.01	0.06	−0.06	0.03	0.11	0.00
9	−0.13	−0.18	−0.10	−0.09	−0.12	−0.13	−0.19	−0.11	−0.09	−0.13
D	0.03	0.03	−0.03	−0.01	−0.03	0.03	0.03	−0.02	−0.03	−0.02
N10	0.33	0.27	0.28	0.37	0.22	0.30	0.26	0.26 (0.22)	0.37 (0.41)	0.22
$CH_3$7′	0.02	0.01	0.02	0.03	0.02	0.02	0.01	0.02	0.03	0.02
$CH_3$8′	0.02	0.02	0.02	0.03	0.02	0.02	0.01	0.02	0.03	0.02
$CH_3$10′	0.01	0.00	0.01	0.01	0.00	0.01	0.00	0.00	0.01	0.00

Table 3. Net charges added for larger parts of the molecule due to π-electrons in units of electronic charge e, calculated with restricted Hartree-Fock (RHF).

	$Lf_{ox}H$	$\dot{L}fH^-$	$\dot{L}fH_2$	$\dot{L}fH_3^+$	$Lf_{red}H_3$
Corrections of W and γ: Calc. A					
Pyrimidine ring with A and B	−0.30	−0.90	−0.49	0.05	−0.25
Middle part: N5, N10 and $CH_3$10′	0.30	0.13	0.62	0.81	0.44
Benzene ring with C and D	0.00	−0.24	−0.13	0.14	−0.19
Pyrimidine part without A and B (1,2,2′,3,4,4′)	−0.39	−0.72	−0.44	0.13	−0.02
Middle ring with A, B, C, and D	0.38	0.02	0.51	0.72	0.18
Benzene ring without C and D (6,7,7′,8,8′,9)	0.00	−0.30	−0.08	0.15	−0.16
A+B	0.09	−0.18	−0.05	−0.08	−0.23
C+D	0.00	0.06	−0.06	−0.01	−0.03
Corrections of W and γ: Calc. B					
Pyrimidine ring with A and B	−0.17	−0.76	−0.37	0.16	−0.22
Middle part: N5, N10 and $CH_3$10′	0.22	0.08	0.54	0.77	0.44
Benzene ring with C and D	−0.05	−0.32	−0.17	0.07	−0.22
Pyrimidine part without A and B (1,2,2′,3,4,4′)	−0.31	−0.63	−0.37	0.18	0.01
Middle ring with A, B, C, and D	0.35	0.01	0.48	0.72	0.19
Benzene ring without C and D (6,7,7′,8,8′,9)	−0.04	−0.38	−0.12	0.11	−0.20
A+B	0.14	−0.13	−0.01	−0.02	−0.23
C+D	−0.01	0.06	−0.05	−0.04	−0.02

from Norrestam – Stensland – v. Glehn (personal communication) and this implies that the reduced form is bent, the angle being 150°. The structure used for the oxidized form is also used for $\dot{I}aH^-$ and $\dot{I}aH_2$. CNDO calculations for $\dot{I}aH_3^+$ did not converge.

PARAMETER VALUES

Most parameters used are the same as in Ref. 1. The one-electron integrals W_μ and the one-center two-electron integrals $\gamma_{\mu\mu}$ have, however, been varied with the charge for those atoms where the calculated charge is >0.2. This implies that W_μ and $\gamma_{\mu\mu}$ have been varied for the oxygen atoms, the carbons bound to the oxygens, and for the nitrogens.

For the carbon and oxygen atoms in the C=O bonds, two different parameter sets have been used. In Calc. A the values of W_μ for neutral atoms and the variation of W_μ with charge are according to Alt. 2 $F_2(Z_{\text{eff}})$ in Ref. 3, and in Calc. B they are according to Alt. 1 $F_1(\varrho)$ in the same reference.

For the nitrogen atoms, the values of W_μ for neutral atoms and the variation of W_μ with charge are according to Alt. 1 $F_2(Z_{\text{eff}})$ in Ref. 3 for pyridine N and according to Alt. 2 F_2 (Z_{eff}) for pyrrole N in the same reference.

For the numerical values of the one-center two-electron integrals $\gamma_{\mu\mu}$ and their variation with charge, see Refs. 2 and 3.

RESULTS

The bond lengths calculated with restricted Hartree-Fock (RHF) are given in Table 1 together with experimental values given by Norrestam *et al.*[6,7] Charges on the atoms calculated with RHF are given in Table 2. The calculations with unrestricted Hartree-Fock (UHF) have in most cases given the same results. When they differ >0.03 from the RHF calculations, they are given in parentheses. To show how the charges are dislocated, charges on larger parts of the molecule are given in Table 3.

Table 4. Spin densities obtained with restricted Hartree-Fock (RHF) and with unrestricted Hartree-Fock (UHF) after annihilation.

Atom	Corrections of W and γ due to charges according to Calc. A RHF			UHF			Calc. B RHF			UHF		
	$\dot{L}fH^-$	$\dot{L}fH_2$	$\dot{L}fH_3^+$	$\dot{L}fH^-$	$\dot{L}fH_2$	$\dot{L}fH_3^+$	$\dot{L}fH^-$	$\dot{L}fH_2$	$\dot{L}fH_3^+$	$\dot{L}fH^-$	$\dot{L}fH_2$	$\dot{L}fH_3^+$
A	0.05	0.01	0.06	0.06	−0.07	0.02	0.05	0.01	0.08	−0.01	−0.11	0.00
N1	0.02	0.06	0.02	0.01	0.25	0.00	0.04	0.08	0.03	0.05	0.25	−0.02
2	0.02	0.02	0.00	0.03	−0.01	0.00	0.01	0.00	0.00	−0.08	−0.11	−0.10
O2′	0.01	0.02	0.00	0.02	0.08	0.01	0.03	0.04	0.01	0.36	0.40	0.22
N3	0.00	0.01	0.00	−0.02	−0.01	−0.01	0.00	0.00	0.00	−0.06	−0.06	−0.06
4	0.04	0.05	0.01	0.04	0.02	0.00	0.02	0.02	0.00	−0.07	−0.09	−0.11
O4′	0.02	0.06	0.02	0.03	0.10	0.04	0.07	0.16	0.04	0.34	0.41	0.41
B	0.09	0.44	0.13	0.02	0.41	0.14	0.14	0.46	0.19	0.04	0.27	0.18
N5	0.51	0.23	0.32	0.47	0.18	0.31	0.36	0.16	0.29	0.22	0.06	0.18
C	0.00	0.00	0.08	−0.08	−0.04	0.06	0.02	0.00	0.06	−0.07	−0.04	0.03
6	0.09	0.01	0.01	0.21	0.05	0.00	0.11	0.01	0.01	0.16	0.04	−0.01
7	0.00	0.00	0.03	−0.08	−0.03	0.03	0.00	0.00	0.02	−0.08	−0.04	0.03
8	0.04	0.01	0.04	0.16	0.05	0.06	0.06	0.01	0.03	0.13	0.04	0.02
9	0.02	0.00	0.00	−0.04	−0.03	−0.02	0.02	0.00	0.00	−0.04	−0.03	0.00
D	0.03	0.01	0.08	0.09	0.04	0.09	0.03	0.01	0.06	0.06	0.04	0.03
N10	0.05	0.05	0.19	0.07	0.01	0.24	0.04	0.03	0.19	0.03	−0.01	0.18
S^2				0.79	0.78	0.75				1.45	1.38	1.15

Spin densities on the CH_3-groups are = 0.00 except on CH_310' in $\dot{L}fH_3^+$, where it is 0.01.

In Table 4 the spin densities obtained with RHF and UHF are given. The expectation values of the S^2 operator after annihilation are also given. The S^2 values in Calc. A are near 0.75, so the wave functions after annihilation are close to spin eigenfunctions, and in these cases the agreement between RHF and UHF values on the charges on the atoms (Table 2) is very good. For Calc. B the deviations of S^2 from 0.75 are large. thus further annihilation is desirable. From Table 2 it is seen that in these cases there are large differences between values obtained from RHF and UHF for charges on some of the atoms. Fjeldstad and Jensen [8] have tested the UHF program on some π-electron radicals. In most of their calculations the values on S^2 are near 0.75, but in two cases they have also obtained large values on S^2 (1.10 and 1.37).

In Table 5 charges on the atoms and spin densities obtained with CNDO calculations on isoalloxazine are given. Convergence was not obtained for Ia H_3^+.

Ionization potentials obtained with restricted HF are given in Table 6 and in Tables 7a-e calculated values on transition energies, oscillator strengths, and direction of the transition moments are given, *viz.* singlet-singlet π-π^* transitions for the molecules with paired spins in the ground state and doublet-doublet π-π^* transitions for the radicals with one unpaired electron in the ground state. Experimental values obtained by different workers are also given, but for more detailed references to experimental values see Ref. 1.

Comparisons with the results in Ref. 1 and with the CNDO calculations

Bond lengths. The results in Calc. A are very close to those obtained in Ref. 1, but in Calc. B the bond lengths in the C=O bonds and C(2)–N(3) are much closer to the experimental values than those obtained in Ref. 1 and in Calc. A.

Table 5. Charges on atoms and spin densities calculated with the CNDO method on isoalloxazine. The notations in accordance with those of lumiflavin.

Atom	Charges								Spin densities	
	$Ia_{ox}H$		$\dot{I}aH^-$		$\dot{I}aH_2$		$Ia_{red}H_3$		$\dot{I}aH^-$	$\dot{I}aH_2$
	total	π	total	π	total	π	total	π		
A	0.21	0.20	0.21	0.23	0.22	0.19	0.18	0.13	0.02	−0.06
N1	−0.25	−0.38	−0.33	−0.47	−0.25	−0.37	−0.24	0.28	0.03	0.12
2	0.32	0.19	0.32	0.22	0.32	0.19	0.37	0.19	−0.01	−0.04
02′	−0.27	−0.39	−0.36	−0.47	−0.28	−0.39	−0.28	−0.43	0.03	0.07
N3	−0.28	0.24	−0.29	0.24	−0.27	0.23	−0.27	0.28	−0.02	−0.04
4	0.28	0.18	0.27	0.21	0.26	0.16	0.29	0.18	−0.03	−0.11
04′	−0.25	−0.35	−0.34	−0.45	−0.26	−0.35	−0.27	−0.42	0.11	0.22
B	−0.09	−0.09	−0.19	−0.34	−0.12	−0.20	−0.13	−0.22	0.17	0.44
N5	0.01	0.12	−0.14	−0.23	−0.08	0.42	−0.12	0.80	0.50	0.32
C	0.00	−0.10	0.05	0.02	0.04	−0.06	0.07	0.03	−0.15	−0.06
6	−0.05	0.05	−0.11	−0.05	−0.09	−0.02	−0.10	−0.04	0.16	0.06
7	−0.10	−0.06	−0.09	−0.04	−0.08	−0.03	−0.06	0.01	−0.12	−0.04
8	−0.02	0.07	−0.09	−0.06	−0.05	0.01	−0.08	−0.02	0.17	0.06
9	−0.13	−0.09	−0.12	−0.07	−0.11	−0.07	−0.08	−0.01	−0.09	−0.04
D	0.12	0.09	0.06	0.00	0.10	0.02	0.04	−0.02	0.14	0.06
N10	−0.16	0.32	−0.18	0.26	−0.19	0.26	−0.18	0.81	0.08	0.05
H1′							0.17			
H3′	0.16		0.11		0.16		0.17			
H5′					0.18		0.11			
H6′	0.09		0.05		0.08		0.08			
H7′	0.08		0.03		0.08		0.07			
H8′	0.08		0.03		0.08		0.08			
H9′	0.08		0.04		0.08		0.07			
H10′	0.16		0.11		0.16		0.14			

Table 6. Vertical ionization potentials of π-electrons calculated with restricted Hartree-Fock (RHF). Notation o singnifies ionization of the odd electron, t = triplet, s = singlet, the state after ionization.

	Corrections of W and γ due to charges according to Calc. A					Calc. B				
	$Lf_{ox}H$	$\dot{L}fH^-$	$\dot{L}fH_2$	$\dot{L}fH_3^+$	$Lf_{red}H_3$	$Lf_{ox}H$	$\dot{L}fH^-$	$\dot{L}fH_2$	$\dot{L}fH_3^+$	$Lf_{red}H_3$
Ionization potential, eV		o 2.29	o 7.64	o 12.73	6.14		o 0.81	o 6.82	o 12.03	5.53
	7.72	t 2.81 s 4.36	t 7.39 s 9.25	t 12.69 s 14.36	8.40	6.91	t 1.68 s 3.86	t 6.67 s 8.16	t 11.95 s 13.47	7.80
	8.89	t 3.94 s 5.88	t 8.90 s 10.92	t 13.19 s 15.30	8.77	8.01	t 2.97 s 4.06	t 7.51 s 9.03	t 12.12 s 12.45	8.08
	9.19	t 4.38 s 4.63	t 8.94 s 9.70	t 13.29 s 13.46	9.47	8.59	t 3.42 s 4.70	t 8.49 s 9.94	t 12.80 s 15.03	8.17
	9.82	t 5.37 s 6.13	t 9.71 s 10.21	t 14.05 s 15.12	9.78	9.26	t 4.70 s 5.51	t 9.20 s 9.66	t 13.43 s 14.60	9.10

Table 7a. Electronic singlet-singlet transitions of $Lf_{ox}H$ below 60 kK with restricted Hartree-Fock (RHF).

Corrections of W and γ according to Calc. A			Calc. B			Observed absorption Riboflavin in dioxane, Koziol [9]			
ν, kK	f	pol. ϕ^a	ν, kK	f	pol. ϕ^a	max. λ, nm	ν, kK	min. ν, kK	$\varepsilon \times 10^{-3}M^{-1}cm^{-1}$
								20 [b]	
26.7	0.51	165	26.7	0.54	167	440	22.7		12.1
								26.5	
34.1	0.02	55	33.6	0.02	123	344	29.1		8.4
35.7	0.01	157	35.4	0.05	80				
								33.5	
39.6	1.17	25	38.8	0.74	27	271	36.9		33.1
40.8	0.07	12	40.8	0.44	16				
44.6	0.17	35	44.2	0.26	24				
								42.1	
47.1	0.11	139	45.9	0.11	158				
48.9	0.32	161	46.6	0.03	49				
50.8	0.54	144	49.6	0.35	151	224	44.6		31.0
51.5	0.10	166	50.4	0.05	91				
51.8	0.12	29	51.3	0.38	3				
54.7	0.01	159	52.7	0.48	101				
56.3	0.81	55	54.0	0.67	53				
57.0	0.13	79	55.1	0.10	172				
57.9	0.21	106	57.0	0.07	107				
59.6	0.00		59.1	0.06	70				

[a] The angle ϕ, see Fig. 1. [b] The start of the band.

Table 7b. Electronic doublet-doublet transitions below 50 kK of the lumiflavin radical $\dot{L}fH^-$ with restricted Hartree-Fock (RHF).

Corrections of W and γ according to Calc. A			Calc. B			Observed absorption Lumiflavin 3-$CH_3COOC_2H_5$ in nonaqueous dimethylformamide, semiquinone anion Ehrenberg, Müller and Hemmerich [10]			
ν, kK	f	pol. ϕ^a	ν, kK	f	pol. ϕ^a	max. λ, nm	ν, kK	min. ν, kK	$\varepsilon \times 10^{-3}M^{-1}cm^{-1}$
14.6	0.00		9.6	0.00					
16.7	0.06	14	11.4	0.00					
21.1	0.02		15.7	0.03	11			18 [b]	1.5
22.7	0.20	176	18.1	0.10	2	477	21.0		5.9
26.3	0.03							23.3	3.5
28.7	0.09	179	22.2	0.22	170	400	25.0 (peak)		11.5
								25.6	11
31.9	0.07	172	25.5	0.04	75	373	26.8		17.6
33.8	0.00		28.2	0.04	2			29 [c]	5
35.9	0.08	109	31.8	0.03	132				
37.9	0.36	36	36.2	0.23	22				
40.5	0.23	7	36.9	0.28	62				
40.7	0.20	40	38.2	0.04	149				

Table 7b. Continued.

41.0	0.06	20	39.4	0.04	48
41.5	0.15	3	41.0	0.17	7
44.0	0.28	154	41.4	0.16	178
45.8	0.01		42.5	0.04	
46.4	0.15	168	45.2	0.34	168
47.2	0.04		45.6	0.03	
48.3	0.01		47.4	0.01	
49.3	0.10	15	47.9	0.02	
			48.7	0.08	160
			49.9	0.08	11

[a] The angle ϕ, see Fig. 1. [b] Start of the band. [c] End of the recorded curve.

Table 7c. Electronic doublet-doublet transitions below 50kK of the lumiflavin radical $\dot{L}fH_2$ with restricted Hartree-Fock (RHF).

Corrections of W and γ according to Calc. A			Calc. B			Observed absorption Neutral semiquinone of glucose oxidase, pH 6.3		Palmer and Massey [11]	
ν, kK	f	pol. ϕ[a]	ν, kK	f	pol. ϕ[a]	max. λ, nm	ν, kK	min. ν, kK	$\varepsilon \times 10^{-3}M^{-1}cm^{-1}$ [b]
10.5	0.06	177	9.6	0.01					
			15.0	0.02				15 [c]	0.3
20.4	0.01		19.3	0.03	172	~600	~17		1.9
22.6	0.00							18.5	1.7
24.6	0.03					450	22.2		5.5
26.1	0.01		25.9	0.00				24	5.1
26.6	0.07	23	27.6	0.00		382 (shoulder)	26.2		9.3
28.3	0.00								
31.6	0.09	166	30.2	0.04		360	27.8		10.1
			32.5	0.01				30 [d]	7.5
35.0	0.18	178	35.6	0.23	161				
37.8	0.13	16	37.5	0.14	18				
38.5	0.45	39	39.1	0.09	75				
39.6	0.06		40.9	0.28	10				
39.8	0.07		42.1	0.06	47				
41.9	0.09	159	42.7	0.04					
42.6	0.06	160	44.7	0.02					
43.4	0.01		45.9	0.05					
44.9	0.36	169	46.7	0.34	167				
45.7	0.04		47.2	0.17	6				
47.4	0.11	106	48.1	0.11	151				
48.3	0.04		50.0	0.04	56				
49.0	0.20	141							
49.6	0.06								

[a] The angle ϕ, see Fig. 1. [b] Estimated from curve in Palmer and Massey,[11] and based on value 14.1 at 450 nm in Massey and Palmer.[12] [c] Start of the band. [d] End of the recorded curve.

Table 7d. Electronic doublet-doublet transitions below 50 kK of the lumiflavin radical $\dot{L}fH_3^+$ with restricted Hartree-Fock (RHF).

Corrections of W and γ according to Calc. A			Calc. B		
ν, kK	f	pol. ϕ^a	ν, kK	f	pol. ϕ^a
16.4	0.05	161	10.4	0.02	
18.5	0.10	20	17.6	0.10	168
19.7	0.06	155	19.4	0.01	
23.7	0.01		20.3	0.08	1
26.0	0.01		21.1	0.04	72
27.2	0.04	156	25.3	0.00	
29.4	0.06	39	26.6	0.03	
31.1	0.01		30.4	0.07	27
34.4	0.03	164	32.7	0.01	
38.4	0.02		34.2	0.03	
39.0	0.00		36.4	0.00	
40.4	0.00		39.1	0.01	
40.9	0.21	48	40.4	0.11	51
41.6	0.29	30	40.6	0.14	41
43.0	0.04		41.8	0.01	
43.8	0.34	176	43.3	0.10	151
44.8	0.01		43.9	0.12	14
45.9	0.26	148	46.1	0.32	169
47.5	0.05		47.1	0.01	
48.1	0.17	168	48.3	0.06	
48.8	0.03		48.6	0.64	180
49.4	0.05	8	50.0	0.03	

[a] The angle ϕ, see Fig. 1.
Absorption spectrum of flavin semiquinone $\dot{F}lH_3^+$ has maxima at about 490 nm (*ca.* 20 kK) and at about 360 nm (*ca.* 28 kK), according to Ehrenberg and Hemmerich.[13]

Table 7e. Electronic singlet-singlet transitions below 60 kK of $Lf_{red}H_3$ with restricted Hartree-Fock (RHF).

Corrections of W and γ according to Calc. A			Calc. B			Observed absorption Flavohydroquinone $Fl_{red}H_3$ in H_2O Ehrenberg and Hemmerich [13] (see also Hemmerich *et al.*[14])			
ν, kK	f	pol. ϕ^a	ν, kK	f	pol. ϕ^a	max. λ, nm	ν, kK	min. ν, kK	$\varepsilon \times 10^{-3} M^{-1}cm^{-1}$
19.6	0.04		20.4	0.04					
30.0	0.20	4	28.8	0.24	2	~400	~25 shoulder		ca. 2
35.1	0.23	114	33.4	0.22	113	~300	~33 »		» 6
39.9	0.14	26	39.0	0.18	22				
			41.1	0.12	174				
42.0	0.83	4	43.1	0.54	172	250	40.0		30
43.9	0.17	132	44.2	0.30	54				
			45.8	0.27	158				
46.5	0.07	146	46.8	0.01				43.5	12
47.2	0.24	75	48.2	0.03					

Table 7e. Continued.

48.1	0.04							
50.1	0.04							
53.1	0.56	88	50.6	0.92	65	204	49.0	30
53.6	0.50	29	52.5	0.19	157			
54.9	0.22	147	53.2	0.08	101			
55.8	0.06		55.1	0.27	131			
56.1	0.04		55.6	0.40	43			
56.8	0.26	44	58.0	0.13	106			
59.4	0.30	96	59.4	0.03				
			59.8	0.02				

[a] The angle ϕ, see Fig. 1.

In the experimental curve given by Ehrenberg and Hemmerich,[13] the absorption ($\varepsilon \times 10^{-3}$) increases continuously from about 1 at 22 kK (450 nm) to about 30 at 40 kK (250 nm). According to Dudley *et al.*,[16] the intensity in the 500—700 nm range appears to be a measure of molecular planarity.

As in Ref. 1 the bond lengths in the benzene ring are alternating long and short in $Lf_{ox}H$, and $\dot{L}fH_3^+$ but approximately equal within the ring in $\dot{L}fH^-$, $\dot{L}fH_2$, and $Lf_{red}H_3$.

Charges on the atoms due to π-electrons. Calc. A gives approximately the same values for charges on the atoms as those obtained in Ref. 1. In Calc. B, however, much smaller charges have been obtained on C(2), O(2′), C(4), and O(4′) than in the other calculations. In CNDO the charges on C(2), O(2′), C(4), and O(4′) are between those obtained with Calc. A and B. The oxygen atoms are the most negatively charged atoms both in Calc. A and B as in Ref. 1. The CNDO calculations give about the same negative values on N(1) as on O(2′) and O(4′) except in $Lf_{red}H_3$ where N(1) is positively charged.

The pyrimidine ring compared to the other parts of the molecule is more negatively charged in $Lf_{ox}H$, $\dot{L}fH^-$ and $\dot{L}fH_2$ as also was obtained in Ref. 1. The values in Calc. B are, however, smaller than those in Calc. A and Ref. 1.

The middle part is positively charged in all the calculations in all molecules. The relatively large variation in charge of the benzene ring in different oxidation and dissociation states, pointed out in Ref. 1, is obtained also in Calc. A and B.

Ionization potentials. Most values on ionization potentials obtained are smaller than those obtained in Ref. 1. In most cases Calc. B gives smaller values than Calc. A.

Electronic spectra. The calculated spectra are compared with experimental ones and with those calculated in Ref. 1. Calc. A gives about equally good agreement with experimental spectra as the calculations in Ref. 1. Calc. B gives poorer agreement with experiments in all the molecules except $Lf_{ox}H$, where the results are equally good.

Spin densities. With the RHF method Calc. A and B give about the same values on spin densities except on N(5) in $\dot{L}fH^-$ (Calc. A 0.51, Calc. B 0.36) and on O(4′) in $\dot{L}fH_2$ (Calc. A 0.06, Calc. B 0.16), in spite of very different values for charges on some atoms.

With the UHF method there are differences between Calc. A and B for N(5), C(2), O(2′), C(4), and O(4′) in all three radicals and on C(A) in $\dot{L}fH^-$ and on C(B) in $\dot{L}fH_2$. Furthermore, the RHF and the UHF methods according to Calc. B give significantly different values for the charges on these atoms. Since the S^2 values in Calc. B (see Table 4) differ a lot from 0.75, these UHF wave functions are not pure eigenfunctions of S^2, and thus the UHF results are uncertain.

According to experimental data the spin density is large on N(5) and small on N(1).[15] From Tables 4 and 5 it is seen that large values on N(5) are obtained in all the calculations except for the UHF Calc. B in $\dot{L}fH_2$ and that small values on N(1) are obtained in all the calculations except for the UHF Calc. A and B in $\dot{L}fH_2$. It is to be pointed out that in Calc. B UHF for $\dot{L}fH_2$, the value of S^2 is 1.38, and thus the wave functions are not pure eigenfunctions, and thus the obtained spin densities are uncertain.

According to experimental data the spin density on N(10) should be about half of the

density on N(5).[15] As is seen from Tables 4 and 5, this result is not obtained by the calculations: for $\dot{L}fH^-$ and $\dot{L}fH_2$ the ratio of spin density on N(10) and N(5) is smaller than 0.5 and for $\dot{L}fH_3^+$ it is larger.

DISCUSSION

From Table 1 it is seen that the parameter values used in Calc. B are the best for determining the bond lengths and that they are better than those used in Ref. 1. The CNDO calculations give values for the charges due to the π-electrons which are between those obtained by Calc. A and B. The spectra are best reproduced with the parameter set used in Calc. A which is in agreement with the results on smaller molecules.[2,3]

Calc. B seems to be preferable as far as ground state properties are concerned, and Calc. A in case of excited states. If possible, both types of calculations should be carried out.

Acknowledgement. The author is indebted to Professor Inga Fischer-Hjalmars for valuable discussions and to Fil. kand. Lars Norén for skilful assistance in the numerical computations. Information about experimental results from Drs. Rolf Norrestam, Birgitta Stensland and Marianne von Glehn is gratefully acknowledged.

The investigation has been supported by grants from the Swedish Natural Science Research Council.

REFERENCES

1. Grabe, B. *Acta Chem. Scand. 26* (1972) 4084.
2. Grabe, B. and Skancke, P. N. *Acta Chem. Scand. 26* (1972) 468.
3. Grabe, B. *Acta Chem. Scand. A 28* (1974) 315.
4. Amos, T. and Snyder, L. C. *J. Chem. Phys. 41* (1964) 1773.
5. Höjer, G. and Meza, S. *Acta Chem. Scand. 26* (1972) 3723.
6. Norrestam, R. and Stensland, B. *Acta Crystallogr. B 28* (1972) 440.
7. Norrestam, R. and von Glehn, M. *Acta Crystallogr. B 28* (1972) 434.
8. Fjelstad, A. and Jensen, H. H. *Acta Chem. Scand. 26* (1972) 1869.
9. Koziol, J. *Photochem. Photobiol. 5* (1966) 41.
10. Ehrenberg, A., Müller, F. and Hemmerich, P. *Eur. J. Biochem. 2* (1967) 286.
11. Palmer, G. and Massey, V. In Singer, Th. P., Ed., *Biological oxidations*, Interscience New York-London-Sidney 1968, p. 263.
12. Massey, V. and Palmer, G. *Biochemistry 5* (1966) 3181.
13. Ehrenberg, A. and Hemmerich, P. In Singer, Th. P., Ed., *Biological oxidations*, Interscience, New York-London-Sidney 1968, p. 239.
14. Hemmerich, P., Ghisla, S., Hartmann, U. and Müller, F. *Flavins and Flavoproteins, 3rd Int. Symp.*, Kamin, H., Ed., Univ. Park Press, Butterworths, London 1971, p. 83.
15. Eriksson, L. E. G. *Personal communication*; Hemmerich, P., Ghisla, S., Hartmann, U. and Müller, F. *Flavins and Flavoproteins, 3rd Int. Symp.*, Kamin, H., Ed., Univ. Park Press, Butterworths, London 1971, p. 107.
16. Dudley, K. H., Ehrenberg, A., Hemmerich, P. and Müller, F. *Helv. Chim. Acta 47* (1964) 1354.

Received October 18, 1973.

Acta Chemica Scandinavica A 28 (1974) 375—384

A Comparative Study of the $AA'A''A'''X_nX_n'$ and $AA'BB'X_nX_n'$ Spin Systems for n=1, 2 and 3

DAGFINN W. AKSNES

Chemical Institute, University of Bergen, N-5000 Bergen, Norway

The combined composite particle-symmetry good quantum number approach has been used to achieve maximum factorization of the secular matrices of the $AA'A''A'''X_nX_n'$ and $AA'BB'X_nX_n'$ systems. The basic molecular wave functions of the composite particle spin states have been classified under the highest possible symmetry. The next step involves the evaluation of the matrix elements in terms of the chemical shifts and coupling constants.

Rather than calculating the transition frequencies directly familiar sub-spectra from which the spectral parameters can be obtained, have been picked out. It is shown that the $AA'BB'$ region of the $AA'BB'X_nX_n'$ system can be completely broken down into $(n+1)$ different aa'bb' sub-spectra and $\sum_{i=1}^{n} i$ different abcd sub-spectra when $J_{xx'}=0$. For the $AA'AA''A'''X_nX_n'$ system these sub-spectra simplify into a_4 and aa'bb' sub-spectra, respectively. The spectral transformations of the contributing sub-spectra have been worked out. When $J_{xx'}\neq 0$, however, only sub-patterns characterized by the extreme values of $m(X_q)$ within a given sub-system, give rise to real sub-spectra.

The experimental 100 MHz spectra of 1,4-dibromobutane and *trans,trans*-2,4-hexadiene and the 270 MHz spectrum of butane are shown as typical examples of the studied spin systems.

NMR spectra of the general types $AA'A''A'''X_nX_n'$ and $AA'BB'X_nX_n'$ have, apart from the $AA'A''A'''XX'$ system, received little attention. However, the combined symmetry-composite particle-good quantum number approach makes it feasible to tackle spectra of such large spin systems.[1]

The $AA'A''A'''X_3X_3'$ system has similar features as the $AA'A''A'''XX'$ system which has been studied by Diehl,[2] Lynden-Bell,[3] and by Kaiser.[15] The algebraic manipulations are more complex, however, due to the four possible spin combinations and increasing dimension of the secular matrices. Jones [4] has shown that the use of the permutation symmetry groups for the non-rigid $AA'A''A'''X_2X_2'$ system leads to identical factorization of the Hamiltonian matrix as does the composite particle method, as expected. The calculations are, however, much simpler using the latter.

The nuclear arrangement $AA'A''A'''X_nX_n'$ of C_{2v} (C_{2h}) symmetry is often found, for instance, in 1,4-difluorobenzene (n=1), 1,4-dibromobutane (n=2),[5] perfluorobutane (n=3), and perfluoro *p*-xylene (n=3).[6] The $AA'BB'X_nX_n'$ spin system of C_2 symmetry can be typified by 1,2-difluorobenzene (n=1), α,α'-dichloro-*o*-xylene (n=2), *cis,cis*-2,4-hexadiene (n=3) and *trans-trans*-2,4-hexadiene (n=3).[7]

The experimental 100 MHz spectra of 1,4-dibromobutane and *trans,trans*-2,4-hexadiene and the 270 MHz spectrum of butane will be shown as typical examples of the studied spin systems.

FACTORIZATION OF THE HAMILTONIAN

Composite particle notation. It is convenient to define the group magnetic quantum numbers

$$m(A_4)=m_A+m_{A'}+m_{A'}+m_{A'''}$$

$$m(A_2B_2)=m_A+m_{A'}+m_B+m_{B'}$$

$$m(X_q)=m_X+m_{X'};\ q=2n$$

and the total quantum number

$$m_T=m(A_4)\ [\text{or } m(A_2B_2)]+m(X_q)$$

The $AA'A''A'''X_nX_n'$ and $AA'BB'X_nX_n'$

spin systems for n = 2 and 3 have each four overall spin states:[1]

DDDD*AA*
DDDD*AB* DDDD*BA*
DDDD*BB*

where the composite particles A = T or Q and B = S or D for n = 2 or 3, respectively. The degeneracy of the D particles of the X_3X_3' nuclei is 2 whereas the remaining particles have a degeneracy of 1. When n = 2 the total relative intensities (normalized to $n \times 2^{n-1}$ for an n-spin system)[1] attributable to these four spin states are 672, 160, 160, and 32. Listed in the same order the four strongly coupled nuclei contribute 288, 96, 96, and 32 intensity units. Similarly, when n = 3 the DDDDQQ, DDDDQD, DDDDDQ and DDDDDD spin states contribute altogether 1792, 1280, 1280, and 768 intensity units. Now, the four strongly coupled nuclei give rise to 512 intensity units for each spin state.

Basic symmetry wave functions. The DDDD*AB* and DDDD*BA* spin states are degenerate and do not mix. It is thus sufficient to treat only one of these states, say DDDD*AB*. The secular matrices of the three different overall spin states can be factorized in accordance with symmetry. The DDDD*AA* and DDDD*BB* states of the $AA'A''A'''X_nX_n'$ and $AA'BB'X_nX_n'$ systems possess C_{2v} (C_{2h}) and C_2 symmetry, respectively. The DDDD*AB* spin state of the former spin system possesses C_2 symmetry.

The four A nuclei have previously been classified according to the symmetry species A_1, A_2, B_1, and B_2 of the C_{2v} point group.[3,9] The symmetrized spin functions $\phi_i\Gamma^\mu$ (A_2B_2) of the AA'BB' nuclei are listed in Ref. 8, p. 400.

The QQ, TT, and DD functions $\psi_j\Gamma^\nu$ (X_q) of the X_nX_n' nuclei have also been classified according to symmetry as shown in Table 1 for the QQ functions.

The basic molecular wave functions $\Phi_k\Gamma^\lambda$ (A_4X_q) can be constructed from the basic group symmetry wave functions (Table 1) by taking all possible products $\phi_i\Gamma^\mu(A_4) \times \psi_j\Gamma^\nu(X_q) = \Phi_k\Gamma^\lambda$ (A_4X_q) and reclassifying these product functions under the total molecular symmetry.[9] The $\Phi_k\Gamma^\lambda$ ($A_2B_2X_q$) functions can be obtained by a similar procedure.

Table 2 shows a schematic energy level diagram for the DDDD*AA* spin states (A = Q, T, D, S) of the general $AA'A''A'''X_nX_n'$ system. It is also readily shown that the DDDDST spin state of C_2 symmetry forms 1:2:4:2:1 (A) + 2:2:2(B) energy level groupings for $m(X_4) = \pm 1$ and 0. The DDDDQD spin state of C_2 symmetry can similarly be factorized into 1:2:4:2:1(A) + 2:2:2(B) and 2:4:8:4:2(A) + 4:4:4(B) energy level groupings for $m(X_6) = \pm 2$ and 0, ± 1, respectively. When $J_{XX'} = 0$, however, the two latter sub-patterns can be further reduced into two sets of 1:2:4:2:1(A) + 2:2:2(B) energy levels. A schematic diagram over the factorization of the secular matrices of the $AA'BB'X_nX_n'$ system is easily obtained by adding together correspond-

Table 1. Basic QQ symmetry wave functions for the X_3X_3' nuclei classified according to C_2 symmetry. The diagonal and non-zero off-diagonal elements of $\mathcal{H}(X_6)$ are also listed.

State	$m(X_6)$	Symmetry species Γ_ν	$\Psi_j\Gamma_\nu(X_6)$	$H(X_6)_{jj}$[a]	$H(X_6)_{jj'}$[b]
1	3	A	$Q^{3/2}Q^{3/2}$	$3\nu_X + 4X$	
2	2	A	$2^{-1/2}(Q^{3/2}Q^{1/2} + Q^{1/2}Q^{3/2})$	$2\nu_X + 4X$	
3		B	$2^{-1/2}(Q^{3/2}Q^{1/2} - Q^{1/2}Q^{3/2})$	$2\nu_X - 2X$	
4	1	A^{11}	$2^{-1/2}(Q^{3/2}Q^{-1/2} + Q^{-1/2}Q^{3/2})$	$\nu_X - 2X$	
5		A^{12}	$Q^{1/2}Q^{1/2}$	ν_X	$H_{45} = 2\sqrt{6}X$
6		B	$2^{-1/2}(Q^{3/2}Q^{-1/2} - Q^{-1/2}Q^{3/2})$	$\nu_X - 2X$	
7	0	A^{01}	$2^{-1/2}(Q^{3/2}Q^{-3/2} + Q^{-3/2}Q^{3/2})$	$-5X$	
8		A^{02}	$2^{-1/2}(Q^{1/2}Q^{-1/2} + Q^{-1/2}Q^{1/2})$	$+3X$	$H_{78} = 3X$
9		B^{01}	$2^{-1/2}(Q^{3/2}Q^{-3/2} - Q^{-3/2}Q^{3/2})$	$-5X$	
10		B^{02}	$2^{-1/2}(Q^{1/2}Q^{-1/2} - Q^{-1/2}Q^{1/2})$	$-9X$	$H_{910} = 3X$

[a] $1/2X = \frac{1}{4}J_{XX'}$ has been subtracted from every diagonal element. [b] For convenience the X_6 index has been omitted in the expressions below.

Table 2. Schematic diagram of the factorization of the composite particle spin states of the $AA'A''A'''X_nX_n'$ spin system using good quantum numbers and C_{2v} symmetry.

$\pm m_T$ [b]	Symmetry species [a] $A_1=A_1\times A_1$ or $B_2\times B_2$						$A_2=A_1\times A_2$ or $B_2\times B_1$						$B_2=A_1\times B_2$ or $B_2\times A_1$						$B_1=A_1\times B_1$ or $B_2\times A_2$					
$F+2$	1																							
$F+1$	1	1					1						1	1					1					
F	3	2	1	1			1	2					1	2	1				1	2				
$F-1$	1	4	2	1	1	1	1	2	2	1			1	4	2	1	1	1	1	2	2	1		
$F-2$	1	2	4	3	2	2		2	2	1	2	2		2	4	1	2	2		2	2	1	2	2
$F-2$		1	2	1	4	4			2	1	2	2		1	2	1	4	4			2	1	2	2
$F-4$			1	1	2	2					2	2			1		2	2					2	2
$F-5$					1	1											1	1						
$\|m(X_q)\|$ [b]	F	$F-1$	$F-2$	$F-3$			F	$F-1$	$F-2$	$F-3$			F	$F-1$	$F-2$	$F-3$			F	$F-1$	$F-2$	$F-3$		

[a] Two entries for a given value of $m(X_q)$ indicate the additional factorization occurring when $J_{XX'}=0$.
[b] $F=3$, 2, 1 and 0 for QQ, TT, DD and SS states, respectively. The factorization above is valid only for $|m(X_q)|\geq 0$.

ing matrix dimensions under the A_1, A_2 and B_1, B_2 symmetry species (Table 2) or A, B symmetry species as appropriate.

Calculation of matrix elements. The total spin Hamiltonian of the $AA'A''A'''X_nX_n'$ system can be written.

$$\mathcal{H}=\mathcal{H}(A_4)+\mathcal{H}(X_q)+\mathcal{H}(AX) \quad (1)$$

The first two terms on the right-hand side represent the A and X parts of the Hamiltonian whereas the final term takes account of coupling between these two groups of nuclei. The Hamiltonian of the $AA'BB'X_nX_n'$ system can, of course, be written in a similar manner.

It is impracticable to tabulate the large number of matrix elements of the present spin systems. The diagonal and off-diagonal matrix elements for the DDDDQQ, DDDDTT, and DDDDDD sub-systems may, however, be obtained from eqns. (2) – (5).

$$H(A_4X_q)_{kk}=H(A_4)_{ii}+H(X_q)_{jj}+m(A_4)m(X_q)K_A \quad (2)$$

$$H(A_4X_q)_{kl}=H(A_4)_{ii'}+H(X_q)_{jj'}+H(AX)_{kl} \quad (3)$$

$$H(A_2B_2X_q)_{kk}=H(A_2B_2)_{ii}+H(X_q)_{jj}+m(A_2)m(X_q)K_A+m(B_2)m(X_q)K_B \quad (4)$$

$$H(A_2B_2X_q)_{kl}=H(A_2B_2)_{ii'}+H(X_q)_{jj'}+H(ABX)_{kl} \quad (5)$$

where $K_i=\frac{1}{2}(J_{iX}+J_{iX'})$ with i = A or B.

The first two terms in eqns. (2) – (5) refer to the appropriate matrix elements of the basic groups. Some of these matrix elements are listed in Table 1 and in Refs. 3 and 8.

The last term in eqn. (3) is given by

$$H(AX)_{kl}=\int\phi_i\Gamma_1(A_4)\psi_j\Gamma_3(X_q)\mathcal{H}(AX)\phi_{i'}\Gamma_3(A_4)\cdot\psi_{j'}\Gamma_4(X_q)d\tau=[2-m(A_4)][F-m(X_q)]L_A \quad (6)$$

A corresponding expression is readily found for the last term in eqn. (5), *viz.*

$$H(ABX)_{kl}=[1-m(A_2)][F-m(X_q)]L_A+[1-m(B_2)][F-m(X_q)]L_B \quad (7)$$

where $F=3$, 2, and 1 for QQ, TT, and DD functions, respectively. $L_i=\frac{1}{2}(J_{iX}-J_{iX'})$ with i = A or B. The off-diagonal elements given by eqns. (6) and (7) are non-zero only when the following conditions are fulfilled:

(1) $\Gamma_1\times\Gamma_3=\Gamma_2\times\Gamma_4=B_2$

(2) $\phi_{i'}\Gamma_3(A_4)$ and $\phi_{i'}\Gamma_3(A_2B_2)$ contain the same basic spin $\frac{1}{2}$ product wave functions as $\phi_i\Gamma_1(A_4)$ and $\phi_i\Gamma_1(A_2B_2)$, respectively. (3) $\psi_{j'}\Gamma_4(X_q)$ contains the same A^{mX} $A^{mX'}$ functions as $\psi_j\Gamma_3(X_q)$.

The diagonal matrix elements for the DDDDQD and DDDDTS sub-states of C_s symmetry follow from eqn. (8)

$$H(A_4X_q)_{kk}=H(A_4)_{ii}+m(X_q)\nu_x+m_xm_{x'}J_{xx'}+m(A_4)m(X_q)K_A+(m_A+m_{A'''}-m_{A'}-m_{A''})\cdot(m_x-m_{x'})L_A \quad (8)$$

The only off-diagonal elements are the group

values for the A functions and $\frac{1}{2}\sqrt{3}J_{XX}$ or $J_{XX'}$ for the QD functions.

It is only necessary to calculate matrix elements for positive values of $m(A_4)$, $m(A_2B_2)$ and $m(X_q)$ since the remaining elements then follow from simple symmetry considerations.

Calculations of transition frequencies. The A and X transitions of the $AA'A''A'''X_nX_n'$ system are picked out in the ordinate and diagonal direction in Table 2 by using the selection rules $\Delta m(A_4)=1$, $\Delta m(X_q)=0$ and $\Delta m(A_4)=0$, $\Delta m(X_q)=1$, respectively. Only transition frequencies corresponding to positive and zero values of $m(A_4)$ and $m(X_q)$ need to be calculated since the remaining lines are obtained by reflecting the whole pattern at the point ν_A for the A spectrum and at ν_X for the X spectrum. The transition frequencies of the $AA'BB'X_nX_n'$ system are found by a similar procedure.

Rather than calculating the transition frequencies directly it is often advantageous to pick out familiar sub-spectra from which the spectral parameters may be obtained.

SUB-SPECTRAL TRANSFORMATIONS

The A and B spectra. The use of symmetry and good quantum numbers show that for the extreme values of $m(X_q)$ within the DDDDAA (A = Q, T, D, S), DDDDQD and DDDDST sub-systems, there is break-down into aa'bb' and abcd sub-spectra for the $AA'BB'$ part of the $AA'BB'X_nX_n'$ system. These sub-spectra simplify into a_4 and aa'bb' sub-spectra, respectively, for the $AA'A''A'''X_nX_n'$ system (Table 2).

The spectral transformations for the sub-spectra characterized by the extreme values of $m(X_q)$ within a given sub-system, have been worked out using the procedure due to Diehl:[2]*

$$\begin{aligned}&\nu_a=\nu_A+m(X_q)K_A-pL_A;\ \nu_b=\nu_B+\\&m(X_q)K_B-pL_B\\&\nu_c=\nu_A+m(X_q)K_A+pL_A;\ \nu_d=\nu_B+\\&m(X_q)K_B+pL_B\\&J_{ac}=J_{AA'};\ J_{ab}=J_{cd}=J_{AB}\\&J_{bd}=J_{BB'};\ J_{ad}=J_{bc}=J_{AB'}\end{aligned} \qquad (9)$$

When $p=0$ and $m(X_q)=\pm3$, ±2, and ±1, the transformations for the a_4 and aa'bb' sub-spectra of the $AA'A''A'''X_nX_n'$ and $AA'BB'X_nX_n'$ systems, respectively, are obtained. Similarly, when $p=1$ and $m(X_q)=\pm2$ and ±1 eqn. (9) gives the transformations for the aa'bb' and abcd sub-spectra arising from the DDDDQD and DDDDST sub-states of the $AA'A''A'''X_nX_n'$ and $AA'BB'X_nX_n'$ systems ($n=3$ or 2).

The remaining recognizable energy level groupings not characterized by extreme values of $m(X_q)$ are 1:2:4:2:1 (A_1, B_2) + 2:2:2 (A_2, B_1) and 1:4:6:4:1 (A, B) for the $AA'A''A'''X_nX_n'$ and $AA'BB'X_nX_n'$ systems, respectively. Examination of these sub-patterns reveals that they cannot be identified with real aa'bb' and abcd sub-spectra unless $J_{XX'}=0$. This anomaly has been noted previously for similar systems containing a group of four chemically equivalent nuclei.[1,4,9]

For most problems of practical interest, however, it can be assumed that the long-range coupling constant $J_{XX'}$ is small or negligible. When $J_{XX'}=0$ the energy level groupings can be further reduced as shown in Table 2. In that case the $AA'BB'$ region of the $AA'BB'X_nX_n'$ system can be completely broken down into $(n+1)$ different aa'bb' sub-spectra and $\sum_{i=1}^{n} i$ different abcd sub-spectra. For the $AA'A''A'''X_nX_n'$ system these sub-spectra simplify into a_4 and aa'bb' sub-spectra, respectively. The sub-spectral transformations are still given by eqn. (9) with the following expression of p for the QQ, TT, DD, and SS spin states:

$$p=m-|m(X_q)| \qquad (10)$$
where $m=F$, $F-2\geq|m(X_q)|$

In addition, the following values of p are allowed for the asymmetrical ST and QD states:

$p=|m(X_4)|$ for ST states and $p=1$ or 2 corresponding to even or odd values of $m(X_6)$, respectively, for QD states.

The transition frequencies of the general aa'bb' system that can be obtained in analytical form are given in Table 3. The relevant spectral lines of a given sub-spectrum can then be found by inserting the appropriate expressions for the spectral parameters from eqn. (9).

The X spectrum. The 1:1:1 (A_1, A) + 1(B_2, B) and 1:2:1 (A_1, A_2, B_1, B_2) energy level groupings found in the DDDDDD sub-state of the $AA'A''A'''X_nX_n'$ and $AA'BB'X_nX_n'$ systems

* Some misprints occur in the invariants listed in Ref. 2.

Table 3. Closed-form transition frequencies for the aa'bb' spin system.

Line	Transition frequencies relative to $\frac{1}{2}(\nu_a+\nu_b)$.[a]
a_1 or b_1	$\mp\frac{1}{2}n\mp\frac{1}{2}[\nu_{ab}^2+n^2]^{\frac{1}{2}}$
a_2 or b_2	$\pm\frac{1}{2}n\mp\frac{1}{2}[\nu_{ab}^2+n^2]^{\frac{1}{2}}$
a_3 or b_3	$\mp\frac{1}{2}[(\nu_{ab}+m)^2+l^2]^{\frac{1}{2}}\mp\frac{1}{2}[m^2+l^2]^{\frac{1}{2}}$
a_4 or b_4	$\mp\frac{1}{2}[(\nu_{ab}-m)^2+l^2]^{\frac{1}{2}}\mp\frac{1}{2}[m^2+l^2]^{\frac{1}{2}}$
a_5 or b_5	$\mp\frac{1}{2}[(\nu_{ab}+m)^2+l^2]^{\frac{1}{2}}\pm\frac{1}{2}[m^2+l^2]^{\frac{1}{2}}$
a_6 or b_6	$\mp\frac{1}{2}[(\nu_{ab}-m)^2+l^2]^{\frac{1}{2}}\pm\frac{1}{2}[m^2+l^2]^{\frac{1}{2}}$

[a] $\nu_{ab}=\nu_a-\nu_b$, $k=J_{aa'}+J_{bb'}$, $m=J_{aa'}-J_{bb'}$, $n=J_{ab}+J_{ab'}$ and $l=J_{ab}-J_{ab'}$.

(n = odd) can be identified with real x_2 and xy sub-spectra.[2] It is not possible, however, to pick out known sub-spectra in the remaining sub-systems since these involve particles with spin $I>\frac{1}{2}$.

The energy level groupings characterized by $m(A_4)=\pm 2$ give rise to the familiar pair of lines located at $\nu_X\pm 2K_A$ or $\nu_X\pm(K_A+K_B)$ for the AA'A''A'''X_nX_n' and AA'BB'X_nX_n' systems, respectively. Other sub-patterns, 1:2:3:2:1 and 1:2:3:4:3:2:1 under the A_1, A_2, B_1, and B_2 symmetry species for the AA'A''A'''X_nX_n' system for n = 2 or 3, respectively, resemble parts of x_2y_2 and x_3y_3 systems. However, because these sub-patterns are incomplete it seems unlikely that they have any significant meaning. Inspection of Table 2 indicates, however, that it may be possible to pick out groups of lines in these sub-patterns [$m(A_4)=\pm 1$] corresponding to real xy sub-spectra when $J_{XX'}=0$. Ten familiar 1:2:1 sub-patterns for $m(A_4)=0$

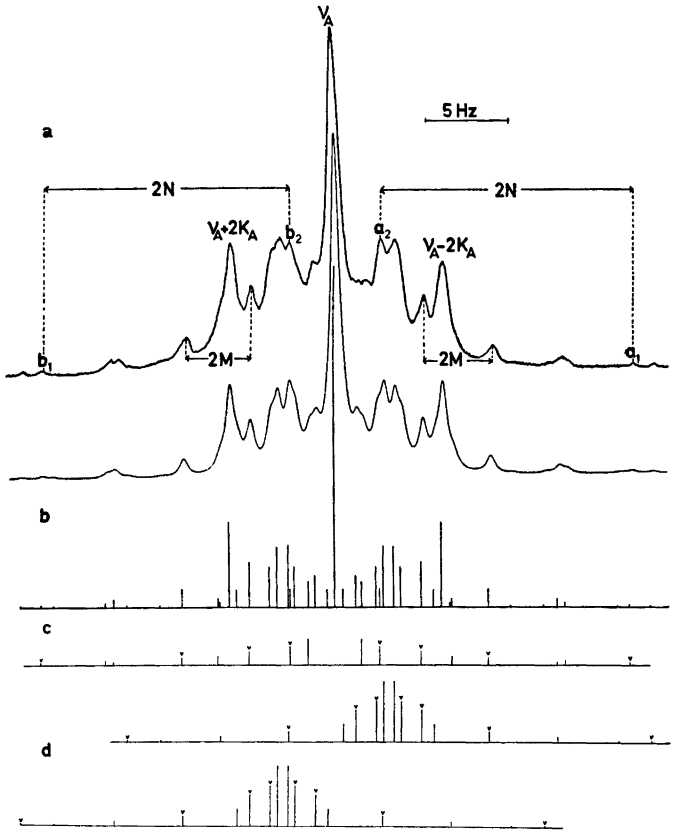

Fig. 1. The 100 MHz methylene proton spectrum of 1,4-dibromobutane; a and b, experimental and theoretical A spectrum; c and d, the three aa'bb' sub-spectra based on eqn. (9) with $p=2$, $m(X_4)=0$ and $p=1$, $m(X_4)=\pm 1$, respectively.

and ± 1 stand out in the DDDDDD state of the AA'A''A'''X_nX_n' system (n = odd).[2] These sub-patterns constitute real xy sub-spectra even if $J_{XX'} \neq 0$. These xy sub-spectra are characterized by the following spectral parameters:

$$\nu_x = \nu_X + m(A_4)(K_A - L_A);\ \nu_y = \nu_X + m(A_4)\ (K_A + L_A)$$
$$J_{xy} = J_{XX'} \pm 2N\ (A_1 \text{ and } B_2 \text{ species}) \qquad (11)$$
$$J_{xy} = J_{XX'} \pm 2M\ (A_2 \text{ and } B_1 \text{ species})$$
where $M = \frac{1}{2}(J_{AA''} - J_{AA'})$; $N = \frac{1}{2}(J_{AA''} + J_{AA'})$

The positive and negative signs in the expression for J_{xy} represent the A_1, B_1 and A_2, B_2 species, respectively. Once the relevant lines of these sub-systems have been identified K_A, L_A, M, N, and $J_{XX'}$ can be found. The xy sub-spectra originating from the 1:2:3:3:2:1 and 1:2:3:4:2:1 sub-patterns also follow from eqn. (11) by putting $J_{XX'} = 0$.

ILLUSTRATIVE EXAMPLES

The 100 MHz spectrum of 1,4-dibromobutane. This spectrum is of the AA'A''A'''X_2X_2' type since the bromomethyl protons at each end of the molecule are magnetically equivalent.[5] The experimental and theoretical spectra are shown in Figs. 1 and 2. The most prominent feature of the A spectrum is the three strong lines at $\nu_A \pm 2K_A$ and ν_A. The central line contributes 128 intensity units (4 a_4 sub-spectra) whereas the two remaining lines give rise to 32 intensity units each, (1 a_4 sub-spectrum). The remaining part of the spectrum can be completely broken down into three aa'bb' sub-spectra as shown in Fig. 1. The aa'bb' transition lines that can be obtained on analytical form have been labelled (*cf.* Table 3).

Again the strong central line and the two lines at $\nu_X + 2K_A$ are the most outstanding features of the X spectrum. The line at ν_X contributes

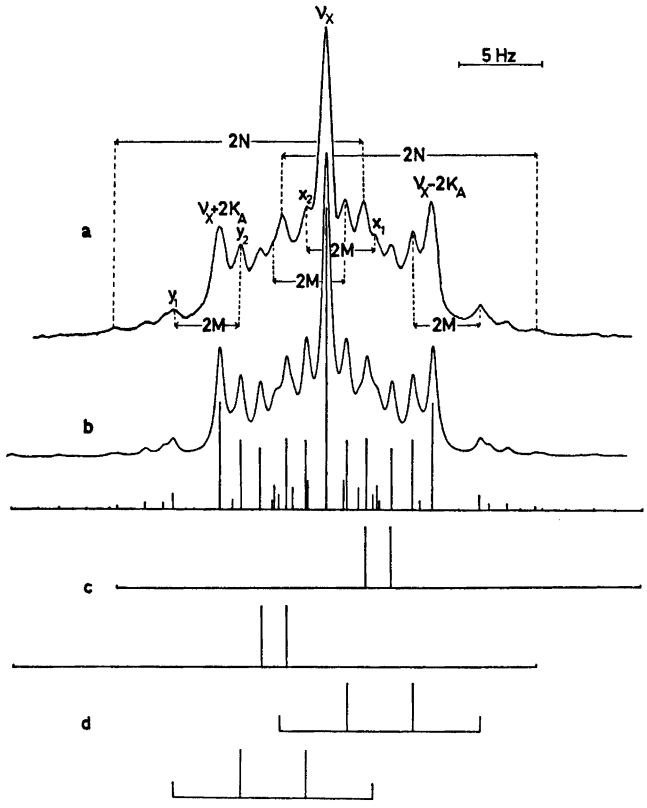

Fig. 2. The 100 MHz bromomethyl proton spectrum of 1,4-dibromobutane; a and b, experimental and theoretical X spectrum; c and d, the four xy sub-spectra based on eqn. (11) with $m(A_4) = \pm 1$.

about 22 % to the total intensity of the X spectrum. The contributing xy sub-spectra are also shown in Fig. 2.

Once the relevant spectral lines of the aa'bb' or xy sub-spectra have been picked out all spectral parameters of the $AA'A''A'''X_2X_2'$ system except $J_{AA'''}$ and L_A, can be obtained directly from the experimental spectrum as demonstrated in Figs. 1 and 2. L_A can be found indirectly by using eqn. (12).

$$L_A = \tfrac{1}{4}[(b_1 - a_1)\,(b_2 - a_2)]^{\frac{1}{2}} = \tfrac{1}{2}[(y_1 - x_1)(y_2 - x_2)]^{\frac{1}{2}} \quad (12)$$

The relevant lines are indicated in Figs. 1 and 2. $J_{AA'''}$ can only be found by diagonalizing 4×4 matrices. However, a precise value of $J_{AA'''}$ is not obtainable from the A spectrum since $J_{AA'''}$ only affects weak combination transitions at the wings or lines near the strong peaks at ν_A and $\nu_A \pm 2K_A$. This follows from the fact that $L_A \approx K_A$ and $|k| \gg |l|$.

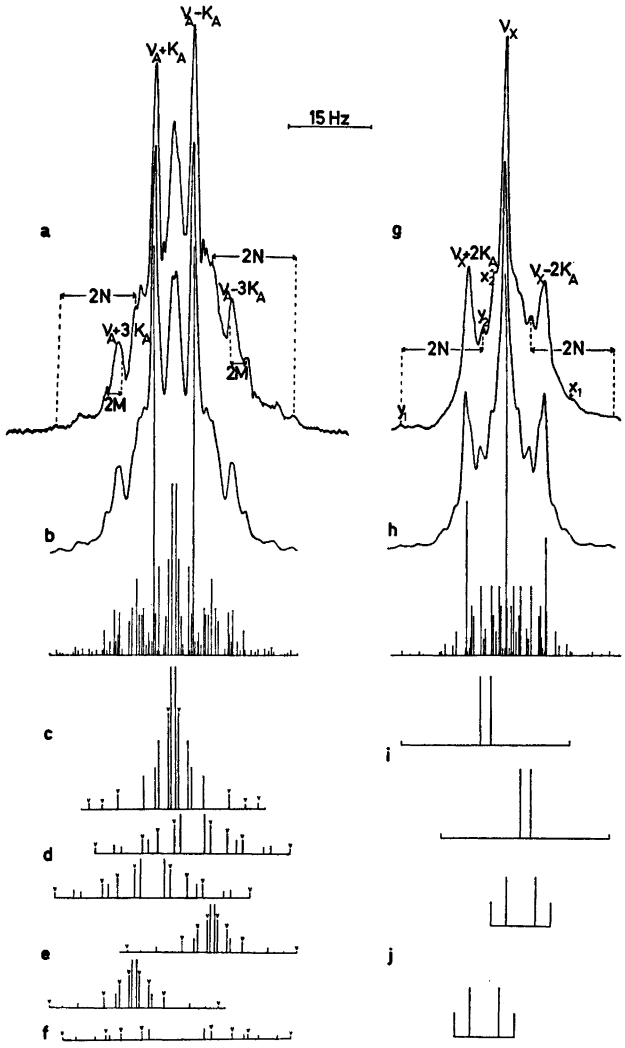

Fig. 3. The 270 MHz spectrum of butane; a and b, experimental and theoretical A spectrum; c–f, the six aa'bb' sub-spectra based on eqn. (9) with c, $m(X_6) = 0$, $p = 1$; d, $m(X_6) = \pm 1$, $p = 2$; e, $m(X_6) = \pm 2$, $p = 1$; f, $m(X_6) = 0$, $p = 3$. g and h, experimental and theoretical X spectrum; i and j, the four xy sub-spectra based on eqn. (11) with $m(A_4) = \pm 1$.

The following averaged values of the spectral parameters (in Hz) have been obtained directly from the experimental spectrum:
$\nu_X - \nu_A = 144.62$ (144.52), $K_A = 3.17$ (3.18), $L_A = 3.43$ (3.43), $M = 2.00$ (2.01), $N = 7.45$ (7.45). The excellent agreement with the values in the parentheses obtained from the iterative analysis,[5] is noteworthy.

The signs of the two AX coupling constants can be determined relative to each other as K_A and L_A are found separately. The observed values of M and N show similarly that the *cis* and *trans* AA coupling constants have the same sign as expected.

The 270 MHz spectrum of butane. This spectrum which is of the AA'A''A'''X_3X_3' type is shown in Fig. 3. The theoretical spectra have been calculated on basis of the 100 MHz spectral parameters.[10] The two strong lines at $\nu_A \pm K_A$ are the most outstanding feature of the A spectrum. Each line contributes 288 intensity units. The two lines at $\nu_A \pm 3K_A$ contributing 32 intensity units each can also be seen. These four lines are also typical of the AA'X_3X_3' system.[1,3] The remaining part of the A spectrum can be broken down into six different aa'bb' sub-spectra (Fig. 3). The labelled lines indicate transitions that can be obtained in explicit form (*cf.* Table 3).

Since the chemical shift difference $\nu_{ab} = -2pL_A$ it follows that all sub-spectra characterized by the same value of p have identical appearance (*cf.* sub-spectra c and e in Fig. 3).

The X spectrum resembles the corresponding spectrum of 1,4-dibromobutane in the sense that the four xy sub-spectra and the three peaks located at ν_X and $\nu_X \pm 2K_A$ make a significant contribution to the total spectrum. This is a consequence of $J_{XX'} = 0$. The central peak contributes *ca.* 20 % to the total intensity of the X spectrum.

Again it is possible to obtain all spectral parameters except $J_{AA'''}$ directly from the spectrum as indicated in Fig. 3. As for 1,4-dibromobutane L_A may be obtained from the sub-spectra using eqn. (12). However, the rather

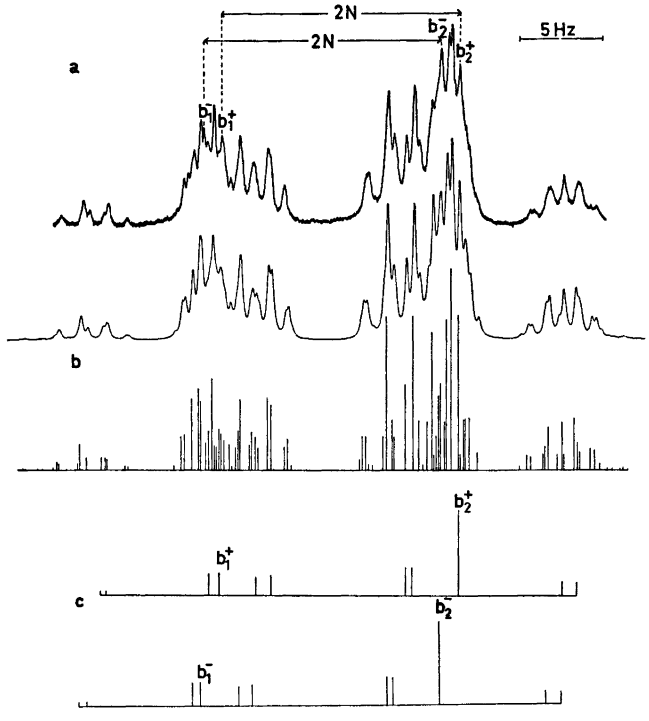

Fig. 4. The 100 MHz spectrum of the diene protons at carbons 3 and 4 in *trans, trans*-2,4-hexadiene; a and b, experimental and theoretical B spectrum; c, the B region of the aa'bb' sub-spectra based on eqn. (9) with $p = 0$ and $m(X_6) = \pm 1$.

poor resolution and limited expansion of the experimental spectrum makes it impossible to measure precise values of M and L_A.

The observed values of K_A, L_A, M, and N imply that the two AX coupling constants are of opposite sign whereas the *cis* and *trans* coupling constants have the same sign as for 1,4-dibromobutane.

The 100 MHz spectrum of trans,trans-*2,4-hexadiene.* The protons of this compound constitute an AA'BB'X_3X_3' spin system (label A refers to the diene proton at the end of the molecule). The experimental and theoretical B spectra are shown in Fig. 4. The B region of the two aa'bb' sub-spectra arising from the DDDDDD sub-state are also displayed. Each of these sub-spectra contributes $4 \times 32 = 128$ intensity units and gives rise to prominent lines.

One can readily assign the intense a_1, b_1, a_2, and b_2 lines listed in Table 3. These lines can then be manipulated to find $N = \frac{1}{2}(J_{AB} + J_{AB'})$, K_A, K_B, and $\nu_{AB} = \nu_A - \nu_B$ as shown in eqns. (13) – (17).

$$2N = a_2^{\pm} - a_1^{\pm} = b_1^{\pm} - b_2^{\pm} \quad (13)$$

$$K_A + K_B = \tfrac{1}{2}[a_2^{+} - a_2^{-} + b_2^{+} - b_2^{-}] \quad (14)$$

$$K_A - K_B = \tfrac{1}{2}[\nu_{ab}^{+} - \nu_{ab}^{-}] \quad (15)$$

$$\nu_{AB} = \tfrac{1}{2}[\nu_{ab}^{+} + \nu_{ab}^{-}] \quad (16)$$

$$\text{where } \nu_{ab}^{\pm} = -[(b_1^{\pm} - a_1^{\pm})\,(b_2^{\pm} - a_2^{\pm})]^{\frac{1}{2}} \quad (17)$$

The + and − superscripts refer to the aa'bb' sub-spectra characterized by $m(X_6) = 1$ and -1, respectively. $M = \frac{1}{2}(J_{AB} - J_{AB'})$ and $G = \frac{1}{2}(J_{AA'} - J_{BB'})$ can be obtained from the b_4 and b_6 lines using a similar procedure. However, $H = \frac{1}{2}(J_{AA'} + J_{BB'})$ can only be obtained by an indirect process involving trial and error fitting or else by iterative computer analysis.

The following averaged values (in Hz) of the spectral parameters were obtained by using eqns. (13) – (17):

$\nu_{AB} = -48.33$, $K_A = 3.02$, $K_B = -0.64$, $N = 7.12$, $M = 7.85$, $G = 9.23$.

$K_A + K_B$ also follows from the strong pair of lines at $\nu_X \pm (K_A + K_B)$ in the X spectrum. The agreement with the refined values listed below is excellent. The theoretical spectra in Fig. 4 are based on the following parameters obtained from the iterative analysis:

$\nu_{AB} = -48.90$, $K_A = 3.00$, $L_A = 3.25$, $K_B = -0.64$, $L_B = 1.06$, $N = 7.12$, $M = 7.85$, $G = 9.47$ and $H = -10.83$.

The root-mean-square deviation was 0.095 for 582 matched lines in the whole spectrum. The calculated probable error for the parameters was 0.022 Hz or less. However, the real error in K_A and L_A is probably larger since it was difficult to make a unique assignment of some lines in the A and X spectra. Although the parameters above differ by less than ±0.2 Hz from those reported by Albriktsen *et al.*[7] the present data reproduce the experimental spectra far better.

The present work shows that the sub-spectral technique is a helpful aid in the analysis of large spin systems possessing some symmetry. Obviously, the more symmetry a system has the further the sub-spectral breakdown can be carried.

NUMERICAL COMPUTATIONS

The plots shown in Figs. 1 – 4 were generated by means of the UEANMR II,[11] LAOCOON II,[12] and KOMBIP [13] computer programs.

The iterative fitting of the experimental and calculated spectra of *trans,trans*-2,4-hexadiene was performed by means of the UEAITR [14] computer program. This program and its non-iterative version UEANMR II make use of magnetic equivalence factoring based on the composite particle method, to reduce the size of the secular matrices.

The computations were performed on the UNIVAC 1110 computer at the University of Bergen. The graphical output was obtained on a Calcomp Plotter.

EXPERIMENTAL

trans, trans-2,4-Hexadiene and 1,4-dibromobutane were obtained from K&K laboratories and Fluka AG, respectively. These compounds were used without further purification. The synthesis of butane has been described in a previous paper.[10] The neat liquids were introduced into 5 mm OD sample tubes and a small quantity of TMS was added to serve as locking and/or reference substance. About 25 % v/v of $CDCl_3$ was used as D-lock signal source for the butane sample. The NMR tubes were degassed and sealed under vacuum.

The 100 MHz and 270 MHz spectra were run on VARIAN HA-100 and BRUKER HX-270 spectrometers, respectively, at ambient probe temperature (*ca.* 30°C). The frequency-calibrated

spectra were recorded at 1 Hz/cm and 3 Hz/cm sweep widths. Line positions were obtained by averaging the results of 2 scans.

Acknowledgements. The author wishes to thank Mr. R. Bosvik at Bruker Spectrospin AB, Sweden, for obtaining the 270 MHz spectra of butane. The author is also indebted to cand. real. P. Albriktsen at the Chemical Institute, University of Bergen, Norway, for his assistance in recording the 100 MHz spectra of *trans,trans*-2,4-hexadiene.

REFERENCES

1. Diehl, P., Harris, R. K. and Jones, R. G. *Progr. Nucl. Magn. Resonance Spectrosc. 3* (1967) 1.
2. Diehl, P. *Helv. Chim. Acta 48* (1965) 567.
3. Lynden-Bell, R. M. *Mol. Phys. 6* (1963) 601.
4. Jones, R. G. *NMR Basic Principles and Progress 1* (1969) 97.
5. Aksnes, D. W. *Acta Chem. Scand. 26* (1972) 164.
6. Ayanbadejo, F. A. M. *Spectrochim. Acta 25 A* (1969) 1009.
7. Albriktsen, P., Cunliffe, A. V. and Harris, R. K. *J. Magn. Resonance 2* (1970) 150.
8. Emsley, J. W., Feeney, J. and Sutcliffe, L. H. *High Resolution Nuclear Magnetic Resonance Spectroscopy*, Pergamon, New York 1965, Vol. 1.
9. Jones, R. G. and Walker, S. M. *Mol. Phys. 10* (1966) 349, 363.
10. Aksnes, D. W. and Albriktsen, P. *Acta Chem. Scand. 26* (1972) 3021.
11. Woodman, C. M. *Personal communication.*
12. Castellano, S. and Bothner-By, A. A. *J. Chem. Phys. 41* (1964) 3863.
13. Aksnes, D. W. *KOMBIP*, Quantum Chemistry Program Exchange, Chemistry Department, Indiana, U.S.A., Program No. 205.
14. Johannesen, R. B., Ferretti, J. A. and Harris, R. K. *J. Magn. Resonance 3* (1970) 84.
15. Kaiser, R. *J. Magn. Resonance 1* (1969) 534.

Received November 13, 1973.

Acta Chemica Scandinavica A 28 (1974) 385—398

The Tris[(±)-1,2-propanediamine]cobalt(III) System*

S. E. HARNUNG, S. KALLESØE, A. M. SARGESON, and C. E. SCHÄFFER

Chemistry Department I (Inorganic Chemistry), University of Copenhagen, The H. C. Ørsted Institute, Universitetsparken 5, DK-2100 Copenhagen Ø, Denmark

The twenty-four isomers, $[Co(\pm)pn_3]Cl_3$ (pn = 1,2-propanediamine), constitute two catoptric (enantiomeric) series with the configurations Δ and Λ, respectively. In each of the series there are two methyl group isomers with the chelate-ring conformations lel_3, four with lel_2ob, four with ob_2lel, and two isomers with the conformations ob_3.

Equilibrium between the isomers can be established at 100°C (charcoal as catalyst, excess of diamine, pH = 7). By ion exchange chromatography (SP-Sephadex; eluent 0.1 M Na_3PO_4) of such an equilibrium mixture of racemic $[Co(\pm)pn_3]Cl_3$ one obtains four racemic fractions which are eluted in the sequence lel_3, lel_2ob, ob_2lel, and ob_3, the relative amounts being 35.0:41.1:18.0:4.0. Each fraction can be separated (SP-Sephadex; eluent 0.15 M (+)-tartrate) into equal amounts of catoptric forms, and the Λ forms are first eluted. Absorption- and circular dichroism spectra are recorded.

Using the figures mentioned, one can calculate the composition of the equilibrium mixture for an arbitrary ratio of [(+)pn]/[(−)pn]. Agreement between calculated and measured values is found.

The free energies at 100°C for the interconversion between the conformational isomers have been analysed. This leads to a ring-pair relationship model, which in terms of the mutual interaction between the chelate rings accounts for the equilibrium data in a two-parameter model.

By combination of paper and column chromatography some of the methyl group isomers have been partly separated. Such fractions show different ^1H NMR spectra whereas their circular dichroism spectra are virtually identical in the visible-ultraviolet spectral region.

1. INTRODUCTION

$[Co(\pm)pn_3]^{3+}$ (pn = 1,2-propanediamine) represents 24 isomers whose properties and relative stabilities have attracted interest [1–3] in connection with optical activity problems [4] and conformational analyses.[5–8] The system has been studied previously [1–3] and some of the isomers, or mixtures of isomers, have been separated. In the present paper further separations are described, equilibrium data analysed and circular dichroism data presented.

In order for the reader to appreciate the discussion of the many isomers a nomenclature symbolism is introduced. This symbolism applies to the unsolvated complex ions and allows at the same time the estimation of their relative probabilities which govern an important part of the entropy terms of the isomer equilibria.

Firstly, we note that a coordinated propanediamine molecule has two conformers, the methyl group being either equatorial or axial. Corey and Bailar [5] asserted that in tris(propanediamine) complexes the former conformer is the more stable one by at least 8 kJ per chelate ring. This means that at most 3 % of the methyl groups will be axial at equilibrium. These numbers have not been confirmed experimentally in a quantitative sense but the pronounced stereospecificity which optically active propanediamine shows, particularly in tris(propanediamine) complexes, is a qualitative indication of the correctness of the above assertion. Unless the opposite is explicitly stated we shall ignore the existence of axial methyl groups in the following and base the discussion upon conformations fixed in the stable form with equatorial methyl groups. This will not in any way change the arguments, and will make the text easier to read.

Secondly, all $[Co(\pm)pn_3]^{3+}$ isomers have a pseudo three-fold axis which only in the case

* This work was communicated at the 14th Nordiska Kemistmötet, Umeå, Sweden 1971.

of four of the isomers [*fac* lel_3 (Δ,Δ) and *fac* ob_3 (Δ,Δ), see below] becomes a true three-fold axis.

2. A NOMENCLATURE SYMBOLISM AND AN ENUMERATION OF THE ISOMERS

The cause of the isomerism may be briefly characterized as an interplay of configurational and conformational isomerism,[9,10] upon which a geometrical isomerism due to the methyl groups is superimposed.

The designation of configuration is, in accordance with IUPAC,[11,12] based upon the edges of the octahedron spanned by the chelate rings. Two such edges form a pair of skew lines describing a screw which may be right-handed (designated delta) or left-handed (designated lambda). Because of the three-fold axis of the octahedron each of the three possible pairs of edges forms screws of the same handedness and this is used to characterize the configurational chirality Δ or Λ. It may be noted that when one of the edges spanned by a chelate ring is taken together with the three-fold axis, defined by the three edges spanned by the three chelate rings, these also form a pair of skew lines of the same chirality (Fig. 1). This was essentially the basis for Piper's original proposal [13] of the symbols Δ and Λ for configuration. So, for tris(bidentate) complexes there is agreement between Piper's nomenclature and that of IUPAC.

The designation of conformation is, also in accordance with IUPAC, based upon the principle of a pair of skew lines. For propanediamine one of these lines is defined by the two chelating nitrogen atoms and the other by the two carbon atoms in the chelate ring, and their chirality is designated by the symbols δ or λ (Fig. 2), IUPAC being in agreement with Liehr's original proposal.[14] The absolute chirality of propanediamine is, also according to IUPAC,[15] given by the *R*, *S*, nomenclature proposed by Cahn and Ingold.[16] So (−)-propanediamine is *R*, and when chelated in the stable conformer with the methyl group equatorial, it is λ.

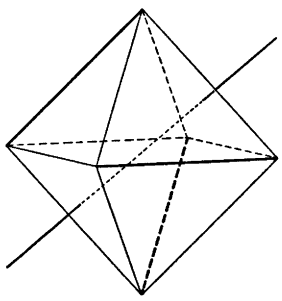

Fig. 1. The configuration Δ. Each pair of chelate rings defines by the edges they span a right-handed pair of skew lines and the same is true if the edge of a chelate ring is taken together with the three-fold axis.

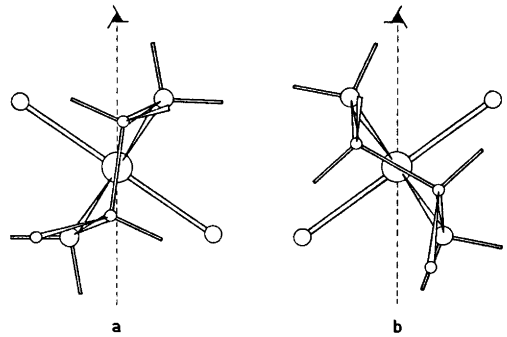

Fig. 2. The conformation λ of the chelate ligand *R*-(−)-1,2-propanediamine. (a) shows a part of a tris complex with the configuration Δ. The diamine connects the corner of the front edge of the octahedron shown in Fig. 1. The C−C bond is nearly parallel to the (pseudo) three-fold axis, which is indicated by the dotted line. (b) shows a part of a tris complex with the configuration Λ. Here the C−C bond of the diamine is oblique relative to the (pseudo) three-fold axis.

The concepts symbolized by Δ, Λ and δ, λ are invariant under proper rotations but are interchanged under improper rotations. The interplay of these concepts, however, gives rise to a characterization of the chelate ring which is invariant to both proper and improper rotations.[10] This characterization, which is the relevant one when discussing stabilities, will be designated lel and ob using an extension [4,9,10] of a nomenclature originally proposed by Corey and Bailar [5] for characterizing a tris(diamine) complex as whole. Letting, for example, $\lambda(\Delta)$ mean a conformation λ associated with a configuration Δ the diastereoisomeric concepts

lel [$\equiv\lambda(\Delta)$ or $\delta(\Lambda)$]
ob [$\equiv\delta(\Delta)$ or $\lambda(\Lambda)$] (1)

may be taken as the definition of lel and ob. A tris(diamine) complex $\Delta\lambda_2\delta$ may then alternatively be characterized by Δlel_2ob and the catoptric (enantiometric) complex $\Lambda\delta_2\lambda$ by Λlel_2ob, so that together they constitute a lel_2ob pair. Corey and Bailar,[5] who pointed out that the C–C bond in the stable conformer of the (−)-propanediamine chelate rings of $[Co(-)pn_3]^{3+}$ could be either parallel (lel) or oblique (ob) to the three-fold axis, used the symbols lel and ob for the isomer pairs which we now call lel_3 and ob_3. These authors also asserted that the lel_3 system was the energetically favoured one.

It should be emphasized that for a single chelate ring, as for example in $[Co\ pn(NH_3)_4]^{3+}$, the concepts lel and ob are not defined. Two or three chelate rings are necessary in order to define a kind of (pseudo) three-fold axis. For two chelate rings one has the conformational isomers lel_2, lel ob, or ob_2, and the relative energies of these systems are associated with the ring pair relationships lel-lel, lel-ob, and ob-ob, respectively.

It is useful to consider the configurational plus conformational isomerism by a building-up process. There are two configurations Δ and Λ and two conformations δ and λ for each of the three chelate rings giving altogether $2\times 2^3 = 16$ possibilities of building-up a complex. Among these possibilities some isomers are represented more than once, the number of times being the statistical weight or relative probability which govern the inner-sphere entropy term for the isomerization reactions. A projection formula [10] for an isomer of the type

$$\Delta[Co(R\text{-pn})_2S\text{-pn}]^{3+} = \Delta R_2S = \Delta\lambda_2\delta = \Delta lel_2ob \quad (2)$$

may, for example, be written as

$$\begin{matrix} R & & S & & R \\ & \Delta\ S \text{ or} & & \Delta\ R \text{ or} & & \Delta\ R \\ R & & R & & S \end{matrix} \quad (3)$$

The situation is equivalent for the Δlel_2ob and for both Δob_2lel and Δob_2lel all of which obtain a statistical weight of 3, thus accounting for 12 of the 16 possibilities stated above. Adding the two lel_3 isomers and the two ob_3 isomers of weight 1 we have 8 isomers of lel_iob_j type $(i+j=3)$.

The projections shown in eqn. (3) have been performed along the (pseudo) three-fold axis of the molecule, onto the plane perpendicular to this axis and containing the central ion. Provided that the symbols (Δ,Λ), (δ,λ), and (R,S) are manipulated properly, the projection formulas have the symmetries of the molecules themselves.[10] A proper manipulation means that the symbols should be left invariant by proper rotations and be permuted within each associated enantiomeric pair of symbols by improper rotations.

We reiterate that as far as the configurational-conformational isomerism is concerned the complexes may be classified as lel_3, lel_2ob, ob_2lel, and ob_3, each class comprising a Δ and a Λ isomer. This classification applies to all tris(bidentate) complexes for which two conformations are possible for each chelate ring. For systems containing three propanediamine or three *trans*-1,2-cyclohexanediamine chelate rings bound to chromium(III),[17] cobalt(III),[18] rhodium(III),[19] and iridium(III),[20] the isomers can be separated, and can be had individually in solution. For tris(ethylenediamine) systems all the isomers of a given configuration are in equilibrium in solution and the individual isomers can only be isolated in certain cases where they become trapped in solids.[21]

Within each of the four classes just mentioned the tris(propanediamine) systems have an additional methyl group isomerism which may now be discussed by the same kind of building-up procedure. Each methyl groups may be either above (a) or below (b) the projection plane containing the central ion giving $2^3 = 8$ possibilities which at once reduce to 4 because the configurational-conformational isomers do not distinguish between up and down

$$\begin{matrix} [1] & \begin{matrix} a & & b \\ & a = & \\ a & & b \end{matrix} & & \begin{matrix} & b \\ = & \\ & b \end{matrix} \\ [2] & \begin{matrix} a & & b \\ & b = & \\ a & & b \end{matrix} & & \begin{matrix} & a \\ = & \\ & b \end{matrix} \\ [3] & \begin{matrix} a & & b \\ & a = & \\ b & & a \end{matrix} & & \begin{matrix} & b \\ = & \\ & b \end{matrix} \\ [4] & \begin{matrix} b & & a \\ & a = & \\ a & & b \end{matrix} & & \begin{matrix} & b \\ = & \\ & b \end{matrix} \end{matrix} \quad (4)$$

These four isomers are different for lel_2ob and ob_2lel systems, but the three last ones are identical for lel_3 and ob_3 systems and are described as meridional and given a statistical weight of 3 as opposed to the first isomer which is described as facial with a weigth of 1. So when the methyl group isomerism is included we have the four lel_3 isomers *fac* Δ, *fac* Λ and *mer* Δ, *mer* Λ and the eight lel_2ob isomers

$$\left[\begin{matrix}\text{lel(a)}\\ \\ \text{lel(a)}\end{matrix}\right.\ \begin{matrix}\text{lel(a)}\\ \text{ob(a)},\\ \text{lel(a)}\end{matrix}\ \begin{matrix}\text{lel(a)}\\ \text{ob(b)},\\ \text{lel(a)}\end{matrix}\ \left.\begin{matrix}\text{lel(a)}\\ \text{ob(a)},\\ \text{lel(b)}\end{matrix}\right.$$

$$\left.\begin{matrix}\text{lel(b)}\\ \\ \text{lel(a)}\end{matrix}\right]\ \begin{matrix}\text{ob(a)}\\ \\ \end{matrix}\ \Big]\ \Delta,\Lambda \qquad (5)$$

plus similarly four ob_3 isomers and eight ob_2lel isomers, all together 24 isomers. If the convention is used that the number of (a)'s in a formula should always exceed the number of (b)'s the formulae of eqn. (5) are unique.

3. EXPERIMENTAL

Paper chromatography. The separations were carried out in the manner described [2,3] previously, using Whatman 3 MM paper and a mixture of butanol, water, and 12 M hydrochloric acid (6:3:1 vol) as eluent.

Ion exchange separations. Based upon the idea of Yoshikawa and Yamasaki [22] the lel_iob_j isomers were separated on Sephadex cation exchanger SP-C25 using columns of 2.5 cm in diameter and packed with the beads suspended in "boiled-out" water. The complexes were sorbed on the column from dilute aqueous solution and then eluted with 0.1 or 0.2 M sodium orthophosphate. Our method of using phosphate for such isomer separations has been used in this laboratory for the tris(*trans*-1,2-cyclopentanediamine)cobalt(III) and chromium(III) systems [23] and for the corresponding complexes with *trans*-1,2-cyclohexanediamine.[17,18]

Resolution into catoptric forms. Here the method of Yoshikawa and Yamasaki [22] was directly used. The columns, 70 cm long, were packed as above and the sorbed complex was eluted with 0.15 M(+)-tartrate. For each fraction lel_3, lel_2ob, ob_2lel, ob_3 two equal and completely separated fractions were obtained. In all cases the two fractions showed catoptric circular dichroism spectra and the Λ-fraction was the first eluted one.

Purification. The samples obtained above were sorbed on Dowex Cation Exchange Resin 50 W – X2, washed with water and eluted with 6 M hydrochloric acid. The eluted samples were then evaporated to dryness. During the evaporation ethanol was added to remove traces of hydrochloric acid.

Equilibrium conditions. Here we describe a typical experiment which has been discussed in detail in section 4. $\Lambda[Co(+)pn_3,lel_3]Cl_3$ (4.70 mmol), (±)pn.2HCl (1.61 mmol), and (−)pn.2HCl (5.99 mmol) in water (90 ml) were mixed with charcoal (70 mg Struer's "Medicinsk A"). Sodium hydroxide (3.8 ml 1 M) was added to pH 7. The mixture was refluxed for 30 min, sucked through a filter from the hot solution, quenched with hydrochloric acid (8.5 ml 1 M) and cooled. Two samples (50 ml and 25 ml) were sorbed on Sephadex SP-C25 columns (2.5 cm × 100 cm) and eluted with 0.1 M sodium phosphate. The four fractions were then acidified to pH 2 and each was resorbed on a separate column and after washing with water resolved by elution with a mixture of ammonia (1 M) and (+)-tartaric acid (0.15 M).

The experiment with racemic compounds was carried out in the same manner except that in this equilibrium experiment the initial four racemic fractions, lel_3, lel_2ob, ob_2lel, and ob_3, were not resolved.

Cobalt analyses. These were carried out with a Perkin Elmer Atomic Absorption Spectrophotometer 403 to an accuracy of ≤ 1 %.

Spectra and circular dichroism. These were measured with a Cary 14 Spectrophotometer and a Jouan Dichrograph 2B. The complex samples were prepared by sorbing the complex on Sephadex SP – C25 and eluting with LiCl (1 M). The eluates were then diluted with LiCl (1 M, prepared by passage through the column) to give a constant cobalt concentration (9×10^{-3} M) for all samples. The measurements in the ultraviolet region were obtained after diluting the LiCl solutions with water up to 250-fold.

Preparative conditions. A racemic mixture of $[Co(\pm)pn_3]Cl_3$ was prepared from cobalt(II) chloride hexahydrate, (±)-propanediamine, and hydrochloric acid in the ratio 1:3:1 by oxidizing an aqueous solution in the presence of charcoal with oxygen at room temperature. The charcoal was filtered off and the mixture of isomers isolated by evaporation. This crude mixture always has the same composition in terms of configurational-conformational isomers and therefore appeared to be an equilibrium mixture.

The equilibrium problem. We tried to establish equilibrium by stirring the lel_3 isomer with charcoal at 25°C under anaerobic conditions. It turned out that conversion of lel_3 into ob_3 took place, and a partial equilibrium (between lel_3 and ob_3) could be established. However, the production of the lel_2ob and

ob_2lel isomers could hardly be detected chromatographically even when the heterogeneous system had been allowed to react during a week. Apparently the charcoal lost activity in time. Even though we tried the charcoals which were commercially available to us and used different propanediamine buffers between pH 7 and 10 we were not able to find conditions under which equilibrium could be established at 25°C. We tested the different charcoals for their ability to racemize the optically active tris(ethylenediamine)cobalt(III) ions and found that the time required for 90 % racemization under equivalent conditions varied by several orders of magnitude. A particular charcoal delivered from Struer's in Copenhagen called "Medicinsk A" was chosen as the best one available to us. This charcoal was used also in an attempt to equilibrate a lel_2ob fraction and it transpired that the partial equilibrium with ob_2lel was almost established before lel_3 was present in significant amounts. It can be concluded that an equilibrium with respect to the propanediamine molecules already bound to a cobalt(III) ion is much faster than one which requires exchange with propanediamine molecules from the outer solution.

4. RESULTS AND DISCUSSION

a. Separation of isomers

The racemic mixture of $[Co(\pm)pn_3]Cl_3$ was separated into four fractions using either paper chromatography or a Sephadex column (0.2 M sodium phosphate eluent). For both methods the ratio of the first moving fraction (lel_3) to the second one (lel_2ob) was the same, whereas the ratios of the last two fractions differed. This difference arose from the fact that portion of the ob_2lel fraction was resolved into Λ and Δ forms on the paper and that one (or some) of the Δ isomers coincided with the ob_3 fraction. However, for the separation on Sephadex all four fractions were optically inactive. These four fractions are $\Delta,\Lambda lel_3$; $\Delta,\Lambda lel_2ob$; $\Delta,\Lambda ob_2lel$; and $\Delta,\Lambda ob_3$ (eluted in this sequence) and we shall show later that these assignments are correct. The slowest moving fraction from the separation on paper was then eluted on the Sephadex column with phosphate and an optically active Δob_2lel fraction and the inactive ob_3 fraction were separated.

The four fractions obtained from the Sephadex separation of the racemic mixture were then resolved into Λ (first eluted) and Δ configurations using Sephadex with (+)-tartrate as eluent. The circular dichroism (CD) of the resolved forms of the fastest and the slowest moving racemic fraction coincided with those obtained from the lel_3 and ob_3 forms of $[Co(-)pn_3]Cl_3$ and $[Co(+)pn_3]Cl_3$. Moreover,

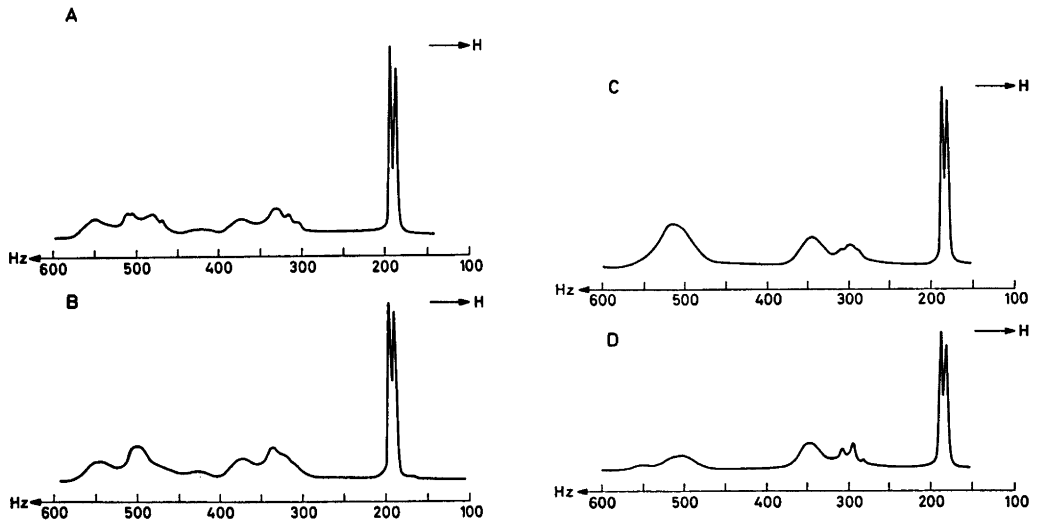

Fig. 3. A, B: 100 MHz ^1H NMR spectra of Δob_2lel isomers in $D_2O+D_2SO_4$ with TMS as external standard. A. The fraction last eluted (paper). B. The fraction first eluted (paper). C, D: 100 MHz ^1H NMR spectra of racemic lel_3 isomers in $D_2O+D_2SO_4$ with TMS as external standard. C. The fraction last eluted (column). D. The fraction first eluted (column).

the Δob_2lel fraction from the column experiments was separated completely on paper into two Δ fractions (first eluted: last eluted $\sim 2:1$) with virtually identical CD curves in the visible and ultraviolet region but different ^1H NMR spectra. These fractions are therefore either a mixture of three methyl isomers and one methyl isomer or two pairs of methyl isomers. The ^1H NMR spectra, Fig. 3a, b, indicate that the first possibility is the more likely one.

All the Λ forms of ob_2lel run together with the fastest moving Δ fraction on paper and the methyl isomers for the Λ fraction could not be separated by these eluents. Similarly the methyl isomers of the lel_2ob fraction were not resolved.

Racemic lel_3 was eluted on Sephadex columns (~ 7 m) with 0.1 M sodium phosphate until a minimum was observed in the sorbed fraction. The first half and the last third of the fraction on either side of the minimum were collected and recovered. The ^1H NMR spectra for these fractions are given in Fig. 3c,d. They show marked differences in the region of the NH (~ 5 ppm) absorption although there is little difference in the CH,CH_2 (~ 3.5 ppm) and CH_3 (~ 2 ppm) absorptions. This result might be anticipated because the chemical shift differences for protons attached to saturated N atoms are usually much larger than those for saturated C atoms. In addition the two fractions showed a large difference in behaviour toward concentrated hydrobromic acid. The faster (less abundant) moving fraction was almost insoluble in concentrated hydrobromic acid but the slower moving fraction did not crystallize at all. On the basis of this evidence and the second experiment (see below) on an active lel_3 fraction we assert that the first fraction which crystallizes is the *fac* isomer and the second, more abundant, fraction is the *mer* isomer.

Δlel_3 was also eluted on Sephadex columns (~ 11 m) with 0.1 M sodium phosphate and two fractions were collected on either side of the observed minimum the less abundant fraction ($\sim 1/4$ of total) gave a crystallized bromide also here and its properties coincide with those of the isomer described previously [24] as Δfac-$[Co(-)pn_3]^{3+}$. The more abundant form is the *mer* isomer and is difficult if not impossible to crystallize as the bromide in keeping with previous observations.[25,26]

The *fac* and *mer* ob_3 isomer have been separated ion exchange chromatographically by Yamasaki *et al.*[27]

b. Energy differences between lel_iob_j isomers

$[Co(-)pn_3]^{3+}$ consists of the configurational-conformational isomers Δlel_3 and Δob_3. The equilibrium constant $K(ob_3 \rightarrow lel_3)$ for the reaction

$$\Delta ob_3 \rightarrow \Delta lel_3 \qquad (6)$$

was determined by separating the isomers from the equilibrium mixture within the $[Co(-)pn_3]^{3+}$ system and simply measuring the relative amounts of Δob_3 and Δlel_3. The same constant was also determined from the equilibrium mixture within $[Co(\pm)pn_3]^{3+}$ but in this case three independent constants were measured at 100°C (Table 1)

$$K(ob_3 \rightarrow lel_3) = \frac{[lel_3]}{[ob_3]} = 8.75$$

$$K(ob_2lel \rightarrow lel_2ob) = \frac{[lel_2ob]}{[ob_2lel]} = \frac{41.1}{18.0} = 2.28 \qquad (7)$$

$$K(lel_2ob \rightarrow lel_3) = \frac{[lel_3]}{[lel_2ob]} = \frac{35.0}{41.1} = 0.852$$

where in eqn. (7) each concentration symbol designates the sum of the concentrations of all the methyl group isomers embodied in the symbol. The corresponding standard free energies $\Delta G^0 = -RT \ln K$ at 100°C are

$$\begin{aligned} \Delta G^\circ(ob_3 \rightarrow lel_3) &= -6.73 \text{ kJ} \\ \Delta G^\circ(ob_2lel \rightarrow lel_2ob) &= -2.56 \text{ kJ} \quad 373 \text{ K} \\ \Delta G^\circ(lel_2ob \rightarrow lel_3) &= +0.50 \text{ kJ} \end{aligned} \qquad (8)$$

These ΔG° values may be corrected for the building-up-statistical inner-sphere entropy terms $T\Delta S'$ mentioned in section 2

$$\begin{aligned} T\Delta S'(ob_3 \rightarrow lel_3) &= 0 \\ T\Delta S'(ob_2lel \rightarrow lel_2ob) &= 0 \quad 373 \text{ K} \\ T\Delta S'(lel_2ob \rightarrow lel_3) &= RT \ln (1/3) = -3.41 \text{ kJ} \end{aligned} \qquad (9)$$

to obtain a kind of ΔH° term which we shall designate $\Delta H'^\circ = \Delta G^\circ + T\Delta S'^\circ$

$$\begin{aligned} \Delta H'^\circ(ob_3 \rightarrow lel_3) &= -6.73 \text{ kJ} \\ \Delta H'^\circ(ob_2lel \rightarrow lel_2ob) &= -2.56 \text{ kJ} \quad 373 \text{ K} \\ \Delta H'^\circ(lel_2ob \rightarrow lel_3) &= -2.91 \text{ kJ} \end{aligned} \qquad (10)$$

Table 1. Equilibrium isomer distribution at 100°C.

Isomer	Experimental composition % $F=1.00$ [a]	$F=1.90$ [b]	$F=1.90$ [c]	Calculated composition % $F=1.90$ [d]
Λlel$_3$	35.0	37.9	37.9	38.0
Δlel$_3$		5.6	5.5	5.5
Λlel$_2$ob	41.1	23.6	22.4	23.5
Δlel$_2$ob		12.4	11.9	12.4
Λob$_2$lel	18.0	5.1	5.1	5.4
Δob$_2$lel		10.2	10.0	10.3
Λob$_3$	4.0	–	–	0.6
Δob$_3$		3.9	4.0	4.3
Total	98.1	98.7	96.8	100.0

[a] The isomer distribution of an equilibrium mixture made by refluxing a mixture of $[Co(\pm)pn_3]^{3+}$:$(\pm)$pn= 1.00:1.50 at 100 °C as described in section 2. Approximately 1 mmol cobalt was placed on the column. [b] By use of the ratios of the β_3 constants of eqn. (23) as determined in experiment (*a*) one can calculate the composition required for the initial mixture in order that F of eqn. (25) is equal to 1.90 when equilibrium is established. Such calculation makes use of the ratio $B=[(+)pn]_b/[(-)pn]_b$ of complex bound diamine. With $[(+)pn]_b=3([\Lambda(+)pn_3]+[\Delta(+)pn_3])+2([\Lambda(+)pn_2(-)pn]+[\Delta(+)pn_2(-)pn])+([\Lambda(-)pn_2(+)pn]+[\Delta(-)pn_2(+)pn])$ and an analogous expression for $[(-)pn]_b$, one obtains

$$B=\frac{3F^3\left(\frac{\beta_3(ob_3)}{\beta_3(lel_3)}+1\right)+(2F^2+F)\left(\frac{\beta_3(lel_2ob)}{\beta_3(lel_3)}+\frac{\beta_3(ob_2lel)}{\beta_3(lel_3)}\right)}{3\left(\frac{\beta_3(ob_3)}{\beta_3(lel_3)}+1\right)+(2F+F^2)\left(\frac{\beta_3(lel_2ob)}{\beta_3(lel_3)}+\frac{\beta_3(ob_2lel)}{\beta_3(lel_3)}\right)}$$

The figures in column (*b*) show the isomer distribution of an equilibrium mixture with the initial composition (*cf.* section 2) $\Lambda[Co(+)pn_3]Cl_3$:$(\pm)$pn:$(-)$pn= 1.00:0.34:1.27. At equilibrium the diamine ratios are $F=1.90$ and $B=2.42$. Approximately 2 mmol cobalt was placed on the column. [c] Equilibrium mixture as described in (*b*) and in section 2. Approximately 1 mmol cobalt was placed on the column. [d] The calculated composition of an equilibrium mixture with $F=1.90$. Use has been made of eqns. (24), (26), (28), and (23) together with the results in column (a).

Equilibrium data have previously been determined at 25°C for the first and the third of the reactions of eqns. (7) – (10). These data, valid at 25°C, are [3]

$$\begin{aligned} &K(ob_3\rightarrow lel_3=15\\ &K(lel_2ob\rightarrow lel_3)=1 \end{aligned} \qquad 298\ K \qquad (11)$$

and from them the corresponding $\Delta H'^\circ$ values can be derived

$$\begin{aligned} &\Delta H'^\circ(ob_3\rightarrow lel_3)=-6.77\ kJ\\ &\Delta H'^\circ(lel_2ob\rightarrow lel_3)=-2.75\ kJ \end{aligned} \qquad 298\ K \qquad (12)$$

It is gratifying that the $\Delta H'^\circ$ values at the two different temperatures [eqns. (10) and (12)] are the same within the experimental uncertainty.

Under the assumption that the full ΔH° values, including all inner-sphere and outer-sphere entropy terms, are also temperature-independent, the relation

$$\Delta H^\circ=R\frac{T_1T_2}{T_2-T_1}\ln\frac{K(T_2)}{K(T_1)} \qquad (13)$$

is valid and gives, using eqns. (7) and (11)

$$\begin{aligned} &\Delta H^\circ(ob_3\rightarrow lel_3=-6.6\ kJ\\ &\Delta H^\circ(lel_2ob\rightarrow lel_3)=-2.0\ kJ \end{aligned} \qquad (14)$$

These ΔH° values are probably not very good, but still it is interesting that they compare so well with the corresponding $\Delta H'^\circ$ values of eqns. (10) and (12), because this comparison does provide some support to the proposition that the building-up-statistical inner-sphere entropy terms are the essential entropy terms for these reactions in solution.

c. $\Delta H'^\circ$ values and the ring pair relationship model

The $\Delta H'^\circ$ data may be used to establish a model based upon the ring pair relationships

lel-lel, lel-ob, and ob-ob, mentioned in section 2. In the ob_3 complexes there are three ob-ob relationships and in the lel_3 complexes three lel-lel relationships. One may now with reference to the practice in conformational analysis,[5,6] try to interpret $\Delta H'^{\circ}(ob_3 \rightarrow lel_3)$ as the energy required to transform 3 (ob-ob) relationships into 3 (lel-lel) relationships so that from the first equation of eqn. (10) one obtains

$$\Delta H'^{\circ}(\text{ob-ob} \rightarrow \text{lel-lel}) = -2.24 \text{ kJ per ring pair} \quad (15)$$

A similar comparison of the ob_2lel and lel_2ob isomers can be made. These isomers have two lel-ob relationships in common and differ only in that ob_2lel has an additional ob-ob relationship and lel_2ob and additional lel-lel relationship. So the second equation of (10) may be rewritten

$$\Delta H'^{\circ}(\text{ob-ob} \rightarrow \text{lel-lel}) = -2.56 \text{ kJ per ring pair} \quad (16)$$

Eqns. (15) and (16), which are completely independent experimentally as well as with respect to the pair relationship model, indicate an approximate additivity of the enthalpies of pair relationship changes. Using this additivity the last equation of eqn. (10) gives

$$\Delta H'^{\circ}(\text{lel-ob} \rightarrow \text{lel-lel}) = -1.45 \text{ kJ} \quad (17)$$

and when this is combined with the average of eqns. (15) and (16):

$$\Delta H'^{\circ}(\text{ob-ob} \rightarrow \text{lel-lel}) = -2.40 \text{ kJ} \quad (18)$$

one obtains

$$\Delta H'^{\circ}(\text{ob-ob} \rightarrow \text{lel-ob}) = -0.95 \text{ kJ} \quad (19)$$

Comparison of eqns. (17) and (19) shows that it costs 50 % more to transform a lel-lel relationship into a lel-ob one, than to transform a lel-ob relationship into an ob-ob one.

It should be emphasized that this result, obtained from the tris(propanediamine)-cobalt(III) complexes, may not apply to the corresponding *cis*-bis(propanediamine) complexes. For example, optically active propanediamine has only a small stereospecific effect [28] in the oxalatobis(propanediamine)cobalt(III) system.

d. Application of the pair relationship model to the tris(ethylenediamine)cobalt(III) system

The assumption of equatorial methyl groups being completely dominant in the tris(propanediamine)cobalt(III) system makes a comparison with the tris(ethylenediamine) system possible. This assumption, which is necessary, not in order to characterize all the $(Co\ pn_3]^{3+}$-isomers as lel_iob_j but in order to give these symbols their literal meaning, implies that the enthalpy-like concepts $\Delta H'^{\circ}$ of the pair relationship model really refer to such pair relationship changes. Therefore this model can be applied to the tris(ethylenediamine) system as well, this system being governed by the same statistical factors as the tris(propanediamine) system as far as lel_iob_j isomers are concerned (*cf.* section 2). Using the data from eqns. (15) and (17) one calculates the equilibrium ratios

$$lel_3{:}lel_2ob{:}ob_2lel{:}ob_3 = 34.9{:}41.1{:}20.0{:}4.0 \quad (20)$$

applicable at 100°C. A different way of evaluating the pair relationship model, which is a two parameter model, is to compare the results of eqn. (20) with the experimental results in column 1 of Table 1, which contain three independent experimental quantities.

The data of eqn. (11) can also be used with the pair relationship model, and give the equilibrium ratios

$$lel_3{:}lel_2ob{:}ob_2lel{:}ob_3 = 40.4{:}40.4{:}16.4{:}2.7 \quad (21)$$

applicable at 25°C.

If one assumes that both the steric interactions involving the equatorial methyl groups and the interactions with the solvent do not influence the relative stability of the lel_iob_j isomers then the results expressed in eqns. (20) and (21) are applicable also to the tris-(ethylenediamine)cobalt(III) system. In this case, however, the ratios will refer to the different lel_iob_j isomers, which for a given configuration about the cobalt ion exist together in equilibrium. These possible consequences of the experimental equilibrium results for the $[Co(\pm)pn_3]^{3+}$ system on the conformational equilibria of $[Co\ en_3]^{3+}$ have previously been discussed by Hawkins.[29]

The data of eqns. (20) and (21), when used for the $[Co\ en_3]^{3+}$ system, agrees well with

some recent NMR data.[30,31] The NMR data allow the determination of the mol fraction of the diamine which exist as lel in the solution. This quantity may be calculated from eqns. (20) and (21) as 0.69, valid at 100°C, and 0.73, valid at 25°C, to be compared with the experimental quantities, 0.79 ± 0.03, valid at 93°C and 0.75 ± 0.07, valid at 17°C. For the $[Rh\ en_3]^{3+}$ system the NMR values are 0.71 ± 0.02 at 93°C and 0.68 ± 0.05 at 17°C. Our calculated values for the mol fraction of the lel decreases with increasing temperature as a consequence of the fact that all reactions involving an increase in lel conformers have negative $\Delta H°$ values [*cf.* eqns. (10), (12), and (14)].

5. THE IDENTIFICATION OF THE ISOMERS

Till now we have assumed that the isomers were already identified. They were in fact identified mainly on the basis of the equilibrium experiments as we shall now see.

The complexity of each of the isomers of $[Co(\pm)pn_3]^{3+}$ can be described by the constant

$$\beta_3 = \frac{[Co\ pn_3]^{3+}}{[Co^{3+}][pn]^3} \tag{22}$$

which is of almost the same magnitude as β_3 for $[Co\ en_3]^{3+}$, *i.e.*[32] about 10^{50} mol^{-3} l^3. The constants of eqn. (22) may be classified according to lel_iob_j

$$\begin{aligned}
\beta_3(lel_3) &= \frac{[\Delta lel_3]}{[Co^{3+}][(-)pn]^3} = \frac{[\Lambda lel_3]}{[Co^{3+}][(+)pn]^3} \\
\beta_3(lel_2ob) &= \frac{[\Delta lel_2ob]}{[Co^{3+}][(-)pn]^2[(+)pn]} = \frac{[\Lambda lel_2ob]}{[Co^{3+}][(+)pn]^2[(-)pn]} \\
\beta_3(ob_2lel) &= \frac{[\Delta ob_2lel]}{[Co^{3+}][(+)pn]^2[(-)pn]} = \frac{[\Lambda ob_2lel]}{[Co^{3+}][(-)pn]^2[(+)pn]} \\
\beta_3(ob_3) &= \frac{[\Delta ob_3]}{[Co^{3+}][(+)pn]^3} = \frac{[\Lambda ob_3]}{[Co^{3+}][(-)pn]^3}
\end{aligned} \tag{23}$$

where, as in eqn. (7), the $[lel_iob_j]$ symbols embrace all possible methyl group isomers.

From eqn. (23) [see also eqn. (7)] the following relationships can be derived

$$\frac{[\Delta lel_3]}{[\Lambda ob_3]} = \frac{[\Lambda lel_3]}{[\Delta ob_3]} = \frac{[lel_3]}{[ob_3]} = \frac{\beta_3(lel_3)}{\beta_3(ob_3)} = K(ob_3 \rightarrow lel_3) \tag{24}$$

$$\frac{[\Delta lel_2ob]}{[\Lambda ob_2lel]} = \frac{[\Lambda lel_2ob]}{[\Delta ob_2lel]} = \frac{[lel_2ob]}{[ob_2lel]} = \frac{\beta_3(lel_2ob)}{\beta_3(ob_2lel)} = K(ob_2lel \rightarrow lel_2ob)$$

Those isomer ratios, not occurring in eqn. (24), depend on the ratio F between the (+) and the (−) propanediamine

$$F = [(+)pn]/[(-)pn] \tag{25}$$

For example,

$$\begin{aligned}
\frac{[\Delta lel_3]}{[\Lambda lel_2ob]} &= \frac{\beta_3(lel_3)}{\beta_3(lel_2ob)} \frac{[(-)pn]^2}{[(+)pn]^2} = K(lel_2ob \rightarrow lel_3)F^{-2} \\
\frac{[\Lambda lel_3]}{[\Delta lel_2ob]} &= \frac{\beta_3(lel_3)}{\beta_3(lel_2ob)} \frac{[(+)pn]^2}{[(-)pn]^2} = K(lel_2ob \rightarrow lel_3)F^2
\end{aligned} \tag{26}$$

where for $F = 1$ the two equations of eqn. (26) may be combined to yield

$$\frac{[\Delta lel_3] + [\Lambda lel_3]}{[\Lambda lel_2ob] + [\Delta lel_2ob]} = \frac{[lel_3]}{[lel_2ob]} = K(lel_2ob \rightarrow lel_3) \tag{27}$$

which is the last equation of eqn. (7), valid only for experiments with racemic diamine, whereas eqn. (24), which corresponds to the two first equations of eqn. (7), is valid independently of F.

Further, equilibrium concentration ratios for catoptromers depend on F only

$$\begin{aligned}
\frac{[\Delta lel_3]}{[\Lambda lel_3]} &= \frac{[\Lambda ob_3]}{[\Delta ob_3]} = F^{-3} \\
\frac{[\Delta lel_2ob]}{[\Lambda lel_2ob]} &= \frac{[\Lambda ob_2lel]}{[\Delta ob_2lel]} = F^{-1}
\end{aligned} \tag{28}$$

Finally, it is noted that the ratios between the eight lel_iob_j isomers depend only on the three constants of eqn. (7), which were determined using racemic diamine, and the ratio F which can be fixed experimentally (Table 1).

The relative concentrations of the methyl isomers do not possess any mass action dependence and will within each lel_iob_j be constants for a given temperature in a given medium. It is the fact that we do find a mass action dependence in agreement with eqn. (23) and

Table 2. Spectral data of Δ[Co pn_3]Cl_3. The measurements were carried out on Δlel_3, Δlel_2ob, Δob_2lel, and Δob_3 in concentrations as stated in the legend to Fig. 4. The molar decadic extinction coefficient, ε, is given for the maxima of the ABS-spectra and correspondingly $\Delta\varepsilon = \varepsilon_l - \varepsilon_r$ is given for the extrema of the CD-spectra.

Δlel_3		Δlel_2ob		Δob_2lel		Δob_3	
ABS kK (ε)	CD kK ($\Delta\varepsilon$)	ABS kK (ε)	CD kK ($\Delta\varepsilon$)	ABS kK (ε)	CD kK ($\Delta\varepsilon$)	ABS kK (ε)	CD kK ($\Delta\varepsilon$)
21.39(100.5)	20.3(−2.66)	21.35(94.6)	20.4(−2.25)	21.33(89.1)	20.7(−2.34)	21.37(90.2)	21.1(−2.49)
	22.8(+0.65)		23.6(+0.05)		25.5(−0.05)		26.0(−0.06)
29.41(96.0)	29.0(−0.35)	29.40(88.9)	28.4(−0.25)	29.41(81.9)	27.8(−0.15)	29.49(80.4)	27.1(−0.07)
							29.4(+0.04)
							31.6(−0.04)
					36 (0)		34.7(−0.01)
					38.4(−0.1)		41.5(−1.7)
47.5(24.7 × 10^3)	46.7(+39)	47.4(26.3 × 10^3)	47.2(+32)	47.2(27.3 × 10^3)	47.2(+28)	47.0(21.4 × 10^3)	47.4(+21)

the derived eqns. (24), (26), (27), and (28) [Table 1], which shows that the lel_iob_j classification is the correct one for characterizing the chromatographically separated fractions.

Regarding the experimental identification of the lel_iob_j isomers the following can be said. The set of isomers, lel_3 and ob_3, can be recognized by their CD spectra as the same isomers which arise as the only isomers when a pure catoptromer of the amine is used for the experiments [see also eqn. (23)]. Further, within this set the lel_3 isomer is here known from the X-ray structure analysis [33,34] on *fac*-$\Lambda(-)_{589}$[Co{(*R*)(−)pn}$_3\lambda\lambda\lambda$]Br_3 and for that matter the ob_3 isomer is also known [18] from *fac*-$\Lambda(-)_{589}$-[Co{(*S*)(+)pn}$_3\delta\delta\delta$]$Co(CN)_6.3H_2O$ but this is a superfluous piece of information from the present point of view. Thus these identifications mean that the lel_3 isomers pass through the column with phosphate first, then comes the set of isomers lel_2ob, ob_2lel in two separate fractions and finally the ob_3 isomers.

The assumption that the second fraction is lel_2ob and the third one is ob_2lel leads to the whole discussion of section 4. It should, however, be noted that equilibrium experiments by themselves do not distinguish between isomers which contain the same ratio of the catoptric forms of diamine bound in them. For example, the mass action behaviour of Λlel_2ob is the same as that of Λob_2lel. On the other hand the assumption that the second fraction is ob_2lel and the third accordingly lel_2ob leads to a complete breakdown of the pair relationship model discussed in section 4c. This is most easily seen by studying the effect that the assumption has on the form of eqns. (15) and (16). Eqn. (15) is derived from the first equation of eqn. (10) and remains unchanged. Eqn. (16) is derived from the second equation of eqn. (10), which now reads

$$\Delta H'^{\circ}(ob_2lel \rightarrow lel_2ob) = +2.56 \text{ kJ} \quad (29)$$

leading to a changed version of eqn. (16)

$$\Delta H'^{\circ}(ob\text{-}ob \rightarrow lel\text{-}lel) = +2.56 \text{ kJ} \quad (30)$$

Even though a quantitatively working additivity model for pair interaction energies could not be expected, it is absurd to make an assumption which does not associate the relative energies of the lel_iob_j isomers with pair relationships at all. We therefore conclude that our first assumption, that lel_2ob precedes ob_2lel on the column is correct. It turns out that a series of other properties of the isomers also exhibit a regular behaviour only on this assumption.

It is natural to add here that the lel_iob_j isomers were correctly identified in the original work on their separation,[3] the assignments being based upon some of the properties to be described below.

6. PROPERTIES OF THE ISOMERS

Absorption (ABS) and circular dichroism (CD) spectra were recorded in the visible (VIS) and ultraviolet (UV) region. Fig. 4 and Table 2. The four lel_iob_j types of isomers were measured under identical conditions in a medium containing lithium chloride. The only effect of the lithium chloride on the spectra is to enhance the extinctions slightly without shifting the absorption frequences. It is seen that the net rotational strength under the first cubic spin-allowed absorption band $^1A_1(O) \rightarrow {}^1T_1(O)$ at 21 − 22 kK is negative for the Δ series. Also the residual wing of the transition $A_1(O)A_1(D_3) \rightarrow T_1(O)A_2(D_3)$ identified on the basis of the assignments in the tris(ethylenediamine)-cobalt(III) ion and observed at 23 kK in the lel_3 complex, gradually vanishes through the series $lel_3 \rightarrow ob_3$. An apparently opposite effect is noted in the circular dichroism under the ultraviolet absorption band.

Solubility of catoptromers. The least soluble chloride(+)-tartrate of $[Coen_3]^{3+}$, $[Copn_3; lel_3]^{3+}$, and $[Copn_3; ob_3]^{3+}$ are known from the X-ray results [24] to be the Λ forms. The catoptromer, which according to the previous investigation gives the least soluble chloride (+)-tartrate in the lel_2ob set, is also Λ. It must be noted, however, that the ob_2lel set has not been resolved in this way, but only on the column.

Outer sphere complexes. Recent investigations [35] show that the association constant K of the pair $[Co\ pn_3; lel_3]^{3+}SO_4^{2-}$ is greater than that of $[Co\ pn_3; ob_3]^{3+}SO_4^{2-}$. Our experiments on the elution of these complexes from the Sephadex cation exchange column show that, even though the cation of course is the im-

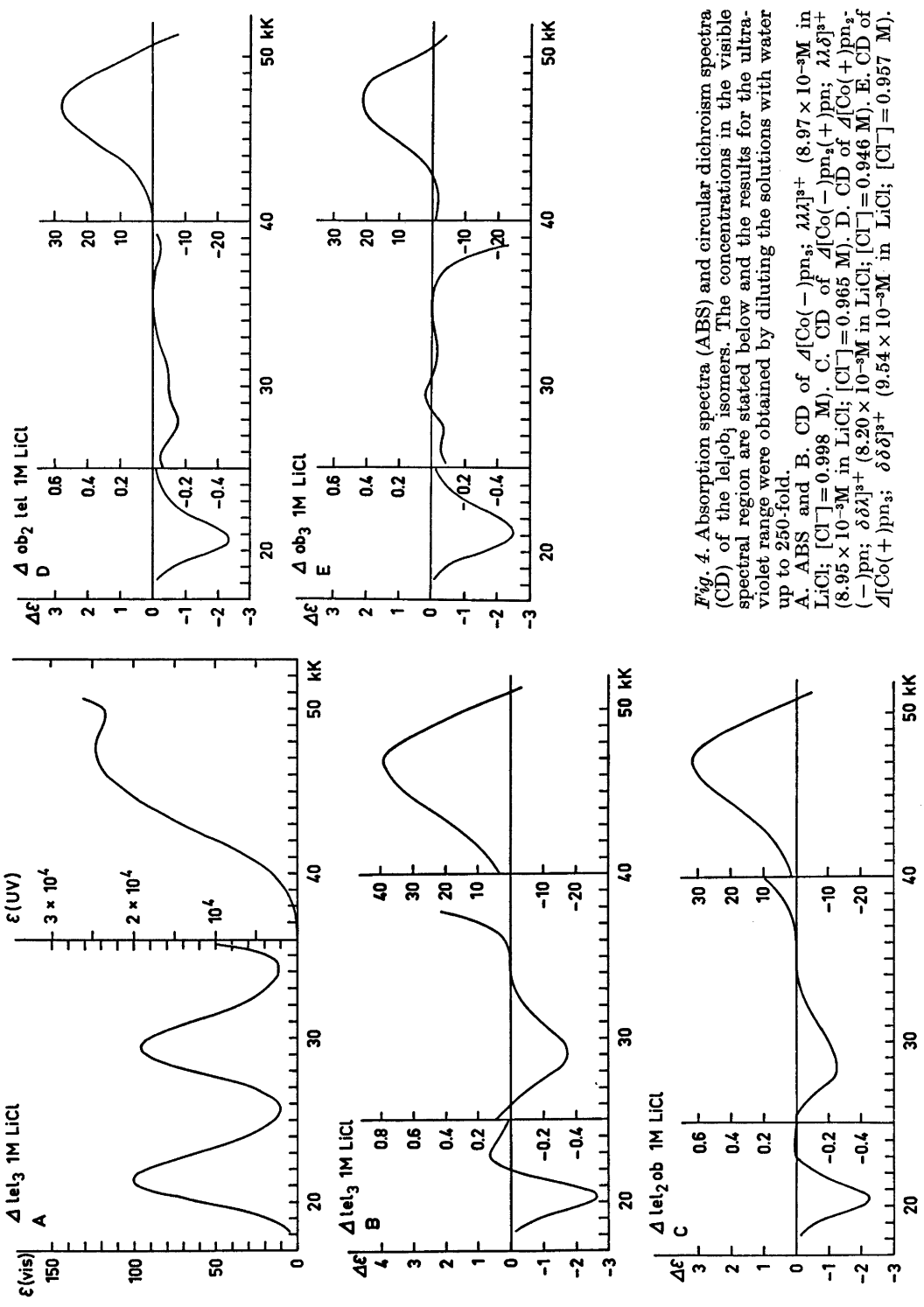

Fig. 4. Absorption spectra (ABS) and circular dichroism spectra (CD) of the lel_2ob_3 isomers. The concentrations in the visible spectral region are stated below and the results for the ultraviolet range were obtained by diluting the solutions with water up to 250-fold.
A. ABS and B. CD of Δ[Co(−)pn$_3$; $\lambda\lambda\lambda$]$^{3+}$ (8.97×10^{-3}M in LiCl; [Cl$^-$] = 0.998 M). C. CD of Δ[Co(−)pn$_2$(+)pn; $\lambda\lambda\delta$]$^{3+}$ (8.95×10^{-3}M in LiCl; [Cl$^-$] = 0.965 M). D. CD of Δ[Co(+)pn$_2$(−)pn; $\delta\delta\lambda$]$^{3+}$ (8.20×10^{-3}M in LiCl; [Cl$^-$] = 0.946 M). E. CD of Δ[Co(+)pn$_3$; $\delta\delta\delta$]$^{3+}$ (9.54×10^{-3}M in LiCl; [Cl$^-$] = 0.957 M).

portant one for driving the complexes through, the relative elution rates depend predominantly on the anion, and using phosphate the order of elution is lel_3, lel_2ob, ob_2lel, ob_3. It seems likely that lel conformations somehow have a greater affinity to phosphate than do ob conformations in agreement with the facts mentioned for sulphate. This is also supported experimentally through the NMR results [30,31] on the tris(ethylenediamine) systems of rhodium(III) and cobalt(III), which show that the equilibrium between the lel_iob_j isomers, which is mobile in the ethylenediamine as opposed to the propanediamine systems, shifts toward a higher mol fraction of lel on increasing the phosphate concentration. It has similarly been found [35] that $K(\Lambda[Co\ pn_3;\ lel_3]^{3+}(+)\text{-tart}) > K(\Delta[Co\ pn_3;\ lel_3]^{3+}(+)\text{tart})$ and that $K(\Lambda[Co\ pn_3;\ ob_3]^{3+}(+)\text{tart}) > K(\Delta[Co\ pn_3;\ ob_3]^{3+}(+)\text{tart})$. Our experiments on the elution of the catoptromers from the Sephadex cation exchange column using (+)-tartrate also agrees with these association constants since it is a general feature that the Λ configurations are eluted first.

7. CONCLUSIONS

The isomers in the $[Co(\pm)pn_3]^{3+}$ system have almost the same standard free energies in solution, the difference between the most and the least abundant ones being at 100°C only about 7 kJ/mol which is of the order of magnitude of small van der Waals energies. The same is true of their enthalpy differences. This is in itself understandable since all the truly chemical bonds are the same in all the isomers and no apparent steric hindrances exist when the methyl groups of the coordinated propanediamine molecules are equatorial. However, the relative free energies, as well as enthalpies, vary with the lel_iob_j-classified isomers in a remarkably regular manner in view of the fact that the solvation processes are involved here as well.

It should be noted that similar regularities also have been found with the mixed tris-diamine cobalt(III) system containing ethylenediamine and (−)-propanediamine [2] and also with the tris-[(±)-*trans*-1,2-cyclohexanediamine]cobalt(III) system [18] and the tris(propanediamine)chromium(III) system.[36]

The absolute configuration of the complexes determines the net rotational strength of the magnetically allowed cubic parentage [4] transition $^1A_1(O) \rightarrow {}^1T_1(O)$, the strength being positive for all Λ isomers, in agreement with the results for the tris(ethylenediamine)-cobalt(III) system and the tris[(±)-*trans*-1,2-cyclohexanediamine]-cobalt(III) systems. In a perturbation model this net rotational strength corresponds to the effect of the term of $A_{1u}(O_h)$ symmetry [4] in a potential expansion and the sign of the net rotational strength to the sign of this term.

The sign of the net rotational strength of the ultraviolet band around 47 kK also depends on the absolute configuration, being positive for the Δ isomers. The $\Delta\varepsilon$ values at the main extremum points can in fact be given within the experimental uncertainty by adding a configurational contribution $(\Delta\varepsilon)_\Delta = +30$ and a conformational contribution $(\Delta\varepsilon)_\lambda = +3$ where the contributions from the catoptromeric situations, of course, have opposite signs. Such an additivity rule has been reported previously [37] but with different numerical values. The present investigation, however, has shown that the circular dichroism spectra of the optically active ob_3-isomer are in fact different from the previously published data. It is noted that the additivity rule does not apply quite so well to the net rotational strengths.

REFERENCES

1. Dwyer, F. P., Garvan, F. L. and Shulman, A. *J. Amer. Chem. Soc. 81* (1959) 290.
2. Dwyer, F. P., MacDermott, T. E. and Sargeson, A. M. *J. Amer. Chem. Soc. 85* (1963) 2913.
3. Dwyer, F. P., Sargeson, A. M. and James, L. B. *J. Amer. Chem. Soc. 86* (1964) 590.
4. Schäffer, C. E. *Proc. Roy. Soc. (London) A 297* (1967) 96.
5. Corey, E. J. and Bailar, J. C. *J. Amer. Chem. Soc. 81* (1959) 2620.
6. Sargeson, A. M. In Carlin, R. L., Ed., *Transition Metal Chemistry*, Dekker, New York 1966, Vol. 3, p. 303.
7. Buckingham, D. K. and Sargeson, A. M. *Conformational Analysis and Steric Effects in Metal Chelates*. In Allinger, N. L. and Eliel, E. L., Eds., *Topics in Stereochemistry*, Wiley-Interscience, New York 1971, Vol. 6, p. 219.
8. Gainsford, G. *Unpublished work.*

9. Andersen, P., Galsbøl, F. and Harnung, S. E. *Acta Chem. Scand. 23* (1969) 3027.
10. Thewalt, U., Jensen, K. A. and Schäffer, C. E. *Inorg. Chem. 11* (1972) 2129.
11. *IUPAC, Information Bulletin No. 33*, Zürich 1968; *Inorg. Chem. 9* (1970) 1.
12. *IUPAC, Nomenclature of Inorganic Chemistry 2nd Ed.*, Butterworths, London 1971, p. 75.
13. Piper, T. S. *J. Amer. Chem. Soc. 83* (1961) 3908.
14. Liehr, A. D. *J. Phys. Chem. 68* (1964) 3629.
15. *IUPAC, Information Bulletin No. 35*, Zürich 1969.
16. Cahn, R. S. and Ingold, C. K. *J. Chem. Soc.* (1955) 612.
17. Harnung, S. E. and Laier, T. *To be published.*
18. Harnung, S. E., Sørensen, B. S., Creaser (nee Olsen) I., Maegaard, H., Pfenninger, U. and Schäffer, C. E. *To be published.*
19. Galsbøl, F., Steenbøl, P. and Sørensen, B. S. *Acta Chem. Scand. 26* (1972) 3605.
20. Galsbøl, F. *To be published.*
21. Raymond, K. N., Corfield P. W. R. and Ibers, J. A. *Inorg. Chem. 7* (1968) 842.
22. Yoshikawa, Y. and Yamasaki, K. *Inorg. Nucl. Chem. Lett. 6* (1970) 523.
23. Toftlund, H. and Pedersen, E. *Acta Chem. Scand. 26* (1972) 4019.
24. Saito, Y. *Pure Appl. Chem. 17* (1968) 21.
25. MacDermott, T. E. *Inorg. Chim. Acta 2* (1968) 81.
26. Craighead, K. L. *J. Amer. Chem. Soc. 95* (1973) 4434.
27. Kojima, M., Yoshikawa Y. and Yamasaki, K. *Inorg. Nucl. Chem. Lett. 9* (1973) 689.
28. MacDermott, T. E. *Thesis*, Australian National University, Canberra 1961.
29. Hawkins, C. J. *Absolute Configuration of Metal Complexes*, Wiley-Interscience, New York 1971, p. 105.
30. Sudmeier, J. L., Blackmer, G. L., Bradley, C. H. and Anet, F. A. L. *J. Amer. Chem. Soc. 94* (1972) 757.
31. Sudmeier, J. L. and Blackmer, G. L. *Inorg. Chem. 10* (1971) 2010.
32. Bjerrum. J. *Metal Ammine Formation in Aqueous Solution*, P. Haase and Son, Copenhagen 1941.
33. Saito, Y., Iwasaki, H. and Ota, H. *Bull. Chem. Soc. Jap. 36* (1963) 1543.
34. Iwasaki, H. and Saito, Y. *Bull. Chem. Soc. Jap. 39* (1966) 92.
35. Ogino, K. *Bull. Chem. Soc. Jap. 42* (1969) 447.
36. Andersen, P. *To be published.*
37. McCaffery, A. J., Mason, S. F., Norman, B. J. and Sargeson, A. M. *J. Chem. Soc. A* (1968) 1304.

Received January 14, 1974.

Acta Chemica Scandinavica A 28 (1974) 399—406

Aqueous Chemistry of Protactinium(IV). 2. Pa(IV) Complexes in Acetylacetone-Sulphate Media

ROBERT LUNDQVIST and JAN RYDBERG

Department of Nuclear Chemistry, Chalmers University of Technology, Fack, 402 20 Göteborg 5, Sweden

Stability and distribution constants for tetravalent protactinium acetylacetone and sulphate complexes were obtained from liquid-liquid distribution measurements of Pa(IV) between acetylacetone (HAA) in C_6H_6 and 0.94 M $(Na,H)ClO_4$ + 0.06 M Na_2SO_4 at 25°C. The constants $\beta_n' = [Pa(OH)(AA)_n^{3-n}][SO_4^{2-}]/[Pa(OH)SO_4^+][AA^-]^n$, and $\lambda_3 = [Pa(OH)(AA)_3]_{org}/[Pa(OH)(AA)_3]$ were calculated to be $\log \beta_2' = 12.3 \pm 0.1$, $\log \beta_3' = 18.34 \pm 0.10$, and $\log \lambda_3 = 2.54 \pm 0.06$.

The addition of sulphate to the extraction system $Pa(IV) - (Na,H)ClO_4 - HAA - C_6H_6$ changed the extraction mechanism from $M^{4+} + 2HAA(org) \rightleftharpoons M(AA)_2(org) + 2H^+$ (where $M = Pa(OH)_2^{2+}$ or PaO^{2+}) to $Pa(OH)SO_4^+ + 3HAA(org) \rightleftharpoons Pa(OH)(AA)_3(org) + 3H^+ + SO_4^{2-}$. The equilibrium constant for the latter reaction was calculated to be $\log K_D = -8.17 \pm 0.06$ with $\Delta H° = 14 \pm 3$ kJ/mol and $\Delta S° = -110 \pm 11$ J/(mol K).

The distribution of Pa(IV) between 1 M $(Na,H)ClO_4$ and benzene in the presence of acetylacetone showed that Pa(IV) is complexed and extracted as a divalent cation.[1] In order to examine this species, assumed to be PaO^{2+} or $Pa(OH)_2^{2+}$, further, the system was investigated in an aqueous sulphate medium. Mitsuji [2] has found a 1:1 $Pa(IV) - HSO_4^-$ complex with sulphate in 0.5 M $(Na,H)ClO_4$ at pH 0.4 − 1.1, and suggested the reaction $Pa(OH)_2^{2+} + HSO_4^- \rightleftharpoons Pa(OH)SO_4^+ + H_2O$. Further, the hydrolysis of Pa(IV) has been studied by a thenoyltrifluoroacetone (TTA) extraction method and the results interpreted as a stepwise formation of the hydrolyzed species $Pa(OH)^{3+}$, $Pa(OH)_2^{2+}$ (or PaO^{2+}), and $Pa(OH)_3^+$ (or $PaO(OH)^+$).[3]

THEORY

The extraction of Pa(IV) from an aqueous sulphate medium into an organic solvent in the presence of acetylacetone involves complexes of the general type $M_mL_n(OH)_pB_q(HL)_r(Org)_s(H_2O)_t$, where in our particular case M stands for Pa(IV), HL for undissociated acetylacetone, H_2B for H_2SO_4 and Org for the organic medium (benzene). Following Rydberg,[4] and neglecting solvent interaction, the general complex can be written $M(HL)_x(H)_y(B)_q$ (where $x = n + r$ and $y = n + p + 2q$), as long as only mononuclear ($m = 1$) complexes are formed.* For $x > -y$ this complex is acidic, white for $x < -y$ it is basic. To simplify our case further we may assume that only one complex is extracted, $M(HL)_a(H)_{-b}(B)_c$. Thus the distribution of tetravalent protactinium may be written

$$D_M = \frac{[M(HL)_a(H)_{-b}(B)_c]_{org}}{\sum^{x,y,q}[M(HL)_x(H)_{-y}(B)_q]} \quad (1)$$

where the organic phase is denoted by the index org, and the aqueous phase is not indexed. It is, of course, necessary to verify experimentally that the conditions for the formation of the species $M(HL)_x(H)_{-y}(B)_q$ are fulfilled. One may decide whether or not $m = 1$ by varying the metal concentration (a constant D_{Pa} implies $m = 1$). To investigate whether or not solvent interactions may be neglected, different solvents may be tried.[4,5]

We may rewrite the above equation

$$D_M = \frac{\lambda_{abc}\beta_{abc}[HL]^a[H]^{-b}[B]^c}{\sum\beta_{xyq}[HL]^x[H]^{-y}[B]^q} \quad (2)$$

* (Footnote: q is used here and not z, as z is used to denote $p+t$ in Ref. 4).

where λ_{abc} is the distribution constant of the species $M(HL)_a(H)_{-b}(B)_c$ between the two phases, and β_{xyq} is the stability constant for the formation of a particular complex. By measuring D_M as a function of each variable separately (*e.g.* D_M $([HL])_{[H],[B]}$) it should in principle be possible to determine explicity all equilibrium constants from a sufficiently large number of experimental points.[6] However, it is easier to approach the problem by the slope analysis technique,[7,8] *i.e.* to determine which of the coefficients a, b, c, x, y, and q have to be considered.

The slope analysis technique involves the determination of the partial derivatives of eqn. 2 at constant (HL], [B], and [H]. If the aqueous phase is assumed to contain a complex with the average composition $M(HL)_{\bar{x}}(H)_{-\bar{y}}(B)_{\bar{q}}$, then the partial derivatives are:

$$\delta \log D_M([HL])_{[H],[B]} = (a - \bar{x})\delta \log [HL] \quad (3a)$$

$$\delta \log D_M([H])_{[HL],[B]} = -(b - \bar{y})\delta \log [H] \quad (3b)$$

$$\delta \log D_M([B])_{[HL],[H]} = (c - \bar{q})\delta \log [B] \quad (3c)$$

Thus slope analysis gives only the difference between the number of ligands bound to the metal atom in the organic phase and the corresponding average number for the aqueous phase. To determine the composition of the species, other information and criteria are therefore required, for example the charge on the metal atom, the fact that only uncharged species dissolve in the organic phase, and the fact that acid and basic ligands may not at the same time occur in the metal complex (such an assumption is of course not valid for very stable basic entities such as UO_2^{2+} in the complex $UO_2AA_2(HAA)$). Such criteria, which limit the number of possible species, depend on the particular chemical system.

In the absence of the second complex former B, the composite complex is reduced to $M(HL)_x(H)_{-y}$ (or $ML_n(OH)_p(HL)_r$). From a plot of log D_M $([H])_{[HL]}$ it is rather easy to get qualitative information about the species formed.[4,9] This is helpful for estimating values for the coefficients x and y. This approach will also be applied in this paper.

With the coefficients in eqn. 2 known, the equilibrium constants λ_{abc} and β_{xyq} may be calculated. If a large number of complexes are formed, such a calculation becomes rather complicated, particularly by graphical methods (*cf.* Ref. 6). We have therefore transformed eqn. 2 into a set of linear equations and solved it explicitly for the coefficients, according to Sullivan, Rydberg and Miller.[10] This provides the coefficients with their standard deviations.

EXPERIMENTAL

The distribution experiments were carried out in a 50 ml glass vessel. The vessel was closed with a tight lid and an oxygen-free atmosphere was maintained with a slow flow of nitrogen. The apparatus was equipped with a magnetic stirrer and thermostated ($\pm 0.05°$) with a stream of water through the mantle of the vessel. Equal volumes (15 ml) of (0.1 H, 0.9 Na)ClO_4 and acetylacetone in benzene were added and the system was prepared for reduction, either electrolytically or with chromous ions.

The electrolytic reduction was carried out, after addition of ^{233}Pa, by electrolysis between a mercury cathode and a platinum anode. The anode compartment was separated from the bulk solution by an almost tight glass fritt. The electrolysis was performed for 1 – 10 h at 10 – 50 mA (10 – 30 V) until the p*h* (p*h* = $-\log[H^+]$) reached about 8.5. After complete reduction, which was obtained for p*h* higher than 7, 1 ml 1 M Na_2SO_4 was added. The p*h* was then decreased with 1 M $HClO_4$ and the system equilibrated by stirring for about 20 – 40 min.

For reducing Pa(V) to Pa(IV) with chromous ions, 3 – 6 ml liquid amalgamated zinc (2 %, by weight, Zn in Hg) and 0.1 ml 1.92 M $Cr(ClO_4)_3$ were added. The green Cr(III) ions were reduced to blue Cr(II) ions before addition of ^{233}Pa and 0.005 – 2 ml 1 M Na_2SO_4, because it was observed to be relatively difficult to reduce (10^{-2} M) Cr(III) in the presence of sulphate. It was unessential whether the sulphate was added prior to or after the addition of the organic phase. The p*h* was adjusted with 1 M NaOH, 0.1 M NaOH + 0.9 M $NaClO_4$ or 1 M (H,Na)ClO_4 and additional acetylacetone was added as required. Distribution equilibrium was reached withiu 10 min of stirring.

In order to investigate the distribution of Pa(IV) at higher sulphate concentrations, experiments were performed with aqueous phase of 0.308 M Na_2SO_4 and 0.005 M $Cr_2(SO_4)_3$. These sulphate phases of unit ionic strength were reduced electrolytically at p*h* 2.36.

In order to measure the distribution of Pa(IV), equal samples (1.31 ± 0.005 ml) were taken from each phase with disposable glass pipettes. The pipettes were crushed in 20 ml glass tubes and the activity from ^{233}Pa was measured with a NaI(Tl) crystal. Only the complex 80 – 110 keV gamma peaks of ^{233}Pa were measured; the total efficiency was calculated to be 24 % using a $^{237}Np - ^{233}Pa$ standard.

The total counts measured for both phases were around 200 000. More than 2000 disintegrations were measured from the least active phase, which was at least twice as active as the background. Thus the radiometric accuracy in D was better than 3 %, so that the logarithm of the distribution factor D_{Pa} has a radiometric spread of ± 0.01. The ph was calculated from the measured EMF of a glass calomel electrode pair with the KCl replaced by 1 M $NaClO_4$. The accuracy of the ph measurements was ± 0.01 ph units. The hydrogen ion activity (pH) in the sulphate phases (0.308 M $Na_2SO_4 + 0.005$ M $Cr_2(SO_4)_3$) was measured with an ordinary glass calomel electrode combination, which was calibrated with standard pH buffer solutions. The acetylacetone concentration was checked by spectrophotometric determination of the absorbance at 490 nm of the Fe(III) acetylacetone complex and was found to agree, within the accuracy (± 2 %) of the method, with the added concentration. One or two drops of the stock solution of ^{233}Pa in 7 M $HClO_4$ were normally added to the system giving a protactinium concentration of $10^{-10.4 \pm 0.2}$ M. The absorption of protactinium on the glass walls of the vessel was low as long as Pa was in the tetravalent state; moreover it was found that desorbed protactinium (that had been absorbed during previous experiments) gave the same distribution values as "fresh" protactinium. This is very different from the behaviour of Pa(V) (*cf.*, *e.g.* Ref. 11). About 5 equilibrium points were determined during each distribution run, after which the vessel was washed with sulphuric acid containing potassium dichromate.

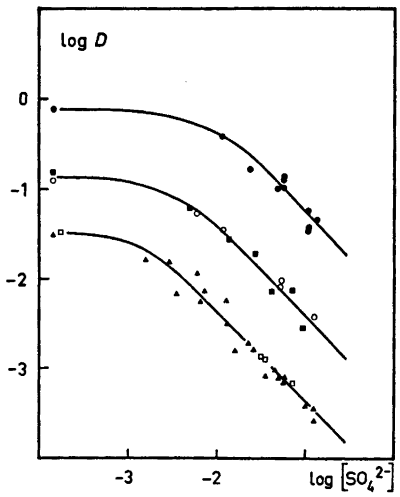

Fig. 1. Distribution of $^{233}Pa(IV)$ between benzene and 1 M $(Na,H)ClO_4$ (at 25°C) as a function of the sulphate concentration, at different ph and initial acetylacetone (C_{AA}) concentrations in the organic phase. (The sulphate concentration was calculated using $K_{HSO_4} = 10$.)

	$[C_{AA}]$	ph	pAA
●	0.50 M	2.40	7.66
○	0.50 M	2.00	8.06
■	2.50 M	1.40	7.96
□	2.50 M	1.00	8.36
▲	0.10 M	2.39	8.37

EXTRACTION WITH ACETYLACETONE IN THE PRESENCE OF SULPHATE

The distribution of Pa(IV) ($D = [Pa(IV)]_{org}/[Pa(IV)]$ between 1 M $(Na,H)ClO_4$ and benzene was studied as a function of the sulphate, the hydrogen ion and the acetylacetone (HAA) concentration, and of the temperature, see Figs. 1 – 5.

The protactinium was kept in its tetravalent state either by 10^{-2} M Cr^{2+} ions at ph 1 – 3, or by electrolytic reduction at ph 2 – 9. Reduction with Cr^{2+} was not possible at ph higher than 3 because of the formation of extractable Cr(III) acetylacetone complexes.

The size of the dots in the figures corresponds approximately to the uncertainties in the measured values.

The distribution experiments were made at different trace concentrations of ^{233}Pa ($10^{-10} - 10^{-11}$ M). No [Pa]-dependence was found, indicating that only mononuclear protactinium complexes were formed.

The sulphate dependence was investigated at different ph and acetylacetone concentrations, see Fig. 1. The concentration of free SO_4^{2-} was calculated from the relations $K_B = [HSO_4^-][H^+]^{-1}[SO_4^{2-}]^{-1}$ and $[SO_4^{2-}] = C_B/(1 + [H^+]K_B)$ where C_B is the total amount of SO_4 present (as added). The dissociation of HSO_4 at unit ionic strength, at 25°C, depends upon the ionic medium. The stability constant K_B is $10^{0.50}$ in H_2SO_4 media,[12] $10^{0.76}$ for mixtures[13] of $NaClO_4$, $HClO_4$ and Na_2SO_4, and $10^{1.02}$ for (0.01 H, 0.99 Na)ClO_4.[14] At p$h \gtrsim 1$ the amount of free H_2SO_4 can be neglected, and in the presence of trace concentrations of Pa the amount of SO_4 complexed by Pa can also be neglected. The dominating sulphate species for p$h > 1.4$ – *i.e.* over almost the entire ph range investigated – was SO_4^{2-}.

The acetylacetone dependence was in-

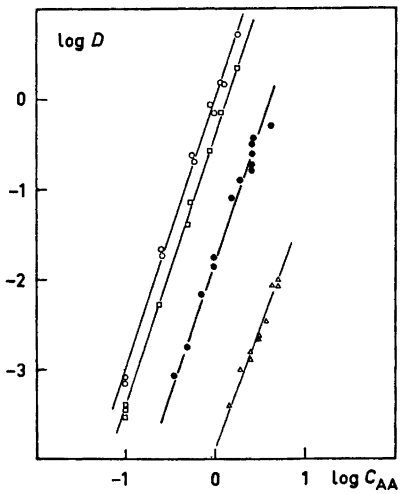

Fig. 2. Distribution of ^{233}Pa(IV) as a function of initial concentration of acetylacetone in the organic phase C_{AA}, at 25°C, for different p*h* and sulphate concentrations. Unfilled symbols denote aqueous phases of $(1-x)$(Na,H)ClO_4 + xNa_2SO_4, and filled symbols denote 0.308 Na_2SO_4 + 0.005 $Cr_2(SO_4)_3$.

○ p*h* 2.39 $x=0.057$
□ p*h* 2.40 $x=0.080$
△ p*h* 1.00 $x=0.059$
● pH 1.36

vestigated at p*h* 1 and 2.4 by varying the initial concentration of acetylacetone in the organic phase between 0.1 and 5 M, see Fig. 2. The dependence of log D_{Pa} on the hydrogen ion concentration at constant Na_2SO_4 concentration is shown in Fig. 3 for different acetylacetone concentrations.

In order to evaluate the extraction mechanism, all data may be put on a common footing by plotting the logarithm of the distribution of Pa(IV) as a function of the aqueous acetylacetone anion concentration [AA^-], see Fig. 4. It is easily shown that for equal phase volumes

$$pAA = -\log [AA^-] = pK_a - ph + \log (K_d + 1 + K_a[H^+]^{-1}) - \log C_{AA}$$

where K_a is the acid dissociation constant, K_d the distribution constant for acetylacetone and C_{AA} is the initial concentration of HAA in the organic phase.

The following constants were used: $pK_a = 9.3027 - 0.01228T$°C [15] and $k_d = 4.80 \pm 0.02$.[16]

The influence of the temperature on the distribution of Pa(IV) was studied by changing

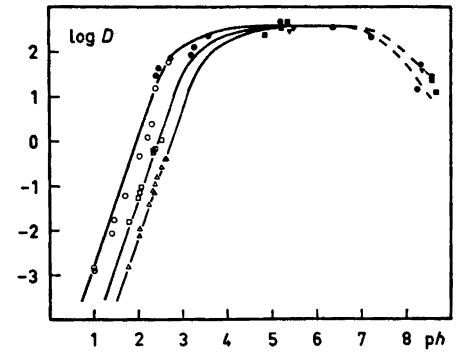

Fig. 3. Distribution of ^{233}Pa(IV) between benzene and 0.937 M (Na,H)ClO_4 + 0.063 M Na_2SO_4 (at 25°C) as a function of p*h*, at different initial acetylacetone C_{AA} concentrations in the organic phase. Filled symbols denote electrolytic reduction and unfilled symbols reduction with Cr^{2+}.

C_{AA}
○ ● 2.50 M
□ ■ 1.00 M
△ ▲ 0.50 M
▼ 0.39 M

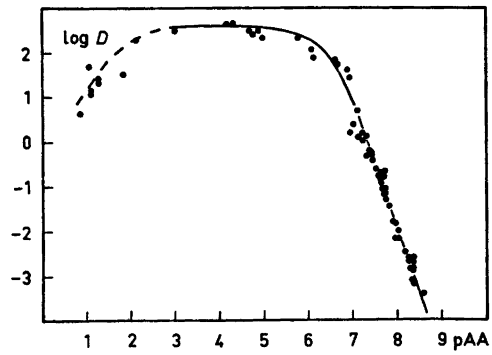

Fig. 4. Distribution of ^{233}Pa(IV) between benzene and 0.941 M (Na,H)ClO_4 + 0.059 M Na_2SO_4 (at 25°C) as a function of pAA (= −log [AA^-]). The solid curve is calculated from estimated stability constants.

the temperature (3 − 48°C) at constant acetylacetone ($C_{AA}=1$ M), sulphate (0.06 M) and hydrogen ion (p*h* 2.01) concentrations, see Fig. 5. The glass electrode combination used to measure the p*h* was pre-calibrated in the proper temperature range. The extraction was carried out with both increasing and decreasing temperature. Some primary experimental data are collected in Table 1.

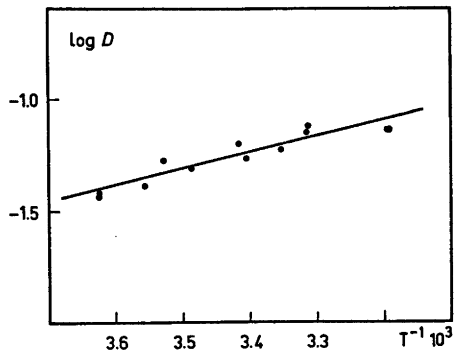

Fig. 5. Distribution of ^{233}Pa(IV) between 1 M acetylacetone in benzene and 0.944 M (Na,H)-ClO_4 + 0.056 M Na_2SO_4, at ph 2.01, as a function of the temperature 3 – 48°C (T = 276 – 321 K).

DERIVATION OF COMPLEXES

The plots of log $D_{Pa}([SO_4])_{[HAA],[H]}$ (Fig. 1), log $D_{Pa}(C_{AA})_{[H][SO_4]}$ (Fig. 2), and log $D_{Pa}([H])_{[HAA],[SO_4]}$ (Fig. 3) show that the formation of complexes of the type $Pa(HAA)_x(H)_{-y}(SO_4)_q$ is to be expected.

In Fig. 1 the gradient of the curves $D_{Pa}([SO_4^{2-}])$ change from zero to -1 with increasing sulphate concentration. In the horizontal part D_{Pa} is independent of $[SO_4^{2-}]$ and thus $c = \bar{q}$, according to eqn. 3c. The simplest assumption is that both c and q are zero. If no $Pa-SO_4$-complexes are formed, only Pa – AA-complexes have to be considered; the plateau values should then vary with pAA as shown by Lundqvist [1] for the system Pa – HAA – H_2O – C_6H_6 for which the following complexes were identified: $Pa(OH)^{3+}$ (or PaO^{2+}), $Pa(OH)_2AA^+$ and $Pa(OH)_3(AA)_2$. Such dependence is in fact found.

For log $[SO_4^{2-}] \gtrsim 10^{-2}$ the slopes of the curves in Fig. 1 are again constant and equal having $c - \bar{q} = -1$. The most reasonable assumption is that $c = 0$, *i.e.* there is no sulphate complex in the organic phase, and $\bar{q} = 1$, *i.e.* one sulphate ion is attached to the aqueous central atom. Another but less likely possibility is that the metal complex in the organic phase contains one sulphate, and that in the aqueous phase two.

In Fig. 2 the slope $\delta \log D_{Pa}/\delta \log C_{AA}$ is +3. Remembering that [HAA] is a linear function of C_{AA} under our conditions, one finds from the theory that $a - \bar{x} = 3$. All lines are for constant $[SO_4^{2-}]$ and ph (p$h \leq 2.4$). The simplest explanation is that $\bar{x} = 0$ and $a = 3$, *i.e.* that under these conditions the aqueous phase contains negligible concentrations of $M(HL)_x(H)_{-y}B$-complexes, while in the organic phase $M(HL)_3(H)_{-b}$-complexes dominate.

From the plot in Fig. 3 of log $D_{Pa}([H^+])$ for various (constant) values of C_{AA} and C_{SO_4} it is seen that at p$h \lesssim 3$ different curves are obtained for different C_{AA} (and consequently different [HAA]), while at ph around 5 – 7 all lines coincide into one horizontal line (plateau). Our theory then leads us to the conclusion that at p$h \lesssim 2.4$, $\bar{y} - b = -3$ and at ph 5 – 7, $\bar{y} - b = 0$. The value of b, which must be the same in both ph-regions, is obtained from the electrostatic neutrality criterion for the extracted complex $M(HL)_3(H)_{-b}$. As the charge on M is 4+ one finds that $b = 4$. Thus for p$h \leq 2.4$, $\bar{y} = 1$ and for ph 5 – 7, $\bar{y} = 4$. The conclusions arrived at so far may be summarized as in Table 2.

To reach a conclusion concerning the nature of the species dominant at ph 5 – 7 one may consider Fig. 4, in which log D_{Pa} is plotted against pAA for various C_{AA} at constant C_B. All points seem to fall on one curve, the slope of which varies from -3 to 0 (and then assumes positive values for pAA < 3). According to the general theory for $ML_n(OH)_p(HL)_r$-complexes,[9] such a curve can only be obtained if $r = 0$ and p is constant throughout the region (of gradient -3 to 0). Consequently one is led to the conclusion that the organic phase contains only $Pa(OH)(AA)_3$, and the aqueous phase $Pa(OH)(AA)_n(SO_4)_v^{3-n-2v}$, where n varies from 0 to +3 and v has the values 0 or +1.

The only complexes required to interpret the experimental results are thus $Pa(OH)SO_4^+$ and $Pa(OH)AA_3$ but it is reasonable to assume that the intermediate complexes $Pa(OH)SO_4AA$, $Pa(OH)AA^{2+}$ and $Pa(OH)AA_2^+$ are also formed. (Though the mixed sulphate and acetylacetone complex is expected to be weak and might therefore be neglected immediately, provision for its existence is made in the calculations below.)

The decrease in log D_{Pa} at ph > 7 (Fig. 3) and at pAA < 3 (Fig. 4) indicates hydrolysis or formation of $Pa(OH)(AA)_4^{-1}$ in the aqueous phase, but the data are not conclusive.

Table 1. Experimental data for the distribution of ^{233}Pa(IV) between acetylacetone in benzene and 0.94 M (Na,H)ClO_4 + 0.06 M Na_2SO_4 at 25.0 ± 0.1°C. About 2000 disintegrations were measured from the least active phase, which was at least twice as active as the background. The total measured activity from both phases was around 200 000 disintegrations. Remarks: C = reduction with Cr^{2+}, E = electrolytic reduction, C_{AA} = initial concentration of HAA in organic phase, C_B = total concentration of sulphate and pAA = $-\log [AA^-]$.

C_{AA}	$-\log C_B$	p*h*	pAA	$\log D_{Pa}$		C_{AA}	$-\log C_B$	p*h*	pAA	$\log D_{Pa}$	
2.50	1.24	1.40	7.96	−2.14	C	0.85	1.23	4.85	4.98	2.35	E
0.10	1.25	2.39	8.37	−3.16	C	0.45	1.24	5.22	4.89	2.50	E
0.10	1.24	2.40	8.36	−3.08	C	0.39	1.21	9.48	0.87	0.63	E
0.59	1.24	2.38	7.61	−0.74	C	0.39	1.21	8.33	1.85	1.54	E
0.50	1.24	2.32	7.74	−1.12	C	0.39	1.21	5.48	4.69	2.50	E
0.50	1.23	2.42	7.64	−0.83	C	0.39	1.21	5.40	4.77	2.41	E
0.50	1.24	2.34	7.72	−1.16	C	1.16	1.21	5.36	4.33	2.68	E
2.50	1.22	1.00	8.36	−2.87	C	0.50	1.24	2.61	7.45	−0.40	C
0.50	1.24	2.02	8.04	−1.97	C	0.50	1.24	2.62	7.44	−0.40	C
0.50	1.23	2.01	8.05	−2.15	C	0.50	1.24	2.52	7.54	−0.59	C
2.50	1.22	1.46	7.90	−1.78	C	0.50	1.24	2.32	7.74	−1.12	C
2.50	1.20	2.39	6.97	0.18	C	0.50	1.23	1.76	8.30	−2.83	C
2.50	1.22	1.72	7.64	−1.20	C	0.50	1.23	2.23	7.83	−1.43	C
2.50	1.22	2.03	7.33	−0.32	C	0.50	1.23	2.42	7.64	−0.83	C
2.50	1.23	2.22	7.14	0.11	C	0.50	1.30	2.36	7.70	−1.10	C
2.50	1.23	2.33	7.03	0.42	C	2.50	1.20	8.32	1.06	1.69	E
2.50	1.22	1.00	8.36	−2.82	C	2.50	1.20	3.22	6.14	1.91	E
2.50	1.20	8.25	1.12	1.13	E	2.50	1.20	2.74	6.62	1.85	E
2.50	1.20	7.22	2.14	2.30	E	2.50	1.20	2.46	6.90	1.64	E
2.50	1.20	6.37	2.99	2.50	E	2.50	1.20	2.40	6.96	1.47	E
2.50	1.20	5.19	4.17	2.66	E	2.50	1.20	3.59	5.77	2.34	E
2.50	1.20	2.69	6.67	1.76	E	2.50	1.20	3.27	6.09	2.08	E
0.97	1.24	2.38	7.39	−0.18	C	0.54	1.24	2.37	7.66	−0.64	C
1.00	1.23	2.35	7.41	−0.21	C	0.86	1.24	2.38	7.45	−0.06	C
1.00	1.23	2.34	7.42	−0.26	C	1.18	1.24	2.37	7.32	0.16	C
1.00	1.23	2.06	7.70	−1.03	C	1.76	1.24	2.40	7.11	0.73	C
1.00	1.23	1.79	7.97	−1.81	C	0.26	1.24	2.40	7.94	−1.72	C
1.00	1.26	2.53	7.23	0.06	C	1.31	1.24	2.41	7.23	0.22	C
1.00	1.24	2.03	7.73	−1.14	C	1.43	1.23	1.00	8.60	−3.40	C
1.00	1.25	2.00	7.76	−1.26	C	3.10	1.25	1.00	8.27	−2.60	C
1.00	1.22	8.66	1.13	1.07	E	3.10	1.25	1.00	8.27	−2.65	C
0.85	1.22	8.56	1.30	1.33	E	3.71	1.25	1.00	8.19	−2.44	C
0.85	1.22	8.56	1.30	1.43	E	5.00	1.24	1.00	8.06	−1.99	C

Table 2. Summary of conclusions.

Conditions (sulphate medium)	Derived coefficients	Assumed species
p*h* $\lesssim$ 2.4, aqueous phase	$\bar{x} = 0$ (Fig. 2)	$M(H)_{-1}(B)_1$
	$\bar{y} = 1$ (Fig. 3)	or
	$\bar{q} = 1$ (Fig. 1)	$Pa(OH)SO_4^+$
organic phase	$a = 3$ (Fig. 2)	$M(HA)_3(H)_{-4}$
	$b = 4$ (Fig. 3)	or
	$c = 0$ (Fig. 1)	$Pa(OH)(AA)_3$
p*h* 5 − 7, aqueous phase	$\bar{y} = 4$ (Fig. 3)	$M(HA)_x(H)_{-4}(B)_q$
organic phase	$b = 4$ (Fig. 3)	$M(HA)_a(H)_{-4}(B)_c$

CALCULATION OF EQUILIBRIUM CONSTANTS

The sulphate extraction system was found to consist of the protactinium complexes $Pa(OH)SO_4^{,+}$ $Pa(OH)SO_4AA$ and $Pa(OH)(AA)_3^{3-n}$, $0 \leq n \leq 3$. If the formation of the acetylacetone complexes $(Pa(OH)SO_4^{+} + AA^{-} \rightleftharpoons Pa(OH)SO_4AA$ and $Pa(OH)SO_4^{+} + nAA^{-} \rightleftharpoons Pa(OH)(AA)_n^{3-n} + SO_4^{2-}$; $0 \leq n \leq 3)$ is described by the formation constants β_1 and β_n' respectively, then the dependence of D_{Pa} upon the variable $[AA^{-}]$, for $pAA > 3$, can be written:

$$D_{Pa}^{-1} = \frac{1 \cdot [AA]^{-3}}{\lambda_3 \beta_3'} + \frac{(\beta'_1 + \beta_1[SO_4])[AA]^{-2}}{\lambda_3 \beta'_3} + \frac{\beta_2'[AA]^{-1}}{\lambda_3 \beta'_3} + \frac{1}{\lambda_3}$$

The coefficients in this equation were calculated with a least-squares program specially designed [10] for solvent extraction data. However, due to the unacceptably large statistical uncertainties in $(\beta_1' + \beta_1[SO_4])$ and β_2' these constants were set equal to zero and calculations were performed with only the two parameters β_3' and λ_3.

When the formation of $Pa(OH)AA^{2+}$ and $Pa(OH)(AA)_2^{+}$ was thus excluded, the values $\log \lambda_3 = 2.54 \pm 0.06$ and $\log \beta_3' = 18.34 \pm 0.10$ were obtained. The exclusion of $Pa(OH)AA^{2+}$ and $Pa(OH)(AA)_2^{+}$ from the calculations changed the S_{min}/K value [10] only slightly (from 0.142 to 0.175) which indicates that those complexes were statistically insignificant. By slope analysis [7] of the distribution function the following values were obtained: $\log \lambda_3 = 2.6$, $\log \beta_2' = 12.3$, and $\log \beta_3' = 18.4$. (The error in the logarithm of these values was estimated graphically to be ± 0.1.)

The distribution of Pa(IV), under conditions where the concentrations of the acetylacetone complexes $Pa(OH)(AA)_n^{3-n}$ may be neglected in comparison with $Pa(OH)SO_4^{+}$, can be described by the extraction reaction

$$Pa(OH)SO_4^{+} + 3HAA(org) \rightleftharpoons Pa(OH)(AA)_3(org) + SO_4^{2-} + 3H^{+}$$

The validity of this equilibrium is demonstrated by the linearity of $\log D_{Pa}$ with $\log [SO_4^{2-}]$ (slope -1), with ph (slope $+3$) and with $\log [HAA]_{org}$ (slope $+3$) for $ph < 2.4$ and $[Na_2SO_4] > 0.05$ M (see Figs. 1, 3 and 2). The equilibrium constant K_D has been calculated to be $\log K_D = -8.17 \pm 0.06$ at 25°C (0.94 M $(Na,H)ClO_4$ + 0.06 M Na_2SO_4). The enthalpy and entropy changes were found from the temperature dependence (see Fig. 5) to be $\Delta H°$ (25°C) $= 14 \pm 3$ kJ/mol and $\Delta S° = -110 \pm 11$ J/(mol K).

DISCUSSION

The extraction mechanism for the system $Pa(IV) - (Na,H)ClO_4 - HAA$ was found to change when sulphate was added. There are good reasons for believing that this change is not associated with a change in the valency of Pa, *i.e.* that complete reduction is obtained even in the presence of sulphate. Firstly, it has been shown that for other extraction systems [17,18] complete reduction of Pa(V) to Pa(IV) is achieved in the presence of $Cr^{2+} \geq 10^{-4}$ M (both in the presence and absence of sulphate). Secondly, as the sulphate complex with Pa(IV) [2] is stronger than the corresponding [19] complex with Pa(V), it ought to be easier to reduce Pa(V) in the presence of sulphate. Thirdly, the distribution of Pa(V) should not be expected to be described by the simple relation $D = f(pAA)$, as the $Pa(V) - HAA$ system was found to be much more complicated.[20]

The change in the extraction mechanism from $M^{2+} + 2HAA(org) \rightleftharpoons M(AA)(org) + 2H^{+}$, where M^{2+} is PaO^{2+} or $Pa(OH)_2^{2+}$, to $Pa(OH)SO_4^{+} + 3HAA(org) \rightleftharpoons Pa(OH)(AA)_3(org) + SO_4^{2-} + 3H^{+}$ may be due to the dehydrolyzation of Pa(IV) with sulphate according to the reaction $Pa(OH)_2^{2+} + HSO_4^{-} \rightleftharpoons Pa(OH)SO_4^{+} + H_2O$ (or $PaO^{2+} + HSO_4^{-} \rightleftharpoons Pa(OH)SO_4^{+}$). This would make it possible for an acetylacetonate to replace the sulphate without rehydrolyzation of the central atom. Such an irreversible mechanism is proposed because $Pa(OH)(AA)_3$ is not formed in absence of sulphate. Consequently, we have not attempted to calculate the formation constant for $Pa(OH)SO_4^{+}$.

The value of the distribution coefficient, λ_3 $([M(AA)_3]_{org}/[M(AA)_3]) = 10^{2.54 \pm 0.06}$, lies as expected between the distribution coefficient for $M(AA)_2$, $\lambda_2 = 10^{2.07 \pm 0.10}$ (Ref. 1) and the theoretical [11] value for $M(AA)_4$, $\lambda_4 = 10^{3.05 \pm 0.05}$.

Finally, the present study did not indicate any further hydrolysis of Pa(IV) in the ph

range 1 to around 6 which agrees with the investigation in absence[1] of sulphate.

Acknowledgement. The authors are grateful to Ing. Martin Ohlson for experimental aid and to Ph.D. Christopher Coombes for linguistic corrections.

REFERENCES

1. Lundqvist, R. *Acta Chem. Scand. A 28* (1974) 243.
2. Mitsuji, T. *Bull. Chem. Soc. Jap. 41* (1968) 115.
3. Guillaumont, R. *C. R. Acad. Sci. Ser. C 260* (1965) 1416.
4. Rydberg, J. *Ark. Kemi 8* (1955) 101.
5. Rydberg, J. *Ark. Kemi 5* (1953) 517.
6. Rydberg, J. *Acta Chem. Scand. 15* (1961) 1723.
7. Rydberg, J. *Acta Chem. Scand. 4* (1950) 1503.
8. Irving, H., Rossotti, F. V. C. and Williams, R. J. P. *J. Chem. Soc.* (1955) 1906.
9. Rydberg, J. *Rec. Trav. Chim. Pays-Bas 75* (1956) 737.
10. Sullivan, J. C., Rydberg, J. and Miller, W. F. *Acta Chem. Scand. 13* (1959) 2023; rewritten into Fortran by Zielen, A., Argonne National Laboratory (U.S.A.), *private communication.*
11. Liljenzin, J. O. and Rydberg, J. *Physicochimie du Protactinium,* Editions du C. N. R. S., No. 154, Paris 1966, p. 255.
12. Kerker, M. *J. Amer. Chem. Soc. 79* (1957) 3664.
13. Reynolds, W. L. and Fukushima, S. *Inorg. Chem. 2* (1963) 176.
14. Eichler, E. and Rabideau, S. *J. Amer. Chem. Soc. 77* (1955) 5501.
15. Liljenzin, J. O. *Acta Chem. Scand. 23* (1969) 3592.
16. Johansson, H. and Rydberg, J. *Acta Chem. Scand. 23* (1969) 2797.
17. Mitsuji, T. *Bull Chem. Soc. Jap. 40* (1967) 2822.
18. Guillaumont, R., Bouissieres, G. and Muxart, R. *Actinides Rev. 1* (1968) 135.
19. Mitsuji, T. and Suzuki, S. *Bull Chem. Soc. Jap. 40* (1967) 821.
20. Liljenzin, J. O. *Acta Chem. Scand. 24* (1970) 1655.

Received January 2, 1974.

Acta Chemica Scandinavica A 28 (1974) 407—414

An Infrared Spectroscopic Study on the Thiocyanato Complexes of Nickel(II) in Non-aqueous Solutions

ATIS MIEZIS

Inorganic Chemistry 1, Chemical Center, University of Lund, Box 740, S-220 07 Lund 7, Sweden

The nickel(II) thiocyanate systems in acetonitrile, propane-1,2-diolcarbonate, trimethylphosphate, dimethylacetamide, and dimethyl sulfoxide have been investigated using infrared spectroscopic techniques. The stability constants of the four first complexes and the molar absorption coefficients of the C—N stretching vibration of the bonded thiocyanate ion have been determined in all the solvents except propane-1,2-diolcarbonate. From an estimated value of the integrated absorption ($\varepsilon \Delta \nu_{1/2}$), it is concluded that there is N-coordination between the metal and the thiocyanate ion.

The order of stability of the nickel(II) thiocyanate system in the various solvents is, with one exception, that presupposed from the donor properties of the solvents.

Recently, Gutmann and Bardy [1] published an investigation on the formation of thiocyanato complexes of nickel(II) in various non-aqueous donor solvents. By using spectrophotometric, conductometric, and potentiometric methods they tried to describe the kind of species existing in solution and their configuration. They also determined how large the excess of ligand to metal has to be to obtain the highest thiocyanate-coordinated form, $Ni(NCS)_6^{4-}$, quantitatively. The results were then used in discussing the donor properties of solvents.[2]

However, in the work of Gutmann and Bardy, no quantitative description of the stability of the complexes was made. As in the case of the thiocyanato complexes of cobalt(II),[3] we believe that a knowledge of the stability constants would be valuable when the donor properties of the solvents are discussed.

It has long been known that there is in most cases a distinct difference in the infrared spectrum of the thiocyanate ion when it is coordinated to a metal as compared to that of the free ion. On the other hand, there are, as a rule, no detectable differences in spectra between the consecutively formed complexes ML_n[4,5] in solution. Of course it is not possible to exclude a small splitting of the bands but this is not so pronounced that it can be used to distinguish between different complexes. But in most cases infrared spectra can be used to determine stability constants of the complexes from the absorption band of the free ligand.[5] Furthermore, from the infrared spectra it can be concluded whether the thiocyanate group is coordinated to the metal *via* the nitrogen or the sulfur atom.[6]

METHOD OF INVESTIGATION

The following notations are used in the present paper:

C_M = total concentration of metal.
C_L = » » » ligand.
[M] = free » » metal.
[L] = » » » ligand.

$\bar{n} = \dfrac{C_L - [L]}{C_M}$ = mean ligand number.

$[ML_n]$ = concentration of the n-th complex.

$\beta_n = \dfrac{[ML_n]}{[M][L]^n}$ = overall stability constant of the n-th complex.

$\beta_0 = 1$

$K_n = \dfrac{[ML_n]}{[ML_{n-1}][L]} = \dfrac{\beta_n}{\beta_{n-1}}$ = stepwise stability constant of the n-th complex.

$X = \sum_{n=0}^{N} \beta_n [L]^n$

$X_n = \frac{X_{n-1} - \beta_{n-1}}{[L]}$

$\alpha_n = \frac{[ML_n]}{C_M} = \frac{\beta_n [L]^n}{X}$

A_ν = absorbance at the band maximum of wave number ν cm^{-1}.

ε_L = molar absorption coefficient of the free ligand.

ε_n = molar absorption coefficient of the complex ML_n.

d = the cell thickness.

The method of investigation used in this work is based on the fact that there is a considerable difference between the C–N stretching vibration frequency of the nickel-thiocyanato complexes (about 2 100 cm^{-1}) and that of the free ligand (about 2 060 cm^{-1}) in all the solvents used. Thus, knowing the molar absorption coefficient of the SCN^- ion one can determine the free ligand concentration from the "free ligand peak". For a series of solutions of general composition C_M $Ni(ClO_4)_2$ and C_L M NaSCN, where C_M is kept constant and C_L varied, it is possible to calculate the mean ligand number, $\bar{n}$. Then the polynomial X can be obtained as

$$\ln X([L]_j) = \int_0^{[L]_j} \bar{n}/[L] \, d[L] \qquad (1)$$

The integration can be carried out graphically and also the determination of the stability constants from the corresponding values of X and [L]. (For a more detailed treatment of this graphical method see, *e.g.*, Ref. 7). The stability constants can also be calculated numerically from the corresponding $\bar{n}$ and [L] values (see below).

In some cases it is possible to use the "complex peak" to obtain $\bar{n}$ and [L] by the method of "corresponding solutions".[8,7] The absorbance at the maximum of this band (A_ν) is measured and by definition

$$\frac{A_\nu}{d} = \sum_{n=1}^{N} \varepsilon_n [ML_n] = \frac{C_M}{X} \sum_{n=1}^{N} \varepsilon_n \beta_n [L]^n \qquad (2)$$

From this equation one can conclude that A_ν/dC_M is a function of [L] only. Corresponding values of [L] and $\bar{n}$ are now obtained in the following way: On the basis of several series with constant C_M but varying C_L, A_ν/dC_M can be plotted against C_L with C_M as a parameter. The curves thus obtained are then cut at a number of constant A_ν/dC_M values and from the points of intersection C_L can be plotted against C_M for every constant A_ν/dC_M chosen. The $C_L - C_M$ curves would then be straight lines with the equations

$$C_L = [L]_j + \bar{n}_j C_M \qquad (3)$$

By extrapolating these lines to $C_M = 0$ one obtains the [L] values and from the slopes the corresponding $\bar{n}$. The determination of [L] in this way can, however, be done only if the complexity of the system is not too strong.

Knowing the stability constants of the complexes, the molar absorption coefficients can be calculated from the measured absorbance of the "complex band". Eqn. (2) can be written

$$\frac{A_\nu}{dC_M} = \sum_{n=1}^{N} \varepsilon_n \alpha_n \qquad (4)$$

Now if $\varepsilon' = A_\nu/dC_M\alpha_1$ is plotted *versus* [L] and the resulting curves extrapolated to $[L] = 0$, ε_1 is obtained. Then ε_2 (*i.e.* $\varepsilon_2\beta_2/\beta_1$) is determined in the same way from a plot of $(\varepsilon' - \varepsilon_1)/[L]$ *versus* [L], and so on.

Numerical calculations of the stability constants. The stability constants obtained graphically were checked by a numerical method developed by Karlsson.[9] The method is based on the principles of Deming as they have been reviewed by Guest.[10] The input data to the computer program CURVEFIT [9] were $\bar{n}_i$, $[L]_i$, $\sigma_{\bar{n}_i}$, $\sigma_{[L]_i}$. The standard deviations $\sigma_{\bar{n}_i}$ and $\sigma_{[L]_i}$ were given by the estimated uncertainties in $\bar{n}_i$ and $[L]_i$. The functional relationship used between $\bar{n}$ and [L] was

$$\bar{n}([L], \beta) = \frac{\sum_{n=1}^{4} n\beta_n [L]^n}{\sum_{n=0}^{4} \beta_n [L]^n} \qquad (5)$$

and the error square sum

$$\mathrm{CHISQ} = \sum_i \left(\frac{\Delta n_i^2}{\sigma_{\bar{n}_i}^2} + \frac{\Delta [L]_i^2}{\sigma_{[L]_i}^2} \right) \qquad (6)$$

was minimized by the subroutine STEPIT.[11] $\Delta\bar{n}_i = \bar{n} - \bar{n}_i$ and $\Delta[L]_i = [L] - [L]_i$ where $(\bar{n}_i, [L]_i)$ refer to the observed point and $(\bar{n}, [L])$

to the adjusted point on the least-squares curve. The slope of the line between these points was given by

$$\tan \theta_i = -1 \Big/ \left(\frac{\sigma_{[L]_i}{}^2 d\bar{n}}{\sigma_{\bar{n}_i}{}^2 d[L]} \right) \quad (7)$$

The errors in the constants were also calculated by STEPIT using the following method: The matrix of the second partial derivatives of the error square sum with respect to the parameters was calculated. Twice the inverse of this matrix would be the covariance matrix assuming that the error square sum is an approximately quadratic function of the parameters over the error range. Then the standard deviations would be given by the square roots of the diagonal elements of this matrix. To check the values of the standard deviation another subroutine was used. Starting from the adjusted values of $\bar{n}$ and [L], all of them were disturbed by a small amount, randomly chosen from a normal distribution with mean zero and the standard deviation $\sigma_{\bar{n}_i}$ or $\sigma_{[L]_i}$. From the new set of points the best set of parameters was found by reminimization. From several sets of parameters obtained in this way the standard deviations could be estimated. No perceptible difference in the results using the two methods could be found.

EXPERIMENTAL CONDITIONS

The nickel(II)-thiocyanate system was investigated in five different solvents. They were acetonitrile (AN), propane-1,2-diolcarbonate (PDC), trimethylphosphate (TMP), *N*,*N*-dimethylacetamide (DMA), and dimethyl sulfoxide (DMSO). The solutions used were made from stock solutions of anhydrous nickel(II) perchlorate and sodium thiocyanate in these solvents. The experimental procedures have been described in detail in a previous paper.[3] As in that work the measurements had to be performed in solutions with uncontrolled ionic strengths because of the low solubilities of supporting electrolytes in these solvents. However, the results of the measurements on silver-thiocyanato complexes in another organic donor solvent, *i.e.* pyridine,[5,12] indicate that the stability constants would hardly be influenced significantly by the change of the activity coefficients that would be caused by the varying ionic strength. The infrared spectra are recorded using a Perkin-Elmer 521 grating spectrophotometer.[3] As could be seen in, *e.g.*, Fig. 1 there is usually some overlap between the "free ligand band" and the "complex band", although not very large. Because of this fact there would be some difficulties in the determination of the baseline, especially for the less intense band. By using both bands in the calculation of the stability constants one can concentrate the absorbance readings to the most intense band. To that end the method of "corresponding solutions" is used at low free ligand concentrations in some systems.

RESULTS *

Measurements on NaSCN

In order to use the "free ligand peak" for free ligand concentration determinations the molar absorption coefficients for the thiocyanate ion in the various solvents must be known. Therefore, measurements on the C–N stretching vibration of NaSCN were made and the results can be seen in Table 1. The wave numbers of the bands and the integrated absorptions are also included in this table.

Measurements on the nickel(II) thiocyanate systems

TMP. Only two bands could be observed in the C–N stretching region of the spectra, one at 2 059 cm^{-1} and the other at 2 102 cm^{-1}. The former was assigned as the vibration of the "free" ion and the latter corresponds to the C–N stretching vibration of the thiocyanate groups coordinated to the metal. From the "free ligand band" the free ligand concentration was obtained and the stability constants determined according to the methods described above. Four complexes could be established and their stability constants are included in Table 2. The "complex band" gave the data needed for the calculation of the molar absorption coefficients and the results can be found in Table 1.

DMSO. Two bands were found at 2056 cm^{-1} and 2092 cm^{-1}. As for TMP, the former was used in the determination of the stability

* The experimental material of this work is very comprehensive and a complete presentation of it would be very space-demanding. According to the editorial rules of Acta Chemica Scandinavica these data could not be included in the paper. A reader, specially interested in the details of this work, is therefore recommended to apply directly to the author for a copy of the experimental data.

Table 1. Infrared spectral data for NaSCN and the thiocyanato complexes of Ni(II) in various solvents. The values of ε_n are calculated per SCN group.

Solvent	NaSCN ν (cm^{-1})	ε ($M^{-1}\,cm^{-1}$)	$\varepsilon\Delta\nu_{1/2}\times10^{-4}$ ($M^{-1}\,cm^{-2}$)	Ni(NCS)$_n$ ν (cm^{-1})	ε_1 ($M^{-1}\,cm^{-1}$)	ε_2	ε_3	ε_4	$\varepsilon_1\Delta\nu_{1/2}\times10^{-4}$ $M^{-1}\,cm^{-2}$
AN	2062	701	1.3	2097		850 ± 400	970 ± 400	750 ± 400	2.0 [b]
TMP	2059	525	0.8	2102	1000 ± 300	870 ± 200	650 ± 400		2.3
DMA	2058	913	1.1	2094	1280 ± 150	770 ± 120	780 ± 150	1100 ± 400	2.6
DMSO	2056	850	1.1	2092	880 ± 100	620 ± 200			2.6
PDC	2057	571	1.3	2089					
H_2O [a]	2066	537	2.0	2119	640				2.1

[a] Values taken from Ref. 6. [b] $\varepsilon_2\Delta\nu_{1/2}\times10^{-4}$.

Table 2. The stability constants of the thiocyanato complexes in various solvents.

Solvent	β_1 (M^{-1})	β_2 (M^{-2})	β_3 (M^{-3})	β_4 (M^{-4})	K_2 (M^{-1})	K_3 (M^{-1})	K_4 (M^{-1})	$\frac{K_1}{K_2}$	$\frac{K_2}{K_3}$	$\frac{K_3}{K_4}$
Graphically determined constants.										
AN	$(5\pm5)\times10^3$	$(1.2\pm0.4)\times10^8$	$(2.8\pm1.0)\times10^{10}$	$(3.0\pm1.0)\times10^{11}$	(24 000)	230	11	(0.2)	(100)	21
TMP	$(2.3\pm0.5)\times10^3$	$(2.0\pm0.4)\times10^5$	$(6.0\pm1.5)\times10^5$	$(1.1\pm0.3)\times10^6$	87	3.0	1.8	26	29	1.7
DMA	$(2.9\pm0.3)\times10^3$	$(1.8\pm0.2)\times10^6$	$(1.3\pm0.2)\times10^8$	$(1.3\pm0.3)\times10^9$	620	72	10	4.7	8.6	7.2
DMSO	$(4.3\pm0.3)\times10^2$	$(4.6\pm0.6)\times10^3$	$(1.2\pm1.0)\times10^4$	$(1.8\pm1.0)\times10^5$	11	2.6	15	39	4.2	0.2
H_2O [a]	15 ± 0.5	44 ± 4	65 ± 10		2.9	1.5		5.1	1.9	
Numerically determined constants										
TMP	$(1.9\pm0.4)\times10^3$	$(1.8\pm0.3)\times10^5$	$(4.4\pm1.4)\times10^5$	$(1.1\pm0.3)\times10^6$	95	2.4	2.5	20	40	1.0
DMA	$(2.8\pm0.4)\times10^3$	$(2.0\pm0.3)\times10^6$	$(1.3\pm0.2)\times10^8$	$(1.3\pm0.2)\times10^9$	710	65	10	3.9	11	6.5
DMSO	$(4.5\pm0.2)\times10^2$	$(4.7\pm0.4)\times10^3$	$(7\pm60)\times10^2$	$(2.6\pm0.3)\times10^5$	10	(0.1)	(370)	45	(100)	–
I	0	0.6×10^8	1.3×10^{10}	1.4×10^{11}						
AN II	5.0×10^3	1.1×10^8	2.8×10^{10}	2.9×10^{11}	22 000	250	10	0.2	88	25
III	1.0×10^4	1.7×10^8	4.4×10^{10}	4.4×10^{11}						

[a] The values in H_2O are taken from Ref. 13 and are determined in solutions with constant ionic strength = 1 M.

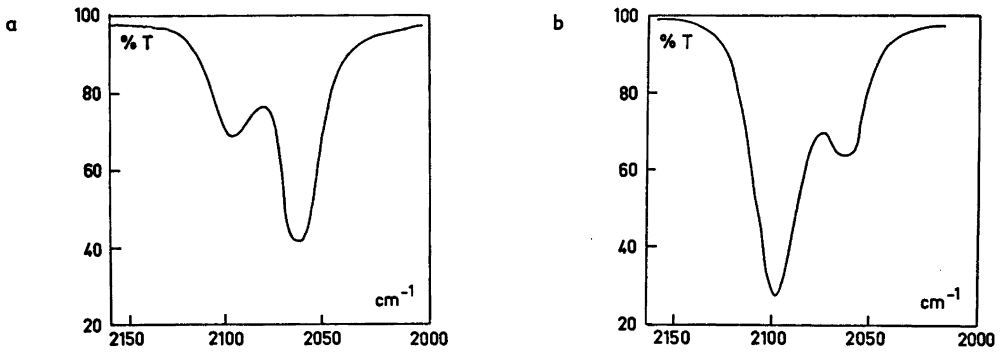

Fig. 1. Spectra of the Ni^{2+}-NCS^- system in *AN*.
a. $C_{Ni^{2+}} = 0.01012$ M, $C_{SCN^-} = 0.1399$ M, $d = 0.0508$ mm.
b. $C_{Ni^{2+}} = 0.01012$ M, $C_{SCN^-} = 0.0401$ M, $d = 0.2167$ mm.

constants and the latter in the determination of the molar absorption coefficients. The resulting constants can be found in Tables 2 and 1.

AN. In AN the two bands were found at 2062 cm^{-1} and 2097 cm^{-1}. Fig. 1 shows two representative examples of the spectra of solutions with different compositions. Both absorption bands were used in the determination of the stability constants according to the methods described above. The overlap of the $\bar{n}$, [L] values as determined from the two absorption bands can be seen in Fig. 2. At the graphical determination of the stability constants in this system the extrapolation of X_1 was somewhat hazardous because of the lack of data for small mean ligand numbers. Therefore the existence of the first complex is uncertain and the stability constants of the following ones inaccurate. The molar absorption coefficient ε_1 could not be determined according to eqn. (4) because of the uncertainty of α_1. But from, *e.g.* Fig. 4a it could be concluded that $\alpha_1 \approx 0$ at least for $[SCN^-] > 0.001$ M. Then ε_2 could be obtained from the extrapolation of $A_{2097}/dC_{Ni}\alpha_2$ *versus* [L] and after that ε_3 and ε_4 in the usual way.

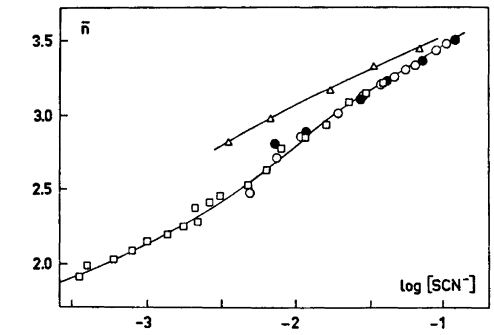

Fig. 2. $\bar{n}$ as a function of log $[SCN^-]$ for *AN* (lower curve) and *PDC* (upper curve). The values in AN are obtained from the 2062 cm^{-1} band with constant $C_{Ni} = 0.01012$ M (○) and $C_{Ni} = 0.02024$ M (●) and from the 2097 cm^{-1} band (□). (See text!) The values in PDC (△) are calculated from the 2057 cm^{-1} band.

DMA. Here the two bands appeared at 2058 cm^{-1} and 2094 cm^{-1}. As in AN, both bands were used in the determination of the stability constants in this solvent. The overlap of the $\bar{n}$, [L] values obtained from the two bands is illustrated in Fig. 3.

PDC. In PDC there was a precipitate, probably of $Ni(NCS)_2$, in solutions with

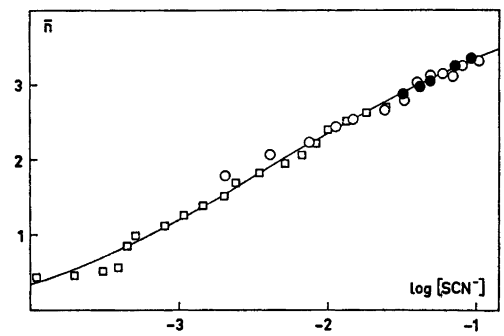

Fig. 3. $\bar{n}$ as a function of log $[SCN^-]$ in DMA. The values are obtained from the 2058 cm^{-1} band with constant $C_{Ni} = 0.01010$ M (○) and $C_{Ni} = 0.02020$ M (●) and from the 2094 cm^{-1} band (□).

$\bar{n} < 2.8$. This means that the stability constants could not be determined because the extrapolation to $[SCN^-] = 0$ was difficult to make. From the complex formation curve for $\bar{n} > 2.8$, which is drawn in Fig. 2, together with the same curve in AN, it can be inferred that complexes in PDC are slightly more stable than those in AN. In PDC the "complex peak" was found at 2089 cm^{-1} and the "free ligand peak" at 2057 cm^{-1}.

A comparison between the graphically and the numerically determined stability constants

The numerically calculated constants are in most cases in good agreement with the graphical ones. For the AN-system, when using four parameters in the calculations, no chemically acceptable β-values could be obtained. The consecutive constants K_3 and K_4 were, however, very similar to those obtained graphically. As mentioned above the graphical determinations of β are very uncertain depending on the lack of data for small mean ligand numbers. Thus, the existence of the first complex is questionable but if it exists the graphical method indicates that β_1 should be $< 10^4$. The constants for this system given in Table 2 are therefore obtained from calculations with some fixed values of the parameters β_1 (between 0 and 10^4 M^{-1}). For the DMSO-system β_3 was very uncertain when determined graphically and this uncertainty is even more accentuated in the numerical calculations. The existence of the complex might be questioned.

DISCUSSION

In the same way as for the cobalt(II) thiocyanate systems,[3] the increased integrated absorption ($\varepsilon \Delta \nu_{1/2}$) of the C–N vibration of the thiocyanate ion upon coordination with the nickel(II) ion (Table 1) indicates that the thiocyanate ion is N-bonded in these solvents. Furthermore, it can be concluded that there is a definite electron exchange between ligand and metal when the complexes are formed. No such electron exchange can be found in aqueous solution,[6] which probably means that the metal-thiocyanate bond in aqueous solution is merely electrostatic. This should be remembered

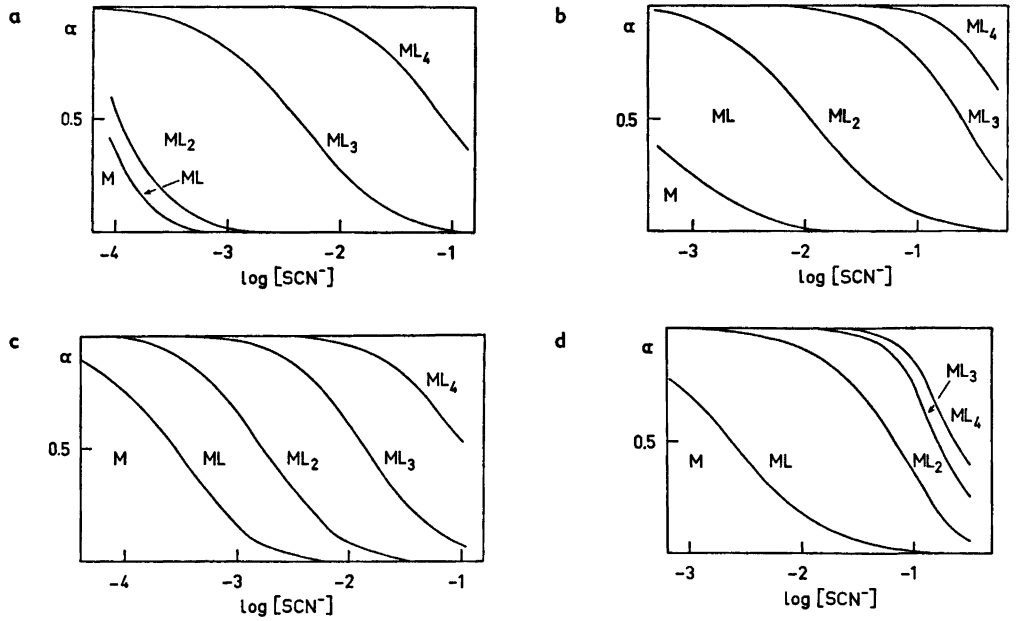

Fig. 4. The distribution of the nickel(II) ion between the mononuclear complexes with varying $[SCN^-]$ in a, AN; b, TMP; c, DMA; d, DMSO.

when the stability of the complexes in different solvents is discussed.

Within the range of concentration investigated, four mononuclear complexes are found in all the systems. All the complexes except $Ni(NCS)^+$ in AN and $Ni(NCS)_3^-$ in DMSO seem to be well established by this investigation (see Fig. 4). Quantitatively this is demonstrated by the values found for the quotients K_n/K_{n+1} (Table 2). With these results in mind it is confusing that Gutmann and Bardy [1] from conductometric measurements have found that generally only $Ni(NCS)_3$ [in DMA $Ni(NCS)^+$], $Ni(NCS)_4^{2-}$, and $Ni(NCS)_6^{4-}$ appear in these solutions.

The relative stabilities of the consecutive complexes are, however, very different in most of the investigated solutions. Usually abrupt changes in K_n/K_{n+1} may indicate differences, *e.g.* in stereochemistry or in the kind of bonding between metal ion and ligand for the stepwise formed complexes.[14] Thus, transitions from, *e.g.*, tetrahedral to octahedral configuration [1] may cause such changes. However, in the infrared spectra of the thiocyanato complexes of nickel(II) only one band is found in the range of the C–N stretching vibration. The frequency of this band is about 10 cm^{-1} higher than that of the octahedral cobalt(II) complex in each solvent. This is a normal shift between nickel and cobalt as found in pyridine and pyridine-chloroform solutions.[15] As the integrated absorptions of the nickel complexes are also nearly the same as those of the octahedral cobalt complexes, one would suggest that all the complexes have the same configuration, *viz.* octahedral. Another possible cause of the changes in K_n/K_{n+1} may be the various steric requirements of the surrounding solvent molecules at the competition for the coordination sites of the metal. How such a steric effect is working in detail is, however, difficult to describe.

The stability of the thiocyanato complexes of nickel(II) may be related to the "donor numbers" [2] of the solvents used (Fig. 5). β_2 is chosen because of the uncertainty of the first stability constant in AN. The expected decrease in stability with increasing "donor number" of the solvent, if the complex formation is regarded as ligand exchange reactions of a solvated metal ion, can be found for all

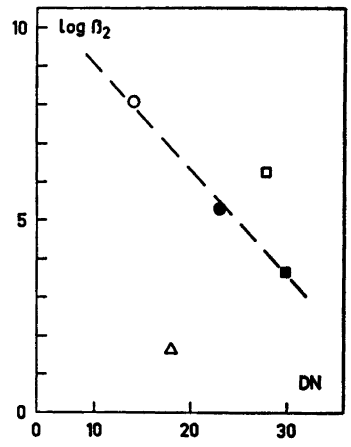

Fig. 5. The dependence of log β_2 on the "donor number" of Gutmann.[2] The line is drawn only to emphasize the trend. ○-AN, ●-TMP, □-DMA, ■-DMSO, and △-H_2O.

solvents investigated except DMA. Thus, the complexes in DMA are more stable than those in TMP, which is in contrast to the situation in the cobalt(II) system in the same solvents.[3] Also when the β_2 value for the thiocyanato complex in water is introduced in Fig. 5 it can be seen that the conformity with the trend shown by the other solvents is not good. This situation was also found for cobalt(II) and is not unexpected. As mentioned above the metal-thiocyanate bonds should be merely electrostatic in aqueous solution and such bonds are influenced strongly also by the dielectric properties of the solvent.

In summary, the concept of donor numbers seems to be rather reliable when predicting the stability of thiocyanato complexes in aprotic solvents. The donor number of a solvent may, however, never become the exclusive factor determining the stability of complexes formed in all kinds of solvents. Especially in highly polar protic solvents, *e.g.* water, it is probable that also factors such as the dielectric constant and the hydrogen bonding ability of the solvent have to be considered.

Acknowledgement. The author is greatly indebted to Dr. Ragnar Larsson and Prof. Sture Fronæus for their kind interest and valuable comments on this work and to Dr. Roland Karlsson for his invaluable assistance

with the numerical calculations. Financial support has been given by Statens Naturvetenskapliga Forskningsråd (Swedish Natural Science Research Council) which is also gratefully acknowledged.

REFERENCES

1. Gutmann, V. and Bardy, H. *Z. Anorg. Allg. Chem. 361* (1968) 213.
2. Gutmann, V. *Coordination Chemistry in Non-aqueous Solutions*, Springer, Wien–New York 1968.
3. Miezis, A. *Acta Chem. Scand. 27* (1973) 3801.
4. Fronæus, S. and Larsson, R. *Acta Chem. Scand. 16* (1962) 1433.
5. Larsson, R. and Miezis, A. *Acta Chem. Scand. 22* (1968) 3261.
6. Fronæus, S. and Larsson, R. *Acta Chem. Scand. 16* (1962) 1447.
7. Fronæus, S. *Determinations of Formation Constants of Complexes*, In Jonassen, H. B. and Weissberger, A., Eds., *Technique of Inorganic Chemistry*, Interscience, New York and London 1963, Vol. 1, Chapter 1.
8. Bjerrum, J. *Kgl. Dan. Vidensk. Selsk. Mat. Phys. Medd. 21* (1944) No. 4.
9. Karlsson, R. *To be published.*
10. Guest, P. G. *Numerical Methods of Curve Fitting*, Cambridge 1961.
11. Chandler, J. P., Physics Dept., Indiana University, STEPIT is available from Quantum Chemistry Program Exchange, I.U. Chemistry Dept., Bloomington, Indiana, USA.
12. Miezis, A. and Larsson, R. *Acta Chem. Scand. 22* (1968) 3293.
13. Fronæus, S. *Acta Chem. Scand. 7* (1953) 21.
14. Rossotti, F. J. C. *The Thermodynamics of Metal Ion Complex Formation in Solutions*, In Lewis, J. and Wilkins, R. G., Eds., *Modern Coordination Chemistry*, Interscience, New York 1960.
15. Larsson, R. and Miezis, A. *Acta Chem. Scand. 19* (1965) 47.

Received January 16, 1974.

Acta Chemica Scandinavica A 28 (1974) 415—422

On the Infrared Spectra of Thiocyanic Acid and some Thiocyanato Complexes of Iron(III)

ATIS MIEZIS

Inorganic Chemistry 1, Chemical Center, University of Lund, P.O. Box 740, S-220 07 Lund 7, Sweden

The infrared spectra in the C–N absorption region have been recorded for (iso)thiocyanic acid extracted into various solvents. The variations in frequency and integrated absorption are related to possible solute-solvent interactions and the use of simple valence-bond models in describing this variation is discussed.

Thiocyanato complexes of iron(III) have also been examined both in the solid state and in solution. There is some evidence from the infrared data that solid octahedral complexes change configuration when dissolved in low-polar solvents. It is suggested that in such solvents they adopt the tetrahedral configuration just as iron(III) thiocyanato complexes extracted from aqueous into organic solutions.

The coordination chemistry of the ambidentate thiocyanate ion has long been a subject of interest. One way to differentiate between the bonding types is offered by infrared spectroscopy. Thus, both frequency shifts and the change of the integrated absorption of the IR-bands of the thiocyanate ion could be used (See Refs. 1–4 and references therein). Fronæus and Larsson [1] have shown that most of the behavior of the C–N stretching vibration upon coordination could be explained qualitatively by a changed distribution between the resonance structures of the thiocyanate ion suggested by Jones.[5] However, the frequency shift of the C–N stretching vibration did not follow the rules. Thus, for the complexes of the first row transition metals in aqueous solution it was obvious from the intensity measurements that no appreciable electron exchange was taking place between ligand and metal. This means that the attraction would be mainly electrostatic and that the distribution between the resonance structures, and consequently the vibrational frequencies of the thiocyanate ion, would be unchanged upon coordination. Nevertheless, a large positive frequency shift was found in these cases, which was ascribed to mechanical squeezing of the C–N group in these complexes. Later Porai-Koshits *et al.*[6] showed theoretically that in complexes of this kind the frequency shift would be positive and an almost linear function of the force constant of the M–N bond.

For more covalent metal ligand bonds (M–NCS bonds) the resonance structure model would predict a negative frequency shift, but a positive one is still found although smaller than before. This may be the result when this "covalent effect" is overbalanced by the "electrostatic effect" described above.

The (iso)thiocyanato complexes of iron(III) are especially interesting in this respect. Among all the transition metal complexes in aqueous solution investigated by Fronæus and Larsson [1] those of iron(III) were the only ones giving a negative frequency shift of the C–N stretching vibration as compared to the free thiocyanate ion (2045 cm^{-1} to 2066 cm^{-1}). Furthermore, the large value of the integrated absorption reported indicates that there is a considerable electron exchange between ligand and metal in these complexes. The analysis of the spectra of the iron(III) system in aqueous solution was, however, complicated by the existence of polynuclear complexes (*cf.* also Ref. 7), resulting in broad and diffuse absorption bands.

There are exceptionally few other reports in the literature on the IR-spectra of the thiocyanato complexes of iron(III). These are usually studies on solid octahedral complexes of the

type $(R_4N)_3Fe(NCS)_6$.[8-12] The C–N stretching frequency is frequently split in these solid-state spectra and varies widely from one compound to another, but is usually found between 2070 and 2050 cm^{-1}. No integrated absorptions have been reported for the vibrations. $(Et_4N)_3Fe(NCS)_6$ has also been studied in solution (acetone).[13] The values of the C–N stretching frequency and the integrated absorption per SCN-group are here 2062 cm^{-1} and 15.2×10^4 M^{-1} cm^{-2}, respectively.

Complex anions formed with pseudohalide ions, such as thiocyanate, can often be extracted from aqueous phases into organic ones. There are also some papers on iron(III) thiocyanate extraction, but the data are conflicting even for a given solvent with a specific aqueous phase. For example, some authors [14] have reported that diethyl ether extracts the neutral molecules $Fe(NCS)_3$ from aqueous solutions, others [15,16] that the extractable species would be $Fe(NCS)_4^-$. Bock [17] has found that both kinds of species are extractable depending on the composition of the aqueous phase. However, the configuration of the species is not settled once the stoichiometric ratio Fe/SCN is determined. Maddock and Medeiros [18] have shown that for an extraction from water into nitrobenzene the extracted species must be the six-coordinated $Fe(NCS)_4S_2^-$, where S represents a molecule of solvent, in this case water rather than nitrobenzene. As there are some indications of a higher covalency in the metal-ligand bond of complexes with tetrahedral configuration than in those with octahedral,[5,1] one would expect a more pronounced negative frequency shift of the C–N stretching frequency upon tetrahedral coordination and perhaps also a larger integrated absorption.

In this work the infrared spectra of the thiocyanato complexes of iron(III) extracted into some different organic solvents are reported, as well as the spectra of tributylammonium- and triphenylmethylarsonium-hexathiocyanato ferrate(III), both in the solid state and in various solutions.

Even if the iron(III) complexes (either octahedral or tetrahedral) in some cases show unusually low C–N stretching frequencies of the thiocyanato group, the M–NCS bond cannot be extremely covalent. As a matter of fact, high covalency would scarcely exist in any transition metal-isothiocyanato complexes. But also in established covalent compounds such as organic isothiocyanates the C–N frequency often is higher than that of the thiocyanate ion.[19,20] Extremely low frequencies, however, are reported for $P(NCS)_3$, $OP(NCS)_3$[21] and for tetraalkyl distannoxanes $(SCN)R_2SnOSnR_2(NCS)$,[22] but at least for the last compound the lowering of the C–N stretching frequency may be interpreted as being caused by the bridging of the thiocyanate nitrogen to another tin atom. The simplest covalent compound that a thiocyanate group can form is HNCS and in gaseous HNCS the pseudoantisymmetric stretching of the NCS part (approximately ν_{CN}) is found at 1963 cm^{-1}.[23] Thiocyanic acid extracts also very well into organic solvents,[24] and may then be investigated by IR-spectroscopy. The frequency and the integrated absorption of the C–N stretching vibration of HNCS as compared to that of NCS^- have been maesured to see if more information can be obtained about the usefulness of the simple valence bond model [1,3] when discussing a thiocyanate group involved in covalent compounds.

EXPERIMENTAL

Extraction of thiocyanic acid. Thiocyanic acid was obtained by extraction from aqueous solutions of sodium thiocyanate and perchloric acid into carbon tetrachloride, benzene, nitrobenzene, diethyl ether, and chloroform. The concentration of the thiocyanic acid in the separated organic phase was determined in the following way: A portion of the phase was added to a known volume of dilute sodium hydroxide in water and the acid was reextracted to the aqueous phase. The excess of sodium hydroxide was then titrated with standard acid, using methyl red as indicator. The thiocyanate concentration was determined gravimetrically as AgSCN. The ratio of hydrogen ions to thiocyanate ions was found to be 1:1, whence it may be concluded that only thiocyanic acid was extracted in these experiments. The same results were also obtained by analysing the aqueous phase and using the known total concentrations of acid and thiocyanate ions.

Extraction of iron(III) thiocyanato complexes. Iron(III) thiocyanato complexes were extracted into diethyl ether from aqueous solutions of iron(III) perchlorate and sodium thiocyanate. Because thiocyanic acid itself extracts very well into this solvent the extraction was made from very slightly acid aqueous solutions, *i.e.* at a pH just below that at which the metal ion hydrolysis begins. The iron(III) concentration in the aqueous phase was determined by titra-

tion with a mercurous nitrate solution (see Ref. 25, p. 399) and the thiocyanate concentration gravimetrically as AgSCN. Knowing the original concentrations those in the organic phase could be obtained.

Extraction with trilaurylamine (TLA). A 35 mM trilaurylamine (tridodecylamine) solution in benzene was pre-equilibrated with an equal volume of 35 mM nitric acid. Sodium thiocyanate and iron(III) nitrate were used in the aqueous phase to form the extractable species. Both the iron and the total thiocyanate concentrations in the aqueous phase were determined as described above, and those in the organic phase were obtained using the values in the aqueous phase and in the original solution.

Preparation of $Fe(NCS)_6^{3-}$ complexes. $(Bu_3HN)_3Fe(NCS)_6$ was prepared from iron(III) chloride, ammonium thiocyanate and a tributylammonium acetate solution as described by Ziegler *et al.*,[26] $(Ph_3MeAs)_3Fe(NCS)_6$ from ammonium thiocyanate, iron(III) ammonium sulfate, and triphenylmethylarsonium chloride according to Dwyer and Gibson.[27] $Ph_3MeAsSCN$ was also obtained as an intermediate. All the compounds were soluble in several organic solvents.

The stoichiometry of the iron compounds was checked by carbon-hydrogen-nitrogen analysis at the Analytical Laboratory, Chemical Center, Lund. Calc. for $(Bu_3HN)_3Fe(NCS)_6$: C 52.36; H 8.79; N 13.08. Found: C 52.5; H 8.70; N 13.2. Calc. for $(Ph_3MeAs)_3Fe(NCS)_6$: C 55.31; H 3.98; N 6.14. Found: C 55.36; H 3.89; N 6.06.

Chemicals. Most of the chemicals were of *p.a.* quality and used as purchased without further purification. Only the chloroform was purified from the stabilizing ethanol (1 %) by means of molecular sieves. Trilaurylamine (tridodecylamine) was of "qualité nucléaire" from Rhône-Poulenc-Paris.

Infrared spectra. The infrared spectra were recorded on a Perkin-Elmer Model 521 grating spectrophotometer. The spectral slit width (resolution) of the spectrophotometer was about 1.5 cm^{-1}. The integrated absorptions were determined by direct graphical integration.[4] The solid samples were examined in KBr pellets and the solutions in CaF_2 cells usually of thickness 0.1 mm. The concentration of the solid sample in a KBr pellet was obtained by accurate weighing of the sample before it was mixed up and by a determination of the volume of the pellet when it had been pressed. The accuracy of the integrated absorption was estimated to be within 10 %.

RESULTS AND DISCUSSION

As a basis for the discussion of the binding type in thiocyanic acid and the thiocyanato complexes of iron(III), the frequencies and integrated absorptions of NaSCN and $Ph_3MeAsSCN$ are given in Table 1. Judging from the frequencies both compounds would be regarded as ionic compounds but the integrated absorptions suggest there are some interactions between the triphenylmethylarsonium ion and the thiocyanate ion which increase the integrated absorption. This effect should be remembered when anionic thiocyanato complexes are investigated. Generally, these are prepared from non-aqueous solvents as salts of large quaternary cations, to avoid the presence of water of solvation that often occurs with the salts of alkali metal cations prepared from aqueous solution. It is then not certain that these cations could be regarded as fully inactive in their relation to the thiocyanate-containing species, and that the infrared absorption of the thiocyanate groups would not be governed only by the interaction between these groups and the central atom.

Table 1. Infrared spectral data of sodium thiocyanate and triphenylmethylarsonium thiocyanate in different solvents.

	Solvent *etc.*	ν_{CN} (cm^{-1})	ε ($M^{-1}\,cm^{-1}$)	$\Delta\nu_{1/2}$ (cm^{-1})	$\varepsilon\Delta\nu_{1/2} \times 10^{-4}$ ($M^{-1}\,cm^{-2}$)	$A \times 10^{-4}$ ($M^{-1}\,cm^{-2}$)
Na^+SCN^+	KBr-pellets	2070	310	39	1.22	3.25
	Pyridine	2059	1020	15	1.53	4.28
	Acetonitrile	2062	700	18.5	1.30	4.29
	Dimethyl sulfoxide	2056	850	13	1.11	3.31
$Ph_3MeAs^+SCN^-$	Pyridine	2055	1270	16	2.03	6.04
	Acetonitrile	2058	1465	15	2.20	7.37
	Nitrobenzene	2056	790	21	1.66	5.37
	Dimethyl sulfoxide	2055	1390	13	1.81	5.34

Table 2. The spectral data of the C–N stretching vibration of HNCS in various solvents.

Solvent	ν_{CN} (cm^{-1})	ε (M^{-1} cm^{-1})	$\Delta\nu_{1/2}$ (cm^{-1})	$\varepsilon\Delta\nu_{1/2} \times 10^{-4}$ (M^{-1} cm^{-2})	w	$A \times 10^{-4}$ (M^{-1} cm^{-2})
Carbon tetrachloride	1980	1110	23	2.6		8.4
Chloroform	1987	390	46	1.8		6.1
Benzene	1992	530	45	2.4		7.0
Nitrobenzene	2021	260	60	1.6		4.2
Diethyl ether	2027	260	54	1.4		3.9

Thiocyanic acid. The infrared spectrum [23] shows that the acid has the structure HNCS and it should therefore be called isothiocyanic. From microwave studies the dimensions of HNCS have been accurately determined.[28] The bond lengths are: C–S 1.56 Å, C–N 1.22 Å and N–H 1.01 Å. The H–N–C bond angle is 136° and the N–C–S group is linear. Probable resonance structures are (*cf.* Pauling [29])

$$H-N^{+}\equiv C-S^{-}, \quad \underset{H}{N=C=S}, \quad \underset{H}{N^{-}-C\equiv S^{+}}$$

116° 108°

a *b* *c*

Using the experimental lengths and Pauling's formulae relating the amount of single-, double-, and triple-bond character to observed bond lengths, one will find that there is approximately equal resonance among the three structures. Also the bond angle would then have the expected value. As mentioned above, ν_{CN} for gaseous HNCS is 1963 cm^{-1}. The deviations from this value found for HNCS in different solvents (Table 2) are too large to be explained by changes in the force fields caused by differences in the dielectric constant *e.g.* by the classical Kirkwood-Bauer-Magat relation.[30] They are therefore likely to depend on specific solute-solvent interactions. High C–N stretching frequencies of HNCS would imply high bond orders of the C–N bond, which means that structure *a* is growing in importance. It is known that the nitrogen in *a* (*sp*-hybridization) is more electronegative than that of *b* (sp^2-hybridization). Therefore, one would interpret such an increase of ν_{CN}(HNCS) as an increase of ionic character of the isothiocyanic acid. In the limit it would lead to a displacement of the electronic structure of the NCS group in HNCS to that of the free NCS^- ion.[5] $\nu_{CN}(SCN^-)$ is usually found at 2055 – 2070 cm^{-1} depending on the solvent used.

It is very difficult to find any general quantitative measure of the form of solute-solvent interactions. Some successful attempts to relate observed frequency changes of a solute to the electron density at likely centers of interaction of the solvents based upon the Taft (Hammett) inductive factors have been made (see, *e.g.*, Ref. 31). Most of the solvents used in this investigation would, however, have different atoms as centers of interaction and therefore a discussion about the inductive factors of the groups bonded to them is not meaningful.

It is reasonable to suggest that the solvent-solute interactions in this case could be a hydrogen bond formation RX···HNCS. Such hydrogen bonds would cause a weakening of the H–N bond, which in the valence bond treatment could be described as a decrease of the covalent character of the bond. It would also increase the bond order of the N–C bond and consequently ν_{CN}. If the solvent-solute interaction in this way is supposed to be directed towards the hydrogen atom of HNCS, a high electron density on the interacting atom of the solvent molecule would promote it.

Carbon tetrachloride and chloroform would use a chlorine atom as the center of interaction, but as could be inferred from the Taft inductive factors of $-CCl_3$ and $-CHCl_2$ (+2.65 and +1.94) this atom would be more negative for chloroform. Benzene is supposed to interact by the π electron cloud of the aromatic ring, whereas nitrobenzene is more likely to use an oxygen of the electronegative nitro group. It is therefore probable that the interaction of nitrobenzene is larger than that of benzene. The last member of the solvents used is diethyl ether,

which apparently is more basic than nitrobenzene (*cf.* the pK_a values reported in Ref. 32). Although the order of the solvents suggested above according to their possibilities to interact with the isothiocyanic acid hydrogen is very approximate, it is nevertheless the same that is given by the experimentally determined ν_{CN}(HNCS) in these solvents.

It is also interesting to see in Table 2 that the integrated absorptions follow an opposite trend as to the frequency. As has been argued before,[3] this is a logical change when a simple fixed charge model is used. This model would suggest that the larger the integrated absorptions for the thiocyanate groups the more covalent the H–NCS bond would be. The absolute values of the integrated absorption are, however, surprisingly small. As could be seen in, *e.g.*, Ref. 33 many N-bonded complexes would have integrated absorptions near 20×10^4 M^{-1} cm^{-2} and for organic thiocyanates they are between 15 and 20×10^4 M^{-1} cm^{-2}.[19] It should, however, be remembered that the model presupposes an almost independent SCN^- group and this is apparently not the case when the group is, for the main part, covalently bound to other atoms.

Iron(III) thiocyanato complexes. Thiocyanato complexes of iron(III) could be extracted into diethyl ether but not in appreciable amounts in the other solvents used when thiocyanic acid was extracted. The extraction into nitrobenzene has been reported by Maddock and Medeiros [18] but it was an extraction of tracer iron with a total iron concentration of 10^{-6} M, which is too small to give observable IR-absorption bands of the complexes extracted. When in this work more concentrated solutions were used, there were some species extracted that showed an intense IR-absorption at 1996 cm^{-1}. This band could hardly be the C–N stretching vibration of a ferric thiocyanato complex. The ratio Fe:SCN in the organic phase, as calculated from the total concentrations and those in the aqueous phase, would be 1:23. NaSCN cannot be extracted into nitrobenzene and therefore it must be suggested that the thiocyanate group has decomposed in some way and that the spectrum has its origin in these degradation products.

The infrared spectrum of the ether solution has an intense absorption band at 2042 cm^{-1} (Fig. 1 and Table 3). The integrated absorption of this band (calculated per SCN group) was 15.1×10^4 M^{-1} cm^{-2}. Analysis gave the stoichiometric ratio $Fe^{3+}:SCN^- = 1:4.5$. This suggests either that more than one ferric thiocyanate species are extracted or that some thiocyanate ions are extracted in another form. The absorption band is, however, somewhat asymmetric at the low frequency side, and as the C–N stretching frequency of HNCS is usually found at 2027 cm^{-1}, the most probable explanation would be that the ferric species is $Fe(NCS)_4^-$ and that HNCS is co-extracted in spite of the precautionary measures (see the experimental part). If this is so, the value of the integrated absorption also contains the contribution from the thiocyanate group in HNCS. Therefore, this quantity for the iron(III) thiocyanates is not known exactly but it may be supposed that it is $> 15 \times 10^4$ M^{-1} cm^{-2}.

Also an extraction of iron(III) thiocyanato complexes with trilaurylamine or rather trilaurylammonium nitrate has been performed. There are indications [7] that the only iron-con-

Table 3. Infrared spectral data of the extracted iron(III) thiocyanato complexes [probably $Fe(NCS)_4^-$] and $TLAH^+$ NCS^-. The values of ε, $\varepsilon\Delta\nu_{1/2}$ and A are calculated per SCN group.

	Solvent	ν_{CN} (cm^{-1})	ε (M^{-1} cm^{-1})	$\Delta\nu_{1/2}$ (cm^{-1})	$\varepsilon\Delta\nu_{1/2} \times 10^{-4}$ (M^{-1} cm^{-2})	$A \times 10^{-4}$ (M^{-1} cm^{-2})
$Fe(NCS)_4^-$	Diethyl ether	2042	1540	35	5.4	15.1
$TLAH^+Fe(NCS)_4^-$	Benzene	2048	790	57	4.5	12
$TLAH^+NCS^-$	Benzene	2042	630	45	2.8	8.4

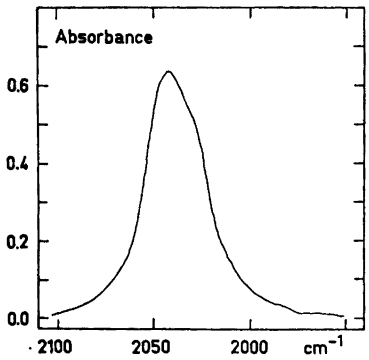

Fig. 1. The infrared spectrum in the C–N stretching range of the iron(III) thiocyanato complexes extracted into diethyl ether. $C_{Fe^{3+}} = 9.0 \times 10^{-3}$ (M) and $C_{SCN^-} = 40.6 \times 10^{-3}$ (M). The cell thickness is 0.10 mm.

taining anion extracted should be $Fe(NCS)_4^-$, but of course also other anions, *e.g.* NCS^-, could be extracted simultaneously.

The extraction of anions or anionic complexes by high molecular weight ammonium salts may be regarded as an anion exchange reaction. If for example an aqueous phase containing Fe^{3+} and SCN^- ion is shaken with a benzene solution of trilaurylammonium nitrate there would be exchanges in the following ways (*cf.* Ref. 7):

$$\overline{R_3NH^+NO_3^-} + Fe(NCS)_4^- \rightleftharpoons \overline{R_3NH^+Fe(NCS)_4^-} + NO_3^- \quad (1)$$

and

$$\overline{R_3NH^+NO_3^-} + SCN^- \rightleftharpoons \overline{R_3NH^+NCS^-} + NO_3^- \quad (2)$$

The ammonium salts, when dissolved in the common low dielectric constant organic solvents, usually exist as ion pairs, but also higher aggregations may occur in special cases. The main feature that characterizes an ion pair is the electrostatic nature of the interaction and no directed valence bonds would be involved. The infrared data of $\overline{TLAH^+NCS^-}$ (Table 3) show, however, a much lower C–N frequency and higher absorption intensity than would be expected from a thiocyanate ion with little electron exchange (*cf.* the values found not only for NaSCN but also for $Ph_3MeAsSCN$). It may be suggested that in the actual case a hydrogen bond formation $R_3NH^+\cdots NCS^-$ is possible, because such bonding would give the effect on the infrared spectra that has been found. This conclusion is supported by the reported [34] ν_{CN} values of $R_4N.NCS$ and R_3NHNCS ($R = C_{10}H_{21}$). For the tetradecylammonium salt, where hydrogen bonding is excluded, $\nu_{CN} = 2050$ cm, but for tridecylammonium thiocyanate the lower value $\nu_{CN} = 2043$ cm^{-1} was found.

The C–N frequency of $\overline{TLAH^+NCS^-}$ is also below that of $\overline{TLAH^+Fe(NCS)_4^-}$ (2042 cm^{-1} and 2048 cm^{-1}, respectively). But the difference is not large enough to let the two bands be fully resolved at the simultaneous extraction of both species. However, by assuming that the ratio Fe^{3+}:SCN^- is 4 the $\overline{TLAH^+SCN^-}$ concentration could be obtained from the total concentrations of iron and thiocyanate. Then a spectrum of $\overline{TLAH^+SCN^-}$ alone with the same concentration was run and the integrated absorption of the ferric complex determined graphically as the difference of the total, unresolved band and the $\overline{TLAH^+SCN^-}$ band. The method is rather rough because it cannot be excluded that there could be any interaction between the ferric species and $\overline{TLAH^+SCN^-}$ and therefore the value of the integrated absorption given in Table 3 (12×10^4 M^{-1} cm^{-2}) should be regarded as approximate. This is still well above that of the unbounded thiocyanate group.

As mentioned above the extracted ferric thiocyanato complexes would probably be four-coordinated. Also six-coordinated complexes, tributylammonium- and triphenylmethylarsonium-hexathiocyanato ferrate(III), were prepared and investigated both in the solid state and in solution, and the results are given in Table 4.

For isolated octahedral ions of the type $M(NCS)_6^{n-}$ belonging to the point group O_h, one would expect a single C–N stretching absorption band. In the solid state, however, splitting could appear owing to site symmetry and correlation effects.[10] This is probably the case for $(Bu_3NH)_3Fe(NCS)_6$ pressed in KBr pellets. The splitting observed when the compounds are dissolved in the various solvents could hardly be due to such effects, but may be caused by a decomposition of the complex. A plausible way is then a partial dissociation:

$$Fe(NCS)_6^{3-} \rightleftharpoons Fe(NCS)_{6-n}^{(3-n)-} + nSCN^- \quad (3)$$

The "free" thiocyanate ion would have about

Table 4. Frequencies and integrated absorptions of the C–N vibration of $(Bu_3NH)_3Fe(NCS)_6$ and $(Ph_3MeAs)_3Fe(NCS)_6$ in various solvents. A is the total integrated absorption over all bands cited and is calculated per SCN group.

Solvent *etc.*	$(Bu_3NH)_3Fe(NCS)_6$		$(Ph_3MeAs)_3Fe(NCS)_6$	
	ν_{CN} (cm^{-1})	$A \times 10^{-4}$ (M^{-1} cm^{-2})	ν_{CN} (cm^{-1})	$A \times 10^{-4}$ (M^{-1} cm^{-2})
KBr	2080, 2055	5.6	2060	6.0
Diethyl ether	2040, 2070sh	[a]	[b]	[b]
Chloroform	2045, 2000sh	13.2	2067	[a]
Pyridine	2038, 2055sh	9.5	2055, 2036sh	7.8
Nitrobenzene	2033, 2060sh, 1995sh	14.4	2059, 2037	12.7
Acetonitrile	2054	13.7	2059	11.7
Dimethyl sulfoxide	2055, 2038sh	6.8	2055, 2038sh	6.8

[a] The solubility of the compound is too low to permit determination of the integrated absorption.
[b] The compound is insoluble in this solvent. sh = shoulder.

the same frequency as $Fe(NCS)_6^{3-}$ and therefore would be difficult to observe. The low frequency band (2040 – 2030 cm^{-1}) in the spectrum could then be assigned to the complex formed through the dissociation of $Fe(NCS)_6^{3-}$. The large frequency shift is a strong indication of different configurations of the two complexes. Of course the infrared spectrum gives no definite evidence that the complex formed is tetrahedral, but, as has been mentioned previously, the frequency shift is that expected from a change from octahedral to tetrahedral configuration. The expected increase of the integrated absorption is more difficult to observe as the equilibrium between the forms changes from solvent to solvent and also depends on the kind of cation present. The solvents in Table 4 are given in an order of increasing dielectric constants and from a theoretical point of view one would expect the equilibrium (3) to be further to the right for solvents of low polarity because highly charged species are disfavoured in such solvents. This seems also to be partly justified by the frequencies given in the table although the dimethyl sulfoxide solutions show an obvious dissociation of the six-coordinated complex. As expected, the cation influence on the equilibrium is also accentuated in solutions of low polarity. Generally $(Ph_3MeAs)_3Fe(NCS)_6$ is less soluble than $(Bu_3NH)_3Fe(NCS)_6$ and it is also less disposed to dissociate. This is best illustrated by the chloroform solutions. The spectra of $(Bu_3NH)_3Fe(NCS)_6$ in chloroform and in nitrobenzene (Fig. 2) reveal another peculiarity, *viz.* traces of absorption peaks at about 2000 cm^{-1}. It may be suggested that this is due to a decomposition of thiocyanate groups like that found above at the extraction of thiocyanato complexes of iron(III) into nitrobenzene.

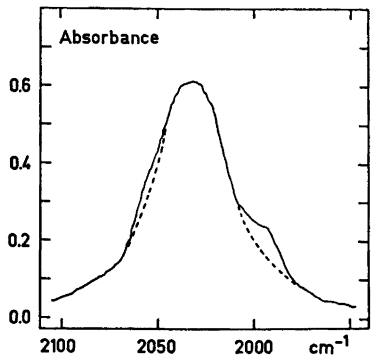

Fig. 2. The infrared spectrum in the C–N stretching range of $(Bu_3NH)_3Fe(NCS)_6$ dissolved in nitrobenzene (8.85×10^{-3} M). The cell thickness is 0.10 mm.

Acknowledgements. The author thanks Dr. Ragnar Larsson for his encouragement and many valuable comments on the work. The investigation has been financially supported by Statens Naturvetenskapliga Forskningsråd (Swedish Natural Science Research Council) which is also gratefully acknowledged.

REFERENCES

1. Fronæus, S. and Larsson, R. *Acta Chem. Scand. 16* (1962) 1447.
2. Larsson, R. and Miezis, A. *Acta Chem. Scand. 19* (1965) 47.
3. Larsson, R. and Miezis, A. *Acta Chem. Scand. 23* (1969) 37.
4. Miezis, A. *Acta Chem. Scand. 27* (1973) 3746.
5. Jones, L. H. *J. Chem. Phys. 25* (1956) 1069.
6. Kharitonov, Yu. Ya., Tsintsadze, G. V. and Porai-Koshits, M. A. *Russ. J. Inorg. Chem. 10* (1965) 427.
7. Burkin, A. R., Rice, N. M. and Rogers, M. J. In Dyrssen, D., Liljenzin, J. O. and Rydberg, J., Eds., *Solvent Extraction Chemistry*, North-Holland, Amsterdam 1967, p. 439.
8. Forster, D. and Goodgame, D. M. L. *J. Chem. Soc.* (1965) 268.
9. Forster, D. and Goodgame, D. M. L. *Inorg. Chem. 4* (1965) 715.
10. Clark, R. J. H. and Goodwin, A. D. J. *Spectrochim. Acta 26 A* (1970) 323.
11. Schmidtke, H.-H. and Garthoff, D. *Helv. Chim. Acta 50* (1967) 1631.
12. Bailey, R. A., Kozak, S. L., Michelsen, T. W. and Mills, W. N. *Coord. Chem. Rev. 6* (1971) 407.
13. Bailey, R. A., Michelsen, T. W. and Mills, W. N. *J. Inorg. Nucl. Chem. 33* (1971) 3206.
14. Mitchell, K. M. and MacDonald, J. Y. *J. Chem. Soc.* (1951) 1310.
15. Mironov, V. E. and Rutkovskii, Yu. I. *Russ. J. Inorg. Chem. 10* (1965) 580.
16. Specker, H., Jackwerth, E. and Hövermann, G. *Z. Anal. Chem. 177* (1960) 10.
17. Bock, R. *Z. Anal. Chem. 133* (1951) 110.
18. Maddock, A. G. and Medeiros, L. O. *J. Chem. Soc. A* (1969) 1946.
19. Ham, N. S. and Willis, J. B. *Spectrochim. Acta 16* (1960) 279.
20. Goubeau, J. and Reyhing, J. *Z. Anorg. Allg. Chem. 294* (1958) 96.
21. Oba, K., Watari, F. and Aida, K. *Spectrochim. Acta 23 A* (1967) 1515.
22. Wada, M. and Okawara, R. *J. Organometal. Chem. 8* (1967) 261.
23. Reid, C. *J. Chem. Phys. 18* (1950) 1512.
24. Diamond, R. M. and Tuck, D. G. *Progr. Inorg. Chem. 2* (1960) 109.
25. Vogel, A. I. *A Text-book of Quantitative Inorganic Analysis*, Longmans, London 1961.
26. Ziegler, M., Glemser, O. and Petri, N. *Z. Anal. Chem. 154* (1957) 81.
27. Dwyer, F. P. and Gibson, N. A. *Analyst (London) 76* (1951) 548.
28. Beard, C. I. and Dailey, B. P. *J. Chem. Phys. 18* (1950) 1437.
29. Pauling, L. *The Nature of the Chemical Bond*, Cornell University Press, Ithaca, New York 1960, Chapter 8.
30. Bauer, E. and Magat, M. *J. Phys. Radium. 9* (1938) 319.
31. Caldow, G. C. and Thompson, H. W. *Proc. Roy. Soc. (London) A 254* (1960) 1.
32. *Dissociation Constants of Organic Bases in Aqueous Solution, Suppl. 1972* Butterworths, London 1972.
33. Bailey, R. A., Kozak, S. L., Michelsen, T. W. and Mills, W. N. *Coord. Chem. Rev. 6* (1971) 407.
34. Vdovenko, V. M., Skoblo, A. I. and Suglobov, D. N. *Radiokhim. 9* (1967) 119.

Received January 16, 1974.

Acta Chemica Scandinavica A 28 (1974) 423—427

The Stability Constants for Complexes between Oxovanadium(IV) and Squaric Acid

DAGMAR ALEXANDERSSON and NILS-GÖSTA VANNERBERG

Department of Inorganic Chemistry, Chalmers University of Technology and the University of Göteborg, P.O. Box, S-402 20 Göteborg 5, Sweden

The formation of complexes between the oxovanadium(IV) ion and squaric acid has been studied at 25°C with spectrophotometric methods in solutions in which the total molarity was held constant at 3 M by the addition of $NaClO_4$. The total concentrations of oxovanadium(IV) perchlorate and sodium squarate ranged from 5 to 100 mM and 0.1 to 2 mM, respectively. The pH range was 1.6 – 2.8. Preliminary constants were obtained graphically. These were then refined with Sillén's generalized least squares program "Letagrop". The experimental data could best be explained in terms of the following equilibrium in the $VO^{2+} - H^+ - C_4O_4^{2-}$ system:

$$VO^{2+} + C_4O_4^{2-} \rightleftharpoons VOC_4O_4 \qquad \log \beta_{101} = 2.47 \pm 0.04$$

The error given corresponds to 3σ in β, where σ is the standard deviation in β.

In connection with studies on complex formation between the squarate ion, $C_4O_4^{2-}$, denoted A^{2-} in the following, and transition metal ions, we have found that nickel(II) forms very weak complexes.[1] According to Tedesco and Walton,[2] however, complexes with metal ions of higher valency [iron(III), aluminium(III), and uranium(VI)] are stronger. As a complement to our investigation on complex formation with nickel(II) with 8 *d*-electrons we have now chosen vanadium(IV) with 1 *d*-electron.

EXPERIMENTAL

Chemicals and analyses. Oxovanadium(IV) perchlorate was prepared from vanadium(IV) oxide (Schuchardt) by dissolving in an excess of 6 M perchloric acid (Merck *p.a.*). The solution was neutralized by adding a solution of sodium hydroxide (Bohus EKA *p.a.*). Oxovanadium hydroxide was then precipitated by the dropwise addition of the sodium hydroxide solution as long as any precipitate was formed. The precipitate was centrifuged, washed and dissolved in a slight excess of perchloric acid, as described by Rossotti and Rossotti.[3] The concentration of vanadium(IV) in the solution was determined by titration with a standardized potassium permanganate solution. The solution was also tested for the presence of vanadium(V) in the way described by Rossotti and Rossotti. No traces of vanadium(V) were found. The free hydrogen ion concentration was determined by Gran titrations.[4]

Perchloric acid, *sodium perchlorate*, and *sodium squarate* solutions were prepared as described elsewhere.[5]

Apparatus. The *ultra-violet absorption measurements* were performed as described previously.[1] The absorbance was measured at 25 different wavelengths ranging from 240 to 300 nm.

The solutions to be examined were prepared by mixing solutions of oxovanadium(IV) perchlorate, sodium squarate and perchloric acid, the total molarity being held constant at 3 M by the addition of a sodium perchlorate solution. The total concentrations of sodium squarate, A, and oxovanadium(IV) perchlorate, B, varied within the ranges 0.1 – 2 mM and 5 – 100 mM, respectively. The concentration of the free squarate ion, A^{2-}, however, ranged from only 0.003 to 0.3 mM, owing to the varying hydrogen ion and VO^{2+} concentrations.

The *free hydrogen ion concentration*, h, was measured in each solution by emf methods, as described previously.[5]

To obtain a reasonable concentration of squarate ions, A^{2-}, it is necessary to work at as high a pH as possible (*cf.* Fig. 1). On the other hand, it is desirable to avoid hydrolysis of VO^{2+}. The pH range was thus chosen so that the concentrations of the hydrolysis complexes were kept $< 10^{-5}$ M, as calculated by means of the formation constants determined by Rossotti and Rossotti.[3] The pH range chosen was therefore $1.6 \leq$ pH ≤ 2.8.

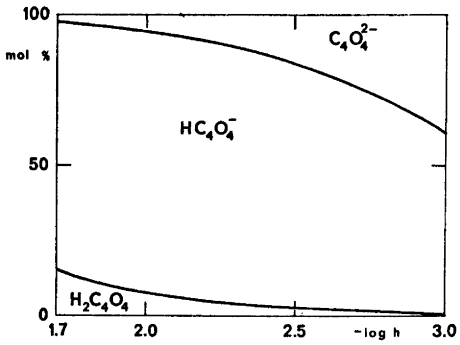

Fig. 1. The distribution of squaric acid species as a function of $-\log h$.

LIST OF SYMBOLS

A total concentration of squaric acid, H_2A
a free concentration of squarate ions, A^{2-}
B total concentration of VO^{2+}
b free concentration of VO^{2+}
H total concentration of hydrogen ions, H^+
h free concentration of hydrogen ions, H^+
c_{pqr} free concentration of $(VO)_pH_qA_r^{(2p+q-2r)+}$
β_{pqr} equilibrium constant for the reaction $pVO^{2+} + qH^+ + rA^{2-} \rightleftharpoons (VO)_pH_qA_r^{(2p+q-2r)+}$ defined so that $c_{pqr} = \beta_{pqr} b^p h^q a^r$
ε_{pqr} molar absorptivity for the complex $(VO)_pH_qA_r^{(2p+q-2r)+}$
A_s absorbance
l optical path length
$\varepsilon = (A_s - l\ \varepsilon_{100} b)/Al$

MEASUREMENTS

Both the components of the squaric acid system and the VO^{2+} ion show strong absorption in the UV region. For the VO^{2+} ion the absorption increases with decreasing wavelength. In Fig. 2 the experimentally determined absorbances of a solution with $A = 1.000$ mM, $B = 20.00$ mM and $-\log h = 2.58$ are shown, as well as the sum of the calculated absorbances of two solutions with the same A and B values, respectively, and the same h value. There are large differences between the curves and thus VO^{2+} would appear to form squarate complexes.

Of the measurements at 25 different wavelengths those at 16 wavelengths were chosen to determine the stability constants and the molar

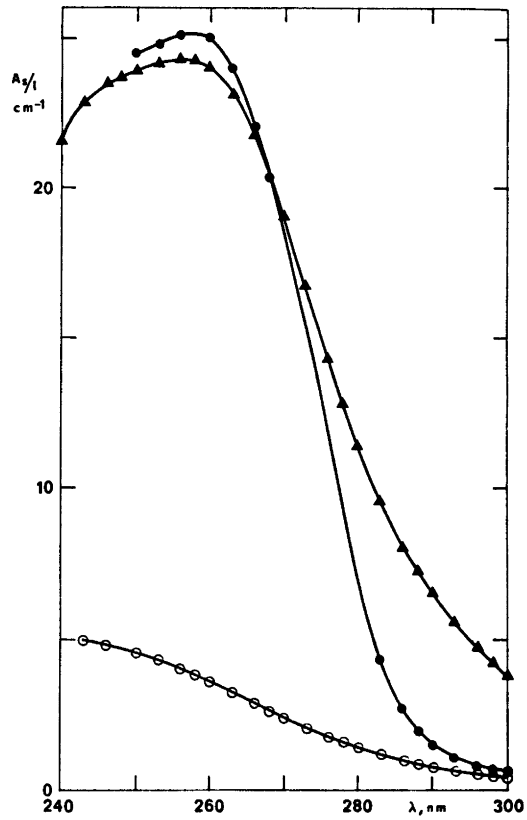

Fig. 2. Experimentally determined absorbances (▲) for a solution with $A = 1.000$ mM, $B = 20.00$ mM, and $-\log h = 2.58$, compared with the sum of the calculated absorbances (●) for two solutions with $A = 1.000$ mM, $B = 0$ mM, $-\log h = 2.58$ and $A = 0$ mM, $B = 20.00$ mM, $-\log h = 2.58$, respectively. The calculated absorbances (○) for the last solution only are also shown.

absorptivities for the complexes. Eight of these correspond to wavelengths in the range 250 – 268 nm, where the HA^- and A^{2-} ions show strong absorption and eight correspond to wavelengths in the range 283 – 300 nm, where the absorption of the VO^{2+} complexes dominate. The other measurements were used only to determine the molar absorptivities at the wavelengths used.

The VO^{2+} squarate solutions were not as stable as those of nickel(II),[1] the absorbances decreasing gradually at all the wavelengths used. The decrease was constant during the 2 months during which the measurements were made and largest in solutions with the highest A and B

values. In all the solutions the decrease was < 0.4 % per day. The pH values were constant or showed a very small decrease. It would seem probable that a redox reaction took place between the VO^{2+} ion and a component of the squaric acid system, and, since $B \gg a$, the decrease in B was negligible. The decrease in absorbance was not affected when a stream of nitrogen gas was passed through the solutions and these were then kept in a nitrogen atmosphere.

In the graphical calculations the first absorbances measured one day after the preparation of the solutions were used, while in the "Letagrop" calculations the measured absorbances were corrected for the estimated decrease.

TREATMENT OF DATA

The absorbance, A_s, at a given wavelength in a solution may be expressed as follows:

$$A_s = l \sum_p \sum_q \sum_r \varepsilon_{pqr} c_{pqr} = l \sum_p \sum_q \sum_r \varepsilon_{pqr} \beta_{pqr} b^p h^q a^r \qquad (1)$$

As is described in the work on nickel(II) squarate complexes,[1] the ε_{021}, ε_{011}, and ε_{001} values were determined by means of the spectrophotometric version of the "Letagrop" program.[6] The stability constants for squaric acid, obtained from the emf measurements [5] were used. The ε_{100} values were determined in solutions where $A = 0$ and $25 \text{ mM} \leq B \leq 100$ mM, also using the "Letagrop" program.

Owing to the low total concentration of squaric acid, $A \leq 2$ mM, complexes with $r = 1$ seem to be the most likely and therefore $q = 0$ or 1 are more probable than higher values of q. With ε defined as

$$\varepsilon = (A_s - l\varepsilon_{100} b)/Al$$

eqn. (1) can be transformed to

$$\varepsilon = (\varepsilon_{001} + \varepsilon_{011}\beta_{011}h + \varepsilon_{021}\beta_{021}h^2 + \sum_p \varepsilon_{p01}\beta_{p01}b^p + \sum_p \varepsilon_{p11}\beta_{p11}b^p h)/ (1 + \beta_{011}h + \beta_{021}h^2 + \sum_p \beta_{p01}b^p + \sum_p \beta_{p11}b^p h) \qquad (2)$$

or

$$\frac{\varepsilon(1 + \beta_{011}h + \beta_{021}h^2) - (\varepsilon_{001} + \varepsilon_{011}\beta_{011}h + \varepsilon_{021}\beta_{021}h^2)}{\varepsilon b} = -\sum_p (\beta_{p01} + \beta_{p11}h)b^{p-1} + \frac{1}{\varepsilon}\sum_p (\varepsilon_{p01}\beta_{p01} + \varepsilon_{p11}\beta_{p11}h)b^{p-1} \qquad (3)$$

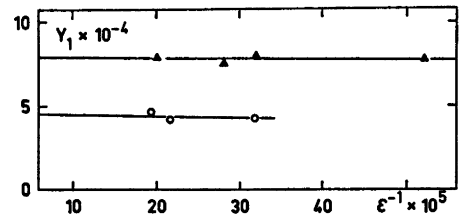

Fig. 3. The left-hand side of eqn. (3) divided by h, Y_1, as a function of ε^{-1} for $\lambda = 293$ nm, $A = 1.000$ mM, and varying h values. The following B values were used: ▲ 20.00 mM and ○ 39.30 mM.

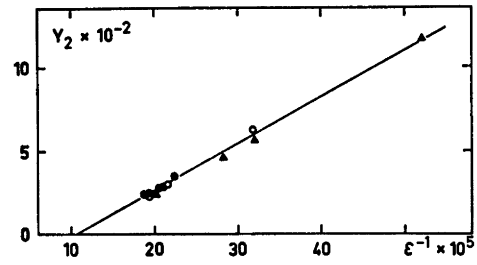

Fig. 4. The left-hand side of eqn. (3), Y_2, as a function of ε^{-1} for $\lambda = 293$ nm, $A = 1.000$ mM, and varying h values. The following B values were used: ▲ 20.00 mM, ○ 39.30 mM, and ● 100.0 mM. From the slope and intercept $\beta_{101} = 298$ M^{-1} and $\varepsilon_{101} = 9440$ M^{-1} cm^{-1} were obtained. For solutions with the same A and B values the concentration of free squarate ions, a, decreases with increasing h as does the concentration of the vanadium(IV) complex. The points for solutions with the highest h values (and thus the lowest ε values at $\lambda = 293$ nm) are to be found to the right in the figure.

In solutions where $B \gg A$, b can be replaced by B. To test whether or not VO^{2+} complexes containing hydrogen ions are formed, those with $q = 0$ were omitted and all terms in eqn. (3) were divided by a factor h. The left-hand side of the equation was then plotted against ε^{-1} (*cf.* Fig. 3). When data from solutions with $A = 1.000$ mM, $B = 20.00$ mM or 39.30 mM, and varying h values were used, it was possible to draw straight lines through the points. These almost horizontal lines imply that $\sum_p \beta_{p11} B^{p-1} < 0$ and thus that $(VO)_p HA_{(2p-1)}^{+}$ would not appear to be the main complexes formed.

VO^{2+} complexes with $q = 1$ were then omitted in eqn. (3) and the left-hand side was plotted against ε^{-1} (*cf.* Fig. 4). Data from solutions with

$A = 1.000$ mM, $B = 20.00$ mM, and varying h values were used and a linear correlation was obtained. Data from solutions with other B values were then inserted and the new points still indicated the same line. $\sum_p \beta_{p01} B^{p-1}$ and $\sum_p \varepsilon_{p01} \beta_{p01} B^{p-1}$ are thus independent of B, *i.e.* $p = 1$. From the slope and intercept of the line the following constants were obtained:

$\beta_{101} = 298$ M^{-1}
$\varepsilon_{101} = 9440$ cm^{-1}M^{-1}
for $\lambda = 293$ nm.

In order to obtain more accurate results, the data were processed with the spectrophotometric version of the "Letagrop" program.[6] The refinement of the constant gave the following best value:

$\beta_{101} = (297 \pm 30)$ M^{-1}
$\log \beta_{101} = 2.47 \pm 0.04$

The error squares sum, defined as

$$U = \sum \left(\frac{A_{s,calc} - A_s}{l} \right)^2$$

was 7.79 for 497 A_s values. Calculations made using "relative errors" and

$$U_r = \sum \left(\frac{A_{s,calc} - A_s}{A_s} \right)^2$$

yielded the same β_{101} value ($\log \beta_{101} = 2.47 \pm 0.03$) but slightly different standard deviations, *i.e.* smaller in β and larger in ε.

Efforts were also made to explain the experimental data by inserting other complexes [*i.e.* $(pqr) = (111)$ or (201), together with (101)] and processing them simultaneously. The improvement in U was, however, small and the standard deviations in β were large. It would therefore seem that no other complexes were present in detectable amounts.

RESULTS AND DISCUSSION

The experimental data could best be explained by the presence of the complex, VOA, with the formation constant

$\log \beta_{101} = 2.47 \pm 0.04$

where the error given corresponds to an error of 3σ in β, σ being the standard deviation. This β value has been used, together with the previously determined [5] $\log \beta_{011} = 3.19$ and $\log \beta_{021} = 4.15$, to calculate the distribution of the squarate ion, A^{2-}, between the different complexes for different vanadium concentrations (*cf.* Figs. 1, 5, and 6). Despite the rather low pH and thus the low percentage of free A^{2-} ions, about 50 % of the squaric acid can be bound in the form of a vanadium(IV) complex.

The UV spectrum of the VO^{2+} complex differs considerably from that of the squarate ion (*cf.* Fig. 7) in contrast to the spectra of the weaker nickel complexes.[1] Complex formation between a VO^{2+} ion and a squarate ion thus affects the electronic structure of the latter so that the absorption maximum occurs at a lower wave-

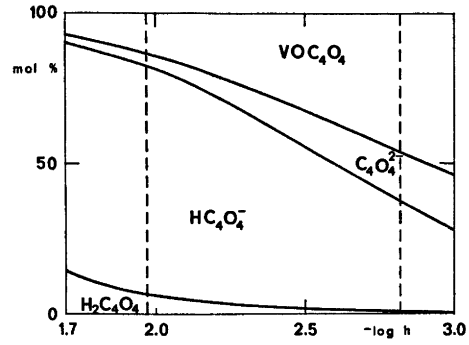

Fig. 5. The distribution of squaric acid species as a function of $-\log h$ for the oxovanadium(IV) squarate system when $B = 10.00$ mM. Only the $-\log h$ values between the dashed lines have been used.

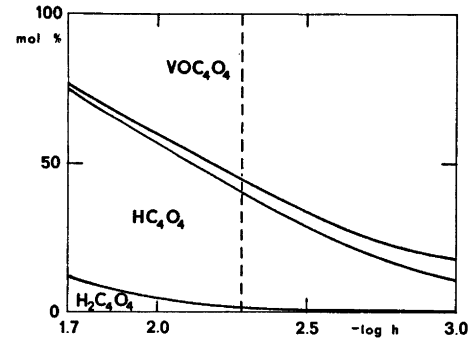

Fig. 6. The distribution of squaric acid species as a function of $-\log h$ for $B = 40.00$ mM. Only the $-\log h$ values to the left of the dashed line have been used.

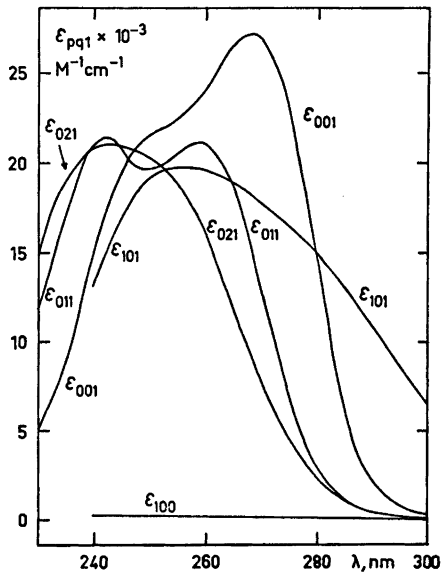

Fig. 7. ε_{pq1} as a function of λ. The ε_{pq1} values have been calculated by the "Letagrop" program.

length, *i.e.* 256 nm. The molar absorptivities are, moreover, also lower (*cf.* Fig. 7). A similar effect is seen when the squarate ion binds two hydrogen ions. The spectrum of squaric acid shows a maximum at 242 nm and a shape similar to that of the VO^{2+} squarate complex.

The authors would like to thank Professor Georg Lundgren for many stimulating discussions and invaluable help during the preparation of this paper. They are indebted to Mr. Ove Lindgren, fil.lic., for help with the computer programs and would also like to thank Dr. Susan Jagner for revising the English text of this paper. Financial support from the Swedish Natural Science Research Council is gratefully acknowledged.

REFERENCES

1. Alexandersson, D. and Vannerberg, N.-G. *Acta Chem. Scand. 27* (1973) 3499.
2. Tedesco, P. H. and Walton, H. F. *Inorg. Chem. 8* (1969) 932.
3. Rossotti, F. J. C. and Rossotti, H. S. *Acta Chem. Scand. 9* (1955) 1177.
4. Gran, G. *Analyst (London) 77* (1952) 661.
5. Alexandersson, D. and Vannerberg, N.-G. *Acta Chem. Scand. 26* (1972) 1909.
6. Sillén, L. G. and Warnqvist, B. *Ark. Kemi 31* (1969) 377.

Received December 10, 1973.

Acta Chemica Scandinavica A 28 (1974) 428—434

Tris-complexes of $(-)_D$- and $(+)_D$-[1-(2-Pyridyl)ethylamine] and Cobalt(III). Preparation and Partial Structural Assignment of Geometrical and Optical Isomers

KIRSTEN MICHELSEN

Chemistry Department I (Inorganic Chemistry), University of Copenhagen, H. C. Ørsted Institute, Universitetsparken 5, DK 2100 Copenhagen Ø, Denmark

Tris-complexes of $(-)_D$and$(+)_D$-[1-(2-pyridyl)-ethylamine] with cobalt(III) were prepared, and three different isomers and their enantiomers were isolated by column chromatography. The absorption spectra, circular dichroism spectra and ^1H NMR spectra of the compounds suggest that they are:

A: *fac*-$\Lambda(+)_D-[Co\{(S)(-)_D\text{-}C_7H_{10}N_2\}_3]Cl_3$, B: *fac*-$\Delta(-)_D$-$[Co\{(S)(-)_D\text{-}C_7H_{10}N_2\}_3]Cl_3$, C: *mer*-$\Lambda(+)_D$-$[Co\{(S)(-)_D\text{-}C_7H_{10}N_2\}_3]Cl_3$, A′: *fac*-$\Delta(-)_D$-$[Co\{(R)(+)_D\text{-}C_7H_{10}N_2\}_3]Cl_3$, B′: *fac*-$\Lambda(+)_D$-$[Co\{(R)(+)_D\text{-}C_7H_{10}N_2\}_3]Cl_3$, C′: *mer*-$\Delta(-)_D$-$[Co\{(R)(+)_D\text{-}C_7H_{10}N_2\}_3]Cl_3$.

In a recent paper [1] tris-complexes of cobalt(III) with the bidentate ligand 2-picolylamine [(2-pyridyl)methylamine] (Fig. 1a) were described. In this work the corresponding complexes of cobalt(III) with the related ligand 1-(2-pyridyl)-ethylamine (Fig. 1 b) have been investigated. Resolution of the racemic form of this amine with tartaric acid gives the two optically active amines, the $(-)_D$-form of which is reported to have the *S*-configuration.[2,3] Theoretically each of the formulas $[Co\{(-)_D\text{-}C_7H_{10}N_2\}_3]X_3$ and $[Co\{(+)_D\text{-}C_7H_{10}N_2\}_3]X_3$ represents several isomers. First, the ligand is unsymmetrical and consequently two geometrical forms of the tris-complexes may occur, namely *facial* and *meridional* forms (Fig. 2). Secondly, the ligands may adopt a Δ or a Λ configuration around the central atom, and thirdly, their conformations may be δ or λ.

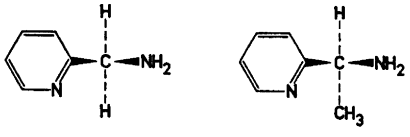

Fig. 1. a. (2-Pyridyl)methylamine (2-picolylamine). b. 1-(2-Pyridyl)ethylamine.

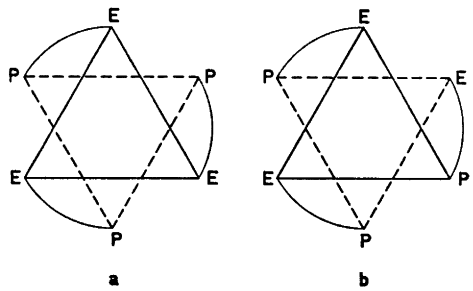

Fig. 2. Geometrical isomers of tris-complexes of 1-(2-pyridyl) ethylamine and cobalt(III). P symbolizes the "pyridine nitrogen", E the "ethylamine nitrogen". a. A *facial* isomer. b. A *meridional* isomer. Both isomers have the configuration Λ.

We succeeded in isolating 3 different tris-complexes (A, B, and C) with $(-)_D$-1-(2-pyridyl)-ethylamine and the corresponding 3 enantiomers (A′, B′, and C′) with the $(+)_D$-amine.

General remarks concerning the preparative methods. Racemic 1-(2-pyridyl)ethylamine was prepared by way of a zinc-acetic acid reduction of 2-pyridylmethyl ketoxime,[4] and the yield was acceptable contrary to the experience of Kolloff *et al.*[5]

Recently the amine has been resolved independently at 3 different laboratories. The methods were in principle the same, tartaric acid being used as the resolving agent. Smith *et al.*[2] and Cervinka *et al.*[3] report to have prepared the $(-)_D$-amine, the latter without giving any experimental details. We have isolated both the $(-)_D$- and the $(+)_D$-amine.

The cobalt complexes were prepared by two different methods. In method 1 [6] *trans*-dichlorotetrakis(pyridine)cobalt(III) chloride reacted with the amine in a convenient medium, and in method 2 a solution of cobalt(II) chloride was oxidized by atmospheric oxygen in the presence of the amine. The crude products obtained from either method were separated in the different isomers on a column, and gave the same 3 tris-complexes, named A (A′), B (B′) and C (C′) in the order of their elution. If activated charcoal was added to the cobalt(II) chloride, A (A′) and B (B′) were formed as before, but the yield of C (C′) was negligible.

EXPERIMENTAL

Reagents. The initial material *trans*$[Co\,py_4Cl_2]$-$Cl.6H_2O$ was prepared by a method developed by Glerup and Schäffer.[7] 2-Acetylpyridine was purchased from Fluka AG, Buchs, Switzerland, Norit SA 1 from Norit Sales Corp. Ltd., Amsterdam and SE-Sephadex C-25 from Pharmacia, Uppsala, Sweden. All other chemicals were of reagent grade and were used without further purification.

Physical measurements. Electronic absorption spectra were recorded on a Cary Model 14 spectrophotometer. The solvent was 0.1 M hydrochloric acid. The spectra are characterized by their maxima and minima (ε, λ), where the molar extinction coefficient ε is in units of 1 mol^{-1} cm^{-1}, and λ is in nm. Circular dichroism was measured on a Roussel-Jouan Dichrographe I. The solvent was 0.1 M hydrochloric acid. The maxima are given below as $(\Delta\varepsilon, \lambda) = (\varepsilon_l - \varepsilon_r, \lambda)$. Optical rotation was measured on a Perkin Elmer Model 141 polarimeter. The amine tartrates were dissolved in water, the cobalt complexes in 0.1 M hydrochloric acid. ^1H NMR spectra were obtained on a Varian Model A-60 spectrometer using sodium 3-trimethyl-silyl-1-propane sulfonate (TPSNa) as an internal standard. The solvents were D_2O and $D_2O + D_2SO_4$.

Analyses. The cobalt analyses were performed on a Perkin Elmer 403 Atomic Absorption Spectrophotometer. The microanalytical laboratory of this institute carried out the carbon and the nitrogen analyses by standard methods. Thermogravimetric determinations of water contents in the cobalt complexes were performed on a thermobalance previously described.[8]

Preparation of the ligand

2-Pyridylmethyl ketoxime. A modification of Pinner's method [9] was used. 60 g of hydroxylamine hydrochloride (0.86 mol) was dissolved in 140 ml of water. 100 g of 2-acetylpyridine (0.90 mol) was added. After 1 h the oxime was set free by the addition of a saturated solution of potassium carbonate (~300 ml). After cooling on ice and stirring, white crystals separated. They were filtered, washed with water and recrystallized from ethanol. Yield: 91 g (78 %), m.p. 115–118° (litt.[9,10] m.p. 120°, 121°).

1-(2-Pyridyl)ethylamine. In principle the method was the same as that used by La Forge [4] for the preparation of 1-(3-pyridyl)ethylamine. 50 g of 2-pyridyl ketoxime (0.37 mol) was dissolved in 700 ml of ethanol (95 %). The solution was placed in a beaker (2 l) equipped with magnetic stirring. 400 g of zinc dust and 400 ml of glacial acetic acid were added alternately in small portions over a period of 7 h. The reaction mixture was left for further 17 h. Then the precipitate of undissolved zinc and zinc acetate was filtered off and carefully washed with ethanol (700 ml). The combined filtrates were evaporated on a vacuum rotatory evaporator, and the acetic acid was removed by repeated additions of water to the residue followed by evaporations. Finally, the amine was set free by the addition of a saturated solution of potassium hydroxide. The separated oil was extracted with ether, the ethereal solution was dried over sodium sulfate, filtered, dried over sodium, and the solvent was evaporated. Distillation of the residue gave an almost colourless oil, $b.p._{16}$ 89° (lit.[2] $b.p._{24}$ 96–97°). The yields varied in different experiments from 37 to 42 g (82–93 %).

$(-)_D$ and $(+)_D$-1-(2-Pyridyl)ethylammonium $(+)_D$-hydrogentartrate. A solution of 75 g of tartaric acid (0.50 mol) in 50 ml of water (80°) was added to a solution of 100 ml of 1-(2-pyridyl)ethylamine (0.84 mol) in 50 ml of water (80°). The mixture was allowed to cool to room temperature, and the following day fraction 1, 40 g of white crystals, $[\alpha]_D^{25} = 4.8°$, could be filtered and washed with ethanol. The mother liquor was heated to 80°, and 45 g of tartaric acid (0.30 mol) was added. When the solution was cooled on ice, fraction 2, 47 g, $[\alpha]_D^{25} = 8.5°$ separated. The filtrate was evaporated on a vacuum rotatory evaporator to give fraction 3, 38 g, $[\alpha]_D^{25} = 24.1°$, fraction 4, 24 g, $[\alpha]_D^{25} = 18.7°$, and several smaller fractions with $[\alpha]_D^{25}$ ranging from 12° to 19°. Fraction 1 was recrystallized once and fraction 2 twice from water to give a total amount of 49 g of $(-)_D$-1-(2-pyridyl)ethylammonium $(+)_D$-hydrogentartrate monohydrate; 40 % (Found: C 45.8; N 9.62; H 6.39. Calc. for $C_{11}N_2H_{18}O_7$: C 45.5; N 9.65; H 6.25). $[\alpha]_D^{25} = +4.3°$ ($c = 0.01$ g/ml), $[\alpha]_D^{25} = +4.8°$ ($c = 0.04$

g/ml). (Lit.[3,2] $[\alpha]_D^{25} = +5.4°$ ($c = 0.04$ g/ml) and $[\alpha]_D^{25} = +5.1°$ ($c = 0.04$ g/ml). Fraction 3 was recrystallized once and fraction 4 twice from water to give a total amount of 36 g of $(+)_D$-1-(2-pyridyl)ethylammonium $(+)_D$-hydrogentartrate monohydrate, 30 %. (Found: C 45.3; N 9.65; H 6.21. Calc. for $C_{11}N_2H_{18}O_7$: C 45.5; N 9.65; H 6.25). $[\alpha]_D^{25} = +24.8°$ ($c = 0.01$ g/ml). This value for $[\alpha]_D^{25}$ could not be improved by further recrystallizations, and the "symmetric" results for molar rotations and circular dichroism of the corresponding cobalt complexes with $(-)_D$- and $(+)_D$-1-(2-pyridyl)ethylamine, respectively, proved that the separation had been complete. The impure fractions mentioned above were recrystallized several times to give 5 to 10 g of each of the pure salts. The pure, optically active amines could be isolated as described above for the racemic amine, but it was not necessary for our special purpose.

Preparation of the cobalt complexes

Tris-{$(-)_D$-1-(2-pyridyl)ethylaminec}cobalt-(III) chloride, $[Co\{(-)_D\text{-}C_7H_{10}N_2\}_3]Cl_3$. Preparation of the crude product by means of method 1: 0.80 g of lithium hydroxide monohydrate (19 mmol) was dissolved in 8 ml of boiling water, and 3.00 g of $(-)_D$-1-(2-pyridyl)ethylammonium $(+)_D$-hydrogentartrate, monohydrate (10.3 mmol) was added. The solution was cooled on ice. The addition of 30 ml of pyridine and 20 ml of ethanol caused the lithium tartrate to precipitate. The filtrate, containing $(-)_D$-1-(2-pyridyl)-ethylamine, was added to a solution of 1.50 g $[Copy_4Cl_2]Cl.6H_2O$ (2.54 mmol) in 30 ml of pyridine. An immediate colour-shift from green to red-brown took place. After 15 min the solution was cooled on ice, and a sticky, yellow-brown solid was precipitated by the addition of ethanol and ether. Washing with ether.

Separation of the isomers: The crude product, a mixture of bis- and tris-complexes, was dissolved in water. The solution was poured on a column of a SE-Sephadex C-25 cation exchanger (length 40 cm, vol. 400 ml), and the adsorbed bands were eluted with 0.1 M sodium sulfate solution. After the elution of 5 reddish bands (the bis-complexes), 2 yellow and one orange band (the tris-complexes) remained. These 3 bands were eluted, and each fraction was treated in the following way: The solution was acidified (pH ~ 4) and poured on a small Sephadex column (length 20 cm, vol. 100 ml). Sodium and sulfate ions were removed by a subsequent elution with 0.1 M hydrochloric acid. When the eluate showed negative sulfate reaction, the complex was eluted with 1 M hydrochloric acid. The concentrated solution was evaporated to dryness on a vacuum rotatory evaporator. The residue was dissolved in ethanol (99 %), the solution was cooled on ice, and the complex was precipitated by the slow addition of ether. Washing with ether. Letters A, B, and C were used to indicate the bands in the order of their first elution.

A = $(+)_D$-$[Co\{(-)_D\text{-}C_7H_{10}N_2\}_3]Cl_3$. Yield: 641 mg of yellow crystals (41 %). (Found: C 9.65; C 41.2; N 13.7. Calc. for $[Co(C_7H_{10}N_2)_3]Cl_3.4.5H_2O$: Co 9.62; C 41.2; N 13.7). The water content was determined by thermogravimetry to be 4.5 mol per mol cobalt. In other experiments the complex crystallized with 5.5 mol of water. (ε, λ)$_{max}$: (149, 461), (156, 338). (ε, λ)$_{min}$: (15.0, 388), (138, 322.5). ($\Delta\varepsilon$, λ): (+2.22, 471.5), (−0.32, 343). $[M]_D^{25} = +947°$ ($c = 1.8$ mg/ml).

B = $(-)_D$-$[Co\{(-)_D\text{-}C_7H_{10}N_2\}_3]Cl_3$. Yield: 400 mg of lemon-yellow crystals (25 %). (Found: Co 9.28; C 39.9; N 13.5. Calc. for $[Co(C_7H_{10}N_2)_3]Cl_3.5.5H_2O$: Co 9.34; C 40.0; N 13.3). The water content was determined by thermogravimetry to be 5.5 mol per mol cobalt. (ε, λ)$_{max}$: (155, 459), (128, 336). (ε, λ)$_{min}$: (15.2, 385), (124, 325). ($\Delta\varepsilon$, λ): (−2.50, 464), (+0.58, 344). $[M]_D^{25} = -544°$ ($c = 1.7$ mg/ml).

C = $(+)_D$-$[Co\{(-)_D\text{-}C_7H_{10}N_2\}_3]Cl_3$. Yield: 262 mg of orange-coloured crystals (18 %). (Found: Co 10.31; C 44.6; N 15.0. Calc. for $[Co(C_7H_{10}N_2)_3]Cl_3.2H_2O$: Co 10.38; C 44.4; N 14.8). The water content was determined by thermogravimetry to be 2.1 mol per mol cobalt. In other experiments the complex crystallized with 3 mol of water. (ε, λ)$_{max}$: (194, 475), (209, 341). (ε, λ)$_{min}$: (19.9, 394), (186, 325). ($\Delta\varepsilon$, λ): (+5.33, 473), (−0.94, 342). $[M]_D^{25} = +1622°$ ($c = 1.2$ mg/ml).

Tris-{$(+)_D$-1-(2-pyridyl)ethylamine}cobalt-(III) chloride, $[Co\{(+)_D\text{-}C_7H_{10}N_2\}_3]Cl_3$. The compounds were prepared from 1.50 g $[Copy_4Cl_2]Cl.6H_2O$ and 3.00 g $(+)_D$-1-(2-pyridyl)ethylammonium $(+)_D$-hydrogentartrate monohydrate, exactly as described above in the case of the complexes with the $(-)_D$-amine.

A′ = $(-)_D$-$[Co\{(+)_D\text{-}C_7H_{10}N_2\}_3]Cl_3$. Yield: 680 mg of yellow crystals (43 %). (Found: Co 9.46; C 40.4; N 13.5. Calc. for $[Co(C_7H_{10}N_2)_3]Cl_3.5H_2O$: Co 9.48; C 40.6; N 13.5). The water content was determined by thermogravimetry to be 4.9 mol per mol cobalt. In other experiments the complex crystallized with 5.5 mol of water. (ε, λ)$_{max}$: (148, 461), (154, 338). (ε, λ)$_{min}$: (15.7, 388), (136, 322). ($\Delta\varepsilon$, λ): (−2.21, 471.5), (+0.28, 343). $[M]_D^{25} = -949°$ ($c = 1.8$ mg/ml).

B′ = $(+)_D$-$[Co\{(+)_D\text{-}C_7H_{10}N_2\}_3]Cl_3$. yield:330 mg of lemon-yellow crystals (21 %). (Found: Co 9.28; C 39.7; N 13.4. Calc. for $[Co(C_7H_{10}N_2)_3]Cl_3.5.5H_2O$: Co 9.34; C 40.0; N 13.3). The water content was determined by thermogravimetry to be 5.5 mol per mol cobalt. (ε, λ)$_{max}$: (156, 459), (130, 336). (ε, λ)$_{min}$: (16.6, 386), (127, 326). ($\Delta\varepsilon$, λ): (+2.48, 464), (−0.57, 344). $[M]_D^{25} = +554°$ ($c = 1.7$ mg/ml).

C′ = $(-)_D$-$[Co\{(+)_D\text{-}C_7H_{10}N_2\}_3]Cl_3$. Yield: 195 mg of orangecoloured crystals (14 %). (Found: Co 10.34; C 44.1; N 14.9. Calc. for $[Co(C_7H_{10}N_2)_3]Cl_3.2H_2O$: Co 10.38; C 44.4; N 14.8). The water content was determined by thermogravimetry to be 1.9 mol per mol cobalt. In other experiments the complex crystallized with 3 mol of

water. $(\varepsilon, \lambda)_{max}$: (193, 475), (206, 341). $(\varepsilon, \lambda)_{min}$: (19.7, 394), (185, 325). $(\Delta\varepsilon, \lambda)$: (−5.30, 473), (+0.95, 342). $[M]_D^{25} = -1632°$ ($c = 1.2$ mg/ml).

Tris-{(+)$_D$-1-(2-pyridyl)ethylamine}cobalt-(III) chloride, $[Co\{(+)_D\text{-}C_7H_{10}N_2\}_3]Cl_3$. Preparation of the crude product by means of method 2: 0.80 g of lithium hydroxide monohydrate (19 mmol) was dissolved in 10 ml of hot water. 3.00 g of (+)$_D$-1-(2-pyridyl)ethylammonium (+)$_D$-hydrogentartrate (10.3 mmol) was added. The solution was cooled on ice, and 40 ml ethanol was added to precipitate lithium tartrate. 3 ml 1 M hydrochloric acid, 0.1 g activated charcoal Norite SA 1, and 0.600 g cobalt chloride hexahydrate (2.52 mmol) was added to the filtrate. The solution was then oxidized, air being drawn through it for 3 h. 2 ml 4 M hydrochloric acid was added, and the solution was filtered and cooled on ice. A sticky, crude product was precipitated with ethanol and ether and poured on a column and separated as described before.
A′ = (−)$_D$-$[Co\{(+)_D\text{-}C_7H_{10}N_2\}_3]Cl_3$. Yield: 480 mg (30 %).
B′ = (+)$_D$-$[Co\{(+)_D\text{-}C_7H_{10}N_2\}_3]Cl_3$. Yield: 490 mg (31 %).

RESULTS AND DISCUSSION

Characterization of the isomers. The compounds A (A′) and C (C′) crystallize easily and well in contrast to the compound B (B′), which is inclined to deliquescence. The yellow compounds A (A′) and B (B′) have nearly the same colour as the *facial* isomer of tris-(2-picolylamine)cobalt(III) bromide,[1] while the orange compound C (C′) has the same colour as the *meridional* isomer. This suggests that A (A′) and B (B′) could be *facial* isomers, while C (C′) is a *meridional* isomer.

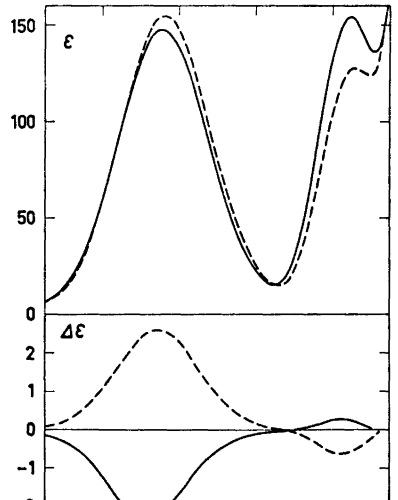

Fig. 3. The absorption spectra (top) and the circular dichroism spectra (bottom) of A′ (——) and B′ (— — —).

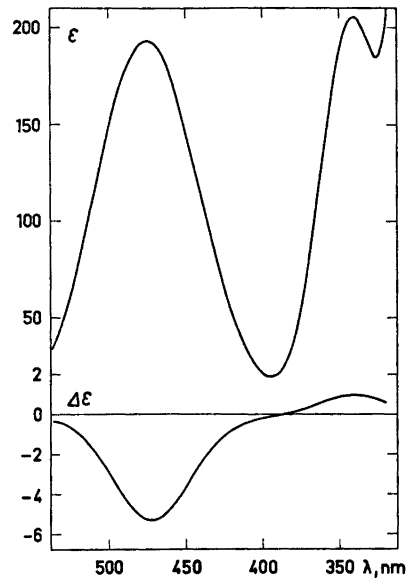

Fig. 4. The absorption spectrum (top) and the circular dichroism spectrum (bottom) of C′.

Electronic spectra The electronic spectra in the visible region of A′ (A), B′ (B), and C′(C) are given in Figs. 3 and 4. A comparison of the long-wavelength bands shows a great similarity between A′, B′ and the *facial* tris-(2-picolylamine)cobalt(III) isomer [1] regarding intensity and position of the band, whereas C′ and the *meridional* isomer of tris-(2-picolylamine)cobalt-(III) bromide [1] are very much alike, both having a higher intensity and occurring at a lower energy than the former (Table 1). Furthermore, the C′-type complex is characterized by a band of greater half-width than the A′ and B′-type bands. This would agree with the assumption that C′ (C) is a *meridional* isomer, and consequently has a lower symmetry than A′ (A) and B′ (B), the *facial* isomers.

Circular dichroism spectra. The CD spectra of A′, B′, and C′ are shown in Figs. 3 and 4. The C′-type spectrum differs from the other spectra

Table 1. The wavelengths λ_{max}, the molar extinction coefficients ε_{max} and the corresponding half-widths δ of the long-wavelength bands of 3 tris-{(+)$_D$-1-(2-pyridyl)ethylamine}cobalt(III) complexes, named A′, B′, and C′, and of *fac*- and *mer*-tris(2-picolylamine)cobalt(III) bromide.[1]

Complex	λ_{max}(nm)	ε_{max}	δ(cm^{-1})
A′. (−)$_D$-[Co{(+)$_D$-$C_7H_{10}N_2$}$_3$]Cl_3.aq.	461	148	3327
B′. (+)$_D$-[Co{(+)$_D$-$C_7H_{10}N_2$}$_3$]Cl_3.aq.	459	156	3301
fac-[Co($C_6H_8N_2$)$_3$]Br_3.aq.	462	130	3360
C′. (−)$_D$-[Co{(+)$_D$-$C_7H_{10}N_2$}$_3$]Cl_3.aq.	475	193	3526
mer-[Co($C_6H_8N_2$)$_3$]Br_3.aq.	471	155	3450

as regards the intensities of the bands, but apart from that, the spectra are all very much alike, showing only one CD band corresponding to the first absorption band. For many tris-(diamine)-cobalt(III) complexes it has been possible to establish a relationship between the CD spectrum and the absolute configuration, a positive dominating CD band in the region of the octahedral $^1T_{1g} \leftarrow {}^1A_{1g}$ absorption band generally being tantamount to a Λ configuration.[11] If this method of assigning the isomers by means of the sign of the dominating CD band can be applied equally successfully to our compounds, the configurations of A′ and C′ should be Δ and the configuration of B′ Λ. Similarly, A and C should have the configurations Λ and B Δ.

Nuclear magnetic resonance. A facial isomer has three equivalent rings and a threefold axis of symmetry and should therefore show one doublet in the methyl region, while an unsymmetrical, *meridional* isomer is expected to show a more complicated spectrum with up to three doublets. Figs. 5, 6, and 7 and Table 2 show the ^{1}H NMR resonances of NH_2, CH and CH_3 protons in A′(A), B′(B), and C′(C) (solvent: $D_2O + D_2SO_4$). In the case of A′ and C′, the signals arising from the NH_2 protons are partly overlapped by bands due to water protons (~5.7 – 5.8 ppm). Contrary to what should be expected, similar spectra were found for all the

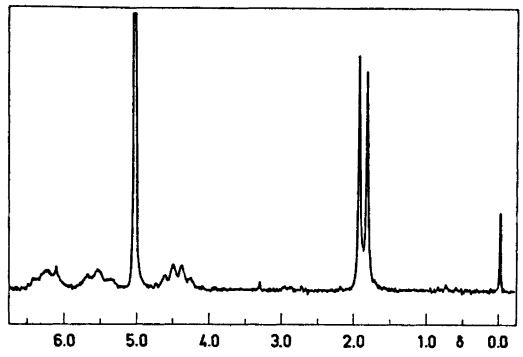

Fig. 6. ^{1}H NMR spectrum of the CH_3, CH and NH_2 protons in B′.

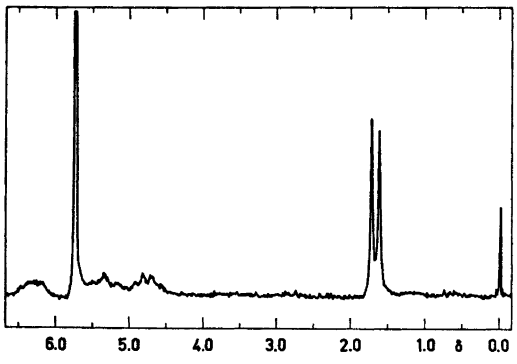

Fig. 5. ^{1}H NMR spectrum of the CH_3, CH and NH_2 protons in A′.

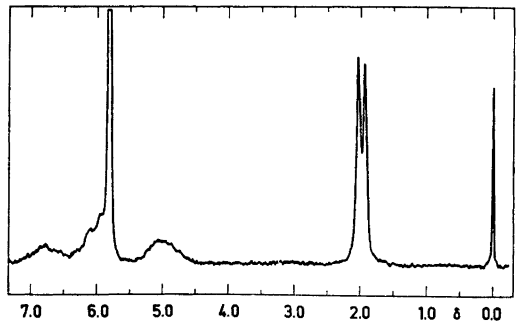

Fig. 7. ^{1}H NMR spectrum of the CH_3, CH and NH_2 protons in C′.

Table 2. Proton chemical shifts (δ ppm) in tris-{(+)$_D$-1-(2-pyridyl) ethylamine}cobalt(III) complexes.[a] The relative areas of the peaks are given in brackets.

Complex	(NH_2)	(CH)	(CH_3)
A'. (−)$_D$-[Co{(+)$_D$-$C_7H_{10}N_2$}$_3$]Cl_3.aq.	6.28 (1) ~ 5.37 (1)	4.75 (1)	1.67 (3)
B'. (+)$_D$-[Co{(+)$_D$-$C_7H_{10}N_2$}$_3$]Cl_3.aq.	6.20 (1) 5.52 (1)	4.42 (1)	1.87 (3)
C'. (−)$_D$-[Co{(+)$_D$-$C_7H_{10}N_2$}$_3$]Cl_3.aq.	6.72 (1) ~ 6.00 (1)	4.98 (1)	1.97 (3)

[a] Measured from TPSNa as an internal standard. All spectra were run in mixed $D_2O-D_2SO_4$ solutions.

isomers, one doublet being observed in the CH_3 region, one broad band in the CH region and two broad bands in the NH_2 region. When the compounds were measured in D_2O, the two broad bands in the region 5.30 − 6.80 ppm disappeared owing to deuteration of the NH_2 groups. Fig. 8 shows the ^1H NMR resonances of the pyridine protons in A'(A), B'(B), and C'(C). It is noticeable that the C' spectrum is more complicated than the A' and B' spectra, which offer points of resemblance. This could be in agreement with the assumption that A'(A) and B'(B) are both *facial* isomers, while C'(C) is a *meridional* isomer.

Conclusion. Results from the physical measurements thus indicate that A: (+)$_D$-[Co{(*S*)-(−)$_D$-$C_7H_{10}N_2$}$_3$]Cl_3 is *fac-Λ*, B: (−)$_D$-[Co{(*S*)-(−)$_D$-$C_7H_{10}N_2$}$_3$]Cl_3 is *fac-Δ*. C: (+)$_D$-[Co{(*S*)-(−)$_D$-$C_7H_{10}N_2$}$_3$]Cl_3 is *mer-Λ*, and that A': (−)$_D$-[Co{(*R*)(+)$_D$-$C_7H_{10}N_2$}$_3$]Cl_3 is *fac-Δ*, B': (+)$_D$-[Co{(*R*)(+)$_D$-$C_7H_{10}N_2$}$_3$]Cl_3 is *fac-Λ*, C': (−)$_D$-[Co{(*R*)(+)$_D$-$C_7H_{10}N_2$}$_3$]Cl_3 is *mer-Δ*. Two important questions remain, namely: Why did only 3 (+3) isomers occur in recognizable amounts? and what are the conformations of the ligands? If, however, as in the case of propylenediamine,[12] there is a preference for the conformation in which the methyl group is equatorial, (*S*)(−)$_D$-1-(2-pyridyl)ethylamine will chelate with the conformation δ and (*R*)(+)$_D$-1-(2-pyridyl)ethylamine with the conformation λ. This hypothetical preference might explain why we obtained 2 (+2) *facial* isomers instead of the theoretical 4 (+4). In the case of the *meridional* isomers, models show that the steric interactions are much smaller for 1 (+1) isomer, namely a *ΔRλ* (*ΛSδ*), than for the others. This might explain the fact that we found only 1 (+1) *meridional* isomer, suggested above to be *ΔR* (*ΛS*).

The structure and absolute configuration of the A-type will now be determined by X-ray analysis at this laboratory, and our work on complexes of cobalt(III) and 1-(2-pyridyl)ethylamine is being continued.

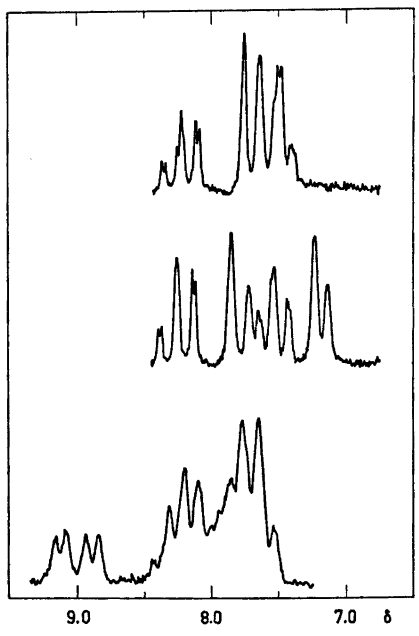

Fig. 8. ^1H NMR spectra of the pyridine protons in A' (top), B' (in the middle) and C' (bott)om.

REFERENCES

1. Michelsen, K. *Acta Chem. Scand. 24* (1970) 2003.
2. Smith, H. E., Schaad, L. J., Banks, R. B., Wiant, C. J. and Jordan, C. F. *J. Amer. Chem. Soc. 95* (1973) 811.
3. Cervinka, O., Belovsky, O. and Rejmanova, P. *Z. Chem. 10* (1970) 69.

4. La Forge, F. B. *J. Amer. Chem. Soc. 50* (1928) 2480.
5. Kolloff, H. G. and Hunter, J. H. *J. Amer. Chem. Soc. 63* (1941) 490.
6. Smirnoff, A. P. *Helv. Chim. Acta 3* (1920) 181.
7. Glerup, J. and Schäffer, C. E. *Acta Chem. Scand. To be published.*
8. Pedersen, E. *J. Sci. Instrum. Ser. 2. 1* (1968) 1013.
9. Pinner, A. *Ber. Deut. Chem. Ges. 34* (1901) 4234.
10. Engler, C. and Rosumoff, P. *Ber. Deut. Chem. Ges. 24* (1891) 2528.
11. McCaffery, A. J., Mason, S. F. and Norman, B. J. *J. Chem. Soc.* (1965) 2883.
12. Corey, E. J. and Bailar, J. C. *J. Amer. Chem. Soc. 81* (1959) 2620.

Received December 14, 1973.

Acta Chemica Scandinavica A 28 (1974) 435—438

Crystal Structure of 5-Chloropyrimidin-2-one

S. FURBERG and J. SOLBAKK

Department of Chemistry, University of Oslo, Oslo 3, Norway

The crystal structure of 5-chloropyrimidin-2-one has been derived from 2287 reflections measured by counter methods. The space group is *Pbca* with 16 molecules in the unit cell. The structure was refined to $R = 0.113$ by full matrix least squares calculations. Hydrogen bonds N – H···N and interactions Cl···O link the molecules together in planar layers (010).

Substituted pyrimidin-2-ones are substances of great biological importance and it would appear to be of interest to investigate the influence of different substituents on the structure of the ring system. We have carried out X-ray crystal structure analyses of a number of such compounds.[1–3] In the present paper the structure of the 5-chloro derivative is described.

EXPERIMENTAL. STRUCTURE ANALYSIS

Crystals were grown by slow evaporation of an ethyl acetate solution. Weissenberg diagrams showed them to be orthorhombic, with space group *Pbca*. Strong thermal diffuse scattering occurs, especially at reflections 040, 080, and 0120. Unit cell dimensions were measured on a diffractometer and found to be $a = 9.310(2)$ Å, $b = 12.611(2)$ Å, and $c = 17.261(2)$ Å. There are 16 molecules in the unit cell.

The intensity measurements were made on a crystal of dimensions about 0.3 mm, using a Picker automatic diffractometer and mono-chromatic Mo$K\alpha$ radiation. The $\omega/2\theta$ scan mode was employed (rate 1°/min). All 2769 independent reflections with $2\theta < 55°$ were measured, of which the 2287 with $I > 0$ were retained for refinement. Of these only 1482 satisfy the condition $I > 2\sigma(I)$. Corrections for absorption, extinction and thermal diffuse scattering were not applied. The atomic form factors used were those of Hanson *et al.*,[4] except for hydrogen.[5]

The structure was solved by vector methods and refined by full-matrix least squares calculations. The weighting scheme was based on standard deviations from counter statistics and 2 % fluctuations in diffractometer stability. The hydrogen atoms were assumed to have the same anisotropic temperature factor as the atom to which they are attached, and only their positional parameters were refined. The final value of R is 0.113 ($R_w = 0.079$) for 2287 reflections. If those with $I < 2\sigma(I)$ are excluded R drops to 0.066 ($R_w = 0.065$). The parameters obtained were not significantly different and the discussion will be based on those derived from the largest data set. They are given in Table 1.

A list of observed and calculated structure factors will be supplied by the authors on request.

The vibrations of all atoms are strongly anisotropic, with maximum amplitudes (ranging from $B = 3.1$ to 7.7 Å^2) in the y direction. The r.m.s. difference between atomic vibration tensor components calculated from Table 1 and those derived from the rigid body model was as high as 0.0036 Å^2. Corrections were therefore not carried out.

The calculations were carried out on CYBER-74.[6]

RESULTS AND DISCUSSION

Molecular structure. Interatomic distances and bond angles are given in Table 2. The differences between the two crystallographically independent molecules A and B are larger than to be expected from the estimated standard deviations, being as large as 6σ for the bond N1 – C6. Maximum deviations from least squares planes are 0.03 – 0.04 Å for non-hydrogen atoms, greater than usually found for pyrimidines. The structure arrived at is therefore not quite satisfactory. We believe that this is related to the fact that all atoms lie very close to planes $y = 0$ or $y = 0.25$. The intensities of about half of the reflections are nearly zero and inaccurately measured. Various refinements starting with slightly different y coordinates were tried, but

Table 1. Positional ($\times 10^5$ for non-hydrogens, $\times 10^4$ for hydrogens) and thermal ($\times 10^5$) parameters with estimated standard deviations. The temperature factor is exp $[-(B11h^2+B22k^2+B33l^2+B12hk+B13hl+B23kl)]$.

ATOM	x	y	z	B11	B22	B33	B12	B13	B23
CL A	-322(9)	24992(14)	-1369(6)	987(12)	982(12)	168(3)	428(27)	6(9)	-28(15)
N1 A	-18329(27)	24575(48)	28746(17)	583(29)	788(29)	284(9)	317(68)	153(27)	-257(44)
N3 A	14714(27)	24612(35)	19917(17)	693(30)	692(26)	237(10)	116(65)	-72(28)	76(43)
C2 A	2784(39)	24832(46)	24552(28)	634(42)	569(47)	214(13)	353(92)	-41(29)	31(45)
C4 A	13441(33)	24625(49)	12475(19)	468(35)	689(31)	222(11)	271(88)	59(30)	-55(51)
C5 A	318(32)	24731(42)	8558(19)	631(36)	588(30)	157(10)	-9(83)	27(28)	62(52)
C6 A	-11692(33)	24797(48)	13038(18)	476(33)	698(32)	208(10)	164(83)	-97(30)	-66(56)
O2 A	3316(31)	24128(40)	31541(15)	1259(39)	1198(37)	173(9)	765(73)	-14(30)	83(44)
CL B	25787(11)	565(17)	-1263(6)	1866(13)	978(14)	175(3)	-28(19)	23(12)	-13(18)
N1 B	36181(30)	375(34)	28879(18)	641(33)	626(33)	199(11)	214(68)	-53(30)	-73(37)
N3 B	18630(31)	-944(35)	20186(19)	692(33)	810(36)	225(12)	-251(62)	121(31)	-28(48)
C2 B	23021(40)	-597(46)	24785(19)	731(48)	421(40)	199(13)	-144(88)	25(35)	88(42)
C4 B	11761(37)	-824(44)	12614(23)	569(40)	734(47)	263(15)	-235(85)	-5(40)	-319(53)
C5 B	25851(39)	-92(49)	8748(19)	691(38)	679(36)	184(10)	-1(57)	16(42)	-457(60)
C6 B	37288(36)	833(42)	13012(22)	615(39)	628(43)	213(13)	232(84)	78(38)	-293(47)
O2 B	22468(30)	-248(41)	31758(16)	1162(42)	1199(37)	197(9)	282(74)	127(32)	79(44)
H4 A	2851(36)	2481(36)	1618(28)						
H6 A	-2071(36)	2434(36)	1122(19)						
H4 B	284(37)	-287(34)	1806(22)						
H6 B	4827(36)	66(31)	1129(22)						
H1 A	-1713(35)	2427(36)	2418(21)						
H1 B	4783(38)	-16(32)	2455(28)						

Table 2. Bond lengths (Å) and bond angles (°). Prime denotes an atom in a neighboring molecule.

Distance	Mol. A	Mol. B	Angle	Mol. A	Mol. B
Cl–C5	1.715(3)	1.730(3)	Cl–C5–C6	122.7(3)	120.5(3)
C5–C6	1.358(4)	1.361(5)	Cl–C5–C4	120.9(2)	120.5(3)
C6–N1	1.338(4)	1.364(5)	C5–C6–N1	119.2(3)	117.9(3)
N1–C2	1.388(4)	1.391(5)	C6–N1–C2	123.7(3)	123.2(3)
C2–N3	1.371(4)	1.393(5)	N1–C2–N3	115.7(3)	117.5(3)
N3–C4	1.290(4)	1.311(5)	C2–N3–C4	120.5(3)	119.4(3)
C4–C5	1.397(4)	1.409(5)	N3–C4–C5	124.2(3)	123.0(3)
C2–O2	1.207(4)	1.219(4)	C4–C5–C6	116.4(3)	118.9(3)
N1–H	0.86	1.20	N1–C2–O2	120.6(4)	120.6(4)
C4–H	0.78	1.02	N3–C2–O2	123.3(4)	121.7(4)
C6–H	0.90	1.07	C5–Cl···O2′	171.4(2)	176.2(2)
Cl···O2′	2.971(3)	2.936(3)	C2–O2···Cl′	171.0(3)	173.6(3)
N1···N3′	2.828(4)	2.761(4)			

it appears that the least squares refinements do not lead unequivocally to the correct deviations from $y=0$ or 0.25. Details in the structure will therefore not be discussed and we do not consider the differences between molecules A and B real.

In Fig. 1 the molecular structure is compared with those of pyrimidin-2-one [1] and 5-fluoropyrimidin-2-one.[3] The external bonding of the chlorine compound is quite different from that of the others but this hardly influences the bonds at the substituted atom C5. The greatest difference between the fluorine and chlorine derivative occurs in the bond C5–C6, which is found to be shortened by 0.016 Å by fluorine substitution and elongated by 0.014 Å by chlorine substitution. Although of doubtful significance, these effects are in general agreement with the view that both halogens withdraw electrons from the ring, but that only fluorine backdonates electrons to the π-system.[6]

The C=O bond is slightly shorter in the chloro-derivative than in the other two compounds. This is presumably related to the differences in intermolecular bonding.

Crystal structure. The crystal consists of nearly planar layers of molecules parallel to the *ac* plane. The distance between layers is $b/4=3.15$ Å. The hydrogen bonding is not of the N–H···O type usually found in pyrimidin-2-ones, the molecules being linked together in planar ribbons along *a* by N1–H···N3 hydrogen bonds of lengths 2.828 Å (A) and 2.761 Å (B) (Fig. 2). The ribbons appear to be held together mainly by a Cl···O interaction, this distance being 2.971 Å and 2.936 Å in layers of molecules A and B,

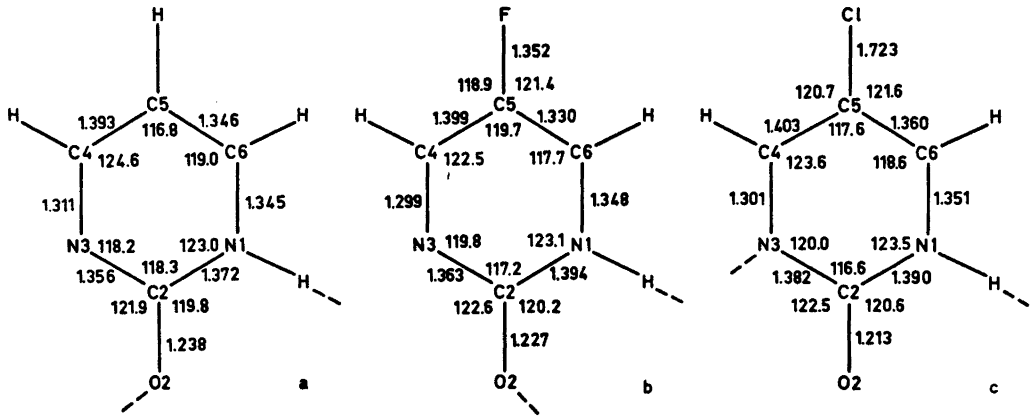

Fig. 1. Bond lengths and angles (uncorrected values) in (a) pyrimidin-2-one, (b) 5-fluoropyrimidin-2-one and (c) 5-chloropyrimidin-2-one (mean value of mols. A and B). E.s.d.'s are 0.003 – 0.005 Å in bond lengths and 0.2 – 0.4° in the angles.

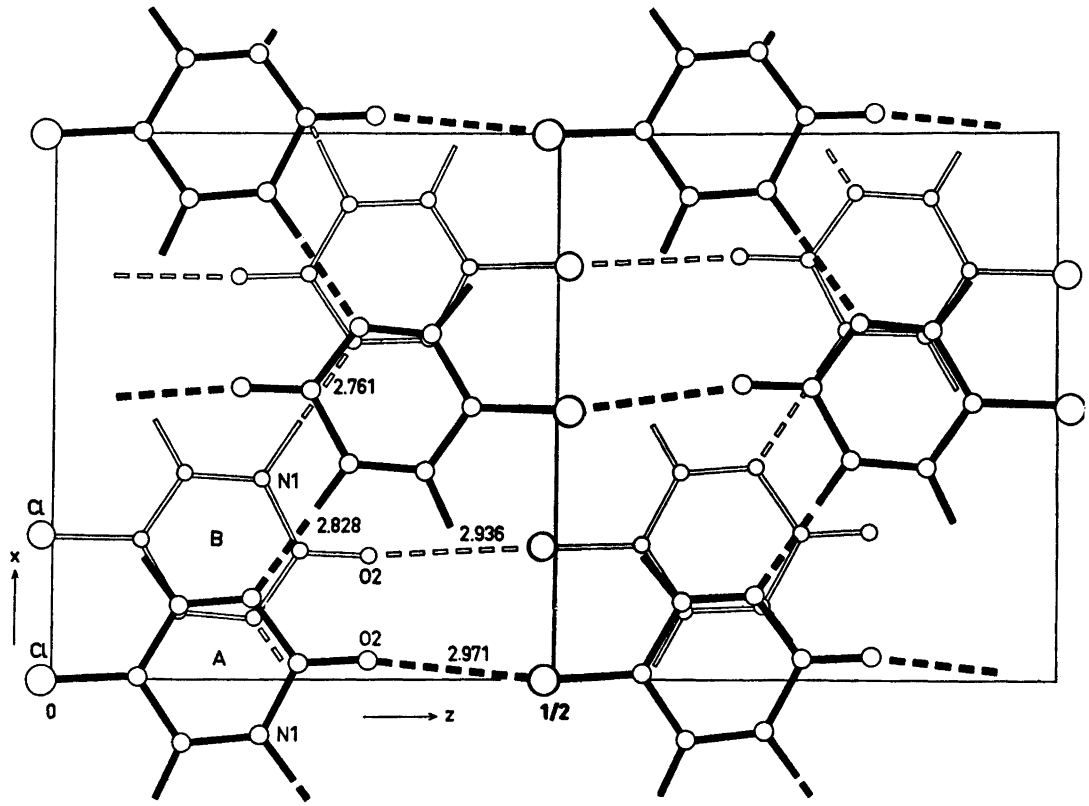

Fig. 2. The structure in *b* projection. One layer of A molecules (heavy lines) and one of B molecules (open lines) are shown. Hydrogen bonds and Cl···O contacts in broken lines.

respectively. This is significantly shorter than the normal van der Waals separation (3.25 Å) between chlorine and oxygen atoms. The C–Cl and C=O bonds are nearly parallel to the Cl···O direction and the interaction may possibly be classified as a charge transfer bond.[7] A similar short Cl···O contact of 2.88 Å is present in the crystal structure of *N*-chloro-succinimide.[8]

We wish to thank Professor S. G. Laland for a sample of the compound and Dr. P. Groth for assistance with the calculations.

REFERENCES

1. Furberg, S. and Solbakk, J. *Acta Chem. Scand. 24* (1970) 3230.
2. Solbakk, J. *Acta Chem. Scand. 25* (1971) 3006.
3. Furberg, S. and Petersen, C. S. *Acta Chem. Scand. 26* (1972) 760.
4. Hanson, H. R., Hermann, F., Lea, J. D. and Skillman, S. *Acta Crystallogr. 17* (1964) 1040.
5. Stewart, R. F., Davidson, E. R. and Simpson, W. T. *J. Chem. Phys. 17* (1964) 3175.
6. Sheppard, W. and Sharts, A. *Organic Fluorine Chemistry*, Benjamin, New York 1969.
7. Hassel, O. and Rømming, C. *Quart. Rev. 16* (1962) 1.
8. Brown, R. N. *Acta Crystallogr. 14* (1961) 711.
9. Groth, P. *Acta Chem. Scand. 27* (1973) 1837.

Received February 13, 1974.

Acta Chemica Scandinavica A 28 (1974) 439—441

Normal Coordinate Analysis of 1,2,4,5-Hexatetraene (Biallenyl)

ANDERS ERIKSSON,[a,*] J. BRUNVOLL,[a] G. HAGEN,[a] S. J. CYVIN,[a] ALF BJØRSETH[b] and D. L. POWELL[b,**]

[a]Division of Physical Chemistry, The University of Trondheim, N-7034 Trondheim-NTH, Norway and [b]Department of Chemistry, University of Oslo, Oslo 3, Norway

Two independent force constant calculations for 1,2,4,5-hexatetraene (biallenyl) are reported. Both results were found to be compatible with the assignment of experimental frequencies in all cases apart from the lowest B_u fundamental. This frequency has later been re-assigned on the basis of the present calculations.

Many hydrocarbons with CC double bonds in different environments have been subjected to structural and spectroscopical studies. The present work on biallenyl (1,2,4,5-hexatetraene) may be considered as a continuation of the studies of allene,[1] 1,3-butadiene,[2] butatriene,[3] and 1,3,5-hexatriene.[4] Biallenyl, C_6H_6, is a structural isomer of benzene [5] and dimethyldiacetylene.[6]

In the present work a normal coordinate analysis was performed on the basis of the recent vibrational spectra of Powell *et al.*[7] A similar analysis has also recently been performed for 1,2,4-pentatriene (vinylallene).[8] It is intended to utilize the developed force fields in computations of mean amplitudes of vibration [9] for both biallenyl and vinylallene.[10] These quantities are of great interest in electron diffraction studies. A structural investigation of biallenyl by electron diffraction has been performed,[11] and the similar work on vinylallene is in progress.[12]

NORMAL COORDINATE ANALYSIS

A molecular structure of the symmetry C_{2h} (see Fig. 1) was adopted. The structural parameters from the electron diffraction work [11] were employed.

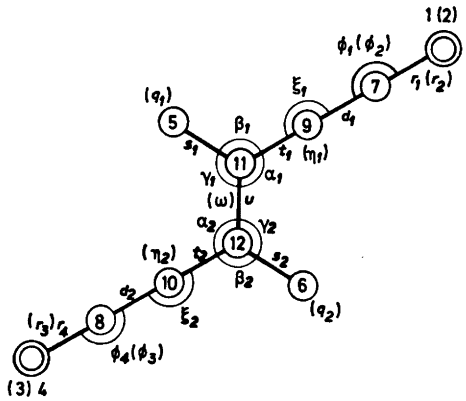

Fig. 1. The biallenyl molecular model showing the numbering of atoms and designation of the valence coordinates. Symmetrically equivalent atoms are numbered consecutively within each of the five sets. The stretchings (r) and bendings (ϕ) given in parentheses involve the atoms below the skeleton plane (Nos. 2 and 3). Otherwise the parenthesized symbols denote out-of-plane valence coordinates: linear bendings (η), out-of plane bendings (q), and torsion (ω). In addition four torsions were introduced as τ_1[1,7,11,12], τ_2[2,7,11,12], τ_3[3,8,12,11], and τ_4[4,8,12,11].

The normal modes of vibration are distributed among the symmetry species of the appropriate point group according to

$$\Gamma_{\text{vib}} = 10A_g + 5B_g + 6A_u + 9B_u$$

Force constant calculations (I). A calculation of the force field was performed in Oslo, utilizing a computer program written by Gwinn.[13] The original version of the program was modified to accept force constants for bending of three colinear atoms. The force field was based on

* Permanent address: Institute of Chemistry, University of Uppsala, S-751 21 Uppsala, Sweden.

** Permanent address: College of Wooster, Wooster, Ohio, USA.

valence coordinates. For the sake of simplicity the terminal hydrogens (Nos. 1, 2, 3, and 4 in Fig. 1) were excluded from the calculations, and the masses of the terminal carbon atoms adjusted accordingly.

The force constants were refined by a procedure of trial and error in order to improve the agreement with observed frequencies. In Table 1 the observed frequencies are compared with the calculated values obtained from a relatively simple force field. The corresponding force constants (stretch-stretch in mdyne/Å, bend-bend in mdyne Å/rad^2 and stretch-bend in mdyne/rad) are given in the following with reference to Fig. 1 for the designation of valence coordinates.

Stretchings: $K_s = 5.05$, $K_t = K_d = 9.5$, $K_u = 6.5$.
Bendings: $H_\alpha = 0.90$, $H_\beta = 0.45$, $H_\gamma = 0.45$.
$H_\xi = 0.37$, $H_\eta = 0.19$.
$H_q = 0.08$.
Torsion: $Y_\omega = 0.055$.
Interactions: $F_{tt} = -0.50$, $F_{td} = 0.50$, $F_{ut} = 1.5$, $F_{ud} = 1.5$, $F_{ss} = -0.35$.
$F_{\alpha\alpha} = 0.4$, $F_{\gamma\gamma} = 0.2$.
$F_{\xi\xi} = 0.10$, $F_{\eta\eta} = 0.15$.
$F_{qq} = 0.03$.
$F_{u\gamma} = 0.7$.

Force constant calculations (II). Independently of the calculations (I) a more elaborate analysis of the force constants was performed in Trondheim. All the hydrogen atoms were included in the twelve-atomic model of the molecule. The secular equation of the vibrational problem was solved in terms of symmetry coordinates, in contrast to the approach of the calculations (I). The well-known GF matrix method of Wilson [14] was applied, utilizing well-established computer programs.

An initial approximate force field was estimated by means of force constants transferred from allene,[1] in part from butatriene,[3] and from hexatriene.[4] Additional force constants were guessed in the first run. Some details of these calculations are reported elsewhere.[8] The calculated frequencies are included in Table 1. The force field was tentatively adjusted to fit the observed frequencies from Powell *et al.*[7] through trials and errors and through several steps of iteration. During these refinements several seemingly meaningful interaction force constants were introduced, and the values of principal force constants were modified. It was found possible to reproduce all of the assigned fundamentals from Powell *et al.*[7] with seemingly reasonable force constants except for one frequency. In the experimental work [7] the 333 cm^{-1} band is assigned as the lowest B_u frequency (ν_{30}). The present calculations suggest rather a value around 130 cm^{-1} or at least below 170 cm^{-1}. In the following we give the list of valence force constants from the final force field. This force field is compatible with the assignment of Powell *et al.*[7] except for $\nu_{30} = 130$ cm^{-1}. All values are in mdyne/Å. The symbols are supposed to be self-explanatory when reference is made to the notation defined in Fig. 1.

Table 1. Observed fundamental frequencies (cm^{-1}) and those from the calculations.

Species	Observed [7,8]	Calculated (I)	(II)
A_g	3005	3010	3019
	2985	–	2994
	1934	1976	1948
	1455	–	1501
	1383	1369	1405
	1352	1316	1257
	1142	1062	1103
	1012	–	867
	525	535	509
	228	282	251
A_u	3070	–	3062
	885	–	964
	793	–	736
	674	690	688
	283	309	268
	90	84	81
B_g	3057	–	3063
	1087	–	1108
	860	–	842
	652	651	684
	311	316	298
B_u	3100	3095	3022
	3000	–	2993
	1957	1990	1933
	1432	–	1462
	1241	1058	1321
	1216	1231	1176
	854	–	825
	522	507	551
	333[a] / 110[b]	130	133

[a] From Ref. 7. [b] Re-assigned in Ref. 8.

Stretchings: $f_{rr}^{(1)}(r_1r_1) = 4.99$, $f_{rr}^{(2)}(r_1r_2) = 0.01$, $f_{rr}^{(3)}(r_1r_3) = -0.03$, $f_{rr}^{(4)}(r_1r_4) = 0.00$.
$f_{ss}^{(1)} = 5.10$, $f_{ss}^{(2)} = -0.15$.
$f_{dd}^{(1)} = 10.83$, $f_{dd}^{(2)} = -0.31$.
$f_{tt}^{(1)} = 10.79$, $f_{tt}^{(2)} = -0.20$.
$f_u = 7.34$.
Bendings (including linear and out-of-plane): $f_{\phi\phi}^{(1)} = 0.64$, $f_{\phi\phi}^{(2)} = 0.30$, $f_{\phi\phi}^{(3)} = 0.03$, $f_{\phi\phi}^{(4)} = -0.02$.
$f_{\beta\beta}^{(1)} = 0.68$, $f_{\beta\beta}^{(2)} = 0.01$.
$f_{\gamma\gamma}^{(1)} = 0.70$, $f_{\gamma\gamma}^{(2)} = 0.04$.
$f_{\xi\xi}^{(1)} = 0.24$, $f_{\xi\xi}^{(2)} = 0.01$.
$f_{\eta\eta}^{(1)} = 0.16$, $f_{\eta\eta}^{(2)} = 0.03$.
$f_{qq}^{(1)} = 0.15$, $f_{qq}^{(2)} = -0.01$.
Torsions: $f_{\tau\tau}^{(1)} = 0.20$, $f_{\tau\tau}^{(2)} = -0.03$, $f_{\tau\tau}^{(3)} = 0.00$, $f_{\tau\tau}^{(4)} = 0.04$.
$f_\omega = 0.0637$.
Interactions for coordinates of different types:
$f_{rd}^{(1)} = 0.18$, $f_{rd}^{(2)} = 0.00$.
$f_{r\phi}^{(1)} = 0.18$, $f_{r\phi}^{(2)} = 0.12$, $f_{r\phi}^{(3)} = -0.02$, $f_{r\phi}^{(4)} = 0.02$.
$f_{s\beta}^{(1)} = 0.15$, $f_{s\beta}^{(2)} = 0.02$.
$f_{s\gamma}^{(1)} = 0.15$, $f_{s\gamma}^{(2)} = 0.05$.
$f_{du} = 0.46$, $f_{tu} = 1.45$.
$f_{d\phi}^{(1)} = 0.33$, $f_{d\phi}^{(2)} = 0.00$.
$f_{t\beta}^{(1)} = 0.29$, $f_{t\beta}^{(2)} = -0.07$.
$f_{t\gamma}^{(1)} = -0.20$, $f_{t\gamma}^{(2)} = 0.16$.
$f_{u\beta} = -0.15$, $f_{u\gamma} = 0.31$.
$f_{\beta\gamma}^{(1)} = 0.33$, $f_{\beta\gamma}^{(2)} = 0.00$.

CONCLUSION

Results obtained from an analysis using Gwinn's program and from programs using Wilson's GF method should of course not differ in the physical sense.

From the both independent calculations (I) and (II) it was concluded that the force constant analysis confirms the assignment of experimental frequencies of Powell *et al.*[7] except for the lowest B_u fundamental, ν_{30} (333 cm^{-1}). It was found impossible to modify the force fields so as to be compatible with $\nu_{30} = 333$ cm^{-1} without introducing unreasonable force constant values. The ν_{30} fundamental was re-assigned [8] on the basis of the present calculations. Three candidates for this fundamental were detected as weak infrared bands at 150, 130, and 110 cm^{-1} with a slight preferance for 110 cm^{-1}. In that case it is easiest to explain 333 cm^{-1} as a combination band. Anyone of the three values proposed as the re-assigned ν_{30} fundamental are compatible with reasonable force constant values.

Acknowledgement. Some of the calculations were performed when one of us (A. B.) stayed at the University of Texas at Austin. He wants to express his appreciation to Professor James E. Boggs for his hospitality and Stan McNeme for skilful assistance.

REFERENCES

1. Cyvin, S. J. *J. Chem. Phys. 29* (1958) 583; Almenningen, A., Bastiansen, O. and Trætteberg, M. *Acta Chem. Scand. 13* (1959) 1699; Andersen, B., Stølevik, R., Brunvoll, J., Cyvin, S. J. and Hagen, G. *Acta Chem. Scand. 21* (1967) 1759.
2. Almenningen, A., Bastiansen, O. and Trætteberg, M. *Acta Chem. Scand. 12* (1958) 1221; Trætteberg, M., Hagen, G. and Cyvin, S. J. *Acta Chem. Scand. 23* (1969) 74; Cyvin, S. J., Trætteberg, M. and Hagen, G. *Acta Chem. Scand. 23* (1969) 1456.
3. Almenningen, A., Bastiansen, O. and Trætteberg, M. *Acta Chem. Scand. 15* (1961) 1557; Cyvin, S. J., Cyvin, B. N., Klæboe, P. and Augdahl, E. *Acta Chem. Scand. 19* (1965) 883; Cyvin, S. J. and Hagen, G. *Acta Chem. Scand. 23* (1969) 2037.
4. Trætteberg, M. *Acta Chem. Scand. 22* (1968) 628, 2294; Cyvin, S. J., Hagen, G. and Trætteberg, M. *Acta Chem. Scand. 23* (1969) 3285.
5. Cyvin, S. J. *Acta Chem. Scand. 11* (1957) 1499; Almenningen, A., Bastiansen, O. and Fernholt, L. *Kgl. Nor. Vidensk. Selsk. Skr.* No. 3 (1958); Kimura, K. and Kubo, M. *J. Chem. Phys. 32* (1960) 1776; Brooks, W. V. F. and Cyvin, S. J. *Acta Chem. Scand. 16* (1962) 820.
6. Almenningen, A., Bastiansen, O. and Munthe-Kaas, T. *Acta Chem. Scand. 10* (1956) 261.
7. Powell, D. L., Klæboe, P., Christensen, D. H. and Hopf, H. *Spectrochim. Acta 29 A* (1973) 7.
8. Klæboe, P., Torgrimsen, T., Christensen, D. H., Hopf, H., Eriksson, A., Hagen, G. and Cyvin, S. J. *Spectrochim. Acta 30 A* (1974). *In press.*
9. Cyvin, S. J. *Molecular Vibrations and Mean Square Amplitudes*, Universitetsforlaget, Oslo and Elsevier, Amsterdam 1968.
10. Eriksson, A., Hagen, G. and Cyvin, S. J. *Chem. Phys. Lett. 17* (1974). *In press.*
11. Trætteberg, M., Paulen, G. and Hopf, H. *Acta Chem. Scand. 27* (1973) 2227.
12. Trætteberg, M. *Private communication.*
13. Gwinn, W. D. *J. Chem. Phys. 55* (1971) 477.
14. Wilson, E. B., Jr., Decius, J. C. and Cross, P. C. *Molecular Vibrations*, McGraw, New York 1955.

Received December 7, 1974.

Acta Chemica Scandinavica A 28 (1974) 442—448

Base Promotion and Intramolecular Catalysis in Acetal Hydrolysis. Reaction of *o*-Hydroxybenzaldehyde Diethyl Acetal

ALPO KANKAANPERÄ, LEENA OINONEN and MARKKU LAHTI

Department of Chemistry, University of Turku, SF-20500 Turku, Finland

The existence of three different routes of hydrolysis has been demonstrated for the reactions of *o*-hydroxybenzaldehyde diethyl acetal. In the first route, the specifically hydronium ion-catalyzed decomposition prevails if the acid concentration is relatively high (pH about 6 or lower). In the second route, the decomposition proceeds mainly by the intramolecular catalysis of the phenolic hydroxy group if the pH varies between 7.9 and 8.6. In the third route, the base-promoted hydrolysis takes place if the solution is relatively basic. Especially, if the sodium hydroxide concentration is higher than 0.15 M, the observed first-order rate coefficients remain constant. The formal kinetics of these different routes has been described. The dissociation constant of the phenol has been estimated from the kinetic data.

The hydrolysis of acetals has been the object of intensive studies. Although the pre-equilibrium protonation and the subsequent unimolecular decomposition of the protonated substrate (an *A*-1 reaction) has been accepted as the general mechanism of acetal hydrolysis,[1] it has recently been shown that in many cases the proton transfer occurs in the rate-determining stage of the reaction.[2] It is by no means justified to assume that only these two routes could exist in the hydrolytic decomposition of acetals. For instance, the reactions of acetals in basic solutions have not been studied in detail. Although it is well-known [1b] that acetals are generally stable in basic solutions, it is reasonable to assume that in particular cases, for instance in the case of *o*-hydroxybenzaldehyde diethyl acetal (I), the structure of the acetal may favor the hydrolytic decomposition in basic solutions.

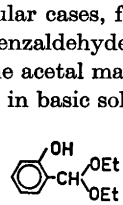

(I)

In solutions of strong bases the proton in the hydroxyl group is dissociated, and the structure of the anion thus formed can be assumed to favor a unimolecular heterolysis of the substrate as the negative charge of the phenolate ion will be easily distributed to the possible leaving group, the alkoxide ion. Moreover, (I) is an excellent model compound to study the possible intramolecular catalysis by a hydroxyl group. This phenomenon may especially appear in the hydrolysis of glycosides.

EXPERIMENTAL

Materials. *o*-Hydroxybenzaldehyde diethyl acetal was prepared from *o*-hydroxybenzaldehyde, triethyl orthoformate, and absolute ethanol using the method described previously by Pauly and Buttlar.[3] The product was purified by distillation. B.p. 98 °C/4 Torr. NMR spectrum: 6 H at δ 1.32 ppm, 4 H at δ 3.49 ppm, 1 H at δ 5.43 ppm, 5 H at δ 6.5 – 7.2 ppm, and 1 H at δ 7.75 ppm. Other signals were not observed.

Kinetic measurements. Kinetic measurements were performed in dilute perchloric acid solutions, in sodium hydroxide solutions, and in the following buffer systems: potassium dihydrogen phosphate-disodium hydrogen phosphate, boric acid-sodium dihydrogen borate, sodium hydrogen carbonate-sodium carbonate, and acetic acid-sodium acetate. Ordinary water was usually employed as solvent in the measurements. Some experiments were also performed in heavy water. The temperatures were between 25 and 80 °C.

The progress of the reaction was followed spectrophotometrically on a Unicam SP 800 (absorption of salicylaldehyde at 255 – 275 nm). The temperature of the cell housing block was adjusted with water circulation from a electronically controlled Lauda thermostat. The concentration of the substrate was about 3×10^{-5} M. First-order kinetics was strictly obeyed in all cases.

The pH values of the reaction mixtures were measured with a Radiometer apparatus. These determinations were performed at 70 °C.

RESULTS AND DISCUSSION

Specific hydronium ion catalysis. To study the nature of the catalysis in the hydrolysis of salicylaldehyde diethyl acetal some measurements were performed in relatively high hydronium ion concentrations (higher than 10^{-7} M) in acetic acid-sodium acetate buffers at 25 °C (Table 1). The kinetic data in 1/2 buffer reveal that the observed rate coefficients are independent of the concentration of the undissociated acid. This observation is in accordance with the A-1 mechanism of acetal hydrolysis (eqn. 1).

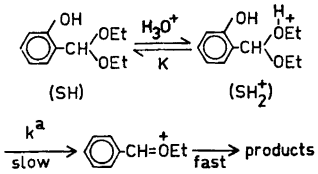

(1)

The rate of reaction (1) can be expressed by eqn. (2)

$$\text{rate} = k^a K_{eq}[H_3O^+][SH] = k_2^a [H_3O^+][SH] = k_1^a [SH] \quad (2)$$

where k_1^a is the measured first-order rate coefficient and k_2^a the corresponding second-order rate coefficient. The calculated second-order rate coefficients were found to be independent of the hydronium ion concentration of the solution, which is in accordance with eqn. (2). For instance, the second-order rate coefficients measured in 1/10, 1/2, and 1/1 acetic acid-sodium acetate buffers are equal within the limits of experimental error. Dilute perchloric acid solutions were also employed in some measurements (Table 2); the second-order rate coefficients were found to be in good agreement with those measured in buffer solutions. This reveals that the contribution of uncatalyzed reactions must be negligible under the above mentioned conditions. Some additional measurements were also performed in potassium dihydrogen phosphate-disodium hydrogen phosphate buffers (Table 1). If only the hydronium ion-catalyzed reaction occurred in these solutions, the ratio of the rate coefficients would correlate with the buffer ratio (HA)/(A^-). It is found that the rate coefficients measured in 19/1 and 9/1 buffers have a ratio of 19/9.6, which is only a little lower than is expected and the rate coefficients measured in 7/3 and 1/1 buffers are, on the contrary, markedly higher than is expected on the basis of the buffer ratios. Thus it is evident that at hydronium ion concentrations lower than 10^{-6} M (19/1 buffer) some additional route must be taken into account.

The acid-catalyzed hydrolysis of salicylaldehyde diethyl acetal was also studied at different

Table 1. Kinetic data for the acid-catalyzed hydrolysis of *o*-hydroxybenzaldehyde diethyl acetal in buffer solutions at 25 °C. HA denotes the more acidic component of the buffer system.

HA	[HA]/[A^-]	[HA]	No. of runs	10^2k s^{-1}	$[H_3O^+]^b$ M	10^2k $M^{-1}s^{-1}$
CH_3COOH	1/1	0.100	4	2.385	4.17×10^{-5}	5.72
CH_3COOH	1/2	0.05	1	1.350	2.087×10^{-5}	6.47
CH_3COOH	1/2	0.0375[a]	1	1.319	2.087×10^{-5}	6.32
CH_3COOH	1/2	0.0250[a]	1	1.309	2.087×10^{-5}	6.27
CH_3COOH	1/2	0.0125[a]	1	1.311	2.087×10^{-5}	6.28
CH_3COOH	1/10	0.0100[a]	2	0.2221	4.17×10^{-6}	5.33
$H_2PO_4^-$	19/1	0.0633	1	0.265		
$H_2PO_4^-$	9/1	0.0600	2	0.1335		
$H_2PO_4^-$	7/3	0.0467	1	0.0458		
$H_2PO_4^-$	1/1	0.0333	1	0.0269		
$H_2PO_4^-$	1/9	0.00667	1	0.01155		
$H_2PO_4^-$	1/19	0.00333	1	0.01220		

[a] The ionic strength was adjusted at 0.1 M with sodium chloride.
[b] The hydronium ion concentration of the buffer solutions was determined kinetically by the method described previously.[4]

Table 2. Kinetic data for the hydronium ion-catalyzed hydrolysis of *o*-hydroxybenzaldehyde diethyl acetal in aqueous solutions at different temperatures. Perchloric acid was employed as the catalyst. $[H_3O^+]^a = 4.179 \times 10^{-5}$ M; No. of runs: 2.

t °C	k $M^{-1}s^{-1}$	$\Delta H^{\ddagger}_{298}$ kcal mol^{-1}	$\Delta G^{\ddagger}_{298}$ kcal mol^{-1}	$\Delta S^{\ddagger}_{298}$ cal $K^{-1}mol^{-1}$
6.6	121.1			
11.4	178.9			
16.2	259.0	12.6 ± 0.2	13.75 ± 0.01	-3.9 ± 0.6
21.2	394.2			
26.0	560.4			

[a] The hydronium ion concentration of the perchloric acid solution was determined kinetically by the medthod described previously.[4]

Table 3. First-order rate coefficients for the hydrolysis of *o*-hydroxybenzaldehyde diethyl acetal in aqueous buffer solutions at 70 °C. HA denotes the more acidic component of the buffer system.

[HA]/[A⁻]	[HA] M	No. of runs	10^3k s^{-1}
HA = $H_2PO_4^-$; pK_a^{25} 7.20 (Ref. 7)			
9/1	0.0600	2	34.8
7/3	0.0467	2	16.6
1/1	0.0333	2	12.84
4/6	0.0267	2	11.6
3/7	0.0200	5	9.48
2/8	0.0133	4	9.16
1/9	0.00667	8	7.98
1/19	0.00333	2	7.82
HA = H_3BO_3; pK_a^{25} 9.23 (Ref. 7)			
5/1	0.100	6	8.41
5/2	0.100	3	7.82
10/7	0.100	2	7.31
1/1	0.100	4	6.66
3/5	0.0600	2	5.76
2/5	0.0400	2	4.86
2/10	0.0200	2	3.69
1/10	0.0100	2	2.75
HA = HCO_3^-; pK_a^{25} 10.33 (Ref. 7)			
1/1	0.100	2	3.35
3/5	0.0600	1	2.58
3/7	0.0429	1	2.09
3/17	0.0176	1	1.462
1/19	0.01111	1	1.162
HA = $D_2PO_4^-$[a]			
1/19	0.00333	2	5.35

[a] In deuterium oxide.

temperatures (Table 2). The parameters of the Arrhenius equation were calculated from the plot log k *versus* $1/T$ by the method of least squares. The activation entropy, $\Delta S^{\ddagger} = -3.9$ cal K^{-1} mol^{-1}, is found to be of the magnitude expected for the A-1 hydrolysis of acetals.[5]

Intramolecular catalysis. As mentioned above, an alternative route must exist in hydronium ion concentrations lower than 10^{-6} M. Further kinetic data are, however, required especially at low hydronium ion concentrations to get information on this mechanistical anomaly. The sensitivity of the studied compound to hydrolytic decomposition is relatively low under these conditions and therefore a higher temperature, 70 °C, was generally employed for the kinetic

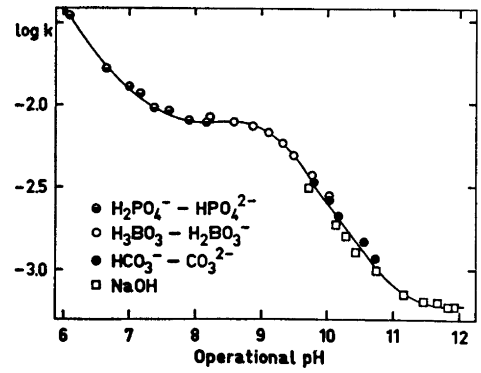

Fig. 1. The logarithms of the first-order rate coefficients of the hydrolysis of *o*-hydroxybenzaldehyde diethyl acetal in water as a function of the operational pH value of the solution. Temperature 70 °C.

measurements. First-order rate coefficients determined in different buffer systems at 70 °C are collected in Table 3. To get an illustration of the variation of the rate coefficients with the hydronium ion concentration of the solution the logarithms of the rate coefficients were plotted against the measured pH values of the reaction mixtures (Fig. 1). Although the pH values are only operative and do not give exact hydronium ion concentrations of the solutions it is reasonable to assume that they are satisfactorily in correlation with the hydronium ion concentrations of the solutions. From this plot it can be seen that in solutions with pH 7.9 – 8.6 the hydrolytic decomposition is actually independent of the hydronium ion concentration of the solution. This situation can best be explained in terms of an intramolecular general acid catalysis (eqn. 3). Although the intramolecular catalysis by a carboxy group has been realized in the hydrolysis of acetals [6] the related intramolecular catalysis by a hydroxy group has not been observed in previous studies. In this particular case, however, structural effects can be assumed to favor the intramolecular catalysis. First, the phenolic hydroxyl group is at a position which enables the hydrogen bond formation with the etheral oxygen atom in the transition state of the reaction. Second, the quinone type structure of the transition state is energetically favorable. The rate of reaction (3) may be expressed by eqn. (4).

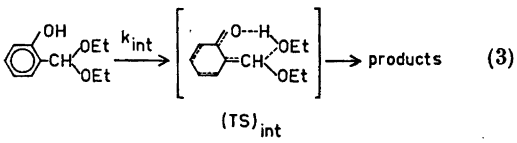

(3)

$$\text{rate} = k_{int}[SH] \quad (4)$$

Naturally the rate of this particular reaction is independent of the hydronium ion concentration of the solution. The contribution of k_{int} decreases with increasing hydronium ion concentration of the solution as shown in eqn. (5).

$$\text{rate} = (k_2^a[H_3O^+] + k_{int})\,[SH] = k_{obs}[SH] \quad (5)$$

Thus k_{int} can be neglected along with the hydronium ion-catalyzed reaction at sufficiently high acid concentrations. As mentioned above this is really the case at hydronium ion concentrations higher than 10^{-6} M. Eqn. (5) also reveals that at low hydronium ion concentrations the contribution of the term $k_2^a[H_3O]^+$ becomes negligible as compared with k_{int}. From the kinetic data in Table 2 a value of $9.6 \times 10^3\,M^{-1}s^{-1}$ can be estimated for k_2^a at 70 °C. If the hydronium ion concentration is 10^{-6} M the term $k_2^a[H_3O^+]$ is $9.6 \times 10^{-5}s^{-1}$ and is thus only about one per cent of the observed rate coefficient. Hence, it is reasonable to assume that in the pH range 7.9 – 8.8 the contribution of the hydronium ion-catalyzed reaction is negligible and consequently the rate coefficients measured under these conditions give directly the value for k_{int}, thus, a value of $(8.01 \pm 0.14) \times 10^{-3}\ s^{-1}$ is obtained from the data in Table 3.

To get additional evidence for the change in the mechanism discussed above some measurements were performed in heavy water. The rate coefficients in 1/19 phosphate buffer give a k_D/k_H value of 0.68 (Table 3). As in the A-1 hydrolysis of acetals this ratio is generally of the magnitude 2 – 3,[1b] the remarkable difference cannot be explained without assuming a change in the reaction mechanism. On the contrary, deuterium solvent isotope effects of unity or lower reflect a general acid catalysis as shown by the kinetic data presented recently for the A-S_E2 hydrolysis of acetals.[2] Thus the measured k_D/k_H value is in accordance with the proposed intramolecular general acid catalysis.

To get information on the temperature dependence of the intramolecular OH-catalyzed reaction some measurements were performed in boric acid-sodium borate and potassium dihydrogen phosphate-disodium hydrogen phosphate buffers at different temperatures (Table 4). The rate coefficients measured in these buffers are equal within the limits of experimental error. If the measured activation entropy is compared with that of the hydronium ion-catalyzed hydrolysis only a small difference is found. This result is not surprising since in the case of A-1 and A-S_E2 reactions the activation entropies have been found to be of the same magnitude.[5]

As mentioned above the rate of the intramolecular OH-catalyzed reaction should be independent of the hydronium ion concentration of the solution. However, if a partial neutralization of the substrate took place, the total rate would be retarded due to the acid-base equilibrium described in eqn. (6).

Table 4. Kinetic data for the hydrolysis of *o*-hydroxybenzaldehyde diethyl acetal at different temperatures in boric acid-sodium borate buffer ([HA] = 0.1 M, [A^-] = 0.1 M), in potassium dihydrogen phosphate-disodium hydrogen phosphate buffer (HA] = 0.00333 M, [A^-] = 0.0633 M) and in 0.2 M sodium hydroxide in water.

t °C	10^3k s^{-1}	$\Delta H^{\ddagger}_{298}$ kcal mol^{-1}	$\Delta G^{\ddagger}_{298}$ kcal mol^{-1}	$\Delta S^{\ddagger}_{298}$ cal $K^{-1}mol^{-1}$
$H_2PO_4^-$-HPO_4^{2-}				
25.0	0.1219			
40.6	0.571			
50.6	1.403	18.3 ± 0.3	22.81 ± 0.02	−15.0 ± 0.8
59.6	3.42			
69.8	7.82			
H_3BO_3-$H_2BO_3^-$				
40.6	0.583			
50.0	1.493			
59.6	3.56	18.9 ± 0.2	22.83 ± 0.02	−13.1 ± 0.5
69.8	8.41			
NaOH				
50.0	0.0802			
59.5	0.224			
69.5	0.601	22.0 ± 0.1	24.78 ± 0.02	−9.5 ± 0.4
80.0	1.591			

$$\text{Products} \xleftarrow[\text{slow}]{k_{int}} SH + OH^- \underset{\text{fast}}{\overset{K}{\rightleftharpoons}} S^- + H_2O \qquad (6)$$

Here the acid-base equilibrium can be assumed to be a diffusion-controlled reaction as a relatively strong acid will be neutralized with a strong base. When the acid-base equilibrium is taken into account the total rate of the reaction can be expressed with eqn. (7).

$$\text{rate} = \frac{k_{int}}{1+K[OH^-]}[SH]_{total} = k_{obs}[SH]_{total} \qquad (7)$$

The form of this equation reveals that the difference between k_{int} and k_{obs} will be increased with increasing hydroxide-ion concentration of the solution, since the term $1+K[OH^-]$ will deviate more and more from unity. Of course, the value of the equilibrium constant K determines in which pH region the difference between k_{obs} and k_{int} becomes observable. The kinetic data (see Fig. 1) reveal that this occurs when the pH value of the solution is higher than 8.6. As the pH measurements were performed at 70 °C, the hydroxide ion concentration of the solution is of the magnitude 10^{-4} M (pK_w is 12.80 at 70 °C [7]).

The equilibrium constant of reaction (6) is $K = K_a/K_w$, where K_a is the dissociation constant of the acid and K_w is the ionic product of water. From the pK_a values of different phenols it can be concluded that in this case K_a is of the magnitude $10^{-9}-10^{-10}$ (Ref. 8). As K_w is of the magnitude 10^{-13} at 70 °C the equilibrium constant K can be assumed to be between 10^3 and 10^4. Thus eqn. (7) can be reduced to eqn. (8) if the hydroxide

$$k_{obs} = k_{int}/K[OH^-] \qquad (8)$$

ion concentration of the solution is higher than 10^{-2} M when $K[OH^-] \gg 1$. Thus eqn. (8) should be valid especially at relatively high hydroxide ion concentrations. When this is the case it is at first sight surprising that at the highest hydroxide ion concentrations employed in this work (Table 5) the observed rate coefficients remain constant although the hydroxide ion concentration of the solutions is varied (see also Fig. 1). This situation is, however, understandable if a third reaction route is followed in the most basic solutions.

Base-promoted hydrolysis. In basic solutions the hydrolysis of salicylaldehyde diethyl acetal may also take place through the anionic form of the substrate as described in eqn. (9). The rate of this reaction is given by eqn. (10). In

Table 5. Kinetic data for the hydrolysis of *o*-hydroxybenzaldehyde diethyl acetal at 70 °C in sodium hydroxide solutions of different concentrations. The equilibrium constants of reaction (6) collected in the table have been calculated from the kinetic data using eqn. (13).

[NaOH] M	No. of runs	$10^3 k$ s^{-1}	$10^{-3} K$ M^{-1}
Solvent: H_2O			
0.00100	3	3.07	2.00
0.00250	2	1.838	1.99
0.00350	2	1.575	1.88
0.00500	3	1.255	2.05
0.0100	1	0.980	1.84
0.0250	1	0.692	(3.08)
0.0500	2	0.642	(3.27)
0.100	2	0.623	–
0.150	1	0.593	–
0.200	2	0.601	–
Solvent: D_2O			
0.096	2	0.292	–

$$SH + OH^- \underset{\text{fast}}{\overset{K}{\rightleftharpoons}} S^- + H_2O \xrightarrow[\text{slow}]{k_b} \text{Products} \quad (9)$$

$$\text{rate} = \frac{k_b K[OH^-]}{1 + K[OH^-]}[SH]_{total} \quad (10)$$

extreme cases, $K[OH^-] \gg 1$, eqn. (10) is reduced to form (11).

$$\text{rate} = k_b[SH]_{total} \quad (11)$$

This expression shows that although the rate of reaction (9) depends on the hydroxide ion concentration of the solution under relatively mild conditions, the rate of the base-promoted reaction is independent of $[OH^-]$ at sufficiently high hydroxide ion concentrations. The kinetic data in Fig. 1 show that this is really the case in solutions in which the hydroxide ion concentration is higher than 0.1 M. Thus the value of k_b can be calculated from the kinetic data in 0.15 and 0.2 M sodium hydroxide solutions and a value of 5.97×10^{-4} s^{-1} is obtained.

In the formal kinetics discussed above it was not taken into account that in reality reactions (6) and (9) can take place simultaneously. The rate coefficient of this total reaction is expressed by eqn. (12). It is easy to find out that eqn. (10) is only a particular case of this expression, as in

$$k_{obs} = (k_{int} + k_b K[OH^-])/(1 + K[OH^-]) \quad (12)$$

the numerator k_{int} was disregarded in comparison with the term $k_b K [OH^-]$. This is naturally the case when the hydroxide ion concentration is sufficiently high. However, in the pH range 8.6 – 11.5 all the terms in eqn. (12) must be taken into account.

Eqn. (12) enables also the determinations of the equilibrium constant K in eqn. (6) in water solutions. From the rate coefficients $k_{int} = 8.01 \times 10^{-3}$ s^{-1} and $k_b = 0.597 \times 10^{-3}$ s^{-1} and from the first-order rate coefficients measured in sodium hydroxide solutions of different concentrations (Table 5) a value for the equilibrium constant can be obtained using eqn. (13).

$$K = (k_{int} - k_{obs})/(k_{obs} - k_b)[OH^-] \quad (13)$$

The results are collected in Table 5. When the equilibrium constant $(1.95 \pm 0.04) \times 10^3$ was calculated, the rate coefficients measured in 0.025 and 0.05 M sodium hydroxide solutions were omitted as the term $(k_{obs} - k_b)$ becomes indeterminate within the limits of experimental error.

In the determination of the dissociation constants of salicylaldehyde diethyl acetal potentiometric titration cannot be applied. First, the acid is relatively weak and consequently the accuracy of the measurements may be low. Second, the substrate undergoes hydrolytic decomposition both in acid and neutral solutions. The dissociation constant K_a can, however, be calculated from the kinetic data. The dissociation constant $K_a = K \times K_w$ and thus a value of $K_a = (3.09 \pm 0.06) \times 10^{-10}$ is obtained at 70 °C from the ionic product of water and from the kinetic value of K. Thus pK_a of the acid is 9.51 ± 0.01 at 70 °C. This pK_a value is found to be a little lower than that of the unsubstituted phenol. This difference is expected as the electronegative diethoxymethyl group in the aromatic ring may increase the acid strength of the substrate.

The hydrolysis of salicylaldehyde diethyl acetal in 0.2 M sodium hydroxide was studied also at different temperatures (Table 4). The activation entropy of this reaction, – 9.5 cal $K^{-1}mol^{-1}$, is only slightly negative and therefore it seems probable that a water molecule has not taken part in the transition state of the reaction. Some additional measurements were performed in 0.1 M sodium hydroxide using different

Table 6. Salt effects in the hydrolysis of *o*-hydroxybenzaldehyde diethyl acetal at 0.1 M sodium hydroxide in water at 70 °C.

Salt	[Salt] M	10^3k s^{-1}
–	0	0.630
NaCl	0.100	0.639
	0.250	0.666
	0.500	0.654
	0.750	0.669
Na_2CO_3	0.100	0.610
	0.300	0.614
Na_3PO_4	0.100	0.636

amounts of added electrolytes (Table 6); the rate coefficients are seen to be equal within the limits of experimental error. Solvent deuterium isotope effect was also studied in basic solutions (Table 5). The ratio k_D/k_H was found to be 0.469.

Although the formal kinetics of the hydrolysis of salicylaldehyde diethyl acetal reveals that in relatively basic solutions the hydrolysis of the compound proceeds through the anionic form of the substrate, the transition state of this reaction cannot be deduced on the basis of the formal kinetics. It is, however, reasonable to assume that in the transition state of this route the negative charge of the phenolate ion will be distributed to the leaving alkoxide ion [structure $(TS)_b$]. The stability of this species can be

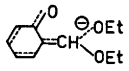

$(TS)_b$

assumed to be relatively high and consequently the observed decomposition in basic solutions is understandable in this particular case, although this kind of reaction has not been observed in previous studies of acetal hydrolysis. All the kinetic data are also in accordance with this mechanism. First, the salt effects are expected to be negligible in this route as the initial state and the transition state differ only in the distribution of the negative charge. Second, the activation entropy of the reaction is in accordance with this mechanism as stated above. Third, the deuterium solvent isotope effect is not unexpected for this kind of unimolecular decomposition. Naturally the mechanism in which the solvent, water, would act as a general acid cannot fully be excluded, but it seems less probable on the basis of the kinetic data. In accordance with this assumption the buffer experiments performed in sodium hydrogen carbonate-sodium carbonate and disodium hydrogen phosphate-sodium phosphate buffers did not give evidence for a general acid catalysis.

Acknowledgement. Grants for support of this work from the Finnish Academy, Division of Sciences, are gratefully acknowledged.

REFERENCES

1. a. Ingold, C. K. *Structure and Mechanism in Organic Chemistry*, 2nd Ed., Cornell University Press, Ithaca, N.Y. 1969, pp. 447–448; b. Cordes, E. H. *Progr. Phys. Org. Chem. 4* (1967) 1.
2. a. Fife, T. H. *Accounts Chem. Res. 5* (1972) 264; b. Fife, T. H. and Jao, L. K. *J. Amer. Chem. Soc. 90* (1968) 4081; c. Kankaanperä, A. and Lahti, M. *Acta Chem. Scand. 23* (1969) 2465; d. Kankaanperä, A. and Lahti, M. *Acta Chem. Scand. 23* (1969) 3266; e. Kankaanperä, A. *Suom. Kemistilehti B 42* (1969) 460; f. Anderson, E. and Capon, B. *J. Chem. Soc. B* (1969) 1033; g. Anderson, E. and Fife, T. H. *J. Amer. Chem. Soc. 91* (1969) 7163; h. Fife, T. H. and Brod, L. H. *J. Amer. Chem. Soc. 92* (1970) 1681; i. Anderson, E. and Fife, T. H. *J. Amer. Chem. Soc. 93* (1971) 1701.
3. Pauly, H. and Buttlar, R. F. *Justus Liebigs Ann. Chem. 383* (1911) 230.
4. Kankaanperä, A., Taskinen, E. and Salomaa, P. *Acta Chem. Scand. 21* (1967) 2487.
5. Schaleger, L. L. and Long, F. A. *Advan. Phys. Org. Chem.* (1963) 27.
6. a. Piszkiewicz, D. and Bruice, T. C. *J. Amer. Chem. Soc. 90* (1968) 2156; b. Capon, B., Smith, M. C., Anderson, E., Dahm, R. H. and Sankey, G. H. *J. Chem. Soc. B* (1969) 1038; c. Dunn, B. M. and Bruice, T. C. *J. Amer. Chem. Soc. 92* (1970) 2410, 6589; d. Capon, B., Anderson, E., Anderson, N. S., Dahm, R. H. and Smith, M. C. *J. Chem. Soc. B* (1971) 1963.
7. Perrin, D. D. *Dissociation Constants of Inorganic Acids and Bases in Aqueous Solution*, Butterworths, London 1969.
8. Kortüm, G., Vogel, W. and Andrussov, K. *Dissociation Constants of Organic Acids in Aqueous Solution*, Butterworths, London 1961.

Received December 12, 1973.

Acta Chemica Scandinavica A 28 (1974) 449—454

Crystal Structure of Cycloalanyltetrasarcosyl Hemihydrate

P. GROTH

Department of Chemistry, University of Oslo, Oslo 3, Norway

The crystals of $C_{15}O_5N_5H_{25}\cdot\frac{1}{2}H_2O$ belong to the monoclinic system with space group $C2/c$ and cell dimensions $a=19.427(5)$ Å, $b=10.804(3)$ Å, $c=17.731(7)$ Å, $\beta=100.27(3)°$. There are eight molecules in the unit cell. The phase problem was solved by direct methods and the R-value arrived at for 1774 observed reflections was 6.3 % ($R_W=5.2$ %). The conformation is *cis, cis, cis, trans, trans*. Inter-molecular N···O hydrogen bonds (2.962 Å) connect centrosymmetrically related molecules, forming dimers. Water molecules, situated at two-fold axes of rotation, link the dimers to endless chains along [001]. The results are compared with those of cyclotetra-, cyclopenta-, and cycloocta-sarcosyl.

Cyclic oligopeptides of sarcosine, glycine, and alanine are studied by Dale and Titlestad, mainly by spectroscopic methods.[1-3] For the sarcosine compounds

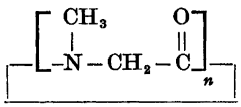

with $n=2$, 4, 5, 8, the crystal structures are known.[4-7] The *cis, cis, cis, trans, trans*-conformation found for cyclopentasarcosyl is also predominant in solution, whereas many other cyclic pentapeptides are conformer mixtures in solution.[3] For example, by dissolving crystals of cycloalanyltetrasarcosyl, (AS4), in $CHFCl_2$ at low temperature (−75°), and slowly heating the solution, drastic changes in the NMR-spectra recorded at different temperatures are observed. A new set of lines due to a second conformer develops at −40°. At the final equilibrium, the crystal conformer spectrum is completely replaced by these lines together with a third set, belonging to the dominant solution conformer. These findings, and a comparison of the (−75°)-spectrum of AS4 with the (−50°)-spectrum of cyclopentasarcosyl, suggest different crystal conformations. In order to settle the conformational problem, and to obtain detailed information of the molecular geometry, an X-ray crystallographic investigation of cycloalanyltetrasarcosyl has been carried out.

The crystals belong to the monoclinic system and the systematic absences lead to the space group $C2/c$.* The cell parameters, measured by means of a four circle diffractometer, and their estimated standard deviations are: $a=19.427(5)$ Å, $b=10.804(3)$ Å, $c=17.731(7)$ Å, $\beta=100.27(3)°$. The unit cell contains eight AS4, and four water molecules. With $2\theta(\max)=50°$ and Mo$K\alpha$-radiation, about 3400 independent reflections were measured on an automatic four circle diffractometer. Using an observed-unobserved cutoff at $2.0\sigma(I)$, 1774 were recorded as observed. No corrections have been made for absorption or secondary extinction effects.

The structure was solved by direct methods [8] and refined by full-matrix least squares technique.[9]** Hydrogen atom positions were calculated. Anisotropic temperature factors were introduced for O, N, and C-atoms, and weights in least squares were calculated from the standard deviations in intensities, $\sigma(I)$, taken as

$$\sigma(I)=[C_T+(0.02C_N)^2]^{\frac{1}{2}}$$

where C_T is the total number of counts and C_N the net count (peak minus background). The conventional R-value arrived at was 6.3 % (weighted value $R_W=5.2$ %) for 1774 observed reflections. The form factors were those of

* Since L-alanine was used in the synthesis, the centrosymmetric space group shows that racemization has occurred.

** All programs used are included in this reference.

Table 1. Final fractional coordinates and anisotropic thermal vibration parameters with estimated standard deviations (multiplied by 10^5 for non-hydrogens and 10^4 for hydrogens). The symbols CC, CM, and OW are used for carbonyl carbons, methyl carbons and water oxygen, respectively. Hmn is bonded to Cm, HMmn to CMm, H4 to N4, and HW to OW.

ATOM	X	Y	Z	B	B11	B22	B33	B12	B13	B23
OW	0(0)	46453(47)	25000(0)		478(24)	937(60)	768(31)	0(0)	440(44)	0(0)
O1	4926(16)	35157(29)	4789(18)		211(11)	718(35)	360(14)	118(33)	96(20)	-171(37)
O2	11057(18)	29460(34)	25890(19)		374(15)	1238(46)	271(14)	25(41)	210(23)	-168(42)
O3	19070(18)	65947(31)	26294(19)		364(14)	763(37)	339(14)	-138(36)	-63(22)	-307(39)
O4	7465(18)	87466(31)	5710(20)		431(15)	597(36)	451(17)	297(38)	223(25)	129(41)
O5	19549(18)	48424(31)	-1265(20)		204(12)	901(40)	488(17)	118(35)	-63(23)	-256(42)
N1	10568(20)	18176(35)	15110(22)		297(15)	644(43)	274(17)	-24(41)	195(25)	-41(45)
N2	20966(21)	45420(38)	22929(22)		276(15)	749(48)	293(17)	98(43)	-107(25)	-94(46)
N3	9986(20)	70501(34)	12895(22)		285(14)	518(40)	298(16)	80(39)	88(24)	-122(44)
N4	18393(18)	61737(35)	-3441(21)		174(12)	639(41)	315(16)	30(37)	31(23)	-30(41)
N5	10457(20)	28841(35)	-4593(22)		271(14)	606(41)	262(17)	121(40)	75(25)	-123(43)
CC1	8708(24)	27624(43)	2379(27)		196(16)	530(48)	261(19)	-98(47)	21(28)	-223(53)
CC2	13198(24)	27344(46)	19906(28)		257(18)	719(53)	229(20)	239(52)	107(31)	108(57)
CC3	17888(24)	56560(50)	21686(28)		217(17)	750(56)	273(21)	-158(51)	18(30)	-11(58)
CC4	10286(25)	77297(47)	6503(29)		257(18)	553(52)	308(21)	-82(50)	-12(31)	-59(59)
CC5	13468(27)	50698(45)	-4050(26)		239(18)	670(54)	234(19)	-36(50)	70(29)	59(51)
C1	12470(24)	17061(42)	7484(27)		246(18)	605(50)	283(20)	-22(49)	144(29)	-109(52)
C2	19245(24)	34921(44)	17872(26)		230(16)	674(53)	263(19)	83(48)	44(28)	-98(53)
C3	12771(25)	58024(41)	14171(26)		290(18)	494(49)	306(20)	6(47)	-16(31)	-81(50)
C4	14387(25)	72077(41)	513(27)		286(18)	470(47)	305(20)	-163(49)	131(30)	-58(54)
C5	8825(25)	40760(45)	-8389(26)		244(17)	712(55)	265(19)	88(48)	-55(30)	-12(53)
CM1	4417(29)	11592(49)	16802(32)		432(21)	911(57)	474(27)	-332(60)	370(39)	-35(65)
CM2	25684(28)	43252(53)	30285(30)		398(21)	1192(69)	349(22)	339(61)	-274(36)	-57(66)
CM3	5745(26)	75193(47)	18304(28)		289(18)	874(62)	359(21)	2(53)	119(32)	-159(59)
CM4	15329(27)	82184(50)	-5178(31)		305(20)	963(67)	439(24)	-209(59)	193(34)	-88(67)
CM5	15169(28)	20379(48)	-7652(27)		443(22)	904(63)	326(20)	246(61)	338(35)	-95(60)
H11	1428(17)	869(32)	535(18)	2,9(,8)						
H12	1729(16)	1703(29)	746(17)	1,7(,7)						
H21	2334(17)	2921(32)	1817(18)	3,1(,8)						
H22	1812(16)	3798(31)	1240(18)	3,0(,8)						
H31	1523(18)	5589(34)	982(19)	4,2(,9)						
H32	890(19)	5215(33)	1381(21)	3,9(,9)						
H51	368(15)	4295(27)	-857(16)	2,1(,7)						
H52	985(15)	3995(29)	-1354(16)	2,0(,7)						
HM11	292(19)	456(36)	1294(23)	10,6(1,0)						
HM12	59(23)	1743(44)	1684(26)	8,3(1,3)						
HM13	569(24)	732(45)	2142(28)	8,8(1,3)						
HM21	2715(27)	3485(54)	3024(31)	10,8(1,6)						
HM22	2327(27)	4584(50)	3422(29)	10,4(1,5)						
HM23	2928(20)	4845(38)	3061(23)	10,7(1,0)						
HM31	436(20)	6815(40)	2136(24)	6,3(1,1)						
HM32	164(21)	7986(38)	1535(23)	6,5(1,1)						
HM33	841(24)	8162(42)	2175(26)	5,6(1,2)						
HM41	1830(22)	8904(41)	-232(24)	6,2(1,2)						
HM42	1074(20)	8616(37)	-758(22)	5,4(1,0)						
HM43	1791(19)	7874(36)	-904(21)	5,8(1,0)						
HM51	1573(20)	2298(37)	-1247(22)	9,6(1,0)						
HM52	1368(25)	1200(49)	-735(26)	9,9(1,5)						
HM53	1965(21)	2025(38)	-414(22)	10,8(1,0)						
H4	580(19)	6248(35)	-473(20)	4,9(1,0)						
HW	382(17)	4212(35)	2642(22)	9,0(1,0)						

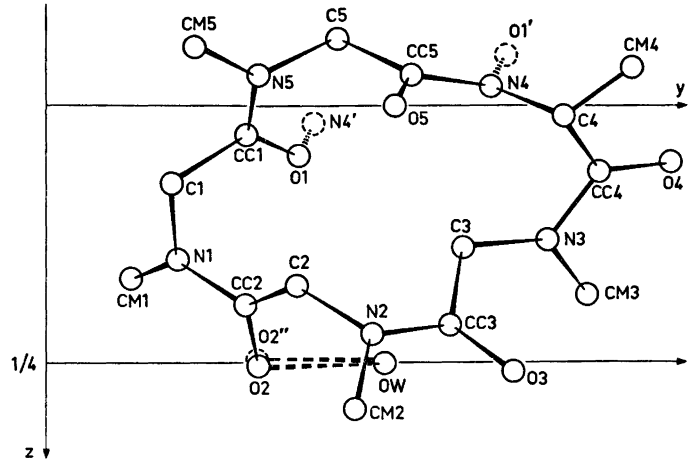

Fig. 1. The molecule viewed along [100].

Table 2. Observed and calculated structure factors on 10 times absolute scale.

K=	0,L=	0
2	184	205
4	4091	4070
6	1149	1146
10	1246	1245
12	499	479
14	524	528
16	158	154
20	416	421
22	142	134
K=	0,L=	2
-20	196	221
-16	646	667
-14	263	295
-12	376	379
-8	428	411
-6	176	232
-4	1160	1209
-2	3189	3178
0	896	834
2	823	807
4	3595	3600
6	1135	1131
8	463	461
10	393	447
14	483	487
16	172	151
18	160	217
20	197	204
K=	0,L=	4
-20	187	210
-16	176	156
-14	157	173
-12	308	323
-8	767	728
-6	861	822
-4	1376	1398
-2	3236	3308
0	2220	2132
2	1058	1140
4	874	879
6	418	391
8	525	508
10	733	731
14	118	65
16	227	200
18	215	175
K=	0,L=	6
-16	211	195
-14	143	172
-12	951	957
-10	823	828
-6	1558	1545
-4	1081	1089
-2	682	703
0	532	521
2	331	356
4	112	102
6	1404	1373
8	236	270
12	359	367
18	301	295
K=	0,L=	8
-18	244	207
-16	130	103
-10	671	699
-8	264	283
-6	836	825
-4	1215	1281
-2	305	319
0	836	834
2	626	619
4	848	809
6	330	358
10	903	909
K=	0,L=	10
-20	236	262
-18	470	462
-16	320	315
-14	817	838
-10	700	699
-8	182	141
-6	454	446
-4	724	712
-2	1105	1144
0	1237	1213
2	402	427
4	717	695
6	397	422
8	191	194
10	206	203
12	397	421
K=	0,L=	12
-18	135	47
-14	166	144
-12	289	304
-8	245	260
-6	332	352
-2	219	285
0	135	67
4	294	300
6	215	235
8	438	428
10	238	289
K=	0,L=	13
8	141	0
K=	0,L=	14
-14	245	204
-8	283	308
-4	423	432
-2	452	477
4	149	98
6	173	198
K=	0,L=	16
-14	169	102
-12	144	169
-10	224	214
-6	715	728
-2	397	411
0	207	176
2	357	388
6	575	542
10	327	280
K=	0,L=	18
-14	145	49
-8	454	419
-4	328	334
2	173	170
6	289	286
K=	0,L=	20
-10	155	106
-6	185	171
-2	274	285
K=	1,L=	0
1	1783	1772
3	1868	1864
5	925	874
7	403	374
9	534	497
11	444	449
13	607	616
15	304	301
19	129	19
21	152	194
K=	1,L=	1
-15	203	232
-13	276	260
-11	624	622
-9	639	665
-7	314	303
-5	587	569
-3	301	313
-1	123	36
1	371	427
5	135	85
7	744	732
9	410	400
13	257	278
21	180	155
K=	1,L=	2
-13	393	395
-11	408	415
-7	441	465
-5	1756	1765
-3	251	217
-1	219	200
1	308	312
3	1096	1142
7	749	724
9	107	140
11	269	269
21	196	187
K=	1,L=	3
-17	274	252
-15	178	202
-13	279	276
-9	641	625
-5	298	308
-1	191	231
1	1259	1218
3	583	549
5	2196	2199
7	315	331
9	929	957
11	356	344
K=	1,L=	4
-21	139	174
-17	189	197
-13	439	446
-11	191	208
-9	972	978
-7	224	202
-5	1747	1774
-3	1486	1447
-1	330	315
1	1768	1759
5	358	352
7	636	602
9	449	458
11	609	600
13	382	370
15	233	235
17	143	135
K=	1,L=	5
-21	147	48
-19	180	233
-11	836	835
-9	602	604
-7	462	413
-5	757	711
-3	461	397
-1	387	368
1	237	297
3	305	255
5	413	381
7	272	210
9	380	386
K=	1,L=	6
-17	201	204
-15	224	225
-11	193	198
-9	127	87
-7	1097	1061
-5	198	239
-3	1318	1301
-1	886	888
1	318	314
5	340	356
7	605	594
K=	1,L=	7
-19	146	115
-13	458	466
-11	173	162
-9	226	220
-5	389	366
-3	406	385
-1	836	857
3	412	411
5	790	809
7	165	165
9	558	538
13	226	206
17	234	220
K=	1,L=	8
-15	136	144
-9	369	389
-7	171	208
-5	423	444
-3	480	484
-1	206	189
1	1023	1020
3	539	541
11	305	319
K=	1,L=	9
-19	175	168
-17	220	227
-15	556	552
-13	259	277
-11	434	439
-9	188	200
-7	488	482
-5	638	635
-3	783	756
-1	717	737
1	160	183
5	300	340
7	146	178
9	250	237
13	159	129
15	147	79
K=	1,L=	10
-17	240	207
-11	131	147
-9	283	300
-7	249	254
-5	356	378
-3	143	155
1	254	245
3	190	200
5	171	177
9	210	207
11	334	337
K=	1,L=	11
-17	243	255
-7	150	150
-5	305	321
-3	225	268
-1	166	168
1	165	170
3	134	126
5	348	334
7	312	320
9	133	86
11	190	198
13	260	231
K=	1,L=	12
-13	277	306
-11	180	213
-7	274	297
-5	305	326
-3	357	355
-1	439	456
3	182	171
5	251	276
7	165	167
11	200	207
K=	1,L=	13
-19	136	30
-15	217	207
-13	202	198
-11	427	455
-9	486	492
-7	292	282
-5	426	446
-1	172	198
1	435	409
3	194	186
5	271	249
11	230	256
15	190	137
K=	1,L=	14
-7	231	212
-5	188	214
-3	160	154
-1	210	197
1	117	140
3	215	206
9	217	203
11	139	104
K=	1,L=	15
-11	148	134
-7	128	149
-3	166	146
-1	199	195
1	132	126
3	128	69
5	343	363
7	159	169
9	309	309
K=	1,L=	16
-9	132	154
-3	287	301
-1	148	143
5	185	236
9	162	125
K=	1,L=	17
-15	171	168
-9	249	230
-7	242	263
-3	331	368
1	183	181
3	384	383
7	274	262
K=	1,L=	18
-7	167	140
-5	170	175
5	210	210
K=	1,L=	19
-1	138	25
1	189	190
3	168	184
5	228	192
K=	1,L=	20
-5	153	133
-3	155	96
K=	1,L=	21
-5	148	167
K=	2,L=	0
0	2315	2271
2	1325	1344
4	2754	2708
6	948	951
8	560	561
14	338	361
16	273	268
18	211	251
20	216	167
22	142	11
K=	2,L=	1
-20	172	187
-16	145	140
-14	222	237
-12	264	265
-10	521	538
-8	300	315
-6	1580	1590
-4	342	399
-2	447	499
0	390	402
2	345	356
4	1297	1285
6	877	875
8	128	112
10	824	834
12	208	216
14	272	289
16	166	174
K=	2,L=	2
-16	405	413
-12	711	726
-8	311	330
-6	223	254
-4	1306	1287
-2	888	921
0	712	717
2	835	862
4	812	858
6	134	153
8	704	723
10	228	226
12	171	209
14	165	161
16	274	289
K=	2,L=	3
-22	151	132
-16	321	311
-10	391	334
-8	1438	1465
-6	197	215
-4	693	650
-2	565	604
0	351	340
2	1048	1015
4	1684	1666
6	243	272
8	882	891
10	364	367
K=	2,L=	4
-20	214	194
-12	268	270
-10	406	413
-8	130	80
-6	215	214
-4	942	905
-2	607	615
0	368	382
2	374	409
4	633	650
6	586	547
8	669	685
10	469	480
K=	2,L=	5
-20	164	149
-18	176	161
-16	283	255
-14	153	169
-12	228	225
-10	276	269
-8	352	356
-6	1288	1311
-4	399	410
-2	1488	1459
0	1335	1324
2	1635	1608
4	1185	1192
6	916	923
8	181	177
10	120	118
12	221	227
14	235	232
18	251	259
K=	2,L=	6
-20	222	193
-16	200	195
-12	188	185
-8	382	397
-6	136	130
-4	746	769
-2	746	729
0	135	126
2	337	350
4	126	105
8	411	436
10	235	243
12	383	419
14	566	541
16	313	336
K=	2,L=	7
-18	315	296
-16	180	175
-10	190	196
-8	989	976
-6	379	367
-4	639	641
-2	859	823
0	917	941
2	994	983
4	559	561
6	423	436
12	135	106
K=	2,L=	8
-18	136	138
-14	177	162
-12	314	297
-4	625	589
-2	655	622
0	588	595
2	696	668
4	275	294
6	595	606
8	402	381
16	188	176
18	147	37
K=	2,L=	9
-18	192	158
-12	193	182
-10	238	237
-6	229	220
-4	312	302
-2	871	861
0	136	96
2	345	321
4	377	360
6	256	246
8	193	198
10	272	269
12	139	132
K=	2,L=	10
-20	312	269
-18	286	296
-16	356	359
-14	711	728
-12	271	258
-10	619	632
-8	349	368
-6	267	232
-4	122	80
0	381	383
2	185	198
6	453	472
10	285	276
14	251	233
K=	2,L=	11
-14	268	256
-12	500	537
-8	579	596
-6	229	240
-4	120	103
-2	115	98
0	288	294
4	168	129
6	464	471
12	204	200
K=	2,L=	12
-16	246	271
-12	185	189
-10	241	284
-8	161	151
-6	353	347
-4	481	478
-2	270	267
0	140	153
2	654	692
4	143	140
6	128	18
8	183	138
10	144	129
14	144	146
K=	2,L=	13
-14	211	260
-10	480	494
-8	546	555
-4	218	232
0	117	70
2	344	349
4	342	335
6	261	258
12	161	125
K=	2,L=	14
-14	264	292
-10	294	300
-8	295	302
-6	144	192
-4	212	181
2	159	142
4	205	204
8	340	321
K=	2,L=	15
-6	186	195
0	439	451
4	311	325
K=	2,L=	16
-8	297	263
-6	122	109
-4	241	220
-2	266	285
0	380	377
2	339	331
4	228	230
8	226	239
K=	2,L=	17
-4	156	154
-2	308	308
2	154	127
4	141	101
K=	2,L=	18
-12	142	101
-10	194	190
-4	165	131
K=	2,L=	19
-4	189	185
K=	3,L=	0
1	312	321
3	418	489
5	437	459
7	643	597
11	211	184
13	328	317
15	288	293
21	228	178
K=	3,L=	1
-19	404	400
-13	185	175
-11	159	132
-9	217	227
-7	1101	1109
-5	273	240
-3	1254	1225
-1	426	446
1	119	97
3	779	797
5	703	728
7	232	202
9	146	139
13	144	140
17	145	141
19	217	196
K=	3,L=	2
-15	255	264
-11	416	429
-9	373	358
-7	516	510
-5	677	701
-3	1144	1120
1	376	398
3	2320	2359
5	109	146
7	789	780
9	177	172
11	190	158
13	394	397
15	391	427
19	372	392
K=	3,L=	3
-21	219	183
-15	244	266
-13	248	245
-11	214	191
-9	505	498
-7	454	486
-5	522	500
-3	151	149
1	448	447
3	1787	1772
5	1253	1232
7	420	423
9	976	957
13	554	542
15	342	365
17	443	434
K=	3,L=	4
-15	206	190
-13	480	463
-11	324	320
-9	497	494
-7	1060	994
-5	1126	1097
-3	269	218
-1	929	898
1	317	329
5	667	671
7	556	566
9	253	289
15	239	280
17	218	187
K=	3,L=	5
-19	144	169
-13	440	430
-11	138	121
-9	420	417
-7	323	292
-1	292	270
1	186	232
3	456	446
5	243	254
7	1088	1117
9	634	645
11	225	240
13	657	648
K=	3,L=	6
-19	221	202
-11	425	436
-9	584	597
-7	1062	1022
-5	258	276
-3	436	393
-1	174	176
7	139	129
9	491	525
13	603	638
17	195	187
K=	3,L=	7
-19	235	199
-15	135	144
-13	412	426
-11	249	257
-9	342	346
-7	485	483
-5	210	190
-3	180	205
-1	337	363
1	720	703
3	253	250
5	560	554
7	180	154
9	192	181
11	273	261
13	285	236
15	161	183
17	233	209
K=	3,L=	8
-21	145	171
-17	166	156
-15	145	149
-9	152	155
-7	880	859
-5	911	907
-3	886	898
-1	1031	1005
1	153	108
3	115	112
5	452	464
7	172	141
9	218	194
13	348	340
17	242	179
K=	3,L=	9
-15	251	264
-11	144	145
-9	351	346
-7	476	482
-5	287	283
-3	171	117
-1	244	232
1	439	429
3	109	107
5	150	114
7	341	333
11	195	215
K=	3,L=	10
-17	144	100
-13	337	371
-11	165	163
-9	153	179
-7	188	165
-3	430	402
1	144	174
3	482	491
5	283	268
7	510	505
11	162	110
13	309	299
K=	3,L=	11
-11	127	119
-9	239	230
-7	150	77
-5	290	294
-3	470	465
-1	179	158
1	127	144
3	508	513
5	291	291
13	128	17
K=	3,L=	12
-19	177	175
-13	233	221
-11	374	374
-9	573	560
-5	120	143
-1	287	303
1	853	900
3	246	249
5	236	271
7	168	148
9	216	188
11	235	238
15	196	190
K=	3,L=	13
-15	153	145
-11	443	449
-9	187	192
-7	444	486
-5	262	259
-3	155	184
-1	347	360
1	393	392
5	213	230
7	164	167
9	248	244
K=	3,L=	14

Table 2. Continued.

-15	280	237	- 4	398	386	- 2	322	327	- 3	394	365	13	151	156	- 2	753	758	K-	7,L=	0	K-	7,L=	10								
-13	337	328	- 2	526	533	2	187	146	- 1	792	799	K-	5,L=	13	0	199	160	1	449	440	-13	135	135								
-11	344	350	0	695	714	4	352	364	1	719	704	-15	143	156	4	113	102	5	890	913	- 9	524	536								
- 9	309	308	2	310	297	6	273	280	3	1030	991	-13	138	120	10	465	457	7	178	183	- 7	133	127								
- 7	177	193	4	185	188	8	141	112	5	142	129	-11	279	234	K-	6,L=	6	9	355	341	- 5	530	528								
- 5	171	179	6	431	412	10	164	125	7	131	119	- 7	161	194	-20	160	116	13	196	202	1	300	328								
- 3	182	180	8	521	514	12	162	188	9	559	560	- 5	387	399	-16	232	261	15	187	113	3	127	138								
- 1	573	592	10	144	141	K-	4,L=	13	11	240	215	- 3	232	237	-14	233	213	K-	7,L=	1	5	142	133								
3	350	338	12	576	577	-14	201	119	13	247	256	- 1	218	216	-12	149	144	-15	270	272	11	226	233								
7	205	182	16	126	115	-10	363	386	K-	5,L=	5	3	343	336	-10	527	540	-11	228	226	K-	7,L=	11								
11	140	101	K-	4,L=	5	- 6	530	566	-19	142	161	5	265	272	- 8	149	118	- 9	355	340	-16	160	68								
K-	3,L=	15	-20	153	161	- 2	571	579	-15	177	182	7	260	235	- 4	393	376	- 3	329	330	-11	131	61								
-13	152	88	-16	156	122	0	185	166	- 9	230	209	K-	5,L=	14	- 2	523	532	1	710	720	- 9	373	354								
-11	173	187	-14	371	369	2	453	477	- 7	141	153	-15	157	114	0	196	197	3	240	235	- 5	429	442								
- 9	134	124	-10	350	325	4	155	153	- 5	611	594	- 5	252	242	2	326	336	5	122	118	- 3	238	222								
- 7	296	314	- 6	503	512	8	132	143	- 3	347	336	- 3	231	223	4	149	157	7	213	214	- 1	375	342								
- 5	142	181	- 4	570	562	12	156	88	- 1	316	305	- 1	378	347	6	250	224	11	291	287	1	323	345								
- 3	139	130	0	118	29	K-	4,L=	14	1	120	108	1	134	149	8	242	243	K-	7,L=	2	7	217	167								
- 1	132	169	2	1082	1056	- 8	264	228	5	143	152	3	163	115	10	235	293	-13	128	127	11	203	188								
1	400	393	6	796	803	- 6	251	249	7	668	682	5	173	131	12	136	174	-11	176	224	K-	7,L=	12								
3	229	228	10	164	195	- 4	171	181	11	448	455	K-	5,L=	15	K-	6,L=	7	- 9	146	106	-11	166	193								
9	178	136	12	394	396	- 2	127	80	15	365	354	- 7	406	397	-18	226	262	- 7	181	220	- 3	428	425								
11	146	119	14	192	200	0	125	84	17	205	147	- 3	188	184	-14	148	146	- 5	472	465	7	217	241								
K-	3,L=	16	16	213	170	2	241	199	K-	5,L=	6	3	177	75	-12	138	119	- 3	294	298	11	250	227								
- 9	157	85	K-	4,L=	6	10	186	200	-15	159	206	K-	5,L=	16	- 8	149	156	1	396	388	K-	7,L=	13								
- 1	211	229	-18	177	199	K-	4,L=	15	-11	386	389	-11	134	95	- 6	364	362	3	113	68	- 7	160	153								
K-	3,L=	17	-16	166	111	-12	234	231	- 9	240	230	- 7	209	219	- 4	138	150	5	301	307	- 5	247	218								
- 9	208	201	-14	372	354	0	176	134	- 5	396	403	- 5	184	229	0	686	679	7	188	155	- 1	295	290								
- 7	168	155	- 6	536	531	2	134	140	- 3	401	390	- 1	255	266	4	210	229	9	166	153	5	178	154								
- 5	252	259	- 6	417	391	K-	4,L=	16	- 1	277	246	3	269	240	6	378	391	11	267	242	9	169	59								
- 3	191	171	- 4	514	522	-14	200	118	1	154	150	7	174	99	8	273	255	13	317	353	K-	7,L=	14								
- 1	422	419	0	480	486	- 6	151	146	3	330	334	K-	5,L=	17	10	625	610	17	172	202	- 7	234	223								
1	255	244	6	148	147	- 4	138	149	9	400	421	- 9	164	119	K-	6,L=	8	K-	7,L=	3	- 5	180	149								
3	145	118	8	260	259	- 2	293	298	11	170	225	- 3	215	166	-16	228	204	-11	135	131	- 3	257	287								
K-	3,L=	18	10	159	146	0	164	112	13	141	159	- 1	134	109	-14	138	110	- 9	138	109	- 1	247	263								
- 9	180	194	18	183	143	4	350	330	17	223	217	K-	5,L=	18	-12	333	350	- 5	359	372	K-	7,L=	15								
7	161	110	K-	4,L=	7	K-	4,L=	17	K-	5,L=	7	-11	184	98	-10	188	163	- 3	287	273	- 9	145	106								
K-	3,L=	19	-18	190	197	- 4	225	207	-19	219	222	K-	6,L=	0	- 8	197	209	- 1	118	95	- 3	172	158								
- 1	200	168	-14	211	173	4	161	90	-15	291	267	0	241	239	- 2	115	98	1	283	319	5	160	108								
K-	3,L=	20	-12	163	155	K-	4,L=	18	-11	128	41	2	345	327	2	110	49	5	252	251	K-	7,L=	16								
- 3	144	38	-10	191	161	-10	185	109	- 9	216	244	4	115	110	4	244	246	7	139	60	- 5	292	245								
K-	4,L=	0	- 8	539	568	2	189	164	- 5	597	600	6	583	605	6	424	422	9	190	167	- 3	229	189								
2	474	458	- 6	198	194	K-	4,L=	19	- 3	360	353	8	247	246	10	317	290	K-	7,L=	4	- 1	197	163								
4	500	478	- 4	533	533	- 2	208	188	- 1	611	628	10	160	140	16	175	172	-17	171	157	1	149	94								
6	290	321	- 2	337	334	2	154	105	1	514	482	12	331	332	K-	6,L=	9	-13	131	166	3	187	179								
8	781	775	2	376	363	K-	5,L=	0	5	352	383	K-	6,L=	1	-18	166	151	-11	179	175	K-	7,L=	17								
10	209	200	4	504	513	1	487	470	7	505	498	-16	192	132	-14	230	227	- 7	142	120	- 5	166	145								
14	294	278	6	251	245	7	338	327	9	134	116	-12	571	586	-12	244	241	- 5	213	212	K-	8,L=	0								
18	138	75	8	565	578	9	180	152	13	479	465	-10	135	170	-10	210	192	- 3	240	258	2	337	344								
K-	4,L=	1	10	312	377	15	215	230	15	289	279	- 8	588	603	- 8	152	114	3	262	251	4	131	153								
-20	162	118	12	389	388	17	148	117	K-	5,L=	8	- 6	216	218	- 6	160	151	7	154	136	6	183	185								
-18	122	37	16	162	216	K-	5,L=	1	-19	156	189	- 4	333	330	- 4	401	400	9	115	39	8	432	422								
-16	229	216	K-	4,L=	8	-17	220	209	-17	260	220	0	443	463	- 2	158	141	11	174	200	14	155	143								
-10	298	278	-20	218	194	-15	154	100	-13	158	168	2	306	317	0	321	324	13	200	231	K-	8,L=	1								
- 8	343	317	-16	153	127	-11	174	150	-11	171	130	4	250	243	2	220	229	15	199	168	-16	131	53								
- 6	1011	994	-14	364	372	- 9	179	737	- 7	148	155	12	197	205	4	251	271	17	214	204	-14	291	271								
- 2	301	249	-12	138	121	- 7	146	144	- 5	131	138	14	234	238	6	492	496	K-	7,L=	5	-12	188	192								
0	142	124	- 8	373	368	- 5	428	443	- 3	356	350	16	153	122	8	246	239	-19	169	70	- 8	517	537								
2	367	365	- 6	571	597	- 3	177	134	1	519	527	K-	6,L=	2	12	194	188	-13	173	124	- 6	360	360								
4	321	321	- 4	227	273	- 1	228	185	3	378	390	-16	155	129	K-	6,L=	10	-11	125	156	- 4	540	547								
6	366	378	- 2	133	161	1	507	506	5	174	177	-14	164	174	-18	143	131	- 9	244	230	2	173	166								
10	368	360	0	579	570	5	490	470	9	217	186	-10	617	629	-12	203	157	- 7	115	94	4	145	108								
12	134	122	2	535	536	7	159	182	11	281	308	- 8	317	302	-10	262	236	- 3	199	218	6	265	274								
20	153	112	6	226	219	9	186	196	13	148	168	- 6	376	342	- 4	488	514	1	320	332	8	253	297								
K-	4,L=	2	8	178	172	13	330	360	K-	5,L=	9	- 4	324	323	- 2	386	378	5	177	156	12	191	205								
-20	143	85	10	158	160	15	504	515	-17	135	112	- 2	147	152	0	525	528	7	188	128	14	142	150								
-18	412	428	14	217	222	17	145	124	-15	221	212	0	363	367	2	281	288	9	227	277	K-	8,L=	2								
-14	179	198	16	166	77	K-	5,L=	2	-13	250	250	4	148	161	4	218	213	11	158	112	-12	219	200								
-10	257	278	K-	4,L=	9	-19	357	324	- 7	311	312	8	224	257	K-	6,L=	11	K-	7,L=	6	- 8	211	198								
- 8	813	630	-18	172	192	-17	198	199	- 3	116	133	10	434	440	-18	228	217	-17	168	152	- 2	202	181								
- 6	340	346	-16	210	180	-15	481	481	1	187	193	12	496	528	-14	314	293	-15	162	136	0	590	602								
- 4	156	113	-12	179	220	-11	247	258	5	659	672	16	271	295	- 6	294	310	-11	288	327	4	304	294								
- 2	1221	1212	- 4	327	324	- 9	332	331	7	187	181	K-	6,L=	3	0	229	215	- 9	276	264	6	511	538								
2	965	956	- 2	434	433	- 7	115	121	11	371	365	-18	133	45	4	220	224	- 7	572	579	8	217	224								
4	297	291	0	432	409	- 5	657	661	13	163	158	-12	535	533	6	125	27	- 5	309	309	10	387	414								
6	1038	1052	2	365	392	- 1	111	85	K-	5,L=	10	-10	145	161	10	221	215	- 3	211	253	12	218	215								
8	229	222	4	120	106	1	263	276	-17	153	156	- 8	601	615	K-	6,L=	12	- 1	187	167	K-	8,L=	3								
10	291	302	6	205	210	3	485	458	-13	133	166	- 6	698	701	-14	135	101	3	132	132	-12	123	121								
12	147	144	8	339	325	5	164	168	- 9	150	180	- 4	209	212	-10	204	233	5	228	206	-10	120	103								
14	302	296	10	410	413	7	342	352	- 7	127	162	- 2	628	638	- 8	153	118	13	176	208	- 8	410	420								
18	256	232	16	175	127	11	467	467	- 5	202	216	0	1301	1274	- 4	278	315	15	139	165	- 6	206	226								
K-	4,L=	3	K-	4,L=	10	13	128	109	- 1	228	221	2	264	261	- 2	249	264	K-	7,L=	7	- 2	210	229								
-20	138	41	-16	134	110	15	127	10	3	297	292	4	167	141	2	206	201	- 9	344	346	0	215	204								
-16	176	183	-14	156	172	K-	5,L=	3	7	399	404	8	627	658	4	274	235	- 5	253	259	4	172	212								
-12	211	189	-10	351	367	-21	160	104	11	259	214	10	504	503	10	225	216	- 3	140	35	6	127	122								
-10	290	269	- 8	497	498	-19	189	156	13	157	122	12	784	836	K-	6,L=	13	- 1	141	89	8	209	227								
- 8	192	196	- 6	133	122	-15	145	166	K-	5,L=	11	14	168	147	- 8	140	100	5	131	110	12	274	271								
- 6	485	491	- 4	156	108	- 9	135	124	-13	190	157	16	234	154	- 6	609	628	9	252	239	14	157	161								
- 4	218	208	- 2	253	275	- 7	118	119	-11	234	211	18	205	185	- 2	599	590	K-	7,L=	8	K-	8,L=	4								
- 2	296	306	0	541	535	- 5	188	214	- 5	276	292	K-	6,L=	4	0	330	323	- 9	150	133	-14	208	184								
2	221	207	6	164	160	- 3	300	311	- 1	228	222	-14	158	119	6	136	118	- 7	256	217	- 4	341	342								
4	1984	1972	12	264	264	- 1	1718	1702	5	429	439	-12	311	325	K-	6,L=	14	- 5	155	172	- 2	229	256								
6	219	183	K-	4,L=	11	1	116	151	7	253	248	- 8	118	77	- 6	490	480	- 1	188	218	0	304	306								
8	1034	1037	-20	177	148	3	736	729	11	133	51	- 6	519	516	- 2	224	234	1	279	279	4	278	291								
10	115	71	-10	137	131	9	857	861	15	147	138	- 4	561	571	K-	6,L=	15	3	309	336	6	171	193								
12	160	173	- 8	217	244	11	156	136	K-	5,L=	12	0	275	287	- 8	175	173	5	270	272	8	233	221								
14	587	572	- 2	265	276	13	595	604	-11	200	181	2	274	238	- 2	204	184	7	425	433	10	274	305								
16	276	266	2	391	398	15	182	153	- 9	123	94	4	284	308	0	132	147	15	187	210	14	205	196								
18	364	362	6	338	338	19	248	235	- 7	440	431	8	295	315	4	144	153	K-	7,L=	9	K-	8,L=	5								
20	165	177	8	402	398	K-	5,L=	4	- 5	244	224	14	247	225	K-	6,L=	16	-13	219	201	-14	211	203								
K-	4,L=	4	10	138	179	-19	150	99	- 3	411	407	16	266	287	-12	146	75	-11	205	158	-12	160	141								
-20	138	54	K-	4,L=	12	-17	184	149	1	355	342	18	172	186	K-	6,L=	17	- 5	207	202	-10	200	167								
-18	363	357	-18	178	172	-15	498	496	3	224	244	K-	6,L=	5	- 2	168	183	- 3	388	387	- 6	207	233								
-14	553	549	-12	144	117	-13	144	167	5	362	397	-10	433	448	0	166	163	- 1	160	182	- 4	891	607								
-12	328	342	- 8	127	97	-11	365	331	7	366	347	- 8	603	621	4	196	136	3	323	314	0	270	260								
-10	127	145	- 6	235	239	- 7	284	293	9	236	221	- 6	172	186	K-	6,L=	18	7	421	436	2	424	434								
- 6	128	142	- 4	664	671	- 5	248	252	11	151	118	- 4	363	370	- 4	208	119	11	256	229	4	171	136								

Table 2. Continued.

6	158	183	8	179	126	7	302	316	-9	145	90	-3	171	170	2	142	110	-2	154	209	9	144	167
8	151	106	10	167	126	9	414	428	-7	161	105	K=	9,L=	11	6	190	234	4	236	219	K=	11,L=	4
10	246	260	K=	8,L=	10	K=	9,L=	1	-3	291	315	-9	179	109	10	176	186	K=	10,L=	8	1	237	237
K=	8,L=	6	-10	267	194	-13	141	63	-1	242	244	-1	207	187	K=	10,L=	3	-6	187	177	K=	11,L=	5
-12	238	270	-8	219	195	-7	174	176	1	300	306	3	231	180	-10	212	196	0	160	136	-11	245	194
-10	177	121	-6	125	63	-3	206	220	7	125	92	K=	9,L=	12	-8	207	203	K=	10,L=	9	-9	200	177
-8	138	128	-2	442	406	1	127	142	9	147	140	-9	138	62	-6	522	527	-6	281	277	6	183	199
-6	125	68	2	318	328	3	316	316	K=	9,L=	6	-3	197	193	-4	405	428	-4	259	238	K=	11,L=	6
-4	432	428	4	231	211	7	373	379	-9	235	233	1	227	226	-2	188	237	4	180	164	-9	147	104
0	264	302	6	189	173	K=	9,L=	2	-3	486	490	K=	9,L=	13	0	341	299	K=	10,L=	10	-5	271	267
2	220	218	K=	8,L=	11	-9	157	187	1	473	484	-8	131	85	8	165	104	-8	206	172	-1	209	193
4	405	427	-14	153	131	-7	147	152	9	134	123	5	174	5	10	154	163	-4	204	215	K=	11,L=	7
6	275	299	-10	137	84	-3	559	556	11	215	255	K=	9,L=	14	K=	10,L=	4	4	145	136	-5	233	213
K=	8,L=	7	4	232	241	-1	216	218	K=	9,L=	7	-3	165	147	-6	204	186	K=	10,L=	11	K=	11,L=	9
-12	301	294	8	149	117	1	399	391	-15	150	80	K=	10,L=	0	-4	240	238	-8	147	81	3	183	188
-10	259	268	K=	8,L=	12	3	258	297	-13	181	189	2	148	131	-2	239	257	-4	159	128	K=	12,L=	0
-6	509	524	-14	182	157	5	241	259	-3	338	343	4	500	523	0	176	205	0	195	152	6	168	138
-4	126	72	-8	145	165	11	132	130	3	159	138	6	201	209	2	267	266	K=	10,L=	12	K=	12,L=	1
-2	353	371	-4	141	142	K=	9,L=	3	5	129	34	8	363	364	4	177	108	2	159	95	-8	153	159
2	241	240	2	135	162	-7	199	205	K=	9,L=	8	12	162	148	10	148	42	K=	11,L=	0	-4	275	276
6	234	220	4	198	193	-5	382	380	-9	286	296	K=	10,L=	1	K=	10,L=	5	1	180	165	-2	135	116
8	261	242	K=	8,L=	13	-1	376	402	-7	205	164	-12	226	175	-10	152	145	3	186	186	0	151	135
K=	8,L=	8	-6	175	190	7	147	169	1	298	254	-10	189	177	-6	239	243	K=	11,L=	1	2	225	214
-10	261	253	-4	287	275	11	152	134	3	160	156	-8	400	404	0	360	348	-3	166	147	4	152	163
-8	200	215	0	145	130	13	150	142	5	144	179	-4	476	472	2	151	138	3	198	181	K=	12,L=	2
-6	703	682	4	171	166	K=	9,L=	4	11	184	155	-2	203	211	4	185	161	K=	11,L=	2	2	157	91
-2	410	407	K=	8,L=	14	-11	171	150	K=	9,L=	9	0	397	415	8	186	189	-9	175	139	4	159	167
0	289	288	-4	181	200	-7	478	484	-11	219	185	2	279	276	12	196	177	-5	138	158	6	183	187
2	171	190	0	309	309	-5	219	225	-9	178	182	4	164	151	K=	10,L=	6	-3	152	111	K=	12,L=	3
4	220	227	4	160	102	-3	427	427	-7	159	167	8	200	183	-12	195	147	5	183	129	-4	264	190
K=	8,L=	9	6	137	73	1	330	323	1	315	312	12	175	115	-2	473	479	7	167	141	-2	154	119
-12	353	330	K=	8,L=	15	3	261	248	3	239	211	K=	10,L=	2	2	349	349	K=	11,L=	3	0	177	193
-10	316	303	0	146	129	5	165	195	5	139	156	-14	178	125	4	180	163	-11	196	187	4	160	119
-8	598	601	4	154	71	7	202	185	K=	9,L=	10	-10	259	237	10	145	127	-9	241	204	K=	12,L=	4
-6	247	300	K=	8,L=	0	11	169	92	-11	225	235	-8	150	152	K=	10,L=	7	-3	249	248	0	142	161
-2	200	198	1	286	280	K=	9,L=	5	-9	188	215	-2	481	449	-6	188	203	-1	255	250	K=	12,L=	7
2	278	316	3	356	362	-11	147	127	-5	313	281	0	441	435	-4	220	180	1	330	318	0	176	204
4	272	278	5	687	681																		

Table 3. Interatomic distances, bond angles and dihedral angles with estimated standard deviations.

DISTANCE	(Å)	DISTANCE	(Å)	DISTANCE	(Å)
O1 - CC1	1,224(5)	O2 - CC2	1,228(5)	O3 - CC3	1,222(5)
O4 - CC4	1,225(5)	O5 - CC5	1,222(5)	N1 - CM1	1,467(6)
N2 - CM2	1,473(6)	N3 - CM3	1,462(6)	C4 - CM4	1,520(7)
N5 - CM5	1,463(6)	CC1 - N5	1,346(5)	CC2 - N1	1,345(6)
CC3 - N2	1,344(6)	CC4 - N3	1,348(6)	CC5 - N4	1,347(6)
CC1 - C1	1,529(6)	CC2 - C2	1,527(6)	CC3 - C3	1,522(6)
CC4 - C4	1,555(7)	CC5 - C5	1,520(6)	N1 - C1	1,438(5)
N2 - C2	1,448(5)	N3 - C3	1,455(5)	N4 - C4	1,466(5)
N5 - C5	1,461(6)	O1 - N4′	2,962(5)	OW - O2	2,809(5)

ANGLE	(°)	ANGLE	(°)
N5 - CC1 - O1	121,4(4)	N1 - CC2 - O2	122,3(5)
N2 - CC3 - O3	122,5(4)	N3 - CC4 - O4	120,6(5)
N4 - CC5 - O5	123,8(5)	C1 - N1 - CM1	117,4(4)
C2 - N2 - CM2	117,5(4)	C3 - N3 - CM3	117,2(4)
C5 - N5 - CM5	118,6(4)	N5 - CC1 - C1	117,8(4)
N1 - CC2 - C2	117,8(4)	N2 - CC3 - C3	116,0(4)
N3 - CC4 - C4	118,7(4)	N4 - CC5 - C5	115,8(4)
CC1 - C1 - N1	110,9(4)	CC2 - C2 - N2	112,1(4)
CC3 - C3 - N3	113,5(4)	CC4 - C4 - N4	108,4(4)
CC5 - C5 - N5	109,2(4)	C1 - N1 - CC2	122,5(4)
C2 - N2 - CC3	123,6(4)	C3 - N3 - CC4	124,3(4)
C4 - N4 - CC5	120,6(4)	C5 - N5 - CC1	116,1(4)
O1 - CC1 - C1	120,6(4)	O2 - CC2 - C2	119,8(5)
O3 - CC3 - C3	121,5(5)	O4 - CC4 - C4	120,7(5)
O5 - CC5 - C5	120,4(5)	CM1 - N1 - CC2	117,3(4)
CM2 - N2 - CC3	118,4(4)	CM3 - N3 - CC4	117,9(4)
CM5 - N5 - CC1	123,8(4)	CC4 - C4 - CM4	109,7(4)
N4 - C4 - CM4	110,2(4)	CC1 - O1 - N4′	134,8(3)
C4 - N4 - O1	113,0(3)	CC5 - N4 - O1′	123,2(3)
OW - O2 - CC2	116,5(3)	O2 - OW - O2″	98,4(2)

DIHEDRAL ANGLE	(°)	DIHEDRAL ANGLE	(°)
C1 - N1 - CC2 - C2	14,4(6)	N1 - CC2 - C2 - N2	-172,5(4)
CC2 - C2 - N2 - CC3	87,9(5)	C2 - N2 - CC3 - C3	4,9(7)
N2 - CC3 - C3 - N3	175,9(4)	CC3 - C3 - N3 - CC4	-125,5(5)
C3 - N3 - CC4 - C4	5,3(6)	N3 - CC4 - C4 - N4	-71,3(5)
CC4 - C4 - N4 - CC5	128,3(4)	C4 - N4 - CC5 - C5	179,8(4)
N4 - CC5 - C5 - N5	141,3(4)	CC5 - C5 - N5 - CC1	-68,1(5)
C5 - N5 - CC1 - C1	163,1(4)	N5 - CC1 - C1 - N1	-170,8(4)
CC1 - C1 - N1 - CC2	68,1(5)		

Hanson *et al.*[10] except for hydrogen.[11] The final fractional coordinates and thermal vibration parameters are given in Table 1. The expression for anisotropic vibration is:

$$\exp[-(B11h^2+B22k^2+B33l^2+B12hk+B13hl+B23kl)]$$

The principal axes of the thermal vibration ellipsoids for oxygen, nitrogen, and carbon atoms were calculated from the temperature parameters of Table 1. Maximum root mean square amplitudes range from about 0.23 Å for ring atoms to about 0.33 Å for methyl carbon atoms and the water oxygen. Due to the size of the molecule, no rigid-body analysis of translational, librational, and screw motion has been carried out. A comparison between observed and calculated structure factors is presented in Table 2.

Interatomic distances, bond angles and dihedral angles are given in Table 3. The standard deviations, given in parentheses, are estimated from the correlation matrix of the last least squares refinement cycle. Fig. 1 shows the molecule viewed along [100].

By averaging bond distances of Table 3, and comparing with the results of the corresponding tetrameric [5] (I), pentameric [7] (II), and octameric [6] (III) compounds of sarcosine, no significant differences are observed:

Distance	(I)	(II)	(III)	AS4
CC–C	1.531 Å	1.527 Å	1.530 Å	1.525 Å
CC–N	1.358	1.344	1.345	1.346
CC–O	1.225	1.228	1.232	1.224
C–N	1.458	1.456	1.453	1.454
CM–N	1.467	1.483	1.487	1.466

The somewhat longer CM–N distances of (II) and (III) are possibly connected with the fact that for these compounds, methyl hydrogens were not included in the calculations. The geometry of the *cis* and *trans* *N*-methyl amide groups, respectively, is also roughly the same:

Angle	(I)	(II)	(III)	AS4
(CM–N–CC)*cis*	119.8°	118.7°	118.6°	117.9
(CM–N–CC)*trans*	124.3	123.9	123.5	123.8
(C–N–CC)*cis*	123.9	123.8	122.8	123.5
(C–N–CC)*trans*	120.1	117.2	117.5	116.1

Fig. 1 shows that the ring conformation is *cis, cis, cis, trans, trans*; quite unexpectedly the same as that of cyclopentasarcosyl [7] (II). Dihedral angles of AS4 and (II) agree closely except for CC3–C3–N3–CC4 (−125.5°) which has a value of −102.8° for the latter compound. Since the shortest CC···N distance across the ring is longer than 3.5 Å, no direct transannular contact can be held resposible for the rigidity of this 15-membered ring. As in the case of cyclooctasarcosyl and cyclopentasarcosyl, the explanation must be sought in the intrinsic conformation of the peptide chain itself.[2]

As indicated in Fig. 1, hydrogen bonds N4···O1′ and O1···N4′ of length 2.962 Å connect centrosymmetrically related molecules, forming dimers. Water molecules, situated at two-fold axes of rotation, link the dimers to endless chains along [001] with OW···O2 bonds of length 2.809 Å, the angle O2···OW···O2″ being 98.4°.

The OW–HW and N4–H4 bonds are 0.88 Å, while the C–H bond distances range from 0.89 Å to 1.03 Å.

Apart from the hydrogen bonds, there are no short inter-molecular contacts.

Acknowledgement. The author thanks cand. real. K. Titlestad for preparing the crystals.

REFERENCES

1. Dale, J. and Titlestad, K. *Chem. Commun.* (1969) 656.
2. Titlestad, K., Groth, P. and Dale, J. *Chem. Commun.* (1973) 346.
3. Titlestad, K., Groth, P. and Dale, J. *Chem. Commun.* (1973) 646.
4. Groth, P. *Acta Chem. Scand. 23* (1969) 3155.
5. Groth, P. *Acta Chem. Scand. 24* (1970) 780.
6. Groth, P. *Acta Chem. Scand. 27* (1973) 3217.
7. Groth, P. *Acta Chem. Scand. 27* (1973) 3419.
8. Germain, G., Main, P. and Woolfson, M. M. *Acta Crystallogr. A 27* (1971) 368.
9. Groth, P. *Acta Chem. Scand. 27* (1973) 1837.
10. Hanson, H. P., Herman, F., Lea, J. D. and Skillman, S. *Acta Crystallogr. 17* (1964) 1040.
11. Stewart, R. F., Davidson, E. R. and Simpson, W. T. *J. Chem. Phys. 43* (1965) 3175.

Received January 21, 1974.

Acta Chemica Scandinavica A 28 (1974) 455—466

Conformational Analysis. III. The Molecular Structure, Torsional Oscillations, and Conformational Equilibria of Gaseous $(CH_2Cl)_2C(CH_3)_2$, 1,3-Dichloro-2,2-dimethylpropane, as Determined by Electron Diffraction and Compared with Semiempirical Calculations

REIDAR STØLEVIK

Department of Chemistry, University of Oslo, Blindern, Oslo 3, Norway

Gaseous $(CH_2Cl)_2C(CH_3)_2$ has been studied by electron diffraction at a nozzle temperature of 60 °C. Three spectroscopically distinguishable conformers *GG*, *AG*, and *AA* (see Fig. 1) were detected. Results are presented with error limits (2σ). The following values for distances (r_a) and bond angles ($\angle\alpha$) are appropriate for the structure of all three conformers: $r(C-H) = 1.101(8)$ Å, $r(C-C) = 1.531(4)$ Å, $r(C-Cl) = 1.792(4)$ Å, $\angle CCCl = 114.3°(0.4)$, $\angle CCH = 109.1°(0.8)$. A tetrahedral carbon-atom framework was assumed. Non-bonded distances were computed as dependent quantities under the constraints of geometrically consistent r_α parameters.

By symmetry, *AA* has a staggered conformation. The conformations of *AG* and *GG* have torsion angles close to staggered values, but the deviations determined are not statistically significant.

The relative amounts of the conformers have been determined, and the composition at 60 °C is: 56 % (*4*) of *GG*, 37 % (*6*) of *AG*, and 7 % (*6*) of *AA*. The conformer with two parallel C—Cl bonds, *GG(1:3)*, is not present in detectable amounts.

Conformational energies have been estimated from the experimental composition. *AG* and *AA* have approximately equal *minimum* energy, while *GG* has about 1.6(±0.6) kcal/mol lower *minimum* energy. The difference in zero-pcint vibrational energy between *GG* and *AG*, due to unequal torsional force constants, may well as large as 1 kcal/mol, in favour of *AG*.

Valence force constants, corresponding to torsion of the $-CH_2Cl$ groups, have been estimated by combining information from electron diffraction and vibrational spectroscopy. Fundamental vibrational frequencies, which approximately correspond to torsional oscillations of the $-CH_2Cl$ groups, are expected in the range $80-170$ cm^{-1}.

Semiempirical calculations of conformational energies, torsional force constants, and geometries have been carried out. The calculated geometry is confirmed by the experimental findings, while the torsional force constants do not agree with those determined from electron diffraction. The greater stability of conformer *GG* is not predicted by the calculations, but no obvious correction in the standard energy parameters seems to be able to improve the theoretical results.

The *semi-empirical* energy model corresponds to simple *molecular mechanics caclulations*, involving atom-atom potentials and valence force constants.

I. INTRODUCTION

The present electron-diffraction work is part of a systematic conformational study of halogenated propanes and related molecules. General information [1,2] relevant to this investigation and to the electron-diffraction method [3] is found (reviewed) in Refs. 1, 2, and 3.

Compounds of the type $(CH_2X)_2C(CH_3)_2$ will be referred to as NDX(X = F, Cl, Br, I), and the title compound $(CH_2Cl)_2C(CH_3)_2$ as NDCL. Classically the possible number of staggered conformers in NDX is *nine*, as indicated in Fig. 1. The conformers *6* and *7* are *enantiomers* and thereby physically distinguishable, but neither spectroscopy nor electron diffraction can distin-

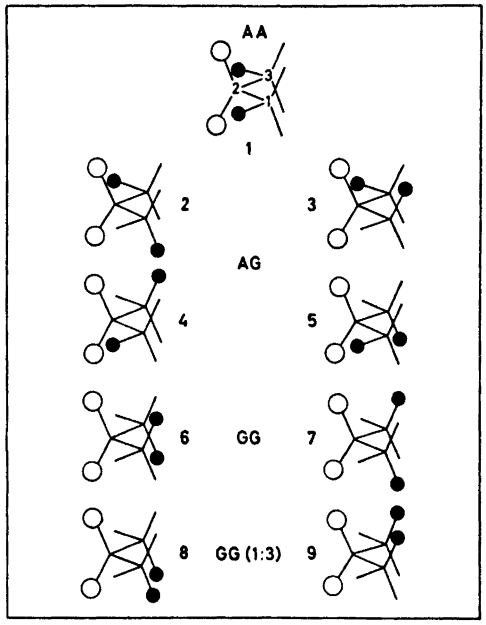

Fig. 1. Staggered conformers of 1,3-dihalo-2,2-dimethylpropane.

Table 1. Characterization of the four spectroscopically distinguishable staggered conformers of 1,3-dihalo-2,2-dimethylpropane. Classically there are *nine* possible staggered conformers. *Six* of the conformers are distinguishable, but only *four* are spectroscopically dinstinguishable (see Fig. 1).

Conformer	Point group	Symmetry number (σ)	M_c	M_d	$2(M_d/\sigma)$
AA	C_{2v}	2	1	1	1
AG	C_1	1	4	2	4
GG	C_2	2	2	2	2
GG(1:3)	C_s	1	2	1	2

guish between them. The conformers *8* and *9* are identical in *all* respects. The conformers *2* and *3* are enantiomers, while *4* and *5* are identical to *2* and *3*, respectively. In conclusion, there are *six* physically different conformers, but only *four* [*AA*, *AG*, *GG*, and *GG(1:3)*] are *spectroscopically* distinguishable, as indicated in Fig. 1 and Table 1.

The spectroscopically distinguishable conformers may be assigned multiplicities in two ways,

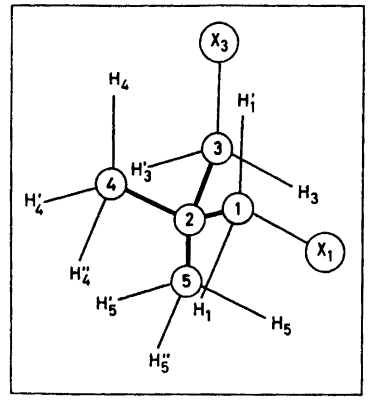

Fig. 2. Numbering of atoms in the conformer *GG*.

as follows: (1) only conformers being distinguishable (*six*) are considered (M_d in Table 1); (2) all classically possible conformers (*nine*) are included (M_c in Table 1). It is noteworthy [4] that $M_c^*/M_c = (M_d^*/M_d)(\sigma^*/\sigma)^{-1}$ for two spectroscopically distinguishable conformers, C and C*, having symmetry numbers σ and σ^*.

The total entropy difference ($\Delta S = S^* - S$) between two spectroscopically distinguishable conformers in the gas phase is:

$$\Delta S_T = \Delta S_T^{vib} + \Delta S^{rot} + \Delta S^{d}$$

ΔS_T^{vib} is the vibrational entropy difference and it is a function of temperature (T). ΔS^{rot} is the rotational entropy difference. If the classical rotational partition functions for the conformers are equal, then $\Delta S^{rot} = R \ln (\sigma^*/\sigma)^{-1}$. The term $\Delta S^{d} = R \ln (M_d^*/M_d)$. Using the relation between M_c, M_d and σ, the sum of ΔS^{rot} and ΔS^{d} is seen to be equal to $R \ln (M_c^*/M_c)$.

There are four X···X distances of different lengths: AA (*anti-anti*), AG (*anti-gauche*), GG (*gauche-gauche*), and GG(1:3) which corresponds to a parallell (1:3)X···X interaction. The symbols A (anti) and G (gauche) thus refer to the plane of the $C_1C_2C_3$ atoms (see Fig. 1).

II. CALCULATION OF CONFORMATIONAL ENERGIES, GEOMETRIES, BARRIERS, AND TORSIONAL FORCE CONSTANTS

The *semi-empirical* energy model corresponds to simple *molecular mechanics calculations*, involving atom-atom potentials and valence force

Table 2. Calculated conformational geometries for 1,3-dichloro-2,2-dimethylpropane. Distances in Å and angles in degrees.

Parameter (normal value)	*AA*	*AG*	*GG*	*GG(1:3)*
C–H(1.094)	1.093	1.094	1.093	1.093
C–C(1.513)	1.534	1.535	1.534	1.537
C–X(1.780)	1.789	1.789	1.789	1.791
$C_1C_2C_3$(109.47)[a]	108.0	109.3	110.5	109.8
CCX(109.47)	113.7	113.3	113.6	116.8
CCH(109.47)	110.2	110.1	110.1	109.8
$\phi_{1-2}(-CH_2X)$[b]	0	+117.4	+121.4	−106.9
$\phi_{3-2}(-CH_2X)$	0	+2.3	+121.4	+106.9
$\phi_{4-2}(-CH_3)$	0	+6.8	−6.7	0
$\phi_{5-2}(-CH_3)$	0	−11.4	−6.7	0

[a] In minimizing the energy, the geometry was constrained in the way described in sect. V-A, except for the torsion angles being adjusted as independent variables. Moreover, the CCC angles were adjusted too. The C-atom framework possesses D_{2d} symmetry with $\angle C_1C_2C_3 = \angle C_4C_2C_5$. [b] $\phi_0 = 60°$ in the expression $V_\phi = \frac{1}{2}V_0\sum_k[1+\cos(3\phi_{k-2}-\phi_0)]$ with $k = 1, 3, 4, 5$,

Table 3. Conformational energies (kcal/mol) for 1,3-dichloro-2,2-dimethylpropane. Details about the energy expression are found in Ref. 5.

Type of energy	*AA*	*AG*	*GG*	*GG(1:3)*
E (bonded)	2.14	2.06	2.13	4.64
E (van der Waals)	4.12	3.78	3.75	4.71
E (polar, Cl···H)	−11.59	−11.46	−11.17	−10.80
E (polar, Cl···Cl)	1.41	1.62	2.01	2.39
E (total)	−3.92	−4.00	−3.28	0.94
E (total) − E (total)$_{AG}$ = ΔE^m	0.08	0.00	0.72	4.94

constants, as described in Ref. 5. Energy parameters (V_0, a, b, c, d) were taken from the work of Abraham and Parry,[6] and diagonal valence force constants from Table 6 were used. "Normal" values [5] of the geometry parameters are given in Table 2.

The conformational geometries derived from the semi-empirical energy model are presented in Table 2. It is noteworthy that, except for *GG(1:3)*, the torsion angles of $-CH_2X$ groups are very nearly staggered for all conformers. Moreover, the deviations from a tetrahedral carbon framework are quite small in all conformers.

The conformational energies are found in Table 3. Contrary to the experimental findings, the conformers *AG* and *AA* are more stable than the conformer *GG*. The conformer [*GG(1:3)*] with two C–X bonds parallel has torsion angles displaced from staggered values. The energy of that conformer is thereby considerably lowered. However, the energy is nearly 5 kcal/mol higher than the energies for *AG* and *AA*.

Considering the conformers *GG*, *AG*, and *AA*, the conformational energy differences (ΔE^m) are largely determined by non-bonded (1:3) interactions. All three conformers (being nearly staggered) have non-bonded (1:2) distances (X···C and C···H) with equal multiplicities and almost equal lengths. The dominant (1:3) contributions are the polar X···H and X···X interactions.

Table 4. Conformational energy minima and torsional barriers in 1,3-dichloro-2,2-dimethylpropane (kcal/mol). Details about the conformational minima corresponding to the stable conformers *AA*, *AG*, *GG*, and *GG(1:3)* are found in Tables 2 and 3. See also explanations given in the text.

ϕ_{2-3}(°) \ ϕ_{1-2}(°)	0	60	120	180
180	6.33[s]	19.22[m]	9.93[s]	(∞)
120	0.00(AG)	6.53[s]	0.72(GG)	9.93[s]
60	6.12[s]	12.85[m]	6.53[s]	19.22[m]
0	0.08(AA)	6.12[s]	0.00(AG)	6.33[s]
−60	6.12[s]	13.14[m]	7.03[s]	19.22[m]
−120	0.00(AG)	7.03[s]	4.94[GG(1:3)]	9.93[s]
−180	6.33[s]	19.22[m]	9.93[s]	(∞)

[m] Corresponding to maximum. [s] Corresponding to "saddle-point".

In Table 4 are shown the conformational energy minima and torsional barriers between the conformers. Each energy value has been obtained by adjusting *all* geometry variables except for values of ϕ_{1-2} and ϕ_{3-2} being $\pm 60°$ and $\pm 180°$. (The latter values of ϕ_{1-2} and ϕ_{3-2} correspond to $-CH_2X$ groups *eclipsing* the C-atom framework.) The actual values of the geometry variables are not shown in Table 4; however, the values of ϕ_{1-2} and ϕ_{3-2} are approximately those in parenthesis (see also Table 2).

Table 5. Calculated torsional force constants for 1,3-dichloro-2,2-dimethylpropane.

(mdyn Å(rad)$^{-2}$)	*AA*	*AG*	*GG*
F ($-CH_2X$)	0.247[a]	0.22 − 4[b]	0.272[c]
F($-CH_3$)	0.135[d]	0.14 − 5[e]	0.130[f]
$-F_{\phi\phi'}$($-CH_2X$/ $-CH_2X$)[g]	0.011	0.062	0.096
$-F_{\phi\phi'}$($-CH_2X$/ $-CH_3$)[g]	0.062	0.01 − 6	0.01 − 6
$-F_{\phi\phi'}$($-CH_3$/ $-CH_3$)[g]	0.010	0.009	0.006

[a] $F_\phi(1-2)=F_\phi(3-2)$, [b] $F_\phi(1-2)\neq F_\phi(3-2)$, [c] $F_\phi(1-2)=F_\phi(3-2)$ [d] $F_\phi(4-2)=F_\phi(5-2)$, [e] $F_\phi(4-2)\neq F_\phi(5-2)$, [f] $F_\phi(4-2)=F_\phi(5-2)$ [g] All interaction force constants $F_{\phi\phi'}$ are negative. The ranges of force constants are indicated.

Torsional force constants may be numerically computed from the semiempirical energy model. The general expression for a quadratic force constant is:

$F_{qq'}=\partial^2 E/\partial q\partial q'$ (q: internal coordinate)

Torsional force constants are given in Table 5.

III. CALCULATION OF VIBRATIONAL QUANTITIES

Valence force constants, except for the torsional part, were taken from works of Schachtschneider [7] and Snyder.[8] The final force constant values used are shown in Table 6.

The normal-coordinate program described by Gwinn [9] was used in computing vibrational frequencies.

Mean amplitudes of vibration were computed as described in Ref. 10. In Table 7 are given u and K values for internuclear distances. Some of these quantities are quite sensitive to the values of torsional force constants, which have been adjusted to fit the experimental intensities, as described in sect. V-B. In Table 8 are shown some u values corresponding to different values of the torsional force constant $F_\phi(-CH_2X)$.

If the torsional force constants estimated from the electron-diffraction data are used, then the torsional oscillations of the $-CH_2X$ groups correspond to vibrational frequencies in the range 80 − 170 cm^{-1}.

IV. EXPERIMENTAL AND DATA REDUCTION

The compound was bought from "K & K" Laboratories. The purity of the sample was better than 97 %.

Electron-diffraction photographs were made at a nozzle temperature of 60°C in the Balzer [11] apparatus [12] under conditions summarized below.

Nozzle-to-plate distance (mm)	500.00	250.00
Electron wavelength (Å)	0.05843	0.05854
Number of plates:	4	5
Range of data, in s (Å^{-1})	1.25 − 15.25	2.25 − 30.50
Data interval, Δs (Å^{-1})	0.125	0.250
Estimated uncertainty in s-scale (%)	0.14	0.14

Table 6. Valence force constants for 1,3-dichloro-2,2-dimethylpropane.

Stretch (mdyn/Å)		Bend (mdyn Å/(rad)²)	
C–H(CH_2X)	4.850	CCH(CH_2X)	0.677
C–H(CH_3)	4.700	CCH(CH_3)	0.640
C–X	3.140	HCH(CH_2X)	0.412
C–C	4.534	HCH(CH_3)	0.500
		HCX	0.860
		CCC	1.086
		CCX	0.980

Stretch/Stretch (mdyn/Å)
C common: C–H/C–C = 0.73, C–C/C–C = 0.101, C–H/C–H = 0.059(CH_2X), C–H/C–H = 0.039(CH_3)

Stretch/Bend (mdyn/rad)
C–C common: C–C/CCC = 0.417, C–C/CCX = 0.075, C–C/CCH = 0.26
C–X common: C–X/HCX = 0.33, C–X/CCX = 0.55

Bend/Bend (mdyn Å/(rad)²); (combination of two angles with C atom common)
HCX/HCX(C–X common) = 0.161, HCC/HCX(C–H common) = 0.089, C–C common: HCC/HCC(CH_2X) = −0.014, HCC/HCC(CH_3) = −0.017; HCC/HCX (C common) = 0.030

Bend/Bend (combination of two angles with C–C common and dihedral angle *anti* or *gauche*)
anti: CCC/CCX = 0.046, HCC/CCC = 0.072
gauche: CCC/CCX = −0.024, HCC/HCC = −0.058

Torsion (mdyn Å/(rad)²)[a]
$F_\phi(-CH_2X)$ = 0.630 and $F_\phi(-CH_3)^b$ = 0.315

[a] The torsional force constants have been defined in the following way: each fragment C–C–C–A (A = H or Cl, see Fig. 2) in a —C(—)—CH_2Cl group has been assigned an equal torsional force constant $f_\phi(-CH_2X)$, while each fragment C–C–C–H in a —C(—)—CH_3 group has been assigned an equal torsional force constant $f_\phi(-CH_3)$. The total force constant for the torsion coordinate ϕ_{i-2} (i = 1, 3) is thus $F_\phi(i-2) = 9f_\phi(-CH_2X)$ and $F_\phi(j-2) = 9f_\phi(-CH)_3$ for j = 4,5. The input to Gwinn's normal coordinate program [9] demands a separate specification for each torsion fragment.
[b] These values were determined from the electron diffraction data, as described in sect. V-B.

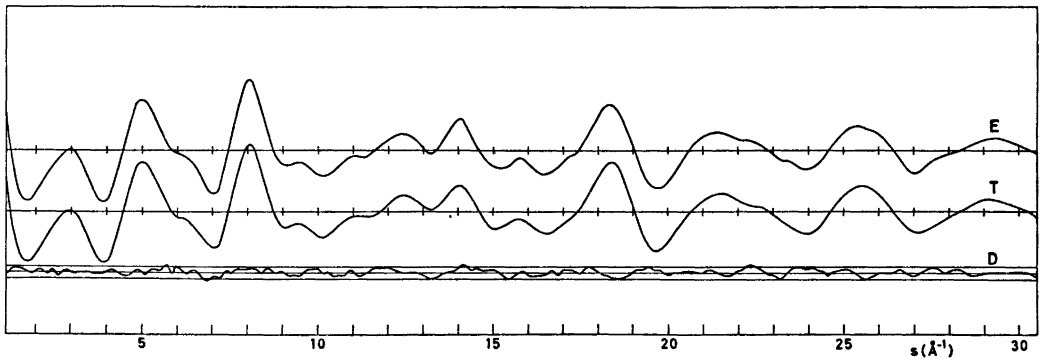

Fig. 3. Intensity curves for 1,3-dichloro-2,2-dimethylpropane at 60°C. Curve E shows the experimental intensity, and curve T the theoretical intensity corresponding to the final least-squares parameters. Curve D is the experimental minus theoretical, and the straight lines the give experimental uncertainty (± 3 × experimental standard deviation).

Table 7. Calculated u- and K-values (Å) in 1,3-dichloro-2,2-dimethylpropane at 60 °C.

Type of distance	Dist. (Å)	u value	K values AA	AG	GG
C – H(in CH_2X)	1.10	0.078	0.0166	0.0170	0.0173
C – H(in CH_3)	1.10	0.079	0.0227	0.0233	0.0234
C – C(C – CH_2X	1.53	0.052	0.0033	0.0032	0.0033
C – C(C – CH_3)	1.53	0.051	0.0041	0.0053	0.0053
$C_1 - X_1$	1.79	0.054	0.0087	0.0080	0.0075
$C_3 - X_3$	1.79	0.054	0.0087	0.0072	0.0075
$C_2 \cdots X$	2.80	0.072	0.0061	0.0043 – 6	0.0044
$C_2 \cdots H$	2.16	0.107 – 9[a]	0.010 – 4	0.011 – 6	0.010 – 6
C···C	2.50	0.071 – 2	0.003 – 4	0.003 – 6	0.003 – 6
X···H	2.36	0.108	0.014 – 5	0.013 – 5	0.013 – 4
H···H	1.80	0.127 – 8	0.020 – 33	0.021 – 32	0.022 – 32
C···X(a)	4.15	0.072	0.0031	0.0020 – 8	0.0029
C···X(g)	3.19	0.131	0.0042 – 9	0.003 – 4	0.003 – 4
C···H(g)	2.73	0.150	0.010 – 1	0.009 – 13	0.008 – 13
C···H(a)	3.46	0.103	0.007 – 11	0.008 – 13	0.007 – 14
X···X	5.59	0.095	0.0002	–	–
X···X	4.95	0.146	–	0.0005	–
X···X	3.96	0.197	–	–	0.0010
X···H(GG)	2.73	0.212 – 9	0.011	0.010 – 2	0.009 – 12
X···H(GG)	3.54	0.19 – 21	0.009	0.007 – 9	0.008
X···H(AG)	4.42	0.152 – 6	0.006	0.005 – 7	0.007
X···H(AG)	4.19	0.154 – 8	0.009	0.007 – 9	0.005 – 8
X···H(AA)	4.96	0.120	–	0.004 – 7	0.007
H···H(AG)	3.74	0.16 – 7	0.011 – 5	0.011 – 8	0.010 – 8
H···H(GG)	3.07	0.19 – 22	0.011 – 6	0.012 – 7	0.011 – 7
H···H(GG)	2.50	0.21 – 3	0.013 – 7	0.014 – 9	0.016 – 9
H···H(AA)	4.30	0.14 – 5	0.012 – 5	0.014 – 8	0.010 – 8

The torsional force constants $F_\phi(-CH_2X) = 0.630$ and $F_\phi(-CH_3) = 0.315$ mdyn Å $(rad)^{-2}$ were used, and the conformational geometries were *staggered*. For definition of F_ϕ, see Table 6.

[a] Range of values: 0.107 – 9 means 0.107 – 0.109.

Table 8. Mean amplitudes of vibration, u (Å), calculated at 60 °C using three different values of $F_\phi(-CH_2X)$.

$F_\phi(-CH_2X)$[a]	0.387[b]	0.630	0.855[c]
X···X(GG)	0.227	0.197	0.182
X···X(AG)	0.154	0.146	0.142
X···X(AA)	0.095	0.095	0.095
X···C(g)	0.139[b]	0.131[b]	0.127[b]

[a] For definition of F_ϕ, see Table 6. [b] Best value for conformer AG. [c] Best value for conformer GG.

The electron wavelength was determined by calibration against ZnO, and corrected by an experiment with CO_2 giving a correction of +0.1 % in the s-scale. The data were reduced in the usual way [13] to yield an intensity curve for each plate. Average curves for each set of distances were formed. A composite curve was then made by connecting the two average curves after scaling. The final experimental intensity curve is shown in Fig. 3. The intensities have been modified by $s/|f_C'||f_{Cl}'|$.

The scattering amplitudes were calculated by the partial wave method [14] using Hartree-Fock atomic potentials.[15]

The radial distribution curve obtained by Fourier transformation [13] of the final experimental intensity is presented in Fig. 4.

V. STRUCTURE ANALYSIS AND REFINEMENTS

The semiempirically calculated conformational energies (see sect. II) suggest that the conformer *GG(1:3)* is not present in detectable amounts at 60 °C. From the experimental RD curve (Fig. 4) it was easily concluded that the conformers AA, AG, and GG are present in

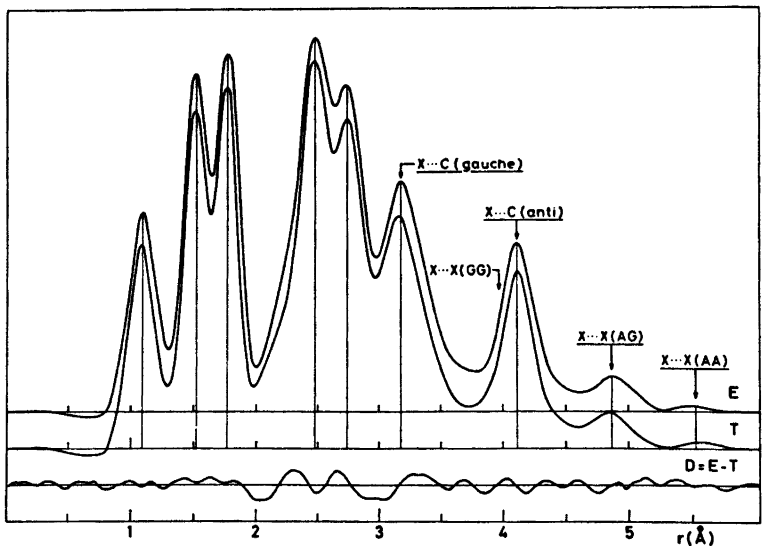

Fig. 4. Radial distribution curves for 1,3-dichloro-2,2-dimethylpropane at 60 °C. Experimental (E) and theoretical (T) radial distribution curves and difference curve (D). The RD curves were calculated from the intensity curves of Fig. 3 with an artificial damping constant 0.0020 Å².

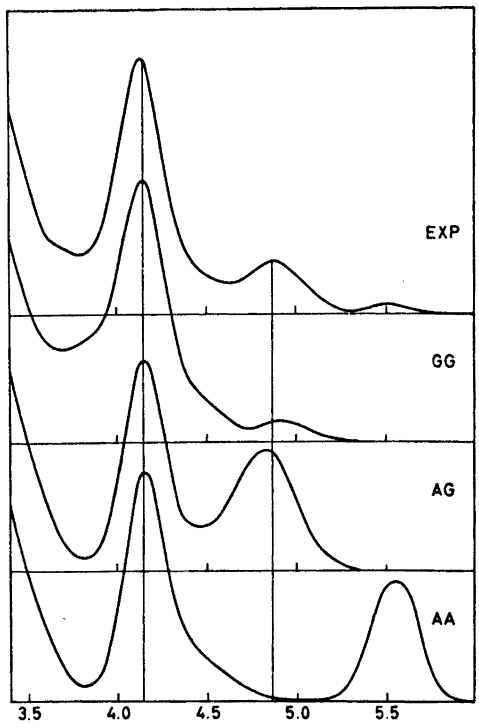

Fig. 5. Theoretical radial distribution curves for the conformers of 1,3-dichloro-2,2-dimethylpropane, and the experimental curve at 60°C. The artificial damping constant was 0.0020 Å².

detectable amounts, and *approximate* composition parameters were estimated. [α(GG) $\simeq$ 60 %, α(AG) $\simeq$ 40 %, and α(AA) < 10 %]. RD curves for the individual conformers are shown in Fig. 5.

A. Least-squares refinements. The least-squares program was written by H. M. Seip, and it is a modified version of the program explained in Ref. 13. Several conformers may be included in the refinements with the present version of the program.

Models for the conformers were constructed with the following geometrical assumptions: (1) the carbon atoms have a tetrahedral arrangement; (2) the two C–CH_2X groups are equal; (3) the two C–CH_3 groups are equal; (4) the C–CH_3 groups possess C_{3v} symmetry; (5) each C–CH_2X group possesses C_s symmetry and the projection of $\angle$HCH′ on a plane perpendicular to C–C is 120°; (6) the C–H bonds are equal; (7) $\angle$CCH in C–CH_2X and C–CH_3 are equal; (8) the conformers have identical structures except for the C–C torsion angles: ϕ_{1-2}, ϕ_{3-2}, ϕ_{4-2}, and ϕ_{5-2}.

Models were defined in terms of the following average parameters: C–H, C–C, C–X, $\angle$CCX, $\angle$CCH, and the four ϕ angles.

Also adjusted were the composition (%) parameters α(AG) and α(GG), with α(AA) = 100 % – α(AG) – α(GG).

Corrections for the Bastiansen-Morino shrinkage [16] effect on non-bonded distances have been included. Non-bonded distances were computed as dependent parameters, restricted under the constraints of geometrically consistent r_α parameters.[17,18]

In the first part of the structure analysis a number of refinements were carried out, in which selected combinations of parameters were allowed to vary, while others were held constant at plausible values. At some stages the background [13] had to be corrected; however, none of the important conclusions about structure and composition were changed thereby.

B. Determination of torsional force constants. The torsional modes of vibration contribute substantially to the mean amplitudes of several distances in a molecule like NDCl (see Table 8). Therefore, since a reasonable force field is known, except for the torsional part, torsional force constants can be adjusted to fit the electron-diffraction data. Determination of all torsional force constants from electron-diffraction data alone is *not* possible. Therefore, the theoretical values of Table 5 were used as a guide, and the following assumptions were made: (1) all interaction constants $F_{\phi\phi'}=0$; (2) in conformer *GG* $F_\phi(1-2)=F_\phi(3-2)=F_\phi(\mathrm{GG})$; (3) in conformer *AG* $F_\phi(1-2)=F_\phi(3-2)=F_\phi(\mathrm{AG})$; (4) in conformer *AA* $F_\phi(1-2)=F_\phi(3-2)=0.5\ [F_\phi(\mathrm{GG})+F_\phi(\mathrm{AG})]$; (5) for all conformers $F_\phi(4-2)=F_\phi(5-2=0.25\ [F_\phi(\mathrm{GG})+F_\phi(\mathrm{AG})]$. Thus two variables, $F_\phi(\mathrm{GG})$ and $F_\phi(\mathrm{AG})$, are considered for adjustment. The following procedure was used: Firstly, an average torsional force constant $[\bar{F}_\phi=F_\phi(\mathrm{GG})=F_\phi(\mathrm{AG})]$ common to all three conformers was determined. Parallel [10] and perpendicular [10] amplitudes for several values of $\bar{F}_\phi$ were computed and included in the least-squares refinements. The value of $\bar{F}_\phi$ which lead to minimum in the error sum (**V'PV**) was obtained for $\bar{F}_\phi=0.63$ mdyn Å (rad)$^{-2}$. The discrepancies between theoretical and experimental RD curves indicated that the torsional force constant $F_\phi(\mathrm{GG})$ is greater than $F_\phi(\mathrm{AG})$. The combination of force constants that lead to a minimum in the error sum (**V'PV**) was determined by a systematic iteration procedure, and the best fit was obtained with $F_\phi(\mathrm{GG})=0.855$ and $F_\phi(\mathrm{AG})=0.387$ mdyn Å (rad)$^{-2}$. The new value of **V'PV** is only 0.4 % less than the value obtained with $F_\phi(\mathrm{GG})=F_\phi(\mathrm{AG})=\bar{F}_\phi$.

Although the values of the individual, parameters $F_\phi(\mathrm{GG})$ and $F_\phi(\mathrm{AG})$ are very uncertain, the average parameter $\bar{F}_\phi$ is determined with less uncertainty. Keeping in mind the assumptions involved, the most probable parameter values [mdynÅ(rad)$^{-2}$] are as follows:

$F_\phi(\mathrm{GG})$ in the range $0.86-0.63$ ($\bar{F}_\phi=0.63$)
$F_\phi(\mathrm{AG})$ in the range $0.63-0.39$ ($\bar{F}_\phi=0.63$)
$F_\phi(-\mathrm{CH_3})\simeq 0.32$ (for all conformers)

The average value of $F_\phi(-\mathrm{CH_2X})$ is not significantly different from the one (0.62) determined for $(\mathrm{CH_2Cl})_4\mathrm{C}$.[19] For both molecules, it seems that the torsional force constants of the detectable conformers have quite different values; a conclusion not predicted by the results of semi-empirical calculations (Sect. II). In adjusting the F_ϕ parameters one has to refine all relevant geometry parameters simultaneously. If that is not done, the F_ϕ values may be quite biased. Moreover, the adjustments ought to be carried out after a reasonable background has been established. Finally, one should keep in mind that systematic errors in the remainder (sect. III) of the force field may be present.

VI. FINAL RESULTS

Results from the least-squares refinements and standard deviations (σ) corrected for correlation in the experimental data [20] are given. All intensities were given equal weights in the final refinements, using a diagonal weight matrix.

Non-bonded distances were restricted under the geometrical constraint of r_α parameters, by including correction terms $D=r_\alpha-r_a$ ($D=(u^2/r)-K$) for all distances. Calculated u and K values, corresponding to the final torsional force constant, are shown in Table 7.

The structure and composition parameters are given in Table 9.

The theoretical values for $\angle \mathrm{C_1C_2C_3}$ in Table 2 suggest that deviation from a tetrahedral arrangement of C atoms is small. Therefore the C atoms were assigned a tetrahedral framework in all refinements.

Torsion angles of the conformers *GG* and *AG* were confined (see also Table 2) as follows: $\phi_{1-2}=\phi_{3-2}=120°+\Delta\phi$ and $\phi_{4-2}=\phi_{5-2}=-5(\Delta\phi)$ *in the conformer GG*; $\phi_{1-2}=120°-\Delta\phi$, $\phi_{3-2}=\Delta\phi$, $\phi_{4-2}=5(\Delta\phi)$, and $\phi_{5-2}=-8(\Delta\phi)$ *in the conformer AG*. ($\Delta\phi=0°$ corresponds to both *GG* and *AG*

Table 9. Structure and composition parameters for 1,3-dichloro-2,2-dimethylpropane at 60 °C. Standard deviations are given in parentheses.

Bond[a] lengths (Å)	Bond[b] angles ∠α(°)	Composition parameters (%)
r_a(C−H) = 1.101(4)	∠CCCl = 114.3(0.2)	α(GG) = 56(2)
r_a(C−C) = 1.531(2)	∠CCH = 109.1(0.4)	α(AG) = 37(3)
r_a(C−Cl) = 1.792(2)	∠CCC = (109.47)[c]	α(AA) = 7(3)[d]

[a] An experiment with CO_2 gave a correction of 0.1 % in the s-scale. The bond lengths are therefore 0.1 % longer than those directly determined by least-squares refinements. The uncertainty (0.14 %) in the s-scale has been included in the standard deviations for bond distances. [b] The bond angles are those of the self-consistent r_α structure. Dependent angles are ∠HCH = 109.9° (σ = 0.5°) and ∠HCCl = 107.2° (σ = 0.3°). [c] Tetrahedral arrangement of C-atoms was assumed. [d] The parameters α(GG) and α(AG) were refined with α(AA) = 100 % − α(GG) − α(AG) and α[GG(1:3)] = 0 %.

Table 10. Mean amplitudes (u) of vibration for 1,3-dichloro-2,2-dimethylpropane at 60 °C.

Type of distance	Dist. (Å)	Calculated[a] u value (Å)	Refined u value (Å)	Standard deviation (σ)
C−H	(1.10)	0.078 − 9	0.075	0.004
C−C	(1.53)	0.051 − 2	0.055	0.003
C−X	(1.79)	0.054	0.052	0.003
C_2···X	(2.79)	0.072	(0.072)[c]	−
C···C	(2.50)	0.071 − 2	0.074	0.004
X···C(a)	(4.13)	0.072	0.077	0.003
X···C(g)	(3.17)	0.131	0.127	0.003
X···X(AA)	(5.57)	0.095	(0.095)[c]	−
X···X(AG)	(4.82)	0.146(0.154)[b]	0.154	0.017
X···X(GG)	(3.93)	0.197(0.182)[b]	0.213	0.019

[a] Calculated with $\bar{F}_\phi$ = 0.63 mdyn Å (rad)$^{-2}$, see also Table 7. [b] Values in parentheses calculated with F_ϕ(GG) = 0.855 and F_ϕ(AG) = 0.387, see also Table 8 for details. [c] Not refined; calculated values were used.

being *staggered*.) The parameter $\Delta\phi$ was refined, including as many as possible of the remaining least-squares parameters simultaneously. The values of the parameter $\Delta\phi$ were always found to be less than 1° (σ = 2°), indicating nearly staggered conformations for *GG* and *AG*. The same conclusion was reached by the semiempirical calculations. (Table 2)

Several mean amplitudes (u values) of vibration have been refined. In Table 10 their values are compared to those computed (sect. III). Both sets of u values are *experimental*, but the calculated values combine information from spectroscopy as well as from electron diffraction. The average deviation between the two sets of u values is less than 6 %, while the average relative, $\langle\sigma/u\rangle$, uncertainty of the refined u values is 6.5 %. In calculating the average deviation between the sets, only u values that have been refined were considered. The large number of mean amplitudes corresponding to non-bonded X···H and C···H distances could not be refined, but their values fit the experimental data well. It is thereby shown that *calculated* u values are reliable for NDCl. Since the u values are reliable, then it is likely that the calculated K values are reliable to the same extent.

Cartesian coordinates for the conformers *GG* and *AG* and principal axes' moments of inertia for the conformers *GG*, *AG*, and *AA* are found in Table 11.

Table 11. Cartesian coordinates (Å) for conformers of 1,3-dichloro-2,2-dimethylpropane (see Fig. 2). The coordinates have been calculated for staggered conformations, using the final structure parameters in Table 9 (r_a and $\angle\alpha$ values). The number of atoms in the conformer *GG* is shown in Fig. 2. The principal axes' moments of inertia are (amuÅ²):
$I_A = 251.58$, $I_B = 384.86$, and $I_C = 524.08$ *for conformer GG.*
$I_A = 182.08$, $I_B = 521.05$, and $I_C = 590.58$ *for conformer AG.*
$I_A = 112.53$, $I_B = 657.14$, and $I_C = 657.24$ *for conformer AA.*

Conformer GG[a] (corresponding to No. 7 in Fig. 1)				Conformer AG[a] (corresponding to No. 2 in Fig. 1)			
	x	*y*	*z*		*x*	*y*	*z*
C_1	0	0	0	C_1	0	0	0
C_2	1.2500	0.8839	0	C_2	1.2500	0.8839	0
X_1	1.3800	1.9762	−1.4147	X_1	1.3800	1.9762	−1.4147
H_1	2.1447	0.2422	0	H_1	2.1447	0.2422	0
H_1'	1.2435	1.5165	0.9011	H_1'	1.2435	1.5165	0.9011
C_3	−1.2500	0.8839	0	C_3	−1.2500	0.8839	0
X_3	−1.3800	1.9762	1.4147	X_3	−2.7947	−0.0244	0
H_3'	−2.1447	0.2422	0	H_3	−1.2435	1.5165	0.9011
H_3	−1.2435	1.5165	−0.9011	H_3'	−1.2435	1.5165	−0.9011
C_4	0	−0.8839	1.2500	C_4	0	−0.8839	1.2500
H_4	0	−0.2422	2.1447	H_4	0	−0.2422	2.1447
H_4''	0.9011	−1.5165	1.2435	H_4''	0.9011	−1.5165	1.2435
H_4'	−0.9011	−1.5165	1.2435	H_4'	−0.9011	−1.5165	1.2435
C_5	0	−0.8839	−1.2500	C_5	0	−0.8839	−1.2500
H_5	0	−0.2422	−2.1447	H_5	0	−0.2422	−2.1447
H_5'	−0.9011	−1.5165	−1.2435	H_5'	−0.9011	−1.5165	−1.2435
H_5''	+0.9011	−1.5165	−1.2435	H_5''	+0.9011	−1.5165	−1.2435

VII. DISCUSSION

Following standard statistical thermodynamics,[21,22] the percentages α^* and α of two conformers (C⇌C*) in equilibrium in the gas phase,[3] are related to the theoretical expression for the equilibrium constant, as given in eqn. (1):

$$\alpha^*/\alpha = (M_c^*/M_c)(Q^*/Q)^{vib} \exp(-\Delta E^m/RT) \quad (1)$$

(The *classical* rotational partition functions for the conformers are approximately equal.) Q^{vib} is the vibrational partition function of a conformer referred to the potential energy *minimum* of that conformer. $\Delta E^m = E^* - E$ is the potential-energy difference between the conformers, and the difference is measured between potential energy minima. The zero-point vibrational energy is thus included in the vibrational partition functions. R and T have their usual thermodynamic meanings, and M_c (Table 1) is the multiplicity of a conformer.

If the vibrational partition functions for the conformers are known, then the quantity ΔE^m may be estimated from eqn. (1). The ratios between the partition functions depend on the differences in force fields between the conformers.[19] Calculations of ΔE^m using two different sets of *torsional* force constants are summarized in Table 12. Both sets of results are equally probable as pointed out in sect. V-B. An approximate estimate of ΔE^m(GG − AG) is therefore -1.6 ± 0.6 kcal/mol.

If the value of ΔE^m (GG − AG) computed from the semiempirical energy model (+0.72 kcal/mol) is accepted, then the quantity q (Table 12) has to be 8.6 according to eqn. (1). Such a large value of q is possible, but only if some of the force constants of the conformer *GG* are much *smaller* than those of *AG*. The torsional force constants of the two conformers could well be different, but the experimental evidence of sect. V-B indicates a difference, if any significant difference at all, in the opposite direction.

Assuming equal vibrational partition functions for the conformers *AA* and *AG*, the quantity ΔE^m(AA − AG) is +0.2 kcal/mol, in agreement with the theoretical estimate (Table 3) of +0.08 kcal/mol.

Thus, the semi-empirical calculations correctly predict the energy difference between the

Table 12. Energy difference (ΔE^m) between the conformers GG and AG of 1,3-dichloro-2,2-dimethylpropane.

	I	II
$F_\phi(-CH_2X)^a$ in GG	0.630 mdyn Å (rad)$^{-2}$	0.855 mdyn Å (rad)$^{-2}$
$F_\phi(-CH_2X)^a$ in AG	0.630 ,, ,,	0.387 ,, ,,
$F_\phi(-CH_3)^a$ in AG and GG	0.315 ,, ,,	0.315 ,, ,,
$q=(Q(GG)/Q(AG))_T^{vib}$	1.04[b]	0.40[b]
$\Delta S_T^{vib}=S(GG)^{vib}-S(AG)^{vib}$	0.00[c] e.u.	−1.54[c] e.u.
$\Delta E^m=E(GG)^m-E(AG)^m$	−1.1[d] kcal/mol	−2.2[d] kcal/mol

[a] F_ϕ: torsional force constant. For definition of F_ϕ see Table 6. [b] $Q(GG)$ and $Q(AG)$: vibrational partition functions referred to the potential energy *minimum* of the conformers.

[c] Calculated according to the standard expression for contribution of entropy associated with vibrational degrees of freedom:

$\Delta S_T^{vib}=R \ln q+RT\, d(\ln q)/dT$.

[d] The force constants in column II lead to a difference (GG−AG) in zero-point vibrational energy of +0.96 kcal/mol. The energy differences were calculated according to eqn. (1) using the experimental equilibrium constant of 1.51.

conformers *AA* and *AG*, but the high conformational energy predicted for *GG* does not agree with the experiment. The conformer *GG(1:3)* has not been experimentally detected, but according to the energy differences in Table 3 that conformer should be present in negligible amounts at 60 °C.

Taking into consideration the symmetry numbers and multiplicities (Table 1) of the conformers, the *total entropy* differences may be expressed as follows:

$$\Delta S(GG-AG)=\Delta S_T^{vib}(GG-AG)-R \ln 2\simeq -2.2\pm 0.8 \text{ cal } K^{-1} \text{ mol}^{-1}$$

$$\Delta S(AA-AG)=\Delta S_T^{vib}(AA-AG)-R \ln 4$$

At present, no estimate of ΔS_T^{vib} (AA−AG) is available, however, the conformer *AA* most probably has a lower entropy than *AG*.

Acknowledgements. I am grateful to K. Brendhaugen for recording the diffraction photographs, and to Prof. O. Bastiansen, Dr. A. Haaland, and Dr. H. M. Seip for helpful discussions. Computer programs made available by Dr. H. M. Seip, Cand. real. S. Rustad, and Prof. W. D. Gwinn have been extensively used in this work. Financial support from Norges almenvitenskapelige forskningsråd is gratefully acknowledged.

REFERENCES

1. Sheppard, N. *J. Mol. Struct. 6* (1970) 5.
2. Bastiansen, O., Seip, H. M. and Boggs, J. E. In Dunitz, J. B. and Ibers, J. A., Eds., *Perspectives in Structural Chemistry*, Wiley, New York 1971, Vol. 4.
3. Seip, H. M. In Sim, G. A. and Sutton, L. E. *Molecular Structure by Diffraction Methods*, (Specialist Periodical Reports), The Chemical Society, London 1973, Vol. 1, part 1, Chapter 1.
4. Bartell, L. S. *Private communication.*
5. Stølevik, R. *Acta Chem. Scand. A 28* (1974) 299.
6. Abraham, R. J. and Parry, K. J. *J. Chem. Soc. B* (1970) 539.
7. Schachtschneider, J. H. and Snyder, R. G. *Vibrational Analysis of Polyatomic Molecules, IV*, (force constants for the haloparaffins). Project No. 31450, Technical Report No. 122−63 of Shell Development Company.
8. Snyder, R. G. and Schachtschneider, J. H. *Spectrochim. Acta 21* (1965) 169.
9. Gwinn, W. D. *J. Chem. Phys. 55* (1971) 477.
10. Stølevik, R., Seip, H. M. and Cyvin, S. J. *Chem. Phys. Lett. 15* (1972) 263.
11. Zeil, W., Haase, J. and Wegmann, L. *Z. Instrumentenk. 74* (1966) 84.
12. Bastiansen, O., Graber, R. and Wegmann, L. *Balzer's High Vacuum Report 25* (1969) p. 1.
13. Andersen, B., Seip, H. M., Strand, T. G. and Stølevik, R. *Acta Chem. Scand. 23* (1969) 3224.
14. Peacher, J. and Willis, J. C. *J. Chem. Phys. 46* (1967) 4809.

15. Strand, T. G. and Bonham, R. A. *J. Chem. Phys. 40* (1964) 1686.
16. Almenningen, A., Bastiansen, O. and Munthe-Kaas, T. *Acta Chem. Scand. 10* (1956) 261.
17. Morino, Y., Kuchitsu, K. and Oka, T. *J. Chem. Phys. 36* (1962) 1108.
18. Kuchitsu, K. *J. Chem. Phys. 49* (1968) 4456.
19. Stølevik, R. *Acta Chem. Scand. A 28* (1974) 327.
20. Seip, H. M. and Stølevik, R. In Cyvin, S. J., Ed. *Molecular Structures and Vibrations*, Elsevier, Amsterdam 1972, p. 171.
21. Glasstone, S. *Theoretical Chemistry*, Van Nostrand, New York 1944.
22. Herzberg, G. *Infrared and Raman Spectra of Polyatomic Molecules*, Van Nostrand, Princeton, N. J. 1945.

Received January 2, 1974.

Acta Chemica Scandinavica A 28 (1974) 467—470

Short Communications

A Carbon-13 NMR Study of Platinum(II) Diamine Complexes

SVEN BAGGER

Chemistry Department A, The Technical University of Denmark, Building 207, DK-2800 Lyngby, Denmark

Platinum(II) chelates with isomeric methyl-substituted 1,2-ethanediamines as ligands have been studied by carbon-13 NMR spectroscopy in an effort to elucidate their conformational behaviour in aqueous solution.

The compounds investigated are the square planar complexes $[Pt(NH_3)_2(mbn)]Cl_2$, $[Pt(NH_3)_2(lbn)]Cl_2$, and $[Pt(NH_3)_2(ibn)]Cl_2$ where mbn and lbn are the *meso*- and the $(-)_D$-form of 1,2-dimethyl-1,2-ethanediamine, and ibn is 1,1-dimethyl-1,2-ethanediamine.

The three *cis*-diammine salts were prepared from the pertinent *cis*-dichloro(diamine)platinum(II) compounds in accordance with the procedures for the corresponding ethylenediamine complexes.[1,2] The yellow *cis*-dichloro compounds were treated with conc. NH_3-water at 100 °C in a stoppered test tube till they dissolved; the solution was filtered and after evaporation *in vacuo* over conc. H_2SO_4 in a desiccator the colourless crystals of $[Pt(NH_3)_2(diamine)]Cl_2$ were collected.

The five-membered, chelate rings may adopt either δ or λ form,[3] the two conformations being interconvertible on ring inversion. From Fig. 1 it appears that the substituted methyl groups may be either equatorially or axially orientated relative to the ring.

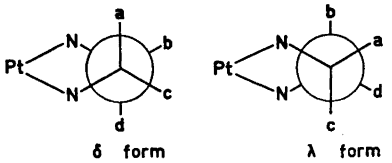

Fig. 1. The 1,2-ethanediamine-platinum moiety of the three complexes as wieved along the C—C bond of the five-membered ring (Newman projection). The conformations of the methyl-substituted 1,2-ethanediamines are obtained by adding methyl groups at two of the sites a, b, c, and d as specified in Table 1.

Table 1. Specification of the two methyl group positions in $[Pt(NH_3)_2(mbn)]^{2+}$, $[Pt(NH_3)_2(lbn)]^{2+}$, and $[Pt(NH_3)_2(ibn)]^{2+}$.

	Methyl position (See Fig. 1)	Orientation in δ-ring	Orientation in λ-ring
mbn	b	equatorial	axial
	a	axial	equatorial
lbn	a	axial	equatorial
	d	axial	equatorial
ibn	a	axial	equatorial
	c	equatorial	axial

The δ and λ forms of each of the complexes $[Pt(NH_3)_2(mbn)]^{2+}$ and $[Pt(NH_3)_2(ibn)]^{2+}$ are mirror images of each other and must therefore have the same potential energy.

But as it is seen from Table 1 the two forms of $[Pt(NH_3)_2(lbn)]^{2+}$ are different; the δ conformation contains two axial and the λ conformation two equatorial methyl groups. In the conformationally related *trans*-1,2-dimethylcyclohexane the energy difference between the diaxial and the diequatorial conformations has been calculated to 2.7 kcal/mol.[4] By analogy it is estimated that the λ ring with lbn is favoured relative to the δ ring by 2—3 kcal/mol. This would mean that less than 4 % of the complex has the δ conformation in a solution at room temperature.

The proton-decoupled 22.63 MHz carbon-13 NMR spectra of the three complexes in D_2O solution were measured in the manner that has been described previously,[5] and the data are shown in Table 2.

The methyl resonances in all three spectra have two well-resolved satellite peaks due to coupling with ^{195}Pt ($I = \frac{1}{2}$, 34 % abundance). The coupling constants, $^3J_{Pt-N-C-C}$, are given in Table 2. It is seen that the value for the lbn complex is about twice that for the other two. ^{195}Pt sidebands were resolved and distinct for the methyl peaks only, so values for $^2J_{Pt-N-C}$ could not be obtained, but they must all be less than 10 Hz.

Platinum-proton three-bond coupling constants in Pt—N—C—H fragments have been rationalized by assuming a Karplus type angular dependence.[6,7] It turns out that the variation of the platinum-carbon coupling constants

Table 2. ^{13}C NMR data.

	$\delta(-CH_3)$	$^3J_{Pt-N-C-C}$ in Hz	$\delta(>CH_2)$	$\delta(-\overset{\vert}{C}H)$	$\delta(-\overset{\vert}{C}-)$
$[Pt(NH_3)_2(mbn)]^{2+}$	13.8	27.3	–	57.7	–
$[Pt(NH_3)_2(lbn)]^{2+}$	18.0	49.8	–	59.9	–
$[Pt(NH_3)_2(ibn)]^{2+}$	24.3	22.4	56.7	–	61.3

found here would similarly be explained if the relationship

$$^3J_{Pt-N-C-C} \approx a \cos^2 \phi$$

is valid, ϕ being the dihedral angle between the planes PtNC and NCC, and a being a constant.

Molecular models reveal that ϕ for equatorial and axial methylcarbons are $\sim 180°$ and $\sim 90°$, respectively, *i.e.* according to the equation above

$$^3J_{Pt-N-C-C_{eq}} \approx a \text{ and } ^3J_{Pt-N-C-C_{ax}} \approx 0$$

In $[Pt(NH_3)_2(mbn)]^{2+}$ and $[Pt(NH_3)_2(ibn)]^{2+}$ the methyl groups spend equal time in equatorial and axial orientations and averaged coupling due to rapid ring inversion would give $^3J \approx \frac{1}{2}a$. As discussed above the methyl groups in $[Pt(NH_3)_2(lbn)]^{2+}$ are predominantly equatorial, giving $^3J \approx a$.

Thus the experimental coupling constants are accounted for by the Karplus-like relationship with $a = 50$ Hz.

From the presence of only one methyl doublet in the proton NMR spectrum of $[Pt(NH_3)_2(mbn)]^{2+}$ it has been concluded [8] that in this complex the conformational inversion is rapid on the NMR time scale.

Considering that the ^{13}C chemical shift differences between equatorial and axial methyl groups in methylcyclohexanes are of the order of 5 – 9 ppm,[9] the observed singularity of the methyl pattern in the ^{13}C spectra of $[Pt(NH_3)_2(mbn)]^{2+}$ and $[Pt(NH_3)_2(ibn)]^{2+}$ is a confirmation of the expected rapid ring inversion in these two complexes.

But in the case of $[Pt(NH_3)_2(lbn)]^{2+}$ the presence of only one methyl resonance does not necessarily imply rapid inversion; slow inversion would also result in a single methyl peak, as the energetically unfavourable δ conformation would scarcely be observable.

Internal molecular motion is one of the factors controlling the ^{13}C spin-lattice relaxation; [10] so any differences in the ring inversion rates of the three isomeric platinum complexes will to some degree influence the spin-lattice relaxation times, T_1. In order to explore this a relaxation study of the methyl carbon atoms was undertaken.

T_1 was determined from proton-decoupled, partially-relaxed Fourier transform spectra obtained by use of the pulse sequence $(T - 180° - \tau - 90°)_n$, [10] where $T = 10$ s, $n = 100$, and $\tau = 3$, 2, 1, and 0.1 s. The concentration of the three complexes was 0.66 g per ml D_2O, the temperature was 30.0 °C, and the solutions were deoxygenated. The T_1 values obtained are estimated to be accurate and reproducible within ± 15 %.

T_1 for $[Pt(NH_3)_2(mbn)]^{2+}$, $[Pt(NH_3)_2(lbn)]^{2+}$, and $[Pt(NH_3)_2(ibn)]^{2+}$ was found to be 1.5, 1.4, and 1.3 s, respectively. So, considering the experimental uncertainty, these measurements do not demonstrate any significant differences between the spin-lattice relaxation times of the methyl carbon atoms.

The Bruker WH 90 spectrometer is placed at our disposal by Statens Naturvidenskabelige Forskningsråd.

1. Johnson, G. L. and Michelfeld, T. A. *Inorg. Syn. 8* (1966) 242.
2. Drew, H. D. K. *J. Chem. Soc.* (1932) 2328.
3. *IUPAC Nomenclature of Inorganic Chemistry*, 2nd Ed., Butterworths, London 1971, p. 80.
4. Eliel, E. L., Allinger, N. L., Angyal, S. J. and Morrison, G. A. *Conformational Analysis*, Interscience, New York 1966, p. 53.
5. Bagger, S., Bang, O. and Woldbye, F. *Acta Chem. Scand. 27* (1973) 2663.
6. Erickson, L. E., McDonald, J. W., Howie, J. K. and Clow, R. P. *J. Amer. Chem. Soc. 90* (1968) 6371.
7. Appleton, T. G. and Hall, J. R. *Inorg. Chem. 10* (1971) 1717.
8. Appleton, T. G. and Hall, J. R. *Inorg. Chem. 9* (1970) 1807.
9. Doddrell, D., Charrier, C., Hawkins, B. L., Crain, W. O., Harris, L. and Roberts, J. D. *Proc. Nat. Acad. Sci. U.S. 67* (1970) 1588.
10. Levy, G. C. *Accounts Chem. Res. 6* (1973) 161.

Received March 1, 1974.

Examples of the Fourier Transform Technique in Sharpening ^{121}Sb Mössbauer Spectra

A. KJEKSHUS and D. G. NICHOLSON

Kjemisk Institutt, Universitetet i Oslo, Blindern, Oslo 3, Norway

The Fourier transform technique has become increasingly more common in the analysis of poorly resolved experimental data. It has also entered the field of Mössbauer spectroscopy where Stone [1] and Ure and Flinn [2] have shown that significant sharpening is obtainable on deconvoluting the source line-shape from ^{57}Fe and ^{125}Te spectra. A major problem associated with ^{121}Sb Mössbauer spectroscopy is the poorly resolved eight or twelve line quadrupole split spectra. For this reason it is considered to be of interest to explore the advantages of the Fourier transform process to this Mössbauer nuclide. In choosing actual data for this trial we conveniently have at hand those recently communicated for $CoSb_3$, $Fe_{0.5}Ni_{0.5}Sb_3$, $RhSb_3$, and $IrSb_3$, which were presented with reservations concerning the values derived for the quadrupole interaction parameters.

The Fourier transform computations were based on the programme of Ure and Flinn [2] and the experimental data least squares fitted to twelve superimposed Lorentzian peaks employing the resonance line coefficients and transition probabilities of Shenoy and Dunlap.[4]

The Fourier transformed reduced spectra for $CoSb_3$ and $Fe_{0.5}Ni_{0.5}Sb_3$ under consideration are shown in Fig. 1. The features revealed include possible evidence for contamination of the $CoSb_3$ sample with antimony.[5,6] The presence of this impurity, which thus must be amorphous because it does not appear on the Guinier photographs, would have gone unnoticed but for the Fourier transform reduction. For the remaining compounds of which the $Fe_{0.5}Ni_{0.5}Sb_3$ transform is a typical example, the sharpening of the absorption envelope permits preliminary estimates as to the input parameters for the least squares procedure. The new values for the quadrupole splittings (Table 1) confirm the validity of the reservations expressed in the previous paper.[3] The small deviations between the present values for the coupling constants would accord with the virtually constant average deviation of the bond angles about Sb from the tetrahedral value of 109.47°. On the other hand the revised quadrupole coupling constants no longer show a significant correlation with the difference $(d_1 - d_2)$ in Sb–Sb bond lengths in these compounds.[7] This inadequacy of the

Table 1. ^{121}Sb Mössbauer parameters (at 4.2 K) for $CoSb_3$, $Fe_{0.5}Ni_{0.5}Sb_3$, $RhSb_3$, and $IrSb_3$. Chemical shifts with respect to $Ba^{121}SnO_3$. Asymmetry parameters (η) lie between 0.9 and 1.0. Probable errors are ± 0.1 mm/s in δ and ± 1 mm/s in $|eQV_{zz}|$.

Compound	δ (mm/s)	$\lvert eQV_{zz}\rvert$ (mm/s)	Γ (mm/s)
$CoSb_3$	−9.9		
$Fe_{0.5}Ni_{0.5}Sb_3$	−10.2	10.0	3.9
$RhSb_3$	−9.5	10.4	3.3
$IrSb_3$	−9.0	10.6	3.1

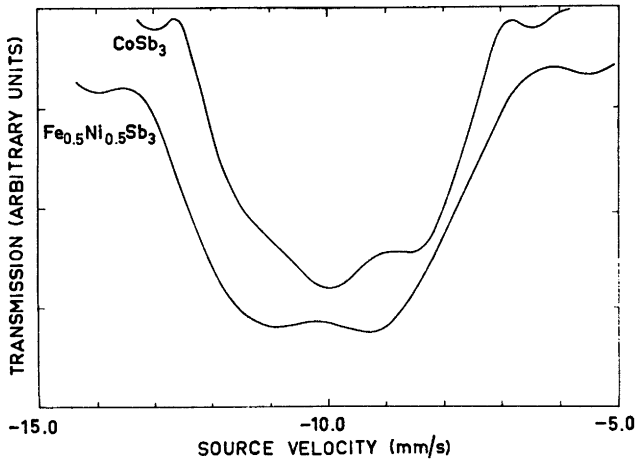

Fig. 1. Fourier transformed reduced spectra of $CoSb_3$ and $Fe_{0.5}Ni_{0.5}Sb_3$.

previous treatment results to some extent from the neglect to take more than eight lines into account (which is particularly inappropriate when $\eta > 0.5$) and the presumably consequent terminations of the least squares procedures at false minima.

In the present instance the Fourier transform technique has proved useful in detecting impurities and providing input parameters for the least squares refinements. However, the advantages of this procedure are even more promising in cases where the spectral envelope consists of more than one profile.

1. Stone, A. J. *Chem. Phys. Lett. 6* (1970) 331.
2. Ure, M. C. D. and Flinn, P. A. *Mössbauer Eff. Methodol. 7* (1969) 245.
3. Kjekshus, A., Nicholson, D. G. and Rakke, T. *Acta Chem. Scand. 27* (1973) 1315.
4. Shenoy, G. K. and Dunlap, B. D. *Nucl. Instrum. Methods 71* (1969) 285.
5. Dokuzoguz, H. Z., Bowen, L. H. and Stadelmaier, H. H. *J. Phys. Chem. Solids 31* (1970) 1565.
6. Avenarius, I. A., Kuz'min, R. N. and Opalenko, A. A. *Soviet Phys. JETP Lett. 14* (1971) 331.
7. Kjekshus, A. and Rakke, T. *Acta Chem. Scand. A 28* (1974) 99.

Received March 14, 1974.

Acta Chemica Scandinavica A 28 (1974) 471—476

Ultrasonic Absorption and Vibrational Relaxation in Liquid Tribromomethane

JØRN THAMSEN

Department of Physical Chemistry, Chemical Laboratory D, The Royal Danish School of Pharmacy, DK-2100 Copenhagen Ø, Denmark

In the present investigation the ultrasonic absorption in tribromomethane has been measured at temperatures from 10 to 50 °C. The absorption measurements were made by a pulse method over the frequency range 12 to 208 MHz.

A pronounced relaxation is found and this is associated with the time delay in deactivation of one of the vibrational modes. The residual absorption, which is greater than the Stokes value, suggests a second relaxation at higher frequencies.

A comparison of the experimental value of the absorption per wavelength μ'_{max} with values calculated from the Raman fundamentals appears to indicate that the ultrasonic relaxation in tribromomethane is associated with the degenerate CBr_3 deformation vibration.

In a very few examples of vibrational relaxation in liquids it has been possible to account for the observed relaxation by the specific heat associated with vibrational modes of the molecules. The absorption of ultrasonic waves in carbon disulphide [1] is thus due to a relaxation of the total vibrational specific heat which is described by a single relaxation time. The observed relaxation in dichloromethane [2-4] on the other hand cannot be accounted for by the specific heat associated with all the vibrational modes. In this case the experimental values are predictable if the specific heat is assumed to be divided in two parts, where one comprising all the vibrational modes except the mode of lowest wavenumber is associated with a frequency of relaxation of 171 MHz at 25 °C. The specific heat corresponding with the mode of lowest wave number is associated with a relaxation at higher ultrasonic frequencies.

Measurements of the ultrasonic absorption in tribromomethane [5,6] and trichloromethane [5,7] at lower frequencies did not give evidence of vibrational relaxation in these liquids. Relaxational behavior has, however, been detected later by measurements at higher frequencies.[8,9]

Commercially available tribromomethane and trichloromethane are stabilized by admixture of approximately 1 % ethanol and it is thus to be expected that this impurity might strongly influence the ultrasonic absorption and the relaxation frequency.

In the present investigation the absorption of ultrasonic waves has been measured in tribromomethane with very low contents of ethanol in the frequency range 12 to 208 MHz and the temperature range 10 to 50 °C. The values of the absorption calculated from the measurements are considerably increased and they are dependent on frequency thus indicating ultrasonic relaxation in tribromomethane in the investigated frequency range.

EXPERIMENTAL

The ultrasonic absorption measurements have been made by a "pulse" method.[10-12]

The tribromomethane was Bromoform reinst Merck, which is stabilized by about 1 % ethanol. The ethanol was removed from the samples by repeated shaking with water, followed by drying with anhydrous calcium chloride and fractionated distillation in vacuum. The "pure" tribromomethane decomposes gradually acquiring a yellow color. The influence of light and oxygen accelerate the decomposition and the purified samples were therefore handled with the necessary precaution. GLC [13,14] on a column of 20 % diethylhexylsebacate, 5 % sebacic acid and 75 % celite C 22 showed that the ethanol

was almost completely removed by this procedure.

The viscosity of the tribromomethane was measured with a Raaschou capillary type viscometer [15] relative to water, which was assumed to have a viscosity 17.938 mP at 0 °C and 8.949 mP at 25 °C.[16] The accuracy of measurement is considered to be of the order of 1 %.

The boiling point of bromoform is 150.5 °C at 760 mmHg and 34.0 °C at 10 mmHg. The melting point is 8.05 °C and $n_D^{20} = 1.5976$. The samples distilled at 34.1 °C at 10 mmHg and had the refractive index $n_D^{20} = 1.5973$.

EXPERIMENTAL RESULTS

Absorption measurements were made over the frequency range 12 to 208 MHz for a number of temperatures between 10 and 50 °C. The results obtained show that the major part of the measured absorption is due to a relaxation process in the frequency region 76 to 106 MHz.

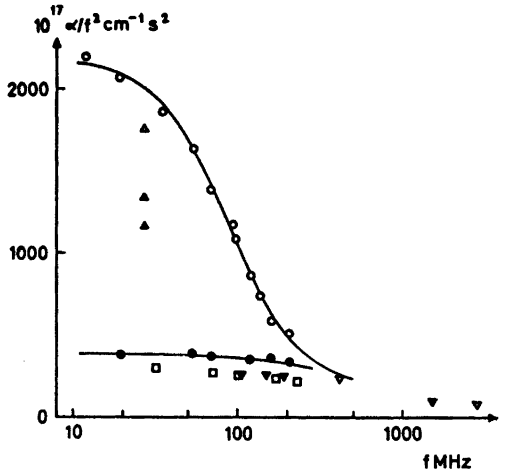

Fig. 1. Ultrasonic absorption in liquid tribromomethane; purified samples: ○ 25 °C (this work), △ 23 – 25 °C (Rasmussen [31]); commercial samples: ● 25 °C (this work), ▲ 23 – 25 °C (Rasmussen), ▼ 25 °C (Heasell and Lamb [5]), □ 26 – 27 °C (Andreae and Joyce [6]), ▽ 20 °C (Plass [5,32]).

The experimental results obtained at 25 °C are shown in Fig. 1. The smooth curve of Fig. 1 was calculated from the equation

$$\alpha/f^2 = A/[1+(f/f_c)^2] + B \qquad (1)$$

which represents the absorption caused by a single relaxation process; α is the ultrasonic absorption coefficient, f is the frequency of the sound wave and f_c the relaxation frequency. A and B are frequency-independent parameters. The parameters A, B, and f_c are, however, generally expected to be depending upon temperature. The term B represents the absorption at frequencies well above the investigated region of relaxation and includes the classical absorption, due to the effects of shear viscosity. The classical absorption (Stokes)

$$(\alpha/f^2)_{cl} = 8\pi^2\eta/3\varrho v_u^3 \qquad (2)$$

has the values given in Table 1 in the temperature range considered. In the table are also listed the viscosity, density, and ultrasonic velocity v_u.[17]

The values of the adjustable parameters A, f_c, and B, which agree with the best fits to the experimental data, have been estimated on an IBM 360 computer by use of a non-linear least squares program.* In Table 3 are the values of the parameters and also the values of the "relaxation strength" r, defined as the ratio of the relaxing part ($\delta\varkappa_s$) of the adiabatic compressibility divided by the value ($\bar{\varkappa}_s$) which the latter assumes at low frequencies, together with the relaxation time $\tau_{p,S}$. r and $\tau_{p,S}$ are calculated from the formulas [18]

$$r = Av_uf_c/\pi - \tfrac{1}{2}(1+2B/A)(Av_uf_c/\pi)^2 - \ldots \qquad (3)$$

$$\text{and } f_c = [2\pi\tau_{p,S}(1-r)^{\frac{1}{2}}]^{-1} \qquad (4)$$

which are valid since the values of r and Z/τ are much less than unity. Z represents the additional effects when the attention is confined to frequencies in the neighbourhood of the relaxation region in question.

From eqn. (1) it follows that the ultrasonic absorption per wavelength $\mu = \alpha v_u/f$ is composed of two terms; the one equal to Bv_uf represents the effects of relaxations at higher frequencies and shear viscosity, the other

$$\mu' = \frac{Av_uf}{1+(f/f_c)^2} = 2\mu'_{max}\frac{(f/f_c)}{1+(f/f_c)^2} \qquad (5)$$

is the absorption per wavelength corresponding to the relaxing component of the specific heat $C_p(a)$, which has the relaxation time $\tau_{p,S} = \tau_a$ such that $\omega\tau_a \simeq 1$, where $\omega = 2\pi f$. The maximum

* The program (Shares DA 3094) is written in Fortran and adapted by Finn Johnsen, Technical University of Denmark.

Table 1. The classical absorption (Stokes) in liquid tribromomethane in the temperature range 10 to 50 °C.

θ °C	η mP [a]	ϱ g cm^{-1} [b]	v_u m s^{-1} 500 KHz [b]	v_u m s^{-1} 4 MHz [a]	$10^{17} \times (\alpha/f^2)_{cl}$. cm^{-1} s^2
50	14.57	2.8118	866	866	21
40	16.41	2.8377	888	891	22
30	18.77	2.8639	910	910	23
25	20.85	2.8772		920	24
20	22.29	2.8904	931	929	25
10	25.34	2.9159	953	952	26

[a] This work. [b] Lagemann *et al.*[17]

Table 2. Experimental values of α/f^2 ($\times 10^{17}$ cm^{-1} s^2) in tribromomethane.

Frequency MHz	50 °C	40 °C	30 °C	25 °C	20 °C	10 °C
12	2698	2423	2365	2194	1961	1737
20	2546	2372	2254	2062	2081	1737
36	2241	2223	2028	1857	1772	1536
54	1903	1855	1661	1624	1528	1374
70	1690	1639	1502	1375	1260	
76	1445	1349	1213		1125	1141
94	1313	1300	1178	1168	1027	
98	1236	1142	1065	1078	1001	991
119	1083	958	919	856	831	819
140	862	803	773	736	728	623
162	797	790	611	579	548	534
184	690	711	595		488	492
208	600	551	501	502	445	344

absorption per wavelength $\mu'_{max} = \frac{1}{2} A v_u f_c$ is attained at the frequcny $f = f_c$.

It has been shown that values of μ'_{max} can be computed from the formula [19]

$$\mu'_{max} = \frac{\pi}{2} \frac{(C_{p_o} - C_{v_o}) C_{ia}}{[C_{p_o}(C_{p_o} - C_{ia}) C_{v_o}(C_{v_o} - C_{ia})]^{\frac{1}{2}}} \quad (6)$$

where C_{ia} is the relaxing specific heat. C_{p_o} and C_{v_o} are the "static" specific heats, and it is

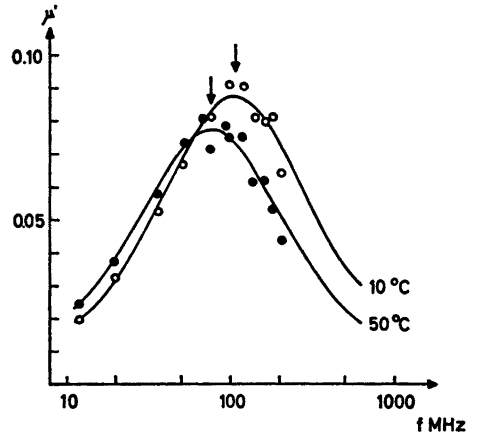

Fig. 2. The absorption per wavelength μ' due to the relaxation process in tribromomethane. The curves are theoretical and the points experimental.

Table 3. Absorption parameters and relaxation time for liquid tribromomethane.

θ °C	$10^{17} A$ cm^{-1} s^2	$10^{17} B$ cm^{-1} s^2	f_c MHz	$\mu'_{max.}$	r	$10^{10}\tau_{p,S}$ s	Z/τ
10	1732	20	106	0.088	0.055	15.2	0.0006
20	1891	191	83	0.073	0.046	19.4	0.0045
25	2007	175	88	0.081	0.051	18.3	0.0043
30	2141	260	77	0.075	0.047	20.9	0.0056
40	2220	291	81	0.080	0.050	19.9	0.0064
50	2357	356	76	0.078	0.049	21.2	0.0072

assumed that C_{po} apply at frequencies below the present relaxation range. μ' is plotted *versus* frequency in Fig. 2 at the temperatures 10 and 50 °C. The curves are calculated from the relaxation parameters, the points correspond to the values of $\alpha'/f^2 = (\alpha/f^2 - B)$.

DISCUSSION OF RESULTS

A comparison of the present results with those recently reported for tribromomethane and those for dichloro- and dibromomethane [20,21] suggests that the behavior of tribromomethane is associated with the time-delay in deactivation of one or more vibrational modes, *i.e.* an ultrasonic relaxation which involves either a part or the whole of the vibrational specific heat.[22] Tribromomethane has a symmetry which belongs to the symmetry group C_{3v} and in agreement with that expected on the symmetrical model there are six Raman fundamentals. The components of the vibrational specific heat C_i can be calculated from the Planck-Einstein relation [23]

$$C_i = gRx^2[e^{-x}/(1-e^{-x})^2] \quad (7)$$

where $x = h\nu/kT$ and g is the degeneracy.

The fundamental vibration frequencies [24] are arranged in Table 4 together with the contributions from the six normal modes of vibration

Table 4. Calculation of the maximum absorption per wavelength μ'_{max} for liquid tribromomethane at 25 °C.

Assignment	ν_i cm^{-1}	$x = h\nu/kT$	C_i
ν_1(CH)A_1	3023	14.59	0.000
ν_2(CBr)A_1	538.6	2.60	1.164
ν_3(CBr$_3$)A_1	222.3	1.07	1.808
ν_4 E	1142	5.51	0.492
ν_5(CBr)E	656	3.17	1.828
ν_6(CBr$_3$)E	153.8	0.74	3.797
$\sum C_i$	C_{ia} cal mol^{-1} deg^{-1}	μ'_{max}	
1. C_3	1.808	0.037	
2. C_6	3.797	0.085	
3. C_{123}	2.972	0.064	
4. C_{456}	6.117	0.151	
5. C_{total}	9.089	0.263	
μ'_{max} (exp.)		0.081	

to the vibrational specific heat C_{ia}. In the table are also the values of μ'_{max} calculated from eqn. (6) using the different values for the specific heat.

The first division is the contribution to the specific heat from the symmetrical vibrational mode of species A_1 having the lowest frequency ($\nu_3 = 222.3$ cm^{-1}). The second division corresponds to the degenerate mode of species E having the lowest frequency ($\nu_6 = 153.8$ cm^{-1}). In the third and fourth divisions the modes 1, 2,3 of species A_1 and 4,5,6 of species E are combined in possible specific heats. Finally is given the total vibrational specific heat.

In Table 5 is given an account of the thermal properties of liquid tribromomethane used for the computations in Table 4.

A comparison of the calculated values of μ'_{max} with the experimental value derived from the absorption measurements entail the conclusion, that it is probable that the ultrasonic relaxation in tribromomethane is associated with the degenerate CBr_3 deformation vibration ν_6, which is the vibrational mode with the lowest frequency. A relaxation time τ_1 is then associated with the deactivation of this mode. The value of the parameter B is equal to the Stokes value at 10 °C and there are no additional effects at this temperature. The value of B increases, however, with increased temperature and the percentage of absorption associated with the relaxation time τ_1 decreases. The experimental behavior suggests that additional effects have to be taken into consideration when the temperature is increased. By analogy with the mechanism proposed for polyatomic gases [26-29] an additional effect might be a relaxation at a very high frequency associated with a complex transition probability, *e.g.* involving the modes ν_6 and ν_3.

Absorption measurements in trichloromethane [30] have in a similar way given results which suggest that the relaxation in this case is associated with the symmetrical CCl_3 deformation vibration ($\nu_3 = 365.9$ cm^{-1}) rather than the degenerate deformation vibration of lowest frequency ($\nu_6 = 262.0$ cm^{-1}). It is rather difficult to appraise the apparent distinction in behavior between these halogenated methanes, but it might be of importance, that the measurements in tribromomethane have been carried out at temperatures rather close to the melting point,

Table 5. Thermal properties of liquid tribromomethane.

Thermal expansion coefficient	a deg^{-1}	0.000907 [a]
Specific heat (constant pressure)	C_{p_0} cal mol^{-1} deg^{-1}	32.10 [25]
Ratio of specific heats	$\gamma = C_{p_0}/C_{v_0}$	1.390 [b]
Specific heat (constant volume)	C_{v_0} cal mol^{-1} deg^{-1}	23.09

[a] Calculated from the densities at different temperatures and the formula $a = -(1/\varrho)\, d\varrho/dT$.[17] [b] Calculated from the formula $\gamma - 1 = Mv_u^2 a^2 T/C_{p_0}$; the molecular weight $M = 252.75$.

whereas the measurements in trichloromethane are at temperatures rather close to the boiling point.

The about 1 % ethanol in the commercial tribromomethane has an effect, which means that the relaxation frequency is displaced to higher frequencies and that the loss decreases as a consequence of higher efficiency of collisions in the deactivation of the molecules. The measurements of Plass [6] support this view.

Several authors have reported values of the ultrasonic absorption in commercial samples of bromoform. From Fig. 1 it can be seen that the values are undoubtedly in disagreement. When the lowest values are found in samples with the highest concentration of ethanol, they are obviously dependent on concentration. Andreae and Joyce have evaluated the relaxation frequency 124 MHz from the measurements, which is reported without further comments. Plass on the other hand has estimated the relaxation frequency to 814 MHz, which gives a relaxation time of $\tau_{obs} = 2.0 \times 10^{-10}$ s. The relaxation is considered as vibrational and the vibrational specific heat calculated from the normal mode spectrum is compared with the value obtained from the ultrasonic absorption measurements. When the values disagree it is suggested that an additional mechanism of energy exchange between degrees of freedom must be supposed. The influence of the ethanol on the measured absorption values has not been taken into consideration.

The commercial samples are in fact dilute solutions of ethanol in bromoform, where the less absorbing component ethanol is asscociated.

The ultrasonic absorption in solutions of alcohols, *e.g.* propanol, butanol, *t*-butanol, and phenol in the non-polar solvents carbon tetrachloride and cyclohexane has been reported by several workers [33–35] and in some of these cases it has been shown, that the curve of α/f^2 plotted against the concentration of alcohol has a maximum at low concentrations of alcohol. The ultrasonic relaxation spectra of solutions of this type have been attributed to the association of the alcohols by hydrogen bonding and the experiments are described by a multistep mechanism.[36,37] Measurements on solutions of ethanol in carbon tetrachloride,[38] however, have not revealed any absorption maximum at low concentration and 25 °C. In Fig. 3 is shown the absorption of ultrasonic waves at 55 MHz and 25 °C in diluted solutions of ethanol in carbon tetrachloride. The absence of the maximum could be a question of too high a temperature so the complexes are depolymerized. It might then be possible to reveal a maximum by measurements at lower temperatures.

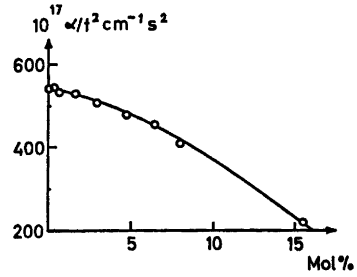

Fig. 3. Ultrasonic absorption in diluted solutions of ethanol in carbon tetrachloride.

In the solutions of alcohols in inert solvents the interactions between the alcohol molecules (monomers and polymers) and the solvent molecules are negligible; this is, however, not the case in polar solvents, *e.g.* benzene, chloroben-

zene or solvents, *e.g.* chloroform, bromoform, where hydrogen bonding between the alcohol complexes and solvent molecules is to be expected.[39,40] In these cases the absorption maximum decreases and is displaced to higher alcohol concentration or vanish completely.

Acknowledgements. The author is indebted to Professor Thor A. Bak for his kind interest in the work. He also wants to thank Professor Sv. Aa. Schou and Professor V. Sten Andersen for support. He finally wishes to express his gratitude to *Den teknisk-videnskabelige Fond* for financial support and to NEUCC, Technical University of Denmark, for allotment of computer time.

REFERENCES

1. Andreae, J. H., Heasell, E. L. and Lamb, J. *Proc. Phys. Soc. (London) B 69* (1956) 625.
2. Andreae, J. H. *Proc. Phys. Soc. (London) B 70* (1957) 71.
3. Andreae, J. H., Joyce, P. L. and Oliver, R. J. *Proc. Phys. Soc. (London) B 75* (1960) 82.
4. Hunter, J. L. and Dardy, H. D. *J. Chem. Phys. 42* (1965) 2961.
5. Heasell, E. L. and Lamb, J. *Proc. Phys. Soc. (London) B 69* (1956) 869.
6. Andreae, J. H. and Joyce, P. L. *Brit. J. Appl. Phys. 13* (1962) 462.
7. Verma, G. S. *J. Chem. Phys. 18* (1950) 1352.
8. Plass, K. G. *Ber. Bunsen-Ges. Phys. Chem. 74* (1970) 343.
9. Khabibullaev, P. K., Khaliulin, M. G. and Parpiev, K. *Russ. J. Phys. Chem. 44* (1970) 717.
10. Jarzynski, J. *Ph. D. Thesis*, Imperial College, London 1962.
11. Andreae, J. H., Bass, R., Heasell, E. L. and Lamb, J. *Acustica 8* (1958) 131.
12. Thamsen, J. *Acta Chem. Scand. 19* (1965) 1939.
13. Gloesener, E. *J. Pharm. Belg. 15* (1960) 297.
14. Gloesener, E. *J. Pharm. Belg. 16* (1961) 379.
15. Raaschou, P. E. *Ind. Eng. Chem. Anal. Ed. 10* (1938) 35.
16. *International Critical Tables*, McGraw, New York 1929, Vol. V, p. 10.
17. Lagemann, R. T., McMillan, Jr., D. R. and Woolf, W. E. *J. Chem. Phys. 17* (1949) 369.
18. Bass, R. and Lamb, J. *Proc. Roy. Soc. (London) A 243* (1957) 94.
19. Andreae, J. H. and Lamb, J. *Proc. Phys. Soc. (London) B 69* (1956) 814.
20. Hunter, J. L., Dardy, H. D. and Bucaro, J. A. *5e Congrès International D'Acoustique*, Liege 1965, D 26.
21. Hunter, J. L. and Dardy, H. D. *J. Chem. Phys. 44* (1966) 3637.
22. Matheson, A. J. *Molecular Acoustics*, Wiley-Interscience 1971, p. 187.
23. Andreae, J. H. and Lamb, J. *Proc. Phys. Soc. (London) B 64* (1951) 1021.
24. Herzberg, G. *Molecular Spectra and Molecular Structure II. Infrared and Raman Spectra of Polyatomic Molecules*, Van Nostrand, Princeton 1945, p. 320.
25. Tschamler, H., Richter, E. and Wettig, F. *Monatsh. Chem. 158* IIb (1949) 856.
26. Dickens, P. G. and Linnett, J. W. *Proc. Roy. Soc. (London) A 243* (1957) 84.
27. Lambert, J. D. and Salter, R. *Proc. Roy. Soc. (London) A 243* (1957) 78.
28. Lambert, J. D. *Quart. Rev. Chem. Soc. 21* (1967) 67.
29. Holmes, R. and Tempest, W. *Proc. Phys. Soc. (London) 78* (1961) 1502.
30. Thamsen, J. *Unpublished.*
31. Rasmussen, R. A. *J. Chem. Phys. 47* (1967) 1871.
32. Plass, K. G. *Acustica 19* (1967/68) 236.
33. Mez, A. and Maier, W. *Z. Naturforsch. 10a* (1955) 997.
34. Musa, R. S. and Eisner, M. *J. Chem. Phys. 30* (1959) 227.
35. Eppler, K. *Z. Naturforsch. 10a* (1955) 744.
36. Rassing, J. and Nordby Jensen, B. *Acta* Chem. Scand. 24 (1970) 855.
37. Garland, F., Rassing, J. and Atkinson, G. *J. Phys. Chem. 75* (1971) 3182.
38. Sette, D. *Atti del Convegno Internazionale di Ultracustica*, Suppl. 2, Vol. 7, Ser. 9 del Nuovo Cimento (1950) 318.
39. Martin, M. *Arch. Sci. 13* (1960) 519.
40. Gordy, W. *J. Chem. Phys. 7* (1939) 163.

Received January 21, 1974.

Acta Chemica Scandinavica A 28 (1974) 477—481

Calcium Phosphates with Apatite Structure. I. Precipitation at Different Temperatures

P. JERVØE and H. E. LUNDAGER MADSEN

Department of Inorganic Chemistry, Royal Veterinary and Agricultural University, Thorvaldsensvej 40, DK-1871 Copenhagen V, Denmark

Precipitation of basic calcium phosphates from aqueous solutions by dropwise addition of ammoniacal calcium chloride and ammonium phosphate in stoichiometric ratio to ammonia buffer at pH ~ 9 and different temperatures from 25 to 98 °C has been studied. The products were investigated by chemical analysis and X-ray diffraction, and were identified as hydroxyapatite, $Ca_5(PO_4)_3OH.aq$, with properties similar to those of biological apatites.

The mineralized or hard tissue of teeth consists of an organic matrix embedding inorganic material. The former contains collagenous fibres and a structureless ground substance, and the latter includes crystallized and noncrystallized inorganic salts; it is often called the mineral. Strictly, a distinction must be made between the mineral phase as such and the inorganic fraction as a whole, since the latter includes any inorganic material associated with the organic or tissue fluid components. The various types of hard tissue, *viz.* enamel, dentine, cementum, and bone, differ slightly in their mineral content as shown in Table 1. The mineral phase of human teeth is essentially calcium phosphate with apatite structure, and the major ion constituents are Ca^{2+}, PO_4^{3-}, OH^-, and CO_3^{2-}.[1,3-6] Much research has been devoted to studies of structure, chemical and physicochemical properties of natural and synthetic basic calcium phosphates, and to comparison of these properties with those of biological apatites.[7-11]

In 1970 Jervøe [12] reported experimental evidence for changes in the crystallinity of mature human teeth irradiated both *in vitro* and *in situ*. The question whether the effect was primary or secondary, *i.e.* caused by products of radiolysis in the non-mineral phase, was let open. Since teeth consist of many different substances of both organic and inorganic nature, it is difficult to identify cause and effect of radiolysis in the crystalline structure. No method for removal of the organic constituents of enamel, dentine, and bone without structural modification of the mineral phase is known at present.[13-19] The literature concerning basic calcium phosphates is extensive. Most experiments described are often performed on purchased specimens with uncertain chemical composition, homogeneity, dispersity, polydispersity, and average crystal-

Table 1. Chemical contents of human enamel, dentine, cementum, and bone, after Orban.[1] Values are percentage dry weight.

Content	Enamel	Dentine	Cementum Bone
Water	2.3	13.2	32
Organic Matter	1.7	17.5	22
Ash	96.0	69.3	46
In 100 g of Ash:			
Calcium	36.1	35.3	35.5
Phosphorus	17.3	17.1	17.1
Carbon dioxide	3.0	4.0	4.4
Magnesium	0.5	1.2	0.9
Sodium	0.2	0.2	1.1
Potassium	0.3	0.07	0.1
Chloride	0.3	0.03	0.1
Fluoride[a]	0.016	0.017	0.015
Ca/P	2.08	2.07	2.28[b]
Ca/P (molar)	1.64	1.64	1.77[b]

[a] Depends on F^- content of drinking water. [b] Calculated from values given by Morse and Looney.[2]

linity. Even authors preparing their own specimens have not published data in such detail that we could use their prescriptions in our radiochemical experiments. For this reason we have synthesized pure calcium phosphate with structure, chemical, and physicochemical properties similar to those of biological apatites for later use in irradiation experiments. The method has been direct precipitation, according to the reaction

$$5Ca^{2+} + 3PO_4^{3-} + OH^- \rightarrow Ca_5(PO_4)_3OH$$

The calcium phosphates described in this paper can presumably be used with advantage in other than radiolytical experiments because they are well-characterized.

EXPERIMENTAL

Apparatus. Examinations of precipitates by X-ray powder diffractometry were carried out using both a Hägg-Guinie rcamera with Cu$K\alpha_1$-radiation and a General Electric diffractometer (type XRD-3) equipped with a scintillation counter, Speedomax recorder, and with Ni-filtered Cu$K\alpha$-radiation. The camera has been calibrated by means of recrystallized NaCl, a scale has been printed on the film before exposing, and an apparatus constant considering these properties has been calculated for the computer program.

Colorimetric determinations were carried out using a Beckman DU spectrophotometer.

Water content was determined using a Stanton automatic Thermo-recording balance, model HT-FS, in combination with a Univel-temperature programmer type TVP-2.

Materials. Calcium phosphate was prepared using C. P. grade chemicals and glass-distilled water. We shall not go into details but draw attention to the fact, that we have wasted a lot of time on unsuccessful experiments because we had not controlled the quality of the water. The samples were prepared by mixing equal volumes of solution A: 0.167 M $CaCl_2$, 0.40 M NH_3, and solution B: 0.10 M $(NH_4)_2HPO_4$, 0.20 M NH_3, with solution C: 0.10 M NH_4Cl, 0.10 M NH_3. The solutions A and B were added dropwise to solution C, which was heated to the desired temperature of precipitation. A pH of about 9 was calculated from the composition of the mixtures, and this value was considered favourable for the formation of hydroxyapatite. Variation of temperature enabled the preparation of fractions with different crystallinities comparable with those of human enamel and dentine. Ageing of the precipitate was allowed to proceed for 24 h. The solid phase was collected on a glass filter with a pore size of 10 – 20 μm, washed 6 times with 3 litre portions of boiled, deionized water, then once with acetone, and finally dried in air. A basic calcium phosphate, prepared by A. Tovborg Jensen, (ATJ), precipitated at 100 °C in 1936 as sample No. 8, allowed to age in a flask until 1942 when washed and dried in air, was used as a reference material in the X-ray diffraction investigation.

Analytical methods. Calcium was determined by complexometric titration,[20] phophorus colorimetrically using the molybdenum-blue method.[21] carbonate as described by Larsen,[22] chloride by potentiometric titration using silver nitrate, and ammonium with Nessler's reagent.

RESULTS

Table 2 shows the data from chemical analyses, expressed as weight %. The amount of calcium phosphate precipitated at 25 °C was too small to be analysed. Water content was calculated from weight loss at 900 °C after substraction of carbonate contribution to this figure. The percentages should add up to 100; however, $Ca_5(PO_4)_3OH$ is stable at 900 °C, which means that, if all phosphate present at this temperature is apatite, a correction of 0.5 mol water per mol apatite should be added. This has been done

Table 2. Results from chemical analysis on basic calcium phosphates with apatite structure precipitated at different temperatures.

Temp. °C	CaO %	P_2O_5 %	CO_2 %	H_2O %	NH_3 %	HCl %	Total %	Total corr. %
35	51.5	37.6	0.725	8.96	3.7×10^{-3}	0.02	98.8	100.5
45	50.6	37.8	0.602	7.51	4.1×10^{-3}	0.02	96.5	98.1
55	52.3	38.0	0.743	6.02	4.4×10^{-3}	0.02	97.0	98.7
65	53.0	39.8	0.387	5.41	4.1×10^{-3}	0.02	98.6	100.3
75	53.1	39.5	0.456	4.81	3.1×10^{-3}	0.01	97.9	99.6
88	54.0	39.5	0.456	3.07	3.4×10^{-3}	0.01	97.1	98.8
98	54.1	40.7	0.178	4.02	6.5×10^{-3}	0.03	99.0	100.7

Table 3. Calculated Ca/P molar ratio, CO_3^{2-} and OH^- contents, and molecular weight, from chemical analysis on basic calcium phosphates with apatite structure precipitated at different temperatures.

Temp. °C	Ca/P mol ratio	$CaCO_3$ mol	$Ca(OH)_2$ mol	H_2O mol	Molecular weight
35	1.73	0.093	0.097	2.72	568
45	1.69	0.077	0	2.35	552
55	1.74	0.094	0.118	1.75	552
65	1.68	0.047	0	1.61	536
75	1.70	0.056	0.040	1.40	536
88	1.73	0.056	0.127	0.79	532
98	1.68	0.021	0.011	1.16	526

in the last column of Table 2, and the total is seen to be correct within a standard deviation of 1 % which is completely satisfactory.

The second column in Table 3 gives the calcium to phosphorus molar ratio, which is $5/3 = 1.67$ in pure hydroxyapatite. All preparations contain a slight excess of calcium, which may be assumed to be present partly as carbonate, partly as hydroxide. In the third and fourth column of Table 3 these amounts are expressed as mol per mol apatite. The figures

Table 4. Unit cell dimensions of basic calcium phosphates with apatite structure precipitated at different temperatures obtained from least-squares refinement of a series of Guinier-film measured 2θ angles, and of human enamel and dentine obtained from least-squares refinement of a series of diffractometer-measured 2θ angles.

Temp. °C	*a*-axis Å	*c*-axis Å	Number of reflections
25	9.420(6)	6.891(4)	12
35	9.432(5)	6.888(3)	15
45	9.434(2)	6.892(2)	26
55	9.433(2)	6.892(2)	34
65	9.435(2)	6.890(2)	35
75	9.438(2)	6.893(1)	46
88	9.439(1)	6.896(1)	50
98	9.441(1)	6.894(1)	53
100 (ATJ)	9.443(2)	6.896(2)	43
Hum. Enamel [a]	9.437(3)	6.883(3)	28
Hum. Dentine [a]	9.434(7)	6.868(9)	18

Values within parenthesis refer to standard deviation in the least significant digits. [a] Values are the average for 23 samples.[23]

Table 5. *d*-Spacings, *hkl*-values from 98 °C precipitated calcium phosphate calculated from Hägg-Guinier photograph and relative intensities (I^x) calculated from diffractogram.[a]

d Å	*hkl*	I^x	*d* Å	*hkl*	I^x	*d* Å	*hkl*	I^x
8.166	100	12	1.945	222	29	1.408	413	6
5.268	101	4	1.891	312	13	1.349	512	8
4.084	200	6	1.872	320	4	1.317	431	4
3.891	111	8	1.842	213	33	1.308	520	6
3.447	002	46	1.808	321	15	1.281	423	6
3.172	102	12	1.782	410	12	1.267	602	4
3.089	210	17	1.755	402	12	1.257	215	6
2.819	211	100	1.722	004	15	1.245	610	4
2.780	112	67	1.645	322	8	1.238	414	6
2.725	300	62	1.612	313	4	1.222	522	6
2.634	202	27	1.574	330	4	1.177	315	6
2.530	301	6	1.543	420	4	1.159	433	4
2.298	212	6	1.531	331	4	1.149	006	4
2.267	310	21	1.504	214	6	1.137	523	4
2.153	311	4	1.476	502	8	1.116	442	4
2.063	113	5	1.454	304	8	1.110	325	4
2.039	400	5	1.453	323	8	1.104	206	4
2.000	203	4	1.434	511	6			

[a] The peak of maximum is arbitrarily assigned a value of 100 and the other peaks are expressed in terms of percentages of this value.

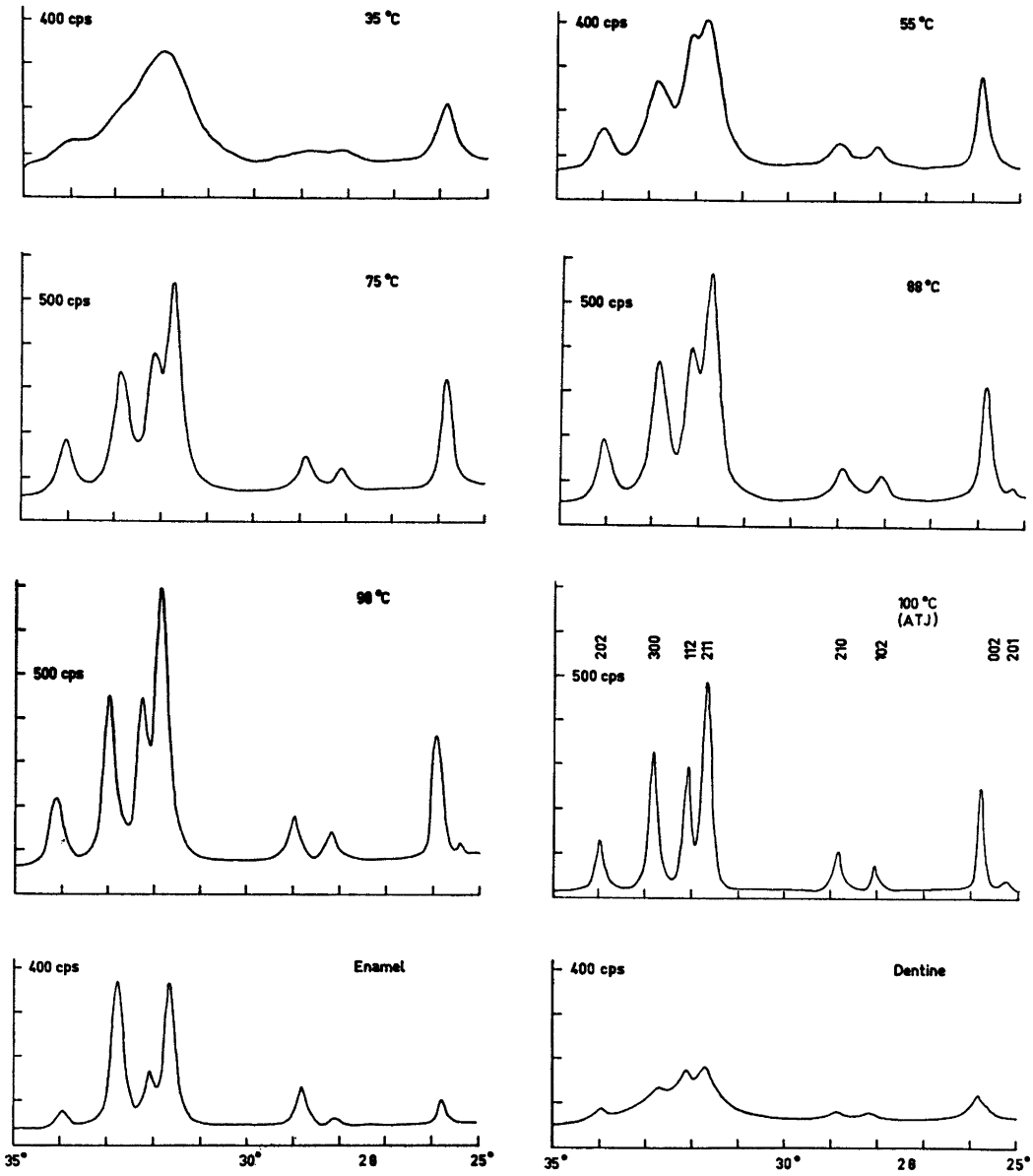

Fig. 1. Diffractograms of basic calcium phosphates with apatite structure precipitated at different temperatures, precipitated at 100 °C in 1936 (ATJ), and of human enamel and dentine.

in the fifth column express the total water content in the samples (water of crystallization or adsorbed water *etc.*) per mol apatite. Finally, the sixth column contains the "molecular weights", *i.e.* the amounts of substance in gram containing 1 mol $Ca_5(PO_4)_3OH$.

All X-ray reflections from both powder photographs and diffractograms were measured, *d*-spacings, *hkl*-values, and *a*- and *c*-axes of the unit cells were calculated. Spacings were compared with values obtained from X-ray powder patterns of the ATJ calcium phosphate, human

enamel, and human dentine.[23] The results are given in Tables 4 and 5. Diffractograms of calcium phosphates, and human enamel and dentine are shown in Fig. 1. in the 2θ range from 25 to 35°, which includes the most important reflections of hydroxyapatite. The diffractograms clearly reflect dependence of crystallinity of calcium phosphates on temperature of precipitation.

DISCUSSION AND CONCLUSION

The data of Tables 3, 4, and 5 as well as Fig. 1 establish the identity of all the prepared samples as hydroxyapatite with composition and crystallinity depending uniquely on the temperature of precipitation. The resemblance with the crystalline constituent of teeth is also obvious; the 55 °C fraction is very similar to dentine, the 75 °C to enamel.

The only important difference between our synthetic samples and biological apatites is the Ca/P ratio. Where the latter in general show a Ca deficiency of about 2 %,[1] see Table 1, the former contain an excess ranging from 0.6 to 4 %. This is of the same order of magnitude as the fraction of calcium ions, which are situated in the surface layer of the crystals. At a pH about 9 absorption of Ca^{2+} by the precipitate is very likely, much more so than in acid solution; presumably, OH^- acts as counterion (to assure electroneutrality), but is more or less exchanged for CO_3^{2-} during filtering, washing, and storage. Precipitation at a lower pH would probably lead to a lower Ca/P ratio, but then the preparation would require much more time, and it would be difficult to avoid contamination of the apatite by other calcium phosphates, in particular $Ca_4H(PO_4)_3$. Though metastable, this substance crystallizes readily from neutral solution and is transformed very slowly to hydroxyapatite, especially at low temperature.

As we would not expect the adsorbed layer to play any role in the behaviour of the synthetic apatites upon irradiation, we shall consider the results of experiments with these to be valid also for biological materials.

Acknowledgements. The authors wish to thank Professor A. Tovborg Jensen, Dr. E. Jensen, and Dr. K. J. Pedersen, for their interest and valuable advice. The investigation was in part supported by a grant from Statens Forskningsråd (Danish State Medical Research Council).

REFERENCES

1. Orban, B. J. *Oral Histology and Embryology*, 3rd Ed., The C. V. Mosby Company, St Louis 1953, p. 52.
2. Morse, W. and Looney, J. M. *Applied Biochemistry*, 2nd Ed., Saunders, Philadelphia, Pa. 1927, p. 357.
3. Gross, R. *Festschr.* Zahnärztl. Inst. Univ. Greifswald, Berlin 1926.
4. De Jong, W. F. *Res. Trav. Chim. Pays-Bas 45* (1926) 445.
5. Mehmel, M. *Z. Kristallogr. 75* (1930) 323.
6. Náray-Szabó, S. *Z. Kristallogr. 75* (1930) 387.
7. Bale, W. F. *Amer. J. Roentgenol. 43* (1940) 735.
8. Jensen, A. T. and Møller, E. *Acta Odontol. Scand. 6* (1944) 7.
9. Carlström, D. *Acta Radiol.* (1955) Suppl. 121.
10. Trautz, O. R. *Ann. N. Y. Acad. Sci. 60* (1955) 696.
11. Posner, A. S. *Norelco Rep. 2* (1955) 26.
12. Jervøe, P. *Acta Odontol. Scand. 28* (1970) 623.
13. Beaulieu, M. M., Dallemagne, M. J., Brasseur, H. and Melon, J. *Arch. Int. Physiol. 57* (1950) 411.
14. Williams, J. B. and Irwine, J. W. *Science 119* (1954) 771.
15. Peckham, S. C., Losee, F. L. and Ethelmann, I. *J. Dent. Res. 35* (1956) 947.
16. Zapanta, R. R. and Trautz, O. R. *J. Dent. Res. 40* (1961) 702.
17. Termine, J. D. and Posner, A. S. *Calcif. Tissue Res. 1* (1967) 8.
18. Swedlow, D. B., Harper, R. A. and Katz, J. L. *Proceeding, Workshop on Biological Scanning Electron Microscopy*, Chicago, ITT Research Institute 1972, p. 335.
19. Termine, J. D., Eanes, E. D., Greenfield, D. J., Nylén, M. U. and Harper, R. A. *Calcif. Tissue Res. 12* (1973) 73.
20. Lundager Madsen, H. E. *Acta Chem. Scand. 24* (1970) 1677.
21. Murphy, J. and Riley, J. P. *Anal. Chim. Acta 27* (1962) 31.
22. Larsen, S. *Acta Chem. Scand. 3* (1949) 967.
23. Jensen, E. and Jervøe, P. *Acta Crystallogr. B 30* (1974). *In press.*

Received February 18, 1974.

Acta Chemica Scandinavica A 28 (1974) 482—490

Conformational Analysis. 1. The Temperature Effect on the Structure and Composition of the Rotational Conformers of 1,2-Dichloroethane as Studied by Gas Electron Diffraction

K. KVESETH

Department of Chemistry, University of Oslo, Blindern, Oslo 3, Norway

Gaseous 1,2-dichloroethane has been studied by electron diffraction at −13, 40, 140, and 300 °C. The relative amount of the *anti*-conformer as compared to *gauche*, showed a marked variation with the temperature, whereas the structure remained almost invariant, with exception for the long distance u-values. A least-squares fit to the estimated equilibrium constants gave $\Delta E = 1.5(0.2)$ kcal mol^{-1} and $\Delta S = 2.0(0.5)$ cal K^{-1} mol^{-1}, which is in good agreement with earlier estimates. The distances (R_a), corrected for shrinkage, and u-values determined are given in Table 4.

It is well established that internal rotation about carbon-carbon single bonds gives rise to a mixture of different conformers, the amount of each depending on the energy difference. The structure of each conformer differs mainly in their torsional angle about the C−C bond.

Table 1. Experimental conditions and photographic plate data.

Temp. (°C)	−13		40	
Apparatus	Balzer		Oslo	
Nozzle-to-plate distance (mm)	500.00	250.00	481.19	201.19
Electron wavelength (Å) [a]	0.05848	0.05849	0.06452	0.06452
Number of plates used	6	5	6	6
Range of data (s) [b]	1.125−15.625	2.250−29.500	1.500−19.375	7.000−43.500
Data interval (Δs)	0.125	0.250	0.125	0.250
Corresponding curves in Figs. 2 and 3	A		B	

140		140 B		300	
Oslo		Balzer		Balzer	
481.19	201.19	500.00	250.00	500.09	248.18
0.06452	0.06452	0.05850	0.05851	0.05850	0.05850
6	6	5	5	4	6
1.500−19.375	7.000−42.250	1.125−15.500	2.250−30.000	1.125−15.500	2.250−30.250
0.125	0.250	0.125	0.250	0.125	0.250
C		D		E	

[a] Determined in separate experiments by calibration to CO_2. [b] $s = 4\pi/\lambda \sin\theta$; 2θ is the scattering angle.

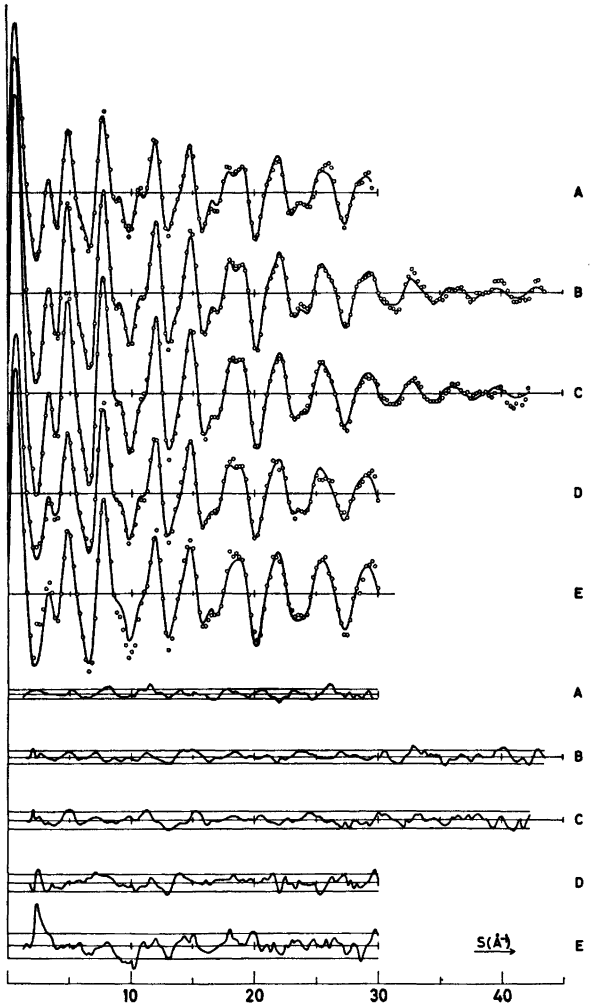

Fig. 1. Intensity and difference curves. The solid curves are theoretically calculated from the parameters given in Table 4. The experimental values are the O. The difference is experimental minus theoretical, and the limits are 3σ, σ being the experimental standard deviation in the observations. The temperature in the different curves are A: − 13, B: 40, C: 140, D: 140 and E: 300 (°C).

Substituted ethanes are thoroughly studied both by spectroscopy and diffraction methods,[1] and exist definitely as the two conformers *anti* and *gauche*. Due to the energy difference one must expect that the relative amount of the two conformers varies with the temperature of the experiment. The variation in composition may be used to evaluate both the difference in energy and entropy between the *gauche* and *anti* conformer, the last quantity usually assumed to be R ln 2, only taking into account the statistical weight of 2 for the *gauche* form.

In a similar study on ethylenechlorohydrin by Bastiansen *et al.*[2], they were able to evaluate these two quantities. 1,2-Dichloroethane ought to be well suited as the Cl − Cl distance in *anti* is well separated from the rest of the structure, and is also fairly well represented because of the scattering power of the two chlorine atoms.

EXPERIMENTAL

The sample of 1,2-dichloroethane was obtained from British Drug Houses (> 98.9 %) and used without further purification. Electron diffraction photographs were obtained with the Oslo apparatus [3] and the Balzer Eldigraph KDG-2 unit. The experimental conditions are summarized in Table 1. The data were corrected in the usual way,[4] obtaining an intensity curve for each photographic plate. The intensities were modified with the function [4]

$s/|f_{Cl}|^2$

The background was subtracted separately from each intensity curve. The average for each set of plates was calculated, and composites made for each temperature by scaling corresponding pair of curves and averaging the intensities in the overlap region. These total intensity curves are drawn in Fig. 1. (The discrepancy at $s = 2$ Å^{-1} in the 300 °C-curve is due to a dust particle in the sector opening.) The amount of the two conformers, as well as the structure, is determined by least squares refinements, carried out either on the composite curves, or simultaneously on data from each nozzle-to-plate distance without connecting them.

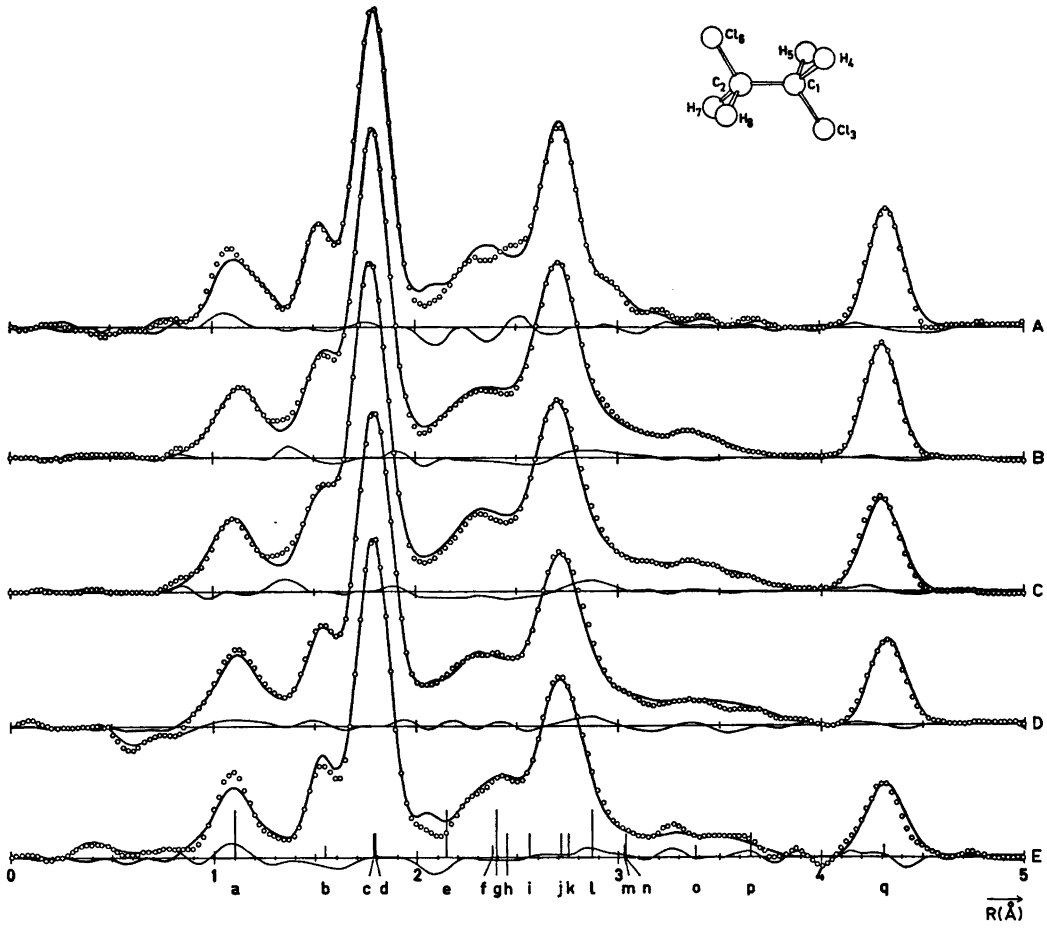

Fig. 2. Radial distribution and difference curves ($k = 0.0015$ Å^2). The solid curves are those theoretically calculated from the parameters given in Table 4. The experimental values are the O. The difference is experimental minus theoretical. The temperature in the different curves are A: −13, B: 40, C: 140, D: 140 and E: 300 (°C).
a C_1-H_4; b C_1-C_2; c C_1-Cl_3; d $H_4\cdots H_5$; e $C_1\cdots H_7$; f $H_5\cdots H_7$g,g; g $Cl_3\cdots H_4$; h $H_4\cdots H_6$a,g; i $H_4\cdots H_7$g,g; j $C_1\cdots Cl_6$; k $Cl_3\cdots H_6$g,g; l $Cl_3\cdots H_7$a,g; m $H_4\cdots H_6$g,a; n $H_4\cdots H_7$a,a; o $Cl_3\cdots Cl_6$g; p $Cl_3\cdots H_7$g,a; q $Cl_3\cdots Cl_6$a.

The theoretical molecular intensities were calculated according to eqn. (10) of Ref. 4. The scattering amplitudes were calculated by the partial wave method,[4,5] using Hartree-Fock atomic potentials.[6]

STRUCTURE ANALYSIS AND REFINEMENT

Radial distribution curves (RD-curves) calculated from the composities by a Fourier transformation, are shown in Fig. 2. The bond distances contribute to the first three peaks, together with the short r(H···H). The peak complex between $R=2$ Å and $R=4$ Å corresponds to all the non-bonded distances, except for the torsional dependant r(Cl···Cl) in *anti*, which gives rise to an isolated peak in the outer part of the curve, the area of which varies with the temperature.

All bond distances, the angles CCCl and CCH and the torsional angle ϕ were chosen as independant parameters. ϕ is defined as 180° in *anti*. For the *gauche* conformation ϕ was refined for each temperature. The torsional independant part of the structure is assumed to be the same for the two conformers. The composition in the gas phase is thus determined from the two torsional dependant r(Cl···Cl)-distances, as the contribution from the long r(Cl···H) is comparatively small.

The molecular structure was calculated in the geometrical consistent R_α-picture, the bond distances transformed by eqn. (1)

$$R_\alpha = R_a + u^2/R - K = R_a + D \qquad (1)$$

K is perpendicular amplitude correction coefficient (see Ref. 8). The distances thus determined are transformed to R_a-values before refining to the intensities by least-squares procedure. The calculated angles will correspond to R_α-structure.

D-values and root-mean-square vibrational amplitudes (u-values) calculated[7,8] from the established valence force field[9] and cartesian displacement coordinates, are given in Table 2 and Table 3, respectively. Both parameters vary considerably with the temperature, with the smallest dependency for the bond distances.

Table 2. The difference, D(Å), between R_α and R_a. The difference is calculated from the valence force field established by Schachtschneider and Snyder, with the torsional force constants from this work; $f_{t,g}=0.253$ mdyn Å rad^{-2} and $f_{t,a}=0.174$ mdyn Å rad^{-2}.

Temp. (° C)	−13	40	140	300
r(C−C)	0.00010	0.00005	−0.00005	−0.00020
r(C−Cl)	−0.00304	−0.00370	−0.00494	−0.00694
r(C−H)	−0.01009	−0.01054	−0.01160	−0.01534
r(C···Cl)a [a]	−0.00155	−0.00191	−0.00258	−0.00363
r(C...Cl)g	−0.00016	−0.00027	−0.00046	−0.00073
r(C···H)a	−0.00122	−0.00137	−0.00170	−0.00228
r(C···H)g	−0.00450	−0.00511	−0.00636	−0.00850
r(Cl···H)	−0.00506	−0.00593	−0.00765	−0.01046
r(H···H)	−0.00963	−0.01030	−0.01186	−0.01489
r(Cl···Cl)a	0.00096	0.00109	0.00135	0.00180
r(Cl···H)a,g [b]	0.00147	0.00149	0.00157	0.00179
r(Cl···H)a,g	0.00147	0.00149	0.00157	0.00179
r(H···H)a,a	−0.00238	−0.00247	−0.00269	−0.00321
r(H···H)a,g	0.00240	0.00230	0.00222	0.00231
r(H···H)a,g	0.00240	0.00230	0.00222	0.00231
r(Cl···Cl)g	0.00534	0.00635	0.00827	0.01138
r(Cl···H)g,g	0.00275	0.00288	0.00323	0.00396
r(Cl···H)g,a	−0.00194	−0.00210	−0.00244	−0.00307
r(H···H)g,g	−0.00268	−0.00334	−0.00460	−0.00661
r(H···H)g,g	−0.00363	−0.00458	−0.00641	−0.00936
r(H···H)g,a	−0.00636	−0.00697	−0.00828	−0.01064

[a] the suffix a and g means *anti* and *gauche*, respectively. [b] in the double suffix the first letter gives the conformation, the second the type of distance involved.

Table 3. Vibrational amplitudes, u (Å), calculated from the valence force field.

Temp. (° C)	−13	40	140	300
u(C−C)	0.052	0.052	0.054	0.056
u(C−Cl)	0.052	0.053	0.056	0.061
u(C−H)	0.078	0.078	0.078	0.078
u(C···Cl)	0.067	0.070	0.076	0.086
u(C···H)	0.109	0.110	0.112	0.116
u(Cl···H)	0.109	0.109	0.111	0.116
u(H···H)	0.128	0.128	0.129	0.131
u(Cl···Cl)a [a]	0.064	0.068	0.075	0.087
u(Cl···H)a,g	0.160	0.167	0.180	0.200
u(Cl···H)a,g	0.160	0.167	0.180	0.200
u(H···H)a,a	0.131	0.131	0.132	0.135
u(H···H)a,g	0.173	0.175	0.180	0.191
u(H···H)a,g	0.173	0.175	0.180	0.191
u(Cl···Cl)g	0.141	0.153	0.175	0.205
u(Cl···H)g,g	0.158	0.163	0.174	0.193
u(Cl···H)g,a	0.102	0.104	0.107	0.113
u(H···H)g,g	0.170	0.172	0.177	0.187
u(H···H)g,g	0.173	0.175	0.180	0.191
u(H···H)g,a	0.129	0.129	0.130	0.133

[a] See captions to Table 2.

Vibrational amplitudes which did not refine, are given the calculated value (see discussion).

The (Cl···Cl)-vibrational amplitudes in *gauche* are, contrary to u(Cl...Cl)a, dependent on the torsional force constant, $f_{t,g}$, which is varied to reproduce the experimental u-value. At 300 °C it was found that $f_{t,g}=0.253$ mdyn Å/rad^2 gave the experimental u-value. The calculated torsional frequency of 117 cm^{-1} is also in excellent agreement with the experimental value of 125 cm^{-1},[10-12] measured in liquid Raman, where a shift to lower frequency may be expected in the gas phase.

To reproduce the torsional frequency in *anti* at 125 cm^{-1}, measured in gas phase IR, the force constant was found to be $f_{t,a}=0.174$ mdyn Å/rad^2, a bit smaller than in *gauche*.

An attempt to estimate the ratio between the two torsional force constants from the extended van der Waals potential curve [13] (as suggested by R. Stølevik), gave the same results as found above. The magnitude agrees with an estimate from the second derivatives of the assumed cosine potential at $\phi=60°$ and 180°, also assuming harmonic motion with small amplitudes. Using an earlier estimate of ΔH, this method gave $f_{t,g}=f_{t,a}=0.17$ mdyn Å/rad.[2] The graphs in Fig. 3 show the excellent over all agreement between the calculated and refined torsional u-values, as well as the linear dependency of $T^{\frac{1}{2}}$.

To get some information about the uncertainty introduced by the parameters kept at fixed values, all parameters were refined one cycle and corresponding standard deviations, σ, were calculated. The fixed parameters were varied in the region of $\pm 3\sigma$ without

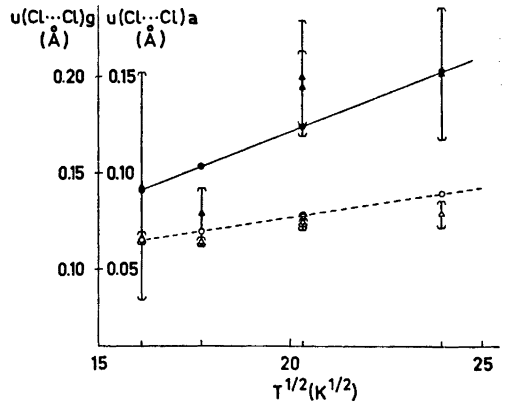

Fig. 3. u(Cl···Cl) as a function of $T^{\frac{1}{2}}$. △: experimental values, ○: calculated values. Open marks in *anti*, closed in *gauche*.

Table 4. Molecular parameters for 1,2-dichloroethane. Distance (r_a) and amplitudes in Å, angles ($\angle\alpha$) in degrees.

Temp. (° C)	−13	40	140	140B	300	[c]
r(C−C)	1.528(6) [a]	1.533(3)	1.533(4)	1.521(8)	1.541(8)	1.531(3)
r(C−Cl)	1.796(3)	1.785(2)	1.786(2)	1.795(3)	1.790(3)	1.790(2)
r(C−H)	1.120(10)	1.128(6)	1.101(6)	1.111(10)	1.100(10)	1.112(5)
∠CCCl	108.9(.3)	108.8(.2)	108.6(.2)	109.5(.4)	109.1(.4)	109.0(.2)
∠CCH	113.0(1.3)	114.5(1.6)	114.0(1.2)	116.0(3.0)	108.4(1.6)	113.2(1.3)
ϕ_g	78.2(4.6)	76.4(1.3)	75.5(2.0)	77.6(3.1)	74.4(3.0)	76.4(.7)
u(C−C)	0.032(10)	0.043(4)	0.053(4)	0.043(9)	0.035(14)	
u(C−Cl)	0.044(3)	0.047(2)	0.050(3)	0.054(3)	0.038(5)	
u(C···Cl)	0.057(4)	0.073(3)	0.080(3)	0.088(5)	0.076(6)	
u(Cl···H)	0.102(14)	0.151(19)	0.115(11)	0.134(25)	0.076(14)	
u(Cl···Cl)a	0.066(5)	0.074(5)	0.074(6)	0.074(6)	0.078(7)	
u(Cl···Cl)g	0.143(59)	0.129(13)	0.194(19)	0.199(30)	0.201(34)	
% *anti*	89.4(4.4)	78.7(3.4)	67.9(3.6)	67.0(5.1)	63.9(5.8)	
% *anti* [b]	87.6(3.1)	77.0(1.7)	67.5(2.2)	65.1(3.4)	64.7(4.3)	
% *gauche*	15.4(4.1)	20.6(2.4)	32.1(3.6)	38.9(5.6)	43.7(6.4)	

[a] The distances are corrected for shrinkage. Standard deviations obtained from the refinement using off diagonal elements in the weight matrix, are given in paranthesis. [b] The % of *anti* and *gauche* are individually refined, the rest of the structural parameters is kept constant. [c] This column gives the average and calculated standard deviations in paranthesis for the geometry parameters.

causing any significant changes in the rest of the refined structure.

Table 4 gives the results obtained from refinements at the different temperatures on average curves. The distances are all R_a-values, the angles correspond to α-values. The standard deviations, given in parenthesis, are those calculated by the least-squares procedure, using non-diagonal elements in the applied weight matrix,[14] and adding 0.1 % R as systematic error.

THERMODYNAMICS

The equilibrium between the two conformers (*anti* ⇌ *gauche*) is described by eqn. (2)

$$K = \frac{n_g}{n_a} = 2\frac{Q_g}{Q_a} e^{-\Delta E^\circ/RT} = e^{-(\Delta E - T\Delta S)/RT} \qquad (2)$$

where n is the percentage of the conformer, Q is the partition function, and ΔE° is the difference in energy between *gauche* and *anti* at the absolute zero point. $\Delta E = \Delta H$ and ΔS are the ordinary thermodynamical quantities for the reaction. The factor 2 is the statistical weight of the *gauche* form.

It is quite common to assume $Q_g = Q_a$, and one aim of this investigation is to test this assumption.

The partition function can be calculated from the moments of inertia, I, and vibrational frequencies, ν, by eqn. (3), as the translational functions are equal in the two forms

$$Q = Q_{rot}Q_{vib} = \frac{1}{\sigma_r h} 8\pi^2 (8\pi^3 I_A I_B I_C)^{\frac{1}{2}} (kT)^{3/2} \times \prod_j [1 - \exp(-h\nu_j/kT)]^{-1} \qquad (3)$$

The torsional frequency is included in the vibrational contribution to Q. σ_r is here the rotational symmetry number, equal to 2 for both conformers.

In the investigation by electron diffraction K is determined as a function of the temperature. Fig. 4 shows how $R \ln (2/K)$ varies with the inverse, absolute temperature, $1/T$.

The straight line fitted to these values by least squares, has an angle coefficient of ΔE° and cuts the $R \ln (2/K)$-axis in $-R \ln (Q_g/Q_a)$. This is true as long as Q_g/Q_a does not vary with the temperature. The fraction $(Q_g/Q_a)_{rot}$ is independant of the temperature, thus Q_g/Q_a is temperature dependant only if $(Q_g/Q_a)_{vib}$ varies with the temperature.

From eqn. (2) and the statistical expression for ΔE and ΔS [eqn. (4)] it is seen that assuming

ΔE and ΔS constant in the reaction interval, implies that Q_g/Q_a is temperature independent, and therefore $\partial/\partial T(\ln\ Q_g/Q_a)=0$. And then $\Delta E=\Delta E^\circ$ and $\Delta S=R\ \ln\ (Q_g/Q_a)+R\ \ln\ 2$. If $\partial/\partial T(\ln\ Q_g/Q_a)$ differs from zero, then assuming $R\ \ln\ (2/K)$ as a linear function of $(1/T)$ implies that the calculated $\ln\ (Q_g/Q_a)$ is the mean value in the actual temperature interval. The calculation of the thermodynamic quantities then requiers a knowledge of $\partial/\partial T(\ln\ Q_g/Q_a)$. Then

$$\Delta E=\Delta E^\circ+RT^2\frac{\partial}{\partial T}(\ln\ Q_g/Q_a)$$

$$\Delta S=R\ \ln\ (Q_g/Q_a)+RT\frac{\partial}{\partial T}(\ln\ Q_g/Q_a)+R\ \ln\ 2 \quad (4)$$

RESULTS AND DISCUSSION

From Table 3 it is seen that the temperature dependency is of major importance in the u-values for the non-bonded distances. This is also confirmed by the refined values in Table 4, though some fluctuations due to experimental errors are seen here. In general, the discrepancies are within one to two standard deviations. But especially $u(C-C)$ from the Balzer plates refines to a much smaller value, probably due to the shorter observation interval (SMAX $\approx$ 30 Å^{-1} contrary to 42 Å^{-1}) and thereby the greater uncertainty introduced in the bond distances. It is also believed that the blackness correction was too small, and therefore generally made the amplitudes too small.

The structural parameters change very little with respect to the temperature (see Table 4). Thus the temperature effect, as demonstrated on the RD-curves (Fig. 2) causes a broadening of the peaks, whereas the positions remain constant.

The structural parameters show quite normal values, and agree very well with earlier investigations by Brunvoll [15] and Karle.[16] The CCH-angles seem to be a bit too large. But the determination of both this angle and $r(C-H)$ is to some extent coupled to the uncertainties in the experimental background.

The torsional angle in *gauche*, ϕ_g, is considerably larger than 60°, which is understood from the relatively strong Cl···Cl-repulsion in this form. Calculations of the van der Waals energy,[13] also including dipol repulsions, gave a minimum at 78°, in excellent agreement with the experimental values.

The agreement between the parameters given in column 140 and 140 B (Table 4), (the latter is the Balzer-recording), shows that there are no camera effects in the structure determination.

As expected, the percentage of the two conformers, *gauche* and *anti*, varies most markedly with the temperature. The presence of the *anti*-form decreases strongly as the temperature increases, in accordance with the increasing population of *gauche*, having higher energy than *anti* but favoured by the statistical weight, equal to 2.

The uncertainties in $R\ \ln\ (2/K)$, marked as vertical lines in Fig. 4, are calculated from the least squares standard deviations, σ, in n. These uncertainties are likely to be too great. By varying the percentage within $\pm\sigma$, the visual change in Cl···Cl-peak is much too great to be acceptable. This implies that the errors in the total structure overestimate the error in the percentage determination.

Also individual refinements at -13 and 300 °C on single plates, and thereby estimation of the means and standard deviations from distribution of the parameters (see Table 5), give much smaller σ's in n, whereas the overall

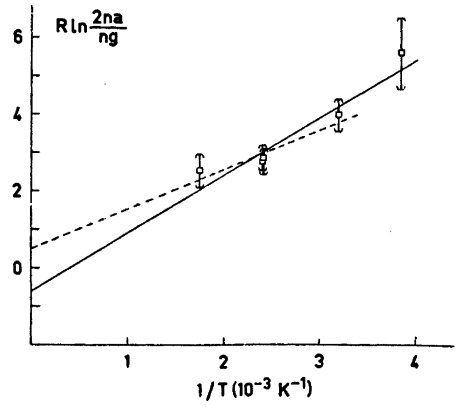

Fig. 4. $R\ \ln\ (2/K) = R\ \ln\ (2n_a/n_g)$ as a function of $1/T$. The standard deviations marked in each point by vertical lines are calculated from those obtained on n_a in the least squares refinement on the total structure. The solid line is calculated from all five observations, the broken line from four observations excluding the point at -13 °C.

Table 5. Average molecular parameters for 1,2-dichloroethane. Distance (r_a) and amplitudes in Å, angles ($\angle_a$) in degrees.

Temp. (° C)	−13	300
r(C−C)	1.528(4)[a]	1.535(2)
r(C−Cl)	1.793(1)	1.789(7)
∠CCCl	109.1(.3)	108.9(.5)
ϕ_g	73.8(3.0)	74.6(.8)
u(C−C)	0.030(6)	0.039−
u(C−Cl)	0.043(2)	0.044(11)
u(C··Cl)	0.056(4)	0.083(6)
u(C··H)	0.210(45)	0.110(10)
u(Cl··H)	0.116(14)	0.089(13)
u(Cl··Cl)a	0.064(3)	0.085(13)
u(Cl··Cl)g		0.196(1)
% *anti*	89.6(2.5)	62.7(.7)

[a] Standard deviations calculated from the individual differences from the mean $\sigma_{\bar{p}}^2 = \sum_n (p-\bar{p})^2/n(n-1)]$ are given in parenthesis. The mean is calculated from 5, respectively 4, individual refinements.

agreement between the structural parameters and standard deviations is very good.

The two bottom rows of Table 4 give the percentage with standard deviations, individually refined, when the rest of the structure is kept constant. Still the σ's are greater than obtained from refinement on individual plates.

The accuracy in the nozzle temperature is at least better than 3 °C. If this temperature reflects the gas temperature, this is sufficiently accurate to assume that the uncertainty due to errors in the temperature can be neglected in the thermodynamic calculations. The overall agreement between the investigations by the Oslo- and the Balzer-apparatus also verifies the this.

The gas is definitely cooled when it comes into vacuum, but this temperature fall in the gas jet is assumed to be only in the translational energy. This is supported by earlier investigations where electron diffraction data agree very well with other experiments,[17] and the reproducibility of the results from the two Oslo-apparatus, as well as the reproducibility reported by Bastiansen/Hedberg.[2] A recent paper by Bauer [18] seems to indicate a temperature fall of as much as 50 °C.

Table 6 shows the calculated values for ΔE and ΔS, assuming the $\partial/\partial T(\ln Q_g/Q_a)$ is negligible, calculated by least squares using all 5 observation points in column A, and only the 4 highest temperature points in column B. If the calculated frequency in *gauche*, 117 cm^{-1}, is correct, the torsional frequency in *anti* is calculated from comparing the theoretical expression for the partition function [eqn. (3)] and the $R \ln (Q_g/Q_a)$ quantity from the least-squares fit.

Fig. 4 gives the five corresponding ($R \ln (2/K)$, $1/T$) values as well as the two least-squares fitted straight lines, the solid line fitted to all five points, the broken excluding the $t = -13$ °C observation. The figure reveals that the observation at $t = -13$°C ($1/T = 3.846 \times 10^{-3}$ K^{-1}) is off the line about which the other observations are grouped. I believe this is due to some condensing phenomena in the nozzle, favouring the *anti* conformer, since the external bath temperature and the nozzle temperature here ary very close to each other. To check this

Table 6. Thermodynamical differences between *gauche* and *anti*, and the torsional frequencies of the two conformers.

	a	*b*	*c*	*d*
ΔE (kcal/mol)	1.5(0.2)[e]	1.0(0.2)		0.89 − 1.27 [15,16,19,20]
ΔS (cal/K mol)	2.0(0.5)	0.8(0.5)	1.4[f]	∼1.4 [21]
ν_g (cm^{-1})	117	117	117[g]	125 [12]
ν_a (cm^{-1})	198(84)	96(28)	125[g]	123 [12]

[a] Least-squares result from electron diffraction data, also including the observation at −13 °C. [b] Least-squares result from electron diffraction data, excluding the observation at −13 °C. [c] Calculated values from normal coordinates and frequencies. [d] Earlier observations. [e] Standard deviations are given in parenthesis. [f] The average in the observation interval ($\Delta S = R \ln 2 + R \ln (Q_g/Q_a)$ [g] The calculated torsional frequensies, $f_{t,g} = 0.253$ mdyn Å rad^{-2} and $f_{t,a} = 0.174$ mdyn Å rad^{-2}.

a new experiment with a slightly higher nozzle temperature is performed.

The normal coordinate calculations have given values for the partition functions and their temperature derivatives, and it shows that the temperature dependency is much too small to explain the apparent non-linearity ($\partial/\partial T(\ln Q_g/Q_a) = 0.36 \times 10^{-3}$).

The apparent non-linearity could be a result of the above mentioned drop in the vibrational temperature.[18] If this is assumed to be constant, and approximately 50 C°, the shift in the $1/T$-scale will be greatest for the lowest temperature point, and thereby making the points closer to a straight line. This shift in the $1/T$-scale, however, will cause very little change in the value of the determined quantities, compared to the calculated standard deviations.

The value $\Delta E° = 1.0$ kcal/mol agrees very well with earlier estimates, while the value calculated from all five observations seems to be too high. But compared with the calculated van der Waals energy difference, $\Delta E_{vdW} = 1.4$ kcal/mol, and adding the difference in zero point energy between the two conformers, 0.23 kcal/mol [calculated in the force field program, $\Delta E° = \Delta E_{vdW} + \frac{1}{2}h\sum_k(\nu_{k,g} - \nu_{k,a})$], the agreement is better with the result in column A.

From this investigation it is quite clear that the partition functions in the two conformers are very similar, and therefore ΔS is very close to R ln 2. Also the assumed temperature invariance of ΔE and ΔS is established within the experimental error limits. Within the calculated standard deviations it is not possible to tell whether ΔS should be smaller or greater than R ln 2. But if the torsional frequency should be smaller in *gauche*, $\nu_g < \nu_a$, there seems to be a discrepancy between the calculated entropy difference from the partition functions (C) and the value estimated from the four best electron diffraction points (B), the latter revealing an entropy smaller than R ln 2 in *gauche*, and therefore $\nu_g > \nu_a$.

Conclusion. This structure determination of 1,2-dichloroethane at different temperatures, has shown that such a temperature study of conformational equilibria by electron diffraction is a suitable tool to estimate energy and entropy values with reasonable certainty.

From the estimated entropy value and the observed frequencies the ratio between the torsional frequencies of the conformers can be determined.

Acknowledgement. I like to express my gratitude to Prof. O. Bastiansen for his support and interest in this project. Also cand. real. R. Stølevik should be thanked for many helpful discussions, as well as Mr. A. Almenningen, Mr. K. Brendhaugen and Siv.ing. R. Seip for recording the diffraction photograps.

REFERENCES

1. Bastiansen, O., Seip, H. M. and Boggs, J. E. In Dunitz, J. D. and Ibers, J. A., Eds., *Conformational Equilibria in the Gas Phase, Perspectives in Structural Chem.*, Wiley, London 1971, Vol. 4, p. 60.
2. Almenningen, A., Bastiansen, O., Fernholt, L. and Hedberg, K. *Acta Chem. Scand. 25* (1971) 1946.
3. Bastiansen, O., Hassel, O. and Risberg, E. *Acta Chem. Scand. 9* (1955) 232.
4. Andersen, B., Seip, H. M., Strand, T. G. and Stølevik, R. *Acta Chem. Scand. 23* (1969) 3224.
5. Peacher, J. and Wills, J. C. *J. Chem. Phys. 46* (1967) 4809.
6. Strand, T. G. and Bonham, R. A. *J. Chem. Phys. 40* (1964) 1686.
7. Gwinn, W. D. *J. Chem. Phys. 55* (1971) 477.
8. Stølevik, R., Seip, H. M. and Cyvin, S. J. *Chem. Phys. Lett. 15* (1972) 263.
9. Schachtschneider, J. H. and Snyder, R. G. *Vibrational Analysis of Polyatomic Molecules IV*, Shell Dev. Company, Tech. Report No. 122–63.
10. Mitchuschima, S. *Structures of Molecules and Internal Rotation*, Academic, New York 1954.
11. Allen, G., Brier, P. N. and Lane, G. *Trans. Faraday Soc. 63* (1967) 824.
12. Shimanouchi, T. *Tables of Molecular Vibrational Frequencies*, Part 1, NSRDS-NBS *6* (1967) 33.
13. Scott, R. A. and Scheraga, H. A. *J. Chem. Phys. 42* (1965) 2209; *44* (1966) 3054.
14. Seip, H. M., Strand, T. G. and Stølevik, R. *Chem. Phys. Lett. 3* (1969) 617.
15. a. Brunvoll, J. *Licenciate-work*, Norwegian Technical College, Trondheim 1962; b. Almenningen, A., Bastiansen, O., Haaland, A. and Seip, H. M. *Angew. Chem. Int. Ed. Engl. 4* (1965) 819.
16. Ainsworth, J. and Karle, J. *J. Chem. Phys. 20* (1952) 425.
17. Hedberg, K. *Ethylene Chlorohydrin. To be published*, and *private communication* on NO_2/N_2O_4.
18. Bauer, S. H. *To be published.*
19. Wyn-Jones, E. and Pethrick, R. A. *Topics in Stereochemistry 5* (1970) 205.
20. Tanabe, K. *Spectrochim. Acta 28 A* (1972) 407.
21. Lowe, J. P. *Progr. Phys. Org. Chem. 6* (1968) 1.

Received February 4, 1974.

Acta Chemica Scandinavica A 28 (1974) 491—498

Infrared Intensity and ESCA Studies on the Polarity of the Nitrosyl Ligand in Some Transition Metal Pentacyanonitrosyl Complexes

BÖRJE FOLKESSON

Inorganic Chemistry 1, Chemical Center, Universty of Lund, Box 740, S-220 07 Lund, 7, Sweden

The infrared absorption intensity of the N—O stretching vibration has been measured for the complexes $Na_2[Fe(CN)_5NO].2H_2O$, $Zn[Mn(CN)_5NO].H_2O$, $K_3[Mn(CN)_5NO].2H_2O$, $K_3[Cr(CN)_5NO].H_2O$, and $K_4[Mo(CN)_5NO]$ in aqueous solution. It was found that the intensity (A_{NO}) increases with decreasing frequency (ν_{NO}), which is in agreement with a model of $d\pi-p\pi^*$ back donation. Thus, it was concluded that the degree of backbonding in the nitrosyl complexes increases in the order Fe(II) < Mn(II) < Mn(I) < Cr(I) < Mo(0).

Nitrogen 1*s* and oxygen 1*s* photoelectron spectra were recorded on the above mentioned nitrosyl complexes and also on $K_3[V(CN)_5NO].2H_2O$. It was found that both the nitrogen 1*s* and oxygen 1*s* electron binding energies for the nitrosyl group decrease with decreasing N—O stretching frequency in the complexes. Thus, when the degree of backbonding in the nitrosyl complexes increases, the effective charge on the nitrogen and oxygen atoms becomes more and more negative. It was found that the total charge on the nitrosyl group in the iron complex is positive (+0.35 a.u.), while the total charge on the nitrosyl group in the other complexes is negative. Most negative is the nitrosyl group in the vanadium complex (−0.41 a.u.).

From the dipole moment derivative, $d\mu/dr$, and the effective charges on the oxygen atoms, it was possible to get a value of the variation of charge with interatomic distance $d|q|/dr$. An estimation of $d|q|/dr$ was also made from experimentally determined charges on the oxygen atoms and experimentally determined interatomic distances. It was found that both the calculation procedures gave the same value of $d|q|/dr$, *viz.* 0.6 a.u. This value agrees with the $d|q|/dr$-value earlier found for the N—N bond in dinitrogen complexes.

The bonding and electronic structures of transition metal nitrosyls have been frequently studied in recent years.[1] A comprehensive study of the infrared spectra of metal nitrosyl complexes has been made by Lewis and Wilkinson and their coworkers.[2,3] They demonstrated that NO complexes absorb in the range from 1045 cm^{-1} to about 1980 cm^{-1}. Complexes which show NO absorption in the range 1200—1980 cm^{-1} have been regarded as NO^+ complexes, whereas NO compounds absorbing in the range 1045—1195 cm^{-1} probably should be formulated as hyponitrito compounds.[1] In the present work a series of pentacyanonitrosyl complexes, in which the N—O stretching frequency varies in the range 1500—2000 cm^{-1}, has been studied by IR and ESCA to get more detailed information about the charge distribution on the nitrosyl ligand. It is well known that the infrared intensity of a stretching vibration is related to the dipole moment derivative ($d\mu/dQ$). This quantity has earlier [4,5] been found to give approximate information about charge distribution within coordination compounds. By means of ESCA [6] effective charges on atoms can be determined. From the combination of these two kinds of measurements the variation of charge with interatomic distance ($d|q|/dr$) can also be determined, as has been done earlier [5] on dinitrogen complexes.

ESCA measurements on two pentacyanonitrosyl complexes, *viz.* $Na_2[Fe(CN)_5NO].2H_2O$ and $K_3[Cr(CN)_5NO].H_2O$, have been performed earlier [7,8] to attempt correlations of nitrogen 1*s* binding energy with the character of the NO-group. It was found [7,8] that the N1*s* binding energy of the NO-group is higher in the iron complex than in the chromium complex. This means that the NO-group is more positive in the

iron complex that in the chromium complex. The N – O stretching frequency is higher in the iron complex than in the chromium complex, which indicates that the degree of $d\pi - p\pi^*$ back donation of electrons from metal to NO-group increases from iron to chromium.

This investigation was started to further substantiate these observations on some more complexes of similar type and also to determine the charge on the oxygen atoms in the nitrosyl group.

EXPERIMENTAL

Preparation of nitrosyl complexes

$Na_2[Fe(CN)_5NO].2H_2O$, which was commercially obtained, was of analytical grade.

$K_3[Mn(CN)_5NO].2H_2O$ was prepared according to the procedure given by Cotton *et al.*[9] from $K_3[Mn(CN)_6]$ and hydroxylamine in potassium cyanide solution. The salt first obtained, $Mn_3[Mn(CN)_5NO]_2$, was converted to the potassium salt by the reaction with K_2CO_3. After repeated recrystallizations the compound was found pure. (Found: C 16.1; H 1.92; N 22.6. Calc. C 16.3; H 1.09; N 22.8).

$Zn[Mn(CN)_5NO].H_2O$ was prepared by oxidation [9] of $[Mn(CN)_5NO]^{3-}$ with nitric acid and precipitation of the salt with Zn^{2+}. The purity of the salt was checked by elemental analysis. It was found that the analysis values corresponded to a water content of the salt of 1 mol H_2O. (Found: C 21.0; H 1.18; N 28.5. Calc. C 20.1; H 0.67; N 28.2).

$K_3[Cr(CN)_5NO].H_2O$ was prepared according to Griffith *et al.*[10] (Found: C 18.3; H 0.51; N 25.2. Calc. C 17.3; H 0.58; N 24.2.)

$K_4[Mo(CN)_5NO]$ was prepared by Nast's method.[11] This purple pentacyanonitrosyl complex has been formulated in various ways, *viz.* as a complex of molybdenum(0), $K_4[Mo(CN)_5NO]$, either with [11] or without [12] water of hydration and as an eight-coordinated complex of molybdenum(II), $K_4[Mo(CN)_5(OH)_2NO]$.[10] In the work of Riley and Ho [12] it is pointed out that the complex partially decomposes in air and that this fact could be the reason for the earlier formulation [10-11] of the complex with water of hydration or as a hydroxy complex of molybdenum(II). Also an X-ray crystallographic investigation of the molybdenum complex by Svedung *et al.*[13] has shown that the complex should be formulated as $K_4[Mo(CN)_5NO]$. The infrared spectrum of the compound used in the present investigation showed absorption in the 3300 – 3600 cm^{-1} and 1600 cm^{-1} regions, which indicates the presence of water in the compound. The elemental analysis values are also in agreement with the formula $K_3[Mo(CN)_5NO].2H_2O$. (Found: C 13.0; H 0.69; N 18.1. Calc. C 13.4; H 0.89; N 18.7). It is therefore reasonable to conclude that the compound investigated here is the partially hydrolysed pentacyanonitrosyl complex and consequently the formula with water of hydration has been used in the calculations of concentrations necessary for the infrared intensity calculations.

$K_3[V(CN)_5NO].2H_2O$ was prepared according to the method of Griffith *et al.*[14] from ammonium vanadate and hydroxylamine in alkaline potassium cyanide solution. The compound could, however, not be obtained analytically pure in spite of several rescrystallizations. Consequently, the infrared intensity measurements have been omitted for this compound (*cf.* Table 1).

Experimental techniques

The infrared spectra were recorded with a Perkin Elmer Spectrophotometer Model 521 equipped with a linear absorbance potentiometer. All spectra on the N – O stretching vibration were recorded with a wavenumber scale expansion, so that 1 cm on the chart corre-

Table 1. The results of the infrared intensity measurements on the nitrosyl complexes.

Nitrosyl complex	Dispersion medium	ν_{NO} cm^{-1}	ε $M^{-1}\,cm^{-1}$	$A_{NO} \times 10^{-4}$ $M^{-1}\,cm^{-2}$
○ $Na_2[Fe(CN)_5NO].2H_2O$	H_2O	1936	1750 ± 75	7.3 ± 0.3
● $Zn[Mn(CN)_5NO].H_2O$	KBr	1890	425 ± 40	6.3 ± 0.6
		1800	280 ± 30	
	H_2O	1880		8.2[a]
□ $K_3[Mn(CN)_5NO].2H_2O$	KBr	1730	310 ± 30	6.0 ± 0.6
	D_2O	1766	1450 ± 50	8.0 ± 0.4
■ $K_3[Cr(CN)_5NO].H_2O$	D_2O	1682	950 ± 50	8.4 ± 0.4
▽ $K_4[Mo(CN)_5NO]$	D_2O	1622	500 ± 50	8.7 ± 0.8
▼ $K_3[V(CN)_5NO].2H_2O$	D_2O	1545		

[a] *Cf.* the text.

sponded to 12.5 cm^{-1}. The measurements on the nitrosyl complexes were performed in aqueous solution but deuterium oxide was used when the N – O absorption coincided with the water absorption. Calibrated cells with CaF_2-windows and 25 μ platinum spacers were used. Some of the complexes (*cf.* Table 1) were examined in the solid state (KBr). For further details about the intensity measurements the reader is referred to Ref. 5.

The ESCA spectra were measured with an AEI ES 100 photoelectron spectrometer. All spectra were obtained with AlKα-radiation (1486.6 eV). The electron binding energy E_b was obtained from the following expression:[15]

$$E_b = 1477.1 - E_{kin}$$

where E_{kin} is the measured kinetic energy of the electrons. The samples were mechanically spread out as a thin film on a platinum foil. Through this sample preparation technique no surface charging effects were obtained during the measurements. As before,[15] the Pt $4f_{7/2}$ electron peak was used as reference peak.

RESULTS AND DISCUSSION

The results of the intensity measurements on the nitrosyl complexes are given in Table 1. The complex $Zn[Mn(CN)_5NO].H_2O$ was not soluble in water and therefore only measured in the solid state. It was found that the infrared spectrum of the compound in the solid state gave two bands assigned to the N – O stretching vibration. This situation has also been pointed out by Cotton *et al.*[9] The intensity of the two bands was measured and the total intensity given. It has earlier [4,16] been found that measurements of the same species in solution and in KBr immersion showed that the intensity was larger in the former by a factor of about 1.3. The intensity value for the zinc salt in solution has been estimated in accordance with these observations.[4,16] The compound $K_3[Mn(CN)_5NO].2H_2O$ has also been measured in KBr immersion and the intensity value was smaller than that in solution by a factor of 1.3. The molar absorption coefficients (ε M^{-1} cm^{-1}) at band maximum are included in Table 1. It can be seen that the ε-values decrease within the series of complexes. The NO-absorption bands became, however, broader and the intensity was found to increase within the series. It can be seen from Table 1 that the intensity increases when ν_{NO} decreases. In accordance with the reasoning in the previous studies [4,5] on dinitrogen complexes, a large infrared intensity means a greater degree of $d\pi - p\pi^*$ back donation of electrons from metal *d*-orbitals to antibonding π-orbitals of the ligand. The largest infrared intensity of the N – O stretching vibration has been found for the molybdenum compound. Thus, the degree of metal-ligand π-bonding should be greatest for this compound within the series of nitrosyl complexes. As mentioned above, the infrared intensity of the N – O stretching vibration in $K_3[V(CN)_5NO].2H_2O$ could not be determined. The N – O stretching frequency in this compound was, however, determined and was found to be lower than in the other investigated nitrosyl complexes. Consequently, the degree of back donation of electrons should be pronounced in this complex as well. This fact has been confirmed through the ESCA measurements, which give evidence of a large negative charge on the NO-group (*cf.* Table 3).

N1*s* and O1*s* photoelectron spectra were recorded on all the compounds. A representative example of a N1*s* electron spectrum for a pentacyanonitrosyl complex is given in Fig. 1. Two peaks show that the complex contains different nitrogen atoms. The O1*s* electron spectrum of the same complex is shown in Fig. 2. Besides the oxygen peak from the oxygen in the nitrosyl group there is also a broad peak with maximum

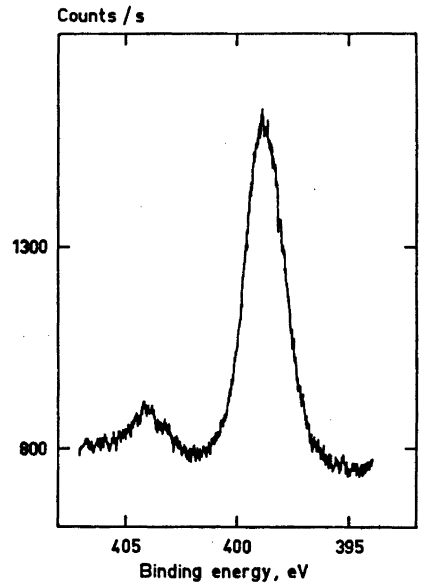

Fig. 1. Nitrogen 1*s* electron spectrum of $Na_2[Fe(CN)_5NO].2H_2O$.

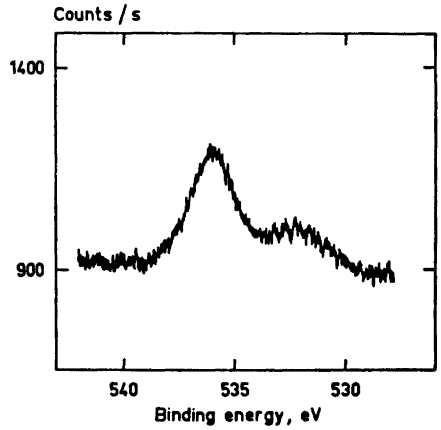

Fig. 2. Oxygen 1*s* electron spectrum of $Na_2[Fe(CN)_5NO].2H_2O$.

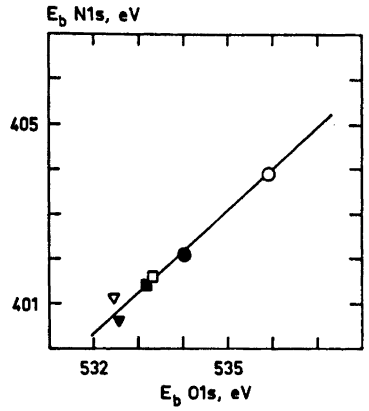

Fig. 3. The nitrogen 1*s* electron binding energy (E_bN1s) as a function of the oxygen 1*s* electron binding energy (E_bO1s) for the nitrosyl group in the various nitrosyl complexes. The same symbols as in Table 2 are used.

at a binding energy of about 532.5 eV. This broad peak probably can be assigned to adsorbed oxygen, as an oxygen peak at a binding energy of about 532 eV is always obtained in our ESCA measurements [17] with our present vacuum ($\geq 10^{-7}$ torr). The measured N1*s* and O1*s* electron binding energies for the nitrosyl complexes are collected in Table 2. It can be seen that the N1*s* electron binding energy for the NO-group is greatest for the iron complex and smallest for the vanadium complex. The corresponding trend has been found for the O1*s* electron binding energy. In Fig. 3 the N1*s* electron binding energy is plotted against the O1*s* electron binding energy. A straight line with a slope of 1 is found, which shows that the change in the binding energy for the N1*s* and O1*s* electrons is the same from one complex to another. It must be pointed out that because of the oxygen peak from adsorbed oxygen the exact determination of the O1*s* electron binding energy for the nitrosyl oxygen in the molybdenum and vanadium complex is somewhat uncertain. Consequently, the error in the O1*s* electron binding energy is greater for these two complexes than for the other four complexes, in which the oxygen peak is well separated from the peak due to adsorbed oxygen. It is obvious from Table 2 that the N1*s* electron binding energy decreases with decreasing ν_{NO} (and increasing infrared intensity). Thus, when the degree of $d\pi - p\pi^*$ back donation of electrons from the metal to the NO-ligand increases (as is indicated by the decrease in ν_{NO}), the charge on the nitrogen atom becomes more and more negative. The same conclusion can be drawn about the charge on the oxygen atom in the NO-ligand.

Table 2. Nitrogen 1*s* and oxygen 1*s* electron binding energies in the various pentacyanonitrosyl complexes. All binding energy values are referred to a binding energy for Pt $4f_{7/2}$ electrons of 71.1 eV.

Nitrosyl complex	E_bN1s(CN) eV	E_bN1s(NO) eV	E_bO1s eV	ν_{NO} cm^{-1}
○ $Na_2[Fe(CN)_5NO].2H_2O$	398.7	403.9	535.9	1936
● $Zn[Mn(CN)_5NO].H_2O$	398.3	402.1	534.0	1880
□ $K_2[Mn(CN)_5NO].2H_2O$	398.3	401.6	533.3	1766
■ $K_2[Cr(CN)_5NO].H_2O$	399.0	401.4	533.2	1682
▽ $K_4[Mo(CN)_5NO]$	398.8	401.1	532.5	1622
▼ $K_2[V(CN)_5NO].2H_2O$	398.8	400.6	532.6	1545

While the N1*s* electron binding energy for the NO-ligand varies from one complex to another the N1*s* electron binding energy for the cyanide ligand is practically constant within the series of pentacyanonitrosyl complexes, as can be seen from Table 2. This means that the degree of π-bonding within the M–C–N group is changed very little compared to the more pronounced change in the degree of π-bonding within the M–N–O group. Such a conclusion can also be drawn from the variations in the C–N stretching frequency and the N–O stretching frequency (*cf.*, *e.g.*, Ref. 1).

The charge on the nitrogen atom in the NO-group in the various nitrosyl complexes has been estimated with the aid of the correlation between N1*s* binding energy and calculated charge, which has been determined earlier (Fig. 5 in Ref. 15). The result is given in Table 3. It can be seen that the nitrogen atom in the NO-group in the iron complex has a positive charge, while the nitrogen atom in the NO-group in the other complexes is negatively charged. It is more difficult to obtain the charge on the oxygen atom, since surprisingly few ESCA data and charge calculations on oxygen compounds exist. However, it seems clear from the figures given by Siegbahn *et al.*[18] that a crude correlation between O1*s* binding energy and calculated charge (q_o), disregarding the potential fields from neighbouring atoms, should result in a slope (dE_b/dq_o) of about 12 eV/a.u. In a recent paper by Larsson *et al.*[19] oxygen atom charges have been estimated for two values of O1*s* electron binding energy from a combination of IR data with ESCA data on some oxinato complexes. The values reported [19] are $q_o = -0.37$ a.u. corresponding to an O1*s* electron binding energy of 530.0 eV and $q_o = -0.27$ a.u. corresponding to 531.5 eV. From ESCA measurements on vanadium compounds [20] the charge on the vanadium atom in V_2O_5 has been estimated to +1.01 a.u. The charge on the oxygen atom can thus easily be calculated to −0.40 a.u. This value corresponds to an O1*s* electron binding energy [20] of 529.6 eV. Furthermore, from ESCA measurements on solid carbon suboxide [21] one can get an oxygen atom charge of −0.28 a.u. corresponding to an O1*s* electron binding energy of 531 eV, if the binding energy is referred to a C1*s* electron binding energy of 285 eV. From the above mentioned corresponding values of O1*s* electron binding energy and oxygen atom charge a correlation has been constructed. This is presented in Fig. 4. The slope of the straight line is about 11.5 eV/a.u., which is in accordance with the crude correlation found by Siegbahn *et al.*[18] From Fig. 4 and the measured O1*s* electron binding energies the charge on the oxygen atom in the NO-group in the nitrosyl complexes has been determined. It can be seen from Table 3 that the oxygen atom charge in the iron complex is positive, while the charge on the oxygen atom in the other nitrosyl complexes is negative.

The total charge on the NO-group has thus been found to be positive (+0.35 a.u.) in the iron complex, while in the other complexes the total charge on the NO-group is negative. The negative charge on the NO-group increases throughout the series of complexes. Thus, in the vanadium complex the charge on the NO-group is −0.41 a.u. There is, consequently, an increase of the electron density over the NO-ligand caused by $d\pi - p\pi^*$ back donation of electrons from metal *d*-orbitals to antibonding π-orbitals of NO. This result confirms and strengthens the result from the infrared intensity measurements.

Table 3. Experimentally obtained charges on the nitrogen and oxygen atoms in the nitrosyl group together with calculated values of $|d\mu/dr|$ and $d|q|/dr$ for the various nitrosyl complexes.

Nitrosyl complex	q_N a.u.	q_O a.u.	$\lvert d\mu/dr\rvert$ a.u.	r_{M-O} Å	$d\lvert q\rvert/dr$ a.u.
○ $Na_2[Fe(CN)_5NO]2H_2O$	+0.22	+0.13	3.35	2.76 [23]	0.58
● $Zn[Mn(CN)_5NO]H_2O$	−0.04	−0.03			
□ $K_3[Mn(CN)_5NO]2H_2O$	−0.11	−0.09	3.50	2.87 [24]	0.59
■ $K_3[Cr(CN)_5NO]H_2O$	−0.14	−0.10	3.58	3.01 [25]	0.58
▽ $K_4[Mo(CN)_5NO]$	−0.18	−0.16	3.69	3.18 [13]	0.56
▼ $K_3[V(CN)_5NO]2H_2O$	−0.26	−0.15		2.95 [26]	

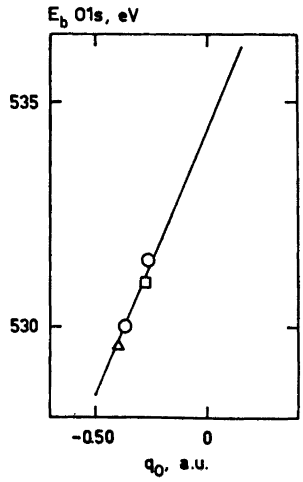

Fig. 4. Plot of oxygen 1*s* electron binding energies (E_bO1*s*) against calculated charge on oxygen atoms. (O) Ref. 19; (△) V_2O_5 Ref. 20; (□) C_3O_3(s) Ref. 21.

From the measured infrared intensities of the N – O stretching vibration it is possible to get approximate information about the polarity of the N – O bond. In this case the fixed charge model has been applied. The complexes are considered as two-atomic molecules, *viz.* consisting of, *e.g.*, $Fe(CN)_5$ N and O. For a two-atomic molecule, the absorption intensity is related to the dipole moment of the molecule by the formula [22]

$$A = \frac{\pi N}{3c^2 \times 10^3 \times \mu_{red}} \left(\frac{d\mu}{dr}\right)^2 \quad (1)$$

Here N and c stand for the Avogadro number and the velocity of light. μ_{red} is the reduced mass and has in the present case been calculated from the above mentioned molecular fragments. μ is the dipole moment and r the interatomic distance. If it is assumed that the charges on the molecular fragments are $+q$ and $-q$ (atomic units), the dipole moment is

$$\mu = r|q| \quad (2)$$

If, as stated in the fixed charge model, it is assumed that q does not change with r, it follows that

$$|d\mu/dr| = |q| \quad (3)$$

If, on the other hand, there is a variation of charge with interatomic distance, a term relating to this, *viz.* $d|q|/dr$, is easily derived from eqn. (2), *i.e.*

$$\left|\frac{d\mu}{dr}\right| = |q| + r\frac{d|q|}{dr} \quad (4)$$

Calculated values of $|d\mu/dr|$ from eqn. (1) are given in Table 3. Calculations have been performed only for those complexes for which it has been possible to measure the infrared intensity of the N – O stretching vibration in aqueous solution. The $|d\mu/dr|$-values are relatively high, so it is reasonable to suppose that the charge varies with the interatomic distance. As the charge on the oxygen atom is determined with ESCA (Table 3) and interatomic distances are known from X-ray crystallographic measurements,[13,23–26] $d|q|/dr$ can be determined from eqn. (4). In the calculation of $d|q|/dr$ the M – O (M – N + N – O) distance has been used and not the N – O distance, since r in eqn. (4) means the distance between two charge centers and it is quite reasonable that the charge center on the big molecular fragment is placed closer to the metal atom than to the nitrogen atom. The M – O distances from the literature [13,23–26] are included in Table 3. The calculated values of $d|q|/dr$ are given in Table 3. It can be seen that $d|q|/dr$ has about the same value for all the nitrosyl complexes. Thus, as $|q_O|$ is small and practically constant, the change in $|d\mu/dr|$, which one observes, depends on the change in the interatomic distance (r_{M-O}).

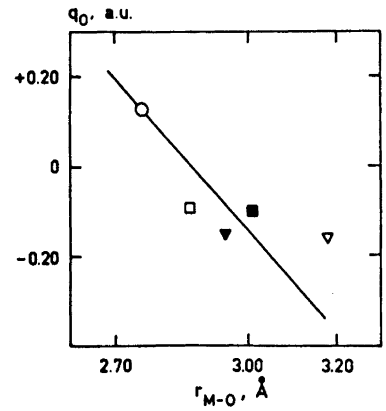

Fig. 5. The charge on the oxygen atom (q_O) in the various nitrosyl complexes plotted against experimentally determined M – O distances. The same symbols as in Table 3 are used.

A more direct way to obtain a value of the charge parameter $d|q|/dr$ is from experimentally determined charges on the oxygen atoms and experimentally determined interatomic distances.[13,23-26] In Fig. 5 the charge on the oxygen atom (q_O) has been plotted against the M–O distance. From the slope of the straight line $d|q|/dr$ has been estimated to 0.6 ± 0.2 a.u., a value in good agreement with the $d|q|/dr$-values calculated from infrared intensity data (*cf.* Table 3).

CONCLUDING REMARKS

The results of the present investigation and the previous studies [5,15] on dinitrogen complexes show that it is possible to get more detailed information from ESCA data about the charge distribution on the M–X≡Y group than from infrared intensity measurements. Through the combination of infrared intensity data with experimentally determined charges on atoms, it has been possible to determine the variation of charge with interatomic distance ($d|q|/dr$). This quantity gives increased characterisation of the electronic structure of a molecule by indicating the degree of mobility of charges over the bond in question. The calculated value of $d|q|/dr$ for the nitrosyl complexes is about the same as the $d|q|/dr$-value earlier found [5] for the N–N bond in the dinitrogen complexes of rhenium and iridium. Consequently, a $d|q|/dr$-value of about 0.6 a.u. may be characteristic for the bond type that exists in the M–X≡Y group.

A further similarity between nitrosyl complexes and dinitrogen complexes is found if one regards the charge distribution on the dinitrogen ligand and the nitrosyl ligand. In the previous work [5] it was found that the inner nitrogen atom in the group M–N–N was the most negative one. In the present investigation it has been found that the nitrogen atom in the nitrosyl group is more negative than the oxygen atom (*cf.* Table 3). This is valid for all the complexes except for the iron complex, in which the nitrogen atom is more positive than the oxygen atom. This means that the degree of π-bonding in the iron complex is very small compared to the degree of π-bonding in the other complexes.

On the basis of the similarities which have been found between dinitrogen complexes and nitrosyl complexes when considering the charge distribution and the charge parameter $d|q|/dr$, it could be of interest also to investigate carbonyl complexes. Carbonyl complexes are isoelectronic with corresponding dinitrogen complexes and are consequently suitable to investigate in this connection. Probably, it can be expected that they will give results which are well comparable with those found for dinitrogen complexes and nitrosyl complexes.

When this manuscript was close to completion it was learned that an ESCA investigation on almost the same nitrosyl complexes had been performed at the University of Gothenburg (Dr. N.-G. Vannerberg). It must be emphasized that these two investigations have been carried out completely independently. The ESCA spectra obtained in both these investigations were essentially identical.

The financial support for this work from the Swedish Board for Technical Development and the Bank of Sweden Tercentenary Fund is gratefully acknowledged. The author wishes to thank Dr. R. Larsson for his kind interest and valuable discussions. The author is also indebted to Mrs. Karin Trankéll for her assistance in the infrared spectroscopic measurements.

REFERENCES

1. Johnson, B. F. G. and McCleverty, J. H. *Progr. Inorg. Chem. 7* (1966) 277.
2. Lewis, J., Irving, R. J. and Wilkinson, G. *J. Inorg. Nucl. Chem. 7* (1958) 32.
3. Griffith, W. P., Lewis, J. and Wilkinson, G. *J. Inorg. Nucl. Chem. 7* (1958) 38.
4. Folkesson, B. *Acta Chem. Scand. 26* (1972) 4008.
5. Folkesson, B. *Acta Chem. Scand. 27* (1973) 276.
6. Siegbahn, K., Nordling, C., Fahlman, A., Nordberg, R., Hamrin, K., Hedman, J., Johansson, G., Bergmark, T., Karlsson, S.-E., Lindgren, I. and Lindberg, B. *ESCA-Atomic, Molecular and Solid State Structure Studied by Means of Electron Spectroscopy*, Almqvist & Wiksell, Uppsala 1967.
7. Hendrickson, D. N., Hollander, J. M. and Jolly, W. L. *Inorg. Chem. 8* (1969) 2642.
8. Finn, P. and Jolly, W. L. *Inorg. Chem. 11* (1972) 893.
9. Cotton, F. A., Monchamp, R. R., Henry, R. J. M. and Young, R. C. *J. Inorg. Nucl. Chem. 10* (1959) 28.
10. Griffith, W. P., Lewis, J. and Wilkinson, G. *J. Chem. Soc. A* (1959) 872.
11. Hieber, W., Nast, R. and Gehring, G. *Z. Anorg. Chem. 256* (1948) 169.

12. Riley, R. F. and Ho, L. *J. Inorg. Nucl. Chem. 24* (1962) 1121.
13. Svedung, D. H. and Vannerberg, N.-G. *Acta Chem. Scand. 22* (1968) 1551.
14. Griffith, W. P., Lewis, J. and Wilkinson, G. *J. Chem. Soc. A* (1959) 1632.
15. Folkesson, B. *Acta Chem. Scand. 27* (1973) 287.
16. Larsson, R. and Miezis, A. *Acta Chem. Scand. 23* (1969) 37.
17. Schön, G. and Lundin, S. T. *J. Electron Spectrosc. 1* (1972/73) 105.
18. Siegbahn, K., Nordling, C., Johansson, G., Hedman, J., Hedén, P. F., Hamrin, K., Gelius, U., Bergmark, T., Werme, L. O., Manne, R. and Baer, Y. *ESCA Applied to Free Molecules*, North Holland, Amsterdam 1969.
19. Larsson, R. and Larsson, L. *Chem. Scr. 5* (1974) 195.
20. Larsson, R., Folkesson, B. and Schön, G. *Chem. Scr. 3* (1973) 88.
21. Gelius, U., Allan, C. J., Allison, D. A., Siegbahn, H. and Siegbahn, K. *Chem. Phys. Lett. 11* (1971) 224.
22. Barrow, G. M. *Introduction to Molecular Spectroscopy*, McGraw, New York 1962.
23. Manoharan, P. T. and Hamilton, W. C. *Inorg. Chem. 2* (1963) 1043.
24. Tullberg, A. and Vannerberg, N.-G. *Acta Chem. Scand. 21* (1967) 1462.
25. Vannerberg, N.-G. *Acta Chem. Scand. 20* (1966) 1571.
26. Jagner, S. and Vannerberg, N.-G. *Acta Chem. Scand. 24* (1970) 1988.

Received January 23, 1974.

Acta Chemica Scandinavica A 28 (1974) 499—506

Structures of Linear Multisulphur Systems. VI. The Crystal and Molecular Structure of 2-*p*-Methoxyphenyl-4,5-[1-(1,3-dithiolane-2-ylidene)-tetramethylene]-1,6,6a-thiathiophthene, $C_{19}H_{18}OS_5$

JORUNN SLETTEN

Chemical Institute, University of Bergen, N-5000 Bergen, Norway

An X-ray crystallographic investigation of the title compound, $C_{19}H_{18}OS_5$, has been carried out. The crystals are triclinic, space group $P\bar{1}$ with four molecules in the unit cell. The cell dimensions are $a = 14.167(5)$ Å, $b = 11.623(5)$ Å, $c = 12.947(4)$ Å, $\alpha = 63.67(4)°$, $\beta = 101.78(5)°$, $\gamma = 100.95(6)°$. 7228 independent reflections with $2\theta \leq 52°$ (Mo$K\alpha$-radiation) were measured on an off-line diffractometer. The structure was solved by the symbolic addition procedure and refined by full-matrix least-squares to an R of 0.052. There are significant differences in bond lengths and angles between the two independent molecules in the asymmetric unit. In each molecule four sulphur atoms are lying on an approximately linear row, the interatomic distances in molecules a and b being S(1)–S(2) = 2.429(1) Å [2.563(1) Å], S(2)–S(3) = 2.225(1) Å, [2.165(1) Å], S(3)–S(4) = 2.920(1) Å, [2.974(1) Å], the numbers in brackets referring to molecule b.

A number of structure investigations of compounds with four and five collinear sulphur atoms have been undertaken.[1-8] Examples of these types of compounds are shown in formulas I–III.

In these molecules S–S distances have been found to lie in the range between a single S–S bond length and van der Waals distance. Because the bonds are weak, they are easily perturbed by the influence of different substituents and by the intermolecular environment.

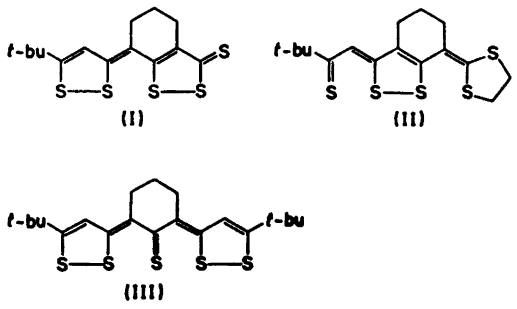

EXPERIMENTAL

The compound was synthesized by Stavaux and Lozac'h.[9] Deep red crystals grew from a toluene solution by slow evaporation at room temperature. The crystal used throughout the data collection had dimensions $0.40 \times 0.40 \times 0.10$ mm^3, and was mounted with the [100] vector along the goniometer head axis. Weissenberg and precession photographs indicated a triclinic space group. Unit cell dimensions were derived from diffractometer measurements of 2θ values for 15 reflections using Mo$K\alpha$ radiation ($\lambda_{\alpha_1+\alpha_2} = 0.71069$ Å).

7228 unique reflections with $2\theta \leq 52°$ were recorded on an off-line four-circle diffractometer employing the $\theta - 2\theta$ scan technique and using niobium filtered MoK radiation. Scan ranges were calculated according to the tangent relationship of Alexander and Smith [10] using constants evaluated by scanning a number of reflections manually. Two reference reflections were monitored throughout the data collection; the repeated measurements were used for scaling the data. 1933 of the reflections were less than twice the estimated error in measurement;

Table 1. Atomic coordinates. The numbers in parentheses are standard deviations, referring to the last decimal places.

Atom	Molecule *a* *X/a*	*Y/b*	*Z/c*	Molecule *b* *X/a*	*Y/b*	*Z/c*
S(1)	0.86195(7)	0.17417(10)	0.63597(8)	0.44703(9)	0.26871(11)	0.50990(9)
S(2)	0.83949(7)	0.03940(9)	0.83773(8)	0.40477(8)	0.11941(10)	0.71465(9)
S(3)	0.81955(7)	−.08810(9)	1.02211(8)	0.36810(8)	−.01535(10)	0.88518(9)
S(4)	0.77973(7)	−.26494(10)	1.25736(8)	0.31310(8)	−.20552(10)	1.11570(9)
S(5)	0.91050(8)	−.46464(10)	1.37938(8)	0.42107(11)	−.42920(12)	1.22723(11)
O	1.14655(19)	0.28538(25)	0.25081(21)	0.76957(20)	0.30971(30)	0.18065(24)
C(1)	0.95757(24)	0.09966(32)	0.64697(28)	0.53456(25)	0.17686(34)	0.52931(30)
C(2)	0.98427(24)	0.00069(32)	0.75280(29)	0.54857(25)	0.07103(35)	0.63343(31)
C(3)	0.93499(23)	−.04234(31)	0.84967(27)	0.49328(24)	0.02883(33)	0.72477(29)
C(4)	0.95797(23)	−.15015(31)	0.95496(27)	0.50575(23)	−.08675(31)	0.82597(28)
C(5)	0.90672(23)	−.18398(31)	1.04644(27)	0.44848(23)	−.12153(32)	0.91173(29)
C(6)	0.92650(24)	−.29279(32)	1.15801(28)	0.45741(27)	−.24000(34)	1.01858(31)
C(7)	0.87689(25)	−.33195(31)	1.25038(28)	0.40320(26)	−.28188(34)	1.10608(30)
C(8)	0.83744(34)	−.44842(43)	1.46734(34)	0.32435(47)	−.43238(52)	1.29959(46)
C(9)	0.75205(32)	−.38428(39)	1.39843(33)	0.29975(40)	−.30868(46)	1.26401(38)
C(10)	1.00898(24)	0.14230(30)	0.54500(27)	0.59567(24)	0.21262(34)	0.43679(28)
C(11)	1.10059(26)	0.10988(34)	0.55434(29)	0.64817(28)	0.12444(36)	0.43424(31)
C(12)	1.14884(25)	0.15442(35)	0.45909(35)	0.70572(28)	0.16074(39)	0.34749(34)
C(13)	1.10516(26)	0.23250(33)	0.35162(30)	0.71156(26)	0.28487(41)	0.26203(33)
C(14)	1.23471(30)	0.24011(44)	0.25542(36)	0.76763(36)	0.43022(51)	0.08323(43)
C(15)	1.01347(27)	0.26548(34)	0.33903(29)	0.66086(28)	0.37339(37)	0.26342(32)
C(16)	0.96667(26)	0.22049(33)	0.43502(28)	0.60334(27)	0.33641(36)	0.34933(33)
C(17)	1.03638(26)	−.22807(35)	0.96555(29)	0.57880(26)	−.17172(36)	0.83734(31)
C(18)	1.02368(30)	−.36322(36)	1.05966(34)	0.56932(45)	−.30175(51)	0.93650(48)
C(19)	1.01095(29)	−.36241(36)	1.17198(31)	0.53505(46)	−.31901(52)	1.02964(45)
H(2)	1.0347(22)	−.0434(29)	0.7605(25)	0.5886(24)	0.0176(32)	0.6432(27)
H(81)	0.8827(47)	−.3759(64)	1.5079(52)			
H(82)	0.8296(38)	−.5222(51)	1.5252(42)			
H(91)	0.7059(40)	−.4522(52)	1.3740(45)			
H(92)	0.7372(40)	−.3266(53)	1.4268(45)			
H(11)	1.1291(30)	0.0528(38)	0.6199(34)	0.6481(29)	0.0252(39)	0.4900(33)
H(12)	1.2068(19)	0.1332(25)	0.4740(22)	0.7369(26)	0.0937(34)	0.3423(29)
H(141)	1.2393(31)	0.1303(43)	0.2899(37)	0.7905(45)	0.5063(62)	0.1088(49)
H(142)	1.2932(29)	0.2646(39)	0.2994(35)	0.8063(43)	0.4148(54)	0.0414(50)
H(143)	1.2445(33)	0.2819(44)	0.1654(40)	0.6945(43)	0.4455(50)	0.0397(43)
H(15)	0.9820(22)	0.3217(30)	0.2617(26)	0.6633(28)	0.4682(37)	0.2023(32)
H(16)	0.9026(29)	0.2384(38)	0.4215(32)	0.5788(24)	0.4022(31)	0.3535(27)
H(171)	1.0965(30)	−.1853(39)	0.9868(34)			
H(172)	1.0298(32)	−.2301(41)	0.8967(37)			
H(181)	0.9667(35)	−.4058(44)	1.0297(38)			
H(182)	1.0807(31)	−.4119(41)	1.0792(36)			
H(191)	1.0098(34)	−.4407(45)	1.2215(38)			
H(192)	1.0780(26)	−.3098(36)	1.1983(30)			

these reflections were given the threshold value of $2\sigma_c$ and were not included in the refinement unless $|F_c| > |F_{threshold}|$. Standard deviations in intensities were calculated as $\sigma_I = k[\sigma_c^2 + (0.02N_{net})^2]^{\frac{1}{2}}$, where k is the appropriate scalefactor, σ_c is the estimated error due to counting statistics and N_{net} is the net count, $(N_{scan} - N_{background})$, of the reflection. Standard deviations in structure factors were calculated as $\sigma_F = \sigma_I/2(I\ Lp)^{\frac{1}{2}}$. The data were corrected for Lorentz and polarization effects according to standard procedures and for absorption using the method described by Coppens *et al.*[11] Extinction correction was not made as no evidence of extinction was detected at the end of the refinement.

Table 2. Thermal parameters with standard deviations, referring to the last decimal places, in parentheses. Anisotropic thermal parameters are of the form: $T_i = \exp[-2\pi^2(U_{11}h^2a^{*2} + U_{22}k^2b^{*2} + U_{33}l^2c^{*2} + 2U_{12}hka^*b^* + 2U_{23}klb^*c^* + 2U_{13}hla^*c^*)]$. The values are multiplied by 10^4.
Isotropic parameters are defined by: $T_i = \exp[-8\pi^2U(\sin^2\theta)/\lambda^2]$. These values are multiplied by 10^3.

Atom	Molecule	U_{11}	U_{22}	U_{33}	U_{12}	U_{23}	U_{13}
S(1)	*a*	663(7)	644(6)	489(5)	257(5)	−166(5)	170(5)
	b	816(8)	729(7)	628(7)	386(6)	−1(6)	239(6)
S(2)	*a*	536(6)	509(5)	479(5)	165(4)	184(4)	131(4)
	b	697(7)	559(6)	605(6)	288(5)	−88(5)	174(5)
S(3)	*a*	579(6)	560(6)	458(5)	203(5)	−146(4)	173(4)
	b	749(7)	558(6)	600(6)	300(5)	−88(5)	240(5)
S(4)	*a*	606(6)	716(7)	436(5)	227(5)	−155(5)	159(4)
	b	709(7)	637(4)	598(6)	307(5)	−84(5)	239(5)
S(5)	*a*	842(8)	594(6)	498(6)	276(6)	−52(5)	230(5)
	b	1380(11)	784(8)	871(9)	649(8)	222(7)	679(8)
O	*a*	765(18)	735(18)	553(15)	145(14)	−201(13)	292(13)
	b	700(19)	972(23)	726(19)	147(16)	−278(18)	249(15)
C(1)	*a*	507(21)	457(20)	485(20)	48(17)	−250(17)	106(16)
	b	477(21)	543(22)	552(22)	76(18)	−194(19)	62(17)
C(2)	*a*	470(20)	489(21)	518(21)	79(17)	−234(18)	126(16)
	b	487(22)	535(23)	564(23)	139(18)	−138(19)	91(18)
C(3)	*a*	451(20)	467(20)	427(19)	75(16)	−230(16)	96(15)
	b	420(20)	517(21)	512(21)	119(17)	−161(18)	34(16)
C(4)	*a*	452(20)	451(20)	470(20)	80(16)	−236(17)	94(16)
	b	382(19)	468(20)	533(21)	86(16)	−185(17)	58(16)
C(5)	*a*	452(20)	429(19)	447(19)	44(15)	−21(16)	117(15)
	b	428(20)	472(20)	582(22)	91(16)	−220(18)	108(16)
C(6)	*a*	497(21)	477(20)	479(20)	79(17)	−230(17)	112(16)
	b	604(24)	515(22)	558(22)	205(18)	−93(18)	177(19)
C(7)	*a*	536(22)	432(20)	457(20)	59(16)	−189(16)	96(16)
	b	585(24)	495(22)	557(22)	181(18)	−120(18)	142(18)
C(8)	*a*	987(33)	888(32)	553(24)	382(27)	4(23)	361(23)
	b	1894(60)	1034(40)	1099(41)	806(41)	187(32)	1039(42)
C(9)	*a*	857(31)	645(26)	601(24)	114(23)	−145(21)	326(22)
	b	1437(47)	840(33)	701(30)	601(32)	146(25)	564(30)
C(10)	*a*	486(21)	426(19)	442(19)	48(16)	−221(16)	110(16)
	b	443(20)	529(22)	469(20)	50(17)	−181(18)	20(16)
C(11)	*a*	585(23)	533(22)	462(20)	163(18)	−192(17)	91(17)
	b	648(25)	581(24)	551(23)	154(20)	−223(19)	50(19)
C(12)	*a*	499(22)	606(23)	544(22)	164(18)	−232(19)	113(17)
	b	662(27)	679(27)	666(26)	190(21)	−299(23)	104(21)
C(13)	*a*	599(24)	478(21)	523(22)	23(18)	−270(18)	194(18)
	b	468(22)	777(29)	585(23)	76(20)	−328(22)	61(18)
C(14)	*a*	665(28)	964(33)	750(28)	36(24)	−392(25)	309(22)
	b	945(36)	1002(38)	945(36)	−5(30)	−328(31)	510(29)
C(15)	*a*	651(25)	526(22)	460(20)	151(19)	−182(17)	122(18)
	b	618(25)	609(25)	606(24)	85(20)	−127(20)	191(20)
C(16)	*a*	554(23)	533(21)	473(20)	133(18)	−210(17)	123(17)
	b	564(24)	551(24)	692(25)	138(19)	−182(21)	140(20)
C(17)	*a*	617(23)	587(23)	494(21)	207(19)	−227(18)	123(18)
	b	514(22)	631(24)	568(22)	217(19)	−115(19)	139(18)
C(18)	*a*	789(28)	549(24)	708(25)	222(21)	−232(21)	252(21)
	b	1624(53)	1009(40)	1200(43)	928(39)	462(33)	933(41)
C(19)	*a*	805(27)	562(24)	532(22)	284(21)	−94(19)	219(20)
	b	1715(53)	1094(40)	1011(38)	1009(39)	314(31)	849(38)

Table 2. Continued.

Atom	U molecule *a*	U molecule *b*	Atom	U molecule *a*	U molecule *b*
H(2)	51(9)	62(10)	H(143)	135(16)	129(20)
H(81)	209(25)		H(15)	60(9)	90(13)
H(82)	113(19)		H(16)	62(13)	62(10)
H(91)	154(21)		H(171)	85(14)	
H(92)	134(21)		H(172)	68(15)	
H(11)	73(14)	85(13)	H(181)	117(16)	
H(12)	13(7)	84(12)	H(182)	74(15)	
H(141)	79(14)	140(25)	H(191)	78(16)	
H(142)	80(13)	135(22)	H(192)	85(12)	

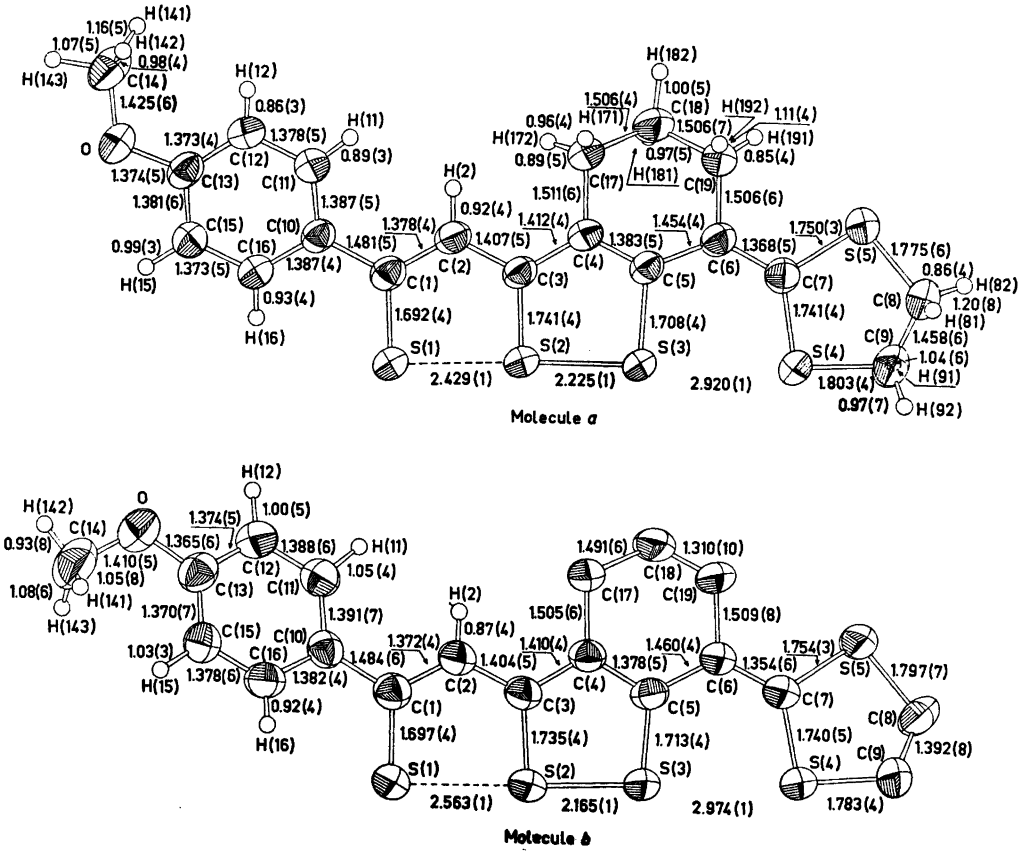

Fig. 1. Intramolecular distances in molecules *a* and *b* together with the standard deviations as calculated based on the least-square parameters. Thermal ellipsoids for non hydrogen atoms are drawn at the 50 % probability level, hydrogen atoms are drawn with a fixed radius. Hydrogens are not included in the disordered regions of *b*.
Figs 1 and 3 are prepared using the ORTEP program.[20]

CRYSTAL DATA

$C_{19}H_{18}OS_5$, M.W. = 422.68
Crystal system triclinic, spacegroup $P\bar{1}$ (or $P1$).
Cell dimensions: $a = 14.167(5)$ Å, $b = 11.623(5)$ Å, $c = 12.947(4)$ Å, $\alpha = 63.67(4)°$, $\beta = 101.78(5)°$, $\gamma = 100.95(6)°$.
$V = 1858(2)$ Å^3, $Z = 4$.
$D_x = 1.511$ g cm^{-3}, $D_m = 1.50$ g cm^{-3} (flotation)
$\mu_{MoK\alpha} = 6.0$ cm^{-1}.

STRUCTURE DETERMINATION AND REFINEMENT

The distribution of E-values clearly indicated a centrosymmetric space group, thus $P\bar{1}$ was chosen rather than $P1$. A Patterson map revealed that the linear sulphur rows of the two independent molecules in the asymmetric unit were approximately parallel, however, the position of each row was not found. In retrospect it is seen that as expected the most dominant peaks in the map are due to intermolecular sulphur-sulphur vectors between the two molecules in the asymmetric unit. Since the S – S vectors between centrosymmetrically related molecules give peaks of approximately the same size as overlapping intermolecular S – C vectors, it was difficult to choose among a number of possible solutions.

A symbolic addition procedure programmed by Long [12] was tried. Two attempts were made with different starting sets, in each case using three variable signs. The most probable set of signs, judging from the internal consistency, was identical in the two runs. The corresponding E-map was not possible to interpret in terms of the structure. Six more sets were tested, none of which gave the correct solution.

The automatic procedure was then abandoned, and the signs of 170 reflections were calculated by hand, in each step including reflections determined with multiple, consistent sign relationships. Four symbolic signs were used. One of the possible solutions had no internal inconsistencies in the sign determination and was identical with the most probable set obtained by the automatic procedure. The second most consistent set was different from any of the sets tested. An E-map based on the 170 reflections clearly revealed 47 out of the 50 non-hydrogen atoms in the asymmetric unit. A structure factor calculation gave $R = 0.49$ ($R = \sum||F_o| - |F_c||/\sum|F_o|$), and the remaining atoms were found in the subsequent Fourier map.

The structure was refined by full-matrix least-squares. The carbon atoms C(8), C(9), C(18) and C(19) of molecule b had fairly high temperature factors, indicating disorder for these atoms. However, an attempt to refine two fractional atoms for each of the four sites were not successful. At an R of 0.07 all hydrogen atoms, except those on C(8), C(9), C(17), C(18), C(19) of molecule b, were located from a difference map. All non-hydrogen atoms were refined anisotropically, and the hydrogen atoms with isotropic temperature factors. The refinement converged, at a conventional R of 0.052, and a weighted R of 0.058. The standard deviation of an observation of unit weight, $[\sum w(|F_o| - |F_c|)^2/(m-n)]^{\frac{1}{2}}$, is 2.87.

The function minimized in the refinement was $\sum w(|F_o| - |F_c|)^2$, where $w = 1/\sigma_F^2$. The atomic scattering factors used were for non-hydrogen atoms those of Hanson *et al.*[13] and for hydrogen those of Stewart *et al.*[14] The final positional and thermal parameters, with standard deviations estimated from the least-squares process, are given in Tables 1 and 2.

Lists of observed and calculated structure factors may be obtained from the author.

The thermal parameters of each molecule were analyzed in terms of rigid body motion using the method of Schomaker and Trueblood.[15] For both molecules the thermal motion of the atoms of rings A + B are described reasonably well by the rigid body approximation. The axis of largest oscillation amplitude is in each case nearly parallel to the S(1) – S(2) – S(3) direction. Bond length corrections according to this model are 0.002 Å for S – S bonds, 0.014 Å for S – C and 0.004 Å for C – C bonds in rings A + B. Bond lengths shown in Fig. 1 are uncorrected for thermal motion.

DESCRIPTION AND DISCUSSION OF THE STRUCTURE

In Fig. 1 the atomic labelling used in this analysis and the intramolecular distances of the two molecules are shown. The intramolecular angles are listed in Table 3.

Table 3. Bond angles with the corresponding standard deviations listed in parentheses.

Angle	Molecule *a*	Molecule *b*	Angle	Molecule *a*	Molecule *b*
S(2)–S(1)–C(1)	92.3(1)	90.3(1)	C(1)–C(10)–C(11)	122.6(2)	122.0(3)
S(1)–S(2)–S(3)	178.65(6)	176.93(7)	C(1)–C(10)–C(16)	120.1(3)	121.0(3)
S(1)–S(2)–C(3)	88.5(1)	86.3(1)	C(11)–C(10)–C(16)	117.3(3)	117.0(3)
S(3)–S(2)–C(3)	90.5(1)	91.8(1)	C(10)–C(11)–C(12)	121.8(3)	120.9(3)
S(2)–S(3)–S(4)	175.58(4)	178.09(5)	C(10)–C(11)–H(11)	122(3)	128(3)
S(2)–S(3)–C(5)	95.6(1)	96.1(1)	C(12)–C(11)–H(11)	116(3)	111(3)
S(4)–S(3)–C(5)	85.5(1)	83.8(1)	C(11)–C(12)–C(13)	119.4(3)	120.4(4)
S(3)–S(4)–C(7)	80.6(1)	80.5(1)	C(11)–C(12)–H(12)	115(2)	119(2)
S(3)–S(4)–C(9)	175.3(2)	170.0(2)	C(13)–C(12)–H(12)	125(2)	120(2)
C(7)–S(4)–C(9)	97.6(2)	96.5(2)	C(12)–C(13)–C(15)	120.3(3)	119.6(4)
C(7)–S(5)–C(8)	97.4(2)	97.2(2)	C(12)–C(13)–O	124.9(3)	115.5(4)
S(1)–C(1)–C(2)	117.4(3)	118.2(3)	C(15)–C(13)–O	114.8(3)	124.9(3)
S(1)–C(1)–C(10)	119.8(2)	120.5(2)	C(13)–O–C(14)	117.0(3)	117.3(4)
C(2)–C(1)–C(10)	122.8(3)	121.2(3)	O–C(14)–H(141)	120(2)	111(3)
C(1)–C(2)–C(3)	123.4(3)	125.1(3)	O–C(14)–H(142)	118(3)	98(3)
C(1)–C(2)–H(2)	119(2)	120(2)	O–C(14)–H(143)	102(3)	111(2)
C(3)–C(2)–H(2)	117(2)	114(2)	H(141)–C(14)–H(142)	101(3)	119(5)
S(2)–C(3)–C(2)	118.3(2)	119.9(2)	H(141)–C(14)–H(143)	106(4)	105(5)
S(2)–C(3)–C(4)	118.6(3)	117.6(3)	H(142)–C(14)–H(143)	109(3)	113(5)
C(2)–C(3)–C(4)	123.1(3)	122.5(3)	C(13)–C(15)–C(16)	119.5(3)	119.7(3)
C(3)–C(4)–C(5)	119.1(3)	119.0(3)	C(13)–C(15)–H(15)	120(2)	123(3)
C(3)–C(4)–C(17)	119.9(3)	119.8(3)	C(16)–C(15)–H(15)	120(2)	117(3)
C(5)–C(4)–C(17)	121.0(2)	121.1(3)	C(10)–C(16)–C(15)	121.7(3)	122.5(4)
S(3)–C(5)–C(4)	116.1(2)	115.5(2)	C(10)–C(16)–H(16)	121(2)	121(2)
S(3)–C(5)–C(6)	121.4(3)	122.6(3)	C(15)–C(16)–H(16)	117(2)	116(2)
C(4)–C(5)–C(6)	122.5(3)	121.9(3)	C(4)–C(17)–C(18)	111.5(3)	113.2(4)
C(5)–C(6)–C(7)	124.9(3)	125.5(3)	C(4)–C(17)–H(171)	106(3)	
C(5)–C(6)–C(19)	116.2(3)	115.4(3)	C(4)–C(17)–H(172)	105(3)	
C(7)–C(6)–C(19)	118.8(3)	119.0(3)	C(18)–C(17)–H(171)	108(2)	
S(4)–C(7)–S(5)	113.3(2)	112.8(2)	C(18)–C(17)–H(172)	110(3)	
S(4)–C(7)–C(6)	127.5(2)	127.5(2)	H(171)–C(17)–H(172)	115(4)	
S(5)–C(7)–C(6)	119.2(2)	119.7(3)	C(17)–C(18)–C(19)	111.4(3)	121.1(5)
S(5)–C(8)–C(9)	111.8(3)	111.3(4)	C(17)–C(18)–H(181)	105(2)	
S(5)–C(8)–H(81)	108(4)		C(17)–C(18)–H(182)	113(2)	
S(5)–C(8)–H(82)	107(5)		C(19)–C(18)–H(181)	111(3)	
C(9)–C(8)–H(81)	104(3)		C(19)–C(18)–H(182)	105(3)	
C(9)–C(8)–H(82)	119(4)		H(181)–C(18)–H(182)	110(4)	
H(81)–C(8)–H(82)	106(5)		C(6)–C(19)–C(18)	112.3(3)	119.7(4)
S(4)–C(9)–C(8)	110.5(3)	113.3(4)	C(6)–C(19)–H(191)	117(4)	
S(4)–C(9)–H(91)	100(3)		C(6)–C(19)–H(192)	108(2)	
S(4)–C(9)–H(92)	98(3)		C(18)–C(19)–H(191)	105(4)	
C(8)–C(9)–H(91)	105(3)		C(18)–C(19)–H(192)	107(2)	
C(8)–C(9)–H(92)	112(3)		H(191)–C(19)–H(192)	107(4)	
H(91)–C(9)–H(92)	130(5)				

The two chemically equivalent molecules are shown to have markedly different sulphur-sulphur bond lengths. Corresponding S–C, O–C, and C–C distances in the two molecules are not significantly different, when bonds involving the disordered atoms C(8), C(9), C(18) of molecule *b* are excluded.

The atoms of rings A, B and C in each molecule show a small but significant deviation from planarity, the atomic deviations being essentially the same for the two molecules (Fig. 2). The atom C(18) of the trimethylene bridge is bent out of the plane in the same direction in the two molecules. In molecule *b* there is a disorder in this part of the molecule which could not be satisfactorily resolved by the refinement procedure. In a related multisulphur compound [8] a disordered structure could be for-

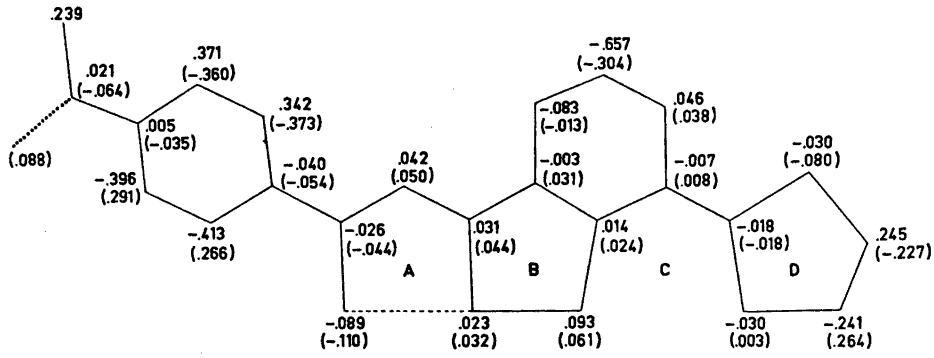

Fig. 2. Deviations (Å) from least-squares planes through the atoms of rings A + B + C for molecules *a* and *b*. Numbers referring to molecule *b* are in parentheses.

mulated in which two sites of approximately equal weight were found for C(18); the two sites being located on opposite sides of the least-squares plane. In the present case one of the configurations evidently is dominant.

The puckering of the 1,3-dithiolane rings are opposite in the two molecules. As mentioned above there are some signs of disorder in C(8) and C(9) of molecule *b*. The positions of these atoms are therefore uncertain. The $Csp^3 - Csp^3$ bond C(8) – C(9) of 1.39 Å is clearly in error. In molecule *a* where there is apparently no disorder, the C(8) – C(9) bond of 1.458 Å is also unusually short. In other molecules containing 1,3-dithiolane rings the $Csp^3 - Csp^3$ bonds have been found to be significantly shorter than the single bond value.[2,16] The tendency of these rings to be more or less disordered may account for this discrepancy.

The ring of the *p*-methoxyphenyl group is inclined at 16.5(5)° from ring A in molecule *a* and at 18.9(5)° in molecule *b*, the torsion angle in *a* being in the opposite direction to that in *b*. The methyl of the methoxy group is oriented *cis* and *trans* relative to C(12) in molecules *a* and *b*, respectively. The dihedral angle between the phenyl ring and the methoxy group is 9.2(5)° in *a* and 8.2(5)° in *b*.

The packing of molecules in the crystal is illustrated in Fig. 3. The crystal environments of the two molecules are similar, though with some noticeable differences. Pairs of centrosymmetrically related molecules overlap to a considerable extent; the interplanar spacing between molecule *a* and its inversion through (1,0,1) being 3.65 Å, and the corresponding distance between *b* and its inversion through ($\frac{1}{2}$,0,1) (*b'*) being 3.90 Å. Another difference between the molecular environments of *a* and *b* is that the oxygen of a *p*-methoxy group is

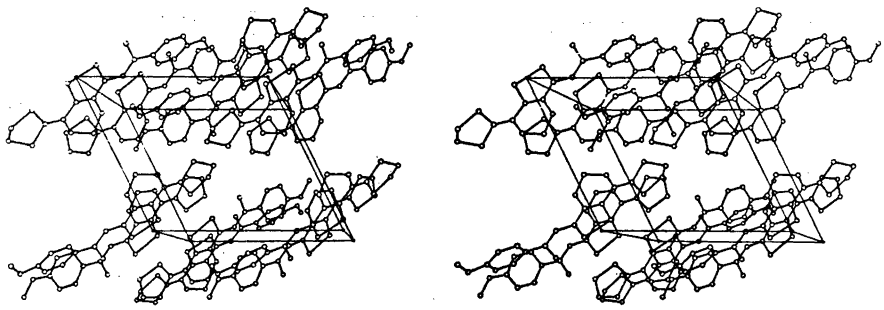

Fig. 3. Stereoscopic view of the molecular packing. The *a*-axis points towards the viewer, the *b* axis is horisontal, left to right, and *c* is vertical, top to bottom.

Table 4. Comparison between S–S distances (Å) in related compounds with four approximately collinear sulphur atoms.

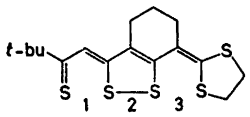

(II)

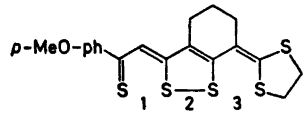

(IV)

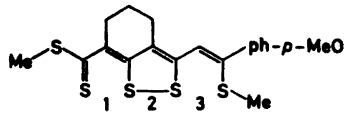

(V)

Molecule	Bonds					References
	1	2	3	1+2	1+2+3	
II	2.482	2.209	2.965	4.691	7.656	2
IV	2.429	2.225	2.920	4.654	7.574	present
	2.563	2.165	2.974	4.728	7.702	investigation
V	2.551	2.156	3.002	4.707	7.709	4

located 3.65 Å above ring C of molecule *b*, while no corresponding short contact is found for molecule *a*. The shortest intermolecular S···S distances occur between pairs of molecules not related by symmetry, *e.g.* between *a* and *b'* where S(2)*a*···S(4)*b'* = 3.45 Å, S(3)*a*···S(3)*b'* = 3.71 Å and S(4)*a*···S(2)*b'* = 3.53 Å.

Intramolecular distances of the collinear sulphur row in chemically related 4-sulphur compounds are given in Table 4. The variation in bonding through the chain is hard to explain in terms of substituent effects only. The large differences between chemically equivalent molecules in the present determination, clearly show that minor packing differences may exert a profound effect in the semi-covalent bonding between sulphur atoms. In a linear three-sulphur compound with two molecules in the asymmetric unit, large differences in S–S distances between chemically equivalent molecules have also been observed.[17] These findings are in agreement with the results from MO calculations on thiathiophthene, where it has been shown that the potential energy curve has a rather flat minimum when plotted as a function of the variation in S–S bond lengths.[18,19]

It is interesting to notice that a short central S–S bond length (2) corresponds to a long chain length and also to a long S(3)···S(4) distance (3). This may imply that the fourth sulphur atom exerts a small but significant influence on the thiathiophthene sulphur sequence, S(1)···S(3).

Thanks are due to Dr. M. Stavaux for supplying a sample of the compound and for valuable help of growing crystals suitable for X-ray work.

REFERENCES

1. Hordvik, A. *Acta Chem. Scand. 19* (1965) 1253.
2. Sletten, J. *Acta Chem. Scand. 25* (1971) 3577.
3. Sletten, J. *Acta Chem. Scand. 26* (1972) 873.
4. Sletten, J. *Acta Chem. Scand. 27* (1973) 229.
5. Flippen, J. L. *J. Amer. Chem. Soc. 95* (1973) 6073.
6. Sletten, J. *Acta Chem. Scand. 24* (1970) 1464.
7. Kristensen, R. and Sletten, J. *Acta Chem. Scand. 25* (1971) 2366, *27* (1973) 2517.
8. Sletten, J. and Velsvik, M. *Acta Chem. Scand. 27* (1973) 3881.
9. Stavaux, M. and Lozac'h, N. *Bull. Soc. Chim. Fr.* (1971) 4419.
10. Alexander, L. E. and Smith, G. S. *Acta Crystallogr. 17* (1964) 1195.
11. Coppens, P., Leiserowitz, L. and Rabinovich, D. *Acta Crystallogr. 18* (1965) 1035.
12. Long, R. E. *Ph. D. Diss.*, University of California, Los Angeles 1965.
13. Hanson, H. P., Hermann, F., Lea, J. D. and Skillmann, S. *Acta Crystallogr. 17* (1964) 1040.
14. Stewart, R. F., Davidson, E. R. and Simpson, W. T. *J. Chem. Phys. 42* (1965) 3175.
15. Schomaker, V. and Trueblood, K. N. *Acta Crystallogr. B 24* (1968) 63.
16. Lee, J. D. and Goodacre, G. W. *Acta Crystallogr. B 27* (1971) 1055.
17. Johnson, S. M., Newton, M. G. and Paul, I. C. *J. Chem. Soc. B* (1969) 986.
18. Gleiter, R. and Hoffman, R. *Tetrahedron 24* (1968) 5899.
19. Hansen, L. K., Hordvik, A. and Sæthre, L. J. *Chem. Commun.* (1972) 222.
20. Johnson, C. K. (1965), *ORTEP*, Report ORNL-3794, Oak Ridge National Laboratory, Oak Ridge, Tennessee.

Received February 13, 1974.

Acta Chemica Scandinavica A 28 (1974) 507—514

Structure of Gaseous and Crystalline 2,2′-Dichlorobiphenyl

CHR. RØMMING, H. M. SEIP and I.-M. AANESEN ØYMO

Department of Chemistry, University of Oslo, Oslo 3, Norway

The structure of 2,2′-dichlorobiphenyl has been examined in the gaseous phase by the electron-diffraction technique and in the crystalline state by X-ray diffraction. The twist angle about the central carbon-carbon bond is approximately 70° and only slightly larger in the gas phase than that in the solid in contrast to what has been found for biphenyl. Only one stable conformer was detected in the gas phase at 300 °C.

Bastiansen and coworkers studied biphenyl [1,2] and a series of ortho-substituted biphenyls (2,2′-difluoro-,[3] 2,2′-dichloro-,[4] 2,2′-dibromo-,[4] and 2,2′-diiodo-biphenyl [4]) by electron-diffraction methods several years ago. More recently other related compounds, including perfluorobiphenyl,[5] have also been studied. (See Ref. 6 for a more detailed discussion). The angle between the ring planes (ϕ) in biphenyl was found to be about 42° in the gaseous phase whereas the molecule is planar ($\phi = 0$) in the crystal.[7–9] The angle ϕ found in some of the biphenyls is given in Table 1.

Semi-empirical calculations [10–12] of the variation in the conjugation and van der Waals energies as a function of ϕ lead to a flat minimum at about 40° from planarity in biphenyl in good agreement with the electron diffraction result. The barrier heights obtained were 2 – 4 kcal/mol, the barrier at $\phi = 0°$ probably being slightly higher than that at $\phi = 90°$.

The CNDO/2 method has also been applied to biphenyl [13,14] and perfluorobiphenyl.[14] The calculations in both cases gave an energy minimum for ϕ close to 90° in contrast to the experimental values.

Table 1. Angle of twist in biphenyl and some substituted biphenyls. $\phi = 0$ corresponds to the *syn* form.

Compound	ϕ (obs), gas phase	ϕ (calc)
Biphenyl	42,[2] 0 (solid)[7]	40[11]
2,2′-Difluorobiphenyl	60[3]	42, 143[5]
2,2′-Dichlorobiphenyl	74[4]	72, 120[5]
2,2′-Dibromobiphenyl	75[4]	82, 112[5]
2,2′-Diiodobiphenyl	79[4]	93[5]
Perfluorobiphenyl	70[5]	46[5]

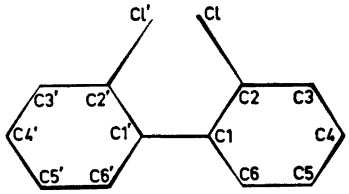

Fig. 1. 2,2′-Dichlorobiphenyl.

The most stable conformers of the 2,2′-dihalobiphenyls are closer to the *syn* ($\phi = 0°$) than to the *anti* ($\phi = 180°$) form. Extension of the semi-empirical calculations which gave promising results for biphenyl, to these compounds,[5,15] yielded two energy minima for the fluoro-, chloro-, and bromocompounds. In contradiction to the experimental results the calculations gave a lower minimum for $\phi > 90°$ than for $\phi < 90°$.

The results of the calculations led us to reinvestigate 2,2′-dichlorobiphenyl by electron diffraction to see if there was evidence for a second conformer with $\phi > 90°$. In order to increase the amount of a possible less stable conformer, the nozzle temperature was as high as 300 °C, though a lower temperature would be

preferable for an accurate determination of the molecular parameters, especially the twist angle ϕ. At the same time we have determined the structure in the solid by X-ray diffraction methods in order to observe any change in the conformation as well as to compare the molecular parameters obtained by the two methods. In the earlier work on the conformation of 2,2′-dihalobiphenyls in the gas phase two assumptions have been made: that each of the chlorophenyl parts are planar and that the C4 – Cl – Cl′ – C4′ arrangement is linear. Deviations from these conditions make at least three definitions of ϕ possible; ϕ may be defined as the angle formed by the best plane through all the atoms of each of the chlorophenyl parts, as the angle between the best planes through the carbon atoms of each ring or it may be defined as the dihedral angle C2ClCl′C2′. In a deformed molecule the three angles are not equal and this must be taken into account when the results from the two methods are discussed.

CRYSTAL STRUCTURE DETERMINATION

Experimental

The sample of 2,2′-dichlorobiphenyl was obtained from Monsanto Chemical Co. Single crystals were formed by slow diffusion of water into a solution of the compound in ethanol. The crystals sublime and had to be kept in a capillary tube during the X-ray experiments. The specimen used was approximately shaped as a cube with edges of about 0.3 mm.

Oscillation, Weissenberg and precession films indicated orthorhombic symmetry. Conditions for the presence of reflections were $h+k$, $k+l$ and $h+l$ even for hkl, $k+l=4n$ for $0kl$, and $l+h=4n$ for $h0l$. This characterizes the space group uniquely to be $Fdd2$.

Unit cell dimensions were determined from diffractometer measurements. A manual Picker four-circle diffractometer with Cu$K\beta$ radiation ($\lambda=1.3922$ Å) was used. The computer program applied for the least-squares calculations as well as other programs applied during the X-ray structure analysis are described in Ref. 16.

Three-dimensional intensity data were recorded on an automatic Picker four-circle diffractometer using graphite crystal monochromated Mo$K\alpha$ radiation. The $\theta-2\theta$ scanning mode with a 2θ scan speed of 1° min^{-1} was applied through the scan range of 0.7° below $2\theta(\alpha_1)$ to 0.8° above $2\theta(\alpha_2)$. Background counts were taken for 25 sec at each of the scan range limits. The take-off angle was 4° and the temperature was kept constant at 18 °C. The intensities of three standard reflections were measured for every 100 reflections of the data set. They showed a variation of up to 5.5 % and the data were accordingly adjusted. The standard deviations in the intensities were taken as the square root of the total counts with the addition of 2 % of the net intensity.

The measurements included 799 reflections with $\sin\theta/\lambda$ less than 0.6 Å^{-1}; of these 734 had intensities larger than twice their standard deviations and were regarded as observed. The remaining reflections were excluded from the refinement procedure.

Atomic form factors used were those of Hansen *et al.*[17] for chlorine and carbon, and of Stewart *et al.*[18] for hydrogen.

Crystal data

2,2′-Dichlorobiphenyl, $C_{12}H_8Cl_2$, orthorhombic. $a=23.913(0.006)$ Å; $b=13.469(0.007)$ Å; $c=6.637(0.004)$ Å.

$V=2137.7$ Å^3; $M=223.10$; $F(000)=912$; $\mu=0.056$ mm^{-1}; $Z=8$.

$D_{obs}=1.33$ g cm^{-3}, $D_{calc}=1.386$ g cm^{-3}.

Absent reflections: hkl: $h+k$ and $k+l$ odd, $0kl$ other than $k+l=4n$, $h0l$ other than $h+l=4n$. Space group $Fdd2$.

Structure determination and refinement

The space group symmetry requires the molecule to possess a two-fold axis of symmetry. The positions of the chlorine atom and the six carbon atoms were readily derived from a sharpened Patterson synthesis. After a preliminary refinement of the coordinates the positions of the four hydrogen atoms were calculated from stereochemical considerations. All positional parameters (except for one origin-fixing z-coordinate), anisotropic thermal parameters for the heavy atoms and isotropic thermal parameters for hydrogen atoms were refined by least-squares calculations minimizing the function $\sum w(F_o-F_c)^2$. The weight w assigned to each reflection was the inverse of the variance of the structure factor. The refinement converged with a final conventional R factor of 0.035, $R_w=0.043$. A difference Fourier map showed no electron density larger than 0.35 e Å^{-3}.

The experimental data may be obtained at request from the authors. Final parameters are listed in Table 2 and interatomic distances and

Table 2. Fractional (crystallographic) atomic coordinates and thermal parameters with estimated standard deviations ($\times 10^5$ for Cl and C; $\times 10^4$ for H). The temperature factor is exp $-(B11h^2 + B22k^2 + B33l^2 + B12hk + B13hl + B23kl)$.

Atom	x	y	z	$B11(B)$	$B22$	$B33$	$B12$	$B13$	$B23$
Cl	7081	−1705	66243	213	740	2389	−14	−404	634
	3	5		1	5	17	4	8	16
C1	1666	4669	32647	133	493	1794	13	60	29
	10	17	41	4	12	55	11	25	46
C2	5702	6794	47117	144	503	1940	36	−36	117
	10	17	42	4	12	56	12	25	46
C3	8896	15290	46498	164	590	2977	−68	−125	−212
	12	20	54	5	15	86	14	34	61
C4	8087	22026	30983	199	594	3564	157	299	239
	13	24	64	5	17	101	15	41	70
C5	4115	20224	16549	236	694	2923	59	119	878
	14	23	64	6	16	86	17	41	73
C6	1024	11637	17378	195	635	2084	47	132	447
	12	22	53	6	16	62	14	34	58
HC3	1174	1636	5677	5.2					
	14	23	65	0.7					
HC4	1005	2799	2912	3.8					
	12	20	56	0.6					
HC5	347	2747	682	5.9					
	14	19	70	0.8					
HC6	−85	953	763	6.8					
	16	28	78	1.0					

Table 3. Interatomic distances (Å) and bond angles (°) found by X-ray diffraction. Estimated standard deviations (in parentheses) apply to the least significant figure.

Distance		Corrected	Angle	
Cl−C2	1.741(3)	1.748	Cl−C2−Cl	120.0(2)
C1−C2	1.392(4)	1.398	C3−C2−Cl	117.6(2)
C2−C3	1.376(4)	1.379	C1−C2−C3	122.4(2)
C3−C4	1.386(5)	1.391	C2−C3−C4	119.3(3)
C4−C5	1.371(6)	1.375	C3−C4−C5	120.0(3)
C5−C6	1.374(4)	1.376	C4−C5−C6	119.6(8)
C1−C6	1.390(4)	1.394	C1−C6−C5	122.6(3)
C1−C1′	1.489(5)	1.493	C2−C1−C6	116.2(2)
Cl−Cl′	3.418(2)		Cl′−C1−C6	120.8(2)
C−H	0.98 (mean value)		Cl′−C1−C2	123.0(2)

bond angles are given in Table 3. The r.m.s. deviation of the experimental U_{ij} values from those calculated from a rigid-body analysis of the molecule was 0.0025 Å². The r.m.s. amplitudes of translation along the principal axes are 0.22, 0.19, and 0.18 Å and the librations have r.m.s. amplitudes of 5.3°, 3.4°, and 2.6° about the principal axes, the largest amplitude being about the axis of the least moment of inertia. Corrections in bond lengths were derived from the rigid-body librations.

Interatomic distances and bond angles are listed in Table 3. Standard deviations were derived from the correlation matrix ignoring standard deviations in cell parameters.

The values obtained for the bond lengths

are discussed in the last section. However, some comments on the bond angles are given here since they were used as input parameters in the gas phase investigation. The internal angles of the phenyl rings deviate significantly from 120°. This is also found for biphenyl itself in which the C2C1C6 angle was found to be 116.8° (117.4 corrected for thermal vibration effects.)[8] The decrease in the corresponding angle in the present structure is 4° from the benzene value, an increase of about 2.5° is found in the internal angles at C2 and C6.

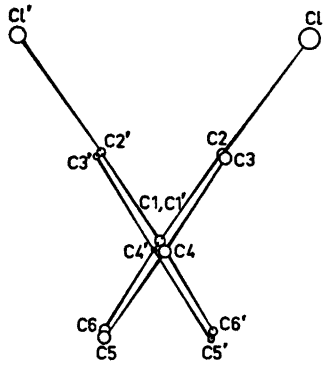

Fig. 2. 2,2′-Dichlorobiphenyl as seen along the central carbon-carbon bond.

The external angles at Cl and C2 are deformed, probably to relieve the strain caused by the fairly short intramolecular Cl – Cl distance (3.42 Å). The Cl′C1C2 angle is thus by 2° larger than Cl′C1C6 and ClC2C1 by 2.5° larger than ClC2C3. Furthermore, the C – Cl bond is bent out of the plane of the benzene ring by 2.3° and the Cl – Cl′ bond forms an angle of 1.9° with this plane. The deformation of the molecule may be seen from Fig. 2 which shows the molecule as seen along the central C – C bond. The carbon atoms of each phenyl ring is strictly coplanar, the largest deviation from a least-squares plane being 0.007 Å

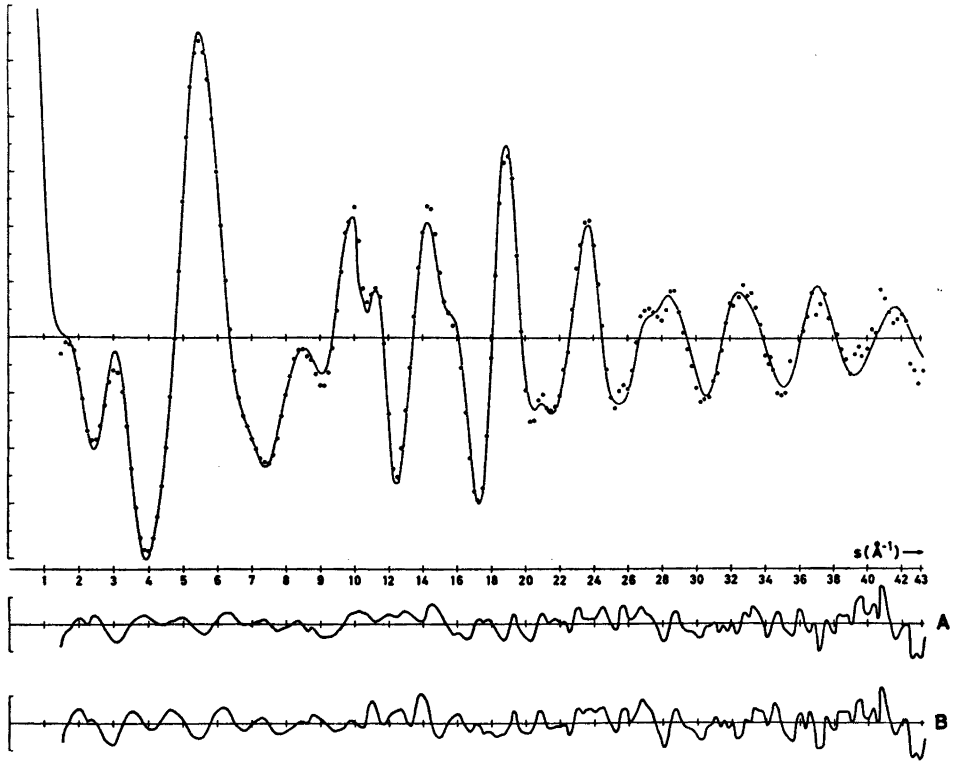

Fig. 3. Experimental (dotted) and theoretical intensity functions for 2,2′-dichlorobiphenyl. The theoretical curve corresponds to model A. The lower part of the curve shows the differences between experimental and theoretical values for model A and model B.

Including the chlorine atom in the least-squares plane the deviations vary between 0.01 and 0.03 Å.

The "twist angle" about the C1 – C1' bond may now be calculated to be as follows (*cf.* the introductory remarks): The angle between the least-squares planes through the chlorophenyl moieties is 68.5°; the angle between the corresponding planes excluding the chlorine atoms is 66.8°; the dihedral angle C2'C1'C1C2 is 69.2°.

ELECTRON DIFFRACTION INVESTIGATION

Experimental

Two sets of diffraction diagrams were recorded by the Oslo unit,[19] with nozzle-to-plate distances of 480.12 mm (set I) and 200.81 mm (set II), respectively. The nozzle temperature was about 300 °C and the electron wave-length 0.06458 Å. The data from five plates from set I (s range 1.50 $Å^{-1}$ to 19.125 $Å^{-1}$) and four plates from the II (s range 7.25 $Å^{-1}$ to 44.0 $Å^{-1}$) were plotted and found satisfactory. A composite intensity curve was then calculated (see Fig. 3).

The data were processed in the usual way.[20] The modified molecular intensities were calculated using the modification function

$$s/(|f_C'||f_{Cl}'|).$$

The elastic scattering amplitudes were calculated for the applied accelerating potentials by the partial wave method.[21] The atomic potentials for carbon and chlorine were from Ref. 22, for hydrogen from Ref. 18.

Structure determination and refinement

An experimental radial distribution (RD) curve [20] (see Fig. 4) was calculated by Fourier transformation of the experimental intensity

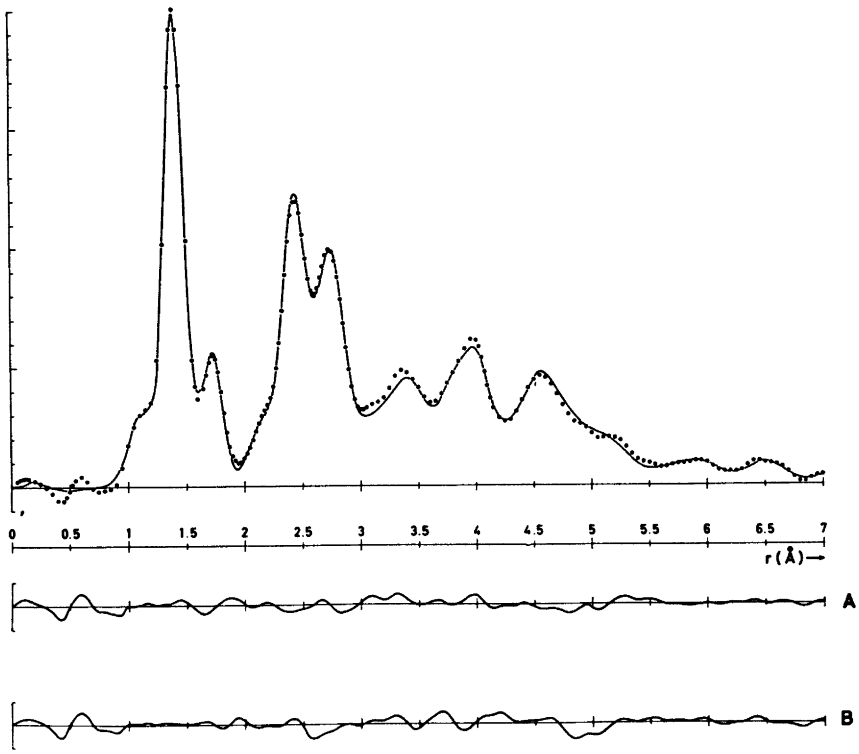

Fig. 4. Experimental (dotted) and theoretical radial distribution functions for 2,2'-dichlorobiphenyl (artificial damping, $k = 0.002$ Å^2) calculated by Fourier inversion of the curves in Fig. 3. Difference curves corresponding to those in Fig. 3 are also shown.

curve in Fig. 3. Comparison with theoretical RD curves showed, in agreement with the previous investigation, that the main conformer is closer to *syn* than to *anti*, and that the amount of a possible second conformer must be small. The structure was therefore refined by the least-squares method, assuming one conformer only.

Two models were considered in the calculations. The independent parameters which may be refined, were the same in both models, *i.e.*

$(C-C)_{ring}$	(all assumed equal)
C–C1′	
C–Cl	
C–H	(all assumed equal)
∠C1C2Cl	
∠C1C6H6	

β: angle between the CCl bond and the ring plane
ϕ: angle of twist about the bridge bond
The models differ in the assumptions about the bond angles.

Model A: All bond angles except those involving Cl and H6 were assumed to be 120°.

Model B: The X-ray results show that the angles in the ring deviate somewhat from 120°. The following values, which are close to the X-ray results, were therefore tried in the electron-diffraction study.

∠C2C1C6 = 116.2°
∠C1C2C3 = C1C6C5 = 122.9°
∠C2C3C4 = C6C5C4 = 119.0°
∠C3C4C5 = 120°.

It was not possible to refine the angles β and ϕ simultaneously. Refinements were therefore carried out with fixed values of β. With $\beta = 0°$ ϕ was found to be 75.0° for model A and 72.2° for model B. With $\beta = 2°$, *i.e.* close to the result obtained in the X-ray investigation, the values were 73.5° (model A) and 70.0° (model B). The results for the bond distances and bond angles did not vary significantly with this change in β.

The results obtained by least-squares refinement of model A with $\beta = 2°$ are given in Table 4. Since the least-squares refinements were carried out with a diagonal weight matrix, the standard deviations have been corrected as described by Seip and Stølevik.[23]

The most important non-bonded distances corresponding to the parameters in Table 4 are given in Table 5.

Only a few of all the mean amplitudes of vibration (u) [24] given as u^{obs} in Tables 4 and 5 were refined with the other parameters. The other values were fitted by additional refinements and by trial and error. To check that the values for the important distances were reasonable, tentative values were computed as described by Stølevik *et al.*[26] These values, which correspond to 300 °C, are included as u^{calc} in Tables 4 and 5, and the force constants used are given in Table 6. The agreement with the values used in the electron-diffraction study, seems quite satisfactory.

DISCUSSION

Table 4 shows that the average of the $(C-C)_{ring}$ bonds is found 0.012 Å longer and

Table 4. Structural parameters for 2,2′-dichlorobiphenyl. The electron diffraction results (ED) were obtained by assuming rings with sixfold symmetry (Model A). The standard deviations given in parentheses apply to the last decimal place.

	ED r_a(Å) [25]	u^{obs}(Å)	u^{calc}(Å)	XD[a] r(Å)		ED angles (degrees)	XD[a] angles (degrees)
$(C-C)_{ring}$	1.398(2)	0.042(3)	0.048	1.386 (average)	∠C1C2Cl	121.4(9)	120.0(2)
C1–C1′	1.495(9)	0.043(15)	0.052	1.493(5)	∠C1C6H6	125.5(35)	
C–Cl	1.732(4)	0.048(4)	0.055	1.748(3)	β	(2.0)[b]	2.3
C–H	1.095(10)	0.072	0.077	0.98	ϕ	73.5(20)	67–69

[a] The distances corrected or thermal motion are given (X-ray diffraction). [b] β, the angle between the C–Cl bond and the ring plane, was not varied.

Table 5. Non-bonded distances and the corresponding mean amplitudes of vibration from electron diffraction. The mean amplitudes calculated with the force constants given in Table 6 are also given.

	r_a(Å)	u^{obs}(Å)	u^{calc}(Å)
C1···C3	2.42	0.062	0.060
C1···C4	2.80	0.069	0.066
C1···C2′	2.51	0.074	0.079
C1···C3′	3.79	0.072	0.078
C1···C4′	4.29	0.070	0.079
C2···C2′	3.24	0.152	0.138
C2···C3′	4.53	0.157	0.146
C2···C4′	5.14	0.142	0.138
C2···C5′	4.71	0.129	0.131
C2···C6′	3.48	0.120	0.121
C3···C3′	5.87	0.157	0.146
C3···C4′	6.50	0.133	0.125
C3···C5′	6.01	0.128	0.131
C4···C4′	7.09	0.115	0.098
C1···Cl2	2.74	0.076	0.078
C3···Cl2	2.70	0.085	0.079
C4···Cl2	4.00	0.085	0.079
C5···Cl2	4.53	0.082	0.080
C6···Cl2	4.03	0.086	0.078
C1···Cl2′	3.05	0.171	0.140
C2···Cl2′	3.38	0.245	0.209
C3···Cl2′	4.38	0.248	0.266
C4···Cl2′	4.98	0.252	0.283
C5···Cl2′	4.76	0.249	0.270
C6···Cl2′	3.86	0.238	0.219
Cl···Cl	3.58	0.314	0.296

the C–Cl bond 0.016 Å shorter in the X-ray than in the electron-diffraction investigation. The reason is probably a small shift in the centre of gravity of the carbon electrons relative to the nuclei towards the ring centre, giving a small systematic error in the X-ray results.

The molecule is found to be in a form closer to the *syn* than to the *anti* form both in the crystalline and in the gaseous state with a twist angle of about 70° in both cases. The twist angle found in the electron-diffraction investigation assuming planar chlorophenyl groups ($\beta = 0$) of 75° (model A) or 72° (model B) may be compared with the X-ray result of 68.5° if the chlorine atoms are included in the definition of the least-squares planes. The assumption of $\beta = 2°$ in the electron-diffraction work gives a twist angle of 73.5° or 70.0° which may be compared to the result from the X-ray analysis of 66.8° between the least-squares planes through the carbon atoms of each ring. The difference of 3–7° found by the two methods may be real. A somewhat larger angle in the gaseous phase seems reasonable; the amplitude of torsional oscillation about the central bond is larger at the nearly 300 °C higher temperature, and the oscillation is probably rather anharmonic, the Cl-Cl′ separation being as small as 3.43 Å (in the solid). However, the twist angle is not well determined by the electron-diffraction method partly because of the large oscillations about the bridge bond

Table 6. Force constants used in the calculation of mean amplitudes of vibration. The number of contributions of each type is given in parentheses.

Stretching force constants (mdyn Å^{-1})

$(C-C)_{ring}$	5.40(12)
C1–C1′	4.60(1)
C–H	4.70(8)
C–Cl	3.40(2)

Coupling constant (mdyn Å^{-1})

C1–C2/C2–C3	0.75 (12)

Bending force constants (mdyn Å rad^{-2})

$(CCC)_{ring}$	0.70(12)
C1′C1C	0.90(4)
HCC	0.38(16)
ClCC	1.15(4)

Repulsion force constants (mdyn Å^{-1})

C1···C3	0.45(12)
C1···C4	0.20(6)
C1···H6	0.34(16)
Cl···Cl	0.05(1)

Torsional force constants (mdyn Å rad^{-2})

C1C2C3C4	0.12(12)
C1C2C3H3	0.09(24)[a]
H3C3C4H4	0.07(12)[a]
C2C1C1′C2′	0.08(4)

[a] The torsional force constants of this type were assumed to be the same also in cases where the H atoms are replaced by C or Cl.

which gave a large u value for the Cl−Cl distance, and partly because the result depends somewhat on the assumptions about the bond angles.

In agreement with the investigation by Bastiansen,[4] the electron-diffraction data give no evidence for more than one conformer even at 300 °C. The amount of a possible second form which can be introduced without destroying the agreement between experimental and theoretical curves, depends on the ϕ angle assumed for the second form. The RD function for a form with $\phi \approx 105°$ does not differ drastically from the function shown in Fig. 3, and up to 25 % of a form of this kind might be difficult to detect. However, a somewhat larger ϕ value is more probable, and changing ϕ to about 120° (*cf.* Table 1) gives a considerable change in the RD curve. If this ϕ value is correct an upper limit for a second conformer seems to be about 15 %.

Acknowledgements. The authors are grateful to Professor O. Bastiansen for helpful discussions and Cand. Real. A. Almenningen for recording the electron-diffraction data.

REFERENCES

1. Bastiansen, O. *Acta Chem. Scand. 3* (1949) 408.
2. Almenningen, A. and Bastiansen, O. *Kgl. Norske Vidensk. Selsk. Skr.* (1958) No. 4.
3. Bastiansen, O. and Smedvik, L. *Acta Chem. Scand. 8* (1954) 1593.
4. Bastiansen, O. *Acta Chem. Scand. 4* (1950) 926.
5. Almenningen, A., Hartmann, Å. O. and Seip, H. M. *Acta Chem. Scand. 22* (1968) 1013.
6. Bastiansen, O., Seip, H. M. and Boggs, J. E. In Dunitz, J. O. and Ibers, J. A., Eds., *Perspectives in Structural Chemistry*, Vol. IV, Wiley, New York 1971.
7. Trotter, J. *Acta Crystallogr. 14* (1961) 1135.
8. Robertson, G. B. *Nature (London) 191* (1961) 593.
9. Hargreaves, A. and Hasan Rizvi, S. *Acta Crystallogr. 15* (1962) 365.
10. Guy, J. *J. Chim. Phys. 46* (1949) 469.
11. Fischer-Hjalmars, I. *Tetrahedron 19* (1963) 1805.
12. Dewar, M. J. S. and Harget, A. J. *Proc. Roy. Soc. (London) A 315* (1970) 443.
13. Tinland, B. *Theor. Chim. Acta 11* (1968) 452.
14. Gropen, O. and Seip, H. M. *Chem. Phys. Lett. 11* (1971) 445.
15. Farbrot, E. M. and Skancke, P. M. *Acta Chem. Scand. 24* (1970) 3645.
16. Dahl, T., Gram, F., Groth, P., Klewe, B. and Rømming, C. *Acta Chem. Scand. 24* (1970) 2232.
17. Hanson, H. P., Herman, F., Lea, J. D. and Skillman, S. *Acta Crystallogr. 17* (1964) 1040.
18. Stewart, R. F., Davidson, E. R. and Simpson, W. T. *J. Chem. Phys. 42* (1965) 3175.
19. Bastiansen, O., Hassel, O. and Risberg, E. *Acta Chem. Scand. 9* (1955) 232.
20. Andersen, B., Seip, H. M., Strand, T. G. and Stølevik, R. *Acta Chem. Scand. 23* (1969) 3224.
21. Peacher, J. and Wills, J. C. *J. Chem. Phys. 46* (1967) 4809.
22. Strand, T. G. and Bonham, R. A. *J. Chem. Phys. 40* (1964) 1686.
23. Seip, H. M. and Stølevik, R. In Cyvin, S. J., Ed., *Molecular Structures and Vibrations*, Elsevier, Amsterdam 1972, Chapter 11.
24. Cyvin, S. J. *Molecular Vibrations and Mean Square Amplitudes*, Universitetsforlaget, Oslo, and Elsevier, Amsterdam 1968.
25. Kuchitsu, K. and Cyvin, S. J. In Cyvin, S. J., Ed., *Molecular Structures and Vibrations*, Elsevier, Amsterdam 1968, Chapter 12.
26. Stølevik, R., Seip, H. M. and Cyvin, S. J. *Chem. Phys. Lett. 15* (1972) 263.

Received February 1, 1974.

Acta Chemica Scandinavica A 28 (1974) 515—527

The Crystal Structures of the Orientationally Disordered, Cubic High-temperature Phases of Univalent Metal Perchlorates

K. O. STRØMME

Department of Chemistry, University of Oslo, Blindern, Oslo 3, Norway

A model of the orientationally disordered crystal structures of the cubic, high-temperature phases of a series of isostructural univalent metal perchlorates has been proposed. The perchlorate ions are found to occupy statistically two distinct sets of orientation in a given frame of the metal ions. Each set comprises a number of crystallographically equivalent orientations separated by potential barriers. X-Ray diffraction and transition entropies are interpreted in terms of the model.

The crystalline perchlorates of sodium, ammonium, potassium, rubidium, cesium, univalent thallium, and silver transform into a cubic high temperature phase [1] at higher temperatures (Table 1). Apart from sodium and (possibly) silver perchlorate, the compounds are isostructural at room temperature, the ratios of the axes of the orthorhombic unit cell being nearly the same for all compounds.[2] The crystal structures of the room-temperature phases of ammonium, potassium, and sodium perchlorate have been reported.[3-7] Sodium perchlorate transforms gradually into the high-temperature phase on heating. The other compounds change rather abruptly into the new phase. Decomposition of most perchlorates occurs at temperatures considerably above the transition points.[8]

The cubic high-temperature phases are face-centred with four formula units per unit cell (Table 1).[9,10] Finbak and Hassel suggested that the anion polyhedra rotate in the high temperature phases.[16] Referring in particular to sodium, ammonium and potassium perchlorate, a plausible rotation model was presented according to which the tetrahedrons rotate about the [100]-, [010]-, and [001]-directions, the chlorine atoms being situated at the origin and the metal ions in $(\frac{1}{2}\frac{1}{2}\frac{1}{2})$ *etc.*, as proposed previously.[9,10] The model was not checked in detail against experimental data. The idea that the high-temperature phases are disordered is supported by other kinds of evidence, such as the high transition heats observed in these solids (Table 1).

In agreement with more recent views,[17,18] the polyatomic anions are in this work assumed to librate in preferred orientations most of the time (Frenkel model of disorder), rather than to rotate more or less freely in the disordered phases (Pauling model). The latter case represents a strongly excited state compatible with relatively high temperatures. Only a few examples of quasi-free rotation are known in the solid state according to Janik *et al.*[19] An example is the ammonium ion in ammonium perchlorate.[19-22]

EXPERIMENTAL

Commercially available sodium and potassium perchlorate were used without further purification. The other compounds were obtained from aqueous solutions prepared by adding together solutions of approximately equimolecular amounts of perchloric acid and one of the metal salts (carbonate or chloride), and evaporating subsequently the excess water. The crystals were purified by repeated crystallizations from aqueous solutions and dried at about 150 °C.

The Bragg reflections of powdered samples of sodium, ammonium, potassium, and rubidium perchlorate were recorded with an automatic X-ray diffractometer, model GEXRD3, equipped with a high-temperature X-ray diffractometer furnace, Model TemPres Sx, using CuKα-radiation. The precision of the temperature

Table 1. Crystallographic data for face-centred cubic phases of univalent metal perchlorates along with transition temperatures, t_t, and heats, ΔH_t. $n=4$ formula units per unit cell.

	$NaClO_4$	NH_4ClO_4	$KClO_4$	$RbClO_4$	$CsClO_4$	$TlClO_4$	$AgClO_4$
a(Å)	7.27[a]	7.66[a]	7.49[a]	7.65[a]	7.98[a]	7.63[a]	6.95[a]
$t_{exp.}$ (°C)	380	270	340	320	250	280	200
a(Å)	7.08± 0.02[b]	7.67± 0.02[b]	7.50± 0.02[b]	7.70± 0.01[b]	7.98± 0.02[b]	7.70± 0.01[b]	7.00± 0.01[b]
$t_{exp.}$ (°C)	314	243	310	300	230	280	160
a(Å)	7.085± 0.005	7.71± 001	7.510± 0.005	7.720± 0.005	7.990± 0.002[c]		
$t_{exp.}$ (°C)	322	249	310	300	320		
t_t(°C)	308[a,b]	240[a,b]	299.5[a,b]	279[a,b]	219[a,b]	266[a,b]	155– 159[a]
	313[d]	240[d]	300[d]	281[d]	224[d]	269	155[b]
	306.5*	240[e]	303[f]	284[f]	225[f]		157 and 175[d]
	307	240	302.3	284	223		97 and 154
ΔH_t(kcal/mol)	2.43**	2.15± 0.18[g]	3.29[h]	3.0± 0.1[f]	2.0± 0.2[f]		0.248 at 97°C
		2.3± 0.2[e]	3.25	2.78	1.80	2.39	0.79 at 154 °C
		2.48					

*C_p-peak position, **ΔH_t= integrated excess heat capacity. [a,b,c,d,e,f,g,h] = Refs. 9, 10, 11, 8, 12, 13, 14, 15, respectively.

reading is about ± 2 °C. Ammonium perchlorate was sealed in (pyrex) capillaries subsequently mounted in the sample holder, to avoid dissociation and sublimation. The other samples were pressed gently into the sample holder to minimize orientational effects. The intensity of certain reflections changed slightly in some cases from one run to the other, possibly due to orientational effects. The intensities of the graphically recorded reflections were obtained by weighing the areas under the intensity peaks and corrected for systematic effects due to multiplicity, orientational and polarization factors in the usual way. Structure factor amplitudes are listed in Table 5.

The heat capacity of sodium perchlorate was measured in the temperature range from 26 to 409 °C, using an adiabatic calorimeter.[23] The polycrystalline sample of about 50 g was preheated in a quartz holder to about 380 °C before the measurements were started. Two series of measurements were made. Peak details were studied in the second run. For some unknown reason, the peak shifted slightly towards higher temperatures in the second run.

Numerical results are listed in Table 2. The precision in single temperature and heat capacity measurements ranges from 0.01 to 0.1 °C and from 0.2 to 0.6 %, respectively.[23] The heat capacity of the first series is plotted against temperature in Fig. 1. The transition starts very slowly between 350 and 400 K. The rate of change of the heat capacity increases gradually with temperature till a maximum and then decreases until the heat capacity approaches a constant value. Then a very strong increase sets in, the curve passes through the maximum at

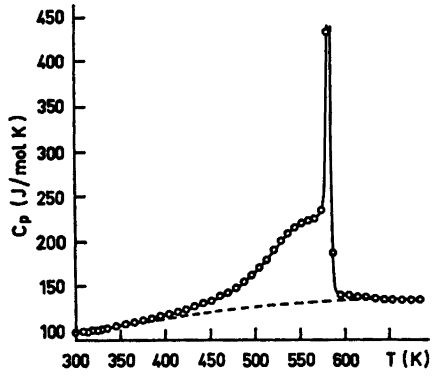

Fig. 1. Heat capacity of sodium perchlorate plotted against temperature.

Table 2. Heat capacity of solid sodium perchlorate from room temperature to about 410 °C. Peak maximum at about 579.6 K according to the second run. Asterisk denotes the first measurement (after a break), which is somewhat uncertain.

First run				Second run (peak details)	
T (K)	C_p (J/K mol)	T (K)	C_p (J/K mol)	T (K)	C_p (J/K mol)
315.0	99.3*	528.6	199.9	299.1	98.5*
325.3	101.2	536.2	207.9	309.5	99.5
335.4	103.3	543.7	214.9	319.7	100.8
345.5	105.5	551.1	220.1	329.9	102.0
355.5	107.2	558.4	222.7	576.2	464.3*
365.4	109.2	565.7	225.1	576.9	450.6
375.3	111.7	573.0	235.2	577.6	478.5
385.0	113.6	578.9	433.0	578.4	464.0
394.8	116.0	585.3	186.6*	578.9	791.8
404.4	118.3	594.2	140.1	579.2	1334.4
414.0	120.7	603.7	139.5	579.5	1623.2
423.5	123.4	613.3	138.0	579.7	1536.1
432.9	127.1	623.0	137.7	579.9	1215.4
442.3	130.3	632.8	136.5	580.4	616.8
451.6	133.1	642.6	135.5	581.1	328.5
460.7	138.3	652.5	135.4		
469.8	142.0	662.4	134.7		
478.7	147.2	672.4	135.5		
487.4	154.1	682.5	134.8		
496.1	161.8				
504.5	170.4				
512.7	178.7				
520.8	189.7				

about 580 K and drops off very quickly to a "normal", approximately constant heat capacity at 650 K. This remarkable behaviour of the heat capacity indicates that the transition is a compound process, occurring in several steps. A further study of this requires more experimental data for the transition region. However, some general comments may be appropriate. The process is presumably an orientational order-disorder process. At room temperature, the *a* and *b*-axes are very similar, the reported values being not significantly different from the cubic axis measured at about 314 °C, while the *c*-axis is considerably shorter. Inspection of the crystal structure and space group indicates that the structure may pass through a tetragonal phase before changing into the cubic structure.

The integrated excess heat capacity was determined by weighing the peak bounded by the heat capacity curve and a smooth curve drawn below the peak in Fig. 1, *etc.* The integrated excess heat capacity divided by the absolute temperature was determined in a similar way. These quantities, put equal to the heat and entropy of the transition, respectively, are given in Table 1 and Table 8, respectively. The actual fraction of the given figures attributable to changes in orientational order alone, is somewhat uncertain because of the arbitrariness associated with drawing the basis line extending over a considerable temperature interval.

Differential scanning calorimetry curves of polycrystalline samples were run for all compounds, using a Perkin Elmer differential scanning calorimeter and indium as reference substance. The peak areas were determined by weighing as in the preceding case. Numerical results are listed in Table 1. Diff. scan. curves are shown in Fig. 2. The standard deviation in the measured peak areas is of the order of 1 %. The diagrams of silver perchlorate contain four endotherms, of which the two small peaks are not represented in Table 1. These endotherms changed in repeated runs, the others not. The origin of the first three peaks is not certain. They have been suggested to originate in absorbed moisture.[8]

SPACE GROUP

The following space groups are compatible with the extinction rules of the X-ray reflections: $F23$, $F\bar{4}3m$, $F432$, $Fm3$, and $Fm3m$, of which the two first ones were chosen in the original model assuming an ordered structure,[10,11] while the last one corresponds to the rotationally disordered structure of Finbak and Hassel.[16] Only the last two space groups are centrosymmetric. Since the ordered room temperature phases are centrosymmetric, the high-temperature phases are probably centrosymmetric too. The difference between the two centrosymmetric space groups is that $Fm3m$ possesses a mirror plane in the (100) plane *etc.*, $Fm3$ not. Since there is apparently no long range order in these high-temperature phases, two positions equivalent *via* this mirror plane must be considered equally probable. This leaves $Fm3m$ as the most probable space group of the statistical structure. The same space group is also found in a number of other, disordered, face-centred cubic structures.[24-26]

MOLECULAR EQUILIBRIUM POSITIONS

The perchlorate ions are assumed to be situated at (000), $(\pm\frac{1}{2},\pm\frac{1}{2},0)$, $(0,\pm\frac{1}{2},\pm\frac{1}{2})$ and $(\pm\frac{1}{2},0,\pm\frac{1}{2})$ *etc.*, with the metal ions in the

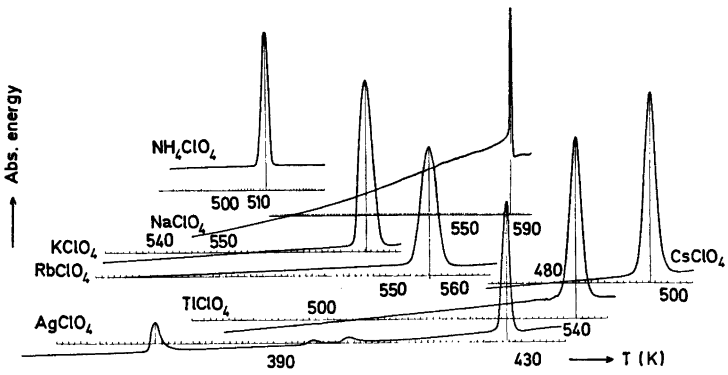

Fig. 2. Differential scanning calorimetry diagrams. Heating rate: 8 °C/min.

average positions $(\pm\frac{1}{2},0,0)$, $(0,\pm\frac{1}{2},0)$, $(0,0,\pm\frac{1}{2})$ and $(\pm\frac{1}{2},\pm\frac{1}{2},\pm\frac{1}{2})$ *etc.*, in agreement with previous assumptions.[9,10] The problem is to locate the statistical equilibrium orientations of the anions at these sites. The main intermolecular attraction originates in neighbouring metal-oxygen interactions, while coulombic repulsions [27] should tend to maximize chlorine-metal separations. The oxygen-metal equilibrium contact distances are assumed to be relatively close to the sum of the van der Waals and ionic radii for these atoms,[28] respectively, in agreement with observations in other orientationally disordered solids,[24,29-32] and in ordered structures,[3-7,33-36] which may, however, show a considerable variation in the metal-oxygen contact distance, as reflected in the lower crystal symmetry.

Furthermore, at least three oxygen atoms of the perchlorate ion are assumed to participate in "bond" formation with metal ions in the equilibrium state. Inspection shows that only a small orientational change is in general needed to turn a perchlorate ion, having only two O-atoms in close contact with neighbouring metal ions, into a position where three or all four oxygens make close contact with the other species.

It seems also reasonable to expect the perchlorate ions to be situated (statistically) in special positions of the space group, given that the metal ions are in special positions. The perchlorate ion is assumed to be tetrahedrally symmetric with a given chlorine-oxygen bond length.

The distinct molecular orientations considered as possible, statistically averaged, equilibrium positions of the anion are given in Fig. 3, including the corresponding numbers of equivalent orientations per site according to *Fm3m*. The positions represent a great variety of orientations, when all equivalent orientations are taken into account. However, a general orientation of the anion is missing because it was difficult to select one such position not closely related to one of those already shown, or which seemed likely as an equilibrium orientation according to the rules mentioned.

The various, equivalent orientations of a given set are in principle separated by potential barriers, since reorientation from one position to another requires breaking original O–Me "bonds" and establishing new ones in the equivalent orientation.

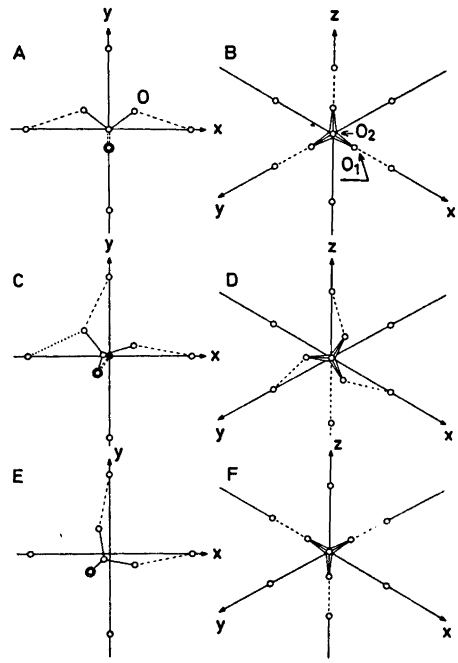

Fig. 3. Various orientations of the perchlorate ion in the face-centred cubic unit cell. Location of molecular symmetry elements and number of crystallographically equivalent orientations per molecule:
A: $\bar{4}\,||\,[010]$, [101] and $[\bar{1}01]$; $g=6$.
B: $\underline{3}\,||\,[111]$; $g=8$.
C: $\bar{4}$ and m in (001); $g=24$.
D: $3\,||\,[111]$; $g=16$.
E: $\bar{4}\,||\,[110]$; $g=12$.
F: $3\,||\,[111]$, $[\bar{1}11]$, $[1\bar{1}1]$ and $[11\bar{1}]$; $g=2$.

Molecular positions A and F are locked with the chlorine atom at the origin. In the other models, the O–Me distances may be adjusted by translation (B, E, D) and/or rotation (C), keeping the molecule in the same special position. A and B were found to satisfy reasonably well the requirements discussed above. O–Me distances are listed in Table 3. The contact distances *calculated* in A are in general not much different from those *assumed* in B, except perhaps for $NaClO_4$. However, reported Na–O contact separations show a relatively wide distribution about the average value. The corresponding distances listed for $CsClO_4$ are con-

Table 3. Metal-oxygen distances referring to perchlorate positions A and B (Fig 3), respectively. $d(Cl-O)=1.42$ Å (ass.), crystallographic data taken from Table 1, tetrahedral symmetry assumed for the perchlorate ion.

	$NaClO_4$ 314 °C (Å)	$NaClO_4$ 380 °C (Å)	NH_4ClO_4 249 °C (Å)	$KClO_4$ 310 °C (Å)	$RbClO_4$ 300 °C (Å)	$CsClO_4$ 320 °C (Å)	$TlClO_4$ 280 °C (Å)	$AgClO_4$ 160 °C (Å)
A								
$O(xy0)-Me(\frac{1}{2}00)$	2.52	2.61	3.82	2.72	2.82	2.95	2.81	2.48
$O(xy0)-Me(0\frac{1}{2}0)$	2.96	3.04	3.25	3.16	3.25	3.38	3.24	2.92
$Cl(000)-Me(\frac{1}{2}00)$	3.54	3.63	3.86	3.75	3.86	4.00	3.85	3.50
B								
$O_1(xyy)-Me(\frac{1}{2}00)$	2.44(ass.)	2.45(ass.)	2.86(ass.)	2.76(ass.)	2.86(ass).	2.96(ass.)	2.82(ass.)	2.46(ass.)
$O_2(xxx)-Me(-\frac{1}{2}00)$	2.91	3.00	3.17	3.08	3.17	3.29	3.17	2.87
$Cl(xxx)-Me(-\frac{1}{2}00)$	3.37	3.52	3.62	3.51	3.62	3.70	3.62	3.29
$Cl(xxx)-Me(\frac{1}{2}00)$	3.73	3.76	4.14	4.03	4.14	4.25	4.11	3.73

siderably less than the sum of the reported contact radii (3.09 Å) and may possibly be too short in the equilibrium state. This would rule out A, in agreement with the result of the entropy analysis, which indicates that A or B is inaccessible.

C is the most asymmetric position shown in Fig. 3. Two O atoms and the Cl atom are placed in the (001) mirror plane. The number of O – Me contacts is generally quite reasonable, the arrangement of such contacts appears, however, to be somewhat arbitrary. C may be changed into A by a relatively small positional shift, establishing a close O2 – Me($-\frac{1}{2}00$) contact at the expence of the O2 – Me($0\frac{1}{2}0$) contact. Although C may not appear likely at equilibrium, it cannot presently be definitely ruled out. The subsequent analysis indicates, however, that C-population is either small or zero.

In B and D, three O atoms are in close contact with three metal ions. D may be transferred into B without breaking any of the Me – O contacts. These two positions are therefore hardly separated by a potential barrier. The O – Me contacts in B resemble the "aragonite-type" found in univalent metal nitrates.[27-30]

Position E, involving two Me – O contacts only, may, for instance, be transferred into one of the A equivalents by rotating an angle of 45° about and translating the group along the [110]-direction, without breaking the O – Me contacts. E represents therefore hardly a potential minimum at all.

In F the O – Cl bonds lie along the four equivalent body diagonals of the unit cell. The O – Me contacts are too long to render the position likely as an equilibrium orientation. The population of F would at any rate be expected to be small. The most probable equilibrium positions are thus A and B, giving rise to a satisfactory interpretation of X-ray and transition entropy data for these compounds.

ANALYSIS OF X-RAY DIFFRACTION DATA

X-Ray structure factor sets were calculated for A and B, assuming all atoms to be neutral. The form factors of Hanson *et al.* were used.[37] Basic positional parameters are listed in Table 4. The Cl – O bond length was assumed equal to 1.42(0.02) Å, which is the average value of recently reported Cl – O distances in perchlorates [6,38,39] (e.s.d. in parenthesis). The positions of the hydrogen atoms in ammonium perchlorate are not known. A spherical [40] distribution of these atoms centred about N at a distance of 1.02 Å (NH bond length) was therefore assumed, corresponding to (quasi) free rotation of the ammonium group. A linear combination of the two sets of structure factors was formed. Thus, $F_C = x_A F_A + x_B F_B$, where F_A is the calculated structure factor based on model A and

Table 4. Positional coordinates for atoms in perchlorate ions in orientations A and B, respectively, derived from Table 2.

A. All O atoms crystallographically equivalent.
$x(\mathrm{Cl}) = y(\mathrm{Cl}) = z(\mathrm{Cl}) = z(\mathrm{O}) = 0$
B. Three O atoms in each ion equivalent through operation of the three-fold symmetry axis.
$x(\mathrm{Cl}) = y(\mathrm{Cl}) = z(\mathrm{Cl})$, $y_1(\mathrm{O}) = z_1(\mathrm{O})$ and $x_2(\mathrm{O}) = y_2(\mathrm{O}) = z_2(\mathrm{O})$.
Metal ions at ($\pm\frac{1}{2}00$) *etc.*

Atomic position	$NaClO_4$ (314 °C)	$NaClO_4$ (380 °C)	NH_4ClO_4	$KClO_4$	$RbClO_4$	$CsClO_4$	$TlClO_4$	$AgClO_4$
A								
$x(\mathrm{O})$	0.164	0.159	0.150	0.154	0.150	0.145	0.151	0.166
$y(\mathrm{O})$	0.116	0.113	0.106	0.109	0.106	0.103	0.106	0.117
B								
$x(\mathrm{Cl})$	−0.026	−0.017	−0.034	−0.035	−0.034	−0.030	−0.031	−0.032
$x_1(\mathrm{O})$	0.167	0.171	0.143	0.147	0.143	0.141	0.146	0.163
$y_1(\mathrm{O})$	−0.064	−0.054	−0.069	−0.071	−0.069	−0.065	−0.067	−0.071
$x_2(\mathrm{O})$	−0.141	−0.129	−0.140	−0.144	−0.140	−0.133	−0.138	−0.149

Table 5. Observed and calculated structure factors based on a combination of A and B. Unobserved and overlapping reflections excluded from the R-value calculations. Overlapping reflections computed according to the formula $(\sum pF^2/\sum p/N)^{\frac{1}{2}}$, where p denotes the multiplicity of the reflections and N is the number of overlapping reflections included in the sum. The listed F_o-values of the non.obs. reflections (n.o.) were computed according to $I_{n.o.}(hkl) < \frac{1}{2} I_{obs.min.}(hkl)$.

	$NaClO_4$(322 °C)			NH_4ClO_4			$KClO_4$			$RbClO_4$		
B(is.):	9.0 Å²			4.0 Å²			7.0 Å²			7.0 Å²		
$x_A A + x_B B$:	$x_A = 0.33$			$x_A = 0.37$			$x_A = 0.68$			$x_A = 0.79$		
	$R = 0.094$			$R = 0.064$			$R = 0.063$			$R = 0.063$		
hkl	F_o	F_c		F_o	F_c		F_o	F_c		F_o	F_c	
111	54.6	55.63		67.1	70.44		33.2	35.68		16.7	−23.26	
200	104.7	97.11		98.7	100.33		123.7	125.71		194.1	191.43	
220	47.6	52.26		56.3	57.51		75.6	77.02		133.5	130.66	
311	≤ 5.1	−3.75		≤ 9.0	3.15		18.6	20.83		62.9	−63.78	
222	28.6	35.32		44.6	40.24		64.3	59.90		101.6	105.82	
400	26.7	24.05		≤22.6	10.93		38.2	35.57		71.3	76.60	
331	≤ 7.0	0.09		17.7	10.19		≤ 6.4	−10.33		34.9	−43.95	
420	20.9	22.63		21.7	21.44		34.0	33.83		69.8	67.44	
422	24.1	19.63		26.6	23.33		31.6	34.63		64.5	64.83	
333	≤11.4	1.48	2.90	≤19.0	9.37	7.07	≤ 9.8	1.01	9.21	41.7	−21.40	41.21
511		2.21			2.02			−7.49			−31.30	
440	≤14.0	12.99		≤24.4	20.60		31.1	21.78		55.4	43.52	
531	≤ 7.0	1.91		≤12.8	6.60		≤ 6.6	− 4.62		≤12.0	−22.99	
600	19.7	11.76	15.38	≤24.4	16.54	26.21	40.0	23.75	33.69	62.9	45.11	63.11
442		10.64			19.00			23.84			45.11	
620	≤10.8	8.80		≤19.4	3.25		15.2	17.10		37.9	35.33	
533	≤10.8	1.51		≤20.2	2.05		≤10.3	0.15		≤19.0	−12.44	
622	≤10.8	7.36		≤20.4	3.52		14.6	15.27		37.9	31.15	

$x_A = 1 - x_B$ is the fraction of anions occupying A-type positions *etc.* The linear coefficient, x_A, was refined by least squares methods, using an invariant temperature factor. The weight factor, w, assigned to each reflection, is given as $w = 1/[2F_o(\min) + F_o + 2F_o^2/F_o(\min)]$. The B-value was varied in a series of refinements. Both R and x_A changed in general considerably with B. Observed and calculated structure factors *etc.*, corresponding to the best agreement obtained between observed and calculated structure factors, are listed in Table 5. Systematic effects due to neglect of anisotropy in the refinement process along with the low rate of change of the $\sum w(\Delta F)^2$-function about the minimum value *etc.*, render the linear coefficient values somewhat uncertain. The weighted R-values, R_w, are from 6 (for $NaClO_4$) to 33 % (for NH_4ClO_4) less than the corresponding R_w-values derived from the single structure giving rise to the best fit between observed and calculated structure factors. The corresponding agreement obtained for the non-observed and overlapping reflections on the basis of the structural combinations is considerably better than those based on the single structures in all cases studied. Finally, the present agreement factors are mostly much less than those obtained on the basis of the free rotation model.

In view of the uncertainty in the Cl – O bond length and the translational position of the anion along the [111]-direction in case B, together with the approximation involved in using a common, isotropic temperature factor for all atoms *etc.*, the agreement between observed and calculated structure factors listed in Table 5 is considered to be satisfactory. *Significant* improvement of the translational position of B in the [111]-direction by least squares techniques appears to be unlikely in view of the present limitations. As to be expected, the B-values are relatively high. This is attributable to relatively large vibrational amplitudes and to the circumstance that the instantaneous equilibrium positions are distributed statistically about the mean values.

INTERPRETATION OF TRANSITION ENTROPY DATA

The number of equivalent orientations of type A and B is 6 and 8 per anion, respectively, according to space group $Fm3m$. Inspection shows that many configurations implied statistically involve intermolecular O – O separations less than the smallest separation attainable, here taken to be twice the van der Waals radius of oxygen, 2.80 Å. Such configurations are therefore sterically blocked and thus thermodynamically inaccessible.

Assigning a common weight factor to all accessible configurations, the configurational entropy, S_c, for such a system may be expressed as [29,31] $S_c = \mathbf{k} \ln [W_o(1-P)]$, where $\mathbf{k}$ = Boltzmann constant and PW_o is the number of sterically blocked configurations among the W_o ones implied statistically. The generally very complicated function P has previously been approximated as $(1-s)^n$, corresponding to breaking the total system down to n identical micro-systems, each of which comprising only a few lattice sites (molecules). Here each microsystem is defined as a central lattice site surrounded by z neighbour sites, which comprise blocked orientations relative to one or several orientations at the central site. Since each of the z neighbour sites also is surrounded by z such sites, each microsystem contains effectively two lattice sites in the present case, so that $n = N/2$, where N is the total number of lattice sites associated with orientationally disordered molecules. The appropriate expressions for w and s are given elsewhere.[31]

Distances less than 2.80 Å between the O-atoms denoted by their chemical symbols in A and B, Fig. 3, and O-atoms in A- and B-type positions at neighbouring lattice sites, are listed in Table 6. The O-positions situated less than 2.80 Å from the *other* O-atoms in A and B, Fig. 3, are obtained by symmetry. The anion orientations comprising these O-positions may be identified by transforming position A or B to the orientation and site in question.

The number of distinct orientations of either kind situated less than 2.80 Å from either A or B in Fig. 3 are given in Table 7, together with the associated sites. Using the results of Table 7 along with g-values quoted previously and the occupation numbers obtained in the preceding analysis, approximate values of the configurational entropy may now be derived in the actual cases. For thallium and silver perchlorate the occupation numbers were somewhat arbitrarily put equal to $x_A = x_B = 0.5$, while $x_A = 0$ or 1.0

Table 6. Intermolecular distances (Å) less than 2.80 Å between the oxygen positions $(xy0)$, $(x_1y_1y_1)$ or $(x_2x_2x_2)$ given in Table 4, respectively, and equivalent oxygen positions at neighbouring sites, L, where $(xy0)$ belongs to the perchlorate ion orientation A and the latter two to B (Fig. 3) at the origin S. O—O-separations slightly less than 2.80 Å are marked with an asterisk.

S	L	$NaClO_4$ (380 °C)	$NaClO_4$ (314 °C)	NH/ClO_4 (243 °C)	$KClO_4$ (310 °C)	$RbClO_4$ (300 °C)	$CsClO_4$ (320 °C)	$TlClO_4$ (280 °C)	$AgClO_4$ (160 °C)
A	A-type								
$O(xy0)$	$O(\frac{1}{2}-x, \frac{1}{2}-y, 0)$	2.39	2.26	2.70	2.56	2.70		2.69	2.20
$O(xy0)$	$O(\frac{1}{2}-y, \frac{1}{2}-x, 0)$	2.34	2.21	2.66	2.51	2.66		2.65	2.15
A	B-type								
$O(xy0)$	$O(\frac{1}{2}+y_1, \frac{1}{2}-x_1, y_1)$	2.64	2.50						2.45
$O(xy0)$	$O(\frac{1}{2}+y_1, \frac{1}{2}-x_1, \bar{y}_1)$	2.64	2.50						2.45
$O(xy0)$	$O(\frac{1}{2}-x_1, \frac{1}{2}+y_1, y_1)$	2.74*	2.60						2.54
$O(xy0)$	$O(\frac{1}{2}-x_1, \frac{1}{2}+y_1, \bar{y}_1)$	2.74*	2.60						2.54
$O(xy0)$	$O(\frac{1}{2}+x_2, \frac{1}{2}+x_2, x_2)$	2.60	2.42	2.76*	2.63	2.76*		2.77*	2.34
$O(xy0)$	$O(\frac{1}{2}+x_2, \frac{1}{2}+x_2, \bar{x}_2)$	2.60	2.42	2.76*	2.63	2.76*		2.77*	2.39
$O(xy0)$	$O(\frac{1}{2}+x_2, \bar{x}_2, \frac{1}{2}+x_2)$								2.79*
$O(xy0)$	$O(\frac{1}{2}+x_2, \bar{x}_2, -\frac{1}{2}-x_2)$								2.79*
B	B-type								
$O(x_1y_1y_1)$	$O(\frac{1}{2}+y_1, -\frac{1}{2}+x_1, y_1)$		2.69						2.63
$O(x_1y_1y_1)$	$O(\frac{1}{2}+y_1, y_1, -\frac{1}{2}+x_1)$		2.69						2.63
$O(x_1y_1y_1)$	$O(\frac{1}{2}-x_1, y_1, -\frac{1}{2}-y_1$								2.79*
$O(x_1y_1y_1)$	$O(\frac{1}{2}-x_1, -\frac{1}{2}-y_1, y_1)$								2.79*
$O(x_1y_1y_1)$	$O(\frac{1}{2}+x_2, x_2, -\frac{1}{2}-x_2)$	2.77*	2.54		2.71				2.42
$O(x_1y_1y_1)$	$O(\frac{1}{2}+x_2, -\frac{1}{2}-x_2, x_2)$	2.77*	2.54		2.71				2.42
$O(x_1y_1y_1)$	$O(\bar{x}_2, -\frac{1}{2}-x_2, -\frac{1}{2}-x_2)$								2.78*
$O(x_2x_2x_2)$	$O(x_2, -\frac{1}{2}-x_2, -\frac{1}{2}-x_2)$	2.48	2.17	2.40	2.25	2.40	2.64	2.44	2.00
$O(x_2x_2x_2)$	$O(-\frac{1}{2}-x_2, x_2, -\frac{1}{2}-x_2)$	2.48	2.17	2.40	2.25	2.40	2.64	2.44	2.00
$O(x_2x_2x_2)$	$O(-\frac{1}{2}-x_2, -\frac{1}{2}-x_2, x_2)$	2.48	2.17	2.40	2.25	2.40	2.64	2.44	2.00

has to be chosen for cesium perchlorate if the computed configurational entropy shall not exceed the experimental value. $x_A = 0$ was chosen for two reasons. The O—Cs contact distance obtained in the A-case is considerably shorter than the sum of the quoted contact radii and is thus possibly inaccessible. In case B, the O—Cs distances may be somewhat adjusted by translation of the perchlorate ion, so that this position is likely to be occupied statistically in any case.

Experimental entropy data associated with the solid phase changes are listed in Table 8, along with calculated configurational entropies for the cubic phases. For silver perchlorate, two transition entropies are listed, corresponding to the two main peaks shown in Fig. 2 for this compound. While the origin of the first peak is not known with certainty,[8] the second is assumed to originate in orientational changes of the perchlorate ions, as are those of the other compounds. Except for silver perchlorate, the transition entropies are rather high, indicating that the entropy changes are dominated by configurational contributions.

The instantaneous equilibrium orientations of the anions deviate probably in general somewhat from the mean positions because of lattice interactions. As a consequence, configurations involving O—O separations which are statistically slightly less than the smallest O—O separation attainable, may actually become accessible through molecular displacements from the mean positions. This is one of the factors complicating in principle the evaluation of the configurational entropy of a given system.

Several configurational entropy values are listed for each compound in Table 8 in most cases. The unmarked S_c-values are based on the assumption that configurations involving O—O separations which are statistically slightly less than 2.80 Å, are inaccessible, while those denoted by an asterisk are based on the assumption that these O—O separations correspond to

Table 7. The number of distinct, assumed sterically blocked orientations of perchlorate ions at neighbour sites, L, relative to a central perchlorate ion, S, in positions A and B (Fig. 3), respectively. The result is based on Table 6, using tetrahedral symmetry for the anion and space group $Fm3m$, *etc.* Binary orientations involving O – O separations slightly less than 2.80 Å, are represented in the numbers denoted by an asterisk only.

S – L	L lattice sites												
	$(\frac{1}{2}\frac{1}{2}0)$	$(0\frac{1}{2}\frac{1}{2})$	$(\frac{1}{2}0\frac{1}{2})$	$(\frac{1}{2}\bar{\frac{1}{2}}0)$	$(0\frac{1}{2}\bar{\frac{1}{2}})$	$(\bar{\frac{1}{2}}0\frac{1}{2})$	$(\bar{\frac{1}{2}}\frac{1}{2}0)$	$(0\bar{\frac{1}{2}}\frac{1}{2})$	$(\frac{1}{2}0\bar{\frac{1}{2}})$	$(\bar{\frac{1}{2}}\bar{\frac{1}{2}}0)$	$(0\bar{\frac{1}{2}}\bar{\frac{1}{2}})$	$(\bar{\frac{1}{2}}0\bar{\frac{1}{2}})$	
A-A-type	2						2	2			2		$NaClO_4$ (380 °C)
	2						2	2			2		$NaClO_4$ (314 °C)
	2						2	2			2		NH_4ClO_4
	2						2	2			2		$KClO_4$
	2						2	2			2		$RbClO_4$
													$CsClO_4$
	2						2	2			2		$TlClO_4$
	2						2	2			2		$AgClO_4$
A-B-type	4,6*						4,6*	4,6*			4,6*		$NaClO_4$
	6						6	6			6		$NaClO_4$
	2*						2*	2*			2*		NH_4ClO_4
	2						2	2			2		$KClO_4$
	2*						2*	2*			2*		$RbClO_4$
													$CsClO_4$
	2*						2*	2*			2*		$TlClO_4$
	6		2*		2*		6	6	2*		6	2*	$AgClO_4$
B-A-type				1,2*	1,2*	1,2*	1,2*	1,2*	1,2*	2	2	2	$NaClO_4$
				2	2	2	2	2	2	2	2	2	$NaClO_4$
										2*	2*	2*	NH_4ClO_4
										2	2	2	$KClO_4$
										2*	2*	2*	$RbClO_4$
													$CsClO_4$
										2*	2*	2*	$TlClO_4$
				2	2	2	2	2	2	2,4*	2,4*	2,4*	$AgClO_4$
B-B-type				1*	1*	1*	1*	1*	1*	1,3*	1,3*	1,3*	$NaClO_4$
				2	2	2	2	2	2	3	3	3	$NaClO_4$
										1	1	1	NH_4ClO_4
				1	1	1	1	1	1	3	3	3	$KClO_4$
										1	1	1	$RbClO_4$
										1	1	1	$CsClO_4$
										1	1	1	$TlClO_4$
				2,3*	2,3*	2,3*	2,3*	2,3*	2,3*	3,5*	3,5*	3,5*	$AgClO_4$

accessible states (Tables 6 and 7). The two O – O distances close to 2.70 Å listed for sodium (314 °C) and potassium perchlorate, refer to B-type orientations of the anions. These distances may become accessible by small adjustments of the anion positions, which have a certain translational and positional freedom, as pointed out previously. This gives rise to the two S_c**-values listed in Table 8. The actual configurational entropies originating in the present model lie probably somewhere between the limits given in Table 8 and are thus considerably uncertain in several cases. The importance of distinguishing between accessible and inaccessible configurations among those implied statistically is clearly demonstrated for $AgClO_4$, for which a configurational entropy far exceeding the experimental value is obtained on ignoring that many of the configurations indicated statistically are actually blocked.

The rather large difference in computed configurational entropy of sodium perchlorate at the two experimental temperatures is attributable to the large difference in the values used for the *a*-axis (Table 1). The actual configurational entropy difference would be expected to be smaller than that indicated in Table 8, since the transition appears to be mostly completed

Table 8. Observed transition entropies and calculated configurational entropies. For $NaClO_4$: $\Delta S_t = \int_{Ti}^{Tj} (\Delta C_p/T)dT$, where ΔC_p denotes the anomalous heat capacity observed in the transition and $T_i - T_f$ is the temperature interval of the transition. For the other compounds: $\Delta S_t = \Delta H_t/T_t$, where ΔH_t and T_t are given in Table 1, $g_A = 6$, $g_B = 8$. x_A, x_B = fraction of anions in A- and B-type positions, respectively (see text).
S_c*-values are based on the assumption that configurations comprising O – O separations only slightly less than 2.80 Å are accessible.
S_c**-values are based on the assumption that configurations comprising O – O separations close to 2.70 Å involving at least one B-type orientation, are accessible. S_c-values: both categories assumed inaccessible.

Compound	ΔS_t (cal/mol K)	x_A	S_c (cal/mol K)	S_c*, S_c** (cal/mol K)
$NaClO_4$	4.24	0.34 (X-ray)	1.80	2.67** (314 °C)
		0.34 (ass.)	2.67	3.93* (380 °C)
NH_4ClO_4	4.83	0.37 (X-ray)	4.36	4.86*
$KClO_4$	5.65	0.65 (X-ray)	3.57	3.83**
$RbClO_4$	4.99	0.82 (X-ray)	3.22	3.68*
$CsClO_4$	3.63	0.0 (ass.)	3.73	
$TlClO_4$	4.41	0.50 (ass.)	4.20	4.80*
$AgClO_4$	0.67			
	1.85	0.50 (ass.)	1.02	2.00*

at the lower temperature (Fig. 1). – Alternative orientations shown in Fig. 3, such as C, may possibly contribute to the state of disorder in the given frame of metal ions, in addition to those already considered. However, even a low percentage of molecules in such positions would increase the configurational entropy by a considerable amount, particularly in case C because of the high statistical factor (Fig. 3), making quickly up for the difference between observed and calculated quantities in Table 8.

Another possibility is that instantaneous equilibrium positions of neighbouring metal ions may be sufficiently displaced from the average positions, so that distinctly different equilibrium orientations become accessible. A certain contribution to the state of disorder may also come from positional disorder of the metal ions.[31]

Inspection of Table 8 indicates that there is little room for further disorder in the case of ammonium, cesium, silver and thallium perchlorate. For the others, the difference between observed and calculated entropy values is considerably larger. The discrepancy may largely originate in changes in the vibrational state associated with the phase transformation.[18,41] A further investigation into this matter seems to be difficult and would evidently require more experimental information.

The computer programs used in the present work are written by the author.

Acknowledgements. The author is indebted to Dr. F. Grønvold and Mr. B. Lyng-Nielsen who measured the heat capacity of sodium perchlorate. Thanks are also due to Dr. B. F. Pedersen, Sentralinstituttet for industriell forskning (S. I.) and Dr. T. Ledaal by whose help the X-ray diffraction and diff. scan. cal. measurements became possible. Technical assistance by Mrs. T. L. Rolfsen (S. I.), Miss G. Teien and Miss A. Mjærum is gratefully acknowledged. Part of the work was financially supported by Norges almenvitenskapelige forskningsråd.

REFERENCES

1. Vorländer, D. and Kaascht, E. *Ber. Deut. Chem. Ges. 56 B* (1923) 1157.
2. Büsen, W. and Herrmann, K. *Z. Kristallogr. 67* (1928) 405.
3. Gottfried, C. and Schusterius, C. *Z. Kristallogr. 84* (1933) 65.
4. Venkatesan, K. *Proc. Indian Acad. Sci. Sect. A 46* (1957) 134.
5. Mani, N. V. *Ibid.* 143.
6. Smith, H. G. and Levy, H. A. *Acta Crystallogr. 15* (1962) 1201.
7. Zachariasen, W. H. *Z. Kristallogr. 73* (1930) 141.
8. Gordon, S. and Campbell, C. *Anal. Chem. 27* (1955) 1102.
9. Herrmann, K. and Ilge, W. *Z. Kristallogr. 75* (1930) 41.

10. Braekken, H. and Harang, L. *Ibid.* 538.
11. Kanellakopulos, B. *J. Inorg. Nucl. Chem. 28* (1966) 813.
12. Markowitz, M. M. and Boryta, D. A. *J. Amer. Rocket Soc. 32* (1962) 1941.
13. Markowitz, M. M. and Boryta, D. A. *J. Phys. Chem. 69* (1965) 1114.
14. Krien, G. *Explosivstoffe 5* (1967) 73.
15. Hoffmann, K. A. and Marian, P. H. *Sitzber. Preuss. Akad. Wiss. Phys. Math. Kl.* (1932) p. 448.
16. Finbak, Chr. and Hassel, O. *Z. Phys. Chem. B 32* (1936) 130.
17. Zimm, B. H., Oriani, R. A. and Hoffman, J. D. *Annu. Rev. Phys. Chem. 4* (1953) 207.
18. Darmon, I. and Brot, C. *Mol. Cryst. 2* (1967) 301.
19. Janik, J. A., Janik, J. H. and Mayer, J. *Phys. Status Solidi 44* (1971) 437.
20. Rensburg, D. J. J. and Schutte, C. J. H. *J. Mol. Struct. 11* (1972) 229.
21. Westrum, Jr., E. F. and Justice, B. H. *J. Chem. Phys. 50* (1969) 5083.
22. Riehl, J. W., Wang, R. and Bernard, H. W., *J. Chem. Phys. 58* (1973) 508.
23. Grønvold, F. *Acta Chem. Scand. 21* (1967) 1695.
24. Solbakk, J. K. and Strømme, K. O. *Acta Chem. Scand. 23* (1969) 300.
25. Kahn, R., Fourme, R., André, D. and Renaud, M. *Acta Crystallogr. B 29* (1973) 131.
26. Strømme, K. O. *Unpublished results.*
27. Johansen, H. *Chem. Phys. Lett. 11* (1971) 466.
28. Slater, J. C., *J. Chem. Phys. 41* (1964) 3199.
29. Strømme, K. O. *Acta Chem. Scand. 23* (1969) 1616.
30. Strømme, K. O. *Ibid.* 1625.
31. Strømme, K. O. *Acta Chem. Scand. 25* (1971) 211.
32. Strømme, K. O. *Acta Chem. Scand. 24* (1970) 1475 and 1477.
33. Andersen, S. and Wadsley, A. D. *Acta Crystallogr. 15* (1962) 194.
34. Wilhelmi, K.-A. *Ark. Kemi 26* (1967) 141.
35. *Structural Reports 9* (1942–44) 228 and *11* (1947–48) 366.
36. Lindley, P. F. and Woodward, P. *J. Chem. Soc. A* (1966) 123.
37. Hanson, H. P., Herman, F., Lea, J. D. and Skillman, S. *Acta Crystallogr. 17* (1964) 1040.
38. de Boer, J. L. and Vos, A. *Acta Crystallogr. B 28* (1972) 839.
39. Anzenhofer, K. and Hewitt, T. G. *Z. Kristallogr. 134* (1971) 54.
40. James, R. W. *The Optical Principles of the Diffraction of X-Rays* S. Bell and Sons, London 1958.
41. Brot, C. *J. Phys. (Paris) Colloq. C5a 32* (1971) 223.

Received January 21, 1974.

Acta Chemica Scandinavica A 28 (1974) 528—530

The Solubility of Ferrocene in Non-polar Solvents

OLE JØNS and J. CHR. GJALDBÆK

The Royal Danish School of Pharmacy, Chemical Laboratory A, Universitetsparken 2, DK-2100 Copenhagen Ø, Denmark

The solubility of ferrocene in perfluoroheptane, iso-octane, heptane, cyclohexane, carbon tetrachloride, bromotrichloromethane, carbon disulphide, and 1,4-dioxane has been determined at 25 °C. Several of the determinations were also carried out at 10 °C and 40 °C. The data are analyzed in terms of the Scatchard-Hildebrand theory. The problems in calculating solubilities of solids with high melting points are discussed.

The Scatchard-Hildebrand theories have led to an understanding of the theory of the thermodynamic properties of solutions of non-electrolytes, including the solubility of solids. Hildebrand and Scott [1,2] have carefully examined the solubility of iodine, sulphur, stannic iodide, phosphorus, and a few other, *e.g.* naphthalene and anthracene, are roughly discussed. Latest Victoria and Walkley [3] have presented the solubility of tetraphenyltin.

In the prediction of the solubility of solids in non-polar solvents the following equation can be used

$$\ln x_2 = \ln x_2^{i} - v_2 \Phi_1^2 (\delta_1 - \delta_2)^2 / RT \qquad (1)$$

where x_2 and x_2^{i} are the solubility and the ideal solubility expressed in mol fractions, Φ_1 the volume fraction and δ the solubility parameter. Index 2 refers to the solute and index 1 to the solvent.

The solubility of ferrocene in eight solvents has been determined and some problems in the theoretical calculation of the solubility of ferrocene are discussed, and it is shown that ferrocene fulfils the assumptions in the solubility parameter theory. The deviations between predicted and experimental values are for seven of the solvents within the usual order of magnitude, but for heptane the predicted value is about 2.5 times smaller than the experimental.

EXPERIMENTAL

Materials

Ferrocene was of same origin and purity as described earlier.[4]

Perfluoroheptane was purified for hydrocarbons as described by Glew and Reeves.[5] Gaschromatographic analysis showed an amount of impurity of about 6 %. Determination of the boiling point gave 82.48 – 82.53 °C. Glew and Reeves found 82.34 °C. A part of the material was further purified by preparative gaschromatography. The boiling point was now 82.38 – 82.40 °C, and a gaschromatographic analysis showed impurities about 0.5 %. The solubility of ferrocene in the two products differed by about 9 %. Only the result from the purest product was used.

Iso-octane, *cyclohexane*, and *carbon disulphide* were of the same origin and purity as described by Thomsen.[6]

Heptane was of the same origin and purity as described by Thomsen and Gjaldbæk.[7]

Carbon tetrachloride (zur Analyse, Merck) showed an amount of about 0.6 % impurity by GLC analysis. The boiling point was 76.67 °C and $n_D^{20} = 1.4606$, Nilsson.[8] Timmermans [9] states 76.75 °C and 1.46023 – 1.46044, respectively. It was used without any purification.

Bromotrichloromethane (Aldrich) was purified by fractional distillation and the purity examined by Harsted.[10] The boiling point was 104.62 °C and $n_D^{20} = 1.5065$. Davidson and Sullivan [11] found 105.2 °C and Stevels [12] found 1.5061. A GLC analysis showed impurities of about 0.1 %.

1,4-Dioxane (zur Analyse, Merck) was kept with sodium and distilled before use. The distilled dioxane showed no content of peroxide.

Measurements

Saturated solutions of ferrocene in the different solvents were established in a water thermostat kept within ±0.02 °C. The great differences in the solubilities of ferrocene in the solvents employed demanded the use of different methods in the determination of the concentration of ferrocene in the saturated solutions.

In the experiments with *cyclohexane*, *iso-octane*, and *heptane* as solvents, a part of the saturated solutions were diluted in a known scale with the solvent. The optical density of these solutions were measured and the concentration of ferrocene was found by using calibration curves. This method was earlier used by Glew and Hildebrand [13] on the iodine-perfluoroheptane system.

In *carbon disulphide*, *dioxane*, *carbon tetrachloride*, and *bromotrichloromethane*, the solvents of samples taken were removed by vacuum evaporation and the residue of ferrocene was weighed. All work with solutions of ferrocene in the two last mentioned solvents took place in the dark; *cf.* below.

In *perfluoroheptane* the solvent was removed in the same way and the residue of ferrocene determined by a micro-quantitative titration used by Renger and Jenik.[14]

Spectra of solutions of ferrocene in the solvents used in this work (except carbon disulphide) were recorded with a Beckman DK-2 spectrophotometer in the range 3000 – 6000 Å. Only the solutions in silicone tetrachloride, carbon tetrachloride, and bromotrichloromethane showed spectra different from that in cyclohexane, with the absorption of ferrocene at 3500 and 4400 Å. Moreover the solutions in CCl_4 and $CBrCl_3$ showed changes with the time after the solutions were placed in daylight. Earlier Brand and Snedden [15] observed that solutions of ferrocene in carbon tetrachloride and in bromotrichloromethane are stable in darkness, but react on irradiation with the formation of phosgene and ferric chloride. They have suggested that the absorption at 307 mμ is attributed to intermolecular charge transfer in which ferrocene serves as the electron donor.

RESULTS AND DISCUSSION

The results of the solubility experiments are given in Table 1 expressed in mol fraction (100 x_2), with the uncertainties stated. Each determination given is the average of 4 – 6 experiments.

The measured solubilities of ferrocene at 25 °C show, in most cases, the expected increase with increasing value of the solubility parameter of the solvent, δ_1.

The ideal solubility of ferrocene, x_2^i, was calculated from

$$\mathrm{d} \ln x_2^i / \mathrm{d}T = \Delta H^{fus} / RT^2 \qquad (2)$$

where ΔH^{fus} is the heat of fusion. Using the heat of fusion and heat capacities for solid and liquid ferrocene, determined in an earlier work,[4] the ideal solubility of ferrocene, $x_2^i = 0.140$, was found. Since our determination of the molal heat capacity of liquid ferrocene was carried out only between 448 and 485 K, we used an empirical value 0.1 for $\mathrm{d}C_p/\mathrm{d}T$ in calculating the heat of fusion at 25 °C. Values of $\mathrm{d}C_p/\mathrm{d}T$ were calculated for about 20 liquids using c_p given by Timmermans.[9] It turned out that the value 0.1 can be considered as a first rough estimation of the temperature coefficient even over large intervals of temperature.

The solubility parameter, δ_2, for ferrocene was calculated from

$$\delta_2 = [(\Delta H^{vap} - RT)/v_2]^{\frac{1}{2}} \qquad (3)$$

where the heat of vaporization, ΔH^{vap}, at 25 °C was calculated as the difference between the heat of sublimation at 25 °C, 17.53 kcal per mol found by Edwards and Kington,[16] and the heat of fusion at 25 °C calculated in the same way as the calculation for the ideal solubility. $\delta_2 = 10.8$ was found.

Table 1. Solubilities of ferrocene. Experimental values expressed in mol fractions ($100x_2$). The ratio (f) between experimental values and values calculated by means of eqn. (1) (25 °C).

Solvent	v_1	δ_1	10 °C	25 °C	40 °C	f
1. Perfluoroheptane	226	5.85		0.044 ± 0.001		0.83
2. Iso-octane [b]	166	6.9	1.50 ± 0.04	2.28 ± 0.02	3.34 ± 0.03	0.51
3. Heptane	148	7.4	1.65 ± 0.02	2.62 ± 0.06	3.79 ± 0.04	2.5
4. Silicone tetrachloride	115	7.6		2.17[a]		1.5
5. Cyclohexane	109	8.2	2.43 ± 0.02	3.88 ± 0.03	5.62 ± 0.04	1.1
6. Carbon tetrachloride	97	8.6	5.04 ± 0.01	6.92 ± 0.06	9.61 ± 0.08	1.3
7. Bromotrichloromethane	99	8.8		9.40 ± 0.02		1.4
8. Carbon disulphide	61	10.0	4.51 ± 0.08	6.69 ± 0.10		0.52
9. 1,4-Dioxane	86	10.0		6.83 ± 0.07		0.54

[a] Uhlig and Hüttenrauch.[17] [b] *i.e.* 2,2,4-trimethylpentane.

The molal volume, v_2, of liquid ferrocene extrapolated to 25 °C is required in the calculations. Determinations of the density of molten ferrocene were carried out by the pycnometer method. Six experiments carried out between about 177 and 206 °C resulted in the following equation for the density (ϱ)

$$\varrho_t = 1.4055 - 0.0011104\ t$$

resulting in the value $v_2 = 135$ ml at 25 °C. Although the extrapolation is carried out over an interval of about 150 °C the error in the value of v_2 is considered to be small since the density changes only slightly with the temperature.

The calculated ratio (f) between experimental values and values calculated by means of eqn. (1) (25 °C) are shown in Table 1. Using this equation the usual maximum error is ± 0.3 in $\log x_2$, *i.e.* the ratio f should lie between 0.5 and 2. This is fulfilled for all the experiments except for the solubility in heptane. Large discrepancies in the calculated solubility in heptane have earlier been observed, see *e.g.* Refs. 18, 19. An empirical value ($\delta_1 = 8.1$) for heptane was used in these two papers in order to get better agreement with the solubility measurements.

If δ_2 is calculated from eqn. (1) using the experimental values for the solubilities at 25 °C we get the mean value 10.78, which is accidentally identical with the theoretical value 10.8. However there are large discrepancies from the mean value for some of the δ_2's. In heptane we thus calculate $\delta_2 = 10.18$, while using the empirical value (8.1) we get $\delta_2 = 10.88$. The theory which has resulted in eqn. (1) is too rough to use for an interpretation of these discrepancies.

It should be pointed out that very carefully made heat capacity measurements are necessary in the calculations of solubilities of solids. If such measurements do not exist, a constant enthalpy of fusion in eqns. (2) and (3) can be used as a first approximation.

In the calculation of the ideal solubility, the molal volume, and the solubility parameter long extrapolations of heat capacities and densities of the melted solid are necessary. This will in many cases introduce a considerable uncertainty in the theoretical calculation of the solubility of solids.

REFERENCES

1. Hildebrand, J. H. and Scott, R. L. *The Solubility of Nonelectrolytes*, 3rd Ed, Dover Publ., New York 1964.
2. Hildebrand, J. H. and Scott, R. L. *Regular Solutions*, Prentice-Hall, New Jersey 1962.
3. Victoria, M. and Walkley, J. *Trans. Faraday Soc. 65* (1969) 57.
4. Jøns, O. and Gjaldbæk, J. Chr. *Dan. Tidskr. Farm. 43* (1969) 151.
5. Glew, D. N. and Reeves, L. W. *J. Phys. Chem. 60* (1956) 615.
6. Thomsen, E. S. *The Energy of Mixing of Non-Polar Liquids*, (Diss. in Danish), The Royal Danish School of Pharmacy, Copenhagen 1965.
7. Thomsen, E. S. and Gjaldbæk, J. Chr. *Acta Chem. Scand. 17* (1963) 127.
8. Nilsson, M. *Private communication* 1967.
9. Timmermans, J. *Physico-Chemical Constants of Pure Organic Compounds*, Elsevier, Vol. I 1950; Vol. II 1965.
10. Harsted, B. *Private communication* 1967.
11. Davidson, N. and Sullivan, J. H. *J. Chem. Phys. 17* (1949) 176.
12. Stevels, J. M. *Trans. Faraday Soc. 33* (1937) 1381.
13. Glew, D. N. and Hildebrand, J. H. *J. Phys. Chem. 60* (1956) 616.
14. Renger, F. and Jenik, J. *Sb. Ved. Pr. Vys. Sk. Chemickotechnol., Pardubice* (1963) 55; *cf. Chem. Abstr. 62* (1965) 8379a.
15. Brand, J. C. D. and Snedden, W. *Trans. Faraday Soc. 54* (1957) 894.
16. Edwards, J. W. and Kington, G. L. *Trans. Faraday Soc. 58* (1962) 1323.
17. Uhlig, E. and Hüttenrauch, J. *Z. Anorg. Allg. Chem. 338* (1965) 47.
18. Gjaldbæk, J. Chr. *Acta Chem. Scand. 6* (1952) 623.
19. Gjaldbæk, J. Chr. *Acta Chem. Scand. 7* (1953) 537.

Received December 20, 1973.

Acta Chemica Scandinavica A 28 (1974) 531—540

NMR Studies of Chemical Exchange Processes in Intramolecularly Hydrogen Bonded *o*-Hydroxy-carbonyl Compounds

ULRICH KOELLE* and STURE FORSÉN

Department of Physical Chemistry 2, Chemical Center, P.O.B. 740, S-220 07 Lund, Sweden

Activation parameters for the restricted internal rotation in phenols with carbonyl residues in the 2- and 6-positions and in resorcinols with a carbonyl function in the 2-position were determined using complete lineshape analysis or coalescence measurements. Variations of the observed barriers with solvent and concentration and the large negative entropies of activation are discussed. A complex mechanism is suggested for the interconversion of the conformers to account for the experimental findings. IR frequencies for the OH-stretching vibration are recorded and compared with values for intermolecular complexes.

In contrast to the vast number of investigations dealing with the strength of intermolecular hydrogen bonds, quantitative data on intramolecular bonds are more sparse. In the case of intermolecular hydrogen bonds it is most straightforward to determine either equilibrium constants, from which the enthalpy changes on complex formation may be calculated, or to record these changes directly by forming the adducts. The $\Delta H°$-values determined in this way are then frequently correlated with IR and PMR data for the chelated proton.[1-4] For intramolecularly chelated hydrogens similar relations are not readily established due to the presence of one overwhelmingly predominant form in the equilibrium. In fact, only in the case of rather weak hydrogen bonds between a phenolic OH-group and an adjacent halogen, was it possible to indirectly determine a value for the strength of this bond.[5-8]

In phenols with donor substituents *ortho* to the OH-group, the intramolecular hydrogen bond should stabilize the planar or nearly planar ground state [9,10] compared to the nonplanar transition state of internal rotation. Rotation of the donor – *i.e.* carbonyl residues – interchanges the chemical environments of H^1 and H^2 (see formulae) and that of the two protons in the *meta* positions with respect to the OH-group,

thus allowing the barrier to internal rotation to be studied by ^1H NMR lineshape analysis. It was anticipated that the height of this rotational barrier as measured by $\Delta G^{\ddagger}$ or $\Delta H^{\ddagger}$ should at least partly reflect the strength of the internal hydrogen bond. Values for *1* and *2* were recently published by Tabei, Tezuka and Hiroita.[11] Our own results, which for *1* are based on the complete lineshape equations, instead of approximate formulas, are included in the publication.

EXPERIMENTAL

Melting and boiling points are not corrected. Melting points were determined on a Kofler microscope. IR spectra were recorded on a Perkin Elmer model 257 double beam grating spectrophotometer, using 0.1 mm or 1.0 mm NaCl cells. Mass spectra were run on an LKB 9000 A mass spectrometer with attached gas chromatography (GC) unit. ^1H NMR shift differences in Hz refer to spectra at 100 MHz.

a. Synthesis of materials

2,6-Diformyl-4-chlorophenol (1) was prepared by a procedure analogous to that described by

* Present address: Anorg. Chem. Inst. der RWTH, D-51 Aachen.

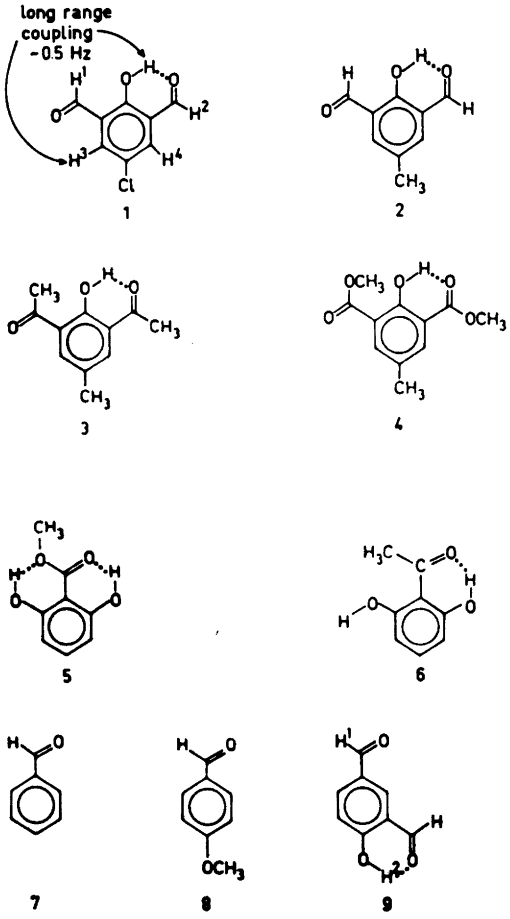

Ullman and Brittner [12] for the 4-methyl compound (*2*) from 4-chlorophenol and formaldehyde, followed by oxidation of the 2,6-bishydroxymethylene intermediate to the bisformylphenol. Pale yellowish crystals, m.p. 122 °C (ethanol). (Found: C 51.9; H 2.8; Cl 19.2. Requ. C 52.0, H 2.7; Cl 19.2). ^{1}H NMR spectrum in CD_2Cl_2 (38 °C): singlet at $\tau = 2.06$ (H^3, H^4), singlet at $\tau = -0.19$ (CHO), singlet at $\tau = -1.58$ (OH). The absorption at $\tau = 2.06$ splits into an AB quartet below -60 °C ($\Delta\nu_{AB} = 15.4$ Hz, $J_{AB} = 2.6$ Hz), and the aldehydic protons emerge as two lines at $\tau = 0.0$ and -0.47 below the coalescence temperature.

2,6-Diacetyl-4-methyl phenol (3). 14.7 g (0.07 mol) of 2-methoxy-4-methyl isophthalic acid [12] was heated with excess thionyl chloride until the acid was completely dissolved. Excess thionyl chloride was stripped and the residue dissolved in benzene. To this solution was added a benzene solution of $Cd(CH_3)_2$ (from 0.34 mol of CH_3MgI and 31 g of anhydrous $CdCl_2$) and the mixture refluxed for 2 h. It was then acidified with dil. HCl, washed with water and aqu. K_2CO_3, dried and the solvent evaporated. The residual oil on distillation gave a fraction of 3 ml with b.p. 100–160 °C/0.1 mmHg which showed strong carbonylic absorption near 1680 cm^{-1} in its IR spectrum. GC/mass spectral analysis (3 % Silicon gum, 160 °C) of this oil revealed among other products with higher molecular weight a GC-peak ($R_t = 3.5$ min) with $m/e = 206$, indicating 2,6-diacetyl-4-methylanisole. The oil was then warmed with 5 ml 20 % HCl to hydrolyze possible esters derived from the starting acid, alkalized and extracted with CH_2Cl_2. The dried CH_2Cl_2-solution was treated with excess $BCl_3(CH_3)_2O$ at room temp., the solvent and excess BCl_3 removed *in vacuo* and the residue extracted with 10 % NaOH at 0 °C. The resulting phenolate solution was washed with ether, acidified and extracted with ether. After drying, evaporation of the solvent left 170 mg of a solid which was purified by thick layer chromatography on Silica gel (Merck HF_{254})/$CHCl_3$ yielding 117 mg pure *3* as yellowish crystals, melting at 70–72 °C after sublimation *in vacuo*. (Found: C 68.7; H 6.3. Requ. C 69.2; H 6.4). IR (CCl_4): ν_{CO} at 1645 and 1685 cm^{-1}. ^{1}H NMR ($CDCl_3$): $\tau = 7.56$ (4-methyl), $\tau = 7.20$ (acetyl), $\tau = 2.04$ (aromatic protons), $\tau = -3.34$ (OH).

2,6-Dicarbomethoxy-4-methyl phenol (4) was prepared from the corresponding acid [12] and diazomethane. The well-protected OH-group does not react with excess diazomethane. The product was white crystals melting at 119 °C after sublimation *in vacuo*. ^{1}H NMR (CD_2Cl_2): $\tau = 7.63$ (4-methyl), $\tau = 6.07$ ($COOCH_3$), $\tau = 2.07$ (aromatic protons), $\tau = -1.84$ (OH).

Methyl γ-resorcylate (5). A solution of γ-resorcylic acid in methanol was saturated with HCl gas and warmed for 5 h on a water bath. The product, which is insoluble in saturated $NaHCO_3$, was collected. After sublimation it had m.p. 68–70 °C.

b. ^{1}H NMR lineshape measurements

^{1}H NMR spectra were recorded on Varian A 60, HA 100, and XL 100 instruments. Complete lineshape analysis was performed only on 100 MHz spectra. Temperatures are 35 °C when not stated otherwise. Low temperature measurement was done with a capillary fixed in the center of the NMR tube and filled with a mixture of methanol and dimethyl ether. The chemical shift difference between the ether CH_3- and the methanol OH-protons was calibrated against the temperature. Temperatures measured in this way are believed to be accurate to at least ±0.3 degrees. When the signals from the capillary interfered with those of the compound or the solvent, as was the case with *3* and *6*, respectively, the same capillary in a separate NMR

tube was used to check the temperature before and after recording the spectrum. Observed temperature differences were within 1 °C. Simulation of experimental ^{1}H NMR line shapes was carried out with computer programs based on McConnell's equations for the interchange of two uncoupled nuclei and on the treatment of Alexander for the strongly coupled cases.[13]

RESULTS

In order to perform a meaningful lineshape analysis, *i.e.* to evaluate the mean life time τ for a conformer at different temperatures by matching theoretical curves to experimental ones in such "simple" cases as coupled or uncoupled AB-systems, the shift difference $\Delta\nu$ and the natural line width $1/\pi T_2$ at any temperature must in principle be known to remove ambiguities. These requirements are never fully met in the present cases. They are best fulfilled by compounds *1* and *5* where it is possible to extend the measurements far enough below the coalescence point to allow an extrapolation of $\Delta\nu$. *2* does not give sharp signals for the aromatic protons and provides little information in addition to that extracted from the spectra of *1*. The difference in activation energy between *1* and *2* is believed to be smaller than the present experimental errors (see also Ref. 11). In *3* and *4* the shift difference between the coalescing methyl signals is too small for a complete separation at low temperature. The resorcinol derivative 2,6-dihydroxyacetophenone (*6*) is not soluble in the relatively inert solvents that can be used for the other compounds. Therefore the activation parameters in these solvents can only be presented for *1* and *5*. In the other cases values for $\Delta G^{\ddagger}$ are given, which were evaluated by fitting calculated to experimental curves near the coalescent point.

To ensure that the signal averaging process can be neither due to nor concerted with an intermolecular proton exchange, the latter was shown to be slow compared with the intramolecular rotation of aldehyde and ester groups in compounds of the type in question. A mixture of the ester *5* with its *p*-methoxy derivative shows separate OH signals up to 90°. This has also been demonstrated for a mixture of the aldehydes *1* and *2* whose OH protons do not rapidly exchange at elevated temperatures.

For compound *1* both the signals from the aromatic protons and those from the aldehyde protons (H^1 and H^2) could be matched with calculated curves, giving essentially the same values for the mean life time τ. Shift differences of both the aromatic and the aldehyde protons increase with temperature and were extrapolated from low temperature measurements. Apparent differences in line width between the aromatic protons at low temperature are attributed to ring proton-side chain long-range couplings such as those observed in similar systems [14] (see formula). The signal due to H^3 (at lower field) is about 0.5 Hz broader than that of H^4 due to a small coupling with the OH proton. The AB quartet from the aromatic protons was thus treated as an ABX case with nuclei A and B interchanging and with a natural line width $1/\pi T_2$ of 1.8 Hz together with coupling constants $J_{AX}=0.5$ $J_{BX}=0$ and $J_{AB}=2.6$ Hz. At higher temperatures gradually larger T_2-values have been used to account for the smaller natural linewidth. Measurements were performed on 0.1 M solutions in 1:1 mixtures of $CD_2Cl_2/CDCl_3$ as a compromise between solubility and low freezing point.

The internal rotation of *5* can only be studied from temperature-dependent linewidths of the OH proton signal(s), the spectral changes in the aromatic region being too small. As a consequence of the very large shift difference between the strongly and the more weakly bonded OH proton at low temperature (255 Hz at -100 °C; see also Table 1), essentially no ^{1}H NMR absorption intensity is observed between -65 °C and -25 °C. The Arrhenius plot thus has a low- and a high-temperature part, covering an overall range of about 120 °C. Also in this case the temperature dependence of the chemical shifts were extrapolated from low temperature data.

The aromatic protons of *3* and *4* are rather strongly coupled to the adjacent methyl group and are thus not suited for a complete lineshape analysis. The shift difference between the lines from the acetyl and carboxymethyl protons in *3* and *4*, respectively, was too small for a complete separation, as mentioned above. The lines from these protons are still broadened at the lowest temperatures that could be reached in the NMR probe (about -130 °C). The $\Delta G^{\ddagger}$ value at the coalescence temperature as given in Table 1 may therefore include a somewhat

Table 1. Activation parameters and chemical shifts of compounds *1* to *9*.

Compound	Solvent	$\Delta\nu^a$ at t °C	$\tau_{OH}{}^b$	E_a kcal/mol	$\Delta H^{\ddagger}$ kcal/mol	$\Delta G^{\ddagger}$ kcal/mol	$\Delta S^{\ddagger}$	t_c °C (coalesc. temp.)
1	$CD_2Cl_2/CDCl_3$	14.3 −107 (H_{arom}) 48.2 −94 (CHO)	−1.58	9.07 ± 0.3^f	8.5	11.4 ± 0.25 at 0 °C 10.6 at −76 °C	-10.5 ± 2	−58 (H_{arom})
3	$CD_2Cl_2/CDCl_3$	4.5 −100 ($COCH_3$)	−3.34			10.6 ± 0.4^g at −76.3 °C		−78.8
4	$CHFCl_2$	6.5 −120 (OCH_3)	−1.84			8.85 ± 0.4^g at −103 °C		−103
5	$CHFCl_2$	255 −100 (OH)	+1.30 −1.25 at −100 °C	7.53 ± 0.12^f	6.8	10.8 ± 0.13 at 0° 9.4 at −103 °C	-14.2 ± 1.5	−
6	$(C_2H_5)_2O$	358 −100 (OH)	+0.35 −3.23 at −100 °C	$5\pm0.5^{c,f}$	4.6^c	8.3 ± 0.4 at −70 °C	$-18^c\pm4$	−
7						7.9^d		−123
8						9.2^d		−99
9	$(CH_3)_2O$	8 ± 1.5^e (CHO) at −130				8.2 ± 0.3		−113

[a] Chemical shift difference in Hz at 100 MHz of the interchanging protons at low temperature. [b] Chemical shift of the chelated OH protons at +35 °C for *1*, *3*, *4*, at −100 °C for *5* and *6*. The high field proton in *5* is the one that is only weakly hydrogen bonded; in *6* the high field value refers to the "free" OH group (see also text). [c] These values are subject to greater uncertainty due to estimations used in their evaluation (see text). Errors given with *1* and *5* are calculated from the least-squares sums from the Arrhenius plots. [d] Values taken from Ref. 15. [e] The uncertainty in $\Delta\nu$ is due to the overlap of the high field part of the temperature-dependent aldehyde signal with the absorption due to the other aldehyde proton. [f] From complete line shape measurements. [g] From fitting of calculated to experimental curves near the coalescent point.

greater uncertainty than for the other compounds.

2,6-Dihydroxyacetophenone (6) has one "free", or non-intramolecularly hydrogen-bonded OH group, which makes this compound insoluble in solvents even of the polarity of chloroform. In acetone, where it is readily dissolved, coalescence does not occur down to the freezing point of the solvent. As a compromise between requirements of "inertness" and solubility, diethyl ether was used as a solvent. The temperature had to be checked separately with the capillary between measurements. Only signals above the coalescence temperature were used for the evaluation of the activation parameters, taking $\Delta\nu$ from a low temperature spectrum where the OH-signals are separated but still exchange-broadened.

The activation parameters of *1* through *6* are collected in Table 1, which also contains the three aldehydes *7*, *8*, and *9* with no internal hydrogen bonds at the interesting moiety, to allow comparisons. The values for benzaldehyde (*7*) and *p*-methoxybenzaldehyde (*8*) are taken from a paper by Anet and Ahmad.[15]

4-Hydroxyisophthalaldehyde (*9*) has an electronic structure close to those of *1* and *2*, but one free aldehyde group. The activation enthalpy for the interconversion of the free aldehyde group in *9* should thus be relevant to the series of interest. Proton H^1 of compound *9* (see formula) splits into a doublet below −113 °C in dimethyl ether as solvent. The high field signal due to H^1 then overlaps with the signal from H^2, which renders $\Delta\nu$ somewhat uncertain. Taking $\Delta\nu = 8 \pm 1.5$ Hz from a spectrum at −130 °C, the $\Delta G^{\ddagger}$ given in Table 1 can be calculated.

The nearly equal values of $\Delta G^{\ddagger}$ for the chloroaldehyde *1* and the ketone *3* initiated an experiment in which the rate of interconversion of an aldehyde and that of the corresponding ketone at a fixed temperature could be directly compared. For exact comparison of k values at the same temperature, the 4-methyl aldehyde *2* was chosen instead of its chloro analogue *1*. The temperature-dependent lines of a 1:1 mixture of *2* and *3* in $CDCl_3/CD_2Cl_2$ were recorded at −70 °C. Simulated spectra could be fit with a k value of 3.3 s^{-1} for *2* and one of 10 s^{-1} for *3* at this temperature, indicating a slower rotation of the aldehyde.

Influence of solvent and concentration

A marked influence of the solvent on the rotational barriers was not unexpectedly noted in many experiments. A solvent which can act as a hydrogen acceptor generally lowers the barrier. Table 2 is a compilation of activation parameters for *5* and *6* in different solvents. Diethyl ether is the only solvent in which the activation parameters of the compounds are directly comparable. *6* is not soluble in chloroform-like solvents (see above). For the ester *5* the rate of interconversion is enhanced on going from $CHFCl_2$ to diethyl ether so that the splitting of the OH signal at low temperature was no longer observable. Assuming a value for $\Delta\nu$ similar to that in $CHFCl_2$, the mean life τ was calculated from the width of the broadened line due to both OH protons at −90 °C. Note that coalescence of *5* in $CHFCl_2$ occurs around −50 °C. Thus the difference in $\Delta G^{\ddagger}$ for the two solvents in the case of compound *5* is about 3 kcal/mol. Coalescence of the OH protons of *6* in ether is observed around −70 °C. In the more strongly proton accepting solvent acetone, only a slight broadening of the OH signal was noted

Table 2. Variation of $\Delta G^{\ddagger}$ with solvent.

Compound	Solvent	$\Delta G^{\ddagger}$ (kcal/mol)	Temp. (°C)	Mean life time τ of rotamer (s)
5	$CHFCl_2$	9.5	−92.3	9×10^{-3}
5	$CHFCl_2$	9.5	+6.1	5.1×10^{-5}
5	$(C_2H_5)_2O$	6.6	−92.3	5.1×10^{-5}
6	$(C_2H_5)_2O$	8.3	−70.0	
6	$(CH_3)_2CO$	no coalescence; broadened signals at −100 °C		

down to −100 °C, when the solvent freezes. It would be difficult to substitute these more qualitative figures by quantitative data because of the low solubility and the very low temperatures that are needed to separate the different OH protons under conditions of slow rotation.

To further substantiate the significance of the strongly negative values for $\Delta S^{\ddagger}$ in Table 1, a study of the dependence of line shape upon concentration at a fixed temperature was performed with two compounds. The aldehyde signal of *1* above coalescence temperature became broader on dilution (Table 3), indicating a slower rotation at lower concentrations. A similar result was obtained with *5*, where the OH signals below coalescence sharpened when the concentration was decreased. The k values for the two experiments, as given in Table 3, are extracted from calculated plots of the linewidth $\Delta\nu_{1/2}$ *vs.* k for the pertinent compounds with all other parameters the same as those used in the evaluation of the activation parameters of Table 1.

Table 3. Concentration dependence of the linewidth of *1* and *5*.

Comp.	Conc.(mol/l)	Temp. (°C)	$\Delta\nu$Hz[a]	$k(s^{-1})$
1	1.02	−2	5.7	10^3
	0.51		9.0	0.5×10^3
5	0.274	−100	11	0.3×10^2
	0.137		9.3	0.19×10^2

[a] Signal width at half height.

Infrared studies

Table 4 collects the IR stretching frequencies of the OH groups of compounds *1* through *6*. Data for salicylaldehyde and *o*-hydroxyacetophenone are included from Ref. 5. For *1*, *3*, and *4* (the spectrum of 2 closely resembles that of *1*), one absorption due to the intramolecularly bonded proton is seen. *6* has a "free" OH absorption at 3590 cm^{-1} and one broad band around 3050 cm^{-1} which must be assigned to the hydrogen bond. The IR spectrum of *5* very nicely shows the difference between the strongly (towards the carbonyl oxygen) and weakly (towards the methoxy oxygen) bonded OH proton with absorptions at 3470 and 3200 cm^{-1}, respectively. Concentrations were kept at 0.01 M, or below. Compound *1* was studied in CCl_4 in the concentration range 0.05 to 0.0025 M and from the absence of any changes in the spectrum it was concluded that the observed bands near 3000 cm^{-1} are due to monomers rather than higher associates.

To see how the spectrum would be influenced by the addition of bases such as pyridine or triethylamine which are known to form strong

Table 4. Activation parameters, IR frequencies (ν_{OH}) and chemical shifts (τ_{OH}).[a]

Compound	Solvent	$\Delta H^{\ddagger}$ (kcal/mol)	$\Delta G^{\ddagger}$ (kcal/mol)	$\nu_{OH}(cm^{-1})$[b]	Solvent	τ_{OH}	Solvent
1	CD_2Cl_2	8.5	10.6	3080b	CCl_4	−1.58	CD_2Cl_2/CD_3Cl
3	CD_2Cl_2		10.6	[c]		−3.34	$CD_2Cl/_2CD_3Cl$
4	$CFHCl_2$		8.8	3150b	CCl_4	−1.84	$CHFCl_2$
5	$CFHCl_2$	6.8	9.4	3470s		−1.12	$CHFCl_2$
				3200b	CCl_4		
5	Et_2O		6.7				
6	Et_2O		8.3	3590s near 3050b	$CDCl_3$	−3.24	Et_2O
Salicylaldehyde[d]				3140	CCl_4[5]	−2.37	
o-Hydroxyacetophenone[d]				3040	CCl_4[5]		

[a] For temperatures to which activation parameters and τ values refer, see Table 1. [b] s, sharp; b, broad. [c] Interfering with methyl-stretch near 3000. [d] From Ref. 5.

intermolecular complexes with phenols in hydrocarbons or CCl_4,[2] spectra were also recorded in the presence of these bases. The samples were added to a solution of the base in CCl_4 using the same solution as reference in the double beam spectrometer. Only the "free" OH group of *6* at 3590 cm^{-1} is broadened and shifted to lower frequencies on addition of base. In no other case was a significant change in the IR spectrum noted on addition of pyridine or triethylamine in great excess. This is especially noteworthy for *5*, whose weak hydrogen bond towards the ether oxygen is obviously not broken by a strong base. On the other hand, the relative strength of hydrogen bonds in pyridine/phenol and carbonyl/phenol complexes is illustrated by the fact that the absorption at 3250 cm^{-1} in a solution of *p*-hydroxybenzaldehyde in chloroform, which must be assigned to the stretching mode of the intermolecular $=O\cdots H-O-$ complexed OH-group is shifted towards 3000 cm^{-1} on addition of pyridine.

Fig. 1 is a plot of $\Delta\nu_{OH}$ *vs.* the chemical shifts of the proton. It is seen that with the exception of *1* the frequently observed correlation [7,8] between IR frequencies and chemical shifts exists also in the present cases.

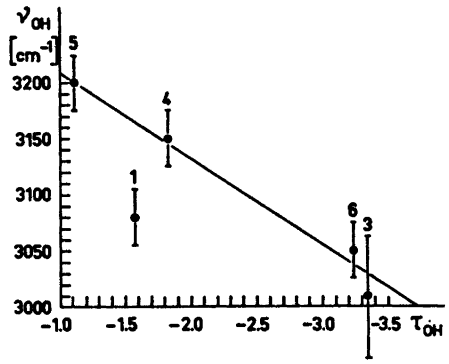

Fig. 1. Plot of the infrared shift $\Delta\nu_{OH}$ *vs.* the chemical shift τ_{OH}.

DISCUSSION

In the initial stages of this work, our main goal was an attempt towards the determination of the strength of intramolecular hydrogen bonds between a phenolic OH group and an adjacent carbonyl function. If the internal rotation of the latter is associated with the rupture and reforming of the intramolecular hydrogen bond, the enthalpy of this bond will make a significant contribution to the overall barrier. This should be corroborated by a variation of the barrier height with the basicity of the carbonyl group acting as the donor.

Comparison of the activation parameters from Table 1 makes it evident that $\Delta G^{\ddagger}$ and $\Delta H^{\ddagger}$ for compounds *1* through *6* are not very much greater than those observed in the structurally related aldehydes *7*, *8*, and *9*, which do not have a hydrogen bond. Apart from the hydrogen bond interaction energy, it would be expected that the presence of one or more OH groups *ortho* or *para* to the carbonyl group would cause a slight increase in the barrier to internal rotation, whereas a second carbonyl group in the *meta* position should exert a minor effect. The measured $\Delta G^{\ddagger}$ values for *7* through *9* indicate the correctness of this assumption.

The strengths of intramolecular bonds in chelated phenols such as *o*-hydroxyacetophenone have never been directly determined. From the low chemical shift of the chelated proton and its broad infrared absorption at low frequencies, as well as the lack of unchelated, "open" conformer in the equilibrium, it was frequently concluded that these hydrogen bonds are rather strong,[16-18] *i.e.* > 5 kcal/mol. A figure of this order of magnitude must be considered a lower limit if the relations between ΔH° and IR as well as ^1H NMR shifts for intermolecular complexes are applied to the intramolecular chelates (see below). If the interconversion process in *1* through *6* would require a complete breaking of the hydrogen bond, the enthalpy change for this process must be added to the enthalpy of activation for the rotation of a non-hydrogen bonded aromatic carbonyl compound. Thus the barriers would be expected to be at least of the order of 13 to 15 kcal/mol. The experimental values in Table 1 are significantly lower. Two alternative conclusions may be drawn from these findings:

(i) The intramolecular hydrogen bond energies in chelated phenols have been greatly overestimated, or

(ii) the interconversion process in *1* through *6* occurs in such a way that the hydrogen bond energy is partly retained, for example through solvent interaction or formation of bimolecular

complexes.*

Significant differences in the activation parameters of Table 1 in the series *1* through *6* are observed between aldehydes and ketones compared with the esters, the latter having barriers lower by roughly 2 kcal/mol (compare *1*, *3* and *5*). The order is the same as that found by Porte, Gutowsky and Hunsberger [16] in a ^{1}H NMR study, where increasing chemical shifts indicated a stronger hydrogen bond in the order ester, aldehyde, ketone. Comparison of the $\Delta G^{\ddagger}$ values in Table 1 and the hydroxylic chemical shifts in *1*, *3*, and *4* makes it clear that these two parameters are not exactly parallel because the greater downfield shift of *3* compared with *1* is not reflected in the barrier (see also below). The lower barrier of the ester *4* may be due to a weaker hydrogen bond or to a less pronounced double bond character of the $C_{aryl}-C=O$ bond. The same trend is revealed again in compounds *5* and *6* in ether solution (Table 2), where the difference between *5* ($\Delta G^{\ddagger}_{-93\,°C} = 6.6$ kcal/mol) and *6* ($\Delta G^{\ddagger}_{-70\,°C} = 8.3$ kcal/mol) can hardly be attributed to the temperature difference of 23 °C. The difference between *4* and *5* as reflected by the $\Delta G^{\ddagger}$ values at -103 °C is indicative of the weak second hydrogen bond present only in *5*.

The greater stabilization of the ketone relative to the aldehyde, which would be expected from ^{1}H NMR and IR data,[14,16] is not observable from the activation energy data in Table 1.

Direct evidence for which group has the greater hydrogen bonding capacity is given by 2-acetyl-6-formylphenol, where the pattern of long-range couplings in a sample in $CDCl_3$ solution at room temperature is only consistent with a conformer that has its hydrogen bond directed exclusively towards the acetyl group.[19] On the other hand, the *k*-values for the mixture of *2* and *3* clearly show a faster rotation in the ketone. From the IR absorption studies of the OH and C=O stretching frequencies of salicylaldehyde and *o*-hydroxyacetophenone, the difference in hydrogen bond energy between a chelated aldehyde and a ketone would be expected to be of the order of 1 kcal/mol, in favor of the ketone, if the equation of Drago and Epley [2] (see eqn. (1) p. 540) is applied to the values given in Ref. 14 (see Table 4). The fact that this difference is not reflected in the rotational barriers of *1*, *2*, and *3* may be rationalized by a bimolecular complex undergoing rotation (see below). Here the assistance of a second molecule parallels its hydrogen bonding capacity, which cancels the stronger stabilisation of the ground state.

The solvent dependence of the barriers demonstrated with compounds *5* and *6* is in accord with the findings of Frankle and Laszlo,[20] who noted a marked decrease of the barrier to internal rotation in Vorländer adducts (di[4,4-dimethylcyclohexanedione(2,6)]methanes) when changing to solvents with a greater hydrogen bonding ability. The authors suggest that in the cases of basic solvents the interconverting species are those whose internal hydrogen bonds are broken by the solvent. The IR absorptions of such complexes should be different from those in the intramolecularly hydrogen bonded molecules, but this could not be confirmed with the present substances. Besides the IR shifts, the ^{1}H NMR shifts also seem to be rather insensitive towards added base. Pyridine for example, added in great excess to a dilute sample of salicylaldehyde, shifts the OH proton not more than a few Hz to lower field, an effect that may reflect solvent anisotropy changes rather than the formation of appreciable amounts of a species with a broken intramolecular hydrogen bond. Considering the very high rates established for the formation of hydrogen bonds,[21] only a small fraction of intermolecularly hydrogen bonded molecules in the equilibrium is necessary to account for the enhanced rotational rates. The influence of concentration on the interconversion rate, which was demonstrated with compounds *1* and *5*, suggests a second-order process. Because of the relatively small range of concentrations accessible, it was not possible to establish quantitative depend-

* *Note added in proof.* A recently performed calorimetric determination of the heats of neutralization for the tetrabutylammonium salts of salicylaldehyde and 4-hydroxybenzaldehyde in butanone as a solvent did give values $\Delta H_{neutr} = -19.8$ kcal/mol for the 2-hydroxy- and $\Delta H_{neutr} = -19.0$ kcal/mol for the 4-hydroxycompound. This minor difference in neutralization enthalpy is corroborating our suggestion that hydrogen bonding of intramolecularly chelated phenols to proton accepting solvents is of major importance.

We are indebted to Doc. G. Olofsson at the Thermochemical Inst., Kemicentr. in Lund for doing the measurements.

ence of the rotational rates upon the concentration and thus evaluating the kinetic order of the process in question. A purely second order process would require the interconversion rate to be proportional to the concentration. The observed effects are slightly smaller and therefore different pathways must also be taken into account, which may be operative to varying extents depending on the compound, the solvent and the concentration.

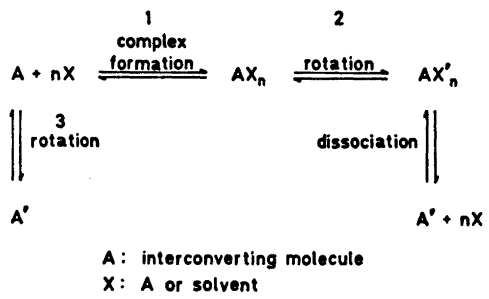

Fig. 2. Possible reaction pathways for the interconversion of *1* through *6*.

Fig. 2 depicts two such pathways, where A is the interconverting molecule and X is either a second A molecule or a solvent molecule. The fraction of AX_n may be small in the equilibrium, but if process 1 is fast enough compared to 2 the latter will still be rate determining. It is further assumed that rotation of the uncomplexed molecules, *i.e.* process 3, is much slower than 2. An overall rate which is composed of individual pathways differing in the association number n and the nature of X may then account for the experimental results.

Although our experimental data seem to be insufficient to describe the exact nature of the interconverting species, two possible models for the complex AX_n are depicted in Fig. 3. Path I (AX_n = Ia) implies that complex formation occurs *prior to and kinetically independent* of the rupture of the intramolecular bond, the latter weakening successively in favour of the intermolecular bond on reaching the transition state of rotation. In II the intramolecular bond is broken *together with* complex formation (IIb) followed by rotation of the carbonyl residue. Both pathways account for the solvent and concentration dependence of the barriers observed. An argument in favour of II is the large

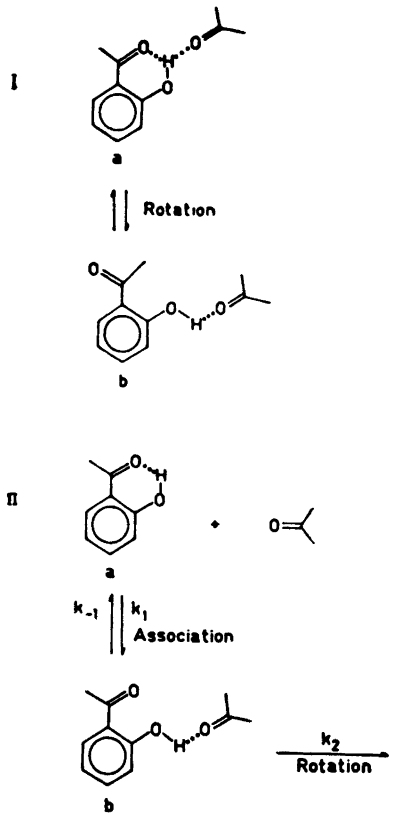

Fig. 3. Possible interconverting species of *1* through *6*.

negative entropy of activation. Complexes of type Ia should make a substancial equilibrium fraction and the degree of ordering of the solvated chelate should not be drastically changed during the interconversion. The net entropy effects should then be small. In contrast, the equilibrium fraction of complexes of type IIb should be small, and as long as $k_{-1} \gg k_2$, the activation entropy, $\Delta S^{\ddagger}$, is largely determined by the association process.

Intermolecular complexes formed by bases like carbonyl compounds or amines with phenols have been the subject of numerous investigations, and ΔH° values for the formation of these complexes have recently been determined by direct thermodynamic measurements of the heat of mixing by Drago and coworkers.[2,4,22] Drago and Epley [2] thus found ΔH° values for the systems phenol-pyridine and phenol/triethylamine to be -7.2 and -8.3 kcal/mol respec-

tively, whereas carbonyl bases like acetone yield enthalpies of only -5 kcal/mol.[3] The fact that no spectral changes occur on addition of pyridine or triethylamine to the phenols *1* through *6* (not even the "weak" hydrogen bond in *5* is altered) may be rationalized by the negative entropies of mixing observed in several cases.[4,23] Part of the enthalpy expected to favour the intermolecular complex is consumed by the entropy change that parallels the breaking of the intramolecular or the formation of the intermolecular bond. This finding is further support for the path II discussed above, where the interconversion process observed in the NMR is connected with a substantial change in entropy.

Drago and Epley [2] present the equation

$$-\Delta H^\circ = (0.015\Delta\nu_{OH} + 3) \text{ kcal/mol} \quad (1)$$

which relates the enthalpy change on formation of the hydrogen bond to the corresponding IR frequency shift. If applied to the intramolecularly hydrogen bonded phenols, a ΔH° value of 8.7 kcal/mol follows for *6* if $\Delta\nu_{OH}$ is equated to the frequency difference between the complexed and the uncomplexed OH group (see Table 4). Similar values are obtained for the other compounds in the series if the absorption of free phenol in dilute solution at 3600 cm^{-1} is taken as reference. Though it appears uncertain if the above equation also gives correct results for intramolecular chelates, it should allow at least an estimate of their strength. From the activation parameters it then appears quite obvious that the major fraction of the hydrogen bond enthalpy must be conserved during the internal rotation by either intermolecular association or through solvation by the polar solvents.

Acknowledgement. We are indebted to Mrs. Annika Raihle for experimental assistance with the syntheses, to Dr. Torbjörn Drakenberg for placing the lineshape computer programs at our disposal and to Dr. Robert E. Carter for unfailing interest and moral support as well as linguistic criticism. We wish to thank Mrs. Berit Rosberg for drawing the original figures. Part of the work was supported by an NFR grant to one of us (U.K.).

REFERENCES

1. For reviews see: a. Pimentel, C. and McClellan, A. L. *The Hydrogen Bond*, Freeman, San Francisco 1960; b. Pimentel, C. and McClellan, A. L. *Annu. Rev. Phys. Chem. 22* (1971); c. Vinogradov, A. N. and Linnell, R. H. *Hydrogen Bonding*, Van Nostrand, New York 1971.
2. Drago, R. S. and Epley, T. D. *J. Amer. Chem. Soc. 91* (1969) 2883.
3. Epley, T. D. and Drago, R. S. *J. Amer. Chem. Soc. 89* (1967) 5770.
4. Joesten, M. D. and Drago, R. S. *J. Amer. Chem. Soc. 84* (1962) 3817; Drago, R. S., O'Bryan, N. and Vogel, G. C. *J. Amer. Chem. Soc. 92* (1970) 3924.
5. Baker, A. W. *J. Amer. Chem. Soc. 80* (1958) 3598.
6. Brown, I., Ellington, G. and Martin-Smith, M. *Spectrochim. Acta 18* (1962) 1593.
7. Reeves, L. W., Allan, E. A. and Strømme, K. O. *Can. J. Chem. 38* (1960) 1249.
8. Allan, E. A. and Reeves, L. W. *J. Phys. Chem. 66* (1962) 613.
9. Jones, N. and Curl, R. F. *J. Mol. Spectrosc. 42* (1972) 65.
10. Diehl, P. and Henrichs, P. M. *J. Magn. Resonance 5* (1971) 134.
11. Tabei, M., Tezuka, T. and Hiroita, M. *Tetrahedron Lett.* (1971) 301.
12. Ullmann, F. and Brittner, K. *Ber. Deut. Chem. Ges. 42* (1909) 2539.
13. See, *e.g.*, Sutherland, I. O. *Annu. Rep. NMR Spectrosc. 4* (1971) 71, and references therein.
14. Forsén, S., Åkermark, B. and Alm, T. *Acta Chem. Scand. 18* (1964) 2313.
15. Anet, F. A. L. and Ahmad, M. *J. Amer. Chem. Soc. 86* (1964) 119.
16. Porte, A. L., Gutowsky, H. S. and Hunsberger, I. M. *J. Amer. Chem. Soc. 82* (1960) 5057.
17. Hay, R. W. and Williams, P. P. *J. Chem. Soc.* (1964) 2270.
18. Magnusson, L. B., Craig, C. A. and Postmus, C. Jr. *J. Amer. Chem. Soc. 86* (1964) 3958.
19. Koelle, U. and Forsén, S. *Unpublished results*; *cf.* Forsén, S. and Åkermark, B. *Acta Chem. Scand. 17* (1963) 1712.
20. Frankle, W. E. *Ph. D. Thesis*, Princeton 1970.
21. See Ref. 1c, p. 264ff.
22. Eyman, D. P. and Drago, R. S. *J. Amer. Chem. Soc. 88* (1966) 1617.
23. Nagakura, S. *J. Amer. Chem. Soc. 76* (1954) 3070.

Received January 7, 1974.

Acta Chemica Scandinavica A 28 (1974) 541—545

The Crystal Structure of Ammonium Dichromate, $(NH_4)_2Cr_2O_7$

G. A. P. DALGAARD, A. C. HAZELL and R. GRØNBÆK HAZELL

Department of Inorganic Chemistry, Aarhus University, DK-8000 Aarhus C, Denmark

The crystal structure of the room temperature form of ammonium dichromate has been redetermined by X-ray diffraction. Least squares refinement with 950 reflections gave a final R-value of 0.039 for 52 parameters. The intensity data were collected on a semi-automatic diffractometer using monochromatized Mo$K\alpha$-radiation.

The dichromate ions are in the eclipsed form with terminal oxygen atoms *trans* to the bridging oxygen atom. The symmetry is approximately C_{2v}. The Cr – O (bridge) distance is 1.781 Å, e.s.d. 0.002 Å and the mean Cr – O (terminal) is 1.634 Å, e.s.d. 0.002 Å. The Cr – O – Cr angle is 121.0°, e.s.d. 0.19°. There is no evidence for an abnormally long Cr – O (bridge) distance.

The crystal structure of the room temperature form of ammonium dichromate has been redetermined to obtain more precise values of the bond lengths and angles. The structure was first solved by Byström and Wilhelmi,[1] henceforth referred to as B and W, who obtained an exceptionally large value, 1.91 Å, for the Cr – O (bridge) distance. Although B and W attributed the apparent lengthening of the bond to errors in the atomic coordinates, Luu and Hillaire [2] claimed from their interpretation of the solid-state Raman-spectrum that the lengthening was real and could be explained by invoking hydrogen bonding.

We now find no evidence for an abnormally long Cr – O bond.

EXPERIMENTAL

Intensity data were collected using a linear diffractometer of the Arndt-Phillips [3] design. Mo$K\alpha$-radiation monochromatized [4] by means of a graphite crystal was employed in conjunction with a scintillation counter and a pulse height analyser. The background – peak – background technique was used. The crystal was mounted with its [010] axis, the needle axis, as rotation axis.

Reflections hkl with $0 \leq k \leq 9$ and for which $\sin\theta/\lambda < 0.7$ were measured giving 1040 independent reflections of which 957 had $I > 2\sigma_c(I)$ where $\sigma_c(I)$ is the square root of the total number of counts for the reflection.

The crystal used was 0.7 mm in length and 0.20 by 0.25 mm in cross section. No correction was made for absorption.

CRYSTAL DATA

$(NH_4)_2Cr_2O_7$, M = 252.1. Monoclinic, $a = 13.26 \pm 0.01$ Å, $b = 7.54 \pm 0.02$ Å, $c = 7.74 \pm 0.02$ Å, $\beta = 93.2°$, $U = 772.6$ Å^3, $Z = 4$, $D_c = 2.17$, $F(0,0,0) = 504$. The cell dimensions are those given by B and W. The possible space groups are $C2/c$ (C_{2h}^6, No. 15) and Cc (C_s^4, No. 9); the morphology shows the space group to be $C2/c$.

The orange crystals are tabular on (100) and bounded by {101} and {111}, the largest dimension is in the [010] direction.

Observed and calculated structure factors, atomic coordinates and thermal vibration parameters are listed in Tables 1 – 3. Bond distances, angles, and torsion angles are given in Tables 4 – 6. The estimated standard deviations do not include the errors in the cell dimensions.

STRUCTURE DETERMINATION AND REFINEMENT

The structure was determined by the heavy atom method. Least-squares refinement of atomic coordinates, thermal parameters, scale factor, and an isotropic extinction parameters gave a final R-value of 0.039 for 950 reflections and 52 parameters, the weighted R-value was $r = 0.062$. Only those reflections for which $\sin\theta/\lambda < 0.7$

Table 1. Observed and calculated structure factors: h, k, l, $10|F_{obs}|$, $10|F_{calc}|$.

Table 2. Atomic coordinates in fractions of cell edges. The estimated standard deviations $\times 10^5$ are given in brackets.

	x	y	z
Cr	0.10148(4)	0.17124(7)	−0.14046(6)
O1	0.05730(21)	0.30327(40)	0.00172(34)
O2	0.17849(19)	0.02802(41)	−0.05279(16)
O3	0.15877(20)	0.28968(38)	−0.28058(34)
O4	0	0.05488(45)	−0.25
NH_4^+	0.35655(23)	0.15412(42)	−0.34526(39)

were used, 7 reflections very close to the rotation axis ($h^2+l^2\leq 2$) were omitted from the refinement.

It was not possible to determine the positions of the hydrogen atoms. Since proton magnetic resonance [5] and inelastic neutron scattering [6,7] both indicate that the ammonium ion is reorienting about random axes the scattering factor for a freely rotating ammonium ion was used. This did not give an appreciably lower R-value than that obtained by refining with a neutral nitrogen atom and no hydrogen atoms ($R=0.040$). Refinement in the lower symmetry space group, Cc, did not give a lower R-value.

COMPUTATIONAL DETAILS

Least squares refinement was carried out using the fullmatrix program LINUS,[8] the quantity minimized was

$$r=\frac{\sum w||F_o|-|F_c||^2}{\sum w|F_o|^2}$$

where $w=1/\sigma^2$, where

$$\sigma=\sqrt{\sigma_c(F_o^2)+(1+K)F_o^2}-|F_o|$$

The parameter K was varied so that $\langle w||F_o|-|F_c||\rangle$ varied as little as possible with the magnitude of F_o.

The atomic scattering factors used were those of Cromer and Waber [9] for chromium and of Cromer and Mann [10] for oxygen and for nitrogen. The scattering factor for the ammonium ion was calculated [11] as

$$f_{NH_4^+}=f_N+3f_H \sin(4\pi rs)/4\pi rs$$

where $r=1.0$ Å, $s=\sin\theta/\lambda$, and f_H is the scattering factor for hydrogen as calculated for a spherically symmetric atom by Stewart, Davidson, and Simpson.[12]

No correction was made for anomalous dispersion or for absorption.

Bond lengths and angles and their standard deviations were calculated using ORFFE,[13] drawings were made using ORTEP.[14]

DISCUSSION

The structure is shown in Fig. 1. The two tetrahedra of the $Cr_2O_7^{2-}$ ion are related by a 2-fold axis through the centre oxygen atom. The compound is isostructural with one of the forms [15] of $Rb_2Cr_2O_7$.

The dimensions of the dichromate ion are very similar to those found for other dichromates. Panagiotopoulos and Brown [16] quote structural data for 12 dichromates for which Cr−O terminal) range from 1.60 Å to 1.62 Å, Cr−O (bridge) from 1.76 Å to 1.80 Å, and the angle Cr−O−Cr from 121° to 141°. We find Cr−O (terminal) = 1.634(2) Å, Cr−O (bridge) = 1.781(3) Å, and Cr−O−Cr = 121.0(2)°. From the torsion angles the mean value of the twist of the CrO_3 groups out of the plane defined by the two chromium

Table 3. Thermal parameters ($\times 10^4$) with their estimated standard deviations. The u_{ij} are defined by: $\exp[-2\pi^2(u_{11}a^{*2}h^2+\cdots 2u_{12}a^*b^*hk+\cdots)]$.

	u_{11}	u_{22}	u_{33}	u_{12}	u_{13}	u_{23}
Cr	237(4)	295(3)	204(3)	41(2)	40(2)	19(2)
O1	409(15)	557(16)	253(13)	59(12)	92(11)	−77(12)
O2	406(14)	477(16)	571(18)	136(12)	−82(13)	92(14)
O3	376(14)	476(14)	278(13)	−96(11)	96(11)	23(11)
O4	277(16)	295(15)	279(19)	0	18(14)	0
NH_4^+	317(15)	446(17)	262(14)	45(12)	33(11)	59(12)

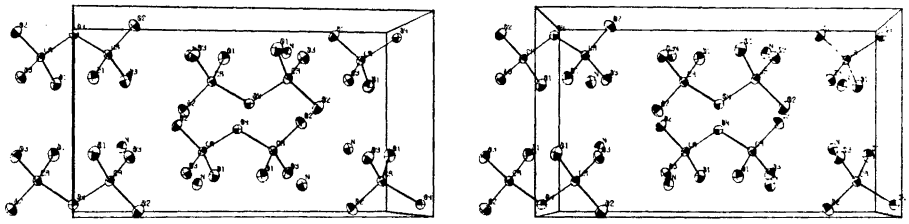

Fig. 1. Stereoscopic view of the unit cell contents as seen down the *c*-axis. The *a*-axis is horizontal.

Table 4. Bond lengths l, and bond lengths corrected for riding motion, l_{corr}, and their estimated standard deviations.

	l	l_{corr}
Cr – O1	1.618(3)	1.632(3)
Cr – O2	1.610(3)	1.632(3)
Cr – O3	1.626(3)	1.637(3)
Cr – O4	1.781(2)	

Table 5. Angles and their estimated standard deviations.

	θ	$\sigma(\theta)$
O1 – Cr – O2	111.8	0.15
O1 – Cr – O3	108.4	0.17
O1 – Cr – O4	109.5	0.12
O2 – Cr – O3	109.9	0.15
O2 – Cr – O4	108.3	0.16
O3 – Cr – O4	108.8	0.11
Cr – O4 – Cr	121.0	0.19

Table 6. Torsion angles (°) and their standard deviations. The torsion angle is defined as 0° when the 4 atoms are coplanar and the two oxygen atoms are *cis* to each other, and as 180° when the two oxygen atoms are in the *trans* position.

	θ	$\sigma(\theta)$
Cr′ – O4 – Cr – O1	56.67	0.12
Cr′ – O4 – Cr – O2	178.86	0.12
Cr′ – O4 – Cr – O3	−61.68	0.11

atoms and the bridging oxygen atoms are $\alpha_1 = 2.05°$ and α_2, the twist of the CrO_3 group related by the 2-fold axis is $-\alpha_1$. Panagiotopoulos and Brown [16] found a correlation between the Cr – O – Cr angle, the antisymmetric twist $(\alpha_1 - \alpha_2)$, and the amplitude of the antisymmetric torsion mode, each of these tending to increase together. For ammonium dichromate $\alpha_1 - \alpha_2$ is very small, 4.1°, the Cr – O – Cr is one of the smallest observed and unlike most of the dichromates studied the thermal vibration of the central oxygen atom is not larger than that of the terminal atoms.

There is no evidence for an abnormally long Cr – O (bridge) bond, the extreme value found by B and W is partly explained by the fact that the reflections were indexed according to a cell with $\beta = 86.8°$ whereas they used $\beta = 93.2°$ in their calculations. The confirmation of the long bond by Raman spectroscopy would seem to call for a reinterpretation of the Raman data.

The nearest neighbour distances to the nitrogen atom are given in Table 7, showing that there are many ways in which the ammonium

Table 7. Nitrogen-oxygen distances less than 3.5 Å. The nitrogen atom has the coordinates as in Table 2, the symmetry operations show how the oxygen positions are related to those in Table 2. The standard deviations are ~0.004 Å.

N – O1	2.853	$\frac{1}{2}-x, \frac{1}{2}-y, -z$
N – O1	2.991	$\frac{1}{2}+x, \frac{1}{2}-y, z-\frac{1}{2}$
N – O1	3.150	$\frac{1}{2}-x, y-\frac{1}{2}, -\frac{1}{2}-z$
N – O2	2.957	$\frac{1}{2}-x, \frac{1}{2}+y, -\frac{1}{2}-z$
N – O2	3.101	$x, -y, -\frac{1}{2}+z$
N – O2	3.493	x, y, z
N – O3	2.885	x, y, z
N – O3	2.923	$\frac{1}{2}-x, \frac{1}{2}-y, z-1$
N – O3	2.926	$\frac{1}{2}-x, y-\frac{1}{2}, -\frac{1}{2}-z$

ion could be hydrogen-bonded to the oxygen atoms so that there is the possibility of either static or dynamic disorder.

Acknowledgement. The linear diffractometer was provided by Carlsbergfondet.

REFERENCES

1. Byström, A. and Wilhelmi, K.-A. *Acta Chem. Scand. 5* (1951) 1003.
2. Luu, D. V. and Hillaire, P. *C. R. Acad. Sci., Ser. B. 270* (1970) 496.
3. Arndt, U. W. and Phillips, D. C. *Acta Crystallogr. 14* (1961) 807.
4. Rasmussen, S. E. and Henriksen, K. *J. Appl. Crystallogr. 3* (1970) 100.
5. Richards, R. E. and Schaefer, T. *Trans. Faraday Soc. 57* (1961) 210.
6. Rush, J. J. *Bull. Amer. Phys. Soc. 9* (1964) 623.
7. Leung, P. S., Taylor, T. I. and Havens, W. W. *J. Chem. Phys. 48* (1968) 4912.
8. Coppens, P. and Hamilton, W. C. *Acta Crystallogr. A 26* (1970) 71.
9. Cromer, D. T. and Waber, J. T. *Los Alamos Scientific Laboratory Report* LA-3056 (1964).
10. Cromer, D. T. and Mann, B. *Acta Crystallogr. A 24* (1968) 321.
11. Zachariasen, W. H. *Theory of X-Ray Diffraction in Crystals*, Dover Publications, New York 1967, p. 223.
12. Stewart, R. F., Davidson, E. R. and Simpson, W. T. *J. Chem. Phys. 42* (1965) 3175.
13. Busing, W. R., Martin, K. O. and Levy, H. A. (1964), *ORFFE*, Report ORNL-TM-306, Oak Ridge National Laboratory, Oak Ridge, Tennessee.
14. Johnson, C. K. (1965), *ORTEP*, Report ORNL-3794, Oak Ridge National Laboratory, Oak Ridge, Tennessee.
15. Löfgren, P. and Waltersson, K. *Acta Chem. Scand. 25* (1971) 35.
16. Panagiotopoulos, N. C. and Brown, I. D. *Acta Crystallogr. B 29* (1973), 890.

Received February 20, 1974.

Acta Chemica Scandinavica A 28 (1974) 546—550

The Crystal Structure of the High-temperature Phases of Ammonium and Potassium Tetrafluoroborate

K. O. STRØMME

Department of Chemistry, University of Oslo, Blindern, Oslo 3, Norway

An approximate model of the crystal structures of the high-temperature phases of ammonium and potassium tetrafluoroborate is presented. The anions are distributed between two sets of statistically equivalent orientations in the frame of the positive ions, resembling that proposed for univalent metal perchlorates. X-Ray diffraction and transition entropy data are interpreted in terms of this model.

Crystalline ammonium and potassium tetrafluoroborate transform from a structurally ordered, orthorhombic room temperature form to a disordered, facecentred, cubic high-temperature structure at elevated temperatures (Table 1). The various phases are closely related to those of the univalent metal perchlorates.[2,11]

Detailed crystal structures of the room-temperature forms have recently been reported.[11–13] (The two published crystal structures of KBF_4 are, however, referred to significantly different unit cell dimensions.) $NaBF_4$ is reported to change into a hexagonal structure [1] and possibly into a cubic [2] phase on further heating. No second transition was, however, apparent from drop calorimetric measurements.[6] The crystal system of the high-temperature phases of the other alkali metal tetrafluoroborates has not yet been determined.

The published values of the transition temperature of NH_4BF_4 (Table 1), show a considerable variation (disregarding the value quoted in Ref. 4 which is almost certainly wrong, as are probably the transition heats quoted in Ref. 10). Other, reported transition heats are rather close to those of the corresponding perchlorates (Table 1, Ref. 14) (except for $NaBF_4$), while the transi-

Table 1. Crystallographic data for the high-temperature phases of alkalimetal tetrafluoroborates along with transition temperatures and heats. n = number of molecules per unit cell, ΔH_t = transition heat, t_t = transition temperature. (The numbers in parentheses are probably erroneous.)

	$NaBF_4$	NH_4BF_4	KBF_4	$RbBF_4$	$CsBF_4$
Cryst. syst.	hex.	f.c. cubic	f.c.c.		
Cryst. axes (Å)	$a(t_{exp}) = 5.00 \pm 0.02$ [1] $c(t_{exp}) = 7.75 \pm 0.03$	7.56,[2] 7.57	7.27,[2] 7.35		
t_{exp} (°C)	265 [1]	260,[2] 260	300,[2] 306		
n	2	4	4		
t_t (°C)	238.2 [3]	199.5 [3]	278.3 [3]		
	240 – 241 [4]	(236 [4])	276 – 280 [4]		
	246 – 247 [5]		278 – 279 [5]	250 – 251 [5]	169 – 170 [5]
	238 – 240 [5]		278 – 280 [5]	245 – 247 [5]	166 – 170 [5]
	243 [6]		283 [6]	243 [6]	170 [6]
	243 [7]	189 ± 5 [8]	283 [7]	245 [7]	169.5 [7]
		203	286	250 [9]	176 [9]
ΔH_t (kcal/mol)	1.61 [6]	2.12	3.30 [6]	2.86 [6]	1.94 [6]
	(0.54 [10])		3.28	(1.14 [10])	(0.70 [10])

tion temperatures are somewhat lower than those observed in the perchlorates, indicating that the transitions are very similar. Spectroscopic studies as well as the magnitude of the transition heats indicate that the transitions are of the order-disorder type. Reorientation of the BF_4^--groups has been detected in the room temperature phases and the reorientation rate studied as a function of temperature.[9,15]

Finbak and Hassel [2] assumed the cubic, high-temperature phases of NH_4BF_4 and KBF_4 to be rotationally disordered with the BF_4^--ions rotating about axes parallel to the cubic axes. This was also proposed for the perchlorate ions in the alkali metal perchlorates.[16]

The present model of the structure is based on the Frenkel model of disorder and is closely related to that recently derived for the perchlorates.[14]

EXPERIMENTAL

Commercially available KBF_4 and NH_4BF_4 (Hopkins and Williams, Ltd.) were used without further purification.

X-Ray and differential scanning calorimetry data were measured as described for the perchlorates.[14] The powder samples for X-ray analysis were sealed in pyrex tubes to avoid dissociation of the salts. Structure factor amplitudes, temperatures and heats of transition are listed in Tables 3 and 1, respectively.

RESULTS AND DISCUSSION

Potassium and nitrogen were assumed to be located at $(\pm\frac{1}{2},0,0)$, $(0,\pm\frac{1}{2},0)$ and $(0,0,\pm\frac{1}{2})$ *etc.*[2,14] The various orientations of the anion shown in Fig. 3, Ref. 14, were considered as possible equilibrium positions in a similar way to that described previously.[14] This showed A and B to be the more likely ones at equilibrium. The corresponding statistical fluorine-potassium and fluorine-nitrogen distances are listed in Table 2a, using a fluorine-boron bond length of 1.406(4) Å, which is the average fluorine-boron bond distance observed in NH_4BF_4 at room temperature, after correcting for effects of librational motion (e.s.d. in parenthesis).[13] The fluorine-potassium (nitrogen) distances are somewhat shorter than the average fluorine-potassium (nitrogen) distance observed in the ordered room temperature phases [11-13] listed for comparison. This may in part be due to the fact

Table 2. a. Statistical F – K(N) distances (Å) referring to anion position A and B, Fig. 3, Ref. 14, respectively. $d(B-F)=1.406$ Å (ass.),[13] symmetry of BF_4^--group: tetrahedral. A is a locked position, B is adjustable by translation along the [111]-direction.
b. Corresponding positional coordinates for the atoms in the BF_4^--group. A: All F-atoms crystallographically equivalent: $x_B=y_B=z_B=0$; $z_F=0$. B: three F-atoms crystallographically equivalent: $x_B=y_B=z_B$; $y_{F_1}=z_{F_1}$ and $x_{F_2}=y_{F_2}=z_{F_2}$.
K(N) in $(\pm\frac{1}{2}00)$ *etc.*

a. Distance	NH_4BF_4 (260 °C)	KBF_4 (306 °C)	*b.*	NH_4BF_4 (206 °C)	KBF_4 (306 °C)
A [at (000)]			A [at (000)]		
F($xy0$) – Me($\frac{1}{2}00$)	2.76	2.65	x_F	0.152	0.156
F($xy0$) – Me($0\frac{1}{2}0$)	3.14	3.08	y_F	0.107	0.110
B(000) – Me($\frac{1}{2}00$)	3.783	3.675			
B [at (000)]			B [at (000)]		
F_1(xyy) – Me($\frac{1}{2}00$)	2.83 (ass.)	2.70	x_B	−0.038	−0.036
F_2(xxx) – Me($-\frac{1}{2}00$)	3.10	3.01	x_{F_1}	0.140	0.148
B(xxx) – Me($-\frac{1}{2}00$)	3.52	3.43	y_{F_1}	−0.074	−0.073
B(xxx) – Me($\frac{1}{2}00$)	4.09	3.96	x_{F_2}	−0.146	−0.147
F – Me (av.) at room temp. (Å) [11-13]	2.932(0.015)				
Sum of contact radii (Å) [18]		2.69			

Table 3. Observed and calculated structure factors based on a combination of A and B. Unobserved and overlapping reflections excluded from R-value calculations. Overlapping reflections are computed according to $(\sum pF^2/\sum p/N)^{\frac{1}{2}}$, where p denotes the multiplicity of the reflections and N is the number of overlapping reflections included in the sum. The listed F_o-values of the non-obs. reflections (n.o.) are computed according to $I_{n.o.}(hkl) = \frac{1}{2}I_{obs.\ min.}(hkl)$.

	KBF_4[a]			NH_4BF_4[b]		
$h\,k\,l$	F_o	F_c		F_o	F_c	
1 1 1	≤7.5	4.36		37.4	37.69	
2 0 0	96.1	92.06		60.8	63.18	
2 2 0	39.5	42.69		21.2	26.41	
3 1 1	39.7	−39.97		23.6	−21.48	
2 2 2	28.7	32.54		18.5	13.60	
4 0 0	≤22.1	16.42		13.4	−14.52	
3 3 1	20.7	−22.52		≤ 6.0	−4.96	
4 2 0	19.3	13.76		≤6.2	1.70	
4 2 2	20.1	18.78		≤6.9	5.81	
3 3 3	≤18.7	−2.13	13.83	≤9.1	−2.72	12.12
5 1 1		−11.23			−9.77	
4 4 0	≤23.8	7.56		≤11.6	−0.08	
5 3 1	≤12.5	−7.99		≤6.1	−1.21	
6 0 0	≤22.6	14.60	18.76	≤11.1	4.16	8.98
4 4 2		12.91			6.79	
6 2 0	≤18.8	8.54		≤9.2	0.67	
5 3 3	≤19.3	−1.23		≤9.5	0.31	
6 2 2	≤19.3	7.25		≤9.6	1.07	

[a] $B(is) = 9.0$ Å^2; $x_A = 0.86$; $R = 0.076$. [b] $B(is) = 7.0$ Å^2; $x_A = 0.35$; $R = 0.071$.

that instantaneous fluorine-potassium (nitrogen) equilibrium separations in the disordered phases are probably on the average somewhat larger than the statistical mean values and that the number of close oxygen-potassium (nitrogen) contacts is smaller in the high-temperature phase. Atomic positional coordinates derived from Table 2a are given in Table 2b.

Structure factors based on anion orientations A and B were calculated using the form factors of Hanson *et al.*[17] and an F−B bond length of 1.382 Å, the mean F−B bond length observed in NH_4BF_4 at room temperature, not corrected for effects of librational effects[18] (e.s.d. in parenthesis). Neutral atoms were assumed for simplicity. A linear combination of the structure factors of A and B was refined by L. S. methods as outlined previously.[14] Observed and calculated structure factors are listed in Table 3. The fraction of molecules in A-type positions, x_A, is considerably uncertain because of the limited number of observable reflections. The relatively high B-values are attributable to large amplitudes of molecular libration and to the circumstance that instantaneous equilibrium positions are distributed statistically about the mean positions.

The weighted R-value, R_w, based on the structural combination is much less than the R_w-values obtained for the individual structures in the case of NH_4BF_4. For KBF_4, the A struc-

Table 4. Statistical F−F separations about or less than 2.70 Å between a BF_4^--group in either the A- or B-position (S) shown in Fig. 3, Ref. 14, and neighbouring BF_4^--groups in either A- or B-type orientations (L). Basic positional coordinates in Table 2b.

Positions S	Positions L	NH_4BF_4 d (Å)	KBF_4 d (Å)
A	A		
$F(xy0) - F(\frac{1}{2}-x,\frac{1}{2}-y,0)$		2.65	2.47
$F(xy0) - F(\frac{1}{2}-y,\frac{1}{2}-x,0)$		2.61	2.43
A	B		
$F(xy0) - F_1(\frac{1}{2}+y,\frac{1}{2}-x,y)$			2.72
$F(xy0) - F_2(\frac{1}{2}+x,\frac{1}{2}+x,x)$		2.69	2.54
$F(xy0) - F_3(\frac{1}{2}+x,\frac{1}{2}+x,x)$		2.69	2.54
B	B		
$F_1(xyy) - F_3(\frac{1}{2}+x,x,-\frac{1}{2}-x)$		2.75	2.61
$F_1(xyy) - F_2(\frac{1}{2}+x,-\frac{1}{2}-x,x)$		2.75	2.61
$F_2(xxx) - F_3(-\frac{1}{2}-x,-\frac{1}{2}-x,x)$		2.26	2.15

Table 5. The number of orientations of neighbouring BF_4^--groups (L) situated less than 2.70 Å from a given BF_4-group (S) in either position A or B, shown in Fig. 3, Ref. 14, listed as a function of the corresponding lattice sites associated with L. Derived from Table 4, using the symmetry operations of the space group ($Fm3m$). The numbers marked with an asterisk represent F—F distances close to 2.70 Å (2.69 Å, Table 4).

S	(at (000))	L	$(\frac{1}{2}\frac{1}{2}0)$	$(0\frac{1}{2}\frac{1}{2})$	$(\frac{1}{2}0\frac{1}{2})$	$(\frac{1}{2}\bar{\frac{1}{2}}0)$	$(0\frac{1}{2}\bar{\frac{1}{2}})$	$(\bar{\frac{1}{2}}0\frac{1}{2})$	$(\bar{\frac{1}{2}}\frac{1}{2}0)$	$(0\bar{\frac{1}{2}}\frac{1}{2})$	$(\frac{1}{2}0\bar{\frac{1}{2}})$	$(\bar{\frac{1}{2}}\bar{\frac{1}{2}}0)$	$(0\bar{\frac{1}{2}}\bar{\frac{1}{2}})$	$(\bar{\frac{1}{2}}0\bar{\frac{1}{2}})$	
A		A-type	2							2	2		2		NH_4BF_4
	»		2							2	2		2		KBF_4
A		B-type	2*							2*	2*		2*		NH_4BF_4
	»		2							2	2		2		KBF_4
B		A-type										2*	2*	2*	NH_4BF_4
	»											2	2	2	KBF_4
B		B-type										1	1	1	NH_4BF_4
	»				1	1	1	1	1	1		3	3	3	KBF_4

ture is found to dominate in the combination, leading to an R_w-value, which is only 5—6 % less than that based on pure A structure.

The van der Waals radius of fluorine is reported as 1.35 Å.[18] Empirical values of the ionic radius are 1.36 Å [18] and 1.33 Å,[19] while a calculated value is 1.40 Å.[20] The minimum, equilibrium intermolecular F—F separation [14] was chosen as 2.70 Å in the present case. (The shortest intermolecular F—F distance in the room temperature phases is much larger than this value.[11–13]) Statistical, intermolecular F—F separations equal to or less than 2.70 Å calculated for the high-temperature phases, are listed in Table 4. The number of neighbouring anions situated less than 2.70 Å from a chosen BF_4-group in either the A or B position in Fig. 3, Ref. 14, is listed as a function of the associated lattice sites in Table 5. The configurational entropies (S_c) were computed as described for the perchlorates,[14] using the results of Tables 3 and 5, *etc.*[14] This gave:

$S_c = 4.40$ cal/mol K and $S_c = 2.93$ cal/mol K,

for NH_4BF_4 and KBF_4, respectively, while the transition entropies, obtained as $\Delta H_t/T_t$, from Table 1, are

$\Delta S_t = 4.45$ cal/mol K and $\Delta S_t = 5.85$ cal/mol K,

respectively. The S_c-values suffer from inaccuracy in the basic x_A-values noted above, in addition to the general uncertainty associated with the evaluation of the configurational entropy discussed in Ref. 14. Thus ignoring the numbers marked with an asterisk in Table 4 in the calculations,[14] leads to an S_c-value of 4.89 cal/mol K for NH_4BF_4, which is even greater than the experimental transition entropy. The findings indicate, however, that the presence of the NH_4^+-ion does not give rise to a particularly large contribution to the transition entropy, as also noted for NH_4ClO_4.[14]

The transition entropies observed in $KClO_4$[14] and KBF_4 are particularly high. Comparison with the results obtained for $KClO_4$ indicates that the x_A-value obtained for KBF_4 may be too high and the S_c-value correspondingly too low. Inspection shows, however, that the discrepancy between ΔS_t and S_c is rather large, irrespectively of the x_A-value. A similar result was also obtained for $KClO_4$. A specific explanation of these relatively large discrepancies has not been found. In general, the difference between observed transition entropies and calculated configurational entropies is ascribed to various factors, such as changes in the vibrational state associated with the transition [21,22] as well as additional (orientational or positional) disorder in the high-temperature phases.[14]

The present high-temperature phases are apparently very similar to those of the corresponding perchlorates. Much of the discussion in Ref. 14 is thus equally valid here. Comparison of Table 1 and Table 1, Ref. 14, indicates that the high-temperature forms of $RbBF_4$ and $CsBF_4$ may have crystal structures similar to those of the perchlorates.[14]

REFERENCES

1. Quist, A. S., Bates, J. B. and Boyd, G. E. *J. Chem. Phys.* *55* (1971) 2836.

2. Finbak, Chr. and Hassel, O. *Z. Phys. Chem. B 32* (1936) 433.
3. Hassel, O. and Hveding, J. A. *Arch. Math. Naturvidensk. B XLV* (1941) No. 2.
4. Vorländer, D., Hollatz, J. and Fischer, J. *Ber. Deut. Chem. Ges. 65* (1932) 535.
5. Marano, R. T. and Shuster, E. K. *Thermochim. Acta 1* (1970) 521.
6. Dvorkin, A. S. and Bredig, M. A. *J. Chem. Eng. Data 15* (1970) 505.
7. Cantor, S., McDermott, D. P. and Gilpatrick, L. O. *J. Chem. Phys. 52* (1970) 4600.
8. Marano, R. T. and McAtee, Jr., J. L. *Thermochim. Acta 4* (1972) 421.
9. Huettner, D. J., Ragle, J. L., Sherk, L., Stengle, T. R. and Yeh, H. J. C. *J. Chem. Phys. 48* (1968) 1739.
10. Marano, R. T. and Shuster, E. R. *Chem. Abstr. 75* (1971) 11463.
11. Clark, M. J. R. and Lynton, B. *Can. J. Chem. 47* (1969) 2579.
12. Brunton, G. D. *Acta Crystallogr. B 25* (1969) 2161.
13. Caron, A. P. and Ragle, J. L. *Acta Crystallogr. B 27* (1971) 1102.
14. Strømme, K. O. *Acta Chem. Scand. A 28* (1974) 515.
15. Caron, A. P., Huettner, D. J., Ragle, J. L., Sherk, L. and Stengle, T. R. *J. Chem. Phys. 47* (1967) 2577.
16. Finbak, Chr. and Hassel, O. *Z. Phys. Chem. B 32* (1936) 130.
17. Hanson, H. P., Herman, F., Lea, J. D. and Skillman, S. *Acta Crystallogr. 17* (1964) 1040.
18. Pauling, L. *Nature of the Chemical Bond*, Cornell University Press, New York 1960.
19. Slater, J. C. *J. Chem. Phys. 41* (1964) 3199.
20. Goldberg, S. Z. *J. Chem. Educ. 45* (1968) 638.
21. Darmon, I. and Brot, C. *Mol. Cryst. 2* (1967) 301.
22. Brot, C. *J. Phys. (Paris) 32, C59* (1971) 223.

Received November 2, 1973.

Acta Chemica Scandinavica A 28 (1974) 551—562

The Crystal Structures of Hexacyanomanganate Decahydrate, $Na_4[Mn(CN)_6].10H_2O$ and Tetrasodium Hexacyanoferrate Decahydrate, $Na_4[Fe(CN)_6].10H_2O$

AINA TULLBERG and NILS-GÖSTA VANNERBERG

Department of Inorganic Chemistry, Chalmers University of Technology and University of Göteborg, P.O. Box, S-402 20 Göteborg 5, Sweden

The crystal structures of the isomorphous compounds $Na_4[Mn(CN)_6].10H_2O$ and $Na_4[Fe(CN)_6].10H_2O$ have been refined by single crystal X-ray diffraction methods. The crystals are monoclinic and belong to space group $P2_1/n$. R-values of 0.09 and 0.08 have been obtained for the manganese and iron compounds, respectively.

The structures are built up of almost regular octahedral $[Me(CN)_6]^{4-}$ ions, linked together in three dimensions by distorted sodium ion coordination octahedra. There are three crystallographically different cyanide groups. In each $[Me(CN)_6]^{4-}$ octahedron the nitrogen atoms of two cyanide groups are thus each linked to three sodium ions, the nitrogen atoms of two other cyanide groups are each linked to one sodium ion, while the nitrogen atoms of the remaining two cyanide groups would appear to participate in hydrogen bonding to water molecules.

The mean Me—C distances are 1.95(3) Å and 1.91(1) Å and the mean C—N bond distances are 1.16(3) Å and 1.17(1) Å for $Na_4[Mn(CN)_6].10H_2O$ and $Na_4[Fe(CN)_6].10H_2O$, respectively.

The chemical bonding in hexacyanido complexes has been subject to much discussion. Many authors believe that the extreme stability and inertness of the complexes are due to appreciable π-bonding between the central ion and the cyanide ligand.[1,2] However, some theoretical calculations show little π-bonding in these complexes.[3] Qualitatively, it should be possible to determine the relative contributions of π- and σ-bonding if the variation in bond lengths of complex ions of the type $Me(CN)_6^{n-}$ can be expressed as a function of the central ion and its oxidation state. This calculation has been performed in order to determine the bond distance in Me(II)—CN, where Me is Mn and Fe. The Me(III)—CN distances have been previously determined by one of the authors.[4,5] A short communication regarding the work has been given previously.[6]

EXPERIMENTAL

Crystals of $Na_4[Mn(CN)_6].10H_2O$ were prepared from $MnCO_3$ and NaCN, according to the method described by Brauer;[7] those of $Na_4[Fe(CN)_6].10H_2O$ were obtained by recrystallizing a commercial sample from water. Both compounds, and particularly $Na_4[Mn(CN)_6].10H_2O$, are unstable in air, due to high water vapor pressure.

Crystal data. The unit cell dimensions for the compounds were determined from Guinier powder photographs taken with $CuK\alpha_1$ radiation, using potassium chloride (Mn) and lead nitrate (Fe) as an internal standard.[8] The manganese compound reacted quantitatively with lead nitrate even in solid phase why potassium chloride has to be used in this case. About 20 lines were indexed and the cell parameters were refined with the program POWDER.[9] The following results were obtained: Mn: $a = 9.818(7)$ Å, $b = 11.460(8)$ Å, $c = 9.093(8)$ Å, $\beta = 97.95(6)°$ and $V = 1013.2$ Å^3, Fe: $a = 9.787(5)$ Å, $b = 11.448(6)$ Å, $c = 9.037(5)$ Å, $\beta = 97.49(4)°$ and $V = 1003.8$ Å^3. Observed and calculated $\sin^2\theta$ values, d-values and the corresponding intensities are listed in Tables 1a and 1b.

The measured density for $Na_4[Fe(CN)_6].10H_2O$, 1.60 g cm^{-3} was determined by the flotation method using carbon tetrachloride (density 1.60 g cm^{-3}). The calculated density,

Table 1a. X-Ray powder diffraction data for $Na_4Mn(CN)_6.10H_2O$. Guinier camera; $CuK\alpha_1$ radiation ($\lambda = 1.54050$ Å).

$h\ k\ l$	$10^5 \sin^2\theta$ obs	$10^5 \sin^2\theta$ calc	d (calc) Å	I_{calc}	I_{obs}
1 1 0	1071	1079	7.443	43	vs
0 1 1	1179	1183	7.094	3	vw
1 0 1	1536	1547	6.215	9	m
0 2 0	1809	1807	5.727	8	m
0 0 2	2906	2926	4.518	9	m
1 2 $\bar{1}$	2959	2979	4.478	3	w
2 1 $\bar{1}$	3301	3318	4.239	5	m
1 1 $\bar{2}$	3619	3631	4.049	15	s
2 1 1	4054	4069	3.826	6	m
0 3 1	4785	4797	3.521	17	s
3 1 0	6088	6099	3.122	10	s
1 0 $\bar{3}$	6647	6649	2.988	7	m
0 4 0	7213	7228	2.868	6	m
3 2 $\bar{1}$	7610	7624	2.792	8	s
2 2 2	7975	7994	2.728	7	s
1 4 $\bar{1}$	8399	8398	2.658	4	m
3 2 1	8745	8749	2.605	5	m
3 2 $\bar{2}$	9242	9256	2.534	4	m
3 3 0	9708	9713	2.472	2	w
3 3 $\bar{1}$	9872	9882	2.451	2	w
1 4 $\bar{3}$	13867	13877	2.068	10	s

Table 1b. X-Ray powder diffraction data for $Na_4Fe(CN)_6.10H_2O$. Guinier camera; $CuK\alpha_1$ radiation ($\lambda = 1.54050$ Å).

$h\ k\ l$	$10^5 \sin^2\theta$	$10^5 \sin^2\theta$	d (calc) Å	I_{calc}	I_{obs}
1 1 0	1093	1083	7.402	45	vs
1 0 $\bar{1}$	1205	1191	7.057	1	vw
0 1 1		1192	7.056	3	
1 0 1	1554	1547	6.193	12	m
0 2 0	1819	1811	5.724	8	m
0 0 2	2964	2954	4.480	9	m
1 2 $\bar{1}$	3013	3002	4.446	3	vw
2 1 $\bar{1}$	3360	3357	4.204	5	m
1 2 1		3358	4.204	4	
1 1 $\bar{2}$	3673	3683	4.013	17	m
2 1 1	4077	4068	3.819	6	w
0 3 1	4814	4813	3.511	10	s
2 2 1	5434	5426	3.307	2	diff.
3 1 0	6128	6124	3.113	11	m
1 0 $\bar{3}$	6758	6748	2.965	10	m
0 4 0	7250	7243	2.862	10	m
3 2 $\bar{1}$	7695	7687	2.778	10	m
2 2 2	8006	7999	2.723	9	m
1 4 $\bar{1}$	8444	8434	2.652	4	vw
1 2 $\bar{3}$	8569	8559	2.633	4	w
3 2 1	8763	8755	2.603	6	w
3 2 $\bar{2}$	9380	9371	2.516	4	w

based on two formula units in the unit cell, is 1.60 g cm^{-3}.

Conditions limiting possible reflections for crystals of both compounds are

$h0l : h+l=2n$
$0k0 : k=2n$

This is in accordance with space group $P2_1/n$.

DETERMINATION OF THE STRUCTURE OF $Na_4[Mn(CN_6].10H_2O$

The structure of $Na_4[Mn(CN)_6].10H_2O$ was determined first. A crystal was mounted in a sealed glass capillary with rotation axis parallel to the *c*-axis and rotation and Weissenberg equi-inclination photographs were registered using multiple film techniques and Cu$K\alpha$ radiation. Only the layers $hk0-hk4$, giving a total of 561 independent reflections, were recorded before the crystal decomposed. Attempts were made to mount other crystals but, before a satisfactory specimen was found, interest was focused on the isomorphous iron compound, which seemed to be more stable to X-ray exposure. Since the linear absorption coefficient for $Na_4[Mn(CN)_6].10H_2O$ in Cu$K\alpha$ radiation is 69.3 cm^{-1}, the data are seriously effected by absorption. However, no corrections were made for this.

The relative intensities of the reflections $hk0-hk4$ were estimated visually by comparison with a logarithmic scale. After correction for Lorentz and polarisation effects, using the program DATA P2,[9] a three dimensional Patterson synthesis was computed with the program DRF.[9] Since the unit cell contains two manganese atoms and the general equivalent positions in space group $P2_1/n$ are fourfold, the manganese atoms must occupy one of the special twofold positions with site symmetry 1. The general positions of the sodium atoms and the orientation of the octahedral $[Mn(CN)_6]^{4-}$ ions were determined from the Patterson synthesis. Some C and N peaks were lower than expected and there was overlapping, probably due to the approximate scaling of the data, which had been carried out assuming that there were no fluctuations in the intensity from the X-ray tube.

Subsequent electron density calculations based on the contributions of the postulated atoms to the structure factor phases revealed the positions of the remaining non-hydrogen atoms. After a few cycles of isotropic block diagonal least squares refinement, using the program BLOCK,[9] the *R*-value converged to 0.089. A difference electron density calculation showed no spurious peaks, the highest being 1 e/Å^3. F_c values were calculated for the unobserved reflections in the five layers registered. All were small.

Bond distances and angles were calculated with the program DISTAN.[9] The Mn–C bond distances vary between 1.91 and 1.98 Å (mean 1.95 Å) and the C–N distances between 1.14

Table 2. Final atomic fractional coordinates and isotropic thermal parameters for $Na_4Mn(CN)_6.10H_2O$. Standard deviations are given in parentheses. The temperature factor is exp $(-B \sin^2\theta/\lambda^2)$.

Atom	*x*	*y*	*z*	*B* Å^2
Mn	0	0	0	2.6(1)
Na(1)	0.0948(6)	0.1419(4)	0.5122(8)	3.9(1)
Na(2)	0.7154(5)	0.1285(4)	0.3992(8)	3.5(1)
C(1)	0.303(1)	0.510(1)	0.431(2)	2.8(2)
C(2)	0.498(1)	0.328(1)	0.476(2)	2.8(2)
C(3)	0.542(1)	0.517(1)	0.300(2)	2.5(2)
N(1)	0.187(1)	0.519(8)	0.391(2)	3.3(2)
N(2)	0.502(1)	0.228(1)	0.472(2)	3.6(2)
N(3)	0.431(1)	0.471(1)	0.823(2)	2.9(2)
O(1)	0.302(1)	0.038(1)	0.444(1)	3.5(2)
O(2)	0.106(1)	0.487(1)	0.700(1)	4.7(2)
O(3)	0.267(1)	0.219(1)	0.715(2)	4.8(2)
O(4)	0.113(1)	0.274(1)	0.317(2)	6.4(3)
O(5)	0.383(1)	0.278(1)	0.099(1)	4.3(2)

and 1.19 Å (mean 1.16 Å). The Mn–C–N angles are 178.2°, 175.5°, and 178.5°. As there is no chemical reason why the $[Mn(CN)_6]^{4-}$ ions should not be close to regular, the observed distortion is probably due to absorption and termination errors in the data. Atomic parameters are listed in Table 2 and bond distances and angles within the complex $Mn(CN)_6^{4-}$ ion are listed in Table 5.

DETERMINATION OF THE STRUCTURE OF $Na_4[Fe(CN)_6].10H_2O$

A crystal of $Na_4[Fe(CN)_6].10H_2O$ was first mounted to rotate about the *c*-axis on an automatic single crystal diffractometer (Philips PAILRED) and the intensities of reflections in layers $hk0-hk9$ were measured with Mo$K\alpha$ radiation. They were reduced to structure amplitudes using the program DATA P1.[5] It was then discovered that due to an instrumental error, several reflections had been wrongly indexed. A preliminary structure report based on selected data from the PAILRED data was published.[6] Refinement of the data gave an *R*-value of 0.13 and a distorted $[Fe(CN)_6]^{4-}$ octahedron with Fe–C bond distances varying between 1.90 and 2.04 Å and Fe–C bond distances between 1.12 and 1.21 Å.

Another crystal was mounted on an in-

Table 3. Atomic coordinates for $Na_4Fe(CN)_6.10H_2O$, expressed as fractions of the cell edges, and their standard deviations.

Atom	*x*	*y*	*z*
Fe	0	0	0
Na(1)	0.0935(4)	0.1396(3)	0.5098(4)
Na(2)	0.7138(4)	0.1285(3)	0.3989(4)
C(1)	0.3086(7)	0.5088(8)	0.4290(8)
C(2)	0.5004(8)	0.3333(6)	0.4776(8)
C(3)	0.5434(7)	0.5174(5)	0.3016(8)
N(1)	0.1896(8)	0.5175(7)	0.3882(9)
N(2)	0.5033(8)	0.2318(6)	0.4680(8)
N(3)	0.4296(8)	0.4705(6)	0.8202(8)
O(1)	0.3023(7)	0.0388(6)	0.4439(7)
O(2)	0.1050(7)	0.4902(7)	0.7013(8)
O(3)	0.2666(7)	0.2201(6)	0.7149(8)
O(4)	0.1138(11)	0.2724(7)	0.3162(9)
O(5)	0.3817(8)	0.2785(6)	0.0979(8)

Table 4. Anisotropic thermal parameters and their standard deviations. The temperature coefficient is expressed as exp $[-(h^2\beta_{11}+k^2\beta_{22}+l^2\beta_{33}+2hk\beta_{12}+2hl\beta_{13}+2kl\beta_{23})]$.

Atom	β_{11}	β_{22}	β_{33}	β_{12}	β_{13}	β_{23}
Fe	0.0045(1)	0.0031(1)	0.0052(2)	−0.0005(3)	0.0017(2)	−0.0006(3)
Na(1)	0.0085(4)	0.0061(3)	0.0101(5)	−0.0001(5)	0.0008(7)	0.0002(6)
Na(2)	0.0084(4)	0.0050(3)	0.0100(5)	0.0009(5)	0.0017(6)	0.0007(5)
C(1)	0.0049(6)	0.0050(6)	0.0055(7)	−0.0006(12)	0.0001(10)	−0.0014(12)
C(2)	0.0045(6)	0.0045(5)	0.0065(10)	−0.0009(11)	0.0017(14)	−0.0002(10)
C(3)	0.0034(6)	0.0023(5)	0.0078(9)	−0.0002(8)	0.0014(10)	0.0011(9)
N(1)	0.0068(7)	0.0067(7)	0.0109(10)	0.0010(12)	0.0039(13)	0.0007(13)
N(2)	0.0072(8)	0.0046(5)	0.0114(2)	−0.0007(11)	0.0045(16)	−0.0029(10)
N(3)	0.0072(8)	0.0055(6)	0.0065(8)	0.0012(9)	0.0039(12)	0.0015(9)
O(1)	0.0104(9)	0.0069(6)	0.0081(8)	−0.0024(10)	0.0037(13)	0.0009(9)
O(2)	0.0069(6)	0.0115(7)	0.0104(8)	0.0037(14)	0.0017(11)	0.0063(14)
O(3)	0.0093(8)	0.0073(6)	0.0132(11)	0.0002(11)	0.0010(14)	−0.0067(12)
O(4)	0.0229(16)	0.0070(6)	0.0137(13)	−0.0067(17)	−0.0050(22)	0.0014(14)
O(5)	0.0117(9)	0.0067(6)	0.0112(10)	−0.0023(12)	0.0029(14)	0.0021(12)

Table 5. Geometry of the $Fe(CN)_6^{4-}$ and $Mn(CN)_6^{4-}$ octahedra. Interatomic distances (in Å) and angles with their standard deviations in parentheses.

Distance		Angle	
Fe – C(1)	1.902(7)	Fe – C(1) – N(1)	177.7(8)
Fe – C(2)	1.920(8)	Fe – C(2) – N(2)	178.0(7)
Fe – C(3)	1.906(7)	Fe – C(3) – N(3)	179.2(6)
C(1) – N(1)	1.180(10)	C(1) – Fe – C(2)	88.1(4)
C(2) – N(2)	1.165(10)	C(1) – Fe – C(3)	89.6(3)
C(3) – N(3)	1.174(10)	C(2) – Fe – C(3)	90.0(3)
Mn – C(1)	1.95(1)	Mn – C(1) – N(1)	178(4)
Mn – C(2)	1.98(1)	Mn – C(2) – N(2)	175(2)
Mn – C(3)	1.93(2)	Mn – C(3) – N(3)	179(1)
C(1) – N(1)	1.15(2)	C(1) – Mn – C(2)	88.4(5)
C(2) – N(2)	1.15(2)	C(1) – Mn – C(3)	88.7(6)
C(3) – N(3)	1.19(2)	C(2) – Mn – C(3)	89.8(6)

Table 6. Geometry of the sodium ion coordination octahedra in $Na_4[Fe(CN)_6].10H_2O$. Interatomic distances (in Å) and angles with their standard deviations in parentheses.

Coordination of Na(1)

Atom	x	y	z
Na(1)	0.0935	0.1396	0.5098
N(3)	0.0704	−0.0295	0.6798
N(3)′	−0.0704	0.0295	0.3202
O(1)	0.3023	0.0388	0.4439
O(3)	0.2666	0.2201	0.7149
O(4)	0.1138	0.2724	0.3162
O(5)	−0.1183	0.2215	0.5979

Distance	
Na(1) – N(3)	2.500(8)
Na(1) – N(3)	2.526(8)
Na(1) – O(1)	2.486(8)
Na(1) – O(3)	2.517(8)
Na(1) – O(4)	2.346(9)
Na(1) – O(5)	2.498(8)
Mean	2.479

Angle	
N(3) – Na(1) – N(3)″	86.0(3)
N(3) – Na(1) – O(1)	86.0(3)
N(3) – Na(1) – O(3)	86.4(3)
N(3) – Na(1) – O(4)	169.6(3)
N(3) – Na(1) – O(5)	87.1(3)
N(3)′ – Na(1) – O(1)	94.3(3)
N(3)′ – Na(1) – O(3)	171.5(3)
N(3)′ – Na(1) – O(4)	85.7(3)
N(3)′ – Na(1) – O(5)	85.6(3)
O(1) – Na(1) – O(3)	81.4(3)
O(1) – Na(1) – O(4)	88.3(3)
O(1) – Na(1) – O(5)	173.1(3)
O(3) – Na(1) – O(4)	101.4(3)
O(3) – Na(1) – O(5)	97.8(3)
O(4) – Na(1) – O(5)	98.6(3)

Coordination of Na(2)

Atom	x	y	z
Na(2)	0.7138	0.1285	0.3989
N(2)	0.5033	0.2318	0.4680
N(3)″	0.9296	0.0295	0.3202
O(1)′	0.6977	−0.0388	0.5561
O(2)	0.6050	0.0098	0.2013
O(3)′	0.7666	0.2799	0.2149
O(5)′	0.8817	0.2215	0.5979

Distance	
Na(2) – N(2)	2.524(8)
Na(2) – N(3)″	2.576(8)
Na(2) – O(1)′	2.402(8)
Na(2) – O(2)	2.382(8)
Na(2) – O(3)′	2.503(8)
Na(2) – O(5)′	2.510(8)
Mean	2.483

Angle	
N(2) – Na(2) – N(3)″	177.6(3)
N(2) – Na(2) – O(1)′	96.2(3)
N(2) – Na(2) – O(2)	98.8(3)
N(2) – Na(2) – O(3)′	94.9(3)
N(2) – Na(2) – O(5)′	95.9(3)
N(3)″ – Na(2) – O(1)′	86.1(3)
N(3)″ – Na(2) – O(2)	81.1(3)
N(3)″ – Na(2) – O(3)′	82.7(3)
N(3)″ – Na(2) – O(5)′	84.3(3)
O(1)′ – Na(2) – O(2)	86.1(3)
O(1)′ – Na(2) – O(3)′	168.7(3)
O(1)′ – Na(2) – O(5)′	90.1(3)
O(2) – Na(2) – O(3)′	90.5(3)
O(2) – Na(2) – O(5)′	165.1(4)
O(3)′ – Na(2) – O(5)′	90.6(3)

tegrating Weissenberg equiinclination camera. The layers $hk0 - hk10$ were recorded using Mo$K\alpha$ radiation. There were 1283 independent reflections. Multiple film techniques were used and the intensities of the reflections were estimated visually by comparison with a logarithmic scale. The data were corrected for Lorentz and polarisation effects with the program DATA P2.[9] No absorption corrections were made. The linear absorption coefficient for $Na_4[Fe(CN)_6].10H_2O$ in Mo$K\alpha$ radiation is 9.2 cm^{-1}. The structure refined to $R = 0.109$ with block diagonal least squares refinement using the program BLOCK [9] and isotropic temperature coefficients. 162 reflections were omitted in this stage of the refinement because their intensities had been estimated with less precision than the others.

The parameters were then further refined with the full matrix least squares program LALS,[9] an R-value of 0.089 being obtained. When anisotropic thermal parameters were assigned to all atoms the R-value dropped to 0.077. After refinement with the 162 reflections mentioned earlier included the R-value was 0.084.

The atomic scattering factors used for Fe^+, Na^+, C, N, and O were those given in the International Tables.[8] The Fe^+ values were corrected for anomalous dispersion according to Cromer and Waber.[10] A weighting scheme of the form proposed by Cruickshank [11] ($s = [10.0 + |F_o| + 0.05|F_o|^2]^{-1}$) was employed.

The 830 unobserved reflections were then assigned values by taking $I = 0.5I_{min}$ for each reciprocal lattice layer. A difference synthesis was calculated with the program DRF with these reflections included. This showed a maximum peak height of 1.4 e/Å^3. No attempts were made to locate the hydrogen atoms.

Atomic parameters for the structure are given in Tables 3 and 4. Bond distances and angles are listed in Tables 5, 6, and 7, and observed and calculated structure factors are listed in Table 8.

Table 7. Water contact distances (in Å) shorter than 3.10 Å in $[Na_4Fe(CN)_6].10H_2O$ with their standard deviations given in parentheses.

Distances	
O(1) – N(1)	3.02(1)
O(1) – N(2)	2.95(1)
O(2) – N(1)	3.07(1)
O(2) – N(1)	2.89(1)
O(2) – O(3)	2.97(1)
O(4) – N(1)	2.95(1)
O(5) – N(1)	3.08(1)

DESCRIPTION AND DISCUSSION OF THE STRUCTURE

The unit cell is body-centered with respect to the nearly octahedral $[Me(CN)_6]^{4-}$ ions. These are linked together in three dimensions by sodium ions in distorted coordination octahedra, each involving two nitrogen atoms of cyanide groups and four oxygen water atoms at a mean distance of 2.5 Å.

Due to the centre of symmetry there are three crystallographically different cyanide groups in the unit cell, so that two opposite cyanide groups in each $[Me(CN)_6]^{4-}$ octahedron are each linked through nitrogen atoms N(3) to three different sodium ions while two other cyanide groups are each linked through nitrogen atoms N(2) to one sodium ion. The remaining two nitrogen atoms N(1) are not coordinated to sodium ions but would appear to participate in hydrogen bonding to water molecules which are corners of sodium ion octahedra (Fig. 1).

The distances and angles within the $[Fe(CN)_6]^{4-}$ octahedron are illustrated in Fig. 2.

There are five water contact distances to nitrogen or oxygen atoms shorter than 3.1 Å, indicating the possibility of hydrogen bonding, as mentioned above. These distances are listed in Table 10.

Few structure investigations of hexacoordinated transition metal cyanide compounds have been described, probably because many of these compounds are unstable and tend to crystallize with disordered structures. However, a neutron diffraction study of $K_4[Fe(CN)_6].3D_2O$ by Taylor, Mueller and Hitterman [12] was published in 1970. The results presented here are in good agreement with those found in that investigation. Fe – C bond distances varying between 1.908(4) and 1.956(4) Å [mean 1.927(3) Å] are reported for $K_4[Fe(CN)_6].3D_2O$. The corresponding distances in $Na_4[Fe(CN)_6].10H_2O$ are 1.907(7), 1.906(7), and 1.920(8) Å. In $K_4[Fe(CN)_6].3D_2O$ the C – N

Table 8. Observed and calculated structure factors for the structure $Na_4[Fe(CN)_6].10H_2O$.

H 0 0		
4	41	41
6	-	7*
8	20	20
10	48	43
12	-	9*

H 1 0		
2	20	-24
3	118	105
4	9	-11
5	-	-1*
6	-	-1*
7	30	31
8	12	12
9	-	3*
10	-	2*
11	13	13
12	-	-3*

H 2 0		
2	23	20
3	14	-16
4	26	26
5	-	4*
6	31	30
7	6	8
8	16	-19
9	-	6*
10	16	16
11	-	2*

H 3 0		
1	21	21
2	8	-9
3	58	56
4	-	7*
5	66	62
6	-	3*
7	-	7*
8	17	18
9	-	5*
10	-	-6*
11	-	-4*
12	-	1*

H 4 0		
0	146	130
1	18	-16
2	52	47
3	13	13
4	22	22
5	23	23
6	38	37
7	7	-8
8	16	16
9	-	2*
10	8	11

H 5 0		
1	35	35
2	57	51
3	42	41
4	-	-6*
5	39	40
6	22	23
7	15	16
8	18	-19
9	8	8

H 6 0		
0	75	71
1	24	-24
2	37	37
3	94	86
4	24	24
5	-	-3*
6	21	20
7	13	-15
8	-	4*
9	-	3*
10	20	19

H 7 0		
1	55	55
2	27	25
3	50	47
4	-	-7*
5	14	18
6	18	19
7	17	16
8	-	-2*
9	-	11*
10	-	0*
11	14	13

H 8 0		
0	84	82
1	13	-15
2	16	17
3	9	-11
4	19	18
5	18	20
6	11	10
7	-	2*
8	11	9
9	9	8
10	18	17

H 9 0		
1	10	10
2	10	-9
3	15	16
4	-	3*
5	7	9
6	8	8
7	11	11
8	11	12

H 10 0		
0	-	11*
1	-	6*
2	12	13
3	9	12
4	15	15
5	-	7*
6	16	16
7	-	0*
8	9	7

H 11 0		
1	17	19
2	-	8*
3	14	15
4	-	7*
5	44	38
6	-	3*
7	10	10
8	-	4*
9	12	12

H 12 0		
0	-	4*
1	-	-2*
2	26	25
3	8	9
4	13	14
5	12	10
6	19	20
7	-	-1*
8	12	11

H 13 0		
1	12	12
2	-	8*
3	-	6*
4	-	5*
5	13	14
6	-	7*

H 14 0		
0	17	18
1	-	-3*
2	-	8*
3	13	13

H 0 1		
-13	16	13
-11	16	13
-9	20	22
-7	36	37
-5	94	87
-3	83	67
3	75	66
5	-	175*
7	-	15*
9	26	27

H 1 1		
-12	15	14
-11	-	6*
-10	19	19
-9	-	9*
-8	12	9
-7	-	10*
-6	33	35
-5	-	5*
-4	26	25
-3	22	-22
2	72	61
3	25	24
4	57	57
5	-	12*
6	70	65
7	-	-6*
8	35	33

H 2 1		
-8	29	27
-7	26	26
-6	-	-8*
-5	15	18
-4	16	-16
-3	149	-103
1	45	40
2	35	36
3	101	86
4	-	-5*
5	14	16
6	-	7*
7	-	2*
8	-	-7*
9	15	15

H 3 1		
-10	21	20
-9	-	8*
-8	14	12
-7	-	-5*
-6	25	-22
-5	21	20
-4	28	27
-3	68	-59
0	136	111
1	-	1*
2	30	28
3	-	2*
4	-	6*
5	-	6*
6	37	40
7	15	-15
8	15	14
9	-	8*
10	22	23

H 4 1		
-11	23	23
-10	-	-4*
-9	-	5*
-8	-	-3*
-7	31	30
-6	16	20
-5	-	1*
-4	-	1*
-3	31	33
-2	15	12
-1	76	70
0	78	-65
1	24	30
2	-	-3*
3	82	74
4	-	5*
5	39	41
6	-	2*
7	15	17
8	-	8*
9	19	19
10	-	3*
11	15	12

H 5 1		
-10	22	23
-9	-	-4*
-8	-	3*
-7	-	0*
-6	-	5*
-5	-	-6*
-4	30	30
-3	47	45
-2	14	16
-1	24	-26
0	75	65
1	-	-7*
2	21	23
3	46	-41
4	32	34
5	-	1*
6	38	38
7	18	20
8	13	14
9	-	4*
10	17	16

H 6 1		
-7	29	29
-6	-	0*
-5	34	31
-4	-	0*
-3	-	-5*
-2	25	21
-1	20	22
0	-	11*
1	28	34
2	76	-74
3	58	57
4	-	9*
5	34	36
6	11	-10
7	15	16
8	32	30
9	15	16
10	-	-1*

H 7 1		
-10	15	12
-9	-	3*
-8	13	12
-7	-	4*
-6	38	35
-5	-	-3*
-4	27	29
-3	-	0*
-2	35	37
-1	14	-17
0	27	30
1	-	3*
2	24	27
3	20	-19
4	36	38
5	-	2*
6	42	44
7	-	7*
8	22	24

H 8 1		
-7	13	14
-6	16	18
-5	32	30
-4	-	-6*
-3	20	22
-2	-	-8*
-1	12	8
0	38	-43
1	25	26
2	18	20
3	19	21
4	-	11*
5	46	47

H 9 1		
-6	13	13
-5	-	9*
-4	-	1*
-3	28	-28
-2	16	17
-1	-	-3*
0	11	13
1	-	-6*
2	-	6*
3	-	9*
4	15	17

H 10 1		
-3	13	14
-2	-	-3*
-1	21	20
0	12	-11
1	19	21
2	-	-2*
3	16	17

H 11 1		
-4	22	22
-3	-	-11*
-2	16	16
-1	-	3*
0	-	50*
1	15	-13
2	13	12
3	-	-7*
4	16	14
5	-	2*
6	18	17
7	-	2*
8	-	10*
9	-	7*
10	21	18

H 12 1		
-3	14	15
-2	-	1*
-1	25	27
0	16	-16
1	14	15
2	-	-5*
3	24	26
4	-	0*
5	-	5*
6	-	3*
7	15	15

H 13 1		
-1	-	-4*
0	15	16
1	-	-5*

H 14 1		
-4	-	-3*
-3	15	14
-2	-	-2*
-1	-	5*

H 0 2		
-12	18	20
-10	22	25
-8	27	25
-6	39	45
-4	87	76
4	22	25
6	58	58
8	15	16
10	52	45
12	10	13

H 1 2		
-11	22	22
-10	-	6*
-9	18	18
-8	15	-16
-7	39	41
-6	19	20
-5	8	8
-4	26	29
-3	-	9*
3	67	55
4	16	13
5	-	-4*
6	-	-5*
7	22	21
8	8	8
9	43	39
10	-	4*
11	21	20
12	-	0*
13	11	10

H 2 2		
-12	8	9
-11	-	4*
-10	14	14
-9	20	-19
-8	-	-3*
-7	-	6*
-6	16	18
-5	15	-14
-4	44	49
-3	77	72
-2	17	13
1	31	-29
2	-	-96*
3	17	-16
4	36	36
5	14	-15
6	44	37
7	19	20
8	22	23
9	-	2*
10	8	9
11	-	3*
12	-	6*

H 3 2		
-9	12	12
-8	10	-5
-7	41	39
-6	21	-22
-5	22	21
-4	34	30
-3	40	36
-2	6	-5
-1	-	-18*
0	28	27
1	-	10*
2	67	-57
3	18	18
4	14	-12
5	49	47
6	-	2*
7	19	19
8	-	2*
9	19	19
10	-	3*
11	13	13

H 4 2		
-10	15	13
-9	-	1*
-8	-	2*
-7	-	5*
-6	-	79*
-5	8	-9
-4	31	33
-3	23	-23
-2	19	22
-1	53	46
0	26	-21
1	3	-5
2	23	25
3	9	10
4	66	63
5	24	-26
6	40	37
7	-	-4*
8	24	24
9	-	1*
10	11	12
11	-	1*
12	-	9*

H 5 2		
-13	9	10
-12	-	0*
-11	8	8
-10	-	-1*
-9	21	20
-8	11	12
-7	28	28
-6	7	9
-5	25	25
-4	8	-9
-3	5	5
-2	10	-10
-1	28	30
0	18	-17
1	42	38
2	67	55
3	17	17
4	11	-11
5	27	26
6	5	-7
7	12	12
8	15	-13
9	27	27
10	-	-3*
11	15	15

H 6 2		
-12	13	14
-11	-	1*
-10	17	18
-9	-	0*
-8	10	11
-7	-	-2*
-6	12	13
-5	10	11
-4	31	32
-3	10	-12
-2	36	33
-1	-	0*
0	45	42
1	7	-8
2	-	-1*
3	-	0*
4	19	21
5	10	12
6	30	29
7	29	-28
8	18	20
9	-	6*
10	17	17
11	-	-1*
12	8	10

H 7 2		
-11	26	25
-10	-	-3*
-9	11	12
-8	-	7*
-7	26	25
-6	7	-7
-5	7	10
-4	7	8
-3	17	19
-2	9	8
-1	73	67
0	10	-11
1	22	21
2	6	8
3	44	41
4	13	-15
5	14	15

Table 8. Continued.

6	-	-1*	7	-	-5*	1	26	28	4	47	47	-3	12	11	H	5	4		
7	16	16	8	12	13	2	76	76	5	-	1*	-2	11	9	-11	15	16		
8	-	-3*				4	14	-13	6	10	10	-1	-	4*	-10	-	3*		
9	25	25	H	13	2	5	21	23	7	-	1*	0	-	6*	-9	-	5*		
10	-	-1*	-1	17	17	6	-	7*	8	15	17	1	-	-2*	-8	-	2*		
11	15	16	0	-	-7*	7	19	-19				2	-	4*	-7	33	33		
			1	15	16	8	-	3*	H	8	3	3	-	3*	-6	10	11		
H	8	2	2	7	8	9	-	-7*	-11	12	10	4	13	14	-5	24	25		
-10	11	11	3	-	7*	10	15	15	-10	-	2*	5	-	-2*	-4	-	-7*		
-9	-	-2*	4	-	-5*	11	-	0*	-9	11	10	6	13	10	-3	45	42		
-8	15	16	5	10	10	12	15	14	-8	13	11				-2	-	-5*		
-7	-	4*							-7	28	26	H	14	3	-1	-	4*		
-6	-	2*	H	14	2	H	4	3	-6	-	2*	5	16	10	0	-	-2*		
-5	-	-1*	-2	9	9	-11	31	30	-5	15	14				1	26	26		
-4	28	31	-1	-	1*	-10	-	-3*	-4	-	-4*	H	15	3	2	-	5*		
-3	6	7	3	10	12	-9	13	14	-3	30	31	3	-	2*	3	28	29		
-2	13	12	1	-	-4*	-8	-	1*	-2	13	15	4	14	13	4	24	25		
-1	41	38	2	14	15	-7	10	12	-1	9	9				5	29	27		
0	33	33				-6	8	-8	0	-	-2*	H	0	3	6	-	-6*		
1	7	-8	H	15	2	-5	16	15	1	22	23	-12	21	21	7	14	13		
2	27	27	-1	15	15	-4	-	4*	2	14	15	-10	14	17					
3	-	-7*	0	6	-8	-3	8	-7	3	9	8	-8	45	42	H	6	4		
4	7	9	1	-	8*	-2	27	23	4	18	20	-6	25	32	-8	25	27		
5	19	-21	2	-	0*	-1	169	161	5	21	22	-4	15	18	-7	-	-1*		
6	24	24	3	11	11	0	9	-12	6	10	-10	-2	91	83	-6	22	20		
7	-	6*				1	11	12	7	15	15	2	98	76	-5	-	-7*		
8	-	7*	H	16	2	2	10	-11				4	45	43	-4	-	11*		
9	-	0*	0	9	10	3	17	18	H	9	3	6	-	2*	-3	-	2*		
10	19	18				4	12	14	-10	12	8	8	17	21	-2	38	36		
			H	0	3	5	-	-3*	-9	12	10				-1	21	-20		
H	9	2	-13	14	14	6	9	-10	-8	-	6*	H	1	4	0	35	34		
-7	11	11	-11	28	27	7	-	7*	-7	-	-5*	-11	21	22	1	11	9		
-6	-	1*	-9	15	18	8	-	5*	-6	15	14	-10	-	-1*	2	-	42*		
-5	10	10	-7	51	46	9	31	31	-5	-	7*	-9	18	21	3	-	3*		
-4	17	18	-5	37	38	10	-	-8*	-4	11	12	-8	-	4*	4	14	14		
-3	13	-15	-3	55	49	11	12	11	-3	11	-11	-7	-	12*	5	-	3*		
-2	-	5*	3	22	25				-2	11	12	-6	11	-12	6	-	4*		
-1	33	33	5	43	42	H	5	3	-1	-	0*	-5	43	39	7	-	2*		
0	10	10	7	30	32	-12	16	15	0	9	10	-4	76	73	8	12	12		
1	-	3*	9	23	22	-11	-	3*	1	22	22	-3	-	30*					
2	18	-18	11	13	17	-10	12	10	2	-	-9*	1	47	40	H	7	4		
3	17	15				-9	-	-3*	3	-	0*	2	33	-33	-11	16	17		
4	8	-7	H	1	3	-8	30	28	4	19	21	3	17	17	-10	-	0*		
5	-	5*	-14	14	13	-7	-	-8*	5	12	12	4	15	17	-9	19	19		
6	-	-4*	-13	-	2*	-6	-	5*	6	-	4*	5	35	33	-8	-	-1*		
7	-	1*	-12	12	10	-5	-	4*	7	11	-9	6	24	25	-7	-	6*		
8	-	5*	-11	-	-2*	-4	50	48				7	-	9*	-6	-	10*		
9	15	15	-10	14	13	-3	13	14	H	10	3	8	-	2*	-5	28	28		
			-9	29	27	-2	32	29	-9	12	10	9	18	17	-4	15	-15		
H	10	2	-8	22	23	-1	35	32	-8	-	7*				-3	15	17		
-9	9	-10	-7	-	-3*	0	21	20	-7	-	9*	H	2	4	-2	-	5*		
-8	7	7	-6	46	45	1	6	-7	-6	-	3*	-9	12	-13	-1	97	81		
-7	-	3*	-5	12	16	2	25	29	-5	-	6*	-8	29	32	0	-	4*		
-6	16	17	-4	72	61	3	17	-18	-4	25	-24	-7	-	2*	1	15	15		
-5	7	-6	-3	45	-36	4	8	11	-3	11	11	-6	23	32	2	-	2*		
-4	10	12	-2	24	30	5	-	-7*	-2	9	7	-5	-	5*	3	11	10		
-3	21	22	1	56	49	6	23	23	-1	26	27	-4	18	-18	4	-	2*		
-2	10	10	2	35	41	7	15	16	0	14	-16	-3	29	28	5	16	18		
-1	-	-6*	3	-	-5*	8	-	7*	1	10	10	-2	29	27	6	-	-3*		
0	-	1*	4	49	49	9	-	-3*	2	25	26	-1	58	30	7	-	11*		
1	15	-14	5	12	13	10	13	13	3	10	9	0	19	16	8	-	5*		
2	9	13	6	18	19	11	-	-3*	4	-	-3*	1	60	-51	9	19	20		
3	9	-10	7	-	-9*	12	13	11	5	-	5*	2	55	49					
4	16	17	8	15	16				6	12	-12	3	9	11	H	8	4		
5	6	-7	9	-	5*	H	6	3	7	-	7*	4	22	24	-8	25	22		
6	18	18	10	-	6*	-11	16	17	8	-	-3*	5	10	-14	-7	-	8*		
			11	-	0*	-10	-	-5*	9	12	10	6	-	-1*	-6	-	10*		
H	11	2	12	14	14	-9	11	11				7	24	24	-5	-	10*		
-9	9	10				-8	-	4*	H	11	3				-4	-	11*		
-8	-	1*	H	2	3	-7	30	28	-3	14	15	H	3	3	-3	18	19		
-7	18	17	-11	22	21	-6	-	-6*	-7	-	-6*	-7	29	28	-2	44	37		
-6	-	1*	-10	-	1*	-5	30	29	-6	17	18	-8	-	-4*	-1	-	-7*		
-5	20	20	-9	-	2*	-4	-	-5*	-5	-	6*	-5	28	28	0	16	16		
-4	-	2*	-8	15	16	-3	24	26	-4	11	10	-4	-	-7*	1	-	2*		
-3	19	19	-7	20	19	-2	-	3*	-3	-	-2*	-3	43	44	2	38	36		
-2	-	-2*	-6	15	16	-1	30	32	-2	18	19	-2	14	-13					
-1	9	10	-5	21	20	0	-	1*	-1	-	1*	-1	17	18	H	9	4		
0	-	-3*	-4	62	-57	1	29	12	0	24	23	0	15	17	-7	15	13		
1	20	20	-3	-	5*	2	9	5	1	-	5*	1	-	4*	-6	-	-2*		
2	-	-4*	-2	19	18	3	18	19	2	25	26	2	7	-9	-5	18	19		
3	18	16	-1	74	64	4	-	-5*	3	-	-8*	3	15	17	-4	21	18		
4	-	-1*	0	36	-30	5	29	32	4	-	11*	4	22	-25	-3	-	7*		
5	33	32	3	-	0*	6	-	-5*	5	-	1*	5	35	34	-2	-	4*		
6	9	-10	4	-	6*	7	-	7*	6	-	10*	6	-	4*	-1	15	14		
7	9	10	5	20	23	8	-	0*				7	24	25	0	-	7*		
8	-	-2*	6	12	-13	9	18	18	H	12	3				1	-	0*		
9	11	11	7	13	-17	10	-	0*	-7	14	14	H	4	4	2	-	-9*		
			8	-	-3*	11	12	9	-6	-	0*	-10	14	13	3	14	13		
H	12	2	9	27	25				-5	16	16	-9	-	1*	4	-	1*		
-8	9	8				H	7	3	-4	-	8*	-8	24	22	5	15	14		
-7	-	5*	H	3	3	-10	15	15	-3	11	11	-6	51	51					
-6	-	16*	-12	14	13	-9	-	-3*	-2	13	12	-7	-	11*	H	10	4		
-5	-	2*	-11	-	-1*	-8	13	13	-1	20	20	-5	-	-3*	-6	15	16		
-4	12	13	-10	10	9	-7	-	-1*	0	-	1*	-4	27	28	-5	-	-4*		
-3	6	-7	-9	-	2*	-6	56	56	1	14	12	-3	-	2*	-4	20	19		
-2	22	20	-8	25	25	-5	-	4*	2	-	-4*	-2	14	13	-3	-	6*		
-1	9	9	-7	9	-10	-4	21	22	3	14	15	-1	34	-29	-2	-	9*		
0	10	13	-6	-	5*	-3	-	3*	4	-	4*	0	23	25	-1	-	4*		
1	-	3*	-5	10	9	-2	18	18	5	11	13	1	7	10	0	-	9*		
2	13	13	-4	31	31	-1	-	-8*				2	13	10	1	18	-18		
3	-	0*	-3	16	-17	0	12	14	H	13	3	3	8	9	2	13	12		
4	23	22	-2	32	30	1	-	7*	-6	13	11	4	83	74	3	-	4*		
5	-	-7*	-1	54	-51	2	26	31	-5	-	2*				4	17	16		
6	12	12	0	26	25	3	-	2*	-4	12	12								

Table 8. Continued.

H 11 4			0 24 22		10 7 7		7 8 7		0 19 20		H 13 6												
-7 18 18			1 - -5*						1 13 9		-1 12 11												
-6 - -5*			2 45 40		H 8 5		H 14 5		2 - -9*		0 - 3*												
-5 16 17			3 13 -13		-7 22 21		1 - 10*		3 42 39		1 - 2*												
-4 - 0*			4 - 4*		-6 - -3*		2 - 2*		4 9 11		2 - 1*												
-3 24 23			5 - 5*		-5 17 17		3 9 10		5 15 16		3 15 14												
-2 - -3*			6 - 2*		-4 - -4*				6 - -2*														
-1 23 23			7 - -1*		-3 26 26		H 15 5		7 17 17		H 0 7												
0 - 1*			8 21 19		-2 14 16		0 9 8				-11 12 13												
1 - 5*			9 - -6*		-1 6 9				H 6 6		-9 14 16												
2 - -1*			10 10 9		0 - 6*		H 0 6		-5 23 -30		-7 40 36												
3 17 15					1 8 9		-12 25 24		-4 9 9		-5 - 6*												
4 - 0*			H 4 5		2 14 17		-10 - 6*		-3 - 2*		-3 - 6*												
5 17 16			-9 13 13		3 31 30		-8 - 6*		-2 45 46		1 9 11												
6 - 1*			-8 - -4*		4 - 2*		-6 - 10*		-1 25 -27		3 65 55												
7 16 15			-7 6 8		5 15 14		-4 - -4*		0 24 24		5 8 8												
			-6 10 -11		6 - 3*		-2 - 107*		1 13 22		7 24 25												
H 12 4			-5 39 36		7 13 14		2 45 41		2 21 21														
-6 15 15			-4 - 1*				4 21 20		3 - 7*		H 1 7												
-5 - 3*			-3 20 20		H 9 5		6 - 4*		4 23 18		-13 12 3												
-4 17 15			-2 23 24		-8 - 9*		8 30 30		5 - -6*		-12 14 14												
-3 - 2*			-1 60 50		-5 - -4*				6 - 9*		-11 - 6*												
-2 16 15			0 9 -8		-4 - -2*		H 1 6		7 - 1*		-10 - 9*												
-1 - -5*			1 42 33		-3 - -1*		-9 15 18		8 19 19		-9 19 6												
0 17 18			2 - 1*		-2 22 24		-8 - 3*				-8 20 20												
1 - 11*			3 11 12		-1 9 -9		-7 - -2*		H 7 5		-7 11 13												
2 - 10*			4 12 -13		0 21 23		-6 - 1*		-9 15 13		-6 13 14												
3 - 8*			5 27 29		1 23 24		-5 21 24		-8 - -6*		-5 - 9*												
4 17 15			6 - 4*		2 9 10		-4 15 10		-7 10 12		-4 26 28												
			7 - 0*		3 - 3*		-3 - 29*		-6 - 4*		-3 - 5*												
H 15 4			8 - 3*		4 - 6*		1 69 83		-5 - 6*		2 23 21												
-1 18 17			9 21 20		5 - 4*		2 - 1*		-4 - -7*		3 30 28												
					6 - 1*		3 15 16		-3 19 17		4 33 30												
H 0 5			H 5 5		7 - -1*		4 15 -16		-2 13 -15		5 - 2*												
-11 9 8			-12 8 8		8 11 10		5 22 21		-1 24 23		6 27 27												
-9 - 2*			-11 - -2*				6 23 24		0 - 9*		7 - 4*												
-7 61 58			-10 10 8		H 10 5		7 9 9		1 43 49		8 10 10												
-5 51 50			-9 6 -9		-9 6 7		8 - 7*		2 - -7*														
-3 50 51			-8 20 21		-8 - -9*		9 13 12		3 11 13		H 2 7												
1 70 61			-7 - -6*		-7 8 7		10 - 4*		4 13 14		-7 12 12												
5 46 44			-6 18 17		-6 - -2*		11 13 11		5 11 11		-6 - 3*												
7 29 27			-5 12 14		-5 7 8						-5 - -2*												
9 9 12			-4 - -2*		-4 12 -14		H 2 6		H 8 6		-4 - 2*												
			-3 - 0*		-3 14 14		-7 10 -9		-3 9 10		-3 14 15												
H 1 5			-2 74 64		-2 - 0*		-6 11 12		-2 35 32		-2 20 -20												
-10 8 8			-1 10 11		-1 20 18		-5 12 11		-1 - -2*		-1 11 10												
-9 6 9			0 26 27		0 - -3*		-4 - 1*		0 14 14		0 15 14												
-8 31 30			1 - 0*		1 19 21		-3 - 4*		1 - 5*		1 22 21												
-7 21 23			2 44 39		2 - -2*		-2 59 56		2 21 19		2 - 6*												
-6 24 25			3 - -3*		3 8 9		-1 13 16		3 13 10		3 33 30												
-5 - -3*			4 - 0*		4 - 5*		0 22 19		4 13 12		4 10 10												
-4 43 42			5 - -2*		5 10 9		1 14 -14		5 - -2*		5 7 8												
1 80 73			6 8 7		6 10 -9		2 16 13		6 - 5*		6 - -2*												
2 32 26			7 - 2*		7 - 5*		3 - -3*		7 - 11*		7 15 13												
3 13 16			8 23 22		8 - 4*		4 31 28		8 17 16		8 - -3*												
4 34 28			9 - 5*		9 7 7		5 - 5*				9 10 11												
5 4 6			10 8 9				6 - 2*		H 9 6														
6 16 18					H 11 5		7 - 6*		-5 13 12		H 3 7												
7 5 -8			H 6 5		-8 9 10		8 24 22		-4 - 4*		-12 14 14												
8 20 20			-11 7 7		-7 8 -6				-3 10 11		-11 - 1*												
9 - 1*			-10 13 -13		-6 10 10		H 3 6		-2 - 2*		-10 - 14*												
10 10 10			-9 - 5*		-5 - -6*		-7 22 23		3 16 17		-9 - 0*												
11 7 7			-8 6 -4		-4 9 9		-6 - -5*		4 - -2*		-8 - 3*												
			-7 28 26		-3 - 3*		-5 15 17		5 12 13		-7 8 8												
H 2 5			-6 14 -15		-2 25 27		-4 - 7*		6 - 12*		-6 9 10												
-11 9 7			-5 33 32		-1 8 -9		-3 15 15		7 - 7*		-5 19 -19												
			-4 18 17		0 15 14		-2 24 -24		8 - 2*		-4 - 1*												
H 1 5			-3 29 30		1 - 6*		-1 - 3*		9 - 5*		-3 6 -7												
-10 - 8*			-2 8 9		2 20 20		0 10 -10				-2 40 35												
			-1 22 20		3 - -2*		1 33 34		H 10 6		-1 - -5*												
H 2 5			0 11 -9		4 15 16		2 - -4*		-7 11 -10		0 13 13												
-9 - -3*			1 13 13		5 - -1*		3 41 38		-6 - 8*		1 5 7												
-8 - 0*			2 6 -6		6 - 4*		4 - 3*		-5 - -7*		2 8 10												
-7 22 22			3 31 29		7 - 2*		5 14 14		-4 13 12		3 7 -8												
-6 13 14			4 13 -14		8 11 11		6 - 1*		-3 - -8*		4 19 17												
-5 33 36			5 29 26				7 15 14		-2 11 12		5 8 -9												
-4 26 -24			6 6 5		H 12 5				-1 - -6*		6 10 12												
-3 27 30			7 15 16		-9 11 9		H 4 6		0 - 6*		7 - -1*												
-2 - 2*			8 - 5*		-5 14 14		-8 14 14		1 - -7*		8 16 16												
-1 - 39*			9 7 6		-4 - 5*		-7 - 1*		2 12 11														
0 7 8					-3 10 12		-6 9 8		3 - -2*		H 4 7												
1 12 -10			H 7 5		-2 7 8		-5 13 -15		4 15 16		-9 21 20												
2 13 14			-12 8 7		-1 14 17		-4 31 29		5 - -2*		-8 - 3*												
3 28 29			-11 - -1*		0 16 3		-3 - -2*		6 12 13		-7 10 12												
4 24 21			-10 - 5*		1 17 16		-2 27 26				-6 - 0*												
5 4 19			-9 - -4*		2 - 1*		-1 14 -14		H 11 6		-5 9 -11												
6 17 -18			-8 19 19		3 12 12		0 21 19		-7 21 20		-4 - 6*												
7 11 12			-7 3 -11		4 - 0*		1 - 9*		-6 - -5*		-3 24 22												
8 5 5			-6 22 23		5 12 12		2 16 17		-5 - 7*		-2 - -3*												
9 6 7			-5 5 6				3 12 13		-4 - -8*		-1 12 12												
			-4 39 38		H 13 5		4 36 31		-3 - 9*		0 13 -11												
H 3 5			-3 - -2*		-8 9 8		5 9 -10		-2 - -6*		1 47 40												
-12 10 10			-2 12 13		-7 - -5*		6 18 19		-1 - 10*		2 - -7*												
-11 - -6*			-1 11 12		-6 - 9*		7 - 1*		0 - -5*		3 10 12												
-10 - 3*			0 21 20		-5 - 2*		8 12 12		1 12 11		4 - -6*												
-9 - 3*			1 7 -8		-4 - 1*				2 - -1*		5 - 3*												
-8 20 21			2 13 14		-3 - 3*		H 5 6		3 23 23		6 - 5*												
-7 14 -17			3 - 1*		-2 17 17		-7 11 12				7 13 15												
-6 - 4*			4 49 44		-1 - 6*		-6 - 4*		H 12 6		8 - 2*												
-5 - -5*			5 - 2*		0 9 9		-5 21 23		-4 16 15		9 12 12												
-4 16 18			6 12 12		1 - -3*		-4 20 -22		-3 - -1*														
-3 - -2*			7 - 3*		2 11 12		-3 22 22		-2 - 4*		H 5 7												
-2 73 58			8 13 13		3 - 4*		-2 - -6*		-1 - -6*		-10 10 10												
-1 6 -4			9 - 1*		4 9 8		-1 21 21		0 13 13		-9 - 1*												

Table 8. Continued.

-8	11	12	0	-	6*	-4	-	0*	-2	8	-9	-9	7	7	6	8	9			
-7	-	-4*	1	-	-8*	-3	21	22	-1	19	19	-8	-	0*		H	7	10		
-6	17	17	2	-	8*	-2	10	-12	0	10	12	-7	8	9	-7	7	7			
-5	19	20	3	-	-4*	-1	15	16	1	11	11	-6	9	11	-6	-	0*			
-4	-	8*	4	-	8*	0	19	20	2	11	11	-5	8	8	-5	5	5			
-3	-	-1*	5	-	-5*	1	-	10*	3	10	8	-4	4	4	-4	-	-1*			
-2	16	13	6	-	7*	2	-	0*	4	-	2*	-3	13	15	-3	20	18			
-1	-	4*	7	-	1*	3	-	6*	5	-	0*	-2	-	8*	-2	-	0*			
0	16	16	8	12	12	4	-	2*	6	-	3*	-1	-	16*	-1	10	9			
1	21	-22				5	-	7*	7	13	13	0	-	-1*	0	-	0*			
2	18	17		H 12	7	6	-	-9*				1	16	16	1	12	12			
3	-	-6*	-3	13	14	7	16	14		H	3 9	2	-	2*	2	-	2*			
4	25	26	-2	-	2*				-4	15	17	3	13	17	3	12	10			
5	-	6*	-1	-	7*		H	6 8	-3	12	-14	4	6	6	4	-	2*			
6	-	7*	0	-	-3*	-8	18	17	-2	12	13	5	8	8	5	-	5*			
7	-	1*	1	14	14	-7	-	5*	-1	-	6*	6	-	4*	6	-	4*			
8	15	16				-6	16	17	0	45	35	7	10	9	7	8	8			
				H 13	7	-5	-	-9*	1	-	-4*									
	H	6 7	-6	11	11	-4	16	17	2	-	7*		H	2 10						
-13	13	10				-3	-	6*	3	11	12	-10	13	11		H	8 10			
-12	-	1*		H 0	8	-2	15	14				-9	-	2*	-10	8	8			
-11	-	8*	-6	24	26	-1	-	2*		H	4 9	-8	9	10	-9	-	2*			
-10	-	-5*	-4	9	13	0	16	15	-3	40	33	-7	-	1*	-8	6	5			
-9	16	17	2	-	5*	1	-	2*	-2	-	-4*	-6	7	7	-7	-	4*			
-8	-	4*	4	19	19	2	12	14	-1	12	13	-5	-	5*	-6	-	2*			
-7	17	16	6	-	4*	3	-	1*	0	-	5*	-4	15	15	-5	-	5*			
-6	-	0*	8	19	19	4	-	10*	1	15	16	-3	5	8	-4	12	12			
-5	12	13				5	14	-13	2	-	4*	-2	9	12	-3	-	4*			
-4	8	10		H 1	8				3	12	12	-1	5	-6	-2	7	7			
-3	14	15	-9	21	23		H	7 8				0	11	12	-1	-	-1*			
-2	-	0*	-8	-	5*	-9	16	14		H	5 9	1	-	5*	0	18	18			
-1	8	8	-7	13	14	-8	-	-2*	-6	14	16	2	29	26	1	-	2*			
0	23	-25	-6	-	11*	-7	-	11*	-5	-	1*	3	-	-4*	2	6	6			
1	17	16	-5	-	9*	-6	-	4*	-4	18	18	4	10	9	3	-	0*			
2	-	3*	-4	-	6*	-5	-	8*	-3	-	5*	5	6	6	4	-	4*			
3	29	27	-3	33	35	-4	-	8*	-2	13	14	6	12	10	5	6	10			
4	12	-14	-2	-	13*	-3	26	23	-1	-	4*				6	5	6			
5	11	12	-1	-	11*	-2	-	0*	0	21	19		H	3 10						
6	-	9*	0	-	9*	-1	-	10*	1	-	-2*	-9	9	8		H	9 10			
7	14	15	1	26	25	0	-	9*	2	26	14	-8	-	-4*	-7	9	9			
			2	-	5*	1	17	15				-7	7	7	-6	-	1*			
	H	7 7	3	-	-2*	2	-	-4*		H	6 9	-6	-	1*	-5	-	6*			
-8	15	14	4	-	3*	3	11	11	-7	16	12	-5	18	16	-4	-	0*			
-7	-	2*	5	-	3*				-6	-	-3*	-4	-	-4*	-3	11	11			
-6	12	13	6	-	1*		H	8 8	-5	-	13*	-3	10	10	-2	-	2*			
-5	-	6*	7	19	18	-6	15	13	-4	-	1*	-2	-	2*	-1	6	7			
-4	20	19				-5	14	13	-3	29	26	-1	5	6	0	-	-1*			
-3	-	-6*		H 2	8	-4	-	10*	-2	-	4*	0	-	-2*	1	10	9			
-2	18	19	-8	27	24	-3	16	17	-1	12	12	1	15	14	2	-	-3*			
-1	-	4*	-7	-	-5*	-2	14	13	0	-	-3*	2	7	-8	3	13	12			
0	-	-1*	-6	27	26	-1	-	6*	1	11	11	3	16	14	4	-	4*			
1	-	-4*	-5	11	12	0	12	11	2	-	2*	4	-	3*	5	-	3*			
2	12	14	-4	19	19				3	11	11	5	13	17	6	-	3*			
3	-	-8*	-3	14	14		H	9 8							7	9	8			
4	19	19	-2	9	9	-3	19	20		H	7 9		H	4 10						
5	-	2*	-1	-	3*	-2	-	11*	-8	15	15	-10	7	6		H	13 10			
6	23	23	0	-	1*	-1	-	7*	-7	-	0*	-9	-	0*	-6	9	8			
			1	-	2*	0	-	0*	-6	12	11	-8	13	12	-5	-	0*			
	H	8 7	2	15	18	1	14	11	-5	-	0*	-7	-	-2*	-4	10	10			
-9	11	10	3	-	-14*				-4	13	13	-6	-	4*	-3	-	-6*			
-8	11	11	4	16	12		H	10 8	-3	-	0*	-5	-	-2*	-2	7	7			
-7	13	14				-4	13	12	-2	11	10	-4	9	9	-1	-	-6*			
-6	-	8*		H 3	8	-3	-	5*	-1	-	5*	-3	4	-4	0	8	8			
-5	-	8*	-9	18	16	-2	-	5*	0	11	11	-2	14	11	1	-	0*			
-4	-	6*	-8	-	-10*	-1	-	0*	1	-	4*	-1	6	-5	2	9	10			
-3	8	8	-7	16	15	0	-	8*	2	16	17				3	-	-3*			
-2	-	-4*	-6	-	5*	1	-	-1*					H	5 10	4	7	5			
-1	10	10	-5	25	27	2	13	10		H	8 9	-9	8	10	5	-	2*			
0	-	2*	-4	-	-1*				-5	17	16	-8	-	4*	6	8	8			
1	-	7*	-3	9	10		H	11 8	-4	-	4*	-7	9	8						
2	-	4*	-2	13	14	2	-	-1*	-3	-	9*	-6	-	-3*		H	11 10			
3	20	19	-1	-	6*	3	17	16	-2	-	-2*	-5	15	14	-5	8	9			
4	-	3*	0	13	-15	4	-	-5*	-1	-	9*	-4	5	-5	-4	-	-4*			
5	-	8*	1	-	0*				0	14	16	-3	9	9	-3	10	9			
6	-	5*	2	-	-8*		H	12 8	1	-	7*	-2	6	-5	-2	-	-3*			
7	11	12	3	15	17	1	-	4*	2	13	13	-1	11	11	-1	-	3*			
			4	-	-5*	2	14	12				0	-	-2*	0	-	-2*			
	H	9 7	5	-	8*	3	-	3*		H	9 9	1	17	14	1	8	7			
-8	12	12	6	-	1*				-2	12	12	2	-	5*	2	-	0*			
-7	-	11*	7	15	14		H	0 9	-1	-	9*	3	14	15	3	-	7*			
-6	-	8*				-9	12	11	0	-	3*	4	-	0*	4	-	1*			
-5	-	-4*		H 4	8	-7	11	12	1	-	3*	5	12	11	5	8	8			
-4	10	10	-8	25	21	-5	24	25	2	14	15	6	-	1*						
-3	-	1*	-7	-	-3*	-3	18	24				7	7	7		H	12 10			
-2	-	5*	-6	20	20	1	8	9		H	10 9				-2	7	7			
-1	-	-4*	-5	-	1*	3	24	22	-3	16	14		H	5 10	-1	-	1*			
0	-	7*	-4	19	22							-10	9	9	0	-	5*			
1	-	1*	-3	-	6*		H	1 9		H	11 9	-9	-	2*	1	-	2*			
2	13	12	-2	10	11	-8	13	13	0	14	13	-8	7	8	2	7	7			
3	-	4*	-1	-	-4*	-7	-	7*				-7	-	-1*						
4	12	12	0	11	-13	-6	16	19		H	0 10	-6	6	6		H	13 10			
			1	-	3*	-5	-	0*	-10	13	11	-5	-	3*	-4	-	1*			
	H	10 7	2	14	17	-4	22	23	-8	13	11	-4	14	14	-3	7	8			
-3	11	12	3	-	-2*	-3	-	5*	-6	6	-6	-3	14	-14	-2	-	-1*			
-2	17	-18	4	13	13	-2	-	13*	-4	9	14	-2	12	12	-1	7	5			
-1	10	11				-1	-	12*	2	15	15	-1	-	-1*	0	-	3*			
0	-	-2*		H 5	8	0	15	17	6	8	9	0	15	15	1	7	7			
1	14	14	-9	18	17	1	-	6*	8	7	7	1	-	2*						
			-8	-	2*	2	22	22				2	17	17						
	H	11 7	-7	14	15					H	1 10	3	-	5*						
-2	28	25	-6	-	2*		H	2 9	-11	8	7	4	-	6*						
-1	-	-6*	-5	14	12	-3	48	41	-10	-	2*	5	-	2*						

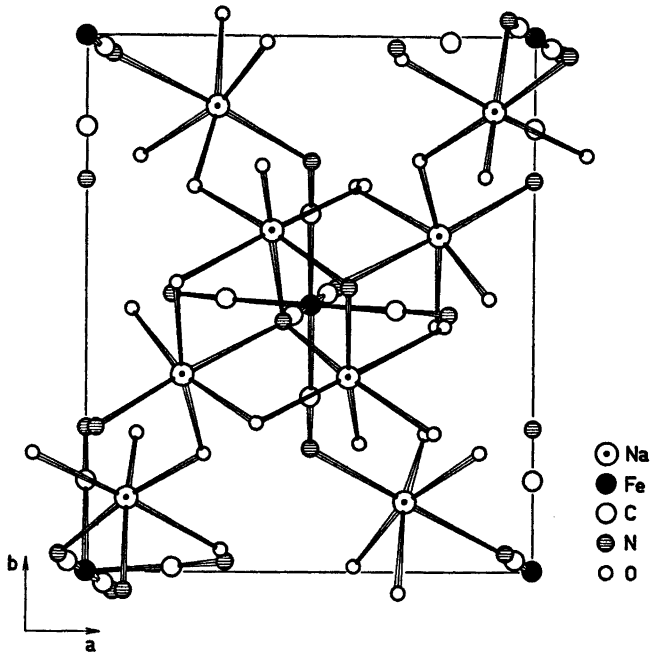

Fig. 1. Perspective view of $Na_4[Fe(CN)_6].10H_2O$ along the *c*-direction. Full lines indicate one unit cell. The atoms shown do not all belong to the same unit cell. Some nitrogen and oxygen atoms belonging to two neighbouring unit cells are drawn double with a small separation in the *a*-direction.

distances vary between 1.147(3) and 1.187(2) Å (mean 1.167 Å), while in $Na_4[Fe(CN)_6].10H_2O$ the C–N distances are 1.180(10), 1.165(10), and 1.174(10) Å. The Fe–C–N atoms are almost linear in both structures; the greatest deviation of a Fe–C–N angle from 180° is 2.6° in $K_4[Fe(CN)_6].3D_2O$.

A report on the structure of $H_4Fe(CN)_6$ has also been published.[13] The $[Fe(CN)_6]^{4-}$ ions are regular octahedra with Fe–C and C–N bond distances of 1.89(1) and 1.15(1) Å, respectively.

As may be seen from Table 9 the Fe–C distances in the Fe(II) compounds are shorter than the Fe–C bond distances found in Fe(III) cyanide compounds. The probability that the mean bond length differ in $Na_4[Fe(CN)_6].10H_2O$ and $K_3[Fe(CN)_6]$ is 99%. However, even if they were equal this result can only be interpreted as a proof of strong π-bonding in the Fe(II)–C bonds.

The mean values of the Mn–C and C–N bond distances found in $Na_4[Mn(CN)_6].10H_2O$, *i.e.* Mn–C = 1.95(3) Å and C–N = 1.16(3) Å, may be compared with those found in $K_3[Mn(CN)_5NO].2H_2O$,[10] *i.e.* Mn–C = 1.98(1) Å and C–N = 1.16(1) Å (mean values) and in $K_3[Mn(CN)_6]$,[11] Mn–C = 2.00(1) Å and C–N = 1.14(1) Å (mean values). Thus even here it is

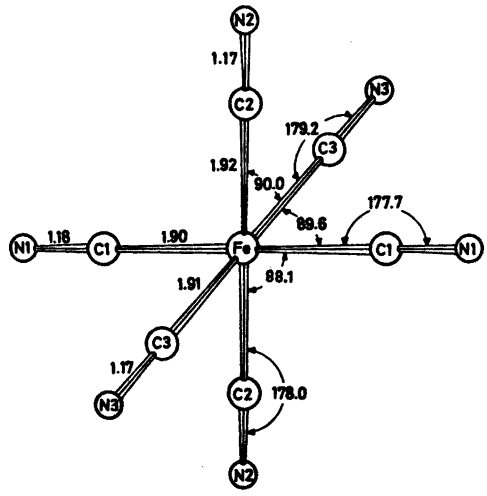

Fig. 2. The $[Fe(CN)_6]^{4-}$ octahedron.

Table 9. Comparison of bond lengths in hexacyanido complex ions.

Central atom	Compound	Me–C distance	Mean	C–N distance	Mean
Fe^{II}	$Na_4[Fe(CN)_6].10H_2O$	1.902(7) 1.906(7) 1.920(8)	1.909	1.180(10) 1.174(10) 1.165(10)	1.173
Fe^{II}	$K_4[Fe(CN)_6].3D_2O$[a]	1.908(4) 1.956(4) 1.920(2) 1.915(2)	1.925	1.184(3) 1.147(3) 1.150(2) 1.187(2)	1.167
Fe^{II}	$H_4[Fe(CN)_6]$	1.88(1) 1.88(1) 1.91(1)	1.89	1.14(1) 1.16(1) 1.15(1)	1.15
Fe^{III}	$K_3[Fe(CN)_6]$	1.93(1) 1.95(2) 1.97(2)	1.95	1.13(2) 1.13(2) 1.17(3)	1.14
Mn^{II}	$Na_4[Mn(CN)_6].10H_2O$	1.91(2) 1.95(1) 1.98(1)	1.95	1.14(2) 1.14(2) 1.19(2)	1.16
Mn^{III}	$K_3[Mn(CN)_6]$	1.98(2) 2.00(1) 2.02(1)	2.00	1.15(2) 1.13(2) 1.14(2)	1.14

[a] The structure of $K_4[Fe(CN)_6].3D_2O$ is disordered [12,15] with a disorder of the so called OD type (for nomenclature, see Ref. 16). Therefore the stated standard deviations may be under-estimated.

evident that the π-bonding in Mn(II)–C is so large that the bonds are equal or even shorter in length than in the Mn(III) complex.

Acknowledgements. The authors would like to thank Dr. Susan Jagner for revising the English text and Mrs. Margareta Biéth for skilful technical assistance. This work has been supported by a grant given from the Swedish Natural Science Research Council (Contract No. 2286–19).

REFERENCES

1. Philips, C. S. G. and Williams, R. J. P. *Inorganic Chemistry*, Clarendon Press, Oxford 1966, Vol. 2, pp. 272–275.
2. Alexander, J. J. and Gray, H. B. *J. Amer. Chem. Soc. 90* (1968) 4260.
3. Alexander, J. J. and Gray, H. B. *Coord. Chem. Rev. 2* (1967) 29.
4. Vannerberg, N.-G. *Acta Chem. Scand. 24* (1970) 2335.
5. Vannerberg, N.-G. *Acta Chem. Scand. 26* (1972) 2863.
6. Tullberg, A. and Vannerberg, N.-G. *Acta Chem. Scand. 25* (1971) 343.
7. Brauer, G. *Handbuch der präparativen anorganischen Chemie*, Ferd. Enke, Stuttgart 1962, Vol. II, p. 1286.
8. *International Tables for X-Ray Crystallography*, 2nd Ed., Kynoch Press, Birmingham 1962, Vol. III.
9. The program library of the Dept. of Inorg. Chem. Göteborg. DATA P1 and BLOCK have been written locally by O. Lindgren, DATA P2 was originally written by Coppens, Leiserowitz and Rabinowich (1965), DRF by A. Zalkin, Berkeley, California and LALS by P. Gantzel, R. Sparks and T. Trueblood.
10. Cromer, D. T. and Waber, J. T. *Acta Crystallogr. 18* (1965) 104.
11. Cruickshank, D. W. J. *The Equations of Structure Refinements*, Glasgow 1964.
12. Taylor, J. C., Mueller, M. H. and Hitterman, R. L. *Acta Crystallogr. A 26* (1970) 559.
13. Pierrot, M., Kern, R. and Weiss, R. *Acta Crystallogr. 20* (1966) 425.
14. Tullberg, A. and Vannerberg, N.-G. *Acta Chem. Scand. 21* (1967) 1426.
15. Pearson, W. B., Ed., *Structure Reports 11* (1947) 421, 424; *24* (1960) 300.
16. Dornberger-Schiff, K. *Lehrgang über OD-Strukturen*, Akademie-Verlag, Berlin 1966.

Received February 4, 1974.

Acta Chemica Scandinavica A 28 (1974) 563—568

An Experimental and Theoretical Investigation of the Salt Bridge in Concentration Cells

ERIK G. B. LINDEBERG[a] and TERJE ØSTVOLD[b]

[a] The University of Trondheim, Norwegian Institute of Technology, Division of Physical Chemistry, Trondheim, Norway and [b] The University of Trondheim, College of Arts and Science, Chemistry Department, Trondheim, Norway

Measured and calculated emfs for the concentration cell

$$\mathrm{Ag}\left|\mathrm{AgCl}\right|\begin{matrix}\mathrm{HCl}\\ \text{aq. } C_1\end{matrix}\Big|\Big|\begin{matrix}\mathrm{HCl},\ \mathrm{KCl}\\ \text{aq. } C_1,\ \text{aq. } C_{\mathrm{K}}\end{matrix}\Big|\Big|\begin{matrix}\mathrm{KCl},\ \mathrm{HCl}\\ \text{aq. } C_{\mathrm{K}},\ \text{aq. } C_2\end{matrix}\Big|\begin{matrix}\mathrm{HCl}\\ \text{aq. } C_2\end{matrix}\Big|\mathrm{AgCl}\left|\mathrm{Ag}\right.$$

are compared. The junction between the two half cells is made such that the concentration of HCl(KCl) is kept close to constant over the range where the KCl(HCl) concentration changes. Adopting this specific experimental arrangement and introducing the assumption of constant mobility ratios, calculated and measured potentials agree within 1 % when C_1 and C_2 are varied between 0.1 M and 0.001 M and C_{K} is varied from 0 to 4 M.

The salt bridge in concentration cells has been discussed in a previous communication.[1] The emf of a concentration cell containing two HCl solutions separated by a KCl salt bridge was calculated assuming ideal electrolyte solutions or Debye-Hückel activity coefficients ($\log \gamma_{\pm} = -A\omega^{\frac{1}{2}}$ where ω is the ionic strength).

In the present paper this discussion will be extended to include also experimental data on concentration cells of the above type. The following cell

$$\mathrm{Ag}\left|\mathrm{AgCl}\right|\begin{matrix}\mathrm{HCl}\\ \text{aq. } C_1\end{matrix}\Big|\Big|\begin{matrix}\mathrm{KCl},\ \mathrm{HCl}\\ \text{aq. } C_{\mathrm{K}},\ \text{aq. } C_1\end{matrix}\Big|\Big|\begin{matrix}\mathrm{KCl},\ \mathrm{HCl}\\ \text{aq. } C_{\mathrm{K}},\ \text{aq. } C_2\end{matrix}\Big|\begin{matrix}\mathrm{HCl}\\ \text{aq. } C_2\end{matrix}\Big|\mathrm{AgCl}\left|\mathrm{Ag}\right.$$

was studied with varying concentrations of HCl in the two half cells and with varying concentrations of KCl in the bridge. Since the cell emf is a function of the form of the concentration gradients between the two electrolytes, the experiment should be arranged in such a way that the concentrations as functions of position in the cell are well defined. It is then possible to calculate in a rigorous manner the chemical work carried out in the salt bridge and its contacts with the two HCl solutions.

In the work of Henderson [2] a mixed boundary is assumed in the emf calculation. Guggenheim [3] showed how such boundaries could be obtained experimentally, and his results indicated that the junctions prepared were reproducible with a probable error of less than 0.2 mV. According to Planck [4] a so called restricted diffusion contact may be formed between the solution in the salt bridge. Using this method a rigorous calculation of the concentration gradients and the cell emf would involve an enormous amount of work.

By assuming a mixed boundary and that the activity coefficients of individual ions of an electrolyte are equal in all cases to the mean activity coefficient of that electrolyte (the Guggenheim assumption [5]), Hamer [6] calculated the liquid junction potentials for HCl – KCl junctions for varying concentrations of HCl and KCl. Using the same approximation for single ion activities Maronny and Valensi [7] estimated the HCl – KCl liquid junction potentials from measured potentials without specifying which type of junction they were using. Picknett [8] calculated the junction potential by a numerical method also involving assumptions regarding single ion activities.

It is well known that varying assumptions regarding single-ion activity coefficients will

lead to varying values of a calculated steady-state junction potential, but these differences must be cancelled by corresponding differences in calculated electrode potentials, so that the overall potential remains constant. The calculated junction and electrode potentials therefore have no absolute values. Instead of calculating separately such immeasurable potentials MacInnes and Longsworth [9] calculated the total cell potential for the cell

Ag|AgCl|HCl(0.1 M)||KCl(0.1 M)|AgCl|Ag

from experimentally determined transport numbers and activity coefficients assuming only a mixed boundary.

In the present work we will in a similar manner calculate the total cell potential and we will introduce assumptions which may or may not be verified experimentally.

In the present work we used a junction between the two half cells similar to the one previously discussed [1] where the concentration of HCl is kept approximately constant over the range where the KCl concentration changes. Similarly C_{KCl} is approximately constant when C_{HCl} is changing. Adopting this specific experimental arrangement, calculated and measured potentials may be compared.

In the present calculation some approximations concerning the mobilities of ions and activity coefficients of neutral components have been introduced. The transport numbers of the ions K^+, H^+, and Cl^- have been measured by Longsworth [10] in the system $HCl-KCl-H_2O$ for a few concentrations at a total concentration of 0.1 M only. It was therefore necessary in the present emf calculations to introduce some simplifying assumptions to obtain transport numbers over the required concentration range. The activity coefficients of HCl and KCl are well known in pure electrolytes and also to some extent in $HCl-KCl-H_2O$ mixtures. The assumptions made with respect to the molar activity coefficients y_{HCl} and y_{KCl} in these mixtures are therefore quite reliable.

The emf of a cell of the above type is frequently expressed by quantities like single electrode potentials, liquid junction potentials, and single ion activities (see MacInnes [11]).

$$E = E_{el} - \frac{1}{F}\int \sum_i \frac{t_i}{z_i} \mathrm{d}\mu_i = E_{el} - \frac{RT}{F}\int \sum_i \frac{t_i}{z_i} \mathrm{d} \ln a_i \quad (1)$$

In this equation E_{el} is the contribution to the emf from the electrode reactions, t_i is the ionic transport number, z_i is the singned number of charges of the i'th ion, μ_i is the chemical potential of that ion, and a_i is the activity of the same ion. The integration is carried out over the whole cell.

For the present cell eqn. (1) may be written

$$E = \frac{1}{F}\Big|_{(1)}^{(2)} \mu_{HCl} t_H + \frac{1}{F}\int_{(1)}^{(2)} (\mu_{HCl} \mathrm{d}t_H + \mu_{KCl} \mathrm{d}t_K) \quad (2)$$

This equation may also be derived in an alternative way on the basis of classical irreversible thermodynamics where only measureable quantities are introduced.[12]

EXPERIMENTAL

The hydrochloric acid solutions were made from Titrisol HCl ampullas containing 1 M, 0.1 M and 0.01 M HCl. The relative error in concentrations given in the text are within ± 0.05 %. The potassium chloride-containing hydrochloric acid solutions were prepared by mixing predried potassium chloride and the content of a Titrisol ampulla and diluting with distilled water to a given volume. The silver-silver chloride electrodes were made by electrode-position of silver on 0.5 cm^2 platinum plates. The electrodes were chloridized by anodization in a dilute solution of HCl. In the same solution the difference in potential between these electrodes never amounted to more than 0.03 mV.

The galvanic cell was made of pyrex. The connection between the two half cells was made through a pyrex tube of 2 cm o.d. split in sections of about 5 cm length by relative coarse pyrex frits (No. 2 porosity $40-60$ μ). Normally ten such sections were used. If we used pyrex frits with fine pores (*e.g.* No. 5 porosity 2 μ), the potentials of the concentration cells containing HCl only, differed systematically ($0.5-4$ %, depending on the total HCl concentrations) from the theoretical value. This phenomen is probably due to a change in the ionic transport numbers inside the fine-sized pores. The concentrations of HCl and KCl in the central sections of the bridge could be changed in the course of the experiment, and by keeping pure HCl of concentration C_1 in the first left and of concentration C_2 in the first right hand sections of the bridge, KCl never entered into the electrode compartments which contained 0.75 l solution. The solutions were deoxygenized by bubbling nitrogen through the cell which was tilted so that the heavy KCl-rich solutions allways were at the lower end of the cell.

The concentrations of the two electrolytes HCl and KCl as functions of the position along

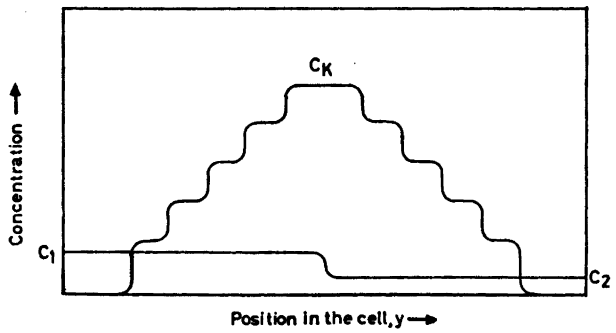

Fig. 1. The concentration of the two electrolytes HCl and KCl as functions of position, y, in the concentration cell

$$\mathrm{Ag}\left|\mathrm{AgCl}\right|\begin{matrix}\mathrm{HCl}\\ \text{aq. } C_1\end{matrix}\Big|\Big|\begin{matrix}\mathrm{HCl} & \mathrm{KCl}\\ \text{aq. } C_1, & \text{aq. } C_K\end{matrix}\Big|\Big|\begin{matrix}\mathrm{KCl} & \mathrm{HCl}\\ \text{aq. } C_K, & \text{aq. } C_2\end{matrix}\Big|\Big|\begin{matrix}\mathrm{HCl}\\ \text{aq. } C_2\end{matrix}\Big|\mathrm{AgCl}\left|\mathrm{Ag}\right.$$

the length of the cell, y, are shown schematically in Fig. 1. When the cell is assembled, there is a relatively large concentration gradient in KCl across each pyrex frit where C_{KCl} is varying. The interdiffusion of K+ and H+ that starts in these concentration gradients may generate "humps" in the HCl concentrations at each step. These concentration changes will have an influence on the cell potential.

RESULTS

In Table 1 the experimental potentials are presented. The standard deviation was 0.025 mV for the pure HCl concentration cells and around 0.12 mV for cells containing KCl. With the above mentioned experimental arrangement the cell potential was normally stable for 3 – 10 h after the cell had been assembled. The potential was normally stable from 10 to 20 h. Three typical potential *versus* time curves are shown in Fig. 2 for $C_{KCl}=0.1$ M, 0.5 M, and 4.0 M in the KCl salt bridges. By constructing cells with approximately constant concentration of HCl throughout the cell and a large KCl gradient on the left and a small KCl gradient on the right side of the bridge, cell potentials around −5 to −7 mV were observed when the cell was assembled. These potentials decreased with time.[13] When a symmetrical KCl gradient was applied 0 ± 0.05 mV was observed after 3 – 10 h.[13] These observations are in agreement with the long times necessary to establish steady state conditions and thus stable potentials in the above concentration cells.

In some cases when the concentration of KCl

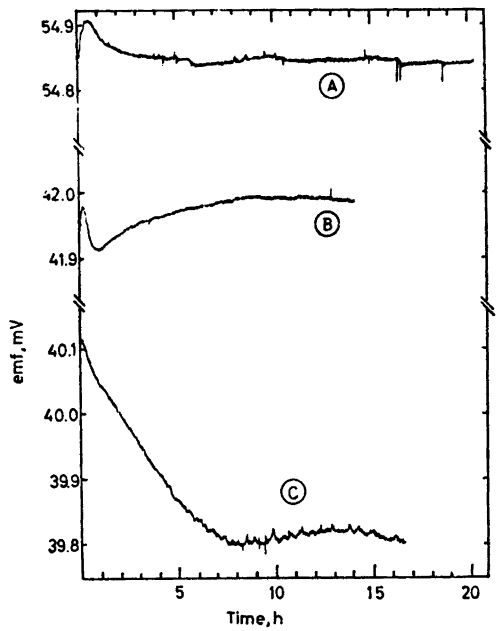

Fig. 2. Potential *versus* time curves for the galvanic cell

$$\mathrm{Ag}\left|\mathrm{AgCl}\right|\begin{matrix}\mathrm{HCl}\\ \text{aq. } C_1\end{matrix}\Big|\Big|\begin{matrix}\mathrm{HCl} & \mathrm{KCl}\\ \text{aq. } C_1, & \text{aq. } C_K\end{matrix}\Big|\Big|\begin{matrix}\mathrm{KCl} & \mathrm{HCl}\\ \text{aq. } C_K, & \text{aq. } C_2\end{matrix}\Big|\Big|\begin{matrix}\mathrm{HCl}\\ \text{aq. } C_2\end{matrix}\Big|\mathrm{AgCl}\left|\mathrm{Ag}\right.$$

at 25 °C.

A: $C_1=0.1$ mol/l, $C_2=0.01$ mol/l, and $C_K=0.5$ mol/l
B: $C_1=0.001$ mol/l, $C_2=0.005$ mol/l, and $C_K=0.1$ mol/l
C: $C_1=0.001$ mol/l, $C_2=0.005$ mol/l, and $C_K=4.0$ mol/l

in the central part of the bridge was low (0.1 M), a steady increase in cell potential was observed after some time ($\simeq 0.05$ mV/h). This increase was due to a dilution of KCl in the central section of the bridge.

DISCUSSION

We will now briefly go through the emf calculation and present the approximations introduced. As mentioned previously, the water framed ionic transport numbers t_{K^+}, t_{H^+}, and t_{Cl^-} are not very well known in the KCl – HCl – H_2O system. We will therefore assume that the ionic transport numbers can be expressed by eqn. (3).

$$t_i = [(u_i/u_{Cl})C_i]/\sum_i (u_i/u_{Cl})C_i \quad (3)$$

In this equation u_i and C_i represent ionic mobilities and concentrations, respectively. In our calculation we will assume that the mobility ratios u_H/u_{Cl} and u_K/u_{Cl} are independent of concentration.

Transport numbers calculated from eqn. (3) agree within 1 % with transport numbers measured by Longsworth [10] for a total concentration of 0.1 M HCl and KCl in the present ternary system. The mobility ratios used in eqn (3) to compare calculated and measured transport numbers, are average values of the mobility ratios in 0.1 M pure electrolytes and at infinite dilution. Using data from Longsworth,[14] these mobility ratios are $u_H/u_{Cl} = 4.773$ and $u_K/u_{Cl} = 0.9605$. We know that the ionic mobilities vary considerably with concentration. The variation in mobility ratios are, however, smaller $u_H/u_{Cl} = 4.618$ at infinite dilution and 4.928 in 0.1 M HCl. $u_K/u_{Cl} = 0.9621$ at infinite dilution and 0.9589 in 0.1 M KCl.

The approximation of constant mobility ratios are questionable at least for HCl solutions where the variation is about 6 % going from infinite dilution to 0.1 M HCl solutions. Even so we believe that a calculation of cell potentials of the above cell using eqn. (3) are worth while doing until accurate experimental transport numbers are known. The activity coefficients of HCl and KCl in water are very well known, and the following expression for y_{HCl} in the system HCl-H_2O was based on the equation given by MacInnes [11] and formation cell data given by Harned and Ehlers [15]

($y_{HCl} = a_{HCl}/C_H C_{Cl}$, $y_{HCl} \to 1$ when $C_{HCl} \to 0$)

$$\ln y_{HCl} = -\frac{2.3284\, C_{HCl}^{\frac{1}{2}}}{1 + 1.1382\, C_{HCl}^{\frac{1}{2}}} + 0.8932\, C_{HCl} \quad (4)$$

The molar activity coefficients calculated from eqn. (4) agree very well with experimental results for concentrations up to 0.1 M.

In the mixed system KCl – HCl – H_2O the following equation for the molar activity coefficient of HCl was used

$$\ln y_{HCl} = -\frac{2.3284\, \omega^{\frac{1}{2}}}{1 + 1.350\, \omega^{\frac{1}{2}}} + 0.4472\, C_{HCl} + 0.3050\, C_{KCl} \quad (5)$$

where ω is the ionic strength of the solution.[11] This equation is based on work of Harned [16] and the coefficients are adjusted to fit experimental activity coefficients in the mixed KCl – HCl – H_2O system at 0.1 M and 0.01 M HCl concentrations at varying ionic strength.[16,17] At concentrations of KCl greater than 3 M, $\ln y_{HCl}$ is roughly constant for constant HCl concentrations. This is accounted for in eqn. (5) by setting $C_{KCl} = 3$ M in solutions of higher potassium chloride concentrations. For KCl the following molar activity coefficient expression was used

$$\ln y_{KCl} = -\frac{2.3444\, \omega^{\frac{1}{2}}}{1 + 1.294\, \omega^{\frac{1}{2}}} + 0.04738\omega + 0.01985\omega^2 \quad (6)$$

Experimental molar activity coefficients of KCl in mixtures with water may be accurately represented by this equations.[18] In the ternary HCl – KCl – H_2O system the experimental activity coefficients will deviate most markedly from coefficients calculated from eqn. (6) in the low potassium chloride concentration regions. Data are not available to construct equations of the form given by eqn. (5) for the KCl activity coefficient.

Introducing eqns. (3, 4, 5, and 6) into the expression for the emf of the cell, eqn. (2), and integrating over the concentration gradient as outlined in a previous communication [1] the following result is obtained

$$E = (RT/F)\Big[(2u_K/u_{Cl}) \ln (C_1/C_2)/[(u_K/u_{Cl}) + 1] + 2\{[(u_H/u_{Cl}) - (u_K/u_{Cl})]/[(u_H/u_{Cl}) + 1] \times [(u_K/u_{Cl}) + 1]\} \times \ln \frac{1 + [(u_H/u_{Cl}) + 1]C_1/[(u_K/u_{Cl}) + 1]C_K}{1 + [(u_H/u_{Cl}) + 1]C_2/[(u_K/u_{Cl}) + 1]C_K} \Big] + E^{corr} \quad (7)$$

Table 1. Emf of the concentration cell

$$Ag|AgCl|\overset{HCl}{aq.\ C_1}||\overset{HCl,\ KCl}{aq.C_1,\ aq.\ C_K}||\overset{KCl,\ HCl}{aq.\ C_K,\ aq.\ C_2}||\overset{HCl}{aq.\ C_2}|AgCl|Ag$$

as a functions of the HCl and KCl concentrations at 25 °C.

Concentrations			Calculated potentials			Observed potentials
HCl		KCl	"Electrode potential"	Ideal	Debye-Hückel	E^{obs}
C_1 mol/l	C_2 mol/l	C_K mol/l	eqn. (8) mV	E(eqn. (7)] $-E^{corr}$ mV	E(eqn. (7)) mV	mV
0.1	0.02	0		68.30	64.59[a]	64.59
		0.1		56.17	53.03	53.21
		4.0	38.95	41.40	35.59	35.51
0.1	0.01	0		98.01	92.63[a]	92.65
		0.1		77.42	73.02	73.22
		0.5		65.06	60.23	60.59
		1.5		60.76	54.51	54.84
		4.0	55.94	59.07	51.81	51.78
0.1	0.005	0		127.28	120.83[a]	120.82
		0.1		96.79	91.74	92.07
		0.4	73.09	76.56	68.48	68.27
0.1	0.001	0		195.66	187.21[a]	187.11
		0.1		139.18	133.42	133.20
		4.0	113.46	117.12	108.19	108.70
0.02	0.01	0		29.41	28.04[a]	28.05
		0.1		20.97	19.98	20.11
		4.0	16.99	17.59	16.22	16.35
0.005	0.001	0		68.09	66.39[a]	66.36
		0.1		42.19	41.61	41.71
		4.0	40.37	40.38	39.71	39.81

[a] The potentials for the pure HCl//HCl concentration cell are calculated from the equation

$$E = \frac{1}{F}\Big|_{(1)}^{(2)} \mu_{HCl} t_H + \frac{1}{F}\int_{(1)}^{(2)} \mu_{HCl} \mathrm{d}t_H$$

using experimental transport numbers [14] and chemical potentials.[15]

In this equation the term E^{corr} is due to activity coefficient corrections. The mobility ratios u_H/u_{Cl} are average values and the numbers used in the present calculations are given in Table 2. The ionic mobility ratio u_K/u_{Cl} seems to be relatively constant with varying concentration of KCl [10] and we have adopted the value 0.96.

C_1 and C_2 are the HCl concentrations in the left and right solution, respectively, and C_K is the concentration of KCl in the salt bridge. In Table 1 the potentials calculated by eqn. (7) are compared with experimental values.

For the above cell the following equation for the cell potential is often written

$$E = (RT/F) \ln [C_{Cl}(1) y_{\pm}(1)/C_{Cl}(2) y_{\pm}(2)] \quad (8)$$

when the liquid junction potential across the salt bridge is neglected [*cf.* eqn. (1)]. This

Table 2. Average ionic mobility ratios at 25 °C in the ternary system HCl – KCl – H_2O calculated from experimental mobilities by Longsworth.[10]

Concentration of HCl in mol/l		Average ionic mobility ratios	
C_1	C_2	u_H/u_{Cl}	u_K/u_{Cl}
0.1	0.01	4.826	0.96
0.1	0.02	4.846	0.96
0.1	0.001	4.775	0.96
0.1	0.005	4.775	0.96
0.01	0.02	4.741	0.96
0.005	0.001	4.62	0.96

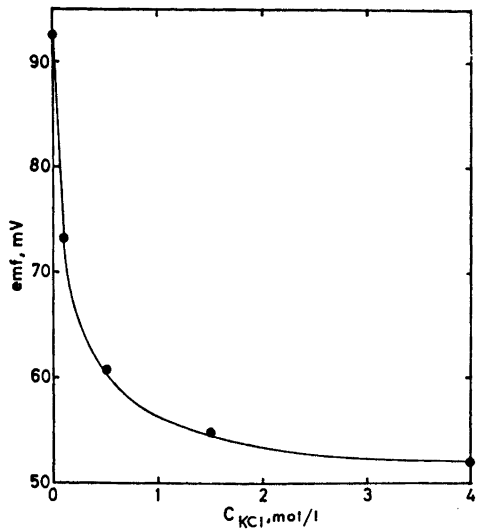

Fig. 3. Potential *versus* concentration of KCl, C_{KCl}, in the salt bridge for the galvanic cell

$$\mathrm{Ag}\,|\,\mathrm{AgCl}\,|\,\frac{\text{HCl}}{0.1\ \text{M}}\,\Big|\,\frac{\text{HCl, KCl}}{0.1\ \text{M},\ C_K}\,\Big|\,\frac{\text{HCl, KCl}}{0.01\ \text{M},\ C_K}\,\Big|\,\frac{\text{HCl}}{0.01\ \text{M}}\,|\,\mathrm{AgCl}\,|\,\mathrm{Ag}$$

at 25 °C. Full drawn line, calculated; ●, experimental.

potential is also compared with experimental potentials in Table 1.

From Table 1 it is observed that while both the potential given by eqn. (8) and the ideal solution potential, E[eqn. (7)] $-E^{corr}$, deviate markedly from the experimental potentials, there is a very good agreement between observed potentials and potentials calculated by eqn. (7).

In Fig. 3 calculated and measured potentials for cells containing 0.1 M HCl and 0.01 M HCl in the two half cells and varying concentration of KCl in the salt bridge are plotted *versus* C_{KCl}. At low potassium chloride concentrations the cell potential is very dependent on C_{KCl} while the variation in emf is rather small at concentrations higher than $C_{KCl} = 2$ M. It is therefore important to use high concentration of KCl in standard salt bridges of the above type.

We know that the mobility ratios u_i/u_{Cl} do vary with concentration, and the use of constant mobility ratios therefore probably represents the most serious error in the above calculations. With experimentally known activities and ionic transport numbers we should probably be able to come even closer to the experimentally obtained potentials than is the case in the present calculation. The degree of consistency between experimentally and theoretically obtained potentials, would then give an indication on the reliability of the assumption regarding the concentration gradients made in the emf calculations.

Acknowledgement. The authors thank professor T. Førland for stimulating advice and discussions and Norges Almenvitenskapelige Forskningsråd for financial support.

REFERENCES

1. Førland, T. and Østvold, T. In Högfeldt, E., Ed., *Contributions to Coordination Chemistry in Solution.* Berlingska Boktryckeriet, Lund 1972, p. 587.
2. Henderson, P. *Z. Phys. Chem. 59* (1907) 118; *63* (1908) 325.
3. Guggenheim, E. A. *J. Amer. Chem. Soc. 52* (1930) 1315.
4. Planck, M. *Ann. Phys. (Leipzig) 39* (1890) 161; *40* (1890) 561.
5. Guggenheim, E. A. *J. Phys. Chem. 34* (1930) 1758.
6. Harner, W. J. *Trans. Electrochem. Soc. 72* (1973) 325.
7. Maronny, G. and Valensi, G. *Proc. 7th. Int. Comm. Electrochem. Thermodynamics and. Kinetics*, Butterworths, London 1957, p. 38
8. Picknett, R. G. *Trans. Faraday Soc. 64* (1968) 1059.
9. MacInnes, D. A. and Longsworth, L. G. *Cold Spring Harbor Symp. Quant. Biol. 4* (1936) 18; Mac Innes, D. A. *The Principles of Electrochemistry*, Dover Publications, New York 1961, pp. 238–243.
10. Longsworth, L. G. *J. Amer. Chem. Soc. 52* (1930) 1897.
11. MacInnes, D. A. *The Principles of Electrochemistry* Dover Publications, New York 1961: a. pp. 222–223; b. p. 166; c. p. 147.
12. Førland, T., Thulin, L. U. and Østvold, T. *J. Chem. Educ. 48* (1971) 741.
13. Lindeberg, E. B. and Østvold, T. *Unpublished results.*
14. Longsworth, L. G. *J. Amer. Chem. Soc. 54* (1932) 2741.
15. Harned, H. S. and Ehlers, R. W. *J. Amer. Chem. Soc. 55* (1933) 2179.
16. Harned, H. S. *J. Amer. Chem. Soc. 48* (1926) 322.
17. Harned, H. S. and Hamer, W. J. *J. Amer. Chem. Soc. 55* (1933) 2194.
18. Monk, C. B. *Electrolytic Dissociation.* Academic, London and New York 1961, p. 33.

Received November 30, 1973.

Acta Chemica Scandinavica A 28 (1974) 569—577

Reaction Rate Studies of the Acid Hydrolysis of Some Chromium(III) Complexes. III. The Acid Hydrolysis of Pentaammineaqua- and Hexaamminechromium(III) Ions in Aqueous Perchloric Acid

L. MØNSTED and O. MØNSTED

Chemistry Department I, Inorganic Chemistry, The H. C. Ørsted Institute, University of Copenhagen, DK-2100 Copenhagen, Denmark

The acid hydrolysis of pentaammineaqua- and hexaamminechromium(III) cations has been investigated in 0.5 to 1.0 M perchloric acid at an ionic strength of 1.0, adjusted by the addition of sodium perchlorate, in the temperature range 60 – 80 °C.

In the possible reaction scheme:

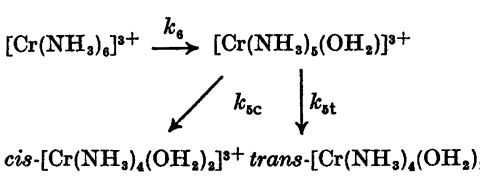

no evidence for the production of the *trans*-tetraamminediaquachromium(III) ion was found. For the well defined kinetic paths rate constants at 70°C and activation energies were found to be:

k_{5c}: $(47.2 \pm 0.8) \times 10^{-6}$ s^{-1}, 27.1 ± 0.4 kcal/mol,
k_6: $(47.5 \pm 1.4) \times 10^{-6}$ s^{-1}, 27.6 ± 0.8 kcal/mol,

whereas for k_{5t} an upper limit for the rate constant at 70 °C of 1.0×10^{-6} s^{-1} (taken as mean value plus twice the standard deviation), was found.

In the acidity range studied no dependence of these rate constants upon the hydrogen ion concentration was found.

It is concluded that the isomerization and ammine hydrolysis reactions of ammineaquachromium(III) complexes proceed *via* an intermediate of increased coordination number with an approximate pentagonal bipyramidal structure, and that the two ligands coordinated along the five fold axes in this intermediate play only a secondary role for the kinetics of the reactions.

Similar charges and almost similar sizes should render the isomeric ammineaquachromium(III) complexes ideal for the study of stereochemical changes by octahedral substitution reactions, since differences in both the solvation and the ion pair formation of these cations should be small. We have earlier studied the acid hydrolysis of the monoamminepentaaqua- and the isomeric diamminetetraaqua-,[1] triamminetriaqua-, and tetraamminediaquachromium(III) ions,[2] and report here the acid hydrolysis of the pentaammineaqua- and the hexaamminechromium(III) ions. The acid hydrolysis and isomerization reactions of all isomers of chromium(III) complexes coordinated with ammonia and water have thus now been investigated.

EXPERIMENTAL

Chemicals. Most chemicals employed have been described earlier.[1] $[Cr(NH_3)_5(OH_2)](NO_3)_3$[3] and $[Cr(NH_3)_6](NO_3)_3$[4] were prepared according to literature methods, and the latter compound transformed into the perchlorate salt by double reprecipitation from water with 70 % perchloric acid.

Preparation of solutions. Solutions of the pentaammineaquachromium(III) ion were prepared as follows: pentaammineaquachromium(III) nitrate was dissolved in water and adsorbed at the top of a 2 × 10 cm Sephadex SE 25C ion exchange column. By use of an ammonium ion-ammonia buffer solution (1.0 M NH_4Cl + 0.1 M NH_3) pentaamminehydroxochromium(III) was eluted free of other chromium species. After

Table 1. Comparison of spectral characteristics of compounds, prepared and purified as described in the text, with literature values.

Complex ion	Medium	λ_1 max (nm)	ε_1 max l/(mol cm)	λ_2 max (nm)	ε_2 max l/(mol cm)	ε_1 max/ ε_2 max	Ref.
$[Cr(NH_3)_6]^{3+}$	0.1 M HCl	465	39.7	351	32.9	1.21	[a]
	0.1 M HNO_3	465	39	345	35	1.1	5[b]
	0.05 M $HClO_4$	466	40.7	354	33.7	1.20	8
	0.05 M $HClO_4$	463	41	355	35	1.2	7[b]
$[Cr(NH_3)_5(OH_2)]^{3+}$	0.5 M $HClO_4$ + 0.5 M $NaClO_4$	480	35.1	359	30.3	1.16	[a]
	0.1 M $HClO_4$	475	34	360	29	1.2	5[b]
	0.05 M $HClO_4$	484	35	360	29	1.2	7,8
	0.1 M $HClO_4$	480	35	360	28.5	1.2	6[b]

[a] This work. [b] Estimated from the graph in this reference.

acidification of the pentaamminehydroxochromium(III) eluate a solution of the pure pentaammineaquachromium(III) ion in perchloric acid was obtained as described previously.[1] Solutions of the hexaamminechromium(III) ion in perchloric acid were obtained by directly dissolving the perchlorate salt in perchloric acid. The limited solubility of hexaamminechromium(III) perchlorate at room temperature in a 1 M perchlorate medium prevented the preparation of solutions with greater chromium(III) concentrations than approximately 10^{-4} M. Spectral characteristics of the hexaamminechromium(III) perchlorate salt dissolved in 0.1 M hydrochloric acid, and of the pentaammineaquachromium(III) solution prepared by the above method are given in Table 1 and Fig. 1.

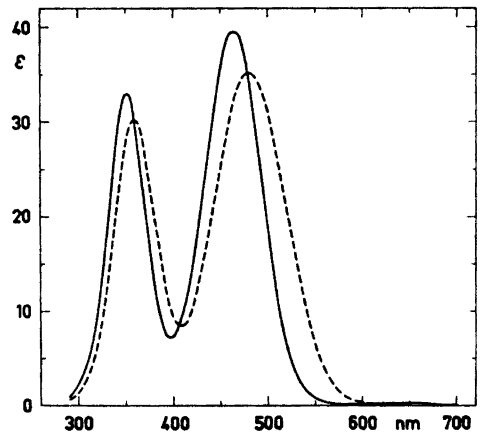

Fig. 1. Visible absorption spectra of compounds prepared and purified as described in the text. – – –, $[Cr(NH_3)_5(OH_2)]^{3+}$; ——, $[Cr(NH_3)_6]^{3+}$. No hydrogen ion dependence of these spectra was observed in the acidity range 0.5 to 1.0 in 1 M $(Na^+ + H^+)ClO_4$ solution.

Kinetic measurements and the *Methods of analysis* and *calculation* were essentially those described previously.[1,2]

RESULTS AND DISCUSSION

Contrary to the kinetic behaviour in acid solution of the previously studied ammineaquachromium(III) complexes, that of the pentaammineaqua- and hexaamminechromium(III) ions is fairly uncomplicated. From the hexaamminechromium(III) ion only the pentaammineaquachromium(III) ion can be formed, and from this latter ion only *cis*- and *trans*-tetra-

Table 2. Initial composition of reaction kinetic experiments started with hexaammine- and pentaammineaquachromium(III) ions.

Exp. No.	[Cr(III)] (mmol/l)	$[H^+]$ (mol/l)	Temp. (°C)	Max. react. time (h)
	$[Cr(NH_3)_5(OH_2)]^{3+}$			
1[a]	2.163 ± 0.005	1.0	60.18	143
2[a]	2.170 ± 0.006	1.0	69.70	143
3	2.975 ± 0.011	1.0	80.15	24
	$[Cr(NH_3)_6]^{3+}$			
4[a]	0.1051 ± 0.0006	1.0	60.00	30
5	0.0238 ± 0.0004	1.0	70.00	6
6[a]	0.1057 ± 0.0009	1.0	70.55	6
7	0.1008 ± 0.0004	1.0	80.25	3
8	0.1018 ± 0.0006	0.5	80.04	5

[a] These four solutions were pairwise prepared from the same stock solutions.

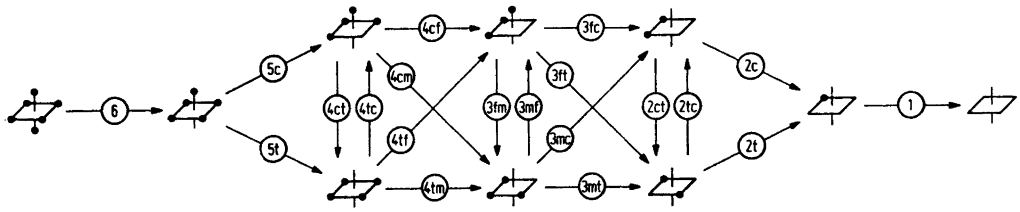

Fig. 2. Isomerization and hydrolysis reactions of ammineaquachromium(III) complexes. Filled circles depict coordinated ammonia, whereas the coordinated water is shown only by the absence of such circles. Reaction pathways are indicated by the subindices of the symbols used for the reaction rate constants.

Table 3. Rate constants at 60, 70, and 80 °C and activation energies for the hydrolysis reactions of the hexaammine- and the pentaammineaquachromium(III) ions calculated from all kinetic experiments and all kinetic experiments in 1 M acid, respectively.

	All experiments				Experiments in 1 M acid	
($\times 10^6$)	60 °C (s^{-1})	70 °C (s^{-1})	80 °C (s^{-1})	E_A (kcal/mol)	80 °C (s^{-1})	E_A (kcal/mol)
k_6	14.2 ± 0.8	47.5 ± 1.4	149 ± 3	27.6 ± 0.8	154 ± 3	28.0 ± 0.9
k_{5c}	14.3 ± 0.4	47.2 ± 0.8	145 ± 3	27.1 ± 0.4	145 ± 3	27.1 ± 0.4
k_{5t}	0.00 ± 0.14	0.0 ± 0.5	0.0 ± 1.4	–	0.3 ± 1.4	–

amminediaquachromium(III) ions are possible reaction products. Rate constants and activation energies from the kinetic experiments of Table 2, and those of our earlier publications in this series of papers,[1,2] interpreted within the reaction scheme of Fig. 2 are shown in Table 3. In agreement with what was found for the complexes with a smaller number of coordinated ammonia molecules, no dependence of the acidity at hydrogen ion concentrations between 0.5 and 1.0 M, upon the rate constants for the hydrolysis of the hexaammine- and the pentaammineaquachromium(III) ions was observed.

In Table 4 kinetic parameters for the total experimental material are exhibited, and the corresponding correlation coefficients are shown in Table 5. From this latter table it is seen that correlation terms are particularly important among rate constants and activation energies that describe different reaction pathways from the same reactant species. These correlation coefficients are collected in blocks along the diagonal in the matrix of Table 5. Outside these blocks correlation is almost non-existent except in very few instances. That correlation terms among the rate constants and the activation

Table 4. Reaction rate constants at 70 °C and activation energies calculated from all ammineaquachromium(III) hydrolysis experiments within the reaction scheme of Fig. 2 in a 1 M perchlorate medium.

Reaction	$10^6 \times$ Rate constant (s^{-1})	Activation energy (kcal/mol)
6	47.5 ± 1.4	27.6 ± 0.8
5c	47.2 ± 0.8	27.1 ± 0.4
5t	0.0 ± 0.5	–
4cf	24.2 ± 0.6	25.7 ± 0.5
4cm	3.3 ± 0.6	26 ± 2
4ct	0.0 ± 0.6	–
4tm	44.4 ± 0.8	26.3 ± 0.5
4tf	0.8 ± 0.6	–
4tc	4.2 ± 0.6	26 ± 4
3fc	7.6 ± 0.3	27.6 ± 0.6
3ft	0.03 ± 0.19	–
3fm	0.3 ± 0.3	–
3mc	23.5 ± 0.4	26.0 ± 0.5
3mt	0.5 ± 0.4	–
3mf	1.1 ± 0.3	26 ± 7
2c	3.39 ± 0.08	27.0 ± 0.4
2ct	0.00 ± 0.14	–
2t	17.5 ± 0.3	26.3 ± 0.4
2tc	5.25 ± 0.19	27.6 ± 1.0
1	1.108 ± 0.011	28.6 ± 0.2

Table 5. Correlation coefficients between the parameters of Table 4.

Rate Constants

	6	5c	5t	4cf	4cm	4ct	4tm	4tf	4tc	3fc	3ft	3fm	3mc	3mt	3mf	2c	2ct	2t	2tc	1
6		-.15	+.05	+.04	.00	.00	.00	.00	.00	.00	.00	.00	.00	.00	.00	.00	.00	.00	.00	.00
5c			-.52	-.39	+.06	+.11	.00	+.05	-.03	+.03	+.01	-.08	.00	.00	-.01	.00	+.01	.00	.00	.00
5t				-.03	-.04	-.20	-.03	-.01	-.03	+.01	-.02	+.03	-.01	+.01	+.01	.00	.00	.00	.00	.00
4cf					-.68	+.53	+.05	-.13	+.10	-.08	-.04	+.25	.00	+.01	+.02	+.04	-.05	.00	.00	+.02
4cm						-.89	-.10	+.09	-.05	-.10	+.08	-.11	+.02	-.02	-.03	.00	+.02	.00	.00	-.02
4ct							+.08	-.06	+.07	+.04	+.01	-.02	-.01	+.01	+.01	+.01	-.02	.00	.00	.00
4tm								-.83	+.71	+.04	-.01	.00	-.09	+.01	+.20	-.06	+.04	.00	.00	+.01
4tf									-.86	.00	+.01	-.05	-.03	-.01	-.22	+.05	-.05	.00	.00	-.01
4tc										-.02	+.01	+.01	+.10	-.04	-.01	-.05	+.05	+.01	.00	+.01
3fc											-.78	-.04	-.11	+.06	+.10	-.25	+.32	+.02	+.04	-.04
3ft												-.56	+.08	-.09	-.17	+.04	-.17	.00	-.05	+.04
3fm													.00	+.07	+.17	+.18	-.13	-.02	+.02	+.04
3mc														-.83	-.66	-.19	+.24	+.02	+.01	-.07
3mt															+.81	-.05	-.11	-.01	-.01	+.09
3mf																+.07	-.09	-.01	.00	+.03
2c																	-.96	-.10	-.02	+.01
2ct																		+.09	+.02	-.14
2t																			+.53	.00
2tc																				+.10
1																				

Activation Energies

	6	5c	4cf	4cm	4tm	4tc	3fc	3mc	3mf	2c	2t	2tc	1
6	-.73	+.04	-.05	+.01	.00	.00	.00	.00	.00	.00	.00	.00	.00
5c	+.02	-.27	+.43	-.22	+.01	+.03	-.02	.00	.00	-.01	.00	.00	.00
5t	+.01	-.07	-.03	+.29	-.03	+.02	-.04	.00	-.01	+.01	.00	.00	.00
4cf	-.04	+.40	+.20	-.29	-.02	-.07	+.10	-.01	-.01	.00	.00	.00	.00
4cm	.00	-.05	-.72	+.30	+.05	+.02	-.03	-.01	+.02	.00	.00	.00	.00
4ct	-.01	+.02	-.04	+.05	-.03	-.03	+.04	.00	.00	-.01	.00	.00	.00
4tm	.00	-.01	-.01	+.06	-.33	-.29	-.02	+.04	-.09	+.03	-.01	.00	-.01
4tf	.00	-.05	+.11	-.06	+.28	+.38	-.02	-.01	+.09	-.02	.00	.00	+.01
4tc	-.01	+.05	-.07	.00	-.29	-.52	+.03	-.02	+.01	+.01	.00	.00	.00
3fc	.00	-.03	+.07	+.02	-.03	+.01	-.19	+.09	-.04	+.05	.00	+.01	-.01
3ft	.00	.00	+.01	-.02	+.02	.00	+.06	-.05	+.06	-.07	+.01	-.01	+.02
3fm	.00	+.04	-.13	+.07	-.01	-.02	+.14	-.03	-.06	+.05	-.01	+.01	-.03
3mc	.00	.00	-.01	-.01	+.05	-.01	+.09	-.09	+.09	-.01	+.01	.00	+.02
3mt	.00	.00	.00	+.01	.00	+.01	-.03	+.06	-.10	+.01	.00	.00	-.02
3mf	.00	.00	-.01	+.03	-.09	+.01	-.02	+.09	-.22	+.01	.00	.00	-.01
2c	.00	.00	+.01	.00	+.03	+.01	-.02	-.03	.00	-.04	-.01	+.01	.00
2ct	.00	.00	.00	.00	-.02	-.01	+.02	+.03	.00	+.04	+.01	.00	+.03
2t	.00	.00	.00	.00	-.01	.00	.00	.00	.00	.00	-.34	-.36	-.02
2tc	.00	.00	.00	.00	.00	.00	.00	.00	.00	+.01	-.35	-.36	-.03
1	.00	.00	.00	.00	-.01	.00	-.01	.00	.00	+.02	-.02	-.03	-.34

Activation Energies

	6	5c	4cf	4cm	4tm	4tc	3fc	3mc	3mf	2c	2t	2tc	1
6		-.16	+.05	.00	.00	.00	.00	.00	.00	.00	.00	.00	.00
5c			-.50	+.08	+.01	-.04	+.06	-.01	.00	.00	.00	.00	.00
4cf				-.56	+.01	-.07	-.19	+.02	+.01	-.01	.00	.00	+.01
4cm					-.06	.00	-.06	+.01	-.02	+.05	.00	+.01	-.02
4tm						+.72	+.03	-.10	+.19	-.04	.00	.00	+.01
4tc							-.03	+.09	.00	-.03	.00	.00	+.01
3fc								-.15	+.03	-.14	+.01	.00	+.02
3mc									-.66	-.02	.00	+.01	-.04
3mf										.00	.00	-.01	+.01
2c											-.06	+.02	-.16
2t												+.45	.00
2tc													+.11
1													

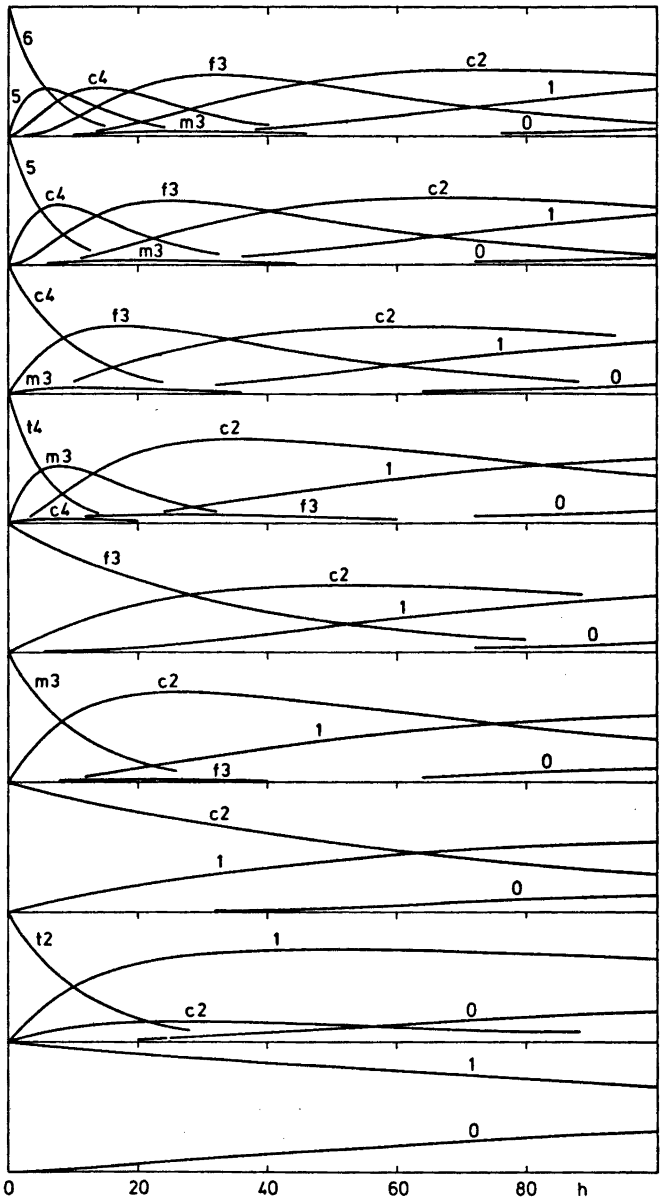

Fig. 3. Calculated time evolution of complex concentrations in 1 M perchloric acid solution at 70 °C started from pure ammineaquachromium(III) isomers. Isomer names are based upon the number of coordinated ammonia molecules, extended where necessary with prepositioned letters to indicate, c, *cis*; t, *trans*; f, *fac*; or m, *mer* isomers.

energies are also on the average of practically no importance, is of course due to the fact that the rate constants are evaluated at a temperature not very far from the average temperature of all the experimental data.

In Fig. 3 the time evolution, of hydrolysis experiments started with the pure ammineaquachromium(III) isomers, is calculated from the reaction rate constants of Table 4. This figure illustrates the complicated nature of the mix-

tures that are produced even after very short reaction times, and also the absence of both the *trans*-tetraamminediaqua- and the *trans*-diamminetetraaquachromium(III) ions as reaction products.

Reactions of some chromium(III) ammine complexes have earlier been studied in media containing nitrate ions.[5,6] In Table 6 these data are compared with those of the present work in a 1 M perchlorate ion medium. The absence of any simple correlation between the reactivity parameters in the two media, and also in most cases the magnitude of the differences in the reaction rate constants, cannot reasonably be attributed only to unspecific medium effects.

Nitrate ions are seen significantly to accelerate the reactions of those chromium(III) ammine complexes that contain coordinated water, while the effect of nitrate ions in the case of the hydrolysis reaction of the hexaamminechromium(III) ion is negligible. This would be expected if inner sphere nitrato complexes are formed from the aqua complexes. Such complexes are probably formed so rapidly compared to the other reactions in the system, that the kinetic pattern of the slower reactions is not seen to be effected. Such fast complex formation between aqua ions and oxyanions has been demonstrated [9] in a number of cases, where the aniono complexes are probably formed without chromium(III) oxygen bond breaking. It is interesting to note that nitrate ions have no similar great effect upon the halide ion hydrolysis reactions of aquahalogenidochromium(III) complexes. This suggest that an intramolecular interaction between coordinated ammonia and coordinated nitrate ions may play an important role for the ammineaquachromium(III) hydrolysis reactions.

Table 6. Comparison between chromium(III) ammine hydrolysis and isomerization rate constants at 40 °C in 0.4 M nitrate [5] and 1 M perchlorate media.

Reaction	$k(ClO_4^-)/k(NO_3^-)$
6	0.73
5c + 5t	0.04
4cf + 4cm + 4ct	0.03
2c + 2ct	0.09
2t	0.04
2tc	0.07
1	0.008

In the literature data on some chromium(III) polyamine hydrolysis reactions has appeared.[10–14] The ammonia displacement reactions investigated by us are found invariably to be slower than the reactions involving the other amines, if chromium(III) complexes equivalently coordinated with amine nitrogen atoms and water are compared.* Except for the hydrolysis of the *mer*-amminetriaqua(1,2-ethanediamine)chromium(III) ion,[11] the rate differences, between complexes with the same configuration of nitrogen and oxygen donor atoms around the chromium center, seem mainly to be associated with differences in the activation energies of the processes. Published data on amine chromium(III) reactions are, however, still rather sparse.

Qualitative intercomparison of the data for the reactions of the chromium(III) complexes, differently coordinated with ammonia and water, suggests that when these reactions take place, major stereochemical ligand movements involve only four coplanar ligands, whereas the two ligands above and below this plane are not intimately involved in the reactions.

A quantitative description in these terms may be obtained, if the octahedron is regarded as composed of three square planes, each of which contains four half ligands and one third of the central atom. If the reaction rate constants for each of these substructural units of the octahedron is assumed to follow an Arrhenius type equation:

$$k = Z \exp(-E/RT)$$

the experimentally observed rate constants may be expressed as:

$$k_{obs} = \sum Z_{ij} \exp(-E_{ij}/RT)$$

The index i is a description of the reaction of the square planar ligand arrangements labelled according to the ligand atom reaction

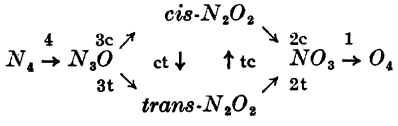

* Investigations on other amine chromium(III) hydrolysis reactions have shown that this behaviour is not generally adopted by chromium(III) complexes, as, *e.g.*, tetraaqua(1,3-propanediamine)-chromium(III) aquates considerably slower at 80 °C than does *cis*-diamminetetraaquachromium(III).

Table 7. Analytical expressions and calculated rate constants at 70 °C for the reaction scheme of Fig. 2, within the model presented in the text.

Reaction	Analytical expression		$10^6 \times k_{calc}$ (s^{-1})	$10^6 \times k_{obs}$ (Table 4) (s^{-1})
6	$3Z_4$	$\times \exp(-E_6/RT)$	48.3	47.5
5c	$(2Z_{3c}+Z_4)$	$\times \exp(-E_5/RT)$	48.5	47.2
5t	$2Z_{3t}$		0.0	0.0
4cf	$2Z_{3c}$		22.7	24.2
4cm	$(Z_{2c}+2Z_{3t})$	$\times \exp(-E_{4c}/RT)$	3.6	3.3
4ct	Z_{ct}		0.0	0.0
4tm	$(2Z_{2t}+Z_4)$		45.2	44.4
4tf	0	$\times \exp(-E_{4t}/RT)$	0.0	0.8
4tc	$2Z_{tc}$		4.8	4.2
3fc	$3Z_{2c}$		7.9	7.6
3ft	0	$\times \exp(-E_{3f}/RT)$	0.00	0.03
3fm	$3Z_{ct}$		0.0	0.3
3mc	$(Z_{2t}+Z_{3c})$		22.3	23.5
3mt	(Z_1+Z_{3t})	$\times \exp(-E_{3m}/RT)$	1.7	0.5
3mf	Z_{tc}		1.9	1.1
2c	$(2Z_1+Z_{2c})$	$\times \exp(-E_{2c}/RT)$	3.34	3.39
2ct	Z_{ct}		0.00	0.00
2t	$2Z_{2t}$	$\times \exp(-E_{2t}/RT)$	17.6	17.5
2tc	$2Z_{tc}$		5.28	5.25
1	$2Z_1$	$\times \exp(-E_1/RT)$	1.125	1.108

The j-index similarly describes the whole complex ion that reacts, named by an integer that reflects the number of nitrogen donor atoms, extended where necessary with a postpositioned letter to indicate *cis*, *trans*, *mer*, or *fac* isomers, respectively.

Initial calculations within this model with the additional empirical requirements:

$$Z_{ij} = Z_{ik} \ (= Z_i)$$

and

$$E_{ij} = E_{kj} \ (= E_j)$$

showed that although no well defined values of ln Z_{3t}* and ln Z_{ct}* could be obtained all the kinetic experiments, previously described with the parameters of Table 4, were equally well described within this simpler model.** Exclusion of Z_{3t} and Z_{ct} from the calculations caused no change in the overall agreement between model and data. In Table 7 analytical expressions for the rate constants of Fig. 2 are tabulated together with a comparison between the rate constants of Table 4 and those calculated in this restricted model from the estimated parameters of Table 8. The linear correlation between the ln Z values in this table for the ammine hydrolysis reactions and the natural logaritm of the number of coordinated nitrogen atoms in the reacting plane, n, with a slope about 2.0 should be noted, as should also the minor difference between ln Z_{2t} and ln Z_{2c}. The

* Since the calculations were performed in a linearized model ln Z's were used as parameters rather than the Z's themselves.

** This statement may be tested rigorously by a variance ratio test. Let x be an n dimensional experiment vector. X the corresponding $n \times n$ experiment variance matrix, and Q a matrix with columns q_i that diagonalizes X. The rank of X, r ($r \leq n$), may then be taken as the number of non negative expressions of the type ($\omega \geq 0$):

$$|q_i^T x| - \omega(q_i^T X q_i)^{\frac{1}{2}} \quad (i = 1, 2, \cdots, n)$$

For the present data and $\omega = 0$, 2, or 3, ranks of the experiment variance matrix, in the last reduction of the data, of 422, 283, or 256 are calculated. Consequently $P\{v^2(f_1,f_2) > s_1^2/s_2^2\}$ [15] is found to be about 1 %, 5 %, and 10 %, respectively, in these three cases.

Table 8. Estimated reaction parameters and correlation coefficients for reactions of the square planar octahedral substructural units presented in the text.

Parameter name	Parameter value	Correlation coefficients																			
Z_4	exp (28.26 ± 0.18) s^{-1}																				
Z_{3c}	exp (28.02 ± 0.13) s^{-1}	−.09																			
Z_{2c}	exp (26.88 ± 0.13) s^{-1}	−.11	.92																		
Z_{2t}	exp (27.07 ± 0.14) s^{-1}	.83	−.03	−.05																	
Z_1	exp (25.79 ± 0.17) s^{-1}	.56	−.19	−.21	.73																
Z_{tc}	exp (25.86 ± 0.14) s^{-1}	.88	−.02	−.04	.97	.73															
E_6	26.87 ± 0.13 kcal/mol	.99	−.09	−.10	.83	.56	.87														
E_5	26.72 ± 0.07 kcal/mol	.67	.67	.59	.59	.28	.63	.67													
E_{4c}	26.87 ± 0.09 kcal/mol	−.10	.99	.94	−.03	−.19	−.03	−.09	.66												
E_{4t}	26.46 ± 0.11 kcal/mol	.98	−.08	−.09	.92	.64	.94	.97	.67	−.08											
E_{3f}	27.09 ± 0.09 kcal/mol	−.11	.90	.99	−.05	−.21	−.04	−.10	.58	.92	−.10										
E_{3m}	26.63 ± 0.07 kcal/mol	.31	.87	.78	.44	.23	.44	.32	.87	.87	.36	.77									
E_{2c}	27.28 ± 0.06 kcal/mol	.34	.61	.65	.51	.60	.53	.34	.69	.62	.40	.65	.82								
E_{2t}	26.40 ± 0.10 kcal/mol	.83	−.03	−.05	.99	.73	.97	.82	.59	−.03	.91	−.05	.44	.51							
E_1	27.40 ± 0.12 kcal/mol	.56	−.19	−.21	.74	.99	.75	.56	.28	−.19	.64	−.21	.23	.60	.73						

regularity of the calculated activation energies should also be noted, and although the differences are yet unexplained attempts will be made to rationalize these data.

From these calculations we concluded that the two ligands perpendicular to the reacting plane play only a secondary role in the formation of the transition state by these reactions. In view of the very similar reactivity parameters for the different hydrolysis and isomerization reactions for the individual complexes, it is not unreasonable to assume a common intermediate for these different types of reactions. If this is accepted we must conclude that ammonia is not lost in the activated complex. Consequently the reactions of the complexes proceed by an associative mechanism *via* an intermediate of increased coordination number. The most plausible geometry of this intermediate is that of five of the ligands situated in a plane, that also contains the chromium atom, and those remaining two ligands of minor importance for the reaction coordinated above and below this plane, *i.e.* a distorted pentagonal bipyramid. Preferential attack of solvent water, hydrogen bonded to a coordinated water molecule, may rationalize the absence of Z_{3t} and Z_{ct} terms, as such attack will not separate neighbouring coordinated ammonia molecules when the reactive intermediate is formed.

From the limited amount of data on water exchange reactions in chromium(III) complexes [16,17] it seems that such reactions proceed so much faster, particularly in the pentaammineaquachromium(III) ion, than both the isomerization and the ammine hydrolysis reactions, that it does seem plausible that the water exchange reactions proceeds *via* a somewhat different intermediate than the other reactions discussed. This is also in favour of an associative mechanism for the hydrolysis and isomerization reactions, as water exchange and isomerization should be expected to parallel each other if a dissociative mechanism is assumed. Probably, however, the transition state in all the types of reactions just discussed contains additional water, in which case the intermediate in the water exchange reactions can be a first and less intimate stage in the just hypothetized attack by the water of the first solvent shell of the complex ion.

It is obvious that a more concise mechanistic picture of the reactions discussed must await further information, especially about water exchange, in a more generous number of chromium(III) aqua complexes.

REFERENCES

1. Mønsted, L. and Mønsted, O. *Acta Chem. Scand. 27* (1973) 2121.
2. Mønsted, L. and Mønsted, O. *Acta Chem. Scand. A 28* (1974) 23.
3. Mori, M. J. *J. Inst. Polytechn. Osaka City Univ. Ser. C. 3* (1952) 41.
4. Audrieth, L. F., Ed., *Inorganic Synthesis*, New York 1950, Vol. 3, p. 153.
5. Jørgensen, E. and Bjerrum, J. *Acta Chem. Scand. 12* (1958) 1047.
6. Bjerrum, J. and Lamm, C. G. *Acta Chem. Scand. 9* (1955) 216.
7. Edelson, M. R. and Plane, R. A. *J. Phys. Chem. 63* (1959) 327.
8. Edelson, M. R. and Plane, R. A. *Inorg. Chem. 3* (1964) 231.
9. Diebler, H. and Bazsa, Gy. *Proc. Int. Conf. Coord. Chem. 15th*, Moscow 1973.
10. Childers, R. F., Vander Zyl, K. G., House, D. A., Hughes, R. G. and Garner, C. S. *Inorg. Chem. 7* (1968) 749.
11. Williams, T. J. and Garner, C. S. *Inorg. Chem. 8* (1969) 1639.
12. Lin, D. K. and Garner, C. S. *J. Amer. Chem. Soc. 91* (1969) 6637.
13. Kamp, D. A., Wilder, R. L., Tang, S. C. and Garner, C. S. *Inorg. Chem. 10* (1971) 1396.
14. Ranney, S. J. and Garner, C. S. *Inorg. Chem. 10* (1971) 2437.
15. Hald, A. *Statistical Tables and Formulas*, New York 1952.
16. Duffy, N. V. and Early, J. E. *J. Amer. Chem. Soc. 89* (1967) 272.
17. Hunt, J. P. and Plane, R. A. *J. Amer. Chem. Soc. 76* (1954) 5960.

Received February 20, 1974.

Acta Chemica Scandinavica A 28 (1974) 578—588

Metal Complexes with Mixed Ligands. 9. The Crystal Structure of Aquatrisimidazolecopper(II) Sulphate, $Cu(H_2O)(C_3H_4N_2)_3SO_4$

GUNNAR FRANSSON and BRUNO K. S. LUNDBERG

Department of Inorganic Chemistry, University of Umeå, S-901 87 Umeå, Sweden

The crystal structure of $Cu(H_2O)(C_3H_4N_2)_3SO_4$ has been determined from three-dimensional X-ray diffraction data. The crystals are monoclinic, spacegroup $P2_1/n$, with unit cell dimensions and corresponding standard deviations (at 25 °C) $a = 14.239(1)$ Å; $b = 8.707(1)$ Å; $c = 11.717(1)$ Å and $\beta = 90.244(5)°$. There are four formula units per unit cell. Intensities were collected and measured with the linear diffractometer PAILRED using Mo$K\alpha$ radiation. The structure was solved by routine heavy-atom methods and refined by full matrix least-squares methods. With positional coordinates of all atoms and anisotropic thermal factors of non-hydrogen atoms as parameters the structure was refined to a conventional R-value of 0.043. The refinement was based on 3032 observations. The distorted octahedron around copper is formed by four short bonds from three imidazole nitrogens and one sulphate oxygen and two longer bonds formed by one sulphate oxygen and the water oxygen. The sulphate group forms a bridge between copper atoms leading to infinite chains along the two-fold screw axes. Both within and between the chains there are hydrogen bonds between the nitrogens not coordinated to copper atoms, the sulphate oxygens, and the water oxygen.

The investigation of metal-imidazole-complexes forms the basis of a research programme at this department which aims at determining the different possible coordinations of the histidine residue imidazole to metal atoms as models for the more complex biological systems where metal atoms interact with histidine residues. The formation of Cu(II)-imidazole complexes with different anions have been studied especially, both in the crystalline state and in solution.[1-8]

When the ratio of imidazole to copper is varied, mononuclear complexes are formed in solution where the number of imidazole rings bound to Cu(II) varies from one to six. If the anion medium is varied, most of the complexes with a composition corresponding to these mononuclear species can crystallize. At this stage the crystal structures of Cu(II)-imidazole complexes with Cl^-, ClO_4^- and SO_4^{2-} have been determined.[2-4] They contain complexes with the ratio $C_3H_4N_2$:Cu = 2:1, 3:1, and 4:1. Two complexes have been crystallized with PO_4^{3-} as anion and the chemical analyses correspond to the formulas $Cu(C_3H_4N_2)_5HPO_4.5H_2O$ and $Cu(C_3H_4N_2)_6(H_2PO_4)_2.2H_2O$. The structure determinations of these are in progress and may possibly confirm the suggested 5:1 and 6:1 coordinations. In the sulphate medium two different species have so far been crystallized; the first was $Cu(C_3H_4N_2)_4SO_4$[3] and the other is $Cu(H_2O)(C_3H_4N_2)_3SO_4$ which is the subject of this communication.

EXPERIMENTAL

Crystal preparation and analysis. In a typical preparation of the crystals 30 ml of a 1 M imidazole solution were added to 10 ml of 1 M $CuSO_4$ solution and the pH of the mixture was adjusted to about 6.5 by adding 0.1 M sulphuric acid. The solution was left to evaporate at room temperature and after a few days blue crystals, in the shape of well-defined prisms, were formed. They were not stable in air. The copper content was determined by titration with EDTA,[9] and the nitrogen content was determined using the Kjeldahl method.[10] With the aid of IR-spectra the presence of H_2O was indicated. Using a thermal balance it could be shown that the crystals lose one water molecule per formula unit after heating to 130 – 140 °C. The following analyses (in weight-%) were obtained. Found: Cu 16.4; N 21.7; H_2O 4.6. Calc. for $Cu(H_2O)$-

$(C_3H_4N_2)_3SO_4$: Cu 16.6; N 22.0; H_2O 4.7. The density of the crystals was determined by flotation (using bromoform and xylene) to be 1.73 g/cm³. With four units of $Cu(H_2O)(C_3H_4N_2)_3SO_4$ in the unit cell the calculated density is 1.74 g/cm³.

Unit cell data and spacegroup. From rotation photographs around the *a*- and *b*-axes and corresponding Weissenberg photographs ($0kl-2kl$ and $h0l-h2l$) taken with Cu$K\alpha$-radiation, it was concluded that the crystals are monoclinic. The systematic extinctions for $h0l$ when $h+l$ is odd and for $0k0$ when k is odd are characteristic for the spacegroup $P2_1/n$ (No. 14).[11] The dimensions of the unit cell were determined with the aid of powder photographs taken with a camera of Guinier-Hägg type using 45 observations in a least-squares refinement. The following parameters and corresponding standard deviations were obtained: $a=14.239(1)$ Å; $b=8.707(1)$ Å; $c=11.717(1)$ Å; and $\beta=90.244(5)°$.

Collection and reduction of intensity data. The intensities were measured with an automatic linear diffractometer (PAILRED) using Mo$K\alpha$-radiation, graphite monochromator and pulse height discriminator. The specimen crystal was enclosed, together with part of the crystallization mother liquid, in a sealed capillary of Lindeman glass. It was mounted around the *b*-axis and about 4300 independent reflexions from ten reciprocal levels ($h0l-h9l$) were measured. All reflexions with counts less than 10 000 were measured up to three times; background radiation was measured for 40 s on each side of every reflexion. For the $h0l$ layer the half-scan ranges were 1.1° and 1.4° for $\theta \geq 22°$ (ω_1) and $\theta < 22°$(ω_2) respectively. The half-scan ranges were then gradually increased to the value of 1.3° and 1.8° for the $h9l$-layer. The scan speed used was 1 deg./min.

The intensities were corrected according to the relation $I=TI/N-\omega(B_1+B_2)/t_Bv$ where $I=$ net intensity, $TI=$ total intensity (peak + background), $N=$ number of scans over the reflexion, $\omega=$ the half-scan range, B_1 and $B_2=$ background intensities, $t_B=$ time for background measurement and $v=$ scan speed. The relative counting statistical error of each reflexion $\Delta I/I$ was calculated using the formula

$$\frac{\Delta I}{I} = \frac{[TI/N^2 + (\omega/t_Bv)^2(B_1+B_2) + (T^2/N^2) \times 0.0001]^{1/2}}{TI/N - [\omega(B_1+B_2)]/t_Bv}$$

where $(T^2/N^2) \times 0.0001$ is a term that corrects for the linear error in the diffractometer. Of 4300 measured reflexions 3032 were significant at the 95 % level, *i.e.* had $\Delta I/I < 0.50$. Lp and absorption corrections were then applied. The linear absorption coefficient is 17.29 cm^{-1} for Mo$K\alpha$-radiation; there was thus a variation in the transmission factors of 11 %.

The calculations were performed with a CDC 3300 computer using modified versions of the programmes mentioned by Ivarsson, Lundberg and Ingri.[4]

STRUCTURE DETERMINATION AND REFINEMENT

The position of the copper atom was found from the three-dimensional Patterson synthesis. Heavy atom Fourier methods allowed the determination of the approximate positions of the other non-hydrogen atoms. However, to distinguish N(2), N(4), and N(6) from C(2), C(5), and C(8) (see Fig. 1 for numbering) all six atoms were refined as carbons and then the group of three atoms with the lower temperature factors was labelled nitrogen prior to further refinement.

The atomic coordinates and anisotropic temperature factors were refined using full matrix least-squares techniques. The reflexions were weighted according to the method suggested by Cruickshank,[12] $\omega = 1/(a+|F_o|+c|F_o|^2+d|F_o|^3)$ using constants $a=100$, $c=-0.02$, $d=0.0006$.

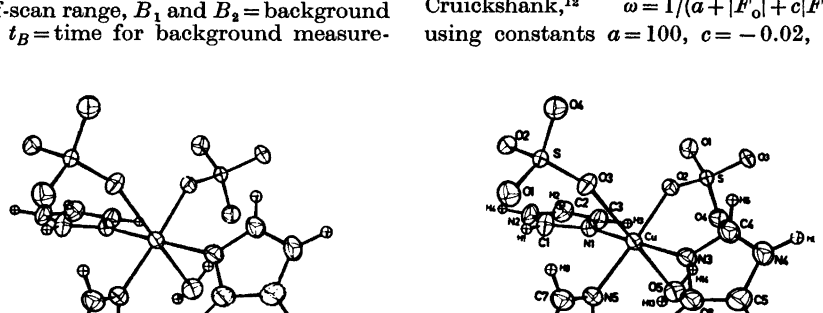

Fig. 1. A stereoscopic illustration of a molecule viewed along the *a*-axis. Thermal ellipsoids are scaled to enclose 50 % probability. The parenthesis around the numbers are omitted in the figure.

Table 1a. Fractional atomic coordinates and anisotropic thermal parameters. Their estimated standard deviations are given in parentheses. All values are multiplied by 10^4. Anisotropic temperature factors have been calculated according to the formula
$\exp[-(h^2\beta_{11}+k^2\beta_{22}+l^2\beta_{33}+hk\beta_{12}+hl\beta_{13}+kl\beta_{23})]$.

	x	y	z	β_{11}	β_{22}	β_{33}	β_{12}	β_{13}	β_{23}
Cu	2792(0.3)	1506(0.5)	746(0.3)	29(0.2)	59(1)	38(0.3)	−15(0.5)	−14(0.3)	22(1)
S	1079(1)	4198(1)	2495(1)	25(0.3)	49(1)	33(0.5)	2(1)	0(1)	−6(1)
01	4572(2)	−148(3)	3356(2)	32(1)	83(4)	63(2)	3(3)	−32(3)	−11(4)
02	3259(2)	423(3)	2158(2)	34(1)	68(3)	41(1)	12(3)	−10(2)	19(4)
03	1586(2)	2901(3)	2011(2)	40(1)	65(3)	46(2)	19(3)	6(2)	−30(4)
04	539(2)	3678(3)	3509(2)	46(1)	84(4)	51(2)	−2(4)	39(3)	−4(4)
05	3896(2)	113(4)	−513(2)	40(1)	117(5)	63(2)	4(4)	6(3)	−8(5)
N1	3734(2)	3159(3)	1056(2)	33(1)	52(4)	46(3)	−9(3)	2(3)	3(4)
N2	4344(3)	5417(4)	1367(3)	55(2)	62(5)	70(3)	−26(5)	13(4)	−33(5)
C1	3564(3)	4640(5)	1096(4)	38(2)	74(5)	72(3)	4(5)	9(4)	−5(6)
C2	5047(3)	4384(5)	1513(4)	37(2)	110(6)	67(3)	−28(5)	−3(4)	−20(7)
C3	4664(2)	2993(5)	1321(3)	33(2)	78(5)	59(3)	−3(4)	−6(3)	−16(6)
N3	1884(2)	−201(3)	441(2)	30(1)	74(4)	34(2)	−13(3)	−1(2)	12(4)
N4	1113(2)	−2372(4)	618(3)	42(2)	82(5)	60(2)	−39(4)	−5(3)	23(5)
C4	1748(3)	−1428(5)	1082(3)	38(2)	87(5)	51(2)	−35(5)	−7(3)	17(6)
C5	811(3)	−1711(5)	−379(3)	47(2)	119(7)	54(3)	−43(6)	−24(4)	−4(6)
C6	1290(3)	−392(5)	−484(3)	46(2)	100(6)	45(2)	−47(5)	−27(4)	16(6)
N5	2315(2)	2685(4)	−597(7)	29(1)	81(4)	40(2)	−7(4)	−2(2)	23(4)
N6	1374(2)	3980(4)	−1710(3)	41(2)	121(5)	50(2)	15(5)	−15(3)	39(5)
C7	1522(2)	3464(5)	−647(3)	34(2)	94(5)	44(2)	−14(5)	−11(3)	15(6)
C8	2101(3)	3506(6)	−2373(3)	53(2)	164(8)	44(3)	11(7)	4(4)	65(7)
C9	2689(3)	2707(5)	−1679(3)	36(2)	122(6)	53(3)	21(5)	15(3)	31(6)

Table 1b. Fractional atomic coordinates and isotropic thermal parameters for the hydrogen atoms. Their estimated standard deviations are given in parentheses. All coordinates are multiplied by 10^4.

	x	y	z	B(Å^2)
H1	2991(33)	5132(62)	951(43)	4.3(1.1)
H2	5655(40)	4678(75)	1655(51)	6.1(1.4)
H3	4935(31)	2016(58)	1287(39)	3.6(1.0)
H4	4413(35)	6335(62)	1446(44)	4.5(1.1)
H5	1998(35)	−1500(61)	1775(43)	4.6(1.2)
H6	336(35)	−2096(66)	−877(44)	4.9(1.2)
H7	1237(29)	379(53)	−1067(37)	3.2(0.9)
H8	906(33)	−3221(59)	980(41)	4.1(1.1)
H9	1151(33)	3743(57)	−2(40)	3.8(1.0)
H10	2142(38)	3762(67)	−3161(46)	5.3(1.3)
H11	3236(30)	2330(54)	−1840(37)	3.3(0.9)
H12	842(31)	4503(58)	−1914(39)	3.8(1.0)
H13	4451(38)	571(74)	−837(48)	5.8(1.4)
H14	4179(41)	−405(79)	23(53)	6.5(1.5)

The atomic scattering factors for Cu^{2+}, S, O, N, and C were taken from the International Tables.[14] Account was taken of the real part of the dispersion correction for Cu^{2+} and S. Refinement, not including hydrogen atoms, was terminated at an R-value $= (\sum||F_o|-|F_c||)/\sum|F_o| = 0.049$.

A difference Fourier map was then calculated and peaks on it could be postulated as being due to hydrogen atoms. Refinement including the hydrogen coordinates and their isotropic thermal parameters was made, using the scattering factors proposed by Stewart, Davidson and Simpson.[13] This was terminated when all param-

Table 2. Observed and calculated structure factors (× 10).

L	H			L	H			L	H			L	H			L	H			L	H		
				6-16	192	188		0	6	333	358	10	6	143	137	6	12	167	160	3	0	1250	1165	15	0	181	189
K=	0			6-14	157	161		0	4	528	554	10	5	141	133	6	10	242	238	3	1	1077	1005	15	-1	109	131
				6-12	330	330						10	4	311	315	6	9	641	641	3	2	561	546	15	-4	97	109
16	-2	83	94	6-10	478	471	K=	1				10	3	214	203	6	8	399	408	3	3	718	700	14	-7	154	158
16	0	158	148	6 -8	98	102						10	2	171	179	6	7	569	569	3	4	253	264	14	-2	91	78
16	4	142	132	6 -6	104	105	17	-2	82	80		10	1	404	405	6	6	314	320	3	6	610	631	14	-1	309	318
16	6	125	117	6 -4	548	528	17	2	77	114		10	0	119	132	6	5	105	100	3	7	260	282	14	0	148	149
15	9	112	109	6 -2	1285	1249	16	4	117	121		10	-2	402	416	6	4	242	229	3	8	187	190	14	1	329	337
15	7	144	140	6 0	1002	991	16	2	110	110		10	-4	240	239	6	2	184	168	3	9	789	783	14	3	76	48
15	5	224	245	6 2	874	824	16	1	138	137		10	-5	348	357	6	1	228	208	3	10	300	306	14	7	102	104
15	3	175	204	6 4	289	300	16	0	155	164		10	-6	98	96	6	0	104	111	3	11	372	381	14	8	76	85
15	1	156	170	6 6	633	641	16	-2	208	213		10	-7	143	145	6	-1	511	498	3	12	568	565	13	10	294	300
15	-3	142	148	6 8	560	549	16	-4	95	113		10	-9	107	104	6	-2	428	426	3	13	190	190	13	8	124	141
15	-7	191	211	6 10	390	384	16	-5	79	93		10	-11	98	95	6	-3	566	545	3	14	166	151	13	7	69	11
14	-10	75	80	6 14	94	96	16	-8	83	24		10	-12	115	98	6	-4	212	221	3	15	222	224	13	6	124	115
14	-4	376	396	6 16	217	215	15	-9	117	110		10	-14	146	147	6	-5	122	120	3	16	152	155	13	4	284	291
14	-2	212	229	6 18	242	221	15	-6	183	189		10	-15	187	186	6	-6	285	303	3	17	74	96	13	3	120	155
14	2	135	128	5 19	136	117	15	-4	172	174		9	-11	171	180	6	-7	124	116	2	20	173	166	13	0	190	192
14	4	218	226	5 17	98	89	15	-3	128	134		9	-10	70	75	6	-8	84	96	2	19	79	83	13	-2	109	112
14	8	143	138	5 15	61	44	15	-1	132	143		9	-9	298	308	6	-9	473	483	2	18	115	120	13	-3	86	108
13	13	194	180	5 13	123	101	15	0	80	88		9	-8	119	115	6	-10	210	218	2	17	142	136	13	-4	78	66
13	9	191	193	5 11	836	824	15	1	83	89		9	-7	339	361	6	-12	285	289	2	16	104	121	13	-6	187	184
13	7	427	434	5 9	582	581	15	4	96	76		9	-6	534	539	6	-14	74	63	2	15	174	183	13	-7	150	155
13	5	186	188	5 7	177	170	15	6	135	121		9	-5	154	144	6	-16	81	71	2	14	142	159	13	-8	227	236
13	1	102	103	5 5	462	442	15	9	131	131		9	-4	284	287	6	-18	68	40	2	13	250	241	13	-10	114	101
13	-1	95	89	5 3	450	419	14	11	90	60		9	-3	571	570	6	-19	105	100	2	12	176	173	12	-9	150	150
13	-3	305	297	5 -1	1014	993	14	10	136	140		9	-1	409	401	5	-18	70	61	2	11	179	184	12	-8	71	70
13	-5	317	317	5 -3	1030	1009	14	8	200	217		9	0	183	183	5	-17	95	91	2	10	139	142	12	-7	196	180
13	-11	172	158	5 -5	127	82	14	7	152	160		9	2	267	256	5	-16	135	152	2	8	530	533	12	-6	98	88
12	-14	102	99	5 -7	688	685	14	6	127	150		9	3	121	126	5	-15	168	160	2	7	139	147	12	-5	94	103
12	-12	284	278	5 -9	120	118	14	5	207	218		9	4	336	352	5	-14	143	146	2	5	265	289	12	-3	193	204
12	-10	159	149	5 -13	203	196	14	4	108	115		9	5	139	142	5	-13	395	401	2	4	442	450	12	-2	187	177
12	-8	102	93	5 -17	205	217	14	3	111	118		9	6	231	231	5	-12	158	148	2	3	441	438	12	-1	119	129
12	-6	67	67	5 -19	160	150	14	2	100	108		9	7	288	290	5	-11	505	522	2	2	1166	1127	12	1	96	104
12	-4	65	47	4 -20	68	41	14	0	69	21		9	9	322	320	5	-10	262	263	2	1	261	250	12	2	240	239
12	0	289	286	4 -18	82	88	14	-1	71	91		9	10	181	173	5	-9	158	160	2	0	319	268	12	3	373	384
12	2	273	276	4 -14	569	565	14	-3	138	128		9	11	161	137	5	-8	299	298	2	-1	1197	1112	12	4	166	174
12	4	368	376	4 -12	650	650	14	-5	206	209		9	12	316	305	5	-7	343	341	2	-2	868	851	12	5	224	223
12	6	580	570	4 -10	151	162	14	-7	82	44		9	13	152	147	5	-6	408	387	2	-3	1517	1512	12	6	72	77
12	8	282	276	4 -8	536	539	14	-8	151	129		9	14	149	140	5	-5	169	172	2	-4	287	308	12	7	89	84
11	13	164	166	4 -6	765	770	14	-10	155	152		9	15	166	166	5	-4	182	181	2	-5	191	200	12	9	147	158
11	11	370	370	4 -2	583	541	14	-11	81	83		9	17	134	121	5	-2	197	177	2	-6	114	100	12	11	123	126
11	9	359	369	4 0	612	566	13	-12	155	145		8	18	115	108	5	-1	217	231	2	-7	316	317	11	13	111	114
11	7	87	77	4 2	119	103	13	-11	76	64		8	17	164	153	5	0	188	186	2	-8	251	250	11	12	170	176
11	5	240	249	4 4	1258	1260	13	-9	160	175		8	14	93	73	5	1	233	233	2	-9	332	346	11	9	134	139
11	3	195	201	4 6	611	628	13	-5	113	125		8	13	187	193	5	2	616	588	2	-10	373	379	11	7	119	115
11	1	237	227	4 8	381	381	13	-3	199	206		8	12	116	98	5	3	710	687	2	-11	256	259	11	6	170	158
11	-1	114	99	4 10	1058	1042	13	-2	204	207		8	11	220	221	5	4	481	477	2	-12	196	184	11	4	214	211
11	-3	180	188	4 12	477	466	13	-1	171	174		8	10	302	298	5	5	974	981	2	-13	305	308	11	3	73	70
11	-5	448	463	4 14	77	44	13	1	286	307		8	9	80	71	5	7	786	791	2	-14	189	179	11	2	454	463
11	-7	384	391	4 20	112	106	13	3	245	247		8	8	632	628	5	8	422	441	2	-15	71	75	11	1	88	98
11	-9	85	80	3 19	159	156	13	4	258	267		8	7	111	107	5	9	270	281	2	-16	213	201	11	0	244	249
11	-11	152	150	3 17	135	126	13	5	145	139		8	6	313	311	5	10	187	176	2	-19	110	101	11	-1	66	39
10	-14	189	188	3 15	232	229	13	6	141	142		8	5	569	565	5	11	178	183	1	-21	138	110	11	-2	425	438
10	-8	354	358	3 13	506	510	13	7	118	128		8	4	170	171	5	12	82	72	1	-20	168	164	11	-3	129	119
10	-6	477	495	3 9	75	52	13	13	107	83		8	3	187	179	5	13	78	48	1	-18	154	146	11	-4	283	278
10	-4	305	314	3 7	378	381	12	14	135	125		8	2	499	506	5	15	75	73	1	-17	213	206	11	-10	139	153
10	-2	107	122	3 5	676	664	12	12	218	214		8	1	307	299	5	19	107	78	1	-16	154	156	11	-14	177	170
10	0	553	553	3 3	1301	1292	12	11	142	133		8	0	451	449	5	20	127	106	1	-15	281	281	10	-13	78	63
10	2	187	201	3 1	85	74	12	10	168	172		8	-1	165	157	4	20	101	71	1	-13	148	149	10	-12	131	124
10	4	468	474	3 -1	1388	1290	12	9	191	194		8	-2	148	148	4	19	82	101	1	-12	268	271	10	-11	283	282
10	8	187	193	3 -3	839	831	12	8	162	168		8	-4	66	62	4	17	79	75	1	-11	76	72	10	-10	112	113
10	10	462	457	3 -5	809	806	12	7	154	150		8	-5	195	178	4	16	222	221	1	-10	145	149	10	-9	324	327
10	12	379	359	3 -7	114	125	12	6	211	215		8	-6	86	108	4	14	325	322	1	-9	583	570	10	-7	226	225
9	17	74	52	3 -9	125	128	12	5	81	76		8	-7	88	83	4	13	222	218	1	-8	74	100	10	-6	143	139
9	15	213	211	3 -11	207	198	12	3	75	20		8	-8	421	421	4	12	233	230	1	-7	287	302	10	-5	184	186
9	9	207	208	3 -13	422	420	12	2	160	167		8	-10	145	135	4	11	284	284	1	-6	479	479	10	-4	294	288
9	7	312	312	3 -15	324	318	12	1	68	67		8	-11	225	246	4	10	409	425	1	-5	900	809	10	-3	287	288
9	5	336	339	3 -17	79	56	12	-1	389	400		8	-12	87	99	4	9	92	79	1	-4	119	112	10	-2	144	153
9	3	532	530	2 -20	138	129	12	-3	260	268		8	-13	204	196	4	8	205	205	1	-3	1379	1386	10	-1	95	98
9	1	188	180	2 -16	141	133	12	-4	335	338		8	-14	84	79	4	7	419	415	1	3	742	744	10	0	254	253
9	-1	496	506	2 -14	225	221	12	-6	196	186		8	-16	104	109	4	6	443	437	1	4	302	295	10	1	202	196
9	-3	714	720	2 -12	402	399	12	-7	90	88		8	-18	72	51	4	5	221	203	1	5	302	294	10	3	71	80
9	-5	141	141	2 -10	457	445	12	-8	79	78		7	-18	84	85	4	4	193	208	1	7	84	76	10	4	84	96
9	-7	314	305	2 -8	456	464	12	-9	172	172		7	-17	151	142	4	3	1103	1081	1	8	264	272	10	5	337	332
9	-9	189	189	2 -6	825	823	12	-12	156	151		7	-16	78	60	4	1	814	769	1	10	455	470	10	6	120	120
9	-13	232	230	2 -4	456	455	12	-13	103	112		7	-15	180	177	4	0	458	431	1	11	313	316	10	7	539	547
9	-15	288	282	2 -2	1533	1488	11	-13	245	233		7	-12	294	288	4	-1	311	326	1	13	324	324	10	8	97	87
8	-16	97	91	2 0	203	199	11	-11	126	125		7	-11	143	134	4	-2	881	871	1	14	80	75	10	9	307	318
8	-14	169	163	2 2	272	258	11	-10	184	196		7	-9	116	107	4	-3	356	358	1	15	206	197	10	11	142	142
8	-10	348	353	2 4	131	128	11	-9	121	118		7	-8	306	305	4	-4	921	897	1	16	288	284	10	13	154	142
8	-8	291	296	2 8	248	259	11	-8	185	185		7	-7	75	67	4	-5	786	792	1	17	131	136	10	14	114	106
8	-6	281	288	2 10	603	582	11	-7	76	76		7	-6	158	175	4	-6	468	458	1	18	72	58	10	15	114	109
8	-4	803	786	2 12	677	676	11	-5	214	218		7	-5	441	454	4	-7	60	36	1	19	158	145	10	16	90	88
8	-2	859	864	2 14	403	395	11	-4	216	219		7	-4	234	233	4	-8	211	211	0	21	86	60	9	16	200	195
8	0	542	525	2 20	108	100	11	-3	158	161		7	-3	606	583	4	-9	279	275	0	19	185	179	9	10	97	97
8	2	567	579	1 19	198	170	11	-2	188	189		7	-2	441	434	4	-10	203	205	0	18	82	57	9	9	259	251
8	6	288	288	1 17	245	235	11	-1	150	159		7	-1	846	813	4	-11	156	154	0	15	300	300	9	8	289	280
8	8	221	217	1 15	176	170	11	0	78	90		7	0	783	757	4	-12	292	302	0	14	102	101	9	7	174	171
8	10	181	168	1 13	263	251	11	1	166	159		7	1	651	633	4	-14	182	175	0	13	73	67	9	6	217	215
8	12	145	145	1 11	258	262	11	2	263	257		7	2	88	75	4	-15	201	198	0	12	148	140	9	5	239	251
8	14	323	321	1 9	540	547	11	3	181	183		7	3	428	415	4	-17	195	187	0	11	290	297	9	4	265	262
8	16	250	231	1 7	342	385	11	4	179	175		7	4	150	150	4	-18	104	87	0	10	422	430	9	3	91	99
7	19	134	114	1 5	597	588	11	5	327	324		7	6	294	300	4	-20	128	116	0	9	458	479	9	2	443	446
7	17	73	46	1 3	1222	1244	11	6	178	189		7	8	275	277	3	-19	93	90	0	8	559	580	9	1	330	334
7	15	104	102	1 -3	588	563	11	7	307	297		7	10	177	169	3	-16	141	136	0	7	458	475	9	0	618	609
7	13	141	128	1 -5	404	410	11	8	224	230		7	11	79	62	3	-15	207	214	0	6	501	526	9	-1	256	256
7	11	96	83	1 -7	906	895	11	9	153	157		7	12	76	77	3	-14	64	15	0	4	387	389	9	-3	180	173
7	9	508	502	1 -9	655	654	11	10	214	210		7	13	262	267	3	-13	92	73	0	3	572	590	9	-5	221	203
7	7	1028	1006	1 -11	603	598	11	11	165	168		7	14	74	81	3	-12	286	292					9	-6	214	224
7	5	188	207	1 -13	152	148	11	13	106	126		7	15	199	196	3	-11	348	356	K=	2			9	-7	74	78
7	1	344	333	1 -15	77	82	10	16	140	156		7	16	171	159	3	-10	259	251					9	-9	78	63
7	-1	918	875	1 -17	276	263	10	15	89	59		7	17	142	141	3	-9	478	506	16	-5	141	145	9	-10	337	347
7	-3	719	736	0 20	115	89	10	14	109	116		7	18	104	86	3	-8	438	431	16	-4	85	80	9	-11	83	89
7	-5	570	553	0 18	337	328	10	13	241	245		7	19	163	166	3	-7	163	180	16	-3	184	196	9	-12	256	258
7	-7	171	163	0 16	232	225	10	12	113	95		6	19	144	110	3	-6	756	760	16	1	78	58	8	-16	97	83
7	-9	250	249	0 14	76	55	10	10	171	177		6	17	73	80	3	-5	665	638	15	8	134	134	8	-12	164	162
7	-11	307	307	0 12	397	410	10	9	195	197		6	15	170	172	3	-3	1152	1117	15	6	141	146	8	-11	191	194
7	-15	79	43	0 10	121	131	10	8	117	112		6	14	116	109	3	-2	1199	1194	15	5	95	77	8	-10	156	151
6	-18	231	217	0 8	284	279	10	7	177	184		6	13	125	130	3	-1	396	382	15	2	154	166	8	-8	317	324

Table 2. Continued.

L	H			L	H			L	H			L	H			L	H			L	H		
					4-15	92	76	1	5	229	252	11	-6	234	237	6	-8	121	126	3-12	239	246	13	10	109	82
K=	2				4-13	75	76	1	4	1242	1275	11	-7	84	90	6	-7	807	812	3-13	67	68	13	9	109	79
					4-12	223	225	1	3	82	50	11	-8	192	200	6	-6	630	627	3-14	67	39	13	8	150	145
8	-7	391	395		4-11	525	537	1	2	1642	1706	11	-10	207	206	6	-5	649	635	3-19	144	144	13	7	141	153
8	-6	159	162		4-10	223	230	1	-2	146	125	11	-12	127	129	6	-4	291	288	2-19	118	103	13	6	129	144
8	-5	425	447		4	-9	675	673	1	-3	89	57	11	-13	152	154	6	-3	366	365	2-17	214	214	13	1	74	72
8	-3	313	327		4	-8	89	110	1	-4	210	189	10	-13	70	59	6	-1	158	97	2-16	157	159	13	0	173	171
8	-1	756	736		4	-7	134	139	1	-5	741	731	10	-12	149	148	6	0	335	315	2-15	224	223	13	-3	113	104
8	0	332	319		4	-6	155	159	1	-6	447	466	10	-11	101	83	6	2	109	100	2-13	337	341	13	-4	169	182
8	1	276	277		4	-5	389	402	1	-7	98	80	10	-3	138	156	6	3	154	143	2-11	293	287	13	-5	144	155
8	2	366	362		4	-4	791	769	1	-8	628	661	10	-2	399	405	6	4	174	157	2-10	471	484	13	-6	85	24
8	6	237	250		4	-3	64	74	1	-9	101	96	10	-1	398	405	6	5	440	453	2	-9	134	134	13	-7	139	136
8	7	72	58		4	-2	230	230	1-10		220	238	10	0	200	203	6	6	311	315	2	-8	200	206	13	-9	114	108
8	9	234	225		4	-1	224	237	1-11		193	199	10	1	490	502	6	7	201	194	2	-7	147	158	13-10		180	162
8	10	222	220		4	0	333	321	1-12		315	313	10	2	170	180	6	8	77	79	2	-6	64	72	13-11		74	100
8	11	414	411		4	1	368	349	1-14		524	521	10	3	347	347	6	9	188	179	2	-4	503	474	12-12		105	98
8	12	87	83		4	2	759	720	1-15		90	96	10	4	304	310	6	11	610	619	2	-3	47	32	12-11		104	98
8	13	203	202		4	3	194	193	1-16		124	120	10	5	332	339	6	12	369	372	2	-1	1058	991	12-10		151	139
8	15	81	101		4	4	506	474	1-18		83	56	10	6	272	277	6	13	328	332	2	0	113	101	12	-9	136	141
8	17	241	222		4	5	805	792	1-19		79	53	10	11	95	105	6	15	190	184	2	1	984	949	12	-6	89	67
7	16	72	41		4	6	382	311	0	2	844	853	10	12	88	82	6	16	87	91	2	2	864	878	12	-4	117	118
7	15	130	124		4	7	1004	1031	0	3	1477	1510	10	13	141	136	6	18	101	84	2	3	537	538	12	-1	257	257
7	12	292	284		4	8	389	401	0	4	670	707	10	15	203	193	5	18	157	153	2	4	254	267	12	0	315	333
7	11	115	108		4	9	314	331	0	5	754	778	9	15	119	119	5	17	158	153	2	5	1090	1119	12	1	249	250
7	10	389	394		4	10	160	168	0	6	261	253	9	14	185	163	5	16	86	89	2	6	155	149	12	2	302	312
7	9	136	140		4	11	67	92	0	8	203	185	9	12	264	261	5	15	148	160	2	7	382	406	12	3	73	84
7	8	129	142		4	13	169	150	0	9	222	213	9	11	83	99	5	11	75	61	2	8	524	534	12	4	74	72
7	7	68	74		4	14	341	349	0	10	142	153	9	10	338	344	5	10	190	195	2	9	238	249	12	5	81	62
7	6	456	449		4	17	115	107	0	13	215	212	9	9	101	124	5	9	386	393	2	10	177	194	12	6	144	140
7	5	390	391		4	19	107	107	0	14	191	192	9	8	331	334	5	8	245	253	2	11	167	167	12	7	158	154
7	4	987	949		3	19	120	114	0	15	298	302	9	6	183	172	5	7	369	363	2	12	67	71	12	8	171	164
7	3	180	186		3	18	250	239	0	16	177	176	9	5	102	86	5	6	363	375	2	13	172	181	12	9	139	133
7	2	555	536		3	17	105	111	0	17	93	91	9	3	304	290	5	5	510	500	2	14	88	77	11	12	74	74
7	1	196	192		3	16	266	258	0	19	149	138	9	1	303	295	5	4	425	443	2	15	75	78	11	11	139	126
7	0	377	355		3	14	181	178	0	20	107	98	9	0	189	190	5	3	101	93	2	17	179	181	11	10	140	145
7	-1	190	172		3	13	89	105					9	-1	304	292	5	2	948	910	2	18	91	93	11	9	102	97
7	-2	375	356		3	12	129	120	K=	3			9	-3	87	77	5	1	152	144	2	19	97	96	11	8	84	84
7	-3	482	462		3	11	561	576					9	-4	494	502	5	0	695	657	1	19	100	75	11	5	97	103
7	-4	78	56		3	10	107	94	16	-2	121	128	9	-5	212	213	5	-1	359	334	1	18	147	141	11	4	79	73
7	-5	224	210		3	9	153	156	16	1	111	120	9	-6	343	353	5	-2	534	498	1	16	180	184	11	3	189	205
7	-6	555	563		3	8	448	452	16	3	172	179	9	-7	96	104	5	-3	378	364	1	14	359	364	11	1	285	290
7	-7	367	369		3	7	255	268	15	5	84	85	9	-8	189	176	5	-4	62	69	1	13	351	364	11	0	473	467
7	-8	530	529		3	6	797	788	15	2	93	90	9	-9	98	107	5	-5	455	448	1	12	309	324	11	-1	308	311
7	-9	128	129		3	5	164	172	15	1	74	78	9	-10	261	266	5	-6	361	353	1	11	188	185	11	-2	260	263
7	-10	213	218		3	4	67	70	15	0	107	87	9	-13	91	94	5	-7	220	217	1	10	129	127	11	-3	149	148
7	-11	64	61		3	2	663	633	15	-1	129	122	8	-15	59	59	5	-8	371	382	1	9	170	167	11	-5	191	190
7	-12	215	213		3	1	324	312	15	-2	157	176	8	-16	116	105	5	-9	432	435	1	8	532	557	11	-6	173	170
7	-13	96	91		3	0	950	892	15	-3	131	124	8	-15	193	192	5	-10	292	294	1	7	326	327	11	-7	166	181
7	-14	224	223		3	-1	625	608	15	-4	129	125	8	-13	142	135	5	-11	97	103	1	6	249	233	11	-8	89	107
7	-15	90	88		3	-2	559	539	15	-6	162	156	8	-11	240	234	5	-13	133	137	1	5	878	922	11	-10	87	79
7	-16	95	81		3	-3	709	685	15	-8	86	93	8	-10	135	131	5	-14	186	185	1	4	769	818	10	-13	118	106
7	-18	73	71		3	-4	468	445	14	-10	102	92	8	-9	301	301	5	-16	137	142	1	3	481	481	10	-12	102	103
6	-17	90	80		3	-5	332	322	14	-9	123	116	8	-8	337	345	5	-17	85	62	1	2	322	341	10	-10	196	196
6	-15	211	221		3	-6	383	398	14	-8	149	151	8	-7	79	78	5	-18	109	97	1	-2	226	257	10	-9	131	132
6	-14	146	133		3	-7	551	563	14	-7	191	192	8	-5	231	236	5	-19	72	42	1	-3	391	377	10	-8	114	107
6	-13	262	266		3	-8	75	72	14	-2	177	160	8	-2	309	293	4	-19	182	172	1	-4	894	897	10	-7	288	279
6	-12	110	106		3	-9	166	178	14	1	178	170	8	-1	124	130	4	-18	533	559	1	-5	828	842	10	-6	154	163
6	-11	81	58		3	-10	345	358	14	2	78	119	8	0	79	92	4	-17	193	178	1	-6	607	611	10	-5	75	76
6	-10	83	76		3	-11	186	186	14	3	146	145	8	1	277	273	4	-15	227	224	1	-8	127	132	10	-4	113	100
6	-9	73	53		3	-12	239	247	14	5	184	178	8	2	371	360	4	-14	84	99	1	-9	259	249	10	-2	179	176
6	-8	290	296		3	-13	65	57	14	6	98	75	8	3	778	798	4	-12	316	320	1	-11	62	79	10	-1	276	281
6	-7	178	190		3	-14	133	128	14	7	104	107	8	4	76	72	4	-10	176	174	1	-12	126	130	10	2	251	244
6	-6	112	94		3	-15	183	192	14	9	135	129	8	5	500	499	4	-9	123	128	1	-13	221	226	10	3	321	319
6	-5	274	268		3	-16	268	269	14	10	93	89	8	6	74	67	4	-8	443	429	1	-14	149	152	10	4	227	228
6	-4	357	361		3	-17	132	127	13	9	74	48	8	7	233	236	4	-7	441	453	1	-15	171	162	10	5	366	360
6	-3	538	533		3	-18	203	191	13	8	113	98	8	8	150	158	4	-6	179	171	1	-16	191	202	10	6	186	188
6	-2	59	59		3	-19	97	82	13	6	131	125	8	9	87	85	4	-5	148	115	1	-17	143	132	10	7	119	122
6	-1	312	305		2	-19	160	124	13	5	105	91	8	10	167	167	4	-3	570	560	1	-18	146	151	10	8	138	136
6	0	268	257		2	-18	124	118	13	4	139	150	8	11	187	170	4	-2	298	301	1	-19	80	69	10	9	152	155
6	1	529	514		2	-17	188	185	13	3	116	125	8	12	88	91	4	-1	1026	996	0	2	480	520	10	10	210	215
6	3	713	699		2	-15	107	102	13	2	229	227	8	13	91	99	4	0	504	465	0	3	698	706	10	11	193	207
6	4	329	331		2	-14	64	70	13	1	194	189	8	15	125	99	4	1	849	805	0	4	995	1020	10	12	148	123
6	5	755	742		2	-11	231	234	13	0	283	291	8	16	87	81	4	2	193	168	0	5	824	873	10	14	118	103
6	6	185	190		2	-10	170	193	13	-2	77	90	7	16	204	189	4	3	656	630	0	6	369	385	9	14	117	102
6	8	208	220		2	-9	307	310	13	-4	119	133	7	14	212	197	4	4	115	108	0	7	508	550	9	13	151	153
6	9	136	142		2	-8	233	228	13-12		113	92	7	13	125	113	4	6	484	492	0	8	125	120	9	10	188	174
6	10	86	89		2	-7	1058	1054	12-12		103	86	7	12	313	321	4	7	63	70	0	9	399	419	9	7	182	190
6	11	143	135		2	-6	753	728	12-10		80	84	7	11	167	167	4	8	175	180	0	10	136	150	9	6	134	129
6	13	301	300		2	-5	1011	1018	12	-9	163	160	7	10	282	298	4	11	143	142	0	11	442	455	9	5	507	511
6	14	117	116		2	-4	97	115	12	-7	230	239	7	9	145	146	4	13	291	296	0	12	248	265	9	4	483	483
6	15	208	204		2	-3	711	695	12	-6	162	160	7	8	176	179	4	14	146	140	0	13	378	405	9	3	512	503
6	17	86	79		2	-2	223	216	12	-5	224	230	7	7	68	65	4	15	238	234	0	14	114	122	9	2	221	215
5	16	219	212		2	-1	317	312	12	-3	144	135	7	6	266	275	4	16	171	176	0	16	91	107	9	1	338	337
5	15	67	70		2	0	487	435	12	-2	130	139	7	4	544	545	4	17	234	232	0	19	80	73	9	0	69	61
5	14	442	444		2	1	1196	1149	12	-1	277	286	7	3	118	113	4	19	124	116					9	-1	64	70
5	13	228	224		2	3	213	212	12	0	160	151	7	2	669	671	3	19	81	82	K=	4			9	-2	129	132
5	12	262	267		2	4	307	298	12	1	201	202	7	1	475	464	3	16	116	119					9	-3	277	279
5	10	79	84		2	5	378	387	12	2	352	360	7	0	73	71	3	15	101	91	16	-2	82	90	9	-4	319	322
5	9	96	88		2	6	167	171	12	6	171	176	7	-2	281	297	3	14	181	185	16	-1	88	72	9	-7	232	233
5	8	587	601		2	7	352	346	12	7	85	91	7	-3	191	190	3	13	80	100	16	0	87	74	9	-8	167	169
5	7	131	123		2	8	66	56	12	9	168	166	7	-4	399	400	3	12	160	162	15	7	88	76	9	-9	94	109
5	6	523	513		2	9	359	384	12	11	142	150	7	-5	378	376	3	10	356	380	15	5	148	146	9-10		112	118
5	4	457	446		2	10	342	353	12	12	107	98	7	-6	332	325	3	9	346	352	15	4	227	218	9-11		115	109
5	3	395	363		2	11	467	469	12	13	246	233	7	-8	88	98	3	8	582	621	15	3	186	197	9-12		92	82
5	2	569	554		2	13	282	293	11	13	76	65	7	-9	277	279	3	7	115	120	15	2	104	119	9-13		84	81
5	0	760	713		2	15	226	221	11	11	76	96	7	-10	65	55	3	6	756	775	15	-7	144	137	9-14		194	186
5	-2	300	319		2	16	128	122	11	10	129	129	7	-12	65	67	3	5	319	326	14	-7	78	67	9-15		147	139
5	-3	71	80		2	17	274	266	11	8	248	248	7	-13	63	50	3	4	443	432	14	-6	122	118	9-16		85	83
5	-4	955	961		2	18	113	86	11	6	196	210	7	-14	108	102	3	3	188	183	14	-5	155	163	8-16		144	132
5	-5	312	312		1	16	67	80	11	5	293	294	7	-15	92	82	3	2	65	22	14	-4	141	154	8-15		70	37
5	-6	425	438		1	15	139	134	11	4	311	305	7	-16	178	181	3	1	109	98	14	-3	170	170	8-14		134	147
5	-7	134	124		1	14	113	115	11	3	121	139	7	-17	81	86	3	0	296	272	14	-2	111	129	8-13		110	106
5	-8	181	190		1	13	144	146	11	2	299	294	7	-18	81	90	3	-1	103	105	14	0	85	82	8-11		100	94
5	-9	125	127		1	12	225	226	11	1	152	152	6	-17	115	119	3	-2	780	754	14	2	124	135	8-10		194	197
5	-10	325	341		1	11	198	192	11	0	250	240	6	-14	93	94	3	-4	403	404	14	3	192	206	8	-8	137	132
5	-13	90	107		1	10	376	388	11	-1	214	207	6	-13	102	92	3	-5	197	193	14	4	180	168	8	-5	347	346
5	-14	160	178		1	9	128	144	11	-2	158	163	6	-12	234	245	3	-6	718	707	14	5	80	51	8	-4	418	425
4	-18	129	112		1	8	415	423	11	-3	96	78	6	-11	110	99	3	-8	825	818	14	7	74	65	8	-3	316	314
4	-17	131	126		1	7	213	229	11	-4	67	45	6	-10	71	56	3	-9	302	312	14	9	85	60	8	-2	70	87
4	-16	85	79		1	6	592	605	11	-5	167	174	6	-9	513	519	3	-10	247	252	14	10	84	70	8	-1	60	79

Table 2. Continued.

L	H		
K=	4		
8	2	331	325
8	3	296	291
8	4	153	145
8	5	131	136
8	6	69	70
8	7	417	428
8	8	252	246
8	10	102	103
8	11	99	95
8	12	180	169
8	13	245	250
8	14	335	328
8	15	144	156
8	16	88	87
8	17	90	72
7	15	110	100
7	14	154	164
7	13	207	202
7	12	150	141
7	11	172	187
7	10	159	155
7	9	356	360
7	8	342	359
7	7	252	238
7	6	397	392
7	5	204	203
7	4	133	130
7	3	124	139
7	2	297	272
7	1	178	165
7	0	181	178
7	-1	112	95
7	-2	126	121
7	-3	407	418
7	-4	318	301
7	-5	389	388
7	-6	220	225
7	-7	326	327
7	-9	403	406
7	-10	296	298
7	-11	225	225
7	-12	245	237
7	-13	86	86
7	-14	79	60
7	-16	88	84
7	-18	85	52
6	-17	148	133
6	-16	146	143
6	-14	99	99
6	-12	94	96
6	-11	307	319
6	-10	177	184
6	-9	84	100
6	-8	92	87
6	-7	259	254
6	-6	134	135
6	-5	348	343
6	-4	129	128
6	-3	110	113
6	-2	56	54
6	-1	259	259
6	0	533	516
6	1	495	486
6	2	749	733
6	3	78	74
6	4	526	547
6	5	99	111
6	6	209	212
6	7	299	300
6	8	87	75
6	10	72	64
6	12	147	138
6	13	78	45
6	16	203	201
6	17	163	165
6	18	181	171
5	18	103	95
5	17	174	175
5	16	165	174
5	15	112	105
5	13	215	222
5	12	225	231
5	11	397	391
5	10	272	282
5	9	227	245
5	6	139	137
5	6	134	123
5	4	396	396
5	3	96	88
5	2	136	139
5	1	381	363
5	0	761	724
5	-1	356	354
5	-2	285	279
5	-3	271	273
5	-4	199	206
5	-5	402	402
5	-6	585	587
5	-7	625	631
5	-8	207	217
5	-9	431	430
5	-12	68	42
5	-14	129	130
5	-17	105	103
5	-18	114	88
4	-15	223	224
4	-14	109	103
4	-13	89	91
4	-10	129	112
4	-9	195	207
4	-8	558	569
4	-7	526	520
4	-6	309	309
4	-5	177	182
4	-4	308	289
4	-3	437	420
4	0	93	96
4	1	53	15
4	2	462	470
4	3	605	597
4	4	444	434
4	5	177	200
4	6	88	96
4	7	119	128
4	8	370	381
4	9	194	200
4	10	210	213
4	11	372	389
4	13	95	95
4	15	71	81
4	17	69	43
3	19	81	77
3	17	93	100
3	16	137	126
3	15	194	197
3	14	218	235
3	13	129	139
3	12	134	148
3	10	213	230
3	9	171	183
3	8	103	115
3	6	77	76
3	5	579	593
3	4	293	316
3	3	1135	1167
3	2	865	837
3	1	606	577
3	0	290	290
3	-1	804	770
3	-2	436	412
3	-3	305	305
3	-4	828	792
3	-5	149	132
3	-6	340	331
3	-8	214	211
3	-9	198	211
3	-10	97	92
3	-11	59	59
3	-12	63	49
3	-13	249	255
3	-14	292	288
3	-15	167	177
3	-16	139	152
3	-17	159	147
3	-19	185	170
2	-19	79	76
2	-18	77	84
2	-16	78	87
2	-15	91	101
2	-14	175	183
2	-12	219	220
2	-11	255	259
2	-10	473	496
2	-9	359	353
2	-8	111	121
2	-7	345	334
2	-6	242	250
2	-5	368	371
2	-4	534	546
2	-3	983	947
2	-2	783	757
2	-1	183	165
2	0	46	30
2	1	366	328
2	2	236	237
2	3	346	364
2	4	357	370
2	5	287	279
2	6	439	463
2	7	423	452
2	8	479	503
2	9	315	334
2	10	152	165
2	12	162	166
2	13	330	342
2	14	202	217
2	15	161	168
2	16	179	183
2	18	71	34
1	19	122	119
1	18	167	166
1	17	74	72
1	16	214	219
1	12	94	95
1	11	152	168
1	10	171	184
1	9	265	274
1	8	590	622
1	7	857	907
1	6	619	662
1	5	774	812
1	4	571	591
1	3	368	389
1	2	64	76
1	-2	64	77
1	-3	67	67
1	-4	151	164
1	-5	167	187
1	-6	158	135
1	-7	186	198
1	-9	461	465
1	-10	434	431
1	-11	420	422
1	-12	306	317
1	-13	93	75
1	-14	199	187
1	-16	105	112
1	-17	124	136
1	-18	77	83
0	2	426	459
0	3	290	291
0	4	303	329
0	5	114	125
0	6	198	216
0	7	449	474
0	10	139	144
0	11	306	315
0	12	150	155
0	13	131	132
0	14	265	263
0	16	179	178
0	17	140	144
0	18	126	128
K=	5		
16	-4	80	47
16	-2	81	60
16	0	110	113
16	2	159	159
15	7	93	101
15	2	136	124
15	1	176	179
15	0	81	49
15	-5	153	151
15	-7	119	111
14	-10	76	83
14	-6	196	188
14	-5	94	76
14	-4	145	139
14	-3	82	96
14	-2	77	91
14	1	113	107
14	3	113	113
14	4	153	141
14	5	99	98
14	6	195	192
14	8	176	180
14	10	177	182
13	9	88	78
13	6	144	161
13	5	126	140
13	3	157	148
13	2	103	81
13	1	143	136
13	-1	251	259
13	-3	205	210
13	-6	105	102
13	-11	110	74
13-12		93	81
12-10		82	92
12	-9	78	54
12	-8	173	170
12	-7	77	78
12	-6	142	135
12	-5	72	58
12	-4	179	206
12	-3	97	104
12	-2	320	327
12	0	115	108
12	1	114	106
12	3	101	106
12	5	222	219
12	7	69	34
12	8	139	148
12	9	111	105
12	10	209	206
11	11	124	137
11	10	77	75
11	9	196	206
11	8	95	92
11	7	257	251
11	6	94	93
11	5	196	204
11	4	89	94
11	3	295	305
11	2	158	160
11	1	185	191
11	-2	153	150
11	-3	149	142
11	-4	84	73
11	-7	130	141
11	-9	216	200
11-11		91	100
11-12		88	94
10-14		114	114
10-12		79	42
10-10		92	84
10	-7	97	86
10	-6	140	140
10	-4	304	301
10	-3	132	138
10	-2	404	403
10	-1	178	181
10	0	409	402
10	1	118	118
10	2	415	416
10	3	110	114
10	4	157	154
10	5	94	104
10	6	91	100
10	8	123	132
10	10	91	74
10	12	126	130
10	13	79	66
10	14	94	56
10	15	86	78
9	15	73	59
9	13	211	215
9	12	80	87
9	11	233	225
9	10	97	96
9	9	136	147
9	7	270	270
9	5	514	515
9	4	180	195
9	2	254	254
9	1	237	240
9	0	81	88
9	-1	243	261
9	-2	204	210
9	-3	176	175
9	-4	239	244
9	-5	184	179
9	-6	106	106
9	-7	153	144
9	-8	125	114
9	-9	83	55
9-11		145	140
9-12		69	74
9-13		145	146
9-15		71	55
9-16		119	119
8-15		94	90
8-14		174	182
8-12		345	348
8-10		177	173
8	-9	91	74
8	-8	79	88
8	-6	296	296
8	-5	298	305
8	-3	178	179
8	-2	169	161
8	-1	242	238
8	0	100	102
8	1	226	231
8	2	116	111
8	3	73	74
8	4	496	494
8	6	592	603
8	8	351	358
8	9	122	123
8	10	174	172
8	12	89	99
8	13	87	81
8	15	129	119
8	16	120	98
8	17	70	58
7	15	205	209
7	13	193	185
7	12	122	111
7	11	66	75
7	10	121	119
7	9	103	109
7	6	135	126
7	5	250	260
7	4	104	99
7	3	227	218
7	2	206	203
7	1	282	274
7	0	116	134
7	-1	625	614
7	-2	422	411
7	-3	405	395
7	-4	162	162
7	-5	210	214
7	-6	311	308
7	-7	240	248
7	-9	165	157
7-10		113	116
7-11		217	224
7-13		270	270
7-15		96	83
7-17		68	63
6-16		109	98
6-14		77	71
6-13		138	143
6-12		85	82
6-11		86	84
6-10		239	238
6	-9	93	88
6	-6	469	467
6	-6	431	450
6	-5	271	266
6	-4	437	446
6	-2	340	325
6	-1	154	151
6	0	219	213
6	1	217	209
6	2	100	98
6	4	65	53
6	5	97	93
6	6	157	164
6	7	157	164
6	8	482	488
6	9	144	139
6	10	443	457
6	11	100	109
6	12	194	182
6	13	154	156
6	14	146	157
6	15	93	98
6	16	177	166
5	17	146	142
5	16	163	157
5	15	89	86
5	13	78	36
5	12	180	177
5	11	132	139
5	10	96	89
5	9	368	389
5	8	221	233
5	7	195	192
5	6	177	182
5	5	363	357
5	3	474	465
5	2	340	333
5	1	701	674
5	0	108	71
5	-1	250	249
5	-2	379	375
5	-4	172	171
5	-5	72	60
5	-6	149	147
5	-7	56	39
5	-8	167	175
5	-9	368	370
5-10		133	145
5-11		244	244
5-12		86	82
5-13		157	149
5-15		141	132
5-16		71	69
5-17		87	84
5-18		79	63
4-18		101	100
4-16		147	154
4-15		82	82
4-14		69	91
4-12		75	92
4-11		74	62
4-10		163	164
4	-9	264	259
4	-7	119	125
4	-6	559	546
4	-5	99	94
4	-4	753	729
4	-2	551	539
4	-1	146	178
4	0	976	918
4	1	118	102
4	2	433	434
4	4	136	138
4	5	186	180
4	7	254	269
4	9	77	76
4	10	199	195
4-11		219	220
4-12		254	263
4-13		83	72
4-14		130	140
4-15		90	82
4-16		124	121
4-18		221	208
4-19		90	92
3-19		72	11
3-16		103	102
3-13		248	263
3-11		298	307
3-10		69	56
3	9	83	80
3	8	279	292
3	7	457	482
3	6	172	165
3	5	627	626
3	4	139	143
3	3	274	273
3	2	59	53
3	1	359	352
3	0	484	443
3	-1	372	366
3	-2	277	257
3	-3	393	389
3	-4	244	238
3	-5	504	502
3	-6	73	91
3	-7	210	215
3	-8	89	86
3	-9	172	179
3-10		91	97
3-11		264	270
3-12		135	139
3-13		197	196
3-14		101	114
2-18		147	134
2-17		75	59
2-16		118	113
2-15		109	109
2-14		268	273
2-13		121	138
2-12		425	443
2-11		61	16
2-10		281	280
2	-9	453	465
2	-8	130	144
2	-7	119	104
2	-6	84	98
2	-5	382	377
2	-3	502	469
2	-2	730	713
2	-1	292	293
2	0	436	413
2	1	139	125
2	2	494	500
2	3	451	476
2	4	772	806
2	5	245	255
2	6	1097	1173
2	7	162	149
2	8	333	362
2	9	108	107
2	10	70	76
2	12	90	95
2	16	147	147
2	18	81	69
1	17	113	112
1	16	92	110
1	15	256	261
1	13	224	236
1	12	140	150
1	11	398	423
1	10	59	65
1	9	342	366
1	8	276	283
1	7	101	104
1	6	113	122
1	5	107	111
1	4	394	416
1	3	71	78
1	2	219	207
1	-2	134	135
1	-3	591	699
1	-4	91	79
1	-5	143	159
1	-6	195	218
1	-7	473	467
1	-8	179	181
1	-9	312	325
1-10		289	300
1-12		267	269
1-13		204	212
1-14		108	102
1-15		94	75
1-17		112	100
1-19		167	149
0	2	140	152
0	3	171	172
0	4	77	104
0	5	333	329
0	6	478	495
0	8	633	638
0	9	215	227
0	10	354	378
0	12	185	165
0	13	171	192
0	14	177	176
0	16	91	92
K=	6		
14	-2	107	93
14	0	138	156
13	6	101	88
13	5	74	72
13	4	100	53
13	3	134	116
13	-2	85	62
13	-4	165	179
13	-5	136	130
13	-6	78	61
12	-9	140	150
12	-8	114	101
12	-6	76	86
12	-4	179	181
12	-2	98	108
12	-1	91	92
12	0	79	31
12	2	194	204
12	4	310	322
12	5	156	171
12	7	73	79
11	8	75	66
11	7	163	158
11	5	154	143
11	3	207	208
11	1	69	45
11	0	121	131
11	-1	79	76
11	-2	215	235
11	-3	354	364
11	-4	103	106
11	-5	302	304
11-10		102	96
10-10		187	197
10	-7	202	205
10	-6	90	75
10	-5	174	175
10	-4	299	302
10	-3	189	206
10	-1	71	66
10	0	173	161
10	2	67	57
10	4	80	71
10	5	124	135
10	6	236	240
10	7	197	187
10	8	349	363
10	9	117	135
10	11	86	93
10	12	90	84
9	11	107	108
9	8	86	71
9	7	379	366
9	6	164	163
9	5	153	157
9	4	151	143
9	3	143	155
9	2	87	80
9	1	373	371
9	0	196	197
9	-1	409	402
9	-2	163	166
9	-4	110	106
9	-5	83	72
9	-7	150	154
9	-8	93	84
9	-9	157	158
9-11		195	200
8-11		104	116
8-9		76	65
8-8		165	160
8-7		130	133
8-6		239	231
8-5		169	170
8-4		104	105
8-3		196	189
8-2		251	249
8-1		308	313
8	0	374	377
8	1	210	211
8	3	191	195
8	4	192	188
8	7	143	131
8	9	97	109
8	10	340	341
8	11	139	140
8	12	155	162
8	13	86	81
7	11	278	291
7	10	113	122
7	9	343	339
7	8	314	324
7	7	223	215
7	6	342	349
7	5	208	206
7	3	251	237
7	2	18	18
7	-1	179	187
7	-5	186	187
7	-6	150	146
7	-7	307	310
7	-9	281	284
7-10		74	88
7-11		96	73
7-12		197	204
7-13		167	169
6-14		277	300
6-15		151	155
6-12		102	86
6-11		187	200
6-10		61	72
6	-9	150	150
6	-8	74	88
6	-7	122	123
6	-6	100	114
6	-5	195	192
6	-4	340	336
6	-3	220	222
6	-2	461	448
6	-1	324	312
6	0	204	206
6	1	184	181
6	2	517	500
6	3	87	90
6	4	407	410
6	7	340	372
6	8	83	85
6	9	158	160
6	10	74	61
6	13	100	97
6	14	240	234
6	15	113	105
5	15	203	215
5	14	140	133
5	13	217	219
5	12	94	111
5	11	71	95
5	10	142	147
5	9	294	309
5	8	86	73
5	7	400	406
5	6	85	89
5	4	177	171
5	3	570	563
5	2	77	78
5	1	198	174
5	0	276	265
5	-1	77	73
5	-2	507	486
5	-3	827	804
5	-4	352	363
5	-5	384	384
5	-6	273	271
5	-8	187	181
5	-9	196	204
5	-11	315	318

Table 2. Continued.

L	H		
K=	6		
5	-13	64	59
5	-15	99	103
4	-16	80	49
4	-15	105	103
4	-13	127	127
4	-12	296	299
4	-11	308	318
4	-10	321	314
4	-7	174	172
4	-5	207	222
4	-4	310	297
4	-3	147	209
4	-2	202	196
4	-1	219	215
4	0	462	430
4	1	359	345
4	2	267	263
4	3	512	495
4	4	56	21
4	5	188	196
4	6	339	341
4	7	179	184
4	8	319	329
4	9	216	219
4	10	149	169
4	11	181	176
4	12	74	83
4	13	66	78
4	14	160	185
4	16	81	51
3	14	87	70
3	11	190	201
3	10	204	219
3	9	63	81
3	7	283	307
3	6	158	171
3	5	342	342
3	3	244	251
3	2	316	317
3	1	761	735
3	0	350	333
3	-1	710	667
3	-2	203	193
3	-3	375	373
3	-4	209	211
3	-5	115	118
3	-6	186	180
3	-7	117	140
3	-8	76	84
3	-9	137	140
3	-11	255	273
3	-12	171	185
3	-13	76	85
3	-14	69	82
3	-15	82	104
3	-16	92	99
2	-14	121	131
2	-12	112	122
2	-10	64	55
2	-9	228	238
2	-8	433	446
2	-6	378	373
2	-5	289	289
2	-3	349	345
2	-2	365	368
2	-1	312	311
2	0	694	677
2	1	387	374
2	3	71	75
2	4	371	388
2	5	103	98
2	8	106	104
2	9	364	394
2	10	475	489
2	11	203	197
2	12	231	241
2	13	127	143
2	14	66	72
1	16	108	119
1	11	415	436
1	10	161	165
1	9	557	570
1	8	283	303
1	6	63	63
1	5	375	382
1	4	253	263
1	3	627	665
1	2	70	77
1	-2	92	95
1	-3	146	132
1	-4	319	315
1	-5	143	150
1	-6	195	196
1	-7	499	503
1	-8	66	60
1	-9	282	303
1	-10	235	251
1	-11	181	198
1	-12	222	240
1	-13	251	248
1	-14	102	135
1	-15	164	178
0	2	400	418
0	3	275	292
0	4	421	438
0	5	97	99
0	7	190	182
0	8	264	271
0	9	129	124
0	10	95	106
0	11	211	211
0	12	154	147
0	13	102	121
0	14	219	219
0	15	138	127
0	16	112	108
0	17	102	101
K=	7		
13	-4	156	170
13	-1	108	113
13	0	82	93
13	2	174	181
13	4	108	112
13	5	100	114
12	8	92	86
12	7	141	129
12	6	77	33
12	5	180	161
12	1	125	123
12	-1	91	63
12	-3	124	138
12	-5	332	336
12	-7	120	108
11	-7	76	54
11	-6	249	248
11	-4	150	136
11	-2	121	135
11	-1	93	92
11	1	67	74
11	2	122	123
11	4	209	215
11	6	261	262
11	7	133	109
10	9	147	151
10	8	95	77
10	6	82	43
10	5	219	222
10	3	175	175
10	2	104	113
10	1	172	177
10	0	90	92
10	-1	153	161
10	-3	227	224
10	-4	141	141
10	-5	87	83
10	-6	111	120
10	-7	78	61
10	-9	101	110
10	-11	76	83
9	-10	145	141
9	-8	347	342
9	-7	75	75
9	-6	134	140
9	-5	148	141
9	-4	285	281
9	-2	339	341
9	-1	143	135
9	0	160	160
9	1	123	112
9	7	73	89
9	8	322	319
9	10	299	307
9	11	104	90
8	12	98	89
8	9	334	332
8	7	206	207
8	6	100	104
8	5	73	58
8	4	75	101
8	3	367	352
8	2	122	124
8	1	411	398
8	0	96	109
8	-1	90	75
8	-2	211	205
8	-3	86	86
8	-4	67	63
8	-5	91	89
8	-6	144	148
8	-7	78	70
8	-9	266	279
8	-11	107	102
8	-12	91	86
7	-12	69	19
7	-11	94	91
7	-10	104	92
7	-9	120	102
7	-6	212	203
7	-5	149	157
7	-4	301	293
7	-3	204	193
7	-2	236	233
7	-1	377	370
7	0	264	257
7	1	61	55
7	2	514	506
7	3	108	98
7	4	84	93
7	5	135	123
7	6	83	66
7	7	95	100
7	8	112	99
7	9	163	158
7	11	73	75
7	12	225	224
7	14	116	126
6	13	266	269
6	11	221	222
6	10	123	128
6	9	140	134
6	8	171	167
6	7	238	238
6	5	379	374
6	2	114	112
6	1	261	262
6	-2	198	197
6	-3	380	374
6	-5	265	256
6	-6	139	139
6	-7	163	168
6	-8	123	115
6	-9	116	106
6	-10	121	119
6	-11	172	175
6	-12	104	94
6	-13	133	123
6	-15	117	125
5	-14	179	176
5	-13	102	74
5	-12	326	331
5	-10	182	176
5	-9	140	133
5	-8	203	215
5	-6	194	197
5	-5	72	79
5	-4	82	74
5	-3	82	82
5	-2	474	461
5	-1	143	143
5	0	285	276
5	1	202	204
5	3	106	122
5	4	539	537
5	5	79	80
5	6	426	434
5	7	215	214
5	8	180	187
5	9	65	72
5	11	72	53
5	12	128	124
5	13	107	100
4	15	233	233
4	14	70	76
4	13	119	98
4	12	150	148
4	11	147	144
4	10	146	141
4	9	199	200
4	8	179	185
4	7	118	120
4	6	185	190
4	5	271	276
4	3	332	328
4	2	165	156
4	0	65	61
4	-1	721	696
4	-3	439	426
4	-4	139	132
4	-6	221	222
4	-7	62	67
4	-8	110	98
4	-9	171	168
4	-10	106	106
4	-13	180	188
4	-14	87	74
4	-16	98	78
3	-16	112	107
3	-15	82	56
3	-14	111	99
3	-13	85	70
3	-11	153	154
3	-10	272	285
3	-8	454	448
3	-7	135	130
3	-6	323	322
3	-5	228	233
3	-4	186	190
3	-3	68	62
3	-2	508	496
3	-1	160	161
3	0	69	64
3	2	292	291
3	5	194	211
3	6	135	138
3	7	79	102
3	8	491	513
3	10	412	431
3	11	132	136
3	12	165	164
3	13	117	115
3	14	103	87
3	16	124	126
2	13	117	125
2	10	137	151
2	9	262	275
2	8	247	262
2	6	168	175
2	4	64	60
2	3	603	606
2	2	98	114
2	1	700	669
2	-1	159	169
2	-2	142	141
2	-3	112	125
2	-5	229	231
2	-6	135	146
2	-7	122	128
2	-8	95	103
2	-9	353	347
2	-11	88	76
2	-12	176	191
2	-13	102	115
2	-15	224	228
1	-16	141	159
1	-14	135	129
1	-12	100	99
1	-11	65	64
1	-9	222	228
1	-7	55	51
1	-6	529	541
1	-5	57	65
1	-4	275	268
1	-3	159	157
1	-2	194	204
1	2	616	625
1	3	130	151
1	4	347	376
1	5	80	93
1	6	211	221
1	10	194	196
1	12	328	323
1	14	113	103
1	15	86	86
0	13	173	173
0	11	373	384
0	10	186	186
0	9	240	244
0	8	131	131
0	7	380	391
0	5	413	430
0	4	192	197
0	3	73	87
0	2	373	391
K=	8		
12	-1	162	160
12	1	207	200
11	2	175	184
11	0	218	221
11	-3	68	53
11	-5	101	101
10	-7	289	283
10	-5	136	137
10	-4	102	103
10	-2	149	134
10	-1	68	57
10	3	175	167
10	5	108	114
10	8	72	61
9	7	120	118
9	4	260	260
9	3	70	44
9	2	340	335
9	1	95	94
9	0	123	112
9	-2	172	176
9	-3	138	131
9	-4	159	156
9	-6	93	85
8	-9	148	142
8	-8	155	158
8	-7	139	129
8	-6	136	142
8	-5	210	199
8	-3	383	376
8	-1	190	187
8	0	305	301
8	1	206	202
8	2	59	42
8	3	245	247
8	6	73	65
8	7	161	153
8	9	130	120
8	10	102	110
7	10	76	50
7	9	96	68
7	8	247	245
7	6	305	300
7	4	288	278
7	3	146	148
7	2	159	160
7	1	65	84
7	-1	212	198
7	-1	159	157
7	-2	66	71
7	-3	166	163
7	-4	215	213
7	-5	69	74
7	-7	104	100
7	-8	128	121
7	-10	252	247
7	-11	94	92
6	-11	206	211
6	-10	68	86
6	-9	126	135
6	-8	66	56
6	-7	123	114
6	-6	117	117
6	-5	56	54
6	-4	113	101
6	-2	100	102
6	-1	397	369
6	0	71	70
6	1	243	235
6	2	152	136
6	3	174	169
6	4	213	214
6	5	383	382
6	7	291	291
6	10	72	42
6	11	157	153
6	12	85	92
5	12	214	225
5	10	220	213
5	7	108	124
5	5	93	74
5	4	209	207
5	3	179	184
5	2	121	108
5	1	75	72
5	0	512	490
5	-2	276	261
5	-3	149	143
5	-4	101	88
5	-5	85	75
5	-6	295	287
5	-8	252	251
5	-13	73	74
4	-13	254	248
4	-12	71	66
4	-11	127	123
4	-10	95	89
4	-9	246	247
4	-8	89	104
4	-7	380	381
4	-6	119	123
4	-5	171	164
4	-4	184	169
4	-3	85	69
4	-2	115	117
4	-1	59	51
4	0	100	97
4	1	69	70
4	2	94	88
4	3	389	379
4	5	551	563
4	6	256	271
4	7	269	283
4	8	67	45
4	9	239	245
4	10	61	11
4	11	192	197
4	12	81	74
3	12	90	66
3	11	99	81
3	10	92	84
3	9	75	69
3	6	60	47
3	4	487	480
3	2	323	314
3	1	335	321
3	0	85	75
3	-1	103	102
3	-2	148	130
3	-4	285	276
3	-5	68	59
3	-6	254	255
3	-7	52	56
3	-9	145	154
3	-11	99	101
3	-12	131	130
3	-14	204	209
2	-14	93	94
2	-13	85	87
2	-11	102	107
2	-10	126	141
2	-9	163	154
2	-8	140	149
2	-7	340	334
2	-6	157	154
2	-5	438	626
2	-3	446	434
2	-1	56	57
2	0	293	280
2	1	80	84
2	2	209	219
2	3	279	282
2	4	180	182
2	6	103	87
2	7	302	314
2	9	131	138
2	10	166	162
2	11	165	169
2	12	77	82
2	13	177	182
1	12	87	81
1	11	66	69
1	8	263	271
1	6	450	441
1	5	146	159
1	4	136	143
1	3	145	139
1	2	339	350
1	-2	69	76
1	-3	103	94
1	-4	268	274
1	-5	116	106
1	-6	214	221
1	-7	286	295
L'	H		
1	-8	185	190
1	-9	80	73
1	-10	277	284
1	-11	63	29
1	-12	129	130
1	-13	83	110
0	2	170	146
0	3	193	197
0	4	202	227
0	5	227	220
0	7	302	309
0	8	120	134
0	10	73	50
0	11	155	162
0	12	93	91
K=	9		
11	-5	97	89
11	0	94	86
11	1	90	102
11	2	111	114
11	3	100	98
11	4	94	97
10	6	86	70
10	5	77	69
10	4	90	89
10	3	107	106
10	2	204	199
10	1	82	83
10	0	169	160
10	-1	91	90
10	-4	128	129
10	-5	74	97
10	-6	183	177
10	-7	99	95
10	-8	150	149
9	-8	167	161
9	-7	129	127
9	-6	200	199
9	-5	277	274
9	-4	90	102
9	-3	77	78
9	-1	80	84
9	1	90	82
9	5	125	124
9	7	91	78
8	8	66	5
8	7	85	85
8	6	257	256
8	5	89	113
8	4	220	223
8	3	145	139
8	2	60	66
8	1	175	169
8	0	107	107
8	-1	173	165
8	-2	60	55
8	-3	81	83
8	-5	64	25
8	-6	188	183
8	-7	101	82
8	-8	87	87
8	-9	74	54
8	-10	73	83
7	-9	88	78
7	7	87	92
7	-4	139	135
7	-3	194	187
7	-2	132	106
7	-1	360	354
7	0	200	191
7	1	105	111
7	2	204	197
7	3	105	99
7	4	130	126
7	5	261	270
7	9	133	124
7	11	68	30
6	10	148	140
6	9	88	82
6	8	251	249
6	7	128	128
6	6	85	65
6	5	144	143
6	4	84	87
6	3	89	90
6	2	250	247
6	1	53	66
6	0	87	92
6	-1	173	176
6	-2	253	248
6	-3	61	56
6	-4	57	69
6	-6	118	113
6	-7	100	71
6	-8	180	175
6	-9	97	112
6	-10	156	142
6	-11	114	103
6	-12	81	79
5	-12	91	90
5	-10	142	146
5	-9	191	193
5	-8	156	142
5	-7	153	143
5	-4	179	176
5	-2	48	53
5	-1	184	187
L	-		
5	1	440	410
5	2	306	288
5	3	305	294
5	4	208	201
5	5	97	88
5	6	202	202
5	7	237	240
5	8	174	172
5	9	193	193
5	11	83	66
5	13	134	116
4	13	142	129
4	12	210	208
4	11	98	97
4	9	70	46
4	3	159	153
4	2	394	383
4	1	180	179
4	0	165	149
4	-2	56	55
4	-3	172	163
4	-4	404	392
4	-5	167	163
4	-6	202	200
4	-7	163	152
4	-8	50	40
4	-9	64	55
3	-13	144	141
3	-12	129	107
3	-11	155	166
3	-10	130	122
3	-8	202	197
3	-7	182	179
3	-6	230	230
3	-5	430	414
3	-4	172	154
3	-3	50	67
3	-1	83	75
3	1	205	206
3	2	107	88
3	3	144	126
3	4	54	65
3	5	322	323
3	6	105	106
3	7	169	150
3	8	183	180
3	10	184	187
3	11	121	122
3	12	84	83
3	13	214	212
3	14	152	146
2	14	160	142
2	13	75	50
2	12	66	58
2	8	54	68
2	6	304	329
2	5	179	185
2	4	261	262
2	3	179	182
2	2	119	114
2	1	108	101
2	-1	102	96
2	-2	293	294
2	-3	157	156
2	-6	221	216
2	-7	69	71
2	-10	101	113
2	-11	114	100
2	-12	194	201
1	-14	69	28
1	-13	91	86
1	-12	80	64
1	-11	93	107
1	-10	123	101
1	-9	186	191
1	-8	119	125
1	-7	133	130
1	-6	136	116
1	-5	134	125
1	-4	285	282
1	-3	557	564
1	-2	254	252
1	2	175	186
1	3	45	55
1	4	147	140
1	5	143	150
1	6	111	97
1	8	97	94
1	10	204	209
1	10	54	42
1	11	58	30
1	14	83	99
0	14	64	63
0	13	87	33
0	10	161	156
0	9	160	157
0	8	281	298
0	7	173	183
0	6	55	43
0	5	167	176
0	4	317	317
0	3	120	121
0	2	319	346

eter shifts were less than 16 % of their corresponding standard deviations. The R-value was now 0.043.

The decrease in the R-value from 0.049 to 0.043 was shown, using the Pawley (1970)[15] simplification of the method proposed by Hamilton,[16] to be significant with a probability greater than 99 %. The R-ratio is 1.140 and should be compared with the calculated ratio $\mathcal{R}_{56,2777,\,0.01} = 1.015$. The indices 56, 2777 and 0.01 refer to the dimension of the hypothesis, the number of degrees of freedom, and the significance level, respectively.

A final difference Fourier map was calculated and no abnormalities could be detected in it. Lists of the final positional and thermal parameters are given in Tables 1a and 1b. The observed and calculated structure factors are given in Table 2.

DESCRIPTION AND DISCUSSION OF THE STRUCTURE

The coordination around the copper atom is a distorted octahedron. One bond is formed to the oxygen [O(5)] of the water molecule, and *trans* to it is a bond to an oxygen [O(3)] of a sulphate group. The remaining four bonds are to nitrogens of the imidazole rings and to an oxygen [O(2)] in a second, symmetry-related sulphate group. Thus infinite chains are formed with the sulphate group bridging successive copper atoms (Fig. 2). The chains run in the b-direction along the two-fold screw axes. The symmetry-related chains are held together by hydrogen bonds and van der Waals forces.

Table 3. Bond lengths and bond angles, and their estimated standard deviations, for the atoms around copper.

Bond length (Å)		Angle (°)	
Cu–N1	1.999(3)	N1–Cu–N3	178.1(1)
Cu–N3	2.002(3)	N5–Cu–O2	176.7(1)
Cu–N5	1.995(3)	O3–Cu–O5	177.6(1)
Cu–O2	2.015(2)	N1–Cu–N5	89.9(1)
Cu–O3	2.578(2)	N5–Cu–N3	91.4(1)
Cu–O5	2.478(3)	N1–Cu–O2	88.2(1)
		N3–Cu–O2	90.6(1)
		O2–Cu–O3	88.1(1)
		O3–Cu–N5	89.2(1)
		O2–Cu–O5	93.0(1)
		N5–Cu–O5	89.9(1)
		O3–Cu–N1	90.2(1)
		O3–Cu–N3	91.2(1)
		O5–Cu–N1	92.0(1)
		O5–Cu–N3	86.7(1)

The coordination around copper. The copper atom is surrounded by three nitrogens and three oxygens. The arrangement is shown in Fig. 1 and distances and angles are given in Table 3. The mean of the three equatorial bond lengths for Cu–N is 1.999(3) Å, which is normal.[1-5] All the Cu–N bonds are within two standard deviations of this value. The fourth equatorial bond Cu–O(2) is 2.015(2) Å long. Of the three imidazole rings one ring is almost coplanar with the coordination plane around copper (counting the atoms N(1), N(3), N(5), O(2), and Cu), one is almost perpendicular to that plane and the third deviates about 45°. Apparently this does not produce any significant differences in the copper-nitrogen bond lengths. The apical bond

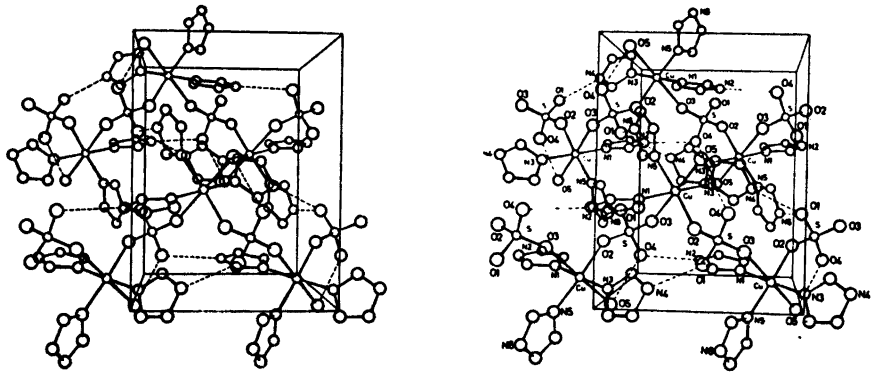

Fig. 2. A stereoscopic illustration of the molecular packing of $[Cu(H_2O)(C_3H_4N_2)_3SO_4]$, viewed along the a-axis. The parenthesis around the numbers are omitted in the figure.

length Cu – O(3) is 2.578(3) Å, which is in good agreement with a recent determination[3] [2.574(4) Å] for a bond between copper and a sulphate oxygen, but much longer than the average 2.41 Å in the same kind of bond in $CuSO_4.5H_2O$.[17] The other apical bond Cu – O(5) is 2.478(3) Å long, which is in good agreement with the range for a copper-water oxygen separation tabulated by Blount *et al.*,[18] but much longer than the 2.19 Å found in $(NH_4)_2Cu(SO_4)_2.6H_2O$,[19] where water oxygens are also in the apical positions in the coordination octahedron around copper. With these four short and two long bond distances the octahedron is seen to be distorted as expected.[20] The octahedron is also angularly distorted which is shown from significant differences for almost all of the angles compared to the ideal ones. The greatest difference is 3.3(1)° [O(5) – Cu – N(3)].

The sulphate group. In the sulphate group the oxygens are arranged in a tetrahedron which is nearly ideal, although three of the six tetrahedral angles differ significantly from the ideal one. The deviations are 1.7(2)° for [O(1) – S – O(2)]; 0.9(2)° for [O(1) – S – O(3)], and 1.0(2)° for [O(2) – S – O(3)]. The differences in sulphur-oxygen bond lengths do not seem to depend on whether the oxygen atoms are coordinated to a copper atom or not.

Bond distances and angles are given in Table 4. The sulphur-oxygen bond distances are in good agreement with those given in the recent tabulation by Andreetti, Cavalca and Musatti.[21]

Water and hydrogen bonds. The distances of the water hydrogens to the water oxygens are 0.96(6) Å for H(13) and 0.87(6) Å for H(14). This is longer than expected when a comparison is made with similar bonds in $MoO_3.2H_2O$,[22] where the range of distances in sixteen O – H bonds is 0.69(5) – 0.84(5) Å, considering that both determinations are from X-ray data. The O – H distances in $CuSO_4.5H_2O$ [17] calculated from neutron diffraction data have a mean value of 0.96 Å and our values should therefore show a reasonable shortening of at least 0.1 Å.[23]

Table 4. Bond lengths and bond angles, and their estimated standard deviations, for the sulphate group.

Bond lengths (Å)		Angle (°)	
S – O1	1.473(3)	O1 – S – O2	107.8(2)
S – O2	1.480(3)	O1 – S – O3	110.4(2)
S – O3	1.457(3)	O1 – S – O4	109.5(2)
S – O4	1.489(3)	O2 – S – O3	110.5(2)
		O2 – S – O4	109.3(2)
		O3 – S – O4	109.5(2)

It seems possible that the distances found in this determination depend on the oxygen coordination to copper and the two hydrogen bonds formed to sulphate oxygens. These hydrogen bond lengths are [O(4)···H(13) – O(5)] = 2.813(4) Å and [O(4)···H(14) – O(5)] = 2.776(4) Å and the deviation of the bonds is such that the angle H(13) – O(5) – H(14) is 97 (5)° which is smaller than those in $MoO_3 \cdot 2H_2O$ [mean value 109(6)°].

The hydrogen atoms on the imidazole nitrogens also take part in a hydrogen bonding scheme. The acceptor atoms are sulphate oxygens which are not copper-coordinated. Hydrogen bonds within the symmetry-related chains are [N(2) – H(4)···O(4)] = 2.847(4) Å, [N(4) – H(8)···O(1)] = 2.871(4) Å and [O(5) – H(14)··· O(4)] = 2.776(4) Å. Those between the chains are [N(6) – H(12)···O(1)] = 2.762(4) Å and [O(5) – H(13)···O(4)] = 2.813(4) Å. No significant difference of the hydrogen bond distances between N – O and O – O can be seen. All hydrogen bond lengths are of the same magnitude as those found in similar structures.[3,4]

The imidazole rings. Interatomic distances and angles for the imidazole rings are given in Table 5. Considering the standard deviations there are no significant differences in the bond distances and angles for the three rings. Bond distances and angles between carbons and nitrogens are also about the same as those found in other structure determinations.[1–5] The bond distance range for hydrogens to carbons and nitrogens is 0.81(5) Å to 0.96(5) Å. Planes through the positions of the nitrogen and carbon atoms in respective imidazole rings were calculated and have the equations

1. $0.2334\,x + 0.0764\,y - 0.9694\,z + 0.2486 = 0$ [N(1), N(2), C(1), C(2), C(3)]
2. $0.7265\,x - 0.4784\,y - 0.4933\,z + 1.7762 = 0$ [N(3), N(4), C(4), C(5), C(6)]
3. $-0.4940\,x - 0.8414\,y - 0.2192\,z - 3.4449 = 0$ [N(5), N(6), C(7), C(8), C(9)]

The maximum deviations of non-hydrogen atoms from the planes are 0.001 Å, 0.004 Å, and 0.003 Å for the first, second, and third imidazole

Table 5. Bond lengths and bond angles, and their estimated standard deviations, for the imidazole rings.

Bond length (Å)		Angle (°)	
N1–C1	1.313(5)	C3–N1–C1	105.9(3)
N1–C3	1.367(5)	N1–C1–N2	110.7(3)
N2–C1	1.337(5)	C1–N2–C2	107.8(3)
N2–C2	1.357(6)	N2–C2–C3	106.1(3)
C2–C3	1.347(6)	C2–C3–N1	109.5(3)
N3–C4	1.321(5)	C6–N3–C4	105.0(3)
N3–C6	1.381(5)	N3–C4–N4	111.5(3)
N4–C4	1.337(5)	C4–N4–C5	107.3(3)
N4–C5	1.369(5)	N4–C5–C6	106.3(4)
C5–C6	1.342(6)	C5–C6–N3	109.9(3)
N5–C7	1.319(5)	C9–N5–C7	106.7(3)
N5–C9	1.377(5)	N5–C7–N6	110.2(3)
N6–C7	1.340(5)	C7–N6–C8	108.2(3)
N6–C8	1.361(6)	N6–C8–C9	106.4(3)
C8–C9	1.358(6)	C8–C9–N5	108.6(3)
H1–C1	0.94(5)	H1–C1–N1	127.1(32)
H2–C2	0.92(6)	H1–C1–N2	122.2(32)
H3–C3	0.94(5)	H2–C2–N2	122.2(41)
H4–N2	0.81(5)	H2–C2–C3	131.5(40)
H5–C4	0.89(5)	H3–C3–N1	119.1(28)
H6–C5	0.95(5)	H3–C3–C2	131.2(28)
H7–C6	0.96(5)	H4–N2–C1	128.8(36)
H8–N4	0.90(5)	H4–N2–C2	123.4(36)
H9–C7	0.96(5)	H5–C4–N3	121.2(34)
H10–C8	0.95(5)	H5–C4–N4	126.7(34)
H11–C9	0.87(4)	H6–C5–N4	126.4(33)
H12–N6	0.92(5)	H6–C5–C6	127.2(34)
		H7–C6–C5	128.6(26)
		H7–C6–N3	121.4(26)
		H8–N4–C4	122.3(31)
		H8–N4–C5	130.1(31)
		H9–C7–N5	124.9(29)
		H9–C7–N6	124.4(29)
		H10–C8–N6	122.2(33)
		H10–C8–C9	131.4(33)
		H11–C9–C8	128.0(30)
		H11–C9–N5	123.2(29)
		H12–N6–C7	122.5(29)
		H12–N6–C8	129.2(29)

rings, respectively. The corresponding maximum deviations of hydrogens are 0.06 Å [H(3)], 0.12 Å [H(5)], and 0.11 Å [H(9)] Å, respectively. None of these hydrogen atoms is involved in hydrogen bonds.

Conclusions. This structure determination has shown that when the anion is sulphate and the ratio of imidazole to copper is 3:1 the coordination around copper in the equatorial plane is formed by three imidazole nitrogens and a sulphate oxygen. The water molecule can thus not compete with the oxygen of the anion. We think that the systematic change of anions and different ratios of imidazole to copper will show (as described in the introduction) differences in coordination of the anions to copper. This in turn will provide us with more variations in copper-imidazole interactions than has hitherto been found.

Acknowledgements. We thank Professor Nils Ingri for his great interest and for the facilities placed at our disposal. The English of the paper has been corrected by Dr. Michael Sharp. This work has been financially supported by the Swedish Natural Science Research Council.

REFERENCES

1. Lundberg, B. K. S. *Acta Chem. Scand. 26* (1972) 3902.
2. Lundberg, B. K. S. *Acta Chem. Scand. 26* (1972) 3977.
3. Fransson, G. and Lundberg, B. K. S. *Acta Chem. Scand. 26* (1972) 3969.
4. Ivarsson, G., Lundberg, B. K. S. and Ingri, N. *Acta Chem. Scand. 26* (1972) 3005.
5. Ivarsson, G. *Acta Chem. Scand. 27* (1973) 3523.
6. Sjöberg, S. *Acta Chem. Scand. 25* (1971) 2149.
7. Sjöberg, S. *Acta Chem. Scand. 26* (1972) 3400.
8. Sjöberg, S. *Acta Chem. Scand. 27* (1973) 3721.
9. Kolthoff, I. M., Sandell, E. B., Meehan, E. J. and Bruckenstein, S. *Quantitative Chemical Analysis*, 4th Ed., Macmillan, London 1969, pp 744–747.
10. Kjeldahl, J. *Z. anal Chem 22* (1883) 366.
11. *International Tables for X-Ray Crystallography*, Kynoch Press, Birmingham 1965, Vol. 1.
12. Cruickshank, D. W. J. *Computing Methods in Crystallography*, Pergamon, London 1965, p. 114.
13. Stewart, R. F., Davidson, E. R. and Simpson, W. T. *J. Chem. Phys. 42* (1965) 3175.
14. *International Tables for X-Ray Crystallography*, Kynoch Press, Birmingham, 1962 Vol. III.
15. Pawley, G. S. *Acta Crystallogr. A 26* (1970) 691.
16. Hamilton, W. C. *Acta Crystallogr. 18* (1965) 502.
17. Bacon, G. E. and Curry, N. A. *Proc. Roy. Soc. (London) A 266* (1962) 95.
18. Blount, J. F., Fraser, K. A., Freeman, H. C., Szymanski, J. T. and Wang, C.-H. *Acta Crystallogr. 22* (1967) 396.
19. Webb, M. W., Kay, H. F. and Grimes, N. W. *Acta Crystallogr. 18* (1965) 740.
20. Orgel, L. E. *An Introduction to Transition-Metal Chemistry, Ligand-Field Theory*, Methuen, London 1960, p. 57.
21. Andreetti, G. D., Cavalca, L. and Musatti, A. *Acta Crystallogr. B 24* (1968) 683.
22. Åsbrink, S. and Brandt, B. G. *Chem. Scr. 1* (1971) 169.
23. Hamilton, W. C. and Ibers, J. A. *Hydrogen Bonding in Solids*. Benjamin, New York and Amsterdam 1968.

Received October 25, 1973.

Acta Chemica Scandinavica A 28 (1974) 589—593

Short Communications

Stabilities of Lanthanoid Complexes of 2-Nitroso-1-naphthol-4,6-disulfonic and 2-Nitroso-1-naphthol-4,7-disulfonic Acids

HEIKKI SAARINEN

Department of Inorganic Chemistry, University of Helsinki, SF-00100 Helsinki 10, Finland

Studies of the lanthanoid complex formation with different sulfonic acid derivatives of 1-nitroso-2-naphthol and 2-nitroso-1-naphthol are in progress in our laboratory. In a previous communication we noted that, compared with other nitrosonaphtholsulfonic acids, 2-nitroso-1-naphthol-4,8-disulfonic acid forms remarkably stable complexes with tervalent lanthanoids.[1] The result was unexpected in view of our observations of nickel(II), zinc(II), and cadmium(II) complex formation with the ligands of 1,2-nitrosonaphthol series.[2,3]

The object of the present work was to learn more about those factors responsible for the stability of lanthanoid complexes of this type of ligand by investigating additional compounds of similar structure to 2-nitroso-1-naphthol-4,8-disulfonic acid. For this purpose 2-nitroso-1-naphthol-4,6-disulfonic and 2-nitroso-1-naphthol-4,7-disulfonic acids were chosen, and stability constants for their Pr(III), Nd(III), Sm(III), Eu(III), Gd(III), Tb(III), and Dy(III) complexes were determined. The choice of the lanthanoid ions for the study was directed by the fact that the stability of the 1:1 lanthanoid complexes of several 1,2-nitrosonaphtholsulfonic acids has been found to have a maximum value at samarium or europium; the lanthanoids represented are just those near this region.

Results. Interpretation of the potentiometric data obtained from titrations of both 2-nitroso-1-naphthol-4,6-disulfonic and 2-nitroso-1-naphthol-4,7-disulfonic acids with each of the lanthanoid ions indicates that only two successive complexes are formed. No protonated or polynuclear complex species could be found. It was also impossible to increase the concentrations of the free ligands to such extent that any reliable data for the possible third complexes would have been found. These results confirm our earlier observations of 1-nitroso-2-naphthol-3,6-disulfonic and 2-nitroso-1-naphthol-4,8-disulfonic acids.[1,4] As pointed out previously, there were no difficulties in producing the third complexes with nitrosonaphthol(mono)sulfonic acids, especially in the case of 1-nitroso-2-naphtholmonosulfonic acids.

The gross stability constants ($\beta_1 = [ML]/[M^{3+}][L^{3-}]$ and $\beta_2 = [ML_2^{3-}]/[M^{3+}][L^{3-}]^2$) of the complexes of 2-nitroso-1-naphthol-4,6-disulfonic and 2-nitroso-1-naphthol-4,7-disulfonic acids are collected in Table 1. The results for the 1:1 complexes are illustrated in Fig. 1, together with the corresponding values for some other nitrosonaphtholsulfonic acids, studied previously. As one can see, the stability order of the lanthanoid

Table 1. Stability constants of the lanthanoid complexes of 2-nitroso-1-naphthol-4,6-disulfonic and 2-nitroso-1-naphthol-4,7-disulfonic acids in aqueous solution at $I = 0.100$ and 25 °C.[a]

	2-Nitroso-1-naphthol-4,6-disulfonic acid		2-Nitroso-1-naphthol-4,7-disulfonic acid	
	$\log \beta_1$	$\log \beta_2$	$\log \beta_1$	$\log \beta_2$
Praseodymium	3.670 ± 0.014	5.893 ± 0.030	3.803 ± 0.012	5.862 ± 0.035
Neodymium	3.759 ± 0.014	6.021 ± 0.023	3.879 ± 0.012	6.000 ± 0.026
Samarium	3.886 ± 0.010	6.383 ± 0.018	4.017 ± 0.014	6.271 ± 0.032
Europium	3.818 ± 0.009	6.349 ± 0.015	3.955 ± 0.016	6.241 ± 0.034
Gadolinium	3.702 ± 0.012	6.259 ± 0.015	3.831 ± 0.017	6.228 ± 0.030
Terbium	3.480 ± 0.011	6.135 ± 0.015	3.651 ± 0.017	6.194 ± 0.033
Dysprosium	3.389 ± 0.009	6.015 ± 0.015	3.589 ± 0.017	6.053 ± 0.026

[a] The uncertainties given are three times the computed least squares standard deviations.

Table 2. Representative data for the determination of β_1 and β_2 from an individual titration of disodium 2-nitroso-1-naphthol-4,6-disulfonate with samarium ions. $C_{Sm} = 8.90 \times 10^{-4}$ M, $C_L = 3.153 \times 10^{-3}$ M, $C_H = 1.5 \times 10^{-5}$ M, titrant 0.100 M NaOH, $v_0 = 100.0$ ml, $\bar{I}$(mean) = 0.333, pK_3 (mean) = 5.863.

Titre (ml)	$-\log [H^+]$	Titre (ml)	$-\log [H^+]$	Titre (ml)	$-\log [H^+]$
0.136	3.981	0.895	4.928	1.658	5.555
0.259	4.174	1.020	5.049	1.780	5.644
0.384	4.351	1.146	5.161	1.912	5.734
0.510	4.514	1.277	5.267	2.039	5.824
0.639	4.661	1.400	5.367	2.160	5.918
0.760	4.799	1.525	5.462		

Calculated values: $\log \beta_1 = 3.823 \pm 0.003$, $\log \beta_2 = 6.313 \pm 0.006$

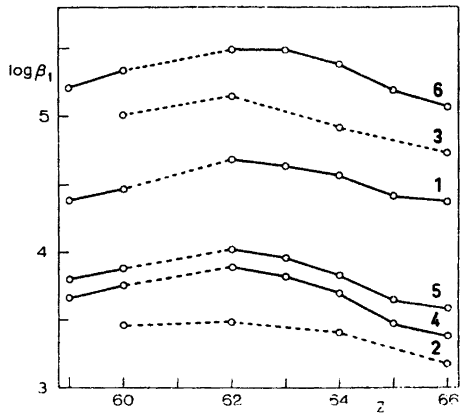

Fig. 1. Stability constants of the first lanthanoid complexes *versus* atomic number for 1-nitroso-2-naphthol-6-sulfonic (1), 2-nitroso-1-naphthol-4-sulfonic (2), 1-nitroso-2-naphthol-3,6-disulfonic (3), 2-nitroso-1-naphthol-4,6-disulfonic (4), 2-nitroso-1-naphthol-4,7-disulfonic (5), and 2-nitroso-1-naphthol-4,8-disulfonic (6) acids at 25 °C and $I = 0.100$.

complexes of these sulfo-substituted ligands is essentially similar; in each case the most stable complexes are formed by samarium or europium.

2-Nitroso-1-naphthol-4,7-disulfonic acid forms stronger 1:1 complexes than does 2-nitroso-1-naphthol-4,6-disulfonic acid. This mutual order of stability, which has also been found for the nickel(II) [2] and zinc(II) [5] complexes of the ligands, is exceptional when one takes the acid strengths of the ligands into consideration (at the ionic strength 0.1, the values of pK_3 for 2-nitroso-1-naphthol-4,7-disulfonic and 2-nitroso-1-naphthol-4,6-disulfonic acids are 5.84 and 5.88, respectively). In producing 1:2 complexes it is no longer valid.

As compared with 2-nitroso-1-naphthol-4,8-disulfonic acid, the complexes of the present ligands are distinctly less stable (Fig. 1). The difference in the stabilities of the complexes is so pronounced that it cannot entirely be explained by the different basicities of the ligand anions (pK_3 for 2-nitroso-1-naphthol-4,8-disulfonic acid at $I = 0.1$ is 6.66 [6]).[2,3] It is obvious that the negative sulfonate group in *peri*-position to the hydroxyl group has a strengthening effect on complex formation with tervalent lanthanoids.

As expected for electrostatic reasons, the 1:1 lanthanoid complexes of nitrosonaphthol(di)sulfonic acids are more stable than those of nitrosonaphthol(mono)sulfonic acids. By contrast, it seems evident that the weakened tendency of the disulfonic acid derivatives of 1,2-nitrosonaphthols to form higher complexes also arises from electrostatic reasons rather than any strict steric grounds. Owing to the different ionic charges of the reacting species, however, the concentration stability constants of the complexes are not directly comparable.

It has been shown previously that 1-nitroso-2-naphthols generally form stronger nickel(II), zinc(II), and cadmium(II) complexes than do 2-nitroso-1-naphthols.[1,2] Since our information about the lanthanoid complexes of these ligands is still quite limited, general conclusions in this respect can hardly be made.

Experimental. The disodium salts of 2-nitroso-1-naphthol-4,6-disulfonic and 2-nitroso-1-naphthol-4,7-disulfonic acids were prepared by treatments of the sodium salts of 1-nitroso-2-naphthol-6-sulfonic and 1-nitroso-2-naphthol-7-sulfonic acids with aqueous $NaHSO_3$ followed by boiling with hydroxylamine hydrochloride in dil. HCl. Methods of the synthesis and analysis of *ortho*-nitrosonaphtholsulfonic acids, including the acids above, have previously been described in detail by the author.[2]

The lanthanoid salts were perchlorates prepared by dissolving the corresponding oxides into warm perchloric acid. The metal concen-

trations of the stock solutions were controlled by complexometric titrations and the acid contents by titrations of the hydrogen ion liberated from an ion-exchange column (Amberlite IR-120).

Apparatus and methods. The apparatus and methods were the same as described in a recent paper.[2] All measurements were carried out at 25 °C.

In the determination of the complex stability constants, several titrations were carried out at ionic strengths near 0.1 using different ligand-metal ratios. The initial estimates of the constants calculated from stoichiometric relationships were refined by a modified version of the programme SCOGS[7] on a Univac 1108 computer. An example of the calculations is presented in Table 2. The final values of the constants given are those obtained by interpolation to the precise value 0.100 of ionic strength.

The values of the naphtholic protonation constants of the ligands needed in the calculations were obtained from the following Debye-Hückel equations: for 2-nitroso-1-naphthol-4,6-disulfonic acid,[2]

$pK_3 = 6.507 - 3.054\sqrt{I}/(1 + 1.394\sqrt{I}) + 0.453\ I$

and for 2-nitroso-1-naphthol-4,7-disulfonic acid,[2]

$pK_3 = 6.451 - 3.054\ \sqrt{I}/(1 + 1.591\ \sqrt{I}) + 0.277\ I.$

Acknowledgement. Financial aid from the Neste Oy Foundation (Neste Oy:n Säätiö) is gratefully acknowledged.

1. Saarinen, H. *Suom. Kemistilehti B 46* (1973) 250.
2. Saarinen, H. *Ann. Acad. Sci. Fenn. Ser. A 2 170* (1973).
3. Mäkitie, O. and Saarinen, H. *Suom. Kemistilehti B 44* (1971) 209.
4. Mäkitie, O., Saarinen, H., Pelkonen, R. and Mäki J. *Suom. Kemistilehti B 44* (1971) 410.
5. Mäkitie, O., Saarinen, H., Jantunen, T., Jyske, P. and Suonpää, M. *Suom. Kemistilehti B 46* (1973) 336.
6. Mäkitie, O. and Saarinen, H. *Suom. Kemistilehti B 42* (1969) 394.
7. Sayce, I. G. *Talanta 18* (1968) 1397.

Received February 25, 1974.

Multicomponent Polyanions. IX. On the Crystal Structure of a Protonized Mannitolodimolybdate Complex

BRITT HEDMAN

Department of Inorganic Chemistry, University of Umeå, S-901 87 Umeå, Sweden

Investigations of equilibria

$$p\mathrm{H}^+ + q\mathrm{MoO_4^{2-}} + r\mathrm{C_6H_{14}O_6} \rightleftharpoons (\mathrm{H}^+)_p(\mathrm{MoO_4^{2-}})_q(\mathrm{C_6H_{14}O_6})_r$$

where $C_6H_{14}O_6$ is D-mannitol, have shown that complexes (2,2,1) and (3,2,1) are formed (the complexes are given in (p, q, r) notation).[1] The study covered the $-\log [H^+]$ range $1 < -\log [H^+] < 9$.

In parallel with this investigation crystallization experiments using molar ratios of H^+, MoO_4^{2-}, and $C_6H_{14}O_6$ corresponding to the composition of the complexes, have also been carried out. Hitherto this preparative work has only resulted in crystals corresponding to a (4, 2, 1) complex, which has not been confirmed in the $-\log [H^+]$ range studied, but is assumed to appear at $-\log [H^+] < 1$.

X-Ray characteristics and a preliminary structure of this crystalline phase is reported in the present communication.

Crystal data.

$H_2Mo_2O_5C_6H_{10}O_6.3H_2O$	F.W. = 506.10
Monoclinic $P2_1$	V = 697.7(1) Å^3
a = 12.2342(6) Å	D_x = 2.409 g cm^{-3}
b = 6.9008(4) Å	D_m = 2.40 ± 0.01 g cm^{-3}
c = 8.3845(5) Å	(flotation method)
β = 99.740(6)°	Z = 2

Experimental. Accurate unit cell dimensions were determined from X-ray powder photographs taken with a Guinier-Hägg camera using Cu$K\alpha_1$-radiation (λ = 1.54051 Å) with $Pb(NO_3)_2$ as internal standard ($a_{Pb(NO_3)_2}$ = 7.8575 Å, 25 °C). Three-dimensional single crystal X-ray diffraction data were collected by the equi-inclination Weissenberg method, using Cu$K\alpha$-radiation (λ = 1.5418 Å). The intensities of 1414 independent reflexions from the $h0l - h6l$ layers were estimated visually using multiple film technique. Correction for Lorentz- and polarization effects was then applied.

From a three-dimensional Patterson synthesis the positions of the two Mo atoms were obtained. Since the y-coordinates for both atoms were the same (≈ 0.37), the phase angles computed were equivalent within the layers and restricted to multiples of $\approx \pi/4$. This resulted in a centre of symmetry induced in the space group $P2_1$, making both the complex and its mirror image appear in a following Fourier map.[2] To obtain non-equivalent phase angle values anomalous scattering was applied, and combined

trations of the stock solutions were controlled by complexometric titrations and the acid contents by titrations of the hydrogen ion liberated from an ion-exchange column (Amberlite IR-120).

Apparatus and methods. The apparatus and methods were the same as described in a recent paper.[2] All measurements were carried out at 25 °C.

In the determination of the complex stability constants, several titrations were carried out at ionic strengths near 0.1 using different ligand-metal ratios. The initial estimates of the constants calculated from stoichiometric relationships were refined by a modified version of the programme SCOGS[7] on a Univac 1108 computer. An example of the calculations is presented in Table 2. The final values of the constants given are those obtained by interpolation to the precise value 0.100 of ionic strength.

The values of the naphtholic protonation constants of the ligands needed in the calculations were obtained from the following Debye-Hückel equations: for 2-nitroso-1-naphthol-4,6-disulfonic acid,[2]

$pK_3 = 6.507 - 3.054\sqrt{I}/(1 + 1.394\sqrt{I}) + 0.453\ I$

and for 2-nitroso-1-naphthol-4,7-disulfonic acid,[2]

$pK_3 = 6.451 - 3.054\ \sqrt{I}/(1 + 1.591\ \sqrt{I}) + 0.277\ I.$

Acknowledgement. Financial aid from the Neste Oy Foundation (Neste Oy:n Säätiö) is gratefully acknowledged.

1. Saarinen, H. *Suom. Kemistilehti B 46* (1973) 250.
2. Saarinen, H. *Ann. Acad. Sci. Fenn. Ser. A 2 170* (1973).
3. Mäkitie, O. and Saarinen, H. *Suom. Kemistilehti B 44* (1971) 209.
4. Mäkitie, O., Saarinen, H., Pelkonen, R. and Mäki J. *Suom. Kemistilehti B 44* (1971) 410.
5. Mäkitie, O., Saarinen, H., Jantunen, T., Jyske, P. and Suonpää, M. *Suom. Kemistilehti B 46* (1973) 336.
6. Mäkitie, O. and Saarinen, H. *Suom. Kemistilehti B 42* (1969) 394.
7. Sayce, I. G. *Talanta 18* (1968) 1397.

Received February 25, 1974.

Multicomponent Polyanions. IX. On the Crystal Structure of a Protonized Mannitolodimolybdate Complex

BRITT HEDMAN

Department of Inorganic Chemistry, University of Umeå, S-901 87 Umeå, Sweden

Investigations of equilibria

$$p\mathrm{H}^+ + q\mathrm{MoO_4^{2-}} + r\mathrm{C_6H_{14}O_6} \rightleftharpoons (\mathrm{H}^+)_p(\mathrm{MoO_4^{2-}})_q(\mathrm{C_6H_{14}O_6})_r$$

where $C_6H_{14}O_6$ is D-mannitol, have shown that complexes (2,2,1) and (3,2,1) are formed (the complexes are given in (p, q, r) notation).[1] The study covered the $-\log [H^+]$ range $1 < -\log [H^+] < 9$.

In parallel with this investigation crystallization experiments using molar ratios of H^+, MoO_4^{2-}, and $C_6H_{14}O_6$ corresponding to the composition of the complexes, have also been carried out. Hitherto this preparative work has only resulted in crystals corresponding to a (4, 2, 1) complex, which has not been confirmed in the $-\log [H^+]$ range studied, but is assumed to appear at $-\log [H^+] < 1$.

X-Ray characteristics and a preliminary structure of this crystalline phase is reported in the present communication.

Crystal data.

$H_2Mo_2O_5C_6H_{10}O_6.3H_2O$	F.W. = 506.10
Monoclinic $P2_1$	V = 697.7(1) Å^3
a = 12.2342(6) Å	D_x = 2.409 g cm^{-3}
b = 6.9008(4) Å	D_m = 2.40 ± 0.01 g cm^{-3}
c = 8.3845(5) Å	(flotation method)
β = 99.740(6)°	Z = 2

Experimental. Accurate unit cell dimensions were determined from X-ray powder photographs taken with a Guinier-Hägg camera using Cu$K\alpha_1$-radiation (λ = 1.54051 Å) with $Pb(NO_3)_2$ as internal standard ($a_{Pb(NO_3)_2}$ = 7.8575 Å, 25 °C). Three-dimensional single crystal X-ray diffraction data were collected by the equi-inclination Weissenberg method, using Cu$K\alpha$-radiation (λ = 1.5418 Å). The intensities of 1414 independent reflexions from the $h0l - h6l$ layers were estimated visually using multiple film technique. Correction for Lorentz- and polarization effects was then applied.

From a three-dimensional Patterson synthesis the positions of the two Mo atoms were obtained. Since the y-coordinates for both atoms were the same (≈ 0.37), the phase angles computed were equivalent within the layers and restricted to multiples of $\approx \pi/4$. This resulted in a centre of symmetry induced in the space group $P2_1$, making both the complex and its mirror image appear in a following Fourier map.[2] To obtain non-equivalent phase angle values anomalous scattering was applied, and combined

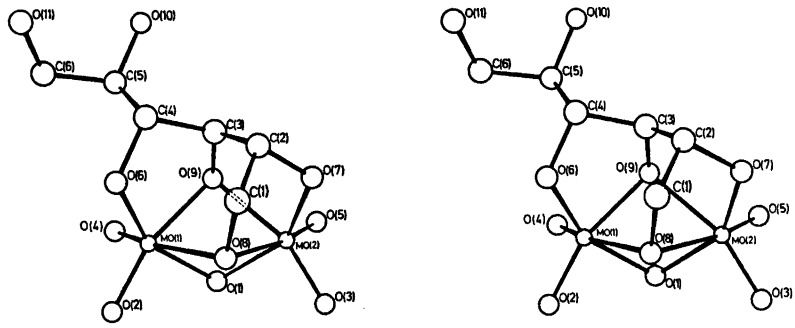

Fig. 1. A stereoscopic view of the non-hydrogen atoms in the $H_2Mo_2O_5C_6H_{10}O_6$-complex.

with very careful weighting of the material during the computational refinements. The positions of eleven oxygen and six carbon atoms of the complex and three water oxygen atoms were then determined stepwise from Fourier calculations. Full-matrix least squares refinement of positional and isotropic thermal parameters has so far yielded an R-value of 0.108, R being defined as $\sum||F_o|-|F_c||/\sum|F_o|$.

Structure description. The structure consists of uncharged mannitolodimolybdate complexes and water molecules linked together by hydrogen bonds forming probably a three-dimensional network. The mannitolodimolybdate complex consists of two MoO_6-octahedra which share a face. Four of the oxygen atoms in this dimolybdate unit are directly bonded to four adjacent carbon atoms in the D-mannitol chain, as shown in Fig. 1. Actually D-mannitol can be considered as a tetradentate ligand with respect to the dimolybdate group. Three five-membered chelate rings Mo(1) – O(9) – C(3) – C(4) – O(6), Mo(2) – O(7) – C(2) – C(1) – O(8), and Mo(2) – O(7) – C(2) – C(3) – O(9) are formed.

Besides these four mannitol-bonded oxygen atoms of the dimolybdate group there are five additional oxygen atoms, of which two are probably part of hydroxyl groups. At the present stage it is impossible to decide which of the oxygens that are protonized.

The Mo – Mo distance is 3.13 Å, considerably shorter than for MoO_6-octahedra which share an edge or a corner. For instance in $Na_4H_2Mo_5P_2O_{23}(H_2O)_{10}$ the average Mo – Mo distance is 3.39 Å when sharing an edge.[3] To our knowledge the coupling of octahedra by sharing a face has not earlier been reported for discrete dimolybdate units. However, for condensed heteropolyanions the occurrence of shared faces has been found in the crystal structure of $(NH_4)_2H_6(CeMo_{12}O_{42}).12H_2O$.[4]

The Mo – O distances can, in both octahedra, be divided into three groups, each containing two distances, the average of which are 1.69, 1.95, and 2.29 Å. They are in agreement with other Mo – O distances reported, for instance in $Na_4H_2Mo_5P_2O_{23}(H_2O)_{10}$[3] and $Na_6Mo_5P_2O_{23}(H_2O)_{13}$.[5]

In the D-mannitol chain the average C – C and C – O distances are 1.53 and 1.45 Å, respectively. The average angle C – C – C is 114° and C – C – O 106°. In the crystal structure determination of the β form of D-mannitol the corresponding distances reported are 1.516 and 1.437 Å.[6]

The variation in distances found in the complex and the corresponding distances in β-D-mannitol are possibly not significantly different from each other.

Collection of a new reflexion data set, measured by diffractometer, is in progress. This should not only permit higher accuracy in positional and thermal parameters, but should also allow an attempt to determine the hydrogen atom positions, of which the two protons of the hydroxyl groups previously mentioned are of special interest. A neutron diffraction study of the compound is also planned.

Acknowledgements. I thank Professor Nils Ingri for much valuable advice, for his great interest and for all the facilities placed at my disposal. The work forms part of a program financially supported by the Swedish Natural Science Research Council.

1. Pettersson, L. *Acta Chem. Scand. 26* (1972) 4067.
2. Stout, G. H. and Jensen, L. H. *X-Ray Structure Determination, A Practical Guide*, Macmillan, London 1968, p. 284.
3. Hedman, B. *Acta Chem. Scand. 27* (1973) 3335.
4. Dexter, D. D. and Silverton, J. V. *J. Amer. Chem. Soc. 90* (1968) 3589.
5. Strandberg, R. *Acta Chem. Scand. 27* (1973) 1004.
6. Berman, H. M., Jeffrey, G. A. and Rosenstein, R. D. *Acta Crystallogr. B 24* (1968) 442.

Received April 5, 1974.

X-Ray Investigation of Potassium *p*-Nitrosophenolate Monohydrate

H. J. TALBERG

Department of Chemistry, University of Oslo, Oslo 3, Norway

The present structure investigation of potassium *p*-nitrosophenolate monohydrate is part of a series of structural investigations of *para* substituted nitrosobenzenes and oximes derived from these by protonation or tautomeric proton exchange. Lüttke [1] has demonstrated the ability of *para* substituted nitrosobenzenes in forming dimers of the azodioxy-type to be heavily dependent upon the electron donating ability of the *para* substituent. An intramolecular charge transfer from the *para* substituent to the nitroso group is probably preventing dimerisation. A comparison of the molecular structure of these nitrosobenzenes and their corresponding oximes should indicate to what degree this intramolecular charge transfer is present.

So far the crystal and molecular structure of *N*,*N*-dimethyl-*p*-nitrosoaniline,[2] its hydrochloride,[3] and quinone-4-oxime [4] have been investigated.

Potassium *p*-nitrosophenolate monohydrate was formed in ethanolic solutions of *p*-nitrosophenol and potassium hydroxide. Recrystallisation from pure acetone gave suitable tabular green crystals. The crystal data are as follows: Potassium *p*-nitrosophenolate monohydrate, $KC_6H_4O_2N.H_2O$, orthorhombic, space group $P2_12_12_1$. Cell dimensions: $a=5.527(4)$ Å, $b=7.558(4)$ Å, $c=18.883(13)$ Å, $V=788.9$ Å^3, $M=179.22$, $F(000)=364$, $Z=4$, $\mu=0.621$ mm^{-1}, $D_{obs}=1.52$ gcm^{-3}, $D_{calc}=1.51$ gcm^{-3}.

The intensity data were collected using an automatic Picker diffractometer with graphite crystal monochromated Mo$K\alpha$ radiation. The crystal used was $0.40\times0.40\times0.12$ mm^3. 404 reflections with $I\geq2\sigma(I)$ (1300 reflections with $2\theta\leq60°$ were measured) were regarded as observed. The intensity data were corrected for absorption effects.

Disregarding 18 small reflections the data are consistent with the space group $Pan2_1$. Fourier refinement of the potassium atom coordinates in this space group revealed all other non-hydrogen atoms but subsequent least squares refinement did not converge ($R=32$ %). Using the space group $P2_12_12_1$ least squares refinements terminated with $R=9.7$ %. Only the potassium and the water oxygen atom were refined anisotropically. Refinement with anisotropic thermal parameters for all non-hydrogen atoms gave unreasonable results. The goodness of fit was approximately 3. The result of the structure analysis is given in Fig. 1. The estimated standard deviations are 0.03 Å in the bond lengths and 2° in the angles.

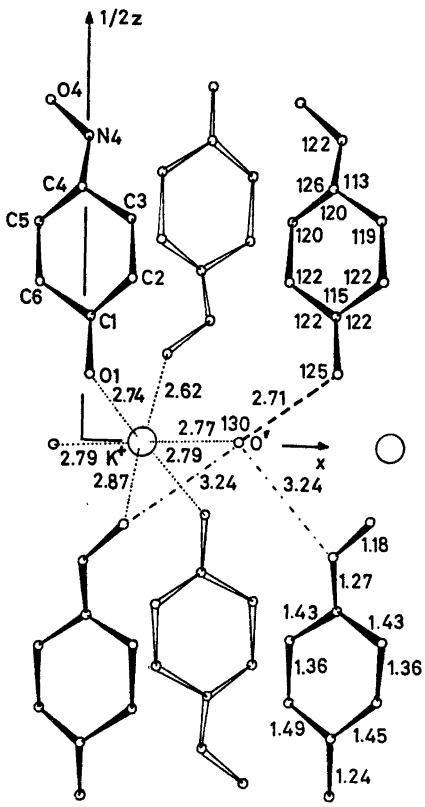

Fig. 1. The potassium salt of *p*-nitrosophenolate. Bond lengths (Å) and angles (°), $R=9.7$ % (the atoms in the anion moiety are refined isotropically). The O1···HO′ hydrogen bond is indicated by broken line, the coordination about the potassium atom by dotted lines and the two shortest contacts to O′ by the — · — · — lines.

The anion is almost planar, and apart from the NO bond length being shorter and the CNO angle larger than expected, the bond lengths and angles are rather similar to the corresponding bond lengths and angles found in quinone-4-oxime.[4] Thus the quinonoid character of the anion seems to be pronounced indicating a strong intramolecular charge transfer.

1. Lüttke, W. *Z. Elektrochem. 61* (1957) 976.
2. Rømming, C. and Talberg, H. J. *Acta Chem. Scand. 27* (1973) 2246.
3. Drangfeldt, O. and Rømming, C. *Acta Chem. Scand. To be published.*
4. Talberg, H. J. *Acta Chem. Scand. To be published.*

Received April 29, 1974.

Acta Chemica Scandinavica A 28 (1974) 595—599

The Activity Coefficients of Formate and Hexanoate Ions in Mixed Aqueous Solutions of Sodium Alkanoate and Sodium Chloride at Constant Sodium Molality (3.0 m)

SUNE BACKLUND and KURT PALM

Department of Physical Chemistry, Åbo Akademi, Porthansgatan 3—5, SF-20500 Åbo 50, Finland

The activity coefficients of the sodium and chloride ions have been calculated from potentiometric measurements at 25 °C in aqueous sodium chloride and sodium formate as well as sodium chloride and sodium hexanoate. In the measurements, the sodium molality was kept constant at 3.0 mol kg^{-1}. On the basis of these data and water activities calculated from vapour pressure measurements, the activity coefficients of the alkanoate ion has been calculated using the Gibbs-Duhem equation. The results show that Harned's rule is valid for the formate mixtures. The hexanoate mixtures, however, deviate strongly from this rule. The investigation is connected with other investigations of the self association of alkali alkanoates in highly concentrated ionic media.

Previous investigations of the activity coefficients in aqueous sodium chloride media [1,2] have been continued with an investigation of the activity coefficients of the formate and hexanoate ions at the constant sodium molality 3.0 mol kg^{-1}. These investigations constitute a part of work to clarify the association and the micelle formation of the alkali salts of short-chain fatty acids.[3] The investigations of these equilibria have been conducted in a highly concentrated ionic medium, Na(Cl), in order to minimize the variations of the activity coefficients. Some caution in the interpretation of these results seems to be necessary, as the activity coefficients of the alkanoate ions change considerably when chloride ions are replaced with alkanoate ions in neutral aqueous solutions of sodium chloride and sodium alkanoate in water at constant total molality.[1,2] The purpose of this series of investigations, is to enable variations of ionic activity coefficients to be used in investigations of the association and the formation of micelles.

EXPERIMENTAL

1. Chemicals. Sodium chloride (E. Merck AG *pro analysi* quality) and sodium formate (J. T. Baker *pro analysi* quality) were dried before use at respectively 140 °C and 90 °C, in vacuum. Sodium hexanoate was synthetized by neutralization of boiling sodium hydroxide solution (E. Merck AG "1 N Titrisol") with hexanoic acid (Fluka AG *purissimum* quality). The molar mass, as determined by titration with perchloric acid in glacial acetic acid, was not allowed to deviate more than 0.5 % from the theoretical value. The distilled water used was passed through an ion exchange resin immediately before use. Its conductivity was about 0.5 μS cm^{-1}.

2. Measurements of electromotive force. Measurements were made after each addition in titrations where a 3.0 mol kg^{-1} sodium chloride solution was added to a sodium alkanoate (NaB) solution of the same molality and *vice versa*. The electrode systems, the bridge and the temperature control described in Ref. 2 were used. The sodium responsive electrode was an E.I.L. glass electrode, type GEA 33 B. The silver-silver chloride electrodes were prepared by a procedure slightly modified from that of Brown.[4] Emf was measured with a "Beckmann Research pH Meter".

3. Vapour pressure osmometry. The water activities a_w in mixtures of sodium chloride, sodium alkanoate and water were measured with a "Perkin-Elmer Model 115" vapour pressure osmometer. All solutions were prepared separately by direct weighing; the molalities of the reference solutions were checked after the measurements.

RESULTS

The water activities found are shown as functions of sodium alkanoate molality in Fig. 1. The water activities of these systems have been investigated previously by Danielsson *et al.*,[3,5] these measurements, however, were made at the constant sodium concentration 3.0 M.

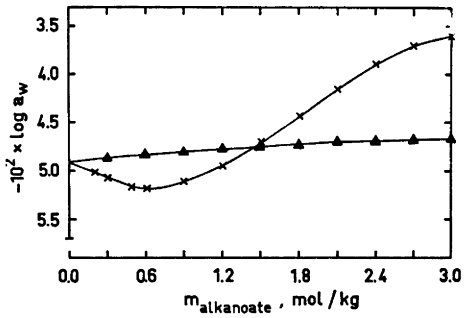

Fig. 1. The logarithm of the water activity as a function of the sodium alkanoate molality for the systems sodium chloride-sodium formate-water and sodium chloride-sodium hexanoate-water at the constant sodium molality 3.0 mol kg^{-1}, temperature 25 °C. ▲, formate; ×, hexanoate.

In Fig. 2 the logarithms of the mean activity coefficients of sodium chloride, $\gamma_{Na,Cl}$, are shown as functions of the alkanoate molality m_{NaB}. These are calculated directly from measured emf values. From $\gamma_{Na,Cl}$, and a_w for the two systems investigated it is possible to calculate the mean activity coefficients for the sodium alkanoates, using the equation

$$2m_{NaCl}d(\log \gamma_{Na,Cl}) + 2m_{NaB}d(\log \gamma_{Na,B}) + m_w d(\log a_w) = 0 \quad (1)$$

where m_w is the molality of water. This equation is the Gibbs-Duhem equation as applied to the system $NaCl - NaB - H_2O$; it has been given by Harned [6] and developed further by Backlund *et al.*[2] The final equation used for calculating the mean activity coefficients, $\gamma_{Na,B}$, of sodium alkanoate was

$$\log \gamma_{Na,B} = \log \gamma^*_{Na,B} + b_0 \ln 10 \log m_{NaB}/m_{Na} + \sum_{i=1}^{n}[b_i(i+1)/i](m^i_{NaB} - m^i_{Na}) \quad (2)$$

$\gamma^*_{Na,B}$ are the mean activity coefficients in the binary system $NaB - H_2O$. The values for these, according to Robinson and Stokes [7] are $\gamma^*_{Na,Fo} = 0.678$ for the formate and $\gamma^*_{Na,Hex} = 0.612$ for the hexanoate. b_i are constants ($i = 0, 1, \ldots n$) which are determined by fitting the polynomial to experimental values of $\gamma_{Na,Cl}$ and a_w by regressional analysis. m_{Na} is the constant sodium molality and thus $m_{Na} = 3.0$ mol kg^{-1}. The standard states are chosen to give $\lim_{\substack{m_{NaCl}\to 0 \\ a_w \to 1}} \gamma^*_{Na,Cl} = \lim_{\substack{m_{NaB}\to 0 \\ a_w \to 1}} \gamma^*_{Na,B} = 1$. It is also assumed that, as postulated by Guggenheim,[8] $\gamma^*_{Na,Cl} = \gamma^*_{Cl^-} = \gamma^*_{Na^+}$ in pure sodium chloride-water systems.

Table 1. Single ion activity coefficients in mixed aqueous solutions of sodium chloride and sodium alkanoate at the constant sodium molality $m_{Na} = 3.0$ mol kg^{-1}, temperature 25 °C.

$m_{alkanoate}$ mol kg^{-1}	Formate			Hexanoate		
	γ_{Na^+}	γ_{Cl^-}	γ_{Fo^-}	γ_{Na^+}	γ_{Cl^-}	γ_{Hex^-}
0.00	0.714	0.714	0.658	0.714	0.714	2.985
0.30	0.694	0.723	0.676	0.723	0.770	2.447
0.60	0.674	0.733	0.695	0.719	0.830	1.996
0.90	0.655	0.741	0.714	0.702	0.886	1.632
1.20	0.637	0.749	0.733	0.675	0.938	1.349
1.50	0.618	0.756	0.753	0.640	0.990	1.137
1.80	0.601	0.762	0.774	0.600	1.044	0.984
2.10	0.584	0.768	0.795	0.558	1.105	0.883
2.40	0.567	0.773	0.816	0.517	1.177	0.827
2.70	0.551	0.776	0.838	0.478	1.267	0.815
3.00	0.535	0.779	0.860	0.441	1.381	0.852

The logarithms of the activity coefficients calculated from eqn. (2) are shown as functions of m_{NaB} in Fig. 3. The experimentally estimated single ion activity coefficient γ_{Na^+} now makes it possible to calculate the alkanoate single ion activity coefficient γ_{B^-} from the defining equality

$$\log \gamma_{B^-} = 2 \log \gamma_{Na,B} - \log \gamma_{Na^+} \quad (3)$$

The calculated values of γ_{B^-} are given in Table 1, together with the experimentally estimated values of γ_{Na^+} and γ_{Cl^-} for both three component systems.

DISCUSSION

Previous investigations of sodium hexanoate in aqueous solutions [9] and in aqueous sodium chloride solutions [3,10] have shown that the hexanoate forms micelles. In a sodium chloride solution of total sodium ion concentration 3.0 M the critical micelle concentration (c.m.c.) of sodium hexanoate is about 0.4 M. In a sodium chloride ionic medium with the same total concentration of sodium ions, Ödberg *et al.*[11] have found a considerable change in the spin relaxation rate of the protons bound to the hydrocarbon chain when the sodium hexanoate concentration exceeds 0.3 M.

Figs. 1 and 2 show that log a_w and log $\gamma_{Na,Cl}$ both depend linearly on molarity up to 0.5 mol kg^{-1} sodium hexanoate. The same linearity is found for molalities < 0.5 mol kg^{-1} if log γ_{Na^+} (Table 1) is plotted against the sodium hexanoate molality. These linear relationships indicate that the components in the mixture behave as simple 1 – 1 electrolytes, *i.e.*, Harned's rule [7] is valid. At the sodium molality 3.0 mol kg^{-1} Na(Cl), an increasing deviation from this rule is observed as the sodium hexanoate molality increases above 0.5 mol kg^{-1}. This is in good agreement with the values for c.m.c. of sodium hexanoate given above. Considering the relatively high aggregation numbers of sodium hexanoate (about 17 anions [3]) one might expect that the deviations from Harned's rule should manifest themselves as well defined breaks in the curves giving log $\gamma_{Na,Hex}$ or log γ_{Hex^-} as functions of the alkanoate molality. This, however, is not the case, as can be seen from Fig. 3 or Table 1. This can be attributed to the method of treatment of the experimental data. These have all been fitted to eqn. (2) using one polynomial in the whole molality range, giving slightly high values for $\gamma^{tr}_{Na,Hex}$ and $\gamma^{tr}_{Hex^-}$. The deviation is probably about 0.02 logarithmic units. γ^{tr} is the trace activity coefficient as defined by $\lim_{m_{NaB} \to 0} \gamma = \gamma^{tr}$ at constant total molality.

The activity coefficients of the chloride ions follow Harned's rule in the whole range of molalities. This is clearly because the chloride ions do not participate in micelle formation, see, among others, Danielsson.[10] Figs. 2 and 3 as

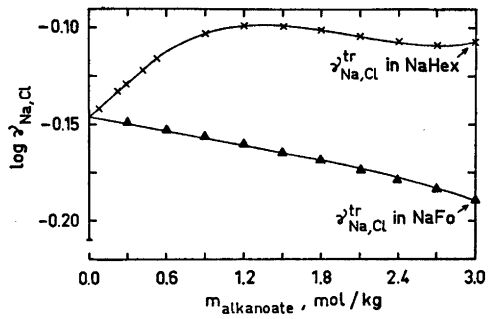

Fig. 2. The logarithm of the mean activity coefficient of sodium chloride as a function of the sodium alkanoate molality in the systems sodium chloride-sodium formate-water and sodium chloride-sodium hexanoate-water at the constant sodium molality 3.0 mol kg^{-1}, temperature 25 °C. ▲, formate; ×, hexanoate.

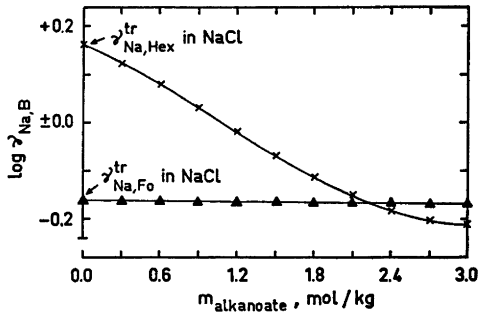

Fig. 3. The logarithm of the mean activity coefficient of sodium alkanoate as a function of the sodium alkanoate molality in the systems sodium chloride-sodium formate-water and sodium chloride-sodium hexanoate-water at the constant sodium molality 3.0 mol kg^{-1}, temperature 25 °C. ▲, formate; ×, hexanoate.

well as Table 1 show that Harned's rule is valid for all formate molalities and that the formate ion behaves quite analogously to singly charged anions of ordinary dimensions. The inclusion of the formate into this investigation is justified by the possibilities of obtaining information about the influence of the carboxylic group (COO^-) on water, an effect which may apply for the higher homologues, acetate, propionate, butyrate, pentanoate, and hexanoate.

There are no experimental data directly comparable to the present investigation. The results, however, are in good agreement with the general picture of the structure of the solutions of other homologues that has been obtained in earlier investigations.[1,2]

The differences in the activity coefficients of formate and hexanoate at low alkanoate molalities (*e.g.*, Table 1 and Fig. 3) merit a short discussion.

Gurney [12] divides ions into structure makers and structure breakers, that is, ions that increase and decrease the hydrogen bonding of water, respectively. Snell and Greyson [13] investigated the whole series of homologues from sodium formate to sodium hexanoate. On the basis of transfer entropies from heavy to normal water they concluded that the formate is a structure breaker and hexanoate is a structure maker. Gurney [12] considers the chloride ion a weak structure breaker. The almost constant water activity shown in Fig. 1 for mixtures of sodium chloride and sodium formate indicates that the formate ion is weakly structure-breaking too. This is also seen from the transfer entropies tabulated by Snell and Greyson.[13] From these it may be concluded that the hexanoate ion is a strong structure maker. On the basis of apparent molal enthalpy data, an increase in structure making effects has also been found by Lindenbaum [14] for the homologues acetate < butyrate < pentanoate. From investigations of the near-infrared spectra of $H_2O - D_2O$ solutions of sodium alkanoates, Worley and Klotz [15] have concluded that the sodium formate has a weakly structure-breaking effect. They found no effect at all for the sodium acetate and an increasing structure-making effect as the number of carbon atoms in the hydrocarbon chain increases.

Gurney [12] considers the sodium ion a weak structure maker. However, it must be stressed that the structure-making effect of the sodium ion is caused by ion-dipole attraction of the water molecules, whereas the structure-making effect of, for example, the hexanoate ion implies the stabilization of water cages around the hydrocarbon chain. Gurney also concludes that the more similar the anion and the cation are with respect to their effects on the structure of water, the smaller is the activity coefficient. Accordingly, $\gamma^{tr}_{Na,B}$ for the formate should be smaller than for the hexanoate, since there is a large difference between the structure-making effect of the sodium ion and that of the hexanoate ion. Since the sodium ion is common for both salts, $\gamma^{tr}_{Fo^-}$ should also be smaller than $\gamma^{tr}_{Hex^-}$. The results of this investigation show that this is the case.

This discussion of the relation between the activity coefficients of the anions and their effect on the structure of the solvent does not, of course, pertain to higher hexanoate molalities where the association to smaller and larger polynuclear aggregates completely dominates the dependence of the activity coefficients on the molalities.

Acknowledgements. The authors thank Professor I. Danielsson, Ph. D. for reading the manuscript, and Mr. Folke Eriksson for helping them with the computer programming.

REFERENCES

1. Backlund, S. *Acta Chem. Scand. 25* (1971) 2070.
2. Backlund, S., Eriksson, F. and Friman, R. *Acta Chem. Scand. 27* (1973) 3234.
3. Danielsson, I. and Stenius, P. *J. Colloid Interface Sci. 37* (1971) 264.
4. Brown, A. S. *J. Amer. Chem. Soc. 56* (1934) 646.
5. Danielsson, I. *Proc. 3rd Scandinavian Symp. Surface Chemistry, Fredensborg 1967*, Nordforsk, pp. 1–7.
6. Harned, H. S. *J. Amer. Chem. Soc. 57* (1935) 1865.
7. Robinson, R. A. and Stokes, R. H. *Electrolyte Solutions*, Butterworths, London 1959, pp. 492–493 and 438–450.
8. Guggenheim, E. A. *J. Phys. Chem. 34* (1930) 1758.
9. Markina, Z. N., Tsikurina, N. N. and Kostovo, N. Z. *Kolloid. Zh. 26* (1964) 76.
10. Danielsson, I. *Proc. 5th Intern. Congr. Surface Active Substances, Barcelona 1968*, Ediciones Unidas, Barcelona 1969, Vol. II, p. 869.
11. Ödberg, L., Svens, B. and Danielsson, I. *J. Colloid Interface Sci. 41* (1972) 298.

12. Gurney, R. W. *Ionic Processes in Solution*, McGraw, New York 1953, pp. 248–261.
13. Snell, H. and Greyson, J. *J. Phys. Chem.* *74* (1970) 2148.
14. Lindenbaum, S. *J. Phys. Chem.* *74* (1970) 3027.
15. Worley, J. D. and Klotz, I. M. *J. Chem. Phys.* *45* (1966) 2868.

Received November 27, 1973.

Acta Chemica Scandinavica A 28 (1974) 600—606

The Crystal and Molecular Structure of 2-(3-Diethylaminopropylthio)-4,5-dichloropyrimidin-6-one

H. J. TALBERG

Department of Chemistry, University of Oslo, Oslo 3, Norway

The crystal structure of 2-(3-diethylaminopropylthio)-4,5-dichloropyrimidin-6-one, $C_{11}H_{17}ON_3SCl_2$, has been determined from three-dimensional X-ray diffraction data and refined by least-squares methods. The space group is $P2_1/c$, $a = 9.471$ Å, $b = 17.634$ Å, $c = 9.006$ Å, $\beta = 80.93°$.

The molecules are forming dimers with hydrogen bonds between the oxygen atom and the aminonitrogen atom. Two nonbonding contacts between atoms in the pyrimidine moiety and atoms in the side chain are rather short (N1···C7 2.943 Å, S2···C9 3.205 Å). The C6−O and C2−S bond lengths (1.262 Å and 1.764 Å, respectively) indicate some double bond character of these bonds.

Berg-Nielsen[1] has shown that 2-(bromoalkylthio)-4,5-dichloropyrimidin-6-ones (I) may cyclicize, thus giving compounds (II) which have potential analgetic activity.

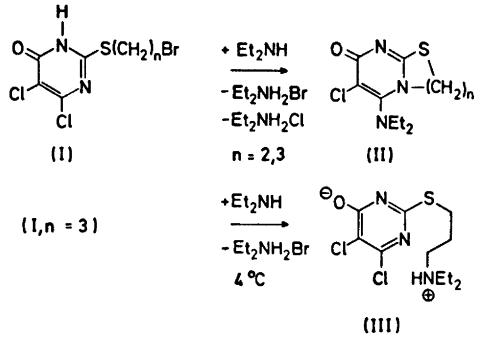

At room temperature the 1,3-thiazole, (II, $n = 2$), is more readily formed than the 1,3-thiazine (II, $n = 3$). At 4 °C the 1,3-thiazine is not formed at all, and reaction with (I, $n = 3$) gives (III). Studies by Reistad and Undheim [2,3] have shown pyridine[2,1-*b*]-1,3-thiazine derivatives to rearrange to their corresponding thiazole analogs. These investigations indicate the 1,3-thiazoles to be more stable than their thiazine analogs.

In order to examine the conformation of these thiazine rings, and to shed some light on conformational changes promoted by ring closure, a crystal structure determination of (II, $n = 3$) and (III) was initiated. The structure of (III) is described in this article.

EXPERIMENTAL

Colourless tabular crystals were obtained by slow evaporation of an acetone solution.

From the systematic absences the space group was determined to $P2_1/c$. Unit cell parameters were calculated using measurements of the four equivalents of twelve unique reflections on a manual Picker diffractometer with Cu$K\beta$ radiation ($\lambda = 1.3922$ Å). Three-dimensional data were collected on a punched card controlled four circle Picker diffractometer with $\omega - 2\theta$ scan technique. The crystal used was approximately $0.35 \times 0.18 \times 0.07$ mm^3, and was mounted with b along the ϕ axis. The Mo$K\alpha$ radiation was monochromated with a highly oriented graphite crystal. The 2θ scan speed was 2° min^{-1}. Three test reflections were measured for every 100 reflections and the intensities accordingly adjusted. Estimated standard deviations in the intensities were taken as the square root of the total counts adding 1 % to allow for the uncertainty in the adjustments.

2185 unique reflections with 2θ less than 50° were measured. 1019 of these had intensities larger than $2\sigma(I)$ and were regarded as observed. The intensity data were corrected for Lorentz, polarization and absorption effects.

Atomic form factors used were those of P. A. Doyle and P. S. Turner [4] for chlorine, sulphur, oxygen, nitrogen, and carbon, and of Stewart *et al.*[5] for hydrogen.

All programs but the *ORTEP* program applied during the structure investigations are described in Ref. 6.

CRYSTAL DATA

2-(3-Diethylaminopropylthio)-4,5-dichloropyrimidin-6-one, $C_{11}H_{17}ON_3SCl_2$, monoclinic, space group $P2_1/c$.
$a = 9.471(1)$ Å, $b = 17.634(4)$ Å, $c = 9.006(1)$ Å, $\beta = 80.93(1)°$, $V = 1485$ Å^3, $M = 309.27$, $F(000) = 648$, $\mu = 0.538$ mm^{-1}, $Z = 4$, D_{obs} (flotation) = 1.37 g cm^{-3}, $D_{calc} = 1.383$ g cm^{-3}.

STRUCTURE DETERMINATION

From a sharpened Patterson function the positions of the sulphur and one of the chlorine

Table 1. Observed and calculated structure factors.

Table 1. Continued.

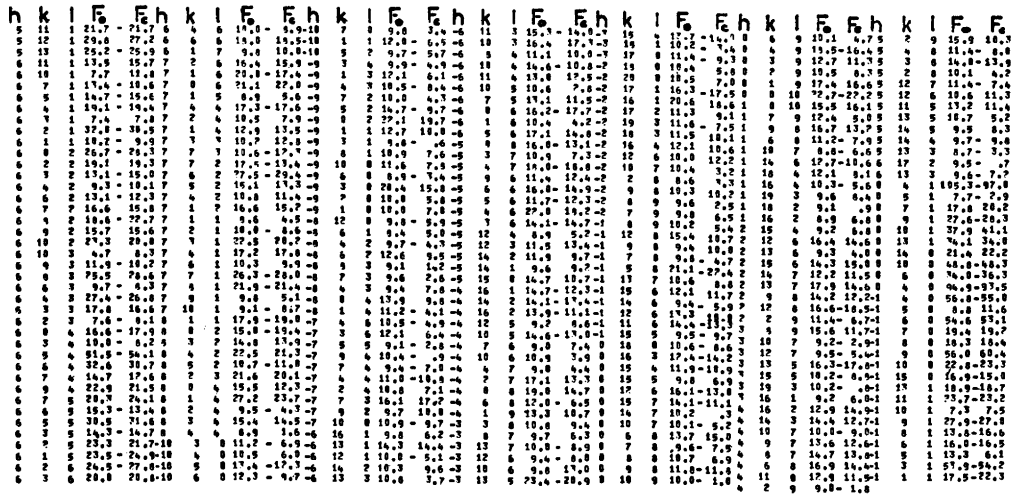

Table 2. Fractional atomic coordinates for non hydrogen atoms, anisotropic thermal vibration parameters and their estimated standard deviations (multiplied by 10^4). The temperature factors are expressed as: $\exp -(\beta_{11}h^2+\beta_{22}k^2+\beta_{33}l^2+\beta_{12}hk+\beta_{13}hl+\beta_{23}kl)$.

Atom		x	y	z	β_{11}	β_{22}	β_{33}	β_{12}	β_{13}	β_{23}
Cl	5	431	1533	1135	136	57	230	25	−49	94
		3	3	3	3	1	8	6	10	7
Cl	4	2905	2387	−1008	212	66	272	15	−92	−165
		4	2	4	7	2	9	7	13	8
S	2	6754	768	921	129	63	145	−10	−61	6
		3	2	4	6	2	6	6	10	7
O	6	1634	411	2988	134	39	140	−5	−15	54
		8	4	9	14	4	16	13	25	14
N	3	4619	1502	107	158	41	143	−20	−83	73
		13	7	12	23	6	21	21	36	19
N	1	3993	584	2046	120	26	143	−11	−86	−3
		13	5	11	19	5	22	17	33	16
C	2	4911	970	1072	100	38	94	−35	−50	−30
		13	8	15	23	8	26	22	39	22
C	6	2562	764	2091	119	39	79	−63	3	−6
		15	8	13	25	7	26	25	40	23
C	5	2152	1330	1118	141	31	100	−2	−27	56
		14	7	15	25	6	24	23	40	21
C	4	3231	1659	199	118	44	141	10	−106	17
		17	8	15	24	8	28	25	45	23
C	7	6878	−24	2200	227	37	145	11	−194	44
		13	7	13	26	6	24	22	42	22
C	8	6763	235	3826	239	46	167	−44	−146	54
		14	8	15	30	7	29	25	48	22
C	9	7973	771	404	194	47	143	−93	−151	57
		14	8	15	25	6	25	25	39	25
N	10	8031	930	5711	141	24	130	−14	−15	−27
		11	5	11	18	5	19	16	31	17
C	11	9407	1346	5782	162	43	239	100	−79	−31
		14	7	15	25	8	32	24	46	26
C	12	9671	1413	−7434	335	64	200	84	−293	−20
		17	8	17	34	9	29	29	53	29
C	13	6698	1291	6640	236	46	260	−117	162	−108
		16	8	16	30	7	43	26	53	27
C	14	6334	2048	6038	367	55	451	−133	25	−74
		18	8	20	40	9	50	33	70	38

atoms were determined. The corresponding Fourier map revealed the positions of all non hydrogen atoms. Fourier and fullmatrix least squares refinements converged with a conventional R factor of 0.100 and a weighted R_w factor ($R_w = (\sum w\Delta^2/\sum wF^2)^{\frac{1}{2}}$) of 0.062. Least squares refinements using 913 reflections with $I \geq 2.5\sigma(I)$ yielded an R of 0.086 and an R_w of 0.060. There were no significant differences between the two parameter sets. Calculated positional parameters and estimated thermal parameters (6 – 8 Å^2) for hydrogen atoms were included, but not refined, in the last refinements.

Observed and calculated structure factors are given in Table 1. [$I \geq 2\sigma(I)$] and final parameters for non-hydrogen atoms in Table 2. Magnitudes and directions of the principal axes of the vibrational ellipsoids and numbering of atoms are given in Fig. 1. Bond lengths and angles with estimated standard deviations are presented in Table 3. The estimated standard deviations were calculated from the correlation matrix. Short intermolecular contacts and deviations from a least squares plane are given in Table 4. The r.m.s. discrepancy between the atomic vibration tensor components obtained in the structure determination and those calculated from a rigid-body analysis were 0.0087 in the pyrimidine moiety and 0.0227 for the entire molecule. The coordinates were accordingly not adjusted for libration.

DISCUSSION

Fig. 3. shows the packing of molecules in the crystal, and Fig. 2. shows how molecules related by inversion centres form dimers with hydrogen bonds between the O4 and the N10 atoms.

The hydrogen bond length (2.688 Å) is identical to that ($NH^+\cdots O^-$) found in the crystal structure of methoxypromazine malonate.[7] The remaining intermolecular contacts are normal van der Waals contacts.

The conformation in the side chain (with two *gauche* interactions) is probably adapted to the ring system arising when the hydrogen bonds are formed.[8] The contact between S2 and C9 is rather short (3.205 Å), while the N1···C8 distance (3.755 Å) is somewhat longer than a normal van der Waals contact.

Bond lengths and angles in the side chain are normal. The N10 – C bond distances (1.52 Å in average) resemble C – N bond distances found in the $Et_2\overset{+}{H}N$-groups of isothiazine,[9] procain,[10] and diethazine.[11] The C13 – C14 bond length is slightly shorter than the other $C_{sp^3} - C_{sp^3}$ bond lengths. This is probably a result of high thermal motion in the side chain.

The pyrimidine moiety seems to be nearly planar. The chlorine atoms deviate significantly from this plane, and together with the oxygen atom they form a system similar to that found

Table 3. Bond lengths (Å) and angles (°) with their estimated standard deviations in parenthesis.

N1 – C2	1.322(13)	C2 – S2	1.764(12)
C2 – N3	1.336(13)	S2 – C7	1.827(11)
N3 – C4	1.334(13)	C7 – C8	1.521(15)
C4 – C5	1.341(14)	C8 – C9	1.516(15)
C5 – C6	1.418(15)	C9 – N10	1.538(13)
C6 – N1	1.388(13)	N10 – C11	1.507(13)
C6 – O6	1.262(11)	N10 – C13	1.537(14)
C5 – C15	1.668(13)	C11 – C12	1.551(16)
C4 – C14	1.743(13)	C13 – C14	1.499(16)
N1 – C2 – N3	127.5(12)	N1 – C2 – S2	119.1(12)
C2 – N3 – C4	114.3(12)	N3 – C2 – S2	113.3(11)
N3 – C4 – C5	126.5(13)	C2 – S2 – C7	105.4(7)
C4 – C5 – C6	115.4(13)	S2 – C7 – C8	111.9(11)
C5 – C6 – N1	120.4(11)	C8 – C9 – N10	112.5(12)
C6 – N1 – C2	115.9(11)	C7 – C8 – C9	111.8(12)
N1 – C6 – O6	118.7(14)	C9 – N10 – C11	107.2(9)
O6 – C6 – C5	120.9(14)	C9 – N10 – C13	116.9(10)
C6 – C5 – C15	120.6(11)	C11 – N10 – C13	114.6(10)
C15 – C5 – C4	124.0(11)	N10 – C11 – C12	110.6(12)
C5 – C4 – C14	120.9(12)	N10 – C13 – C14	112.8(12)
C14 – C4 – N3	112.6(12)		

Table 4. Deviation (Å) of atoms from a least squares plane through the atoms N1, C2, N3, C4, C5, C6.

N1	−0.002	C7	−0.120
C2	0.008	S2	−0.017
N3	−0.007		
C4	0.004	C14	0.069
C5	0.001	C15	−0.035
C6	−0.001	O6	−0.022

Intramolecular contacts		Intermolecular contacts	
N1···C7	2.943	C15···C9(a)	3.487
S2···C9	3.205	C15···C12(b)	3.526
C8···C13	3.136	C15···S2(a)	3.768
C15···C14	3.170	C14···C5(c)	3.592
C15···O6	2.934		

Hydrogen bond

O6−N10(d)	2.688	(a) $-1+x,y,z$
		(b) $-1+x,y,-1+z$
		(c) $x,\frac{1}{2}-y,-\frac{1}{2}+z$
		(d) $1-x,-y,1-z$

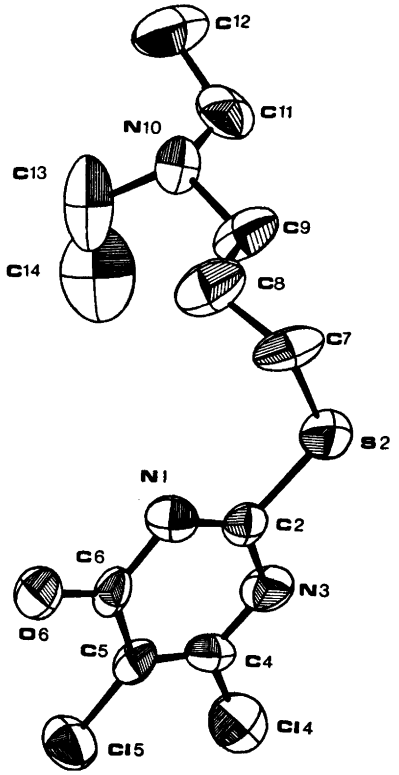

Fig. 1. The molecule viewed along *b*. 50 % probability ellipsoids.

in benzene derivatives possessing molecular overcrowding.[12–14]

It is interesting to compare corresponding bond lengths and angles with those found in disodium 4-oxypyrimidine-2-sulphinal hexahydrate [15] (IV):

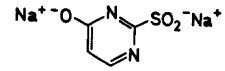

(IV)

Apart from the C−S bonds there is a remarkable similarity between corresponding bond lengths and angles. No significant differences are observed. Thus, the pertubation of the ring system seems to be negligible when chlorine atoms are introduced at position 4 and 5. The observed bond lengths in the pyrimidine moiety are approximately (∓0.03 Å) simulated by CNDO/2 calculations [16] and empirical bond length-π-bond order relationships.[17] The calculations indicates a π-bond order of 0.73 in the C−O bond. Thus, a zwitterionic state of the molecule seems very probable. The following charge density were found: N1 −0.28; C2 0.26; N3 −0.31; C4 0.31; C5 −0.08; C6 0.25; O6 −0.47; C15 −0.22; C14 −0.26; S2 −0.18.

As to the C2−S2 bond length (1.764 Å) it is very similar to $C_{sp^3}-S$ bonds in 1,4-thiazine derivatives.[9,18,19] A calculated π-bond order of 0.20 indicates a barrier against rotation about this bond. This barrier probably forces C7 into the plane through the ring atoms. The N1···C7 contact (2.943 Å), the C2−S and S−C7 bond lengths, the C−S−C angle and the dihedral angle about the C2−S bond are in agreement with those for *S*-methyl-thiourea sulphate [20] (2.99 Å, 1.743(7) Å, 1.790(9) Å, 104.1(4)°, 18°).

The C4−C14 bond length (1.743 Å) is similar to the average value 1.737(∓0.016) Å of 26 $C_{arom.}-Cl$ bond lengths reported by Palenik, Donohue and Trueblood(1968).[21] Comparing the C4−C14 bond length with the C4−C14 bond lengths in 6-amino-2,4-dichloropyrimidine [22] [1.76(1) Å] and 2-amino-4,6-dichloropyrimidine [22] [1.77(1) Å] it seems to be somewhat short.

The C5−C15 bond length (1.668 Å) is significantly shorter than both the C4−C14 bond length and the average value.

The observation of two short C−Cl bonds in (III) is not surprising as C−Cl bonds in molecules with chlorine atoms in adjacent positions

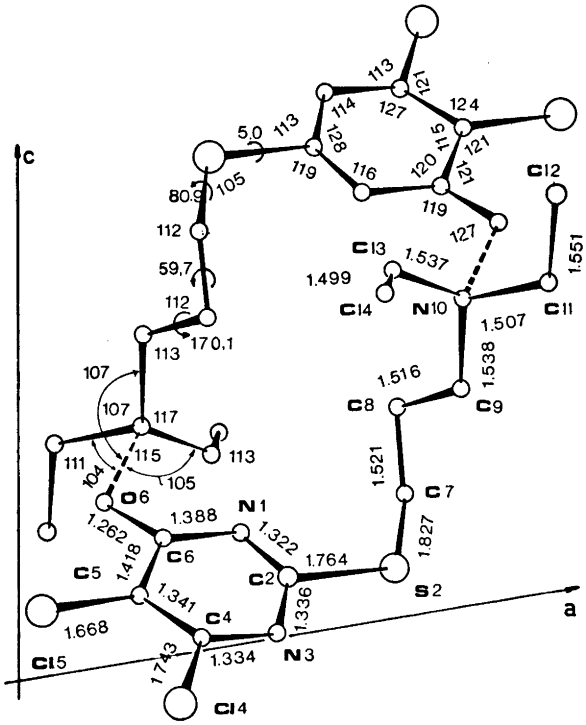

Fig. 2. The dimeric unit. Bond lengths, bond angles, and dihedral angles.

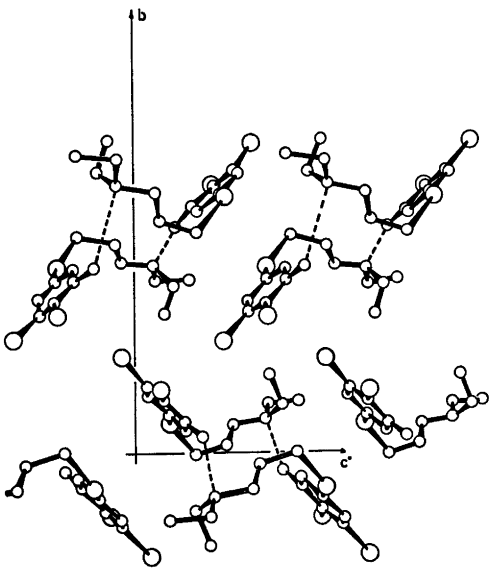

Fig. 3. Packing of molecules. The view is down the *a* axis.

usually are found to be somewhat short (discussed by Rudman 1971).[12] The difference between the two C–Cl bond lengths may possibly be attributed the overall shape of the pyrimidine ring. Corresponding pyrimidine rings (including IV) have wide internal angles at the C2, C4, and C6 atoms and narrow angles at the N1, N3, and C5 atoms.[22–25] Thus C5–Cl bonds probably get a greater *s*-character than the C4–Cl bonds in pyrimidines.

Morino *et al.* (1967) [26] and Boer and North (1971) [27] attribute the shortening of these C–Cl bonds to an inductive effect from the chlorine atoms lowering the charge densities or increasing the electronegativity (according to Walsh [28] and Dewar [29]) in the adjacent positions.

The author thanks K. Berg-Nielsen for supplying the title compound, and E. Hough for extended advice when using the *ORTEP* [30] program.

REFERENCES

1. Berg-Nielsen, K., *Acta Chem. Scand. To be published.*
2. Undheim, K. and Reistad, K. R. *Acta Chem. Scand. 24* (1970) 2949.
3. Undheim, K. and Reistad, K. R. *Acta Chem. Scand. 26* (1972) 1620.
4. Doyle, P. A. and Turner, P. S. *Acta Crystallogr. A 24* (1968) 390.
5. Stewart, R. E., Davidson, E. R. and Simpson, W. T. *J. Chem. Phys. 42* (1965) 3175.
6. Dahl, T., Gram, F., Groth, P., Klewe, B. and Rømming, C. *Acta Chem. Scand. 24* (1970) 2232.
7. Marsau, P. and Gauthier, J. *Acta Crystallogr. B29* (1973) 992.
8. Eliel, E. L., Allinger, N. L., Angyal, S. J. and Morrison, G. A. *Conformational Analysis*, Interscience, New York, London, Sidney 1967, p. 217.
9. Marsau, P. and Calas, M. *Acta Crystallogr. B 27* (1971) 2058.
10. Dexter, D. D. *Acta Crystallogr. B 28* (1972) 49.
11. Marsau, P. *Acta Crystallogr. B 27* (1971) 42.
12. Rudman, R. *Acta Crystallogr. B 27* (1971) 262.
13. Gafner, G. and Herbstein, F. H. *Acta Crystallogr. 15* (1962) 1081.
14. Sakurai, T. *Acta Crystallogr. 15* (1962b) 1164.
15. Sletten, J. *J. Amer. Chem. Soc. 91* (1969) 4545.
16. Pople, J. A. and Segal, G. A. *J. Chem. Phys. 44* (1166) 3289.
17. Gropen, O. and Skancke, P. N. *Acta Chem. Scand. 23* (1969) 2685.
18. McDowell, J. J. H. *Acta Crystallogr. B 25* (1969) 2175.
19. Chu, S. S. C. *Acta Crystallogr. B 28* (1972) 3625.
20. Stam, C. H. *Acta Crystallogr. 15* (1962) 317.
21. Palenik, G. H., Donohue, J. and Trueblood, K. N. (1968) *Acta Crystallogr. 12* (1959) 600.
22. Cochran, W. and Clews, C. J. B. *Acta Crystallogr. 9* (1956) 586.
23. Pletcher, J. Sengupta, S., Sax, M., Chu, I. and Yoo, C. S. *Acta Crystallogr. B 28* (1972) 2928.
24. Clews, C. J. B. and White, N. E. *Acta Crystallogr. 9* (1956) 586.
25. Wheatley, P. I. *Acta Crystallogr. 13* (1960) 80.
26. Monno, Y., Toyama, M., Itoh, K. and Kyono, S. *Bull. Chem. Soc. Jap. 35* (1962) 1667.
27. Boer, F. P. and North, P. P. *Acta Crystallogr. B 28* (1972) 1613.
28. Walsh, A. D. *J. Chem. Soc.* (1948) 390.
29. Dewar, M. J. S. *The Molecular Orbital Theory of Organic Chemistry*, McGraw-Hill, New York 1969, p. 150.
30. Johnson, C. K. (1965) *ORTEP*, Report ORNL-3795, Oak Ridge National Laboratory, Oak Ridge, Tennessee.

Received February 4, 1974.

Acta Chemica Scandinavica A 28 (1974) 607—611

The Donnan Potential. I

TORMOD FØRLAND[a] and TERJE ØSTVOLD[b]

[a]The University of Trondheim, Norwegian Institute of Technology, Division of Physical Chemistry, Trondheim, Norway and [b]The University of Trondheim, College of Arts and Science, Chemistry Department, Trondheim, Norway

The Donnan potential is calculated on the basis of classical irreversible thermodynamics for the following galvanic cell:

$$\mathrm{Ag}\left|\mathrm{AgCl}\left|\begin{matrix}\mathrm{KCl}\\ C_{(3\mathrm{M})}\end{matrix}\right|\right|\begin{matrix}\mathrm{KCl} & \mathrm{KR}\\ C_{(1)} & C_{\mathrm{R}}\end{matrix}\Bigg|\mathrm{Membrane}\left|\begin{matrix}\mathrm{KCl}\\ C_{(2)}\end{matrix}\right|\left|\begin{matrix}\mathrm{KCl}\\ C_{(3\mathrm{M})}\end{matrix}\right|\mathrm{AgCl}\left|\mathrm{Ag}\right|$$

The membrane is permeable to water, K^+ and Cl^- ions, but impermeable to R^- ions. When chemical equilibrium has been established across the membrane for KCl and H_2O, the emf calculated for the present cell may be approximated by the equation:

$$E=\frac{RT}{F}\left\{\ln\frac{C_{(\mathrm{K}1)}}{C_{(\mathrm{K}2)}}+\ln\left(1+\frac{(u_{\mathrm{R}}-u_{\mathrm{Cl}})\,C_{\mathrm{R}}}{(u_{\mathrm{K}}+u_{\mathrm{Cl}})\,C_{\mathrm{K}(3\mathrm{M})}}\right)\right\}$$

where the subscripted C's and u's denote, respectively, the concentrations and mobilities of the different ions in the solution. It is important to note that the potential given by this equation, according to the formalism applied in the present paper, is created in the two KCl salt bridges and not as usually stated in the area of the membrane.

The Donnan potential is a concept very commonly used in biophysics, and it is frequently used in calculations on transport processes across biological membranes. It is defined as the electric potential difference between membrane and solution at the membrane-solution interface. In a recent paper Førland and Østvold (1973)[1] calculated the total potential for the cell

$$\mathrm{Ag}\left|\mathrm{AgCl}\left|\begin{matrix}\mathrm{KCl}\\ C_{\mathrm{K}(3\mathrm{M})}\end{matrix}\right|\right|\begin{matrix}\mathrm{KCl} & \mathrm{K_2SO_4} & \mathrm{HCl}\\ C_{\mathrm{KCl}(1)} & C_{\mathrm{K_2SO_4}} & C_{\mathrm{HCl}}\end{matrix}\Bigg|$$
$$\mathrm{Membrane}\left|\begin{matrix}\mathrm{KCl} & \mathrm{Sugar}\\ C_{\mathrm{KCl}(2)} & C_{\mathrm{S}}\end{matrix}\right|\left|\begin{matrix}\mathrm{KCl}\\ C_{\mathrm{K}(3\mathrm{M})}\end{matrix}\right|\mathrm{AgCl}\left|\mathrm{Ag}\right|$$

The membrane was considered permeable to water and K^+ and Cl^- ions. Chemical equilibrium was assumed established for KCl and H_2O across the membrane.

Since it is generally assumed that the liquid junctions at the two salt bridges do not create any emf, it is supposed that the emf is created across the membrane. Since there is a concentration gradient of K^+ (and Cl^-) ions over the membrane, it has, of course, been tempting to apply the Nernst equation to this concentration gradient and calculate the corresponding potential difference, which immediately leads to the equation

$$E=\frac{RT}{F}\ln\frac{C_{\mathrm{K}(1)}}{C_{\mathrm{K}(2)}} \qquad (1)$$

This equation was derived by Donnan and by Guggenheim (1932)[2] and is in agreement with the results obtained for the above mentioned cell by the present authors.[1] The extensive agreement between theory and experiment has made this emf calculation widely accepted. However, since it inherently contains some not well defined quantities, a critical analysis of the above method of calculation ought to be made.

The only measurable potential difference is the total emf of the cell, but in the above treatment this has been split up into two liquid junctions and one membrane potential (in addition to the potentials of the two identical electrodes), which are not measurable quantities. Furthermore, the ratio $C_{\mathrm{K}(1)}/C_{\mathrm{K}(2)}$ is an approximation for the activity ratio of potassium ions, and activities of ions are also immeasurable.

The fundamental equation for calculating the emf of a reversible galvanic cell is:

$$\Delta G + FE = 0 \qquad (2)$$

where ΔG is the total change in Gibbs energy in the cell per Faraday transferred. Eqn. (2) is based on the first and second law of thermodynamics.

If, in addition to the process connected to the charge transfer, an irreversible diffusion process takes place in the cell, the problem can be dealt with within the framework of irreversible thermodynamics.

Due to the irreversible diffusion that takes place and due to the charge transfer itself, the Gibbs energy of the cell will change during charge transfer. It may be shown from the postulated of irreversible thermodynamics [Førland (1960)[3] and Førland, Thulin and Østvold (1971)[4]] that the Gibbs energy change can be separated into two parts, one time dependent, $\Delta G_{(t)}$, and one dependent on the electric charge transferred, $\Delta G_{(Q)}$, and that only the last one is connected to the external emf, E:

$$\Delta G_{(Q)} + FE = 0 \qquad (3)$$

This equation is the same as eqn. (2) for a cell with reversible reactions only.

The main difference between the method of emf calculation expressed by eqn. (3) and that expressed by an equation like eqn. (1), is that in the former no attempt is made to calculate any quantity that cannot be measured, whereas in the latter operations concerning immeasurable quantities are introduced. In most cases these immeasurable quantities will be combined in the final result yielding a measurably quantity, the calculated emf of the cell, so that the two approaches give the same final answer. However, problems may arise in applications of the latter method whenever it is desirable to include physical interpretations in the course of the calculations, *e.g.* in connection with the introduction of approximations.

Equations like eqn. (1) give detailed information on the sources of the electric potential difference. In the case of the present cell, this is across the membrane, even though it cannot be verified by measurements. Eqn. (3), on the other hand, can tell us in an exact way the siatuation in cell where the cause of the measured emf is to be found, since contributions to $\Delta G_{(Q)}$ are well defined measureable quantities in any section of the cell.

The statement that the electrical potential difference over the cell according to eqn. (1) is created over the membrane, is in contradiction with the results obtained using the more fundamental eqns. (2) or (3).

Let us in the following discussion try to resolve this contradiction and let us use the following galvanic cell to demonstrate our ideas:

$$\mathrm{Ag}\,|\,\mathrm{AgCl}\,|\,\underset{C_{(3M)}}{\mathrm{KCl}}\,||\,\underset{C_{(1)}}{\mathrm{KCl}}\;\underset{C_{(R)}}{\mathrm{KR}}\,|\,\mathrm{Membrane}\,|\,\underset{C_{(2)}}{\mathrm{KCl}}\;\underset{C_S}{\mathrm{Sugar}}\,||\,\underset{C_{(3M)}}{\mathrm{KCl}}\,|\,\mathrm{AgCl}\,|\,\mathrm{Ag}$$

The membrane is permeable to water and K^+ and Cl^- ions but impermeable to the larger anion R^-. Chemical equilibrium is assumed established for KCl and H_2O across the membrane. This cell is also shown schematically in Fig. 1.

Since the membrane is permeable to K^+ and Cl^- only (the transport of water may be disregarded at the moment), charge transfer across the membrane will be connected with a change in the content of KCl in the electrolyte on the two sides of the membrane. The extent of the change in KCl content on each side is dependent on the transport numbers in the

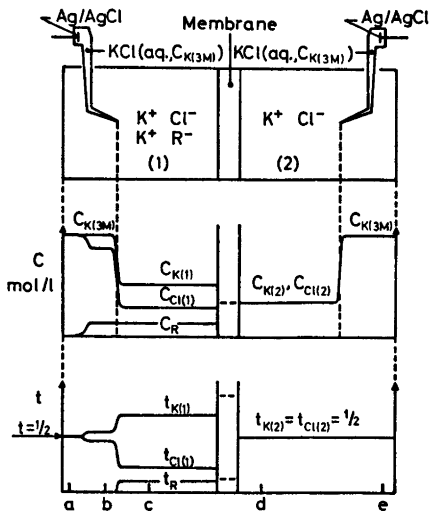

Fig. 1. A schematic diagram of a special galvanic cell constructed to study the Donnan potential together with diagrams of the variations of the concentration of the K^+, Cl^-, and R^- ions and the transport numbers of the K^+, Cl^-, and R^- ions throughout the cell.

membrane. However, these transport numbers are of no interest in the emf calculation, since transport of KCl in this region occurs over ranges with constant chemical potential ($\mu_{KCl(1)} = \mu_{KCl(2)}$). Thus, the contribution to $\Delta G_{(Q)}$, and therefore also to the emf, by charge transfer is zero in the electrolyte close to the membrane and in the membrane.

This has been a problem to several scientists working in the field of membrane potentials [see Babcock and Overstreet (1953) [5] and Bull (1971) [6]]. When there is no contribution to $\Delta G_{(Q)}$ in the region of the membrane, the next question arise; Where is the measured electric work generated? The only source left is the liquid junction to the KCl bridge, even though such contacts are generally believed not to contribute to an emf.

We will consider the transport of components from the left hand side of the cell. The mobilities of K^+ and Cl^- ions are approximately equal. The ratio C_K/C_{Cl} is unity in the 3 M solution, but it is greater than unity in the KCl-KR mixture. Therefore the transport number of K^+ ions is increasing from left to right in the liquid junction (water is chosen as frame of reference). Consequently KCl must be transported from a high to a low concentration region when a positive charge is passed from left to right in the cell. This must be the main contribution to $\Delta G_{(Q)}$ and thus to the observed emf.

The following derivation is carried out for the sake of the scientist interested in the alternative approach to emf calculations making use of well defined measurable quantities only.

The cell considered is the one shown in Fig. 1. In the following calculation the assumption of ideal solution and constant ionic mobilities will be introduced. However, the method of calculation posesses the same rigidity as the laws of thermodynamics themselves. Since only measurable quantities are dealt with, it is always possible to check the approximations introduced in the calculation by measurements.

The change in Gibbs energy due to charge transfer and the emf are connected by eqn. (3). Calculation of $\Delta G_{(Q)}$ requires knowledge of the transport numbers and chemical potential of the components along the whole length of the cell [see, *e.g.*, Førland, Thulin and Østvold (1971) [4]],

$$\Delta G_{(Q)} = \Delta G_{el} - \int_{\substack{over \\ cell}} \sum_i \mu_i dt_i \qquad (4)$$

where ΔG_{el} is the change in Gibbs energy in the vicinity of the electrodes. In the present cell the two electrodes and their surroundings are identical, so $\Delta G_{el} = 0$. The integral $-\int \sum_i \mu_i dt_i$ is the change in Gibbs energy due to change in composition by the charge transfer in the different sections of the cell. In any region where all transport numbers t_i, are constant, the change in Gibbs energy is zero.

If we are to strictly restrain ourselves to measured quantities in our derivation of the emf, and not introduce and unnecessary assumptions about the ionic species present in our system, both μ_i and t_i should refer to neutral components. The transport coefficient, t_i, simply expresses the result of an Hittorf transport experiment, where it is found by chemical analysis that a quantity t_i of component i has moved from left to right in a Hittorf cell, when 1 Faraday is passed through the cell. Such a transport coefficient for a neutral componet will depend on the kind of electrodes used.

In a transport experiment it is necessary to define a frame of reference relative to which the movements of the components are expressed. The most commonly used reference frame in experiments on aqueous solutions is the water itself. For systems with a membrane it may sometimes be more practical to use the membrane as a frame of reference. The correlation between the two kinds of corresponding transport coefficients is of course given by the transpost of water through the membrane during charge transfer.

For the present cell, where the Gibbs energy charge during charge transfer is zero in the region of the membrane, it is most practical to use the water as frame of reference.
From eqn. (4) we have:

$$\Delta G_{(Q)} = -\int (\mu_{KCl} dt_{KCl} + \mu_{KR} dt_{KR}) \qquad (5)$$

Here t_{KCl} and t_{KR} are, respectively, the number of moles of KCl and KR transported from left to right per Faraday transferred in a Hittorf cell with electrodes reversible to the Cl^- ion as shown in Fig. 2.

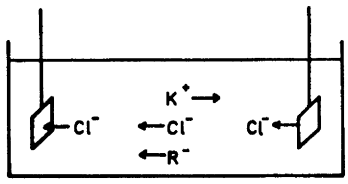

Fig. 2. The Hittorf experiment with electrodes reversible to the Cl^- ion.

Wanting to express the result of the Hittorf experiment in terms of the ionic transport numbers, it may easily be seen that:

$$t_{KCl} = t_K + t_R = 1 - t_{Cl}$$
and
$$t_{KR} = -t_R$$
thus
$$dt_{KCl} = -dt_{Cl} \text{ and } dt_{KR} = -dt_R \quad (6)$$

Introducing eqn. (6) into eqn. (5) we obtain

$$\Delta G_{(Q)} = \int_{a\to e} \mu_{KCl} dt_{Cl} + \int_{a\to e} \mu_{KR} dt_R \quad (7)$$

Fig. 1 shows how the concentration changes along the length of the cell. It should be noticed that the liquid junction for the KCl bridge on the left hand side is made in a special way. Some KR is dissolved into the 3 M KCl solution. Thus, in this liquid junction the content of one component (with respect to the water content) remains approximately constant while the other one is changing. This makes it possible to calculate the contribution to $\Delta G_{(Q)}$ in the liquid junction without introducing the Henderson (1907, 1908) [7] or Planck (1890) [8] approximations. In a recent paper experimental and calculated potentials for concentration cells containing the above mentioned type of gradients were compared.*

Calculation of $\Delta G_{(Q)}$ in eqn. (7) may be simplified by the use of partial integration:

$$\Delta G_{(Q)} = |_{a\to e} t_{Cl}\mu_{KCl} - \int_{a\to e} t_{Cl} d\mu_{KCl} + |_{a\to e} t_R \mu_{KR} - \int_{a\to e} t_R d\mu_{KR} \quad (8)$$

Since the two electrodes are identical the terms $|_{a\to e} t_{Cl}\mu_{KCl} = 0$.

Since $\lim_{x\to 0} x \ln x = 0$ the term $|_{a\to e} t_R \mu_{KR} = 0$

*To be published.

Furthermore, the integral over the range c→d

$\int_{c\to d} t_{Cl} d\mu_{KCl} = 0$ because $d\mu_{KCl} = 0$ in this range

and

$\int_{c\to d} t_R d\mu_{KR} = 0$ because $d\mu_{KR} = 0$ in the range

where $t_R \neq 0$

The terms left in eqn. (8) are:

$$\Delta G_{(Q)} = -\int_{a\to c} t_{Cl} d\mu_{KCl} - \int_{d\to e} t_{Cl} d\mu_{KCl} - \int_{a\to c} t_R d\mu_{KR} \quad (9)$$

Using the present formalism it is evident that no contribution to $\Delta G_{(Q)}$ is created in the area of the membrane and therefore no emf can be produced in this section of the cell.

From eqn. (9) an exact calculation of $\Delta G_{(Q)}$, and thus of the emf, may be carried out when the chemical potential and transport numbers are known as functions of composition.

When such data are not at hand, an approximate calculation may be carried out by assuming ideal solutions and constant ionic mobilities. Since the mobilities of K^+ and Cl^- are approximately equal, $t_{Cl} \simeq \frac{1}{2}$ in the range d→e. The transport numbers of Cl^- and R^- may be expressed as:

$$t_{Cl} = \frac{u_{Cl}C_{Cl}}{\sum_i u_i C_i} \text{ and } t_R = \frac{u_R C_R}{\sum_i u_i C_i}$$

where

$$\sum_i u_i C_i = u_K C_K + u_{Cl} C_{Cl} + u_R C_R = (u_K + u_{Cl}) C_K + (u_R - u_{Cl}) C_R$$

The assumption of ideal solution gives:

$$d\mu_{KCl} = RT\, d \ln C_K C_{Cl} \text{ and } d\mu_{KR} = RT\, d \ln C_K C_R$$

In the following integration this approximation is applied over a very large concentration range. However, the major contribution to the integrals will lie in the range of low concentrations. (This may also be observed from the final result of this calculation.)

In the range a→b C_R and C_{Cl} vary, and $dC_R = -dC_{Cl}$

In the range b→c C_K and C_{Cl} vary, and $dC_K = dC_{Cl}$

Introducing the above approximations into eqn. (9) we obtain

$$\frac{\Delta G_{(Q)}}{RT} = -\int_{a\to b} t_{Cl}\frac{dC_{Cl}}{C_{Cl}} - \int_{a\to b} t_R\frac{dC_R}{C_R} - \int_{b\to c} t_{Cl}\times \left(\frac{dC_K}{C_K}+\frac{dC_{Cl}}{C_{Cl}}\right) - \int t_R\frac{dC_K}{C_K} - \tfrac{1}{2}\ln C_{K(3M)}{}^2 + \tfrac{1}{2}\ln C_{K(2)}{}^2$$

and

$$\frac{\Delta G_{(Q)}}{RT} = -\int_{a\to b}\frac{(u_R-u_{Cl})dC_R}{(u_K+u_{Cl})c_{K(3M)}+(u_R-u_{Cl})C_R} - \int\frac{u_{Cl}-u_K}{\sum u_i C_i}dC_K - \int\frac{dC_K}{C_K} - \ln C_{K(3M)} + \ln C_{K(2)}$$

Since $u_{Cl}=u_K$, we obtain

$$\frac{\Delta G_{(Q)}}{RT} = \int_{C_R=0}^{C_R=C_R} \ln\{(u_K+u_{Cl})C_{K(3M)}+(u_R-u_{Cl})C_R\} - \int_{C_{K(3M)}}^{C_{K(1)}} \ln C_K - \ln C_{K(3M)} + \ln C_{K(2)}$$

and

$$\frac{\Delta G_{(Q)}}{RT} = -\ln\left\{1+\frac{(u_R-u_{Cl})C_R}{(u_K+u_{Cl})C_{K(3M)}}\right\} + \ln\frac{C_{K(2)}}{C_{K(1)}} \quad (10)$$

The emf of the Donnan cell will therefore be equal to

$$E = \frac{RT}{F}\left[\ln\frac{C_{K(1)}}{C_{K(2)}} + \ln\left\{1+\frac{(u_R-u_{Cl})C_R}{(u_K+u_{Cl})C_{K(3M)}}\right\}\right] \quad (11)$$

The last term will generally be very small since $C_{K(3M)} \gg C_R$, and the expression for the emf will be the same as eqn. (1). It is, however, important to note that the potential given by eqn. (11), according to the present formalism, is created in the two KCl salt bridges and not in the area of the membrane.

This surprising result, namely that the potential created across the membrane is zero, is a consequence of the alternative way proposed for splitting the total cell potential in electrode and junction contribution which now are expressed by measurable and thermodynamically well defined quantities.

The advantage of the above derivation of eqn. (11) lies in the fact that only quantities which are well defined by measurements are used, that each operation in the derivation is easily visualized physically, that the approximations introduced may be judged experimentally, and that one can see how the calculation can be carried out more accurately when better data are available.

REFERENCES

1. Førland, T. and Østvold, T. *Acta Chem. Scand. 27* (1973) 2199.
2. Donnan, F. G. and Guggenheim, E. A. *Z. Phys. Chem. (Leipzig) 162* (1932) 346.
3. Førland, T. *Acta Chem. Scand. 14* (1960) 1381.
4. Førland, T., Thulin, L. U. and Østvold, T. *J. Chem. Educ. 48* (1971) 741.
5. Babcock, K. L. and Overstreet, R. *Science 117* (1953) 686.
6. Bull, H. B. *An Introduction to Physical Biochemistry*, F. H. Davis Company, Philadelphia, 1971, p. 178.
7. Henderson, P. *Z. Phys. Chem. (Leipzig) 59* (1907) 118; *63* (1908) 325.
8. Planck, M. *Ann. Phys. (Leipzig) 39* (1890) 161; *40* (1890) 561.

Received January 21, 1974.

Acta Chemica Scandinavica A 28 (1974) 612—622

Conformational Analysis. IV. The Molecular Structure, Torsional Oscillations, and Conformational Equilibria of Gaseous $(CH_3)C(CH_2Cl)_3$, 1,1,1-Tris(chloromethyl)ethane, as Determined by Electron Diffraction and Compared with Semiempirical Calculations

REIDAR STØLEVIK

Department of Chemistry, University of Oslo, Blindern, Oslo 3, Nowray

Gaseous 1,1,1-tris(chloromethyl)ethane has been studied by electron diffraction at a nozzle temperature of 88 °C. Three spectroscopically distinguishable conformers *CS*, *C1*, and *C3* were detected (see Fig. 1 and Table 1). Results are presented with error limits (2σ). The following values for bond lengths (r_a) and bond angles ($\angle_\alpha$) are average parameters for the conformers: $r(C-H)=1.100(14)$ Å, $r(C-C)=1.532(6)$ Å $r(C-Cl)=1.792(6)$ Å, $\angle CCCl=113.9°(0.6)$, $\angle CCH=110.2°(1.4)$, $\angle HCH=108.7°(1.8)$, and $\angle HCCl=106.8°(1.6)$. A tetrahedral arrangement of carbon atoms was assumed. Non-bonded internuclear distances were computed as dependent qualities under the constraints of geometrically consistent r_α parameters. The conformers have torsion angles close to staggered values.

The composition at *ca.* 88 °C is: 45 %(6) of *CS*, 34 %(16) of *C1*, and 21 %(14) of *C3*. Conformers with C—Cl bonds parallel are not present in detectable amounts.

According to the semi-empirical calculations, *C3* is the conformer of lowest minimum energy. The large percentage of *CS* encountered can be explained if it is assumed that the force field of *CS* is quite different from that of *C3* and *C1*. This point has been discussed.

Torsional force constants and frequencies corresponding to the torsional modes of the $-CH_2Cl$ groups have been estimated by combining information from electron diffraction and vibrational spectroscopy.

The characteristic structure parameters of molecules of the type $(CH_3)_{4-n}C(CH_2Cl)_n$ with $n=2$, 3, 4, have been compared in Table 10.

I. INTRODUCTION

The present electron-diffraction work is part of a systematic conformational study of halogenated propanes and related molecules. General [1] information [2] relevant to this investigation and to the electron-diffraction method [3] is found in Refs. 1, 2, and 3. The compounds $C(CH_2Cl)_4$[4] and $(CH_3)_2C(CH_2Cl)_2$[5] have recently been investigated by electron diffraction.

Compounds of the type $(CH_3)C(CH_2X)_3$ will be referred to as TEX, and the title compound as TECL. Classically the possible number of staggered conformers for TEX is 27 (3^3), but only *seven* are spectroscopically distinguishable as indicated in Fig. 1 and Table 1. Including *enantiomeric* conformers, there are 11 *physically* distinguishable staggered conformers.

The conformational names (Table 1) have been chosen to indicate the symmetries of the conformers. The conformers *CS*, *C1*, and *C3* are expected to be the most stable ones and the conformers *C1(1:3)**, *C1(1:3)***, and *CS(1:3)* less stable because of parallel (1:3)X···X interactions.[1] The conformational energy of *C3(1:3)* has to be very high because of the very unfavourable X-atom arrangement.

The spectroscopically distinguishable conformers may be assigned *multiplicities* (M) in two ways, as follows:

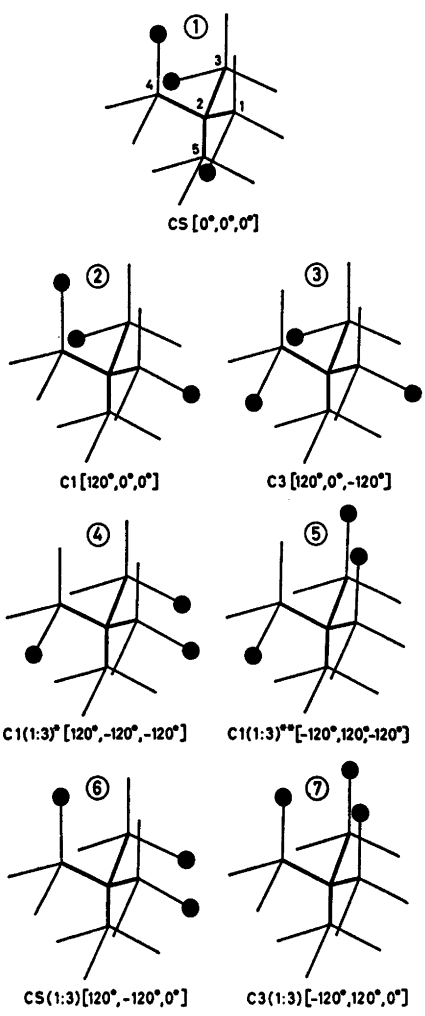

Fig. 1. Spectroscopically distinguishable staggered conformers of $(CH_3)C(CH_2X)_3$. If a conformer has C–X bonds parallel, that is indicated in the name as (1:3). Numbers in brackets are values of the torsion angles ϕ_{1-2}, ϕ_{3-2}, and ϕ_{4-2} ($\phi_{5-2}=0°$).

(1) only distinguishable conformers (11) are considered (M_d in Table 1)

(2) all classically possible conformers (27) are considered (M_c in Table 1).

For two spectroscopically distinguishable conformers C and C*, having symmetry numbers σ and σ^*, it is noteworthy [6] that $M_c^*/M_c = (M_d^*/M_d)\,(\sigma^*/\sigma)^{-1}$.

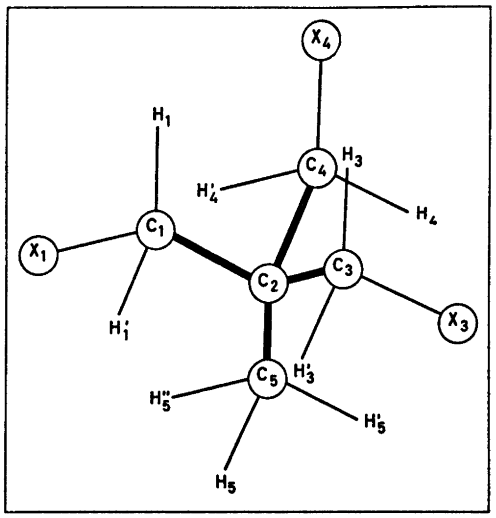

Fig. 2. Numbering of atoms in the conformer *CS*. The conventional name 1,1,1-tris(chloromethyl)ethane does not correspond to the numbering here.

II. CALCULATION OF CONFORMATION ENERGIES, GEOMETRIES, AND TORSIONAL FORCE CONSTANTS

The method of classical mechanics was used. The semiempirical energy calculations were carried out as described in Ref. 7. Energy parameters were taken from the work of Abraham and Parry,[8] and the diagonal valence force constants in Table 6 of Ref. 4 were used. In minimizing the energy, the geometry was constrained in the same way as described in Sect. V-A, except that all torsional angles (ϕ) were adjusted as independent variables.

The conformational geometries derived from the semiempirical energy model are presented in Table 2 together with "normal" values [7] of the geometry parameters.

In Table 3 are the results for conformational energies. According to the present energy model, *C3* is the most stable conformer. Most of the staggered conformers, except for *CS*, *C1*, and *C3*, have high conformational energies due to parallel (1:3)X···X interactions (see Fig. 1). All conformers with parallel (1:3)X···X interactions have their torsion angles displaced from staggered values. The energy of these conformers is thereby considerably lowered, but the

Table 1. Characterisation of the seven spectroscopically distinguishable staggered conformers of $(CH_3)C(CH_2X)_3$.

There are four X···X distances of different lengths: GG, AG, AA, and GG(1:3). The symbols A(*anti*) and G(*gauche*) have been used to characterize C–X bonds (*anti* or *gauche* to the CCC framework) of a X–CCC–X fragment. Lower case letters a(*anti*) and g(*gauche*) have been used to characterize the C–X bond (*anti* or *gauche* to the CCC framework) of a C–C–C–X fragment. The type of X···X distance corresponding to a *parallel* (1:3)X···X interaction (two C–X bonds parallel) has been specified as GG(1:3). All staggered conformers possess *three* C···X(a) and *six* C···X(g) distances.

	Name of conformer	Point group (symmetry number)	Multiplicities M_d	M_c	Type of X···X distances GG	AG	AA	GG(:3)
(1)	*CS*	$C_s(1)$	1	3	2	0	1	0
(2)	*C1*	$C_1(1)$	2	6	1	2	0	0
(3)	*C3*	$C_3(3)$	2	2	0	3	0	0
(4)	*C1(1:3)**	$C_1(1)$	2	6	0	1	1	1
(5)	*C1(1:3)***	$C_1(1)$	2	6	1	1	0	1
(6)	*CS(1:3)*	$C_s(1)$	1	3	0	2	0	1
(7)	*C3(1:3)*	$C_{3v}(3)$	1	1	0	0	0	3

Table 2. Calculated conformational geometry for $(CH_3)C(CH_2Cl)_3$. Distances in Å and angles in degrees.

Parameter (normal value)	*CS*	*C1*	*C3*
C–H (1.094)	1.093	1.093	1.093
C–C (1.513)	1.540	1.538	1.538
C–X (1.780)	1.790	1.790	1.789
CCC (109.47)[a]	(109.47)[a]	(109.47)[a]	(109.47)[a]
CCX (109.47)	113.9	113.5	113.4
CCH (109.47)	110.1	110.1	110.1
$\phi_{1-2}(-CH_2X)$[b]	−1.6	113.9	120.4
$\phi_{3-2}(-CH_2X)$	+1.6	1.6	0.4
$\phi_{4-2}(-CH_2X)$	0	1.0	−119.6
$\phi_{5-2}(-CH_3)$	0	−12.7	−15.0

[a] In minimizing the energy, the geometry was constrained in the way described in Sect. V-A, except for the torsion angles being adjusted as independent variables. [b] $\phi_0 = 60°$ in the expression $V_\phi = \frac{1}{2}V_0\sum(1+\cos(3\phi_{k-2}-\phi_0))$ with $k = 1, 3, 4, 5$.

lowest energy obtained [for *CS(1:3)*] was still 4 kcal/mol higher than the energy for *CS*.

Some of the torsional barriers within TECL have to be very high, but the *lowest* torsional barriers separating the conformers *CS*, *C1*, and *C3* are *ca.* 5–6 kcal/mol.

The staggered conformer *C3(1:3)(−120°, 120°, 0°)*, with three C–X bonds parallel, corresponds to a *maximum* on the potential energy surface. If the C_{3v} symmetry is reduced to C_3 by a simultaneous change of the torsion angles ϕ_{1-2}, ϕ_{3-2}, and ϕ_{4-2}, then a conformation, *C3(1:3)(−100°, 140°, 20°)*, corresponding to a *minimum* on the energy surface is obtained. That minimum is still several kcal/mol above the minima of the remaining conformers.

The results of the energy calculations therefore suggest that the three conformers *CS*, *C1*, and *C3* ought to be present in detectable amounts at 88 °C.

Torsional force constants may be numerically

Table 3. Conformational energies (kcal/mol) in $(CH_3)C(CH_2Cl)_3$. Details about the energy expression are found in Ref. 7.

Type of energy	*CS*	*C1*	*C3*
E(bonded)	3.12	3.03	2.95
E(van der Waals)	5.02	4.66	4.71
E(polar, Cl···H)	−14.93	−15.07	−15.33
E(polar, Cl···Cl)	5.40	5.23	4.88
E(total)	−1.40	−2.16	−2.80
ΔE^m(total) $= E - E$(C3)	1.40	0.64	0.00

Table 4. Calculated torsional force constants for $(CH_3)C(CH_2Cl)_3$.

mdyn Å (rad)$^{-2}$	*CS*	*C1*	*C3*
$F_\phi(-CH_2X)$[a]	0.28 – 0.32	0.25 – 0.28	0.26
$F_\phi(-CH_3)$[b]	0.14	0.16	0.16
$-F_{\phi\phi'}(-CH_2X/-CH_2X)$[c]	0.01 – 0.12	0.05 – 0.11	0.06 – 0.07
$-F_{\phi\phi'}(-CH_2X/-CH_3)$[c]	0.01 – 0.06	0.01 – 0.04	0.03 – 0.04

[a] The range of values corresponding to $F_\phi(1-2)$, $F_\phi(3-2)$, and $F_\phi(4-2)$. [b] $F_\phi(-CH_3)=F_\phi(5-2)$. [c] All interaction force constants ($F_{\phi\phi'}$) are negative.

computed from the semiempirical energy model. The general expression for a quadratic force constant is:

$F_{qq'}=\partial^2E/\partial q\partial q'$ (q: internal coordinate)

Torsional force constants are given in Table 4. Experimental values are found in Sect. V-B.

III. CALCULATION OF VIBRATIONAL QUANTITIES

Valence force constants, except for the torsional part, were taken from the works of Schachtschneider [9] and Snyder.[10] The force constants for $(CH_3)_2C(CH_2Cl)_2$ were also used for TECL, and their values are found in Table 6 of Ref. 4.

The normal coordinate program described by Gwinn [11] was applied in computing vibrational frequencies.

Mean amplitudes of vibration (u and K values) were computed as described in Ref. 12. For the molecules $(CH_2Cl)_4C$ and $(CH_3)C(CH_2Cl)_3$, mean amplitudes of vibration at 105 and 60 °C, respectively, have already been published.[4,5] Therefore, only u values relevant for discussion and comparison with least-squares refined values are given here (Sect. VI). In Table 5 are shown some u values corresponding to different values of the torsional force constant $F_\phi(-CH_2X)$.

If the torsional force constants estimated from the electron diffraction data are used, then the torsional oscillations of the $-CH_2X$ groups correspond to vibrational frequencies in the range 70 – 200 cm^{-1}. The lowest frequency (*ca.* 70 cm^{-1}) is expected for the confomer *CS*, while the conformers *C1* and *C3* may have frequencies as low as 100 cm^{-1}.

Table 5. Mean amplitudes of vibration, u(Å), for $(CH_3)C(CH_2X)_3$ calculated at 88 °C using three different values of the torsional force constant $F_\phi(-CH_2X)$; X = Cl.

$F_\phi(-CH_2X)$[a]	0.36	0.63	0.90
X···X(GG)[b]	0.242	0.204	0.186
X···X(AG)[c]	0.161	0.151	0.146
X···X(AA)[d]	0.101	0.100	0.100
C···X(*gauche*)[e]	0.146	0.136	0.131

[a] Values of the valence force constants are found in Table 6 of Ref. 4. The value of $F_\phi(-CH_3)$ was 0.315 mdyn Å (rad)$^{-2}$. The torsional force constant F_ϕ were defined as follows: each fragment C–C–C–A (A=H or Cl) in a $-\overset{|}{\underset{|}{C}}-CH_2Cl$ group has been assigned an equal torsional force constant $f_\phi(-CH_2X)$, while each fragment C–C–C–H in a $-\overset{|}{\underset{|}{C}}-CH_3$ group has been assigned an equal torsional force constant $f_\phi(-CH_3)$. The total force constant for the torsion coordinate ϕ_{i-2} (i = 1, 3, 4) is thus $F_\phi(i-2)=9f_\phi(-CH_2X)$ and $f_\phi(5-2)=9f_\phi(-CH_3)$. [b] Present in the conformers *CS* and *C1*. [c] Present in the conformers *C1* and *C3*. [d] Only present in conformer *CS*. [e] Present in all conformers.

The conformational analysis of a molecule like TECL would be greatly simplified if the lowest frequencies could be independently obtained by vibrational spectroscopy (see Sect. VII).

IV. EXPERIMENTAL AND DATA REDUCTION

The compound was obtained from "K & K" laboratories. The purity of the sample was better than 98 %.

Electron-diffraction photographs were made

at a nozzle temperature of 88 °C in the Oslo apparatus [13] under conditions summarized below.

Nozzle-to-plate distance (mm)	480.74	200.60
Electron wavelength (Å)	0.06458	0.06458
Number of plates	4	4
Range of data, in s (Å^{-1})	1.50 – 19.875	7.25 – 44.25
Data interval, Δs (Å^{-1})	0.125	0.250
Estimated uncertainty in s-scale (%)	0.14	0.14

The electron wavelength was determined by calibration against gold and corrected by an experiment with CO_2 giving a correction of +0.1 % in the s-scale. The data were reduced in the usual way [14] to yield an intensity for each plate.

Average curves for each set of distances were formed. A composite curve was then made by connecting the two average curves after scaling. The final experimental intensity curve is shown in Fig. 3. The intensities have been modified by $s/|f'_{Cl}|^2$.

The scattering amplitudes were calculated by the partial wave method [15] using Hartree-Fock atomic potentials.[16]

Contributions to the theoretical intensities from H···H distances, the H atoms bonded to different carbon atoms, were not included.

The radial distribution (RD) curve obtained by Fourier transformation [14] of the final experimental intensity is presented in Fig. 4.

V. STRUCTURE ANALYSIS AND REFINEMENTS

From the experimental RD curve (Fig. 4) it was concluded that the conformers *CS*, *C1*, and *C3* are present, and approximate composition parameters (α) were estimated. [$\alpha(CS) \simeq \alpha(C1) + \alpha(C3) \simeq 50$ %]. The relative amounts of *C1* and *C3* can not easily be obtained from the RD curve alone. RD curves for the individual conformers are found in Fig. 5.

A. Least squares refinements. The least-squares program was written by H. M. Seip, and it is a modified version of the program explained in Ref. 14. Several conformers may be included in the refinements with the present version of the program. Models for the conformers were constructed with the following geometrical assumptions: (1) the carbon atoms have a tetrahedral arrangement; (2) the three C – CH_2X groups are equal; (3) each C – CH_2X group possesses C_s symmetry and the projection of ∠HCH′ on a plane perpendicular to the C – C axis is 120°;

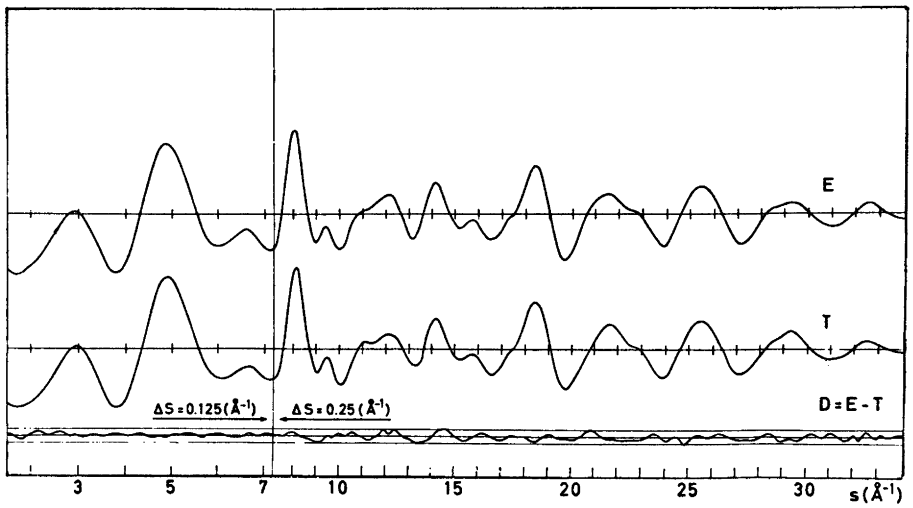

Fig. 3. Intensity curves for $(CH_3)C(CH_2Cl)_3$ at 88 °C. Experimental (E) and theoretical (T) intensity corresponding to the final least-squares parameters. Curve D represents E – T, and the straight lines give the experimental uncertainty (± 3 × experimental standard deviation).

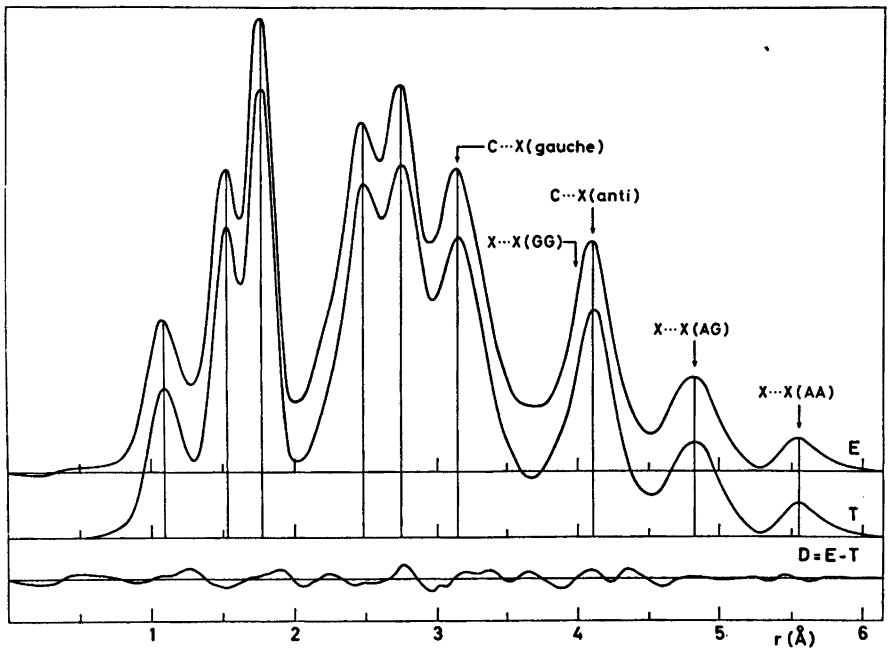

Fig. 4. Radial distribution curves for $(CH_3)C(CH_2Cl)_3$ at 88 °C. Experimental (E) and theoretical (T) radial distribution curves, and difference curve (D). The RD curves were calculated from the intensities of Fig. 3 with an artificial damping constant equal to 0.0020 Å^2.

(4) the $C-CH_3$ group possesses C_{3v} symmetry; (5) all C–H bonds are equal; (6) all CCH angles are equal; (7) the conformers have identical structures except for the C–C torsion angles (ϕ_{1-2}, ϕ_{3-2}, ϕ_{4-2}, and ϕ_{5-2}).

Models were defined in terms of the following average parameters: C–H, C–C, C–X, ∠CCX, ∠CCH, and the four ϕ angles. Also adjusted were the composition (%) parameters α(CS) and α(Cl), with $\alpha(C3) = 100\ \% - \alpha(CS) - \alpha(Cl)$.

Corrections for the "Bastiansen-Morino" shrinkage [17] effect on non-bonded distances have been included; non-bonded distances were computed as dependent parameters, restricted under the constraints of geometrically consistent r_α parameters.[18,19]

B. Determination of torsional force constants. The torsional modes of vibration contribute substantially to the mean amplitudes of several internuclear distances in a molecule like TECL Since a reasonable force field is known, except for the torsional part, torsional force constants can be adjusted to fit the electron-diffraction data. Determination of all torsional force constants from electron-diffraction data alone is not possible. Therefore, the theoretical values of Table 4 were used as a guide, and the following assumptions were made:

(1) all interaction constants $F_{\phi\phi'} = 0$; (2) in the conformer *CS*: $F_\phi(1-2) = F_\phi(2-3) = F_\phi(4-2) = F_\phi(CS)$; (3) in the conformer *C1*: $F_\phi(1-2) = F_\phi(3-2) = F_\phi(4-2) = F_\phi(Cl)$; (4) in the conformer *C3*: $F_\phi(1-2) = F_\phi(3-2) = F_\phi(4-2) = F_\phi(C3)$; (5) for all three [4] conformers $F_\phi(5-2) = F_\phi(-CH_3) = 0.135$ mdyn Å (rad)$^{-2}$. Thus, three variables, F_ϕ(CS), F_ϕ(Cl), and F_ϕ(C3) were considered as independent variables. An average torsional constant ($F_\phi(CS) = F_\phi(Cl) = F_\phi(C3) = \bar{F}_\phi$) equal to 0.63 mdyn Å (rad)$^{-2}$ was tried. (That value of $\bar{F}_\phi$ was obtained for the molecules $C(CH_2Cl)_4$ [4] and $(CH_3)_2C(CH_2Cl)_2$ [5]). Parallel and perpendicular amplitudes corresponding to $\bar{F}_\phi = 0.63$ were computed and included in the least-squares refinements. The structure and composition parameters were refined simultaneously. The fit obtained between theoretical and experimental intensities was practically as good as shown in Fig. 3. The discrepancies between

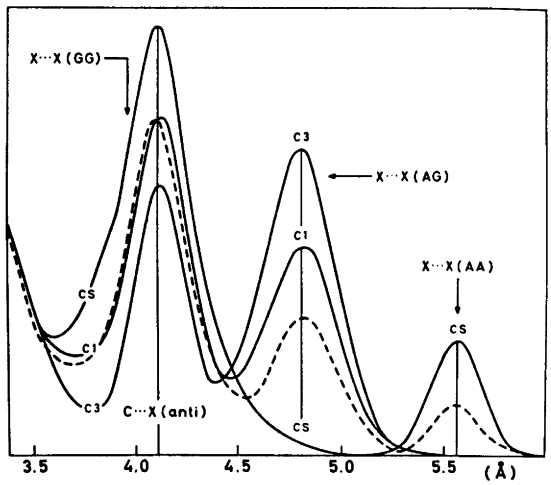

Fig. 5. Radial distribution curves for conformers of $(CH_3)C(CH_2Cl)_3$. Experimental curve (- - -), and theoretical curves (——) for the conformers *CS*, *C1* and *C3*. An artificial damping constant equal to 0.0022 Å^2 was used.

calculated u values for X···X distances of the type GG and AG (see Table 1) may be compared with the best least-squares estimates of Table 7. Although the individual least-squares estimates are quite uncertain, the discrepancies indicate that *C1* and *C3* may have greater average torsional force constants than *CS*.

Several combinations of F_ϕ values with $F_\phi(CS) < 0.63$ and $F_\phi(C1) = F_\phi(C3) > 0.63$ were then tried. Many combinations with $F_\phi(CS)$ in the range $0.30 - 0.63$ and $F_\phi(C1)$ in the range $0.63 - 0.90$ lead to a slight improvement, but not significantly better than the fit obtained with $F_\phi(CS) = F_\phi(C1) = F_\phi(C3) = 0.63$. Although a definite conclusion could not be reached in this way, the most probable estimates for the F_ϕ values are presented as follows: $F_\phi(CS)$ in the range $0.30 - 0.60$, $F_\phi(C1)$ and $F_\phi(C3)$ in the range $0.70 - 0.90$. The torsional force constants, $F_\phi(-CH_2X)$, predicted by the semiempirical energy model are found in Table 4. Clearly, the calculated $F_\phi(-CH_2X)$ values for the conformers *C1* and *C3* are too small, while the value (*ca.* 0.30) calculated for *CS* is not unlikely.

Table 6. Structure and composition parameters for $(CH_3)C(CH_2Cl)_3$ at 88 °C. Standard deviations are given in parentheses.

Parameter correlation: $|\varrho| > 0.49$.
$\varrho[\angle CCX/r(C-C)] = -0.50$, $\varrho[r(C-C)/u(X_1\cdots H_1)] = -0.52$, $\varrho[\alpha(Cl)/\alpha(CS)] = -0.94$.

Bond[a] lengths (Å)	Bond[b] angles ($\angle\alpha$; deg.)	Composition parameters
$r_a(C-H) = 1.000(7)$	$\angle CCCl = 113.9\ (0.3)$	$\alpha(CS) = 45\ \%(3)$
$r_a(C-C) = 1.532(3)$	$\angle CCH = 110.2(0.7)$	$\alpha(C1) = 34\ \%(8)$
$r_a(C-Cl) = 1.792(3)$	$\angle CCC = (109.47)^c$	$\alpha(C3) = 21\ \%(7)^d$

[a] An experiment with CO_2 gave a correction of 0.1 % in the s-scale. The bond lengths are therefore 0.1 % longer than those directly determined by least-squares refinements. The uncertainty (0.14 %) in the s-scale has been included in the standard deviations for bond distance. [b] Bond angles are those of the self-consistent r_α structure. Dependent angles are: $\angle HCH = 108.7°$ ($\sigma = 0.9°$) and $\angle HCCl = 106.8°$ ($\sigma = 0.5°$). [c] Tetrahedral arrangement of C-atoms was assumed. [d] The parameters $\alpha(CS)$ and $\alpha(C1)$ were refined with $\alpha(C3) = 100\ \% - \alpha(CS) - \alpha(C1)$.

VI. FINAL RESULTS

Parameters from the least-squares refinements [14] and standard deviations (σ) corrected for correlation in the experimental data [20] are given. In the final refinements, intensities beyond $s = 34.0$ Å^{-1} were not included and, using a diagonal weight matrix, all intensities were given equal weights.

Non-bonded distances were restricted under the geometrical constraints of r_α parameters, by including correction terms $D = r_\alpha - r_a$ [$D = (u^2/r) - K$] for all distances.

Parameters correlation coefficients (ϱ) are included in Tables 6 – 7. The structure and composition parameters are found in Table 6.

It is not possible to refine all torsion angles of the three conformers simultaneously as independent parameters. The results in Table 2 were used as a guide and the torsion angles were confined, as follows.

Conformer CS:
$\phi_{1-2} = -\phi°$, $\phi_{3-2} = +\phi°$, and $\phi_{4-2} = \phi_{5-2} = 0°$

Conformer C1:
$\phi_{1-2} = 120° - 4\phi°$, $\phi_{3-2} = \phi_{4-2} = \phi°$, and $\phi_{5-2} = -8\phi°$

Conformer C3:
$\phi_{1-2} = 120° + \phi°/4$, $\phi_{3-2} = \phi°/4$, $\phi_{4-2} = -120° + \phi°/4$, and $\phi_{5-2} = -9\phi°$

($\phi° = 0$ corresponds to staggered conformations.) The parameter $\phi°$ was refined, including as many as possible of the remaining least-squares parameters simultaneously. The absolute value of $\phi°$ was always found to be less than *one* standard deviation (σ) of that parameter ($\sigma = 1°$). The expected value of $\phi°$ according to Table 2 is *ca.* $+1.6°$. Keeping in mind the assumptions involved, the theoretical value is in reasonable agreement with the experimental evidence.

Several mean amplitudes of vibration (u values) have been refined. In Table 7 their values are compared to those computed. (Sect. III) Both sets of u values are experimental, but the calculated values combine information from spectroscopy as well as from electron diffraction. The average relative deviation between the two

Table 7. Mean amplitudes (u) of vibration for $(CH_3)C(CH_2Cl)_3$ at 88 °C. Parameter correlation:

$|\varrho| \geq 0.5$.
$\varrho[u(AG)/u(GG)] = -0.82$, $\varrho[\alpha(Cl)/u(AG)] = -0.81$, $\varrho[\alpha(Cl)/u(GG)] = -0.98$,
$\varrho[\alpha(CS)/u(AA)] = +0.50$, $\varrho[\alpha(CS)/u(AG)] = +0.66$, $\varrho(\alpha(CS)/u(GG)) = +0.95$.
The symbols AA, AG, and GG represent the three different kinds of X···X distances.

Type of distance	Dist. (Å)	Calculated[a] u value (Å)	Refined u value (Å)	Standard deviation (Å)
C–H	(1.10)	0.078	0.073	0.007
C–C	(1.53)	0.052	0.053	0.003
C–X	(1.79)	0.054	0.040	0.003
C_2···X	(2.80)	0.074	0.071	0.003
C···C	(2.50)	0.073	0.067	0.005
X_1···H_1	(2.36)	0.108	0.103	0.008
C···H(g)	(2.74)	0.146	(0.146)[b]	–
C···H(a)	(3.46)	0.104	(0.104)[b]	–
C···X(g)	(3.16)	0.136	0.130	0.002
C···X(a)	(4.13)	0.074	0.074	0.003
X···X(AA)	(5.56)	0.100	0.101	0.014
X···X(AG)	(4.82)	0.151	0.130	0.019
X···X(GG)	(3.94)	0.204	0.280	0.071

[a] Calculated with $\bar{F}_\phi = 0.63$ mdyn Å (rad)$^{-2}$. [b] Not refined; calculated values were used.

sets of u values is *ca.* 7 % (u_{C-X} not included). The average relative uncertainty, $\langle\sigma/u\rangle$, of the refined u values is *ca.* 9 %. Since the calculated u values are reliable, then it is likely that the calculated K values are reliable to the same extent.

The u value for the bond C–X obtained by direct refinement is too small compared to the calculated value of 0.054 Å. The low value is most probably due to an error [5] in the blackness correction,[14] however, the remaining u values seem unaffected by that error.

Cartesian coordinates and principal axes' moments of inertia for the conformers are found in Table 8.

Table 8. Cartesian coordinates (Å) for the conformers *CS*, *C1*, and *C3* of $(CH_3)C(CH_2X)_3$, X = Cl.

The coordinates have been calculated for staggered conformations, using the final bond angles ($\angle\alpha$) of Table 6 and r_g values for the bond lengths (see Table 10). The numbering of atoms in the conformer *CS* is shown in Fig. 2. The principal axes' moments of inertia are (amuÅ²):

$I_A = 331.98$, $I_B = 657.17$, and $I_C = 875.87$ *for conformer CS*
$I_A = 418.58$, $I_B = 603.80$, and $I_C = 842.64$ *for conformer C1*
$I_A = 521.35$, $I_B = 521.35$ and $I_C = 929.16$ *for conformer C3*

The coordinates for the conformer *C1* are equal to those of the conformer *CS*, with the following exceptions: X_1($x = 1.3724$, $y = 1.9749$, $z = -1.4204$) and H_1' ($x = 2.1636$, $y = 0.2586$, $z = 0$). The coordinates for the conformer *C3* are equal to those of the conformer *C1*, with the following exceptions: X_4 ($x = 1.4204$, $y = -1.9749$, $z = 1.3724$) and H_4($x = 0$, $y = -0.2586$, $z = 2.1636$).

CS	*x*	*y*	*z*
C_1	1.2525	0.8857	0.0000
X_1	2.7929	−0.0339	0.0000
H_1	1.2645	1.5299	0.8989
H_1'	1.2645	1.5299	−0.8989
C_2	0.0000	0.0000	0.0000
C_3	−1.2525	0.8857	0.0000
X_3	−2.7929	−0.0339	0.0000
H_3	−1.2645	1.5299	0.8989
H_3'	−1.2645	1.5299	−0.8989
C_4	0.0000	−0.8857	1.2525
X_4	0.0000	0.0339	2.7929
H_4	0.8989	−1.5299	1.2646
H_4'	−0.8989	−1.5299	1.2646
C_5	0.0000	−0.8857	−1.2525
H_5	0.0000	−0.2586	−2.1636
H_5'	−0.8989	−1.5299	−1.2646
H_5''	0.8989	−1.5299	−1.2646

VII. DISCUSSION

The percentages α^* and α of two conformers ($C \rightleftharpoons C^*$) in equilibrium in the gas phase, are related to the theoretical [21] expression [22] for the equilibrium constant, as given in eqn. (1):

$$\alpha^*/\alpha = (M^*/M)(Q^*/Q)^{vib} \exp(-\Delta E^m/RT) \quad (1)$$
with $M^*/M = (M_d^*/M_d)(\sigma^*/\sigma)^{-1} = M_c^*/M_c$
(see Table 1)

(The classical rotational partition functions for the conformers are approximately equal.) Q^{vib} is the vibrational partition function of a conformer referred to the potential energy minimum of that conformer. $\Delta E^m = E^* - E$ is the potential-energy difference between the conformers, and the difference is measured between potential-energy minima. The zero-point vibrational energy is included in the vibrational partition function. R and T have their usual thermodynamic meanings.

If the vibrational partition functions are known, then the quantity ΔE^m may be computed from eqn. (1). Conversely, if the quantity ΔE^m is known, then the *ratios* (q) between vibrational partition functions may be estimated from eqn. (1). Assuming the values of Table 3 for ΔE^m, q values have been computed and their values are found in Table 9.

If *equal* vibrational partition functions ($q = 1$) are assumed, then eqn. (1) yield the values $\Delta E^m(q = 1)$ of Table 9. According to the last set of ΔE^m values, the conformer *CS* is more stable than the conformers *C1* and *C3*. If the results from the semiempirical calculations were correct, then *C3* is the most stable conformer, and *ca.* 1.4 kcal/mol more stable than *CS*.

The great relative amount of the conformer *CS* encountered can be explained in at least two different ways: (1) the conformer *C3* has the lowest minimum energy as suggested by the semi-empirical calculations, but part of the force field for *CS* is quite different ($q \neq 1$) from that of *C1* and *C3*; (2) the force fields of the conformers are approximately equal ($q = 1$) and *CS*

Table 9. Energy differences and ratios between vibrational partition functions for the conformers, *CS*, *C1*, and *C3* or $(CH_3)C(CH_2Cl)_3$.

Difference or ratio	*CS* = *C1*	*CS* = *C3*	*C1* = *C3*
(1) ΔE^m(CALC)[a] in kcal/mol	+0.76	+1.40	+0.64
Ratio between vibrational partition functions (q)	7.6	10.0	1.3
(2) $\Delta E^m(q=1)$ in kcal/mol	−0.70	−0.25	+0.45
$\Delta E^m(q=1) - \Delta E^m$(CALC)	−1.46	−1.65	−0.19

[a] Difference between conformational minima as predicted by the semiempirical energy model (Sect. II).

has the lowest minimum energy contrary to the results of semi-empirical calculations.

The experimental information available for TECL alone does not make a definite choice between the two alternatives possible. However, there is a certain evidence for the *torsional* force constants of *CS* being smaller than those of *C1* and *C3*.

The values [mdyn Å (rad)$^{-2}$] of the torsional force constants (F_ϕ) were confined as follows: $F_\phi(CS) = 0.63 - \Delta F_\phi$, and $F_\phi(Cl) = 0.63 + \Delta F_\phi = F_\phi(C3)$. The value of ΔF_ϕ which leads to the q values of Table 9 is 0.15, corresponding to $F_\phi(CS) = 0.48$ and $F_\phi(Cl) = F_\phi(C3) \simeq 0.78$. Such a difference between the torsional force constants is not contradicted by the experimentally determined mean amplitudes. The calculated values (Table 5) for u[X···X(GG)] and u[X···X(AG)] are 0.204 Å and 0.150 Å, respectively, if a force constant $F_\phi = 0.63$ is used for all three conformers. The best least-squares estimates (Table 7) are 0.280 Å and 0.130 Å. The calculated u value for X···X(GG) is too small and the one for X···X(AG) is too large compared to the least-squares estimates. The discrepancies between the two sets of u values are *partly* removed if $F_\phi(CS) = 0.48$ and $F_\phi(Cl) = F_\phi(C3) = 0.78$. Unfortunately, the least-squares values are very uncertain quantities and no further conclusions about the value of ΔF_ϕ can reasonably be arrived at from u values alone. (If observed frequencies were available, then hopefully the difference between the force constants of the conformers could be determined.)

It is thereby demonstrated that a reasonable value of ΔF_ϕ could easily lead to q values as large as 7.6 and 10.0 in a molecule like TECL. In the molecules $C(CH_2Cl)_4$ [5] and $(CH_3)_2C(CH_2Cl)_2$ [14] similar situation swere encountered. For $C(CH_2Cl)_4$, a q value as large as 50, corresponding to a large difference in zero-point vibrational energy between the two abundant conformers, is possible.

The characteristic structure parameters for

Table 10. Structure parameters for molecules of the type $(CH_3)_{4-n}C(CH_2X)_n$, $n = 2$, 3, and 4.

[X = Cl]	$(CH_3)_2C(CH_2X)_2$	$(CH_3)C(CH_2X)_3$	$C(CH_2X)_4$	$\bar{M}$(calc.)[b]
r_g(C−H)[a]	1.107(4)[c]	1.106(7)	1.133(9)	(1.093 − 1.094)
r_g(C−C)	1.533(2)	1.534(3)	1.541(4)	(1.534 − 1.544)
r_g(C−X)	1.794(2)	1.794(3)	1.794(3)	(1.789 − 1.790)
$\angle_\alpha$CCX	114.3(0.2)	113.9(0.3)	113.5(0.4)	(113.3 − 113.9)
$\angle_\alpha$CCH	109.1(0.4)	110.2(0.7)	108.0(1.0)	(110.1 − 110.2)
$\angle_\alpha$CCC	(≃109.47)[d]	(≃109.47)[d]	(≃109.47)[e]	

[a] $r_g = r_a + u^2/r$; the spectroscopic u values were used in computing the u^2/r term. [b] $\bar{M}$(calc.); represents the range of the (average) parameter as predicted by the semi-empirical calculations. [c] Standard deviations for the experimental parameters are found in parentheses. [d] Tetrahedral arrangements of C atoms were assumed. [e] Small, but significant, deviations from a tetrahedral arrangement of C atoms were detected.

molecules of the type $(CH_3)_{4-n}C(CH_2Cl)_n$, with $n = 2, 3, 4$, have been compiled in Table 10. The parameters are average values for the molecules, but conformers of the same molecule may have unequal structure parameters as indicated by the semi-empirical calculations (see Table 2 and Refs. 4 and 5) Small, and in some cases experimentally significant, deviations from a tetrahedral arrangement of C atoms are likely. The abundant conformers of these molecules have torsion angles close to staggered values. Larger deviations ($10-20°$) are only likely for $-CH_3$ groups. The values predicted by the semi-empirical model reasonably agree with the experimental values. Although small adjustments in the force constants and the "normal" parameter values (Table 2) would remove most of the discrepancies, it was felt that results from additional molecules ought to be included before such corrections were considered. Reasonable adjustments of this kind would change the values of the conformational energy differences very little.

Acknowledgements. I am grateful to Cand.real. A. Almenningen for recording the diffraction photographs, and to Prof. O. Bastiansen, Dr. A. Haaland, and Dr. H. M. Seip for helpful discussions. Computer programs made available by Dr. H. M. Seip, Cand.real. S. Rustad, and Prof. W. D. Gwinn have been extensively used in this work. Financial support from Norges almenvitenskapelige forskningsråd is gratefully acknowledged.

REFERENCES

1. Sheppard, N. *J. Mol. Struct. 6* (1970) 5.
2. Bastiansen, O., Seip, H. M. and Boggs, J. E. In Dunitz, J. D. and Ibers, J. A., Eds., *Perspectives in Structural Chemistry*, Wiley, New York 1971, Vol. IV.
3. Seip, H. M. In Sim, G. A. and Sutton, L. E., Eds. *Molecular Structure by Diffraction Methods*, Specialist Periodical Reports, The Chemical Society, London 1973, Vol. 1, Part 1, Chapter 1.
4. Stølevik, R. *Acta Chem. Scand. A 28* (1974) 327.
5. Stølevik, R. *Acta Chem. Scand. A 28* (1974) 455.
6. Bartell, L. S. *Private communication.*
7. Stølevik, R. *Acta Chem. Scand. A 28* (1974) 299.
8. Abraham, R. J. and Parry, K. J. *J. Chem. Soc. B* (1970) 539.
9. Schachtschneider, J. H. and Snyder, R. G. *Vibrational Analysis of Polyatomic Molecules. IV.* Force constants for the haloparaffins. Project No. 31450, Technical Report No. 122 – 63 of Shell Development Company.
10. Snyder, R. G. and Schachtschneider, J. H. *Spectrochim. Acta 21* (1965) 169.
11. Gwinn, W. D. *J. Chem. Phys. 55* (1971) 477.
12. Stølevik, R., Seip, H. M. and Cyvin, S. J. *Chem. Phys. Lett. 15* (1972) 263.
13. Bastiansen, O., Hassel, O. and Risberg, E. *Acta Chem. Scand. 9* (1955) 232.
14. Andersen, B., Seip, H. M., Strand, T. G. and Stølevik, R. *Acta Chem. Scand. 23* (1969) 3224.
15. Peacher, J. and Willis, J. C. *J. Chem. Phys. 46* (1967) 4809.
16. Strand, T. G. and Bonham, R. A. *J. Chem. Phys. 40* (1964) 1686.
17. Almenningen, A., Bastiansen, O. and Munthe-Kaas, T. *Acta Chem. Scand. 10* (1956) 261.
18. Morino, Y., Kuchitsu, K. and Oka, T. *J. Chem. Phys. 36* (1962) 1108.
19. Kuchitsu, K. *J. Chem. Phys. 49* (1968) 4456.
20. Seip, H. M. and Stølevik, R. In Cyvin, S. J. Ed., *Molecular Structures and Vibrations*, Elsevier, Amsterdam 1972, p. 171.
21. Glasstone, S. *Theoretical Chemistry*, Van Nostrand, New York 1944.
22. Herzberg, G. *Infrared and Raman Spectra of Polyatomic Molecules*, Van Nostrand, Princeton 1945.

Received February 25, 1974.

Acta Chemica Scandinavica A 28 (1974) 623—630

The Crystal Structure of Potassium Hexacyanochromate(III), $K_3[Cr(CN)_6]$

SUSAN JAGNER,* EVERT LJUNGSTRÖM and NILS-GÖSTA VANNERBERG

Department of Inorganic Chemistry, University of Göteborg and Chalmers University of Technology, Fack, S-402 20 Göteborg 5, Sweden

The crystal structure of potassium hexacyanochromate(III), $K_3[Cr(CN)_6]$, has been determined by single crystal X-ray methods. $K_3[Cr(CN)_6]$ crystallizes with an OD structure characterized by the OD groupoid symbol.

$Pma(n)$
$\{c_2\ n_{2,\frac{1}{2}}\ (n_{\frac{1}{2},1})\}$

The ordered orthorhombic form (MDO_1) has a unit cell with the dimensions $a = 8.5256(9)$ Å, $b = 10.6000(12)$ Å, and $c = 13.6840(13)$ Å, belonging to space group $Pcan$, with $Z = 4$. Its crystal structure has been solved from diffractometer data and refined by the method of least squares to a final R value of 0.046 based on 694 independent reflections. The complex ion has octahedral symmetry with Cr—C bond lengths of 2.057(12) Å, 2.075(7) Å, and 2.100(10) Å.

Much attention has been given in recent years to σ and π contributions to metal-ligand bonds in transition metal cyanocomplexes. Correlation of the bond lengths and geometries of the complex ions and information concerning the charges on the central metal atoms and ligands, obtained from crystal structure studies and X-ray photoelectron spectra, with existing semi-empirical molecular orbital calculations [1-4] ought to permit a determination of the relative variations of these contributions. In connection with such an investigation, in progress at this department, the crystal structures of several hexacyanides [5-8] and monosubstituted hexacyanides, *e.g.* pentacyanonitrosyls [9-11], have been studied. In the transition metal pentacyanonitrosyls, metal-cyanide π bonding is effectively prevented by the strong Me $\rightarrow \pi^*$ (NO) transfer, the strength of which varies in a predictable way with Me.[2-4, 12] π Bonding contributions to Me—CN bonds would, however, appear to be slight even in some hexacyanides, and, in order to examine their variation more closely, hexacyanides of the same transition metal atom with different formal oxidation numbers [5-8] have been studied as well as hexacyanides of different transition metals.

Since the majority of transition metal hexacyanides appear to crystallize with disordered crystal structures, it has not until fairly recently [13] been possible to determine their structures by appropriate methods. Previous crystallographic work has consisted mainly of determinations of unit cell dimensions and space groups (*cf.* Ref. 7). The crystal structures of $K_3[Me(CN)_6]$, where Me = Mn, Fe, and Co, have recently been determined.[7,8] To complete this series for the first row of transition metals, the crystal structures of $K_3[Cr(CN)_6]$ and $K_3[V(CN)_6]$ were of interest. The crystal structure of the former is presented in this paper. Attempts by Bennett and Nicholls [14] to prepare the latter compound yielded, however, $K_4[V(CN)_7].2H_2O$ whose crystal structure has now been determined.[15,16]

Attempts are now being made by the authors to prepare suitable single crystals of $K_4[Cr(CN)_6]$, in order to be able to compare Cr(III) with Cr(II) and $[Cr(CN)_6]^{4-}$ with other first row $[Me(CN)_6]^{4-}$.

* Temporary address: Department of Inorganic Chemistry, University of Aarhus, DK-8000 Aarhus C, Denmark.

PREPARATION AND ANALYSIS

Potassium hexacyanochromate(III) was prepared according to the method described by Brauer.[17] Crystals suitable for single crystal X-ray work were obtained by precipitating $K_3[Cr(CN)_6]$ from aqueous solution with ethanol, instead of evaporating the solution, and then recrystallizing the crude product twice from aqueous solution.

The *chromium* content was determined gravimetrically as $PbCrO_4$ by oxidation of the compound to chromate with boiling conc. perchloric acid and subsequent precipitation with an aqueous solution of lead nitrate. The *potassium* content was determined by means of atomic absorption spectroscopy using a Perkin Elmer 403 spectrometer (Found: Cr 15.97; K 35.8. Calc. for $K_3[Cr(CN)_6]$: Cr 15.98; K 36.0).

The infra-red spectrum, registered with a Beckman IR 9 spectrophotometer, showed complete agreement with that given by Jones.[18]

OD STRUCTURE

Crystals of $K_3[Cr(CN)_6]$ were mounted along the needle-axis which will, in the following, be defined as the crystallographic a axis. Rotation photographs taken about this axis showed layer lines composed of discrete reflections for $A \approx 4.25$ Å and weak streaks corresponding to $a = 2A \approx 8.5$ Å. It was thus apparent that $K_3[Cr(CN)_6]$ crystallized with an OD structure,[13] *i.e.* a structure which can be described in terms of ordered layers whose mode of stacking is disordered. Weissenberg photographs of the weak layer lines showed that there were intensity maxima on the streaks, the majority of which had orthorhombic symmetry while the remainder had monoclinic symmetry. The orthorhombic intensity maxima corresponded to a unit cell with the approximate dimensions $a = 8.5$ Å, $b = 10.6$ Å and $c = 13.6$ Å, the monoclinic maxima requiring an apparent doubling of the c-axis, *i.e.* $c \approx 27.2$ Å.

If, as is usual in OD structures,[13] the c direction is assumed to be that of non-periodicity, the conditions limiting reflection for $K_3[Cr(CN)_6]$ may be summarized:

(i) discrete reflections, hkl, for $h = 2H$
diffuse streaks, $hk\zeta$, for $h = 2H + 1$, where ζ can take any value

(ii) Hkl: $H + l = 2n$

(iii) $hk0$: $h + k = 2n$

(iv) $h0\zeta$: $h = 2n$

$K_3[Cr(CN)_6]$ thus crystallizes as a family of structures characterized by the same OD groupoid as that which characterizes the structures of $K_3[Mn(CN)_6]$,[7] $K_3[Fe(CN)_6]$, and $K_3[Co(CN)]_6$.[8]

As described in detail in Ref. 7, reflection conditions (i) and (ii) indicate that the superposition structure, corresponding to the family reflections, Hkl, has an a axis of one-half 8.5 Å and is B face-centred with $Bmmb$ and $B2_1mb$ as possible space groups [*cf.* also reflection condition (iii)]. According to reflection conditions (iii) and (iv), the minimum layer symmetry is $P2a(n)$, but for the same reasons as given in Ref. 7, *i.e.* the high symmetry of the building units, the layer symmetry has here been assumed to be $Pma(n)$.

The B face-centring of the superposition structure requires that one layer be related to the next by the translation $-\vec{a}/4 + \vec{c}_0$ or $+\vec{a}/4 + \vec{c}_0$, where $\vec{c}_0$ is the unit vector perpendicular to the layers in the direction of non-periodicity [13] and $c_0 \approx 6.8$ Å. This means that the symmetry elements converting one layer, L_0, into the next, L_1, can be expressed as ${}_{0,1}[c_2\, n_{2,\frac{1}{4}}\, (n_{\frac{1}{4},1})]$ or ${}_{0,1}[c_2\, n_{2,\bar{\frac{1}{4}}}\, (n_{\bar{\frac{1}{4}},1})]$, respectively. These symmetry elements are illustrated by means of asymmetric triangles in Fig. 1.

$K_3[Cr(CN)_6]$ may thus be said to crystallize as a family of structures characterized by the OD groupoid

$$Pma(n)$$
$$\{c_2\, n_{2,\frac{1}{4}}\, (n_{\frac{1}{4},1})\}$$

the symbol giving the total symmetry of any pair of consecutive layers, L_p and L_{p+1}.

Successive layers may thus, alternatively, be regarded as being related to one another by the translation $\alpha\vec{a}/4$ where α can take the value $+1$ or -1. As described in Ref. 7, there are two ordered extreme structures, or "structures of maximum degree of order" (MDO),[13] one orthorhombic, MDO_1, obtained by a zig-zag stacking of layers, *i.e.* α = alternately -1 and, $+1$ (*cf.* Fig. 1), and the other monoclinic, MDO_2 obtained by an oblique stacking of layers ($\alpha = +1$ or -1, only). The unit cell of the MDO_1 structure has the approximate dimensions $a = 8.5$ Å, $b = 10.6$ Å, and $c = 2c_0 = 13.6$ Å, the space group being $Pcan$, while the unit cell of the MDO_2 structure [7,8] is defined by $\vec{a}_{mon} = \vec{a}$, $\vec{b}_{mon} = \vec{b}$, $\vec{c}_{mon} = \vec{a}/4 + \vec{c}_0$ with $\beta \approx 107°$, the

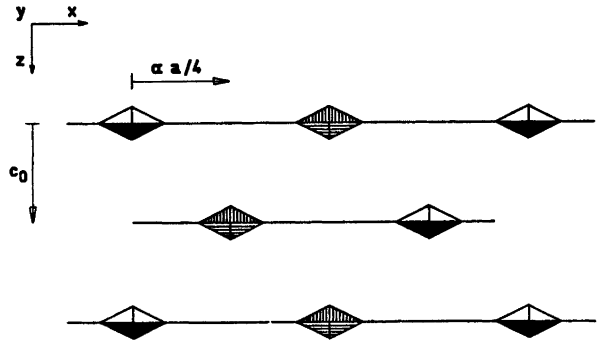

Fig. 1. Schematic representation of the ordered orthorhombic structure of $K_3[Cr(CN)_6]$, space group *Pcan*. $\vec{c}_0$ is the unit vector perpendicular to the layers in the non-periodic direction, while α is a factor which can take the value $+1$ or -1. *Notation:* empty triangles: y, filled triangles: $-y$, vertically shaded triangles: $\frac{1}{2}-y$, and horizontally shaded triangles: $\frac{1}{2}+y$.

space group being $P2_1/a$. In principle, each crystal of $K_3[Cr(CN)_6]$ can exhibit a different stacking sequence and thus be described in terms of larger or smaller contributions from the different MDO structures.

The fictitious superposition structure, $\hat{\varrho}(x,y,z)$, which is the same for all members of the OD groupoid family, is related to the real structure, $\varrho(x,y,z)$ by

$$\hat{\varrho}(x,y,z) = \tfrac{1}{2}[\varrho(x,y,z) + \varrho(x+\tfrac{1}{2},y,z)].$$

It has the approximate cell dimensions $a = 4.25$ Å, $b = 10.6$ Å, and $c = 13.6$ Å and belongs to space group *Bmmb*.

Unlike the crystals of $K_3[Mn(CN)_6]$,[7] $K_3[Fe(CN)_6]$, and $K_3[Co(CN)_6]$,[8] the crystals of $K_3[Cr(CN)_6]$ studied showed a predominance of more or less discrete non-family reflections with orthorhombic symmetry, the streaks joining them being exceedingly weak. This indicates the presence of large regions of MDO_1 type structure.[13] The intensity maxima with mono-

Table 1. X-Ray powder diffraction data for $K_3[Cr(CN)_6]$. Guinier camera, $CuK\alpha_1$ radiation ($\lambda = 1.54050$ Å).

h k l	$10^5 \sin^2\theta_{obs}$	$10^5 \sin^2\theta_{calc}$	I_{calc} (relative scale)	I_{obs}
0 0 2	1261	1267	35	vvw
0 2 2	3380	3379	1450	vvs
0 0 4	5078	5069	68	w
2 2 1	5689	5694	100	w
0 3 2	6022	6020	435	s
2 2 3	8233	8228	445	s
2 3 1	8338	8334	75	w
0 4 0	8444	8448	27	vw
0 4 2	9715	9716	10	vvw
2 3 3	10870	10869	45	w
2 4 1	12033	12030	175	m
4 0 0	13059	13060	53	w
4 2 2	16443	16439	91	w
4 0 4	18125	18129	12	vvw
2 4 5	19629	19634	24	vw
0 0 8	20277	20278	50	w
2 2 7	20904	20902	30	vw
4 6 2	33338	33336	24	vw

clinic symmetry were so few in number that it was not considered profitable to attempt to determine the MDO_2 structure.

ACCURATE UNIT CELL DIMENSIONS

Powder photographs of $K_3[Cr(CN)_6]$ were taken in a Guinier focusing camera with Cu$K\alpha_1$ radiation, using lead nitrate as an internal standard ($a = 7.8564$ Å).[19] $\sin^2\theta_{obs}$ values were obtained from the measured s values by means of the program PEPP [20] and eighteen family reflections were indexed and used to refine the cell dimensions of the MDO_1 structure with the program POWDER.[20] The following values were obtained (standard deviations, $\times 10^4$, in parentheses): $a = 8.5256(9)$ Å, $b = 10.6000(12)$ Å, and $c = 13.6840(13)$ Å. Observed and calculated $\sin^2\theta$ values are listed in Table 1. The calculated density corresponding to a cell content of four formula units is 1.75 g cm^{-3}. The experimental density, as determined by the method of flotation using bromoform and carbon tetrachloride is 1.74 g cm^{-3}.

DETERMINATION OF THE MDO_1 STRUCTURE

A crystal of $K_3[Cr(CN)_6]$ with the approximate dimensions $0.05 \times 0.02 \times 0.01$ cm was mounted along the a axis and the intensities of the family reflections (hkl, $h = 2H$) and the streaks, $hk\zeta$, at the reciprocal lattice points corresponding to the unit cell of the MDO_1 structure, were measured with an Arndt-Phillips linear diffractometer at the Department of Inorganic Chemistry, University of Aarhus. Mo$K\alpha$ radiation selected by a graphite monochromator was employed, data being collected for the layers $0kl - 10kl$. Symmetry related reflections were averaged and correction was made for Lorentz and polarisation effects, assuming the graphite monochromator to behave as an ideal mosaic crystal, using the program G4.[21] A total of 694 independent reflections for which $F_o^2 > 2.5\,\sigma(F_o^2)$, according to counting statistics, were regarded as being observed and were used in the subsequent calculations. No correction was made for absorption (linear absorption coefficient for $K_3[Cr(CN)_6]$ in Mo$K\alpha$ radiation = 19.3 cm^{-1}).

A Patterson function and subsequent electron density calculations based on the family reflections only, using the program FORDAP,[21] confirmed that the superposition structure of $K_3[Cr(CN)_6]$ was isomorphous with those of $K_3[Mn(CN)_6]$,[7] $K_3[Fe(CN)_6]$,[8] and $K_3[Co(CN)_6]$.[8] No attempt was made to refine the atomic and thermal parameters of this structure.

A Patterson function based on the non-family reflections (hkl, $h = 2H + 1$) only, was then calculated. Since such a calculation [13] yields vectors between atoms within a single layer, it was possible to obtain the positions of the potassium atoms relative to chromium and thus eliminate the other potential relative positions afforded by the superposition structure. The chromium atom, which is situated at the origin of the superposition structure, was assigned the position *Pcan*,* 4*c*, with $x = 1/8$, $y = 0$, and $z = 1/4$, and the two potassium atoms were assigned a fourfold and an eight-fold position in accordance with the vectors obtained from the Patterson synthesis. An electron density calculation using the signs obtained with the chromium and potassium atoms in these positions revealed the positions of all the ligand atoms.

Atomic and anisotropic thermal parameters were then refined using the full matrix least squares program LINUS [21] and assigning the reflections unit weights. The atomic scattering factors due to Cromer and Mann [22] were used for all atoms. As is necessary in OD structures, the family and non-family reflections were assigned separate scale factors. No layer scale factors were, however, refined. An isotropic extinction coefficient was refined assuming unit path length for all reflections, a final g value of $4.1(5) \times 10^{-7}$ being obtained. During the refinement, x_{Cr} was held fixed at 0.125 in order to obtain convergence. If this parameter was refined extremely large shifts were obtained for x_{Cr} and x_{K1} and the standard deviations for all parameters were considerably larger than when x_{Cr} was fixed. This is probably because the origin is not properly defined for the family reflections unless either x_{Cr} or x_{K1} is fixed. As expected, there were large correlations between many of the x parameters.

A final R value of 0.046 was obtained ($R = 0.037$ for the 372 family reflections and $R = 0.074$

* Equipoints of general position of *Pcan* (conventional setting,[19] No. 60, *Pbcn*): $\pm(x,y,z;\ \frac{1}{2}-x, \frac{1}{2}-y, \frac{1}{2}+z;\ \frac{1}{2}-x, \frac{1}{2}+y,\bar{z};\ x,\bar{y}, \frac{1}{2}-z)$.

Table 2. Atomic coordinates, expressed as fractions of the cell edges, and mean square vibration amplitudes, U_{ij}, ($Å^2$) for $K_3[Cr(CN)_6]$. The estimated standard deviations of the parameters ($\times 10^4$) are given in parentheses.

Atom	Site	x	y	z	U_{11}	U_{22}	U_{33}	U_{12}	U_{13}	U_{23}
Cr	4*c*	0.1250	0.0000	0.2500	0.0168(7)	0.0256(8)	0.0235(8)	0.0000	0.0000	0.0012(7)
K(1)	4*c*	0.6297(4)	0.0000	0.2500	0.0232(12)	0.0372(13)	0.0408(15)	0.0000	0.0000	0.0070(12)
K(2)	8*d*	0.6263(30)	0.2329(3)	0.5021(1)	0.0249(7)	0.0722(16)	0.0358(8)	0.0074(55)	0.0008(32)	−0.0100(10)
N(1)	8*d*	0.1254(28)	0.2730(7)	0.1474(4)	0.0458(37)	0.0368(43)	0.0391(33)	0.0064(81)	−0.0056(89)	0.0057(30)
N(2)	8*d*	0.3991(18)	0.0857(9)	0.3980(7)	0.0227(95)	0.0629(52)	0.0469(46)	−0.0114(46)	−0.0110(53)	−0.0081(41)
N(3)	8*d*	0.3623(32)	0.4108(9)	0.4019(6)	0.0450(74)	0.0687(54)	0.0387(42)	0.0096(66)	0.0011(82)	0.0080(41)
C(1)	8*d*	0.1248(17)	0.1771(6)	0.1853(5)	0.0309(34)	0.0354(37)	0.0260(32)	0.0069(62)	−0.0037(56)	−0.0004(29)
C(2)	8*d*	0.2971(12)	0.0565(10)	0.3458(8)	0.0312(58)	0.0397(53)	0.0296(58)	0.0033(40)	0.0020(44)	0.0002(46)
C(3)	8*d*	0.4519(10)	0.4431(9)	0.3499(7)	0.0192(47)	0.0309(45)	0.0357(62)	0.0046(35)	0.0020(41)	0.0057(43)

Table 3. Observed and calculated structure factors (× 10) for the MDO_1 structure of $K_3[Cr(CN)_6]$.

K	L	FOBS	FCALC
*	H=	0	*
0	4	948	969
0	6	176	156
0	8	1597	1657
0	10	195	-164
0	12	1818	1859
0	14	124	-100
0	16	346	366
1	4	551	530
1	6	278	-268
1	8	362	-351
2	2	2362	-2403
2	4	73	-53
2	6	2823	-2857
2	8	265	293
2	10	1847	-1882
2	12	197	193
2	14	585	-628
3	2	1688	1627
3	4	82	-105
3	6	493	-494
3	8	128	111
3	14	175	210
4	0	1981	1968
4	2	511	-504
4	4	1705	1732
4	6	1167	1288
4	10	434	-449
4	12	685	705
4	16	345	399
5	2	442	449
5	4	166	-174
5	14	134	76
5	16	291	-33
6	*	83	-94
6	2	1408	-1416
6	4	818	826
6	6	914	-924
6	8	106	74
6	10	617	-643
6	12	122	128
6	14	448	-462
6	16	173	258
7	4	98	-185
7	6	185	187
7	12	242	-245
8	0	529	536
8	2	319	-305
8	4	882	911
8	6	452	-483
8	8	628	648
8	10	198	-203
8	12	304	319
8	14	165	-145
9	2	111	-113
9	4	186	-183
9	6	124	143
10	0	275	288
10	2	496	-481
10	4	361	379
10	6	567	-575
10	8	234	237
10	10	188	-198
10	12	180	199
11	2	92	-81
12	0	336	366
12	2	264	-267
12	4	313	318
12	6	257	-285
12	8	181	224
12	12	96	-59
13	2	191	211
14	0	185	-196
*	H=	1	*
1	2	482	-485
1	3	183	187
1	7	96	-36
1	9	257	-154
1	10	283	-196
1	11	127	133
1	12	187	95
1	13	184	-182
1	17	114	-62
1	18	183	-93
2	1	179	-181
2	3	282	-192
2	4	84	73
2	5	289	-195
2	6	122	-181
2	7	185	66
2	8	139	126
2	9	131	-123
2	11	151	-162
2	12	92	-83
3	0	388	378
3	1	115	-108
3	2	188	165
3	4	281	222
3	6	67	35
3	7	218	229
3	8	378	389
3	9	212	-196
3	10	121	-138
3	11	161	196
3	12	171	168
4	1	310	313
4	2	101	93
4	4	282	-196
4	5	342	350
4	7	184	178
4	9	94	36
4	10	113	-118
4	11	191	205
5	0	164	-143
5	1	135	-128
5	2	488	-413
5	3	141	138
5	5	226	-238
5	6	333	-338
5	8	118	-188
5	10	137	-123
5	12	142	-157
5	14	194	-197
6	1	113	-124
6	2	172	162
6	3	353	-354
6	5	233	-237
6	6	89	-82
6	8	198	163
6	9	178	-188
6	11	148	-151
7	0	391	385
7	1	137	-127
7	2	181	91
7	3	122	94
7	4	251	248
7	6	85	69
7	7	128	128
7	8	236	248
7	12	148	134
8	1	134	129
8	2	89	-84
8	3	243	255
8	5	187	189
8	9	126	122
8	11	132	112
9	0	225	-242
9	2	137	-158
9	3	111	-98
9	4	85	91
9	5	218	-216
9	6	278	-318
9	10	111	-87
10	2	98	-81
10	3	177	-185
10	9	124	-114
11	0	215	199
11	1	153	-159
11	4	142	138
12	3	129	145
*	H=	2	*
0	3	2162	2137
0	5	697	-714
0	7	428	443
0	9	713	-728
0	11	676	674
0	13	257	-248
0	15	473	444
0	17	340	-327
1	3	1959	1916
1	5	1042	1029
1	7	573	593
1	9	597	598
1	11	351	334
1	13	334	314
1	15	291	264
1	17	223	210
2	1	444	-448
2	3	1616	1595
2	5	1601	-1583
2	7	828	827
2	9	685	-681
2	11	408	393
2	13	439	-418
2	15	346	327
2	17	324	-285
3	1	1443	-1388
3	3	779	-752
3	5	279	-268
3	7	468	-474
3	9	626	-617
3	11	918	-913
3	13	282	-258
3	15	146	-105
4	1	1418	-1373
4	3	674	684
4	5	719	-719
4	7	948	941
4	9	619	-683
4	11	496	481
4	13	383	-363
4	15	201	265
5	1	287	276
5	3	782	773
5	5	697	691
5	7	183	167
5	9	361	364
5	11	329	319
5	13	136	77
5	15	187	185
6	1	1116	-1187
6	3	587	578
6	5	676	-659
6	7	673	651
6	9	318	-318
6	11	335	326
6	13	437	-443
6	15	291	281
7	1	225	-228
7	3	249	-233
7	5	468	-462
7	7	227	-238
7	11	196	-206
7	15	164	-145
8	1	672	-673
8	3	441	431
8	5	455	-434
8	7	496	497
8	9	518	-498
8	11	377	374
8	13	266	-243
9	1	227	245
9	9	124	148
9	11	179	194
10	1	428	-437
10	3	464	468
10	5	297	-305
10	7	272	267
10	9	273	-289
10	11	318	321
11	3	126	-119
12	1	311	-311
12	2	218	224
12	5	228	-249
12	7	174	166
12	9	254	-232
14	1	153	-159
14	5	289	-188
*	H=	3	*
1	2	58	57
1	3	151	167
1	4	1167	-1192
1	5	381	-398
1	6	387	396
1	7	222	237
1	8	115	-93
*	H=	3	*
1	13	145	-139
1	14	178	179
1	15	178	168
1	17	113	-102
2	1	211	-218
2	2	117	118
2	3	98	63
2	4	303	-294
2	5	328	-322
2	7	149	-155
2	8	133	127
2	10	713	722
2	12	828	804
2	14	689	684
2	16	713	722
3	2	210	-197
3	3	128	139
3	4	306	-314
3	5	217	-228
3	6	74	84
3	7	269	273
3	8	261	-271
3	9	128	-118
3	11	134	128
3	12	113	-104
3	13	105	72
4	1	142	144
4	2	184	179
4	3	376	383
4	4	108	-95
4	5	196	168
4	6	149	-122
4	7	102	-73
4	8	250	256
4	9	237	238
4	10	99	92
4	11	240	235
4	12	166	-156
4	13	107	-94
4	14	101	112
5	0	163	168
5	1	142	-143
5	2	363	367
5	3	216	215
5	5	175	-173
5	6	166	165
5	8	132	135
5	9	91	-84
5	10	598	-580
5	11	91	58
5	12	122	-125
5	14	138	148
6	1	271	-277
6	2	102	93
6	3	189	-196
6	4	92	-189
6	5	215	-228
6	7	204	-199
6	9	99	-98
6	10	195	-177
6	13	134	-108
7	0	411	-431
7	1	258	-255
7	3	121	114
7	4	108	-112
7	6	223	-221
7	8	218	-217
7	9	151	-143
7	11	204	226
7	12	166	-157
8	2	178	173
8	3	297	305
8	5	146	137
8	7	86	65
8	9	129	124
8	11	88	-93
9	2	175	175
9	4	95	98
9	6	129	152
9	8	148	-158
9	10	178	171
10	1	220	-217
10	8	115	-102
10	9	146	-147
11	0	274	-288
11	1	187	-188
11	2	129	-143
11	5	145	-188
*	H=	4	*
0	4	1279	-1323
0	6	286	284
0	8	1161	-1175
0	12	792	-787
0	14	169	179
0	16	437	-434
1	2	283	296
1	4	381	-375
1	6	100	95
1	8	317	328
2	2	1594	1532
2	4	305	-315
2	6	1698	1718
2	8	179	-178
2	10	713	722
2	12	804	804
2	14	679	684
2	16	713	722
3	2	477	-469
3	4	171	-154
3	6	143	138
3	8	126	137
3	12	132	-116
4	0	1296	-1349
4	2	344	341
4	4	1316	-1323
4	6	112	61
4	8	954	-953
4	10	316	308
4	12	688	-687
4	14	378	-361
5	4	182	-66
5	6	116	-124
5	8	219	206
5	9	185	-116
5	12	145	-119
6	0	250	256
6	2	1162	1132
6	4	482	-488
6	6	656	646
6	8	141	-99
6	10	636	621
6	12	148	-145
6	14	384	387
6	16	181	-169
7	2	172	168
7	12	152	126
8	0	673	-675
8	2	331	322
8	4	586	-582
8	6	238	234
8	8	598	-580
8	10	318	303
8	12	333	-333
9	2	95	78
9	4	187	85
10	0	378	-399
10	2	448	443
10	4	229	-218
10	6	389	374
10	8	247	-231
10	10	298	278
10	12	126	-177
12	0	361	-378
12	2	272	258
12	4	239	-229
12	6	197	187
12	8	238	-218
*	H=	5	*
1	2	349	323
1	3	173	-171
1	4	125	-102
1	7	84	88
1	9	143	149
1	10	233	224
1	11	127	-123
1	12	174	-182
2	1	163	153
2	3	96	91
2	7	78	-63
2	8	145	-153
2	9	123	128
2	11	161	151
2	12	93	97
*	H=	5	*
3	0	314	-313
3	2	96	-43
3	4	182	-198
3	7	156	-152
3	8	129	-139
3	9	139	143
3	10	184	188
3	11	149	-128
3	12	143	-161
4	1	149	-134
4	5	172	178
4	6	268	-262
4	7	168	-167
4	8	80	-72
5	1	115	111
5	2	294	296
5	5	118	138
5	6	284	314
5	7	86	-68
5	11	93	98
5	13	126	135
5	14	196	185
6	2	98	-120
6	3	236	240
6	5	178	174
6	8	114	-117
6	9	121	118
6	11	117	136
7	8	321	-307
7	1	96	68
7	4	286	-218
7	5	81	47
7	7	88	-131
7	8	195	-204
7	12	121	-138
8	1	129	-125
8	3	153	-158
8	6	86	50
8	9	185	-116
8	10	186	-165
9	2	122	133
9	5	184	182
9	6	262	266
9	10	185	94
10	3	142	127
11	8	158	-151
11	4	132	-135
12	2	97	74
*	H=	6	*
0	3	859	-877
0	5	228	222
0	7	286	-276
0	9	648	618
0	11	682	-608
0	13	196	198
0	15	236	-221
1	3	731	-738
1	5	548	-534
1	7	471	-456
1	9	361	-349
1	11	212	-208
1	13	292	-282
1	15	206	-178
2	1	658	667
2	3	721	-721
2	5	613	618
2	7	468	-467
2	9	611	595
2	11	415	-405
2	13	305	291
2	15	158	-155
3	1	462	457
3	3	734	726
3	5	268	236
3	7	132	108
3	9	584	494
3	11	424	405
4	1	762	772
4	3	478	-471
4	5	454	-443
4	7	568	-574
4	9	448	436
4	11	392	-373
4	13	278	284
4	15	188	-187
5	1	483	-393
*	H=	6	*
5	3	139	-156
5	9	116	-114
5	7	351	-337
5	9	167	-134
5	11	158	-153
5	13	115	-118
5	15	124	-97
6	1	547	544
6	3	469	-461
6	5	373	344
6	7	468	-468
6	9	167	176
6	11	196	-189
6	13	123	122
6	15	94	-73
7	3	291	274
7	5	283	266
7	9	104	101
7	11	192	196
8	1	291	281
8	3	370	-374
8	5	506	498
8	7	408	-413
8	9	282	266
8	11	192	-179
9	1	136	-147
9	11	132	-97
10	1	212	207
10	3	388	-371
10	5	358	356
10	7	251	-253
10	9	168	157
11	7	109	99
12	1	196	284
12	3	253	-254
12	5	218	233
*	H=	7	*
1	4	55	-74
1	5	61	78
1	6	85	-105
1	7	127	-128
2	2	87	103
2	3	94	108
2	4	84	98
2	5	178	197
2	6	106	-97
3	8	124	119
3	1	88	85
3	2	62	61
3	3	91	-98
3	4	101	108
3	5	85	76
3	7	163	-146
3	8	151	153
3	9	135	135
3	11	148	-136
4	1	212	-217
4	2	112	99
4	3	67	-63
4	5	92	-102
4	7	85	-69
4	9	109	-94
4	10	102	-74
5	8	157	-131
5	1	72	73
5	2	199	-192
5	3	169	-173
5	5	148	132
5	6	88	-78
5	8	119	-106
5	9	106	83
5	10	116	-108
6	1	96	117
6	3	154	172
6	4	75	15
6	5	139	125
6	9	137	128
7	8	127	126
7	1	83	77
7	3	136	-128
7	4	159	147
7	8	108	116
8	2	82	-85
8	3	153	-163
8	5	116	-108
8	7	114	-99
9	8	117	-114
9	5	148	136
9	6	147	-147
9	7	116	-101
10	3	116	119
*	H=	8	*
0	4	785	846
0	6	169	-163
0	8	511	528
0	12	478	483
1	2	110	-124
1	4	133	142
1	8	120	-195
2	2	765	-786
2	4	198	215
2	6	894	-917
2	8	96	93
2	10	449	-451
3	2	82	54
3	4	68	84
3	8	106	-98
4	0	792	734
4	2	172	-174
4	4	711	711
4	6	108	-87
4	8	573	578
4	10	145	-167
4	12	367	379
5	2	97	-89
5	6	108	108
5	8	116	-132
6	8	229	219
6	2	670	-649
6	4	213	201
6	6	410	-391
6	10	412	-406
7	2	116	-94
8	0	516	472
8	2	207	-210
8	4	343	325
8	6	142	-134
8	8	391	385
8	9	299	276
8	2	311	-298
8	4	156	131
*	H=	9	*
1	2	185	-127
1	4	169	188
1	6	145	-128
1	8	191	-135
2	1	74	-148
2	2	138	-138
3	8	78	109
3	4	171	181
3	7	92	91
3	8	168	171
4	2	117	-118
4	3	182	158
4	5	159	191
4	6	89	72
4	8	96	-65
5	8	87	58
5	1	189	-92
5	2	193	-189
5	6	173	-181
6	1	113	-109
6	5	145	-98
6	7	113	-72
7	8	262	268
7	1	121	-107
7	4	95	98
8	3	182	182
9	2	124	-133
*	H=	10	*
0	3	336	418
0	5	257	-261
0	7	254	256
0	9	233	-245
1	3	332	357
1	5	228	236
1	7	216	215
1	9	215	222
2	3	336	354
2	5	373	-389
2	7	293	304
2	9	280	-276
3	1	224	-258
3	3	267	-264
3	5	171	-181
3	7	162	-163
3	9	172	-176
4	1	337	-343
4	3	288	288
4	5	268	-282
4	7	298	302
4	9	246	-229
5	1	152	163
5	3	175	171
5	5	191	198
5	7	186	182
6	1	313	-313
6	3	275	275
6	5	268	-269
6	7	234	216
7	1	134	-103
7	3	99	-75
7	5	197	-141
8	1	228	-219

for the 322 non-family reflections. The corresponding R_w values were 0.049, 0.044, and 0.093, respectively. The final ratio between the scale factors for the non-family and family reflections was 1.04, which is in accordance with the observation that the structure of the crystal studied closely approximated the MDO_1 structure. An $F_o - F_c$ Fourier synthesis, calculated with the program JIMDAP,[21] showed a maximum electron density of 0.5 e/Å^3.

Atomic and thermal parameters are listed in Table 2 and observed and calculated structure factors in Table 3. Distances and angles within the $[Cr(CN)_6]^{3-}$ complex ion, as calculated by the program ORRFE,[21] are given in Table 4.

DESCRIPTION OF THE STRUCTURE AND DISCUSSION

A projection of a unit cell of $K_3[Cr(CN)_6]$ along [010], drawn by the program ORTEP,[21] is shown in Fig. 2. By comparing Fig. 2 with Fig. 1 it is seen that a layer of the OD structure is composed of the two $[Cr(CN)_6]^{3-}$ complex

Table 4. Bond distances (Å) and angles (°) within the $[Cr(CN)_6]^{3-}$ complex ion. Standard deviations of the distances ($\times 10^3$) and the angles are given in parentheses.

Distances			
Cr – C(1)	2.075(7)	C(1) – N(1)	1.141(9)
Cr – C(2)	2.057(12)	C(2) – N(2)	1.167(17)
Cr – C(3)	2.100(10)	C(3) – N(3)	1.099(22)
Angles			
Cr – C(1) – N(1)	178.2(0.6)	C(1) – Cr – C(3)	91.0(0.4)
Cr – C(2) – N(2)	177.3(1.0)	C(1) – Cr – C(3)	90.0(0.4)
Cr – C(3) – N(3)	178.5(1.0)	C(2) – Cr – C(2)	88.9(0.5)
C(1) – Cr – C(1)	179.9(0.8)	C(2) – Cr – C(3)	90.2(0.2)
C(1) – Cr – C(2)	90.5(0.4)	C(2) – Cr – C(3)	179.0(0.5)
C(1) – Cr – C(2)	89.5(0.4)	C(3) – Cr – C(3)	90.7(0.5)

ions in the upper half ($0 < z < 0.5$) of the unit cell, together with the four K(2) ions directly above and below the K(1) and Cr atoms in the c direction. The second layer, which is identical with the first, is obtained from the latter by a translation of $-\vec{a}/4+\vec{c}_0$, while the third layer is obtained from the second by the translation $\vec{a}/4+\vec{c}_0$.

As is apparent from Table 4, the $[Cr(CN)_6]^{3-}$ ions are not significantly distorted from octahedral symmetry. Although there is no significant difference between them, the three Cr – C bonds show a spread in length [2.057(12) Å, 2.075(7) Å, and 2.100(10) Å] similar to that found for $K_3[(Mn(CN)_6]$, $K_3[Fe(CN)_6]$, and $K_3[Co(CN)_6]$.[7,8] The mean Cr – C bond length, 2.077(5) Å, is in agreement with mean Cr – C bond lengths found in $Cd_3[Cr(CN)_6]_2.xH_2O$ [2.047(19) Å],[23] $Mn_3[Cr(CN)_6]_2.6H_2O$ [2.063(11) Å],[24] and $[Co(C_2H_8N_2)_3][Cr(CN)_5NO].2H_2O$ [Cr – C_{eq} 2.033(7) Å and Cr – C_{ax} 2.075(14) Å].[25] A mean Cr – C bond length of 1.99(3) Å was found in $[K_3Cr(CN)_5NO]$.[10] This value represents, however, the mean including Cr – N(O), since $K_3[Cr(CN)_5NO]$ crystallizes with an OD structure and it was possible, at that time, only to solve the superposition structure. The cyanide bond lengths, which range from 1.099 – 1.167 Å with a mean value of 1.136(7) Å, are also in agreement with C – N distances found in other transition metal cyanocomplexes.[5–11,16,23–25]

Accompanying the increase in effective nuclear charge on the central metal atom from chromium(III) to cobalt(III), there is a decrease in Me – C bond length and an increase in the Me – C≡N bending and Me – C stretching frequencies, whereas the C≡N stretching frequencies and bond lengths are fairly constant (*cf.* Table 5). This would appear to indicate

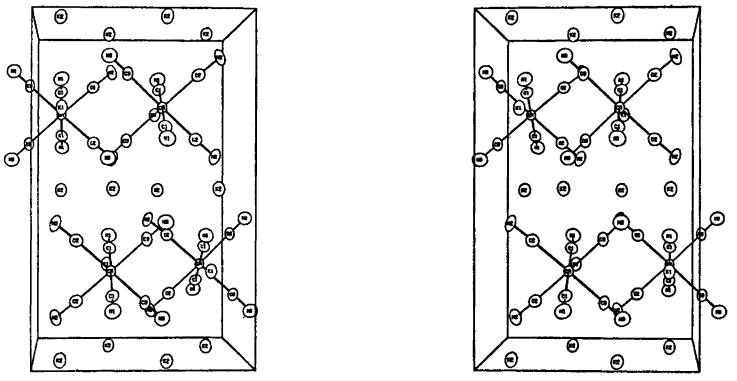

Fig. 2. Stereoscopic projection of the unit cell of $K_3[Cr(CN)_6]$ along [010]. The a axis is horizontal.

Table 5. Infra-red data [18] and bond distances (Å) for some Me(III) hexacyanides.

Compound	Mean Me–C (Å)	ν_7 cm^{-1} (Me–C≡N bend)	ν_8 cm^{-1} (Me–C stretch	Mean C≡N (Å)	ν_6 cm^{-1} (C≡N stretch
$K_3[Cr(CN)_6]$	2.08[a]	458	339	1.14[a]	2128
$K_3[Mn(CN)_6]$	2.00[7]	483	361	1.14[7]	2112
$K_3[Fe(CN)_6]$	1.95[8]	506	389	1.14[8]	2118
$K_3[Co(CN)_6]$	1.89[8]	564	416	1.15[8]	2129

[a] Present work.

that the π-bonding contribution to the Me–C bond is very slight, which is in accordance with molecular orbital calculations[1] on $[Co(CN)_6]^{3-}$. Moreover, there is no significant difference between the C≡N distances in the Me(III) hexaxyanides and those found in the corresponding pentacyanonitrosyls, in which Me–C π-bonding is regarded as being negligible.[2–4,12]

Acknowledgements. The authors wish to thank Dr. R. G. Hazell for valuable discussions concerning all aspects of the work, and Professor S. E. Rasmussen for facilities placed at their disposal. A grant from the Swedish Natural Science Research Council (Contract No. 2286 – 18) is gratefully acknowledged.

REFERENCES

1. Alexander, J. J. and Gray, H. B. *Coord. Chem. Rev. 2* (1967) 29.
2. Manoharan, P. T. and Gray, H. B. *J. Amer. Chem. Soc. 87* (1965) 3340.
3. Manoharan, P. T. and Gray, H. B. *Inorg. Chem. 5* (1966) 823.
4. Fenske, R. F. and DeKock, R. L. *Inorg. Chem. 11* (1972) 437.
5. Tullberg, A. and Vannerberg, N.-G. *Acta Chem. Scand. 25* (1971) 343.
6. Tullberg, A. and Vannerberg, N.-G. *Acta Chem. Scand. To be published.*
7. Vannerberg, N.-G. *Acta Chem. Scand. 24* (1970) 2335.
8. Vannerberg, N.-G. *Acta Chem. Scand. 26* (1972) 2863.
9. Jagner, S. and Vannerberg, N.-G. *Acta Chem. Scand. 24* (1970) 1988.
10. Vannerberg, N.-G. *Acta Chem. Scand. 20* (1966) 1571.
11. Svedung, D. H. and Vannerberg, N.-G. *Acta Chem. Scand. 22* (1968) 1551.
12. Vannerberg, N.-G. and Jagner, S. *Chem. Scr. 6* (1974) 19.
13. Dornberger-Schiff, K. *Lehrgang über OD-Strukturen*, Akademie-Verlag, Berlin 1966.
14. Bennett, B. G. and Nicholls, D. *J. Chem. Soc. A* (1971) 1204.
15. Towns, R. L. R. and Levenson, R. A. *J. Amer. Chem. Soc. 94* (1972) 4345.
16. Towns, R. L. R. and Levenson, R. A. *Inorg. Chem. 13* (1974) 105.
17. Brauer, G. *Handbuch der Präparativen Anorganischen Chemie*, Ferd. Enke, Stuttgart 1962, Vol. II, p. 1202.
18. Jones, L. H. *Inorg. Chem. 2* (1963) 777.
19. *International Tables for X-Ray Crystallography*, Kynoch Press, Birmingham 1959.
20. Program library of Department of Inorganic Chemistry, University of Göteborg and Chalmers University of Technology: PEPP written by Berggren, J. and POWDER by Lindqvist, O. and Wengelin, F.
21. Program library of Department of Inorganic Chemistry, University of Aarhus: G4 written by Hazell, R. G., FORDAP by Zalkin, A., LINUS by Hamilton, W. C. and Ibers, J. (modification of the Busing-Martin-Levy program ORFLS), JIMDAP by Zalkin, A., ORRFE by Busing, W. R., Martin, K. O., and Levy, H. A., and ORTEP by Johnson, C. K.
22. Cromer, D. T. and Mann, J. B. *Acta Crystallogr. A 24* (1968) 321.
23. Güdel, H. U. *Acta Chem. Scand. 26* (1972) 2169.
24. Güdel, H. U., Stucki, H. and Ludi, A. *Inorg. Chim. Acta 7* (1973) 121.
25. Enemark, J. H., Quinby, M. S., Reed, L. L., Steuck, M. J. and Walthers, K. K. *Inorg. Chem. 9* (1970) 2397.

Received February 26, 1974.

Acta Chemica Scandinavica A 28 (1974) 631—637

Equilibrium Studies of L-Ascorbate Ions. IX. Equilibria between Iron(II) Ions, Ascorbate Ions, and Protons in 3 M $(Na)ClO_4$ Medium

PER ULMGREN and OLOF WAHLBERG

Departments of Inorganic and Structural Chemistry, Arrhenius Laboratory, University of Stockholm, S-104 05 Stockholm, Sweden and Department of Inorganic Chemistry, Royal Institute of Technology, S-100 44 Stockholm, Sweden

Potentiometric titrations, giving 154 experimental points, have been carried out for the system Fe(II)-ascorbic acid-H^+ using glass electrodes. The concentrations ranges studied were $0.01\ M \leq [Fe^{2+}]_{tot} \leq 1\ M$, $0.02\ M \leq [H_2Asc]_{tot} \leq 0.2\ M$ and $-7.1 \leq \log [H^+] \leq -1.1$, where $H_2Asc \equiv$ ascorbic acid. Special precautions were taken to keep the system in a reduced state. The following equilibria and equilibrium constants (β_i) are valid in 3 M $(Na)ClO_4$ and at 25 °C:

$HAsc^- + H^+ \rightleftharpoons H_2Asc$
$\log (\beta_1 \pm 3\sigma) = 4.377 \pm 0.011$

$Fe^{2+} + HAsc^- \rightleftharpoons FeHAsc^+$
$\log (\beta_2 \pm 3\sigma) = 0.21 \pm 0.05$

$Fe^{2+} + HAsc^- \rightleftharpoons FeAsc + H^+$
$\log (\beta_3 \pm 3\sigma) = -6.58 \pm 0.09$

Solutions with $\log [H^+] > -1.0$ are green or pale green. When NaOH solution is added the colour turns violet. The experimental data for $\log [H^+] \geq -5.5$ can be explained by the presence of H_2Asc, $HAsc^-$, Fe^{2+}, and $FeHAsc^+$ participating in rapid equilibrium reactions. In solutions with $\log [H^+] < -5.5$, however, the equilibria are approached slowly. These solutions are black, and seem to contain the species FeAsc, possibly together with polynuclear complexes of the type Fe_qAsc_r.

The complex formation between Fe(II) and ascorbic acid is of considerable biological interest. For example, the uptake of iron(II) by the human body is more efficient if ascorbic acid is consumed together with iron(II). Ascorbic acid plays an important role in some biochemical processes, where acid-base and redox properties are essential.[1]

We first studied the complex formation between ascorbate and Cd^{2+} and Ca^{2+}, respectively,[2] which are also of biological interest.[1] Violet iron—ascorbate complexes have been reported.[3] Iron(II) is an easily oxidized metal ion, which may take part in redox equilibria with ascorbic acid; this fact necessitates some precautions.

In this paper an equilibrium study of the complex formation between ascorbate and Fe^{2+} is reported. Special care has been taken to keep the system in a reduced state by using H_2, H^+ as a redox buffer with freshly platinized Pt-foils as a catalyst.

SYMBOLS

The most common symbols are H, B, C for H^+, Fe^{2+}, and $HAsc^-$. H = the analytical (excess) concentration of H^+ over H_2O, Fe^{2+}, and $HAsc^-$. The total concentrations of Fe^{2+} and $HAsc^-$ are written as B and C, respectively. The concentrations of free H^+, Fe^{2+}, and $HAsc^-$ are denoted by h, b, and c. The concentration of $H_pB_qC_r$ is written as c_{pqr}. β_{pqr} is the equilibrium constant for the formation of $H_pB_qC_r$. The following Z-functions are used:
$Z_{H/C}$ = the average number of H^+ per C, *i.e.* H^+ per $HAsc^-$.
$Z_{C/B}$ = the average number of C per B, *i.e.* $HAsc^-$ per iron(II).

A more complete list of symbols has been given elsewhere.[4]

EXPERIMENTAL

Chemicals and analysis. Solutions of $NaClO_4$, $HClO_4$, NaOH, and NaCl were prepared and analysed as reported earlier.[2,4] Samples of ascorbic acid (*p.a.* from Merck, Darmstadt, Germany) were weighed out for each experiment.

$Fe(ClO_4)_2.6H_2O$ was prepared from the following chemicals: Analysed $FeSO_4.7H_2O$ from I. T. Baker Chemical, Deventer, Holland; Analytical grade $BaCO_3$ and analytical grade $HClO_4$ both from Merck, Darmstadt. First $Ba(ClO_4)_2$ was prepared by neutralizing $HClO_4$ with $BaCO_3$. $FeSO_4.7H_2O$ and $Ba(ClO_4)_2$, respectively, were then recrystallized once from water and mixed in water to give solid $BaSO_4$(s) and a solution of $Fe(ClO_4)_2$. The amount of Ba^{2+} was adjusted to be slightly in excess ($\sim$0.1 %). A centrifuging with 10 000 rpm was used to separate the solid phase from the solution. The iron(II) perchlorate was recrystallized once. A stock solution made from these crystals was analyzed for Cl^- and SO_4^{2-} by adding $AgNO_3$ and $BaCl_2$ respectively. No precipitation could be detected. The amount of Ba^{2+} was very small (less than 0.1 % of Fe^{2+}). The iron(II) perchlorate solution was treated with hydrogen gas in an acid solution with platinum black as a catalyst. The solution was stored under CO_2(g).

The stock solution of iron(II) perchlorate was analysed by potentiometric titrations with potassium permanganate. The equivalence point was determined by Gran's extrapolation method.[5] The $KMnO_4$-solution (Merck's ampoule) was standardized in two ways: (a) against Merck's *p.a.* As_2O_3 and (b) against 4N8 pure iron wire from Halewood Chemicals Ltd. Different determinations always agreed within 0.1 %.

Apparatus; The salt bridge and electrodes have been described elsewhere.[4]

The titration procedure and emf measurements. For each titration a solution containing iron(II) perchlorate, ascorbic acid, and perchloric acid with log $h = -1.0$ was prepared and its redox potential decreased by passing a stream of hydrogen gas through it. A freshly platinized platinum foil was used as a catalyst. This

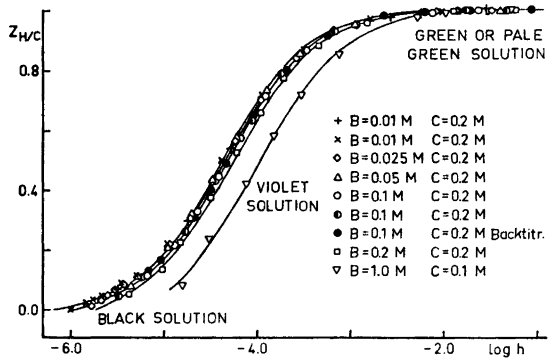

Fig. 1a. $Z_{H/C}$ (= the average number of H^+ bound per C) as a function of log h. The curves have been calculated with the final values of the formation constants using HALTAFALL.[11]

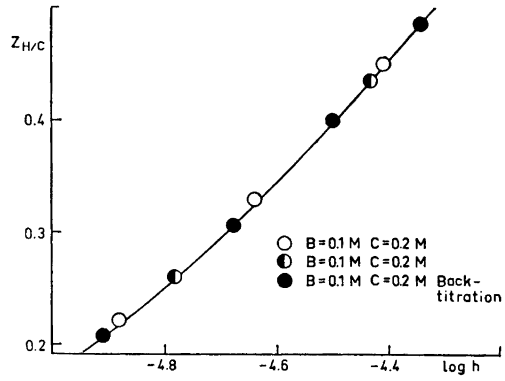

Fig. 1b $Z_{H/C}$ as a function of log h. Part of the data in Fig. 1a are shown in a larger scale to demonstrate the reproducibility of the data.

"reduced" solution was used in one buret and a NAOH-solution in the other. Equal volumes from the two burets were added to a solution made from 15.00 ml reduced solution and 15.00 ml distilled and deaerated water (*cf.* Ref. 4). Hydrogen gas was bubbled through the equilibrium solution during the whole titration (in the presence of platinum catalyst). Two glass electrodes, with catalog numbers 39303 and 40495, respectively, from Beckman Instruments, Fullerton, California, were used. For $\log h > -5.5$ (violet solution) the emf became stable within a few minutes, but for $\log h < -5.5$ (black solution) the emf approached a stable value very slowly. However, no precipitate could be detected with a microscope.

We tried to use a hydrogen electrode to measure h in the equilibrium solution. Down to $\log h = -3.5$ there was a very good agreement between glass and hydrogen electrode data, but not for $\log h < -3.5$. The value of E_0 for the hydrogen electrode, however, determined from the most acid points with $0.010\ \text{M} \leq h \leq 0.050\ \text{M}$, was -293 mV, while the expected value is -320 mV (*cf.* Refs. 2 and 6).

The reproducibility of the glass elctrode measurements is within ± 0.2 mV. The reversibility of the equilibria was confirmed by one back titration. As seen in Fig. 1b the different titrations agree within ± 0.007 in Z.

Table 1a. Experimental data (computer output from LETAGROP). For each point in a titration (≡'Sats') are given V = the volume of the buret solution, with total concentrations H_T, B, and C added to V_0 ml of a solution with total concentrations H_0, B, and C (*cf.* Table 1b); E (≡'E'); $\log [H^+]$ (≡'LOGA'); H (≡'ATOT') and $(H_{calc} - H)10^3$ (≡'DATOT'). H_{calc} has been calculated using the final equilibrium constants. 19 points measured in black solutions with slow equilibria are marked with *.

Sats 1 B=0.01M C=0.02M V_0=30.40ml

V	EA(FV)	LOGA	ATOT(MM)	DATOT
0.000	313.70	-1.301	69,62	0,39
0.800	311.20	-1.344	65,12	0,10
2.300	306.30	-1.430	57,29	-0,12
4.300	298.90	-1.557	47,89	-0,22
6.300	289.80	-1.714	39,52	-0,23
8.300	277.50	-1.924	32,01	-0,16
10.300	257.50	-2.264	25,24	0,05
11.300	238.60	-2.584	22,18	0,18
13.300	171.40	-3.721	16,25	0,27
15.300	138.30	-4.281	10,91	0,16
17.300	111.10	-4.741	6,02	-0,03
19.300	66.40	-5.500	1,53	-0,14

Sats 2 B=0.01M C=0.2M V_0=30.00ml

0.000	327.60	-1.287	250,91	0,59
0.820	325.10	-1.331	246,17	0,37
2.200	321.00	-1.402	238,73	0,70
4.200	314.10	-1.521	229,01	0,82
6.400	304.90	-1.679	219,56	0,95
8.200	295.10	-1.847	212,64	0,99
9.800	283.60	-2.043	207,01	1,12
New buret				
0.700	238.00	-2.816	194,73	1,36
1.980	196.40	-3.520	173,35	2,23
4.020	169.90	-3.968	141,85	1,56
7.200	144.80	-4.392	98,21	-0,63
10.180	124.80	-4.731	62,35	-1,52
12.000	110.90	-4.966	42,48	-1,94
13.980	90.40	-5.314	22,39	-1,91
New buret				
1.120	86.30	-5.384	19,34	-1,63
2.200	82.00	-5.457	16,52	-1,35
4.120	73.10	-5.609	11,76	-0,82
5.120	67.80	-5.700	9,40	-0,44
6.020	63.20	-5.779	7,34	0,18
* 7.120	62.80	-5.772	6,09	1,30
* 8.000	59.90	-5.822	4,20	2,35
*10.120	49.10	-6.009	-0.11	4,20

Sats 3 B=0.025M C=0.2M V_0=30.70ml

0.000	312.00	-1.325	248,10	-1,00
1.400	308.20	-1.391	242,42	-0,83
3.520	300.80	-1.520	229,98	-0,83
5.400	292.70	-1.659	221,74	-0,20
7.500	281.00	-1.859	213,51	-0,30
9.400	265.90	-2.116	206,80	-0,27
New buret				
1.120	203.10	-3.180	187,43	0,85
2.300	178.80	-3.591	168,14	3,98
4.100	156.10	-3.974	140,69	1,21
6.100	140.20	-4.243	112,70	0,90
8.200	125.90	-4.485	85,80	0,16
10.300	111.70	-4.726	61,15	-0,64
11.980	98.90	-4.942	42,85	-1,15
14.000	78.80	-5.284	22,36	-0,91
New buret				
1.200	74.50	-5.357	19,06	-0,62
* 3.020	68.60	-5.434	16,32	-0,97
* 4.500	63.20	-5.526	12,68	-0,19
* 5.800	58.90	-5.600	9,63	0,92
* 7.820	54.90	-5.668	6,89	2,07
* 9.100	46.30	-5.782	2,46	4,29

Sats 4 B=0.05M C=0.2M V_0=30.00ml

0.000	318.10	-1.280	250,70	1,63
0.700	315.80	-1.320	246,68	0,99
2.100	311.20	-1.400	239,17	0,40
4.100	304.20	-1.521	229,51	0,30
6.400	293.80	-1.700	219,72	-0,22
8.100	284.30	-1.862	213,24	-0,17
10.100	269.10	-2.121	206,32	0,05
New buret				
0.800	220.50	-2.944	192,44	1,02
2.000	185.90	-3.530	172,61	1,12
3.600	164.90	-3.885	147,86	0,84
5.800	146.10	-4.203	116,65	-0,14
8.000	130.80	-4.462	88,30	-1,26
10.000	117.50	-4.687	64,68	-1,71
12.000	102.30	-4.944	42,88	-2,31
14.000	83.50	-5.263	22,68	-0,91
New buret				
* 2.000	78.40	-5.344	15,16	2,78

Sats 5 B=0.1M C=0.2M V_0=30.00ml

0.000	320.00	-1.310	249,70	-0,87
0.900	317.60	-1.351	244,57	-0,27
3.100	310.10	-1.482	233,20	-0,50
5.100	302.40	-1.614	224,10	-0,19
7.100	292.50	-1.784	215,98	-0,12
9.980	270.70	-2.155	205,72	-0,10
New buret				
1.120	209.80	-3.186	186,37	0,39
2.920	176.10	-3.756	157,39	-0,45
5.020	157.90	-4.064	126,51	1,97
8.020	136.10	-4.433	87,98	0,09
11.020	115.40	-4.783	52,30	-0,83
14.020	88.30	-5.243	21,37	0,17
*15.520	73.00	-5.484	8,53	3,33
*17.020	33.90	-6.160	-4,93	2,86
*18.520	-5.10	-6.910	-17,70	+3,43
*20.020	-14.80	-7.159	-29,63	+1,91

Sats 6 B=0.1M C=0.2M V_0=30.00ml

0.000	84.90	-5.265	20,70	-0,11
0.200	90.10	-5.170	25,01	-0,03
0.600	98.30	-5.031	33,47	-0,62
1.000	105.20	-4.914	41,71	-0,82
2.000	119.10	-4.678	61,41	-0,23
3.000	129.50	-4.502	79,91	-0,44
4.000	138.90	-4.343	97,32	0,04
6.000	156.40	-4.047	129,25	1,80
8.180	177.60	-3.689	160,24	1,74
10.000	202.80	-3.262	183,53	0,49
11.200	238.20	-2.664	197,75	0,03
12.000	270.20	-2.121	206,79	-0,50
13.000	291.60	-1.756	217,60	-0,64
14.000	303.20	-1.557	227,93	-0,58
16.000	316.80	-1.322	247,24	0,22
17.000	320.90	-1.250	256,28	+0,22
18.000	324.30	-1.190	264,94	-0,55
19.000	327.40	-1.135	273,24	-0,14
20.000	329.90	-1.091	281,22	-0,19

Sats 7 B=0.1M C=0.2M V_0=30.00ml

0.000	317.60	-1.289	251,10	0,26
0.800	315.20	-1.331	246,42	0,09
2.180	310.70	-1.409	239,06	-0,40
3.800	305.10	-1.506	231,19	-0,39
5.800	296.80	-1.649	222,45	-0,42
8.100	284.50	-1.859	213,54	-0,40
10.200	268.50	-2.131	206,29	-0,21
New buret				
0.800	220.20	-2.950	192,45	0,37
1.900	189.80	-3.464	174,28	1,33
3.880	164.20	-3.897	143,86	1,16
5.900	147.70	-4.176	115,52	0,55
7.900	133.70	-4.412	89,80	-0,33
9.900	120.30	-4.639	66,13	-1,10
11.900	105.90	-4.883	44,29	-1,48
13.900	88.10	-5.185	24,05	0,18
N14,900	85.20	-5.214	16,63	5,59
N15,440	77.20	-5.350	11,61	4,80

Sats 8 B=0.2M C=0.2M V_0=30.00ml

0.000	335.10	-1.243	256,20	0,75
0.800	332.70	-1.285	251,62	0,44
4.200	322.40	-1.464	234,52	-0,51
2.100	329.10	-1.348	244,65	-0,12
6.200	315.40	-1.585	225,97	-0,49
8.100	307.00	-1.729	218,68	-0,41
10.060	296.70	-1.905	211,88	-0,32
New buret				
1.040	242.20	-2.829	193,92	0,36
2.040	211.70	-3.345	177,49	1,20
3.440	190.10	-3.711	155,76	0,53
5.020	175.00	-3.966	132,85	0,29
7.020	160.10	-4.218	106,06	-0,34
9.540	143.90	-4.492	75,38	-0,31
12.240	124.20	-4.826	45,79	-1,94
14.040	110.70	-5.054	27,70	0,42
#16,040	91.20	-5.372	10,34	2,96
#18,040	43.90	-6.190	-7,11	-0,06
#20,040	22.90	-6.975	-23,39	3,43

Sats 9 B=1.0M C=0.1M V_0=30.00ml

0.000	326.80	-1.257	193,70	1,43
0.600	324.20	-1.303	186,25	-0,44
1.800	320.70	-1.364	143,73	-0,69
3.600	315.00	-1.463	134,82	-0,66
5.100	309.90	-1.551	128,10	-0,34
7.600	299.10	-1.736	118,09	-0,31
10.300	283.10	-2.009	108,67	0,03
New buret				
0.800	265.00	-2.316	102,22	0,49
2.900	216.60	-3.136	86,45	1,34
5.000	192.50	-3.543	72,14	0,72
7.320	175.20	-3.836	57,79	-0,08
10.180	158.00	-4.127	41,92	-0,72
14.020	134.10	-4.531	23,24	-1,60
#17,800	117,10	-4,808	8,22	4,12

Table 1. For each titration are given: the total concentrations, E_0 estimated from a few acid points, the final value of E_0 and δH obtained in the refinement using LETAGROP.[9] Concentrations are given in M and emf values in mV. H is defined by: H (final) = H [calculated from eqn. (2)] + δH. H_0 is the value of H in the starting solution and H_T is the value of H in the buret solution [*cf.* eqn. (2)].

Titration No.	B	C	H_0	H_T 1st buret	2nd buret	3rd buret	E_0 from acid points	$E_0 \pm 3\sigma$	$(\delta H \pm 3\sigma) \times 10^3$
1	0.01	0.02	0.06925	−0.1061			391.8	391.5 ± 0.3	0.37 ± 0.27
2	0.01	0.2	0.2521	0.0738	−0.5020	−0.1259	404.2	404.6 ± 1.5	−1.2 ± 1.8
3	0.025	0.2	0.2482	0.0720	−0.5058	−0.1297	390.9	391.2 ± 1.7	−0.1 ± 2.2
4	0.05	0.2	0.2498	0.0736	−0.5042	−0.2028	395.7	394.7 ± 1.6	0.9 ± 2.2
5	0.1	0.2	0.2500	0.0738	−0.5040		397.9	398.3 ± 1.3	−0.3 ± 1.7
6[b]	0.1	0.2	0.0212	0.6725			395.6	395.8 ± 0.6	−0.5 ± 0.9
7	0.1	0.2	0.2504	0.0742	−0.5036		395.1	394.7 ± 1.0	0.6 ± 1.4
8	0.2	0.2	0.2554	0.0789	−0.4986		410.0	409.6 ± 1.0	0.8 ± 1.5
9	1.0	0.1	0.1540	−0.02220	−0.2220		401.7	402.1 ± 1.3	−0.3 ± 1.5

[b] = back titration.

SURVEY OF EXPERIMENTAL DATA

For each titration values of E_0, H_0, and H_T were calculated from the most acid points. $(V,E)_{B,C}$ with $[H^+] \geq 0.010$ M, by means of the computer program TRAVE.[7] The primary data were then transformed to $(H,h)_{B,C}$ (Table 1a) and $Z(\log h)_{B,C}$ (Fig. 1).

The total concentrations of iron(II) perchlorate ($=B$) and ascorbic acid ($=C$) were kept constant during each titration, but the analytical hydrogen ion concentration ($=H$) was varied. In the initial and buret solutions $[H^+]_{tot}$ equals H_0 and H_T, respectively. The value of H in a solution prepared from V ml of buret solution and V_0 ml of starting solution is given by eqn. (2). Z was calculated from eqn. (3). In Table 1 we have given H_{calc} obtained from eqns. 4(a–d) with known equilibrium constants. Z_{calc} was calculated from eqn. (3) using the complexes and equilibrium constants finally obtained.

$$E = E_0 + 59.155 \log h - 17h \quad (1)$$

$$H = (V_0H_0 + VH_T)/(V_0 + V) \quad (2)$$

$$Z = (H - h + K_w h^{-1})/C \quad (3)$$

$$H = h + \sum p c_{pqr} \quad (4a)$$

$$B = b + \sum p c_{pqr} \quad (4b)$$

$$C = c + \sum r c_{pqr} \quad (4c)$$

where $c_{pqr} = \beta_{pqr} h^p b^q c^r$ (4d)

and K_w = the ionic product of water ($\log K_w = -14.22$ [2d])

TREATMENT OF THE DATA

The equilibria studied can be written as

$$pH^+ + qFe^{2+} + rHAsc^- \rightleftharpoons H_pB_qC_r \quad (5)$$

In this study we have neglected the hydrolysis of Fe^{2+} (*cf.* Ref. 8). First we have treated the data for $\log h > -5.5$ (135 points in violet solution). Then a rough estimation of the complex formation for $\log h < -5.5$ (19 points in black solution) was made.

Complex formation in the range log $h \geq -5.5$. As seen in Fig. 1 the effects are rather small. It is reasonable to assume that the complexes formed have the general formula $Fe_q(HAsc)_r$ (*cf.* Ref. 4). The data in Fig. 1 have been transformed to $Z_{C/B}$ (log c), where $c = [HAsc^-]$ (*cf.* eqn. (6a) and Fig. 2). $Z_{C/B}$ (log c) has been calculated in the same way as in Ref. 2a p. 1052.

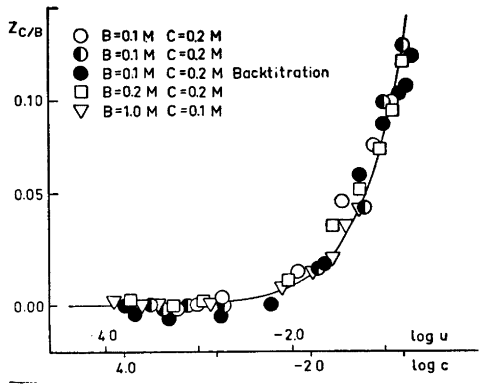

Fig. 2 $Z_{C/H}$ (= the average number of ascorbic acid molecules bound per B) as a function of log c, where $c = [HAsc^-]$. The solid curve is the normalized function $u/(1+u)$ as a function of log u corresponding to $\log \beta_{011} = 0.20$.

$$Z_{C/B} = \sum r \beta_{pqr} b^q c^r / (b + \sum q \beta_{pqr} b^q c^r) \quad (6a)$$

$Z_{C/B}$ (log c)$_{B,C}$ is independent of B (*cf.* Fig. 2). This indicates that $q = 1$ (*cf.* eqn. (6a)]. The experimental data can be very well explained by assuming one single iron ascorbate complex with $q = 1$ and $r = 1$, *i.e.* $FeHAsc^+$. By fitting the normalized curve $u/(1+u) = f(\log u)$ to the data, it was found that

$$\log \beta_{011} = 0.20 \pm 0.05 \quad (6b)$$

By using the least squares program LETAGROP,[9] minimizing $U = \sum (H_{calc} - H)^2$, we obtained

$$\log(\beta_{101} \pm 3\sigma) = 4.377 \pm 0.011 \quad (6c)$$
$$\log(\beta_{011} \pm 3\sigma) = 0.21 \pm 0.05$$

with $\sigma Z = 0.006$; where σ is the standard deviation, and (101) symbolizes H_2Asc. In the last refinement we have assumed small errors in H ($= \delta H$) and E_0 ($= \delta E_0$). The adjusted parameters δH indicate analytical errors of the expected order of magnitude (~ 0.5 %) and they show no trend. Moreover, the values of E_0 agree with those determined in acid solutions (by TRAVE [7]). (*cf.* Table 1b).

Complex formation in the range log $h < -5.5$. A few points (19) were taken in the range of

acidity of the black solutions. The equilibria are slow in this range. No precipitate could be detected, however. For the most basic points stable emf values were obtained after about one hour. The effects are rather large and could be explained by assuming the presence of $FeHAsc^+$ together with at least one species of the type Fe_qAsc_r.

By assuming either FeAsc or Fe_3Asc_3 we obtained the following values:

$$\log(\beta_{\bar{1}11} \pm 3\sigma) = -6.58 \pm 0.09; \quad \sigma Z = 0.009; \quad U_Z = 12 \times 10^3 \qquad (6d)$$
$$\log(\beta_{\bar{3}33} \pm 3\sigma) = -16.98 \pm 0.19; \quad \sigma Z = 0.011; \quad U_Z = 17.10^3$$

Thus FeAsc gives the "best" fit with the data. The fit was not improved significantly if both FeAsc and Fe_3Asc_3 were assumed. The value of $\log \beta_{\bar{1}11}$ should be regarded as tentative, in view of the very limited experimental material available.

RESULTS AND DISCUSSION

As the final description of our data we propose the following reactions and constants valid in 3 M $(Na)ClO_4$ medium at 25 °C.

$$HAsc^- + H^+ \rightleftharpoons H_2Asc$$
$$\log(\beta_{101} \pm 3\sigma) = 4.377 \pm 0.011$$
$$Fe^{2+} + HAsc^- \rightleftharpoons FeHAsc^+$$
$$\log(\beta_{011} \pm 3\sigma) = 0.21 \pm 0.05 \qquad (7)$$
$$Fe^{2+} + HAsc^- \rightleftharpoons FeAsc + H^+$$
$$\log(\beta_{\bar{1}11} \pm 3\sigma) = -6.58 \pm 0.09$$

Solutions with $\log[H^+] \geq -1.0$ containing the main species H_2Asc and Fe^{2+} are green or pale green. In solutions with $-1.0 > \log[H^+] > -5.5$ H_2Asc, $HAsc^-$, Fe^{2+}, and $FeHAsc^+$ predominate. These solutions are violet. At $\log[H^+] \sim -5.5$ the solution turns black. The data for $\log[H^+] < -5.5$ could be explained by assuming the formation of FeAsc. Since the equilibria are slow only a few points were measured and we cannot say anything definite about further complexes, $Fe_q(HAsc)_rH_p$, although the slowless of the equilibria imply that polynuclear complexes might well be formed.

Pfeilsticker [1c] has, by potentiometric titrations, determined a formal value $\log \beta_{\bar{1}11} = -5.8$ for FeAsc which would suggest a stronger complex than our value does. From IR measurements Pfeilsticker [1c] suggests that the complex is Fe_3Asc_3.

The value of pK_{a1} for ascorbic acid in this study agrees reasonably well with the value determined by us earlier, *viz.* $\log(\beta_{101} \pm 3\sigma) = 4.359 \pm 0.006$.[10] The distribution of ascorbic acid over the different species is shown in Fig. 3.

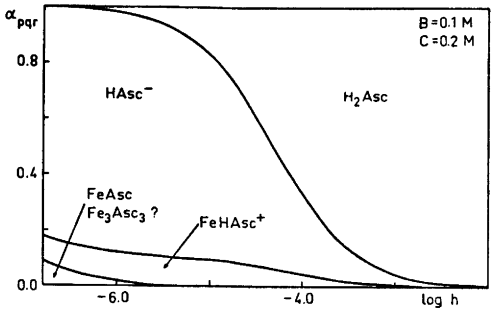

Fig. 3. The distribution of ascorbic acid on different species as a function of $\log h$. $B = 0.1$ M and $C = 0.2$ M. The calculations have been performed by a computer program HALTAFALL [11] with the final equilibrium constants.

The complexes formed between L-ascorbate ions and Cd(II) [2a,b,c] as well as Ca(II) [2d,e] have been studied by our group. In those cases weak colourless complexes of type $Me_q(HAsc)_r$ are formed for $\log[H^+] \geq -5.5$, while at lower $\log[H^+]$ values yellow complex species of type Me_qAsc_r and Me_qAsc_rOH occur. Rather strong cadmium complexes with 3 – 5 Cd^{2+} and 3 – 6 ascorbic acid molecules predominate in solutions with $-5.5 \leq \log[H^+] \leq -8.5$. The cadmium complexes of ascorbic acid are stronger than the corresponding calcium species, which contain 3 – 4 Ca^{2+} and 3 – 4 ascorbic acid molecules and predominate at $-12.5 \leq \log[H^+] \leq -9.5$. The mononuclear complex CaAsc has been observed but not CdAsc.

The order of strength of the metal ascorbate complexes studied are $Cd^{2+} > Fe^{2+} > Ca^{2+}$. Ahrland, Chatt and Davies [12] have classified ligands and central atoms. Pearson [13] has introduced the terms soft and hard acids and bases. The term soft roughly characterises a high degree of polarization in the chemical bonds, while the term hard indicates a lower degree of

polarization. The notation acids and bases are generalized to include central atoms (acids) and ligands (bases). Thus Cd^{2+} is classified as a soft acid, Ca^{2+} as a hard acid and Fe^{2+} as an intermediate acid. Soft acids in general bind soft bases stronger than hard bases. Binding oxygen atoms mostly constitute hard ligands.[12-14] However, in the case of ascorbic acid delocalized π-electrons probably give the ligand a rather soft character.

Thus, for all the metal ions studied we have found acid species $MeHAsc^+$ with weak interactions between the metal ions and the ascorbate ions. In more alkaline solutions, we have found stronger complexes, which are mainly polynuclear in solutions of Ca(II) and ascorbate and and in solutions of Cd(II) and ascorbate and probably also in solutions of Fe(II) and ascorbate ions. We have found evidence for small amounts of CaAsc and FeAsc but not for CdAsc. The trinuclear species Me_3Asc_3 seem to be important in the case of Ca(II) and Cd(II) and it might be so for Fe(II) too.

So far, it has not been possible to prepare crystals of metal ascorbates of type Me_qAsc_p. Hvoslef has investigated the structure of H_2Asc and $HAsc^-$ in the crystals of ascorbic acid and sodium ascorbate by X-ray and neutron diffraction methods.[15] He also has studied $Ca(HAsc)_2.2H_2O$.[15d] Hughes has determined the structure of TlHAsc.[16] These investigations do not contradict that three oxygen atoms in ascorbic acid may be available for the formation of tridentate chelated complexes as suggested by Pfeilsticker[1c] for the metal ascorbate complex Me_3Asc_3.

Acknowledgements. We thank Professor Peder Kierkegaard for his helpful suggestions in connection with this work. Thanks are due to Docent Derek Lewis for revising the English text. This investigation was financially supported by the Swedish Natural Science Research Council.

REFERENCES

1. a. Boyer, P. D., Lardy, H. and Myrbäck, K. *The Enzymes*, Academic, New York 1960, p. 387; b. Sjöstrand, S. E. *Acta Physiol. Scand.* (1970) *Suppl.* Nol 356; c. Pfeilsticker, K. *Deut. Lebensm.-Rundsch. 65* (1969) 348; Björn-Rasmussen, E. *Thesis*, University of Gothenburg, Gothenburg 1974.
2. a. Wahlberg, O. *Acta Chem. Scand. 25* (1971) 1045; b. Ulmgren, P. and Wahlberg, O. *Acta Chem. Scand. 25* (1971) 1063, 1079; c. Ulmgren, P. and Wahlberg, O. In Högfeldt, E., Ed., *Contribution to Coordination Chemistry in Solution*, Berlingska, Lund 1972. *Pure and Applied Chem.* (1972) Vol. 34; d. Forsberg, O., Johansson, K., Ulmgren, P. and Wahlberg, O. *Chem. Scr. 3* (1973) 153; e. Ulmgren, P. and Wahlberg, O. *Chem. Scr. 3* (1973) 159, 193.
3. Stolyarev, L. P. and Amantova, J. A. *Vestn. Leningrad Univ. Ser. Fiz. Khim.* (1964) No. 4, p. 141.
4. Ulmgren, P. and Wahlberg, O. *Acta Chem. Scand. 25* (1971) 1000.
5. Gran, G. *Analyst 77* (1952) 661.
6. Baldwin, W. G. and Sillén, L. G. *Ark. Kemi 31* (1969) 391.
7. Ulmgren, P. and Wahlberg, O. *Chem. Commun. Univ. Stockholm* (1970), No. IV.
8. Hedström, B. O. A. *Ark. Kemi 5* (1952) 457.
9. a. Arnek, R., Sillén, L. G. and Wahlberg, O. *Ark. Kemi 31* (1968) 953; b. Brauner, P., Sillén, L. G. and Whiteker, R. *Ark. Kemi 31* (1968) 377.
10. Wahlberg, O. and Ulmgren, P. *Acta Chem. Scand. 21* (1967) 2759.
11. Ingri, N., Kakolowicz, W., Sillén, L. G. and Warnqvist, B. *Talanta 14* (1967) 1261.
12. Ahrland, S., Chatt, J. and Davies, N. R. *Quart. Rev. Chem. Soc. 12* (1958) 265.
13. Pearson, R. *J. Amer. Chem. Soc. 85* (1963) 3533.
14. Sillén, L. G. and Martell, A. E. *Stability Constants of Metal-ion Complexes*, The Chemical Society, London 1964. Chem. Soc. Spec. Publ. No. 17.
15. a. Hvoslef, J. *Thesis*, University of Oslo, Norway 1972; b. *Acta Crystallogr. B 24* (1968) 23; c. *Acta Crystallogr. B 25* (1969) 2214; d. *Personal communication*, 1974.
16. Hughes, D. *J. Chem. Soc. Dalton 2* (1973) 2709.

Received February 18, 1974.

Acta Chemica Scandinavica A 28 (1974) 638—646

Exchange Reactions of *trans*-1,2-Diaminocyclohexanetetraacetate Complexes of Magnesium, Calcium, Strontium, and Lanthanum Ions in Aqueous Alkaline Solution

NIELS RHOD LARSEN and ARNE JENSEN

The Royal Danish School of Pharmacy, Chemical Laboratory A, DK-2100 Copenhagen Ø, Denmark

The rate of transfer of magnesium, calcium, strontium, and lanthanum ions from D-(−)-*trans*-1,2-diaminocyclohexane-*N*,*N*,*N*′,*N*′-tetraacetate ≡ D-CDTA^{4-} to D,L-CDTA^{4-} has been studied in alkaline solution. The rate of reaction is independent of the HCDTA^{3-} and CDTA^{4-} concentrations for all the ions studied with the exception of the lanthanum ion for which a first order dependence on the CDTA^{4-} concentration is observed. The [H$^+$] profile of the rate constants of the dissociation reactions has been determined and a mechanism consistent with the observed [H$^+$] profile is given. This mechanism is valid for the CDTA complexes of both the alkaline earth ions and the lanthanum ion. The activation parameters for the resolved rate constants have also been determined and support the stated mechanism.

The kinetics of the dissociation of the alkaline earth ion complexes of *trans*-1,2-diaminocyclohexane-*N*,*N*,*N*′,*N*′-tetraacetate (CDTA) have in a previous paper [1] been shown to be dependent on [H$^+$] in a complex way. Glentworth *et al.*,[2] Brücher and Szarvas,[3] and Nyssen and Margerum [4] have studied the kinetics of the dissociation of the lanthanide ion complexes of CDTA in neutral or acidic solution. Glentworth *et al.* and Nyssen and Margerum have shown that the [H$^+$] independent term in the rate law for the dissociation is too large to be equal to the direct dissociation of the complexes to Ln^{3+} and CDTA^{4-}; however, the mechanisms proposed for the reaction path independent of [H$^+$] are not in agreement (*cf.* Ref. 2b).

The present studies deal with the kinetics of dissociation at hydrogen ion concentrations where the usual first order dependence on [H$^+$] is not observed. The dissociation refers to the reaction scheme in (1).

$$\mathrm{MCDTA} \xrightarrow[\mathrm{H^+}]{k_d} \mathrm{M} + \mathrm{CDTA} \qquad (1)$$

The [H$^+$] range has been expanded and studies on the dissociation of LaCDTA have been included (*cf.* Ref. 1). The mechanism of dissociation of MCDTA at low [H$^+$] is found to be similar for M = Mg, Ca, Sr, or La. The stated mechanism agrees with that suggested by Nyssen and Margerum [4] for the dissociation of the lanthanide complexes of CDTA.

The overall reactions studied are shown in (2a) (M = Mg, Ca, Sr or La) and (2b). Reaction (2b) has been included in the investigation since a pronounced dependence on [CDTA^{4-}] exists for La(D-CDTA) in reaction (2a). The charges, protons, and nomenclature for the optical rotation have been omitted for clarity in (2a) and (2b). Each one of the enantiomers L-CDTA and D-CDTA forms only one of the two possible isomeric complexes due to the stereospecificity of this ligand.[5,6]

$$\mathrm{M(D\text{-}CDTA) + D,L\text{-}CDTA \rightarrow M(D,L\text{-}CDTA) + D\text{-}CDTA} \qquad (2a)$$

$$\mathrm{La(D\text{-}CDTA) + Sr(D,L\text{-}CDTA) \rightarrow La(D,L\text{-}CDTA) + Sr(D\text{-}CDTA)} \qquad (2b)$$

EXPERIMENTAL

Chemicals. D,L-H_4CDTA, the racemic form of *trans*-1,2-diaminocyclohexane-*N*,*N*,*N*′,*N*′-tetraacetic acid (Fluka *p.a.*) was recrystallized by

dissolving in dilute NaOH followed by the addition of HNO_3. D-H_4CDTA (D(−)H_4CDTA) was contributed by Professor K. H. Pearson, Cleveland State University, Cleveland, Ohio, U.S.A., and was used without further purification. The metal salts used were the nitrates of analytical grade. D,L-H_4CDTA and nitrates of Mg, Ca, Sr, and La were quantitatively analyzed by complexometric titrations.

Weighed amounts of the metal nitrate and H_4CDTA were dissolved to give the desired concentrations of the reactants. 2,6-Lutidin, tris(hydroxymethyl)methylamine, borate, and *N*-ethylpiperidine of the highest available purity were used and the solutions were adjusted to the desired pH by adding a solution of CsOH to the acidic form of these bases. CsOH was prepared by ion exchange of $CsNO_3$ on an IRA 400 resin (BDH). $[CO_3^{2-}]$ constituted less than 1 % of $[OH^-]$ in the CsOH solutions, as determined by titration with acid. The ionic strength was adjusted using $CsNO_3$ instead of nitrates of Li^+, Na^+ or K^+ as it has been shown that complexes are formed between these metal ions and CDTA, whereas Cs^+ has not been observed to form CDTA complexes in the pH ranges used.[7,8]

Apparatus. A Perkin-Elmer Model 141 photoelectric polarimeter (with potentiometric readout) in combination with a "Servograph REC 51" recorder equipped with a high sensitivity unit "REA 112" (Radiometer, Copenhagen) was used to monitor the change in optical rotation as a function of time during the reactions. The polarimeter had the following five wavelengths available: 589, 578, 546, 436, and 365 nm. However, in this work, 365 nm was used exclusively because of the greater change in optical rotation at this wavelength during reaction (2). The 1 dm polarimeter cell with quartz windows was thermostated to a precision of ± 0.1 °C. The "rapid" reactions were followed by means of a simple mixing device consisting of a Y-formed glass tube which was connected to two calibrated glass syringes containing the reactants. A water bath of the desired temperature was used to thermostate the glass syringes and the Y-formed glass tube. The mixing of the reactants was completed within 5 s, and the response time of the polarimeter and recorder was about 10 s following the initial mixing.

The pH of the reaction mixture was measured after the completion of the reaction with a "pH Meter 4" equipped with a calomel electrode, K 401, and a glass electrode, G 202 B (Radiometer, Copenhagen).

Rate measurements. The pH ranges used in the study of reaction (2) are shown in Figs. 2, 3, 4, and 6. Titrations of the complexes to be discussed have shown that protonated forms as well as the hydroxo forms of these complexes are found in negligible concentrations in the pH ranges studied (*cf.* Ref. 1). The formula for the investigated CDTA complexes is therefore $MCDTA^{(4-n)-}$ where n is the charge of the metal ion.

Table 1. Molar rotations (deg. M^{-1} cm^{-1}) of D-CDTA and the D-CDTA complexes investigated.[a]

CDTA	MgCDTA	CaCDTA	SrCDTA	LaCDTA
−5.4	5.3	2.5	1.3	8.7

[a] pH 10.0; *N*-ethylpiperidine buffer 5×10^{-3} M; 25 °C; 365 nm.

Table 1 shows the values of the molar rotations of the optically active species employed in reaction (2). The molar rotations are calculated from measurements performed on 10^{-3} M solutions with pH adjusted to 10.0 with CsOH. The total change in rotation during reaction (2) is 0.07 − 0.11° for the concentrations used. Different initial concentrations of the decomposing species were used; in each case a tenfold to fiftyfold excess of entering ligand was present, which was found to be sufficient to make the overall reaction to go to completion.

As opposed to the exchange reactions with Cu(II) ion in NH_4^+/NH_3 solutions,[1] changes in $[H^+]$ do not occur for reaction (2). Buffer concentrations of 5×10^{-3} M are therefore sufficient for maintaining the desired pH in the present investigation. For M = La in reaction (2a) at low pH, no buffer is required since the excess of CDTA supplies the solution with a buffer capacity in this pH range. In some kinetic runs, it is possible to maintain a given pH with different buffers, all of which yield identical rate constants; *i.e.*, no buffer effect is observed. The hydrogen ion concentration is calculated as log $[H^+]$ = −pH; that is, the activity coefficient which is a constant at the ionic strength maintained here has been omitted.

A least squares analysis performed on a "Wang" desk computer was used to obtain the best linear dependence.

The stability constants used in the present work are given in Table 2.

Table 2. Stability constants.

Complex	log K (M^{-1})
H_2CDTA	(6.1)[a]
HCDTA	(13.2)[b]
MgCDTA	(11.0)[a]
CaCDTA	(13.1)[a]
SrCDTA	(10.5)[a]
LaCDTA	(16.9)[a]

[a] Ref. 10; $\mu = 0.1$ (KNO_3); corrected to 25 °C by the thermodynamic values from Ref. 10. [b] Ref. 7; $\mu = 0.1$ ($CsNO_3$); 25 °C.

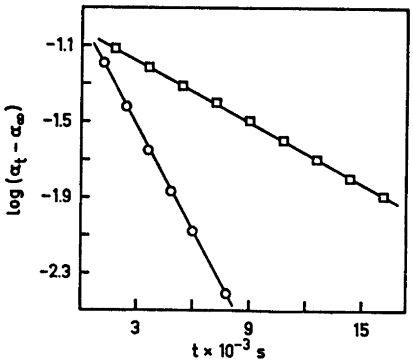

Fig. 1. First order plots. ○ reaction (2a); $[Mg(D\text{-}CDTA)]_0 = 1.0 \times 10^{-3}$ M; $[D,L\text{-}CDTA]_0 = 5.0 \times 10^{-2}$ M; pH 8.29; 25.0 °C; $\mu = 0.5$. □ reaction (2b); $[La(D\text{-}CDTA)]_0 = 1.0 \times 10^{-3}$ M; $[Sr(D,L\text{-}CDTA)]_0 = 1.0 \times 10^{-2}$ M; pH 9.38; 25.0 °C; $\mu = 0.1$.

The exchange reactions studied are all carried out under conditions which make them pseudo first order. Two first order plots representing, respectively, reactions (2a) and (2b) are shown in Fig. 1. $[]_0$ indicates initial concentration.

RESULTS

Magnesium, calcium, strontium. The kinetics of dissociation for the CDTA complexes according to reaction (2a) have been examined as a function of hydrogen ion concentration as well as temperature.

The results are shown in Figs. 2, 3, and 4 where k_d is the observed first order rate constant. The log k_d *versus* pH plot is chosen in order to be able to include all the experimental results for the dissociation reactions of a given complex in one figure. Log k_d shows a linear dependence on pH at low values of pH with a slope of approximately −1 thereby indicating that a first order dependence on hydrogen ion concentration dominates in this pH range. Furthermore, zero order dependence on [D,L-$HCDTA^{3-}$] or [D,L-$CDTA^{4-}$] is observed as illustrated from the experiments with different concentrations of D,L-CDTA. k_d is accordingly the rate constant of the dissociation reaction, k_d being a function only of $[H^+]$ and the medium.

Figs. 2, 3, and 4 give, on the other hand, no distinct information on the $[H^+]$ profile at high values of pH. Plots of k_d *versus* $[H^+]$ for high

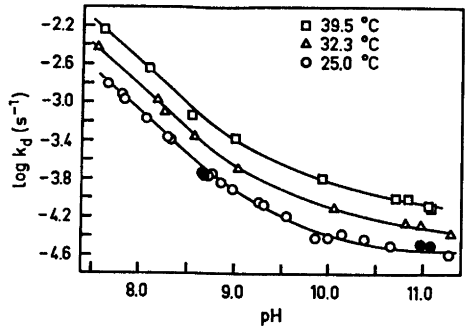

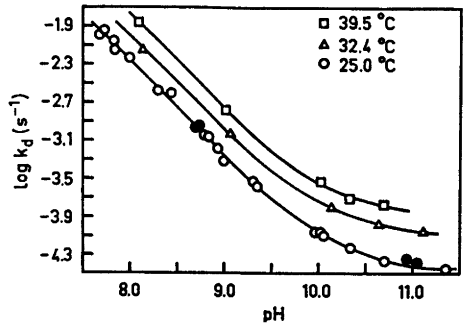

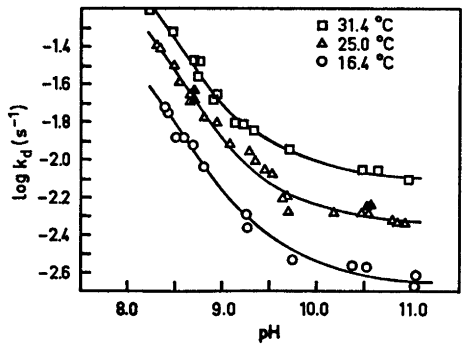

Figs. 2–4. Log k_d *versus* pH for M = Mg, Ca, and Sr, respectively. $[M(D\text{-}CDTA)]_0 = 1.0 \times 10^{-3}$ M; $[D,L\text{-}CDTA]_0 = 5.0 \times 10^{-2}$ M. The symbols, ● and ▲, indicate $[D,L\text{-}CDTA]_0 = 1.0 \times 10^{-2}$ M; 25.0 °C. $\mu = 0.5$.

values of pH (*cf.* Fig. 5) yield profiles similar to those found in Ref. 1.

The straight lines in Fig. 5 display the results of a linear regression analysis of k_d *versus* $[H^+]$ at higher $[H^+]$ (*cf.* the following section, "Discussion").

Lanthanum. The observed first order rate constants for reaction (2a) (M = La) and (2b) are designated k_c and k_s, respectively. The deter-

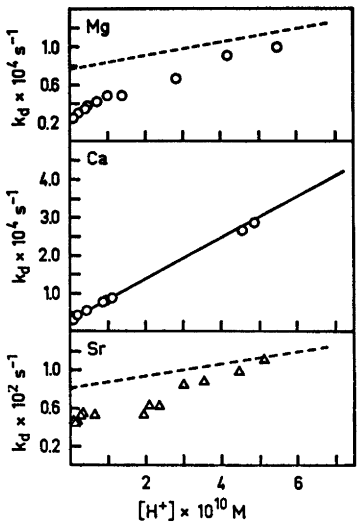

Fig. 5. Dependence of k_d on $[H^+]$ for pH 9.2 – 11.4 for M = Mg, Ca, and Sr respectively; 25.0 °C; $\mu = 0.5$.

mination of k_s from the double exchange in reaction (2b) is feasible only if k_d for the dissociation of SrCDTA is much larger than k_s. Otherwise, k_s will necessarily be dependent on the rate of dissociation of the scavenger, SrCDTA. From Figs. 4 and 6 it is seen that k_d for SrCDTA is indeed much larger than k_s. Reaction (2b) will proceed to completion only if [D,L-CDTA] is considerably higher than [D-CDTA]. This condition is fulfilled when using an excess of Sr(D,L-CDTA) since the ratio between the stability constants for SrCDTA and

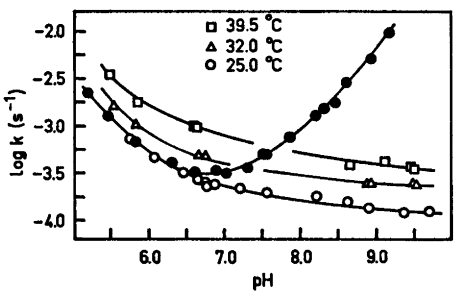

Fig. 6. Log k_s and log k_c *versus* pH for M = La. The symbols □△○ are used for k_s; $[La(D\text{-}CDTA)]_0 = 1.0 \times 10^{-3}$ M; $[Sr(D,L\text{-}CDTA)]_0 = 1.0 \times 10^{-2}$ M. The symbol ● is used for k_c; $[La(D\text{-}CDTA)]_0 = 5.0 \times 10^{-4}$ M; $[D,L\text{-}CDTA]_0 = 1.0 \times 10^{-2}$ M; 25.0 °C. $\mu = 0.1$.

LaCDTA are of the correct order of magnitude (*cf.* Table 2).

From Fig. 6 it is seen that for LaCDTA the reactions approach first order in $[H^+]$ at low values of pH and that the exchange reaction of the ligand is faster than the double exchange reaction with SrCDTA at pH > 6.5. The plot of log k_c *versus* pH in Fig. 6 indicates that k_c depends specifically on $[D,L\text{-}CDTA^{4-}]$ and is independent of $[D,L\text{-}HCDTA^{3-}]$ and $[D,L\text{-}H_2CDTA^{2-}]$. That k_c has this particular form for dependence is evident from the fact that k_c is equal to k_s for pH < 6.5 and from the fact that k_s, for steric reasons, must be independent of [SrCDTA] (*cf.* Margerum [9]). Furthermore, k_c and k_s must be equal to k_d for pH < 6.5, k_d being the rate constant of dissociation analogous to the similar rate constant of dissociation of the alkaline earth complexes. k_d is included in both k_c and k_s, the concentration of $D,L\text{-}CDTA^{4-}$ being negligible in the experiments with the double exchange of SrCDTA as compared with the experiments with the ligand exchange (*cf.* the magnitude of the stability constant of SrCDTA in Table 2). Furthermore, the exchange reaction between La(D-CDTA) and $D\text{-}CDTA^{4-}$ does not give rise to a change in rotation which means that the exchange reaction between La(D-CDTA) and $L\text{-}CDTA^{4-}$ is the only one being observed.

The difference between k_c and k_s is calculated according to eqn. (3). ${k_{CDTA}}^{LaCDTA}$ is the rate constant of the reaction between La(D-CDTA) and $L\text{-}CDTA^{4-}$ where c indicates $[L\text{-}CDTA^{4-}]$ in the ligand exchange.

$$k_c - k_s = {k_{CDTA}}^{LaCDTA}[L\text{-}CDTA^{4-}]_c \qquad (3)$$

$[L\text{-}HCDTA^{3-}]_c$ can, in the pH range 7.5 – 9.2, be set equal to the total concentration of free L-CDTA (*cf.* Table 2); *i.e.*, $[L\text{-}HCDTA^{3-}]_c$ is half the free ligand concentration. $k_c - k_s$ may then be stated as in eqn. (4).

$$k_c - k_s = {k_{CDTA}}^{LaCDTA}\frac{[L\text{-}HCDTA^{3-}]_c}{K_{HCDTA}[H^+]} \qquad (4)$$

Fig. 7 shows a plot of $k_c - k_s$ *versus* $[H^+]^{-1}$ where the slope of the straight line obtained is used for the calculation of ${k_{CDTA}}^{LaCDTA}$. For the calculation of $k_c - k_s$ the observed values of k_c are used whereas an estimated value for k_s at the same $[H^+]$ as k_c is obtained by interpolation between the observed values of k_s. The vanish-

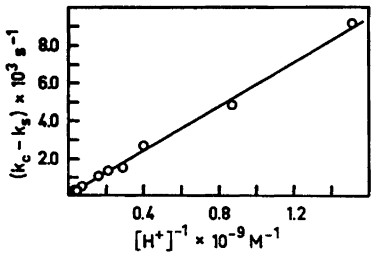

Fig. 7. $k_c - k_s$ *versus* $[H^+]^{-1}$ for the calculation of k_{CDTA}^{LaCDTA}; 25.0 °C; $\mu = 0.1$.

ing intercept for the straight line in Fig. 7 corroborates eqn. (4). The low $[Sr^{2+}]$ in connection with reaction (2b) does not result in a contribution to k_s since a dependence of k_s on $[Sr^{2+}]$ would give rise to a negative intercept and non-linearity in Fig. 7. k_{CDTA}^{LaCDTA} is calculated from the slope to be $1.9 \times 10^4\ M^{-1}\ s^{-1}$ when using $K_{HCDTA} = 10^{13.2}\ M^{-1}$ (*cf.* Table 2) and $[L\text{-}HCDTA^{3-}]_c = 5.0 \times 10^{-3}$ M. The value of k_{CDTA}^{LaCDTA} is surprisingly large compared with the rate constant of the reaction between Pb(L-CDTA) and D-$CDTA^{4-}$ which according to Carr and Baker [8] is equal to $3.77 \times 10^{-2}\ M^{-1}\ s^{-1}$. Otherwise, the work done by these authors and that done in the present study agree inasmuch as no dependence on $[HCDTA^{3-}]$ is observed. The observed rate of both the ligand and double exchange reaction is expressed by eqn. (5) where the bracket is equal to the observed first order rate constants k_c or k_s.

$$-\frac{d[LaCDTA]}{dt} = \{k_{CDTA}^{LaCDTA}[L\text{-}CDTA^{4-}] + k_d\}[LaCDTA] \quad (5)$$

$[L\text{-}CDTA^{4-}]$ in the double exchange, indicated by s, is calculated from eqn. (6) which is valid in the pH range 7.5 – 9.7.

$$[L\text{-}CDTA^{4-}]_s = \left(\frac{[Sr(L\text{-}CDTA)]}{K_{SrCDTA}K_{HCDTA}[H^+]}\right)^{\frac{1}{2}} \quad (6)$$

The rate constant k_d for the dissociation of LaCDTA is calculated from k_s using eqns. (5) and (6) (*cf.* Table 3).

Table 3 shows k_d as being negative at pH 9.71. This inconsistency may be attributed to the fact that the value of the stability constant for SrCDTA ($10^{10.5}\ M^{-1}$) is too low. This value has been determined with K^+ present. The presence of K^+ causes an error since this ion is known to coordinate with CDTA (*cf.* Ref. 7). It can, however, be stated with certainty that k_d extrapolated to $[H^+] = 0$ is negligible. Qualitatively both k_s and k_d have the same dependence on $[H^+]$ as that of k_d in the dissociation reaction of the alkaline earth complexes. Furthermore, k_s is equal to k_d at pH < 7.5.

DISCUSSION

Fig. 8 shows qualitatively the dependence of k_d on $[H^+]$ for MCDTA in the pH range investigated (M = Mg, Sr or La). A similar $[H^+]$ profile of k_d for BaCDTA has also been found (*cf.* Jensen and Larsen [1]). The $[H^+]$ profile of k_d for CaCDTA is, on the other hand, found to be a straight line. The mechanism of the dissociation reaction for CaCDTA is, however, assumed to be the same as that for the dissociation reactions of the other alkaline earth and lanthanum complexes. This assumption is main-

Table 3. Calculation of k_d for M = La in the pH range 7.5 – 9.7.[a]

pH	$k_s \times 10^4$ s^{-1}	$k_{CDTA}^{LaCDTA}[L\text{-}CDTA^{4-}]_0 \times 10^4$ s^{-1}[b]	$k_d \times 10^4$ s^{-1}
7.56	1.92	0.11	1.81
8.21	1.75	0.24	1.51
8.62	1.56	0.38	1.18
8.91	1.33	0.53	0.80
9.38	1.17	0.91	0.26
9.71	1.22	1.33	(−0.11)

[a] 25.0 °C; $\mu = 0.1$. [b] $[L\text{-}CDTA^{4-}]_0$ is calculated from eqn. (6); $[Sr(L\text{-}CDTA)]_0 = 5.0 \times 10^{-3}$ M; K_{SrCDTA} and K_{HCDTA} from Table 2.

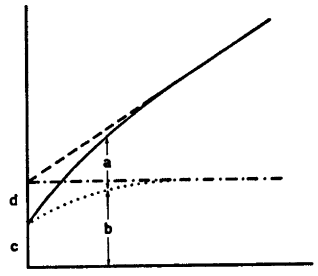

Fig. 8. Typical form of the curve of k_d *versus* $[H^+]$; for M = Ca see text. a = $k_H^{MCDTA}[H^+]$; b = $k_d - k_H^{MCDTA}[H^+]$; c = k_1^{MCDTA}; d = k_2^{MCDTA}; $k^{MCDTA} = k_1^{MCDTA} + k_2^{MCDTA}$. The solid curve is the observed k_d. – – – is the extrapolated straight line for the observed first order $[H^+]$ dependence at low values of pH. · · · is the $[H^+]$ profile for the reaction rate according to the proposed mechanism in (8). –·–·– shows how this mechanism is independent of $[H^+]$ for $[H^+]$ greater than a given value corresponding to the straight line for k_d.

ly based upon the magnitude of the activation parameters.

Fig. 8 shows both that k_d is given by eqn. (7) at low values of pH, and that this equation is invalid at higher pH values; at high pH the difference between k_d and $k_H^{MCDTA}[H^+]$ is

$$k_d = k^{MCDTA} + k_H^{MCDTA}[H^+] \quad (7)$$

smaller than k^{MCDTA}. The deviation from the straight line in Fig. 8 is explained by the mechanism depicted in scheme (8) where the rate determining step is 1→2. Mechanism (8) gives the direct dissociation of $MCDTA^{(4-n)-}$

$$\begin{array}{ccc} M'CDTA^{(4-n)-} & \xrightarrow{k_{23}} & M^{n+} + CDTA^{4-} \\ 2 & & 3 \\ k_{12} \uparrow\downarrow k_{21} & \overset{H^+}{\searrow}\ k_{24} & \uparrow\downarrow H^+ \\ MCDTA^{(4-n)-} & & M^{n+} + HCDTA^{3-} \\ 1 & & 4 \end{array} \quad (8)$$

along the paths 1→2→3. Furthermore, this mechanism also explains the k^{MCDTA} part of k_d (*i.e.*, paths 1→2→3 and 1→2→4) and, as regards this aspect, is in accordance with the mechanism assumed by Nyssen and Margerum.[4]

Jensen and Larsen [1] concluded that k_H^{MCDTA} is $[H^+]$ dependent and accordingly interpreted k^{MCDTA} as the rate constant for the direct dissociation of the CDTA complexes. Both k_H^{MCDTA} and k^{MCDTA} are assumed to be $[H^+]$ independent in the present investigation.

The difference between k_d and $k_H^{MCDTA}[H^+]$ may be expressed as in eqn. (9) when applying the "Steady State" approximation to species 2 in mechanism (8).

$$k_d - k_H^{MCDTA}[H^+] = \frac{k_{23} + k_{24}[H^+]}{k_{21} + k_{23} + k_{24}[H^+]} k_{12} \quad (9)$$

Basolo and Pearson [11] have treated complexes of the chelate type in an analogous fashion and have arrived at a mechanism similar to (8).

The dependence of the reaction rate on $[H^+]$ is, according to mechanism (8), determined by the magnitude of k_{21} relative to $k_{24}[H^+]$. Eqn. (9) is reduced to eqn. (10) if k_{21} is negligible compared with $k_{24}[H^+]$. Eqn. (7) shows that in this case k_{12} is identical to k^{MCDTA}.

$$k_d - k_H^{MCDTA}[H^+] = k_{12} = k^{MCDTA} \quad (10)$$

Eqn. (9) is, on the other hand, reduced to eqn. (11) if $k_{24}[H^+]$ is negligible as compared to k_{21}.

$$k_d - k_H^{MCDTA}[H^+] = \frac{k_{23} + k_{24}[H^+]}{k_{21} + k_{23}} k_{12} \quad (11)$$

If $[H^+]$ is small, a first order dependence on the hydrogen ion concentration is to be expected. Upon extrapolating to the k_d-axis in the plot of k_d *versus* $[H^+]$ (*cf.* Fig. 8), it is seen that k_d can be expressed as in eqn. (12).

$$k_d = \frac{k_{23} k_{12}}{k_{21} + k_{23}} \equiv k_1^{MCDTA} \quad (12)$$

It is furthermore seen from this figure that $k^{MCDTA} = k_1^{MCDTA} + k_2^{MCDTA}$.

k_H^{MCDTA}, k^{MCDTA}, k_1^{MCDTA}, and k_2^{MCDTA} are thus determined from the experimental results. k_H^{MCDTA} and k^{MCDTA} are – as shown in previous sections – the slope and the intercept, respectively, of the straight line found at low values of pH when plotting k_d *versus* $[H^+]$. k_1^{MCDTA} is the intercept of the straight line obtained when plotting k_d *versus* $[H^+]$, *but* only at high values of pH. k_2^{MCDTA} is calculated as described in the preceding paragraph. It has to be emphasized, however, that $[H^+]$ must be one to two orders of magnitude greater when determining k^{MCDTA} than when determining k_1^{MCDTA}. This condition arises as a consequence of the approximations leading to eqns. (10) and (12).

Table 4. The resolved rate constans for the dissociation of MCDTA complexes.[a]

M	t °C	k^{MCDTA} s^{-1}	k_H^{MCDTA} $M^{-1}s^{-1}$	pH range	k_1^{MCDTA} s^{-1}	k_2^{MCDTA} s^{-1}	pH range
Mg	25.0	7.7×10^{-5}	7.1×10^{4}	7.7 – 8.4	2.4×10^{-5}	5.3×10^{-5}	10.4 – 11.0
		$(5.2 \times 10^{-4})^{b}$	$(3.8 \times 10^{4})^{b}$	$(8.5 - 9.2)^{b}$			
		$(0)^{c}$	$(6.33 \times 10^{4})^{c}$	$(5.5 - 7.6)^{c}$			
	32.3	1.2×10^{-4}	1.3×10^{5}	7.6 – 8.6	3.6×10^{-5}	8.1×10^{-5}	11.0 – 11.3
	39.5	1.9×10^{-4}	2.4×10^{5}	7.6 – 9.0	5.7×10^{-5}	1.3×10^{-4}	10.8 – 11.1
Ca							
	25.0	3.1×10^{-5}	5.4×10^{5}	7.6 – 11.4			
		$(2.1 \times 10^{-4})^{b}$	$(4.2 \times 10^{5})^{b}$	$(8.5 - 10.5)^{b}$			
		$(0)^{c}$	$(4.14 \times 10^{5})^{c}$	$(5.5 - 7.6)^{c}$			
	32.4	7.1×10^{-5}	1.0×10^{5}	8.2 – 11.1			
	39.5	1.1×10^{-4}	1.7×10^{5}	8.0 – 10.7			
Sr							
	16.4	3.9×10^{-3}	3.5×10^{6}	8.4 – 8.8	2.2×10^{-3}	1.7×10^{-3}	10.4 – 11.0
	25.0	8.0×10^{-3}	6.4×10^{6}	8.3 – 8.9	4.2×10^{-3}	3.8×10^{-3}	10.5 – 10.9
		$(1.4 \times 10^{-2})^{b}$	$(6.7 \times 10^{6})^{b}$	$(8.5 - 9.2)^{b}$			
		$(3.0 \times 10^{-2})^{c}$	$(6.06 \times 10^{6})^{c}$	$(5.5 - 7.6)^{c}$			
	31.4	1.5×10^{-2}	8.4×10^{6}	8.2 – 8.9	7.9×10^{-3}	6.6×10^{-3}	10.5 – 11.0
La							
	25.0	2.1×10^{-4}	2.8×10^{2}	5.7 – 7.7	(0)	2.1×10^{-4}	
		$(0)^{d}$	$(1.66 \times 10^{2})^{d}$	$(3.9 - 5.3)^{d}$			
		$(0)^{e}$	$(2.34 \times 10^{2})^{e}$	$(4.6 - 5.5)^{e}$			
	32.0	3.8×10^{-4}	4.1×10^{2}	5.5 – 7.7	(0)	3.8×10^{-4}	
	39.5	7.9×10^{-4}	7.5×10^{2}	5.5 – 7.6	(0)	7.8×10^{-4}	

[a] $\mu = 0.5$ ($CsNO_3$) for M = Mg, Ca, and Sr; $\mu = 0.1$ ($CsNO_3$) for M = La. [b] Ref. 1; $\mu = 0.5$ (NH_4NO_3). [c] Ref. 15; $\mu = 0.5$ (Na-acetate). [d] Ref. 4; $\mu = 0.1$ ($NaClO_4$). [e] Ref. 3; $\mu = 0.1$ ($NaClO_4$).

Table 4 shows the resolved rate constants calculated in accordance with the procedure described in the previous paragraphs as well as the corresponding rate constants from the literature. Satisfactory agreement is found for k_H^{MCDTA} even in the event that the pH range in the present investigation is not the same as that in the cited studies. k_1^{MCDTA} and k_2^{MCDTA} cannot be calculated in the case of CaCDTA since no deviation from eqn. (7) is observed in the investigated pH range. The dissociation reaction of CaCDTA, on the other hand, may well follow mechanism (8). It is a possibility that the deviation from eqn. (7) appears at a higher value of pH which would indicate that k_{21} is larger than k_{23} but relatively small compared with $k_{24}[H^+]$. It is remarkable that k^{MCDTA} for the exchange reactions between the CDTA complexes of the alkaline earth ions and metal ions is considerably larger than the corresponding rate constants obtained in the present investigation (*cf.* Jensen and Larsen [1]). This fact may be related to a dependence on the metal ion concentration similar to the dependence on $[H^+]$ in mechanism (8) (*cf.* Nyssen and Margerum [4]). Another explanation for the difference between the values obtained for k_M^{CDTA} in the present work and the work by Jensen and Larsen [1] may involve the NH_4^+/NH_3 buffer used in that investigation in a manner similar to an effect observed with ammonium acetate in a study on isotopic Ce(III)exchange in Ce(III)polyaminocarboxylic acid chelates by Balcombe and Wiseall.[12]

The direct dissociation of the CDTA complexes according to mechanism (8) proceeds along reaction path 1→2→3. A necessary condition for this dissociation mechanism is that the rate of the reverse reaction be slower than the diffusion controlled rate of the reaction between two ions, *i.e.*, about 10^{10} $M^{-1}s^{-1}$ (*cf.* Caldin [13]). Furthermore, the rate of the reverse reaction where the rate determining step (*rds*) is 2→1 must be slower than the rate of formation for the water exchange mechanism of the aquo metal ion.[14]

Eqn. (13) shows how the rate constant

Table 5. Comparison of calculated rate constants for the formation of MCDTA from M^{n+} and $CDTA^{4-}$ at 25 °C with values predicted from the rate constants of water exchange.

M	k_M^{CDTA} $M^{-1}s^{-1}$	$k_M^{-H_2O}$ s^{-1}	$K_{OS}k_M^{-H_2O}$ $M^{-1}s^{-1}$
Mg	2.5×10^6	$(1.4 \times 10^5)^b$	7.0×10^6
Ca	$(3.9 \times 10^8)^a$	$(3.0 \times 10^8)^c$	1.5×10^{10}
Sr	1.3×10^8	$(3.5 \times 10^8)^c$	1.8×10^{10}
La		$(5.2 \times 10^8)^d$	$> 2.6 \times 10^{10}$

[a] k_1^{CaCDTA} is assumed equal to k^{CaCDTA}. [b,c,d] Ref. 16, 17, and 18, respectively.

k_M^{CDTA} for the formation of $MCDTA^{(4-n)-}$ from M^{n+} and $CDTA^{4-}$ has been calculated from k_1^{MCDTA} and the stability constant for the corresponding complex $MCDTA^{(4-n)-}$.

$$k_M^{CDTA} = k_1^{MCDTA} K_{MCDTA} \quad (13)$$

Table 5 shows values for k_M^{CDTA} calculated from eqn. (13) as well as the values predicted from the water exchange rate of the outer sphere complex. K_{OS} is the outer-sphere association constant; a value of 50 M^{-1} has been used for the 2+ metal and the 4− ligand [15] whereas a value larger than 50 M^{-1} has been used for the 3+ metal ion (La^{3+}) and the 4− ligand (*cf.* Table 5). It is seen that the values of $K_{OS}k_M^{-H_2O}$ are larger than the values of k_M^{CDTA}. k_1^{LaCDTA} is found to be negligible (*cf.* Table 4). A calculation by means of eqn. (13) using the diffusion controlled value, $k_{La}^{CDTA} = 10^{10}$ M^{-1} s^{-1}, yields a $k_1^{LaCDTA} \leq 10^{-7}$ s^{-1}. The values of k_1^{MCDTA}, as calculated in the preceding section, are therefore consistent with mechanism (8).

Activation parameters. The *rds* in mechanism (8) is assumed to be 1→2. Accordingly, the activation parameters for k_1^{MCDTA} and k_2^{MCDTA} must be the same. The dependence of the resolved rate constants on temperature is shown in Table 4. Arrhenius plots of log k *versus* T^{-1} show satisfactory linearity, even in the case of $k = k_2^{MgCDTA}$ or k_2^{SrCDTA} where k is determined with some uncertainty because of the rather large values of k_d. $\Delta H^{\ddagger}$, $\Delta S^{\ddagger}$, and $\Delta G^{\ddagger}$ are calculated using the Arrhenius plots (*cf.* Table 6). Table 6 indicates that the requirements for identical activation parameters for k_1^{MCDTA} and k_2^{MCDTA} is fulfilled. The value of $\Delta G^{\ddagger}$ and the pronounced negative value of $\Delta S^{\ddagger}$ for k^{CaCDTA} resemble the parameters obtained for the corresponding reactions with magnesium, strontium, and lanthanum complexes. Mechanism (8) would therefore appear to account for all the reactions examined in a very convincing manner.

Table 6. Activation parameters for the resolved rate constants; 25 °C.

M	$\Delta H^{\ddagger}$ kJ mol^{-1}	$\Delta S^{\ddagger}$ J (deg $mol)^{-1}$	$\Delta G^{\ddagger}$ kJ mol^{-1}
Mg			
k_1	44	−187	100
k_2	46	−172	97
k_H	66	61	46
Ca			
k^a	72	−92	99
k_H	62	72	41
Sr			
k_1	61	−88	87
k_2	65	−74	87
k_H	41	24	34
La			
k_2	83	−45	96
k_H	53	−20	59
	$(54)^b$	$(-22)^b$	$(61)^b$
	$(80)^c$	$(79)^c$	$(56)^c$

[a] k^{CaCDTA}. [b,c] Ref. 4 and 3, respectively.

It is seen from Table 6 that all the reactions related to (8) show a pronounced negative entropy of activation which may be related to a solvation of the transition state. Solvation could come about if step 1→2 in mechanism (8) involves the breaking of a metal ion chelate bond followed by the solvation of the free coordination site of the metal ion. Such a solvation gives rise to a change of the solvation of the complex as a whole.

The free energies of activation are remarkably constant for step 1→2 for the MCDTA complexes investigated. Nyssen and Margerum [4] have proposed that step 1→2 is a slow distortion of the complex which is consistent with an angular displacement instead of a linear displacement in preparation for opening the chelate rings (*cf.* Margerum [19]). Assuming the angular displacement theory, the free energy of activation is related to the rotational barriers of the chelate which again is related to the type of ligand. Furthermore, Day and Reilley [21] have

used an NMR technique in their studies on these complexes and suggest that the relatively long lifetime of the N−M bond is correlated with the steric hindrance caused by this ligand. This hindrance would make the support of a water molecule in the bond breaking impossible. The constant free energy of activation may then be rendered comprehensible in terms of these theories.

The rate constant of dissociation k_d is given by eqn. (7) at low values of pH. k_H^{MCDTA} has been accurately determined in the studies by Margerum *et al.* [20] and Nyssen and Margerum.[4] The activation parameters found in the present investigation for this pathway of the dissociation reaction of LaCDTA agree with the values found by Nyssen and Margerum,[4] whereas Brücher and Szarvas [21] find different values for $\Delta H^{\neq}$ and $\Delta S^{\neq}$, but the same value for $\Delta G^{\neq}$.

It has been found that k_H^{MCDTA} represents an *rds* which involves a proton attack on one of the nitrogen atoms. This attack results in an intermediate with the metal ion outside the coordination cage of the ligand (*cf.* Margerum *et al.*[20] and Nyssen and Margerum [4]). Mechanism (8) has accordingly to be extended to that shown in (14) which is valid at both the low and high values of pH used in this work. M*HCDTA in mechanism (14) has been observed by Nyssen

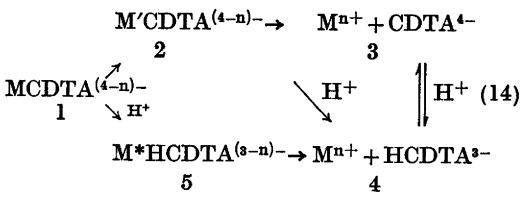

and Margerum [4] in their study on the rate of formation of LaCDTA. Studies [1] on the rate of dissociation of this type of complexes all show a similar $[H^+]$ profile for these reactions with M=Mg, Sr, or Ba; the present study shows this same $[H^+]$ profile for M=Mg, Sr, or La.

The dissociation reaction for these MCDTA complexes is therefore assumed to follow mechanism (14) in the investigated pH range and for M=Mg, Ca, Sr, Ba, or La (*cf.* the preceding discussion). The *rds* are 1→2 and 1→5 for the spontaneous and the H^+ activated dissociation, respectively. The *rds* 1→5 dominates at low values of pH and *rds* 1→2 dominates at relatively high values of pH.

Acknowledgements. The authors wish to thank Professor K. H. Pearson, Cleveland State University, Cleveland, Ohio, U.S.A., for a sample of optically active H_4CDTA, Dr. O. Farver of this institution for fruitful and instructive discussions and Dr. D. Bennett of this institution for linguistic help.

REFERENCES

1. Jensen, A. and Larsen, N. R. *Acta Chem. Scand. 27* (1973) 1838.
2. a. Glentworth, P., Wiseall, B., Wright, C. L. and Mahmood, A. J. *J. Inorg. Nucl. Chem. 30* (1968) 967; b. Glentworth, P. and Newton, D. A. *J. Inorg. Nucl. Chem. 33* (1971) 1701.
3. Brücher, E. and Szarvas, P. *Acta Chim. (Budapest) 67* (1971) 449.
4. Nyssen, G. A. and Margerum, D. W. *Inorg. Chem. 9* (1970) 1814.
5. Dwyer, F. P. and Garvan, F. L. *J. Amer. Chem. Soc. 83* (1961) 2610.
6. Reinbold, P. E. and Pearson, K. H. *Inorg. Chem. 9* (1970) 2325.
7. Carr, J. D. and Swartzfager, D. G. *Anal. Chem. 43* (1971) 1520.
8. Carr, J. D. and Baker, D. R. *Inorg. Chem. 10* (1971) 2249.
9. Margerum, D. W. *Rec. Chem. Progr. 24* (1963) 237.
10. Anderegg, G. *Helv. Chim. Acta 46* (1963) 1833.
11. Basolo, F. and Pearson, R. G. *Mechanisms of Inorganic Reactions*, 2. Ed., Wiley, New York 1967, p. 218.
12. Balcombe, C. I. and Wiseall, B. *J. Inorg. Nucl. Chem. 35* (1973) 2859.
13. Caldin, E. F. *Fast Reactions in Solution*, Blackwell, Oxford 1964, p. 279.
14. Eigen, M. and Wilkins, R. G. *Mechanisms of Inorganic Reactions*, American Chemical Society, Washington, D. C. 1965, p. 55.
15. Pausch, J. B. and Margerum, D. W. *Anal. Chem. 41* (1969) 226.
16. Petrucci, S. and Atkinson, G. *J. Phys. Chem. 70* (1966) 3122.
17. Eigen, M. and Maass, G. *Z. Phys. Chem. (Frankfurt am Main) 49* (1966) 163.
18. Purdie, N. and Vincent, C. A. *Trans. Faraday Soc. 63* (1967) 2745.
19. *Ref.* 14, p. 75.
20. Margerum, D. W., Menardi, P. J. and Janes, D. L. *Inorg. Chem. 6* (1967) 283.
21. Day, R. J. and Reilley, C. N. *Anal. Chem. 37* (1965) 1326.

Received February 14, 1974.

Acta Chemica Scandinavica A 28 (1974) 647—655

A ^{1}H and ^{121}Sb NMR Study of Ionization Reactions in Antimony Pentachloride Donor—Acceptor Adduct Systems in Solution

P. STILBS [a] and G. OLOFSSON [b]

[a] Division of Physical Chemistry 2 and [b] Thermochemistry Laboratory, Chemical Center, University of Lund, S-220 07 Lund, Sweden

The occurrence of ionization reactions in the donor-acceptor adduct systems tetramethylurea (TMU) – $SbCl_5$ (I) and dimethyl sulphoxide (DMSO) – $SbCl_5$ (II) in 1,2-dichloroethane or dichloromethane solution and hexamethylphosphorustriamide (HMPT) – $SbCl_5$ in nitrobenzene solution (IV) has been established by direct observation of the $SbCl_6^-$ ion by ^{121}Sb magnetic resonance. Indirect evidence for the $(donor)_2SbCl_4^+$ ion is obtained from ^{1}H magnetic resonance spectra. Fast exchange reactions involving antimony as well as the donors are indicated from both ^{121}Sb and ^{1}H resonance. While the weaker ethyl acetate $SbCl_5$ adduct in 1,2-dichloroethane solution is shown to be nonionizing, the measured $SbCl_6^-$/adduct ratios in the systems, II, I, and IV are roughly 0.05, 0.1, and 0.3. Results from systems I and II can satisfactorily be interpreted in terms of the autoionization equation $2(donor)SbCl_5 \rightleftharpoons SbCl_6^- + (donor)_2SbCl_4^+$, but system IV shows more complex behaviour and the degree of ionization increases markedly with donor in excess of the ratio $HMPT/SbCl_5 = 1.0$.

Antimony pentachloride is a strong electron pair acceptor which forms numerous donor-acceptor adducts with electron-pair donating molecules. A number of adducts have been shown by X-ray diffraction studies to exist as discrete molecular adducts in the solid state.[1-3] Ionic salts containing the $SbCl_6^-$ anion can result from interaction with acid chlorides which contain an easily ionizable chlorine atom.[4]

Evidence for the structure of the adducts in solution is less conclusive, but what is known is consistent with the assumption that they exist predominantly as molecular adducts in solvents of low dielectric constant.[1,5,6] Autoionization reactions resulting in the formation of $D_2SbCl_4^+$ and $SbCl_6^-$ ions * have been deduced from conductometric measurements on, *e.g.*, $SbCl_5$ – CH_3CN,[7-10] $SbCl_5$ – HMPT in nitrobenzene solution,[11] and $SbCl_5$ – 2,2,6,6-tetramethylpiperidine-*N*-oxyl or $(C_2H_5)_2S$ in 1,2-dichloroethane solution.[12] The conductometric measurements are very sensitive to contamination especially of water, which has been amply demonstrated in the work by Beattie and coworkers [13] on the $SbCl_5$ – CH_3CN system. These later measurements showed $SbCl_5$ to be nonconducting in CH_3CN, thus invalidating the conclusions about autoionization reached in Refs. 7 – 10. Consequently, results of conductometric measurements in this kind of systems must be treated with great caution.

The only previous NMR work on $SbCl_5$ adduct ionization seems to be Ref. 11 and the recent paper by Ahmed and Schmulbach.[14] In the latter publication it is stated that $SbCl_5$ in acetonitrile solution is entirely or predominantly ionized to $SbCl_6^-$ and $(acetonitrile)_2SbCl_4^+$. No real ^{1}H NMR evidence for this is presented and the measurements can equally well be interpreted in terms of simple donor-acceptor adducts.

In a ^{1}H NMR study of exchange processes in $SbCl_5$-alkylurea adducts,[15] varying chemical shifts of the donors present in excess were observed. Water contamination was suspected

* The following abbreviations will be used in this article: TMU = tetramethylurea, DMSO = dimethyl sulphoxide, HMPT = hexamethylphosphorustriamide, EtOAc = ethyl acetate, D = donor, A = $SbCl_5$ (acceptor), X = halogen and MX_n = metal halide. Concentrations are expressed in mol l^{-1} (M).

to be the cause but subsequent studies on the ternary adduct systems $H_2O-SbCl_5-D$ [16] and $HCl-SbCl_5-D$ [17] have shown that this interpretation is not satisfactory. An alternative cause for the observed effect could be ionization reactions in the binary adduct system. The present ^1H and ^{121}Sb magnetic resonance study was undertaken to obtain a reasonable description of the $SbCl_5$-alkylurea systems and to gain some information about ionization reactions of $SbCl_5$ adducts in solution.

During the study we learned about the careful work of Hartman and Schrobilgen [18] on the analogous $TMU-BX_3$ systems in dichloromethane solution. These authors have, from ^1H, ^{11}B, and ^{19}F magnetic resonance studies, obtained direct evidence for the presence of $(TMU)_2BF_2^+$ and BF_4^-, arising from autoionization of the adduct.

EXPERIMENTAL

Samples. The samples for the low-concentration study of the $TMU-SbCl_5-$dichloroethane system were prepared in a glove box in P_2O_5-dried air from stock solutions (0.2 M) of TMU and $SbCl_5$. The TMU solution was determined by a chromatographic method [19] to contain less than 0.01 % water by weight (2 mM). These solutions were dispensed with two Metrohm precision burets *via* an all glass-teflon tubing system. All other samples were prepared in a polyethylene glove bag in a dry N_2 atmosphere. The neat donors were slowly dispensed from an all glass-teflon syringe into weighed amounts of $0.2-1.9$ M $SbCl_5$ solutions kept in the 10 mm i.d. teflon screwcap tubes used for the ^{121}Sb NMR measurements. For the ^1H NMR measurements 0.5 ml of these solutions were transferred to 5 mm o.d. tubes. The two sets of tubes were stored under identical conditions. All glassware had been dried at temperatures above 120 °C overnight. The presence of water or acidic impurities in the samples had been tested for in the low-field region of ^1H NMR, where signals from these acidic protons would occur.[16,17,20] Within the sensitivity of the instrument no such signals could be seen in any sample. In analogy with the BF_3 adduct systems,[20] signals from the D part of species such as $DH^+SbCl_6^-$ would have been expected in the vicinity of the normal adduct signals in samples having acceptor in excess.[17]

The relatively high concentrations used and the methods of sample preparation employed were chosen to minimize water contamination effects.

Under conditions of rapid addition of TMU to the $SbCl_5$ solution (the solution temperature rising to the boiling point) a small extra signal 0.05 ppm to low field of the adduct signal could be observed. No such signal was seen in samples prepared by mixing the two components under milder conditions as dilute solutions. The nature of this species has not been investigated further but it is probably a decomposition product derived from the adduct. No exchange with other species in solution with any sample composition is indicated in ^1H NMR spectra at 40 °C.

Reagents. 1,2-Dichloroethane (Fisher Certified reagent), dichloromethane (BDH, redistilled) and nitrobenzene (BDH, Analar) were pure as judged from ^1H NMR spectra and were dried with 4A molecular sieves prior to use. Tetramethylurea (Fluka) was vacuum distilled on a Nester-Faust spinning band column and was more than 99.5 % pure according to GLC. Hexamethylphosphorustriamide (BDH) was distilled from CaH_2. Ethyl acetate and dimethyl sulphoxide were dried at least 3 h with freshly regenerated 4A molecular sieves just prior to use and were pure as judged from ^1H NMR.

Synthesis. Triphenylmethylhexachloroantimonate was prepared according to Cowell *et al.*[21]

Instrumentation. ^1H NMR spectra were recorded on a Varian Associates A-60A spectrometer equipped with a V-6040 temperature controller. ^{121}Sb spectra were recorded on a V-4200 wide-line spectrometer from the same manufacturer. These spectra were registered as the derivative of the absorption signal at 14.98 MHz.

All quantitative measurements were made at 20 °C.

CALCULATIONS

A numerical cyclic relaxation method has been used to solve the equations for coupled equilibria and simultaneously adjust equilibrium constants for best agreement with the conversion data. The procedure is best illustrated with an example. Consider the following coupled equilibria:

$$\underset{(a-x)}{A} + \underset{(b-x)}{B} \overset{K_1}{\rightleftharpoons} \underset{x}{C}$$

and

$$\underset{(x-y)}{C} + \underset{(d-y)}{D} \overset{K_2}{\rightleftharpoons} \underset{y}{E} + \underset{y}{F}$$

For each data point (with initial concentrations a, b, and d) three equations are obtained:

Table 1. Summary of quantitative measurements on systems I and IV.

$SbCl_5$ adduct/solvent	D_{tot}/[M]	A_{tot}/[M]	$SbCl_6^-$(obs)[a]/[M]	$SbCl_6^-$(calc)[b]/[M]	^{1}H NMR shifts of the excess donor+cation signal [c,d] ν_{obs}/Hz	ν_{calc}/Hz
TMU/CH_2Cl_2 (Ia)	1.3	0.83	0.11	0.097	21.9	21.9
	1.1	0.85	0.10	0.099	15.5	17.2
	1.2	0.83	0.12	0.097	23.8	20.3
	1.4	0.80	0.11	0.092	25.3	23.7
	1.2	0.66	0.06	0.077	26.6	24.1
	1.4	0.64	0.05	0.075	27.2	26.6
	1.6	0.66	0.07	0.077	27.2	26.6
	2.3	0.58	0.06	0.068	28.6	28.7
TMU/CH_2ClCH_2Cl (Ib)	0.105	0.099	—[e]	0.0109	8.0	5.8
	0.111	0.097	—	0.0101	13.7	13.1
	0.115	0.097	—	0.0094	16.6	16.6
	0.120	0.079	—	0.0087	17.9	19.0
	0.124	0.074	—	0.0082	19.5	20.3
	0.127	0.070	—	0.0077	19.5	21.3
	0.130	0.066	—	0.0073	21.3	22.0
	0.135	0.059	—	0.0067	22.2	22.9
	0.137	0.057	—	0.0063	22.2	23.3
	2.7	1.5	0.20	0.16	27.6	—
	2.2	1.9	0.20	0.20	19.0	—
HMPT/nitrobenzene (IV)	0.18	0.27	0.02	0.039	—	—
	0.32	0.28	0.05 (0.05)	0.044	8.5	8.2
	0.36	0.27	0.06 (0.05)	0.056	12.3	10.2
	0.48	0.28	0.10 (0.07)	0.073	13.0	12.1
	0.60	0.26	0.10 (0.08)	0.076	13.5	13.7
	0.70	0.25	0.10 (0.08)	0.079	14.0	14.3
	0.94	0.24	0.09 (0.08)	0.082	14.9	15.3
	0.19	0.27	0.03	0.041	—	—
	0.40	0.26	0.09 (0.06)	0.061	12.0	11.4
	0.68	0.24	0.09 (0.08)	0.073	14.0	14.5
	0.94	0.24	0.10 (0.08)	0.081	14.0	15.3

[a] From intensity measurements in ^{121}Sb spectra. Values in parenthesis are from ^{1}H NMR spectra and have been calculated with the aid of eqn. (9). [b] Calculated from the experimentally estimated equilibrium constants (see the text) and the concentrations given in columns 2 and 3. $K_2 = 0.023$ in the Ia system, 0.02 in the Ib system, and 0.14 in the IV system where K_3 is also 3.3 l mol^{-1}. [c] Shifts are expressed relative to the adduct ^{1}H NMR signal at 60 MHz. The averaged excess donor+cation signal is upfield. [d] Calculated with the aid of eqn. (7) and the ion concentrations shown in column 5. The assumed shifts are given in the text. [e] These concentrations are too low to be measured by ^{121}Sb magnetic resonance.

$$x - K_1(a-x)(b-x) = Q_1$$
$$y^2 - K_2(x-y)(d-y) = Q_2$$
$$(y_{obs} - y)^2 = Q_3$$

Totally there will be $3n$ such equations for n samples and there will be $2n$ parameters for the x and y and 2 parameters for the equilibrium constants. These $2n+2$ parameters are then varied to make the sum of all $(Q_1+Q_2+Q_3)$ a minimum. The $2n$ parameters are completely orthogonal to all other parameters so when the procedure has converged all Q_1 and Q_2 are zero.

The procedure outlined here is time consuming and tedious for a manual calculation, but it lends itself nicely to a computer treatment. The FORTRAN subroutine STEPIT [22] is ideally suited for this purpose and a calculation for 10 samples only takes a few seconds on a UNIVAC 1108 computer. The procedure may be extended to more complicated equilibria, and no complicated explicit concentration expressions have to be derived.

RESULTS AND DISCUSSION

The following $SbCl_5$ adduct systems were studied by ^1H and ^{121}Sb magnetic resonance spectroscopy: the adduct with TMU in CH_2Cl_2 (Ia) and in $C_2H_4Cl_2$ (Ib), the adduct with DMSO in CH_2Cl_2 (II) and with EtOAc in CH_2Cl_2 (III) and finally the adduct with HMPT in nitrobenzene (IV). System IV has previously been studied by Gutmann *et al.*[11]

The solvent properties of CH_2Cl_2 and $C_2H_4Cl_2$ are similar, the dielectric constants at 20 °C being 9.08 and 10.7, respectively, while the dielectric constant of nitrobenzene is appreciably higher (35.7).[23]

^1H NMR spectra of solutions containing $SbCl_5$ in excess show one set of signals ascribed to donor bound in the $DSbCl_5$ adduct. In samples containing donor in excess, that is with concentration ratios D/A > 1, an additional set of donor signals appears at higher field. However, for the EtOAc system (III), the temperature must be lowered below 0 °C to give a separation of the signals. In this system both the adduct and excess donor chemical shifts are almost independent of the composition of the sample, and furthermore the excess donor signals coincide with the signals observed in samples of EtOAc in CH_2Cl_2. Thus ^1H NMR spectra give indications of only EtOAc-adduct molecules when D/A < 1, and only adduct molecules and unbound EtOAc molecules when D/A > 1, the donor exchange between the latter being slow on the ^1H NMR time scale below 0 °C.

For systems I and II the chemical shifts of the adducts remained unchanged over the concentration ranges studied ($D/A \gtrsim 1$), while the shifts of the "excess" donors were observed to vary with the composition of the samples. Results for systems Ia, Ib, and IV are shown in column 6 of Table 1. No quantitative ^1H NMR shift measurements were made on system II. For concentration ratios $D/A \gg 1$ the "excess donor" shifts approached the shifts observed for a solution of the donor. Thus in these systems there are indications of an additional species containing donor molecules in rapid exchange with unbound donors, but slowly exchanging with adducts.

The HMPT system (IV) shows more complex behaviour and some typical ^1H NMR spectra from this system are shown in Fig. 1. These spectra show the effect of adding donor incrementally to a = 0.3 M solution of $SbCl_5$ in nitrobenzene containing a small amount of 1,2-dichloroethane reference. The excess donor signal has a variable chemical shift (see column 6, Table 1), and in addition the intensities

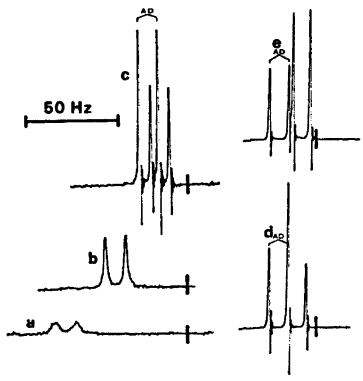

Fig. 1. Some representative 60 MHz ^1H NMR spectra from the HMPT region of the HMPT – $SbCl_5$ – nitrobenzene system (IV) at 40 °C. The solid line is 90 Hz upfield from an internal 1,2-dichloroethane reference signal. The D/A ratio increases in the series a – e, the a and b samples containing excess $SbCl_5$ and the c – e samples excess donor. The 1:1 doublet structure arises from $^1H - ^{31}P$ spin-spin coupling ($J \simeq 10$ Hz).

of the excess donor signals relative to the adduct signals differed markedly from the ratio $([D]_{init}-[A]_{init})/[A]_{init}$, which is the ratio expected for the simple adduct formation reaction. In samples with D/A < 1, the signal of the HMPT adduct was quite broad and the chemical shift was observed to vary with the excess of $SbCl_5$. For samples containing D/A > 1 the adduct signal is sharp and has a constant ^{1}H NMR shift.

Although there certainly must be small amounts of water or acidic impurities in the samples (which will cause similar effects in ^{1}H NMR spectra) [16,17,20] we are convinced that this only gives a minor contribution to the observed shift effects, even in the most dilute samples. Experiments have been made with additions of controlled amounts of water and were found to cause large changes in the spectra as well as the appearance of an "acid proton" signal [16,17,20] in the low field ^{1}H NMR region.

In ^{121}Sb NMR spectra of systems I and II no signals were observed for D/A < 1, while a narrow signal ascribed to $SbCl_6^-$ was observed in samples containing donor in excess. In the HMPT system the $SbCl_6^-$ signal was observed in samples with donor in excess but also in samples containing a slight excess of $SbCl_5$.

^{121}Sb spectra of samples of system III showed a broad signal ascribed to $SbCl_5$ in samples with concentration ratios D/A < 1, and no ^{121}Sb signal in samples containing EtOAc in excess. This confirms the findings from the ^{1}H NMR experiments that in this system there is quantitative formation of the molecular $SbCl_5$–EtOAc adduct with no further reactions taking place in solution.

The assignment of the two ^{121}Sb signals has been made by comparison with signals from 1,2-dichloroethane solutions of $SbCl_5$ and $(C_6H_5)_3C^+SbCl_6^-$, respectively. The $SbCl_6^-$ signal ($\simeq$0.075 mT peak-to-peak linewidth on the derivative spectrum)* is 380 ppm upfield from the $SbCl_5$ signal ($\simeq$1.8 mT linewidth).

A few preliminary measurements have been made on the *N*,*N*-dimethylformamide and 1,3-dimethylurea adducts, and the results were in all respects similar to those found in the TMU systems.

The ^{121}Sb NMR linewidths will be determined by two factors: the linewidth of individual species and the rates of exchange among all antimony-containing species in solution. Since the ^{121}Sb nucleus has an electric quadrupole moment, its linewidths will be dominated by the rate of quadrupolar relaxation.[24]

The relation between the transverse relaxation time (T_2) and the derivative peak-to-peak linewidth (ΔB) for a Lorentzian bandshape [24] is given by (1).

$$\Delta B = 2/T_2\sqrt{3} \tag{1}$$

When the product of the resonance frequency in rad/s (ω) and the rotational correlation time (τ_c) in s is $\ll 1$, (the so-called extreme narrowing case) T_2 is approximately given by (2).[24]

$$\frac{1}{T_2} = \frac{24}{1000}\left(\frac{e^2qQ}{\hbar}\right)^2 \tau_c = kq^2\tau_c \tag{2}$$

This formula applies for a nucleus with $I = 5/2$, such as ^{121}Sb, under the conditions in the present work. In eqn. (2) e stands for the electron charge, q represents the electric field gradient at the nucleus and Q is the quadrupole moment of the nucleus.

q is strongly correlated to molecular symmetry around the antimony atom and consequently sharp resonances are expected for the $SbCl_6^-$ ion and broader ones (perhaps undetectable) for the donor-acceptor adducts. The averaged linewidth of all species in fast exchange with each other will be given by eqn. (3).*

$$\Delta B = \sum_i p_i \Delta B_i \tag{3}$$

Here the p_i represent fractions of antimony content. In case of fast exchange among antimony compounds with very different linewidths, the linewidth will be of the order of that of the broadest line and in case of slow exchange only the sharpest line will be seen since it is difficult to observe broad lines superimposed on sharp lines.

For an accurate quantitative description of the ionization equilibria one must consider the possible importance of solvent separated ions, ion pairs, higher ion aggregates, the composition-dependent dielectric constants of the solutions and a whole spectrum of cations related

* T stands for Tesla (1 Tesla = 10 000 Gauss).

* See, *e.g.*, Ref. 33.

to the $D_2SbCl_4^+$ ion. To test if a description of the equilibria is possible with a minimum number of parameters the simple autoionization scheme (4) was assumed as a working hypothesis.

$$2DSbCl_5 \overset{K_2}{\rightleftharpoons} D_2SbCl_4^+ + SbCl_6^- \quad (4)$$

In conjunction with the equation for the normal donor-acceptor formation (5), this leads to expression (6), where $x = [SbCl_6^-] = [D_2SbCl_4^+]$, and which can be solved for x.

$$D + SbCl_5 \overset{K_1}{\rightleftharpoons} DSbCl_5 \quad (5)$$

$$x^3 \frac{K_1(2\sqrt{K_2}+1)^2}{\sqrt{K_2}} - x\left[K_1([D]_{tot}+[A]_{tot})(2\sqrt{K_2}+1)+1\right] + \sqrt{K_2}K_1[D]_{tot}[A]_{tot} = 0 \quad (6)$$

In the systems studied adduct formation is essentially complete so K_1 is very large [5] and eqn. (6) leads to a constant adduct/x ratio irrespective of the donor/acceptor ratio, as illustrated in Fig. 2.

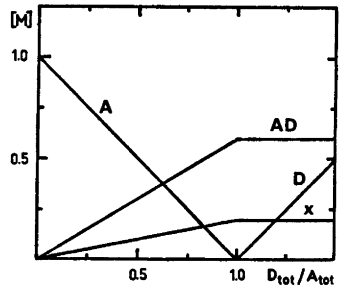

Fig. 2. Calculated concentration dependence of the autoionization reaction (4) for $K_2 = 0.111$ and a large K_1. $[A]_{tot} = 1$ M is constant.

When a ^{121}Sb NMR signal from the species $SbCl_6^-$ is observed measurements of the degree of ionization are straightforward. The concentration of this ion can be obtained by comparison with samples of known concentrations of hexachloroantimonate, assuming that the height × (linewidth)^2 of the peak is proportional to the intensity at constant spectrometer settings. Unless the signals are overmodulated or the lineshape is different this quantity is proportional to the integrated area of the absorption signal. The relatively low signal to noise ratio in the ^{121}Sb NMR spectra precluded a more accurate intensity measurement *via* numerical double integration of the derivative spectrum. The $SbCl_6^-$ concentrations determined from ^{121}Sb spectra are shown in column 4 of Table 1. From these ion concentrations equilibrium constants can be evaluated. The Ia system fits well with the simple autoionization scheme (4) with a value of 0.023 for K_2. This is also the case with the Ib and II systems and the corresponding values are 0.02 and 0.005, respectively. The latter values are, however, based on a small number of samples (4) and the determination is correspondingly less accurate.

The HMPT system (IV), however, does not fit into the simple scheme and, as further discussed below, another equilibrium process has to be considered. From the appropriate equilibrium constants "smoothed" values for the ion concentrations can be calculated. These are given in column 5 of Table 1.

A check on the self-consistency of the models can be made *via* the PMR spectra. The variable chemical shift of the "excess donor" signal in ^1H NMR spectra is a result of the variable proportions of unbound donor and cation. The variation in the observed chemical shift ν_{obs} relative to suitable reference can be simulated by the application of eqn. (7) under the assumption that the chemical shifts ν_D and ν_{ion} are constant.

$$\nu_{obs} = \frac{[D]\nu_D + 2[ion]\nu_{ion}}{[D] + 2[ion]} \quad (7)$$

ν_D should be close to the value observed for a solution of D in the same solvent and ν_{ion} is an unknown which has to be adjusted to obtain the "best fit". The chemical shifts in column 7 of Table 1 have been calculated in this way from the calculated ion concentrations in column 5 of the same table. The agreement is reasonably good, considering the fact that ν_D and ν_{ion} are not necessarily constants over a larger concentration range and that acidic impurities may interfere. For the TMU adduct in 1,2-dichloroethane (Ib) a value of 0 Hz for the ion and 27 Hz upfield for unbound donor reproduces the ν_{obs} values quite well. ^1H NMR shifts are expressed

relative to the shift of the adduct. The donor shift is in good agreement with the shift observed in a solution of TMU in dichloroethane. Provided that there is an exchange process between TMU in cation and adduct when D/A < 1, the former value explains the initially confusing fact that the adduct ^1H NMR shift is the same under conditions of excess donor and excess acceptor and that no separate cation ^1H NMR signal is ever observed. Evidence for such an exchange process is indeed found in ^{121}Sb spectra as further discussed below. In the Ia and IV systems the shifts (cation/unbound donor) 0/31 and 4/18 Hz were found.

As a consequence of ionization the adduct will be consumed and converted to ions. This should affect the relative areas of the adduct signal and the "excess donor" + cation signal in samples having donor in excess. For each cation formed, two adduct molecules are required. Taking the $D_2SbCl_4^+$ concentration to be x, the observed ^1H NMR signal intensity ratio, R, between the averaged signal of unbound donor + cation and the adduct signal will be given by (8).

$$R_{obs} = \frac{[D]_{init} - [A]_{init} + 2x}{[A]_{init} - 2x} \quad (8)$$

Rearranging leads to (9), from which the degree of ionization can be estimated.

$$x = \frac{R_{obs}[A]_{init} + [A]_{init} - [D]_{init}}{2(1 + R_{obs})} \quad (9)$$

Since only deviations are measured, fairly accurate values of the initial concentrations of donor and $SbCl_5$ are required if a reasonable precision of the determination is to be obtained. For this reason this method has only been used for the HMPT adduct (IV) where the conversion to ions is extensive. These results are shown within parenthesis in column 4 of Table 1. The observed degrees of ionization from ^{121}Sb spectra and from ^1H spectra (with the aid of eqn. (9)) agree satisfactorily considering the probable errors of these measurements.

It can be seen that the ionization data for system IV cannot be interpreted according to the simple autoionization scheme since the $SbCl_6^-$ concentration increases significantly with the D/A ratio. One model for this situation involves the assumption of a simultaneous induced autoionization as a result of solvation effects of the excess donor. Formally this can be expressed as (10), where the third D in the ion is assumed to be more weakly bonded.

$$D + 2DSbCl_5 \overset{K_3}{\rightleftharpoons} SbCl_6^- + D_3SbCl_4^+ \quad (10)$$

Values of K_2 (0.14) and K_3 (3.3 l mol^{-1}) can be found which satisfactorily reproduce the ionizations in this adduct system, as shown in columns 5 and 7 of Table 1, which give the $SbCl_6^-$ concentrations and ^1H NMR shifts calculated using the above values for the equilibrium constants. The difference in ionization behaviour between the HMPT adduct system in nitrobenzene and the other systems may reflect the stronger donor-acceptor interaction in the adduct [25] and the higher dielectric constant of the solvent (35.7).[23] It is also known that HMPT is an effective solvent for organic ions.[26] As illustrated in Fig. 1 this adduct system also exhibits a variable ^1H NMR shift of the signal from the HMPT adduct with $SbCl_5$ in varying excess. This might be due to coordination of excess $SbCl_5$ to the nitrogen atoms in the donor molecule. The HMPT signal in this region is quite broad, revealing the existence of an exchange process, which has not been further investigated. Above a D/A ratio of unity the adduct signal suddenly sharpens and remains at a constant shift. Now instead the excess donor signal shows the same type of shift variation as the excess TMU signal.

It has not been possible to directly observe the $D_2SbCl_4^+$ ions in solutions containing $SbCl_4^+$ in excess in any of the systems studied. However, it seems reasonable to assume that autoionization takes place and that donor in the cation is in rapid exchange with donor in the adduct below the ratio D/A = 1.0. In solutions with D/A > 1 the exchange between cation and excess donor is rapid while the donor exchange with the adduct is slow. The following experiment illustrates this point further. To a 0.5 M solution of $SbCl_5$ in CH_2Cl_2 (showing a broad $SbCl_5$ signal in ^{121}Sb spectra), tetrabutylammonium chloride was added in order to make the solution 0.2 M with respect to $SbCl_6^-$, (which should readily form). The ^{121}Sb signal observed after the addition was shifted upfield, but was as broad as the original $SbCl_5$ signal and no $SbCl_6^-$ signal was seen. Addition of a few mol % of TMU to this sample washes out the ^{121}Sb

signal completely. Combined with the observation that the weaker and probably nonionizing EtOAc adduct system shows a $SbCl_5$ signal when $SbCl_5$ is in excess but no $SbCl_6^-$ signal when EtOAc is in excess, this suggests that the presence of $SbCl_6^-$ and $D_2SbCl_4^+$ in the solution provides an exchange pathway between these ions, $SbCl_5$ and the adduct. The averaged linewidth will be given by (3) and should be of the order of the adduct linewidth. This is expected to be broad enough to make the line unobservable. The same argument explains the paradox that no ^{121}Sb signal at all is seen in systems I, II, and IV when $SbCl_5$ is in excess. Closely below the D/A ratio of unity in the HMPT adduct system a $SbCl_6^-$ signal is, however, seen. This could be an effect of the above-mentioned coordination of excess $SbCl_5$ to the HMPT nitrogens whereby the exchange pathway is interrupted.

The equilibria under consideration also include ion pairs, and an alternative to eqn. (4) is

$$2DSbCl_5 \rightleftharpoons SbCl_6^- D_2SbCl_4^+ \quad (11)$$

An alternative to eqn. (10) is an equation which describes a separation of the ion pairs in (11) into ions whereby the equilibrium in (11) is driven further to the right. The available data can, however, be satisfactorily described with eqns. (4) and (10). For instance, eqn. (4) describes the Ib ionization data in Table 1 better than eqn. (11), which leads to a concentration dependent degree of ionization.

^{121}Sb linewidths of the free $SbCl_6^-$ ion and $SbCl_6^-$ in an ion pair possibly differ due to distortions of the octahedron in the ion pair and the different rotation correlation times of the two species. This effect is noticeable for small ions such as the sodium ion.[27] Linewidth considerations could therefore be useful for the estimation of the relative abundances of free ions and ion pairs. The observed $SbCl_6^-$ linewidths in the present work are essentially the same as in the triphenylmethylhexachloroantimonate reference samples. Bowyer *et al.* state that in 1,2-dichloroethane this salt is almost completely in the ion pair form.[28] On the other hand, the linewidths are smaller ($\simeq 50$ %) than those corresponding to T_2 data for $SbCl_6^-$ ions in 5 M HCl [29] where predominantly free ions should exist, so no conclusions can be drawn from these data.

The ^{121}Sb spectra of $SbCl_5$ deserve special comment since the linewidth of neat $SbCl_5$ (0.75 mT) is smaller than in 1 M 1,2-dichloroethane solutions (1.8 mT p−p). Neat $SbCl_5$ seems to have a greater viscosity than the solutions, so a change in τ_c does not explain the difference. Possible explanations include rapid exchange between $SbCl_5$ and small amounts of $SbCl_5-H_2O$, which may be present as an impurity, and solute−solvent interaction. The enthalpy of solution of $SbCl_5$ in 1,2-dichloroethane is −1.80 kJ/mol.[17] Although $SbCl_5$ is invariably reported as monomeric in the literature (solid, Ref. 30 and gas phase, Ref. 31), halogen bridges in related compounds such as Al_2Cl_6 and SbF_5 are well known.[32] If $SbCl_5$ is to some extent dimeric or polymeric at higher concentrations, the electric field gradient factor q in eqn. (2) could be reduced, thereby making the lines sharper. A careful variable solvent study should provide conclusive evidence for the correct explanation.

Added in proof: Preliminary results indicate that the ^1H NMR signal from the $D_2SbCl_4^+$ ion can be observed in TMU−$SbCl_5$−CH_2Cl_2 samples, where an initial excess of $SbCl_5$ has been scavenged with EtOAc. The signal has the correct intensity (≈ 20 % of the adduct signal) and coalesces with the adduct signal above ≈ 0 °C (composition dependent). The shift of this signal is ≈ 3 Hz (60 MHz) upfield from the adduct signal.

Acknowledgements. We wish to thank Professor J. S. Hartman for a stimulating and helpful discussion and for making results available to us prior to publication. We are also grateful for suggestions and helpful comments from Professors S. Forsén and I. Lindqvist.

Dr. R. E. Carter kindly helped to improve the language.

REFERENCES

1. Lindqvist, I. *Inorganic Adduct Molecules of Oxo-Compounds*, Springer, Berlin 1963.
2. Brun, L. and Brändén, C.-I. *Acta Crystallogr. 20* (1966) 749.
3. Binas, H. *Z. Anorg. Chem. 352* (1967) 271.
4. Chevrier, B., Carpentier, J.-M. and Weiss, R. *J. Amer. Chem. Soc. 94* (1972) 5718.
5. Olofsson, G. *Acta Chem. Scand. 22* (1968) 377.
6. Gutmann, V. and Czuba, H. *Monatsh. Chem. 100* (1969) 708.
7. Zuur, A. P. and Groenveld, W. L. *Rec. Trav. Chim. Pays-Bas 86* (1967) 1089.

8. Kolditz, L. and Preiss, H. *Z. Anorg. Chem. 310* (1964) 172.
9. Beattie, I. R. and Webster, M. *J. Chem. Soc.* (1963) 38.
10. Schmulbach, C. D. and Ahmed, I. Y. *J. Chem. Soc. A* (1968) 3008.
11. Gutmann, V. and Imhof, J. *Monatsh. Chem. 101* (1970) 7.
12. Lim, Y. Y. and Drago, R. S. *Inorg. Chem. 11* (1972) 202.
13. Beattie, I. R., Jones, P. J. and Webster, M. *J. Chem. Soc. A* (1969) 218.
14. Ahmed, I. Y. and Schmulbach, C. D. *Inorg. Chem. 11* (1972) 228.
15. Olofsson, G., Stilbs, P., Drakenberg, T. and Forsén, S. *Tetrahedron 27* (1971) 4583.
16. Olofsson, G. and Olofsson, I. *Tetrahedron 29* (1973) 1711.
17. Appleton, Q., Bernander, L., and Olofsson, G. *Tetrahedron 27* (1971) 5291.
18. Hartman, J. S. and Schrobilgen, G. J. *Inorg. Chem. 13* (1974) 874.
19. Sellers, P. *J. Chem. Thermodyn. 2* (1970) 211.
20. Hartman, J. S. and Schrobilgen, G. J. *Can. J. Chem. 50* (1972) 713.
21. Cowell, G. W., Ledwith, A., White, A. C. and Woods, H. J. *J. Chem. Soc. B* (1970) 227.
22. Chandler, J. P., *Program No.* 66:2, Quantum Chemistry Program Exchange, Department of Chemistry, Indiana University, Bloomington, Ind., U.S.A.
23. Maryott, A. A. and Smith, F. A. *Nat. Bur. Stand. (U.S.), Circ. 514* (1951).
24. Abragam, A. *The Principles of Nuclear Magnetism*, Oxford Univ. Press, Oxford 1961.
25. Gutmann, V. *Chimia 23* (1969) 285.
26. Fieser, L. F. and Fieser, M. *Reagents for Organic Synthesis*, Wiley, New York 1967.
27. Erlich, R. H. and Popov, A. I. *J. Amer. Chem. Soc. 93* (1971) 5620.
28. Bowyer, P. M., Ledwith, A. and Sherrington, D. C. *J. Chem. Soc. B* (1971) 1511.
29. Kok, G. L., Morris, M. D. and Sharp, R. R. *Inorg. Chem. 12* (1973) 1709.
30. Ohlberg, S. *J. Amer. Chem. Soc. 81* (1959) 811.
31. Wilmshurst, J. K. *J. Mol. Spectrosc. 5* (1960) 343.
32. Cotton, F. A. and Wilkinson, G. *Advanced Inorganic Chemistry*, 3rd Ed. Interscience, New York 1972.
33. Zimmermann, J. R. and Britten, W. E. *J. Phys. Chem. 61* (1957) 1328.

Received February 21, 1974.

Acta Chemica Scandinavica A 28 (1974) 656—660

Hydrolysis of Anilides. XII. Alkaline and General Acid Catalyzed Alkaline Hydrolysis of Two *ortho*-Substituted Trifluoroacetanilides

URVE MERESAAR

Department of Inorganic and Physical Chemistry, Faculty of Pharmacy, University of Uppsala, Box 574, S-751 23 Uppsala, Sweden

Rate-pH-profiles are given for the alkaline hydrolysis of trifluoroacet-2,4-dimethylanilide and trifluoroacet-2,6-dimethyl-3-nitroanilide at 45 °C and ionic strength 1 in an aqueous medium containing 20 v/v % dimethyl sulfoxide. The pK_a values of these anilides have been determined in the same medium.

The rate constants for the formation of the tetrahedral amide-hydroxide ion intermediates (k_1) are given as well as the ratios of the rate constants for the uncatalyzed breakdown (k_2) of the intermediates and for the reversion to reactants (k_{-1}). A very low k_2/k_{-1} value (0.00060) is found for the trifluoroacet-2,6-dimethyl-3-nitroanilide. The corresponding ratios for the hydroxide ion ($k_{3,OH}/k_{-1}$) and for the hydrogencarbonate ion ($k_{3,HCO_3^-}/k_{-1}$) catalyzed product formation from the intermediates have also been determined.

To obtain information on the effect of dimethyl sulfoxide on the rate constants, trifluoroacetanilide was hydrolyzed at 25 °C in an aqueous alkaline medium of ionic strength 1 containing 5 or 20 v/v % dimethyl sulfoxide. Some increase with increasing dimethyl sulfoxide contents was found in the k_1 values while the k_2/k_{-1} ratios were almost unchanged.

In the previous work in this series [1] a sterically highly hindered amide, trifluoroacet-2,6-dimethylanilide, was studied and an extremely low ratio (0.0008) of k_2/k_{-1} (*cf.* Scheme 1) was found. To get more information concerning the basis for low k_2/k_{-1} values two other *ortho*-substituted anilides have now been studied, one of them with an electron-attracting ring substituent (NO_2). The NO_2-group decreases pK_a and increases k_1 and $k_{3,OH}/k_{-1}$, factors profitable for obtaining high accuracy in the calculation of rate parameters. The experiments were run in 20 v/v % dimethyl sulfoxide solution, and in order to learn how the DMSO content affects the rate constants, the previously studied [2] trifluoroacetanilide has been hydrolyzed at two different DMSO concentrations.

MATERIALS AND METHODS

Materials. The trifluoroacet-2,4-dimethylanilide was prepared from 2,4-dimethylaniline and trifluoroacetic anhydride and recrystallized from aqueous ethanol; m.p. 93 – 94 °C (Ref. 3 gives 91 °C).

The trifluoroacet-2,6-dimethyl-3-nitroanilide, obtained by nitration of trifluoroacet-2,6-dimethylanilide with mixed acid, had melting point 108 – 110 °C and analysis gave: C 46.2, H 3.39, N 10.9. (Calc. C 45.8, H 3.46; N 10.7). To determine the site of nitration, the anilide was hydrolyzed in 1 M hydrochloric acid and the substituted aniline was isolated. It consisted of yellow crystals with m.p. 80 – 81 °C. Ref. 4 gives m.p. 81 – 82 °C for 2,6-dimethyl-3-nitroaniline while 2,6-dimethyl-4-nitroaniline melts at 158 – 160 °C.

The trifluoroacetanilide was of the quality used earlier by Eriksson and Holst.[2] All other chemicals were of reagent grade. In order to remove protolytic impurities from the potassium chloride, it was recrystallized from 0.1 M hydrochloric acid.

Hydrolysis experiments. The experiments with the ring-substituted anilides were run at 45 ± 0.1 °C in an aqueous solution containing 20 v/v % dimethyl sulfoxide and having an ionic strength of 1, obtained by addition of potassium chloride. The trifluoroacetanilide was hydrolyzed at 25 ± 0.05 °C and ionic strength 1 in solutions of 5 and 20 v/v % dimethyl sulfoxide in water. The concentration of the anilides varied between 5×10^{-4} and 0.01 M. The experiments were run at constant pH as described

previously.[1] Carbon dioxide was excluded when hydrolyzing at the lowest pH values by performing the experiments under nitrogen.

The stoichiometric pK_a and pK_w values were determined potentiometrically in the same way as described earlier [2,5] and are given in Table 1. Hydrogencarbonate ions were used as catalyzing species for the ring-substituted anilides.

Assay. The hydrolyses were followed by determining the anilines by diazotisation and coupling with *N*-(1-naphthyl)ethylenediamine as described earlier.[2] The 2,4-dimethylaniline couples very slowly and the previously used method had to be modified. Thus the coupling reaction was allowed to proceed during 72 h in a refrigerator and the coloured product was measured at 560 nm. The molar absorption coefficient of about 30 000 varied somewhat from time to time. Thus reference samples were always run concurrently. The coupled product of diazotized 2,6-dimethyl-3-nitroaniline has a molar absorption coefficient of 38 100 at 500 nm.

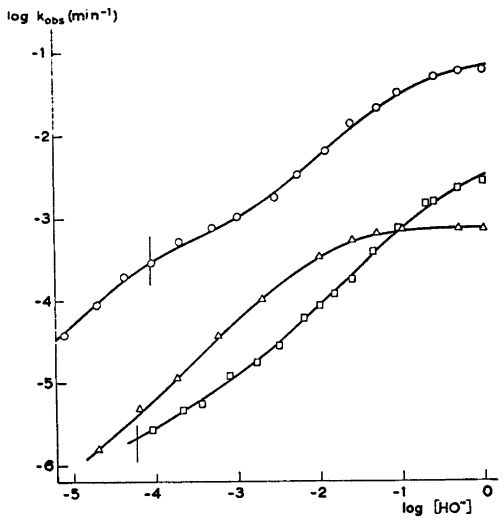

Fig. 1. Plot of log k_{obs} against log [HO$^-$] for trifluoroacet-2,4-dimethylanilide ○, trifluoroacet-2,6-dimethyl-3-nitroanilide △, and trifluoroacet-2,6-dimethylanilide (from Ref. 1) □ at 45 °C in a 20 v/v % DMSO solution of ionic strength 1. The fully drawn lines are calculated from eqn. (1) and parameter values given in Table 1. The bars denote the values of log [HO$^-$] corresponding to the stoichiometric pK_a values in Table 1.

RATE EQUATIONS AND RESULTS

The results are consistent with the reactions in Scheme 1, where B denotes hydroxide or hydrogencarbonate ions (substituents in the aromatic ring are omitted). Using the steady-state approximation, eqn. (1) can be derived, where k_{obs} is the pseudo first-order rate constant at constant pH.

$$k_{obs} = \frac{k_1 K_w}{K_a + [H^+]} \times \frac{k_2 + \sum k_{3,i}[B_i]}{k_{-1} + k_2 + \sum k_{3,i}[B_i]} \quad (1)$$

When $(k_{-1} + k_2)$ is negligible compared to $k_{3,i}[B_i]$, the equation simplifies to

$$k_{obs} = k_1 K_w / (K_a + [H^+]) \quad (2)$$

Thus, under these presumptions, k_{obs} reaches a limiting value from which k_1 can be obtained. According to Figs. 1 and 2 the experiments in alkaline medium could be used for the calculation of k_1. For trifluoroacet-2,4-dimethylanilide the experiments with hydrogencarbonate ion catalysis could also be used for this purpose (*cf.* Fig. 3). With k_1 known, k_2/k_{-1} and $k_{3,oh}/k_{-1}$ were calculated as described previously using a Hewlett-Packard 9810A model 10 calculator.[1] The values giving the best fit to experimental data are given in Table 1 and were used when calculating the curves in Figs. 1 and 2.

The curves in Fig. 4 for hydrogencarbonate ion catalysis of the nitro compound almost coincide. The experiments were run at pH values above the pK_a, and from eqn. (1) it is apparent that graphs of k_{obs} as a function of $[HCO_3^-]$ will be pH-independent when $K_a \gg [H^+]$ and $k_{3,HCO_3^-}/k_{-1}$ is a real constant. No approach to a limiting rate was reached and so

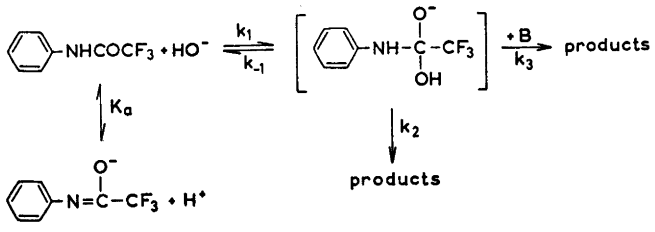

Scheme 1.

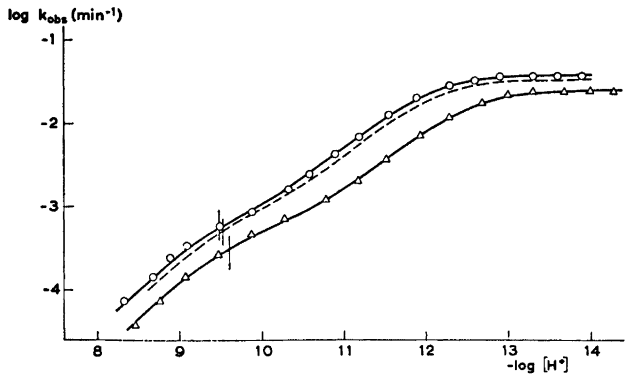

Fig. 2. Plot of log k_{obs} against $-\log [H^+]$ for trifluoroacetanilide at 25 °C and ionic strength 1 in 5 v/v % (○) and 20 v/v % (△) DMSO solution. The dashed curve is for 9.6 v/v % ethanol solution and taken from Ref. 2. The fully drawn lines are calculated from eqn. (1) and parameter values given in Table 1. The bars denote the values of $-\log [H^+]$ corresponding to the stoichiometric pK_a values in Table 1.

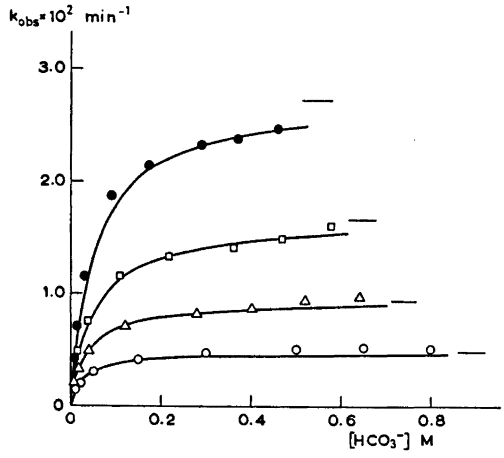

Fig. 3. Plot of k_{obs} against concentration of hydrogencarbonate ions for trifluoroacet-2,4-dimethylanilide at 45 °C and ionic strength 1 in 20 v/v % DMSO solution. The curves are calculated from eqn. (1) and parameter values given in Table 1 and $k_{3,HCO_3^-}/k_{-1}$ values given below. The bars denote limiting values of k_{obs}.

	[H$^+$]	[HCO$_3^-$]/[CO$_3^{2-}$]	$k_{3,HCO_3^-}/k_{-1}$M^{-1}
○	$10^{-8.43}$	32	35
△	$10^{-8.74}$	16	30
□	$10^{-9.04}$	8	20
●	$10^{-9.34}$	4	20

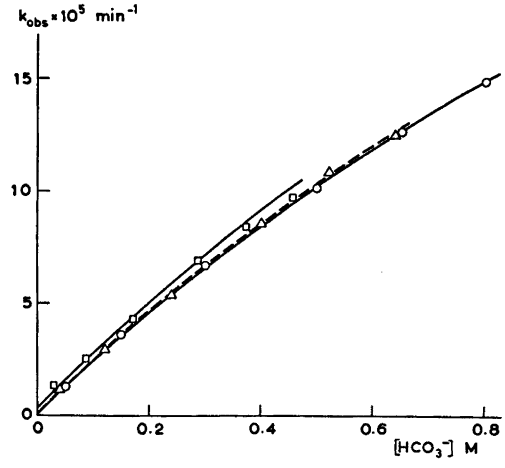

Fig. 4. Plot of k_{obs} against concentration of hydrogencarbonate ions for trifluoroacet-2,6-dimethyl-3-nitroanilide at 45 °C and ionic strength 1 in 20 v/v % DMSO solution. The curves are calculated from eqn. (1) and parameter values given in Table 1 and $k_{3,HCO_3^-}/k_{-1}$ values given below.

	[H$^+$]	[HCO$_3^-$]/[CO$_3^{-2}$]	$k_{3,HCO_3^-}/k_{-1}$M^{-1}
○	$10^{-8.43}$	32	0.39
△	$10^{-8.74}$	16	0.35 dashed curve)
□	$10^{-9.34}$	4	0.34

the experiments could not be used for the calculation of k_1. $k_{3,HCO_3^-}/k_{-1}$ values given in the text to Figs. 3 and 4 are obtained from the experiments shown in these figures and are used together with parameter values in Table 1 when calculating the theoretical curves from eqn. (1).

DISCUSSION

The k_1 values in Table 1 for the ring-substituted anilides follow the expected pattern, *i.e.* *ortho*-substitution with methyl groups decreases k_1 and an electron-attracting nitro group in a position other than *ortho* increases the constant. This increase is about seven times, which is somewhat less than the thirteenfold increase found when *N*-methyltrifluoroacetanilide is *m*-nitro-substituted.[6] The low ratios of k_2/k_{-1} for the ring-substituted anilides may undoubtedly be related to highly hindered proton transfers in the tetrahedral intermediates. Electron-releasing ring substituents, such as CH_3, in *meta* or *para* position, have been shown to increase the value of k_2/k_{-1}, the effect, however, being rather small.[6] The values reported here for the 2,6-substituted compounds seem to be by far the lowest hitherto found in amide hydrolysis.

The steric hindrance also decreases the $k_{3,oh}/k_{-1}$ and $k_{3,HCO_3^-}/k_{-1}$ ratios. In accordance with results obtained recently for *p*-nitrotrifluoroacetanilide,[7,8] the $k_{3,oh}/k_{-1}$ value is also here found to be significantly increased by a nitro substituent. The larger dependence on nitro-substitution of $k_{3,oh}/k_{-1}$ than of k_2/k_{-1} was interpreted by Pollack and Dumsha [7] to signify that, contrary to the mechanism of the k_2-step, a negative charge is formed on the amide nitrogen in the transition state of the $k_{3,oh}$-step for the nitro-substituted anilide. According to them, the mechanism with a negatively charged leaving aniline group then should be specific for anilides with strongly electron-attracting groups in the ring.

The $k_{3,HCO_3^-}/k_{-1}$ ratios increased slightly with increasing concentration of hydrogen ions as has been noticed earlier and discussed for other compounds.[1,9]

According to Table 1, the k_1 value of trifluoroacetanilide increases somewhat with increasing concentration of dimethyl sulfoxide. This was expected because of the desolvation of hydroxide ions in DMSO-water mixtures. The same effect has been found earlier for the second-order rate constants for the alkaline hydrolyses of, *e.g.*, ethyl acetate [10] and aliphatic dicarboxylic esters.[11] Gani and Viout [12] found that second order rate constants for the alkaline hydrolyses of *p*-chlorophenoxyacetamide and acetamide decreased with increasing concentration of DMSO. In the present work an increase of the second-order rate constant of the alkaline hydrolysis (k_{oh}) is, however, found, when the DMSO concentration is increased, this being due to the increase of k_1, while the ratio k_2/k_{-1} remains almost constant. It is hard to draw any general conclusions from this as only two mixtures were investigated, both with rather small concentrations of DMSO. Our main purpose with these experiments was to establish how the used concentrations of DMSO influence the values of k_2/k_{-1}. The results seem to permit the conclusion that the influence is small.

Table 1. Experimentally determined dissociation constants and rate parameters used in the construction of Figs. 1–4. The solvent was 20 v/v % DMSO unless otherwise noted and the ionic strength was 1. $pK_w = 14.27$ (25 °C) and 13.64 (45 °C).

	Temp. °C	pK_a	k_{oh}[a] M^{-1} min^{-1}	k_1 M^{-1} min^{-1}	k_2/k_{-1}	$k_{3,oh}/k_{-1}$ M^{-1}
Trifluoroacet-2,6-dimethylanilide [b]	45	9.40	0.0660	83	0.00080	1.8
Trifluoroacet-2,6-dimethyl-3-nitroanilide	45	7.77	0.340	570	0.00060	80
Trifluoroacet-2,4-dimethylanilide	45	9.59	5.91	850	0.0070	7.3
Trifluoroacetanilide	25	9.60	29.3	1200	0.024	85
Trifluoroacetanilide [c]	25	9.47	25.6	1050	0.025	100
Trifluoroacetanilide [d]	25	9.51	22.7	930	0.025	93

[a] $k_{oh} = k_1k_2/(k_{-1}+k_2)$. [b] The values are taken from Ref. 1. [c] In 5 v/v % DMSO ($pK_w = 13.88$). [d] In 9.6 v/v % ethanol ($pK_w = 13.92$) (from Ref. 2).

Acknowledgements. I wish to thank Dr. Sven O. Eriksson for his interest in this work and for valuable comments on the manuscript. The skilful technical assistance given by Mrs. Barbro Johansson is also acknowledged. Financial support from the Swedish Natural Science Research Council to Sven O. Eriksson for this project is gratefully acknowledged.

REFERENCES

1. Meresaar, U. and Eriksson, S. O. *Acta Chem. Scand. 26* (1972) 4186.
2. Eriksson, S. O. and Holst, C. *Acta Chem. Scand. 20* (1966) 1892.
3. Pailer, M. and Hübsch, W. J. *Monatsh. Chem. 97* (1966) 1541.
4. Wepster, B. M. *Rec. Trav. Chim. Pays-Bas 73* (1954) 809.
5. Eriksson, S. O. and Meresaar, U. *Acta Chem. Scand. 25* (1971) 2688.
6. Kershner, L. D. and Schowen, R. L. *J. Amer. Chem. Soc. 93* (1971) 2014.
7. Pollack, R. M. and Dumsha, T. C. *J. Amer. Chem. Soc. 95* (1973) 4463.
8. Segretain, A.-M., Beugelmans-Verrier, M. and Laloi-Diard, M. *Bull. Soc. Chim. Fr.* (1972) 3367.
9. Eriksson, S. O., Meresaar, U. and Wahlberg, U. *Acta Chem. Scand. 22* (1968) 2773.
10. Tommila, E. and Murto, M.-L. *Acta Chem. Scand. 17* (1963) 1947.
11. Venkoba Rao, G. and Venkatasubramanian, N. *Indian J. Chem. 10* (1972) 178.
12. Gani, V. and Viout, P. *C. R. H. Acad. Sci. Ser. C 274* (1972) 1746.

Received February 4, 1974.

Acta Chemica Scandinavica A 28 (1974) 661—665

The Crystal and Molecular Structure of 1-Methyl-3,6-pyridazinedione

T. OTTERSEN

Department of Pharmacy, University of Oslo, Oslo 3, Norway

The crystal and molecular structure of 1-methyl-3,6-pyridazinedione has been determined by X-ray methods using 2473 reflections above background level collected by counter methods. The crystals are monoclinic, space group $P2_1/c$, with cell dimensions: $a = 3.89_7$ Å; $b = 13.95_5$ Å; $c = 10.61_7$ Å; $\beta = 99.5_4°$. Estimated standard deviations in bond lengths are about 0.001 Å, and in angles 0.1°. The molecule is found to exist as the monolactim and is planar. The bond lengths indicate a resonance stabilization of the heterocycle, although less than what was found in 4,5-dichloro-3,6-pyridazinedione.

The structure determination of 1-methyl-3,6-pyridazinedione was carried out as part of a series of structure investigations of 3,6-pyridazinediones and related compounds.[1-4]

Significant differences were found in the pyridazine moieties of 4,5-dichloro-3,6-pyridazinedione [1] (I), DCMH, and 1-methyl-3-methoxy-6-pyridazone [3,4] (III), MDMH. The bond lengths indicated a larger resonance stabilization of DCMH than of MDMH. The hydrogen bonds in DCMH, which involve N1 and both oxygens, may imply a structure intermediate between the monolactim (I) and the dilactim (II). 1-Methyl-3,6-pyridazinedione, MMH, was, on the basis of the structure found for DCMH, assumed to exist as the monolactim (IV) with an oxygen-oxygen hydrogen bond in the solid state. It was of interest to determine if the pyridazine moiety of MMH corresponds to that of DCMH or that of MDMH. Structural parameters available for formamide [5,6] indicate that N−H···O hydrogen bonds have a large effect on the resonance stabilization of the peptide moiety (O=C−N<). Significant differences were also found in the O1−C6 and C6−N1 bond lengths of DCMH [1] and MDMH.[3,4] The introduction of a methyl-group at the 1-position of the pyridazine moiety in the 3,6-pyridazinedione should therefore be expected to have a significant effect on the resonance stabilization of the heterocycle.

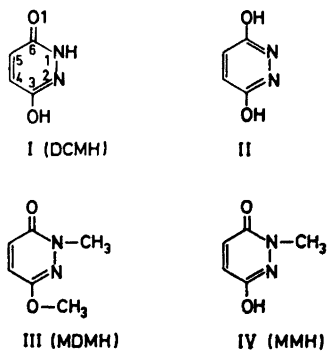

EXPERIMENTAL

MMH was synthesized from 3,6-pyridazinedione by the method of Eichenberger *et al.*[7] The product was recrystallized by slow evaporation of a water solution. Rectangular, colorless crystals were formed. A crystal of dimensions 0.6 × 0.3 × 0.3 mm. was selected for the crystallographic work.

Oscillation, Weissenberg and precession photographs indictated monoclinic symmetry; all reflections ($h0l$) for l odd, and ($0k0$) for k odd, were systematically absent. This uniquely defines the space group as $P2_1/c$. Unit cell parameters were determined on a Syntex-P$\bar{1}$ diffractometer using Mo$K\alpha$ ($\lambda = 0.71069$ Å) radiation. The angular coordinates of fifteen symmetry-independent reflections were utilized

in the least-squares refinement of cell dimensions. The computer program used is part of the diffractometer program library.

Three-dimensional intensity data were recorded using a computer-controlled Syntex-P$\bar{1}$ four-circle diffractometer with graphite monochromated Mo$K\alpha$ radiation. The temperature was kept constant within 1 °C at 20 °C. The $\omega - 2\theta$ scan was utilized with scan speed variable from 1 to 12° min^{-1}, depending on the peak intensity of the reflections. Background was counted for half the scanning time at each end of the scan range. Reflections for which the counts exceeded 10^5 cps were remeasured with reduced primary beam intensity. The intensities of three standard reflections were measured after every 100 reflections, the variations in the check reflection intensity were less than 2 %. No corrections for these variations were applied to the intensity data.

The estimated standard deviations were taken as the square root of the total count with a 2 % addition for experimental uncertainties. Of the 4977 unique reflections measured ($2\theta_{max} = 92°$), 2473 had intensities larger than twice their standard deviations. These were regarded as "observed" reflections, and the remaining reflections were excluded from further calculations. The intensities were corrected [8] for Lorentz and polarization effects.

The atomic scattering factors used were those of Doyle and Turner [9] for oxygen, nitrogen, and carbon, and of Stewart *et al.*[10] for hydrogen.

CRYSTAL DATA

1-Methyl-3,6-pyridazinedione, $C_5H_6N_2O_2$, monoclinic.

$a = 3.897$ (0.0005) Å; $b = 13.955$ (0.002) Å; $c = 10.617$ (0.002) Å; $\beta = 99.54°$ (0.01°).

Figures in parentheses are estimated standard deviations.

$V = 569.3$ Å^3; $M = 126.1$ amu; $Z = 4$; $D_{calc} = 1.471$ g/cm^3; $F(000) = 264$.

Absent reflections: ($h0l$) for l odd; ($0k0$) for k odd; space group $P2_1/c$.

STRUCTURE DETERMINATION AND REFINEMENTS

The phase problem was solved by a computer procedure [11] based on direct methods, utilizing Sayre's equation.[12]

All programs used in subsequent calculations are part of a local assembly of computer programs for CYBER-74 and are described in Ref. 13.

The structure model was refined to a conventional R of 0.20. Introduction of anisotropic thermal parameters for all non-hydrogen atoms and least-squares refinement yielded an R of 0.082. All six hydrogens were located in a difference fourier synthesis. These were included in the least-squares refinement with isotropic thermal parameters. Results from the full-matrix least-squares refinements using various parts of the data set are summarized in Table 1.

It is worth noting that only marginal shifts are found for the N1 – N2 bond length, and also for the nitrogen positions. A significant shortening is usually found for the nitrogen-nitrogen bond

Table 1. Results from the least-squares refinements. R, R_w and R_t are the conventional, the weighted and the conventional for the total data-set correlation factors, respectively (for a more detailed explanation see Ref. 4). G is the "goodness-of-fit". The estimated standard deviation of the scale factor is given in parentheses. The bond lengths are corrected for librational motion (see Fig. 1 for the numbering of the atoms).

No.	sin θ/λ limit on the data (Å^{-1})	Number of reflections used in the refinement	R	R_w	R_t	G	Scale	Mean e.s.d in bond ($\times 10^4$)	Bond lengths (Å) N1 – N2	C4 – C5
I[a]	<0.65	1140	.043	.051	.071	2.30	.077(5)	16	1.373	1.345
II[a]	–	2473	.067	.063	–	2.54	.082(3)	12	1.372	1.352
III[b]	>0.50	1906	.067	.058	.077	2.35	.085(5)	13	1.371	1.356
IV[a]	>0.60	1533	.077	.063	.075	2.43	.084(8)	17	1.371	1.356
V[b]	>0.65	1333	.083	.066	.077	2.52	.085(10)	21	1.370	1.356
VI[b]	>0.70	1103	.090	.072	.088	2.59	.087(14)	29	1.373	1.359

[a] All positional and thermal parameters refined. [b] All positional and thermal parameters refined for non-hydrogen atoms.

when the low-angle data (sin $\theta/\lambda < 0.6$) are excluded from the refinement.[1,3,4] The lengthening of the carbon-carbon double bond is as expected.[4] The other bond lengths show no dependence on the lower sin θ/λ-cut of the data, this has been noted earlier.[1,4]

Only marginal differences are found in the thermal parameters from refinements III, IV, and V, while those from refinements I and II are generally larger and those from refinement VI are generally smaller than these. This is probably coupled with the changes in the scale factor. The total discrepancy between the atomic vibration tensor components and those calculated from the rigid-body parameters found by analysis of the librational, translational and screw motion of the molecule is 0.0013 Å^2 for refinement I, 0.0011 Å^2 for II, III, and IV, 0.0012 Å^2 for V, and 0.0015 Å^2 for VI. This indicates that the molecular model in all cases may be regarded as a rigid body. The atomic coordinates were accordingly corrected for the librational motion.

The results indicate that the valence electrons in this case have no significant effect on the structure model when all data with sin $\theta/\lambda < 0.50$ is excluded from the refinement. Results from refinement III will therefore be used in the discussion. A listing of structure amplitudes is available from the author upon request. The final parameters for non-hydrogen atoms are listed in Table 2. Atomic parameters for hydrogen atoms, from refinement II, are given in Table 3. The eigenvalues of **T** are 0.18, 0.16, and 0.14 Å^2. The r.m.s. librational amplitudes are 5.2, 4.6, and 2.0° with the major axis nearly parallel to a line through C4–C6 (see Fig. 1 for the numbering of the atoms).

Standard deviations in molecular dimensions were calculated from the correlation matrix ignoring standard deviations in cell parameters.

DISCUSSION

Bond lengths and bond angles are listed in Fig. 1 where the numbering of the atoms is indicated.

The heterocycle is planar, the atoms being displaced from a least-squares plane through the six ring atoms by less than 0.009 Å (see Table 4). O2 deviates significantly from the plane, similar displacements have been found both in DCMH [1] and MDMH.[3,4]

Both the N1–N2 and the C4–C5 bond lengths are similar to those found in MDMH.[4] The other bond lengths, however, indicate a slightly larger resonance stabilization of MMH than of MDMH. The C3–C4 and the C5–C6

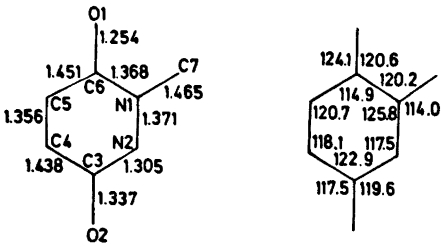

Fig. 1. Bond lengths (Å) (corrected for thermal vibration effects) and bond angles (°). Estimated standard deviations in bond lengths are 0.001 Å and in angles 0.1°. Structure model obtained from the refinement using high-angle data (III).

Table 2. Fractional atomic coordinates and thermal parameters with estimated standard deviations (× 10^5) for non-hydrogen atoms. The temperature factor is given by exp $-(B_{11}h^2+B_{22}k^2+B_{33}l^2+B_{12}hk+B_{13}hl+B_{23}kl)$.

Atom	X	Y	Z	B_{11}	B_{22}	B_{33}	B_{12}	B_{13}	B_{33}
O1	96119(41)	12057(7)	60217(11)	7951(93)	316(3)	665(7)	587(30)	−1678(42)	41(8)
O2	32460(44)	41070(7)	32861(10)	9453(109)	267(3)	615(7)	576(28)	−1581(45)	0(7)
N1	61950(29)	18016(6)	42547(8)	4746(58)	243(3)	442(5)	14(21)	−344(26)	−6(6)
N2	44993(32)	25170(7)	35236(9)	5334(64)	257(3)	442(5)	80(22)	−517(28)	−5(6)
C3	48873(37)	33874(7)	39621(10)	5467(74)	257(3)	460(6)	187(25)	−411(33)	−22(7)
C4	69703(42)	36173(8)	51660(11)	6584(94)	273(4)	547(7)	163(28)	−872(41)	−108(8)
C5	85674(40)	28914(8)	58770(11)	5802(81)	308(4)	501(7)	197(29)	−886(37)	−100(8)
C6	82042(33)	19139(7)	54235(9)	4588(65)	285(4)	457(6)	120(25)	−448(29)	5(7)
C7	56059(49)	8467(8)	36957(14)	7653(109)	248(3)	669(9)	32(31)	−912(49)	−76(9)

Table 3. Fractional atomic coordinates ($\times 10^3$) and isotropic thermal parameters for hydrogen atoms. The e.s.d. is given in parentheses and are in the last digit of the corresponding parameter. H11, H12, and H13 are the three hydrogens in the methyl group.

Atom	x	y	z	B
H8	199(7)	391(2)	258(3)	4.7(5)
H9	715(7)	429(2)	543(2)	4.1(4)
H10	995(6)	297(2)	671(2)	3.5(4)
H11	728(8)	50(2)	397(3)	5.0(5)
H12	556(9)	86(3)	284(3)	6.3(7)
H13	379(11)	55(3)	403(4)	7.1(8)

Table 4. Deviations from a least-squares plane through the six ring atoms. Plane equation: $(-0.2085x - 0.0084y + 0.0426z)R - 0.221 = 0$.

Atom	Deviation (Å $\times 10^3$)	Atom	Deviation (Å $\times 10^3$)
N1	−9	C6	6
N2	5	C7	3
C3	2	O1	7
C4	−6	O2	31
C5	3		

bonds are in MMH 1.438 Å and 1.451 Å, respectively, while they in MDMH were found to be 1.430 Å and 1.460 Å. Also, the N2−C6 bond length is slightly shorter in MMH (1.368 Å) than in MDMH (1.374 Å), and a lengthening of the C6−O1 bond is found (1.254 Å in MMH, 1.245 Å in MDMH). This bond is similar to that in DCMH (1.257 Å), but significantly longer than the carbon-oxygen bond lengths of 1.236 Å and 1.241 Å found in 1,2-dimethyl-3,6-pyridazindione,[2] while the N1−C6 bond is of the same length as the nitrogen-carbon bonds in that molecule. The differences found in the pyridazine moieties of MDMH and MMH may be due to the oxygen-oxygen hydrogen bond which the latter is found to have (see Fig. 2).

However, significant differences are found between the MMH and the DCMH [1] molecules, indicating a much larger resonance stabilization of the latter. The N1−C6 bond is in DCMH only 1.345 Å, much shorter than in both MMH and MDMH. The C3−C4 and C4−C5 bonds

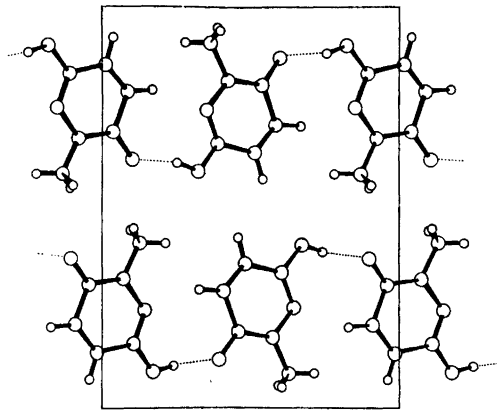

Fig. 2. The crystal structure as seen along the a-axis. Hydrogen bonds are indicated by dotted lines.

in DCMH are equal in length (1.451 Å), and the N1−N2 bond is significantly shorter than in MMH (1.353 Å in DCMH, 1.371 Å in MMH), while the C4−C5 bond is longer (1.362 Å in DCMH, 1.356 Å in both MMH and MDMH). These differences in the pyridazine moieties of the three molecules (DCMH, MMH and MDMH) imply that the N1−O1 hydrogen bond, which is found in DCMH, have a large effect on the resonance stabilization of these systems. This is also indicated by the large differences in molecular dimensions found for formamide [5,6] and acetamide [14–16] in the crystalline and gas state. The differences found between DCMH, MMH, and MDMH indicate that the O1−O2 hydrogen bond has only a small effect on the resonance stabilization of the pyridazine moiety.

The molecular arrangement in the crystal is visualized in Fig. 2, and may be described as layers perpendicular to (102). Within these layers the molecules are hydrogen bonded. The hydrogen bond length from O2 to O1, in position $(-1.0+x, 0.5-y, -0.5+z)$ is 2.616 Å.

Acknowledgement. The author thanks Professor K. Seff for the use of the X-ray diffraction equipment at the Chemistry Department, University of Hawaii.

REFERENCES

1. Ottersen, T. *Acta Chem. Scand. 27* (1973) 797.

2. Ottersen, T. *Acta Chem. Scand. 27* (1973) 835.
3. Ottersen, T. and Seff, K. *Acta Chem. Scand. 27* (1973) 2524.
4. Ottersen, T. *Acta Chem. Scand. A 28* (1974) 666.
5. Ladell, J. and Post, B. *Acta Crystallogr. 7* (1954) 559.
6. Costain, C. C. and Dowling, J. M. *J. Chem. Phys. 32* (1960) 158.
7. Eichenberger, K., Staehelin, A. and Druey, J. *Helv. Chim. Acta 37* (1954) 837.
8. Ottersen, T. *LP-73 comp. prog.*, Chem. Dept., University of Hawaii (1973).
9. Doyle, P. A. and Turner, P. S. *Acta Crystallogr. A 24* (1968) 390.
10. Stewart, R. F., Davidson, E. R. and Simpson, W. T. *J. Chem. Phys. 42* (1965) 3175.
11. Long, R. E. *Ph. D. Thesis*, University of California at Los Angeles (1965) Part III, pp. 87 – 126.
12. Karle, J. *Advan. Struct. Res. Diffr. Methods 1* (1964) 55.
13. Groth, P. *Acta Chem. Scand. 27* (1973) 1837.
14. Senti, F. and Harker, D. *J. Amer. Chem. Soc. 62* (1940) 2008.
15. Hamilton, W. C. *Acta Crystallogr. 18* (1965) 866.
16. Kitano, M. and Kuchitsu, K. *Bull. Chem. Soc. Jap. 46* (1973) 3048.

Received April 25, 1974.

Acta Chemica Scandinavica A 28 (1974) 666—670

The Structure of 1-Methyl-3-methoxy-6-pyridazon at —165 °C

T. OTTERSEN

Department of Pharmacy, University of Oslo, Oslo 3, Norway

The crystal structure of 1-methyl-3-methoxy-6-pyridazon has been determined by X-ray methods using 2402 reflections above background level collected by counter methods. The crystals are monoclinic, space group $P2_1/c$, with cell dimensions $a = 4.01_9$ Å; $b = 11.46_8$ Å; $c = 14.85_2$ Å; $\beta = 98.6_3°$ at −165 °C. Estimated standard deviations in bond lengths are about 0.002 Å and in angles 0.1°. Significant differences were found between the pyridazine moieties of the title compound and of 4,5-dichloro-3,6-pyridazindione. The dependence of the bond lengths on the lower sin θ/λ cutoff has been studied.

X-Ray crystallographic structure determinations of 1-methyl-3-methoxy-6-pyridazon,[1] MDMH, (I) and 4,5-dichloro-3,6-pyridazinedione,[2] DCMH, (II) indicated considerable differences in the ring systems of the two molecules. DCMH was found to have a large contribution from the aromatic resonance structure

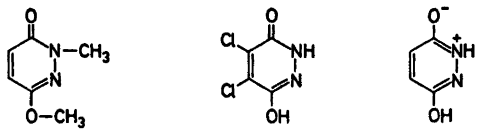

I MDMH II DCMH III

III. This was probably furthered by the formation of intermolecular hydrogen bonds from the nitrogen and the hydroxyl-oxygen to the carbonyl-oxygen. On the other hand the bond lengths of MDMH imply only a small contribution from a resonance structure similar to III.

The estimated standard deviations in the molecular dimensions found in the earlier determination of MDMH were rather large (about 0.007 Å in bond lengths), and in order to obtain sufficient observations for refinement with high-angle data, the lower sin θ/λ limit was set at 0.4 Å^{-1}. It was therefore decided to repeat the structure determination to obtain a more accurate structure. It was further hoped that a new dataset would give the opportunity to study the dependence of the observed nitrogen-nitrogen bond length on the lower sin θ/λ cutoff for the data used in least squares refinement.

EXPERIMENTAL

A Syntex-P$\bar{1}$ computer controlled diffractometer with graphite-monochromatized Mo$K\alpha$ radiation ($K\alpha_1$, $\lambda = 0.70926$ Å; $K\alpha_2$, $\lambda = 0.71354$ Å) and a pulse-height analyzer was used for preliminary experiments and for the measurement of diffraction intensities. The diffractometer was equipped with an Enraf-Nonius liquid nitrogen cooling device (modified by H. Hope). Cell constants and their standard deviations were determined by a least-squares treatment of the angular coordinates of fifteen independent reflections with 2θ-values from 11 to 25°. The temperature at crystal site was −165 °C. The work was carried out using a crystal of dimensions $0.4 \times 0.25 \times 0.25$ mm.

Three-dimensional intensity data were recorded utilizing the $\omega - 2\theta$ scanning mode with scan speed varying from 2 to 24° min^{-1}. The scan range was from 1.0° below the $K\alpha_1$-peak to 1.0° above the $K\alpha_2$-peak. Background was measured for half the scan-time at each end of the scan-range. Reflections with 2θ-values higher than 45°, which had integrated counts of less than 7, determined in a $2s$ scan over the peak, were not measured. The variations in the intensities of three standard reflections, which were remeasured after every 50 reflections, were random and less than three times their estimated standard deviations. Accordingly no correction for these variations was applied to the intensity data.

Standard deviations were assigned to the reflections according to the formula,

$$\sigma(I) = [s^2(CT + B_1 + B_2) + (pI)^2]^{\frac{1}{2}}$$

where s is the scan speed, CT is the integrated count, B_1 and B_2 are the background counts, and the intensity is $I = s(CT - B_1 - B_2)$. A value

of 0.02 was assigned to the empirical parameter p to account for experimental uncertainties. Out of the 3358 unique reflections measured ($2\theta_{max} = 90°$), 2402 had intensities larger than twice their standard deviations, the remainder being excluded from further calculations.

The intensities were corrected for Lorentz and polarization effects. This program together with those employed for all the subsequent calculations, is part of an assembly of programs for CYBER-74 computer, which is described in Ref. 3.

Atomic form factors used were those of Doyle and Turner [4] for oxygen, nitrogen, and carbon, and of Stewart *et al.*[5] for hydrogen. Core and valence electron scattering factors utilized for carbon, nitrogen, and oxygen are those given by Stewart (Tables I and III in Ref. 6).

CRYSTAL DATA

1-Methyl-3-methoxy-6-pyridazon, $C_6H_8N_2O_2$, monoclinic, space group $P2_1/c$. $a = 4.019$ (0.001) Å [4.074 (0.002)], $b = 11.468$ (0.004) Å [11.541 (0.006)], $c = 14.852$ (0.005) Å [14.971 (0.007)], $\beta = 98.63°$ (0.03°) [97.33 (0.04)].* Results from the earlier investigation [1] are given in brackets. Figures in parentheses are estimated standard deviations. $V = 676.8$ Å^3; $M = 140.1$ amu; $Z = 4$; $D_{calc} = 1.375$ g/cm^3; $F(000) = 296$.

* This value was erroneously given in Ref. 1.

REFINEMENT PROCEDURE

The structure model [1] was refined with anisotropic thermal parameters for all nonhydrogen atoms to a conventional R factor of 0.08 and a weighted R_w of 0.11, using the 1382 structure factors with $\sin\theta/\lambda < 0.7$. Attempts to locate the hydrogen atoms in a difference Fourier synthesis were not successful. Their positions were therefore calculated, one hydrogen in each methyl group was assumed to be *anti* to C3 and C6, respectively (see Fig. 1 for the numbering of the atoms). These atoms were included in the least-squares refinement with isotropic thermal parameters.

Results from the full-matrix least-squares refinements using various parts of the data set, are summarized in Table 1 (I–VIII). Standard deviations in molecular dimensions were calculated from the correlation matrix ignoring standard deviations in cell dimensions.

Errors in parameters connected with the asphericity of the electron density have been discussed.[2,7–11] The contribution from valence-electrons to the atomic form factors at $\sin\theta/\lambda$-values > 0.6 Å^{-1} is very small,[12] and it may be assumed that the core-electrons do not participate in the bonding.[11] For most of the bond lengths in the present structure differences in the results obtained with low- and high-angle

Table 1. Results from the least-squares refinements. $R_w = |\sum w(F_o| - |F_c|)^2/\sum wF_o^2|^{\frac{1}{2}}$, $R = (\sum|F_o| - |F_c||)/\sum F_o$, R_1 is for the observations used in the refinement, R_t is for the total number of observations. G is the "goodness-of-fit": $(|\sum w(F_o - |F_c|)^2|/(m-s))^{\frac{1}{2}}$, where m is the number of observations and s is the number of parameters refined. The e.s.d. given is the average estimated standard deviation in nonhydrogen bond lengths. Only those reflections which had $\sin\theta/\lambda$-values less than or larger than (as indicated) the figure given in the first column were used in the refinement. The e.s.d. of the scale factor is in the last digit and is given in parentheses.

No.	$\sin\theta/\lambda$ (Å^{-1})	Number of observations	R_w	R_1	R_t	G	Scale	Bond lengths (Å) N1–N2	C4–C5	E.s.d. (Å × 10^4)
I[a]	<0.7	1382	.044	.042	.062	1.92	.170(2)	1.374	1.341	18
II[b]	All data	2402	.051	.055	—	1.73	.172(2)	1.372	1.343	15
III[b]	>0.4	2071	.049	.057	.059	1.40	.180(3)	1.370	1.350	15
IV[b]	>0.5	1793	.053	.062	.060	1.28	.182(4)	1.370	1.353	16
V[b]	>0.55	1613	.054	.064	.057	1.21	.178(5)	1.368	1.355	17
VI[b]	>0.6	1427	.055	.065	.056	1.17	.173(7)	1.365	1.354	19
VII[b]	>0.7	1020	.063	.073	.059	1.17	.169(13)	1.363	1.353	30
VIII[b]	>0.75	802	.071	.079	.068	1.20	.183(20)	1.362	1.350	43

[a] All positional and thermal parameters refined. [b] All positional and thermal parameters refined for non-hydrogen atoms.

Table 2. Fractional atomic coordinates and thermal parameters ($\times 10^5$) for nonhydrogen atoms. The estimated standard deviations are in parentheses and are in the last digit given for the corresponding parameter. Results from refinement VI are given on the first line, while the second line is results from refinement II. The temperature factor is given by exp $-(B_{11}h^2+B_{22}k^2+B_{33}l^2+B_{12}hk+B_{13}hl+B_{23}kl)$.

Atom	x	y	z	B_{11}	B_{22}	B_{33}	B_{33}	B_{12}	B_{23}
O1	2121(49)	17377(13)	48981(10)	4340(93)	310(7)	172(4)	−409(43)	929(32)	−22(9)
	2056(25)	17354(8)	48944(6)	4341(69)	324(6)	174(4)	−374(35)	909(25)	−38(8)
O2	61179(50)	11461(11)	19417(10)	4455(96)	239(7)	186(4)	127(35)	991(34)	30(8)
	61058(24)	11448(8)	19407(6)	4519(72)	245(6)	182(4)	124(31)	1009(26)	51(7)
N1	24982(42)	24605(11)	37045(9)	2832(72)	189(6)	153(4)	−1(32)	570(27)	8(8)
	24855(26)	24599(8)	37050(7)	2938(66)	203(6)	153(4)	−29(32)	549(25)	−5(8)
N2	39875(40)	23670(12)	29397(9)	2650(77)	216(6)	144(4)	13(33)	475(28)	17(7)
	39882(26)	23699(9)	29369(6)	2753(67)	248(6)	140(4)	−35(32)	483(25)	15(8)
C3	46836(48)	13192(13)	26940(11)	2999(84)	207(7)	146(4)	44(38)	546(31)	28(9)
	46734(32)	13202(11)	26973(8)	2761(73)	253(7)	140(4)	−38(39)	434(28)	32(9)
C4	40327(50)	2857(13)	31750(11)	3176(96)	215(7)	176(5)	−37(39)	522(34)	40(9)
	40231(33)	2884(10)	31784(8)	3242(86)	195(7)	177(5)	10(38)	444(31)	27(10)
C5	25463(48)	3971(13)	39304(10)	3074(91)	224(7)	155(5)	−123(39)	440(33)	35(9)
	25494(33)	4009(11)	39273(8)	3238(84)	225(7)	160(5)	−229(38)	418(32)	43(9)
C6	16544(49)	15522(12)	42276(10)	2827(86)	232(7)	136(4)	−163(37)	430(29)	16(9)
	16499(33)	15501(10)	42266(8)	2709(76)	250(7)	137(4)	−244(37)	292(28)	27(9)
C7	16707(57)	36445(14)	39490(13)	3923(107)	224(7)	229(6)	−21(44)	830(41)	−19(10)
	16633(36)	36477(11)	39475(9)	4295(94)	215(7)	238(5)	−25(44)	913(37)	−16(10)
C8	67345(54)	21548(15)	14163(12)	3410(93)	325(8)	167(5)	5(45)	615(32)	105(10)
	67278(36)	21586(11)	14159(8)	3809(85)	310(8)	174(5)	14(44)	715(31)	119(10)

Table 3. Fractional atomic coordinates ($\times 10^3$) and isotropic thermal parameters for hydrogen atoms. The estimated standard deviations are in the last digit of the corresponding parameter and are given in parentheses.

Atom	x	y	z	B
H4	468(4)	−42(2)	294(1)	1.6(3)
H5	192(5)	−23(2)	426(1)	2.5(4)
H71	253(5)	417(2)	355(1)	3.8(5)
H72	256(6)	382(2)	457(2)	4.9(5)
H73	−81(6)	373(2)	393(1)	4.7(5)
H81	783(4)	184(2)	93(1)	1.7(3)
H82	833(4)	270(1)	178(1)	1.9(4)
H83	463(4)	256(1)	118(1)	1.6(3)

data refinements are small, and of the same order as the standard deviations. However, the N1 – N2 and the C4 – C5 bonds are significantly altered (see Table 1). This has been noted earlier.[1,2] The C4 – C5 double bond is not changed significantly when structure factors with sin θ/λ-values down to 0.5 Å^{-1} are included in the refinement, while the nitrogen-nitrogen bond seems to be affected up to a sin θ/λ-value of 0.7 Å^{-1}. The standard deviations rise sharply between refinement VI (structure factors > 0.6 Å^{-1}) and refinement VII (structure factors > 0.7 Å^{-1}), it is doubtful that the differences in molecular dimensions in these two refinements have any physical meaning. Parameters obtained from refinement VI will therefore be used in the discussion. A listing of structure amplitudes is available from the author upon request. Final parameters obtained in refinement VI and II are listed in Table 2, parameters for hydrogen atoms (from refinement I) are in Table 3.

Only small changes are found in thermal parameters obtained from the different high-angle data refinements (III – VIII), while those from refinement I and II are larger. The total discrepancy, Δ, between the atomic vibration tensor components and those calculated from the rigid-body parameters found by analysis of the librational, translational, and screw motion of the molecules is 0.0017 Å^2 for the low-angle data refinement (I), 0.0011 Å^2 for refinement II, and 0.0009 Å^2 for the high-angle data refinements (III – VI), while refinement VII and VIII yielded 0.0010 Å^2. The difference between the results obtained in refinement I and VI may indicate a tendency of the thermal parameters

to reflect some of the asphericity of the valence electrons.

The thermal motion analysis based on the parameters from refinement VI showed rather large discrepancies for C8 and yielded one slightly negative libration axis. It was therefore decided to exclude C8 from the analyses. The total discrepancy, Δ, is 0.0006 Å^2, and the atomic positions were corrected for the librational motion. The eigenvalues of **T** are 0.14, 0.12, and 0.11 Å^2. The r.m.s. librational amplitudes are 3.1, 2.3, and 1.5° with the direction of the major axis nearly parallel to the C6–N1 bond.

In order to study the valence electron distribution in the MDMH and DCMH [2] molecules, *L*-shell [6] and extended *L*-shell refinements [13] were carried out. Differences found between corresponding atoms in the two symmetry-independent DCMH molecules were large and of the same order as the differences between the MDMH and DCMH molecules.

DISCUSSION

Bond lengths and bond angles are listed in Fig. 1, where the numbering of the atoms is indicated. Only the C3–N2 and C6–O1 bond lengths deviate significantly from those found earlier.[1] This may be due to errors in the data collected at room temperature.

The heterocycle is planar, the atoms being displaced from a least-squares plane through the six ring atoms by less than 0.01 Å (see Table 4), and the bond lengths indicate a resonance stabilization of the molecule. The

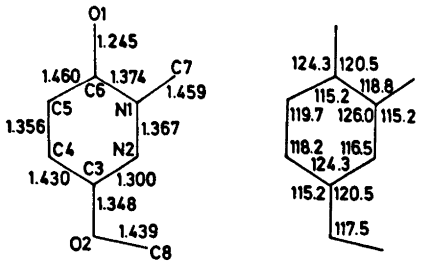

Fig. 1. Bond lengths (Å) (corrected for thermal vibration effects) and bond angles (°). The estimated standard deviations in bond lengths are 0.002 Å and in angles 0.1°. Structure model obtained from the refinement using high-angle data (VI).

Table 4. Deviations (Å) from a least-squares plane through the six ring atoms. Plane eqn.: $(0.2263\,X + 0.0000\,Y + 0.0383\,Z)\cdot R - 3.391 = 0$.

Atom	Deviation	Atom	Deviation
N1	.006	O1	−.043
N2	.002	O2	−.028
C3	−.008	C7	−.018
C4	.004	C8	−.082
C5	.004	H4	.009
C6	−.010	H5	−.038

N1–N2 bond of 1.367 Å is considerably shorter and the C4–C5 double bond of 1.356 Å considerably longer than the corresponding bond lengths (1.406 Å and 1.337 Å, respectively) found in 1,2-dimethyl-3,6-pyridazindione.[14] Also, the C3–N2 double bond of 1.300 Å is significantly longer than the pure C–N double bond length of 1.278 Å.[15]

However, difference in molecular dimensions found for DCMH [2] and the present structure are significant. The N1–C6 bond of 1.374 Å, which is equal to the N–C bond found in the microwave investigation of formamide,[16] was 1.345 Å in DCMH. The bond lengths C5–C6, C6–N1, N1–C1, and C6–O1 are of the same order as those found in 1,2-dimethyl-3,6-pyridazindione,[14] which is a nonplanar molecule. The C3–C4 bond, on the other hand, is short in comparison with that in DCMH (1.430 Å in the present structure and 1.450 Å in DCMH). Other bond lengths also imply a larger resonance stabilization of DCMH than of MDMH. This may indicate that hydrogen bonds, which in DCMH involve N1 and both oxygen atoms, are important in the resonance stabilization of these and similar compounds. The hydrogen bonds in DCMH may imply a structure intermediate between the monolactim and the dilactim. Large difference are also found in the bond lengths of formamide in the non-hydrogen-bonded [16] and hydrogenbonded [17] case. However, corresponding C–N and C–O bond lengths of 1.374 Å and 1.235 Å, respectively, were found in 1,2,3-benzotriazin-4(3*H*)-one,[18] which has an N–H···O hydrogen bond. These bond lengths are similar to those found in 1,2-dimethyl-3,6-pyridazindione,[14] and may imply that the hydrogen bond has little, if any, effect on the resonance stabilization.

REFERENCES

1. Ottersen, T. and Seff, K. *Acta Chem. Scand. 27* (1973) 2524.
2. Ottersen, T. *Acta Chem. Scand. 27* (1973) 797.
3. Groth, P. *Acta Chem. Scand. 27* (1973) 1887.
4. Doyle, P. A. and Turner, P. S. *Acta Crystallogr. A 24* (1968) 390.
5. Stewart, R. F., Davidson, E. R. and Simpson, W. T. *J. Chem. Phys. 42* (1965) 3175.
6. Stewart, R. F. *J. Chem. Phys. 53* (1970) 205.
7. Dawson, B. *Acta Crystallogr. 17* (1964) 990.
8. Coppens, P. and Coulson, C. A. *Acta Crystallogr. 23* (1967) 718.
9. Stevens, E. D. and Hope, H. *Abstract Amer. Cryst. Assoc. Summer Meeting*, 1971.
10. Coppens, P. *Acta Crystallogr. A 25* (1969) 180.
11. Groenewegen, P. P. M., Zeevalkink, J. and Feil, D. *Acta Crystallogr. A 27* (1971) 487.
12. Stewart, R. F. *J. Chem. Phys. 48* (1968) 4882.
13. Coppens, P., Pautler, D. and Griffin, J. F. *J. Amer. Chem. Soc. 93* (1971) 1051.
14. Ottersen, T. *Acta Chem. Scand. 27* (1973) 835.
15. Fischer-Hjalmars, I. and Sundbom, M. *Acta Chem. Scand. 22* (1968) 2237.
16. Costain, C. C. and Dowling, J. M. *J. Chem. Phys. 32* (1960) 158.
17. Ladell, J. and Post, B. *Acta Crystallogr. 7* (1954) 559.
18. Hjortås, J. *Acta Crystallogr. B 29* (1973) 1916.

Received February 25, 1974.

Acta Chemica Scandinavica A 28 (1974) 671—674

An Electron Diffraction Investigation of 2,2,6,6-Tetramethyl-4-piperidone-1-hydroxyl

PER ANDERSEN,[a] E. E. ASTRUP,[a] P. S. FREDERICHSEN[a] and K. F. NAKKEN[b,*]

[a] Department of Chemistry, University of Oslo, Oslo 3, Norway and [b] Norsk Hydro's Institute for Cancer Research, Montebello, Oslo 3, Norway

The molecular structure of 2,2,6,6-tetramethyl-4-piperidone-1-hydroxyl has been determined in the gas phase by electron diffraction. The molecule has a chair conformation which is considerably distorted. The N – O bond is in an equatorial position and the bond length is 1.46 Å. The dihedral angles in the ring are: N – C(2) – C(3) – C(4) = 53°, C(2) – C(3) – C(4) – C(5) = 66°, and C(5) – C(6) – N – C(2) = 47°. The molecular C, N, O skeleton has a plane of symmetry through the nitrogen and C(4) carbon atom.

At the present time organic nitroxyl free radicals are of great interest in radiobiology due to their ability to sensitize bacteria and mammalian cells to ionizing radiation when present during irradiation in absence of oxygen.[1] It has been demonstrated that these compounds may exert their effect, as other oxygen mimics, through interaction with DNA radicals, giving either rise to covalent binding [2–4] or to red-ox reactions with such DNA radicals.[5]

In the present paper the structure of 2,2,6,6-tetramethyl-4-piperidone-1-hydroxyl (TAN-H) has been studied by the electron diffraction method in order to get insight into the possible sterical configuration of the TAN-DNA complexes, in which TAN mainly is bound through its 1-oxyl group to the 5 (or 6) position of the pyrimidin bases within DNA.[6]

For the subsequent structure determination of the organic nitroxyl free radical 2,2,6,6-tetramethyl-4-piperidone-1-oxyl (TAN) it will be of great importance to know the structure of its reduction product TAN-H. The difference in the two structures could be expected to be mainly associated with the difference between the $>N-O\cdot$ and the $>N-O-H$ arrangement.

EXPERIMENTAL

2,2,6,6-Tetramethyl-4-piperidone-1-hydroxyl (TAN-H) was obtained by reduction of 2,2,6,6-tetramethyl-4-piperidone-1-oxyl (TAN) with hydrogen in absolute alcohol, with platinum as a catalyst. The product could be recrystallized as TAN-H.HCl from absolute alcohol – ether – HCl (dry) (m.p. 179 °C). Since TAN-H is easily autoxidized in presence of O_2, it was found necessary to synthesize this compound immediately before use. When the theoretical amount of H_2 had reacted with TAN, the reaction was interrupted, the solution rapidly filtered in N_2-atm., and the solvent removed by evaporation in vacuum at room temperature. The residuum was dissolved in alcohol and once more evaporated in vacuum to dryness. The compound was kept at low temperature in vacuum until used for the diffraction experiment. In various runs TAN-H was formed in nearly quantitative yield. A recrystallized sample of TAN-H.HCl had a $pK_1 = 4.2$.

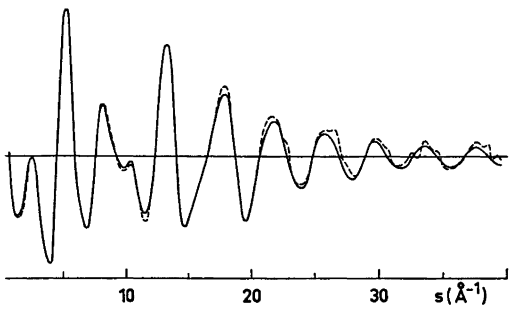

Fig. 1. 2,2,6,6-Tetramethyl-4-piperidone-1-hydroxyl (TAN-H). Calculated (solid line) and experimental (dotted line) molecular intensity curve.

* Present address: Radiotherapy and Isotope Department, Ullevål Hospital, Oslo, Norway.

The diffraction data were recorded on photographic plates at two nozzle-plate distances of 202 mm and 481 mm. The electron wave length was 0.06454 Å and the temperature of the nozzle 120 °C. The microphotometer curves of four long-distance plates covering an s range from 1.375 Å^{-1} to 19.25 Å^{-1} and five short-distance plates covering an s range from 7.00 Å^{-1} to 42.75 Å^{-1} were used. The resulting modified molecular intensity curve has an s range from 1.625 Å^{-1} to 39.75 Å^{-1} and is reproduced in Fig. 1. All calculations were carried out using the programs available in Oslo.[9]

STRUCTURE ANALYSIS

Of the 29 atoms in TAN-H 17 are hydrogen atoms which are difficult to detect. The carbon, oxygen, and nitrogen skeleton of the molecule was initially assumed to have a plane of symmetry through O(7), N(1), C(4), and O(8) (Fig. 2). The experimental radial distribution (RD) curve is reproduced in Fig. 3 and the starting parameters for the bond distances could

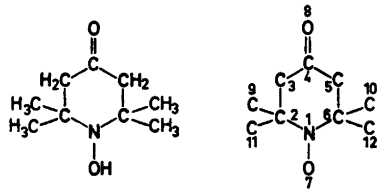

Fig. 2. 2,2,6,6-Tetramethyl-4-piperidone-1-hydroxyl (TAN-H) and the numbering system of the carbon, nitrogen, and oxygen atoms.

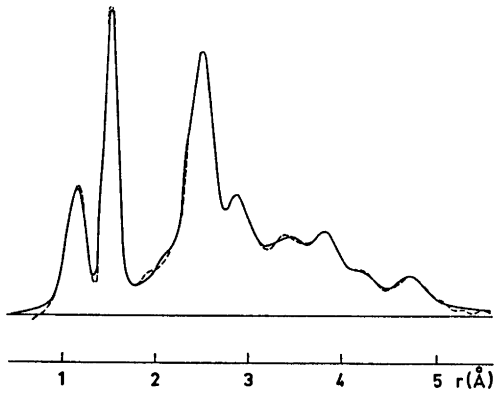

Fig. 3. 2,2,6,6-Tetramethyl-4-piperidone-1-hydroxyl (TAN-H). Calculated (solid line) and experimental (dotted line) radial distribution curve. Artificial damping constant $k = 0.0009$ Å.

be deduced from the two first peaks on the RD curve. The part of the curve outside 2 Å contains information about the longer distances, which also determine the conformation. A preliminary analysis of the RD curve indicated that the assumed chair form of the ring could be present. However, one could not neglect to investigate the possibility of a twisted boat conformation of the ring.

The crystal structure of cyclohexane-1,4-dione [10] shows that a twisted boat form is preferred in the crystalline state, and Rozantsev [8] has proposed on basis of measured and calculated dipole moments of TAN that this molecule should have a twisted boat conformation. Crystal structure determinations of similar molecules [11–13] show that the chair conformation is present in the solid state. That these molecules should have another conformation in the gas phase is possible but probably not likely. In the case of TAN-H the two CH_3 groups in the axial positions on the C(2) and C(6) atoms would come too close together if an ideal sixmembered ring with a chair conformation is present, and considerable deviations in the ring and methyl group positions could be expected.

Preliminary sets of molecular parameters assuming both a chair and a twisted boat conformation, were derived from the RD curve. Independent successive refinements of the parameters of the two forms using the least squares procedure, showed that only the chair conformation parameters could be successfully refined. The experimental and calculated RD curves and the difference between the two is shown in Fig. 3 and the experimental and calculated molecular intensity curves in Fig. 1. The molecular parameters used in calculating the curves are those which gave the best fit of the intensity curves without having unacceptable interatomic distances.

RESULTS AND DISCUSSION

The final molecular parameters, the corresponding u-values (vibrational amplitudes), and standard deviations are listed in Table 1. The numbering of atoms is shown in Fig. 2. All bond lengths and angles are reasonable except for the C(2)–C(3) bond which is 1.56 Å. Similar lengthening of this type of bond has been found in other structures. In, for instance, cyclo-

Table 1. Structure parameters for 2,2,6,6-tetramethyl-4-piperidone-1-hydroxyl (TAN-H) obtained by least squares refinement on the intensity data. Distances (r_a-values) and mean amplitudes of vibration (u-values) are given in Å, angles in degrees. The standard deviations given in parentheses have been corrected to take into account data correlation. The uncertainty arising from error in the electron wave length is included. (For numbering system of the atoms see Fig. 2).

Distances	r	u
N(1)–O(7)	1.465 (18)	0.046
N(1)–C(2)	1.500 (20)	0.048
C(2)–C(3)	1.560 (38)	0.047
C(3)–C(4)	1.510 (39)	0.047
C(4)–O(8)	1.212 (9)	0.036
C(2)–C(9)	1.530 (20)	0.050
C(2)–C(11)	1.530 (20)	0.050
C–H	1.108 (7)	0.070
Angles	deg.	
C(2)–N(1)–C(6)	118 (3.5)	
C(2)–N(1)–O(7)	114 (1.8)	
N(1)–C(2)–C(3)	111 (1.8)	
C(3)–C(2)–C(9)	103 (1.8)	
C(3)–C(2)–C(11)	107 (1.8)	
C(2)–C(3)–C(4)	106 (1.8)	
C(3)–C(4)–C(5)	113 (1.8)	
C(3)–C(4)–O(8)	122 (1.7)	
N(1)–C(2)–C(9)	117 (1.8)	
N(1)–C(2)–C(11)	104 (1.9)	
C(2)–C(9)–H	107 (1.8)	

hexane-1,4-dione [10] is the corresponding bond 1.56 Å. In the ring the angle at the nitrogen atom is 118° whereas the angle at C(4) is 113°, this makes the C(3)···C(5) distance 2.52 Å and the C(2)···C(6) distance 2.57 Å. This is a favourable increase for the methyl groups in axial positions on C(2) and C(6), in addition are these methyl groups bent out to make the C(9)··· C(10) distance 3.35 Å. The dihedral angles in a regular sixmembered ring should be 60°, the following angles have been found in this ring: C(5)–C(6)–N–C(2) = 47°, N–C(2)–C(3)–C(4) = 53°, C(2)–C(3)–C(4)–C(5) = 66°. An INDO closed shell calculation gave a dipole moment of 2.87 D while the measured value is 2.86 D.

In model experiments it has been found that radiation induced binding of TAN to deoxynucleotides takes place at the 5–6 position of the pyrimidin nucleus.[5,6] The data indicate that nearly all radiation-induced radicals located in the 5–6 position of the thymine residue bind TAN covalently, and that a high fraction of radicals located in the 5–6 position of cytosine induced by OH bind TAN.

The very high yield of binding of TAN to thymine radicals is surprising in view of the sterical hindrance around the organic nitroxyl radical and the presence of the methyl group in 5-position of thymine. It has been calculated that the free valence of the pyrimidine nucleotides to a large extent is located at the 6-position and that thus OH may add to position 6 of the pyrimidine nucleus.[7] The resulting nucleotide radicals may exist in at least two stereoisomers. The 5-methyl group of the thymine radicals may cause less sterical hindrance than in the parent residue.

In TAN approximately 70 % of the free electrons are located on the oxygen atom of the nitroxyl group.[8] On a model of double stranded DNA it can be shown that TAN, with a conformation as in TAN-H, may be bound through its nitroxyl oxygen atom to the 5 or 6 position of the pyrimidines being located in the minor groove of the double helix without sterical hindrance from neighbouring groups in DNA.

Acknowledgement. The authors are grateful to Dr. A. Almenningen for doing the electron diffraction experiment.

REFERENCES

1. Emmerson, P. T. and Howard-Flanders, P. *Nature (London) 204* (1964) 1005.
2. Nakken, K. F., Sikkeland, T. and Brustad, T. *FEBS Lett. 8* (1970) 33.
3. Nakken, K. F. and Pihl, A. In Teply, J., Ed., *International Discussion on Progress and Problems in Contemporary Radiation Chemistry*, Prague 1971, p. 678.
4. Brustad, T., Jones, W. B. G. and Nakken, K. F. *Int. J. Radiat. Phys. Chem. 3* (1971) 55.
5. Nakken, K. F., Tomas, E. and Brustad, T. *Ninth Annu. Meeting of the European Society for Radiation Biology, Book of Abstr.* (1972) 122.
6. Nakken, K. F., Tomas, E. and Brustad, T. *I. A. E. A. Panel on Modification of Radiosensitivity in Biological Systems*, Stockholm June 1973. *To be published.*
7. Nofre, C. and Cier, A. In Pullman, B., Ed., *Electronic Aspects of Biochemistry*, Academic, New York 1964.

8. Rozantsev, E. G. In Ulrich, H., Ed., *Free Nitroxyl Radicals*, Plenum, New York 1970.
9. Andersen, B., Seip, H. M., Strand, T. G. and Stølevik, R. *Acta Chem. Scand. 23* (1969) 3224.
10. Groth, P. *Acta Chem. Scand. 18* (1964) 923.
11. Lajzerowicz-Bonneteau, P. J. *Acta Crystallogr. B 24* (1968) 196.
12. Berliner, L. J. *Acta Crystallogr. B 26* (1970) 1198.
13. Hawley, D. M., Ferguson, G. and Robertson, J. M. *J. Chem. Soc. B* (1968) 1255.

Received October 17, 1973.

Acta Chemica Scandinavica A 28 (1974) 675—679

The Molecular Structure of 2,2,6,6-Tetramethyl-4-piperidone-1-oxyl Free Radical Determined by Electron Diffraction in the Gas Phase

PER ANDERSEN,[a] E. E. ASTRUP,[a] P. S. FREDERICHSEN[a] and K. F. NAKKEN[b,*]

[a]Department of Chemistry, University of Oslo, Oslo 3, Norway and [b]Norsk Hydro's Institute for Cancer Research, Montebello, Oslo 3, Norway

The structure determination of 2,2,6,6-tetramethyl-4-piperidone-1-oxyl free radical has been carried out in the gas phase using the electron diffraction method. The N – O bond length has been found to be 1.247 (11) Å and the angle of this bond with the C(2) – N – C(6) plane is 14°. All bond lengths and angles have acceptable values, only the C(2) – C(3) bond (Fig. 2) of 1.570 (36) Å is longer than what is usually found. The ring has a chair conformation. Attempts to refine a twisted boat conformation resulted in unacceptable non-bonded distances.

2,2,6,6-Tetramethyl-4-piperidone-1-oxyl (TAN) is a stable free radical of relatively low toxicity, high solubility, and strong radiosensitizing effect in a number of biological systems.[1,2] Organic nitroxyl free radicals may be stabilized by a low ground state energy of the three-electron bond and by sterical hindrance of the nitroxyl group from alkyl substituents in the α positions.[3] Such sterical hindrance may affect the radiosensitizing effect of the different nitroxyl free radicals when these are used in low molar concentration.[2]

TAN has previously been shown to interact with approximately 50 % of radiation induced DNA radicals through covalent binding [4,5] or through red-ox reactions.[5] Due to low reactivity or sterical hindrance or both, a significant fraction of DNA radicals are unable to interact with TAN.

The advantage of having solved the structure of 2,2,6,6-tetramethyl-4-piperidone-1-hydroxyl (TAN-H) [6] using the electron diffraction method in the gas phase has been utilized in the structure determination of TAN. By comparing the radial distribution (RD) curves and interpreting the difference between the two curves, which on beforehand was assumed mainly to be associated with the difference between the two groups >N–O–H and >N–O·, one could more easily arrive at reliable molecular parameters. A number of structure determinations of different nitroxyl radicals [7–15] have been carried out using X-ray crystallographic and electron diffraction methods. There is still some doubt as to the planarity of the >N–O· group and we felt that the structure determination in the gas phase could be of some value while the molecules are removed from the effect of their surroundings in the crystal. The comparison of TAN with TAN-H should make it possible to get a good estimate of the N – O bond angle with the >N plane.

EXPERIMENTAL

2,2,6,6-Tetramethyl-4-piperidone-1-oxyl (TAN) was synthesized from 2,2,6,6-tetramethyl-4-piperidone-HCl (Fluka AG) according to published procedures [3,8] with some minor modifications. The sample, after recrystallization from light petroleum, had a m.p. of 36.7 °C.

The intensity of the scattered electrons were recovered on photographic plates in the usual

* Present address: Radiotherapy and Isotope Department, Ullevål Hospital, Oslo, Norway

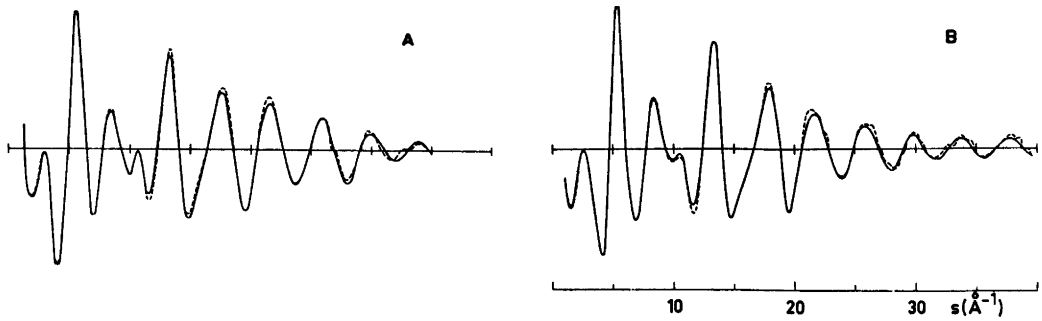

Fig. 1. Calculated (solid line) and experimental (dotted line) molecular intensity curves. A: 2,2,6,6-tetramethyl-4-piperidone-1-oxyl (TAN), B: 2,2,6,6-tetramethyl-4-piperidone-1-hydroxyl (TAN-H).

way at two nozzle-plate distances. One set of six plates at 480 mm and a nozzle temperature of 125 °C and a second set of eight plates at 200 mm and a nozzle temperature of 125 °C were used. The electron wave length was for both sets 0.06457 Å. The first set covered an s range of 1.625 – 19.875 Å^{-1} and the second an s range of 7.50 – 43.00 Å^{-1}. The total modified molecular intensity curve is reproduced in Fig. 1 and extends over an s range from 1.625 Å^{-1} to 35.00 Å^{-1}.

The RD curve of TAN was compared with the RD curve of TAN-H and analyzed to determine approximate molecular parameters for the structure. The parameters were refined by a least squares method in the usual way. The computer programs available in Oslo [17] were used throughout this investigation.

STRUCTURE ANALYSIS

It was initially assumed that TAN and TAN-H would both have a chair conformation and that there should be a plane of symmetry through N and C(4) (Fig. 2). In Fig. 1 are shown the molecular intensity curves of TAN and TAN-H and in Fig. 3 are shown the RD curves of the two compounds. The curves showed that not only the parameters for the free radical part of the molecule had to be changed but also other molecular parameters

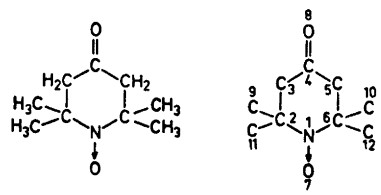

Fig. 2. 2,2,6,6-Tetramethyl-4-piperidone-1-oxyl (TAN) and the numbering system of the carbon, nitrogen and oxygen atoms.

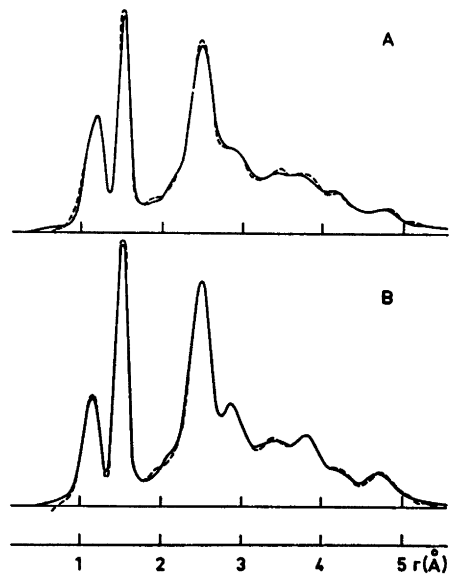

Fig. 3. Calculated (solid line) and experimental (dotted line) radial distribution curves. A: 2,2,6,6-tetramethyl-4-piperidone-1-oxyl (TAN), B: 2,2,6,6-tetramethyl-4-piperidone-1-hydroxyl (TAN-H). Artificial damping constant k = 0.0009 Å.

had to be modified somewhat. However, it could be shown that a chair conformation could be present according to the experimental RD curve.

Rozantsev [3] has proposed that TAN should have a twisted boat conformation. His assumption is based on calculated values of the dipole moment. There are also other indications that TAN could have this form. A recent crystal structure investigation of TAN by Shibaeva and coworkers in the U.S.S.R.[15] shows that

TAN has a twisted boat conformation with a 180° angle between the N–O and C=O directions. The structure is refined to an R value of 0.13 and the parameters should probably be further refined to obtain more accurate bond distances and angles. A crystal structure determination of cyclohexane-1,4-dione [18] showed that this molecule had a twisted boat conformation. TAN is probably more analogous to cyclohexane-1,4-dione than TAN-H because of the sp^2 hybridized atoms in 1,4 positions. It was therefore also assumed that TAN should have this conformation, and the bond lengths mentioned above and the angles from cyclohexane-1,4-dione were used as starting parameters. There were indications that calculated RD curves of both conformations had a shape fairly similar to the experimental RD curve.

Least squares refinements on the chair form proceeded satisfactorily while the refinements on the twisted boat always resulted in unacceptable non-bonded interatomic distances. No matter what was tried, some interatomic distances would always come out too short.

Calculated and experimental molecular intensity curves are reproduced in Fig. 1. A comparison of the experimental and calculated RD curves is shown in Fig. 3.

Table 1. Structure parameters for 2,2,6,6-tetramethyl-4-piperidone-1-oxyl (TAN) obtained by least squares refinement on the intensity data. Distances (r_a-values) and mean amplitudes of vibration (u-values) are given in Å, angles in degrees. The standard deviations given in parentheses have been corrected to take into account data correlation. The uncertainty arising from error in the electron wave length is included. (For numbering system of the atoms see Fig. 2).

Distances	r	u
N(1)–O(7)	1.247 (11)	0.045
N(1)–C(2)	1.500 (20)	0.044
C(2)–C(3)	1.570 (36)	0.047
C(3)–C(4)	1.500 (38)	0.046
C(4)–O(8)	1.204 (11)	0.037
C(2)–C(9)	1.520 (20)	0.048
C(2)–C(11)	1.520 (20)	0.048
C–H	1.094 (9)	0.068
Angles	deg.	
C(2)–N(1)–C(6)	110 (5.3)	
C(2)–N(1)–O(7)	123 (3.5)	
N(1)–C(2)–C(3)	109 (5.4)	
C(3)–C(2)–C(9)	112 (3.6)	
C(3)–C(2)–C(11)	104 (3.6)	
C(2)–C(3)–C(4)	114 (3.6)	
C(3)–C(4)–C(5)	111 (7.0)	
C(3)–C(4)–O(8)	124 (3.5)	
N(1)–C(2)–C(9)	114 (3.6)	
N(1)–C(2)–C(11)	112 (3.6)	
C(2)–C(9)–H	112 (1.9)	

Table 2. Correlation matrix (× 100) for the parameters. (The coefficients having absolute values less than 0.6 are not given.)

Parameters	R_1	R_2	R_3	R_4	R_5	R_6	R_7	R_8	R_9	R_{10}	R_{11}	R_{12}	R_{13}	R_{14}	R_{15}	R_{16}	R_{17}	R_{18}
R_1 N(1)–O(7)	100																	
R_2 N(1)–C(2)		100																
R_3 C(2)–C(3)			100															
R_4 C(3)–C(4)		−86		100														
R_5 C(4)–O(8)					100													
R_6 C(2)–C(9)			−77			100												
R_7 C(2)–N(1)–C(6)		−72					100											
R_8 C(2)–N(1)–O(7)							−85	100										
R_9 N(1)–C(2)–C(3)							−85	94	100									
R_{10} C(3)–C(2)–C(9)							−79	74	70	100								
R_{11} C(3)–C(2)–C(11)								72	71		100							
R_{12} C(2)–C(3)–C(4)							74			−76		100						
R_{13} C(3)–C(4)–C(5)							−74					−88	100					
R_{14} C(3)–C(4)–O(8)													−73	100				
R_{15} C(9)–C(2)–N(1)								−81	−83	−75	−72				100			
R_{16} C(11)–C(2)–N(1)							89		−72	−72		71	−75			100		
R_{17} C(2)–C(9)–H																	100	
R_{18} C–H																		100

Table 3. Nitroxyl group parameters of free radicals whose structures have been determined. TAN-H is added for comparison.

Molecule	Ref.		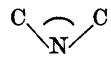	N–O	N–C	Method
I	7	planar	114.5	1.26	1.50	X-ray
II	8	planar	114.8	1.267	1.48	X-ray
III	(9) 10	15.8	125.4	1.291	1.499	X-ray
IV	11	planar	121	1.308	1.496	X-ray
V	12	planar	136	1.28	1.512	el. diffr.
VI	15	planar	–	1.278	1.501	X-ray
VII	13	planar	124	1.23	1.44	X-ray
VIII	14	planar	121	1.30	1.46	X-ray
	this work	14	110	1.247	1.50	el. diffr.
IX	6	37	118	1.465	1.50	el. diffr.

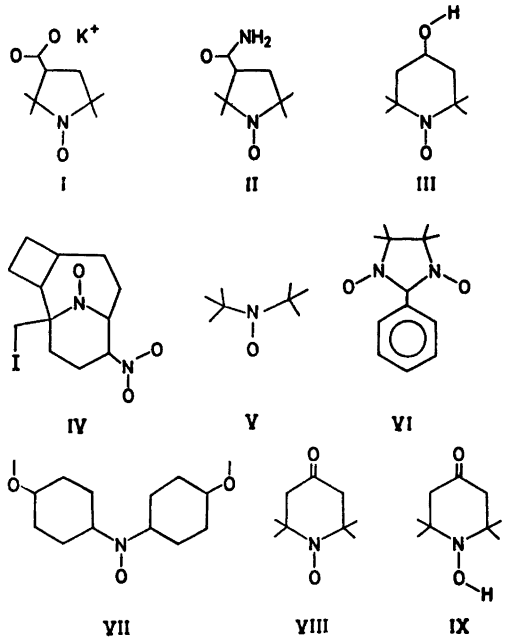

RESULTS AND DISCUSSION

The bond lengths, angles, standard deviations, and u-values (vibrational amplitudes) are listed in Table 1. The correlation between parameters decides how well these parameters may be determined.[19] In Table 2 the correlation coefficients $|\varrho_{ij}| > 0.6$ are listed and the R_i, R_j refers to parameters shown in Table 1. The correlation between R_1 and the 17 other parameters is less than 0.6 and the same is the case for R_5 and R_{18}. These parameters are determined with greater accuracy than the other bond-distance parameters. R_2 and R_4 as well as R_3 and R_6 are greatly correlated and this explains why these are less accurately determined. The correlation between bond distances in TAN is greater than in TAN-H which makes the structure determination of the latter more accurate.

Except for the C(2)–C(3) the bond lengths are about what could be expected. The poor accuracy makes it doubtful to discuss the significance of this lengthening, but it may be pointed out that the 1.570 Å found here is close

to the 1.560 Å found in both TAN-H [6] and cyclohexane-1,4-dione [18] for the same distance. The C(2) – N – C(6) and C(3) – C(4) – C(5) angles are about equal in this structure while C(2) – N – C(6) was 118° in TAN-H. This change in angle contributes to the shortening of the distance between the axial methyl groups which in TAN is C(9)···C(10) = 2.91 Å. The two distances from the nitroxyl oxygen to the methyl groups are O(7)···C(9) = 3.35 Å and O(7)···C(11) = 2.83 Å. The dihedral angles in the ring are C(5) – C(6) – N – C(2) = 60°, N – C(2) – C(3) – C(4) = 54°, and C(2) – C(3) – C(4) – C(5) = 47°. The angle between the N – O bond and the plane defined by C(2) – N – C(6) is found to be 14°. A comparison of the  parameters in the structures determined so far is shown in Table 3.

Pulse radiolysis studies have revealed that organic nitroxyl free radicals might have different sterical hindrance in reactions with deoxynucleotide radicals.[2] Sterical hindrance seems also to be involved in the radiosensitizing effect of nitroxyls in bacteria.[2] Thus, in one bacterial species, where different nitroxyls had nearly equal sensitizing effects at high concentrations, the effect differed strongly at low concentrations of sensitizers.[2]

Evidence is accumulating that DNA is the vital target in irradiated bacteria and cells.[21] It is therefore of interest that TAN may be bound covalently to irradiated native DNA, to the extent expected from the observed yield values in experiments where the four separate deoxynucleotides were irradiated in the presence of TAN.[20]

Nearly all radiation induced binding of TAN to DNA seems to take place at the 5 – 6 position of the pyrimidine bases of DNA.[20] On a model of double stranded DNA it can be shown that TAN may interact with DNA radicals, located at such sites, without restrictive sterical hindrance. It can also be shown that TAN, when bound to DNA with a conformation as in TAN-H (*i.e.* as a hydroxylamine derivative) may be located in the minor groove of the double helix of DNA without sterical hindrance from neighbouring groups of DNA.

Acknowledgement. The authors are grateful to Dr. A. Almenningen for doing the electron diffraction experiments.

REFERENCES

1. Emmerson, P. T. and Howard-Flanders, P. *Nature (London) 204* (1964) 1005.
2. Emmerson, P. T., Fielden, E. M. and Johansen, I. *Int. J. Radiat. Biol. 19* (1971) 229.
3. Rozantsev, E. G. *Free Nitroxyl Radicals*, Plenum, New York 1970.
4. Nakken, K. F., Sikkeland, T. and Brustad, T. *FEBS Lett. 8* (1970) 33.
5. Nakken, K. F., Tomas, E. and Brustad, T. *Ninth Annual Meeting of the European Soc. for Radiation Biology; Book of Abstr.* (1972) 122.
6. Andersen, P., Astrup, E. E., Frederichsen, P. S. and Nakken, K. F. *Acta Chem. Scand. A 28* (1974) 671.
7. Boeyens, J. C. A. and Kruger, G. J. *Acta Crystallogr. B 26* (1970) 668.
8. Turley, W. and Boer, F. P. *Acta Crystallogr. B 28* (1972) 1641.
9. Lajzerowicz-Bonneteau, P. J. *Acta Crystallogr. B 24* (1968) 196.
10. Berliner, L. J. *Acta Crystallogr. B 26* (1970) 1198.
11. Hawley, D. M., Ferguson, G. and Robertson, J. M. *J. Chem. Soc. B* (1968) 1255.
12. Andersen, B. and Andersen, P. *Acta Chem. Scand. 20* (1966) 2728.
13. Hanson, A. W. *Acta Crystallogr. 6* (1953) 32.
14. Shibaeva, R. P., Atovmyan, L. O., Neigauz, M. G., Novakovskaya, L. A. and Ginzburg, S. L. *Zh. Strukt. Khim. 13* (1972) 887.
15. Hope, H. *Private communication.*
16. Briere, R., Lemarie, H. and Rassat, A. *Bull. Soc. Chim. Fr.* (1965) 3273.
17. Andersen, B., Seip, H. M., Strand, T. G. and Stølevik, R. *Acta Chem. Scand. 23* (1969) 3224.
18. Groth, P. and Hassel, O. *Acta Chem. Scand. 18* (1964) 923.
19. Seip, H. M., Strand, T. G. and Stølevik, R. *Chem. Phys. Lett. 3* (1969) 617.
20. Nakken, K. F., Tomas, E. and Brustad, T. *IAEA Panel on Modification of Radiosensitivity in Biological Systems*, Stockholm 1973. *To be published.*
21. Ginoza, W. *Annu. Rev. Microbiol. 21* (1967) 325.

Received October 17, 1973.

Acta Chemica Scandinavica A 28 (1974) 680—692

Conformational Analysis. V. The Molecular Structure, Torsional Oscillations, and Conformational Equilibria of Gaseous 1,3-Dibromopropane, $(CH_2Br)_2CH_2$, as Determined by Electron Diffraction and Compared with Semi-empirical (Molecular Mechanics) Calculations

PER ERIK FARUP and REIDAR STØLEVIK

Department of Chemistry, University of Oslo, Blindern, Oslo 3, Norway

Gaseous 1,3-dibromopropane has been studied by electron diffraction at a nozzle temperature of 65 °C. Three spectroscopically distinguishable conformers *GG*, *AG*, and *AA* (see Fig. 1) were detected. Results are presented with error limits (2σ). The following values for bond lengths (r_a) and bond angles ($\angle_\alpha$) are average parameters for the conformers: $r(C-H) = 1.126(18)$ Å, $r(C-C) = 1.527(10)$ Å, $r(C-Br) = 1.959(4)$ Å, $\angle CCC = 111.4°$ (3.2), and $\angle CCBr = 112.0°(0.6)$. Non-bonded distances were computed as dependent quantities under the constraints of geometrically cosistent r_α parameters.

By symmetry *AA* has a staggered conformation. The conformers *AG* and *GG* have torsion angles close to staggered values (Table 11).

The relative amounts of the conformers have been determined, and the composition at 65 °C is: 67 %(4) of *GG*, 30 %(4) of *AG*, and 3 %(4) of *AA*. The radial distribution curves show that a small relative amount of *AA* is present, in spite of the large error limit (4 %) estimated by the least-squares procedure. The conformer with two C–Br bonds parallel, *GG(1:3)*, is not present in detectable amounts. According to the semiempirical calculations, *AA* is the conformer of lowest minimum energy, but this result is only possible if the zero-point vibrational energies of *GG* and *AG* are significantly smaller than that of *AA*. This question has been discussed.

Torsional force constants and frequencies corresponding to torsional modes have been estimated by combining information from electron diffraction and vibrational spectroscopy. The spectroscopic assignment of low frequencies for the conformer *GG* has to be changed in order to get agreement with the vibrational quantities determined by electron diffraction. A new assignment has been proposed.

I. INTRODUCTION

The present electron diffraction work is part of a systematic conformational study of halogenated propanes and related molecules. General [1] information [2] relevant to this investigation and to the electron diffraction method [3] is found in Refs. 1–3.

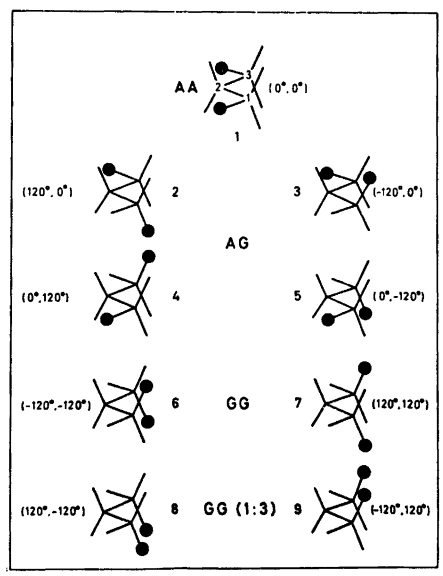

Fig. 1. The numbering and names of staggered conformers in 1,3-dibromopropane. The torsion angles (ϕ_{1-2}, ϕ_{2-3}) are shown in parentheses.

Table 1. Characterization of the four spectroscopically distinguishable staggered conformers of 1,3-dihalopropane. Classically there are *nine* possible staggered conformers. *Six* of the conformers are distinguishable, but only *four* are spectroscopically distinguishable (see Fig. 1).

Conformer	Point group	Symmetry number (σ)	M_c	M_d	$2(M_d/\sigma)$
AA	C_{2v}	2	1	1	1
AG	C_1	1	4	2	4
GG	C_2	2	2	2	2
GG(1:3)	C_s	1	2	1	2

Compounds of the type $(CH_2X)_2CH_2$ will be referred to as DXP (X = F, Cl, Br, I), and the title compound as DBP. Classically the possible number of staggered conformers in DXP is *nine*, as indicated in Fig. 1. The conformer *6* and *7* are *enantiomers* and thereby physically distinguishable, but neither spectroscopy nor electron diffraction can distinguish between them. The conformers *8* and *9* are identical in all respects. The conformers *2* and *3* are enantiomers, while *4* and *5* are identical to *2* and *3*, respectively. In conclusion, there are *six* physically different conformers, but only *four* [*AA*, *AG*, *GG*, and *GG(1:3)*] are spectroscopically distinguishable, as indicated in Fig. 1 and Table 1.

Whenever torsion-angle dependent quantities have to be specified, the conformers *1*, *2*, *7*, and *8* will be taken to represent *AA*, *AG*, *GG*, and *GG(1:3)*, respectively.

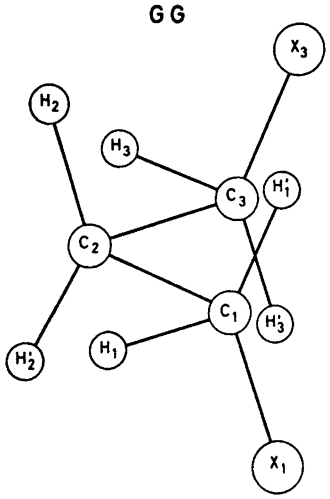

Fig. 2. Numbering of atoms in the conformer *GG* of 1,3-dibromopropane.

There are four X···X distances of different lengths: AA(*anti-anti*), AG(*anti-gauche*) GG(*gauche-gauche*), and GG(1:3) which corresponds to a parallel (1:3)X···X interaction. The symbols A(*anti*) and G(*gauche*) thus refer to the plane of the CCC atoms (see Fig. 1).

The spectroscopically distinguishable conformers may be assigned multiplicities in two ways, as follows:

(1) only conformers being distinguishable (*six*) are considered. (M_d in Table 1).

(2) all classically possible conformers (*nine*) are included. (M_c in Table 1).

It is noteworthy [4] that $M_c^*/M_c = (M_d^*/M_d) \times (\sigma^*/\sigma)^{-1}$ for two spectroscopically distinguishable conformers, C and C*, having symmetry numbers σ and σ^*.

Brown and Sheppard [5] and later on Dempster, Price, and Sheppard [6] studied DBP by vibrational spectroscopy. Based upon infrared spectra they concluded that DBP crystallizes in the *GG* conformation at low temperatures. An extended vibrational spectral study of DBP as liquid, in solution, and in the crystalline state at low temperatures and at high pressure has been published by Thorbjørnsrud *et al.*[7] The three conformers *GG*, *AG*, and *AA* were observed in the liquid. They also found that DBP crystallizes in the *GG* conformation at high pressure.

II. CALCULATION OF CONFORMATIONAL ENERGIES, GEOMETRIES, BARRIERS, AND TORSIONAL FORCE CONSTANTS.

(Molecular Mechanics Calculations)

The semiempirical energy calculations were carried out as described in Ref. 8. Energy parameters (V_0, *a*, *b*, *c*, *d*) were taken from the work of Abraham and Parry,[8] and diagonal valence force constants from Table 2 were used. "Normal" values of the geometry parameters are given in Table 2.

The conformational geometries derived from the semiempirical energy model are presented in Table 2. According to the results in Table 2, *GG* and *AG* have nearly staggered conformations, while *AA* is exactly staggered. Small differences in bond angles and practically no

Table 2. Calculated conformational geometries for 1,3-dibromopropane. Distances in Å, angles in deg.

Parameter (normal value)	*GG*	*AG*	*AA*	*GG(1:3)*
r(C−H), (1.094)	1.094	1.094	1.094	1.094
r(C−C), (1.513)	1.524	1.522	1.520	1.527
r(C−X), (1.935)	1.940	1.939	1.937	1.940
∠CCC (110.0)	113.3	112.0	110.7	113.9
∠CCX (109.47)	110.9	110.5	110.0	112.4
∠CC_2H (109.47)	108.9	109.1	109.3	108.8
∠C_2CH (109.47)	109.9	109.8	109.8	109.6
ϕ_{1-2}[a]	112.7	113.2	0.0	(98.0)[b]
ϕ_{3-2}[a]	112.7	3.0	0.0	(−98.0)[b]

In minimizing the energy the geometry was constrained as described in Sect. V-A: [a] $\phi_0 = 60°$ in the expression $V_\phi = \frac{1}{2}V_0\sum_k\{1+\cos[3(\phi_{k-2}-\phi_0)]\}$, k = 1, 3. [b] The conformer *GG(1:3)* does not correspond to a well defined energy minimum (see also Table 4).

Table 3. Conformational energies (kcal/mol) for 1,3-dibromopropane. Details about the energy expression are found in Ref. 8. Zero-point vibrational energies for the conformers are not included.

Type of energy	*GG*	*AG*	*AA*	*GG(1:3)*
E (bonded)	0.69	0.35	0.08	2.58
E (van der Waals)	0.90	0.77	0.57	1.35
E (polar, X···H)	−5.65	−5.50	−5.29	−5.20
E (polar, X···X)	1.48	1.30	1.16	1.87
E (total)	−2.58	−3.09	−3.47	0.60
E (total) − *E*(AA) = ΔE^m	0.89	0.38	0.00	4.07

Table 4. Conformational energies and torsional barriers in 1,3-dibromopropane. Details about the conformational minima corresponding to the stable conformers *AA*, *AG*, and *GG* are found in Table 2 and Table 3.

ϕ_{1-2} / ϕ_{2-3}	(−180°)	(−120°)	(−60°)	(0°)	(60°)	(120°)	(180°)
(180°)	∞	8.5	12.2	5.6	12.2	8.5	∞
(120°)	8.5	GG(1:3) 4.1	4.1	AG 0.4	3.6	GG 0.9	8.5
(60°)	12.2	4.1	7.7	3.5	7.5	3.6	12.2
(0°)	5.6	AG 0.4	3.5	AA 0.0	3.5	AG 0.4	5.6
(−60°)	12.2	3.6	7.5	3.5	7.7	4.1	12.2
(−120°)	8.5	GG 0.9	3.6	AG 0.4	4.1	GG(1:3) 4.1	8.5
(180°)	∞	8.5	12.2	5.6	12.2	8.5	∞

differences in bond lengths, between the conformers, are predicted by these calculations.

According to the calculated conformational energies of Table 3, *AA* is the most stable conformer. The conformer *GG(1:3)*, which does not correspond to a well defined energy minimum (see Table 4), is *ca.* 4 kcal/mol less table than *AA*.

Conformational energy minima and torsional barriers between the conformers are shown in

Table 5. Calculated torsional force constants for 1,3-dibromopropane.
$F_\phi = \partial^2 E/\partial\phi^2$ and $F_{\phi\phi'} = \partial^2 E/\partial\phi\partial\phi'$ were numerically computed.

(mdyn Å(rad)$^{-2}$)	*GG*	*AG*	*AA*
$F_\phi(1-2)$	0.159	0.141	0.114
$F_\phi(3-2)$	0.159	0.114	0.114
$F_{\phi\phi'}(1-2,3-2)'$	−0.038	−0.033	−0.009

Table 4. Each energy value has been obtained by adjusting *all* geometry variables except for the values of ϕ_{1-2} and ϕ_{2-3} being $\pm 60°$ or $\pm 180°$. Such values of the torsion angles correspond to exlipsed conformations.

The torsional force constants given in Table 5 were numerically computed. The calculated values here are too low compared to the experimentally determined values of Sect. V-B.

III. CALCULATION OF VIBRATIONAL QUANTITIES

Valence force constants, except for the torsional part, were taken from works of Schachtschneider [10] and Snyder.[11] The final force constant values used here are schown in Table 6.

Since observed frequencies are available,[7] it is possible to adjust most force constants of Table 6 to fit DBP even better. However, this was not done for several reasons. The aim was to calculate mean amplitudes of vibration to be used in the structure analysis. The force field required for this purpose may be rather approximate. Mean amplitudes (u and K values) of DBP are quite insensitive to moderate errors in the force field, except for the torsional part of it, which has been adjusted (Sect. V-B). Moreover, it is important to use typical force constants as much as possible in order to test the transferability in various situations. The works by Schachtschneider [10] and Snyder [11] in this respect are extremely valuable for electron diffraction studies.

The normal-coordinate program described by Gwinn [12] was used in computing vibrational frequencies (Table 7). The fit between observed spectroscopic frequencies and those calculated is good. If the first three (ω_1, ω_2, and ω_3) frequencies are left out, the deviation between the

Table 6. Valence force constants for 1,3-dibromopropane.

Stretch (mdyn Å^{-1})		Bend [mdyn Å (rad)$^{-2}$]	
C−C	4.73	CCC	0.90
C_1−H	4.85	CCH	0.67
C_2−H	4.55	HCH	0.53
C−X	2.63	CCX	0.91
		HCX	0.69
Stretch/Stretch (mdyn Å^{-1})		Stretch/Bend [mdyn(rad)$^{-1}$]	
(C−C common)		(C−X common)	
C−X/C−C	0.35	C−X/CCX	0.49
C−C/C−C	0.064	C−X/HCX	0.26
		(C−C common)	
Bend/Bend (mdyn Å (rad)$^{-2}$)		C−C/CCX	0.30
(C−C common)		C−C/CCC	0.29
HCC/CCC	−0.12	C−C/CCH	0.26

Torsion [mdyn Å (rad)$^{-2}$]			
Conformer:	*GG*	*AG*	*AA*
$F_\phi(1-2)^a$	0.243	0.225	0.198
$F_\phi(2-3)^a$	0.243	0.198	0.198

[a] The torsional force constants have been defined as follows: each fragment A′−C_1−C_2−A″ (A=H, C, X, see Fig. 2) has been assigned an equal force constant. Each fragment A′−C_2−C_3−A″ has been assigned an equal force constant, but generally different from those of fragments A′−C_1−C_2−A″. The total force constant for the torsional coordinate ϕ_{i-2} (i=1,3) is thus the sum of *nine* equal contributions. The input to Gwinn's normal-coordinate program demands a separate specification for each torsional fragment.

Table 7. Vibrational frequencies in 1,3-dibromopropane. The valence force field of Table 6 was used.

Approximate mode	Spectroscopic value (GG) [7]	*GG*	*AG*	*AA*
Torsion (ω_1)	176	47	71	100
Torsion (ω_2)	186	149	107	115
CCX bend (ω_3)	310	189	214	159
CCX bend (ω_4)	324	371	266	220
CCC bend	425	420	358	342
C – X stretch	549	566	570	581
C – X stretch	591	578	649	705
CH_2 rock	763	805	807	812
CH_2 rock	854	849	844	820
C – C stretch	958	996	984	996
CH_2 rock	943	1018	1019	1024
C – C stretch	1073	1104	1094	1082
CH_2 twist	1122	1195	1205	1210
CH_2 twist	1133	1215	1223	1219
CH_2 twist	1240	1243	1239	1252
CH_2 wag	1232	1317	1306	1285
CH_2 wag	1294	1321	1322	1342
CH_2 wag	1349	1351	1349	1346
CH_2 scissor	1417	1453	1441	1433
CH_2 scissor	1430	1454	1453	1450
CH_2 scissor	1450	1519	1516	1520
C – H stretch	2850	2817	2817	2817
C – H stretch	2908	2955	2955	2956
C – H stretch	2924	2956	2956	2956
C – H stretch	2969	2962	2961	2960
C – H stretch	3010	3008	3008	3009
C – H stretch	3010	3010	3009	3009

two sets is less than 3 %. (See also discussion in Sect. VII.)

Mean amplitudes of vibration were computed as described in Ref. 13. In Table 8 are given u and K values for internuclear distances.

Some of these quantities are quite sensitive to the values of the torsional force constants, which have been adjusted to fit the experimental intensities (Sect. V-B). In Table 9 are shown vibrational quantities corresponding to different values of the torsional force constants.

IV. EXPERIMENTAL AND DATA REDUCTION

A commercial sample of DBP was obtained from Fluka. The sample was purified by distillation under reduced pressure.[7] The final purity was *ca.* 99 %.

Electron-density photographs were made at a nozzle temperature of 65 °C in the Balzer [14] apparatus [15] under conditions summarized below:

Nozzle-to-plate distance (mm)	500	250
Electron wavelength (Å)	0.05848	0.05845
Number of plates	5	5
Range of data, in s(Å^{-1})	1.125 – 14.75	2.25 – 21.00
Data interval, Δs(Å^{-1})	0.125	0.250
Uncertainty in s-scale (%)	0.14	0.14

The electron wavelength was determined by calibration against ZnO and corrected by an experiment with CO_2 giving a correction of

Table 8. Mean amplitudes of vibration in 1,3-dibromopropane at 65 °C.

Type of distance	Dist.[a] (Å)	Conformer *GG*[b] u (Å)	K (Å)	Conformer *AG*[b] u (Å)	K (Å)
C_2-H	(1.11)	0.0792	0.0166	0.0792	0.0210 – 4[c]
C_1-H	(1.11)	0.0780	0.0213 – 23[c]	0.0780	0.0189 – 93[c]
C_3-H	(1.11)	0.0780	0.0213 – 23[c]	0.0780	0.0285 – 96[c]
C_1-C_2	(1.52)	0.0505	0.0056	0.0505	0.0073
C_2-C_3	(1.52)	0.0505	0.0056	0.0505	0.0099
C_1-X	(1.95)	0.0546	0.0130	0.0547	0.0075
C_3-X	(1.95)	0.0546	0.0130	0.0546	0.0154
$C_2\cdots X$	(2.88)	0.0761	0.0080	0.0760	0.0066
$C_2\cdots H$	(2.22)	0.1054	0.0153	0.1054	0.0214
$C\cdots C$	(2.52)	0.0751	0.0054	0.0751	0.0085
$C\cdots H_2$	(2.09)	0.1098	0.0119	0.1099	0.0185
$H_1\cdots X_1$	(2.49)	0.1130	0.0227	0.1131	0.0229
$H_1\cdots H_1'$	(1.75)	0.1292	0.0301	0.1293	0.0317
$H_2\cdots H_2'$	(2.00)	0.1197	0.0203	0.1199	0.0290
X···H(*anti*)	(3.83)	0.1064	0.0098	0.1071	0.0099
X···H(*gauche*)	(2.83)	0.1678	0.0114	0.168 – 72[c]	0.009 – 13[c]
X···C(*gauche*)	(3.33)	0.1575	0.0062	0.1608	0.0081
X···C(*anti*)	(4.26)	–	–	0.0777	0.0019
X···X(GG)[d]	(4.41)	0.2680	0.0000	–	–
X···X(AG)[d]	(5.13)	–	–	0.1656	0.0000
X···H(GG)[d]	(2.90 – 5)	0.2525	0.0170	0.2548	0.0249
X···H(AG)[d]	(4.3 – 6)	0.1865	0.0082	0.1723	0.0044
X···H(AG)[d]	(3.53)	–	–	0.2685	0.0143
X···H(AA)[d]	(5.09)	–	–	0.1240	0.0040

[a] The distances here correspond to a set of cartesian coordinates slightly different from those in Table 13. [b] The valence force field of Table 6 was used. [c] The range of values corresponding to distances of this kind has been given. [d] A(*anti*) and G(*gauche*). The combination X···H(AG) thus represents the X···H distance of a fragment X – C – C – C – H having one of the end bonds *anti*(A) and the other one *gauche* (G) to the CCC framework. The longest X···H(AG) distance has C – X *anti*.

+0.1 % in the s-scale. The data were reduced in the usual way [16] to yield an intensity curve for each plate. Average curves for each set of distances were formed. A composite curve was then made by connecting the two average curves after scaling. The final experimental intensity curve is shown in Fig. 3. The intensities have been modified by $s/|f_{Br}'||f_C'|$.

Scattering amplitudes were calculated by the partial wave method [17] using Hartree-Fock atomic potentials.[18]

Contributions to the theoretical intensities from H···H distances, the H atoms bonded to different C atoms, were not included.

The radial distribution (RD) curve, obtained by Fourier transformation [16] of the final experimental intensity, is presented in Fig. 4.

V. STRUCTURE ANALYSIS

Radial distribution (RD) curves for the conformers *GG*, *AG*, *AA*, and the experimental curve, are shown in Fig. 5. The conformers *GG* and *AG* are clearly present in considerable amounts, and *GG* is the most abundant conformer. The small peak in the experimental RD curve at *ca.* 5.75 Å corresponds to a small contribution from the X···X distance of the conformer *AA*. Approximate composition parameters (α) were estimated from these RD curves: $\alpha(GG) \simeq 60-70$ %, $\alpha(AG) \simeq 20-40$ %, and $\alpha(AA) \simeq 0-10$ %.

Theoretical RD curves corresponding to 0, 3, and 9 % of the conformer *AA*, are shown in Fig. 6 together with the final experimental curve. The conformer *AA* is clearly present in detectable amounts at 65 °C.

A. Least-squares analysis. The least-squares program was written by H. M. Seip, and it is a modified version of the program explained in Ref. 16. Several conformers may be included in the refinements with the present version of the program. Models for the conformers were

Table 9. Vibrational quantities in 1,3-dibromopropane at 65 °C.

Torsional force constant[a]			
$F\phi(1-2)=F\phi(2-3)=\bar{F}\phi$ [mdyn Å(rad)$^{-2}$]	0.120	0.243	0.480
Torsional frequencies for the conformer *GG* (cm^{-1})[b]	33	47	57
	125	149	181
Ratios (q)[c] between vibrational partition functions[d]			
$Q_{GG}(0.24)/Q_{AG}(\bar{F}\phi)$	0.33	1.17	5.48
$Q_{GG}(0.24)/Q_{AA}(\bar{F}\phi)$	0.33	1.17	5.48
$Q_{AG}(0.24)/Q_{AA}(\bar{F}\phi)$	0.28	1.00	4.68
Mean amplitudes (u values)[e] for the X···X distance (Å)			
in conformer *GG*	0.386	0.268	0.232
in conformer *AG*	0.203	0.166	0.159
in conformer *AA*	0.113	0.113	0.112
u value[e] for the distance C···X (*gauche* (Å)			
in *GG* and *AG*	0.187	0.159	0.144

[a] The remaining force constants are found in Table 6. [b] See also Table 7. [c] The differences in zero-point vibrational energy are included in the q values. [d] Q: vibrational partition function. [e] See also Table 8.

constructed with the following geometrical assumptions: (1) the two C−CH_2X groups are equal; (2) each C−CH_2X group possess C_s symmetry; (3) the plane of the $H_2C_2H_2'$ group is perpendicular to the C-atom plane and bisects the CCC angle; (4) all C−H bonds are equal; (5) the conformers have identical structures except for the C−C torsion angles (ϕ_{1-2} and ϕ_{2-3}). The models were defined in terms of the following average parameters: r(C−H), r(C−C), r(C−X), ∠CCC, ∠C_2CX, ∠C_2CH, ∠CC_2H, ϕ_{1-2}, ϕ_{2-3}, and ∠(HC_1H')* which is the projec-

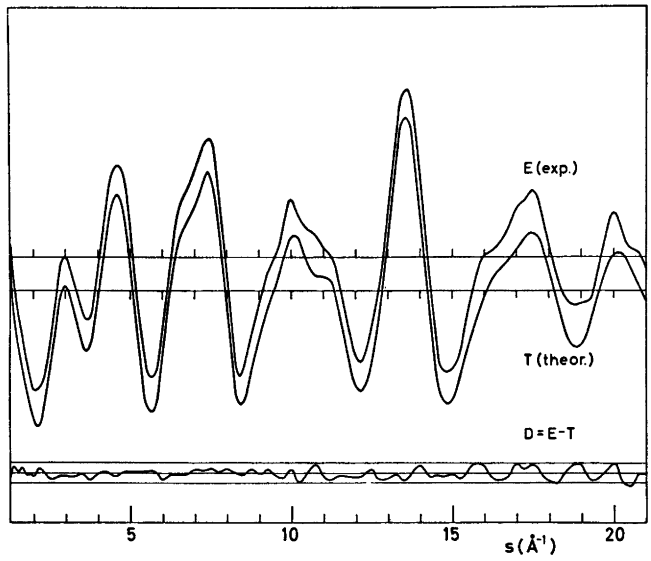

Fig. 3. Intensity curves for 1,3-dibromopropane at 65 °C. Experimental (E) and theoretical (T) intensity curves corresponding to the final least-squares parameters, and D = E − T. The straight lines give the experimental uncertainties (± 3 × experimental standard deviation).

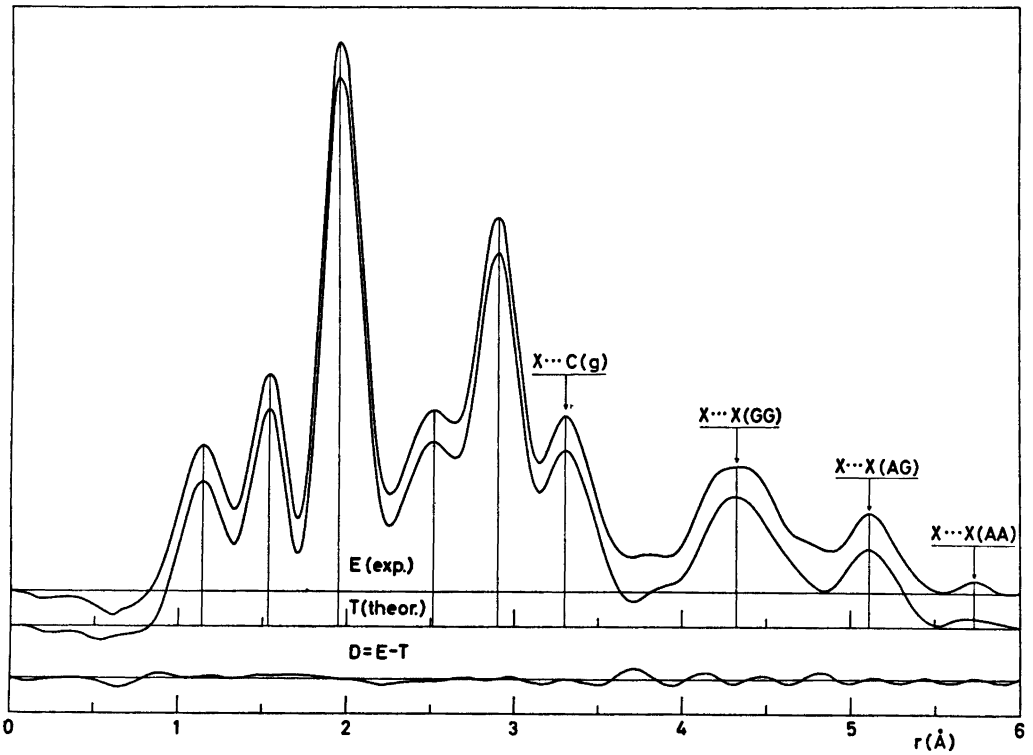

Fig. 4. Radial distribution curves for 1,3-dibromopropane at 65 °C. Experimental (E) and theoretical (T) radial distribution curves, and D = E − T. The RD curves were calculated from the intensity curves of Fig. 3 with an artificial damping constant of 0.0020 Å^2.

tion of the HC_1H' angle on a plane perpendicular to the C_2-C_1 axes. Also adjusted were the composition (%) parameters α(GG) and α(AG) with α(AA) = 100 % − α(GG) − α(AG).

Corrections for the "Bastiansen-Morino" shrinkage [19] effect on non-bonded distances have been included. Non-bonded distances were computed as dependent parameters, restricted under the constraints of geometrically consistent r_α parameters.[20,21]

B. Determination of torsional force constants. The torsional modes of vibration contribute substantially to the mean amplitudes (Sect. III) of several internuclear distances in a molecule like DBP. Since a reasonable force field was known, except for the torsional part, torsional force constants can be adjusted to fit the electron-diffraction data. Determination of all torsional force constants from electron-diffraction data alone is not possible. The values in Table 5 were used as a guide, and the following assumptions were made:

[F_ϕ in mdyn Å (rad)$^{-2}$] $F_{\phi\phi'}(1-2; 3-2) = 0$ for all conformers.

in *GG*: $F_\phi(1-2) = F_\phi(2-3) = 0.159 + \Delta F_\phi$

in *AG*: $F_\phi(1-2) = 0.141 + \Delta F_\phi$, $F_\phi(2-3) = 0.114 + \Delta F_\phi$

in *AA*: $F_\phi(1-2) = F_\phi(2-3) = 0.114 + \Delta F_\phi$

ΔF_ϕ was considered as a variable to be adjusted. K values and u values were computed for several values of ΔF_ϕ and then included in the least-squares refinements. The structure and composition parameters were adjusted for each new value of ΔF_ϕ. The best fit between experimental and theoretical intensities was obtained for $\Delta F_\phi = 0.084$, corresponding to the lowest value of the error sum (**V'PV**).[16] A slight improvement was obtained if individual u values were refined (Sect. VI).

The error limits of ΔF_ϕ were estimated by direct inspection of the fit between theoretical and experimental RD curves computed for each value of ΔF_ϕ. Keeping in mind the assumptions

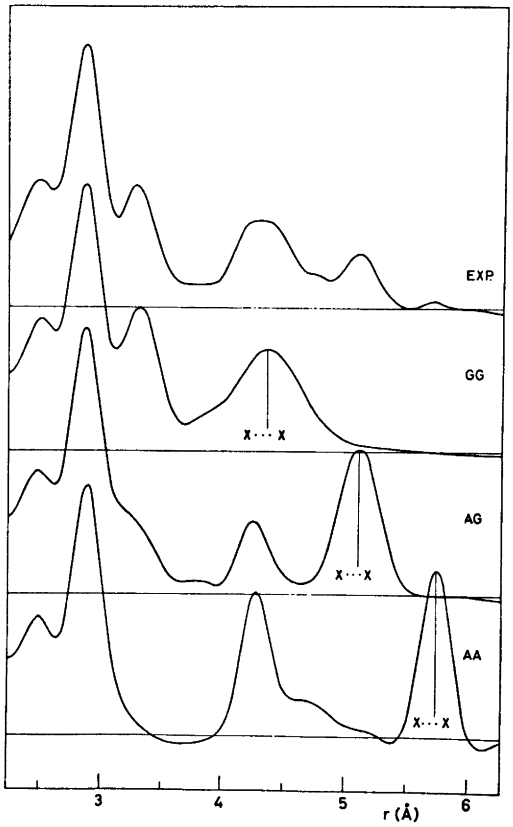

Fig. 5. Radial distribution curves for conformers of 1,3-dibromopropane at 65 °C. Theoretical RD curves of the conformers *AA*, *AG*, and *GG* are shown together with the final experimental curve. The artificial damping constant was equal to 0.0020 Å^2.

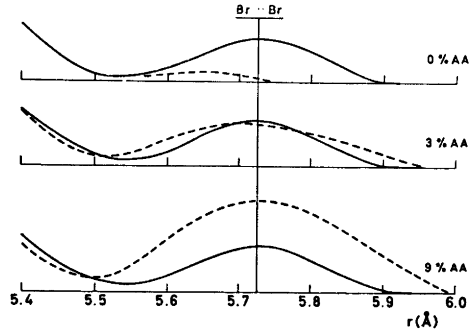

Fig. 6. Radial distribution curves for 1,3-dibromopropane at 65 °C. Experimental and theoretical (– – –) RD curves, computed with the ratio $\alpha(GG)/\alpha(AG) = 67/30$ for the theoretical curves. An artificial damping constant equal to 0.0020 Å^2 was used.

above, the most probable values of the torsional force constants [mdyn Å (rad)$^{-2}$] are:

$F_\phi(1-2) = F_\phi(2-3) = 0.243^{+0.10}_{-0.05}$ in conformer *GG*

$F_\phi(1-2) = 0.225^{+0.10}_{-0.05}$ and $F_\phi(2-3) = 0.198^{+0.10}_{-0.05}$ in conformer *AG*

$F_\phi(1-2) = F_\phi(2-3) = 0.198^{+0.10}_{-0.05}$ in conformer *AA*

(The conformational *differences* in the torsional force constants thus correspond to the theoretical values of Table 5.)

The present electron-diffraction data do not justify any further adjustment of torsional force constants. However, the value of F (0.243) for *GG* seems reasonable compared to the values determined for the conformer *GG* (*ag*) of 1,2,3-tribromopropane [8] ($\bar{F}_\phi = 0.30$, $F_\phi(1-2) = 0.20$ and $F_\phi(2-3) = 0.40$).

VI. FINAL RESULTS

Parameters from the least-squares refinements [16] and standard deviations (σ) corrected for correlation in the experimental data [22] are given. In the final refinements, intensities beyond $s = 21.00$ Å^{-1} were not included and, using a diagonal weight matrix, all intensities were given equal weights.

Non-bonded distances were restricted under the geometrical constraints of r_α parameters, by including correction terms $D = r_\alpha - r_a$ ($D = u^2/r - K$) for all distances.

Parameter correlation coefficients (ϱ) [16] with $|\varrho| > 0.49$ are included in Tables 10–12. Bond lengths and bond angles are found in Table 10. Torsion angles and composition parameters are found in Table 11.

The value of $\angle CCC = 111.4°$ seems somewhat low compared with the calculated values of 113.3° (*GG*) and 112.0° (*AG*), but the uncertainty ($\sigma = 1.6°$) of this parameter does not exclude values as large as 113–114°.

Within their standard deviations the torsion angles of Table 11 agree with those calculated according to the semiempirical energy model (Table 2), and the deviation from staggered values are significant at least for the conformer *GG*.

Table 10. Average bond lengths (Å) and bond angles (deg.) in the conformers of 1,3-dibromopropane. Standard deviations are given in parenthesis.

Bond lengths (r_a)[a]	Bond angles ($\angle\alpha$)[b]	
r_a(C−H) = 1.126(9)	∠CCC	= 111.4(1.6)
	∠C_2CBr	= 112.0(0.3)
r_a(C−C) = 1.527(5)	∠C_2CH	= 115.4(3.6)[c]
	∠CC_2H	= 103.0(2.0)[c]
r_a(C−Br) = 1.959(2)	∠(HC_1H')[d]	= 116.3(7.2)[c]

[a] An experiment with CO_2 gave a correction of 0.1 % in the *s*-scale. The bond lengths are therefore 0.1 % longer than those directly determined by the least-squares refinements. The uncertainty in the *s*-scale (0.14 %) has been included in the standard deviations for bond distances. [b] The bond angles are those of the self-consistent r_α structure. [c] These values are the results of a refinement where torsion angles, ∠CCC, ∠C_2CX, and *u* values of non-bonded distances were not refined. [d] The projection of the angle $H_1C_1H_1'$ in a plane perpendicular to the C_1-C_2 axes (see Sect. V-A).

Parameter correlation, $|\varrho| > 0.49$. $\varrho(\theta/C_2CX) = -0.57$, $\varrho[\theta/\phi_{1-2}(AG)] = 0.83$, $\varrho[\theta/\phi_{2-3}(AG)] = 0.68$, $\varrho(\theta/\phi(GG)) = 0.94$, and $\theta = \angle CCC$.

Table 11. Composition (at 65 °C) parameters (α) and torsion angles (a) for 1,3-dibromopropane. Standard deviations are given in parenthesis.

Conformer	α(%)	ϕ_{1-2}(deg.)	ϕ_{2-3}(deg.)
GG	67(2)	113.4(2)[b]	113.4(2)[b]
AG	30(2)	119.2(6)	11.5(6)
AA	3(2)[a]	(−)[c]	(−)[c]

[a] The parameters α(GG) and α(AG) were refined with $\alpha(AA) = 100\ \% - \alpha(GG) - \alpha(AG)$. [b] $\phi_{1-2} = \phi_{2-3} = 120° - \phi(GG)$; $\phi(GG)$ was refined. [c] $\phi_{1-2} = \phi_{2-3} = 0°$, see Fig. 1.

Parameter correlation. $|\varrho| > 0.49$. $\varrho[\alpha(AG)/\alpha(GG)] = -0.73$, $\varrho[\phi_{1-2}(AG)/\phi_{2-3}(AG)] = 0.96$, $\varrho[\phi(GG)/\phi_{1-2} \times (AG)] = 0.79$, $\varrho[\phi(GG)/\phi_{2-3}(AG)] = 0.62$.

Mean amplitudes of vibration (*u*) from least-squares refinements and those determined by adjusting the torsional force constants (Sect. V-B) are compared in Table 12. The *u* values which are not found in Table 12 could not be refined as individual parameters, but their values have been adjusted in adjusting the torsional force constants as described in Sect. V-B. Those *u* values and the corresponding *K* values are found in Table 8.

The mean amplitudes of the distances X···C(g), X···X(AG) and in particular the amplitudes of the distances X···X(GG) are sensitive to the value of the torsional force constants. Keeping in mind the uncertainties, the refined and calculated *u* values generally agree.

Unfortunately the refined *u* values for C−X, C_2···X and C···X(gauche) are *systematically* lower than those calculated. This might indicate that the applied force constants (F(CCX), F(CCC), F(C−C), F(C−X), and interaction constants among these) are not good enough. Comparison of frequencies in Table 7 lead to the conclusion that this is not the case.

The average relative deviation between the two sets of *u* values is *ca.* 10 %, while the average relative uncertainty of the refined *u* values is *ca.* 14 %.

In conclusion, the mean amplitudes calculated with the final torsional force constants seem the more reliable set of *u* values.

The final intensities and radial distribution curves are found in Fig. 3 and Fig. 4, respectively.

Cartesian coordinates for the conformers *GG* and *AG* together with the principal axes' moments of inertia are given in Table 13.

VII. DISCUSSION

The percentage α^* and α of two conformers (C⇌C*) in equilibrium in the gas phase, are related to the theoretical [23] expression [24] for the equilibrium constant, as given in eqn. (1):

$$\alpha^*/\alpha = (M^*/M)(Q^*/Q)^{vib} \exp(-\Delta E^m/RT) \quad (1)$$

with $M^*/M = (M_d^*/M_d)(\sigma^*/\sigma)^{-1} = M_c^*/M_c$ (see Table 1)

(The *classical* rotational partition functions of the conformers are approximately equal.) Q^{vib} is the vibrational partition function of a conformer refered to the potential-energy minimum of that conformer. $\Delta E^m = E^* - E$ is the potential-energy difference between the conformer C and C*, and the difference is measured between energy minima. The zero-point vibrational energy is included in the quantity Q^{vib}. R and T have their usual thermodynamic meanings.

If the vibrational partition functions are

Table 12. Mean amplitudes of vibration (u) for 1,3-dibromopropane at 65 °C.

Distance type	Dist. (Å)	Refined u-value (Å)	Standard deviation	Calculated[a] u-value (Å)
C–H	(1.11)	0.080	0.011	0.078–9
C–C	(1.52)	0.051	0.008	0.051
C–X	(1.95)	0.041	0.006	0.055
$C_2\cdots X$	(2.88)	0.063	0.007	0.076
$X_1\cdots H_1$	(2.49)	0.109	0.013	0.113
X···X(GG)	(4.41)	0.279	0.010	0.268
X···C(g) in *GG*	(3.33)	0.124[b]	0.052	0.158
X···X(AG)	(5.13)	0.145	0.020	0.166
X···C(g) in *AG*	(3.33)	0.129[b]	0.052	0.161

[a] The valence force constants are found in Table 6. [b] refined as *one* parameter.

Parameter correlation, $|\varrho| > 0.49$. $\varrho[CC_2H/u(C_1\cdots X_1)] = 0.63$, $\varrho[CCX/u(X_1\cdots H_1)] = 0.65$, $\varrho(CC_2H/u(X_1\cdots H_1)] = -0.76$, $\varrho[\alpha(AG)/u(AG)] = 0.59$, $\varrho[SCALE/u(GG)] = 0.55$, with u(AG) and u(GG) representing the u values of the X···X distances.

Table 13. Cartesian coordinates (Å) for conformers of 1,3-dibromopropane. The coordinates have been calculated using the final $\angle_\alpha$ values for angles and $r_g(r_g = r_a + u^2/r)$ values (C–H: 1.132 Å, C–C: 1.529 Å, C–Br: 1.961 Å) for the bond lengths. The numbering of atoms in the conformer *GG* is shown in Fig. 2. The principal axes' moment of inertia (amu Å²) are:
$I_A = 100.7$, $I_B = 843.0$, $I_C = 877.4$ for *GG*
$I_A = 65.0$, $I_B = 1111.8$, $I_C = 1157.2$ for *AG*
$I_A = 41.1$, $I_B = 1390.5$, $I_C = 1142.2$ for *AA*

Conformer *GG*:			Atom	Conformer *AG*		
(x)	(y)	(z)		(x)	(y)	(z)
1.2627	0.8617	0.0000	C_1	1.2627	0.8617	0.0000
1.4638	1.8721	−1.6684	Br_1	1.3709	2.0083	−1.5870
2.2333	0.2998	0.1509	H_1	2.2389	0.2915	0.0479
1.3347	1.6166	0.8399	H_1'	1.3842	1.5440	0.8945
0.0000	0.0000	0.0000	C_2	0.0000	0.0000	0.0000
0.0000	−0.4510	1.0378	H_2	0.0000	−0.4510	1.0378
0.0000	−0.4510	−1.0378	H_2'	0.0000	−0.4510	−1.0378
−1.2627	0.8617	0.0000	C_3	−1.2627	0.8617	0.0000
−1.4638	1.8721	1.6684	Br_3	−2.8743	−0.1947	0.3623
−2.2333	0.2998	−0.1509	H_3	−1.4627	1.4289	−0.9585
−1.3347	1.6166	−0.8399	H_3'	−1.2676	1.7149	0.7433

known, then the quantity ΔE^m may be computed from eqn. (1). Conversely, if the quantity ΔE^m is known, then the *ratio* between Q^{vib} values may be calculated from eqn. (1).

According to the semiempirical energy model, *AA* is the conformer of lowest minimum energy, while the conformers *GG* and *AG* are 0.89 and 0.38 kcal/mol less stable than *AA*, respectively. If these values of ΔE^m are accepted, then the ratios (q) between the vibrational partition functions of the conformers have to be quite different from 1.0, as shown in Table 14 (I). On the other hand, if the conformers have equal vibrational partition functions ($q = 1$) the ΔE^m values of Table 14 (II) show that *GG* is the most stable conformer.

In order to explain the experimental composition (Table 11) two possibilities have to be considered: (I) the conformational energies (ΔE^m) predicted by the semiempirical calculations are approximately correct, but the conformer *GG* has a much lower zero-point vibrational energy ($q \gg 1$) than *AG* and *AA*; (II) the conformers have approximately equal zero-point vibrational energies ($q = 1$), but then the ΔE^m values of the conformers have to be quite different from those calculated from the semiempirical energy model.

Table 14. Energy differences, ΔE^m (kcal/mol), and ratios (q) between vibrational partition functions of the conformers *GG*, *AG*, and *AA* of 1,3-dibromopropane at 65 °C.

Difference or ratio	*GG/AG*	*GG/AA*	*AG/AA*
ΔE^m(CALC.)[a], see Table 3	+0.51	+0.89	+0.38
(I) Ratio (q)[b] between vibrational partition functions if ΔE^m(CALC.) values are used	9.45	24.1	3.96
(II) ΔE^m values[c] if $q=1$	−0.94	−1.62	−0.62

[a] ΔE^m (CALC.) are the conformational-energy differences (between energy minima) predicted by the semiempirical calculations. [b] $q=(Q^*/Q)^{vib}$, calculated according to eqn. (1). [c] Calculated according to eqn. (1). The nozzle temperature (65 °C) and the composition parameters of Table 11 were used.

The conformational force fields have to be very different for the first (I) possibility to be correct. Is there any additional experimental evidence that can support this point? Most probably, the conformational differences in force fields are due to different torsional force constants. A complete set of experimental frequencies for each conformer does not exist, therefore vibrational spectroscopy can not, at present, prove or disprove the first possibility. If the torsional force constant of *GG* [$F_\phi=0.243$ mdyn Å (rad)$^{-2}$] is accepted, then the average value ($\bar{F}_\phi$) of *AG* had to be unreasonably large to yield a q value (GG/AG) of 9.45. With F_ϕ(GG) = 0.243 and $\bar{F}_\phi$(AG) = 0.480 the q value is 5.48 as shown in Table 9. The values of q(GG/AA) and q(AG/AA) critically depend on the value of the composition parameter α(AA). In conclusion, the first possibility seems unlikely, but the second possibility is not thereby proved. The correct ΔE^m values are probably a compromise between the two sets (I and II in Table 14).

The torsional frequencies reported for the conformer *GG* ($\omega_1=176$ and $\omega_2=186$ cm^{-1}) in Ref. 7 are not consistent with those derived from the electron diffraction data: $\omega_1=47^{+10}_{-5}$ cm^{-1} and $\omega_2=149^{+15}_{-10}$ cm^{-1}. The error limits here correspond to the error limits of the torsional force constant (Sect. V-B). Although the spectroscopic values (liquid) ought to be somewhat larger than those from electron diffraction (gas), the shift could not be that great. In conclusion, the lowest frequency (ω_1) has not been detected.[7] This was also the conclusion in the case of 1,2,3-tribromopropane.[8] The spectroscopic value of ω_2 is not excluded, since a shift in going from gas to liquid is possible.

The difference $\Delta\omega_{43}=\omega_4-\omega_3$ according to the present normal-coordinate analysis is 182 cm^{-1}, but the observed difference is only 14 cm^{-1}. The force field in Table 6 would have to be changed drastically in order to account for this observation. On the other hand, the assignment of ω_3 could be wrong. Moreover, the large discrepancies would be removed if the assignment were changed as follows: ω_1 (not observed), $\omega_2=176$ and $\omega_3=186$ cm^{-1}. The value of 310 cm^{-1} for ω_3 then must be given a new interpretation.

Acknowledgements. We are grateful to K. Brendhaugen for recording the diffraction photographs, and to Prof. O. Bastiansen and Dr. P. Klæboe for helpful discussions. Computer programs made available by Dr. H. M. Seip, Cand. real. S. Rustad, and Prof. W. D. Gwinn have been extensively used in this work. Financial support from Norges almenvitenskapelige forskningsråd is gratefully acknowledged.

REFERENCES

1. Sheppard, N. *J. Mol. Struct. 6* (1970) 5.
2. Bastiansen, O., Seip, H. M. and Boggs, J. E. In Dunitz, J. D. and Ibers, J. A., Eds.,

Perspectives in Structural Chemistry, Wiley, New York 1971, Vol. IV.
3. Seip, H. M. In Sim, G. A. and Sutton, L. E., Eds., *Molecular Structure by Diffraction Methods*, Specialist Periodical Reports, The Chemical Society, London 1973, Vol. 1, Part 1, Chapter 1.
4. Bartell, L. S. *Private communication.*
5. Brown, J. K. and Sheppard, N. *Proc. Roy. Soc. (London) A 231* (1955) 555.
6. Dempster, A. B., Price, K. and Sheppard, N. *Spectrochim. Acta Part A 25* (1969) 1381.
7. Thorbjørnsrud, J., Ellestad, O. H., Klæboe, P. and Torgrimsen, T. *J. Mol. Struct. 15* (1973) 61.
8. Stølevik, R. *Acta Chem. Scand. A 28* (1974) 299.
9. Abraham, R. J. and Parry, K. J. *J. Chem. Soc. B* (1970) 539.
10. Schachtschneider, J. H. and Snyder, R. G. *Vibrational Analysis of Polyatomic Molecules. IV* (force constants for the haloparaffins). Project No. 31450, Technical Report No. 122–63 of Shell Development Company.
11. Snyder, R. G. *J. Mol. Spectrosc. 28* (1960) 273.
12. Gwinn, W. D. *J. Chem. Phys. 55* (1971) 477.
13. Stølevik, R., Seip, H. M. and Cyvin, S. J. *Chem. Phys. Lett. 15* (1972) 263.
14. Zeil, W., Haase, J. and Wegmann, L. *Z. Instrumentenk. 74* (1966) 84.
15. Bastiansen, O., Graber, R. and Wegmann, L. *Balzer's High Vacuum Report 25* (1969) p. 1.
16. Andersen, B., Seip, H. M., Strand, T. G. and Stølevik, R. *Acta Chem. Scand. 23* (1969) 3224.
17. Peacher, J. and Willis, J. C. *J. Chem. Phys. 46* (1967) 4809.
18. Strand, T. G. and Bonham, R. A. *J. Chem. Phys. 40* (1964) 1686.
19. Almenningen, A., Bastiansen, O. and Munthe-Kaas, T. *Acta Chem. Scand. 10* (1956) 261.
20. Morino, Y., Kuchitsu, K. and Oka, T. *J. Chem. Phys. 36* (1962) 1108.
21. Kuchitsu, K. *J. Chem. Phys. 49* (1968) 4456.
22. Seip, H. M. and Stølevik, R. In Cyvin, S. J., Ed., *Molecular Structures and Vibrations*, Elsevier, Amsterdam 1972, p. 171.
23. Glasstone, S. *Theoretical Chemistry*, Van Nostrand, New York 1944.
24. Herzberg, G. *Infrared and Raman Spectra of Polyatomic Molecules*, Van Nostrand, Princeton, N. J. 1945.

Received March 5, 1974.

Acta Chemica Scandinavica A 28 (1974) 693—702

Short Communications

Polythionates. I. The Reaction between the Tetrathionate Ion and the Cyanide Ion in Acetonitrile

TOR AUSTAD

Chemical Institute, University of Bergen, N-5000 Bergen, Norway

It is known that the tetrathionate ion in aqueous solution reacts rapidly and quantitatively with the cyanide ion, giving ionic thiocyanate, thiosulfate, and sulfate, eqn. (1),[1]

$$S_4O_6^{2-} + CN^- + OH^- \longrightarrow S_2O_3^{2-} + SCN^- + SO_4^{2-} + H^+ \quad (1)$$

a reaction which forms the basis of the well-known cyanide method for the analysis of polythionates.[2,3]

Kinetic studies by Davis [4] suggest the mechanism to be in consistence with the one postulated by Foss,[5] involving a nucleophilic displacement of ionic thiosulfate by the cyanide ion, eqn. (2),

$$^-O_3S-S-S-SO_3^- + CN^- \xrightarrow{\text{slow}} {}^-O_3S-SCN + S_2O_3^{2-} \quad (2)$$

followed by a fast hydrolysis, eqn. (3).

$$^-O_3S-SCN + OH^- \xrightarrow{\text{fast}} SO_4^{2-} + SCN^- + H^+ \quad (3)$$

The dielectric constant of the solvent and the solvation of the leaving group are probably very important in the reaction between ionic tetrathionate and the cyanide ion. The rate of the reaction between ionic trithionate and the cyanide ion being about 50 times faster in water [6] than in a 50 % water-methanol solution,[7] seems to confirm this view.

To get a better insight into the solvation effects and the intermediates of the tetrathionate-cyanide reaction, this reaction has been studied in the dipolar aprotic solvent, acetonitrile. Tetraphenylarsonium tetrathionate was used as the substrate and tetraphenylphosphonium cyanide was used as the nucleophilic reagent. Results from conductivity measurements suggested these salts to be completely dissociated in acetonitrile in the concentration range used in the kinetic runs.

Product analysis showed that when reacting 1 mol of ionic tetrathionate and 2 mol of cyanide ion, 1 mol of ionic thiocyanate and 1 mol of ionic thiosulfate were obtained. The reaction, followed by measuring the formation of ionic thiocyanate, showed good second-order kinetics up to three half-lives. These observations would be in accordance with a rate determining step similarly to what is the case in aqueous solution (eqn. 2). The thiocyanatosulfonate ion, $^-O_3SSCN$, might then react with a second cyanide ion to give ionic thiocyanate and the cyanosulfonate ion (eqn. 4).

$$^-O_3SSCN + CN^- \longrightarrow {}^-O_3SCN + SCN^- \quad (4)$$

This reaction (eqn. 4) is, according to the kinetics, a much faster step. The rate constant of this step has been observed to be about 10 times higher than the rate constant of the first step.[8] The unstable thiocyanatosulfonate ion is converted, probably by a direct nucleophilic substitution by the cyanide ion, to a more stable cyanosulfonate ion. Stable salts, however, of the cyanosulfonate ion have not been isolated. Jander [9] and co-workers have found the cyanosulfonic acid to exist from potentiometric titration of a mixture of sulfur trioxide in excess hydrogen cyanide. From the present kinetic investigation the cyanosulfonate ion may be stable in acetonitrile, but several attempts to prepare the tetraphenylarsonium salt of this anion, using different synthetic routes, were unsuccessful.

The existence of the thiocyanatosulfonate ion as a reaction intermediates has further been postulated in the sulfur dicyanide-thiosulfate reaction in acid aqueous solution.[10] Schmidt [11] has been able to prepare the thiocyanatosulfonic acid *in situ* in ether at −78 °C, but at room temperature neither the acid nor the sodium salt is stable.

The second-order rate constants and the activation parameters for the reaction between ionic tetrathionate and the cyanide ion in acetonitrile and in water are listed in Table 1.

The rate constant in water is about 400 times greater than in acetonitrile even though the nucleophilicity of the cyanide ion towards methyl iodide is 4.1×10^4 times greater in a dipolar aprotic than in a protic solvent.[12] The solvation of the leaving group may, however, be responsible for the large fall in the rate constant observed in acetonitrile relative to water. The sulfate ion is one of the anions which interacts

Table 1. Second-order rate constants k_2, and activation parameters for the reaction between ionic tetrathionate and the cyanide ion in acetonitrile and in water.

	k_2 M^{-1} s^{-1} 25 °C	35 °C	45 °C	ΔH^* kcal/mol	ΔS^* cal/mol deg	ΔG^* kcal/mol
MeCN [a]	2.9×10^{-3}	5.0×10^{-3}	9.0×10^{-3}	9.8	−37	20.8
H_2O [b]	1.2			11.0	−22	17.5

[a] Ionic strength $\mu = 2.55 \times 10^{-2}$, this work. [b] Ionic strength $\mu = 1.77 \times 10^{-2}$, Ref. 4.

most strongly with protic solvents,[13] and Kolthoff [14] has stated that the sulfate ion is virtually unsolvated in acetonitrile and dimethyl sulfoxide. The thiosulfate ion, which is the leaving group in eqn. (2), probably exhibits much the same solvation properties as does the sulfate ion.

When considering the significance of the activation parameters, which are also presented in Table 1, it is seen that the decrease in the second-order rate constant in going from water to acetonitrile, is governed by a more unfavourable entropy of activation in the dipolar aprotic solvent,

$$\Delta S^*(\mathrm{MeCN}) - \Delta S^*(\mathrm{H_2O}) = -15 \text{ cal/mol deg.}$$

The large negative entropy of activation observed in acetonitrile may be caused by a more tight transition state in this solvent,[15] which provides no hydrogen bonding stabilization of the leaving group. Because of the large difference between the dielectric constants of water and acetonitrile, it is difficult to compare the results any further. However, it seems probable that the transition state is much better solvated in water than in acetonitrile.

The second-order rate constant, k_2, is a function of the ionic strength, μ. The addition of an inert salt, tetraphenylarsonium perchlorate, increases the rate (see Table 2). The data are in accordance with the predictions of the Brønsted-Christiansen-Scatchard equation

$$\log k = \log k_0 + 2AZ_1Z_2\sqrt{\mu}$$

When using $\varepsilon_{\mathrm{MeCN}} = 35.8$, the Debye-Hückel constant A in acetonitrile at 25 °C was calculated to be 3.756. The experimental value of A was found to be 3.9 ± 0.2. This appears to be a rare case of verification of the Debye-Hückel limiting law in a non-aqueous solvent.[16]

Table 2. Salt effects on the rate constant of the tetrathionate-cyanide reaction in acetonitrile at 25 °C. (Ph_4AsClO_4 as inert salt).

$\mu \times 10^2$	2.55	3.05	3.55	4.55
$k_2 \times 10^3$ M^{-1} s^{-1}	2.90	3.43	3.79	4.63

Acetonitrile was purified as reported previously.[17] Tetraphenylphosphonium cyanide was prepared in the same way as reported for tetraphenylarsonium cyanide.[17] Acetone, "Baker Analyzed" reagent, was used without further purification. Potassium tetrathionate was prepared by the method of Kurtenacker and Laszlo.[18]

Tetraphenylarsonium tetrathionate was precipitated from an aqueous solution of potassium tetrathionate, $K_2S_4O_6$, with tetraphenylarsonium chloride, Ph_4AsCl, in nearly quantitative yield. After filtration and washing several times with cold water, the product was washed with cold acetone to remove water and finally washed with ether. The product was recrystallized from acetonitrile by the addition of an equal amount of acetone. Dec. 253 °C. (Found: C 58.53; H 4.24; S 12.94. Calc. for $C_{48}H_{40}O_6S_4As_2$: C 58.20; H 4.04; S 12.95).

Product analysis. Two solutions of tetraphenylarsonium tetrathionate and tetraphenylarsonium cyanide, 1.00×10^{-2} M and 3.00×10^{-2} M respectively, were prepared, and 10 ml of each solution were pipetted out and mixed. After 4½ h at about 30 °C, two portions of 5 ml of the solution were pipetted out. The first was immediately analysed for ionic thiocyanate using IR [17] and found to contain 3.32×10^{-5} mol. The other solution was analysed for ionic thiosulfate, yield 3.48×10^{-5} mol, by iodometric titration.[3] The amounts of ionic thiocyanate and ionic thiosulfate in the reaction mixture were thus found to be the same within the experimental error.

Kinetic experiments. The rate was followed by measuring the formation of ionic thiocyanate, applying IR liquid cells with a path length of 1 mm.[17] The kinetic plots were analysed according to the rate-equation:

$$dx/dt = k_2(a-x)(b-2x)$$

where x is the concentration of ionic thiocyanate and a and b are the initial concentration of ionic tetrathionate and cyanide, 5.0×10^{-3} M and

1.0×10^{-2} M, respectively. The rates were determined with a Unicam SP 200 G Infrared Spectrophotometer and the rate constants were reproduced with an accuracy better than ± 3 %.

Conductivity measurements. When using $\lambda^{\circ}_{Ph_4As^+} = 55.8$ ohm^{-1} cm^{-2} mol^{-1} [19] the following equivalent conductivities at infinite dilution in acetonitrile at 25 °C were found:

$\lambda^{\circ}_{(Ph_4As)_2S_4O_6} = 172$ ohm^{-1} cm^{-2} mol^{-1}
$\lambda^{\circ}_{S_4O_6^{2-}} = 60.4$ ohm^{-1} cm^{-2} mol^{-1}
$\lambda^{\circ}_{Ph_4AsCN} = 150$ ohm^{-1} cm^{-2} mol^{-1}
$\lambda^{\circ}_{CN^-} = 94.2$ ohm^{-1} cm^{-2} mol^{-1}

From the plots, λ *versus* $\sqrt{c}$, the salts appeared to be completely dissociated in acetonitrile. The conductivity measurements were performed on a conductivity meter type CD M3 with a conductivity cell, type CDC 304 (immersion type) with a cell constant 1.00 cm ± 10 %.

Acknowledgement. The author wishes to expresss his thanks to The Norwegian Research Council for Science and the Humatities for a grant.

1. Kurtenacker, A. *Z. Anorg. Allg. Chem. 116* (1921) 243.
2. Kurtenacker, A. and Goldbach, E. *Z. Anorg. Allg. Chem. 166* (1927) 177.
3. Foss, O. *Kgl. Nor. Vidensk. Selsk. Skr.* (1945) No. 2, p. 20.
4. Davis, R. E. *J. Phys. Chem. 62* (1958) 1599.
5. Foss, O. *Acta Chem. Scand. 4* (1950) 404.
6. Davis, R. E., Louis, J. B. and Cohen, A. *J. Amer. Chem. Soc. 88* (1966) 1.
7. Ritter, R. D. and Krueger, J. H. *J. Amer. Chem. Soc. 92* (1970) 2316.
8. Austad, T. *Acta Chem. Scand. A 28* (1974). *In press.*
9. Jander, G., Grüttner, B. and Scholz, G. *Chem. Ber. 80* (1947) 279.
10. Kerr, D. F. and Wilson, I. R. *J. Chem. Soc. Dalton Trans.* (1973) 459.
11. Schmidt, M. and Talsky, G. *Chem. Ber. 93* (1960) 719.
12. Austad, T., Engemyr, L. B. and Songstad, J. *Acta Chem. Scand. 25* (1971) 3535.
13. Taylor, R. P. and Kuntz, Jr., I. D. *J. Amer. Chem. Soc. 94* (1972) 7963.
14. Kolthoff, I. M. and Chantooni, Jr., M. K. *J. Amer. Chem. Soc. 90* (1968) 5961.
15. Haberfield, P., Nudelman, A., Bloom, A., Romm, R. and Ginsberg, H. *J. Org. Chem. 36* (1971) 1792.
16. McLennan, D. J. *J. Chem. Soc. B* (1966) 709.
17. Austad, T., Songstad, J. and Åse, K. *Acta Chem. Scand. 25* (1971) 331.
18. Kurtenacker, A. and Laszlo, G. *Z. Anorg. Allg. Chem. 237* (1938) 359.
19. Springer, C. H., Coetzee, J. F. and Kay, R. L. *J. Phys. Chem. 73* (1969) 471.

Received May 6, 1974.

Hydrogen Bonding of Diphenylamine. Part 1. A Near Infrared Study of Its Complexes with Some Proton Acceptors

ANTTI KIVINEN,[a] JUHANI MURTO [b] and BIRGITTA SILVENNOINEN [a]

[a] Department of Pharmacy, University of Helsinki, Fabianinkatu 35, SF-00170 Helsinki 17, Finland and [b] Department of Physical Chemistry, University of Helsinki, Meritullinkatu 1 C, SF-00170 Helsinki 17, Finland

In the literature two quite different series of equilibrium constants K_c have been reported for the hydrogen bonded complexes formed by diphenylamine (DPA) with some proton acceptors. The values of Bhowmik and Basu [1] are appreciably greater than the values obtained by Sannigrahi and Chandra [2] by the same method (UV) and in similar conditions (Table 1). The proton acceptors used in the two studies mentioned above were not the same, but their proton-accepting power should be of the same order of magnitude.

To obtain a more reliable estimate of the proton donor strength of diphenylamine, we have measured the equilibrium constants for some diphenylamine–proton acceptor complexes by the IR method.

Experimental. Chemicals. Diphenylamine (*purum* grade, Schering-Kahlbaum AG) and benzophenone (zur Synthese, E. Merck AG) were used as received. 1,4-Dioxan (Uvasol grade, E. Merck AG) and dimethyl sulfoxide (DMSO, *purum* grade, Fluka AG) were purified by fractional crystallization. Hexamethylphosphoric triamide (HMPA, zur Synthese, E. Merck AG) was boiled with calcium oxide at diminished pressure for about 15 h and then distilled through a Vigreux column (b.p. 80 °C/2 mmHg). *N,N*-Dimethylacetamide (*purissimum* grade, Fluka AG) and carbon tetrachloride (Uvasol grade, E. Merck AG) were dried with molecular sieves 4A.

Table 1. Literature values of the equilibrium constants for the hydrogen bonding of diphenylamine with proton acceptors. Method UV, solvent cyclohexane, temperature 27 °C.

Proton acceptors	K_c / M^{-1}	Ref.
Benzophenone	14.4	1
Quinoxaline	17.4	1
Diethylnitrosoamine	28.2	1
Diethyl ether	0.28	2
Dioxan	0.58	2
Tetrahydrofuran	0.40	2

1.0×10^{-2} M, respectively. The rates were determined with a Unicam SP 200 G Infrared Spectrophotometer and the rate constants were reproduced with an accuracy better than ± 3 %.

Conductivity measurements. When using $\lambda^{\circ}_{Ph_4As^+} = 55.8$ ohm^{-1} cm^{-2} mol^{-1} [19] the following equivalent conductivities at infinite dilution in acetonitrile at 25 °C were found:

$\lambda^{\circ}_{(Ph_4As)_2S_4O_6} = 172$ ohm^{-1} cm^{-2} mol^{-1}
$\lambda^{\circ}_{S_4O_6^{2-}} = 60.4$ ohm^{-1} cm^{-2} mol^{-1}
$\lambda^{\circ}_{Ph_4AsCN} = 150$ ohm^{-1} cm^{-2} mol^{-1}
$\lambda^{\circ}_{CN^-} = 94.2$ ohm^{-1} cm^{-2} mol^{-1}

From the plots, λ *versus* $\sqrt{c}$, the salts appeared to be completely dissociated in acetonitrile. The conductivity measurements were performed on a conductivity meter type CD M3 with a conductivity cell, type CDC 304 (immersion type) with a cell constant 1.00 cm ± 10 %.

Acknowledgement. The author wishes to expresss his thanks to The Norwegian Research Council for Science and the Humatities for a grant.

1. Kurtenacker, A. *Z. Anorg. Allg. Chem. 116* (1921) 243.
2. Kurtenacker, A. and Goldbach, E. *Z. Anorg. Allg. Chem. 166* (1927) 177.
3. Foss, O. *Kgl. Nor. Vidensk. Selsk. Skr.* (1945) No. 2, p. 20.
4. Davis, R. E. *J. Phys. Chem. 62* (1958) 1599.
5. Foss, O. *Acta Chem. Scand. 4* (1950) 404.
6. Davis, R. E., Louis, J. B. and Cohen, A. *J. Amer. Chem. Soc. 88* (1966) 1.
7. Ritter, R. D. and Krueger, J. H. *J. Amer. Chem. Soc. 92* (1970) 2316.
8. Austad, T. *Acta Chem. Scand. A 28* (1974). *In press.*
9. Jander, G., Grüttner, B. and Scholz, G. *Chem. Ber. 80* (1947) 279.
10. Kerr, D. F. and Wilson, I. R. *J. Chem. Soc. Dalton Trans.* (1973) 459.
11. Schmidt, M. and Talsky, G. *Chem. Ber. 93* (1960) 719.
12. Austad, T., Engemyr, L. B. and Songstad, J. *Acta Chem. Scand. 25* (1971) 3535.
13. Taylor, R. P. and Kuntz, Jr., I. D. *J. Amer. Chem. Soc. 94* (1972) 7963.
14. Kolthoff, I. M. and Chantooni, Jr., M. K. *J. Amer. Chem. Soc. 90* (1968) 5961.
15. Haberfield, P., Nudelman, A., Bloom, A., Romm, R. and Ginsberg, H. *J. Org. Chem. 36* (1971) 1792.
16. McLennan, D. J. *J. Chem. Soc. B* (1966) 709.
17. Austad, T., Songstad, J. and Åse, K. *Acta Chem. Scand. 25* (1971) 331.
18. Kurtenacker, A. and Laszlo, G. *Z. Anorg. Allg. Chem. 237* (1938) 359.
19. Springer, C. H., Coetzee, J. F. and Kay, R. L. *J. Phys. Chem. 73* (1969) 471.

Received May 6, 1974.

Hydrogen Bonding of Diphenylamine. Part 1. A Near Infrared Study of Its Complexes with Some Proton Acceptors

ANTTI KIVINEN,[a] JUHANI MURTO [b] and BIRGITTA SILVENNOINEN [a]

[a] Department of Pharmacy, University of Helsinki, Fabianinkatu 35, SF-00170 Helsinki 17, Finland and [b] Department of Physical Chemistry, University of Helsinki, Meritullinkatu 1 C, SF-00170 Helsinki 17, Finland

In the literature two quite different series of equilibrium constants K_c have been reported for the hydrogen bonded complexes formed by diphenylamine (DPA) with some proton acceptors. The values of Bhowmik and Basu [1] are appreciably greater than the values obtained by Sannigrahi and Chandra [2] by the same method (UV) and in similar conditions (Table 1). The proton acceptors used in the two studies mentioned above were not the same, but their proton-accepting power should be of the same order of magnitude.

To obtain a more reliable estimate of the proton donor strength of diphenylamine, we have measured the equilibrium constants for some diphenylamine–proton acceptor complexes by the IR method.

Experimental. Chemicals. Diphenylamine (*purum* grade, Schering-Kahlbaum AG) and benzophenone (zur Synthese, E. Merck AG) were used as received. 1,4-Dioxan (Uvasol grade, E. Merck AG) and dimethyl sulfoxide (DMSO, *purum* grade, Fluka AG) were purified by fractional crystallization. Hexamethylphosphoric triamide (HMPA, zur Synthese, E. Merck AG) was boiled with calcium oxide at diminished pressure for about 15 h and then distilled through a Vigreux column (b.p. 80 °C/2 mmHg). *N,N*-Dimethylacetamide (*purissimum* grade, Fluka AG) and carbon tetrachloride (Uvasol grade, E. Merck AG) were dried with molecular sieves 4A.

Table 1. Literature values of the equilibrium constants for the hydrogen bonding of diphenylamine with proton acceptors. Method UV, solvent cyclohexane, temperature 27 °C.

Proton acceptors	K_c / M^{-1}	Ref.
Benzophenone	14.4	1
Quinoxaline	17.4	1
Diethylnitrosoamine	28.2	1
Diethyl ether	0.28	2
Dioxan	0.58	2
Tetrahydrofuran	0.40	2

Table 2. Equilibrium constants K_c and frequency shifts $\Delta\nu$NH for hydrogen bonding of diphenylamine (about 0.15 M in CCl_4) with proton acceptors. Temperature 25 °C.

Proton acceptor	K_c / M^{-1}	$\Delta\nu$NH / cm^{-1}	Concentration range/M
Benzophenone	0.622	48	0.19 – 0.49
1,4-Dioxan	0.608	73	0.54
N,*N*-Dimethylacetamide	4.18	102	0.080 – 0.125
DMSO	6.85	117	0.069 – 0.138
HMPA	19.4	155	0.054 – 0.066

Spectrometric measurements. These were carried out with a Beckman DK-2A spectrophotometer as described previously.[3,4] The concentrations were corrected for the thermal expansion of the solvent. The $\Delta\nu$-values are believed to be accurate within $\pm 3-5$ cm^{-1}, ΔH-values within ± 2 kJ mol^{-1} and K_c-values within 10 %.

The non-SI units used were: 1 M = 1 mol dm^{-3}; 1 mmHg = 133.322 Pa.

Results and discussion. The results given in Table 2 reveal that the proton donor strength of DPA is relatively low. This is to be expected, because phenyl groups reduce the basicity of amines. The values of K_c for DPA – benzophenone and DPA – 1,4-dioxan complexes are approximately equal, the frequency shift $\Delta\nu$NH being somewhat smaller in the former case. Our value $K_c = 0.608$ M^{-1} is close to the value 0.58 M^{-1} (27 °C, cyclohexane) reported by Sannigrahi and Chandra [2] for the DPA – dioxan complex. No drastic changes in spectrometric quantities are expected on going from carbon tetrachloride solutions to cyclohexane solutions, and thus we conclude that our results are in accordance with those reported by Sannigrahi and Chandra. The value $K_c = 14.4$ M^{-1} (27 °C, cyclohexane) reported by Bhowmik and Basu [1] for the DPA – benzophenone complex, on the other hand, is remarkably greater than our value $K_c = 0.622$ M^{-1} (25 °C, CCl_4). Thus it would seem that the values reported by Bhowmik and Basu for various hydrogen bonded complexes of DPA are indeed much too great.

Table 3. Spectrometric quantities for the hydrogen bonded 1:1 diphenylamine – hexamethylphosphoric triamide complex.

t / °C	K_c / M^{-1}	$-\Delta H$ / kJ mol^{-1}	$\Delta\nu$NH / cm^{-1}
0	46.1		
25	19.4	21.4	155
50	10.5		

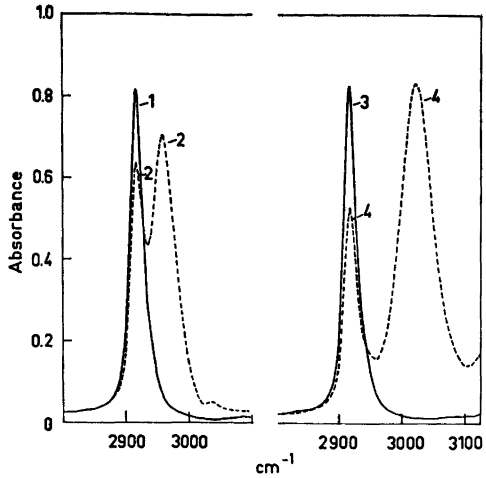

Fig. 1. Representative spectra of DPA – base systems. Solvent CCl_4, temperature 25 °C, path length 1 mm. Curve *1*, 0.148 M DPA, CCl_4 in the reference beam; curve *2*, 0.148 M DPA + 0.491 M benzophenone, 0.491 M benzophenone in the reference beam; curve *3*, 0.149 M DPA, CCl_4 in the reference beam; curve *4*, 0.149 M DPA + 0.138 M DMSO, 0.138 M DMSO in the reference beam.

The experimental data of Bhowmik and Basu are too meagre to conclude what is the reason for the discrepancies between their and our values.

The enthalpy of complexation was measured for the DPA – HMPA complex (Table 3), since HMPA is the most strongly complexing proton acceptor studied in this work. The value we obtained, $-\Delta H = 21.4$ kJ mol^{-1}, is somewhat greater than expected from the relatively small frequency shift (155 cm^{-1}); this enthalpy value indicates medium strong bonding. The values of the other thermodynamic parameters for the DPA – HMPA complex are $-\Delta G° = 7.36$ kJ mol^{-1} and $-\Delta S° = 47.1$ J mol^{-1} K^{-1}.

In Fig. 1 are shown two representative spectra of DPA complexes.

Acknowledgement. We gratefully acknowledge financial support from the Finnish National Research Council for Sciences.

1. Bhowmik, B. B. and Basu, S. *Trans. Faraday Soc. 58* (1962) 48.
2. Sannigrahi, A. B. and Chandra, A. K. *J. Phys. Chem. 67* (1963) 1106.
3. Kivinen, A. and Murto, J. *Suom. Kemistilehti B 40* (1967) 6.
4. Kivinen, A., Murto, J. and Kilpi, L. *Suom. Kemistilehti B 40* (1967) 301.

Received May 13, 1974.

Hydrogen Bonding Features of Hexachloro-2-propanol. Part 1. A Near Infrared Study of Its Hetero-association with Oxygen-containing Bases

ANTTI KIVINEN,[a] JUHANI MURTO[b] and BIRGITTA SILVENNOINEN[a]

[a] Department of Pharmacy, University of Helsinki, Fabianinkatu 35, SF-00170 Helsinki 17, Finland and [b] Department of Physical Chemistry, University of Helsinki, Meritullinkatu 1 C, SF-00170 Helsinki 17, Finland

In a recent, rather extensive study of fluorinated alcohols, special attention was paid to spectral and association properties.[1,2] Now the investigation has been extended to the analogous chlorinated alcohols to discover what influence the substitution of chlorine for fluorine has on the hydrogen bonding ability. 1,1,1,3,3,3-Hexachloro-2-propanol (HCP) was chosen as the model compound since its fluoro-analogue, 1,1,1,3,3,3-hexafluoro-2-propanol (HFP), has been extensively studied by us.

Earlier we have published a study on the hetero-association of HFP.[2] Here we report experimental data for the hetero-association of HCP with some proton acceptors.

Experimental. Chemicals. Hexachloro-2-propanol (Hynes Chemical Research Corp.) was purified by crystallization from hexane and dried in a desiccator with P_2O_5. Diphenyl sulfoxide (Aldrich Chemical Co.) was crystallized from hexane. The purification of the other chemicals has been reported previously.[2]

Measurements. The spectra were recorded on a Beckman DK-2A spectrophotometer equipped with a thermostated cell holder as described previously.[2] The path lengths of the cells were 20 mm. CCl_4 was used as solvent and the alcohol concentrations were sufficiently low to ensure that the alcohol was almost completely in the monomeric form. The concentrations were corrected for the thermal expansion of the solvent. At least two independent series of measurements were made for each alcohol–base pair.

Results and discussion. The free νOH absorption of HCP is a doublet (Fig. 1), the two peaks being somewhat more separated than in the case of HFP whose νOH absorption also comprises two peaks. The doublet nature of the νOH absorption is obviously due to the presence of two different conformers.[1] The experimental results obtained for various HCP–base systems are presented in Table 1, which includes also the corresponding values for HFP–base systems. The frequency shifts $\Delta\nu$OH are reported relative to the upper frequency of absorption of the free OH group occurring at about 3596 cm^{-1} in CCl_4 (the other peak of the doublet is at 3545 cm^{-1}). The equilibrium constants K_c (M^{-1}) were calculated as described previously from absorbance values observed before and after complex formation.[2]

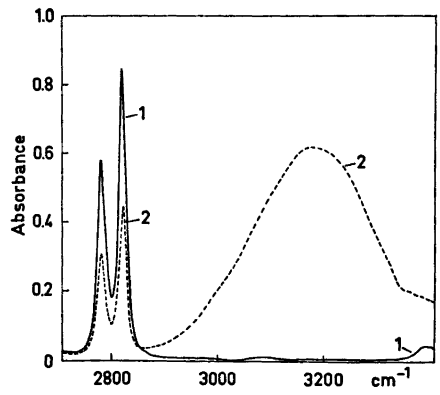

Fig. 1. Illustrative spectra for the system HCP–DMSO. Solvent CCl_4, temperature 25 °C, path length 20 mm. Curve *1*, 0.00418 M HCP, CCl_4 in the reference beam; curve *2*, 0.00418 M HCP + 0.00401 M DMSO, 0.00401 M DMSO in the reference beam.

When *N,N*-dimethylacetamide, tetramethylurea, diphenyl sulfoxide, or dimethyl sulfoxide was used as a base, the absorptions of the bonded νOH were uniform and the estimation of the frequency shifts ($\Delta\nu$) was easy. The absorption due to the bonded OH group of the HCP–acetone complex has a pronounced shoulder on the high-frequency side of the main band. This kind of band form is common when there is hydrogen bonding to a carbonyl oxygen. A reasonable explanation is the one given by Joris and Schleyer,[5] *viz.*, that there are two bonding sites to which the proton can attach. The frequency shift for the HCP–acetone system is estimated from the main maximum.

When hexamethylphosphoric triamide (HMPA) was used as the proton acceptor, only a lower limit for $\Delta\nu$OH could be estimated because of the irregular form of the complex absorption. A similar irregularity in the hydrogen-bonded OH absorption is observed also in other HMPA complexes with alcohols or phenols of relatively great acidity.[4] The obvious reason for this is the relatively strong hydrogen bonds formed by HMPA; these will be discussed later in another connection.

The data in Table 1 reveal that the hydrogen bonds formed by HCP are relatively strong. However, the proton donating power of HFP is still somewhat more pronounced than that of HCP, as indicated by the greater values of K_c and $-\Delta H$ for the former compound. In Fig. 2 the values of $\Delta\nu$OH for the HCP–base complexes are plotted against the values of

Table 1. Values of spectrometric quantities for hydrogen bonding between hexachloro-2-propanol or hexafluoro-2-propanol (from Ref. 2) and various bases. Solvent CCl_4. Abbreviations: DMA = *N*,*N*-dimethylacetamide, TMU = tetramethylurea, DPSO = diphenyl sulfoxide, DMSO = dimethyl sulfoxide, HMPA = hexamethylphosphoric triamide.

Base	t / °C	HCP K_c / M^{-1}	HCP $-\Delta H$ / kJ mol^{-1}	HCP $\Delta\nu$OH / cm^{-1}	HFP K_c / M^{-1}	HFP $-\Delta H$ / kJ mol^{-1}	HFP $\Delta\nu$OH / cm^{-1}
Acetone	0	23.7			118		
	25	11.1	21.0	300	49.0	24.9	297
	50	5.65			22.1		
DMA	0	509			5270		
	25	188	27.6	418	1520	32.1	405
	50	77.9			550		
TMU	0	688			4470		
	25	233	28.7	413	1300	33.7	390
	50	97.1			432		
DPSO[a]	0	183			1380		
	25	78.2	22.1	379	448	30.7	378
	50	40.7			172		
DMSO	0	826			3730		
	25	292	27.3	449	1430	29.2	437
	50	129			609		
HMPA[b]	15	6050			37 000		
	25	3960	33.3	> 552	23 600	37.3	> 519
	50	1360			7140		

[a] Ref. 3. [b] Ref. 4.

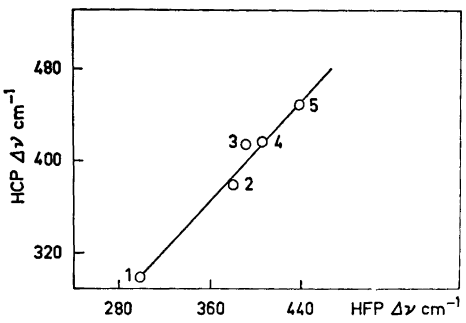

Fig. 2. The values of $\Delta\nu$OH for the HCP – base systems plotted against the values of $\Delta\nu$OH for the HFP – base systems. Base: 1 acetone, 2 diphenyl sulfoxide, 3 tetramethylurea, 4 *N*,*N*-dimethylacetamide, 5 dimethyl sulfoxide. The radii of the circles are of the order of experimental uncertainty.

$\Delta\nu$ for HFP – base complexes. The relationship is seen to be linear within experimental accuracy.

The values of $-\Delta H$, $-\Delta G°$, and $-\Delta S°$ (Table 2) for the HCP – diphenyl sulfoxide system are somewhat smaller than would be expected when compared for instance with the related values for HCP – acetone or HFP – diphenyl sulfoxide systems. This may be due, at least in part, to steric hindrance of the relatively bulky trichloromethyl groups of HCP or of the phenyl groups of diphenyl sulfoxide.

Table 2. Values of $\Delta G°$ and $\Delta S°$ for the hydrogen bonding between HCP and bases. For abbreviations, see Table 1.

Base	$-\Delta G°$ / kJ mol^{-1}	$-\Delta S°$ / J mol^{-1} K^{-1}
Acetone	5.68	50.5
DMA	12.9	47.3
TMU	13.4	49.9
DPSO	10.9	35.3
DMSO	13.9	42.5
HMPA	20.1	40.3

Acknowledgement. We gratefully acknowledge financial support from the Jenny and Antti Wihuri Foundation of the Finnish Academy of Sciences.

1. Murto, J., Kivinen, A., Viitala, R. and Hyömäki, J. *Spectrochim. Acta A 29* (1973) 1121.

2. Kivinen, A., Murto, J. and Kilpi, L. *Suom. Kemistilehti B 40* (1967) 301.
3. Kivinen, A., Murto, J. and Liljeqvist, S. *Unpublished results.*
4. Kuopio, R., Kivinen, A. and Murto, J. *Unpublished results.*
5. Joris, L. and Schleyer, P. von R. *J. Amer. Chem. Soc. 90* (1968) 4599.

Received May 13, 1974.

Additivity Relations of Partial Molal Volumes in Carboxylic Acid Series

HARALD HØILAND

Department of Chemistry, University of Bergen, N-5000 Bergen, Norway

It has been shown by a number of workers that the partial molal volumes of electrolytes at infinite dilution are equal to the sum of the ionic components (see Ref. 1). Clearly, as Millero [1] points out, the utility of partial molal volumes to study ion – water interactions lies in the additivity principle.

Only a CH_2-group, with its volume requirements, separates two successive members of a homologous series of carboxylic acids. As early as 1899 Traube [2] found that the partial molal volume of a CH_2-group in aqueous solution was on the average 16.0 ml mol^{-1}. This has been verified by the data of Sakurai.[3] In this paper data at 25 °C obtained by King,[4] Sakurai,[3] and Høiland [5] have been used to investigate the additivity of the partial molal volumes of the groups comprising the carboxylic acid or the acid anion.

Results. Two requirements must be fulfilled in order to calculate the partial molal volumes of the different groups involved. First, the well documented starting point that the partial molal volume of a CH_2-group is 16.0 ml mol^{-1}. Second, the partial molal volume of the sodium ion is required in order to obtain the partial molal volume of the carboxylate ion. The best value of $\bar{V}^0(Na^+)$ is probably found by taking Zana and Yeager's [6] value for $\bar{V}^0(H^+) = -5.4 \pm 0.2$ ml mol^{-1}, and add the experimentally determined difference $\bar{V}^0(H^+) - \bar{V}^0(Na^+) = -1.2$ ml mol^{-1}. Thus $\bar{V}^0(Na^+) = -6.6$ ml mol^{-1}. This was used, and the experimental data are given in Table 2. The value of $\bar{V}^0(Na^+)$ does not affect the additivity principle, only the partial molal volume of the COO^- group.

Table 1. Partial molal volumes, infinite dilution, 25 °C, ml mol^{-1}.

$-COOH$	25.9	
$-CH_3$	26.1	
$-CH_2-$	16.0	
$-CH_2COO^-$	33.7	(13 + 20.7)

Table 2. Partial molal volumes at infinite dilution, 25 °C, ml mol^{-1}.

n	Exp.	Calc.	Diff.
A; $CH_3(CH_2)_nCOOH$			
0	51.9	52.0	−0.1
1	67.9	68.0	−0.1
2	84.6	84.0	0.6
3	100.5	100.0	0.5
4	116.0	116.0	0
B; $(CH_2)_n(COOH)_2$			
0	50.2	51.8	−1.6
1	67.2	67.8	−0.6
2	82.9	83.8	−0.9
3	99.1	99.8	−0.7
4	115.7	115.8	−0.1
5	131.9	131.8	0.1
C; $CH_3(CH_2)_nCOO^-$			
0	45.8		
1	60.3	59.8	0.5
2	75.8	75.8	0
3	91.7	91.8	−0.1
4	107.2	107.8	−0.6
D; $COOH(CH_2)_nCOO^-$			
0	45.7	(46.6)	(1.2)
2	75.5	75.6	−0.1
3	91.4	91.6	−0.2
4	107.6	107.6	0
5	123.2	123.6	−0.4
E; $(CH_2)_n(COO^-)_2$			
0	41.3	(41.4)	(−0.1)
2	67.3	67.4	−0.1
3	83.2	83.4	−0.2
4	99.4	99.4	0
5	115.0	115.4	−0.4

With $\bar{V}^0(CH_2) = 16.0$ ml mol^{-1} average values of the partial molal volume of the COOH group were calculated from series A and B, Table 2, CH_3 group values from A and C. Results are summarized in Table 1. A charged carboxyl group influences the hydration sphere of the nearest neighbouring CH_2 group substantially.[7] Separation of the partial molal volumes of the COO^- group and the nearest CH_2 group will therefore be ambiguous. The partial molal volumes from series C, D, and E (Table 2) are given as $\bar{V}^0(CH_2COO^-)$ in Table

2. Kivinen, A., Murto, J. and Kilpi, L. *Suom. Kemistilehti B 40* (1967) 301.
3. Kivinen, A., Murto, J. and Liljeqvist, S. *Unpublished results.*
4. Kuopio, R., Kivinen, A. and Murto, J. *Unpublished results.*
5. Joris, L. and Schleyer, P. von R. *J. Amer. Chem. Soc. 90* (1968) 4599.

Received May 13, 1974.

Additivity Relations of Partial Molal Volumes in Carboxylic Acid Series

HARALD HØILAND

Department of Chemistry, University of Bergen, N-5000 Bergen, Norway

It has been shown by a number of workers that the partial molal volumes of electrolytes at infinite dilution are equal to the sum of the ionic components (see Ref. 1). Clearly, as Millero [1] points out, the utility of partial molal volumes to study ion – water interactions lies in the additivity principle.

Only a CH_2-group, with its volume requirements, separates two successive members of a homologous series of carboxylic acids. As early as 1899 Traube [2] found that the partial molal volume of a CH_2-group in aqueous solution was on the average 16.0 ml mol^{-1}. This has been verified by the data of Sakurai.[3] In this paper data at 25 °C obtained by King,[4] Sakurai,[3] and Høiland [5] have been used to investigate the additivity of the partial molal volumes of the groups comprising the carboxylic acid or the acid anion.

Results. Two requirements must be fulfilled in order to calculate the partial molal volumes of the different groups involved. First, the well documented starting point that the partial molal volume of a CH_2-group is 16.0 ml mol^{-1}. Second, the partial molal volume of the sodium ion is required in order to obtain the partial molal volume of the carboxylate ion. The best value of $\bar{V}^0(Na^+)$ is probably found by taking Zana and Yeager's [6] value for $\bar{V}^0(H^+) = -5.4 \pm 0.2$ ml mol^{-1}, and add the experimentally determined difference $\bar{V}^0(H^+) - \bar{V}^0(Na^+) = -1.2$ ml mol^{-1}. Thus $\bar{V}^0(Na^+) = -6.6$ ml mol^{-1}. This was used, and the experimental data are given in Table 2. The value of $\bar{V}^0(Na^+)$ does not affect the additivity principle, only the partial molal volume of the COO^- group.

Table 1. Partial molal volumes, infinite dilution, 25 °C, ml mol^{-1}.

$-COOH$	25.9	
$-CH_3$	26.1	
$-CH_2-$	16.0	
$-CH_2COO^-$	33.7	(13 + 20.7)

Table 2. Partial molal volumes at infinite dilution, 25 °C, ml mol^{-1}.

n	Exp.	Calc.	Diff.
A; $CH_3(CH_2)_nCOOH$			
0	51.9	52.0	−0.1
1	67.9	68.0	−0.1
2	84.6	84.0	0.6
3	100.5	100.0	0.5
4	116.0	116.0	0
B; $(CH_2)_n(COOH)_2$			
0	50.2	51.8	−1.6
1	67.2	67.8	−0.6
2	82.9	83.8	−0.9
3	99.1	99.8	−0.7
4	115.7	115.8	−0.1
5	131.9	131.8	0.1
C; $CH_3(CH_2)_nCOO^-$			
0	45.8		
1	60.3	59.8	0.5
2	75.8	75.8	0
3	91.7	91.8	−0.1
4	107.2	107.8	−0.6
D; $COOH(CH_2)_nCOO^-$			
0	45.7	(46.6)	(1.2)
2	75.5	75.6	−0.1
3	91.4	91.6	−0.2
4	107.6	107.6	0
5	123.2	123.6	−0.4
E; $(CH_2)_n(COO^-)_2$			
0	41.3	(41.4)	(−0.1)
2	67.3	67.4	−0.1
3	83.2	83.4	−0.2
4	99.4	99.4	0
5	115.0	115.4	−0.4

With $\bar{V}^0(CH_2) = 16.0$ ml mol^{-1} average values of the partial molal volume of the COOH group were calculated from series A and B, Table 2, CH_3 group values from A and C. Results are summarized in Table 1. A charged carboxyl group influences the hydration sphere of the nearest neighbouring CH_2 group substantially.[7] Separation of the partial molal volumes of the COO^- group and the nearest CH_2 group will therefore be ambiguous. The partial molal volumes from series C, D, and E (Table 2) are given as $\bar{V}^0(CH_2COO^-)$ in Table

1 with approximate individual values in parenthesis.

Conclusion. Calculations of partial molal volumes by adding the partial molal volumes of the groups comprising the molecule or ion, agree well with the experimental values for the carboxyl series, Table 2. The additivity relations thus established make possible a simplified treatment of solute solvent interactions, reducing the effective number of systems. It would mean that investigations of microscopic relations in solution may be concentrated to one or two of the groups of the molecule. The search for realistic models for statistical simulation calculations would also be simplified.

1. Millero, F. J. In Horne, R. A., Ed., *Water and Aqueous Solutions*, Wiley-Interscience, New York 1971, p. 519.
2. Traube, J. *Samml. Chem. Vortr. 4* (1899) 255.
3. Sakurai, M. *Bull. Chem. Soc. Jap. 46* (1973) 1596.
4. King, E. J. *J. Phys. Chem. 73* (1969) 1220.
5. Høiland, H. *Manuscript in preparation.*
6. Zana, R. and Yeager, E. *J. Phys. Chem. 71* (1967) 521.
7. Høiland, H. *J. Chem. Soc. Faraday Trans. 1* (1974) 1180.

Received June 6, 1974.

Aqueous Chemistry of Protactinium(IV). 4. Complex Formation between Pa(IV) and EDTA

ROBERT LUNDQVIST and JAN-ERIK ANDERSSON

Department of Nuclear Chemistry, Chalmers University of Technology, Fack, S-402 20 Göteborg 5, Sweden

In studying the aqueous chemistry of Pa(IV) it was concluded [1] that Pa(IV) exists as a doubly charged cation PaO^{2+} (or $Pa(OH)_2^{2+}$). To obtain further information on this species, complex formation with ethylenediaminetetraacetic acid (EDTA) was investigated. To study the complexation with EDTA, the liquid–liquid distribution system $^{233}Pa(IV)$ – acetylacetone in benzene – 1 M $(Na,H)ClO_4$ was chosen since this system had been used previously.[2] The influence of EDTA (added to the aqueous phase of the extraction system) on the distribution of Pa(IV) will then provide information on Pa(IV) – EDTA complexes.

Experimental. The extraction technique and the preparation of most chemicals have been previously described.[2,3] The distribution system, 2.16 M acetylacetone in benzene – 1 M (Na,H,-0.01 Cr^{3+})ClO_4 was reduced electrolytically in an atmosphere of argon gas before addition of ^{233}Pa and EDTA (EDTA was always added after the ^{233}Pa). EDTA (Merck, *p.a.*) was added as a 10^{-2} M solution in 1 M $NaClO_4$. The system was stirred during electrolysis until the D-values ($D = [Pa]_{org}/[Pa]$) were constant, which usually occurred within 15 min.

The extraction system was found to be independent of the Cr^{2+} concentration for concentrations up to at least 0.02 M, at ph ($= -\log [H^+]$) = 1. Moreover, the degree of complexation between Cr^{2+} and EDTA was calculated using literature data [4] and was found negligible for the ph range examined.

Evaluation of the species involved in the extraction. In order to derive the ionic forms of the complexes formed in the reactions between Pa(IV) and EDTA the following general reaction is considered: $PaO^{2+} + H_nY^{(n-4)+} \rightleftharpoons Pa(OH)_rYH_b^{(b-r)+} + (n-b-2+r)H^+ + (1-r)H_2O$; $b = 0,1,2$; $n = 0,1,\ldots 6$.

Here Pa(IV) is denoted with PaO^{2+} but a similar reaction may be set up with $Pa(OH)_2^{2+}$. Since EDTA, denoted by H_4Y, is expected to have a maximum of 6 chelate positions, of which at least 4 are assumed to be occupied by Pa(IV) in the complex $Pa(OH)_rYH_b^{(b-r)+}$, b can have the values 0, 1 or 2. In the above equation provision is made for a change in the extent of hydrolysis of the central atom.

The number of protons participating in the reaction may be derived from the experimentally determined ph dependence of the extraction reaction. The extraction reaction formula is obtained by combination of the above reaction formula and the extraction reaction formula valid for Pa(IV) in the absence of EDTA:

$$PaO^{2+} + 2HAA(org) \rightleftharpoons PaO(AA)_2(org) + 2H^+,$$

(HAA = acetylacetone); equilibrium constant K_D. The following overall extraction reaction is thus obtained:

$$Pa(OH)_rYH_b^{(b-r)+} + 2HAA(org) + (n-b-4+r)H^+ + (1-r)H_2O \rightleftharpoons PaO(AA)_2(org) + H_nY^{(n-4)+}$$

This reaction mechanism was studied experimentally under conditions where the Pa-EDTA complex was the dominating protactinium species. The observed dependence of the distribution ratio on the concentrations of HAA ($\partial \log D/\partial \log [HAA] = 2$) and EDTA ($\partial \log D/\partial \log [EDTA] = -1$) verifies the proposed extraction mechanism.

From the limiting ph-dependence $\partial \log D/\partial \log ph = -2$ (see Fig. 1), one concludes that the average number of protons $(n-b-4+r)$

1 with approximate individual values in parenthesis.

Conclusion. Calculations of partial molal volumes by adding the partial molal volumes of the groups comprising the molecule or ion, agree well with the experimental values for the carboxyl series, Table 2. The additivity relations thus established make possible a simplified treatment of solute solvent interactions, reducing the effective number of systems. It would mean that investigations of microscopic relations in solution may be concentrated to one or two of the groups of the molecule. The search for realistic models for statistical simulation calculations would also be simplified.

1. Millero, F. J. In Horne, R. A., Ed., *Water and Aqueous Solutions*, Wiley-Interscience, New York 1971, p. 519.
2. Traube, J. *Samml. Chem. Vortr. 4* (1899) 255.
3. Sakurai, M. *Bull. Chem. Soc. Jap. 46* (1973) 1596.
4. King, E. J. *J. Phys. Chem. 73* (1969) 1220.
5. Høiland, H. *Manuscript in preparation.*
6. Zana, R. and Yeager, E. *J. Phys. Chem. 71* (1967) 521.
7. Høiland, H. *J. Chem. Soc. Faraday Trans. 1* (1974) 1180.

Received June 6, 1974.

Aqueous Chemistry of Protactinium(IV). 4. Complex Formation between Pa(IV) and EDTA

ROBERT LUNDQVIST and JAN-ERIK ANDERSSON

Department of Nuclear Chemistry, Chalmers University of Technology, Fack, S-402 20 Göteborg 5, Sweden

In studying the aqueous chemistry of Pa(IV) it was concluded [1] that Pa(IV) exists as a doubly charged cation PaO^{2+} (or $Pa(OH)_2^{2+}$). To obtain further information on this species, complex formation with ethylenediaminetetraacetic acid (EDTA) was investigated. To study the complexation with EDTA, the liquid–liquid distribution system $^{233}Pa(IV)$ – acetylacetone in benzene – 1 M $(Na,H)ClO_4$ was chosen since this system had been used previously.[2] The influence of EDTA (added to the aqueous phase of the extraction system) on the distribution of Pa(IV) will then provide information on Pa(IV) – EDTA complexes.

Experimental. The extraction technique and the preparation of most chemicals have been previously described.[2,3] The distribution system, 2.16 M acetylacetone in benzene – 1 M (Na,H,-0.01 Cr^{3+})ClO_4 was reduced electrolytically in an atmosphere of argon gas before addition of ^{233}Pa and EDTA (EDTA was always added after the ^{233}Pa). EDTA (Merck, *p.a.*) was added as a 10^{-2} M solution in 1 M $NaClO_4$. The system was stirred during electrolysis until the D-values ($D = [Pa]_{org}/[Pa]$) were constant, which usually occurred within 15 min.

The extraction system was found to be independent of the Cr^{2+} concentration for concentrations up to at least 0.02 M, at ph ($= -\log [H^+]$) = 1. Moreover, the degree of complexation between Cr^{2+} and EDTA was calculated using literature data [4] and was found negligible for the ph range examined.

Evaluation of the species involved in the extraction. In order to derive the ionic forms of the complexes formed in the reactions between Pa(IV) and EDTA the following general reaction is considered: $PaO^{2+} + H_nY^{(n-4)+} \rightleftharpoons Pa(OH)_rYH_b^{(b-r)+} + (n-b-2+r)H^+ + (1-r)H_2O$; $b = 0,1,2$; $n = 0,1,\ldots 6$.

Here Pa(IV) is denoted with PaO^{2+} but a similar reaction may be set up with $Pa(OH)_2^{2+}$. Since EDTA, denoted by H_4Y, is expected to have a maximum of 6 chelate positions, of which at least 4 are assumed to be occupied by Pa(IV) in the complex $Pa(OH)_rYH_b^{(b-r)+}$, b can have the values 0, 1 or 2. In the above equation provision is made for a change in the extent of hydrolysis of the central atom.

The number of protons participating in the reaction may be derived from the experimentally determined ph dependence of the extraction reaction. The extraction reaction formula is obtained by combination of the above reaction formula and the extraction reaction formula valid for Pa(IV) in the absence of EDTA:

$$PaO^{2+} + 2HAA(org) \rightleftharpoons PaO(AA)_2(org) + 2H^+,$$

(HAA = acetylacetone); equilibrium constant K_D. The following overall extraction reaction is thus obtained:

$$Pa(OH)_rYH_b^{(b-r)+} + 2HAA(org) + (n-b-4+r)H^+ + (1-r)H_2O \rightleftharpoons PaO(AA)_2(org) + H_nY^{(n-4)+}$$

This reaction mechanism was studied experimentally under conditions where the Pa-EDTA complex was the dominating protactinium species. The observed dependence of the distribution ratio on the concentrations of HAA ($\partial \log D/\partial \log [HAA] = 2$) and EDTA ($\partial \log D/\partial \log [EDTA] = -1$) verifies the proposed extraction mechanism.

From the limiting ph-dependence $\partial \log D/\partial \log ph = -2$ (see Fig. 1), one concludes that the average number of protons $(n-b-4+r)$

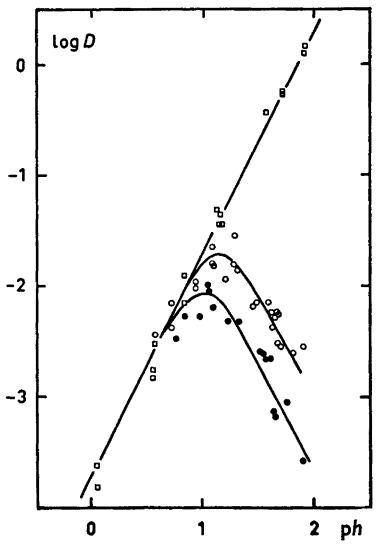

Fig. 1. Distribution of ^{233}Pa(IV), at 25 °C, between 2.16 M acetylacetone in benzene and dilute solutions of EDTA in 1 M (Na,H)ClO_4 as a function of ph (= −log [H$^+$]). The line and curves are calculated from estimated stability constants. □, [EDTA] = 0 M; ○, [EDTA] = $10^{-3.92}$ M; ●, [EDTA] = $10^{-3.25}$ M.

involved in the extraction reaction is equal to 2. Thus $r = 6 + b - n$. The values of n are obtained by considering the presence of three EDTA species H_3Y^-, H_4Y, and H_5Y^+ ($n = 3$, 4, and 5) in the appropriate ph range (1.2 − 1.7) according to the reported protonisation constants [5] for EDTA; $H_{n-1}Y^{(n-5)+} + H^+ \rightleftharpoons H_nY^{(n-4)+}$, $K_1 = 10^{2.85}$, $K_2 = 10^{6.28}$, $K_3 = 10^{2.3}$, $K_4 = 10^{2.2}$, $K_5 = 10^{1.4}$, and $K_6 = 10^{-0.12}$. Formally, r-values ranging from 1 to 5 are obtained. However, Pa(IV) is not expected to be further hydrolyzed due to the complexation with EDTA and hence r-values greater than 2 are not considered. Of the remaining two possible values, r equal to 1 or 2, one concludes that, on the average, $r = 2$ must be the most probable value since the value $r = 1$ is limited to a reaction ($n = 5$, $b = 0$) with only one EDTA species, H_5Y^+, which furthermore represents only a minor portion of the EDTA species. Since only the average number $(n - b - 4 + r)$ of protons participating in the reaction is known, one cannot exclude reactions other than those outlined above. However, one may expect the following species to be the main ones in the extraction system M^{2+}, $M(AA)_2$(org), MY^{2-} and MYH^-, where $M^{2+} = Pa(OH)_2^{2+}$ or PaO^{2+}.

Calculation of formation constants. Having evaluated the main species of the extraction system one can write the distribution constant $D = [Pa(IV)(org)]/[Pa(IV)]$ as

$$D = \frac{[M(AA)_2org]}{[M^{2+}] + [MY^{2-}] + [MYH^-]}$$

The distribution of Pa(IV) in the absence of EDTA, given by D_0, may be obtained from the extraction constant K_D;

$$K_D = \frac{[M(AA)_2(org)][H^+]^2}{[M^{2+}][HAA(org)]^2} = \frac{D_0[H^+]^2}{[HAA(org)]^2}$$

The value of K_D, calculated from the straight line in Fig. 1 was found to be $10^{-4.38 \pm .10}$. This value is slightly different from that reported before,[2] *i.e.* $10^{-4.13 \pm 05}$. The small difference is probably due to the more acidic media in the present investigation and to only one HAA concentration being used. The former value was used in the calculation below. As Pa(IV) is present in trace concentrations ([Pa] ≈ 10^{-10} M), the amount of EDTA complexes with Pa(IV) can be neglected. The concentrations of $H_nY^{(n-4)+}$ may then be calculated from the total concentration of EDTA and H$^+$.

Knowing the main Pa-EDTA species, the concentrations of Y^{4-} and H$^+$ and their effect on the distribution of Pa(IV), it is possible to calculate the complex formation constants K_1 and K_1* for the reactions $M^{2+} + Y^{4-} \rightleftharpoons MY^{2-}$ and $M^{2+} + Y^{4-} + H^+ \rightleftharpoons MYH^-$, respectively. The following equation may be derived $D_0/D - 1 = [Y^{4-}](K_1 + K_1^*[H^+])$. The values of $(K_1 + K_1^*[H])$ were calculated for each experimental point (D,[H$^+$]) and the regression of $(K_1 + K_1^*[H^+])$ as a function of [H$^+$] was calculated using the weighted least squares method. The values obtained were $K_1 = 10^{19.0 \pm 0.2}$ and $K_1^* = 10^{20.5 \pm 0.3}$. (Since the accuracy of the $(K_1 + K_1^*[H^+])$ values is proportional to $(D_0/D - 1)$ the error square sum was weighted with this factor). The calculated functions log $D = f($p$h)$ for [EDTA] = $10^{-3.92}$ M and $10^{-3.25}$ M are shown together with experimental data in Fig. 1. Due to the large uncertainty in the K_1* value, calculations were also carried out with $K_1^* = 0$ (*i.e.* the MHY^- complex was neglected). The value $K_1 = 10^{19.2 \pm 0.1}$ was then obtained.

Discussion. The present investigation shows that PaO^{2+} (or $Pa(OH)_2^{2+}$) is the dominating Pa(IV) species also under rather acidic conditions, ph 0 − 2 (Fig. 1). In the presence of EDTA the species $PaOY^{2-}$ (or $Pa(OH)_2Y^{2-}$) and possibly also $PaOYH^-$ (or $Pa(OH)_2YH^-$) are formed. The formation constant $K_1 = 10^{19.2 \pm 0.1}$ for $PaOY^{2-}$ (or $Pa(OH)_2Y^{2-}$) may be compared to the corresponding constant [6] $K = 10^{22.1 \pm 0.1}$ for the complex $Pa(OH)_2Y^-$ of Pa(V) and EDTA ($\mu = 1$, 20 °C, chloride media). The complexation is as expected stronger with the higher charged Pa(V) ion. However, in comparison with other divalent cations [7] (*e.g.* UO_2^{2+}, VO^{2+}, TiO^{2+}, PuO^{2+}, the first transition series $V^{2+} - Zn^{2+}$, and Group IIA $Be^{2+} - Ba^{2+}$) the complexation between Pa(IV) and EDTA is strong.

Acknowledgement. The authors are indebted to Professor Jan Rydberg for many valuable suggestions and to Enrica Ratti-Moberg for revising the English text.

1. Lundqvist, R. *International Solvent Extraction Conference*, Lyon 8–14 Sept. 1974. *Chem. Soc. Ind. London* (1974) 469.
2. Lundqvist, R. *Acta Chem. Scand. A 28* (1974) 243.
3. Lundqvist, R. and Rydberg, J. *Acta Chem. Scand. A 28* (1974) 399.
4. Pecsok, R. L., Shields, L. D. and Schaefer, N. P. *Inorg. Chem. 3* (1964) 114.
5. Anderegg, G. *Helv. Chim. Acta, 50* (1967) 2333.
6. Shiokawa, T., Kikuchi, M. and Omori, T. *Inorg. Nucl. Chem. Lett. 5* (1969) 105.
7. Sillén, L. G. and Martell, A. E. *Stability Constants of Metal Ion Complexes*, Burlington House, London 1964 and 1971.

Received June 26, 1974.

Acta Chemica Scandinavica A 28 (1974) 703—707

Multicomponent Polyanions. X. A Stopped-flow Study of the Kinetics of the Decomposition of Pentamolybdodiphosphates and Heptamolybdates in Alkaline 3.0 M $Na(ClO_4)$

ROLF MELLSTRÖM and NILS INGRI

Department of Inorganic Cemistry, University of Umeå, S-901 87 Umeå, Sweden

The decomposition of the aqueous pentamolybdodiphosphates, $Mo_5P_2O_{23}^{6-}$, $HMo_5P_2O_{23}^{5-}$, and $H_2Mo_5P_2O_{23}^{4-}$, in alkaline 3.0 M $Na(ClO_4)$, has been studied at 25 °C by using spectrophotometric stopped-flow measurements. It was found that the protonized species were instantaneously neutralized to $Mo_5P_2O_{23}^{6-}$ and that the decomposition of $Mo_5P_2O_{23}^{6-}$ followed the rate equation $-d[Mo_5P_2O_{23}^{6-}]/dt = k[Mo_5P_2O_{23}^{6-}]\cdot[OH^-]$, where the rate constant k was determined to be 16.7 ± 0.9 M^{-1} s^{-1}. This result strongly supports emf-equilibrium measurements which suggest the mentioned protonized series. Equilibrium solutions corresponding to the heptamolybdates $Mo_7O_{24}^{6-}$, $HMo_7O_{24}^{5-}$, $H_2Mo_7O_{24}^{4-}$, and $H_3Mo_7O_{24}^{3-}$ have also been studied. The proton series could not be verified through the measurements. However, for $Mo_7O_{24}^{6-}$ a bimolecular rate constant could be determined to be $13\,000 \pm 1\,300$ M^{-1} s^{-1}. At compositions corresponding to the protonized species no instantaneous neutralization could be observed. Instead, a rather slow reaction occurred. Whether this reaction is caused by silicate impurities or by an octamolybdate could not be decided. However, a bimolecular rate constant with the value of 260 ± 30 M^{-1} s^{-1} was determined. Some preliminary observations of the protonization reactions are also reported.

In recent investigations [1-3] the three component equilibria $pH^+ + qMoO_4^{2-} + rHPO_4^{2-} \rightleftharpoons (H^+)_p(MoO_4^{2-})_q(HPO_4^{2-})_r$ were studied using emf methods (25 °C, 3.0 M $Na(ClO_4)$ medium). In the range $1.5 < -\log [H^+] < 9$ and with phosphate ions in excess ($Mo/P < 2.5$) it was found that the main ternary complexes formed are $Mo_5P_2O_{23}^{6-}$, $HMo_5P_2O_{23}^{5-}$, and $H_2Mo_5P_2O_{23}^{4-}$ (coordinated sodium ions and water have been omitted in the formula). At higher Mo/P ratios also protonized enneamolybdomonophosphates are present and the species $H_3Mo_9PO_{34}^{6-}$, $H_4Mo_9PO_{34}^{5-}$, $H_5Mo_9PO_{34}^{4-}$, and $H_6Mo_9PO_{34}^{3-}$ have been proposed. At these higher Mo/P ratios considerable amounts of binary H^+-MoO_4^{2-} complexes are also present, and the most probable species may be $Mo_7O_{24}^{6-}$, $HMo_7O_{24}^{5-}$, $H_2Mo_7O_{24}^{4-}$, $H_3Mo_7O_{24}^{3-}$, $HMoO_4^-$, and H_2MoO_4.[4,5] However, instead of or in addition to the protonized heptamolybdate series different octamolybdates may also be present. From emf-measurements alone it is very difficult to make a decision between these possibilities, and support from other measurements is needed.

Exact knowledge of the mechanism for formation and decomposition of all the ions mentioned is of greatest importance. It is a difficult task to obtain a complete picture directly. Many different experimental approaches are surely necessary. A suitable starting point would be a spectrophotometric stopped-flow study. The aim of the present work is to study the decomposition of the above mentioned pentamolybdodiphosphates and the heptamolybdates in alkaline 3.0 M $Na(ClO_4)$. In this way we hope to be able to further confirm the proposed protonized series. Some preliminary kinetic measurements will also be performed on the formation reactions for these ions. Concerning the enneamolybdomonophosphates their decomposition has not yet been completely studied but will, as we hope, be presented in a forthcoming paper.

Previous studies. Lagrange and Schwing [6] have studied the decomposition of $Mo_7O_{24}^{6-}$ in four different alkaline NaCl media of total

concentrations 1, 2, 3, and 4 M at 15, 25, 35, and 45 °C. Their experiments showed that the reaction is of first order with respect to each of the reagents $Mo_7O_{24}^{6-}$ and OH^-. It was also found that the logarithm of the rate constant is a decreasing linear function of the medium concentration. For the rate constant in 3.0 M NaCl and at 25 °C they determined the value to be $8\,500 \pm 300$ M^{-1} s^{-1}. Schwarzenbach and Meier [7] have studied condensation reactions of molybdates in aqueous solutions with a continuous flow apparatus. They concluded that the condensation reactions are very fast and they estimated that eventual bimolecular reactions must run with the rate constant of the order of at least 10^5 M^{-1} s^{-1}. For low MoO_4^{2-} concentrations ($< 2 \times 10^{-4}$ M) they were able to measure the protonation of MoO_4^{2-} ions before condensation reactions occurred.

No kinetic studies of pentamolybdodiphosphates seem to have been carried out.

EXPERIMENTAL

The present work has been carried out in close connection to emf work by Pettersson.[1-3] The chemicals used, the preparation of solutions and the measurements of $-\log [H^+]$ have been described earlier.[1]

The stopped-flow measurements were carried out using a Durrum stopped-flow spectrophotometer type 13000 and the cuvette used had a length of 0.2 cm (calibrated to 0.193 cm). The transmittance-time data were recorded on a photographic film and the oscilloscope was equipped with a special measuring screen grid. The arrangement with the grid made it possible to measure out transmittance-time points with good accuracy. It also allowed a comparison between different films. Another advantage with the screen grid is that it is finer than the standard grid, and thereby more points of one film can be measured. During the reaction runs the cathodic ray of the oscilloscope was directly recorded on the film without using the storage screen.

Some complementary absorbance measurements and the determinations of molar absorption coefficients were made on a Bausch and Lomb Spectronic 505 spectrophotometer and a cuvette with a path-length of 0.1 cm (QS-HELLMA) was used.

Method

Equal volumes of an equilibrium solution and a sodium hydroxide solution were rapidly (within less than 10 ms) mixed in the stopped-flow spectrophotometer. The temperature was kept at 25 ± 0.1 °C and a background medium of 3.0 M $Na(ClO_4)$ was used. In the equilibrium solution the total concentrations of molybdenum, phosphorus, and protons over the zero level (MoO_4^{2-}, HPO_4^{2-}, and H_2O) were exactly known. On mixing it was assumed that the free protons and the protons in the protonized species HPO_4^{2-}, $H_2PO_4^-$, H_3PO_4, $HMo_5P_2O_{23}^{5-}$, $H_2Mo_5P_2O_{23}^{4-}$, $HMo_7O_{24}^{5-}$, $H_2Mo_7O_{24}^{4-}$, $H_3Mo_7O_{24}^{3-}$, $HMoO_4^-$ and H_2MoO_4, were instantaneously neutralized by the excess of OH^-. Hence at the start of the reaction ($t = 0$) we have in the molybdophosphate case the species $Mo_5P_2O_{23}^{6-}$, PO_4^{3-}, MoO_4^{2-}, OH^-, and in the heptamolybdate case the species $Mo_7O_{24}^{6-}$, MoO_4^{2-}, OH^-. By using available equilibrium constants the concentrations of these species after mixing were calculated. The total OH^- concentration was adjusted for the above mentioned proton reactions. Thus the overall reactions that will be studied are:

$$Mo_5P_2O_{23}^{6-} + 10\ OH^- \rightarrow 5\ MoO_4^{2-} + 2\ PO_4^{3-} + 5\ H_2O$$

$$Mo_7O_{24}^{6-} + 8\ OH^- \rightarrow 7\ MoO_4^{2-} + 4\ H_2O$$

The rate of decomposition was followed on an oscilloscope screen and recorded on a photographic film. From each film a suitable number of transmittance-time (T-t) data were picked out (mostly about 20 pairs). These data together with the species concentrations, c_i, at $t = 0$, are the primary data of each experiment. To make the measurements as accurate as possible and also to follow the different species concentra-

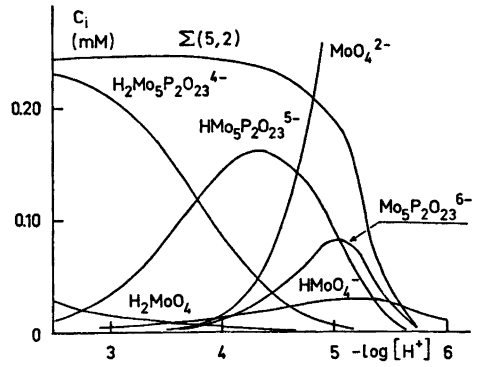

Fig. 1. Distribution diagram for $[Mo]_{tot} = 1.25$ mM and $[P]_{tot} = 1.00$ mM showing concentrations (c_i) of complexes containing molybdenum, as a function of $-\log [H^+]$. In the calculation the binary $H^+ - MoO_4^{2-}$ species and formation constants proposed by Sasaki and Sillén,[4] and the ternary $H^+ - MoO_4^{2-} - HPO_4^{2-}$ species and formation constants proposed by Pettersson [1] were used.

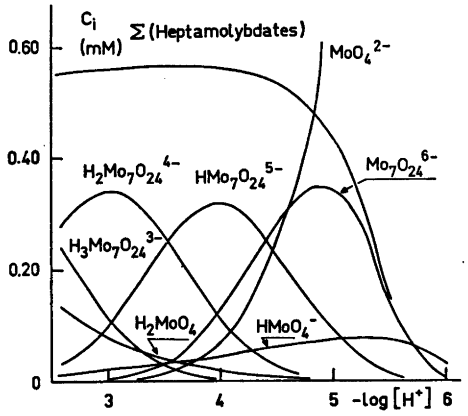

Fig. 2. Distribution of $H^+ - MoO_4^{2-}$ complexes as a function of $-\log [H^+]$ for $[Mo]_{tot} = 4.00$ mM. In the calculation species and formation constants proposed by Sasaki and Sillén [4] were used.

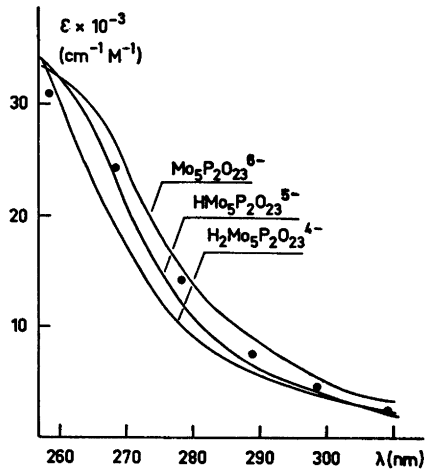

Fig. 3. Molar absorption coefficient curves for the pentamolybdodiphosphate complexes. The values have been taken from a work by Lyhamn.[8] "Best" values obtained at the six wavelengths studied in this work are plotted with the symbol ●.

tions, we have performed the measurements at a number of suitable wavelengths.

Species distributions and molar absorption coefficients. The distributions of molybdophosphate and heptamolybdate complexes as functions of $-\log [H^+]$ are given in Figs. 1 and 2. The total concentrations have been chosen so that the diagrams give a representative picture of the concentration conditions during our stopped-flow experiments.

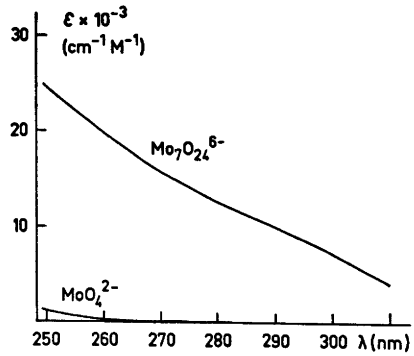

Fig. 4. Molar absorption coefficient curves for MoO_4^{2-} and $Mo_7O_{24}^{6-}$. The values have been taken from a work by Lyhamn.[8]

Curves of molar absorption coefficients of the actual species in the UV range 250 – 310 nm are shown in Figs. 3 and 4. The values have been taken from a work by Lyhamn.[8] None of the phosphate species absorbs in the wavelength range studied.

Choice of wavelengths and concentrations. The wavelength range was chosen to be 260 – 310 nm. In this range the molar absorption coefficient of MoO_4^{2-} is negligible in comparison to the high molar absorption coefficient values of the molybdophosphates and heptamolybdates (see Figs. 3 and 4). For the pentamolybdodiphosphate measurements the wavelengths 259, 269, 279, 289, 299, and 309 nm were used. Due to the high molar absorption coefficients, the concentrations of studied species have to be relatively low. By using the smallest cuvette length available for stopped-flow measurements (0.2 cm) the total concentrations of molybdenum could be held at 1 – 4 mM (before mixing).

Treatment of experimental data. The relation between measured transmittance, T, and concentrations, c_i, of light absorbing species is given by Lambert-Beers law; $A = -\log T = l\sum \varepsilon_i c_i$, where A is the absorbance, ε_i the molar absorption coefficient of the i:th species, and l is the cuvette length. Now, if the species concentrations, at $t = 0$, are exactly known or estimated rate constants and molar absorption coefficients are available, a calculated absorbance value A_{calc} can be obtained for each measured T-t value. Using the least squares principle the rate constant, k, is then determined so that the error squares sum $U = \sum (A_{calc} - A)^2$ is minimized. A Letagrop version for this calculation has been worked out.[9]

CALCULATIONS AND RESULTS

Decomposition of $Mo_5P_2O_{23}^{6-}$. It was found that the decomposition of $Mo_5P_2O_{23}^{6-}$ obeyed

the rate expression $-d[Mo_5P_2O_{23}^{6-}]/dt = k[Mo_5P_2O_{23}^{6-}][OH^-]$, where k is the rate constant. The reaction was studied for several combinations of $[Mo_5P_2O_{23}^{6-}]$ and $[OH^-]$, and three series of experiments were carried out. In two of the series $[Mo]_{tot}$ and $[P]_{tot}$ were 2.50 mM and 1.50 mM, respectively. In the third series the concentrations were 1.25 mM and 1.00 mM. (The values given refer to concentrations before mixing). Within each of the series the $-\log[H^+]$ values in the equilibrium solutions have been chosen within the limits $2.0 < -\log[H^+] < 5.5$. The choice has been made so that all the three species $Mo_5P_2O_{23}^{6-}$, $HMo_5P_2O_{23}^{5-}$, and $H_2Mo_5P_2O_{23}^{4-}$ are well represented in the final data material. The total OH^- concentrations used in the three series were 98.60 mM, 199.7 mM, and 150.2 mM (before mixing). With such an excess of OH^- ions it was found that for each solution investigated, the reaction rate became monomolecular with respect to $Mo_5P_2O_{23}^{6-}$. A monomolecular rate constant, k_{obs}, was calculated for each solution and then, by using the relation $k_{obs} = k[OH^-]$, a bimolecular rate constant, k, was determined. Examining these values we found that the k values were independent of both the total concentrations and the wavelengths used. A mean value of k for all data gave $k = 16.7 \pm 0.9\ M^{-1}\ s^{-1}$ (based on 80 different measurements).

In another Letagrop calculation a variation of k together with the molar absorption coefficient of $Mo_5P_2O_{23}^{6-}$ at the six wavelengths studied was made. The calculation gave $k = 16.8 \pm 0.6\ M^{-1}\ s^{-1}$ and the molar absorption coefficients 30.4 ± 1.3, 24.6 ± 0.9, 14.1 ± 0.4, 7.4 ± 0.5, 4.3 ± 0.1, and 2.4 ± 0.1 ($10^{-3}\ cm^{-1}\ M^{-1}$) at 259, 269, 279, 289, 299, and 309 nm, respectively. A comparison between these values and those obtained by Lyhamn [8] is given in Fig. 3. The agreement is that expected from the experimental accuracy of the measurements.

The main conclusion of the present measurements is that the decomposition rate constant is independent of whether the original equilibrium solution contains $Mo_5P_2O_{23}^{6-}$, $HMo_5P_2O_{23}^{5-}$ or $H_2Mo_5P_2O_{23}^{4-}$. This strongly verifies the results from the equilibrium analyses and provides good support for the existence of a series of protonized pentamolybdodiphosphate anions.

Decomposition of $Mo_7O_{24}^{6-}$. A number of equilibrium solutions were studied with $[Mo]_{tot}$ being 4.00 mM and with different Z-values covering the range $0 < Z < 1.5$. Z is the average number of H^+ bound per MoO_4^{2-}. The OH^- concentration used was 8.91 mM. The values given refer to concentrations before mixing. It was found that as long as the Z-values were within the limits $0 < Z < 0.6$ the rate of the decomposition of $Mo_7O_{24}^{6-}$ could be written $-d[Mo_7O_{24}^{6-}]/dt = k[Mo_7O_{24}^{6-}][OH^-]$, with $k = 13000 \pm 1300\ M^{-1}\ s^{-1}$ (a mean value obtained from seven different experiments). There is a considerable difference between this value and the value obtained by Lagrange and Schwing [6] who reported 8500 $M^{-1}\ s^{-1}$ in 3 M NaCl at 25 °C. The difference may, however, be due to medium effects. For solutions with higher Z-values it was found that an additional comparatively slow decomposition reaction occurred. The contribution from the slow reaction was found to increase when $-\log[H^+]$ was lowered. By making measurements at very high OH^- concentrations we were able to study this slow reaction separately. The study was made using solutions with $[Mo]_{tot} = 1.00$ mM and 4.00 mM and in the range $2.6 < -\log[H^+] < 4.7$. The OH^- concentrations used were 49.67 mM and 99.76 mM. In this great excess of OH^- the slow reaction could be explained with the rate equation $-dc/dt = kc[OH^-]$, where c is the concentration of an undefined species and k is the rate constant determined to be $260 \pm 30\ M^{-1}\ s^{-1}$. We suspected that the solutions could contain silicate impurities and that the species probably was a molybdosilicate complex. This was partly verified through separate studies where silicate ions were added to the solutions. That the silicate ions did not disturb the pentamolybdodiphosphate studies depended probably on the fact that an excess of phosphate ions was used and that the complex formation between molybdate and phosphate ions is stronger than between molybdate and silicate ions. Instead of a silicomolybdate complex the observed unknown species may be, for instance, an octamolybdate, and thus the measurements do not seem to confirm a protonized heptamolybdate series.

Some preliminary measurements of formation reactions. When molybdate solutions with $[MoO_4^{2-}] = 2.00$ mM were rapidly mixed with H^+-solutions with concentrations between 10^{-3} and 10^{-5} M, it was found that the absorbance

and thus the concentration of the formed heptamolybdates, increased proportionally with the initial H^+-concentration. The overall reactions were finished after about 0.1 s. This fast condensation reaction also occurred when HPO_4^{2-} ions were present together with MoO_4^{2-}, but in this case it was followed by a slow reaction, which was completed after about 10 min.

Acknowledgements. The English of the present paper has been corrected by Dr. Michael Sharp. The authors wish to thank Fil.lic. Lage Pettersson for valuable help and discussions. The work forms part of a program financially supported by the Swedish Natural Science Research Council.

REFERENCES

1. Pettersson, L. *Acta Chem. Scand. 25* (1971) 1959.
2. Pettersson, L., Andersson, I., Lyhamn, L. and Ingri, N. *Trans. Roy. Inst. Technol., Stockholm 1972, No. 256.*
3. Pettersson, L. *Chem. Scr. In press.*
4. Sasaki, Y. and Sillén, L. G. *Acta Chem. Scand. 18* (1964) 1014.
5. Sasaki, Y. and Sillén, L. G. *Ark. Kemi 29* (1968) 253.
6. Lagrange, P. and Schwing, J. P. *Bull. Soc. Chim. Fr.* (1970) 1340.
7. Schwarzenbach, G. and Meier, J. *J. Inorg. Nucl. Chem. 8* (1958) 302.
8. Lyhamn, L. *To be published.*
9. Wennerholm, H., Mellström, R., Rehnberg, O. and Ingri, N. *Chem. Scr. In press.*

Received April 5, 1974.

Acta Chemica Scandinavica A 28 (1974) 708—714

Outer-sphere Complex Formation between the Tris(propylenediamine)cobalt(III) Ion and Iodide Ion in Aqueous Solution

LARS JOHANSSON

Division of Inorganic Chemistry 1, Chemical Center, University of Lund, P. O. Box 740, S-220 07 Lund 7

The complex formation between racemic Co pn_3^{3+} and I^- has been studied at 25 °C at the constant ionic strengths ($NaClO_4$) $I = 1$ M and 4 M by potentiometric, spectrophotometric, and solubility methods. The following stability constant values were found (errors within parentheses), $I = 1$ M: $\beta_1 = 1.7(1)$ M^{-1}; $I = 4$ M: $\beta_1 = 1.9(1)$ M^{-1}, $\beta_3 = 0.62(15)$ M^{-3}. The results are compared with those reported earlier for tris(ethylenediamine)cobalt and hexaamminecobalt halide systems.

This study is part of a series of investigations on outersphere complexes formed by inert complex cations, with the emphasis on high ligand concentrations. Studies on Co $en_3^{3+} - I^-$, Co$(NH_3)_6^{3+} - I^-$ and Co$(NH_3)_6^{3+} - Br^-$ complexes have been reported earlier.[1-3] These systems differ in the respect that Co en_3^{3+} prefers one or three iodide ions, while Co$(NH_3)_6^{3+}$ adds ligands more regularly. If this is due to the different symmetries of the cations, Co pn_3^{3+} is expected to behave like Co en_3^{3+}. No detalied studies on the Co $pn_3^{3+} - I^-$ system have appeared in the literature.[4]

In the present investigation, potentiometric and spectrophotometric methods and solubility measurements have been employed, at the constant ionic strengths 1 M and 4 M, $NaClO_4$ being used as supporting electrolyte. By ionic strength is as before [1-3] meant the sum of perchlorate and ligand concentrations.

EXPERIMENTAL

Chemicals. Analytical grade chemicals were used when available. Racemic Co pn_3Cl_3 was prepared as described in the literature.[5] Co pn_3I_3 was prepared from the chloride by repeated precipitation with NaI. Co $pn_3(ClO_4)_3$ was obtained from the chloride by repeated precipitation with $HClO_4$ until the salt was chloride free. It was recrystallized in ca 97 % ethanol. The potential *explosion risk* of Co $pn_3(ClO_4)_3$ should be noted.[6]

The iodide was analyzed for I as described.[1] Found 57.3 % (calc. 57.50 %). In the visible, solutions of the iodide and perchlorate salts showed identical spectra, well in accord with literature data.[7]

Potentiometric measurements. In principle, the change in iodide concentration upon the addition of Co pn_3^{3+} was measured using the I^-, I_3^-/Pt electrode.[8] The element was constituted as follows (the same notation is used as in previous papers [1-3])

$$\mathrm{Ag,AgCl} \;\Big|\; \begin{array}{l|l} \text{0.01 M NaCl} & I \text{ M} \\ & \\ I - \text{0.01 M } NaClO_4 & NaClO_4 \end{array}$$

$$\Big|\; \begin{array}{l|l} C_L \text{ M NaI} & \\ C_T \text{ M } NaI_3 & \\ C_M \text{ M Co } pn_3(ClO_4)_3 & \\ (I - C_L - C_T - 3C_M) \text{ M } NaClO_4 & \text{Pt} \end{array}$$

$C_T \approx 1$ mM was obtained by adding a weighed amount of I_2. Bright platinum foils were used as electrodes. C_L and C_M ranged from 0 to 0.1 M. The test solution was oxygen free, and the electrode vessel was kept stoppered to prevent iodine vapour leakage. The whole element was thermostated. The emf was measured by a Radiometer PHM 52 potentiometer.

The I^-, I_3^-/Pt electrode is known to behave well.[8] The various electrode combinations normally gave identical and stable emfs.

Spectrophotometric measurements. The M-method, described earlier,[1,9] was employed. The solutions contained C_L M NaI, $0 \leq C_L \leq 0.01$ M, C_M M Co $pn_3(ClO_4)_3$, $0 \leq C_M \leq 0.1$ M and $(I - C_L - 3C_M)$ M $NaClO_4$. The absorbances were measured at the wavelengths 280, 290, 300, and 310 nm. For experimental details, see Ref. 1.

Solubility measurements. Solutions of the composition C_L M NaI, $(I - C_L)$ M $NaClO_4$,

Table 1. Iodide content w_1 (weight percent; error ±0.2 %) and mol fraction x_2 of Co $pn_3(ClO_4)_3$ in the salt equilibrated with solutions of various C_L ($I = 4$ M).

C_L M	w_1 %	$x_2 \times 10^3$
Theory	57.50	0
4.0	57.5	0
3.0	57.1	8
2.6	57.0	10
2.2	56.8	14
1.8	56.0	30
1.4	55.6	38
1.0	55.1	47
0.8	53.7	75

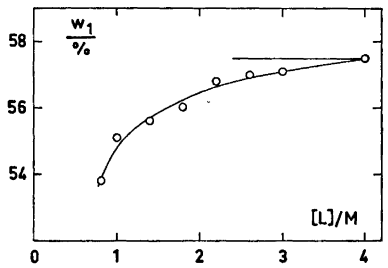

Fig. 1. Solubility measurements at 4 M ionic strength. Iodide content of solid phase *versus* iodide concentration in solution. Points: experimentally observed values. Best curve drawn. Horizontal line: theoretical value for Co pn_3I_3.

$1 \leq C_L \leq 4$ M, ($I = 4$ M only), were equilibrated with Co pn_3I_3(s) in a solubility column, as described earlier.[1,10] Samples of the solid were frequently withdrawn and analyzed for the iodide content. As shown in Table 1 and Fig. 1, Co pn_3I_3(s) is not stable; the iodide content decreases as C_L is decreased. It is natural to assume that some iodide is replaced by perchlorate. To confirm this it was shown (by an ion exchanger) that the solid phase contained the expected number of equivalents. As I^- and ClO_4^- are the only anions present, the missing I^- ions must necessarily have been replaced by ClO_4^-. The same behaviour was observed with Co en_3I_3,[1] but there the change set in at a much lower C_L. As a consequence of the solid solution formation, the equilibria were attained slowly. Care was taken to assure that equilibrium was really reached. Below $C_L = 1$ M, no reproducible solubilities were obtained.

The saturated solutions were analyzed spectrophotometrically at 340 and 470 nm.

RESULTS, CALCULATIONS

Potentiometric measurements

If activity coefficients and liquid junction potentials are constant, the emf E of the described element may be written

$$E = (E' + 0.5k \log [I_3^-]) - 1.5k \log [L] \quad (1)$$

where E' and $k = RTF^{-1}$ ln 10 are constants. Provided $[I_3^-]$ is constant, the expression within parentheses is a constant. If E is measured for a particular C_L with and without M present in the solution, the difference may be taken

$$E_L = E(C_M > 0) - E(C_M = 0) \quad (2)$$

According to eqn. (1), then

$$E_L = 1.5k \log C_L/[L] \quad (3)$$

The triiodide ion is actually dissociated, although very slightly [8,11]

$$I_3^- \rightleftharpoons I_2 + I^-$$

If this dissociation is different for $C_M > 0$ and $C_M = 0$, eqn. (3) is no longer valid. A small correction has to be introduced:

$$E_L = 1.5k \log \delta C_L/[L] \quad (4)$$

where

$$\delta = \left(\frac{1 - (K_{tri}[L])^{-1}}{1 - (K_{tri}C_L)^{-1}}\right)^{\frac{1}{3}} \quad (5)$$

The correction may be calculated from known [8,11] values of K_{tri} and preliminary values of [L] obtained by eqn. (3).

Thus, from E_L we may compute [L], as well as the ligand number,

$$\bar{n}/[L] = (C_L/[L] - 1)/C_M \quad (6)$$

The possible formation of Co $pn_3^{3+} - ClO_4^-$ complexes is neglected (*cf.* Discussion). Since $\bar{n}/[L]$ approaches β_1 for small [L], it follows from eqns. (3) and (6) that

$$E_L \approx 1.5k \log (\beta_1 C_M + 1) \approx \text{const. } C_M$$

Thus, E_L is roughly independent of [L], but roughly proportional to C_M. The precision of β_1 is thus favoured by high C_M, but not by high C_L. It has not been possible to study complexes higher than ML by this method, primarily due to the limited solubility of Co pn_3 salts. From $\bar{n}$, the stability constants can in principle be extracted by standard methods. However, at the low C_L used here, higher

Table 2. Potentiometric measurements, 1 M ionic strength.

$C_L \times 10^3$ M	$C_M \times 10^3$ M	E_L mV	[L] $\times 10^3$ M	δ	$\bar{n}$/[L] M^{-1}	β_1 M^{-1}
49.0	100.0	5.1	42.9	0.9987	1.430	1.52
49.0	50.0	2.75	45.6	0.9993	1.495	1.60
39.0	100.0	3.8	33.6	0.9981	1.646	1.74
39.0	50.0	2.6	36.5	0.9992	1.413	1.49
29.0	100.0	5.9	24.9	0.9973	1.685	1.76
29.0	50.0	3.0	26.8	0.9987	1.648	1.72
19.0	100.0	5.8	16.2	0.9958	1.673	1.72
19.0	50.0	3.0	17.5	0.9978	1.668	1.72

complexes than ML may certainly be neglected. A value of β_1 may then be readily computed from each value of E_L.

The triiodide ion might also be complexed to Co pn_3^{3+}, and although we have to assume that such complexes are absent, it may be of interest to look at their consequences. If a complex $M(I_3)$ is formed, stability constant β_1', eqn. (4) takes the form

$$E_L = 1.5k \log \frac{\delta C_L/[L]}{(C_T/[I_3^-])^{1/3}} \quad (7)$$

or, roughly

$$E_L = 1.5k \log \delta \frac{1+\beta_1 C_M}{1+\frac{1}{3}\beta_1' C_M} \quad (8)$$

Thus, triiodide complexes cannot be revealed by variation of C_L or C_T.

In Table 2, the results of the measurements at $I = 1$ M are reported. Only random variation in β_1 is shown. The average value is 1.66(10) M^{-1}. (Throughout this paper, the errors given refer to the 99 % confidence level.)

At 4 M ionic strength, the E_L values were generally lower, and decreased with increasing C_L (up to $C_L = 0.1$ M) at a rate that could not possibly be due to complex formation only. At low [L] a value $\beta_1 \approx 1$ M^{-1} was approached, but no significance should be attached to this value.

Spectrophotometric measurements

The pertinent equations for the M-method have been derived in an earlier paper.[1] In Tables 3–4 the observed absorbances are given as well as the β_1 values obtained. No significant variation of β_1 with the wavelength or with C_L was observed. The random errors, however, have a minimum at 290 – 300 nm.

Table 3. Spectrophotometric measurements at 1 M ionic strength. Absorbances (cell length 1.000 cm) for the ligand concentrations $C_L = 0$ (A_0) and 4.95×10^{-3} M (A_5). Each value is the average of at least two measurements. The absorbances are corrected for the slight absorption by I^-. Values of β_1 with errors within parentheses referring to the 99 % confidence level.

$C_M \times 10^3$ M	280 nm A_0	280 nm A_5	290 nm A_0	290 nm A_5	300 nm A_0	300 nm A_5	310 nm A_0	310 nm A_5
15.0	0.294	0.415	0.126	0.234	0.204	0.296	0.420	0.492
20.0	0.384	0.548	0.157	0.299	0.262	0.383	0.542	0.636
39.3	0.707	1.031	0.270	0.546	0.483	0.714	1.047	1.227
45.0	0.847	1.200	0.302	0.612	0.540	0.803	1.184	1.388
59.5	1.054	1.515	0.392	0.795	0.711	1.052	1.555	1.822
75.0	1.303	1.853	0.480	0.978	0.880	1.298	1.949	2.272
79.1	1.381	1.979	0.507	1.032	0.936	1.378		
105.0			0.653	1.307				
β_1/M^{-1}		1.56(40)		1.65(15)		1.54(10)		1.62(30)

Table 4. Spectrophotometric measurements at 4 M ionic strength. Ligand concentrations: 0 (A_0), 5.00×10^{-3} M (A_5) and 10.00×10^{-3} M (A_{10}). *Cf.* Table 3.

$C_M \times 10^3$ M	290 nm			300 nm			310 nm		
	A_0	A_5	A_{10}	A_0	A_5	A_{10}	A_0	A_5	A_{10}
20.0	0.164	0.271	0.370	0.261	0.355	0.444	0.538	0.608	0.680
39.9	0.293	0.491	0.688	0.487	0.659	0.834	1.040	1.174	1.314
60.1	0.424	0.718	–	0.718	0.972	–	1.549	1.745	–
61.5	0.441	–	1.027	0.730	–	1.241	1.560	–	1.964
79.9	0.553	0.933	1.324	0.942	1.273	1.619	2.050	2.300	2.588
β_1/M^{-1} →		1.89(15)	1.95(15)		1.86(30)	2.01(30)		2.04(20)	1.94(30)

Solubility measurements

As Table 1 shows, the iodide content of the solid decreases as the ratio of ClO_4^- to I^- in the solution increases. Evidently a *solid solution* of Co $pn_3(ClO_4)_3$ (MA_3, mol fraction x_2, Table 1) in Co pn_3I_3 (ML_3, mol fraction x_1) is formed. The complex formation in the aqueous solution can nevertheless be elucidated if the data are treated in the following way (*cf.* Holmberg [12]).

The activities of the components of the solid phase are denoted a_1 and a_2. Then for the equilibria

$ML_3(s, a_1) \rightleftharpoons M + 3L$

and $MA_3(s, a_2) \rightleftharpoons M + 3A$

the equations apply

$$K_{s1} = [M][L]^3/a_1 \quad (9)$$

and $$K_{s2} = [M][A]^3/a_2 \quad (10)$$

where K_{s1} and K_{s2} are constants. As before it is assumed that activity coefficients are constant *in the aqueous solution*. As expressed by eqn. (9), the product $[M][L]^3$ is now variable, in contrast to the more common situation of pure ML_3, when a_1 is constant (usually taken as unity) and $[M][L]^3$ consequently also constant (= the solubility product).

Since the solubility S is expressed by

$$S = [M]X \quad (11)$$

or $$S[L]^3/a_1 = K_{s1}X \quad (12)$$

where $$X = 1 + \beta_1[L] + \cdots \quad (13)$$

the stability constants can be computed once a_1 is known.

The two activities are connected by the Gibbs-Duhem equation

$$x_1 \, d \ln a_1 + x_2 \, d \ln a_2 = 0 \quad (14)$$

or $$-d \ln a_2 = x_1/x_2 \, d \ln a_1 \quad (15)$$

Eqns. (9) and (10) yield, upon combination, taking logarithms and differentiating

$$d \ln a_1 - d \ln a_2 = 3 \, d \ln [L]/[A] \quad (16)$$

Eqn. (15) is inserted

$$d \ln a_1 = 3x_2 \, d \ln [L]/[A] \quad (17)$$

In integral form

$$\int_1^2 d \log a_1 = 3 \int_1^2 x_2 \, d \log [L]/[A] \quad (18)$$

The integration was performed graphically. The fraction x_2 (Table 1) was plotted *vs.* log [L]/[A]. The area under the curve between any two points yields the difference in log a_1 between these points. Since log [L]/[A] grows infinitely as [L] approaches 4.0 M, it was difficult to estimate the "tail" of the integral between [L] = 3.8 M and [L] = 4.0 M. However, when (log a_1 − log a_1 (3.8)) was plotted *vs.* [L], a practically linear curve resulted, which could be easily extrapolated the short path to [L] = 4.0 M, hence giving a reliable value of $a_1(3.8)/a_1(4.0)$. The a_1 values of Table 5 are calculated setting $a_1(4.0) = 1.000$. It may be noted that the values of a_1 are not very sensitive to the random errors in x_2.

[L] and C_L are equal except at the lowest C_L. Strictly, [L] is given by the expression

$$[L] = C_L + (3x_1 - \bar{n})S \quad (19)$$

The perchlorate concentration, [A], is not significantly different from its initial concentration (*cf.*, however, Discussion).

$K_{s1}X$ was computed according to eqn. (12). The function could be fitted using the constants

Table 5. Solubility at 4 M ionic strength. Observed solubilities, S_o, and solubilities calculated from the constants given in the text, S_c. Deviation = $100(S_o - S_c)/S_c$. The activity a_1 was calculated according to eqn. (18) and [L] according to eqn. (19).

C_L M	[L] M	a_1	$S_o \times 10^3$ M	$S_c \times 10^3$ M	Dev %	$K_{s1}X$ M^4
4.0	$=C_L$	1.000	0.681	0.674	+1.1	43.6
3.8		0.994	0.680	0.683	−0.5	37.5
3.6		0.987	0.695	0.694	+0.1	32.9
3.4		0.980	0.702	0.708	−0.9	28.2
3.0		0.966	0.741	0.747	−0.9	20.7
2.6		0.950	0.815	0.810	+0.6	15.1
2.2		0.932	0.927	0.917	+1.1	10.59
1.8	1.801	0.910	1.112	1.112	±0.0	7.17
1.4	1.402	0.876	1.514	1.513	+0.1	4.76
1.0	1.004	0.822	2.519	2.542	−0.9	3.10

$K_{s1} = 0.9(2) \times 10^{-3}$ M^4, $K_{s1}\beta_1 = 1.65(10) \times 10^{-3}$ M^3, and $K_{s1}\beta_3 = 0.56(2) \times 10^{-3}$ M. Hence $\beta_1 = 1.8(4)$ M^{-1} and $\beta_3 = 0.62(15)$ M^{-3}. (The large errors in β_1 and β_3 are thus due mainly to the uncertainty in K_{s1}.) As shown by Fig. 2, the formation of ML_2 or ML_4 is not needed to explain the data.

For comparison, the calculation of stability constants was also attempted neglecting the solid solution formation, *i.e.* the solid phase was assumed to be Co pn_3I_3(s). Then, $K_{s1} < 0.2 \times 10^{-3}$ and hence $\beta_1 \geq 10$ M^{-1} were obtained. Moreover, the formation of ML_4 had to be assumed in order to fit the data at high [L]. Evidently, when the solid solution formation is taken into consideration, the overall picture of the system is much improved.

At 1 M ionic strength, the solubility was so high already when $C_L = 1$ M ($S \approx 15 \times 10^{-3}$ M) that it was judged impracticable to study the system with the solubility method.

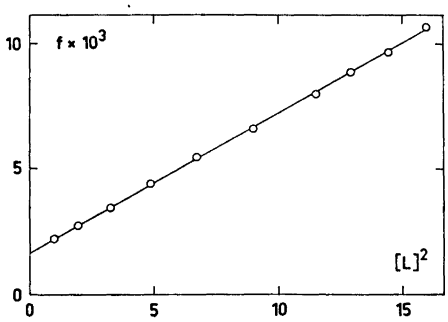

Fig. 2. Solubility measurements at 4 M ionic strength. $f = (K_{s1}X - K_{s1})[L]^{-1}$ *vs.* [L].[2]

DISCUSSION

The results of the present study are summarized in Table 6. At both ionic strengths, different methods gave β_1 values that agree within the limits of error. These values may thus be regarded with confidence. It seems reasonable to assume that this conclusion is valid also for the higher complexes studied although only the solubility method was applicable in the region of high ligand concentration.

As discussed in previous papers,[1-3,13] ClO_4^- quite probably forms complexes with cobaltammine cations to some degree. If this is the case, methods like the potentiometric and spectrophotometric methods used here would give higher β_1 values than the solubility method.[13] The difference found at 4 M ionic strength is, however, although in the right direction, far from being significant. As moreover the precision of the β_1 value from the solubility method is rather low, no safe conclusion about perchlorate complex may be drawn.

Table 6. Stability constant values of the Co $pn_3^{3+} - I^-$ system obtained in the present study.

I M	Method	β_1 M^{-1}	β_3 M^{-3}
1	Pot.	1.7(1)	
	Spectr.	1.6(1)	
4	Spectr.	1.9(1)	
	Soly.	1.8(4)	0.62(15)

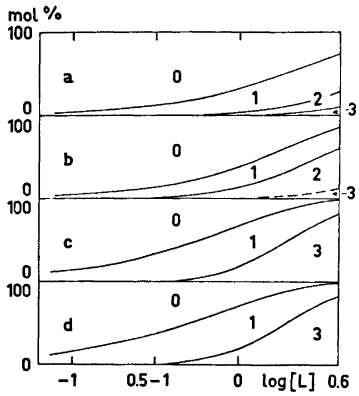

Fig. 3. Distribution of C_M between different species ML_n (n given in the figure). (*a*). $Co(NH_3)_6^{3+} - Br^-$. (*b*). $Co(NH_3)_6^{3+} - I^-$. Dashed curve: only qualitative evidence of ML_3. (*c*). $Co\ en_3^{3+} - I^-$. (*d*). $Co\ pn_3^{3+} - I^-$. Ionic strength: 4 M, temperature: 25 °C.

Anyhow, perchlorate association may affect the value of β_1 slightly; it is not thought to have any influence on the formation of higher complexes.[2]

As discussed in Ref. 2, no serious medium effects should occur when I^- is substituted for ClO_4^-.

The studies on cobaltammine halides may now be summarized. Fig. 3 clearly shows the difference between the hexaamminecobalt systems on the one hand and the trisdiaminecobalt systems on the other. In the first place, the hexaamminecobalt complexes are significantly weaker. Secondly, in the hexaamminecobalt systems, the data are best fitted if it is assumed that halide ions are added successively and regularly. In the trisdiaminecobalt systems, on the other hand, only the first and third complexes are needed to fit the data well. It should perhaps be pointed out that although also this difference is statistically significant, only quite modest systematic errors are required to change the picture appreciably. However, the consistency of the four systems speaks against systematic errors, and the difference between the systems is thought to be real. It is reasonable to ascribe this difference to the difference in shape between the hexaamminecobalt ion and the trisdiaminecobalt ions. This would imply that forces other than electrostatic ionic attraction are involved.

Although it is shown beyond doubt for all systems that complexes higher than the first are formed, the question of the maximum coordination number is not settled. In the hexaamminecobalt systems complex formation is evidently far from completed even at [L] = 4 M. In the trisdiaminecobalt systems, however, ML_3 is formed to about 80 % at 4 M iodide concentration. Nevertheless, in neither system was there any indication of the formation of ML_4. Thus, one tends to conclude that here ML_3 is the final complex, or at least that the complex formation function has a pronounced halt at 3, the negatively charged ML_4 being formed only very reluctantly. This of course indicates that electrostatic forces are important.

All four systems were studied at different ionic strengths. The original intention was to study variations with the ionic strength in some detail. However, the changes in the range studied, 0.5 – 4 M, are not very spectacular. Stability constants of outer-sphere complexes often pass through a shallow minimum [1,14–16] or stay constant within the limits of error;[2] more rapid changes may occur for very low and very high I. Different ionic strengths have therefore primarily been used as a means of providing different series of measurement of essentially the same quantities. Results in accord have increased the confidence in the conclusions drawn.

As far as possible the results have also been tested by using more than one experimental method. The agreement has as a rule been good. In the region of high [L], of particular interest in these studies, unfortunately only the solubility method has been applicable. However, when this method gives results at low [L] in accord with other methods, it is reasonable to assume it to be reliable at high [L] as well.

This work was supported by a grant from the Swedish Natural Science Research Council. The skilful technical assistance of Mrs. Agneta Nilsson is gratefully acknowledged.

REFERENCES

1. Johansson, L. *Acta Chem. Scand. 25* (1971) 3752.
2. Johansson, L. *Acta Chem. Scand. 27* (1973) 1637.
3. Johansson, L. *Acta Chem. Scand. 27* (1973) 2335.

4. Martell, A. E. and Sillén, L. G. *Stability Constants*, The Chemical Society, London 1964; *Suppl. 1*, The Chemical Society, London 1971.
5. Jenkins, I. L. and Monk, C. B. *J. Chem. Soc.* (1951) 68.
6. Tomlinson, E. R., Ottoson, K. G. and Audrieth, L. F. *J. Amer. Chem. Soc. 71* (1949) 375.
7. Mathieu, J.-P. *Bull. Soc. Chim. Fr.* (1936) 463.
8. Johansson, L. *Acta Chem. Scand. 20* (1966) 2156.
9. Johansson, L. *Acta Chem. Scand. 25* (1971) 3569.
10. Johansson, L. *Coord. Chem. Rev. 3* (1968) 293.
11. Håkansson, Å. and Johansson, L. *Chem. Scr. To be published.*
12. Holmberg, B. *Acta Chem. Scand. 27* (1973) 3657.
13. Johansson, L. *Coord. Chem. Rev. 12* (1974) 241.
14. Näsänen, R. *Acta Chem. Scand. 3* (1949) 179.
15. Newton, T. W. and Arcand, G. M. *J. Amer. Chem. Soc. 75* (1953) 2449.
16. Posey, F. A. and Taube, H. *J. Amer. Chem. Soc. 78* (1956) 15.

Received March 7, 1974.

Acta Chemica Scandinavica A 28 (1974) 715—722

Hydrolysis of Amides. Alkaline and General Acid Catalyzed Alkaline Hydrolysis of Some Substituted Acetamides and Benzamides

URVE MERESAAR and LOUISE BRATT

Department of Inorganic and Physical Chemistry, Faculty of Pharmacy, University of Uppsala, Box 574, S-751 23 Uppsala, Sweden

Acetamide, trifluoroacetamide, trichloroacetamide, trimethylammonioacetamide cation, triethylammonioacetamide cation, benzamide, 4-nitrobenzamide, *N*,*N*-dimethyltrifluoroacetamide, *N*,*N*-diethyltrifluoroacetamide, *N*-cyclohexyltrifluoroacetamide, and *N*-benzyltrifluoroacetamide have been hydrolyzed at 25 °C or 45 °C in alkaline solution at ionic strength 1.

The pH-rate profiles show that the rate at high pH values is more than first-order in hydroxide ion concentration for the trialkylammonioacetamide cations, the benzamides, and the *N*-benzyltrifluoroacetamide, which can be interpreted as hydroxide ion catalyzed breakdown of a substrate-hydroxide ion intermediate. In accordance with a mechanism involving acid catalyzed breakdown of this intermediate to products, the rate of hydrolysis of these amides and of the *N*,*N*-diethyltrifluoroacetamide and the *N*-cyclohexyltrifluoroacetamide is enhanced by the presence of hydrogenphosphate or hydrogencarbonate ions. This makes it possible to determine the rate constants for the formation of the tetrahedral intermediates (k_1), and the ratios of the rate constants for the uncatalyzed breakdown of the intermediates to products and for their reversion to reactants (k_2/k_{-1}). The k_2/k_{-1} values are found to be largely independent of electronic effects in the acylic part but dependent on such effects from substituents in the amine part. The corresponding parameters (k_3/k_{-1}) for the hydroxide ion catalyzed breakdown of the intermediates have also been determined.

Many investigations have been carried out on the alkaline hydrolysis of aliphatic amides. Most of this work is summarized in the review of O'Connor [1] and in the work of DeWolfe and Newcomb.[2] The recent papers of Bolton and Jackson [3] and Yamana *et al.*[4] can also be mentioned, which deal with the effects of amide structure and temperature on the second order rate constant of the alkaline hydrolysis. The hydrolyses of, *e.g.*, chloroacetamide,[5] trialkylammonioacetamide cations,[6] glycinamide,[7] and some *N*-substituted acetamides [4] showed at high pH values a dependence on hydroxide ion concentration larger than first order. The performed experiments did not, however, permit a detailed discussion of the mechanism. The mechanism of the hydrolysis of benzamide has earlier been investigated by measuring the hydrolysis rate and the oxygen exchange between carbonyl-^{18}O-labeled amide and water.[12,13]

In previous papers from this laboratory [8,9] rate equations have been derived from a mechanism (Scheme 1) shown to be applicable to the hydrolysis of anilides. As far as the mechanism refers to pure alkaline hydrolysis, it was also suggested by Mader [10] and Schowen *et al.*[11] The present investigation was undertaken to decide its validity in amide hydrolysis and when valid, to determine rate parameters corresponding to those already known for anilide hydrolysis.

MATERIALS AND METHODS

Materials. Benzamide, 4-nitrobenzamide, trifluoroacetamide, and trichloroacetamide of commercial grade were recrystallized from water. The acetamide was of reagent grade.

Trimethylammonioacetamide chloride was prepared from chloroacetamide and trimethylamine [14] and recrystallized from ethanol-ether;

m.p. 192 – 194 °C (Ref. 14: 199 °C). The equivalent weight was determined by argentometric titration using 4,5-dichlorofluorescein as indicator (found 153.9; calc. 152.6). Triethylammonioacetamide iodide was synthesized from diethylaminoacetamide and ethyl iodide in acetone solution (one week at room temperature) and recrystallized from ethanol-ether; m.p. 150 – 152 °C (Ref. 6: 155 °C). Equiv. weight (argentometric titration): 286.9; calc. 286.2. The diethylaminoacetamide was prepared from chloroacetamide and diethylamine in ethanol-water (24 h at room temperature); m.p. 74 – 75 °C (Ref. 15: 76 °C). *N*,*N*-Dimethyltrifluoroacetamide (Found: C 34.6; H 4.49; N 9.98. Calc.: C 34.1; H 4.29; N 9.93) (b.p. 48 °C/16 mmHg; Ref. 16: 134.5 – 136.0 °C) and *N*,*N*-diethyltrifluoroacetamide (Found: C 42.5; H 5.89; N 8.06. Calc.: C 42.6; H 5.96; N 8.28) (b.p. 60 °C/10 mmHg; Ref. 17: 30 °C/2 mmHg) were prepared from the ethyl ester of trifluoroacetic acid and the appropriate amine.[16,17] *N*-Cyclohexyltrifluoroacetamide (m.p. 93 – 94 °C; Ref. 18: 94 – 95 °C) and *N*-benzyltrifluoroacetamide (m.p. 72 – 75 °C; Ref. 18: 73.5 – 75 °C) were obtained from trifluoroacetic anhydride and the appropriate amine.[18]

All other chemicals used were of reagent grade. In order to remove protolytic impurities from the potassium chloride (reagent grade) it was recrystallized from 0.1 M hydrochloric acid.

Hydrolysis experiments. The kinetic experiments with trichloroacetamide and the trifluoroacetic acid derivatives were performed at 25 ± 0.05 °C. The other amides were hydrolyzed at 45 ± 0.1 °C. The concentration of the amides varied between 0.002 and 0.04 M. The ionic strength was 1, obtained by addition of potassium chloride. Some experiments with benzamide were run at ionic strength 3. Water was used as solvent except in the case of *N*-benzyltrifluoroacetamide and *N*-cyclohexyltrifluoroacetamide, when a solution of 9.6 v/v % ethanol in water was used.

The experiments were performed as described earlier.[8] The pH was maintained constant either automatically with a Radiometer SBR titrigraph combined with an SBU syringe burette and a TTT titrator or manually with an Agla microburette.[8] The rates of hydrolysis vary considerably for the compounds. Thus, in some experiments the hydrolysis was followed to about 90 % completion, in others to less than 1 %. No loss of ammonia or amines due to evaporation was noticed throughout the experiments. The loss of chloride ions from trichloroacetamide has been shown to take place about 100 times slower than the hydrolysis.[5]

Hydrogenphosphate ions were used as catalyzing species for the amides unsubstituted at the amide nitrogen. Hydrogencarbonate ions could not be employed for these amides because they interfered in the assay method for ammonia. For the *N*-substituted amides, however, hydrogencarbonate ions were used.

The stoichiometric pK_w values have been determined earlier and found to be 13.78 (25 °C, $\mu = 1$),[19] 13.92 (25 °C, 9.6 v/v % ethanol, $\mu = 1$)[8] and 13.16 (45 °C, $\mu = 1$).[20]

Assay. The ammonia formed in the hydrolysis of the *N*-unsubstituted amides was determined by a method – somewhat modified – used by Kawamura.[21] It consists in oxidative condensation of aminopyrine and phenol in the presence of potassium hexacyanoferrate(III) and ammonium ions at pH 8. An aliquot of the hydrolysate at pH 8 was diluted to 15.00 ml with 1 M KCl. To this solution ($0.5 \times 10^{-4} - 4 \times 10^{-4}$ M in ammonium ions) 25.00 ml of a 0.1 M tris(hydroxymethyl)aminomethane buffer of pH 8.0 was added together with 4.00 ml of a solution of 0.2 % phenol and 0.4 % aminopyrine and 3.00 ml of 5 % potassium hexacyanoferrate(III). After exactly 30 min at room temperature the solution was extracted with 10.00 ml of chloroform and the absorbance of the extract read at 455 nm in a 1 cm cell against a reagent blank. The colour produced is stable for at least 1 h. It is essential to have a fixed pH value and ionic strength during the development of the colour. The molar absorption coefficient was 1400. The rate constants (k_{obs} values) were calculated from the slopes of the straight lines obtained when plotting log [residual amide] against time.

The hydrolysis of trifluoroacetamide was also followed by UV measurements. The absorbance of the amide in 0.1 M hydrochloric acid was measured at 230 nm, where the absorbances of the hydrolysis products are small. The rate constants were obtained as described by Eriksson and Holst.[8] The results were in accordance with those obtained by ammonia determination. The UV method was also used for *N*-benzyltrifluoroacetamide and *N*-cyclohexyltrifluoroacetamide, the absorbances being measured at 228 nm and 225 nm, respectively.

To determine the dimethylamine and diethylamine formed by hydrolysis of the *N*,*N*-dialkyl-substituted amides, a method described by Dahlgren[22] was used. The amines were chlorinated at pH 8.1 and 25 °C with hypochlorite (solution containing 9.5×10^{-3} % active chlorine) and the excess hypochlorite was destroyed by nitrite. The chloroamines then oxidized iodide ions in a starch-potassium iodide reagent and the colour produced was measured at 580 nm. The molar absorption coefficient in the case of dimethylamine was 31 000 and of diethylamine 29 000. Some experiments at high pH values with *N*,*N*-dimethyl- and *N*,*N*-diethyltrifluoroacetamide were followed by UV measurements at 230 nm as described above, giving results agreeing with those obtained by amine determination.

RATE EQUATIONS AND RESULTS

The reaction scheme proposed for the alkaline hydrolysis of anilides[8,9] is found to be applicable

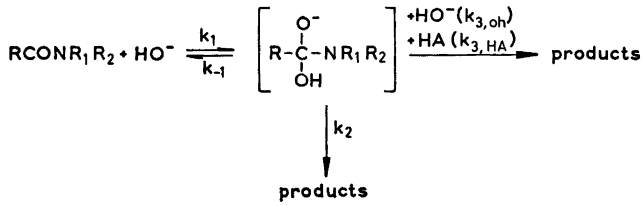

Scheme 1.

also here, *cf.* Scheme 1.
HA denotes weak acids. From the scheme, the following equation is derived, where k_{obs} is a pseudo first-order rate constant at constant pH.

$$k_{obs} = k_1[HO^-] \times \frac{k_2 + k_{3,oh}[HO^-] + k_{3,HA}[HA]}{k_{-1} + k_2 + k_{3,oh}[HO^-] + k_{3,HA}[HA]} \quad (1)$$

Acetamide, trifluoroacetamide, and trichloroacetamide. As can be seen in Figs. 1 and 2, the pH-rate profiles for these compounds are straight lines with slope 1 in the pH-range used. Hence, no $k_{3,oh}$-step was found, and eqn. (1) simplifies to

$$k_{obs} = \frac{k_1 k_2 [HO^-]}{k_{-1} + k_2} = k_{oh}[HO^-] \quad (2)$$

The rate enhancing effect of hydrogencarbonate and hydrogenphosphate ions was also too small to permit an estimation of k_1 and k_2/k_{-1}.

Trimethylammonioacetamide and triethylammonioacetamide cations, benzamide, and 4-nitrobenzamide. According to Fig. 2, a more than first order dependence on hydroxide ion concentration is found at high pH values. With benzamide some experiments have been run at ionic strength 3 in order to be able to use high hydroxide ion concentrations to confirm the deviation from slope 1. For pure hydroxide ion catalysis eqn. (1) can be written in the form

$$k_{obs} = k_1[HO^-] \times \frac{k_2 + k_{3,oh}[HO^-]}{k_{-1} + k_2 + k_{3,oh}[HO^-]} \quad (3)$$

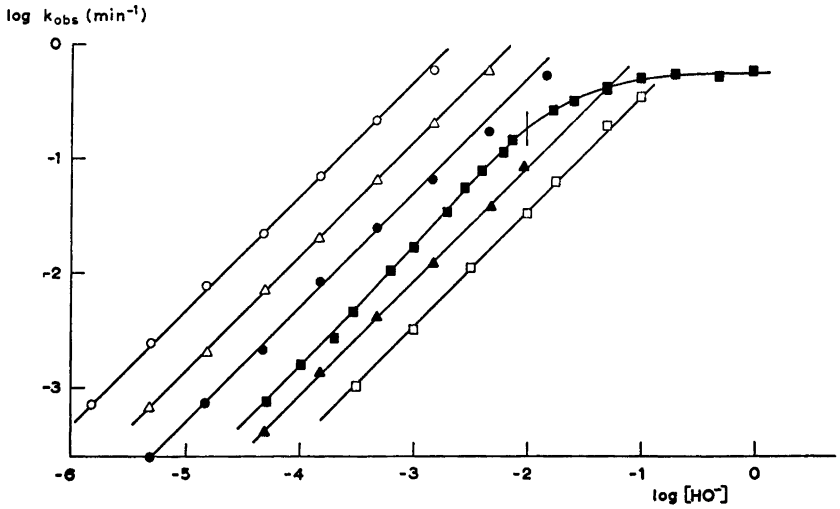

Fig. 1. Plot of log k_{obs} against log [HO^-] for trifluoroacetamide ○, trichloroacetamide ●, *N,N*-dimethyltrifluoroacetamide △, *N,N*-diethyltrifluoroacetamide ▲, *N*-cyclohexyltrifluoroacetamide □, and *N*-benzyltrifluoroacetamide ■ at 25 °C, $\mu = 1$. For the last two compounds the medium consisted of 9.6 v/v % ethanol. The fully drawn lines are calculated from eqns. (2) or (5) and parameter values given in Table 1. The bar denotes the value of [HO^-] corresponding to the $pK_a = 11.92$ for *N*-benzyltrifluoroacetamide.

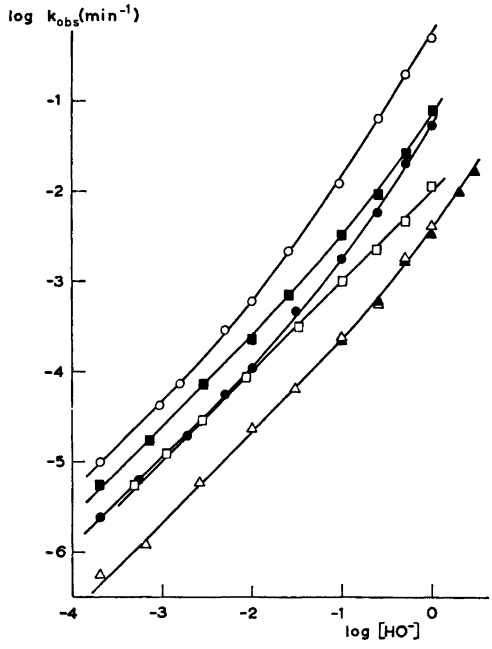

Fig. 2. Plot of log k_{obs} against log [HO$^-$] for acetamide □, trimethylammonioacetamide cation ○, triethylammonioacetamide cation ●, benzamide △, and 4-nitrobenzamide ■ at 45 °C, $\mu = 1$ and benzamide ▲ at 45 °C, $\mu = 3$. The fully drawn lines are calculated from eqns. (2) or (3) and parameter values given in Table 1.

Figs. 3 and 4 show some experiments in the presence of hydrogen phosphate ions. $k_{3,oh}$[HO$^-$] in eqn. (1) is negligible at the pH values used and thus the following equation is valid

$$k_{obs} = k_1[HO^-] \times \frac{k_2 + k_{3,phosph}[phosphate]}{k_{-1} + k_2 + k_{3,phosph}[phosphate]} \quad (4)$$

From the limiting rates, k_1 can be determined with fairly good accuracy, $(k_{-1} + k_2)$ being negligible compared with $k_{3,phosph}$ [phosphate]. With k_1 known, k_2/k_{-1} is obtained from the experiments at low pH values in Fig. 2, where $k_{3,oh}[HO^-] \ll k_2$, $k_{3,oh}/k_{-1}$ is obtained from the experiments at the largest values of [HO$^-$].

Compounds substituted at the amide nitrogen. The pH-rate profiles in Fig. 1 for the *N*-substituted amides are straight lines except for *N*-benzyltrifluoroacetamide, where a small curvature upwards can be noticed at [HO$^-$] = 2.5×10^{-3} – 2.5×10^{-2} M. This depends on hydroxide ion catalysis in the k_3-step. At still higher hydroxide ion concentrations, k_{obs} reaches a limiting value, indicating the existence of a pK_a value for this amide. Assuming that the amide anion is stable to hydrolysis, it can be shown that the following equation is valid, as has earlier been found for anilides.[8,19]

$$k_{obs} = \frac{k_1 K_w}{K_a + [H^+]} \times \frac{k_2 + k_{3,oh}[HO^-]}{k_{-1} + k_2 + k_{3,oh}[HO^-]} \quad (5)$$

At high pH values, where $k_{3,oh}[HO^-] \gg (k_{-1} + k_2)$ and $K_a \gg [H^+]$, the equation simplifies to

$$k_{obs} = k_1 K_w / K_a \quad (6)$$

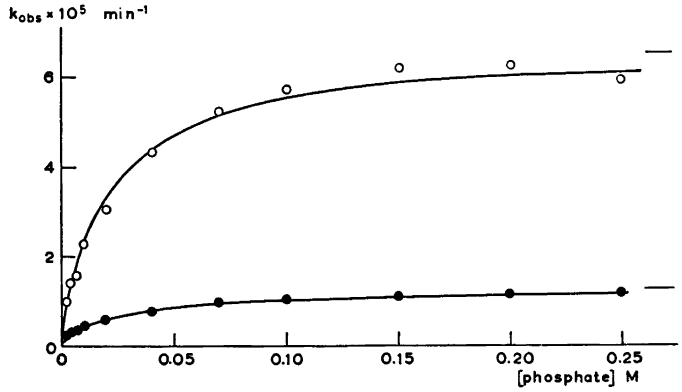

Fig. 3. Plot of k_{obs} against total concentration of phosphate at 45 °C, $\mu = 1$ for trimethylammonioacetamide cation ○ and triethylammonioacetamide cation ● at [H$^+$] = $10^{-8.96}$. The lines are calculated from eqn. (4) with parameter values given in Table 1 and the following $k_{3,phosph}/k_{-1}$ values: ○ 50 M^{-1}, ● 45 M^{-1}. The bars denote limiting values of k_{obs}.

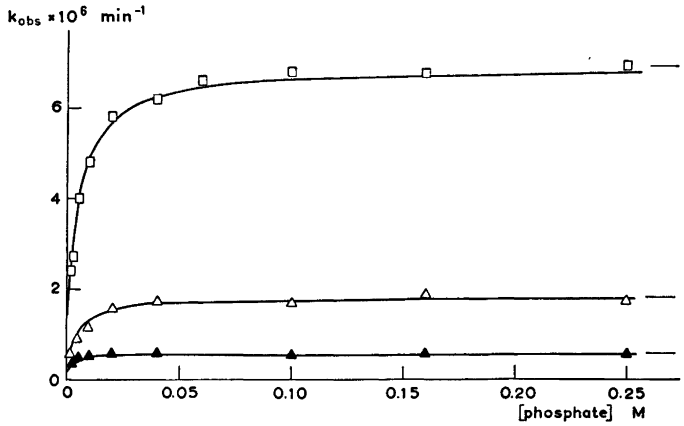

Fig. 4. Plot of k_{obs} against total concentration of phosphate at 45 °C, $\mu = 1$ for 4-nitrobenzamide □ and benzamide ▲ at $[H^+] = 10^{-8.96}$ and for benzamide at $[H^+] = 10^{-9.46}$ △. The lines are calculated from eqn. (4) with parameter values given in Table 1 and the following $k_{3,phosph}/k_{-1}$ values: □ 220 M^{-1}, △ 250 M^{-1}, and ▲ 700 M^{-1}. The bars denote limiting values of k_{obs}.

thus giving a constant value of k_{obs}.

The experiments with hydrogencarbonate ions showed no catalytic effect for *N*,*N*-dimethyltrifluoroacetamide. Thus for this amide only $k_{oh} = k_1k_2/(k_{-1}+k_2)$ could be calculated. The k_1 values for the other *N*-substituted compounds were obtained from the experiments with hydrogencarbonate ions (Figs. 5 – 7) at low pH values as described above for hydrogenphosphate catalysis. With k_{oh} and k_1 known, k_2/k_{-1} is calculated using eqn. (2) and $k_{3,HCO_3^-}/k_{-1}$ from the experiments in Figs. 5 – 7 using eqn. (1), $k_{3,oh}[HO^-]$ being negligible. The stoichiometric pK_a value of 11.92 for *N*-benzyltrifluoroacetamide is obtained from eqn. (6) using the limiting value of k_{obs} at the highest hydroxide ion concentrations.

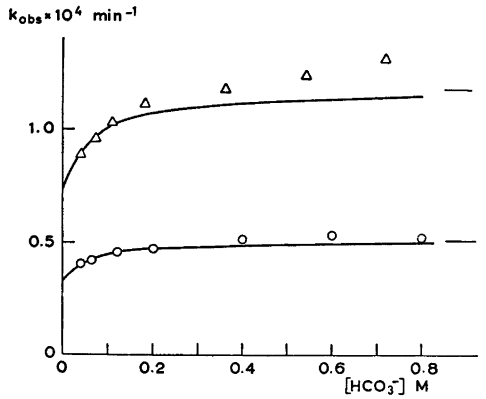

Fig. 5. Plot of k_{obs} against concentration of hydrogencarbonate ions at 25 °C, $\mu = 1$ for *N*,*N*-diethyltrifluoroacetamide at $[H^+] = 10^{-8.36}$ ($[HCO_3^-]/[CO_3^{2-}] = 18$) ○ and at $[H^+] = 10^{-8.72}$ ($[HCO_3^-]/[CO_3^{2-}] = 8$) △. The curves are calculated from eqn. (1) with parameter values given in Table 1 and the following $k_{3,HCO_3^-}/k_1$ values: ○ 45 M^{-1} and △ 40 M^{-1}. The bars denote limiting values of k_{obs}.

DISCUSSION

Pure alkaline hydrolysis. In anilide hydrolysis the breakdown of the substrate-hydroxide ion complex to products is thought to be preceded by a proton transfer to the anilide nitrogen.[9,23] In a recent work by Kershner and Schowen [24] on the hydrolysis of *N*-methylanilides it is suggested that the breakdown of the tetrahedral intermediate proceeds along two different rate-determining pathways, one involving proton transfer from catalyst to nitrogen giving an ammonium intermediate and the other involving C-N-bond cleavage to give a hydrogen-bonded anilide ion intermediate. The former is favoured by poor leaving groups (pK_b of the corresponding aniline < 9) and the latter by good leaving groups (pK_b of the corresponding aniline > 9). If this is true also for other amides, the compounds studied in this work require a proton transfer to the amide nitrogen before

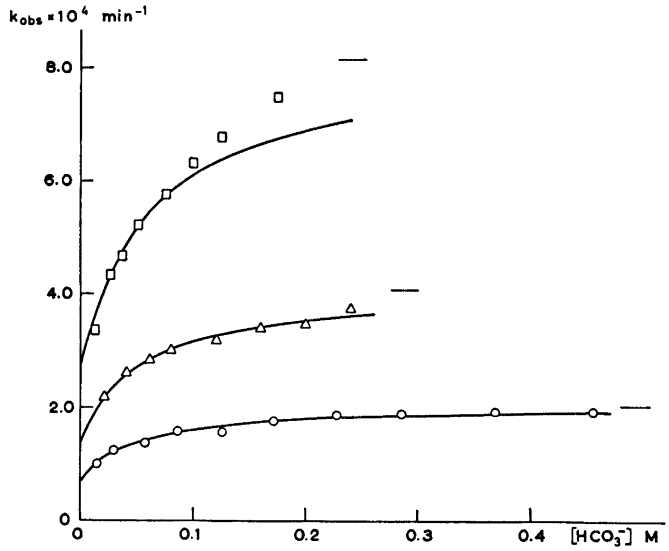

Fig. 6. Plot of k_{obs} against concentration of hydrogencarbonate ions at 25 °C, $\mu = 1$ in 9.6 v/v % ethanol for *N*-cyclohexyltrifluoroacetamide. The curves are calculated from eqn. (1) and parameter values given in Table 1. Values of $k_{3,HCO_3^-}/k_{-1}$ are given below. The bars denote limiting values of k_{obs}.

	[H$^+$]	[HCO$_3^-$]/[CO$_3^{2-}$]	$k_{3,HCO_3^-}/k_{-1}$ M^{-1}
○	$10^{-9.21}$	4:1	32
△	$10^{-9.51}$	2:1	29
□	$10^{-9.81}$	1:1	25

product formation from the intermediate. The ease of this transfer and hence the k_2/k_{-1} ratio seems to be insensitive to inductive effects of acyl substituents but decreased by steric hindrance.[8,25,26]

No or a very small general acid catalytic effect was found for the hydrolyses of acetamide, trifluoroacetamide, trichloroacetamide, and *N*,*N*-dimethyltrifluoroacetamide, indicating a high value of the partitioning ratio k_2/k_{-1}. This is to be expected, because the steric hindrance for the proton transfer to the amide nitrogen is small. For these compounds, only the second order rate constant for the alkaline hydrolysis (*cf.* k_{oh} in Table 1) could be determined. As k_2/k_{-1} is large, k_1 is approximately equal to k_{oh} according to eqn. (2), and the value increases as expected with increasing electron-attracting power of the substituents. The value for trichloroacetamide is almost in accordance with that obtained by Kezdy and Bruylants[5] (46.8 M^{-1} min^{-1}), who followed the hydrolysis with UV measurements. Yamana *et al.*[4] found that the alkaline hydrolysis of acetamide was more than first-order in hydroxide ion concentration at high pH values. We, however, have not been able to confirm this.

The k_1 values, given in Table 1, for the benzamides and trialkylammonioacetamide cations are reasonable, considering the influence of steric and inductive effects on the formation of the intermediate. Bender *et al.*[12] have determined k_1 for benzamide to 1.15×10^{-2} M^{-1} min^{-1} at 40.7 °C (this work 0.92×10^{-2} M^{-1} min^{-1} at 45 °C) from hydrolysis rate measurements together with oxygen exchange data. Their k_2/k_{-1} ratio was 0.263 (this work 0.30). The ratios k_2/k_{-1} for the two benzamides are almost the same, showing no influence from the different inductive effects of the acyl parts, which confirms the earlier results with anilides.[8] The values are larger than that for acetanilide (0.084 at 25 °C),[27] probably due to the larger basicity of the amide nitrogen compared with the anilide nitrogen and less steric hindrance, both being favourable for the proton transfer to nitrogen. For the trialkylammonioacetamide cations the k_2/k_{-1} ratios are

Table 1. Experimentally determined rate parameters, used in the construction of Figs. 1 – 7. The solvent was water except for the last two compounds, where 9.6 v/v % ethanol in water was used. The ionic strength was 1.

Compound	Temp. °C	k_{oh}[a] M^{-1} min^{-1}	k_1 M^{-1} min^{-1}	k_2/k_{-1}	$k_{3,oh}/k^{-1}$ M^{-1}
CH_3CONH_2	45	0.0100			
CF_3CONH_2	25	470			
CCl_3CONH_2	25	50.5			
$(CH_3)_3N^+CH_2CONH_2$	45	0.0470	1.05	0.047	1.00
$(C_2H_5)_3N^+CH_2CONH_2$	45	0.0110	0.20	0.059	0.34
$PhCONH_2$	45	0.00212	0.0092	0.30	0.50
4-NO_2-Ph-$CONH_2$	45	0.0240	0.11	0.28	1.30
$CF_3CON(CH_3)_2$	25	140			
$CF_3CON(C_2H_5)_2$	25	8.60	13.5	1.75	
CF_3CONH-C_6H_{10}	25	3.50	10.5	0.50	
$CF_3CONHCH_2$-Ph	25	15.0	60	0.33	130

[a] $k_{oh} = k_1k_2/(k_{-1}+k_2)$.

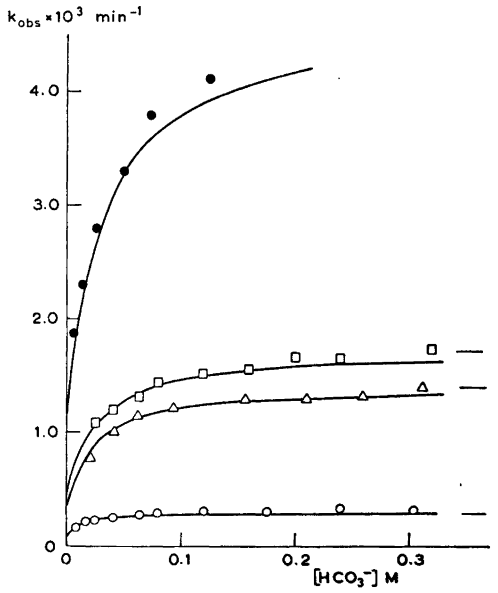

Fig. 7. Plot of k_{obs} against concentration of hydrogencarbonate ions at 25 °C, $\mu = 1$ in 9.6 v/v % ethanol for *N*-benzyltrifluoroacetamide. The curves are calculated from eqn. (1) and parameter values given in Table 1. Values of $k_{3,HCO_3^-}/k_{-1}$ are given below. The bars denote limiting values of k_{obs}.

	[H$^+$]	[HCO_3^-]/[CO_3^{-2}]	$k_{3,HCO_3^-}/k_{-1}$ M^{-1}
○	$10^{-8.61}$	16:1	120
△	$10^{-9.21}$	4:1	60
□	$10^{-9.38}$	8:3	50
●	$10^{-9.81}$	1:1	40

smaller, the acyl substituents being bulkier than in the benzamides.

According to Taft-type steric parameters [4,28] and Stuart molecule models, the *N*,*N*-diethyltrifluoroacetamide ought to be more sterically hindered at the carbonyl group than the cyclohexyl compound, which in turn should be more hindered than the amide with a benzyl substituent. Comparing molecule models of the tetrahedral intermediates with regard to the hindrance at the nitrogen, the differences seem to be smaller. Despite the larger steric hindrance and the somewhat larger electron-releasing power of the diethyl compound compared with the cyclohexyl one, the k_1 value is higher for the former. The latter amide is hydrolyzed in 9.6 v/v % ethanol solution and some decrease of k_1 can be expected, as has been noticed before for acetanilide (0.0047 and 0.0039 M^{-1} min^{-1}, resp.).[27] The decrease here is almost equally as large. Thus it seems that the k_1 values in water solution are about the same. The differences between the k_2/k_{-1} values of these amides substituted at the amide nitrogen might be explained as due to the different nitrogen electron availabilities, which will influence the protonation before breakdown to products. k_2/k_{-1} for trifluoroacetanilide [8] is twenty times lower than that for *N*-cyclohexyltrifluoroacetamide (0.025 and 0.50, resp.) and eight times lower than the value for *N*-methyltrifluoroacetanilide (0.205).[24] Some increase in k_2/k_{-1} values has also been found for *N*-methyltri-

fluoroacetanilides with electron-donating ring substituents.[24] The electron-attracting power of the substituents is reflected in the $k_{3,oh}/k_{-1}$ values, as has been found previously for, *e.g.*, trifluoroacetanilide and trichloroacetanilide ($k_{3,oh}/k_{-1} = 93$ and 34 M^{-1}, resp.).[8]

Catalysis by weak acids. The experiments with hydrogenphosphate and hydrogencarbonate ions have been run mainly to enable the k_1 values to be calculated. Only the experiments giving limiting rates with hydrogenphosphate ions are given in Figs. 3 and 4. Some preliminary experiments not reaching limiting rates were run at $[H^+] = 10^{-9.46}$ also for the other amides in the figures beside benzamide and showed that $k_{3,phosph}/k_{-1}$ decreased with decreasing concentration of hydrogen ions. The same tendency is noticed in Figs. 5 – 7, where hydrogencarbonate ions were used as catalyst. An explanation might be the existence of more than one intermediate as suggested for the hydrogencarbonate ion catalysis of anilides.[9,19] At high pH values and high concentrations of the carbonate system the calculated curves in Figs. 5 – 7 deviate somewhat from the experimental results. This might be due to carbonate ion acting as a nucleophile or catalyzing the water attack on the amide when forming the tetrahedral intermediate, as described earlier.[19,29]

Acknowledgements. We wish to thank Dr. Sven O. Eriksson for his interest in this work and for valuable comments on the manuscript. The skilful technical assistance given by Mrs. Barbro Johansson is also acknowledged. Financial support from the Swedish Natural Science Research Council to Sven O. Eriksson for this project is gratefully acknowledged.

REFERENCES

1. O'Connor, C. *Quart. Rev. Chem. Soc. 24* (1970) 553.
2. DeWolfe, R. H. and Newcomb, R. C. *J. Org. Chem. 36* (1971) 3870.
3. Bolton, P. D. and Jackson, G. L. *Aust. J. Chem. 24* (1971) 969.
4. Yamana, T., Mizukami, Y., Tsuji, A., Yasuda, Y. and Masuda, K. *Chem. Pharm. Bull. 20* (1972) 881.
5. Kezdy, F. and Bruylants, A. *Bull. Soc. Chim. Belg. 69* (1960) 602.
6. Luten, Jr., D. B. and Stewart, T. D. *J. Amer. Chem. Soc. 56* (1934) 2151.
7. Regårdh, C.-G. *Acta Pharm. Suecica 4* (1967) 335.
8. Eriksson, S. O. and Holst, C. *Acta Chem. Scand. 20* (1966) 1892.
9. Eriksson, S. O. *Acta Pharm. Suecica 6* (1969) 139.
10. Mader, P. M. *J. Amer. Chem. Soc. 87* (1965) 3191.
11. Schowen, R. L., Jayaraman, H. and Kershner, L. *J. Amer. Chem. Soc. 88* (1966) 3373.
12. Bender, M. L., Ginger, R. D. and Unik, J. P. *J. Amer. Chem. Soc. 80* (1958) 1044.
13. Bunton, C. A., Nayak, B. and O'Connor, C. *J. Org. Chem. 33* (1968) 572.
14. Steger, E. and Lorenz, J. *J. Pract. Chem. 13* (1961) 272.
15. Backes, M. *C. R. Acad. Sci. 239* (1954) 1520.
16. Middaugh, R. L., Drago, R. S. and Niedzielski, R. J. *J. Amer. Chem. Soc. 86* (1964) 388.
17. Joullié, M. M. *J. Amer. Chem. Soc. 77* (1955) 6662.
18. Bourne, E. J., Henry, S. H., Tatlow, C. E. M. and Tatlow, J. C. *J. Chem. Soc. London* (1952) 4014.
19. Eriksson, S. O., Meresaar, U. and Wahlberg, U. *Acta Chem. Scand. 22* (1968) 2773.
20. Eriksson, S. O. and Regårdh, C.-G. *Acta Pharm. Suecica 5* (1968) 457.
21. Kawamura, K. *Chem. Pharm. Bull. 16* (1968) 626.
22. Dahlgren, G. *Anal. Chem. 36* (1964) 596.
23. Bender, M. L. and Thomas, R. J. *J. Amer. Chem. Soc. 83* (1961) 4183.
24. Kershner, L. D. and Schowen, R. L. *J. Amer. Chem. Soc. 93* (1971) 2014.
25. Eriksson, S. O. and Meresaar, U. *Acta Chem. Scand. 25* (1971) 2697.
26. Meresaar, U. and Eriksson, S. O. *Acta Chem. Scand. 26* (1972) 4186.
27. Eriksson, S. O. *Acta Pharm. Suecica 6* (1969) 121.
28. Bolton, P. D., Ellis, J., Frier, R. D. and Nancarrow, P. C. *Aust. J. Chem. 25* (1972) 303.
29. Eriksson, S. O. and Bratt, L. *Acta Chem. Scand. 21* (1967) 1812.

Received February 4, 1974.

Acta Chemica Scandinavica A 28 (1974) 723—730

The Crystal Structure of $Sb_4O_5(OH)ClO_4 \cdot \frac{1}{2}H_2O$

JAN-OLOV BOVIN

Division of Inorganic Chemistry 2, Chemical Center, The Lund Institute of Technology, P. O. Box 740, S-220 07 Lund 7, Sweden

The crystal structure of the compound, $Sb_4O_5(OH)ClO_4 \cdot \frac{1}{2}H_2O$, has been determined from three-dimensional X-ray data measured on an automatic diffractometer. The crystals are monoclinic (space group $I2/c$). The unit cell contains eight formula units and has the dimensions $a = 20.969(5)$, $b = 5.7051(8)$, $c = 17.872(4)$ and $\beta = 99.84(2)°$. The structure was refined by a full-matrix least-squares technique using 1811 observed reflections to an unweighted R value of 0.037. It contains distorted trigonal bipyramidal SbO_4- and tetrahedral SbO_3-polyhedra, with the lone pairs of electrons of antimony at one of the equatorial corners of the bipyramids and at one corner of each tetrahedron, respectively. Four SbO_4-polyhedra share edges with each other and form a short chain. In both ends of the chain an SbO_3-polyhedron shares edges with a SbO_4-polyhedron. The chain is then terminated in each end by an additional SbO_3-polyhedron sharing corners. The short chains are linked, by sharing oxygen atoms with other chains, to infinite layers parallel to the bc-plane. The perchlorate ions and the water molecules are situated between the layers. The Sb—O bond distances vary between 1.952(9) and 2.378(9) Å.

During an investigation of the solubility of antimony(III) oxide (cubic and orthorhombic) in perchloric acid and nitric acid,[1] undertaken in order to elucidate which species of antimony(III) that exist in such solutions, it was found that the oxide phases were under certain conditions converted into different basic salts. The compositions of these solid phases in stable or metastable equilibrium with solutions of various acidities must be exactly known to make a correct interpretation of the solubility measurements possible. Complete determinations of their structures would have the added advantage that a comparison would be possible between the hydroxo complexes indicated in the solutions and the aggregates that can be discerned in the solid phases. Such structural studies have therefore been started and the result of the first one concerning the nitrate, $Sb_4O_4(OH)_2(NO_3)_2$,[2] has already been published. In this paper, the structure of a perchlorate, $Sb_4O_5(OH)ClO_4 \cdot \frac{1}{2}H_2O$, is reported. This phase has previously been proposed and described by Jander and Hartmann [3] as $4Sb_2O_3 \cdot Cl_2O_7 \cdot 2H_2O$. Further studies completed or in progress include Sb_2O_3(ortho.),[4] Sb_2O_3(cubic) and $Sb(OH)_2ClO_4 \cdot 3H_2O$.

EXPERIMENTAL

Crystal preparation and analysis. Crystals of $Sb_4O_5(OH)ClO_4 \cdot \frac{1}{2}H_2O$ were prepared by the following method: 5 M perchloric acid was heated in an Erlenmeyer flask to 110 °C and orthorhombic Sb_2O_3 was added until a saturated solution was obtained. The flask was stoppered and its temperature was decreased 5 – 10 °C per day to room-temperature. $Sb_4O_5(OH)ClO_4 \cdot \frac{1}{2}H_2O$ crystallized as thin, colourless and transparent plates. The homogeneity of the sample was checked by X-ray Guinier-Hägg powder photographs. The crystals thus prepared were analysed titrimetrically for antimony(III) by a method according to Belcher.[5] The perchlorate analysis was made according to Hoffman *et al.*[6] and the water analysis according to a modification of the method of Fischer.[7,8] The results of the analyses were in good agreement with the calculated values for $Sb_4O_5(OH)ClO_4 \cdot \frac{1}{2}H_2O$. (Found: 70.3 % antimony(III), 14.9 % perchlorate, and 2.2 % water. Calc.: 70.3 %, 14.2 %, and 2.6 %).

Crystal data. Preliminary Weissenberg photographs showed the crystals to be monoclinic and the systematic absences found were: hkl with $h+k+l = 2n+1$, $h0l$ with $l = 2n+1$ which are characteristic of the space group $I2/c$. This space group is not given in the *International Tables*. The general point position:

x,y,z; $\bar{x},\bar{y},\bar{z}$; $\bar{x},y\frac{1}{2}-z$; $x,\bar{y},\frac{1}{2}+z$;
$\frac{1}{2}+x,\frac{1}{2}+y,\frac{1}{2}+z$; $\frac{1}{2}-x,\frac{1}{2}-y,\frac{1}{2}-z$; $\frac{1}{2}-x,\frac{1}{2}+y,z$;
$\frac{1}{2}+x,\frac{1}{2}-y,z$;

Table 1. Guinier-Hägg powder photograph of $Sb_4O_5(OH)ClO_4 \cdot \frac{1}{2}H_2O$ using Cu$K\alpha_1$ radiation.

$h\,k\,l$	$10^5 \sin^2\theta$ obs	$10^5 \sin^2\theta$ calc	I obs
2 0 0	553	556	m
2 0 2	1 537	1 544	vvw
$\bar{1}$ 1 0	1 962	1 962	vvw
$\bar{2}$ 1 1	2 458	2 459	m
$\bar{4}$ 0 2	2 538	2 543	vvw
$\bar{1}$ 1 2	2 613	2 616	vvw
$\bar{1}$ 1 2	2 833	2 839	vvw
$\bar{4}$ 1 1	4 005	4 015	vw
$\bar{2}$ 1 3	4 430	4 435	vvw
$\bar{1}$ 1 4	4 793	4 800	w
$\bar{4}$ 1 3 / $\bar{6}$ 0 2	5 102	5 100	vw
$\bar{1}$ 1 4	5 243	5 246	vw
$\bar{5}$ 1 2	5 500	5 505	m
4 1 3 / $\bar{6}$ 0 2	6 443	6 438	w
$\bar{2}$ 1 5 / 0 1 5	6 604	6 605 / 6 606	vw
3 1 4	6 807	6 804	m
$\bar{0}$ 2 0	7 291	7 291	vs
$\bar{1}$ 2 1	7 563	7 566	vw
$\bar{4}$ 0 6	7 780	7 774	m
2 2 0	7 847	7 847	w
$\bar{7}$ 1 0	8 625	8 633	w
$\bar{1}$ 2 3	9 001	8 985	w
$\bar{4}$ 2 0	9 523	9 515	vvw
$\bar{6}$ 0 6	9 878	9 884	vw
$\bar{7}$ 1 2	10 187	10 179	vw
$\bar{5}$ 1 6	10 527	10 513	vw
$\bar{0}$ 0 8	12 256	12 245	vw
$\bar{6}$ 2 2	12 404	12 391	vvw
$\bar{6}$ 2 2	13 711	13 729	s
$\bar{4}$ 2 6	15 060	15 065	m
$\bar{6}$ 2 6	17 157	17 176	vvw
$\bar{4}$ 3 1	18 586	18 589	w
10 0 4	19 204	19 191	vw
$\bar{1}$ 3 4	19 839	19 829	m
$\bar{5}$ 3 2	20 104	20 090	vw
$\bar{1}$ 1 10	20 527	20 538	m
8 2 4	21 025	21 032	w
5 3 2	21 193	21 203	vw
$\bar{3}$ 3 4	21 398	21 387	vvw
$\bar{10}$ 0 8	21 962	21 684	vvw

Space group $I2/c$ was chosen instead of $C2/c$ because the unit cell dimensions were more suitable in $I2/c$.

The unit cell dimensions were determined by least-squares refinement using as data the diffraction angles of 40 lines on the Cu$K\alpha_1$ ($\lambda = 1.54051$ Å) powder pattern collected at room temperature in a Guinier-Hägg focusing camera equipped with a quartz monochromator and using KCl (cubic, $a = 6.2929$ Å) as internal standard, *cf.* Table 1. The density determined by measuring the loss of weight in benzene was in good agreement with the calculated value for eight formula units $Sb_4O_5(OH)ClO_4 \cdot \frac{1}{2}H_2O$ per unit cell. Some crystallographic data are presented in Table 2.

Table 2. Crystallographic data for $Sb_4O_5(OH)ClO_4 \cdot \frac{1}{2}H_2O$.

Unit cell:	a	= 20.969(5) Å
	b	= 5.7051(8) Å
	c	= 17.872(4) Å
	β	= 99.84(2)
	V	= 2106.9 Å^3
	Z	= 8
Formula weight:	M	= 692.46
Density, 20 °C:	D_m	= 4.28 g cm^{-3}
	D_x	= 4.39 g cm^{-3}
Space group:	$I2/c$	

Collection of intensity data. Three-dimensional intensity data from a single crystal (*cf.* Table 3) were collected on an Enraf-Nonius computer controlled four-circle diffractometer, CAD4, using graphite monochromatized Mo$K\alpha$ radiation ($\lambda = 0.71069$ Å). The intensities were recorded at a take off angle of 5°. The $\omega - 2\theta$ scan technique was used with an ω range of $(0.9 + 0.5\ \mathrm{tg}\theta)°$. A minimum net count of 2000 for each reflection was attained within the maximum measuring time of 3 min. The scan speed thus required was calculated from the net intensity after a fast pre-scan. Two octants of the reciprocal space out to $(\sin\lambda)/\theta = 0.65$ Å^{-1} were examined. The total number of reflections was 2496 of which 33 were considered not above background by giving net counts less than 10 in the fast pre-scan of totally 9 seconds and another 652 were rejected as being considered unobserved since their intensities were less than $3\sigma(I)$, where $\sigma(I)$ is the standard deviation of the intensity estimated from counting statistics. The intensities of the remaining 1811 reflections were corrected for Lorentz, polarization and absorption (*cf.* Table 3) effects. The linear absorption coefficient [9] for the compound with Mo$K\alpha$ is 108 cm^{-1}. The transmission factors

Table 3. Crystal dimensions. Boundary planes and their distances from an internal origin.

Plane	d (cm)
(1$\bar{0}$0)	0.00097
($\bar{1}$00)	0.00097
($\bar{1}$01)	0.00395
(10$\bar{1}$)	0.00395
(0$\bar{1}$0)	0.01175
(0$\bar{1}$0)	0.01175

Crystal volume: 0.17×10^{-3} mm^3.

Table 4. Final positional and thermal parameters in $Sb_4O_5(OH)ClO_4 \cdot \frac{1}{2}H_2O$. The form of anisotropic temperature factor is $\exp[-(h^2\beta_{11}+k^2\beta_{22}+l^2\beta_{33}+2hk\beta_{12}+2hl\beta_{13}+2kl\beta_{23})]$. Standard deviations are given within parentheses.

Atom	x	y	z	β_{11}	β_{22}	β_{33}	β_{12}	β_{13}	β_{23}
Sb(1)	.21675(4)	.04352(16)	.07538(4)	.00095(2)	.00778(24)	.00091(2)	−.00018(5)	.00020(2)	−.00020(6)
Sb(2)	.29647(4)	.03243(16)	.29368(4)	.00077(2)	.00875(24)	.00101(2)	.00032(5)	.00023(2)	.00050(6)
Sb(3)	.14115(4)	−.04377(16)	.34515(4)	.00085(2)	.01087(25)	.00085(2)	.00052(6)	.00017(2)	.00040(6)
Sb(4)	.37048(4)	−.03307(16)	.02440(4)	.00074(2)	.00991(25)	.00089(2)	−.00046(5)	.00012(2)	−.00017(6)
O(1)	.3168(4)	.1269(15)	.4235(4)	.0011(2)	.0093(26)	.0004(2)	.0010(6)	.0000(2)	−.0002(6)
O(2)	.2447(4)	.1562(15)	.1872(5)	.0012(2)	.0069(25)	.0011(3)	.0013(6)	−.0002(2)	.0002(7)
O(3)	.1667(4)	−.1594(14)	.4514(4)	.0011(2)	.0071(24)	.0004(2)	−.0004(6)	.0000(2)	.0011(6)
O(4)	.3910(5)	−.1317(19)	.1669(5)	.0016(3)	.0151(32)	.0015(3)	−.0014(8)	.0000(2)	.0007(8)
O(5)	.2228(4)	−.1511(15)	.3141(5)	.0009(2)	.0068(24)	.0013(3)	.0007(6)	0.002(2)	−.0003(7)
O(6)	.2993(4)	.1555(15)	.0528(5)	.0009(2)	.0084(25)	.0013(3)	.0019(6)	0.003(2)	−.0001(7)
Cl	.0498(2)	.0461(10)	.6202(3)	.0012(1)	.0387(18)	.0032(2)	.0008(3)	.0006(1)	−.0004(5)
O(7)	.104(1)	.006(4)	.677(1)	.004(1)	.089(11)	.002(4)	.006(2)	−.0003(4)	−.001(2)
O(8)	.068(1)	.035(4)	.051(1)	.0028(5)	.103(12)	.0030(5)	−.005(2)	.0008(4)	.006(2)
O(9)	−.006(1)	−.046(5)	.637(2)	.0030(5)	.109(16)	.014(2)	.002(3)	.0053(8)	.008(4)
O(10)	.039(2)	.291(4)	.612(2)	.008(1)	.047(10)	.015(2)	.004(3)	.003(1)	.003(3)
O(11)	½	.0660(29)	¼	.0016(4)	.018(5)	.0029(6)	0	−.0004(4)	0

Table 5. Coordination distances (Å) and angles (°) with standard deviations (in parentheses) in $Sb_4O_5(OH)ClO_4 \cdot \frac{1}{2}H_2O$. Notations of the atoms, *cf.* Table 4.

The Sb(1) – O-polyhedron			
Sb(1) – O(6)	1.952(9)	∠O(1) – Sb(1) – O(2)	75.2(3)
Sb(1) – O(1)	2.009(9)	∠O(1) – Sb(1) – O(3)	69.5(3)
Sb(1) – O(2)	2.085(9)	∠O(1) – Sb(1) – O(6)	91.2(4)
Sb(1) – O(3)	2.378(8)	∠O(2) – Sb(1) – O(3)	144.5(3)
O(1) – O(2)	2.498(12)	∠O(2) – Sb(1) – O(6)	89.0(4)
O(1) – O(3)	2.517(11)	∠O(3) – Sb(1) – O(6)	89.0(3)
O(1) – O(6)	2.829(12)		
O(2) – O(6)	2.832(12)		
O(3) – O(6)	3.049(12)		
The Sb(2) – O-polyhedron			
Sb(2) – O(5)	1.952(9)	∠O(2′) – Sb(2) – O(2)	72.3(4)
Sb(2) – O(2)	2.030(9)	∠O(1) – Sb(2) – O(2)	69.1(3)
Sb(2) – O(2′)	2.143(9)	∠O(2) – Sb(2) – O(5)	93.7(4)
Sb(2) – O(1)	2.350(8)	∠O(1) – Sb(2) – O(2′)	141.3(3)
O(1) – O(2)	2.498(12)	∠O(2′) – Sb(2) – O(5)	92.7(4)
O(1) – O(5)	2.985(12)	∠O(1) – Sb(2) – O(5)	87.4(3)
O(2) – O(2′)	2.464(17)		
O(2) – O(5)	2.905(12)		
O(2′) – O(5)	2.963(12)		
The Sb(3) – O-polyhedron			
Sb(3) – O(4)	1.969(11)	∠O(3) – Sb(3) – O(4)	79.9(4)
Sb(3) – O(5)	1.985(9)	∠O(3) – Sb(3) – O(5)	93.5(4)
Sb(3) – O(3)	1.995(8)	∠O(4) – Sb(3) – O(5)	88.5(4)
O(3) – O(4)	2.545(13)		
O(3) – O(5)	2.898(12)		
O(4) – O(5)	2.760(14)		
The Sb(4) – O-polyhedron			
Sb(4) – O(6)	1.975(9)	∠O(1) – Sb(4) – O(3)	77.5(3)
Sb(4) – O(3)	1.997(8)	∠O(3) – Sb(4) – O(6)	94.8(4)
Sb(4) – O(1)	2.027(8)	∠O(1) – Sb(4) – O(6)	92.5(4)
O(1) – O(3)	2.517(11)		
O(1) – O(6)	2.890(12)		
O(3) – O(6)	2.966(12)		
The perchlorate ion			
Cl – O(9)	1.36(2)	∠O(7) – Cl – O(8)	106(1)
Cl – O(7)	1.40(2)	∠O(7) – Cl – O(9)	113(1)
Cl – O(10)	1.42(3)	∠O(7) – Cl – O(10)	109(2)
Cl – O(8)	1.44(2)	∠O(8) – Cl – O(9)	116(1)
O(7) – O(8)	2.27(2)	∠O(8) – Cl – O(10)	107(2)
O(7) – O(9)	2.30(3)	∠O(9) – Cl – O(10)	106(2)
O(7) – O(10)	2.30(3)		
O(8) – O(9)	2.37(3)		
O(8) – O(10)	2.29(4)		
O(9) – O(10)	2.22(4)		
Possible hydrogen bonds			
O(11)···O(4)	2.75(1)	∠O(4)···O(11)···O(4′)	132(1)
O(11)···O(9)	2.98(3)	∠O(4)···O(11)···O(9)	127(1)
		∠O(4)···O(11)···O(9′)	90(1)
		∠O(9)···O(11)···O(9′)	84(1)
Sb – Sb distances			
Sb(1) – Sb(4)	3.353(1)		
Sb(1) – Sb(2)	3.410(1)		
Sb(1) – Sb(4)	3.524(1)		
Sb(2) – Sb(2)	3.370(2)		
Sb(2) – Sb(3)	3.559(1)		
Sb(3) – Sb(4)	3.394(1)		

were in the range 0.40 – 0.82. Two control reflections, $3\bar{4}5$ and 408, were measured with 90 min intervals to check for crystal decomposition and radiation stability. The mean decrease in intensity over the whole exposure time was 6 % for both control reflections. All intensities were therefore scaled with a first-order polynomial determined by least-squares.

STRUCTURE DETERMINATION AND REFINEMENT

From a three-dimensional Patterson synthesis the antimony atoms of the unit cell were found to occupy four eightfold positions in *I2/c*. A least-squares refinement was performed based on the deduced antimony atom positions. Subsequent three-dimensional electron density difference synthesis revealed the positions of all other non-hydrogen atoms. All atoms occupy eightfold point positions except the water oxygens which occupy a fourfold point position.

A preliminary full matrix least-squares refinement was now performed with isotropic temperature factors for all atoms. The refinement converged to an R-value of 0.102 ($R = \sum||F_o| - |F_c||/\sum|F_o|$). When the isotropic refinement was repeated with the data corrected for absorption effects the R-value was 0.060. Then anisotropic temperature factors were introduced for all atoms and the positional and thermal parameters were refined together with an overall scale factor. The R-value was now reduced to 0.045. Correction was then made for isotropic secondary extinction with the full matrix least-squares program *LINUS*.[10] The function minimized was $\sum w_i(|F_o| - |F_c|)^2$, where the weights, w_i, were calculated from the expression $w_i^{-1} = \sigma^2(F_o^2)/4F_o^2 + cF_o^2 + d$. The values of the constants c and d were chosen so as to give the most constant averages of $w_i(|F_o| - |F_c|)^2$ over ranges of F and $\sin\theta$. The values $c = 0.0003$ and $d = 0.55$ were used in the last refinement, which converged to $R = 0.037$ and $R_w = 0.051$, where $R_w = [\sum w(|F_o| - |F_c|)^2/\sum w|F_o|^2]^{1/2}$. The atomic scattering factors used were those given by Hansen *et al.*[11] The final value of the isotropic extinction parameter g was $0.08(2) \times 10^4$. The value of S defined by $S = [\sum w(|F_o| - |F_c|)^2/(m-n)]^{1/2}$, where m and n are the number of observations and parameters varied, respectively, was 1.009. The final positional and thermal parameters are given in Table 4. Lists of observed and calculated structure amplitudes are available by request to the author. Selected interatomic distances and angles are presented in Table 5. The drawings (Figs. 1 – 5) were obtained with the program ORTEP.[12]

DESCRIPTION AND DISCUSSION OF THE STRUCTURE

The $Sb_4O_5(OH)ClO_4 \cdot \frac{1}{2}H_2O$ structure contains distorted SbO_4- and SbO_3-polyhedra. The coordination spheres of Sb(1) and Sb(2) (notations of the atoms, *cf.* Table 4) could be described as trigonal bipyramids with the lone pair of electrons of antimony in one of the equatorial corners (*cf.* Fig. 1). The SbO_3-polyhedra of Sb(3) and Sb(4) are tetrahedral with the lone pair in one of the corners (*cf.* Fig. 1).

Four SbO_4-polyhedra share edges and build up a short chain (the coordination polyhedra around the atoms Sb(1) and Sb(2) in Fig. 1). In both ends of the chain an $Sb(4)O_3$-polyhedron shares edges with an SbO_4-polyhedron. The chains are terminated in both ends by one $Sb(3)O_3$-polyhedron sharing corners. The chains are linked to each other, by sharing the oxygen

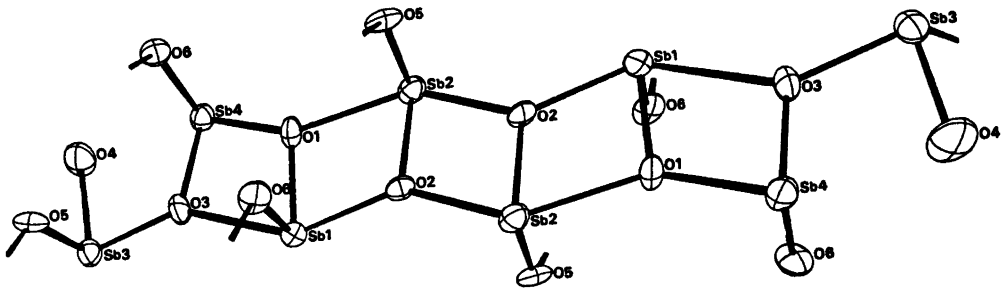

Fig. 1. The short chain of Sb – O polyhedra.

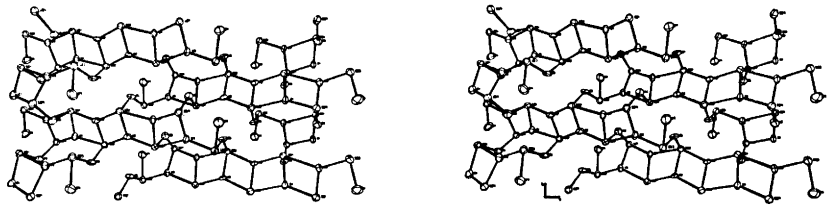

Fig. 2. Stereoview of the infinite layers of Sb – O.

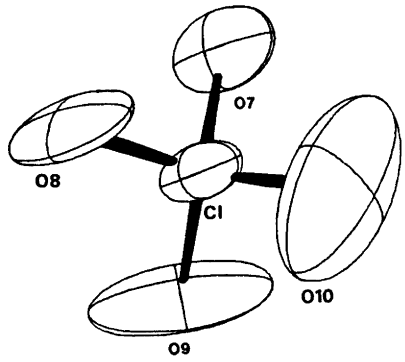

Fig. 3. The perchlorate ion. The thermal ellipsoids are drawn to enclose a 50 % probability.

atoms O(5) and O(6), to infinite layers parallel to the *bc*-plane (*cf.* Fig. 2). The four oxygen atoms O(7), O(8), O(9), O(10) and the chlorine atoms form the tetrahedral ClO_4^--ion (*cf.* Fig. 3). The distances Cl – O and angles O – Cl – O (*cf.* Table 5) are normal (*cf.* International Tables,[9] Lee and Carpenter,[13] Nordman,[14] and Almlöf [15]). The oxygen atoms in the ClO_4^--ion have large thermal motions, however. The r.m.s.-components (R1,R2,R3) of the thermal vibrations for O(7), O(8), O(9), and O(10) are (0.41, 0.16, 0.24), (0.44, 0.13, 0.24), (0.55, 0.11, 0.42) and (0.54, 0.22, 0.41).

The perchlorate ions and the water molecules are situated between the layers described above (*cf.* Fig 4).

For the interpretation of the solubility function of Sb(III) in perchloric acid with $Sb_4O_5(OH)ClO_4.\frac{1}{2}H_2O$ as solid phase it was necessary to verify the existence of the OH^- -ion in the structure. Since the hydrogen atoms could not be located from the available X-ray data it was difficult to distinguish O^{2-}, OH^-, and water from each other. In order to establish the nature of the oxygen atoms O(1), O(2), O(3), O(4), O(5), O(6), and O(11) a procedure based on the principle of local neutralization of charge was used, according to Donnay *et al.*[16] A calculation of cation to anion distances and associated bond valences leads to valence sums $\sum v$ for the oxygen atoms. For O^{2-}, OH^-, and H_2O $\sum v$ is approximately 2.0, 1.0, and 0.0, respectively. The calculated values of $\sum v$ varied between 1.8 and 2.4 for the atoms O(1), O(2), O(3), O(5), O(6), indicating that these are oxide ions. $\sum v$ for O(4) and O(11) was 1.0 and 0.0. Thus O(4) should be an OH^--ion and O(11) a water molecule. The distance O(4) – O(11) between hydroxide and water is 2.74 Å (*cf.* Table 5) which agrees very well with previously determined hydroxide to water distances in the mineral Colemanit, $CaB_3O_4(OH)_3.H_2O$ (2.76 ± 0.03 Å) [17] and in $Zn_5(OH)_8Cl_2.H_2O$ [18] (2.79 Å). It

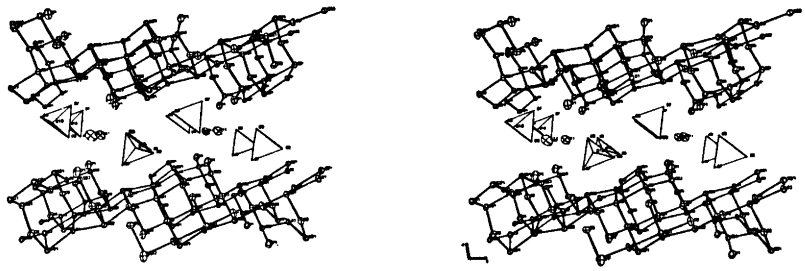

Fig. 4. Stereoview down the *b*-axis. The perchlorate ions are drawn with tetrahedra.

also agrees well with hydrogen bond distances in inorganic solids given in the International Tables.[9] The water molecules are thus hydrogen bonded to two different Sb – O-layers (*cf.* Fig. 4). Possible hydrogen bonds also exist between the water molecule and two perchlorate ions (*cf.* Table 5). The distance O(11) – O(9), 2.98 Å, is in agreement with that which Lee *et al.*[13] found in perchloric acid monohydrate, where hydrogen bonds have been certainly proved. The angle O(9) – O(11) – O(9) (*cf.* Fig. 5, Table 5) differs from the angle in water, but according to Hamilton and Ibers [19] the distribution of the O – O – O angles could be from 80° to 150° in hydrogen bonded hydrates.

A knowledge of the crystal structures of oxide salts can be useful for deducing the coordination of the complexes in solution, as has been shown in many instances. Thus, the dimeric $Th(OH)_2Th$ has been identified both in solution and solid state by X-ray investigations by Johansson.[20–21] Olin and Söderquist [22] found the complex $Pb_6O(OH)_6^{4+}$ as discrete groups in the oxide salt β-$[Pb_6O(OH)_6](ClO_4)_4.H_2O$ and Hong and Olin [23,24] has identified the complex $Pb_4(OH)_4^{4+}$ in the oxide salts $Pb_4(OH)_4(ClO_4)_4.2H_2O$ and $[Pb_4(OH)_4]_3(CO_3)(ClO_4)_{10}.6H_2O$.

From solubility measurements in perchloric acid solutions Ahrland and Bovin [1] found that the complex $Sb_2(OH)_2^{4+}$ exists in metastable equilibria with the solid phases orthorhombic or cubic Sb_2O_3. After a few days of agitation the stable phase $Sb_4O_5(OH)ClO_4.\frac{1}{2}H_2O$ is formed. If $Sb_2(OH)_2^{4+}$ is a fragment in the Sb – O-layers of this compound it is reasonable to expect that the distance between the antimony atoms within the group is significantly shorter than any other Sb – Sb-distances in the structure. In the Sb – O-layers Sb(2) is joined to Sb(2′) by two oxygens O(2) with the longest Sb – O-distances 2.143(9) Å. The Sb(2) – Sb(2′)-distance is 3.370(1) Å which is significantly shorter than the distance from Sb(2) to Sb(3) in an other short chain (*cf.* Fig. 2 and Table 5). Also Sb(1) and Sb(4) are joined over two oxygens O(3) and O(1) with the longest Sb – O-distance 2.378(8) Å. The Sb(1) – Sb(4)-distance is almost the same (3.343(1) Å) as in the other group. It seems possible that these groups are fragments of the complex $Sb_2(OH)_2^{4+}$ found in solution. Also in other solid compounds of Sb(III), Bi(III) and Te(IV) the shortest metal to metal distance exists between metal atoms joined by two oxygens. In $Sb_4O_4(OH)_2(NO_3)_2$ (Ref. 2) the two shortest Sb – Sb distances are 3.437(1) Å and 3.464(1) Å and $Sb_4O_5Cl_2$ [25,26] 3.418(1) Å. Aurivillius [27,28] found in $Bi(OH)CrO_4$ and $Bi(OH)SeO_4.H_2O$ aggregates of the formula $Bi_2(OH)_2^{4+}$ and the shortest Bi to Bi distances, 3.667(3) Å and 3.664(3) Å, respectively, are within these groups. In the structures of $Te_2O_3(OH)NO_3$[29] and β-TeO_2[30] two Te(IV) are joined by two oxygens in the same way with the shortest Te to Te distances 3.270(2) Å and 3.17 ± 0.003 Å, respectively.

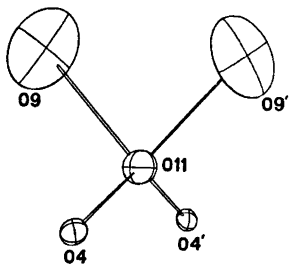

Fig. 5. Possible hydrogen bonds to the water oxygen. The thermal ellipsoids enclose areas with an atomic probability of 50 % (*cf.* Table 5).

It has been shown by Andersson, Åström, Galy and Meunier [31] that for many solid oxides, or oxide fluorides of Sb(III), Pb(II), Bi(III), and Te(IV), the volume of the lone pair and its cation is very nearly the same as that of an anion. If the volume of the unit cell is divided by the number of anions and lone pairs of antimony in $Sb_4O_5(OH)ClO_4.\frac{1}{2}H_2O$, the result is 18.1 Å^3. This value, compared with data (15.2 – 19.4 Å^3) from Andersson and Åström,[32] indicates that the total structure has an approximate closepacked arrangement of oxygens and lone pairs of electrons. The structure of $Sb_4O_4(OH)_2(NO_3)_2$ (Ref. 2) is more effectively closepacked than $Sb_4O_5(OH)ClO_4.\frac{1}{2}H_2O$ since the corresponding value is 16.3 Å^3. In the structure of $Sb_4O_4(OH)_2(NO_3)_2$ the oxygen and lone pairs of electrons in the Sb – O layers with one oxygen from the nitrate group was nearly cubic closepacked. If only the Sb – O layers and one oxygen atom, O(7), from the perchlorate ion are considered, the arrangement of oxygens and lone pairs of electrons has some similarity to the structure of $Sb_4O(_4OH)_2(NO_3)_2$. If in $Sb_4O_5(OH)ClO_4.\frac{1}{2}H_2O$ the infinite ribbons of octahedra, which are held together by tetrahedra

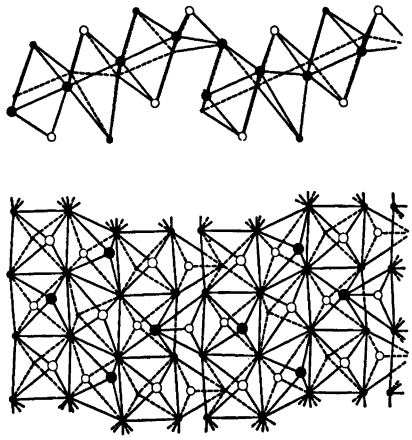

Fig. 6. The packing of oxygen atoms and lone pair of electrons of antimony in the layer parallel to the *bc*-plane. The upper view is along the *b*-axis and the lower is perpendicular to the *bc*-plane.

(*cf.* Fig. 6), are joined together by octahedral edge-sharing, infinite layers of octahedra are obtained similar to those in $Sb_4O_4(OH)_2(NO_3)_2$.

Acknowledgement. The author thanks Professor Bengt Aurivillius for his valuable help during this work. The author is also indebted to Professor Sten Arhland, Dr. Karin Aurivillius and Dr. Sten Andersson for their kind interest. Kerstin Renhult Aspelin and Christer Svensson are thanked for their assistance with the data collection. This work received financial support from the Swedish Natural Science Research Council.

REFERENCES

1. Ahrland, S. and Bovin, J.-O. *Acta Chem. Scand. A. In press.*
2. Bovin, J.-O. *Acta Chem. Scand. A 28* (1974) 267.
3. Jander, G. and Hartmann, H.-J. *Z. Anorg. Chem. 339* (1965) 239.
4. Svensson, C. *Acta Crystallogr. B 30* (1974) 458.
5. Belcher, R. *Anal. Chim. Acta 3* (1949) 578.
6. Hoffman, K. A., Metzler, A. and Höbold, K. *Ber. Deut. Chem. Ges. 43* (1910) 1080.
7. Vogel, A. T. *A Textbook of Quantitative Inorganic Analysis*, 3rd Ed., Longmans, London 1961, p. 944.
8. Karlsson, R. *Talanta 19* (1972) 1639.
9. *International Tables for X-Ray Crystallography*, Kynoch Press, Birmingham 1962, Vol. III.
10. Coppens, P. and Hamilton, W. *Acta Crystallogr. A 26* (1970) 71.
11. Hansen, H. P., Herman, F., Lea, I. D. and Skillmans, S. *Acta Crystallogr. 17* (1964) 1040.
12. Johnson, C. K. *A Fortran Thermal-Ellipsoid Plot-Program for Crystal Structure Illustration*, Oak Ridge National Laboratory, Chemistry Division, Oak Ridge, Tennessee 1965.
13. Lee, F. S. and Carpenter, G. B. *J. Phys. Chem. 63* (1959) 279.
14. Nordman, C. E. *Acta Crystallogr. 15* (1962) 18.
15. Almlöf, J. *Chem. Scr. 3* (1973) 73.
16. Donnay, G. and Allman, R. *Amer. Mineral. 55* (1970) 1003.
17. Christ, C. L., Clark, J. R. and Evands, H. T. *Acta Crystallogr. 11* (1958) 761.
18. Nowacki, W. and Silverman, J. *Acta Crystallogr. 10* (1957) 787.
19. Hamilton, W. C. and Ibers, J. A. *Hydrogen Bonding in Solids*, Benjamin, New York 1969, p. 213.
20. Johansson, G. *Acta Chem. Scand. 22* (1968) 389.
21. Johansson, G. *Acta Chem. Scand. 22* (1968) 399.
22. Olin, Å. and Söderquist, R. *Acta Chem. Scand. 26* (1972) 3505.
23. Hong, S.-H. and Olin, Å. *Acta Chem. Scand. 27* (1973) 2309.
24. Hong, S.-H. and Olin, Å. *Acta Chem. Scand. A 28* (1974) 233.
25. Edstrand, M. *Acta Chem. Scand. 1* (1947) 178.
26. Särnstrand, C. *Private communications.*
27. Aurivillius, B. and Löwenhielm, A. *Acta Chem. Scand. 18* (1964) 1937.
28. Aurivillius, B. *Acta Chem. Scand. 18* (1964) 2375.
29. Swink, L. N. and Carpenter, G. B. *Acta Crystallogr. 21* (1966) 578.
30. Beyer, H. *Z. Kristallogr. 124* (1967) 228.
31. Andersson, S., Åström, A., Galy, J. and Meunier, G. *J. Solid. State Chem. 6* (1973) 187.
32. Andersson, S. and Åström, A. *NBS Special Publication 364, Solid State Chemistry*, Proceedings of 5th Materials Research Symposium, issued July 1972.

Received April 5, 1974.

Acta Chemica Scandinavica A 28 (1974) 731—739

The Crystal Structure of the Adduct between Quinuclidine and the NMR Shift Reagent Eu(DPM)$_3$

ERIK BYE

Department of Chemistry, University of Oslo, Oslo 3, Norway

The molecular and crystal structure of the quinuclidine adduct of tris-(2,2,6,6-tetramethylheptan-3,5-dionato)Eu(III), Eu(DPM)$_3$, has been determined by X-ray methods. The crystals are monoclinic, space group $P2_1/n$ with unit cell dimensions $a = 10.718$ (1) Å; $b = 20.417$ (3) Å; $c = 21.368(3)$ Å; $\beta = 106.94(1)°$. The phase problem was solved by the heavy atom method and the model refined to an R-value of 0.046 for 4151 observed reflections. Estimated standard deviations in bond lengths and angles involving the europium ion are 0.006 Å and 0.2 – 0.6°, respectively.

The coordination polyhedron is best described as a distorted octahedron with the nitrogen atom located above the center of one of the faces, and the adduct has threefold symmetry. The Eu – N distance is 2.60 Å, the average Eu – O distance is 2.33 Å, and the europium ion is situated 0.54 Å, in average, from the three planar chelate rings.

Since the discovery by Hinckley[1] of lanthanide shift reagents, their use have been widespread. Several investigators have postulated relations between the induced chemical shifts and structural parameters of the substrates. The geometric factor 3 $\cos^2\theta$-1/r^3 given by Horrocks *et al.*,[2] valid for molecules having axial symmetry ($n \geq 3$) only, has been the most successful so far. Many structure determinations have been reported.[3–8] None of them, however, has been concerned with substrates having threefold axial symmetry. As such a substrate quinuclidine was thought to be suitable combined with the symmetric and frequently used shift reagent Eu(DPM)$_3$. The present work is a part of the investigations of shift reagents being carried out in this laboratory.[9–11] Fig. 1 shows the molecule with the numbering of atoms.

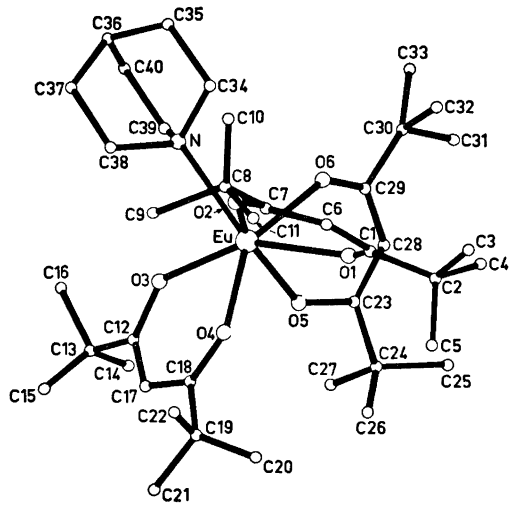

Fig. 1. The adduct between quinuclidine and Eu(DPM)$_3$ with the numbering of atoms.

EXPERIMENTAL

Single crystals of the 1:1 adduct were obtained by slow evaporation of a benzene solution with equimolecular amounts of Eu(DPM)$_3$ and quinuclidine. The crystals are colourless, transparent, parallelepipedes. A single crystal of dimensions 0.5 mm × 0.2 mm × 0.2 mm, sealed in a thin-walled capillary was used for the experiments.

Oscillation and Weissenberg photographs indicated monoclinic symmetry; systematically absent reflections are $h0l$ and $0k0$ for $h+l$ and k odd, respectively. The space group is thus $P2_1/n$. Unit cell dimensions were determined on a Syntex P$\bar{1}$ diffractometer with graphite crystal monochromated Mo$K\alpha$-radiation. Three-dimensional intensity data were collected using the $2\theta - \theta$ autocollection program with variable

scan rate and a cut-off for low intensities. The scan range was from 0.7° below $2\theta(\alpha_1)$ to 0.7° above $2\theta(\alpha_2)$, and the background was counted 0.7 times the intensity measuring time. The intensities of three standard reflections were measured periodically during the data collection. They showed an average decrease of 5 % and the intensities were amended according to this. E.s.d's in the intensities were taken as the square root of the total counts with a 2 % addition for instrumental instability.

A total of 4332 independent reflections were recorded within the limit of 0.60 for sin θ/λ of which 4151 had a net count larger than $3\sigma_I$.

The data were corrected for Lorentz and polarization effects and for absorption according to a μ-value of 14.3 cm^{-1} (Mo$K\alpha$).

All the calculations were performed on a CDC 3300 computer using the programs described in Ref. 12. Atomic form factors were those of Hanson *et al.*[13] for Eu, O, N, and C, and of Stewart *et al.*[14] for H.

CRYSTAL DATA

Quinuclidine adduct of tris-(2,2,6,6-tetramethylheptan-3,5-dionato)europium(III), Eu-$C_{33}H_{57}O_6.C_7H_{13}N$, monoclinic. $a = 10.718$ (1) Å, $b = 20.417$ (3) Å, $c = 21.368$ (3) Å, $\beta = 106.94(1)°$. $V = 4473.0$ Å^3, $M = 812.96$, $Z = 4$. $D_{obs} = 1.20$ g cm^{-3} (flotation). $D_{calc} = 1.21$ g cm^{-3}.

Systematic absences: $h0l$ and $0k0$ for $h+l$ and k odd, respectively; space group $P2_1/n$.

STRUCTURE DETERMINATION

The coordinates of the europium ions were obtained from a three-dimensional Patterson synthesis based on 1628 reflections within the limit of 0.36 for sin θ/λ. A Fourier map revealed 38 of the 48 atomic positions. Two Fourier refinement including all the 4151 reflections served to establish a model of all the non-hydrogen atoms. Successive cycles of full matrix least-squares refinement with isotropic thermal parameters gave an R-factor of 0.07. The data were then corrected for absorption effects, and anisotropic thermal parameters were introduced for the six t-butyl groups. The positional parameters of the 13 quinuclidine hydrogen atoms were calculated from stereochemical con-

Table 1. Fractional coordinates ($\times 10^4$) and isotropic thermal parameters (Å^2) with e.s.d's.

Atom	x	y	z	B
Eu[a]	3147(5)	5553(2)	20647(2)	3.30(01)
O1	1921(6)	674(3)	3062(3)	4.9(1)
O2	2237(6)	137(3)	1932(3)	4.7(1)
O3	−1208(6)	1003(3)	1159(3)	4.3(1)
O4	1209(6)	1506(3)	1790(3)	5.2(1)
O5	−857(6)	1214(3)	2577(3)	4.8(1)
O6	−553(6)	−117(3)	2718(3)	4.2(1)
N	−461(7)	−471(3)	1331(3)	3.7(1)
C1	3150(9)	668(5)	3251(4)	4.4(2)
C6	3907(10)	471(5)	2850(5)	5.1(2)
C7	3433(9)	226(5)	2225(4)	4.2(2)
C12	−1435(9)	1593(5)	931(5)	4.5(2)
C17	−506(10)	2081(5)	1064(5)	5.2(2)
C18	770(10)	2021(5)	1471(5)	5.6(2)
C23	−1118(9)	1176(5)	3123(4)	4.1(2)
C28	−1141(9)	592(5)	3445(4)	4.4(2)
C29	−890(9)	−22(5)	3237(4)	4.0(2)
C34	257(10)	−1052(5)	1652(5)	5.0(2)
C35	−173(11)	−1683(6)	1232(5)	6.3(3)
C36	−1196(11)	−1507(6)	626(6)	6.3(3)
C37	−661(11)	−995(5)	249(5)	6.0(3)
C38	−223(9)	−386(5)	676(5)	4.6(2)
C39	−1879(9)	−582(5)	1228(5)	4.8(2)
C40	−2346(13)	−1195(6)	794(6)	7.5(3)

[a] The parameters of the Eu ion ($\times 10^5$).

Table 2. Fractional coordinates and anisotropic thermal parameters ($\times 10^4$) with e.s.d's.

Atom	x	y	z	$B11$	$B22$	$B33$	$B12$	$B13$	$B23$
C2	3775(11)	922(6)	3959(5)	126(14)	56(6)	19(2)	−4(13)	13(10)	−12(6)
C3	5165(13)	628(9)	4255(6)	154(18)	99(8)	36(4)	48(21)	−41(14)	−23(10)
C4	2926(15)	721(10)	4389(6)	224(23)	135(11)	29(4)	−122(26)	72(16)	−23(11)
C5	3903(18)	1657(7)	3910(7)	439(36)	34(4)	42(5)	−50(22)	38(21)	−16(8)
C8	4360(10)	144(6)	1824(5)	90(12)	44(4)	39(4)	−10(12)	52(11)	−24(7)
C9	3794(13)	278(7)	1111(6)	165(17)	74(6)	29(4)	−1(16)	59(13)	4(7)
C10	4379(15)	−728(6)	1819(7)	256(24)	36(6)	64(6)	34(16)	141(20)	−20(8)
C11	5770(11)	329(7)	2110(7)	96(13)	75(7)	59(6)	−44(14)	73(14)	−51(9)
C13	−2815(10)	1701(5)	487(5)	120(13)	36(4)	35(4)	50(12)	13(11)	16(6)
C14	−3619(16)	1871(14)	926(10)	160(23)	220(19)	77(9)	143(35)	82(23)	−57(21)
C15	−2903(17)	2226(14)	61(15)	177(27)	201(19)	210(20)	−155(36)	−192(37)	329(34)
C16	−3413(17)	1083(9)	171(11)	238(27)	83(9)	133(12)	92(25)	−210(29)	−110(17)
C19	1752(13)	2605(6)	1562(7)	196(20)	39(5)	59(5)	−107(16)	30(17)	7(8)
C20	2147(27)	2796(12)	2109(9)	744(69)	140(14)	65(8)	−541(55)	156(39)	−122(18)
C21	1232(23)	3155(10)	1162(15)	432(47)	76(10)	211(19)	−281(36)	−262(48)	184(23)
C22	2876(22)	2350(11)	1360(17)	403(44)	88(10)	295(26)	−228(36)	526(60)	−101(27)
C24	−1453(11)	1841(5)	3371(5)	159(15)	24(3)	39(4)	20(11)	61(13)	−9(5)
C25	−1444(18)	1832(6)	4102(7)	424(35)	40(5)	44(5)	17(21)	163(22)	−18(8)
C26	−452(16)	2365(6)	3284(8)	326(29)	30(4)	81(7)	−86(18)	192(22)	−36(9)
C27	−2818(15)	2041(7)	2908(8)	245(24)	58(6)	68(6)	144(20)	1(20)	−23(10)
C30	−972(11)	−634(5)	3627(5)	182(16)	25(3)	32(3)	4(12)	81(12)	7(5)
C31	−1747(21)	−540(8)	4114(9)	503(44)	52(8)	88(8)	51(26)	344(34)	39(12)
C32	383(15)	−844(8)	3966(9)	219(24)	64(6)	99(8)	72(21)	79(24)	95(13)
C33	−1516(21)	−1182(7)	3172(8)	552(46)	45(6)	51(6)	−146(26)	135(26)	4(9)

Table 3. Fractional coordinates ($\times 10^3$) for the quinuclidine hydrogen atoms.[a]

Atom	x	y	z	Atom	x	y	z
H1	8	−112	212	H8	−77	3	42
H2	129	−98	172	H9	81	−30	75
H3	−58	−203	151	H10	−243	−16	99
H4	65	−190	111	H11	−205	−66	170
H5	−147	−195	32	H12	−307	−105	35
H6	−143	−86	−19	H13	−276	−154	106
H7	17	−120	12				

[a] The hydrogen atoms were given B-values of 7.0 Å^2.

Table 4. Bond lengths (Å) with e.s.d.'s.

Eu−O1	2.327(6)		
Eu−O2	2.323(6)	C2−C3	1.56(2)
Eu−O3	2.322(6)	C2−C4	1.53(2)
Eu−O4	2.316(6)	C2−C5	1.51(2)
Eu−O5	2.322(6)	C8−C9	1.56(2)
Eu−O6	2.337(6)	C8−C10	1.52(2)
		C8−C11	1.59(2)
Eu−N	2.603(7)	C13−C14	1.49(2)
		C13−C15	1.39(2)
O1−C1	1.26(1)	C13−C16	1.49(2)
O2−C7	1.26(1)	C19−C20	1.36(2)
O3−C12	1.29(1)	C19−C21	1.42(2)
O4−C18	1.27(1)	C19−C22	1.48(3)
O5−C23	1.28(1)	C24−C25	1.56(2)
O6−C29	1.28(1)	C24−C26	1.56(2)
C1−C6	1.40(2)	C24−C27	1.56(2)
C6−C7	1.38(1)	C30−C31	1.52(2)
C12−C17	1.38(1)	C30−C32	1.48(2)
C17−C18	1.39(2)	C30−C33	1.49(2)
C23−C28	1.38(1)		
C28−C29	1.38(1)	N−C34	1.47(1)
		N−C38	1.50(1)
		N−C39	1.49(1)
C1−C2	1.55(1)	C34−C35	1.56(2)
C7−C8	1.55(1)	C35−C36	1.47(2)
C12−C13	1.52(1)	C36−C37	1.53(2)
C18−C19	1.57(2)	C36−C40	1.52(2)
C23−C24	1.54(1)	C37−C38	1.53(2)
C29−C30	1.52(1)	C39−C40	1.55(2)

siderations, given B-values of 7.0 Å,^{2} but not refined. No attempts were made to include the other hydrogen atoms in the calculations. The refinement converged at an conventional R-value of 0.046 ($R_w = 0.062$).

A complete list of the structure factors may be obtained from the author on request.

The atomic parameters are given in Tables 1−3; the anisotropic thermal parameters are given by

$$\exp -(B11h^2 + B22k^2 + B33l^2 + B12hk + B13hl + B23kl)$$

The e.s.d's in bond lengths and angles involving the europium ion were calculated to be 0.006 Å and 0.2−0.6°, respectively. For the

Table 5. Bond angles (°) with e.s.d's.

Angles		Angles	
O1 – Eu – O2	72.9(2)	C1 – C6 – C7	126(1)
O3 – Eu – O4	72.5(2)	C12 – C17 – C18	126(1)
O5 – Eu – O6	72.1(2)	C23 – C28 – C29	126(1)
O1 – Eu – O4	84.0(2)	O1 – C1 – C2	115(1)
O1 – Eu – O5	82.2(2)	O2 – C7 – C8	114(1)
O2 – Eu – O3	118.4(2)	O3 – C12 – C13	114(1)
O2 – Eu – O4	80.1(2)	O4 – C18 – C19	116(1)
O4 – Eu – O5	87.4(2)	O5 – C23 – C24	113(1)
O3 – Eu – O5	79.6(2)	O6 – C29 – C30	115(1)
O3 – Eu – O6	115.1(2)		
O1 – Eu – O6	80.3(2)	C2 – C1 – C6	122(1)
O2 – Eu – O6	112.3(2)	C6 – C7 – C8	122(1)
O2 – Eu – O5	153.1(2)	C13 – C12 – C17	122(1)
O1 – Eu – O3	150.8(2)	C17 – C18 – C19	121(1)
O4 – Eu – O6	155.6(2)	C24 – C23 – C28	123(1)
O1 – Eu – N	131.0(2)	C28 – C29 – C30	121(1)
O2 – Eu – N	76.6(2)		
O3 – Eu – N	78.0(2)	C1 – C2 – C3	111(1)
O4 – Eu – N	127.2(2)	C1 – C2 – C4	110(1)
O5 – Eu – N	129.0(2)	C1 – C2 – C5	107(1)
O6 – Eu – N	77.0(2)	C3 – C2 – C4	109(1)
Eu – O1 – C1	135.7(6)	C3 – C2 – C5	108(1)
Eu – O2 – C7	134.0(6)	C4 – C2 – C5	113(1)
Eu – O3 – C12	133.5(6)	C7 – C8 – C9	108(1)
Eu – O4 – C18	135.7(6)	C7 – C8 – C10	107(1)
Eu – O5 – C23	133.5(6)	C7 – C8 – C11	111(1)
Eu – O6 – C29	133.9(6)	C9 – C8 – C10	110(1)
		C9 – C8 – C11	107(1)
		C10 – C8 – C11	113(1)
Eu – N – C34	109.6(6)	C12 – C13 – C14	106(1)
Eu – N – C38	110.9(6)	C12 – C13 – C15	113(1)
Eu – N – C39	110.2(6)	C12 – C13 – C16	112(1)
		C14 – C13 – C16	103(2)
O1 – C1 – C6	123(1)	C15 – C13 – C16	115(2)
O2 – C7 – C6	124(1)	C18 – C19 – C20	110(1)
O3 – C12 – C17	123(1)	C18 – C19 – C21	113(1)
O4 – C18 – C17	123(1)	C18 – C19 – C22	106(1)
O5 – C23 – C28	123(1)	C20 – C19 – C21	109(2)
O6 – C29 – C28	123(1)		
C20 – C19 – C22	111(2)	C34 – N – C38	109(1)
C21 – C19 – C22	108(2)	C34 – N – C39	109(1)
C23 – C24 – C25	114(1)	C38 – N – C39	109(1)
C23 – C24 – C26	109(1)		
C23 – C24 – C27	107(1)	N – C34 – C35	112(1)
C25 – C24 – C26	109(1)	N – C38 – C37	111(1)
C25 – C24 – C27	111(1)	N – C39 – C40	111(0)
C26 – C24 – C27	107(1)		
C29 – C30 – C31	114(1)	C34 – C35 – C36	109(1)
C29 – C30 – C32	107(1)	C35 – C36 – C37	109(1)
C29 – C30 – C33	110(1)	C35 – C36 – C40	110(1)
C31 – C30 – C32	111(1)	C37 – C36 – C40	107(1)
C31 – C30 – C33	111(1)	C36 – C37 – C38	110(1)
C32 – C30 – C33	104(1)	C36 – C40 – C39	110(1)

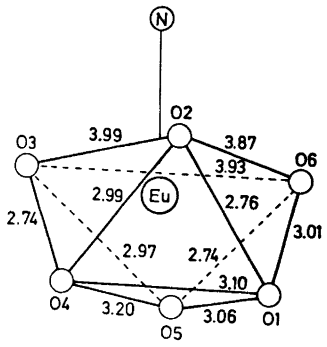

Fig. 2. The coordination polyhedron of the Eu(III) ion.

other atoms the e.s.d's in bond lengths and angles are 0.01 – 0.02 Å and 1.0 – 2.0°, respectively.

DISCUSSION

Interatomic distances and angles are given in Tables 4 and 5.

In the present structure the Eu(III) ion has seven-coordination, and Fig. 2 shows that the coordination polyhedron is best described as a distorted octahedron with the quinuclidine nitrogen atom located above the center of one of the faces. This model is called "1:3:3" according

Table 6. Interatomic distances (Å) of the coord nation polyhedron ($\sigma = 0.01$ Å).

O1 – O6	3.01	O5 – O1	3.06
O6 – O3	3.93	O5 – O6	2.74
O3 – O4	2.74	O5 – O3	2.97
O4 – O1	3.11	O5 – O4	3.21
O2 – O1	2.76	N – O2	3.06
O2 – O6	3.87	N – O6	3.08
O2 – O3	3.99	N – O3	3.11
O2 – O4	3.99	N – O1	4.49
		N – O4	4.41
		N – O5	4.45

Table 7. Equations of least-squares planes through the three chelate rings, with the deviations (Å × 10^3) of individual atoms from these planes.

Plane	Equation
A	$(0.0020a + 0.454b + 0.0178c)R - 1.028 = 0$
B	$(-0.0293a + 0.0147b + 0.0381c)R - 3.622 = 0$
C	$(0.0940A + 0.0057c + 0.0250c)R - 0.854 = 0$

Plane A	Deviations	Plane B	Deviations	Plane C	Deviations
Eu[a]	−458	Eu[a]	527	Eu[a]	629
O1	−40	O3	−52	O5	20
O2	42	O4	48	O6	15
C1	4	C12	2	C23	14
C2	31	C13	25	C24	−6
C6	−16	C17	10	C28	21
C7	−7	C18	7	C29	−2
C8	−15	C19	40	C30	−21

[a] The Eu ions do not define the plane.

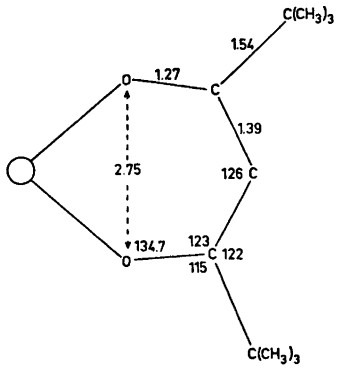

Fig. 3. Averaged bond lengths (Å) and angles (°) of the three planar chelate rings.

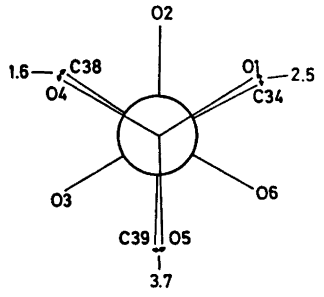

Fig. 4. The orientation of the quinuclidine molecule relative to the oxygen atoms, viewed along the Eu–N line.

to Gillespie.[15] The metal ion is surrounded by six chelate-oxygen atoms at an average distance of 2.325 Å and the nitrogen atom at 2.603 Å. The average Eu–O distance is in agreement with the value 2.347 Å reported by Cramer *et al.*[8] The slight shortening of the present Eu–N bond length compared to the value 2.649 Å found in the dipyridine adduct of Eu(DPM)$_3$[8] is probably significant and may be attributed to the coordination of only one nitrogen atom in the present case.

Adapting the "1:3:3" model[15] the coordination polyhedron is different, for instance, compared with the "1:4:2" model[15] found in Dy(THD)$_3$H$_2$O,[7] with the same coordination number. The preference for the former polyhedron in the present structure is probably due to the non-equivalence of one of the electron pairs and to the space requirements of the quinuclidine molecule.

Some of the interatomic distances of the coordination polyhedron are given in Table 6. The Eu ion is situated 0.51 Å and 1.46 Å from the faces (O2,O3,O6) and (O1,O4,O5), respectively, and the dihedral angle between the two faces is only 3.1°.

As found in acetylacetonato complexes without bridging ligands, the chelate rings are planar. The europium ion is displaced 0.46 Å, 0.53 Å, and 0.63 Å from the three planes A, B, C listed in Table 7 (0.54 Å in average). The bond lengths and angles may be compared to earlier reported dimensions of similar ring

Table 8. Dihedral angles (°), ($\sigma = 0.7°$).

O1–Eu–N–C34	2.5	O3–Eu–N–C34	−178.4
O4–Eu–N–C38	1.6	O6–Eu–N–C34	−178.1
O5–Eu–N–C39	3.7	O2–Eu–N–C39	−174.5

Table 9. Average (r,θ)-values together with those derived from NMR experiments.[18]

	r(distance, Å) X-ray	NMR		θ(angle, °) X-ray	NMR
Eu–α	3.5	3.4	γ–Eu–α	37	39
Eu–β	5.5	5.5	γ–Eu–β	23	28
Eu–γ	6.3	6.3	γ–Eu–γ	0	0

systems,[5,7,8,16,17] and the average values are shown in Fig. 3. The mean "bite" distance of 2.75 Å agrees well with the value 2.734 Å found by Cramer *et al.*[8] They are, however, somewhat shorter than the value 2.87 Å, predicted by Lingafelter *et al.*[16–17]

Fig. 4 shows the orientation of the quinuclidine moiety relative to the oxygen atoms. The dihedral angles O – Eu – N – C are listed in Table 8, and indicate the threefold axial symmetry of the complex. The axis is passing through the europium and nitrogen atoms, and the three dihedral angles O1 – Eu – N – C34 (2.5°), O4 – Eu – N – C38 (1.6°) and O5 – Eu – N – C39 (3.7°) are equal within the limits of experimental error.

The present calculated (r,θ)-values are listed in Table 9 together with those derived from NMR experiments,[18] utilizing the $3\cos^2\theta - 1/r^3$ relation. The α-, β-, and γ-hydrogen atoms of quinuclidine are as follows.

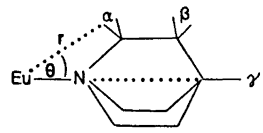

Bearing in mind the large experimental errors in the parameters of the hydrogen atoms, the agreement between corresponding values in Table 9 probably indicates that the complex maintains the same structure in solution.

Fig. 5 illustrates the crystal structure as seen along the a-axis.

Acknowledgement is made to T. Ledaal for supplying the crystals.

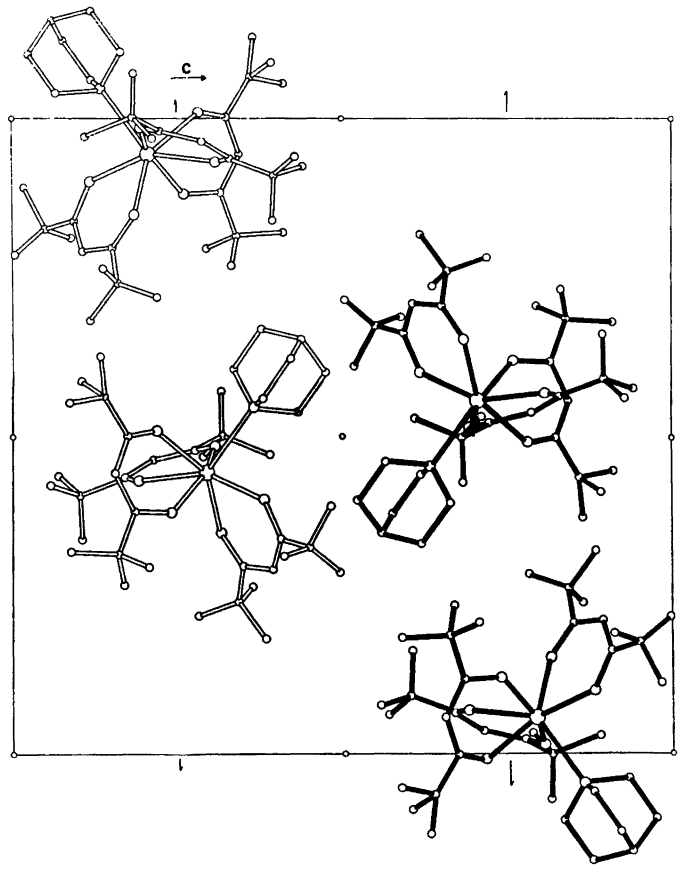

Fig. 5. The crystal structure as seen along the a-axis.

REFERENCES

1. Hinckley, C. C. *J. Amer. Chem. Soc. 91* (1969) 5160.
2. Horrocks, W. DeW., Jr. and Sipe, J. P., III *J. Amer. Chem. Soc. 93* (1971) 6800.
3. Phillips, T., II, Sands, D. E. and Wagner, W. F. *Inorg. Chem. 7* (1968) 2295.
4. Burns, J. H. and Danford, M. D. *Inorg. Chem. 8* (1969) 1780.
5. Erasmus, C. S. and Boeyens, J. C. A. *Acta Crystallogr. B 26* (1970) 1843.
6. Horrocks, W. DeW., Jr., Sipe, J. P., III and Luber, J. R. *J. Amer. Chem. Soc. 93* (1971) 5258.
7. Erasmus, C. S. and Boyens, J. C. A. *J. Cryst. Mol. Struct. 1* (1971) 83.
8. Cramer, R. E. and Seff, K. *Acta Crystallogr. B 28* (1972) 3281.
9. Kristiansen, P. and Ledaal, T. *Tetrahedron Lett. 30* (1971) 2817.
10. Kristiansen, P. and Ledaal, T. *Tetrahedron Lett. 46* (1971) 4457.
11. Kjekshus, A. and Ledaal, T. *Acta Chem. Scand. 27* (1973) 2665.
12. Dahl, T., Gram, F., Groth, P., Klewe, B. and Rømming, C. *Acta Chem. Scand. 24* (1970) 2232.
13. Hanson, H. P., Herman, F., Lea, J. D. and Skillmann, S. *Acta Crystallogr. 17* (1964) 1040.
14. Stewart, R. F., Davidson, E. R. and Simpson, W. T. *J. Chem. Phys. 42* (1965) 3175.
15. Gillespie, R. J. *Can. J. Chem. 38* (1960) 818.
16. Lingafelter, E. C. *Coord. Chem. Rev. 1* (1966) 151.
17. Lingafelter, E. C. and Braun, R. L. *J. Amer. Chem. Soc. 88* (1966) 2951.
18. Ledaal, T. *To be published.*

Received March 7, 1974.

Acta Chemica Scandinavica A 28 (1974) 740—746

Studies on Gold Complexes. I. Robustness, Stability and Acid Dissociation of the Tetramminegold(III) Ion

L. H. SKIBSTED* and JANNIK BJERRUM

Chemistry Department I, Inorganic Chemistry, H. C. Ørsted Institute, University of Copenhagen, DK-2100 Copenhagen Ø, Denmark

This paper presents a study of the stability and robustness of the tetramminegold(III) ion. The acidic character of this complex ion has been demonstrated; pK_a has been determined to be 7.48 ± 0.04 in 1 M (Na, NH_4)ClO_4 at 25 °C. The slow hydrolysis of the tetrammine complex in acid solution leads to a stationary equilibrium between this complex and hydroxotriamminegold(III) in the pH-range 2 – 5. The kinetics of this reaction was studied spectrophotometrically, and the hydrolysis equilibrium constant K_h estimated to be 0.7 mol/l at 25 °C. The aquatriamminegold(III) ion is a strong acid, the pK_a of which was found to be ≈ -0.7. Combining this value with K_h, the 4th consecutive stability constant is determined to be 2×10^{10} l/mol, which by generalization from other square planar tetrammine complexes gives an estimate of the cumulative constant $\beta_4 \approx 10^{46}$ l^4/mol^4 for the tetramminegold(III) ion.

The first to prepare tetramminegold(III) salts was Weitz [1] in 1915. He prepared the nitrate by leading gaseous ammonia into a solution of $AuCl_4^-$ in concentrated NH_4NO_3. However, the conditions are critical, and this is probably the reason why Addison *et al.*[2] had no success when they recently tried to prepare the salt by this method. According to our experience the preparation runs successfully when a supersaturated solution of NH_4NO_3 is used and addition of ammonia is stopped at pH 7 – 8.

The tetramminegold(III) ion has a certain robustness, but is slowly irreversibly hydrolyzed even in 10 M NH_4NO_3. However, the first hydrolysis product $Au(NH_3)_3OH^{2+}$ seems to be in a stationary equilibrium with the tetrammine ion in the pH-range 2 – 5. The kinetics of this reaction was studied spectrophotometrically in the temperature range 50 – 80 °C, and the hydrolysis constant K_h was estimated. At higher pH there is an instantaneous equilibrium between the tetrammine ion and $Au(NH_3)_3NH_2^{2+}$. The acid dissociation constant K_a as well as the absorption spectrum of the amide complex was determined. At pH lower than ≈ 1, $Au(NH_3)_3OH^{2+}$ begins to be protonated forming the corresponding aqua ion $Au(NH_3)_3H_2O^{3+}$. It was therefore possible also to obtain an estimate of K_4, the 4th consecutive stability constant of the tetramminegold(III) ion.

EXPERIMENTAL

Chemicals and solutions. "Goldtrichloride" from H. Drijfhout & Zoon's, Amsterdam, was used as the starting gold compound. The ammonia was taken from a cylinder and purified by passing through a sodium hydroxide solution. A stock solution of ammonia perchlorate was prepared from ammonia and perchloric acid and the neutralization was checked by pH measurements according to the procedure described by one of the authors.[3] All other chemicals used were of analytical grade.

Preparation of $Au(NH_3)_4(NO_3)_3$. The following procedure was found to give maximum yield of tetramminegold(III) nitrate: "Goldtrichloride" corresponding to 0.5 g of gold was dissolved in a supersaturated solution of 95 g NH_4NO_3 and 70 ml water. To this solution gaseous NH_3 is passed until pH ~ 7 with simultaneous cooling with icewater. The reaction mixture is left overnight in a stoppered flask and a white precipitate of tetramminegold(III) nitrate is formed. The crude product is obtained in a yield of ~ 95 %. Recrystallization at 50 °C from 12 ml 10^{-3} M HNO_3 per g

* Chemical Laboratory A, The Royal Danish School of Pharmacy.

gold salt gives a residue which consists of hydrolyzed species having a too high gold content (~50 %). The filtered solution is acidified with 1 ml 4 M HNO_3 for each 12 ml and cooled with icewater. A second fraction can be obtained on precipitation with an equal volume of ethanol. The two fractions show no systematical deviation on analysis. The product is washed with a little icewater and icecooled ethanol and dried at room temperature. The yield after recrystallization is ~65 %. The complex contains less than 0.5 % water determined by drying at 105 °C. (Typical analyses were: Au 43.40; N 21.59; H 2.57; NH_3 14.6, and Au 43.81; N 20.78; H 2.53; NH_3 14.4. Calc. for $Au(NH_3)_4(NO_3)_3$: Au 43.68; N 21.73; H 2.69; NH_3 15.10). Total N and H was determined in the microanalytical laboratory of this institute. Au was determined by weighing in a silica crucible after ignition, and NH_3 by a micro Kjeldahl distillation. Thermogravimetric analysis showed no decomposition of the complex up till ≈230 °C, then decomposition to metallic gold occurs over a short temperature range and not stepwise.

Preparation of $Au(NH_3)_4(ClO_4)_3$. The tetramminegold(III) nitrate was converted into the perchlorate as already described by Weitz.[1] (Found: Au 35.5; N 10.7; H 2.25; Cl 18.2. Calc. for $Au(NH_3)_4(ClO_4)_3$: Au 35.0; N 10.0; H 2.15; Cl 18.9). (*Warning:* The perchlorate explodes easily on heating).

pH-measurements were performed with a digital pH-meter Radiometer PHM 52 with Radiometer's glass electrode type G 202 B selected to have almost theoretical slope in the actual medium. A commercial saturated potassium chloride calomel electrode was modified to 1 M sodium chloride and used as reference electrode. This modification was necessary in order to avoid precipitation of $KClO_4$ in the boundary between the medium and the electrode. The definition $pH = -\log [H^+]$ was employed throughout, and *concentration* pH-standards were made in the actual salt medium.

Spectrophotometric measurements were all made on a Cary 14 spectrophotometer in 1 cm silica cells at 25 °C.

Acid dissociation constant of $Au(NH_3)_4^{3+}$ and spectrum of $Au(NH_3)_3NH_2^{2+}$

The tetramminegold(III) ion is a weak acid forming amidotriamminegold(III) in basic solution, the latter being rather sensitive to further decomposition. A direct titration with strong base gives the correct S-shaped titration curve, but at the end of the titration precipitation occurs. The acid-base equilibrium was therefore studied in 1 M $(Na,NH_4)ClO_4$-ammonia buffer solutions in order to determine the constant

$$K_{amid} = \frac{[NH_4^+][Au(NH_3)_3NH_2^{2+}]}{[NH_3][Au(NH_3)_4^{3+}]}$$

which is connected by the acid dissociation constant of $Au(NH_3)_4^{3+}$ by the relationship

$$K_a(Au(NH_3)_4^{3+}) = K_{amid} \times K_a(NH_4^+)$$

Table 1. Determination of the acid-base constant of $Au(NH_3)_4^{3+}$ in 1 M $(Na,NH_4)ClO_4$-ammonia buffer solutions at 25 °C.

$C^0_{Au(NH_3)_4^{3+}}$	$C^0_{NH_3}$	$C^0_{NH_4^+}$	$pH = -\log[H^+]$	$pK_a(NH_4^+)$	α	K_{amid}
0.00937	0.01195	0.0999	8.094	9.463	0.787	87
0.00936	0.0378	1.000	7.903	9.420	0.769	109
0.0200	0.0378	1.000	7.783	9.420	0.721	112
0.00922	0.00574	0.1088	7.461	9.463	0.500	100
0.0192	0.00909	0.1007	7.349	9.463	0.430	98
0.00938	0.00384	0.1652	7.162	9.460	0.319	93
0.0117	0.00288	0.1000	6.963	9.463	0.219	89
0.0169	0.00384	0.1652	6.902	9.460	0.200	91
0.0185	0.00288	0.1000	6.713	9.463	0.146	96
						$K_{amid} = 97 \pm 4$

C^0_x denotes the initial concentrations of $Au(NH_3)_4^{3+}$, NH_3 and NH_4^+. As $[H^+]$ and $[OH^-]$ are less than 10^{-6} M, then the following relationships are valid:

$[NH_3] = K_a(NH_4^+) \times [NH_4^+]/[H^+]$,

$[NH_4^+] = C^0_{NH_4^+} + \alpha C^0_{Au(NH_3)_4^{3+}}$,

$\alpha = (C^0_{NH_3} - [NH_3])/C^0_{Au(NH_3)_4^{3+}}$, and finally $K_{amid} = \alpha[NH_4^+]/(1-\alpha)[NH_3]$.

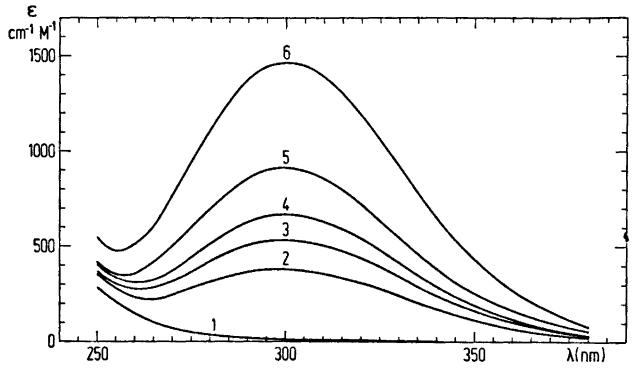

Fig. 1. Spectra of tetramminegold(III) nitrate in 1.0 M $NH_4ClO_4-NH_3$ buffer solutions. Curve 1 is the spectrum of $Au(NH_3)_4^{3+}$ obtained from measurements of solutions of the nitrate in 1.0 M NH_4ClO_4 at pH 2.0. The spectra recorded in NH_4^+, NH_3 buffer solutions have the following values for $\alpha=[Au(NH_3)_3NH_2^{2+}]/C_{Au(III)}$: Curve 2, $\alpha=0.25$; 3, $\alpha=0.36$; 4, $\alpha=0.45$; and 5, $\alpha=0.62$. Curve 6 is the spectrum of $Au(NH_3)_3NH_2^{2+}$ calculated from the mixed spectra. All spectra were recorded immediately after mixing the solutions, and the absorption curves given are corrected for the nitrate absorption. The maximum at 300 nm has a molar absorptivity of 1467 ± 15 cm^{-1} M^{-1}.

Glass electrode measurements were performed in solutions in which the NH_4^+-concentration was varied between 0.1 and 1 M. There was a small drift towards higher pH (especially in the solutions with lowest ammonium concentration) and therefore pH was in all cases extrapolated back to the time of mixing. The possibility of $Au(NH_3)_3OH^{2+}$ formation was excluded because hydroxo complex formation will cause only infinitesimally small changes in pH in a medium containing excess ammonium ions. The acid dissociation constant for NH_4^+ at ionic strength 1.0, necessary to calculate pK_a for $Au(NH_3)_4^{3+}$, was determined in 0.1 M as well as in 1 M NH_4^+ solution, and the following interpolation formula was derived

$$pK_a(NH_4^+) = 9.468 - 0.048[NH_4^+]$$

The experimental data are given in Table 1. K_{amid} was found to be 97 ± 4 at 25 °C in 1 M $(Na,NH_4)ClO_4$, and $pK_a(Au(NH_3)_4^{3+})$ to be 7.48 ± 0.04. The value found for pK_a is compared in Table 4 with the few known values for other metal ammine complexes. The absorption spectrum for amidotriamminegold(III) shown in Fig. 1 was calculated from the mixed absorption spectra of tetramminegold(III) in 1 M $(Na,NH_4)ClO_4$-ammonia buffer solutions.

Hydrolysis of $Au(NH_3)_4^{3+}$ in acid solution

The tetramminegold(III) ion hydrolyzes rapidly in alkaline solution forming an orange-brown, amorphous, and highly explosive precipitate known as fulminating gold. In acid solution the tetramminegold(III) ion is stabilized and the hydrolysis is slow.

The change in the absorption spectrum as function of time in acid ammonium solutions corresponds to first order kinetics. The rate and the degree of hydrolysis depend on the ammonium concentration but not on the hydrogen ion concentration in the pH-range 2 – 4 as illustrated by an example in Table 2. The

Table 2. Hydrogen ion concentration influence on the rate and on the degree of hydrolysis of $Au(NH_3)_4^{3+}$ in 1.0 M $(Na,NH_4)ClO_4$ at 80.0 °C from calculations at $\lambda=320$ nm. $C_{Au} \approx 0.003$ M. ε_{eq} is the formal molar absorptivity at equilibrium obtained from the regression analysis; see text.

$[NH_4^+]$	pH	10^3 k_{obs} s^{-1}	ε_{eq} cm^{-1} M^{-1}
1.0	2.0	1.74 ± 0.05	88
1.0	3.0	1.80 ± 0.08	86
0.50	2.0	1.38 ± 0.06	102
0.50	3.0	1.32 ± 0.12	103

experimental observations fit with the following reaction scheme:

$$Au(NH_3)_4^{3+} + H_2O \underset{k_{-1}}{\overset{k_{+1}}{\rightleftharpoons}} Au(NH_3)_3OH^{2+} + NH_4^+$$

This reaction was investigated in the temperature range 50 – 80 °C by spectrophotometric measurements. Aliquots, removed at known times from thermostated acid solutions (~3 mM in $Au(NH_3)_4(NO_3)_3$ in 1.0 M $(Na,NH_4)ClO_4$) were cooled in icewater, and the spectra recorded at room temperature. The absorption spectrum changes to an almost constant spectrum, which, however, continues to change especially at low ammonium concentration due to irreversible hydrolysis processes. As no final reading could be obtained, the reaction was studied kinetically. The over-all rate constant k_{obs} of the equilibrating process was determined at varying ammonium ion concentrations at pH = 2.0 in 1.0 M $(Na,NH_4)ClO_4$. From the absorbance as a function of time the pseudo first order rate constant k_{obs} was calculated at the wavelengths 310, 320, and 330 nm by means of nonlinear regression analysis as shown in Fig. 2. A final reading is not necessary in this method of calculation, and values corresponding to the slowly increasing absorbance were excluded in the calculations. At a fixed temperature the rate constant k_{obs} obeys the expression

$$k_{obs} = k_{+1} + k_{-1}[NH_4^+]$$

In Fig. 3 k_{obs} determined at varying ammonium ion concentrations is shown. By means of weighted linear regression analysis values of k_{+1} and k_{-1} were calculated at 80.0, 70.0, 60.0, and 50.0 °C as given in Table 3 together with the calculated equilibrium constant, K_h. The values of k_{+1} and k_{-1} at the same temperature are strongly negative correlated, and in the final calculations of the equilibrium constant and the activation energies the non-diagonal elements in the experiment variance matrix must be included. Therefore the activation parameters cannot be obtained from a conventional Arrhenius plot as such a plot neglects the correlation between the rate constants. When the rate constants were fitted to the equation $k = Z \exp(-E_a/RT)$, activation energies of $E_{a(+1)} = 24 \pm 6$ kcal/mol and $E_{a(-1)} = 20 \pm 16$ kcal/mol, respectively, were calculated, whereas when the logarithm of the rate constant was fitted to $\ln k = \ln Z - E_a/RT$, $E_{a(+1)} = 27 \pm 3$ kcal/mol and $E_{a(-1)} = 17 \pm 8$ kcal/mol were obtained. These two sets of parameters are, within the estimated standard deviations, identical. The conclusion is, however, that the experiments do not allow one to get usable values for the activation energies and for $\Delta H°$ for the reaction. By analogy with the corresponding reaction for Hg(II), it is, however, possible to estimate a value for $\Delta H°$; see discussion.

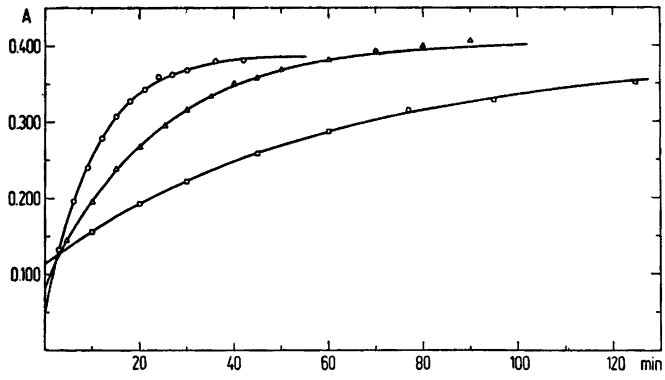

Fig. 2. Determinations of the rate of hydrolysis of $Au(NH_3)_4^{3+}$ from plots of absorbance *versus* time. Solutions ~ 3 mM in $Au(NH_3)_4^{3+}$ were hydrolyzed in 1.0 M $(Na,NH_4)ClO_4$ at pH = 2.0. The absorbance at the wavelengths 310, 320, and 330 nm as function of time was fitted to the expression $A = a_1 + a_2 \times \exp -(k_{obs}t)$ by means of nonlinear regression analysis. The examples given in the figure are experiments with $[NH_4^+] = 0.80$ M at 80.0 °C, 70.0 °C and 60.0 °C monitored at $\lambda = 310$ nm.

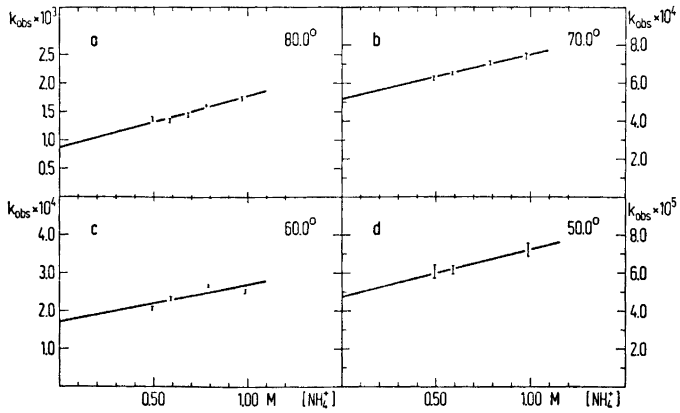

Fig. 3a–d. The influence of ammonium ion concentration on the rate of hydrolysis of $Au(NH_3)_4^{3+}$ at four temperatures. The values of k_{obs} in s^{-1}, determined in 1.0 M $(Na,NH_4)ClO_4$ at pH = 2.0 as shown in Fig. 2, are split up into k_{+1} and k_{-1} by means of weighted linear regression analysis according to the expression: $k_{obs} = k_{+1} + k_{-1}[NH_4^+]$.

Table 3. Summary of the results of the kinetic experiments on the hydrolysis of $Au(NH_3)_4^{3+}$ in 1.0 M $(Na,NH_4)ClO_4$ at pH = 2.0.
The rate constants of the forward reaction k_{+1} and the reverse reaction k_{-1} of the hydrolytic equilibrating process:

$$Au(NH_3)_4^{3+} + H_2O \underset{k_{-1}}{\overset{k_{+1}}{\rightleftharpoons}} Au(NH_3)_3OH^{2+} + NH_4^+.$$

The correlation coefficients, r, illustrate the strong negative correlations between the determined rate constants at the same temperature; see Fig. 3.

t °C	k_{+1} s^{-1}	k_{-1} M^{-1} s^{-1}	$r(k_{+1},k_{-1})$	K_h mol/l
80.0	$(8.72 \pm 0.87) \times 10^{-4}$	$(9.2 \pm 1.1) \times 10^{-4}$	−0.984	1.0 ± 0.2
70.0	$(5.10 \pm 0.30) \times 10^{-4}$	$(2.42 \pm 0.43) \times 10^{-4}$	−0.977	2.1 ± 0.5
60.0	$(1.72 \pm 0.23) \times 10^{-4}$	$(9.8 \pm 2.9) \times 10^{-5}$	−0.970	1.8 ± 0.8
50.0	$(4.73 \pm 0.58) \times 10^{-5}$	$(2.48 \pm 0.83) \times 10^{-5}$	−0.964	1.9 ± 0.9

Acid dissociation constant of $Au(NH_3)_3H_2O^{3+}$

The spectrum of a partially hydrolyzed solution of $Au(NH_3)_4^{3+}$ changes when acidified below pH ≈ 1. The spectral data of such an experiment performed with $Au(NH_3)_4(ClO_4)_3$ in perchloric acid solutions are shown in Fig. 4. The hydrogen ion activity in the concentrated $HClO_4$ solution was expressed in the Hammett acidity function [5] redefined with standard state in 1 M $HClO_4$, which corresponds to the medium used in the hydrolysis experiments. Plotting the absorptivity against the Hammett acidity function, one gets an S-shaped "titration curve" with $pK_a \approx -0.7$. In Table 4 this value found for the aquatriamminegold(III) ion is compared with known values for some ammine and aquaammine complexes, and it will be seen that the difference between the pK_a of $Au(NH_3)_4^{3+}$ and $Au(NH_3)_3H_2O^{3+}$ is of expected order of magnitude. The red shift in the absorption curve upon exchanging NH_3 with H_2O and OH^- is in accordance with the spectrochemical series.

DISCUSSION

Combining thermochemical data from Yatsimirskii and Milyukov [16] and Anderegg *et al.*[17] one can calculate for the enthalpy change of the reaction

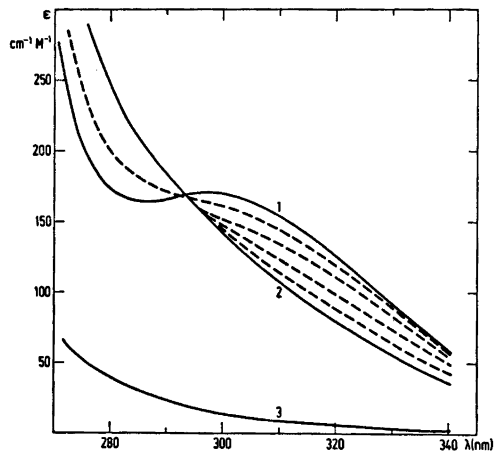

Fig. 4. Spectra and acid dissociation constant of the aquatriamminegold(III) system at 25 °C. A solution with $C_{Au(NH_3)_4(ClO_4)_3} = 0.00293$ M and pH = 2.0 was hydrolyzed at 80 °C for 15 min. From the spectrum the following concentrations after dilution to the double volume could be calculated:

$[Au(NH_3)_4^{3+}] = 0.00080$ M; $[Au(NH_3)_3OH^{2+}] = 0.00070$ M.

Spectra of solutions of this composition with increasing acidity were measured. The absorption curves corrected for the $Au(NH_3)_4^{3+}$ absorption (curve 3) are given in the figure.

Absorption curve 1 with $\varepsilon_{max} \approx 170$ at 297 nm recorded at pH = 2.0 represents the molar absorptivity of $Au(NH_3)_3OH^{2+}$. Curve 2 is the absorption spectrum in 5.89 M $HClO_4$ ($H_0' = -2.65$), which corresponds to a solution of $Au(NH_3)_3H_2O^{3+}$. The dotted curves are mixed spectra at the following concentration of $HClO_4$: 1.00 M ($H_0' = 0.00$), 1.94 M ($H_0' = -0.55$), 2.88 M ($H_0' = -1.00$) and 4.41 M ($H_0' = -1.73$). H_0' given in the brackets is the Hammett acidity function defined with standard state in 1 M $HClO_4$. From the spectral changes as a function of H_0' one calculates $pK_a \approx -0.7$.

$$Hg(NH_3)_2^{2+} + 2\,OH^- \rightleftharpoons Hg(OH)_2 + 2\,NH_3$$

in homogeneous solution, $\Delta H° = 8.7$ kcal/mol, or on an average 4.4 kcal/mol for the exchange of an ammonia molecule with a hydroxide ion. The endothermic character of this reaction is that expected from a consideration of Hg(II) as a soft metal, and therefore according to the HSAB criterion as preferring ammonia to hydroxide ion. For the analogous hydrolysis reaction for Au(III), a metal with a softness greater than but comparable to that of Hg(II), an estimate of $\Delta H° \approx 5$ kcal/mol seems reasonable for the reaction:

$$Au(NH_3)_4^{3+} + OH^- \rightleftharpoons Au(NH_3)_3OH^{2+} + NH_3$$

Combination of this value with the protonation enthalpies for ammonia −12.4 kcal/mol,[14] and for OH^- −13.4 kcal/mol,[15] gives $\Delta H° \approx 6$ kcal/mol for the reaction

$$Au(NH_3)_4^{3+} + H_2O \rightleftharpoons Au(NH_3)_3OH^{2+} + NH_4^+$$

On extrapolation of the hydrolysis constant K_h determined at elevated temperatures to 25 °C by means of $\Delta H° \approx 6$ kcal/mol, one gets $K_h \approx 0.7$ mol/l. The corresponding constant for the hexamminechromium(III) ion $K_h = 150$ mol/l (4.5 M NH_4Cl) [4] and for the hexamminecobalt(III) ion $K_h = 0.032$ mol/l (1.0 M NH_4Cl).[3]

The fourth consecutive stability constant of $Au(NH_3)_4^{3+}$ is given by the expression

$$K_4 = K_a(Au(NH_3)_3H_2O^{3+})/(K_h \times K_a(NH_4^+))$$

Introducing the estimated values for $K_h \approx 0.7$ mol/l in 1 M $(NH_4,Na)ClO_4$ at 25 °C, and the corresponding K_a values, K_4 is calculated to be 2×10^{10} l/mol. An estimate of β_4 ($Au(NH_3)_4^{3+}$) can be obtained in the following way. The

Table 4. Comparison of acidities of ammine and aquaammine metal complexes at room temperature.

	pK_a	I	Ref.		pK_a	I	Ref.
$Au(NH_3)_4^{3+}$	7.48	1.0		$Au(NH_3)_3H_2O^{3+}$	−0.7	(1.0)	
$Pt(NH_3)_6^{4+}$	7.75	0.1	6	$Pt(NH_3)_5H_2O^{4+}$	?		
$Ru(NH_3)_6^{3+}$	12.4	var.	7	$Ru(NH_3)_5H_2O^{3+}$	4.2	var.	10
$Rh(NH_3)_6^{3+}$	> 14		8	$Rh(NH_3)_5H_2O^{3+}$	6.40	0.1	11
$Co(NH_3)_6^{3+}$	> 14		8	$Co(NH_3)_5H_2O^{3+}$	6.40	1.0	3
				$Co(NH_3)_5H_2O^{3+}$	6.03	0.1	3
				$Cr(NH_3)_5H_2O^{3+}$	5.10	0.1	12
$Au\ en_2^{3+}$	6.8	var.	9				
$Au\ pn_2^{3+}$	6.6	var.	9				

tetramminegold(III) complex has the same square planar configuration as the tetrammines of Cu(II) and Pd(II), and the properties of the three complexes may also in other respect be comparable. The spreading of the consecutive constants (especially K_2/K_3), although larger in the Pd(II)- than in the Cu(II)-system, are of the same order of magnitude in the two systems. Thus the ratio $\sqrt[4]{\beta_4}/K_4$ has in the Cu(II)-system [3] the value $10^{1.03}$ and in the Pd(II)-system [13] the value $10^{1.4}$. Combining the average value $10^{1.2}$ with the estimated value for K_4(Au(III)) at 25 °C, the stability constant β_4(Au(III)) is calculated to be about 10^{46} l^4/mol^4 as compared with $\beta_4(Cu(II)) = 10^{12.61}$ l^4/mol^4 (in 1 M NH_4NO_3 at 25 °C) and β_4-(Pd(II)) $\approx 10^{32.8}$ l^4/mol^4.

Acknowledgement. We are most grateful to Mr. Ole Mønsted for his assistance in connection with some computing problems.

REFERENCES

1. Weitz, E. *Justus Liebigs Ann. Chem. 410* (1915) 117.
2. Addison, C. C., Brownlee, G. S. and Logan, N. *J. Chem. Soc. Dalton Trans.* (1972) 1440.
3. Bjerrum, J. *Metal Ammine Formation in Aqueous Solution*, 2nd Ed., P. Haase and Son, Copenhagen 1957.
4. Andersen, P. *14de Nordiska Kemistmötet, Resuméer*, Umeå 1971.
5. Bascombe, K. N. and Bell, R. P. *Discuss. Faraday Soc. 24* (1957) 158.
6. Jørgensen, C. K. *Acta Chem. Scand. 10* (1956) 518.
7. Waysbort, D. and Navon, G. *Chem. Commun.* (1971) 1410.
8. Basolo, F. and Pearson, R. G. *Mechanisms of Inorganic Reactions*, 2nd Ed., Wiley, New York 1967.
9. Block, B. P. and Bailar, J. C. *J. Amer. Chem. Soc. 73* (1951) 4722.
10. Broomhead, J. A., Basolo, F. and Pearson, R. G. *Inorg. Chem. 3* (1964) 826.
11. Brønsted, J. N. and Volqvartz, K. *Z. Phys. Chem. 134* (1927) 97.
12. Chan, S. C. and Hai, K. Y. *Aust. J. Chem. 21* (1968) 3061.
13. Rasmussen, L. and Jørgensen, C. K. *Acta Chem. Scand. 22* (1968) 2313.
14. Everett, D. H. and Landsman, D. A. *Trans. Faraday Soc. 48* (1952) 531.
15. Pitzer, K. H. *J. Amer. Chem. Soc. 59* (1937) 2365.
16. Yatsimirskii, K. B. and Milyukov, P. M. *Zh. Neorg. Khim. 2* (1957) 1046.
17. Anderegg, G., Schwarzenbach, G., Padmoyo, M. and Borg, Ö. F. *Helv. Chim. Acta 41* (1958) 988.

Received March 11, 1974.

Acta Chemica Scandinavica A 28 (1974) 747—752

Isotope Effects in Proton-transfer Reactions. V.* Deuterium Solvent Isotope Effect on the Racemization of (+)-2-Methyl-3-phenylpropionitrile in Methanol

NILS-ÅKE BERGMAN and LARS MELANDER

Department of Organic Chemistry, University of Göteborg and Chalmers University of Technology, Fack, S-402 20 Göteborg 5, Sweden

The deuterium solvent isotope effect on the methoxide-ion catalyzed racemization of (+)-2-methyl-3-phenylpropionitrile and the isotopic -2-*d* compound has been measured for different mixtures of methanol and methanol-*O*-*d* at 60 °C, and the effect has been found to be the same (within the experimental accuracy) for the two substrates. The limiting value of the ratio of the rate constants is $k_{MeOD}/k_{MeOH} = 2.11 \pm 0.05$. The magnitude of the effect is discussed with reference to the picture obtained earlier for the transition state of this reaction. The usefulness of the magnitude of the solvent isotope effect and the curvature of the isotope-effect curve as mechanistic tools is discussed briefly.

The primary hydrogen isotope effect for the methoxide-ion catalyzed racemization of 2-methyl-3-phenylpropionitrile has previously been measured and was found to be very weak.[1] This weak isotope effect was interpreted in terms of a highly unsymmetric transition state,[2] the proton being almost completely transferred to the methoxide ion. The relatively simple model used for this reaction took no explicit account of the solvation of the methoxide ion and the transition state by methanol molecules. Thus the transition state was considered as a carbanion, formed from the nitrile by abstraction of a proton, and a methanol molecule, formed from the methoxide ion and the abstracted proton.

An attempt has now been made to gain further information about the structure of the transition state by means of the deuterium solvent isotope effect.

* For Part IV of this series, see Ref. 2.

EXPERIMENTAL

(+)-2-Methyl-3-phenylpropionitrile and -2-d. The preparation of the substrates has been described elsewhere.[1]

Methanol. The drying of the methanol was performed as in Ref. 3, but Linde type 3 A molecular sieves was used in the present case.

Methanol-O-d. Commercial methanol-*O*-*d* (CIBA, isotopic purity 99 atom % D according to NMR) was used without further purification.

Solutions for kinetic runs were prepared as before.[1]

Kinetic runs were performed on a Perkin-Elmer 141 polarimeter (in some later runs a Zeiss Old 5 digital polarimeter) in thermostated polarimeter cells of 10.0 cm length and a volume of 1 ml. One run (the first one in 64.2 % MeOD), however, was performed in sealed glass ampoules which were not broken until the polarimetric measurement was made, but, as that method showed no advantages over keeping the sample in the polarimeter cell, the latter method was used in all other runs. All runs were performed at 60.0 ± 0.1 °C. The evaluation of the rate constants was performed by the method of least squares.

RESULTS

The results from the measurements of the kinetic solvent isotope effect on the racemization of 2-methyl-3-phenylpropionitrile in mixtures of methanol and methanol-*O*-*d* are shown in Table 1. Light as well as heavy substrate was used in the measurements.

The ratios k_n/k_0 between the rate in a solvent with the fractional content n of methanol-*O*-*d* and that in ordinary methanol, respectively, refer to experiments with the same isotopic

Table 1. Summary of the rate-constant data in the racemization of (+)-2-methyl-3-phenylpropionitrile and -2-*d* in mixtures of methanol and methanol-*O*-*d* with sodium methoxide as base. Substrate concentration 0.15–0.35 M. Temperature 60.0±0.1 °C.

Substrate[a]	Mol fraction (*n*) of methanol-*O*-*d*	Base M	$k \times 10^6$[b] M^{-1} s^{-1}	k_n/k_0[c]	$(k_n/k_0)_{av}$[c]
+H	0	0.273	7.55±0.27[d]	1	1
+D	0	0.273	6.60±0.19[d]	1	1
+H	0.292	0.328	9.23±0.30	1.22	
+D	0.292	0.328	8.09±0.27	1.23	1.22±0.01
+D	0.292	0.320	8.04±0.23	1.22	
+H	0.483	0.311	10.88±0.22	1.44	
+H	0.483	0.310	11.04±0.17	1.46	1.43±0.04
+D	0.483	0.313	9.37±0.12	1.42	
+D	0.483	0.315	9.17±0.12	1.39	
+H	0.642	0.306	12.06±0.32	1.60	
+H	0.642	0.307	12.13±0.32	1.61	1.60±0.01
+D	0.642	0.307	10.50±0.33	1.59	
+H	0.990	0.310	15.40±0.56	2.04	
+H	0.990	0.307	15.69±0.39	2.08	2.09±0.05
+H	0.990	0.230	15.91±0.26	2.11	
+H	0.990	0.223	16.07±0.32	2.13	

[a] +H=(+)-2-Methyl-3-phenylpropionitrile; +D=(+)-2-Methyl-3-phenylpropionitrile-2-*d*. [b] *k* denotes second-order rate constant. Errors include uncertainty in the base concentration. [c] k_n denotes the rate constant for the racemization in a solvent with the fractional content *n* of deuterium. k_0 denotes the rate constant for racemization in methanol. [d] Value from Ref. 1.

composition of the substrate in both cases, *i.e.*, either to ordinary 2-methyl-3-phenylpropionitrile or to its -2-*d* derivative. There seemed to be no significant difference in k_n/k_0 between the two sets of experiments, and hence the average of k_n/k_0 was taken regardless of the mass of the hydrogen atom of the substrate. In order to obtain the limiting kinetic solvent isotope effect a polynomial was fitted to the experimental points by the method of least squares. The polynomial has the form: $k_n/k_0 = 1.000 + 0.655n + 0.451n^2$, and a graphical representation can be seen in Fig. 1. The value for $n=1$ is $k_1/k_0 = 2.1_{06}$, or, in view of the accuracy of the determination in 99 % methanol-*O*-*d*, $k_{MeOD}/k_{MeOH} = 2.11 \pm 0.05$.

From the rate-constant data in Table 1 primary isotope-effect data in different mixtures of methanol and methanol-*O*-*d* can be obtained. These results are shown in Table 2.

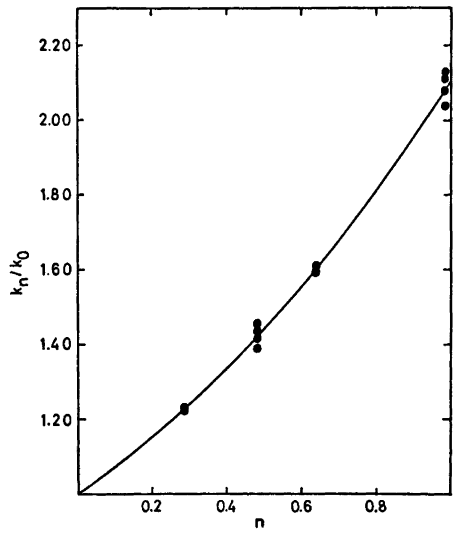

Fig. 1. Plot of k_n/k_0 against isotope composition of the medium. The filled circles denote experimental values. The curve represents the polynomial $k_n/k_0 = 1.000 + 0.655n + 0.451n^2$. Temperature 60.0±0.1 °C.

DISCUSSION

The plot of equilibrium or rate constants *versus* the isotopic composition of the medium is generally curved. This was detected long ago

Table 2. Primary kinetic isotope-effect data for different mixtures of methanol and methanol-*O*-*d* as solvent. Temperature 60.0 ± 0.1 °C.

Solvent composition, mol fraction methanol-*O*-*d*	k_D/k_H[a]
0	0.87 ± 0.04[b]
0.292	0.87
0.483	0.85
0.642	0.87

[a] Ratio of rate constant for heavy and light substrate, respectively. [b] From Ref. 1.

by La Mer and Chittum [4] in an investigation of the variation of the dissociation constant of acetic acid in mixtures of H_2O and D_2O. Since then a great number of results concerning solvent isotope effects in mixtures of H_2O and D_2O have been published. The observed phenomena have been thoroughly interpreted in terms of the mechanism of the reactions, and the use of the curvature of a solvent isotope-effect plot and the limiting solvent isotope effect as mechanistic tools has been discussed.[5-8] The investigations have mainly been concerned with reactions in mixtures of H_2O and D_2O, but in recent years some investigations of the variation of the solvent isotope effect in mixtures of methanol and methanol-*O*-*d* have appeared.[9] Solvent isotope effects in other alcohols have also been investigated.[10,11]

The discussion of solvent isotope effects and their variation with the isotopic composition of the solvent is most conveniently carried through in terms of fractionation factors for the transition state (in the case of kinetic solvent isotope effects) and for the initial state.[5,6] The fractionation factor for a particular site in a molecule is defined as the ratio of its deuterium/protium ratio and that in the bulk of the solvent. In the present case the hydrogen in the reactant carbon acid and the hydrogen in transit in the transition state are not available for equilibration, because there is no way for them to exchange with the medium except *via* the reaction being studied. The only exchangeable hydrogen in addition to that in the bulk of the solvent occurs in the methanol molecules solvating the reactant methoxide ion and in those solvating the transition state. (The reactant nitrile can hardly perturb the surrounding solvent to such an extent that appreciable fractionation takes place.)

The only fractionation factors $(D/H)_{solute}/(D/H)_{solvent}$ to be taken into account in the following are thus those in which $(D/H)_{solute}$ refers to the isotopic composition of methanol solvating either the methoxide ion or the transition state, respectively. The former fractionation factor has been determined to $\phi_{MeO} = 0.73_6$ at 33.5 °C,[9a] and, assuming a pure zero-point-energy effect, the value at 60 °C would be 0.75_4, which will be used throughout the present paper.

Reaction Scheme 1 shows the present model of the proton-abstraction reaction. RH denotes the (+)-2-methyl-3-phenylpropionitrile, and m and p are the numbers of methanol molecules solvating the methoxide ion and the transition state, respectively.

In terms of fractionation factors, the ratio between the rate constant for the reaction in a solvent with the fractional deuterium content n and the rate constant for the same reaction in non-deuterated solvent is given by [6]

$$k_n/k_0 = (1-n+n\phi^{\ddagger})^p/(1-n+n\phi_{MeO})^m$$

Assuming a value of $\phi^{\ddagger}$ between 0.75_4 and 1.0, the maximum limiting isotopic rate ratio is given by

$$k_1/k_0 = 1/0.754^m$$

This ratio equals 1.326, 1.759, 2.333 for $m = 1$, 2, 3, respectively. Because of the magnitude of the experimental limiting rate ratio ($k_1/k_0 = 2.11 \pm 0.05$) obtained in this investigation, $m = 3$ seems most likely. This is also in agreement with results obtained in similar investigations

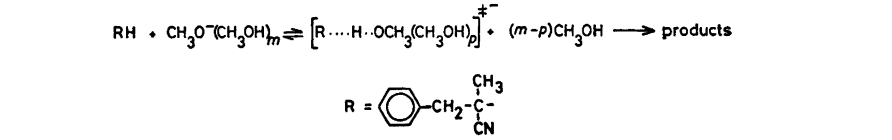

Scheme 1.

Table 3. Comparison of experimentally determined k_n/k_0 values for different n's with values from trial calculations. $\phi_{MeO}=0.75_4$. $k_1/k_0=2.1_{06}$.

n	$(k_n/k_0)_{11}$[a]	$(k_n/k_0)_{21}$	$(k_n/k_0)_{22}$	$(k_n/k_0)_{32}$	$(k_n/k_0)_{33}$	$(k_n/k_0)_{exp}$
0	1	1	1	1	1	1
0.292	1.26	1.23	1.23	1.21	1.21	1.22±0.01
0.483	1.46	1.41	1.41	1.39	1.39	1.43±0.04
0.642	1.64	1.59	1.59	1.57	1.57	1.60±0.01
0.990	2.09	2.09	2.09	2.09	2.09	2.09±0.05
1	2.11	2.11	2.11	2.11	2.11	2.11[b]
$\phi\ddagger$[c]	1.59	1.20	1.09	0.95	0.97	

[a] Subscripts denote the assumed values of m and p, respectively. [b] Extrapolated value. [c] $\phi\ddagger=[2.1_{06}(0.75_4)^m]^{1/p}$.

of methoxide-ion catalyzed reactions.[9c] The existence of three lone pairs of electrons in the oxygen part of MeO^- also makes such a solvation number plausible. Irrespective of the number p, this assumption leaves a very small interval for the fractionation factor $\phi\ddagger$, because $\phi\ddagger^p=2.1_{06}(0.75_4)^3=0.90$.

Some trial calculations were undertaken in order to see whether it is possible to deduce some definite values for m and p from the results obtained in this investigation. The resulting figures are gathered in Table 3 together with the experimental values of k_n/k_0. The stated values for different m and p are calculated from the limiting isotopic rate ratio $k_1/k_0=2.1_{06}$ and $\phi_{MeO}=0.75_4$.

As can be seen from Table 3, high accuracy in the experimental k_n/k_0 values is required to discriminate between different values of m and p. With the results obtained here this is not possible. The calculated values for $m=2$, $p=1$ or 2 seem to agree very well with the experimentally determined values, but it is doubtful whether any value of $\phi\ddagger$ above unity is reasonable. Inescapable facts are that the methoxide ion has to be solvated by methanol molecules and that the most probable number of solvating molecules is three.

It has been suggested that proton-transfer reactions of the present type, showing very weak primary isotope effects, should proceed *via* a pre-equilibrium, in the present case followed by a rate-determining racemization step. Such a mechanism would easily explain the weak dependence upon isotopic mass. According to Cram [12] a possible reaction sequence would be as in Scheme 2.

The expression given above for k_n/k_0 would still be valid for the two cases $k_{-1}\gg k_2$ and $k_{-1}\ll k_2$ if p denotes the solvation number of the rate-determining transition state (transition state 2 and transition state 1, respectively). There is no obvious difference in the most likely assumptions concerning the solvation numbers in the two cases. The charge on the carbanion must be more fully developed in transition state 2 than in transition state 1. Irrespective of the assumption of one or more kinds of methanol molecules solvating the transition state, the limiting solvent isotope effect leaves little room for a high power of fractionation factors appreciably inferior to unity. Introduction of more fractionation factors for the transition state, accounting for possible solvation of the charge on the carbanion, makes therefore little sense.

It may be questioned whether there is a real difference between the strongly endothermal single-step model [2] and the one with two reaction steps, the second of which is rate-determining. In the way Cram [12] writes it, *cf.* Scheme 2, the rate-determining process is nothing but a separation of the two reaction products. The reaction coordinate has conse-

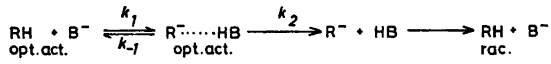

Scheme 2.

quently the same nature in both models. In such a case there is little hope of distinguishing between the models.

Transition-state fractionation factors are thought to be intermediate between reactant and product fractionation factors and can possibly be used to give some information about the transition-state structure.[8] Let x be some measure of the degree of resemblance of the "methanolic" part of the transition state to the bulk solvent, thus $0 \leq x \leq 1$. Then it may be assumed that $\phi^{\ddagger} = \phi_{MeO}{}^{1-x}$.[6]

The limiting kinetic solvent isotope effect k_1/k_0 is thus related to x through the relationship:

$$k_1/k_0 = \phi_{MeO}{}^{(1-x)p}/\phi_{MeO}{}^{m} = \phi_{MeO}{}^{p(1-x)-m}$$

Assuming $m=3$ and $p=2$ the calculated value of x for $k_1/k_0 = 2.1_{06}$ is 0.82, and $m=p=3$ gives $x=0.88$. These values are somewhat smaller than the Brønsted β which has been estimated previously [1] at about unity. The latter value was thought to reflect the product-like nature of the transition state for this reaction.

The interpretation of kinetic solvent isotope effects in simple terms of transition-state symmetry is perhaps not so straight-forward.[13] This is also underlined by some collected data from the present literature on the magnitude of primary kinetic isotope effects and solvent isotope effects for methoxide-catalyzed proton-abstraction reactions in methanol, given in Table 4. The reactions in Table 4, except for those of 2-nitropropane and phenyl 2,2-diphenylcyclopropyl ketone, are all thought to be endothermal, which can be concluded from the pK values of the compounds relative to that of methanol. It is hard to see any correlation between the strength of the primary kinetic isotope effect and that of the kinetic solvent isotope effect. The most striking feature of the presented data is perhaps that several examples are found where the primary isotope effect is very strong, indicating a fairly symmetric transition state, but still the kinetic solvent isotope effect has almost reached its maximum value corresponding to $m=3$.

The primary kinetic isotope effect for 2-methyl-3-phenylpropionitrile in different mixtures of methanol and methanol-*O-d* (Table 2) shows no detectable variation. The values of k_D/k_H for the three mixtures in Table 2 all agree within the experimental errors with the value found for undeuterated methanol.[1]

This constancy of the primary isotope effect in different mixtures of methanol and methanol-*O-d* also implies that the equilibrium constant for the exchange equilibrium between nitrile and methanol should be expected to have a nearly constant value.[18] This rather reasonable result is at variance with the results in Ref. 3, where a supposed variation of the K_H/K_D ratio with the deuterium content of the medium was found.

Acknowledgements. It is a pleasure to acknowledge the interesting discussions between Dr. John Albery and one of us (L. M.) during a most pleasant visit at Oxford University. Financial support from The Swedish Natural Science Research Council is gratefully acknowledged.

Table 4. Methoxide-catalyzed proton-abstraction reactions in methanol. A comparison between primary kinetic isotope effects and kinetic solvent isotope effects.

Substrate	Temp. °C	Isotopic rate ratio primary k_D/k_H	Isotopic rate ratio solvent k_{MeOD}/k_{MeOH}	Reference
2-Nitropropane	24.8	0.135	2.28	9c
2-(*N*,*N*-Dimethylcarboxamido)-9-methylfluorene	24.9	0.15	2.3	14
9-Methylfluorene	44.7	0.19	2.2	15
Phenyl 2,2-diphenylcyclopropyl ketone	50	0.286	2.08	10
1-*H*-perfluoroheptane	60	0.48	1.52	16
2-Methyl-3-phenylpropionitrile	60	0.87	2.11	1 and present investigation
Pentafluorobenzene	25.02	1.0	2.3	17

REFERENCES

1. Melander, L. and Bergman, N.-Å. *Acta Chem. Scand. 25* (1971) 2264.
2. Bergman, N.-Å., Saunders, W. H., Jr. and Melander, L. *Acta Chem. Scand. 26* (1972) 1130.
3. Bergman, N.-Å. *Acta Chem. Scand. 25* (1971) 1517.
4. La Mer, V. K. and Chittum, J. P. *J. Amer. Chem. Soc. 58* (1936) 1642.
5. Gold, V. a. *Trans. Faraday Soc. 56* (1960) 255; b. *Advan. Phys. Org. Chem. 7* (1969) 259.
6. Kresge, A. J. *Pure Appl. Chem. 8* (1964) 243.
7. Albery, W. J. and Davies, M. H. *J. Chem. Soc. Faraday Trans. 1* (1972) 167.
8. Showen, R. L. *Progr. Phys. Org. Chem. 9* (1972) 275.
9. Gold, V. and Grist, S. *J. Chem. Soc. B* (1971) a. 1665; b. 2272; c. 2282; d. 2285.
10. Levin, J.-O. and Rappe, C. *Chem. Scr. 1* (1971) 233.
11. Levin, J.-O. *Chem. Scr. 4* (1973) 85.
12. Cram, D. J. *Fundamentals of Carbanion Chemistry*, Academic, New York and London 1965, pp. 28–29.
13. Gold, V. and Grist, S. *J. Chem. Soc. Perkin Trans. 1* (1972) 89.
14. Ford, W. T., Graham, E. W. and Cram, D. J. *J. Amer. Chem. Soc. 89* (1967) 4661.
15. Streitwieser, A., Jr., Hollyhead, W. B., Pudjaatmaka, A. H., Owens, P. H., Kruger, T. L., Rubenstein, P. A., MacQuarrie, R. A., Brokaw, M. L., Chu, W. K. C. and Niemeyer, H. M. *J. Amer. Chem. Soc. 93* (1971) 5088.
16. Andreades, S. *J. Amer. Chem. Soc. 86* (1964) 2003.
17. Streitwieser, A., Jr., Hudson, J. A. and Mares, F. *J. Amer. Chem. Soc. 90* (1968) 648.
18. Melander, L. *Acta Chem. Scand. 25* (1971) 3821.

Received April 8, 1974.

Acta Chemica Scandinavica A 28 (1974) 753—763

The Mechanisms behind Peak Broadening in a Gel Chromatographic Column

TORBEN SMITH SØRENSEN

Fysisk-Kemisk Institut, Technical University of Denmark, DK-2800 Lyngby, Denmark

An equation for the elution profile in a linear chromatographic system derived in a previous paper is tested by recirculation experiments in a column packed with Sephadex G-25 Medium gel beads. As the elution velocity normally varied somewhat during the recirculation runs the details about the form of the elution curves could not be checked, but assuming that the elution profiles are approximately Gaussian it is possible to calculate apparent diffusion coefficients for different species at different elution velocities. Analysis shows that for substances excluded from the gel there exists a common eddy diffusion coefficient increasing in value with elution velocity. For the substances penetrating the gel beads the expression $D_{app}=D_{eddy}/(1+K)$, where K is the equilibrium distribution coefficient of the substance between the stationary and mobile phase, is a valid approximation at low elution velocities in accordance with simple quasi-equilibrium theory. At higher elution velocities there is an additional non-equilibrium contribution to D_{app} from which it is possible to estimate the relaxation time τ of equilibration between mobile and stationary phase. The order of magnitude of the calculated τ-values is controlled by comparison with a well known formula for the diffusion into or out of a sphere maintained in a bath of constant concentration.

In a preceding paper [1] it was shown that the asymptotic solution (large elution times) to the phenomenological equations governing a linear chromatographic system (linear or linearized "adsorption" and "desorption" kinetics) is given by the expression

$$c_{tot}(x',t')=c(o)+c(s)=$$
$$\frac{s}{\sqrt{2\pi}\,\sigma_x}\exp\left(\frac{-x'^2}{2\,\sigma_x^2}\right)\left[\left(1+\frac{A-2B^2}{\sigma_x^2}\right)+\frac{B}{\sigma_x^2}x'-\frac{A-2B^2}{\sigma_x^4}x'^2\right] \quad (1)$$

c_{tot} is the sum of the concentration in the mobile and the stationary phase based upon total column volume in a slice of column centered at the specific position x. The total number of moles in the chromatographic peak is s. The x'-variable is a Galilei-transformed position

$$x'=x-u_{cm}t' \quad (2)$$

The center of mass velocity is given by

$$u_{cm}=[1/(1+K)]u_{max} \quad (3)$$

where u_{max} is the mean velocity of the mobile phase and K is the "adsorption" equilibrium constant given by

$$K=k_1/k_2 \quad (4)$$

k_1 is the number of moles passing from the mobile to the stationary phase per unit of total column volume in the given slice and per unit of the number of moles in mobile phase per cm³ total column volume, *i.e.* per unit of $c(o)$. Analogously k_2 is the rate constant for "desorption". Finally in (1) the parameters A, B and σ_x are given by

$$A=-\tfrac{1}{2}D_{eddy}\frac{k_1-k_2}{(k_1+k_2)^2}+\frac{k_1k_2}{(k_1+k_2)^4}u_{max}^2 \quad (5)$$

$$B=\frac{k_1-k_2}{2(k_1+k_2)^2}u_{max} \quad (6)$$

$$\sigma_x=\sqrt{2\,D_{app}\cdot t'} \quad (7)$$

with the apparent diffusion coefficient

$$D_{app}=\frac{D_{eddy}}{1+K}+\frac{k_1k_2}{(k_1+k_2)^3}u_{max}^2 \quad (8)$$

The time t' corresponds to an initial condition of a Dirac's δ-function positioned at $x=0$

at $t'=0$. As the initial condition in an actual experiment is some irregular, though narrow, distribution we write

$$t'=t+t_0 \tag{9}$$

where the additive constant t_0 relating actual time to "Gaussian" time t' is to be found in each experiment. The parameter D_{eddy} in (8) is an eddy diffusion coefficient describing the spreading out of the zone due to the many possible routes by which the molecules can pass through the mobile phase. It is assumed to be concentration independent, but it may be a function of u_{max}, and if so it is anticipated that it will increase with u_{max}.

Eqn. (8) has previously been derived by Bak [2] in a study primarily dealing with the electrodiffusion phenomena. It can be shown too that the random walk theory of Giddings and Eyring [3,4] yields a solution with the same center of mass velocity and a D_{app} equal to the second term in (8) when the solution is power expanded to the second degree in the argument of the exponential function to yield a Gaussian distribution.[1,5] However, their calculations of k_1 and k_2 from experimental elution curves are in error, because of their neglect of eddy diffusion.[1] Several authors have used integral transformations with respect to *time* [eqn. (1) is obtained by complex Fourier transformation with respect to position] to obtain solutions to the chromatographic transport equations, *e.g.* Lapidus and Amundson,[6] Kučera,[7] and Kubin [8] (Laplace-Carson transform). The solutions given by these authors are very complicated, however, and not immediately suited for practical applications. Van Deemter *et al.*[9] have made a Gaussian approximation to the solution of Lapidus and Amundson, and their formulae may be translated to our equations (3), (7), and (8) after a rather long series of tedious transformations. The latter authors have checked the formulae on experimental elution curves from ion exclusion and gas-liquid partition chromatographic columns. The arguments in the present article are strengthened by the use of recirculation chromatography. Also, it seems to be the first time that peak broadening has been investigated in gel chromatographic columns by appropriate methods. In this connection it should be mentioned that the formulae derived by Ackers [10] are not sufficient to describe gel chromatography at higher flow rates, because the transport equations used by him are based upon quasi-equilibrium and do not take into account the additional contribution of peak broadening from the finite rate of mass transfer between the stationary and the mobile phase. Vink [11] has solved the chromatographic transport equations proposed by himself by the method of moments. His expression for u_{cm} is identical to eqn. (3), and for the second moment he gets a result similar – but not quite identical – to eqn. (7) and (8). However, his transport equation contains a rather unrealistic assumption on longitudinal diffusion in the stationary phase besides the exchange out of and into the gel beads. The most serious mistake in his equations is that he puts $D_{eddy}/(1+K)$ in eqn. (8) equal to a constant (D_1) which is independent of the partition coefficient K. Thus, he does not correct for the fact that molecules in the stationary phase do not contribute to eddy diffusion. Of course, this assumption has most serious consequences for his theory of determination of molecular weight distributions by gel chromatography.[12] The theoretical conclusions of the previous article [1] and the experimental results in the present are not in accordance with Vink's assumption.

The purpose of the present is to test eqs. (1), (3), (7), and (8) as far as possible for a gel chromatographic column. Seven substances with K-values from 0 to 5.1 were subjected to recirculation chromatography in a column packed with beads of cross-linked dextran (Sephadex). Values of u_{max} ranging from 0.75 to 4.7 cm/min were applied. The spread in parameters is sufficient to sort out approximately the u_{max} dependence of D_{eddy} from the contribution from the second term in (8). Values for the relaxation time of equilibration between stationary and mobile phase

$$\tau=(k_1+k_2)^{-1} \tag{10}$$

can therefore be calculated and because the separating principle in gel-chromatography is diffusion into and out of spherical beads with known upper and lower limits for the radius, it is even possible to check the order of magnitude of these relaxation times.

However, the nomenclature used in the literature concerning gel chromatography appears to be somewhat confusing. Therefore it was found appropriate to start by covering the definitions and symbols used here in order to make the present paper self-consistent.

DEFINITIONS AND INTERRELATIONS IN GEL CHROMATOGRAPHY

In Fig. 1 a schematic subdivision of the inner space of a gelchromatographic column is shown. The primed concentrations refer to that section of the volume in which the molecule is positioned. Thus $c_k'(i)_{x,t}$ is the concentration of substance k at a position x and time t in mol/cm³ of solvent imbibed in the gel. The primed concentrations should be carefully distinguished from the unprimed concentrations based upon total column volume. We define a "molecular sieving" equilibrium constant by

$$K_{ms} = c'(i)/c'(o) \tag{11}$$

In the pure molecular sieve case (without any differences in activity coefficients in V_i and V_0) K_{ms} ranges from 0 for big molecules which cannot enter the network of crosslinked polymer chains to 1 for small molecules which can move freely everywhere in V_i. Many substances show a specific adsorption to the polymer chains in the gel, and we therefore define an adsorption coefficient

$$K_{ads} = c'(g)/c'(i) \tag{12}$$

The equilibrium constant K defined in eqn. (4) can also be expressed as

$$K = \frac{c(i)+c(g)}{c(o)} = \frac{V_i + V_g K_{ads}}{V_0} K_{ms} \tag{13}$$

It is still possible to maintain the picture of linear "adsorption" and "desorption" kinetic given in the introduction, if the diffusion process in the gel beads can be properly linearized and the adsorption process is rapid in comparison to the diffusion process. It should be carefully noted that the concentrations used in (11), (12), and (13) are the *equilibrium concentrations* and not the concentrations at the same x and t in an actual chromatographic experiment. The value of u_{max} may be small enough to make that difference insignificant. In this "quasi-equilibrium" solution to the chromatographic problem, D_{app} is given by the first term in (8) only. The second term, however, reflects the deviation from quasi-equilibrium. In any case it can be shown that in a linear chromatographic system the center of mass velocity is given by (3), whether or not quasi-equilibrium can be used as an approximation. For a detailed discussion of these subjects the reader is refered to the preceding theoretical paper.[1] Combination of (3) and (13) yields

$$u_{max}/u_{cm} = 1 + K_d V_i/V_0 \tag{14}$$

with the *definition*

$$K_d = K_{ms}(1 + V_g K_{ads}/V_i) \tag{15}$$

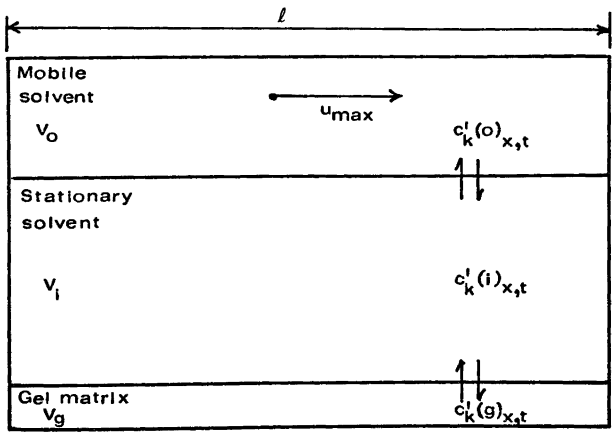

Fig. 1. Schematic subdivision of a gelchromatographic column. Total volume $V_t = V_0 + V_i + V_g$. Cross-sectional area A.

In many gelchromatographic experiments u_{max} and u_{cm} will not be constant in time because of fluctuations or systematic variations. In such cases it is much more practical to measure *elution volumes* than velocities. To prove this we note that the differential increment of the elution volume when the peak advances the distance dx_{cm} in the column is

$$dV_e/dx_{cm} = (dV_e/dt)u_{cm}^{-1} = (V_0/V_t)A(u_{max}/u_{cm})$$

wherein A is the area of column cross section. The instantaneous value of the ratio u_{max}/u_{cm} is still given by (14) and is consequently time independent. By integration through the column

$$V_e = \int_0^l (dV_e/dx_{cm})dx_{cm} = V_0 + K_d V_i \qquad (16)$$

In practice it is indeed found that the elution volumes are independent or nearly independent of elution velocity showing that a gelchromatographic system in this respect behaves as a linear chromatographic system. This fact has been of immense value for the practical utilisation of the technique, and equations based upon elution volumes such as (16) first stated by Wheaten and Baumann [13] pervade the literature about the subject. The present work will make it clear, however, that if the phenomena of peak broadening shall be properly described in order to assess the resolution power of the column, it is *not* sufficient with an elution volume description.

Still another distribution coefficient has been widely used in the literature. It is defined as the ratio between the equilibrium concentration in the gel based upon the volume $V_i + V_g$ and the equilibrium concentration in the mobile phase based upon the volume V_0:

$$K_{av} = \frac{c(i)(V_t/V_i + V_g) + c(g)(V_t/V_i + V_g)}{c(o)(V_t/V_0)} = \frac{V_0}{V_i + V_g} K \qquad (17)$$

The importance of that equilibrium constant rests upon the possibility of a direct theoretical calculation within the framework of statistical mechanics as a ratio between two molecular configuration integrals as has been done in a number of cases, *e.g.* by Giddings *et al.*[14] Explicitly

$$K_{av} = \frac{\int dr \int d\psi \int d\lambda \exp(-\varepsilon_{i+g}/kT)}{\int dr \int d\psi \int d\lambda \exp(-\varepsilon_0/kT)} \qquad (18)$$

wherein r denotes the position of the center of mass of the molecule, ψ the rotation coordinates and λ the possible internal conformation coordinates. The energies ε_{i+g} and ε_0 are the molecular energies of a given configuration in $V_i + V_g$ and V_0, respectively, and the r integration is taken over the same volumes. Typical molecular sieving problems focus upon "on-off" potentials, *i.e.* $\varepsilon_{i+g} = 0$ or ∞, For example Giddings *et al.* were able to derive as a special case the Ogston expression [15] for spherical molecules in a network of randomly oriented fibers

$$K_{av} = \exp[-\pi L(r + r_0)^2] \qquad (19)$$

where L is the total length of fibers per cm^3, r is the molecular radius and r_0 is the radius of the gel-fibers. As well known this equation has been successfully applicated by Laurent and Killander [16] to describe the elution of proteins from Sephadex gels using Stokes radii (from diffusion coefficients) as r.

Also the distribution coefficients K and K_{av} can, of course, be calculated as simple functions of the elution volume as well as K_d. Comparison of eqns. (13) and (15) yields

$$K = (V_i/V_0)K_d \qquad (20)$$

Insertion of (16) in this equation yields

$$K = (V_e - V_0)/V_0 \qquad (21)$$

Application of (21) to (17) yields finally

$$K_{av} = (V_e - V_0)/(V_i + V_g) = (V_e - V_0)/(V_t - V_0) \qquad (22)$$

Eqn. (16) and derived equations are based upon the assumption that the imbibed solvent in the gel does not move, *i.e.* no solvent is forced through the gel beads by the pressure drop in the column. If this assumption were not correct it would show up in variations in the elution volume of excluded molecules with the rate of elution.

EXPERIMENTAL

Materials. The substances used were: DL-tryptophan, L-tyrosine (BDH Chemicals, chromatographically homogeneous), *N*-acetyl-L-tryptophan methyl ester (Mann Res. Lab., chrom. hom.), myoglobin (Seravac, Horse skeletal muscle, 1 × cryst), ovalbumin (Sigma Chem. Comp., cryst. and lyophil., salt free,

electrophoretic purity 99 %), methylene blue (3,9-bisdimethylamino-phenazothionium chloride, Merck) and "Blue Dextran 2000" (Pharmacia). The last substance is dextran with an average molecular weight $M_n \sim 2 \times 10^6$ bound to a polycyclic chromophor. The gel used was Sephadex G-25 Medium (Pharmacia) swollen in 0.1 M KCl. This gel allows for relatively wide variations in elution rate without crack-formation in the gel bed at the high velocities. The eluent was 0.1 M KCl throughout to reduce ionic association of the substances (especially the amino acids and methylene blue) with the gel.

Apparatus. The column used was manufactured in the laboratory workshop of a perspex tube with two adjustable perspex plungers with filter caps for the inlet and outlet of eluent introduced into each column end and tightened against the inside surface of the tube by two O-rings each. The construction follows very nearly the one used in commercial available columns, *e.g.* the type supplied by LKB-Produkter AB (Stockholm-Bromma, Sweden). The bed was packed by decanting small portions of a well-stirred slurry of Sephadex G-25 in 0.1 M KCl into the column. After the total amount of gel had been transferred to the column the gel bed was slightly compressed by the upper plunger to prevent crack formation at the high elution velocities. The final data for the gel bed are the following: length = 30.5 ± 0.2 cm, diameter = 3.19 ± 0.01 cm, volume $V_t = 243.6 \pm 1.8$ cm^3, amount of dry gel = 55.0 ± 0.1 g.

The metering pump was a peristaltic pump "Minimet metering pump, type B" (Protech). By means of a "Recychrom, selector valve, type 4911 B" from LKB the chromatographic system was able to function in two ways. In the "open" state the sample was sucked into a polythene tube leading to the metering pump and from there to the bottom of the column. From the top of the column the eluent was let out of the system in the same rate as sample is introduced. In state "closed" the eluent was lead back to the pump and once more to the bottom of the column so that the sample might be recirculated as many times as desired. The external tubing was made as short as possible. The volume in the external circuit was estimated to be less than 2 % of the column volume. Most of the external volume was located in the tube in the peristaltic pump.

To make possible a registration of the elution profile a spectrophotometer "Uvicord" from LKB was introduced between the top of the column and the selector valve. The light path is 0.3 mm and the wavelength used 280 nm. The supplied signal in percent transmission was converted to absorbance in the Servogor recorder.

Recirculation experiments. The room temperature was 25°C within 1 – 2 °C. The elution rates were varied between 3 ml/min to 11 ml/min. The sample volumes from 1.2 ml to 7.8 ml. The samples were 1 wt % in 0.1 M KCl in the case of ovalbumin, myoglobin, and methylene blue (exp. 7), 10 wt % in the case of exp. 8 (methylene blue) and saturated solutions in the other cases. The gel bed was tested for homogeneity by the direct observation of a zone of blue dextran. During the first passage of the column the zone was irregular, but at the end of the second passage it had become a regular horizontal ring. The center of mass of the zone was moving upwards in the column with a uniform velocity.

RESULTS AND DISCUSSION

Treatment of elution peaks. Fig. 2 shows the outcome of a recirculation experiment with DL-tryptophan. It is noticed that the time difference between the maxima is not quite constant (*cf.* Table 1). It was not possible with the equipment used to maintain a strictly constant flow in the experiments of long duration. Therefore we cannot expect to test eqn. 1 in the most rigorous way in all details and we have to do some approximations. It is seen that even if we assume the instantaneous profile to be Gaussian ($A = B = 0$), the elution curve – *i.e.* c_{tot} as a function of t at constant x given also by (1) – is not a Gaussian curve

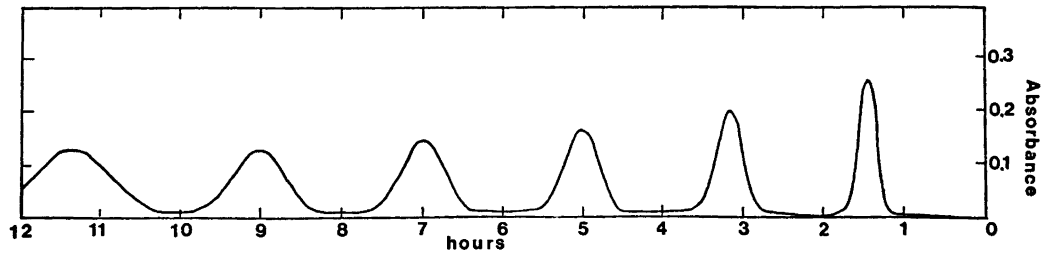

Fig. 2. Absorbance *vs.* time in a recirculation experiment.

Table 1. Analysis of a recirculation experiment. Exp. 18. D,L-Tryptophan. 3.00 ml sat. sol.

Peak No.	t_{max} min	Δt_{max} min	A_{max} abs	h abs	σ_t min	σ_t(corr) min	s abs min	Elution flux ml/min
1	86	86	0.255	0.319	6.50	8.16	5.38	4.03
2	190	104	0.200	0.227	11.0	11.5	5.38	
3	300	110	0.162	0.192	13.5	13.3	5.27	
4	420	120	0.142	0.170	16.5	14.8	5.20	
5	540	120	0.127	0.147	20.8	18.7	5.70	
Mean		108						

Regressions:
$\sigma_t^2(\text{corr}) = (0.578 \pm 0.076) t_{max} + 11.32$
$t_{max} = (1.65 \pm 0.21) \sigma_t^2(\text{corr}) - 3.69$

V_e (directly measured between the two last recorded peaks $= 338.5 \pm 5$ ml
$u_{cm} = 0.282$ cm/min
$K = (V_e - V_0)/V_0 = 2.47 \pm 0.06$
($V_0 = 97.5 \pm 0.8$ ml)
$u_{max} = (1+K) u_{cm} = 0.979$ cm/min

because of the time-dependence of σ_x (*cf.* eqn. 7). As the instantaneous profile broadens and becomes more flat during elution, the ascending limb of the elution curve is steeper than the descending limb. This is observed in Fig. 2 and was indeed observed for all the elution curves observed in this work. If we want to approximate the elution curve by a Gaussian distribution, however, we can do this by substituting for t' in σ_x in the Gaussian x-distribution a suitable mean time, *e.g.* the time of elution maximum. The t-distribution is now given by the Gaussian distribution

$$c_{tot}(l,t') \cong \frac{s}{\sqrt{2\pi}\sigma_t} \exp(-\{t' - t_{max}'\}^2/2\sigma_t^2) \qquad (23)$$

with the root mean square of time of arrival given by

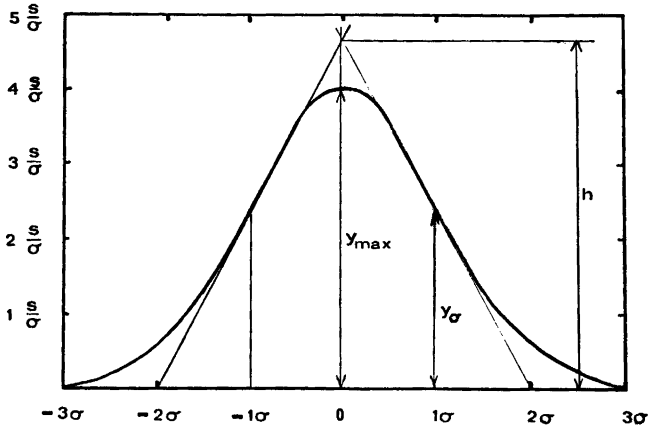

Fig. 3. Geometrical relations in a Gaussian peak with areas s and standard deviation σ.

$h = (2/\pi e)^{\frac{1}{2}}(s/\sigma) \simeq 0.484 s/\sigma$
$y_{max} = [1/(2\pi)^{\frac{1}{2}}](s/\sigma) \simeq 0.399 s/\sigma$
$y_\sigma = [1/(2\pi e)^{\frac{1}{2}}](s/\sigma) \simeq 0.242 s/\sigma$
Area of triangle $= (8/\pi e)^{\frac{1}{2}} s \cong 0.968 s$

$$\sigma_t \cong \sqrt{2D_{app}t_{max}}\,\frac{1+K}{u_{max}} \qquad (24)$$

In Fig. 3 some simple geometry of the Gaussian distribution is shown. It is seen that the turning tangents are well determined and the distance between their intersection with the base-line is simply 4σ. We determine σ_t by this method from the elution peaks and it is seen that this method corrects somewhat for the asymmetry. Eqn. (24) may be written

$$\sigma_t^2 = 2D_{app}u_{cm}^{-2}(t_{max}+t_0) \qquad (24a)$$

so that t_0 and D_{app} can be determined by linear regression of σ_t^2 upon t_{max}. The following factors are responsible for the uncertainty in the determination of these parameters:

(1) The elution curves are not Gaussian. The applied geometrical method corrects roughly for the asymmetry.

(2) Beer's law is not exactly fulfilled. It should be mentioned that the band of the "Uvicord" at 280 nm is rather wide ($\pm$ 10 nm).

(3) The elution velocity is not constant; especially not within experiments of long duration (small and binding molecules). A suitable mean value for u_{cm} is found as the ratio between column length and the mean value of time difference between subsequent elution maxima, in a single recirculation experiment. By means of the K-values determined from the elution volumes (eqn. 21) we find simultaneously a mean value for u_{max} in the recirculation experiment.

(4) The first peak(s) may still be somewhat irregular, and the maximal absorbances may fall outside the domain of Beer's law. The last peaks show an increasing amount of overlap and the background concentration in the column will eventually become too high for the geometrical determination according to Fig. 3 to be permissible. Furthermore the uncertainty in the determination of $4\sigma_t$ in all cases becomes very great when the peak is very flat.

A total of 109 peaks distributed over 21 experiments has been investigated. Table 1 shows the analysis of the experiment shown in Fig. 2. The values of σ_t are corrected for systematic variation in elution velociy by multiplying with $(\Delta t)_{mean}/(\Delta t)_{preceding}$. The area of the peaks is calculated as $2.066h\sigma_t(corr)$ according to Fig. 3 as a control. Preliminary plots were made to determine the number of peaks which should be included in the regression. The number of subsequent peaks showing good linearity was mostly between 5 and 7. In experiments with less than 5 peaks (3 and 4 peaks) all peaks are included. Fig. 4 shows the

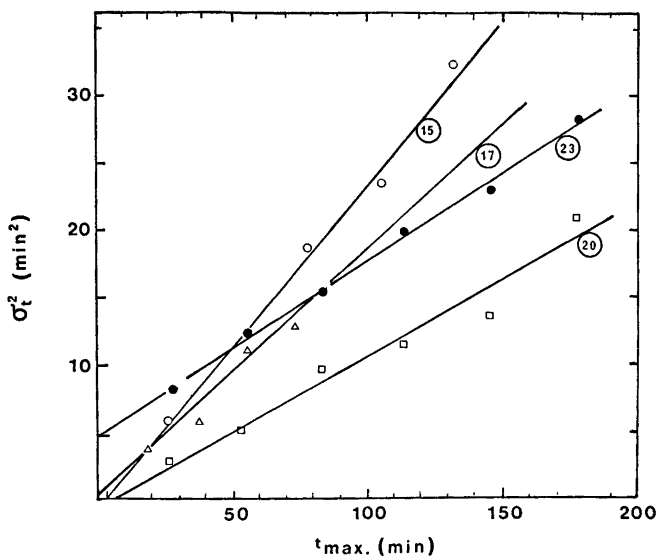

Fig. 4. Plots for determination D_{app}. ○ exp. 15; △ exp. 17; □ exp. 20; ● exp. 23.

σ_t^2(corr) *vs.* t_{max} plots in a number of experiments. It is difficult to judge *a priori* whether the conditions for the correctness of a regression of σ_t^2 upon t_{max} are fulfilled or not. Of course the uncertainty of the measured t_{max} relative to the span in t_{max}-values is much smaller than the corresponding relative uncertainty in σ_t^2, but the "effective" uncertainty in t_{max} must be greater because u_{cm} is not a constant throughout the experiments. Therefore, the regression of t_{max} upon σ_t^2 was also calculated. The straight lines shown in Fig. 4 are the mean of these two regressions. The estimate of the standard deviation of the slope calculated from the regression of σ_t^2 upon t_{max} showed up to be greater than the difference between the slope and reciprocal slope of the two regressions, however, so that the former standard deviation can be used as uncertainty.

Calculation of apparent diffusion coefficients. Table 2 shows the outcome of the least squares treatment of the recirculation experiments. The numbering refers to the chronological sequence of experiments. The calculated K-values and mean values of u_{max} are also tabulated. The minimum elution volume V_0 of the three excluded substances (Blue Dextran, myoglobin and ovalbumin) determined at various velocities is 97.5 ± 0.8 ml with an estimate of the standard error of a single determination ± 2 ml. Therefore, no eluent is forced through the gel beads by the pressure drop. The following conclusion can be drawn from an inspection of Table 2:

(1) The K-values of a single substance do not vary significantly with the elution velocity. Thus, in this respect the system behaves as a linear chromatographic system.

(2) There is no significant difference between

Table 2. Summary of recirculation experiments. BD = blue dextran, Tryp = DL-tryptophan, Ov = ovalbumin, Myo = myoglobin, Me = methylene blue, Tyr = L-tyrosine, and ATM = *N*-acetyl-L-tryptophan methyl ester.

Subst.	Exp.	u_{max}	K	$2D_{app}/u_{cm}^2$	t_0	$10^3 D_{app}$	$10^3 D_{app}(1+K)$	$10^3 D_{term}$
		cm/min		min	min	cm²/min	cm²/min	cm²/min
Elution velocity: medium								
BD	2	1.72	0	0.040±.006	−8 ±2	5.9 ±0.9	5.9±0.9	
Tryp	3	1.58	(2.54±.07)	0.35±.04	−22 ±2	3.5 ±0.4	12.3±1.4	0.0395 [a]
Tryp	4	1.32	(2.54±.07)	0.41 ±.04	−2 ±2	2.8 ±0.3	10.1±1.0	0.0395
Ov	5	1.85	0	0.037±.004	+5 ±2	6.3 ±0.7	6.3±0.7	0.00468 [b]
Myo	6	2.03	0	0.031±.003	−5 ±2	6.4 ±0.6	6.4±0.6	0.00678 [b]
Me	7	2.31	(5.11±.06)	0.61 ±0.4	+43.8±.5	4.4 ±0.3	26.6±1.8	
Me	8	2.46	5.11±.06	0.80 ±.12	+30 ±5	6.5 ±1.0	39.5±6.0	
Tyr	9	2.26	1.72±.09	0.32 ±.07	−9 ±2	11.0 ±2.4	30.0±6.5	
ATM	10	2.30	2.70±.03	0.36 ±.02	−0.9 ±.8	7.0 ±0.4	25.8±1.5	
Elution velocity: high								
Myo	11	4.55	0	0.0247±.0014	−3.2 ±.1	25.5 ±1.5	25.5±1.5	0.00678
Ov	13	4.48	0	0.0244±.0012	+4.8±.1	24.5 ±1	24.5±1	0.00468
Myo	14	4.42	0	0.0268±.0014	+4.2 ±.1	26.0 ±1.5	26.0±1.5	0.00678
Tryp	15	4.15	2.61±.06	0.244±.012	−3.3 ±.3	16.1 ±0.8	58 ±3	0.0395
ATM	16	4.20	2.53±.06	0.26 ±.08	−3 ±6	18 ±6	65 ±20	
Tyr	17	4.66	1.81±.05	0.184±.016	+1.5 ±2.3	25.5 ±2	71.5±6.5	
Elution velocity: low								
Tryp	18	0.979	2.47±.06	0.59 ±.08	+12 ±8	2.3 ±.3	8.1±1.1	0.0395
ATM	19	0.841	2.50±.06	0.62 ±.21	+86.6±.7	1.8 ±.6	6.3±2.1	
Myo	20	1.03	0	0.114±.011	−6 ±2	6.0 ±.6	6.0±0.6	0.00678
Tyr	21	0.750	1.63±.05	0.48 ±.09	+53 ±11	1.95±.35	5.1±1.0	
Ov	22	1.05	0	0.138±.009	−19.5±1	7.6 ±.5	7.6±0.5	0.00468
BD	23	1.03	0	0.130±.004	+36.4±.4	6.9 ±.2	6.9±0.2	

[a] 25 °C Ref. 17. [b] 20 °C Ref. 18.

the K-values of DL-tryptophan and N-acetyl-L-tryptophan methyl ester.

(3) As $V_0 = 97.5$ ml and $V_i = W_r \times$ (gram dry gel) $= 2.5 \times 55 = 137$ ml, wherein W_r is the water regain (ml water taken up per g dry gel) given, *e.g.*, in Ref. 19, p. 28, K-values greater than $V_i/V_0 = 1.41$ correspond to K_d-values greater than 1 according to eqn. (20). All the small molecules investigated here are therefore adsorbed to the dextran chains. If the molecular sieving distribution coefficient is assumed to be 1, we can calculate K_{ads} from eqn. (15). For example we have for DL-tryptophan $K_{ads} V_g/V_i = 0.80$ and with a dry density of the gel 1.64 g/ml [19] we find $K_{ads} = 3.28$.

(4) The apparent diffusion coefficients bear no relation to the ordinary coefficients of diffusion. They are 10^2 to 10^3 times as great.

(5) There is no significant difference between the values of D_{app} for the experiments 2, 5, 6, 20, 22, and 23 corresponding to substances with $K = 0$ at low and medium elution velocities (approximately 1 – 2 cm/min). Thus, at these velocities we have a constant eddy diffusion coefficient independent of molecular size and flexibility (Blue Dextran, myoglobin, ovalbumin). This eddy diffusion apparently is caused by "trajectory splittings" in V_0 of macroscopic dimensions compared with the dimensions of the macromolecules. The mean value of D_{eddy} is 6.5×10^{-2} cm²/min with a standard deviation of the single values ± 0.8 cm²/min. Furthermore it is seen that there is no significant difference between the D_{app} values for the experiments 11, 13, and 14, *i.e.* $K = 0$ and high elution velocities. But here the common D_{eddy} has increased to a value of 25.3×10^{-2} cm²/min with an uncertainty $\pm 0.8 \times 10^{-2}$ for a single determination.

(6) By comparison of the columns D_{app} and $D_{app}(1+K)$ for the group "low elution velocity", it appears that the variation within the latter (relative to the errors) are considerable smaller than within the former. All the values of $D_{app}(1+K)$ fall within the interval determined by the found mean value of D_{eddy} 6.5×10^{-2} cm²/min $\pm$ two times the estimate of the standard deviation of a single determination of D_{eddy} (0.8 cm²/min). Thus, quasi-equilibrium is a reasonable approximation in the estimation of peak broadening at low elution velocities.

(7) In the groups "medium" and "high elution velocity" it is apparent that the values of $D_{app}(1+K)$ for the species entering the gel are significantly *higher* than for the species with $K = 0$. Furthermore it is seen that the values for *different* species deviate significantly from each other and that the values for the *same* species at *different velocities* differ significantly too in such a way that the deviation from quasi-equilibrium is larger for larger velocities.

Calculation of relaxation times. The last observation makes natural the assumption that the deviation from quasi-equilibrium is due to the second term in eqn. (8). For the purpose of analysis we rewrite this expression in the following way:

$$(1+K)D_{app} = D_{eddy} + \Delta \qquad (8a)$$

Table 3. Calculation of relaxation times of diffusion equilibration.

Exp.	Substance	$D_{eddy} \times 10^2$ cm²/min	$\Delta \times 10^2$ cm²/min	$(1+K/K)u_{max}^{-2}$ (min/cm)²	$\tau \times 10^2$ min
3	DL-Tryptophan		5.8 ± 1.6	0.558	3.2 ± 0.9
4	DL-Tryptophan		3.6 ± 1.3	0.800	2.9 ± 1.0
7	Methylene blue		20 ± 2	0.224	4.5 ± 0.5
8	Methylene blue	6.5 ± 0.8	33 ± 6	0.1976	6.5 ± 1.2
9	L-Tyrosine		23.5 ± 6.5	0.310	7.5 ± 2
10	*N*-Ac.-L-tryp. methyl ester		19.3 ± 1.7	0.260	5.0 ± 0.4
15	DL-Tryptophan		32.7 ± 3	0.0803	2.6 ± 0.2
16	*N*-Ac.-L-tryp. methyl ester	25.3 ± 0.8	40 ± 20	0.0791	3.2 ± 1.6
17	L-Tyrosine		46 ± 6.5	0.0715	3.3 ± 0.5

$$\Delta = K\tau u_{max}^2/(1+K) \quad (8b)$$

with the relaxation time of equilibration between stationary and mobile phase given by (10).

Table 3 features the calculation of τ from the deviation term Δ. The correspondence of τ's for the experiments 3, 4, and 15 is remarkable in view of the widely differing values of Δ. Also the experiments 7, 8; and 9, 17 have τ-values which are (in relation to the uncertainty of the difference) a little closer to each other than the Δ-values. The uncertainty in Δ in exp. 16 is too large for a reasonable comparison between exp. 10 and 16, but τ in exp. 10 is significantly greater than τ in exp. 3, 4, and 15 in accordance with the lower diffusion coefficient of *N*-acetyl-L-tryptophan methyl ester compared to tryptophan.

Check of the order of magnitude of relaxation times. The large uncertainties of these calculations make it desirable to judge in some other way the correctness of the values found for the relaxation times. Jost cites in his monograph on diffusion [20] the following formula for the time dependence of the mean concentration c in a sphere which at time $t=0$ is surrounded by a reservoir with a constant concentration

$$\frac{c(t)-c_\infty}{c_0-c_\infty} = \frac{6}{\pi^2}\sum_{\nu=1}^{\infty}\frac{1}{\nu^2}\exp\{-\nu^2\pi^2 Dt/r^2\} \quad (25)$$

wherein c_0 is the position independent initial concentration in the sphere, c_∞ is the final concentration in the sphere and D is the diffusion coefficient in the sphere. Apart from a short transient period the solution (25) can be approximated by the first term in the sum

$$\frac{c(t)-c_\infty}{c_0-c_\infty} \cong \frac{6}{\pi^2}\exp\{-t/\tau\} \quad (26)$$

so that the kinetics are linear with a relaxation time of equilibration

$$\tau = r^2/\pi^2 D \quad (27)$$

If this relaxation time is taken as a reasonable approximation to the one defined in (10) it is possible from the values in Table 3 to calculate the diffusion coefficients in the gel beads. Because the distribution of radii in Sephadex G-25 Medium is rather broad (dry radii from 25 to 75 μ [19]) and the relaxation time according to (27) is very sensitive to variations in r, we shall prefer in a single case to make as good an estimation on the diffusion coefficient in the gel beads as possible. Then from (27) and the determined values of τ we calculate an "effective" radius which should have a value within the "wet radius" interval $45-130\mu$ ($W_r=2.5$ g H_2O/g dry gel and density 1.64 g/ml dry gel [19]). For tryptophan Longsworth [17] has determined the diffusion coefficient in crosslinked dextran gel beads ($W_r=3$, 4″) swelled in water for a number of substances (monovalent alifatic alcohols, acetamid, urea, thiourea, glycerol, and tritiated water). They used (for an isolated bead) the formula (26) in the limit $t \to \infty$. At 25 °C the ratio between these diffusion coefficients and the free diffusion coefficients was found to lie in the interval 0.59 to 0.73. Assuming that none of the above substances are absorbed significantly to the dextran chains we may put this ratio equal to about 2/3 and ascribe it to the combined effect of the reduced cross sectional area and a tortuosity factor both due to the presence of the gel chains. The latter is an expression of the mean value of $\cos^2\phi$ with ϕ being the angle between the mean direction of movement in a small (but macroscopic) volume of V_i and the overall driving force (for pure diffusion the negative overall concentration gradient). The investigated gel does not differ very much in degree of crosslinking from Sephadex G-25, and we assume a factor 2/3 in G-25 too. We have seen, however, that the aromatic small molecules used here have a specific adsorption to the gel matrix. If the adsorption-desorption exchange is rapid compared to the diffusion process, the diffusion coefficient will simply be lowered by a factor $(1+K_{ads}')$ where the modified adsorption constant $K_{ads}' = K_{ads}(V_g/V_i)$ is the ratio between the concentrations of bound and free component on the basis of the volume V_i+V_g. For tryptophan we have found in the present case (*cf.* point 3 above) $K_{ads}'=0.80$, and we have the final estimation of the diffusion coefficient in a G-25 gel bead

$$D=(2/3)\times 3.95\times 10^{-4}/1.80 = 1.46\times 10^{-4}\ \mathrm{cm^2/min}$$

From Table 3 it appears that τ is approximately 3×10^{-2} min, and we find from eqn. (27)

$$r_{eff} = 66\mu$$

a value well within the wet radius interval of Sephadex G-25.

The resolution power of a gelchromatographic column. By following the preceding train of arguments in reverse direction it is now possible to describe a procedure for estimation of the separation power of some given substances in a given column:

(1) Determine the *eddy diffusion characteristic* of the column, *i.e.* the eddy diffusion coefficients of excluded substances as a function of u_{max}. The best thing is to make recirculation experiments as done here, but if this is not feasible the initial zone should be made as possible and the correction time t_0 put equal to zero as a crude approximation.

(2) Estimate the K-values from literature calibration curves, Ogston-Laurent-Killander theory or another adequate theory.

(3) Calculate τ from (27) with the mean radius of the gel beads and some estimate of the diffusion coefficient in the gel inserted.

(4) Calculate the apparent diffusion coefficient at a given u_{max} from eqns. (8a – b).

(5) Estimate the time corresponding to elution maximum by $t_{max} \sim l(1+K)/u_{max}$.

(6) Calculate the root mean square time of arrival to the column end σ_t from eqn. (24) with $t_0 \sim 0$.

(7) Comparison of the difference between t_{max} with $4\sigma_t$ for two substances indicates whether the column will separate these or not.

Acknowledgement. Dr. phil. H. Waldmann-Meyer, Fysisk Kemisk Institut, is thanked for stimulating discussions about gel chromatography.

REFERENCES

1. Sørensen, T. S. *J. Chromatogr. 88* (1974) 197.
2. Bak, T. A. *Contributions to Chemical Kinetics*, 2nd Ed., Benjamin, New York 1963, pp. 53 – 54 and 64.
3. Giddings, J. C. and Eyring, H. *J. Phys. Chem. 59* (1955) 416.
4. Giddings, J. C. *J. Chem. Phys. 26* (1957) 169.
5. Giddings, J. C. *J. Chem. Phys. 26* (1957) 1755.
6. Lapidus, L. and Amundson, N. R. *J. Phys. Chem. 56* (1952) 984.
7. Kučera, E. *J. Chromatogr. 19* (1965) 237.
8. Kubín, M. *Collect. Czech. Chem. Commun. 30* (1965) 1104.
9. van Deemter, J. J. *et al. Chem. Eng. Sci. 5* (1956) 271.
10. Ackers, G. K. *Advan. Protein Chem. 24* (1970) 343.
11. Vink, H. *J. Chromatogr. 20* (1965) 305.
12. Vink, H. *Makromol. Chem. 116* (1968) 241.
13. Wheaten, R. M. and Baumann, W. C. *Ann. N. Y. Acad. Sci. 57* (1953) 159.
14. Giddings, J. C. *et al. J. Phys. Chem. 72* (1968) 4397.
15. Ogston, A. G. *Trans. Faraday Soc. 54* (1958) 1754.
16. Laurent, T. C. and Killander, J. *J. Chromatogr. 14* (1964) 317.
17. Longsworth, L. G. *J. Amer. Chem. Soc. 75* (1953) 5705.
18. *Handbook of Biochemistry*, Chemical Rubber Co., 1968, C-10 Table I and C-28 Table VI.
19. Flodin, P. *Dextran Gels and their Applications in Gel Filtration*, Dissertation, Uppsala 1962.
20. Jost, W. *Diffusion in Solids, Liquids, Gases*, 3rd Ed., Academic, New York 1960, p. 46.
21. Horowitz, S. B. and Fenickel, I. R. *J. Phys. Chem. 68* (1964) 3378.

Received January 20, 1974.

Acta Chemica Scandinavica A 28 (1974) 764—770

Studies on Gold Complexes. II. The Equilibrium between Gold(I) and Gold(III) in the Ammonia System and the Standard Potentials of the Couples Involving Gold, Diamminegold(I), and Tetramminegold(III)

L. H. SKIBSTED* and JANNIK BJERRUM

Chemistry Department I, Inorganic Chemistry, H. C. Ørsted Institute, University of Copenhagen, DK-2100 Copenhagen Ø, Denmark

The three standard potentials involving gold, gold(I), and gold(III) in the ammonia system are determined in 10 M ammonium nitrate at 25 °C by potential measurements with gold and platinum electrodes. The values obtained are

$Au(NH_3)_2^+ + e^- \rightleftharpoons Au + 2\ NH_3$
$E^0_{1,0} = +563 \pm 6$ mV

$Au(NH_3)_4^{3+} + 2\ e^- \rightleftharpoons Au(NH_3)_2^+ + 2\ NH_3$
$E^0_{3,1} = +206 \pm 3$ mV

$Au(NH_3)_4^{3+} + 3\ e^- \rightleftharpoons Au + 4\ NH_3$
$E^0_{3,0} = +325 \pm 3$ mV

This leads to an equilibrium constant of $10^{-12.1}$ for the reaction $Au(NH_3)_4^{3+} + 2\ Au + 2\ NH_3 \rightleftharpoons 3\ Au(NH_3)_2^+$ and under certain assumptions to a cumulative stability constant $\beta_2 = 10^{26.5}$ l²/mol² for the diamminegold(I) ion.

The three standard potentials of gold couples involving gold, gold(I), and gold(III) have been determined for the chloride,[1-3] the bromide,[4-6] and for the thiocyanate systems.[7-9] For several other gold systems the standard potential of the gold(I),gold couple is also known,[10,11] but no investigations of standard potentials for gold ammine complexes have been reported. Gold potentials for the aqua ions cannot be measured for the obvious reason that neither gold(I) nor gold(III) aqua ions exist in measurable amounts. This means that stability constants relative to the aqua gold complexes cannot be directly determined; one can only measure the relative stability of one complex to another. In such a series of stability constants for gold complexes the place of gold ammines is unknown.

Several attempts have been made to estimate the standard potentials for the aqua gold couples and the stability constants relatively to aqua ions from extrapolations in the Periodic Table and from linear free energy relationships.[11-14,26] Knowledge of the standard potentials for different ligand systems are therefore also of interest in order to increase our knowledge of the standard potentials of the aqua couples. The present investigation contributes to this purpose with a determination of the standard potentials of the gold ammines.

Equilibrium between metallic gold and its complexes is attained relatively slowly and equilibrium between gold(I) and gold(III) must be established before measurements with gold electrodes provide reliable values. Gold(I) will disproportionate in systems with gold(I) concentrations greater than the equilibrium concentration, and in systems with a gold(III) concentration greater than that of equilibrium the gold electrode will dissolve. In halide and pseudohalide gold systems with excess of ligand the following equilibrium has been found to be dominating:

$AuX_4^- + 2\ Au + 2\ X^- \rightleftharpoons 3\ AuX_2^-$

* Chemical Laboratory A, The Royal Danish School of Pharmacy.

In the ammonia system the corresponding equilibrium would be:

$$Au(NH_3)_4^{3+} + 2\ Au + 2\ NH_3 \rightleftharpoons 3\ Au(NH_3)_2^{+}$$

However, as discussed below, the situation turns out to be a little more complicated in the ammonia system than in the aniono systems.

The tetramminegold(III) ion is a robust complex and a weak acid with $pK_a = 7.48$, but subject to hydrolysis and further decomposition especially at high pH.[16] The present investigation was therefore carried out in 10 M ammonium nitrate in order to make it possible to have a sufficiently high ammonia concentration without greatly increasing the pH. In this way reliable values for the standard potentials involving $Au(NH_3)_2^+$ and $Au(NH_3)_4^{3+}$ could be obtained.

EXPERIMENTAL

Solutions and materials. The gold(III) complex used in all experiments was $Au(NH_3)_4(NO_3)_3$, synthesized as described earlier.[16] This complex was weighed into measuring flasks and dissolved in 10 M ammonium nitrate solutions containing varying ammonia concentrations. The gold powder used was prepared by reduction of gold(III) chloride with sodium pyrosulphite. All other reagents were of Analytical Reagent quality and were used without further purification. Ion exchanged water, distilled from alkaline permanganate in an all quartz apparatus, was employed throughout.

Analytical determination. Total gold concentrations were measured by atomic absorption spectrophotometry on a Perkin Elmer apparatus model 403 with a hollow cathode lamp using standard conditions. The standard gold solutions were prepared from the same gold salt and with almost the same concentrations as the solutions to be analyzed.

Electrodes and potential measurements. In the Au(III) – Au(I) redox titration experiments a plate of platinum (4 × 4 mm) was used as an inert metal electrode. Before use the platinum electrode was cleaned in concentrated nitric acid to which has been added one drop of concentrated hydrochloric acid and was then washed with water. During the titration experiments the platinum electrode became covered with a thin layer of gold. This coated platinum electrode was used as a gold electrode in the equilibrium experiments. The EMF titrations were carried out under nitrogen in a water thermostated cell at 25.0 ± 0.1 °C. A Radiometer pH-meter model PHM 52 was used.

All potentials were measured relative to a saturated potassium sulphate mercurous sulphate electrode to avoid traces of chloride in the solution of the complex. A Radiometer model K 601 electrode was used and was measured relative to a 0.1 M potassium chloride calomel before and after each measurement. The calomel electrode was prepared according to Gjaldbæk,[17] the potential of this electrode against the normal hydrogen electrode was taken to be + 335.6 mV at 25.0 °C,[19] a value which was controlled by comparison with the silver-silver chloride electrode in 0.1 M potassium chloride [19,20] to be correct within one mV.

The liquid junction potential between the 10 M ammonium nitrate-gold solutions and the saturated potassium sulphate solution of the reference cell was partly eliminated as the reference cell again was measured against the 0.1 M calomel electrode with 10 M ammonium nitrate as an intermediate solution. This reduces the total liquid junction potential to one between 10 M ammonium nitrate and 0.1 M potassium chloride. A diffusion potential which is believed to be very small as the ammonium and the nitrate and the potassium and the chloride ions, respectively, have almost identical ionic mobilities. No correction was therefore introduced for liquid junction potentials. This is also justified from the reproducibility of the potentials.

Gold potentials are generally reported [7,18,21] to be difficult to obtain with reproducible results because of a low exchange current and slow establishment of equilibrium in case of Au(III). The electrodes normally used are gold wires [22] or platinum plates coated with gold by an electrolytical method.[1,13] Gold electrodes without strain should be preferred, and the use of gold pieces or gold wires must therefore be avoided. If an electrolytical method is used to coat a platinum plate, a low current density must be chosen. N. Bjerrum [21] used a titration procedure like the one described here, starting with a smooth platinum electrode which during the titration is converted into a gold electrode, but did not point out the advantage of such a strainfree electrode.

Au(III) – Au(I) redox titration with platinum electrode

Solutions of tetramminegold(III) nitrate ≈ 10^{-3} M in 10 M ammonium nitrate, with ammonia concentrations from 0.2 M to 2 M, were titrated with hydrazine solutions with the same ammonium nitrate and ammonia concentrations as the complex gold solution. Hydrazine acts as a four electron donor in basic solutions,[23] so the reaction with gold(III) under the conditions mentioned is supposed to be:

$$4\ OH^- + NH_2NH_2 + 2\ Au(NH_3)_4^{3+} \rightarrow$$
$$2\ Au(NH_3)_2^+ + N_2 + 4\ H_2O + 4\ NH_3$$

Table 1. Titration of $Au(NH_3)_4^{3+}$ in 10 M NH_4NO_3 and varying NH_3 concentration with NH_2NH_2. The gold complex was dissolved in 20.0 ml of the solvent medium and titrated with a solution of NH_2NH_2 in the same medium. The titrations were performed at 25.0 ± 0.1 °C under a nitrogen atmosphere. The potentials were measured with a platinum electrode and are given (mV) relative to the normal hydrogen electrode. From each titration experiment a mean value of the apparent standard potential $'E^0 = E - 29.6 \log [C_{Au(III)}/C_{Au(I)}]$ was calculated. The standard potential $E^0_{3,1}$ was calculated by means of the expression derived with K_{amid} inserted (see text). The table gives the initial concentration of $Au(NH_3)_4^{3+}$, C^0_{Au} in mM and $C_{NH_3} = [NH_3]$ in M. Full experimental data for titration No. 5 are given in Table 2. For the two experiments marked with an asterisk the final potential measured with a gold electrode (after an equivalent amount of NH_2NH_2 was added) is used to calculate $E^0_{1,0}$; see Table 3.

No.	C^0_{Au}	C_{NH_3}	$'E^0$	$29.6 \log \left[\frac{K_{amid}[NH_3]^3}{[NH_4^+]} + [NH_3]^2\right]$	$E^0_{3,1}$
1	2.09	0.195	+250	−33	+217
2	1.35	0.228	+225	−28	+197
3	1.23	0.338	+217	−15	+202
4	1.33	0.417	+214	− 8	+202
5	2.43	0.417	+217	− 8	+209
6*	2.13	0.906	+194	+19	+213
7*	1.48	2.17	+147	+52	+199
					$E^0_{3,1} = +206 \pm 3$ mV [a]

[a] It must be noted that this standard deviation applies to the mean value of the observed distribution under the assumption of a normal distribution. The standard deviation of the distribution itself is obtained from this figure by multiplication by the square root of the number of experiments. This remark applies also to the standard deviation of Tables 2 and 3.

Table 2. A typical titration experiment, No. 5 of Table 1. 20.0 ml of a 0.00243 M $Au(NH_3)_4^{3+}$ solution in 10 M NH_4NO_3 and 0.417 M NH_3 was titrated with a 0.00130 M NH_2NH_2 solution containing the same ammonium nitrate and ammonia concentration. The titration was performed at 25.0 ± 0.1 °C under a nitrogen atmosphere. 18.7 ml of the hydrazine solution is equivalent to the titrated gold(III).

ml NH_2NH_2	mmol Au(I)	mmol Au(III)	E	$'E^0$
3.00	0.00775	0.0407	+242	(+221)
4.00	0.0104	0.0381	+235	+218
5.00	0.0130	0.0355	+230	+217
6.00	0.0155	0.0330	+225	+215
7.00	0.0181	0.0304	+222	+216
8.00	0.0207	0.0278	+219	+215
9.00	0.0233	0.0252	+216	+215
10.00	0.0259	0.0226	+214	+216
11.00	0.0285	0.0200	+211	+216
12.00	0.0311	0.0174	+209	+217
13.00	0.0337	0.0148	+208	+219
14.00	0.0363	0.0122	+206	+220
15.00	0.0388	0.0097	+205	(+223)
				$'E^0 = 217 \pm 1$ mV

The concentration of the tetramminegold(III) ion must be corrected for amido formation. The equilibrium constant for the reaction:

$$Au(NH_3)_4^{3+} + NH_3 \rightleftharpoons Au(NH_3)_3NH_2^{2+} + NH^+_4$$

$$K_{amid} = \frac{[Au(NH_3)_3NH_2^{2+}][NH_4^+]}{[Au(NH_3)_4^{3+}][NH_3]}$$

has been determined in 1 M ammonium perchlorate to be 97.[16] An estimation using the salt dependence of the reaction:[37]

$$Co(NH_3)_6^{3+} + H_2O \rightleftharpoons Co(NH_3)_5OH^{2+} + NH_4^+$$

gives for K_{amid} in 10 M ammonium nitrate the value ≈ 50. The potential E of the redox reaction:

$$Au(NH_3)_4^{3+} + 2\ e^- \rightleftharpoons Au(NH_3)_2^+ + 2\ NH_3$$

with K_{amid} included in the expression can be written:

$$E = E^0_{3,1} + \frac{RT}{2F} \ln \frac{C_{Au(III)}}{C_{Au(I)}} - \frac{RT}{2F} \ln \left[\frac{K_{amid}[NH_3]^3}{[NH_4^+]} + [NH_3]^2 \right]$$

where $C_{Au(III)} = [Au(NH_3)_4^{3+}] + [Au(NH_3)_3NH_2^{2+}]$ and $C_{Au(I)} = [Au(NH_3)_2^+]$ are the total concentrations of gold(III) and gold(I), respectively.

The results of the redox titration experiments are given in Table 1; full experimental details of one of the experiments are found in Table 2.

Discussion of the potential measurements. Hydrazine titrations of solutions with ammonia concentrations lower than ≈ 0.2 M gave uncertain results. The potentials were stable only in the beginning of the titration, then they started drifting and gold precipitation first on the electrode then in the solution occurred. In titrations with ammonia concentrations higher than ≈ 0.2 M, the potentials obeyed the Nernst equation except in the beginning of the titration and near the equivalent points, and were stable within a few mV. The higher the ammonia concentration, the more stable were the observed potentials. When an excess of hydrazine was added, the potentials started drifting and the platinum electrode was coated with a thin gold layer before the potentials were stabilized. Analysis of such a solution showed that the gold concentration was lowered by less than 2 %. In solutions with ammonia concentrations greater than ≈ 1 M the potentials became stable overnight. The results of the titrations of tetramminegold(III) ion with hydrazine can be summarized as follows. With ammonia concentrations lower than ≈ 0.2 M, titration gives undefined results because the formed diamminegold(I) complex is not sufficiently stabilized towards disproportionation. Titrations with ammonia concentrations between ≈ 0.2 M and ≈ 1 M followed reasonably well the Nernst expression, but after reduction of all gold(III) to gold(I) no final potential on the electrode coated with a thin layer of gold could be obtained. This was possible, however, in systems with ammonia concentration greater than ≈ 1 M. To assure that the gold couple and not a couple including the hydrazine is potential determining, a titration under the same conditions but without gold complex was performed. The potential obtained during such a titration drifted and showed that an irreversible hydrazine couple has no direct effect on the potential. This is also supported from the fact that there was no drop in the potential at the equivalent point like that to be seen in usual redox titrations. When all the gold(III) is converted into gold(I), the hydrazine as the part of an irreversible couple cannot give a defined potential. In the investigations on the gold aniono systems,[2,9,21] sulphite has been used as titrator in the experiments which were all carried out in acidic solutions. The sulphite ion coordinates strongly with gold(I) and gold(III) and therefore it cannot be recommended in basic solution. The choice of hydrazine in this investigation gives a reducing agent with approximately the same coordinating properties as ammonia. With ammonia present in excess it will have no influence on the complex formation.

If gold system is in equilibrium, the potentials of all of the three gold couples are identical. In the titrations with a platinum electrode only the equilibrium with respect to electron transfer between gold(III) and gold(I) at the electrode exists. Therefore the platinum electrode must be free of gold. With gold precipitated on the electrode, then this also responds to the gold, gold(I) couple. Lingane [1,4] and Pouradier *et al.*[2] have shown that in gold chloride and bromide systems not in equilibrium, the gold(I) will be the potential determining concentration on a gold electrode. This phenomenon can be correlated with the fact that while complex of gold(I) are labile, the gold(III) complexes are more robust. Further, it should be considered that the gold(I) complexes have a different configuration from that of the gold(III) complexes. It is therefore not, as might be expected,[21] the gold(III),gold(I) couple but the exchange current of the gold(I) which determines the potential.

Experiments with gold solutions equilibrated with metallic gold

Experiments in order to try to establish equilibrium with metallic gold were performed as follows. A series of solutions of tetramminegold(III) nitrate in 10 M ammonium nitrate with varying ammonia concentration were shaken with gold powder for 15 days. The change in gold concentration was followed with time. The gold concentration remained constant after about one week.

Another series was started with gold(I) initially present using solutions prepared from tetramminegold(III) nitrate which had been reduced with an equivalent amount of hydrazine. After a few hours the gold(I) disproportionated to some extent and a gold precipitate was formed. The solutions were allowed to equilibrate for four days, and the total gold concentrations were then determined.

The potentials of the equilibrated solutions were measured with a gold electrode generated in the titration experiments. The potentials became stable after about an hour. It was now assumed that $C_{Au(I)} = [Au(NH_3)_2^+]$ and $C_{NH_3} = [NH_3]$. The standard potential for the $Au(NH_3)_2^+$, Au couple is therefore given by the expression:

$$E = E^0_{1,0} + \frac{RT}{F} \ln [C_{Au(I)}/C_{NH_3}^2]$$

$C_{Au(I)}$ was calculated from the knowledge of both the initial and the final total gold concentrations, C^0_{Au} and C_{Au} (eq.), respectively. In Table 3 the compositions of the solutions are given together with the measured potentials and the calculated values for $E^0_{1,0}$. The table contains the final potentials from the two titration experiments in solutions with ammonia concentration higher than ≈ 1 M. The uncertainty in $E^0_{1,0}$ is relatively high but in fair agreement with the assumption that Au(I) is present as a diammine complex. The Nernstian plot given in Fig. 1 shows this directly.

DISCUSSION OF RESULTS

From the two standard potentials determined, $E^0_{3,1}$ and $E^0_{1,0}$, the third standard potential is given by the relationship

$$3\,E^0_{3,0} = 2\,E^0_{3,1} + E^0_{1,0}$$

Table 3. Potential measurements with a gold electrode in solutions equilibrated with metallic gold in 10 M NH_4NO_3 at 25 °C. All potentials are relative to the normal hydrogen electrode in mV. Concentrations are in M.

In solutions prepared from tetramminegold(III) ions the $C_{Au(I)}$ are calculated from the initial gold concentration C^0_{Au} and the "equilibrium" total gold concentration C_{Au}(eq.) by the equation $C_{Au(I)} = 1.5\,C_{Au}(eq.) - 1.5\,C^0_{Au}$

In the solutions where the starting solution is gold(I), the gold(I) "equilibrium" concentrations are related to the initial and the equilibrium concentrations by $C_{Au(I)} = 1.5\,C_{Au}(eq.) - 0.5\,C^0_{Au}$.

C_{NH_3}	C^0_{Au}	C_{Au}(eq.)	$C_{Au(I)}$	E	$E^0_{1,0}$
a. Solutions prepared from $Au(NH_3)_4^{3+}$ with Au					
0.231	0.000930	0.001202	0.000408	+449	+574
0.216	0.000959	0.001149	0.000285	+446	+577
0.0851	0.000968	0.001118	0.000225	+477	+566
0.0369	0.000814	0.000954	0.000210	+501	+549
b. Solutions prepared starting with gold(I)					
0.443	0.001092	0.000634	0.000405	+383	+541
0.248	0.001249	0.000649	0.000350	+416	+549
0.158	0.001148	0.000584	0.000302	+473	+586
0.0710	0.001258	0.000604	0.000277	+499	+573
c. Final potentials from redox titrations					
0.906			0.000946	+414	+587
2.17			0.000800	+319	+542
					$E^0_{1,0} = +563 \pm 6$ mV

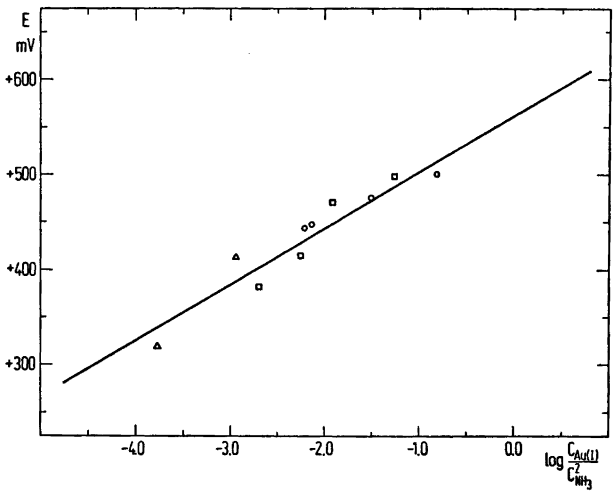

Fig. 1. Nernst plot of the gold(I), gold potentials in 10 M ammonium nitrate solutions with varying ammonia concentration with a gold electrode in solutions with equilibrium between gold(I) and gold(III). The straight line has the theoretical slope, 59.1 mV for 25 °C.
○: Potentials in solutions equilibrated from the gold(III) side. □: Potentials in solutions equilibrated from the gold(I) side. △: Final potentials from redox titration experiments.

so that the results obtained in 10 M ammonium nitrate at 25 °C are the following

$Au(NH_3)_2^+ + e^- \rightleftharpoons Au + 2\ NH_3$
$E^0_{1,0} = +563 \pm 6$ mV
$Au(NH_3)_4^{3+} + 2\ e^- \rightleftharpoons Au(NH_3)_2^+ + 2\ NH_3$
$E^0_{3,1} = +206 \pm 3$ mV
$Au(NH_3)_4^{3+} + 3\ e^- \rightleftharpoons Au + 4\ NH_3$
$E^0_{3,0} = +325 \pm 3$ mV

The standard deviations on the potentials seem to be high, but they are of the same magnitude as ordinarily obtained from measurements of gold potentials,[22,24] except in case of the chloride, bromide, and thiocyanate systems. The situation in these systems is simpler than in the ammonia system because deprotonation, hydrolysis, and further decomposition of the tetramminegold(III) complex influence the result in this system.[16,25] Contrary to what is the case for the gold(III) complex, Au(I) most likely is present exclusively as $Au(NH_3)_2^+$ under the conditions of the measurements.

The data given in Table 3 show qualitatively that Au(III) ammonia solutions dissolve gold,

Table 4. Equilibrium between gold(I) and gold(III) in different ligand systems at 25 °C. In the thiocyanate, the bromide, and the chloride the equilibrium is
$AuX_4^- + 2\ Au + 2\ X^- \rightleftharpoons 3\ AuX_2^-$
and in the ammonia system
$Au(NH_3)_4^{3+} + 2\ Au + 2\ NH_3 \rightleftharpoons 3\ Au(NH_3)_2^+$

	SCN^-	Br^-	Cl^-	NH_3
$K_{3,1}$	4.8×10^{-1}	4.7×10^{-6}	1.8×10^{-8}	8×10^{-13}
Medium	$I \rightarrow 0$	$I \rightarrow 0$	$I \rightarrow 0$	10 M NH_4NO_3
Method	Calc. from potentials	Direct analyt. determination	Direct analyt. determination	Calc. from potentials
Reference	Pouradier and Gadet [8]	Evans and Lingane [4]	Lingane [1]	Present investigation

and that diamminegold(I) solutions disproportionate to Au(III) and gold. But as the gold(III) system is rather undefined and probably not in equilibrium with gold, these data were not used for a direct calculation of the equilibrium constant $K_{3,1}$ of the reaction:

$$Au(NH_3)_4^{3+} + 2\ Au + 2\ NH_3 \rightleftharpoons 3\ Au(NH_3)_2^+$$

A reliable value for this constant is calculated from the standard potentials to be $10^{-12.1}$ in 10 M ammonium nitrate at 25 °C.

This constant is compared in Table 4 with the corresponding constants for the three aniono systems previously investigated. It will be seen that $K_{3,1}$, as could be expected, increases with the tendency of the ligands to be oxidized in the series: $SCN^- > Br^- > Cl^- > NH_3$. This means that the gold(III) ammonia complex is stabilized relatively to the gold(I) complex. However, the standard potentials show that this stabilization of the gold(III) ammonia complex is not sufficient to change the order of stabilities of the gold complexes which in both valence steps are: $NH_3 > SCN^- > Br^- > Cl^-$.

The standard potentials of the gold amines give only relative values for the stability constants of the complexes. As mentioned in the introduction, the standard potential of the aqua couples cannot be directly measured but only estimated from empirical rules. Using the value +2.12 V for the $Au(H_2O)_2^+$, Au couple previously suggested by one of the authors,[13,14,26] one gets the value $\log \beta_2 = 26.5$ for $Au(NH_3)_2^+$. This value is close to J. Bjerrum's prediction in 1950:[14] $\log \beta_2 = 27$. Other suggestions for the $Au(H_2O)_2^+$, Au couple are considerably lower: Latimer [23] together with Hancock and Finkelstein [11] gives a value close to +1.70 V, which leads to $\log \beta_2 = 19.5$. Improved attempts to solve this discrepancy will appear in a forthcoming paper in this series.

Comparing both of these values with those for the two other diammine complexes in group I B of the Periodic Table: $Cu(NH_3)_2^+$, $\log \beta_2 = 10.9$,[15] and $Ag(NH_3)_2^+$, $\log \beta_2 = 7.1$,[27] one finds the usual trend within this group.

REFERENCES

1. Lingane, J. J. *J. Electroanal. Chem. 4* (1962) 332.
2. Pouradier, J., Gadet, M. -C. and Chateau, H. *J. Chim. Phys. 62* (1965) 203.
3. Tschappat, C. and Robert, E. *Helv. Chim. Acta 37* (1954) 333.
4. Evans, D. H. and Lingane, J. J. *J. Electroanal. Chem. 6* (1963) 1.
5. Grube, G. and Morita, T. *Z. Electrochem. 38* (1932) 120.
6. Pouradier, J. and Gadet, M.-C. *J. Chim. Phys. 62* (1965) 1181.
7. Bjerrum, N. and Kirschner, Aa. *Kgl. Dan. Vidensk. Selsk. Skr., Naturv. og Mat. Afd.* (8) *5* (1918) No. 1.
8. Pouradier, J. and Gadet, M.-C. *J. Chim. Phys. 63* (1966) 1467.
9. Peshchevitskii, B. I., Kazakov, V. P. and Erenburg, A. M. *Russian J. Inorg. Chem. 8* (1963) 437.
10. Jørgensen, C. K. and Pouradier, J. *J. Chim. Phys. 67* (1970) 124.
11. Hancock, R. D. and Finkelstein, N. P. *Inorg. Nucl. Chem. Lett. 7* (1971) 477.
12. Erenburg, A. M. and Peshchevitskii, B. I. *Russian J. Inorg. Chem. 14* (1969) 1429.
13. Hawkins, C. J., Mønsted, O. and Bjerrum, J. *Acta Chem. Scand. 24* (1970) 1059.
14. Bjerrum, J. *Chem. Rev. 46* (1950) 381.
15. Bjerrum, J. *Kgl. Dan. Vidensk. Selsk., Mat.-Phys. Medd. 12* (1934) No. 15.
16. Skibsted, L. H. and Bjerrum, J. *Acta Chem. Scand. A 28* (1974) 740.
17. Gjaldbæk, J. K. *Kgl. Dan. Vidensk. Selsk., Mat.-Phys. Medd. 5* (1924) No. 9.
18. Convington, A. K. In Durst, R. A., Ed., *Ion-Selective Electrodes. National Bureau of Standards Special Publication 314*, Washington 1969.
19. Bates, R. G. *Determination of pH*, Wiley, New York 1964.
20. Robinson, R. A. and Stokes, R. H. *Electrolyte Solutions*, 2nd Ed., Butterworths, London 1959.
21. Bjerrum, N. *Bull. Soc. Chim. Belg. 57* (1948) 432.
22. Hancock, R. D., Finkelstein, N. P. and Evers, A. *J. Inorg. Nucl. Chem. 34* (1972) 3747.
23. Latimer, W. M. *Oxidation Potentials*, 2nd Ed., Prentice-Hall, London 1952.
24. Kazakov, V. P., Lapshin, A. I. and Peshchevitskii, B. I. *Russian J. Inorg. Chem. 9* (1964) 708.
25. Weitz, E. *Justus Liebigs Ann. Chem. 410* (1915) 117.
26. Bjerrum, J., George, R. S., Hawkins, C. J. and Olson, D. C. *Proceedings of the Symposium on Coordination Chemistry*, Tihany 1964, Akadémiai Kiadó, Budapest 1965.
27. Bjerrum, J. *Metal Ammine Formation in Aqueous Solution*, 2nd Ed., Haase and Son, Copenhagen 1957.

Received March 11, 1974.

Acta Chemica Scandinavica A 28 (1974) 771—778

The Structure of a High-temperature Polymorph of V_4As_3

ROLF BERGER

Institute of Chemistry, University of Uppsala, Box 531, S-751 21 Uppsala, Sweden

The crystal structure of a high-temperature modification of V_4As_3 has been determined using single-crystal methods. The symmetry is monoclinic (space group $C2/m$), and the compound is isotypic with Cr_4As_3. The cell dimensions are: $a = 13.725$ Å, $b = 3.393$ Å, $c = 9.230$ Å, $\beta = 100.52°$. The two polymorphs are structurally related and can be described in terms of different arrangements of a common structural unit.

Several intermediate phases in the vanadium-arsenic system have been reported earlier, namely V_3As, V_5As_3, V_4As_3, VAs, and VAs_2, and indications are given as to the presence of still more.[1-5] They were all prepared by direct combination of the elements in sealed silica tube syntheses.

In a general survey on the metal-rich part of this system using the same technique, the existence of these phases has been confirmed. In addition, a phase of composition V_3As_2 has been found. It is probably tetragonal, space group $P4/m$, $Z = 4$, with the axes $a = 9.419$ Å and $c = 3.340$ Å. A crystal structure determination is in progress.

In the present study, the work has been extended to higher temperatures than those attainable in silica tube synthesis, by means of an argon arc furnace, and a high-temperature modification of V_4As_3 has thus been discovered. The crystal structure determination and refinement of this phase is described, and the structural relationship between the two polymorphs is discussed.

EXPERIMENTAL

Preparation. An alloy with the nominal composition $VAs_{0.96}$ was prepared by reacting turnings from arc-melted vanadium (Materials Research Corp., claimed purity 99.95 %) and arsenic (Koch-Light Laboratories Ltd., claimed purity better than 99.99 %) in a sealed evacuated silica ampoule. The vanadium, which was contained in an alumina boat to inhibit reaction with the silica, was placed at one end of the tube and heated to 1000 °C. The arsenic, which had previously been freed from superficial oxide by means of gentle sublimation *in vacuo*, was kept at 550 °C at the other end of the tube during the synthesis to avoid too high arsenic pressure. After 20 days the product was allowed to cool. All the arsenic had by then reacted. A powder photograph showed the presence of VAs and the orthorhombic V_4As_3. Part of the sintered product was arc-melted in an atmosphere of purified argon. Powder diffraction analysis of the final alloy showed diffraction lines of a new phase in addition to those of VAs. The lines of the orthorhombic V_4As_3 had disappeared completely. The specimen contained several needle-shaped, mostly intergrown crystals. The crystal picked for collecting the intensity data was a very well shaped parallelepiped of the dimensions $0.104 \times 0.026 \times 0.026$ mm.

X-Ray investigations. The cell dimensions were determined with a Guinier-Hägg type focusing camera, using strictly monochromatic $CrK\alpha_1$ radiation [$\lambda(CrK\alpha_1) = 2.28962$ Å] and germanium ($a = 5.65771$ Å) as internal calibration standard. The powder photograph was indexed using approximate cell dimensions obtained from preliminary Weissenberg and rotation photographs. Powder diffraction data from a least-squares refinement are given in Table 1.

The intensity data were recorded on a computer-controlled Stoe-Philips four-circle diffractometer using graphite monochromatized $MoK\alpha$ radiation and a NaI scintillation detector. Reflexions from a quarter of a sphere in reciprocal space were recorded to a maximum in 2θ of 80° using a $\theta - 2\theta$ step-scan procedure. Instrumental stability and crystal setting were checked using three standard reflexions remeasured every 50 reflexions.

Calculations. The calculations were performed on an IBM 370/155 or an IBM 1800 computer using programs listed in Ref. 6. Absorption corrections were applied to the intensity data

using six limiting faces of the forms {100}, {010} and {001}. The crystal was 0.104 mm along the ⟨010⟩-direction. The minimum and maximum transmission factors were 0.349 and 0.477 with a calculated linear absorption coefficient of 334 cm^{-1}.

DETERMINATION OF THE STRUCTURE

The preliminary data obtained from Weissenberg films indicated a centered monoclinic symmetry. The unit cell dimensions were similar to those of Cr_4As_3,[7] and the cell volume was very nearly one half of that of the orthorhombic V_4As_3.[5] It was therefore suspected that the new vanadium arsenide might be a high-temperature modification of V_4As_3. This hypothesis was substantiated by an experiment, where the arc-melted product was heated in a sealed evacuated silica tube at 1050 °C for seven days. Powder diffraction analysis showed that the monoclinic phase had disappeared completely and was replaced by the orthorhombic V_4As_3. In the following, the orthorhombic low-temperature form is denoted α-V_4As_3 and the monoclinic high-temperature form β-V_4As_3.

The structure refinement of β-V_4As_3 was performed by a full-matrix least-squares method. Space-group symmetry *Cm* was assumed, and the starting values for the coordinates were taken from the structure of Cr_4As_3.[7] Initially, the following parameters were refined: 1 scale factor, 26 positional parameters, and 14 isotropic

Table 1. Powder diffraction data for β-V_4As_3 as measured with a Guinier-Hägg camera, using Cr$K\alpha_1$ radiation.

h k l	$Q \times 10^5$ (Å^{-2}) obs.	calc.	Int. obs.	calc.	d_{obs} (Å)
0 0 1		1 214		1.9	
2 0 0		2 197		0.3	
−2 0 1		2 815		0.0	
2 0 1		4 007		0.0	
0 0 2	4 852	4 858	vvw	0.7	4.540
−2 0 2		5 861		0.3	
2 0 2	8 247	8 247	w	3.8	3.482
4 0 0		8 786		3.0	
	8 792		w		3.372
−4 0 1		8 808		2.6	
1 1 0	9 237	9 236	vw	4.7	3.290
−1 1 1	10 147[a]	10 153	vw	0.3	3.139
1 1 1	10 747	10 749	w	12.3	3.050
0 0 3	10 928	10 929	m	18.8	3.025
4 0 1	11 193	11 194	w	4.2	2.989
−4 0 2	11 255	11 258	m	18.4	2.981
−2 0 3	11 342	11 337	vvw	0.1	2.969
−1 1 2	13 502	13 498	vvw	10.0	2.721
3 1 0	13 633	13 630	vw	10.0	2.708
−3 1 1	13 945	13 949	vst	43.2	2.678
1 1 2	14 694	14 690	vst	63.6	2.609
2 0 3	14 922	14 915	vvw	1.8	2.589
3 1 1	15 737	15 739	vvw	2.5	2.521
4 0 2		16 030		0.2	
−4 0 3	16 139	16 137	w	15.8	2.489
−3 1 2	16 699	16 698	w	24.4	2.447
−6 0 1		19 195		0.8	
−2 0 4		19 241		1.3	
−1 1 3	19 267	19 271	w	16.7	2.278
0 0 4	19 429	19 430	m	20.6	2.269
6 0 0	19 772	19 770	vvw	4.1	2.249
3 1 2	20 278	20 277	st	89.7	2.221
−6 0 2		21 048		59.5	
	21 053		st		2.179
1 1 3		21 061		11.1	
−3 1 3	21 881[a]	21 875	w	14.6	2.138
−5 1 1	22 136	22 139	m	51.1	2.125
5 1 0	22 418	22 416	w	19.7	2.112
6 0 1		22 773		1.6	
4 0 3	23 299	23 295	vvw	4.1	2.072
−4 0 4	23 453	23 445	vvw	4.5	2.065
2 0 4	24 018	24 013	m	40.5	2.040
−5 1 2		24 291		1.6	
5 1 1	25 127	25 122	m	33.6	1.995
−6 0 3	25 324	25 331	vvw	1.7	1.987
3 1 3	27 245	27 243	w	8.1	1.916
−1 1 4		27 474		0.2	
6 0 2	28 204	28 206	vw	9.6	1.883
−5 1 3		28 872		0.5	
−3 1 4	29 475	29 481	st	100.0	1.842
−2 0 5		29 574		0.0	
1 1 4		29 859		0.0	'
5 1 2	30 255	30 256	m	17.2	1.818
0 0 5		30 360		0.9	
−6 0 4	32 034	32 042	vvw	2.4	1.767
4 0 4	32 990	32 988	vw	12.0	1.741
−4 0 5	33 182	33 181	vvw	4.1	1.736
−8 0 1		33 974		0.6	
−7 1 1		34 723		16.0	
	34 752		st		1.696
0 2 0		34 749		92.9	
8 0 0		35 146		3.2	
−8 0 2	35 233	35 232	w	19.3	1.685
2 0 5		35 538		19.7	
	35 579		m		1.677
7 1 0		35 596		21.1	
−5 1 4		35 882		1.1	
0 2 1		35 964		0.1	
6 0 3	36 061	36 067	vw	5.5	1.665
−7 1 2	36 274	36 278	vw	5.2	1.660
3 1 4	36 635	36 639	vw	4.7	1.652
2 2 0		36 946		0.0	
−2 2 1		37 564		0.0	
5 1 3	37 806	37 819	w	14.7	1.626
−1 1 5		38 105		0.1	

[a] Overlapped by a monoarsenide line.

temperature factors. The atomic scattering factors were taken from Ref. 8 and the dispersion correction factors from Ref. 9. Reflexions with $|F_o|$ less than $3\sigma(|F_o|)$ were given zero weight, which reduced the material from 1533 to 1247 independent reflexions. The remaining reflexions were weighted according to the formula

$$w^{-1} = \sigma^2 + (0.009|F_o|)^2$$

where σ is based on counting statistics. The refinement converged to an R-value of 0.029, where

$$R = \sum||F_c| - |F_o||/\sum|F_o|$$

Extinction correction according to Coppens and Hamilton [10] was tried, but the strongest reflexion, (020), remained much weaker than the calculated value. The (020) reflexion was then excluded from the refinement, which thus converged to an R-value of 0.025. Anisotropic temperature factors were finally introduced. The convergence was very slow, and the refinement was stopped after seven cycles at which an R-value of 0.016 was obtained. An inspection of the correlation matrix showed that there were extremely strong correlations (up to 0.98) between the parameters. The values of the positional parameters indicated that the structure was very nearly centrosymmetric, which would cause this behaviour. A second series of refinements based on the centrosymmetric $C2/m$ space-group symmetry was then performed. The refinements converged rapidly, and the final R-values obtained were 0.028 and 0.017, for isotropic and anisotropic thermal parameters, respectively (1189 reflexions).

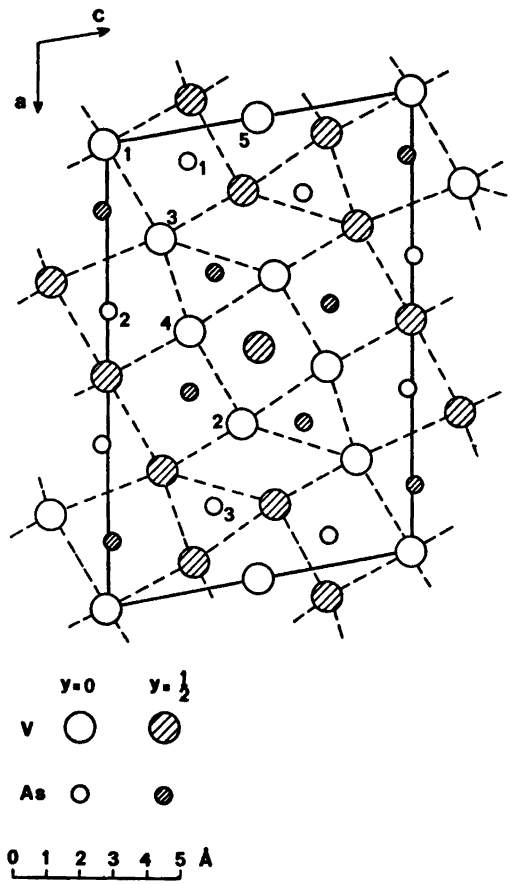

Fig. 1. The crystal structure of β-V_4As_3 projected on (010).

Table 2. Structure data for β-V_4As_3, including anisotropic thermal parameters β_{ij}. The form of the temperature factor is $\exp[-\beta_{11}h^2 \cdots -\beta_{12}hk \cdots]$.
Space group $C2/m$, $Z=4$, $a=13.7251(5)$ Å, $b=3.3928(2)$ Å, $c=9.2297(4)$ Å, $\beta=100.521(3)°$.

Atom	Position	x	y	z	$\beta_{11}\times10^5$	$\beta_{22}\times10^5$	$\beta_{33}\times10^5$	$\beta_{13}\times10^5$	$\beta_{12}=\beta_{23}$
V(1)	2*a*	0	0	0	73(3)	1335(49)	115(6)	9(3)	0
V(2)	4*i*	0.65796(4)	0	0.44440(5)	68(2)	1220(35)	139(4)	19(2)	0
V(3)	4*i*	0.22512(4)	0	0.17747(6)	59(2)	1633(38)	279(5)	21(3)	0
V(4)	4*i*	0.43820(4)	0	0.27309(5)	55(2)	1108(33)	155(4)	20(2)	0
V(5)	2*c*	0	0	1/2	45(2)	1587(50)	84(5)	9(3)	0
As(1)	4*i*	0.06945(2)	0	0.26623(3)	65(1)	1084(21)	106(3)	19(1)	0
As(2)	4*i*	0.35916(2)	0	0.01043(3)	92(1)	1092(21)	130(3)	27(1)	0
As(3)	4*i*	0.82122(2)	0	0.34827(3)	62(1)	951(21)	148(3)	17(1)	0

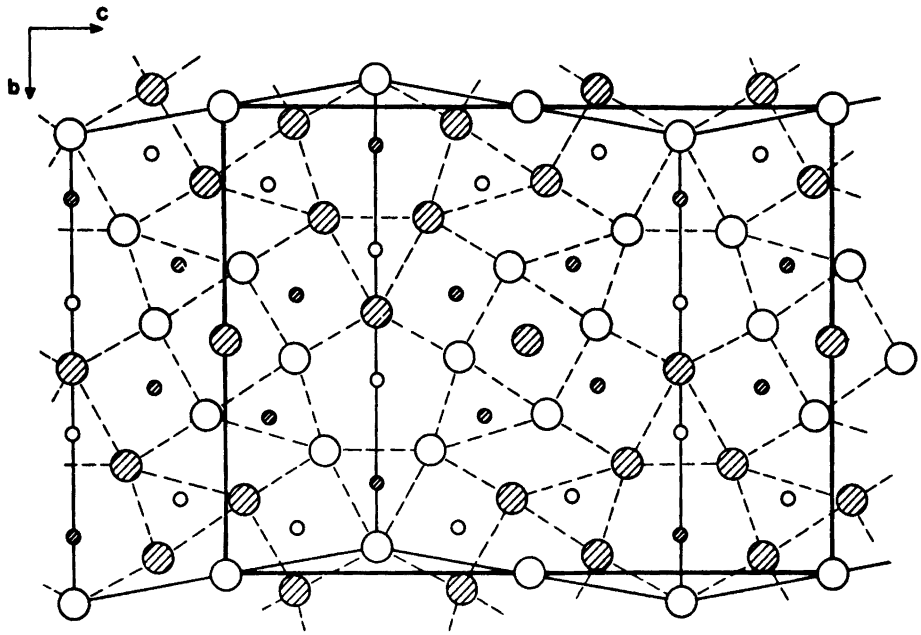

Fig. 2. The α-V_4As_3 structure projected on (100). Sub-unit arrangement indicated by thin full lines. Notation similar to Fig. 1 (Atoms at $x=0$ and $x=\frac{1}{2}$).

The agreement is very good for both the *Cm* and the *C2/m* refinements, and it seems very difficult to reach a decisive conclusion as to the correct choice of space-group symmetry. An application of the Hamilton test [11] would probably not be valid, since uncorrected systematic errors are likely to contribute considerably to the differences between F_o and F_c. Furthermore, the strong correlations among the parameters in *Cm* symmetry indicate that the least-squares refinement procedure is less satisfactory, and the standard deviations are about ten times greater for the lower symmetry. The final structure is accordingly described in the terms of space-group *C2/m* symmetry as presented in Table 2. The observed and calculated structure factors are listed in Table 3.

DESCRIPTION AND DISCUSSION

A projection of the β-V_4As_3 structure along the *b*-axis is illustrated in Fig. 1. The coordination of vanadium around arsenic is essentially trigonal prismatic. The coordination numbers are 6, 7, and 8 for As(2), As(1), and As(3), respectively. The structure may be considered isotypic with Cr_4As_3, although Baurecht, Boller and Nowotny [7] used a non-centrosymmetric description.

It is interesting to compare the structural data for the two V_4As_3 polymorphs. The cell parameters for α-V_4As_3 as determined by the author are:

$a=3.4139(2)$ Å; $b=13.6798(7)$ Å; $c=18.0598(11)$ Å; $V=843.4$ Å^3.

Thus, the cell-volume of β-V_4As_3 (422.6 Å^3) is only slightly more than half of that of the low-temperature form. Both polymorphs can formally be described on a basis of different arrangement of a common sub-unit as depicted in Fig. 2. The sub-unit constitutes one unit cell of the β-form, while the unit cell of the α-form is composed of two sub-units, one being the mirror image of the other one. Consequently, the main differences between the two structures appear at the boundaries between the sub-units. The As(2) site in the β-V_4As_3 structure corresponds to two sites in α-V_4As_3, both of coordination number six. One retains the prismatic coordination while the other one is

Table 3. Observed and calculated structure factors (× 10) for β-V_4As_3. F_o-values for weak reflexions not included in the refinement are omitted from the table. The columns are h, l, $|F_o|$ and $|F_c|$.

H,0,L

2	0	118	85
4	0	630	614
6	0	1040	1032
8	0	898	907
10	0	1009	1022
12	0	1101	1110
14	0	1404	1420
16	0	795	790
18	0	584	577
20	0	350	342
22	0	274	289
24	0	509	495
-24	1	695	682
-22	1	507	509
-20	1	574	560
-18	1	615	604
-16	1	340	339
-14	1	1382	1382
-12	1	1908	1937
-10	1	282	264
-8	1	400	407
-6	1	444	449
-4	1	586	577
-2	1		13
0	1		169
2	1		13
4	1	865	826
6	1	655	671
8	1	2256	2269
10	1	797	800
12	1	141	144
14	1	275	259
16	1	576	577
18	1	418	414
20	1		102
22	1	535	536
24	1	236	231
-24	2	1021	1016
-22	2	345	360
-20	2	766	779
-18	2	198	201
-16	2	1199	1220
-14	2	211	202
-12	2	494	490
-10	2	136	137
-8	2	2226	2223
-6	2	4012	4061
-4	2	1737	1722
-2	2	160	157
0	2	217	220
2	2	693	665
4	2	211	201
6	2	1651	1665
8	2	2853	2875
10	2	254	254
12	2	411	405
14	2	274	267
16	2		52
18	2	928	925
20	2	1156	1165
22	2	605	631
-24	3	311	293
-22	3	494	513
-20	3	164	166
-18	3	1142	1145
-16	3	597	612
-14	3	134	119
-12	3	245	244
-10	3	226	231
-8	3	144	142
-6	3	703	696
-4	3	1907	1881
-2	3	122	147
0	3	1809	1717
2	3	616	609
4	3	1076	1077
6	3	1182	1176
8	3	1304	1305
10	3	668	665
12	3	134	161
14	3	118	110
16	3	1125	1136
18	3		28
20	3	337	351
22	3		41
-24	4	436	429
-22	4	346	343
-20	4	448	441
-18	4		94
-16	4	1161	1156
-14	4	1179	1182
-12	4	627	631
-10	4	836	852
-8	4		74
-6	4	799	816
-4	4	1121	1124
-2	4	592	588
0	4	2357	2293
2	4	3508	3390
4	4	1832	1804
6	4	137	109
8	4	895	894
10	4	775	776
12	4	152	149
14	4	2163	2155
16	4	132	162
18	4		33
20	4	457	466
22	4	226	208
-24	5	360	351
-22	5	1205	1126
-20	5	265	264
-18	5		127
-16	5	816	830
-14	5	526	533
-12	5		69
-10	5	1995	1996
-8	5	1999	2017
-6	5	1205	1126
-4	5	1074	1056
-2	5		31
0	5	507	516
2	5	2281	2235
4	5	153	154
6	5	539	533
8	5	596	597
10	5	1160	1169
12	5	766	771
14	5		27
16	5	405	409
18	5	582	598
20	5		48
-24	6	213	194
-22	6	1428	1421
-20	6		120
-18	6		109
-16	6	214	214
-14	6	378	377
-12	6		42
-10	6	1267	1279
-8	6	621	617
-6	6	2204	2204
-4	6	1001	1003
-2	6	2244	2228
0	6	1196	1184
2	6		92
4	6	358	367
6	6	1296	1281
8	6	1799	1796
10	6		97
12	6		30
14	6	131	130
16	6	152	155
18	6		44
20	6		34
-24	7	326	325
-22	7	467	469
-20	7	582	574
-18	7	532	538
-16	7	522	524
-14	7	1882	1915
-12	7	319	318
-10	7	602	609
-8	7		48
-6	7	358	344
-4	7	1199	1186
-2	7	300	314
0	7	1264	1260
2	7	1161	1147
4	7	369	358
6	7	804	795
8	7	372	372
10	7	1556	1560
12	7		41
14	7	829	841
16	7	329	346
18	7	227	220
20	7		41
-24	8	197	194
-20	8		48
-18	8	368	371
-16	8	723	710
-14	8	990	990
-12	8	791	793
-10	8	722	717
-8	8	417	423
-6	8	937	933
-4	8	663	653
-2	8	1376	1365
0	8	1116	1118
2	8	817	826
4	8	138	127
6	8	490	478
8	8	369	354
10	8	595	595
12	8	190	208
14	8	483	480
16	8	1131	1144
18	8	162	178
-22	9	329	324
-20	9	692	694
-18	9	535	535
-16	9	1688	1683
-14	9	614	610
-12	9		72
-10	9	396	404
-8	9	276	275
-6	9	1880	1876
-4	9		40
-2	9	1400	1393
0	9	172	172
2	9	298	295
4	9	1775	1770
6	9	1526	1513
8	9	842	843
10	9		17
12	9	221	202
14	9	379	387
16	9	567	560
18	9	272	273
-22	10	650	637
-20	10	833	839
-18	10	788	811
-16	10	314	323
-14	10	527	546
-12	10		4
-10	10		15
-8	10	1715	1724
-6	10		48
-4	10	471	460
-2	10		80
0	10	385	369
2	10	935	946
4	10	224	224
6	10		67
8	10	952	955
10	10	388	384
12	10	693	691
14	10	707	706
16	10	239	257
-20	11	491	476
-18	11	469	473
-16	11	261	255
-14	11	638	645
-12	11	1163	1172
-10	11	1106	1117
-8	11	715	713
-6	11	254	240
-4	11	788	805
-2	11	414	416
0	11	1843	1845
2	11	311	313
4	11		84
6	11	397	396
8	11	433	444
10	11	355	360
12	11	459	457
14	11	689	678
-20	12	342	328
-18	12		93
-16	12	488	483
-14	12	947	949
-12	12	217	197
-10	12	172	180
-8	12	195	190
-6	12	492	490
-4	12	560	566
-2	12	148	130
0	12	919	929
2	12	258	291
4	12	266	259
6	12	166	132
8	12	616	615
10	12		117
12	12	464	464
-18	13		14
-16	13	920	909
-14	13		73
-12	13	305	308
-10	13		121
-8	13	483	476
-6	13	1001	1015
-4	13	133	115
-2	13	484	488
0	13	791	791
2	13		82
4	13	456	444
6	13	162	194
8	13	1404	1413
10	13		19
-16	14		161
-14	14	265	279
-12	14	733	724
-10	14	236	230
-8	14	597	604
-6	14	954	968
-4	14	661	665
-2	14	200	205
0	14	634	625
2	14	277	250
4	14	288	292
6	14	393	418
8	14	163	149
-14	15	316	301
-12	15	381	401
-10	15		98
-8	15	805	813
-6	15	385	380
-4	15	274	254
-2	15	441	427
0	15	529	545
2	15	1134	1140
4	15	649	660
6	15	245	238
-10	16	609	627
-8	16	684	686
-6	16	458	467
-4	16	211	220
-2	16		29
0	16	196	185
2	16		42

H,1,L

1	0	565	558
3	0	986	983
5	0	1623	1648
7	0	1627	1633
9	0	786	757
11	0	1615	1618
13	0	1775	1768
15	0		74
17	0	1204	1224
19	0	477	474
21	0	273	264
23	0	574	567
-23	1	260	253
-21	1		72
-19	1	1162	1167
-17	1	332	335
-15	1		37
-13	1	1075	1084
-11	1	785	783
-9	1		40
-7	1	1429	1444
-5	1	2593	2649
-3	1	2073	2064
-1	1	156	141
1	1	1017	976
3	1	532	524
5	1	2185	2194
7	1	112	113
9	1	506	500
11	1	737	747
13	1	1579	1611
15	1	1073	1078
17	1	257	250
19	1		20
21	1	669	673
23	1	255	244
-23	2	475	495
-21	2	190	195
-19	2	875	887
-17	2	218	214
-15	2		82
-13	2		95
-11	2	747	754
-9	2	921	919
-7	2	791	802
-5	2	461	471
-3	2	1670	1674
-1	2	963	979
1	2	2613	2562
3	2	3471	3428
5	2	1567	1566
7	2	682	686
9	2	883	878
11	2	930	944
13	2	1158	1162
15	2	175	166
17	2	800	814
19	2	377	365
21	2	706	703
23	2		48
-23	3	202	202
-21	3	715	717
-19	3	829	840
-17	3	339	331
-15	3	507	504
-13	3	276	277
-11	3	3093	3116
-9	3	389	388
-7	3	998	991
-5	3	258	275
-3	3	1416	1410
-1	3	1434	1455
1	3	1222	1217
3	3	1089	1081
5	3	1315	1310
7	3	456	479
9	3	1727	1728
11	3	363	367
13	3	815	829
15	3	368	362
17	3	634	632
19	3	578	570
21	3		48
-23	4	440	452
-21	4	446	462
-19	4	176	174
-17	4	394	397
-15	4	815	820
-13	4		17
-11	4	103	91
-9	4	1155	1150
-7	4	502	470
-5	4	374	375
-3	4	3735	3789
-1	4	175	170
1	4		71
3	4	772	761
5	4	169	57
7	4	667	668
9	4	419	427
11	4	1454	1453
13	4	910	917
15	4		72
17	4		3
19	4	486	498
21	4	886	895
-23	5	267	269
-21	5	361	369
-19	5	698	701
-17	5	1479	1488
-15	5	1245	1242
-13	5	443	436
-11	5	568	573
-9	5	583	575
-7	5	195	207
-5	5	984	993
-3	5	1984	1976
-1	5	111	103
1	5	1294	1269
3	5	496	506
5	5		93
7	5	1611	1611
9	5	1287	1294
11	5	695	691
13	5		34
15	5		161
17	5	457	458
19	5	177	187
21	5		18
-23	6	427	429
-21	6		130
-19	6		109
-17	6	446	442
-15	6		86
-13	6		69
-11	6	1269	1266
-9	6	1408	1419
-7	6	485	492
-5	6	796	797
-3	6	628	637
-1	6	260	268
1	6	158	154
3	6	606	606
5	6	2538	2511
7	6	336	368
9	6	598	600
11	6	513	519
13	6		37
15	6	1103	1091
17	6	1211	1273
19	6	760	767
-23	7	256	238
-21	7	715	712
-19	7	358	350
-17	7	446	450
-15	7	407	407
-13	7	218	211
-11	7	953	969
-9	7	1557	1574
-7	7	1752	1766
-5	7	811	805
-3	7	598	597
-1	7	967	956
1	7	616	622
3	7	2355	2325
5	7	261	272
7	7	247	224
9	7		31
11	7	610	611
13	7		125
15	7	174	181
17	7	168	154
19	7	277	283
-23	8	279	244
-21	8	414	396
-19	8	986	973
-17	8	808	815
-15	8		17
-13	8		60
-11	8	262	259
-9	8	818	833
-7	8	816	822
-5	8	377	366
-3	8	1311	1302
-1	8	2015	2010
1	8	933	920
3	8		74
5	8	290	290
7	8	594	596
9	8		9
11	8	1751	1750
13	8	484	508
15	8	274	295
17	8		53
19	9	442	434
-19	9	239	224
-17	9	961	964
-15	9	196	197
-13	9	1671	1705
-11	9	384	383
-9	9		104
-7	9	662	672
-5	9	572	559
-3	9	1405	1406
-1	9	644	649
1	9	397	386
3	9	337	326
5	9		106
7	9		66
9	9	360	343
11	9	950	952
13	9	270	244
15	9	387	386
17	9		130
-21	10		103
-19	10		37
-17	10		37
-15	10	161	180
-13	10	629	645
-11	10	722	738
-9	10	1331	1345
-7	10	146	151
-5	10	766	766
-3	10	515	513
-1	10	721	718
1	10	240	239
3	10	1142	1139
5	10	1177	1186
7	10	493	480
9	10		37
11	10	444	439
13	10		107
15	10		75
-19	11	600	603
-17	11	406	393
-15	11	309	294
-13	11	235	244
-11	11	290	291
-9	11	485	482
-7	11	428	422
-5	11	749	749
-3	11	1160	1160
-1	11	559	560
1	11	678	681
3	11	271	247
5	11	1065	1066
7	11	1203	1208
9	11	202	48
11	11	475	460
13	11	220	219
-19	12	449	448
-17	12	1046	1054
-15	12	338	347
-13	12	678	677
-11	12	158	147
-9	12		120
-7	12	742	759
-5	12	1430	1415
-3	12	939	957
-1	12	575	570
1	12	304	301
3	12	442	440
5	12	294	288
7	12	245	214
9	12		38
11	12	709	701
-13	13	1138	1133
-11	13	219	213
-9	13	302	299
-7	13	450	434
-5	13	488	499
-3	13	656	674
-1	13		37
1	13	565	563
3	13	675	695
5	13	137	161
7	13	1167	1174
9	13	1579	1578
11	13	251	239
13	13		120
15	13		79
-11	14	150	97
-9	14		167
-7	14		46
-5	14	1433	1421
-3	14	397	411
-1	14	240	239
1	14	272	259
3	14	240	255
5	14		65
7	14	118	36
9	14	717	723
11	14	970	983
13	14	323	305
-13	15	296	319
-11	15		69
-9	15	215	202
-7	15	341	340
-5	15	335	324
-3	15	525	490
-1	15		94
1	15		107
3	15	376	352
5	15	179	134
-9	16	350	333
-7	16		53
-5	16		137
-3	16	1327	1333
-1	16	299	309
1	16	208	224

H,2,L

0	0	3766	4917*
2	0		42
4	0	523	516
6	0	769	782
8	0	746	751
10	0	838	839
12	0	919	924
14	0	1204	1203
16	0	678	686
18	0	531	519
20	0	301	301
22	0	269	257
-22	1	197	189
-20	1	297	312
-18	1	530	536
-16	1	294	297
-14	1	1166	1175
-12	1	1590	1612
-10	1	146	179
-8	1	351	342
-6	1	309	313
-4	1	472	466
-2	1		9
0	1		83
2	1		26
4	1	754	740
6	1	484	499
8	1	1806	1819
10	1	650	654
12	1	149	122
14	1	227	225
16	1	597	596
18	1	358	358
20	1	139	88
22	1	509	490
-22	2	317	298
-20	2	687	694
-18	2	176	182
-16	2	1061	1060
-14	2	177	177
-12	2	414	409
-10	2	168	157
-8	2	1773	1794
-6	2	2916	2977
-4	2	1287	1304
-2	2		84
0	2	175	171
2	2	258	255
4	2	176	167
6	2	1261	1269
8	2	2262	2279
10	2	537	536
12	2	556	558
14	2	243	232
16	2		30
18	2	808	810
20	2	1053	1044
22	2	565	569
-22	3	459	466
-20	3	298	288
-18	3	998	999
-16	3	520	535
-14	3	122	103
-12	3	201	211
-10	3	189	170
-8	3	147	127
-6	3	556	553
-4	3	1411	1434
-2	3	100	76
0	3	1342	1346
2	3	456	456
4	3	806	814
6	3	951	962
8	3	1046	1045
10	3	575	566
12	3		94
14	3		99
16	3	991	999
18	3		27
20	3	313	323
-22	4	300	312
-20	4	378	388
-18	4		77
-16	4	991	1007
-14	4	1353	1356
-12	4	541	510
-10	4	699	707
-8	4		69
-6	4	654	658
-4	4	833	831
-2	4	442	447
0	4	1705	1715
2	4	2567	2558
4	4	1447	1452
6	4	153	134
8	4	756	747
10	4	667	667
12	4		128
14	4	1868	1873
16	4	156	147
18	4		36
20	4	423	429
-22	5	249	240
-20	5	241	233
-18	5		105

Table 3. Continued.

-16	5	722	725
-14	5	457	460
-12	5	117	60
-10	5	1663	1662
-8	5	1625	1623
-6	5	962	957
-4	5	851	842
-2	5	92	42
0	5	446	402
2	5	1754	1764
4	5	104	99
6	5	422	422
8	5	509	508
10	5	983	992
12	5	671	663
14	5		32
16	5	345	365
18	5	523	527
20	5		42
-22	6	1305	1287
-20	6		106
-18	6		92
-16	6	205	183
-14	6	354	334
-12	6		35
-10	6	1063	1062
-8	6	500	500
-6	6	1780	1792
-4	6	734	746
-2	6	1803	1817
0	6	936	944
2	6		25
4	6	307	314
6	6	1090	1082
8	6	1500	1506
10	6		83
12	6		24
14	6	145	121
16	6		137
18	6		70
-22	7	444	425
-20	7	510	522
-18	7	449	467
-16	7	467	456
-14	7	1662	1659
-12	7	269	270
-10	7	514	517
-8	7		31
-6	7	311	304
-4	7	952	963
-2	7	243	241
0	7	1027	1022
2	7	958	975
4	7	298	303
6	7	663	651
8	7	292	316
10	7	1343	1347
12	7		64
14	7	745	744
16	7	331	310
18	7	184	204
-22	8	169	179
-20	8		37
-18	8	300	329
-16	8	639	641
-14	8	867	863
-12	8	687	687
-10	8	629	620
-8	8	358	357
-6	8	760	777
-4	8	546	551
-2	8	1131	1126
0	8	959	941
2	8	664	671
4	8		110
6	8	424	412
8	8	301	304
10	8	521	519
12	8	179	190
14	8	423	424
16	8	1041	1035
-20	9	634	624
-18	9	497	479
-16	9	191	168
-14	9	541	535
-12	9		72
-10	9	359	341
-8	9	267	235
-6	9	1581	1596
-4	9		40
-2	9	1187	1183
0	9	165	152
2	9	251	254
4	9	1509	1515
6	9	1317	1315
8	9	747	737
10	9		3
12	9	196	184
14	9	371	349
16	9	517	512
-20	10	770	761
-18	10	447	428
-16	10	299	280
-14	10	480	478
-12	10		7
-10	10		14
-8	10	1470	1489
-6	10		41
-4	10	398	396
-2	10		68
0	10	337	323
2	10	813	813
4	10	180	195
6	10		63
8	10	836	839
10	10	360	356
12	10	610	611
14	10	666	639
-18	11	447	436
-16	11	228	224
-14	11	578	571
-12	11	1031	1036
-10	11	968	981
-8	11	625	627

-6	11	217	210
-4	11	699	695
-2	11	341	358
0	11	1588	1609
2	11	265	276
4	11		83
6	11	339	348
8	11	394	395
10	11	342	327
12	11	425	409
-18	12		90
-16	12	450	436
-14	12	858	855
-12	12	187	171
-10	12	197	173
-8	12	155	160
-6	12	447	424
-4	12	490	491
-2	12		113
0	12	804	813
2	12	255	250
4	12	185	215
6	12		125
8	12	562	549
10	12		107
-16	13	809	823
-14	13		72
-12	13	273	273
-10	13		102
-8	13	408	420
-6	13	902	904
-4	13		107
-2	13	434	435
0	13	711	704
2	13		73
4	13	411	399
6	13	175	173
8	13	1283	1279
-14	14	267	254
-12	14	644	647
-10	14	194	212
-8	14	275	276
-6	14	874	867
-4	14	590	589
-2	14	200	199
0	14	551	563
2	14	217	219
4	14	249	263
6	14	375	376
-10	15		84
-8	15	744	737
-6	15	349	346
-4	15	228	231
-2	15	393	385
0	15	504	492
2	15	1037	1036

H,3,L

1	0	347	348
3	0	550	544
5	0	980	983
7	0	1111	1105
9	0	439	444
11	0	1158	1164
13	0	114	110
15	0		58
17	0	928	943
19	0	384	385
21	0	207	203
-21	1		53
-19	1	953	940
-17	1	244	259
-15	1		33
-13	1	781	793
-11	1	565	551
-9	1		19
-7	1	979	966
-5	1	1585	1613
-3	1	1367	1372
-1	1	202	193
1	1	570	567
3	1	275	278
5	1	1383	1386
7	1		72
9	1	350	353
11	1	548	543
13	1	1191	1202
15	1	801	810
17	1	181	198
19	1		20
-21	2		155
-19	2	700	702
-17	2	166	174
-15	2		80
-13	2		60
-11	2	511	516
-9	2	622	622
-7	2	557	539
-5	2	304	312
-3	2	976	985
-1	2	446	467
1	2	1615	1620
3	2	2039	2049
5	2	1040	1039
7	2	497	499
9	2	631	627
11	2	661	669
13	2	855	867
15	2	139	147
17	2	661	659
19	2	286	293
-21	3	597	587
-19	3	678	666
-17	3	271	255
-15	3	374	383
-13	3	186	194
-11	3	2189	2219
-9	3	245	242
-7	3	715	707
-5	3	159	144
-3	3	869	884
-1	3	859	856
1	3	741	751

3	3	703	689
5	3	917	913
7	3	280	291
9	3	1204	1219
11	3	321	263
13	3	609	620
15	3	284	281
17	3	500	485
19	3	501	466
-21	4	417	397
-19	4		140
-17	4	305	293
-15	4	626	620
-13	4		19
-11	4		76
-9	4	797	793
-7	4	419	408
-5	4	270	249
-3	4	2349	2420
-1	4		124
1	4		29
3	4	537	536
5	4	116	71
7	4	471	477
9	4	303	305
11	4	1078	1076
13	4	693	695
15	4		52
17	4		3
19	4	399	399
-21	5	291	298
-19	5	566	563
-17	5	1189	1173
-15	5	937	942
-13	5	328	324
-11	5	416	409
-9	5	426	413
-7	5	126	111
-5	5	639	650
-3	5	1318	1315
-1	5		103
1	5	926	925
3	5	305	316
5	5		73
7	5	1122	1142
9	5	958	945
11	5	503	516
13	5		37
15	5	145	152
17	5	377	367
-21	6		105
-19	6		84
-17	6	343	346
-15	6		55
-13	6		67
-11	6	933	930
-9	6	998	999
-7	6	342	351
-5	6	534	543
-3	6	429	438
-1	6		128
1	6		93
3	6	412	405
5	6	1761	1774
7	6	257	254
9	6	458	461
11	6	393	394
13	6	158	34
15	6	869	861
17	6	1060	1043
-19	7	284	288
-17	7	360	358
-15	7	301	312
-13	7		162
-11	7	737	725
-9	7	1154	1156
-7	7	1264	1259
-5	7	585	587
-3	7	445	447
-1	7	676	680
1	7	429	422
3	7	1649	1663
5	7	179	193
7	7	145	156
9	7		33
11	7	490	476
13	7		90
15	7		145
-19	8	797	801
-17	8	648	637
-15	8		15
-13	8		50
-11	8	167	186
-9	8	631	619
-7	8	613	607
-5	8	249	249
-3	8	910	931
-1	8	1441	1444
1	8	659	672
3	8		69
5	8	220	219
7	8	438	445
9	8		10
11	8	1349	1378
13	8	423	418
15	8		190
-19	9	180	184
-17	9	803	781
-15	9	187	174
-13	9	1328	1318
-11	9	288	289
-9	9		78
-7	9	495	512
-5	9	412	420
-3	9	1038	1038
-1	9	474	469
1	9	240	275
3	9	247	236
5	9		75
7	9		51
9	9	280	269
11	9	772	751
13	9	224	197
-17	10		35

-15	10		138
-13	10	540	531
-11	10	584	580
-9	10	1011	1021
-7	10		119
-5	10	576	579
-3	10	364	374
-1	10	532	537
1	10	204	199
3	10	849	871
5	10	909	921
7	10	387	390
9	10		27
11	10	355	360
-15	11	243	238
-13	11	191	190
-11	11	223	233
-9	11	391	394
-7	11	309	309
-5	11	557	570
-3	11		125
-1	11	407	422
1	11	522	540
3	11	192	191
5	11	839	844
7	11	962	951
9	11		46
-15	12	266	276
-13	12	537	543
-11	12		120
-9	12		88
-7	12	569	571
-5	12	1123	1128
-3	12	744	748
-1	12	453	450
1	12	230	251
3	12	354	352
5	12	243	240
7	12	170	181
-13	13	338	340
-11	13	395	409
-9	13	561	535
-7	13		29
-5	13	466	460
-3	13	550	554
-1	13	158	148
1	13	904	928
3	13	486	474
5	13	202	197
-9	14	343	335
-7	14	238	195
-5	14	176	202
-3	14	178	211
-1	14		46
1	14		34

H,4,L

0	0	2480	2701
2	0		19
4	0	355	347
6	0	465	465
8	0	478	483
10	0	534	539
12	0	617	615
14	0	805	822
16	0	480	483
18	0	405	401
-18	1	392	400
-16	1		215
-14	1	809	803
-12	1	1051	1041
-10	1	138	128
-8	1	224	224
-6	1	196	185
-4	1	288	300
-2	1		12
0	1		39
2	1		40
4	1	502	497
6	1	272	264
8	1	1117	1119
10	1	401	411
12	1		66
14	1		136
16	1	319	335
18	1	274	244
-18	2		143
-16	2	750	748
-14	2		100
-12	2	297	277
-10	2		113
-8	2	1103	1112
-6	2	1711	1731
-4	2	770	775
-2	2		26
0	2		111
2	2	360	349
4	2		104
6	2	753	753
8	2	1413	1412
10	2	285	150
12	2	220	228
14	2	172	166
16	2		15
-18	3	728	706
-16	3	408	389
-14	3		67
-12	3		122
-10	3	143	109
-8	3		82
-6	3	323	339
-4	3	823	836
-2	3		96
0	3	835	838
2	3	276	257
4	3	481	474
6	3	579	590
8	3	669	663
10	3	354	350
12	3		120
14	3		65
16	3	714	725
-18	4		47

-16	4	728	720
-14	4	915	919
-12	4	352	351
-10	4	462	442
-8	4		60
-6	4	407	412
-4	4	476	480
-2	4	250	259
0	4	994	998
2	4	1528	1511
4	4	921	886
6	4		102
8	4	467	484
10	4	455	456
12	4	145	98
14	4	1326	1323
16	4		115
-18	5		64
-16	5	539	519
-14	5	330	328
-12	5		55
-10	5	1071	1061
-8	5	1008	1032
-6	5	607	609
-4	5	518	530
-2	5		48
0	5	231	235
2	5	1091	1075
4	5		78
6	5	286	281
8	5	331	329
10	5	666	672
12	5	458	457
14	5		45
-16	6		122
-14	6	224	250
-12	6		19
-10	6	708	708
-8	6	316	315
-6	6	1135	1135
-4	6	527	466
-2	6	1133	1130
0	6	567	572
2	6		16
4	6	214	217
6	6	697	699
8	6	1006	1017
10	6		45
12	6		22
14	6		105
-16	7	344	320
-14	7	1200	1163
-12	7	205	194
-10	7	360	362
-8	7		25
-6	7	208	198
-4	7	600	602
-2	7	175	169
0	7	634	658
2	7	636	627
4	7	203	201
6	7	410	433
8	7	172	199
10	7	948	936
12	7		75
-16	8	499	481
-14	8	614	614
-12	8	505	487
-10	8	395	390
-8	8	229	239
-6	8	487	492
-4	8	368	361
-2	8	735	730
0	8	615	610
2	8	474	462
4	8		107
6	8	254	276
8	8	205	214
10	8	372	367
12	8		154
-14	9	382	385
-12	9		74
-10	9	224	224
-8	9	199	172
-6	9	1077	1084
-4	9		29
-2	9	788	800
0	9		104
2	9	178	176
4	9	993	1030
6	9	953	939
8	9	523	526
10	9		3
-14	10	339	340
-12	10		25
-10	10		14
-8	10	1053	1043
-6	10		27
-4	10	300	304
-2	10		41
0	10	211	230
2	10	543	554
4	10	154	138
6	10		31
8	10	591	602
-12	11	751	757
-10	11	721	708
-8	11	460	459
-6	11		151
-4	11	491	478
-2	11	275	247
0	11	1149	1149
2	11	204	203
4	11		63
6	11	259	250
-8	12		102
-6	12	282	289
-4	12	341	339
-2	12		78
0	12	575	578
2	12	185	185

H,5,L

1	0	187	176
3	0	312	296
5	0	561	556
7	0	609	614
9	0	325	300
11	0	711	716
13	0		57
-13	1	504	491
-11	1	352	344
-9	1		25
-7	1	525	536
-5	1	929	917
-3	1	764	770
-1	1		111
1	1	279	292
3	1	198	169
5	1	785	792
7	1		55
9	1	218	204
11	1	327	332
13	1	808	793
-13	2		22
-11	2	321	303
-9	2	354	364
-7	2	280	298
-5	2		196
-3	2	562	556
-1	2	244	272
1	2	865	887
3	2	1165	1154
5	2	588	595
7	2	327	313
9	2	332	367
11	2	433	414
13	2	564	550
-13	3		106
-11	3	1362	1375
-9	3		144
-7	3	389	402
-5	3		69
-3	3	511	517
-1	3	492	482
1	3	446	436
3	3	399	387
5	3	556	534
7	3	200	209
9	3	728	730
11	3		147
-13	4		17
-11	4		59
-9	4	511	502
-7	4	223	212
-5	4	188	136
-3	4	1379	1375
-1	4		71
1	4		7
3	4	314	299
5	4		48
7	4	293	269
9	4	230	210
11	4	695	706
-13	5	177	206
-11	5	249	254
-9	5	299	266
-7	5		75
-5	5	400	395
-3	5	767	769
-1	5		72
1	5	512	514
3	5	197	182
5	5		28
7	5	715	700
9	5	601	593
-11	6	575	576
-9	6	617	605
-7	6	239	208
-5	6	321	305
-3	6	280	267
-1	6		111
1	6		80
3	6	259	249
5	6	1100	1099
7	6		158
9	6	298	310
-11	7	497	477
-9	7	752	741
-7	7	768	762
-5	7	350	342
-3	7	275	265
-1	7	436	435
1	7	287	262
3	7	1032	1028
5	7		121
7	7		76
-9	8	400	392
-7	8	416	423
-5	8		177
-3	8	572	568
-1	8	905	902
1	8	410	416
3	8		66
5	8	178	141
-7	9	360	343
-5	9	262	260
-3	9	674	673
-1	9	292	281
1	9	171	154

H,6,L

0	0	1476	1502
2	0		21
4	0	190	187
-4	1		157
-2	1		5
0	1		41
2	1		45
4	1	273	231
-4	2	406	414
-2	2		8
0	2		63
2	2	228	195

Table 4. Interatomic distances and standard deviations for β-V_4As_3 (Å). Distances shorter than 3.5 Å are listed.

V(1) –	2 As(1)	2.468 (0)	V(5) –	2 As(1)	2.513 (0)
	4 As(2)	2.587 (0)		2 As(3)	2.594 (0)
	2 V(3)	3.222 (0)		4 V(4)	2.708 (0)
	4 V(4)	3.276 (0)		4 V(2)	2.872 (0)
	2 V(1)	3.393 (0)		2 V(5)	3.393 (0)
V(2) –	2 As(1)	2.516 (0)	As(1) –	V(3)	2.424 (1)
	2 As(3)	2.534 (0)		V(1)	2.468 (0)
	As(3)	2.556 (1)		2 V(4)	2.484 (0)
	2 V(5)	2.872 (0)		V(5)	2.513 (0)
	2 V(2)	3.061 (1)		2 V(2)	2.516 (0)
	V(4)	3.130 (1)		2 As(2)	3.357 (0)
	V(4)	3.140 (1)		2 As(1)	3.393 (0)
	2 V(3)	3.260 (1)			
	2 V(2)	3.393 (0)			
V(3) –	As(1)	2.424 (1)	As(2) –	V(4)	2.469 (1)
	2 As(3)	2.519 (0)		2 V(3)	2.548 (0)
	2 As(2)	2.548 (0)		2 V(1)	2.587 (0)
	As(2)	2.607 (1)		V(3)	2.607 (1)
	V(4)	2.897 (1)		2 As(1)	3.357 (0)
	V(1)	3.222 (0)		2 As(2)	3.393 (0)
	2 V(2)	3.260 (1)		2 As(2)	3.418 (1)
	2 V(3)	3.393 (0)			
V(4) –	As(2)	2.469 (1)	As(3) –	2 V(3)	2.519 (0)
	2 As(1)	2.484 (0)		2 V(4)	2.519 (0)
	2 As(3)	2.519 (0)		2 V(2)	2.534 (0)
	2 V(5)	2.708 (0)		V(2)	2.556 (1)
	V(3)	2.897 (1)		V(5)	2.594 (0)
	V(2)	3.130 (1)		2 As(3)	3.393 (0)
	V(2)	3.140 (1)			
	2 V(1)	3.276 (0)			
	2 V(4)	3.393 (0)			

characterized by an irregular coordination polyhedron first found in Nb_4As_3.[12] Despite this change in geometrical arrangement, no drastic change in coordination number for near neighbours is found. Only in coordination spheres more remote than the first are neighbours affected. Interatomic distances for β-V_4As_3 are given in Table 4. The interatomic distances within the sub-unit are similar for the two polymorphs, with a maximum difference of 0.1 Å, taking data for α-V_4As_3 from Ref. 5.

Common to both forms is the appearance of a body-centered cubic arrangement of some of the metal atoms, which is found in many other metal-rich compounds between transition metals and pnictides. The structure of Mo_4P_3[13] is closely related to that of β-V_4As_3 with respect to the stacking of the triangular prismatic building blocks, but it contains no counterpart to the body-centered cubic metal atom arrangement in β-V_4As_3, although of the same stoichiometry.

Acknowledgements. The author thanks Professor I. Olovsson for all facilities put at disposal and is also deeply grateful to Professor S. Rundqvist for his encouragement and valuable advice. Thanks are also due to various colleagues for their help with programming and instrumental operation. This work has been financially supported by the Swedish Natural Science Research Council.

REFERENCES

1. Bachmayer, K. and Nowotny, H. *Monatsh. Chem. 86* (1955) 741.
2. Hulliger, F. *Nature 204* (1964) 775.
3. Meissner, H.-G. and Schubert, K. *Z. Metallk. 56* (1965) 523.

4. Boller, H. and Nowotny, H. *Monatsh. Chem. 97* (1966) 1053.
5. Yvon, K. and Boller, H. *Monatsh. Chem. 103* (1972) 1643.
6. Lundgren, J. O., Ed., *Crystallographic Computer Programs*, Institute of Chemistry, University of Uppsala, Uppsala 1974, UUIC–B13–4–01.
7. Baurecht, H.-E., Boller, H. and Nowotny, H. *Monatsh. Chem. 101* (1970) 1696.
8. Hanson, H. P. *et al. Acta Crystallogr. 17* (1964) 1040.
9. *International Tables for X-Ray Crystallography*, Kynoch Press, Birmingham 1962, Vol. III.
10. Coppens, P. and Hamilton, W. C. *Acta Crystallogr. A 26* (1970) 71.
11. Hamilton, W. C. *Acta Crystallogr. 18* (1965) 502.
12. Carlsson, B. and Rundqvist, S. *Acta Chem. Scand. 25* (1971) 1742.
13. Rundqvist, S. *Acta Chem. Scand. 19* (1965) 393.

Received April 9, 1974.

Acta Chemica Scandinavica A 28 (1974) 779—786

The Crystal and Molecular Structure of Bis(acetophenone thioacethydrazonato)nickel(II)

SINE LARSEN *

Chemical Laboratory B, Technical University of Denmark, DK-2800 Lyngby, Denmark

The crystal structure of bis(acetophenone thioacethydrazonato)nickel(II) has been determined by X-ray diffraction methods. The crystals are monoclinic, space group $C2/c$, $Z=4$, with unit cell dimensions: $a=21.071(8)$ Å, $b=8.537(3)$ Å, $c=13.269(5)$ Å, $\beta=118°36(2)'$. The reflection data were measured on an automated equi-inclination diffractometer. The 2271 reflections with intensities greater than their standard deviation were used to solve and refine the structure including all hydrogen atoms by Patterson, difference Fourier, and least squares procedures to final unit weighted and weighted residuals of 0.045 and 0.0[illegible] respectively.

The nickel atom is in the special position having the point symmetry of the twofold axis. The molecular geometry of the inner complex can be described as a tetrahedrally distorted *cis*-planar isomer with the phenyl groups in a *syn*-configuration. The chelate rings are planar and the angle between the two planes is 19°. The Ni-atom is displaced 0.60 Å from the ligand planes.

Structural studies of many nickel thiosemicarbazide complexes have been carried out during the last decade.[1–5] Recently, the synthesis and crystal structure of bis(thioacethydrazidato)-nickel(II) were reported, although the free ligand, which differs only at the methyl-group from thiosemicarbazide, is too unstable to be isolated.[6] It is also possible to synthesize diamagnetic thioacethydrazonate complexes of nickel(II) [7] similar to the thiosemicarbazonate complexes first prepared by Ablov and Gerbeleu.[8] The structure determinations of chloro-bis(acetone thiosemicarbazone)nickel(II) chloride monohydrate and nitratobis(acetone thiosemicarbazone)nickel(II) nitrate monohydrate [9] showed that these paramagnetic nickel thiosemicarbazone complexes have the configuration of a trigonal bipyramid.

Since information about the structures of the diamagnetic inner-complexes of nickel with molecules of thioacethydrazones of various ketones could not be obtained from the results of related thiosemicarbazone complexes, it was decided to undertake a crystal structure analysis of one of these compounds. The complexes derived from unsymmetrical ketones have the possibility of a *syn-anti-amphi* configuration of the two ketone parts in addition to the *cis-trans* isomerism.

The compound chosen for this investigation was bis(acetophenone thioacethydrazonato)nickel(II) as it has been shown from thin layer and column chromatography that only a single isomer is formed.[7] Schematical drawings of the six possible isomers, assuming a planar configuration, are shown in Fig. 1. However, ^{1}H NMR spectra of the complex in common solvents [7] indicated that it possesses a twofold axis of symmetry, which would exclude isomers III and IV.

EXPERIMENTAL

Bis(acetophenone thioacethydrazonato)nickel(II) crystallized from a mixture of heptane and dichloromethane was supplied by Erik Larsen. The crystals are irregularly shaped polyhedra and prismatic needles, which exhibit pleochroism with colour changes from red to green. Preliminary oscillation, Weissenberg, and precession photographs showed that the crystals are monoclinic with the crystallo-

* Present address: Chemical Laboratory IV, H. C. Ørsted Institute, The University of Copenhagen, DK-2100, Copenhagen Ø, Denmark.

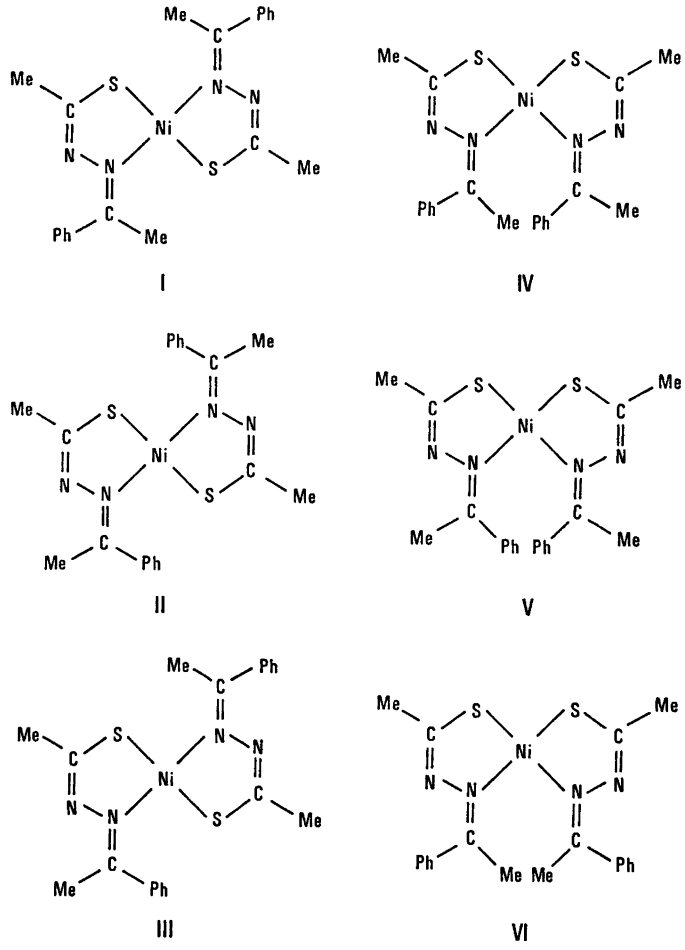

Fig. 1. Schematic drawings of the six isomers of planar bis(acetophenone thioacethydrazonato)-nickel(II).

graphic two-fold axis parallel to the needle axis. The possible space groups were determined from systematically absent reflections. The test for the piezoelectric effect on a sample of relatively large crystals (2 – 3 mm) was negative.

A single crystal of dimensions $0.30 \times 0.15 \times 0.25$ mm^3 was selected for data collection and the determination of cell constants. This crystal was mounted so that the two-fold axis was parallel to the rotation axis of the goniometer head. The unit cell dimensions were determined on a four-circle Picker FACS-1 diffractometer using Mo$K\alpha$ radiation. 30 reflections in the region of 2θ between 30° and 38° were used in a least squares refinement of the unit cell dimensions and the orientation matrix. The density of the crystals was measured by flotation in an aqueous solution of zinc chloride.

Intensity data were collected on a STOE automatic Weissenberg diffractometer using Mo$K\alpha$ radiation obtained by a graphite monochromator. Harmonics were excluded by proper settings of the pulse height discriminator. The relative intensities were measured by an ω-scan technique for all reflections included in reciprocal space between a hemisphere ($k \geq 0$) with $\sin\theta/\lambda \leqq 0.7044$ and a cylinder parallel to the rotation axis with radius $\sin\theta/\lambda = 0.073$. The scans were performed at a constant rate of 1°/min and with the ω-scan range increasing from 2° to 4° with layer number. Background counts were made at both ends of each ω-scan range, each count being for half of the scan count time. A standard reflection on each individual layer line was measured for every 75 reflections, and an equator standard reflection was monitored twice between the layer lines.

These measurements of intensities of the standard reflections showed that no deterioration or misalignment of the crystal had occurred during data collection.

The intensities of symmetry related reflections were averaged. Corrections for Lorentz and polarisation effects but not for absorption were applied. Of the 2956 independent reflections so obtained, 685 had net intensities less than twice their standard deviation, $\sigma(I) = \{\sum_{i=1}^{n} \sigma_i^2\}^{\frac{1}{2}}/n$, where σ_i is the standard deviation of an individual observation based on counting statistics and n is the total number of measurements.

The following computer programs were employed in this work: V-72 (an algol 5 program for calculating diffractometer setting angles), a locally written Fortran program (for data reduction), ORTEP II [10] (the thermal ellipsoid plotting program by C. K. Johnson for illustrations), and the X-Ray System (the crystallographic program package by Stewart *et al.*[11] for the crystal structure analysis).

The X-ray atomic scattering factors used in these calculations were taken from Cromer and Mann [12] for Ni, S, C, and N and from Stewart *et al.*[13] for H. The anomalous dispersion corrections of Cromer [14] were applied to Ni and S.

The computations were performed at the Technical University of Denmark; the algol 5 program on the RC 4000 computer and Fortran programs on the IBM 370/165 computer.

CRYSTAL DATA

Bis(acetophenone thioacethydrazonato)nickel(II). $NiS_2C_{20}N_4H_{22}$; M = 441.01. Monoclinic (*b* unique), a = 21.071(8) Å, *b* = 8.537(3) Å, *c* = 13.269(5) Å, $\beta = 118°36(2)'$; $V = 2096$ Å^3; $d_{obs} = 1.409$ g/cm^3; $Z = 4$; $d_{cal} = 1.399$ g/cm^3. Linear absorption coefficient for X-rays (λ(Mo$K\alpha$) = 0.71069 Å), $\mu = 11.31$ cm^{-1}. Number of electrons in the unit cell, $F(000) = 920$. Systematically absent reflections; *hkl* when $h+k$ odd, *h*0*l* when *h* and *l* odd, 0*k*0 when *k* odd; space groups *Cc* or *C*2/*c* (No. 9, C_s^4 or No. 15, C_{2h}^6). Developed faces are {100}, {001}, {101} and {111} for the prismatic needles.

STRUCTURE DETERMINATION AND REFINEMENT

Due to the negative test for the piezoelectric effect and the statistical distribution of *E*-values, it was assumed that the compound being investigated crystallized in the centric space group *C*2/*c*. From the unit cell volume, density and the possible symmetry of the ligand, it was concluded that in this space group the Ni atom has to be in the special position (0,*y*,1/4) with the point symmetry of a two-fold axis. As mentioned in the introduction, the ^{1}H NMR spectrum of the complex in solution indicates the presence of a two-fold axis of symmetry.

The Harker line (0,*v*,½) in the Patterson map revealed the *y* coordinate for the Ni atom, and a Fourier map phased on the nickel atom showed the position of the sulfur, carbon, and two nitrogen atoms of the ligand ring. The positions of the rest of the non-hydrogen atoms in the complex were located in the Fourier synthesis phased from these five atoms.

This structure was refined by full matrix least squares method using all the 2271 reflections with intensities greater than their standard deviation. The scale factor, the atomic parameters and individual temperature factors were varied in a refinement using unit weights. In the initial stage, isotropic temperature factors were used, later anisotropic temperature factors were employed. After a refinement using anisotropic temperature factors with the conventional residual of $R = 0.06$, a difference Fourier synthesis showed only 11 peaks outside the region of the Ni atom. These were in positions to be expected for the hydrogen atoms of the structure. The hydrogen atoms of the methyl groups were localized to peaks where the maximum density was only two-thirds of the corresponding density of the hydrogen atoms of the phenyl groups. This indicates larger temperature factors for the methyl groups.

The coordinates and individual temperature factors of the hydrogen atoms were also included in the final cycles of the full matrix least squares refinement, minimizing $\sum w(|F_o| - k|F_c|)^2$. The weights used in the final refinement were of the form

$$w = 1/\{2[\sigma(F)]^2 + 0.01|F| + 0.001F^2\}.$$

During the last cycle of least squares refinement no parameter shifted more than 0.138σ, the average shift being 0.012σ. The corresponding residuals were

$$R = \sum||F_o| - |F_c||/\sum|F_o| = 0.044 \text{ and}$$
$$R_w = \{\sum w||F_o| - |F_c||^2/\sum w|F_o|^2\}^{\frac{1}{2}} = 0.052.$$

Table 1. Final atomic coordinates in fractions for the heavier atoms in bis(acetophenone thioacethydrazonato)nickel(II). Standard deviations $\times 10^4$ in parentheses. The other half of the molecule can be generated by the symmetry operation $(1-x,y,\frac{1}{2}-z)$.

Atom	x	$\sigma(x)$	y	$\sigma(y)$	z	$\sigma(z)$
Ni	0.500	(0)	0.4071	(0.4)	0.2500	(0)
S	0.4228	(0.5)	0.2316	(1)	0.2351	(1)
Cl	0.3546	(1)	0.3634	(3)	0.2135	(2)
N2	0.3649	(1)	0.5111	(2)	0.2334	(2)
N1	0.4395	(1)	0.5503	(2)	0.2792	(2)
C11	0.2794	(2)	0.3005	(5)	0.1704	(3)
C2	0.4582	(1)	0.6773	(2)	0.3404	(2)
C3	0.4049	(2)	0.7835	(4)	0.3496	(4)
C21	0.5363	(1)	0.7148	(2)	0.4076	(2)
C22	0.5602	(2)	0.8684	(3)	0.4125	(2)
C23	0.6330	(2)	0.9032	(4)	0.4753	(3)
C24	0.6820	(2)	0.7883	(4)	0.5368	(3)
C25	0.6586	(2)	0.6360	(4)	0.5345	(2)
C26	0.5857	(2)	0.6001	(3)	0.4706	(2)

Table 2. Thermal parameters for the heavier atoms in bis(acetophenone thioacethydrazonate)nickel(II). The expression for the temperature factor is exp $\{-2\pi^2(U_{11}h^2a^{*2}+U_{22}k^2b^{*2}+U_{33}l^2c^{*2}+2U_{12}hka^*b^*+2U_{13}hla^*c^*+2U_{23}klb^*c^*\}$. The anisotropic temperature factor constants. U_{ij}, are in units of Å$^2 \times 10^{-4}$. The estimated standard deviations from the least squares refinement are given in parentheses in units of the last significant figure in the parameter value.

Atom	U_{11}	U_{22}	U_{33}	U_{12}	U_{13}	U_{23}
Ni	443(3)	259(2)	541(3)	0	309(2)	0
S	701(5)	323(3)	1035(7)	−112(3)	541(5)	− 47(3)
Cl	470(14)	509(12)	478(14)	−115(11)	260(12)	3(11)
N2	359(10)	453(10)	480(12)	− 40(8)	218(9)	25(9)
N1	352(9)	315(8)	421(10)	6(7)	219(8)	39(7)
C11	546(18)	792(22)	621(21)	−275(17)	260(16)	− 47(18)
C2	433(12)	323(9)	457(13)	26(9)	271(11)	18(9)
C3	587(19)	487(15)	929(28)	76(14)	473(20)	−120(16)
C21	449(13)	357(10)	377(12)	14(9)	237(11)	− 36(9)
C22	518(15)	373(11)	520(15)	− 28(11)	193(13)	− 19(11)
C23	594(17)	560(15)	615(18)	−174(15)	226(15)	− 88(14)
C24	476(16)	823(21)	514(17)	− 92(16)	194(14)	−122(15)
C25	523(16)	639(16)	456(15)	156(14)	146(13)	6(13)
C26	548(15)	419(12)	424(13)	44(11)	244(12)	20(10)

The final atomic parameters are listed in Tables 1 – 3. The labelling of the non-hydrogen atoms is given in Fig. 2, which also contains bond lengths and angles, except for the benzene ring and the carbon hydrogen bonds. The rule used in the numbering scheme for the hydrogen atoms is such that the first two numbers indicate to which carbon atom it is bonded and the third distinguishes between hydrogen atoms attached to the same carbon atom.

A list of observed structure amplitudes and calculated structure factors may be obtained from the author upon request.

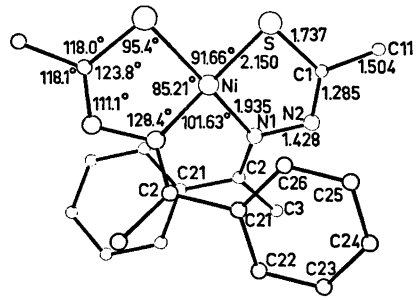

Fig. 2. A perspective view of bis(acetophenone-thioacethydrazonato)nickel(II) showing the labels of the atoms and part of the bond lengths and angles.

Table 3. Refined parameters for the hydrogen atoms in bis(acetophenone thioacethydrazonato)nickel(II). The temperature factor is expressed as exp $(-8\pi^2U \sin^2 \theta/\lambda^2)$. The standard deviations in units of the last significant figure in the parameter value are given in parentheses.

Atom	x	y	z	$U \times 10^2$
H111	0.276(2)	0.223(5)	0.218(3)	10(1)
H112	0.262(2)	0.255(5)	0.094(4)	10(1)
H113	0.253(3)	0.375(6)	0.178(4)	11(2)
H31	0.355(3)	0.755(7)	0.306(5)	16(2)
H32	0.407(3)	0.867(7)	0.330(5)	13(2)
H33	0.420(3)	0.973(6)	0.420(5)	12(2)
H22	0.528(2)	0.946(4)	0.373(3)	5.6(8)
H23	0.649(2)	1.014(4)	0.472(3)	8.3(10)
H24	0.732(2)	0.816(5)	0.580(3)	8.5(11)
H25	0.689(2)	0.552(4)	0.571(3)	7.3(10)
H26	0.571(2)	0.504(4)	0.472(2)	5.2(8)

DESCRIPTION AND DISCUSSION OF THE STRUCTURE

The molecular structure of bis(acetophenone thioacethydrazonato)nickel(II) can be described as a *cis-syn* configuration indicating that the sulfur atoms are *cis* and that phenyl groups are *syn*. The structure is illustrated by V in Fig. 1. From the schematic drawings one would imagine this structure to be one of the least likely due to the bulkiness of the phenyl groups.

However, Fig. 3, which is an ORTEP [10] plot of the molecule viewed down the two-fold axis shows it is possible for this diamagnetic inner complex to have the *cis-syn* configuration and not have any close contacts. The arrangement of the two sulfur atoms and the two coordinating nitrogen atoms, which form a tetrahedrally distorted planar configuration, is also seen from this drawing.

Using the coordinates in Table 1, mean planes for characteristic groups of atoms within the molecule were calculated, in order to describe the non-planarity of this complex. The equations defining these planes and the distances of the atoms to the planes are listed in Table 4.

The ligand ring formed by the atoms S, C1, N1, and N2 approximately form a plane. The nickel atom is not in this plane (plane II, Table 4), but is displaced 0.60 Å from the plane. The angle between the ligand plane and its symmetry related forming the other half of the molecule is found to be 19°. This considerable deviation from planarity can also be illustrated

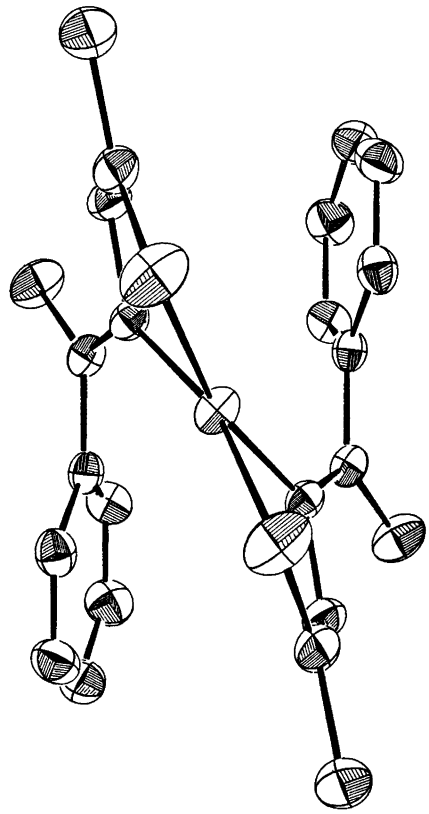

Fig. 3. A perspective view of one molecule from its two-fold axis. The thermal ellipsoids are scaled to enclose 33 % probability.

Table 4. Least squares planes calculated for some characteristic groups of atoms in bis(acetophenone thioacethydrazonato)nickel(II).

Plane	Equation for the least squares plane in direct space [a]
I	$1.5125\,x - 1.5975\,y + 10.9568\,z = 2.8451.$
II	$-7.0048\,x - 1.3949\,y + 12.9318\,z = -0.2401$
III	$-12.1877\,x + 1.6585\,y + 12.9029\,z = -0.0775$

Atom	Distances in Å of the atoms from the planes.		
	I	II	III
Ni	0.000*	−0.597	−2.115
S	0.000*	−0.005*	−1.658
C1	−0.550	0.010*	−0.887
N2	−0.552	0.005*	−0.510
N1	0.000*	−0.010*	−0.763
C11	−1.035	0.068	−0.630
C2	0.496	0.488	0.008
C3	0.346	0.832	0.952
C21	1.290	0.758	−0.013*
C22	1.135	0.439	0.013*
C23	1.877	0.693	−0.006*
C24	2.808	1.304	−0.001*
C25	2.991	1.651	0.001*
C26	2.238	1.385	0.006*

* The starred displacements are those of the atoms used in determining the least squares plane. [a] The equations for the least squares planes for the other half of the molecule may be generated by the symmetry operation $(1-x,\ y,\ \frac{1}{2}-z)$.

by the angle between the two coordination planes (plane I and its symmetry equivalent) defined by the two S−Ni−N1 groups. This has been calculated to 21.6°.

The phenyl groups are tilted relative to the ligand rings. The mean plane (plane III) calculated from the carbon atoms of the benzene ring form an angle of 26° with the ligand ring (plane II) to which it is attached, and an angle of 16° with the ligand plane of the other half of the molecule.

All bond lengths and angles within the molecule and their estimated standard deviations (but not corrected for the effect of thermal vibration) are listed in Table 5. The Ni−S and Ni−N1 bond lengths of 2.150 Å and 1.935 Å are similar to those found in other planar nickel complexes having thiosemicarbazide or related compounds as ligands.[1-6].

However, it should be noted that the Ni−S bond in this *cis* complex is significantly shorter than the Ni−S bond found in similar *trans* complexes. This was also noticed by R. Grønbæk Hazell in the investigation of the structures of β-$Ni(tscH)_2SO_4$[3] and *cis* and *trans* isomers of $Ni(tscH)_2(NO_3)_2$.[5] The structures of the *cis* and *trans* isomers of bis(thioacethydroxamato)nickel(II) [15-16] seem also to confirm the general observation that a *cis* Ni−S complex deviates more from planarity than the equivalent *trans* complex. The Ni−S bond length from 2.145 to 2.155 Å in *cis* complexes are significantly shorter than the Ni−S bonds found in similar trans complexes varying between 2.165 and 2.184 Å.

Looking at the molecular dimensions of the ligand it is remarkable that nearly all the bonds outside the phenyl group can be described as single or double bonds. The two C=N bonds do not vary much from their mean value of 1.291 Å, which is comparable to the bondlength of a C=N double bond of 1.28 Å.[17] The N−N bondlength of 1.428 Å is very similar to the magnitude of the N−N bondlength found in hydrazine derivatives. Finally, the C1−C11 and C2−C3 bondlengths of 1.504 Å and 1.493

Table 5. Bond lengths (Å) and bond angles (°) in bis(acetophenone thioacethydrazonato)nickel(II). The standard deviations in terms of the last digit are in parentheses.

Ni–S	2.150(1)	S–Ni–S′	91.66(5)
Ni–N1	1.935(2)	S–Ni–N1	85.21(7)
S–C1	1.737(3)	N1–Ni–N1′	101.63(9)
C–N2	1.285(3)	Ni–S–C1	95.4(1)
N–N1	1.428(3)	S–C1–C2	123.8(2)
C–C11	1.504(5)	S–C1–C11	118.0(2)
N–C2	1.298(3)	C11–C1–N2	118.1(4)
C–C3	1.493(6)	C1–N2–N1	111.1(2)
C–C21	1.483(3)	N2–N1–Ni	117.6(1)
C21–C22	1.395(3)	N2–N1–C2	113.9(2)
C22–C23	1.382(4)	Ni–N1–C2	128.4(2)
C23–C24	1.375(4)	N1–C2–C3	122.9(2)
C24–C25	1.386(5)	N1–C2–C21	118.3(2)
C25–C26	1.387(4)	C3–C2–C21	118.7(2)
C26–C21	1.382(3)	C2–C21–C22	120.2(2)
C11–H111	0.94(5)	C2–C21–C26	120.6(2)
C11–H112	0.97(5)	C22–C21–C26	119.1(1)
C11–H113	0.88(5)	C21–C22–C23	120.2(2)
C3–H31	0.96(6)	C22–C23–C24	120.4(3)
C3–H32	0.77(6)	C23–C24–C25	119.9(3)
C3–H33	0.83(6)	C24–C25–C26	119.9(3)
C22–H22	0.91(3)	C25–C26–C21	120.5(3)
C23–H23	1.00(4)		
C24–H24	0.95(4)		
C25–H25	0.93(3)		
C26–H26	0.88(3)		

Å indicate that these bonds can be described as single C–C bonds. By comparison of these results with their analogs obtained from structures of other "planar" nickel complexes having thiosemicarbazides or related compounds as ligands,[1–6,9] one finds that the only examples having similar localized bonds are the inner complexes bis(thioacethydrazidato)nickel(II) [6] and bis(thiosemicarbazidato)nickel(II).[1] However, the C–S bond length has approximately the same magnitude in the charged and inner complexes with a value from 1.70 Å to 1.73 Å.

The relative arrangement of the molecules in the crystal is shown in Fig. 4, which is a stereo pair illustrating the packing as seen from the crystallographic *b* axis. The molecules are arranged so that the average plane between plane II in Table 4 and its symmetry equivalent is nearly parallel to the $a-b$ plane. There are van der Waals interactions between adjacent molecules in the direction of the *c* axis. The atoms C11, C1, N2, C2, and C3 of the ligand ring of one molecule have distances between 3.28 Å and 3.82 Å to the atoms C26, C26, C24 of the phenyl group of the nearest molecule, which interacts with a phenyl group from the first molecule. All other intermolecular distances are larger than the sum of the van der Waals radii [18] of the atoms.

The strong pleochroism of the crystals can be derived from the molecular packing. The crystals are red when the electric vector of the polarized light is parallel to the two-fold axis of the crystal and the molecules and green when

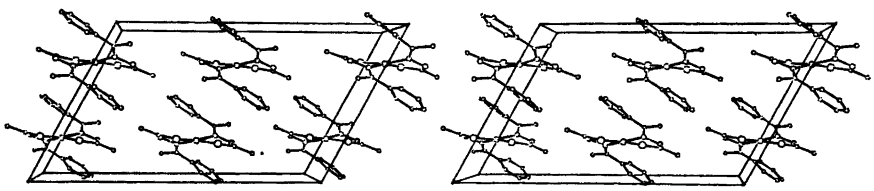

Fig. 4. An ORTEP stereo drawing of a full unit cell as viewed down the *b*-axis.

the electric vector is perpendicular to the two-fold axis.

Unfortunately, it is not possible from this single crystal structure analysis to explain why the molecular structure of bis(acetophenone thioacethydrazonato)nickel(II) approaches a *cis* configuration of the sulfur atoms and why the phenyl group does not enhance conjugation within the ligand. It is the hope, however, that structural determination of related complexes having other thiohydrazones as ligands may elucidate these problems.

Acknowledgements. The author is indebted to Mr. F. Hansen and Dr. K. J. Watson for performing the determination of the unit cell dimensions on the four circle diffractometer.

REFERENCES

1. Cavalca, L., Nardelli, M. and Fava, G. *Acta Crystallogr. 15* (1962) 1139.
2. Grønbæk, R. and Rasmussen, S. E. *Acta Chem. Scand. 16* (1962) 2325.
3. Hazell, R. G. *Acta Chem. Scand. 22* (1968) 2171.
4. Hazell, R. G. *Acta Chem. Scand. 22* (1968) 2809.
5. Hazell, R. G. *Acta Chem. Scand. 26* (1972) 1365.
6. Larsen, E., Trinderup, P., Olsen, B. and Watson, K. J. *Acta Chem. Scand. 24* (1970) 261.
7. Larsen, E. and Trinderup, P. *Unpublished results.*
8. Ablov, A. V. and Gerbeleu, N. V. *Russ. J. Inorg. Chem. 9* (1964) 46.
9. Mathew, M., Palenik, G. J. and Clark, G. R. *Inorg. Chem. 12* (1973) 446.
10. Johnson, C. K. *ORTEP*: A Fortran Ellipsoid Plot Program for Crystal Structure Illustrations. ORNL-3794 (Second Rev.) Report (1970).
11. Stewart, J. M. *et al. The X-Ray System 1972*, Technical Report TR-192, Computer Science Center; University of Maryland.
12. Cromer, D. T. and Mann, J. B. *Acta Crystallogr. A 24* (1968) 321.
13. Stewart, R. F., Davidson, E. R. and Simpson, W. T. *J. Chem. Phys. 42* (1965) 3175.
14. Cromer, D. T. *Acta Crystallogr. 18* (1965) 17.
15. Sato, T., Shiro, M. and Koyama, H. *J. Chem. Soc. B* (1968) 989.
16. Sato, T., Tsukuda, Y. and Koyama, H. *J. Chem. Soc. B* (1969) 125.
17. Pauling, L. *The Nature of the Chemical Bond*, 3rd Ed., Cornell University Press, Ithaca, N. Y. 1960.
18. Bondi, A. *J. Phys. Chem. 68* (1964) 441.

Received March 14, 1974.

Acta Chemica Scandinavica A 28 (1974) 787—796

Crystal and Molecular Structure of 3-Hydroxybiuret Potassium Salt (2:1), $KH(C_2H_4N_3O_3)_2$

INGRID KJØLLER LARSEN

The Royal Danish School of Pharmacy, Chemical Laboratory C, Universitetsparken 2, DK-2100 Copenhagen, Denmark

The structure of the 3-hydroxybiuret potassium salt (2:1) ($C_2H_4KN_3O_3$, $C_2H_5N_3O_3$) has been determined, using three-dimensional diffractometer-collected X-ray data. The salt crystallizes in the space group $P2_1/c$ with 4 formula units $C_4H_9KN_6O_6$ in the unit cell with the dimensions $a = 3.868(2)$, $b = 20.38(1)$, $c = 12.400(7)$ Å, $\beta = 90.38(7)°$. The structure was solved by the heavy-atom method and refined by full-matrix least-squares calculations to a conventional R of 0.032.

The crystals are built up of K^+ ions and $H(C_2H_4N_3O_3)_2^-$ ions. The two 3-hydroxybiuret residues are joined by a very short hydrogen bond (2.442(3) Å) between the hydroxyl oxygen atoms. In addition the anions are connected by several NH···O hydrogen bonds. Each potassium ion is coordinated to eight oxygen atoms. The K···O distances lie in the range 2.663–3.026 Å.

The structure determination of 3-hydroxybiuret, $H_2N-(C=O)-N(OH)-(C=O)-NH_2$, was undertaken as part of an X-ray study of organic hydroxylamine derivatives, which are inhibitors of DNA synthesis in several cell systems. 3-Hydroxybiuret (3-HB) and 1-hydroxybiuret (1-HB) were by Gale *et al.*[1] shown to inhibit DNA synthesis in an *in vitro* Ehrlich ascites tumor test system. The 3-HB used in these experiments was prepared by the method described by Exner,[2] but following the same method the present author obtained a compound with a different melting point (138–139 °C decomp.; Exner: 133 °C decomp.). The elementary analysis suggested the compound to be a 3-HB potassium salt (2:1), and this assumption was verified by the present structure determination. The *CA* name of the compound for the present collective-index period (1972–76) is 2-hydroxyimidodicarbonic diamide potassium salt (2:1). By treatment of the potassium salt with a strongly acidic ion-exchange resin a compound was obtained which is presumed to be 3-HB, but the melting point of 158–160 °C decomp. does still not agree with that reported by Exner. X-Ray structure determination of this compound and of 1-HB are in progress.

EXPERIMENTAL

The potassium acid salt of 3-HB was synthesized from hydroxyurea and potassium cyanate following the method described by Exner [2] for preparation of 3-HB. The yield was 48 % of a crystalline crude product. Recrystallization by precipitation with absolute ethanol from a saturated aqueous solution of the crude product yielded thin, colourless needles, m.p. 138–139 °C (decomp.). (Found: C 17.35; H 3.34; N 30.16. Calc. for $C_4H_9KN_6O_6$: C 17.40; H 3.28; N 30.20).

Table 1. Crystal data for the 3-HB potassium salt (2:1).

Mol. formula	$C_4H_9KN_6O_6$
Mol. weight	276.3
Melting point	138–139 °C (decomp.)
Space group	$P2_1/c$
a	3.868(2) Å
b	20.38(1) Å
c	12.400(7) Å
β	90.38(7)°
V	977.5 Å^3
Z	4
D_x	1.87 g/cm^3
D_m	1.85 g/cm^3
μMo$K\alpha$	5.78 cm^{-1}
Crystal size	0.10 × 0.12 × 0.50 mm^3
Rot. axis	a

Crystals suitable for X-ray work were obtained by diffusion at room temperature of absolute ethanol into a saturated solution of the salt in aqueous ethanol. Some crystal data of the compound are given in Table 1. The density was measured by flotation in a mixture of carbon tetrachloride and methyl iodide. The melting points were determined with a hot stage microscope (Mikroskop Heiztisch Ernst Leitz G.m.b.H., Wetzlar). The microanalysis was performed by Preben Hansen, Microanalytical Laboratory, University of Copenhagen.

The lattice parameters were calculated from a series of diffractometer-measured θ-values. The intensity data were collected with a NONIUS 3-circle automatic diffractometer by the moving crystal-stationary detector technique, using graphite monochromatized Mo$K\alpha$-radiation ($\lambda = 0.71069$ Å). The scan speed was 0.6°/min and each reflexion was scanned over a range of 1.2°. The background was measured on each side of the reflexion for half the scanning time. The background count was in the data reduction set equal to twice the lowest count obtained in order to avoid weak satellite peaks, observed on one side of the strong reflexions. Intensities of reflexions were measured in the range $2.5° < \theta < 25°$, and the intensity of a reference reflexion was measured for every 25 reflexions. Thus 1663 independent reflexions were measured. A reflexion was considered unobserved and was omitted when the intensity observed was less than 2.5 times its estimated standard deviation. The number of observed reflexions was reduced to 1446. These data were corrected for Lorentz and polarization effects, but no corrections for absorption or extinction were made.

STRUCTURE DETERMINATION

The structure was solved from the three-dimensional Patterson map by the heavy-atom method. The electron density map, based on the position of the potassium ion only, revealed the positions of all 16 non-hydrogen atoms of the two 3-HB residues in the asymmetric unit. The conventional R-value was 0.31 at this stage. Three cycles of full-matrix least-squares refinement, in which positional as well as individual atomic, isotropic thermal parameters were varied, reduced the R-value to 0.074.

The difference Fourier map, calculated at this stage of the refinement, revealed the 8 hydrogen atoms of the NH_2-groups unambiguously (*cf.* Fig. 1). The 9th hydrogen atom is situated between the hydroxyl oxygen atoms O(3) and O(3′), apparently either symmetrically or statistically disordered.

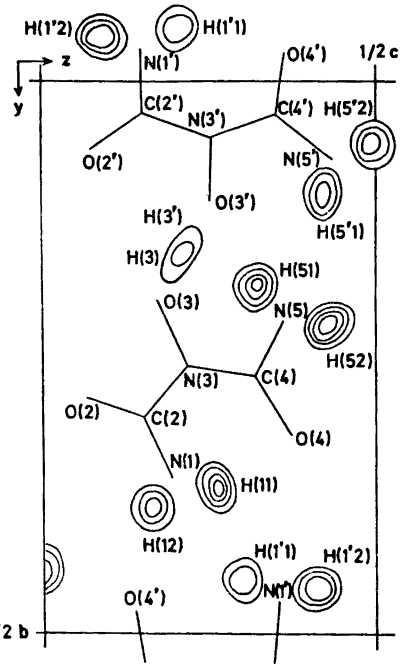

Fig. 1. Projection along the a-axis of sections of the difference Fourier map. Contours are at intervals of about 0.1 e Å^{-3}.

In the following refinement this hydrogen atom was treated as 2 half hydrogen atoms, H(3) and H(3′), *i.e.* each with a population parameter of 0.5 and situated in either end of the elongated peak, about 0.8 Å apart.

Two cycles of anisotropic least-squares refinement with all H-atom parameters fixed, reduced the R-value to 0.042. In the remaining two cycles of refinement the positional parameters of the H-atoms were also varied, but the isotropic thermal parameters of 2.0 Å^2 were still fixed. The final R-value was 0.032. Refinement of the population parameters of H(3) and H(3′) was also carried out, but the shifts were not significant, and these parameters were therefore fixed on 0.5.

In another attempt of refinement the hydrogen atom H(3) was included with a position midway between the oxygen atoms O(3) and O(3′) and allowed to vibrate isotropically. Only these four parameters of H(3) and the scale factor were refined, and at convergence ($R = 0.031$) the hydrogen atom had moved toward the oxygen atom O(3′). The dimensions corre-

Table 2. Observed and calculated structure factors. The columns are l, $10 \times F_o$ and $10 \times F_c$.

	0,0,L		8	318	-317	3	67	-60	-10	290	283	13	102	-109		1,9,L			
			9	28	22	4	180	-190	-12	272	-276	-13	52	56					
2	412	-448	10	81	76	5	126	-131	-12	209	205	14	107	114	0	336	-337		
4	294	-286	11	208	-206	6	110	-109	14	100	91	-14	113	-112	1	155	-136		
6	439	457	12	132	-133	7	74	-79	-14	145	140				-1	353	342		
8	128	139	13	30	24	8	192	-189					1,5,L		2	450	-443		
10	592	-598	14	116	-98	9	36	33		1,1,L					-2	410	-411		
12	44	35				10	170	-169				0	1350	1376	3	366	364		
14	123	126		0,8,L		11	36	15	0	541	520	1	112	108	4	118	-125		
									1	713	717	-1	164	161	-4	180	170		
	0,1,L		0	422	-416		0,16,L		-1	524	-520	2	314	307	-5	170	161		
			1	203	181				-2	117	-120	-2	239	229	6	103	96		
2	316	-315	2	436	-425	0	266	-262	-2	1409	-1479	3	226	-219	-6	253	-266		
3	300	303	3	208	-217	1	125	121	-3	330	-327	-3	194	188	7	53	52		
4	139	-136	4	337	334	2	253	-247	4	571	-576	4	612	595	-7	277	-278		
5	165	159	5	519	-514	3	107	-109	-4	426	-428	-4	528	521	8	59	-58		
6	814	-812	6	129	121	4	30	-22	5	33	13	5	167	-160	9	152	150		
7	97	96	7	420	-414	5	111	113	-5	117	119	-5	283	275	-9	320	-325		
8	216	-225	8	56	57	6	327	-328	6	39	37	6	31	-28	10	64	-66		
10	107	-105	9	146	-141	7	157	-150	-6	210	-215	-6	107	113	-10	100	90		
12	99	-93	10	205	209	8	158	-154	7	213	-207	-7	136	-134	11	320	323		
14	168	-163	11	187	-179	9	132	135	-8	283	-279	8	65	-64	-11	222	-230		
			12	97	-86	10	115	117	9	213	-213	-8	77	-77	12	124	128		
	0,2,L		13	164	-163	11	68	-72	-10	99	-105	9	120	-122	-12	121	-111		
									11	337	-336	-9	155	-151	13	65	66		
1	329	-334		0,9,L			0,17,L		-11	431	436	10	141	-144					
2	50	-45							13	118	-114	11	107	-116		1,10,L			
3	110	-119	1	769	-783	1	27	6	-13	138	136	-11	109	104					
4	200	-206	2	115	-109	2	79	-78	14	56	59	12	47	-45	0	45	35		
5	852	-855	3	195	-207	3	208	-210	-14	137	140	-12	128	128	1	164	176		
6	361	-359	4	123	-117	4	337	335				13	90	93	-1	37	38		
7	137	-143	6	166	-164	5	148	-149		1,2,L					2	125	127		
8	201	188	7	135	-144	6	156	155					1,6,L		-2	93	-87		
9	328	-331	8	82	70	7	53	-45	0	464	448				3	32	29		
10	217	-215	10	335	-339	8	83	80	1	254	-274	0	239	224	-3	305	303		
11	63	61	11	190	189	9	63	-71	-1	298	-293	1	414	407	-4	49	-40		
12	153	162	12	120	-120	10	112	112	2	212	206	-1	586	576	5	31	-24		
13	268	-269							-2	188	187	2	389	-378	-5	240	253		
14	115	106		0,10,L			0,18,L		3	889	-905	-2	127	113	6	283	291		
									-3	601	-598	3	179	-181	-6	56	-47		
	0,3,L		0	438	-439	0	105	-97	4	113	110	-3	61	61	7	75	-80		
			1	236	230	1	211	211	-4	589	-579	4	328	-332	-7	90	96		
1	493	-490	2	278	-292	2	190	186	-5	631	-627	-4	112	118	8	334	339		
2	73	-71	3	244	242	3	46	-38	6	160	160	5	116	-119	-8	390	-394		
3	398	-425	4	587	-576	4	342	336	-6	119	112	-5	211	217	-9	118	-124		
4	85	79	5	324	323	5	68	-69	7	309	-310	6	335	-334	10	179	169		
5	233	-240	7	302	317	6	321	-317	-7	155	156	-6	82	87	-11	73	70		
6	186	179	8	83	84	7	86	86	8	120	117	7	98	107	12	145	156		
7	413	-420	9	166	-168	8	279	271	-8	117	-113	-7	132	133	-12	247	-245		
8	97	-89	10	172	-162				9	99	94	-8	257	253	-13	68	-70		
9	172	-167	12	72	64		0,19,L		-9	282	-287	9	207	-213					
10	63	-59							10	82	-86	-9	52	50		1,11,L			
11	42	22		0,11,L		1	116	114	-10	180	-177	10	518	-525					
12	134	-141				2	145	152	-11	41	38	-10	211	214	0	140	136		
13	113	112	1	105	99	3	240	237	12	47	48	11	120	118	1	166	-177		
			2	53	-41	4	168	-176	-12	189	-194	-11	101	-104	-1	93	89		
	0,4,L		3	273	-271	5	170	166	13	143	147	12	69	72	2	307	312		
			4	183	184	6	72	69	-13	45	-37	-12	136	131	-2	156	159		
0	577	609	5	42	-37	7	44	-37	14	107	102				3	57	-56		
1	605	-633	6	271	272	8	89	87	-14	134	135		1,7,L		-3	89	87		
2	445	-473	7	34	-2	9	86	84							4	130	132		
3	141	-137	8	35	36	10	91	28		1,3,L		0	286	270	-4	47	-32		
4	952	-983	9	34	34							1	394	-382	5	89	-88		
5	464	-441	10	292	285		0,20,L		0	118	108	-1	139	-138	-5	115	-112		
6	235	235	11	86	86				1	429	436	2	227	-233	6	413	421		
7	357	363	12	188	188	0	115	111	-1	748	-750	-2	233	-242	-6	526	527		
8	73	-69	13	31	-26	1	216	-223	2	27	14	3	544	-529	7	342	355		
9	184	186				2	34	9	-2	698	702	-3	205	203	-7	62	-59		
10	229	-227		0,12,L		4	342	343	3	760	757	4	363	-363	8	155	202		
11	342	342				5	154	-146	-3	172	-175	-4	531	-534	-8	162	164		
12	32	-21	0	304	-287	6	39	-26	4	206	-204	5	537	-528	9	66	-68		
13	216	215	2	322	323	7	34	-39	-4	99	83	-5	597	594	-9	145	153		
14	235	233	3	609	596	8	36	25	5	129	140	6	67	-70	10	57	-57		
			4	348	340				-5	161	-166	7	202	-211	11	56	66		
	0,5,L		5	95	94		0,21,L		6	373	-357	-7	238	242	-11	154	-160		
			7	42	-31				-6	467	-462	8	147	146	12	139	-145		
1	25	-13	8	32	-30	1	103	97	7	206	198	-8	46	43	-12	137	132		
2	230	251	9	325	322	2	251	-256	-7	95	93	9	36	-31					
3	154	-146	10	271	274	3	45	-36	8	164	-166	-9	230	239		1,12,L			
4	70	-60	11	78	69	5	87	-90	-8	30	7	10	200	-199					
5	199	200	12	129	-125	6	79	-79	9	564	564	-10	259	-268	0	29	19		
6	320	331				7	45	53	-9	373	-376	11	55	59	1	546	546		
7	100	96		0,13,L					10	177	-188	-11	44	36	-1	40	46		
8	410	413					0,22,L		-10	198	-194	12	105	108	2	213	-219		
10	114	118	1	146	153				11	132	139	-12	124	127	-2	150	156		
11	166	168	2	163	158	0	325	-323	-11	139	-140	13	152	-156	3	67	67		
12	302	304	3	425	430	1	34	26	12	211	215	-13	110	108	-3	93	99		
13	69	-75	4	52	56	2	136	-137	13	77	76				4	30	21		
14	161	152	5	190	186	3	36	-31	14	139	136		1,8,L		-4	205	219		
			6	48	42	4	39	-36	-14	46	30				5	111	112		
	0,6,L		7	132	133	5	235	-236				0	44	-35	-5	167	176		
			8	65	60	6	90	-84		1,4,L			222	-223	6	164	-167		
0	392	396	9	35	30							-1	666	-664	-6	91	-102		
1	93	-99	10	169	-170		0,23,L		0	984	981	2	143	134	7	76	76		
2	383	399	11	45	45				-1	661	-642	-2	241	235	-7	298	299		
3	149	155				1	179	-177	2	280	-272	3	165	152	8	325	-337		
4	312	-301		0,14,L		2	48	51	-2	724	-713	-3	817	-805	-8	150	151		
5	165	167				3	100	-107	3	765	768	4	127	-123	9	165	176		
6	793	781	0	31	26				-3	529	518	-4	226	-212	10	69	-73		
8	335	331	1	270	263		0,24,L		4	77	-61	5	463	-474	-10	45	37		
9	228	235	2	487	484				-4	250	-243	-5	96	-94	11	90	-97		
10	39	-30	3	191	-170	0	203	-205	5	83	84	6	107	98	12	64	-64		
11	195	195	4	139	143				-5	263	266	7	90	-77	-12	97	100		
12	128	-122	5	64	-69		1,0,L		6	527	523	-7	294	-292					
14	58	-56	6	39	-35				-6	44	-60	8	135	-139		1,13,L			
			7	137	-132	0	123	-117	7	44	-40	-8	138	136					
	0,7,L		8	274	-284	-2	273	-265	-7	64	-60	9	248	260	0	82	-70		
			9	202	-200	-2	170	169	8	313	314	-9	186	-190	1	360	-348		
1	602	614	10	74	78	4	1360	-1390	-8	50	49	10	103	111	-1	137	138		
2	116	-123	11	245	-243	-4	495	-474	9	194	201	-10	275	-267	2	325	-324		
3	639	647				6	419	402	10	121	141	11	78	-83	-2	65	61		
4	141	-148		0,15,L		-6	670	646	-10	348	-348	12	48	-45	3	91	82		
5	69	76				8	160	-166	11	201	-199	-12	50	55	4	139	-138		
6	156	-151	1	174	-175	-8	485	463	-11	198	194	13	52	-52					
7	139	143	2	146	-144	10	339	-344	12	112	107	-13	176	179					

Table 2. Continued.

	1,13,L		-7	112	113	-2	106	-101	-8	313	-307	-4	182	176	-7	92	89
			8	134	-136	3	362	357	9	30	35	6	148	137	8	138	-139
-4	115	-120	10	51	99	-3	376	-373	-9	166	-167	6	341	-338	-8	142	143
5	32	17				-4	179	160	10	58	57	-6	124	119			
-5	81	20		1,19,L		5	271	271	-10	38	26	7	64	-61		2,18,L	
6	164	165				-5	135	-129	11	365	-370	-7	103	-106			
-6	131	135	-1	75	-79	6	207	210	-11	390	381	8	164	-162	1	106	-101
7	463	-476	2	131	130	-6	227	224	12	154	153	-8	36	33	-1	66	63
-7	136	137	-2	202	207	7	562	560	-12	110	-108	9	107	-106	2	56	-54
9	216	-222	3	78	-81	-7	313	-311				10	270	-258	-2	118	-108
-9	240	248	-3	180	187	8	84	79		2,7,L		-10	155	156	3	109	-110
10	42	56	4	121	119	-8	203	213							-3	73	68
-10	74	79	-4	42	29	9	60	63	0	45	44		2,12,L		-4	69	-71
11	51	-53	5	69	-71	-9	105	-102	-1	169	-177				5	79	-81
-11	157	158	6	79	-79	10	126	127	2	91	86	0	384	-388	-6	38	-21
12	49	-45	-6	74	-73	-10	191	184	-2	170	170	1	54	-48	-7	76	74
-12	154	-150	7	218	-220	11	41	28	3	154	-141	-1	35	-3			
			-7	135	130	-11	75	-74	-3	436	-430	2	206	-204		2,19,L	
	1,14,L		-8	47	-55	12	90	-85	4	101	94	-2	79	-72			
						-12	89	-92	-4	168	-168	3	186	-187	0	55	-58
0	182	-184		1,20,L		13	88	85	5	146	-136	-3	68	-66	1	232	-234
1	159	-169				-13	71	-66	-5	424	-422	-4	219	-207	-1	152	-146
-1	477	-481	0	244	-250				6	312	311	5	596	-591	3	160	-155
2	62	-72	1	65	-62		2,3,L		-6	85	-79	-5	467	461	-3	164	-165
-2	145	-147	-1	170	-170				-7	43	-51	-6	79	-76	-4	47	29
3	79	-81	2	165	170	0	153	-141	8	155	150	-5	40	-30	5	58	-54
-3	254	-259	3	134	-136	1	764	738	-8	143	-142	9	35	-25	-5	137	-137
4	72	75	-3	46	48	-1	581	571	9	56	-56	10	91	64			
-4	168	160	4	54	-54	2	43	43	-9	257	-254	11	138	-121		2,20,L	
5	328	-337	-4	189	192	3	76	75	10	36	-38	-11	60	57			
-5	43	46	5	36	-22	-3	85	-86	-10	78	79				0	135	-132
6	359	-369	-5	132	-128	4	292	288	11	57	-44		2,13,L		-2	115	-114
-6	106	110	6	149	-156	-4	274	-272	-11	66	-59				3	208	202
7	73	83	7	125	-125	5	32	15	12	82	74	0	104	103	-3	71	-73
-7	177	-177	-7	90	-85	-5	514	506	-12	143	-149	1	353	-342	4	144	-140
8	124	132				6	90	82				2	65	-65	-4	89	-92
-8	149	152		1,21,L		-6	49	34		2,8,L		3	254	-257	5	171	167
9	56	52				7	166	158				-3	261	-258	-5	156	-156
-9	98	-102	0	110	-106	-7	323	324	0	435	420	-4	57	53			
10	42	-53	1	51	-47	8	204	208	1	569	556	-5	368	-371		2,21,L	
-10	49	55	2	181	-182	9	92	-90	-1	383	-365	6	185	186			
			-2	112	-117	10	34	-23	2	101	-102	-6	203	-210	1	62	-56
	1,15,L		3	217	-213	-10	60	63	-2	42	44	7	104	-107	-1	66	73
			-3	48	-45	11	110	-106	3	246	242	-7	41	34	2	134	133
0	526	-533	-4	89	-82	-12	86	-82	-3	275	267	-8	87	87			
1	237	243	5	100	96	13	202	-199	-4	127	-124	-9	85	-81		3,0,L	
-1	49	-46	-5	147	-139	-13	88	87	5	47	-46	10	59	-64			
-2	193	-200	-6	197	-196				6	220	-216	-10	67	-60	0	48	-46
-3	100	-103					2,4,L		-6	65	-67				2	314	313
4	138	-139		1,22,L					7	161	163		2,14,L		-2	203	204
-4	226	-230				0	126	123	-8	38	43				4	272	274
5	299	295	-1	71	-72	1	80	75	9	416	407	8	39	32	-4	54	46
-5	232	-221	-2	84	83	-1	450	-432	-9	300	-288	1	34	22	6	111	-106
6	60	57	3	84	-73	2	537	527	10	49	-49	-1	137	129	8	394	393
-6	130	-137	-3	119	-113	-2	754	734	-10	202	-196	2	55	-50	-8	134	-136
7	166	169	4	223	221	3	307	301	11	65	71	-2	264	-261	10	229	226
-7	131	-136	-4	41	-49	-3	38	-33	-11	153	-145	3	230	231	-10	150	-155
8	48	-49	-5	138	-139	4	73	-75	12	61	65	-3	62	-59			
-8	168	-171				-4	202	-201	-12	104	96	4	168	-169		3,1,L	
9	87	-91		1,23,L		5	352	-349				-4	227	-219			
-9	47	52				-5	94	91		2,9,L		5	64	65	0	105	-109
-10	46	38	0	60	65	6	102	97				-5	76	71	-1	125	118
-11	59	-54	2	70	63	-6	325	321	0	39	42	6	143	145	2	298	309
			-2	74	73	7	466	-469	1	207	209	-6	65	59	-2	154	148
	1,16,L		3	47	47	-7	83	83	-1	123	115	7	104	105	3	120	123
						8	46	45	2	189	182	-7	85	-78	-3	83	77
0	97	-102		2,0,L		-8	119	120	3	95	91	8	40	-36	4	97	98
1	257	-264				-9	78	74	-3	338	334	-8	246	242	-4	238	234
-1	184	183	0	467	-455	10	133	-135	4	204	203	-9	173	-169	5	71	66
2	224	231	2	375	-366	11	193	-194	-4	130	-125	10	45	29	-5	125	124
-2	33	32	-2	551	-547	-11	178	181	5	183	179				6	69	69
3	70	67	4	120	-118	12	166	-165	-5	137	130		2,15,L		-6	238	239
-3	171	-168	-4	452	-440	-13	203	202	6	197	190				7	94	96
4	273	289	6	101	104				7	149	-145	0	104	105	-7	56	-59
-4	99	100	-6	269	-266		2,5,L		-7	180	180	2	72	65	8	62	61
5	33	-31	8	160	160				8	48	45	3	163	157	-8	62	65
-5	105	107	-8	76	-68	1	299	-277	-8	120	-116	-3	255	257	9	107	107
6	197	199	10	86	-73	-1	496	-499	9	93	90	4	236	228	-9	82	-82
-6	351	-358	-10	89	-89	-2	176	-170	-9	109	108	-4	75	77	10	77	-80
7	47	-51	12	45	29	3	244	234	10	196	197	5	61	-64	-10	143	145
-8	219	-224	-12	33	-23	-3	151	152	-10	185	-180	-5	96	93	11	199	205
10	183	183				4	498	-489	11	68	-65	6	84	-84	-11	175	-177
				2,1,L		-4	170	166	-11	96	94	7	65	72			
	1,17,L					5	110	-106				8	168	164		3,2,L	
			0	320	306	-5	206	200		2,10,L		-8	193	-192			
0	366	372	1	328	-320	6	130	-127				9	51	-49	0	153	152
1	170	-166	-1	475	-458	-6	215	214	0	641	612	-9	143	133	1	168	161
-1	114	119	2	86	74	7	88	-89	1	34	22				-1	200	202
2	74	76	-2	85	75	-7	264	-264	-1	141	-137		2,16,L		2	195	-192
-2	261	267	3	63	56	8	404	-397	2	201	202				3	81	75
3	132	129	-3	146	-140	-8	156	161	-2	163	163	0	113	-109	-3	349	354
-4	133	134	4	97	82	9	152	139	3	46	-39	1	277	278	4	155	-155
5	331	334	-4	34	29	10	115	-108	-3	203	-195	-1	232	-232	5	62	61
-5	369	-380	5	325	-306	-10	169	167	4	212	214	2	101	101	-5	300	303
6	77	82	-5	145	133	11	81	84	-4	442	431	-2	229	233	6	91	93
-6	101	105	6	379	372	-11	167	165	5	337	-336	4	135	137	-6	102	-112
8	81	-81	-6	49	-35	12	141	-142	-5	370	359	-4	218	217	7	99	-96
-8	47	37	-7	201	-199	-12	210	212	6	70	-72	5	110	-107	-7	151	156
9	89	89	8	65	57				-6	63	-63	6	153	150	8	216	-217
10	55	-42	-8	213	-215		2,6,L		-7	60	50	-6	237	232	-8	38	35
			9	163	156				8	54	58	7	133	131	-9	74	72
	1,18,L		-9	142	-139	0	113	-110	-8	182	162	-8	132	132	10	147	-143
			10	211	207	1	481	461	9	88	90	-9	72	-68	11	123	-116
0	171	-172	-10	147	-146	-1	294	-284	-9	84	-90				-11	123	127
1	321	332	12	146	138	2	288	-279	10	268	-274		2,17,L				
-1	127	127	-12	100	-97	-2	313	-302	-10	42	-37					3,3,L	
-2	58	58	13	53	61	3	265	-253				0	50	-50			
3	201	213	-13	47	48	-3	426	-415		2,11,L		1	41	-45	0	71	-71
4	65	65				4	245	-241				-1	301	303	1	208	-209
-4	99	-107		2,2,L		-4	58	-102	1	230	225	2	199	-203	-1	72	-74
5	39	-43				5	52	51	-1	37	-40	-3	103	102	-2	40	39
-5	201	202	0	30	35	-5	32	9	2	254	-246	4	138	-134	3	343	-359
6	36	-39	1	507	500	-6	387	-378	3	57	60	5	244	243	-3	91	-90
-6	136	140	-1	33	34	-7	158	169	-3	217	217	-5	58	57	-4	143	142
7	188	200	2	213	-207	8	152	-154	4	249	-245	7	43	-36			

Table 2. Continued.

	3,3,L		-6	93	-99		3,10,L		-7	98	-93	-6	75	75	2	149	150
			7	108	99										-2	137	141
5	325	-323	-7	224	-227	0	302	-298		3,14,L			4,1,L		-3	41	42
-5	122	124	-8	51	-47	1	165	167							4	264	252
6	102	103	10	163	165	-1	44	-56	0	103	98	0	207	-210	-4	153	164
7	132	-130	-10	131	-132	-2	66	-80	1	277	288	1	108	112	5	63	-58
-7	153	152				3	88	-93	-1	169	168	-1	68	62	-5	49	50
8	65	-66		3,7,L		-3	195	-205	2	41	19	2	142	-146	-6	110	-116
-8	121	119				4	326	-327	-3	41	34	-3	135	140			
9	119	-123	0	43	-46	5	103	-100	5	37	20	4	48	43		4,6,L	
-9	70	72	1	325	326	6	57	-55	-5	139	144	-4	72	64			
10	45	48	2	110	112	-6	132	131	6	89	83	5	69	67	0	106	105
-10	135	134	-2	40	22	8	239	-232	-6	64	-62	6	399	-407	1	68	66
-11	147	146	3	96	98	-8	65	64	-7	209	212	7	110	-119	-2	174	172
			-3	178	-182	9	160	157				-7	150	155	-3	50	51
	3,4,L		4	108	112	-9	164	-172		3,15,L					5	79	75
			-4	399	403								4,2,L		6	72	74
-1	295	-285	5	243	238		3,11,L		0	143	138				-6	251	261
2	316	-322	-5	58	56				1	111	-110	1	196	-204			
-2	146	-149	6	44	-34	0	164	-165	2	126	129	-1	124	-128		4,7,L	
3	75	-70	7	198	193	1	56	-54	3	178	-176	2	80	-85			
-3	362	-368	-7	75	-77	-1	66	-69	4	112	106	3	129	-135	0	225	-235
4	101	-96	8	34	-26	-2	295	-287	-4	194	192	-3	58	-54	1	67	67
-4	83	85	9	131	134	-3	65	-65	5	64	-60	4	64	-57	-1	166	152
5	236	-235	-9	138	-144	4	59	-54	-5	71	72	-4	68	-67	-2	52	-59
6	318	-313	10	44	-32	5	86	-90	6	36	-25	5	251	-262	3	51	57
7	174	173	-10	200	205	-5	66	69	-6	72	69	7	77	-76	-3	68	70
-8	152	157				6	105	-108							-4	175	169
9	186	187		3,8,L		-6	271	-273		3,16,L			4,3,L		-5	180	185
-9	170	-171				7	65	-64									
10	131	-131	1	231	223	-7	72	78	0	77	-76	0	66	63		4,8,L	
-10	97	93	-1	105	100	8	45	35	1	70	76	1	58	-59			
			-2	162	166	-8	291	-286	2	129	-127	-1	131	-136	1	65	-66
	3,5,L		3	280	282				3	60	58	2	78	-82	-1	162	-160
			4	55	-48		3,12,L		4	48	-50	-2	92	-95	2	42	-30
0	492	-480	-4	272	-281				-4	36	38	3	101	-98	-2	132	-131
2	162	-160	5	152	-150	0	166	169	5	100	-104	-3	166	-175	3	166	-163
-2	256	-254	-5	424	435	1	111	114	-5	58	58	4	56	-59	-4	141	149
3	253	256	6	170	166	-1	463	-471				-4	76	79			
-3	119	117	-6	109	108	2	72	78		3,17,L		5	100	108		4,9,L	
4	62	56	7	113	111	-2	72	75				-5	195	-203			
-4	334	-335	-7	104	110	4	198	201	0	122	-120	-6	70	-72	0	78	-84
5	142	138	9	43	35	-4	99	-108	1	99	-99	-7	167	-173	-1	139	-140
-5	177	-175	-9	64	69	5	116	-120	-1	91	-95				2	183	-187
-6	71	-68	-10	87	77	-5	144	-142	2	70	-73		4,4,L		-2	43	-38
7	121	-119				6	169	166	-2	130	-133				-3	48	-44
8	100	101		3,9,L		-7	45	41	3	45	-54	0	78	-81			
-8	177	-178				-7	173	-178	-3	65	57	1	61	64		4,10,L	
10	219	219	0	48	43	8	50	46	4	69	-63	-1	170	176			
			-1	95	-97	-8	105	-100	-4	75	-68	-2	90	-92	0	97	-100
	3,6,L		2	112	112							-3	69	71	1	73	70
			-2	329	331		3,13,L			3,18,L		4	75	-73	-1	80	72
0	81	70	4	121	116							-4	196	-198	2	85	-138
1	128	-117	-4	141	135	1	170	167	0	121	125	5	81	87	-2	85	-89
-1	75	-76	5	68	-73	2	34	-31	1	130	-125	-5	85	92	3	63	70
2	260	257	-5	174	-172	-2	257	254	-1	124	-131	6	78	80	-4	242	-246
3	36	21	6	110	-112	3	96	93				-6	105	-120			
-3	104	-107	7	172	-177	-3	115	118		4,0,L						4,11,L	
4	242	237	8	115	-114	4	81	84					4,5,L				
-4	60	63	-8	83	79	-4	37	36	0	396	423				0	83	-91
5	274	-267	9	205	-207	5	160	155	2	38	45	0	105	107	2	244	257
-5	156	158	-9	144	146	6	107	-103	-2	117	113	1	68	-64	-2	87	94
6	221	222				7	189	192	-4	148	148	-1	43	31			

sponding to this refinement are also given in the description of the structure.

The above refinements were based on F, minimizing the function $\sum w(|F_o|-|F_c|)^2$. The weights for all observed reflexions were unity. The weight analysis, *i.e.* the plot of the $\langle w(|F_o|-|F_c|)^2\rangle$ values as a function of F_o and $\sin\theta$ for groups of reflexions, indicated that this choice was satisfactory. The atomic scattering factors for K^+ and neutral O, N, C, and H, respectively, were taken from *International Tables for X-Ray Crystallography*.[3] Observed and calculated structure factors are listed in Table 2. Table 3 lists the fractional coordinates of the atoms, and Table 4 the thermal parameters of the non-hydrogen atoms.

The input tapes for the diffractometer were produced on a GIER computer using a program written by Sørensen.[4] The rest of the calculations were performed on the IBM 360/75 computer at NEUCC, Lundtofte, Denmark, using a local version of the N.R.C. 2A Picker data reduction program,[5] and *The X-Ray System*.[6] The drawings were prepared by *ORTEP*.[7]

DISCUSSION

The structure of the 3-HB potassium salt (2:1) is built up of K^+ ions and $H(C_2H_4N_3O_3)_2^-$ ions. As illustrated in Fig. 2 the potassium ions form slightly puckered layers, which are perpendicular to the c-axis and nearly at $z=0$ and $\frac{1}{2}$. The 3-HB anions are situated between these layers. The anion is composed of the two crystallographically nonequivalent 3-HB residues, which are joined by a short hydrogen bond between the hydroxyl oxygen atoms, O(3) and O(3′), and are linked to the metal ions by ionic interactions. In addition the anions are linked to a three-dimensional network by several NH···O hydrogen bonds. The lengths of these bonds are given in Fig. 2, and the angles concerning the hydrogen bonding system are given in Table 7.

Table 3. Fractional atomic coordinates.

	x	*y*	*z*
K^+	0.2825(1)	0.1554(1)	0.0242(1)
N(1)	0.4725(7)	0.3586(1)	0.1933(2)
C(2)	0.5465(7)	0.3006(1)	0.1491(2)
O(2)	0.4649(6)	0.2852(1)	0.0571(1)
N(3)	0.7314(6)	0.2564(1)	0.2146(1)
O(3)	0.8180(5)	0.1970(1)	0.1667(1)
C(4)	0.8479(7)	0.2660(1)	0.3193(2)
O(4)	0.7810(5)	0.3168(1)	0.3709(1)
N(5)	1.0356(6)	0.2167(1)	0.3594(2)
N(1′)	0.9760(7)	−0.0274(1)	0.1482(2)
C(2′)	0.8047(6)	0.0298(1)	0.1502(2)
O(2′)	0.7428(5)	0.0618(1)	0.0683(1)
N(3′)	0.6879(5)	0.0520(1)	0.2504(1)
O(3′)	0.4831(5)	0.1083(1)	0.2475(1)
C(4′)	0.7963(7)	0.0300(1)	0.3509(2)
O(4′)	0.9568(5)	−0.0224(1)	0.3610(1)
N(5′)	0.7118(7)	0.0680(1)	0.4339(2)
H(11)	0.517(10)	0.366(1)	0.262(3)
H(12)	0.345(10)	0.386(1)	0.158(3)
H(3)	0.717(22)	0.166(4)	0.198(6)
H(51)	1.078(10)	0.182(2)	0.317(3)
H(52)	1.113(09)	0.217(1)	0.430(3)
H(1′1)	1.036(10)	−0.044(1)	0.208(3)
H(1′2)	1.063(10)	−0.038(1)	0.087(3)
H(3′)	0.574(24)	0.140(4)	0.219(7)
H(5′1)	0.604(10)	0.107(2)	0.420(3)
H(5′2)	0.795(10)	0.057(1)	0.497(3)

The 3-HB anions. Fig. 3 shows the geometry of the anion together with the bond lengths and angles. No significant differences in the dimensions of the two non-equivalent 3-HB residues were found, and in addition the bond lengths and angles are in agreement with literature values for comparable molecules, *e.g.* biuret,[8-9] and hydroxyurea.[10]

An analysis of planarity of the 3-HB residues was carried out by calculation of the best plane through the non-hydrogen atoms of each residue and in addition through the N, C, and O atoms of each half of the residues (*cf.* Table 5). The analysis clearly shows that the atoms defining plane 1 is more coplanar than the atoms defining plane 2. In residue 1 there is a twist of only 3.4° between the two $H_2N-(C=O)-N-$ moieties; the corresponding angle of residue 2 is 13.2°. Both residues have adapted the conformation that gives rise to an *intra*molecular NH···O hydrogen bond (*cf.* Fig. 2). The same conformation was found in the biuret molecule [8] and the perdeuterated biuret molecule,[9] where the length of the *intra*molecular hydrogen bond was found to be 2.72 Å and the twisting angle 6.3°.

The environment of the potassium ion. The potassium ion has eight oxygen neighbours belonging to six different 3-HB residues, with K−O distances in the range 2.663−3.026 Å (*cf.* Fig. 4). These values are in good agreement

Table 4. Thermal parameters for the non-hydrogen atoms. $T_i = \exp[-1/4\ (B_{11}h^2a^{*2} + \cdots + 2B_{23}klb^*c^*)]$.

	B_{11}	B_{22}	B_{33}	B_{12}	B_{13}	B_{23}
K^+	1.62(02)	2.12(02)	1.81(03)	0.19(02)	−0.07(02)	0.09(02)
N(1)	3.56(11)	1.95(09)	2.56(06)	0.65(10)	−0.44(10)	−0.14(09)
C(2)	1.71(11)	1.79(10)	1.76(11)	−0.22(06)	0.12(09)	0.09(09)
O(2)	3.75(11)	2.71(10)	1.91(09)	0.21(08)	−0.84(08)	−0.10(07)
N(3)	1.95(10)	1.51(09)	1.48(09)	0.13(08)	−0.03(07)	−0.35(07)
O(3)	2.55(09)	1.77(08)	1.86(08)	0.44(07)	0.28(07)	−0.38(07)
C(4)	1.58(11)	2.00(12)	1.72(11)	−0.59(10)	0.20(09)	−0.01(07)
O(4)	2.81(09)	2.15(09)	1.81(08)	−0.08(07)	−0.13(07)	−0.60(07)
N(5)	2.63(12)	2.37(11)	1.95(10)	0.25(09)	−0.47(09)	−0.02(09)
N(1′)	3.28(09)	2.01(11)	1.89(10)	0.89(10)	0.27(09)	0.08(09)
C(2′)	1.60(11)	1.69(11)	1.88(11)	−0.18(09)	−0.07(09)	−0.17(09)
O(2′)	2.89(09)	2.07(08)	1.52(08)	0.50(07)	0.02(07)	0.27(06)
N(3′)	1.82(10)	1.58(09)	1.69(09)	0.33(08)	0.05(08)	0.22(07)
O(3′)	2.15(09)	1.94(09)	2.15(09)	0.70(07)	0.29(07)	0.13(07)
C(4′)	1.77(11)	1.80(12)	1.86(11)	−0.30(09)	0.00(08)	0.13(09)
O(4′)	3.17(10)	1.98(09)	2.03(08)	0.44(08)	−0.29(07)	0.20(07)
N(5′)	3.44(13)	2.62(12)	1.72(10)	0.68(10)	−0.04(09)	−0.10(09)

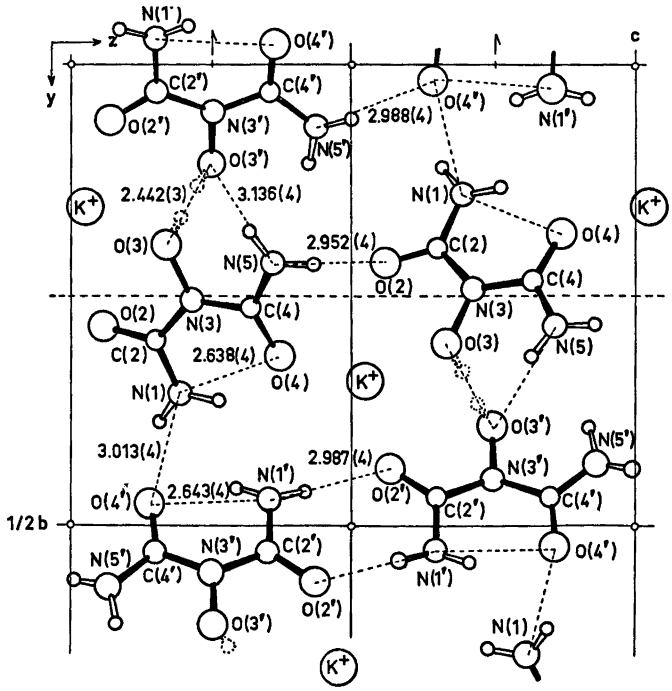

Fig. 2. The structure viewed along the *a*-axis.

Table 5. Least-squares planes. The equations of the planes can be expressed as $Px+Qy+Rz=S$ in direct space.

	Plane 1	Plane 2	Plane 3	Plane 4	Plane 5	Plane 6
P	3.304	3.253	3.343	3.227	3.326	3.337
Q	8.054	11.019	7.584	8.706	10.059	10.099
R	−4.258	0.083	−4.270	−4.391	1.546	−1.314
S	3.591	2.939	3.472	3.650	3.201	2.494

Distances in Å of the atoms from the planes.

Plane 1		Plane 2		Plane 3		Plane 4		Plane 5		Plane 6	
N(1)	0.03	N(1′)	−0.05	N(1)	0.001	N(3)	0.000	N(1′)	−0.003	N(3′)	−0.002
C(2)	0.00	C(2′)	0.02	C(2)	−0.003	C(4)	0.000	C(2′)	0.008	C(4′)	0.005
O(2)	0.00	O(2′)	0.16	O(2)	0.001	O(4)	0.000	O(2′)	−0.003	O(4′)	−0.002
N(3)	−0.02	N(3′)	−0.11	N(3)	0.001	N(5)	0.000	N(3′)	−0.002	N(5′)	−0.002
O(3)	−0.01	O(3′)	−0.15								
C(4)	−0.01	C(4′)	0.01								
O(4)	−0.04	O(4′)	−0.04								
N(5)	0.05	N(5′)	0.16								

Additional atoms:				Angles between normals to planes:	
H(11)	−0.04	H(1′1)	−0.04	1:2	21.9°
H(12)	−0.01	H(1′2)	0.10	3:4	3.6°
H(51)	0.09	H(5′1)	0.25	5:6	13.2°
H(52)	0.01	H(5′2)	0.32		
H(3)	−0.72	H(3′)	0.50		

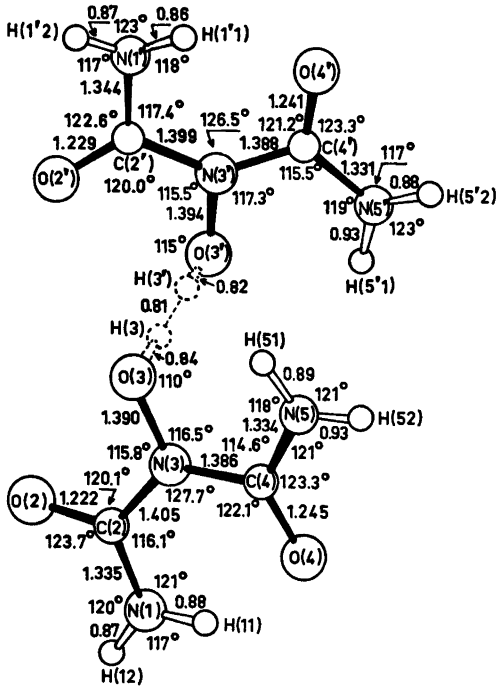

Fig. 3. Bond lengths and valency angles. The standard deviations on bonds between non-hydrogen atoms are 0.003 – 0.004 Å, and on the angles 0.2 – 0.3°. The standard deviations on bonds to hydrogen atoms are 0.03 – 0.04 Å and on angles including hydrogen atoms 2 – 6°.

with those earlier reported for eight-coordinated potassium,[3] *e.g.* in the structure of potassium hydrogen diformate.[11] As in this structure there is no regular geometry of the arrangement (*cf.* Table 6). It seems likely that the reason for this is the intensive *inter*molecular hydrogen bonding in the structure.

Two of the coordinating oxygen atoms, O(2) and O(3), belong to residue 1, and other two, O(2′) and O(3′), belong to residue 2 (*cf.* Fig. 4), but the planes through the chelate ligands do not pass through the central potassium ion. The displacements of K^+ from the planes defined by O(2) – (C2) – N(3) – O(3) and O(2′) – C(2′) – N(3′) – O(3′) are −1.51 and −0.47 Å, respectively. A similar situation was found in the potassium acid salts of isonitrosoacetophenone,[12] and the cyclic hydroxamic acid 5-bromo-3-hydroxy-6-methyl-uracil,[13] and is not a matter for surprise considering the electrostatic nature of the bonding. Nevertheless, the chelate rings in the structures of the potassium acid salts of carboxylic acids are often found to be planar.[11]

The number of ionic contacts to potassium is different for the two 3-HB residues: residue 1 has five and residue 2 has three contacts to K^+. This may mean that there is a tendency towards less ionization in residue 2 than in residue 1.

The distance between the layers of the potassium ions is about 6 Å ($\sim \frac{1}{2}c$). The nearest potassium-potassium contact is 3.868 Å ($=a$).

The short hydrogen bond. In most structures with very short hydrogen bonds, *e.g.* the acid salts of carboxylic acids, the short hydrogen bond has to be symmetric, because the acidic residues are crystallographically symmetry related. In the present structure the hydrogen bond, which links the 3-HB residues to a "dimer", has no crystallographical symmetry.

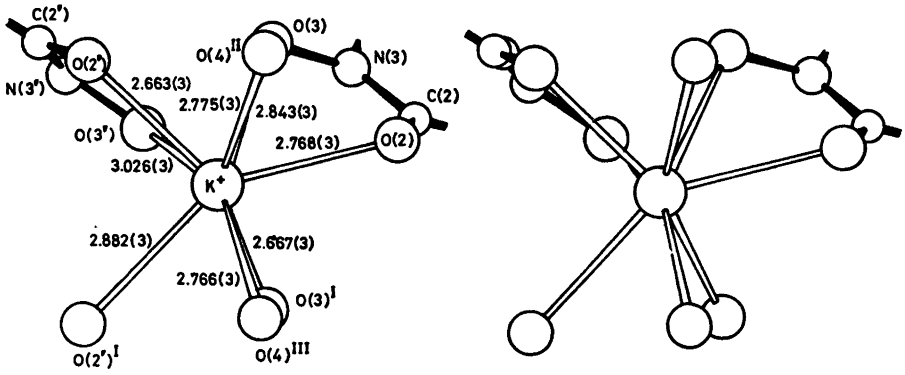

Fig. 4. Stereoscopic view of the potassium ion with its eight oxygen neighbours. In addition the chelate ligands of each 3-HB residue are indicated.

Table 6. The 28 independent O – K – O angles (°). The standard deviations are 0.05 – 0.07°.

O(2) – K$^+$ – O(3)	55.9	O(2′) – K$^+$ – O(3)^{I}	123.0
O(2) – K$^+$ – O(2′)	119.0	O(2′) – K$^+$ – O(2′)^{I}	88.4
O(2) – K$^+$ – O(3′)	96.0	O(2′) – K$^+$ – O(4)^{II}	79.6
O(2) – K$^+$ – O(3)^{I}	76.7	O(2′) – K$^+$ – O(4)^{III}	138.8
O(2) – K$^+$ – O(2′)^{I}	142.1	O(3′) – K$^+$ – O(3)^{I}	70.4
O(2) – K$^+$ – O(4)^{II}	74.3	O(3′) – K$^+$ – O(2′)^{I}	78.4
O(2) – K$^+$ – O(4)^{III}	94.8	O(3′) – K$^+$ – O(4)^{II}	121.1
O(3) – K$^+$ – O(2′)	66.6	O(3′) – K$^+$ – O(4)^{III}	150.2
O(3) – K$^+$ – O(3′)	49.1	O(3)^{I} – K$^+$ – O(2′)^{I}	66.0
O(3) – K$^+$ – O(3)^{I}	89.1	O(3)^{I} – K$^+$ – O(4)^{II}	149.7
O(3) – K$^+$ – O(2′)^{I}	127.2	O(3)^{I} – K$^+$ – O(4)^{III}	85.3
O(3) – K$^+$ – O(4)^{II}	81.9	O(2′)^{I} – K$^+$ – O(4)^{II}	140.5
O(3) – K$^+$ – O(4)^{III}	150.6	O(2′)^{I} – K$^+$ – O(4)^{III}	76.1
O(2′) – K$^+$ – O(3′)	54.4	O(4)^{II} – K$^+$ – O(4)^{III}	88.6

Roman numerals as superscripts denote the following equivalent positions relative to the reference molecule of x, y, z: I $x-1, y, z$; II $x, -y+\frac{1}{2}, z-\frac{1}{2}$; III $x-1, -y+\frac{1}{2}, z-\frac{1}{2}$.

*Table 7. Intera*tomic angles (°) concerning the hydrogen bonding system.

N(1) – H(11) – O(4)	131(3)
N(1) – H(12) – O(4′)^{IV}	156(3)
O(3) – H(3) – O(3′)	172(9)
O(3) – H(3′) – O(3′)	170(9)
N(5) – H(51) – O(3′)^{V}	148(3)
N(5) – H(52) – O(2)^{VI}	158(3)
N(1′) – H(1′1) – O(4′)	134(4)
N(1′) – H(1′2) – O(2′)^{VII}	176(4)
N(5′) – H(5′2) – O(4′)^{VIII}	172(4)

Roman numerals as superscripts denote the following equivalent positions relative to the reference molecule of x, y, z: IV $-x+1, y+\frac{1}{2}, -z+\frac{1}{2}$; V $x+1, y, z$; VI $x+1, -y+\frac{1}{2}, z+\frac{1}{2}$; VII $-x+2, -y, -z$; VIII $-x+2, -y, -z+1$.

But the short O···O distance of 2.442(3) Å, the favourable N – O···O angles of 109.8(3)° and 108.5(2)°, respectively, and the almost identical geometry of the 3-HB-residues being connected, are consistent with the existence of a virtually symmetrical hydrogen bond.[14–16] Symmetry due to statistical disorder is also possible. The rather elongated peak between the oxygen atoms of the difference map could perhaps be interpreted as an unresolved peak due to two half H-atoms about 0.4 Å on either side of the midpoint. The final refinement ($\sim R = 0.032$) was based on this assumption.

But the X-ray data were also consistent with an asymmetric hydrogen bond. Refinement of the positional parameters of the hydrogen atom, with a start position midway between the oxygen atoms, led to the following, perhaps most reliable, arrangement of the system: O(3) – H(3) = 1.31(4) Å, O(3′) – H(3) = 1.13(4) Å and the angle O(3) – H(3) – O(3′) = 179(3)°. In fact the O(3′) – H(3) bond has just the length corresponding to an O···O distance of 2.44 Å, using the curve, given by Lundgren,[16] of O – H distance as a function of O···O distance.

The conclusion must be that it is not possible from the X-ray data to establish whether this hydrogen bond is symmetric or slightly asymmetric.

REFERENCES

1. Gale, G. R., Smith, A. B. and Hynes, J. B. *Proc. Soc. Exp. Biol. Med. 127* (1968) 1191.
2. Exner, O. *Collect. Czech. Chem. Commun. 26* (1961) 701.
3. *International Tables for X-Ray Crystallography*, Kynoch Press, Birmingham 1963, Vol. III.
4. Sørensen, A. M. *INDIFF. GIER ALGOL Program for the NONIUS 3-Circle Diffractometer*, Chemical Laboratory C, The Royal Danish School of Pharmacy, Copenhagen 1967.
5. Ahmed, F. R. *N. R. C. Crystallographic Program System*, National Research Council, Ottawa, Canada 1968.
6. Stewart, J. M., Kundell, F. A. and Baldwin, J. C. *The X-Ray System* (1970), University of Maryland, College Park, Maryland.
7. Johnson, C. K. (1965), *ORTEP*, ORNL-3794, Oak Ridge National Laboratory, Oak Ridge, Tennessee.
8. Hughes, E. W., Yakel, H. L. and Freeman, H. C. *Acta Crystallogr. 14* (1961) 345.

9. Craven, B. M. *Acta Crystallogr. B 29* (1973) 1525.
10. Larsen, I. K. and Jerslev, B. *Acta Chem. Scand. 20* (1966) 983.
11. Larsson, G. and Nahringbauer, I. *Acta Crystallogr. B 24* (1968) 666.
12. Bush, M. A., Lüth, H. and Truter, M. R. *J. Chem. Soc. A* (1971) 740.
13. Truter, M. R. and Vickery, B. L. *J. Chem. Soc. A* (1971) 2077.
14. Currie, M. and Speakman, J. C. *J. Chem. Soc. A* (1970) 1923.
15. Blain, J., Speakman, J. C., Stamp, L. A., Golić, L. and Leban, I. *J. Chem. Soc. Perkin Trans. 2* (1973) 706.
16. Lundgren, J. O. *Acta Universitatis Upsaliensis*, Abstracts of Uppsala Dissertations from the Faculty of Science *271* (1974) 30.

Received March 11, 1974.

Acta Chemica Scandinavica A 28 (1974) 797—802

The Crystal Structure of Pd_6P

YVONNE ANDERSSON, VALAPHA KAEWCHANSILP,* MARIA del ROSARIO CASTELEIRO SOTO** and STIG RUNDQVIST

Institute of Chemistry, University of Uppsala, Box 531, S-751 21 Uppsala, Sweden

The crystal structure of Pd_6P has been investigated by powder diffraction methods. The unit cell is monoclinic of dimensions $a = 2.837$ Å, $b = 9.441$ Å, $c = 7.695$ Å, $\beta = 90.20°$ and contains 12 palladium and 2 phosphorus atoms. The structure is closely related to the Re_3B-type structure.

The Pd–P equilibrium diagram has been throroughly investigated by Gullman.[1] He found two very palladium-rich intermediate phases, Pd_8P and Pd_6P, both being formed peritectically at 799 °C and 792 °C, respectively. Gullman was unable to prepare these compounds in single crystal form, and the powder diffraction patterns were too complex for indexing. Since Pd_8P and Pd_6P represent the most metal-rich intermediate phases known in any transition metal-phosphorus system, it would seem to be of great interest to study the properties of these phases more closely. We decided to start an X-ray crystallographic examination of the two phosphides, and in the present paper we give an account of our work on Pd_6P.

EXPERIMENTAL DETAILS

Preparation and X-ray diffraction work. We prepared Pd–P samples by the silica tube technique in exactly the same manner as described by Gullman,[1] using red phosphorus of purity higher than 99 % and palladium powder (claimed purity 99.9 %) from Johnson, Matthey & Co, Ltd., London, as starting materials. As mentioned by Gullman it is difficult to attain equilibrium conditions in palladium-rich alloys, and in spite of long and careful heat treatments we could not obtain Pd_6P samples completely free from palladium or other Pd-P phases. The alloys were very ductile, and the powders used for X-ray diffraction work were prepared by filing with fine-toothed files and sieving. To remove the effects of cold work the filings were annealed at 650 °C for one hour. The annealing time and temperature was found to be critical, since the powders sintered at higher temperatures and longer annealing times, and sharp diffraction lines were not obtained for powders annealed at lower temperatures. Attempts to obtain Pd_6P crystals suitable for X-ray work were unsuccessful. The fragments extracted from the alloys invariably consisted of conglomerates of several crystallites, which were mechanically deformed and exhibited stacking faults and twinning. Annealing treatments of such fragments produced only minor improvements in the crystalline perfection.

Powder diffraction patterns were recorded in Hägg-Guinier-type cameras using $CrK\alpha_1$ or $CuK\alpha_1$ radiation and silicon ($a = 5.43054$ Å) as internal calibration standard. Unit cell dimensions were refined by the least squares method using the local program CELNE [2] on an IBM 1800 computer.

Powder diffraction intensities were measured by two methods. In the first method the intensities were obtained by direct summation on the read-out scaler, using a Philips powder diffractometer PW 1050 with CuK radiation and a lithium fluoride monochromator between the sample and the proportional counter. In the second method Hägg-Guinier photographs, recorded in a Philips XDC 700 camera with strictly monochromatized $CrK\alpha_1$ radiation, were measured by means of an automatic drum densitometer (SAAB model 2) connected to an IBM 1800 computer in the same manner as described by Malmros and Werner.[3] Evaluation of the integrated intensities was made using the program PILT [3] in a locally modified version.[2] This version included the correction factor $\{1 - \exp -[\mu_l h/\cos(2\theta - \phi)]\}$, ($\mu_l$ = absorption coefficient for the film emulsion, h = thickness of emulsion, θ and ϕ as in Ref. 3) allowing for the

* On leave from the Department of Chemistry, Chulalongkorn University, Bangkok, Thailand.

** On leave from the Department of Physics, Universidad de Oriente, Santiago de Cuba.

variation of the film blackening due to the oblique incidence of the diffracted beam.[4]

Least squares refinements using the intensity data were performed by means of the program POWOW, originally written by the late W. C. Hamilton, Brookhaven National Laboratory, USA, and modified locally for an IBM 370/155 computer.[5] The program permits the use of sums of intensities for unresolved overlapping reflexions as input data.

STRUCTURE ANALYSIS

Our powder diffraction data obtained for Pd_6P were in good agreement with Gullman's results.[1] It was found, however, that some of the weaker diffraction lines listed by Gullman actually belong to the Pd_8P phase, which was present in small amounts in his Pd_6P sample.

Table 1. Powder diffraction data for Pd_6P. (Guinier-Hägg camera, $CuK\alpha_1$ radiation, internal calibration standard silicon $a = 5.43054$ Å, intensities from film scanner.)

$h\,k\,l$	$Q \times 10^5$ obs	$Q \times 10^5$ calc	d_{obs}	I_{obs}
0 0 1		1 689		
0 2 0	4 485	4 488	4.722	–
0 2 1		6 177		
0 0 2	6 754	6 756	3.848	–
0 2 2	11 244	11 244	2.982	7
$\bar{1}$ 1 0	13 543	13 547	2.717	6
$\bar{1}$ 1 1	15 206	15 204	2.564	40
1 1 1	15 266	15 267	2.559	
0 4 0	17 947	17 951	2.360	41
0 4 1 / 0 2 3	19 664	19 640 / 19 689	2.255	100
$\bar{1}$ 1 2	20 240	20 240	2.223	73
1 1 2	20 370	20 366	2.216	
$\bar{1}$ 3 0	22 515	22 522	2.107	33
$\bar{1}$ 3 1	24 174	24 180	2.034	58
1 3 1	24 248	24 243	2.031	
0 4 2	24 698	24 707	2.012	11
0 0 4	27 018	27 025	1.924	3
$\bar{1}$ 1 3	28 646	28 653	1.868	9
1 1 3	28 835	28 843	1.862	8
$\bar{1}$ 3 2	29 207	29 215	1.850	12
1 3 2	29 334	29 342	1.846	8
0 2 4	31 512	31 513	1.781	1
0 4 3	33 155	33 153	1.737	1
$\bar{1}$ 3 3		37 629		
1 3 3		37 819		
0 6 0		40 390		
$\bar{1}$ 1 4	40 442	40 445	1.572	5
1 5 0		40 473		
1 1 4	40 702	40 698	1.567	4
0 6 1	42 083	42 079	1.542	4
$\bar{1}$ 5 1		42 131		
1 5 1		42 194		
0 4 4		44 976		
0 2 5	46 709	46 714	1.463	3
0 6 2 / $\bar{1}$ 5 2	47 142	47 146 / 47 166	1.456	28
1 5 2	47 273	47 293	1.454	
$\bar{1}$ 3 4		49 420		
1 3 4		49 674		
2 0 0	49 694	49 699	1.418	20
2 2 0		54 187		
$\bar{1}$ 5 3 / 0 6 3 / $\bar{1}$ 1 5	55 561	55 580 / 55 592 / 55 615	1.342	
1 5 3	55 749	55 770	1.339	49
$\bar{2}$ 2 1		55 812		
1 1 5	55 936	55 931	1.337	
2 2 1		55 939		
$\bar{2}$ 0 2		56 328		
2 0 2		56 582		
0 4 5	60 161	60 178	1.289	5
0 0 6	60 795	60 806	1.282	10
$\bar{2}$ 2 2		60 816		
2 2 2		61 070		
$\bar{1}$ 3 5	64 585	64 590	1.244	11
1 3 5	64 901	64 907	1.241	10
0 2 6		65 294		
$\bar{1}$ 5 4 / 1 7 0 / 0 6 4	67 379	67 372 / 67 400 / 67 415	1.218	44
1 5 4 / 2 4 0	67 647	67 625 / 67 650	1.216	
$\bar{1}$ 7 1		69 058		
1 7 1		69 121		
$\bar{2}$ 2 3	69 192	69 198	1.202	24
$\bar{2}$ 4 1		69 276		
2 4 1		69 402		
2 2 3	69 594	69 578	1.199	19
0 8 0	71 778	71 805	1.180	3
0 8 1	73 471	73 494	1.167	6
$\bar{1}$ 7 2		74 093		
$\bar{1}$ 1 6		74 163		
1 7 2		74 220		
$\bar{2}$ 4 2	74 272	74 280	1.160	4
2 4 2	74 512	74 533	1.158	3
1 1 6		74 543		
$\bar{2}$ 0 4	76 462	76 470	1.144	2
2 0 4	76 953	76 977	1.140	1
0 8 2	78 542	78 561	1.128	22
0 4 6	78 752	78 757	1.127	
$\bar{2}$ 2 4		80 958		
2 2 4		81 465		
$\bar{1}$ 7 3 / $\bar{1}$ 5 5 / 0 6 5 / $\bar{2}$ 4 3 / 1 7 3	82 576	82 507 / 82 542 / 82 617 / 82 662 / 82 697	1.100	36
1 5 5		82 858		
2 4 3		83 042		
$\bar{1}$ 3 6		83 138		
1 3 6		83 518		

For identification purposes, revised diffraction data for Pd_6P as obtained in our study are given in Table 1.

In order to analyze the Pd_6P structure we started with an attempt to use single crystal methods. As mentioned above, the "crystals" available were of extremely poor quality. However, from the best crystal conglomerates that we found, oscillation films were obtained, which indicated a rotation axis of about 2.8 Å. Weissenberg recordings of the zero, first and second layer lines indicated that Pd_6P might have an orthorhombic symmetry, with lengths of the remaining two axes of about 9.4 and 7.7 Å. An attempt to index the powder pattern on this basis was partially successful, but at several positions, where we expected to find only one single diffraction line, we observed pairs of closely spaced lines. We therefore tentatively assumed a monoclinic symmetry with the monoclinic angle differing only slightly from 90°. With this assumption all lines in the powder pattern could be accounted for in a very satisfactory manner. The indexed powder data are presented in Table 1.

On re-inspection of the "single crystal" films we found that the distribution of diffraction spots might well be compatible with a monoclinic symmetry. The deviations from orthorhombic symmetry were most probably masked by satellite spots, stacking fault effects, and by the very small deviation from 90° for the monoclinic angle in combination by twinning on (100).

The unit cell dimensions of Pd_6P at 24 ° C as derived from the powder diffraction data were: $a = 2.8370(2)$ Å, $b = 9.4409(6)$ Å, $c = 7.6945(5)$ Å, $\beta = 90.198(4)°$ (numbers in parentheses following numerical values are the calculated standard deviations referring to the least significant digits). The standard deviations as returned by the CELNE program include no allowance for systematic errors. The absolute errors are estimated to be less than 0.04 %.

In agreement with Gullman [1] we observed no significant variations in the cell dimensions between samples of different compositions and heat treatments. The cell volume of 206.1 $Å^3$ is consistent with a cell content of 12 palladium and 2 phosphorus atoms. Both the powder and the "single crystal" diffraction data indicated face centering. Furthermore, no reflexions with $l = 2n + 1$ were observed among the $(h0l)$ reflexions. This indicates Cc or $C2/c$ as the most probable space groups. However, among the equivalent positions in these space groups there are no sets of a multiplicity lower than fourfold, while there are only two phosphorus atoms in the unit cell. If the atoms occupy ordered positions in the structure, the space group symmetry can therefore be no higher than $C2$, Cm or $C2/m$.

The numerous overlaps in the powder diffraction patterns and the extremely poor single crystal data precluded the use of X-ray intensities for obtaining an initial structure proposal for Pd_6P. An attempt was therefore made to derive the atomic arrangement by simple space considerations. Accordingly, we assumed that no Pd – Pd and Pd – P distances in Pd_6P should be shorter than 2.7 Å and 2.2 Å, respectively, as inferred from the structure data known for $Pd_{4.8}P$ (Sellberg [6]) and Pd_3P (Rundqvist and Gullman [7]). Furthermore, we assumed that the atomic arrangement was ordered. An analysis of the various possibilities showed that there was only one principal way of arranging the atoms in accordance with the assumed spatial requirements. This structure proposal had $C2$ symmetry, with the following approximate atomic positions: 4 Pd in 4c: $x \sim 0$, $y = 0$ (arbitrarily), $z \sim 0.32$; 4 Pd in 4c: $x \sim 0$, $y \sim 0.73$, $z \sim 0.19$; 2 Pd in 2b: $y \sim 0.28$; 2 Pd in 2a: $y \sim 0.44$; 2 P in 2b: $y \sim 0.58$. With this structure proposal as the starting point we proceeded to make refinements based on powder diffraction intensities.

In the powder diffractometer work, we recorded intensities up to a maximum in θ of about 45°. For diffraction angles higher than this value the overlapping becomes so extensive that we considered an extension of the intensity measurements to be of very little value. The powder sample used contained small amounts of palladium. Within the θ-range recorded, the three palladium reflexions (111), (311), and (222) overlap reflexions from Pd_6P. From measurements of the intensities of the remaining well resolved palladium reflexions we could calculate the intensities for (111), (311), and (222). In the case of (111) and (222), the calculated intensities amounted only to 4.4 and 8.6 %, respectively, of the total integrated intensities for the overlapping palladium and Pd_6P reflexions. For each of these two cases of overlap we subtracted the calculated palladium intensity from the total intensity and used the resulting value as the Pd_6P intensity in the subsequent calculations. The palladium reflexion (311), which overlaps

Table 2. Structure data for Pd_6P based on space group $C2/c$.

		x	y	z
8 Pd(1)	in 8*f*	0.997(5)	0.133(1)	0.064(2)
4 Pd(2)	in 4*e*	0	0.422(2)	¼
2 P(randomly)	in 4*e*	0	0.715(12)	¼

Isotropic overall temperature factor $B = 0.8(3)$ Å^2.

the Pd_6P (081) reflexion, had a calculated intensity which amounted to a considerable fraction of the measured total intensity. Any correction for this overlap would therefore be very uncertain, and accordingly we omitted the Pd_6P (081) reflexion from the intensity data. The intensity material finally obtained comprised 23 data, seven of which consisting of intensities for single, non-overlapped Pd_6P reflexions, the remainder being sums of overlapping Pd_6P reflexions.

For the intensity calculations we assumed the lithium fluoride monochromator crystal to be ideally imperfect. This leads to the expression

$$(1 + \cos^2 2\theta \cos^2 2\theta_M)/\sin^2\theta \cos\theta$$

for the Lorentz-polarization correction, where θ is the Bragg angle for the sample, and θ_M that for the monochromator.[8] The weights w assigned to the observed intensities in the refinement procedure were based essentially on counting statistics but modified according to the formula

$$w = [N_T + N_B + 0.02(N_T - N_B)^2]^{-1}$$

where N_T is the total integrated intensity, and N_B the background intensity, in order to reduce the emphasis on the strongest intensities. In the structure factor calculations, atomic scattering factors for palladium were taken from Cromer and Waber,[9] for phosphorus from Hanson *et al.*[10] and dispersion correction from Cromer.[11]

The refinements based on space group $C2$ never reached a state of complete convergence, and the parameters oscillated slightly between successive cycles. At the termination of the refinement the weighted agreement factor R_w, defined as

Table 3. Observed and calculated intensities for Pd_6P. (Diffractometer data, Cu$K\alpha$ radiation).

h k l	I_o	I_c	*h k l*	I_o	I_c	*h k l*	I_o	I_c
0 2 2	1 426	1 551	0 2 5			$\bar{1}$ 7 1		
1 1 0	805	688	0 6 2	3 648	3 444	1 7 1		
$\bar{1}$ 1 1	5 481	5 243	$\bar{1}$ 5 2			$\bar{2}$ 2 3	4 016	4 536
1 1 1			1 5 2			$\bar{2}$ 4 1		
0 4 0	6 415	6 284	$\bar{1}$ 3 4			2 4 1		
0 4 1			1 3 4	1 739	2 304	$\bar{2}$ 2 3		
0 2 3	33 410	32 400	2 0 0			$\bar{2}$ 0 4	349	258
$\bar{1}$ 1 2			$\bar{1}$ 5 3			2 0 4		
1 1 2			0 6 3			0 8 2	1 944	1 540
1 3 0	4 598	4 715	$\bar{1}$ 1 5			0 4 6		
$\bar{1}$ 3 1	9 430	9 629	1 5 3			$\bar{1}$ 7 3		
1 3 1			$\bar{2}$ 2 1	6 784	6 927	1 5 5		
0 4 2			1 1 5			0 6 5		
0 0 4	841	759	$\bar{2}$ 2 1			$\bar{2}$ 4 3		
$\bar{1}$ 1 3	5 638	5 436	$\bar{2}$ 0 2			1 7 3	2 122	1 911
1 1 3			2 0 2			0 0 7		
$\bar{1}$ 3 2			0 4 5			1 5 5		
1 3 2			0 0 6	2 528	1 989	$\bar{2}$ 4 3		
0 2 4	277	202	$\bar{2}$ 2 2			$\bar{1}$ 3 6		
0 4 3	280	431	2 2 2			1 3 6		
0 6 0	1 542	1 410	$\bar{1}$ 3 5	3 075	2 830			
$\bar{1}$ 1 4			1 3 5					
1 5 0			0 2 6					
1 1 4			$\bar{1}$ 5 4					
0 6 1	446	444	1 7 0	3 916	4 235			
$\bar{1}$ 5 1			0 6 4					
1 5 1			1 5 4					
			2 4 0					

$$R_w = \sum w||I_o| - k|I_c||/\sum|I_o|$$

(where k is the scale factor and I_o and I_c denote intensity values for separate, resolved reflexions or sums of non-resolved, overlapping reflexions) oscillated between 0.11 and 0.12. The good agreement between observed and calculated intensities substantiated the essential features of the proposed structure. It was furthermore observed that the magnitude of the calculated intensities for all ($h0l$) reflexions with l odd was far below the limit of detection in the powder diffractometer measurements.

A study of the correlation matrix revealed strong correlations between some of the parameters refined. This indicates that the oscillatory behaviour of the refinement might be due to the fact that the structure proposed very nearly conforms to an atomic arrangement of higher symmetry. A description in terms of $C2/c$ symmetry would involve one eightfold and one fourfold palladium position, and one fourfold position randomly occupied by two phosphorus atoms. This would lead to a reduction in the number of positional parameters from eight in $C2$ symmetry to five in $C2/c$ symmetry.

A refinement based on $C2/c$ symmetry converged satisfactorily to a final R_w of 0.113. The corresponding value for the unweighted agreement factor R was 0.058. The sign of the x parameter for the eightfold palladium position remained ambiguous, however, due to the fact that every pair of corresponding (hkl) and($\bar{h}kl$) reflexions was overlapping in the powder diffractometer data. The higher resolution in the Hägg-Guinier films afforded a possibility of resolving this ambiguity. A refinement based on film scanner intensity data as obtained from $CrK\alpha_1$ powder films was therefore carried out. The final R_w and R values for this refinement were both 0.058, and the value obtained for the x parameter turned out to be insignificantly different from zero.

The final structure data as obtained from the $C2/c$ refinements are given in Table 2. Lists of observed and calculated intensities are given in Tables 3 and 4.

Table 4. Observed and calculated intensities for Pd_6P. (Film scanner data, $CrK\alpha_1$ radiation).

$h\,k\,l$	I_o	I_c	$h\,k\,l$	I_o	I_c
0 2 2	35	30	$\bar{1}$ 3 0	156	146
$\bar{1}$ 1 0	21	22	$\bar{1}$ 3 1	261	240
$\bar{1}$ 1 1	84	70	1 3 1		
1 1 1	67	62	0 4 2	44	51
0 4 0	181	175	$\bar{1}$ 1 3	46	45
0 4 1	470	490	$\bar{1}$ 1 3	49	43
0 2 3			$\bar{1}$ 3 2	51	47
$\bar{1}$ 1 2	182	182	1 3 2	51	50
1 1 2	181	188			

DESCRIPTION AND DISCUSSION OF THE Pd_6P STRUCTURE

The structure of Pd_6P is shown in projection on the (100) plane in Fig. 1. Calculated interatomic distances are given in Table 5.

The structure can conveniently be described in terms of triangular prismatic building blocks. Four Pd(1) and two Pd(2) atoms are situated at the corners of a slightly deformed trigonal prism. The phosphorus atoms are situated at the centres of every second Pd_6 prism. The prisms are stacked into a closely packed network, where each palladium atom coordinates 12 – 15 palladium and phosphorus neighbours. In addition to the six palladium atoms at the corners of the prism, each phosphorus atom has three more remote palladium neighbours situated outside the quadrilateral faces of the prism. The augmented trigonal prismatic nine-coordination for phosphorus is very common with metal-rich transition metal phosphide structures and has been discussed at length earlier.[12,13] In particular, this coordination oc-

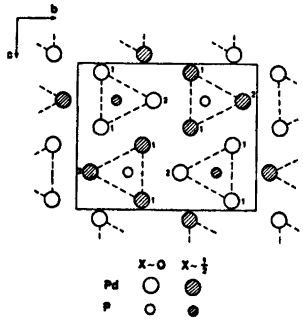

Fig. 1. The crystal structure of Pd_6P projected on (100). Only half of the phosphorus positions as indicated in the figure are occupied by phosphorus atoms.

Table 5. Interatomic distances (Å) in Pd_6P. Distances up to 3.8 Å are included. When greater than one, the number of equivalent distances from a central atom to its neighbours precedes the notation for the neighbouring atoms.

Pd(1) –	P	2.16(5)	Pd(2) –	2P	2.42(10)
	P	2.16(5)		P	2.76(12)
	Pd(1)	2.69(2)		2Pd(1)	2.83(2)
	Pd(1)	2.80(2)		2Pd(1)	2.83(2)
	P	2.81(6)		2Pd(2)	2.84(0)
	Pd(1)	2.82(2)		2Pd(1)	2.84(1)
	Pd(2)	2.83(2)		2Pd(1)	2.86(1)
	Pd(2)	2.83(2)		2Pd(1)	3.09(2)
	2Pd(1)	2.84(0)			
	Pd(2)	2.84(1)			
	Pd(2)	2.86(1)	P –	2Pd(1)	2.16(5)
	Pd(1)	2.86(2)		2Pd(1)	2.16(5)
	Pd(2)	3.09(2)		2Pd(2)	2.42(10)
				Pd(2)	2.76(12)
				2Pd(1)	2.81(6)
				2P	2.84(0)

curs [6,7] in the two palladium phosphides $Pd_{4.8}P$ and Pd_3P.

As regards the twinning observed for the Pd_6P crystals it is evident from the structural results that twinning on (100) requires very small distortions of the structure at the twin boundaries. The stacking faults may be connected with the distribution of the two phosphorus atoms among the four positions available. The distribution might have a certain degree of order, and it is conceivable that Pd_6P might ideally crystallize with $C2$ symmetry as we assumed in our preliminary structure analysis. In the real structure, stacking faults may occur among the sheets of filled and unfilled triangular prisms traversing the structure parallel to (001), and the diffraction data would accordingly correspond to $C2/c$ symmetry.

The atomic arrangement in Pd_6P resembles very closely that occurring in the boride Re_3B. This compound crystallizes with the orthorhombic *Cmcm* symmetry.[14] The unit cell contains twelve rhenium and four boron atoms, and the unit cell dimensions: $a = 2.890$ Å, $b = 9.313$ Å, $c = 7.258$ Å, are not much different from those of Pd_6P. A projection on (100) of the Re_3B structure would look very nearly the same as Fig. 1, with rhenium atoms at the palladium positions and boron atoms filling all triangular Re_6 prisms.

The Re_3B-type metal skeleton is apparently very stable with respect to changes in the non-metal sublattice. In the so-called "filled" Re_3B-type structure, as investigated and discussed thoroughly by Boller and Nowotny,[15-19] the triangular prismatic holes as well as octahedral holes, which also occur between the metal atoms, are filled with non-metal atoms. In contrast, Pd_6P exhibits an Re_3B-type metal sublattice with none of the octahedral, and only half of the triangular prismatic holes, filled.

Acknowledgements. The authors thank Mr. J. Gullman and Mr. N.-O. Ersson for valuable help in computer programming and handling the powder diffractometer and the film scanner. V. K. and M.R.C.S. are indebted to the International Seminar in Chemistry, Uppsala, and the Swedish International Development Authority (SIDA) for financial support. The financial support for this work provided by the Swedish Natural Science Research Council is gratefully acknowledged.

REFERENCES

1. Gullman, L.-O. *J. Less-Common Metals 11* (1966) 157.
2. Ersson, N.-O. Institute of Chemistry, Uppsala 1973. *Unpublished.*
3. Malmros, G. and Werner, P.-E. *Acta Chem. Scand. 27* (1973) 493.
4. Hägg, G. and Regnström, G. *Ark. Kemi Mineral. Geol. A 18* (1944) No. 5.
5. Gullman, J. Institute of Chemistry, Uppsala 1973. *Unpublished.*
6. Sellberg, B. *Acta Chem. Scand. 20* (1966) 2179.
7. Rundqvist, S. and Gullman, L.-O. *Acta Chem. Scand. 14* (1960) 2246.
8. Azaroff, L. V. *Acta Crystallogr. 8* (1955) 701.
9. Cromer, D. T. and Waber, J. T. *Acta Crystallogr. 18* (1965) 104.
10. Hanson, H. P., Herman, F., Lea, J. D. and Skillman, S. *Acta Crystallogr. 17* (1964) 1040.
11. Cromer, D. T. *Acta Crystallogr. 18* (1965) 17.
12. Rundqvist, S. *Ark. Kemi 20* (1962) 67.
13. Lundström, T. *Ark. Kemi. 31* (1969) 227.
14. Aronsson, B., Bäckman, M. and Rundqvist, S. *Acta Chem. Scand. 14* (1960) 1001.
15. Boller, H. and Nowotny, H. *Monatsh. Chem. 98* (1967) 2127.
16. Boller, H. and Nowotny, H. *Monatsh. Chem. 99* (1968) 721.
17. Nowotny, H., Boller, H. and Beckmann, O. *J. Solid State Chem. 2* (1970) 462.
18. Boller, H. *Monatsh. Chem. 102* (1971) 431.
19. Boller, H. *Monatsh. Chem. 104* (1973) 545.

Received March 29, 1974.

Acta Chemica Scandinavica A 28 (1974) 803—805

On the Structural and Magnetic Properties of $V_{1-t}Fe_tAs$

KARI SELTE, ARNE KJEKSHUS and TOR A. OFTEDAL

Kjemisk Institutt, Universitetet i Oslo, Blindern, Oslo 3, Norway

The pseudo-binary VAs-FeAs system has been investigated by X-ray diffraction, magnetic susceptibility, and magnetization measurements. VAs and FeAs are completely soluble in each other, and the structure of the ternary, random solid solution phase is of the MnP type. The paramagnetic susceptibilities do not follow the Curie-Weiss Law over an appreciable range of temperature for any of the ternary samples.

The present contribution on the structural and magnetic properties of the $V_{1-t}Fe_tAs$ phase is a link in continued studies at this Institute on ternary phases with the MnP type structure. The properties of VAs and FeAs have been reported earlier.[1-4]

EXPERIMENTAL

Samples of VAs and FeAs were prepared by heating weighed quantities of the elements (99.5 % V (A. D. Mackay), 99.99 % Fe (Johnson, Matthey & Co; turnings from rods), and 99.9999 % As (Koch-Light Laboratories)) in evacuated, sealed quartz tubes, as described in Refs. 1 – 3. The desired $V_{1-t}Fe_tAs$ samples were prepared by mixing appropriate proportions of VAs and FeAs and subjecting the mixtures to a series of annealings at 850 °C, interrupted by intermediate crushings. The samples were finally cooled to room temperature over a period of 3 days.

The experimental details concerning X-ray diffraction, magnetic susceptibility, and magnetization measurements have been presented in Refs. 2 and 3.

RESULTS

The orthorhombic unit cell dimensions of $V_{1-t}Fe_tAs$ (as determined from room temperature X-ray powder diffraction (Guinier) diagrams) are presented in Fig. 1 as functions of t.

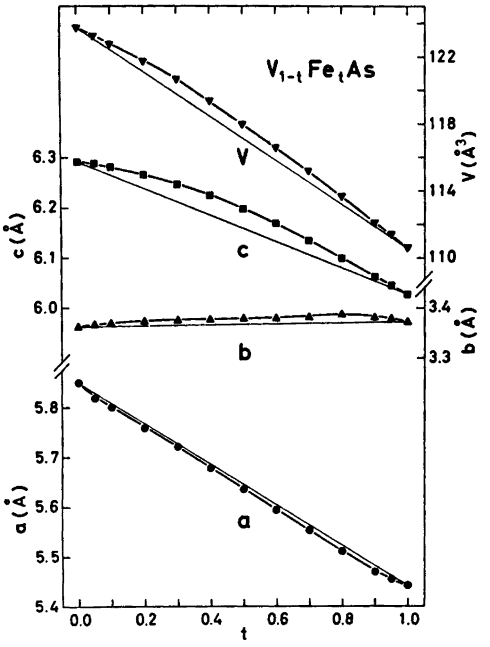

Fig. 1. Unit cell dimensions of the ternary solid solution series VAs-FeAs as functions of composition.

The continuous variations in all unit cell dimensions with composition, from $t=0$ to $t=1$, show that VAs and FeAs are completely soluble in each other. The curves for a and b follow closely Vegard's Law over the whole range of t-values. The well defined stoichiometric nature of both VAs and FeAs has been confirmed earlier.[1,3] The possibility of an extension of the homogeneity range of $V_{1-t}Fe_tAs$ to metal/non-metal (atomic) ratios different from 1.00 has not been examined for $t \neq 0$ and 1, and, thus, cannot be excluded.

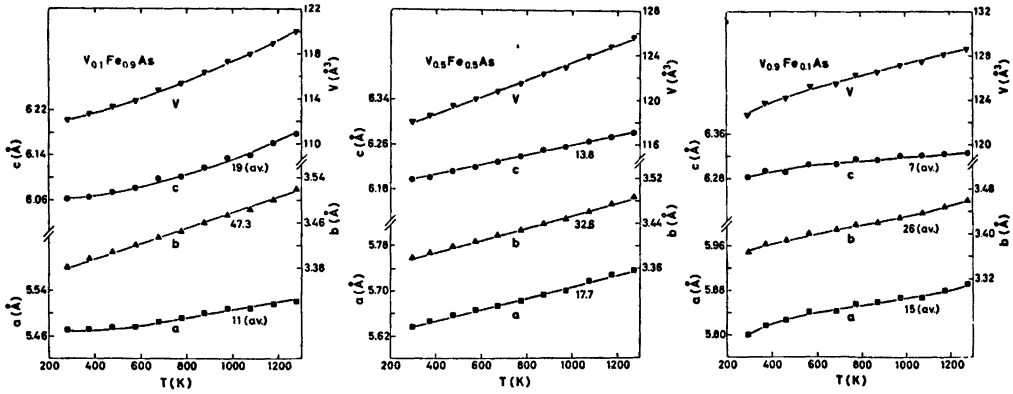

Fig. 2. Unit cell dimensions of three $V_{1-t}Fe_tAs$ samples as functions of temperature. The relative expansion coefficients $\alpha_a(=(a_T-a_{T'})/a_{300}(T-T'))$ α_b, α_c multiplied by 10^6 K are positioned below the appropriate curves. Corresponding triplets for VAs and FeAs are 12.2, 20.8, 7.7, and 11 (av.), 44 (av.), 22 (av.), respectively, *cf.* Ref. 5.

The MnP type structure, with random distribution of the two kinds of metal atoms, is easily confirmed for the $V_{1-t}Fe_tAs$ phase ($0.00 \leqq t \leqq 1.00$) at room temperature. In order to examine whether the phase undergoes a crystallographic transformation to the NiAs type structure at higher temperatures, three representative samples with compositions $t=0.10$, 0.50, and 0.90 were studied in the interval 293 – 1273 K. In conformity with earlier data for VAs [5] and FeAs [2] no such transformation was observed. The unit cell dimensions for the three samples as functions of temperature are shown in Fig. 2. The relative, linear expansion coefficients of the samples are included on the diagram. Also these parameters are seen to vary continuously with t.

The reciprocal magnetic susceptibility curves for different $V_{1-t}Fe_tAs$ samples are shown as functions of temperature in Fig. 3. No field strength dependent susceptibilities were observed. It is seen that the $\chi^{-1}(T)$ curve for $t=0.00$ is unique. The characteristics for $0.1 \leqq t \leqq 0.9$ are very similar, and none of these curves is seen to obey the Curie-Weiss Law relationship over an appreciable temperature range. There is a gradual progression in the data as evidenced by the reduction in χ^{-1} with increasing t. This trend is interrupted in the vicinity of $t=0.8$ where the overall value of χ^{-1} begins to increase, and the shape of $\chi^{-1}(T)$ undergoes gradually more and more rapid

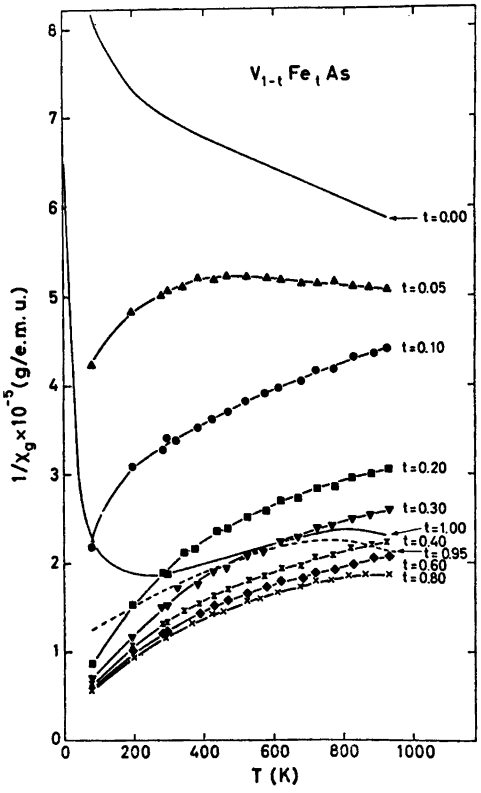

Fig. 3. Reciprocal magnetic susceptibility *versus* temperature for various $V_{1-t}Fe_tAs$ samples.

changes until $t = 1.00$. The latter variation is somewhat peculiar, and, if it had not been for the definite resemblance between curves for $t = 0.95$ and 1.00 (data points omitted in Fig. 3 for clarity), one would have been tempted to search for experimental errors.

The rapid change in characteristic near $t = 1.00$ suggests that small amounts of VAs have radical effects on the electronic band structure of FeAs. The fact that the $\chi^{-1}(T)$ curve for $t = 0.95$ continues to fall below $T = \sim 200$ K (as opposed to that for $t = 1.00$) indicates that the helimagnetic ordering in FeAs [2] may be destroyed already with a small substitution of V for Fe. (A corresponding observation has, more surprisingly, been made for $Mn_{0.05}Fe_{0.95}As$.[6]) In view of the very small ordered moment, corresponding to 0.5 unpaired electron per metal atom, in FeAs it has been considered worthless to prepare large scale samples of $V_{1-t}Fe_tAs$ for neutron diffraction experiments.

REFERENCES

1. Selte, K. and Kjekshus, A. *Acta Chem. Scand. 23* (1969) 2047.
2. Selte, K., Kjekshus, A. and Andresen, A. F. *Acta Chem. Scand. 26* (1972) 3101.
3. Selte, K., Kjekshus, A. and Andresen, A. F. *Acta Chem. Scand. 26* (1972) 4057.
4. Selte, K. and Kjekshus, A. *Acta Chem. Scand. 27* (1973) 1448.
5. Selte, K. and Kjekshus, A. *Acta Chem. Scand. 27* (1973) 3195.
6. Selte, K., Kjekshus, A. and Andresen, A. F. *Acta Chem. Scand. A 28* (1974) 61.

Received March 17, 1974.

Acta Chemica Scandinavica A 28 (1974) 806—810

Short Communications

The Reaction between $(XCN)_2$ (X = S and Se) and the Cyanide Ion in Acetonitrile. A Study of the Mechanism using Ionic ^{13}C Cyanide

TOR AUSTAD

Department of Chemistry, University of Bergen, N-5014 Bergen, Norway

As part of a study of polythionic compounds in dipolar aprotic solvents, it was found necessary to study the action of ionic cyanide on thiocyanogen and selenocyanogen in acetonitrile.[1] In a previous paper we have studied the reaction between chalcogen dicyanides, $X(CN)_2$ (X = S, Se and Te), and the cyanide ion in acetonitrile.[2] In all cases the chalcogen atom was found to be the electrophilic centre.

Selenocyanogen has been found to react with ionic selenocyanate to form the triselenocyanate ion, $(SeCN)_3^-$.[3] Likewise, the trithiocyanate ion, $(SCN)_3^-$, is formed when thiocyanogen and ionic thiocyanate are mixed.[4] The trithiocyanate ion is far more unstable than the triselenocyanate ion and it has not yet been isolated as stable salts. In the dipolar aprotic solvent, acetonitrile, the cyanide ion is believed to be a more powerful nucleophile towards divalent sulfur and selenium than is the thiocyanate ion and the selenocyanate ion. Consequently, a displacement reaction is to be expected upon mixing ionic cyanide with the two pseudohalogens, $(SCN)_2$ and $(SeCN)_2$, in acetonitrile.

The stoichiometry of the thiocyanogen-cyanide reaction and the selenocyanogen-cyanide reaction was found by varying the amount of the nucleophilic reagent, tetraphenylarsonium cyanide, and measuring the yield of the corresponding pseudohalide ion applying IR ($\nu_{SCN^-} = 2059$ cm^{-1} and $\nu_{SeCN^-} = 2068$ cm^{-1}).[5] The nucleophilic reagent was always added to the substrate. The results are collected in Table 1.

Four mol of cyanide ions are consumed per mol of the substrate in order to give 2 mol of the corresponding pseudohalide ion. Table 1 further indicates that one mol of each of the reactants forms one mol of the pseudohalide ion, and in addition 3 mol of cyanide ions have to be used to form the second mol of the pseudohalide ion.

Table 1. Determination of the stoichiometry of the reaction $(XCN)_2 + nCN^- \rightarrow$ Products where X = S or Se in acetonitrile at room temperature.

n	Amount of XCN^- formed (mol)
2	1 1/3
3	1 2/3
4	2

A mechanism satisfying these observations involves a fast substitution by the cyanide ion at one of the chalcogen atoms displacing ionic thiocyanate (selenocyanate) in the first step, eqn. (1).

$$(XCN)_2 + CN^- \xrightarrow{\text{fast}} XCN^- + X(CN)_2 \quad (1)$$

(X = S and Se).

The chalcogen dicyanide that is being formed, is believed to react with ionic cyanide in acetonitrile according to eqns. (2) and (3).[2]

$$X(CN)_2 + CN^- \xrightarrow{\text{slow}} XCN^- + (CN)_2 \quad (2)$$

$$(CN)_2 + 2\,CN^- \xrightarrow{\text{fast}} \underset{(DISN)^{2-}}{\text{NC}(\text{N}^-)\text{C}=\text{C}(\text{N}^-)\text{CN}} \quad (3)$$

IR of the reaction mixture showed a sharp peak at 2140 cm^{-1} which has been attributed to the postulated diiminosuccinonitrile dianion, $(DISN)^{2-}$.[2]

To verify this mechanism, ionic ^{13}C cyanide has been used as the nucleophilic reagent. The reactions were performed by adding 4 mol of ^{13}C cyanide ions to the substrates. The sharp peaks in IR of the ^{12}C-pseudohalides and the ^{13}C-pseudohalides were sufficiently apart for quantitative measurements ($\nu_{S^{13}CN^-} = 2010$ cm^{-1} and $\nu_{Se^{13}CN^-} = 2022$ cm^{-1}).[2] The data are listed in Table 2. The data of the isotopic

Table 2. Isotopic experiments on the reaction $(XCN)_2 + 4\,^{13}CN^- \rightarrow$ Products where X = S or Se in acetonitrile at room temperature.

X	Amounts formed (mol) XCN^-	$X^{13}CN^-$
S	1 1/3	2/3
Se	1 1/5	4/5

experiments are in complete accordance with the mechanism previously reported for the sulfur dicyanide-cyanide reaction and the selenium dicyanide-cyanide reaction.[2] The overall reaction between thiocyanogen and ionic ^{13}C cyanide may then be pictured by Scheme 1.

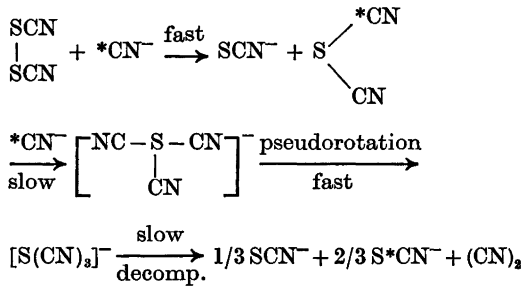

Scheme 1.

The cyanogen formed in the last step adds 2 mol of cyanide ions in a fast reaction, eqn. (3).

The mechanism of the selenocyanogen-cyanide reaction is schematically shown by Scheme 2.

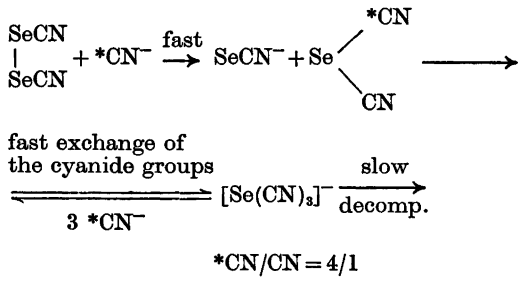

Scheme 2.

Finally some comment concerning the first step of the Schemes 1 and 2 will be given. The first steps in both reactions are irreversible, and the data of Table 2 are in agreement with such reactions. In aqueous solution Hauge [3] has, however, found the cyanide ion and the selenocyanate ion to be of comparable nucleophilicity toward divalent selenium. The data in this paper may be explained by the fact that the nucleophilicity of the cyanide ion toward methyl iodide is 4.1×10^4 times greater in acetonitrile than in methanol.[8] The increase in the nucleophilicity of the thiocyanate ion and the selenocyanate ion toward the same substrate when going from methanol to acetonitrile is, however, 36 and 19, respectively.[8] Thus in a dipolar aprotic solvent the nucleophilicity of the cyanide ion toward divalent sulfur and selenium appears to be much greater than the nucleophilicity of the thiocyanate ion and the selenocyanate ion toward the same substrates.

Experimental. Acetonitrile and tetraphenylarsonium cyanide, Ph_4AsCN, were purified as reported previously.[5] $Ph_4As^{13}CN$ was prepared from $K^{13}CN$, British Oxygen Limited, and contained more than 90 % ^{13}C.

A standard solution of thiocyanogen in acetonitrile was made by the method of Jenkins and Kochi [6] applying bromine and excess of lead thiocyanate, $Pb(NCS)_2$. The solution was stored in a refrigerator.

Selenocyanogen was made from silver selenocyanate and iodine in dry ether.[7]

The thiocyanogen-cyanide reaction was quantitatively studied by measuring the amount of ionic thiocyanate formed applying IR.[5] The reaction was studied using 1.54×10^{-3} M of the substrate and varying the concentration of the nucleophile up to four times the concentration of the substrate. During all the experiments the nucleophilic reagent was always added to the thiocyanogen solution. The IR of the solution further showed a sharp peak at 2140 cm^{-1} which is supposed to be due to the diiminosuccinonitrile dianion, $(DISN)^{2-}$.

The selenocyanogen-cyanide reaction was studied in the same way as described for the thiocyanogen-cyanide reaction. 3.0×10^{-3} M of selenocyanogen was applied.

Both of the reactions were found to be very fast, and the amounts of XCN^- (X = S and Se) were measured shortly after mixing the reactants.

The amounts of XCN^- and $X^{13}CN^-$ were reproduced within ± 3 % of the exact figures which are presented in Tables 1 and 2.

The IR measurements were performed on a Unicam SP 200 G Infrared Spectrophotometer applying 0.1 cm liquid cells.

Acknowledgement. The author is indebted to The Norwegian Research Council for Science and Humanities for a grant.

1. Austad, T. *Acta Chem. Scand. Ser. A.*
2. Austad, T. and Esperås, S. *Acta Chem. Scand. Ser A 28* (1974). *In press.*

3. Hauge, S. *Acta Chem. Scand. 25* (1971) 3081.
4. Seel, F. and Müller, E. *Chem. Ber. 88* (1955) 1747.
5. Austad, T., Songstad, J. and Åse, K. *Acta Chem. Scand. 25* (1971) 331.
6. Jenkis, C. L. and Kochi, J. K. *J. Org. Chem. 36* (1971) 3053.
7. Birckenbach, L. and Kellermann, K. *Ber. 58* (1925) 2378.
8. Austad, T., Engemyr, L. B. and Songstad, J. *Acta Chem. Scand. 25* (1971) 3535.

Received July 29, 1974.

The Crystal Conformation of 1,1,9,9-Tetramethylcyclohexadecane

P. GROTH

Department of Chemistry, University of Oslo, Oslo 3, Norway

By semiempirical calculations of cyclohexadecane Dale[1] has found the square, diamond

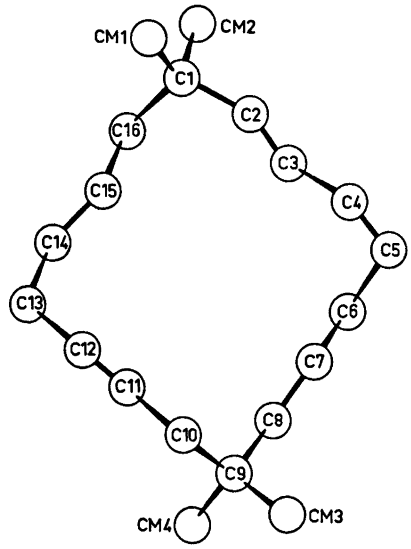

Fig. 1. Schematical drawing showing the molecular conformation.

Table 1. Final fractional coordinates and anisotropic thermal vibration parameters with estimated standard deviations (multiplied by 10^4) for carbon atoms. The symbol CM is used for the methyl carbons.

ATOM	X	Y	Z	B11	B22	B33	B12	B13	B23
C1A	506(11)	3460(4)	2755(4)	263(23)	26(3)	27(3)	41(15)	34(14)	-1(5)
C2A	1383(11)	3328(4)	3366(4)	321(24)	28(3)	23(3)	10(14)	15(14)	-9(4)
C3A	3197(11)	3114(4)	3374(4)	238(23)	28(3)	23(3)	-16(14)	-3(13)	-4(5)
C4A	3957(12)	2958(4)	3983(4)	334(27)	27(3)	26(3)	17(16)	-36(15)	-7(5)
C5A	5738(13)	2741(5)	4029(4)	360(28)	46(5)	29(3)	-24(19)	-75(16)	-8(6)
C6A	6083(10)	2154(5)	3687(4)	181(21)	38(4)	31(3)	-23(15)	-46(13)	-4(6)
C7A	5139(10)	1559(4)	3835(4)	237(23)	36(4)	24(3)	-1(15)	2(13)	-2(5)
C8A	5561(9)	976(4)	3511(3)	167(19)	29(3)	22(2)	21(13)	-9(11)	4(5)
C9A	4622(11)	348(4)	3616(4)	243(23)	27(4)	21(3)	58(15)	-4(14)	9(5)
C10A	2739(11)	433(4)	3525(4)	282(25)	22(3)	24(3)	4(14)	7(14)	3(5)
C11A	2023(10)	679(4)	2948(4)	208(21)	34(3)	24(3)	23(14)	5(13)	-5(5)
C12A	145(10)	816(4)	2912(4)	147(20)	28(3)	42(3)	-8(13)	12(13)	-9(5)
C13A	-640(10)	1080(4)	2347(4)	195(21)	31(4)	41(3)	5(15)	-42(14)	-22(6)
C14A	58(10)	1719(4)	2166(4)	230(22)	21(3)	35(3)	-12(14)	-72(13)	-12(5)
C15A	-129(10)	2254(4)	2575(3)	194(20)	28(3)	23(3)	-13(14)	-2(12)	-9(5)
C16A	548(9)	2872(4)	2374(3)	199(19)	24(3)	23(3)	23(13)	5(12)	6(5)
CM1A	1329(13)	4028(4)	2489(4)	508(33)	29(4)	29(3)	2(18)	6(17)	22(5)
CM2A	-1288(12)	3628(5)	2846(4)	339(27)	47(4)	39(3)	79(19)	-18(17)	-21(6)
CM3A	5869(12)	131(4)	4238(4)	395(29)	39(4)	31(3)	63(18)	-3(15)	24(5)
CM4A	5203(11)	-164(5)	3228(4)	332(27)	53(5)	34(3)	167(18)	39(15)	-18(6)
C1B	-401(11)	6475(4)	9728(3)	269(21)	24(4)	21(3)	4(14)	8(13)	7(5)
C2B	-2273(10)	6588(4)	9652(4)	166(18)	27(3)	25(3)	-31(13)	21(12)	-1(5)
C3B	-3029(10)	6940(4)	9989(4)	169(19)	31(3)	24(3)	-2(13)	14(12)	-3(5)
C4B	-4885(10)	6954(4)	9975(4)	177(22)	24(3)	37(3)	-37(14)	3(14)	2(5)
C5B	-5696(11)	7188(4)	8504(5)	195(22)	34(4)	48(4)	-15(16)	-7(15)	-14(6)
C6B	-5033(10)	7834(4)	8286(4)	183(21)	30(4)	31(3)	37(14)	-68(13)	-12(5)
C7B	-5187(10)	8385(4)	8699(4)	175(20)	29(4)	23(2)	-5(14)	13(12)	-8(5)
C8B	-4531(9)	9317(4)	8451(3)	178(19)	29(3)	17(2)	-14(13)	-3(11)	-3(4)
C9B	-4526(10)	9501(4)	8863(3)	208(21)	28(3)	13(2)	17(14)	11(12)	4(4)
C10B	-3601(10)	9178(4)	9439(3)	234(21)	24(3)	15(2)	8(13)	30(12)	-4(4)
C11B	-1811(10)	9253(4)	9440(3)	210(21)	31(3)	21(2)	-11(14)	-2(12)	3(4)
C12B	-1044(10)	9110(4)	10039(4)	186(21)	27(3)	23(3)	-25(14)	1(12)	-1(4)
C13B	798(11)	8899(4)	10087(4)	262(23)	30(4)	29(3)	-37(15)	-11(14)	4(5)
C14B	1956(9)	8284(4)	9755(3)	163(18)	35(3)	19(2)	-5(13)	-5(11)	1(5)
C15B	142(10)	7693(4)	9932(4)	193(20)	23(3)	27(3)	-31(13)	49(12)	-9(5)
C16B	553(9)	7983(4)	9489(3)	201(19)	32(3)	22(2)	23(14)	32(11)	-7(5)
CM1B	114(11)	6254(4)	10343(4)	308(25)	31(4)	29(3)	-13(16)	-4(15)	14(5)
CM2B	96(11)	5953(4)	9336(4)	254(22)	35(4)	40(3)	50(15)	1(14)	-9(6)
CM3B	-6333(11)	9791(4)	8929(4)	253(24)	39(4)	26(3)	76(15)	-11(14)	-2(5)
CM4B	-3686(11)	10168(4)	8557(3)	346(27)	26(3)	24(3)	-19(15)	5(14)	-1(5)

3. Hauge, S. *Acta Chem. Scand. 25* (1971) 3081.
4. Seel, F. and Müller, E. *Chem. Ber. 88* (1955) 1747.
5. Austad, T., Songstad, J. and Åse, K. *Acta Chem. Scand. 25* (1971) 331.
6. Jenkis, C. L. and Kochi, J. K. *J. Org. Chem. 36* (1971) 3053.
7. Birckenbach, L. and Kellermann, K. *Ber. 58* (1925) 2378.
8. Austad, T., Engemyr, L. B. and Songstad, J. *Acta Chem. Scand. 25* (1971) 3535.

Received July 29, 1974.

The Crystal Conformation of 1,1,9,9-Tetramethylcyclohexadecane

P. GROTH

Department of Chemistry, University of Oslo, Oslo 3, Norway

By semiempirical calculations of cyclohexadecane Dale[1] has found the square, diamond

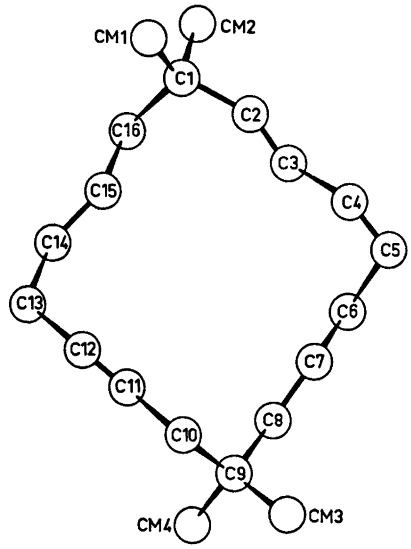

Fig. 1. Schematical drawing showing the molecular conformation.

Table 1. Final fractional coordinates and anisotropic thermal vibration parameters with estimated standard deviations (multiplied by 10^4) for carbon atoms. The symbol CM is used for the methyl carbons.

ATOM	X	Y	Z	B11	B22	B33	B12	B13	B23
C1A	506(11)	3460(4)	2755(4)	263(23)	26(3)	27(3)	41(15)	34(14)	-1(5)
C2A	1383(11)	3328(4)	3366(4)	321(24)	28(3)	23(3)	10(14)	15(14)	-9(4)
C3A	3197(11)	3114(4)	3374(4)	238(23)	28(3)	23(3)	-16(14)	-3(13)	-4(5)
C4A	3957(12)	2958(4)	3983(4)	334(27)	27(3)	26(3)	17(16)	-36(15)	-7(5)
C5A	5738(13)	2741(5)	4029(4)	360(28)	46(5)	29(3)	-24(19)	-75(16)	-8(6)
C6A	6083(10)	2154(5)	3687(4)	181(21)	38(4)	31(3)	-23(15)	-46(13)	-4(6)
C7A	5139(10)	1559(4)	3835(4)	237(23)	36(4)	24(3)	-1(15)	2(13)	-2(5)
C8A	5561(9)	976(4)	3511(3)	167(19)	29(3)	22(2)	21(13)	-9(11)	4(5)
C9A	4622(11)	348(4)	3616(4)	243(23)	27(4)	21(3)	58(15)	-4(14)	9(5)
C10A	2739(11)	433(4)	3525(4)	282(25)	22(3)	24(3)	4(14)	7(14)	3(5)
C11A	2023(10)	679(4)	2948(4)	208(21)	34(3)	24(3)	23(14)	5(13)	-5(5)
C12A	145(10)	816(4)	2912(4)	147(20)	28(3)	42(3)	-8(13)	12(13)	-9(5)
C13A	-640(10)	1080(4)	2347(4)	195(21)	31(4)	41(3)	5(15)	-42(14)	-22(6)
C14A	58(10)	1719(4)	2166(4)	230(22)	21(3)	35(3)	-12(14)	-72(13)	-12(5)
C15A	-129(10)	2254(4)	2575(3)	194(20)	28(3)	23(3)	-13(14)	-2(12)	-9(5)
C16A	548(9)	2872(4)	2374(3)	199(19)	24(3)	23(3)	23(13)	5(12)	6(5)
CM1A	1329(13)	4028(4)	2489(4)	508(33)	29(4)	29(3)	2(18)	6(17)	22(5)
CM2A	-1288(12)	3628(5)	2846(4)	339(27)	47(4)	39(3)	79(19)	-18(17)	-21(6)
CM3A	5869(12)	131(4)	4238(4)	395(29)	39(4)	31(3)	63(18)	-3(15)	24(5)
CM4A	5203(11)	-164(5)	3228(4)	332(27)	53(5)	34(3)	167(18)	39(15)	-18(6)
C1B	-401(11)	6475(4)	9728(3)	269(21)	24(4)	21(3)	4(14)	8(13)	7(5)
C2B	-2273(10)	6588(4)	9652(4)	166(18)	27(3)	25(3)	-31(13)	21(12)	-1(5)
C3B	-3029(10)	6940(4)	9989(4)	169(19)	31(3)	24(3)	-2(13)	14(12)	-3(5)
C4B	-4885(10)	6954(4)	9975(4)	177(22)	24(3)	37(3)	-37(14)	3(14)	2(5)
C5B	-5696(11)	7188(4)	8504(5)	195(22)	34(4)	48(4)	-15(16)	-7(15)	-14(6)
C6B	-5033(10)	7834(4)	8286(4)	183(21)	30(4)	31(3)	37(14)	-68(13)	-12(5)
C7B	-5187(10)	8385(4)	8699(4)	175(20)	29(4)	23(2)	-5(14)	13(12)	-8(5)
C8B	-4531(9)	9317(4)	8451(3)	178(19)	29(3)	17(2)	-14(13)	-3(11)	-3(4)
C9B	-4526(10)	9501(4)	8863(3)	208(21)	28(3)	13(2)	17(14)	11(12)	4(4)
C10B	-3601(10)	9178(4)	9439(3)	234(21)	24(3)	15(2)	8(13)	30(12)	-4(4)
C11B	-1811(10)	9253(4)	9440(3)	210(21)	31(3)	21(2)	-11(14)	-2(12)	3(4)
C12B	-1044(10)	9110(4)	10039(4)	186(21)	27(3)	23(3)	-25(14)	1(12)	-1(4)
C13B	798(11)	8899(4)	10087(4)	262(23)	30(4)	29(3)	-37(15)	-11(14)	4(5)
C14B	1956(9)	8284(4)	9755(3)	163(18)	35(3)	19(2)	-5(13)	-5(11)	1(5)
C15B	142(10)	7693(4)	9932(4)	193(20)	23(3)	27(3)	-31(13)	49(12)	-9(5)
C16B	553(9)	7983(4)	9489(3)	201(19)	32(3)	22(2)	23(14)	32(11)	-7(5)
CM1B	114(11)	6254(4)	10343(4)	308(25)	31(4)	29(3)	-13(16)	-4(15)	14(5)
CM2B	96(11)	5953(4)	9336(4)	254(22)	35(4)	40(3)	50(15)	1(14)	-9(6)
CM3B	-6333(11)	9791(4)	8929(4)	253(24)	39(4)	26(3)	76(15)	-11(14)	-2(5)
CM4B	-3686(11)	10168(4)	8557(3)	346(27)	26(3)	24(3)	-19(15)	5(14)	-1(5)

Table 2. Interatomic distances, bond angles and dihedral angles with estimated standard deviations.

DISTANCE	(Å)	DISTANCE	(Å)	DISTANCE	(Å)
C1A - C2A	1,55(1)	C2A - C3A	1,51(1)	C3A - C4A	1,53(1)
C4A - C5A	1,48(1)	C5A - C6A	1,50(1)	C6A - C7A	1,50(1)
C7A - C8A	1,48(1)	C8A - C9A	1,54(1)	C9A -C10A	1,51(1)
C10A -C11A	1,52(1)	C11A -C12A	1,52(1)	C12A -C13A	1,51(1)
C13A -C14A	1,51(1)	C14A -C15A	1,48(1)	C15A -C16A	1,49(1)
C16A - C1A	1,51(1)	C1A -CM1A	1,50(1)	C1A -CM2A	1,51(1)
C9A -CM3A	1,53(1)	C9A -CM4A	1,51(1)	C1B - C2B	1,51(1)
C2B - C3B	1,51(1)	C3B - C4B	1,50(1)	C4B - C5B	1,51(1)
C5B - C6B	1,55(1)	C6B - C7B	1,51(1)	C7B - C8B	1,55(1)
C8B - C9B	1,55(1)	C9B -C10B	1,49(1)	C10B -C11B	1,51(1)
C11B -C12B	1,50(1)	C12B -C13B	1,53(1)	C13B -C14B	1,52(1)
C14B -C15B	1,51(1)	C15B -C16B	1,53(1)	C16B - C1B	1,51(1)
C1B -CM1B	1,52(1)	C1B -CM2B	1,50(1)	C9B -CM3B	1,52(1)
C9B -CM4B	1,55(1)				

ANGLE	(°)	ANGLE	(°)
C1A - C2A - C3A	114,2(7)	C2A - C3A - C4A	111,4(6)
C3A - C4A - C5A	114,9(8)	C4A - C5A - C6A	116,8(8)
C5A - C6A - C7A	114,7(8)	C6A - C7A - C8A	114,8(8)
C7A - C8A - C9A	118,8(7)	C8A - C9A -C10A	112,1(6)
C9A -C10A -C11A	116,8(7)	C10A -C11A -C12A	113,1(8)
C11A -C12A -C13A	115,6(8)	C12A -C13A -C14A	115,4(7)
C13A -C14A -C15A	114,2(8)	C14A -C15A -C16A	112,2(7)
C15A -C16A - C1A	118,5(7)	C16A - C1A - C2A	111,8(7)
C16A - C1A -CM1A	110,1(8)	C16A - C1A -CM2A	110,2(7)
C2A - C1A -CM1A	110,4(7)	C2A - C1A -CM2A	105,1(8)
CM1A - C1A -CM2A	110,8(8)	C1B - C2B - C3B	117,7(7)
C2B - C3B - C4B	111,7(7)	C3B - C4B - C5B	113,3(8)
C4B - C5B - C6B	116,8(7)	C5B - C6B - C7B	113,1(8)
C6B - C7B - C8B	110,4(7)	C7B - C8B - C9B	114,2(6)
C8B - C9B -C10B	113,4(6)	C9B -C10B -C11B	116,1(7)
C10B -C11B -C12B	111,2(7)	C11B -C12B -C13B	115,2(7)
C12B -C13B -C14B	112,4(7)	C13B -C14B -C15B	116,7(7)
C14B -C15B -C16B	113,8(7)	C15B -C16B - C1B	117,5(7)
C16B - C1B - C2B	111,2(6)	C16B - C1B -CM1B	108,6(7)
C16B - C1B -CM2B	108,6(7)	C2B - C1B -CM1B	109,2(7)
C2B - C1B -CM2B	111,2(7)	CM1B - C1B -CM2B	107,9(7)
C8B - C9B -CM3B	108,8(6)	C8B - C9B -CM4B	105,8(6)
C10B - C9B -CM3B	110,1(7)	C10B - C9B -CM4B	110,2(7)
CM3B - C9B -CM4B	108,3(7)		

DIHEDRAL ANGLE	(°)	DIHEDRAL ANGLE	(°)
C1A - C2A - C3A - C4A	-177,6(7)	C2A - C3A - C4A - C5A	179,8(7)
C3A - C4A - C5A - C6A	-58,1(11)	C4A - C5A - C6A - C7A	-59,3(11)
C5A - C6A - C7A - C8A	-177,4(7)	C6A - C7A - C8A - C9A	-178,1(7)
C7A - C8A - C9A -C10A	54,6(10)	C8A - C9A -C10A -C11A	55,1(10)
C9A -C10A -C11A -C12A	-175,6(7)	C10A -C11A -C12A -C13A	-179,9(7)
C11A -C12A -C13A -C14A	-58,8(10)	C12A -C13A -C14A -C15A	-60,3(10)
C13A -C14A -C15A -C16A	179,0(6)	C14A -C15A -C16A - C1A	-177,8(7)
C15A -C16A - C1A - C2A	54,5(10)	C16A - C1A - C2A - C3A	58,8(10)
C1B - C2B - C3B - C4B	-177,6(7)	C2B - C3B - C4B - C5B	-178,3(7)
C3B - C4B - C5B - C6B	-60,5(10)	C4B - C5B - C6B - C7B	-57,8(10)
C5B - C6B - C7B - C8B	179,8(6)	C6B - C7B - C8B - C9B	-176,8(6)
C7B - C8B - C9B -C10B	54,1(9)	C8B - C9B -C10B -C11B	55,8(10)
C9B -C10B -C11B -C12B	-176,9(7)	C10B -C11B -C12B -C13B	-178,8(6)
C11B -C12B -C13B -C14B	-60,7(9)	C12B -C13B -C14B -C15B	-60,4(9)
C13B -C14B -C15B -C16B	-176,8(7)	C14B -C15B -C16B - C1B	-175,7(6)
C15B -C16B - C1B - C2B	53,1(10)	C16B - C1B - C2B - C3B	56,5(10)

lattice conformation to be of lowest enthalpy. Infrared spectroscopy of the low temperature crystal indicated the same conformation.[2] As part of a study of conformational problems in *gem*-dimethylsubstituted cyclohexadecanes,[3] the 1,1,9,9-tetramethylcyclohexadecane has been synthesized. Its crystal structure is now reported.

The crystals of $C_{20}H_{40}$ belong to the monoclinic system with space group $P2_1/c$ and cell dimensions $a = 8.001(3)$ Å, $b = 20.741(7)$ Å, $c = 23.388(9)$ Å, $\beta = 95.68(3)°$. There are two independent molecules in the asymmetric unit. 1873 observed reflections were measured on an automatic four circle diffractometer at room temperature (Mo$K\alpha$-radiation).

The structure was solved by direct methods [4] and refined by full-matrix least squares technique.[5] * Anisotropic temperature factors were introduced for carbon atoms. Hydrogen positions were calculated, but not refined. Weights in least squares were obtained from the standard deviations in intensities, $\sigma(I)$, taken as

* All programs used (except those for phase determination) are included in this reference.

$$\sigma(I) = [C_T + (0.02C_N)^2]^{\frac{1}{2}}$$

where C_T is the total number of counts, and C_N the net count. The R-value arrived at was 9.5 % (weighted value $R_w = 6.8$ %) for 1873 observed reflections.

Final fractional coordinates and thermal parameters with estimated standard deviations for carbon atoms are given in Table 1. The expression for anisotropic vibration is:

$$\exp[-(B11h^2 + B22k^2 + B33l^2 + B12hk + B13hl + B23kl)].$$

The principal axes of the thermal vibration ellipsoids were calculated from the temperature parameters of Table 1. Maximum r.m.s. amplitudes range from 0.26 to 0.43 Å. Due to the size of the molecule, no rigid-body analysis of translational, librational and screw motion has been carried out.

Interatomic distances, bond angles and dihedral angles are listed in Table 2. The standard deviations, in parentheses, are estimated from the correlation matrix of the last least squares refinement cycle. A list of observed structure factors is available by request to the author.

The two independent molecules, A and B, have the same square, diamond lattice conformation shown in Fig. 1. Bond distances and angles are normal.

Acknowledgement. The author would like to thank cand.real. G. Borgen for supplying the crystal, and A. Aasen for carrying out data collection.

1. Dale, J. *Acta Chem. Scand. 27* (1973) 1115.
2. Borgen, G. and Dale, J. *Chem. Commun.* (1970) 1340.
3. Bjørnstad, S. L., Borgen, G. and Dale, J. *Acta Chem. Scand. To be published.*
4. Germain, G., Main, P. and Woolfson, M. M. *Acta Crystallogr. A 27* (1971) 368.
5. Groth, P. *Acta Chem. Scand. 27* (1973) 1837.

Received August 19, 1974.

Acta Chemica Scandinavica A 28 (1974) 811—814

Potential Functions of 5-Membered Ring-molecules. II. Normal Coordinate Analysis of the Non-planar Vibrations of 1,3,4-Oxadiazole, 1,2,5-Oxadiazole and 1,2,5-Thiadiazole

T. STROYER-HANSEN

Chemistry Department, Odense University, DK-5000 Odense, Denmark

Harmonic potential functions of the non-planar vibrations of 1,3,4-oxadiazole, 1,2,5-oxadiazole, and 1,2,5-thiadiazole have been calculated by using deuterium isotopic frequency data. The results are compared with the potential functions of 1,3,4-thiadiazole, thiophene, and furane.

The normal coordinate analysis of the non-planar vibrations of 1,3,4-thiadiazole (I) has been described in a previous paper.[1] Using the same technique the normal coordinate analysis of 1,3,4-oxadiazole (II), 1,2,5-oxadiazole (III), and 1,2,5-thiadiazole (IV) will be carried out in this work.

The complete assignments of the fundamental vibration frequencies of (II),[2-4] (III),[5,6] and (IV) [7] and their deuterated species are recently made. Sufficient frequency data are, therefore, available to determine the harmonic potential functions of the non-planar vibrations of these molecules.

The geometrical structure of (II),[8] (III),[9] and (IV) [10] to be used in the calculations, are known from previous microwave spectroscopy investigations. It was shown that the molecules are planar. The parent molecules and the dideuterated species, therefore, belong to the C_{2v} point group and the four non-planar fundamental vibrations may be classified as $2A_2 + 2B_2$. The monodeuterated species belong to the C_s point group and the four non-planar fundamental vibrations may be classified as $4A''$.

CALCULATIONS

An earlier attempt to calculate the harmonic force fields of these molecules was made by Cyvin *et al.*[11] on the base of the frequency data from the parent molecules only. From an initial force field they calculated the normal frequencies, which for some of the molecules fitted rather poor to the observed frequencies. The deviations were from -23 % to $+19$ %. From these approximate force fields they calculated the vibration pictures (the **L**-matrices), *i.e.* the directions and amplitudes of the atomic motions in the normal vibrations. Keeping the **L**-matrices fixed they fitted the force constants to the observed frequencies. They determined the 6 constants from 4 data with all the uncertainty that implies.

In this investigation the 6 force constants are determined from 6 independent normal frequencies from the parent molecule and the dideuterated species. The 2 normal frequencies left are not independent because of the product rules. Unfortunately a direct comparison with the results of Cyvin *et al.*[11] is not straightforward because of the different symmetry coordinates used. Also, the assignments of the A_2 vibration frequencies have been changed radically for all of the four molecules in question.

The procedure used for the exact solution of the two-dimensional vibration problem is described in detail in Ref. 1. The two kinds of symmetry coordinates, the CH out-of-plane bending coordinates, **S**, and the ring deformation coordinates, **T**, used in this work are

Table 1. 1,3,4-Oxadiazole and its deuterated species. Assigned and adjusted frequencies (cm^{-1}).

	$C_2H_2N_2O$		C_2HDN_2O		$C_2D_2N_2O$	
	ass.	adj.	ass.	adj.	ass.	adj.
ν_7	825	825.9	727	726.2	709	709.1
ν_8	653	653.7	646	646.3	585	583.2
ν_{14}	852	851.8	840	840.6	747	747.0
ν_{15}	625	625.4	544	543.6	517	516.8

Table 2. 1,2,5-Oxadiazole and its deuterated species. Assigned and adjusted frequencies (cm^{-1}).

	$C_2H_2N_2O$		C_2HDN_2O		$C_2D_2N_2O$	
	ass.	adj.	ass.	adj.	ass.	adj.
ν_7	888	887.8	868	868.2	757	757.0
ν_8	641	642.3	631	631.4	552	552.8
ν_{14}	838	838.7	712	711.7	640	639.2
ν_{15}	631	631.4	579	578.4	631	630.2

Table 3. 1,2,5-Thiadiazole and its deuterated species. Assigned and adjusted frequencies (cm^{-1}).

	$C_2H_2N_2S$		C_2HDN_2S		$C_2D_2N_2S$	
	ass.	adj.	ass.	adj.	ass.	adj.
ν_7	908	908.2	883	883.3	781	780.9
ν_8	612	612.1	558	558.4	519	518.9
ν_{14}	838	838.8	719	718.5	651	650.4
ν_{15}	521	521.5	509	508.5	507	506.5

analogous with those used for (I), and similar to the symmetry coordinates previously used of Orza *et al.* in a normal coordinate analysis of the non-planar vibrations of thiophene (V)[12] and furane (VI).[13] The adjustment of the experimental vibration frequencies is made according to the principles earlier described.[1] The experimental and adjusted vibration frequencies for (II), (III), and (IV) are shown in Tables 1, 2, and 3, respectively. It is thus possible to calculate the three symmetry coordinate force constants, F_{SS}, F_{ST}, and F_{TT} in the harmonic potential function:

$$2V = F_{SS}S^2 + 2F_{ST}ST + F_{TT}T^2$$

in each of the two symmetry species A_2 and B_2 of each of the molecules (II), (III), and (IV).

Also, it is possible to calculate the valence coordinate force constants of the CH out-of-plane bending vibration of the three molecules:

$f_{\gamma\gamma} = \frac{1}{2}(F_{SS(B_2)} + F_{SS(A_2)})$ and $f_{\gamma\gamma'} = \frac{1}{2}(F_{SS(B_2)} - F_{SS(A_2)})$

Furthermore, one can calculate the interaction constants between the CH-valence coordinates γ and γ' and the ring deformation coordinates T in each symmetry species, A_2 and B_2:

$$f_{\gamma T} = 2^{-\frac{1}{2}}F_{ST}$$

The values of these constants are shown in Table 4, which also shows the values of the force constants of (I).[1] For comparison the corresponding values for (V) and (VI), calculated by Orza *et al.*[12,13] are included too. The uncertainties of the values are all from 0.001 to 0.002 mdyn Å/rad².

Unfortunately, there are double solutions in the determinations of the ring deformation constants F_{TT}, and the interaction constants F_{ST}. Only the CH out-of-plane bending force constants F_{SS} are unambiguously determined. This problem is well known, and has recently been treated by Fadini.[14] When expanding the secular determinant, one obtains a first-order equation and a second-order equation. The latter is the cause of the double solution. However, in order to compare the results for all of the six molecules (I) – (VI) we selected (as in Ref. 1), somewhat arbitrarily, but in agreement with Orza *et. al.*,[12,13] the set of force constants which yield the most characteristic normal modes, as those with physical significance. That is Q_7 and Q_{14} are mainly CH out-of-plane bending coordinates and Q_8 and Q_{15} are mainly ring deformation coordinates as shown of the L-matrices which have been calculated for each set of force constants of each molecule. The physical significant values are given in the upper part of Table 4, and the alternative ones are given in the lower part of the table. As will be seen the choice also gives the most similar force constants for the six molecules in question.

DISCUSSION

Since the geometry of furane, 1,2,5-oxadiazole, and 1,3,4-oxadiazole are very similar and the same is true for thiophene, 1,2,5-thiadiazole, and 1,3,4-thiadiazole it is possible to compare

Table 4. Non-planar vibration force constants of some five-membered ring molecules. (mdyn Å/rad²).

	 VI	 II	 III	 V	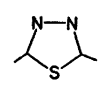 I	 IV
	VI[a]	II[b]	III[b]	V[c]	I[d]	IV[b]
$f_{\gamma(\alpha)\gamma(\alpha)}$	0.339	0.384	–	0.339	0.382	–
$f_{\gamma(\alpha)\gamma'(\alpha)}$	0.032	0.017	–	0.046	0.023	–
$f_{\gamma(\beta)\gamma(\beta)}$	0.387	–	0.425	0.395	–	0.426
$f_{\gamma(\beta)\gamma'(\beta)}$	−0.025	–	−0.018	−0.031	–	−0.017
$F_{T(A_2)T(A_2)}$	0.523	0.391	0.475	0.440	0.310	0.404
$F_{T(B_2)T(B_2)}$	0.420	0.413	0.350	0.443	0.423	0.395
$f_{\gamma(\alpha)T(A_2)} = -f_{\gamma'(\alpha)T(A_2)}$	0.115	0.115	–	0.123	0.120	–
$f_{\gamma(\alpha)T(B_2)} = f_{\gamma'(\alpha)T(B_2)}$	−0.140	−0.139	–	−0.169	−0.160	–
$f_{\gamma(\beta)T(A_2)} = -f_{\gamma'(\beta)T(A_2)}$	−0.193	–	−0.190	−0.179	–	−0.171
$f_{\gamma(\beta)T(B_2)} = f_{\gamma'(\beta)T(B_2)}$	0.078	–	0.085	0.091	–	0.086
Alternative value						
$F_{T(A_2)T(A_2)}$	0.987	0.527	0.827	0.945	0.331	0.843
$F_{T(B_2)T(B_2)}$	0.673	0.731	0.354	1.132	0.935	0.550
$f_{\gamma(\alpha)T(A_2)} = -f_{\gamma'(\alpha)T(A_2)}$	0.203	0.196	–	0.178	0.135	–
$f_{\gamma(\alpha)T(B_2)} = f_{\gamma'(\alpha)T(B_2)}$	−0.254	−0.288	–	−0.361	−0.360	–
$f_{\gamma(\beta)T(A_2)} = -f_{\gamma'(\beta)T(A_2)}$	0.332	–	0.338	0.367	–	0.355
$f_{\gamma(\beta)T(B_2)} = f_{\gamma'(\beta)T(B_2)}$	0.102	–	0.090	0.235	–	0.198

[a] From Ref. 13. [b] This work. [c] From Ref. 12. [d] From Ref. 1.

the force constants of these molecules. From Table 4 it can be seen that the CH out-of-plane bending force constants are of equal size in the analogous oxygen and sulfur compounds of these five-membered ring molecules. However, it also shows that introducing two N-atoms in the furane or thiophene ring causes an increase of these force constants. Contrarily, introducing the two N-atoms in the furane or thiophene ring causes a decrease of the ring deformation force constants, especially the force constants of the symmetry coordinates that mainly involve torsional motion of a N–N, N–O, or an N–S bond, *i.e.* T_{A_2} of the 1,3,4-compounds and T_{B_2} of the 1,2,5-compounds. In other words, it is easier to twist a bond between heteroatoms than a C–C bond in these five-membered heteroatomic ringmolecules.

Acknowledgement. The author wishes to thank Dr. D. Christensen and co-workers at the Chemical Laboratory V, University of Copenhagen, for kind permission to use their preliminary and final results of the vibrational assignments for the three ring molecules studied before publication.

REFERENCES

1. Christensen, D. H. and Stroyer-Hansen, T. *Acta Chem. Scand. 26* (1972) 923.
2. Christensen, D. H., Tormod Nielsen, J. and Nielsen, O. F. *J. Mol. Spectrosc. 24* (1967) 225.
3. Christensen, D. H., Tormod Nielsen, J. and Nielsen, O. F. *J. Mol. Spectrosc. 25* (1968) 197.
4. Antonsen, J., Christensen, D. H. and Nielsen, O. F. *To be published.*
5. Christensen, D. H. and Nielsen, O. F. *J. Mol. Spectrosc. 24* (1967) 477.
6. Christensen, D. H., Jensen, P. W. and Nielsen, O. F. *Spectrochim. Acta A 29* (1973) 1393.
7. Christensen, D. H., Lund, P. A., Nielsen, O. F. and Tormod Nielsen, J. *To be published.*
8. Nygaard, L., Hansen, R. L., Tormod Nielsen, J., Rastrup-Andersen, J., Sørensen, G. O. and Steiner, P. A. *J. Mol. Struct. 12* (1972) 59.

9. Saegebarth, E. and Cox, A. P. *J. Chem. Phys. 43* (1965) 166.
10. Dobyns, V. and Pierce, L. *J. Amer. Chem. Soc. 85* (1963) 3553.
11. Cyvin, B. N. and Cyvin, S. J. *Acta Chem. Scand. 23* (1969) 3139.
12. Orza, J. M., Rico, M. and Biarge, J. F. *J. Mol. Spectrosc. 19* (1966) 188.
13. Orza, J. M., Rico, M. and Barrachina, M. *J. Mol. Spectrosc. 20* (1966) 233.
14. Fadini, A. *Z. Naturforsch. 24* (1969) 208.

Received May 8, 1974.

Acta Chemica Scandinavica A 28 (1974) 815—822

Protolytic Reactions of Orthoesters and Ketene Acetals in Ethanol. Mechanistic Implications of Isotope Exchange Studies

A. KANKAANPERÄ, M. KANTANEN, P. ALAKUIJALA and L. OINONEN

Department of Chemistry, University of Turku, SF-205 00 Turku 50, Finland

Protolytic reactions in ethanol of triethyl orthoesters and the corresponding ketene acetals were studied. Firstly, the rate of the exchange of the ethoxy group in different orthoesters was measured using carbon-14 labeling. A linear correlation was observed between the logarithms of the rate coefficients and the σ^*-values of the substituents attached to the reaction center. Secondly, the detritiation of the orthoesters labeled at the α-position of the acid component was studied in ethanol. Thirdly, the acid-catalyzed ethanolysis of ketene acetals was subjected to a kinetic study. On the basis of the kinetic results the energetics of the total reaction from orthoesters to the corresponding ketene acetals is discussed.

In a recent work [1] isotope exchange studies have been found to be an excellent method to study the energetics of the partial reactions between acetals and vinyl ethers. Thus it is reasonable to assume that this method can also be applied to the study of the protolytic reactions of structurally related compounds, the orthoesters (I) and the ketene acetals (II), Although the hydrolytic decomposition of these

$R_1R_2CHC(OR)_3$ (I) $R_1R_2C=C(OR)_2$ (II)

compounds has been studied in detail [2,3] no quantitative data are available on the energetics of the reaction from orthoesters to the corresponding ketene acetals, a reaction which evidently takes place since dioxo-carbenium ions are intermediates in the hydrolysis of both orthoesters and ketene acetals (eqn. 1). In aqueous solution the dioxo-carbenium ion is rapidly decomposed to a carboxylic acid ester and alcohol and thus the interconversion of an orthoester and a ketene acetal through

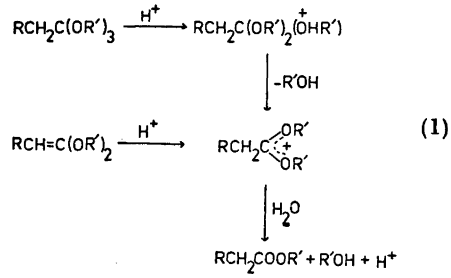

(1)

their common intermediate cannot be studied kinetically. In alcohol solution, however, this interconversion can be investigated by means of isotope labeling. Schroeder [4] has previously studied in ethanol the hydrogen exchange reactions of orthoesters using NMR and mass-spectral methods. These data show qualitatively that the acid-catalyzed protolysis of an orthoester leads to a hydrogen isotope exchange in the methyl group attached directly to the carbenium ion center of the reaction. Detailed kinetic data are, however, required to get information on the energetics of the process.

The protolytic reactivity of orthoesters [2] and ketene acetals [3] is generally quite high. Therefore, great experimental difficulties are encountered when protolytic reactions of structurally different compounds are studied in water. However, if ethanol is employed as the solvent, the measurements can be extended to temperatures markedly below 0 °C and under these conditions even highly reactive compounds can be studied. In the present work the following triethyl orthoesters were subjected to a kinetic study in ethanol: the orthopro-

pionate, the orthoacetate, the orthoformate, the orthobenzoate, the monochloro-orthoacetate, and the dichloro-orthoacetate.

EXPERIMENTAL

Materials. The following orthoesters were commercial products: ethyl orthopropionate (Fluka), ethyl orthoacetate (Fluka), ethyl orthoformate (E. Merck), and ethyl orthobenzoate (Fluka).

1-Chloro-2,2-diethoxyethene was prepared by refluxing 1,1-dichloro-2,2-diethoxyethane with potassium *tert*-butoxide in *tert*-butyl alcohol.[2c,5] The potassium chloride formed in the reaction was filtered off and the solvent and the ketene acetal were separated by distillation. B.p. 75 °C/35 Torr. NMR spectrum: δ 4.50 (1 H), 4.00 and 3.78 (4 H), and 1.30 (6 H).

1,1,1-Trichloro-2,2-diethoxyethane was prepared from trichloroacetaldehyde and ethanol using a large excess of concentrated sulfuric acid as the catalyst.[2c,5] B.p. 153 °C/95 Torr. NMR spectrum: δ 4.60 (1 H), 3.80 (4 H) and 1.25 (6 H).

1,1-Dichloro-2,2-diethoxyethene was prepared from the corresponding acetal by refluxing with potassium *tert*-butoxide in *tert*-butyl alcohol.[2c,5] After potassium chloride had been filtered off, the residue was fractionated. B.p. 85–90 °C/34 Torr. NMR spectrum: δ 3.90 (4 H) and 1.30 (6 H).

Carbon-14 labeling. Two alternative methods were employed in the present work. Most of the orthoesters were labeled through an acid-catalyzed transesterification (eqn. 2). In reaction (2) only the transfer of the carbon-14 labeling from the solvent to the

$$RC(OEt)_3 \xrightarrow[H^+]{Et^*OH} RC(OEt)_2OEt^* \qquad (2)$$

orthoester took place. This method was applied in the case of the orthopropionate, the orthoacetate, the orthoformate, and the orthobenzoate. About 10 vol. % of ethanol with about 20 μCi of the labeled ethanol (The Radiochemical Centre), and a small amount of *p*-toluenesulfonic acid as catalyst was added to 10 ml of the orthoester. The mixture was refluxed for about 3 h, whereupon the catalyst was neutralized with sodium ethoxide, and the product purified by distillation in vacuum. The purity of the orthoester was checked by NMR spectroscopy. The degree of the carbon-14 labeling was determined with an LKB-81000 liquid scintillation counter. The activity of the labeled orthoesters varied from 2000 to 10 000 cpm per μl.

The monochloro-orthoacetate and dichloro-orthoacetate were labeled by alcoholysing the corresponding ketene acetals in ethanol labeled with carbon-14 (eqn. 3). In the case of the mono-

$$R_1R_2C=C(OEt)_2 \xrightarrow{Et^*OH} R_1R_2CHC(OEt)_2OEt^* \qquad (3)$$

chloro derivative the reaction mixture contained 3.3 g of 1-chloro-2,2-diethoxyethene, 1.1 g of absolute ethanol and 15 μCi of carbon-14 labeled ethanol. After refluxing for 15 min the formed 1-chloro-2,2,2-triethoxyethane was purified by distillation. B.p. 85–90 °C/25 Torr. NMR spectrum: δ 3.76 (6 H), 3.46 (2 H), and 1.20 (9 H). The labeled 1,1-dichloro-2,2,2-triethoxyethane was synthesized by refluxing for 15 min a mixture of 2.9 g of 1,1-dichloro-2,2-diethoxyethene, 0.8 g of absolute ethanol, and 15 μCi of the carbon-14 labeled ethanol. A fraction at 100–105 °C/42 Torr was collected. NMR spectrum: δ 5.73 (1 H), 3.78 (6 H), and 1.23 (9 H). The labeled substrates gave from 3000 to 7000 cpm per μl.

Tritium labeling of orthoesters. Two alternative methods were also employed in the tritium labeling of the orthoesters. In the case of the orthoacetate and the orthopropionate the orthoester was sealed in an ampoule with about ten vol. per cent of absolute ethanol and a few μl of tritiated water. *p*-Toluenesulfonic acid was used as the catalyst. The ampoule was kept at 120 °C for about one day whereupon the reaction mixture was neutralized with sodium ethoxide and fractionated. The purity of the product was checked by NMR spectroscopy. In scintillation counting 1 μl of the product gave about 10^5 cpm.

In the tritiation of monochloro-orthoacetate and dichloro-orthoacetate an alternative route (eqn. 4) was followed. A mixture of 2.5 g

$$R_1R_2C=C(OEt)_2 \xrightarrow{EtOH^*} R_1R_2CH^*C(OEt)_3 \qquad (4)$$

of 1-chloro-2,2-diethoxyethene and 0.8 g of absolute ethanol was refluxed with tritiated water for 15 min. The product, 1-chloro-2,2,2-triethoxyethane, was purified by distillation. In the case of 1,1-dichloro-2,2,2-triethoxyethane, 2.2 g of 1,1-dichloro-2,2-diethoxyethene and 0.6 g of absolute ethanol was employed. The practical performance of the synthesis was identical with that of the monochloro derivative. The purity of the orthoester was checked by NMR spectroscopy.

Kinetic measurements. All the kinetic measurements were performed in absolute ethanol. The commercial alcohol (99.5 %) was dried by a standard method.[6] Perchloric acid was used as catalyst in the kinetic measurements. If the amount of the added acid was rather low (lower than 10^{-3} M) the oxonium ion concentration of the solution was measured by a kinetic method using as standard reaction the acid-catalyzed exchange of the ethoxy group

of the carbon-14 labeled acetaldehyde diethyl acetal (see Ref. 7). The rate of the carbon-14 exchange of this acetal had been measured previously.[1]

The isotope exchange studies were performed as follows: The acid solution (generally 60 ml) was kept in an electronically controlled Lauda thermostat to attain the desired temperature. Depending on the activity of the substrate from 0.05 to 0.5 vol. % of the orthoester was added and after vigorous shaking 5 ml samples were taken from the reaction mixture at suitable intervals. The reaction was stopped by transferring the samples into an aqueous solution (20 ml) which contained sodium hydroxide in sufficient amount to neutralize the catalyst. The progress of the reaction was followed by measuring the activity of the substrate, the orthoester, which was extracted into an organic solvent prior to the scintillation counting. In the case of the acetals [1] the best results were obtained when using a 2/1 mixture of cyclohexane and anisole, and this mixture was also employed in the case of the orthoesters. The extraction was performed immediately after the sample had been taken from the reaction mixture to prevent possible side-reactions. Sodium chloride was added to the aqueous solution to increase the efficiency of the extraction process. Under these conditions most of the orthoester could be extracted into the organic layer and the amount of the solvent, ethanol, transferred into the organic layer was found to be negligible. The amount of the orthoester extracted into the organic phase was found to be quite constant by this procedure, about 95 %. After the two phases had been separated, 5 ml samples were transferred from the organic layer into the vials of the scintillation counter. Before counting 10 ml of the scintillation liquid (4 g of diphenyloxazole and 0.1 g of *p*-bis(*o*-methylstyryl) benzene in 1 l of toluene) was added into the vials. In some cases the increase of the activity in the water solution was also followed. In these measurements permafluor II was used as the scintillation liquid. The measured activities were corrected using the external standardization method.

The alcoholysis of the ketene acetals was followed with a Unicam SP 800 spectrophotometer. In the case of 1,1-dichloro-2,2-diethoxyethene the perchloric acid solution was kept in the cell housing block of the spectrophotometer to attain the desired temperature. After 1 μl of the ketene acetal had been added, its alcoholysis was followed by measuring the disappearance of the absorption of the carbon-carbon double bond at 245 nm. In the case of 1-chloro-2,2-diethoxyethene direct measurements in the cell could not be performed since, the measurements had to be carried out at temperatures lower than 0 °C due to the high rate of hydrolysis of this ketene acetal. Under these conditions, however, the measurements were difficult to perform since moisture from the air would condense on the surfaces of the cells. The measurements were therefore performed in separate reaction flasks which had been kept at temperatures between -10 and -30 °C. After the perchloric acid solution (60 ml) had reached the temperature of the thermostat, 3 μl of the ketene acetal was added. 5 ml samples were withdrawn at suitable intervals from the reaction mixture and transferred immediately into flasks which contained a sufficient amount of sodium ethoxide to neutralize the catalyst. Finally, the samples were analyzed spectrophotometrically at 213 nm.

RESULTS AND DISCUSSION

Rates of formation of dioxo-carbenium ions from orthoesters. Although the acid-catalyzed alcoholysis of orthoesters has not previously been subjected to kinetic studies, it can be concluded on the basis of the kinetic results for the related reaction, the hydrolysis of orthoesters,[3] that dioxo-carbenium ions are formed in the rate-determining stage of this reaction. In other words, the rate of the dioxo-carbenium ion formation is equal to that of the formation of the final product. When the transesterification of triethyl orthoesters (eqn. 5) is studied using carbon-14 labeling at the ethoxy group, the isotope effects can be assumed to be negligible.[1]

$$RC(OEt)_3 \xrightarrow[-EtOH]{H^+} RC\overset{OEt}{\underset{OEt}{\overset{|}{\overset{+}{}}}} \xrightarrow[-H^+]{EtOH} RC(OEt)_3 \qquad (5)$$

The kinetic data for the acid-catalyzed transesterification (carbon-14 exchange) of different orthoesters are collected in Table 1. Depending on the reaction rate temperatures between 204 and 298 K were used in the measurements and for each compound the measurements were performed at 3 to 5 temperatures. Except in the case of the rate coefficients determined at the lowest temperatures (lower than 230 K) the standard errors of the rate coefficients are lower than two per cent. The larger standard errors of the rate coefficients measured at temperatures lower than 230 K are probably due to experimental difficulties since under these conditions the reaction does not stop immediately after the withdrawal of the sample. Although the pipette had been cooled to the temperature of the reaction mixture, the relatively large temperature

Table 1. Kinetic data for the oxonium ion-catalyzed isotope exchange of triethyl orthoesters $RC(OEt)_2OEt^*$ in ethanol at different temperatures. The asterisk denotes the carbon-14 labeling. The activation parameters are calculated at 273.15 K.

R	Temperature K	k M^{-1} s^{-1}	$\Delta H^{\neq}$ kcal mol^{-1}	$\Delta S^{\neq}$ cal $K^{-1}mol^{-1}$	$\Delta G^{\neq}$ kcal mol^{-1}	k_{273} M^{-1} s^{-1}
CH_3CH_2	212.6	7.21 ± 0.18				
	223.7	36.8 ± 1.6	12.3 ± 0.3	4.2 ± 1.2	11.17 ± 0.06	6580 ± 680
	223.7	36.8 ± 1.5				
	253.7	1038 ± 20				
CH_3	204.6	5.27 ± 0.19				
	212.6	19.6 ± 0.5				
	223.7	87.5 ± 3.0	12.2 ± 0.3	5.5 ± 1.5	10.72 ± 0.08	14910 ± 2230
	223.7	78.1 ± 1.0				
	232.9	245 ± 2				
H	232.6	1.530 ± 0.007				
	242.0	5.00 ± 0.18				
	242.0	4.52 ± 0.10	12.8 ± 0.2	−2.3 ± 0.9	13.39 ± 0.02	110.6 ± 5.0
	251.9	13.55 ± 0.09				
	251.9	14.21 ± 0.27				
	261.7	38.0 ± 0.2				
Phenyl	253.2	0.695 ± 0.004				
	263.2	2.27 ± 0.02				
	273.2	7.33 ± 0.04	16.4 ± 0.5	5.6 ± 1.7	14.83 ± 0.02	7.71 ± 0.31
	283.2	24.6 ± 0.2				
$ClCH_2$	263.2	3.58 ± 0.02				
	263.2	3.09 ± 0.06				
	273.2	11.96 ± 0.17	16.3 ± 0.9	6.1 ± 3.3	14.64 ± 0.03	10.97 ± 0.57
	283.2	31.7 ± 0.4				
Cl_2CH	278.2	0.0620 ± 0.0004				
	283.2	0.1098 ± 0.0011				
	288.2	0.199 ± 0.003				
	293.2	0.302 ± 0.002	15.6 ± 0.8	−7.7 ± 2.9	17.71 ± 0.05	0.0382 ± 0.0033
	298.2	0.431 ± 0.004				

gradient would raise the temperature of the solution in the pipette before its content was added to the quenching solution.

The activation entropies for the transesterification of the studied compounds vary between +6 and −8 cal K^{-1} mol^{-1}. Correlation with the polar nature of the acid component of the orthoester cannot be observed. The values of this magnitude are in accordance with a mechanism in which the solvent has not taken part in the transition state of the reaction.[8] Conclusions cannot, however, be drawn with regard to the timing of the proton transfer in the transition state of the reaction; the proton transfer process may be a pre-equilibrium or a rate-determining stage of the reaction.

In order to get an improved understanding of the structural effects in the studied exchange reaction, the rate coefficients were extrapolated to a certain temperature. To minimize the errors caused by the extrapolation 273 K was used as a reference temperature as it lies in the middle of the temperature range in which the measurements were performed. The logarithms of the rate coefficients at 273 K were plotted against the polar constants of the substituents [9] attached to the reaction center (Fig. 1). Except in the case of the phenyl substituted derivative there is a satisfactory linear free energy correlation (corr. coeff. 0.995): $\log k_{obs} = (-2.6 \pm 0.2)\sigma^* + (3.6 \pm 0.2)$. This dependence reveals that the structural effects are comparable with those found in the hydrolysis of structurally related acetals. The only difference is the slightly diminished influence of the structure as shown by the ϱ^*-value of -2.6 ± 0.2, which is somewhat more positive than the value of −3.8 observed for the hydrolysis of acetals.[10]

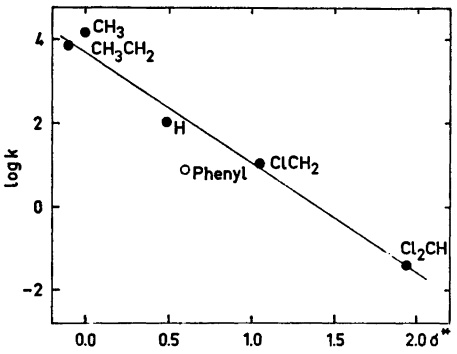

Fig. 1. The logarithms of the rate coefficients for the oxonium ion-catalyzed transesterification of triethyl orthoesters $RC(OEt)_2OEt^*$ in ethanol *versus* the polar constants of the substituents R. The points with filled circles were used in the linear free energy correlation.

This similarity is understandable since it is reasonable to assume that the stabilizing effect of the substituent attached to the carbenium ion center is somewhat similar in oxo-carbenium and dioxo-carbenium ions, the intermediates in the protolytic decomposition of acetals and orthoesters, respectively. In one particular case, in the hydrolysis of diethyl 2,2,2-trichloroethyl orthoesters, structural effects in the orthoester hydrolysis have been studied in detail.[5] In this series the ϱ^*-value was found to be -2.2, which is only slightly more positive than the one observed in the present work for the alcoholysis of orthoesters.

Of the compounds studied in the present work the phenyl-substituted derivative seems to be an exception since this compound is alcoholysed markedly slower than is expected on the basis of the linear free energy correlation (Fig. 1). A similar phenomenon has previously [5] been observed in the hydrolysis of unsymmetrical orthoesters. The exceptional reactivity of the phenyl-substituted derivative is even more marked than shown in Fig. 1 since conjugation effects should be significant in the transition state of this reaction. The relatively low rate of this derivative is understandable if, as a result of steric effects, the conjugation in the dioxo-carbenium like transition state is lower here than in protolytic reactions of aliphatic orthoesters.

Alcoholysis of ketene acetals. Ketene acetals are generally highly reactive and in water the hydronium ion-catalyzed reactions are so fast that the progress of the hydrolysis cannot be followed by conventional methods even at low temperatures.[2b] When the oxonium ion-catalyzed reaction is performed in ethanol, the ketene diethyl acetals derived from the orthoacetate and the orthopropionate are also too reactive for a study of the oxonium ion-catalyzed reaction. Since ketene acetals derived from the orthoformate and the orthobenzoate do not exist, only the alcoholysis of ketene acetals derived from monochloro- and dichloro-orthoacetate could be subjected to kinetic studies in ethanol. The obtained data are collected in Table 2.

The activation entropies for the alcoholysis of the studied ketene acetals are $+8$ and -15 cal K^{-1} mol^{-1}. Values of this magnitude are typical of reactions in which the proton transfer to the carbon atom takes place in the rate-determining stage of the reaction, as is the case in the hydrolysis of vinyl ethers [11] and

Table 2. Kinetic data for the oxonium ion-catalyzed alcoholysis of ketene diethyl acetals $R_1R_2C=C(OEt)_2$ in ethanol. Perchloric acid was used as catalyst. The parameters of activation are given at 273.15 K.

R_2	R_2	Temperature K	k M^{-1} s^{-1}	$\Delta H^{\neq}$ kcal mol^{-1}	$\Delta S^{\neq}$ cal K^{-1} mol^{-1}	$\Delta G^{\neq}$ kcal mol^{-1}	k_{273} M^{-1} s^{-1}
H	Cl	244.2	67.5 ± 2.1				
		245.2	70.5 ± 1.4				
		253.2	208 ± 5	14.1 ± 0.6	8.0 ± 2.4	11.92 ± 0.06	1620 ± 170
		263.2	567 ± 11				
Cl	Cl	280.2	0.0382 ± 0.0003				
		288.2	0.0805 ± 0.0009				
		298.2	0.186 ± 0.002	13.9 ± 0.1	−15.3 ± 0.4	18.07 ± 0.01	0.01980 ± 0.0003
		308.2	0.404 ± 0.003				

ketene acetals.[2] Although the activation entropy is a poor criterion of the reaction mechanism there is no reason to assume that the closely related reactions, the hydrolysis and the alcoholysis of ketene acetals, proceed through different routes.

Detritiation of orthoesters. In these experiments great difficulties were encountered. As first-order kinetics was not strictly obeyed, the kinetic data for reaction (6) are only approximate.

$$R_1R_2CTC(OEt)_3 \xrightarrow[-EtOH]{H^+} R_1R_2CTC\overset{OEt}{\underset{OEt}{\overset{+}{\diagdown\diagup}}} \xrightarrow{-T^+}$$

$$R_1R_2C{=}C(OEt)_2 \xrightarrow[EtOH]{H^+} R_1R_2CHC(OEt)_3 \qquad (6)$$

In preliminary experiments reaction (6) could not be observed although the substrate, triethyl orthoacetate, and the solvent, ethanol, were extracted into different phases. The main reason for the apparent lack of reaction appear to be parallel side-reactions. The fact that the solvent contains small amounts of water, although the applied ethanol was carefully dried, hydrolytic decomposition as described in eqn. 7 will occur.

$$CH_2TC(OEt)_3 \xrightarrow[-EtOH]{H^+} CH_2TC\overset{OEt}{\underset{OEt}{\overset{+}{\diagdown\diagup}}} \xrightarrow[-EtOH]{H_2O} CH_2TCOOEt \qquad (7)$$

If the substrate decomposes mainly through this route no changes can be observed when the activity of the water layer and the organic layer are followed, since the product of reaction (7) also remains in the organic layer as does the initial substrate. Side-reaction (7) is favored under the conditions employed as the rate of this reaction must be markedly higher than the rate of the triton abstraction from the dioxocarbenium ion (eqn. 6). Furthermore it can be assumed that the equilibrium of reaction (7) is mainly on the side of the product even in solutions in which the amount of water is relatively low since orthoesters have been found to be excellent agents for quantitative removal of water from reaction mixtures.[12] In the present reaction water could thus be removed from the reaction mixture by using the substrate in excess. 2 – 10 vol. % of the unlabeled triethyl orthoacetate was therefore added to the reaction mixture prior to the detritiation reaction. Although the detritiation reaction in this way could be followed, the accuracy of the kinetic results was rather low; the standard errors of the measured rate coefficients varied from 2 to 6 % and the variation in the parallel experiments was relatively high; for instance, at 298 K values of rate coefficients between 10^{-2} and 4×10^{-2} M^{-1} s^{-1} were observed. On the basis of the transition state theory the free energy of activation can be calculated to be of the magnitude of 20 kcal mol^{-1}. For the detritiation of triethyl orthopropionate the values of $\Delta G^{\neq}$ were found to be of the same order of magnitude. The detritiation studies could not be performed on formic acid and benzoic acid derivatives due to the lack of exchangeable α-hydrogen atoms. In the case of triethyl monochloro-orthoacetate and triethyl dichloro-orthoacetate approximate values of 22 and 24 kcal mol^{-1} were obtained for the free energy of activation, respectively.

Total reaction from orthoester to ketene acetal. The kinetic data in the present work give information on the energetics of the reaction from triethyl orthoesters to the corresponding ketene acetals (Fig. 2) if the possible isotope effects can be excluded. As discussed above in the case of carbon-14 exchange this assumption appears to be justified. In addition it can be

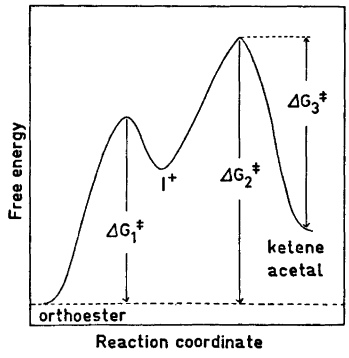

Fig. 2. Free energy profile for the protolytic decomposition of orthoesters to ketene acetals in ethanol. The intermediate I^+ is the dioxocarbenium ion. Notations: (1) the transacetalization of the orthoester, (2) the detritiation of the orthoester, and (3) the alcoholysis of the ketene acetal.

concluded that in the withdrawal of hydrogen nucleus the primary tritium isotope effect cannot be significant if the uncertainty of the experimental data is taken into consideration.

For the first stage of the total reaction from orthoesters to ketene acetals, the formation of the dioxo-carbenium ion, quantitative kinetic data in ethanol are available (Table 1). It is found that the rate of this partial reaction is relatively high since the second-order rate coefficients at 273 K vary between 0.04 and 15 000 M^{-1} s^{-1}.

In the second stage of the total reaction, the proton is abstracted from the methyl group attached directly to the carbenium ion center. When the approximate $\Delta G^{\ddagger}$ values for the detritiation of the orthoacetate and the monochloro-orthoacetate are compared, it is found that $\Delta(\Delta G^{\ddagger})$ is of the magnitude of 2 kcal mol^{-1}, which is less than the corresponding difference between the carbon-14 exchange reactions ($\Delta(\Delta G^{\ddagger}) = 3.92$ kcal mol^{-1}). This observation may suggest that the chlorine substitution makes the hydrogen atoms attached to the same carbon atom more acidic and thus accelerate the following proton withdrawal although the dioxo-carbenium ion formation is retarded by the chlorine substituent. A similar effect can also be observed when the reactions of triethyl orthoacetate and triethyl dichloro-orthoacetate are compared: $\Delta(\Delta G^{\ddagger}) = 4$ kcal for the detritiation is less than $\Delta(\Delta G^{\ddagger}) = 6.99$ kcal observed for the carbon-14 exchange reaction. The free energy difference between the transition states of the carbon-14 exchange reaction and the detritiation reaction thus appear to decrease with the number of the electronegative substituents attached at the carbon atom adjacent to the carbenium ion. However, in spite of this tendency the energy difference between the different transition states is still about 6 kcal in the case of the dichloro derivative. It is interesting to note that for the related reactions of acetals and vinyl ethers [1] the energy levels of the different transition states are almost equal in the case of the dichloro derivative. In the total reaction from orthoesters to ketene acetals the dioxo-carbenium ion formation seems always to be a pre-equilibrium process. Although the kinetic data discussed above refer to dilute solutions in ethanol the observed energy difference can be assumed to be of the same magnitude also in other solvent systems.

When discussing the energetics of the total reaction from orthoesters to the corresponding ketene acetals, the kinetic data for the alcoholysis of ketene acetals can also be applied since the proton abstraction from the dioxo-carbenium ion and the proton transfer to the ketene acetal are reverse reactions. For the alcoholysis of 1-chloro-2,2-diethoxyethene the free energy of activation was found to be 11.92 kcal mol^{-1} (Table 2). When this $\Delta G^{\ddagger}$ value is compared with that of the corresponding detritiation reaction, it can be concluded that the ketene acetal is on an energy level which is approximately 10 kcal higher than that of the corresponding orthoester. In the case of the dichloro derivative the free energy difference between the orthoester, and the ketene acetal is about 6 kcal. This means that in both cases equilibrium concentrations of the ketene acetals are relatively low.

On the basis of the kinetic results of the present work it can be concluded that the route from orthoesters to ketene acetals has limited practical importance and especially when taken into account the facile polymerization of ketene acetals in acid solutions. The reverse reaction, however, the alcoholysis of ketene acetals, appears to be an important synthetic route to the corresponding orthoesters in which they can be obtained in nearly quantitative yield.

Acknowledgement. Grants for support of this work from the Finnish Academy, Division of Sciences, are gratefully acknowledged.

REFERENCES

1. Kankaanperä, A., Salomaa, P., Juhala, P., Aaltonen, R. and Mattsen, M. *J. Amer. Chem. Soc. 95* (1973) 3618.
2. a. Gold, V. and Waterman, D. *J. Chem. Soc. B* (1968) 839, 849; b. Kankaanperä, A. and Tuominen, H. *Suom. Kemistilehti B 40* (1967) 271; c. Straub, T. S. *Ph.D. Thesis*, Illinois Institute of Technology, Chicago 1970; d. Kankaanperä, A. and Aaltonen, R. *Acta Chem. Scand. 26* (1972) 1698.
3. a. Cordes, E. H. *Progr. Phys. Org. Chem. 4* (1967) 1, and references therein; b. Cordes, E. H. In Patai, S., Ed., *The Chemistry of the Carboxylic Acids and Esters*, Interscience, London 1969, pp. 623–667.

4. Schroeder, L. R. *J. Chem. Soc. B* (1970) 1789.
5. Kankaanperä, A., Lahti, M. and Aaltonen, R. *Acta Chem. Scand. 27* (1973) 1444.
6. Vogel, A. I. *Practical Organic Chemistry*, 3rd Ed., Longmans, London 1967, p. 167.
7. Kankaanperä, A., Taskinen, E. and Salomaa, P. *Acta Chem. Scand. 21* (1967) 2487.
8. Schalegar, L. L. and Long, F. A. In Gold, V. *Advances in Physical Organic Chemistry*, Academic, London 1963, pp. 27–29.
9. Taft, Jr., R. W. *J. Amer. Chem. Soc. 75* (1953) 4231.
10. Kreevoy, M. M. and Taft, Jr., R. W. *J. Amer. Chem. Soc. 77* (1955) 5590.
11. a. Kresge, A. J. and Chiang, Y. *J. Chem. Soc. B* (1967) 53, 58; b. Salomaa, P., Kankaanperä, A. and Lajunen, M. *Acta Chem. Scand. 20* (1966) 1790.
12. DeWolfe, R. H. *Carboxylic Acid Ortho Ester Derivatives*, Academic, New York 1970, p. 154.

Received March 27, 1974.

Acta Chemica Scandinavica A 28 (1974) 823—828

Metal Halide and Pseudohalide Complexes in Dimethylsulfoxide Solution. I. Dimethyl Sulfoxide Solvates of Silver(I), Zinc(II), Cadmium(II). and Mercury(II)

STEN AHRLAND and NILS-OLOF BJÖRK

Inorganic Chemistry 1, Chemical Center, University of Lund, P.O.B. 740, S-220 07 Lund, Sweden

Solid dimethyl sulfoxide solvates of silver(I), zinc(II), cadmium(II), and mercury(II) have been prepared. Their infrared spectra indicate that in all the solvates studied DMSO is coordinated *via* oxygen. The solvates have also been characterized by thermogravimetric measurements. The paper also contains an introduction to the investigations of solution equlibria in DMSO which are presently in progress.

The nature of the solvent has a great influence upon the formation of complexes between chemical species in solution. The solvent acts in two ways. First, it provides a medium of which the dielectric constant, D, determines the electrostatic forces of interaction between ions and dipoles present. Second, it forms solvates, thus competing with other coordination reactions which may take place in the solution.

The aim of the present series of investigations is to study the effect of a drastic change of solvent upon a number of complex formation reactions involving acceptors and donors of different bonding characteristics. As the large majority of existing data refers to aqueous solutions, water should evidently be chosen as the solvent of reference and the other solvent should thus have properties very different from those of water. This is certainly achieved if an aprotic solvent is chosen. In such a solvent the solvation of all ligands forming strong hydrogen bonds with water must be much weaker than in aqueous solution. This inference is supported by evidence gathered from very diverse experimental approaches, *viz.* from solvent activity coefficients, mainly determined by solubility measurements,[1–4] from Stokes ionic radii, calculated from ionic mobilities,[5] and from infrared spectra.[6] On the other hand, large and strongly polarizable ligands may well be more strongly solvated in an aprotic solvent.[1–4] Complexes formed by ligands able to form strong hydrogen bonds should therefore be much more stable in aprotic solvents than in water relative to complexes formed by ligands not able to form such bonds. Further, if the solvation of the metal ion is not much stronger in the aprotic solvent, the complexes formed by hydrogen bonding ligands must be not only relatively but also absolutely much stronger in aprotic solvents than in water. This tendency is further strengthened if, as is usually the case, the aprotic solvent has a lower D than water, resulting in a stronger electrostatic interaction.

Once it is recognized that hydrogen bonding ligands form stronger complexes in aprotic than in protic solvents, mainly because of the decrease of the desolvation energies, it is evident that the complex formation reactions should generally be rather more exothermic in the aprotic solvents. Also the increase in electrostatic interaction due to the lower D should act in the same direction. On the other hand, the desolvation accompanying the complex formation should involve a much smaller increase of the entropy in the aprotic than in the protic solvents. The decrease of $\Delta G°$ foreseen for the formation of complexes of hydrogen bonding ligands in aprotic solvents relative to protic ones should thus generally be brought about by a large decrease of $\Delta H°$, while a

simultaneous decrease of $\Delta S°$ will to some extent act in the opposite direction.

For ligands forming no hydrogen bonds the desolvation energy may, on the other hand, be much the same in protic and aprotic solvents. Again provided that the solvation energies of the metal ions are not of very different strength in the various solvents, no large difference in the values of $\Delta H°$ and $\Delta S°$, and consequently in the stability of the complexes, are to be expected. It is possible, however, that the ligand and/or the metal ion are selectively solvated by, *e.g.*, the aprotic solvent. In such case, great differences between the strengths of the complexes formed in the two solvents are of course bound to occur.

A thorough analysis of the various influences exerted by the solvent obviously demands the determination of both the stepwise stability constants, K_n, which directly yield values of $\Delta G°_n$, and the enthalpy changes, $\Delta H°_n$, for the formation of each consecutive complex. The present investigations will thus include equilibrium measurements as well as calorimetric determinations of the corresponding enthalpies of reaction.

The halide ions provide a suitable series of ligands for the test of the conclusions drawn above as their hydrogen bonding properties strongly decrease from the fluoride to the iodide ion as is also clearly reflected by the decrease of the hydration enthalpies along the series.[7]

In order to ensure the intended comparison, a number of complex systems already investigated in aqueous solution must be sufficiently soluble also in the aprotic solvent to be chosen, *i.e.* the species involved must be so strongly solvated that the formation of solid phases does not become the predominating feature. Further, as an ionic medium must be provided in order to keep the activity conditions at least reasonably constant, the solvent must also be able to dissolve suitable "inert" salts in fairly large amounts.

As an aprotic solvent fulfilling these conditions, dimethyl sulfoxide (DMSO) has been chosen.* This solvent has the further interesting feature that it might coordinate either *via* oxygen or *via* sulfur though the latter mode of coordination is sterically less favoured. In spite of this, very soft acceptors do in fact coordinate *via* the sulfur atom, evidently forming a bond of markedly covalent character.[8] This kind of selective solvation has of course no counterpart in aqueous solutions.

The dielectric constant of DMSO is 46.4, as against 78.5 for water, at 25 °C.[8] The electrostatic interactions are thus stronger in DMSO, implying *per se* a stronger complex formation. The increase will of course be more marked the higher the charges and the smaller the radii of the interacting species.

DMSO is also a suitable solvent from some essential practical points of view. The wide and conveniently situated liquid range, between 18.5 °C and 189.0 °C under normal pressure, very much facilitates its use.[8] It is also fairly easy to obtain and keep in a sufficiently pure and dry state though its hygroscopic properties require that precautions are taken to avoid contamination with water during storage and use. Also the marked ability of DMSO to dissolve or penetrate the most diverse organic substances, such as many plastics, rubber and living tissues, poses some practical problems. Chemically, DMSO is fairly inert, though it reacts with strong reducing and oxidizing agents. Often such reactions stop at the corresponding sulfide and sulfone, respectively,[9,10] but very strong oxidizing agents, such as perchloric acid and perchlorates, may bring about a rapid complete oxidation, resulting in an often very violent explosion.[8] Also solid metal perchlorate solvates of DMSO are sometimes highly explosive as will be further discussed below.

As to the choice of complex systems to be investigated, halides of zinc(II), cadmium(II), and mercury(II) seem to be very suitable, for several reasons.

First, these halides are all fairly soluble in DMSO, with the exception of the fluorides. Equally important, the corresponding perchlorates are not difficult to prepare water-free as well-defined and fairly stable DMSO-solvates which are readily soluble in DMSO. These solvates can thus serve as convenient sources for the metal ions. The halide ions, agian with the exception of the fluoride ion, also fulfil the necessary conditions that they form salts easily soluble in DMSO with several cations (Li^+,

* A very informative survey of the physical and chemical properties of DMSO, and particularly of its interaction with inorganic compounds, has recently been compiled by Reynolds.[8]

NH_4^+, tetraalkylammonium ions) which may conceivably be used in order to make up the ionic medium.[6,11]

Second, the acceptors as well as the donors involved show a wide variation in their preferences for coordination partners. The metal ions range from the fairly hard zinc(II) *via* cadmium(II), of a typical border-line behaviour, to the markedly soft mercury(II) while the properties of the ligands change considerably from the mildly soft chloride to the very soft iodide ion.[12,13]

Third, the complex formation in aqueous solution is well known for all these halide systems from a large number of reliable investigations.

The zinc and cadmium systems have not previously been systematically studied in DMSO. On the other hand, the chloride, bromide, and iodide systems of mercury(II), and also of silver(I) and copper(I) have been rather extensively investigated.[2,14-18] In all these systems except copper(I) iodide, more stable complexes are formed in DMSO than in water, but the increase of stability becomes, as expected, much smaller in the sequence $Cl^- > Br^- > I^-$. Especially interesting comparisons should be possible between the monovalent d^{10} acceptors silver(I), and copper(I), of very soft behaviour, and the divalent d^{10} acceptors of the zinc group once the results of the presently planned measurements have emerged. In view of the special interest attached to this comparison, it might even be worthwhile to redetermine *e.g.* the silver halide systems in one or more of the media employed in the present investigation. Anhydrous silver perchlorate and nitrate can easily be prepared and used as sources of silver ions in such a study. In order to make the picture complete, however, the formerly unknown DMSO-solvates of these salts have also been prepared.

The experimental part of this first paper describes the preparation, analysis and characterization of a number of solid metal DMSO solvates of interest for the intended measurements. In all, six well-defined compounds have been prepared, *viz.* perchlorates of zinc (two solvates), cadmium, mercury, and silver, and a nitrate of silver. Of these only two have been identified beyond doubt with compounds described previously, *viz.* $Zn(DMSO)_5(ClO_4)_2$ and $Hg(DMSO)_6(Cl_4)_2$.[19,20]

EXPERIMENTAL

Chemicals. The *metal perchlorates* (G. F. Smith Chemical Co) and the *silver nitrate* (Baker & Adamson) were used for the preparations without further purification. The *DMSO* (BDH laboratory reagent) was distilled in vacuum over calcium hydride and kept in a dark bottle over Union Carbide molecular sieves 3A (diameter of pores ≈3 Å). The product thus obtained had a melting point of 18.55 °C (*cf.* Ref. 8, p. 4) and a water content of 0.02 %. The *hexadeuterio-DMSO*, used in order to confirm IR-assignments, was obtained from Merck.

Preparations. *$Ag(DMSO)NO_3$* was prepared by addition of silver nitrate to DMSO and evaporation of excess DMSO in vacuum. The oil obtained crystallized on rubbing with a glass rod.

$Ag(DMSO)_2ClO_4$. Anhydrous silver perchlorate (0.05 mol) was dissolved in acetone (10 ml) and DMSO (0.20 mol) was added. Acetone and excess DMSO were evaporated in vacuum. On cooling the oily liquid solidified to a glass which was dissolved in dry acetone. On slow evaporation of the solvent, crystals precipitated. *Extreme caution must be exercised when these crystals are handled.* On rubbing or scratching, they explode with extreme violence. This compound is by far the most unstable of the solvates described in this paper.

$Zn(DMSO)_5(ClO_4)_2$ was prepared according to Currier and Weber,[19] with the modification that a temperature of 25 °C was used instead of 40 °C.

$Zn(DMSO)_6(ClO_4)_2$. The zinc perchlorate hexahydrate (0.02 mol) was dissolved in a minimum amount of acetone and DMSO (0.12 mol) was added. On cooling to −20 °C crystals were obtained. The crystals were recrystallized at least twice from dry acetone. Attempts to prepare this compound according to Cotton and Francis [21] always resulted in crystals containing more than 6 DMSO per Zn. The method used here is almost identical with that reported by Selbin *et al.*[22] to yield $Zn(DMSO)_4(ClO_4)_2$.

$Cd(DMSO)_6(ClO_4)_2$. The cadmium perchlorate (0.02 mol) hexahydrate was dissolved in a minimum amount (12 ml) of acetone. After addition of 2,2-dimethoxypropane [23] (0.12 mol) the solution was shaken for 2 h. DMSO (0.12 mol) was then added and the resulting mixture shaken for another 0.5 h. On cooling to −20 °C crystals were formed which were recrystallized from acetone.

$Hg(DMSO)_6(ClO_4)_2$. The mercury(II) perchlorate trihydrate (0.01 mol) was dissolved in ethanol (17 ml). Sometimes, it was necessary to decant the solution in order to remove a slight residue of insoluble matter. When DMSO (0.06 mol) was added, precipitation occurred immediately. The crystals were filtered in a dry nitrogen atmosphere and dried in vacuum over night. On standing, mercury(I) was formed in the ethanol solution with production of acetal-

dehyde. The addition of DMSO should therefore be done without delay.

Chemical analyses. Zinc, cadmium, and *mercury* were titrated with EDTA. *Silver* was titrated according to Volhard.

DMSO was analyzed by a procedure described by Douglas[10] and the *water* content determined by a modified Karl Fischer method.[24] The water determinations, as well as the conventional carbon, hydrogen, and sulfur analyses were performed by the Dept. of Analytical Chemistry of this Chemical Center.

Melting points were determined with a Büchi melting point apparatus.

Infrared spectra were recorded on a Perkin-Elmer Model 221. All spectra were obtained using KBr pellets.

Thermogravimetric analyses were performed by means of a Mettler thermogravimetric balance, at the Dept. of Inorganic Chemistry, University of Gothenburg.

RESULTS AND DISCUSSION

Analytical data, water contents, and melting points of the solvates prepared are presented in Table 1. Zinc and cadmium both form hexasolvates of fairly high melting points. Mercury also forms a hexasolvate that decomposes at a considerably lower temperature. In the case of zinc, a pentasolvate is also easily prepared. The silver perchlorate is a disolvate, the nitrate a monosolvate, both melting considerably lower than the zinc group solvates. Especially the nitrate has quite a low melting point, 50 – 51 °C.

For the mercury compound the thermogravimetric measurements showed no weight loss and no reliable melting point before the decomposition at 130 °C. None of the other solvates lost solvate molecules before melting, except the zinc hexasolvate which lost 1 DMSO. The melting point found thermogravimetrically for the resulting compound is identical with that of the directly prepared zinc pentasolvate.* All compounds, except the mercury one, disintegrated around 200 °C.

For steric reasons, the hexasolvates are most certainly oxygen coordinated, even in the case of mercury(II) which has *per se* a high affinity for sulfur. In the case of the di- and monosolvates of silver(I) no such steric hindrance occurs.

The mode of coordination may be inferred from infrared spectra, as the bond order, and hence the stretching frequency of the sulfur to oxygen bond, is affected very differently depending upon whether the metal ion is coordinated to the oxygen or to the sulfur atom. In the case of oxygen coordination, a lowering of the bond order and hence a decrease of the stretching frequency should occur. Conversely, coordination to the sulfur atom should result in a higher bond order and hence in an increase of the stretching frequency. This effect has been intensively studied especially for the DMSO complexes of the first row transition metals.[19–22,25–29] The deductions drawn have later also been verified by determinations of the structures of several of the complexes, *e.g.* the sulfur coordinated *trans*-$Pd(DMSO)_2Cl_2$[30] and the oxygen coordinated $La(DMSO)_4(NO_3)_3$.[31]

The interpretation of the infrared spectra of oxygen bonded DMSO-complexes has been somewhat in doubt because of the coupling that most probably exists between the SO stretching and the methyl rocking frequencies.[27,32] Some authors [22,25] assign the bands near 1000 and 930 cm^{-1} to the SO stretching

* In the Büchi apparatus, on the other hand, the hexasolvate seemed to keep practically all DMSO until its admittedly not very sharp melting point (Table 1).

Table 1. Analytical data (%).

	Mp °C	DMSO Calc.	DMSO Found	Metal Calc.	Metal Found	Water
$Ag(DMSO)NO_3$	50 – 51	31.50	29.14	43.50	44.11	–
$Ag(DMSO)_2ClO_4$	91 – 92	42.98	43.87	29.67	29.01	–
$Zn(DMSO)_5(ClO_4)_2$	182 – 184	59.65	60.10	9.98	9.95	1.2
$Zn(DMSO)_6(ClO_4)_2$	165 – 175	63.95	63.02	8.92	8.96	0.2
$Cd(DMSO)_6(ClO_4)_2$[a]	188 – 190			14.41	14.45	< 0.1
$Hg(DMSO)_6(ClO_4)_2$[b]	125 – 128 dec.			23.10	22.57	0.25

[a] Calc.: S 24.66; C 18.47, H 4.65. Found: S 23.0, C 18.6, H 4.75. [b] Calc.: S 22.15. Found: S 22.05.

Table 2. Infrared spectra of the DMSO-complexes.[a]

	SO-stretch.	CH_3-rock.
$Ag(DMSO)NO_3$	1018 vs	949 s
$Ag(DMSO)_2ClO_4$	1020 vs	950 s
$Zn(DMSO)_5(ClO_4)_2$	1018 vs	950 s
$Zn(DMSO)_5(ClO_4)_2$	1018 vs	948 s
$Cd(DMSO)_6(ClO_4)_2$	1015 vs	948 s
$Hg(DMSO)_6(ClO_4)_2$	1018 vs	949 s

[a] In Tables 2 and 3, the intensities are indicated as follows: w = weak, m = medium, s = strong, sh = shoulder and v = very.

and the methyl rocking, respectively. Others [26,28] reverse these assignments.

In the pure solvent the band at about 950 cm^{-1} can be fairly safely identified by coordinate analysis as due to the methyl rocking.[26,32] The strong band at 1055 cm^{-1} can no doubt be assigned to the SO stretch. These assignments are in line with the band shifts observed on deuteration of the DMSO.[26,32] For the deuterated compound (DMSO-d_6) the wave number of the methyl rocking should be much lower, while that of the SO stretch should not be much affected. In fact the band at 950 cm^{-1} has moved down to 800 cm^{-1}, while the other band has moved only about 10 cm^{-1}, and moreover upwards.

All spectra in this investigation are very similar. The interesting parts of them are listed in Table 2. The very strong band around 1020 cm^{-1} has been assigned to the SO stretch involving a lowering from 1055 cm^{-1} as expected for oxygen bonded solvates. The wave number of the methyl rocking stays around 950 cm^{-1}, as is also to be expected. In all cases this band is less intense than the SO band.

To get further information two of the complexes have been synthesized with DMSO-d_6, *viz.* $Zn(DMSO\text{-}d_6)_5(ClO_4)_2$ and $Hg(DMSO\text{-}d_6)_6(ClO_4)_2$. Because of the marked similarity between the spectra, the results should be valid for all the complexes studied. The assignments follow Cotton,[26,32] except for the SO stretching where we prefer the alternative interpretation suggested by Drago and Meek.[27] The wave numbers of the principal bands are given in Table 3. Unfortunately, some bands presumably due to CD_3 deformations enter the region of interest, but the fact that all the bands between 900 and 1000 cm^{-1} are of low intensity shows that the SO stretch must give rise to one of the strong bands at 1020 and 1045 cm^{-1}. Most likely the strongest of them should be assigned to the SO stretch.

It is obvious (Table 2) that in all complexes prepared the SO stretching frequency is lower than in uncoordinated DMSO. The magnitude of this shift is $35-40$ cm^{-1}. In all the solvates prepared, DMSO is thus coordinated *via* oxygen. It may be inferred that this is the case also in DMSO solutions.

It is striking that the DMSO solvates of silver(I) and mercury(II) are coordinated *via* oxygen and not *via* sulfur which might have been expected since both are quite soft d^{10} acceptors. In order to investigate this further, complete structure determinations of $Ag(DMSO)_2ClO_4$ and $Hg(DMSO)_6(ClO_4)_2$ are now in progress. As to the silver compound the determination is so far advanced that the main features of the structure are evident, confirming

Table 3. Infrared spectra of $Zn(DMSO\text{-}d_6)_5(ClO_4)_2$ and $Hg(DMSO\text{-}d_6)_6(ClO_4)_2$.

$Zn(DMSO\text{-}d_6)_5(ClO_4)_2$	$Hg(DMSO\text{-}d_6)_6(ClO_4)_2$	Assignment
2240 m	2238 m	Asym CD stretch
–	2104 w	Sym CD stretch
1046 s	1043 s	Sym CD_3 def.
1019 vs	1015 vs	SO stretch
1002 w sh	998 w sh	
959 m	963 m	CD_3 def.
	948 m	
816 m	814 m	
755 m	752 m	CD_3 rocks

the oxygen coordination. The silver atoms are in fact joined to chains by double bridges of 2 DMSO. A detailed report will soon be published.[33]

Acknowledgements. We are indebted to Professor Nils-Gösta Vannerberg and Dr. Inge Svedung for the thermogravimetric measurements and to Dr. Ronald Karlsson for the water determinations in DMSO. The support of Statens naturvetenskapliga forskningsråd (The Swedish Natural Science Research Council) is also gratefully acknowledged.

REFERENCES

1. Parker, A. J. *Quart. Rev. Chem. Soc. 16* (1962) 163.
2. Alexander, R., Ko, E. C. F., Mac, Y. C. and Parker, A. J. *J. Amer. Chem. Soc. 89* (1967) 3703.
3. Alexander, R. and Parker, A. J. *J. Amer. Chem. Soc. 89* (1967) 5549.
4. Kolthoff, I. M. and Chantooni, M. K., Jr. *J. Phys. Chem. 76* (1972) 2024.
5. Prue, J. E. and Sherrington, P. J. *Trans. Faraday Soc. 57* (1961) 1795.
6. Maxey, B. W. and Popov, A. I. *J. Amer. Chem. Soc. 89* (1967) 2230; *91* (1969) 20.
7. Halliwell, H. F. and Nyburg, S. C. *Trans. Faraday Soc. 59* (1963) 1126.
8. Reynolds, W. L. *Progr. Inorg. Chem. 12* (1970) 1.
9. Amonoo-Neizer, E. H., Ray, S. K., Shaw, R. A. and Smith, B. C. *J. Chem. Soc.* (1965) 4296.
10. Douglas, T. B. *J. Amer. Chem. Soc. 68* (1946) 1076.
11. Kenttämaa, J. *Suom. Kemistilehti B 33* (1960) 179.
12. Pearson, R. G. *J. Chem. Educ. 45* (1968) 581, 643.
13. Ahrland, S. *Chem. Phys. Lett. 2* (1968) 303.
14. Luehrs, D. C., Iwamoto, R. T. and Kleinberg, J. *Inorg. Chem. 5* (1966) 201.
15. Luehrs, D. C. and Abate, K. *J. Inorg. Nucl. Chem. 30* (1968) 549.
16. Le Demézét, M., Madec, C. and L'Her, M. *Bull. Soc. Chim. Fr.* (1970) 365.
17. Chantooni, M. K., Jr. and Kolthoff, I. M. *J. Phys. Chem. 77* (1973) 1.
18. Foll, A., Le Demézét, M. and Courtot-Coupez, J. *Bull. Soc. Chim. Fr.* (1972) 1207; *J. Electroanal. Chem. 35* (1972) 41.
19. Currier, W. F. and Weber, J. H. *Inorg. Chem. 6* (1967) 1539.
20. Carlin, R. L., Roitman, J., Dancleft, M. and Edwards, J. O. *Inorg. Chem. 1* (1962) 182.
21. Cotton, F. A. and Francis, R. *J. Amer. Chem. Soc. 82* (1960) 2986.
22. Selbin, J., Bull, W. E. and Holmes, L. H., Jr. *J. Inorg. Nucl. Chem. 16* (1961) 219.
23. Starke, K. *J. Inorg. Nucl. Chem. 11* (1959) 77.
24. Karlsson, R. and Karrman, K. J. *Talanta 18* (1971) 459.
25. Meek, D. W., Straub, D. K. and Drago, R. S. *J. Amer. Chem. Soc. 82* (1960) 6013.
26. Cotton, F. A., Francis, R. and Horrocks, W. D., Jr. *J. Phys. Chem. 64* (1960) 1534.
27. Drago, R. S. and Meek, D. *J. Phys. Chem. 65* (1961) 1446.
28. Holah, D. G. and Fackler, J. P., Jr. *Inorg Chem. 4* (1965) 1721.
29. Edwards, J. O., Goetsch, R. J. and Stritar, J. A. *Inorg. Chim. Acta 1* (1967) 360.
30. Bennett, M. J., Cotton, F. A. and Weawer, D. L. *Acta Crystallogr. 23* (1967) 788.
31. Krishna Bhandary, K. and Manohar, W. *Acta Crystallogr. B 29* (1973) 1093.
32. Cotton, F. A. and Horrocks, W. D., Jr. *Spectrochim. Acta 17* (1961) 134.
33. Björk, N. O. and Cassel, A. *To be published.*

Received April 4, 1974.

Acta Chemica Scandinavica A 28 (1974) 829—838

Thermodynamics of Metal Complex Formation in Aqueous Solution. V. Equilibrium and Enthalpy Measurements on the Copper(II) and Nickel(II) Thiocyanate Systems

LENNART KULLBERG

Inorganic Chemistry 1, Chemical Center, University of Lund, P.O.B. 740, S-220 07 Lund 7, Sweden

The stability constants and the enthalpy changes for the formation of copper(II) and nickel(II) thiocyanate complexes in aqueous solution have been determined by means of a calorimetric titration method. For the copper(II) thiocyanate system the stability constants have also been determined spectrophotometrically. From the measured enthalpy changes, and the free energy changes computed from the stability constants, the entropy changes have been calculated. All data refer to 25.0 °C and an aqueous sodium perchlorate medium of ionic strength 1.00 M.

In the thiocyanate systems studied, all the species are formed in modestly exothermic reactions. The entropy terms are all negative.

In previous papers of this series [3,4] the changes of free energy, enthalpy, and entropy accompanying the formation of a number of thiocyanate complexes have been reported. Besides the uranyl(VI) ion the metals used have been the divalent ions of electron configuration d^{10}, *viz.* Zn^{2+}, Cd^{2+}, and Hg^{2+} of which Zn^{2+} is classified as a hard acceptor, Cd^{2+} as mildly soft and Hg^{2+} as a very soft one.[5]

It should also be of interest to study how the thermodynamic functions for the formation of thiocyanate vary along the long rows of the Periodic Table. In this work the complexes of copper(II) and nickel(II) have been studied, making it possible to compare the coordination of SCN^- to the three acceptors Zn^{2+}, Cu^{2+}, and Ni^{2+}, all on the borderline between hard and soft.[5]

Like the earlier investigations in this series,[1-4] the present one was performed at 25.0 °C and in an aqueous medium of unit ionic strength with sodium perchlorate as supplementary electrolyte.

The stability constants of the copper(II)

Table 1. Comparison of reported values of stability constants and enthalpy changes for the copper(II) and nickel(II) thiocyanate systems. The values given are the overall standard changes.

System		$Cu^{2+}-SCN^-$			$Ni^{2+}-SCN^-$							
Ref.		6	7	8	9	10	7	11	13	8	12	14
Temp./°C		25	25	25	20		25	25	20	25	25	25
I/M		0.5[a]	0.2	$I\rightarrow 0$	1.0[b]	varying	0.2	1.0[b]	1.5[b]	$I\rightarrow 0$	0.7[c]	$I\rightarrow 0$
β_j/M^{-j}	$j=1$	55.1	52.9	213	15.0	15.0	15.7	14.9	13.8	58	17.5	95
	2	347			44				56			
	3	490			65				50			
	4	970							100			
$-\Delta H°_1$/ kJ mol^{-1}				12.6						9.4	14.4	21.5

[a] KNO_3, [b] $NaClO_4$, [c] $HClO_4$

thiocyanate system have previously been determined spectrophotometrically,[6,7] Table 1. For the same system a value of ΔH°_1 at $I=0$ has been obtained from calorimetric measurements.[8]

Several experimental methods have been used in the study of nickel thiocyanate complexes, Table 1, *viz.* cation exchange,[9] spectrophotometry, [7,10] polarography,[11,12] extraction measurements,[13] and potentiometric measurements by means of a silver – silver thiocyanate electrode.[14] The enthalpy change, ΔH°_1, for the first step has been determined both calorimetrically [8] and from the temperature dependence of β_1.[12,14]

For weak or moderately strong complexes, $0<\log K<3$, a titration calorimeter may be a good tool to determine equilibrium constants as well as enthalpy changes provided the enthalpy changes are not too small.[3,15] It is evident from Table 1 that for both the copper(II) and nickel(II) systems β_j and ΔH_j are of the right magnitude to allow a calorimetric determination of these quantities. Such a determination has therefore been undertaken. In order to check the stability constants obtained a spectrophotometric study of the copper(II) thiocyanate has also been performed. From cation exchange and spectrophotometric measurements the stability constants of the nickel thiocyanate system have been determined by Fronæus [9] for the medium used in this study. These constants refer admittedly to 20 °C but they can be recalculated to 25 °C by an iterative procedure once preliminary values of ΔH_j have been found.[3]

CALCULATIONS

The notation is the same as in parts I and II of this series [1,2] with the following additions:

A = absorbance

l = sample path length

λ = wavelength

$a = A/l$

ε_M, ε_L, ε_j = the molar absorptivities of M, L, and the complex ML_j

$$\varepsilon = (a - \varepsilon_M C_M - \varepsilon_L C_L)/C_M \quad (1)$$

$\varepsilon^* = a/C_M$

Q_{exp} = heat change after addition of titrant (>0 if heat is evolved)

Q_{corr} = heat change corrected for heat of dilution

Calculation of stability constants from spectrophotometric measurements. One graphical and one numerical method of calculation have been used. The graphical method has been described previously.[16] Only its main points will therefore be given here.

Assuming that only mononuclear complexes are formed and that Beer's law can be applied to the complex solutions, we get

$$a = \varepsilon_M[M] + \varepsilon_L[L] + \sum_{j=1}^{N} \varepsilon_j[ML_j] \quad (2)$$

Introducing the stability constants we obtain from eqns. (1) and (2):

$$\varepsilon = \left[\sum_{j=1}^{N} (\varepsilon_j - \varepsilon_M - j\varepsilon_L)\beta_j[L]^j\right] \Big/ \left(1 + \sum_{j=1}^{N} \beta_j[L]^j\right) \quad (3)$$

From eqn. (3) it is evident that a constant value of ε implies a constant value of [L] and hence a constant ligand number $\bar{n}$, *cf.* Ref. 1. From the definition of $\bar{n}$

$$C_L = \bar{n}C_M + [L] \quad (4)$$

If ε is measured as a function of C_L for a number of different C_M, a family of curves is obtained where the same value of ε in the different curves means the same value of [L] and also of $\bar{n}$. Cutting the curves at a constant value of ε and plotting corresponding values of C_L and C_M should result, according to eqn. (4), in a straight line with the intercept on the C_L-axis = [L] and the slope = $\bar{n}$. Once corresponding values of $\bar{n}$ and [L] are known, the stability constants are graphically evaluated.[1]

For the numerical calculations the least-squares programme "Letagrop Spefo" developed by Sillén and Warnqvist [17] has been used. The input data were the total concentrations C_M and C_L and the molar absorptivity, ε^*, of each solution. The error square sum to be minimized was

$$U_{rel} = \sum_i (\varepsilon^*_{i,calc} - \varepsilon^*_{i,exp})^2 (\varepsilon^*_{i,exp})^{-2} \quad (5)$$

The calculation gives the stability constants, β_j, and the molar absorptivities of the absorbing species. The molar absorptivities of free ligand and free metal were determined separately (see "Measurements and results") and then regarded as known parameters during the calculations.

Calculation of enthalpy changes and stability constants from calorimetric measurements. Assuming only mononuclear complexes, ML_j, the total heat of reaction between M and L in solution is given by

$$Q_{calc} = -V \sum_{j=1}^{N} [ML_j] \Delta H_j \quad (6)$$

ΔH_j is the overall enthalpy of formation. Introduction of the expressions for the stability constants β_j in eqn. (6) yields

$$Q_{calc} = -V[M] \sum_{j=1}^{N} \beta_j [L]^j \Delta H_j \quad (7)$$

Knowing the total concentrations of metal, C_M, and ligand, C_L, the concentrations [M] and [L] can be calculated once the β_j-values are known. Thus Q_{calc} is a function of only β_j and ΔH_j.

By making a least-squares analysis of the error square sum equation

$$U(\beta_j, \Delta H_j) = \sum_{i=1}^{N} w_i (Q_{i,calc} - Q_{i,corr})^2 \quad (8)$$

where w_i is a weighting term and Q_{corr} the measured heat effects corrected for heats of dilution, a set of unknown parameters β_j and ΔH_j, which minimizes the error square sum U, can be found.

For the calculation of ΔH_j from eqn. (8) in cases where values of β_j are known the least-squares programme "Letagrop Kalle" [18] has previously been used.[2] This programme fails, however, if asked to produce simultaneously all the unknown parameters ΔH_j and β_j. Therefore we decided to construct a new least-squares programme called "Kalori" which could treat both the enthalpy changes and the equilibrium constants as unknown parameters simultaneously. For details of this programme, see Ref. 19.

EXPERIMENTAL

Chemicals. Nickel perchlorate was prepared by dissolving nickel carbonate (Merck's *p.a.*) in perchloric acid (Baker's Analyzed) and was recrystallized a few times from water. The nickel(II) concentration of the stock solution was determined by electrolysis in ammonical solution according to Okáč.[20] In order to avoid hydrolysis of nickel [21] a small excess (about 1/10 of the nickel(II) concentration) of perchloric acid was added to the stock solution. The concentration of free acid was determined potentiometrically.[22] *Copper(II) perchlorate* (G. F. Smith) was recrystallized three times from water. The stock solution was analyzed by electrodeposition. Also to this solution, excess acid (about 1/10 of the copper(II) concentration) was added in order to prevent hydrolysis.[23] *The sodium thiocyanate* (Baker's Analyzed) stock solution was standardized both by Volhard titration and gravimetrically (precipitation of AgSCN). *Sodium perchlorate* was prepared and analyzed as before.[1]

The spectrophotometric measurements were carried out mainly with a Zeiss PMQ II Spectrophotometer. Suitable wavelengths for the measurements were selected from absorption curves of copper(II) solutions with and without thiocyanate, recorded with a Hitachi recording spectrophotometer, Fig. 1. The thiocyanate curve, B, has a relative maximum at 348 nm, where the absorption differs considerably from that of the hydrated copper(II) ion, curve A. As the systematic error in the measured absorbance caused by imperfectly monochromatic light disappears where the curve has a horizontal tangent, this wavelength was selected. Curve B has another absorption peak at 800 nm, Fig. 1, but here also curve A shows high values of ε, which lowers the precision of the measurements undertaken at this wavelength. As measurements carried out at different absorption bands are likely to reveal the possible existence of polynuclear complexes,[16] some measurements have nevertheless been performed at 800 nm.

The solutions were made up in 50 cm³ measuring flasks from stock solutions of copper(II) perchlorate, sodium perchlorate, and sodium thiocyanate. The absorbance was meas-

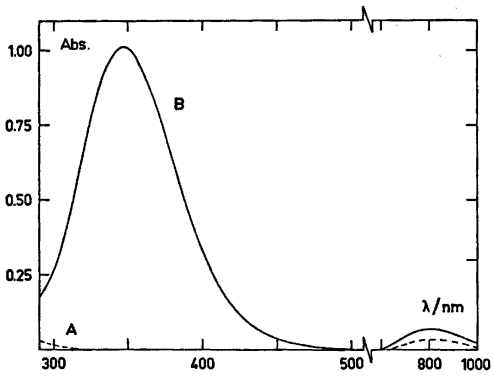

Fig. 1. Absorption curves of free copper(II) ions and a mixture of copper(II) and thiocyanate ions at 25 °C and at ionic strengths of 1.0 M and a cell thickness of 4.00 cm. A. 1.00 mM $Cu(ClO_4)_2$. B. 1.00 mM $Cu(ClO_4)_2$ + 16.00 mM NaSCN.

ured immediately after mixing, as copper(II) thiocyanate on standing disintegrates with the formation of slightly soluble copper(I) thiocyanate.[24]

In each series of measurements, C_M and the cell thickness l were kept constant. For each wavelength all series had a constant product lC_M, *viz.* 0.00200 and 0.0200 cm M for 348 and 800 nm, respectively. For each wavelength, solutions of the same value of ε are thus measured at the same total absorbance which eliminates several systematic errors in the determination of $\bar{n}$. These include errors due to reflections in the end-plates of the absorption cells, and also errors due to imperfect monochromaticity, inasmuch as these have not already been eliminated by selecting an absorption maximum for measurement.[16]

At $\lambda = 348$ nm, series have been carried out with $l = 0.1$, 0.2, 0.5, and 1.0 cm and at 800 nm with $l = 1.0$, 2.0, and 4.0 cm. As the true absorbances of the solutions are not essential, the absolute path lengths of the quartz cells used are not required but only the ratios between them. These ratios were determined by measurements on alkaline picrate solutions.[25] The thickness of the 1 cm cell was set equal to 1.000 cm.

All measurements were repeated at least three times. The solution to be measured and the cell compartment of the spectrophotometer were thermostated at 25.0 ± 0.1 °C.

Calorimetric measurements. The calorimeter and the technique of measurement have been described previously.[2] In each titration series, the reaction vessel initially contained V_0 cm³ of a solution S and a titrant T was then added. When the vessel had been almost filled solution was removed so that the initial volume V_0 was restored. The compositions of the solutions S and T are given in Tables 4 and 5. In order to determine the corrections for the heats of dilution, series analogous to those of the main measurements were performed except that only one of the two reactants was present.

Electrical calibration showed that the heat equivalent, ε_v, was a linear function of the total volume, V, according to

$$\varepsilon_v = 2.091 + 0.0226(V - 90.0)$$

The titration series were repeated once and the reproducibility was generally within 0.05 J.

MEASUREMENTS AND RESULTS

Spectrophotometric measurements on copper(II) thiocyanate. The experimental data are collected in Table 2. At high thiocyanate concentrations the disintegration of the copper(II) thiocyanate solutions mentioned above proceeds quite rapidly which makes the measurements difficult. The highest C_L-value yielding reasonably reproducible results was 80 mM.

Table 2. Experimental values of ε^*_{Cu} cm^{-1}M^{-1} at different values of C_L and C_M at 348 and 800 nm.

λ/nm	348				800		
C_M/mM	2	4	10	20	5	10	20
C_L/mM							
1	22.0	20.2	16.3	12.1	12.45	12.25	12.10
2	43.5	39.4	31.7	23.5	13.15	12.84	12.51
3	64.0	57.9	47.3	35.3	13.75	13.38	12.96
5	101.5	93.8	76.6	58.2	14.95	14.38	13.75
7	137.0	126.7	104.9	80.3	16.07	15.35	14.50
10	184.5	172.1	145.2	112.8	17.74	16.80	15.63
12	212.0	200.0	170.7	134.2	18.55	17.75	16.40
15	253.5	239.4	207.1	164.0	20.05	19.01	17.48
17	279.8	264.1	229.1	183.2	20.80	19.80	18.10
20	313.8	298.8	262.0	212.7	22.12	20.95	19.18
25	364.8	350.2	311.2	257.5	24.00	22.84	20.69
30	411.0	396.0	356.5	299.2	25.75	24.51	22.34
35	451.5	436.2	398.1	339.2	27.20	26.04	23.74
40	489.3	474.9	437.2	375.2	28.70	27.77	25.19
45	522.3	508.3	472.5	410.0	30.00	29.19	–
50	553.0	540.2	505.2	441.4	31.15	30.29	27.74
55	580.0	567.6	534.4	470.9	–	–	–
60	605.5	595.3	562.1	500.2	33.45	32.45	30.38
70	650.5	641.0	610.6	–	35.65	34.39	–
80	689.0	682.4	653.1	–	–	–	–

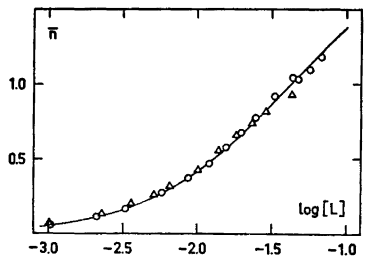

Fig. 2. The complex formation function of the copper(II)thiocyanate system. The fulldrawn curve has been computed from eqn. (4) of Ref. 4 using $\beta_1 = 55$ M^{-1} and $\beta_2 = 550$ M^{-2}. The values of $\bar{n}$ obtained from the slopes of the (C_M, C_L)-lines are denoted by (○), for $\lambda = 348$ nm, and (△), for $\lambda = 800$ nm. [(L) in M].

The molar absorptivities for the copper(II) ion, ε_{Cu}, and the thiocyanate ion, ε_L, were determined separately. The value of ε_{Cu} was considerable ($= 11.70$ cm^{-1} M^{-1}) at 800 nm but negligible at 348 nm. The value of ε_L was low at both wavelengths (0.007 cm^{-1} M^{-1} at 348 nm; < 0.001 cm^{-1} M^{-1} at 800 nm).

From the graphical evaluation the stability constants of the first two complexes were found, Table 3. In the range investigated ($C_L < 80$ mM) there was no sign of a third complex. Values of $\bar{n}$ obtained from the slopes of (C_M, C_L)-lines have been plotted in Fig. 2.

The results of the computer calculations with the least-squares programme "Letagrop Spefo" are also given in Table 3. The experiments are well described by a model including two complexes but as seen from the error square sum, U, a somewhat better fit results for the data at 348 nm if a third complex is introduced. The values of σ, the standard deviation for the relative differences between experimental and calculated values of ε^*, are quite small, Table 3. Due to the high absorption of Cu^{2+} at 800 nm the results derived from the measurements at this wavelength are not very precise. This is indicated by the relatively large standard deviations in the β_j-values. In view of this the agreement between the two sets of β_j obtained at 348 nm and 800 nm is quite satisfactory, Table 3.

Calorimetric measurements on copper(II) thiocyanate. The experimental data are collected in Table 4. The value of C_M varied from 5 to 20 mM. As these measurements were more time-consuming than the spectrophotometric ones the highest value of C_L which could be reached without a significant decomposition of copper(II) thiocyanate was only 60 mM. The spectrophotometric measurements show that only two complexes exist in the concentration range studied and that the second one never exceeds $\simeq 25$ % of the total. The complex formation is moreover fairly weak. A determination of the stability constants from calorimetric data should thus be feasible.

Using the computer programme "Letagrop Kalle" the error square sum, U, was calculated for different sets of β_1 and β_2. Starting with

Table 3. Stability constants for the copper(II) thiocyanate system obtained from spectrophotometric and calorimetric measurements. The errors given correspond to three standard deviations given by the computer or to estimated errors.

Method	β_1/M^{-1}	β_2/M^{-2}	β_3/M^{-3}	U	σ
Spectr. at $\lambda = 348$ nm					
Letagrop	55.9 ± 0.9	500 ± 30		0.00223	0.0055
Letagrop	54.6 ± 1.2	580 ± 60	640 ± 70	0.00137	0.0043
Graphically	55.0 ± 0.5	600 ± 50			
Spectr. at $\lambda = 800$ nm					
Letagrop	67 ± 7	420 ± 100		0.00070	0.0038
Graphically	65 ± 8	460 ± 150			
Calorimetrically					
Kalori	53.4 ± 6.3	520 ± 90		0.00506	0.020
Graphically	53.5 ± 4	520 ± 60			
'Best' values	55 ± 2	550 ± 50			

Table 4. Determination of the heats of formation for the copper(II) thiocyanate complexes.[a] For all the series: $V_0 = 100.0$ cm³ and $V = (V_0 + v)$ cm³.

(a) ○ S: $C_M = 0.02000$ M, $C_{NaClO_4} = 0.940$ M. T: $C_L = 0.500$ M, $C_{NaClO_4} = 0.500$ M.
v/cm³, Q_{exp}/J, Q_{corr}/J, ΔQ_{corr}/J: 2.000, 5.995, 6.059, 0.001; 4.000, 4.973, 5.038, −0.021; 6.000, 4.070, 4.136, −0.008; 8.000, 3.280, 3.347, 0.052;

(b) □ S: $C_M = 0.01000$ M, $C_{NaClO_4} = 0.970$ M. T: $C_L = 0.500$ M, $C_{NaClO_4} = 0.500$ M.
v/cm³, Q_{exp}/J, Q_{corr}/J, ΔQ_{corr}/J: 2.000, 3.803, 3.867, −0.012; 4.000, 2.804, 2.869, −0.014; 6.000, 2.117, 2.183, −0.019; 8.000, 1.629, 1.696, −0.013;

(c) △ S: $C_M = 0.005000$ M, $C_{NaClO_4} = 0.985$ M. T: $C_L = 0.500$ M, $C_{NaClO_4} = 0.500$ M.
v/cm³, Q_{exp}/J, Q_{corr}/J, ΔQ_{corr}/J: 2.000, 2.152, 2.216, −0.003; 4.000, 1.439, 1.504, −0.004; 6.000, 1.011, 1.077, 0.005; 8.000, 0.752, 0.819, −0.001;

(d) ▽ S: $C_M = 0.005000$ M, $C_{NaClO_4} = 0.985$ M. T: $C_L = 1.000$ M.
v/cm³, Q_{exp}/J, Q_{corr}/J, ΔQ_{corr}/J: 3.000, 4.479, 4.846, 0.022; 6.000, 1.722, 2.073, −0.013;

(e) ◇ S: $C_M = 0.005000$ M, $C_{NaClO_4} = 0.985$ M. T: $C_L = 1.000$ M.
v/cm³, Q_{exp}/J, Q_{corr}/J, ΔQ_{corr}/J: 2.000, 3.489, 3.734, 0.022; 5.000, 2.296, 2.649, −0.019;

[a] The values of ΔQ_{corr} refer to the deviations ($Q_{calc} - Q_{corr}$) obtained using the 'best' set of constants, *i.e.* $\beta_1 = 55$ M^{-1} and $\beta_2 = 550$ M^{-2}.

the set of constants found spectrophotometrically, new combinations of β_1 and β_2 were systematically tried. The dependence of $U(\beta_j, \Delta H_j)$ on the values of β_1 and β_2 chosen is summarized in Fig. 3. The two constants giving the minimum of the error square sum according to the graph are given in Table 3.

An analysis of the calorimetric data was also made using the new computer programme "Kalori" which could treat both β_j and ΔH_j as unknown parameters simultaneously. The β_1 and β_2 values obtained by the computer are collected in Table 3, from which it can be seen that the two evaluation methods applied on the calorimetric data give identical β_j-values. This shows that the new programme "Kalori" works well.

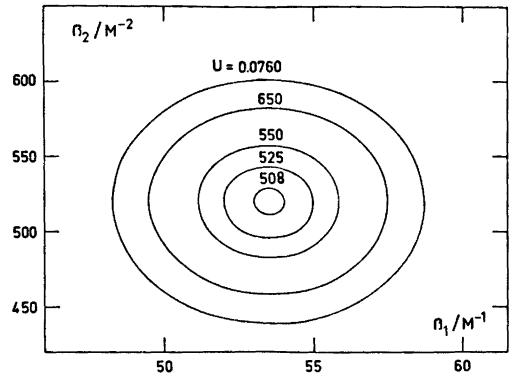

Fig. 3. Plot of assumed values of U *vs.* β_1 and β_2 for the copper(II) thiocyanate system.

It is also evident from Table 3 that the spectrophotometric (at 348 nm) and the calorimetric measurements give very consistent β_j-values. The set of constants considered to be the 'best' one is listed in Table 7. Using these constants, values of $\Delta G°_j$, $\Delta H°_j$ and $\Delta S°_j$ have been calculated and are collected in Table 7. In Fig. 4 the Δh_v-function is plotted *versus* $\bar{n}$, calculated from the 'best' values of β_j (see above). The Δh_v-function is independent of C_M, which proves that no polynuclear complexes exist. The fulldrawn curve is calculated from the stability constants and enthalpy changes listed in Table 7.

Calorimetric measurements on nickel(II) thiocyanate. Seven titration series have been carried out, Table 5. In three of these, a−c, ligand was added to a solution of the metal ion. In order to reach higher values of [L] and hence of $\bar{n}$, four series, d−g, have been performed by adding a metal solution to ligand solutions. As mentioned on p. 831 the nickel

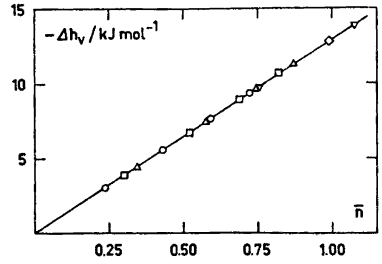

Fig. 4. The total molar enthalpy change, Δh_v, as a function of $\bar{n}$, for the copper(II)-thiocyanate system, *cf.* Table 4.

Table 5. Determination of the heats of formation for the nickel thiocyanate complexes.[a] For all the series: $V_0 = 90.00$ cm³ and $V = (V_0 + v)$ cm³.

(a) ○ S: $C_M = 0.05000$ M, $C_{NaClO_4} = 0.850$ M. T: $C_L = 1.000$ M

v/cm³, Q_{exp}/J, Q_{corr}/J, ΔQ_{corr}/J: 3.000, 12.605, 12.950, −0.020; 6.000, 9.732, 10.066, 0.055; 9.000, 7.704, 8.025, 0.022; 12.000, 6.231, 6.543, −0.022; 15.000, 5.082, 5.383, 0.002; 18.000, 4.240, 4.532, −0.008; 21.000, 3.594, 3.876, −0.017; 24.000, 3.054, 3.325, 0.010; 27.000, 2.659, 2.921, −0.007;

(b) ○ S: $C_M = 0.03846$ M, $C_L = 0.2308$ M, $C_{NaClO_4} = 0.654$ M. T: $C_L = 1.000$ M.

v/cm³, Q_{exp}/J, Q_{corr}/J, ΔQ_{corr}/J: 3.000, 2.327, 2.539, −0.013; 6.000, 1.934, 2.132, 0.047; 9.000, 1.676, 1.864, 0.037; 12.000, 1.461, 1.638, 0.037; 15.000, 1.294, 1.464, 0.025; 18.000, 1.149, 1.314, 0.020;

(c) □ S: $C_M = 0.03000$ M, $C_{NaClO_4} = 0.910$ M. T: $C_L = 1.000$ M.

v/cm³, Q_{exp}/J, Q_{corr}/J, ΔQ_{corr}/J: 3.000, 8.555, 8.900, −0.016; 6.000, 6.131, 6.465, 0.056; 9.000, 4.675, 4.996, −0.026; 12.000, 3.626, 3.938, −0.020; 15.000, 2.903, 3.204, −0.025; 18.000, 2.363, 2.655, −0.016; 21.000, 1.968, 2.250, −0.017; 24.000, 1.651, 1.922, −0.002; 27.000, 1.438, 1.700, −0.028;

(d) □ S: $C_M = 0.02308$ M, $C_L = 0.2308$ M, $C_{NaClO_4} = 0.700$ M. T: $C_L = 1.000$ M.

v/cm³, Q_{exp}/J, Q_{corr}/J, ΔQ_{corr}/J: 3.000, 1.214, 1.426, 0.020; 6.000, 1.049, 1.247, −0.003; 9.000, 0.891, 1.079, 0.005; 12.000, 0.748, 0.925, 0.029; 15.000, 0.662, 0.832, 0.016; 18.000, 0.595, 0.760, −0.001;

(e) △ S: $C_M = 0.01500$ M, $C_{NaClO_4} = 0.955$ M. T: $C_L = 1.000$ M.

v/cm³, Q_{exp}/J, Q_{corr}/J, ΔQ_{corr}/J: 3.000, 4.655, 5.000, −0.036; 6.000, 3.073, 3.407, 0.010; 9.000, 2.198, 2.519, −0.006; 12.000, 1.637, 1.949, −0.008; 15.000, 1.276, 1.577, −0.022; 18.000, 1.014, 1.306, −0.024; 21.000, 0.799, 1.081, −0.001; 24.000, 0.689, 0.960, −0.035; 27.000, 0.548, 0.810, −0.006;

(f) △ S: $C_M = 0.01154$ M, $C_L = 0.2308$ M, $C_{NaClO_4} = 0.735$ M. T: $C_L = 1.000$ M.

v/cm³, Q_{exp}/J, Q_{corr}/J, ΔQ_{corr}/J: 3.000, 0.502, 0.714, −0.020; 6.000, 0.411, 0.609, −0.012; 9.000, 0.333, 0.521, −0.001; 12.000, 0.274, 0.451, 0.007; 15.000, 0.219, 0.389, 0.018; 18.000, 0.199, 0.364, 0.000;

(g) ▼ S: $C_L = 0.4000$ M, $C_{NaClO_4} = 0.600$ M. T: $C_M = 0.1000$ M, $C_{NaClO_4} = 0.700$ M.

v/cm³, Q_{exp}/J, Q_{corr}/J, ΔQ_{corr}/J: 3.000, 4.934, 5.143, 0.039; 6.000, 4.767, 4.974, 0.038; 9.000, 4.618, 4.822, 0.027;

(h) ▲ S: $C_L = 0.5000$, $C_{NaClO_4} = 0.500$ M. T: $C_M = 0.1000$, $C_{NaClO_4} = 0.700$ M.

v/cm³, Q_{exp}/J, Q_{corr}/J, ΔQ_{corr}/J: 3.000, 5.375, 5.617, −0.001; 6.000, 5.230, 5.471, −0.019; 9.000, 5.084, 5.323, −0.029;

(i) ■ S: $C_L = 0.6000$ M, $C_{NaClO_4} = 0.400$ M. T: $C_M = 0.1000$ M, $C_{NaClO_4} = 0.700$ M.

v/cm³, Q_{exp}/J, Q_{corr}/J, ΔQ_{corr}/J: 3.000, 5.687, 5.970, 0.003; 6.000, 5.534, 5.817, −0.005; 9.000, 5.384, 5.666, −0.007;

(j) ● S: $C_L = 0.8000$ M, $C_{NaClO_4} = 0.200$ M. T: $C_M = 0.1000$ M, $C_{NaClO_4} = 0.700$ M.

v/cm³, Q_{exp}/J, Q_{corr}/J, ΔQ_{corr}/J: 3.000, 6.123, 6.512, 0.020; 6.000, 6.036, 6.399, −0.020; 9.000, 5.928, 6.284, −0.051;

[a] The values of ΔQ_{corr} refer to the deviations $(Q_{calc} - Q_{corr})$ for the set of constants giving the minimum of the error square sum.

solutions contained perchloric acid in order to avoid hydrolysis.

From spectrophotometric and cation exchange measurements Fronæus [9] found three complexes for this system. The stability constants determined at 20.0 °C have been recalculated to 25.0 °C by an iterative method.[3] The values of β_j valid at 25.0 °C are given in Table 6.

A determination of the stability constants from the calorimetric data has been performed. As there are evidently three complexes in this system a determination of the β_j-values by the 'schematic map' method is a little more complicated in this case. However, starting with the set of constants found by Fronæus the error square sum, U, was calculated for a number of different sets of β_2 and β_3 (β_1 was kept constant). From the plot of $U(\beta_j, \Delta H_j)$ *versus* β_2 and β_3 the values of these two parameters giving the minimum of the error square sum was found. In the next approximation $\beta_3 (= 18\ M^{-3})$ was kept constant while $U(\beta_j, \Delta H_j)$ was calculated for various values of β_1 and β_2, see Fig. 5. The graphically obtained set of constants giving the minimum of the error square sum is given in Table 6. In the same

Table 6. Stability constants for the nickel(II) thiocyanate system obtained from calorimetric and cation exchange measurements. The errors given correspond to three standard deviations given by the computer or to estimated errors.

Method	β_1/M^{-1}	β_2/M^{-2}	β_3/M^{-3}
Calorimetrically			
Kalori	13.3 ± 1.2	37 ± 10	19 ± 18
Graphically	13.4 ± 0.7	37 ± 5	18 ± 12
By cation exchange [a]	13.8 ± 0.5	38 ± 4	54 ± 10
'Best' values	13.8 ± 0.5	38 ± 4	40 ± 15

[a] Values taken from Ref. 9, recalculated to 25.0 °C.

Table the stability constants computed by the programme "Kalori" are also included. The standard deviation, σQ_{corr}, was found to be equal to 0.024 J. As seen, the two calculation methods give almost identical results, once more indicating that the programme "Kalori" works properly.

The stability constants of the nickel(II) thiocyanate system obtained from calorimetric measurements are quite in line with those found by ion exchange, Table 6. The two methods give practically the same values of β_1 and β_2, respectively, while the value of β_3 determined in this study is lower than that found before. It is difficult to find a good value of β_3 by any method as the third complex is very weak ($K_3 = \beta_3/\beta_2 \approx 1$). The values of β_j obtained calorimetrically have somewhat higher random errors than those found by the cation exchange method. The set of 'best' values of β_j has been selected with due consideration to this, Table 6. These constants have then been used for the calculation of $\Delta H°_j$. The standard deviation, σQ_{corr}, was found to be equal to 0.035 J. In Fig. 6, Δh_v is plotted *versus* $\bar{n}$ (calculated from the 'best' constants). No variation of Δh_v with C_M can be discerned. Consequently no polynuclear complexes are formed. The β_j-values used, together with corresponding values of $\Delta G°_j$, $\Delta H°_j$ and $\Delta S°_j$, are listed in Table 7.

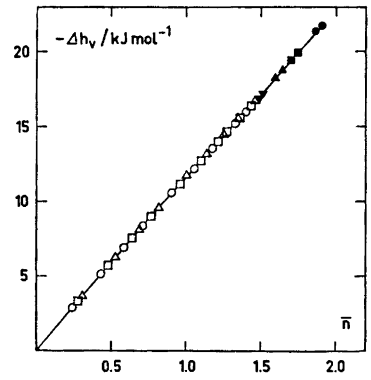

Fig. 6. The total molar enthalpy change, Δh_v, as a function of $\bar{n}$, for the nickel(II)-thiocyanate system; *cf.* Table 5.

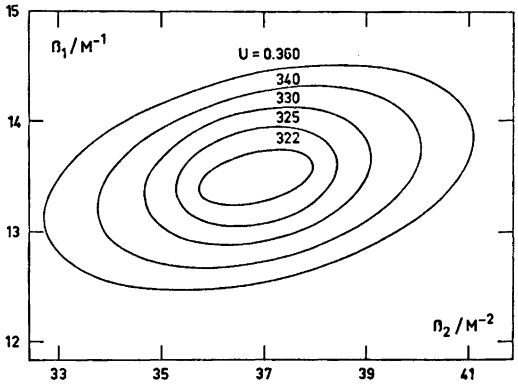

Fig. 5. Plot of assumed values of U *vs.* β_1 and β_2 for the nickel(II) thiocyanate system. $\beta_3 = 18\ M^{-3}$.

DISCUSSION AND CONCLUSIONS

For the copper(II) thiocyanate system our value of β_1 (55 M^{-1}) agrees very well with those

Table 7. The stability constants used and the computed values of $\Delta G°_j$, $\Delta H°_j$ and $\Delta S°_j$ for the stepwise reactions of the nickel, copper(II) and zinc thiocyanate systems. The data for the zinc system are taken from Ref. 4. The errors given correspond to three standard deviations or to estimated errors.

Metal		Ni^{2+}	Cu^{2+}	Zn^{2+}
β_j/M^{-j}	$j=1$	13.8 ±0.5	55 ±2	5.10 ±0.03
	2	38 ±4	550 ±50	11.0 ±0.6
	3	40 ±15		15.0 ±3.6
	4			32 ±5
$-\Delta G°_j/$ kJ mol^{-1}	1	6.51 ±0.10	9.93 ±0.09	4.04 ±0.02
	2	2.51 ±0.30	5.71 ±0.25	1.91 ±0.14
	3	0.1 ±0.9		0.76 ±0.6
	4			1.87 ±0.8
$-\Delta H°_j/$ kJ mol^{-1}	1	12.02 ±0.15	12.65 ±0.20	5.80 ±0.15
	2	8.9 ±1.0	13.1 ±1.5	1.8 ±1.0
	3	8.2 ±4.0		0.8 ±3.0
	4			7.7 ±3.5
$\Delta S°_j/$ J mol^{-1} K^{-1}	1	−18.5 ±0.6	−9.1 ±0.7	−5.9 ±0.5
	2	−21.5 ±3.5	−25 ±5	0 ±4
	3	−27 ±13		0 ±10
	4			−19 ±12

reported by Tanaka and Takamura [6] and by Kodama and Hanawa,[7] see Table 1. The value of β_2 given in Ref. 6, on the other hand, is lower than ours which may be due to the difference in ionic medium.

For the nickel(II) thiocyanate system our calorimetrically determined β_j-values agree very well with those reported by Fronæus, as already mentioned. On the whole they are also compatible with the set of constants found by Tribalat and Caldero, Table 1.

Nancollas and Torrance [8] have calorimetrically determined $\Delta H°_1$ for the formation of thiocyanate complexes of some transition metals at $I=0$. As previously pointed out,[4] their values for the cadmium and zinc thiocyanate systems are considerably less exothermic than those found by Gerding and Johansson [26] and by us. Similarly, for the nickel(II) thiocyanate system our value of $\Delta H°_1$, −12.02 kJ mol^{-1}, is more negative than that found by Nancollas and Torrance, −9.4 kJ mol^{-1}. For the copper(II) thiocyanate system, however, their value of $\Delta H°_1$, −12.6 kJ mol^{-1}, is consistent with ours, −12.65 kJ mol^{-1}. The discrepancies between the values given by Nancollas and Torrance and those obtained at $I=1.0$ M can hardly be due only to the difference in ionic medium.

A more likely explanation is no doubt that for these fairly weak complexes the introduction of even modestly erroneous values of β_j results in relatively large errors in the calculated amounts of the various complexes formed in a given solution. As, for a certain complex, the measured heat change is the product of the amout of the complex formed and the enthalpy change of the complex formation, $\Delta H°_j$, a corresponding error will be introduced in $\Delta H°_j$. For their determinations, Nancollas and Torrance recalculated thermodynamic constants K_1 taken from various sources to the actual ionic strengths ($I<0.06$ M) of their experiments by means of a Debye-Hückel formula. This approach is no doubt likely to introduce errors and inconsistencies serious enough to impair the validity of a comparison between the various systems investigated. The method adopted here, *viz.* to determine the values of K together with the heat changes, or at least determination of the two quantities under identical conditions, should be preferable. Especially the values of K_1 chosen by Nancollas and Torrance for the zinc and cadmium thiocyanate systems, 71.4 M^{-1} and 322 M^{-2}, respectively, seem to be too high, *cf.* Ref. 14. Their values of $\Delta H°_1$ also differ most from ours in these two instances.

From the variation of β_1 with the temperature Das *et al.*[14] and Malyavinskaya and Turyan [12] have determined $\Delta H°_1$ of the nickel(II) thiocyanate system. The value reported by Das *et al.* is considerably more exothermic than ours while that of the latter investigators agrees fairly well, *cf.* Tables 1 and 7.

The three divalent first row transition metal ions Ni^{2+}, Cu^{2+}, and Zn^{2+} all generally behave as mildly hard acceptors with Cu^{2+} closest to the borderline between hard and soft.[5] It is then to be expected that the thiocyanate complexes of Cu^{2+} should be formed in more exothermic reactions than those of Ni^{2+} and Zn^{2+}. As seen from Table 7, this is the case. The difference between Cu^{2+} and Ni^{2+} is perhaps smaller than expected, however. Also the thiocyanate complexes of Cd^{2+}, considered to be an acceptor just on the soft side of the borderline, are in fact formed in less exothermic reactions than those of Ni^{2+}, Table 5 of Ref. 4.

The entropy changes are small and negative. As may be expected,[27] the values become on the whole more negative for each consecutive step.

The thiocyanate ion exhibits linkage isomerism, bonding to the metal ion either through its sulfur or nitrogen atom. Soft acceptors prefer the softer S and hard acceptors prefer the harder N. The metals of this study Ni^{2+}, Cu^{2+}, and Zn^{2+} are probably all N-bonded.[27,28]

Further discussion will be postponed until the complete results of this investigation have been reported.

Acknowledgements. I am most grateful to Professor Sten Ahrland for his encouraging interest and generous advice. My thanks are also due to Dr. Efraim Avsar for doing part of the experimental work.

REFERENCES

1. Ahrland, S. and Kullberg, L. *Acta Chem. Scand. 25* (1971) 3457.
2. Ahrland, S. and Kullberg, L. *Acta Chem. Scand. 25* (1971) 3471.
3. Ahrland, S. and Kullberg, L. *Acta Chem. Scand. 25* (1971) 3677.
4. Ahrland, S. and Kullberg, L. *Acta Chem. Scand. 25* (1971) 3692.
5. Ahrland, S. *Struct. Bonding 5* (1968) 118.
6. Tanaka, N. and Takamura, T. *J. Inorg. Nucl. Chem. 9* (1959) 15.
7. Kodama, M. and Hanawa, K. *Ibaraki Daigaku Bunrigakubu Kiyo* (Shizen Kagaku) *13* (1962) 9, as quoted in *Chem. Abstr. 60* (1964) 2382b.
8. Nancollas, G. H. and Torrance, K. *Inorg. Chem. 6* (1967) 1567.
9. Fronæus, S. *Acta Chem. Scand. 7* (1953) 21.
10. Fronæus, S. and Larsson, R. *Acta Chem. Scand. 16* (1962) 1433.
11. Tribalat, S. and Caldero, J. M. *J. Electroanal. Chem. 5* (1963) 176.
12. Malyavinskaya, O. N. and Turyan, Ya. I. *Russ. J. Phys. Chem. 42* (1968) 144.
13. Tribalat, S. and Caldero, J. M. *Compt. Rend C.R. Acad. Sci. 258* (1964) 2828.
14. Das, R. C., Dash, A. C., Satyanarayan, D. and Dash, U. N. *Thermochim. Acta 2* (1971) 435.
15. Eatough, D. J., Izatt, R. M. and Christensen, J. J. *Thermochim. Acta 3* (1972) 233.
16. Fronæus, S. In Jonassen, H. B. and Weissberger, A. *Techniques of Inorg. Chem.* Interscience, New York, London 1963, Vol. 1, Chapter 1.
17. Sillén, L. G. and Warnqvist, B. *Ark. Kemi 31* (1969) 377.
18. Arnek, R. *Ark. Kemi 32* (1970) 81.
19. Karlsson, R. and Kullberg, L. *To be published.*
20. Okáč, A. *Z. Anal. Chem. 88* (1932) 189.
21. Burkov, K. A., Lilič, L. S. and Sillén, L. G. *Acta Chem. Scand. 19* (1965) 14.
22. Ahrland, S., Larsson, R. and Rosengren, K. *Acta Chem. Scand. 10* (1956) 705.
23. Berecki-Biedermann, C. *Ark. Kemi 16* (1955) 175.
24. Sidgwick, N. V. *The Chemical Elements and Their Compounds*, Oxford 1950, Vol. 1, p. 149.
25. v. Halban, H., Kortüm, G. and Szigeti, B. *Z. Electrochem. 42* (1936) 628.
26. Gerding, P. and Johansson, B. *Acta Chem. Scand. 22* (1968) 2255.
27. Ahrland, S. *Struct. Bonding 15* (1973) 167.
28. Fronæus, S. and Larsson, R. *Acta Chem. Scand. 16* (1962) 1447.

Received April 9, 1974.

Acta Chemica Scandinavica A 28 (1974) 839—845

Thermodynamics of Transfer of Nonelectrolytes from Light to Heavy Water. I.* Linear Free Energy Correlations of Free Energy of Transfer with Solubility and Heat of Melting of a Nonelectrolyte

ANTTI VESALA

Department of Chemistry, University of Turku, SF-20500 Turku 50, Finland

The solubilities of twenty-four slightly soluble nonelectrolytes were measured in light and heavy water. From these solubility values the changes in the standard free energy of transfer from H_2O to D_2O could be calculated for all compounds at 298.15 K. The determined transfer free energies are generally rather small in magnitude and positive in sign. They are, however, significant having a standard error less than 10 %.

A satisfactory linear free energy correlation was obtained between the free energy of transfer of nonelectrolytes from H_2O to D_2O and the free energy of transfer of the corresponding nonelectrolytes from the gas phase to the hypothetical one aquamolal solution in H_2O. In addition, a linear correlation was found between the free energy of transfer from H_2O to D_2O and the heat of melting at the melting point of the various compounds.

When studying the structure of aqueous solutions, further informations are obtained from additional studies in deuterium oxide.[2] Among the earliest studies in this field with nonelectrolytes as solutes is that of Swain and Thornton,[3] who employed methyl halides and determined their thermodynamic transfer properties from H_2O to D_2O in order to get their kinetic studies more complete. Gaseous nonelectrolytes have been studied by Scheraga *et al.*[4] and by Ben Naim.[5] Some interesting works in this field have recently been published by Dahlberg,[6] by Ben Naim *et al.*,[7] and by Jolicoeur and Lacroix.[8] These all are dealing with thermodynamic parameters of transfer of nonelectrolytes from H_2O to D_2O with special reference to the free energy of transfer. The survey by Jolicoeur and Lacroix [8] is interesting in the sense that it deals with a series of isomeric ketones and attaches importance also to the structural changes of solutes. Transfer and exchange effects have not been adequately separated in some of these surveys.[2,6]

In the present study the solubilities of twenty-four slightly soluble nonelectrolytes were determined in H_2O and D_2O. From these solubility values the standard free energy change of dissolution could be calculated for each solute separately in H_2O and D_2O. The difference in the obtained values represents the change in the free energy of transfer of the various nonelectrolytes from H_2O to D_2O. One of the most important criteria when choosing the solutes was that they did not contain any exchangeable hydrogen atoms. The group of nonelectrolytes which was chosen for this study consisted therefore of compounds having moderately different structures and internal polarizabilities.

The main aspect of this work was the search for possible linear free energy correlations where the free energy of transfer from H_2O to D_2O would participate. This type of possible correlations would indoubtedly be useful when solute-solvent interactions in nonelectrolyte-water solutions are considered.

* An abridgement of A. Vesala's dissertation.[1]

EXPERIMENTAL

Reagents. The water employed in the experiments was distilled water which was passed through an Amberlite CG 120+CG 400 ion-exchange column. The deuterium oxide used in the experiments with sulfur dioxide, iodine, and triethylamine was a product of the Norsk Hydro-elektrisk Kvaelstofaktieselskab. In the remaining experiments heavy water from the New England Nuclear Company was employed. The deuterium content in both these waters was 99.7 %. Some portions of solutions containing deuterium oxide were distilled and the distillate reused. The deuterium content of the distillate was determined from its density according to the method proposed by Kirshenbaum.[9a] Both light and heavy water were degassed by boiling under reduced pressure prior to the equilibration experiments.

The reagents used in the solubility measurements were commercial except 1,3-dinitrobenzene which was synthesized from benzene in a nitric acid – sulfuric acid mixture in the usual way.[10] The commercial reagents were at least of analytical grade. The solid compounds were recrystallized twice and sublimated if possible. The liquids were generally distilled through a column. All the organic compounds were checked by gas chromatography and found more than 99 % pure. Sulfur dioxide was bubbled through conc. H_2SO_4 before equilibration. The radioactive naphthalene-1-C-14 was purchased from the Radiochemical Centre and had a specific activity of 200 mCi/mmol and a radiochemical purity of 99 %. The naphthalene used in the experiments was prepared by mixing inactive naphthalene and active naphtalene and by recrystallizing the mixture from absolute ethanol.

Equilibrations. The equilibrations were carried out in vessels which were modified from those constructed by Franks *et al.*[11] The stirring was arranged with the aid of a magnetic stirrer. When liquids were treated, equilibrium was usually obtained in 48 h, whereas it took several days to reach the equilibrium state for the solid substances. The samples were filtered through glass-wool plugs prior to analysis.

The temperature of the water baths was maintained constant with Lauda or Termomix thermostats, the temperature varying within ± 0.05 K. The apparatus and flasks were kept in darkness to prevent possible decomposition of solutes by light.

A simple vacuum line system was applied when the solubility (the constant of Henry's law) of sulfur dioxide was determined. In this case the equilibrating vessel was directly connected to a vacuum pump and a manometer by which the pressure of the system, *i.e.* the sum of partial pressures of water and sulfur dioxide. could be measured.

Methods of analyzing solutes in saturated solutions. Three different methods were applied when the solubilities were determined, titrimetry, spectrophotometry, and radiochemistry. The solutes which were analyzed titrimetrically were sulfur dioxide, iodine, the tertiary amines, and the nitrobenzenes.

The samples of sulfur dioxide were titrated with a standard iodine solution in a phosphate buffer of pH 7. The end point of the titrations was determined visually. The pressure readings were corrected with respect to the vapor pressure of water. The vapor pressure of D_2O used in the calculations was that given by Kirshenbaum.[9b] The system followed Henry's law provided the concentration of the formed dissociation products of sulfurous acid was subtracted from the total concentration of SO_2.[12] This correction was carried out by means of the dissociation constant of sulfurous acid previously determined.[13]

Water samples containing iodine were titrated with a standard sodium thiosulfate solution. The end point of the titration was indicated by the dead-stop method using a Metrohm 350 B potentiometer equipped with a Metrohm Polarizer E 371.

The tertiary amines were titrated with standard HCl solutions. The titration mixture comprising tripropylamine and tributylamine contained about 75 % of acetone. All the amine titrations were performed with a Metrohm Combi titrator type 3 D.

The concentrations of the nitrobenzenes were also determined by a volumetric method.[14] In this procedure the nitro group was reduced by the Ti^{3+} ion. The titrations were carried out manually.

Most of the studied water solubilities were analyzed spectrophotometrically using a direct method of measurements or an extraction method. The employed procedures principally resembled those of Bohon and Claussen [15] and Wauchope and Getzen.[16] The standard solutions were prepared in water or in 2,2,4-trimethylpentane for the direct method and the extraction method, respectively. The measured molar and molal absorptivities are presented in Table 1.

The solubility of naphthalene was determined radiochemically using the technique of liquid scintillation counting. The measuring apparatus was an LKB-Wallac 81000 liquid scintillation counter in which it was possible to choose the counting channels so that the tritium in D_2O could be dropped down to the lower channel. The C-14 pulses in the upper channel were proportional to the concentration of naphthalene-C-14 in the sample. The cpm values were corrected to the same quenching using the method proposed by Reunanen and Soini.[17] The cpm value of the naphthalene used in the solubility experiments was measured in a standard solution in ethanol.

At least five parallel determinations were performed in each case, or alternatively two or

Table 1. Molar and molal absorptivities and values of λ_{max} for solutes at 298.15 K.

Solute	λ_{max} /nm	ε	Solvent	N[a]
Methylbenzene	261.0	248.8 ±2.0[b]	Water	6
Ethylbenzene	260.0	233.5 ±2.7	»	3
1,3-Dimethylbenzene	264.0	249.1 ±8.5	»	4
1,3,5-Trimethylbenzene	264.0	299 ±15	»	7
Diphenyl	247.0	16810 ±590	»	5
Benzene	254.0	150.0[c] ±5.5	2,2,4-Tri-	8
Chlorobenzene	264.5	198.7[c] ±1.5	methylpen-	10
Bromobenzene	265.0	141.3[c] ±0.92	tane	7
Iodobenzene	257.5	471.7[c] ±6.5	»	5
1,3-Dichlorobenzene	270.5	325.1[c] ±4.5	»	9
1,4-Dichlorobenzene	273.0	371.6[c] ±4.0	»	9
Methoxybenzene	277.5	1633*c* ±6	»	4
Ethoxybenzene	271.0	1382*c* ±8	»	4
Diphenylether	271.0	1385*c* ±16	»	4
Acenaphthene	288.5	4676*c* ±24	»	4
Phenanthrene	292.0	9822*c* ±91	»	4

[a] Number of measurements. [b] Mean and standard deviation. [c] Molal absorptivity.

three measurements at five or more temperatures, from which the values at 298.15 K could be calculated by the method of least squares.

RESULTS

The measured solubilities in H_2O as well as those reported previously are presented in Table 2. It is seen that the agreement of the determined values with the literature values is good. The solubilities are expressed in aquamolal units, *i.e.* in numbers of mol of solute dissolved in 55.51 mol of water. This unit is comparable with the mol fraction and has the advantage of being free from temperature and density effects.

When the solubility of a substance is relatively low, nearly ideal conditions can be assumed to exist in the solution. In this case the change in the free energy when the substance is transferred from the gas phase to the solution is

$$\Delta G^\circ_s = -RT \ln m \quad (1)$$

The standard state for a solute is defined as a hypothetical one-aquamolal solution, where the vapour pressure of the solute is one atmosphere (1 atm = 101.325 kPa). The letter m denotes thus aquamolality in the above equation. ΔG°_s can then be considered as the standard free energy change of the process

substance (g, 1 atm) = substance (aq, hypoth. 1 m soln) (2)

When the solute is a gas, both its vapor pressure and solubility have to be determined. In the case of the solute being a solid or a liquid at 298.15 K, the ΔG° values for processes (3) and (4) must be known to allow the desired changes in free energy for process (2) to be calculated from the measured free energy changes in processes (5) and (6).

substance (l) = substance (g, 1 atm) (3)

substance (s) = substance (g, 1 atm) (4)

substance (l) = substance (aq, hypoth. 1 m soln) (5)

substance (s) = substance (aq, hypoth. 1 m soln) (6)

The changes in the free energy of transfer of a solute from H_2O to D_2O in process (7) is simply defined by eqn. (8).

subst. (H_2O, hypoth. 1 m soln) = subst. (D_2O, hypoth. 1 m soln) (7)

$$\Delta G^\circ_t = \Delta G^\circ(D_2O) - \Delta G^\circ(H_2O) \quad (8)$$

ΔG°_t can as well be calculated by eqn. (9)

$$\Delta G^\circ_t = -RT \ln (m_{D_2O}/m_{H_2O}) \quad (9)$$

Table 2. Solubilities of nonelectrolytes in light water determined in this work and reported in literature, respectively. (The values refer to 298 K if not otherwise stated.)

Solute	Solubility/mol 10^{-6} g^{-1} This work[a]		Previously reported	Ref.
1. Sulfur dioxide	1100	±20	1230	12
			1270	18
2. Iodine	1.29	±0.01	1.33	19
3. Nitrobenzene	14.6	±0.4	16.7[b]	20
4. 1,3-Dinitrobenzene	5.12	±0.05	3.98[b]	20
			4.82	21
5. Triethylamine	728	±28	762	22
6. Tripropylamine	5.22	±0.10		
7. Tributylamine	0.765	±0.015	0.2[c]	23
8. Benzene	24.4	±0.1	22.0	24
			23.0	15
			22.4	25
			22.9	26
9. Methylbenzene	6.81	±0.08	6.2	20
			6.84	15
			5.78	25
			6.00	27
			5.62	26
10. 1,3-Dimethylbenzene	1.94	±0.01	1.86	15
			1.48	28
11. 1,3,5-Trimethylbenzene	0.328	±0.005		
12. Ethylbenzene	1.91	±0.02	1.97	15
			1.43	26
13. Chlorobenzene	4.11	±0.07	4.45	27
			4.95	29
			4.33[b]	20
14. Bromobenzene	2.84	±0.03	2.84[b]	20
15. Iodobenzene	1.12	±0.03	1.7[b]	30
16. 1,3-Dichlorobenzene	0.700	±0.007	0.840	31
17. 1,4-Dichlorobenzene	0.580	±0.008	0.565	16
			0.52	20
18. Methoxybenzene	14.2	±0.4	14	32
19. Ethoxybenzene	4.66	±0.04	4.5	32
20. Diphenylether	0.110	±0.005		
21. Diphenyl	0.0491	±0.0004	0.0459	16
			0.0486	15
22. Naphthalene	0.251	±0.002	0.244	16
			0.270	15
23. Acenaphthene	0.0233	±0.0003	0.0252	16
24. Phenanthrene	0.00677	±0.00008	0.00662	16

[a] Mean and standard deviation. [b] 303 K. [c] 291 K.

The results are listed in Table 3, where as well $\Delta G°_t$ values obtained by other investigators are collected.

DISCUSSION

It is seen that the values of $\Delta G°_t$ for nonelectrolytes are rather small and varying in sign and it is difficult to draw any direct conclusions from these values. When the free energies of transfer are plotted against the free energies of dissolution for the thirty-four different nonelectrolytes, a fairly good linear correlation is obtained (Fig. 1). The $\Delta G°$ values for process (2) were evaluated from the values determined in this study and from values found in literature.[37-39] When the $\Delta G°$ values for processes (3) or (4) were not found in literature, they were evaluated by means of the values of vapor pressure. For three of the compounds,

Table 3. Free energies of transfer of nonelectrolytes from light to heavy water at 298.15 K.

Solute	ΔG°_t/J mol^{-1}	Ref.
1. Sulfur dioxide	93 ± 150[a]	This work
2. Iodine	544 ± 33	»
	451	19
3. Nitrobenzene	218 ± 92	This work
	238	33
4. 1,3-Dinitrobenzene	314 ± 46	This work
5. Triethylamine	533 ± 93	»
6. Tripropylamine	138 ± 33	»
7. Tributylamine	−188 ± 25	»
8. Benzene	195 ± 25	»
	0 ± 63	6
	196 ± 73	7
9. Methylbenzene	287 ± 12	This work
	105 ± 63	6
10. 1,3-Dimethylbenzene	203 ± 25	This work
	188 ± 50	6
11. 1,3,5-Trimethylbenzene	463 ± 46	This work
12. Ethylbenzene	135 ± 17	»
13. Chlorobenzene	103 ± 125	»
14. Bromobenzene	322 ± 33	»
15. Iodobenzene	429 ± 29	»
16. 1,3-Dichlorobenzene	246 ± 33	»
17. 1,4-Dichlorobenzene	278 ± 50	»
18. Methoxybenzene	660 ± 134	»
19. Ethoxybenzene	290 ± 33	»
20. Diphenylether	460 ± 138	»
21. Diphenyl	574 ± 46	»
	−109 ± 148	7
22. Naphthalene	343 ± 38	This work
	452 ± 63	6
23. Acenaphthene	468 ± 46	This work
24. Phenanthrene	804 ± 58	»
25. Argon	−211	5
26. Methane	−134	7
27. Ethane	−147	7
28. Propane	−60	4
29. Butane	−73	4
30. Carbon dioxide	2	34
	8	13
31. Methyl fluoride	−58[b]	3
32. Methyl chloride	76[b]	3
33. Methyl bromide	151[b]	3
34. Methyl iodide	230[b]	3
35. *t*-Butyl chloride	−68[c]	35
36. 1,2-Dimethylbenzene	351	6
37. 1,3,5-Trinitrobenzene	481	36

[a] Standard error. [b] 302.5 K. [c] 287 K.

namely, 1,3-dinitrobenzene, 1,3,5-trinitrobenzene, and tributylamine, the ΔG° values could not be estimated because their vapor pressures at 298 K were difficult to evaluate and no reliable values could be found in the literature. It must also be noted that some points in the plot do not refer to measurements at 298 K.

When taken into account the varying type of compounds studied the correlation may appear satisfactory. The correlation becomes still better when the compounds which are highly polarizable like sulfur dioxide and nitrobenzene are omitted.

A correlation that closely resembles the free

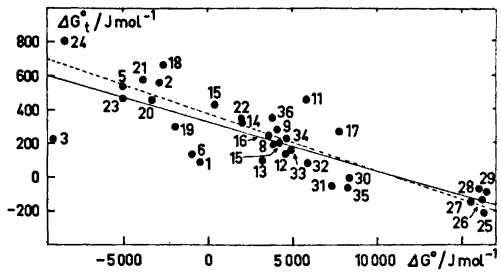

Fig. 1. Correlation between the free energy of transfer from H_2O to D_2O ($\Delta G°_t$) and the free energy of dissolution ($\Delta G°$) of some nonelectrolytes (For numbers, see Table 3)

slope	−0.0287	−0.0338[a]
intercept	331	380[a]
corr. coeff.	−0.814	−0.902[a]

[a] Dotted line (points 1, 3, and 6 omitted).

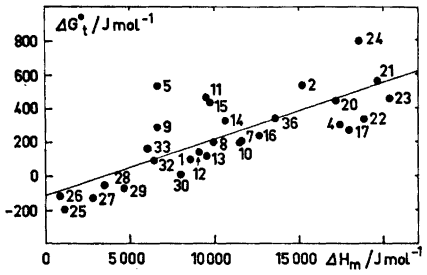

Fig. 2. Correlation between the free energy of transfer from H_2O to D_2O ($\Delta G°_t$) and the heat of melting (ΔH_m) of some nonelectrolytes (For numbers, see Table 3)

slope	0.0332
intercept	−113
corr. coeff.	0.774

energy correlation mentioned above is that between partition coefficients and aqueous solubility of organic liquids reported by Hansch *et al.*[40] in their study on partition coefficients between water and octanol. Different slopes and intercepts are found for the different types of organic liquids but the overall correlation is good.

It is to be expected that in this kind of ideal case there exists a linear correlation between solubilities and heats of melting. It is therefore natural to assume that there must exist a linear correlation between the free energies of transfer and the heats of melting. It is, however, to be expected that polarization effects do not appear in this kind of correlation. The heats of melting at melting points for twenty-nine compounds were taken from literature.[37b,39] When plotting $\Delta G°_t$ against ΔH_m a fairly good linear correlation is indeed obtained (Fig. 2). The values for sulfur dioxide and nitrobenzene (and 1,3-dinitrobenzene) appear to fit satisfactorily into the plot. Since the value of the heat of melting for 1,3,5-trinitrobenzene was not found in literature the value of ΔH_m for trinitrotoluene (22 500 J mol^{-1}) may be considered as a rough estimate. By so doing, a rather good fit is obtained ($\Delta G_t°$ for 1,3,5-trinitrobenzene is 481 J mol^{-1}). The point for triethylamine deviates most from the correlation line. If the ΔH_m value for triethylamine were replaced by that for $(C_2H_5)_3N.3H_2O$, 15 000 − 16 000 J mol^{-1}, evaluated by Kohler *et al.*,[41] a better fit could be obtained. As for the other deviations there is no such uniform group of compounds whose members would systematically deviate. The anomalies observed may thus be regarded as fortuitous.

Acknowledgements. The author wishes to thank Mr. Sulo Piepponen, Ph.M., and Mr. Jouko Leivo, Nat.cand., who gave valuable assistance in the performance of some of the solubility determinations. A grant obtained from the Emil Aaltonen Foundation is gratefully acknowledged.

REFERENCES

1. Vesala, A. *Thermodynamics of Transfer of Nonelectrolytes from Light to Heavy Water*, Diss., University of Turku, Turku 1973.
2. Arnett, E. M. and McKelvey, D. R. In Coetzee, J. F. and Ritchie, C. D. *Solute–Solvent Interactions*, Dekker, New York 1969, Chapter 6.
3. Swain, C. G. and Thornton E. R. *J. Amer. Chem. Soc. 84* (1962) 822.
4. Kresheck, C. G., Schneider, H. and Scheraga, H. A. *J. Phys. Chem. 69* (1965) 3132.
5. Ben Naim, A. *J. Chem. Phys. 42* (1965) 1512.
6. Dahlberg, D. B. *J. Phys. Chem. 76* (1972) 2045.
7. Ben Naim, A., Wilf, J. and Yaacobi, M. *J. Phys. Chem. 77* (1973) 95.
8. Jolicoeur, C. and Lacroix, G. *Can. J. Chem. 51* (1973) 3051.
9. Kirshenbaum, I. *Physical Properties and Analysis of Heavy Water*, McGraw, New York 1955, *a.* p. 16, *b.* p. 20.
10. Vogel, A. I. *Practical Organic Chemistry*, 3rd Ed., Longman Group Ltd., London 1970, p. 526.

11. Franks, F., Gent, M. and Johnson, H. H. *J. Chem. Soc.* (1963) 2716.
12. Johnstone, H. F. and Leppla, P. W. *J. Amer. Chem. Soc. 56* (1934) 2233.
13. Salomaa, P., Vesala, A. and Vesala, S. *Acta Chem. Scand. 23* (1969) 2107.
14. Kolthoff, I. M. and Belcher, R. *Volumetric Analysis*, Interscience, New York and London 1957, Vol. III, p. 610.
15. Bohon, R. L. and Claussen, V. F. *J. Amer. Chem. Soc. 73* (1951) 1571.
16. Wauchope, R. D. and Getzen, F. W. *J. Chem. Eng. Data 17* (1972) 39.
17. Reunanen, M. A. and Soini, E. J. *Liquid Scintillation Counting 3.*, Heyden and Son, London. *In press.*
18. Vosolsobe, J., Simecek, A., Michalek, J. and Kadlec, B. *Chem. Prum. 15* (1965) 401; Ref. *Chem. Abstr. 63* (1965) 14124c.
19. Ramette, R. W. and Sandford, R. W., Jr. *J. Amer. Chem. Soc. 87* (1965) 5001.
20. Gross, P. M. and Saylor, J. H. *J. Amer. Chem. Soc. 53* (1931) 1744.
21. Shikata, M. and Hozaki, N. *Mem. Coll. Agric. Kyoto 17* (1931) 18; Ref. *Chem. Zentralbl. 108* (1937) II 2817.
22. *International Critical Tables*, McGraw, New York 1928, Vol. III, p. 390.
23. Damsgaard-Sörensen, P. and Unmack, A. *Z. Phys. Chem. Abt. A 172* (1935) 289.
24. Arnold, D. S., Plank, C. A., Erickson, E. E. and Pike, F. P. *Chem. Eng. Data Ser. 3* (1958) 253.
25. Andrews, L. J. and Keefer, R. M. *J. Amer. Chem. Soc. 71* (1949) 3644.
26. McAuliffe, C. *J. Phys. Chem. 70* (1966) 1267.
27. Dreisbach, R. R. *Advan. Chem. Ser. 15* (1955) 134.
28. Hermann, R. B. *J. Phys. Chem. 76* (1972) 2754.
29. Chey, W. and Calder, G. V. *J. Chem. Eng. Data 17* (1972) 199.
30. Gross, P. M., Saylor, J. H. and Gorman, M. A. *J. Amer. Chem. Soc. 55* (1933) 650.
31. Ginnings, P. M., Hering, E. and Coltrane, D. *J. Amer. Chem. Soc. 61* (1939) 807.
32. McGowan, J. C., Atkinson, P. N. and Ruddle, L. H. *J. Appl. Chem. 16* (1966) 99.
33. Vermillion, H. E., Werbel, B., Saylor, J. H. and Gross, P. M. *J. Amer. Chem. Soc. 63* (1941) 1346.
34. Curry, J. and Hazelton, C. L. *J. Amer. Chem. Soc. 60* (1938) 2771.
35. Clarke, G. A., Williams, T. R. and Taft, R. W., Jr. *J. Amer. Chem. Soc. 84* (1962) 2292.
36. Salomaa, P. *Suom. Kemistilehti B 45* (1972) 149.
37. Weast, R. C., Ed., *Handbook of Chemistry and Physics*, 50th Ed., The Chemical Rubber Company, Ohio 1969, *a.* p. D-148, *b.* p. C-717.
38. Jordan, T. E. *Vapor Pressures of Organic Compounds*, Interscience, New York 1954.
39. Dreisbach, R. R., Ed., *Physical Properties of Chemical Compounds*, The American Chemical Society, Washington D. C. 1955, Vol. I; 1959, Vol. II; 1961, Vol. III.
40. Hansch, C., Quinlan, J. E. and Lawrence, G. L. *J. Org. Chem. 33* (1968) 347.
41. Kohler, F., Arnold, H. and Munn, R. J. *Monatsh. Chem. 92* (1961) 876.

Received April 22, 1974.

Acta Chemica Scandinavica A 28 (1974) 846—850

The Interpretation of the ^1H NMR Spectrum of 1,2,4,5-Hexatetraene Oriented in a Nematic Solvent

BJÖRN PEDERSEN,[a]* JAN SCHAUG[a] and HENNING HOPF[b]

[a] Kjemisk institutt, Universitetet i Oslo, Oslo 3, Norway and [b] Institut für Organische Chemie der Universität Karlsruhe, Postfach 6380, 7500 Karlsruhe 1, German Federal Republic

The proton magnetic resonance spectrum of 1,2,4,5-hexatriene (biallenyl) dissolved in a nematic solvent at room temperature has been recorded and interpreted in detail. The interpretation is based on a planar *trans* structure of biallenyl with symmetry C_{2h} with the terminal CH_2 groups orthogonal to the plane formed by the other atoms. Six different dipolar coupling constants are obtained from the spectral analysis. This is not sufficient to determine the relative positions completely, but some structural information, supporting the assumed structure, is obtained.

From the vibrational spectra Powel *et al.*[1] conclude that 1,2,4,5-hexatetraene (biallenyl) has the planar *trans* structure (I).

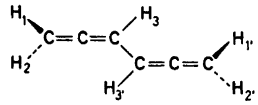

(I)

The symmetry of (I) is C_{2h} and the terminal CH_2 groups are twisted out of the molecular plane by 90°.

The geometry of the carbon skeleton in (I) has been determined quantitatively in the vapour phase by means of electron diffraction by Trætteberg *et al.*[2] The C–C double bond distances are found to be equal to the C–C distance in allene,[3,4] 1.31 Å. The central C–C bond is found to be 1.47 Å as also found in 1,3-butadiene.[5] The hydrogen atoms were not located very precisely. In the terminal CH_2 groups the C–C–H angles were assumed to be 120° and for the inner H atoms the C–C–H angle was assumed to be 118°. The C–H distances were assumed to be equal and found to be 1.10 Å.

Information on the position of the hydrogen atoms can be obtained from the ^1H NMR spectrum of biallenyl dissolved in a nematic solvent.[6] We have recorded such a spectrum and we will give the detailed interpretation of the spectrum below. It turns out that it is not possible from the ^1H NMR spectrum alone to get sufficient information to determine completely the five parameters needed to specify the position of the hydrogen atoms in (I), but partial information is obtained supporting the proposed structure (I).

EXPERIMENTAL

Biallenyl was synthesized as described earlier.[7] After degassing, 45 mg biallenyl was distilled into 595 mg of the liquid crystal *N*-(*p*-ethoxybenzylidene)-*p*-*N*-butylaniline contained in an NMR-tube supplied with a capillary with trifluoroacetic acid (TFA), and sealed under vacuum.

The spectrum was run on a Varian HA-100 spectrometer operating at 98 MHz in the frequency mode locked on the TFA line. The total spectral width was 7400 Hz and close to 90 lines were resolved with a width at half-height of approximately 5 Hz in the center of the spectrum. A complete spectrum is shown in Fig. 1. The analysis was carried out on the basis of an expanded spectrum recorded under slightly different experimental conditions. The calculated spectrum, also given in Fig. 1, is therefore based on slightly different coupling constants than those obtained below.

* Also at the Central Institute for Industrial Research, Oslo 3, Norway.

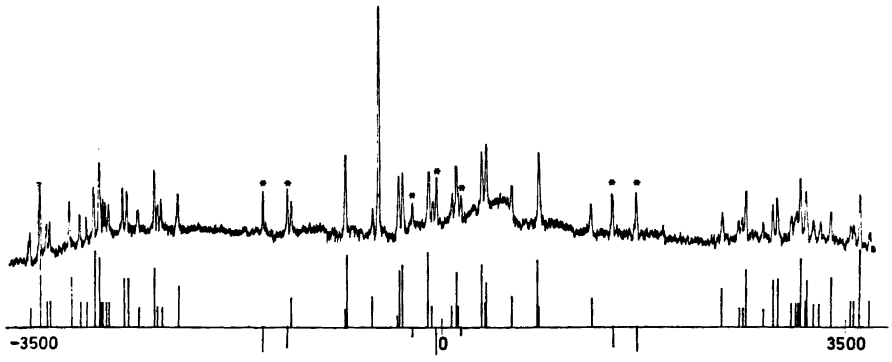

Fig. 1. The 98 MHz NMR spectrum of 1,2,4,5-hexatriene dissolved in *N*-(*p*-ethoxybenzylidene)-*p*-*N*-butylaniline (22 mol %). The calculated spectrum is given as a stick plot below. The lines marked with a star are from an impurity. The lines can be matched to the calculated lines from a A_2B system given below as an inverted stick plot.

INTERPRETATION

The six protons in (I) form a AA'A''A'''BB' spin system. The direct magnetic dipole-dipole coupling D_{ij} is the dominating coupling in the spectrum of an anisotropically reorienting molecule.[6] In this case there are six different D coupling constants to determine. As a first approximation we can ignore the chemical shift and the indirect spin-spin coupling and regard the spin system as A_4X_2. The four terminal protons constitute a weakly coupled two pair system. The spectrum of such a system is well known.[6,8] It consists of two multiplets split by the dominating pair coupling D^{12}. The low field half of the spectrum is shown in Fig. 2. The only effect of the indirect spin-spin coupling is to split the strongest line into a narrow doublet also shown in Fig. 2. This last spectrum is exactly the spectrum observed for allene.[9]

In biallenyl the coupling to the X_2 protons gives rise to a more complex multiplet. But as seen in Fig. 1 the high and low field part of the spectrum consists of a superposition of four simple A_4 multiplets as expected from the X-approximation. On the other hand, each line in the doublet from the X_2 protons is split to a pentet due to the coupling to the four A-protons. This accounts for ten lines in the central part of the spectrum shown in Fig. 1.

We see that the main features of the spectrum in Fig. 1 can be understood on the basis of this simple A_4X_2 approximation. From this

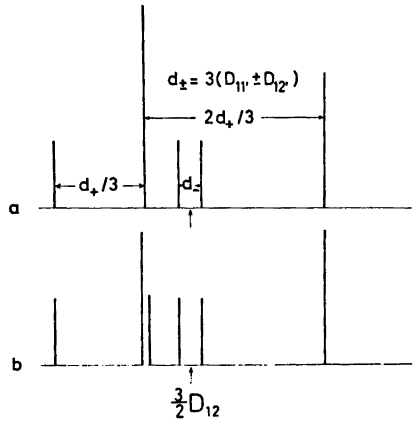

Fig. 2. The low-field half of the calculated spectrum of an oriented A_4 spin system (two weakly coupled proton pairs). (a) Dipole-dipole coupling only, (b) dipole-dipole coupling + indirect spin-spin coupling.

analysis we derive approximate values for D_{12}, $D_{11'}$, $D_{12'}$, $D_{33'}$, and $(D_{13}+D_{13'})$. D_{13} and $D_{13'}$ were assumed to be equal as a first approximation. The thus derived values for the direct coupling constants were then used as input parameters in the LAOCOONOR program.[10] The indirect spin-spin coupling constants and the chemical shift were taken from the analysis of the isotropic ^1H NMR spectrum.[11] During the iteration only the chemical shift and the D's were varied simultaneously. The

Table 1. 98 MHz NMR parameters of 1,2,4,5-hexatetraene partially oriented in *N*-(*p*-ethoxybenzylidene)-*p*-*N*-butylaniline. (Coordinates in Å).

Observed (Hz)	Calculated (Hz)	Observed[a] (Hz)
$D_{12} = 2021.17 \pm 0.12$	2021.17	$J_{12} = -10.0$
$D_{11'} = -63.73 \pm 0.12$	−64.70	$J_{12'} = 3.5$
$D_{12'} = -53.74 \pm 0.12$	−52.60	$J_{11'} = 3.5$
$D_{13} = -235.6 \pm 1.2$	−235.62	$J_{13} = -6.7$
$D_{13'} = -242.0 \pm 1.2$	−242.03	$J_{13'} = 1.2$
$D_{33'} = 254.6 \pm 0.11$	254.67	$J_{33'} = 10.5$
$D_{13} + D_{13'} = = 477.65 \pm 0.15$ Hz		$\nu_1 - \nu_3 = 74.39 \pm 0.18$ Hz

		x	y	z
$S_{xx} = -0.07405 \pm 0.00058$	H_1:	0.6086	3.5693	0.9519
$S_{zz} = -0.11616 \pm 0.00001$	H_3:	1.6777	−0.0921	0
$S_{xy} = 0.06607 \pm 0.00136$				

[a] Ref. 11.

iteration converged to a final r.m.s. error of 1.2 Hz. In Table 1 the final direct coupling constants and chemical shift are given together with the indirect spin-spin coupling constants used.

From the data in Table 1 it is clear that the separation of D_{13} and $D_{13'}$ is still uncertain and the values of the two are correlated. The estimated error in the sum is only 1/10 of the error in the individual values. Otherwise the final values are satisfactory and the agreement between the observed and the calculated spectrum is very good.

The chemical shift difference, 74.4 ± 0.2 Hz, between the terminal and the inner protons is 3.0 Hz larger than observed in the isotropic spectrum.[11] This can be due to the difference between the solvents or might indicate anisotropy of the chemical shift.[6]

Seven of the lines in the observed spectrum could not be matched by a line in the calculated spectrum. These lines are marked in Fig. 1. The lines are probably from an impurity. The interpretation of the spectrum is straightforward. It is the spectrum of an A_2X system where the two outermost doublets are from the A_2 protons and the central triplet is from the X-proton. The obtained chemical shifts are $\nu_A = 74$ Hz, $\nu_X = 49$ Hz (to low field relative to ν_3), $D_{AA} = 1030$ Hz and $D_{AX} = 109$ Hz.

The impurity is most likely $CH_2=C=CHX$ oriented in the nematic solvent similarly to biallenyl. X is probably Br and the same impurity was also detected in the isotropic spectrum.[11] However, in the isotropic spectrum only the low field triplet from $=CHBr$ could be seen, but here all lines are separated. Furthermore, as biallenyl contributes to many more lines the relative intensities of the impurity lines are comparable to the intensities of the lines from biallenyl. The only symmetry for bromoallene is a mirror plane. It is therefore necessary with three elements in the **S**-matrix to specify the orientation of the molecule, and with only two direct coupling constants no structural information can be obtained.

STRUCTURAL INFORMATION

The good agreement between the calculated and observed spectrum is a further support for the structure (I). However, the direct coupling constants also carry quantitative information on the molecular structure of biallenyl. The direct coupling constant between proton i and j is given as [6]

$$D_{ij} = -\frac{h\gamma^2}{4\pi^2 r^3_{ij}} S_{ij}$$

γ is the gyromagnetic ratio of the proton, r_{ij} the distance between proton i and j and S_{ij} is the degree of orientation of the axis passing through i and j. For a molecule of symmetry C_{2h}, S_{ij} can be calculated from an **S**-matrix containing three independent elements: S_{xx}, S_{zz} and S_{xy}. (The coordinate system used has its origin at the centre of symmetry with the z-axis normal to the molecular plane and the y-axis parallel to the double bonds.)

The positions of the protons are determined completely by five coordinates: xyz for H_1 and xy for H_3. The positions of the other protons then follow from the symmetry. The direct coupling constants therefore depend on eight unknowns: five position coordinates and three **S**-matrix elements. We have only six different direct coupling constants, and two of these might be coupled, hence, we can only determine three, or two, proton coordinates. It is therefore necessary to find two or three reasonable constraints. After trying several alternatives we have settled on the following: we have varied x and y for H_3 and used the coordinates calculated from the electron diffraction study for H_1.

The calculations were done using the least squares program SHAPE.[12] The observed direct coupling constants were given weights inversely proportional to the estimated standard deviations. The final calculated direct coupling constants are given in Table 1 together with the obtained coordinates for H_3 and the assumed coordinates for H_1. The largest differences between calculated and observed coupling constants are for the coupling between the terminal protons across the molecule, $D_{12'}$ and $D_{11'}$, where the difference is about eight standard deviations.

In the refinement the H_3-C distance is stretched from 1.10 Å to 1.18 Å and the $H_3-C=C$ angle is reduced from 118° to 115.2°. These changes are not physically reasonable. Extrapolating from related structures [4,5] it is expected that the C–H distance should be about 1.1 Å and the H–C=C angle somewhat larger than 120°. This displacement of H_3 relative to the carbon skeleton probably follows from keeping the position of the terminal atoms fixed.* As the direct coupling constants depend only on the inter-proton distances it is more appropriate to look directly at the proton-proton distances calculated from the final coordinates. These distances are given in Table 2 together with corresponding distances in the related molecules allene and 1,3-butadiene.

The best comparison between allene and biallenyl is probably made by comparing the ratio R_{13}/R_{12}. This ratio is 2.065 for biallenyl and 1.961 for allene [9] (both values from NMR data) indicating that R_{13} is larger in biallenyl. A similar but much larger effect is found comparing 1,3-butadiene [13] and ethene [14] where the ratio R_{trans}/R_{gem} is 1.677 and 1.320, respectively.

The distance between the inner protons, $R_{33'}$, is found to be 0.2 Å larger here than in the electron diffraction study.[2] This difference might not be significant, but, at least, it is a support for the assumed structure as any contribution from another conformer would lead to a reduction in this distance.

* However, this unreasonable distortion of the geometry indicates that the conclusions we can draw are at most semiquantitative.

Table 2. Comparison of corresponding distances (Å) in biallenyl, allene, and 1,3-butadiene obtained by electron diffraction and NMR.

Distance	Biallenyl NMR	ED[a]	Allene NMR[b]	ED[c]	1,3-Butadiene NMR[d]	ED[e]
R_{13}	3.931	3.918	3.7782	3.7250		
$R_{13'}$	4.269	4.206				
$R_{33'}$	3.360	3.167			3.188	3.095
R_{12}	(1.9038)	1.9038	1.9269	1.8582	1.806	1.853

[a] Ref. 2. [b] Ref. 9. [c] Ref. 3. [d] Ref. 5.

REFERENCES

1. Powell, D. L., Klæboe, P., Christensen, D. H. and Hopf, H. *Spectrochim. Acta A 29* (1973) 7.
2. Trætteberg, M. and Paulen, G. *Acta Chem. Scand. To be published.*
3. Almenningen, A., Bastiansen, O. and Trætteberg, M. *Acta Chem. Scand. 13* (1959) 1699.
4. Maki, A. G. and Toth, R. A. *J. Mol. Spectrosc. 17* (1965) 136; Hirota, E. and Matsumura, C. *J. Chem. Phys. 59* (1973) 3038.
5. Haugen, W. and Trætteberg, M. *Acta Chem. Scand. 20* (1966) 1726; Kuchitsu, K., Fukuyama, T. and Morino, Y. *J. Mol. Struct. 1* (1967) 463.
6. For a review, see Diehl, P. and Khetrapal, C. L. In Diehl, P., Fluck, E. and Kosfeld, R., Eds., *NMR-Basic Principles and Progress*, Springer, Berlin 1969, Vol. 1.
7. Hopf, H. *Angew. Chem. 17* (1970) 703.
8. Pedersen, B. *Chem. Phys. Lett. 1* (1967) 373.
9. Sackman, E. *J. Chem. Phys. 51* (1969) 2984.
10. Diehl, P., Khetrapal, C. L. and Kellerhals, H. P. *Mol. Phys. 15* (1968) 333.
11. Pedersen, B., Schaug, J. and Hopf, H. *To be published.*
12. Diehl, P. *Private communication.*
13. Segre, A. L. and Castellano, S. *J. Magn. Resonance 7* (1972) 5.
14. Bovée, W., Hilbers, C. W. and Maclean, C. *Mol. Phys. 17* (1969) 75.

Received March 18, 1974.

Acta Chemica Scandinavica A 28 (1974) 851—854

Thermodynamics of Transfer of Nonelectrolytes from Light to Heavy Water. II. Evaluation of Solvation Energy of Transfer Applying the Internal Charge Distribution of Solute Molecule Estimated by CNDO Calculations

ANTTI VESALA

Department of Chemistry, University of Turku, SF-20500 Turku 50, Finland

A part of the transfer energy of solvation was estimated on the basis of the internal charge distribution of the solute molecule calculated by the CNDO molecular orbital method for some aromatic hydrocarbons, aromatic ethers, and nitrobenzenes. The magnitude of this energy was about 30 % of the transfer free energy from H_2O to D_2O for nitrobenzenes. Nonelectrolytes like nitrobenzenes are so called "structure breakers" which closely resemble electrolytes.

Many theories have been created to clarify the conceptions that deal with the structure of aqueous nonelectrolyte solutions, but the problem is not easily solved. The common laws and rules that hold in liquids are not valid in water and aqueous solutions. There is a unanimous agreement about the fact that a nonreacting solute increases the waterlike structure in its immediate neighborhood.[1] In this respect, the aliphatic hydrocarbons are ideal compounds.

The water layer just around the solute is of greatest importance and most of the attention must be paid to it. The usual concept of the constitution of the energy that is needed when a solute is transferred from the gas phase to solution can be applied to this case. First of all, there is an energy component which a solute needs to create a proper hole or cavity into the solvent. Secondly, the solute brings about a certain arrangement of solvent molecules around the solute. If this occurs in a waterlike manner in water, the solute is known as "structure maker". The effects of another kind are regarded as "structure breaking". Thirdly, there is an energy component which is associated with interactions between the solute molecule and water. There are three kinds of interactions, namely, isotropic, anisotropic, such as caused by hydrogen bonds, and those caused by dispersion forces.

The most proper quantities to illustrate the energy effects mentioned above would, no doubt, be the changes in enthalpy and entropy when the solute is transferred from the gas phase to solution. It is to be expected that the respective quantities of transfer for the solute from H_2O to D_2O would reflect this phenomenon still more profoundly. The values of enthalpy and entropy of transfer determined with the aid of the van't Hoff method have generally a very low accuracy for drawing further conclusions. It is, however, to be anticipated that some of the effects mentioned above will appear when they are studied by the aid of the values of transfer free energies.

CALCULATIONS

The isotropic component can be described in the following way. The change in the isotropic energy component when the solute is transferred from vacuum into water can be estimated by eqn. (1) of Born [2] and Hoijtink *et al.*[3] This equa-

$$\Delta E = -\sum \frac{Q_i Q_j}{2r_{ij}}\left(1 - \frac{1}{D_{H_2O}}\right) \qquad (1)$$

tion has later been widely applied by Daudel.[4] In the equation Q_i and Q_j are the apparent charges of atoms i and j, r_{ij} is the distance between them except in the case when i and j are identical. In this latter case r_i represents the estimated covalent radius according to Pauling.[5] Furthermore, D_{H_2O} is an effective dielectric constant of water.

When a solute is transferred from light to heavy water, the corresponding form for eqn. (1) is expressed by equation (2). When the values of D_{H_2O} and D_{D_2O} are 78.39 and 78.06,

$$\Delta E_t = -\sum \frac{Q_i Q_j}{2r_{ij}} \left(\frac{1}{D_{H_2O}} - \frac{1}{D_{D_2O}} \right) \quad (2)$$

respectively,[6] and joule/mol is chosen as the energy unit, eqn. (3) is obtained. This equation gives information of the isotropic interaction energy for the transfer of a solute from H_2O

$$\Delta E_t = 75 \sum \frac{Q_i Q_j}{2 r_{ij}} \quad (3)$$

to D_2O. However, this energy represents only a part of the whole transfer energy.

The changes in free energy of transfer from H_2O to D_2O for the solutes have been reported earlier.[7]

Atomic populations of the solutes were calculated applying the CNDO treatment formulated by Pople and Segal.[8a,b,c] The calculations were carried out on a Univac 1108 computer, with the aid of the program described by Pople and Beveridge.[9] The data needed for the computer consisted of the cartesian coordinates and atomic numbers of each atom in the solute molecule. This program yields atomic populations from which the apparent charges of atoms could be calculated. Only atoms with an atom number below 18 could be treated in this way.

Bond lengths and angles were taken from literature.[10a,b] All aromatic compounds were assumed to be planar, with the exception of diphenyl, in which the plane of the second ring was assumed to be twisted by an angle of 45° with respect to the first ring. This evidently had no effect on the calculated charges. The methyl group was supposed to have its normal tetrahedral structure. The ethyl group in ethoxybenzene was assumed to have a staggered conformation. The difference in ΔE_t values between staggered and eclipsed conformations is negligible in this case. The calculated apparent charges on various atoms of the solutes are presented in Scheme 1 (only the mean values of the charges have been reported for symmetrical molecules).

RESULTS AND DISCUSSION

This kind of investigation has, of course, a semiquantitative character. When the same molecular orbital method is applied to compounds having nearly similar structures, the possible correlations are reliable. Using the CNDO method it was possible to calculate the apparent charges for all the atoms in the solute molecule. Therefore, the summation could also be made over all the atoms in the solute compound. The dipole moments obtained in

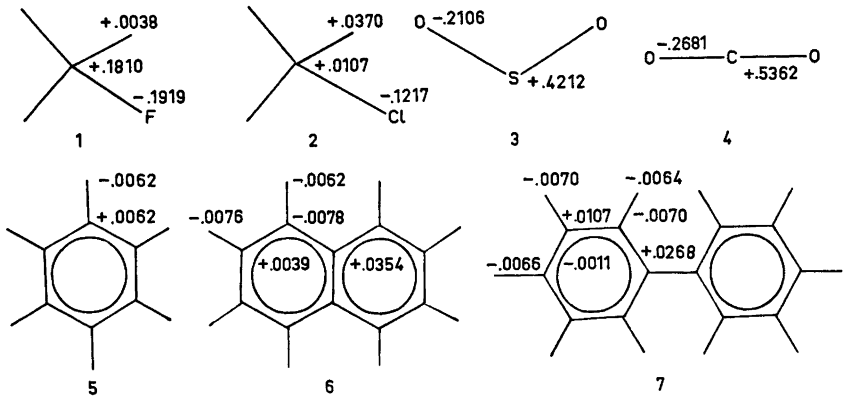

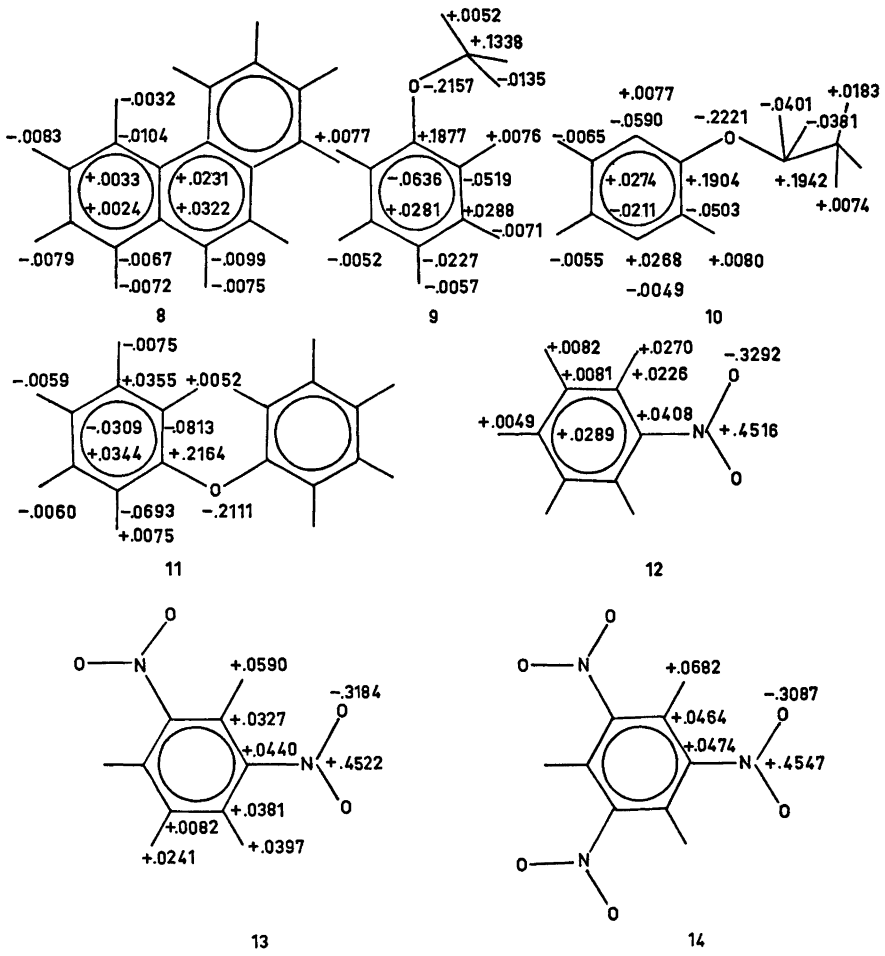

Scheme 1.

connection with the calculations of the internal charge distribution agree satisfactorily with those reported in literature.[11] For instance, for methoxybenzene the values were 1.47 D and 1.38 D, respectively (1 D = 3.33 10^{-30} A s m). Nitrobenzene had the largest deviation when compared with the literature value, namely, 5.08 D and 4.22 D, respectively. For the compounds which by symmetry should have the zero dipole moment this method gave values from 0.00009 D (naphthalene) to 0.0398 D (1,3,5-trinitrobenzene).

The plot of the transfer free energy, ΔG°_t, *versus* ΔE_t is presented in Fig. 1. In the first place, it can be noticed that normal aromatic hydrocarbons like benzene, naphthalene, di-

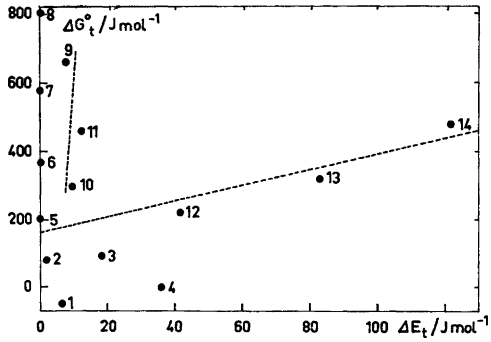

Fig. 1. Plot of the transfer free energy from H_2O to D_2O (ΔG°_t) *versus* the solvation energy (ΔE_t) for some nonelectrolyte solutes (For numbers, see Scheme 1).

phenyl, and phenanthrene show no sign of isotropic interactions. Aromatic ethers seem to have a nearly similar behavior. On the basis of the plot ΔE_t would contribute at the most only a few percentages of $\Delta G°_t$. On the other hand, when nitrobenzenes are examined, there is found an evident linear correlation, the contribution of ΔE_t to $\Delta G°_t$ being about 30 %. It seems quite obvious that there does not exist any overall correlation between $\Delta G°_t$ and ΔE_t. This can especially be seen by studying the points for methyl halides (*1,2*) sulfur dioxide (*3*), carbon dioxide (*4*), and aromatic ethers (*9,10,11*).

When the changes in free energy of transfer of nitrobenzenes from H_2O to D_2O are calculated by adding the $\Delta G°_t$ value of benzene and the corresponding ΔE_t values of nitrobenzenes, and the resulting values are compared with the experimental $\Delta G°_t$ values, then it is seen if the difference between benzene and its nitro derivatives could be wholly assigned to these interactions. The results of these calculations are shown in Table 1. As it is seen the agreement of the two values, namely, the calculated and the experimental ones for nitrobenzenes is rather rough but relevant. The great deviation in trinitrobenzene gives rise to the assumption that besides ΔE_t there are evidently other factors which contribute to the growth of the $\Delta G°_t$ value. Because the molecule of 1,3,5-trinitrobenzene is very symmetric, the main factor for the deviation may be the entropy effect. Of course, the assumption which is made here that the $\Delta S°_t$ values are similar for all nitrobenzenes is very rough.

It is to be expected that there will be an overall correlation between $\Delta G°_t$ and ΔE_t for solutes whose internal molecular polarizability is relatively high if the changes in transfer entropy are assumed to be equal. The behavior of this kind of solutes in water resembles closely that of electrolytes. It is fully believable that also in these compounds the structure breaking effects dominate when the compounds are dissolved in water.

Very accurate measurements of $\Delta H°_t$ would evidently cast more light on the dissolution phenomenon and on the role of ΔE_t in it. The experimental difficulties could be overcome by carrying out calorimetric measurements on compounds that have a relatively high solubility in water. On the other hand, very careful measurements applying the van't Hoff method might give more information on the problem on solutes employed in this work. This investigation is in progress in our laboratory.

Table 1. The $\Delta G°_t$ values for nitrobenzenes calculated by adding up the $\Delta G°_t$ values for benzene ($\Delta G°_{t,B}$) and the ΔE_t values.

Solute	Calculated ($\Delta G°_{t,B} + \Delta E_t$) /J mol^{-1}	Experimental $\Delta G°_t$/J mol^{-1}
Benzene	195	195
Nitrobenzene	237	218
1,3-Dinitrobenzene	278	314
1,3,5-Trinitrobenzene	317	481

REFERENCES

1. Frank, H. S. and Evans, M. W. *J. Chem. Phys. 13* (1945) 507.
2. Born, M. *Z. Phys. 1* (1920) 45.
3. Hoijtink, G. J., DeBoer, E., Van der Meij, P. M. and Weijland, W. P. *Rec. Trav. Chim. Pays-Bas 75* (1956) 487.
4. Daudel, R. In Löwdin, P.-O. *Advan. Quantum Chem. 3* (1967) 186.
5. Pauling, L. *The Nature of the Chemical Bond*, 3rd Ed., Cornell University Press, New York 1960, pp. 257 – 264.
6. Vidulich, G. A., Evans, D. F. and Kay, R. L. *J. Phys. Chem. 71* (1967) 656.
7. Vesala, A. *Acta Chem. Scand. A 28* (1974) 839.
8. a. Pople, J. A., Santry, D. P. and Segal, G. A. *J. Chem. Phys. 43* (1965) 5129; b. Pople, J. A. and Segal, G. A. *Ibid. 43* (1965) 5236; c. *Ibid. 44* (1966) 3289.
9. Pople, J. A. and Beveridge, D. L. *Approximate Molecular Orbital Theory*, McGraw, New York 1970.
10. a. *Tables of Interatomic Distances and Configuration in Molecules and Ions*, The Chemical Society, London 1958; b. Supplement, London 1965.
11. Weast, R. C., Ed., *Handbook of Chemistry and Physics*, 50th Ed., The Chemical Rubber Company, Ohio 1969, p. E-69.

Received April 22, 1974.

Acta Chemica Scandinavica A 28 (1974) 855—865

Thermodynamics of Metal Complex Formation in Aqueous Solution. VI. Equilibrium and Enthalpy Measurements on the Zinc and Cadmium Selenocyanate Systems

STEN AHRLAND, EFRAIM AVSAR and LENNART KULLBERG

Inorganic Chemistry 1, Chemical Center, University of Lund, P.O.B. 740, S-220 07 Lund 7, Sweden

The stability constants and the enthalpy changes accompanying the formation of zinc and cadmium selenocyanate complexes have been determined by potentiometric and calorimetric measurements. From the enthalpy changes measured, and the free energy changes computed from the stability constants, the entropy changes have been calculated. All data refer to 25.0 °C and an aqueous sodium perchlorate medium of ionic strength 1.00 M.

Of the two selenocyanate systems investigated that of cadmium is the strongest one. In the systems studied most of the species are formed in exothermic reactions having entropy terms counteracting the complex formation.

Complexes of ligands coordinating *via* selenium have hitherto received relatively little attention, mainly due to experimental difficulties. Measurements have been performed with organic selenium ligands also containing sulfonate or carboxylate groups in order to make them water-soluble.[1,2] Also selenium semicarbazides have been employed.[3] The environment of the selenium atom may differ considerably between these various ligands and hence also its donor properties. Generally, the ligands have also other potential donor atoms competing with the selenium. This may obscure the interpretation of the results and thus limit the possibilities to study the donor properties of selenium.

The selenocyanate ion, $SeCN^-$, is certainly among the simplest selenium donors and a few complexes of this ligand have also been studied. Unfortunately $SeCN^-$ is not very stable in aqueous solution. Solutions of alkali selenocyanates start to decompose as the pH becomes $\lesssim 5$.[4] In the presence of transition metal ions the disintegration starts at even higher values of pH, the value depending both on the metal ion present and the concentrations used. On the other hand, most transition metal ions are perceptibly hydrolyzed already at pH = 5. It is therefore difficult, or even impossible, to investigate their selenocyanate complexes in aqueous solution.

The selenocyanate ion is a homologue to the thiocyanate ion. Metals can be linked to selenocyanate either through the selenium atom or through the nitrogen atom while coordination to thiocyanate may occur either *via* sulfur or *via* nitrogen. From a comparison of the thermodynamics for the formation of thiocyanate and selenocyanate complexes, it should be possible to draw conclusions about the nature of the bonds formed in various complex systems.

The thiocyanate complexes of the divalent zinc group ions Zn^{2+}, Cd^{2+}, and Hg^{2+} have been studied previously.[5,6] Of these ions, Zn^{2+} and Cd^{2+} are not appreciably hydrolyzed for pH < 5.[8,9] A complete study of their selenocyanate complexes is therefore feasible and will be described in this paper. As to Hg^{2+}, its rather strongly acidic properties [7] prevents the formation of stable selenocyanate complexes except at quite high ligand concentrations where the hydrolysis is sufficiently suppressed. This is in fact achieved only when the final, *i.e.* the fourth complex is the predominating one as will be discussed in Part VIII of this series.

The stability constants were determined from potentiometric measurements and the enthalpy

Table 1. Comparison of reported values of stability constants for the zinc and cadmium selenocyanate systems. The measurements refer to KNO_3 media.

Metal		Zn^{2+}	Cd^{2+}		
Ref		10	10	11	12
Temp/°C		30	30	25	20
I/M		2.0	2.0	0.8	1.5
β_j/M^{-j}	$j=1$	5.8	20		22
	2	10	100		182
	3		440		1000 [a]
	4		1000	4000	1800
	5				8000

[a] The authors gave $\beta_3 = 10\,000$ M^{-3}. According to the graphs in the paper β_3 should rather be 1 000 M^{-3}.

changes, ΔH°_j, were measured calorimetrically. From the stability constants the free energy changes were computed. Finally, the entropy changes, ΔS°_j, were obtained from the relation

$$\Delta G^\circ_j = \Delta H^\circ_j - T\Delta S^\circ_j \quad (1)$$

Previously, a polarographic study of the zinc and cadmium selenocyanate systems has been performed by Humffray *et al.*,[10] Table 1. By the same method Toropova [11] determined β_4 of the cadmium selenocyanate system. From a potentiometric investigation Golub and Andreichenko [12] found five mononuclear cadmium selenocyanate complexes. No determination of the enthalpy changes for the formation of zinc and cadmium selenocyanate complexes seems to have been published so far.

Like the previous investigations in this series, the present one was performed at 25.0 °C and in an aqueous medium of unit ionic strength, with sodium perchlorate as supplementary electrolyte.

CALCULATIONS

The notation is the same as in previous papers of this series.[13,14]

Calculation of stability constants from potentiometric measurements of the free central ion concentration. The stability constants have been calculated both graphically and numerically. The graphical method has been described in an earlier paper.[5] Only some final expressions are given here.

If only mononuclear complexes exist, the following relations hold

$$X([L]) = C_M/[M] = 1 + \sum_{j=1}^{N} \beta_j [L]^j \quad (2)$$

$$E_M = RT/2F \ln X([L]) \quad (3)$$

where E_M is the difference between the emf, E, of the cell given on p. 857 and the emf, E_0, of the same cell with $C_L = 0$, *i.e.* $[M] = C_M$.

The ligand number $\bar{n}$ for the mononuclear complexes can be calculated according to

$$\bar{n} = \sum_{j=1}^{N} j\beta_j [L]^j / X \quad (4)$$

and also by means of the approximate equation

$$\bar{n} = \frac{\Delta E_M}{(RT/2F)\Delta \ln [L]} \quad (5)$$

Furthermore, n can be obtained from the slopes, k, of the straight (C_L, C_M)-lines of constant E_M used for the extrapolation to $C_M = 0$. The numerical calculations have been performed by a least-squares program "EMK" which minimizes the following error square sum

$$U(\beta_j) = \sum_{i=1}^{N} w_i (E_{M,i,calc} - E_{M,i})^2 \quad (6)$$

where w_i is a weighting term.[15]

Calculations from the calorimetric measurements have been performed by the least-squares computer program "Kalori",[15] which minimizes the error square sum

$$U(\beta_j, \Delta H^\circ_j) = \sum_{i=1}^{N} w_i (Q_{i,calc} - Q_{i,corr})^2 \quad (7)$$

By this program it is possible to treat both the enthalpy changes and the equilibrium constants as unknown parameters.

EXPERIMENTAL

Chemicals. Cadmium perchlorate was prepared by dissolving cadmium carbonate (Merck, *p.a.*) in perchloric acid (Baker Analyzed, *p.a.*). In order to avoid hydrolysis a small excess of the acid was used.[8] The cadmium concentration

was determined by titration with EDTA using Erio-T as an indicator.

Cadmium amalgam, ca 9 % by weight, was prepared by dissolving sticks of cadmium metal (Baker Analyzed, *p.a.*) in mercury (*p.a.*) at 70 °C in an evacuated preparation vessel. Before use the cadmium metal was cleaned in sulfuric and perchloric acids. The amalgam was stored under nitrogen in a special storage vessel.[16]

Sodium selenocyanate was prepared from potassium selenocyanate (B.D.H.), which was first purified by three successive recrystallisations from a mixture of acetone and anhydrous ether. An approximately 5 M potassium selenocyanate solution was prepared and passed through a sodium saturated cation exchanger (Dowex 50W). The sodium selenocyanate stock solution was analyzed by potentiometric titration with silver nitrate.[17]

Zinc perchlorate, *zinc amalgam*, and *sodium perchlorate* were prepared and analyzed as described before.[5,13]

The potentiometric measurements. The emf of the following galvanic cell was measured.

$$-\ \mathrm{M(Hg)}\left|\begin{matrix} C_{\mathrm{M}}\ \mathrm{M\ M(ClO_4)_2} \\ C_{\mathrm{L}}\ \mathrm{M\ NaSeCN} \\ \mathrm{NaClO_4\ to}\ I = 1.00\ \mathrm{M} \end{matrix}\right|$$

$$1.00\ \mathrm{M\ NaClO_4}\left|\begin{matrix} 0.025\ \mathrm{M\ NaCl} \\ 0.975\ \mathrm{M\ NaClO_4} \end{matrix}\right|\mathrm{Ag,AgCl} +$$

where $\mathrm{M} = Zn^{2+}$, Cd^{2+}.

A Leeds and Northrup Type K-5 Potentiometer was used, in connexion with a Leeds and Northrup Electronic D-C Null Detector, specifying a precision of ± 0.01 mV. The Ag,AgCl electrodes were prepared according to Brown.[18]

The measurements were arranged as titrations. The solutions in the left-hand half-cell were obtained by adding a volume v cm³ of a solution T to $V_0 = 15.00$ cm³ of a solution S, where S and T had the compositions:

$$\mathrm{S:}\ \begin{cases} C_{\mathrm{M}}' & \mathrm{M\ M(ClO_4)_2} \\ (1.00 - 3C_{\mathrm{M}}') & \mathrm{M\ NaClO_4} \end{cases}$$

$$\mathrm{T:}\ \begin{cases} C_{\mathrm{L}}' & \mathrm{M\ NaSeCN} \\ (1.00 - C_{\mathrm{L}}') & \mathrm{M\ NaClO_4} \end{cases}$$

At every point during the titrations C_{M} and C_{L} were known from the compositions of the S and T solutions. As the T-solution did not contain any metal ions, C_{M} continuously decreased as C_{L} increased. The difference between the emf, E, at a certain point and the initial emf, E_0', was therefore due to dilution, as well as to the formation of complexes. To find the difference E_{M}, defined in eqn. (3), as due only to the formation of complexes, the following correction was applied.

The initial emf, E_0', is given by

$$E_0' = E_{\mathrm{k}} - (RT/2F) \ln C_{\mathrm{M}}' \qquad (8)$$

where E_{k} is a constant. From E_0' and the actually measured emf E of the cell after addition of v ml, the following expression for E_{M} is easily deduced:[5]

$$E_{\mathrm{M}} = E - E_0' - (RT/2F) \ln [(V_0 + v)/V_0] \qquad (9)$$

The solutions were swept by a stream of oxygen-free nitrogen to prevent oxidation of the amalgam. To obtain the correct pressure of water vapour, the nitrogen was bubbled through 1 M $NaClO_4$ before entering the solutions. The potentials attained equilibrium in less than 5 min after each addition.

All titrations were repeated at least once and the reproducibility was in general within 0.15 mV for both the zinc and cadmium measurements.

As a check that the two amalgam electrodes behaved according to Nernst's law, the emf, E_0, for the cell without ligand present was measured as a function of $C_{\mathrm{M}} = [\mathrm{M}]$. These measurements were arranged as titrations where a 1.00 M $NaClO_4$ solution was titrated with zinc and cadmium perchlorate solutions, respectively. For zinc the solution had a composition of $C_{\mathrm{M}} = 0.100$ M, pH = 3.6 and $I = 1.00$ M. The E_{k}-value calculated from eqn. (8) was found to be constant within ± 0.05 mV for 3 mM $\leq [Zn^{2+}] \leq$ 50 mM. For cadmium two different cadmium perchlorate solutions were used. The two solutions had $C_{\mathrm{M}} = 0.100$ and 0.010 M and pH = 3.5 and 5.1, respectively. Both of them had an ionic strength of 1.00 M. The E_{k}-value calculated from eqn. (8) was constant within ± 0.10 mV for 0.8 mM $\leq [Cd^{2+}] \leq$ 40 mM.

The calorimetric measurements. The calorimeter and the measurement technique have been described previously.[14] In each titration series, the reaction vessel initially contained V_0 cm³ of a solution S and a titrant T was then added.

In order to determine the corrections for the heats of dilution, series analogous to those of the main measurements were performed, except that only one of the two reactants was present.

Electrical calibration showed that the heat equivalent was the same linear function of the volume added as had been found before.[19] The titration series were repeated once and the reproducibility was generally within 0.04 J.

MEASUREMENTS AND RESULTS

Potentiometric measurements on zinc selenocyanate. Four different titration series with values of C_{M}' varying from 10 to 30 mM were performed. Corresponding values of C_{L} and E_{M} from these series are collected in Table 2.

Table 2. Corresponding values of C_L and E_M for the zinc selenocyanate system.

v/ml	C_L/ mM	E_M/mV for C_M' = 10.00 mM	15.00 mM	20.00 mM	30.00 mM
0.25	13.1	0.47	0.46	0.45	0.44
0.50	25.8	0.92	0.90	0.89	0.88
0.75	38.1	1.36	1.33	1.31	1.29
1.00	50.0	1.79	1.76	1.73	1.67
1.50	72.7	2.60	2.52	2.51	2.43
2.00	94.1	3.34	3.25	3.20	3.07
2.50	114.3	4.04	3.94	3.88	3.72
3.00	133.3	4.70	4.60	4.52	4.34
3.50	151.4	5.34	5.21	5.11	4.93
4.00	168.4	5.94	5.78	5.67	5.46
5.00	200.0	7.03	6.80	6.68	6.43
6.00	228.6	8.00	7.74	7.62	7.33
7.00	254.5	8.83	8.60	8.46	8.12
8.00	278.3	9.67	9.39	9.21	8.79
9.00	300.0	10.26	10.10	9.94	9.48
10.00	320.0	10.99	10.74	10.60	10.09
12.00	355.6	12.05	11.90	11.71	11.23
14.00	386.2	13.03	12.74	12.66	12.11

Values of E_M obtained at $C_M = 2$ and 5 mM were not consistent with those of Table 2. This is certainly due to contamination of the solutions by cyanide which is formed together with red selenium, at the disintegration of selenocyanate.[4] As the cyanide complexes are much stronger than the selenocyanate ones [20] the presence of even minute amounts of cyanide ions in the selenocyanate solutions may give rise to erroneous results. The values of E_M ought moreover to be too high and increasingly so as the value of C_M decreases. This was in fact observed. In view of this it would *per se* be desirable to measure at even higher values of C_M than has in fact been done. This was not possible, however, as it would lead to an unacceptable increase in the disintegration of selenocyanate.

The pH of the solutions used had to be carefully adjusted so that decomposition of selenocyanate would not occur while the hydrolysis of the zinc ions would still be negligible. When the pH of the initial zinc solutions (S) was $\simeq 4$, no selenium was precipitated during the titrations. At the end of the titration the pH of the zinc solutions had increased from ~ 4 to ~ 7. In this range the hydrolysis of the zinc ion is slight for the concentrations used.[9]

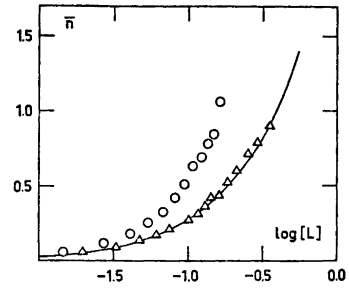

Fig. 1. The complex formation function of the zinc selenocyanate system. The fulldrawn curve has been computed from eqn. (4) while the symbols (△) refer to $\bar{n}$ found by means of eqn. (5). The values of $\bar{n}$ obtained from the slopes of the (C_M,C_L)-lines are denoted by (○) ([L] in M).

The graphical evaluation of the stability constants indicated three mononuclear complexes. In the numerical calculations, on the other hand, a good fit of the experimental data was obtained by a model including only two mononuclear complexes. The following constants were obtained.

	Graphical	Numerical
β_1/M^{-1}	2.90 ± 0.08	2.74 ± 0.09
β_2/M^{-2}	3.90 ± 0.8	4.4 ± 0.4
β_3/M^{-3}	4.5 ± 2.0	

The errors given for the graphically calculated constants are subjectively estimated. For the numerical determination they correspond to three standard deviations. In the range of [L] studied the concentration of a hypothetical complex ML_3 will not exceed 5 % of C_M. It is thus not possible to decide with certainty from these measurements whether a third complex is formed or not.

The numerically found set of constants is considered to be the 'best' one and is used in the following. The complex formation function, $\bar{n}([L])$, computed according to eqn. (4), is given in Fig. 1 as a fulldrawn curve. The values of $\bar{n}$ obtained from the slopes of the (C_M,C_L)-lines deviate. This can be explained, however, by the contamination by cyanide ions, which will give too high E_M-values, especially for the series with the lowest value of C_M ($= 10$ mM). This could also be seen in the numerical calculations where the deviations $(E_M - E_{M,calc})$ have mainly positive signs in this series. The

Table 3. Determination of heats of dilution for sodium selenocyanate. $V_0 = 90.00$ cm³ and $V = (V_0 + v)$ cm³.

S: $C_{NaClO_4} = 1.000$ M. T: $C_{NaSeCN} = 1.000$ M.

v/cm³, $-Q_{dil}$/J: *3.000*, 0.594; *6.000*, 0.551; *9.000*, 0.516; *12.00*, 0.484; *15.00*, 0.462; *18.00*, 0.440; *21.00*, 0.424; *24.00*, 0.406; *27.00*, 0.390.

relatively low value of the standard deviation, 0.14 mV, indicates that the influence of the cyanide ions in the measurements has been satisfactorily suppressed.

Calorimetric measurements on zinc selenocyanate. Three different titration series with $C_M = 20$, 30, and 50 mM have been carried out, Tables 3 and 4. In all series ligand was added to a solution of the metal ion. In this way a total selenocyanate concentration of $\simeq 200$ mM could be reached before selenium was precipitated. In an attempt to reach higher values of [L] a metal solution was added to a ligand solution. This titration, however, was unsuccessful. When the pH was low enough to prevent hydrolysis of the zinc ion, the selenocyanate ion disintegrated rapidly. From the stability constants obtained before it was evident that the concentration of a third complex, if formed, was negligible in the range of concentration used. Due to weak complex formation and low values of $\Delta H°_j$, the measured heat effects were small. It was therefore impossible to determine the stability constants from the calorimetric data. In the calculation of the enthalpy changes by the program "Kalori", sets of stability constants including two as well as three complexes were tried. A good fit, $\sigma Q_{corr} = 0.032$ J, was achieved with the two stability constants obtained in the numerical calculation of the potentiometric measurements. Introduction of a third complex did not give any significantly better fit ($\sigma Q_{corr} = 0.028$ J). The numerically obtained values of β_1 and β_2 together with computed values of $\Delta G°_j$, $\Delta H°_j$ and $\Delta S°_j$ are given in Table 8. In Fig. 2, Δh_v is plotted *versus* $\bar{n}$. Evidently no variation of Δh_v with C_M can be discerned, which indicates that no polynuclear complexes are formed. The fulldrawn curve is calculated from the stability constants and enthalpy changes given in Table 8.

Table 4. Determination of the heats of formation for the zinc selenocyanate complexes. For all the series: $V_0 = 90.00$ cm³ and $V = (V_0 + v)$ cm³.

(a) ○ S: $C_M = 0.05000$ M, $C_{NaClO_4} = 0.850$ M.
T: $C_L = 0.800$ M, $C_{NaClO_4} = 0.200$ M.
v/cm³, Q_{corr}/J, ΔQ_{corr}/J: *3.000*, 1.697, −0.067; *6.000*, 1.437; 0.025; *9.000*, 1.283, 0.030; *12.00*, 1.188, −0.006; *15.00*, 1.071, −0.006; *18.00*, 0.996, −0.033; *21.00*, 0.894, −0.021; *24.00*, 0.810, −0.017; *27.00*, 0.746, −0.024;

(b) □ S: $C_M = 0.03000$ M, $C_{NaClO_4} = 0.910$ M.
T: $C_L = 0.800$ M, $C_{NaClO_4} = 0.200$ M.
v/cm³, Q_{corr}/J, ΔQ_{corr}/J: *3.000*, 1.038, −0.013; *6.000*, 0.883, 0.032; *9.000*, 0.791, 0.026; *12.00*, 0.705, 0.026; *15.00*, 0.633, 0.022; *18.00*, 0.568, 0.021; *21.00*, 0.523, 0.008; *24.00*, 0.466, 0.015; *27.00*, 0.448, −0.012;

(c) △ S: $C_M = 0.02000$ M, $C_{NaClO_4} = 0.940$ M.
T: $C_L = 0.800$ M, $C_{NaClO_4} = 0.200$ M.
v/cm³, Q_{corr}/J, ΔQ_{corr}/J: *3.000*, 0.743, −0.043; *6.000*, 0.581, 0.042; *9.000*, 0.506, 0.049; *12.00*, 0.450, 0.045; *15.00*, 0.396, 0.046; *18.00*, 0.384, 0.013; *21.00*, 0.370, −0.013; *24.00*, 0.362, −0.040; *27.00*, 0.349, −0.058;

Potentiometric measurements on cadmium selenocyanate. The experimental results are collected in Tables 5a and 5b. Two different ligand solutions with $C_L = 0.200$ and 1.000 M, respectively, were added to four different cadmium solutions, with values of C_M' varying from 5 to 40 mM. The values of the pH of these solutions were 5 − 5.5. It is possible to use higher values of pH in cadmium than in zinc solutions.

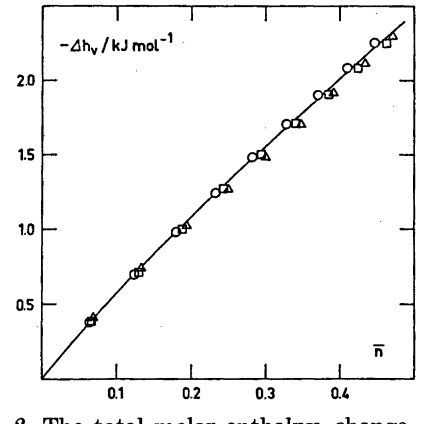

Fig. 2. The total molar enthalpy change, Δh_v, as a function of $\bar{n}$, for the zinc selenocyanate system, *cf.* Table 4.

Table 5a. Corresponding values of C_L and E_M for the cadmium selenocyanate system.

v/ml	C_L/ mM	E_M/mV for C_M' = 5.00 mM	10.00 mM	20.00 mM	40.00 mM
0.25	3.28	1.07	0.97	0.80	0.60
0.50	6.45	2.06	1.87	1.56	1.18
0.75	9.52	2.99	2.73	2.29	1.75
1.00	12.50	3.89	3.55	3.01	2.33
1.25	15.38	4.73	4.34	3.71	2.89
1.50	18.18	5.55	5.10	4.39	3.45
1.75	20.9	6.31	5.81	5.04	3.98
2.00	23.5	7.03	6.51	5.67	4.50
2.50	28.6	8.42	7.82	6.88	5.54
3.00	33.3	9.67	9.02	8.00	6.52
3.50	37.8	10.83	10.16	9.07	7.47
4.00	42.1	11.90	11.19	10.05	8.35
4.50	46.2	12.91	12.18	10.99	9.21
5.00	50.0	13.85	13.10	11.89	10.01
5.50	53.7	14.75	13.98	12.73	10.79
6.00	57.1	15.60	14.81	13.53	11.54
6.50	60.5	16.39	15.59	14.30	12.26
7.00	63.6	17.17	16.32	15.01	12.94
8.00	69.6	18.57	17.71	16.35	14.22
9.00	75.0	19.83	18.96	17.58	15.40
10.00	80.0	20.99	20.10	18.71	16.50
11.00	84.6	22.05	21.15	19.74	17.51
12.00	88.9	23.07	22.13	20.71	18.46
13.00	92.9	23.97	23.02	21.61	19.35
14.00	96.6	24.81	23.86	22.44	20.18
15.00	100.0	25.60	24.55	23.24	20.97

Table 5b. Corresponding values of C_L and E_M for the cadmium selenocyanate system.

v/ml	C_L/mM	E_M/mV for C_M' = 5.00 mM	10.00 mM	20.00 mM
0.25	16.4	4.98	4.58	3.84
0.50	32.3	9.18	8.53	7.43
0.75	47.6	12.99	12.15	10.72
1.00	62.5	16.45	15.46	13.82
1.25	76.9	19.73	18.62	16.74
1.50	90.9	22.73	21.54	19.47
1.75	104.5	25.62	24.31	22.06
2.00	117.6	28.39	26.98	24.54
2.25	130.4	31.04	29.57	26.96
2.50	142.9	33.61	32.00	29.28
2.75	154.9	36.03	34.36	31.50
3.00	166.7	38.30	36.64	33.65
3.25	178.1	40.52	38.82	35.76
3.50	189.2	42.68	40.88	37.77
3.75	200.0	44.67	42.88	39.70
4.00	210.5	46.58	44.79	41.59
4.25	220.8	48.47	46.66	43.42
4.50	230.8	50.21	48.41	45.15
5.00	250.0	53.49	51.71	48.47
5.50	268.3	56.51	54.77	51.58
6.00	285.7	59.27	57.57	54.46
6.50	302.3	61.82	60.18	57.14
7.00	318.2	64.17	62.57	59.61
7.50	333.3	66.31	64.79	61.94
8.00	347.8	68.31	66.89	64.10
8.50	361.7	70.24	68.81	66.12
9.00	375.0	71.99	70.62	68.01
9.50	387.8	73.62	72.30	69.79
10.00	400.0	75.14	73.86	71.45
11.00	423.1	77.88	76.73	74.48
12.00	444.4	80.37	79.29	77.18
13.00	464.3	82.63	81.57	79.58
14.00	482.8	84.63	83.63	81.75
15.00	500.0	86.36	85.46	83.72

First, a higher initial value could be applied as the cadmium ion is a weaker acid than the zinc ion. Second, stronger selenocyanate complexes are formed by cadmium than by zinc. As the complexes are certainly less acidic than the hydrated ions this means that the hydrolysis is more completely suppressed in the cadmium solutions. The relatively high values of pH that could be used in the cadmium selenocyanate solutions also ensured that these became completely stable. This is indicated by the fact that the results from the titration series with lowest cadmium ion concentration ($C_M' = 5$ mM) are quite in line with the results from the other series.

Both the graphical and numerical calculation of the stability constants indicated four mononuclear complexes, Table 7. In the graphical determination of the β_j-values the X_3-function was linear up to [L] = 300 mM, but showing a positive deviation at higher values of [L]. This may of course be interpreted as a fifth complex. It is more likely, however, that the deviation is due to changes in the activity coefficients brought about by complex formation and by the progressive exchange of ClO_4^- for $SeCN^-$. Furthermore, at high ligand concentration there may be some disintegration of $SeCN^-$, giving cyanide ions (*cf.* p. 858). At [L] = 300 mM more than 60 % of the total amount of cadmium is in the form of the fourth complex. This means that a good value of β_4 should be obtained from the measurements up to [L] = 300 mM. Data from higher values of [L] were not considered in the graphical evaluation of the β_j-values. Results from two different numerical calculations are also given in Table 7. In the first of these all measured data are included and in the

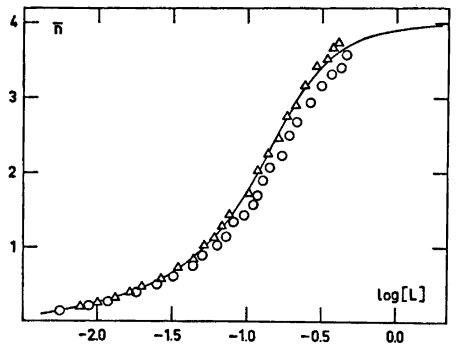

Fig. 3. The complex formation function of the cadmium selenocyanate system. The fulldrawn curve has been computed from eqn. (4) while the symbols (△) refer to $\bar{n}$ found by means of eqn. (5). The values of $\bar{n}$ obtained from the slopes of the (C_M,C_L)-lines are denoted by (○) ([L] in M).

second only those for $C_L < 380$ mM. As expected the results from the latter calculation agree quite well with the results found graphically, while the former calculation naturally yields a higher value of β_4, and a correspondingly lower value of β_3.

The complex formation curve, $\bar{n}$[L]), computed from the graphically obtained set of constants according to eqn. (4) is given in Fig. 3 as a fulldrawn curve. The values of $\bar{n}$ obtained from eqn. (5) agree very well with this curve and also those obtained from the slopes of the (C_M, C_L)-lines fit quite satisfactorily. Only a minor systematic deviation is observed.

Calorimetric measurements on cadmium selenocyanate. In three of the seven titration series carried out ligand was added to a solution of the metal ion (Table 6, a – e). In four series (d – g), metal ions were added to a solution of the ligand, in order to bring about a larger formation of the higher complexes. The metal ion solutions had a pH ≃ 5.5. When ligand was added to cadmium solution the corrected heats, Q_{corr}, were obtained by subtracting the heats of dilution for the ligand (given in Table 3) from the experimentally measured heat effects, as the heats of dilution of the metal ions were negligible in these cases. When cadmium solution was added to the ligand solution, heats of dilution for both metal and ligand had to be introduced.

As the complexes formed are moderately

Table 6. Determination of the heats of formation for the cadmium selenocyanate complexes. For all series: $V_0 = 90.00$ cm³ and $V = (V_0 + v)$ cm³.

(a) ▽ S: $C_M = 0.02000$ M, $C_{NaClO_4} = 0.940$ M.
T: $C_L = 1.000$ M.

v/cm³, Q_{corr}/J, ΔQ_{corr}/J: *3.000*, 9.625, −0.037; *6.000*, 7.053, 0.030; *9.000*, 5.817, −0.042; *12.00*, 5.094, −0.030; *15.00*, 4.496; 0.029; *18.00*, 3.945, 0.071; *21.00*, 3.480, 0.036; *24.00*, 3.014, 0.025; *27.00*, 2.573, 0.032;

(b) □ S: $C_M = 0.01500$ M, $C_{NaClO_4} = 0.955$ M.
T: $C_L = 1.000$ M.

v/cm³, Q_{corr}/J, ΔQ_{corr}/J: *3.000*, 7.677, 0.014; *6.000*, 5.436, 0.071; *9.000*, 4.541, −0.056; *12.00*, 3.960, −0.033; *15.00*, 3.494, −0.020; *18.00*, 3.032, 0.003; *21.00*, 2.579, 0.032; *24.00*, 2.209, 0.012; *27.00*, 1.900, −0.022;

(c) ○ S: $C_M = 0.01000$ M, $C_{NaClO_4} = 0.970$ M.
T: $C_L = 1.000$ M.

v/cm³, Q_{corr}/J, ΔQ_{corr}/J: *3.000*, 5.479, 0.022; *6.000*, 3.757, 0.052; *9.000*, 3.143, −0.038; *12.00*, 2.742, −0.036; *15.00*, 2.355, 0.005; *18.00*, 2.047, −0.025; *21.00*, 1.713, −0.007; *24.00*, 1.422, 0.005; *27.00*, 1.303, −0.112;

(d) ▲ S: $C_L = 0.500$ M, $C_{NaClO_4} = 0.500$ M.
T: $C_M = 0.1000$ M, $C_{NaClO_4} = 0.700$ M.

v/cm³, Q_{exp}/J, Q_{corr}/J, ΔQ_{corr}/J: *3.000*, 9.987, 10.314, −0.021; *6.000*, 9.812, 10.103, −0.026; *9.000*, 9.624, 9.888, −0.045; *12.00*, 9.347, 9.607; −0.014; *15.00*, 9.126, 9.367, −0.040;

(e) ● S: $C_L = 0.400$ M, $C_{NaClO_4} = 0.600$ M.
T: $C_M = 0.1000$ M, $C_{NaClO_4} = 0.700$ M.

v/cm³, Q_{exp}/J, Q_{corr}/J, ΔQ_{corr}/J: *3.000*, 9.547, 9.810, 0.004; *6.000*, 9.297, 9.521, −0.012; *9.000*, 8.980, 9.175, 0.007; *12.00*, 8.540, 8.729, 0.104; *15.00*, 8.363, 8.530, −0.064;

(f) ▼ S: $C_L = 0.300$ M, $C_{NaClO_4} = 0.700$ M.
T: $C_M = 0.1000$ M, $C_{NaClO_4} = 0.700$ M.

v/cm³, Q_{exp}/J, Q_{corr}/J, ΔQ_{corr}/J: *3.000*, 8.792, 8.964, 0.031; *6.000*, 8.349, 8.502, 0.043; *9.000*, 7.903, 8.043, 0.030; *12.000*, 7.494, 7.610, −0.021; *15.00*, 6.992, 7.091, 0.013;

(g) ■ S: $C_L = 0.200$ M, $C_{NaClO_4} = 0.800$ M.
T: $C_M = 0.1000$ M, $C_{NaClO_4} = 0.700$ M.

v/cm³, Q_{exp}/J, Q_{corr}/J, ΔQ_{corr}/J: *3.000*, 7.284, 7.413, 0.046; *6.000*, 6.687, 6.809, 0.019; *9.000*, 6.127, 6.237, −0.014; *12.00*, 5.548, 5.657, 0.010; *15.00*, 5.149, 5.241, −0.078;

Table 7. Stability constants for the cadmium selenocyanate system obtained from potentiometric and calorimetric measurements. The errors correspond to three standard deviations given by the computer or to estimated errors. Parameters printed in italics were not varied.

Method	β_1/M^{-1}	β_2/M^{-2}	β_3/M^{-3}	β_4/M^{-4}	U	
Pot., graphically	29.0 ± 0.5	200 ± 30	700 ± 200	11 000 ± 1 000		
Pot., by computer	29.6 ± 0.9	235 ± 30	350 ± 250	12 300 ± 600		all points incl.
Pot., by computer	30.1 ± 0.9	210 ± 30	650 ± 300	11 300 ± 900		$C_L \leq 375$ mM
Cal.	*29.5*	228	800	*11 000*	0.0746	
Cal.	*29.5*	*228*	760	10 400	0.0740	
Cal.	*29.5*	140	680	8 800	0.0634	
Proposed values	29.5 ± 0.5	200 ± 30	700 ± 200	11 000 ± 1 000	0.0778	

strong, and the heat effects fairly large, a determination of the stability constants from the calorimetric data should be possible. Nevertheless, a complete determination of the stability constants in this manner turned out to be impossible, because of the narrow range of existence of especially the third complex. We have therefore to introduce one or two of the constants calculated from the potentiometric measurements as known parameters in the "Kalori" calculation thereby reducing the number of unknown parameters. In the first hand the value of β_1 ($= 29.5$ M^{-1}) seems to be well established and was therefore not varied in the computations. The constants $\beta_2 - \beta_4$ were on the other hand treated as either known or unknown parameters in different combinations. The results from some of these calculations are given in Table 7. As can be seen the calorimetrically obtained values of $\beta_2 - \beta_4$ are quite in line with those obtained potentiometrically. A 'best' set of values has been proposed, Table 7. These β_j-values and corresponding values of $\Delta G°_j$, $\Delta H°_j$ and $\Delta S°_j$ are listed in Table 8. In Fig. 4 the Δh_v-function is plotted *versus* $\bar{n}$, calculated from the 'best' β_j-values. The function is independent of C_M, which once more proves that no polynuclear complexes

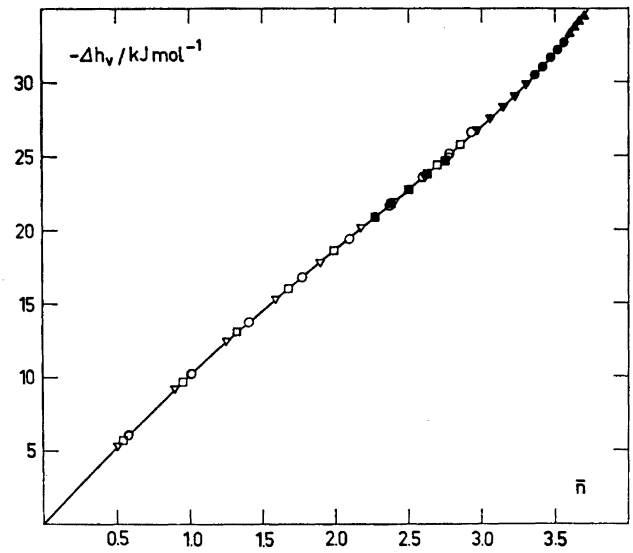

Fig. 4. The total molar enthalpy change, Δh_v, as a function of $\bar{n}$, for the cadmium selenocyanate system, *cf.* Table 6.

Table 8. The stability constants used and the computed values of $\Delta G°_j$, $\Delta H°_j$ and $\Delta S°_j$ for the stepwise reactions of the zinc and cadmium selenocyanate and thiocyanate systems. The data for the thiocyanate systems are taken from Ref. 5. The errors given correspond to three standard deviations or to estimated errors.

System		$Zn^{2+} - SeCN^-$	$Zn^{2+} - SCN^-$	$Cd^{2+} - SeCN^-$	$Cd^{2+} - SCN^-$
	$j=1$	2.74 ± 0.09	5.10 ± 0.03	29.5 ± 0.5	20.7 ± 0.5
	2	4.4 ± 0.4	11.0 ± 0.6	200 ± 30	97 ± 5
β_j/M^{-j}	3		15.0 ± 3.6	700 ± 200	107 ± 20
	4		32 ± 5	11 000 ± 1 000	75 ± 30
	1	2.50 ± 0.08	4.04 ± 0.02	8.39 ± 0.04	7.53 ± 0.08
$-\Delta G°_j$	2	1.17 ± 0.25	1.91 ± 0.14	4.7 ± 0.4	3.85 ± 0.08
kJ mol^{-1}	3		0.76 ± 0.6	3.1 ± 0.9	0.3 ± 0.7
	4		1.9 ± 0.8	6.8 ± 0.9	−0.9 ± 1.6
	1	5.95 ± 0.17	5.80 ± 0.15	10.05 ± 0.10	9.58 ± 0.04
$-\Delta H°_j$	2	0.4 ± 0.6	1.8 ± 1.0	16.3 ± 1.0	8.08 ± 0.38
kJ mol^{-1}	3		0.8 ± 3.0	13.5 ± 1.0 [a]	9.2 ± 3.8
	4		7.7 ± 3.5		
	1	−11.6 ± 0.7	−5.9 ± 0.5	−5.6 ± 0.3	−6.7 ± 0.4
$\Delta S°_j$	2	3 ± 3	0 ± 4	−39 ± 4	−14 ± 1.3
J mol^{-1} K^{-1}	3		0 ± 10	−12 ± 4 [a]	−30 ± 13
	4		−19 ± 12		

[a] For the individual steps of the third and fourth steps we obtain $\Delta H°_3 = 23 \pm 7$, $\Delta H°_4 = -37 \pm 7$, $\Delta S°_3 = 90 \pm 20$, $\Delta S°_4 = -100 \pm 30$.

exist. The fulldrawn curve is calculated from the stability constants and enthalpy changes given in Table 8.

DISCUSSION

In agreement with Humffray *et al.*[10] we find two complexes in the zinc selenocyanate and four in the cadmium selenocyanate system. For the zinc selenocyanate our values of β_j are lower, however, than those given by Humffray *et al.*[10] while for the cadmium selenocyanate the situation is reversed. With the exception of β_4 of the cadmium selenocyanate system, the differences of the β_j-values of the two investigations are not very large, however, and they may be explained by differences in medium and temperature of the two investigations. For the cadmium selenocyanate system our values of $\beta_1 - \beta_3$ are in line with those reported by Golub and Andreichenko.[12] while the value of β_4 given by these authors is considerably lower than ours. Golub and Andreichenko [12] also postulate a fifth complex but this seems hazardous in view of the rather scarce experimental material.

Thiocyanate and selenocyanate are ambidentate ligands coordinating *via* N or S and *via* N or Se, respectively. Soft metals prefer the S and Se atoms, while hard metals prefer the harder N-atom. Selenium donors are generally found to be softer than analogous sulfur donors [21] and should therefore give stronger complexes with soft acceptors. Therefore, if an acceptor is coordinated *via* the S and Se atoms, the selenocyanate complexes should be stronger than the thiocyanate ones. If, on the other hand, the N-atoms are coordinated, the strengths of the thiocyanate and selenocyanate complexes should be much the same.

The selenocyanate complexes of cadmium are somewhat stronger than the thiocyanate complexes, while the reverse holds for the corresponding zinc complexes, Table 8, though the differences are not very large. The results clearly support the deductions drawn from infrared spectroscopy [22] that the thiocyanate and selenocyanate ions are bonded to the borderline acceptor Cd^{2+}, at least partly, *via* the S and Se atoms, respectively, while coordination to the hard Zn^{2+} occurs *via* the N-atoms.

In the discussion of the enthalpy and entropy

changes accompanying the complex formation, the strength of the bond formed between metal and ligand as well as hydration effects have to be considered. The two donor atoms in the thiocyanate and selenocyanate ions are both negatively charged and should consequently be more or less hydrated. From MO-calculations Wagner [23] has found that the nitrogen atoms in the two ligands have the same atomic charge of ≈ -0.4 while the sulfur and selenium atoms have charges of -0.71 and -0.84, respectively. The ratio atomic charge/radius for the sulfur and selenium atoms is about the same (0.58). Thus, it is reasonable to assume that in the free ligands the S and Se atoms are about equally hydrated, as are the two nitrogen atoms.

For both thiocyanate and selenocyanate the charge density on the non-bonding end decreases upon coordination. Wagner [23] has shown by calculations on the corresponding acids that upon coordination *via* the N-atoms the decrease of charge is larger on the sulfur atom than on the selenium atom. Thus if an acceptor is coordinating *via* the N-atoms, more water should be liberated from the S atom in thiocyanate than from the Se atom in selenocyanate. Consequently, the entropy term should be more positive or less negative for the thiocyanate reaction than for the selenocyanate reaction. If coordination, on the other hand, occurs through the S or Se atoms, the same amount of water should be set free from the non-bonding N atom for both ligands. Thus the entropy terms for the two reactions should be about the same.

As seen from Table 8, ΔS°_1 for the formation of zinc thiocyanate is less negative than ΔS°_1 for the formation of zinc selenocyanate. In the reactions with Cd^{2+}, on the other hand, the two ligands give about the same value of ΔS°_1. This evidently fits with the postulated N-bonding of Zn^{2+}, and the preferred S and Se bonding of Cd^{2+}.

The preference for selenium donors over analogous sulfur donors generally exhibited by soft acceptors (p. 863) is mainly due to more negative values of ΔH°_j.[21] This indicates that the Se donors are preferred because of their stronger covalent bonding capacity. Thus if an acceptor coordinates thiocyanate and selenocyanate ions *via* their S and Se donor atoms, respectively, the selenocyanate complexes should be formed in more exothermic reactions than the thiocyanate complexes. If, on the other hand, an acceptor prefers to coordinate these ligands *via* their harder N-atoms, the reactions will be less exothermic than in the case of S or Se coordination. Moreover, the strength of the bonds will be little influenced by an exchange of S for Se and about the same values of ΔH°_j may therefore be expected for thiocyanate and selenocyanate complexes.

The enthalpy changes are much the same for zinc thiocyanate and selenocyanate, Table 8. The complexes are formed in weakly exothermic reactions. For cadmium the enthalpy changes are more exothermic for selenocyanate than for thiocyanate. The complexes are formed in more exothermic reactions than the corresponding zinc complexes. This once more indicates that thiocyanate and selenocyanate are coordinated to Cd^{2+}, at least partly, *via* the S and Se atoms, respectively, and to Zn^{2+} *via* the N-atoms.

For complexes formed between hard or borderline acceptors and donors a fairly regular decrease of ΔS°_j generally occurs for each consecutive step.[24] For the zinc selenocyanate and thiocyanate systems this is obviously not the case, Table 8. In both systems ΔS°_2 is higher than ΔS°_1. This deviation is probably caused by a change of coordination at the second step.[24] The switch most probably takes place between the octahedral coordination represented by the initial hexaquo ion $Zn(H_2O)_6^{2+}$ and the tetrahedral coordination represented by the final complex ZnL_4^{2-}. Such a change of coordination should be followed by a liberation of a large amount of water from the hydration shell, resulting in especially high values of both ΔH°_2 and ΔS°_2. For the halide and acetate systems of Zn^{2+} an even more pronounced increase of ΔH°_2 and ΔS°_2 is observed,[25] strongly suggesting a change of coordination configuration at this very step also for these systems.

For the cadmium selenocyanate system the values of ΔH°_3 and ΔS°_3 are abnormally high. Also the hexaaquo ion $Cd(H_2O)_6^{2+}$ has most likely an octahedral coordination while the final complex, $Cd(SeCN)_4^{2-}$, is tetrahedral. The high values of ΔH°_3 and ΔS°_3 are most probably due to the fact that at least the main part of this change of coordination takes place at the third

step. For the halide systems of Cd^{2+} a similar but less marked reversal of the enthalpy and entropy changes at the third step is observed.[25] Also for these systems the same switch of coordination seems to occur at the same stage.

Remarkably enough no reversal is observed for the cadmium thiocyanate system. The switch from octahedral to tetrahedral coordination which most likely takes place also in this system cannot therefore occur more or less exclusively at the third or any other particular step. Rather it must be spread out over several steps as has been postulated before for other systems where no drastic reversals between consecutive values of $\Delta S°_j$ and $\Delta H°_j$ are observed, in spite of the fact that a change of coordination no doubt takes place between the initial and final complexes.[24]

REFERENCES

1. Ahrland, S., Chatt, J., Davies, N. R. and Williams, A. A. *J. Chem. Soc.* (1958) 264.
2. Barnes, D., Ford, G. J., Pettit, L. D. and Sherrington, C. *J. Chem. Soc. A* (1971) 2883.
3. Sunday, O. A. and Goddard, D. R. *J. Chem. Soc. Dalton Trans.* (1973) 1751.
4. Golub, A. M. and Skopenko, V. V. *Russ. Chem. Rev. 34* (1965) 901.
5. Ahrland, S. and Kullberg, L. *Acta Chem. Scand. 25* (1971) 3692.
6. Gerding, P. and Johansson, B. *Acta Chem. Scand. 22* (1968) 2255.
7. Hietanen, S. and Sillén, L. G. *Acta Chem. Scand. 6* (1952) 747.
8. Biedermann, G. and Ciavatta, L. *Acta Chem. Scand. 16* (1962) 2221.
9. Schorsch, G. *Bull. Soc. Chim.* (1964) 1456.
10. Humffray, A. A., Bond, A. M. and Forrest, J. S. *J. Electroanal. Chem. 15* (1967) 67.
11. Toropova, V. F. *Zh. Neorg. Khim. 1* (1956) 243.
12. Golub, A. M. and Andreichenko, O. E. *Russ. J. Inorg. Chem. 7* (1962) 279.
13. Ahrland, S. and Kullberg, L. *Acta Chem. Scand. 25* (1971) 3457.
14. Ahrland, S. and Kullberg, L. *Acta Chem. Scand. 25* (1971) 3471.
15. Karlsson, R. and Kullberg, L. *To be published.*
16. Persson, H. *Acta Chem. Scand. 24* (1970) 3739.
17. Ripan, R. *Z. Anal. Chem. 94* (1933) 331.
18. Brown, A. S. *J. Amer. Chem. Soc. 56* (1934) 646.
19. Kullberg, L. *Acta Chem. Scand. A 28* (1974) 829.
20. Persson, H. *Acta Chem. Scand. 25* (1971) 543.
21. Ahrland, S. *Proc. XIV Intern. Conf. Coord. Chem.*, Toronto 1972, p. 185.
22. Bailey, R. A., Kozak, S. L., Michelsen, T. W. and Mills, W. N. *Coord. Chem. Rev. 6* (1971) 407.
23. Wagner, E. L. *J. Chem. Phys. 43* (1965) 2728.
24. Ahrland, S. *Struct. Bonding 15* (1973) 167.
25. Gerding, P. *Termokemiska studier av metallkomplex*, Diss., University of Lund, Lund 1969.

Received April 9, 1974.

Acta Chemica Scandinavica A 28 (1974) 866—870

^{121}Sb Mössbauer Studies on Mo_3Sb_7 and $Nb_3Sb_2Te_5$

J. D. DONALDSON,[a] A. KJEKSHUS,[b] D. G. NICHOLSON [b] and J. T. SOUTHERN [a]

[a] Department of Chemistry, Chelsea College of Science and Technology, Manresa Road, London S.W.3, England and [b] Department of Chemistry, University of Oslo, Blindern, Oslo 3, Norway

^{121}Sb Mössbauer data for Mo_3Sb_7 and $Nb_3Sb_2Te_5$ have been obtained at 4.2 K and are discussed in relation to their crystal structures. The resolution of overlapping profiles arising from the two distinct Sb sites in Mo_3Sb_7 has been achieved through the use of a Fourier transform treatment. Sb has been assigned to the X_{II} site of the crystallographic formula $T_3(X_I)_3(X_{II})_4$ for $Nb_3Sb_2Te_5$.

By far the largest amount of experimental information on compounds in the solid state is concerned with structural data because any approach to bonding must begin with the atomic arrangement. For the transition metal pnictides and chalcogenides the amount of structural data at hand has attained a level where it is desirable to acquire supplementary information in order to proceed further with interpretations as to their bonding characteristics. Among the experimental techniques employed for this purpose, Mössbauer spectroscopy is particularly attractive because the probe nucleus reflects the electronic situation at the relevant site in the compound. Although the major part of such studies has been performed on ^{57}Fe and ^{119}Sn, the progress in data reduction (notably least squares fitting and Fourier transform procedures) is changing the situation and there is an increasing interest among chemists in alternative nuclei. The advances being made in ^{121}Sb Mössbauer methodology are typical of the development which is taking place. Even the complicating feature of a twelve line unresolved spectrum arising from a quadrupole splitting interaction of the $7/2 \rightarrow 5/2$ transition has its advantage in permitting the determination of the asymmetry parameter and sign of the quadrupole interaction.

The employment of the Fourier transform technique in the deconvolution of the source line-shape from the experimental absorption envelope provides the opportunity for examining antimonides which have structurally non-equivalent Sb atoms. Hence, as a continuation of previous studies [1-3] on transition metal antimonides we present here the results of an investigation of the isostructural [4,5] compounds Mo_3Sb_7 and $Nb_3Sb_2Te_5$.

EXPERIMENTAL

The experimental details concerning the purity of the elemental starting materials, sample preparation, characterization by X-ray diffraction, Mössbauer spectroscopic measurements and data reduction have been presented in previous communications.[1,6-9] (The Fourier transform computations were performed according to the programme of Ure and Flinn [10] and the experimental data least squares fitted to eight or twelve superimposed Lorentzian peaks employing the resonance line coefficients and transition probabilities of Shenoy and Dunlap.[11])

RESULTS AND DISCUSSION

Fig. 1 shows the ^{121}Sb Mössbauer spectra of Mo_3Sb_7 and $Nb_3Sb_2Te_5$. The Fourier transformed sharpened spectra (Fig. 2) reveal the presence of two different Sb sites in Mo_3Sb_7, but only one site in $Nb_3Sb_2Te_5$. In order to facilitate the discussion, a brief description is presented of the crystal structures of the compounds.

The Ir_3Ge_7 type structure of Mo_3Sb_7 and $Nb_3Sb_2Te_5$ contains two non-equivalent X atoms and the crystallographic formula is $T_3(X_I)_3(X_{II})_4$.[4,5] Those interatomic distances

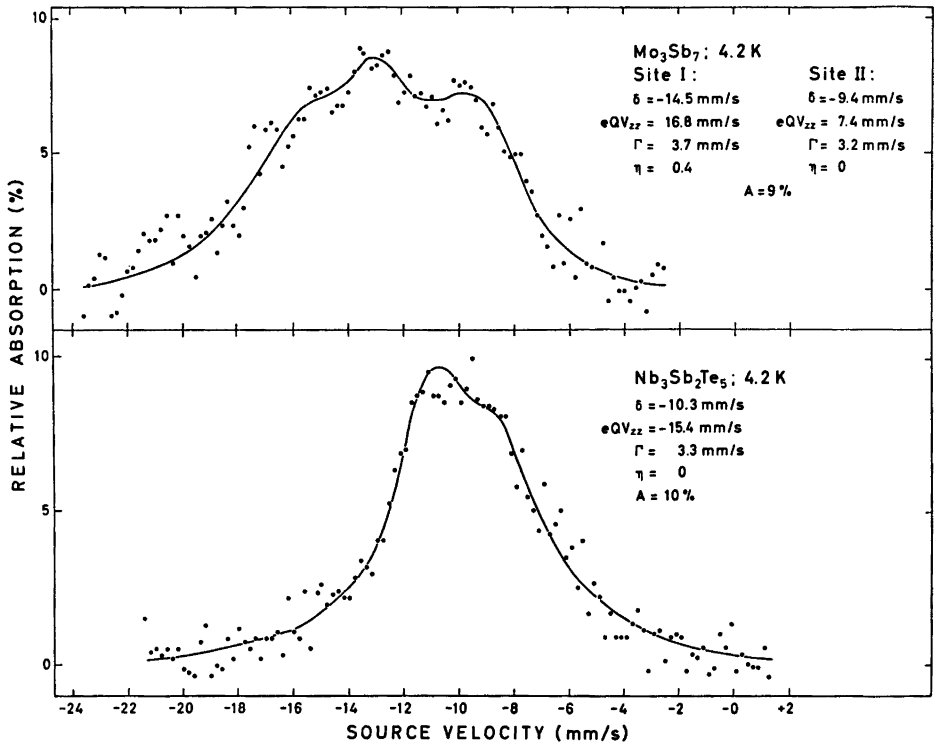

Fig. 1. ^{121}Sb Mössbauer spectra for $Nb_3Sb_2Te_5$ and Mo_3Sb_7. Smooth curves give calculated profiles.

Table 1. Bond distances and angles in $Nb_3Sb_2Te_5$, Mo_3Sb_7, and Re_3As_7, including average distortions from the tetrahedral angle of 109.47 for the bonds around X_I and X_{II}.

Distance (Å)	$Nb_3Sb_2Te_5$	Mo_3Sb_7	Re_3As_7
$4\ T-X_I$, $4\ X_I-T$	2.900(5)	2.828(7)	2.584(4)
$4\ T-X_{II}$, $3\ X_{II}-T$	2.878(8)	2.793(10)	2.559(19)
$1\ T-T$	3.090(20)	3.015(25)	2.779(11)
$1\ X_{II}-X_{II}$	2.890(13)	2.905(14)	2.482(26)

Angle (°)	$Nb_3Sb_2Te_5$	Mo_3Sb_7	Re_3As_7
$2\ T-X_I-T$	64.4(3)	64.4(4)	65.0(2)
$4\ T-X_I-T$	135.7(2)	135.7(3)	135.3(1)
Deviation ξ_I	32.5	32.5	32.0
$3\ T-X_{II}-T$	111.4(3)	112.2(2)	110.3(7)
$3\ T-X_{II}-X_{II}$	107.5(3)	106.6(3)	108.7(8)
Deviation ξ_{II}	2.0	3.0	0.8
$4\ X_I-T-X_I$	73.5(1)	73.5(2)	73.2(1)
$8\ X_I-T-X_{II}$	81.2(1)	81.8(1)	80.5(4)
$4\ X_{II}-T-X_{II}$	68.5(3)	67.6(3)	69.7(6)

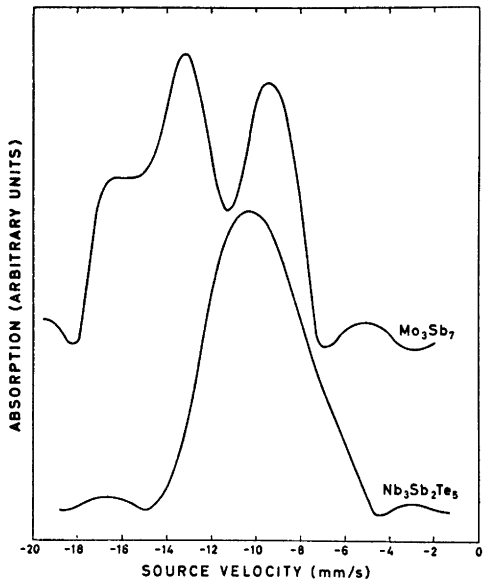

Fig. 2. The Fourier transform sharpened spectra from Fig. 1.

which are presumed to be bond lengths are summarized in Table 1 together with the relevant angles. The corresponding data for Re_3As_7 [12] are included for the purpose of comparison. Each T is coordinated to eight near X (four X_I and four X_{II}) at the corners of a somewhat distorted square antiprism. Each X_I is surrounded by four near T tetrahedrally arranged. The distortion of these T_4 tetrahedra produces $T-T$ pairs, and although their interatomic distance is about 2 – 10 % longer than the shortest interatomic distances in the corresponding metals [13] a $T-T$ bonding interaction within the pairs strongly suggests itself as the cause of the distortion. The X_{II} atoms are coordinated to three near T and one near X_{II} and the resulting $X_{II}-X_{II}$ pairs have short interatomic distances closely matching the corresponding expectation values [14] for single $X-X$ bonds.

The composition $Nb_3Sb_2Te_5$ raises an interesting crystallographic problem associated with the distribution of Sb on the positions X_I and X_{II}. Due to the very small difference in the X-ray scattering factors of Sb and Te it could not be distinguished (*viz.* significantly) between the three simple alternatives: all Sb in X_I, all Sb in X_{II}, and a statistical distribution of Sb over the X_I and X_{II} sites. However, the least squares refinements appeared [5] to show a slight preference for the second alternative.

In addition to revealing the presence of two sites in Mo_3Sb_7 the Fourier transform reduced spectra (Fig. 2) provide preliminary estimates for input parameters for the least squares fitting procedure. The final values for the chemical shifts (δ), quadrupole splittings (eQV_{zz}), line widths (Γ), and asymmetry parameters (η) are contained on Fig. 1, probable experimental errors being ± 0.1 mm/s in δ, ± 0.5 mm/s in eQV_{zz} (± 1 mm/s for site II in Mo_3Sb_7), ± 0.2 mm/s in Γ (± 0.4 mm/s for site II in Mo_3Sb_7), and ± 0.2 in η for site I in Mo_3Sb_7 ($\eta < 0.2$ for site II in Mo_3Sb_7 and in $Nb_3Sb_2Te_5$; fixed at zero during the final computations). (A δ value of -9.0 mm/s is obtained for the reference compound InSb at 4.2 K.)

The chemical shift which is directly governed by the *s* electron distribution over the bonds originating from Sb, is expected to be quite different for Sb_I and Sb_{II} in Mo_3Sb_7 (*vide supra*). This expectation is indeed confirmed by the shifts for the two sites in this compound which take the values -14.5 and -9.4 mm/s, both being in the region for Sb(III) valence states.[8,15]

At first sight it might have seemed natural to attempt an identification of the two contributions to the overall profile on the basis of the relative concentration of Sb atoms in the individual sites. However, such a naive approach appears somewhat dubious in this case where the bonding situations for the two kinds of Sb atoms are substantially different. This environmental distinction is bound to be reflected in the recoil free fractions for the two sites. The fact that X-ray diffraction sees [4] (within standard deviation) equal isotropic thermal vibration at room temperature is misleading in this connection. The Mössbauer experiments were performed at 4.2 K and on going from room to liquid helium temperature the vibrational characteristics for the two Sb sublattices are almost certainly no longer equal. Hence, identification must be based on the expected quadrupole interactions for the two sites.

In covalent compounds of the type studied here, the major contribution to quadrupole interactions at the Sb probe nuclei arises from the imbalances in 5*p* orbital occupation caused by deviations of the electronic environment

from cubic symmetry. It has previously been shown [1] that, for a series of ten structurally closely related antimonides, the average angular distortion (ξ) from the tetrahedral value of 109.47° for the bond angles subtended at Sb provides a relative measure for the deformation through its correlation with the eQV_{zz} values.

The coordination around Sb_{II} (*cf.* Table 1) takes C_{3v} symmetry and hence this site can be unambiguously identified with that having a calculated η value of zero and the small eQV_{zz}, V_{zz} being located along the $Sb_{II}-Sb_{II}$ bond. The actual value for the coupling constant for this site should be regarded as somewhat inaccurately determined because of its small magnitude and the appreciable overlap of a significant part of the envelope. Nevertheless, it is interesting to note that the definitely small eQV_{zz} value is consistent with an almost negligible ξ value of 3.0° for this site. Although the crystallographic symmetry of Sb_{II} is lowered from T_d to C_{3v} the p electron imbalance is not substantial because of the small eQV_{zz}. This suggests that there is no great difference between the p characters of the $Sb_{II}-Sb_{II}$ and $Sb_{II}-Mo$ bonds.

Although the four Sb_I-Mo bond lengths are constrained by symmetry to be equal, the coordination around Sb_I is heavily deformed from T_d symmetry in the bond angles. Moreover, since the six $Mo-Sb_I-Mo$ bond angles split into two groups of two and four, C_{3v} symmetry no longer applies. In line with this a finite η value has been derived for this site. Stronger evidence is provided by the large quadrupole coupling constant which is fully consistent with the remarkably high ξ value of 32.5° for the Sb_I site.

When the absorption envelope is unsymmetrical, the sign of eQV_{zz}, and hence, that of V_{zz} can be deduced. For Mo_3Sb_7 the sign of the quadrupole coupling constant is positive for the Sb_I site whereas that for Sb_{II} cannot be considered reliably determined. Since Q for ^{121}Sb is negative, V_{zz} for the Sb_I site is negative, which implies that the degree of electron delocalization from the Sb_I $5p_z$ orbital into the relevant "molecular orbitals" is lower than those from the $5p_x$ and $5p_y$ atomic orbitals.

It is worth noting that the small, but significant shortening of the Sb–Mo bond on going from Sb_I to Sb_{II} corresponds to an increase in the overall contribution from the Sb (in particular s) electrons to the bonding. This would effectively lower the total s electron density at the Sb nucleus and matches the smaller negative shift assigned to site II.

Turning now to the data for $Nb_3Sb_2Te_5$, the fact that its spectrum (*cf.* Figs. 1 and 2) shows apparently only one site eliminates the possibility of a statistical distribution of Sb on sites X_I and X_{II}. The question then arises as to which of these is occupied by Sb. The decision is taken on the basis of the reasonably close proximity of the δ values for $Nb_3Sb_2Te_5$ with that for the Sb_{II} site in Mo_3Sb_7. Hence, the conclusion from the ^{121}Sb Mössbauer data concurs with the indications from X-ray diffraction (*cf.* Ref. 5 and *vide supra*). Support for Sb being located in the X_{II} site is also provided by assuming similar electronic configurations of Mo in Mo_3Sb_7 and Nb in $Nb_3Sb_2Te_5$.

The accurately determined crystal structures of $Nb_3Sb_2Te_5$, Mo_3Sb_7, and Re_3As_7 show that the X_{II} sites are very similar in the crystallographic sense (*cf.* Table 1). Hence, the larger and positive value of V_{zz} for $Nb_3Sb_2Te_5$ must arise from electronic differences at the Sb_{II} site. This would indicate that the Sb $5p_z$ orbital is participating more strongly in Sb–Te bonding in $Nb_3Sb_2Te_5$ than in Sb–Sb bonding in Mo_3Sb_7, which, in turn, would be consistent with the slightly higher s electron density at Sb_{II} in $Nb_3Sb_2Te_5$ than Mo_3Sb_7 as reflected by the δ values. (We have also observed a positive sign for V_{zz} in the ^{121}Sb Mössbauer spectrum of SbTeI.[16])

REFERENCES

1. Donaldson, J. D., Kjekshus, A., Nicholson, D. G. and Tricker, M. J. *Acta Chem. Scand.* *26* (1972) 3215.
2. Donaldson, J. D., Kjekshus, A., Mukherjee, A. D., Nicholson, D. G. and Southern, J. T. *Acta Chem. Scand.* *26* (1972) 4063.
3. Kjekshus, A., Nicholson, D. G. and Rakke, T. *Acta Chem. Scand.* *27* (1973) 1315.
4. Jensen, P. and Kjekshus, A. *Acta Chem. Scand.* *20* (1966) 417.
5. Jensen, P. and Kjekshus, A. *J. Less-Common Metals* *13* (1967) 357.
6. Furuseth, S. and Kjekshus, A. *Acta Chem. Scand.* *20* (1966) 245.
7. Jensen, P., Kjekshus, A. and Skansen, T. *Acta Chem. Scand.* *20* (1966) 403.

8. Donaldson, J. D., Tricker, M. J. and Dale, B. W. *J. Chem. Soc. Dalton Trans.* (1972) 893.
9. Kjekshus, A. and Nicholson, D. G. *Acta Chem. Scand. A 28* (1974) 469.
10. Ure, M. C. D. and Flinn, P. A. *Mössbauer Eff. Methodol. 7* (1969) 245.
11. Shenoy, G. K. and Dunlap, B. D. *Nucl. Instrum. Methods 71* (1969) 285.
12. Jensen, P., Kjekshus, A. and Skansen, T. *J. Less-Common Metals 17* (1969) 455.
13. Pearson, W. B. *A Handbook of Lattice Spacings and Structures of Metals and Alloys*, Pergamon, Oxford-London-Edinburgh-New York-Toronto-Paris-Braunschweig 1967, Vol. II.
14. Furuseth, S., Selte, K. and Kjekshus, A. *Acta Chem. Scand. 19* (1965) 735.
15. Bowen, L. H., Stevens, J. G. and Long, G. G. *J. Chem. Phys. 51* (1969) 2016.
16. Donaldson, J. D., Kjekshus, A., Nicholson, D. G. and Southern, J. T. *To be published.*

Received April 30, 1974.

Acta Chemica Scandinavica A 28 (1974) 871—884

Conformational Analysis. VI. The Molecular Structure, Torsional Oscillations, and Conformational Equilibria of Gaseous 1,2,3-Trichloropropane as Determined by Electron Diffraction and Compared with Semi-empirical (Molecular Mechanics) Calculations

PER ERIK FARUP and REIDAR STØLEVIK

Department of Chemistry, University of Oslo, Blindern, Oslo 3, Norway.

Gaseous 1,2,3-trichloropropane has been studied by electron diffraction at a (nozzle) temperature of 63 °C. Three spectroscopically distinguishable conformers were detected. Results are presented with error limits (2σ). The following values for bond lengths (r_g) and bond angles ($\angle_\alpha$) are average parameters for the conformers: r(C—H) = 1.137(22) Å, r(C—C) = 1.526(8) Å, r(C—Cl) = 1.792(4) Å, $\angle C_1C_2C_3 = 115.2°(2.6)$, $\angle C_2CCl = 110.7°(2.4)$, $\angle CC_2Cl = 110.4°(2.2)$. The torsion angles of the most abundant conformers have been determined.

The composition parameter (α) are: α_4[GG(ag) + GG(ga)] = 69 % (6), α_3[AG(gg) + GA(gg)] = 5 % (8), α_2[GA(ag) + AG(ga)] = 26 % (4). The numbering and names of the conformers are shown in Fig. 1. The conformers AA(gg), GG(aa), and GG(gg) are not present in detectable amounts.

It has been demonstrated that torsional force constants can be estimated from the electron diffraction data, if the remainder of the force field is approximately known. The low frequencies (< 150 cm^{-1}), derived from the electron diffraction data, are in agreement with those spectroscopically observed.

Although the conformational energies predicted by the semi-empirical model seem unlikely, the structure parameters and torsional force constants derived, generally agree with the experimental results.

I. INTRODUCTION

The present work is one of several in a series of electron diffraction studies concerned with substituted propanes and related molecules in an attempt to understand and quantitatively describe the conformational equilibria in these molecules in the gas phase.

General [1] information [2] relevant to this investigation and to the electron diffraction method [3] is found in Refs. 1, 2, and 3.

The numbering and system of naming for conformers of 1,2,3-trihalopropanes (Fig. 1) was introduced in a previous paper concerned with 1,2,3-tribromopropane (TBP).[4] The numbering of atoms in the conformer GG(ag) is shown in Fig. 2. Unfortunately there is no general agreement about the nomenclature in this type of compounds.

Various authors have reported vibrational spectra of TCP. From Raman spectra [5] it was concluded that only one conformer of TCP was present in the liquid. From infrared spectra [6,7] the presence of at least two conformers in TCP was established. An extended spectroscopic study [8] of 1,2,3-trihalopropanes verified the existence of three or possibly four conformers in the liquids at room temperature. Combined with information from electron diffraction (this work and Ref. 4) of the vapours, the spectra [8] demonstrated the conformer *4* to be present in the low temperature and high pressure crystals of both compounds. This conformer was not the one suggested by earlier authors.[6]

In conclusion, the abundant conformers of TCP and TBP could not be identified by vibrational spectroscopy alone, however, it can be concluded [8] with certainty that the most abundant conformers of the vapours also dominate in the liquids and remain in the crystals.

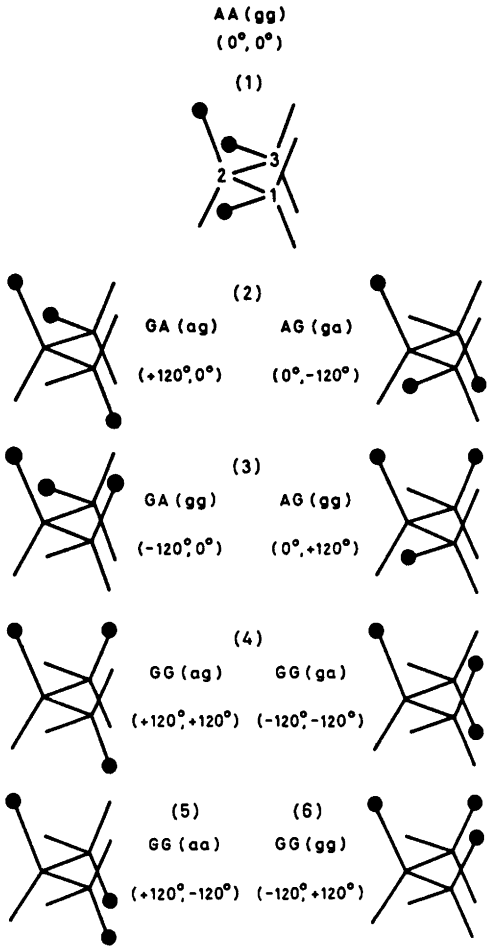

Fig. 1. The numbering and names of staggered conformers in 1,2,3-trichloropropane.

II. MOLECULAR MECHANICS CALCULATIONS OF CONFORMATIONAL ENERGIES, GEOMETRIES, BARRIERS, AND TORSIONAL FORCE CONSTANTS

The method of calculation (the semi-empirical energy model) is described in Ref. 4. Energy parameters (a,b,c,d, and V_0) were taken from the paper [9] by Abraham and Parry, and the force constants of Table 5 were used. In minimizing the energy, the geometry was constrained in the same way as described in Sect. V-A.

The conformational geometries derived from the semi-empirical model are presented in Table 1.

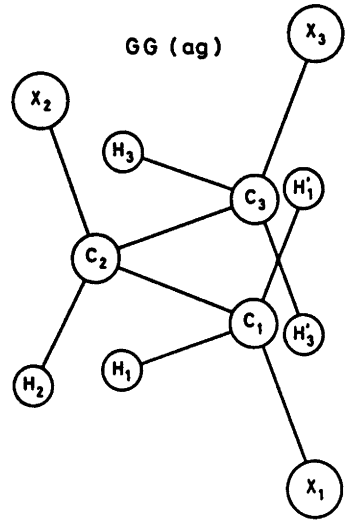

Fig. 2. Numbering of atoms in the conformer GG(ag).

Conformational energies of the six spectroscopically distinguishable conformers of TCP are found in Table 2. According to the present energy model *2* is the conformer of lowest minimum energy.

The destabilizing effect of parallel (1:3) Cl···Cl interactions [1] in conformers like GG(aa) and GG(gg) is reproduced by the calculations. The minima of these conformers are considerably displaced from exact staggered torsion angles (Fig. 1).

Torsional barriers may be estimated from the energy values of Table 3. Each energy value of Table 3 corresponds to a conformer having all structure parameters adjusted, except for one or two torsion angles (ϕ) being kept at constant values. Eclipsed conformers correspond to values of ϕ being $\pm 60°$ or $\pm 180°$. The actual values of the geometry variables are not shown in Table 3; however, the values of ϕ_{1-2} and ϕ_{2-3} are approximately those given in parenthesis. Details about the staggered conformers are found in Tables 1 and 2. The staggered conformers correspond to well defined minima of the potential energy surface.

Valence torsional force constants were computed according to their definitions:

$$F_\phi(1-2) = \partial^2 E/\partial\phi_{1-2}^2,\ F_\phi(2-3) = \partial^2 E/\partial\phi_{2-3}^2,$$
$$F_\phi(1-2,\ 2-3) = \partial^2 E/\partial\phi_{1-2}\partial\phi_{2-3}$$

Table 1. Calculated conformational geometries for 1,2,3-trichloropropane. In minimizing the energy the geometry was constrained as described in Sect. V-A.

Parameter (normal value)	*4* GG(ag)	*3* AG(gg)	*2* GA(ag)	*1* AA(gg)	*5* GG(aa)	*6* GG(gg)
r(C−H), (1.094 Å)	1.095	1.095	1.095	1.095	1.095	1.094
r(C−C), (1.513 Å)	1.534	1.532	1.532	1.530	1.535	1.536
r(C−X), (1.780 Å)	1.792	1.793	1.792	1.794	1.789	1.793
∠CCC (110.0°)	114.1	111.8	111.2	109.0	113.8	115.2
∠C_2CX (109.47°)	112.1	112.1	111.7	111.7	112.9	114.4
∠CC_2X (109.47°)	110.5	111.1	109.6	110.3	108.9	112.3
∠C_2CH (109.47°)	110.0	109.8	110.0	109.8	109.8	109.0
∠CC_2H (109.47°)	107.2	107.6	109.1	109.2	109.0	105.2
ϕ_{1-2}[a]	+119.0	+14.4	+110.9	+9.3	+103.4	−107.7
ϕ_{2-3}[a]	+122.3	+122.3	−8.5	−9.3	−103.4	+107.7

[a] $\phi_0 = 60°$ in eqn. (1) in Ref. 4.

Table 2. Conformational energies (kcal/mol) for 1,2,3-trichloropropane. Details about the energy expression are found in Ref. 4. The zero-point vibrational energies of the conformers are not included.

Type of energy	Type of conformer *4*	*3*	*2*	*1*	*5*	*6*
E (bonded)	1.68	1.64	1.11	1.10	2.62	4.38
E (van der Waals)	2.58	2.60	2.88	2.69	3.02	2.45
E (polar, X···H)	−8.09	−7.68	−7.97	−7.43	−8.03	−7.14
E (polar, X···X)	6.07	6.19	5.77	6.06	5.98	7.03
E (total)	2.24	2.75	1.80	2.43	3.59	6.71
E (tot.) − $E(2) = \Delta E^m$	0.44	0.96	0.00	0.63	1.79	4.91

Table 3. Calculated conformational energies and torsional barriers in 1,2,3-trichloropropane. Details about the conformational minima corresponding to stable conformers are given in Tables 1 and 2.

ϕ_{2-3}(°)	ϕ_{1-2}(°) −180	−120	−60	0	60	120	180
180	∞	8.9 GG(gg)	18.6	6.7 AG(gg)	13.7	7.6 GG(ag)	∞
120	8.9	4.9	10.1	1.0	4.3	0.4	8.9
60	18.6	10.1 GA(gg)	17.0	10.0 AA(gg)	13.8	9.2 GA(ag)	18.6
0	6.7	1.0	10.0	0.6	3.9	0.0	6.7
−60	13.7	4.3 GG(ga)	13.8	3.9 AG(ga)	7.9	3.2 GG(aa)	13.7
−120	7.6	0.4	9.2	0.0	3.2	1.8	7.6
−180	∞	8.9	18.6	6.7	13.7	7.6	∞

Table 4. Calculated torsional force constants (F_ϕ) for 1,2,3-trichloropropane. The F_ϕ values have been numerically computed according to the semi-empirical energy expression.

Force constant [mdyn Å (rad)$^{-2}$]	(4) GG(ag)	(3) AG(gg)	(2) GA(ag)	(1) AA(gg)
$F_\phi(1-2)$	0.189	0.196	0.188	0.193
$F_\phi(2-3)$	0.270	0.220	0.188	0.193
$F_\phi(1-2;\ 2-3)$	−0.069	−0.032	−0.039	−0.012

Table 5. Valence force constants for 1,2,3-trichloropropane.

Stretch (mdyn Å^{-1})		Bend [mdyn Å (rad)$^{-2}$]	
C−C	4.43[a]	CCC	0.90
C_1−H	4.85	CCH	0.67
C_2−H	4.55	HCH	0.53
C−X	3.18	CCX	1.17
		HCX	0.79
Stretch/stretch (mdyn Å^{-1}) (C−C common)		Stretch/bend [mdyn (rad)$^{-1}$] (C−X common)	
C−X/C−C	0.35	C−X/CCX	0.55
C−C/C−C	0.064	C−X/HCX (C−C common)	0.33
Bend/bend [(mdyn Å rad)$^{-2}$] (C−C common)		C−C/CCX	0.29
HCC/CCC	−0.12	C−C/CCC	0.35
		C−C/CCH	0.26

Torsion [(mdyn Å rad)$^{-2}$] [b]

	4	*3*	*2*	*1*
Conformer	GG(ag)	AG(gg)	GA(ag)	AA(gg)
$F_\phi(1-2)$[c]	0.212	0.219	0.211	0.216
$F_\phi(2-3)$[c]	0.293	0.243	0.211	0.216

[a] Probably, 4.73 would have been a slightly better value for F(C−C). [b] The torsional force constants have been defined in the following way: each fragment of type A′−C_1−C_2−A″ (A=H, C, X, see Fig. 2) has been assigned an equal torsional force constant. Each fragment of type A′−C_2−C_3−A″ has been assigned an equal force constant but different from those of fragments A′−C_1−C_2−A″. The total force constant for the torsional coordinate ϕ_{1-3} (i=1,3) is thus the sum of *nine* equal contributions. The input to Gwinn's normal coordinate program demands a separate specification for each torsional fragment. Moreover, all interaction force constants have to be multiplied by two if Gwinn's program is used. [c] These values were estimated from the electron diffraction data as described in Sect. V-B.

The derivatives were calculated numerically at the minimum of potential energy. The values of the force constants are given in Table 4. The interaction force constant $F_\phi(1-2,\ 2-3)$ is always negative and much smaller in absolute value than any of the diagonal ones.

III. CALCULATION OF VIBRATIONAL QUANTITIES

Valence force constants, except for the torsional part of the force field, were taken from the work [10] of Schachtschneider and Snyder. Certain compromises between force constant values had to be made. The final values selected for TCP are given in Table 5.

The normal-coordinate program described by Gwinn [11] was used in computing vibrational frequencies. Results for some staggered conformers are presented in Table 6 together with the observed spectroscopic frequencies.[8] The torsional part of the force field has been adjusted as described in Sect. V-B.

Keeping in mind the fact that only torsional force constants have been adjusted, the fit between observed and calculated frequencies is very satisfactory. Adjustments of the remainder of the force field were not undertaken. Such

Table 6. Fundamental vibrational frequencies (cm^{-1}) in conformers (*4,3,2,1*) of 1,2,3-trichloropropane. The force constants of Table 5 were used in calculating frequencies. Structure parameters slightly different from the final ones were used.

Approximate mode	Observed value [8]	Calculated values *4*	*3*	*2*	*1*
Torsion	75	68	84	78	76
Torsion	154	131	103	114	121
CCX bend	206	190	144	182	131
CCX bend	224	223	246	234	240
CCX bend	288	298	335	308	284
CCX bend	356	386	388	406	415
CCC bend	522	534	541	426	498
C–X stretch	622	674	629	679	619
C–X stretch	720	725	706	732	704
C–X stretch	753	755	758	749	778
CH_2 rock	872	827	878	851	864
CH_2 rock	909	925	925	947	953
C–C stretch	990	979	975	991	974
C–C stretch	1092	1125	1116	1115	1092
CH_2 twist	1145	1241	1241	1244	1230
CH_2 twist	1200	1264	1261	1248	1240
CH def.	1219	1303	1296	1312	1286
CH_2 wag	1282	1321	1323	1322	1305
CH def.	1340	1344	1340	1331	1328
CH_2 wag	1292	1369	1381	1369	1386
CH_2 scissor	1427	1467	1466	1464	1435
CH_2 scissor	1440	1483	1473	1467	1438
C–H stretch	2925	2891	2891	2891	2890
C–H stretch	2960	2945	2944	2945	2947
C–H stretch	2973	2945	2945	2945	2947
C–H stretch	3010	3020	3020	3020	3018
C–H stretch	3020	3021	3021	3020	3018

adjustments could not lead to any significant changes in mean amplitudes for TCP. Contrary to the situation for TBP,[4,8] the observed spectroscopic torsional frequencies (liquid phase) of TCP agree with the results from electron diffraction. The liquid-phase frequencies are expected to be lower than the gas phase values for torsional modes.

Mean amplitudes of vibration (u) and perpendicular amplitude corrections (K) were calculated as explained in Ref. 12. The u- and K values in conformer GG(ag) are found in Table 7.

Several vibrational quantities in a molecule like TCP varies with the values of the torsional force constants. To illustrate this point, some of these quantities have been calculated using three different values of the average ($F_\phi(1-2) = F_\phi(2-3) = \overline{F}_\phi$) torsional force constant. The results are found in Table 8.

IV. EXPERIMENTAL AND DATA REDUCTION

TCP was obtained from Fluka, and the purity of the actual sample used was better than 98 %. Electron diffraction photographs were made at a nozzle temperature of 63 °C in the Balzer [13] apparatus,[14] under conditions summarized below.

Table 7. Mean amplitudes (u) and K values for the conformer GG(ag) of 1,2,3-trichloropropane at 63 °C. K- and u values in Å (See also the text of Table 6). The symbols (a) and (g) means *anti* (a) and *gauche* (g). The numbering of atoms is shown in Fig. 2.

Distance	u Value (Å)	K Value (Å)	Distance	u Value (Å)	K Value (Å)
C_2-H_2	0.0792	0.0141	$X_1\cdots X_3$(a)	0.0743	0.0034
C_1-H_1'	0.0780	0.0230	$X_2\cdots X_3$(g)	0.1524	0.0051
C_1-H_1	0.0780	0.0226	$X_1\cdots H_3$(g)	0.1603	0.0107
C_3-H_3'	0.0780	0.0206	$X_3\cdots H_1'$(g)	0.1575	0.0119
C_1-C_2	0.0528	0.0045	$X_2\cdots H_1$(g)	0.1575	0.0140
C_2-C_3	0.0528	0.0043	$X_2\cdots H_3$(g)	0.1564	0.0098
C_2-X_2	0.0551	0.0054	$X_3\cdots H_3$(a)	0.1036	0.0095
C_1-X_1	0.0533	0.0143	$X_3\cdots H_3'$(a)	0.1030	0.0103
C_3-X_3	0.0534	0.0131	$C_3\cdots X_1$(g)	0.1480	0.0049
$C_2\cdots X_1$	0.0709	0.0081	$C_1\cdots X_3$(g)	0.1401	0.0060
$C_1\cdots X_3$	0.0707	0.0047	$X_1\cdots X_3$	0.2516	0.0012
$C_3\cdots H_1$	0.1079	0.0145	$H_3'\cdots X_1$	0.2387	0.0138
$C_1\cdots H_3$	0.1081	0.0092	$H_3\cdots X_1$	0.1625	0.0072
$C_1\cdots C_3$	0.0723	0.0039	$H_1'\cdots X_3$	0.2290	0.0177
$H_1\cdots X_1$	0.1071	0.0239	$H_1\cdots X_3$	0.1686	0.0086
$H_2\cdots X_2$	0.1079	0.0098	$H_1\cdots H_1'$	0.1265	0.0301

Table 8. Vibrational quantities in 1,2,3-trichloropropane at 63 °C.

Torsional force constants [a]			
$F_\phi(1-2)=F_\phi(2-3)=\overline{F}_\phi$, [mdyn Å (rad)$^{-2}$]	0.12	0.25	0.48
Torsional frequencies [b] for conformer (*4*), [cm^{-1}]	49 100	67 132	85 154
Ratios (q) between vibrational partitions functions [c] (Q) of conformers *1,2,3,4*			
$Q_4(0.25)/Q_3(\overline{F}_\phi)$	0.31	0.97	3.82
$Q_4(0.25)/Q_2(\overline{F}_\phi)$	0.36	1.14	4.51
$Q_4(0.25)/Q_1(\overline{F}_\phi)$	0.36	1.00	3.92
u Values [d] for the distance $X_1\cdots X_3$, (Å)			
In conformer *4*	0.346	0.259	0.207
In conformer *3*	0.262	0.173	0.146
In conformer *2*	0.261	0.171	0.144
In conformer *1*	0.105	0.105	0.104
u Value for the distance $X_2\cdots X_3$(gauche) in conformer *4*	0.194	0.159	0.140

[a] See also Table 5. [b] See also Table 6. [c] The Q value of a conformer is referred to the potential-energy minimum of that conformer. [d] See Table 7.

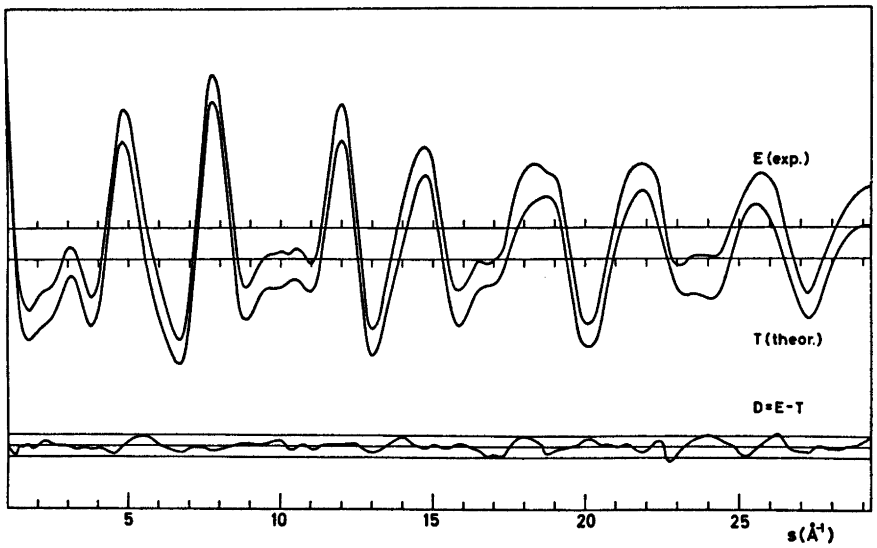

Fig. 3. Intensity curves for 1,2,3-trichloropropane at 63 °C. Curve E shows the experimental intensity, and curve T the theoretical intensity corresponding to the final least-squares parameters. Curve D is the experimental minus the theoretical. The straight lines give the experimental uncertainty (±3 × experimental standard deviation).

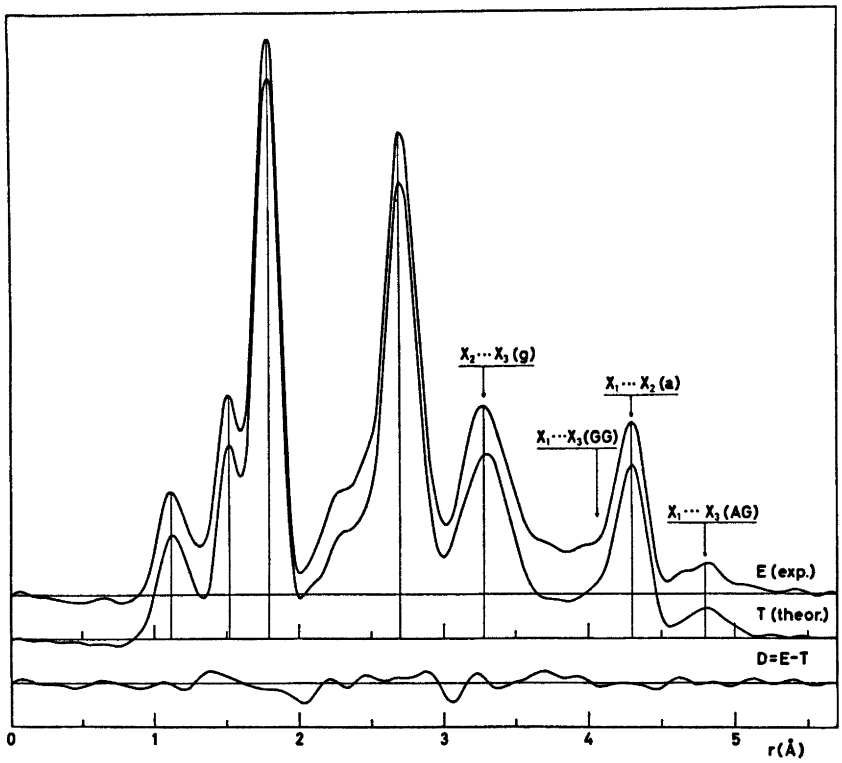

Fig. 4. Radial distribution curves for 1,2,3-trichloropropane at 63° C. Experimental (E) and theoretical (T) radial distribution curves and difference curve (D). The RD curves were calculated from the intensity curves of Fig. 3 with and artificial damping constant 0.0020 Å².

Nozzle-to-plate distance (mm)	500.0	250.0
Electron wavelength (Å)	0.05850	0.05850
Number of plates	6	6
Range of data, in s(Å^{-1})	1.00 – 15.50	2.25 – 29.25
Data interval, Δs(Å^{-1})	0.125	0.250
Uncertainty in s-scale (%)	0.14	0.14

The electron wavelength was determined by calibration against ZnO.

The data were reduced in the usual way [15] to yield an intensity curve for each plate. Average curves for each set of distances were formed. A composite curve was then made by connecting the two average curves after scaling.

The final experimental intensity curve is shown in Fig. 3. The intensities have been modified [15] by $s/|f_C'|\cdot|f_{Cl}'|$. Scattering amplitudes were calculated by the partial wave method [16] using Hartree-Fock atomic potentials.[17]

Radial distribution curves [15] corresponding to Fourier transformation of the final intensity curves are shown in Fig. 4.

V. STRUCTURE ANALYSIS

The conformational energies computed from the semi-empirical energy model (Sect. II) suggest that the relative amount of conformer *6* is negligible at 63 °C. Conformers *2* and *4* must be expected to be present in detectable amounts. The fact that *4* is the most abundant conformer, and not *2* as suggested by the calculated energies, is obvious from the radial distribution (RD) curves in Fig. 5. From the RD curves it also follows that conformer *1* can hardly be present in detectable amounts. Conformer *3* might be present but in small amounts. The energy calculations suggest that conformer *5* is not present in detectable amounts. In conclusion, it was decided to include the conformers *4*, *3*, and *2* in calculating the theoretical intensities. By trial and error, approximate values for the percentages (α) of the conformers were estimated from the experimental RD curve. ($\alpha_4 = 60-70$ %, $\alpha_3 = 0-10$ %, $\alpha_2 = 20-30$ %).

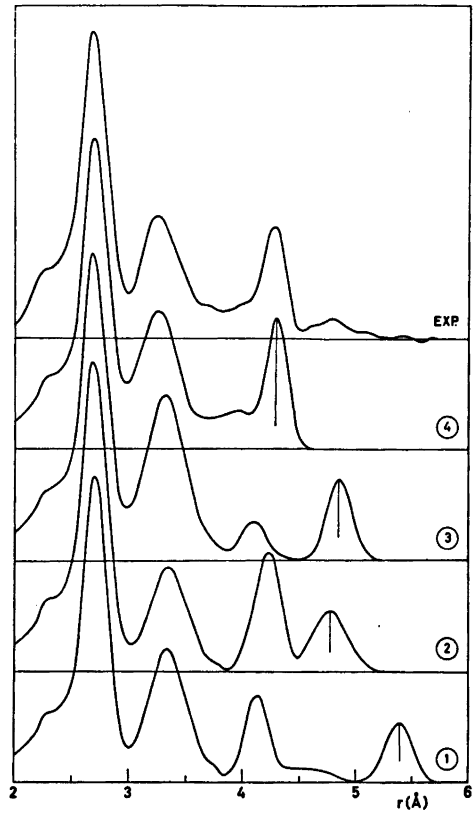

Fig. 5. Radial distribution curves for conformers of 1,2,3-trichloropropane at 63 °C. Theoretical RD curves of four conformers and the final experimental one are shown. The theoretical curves have been labelled in the same way as the conformers in Fig. 1. The artificial damping constant was equal to 0.0020 Å^2.

A. Least-squares refinements. The least-squares program, which is a modified version of the one explained in Ref. 15, was written by H. M. Seip. Several conformers can be included in the refinements with the present version of the program.

Models for the conformers were constructed with the following geometrical assumptions: (1) the plane of the $H_2C_2X_2$ group is perpendicular to the plane of the C atoms and bisect the CCC angle; (2) the two $C-CH_2X$ groups are equal; (3) the $C-CH_2X$ groups possess C_s symmetry and, the projection of $\angle H_1C_1H_1$ on the plane perpendicular to the C_1-C_2 axis is 120°; (4) all C–H bond lengths are equal; (5) all C–X bond lengths are equal; (6) the conformers have

identical structures except for the C−C torsion angles (ϕ); see Fig. 1.

The last assumption is partly justified by the results of Table 1, remembering that the conformers AA(gg), GG(aa), and GG(gg) are not present in detectable amounts.

Models were defined in terms of the following parameters: r(C−H), r(C−C), r(C−X), ∠CCC, ∠C_2CX, ∠CC_2X, ∠C_2CH, ∠CC_2H, and the two torsion angles ϕ_{1-2} and ϕ_{2-3}. The torsion angles of the conformers were refined, but not all of them independently. Also adjusted were the composition parameters (α_4, α_3, and α_2), the percentages of the conformers *4*, *3*, and *2*. It was assumed that $\alpha_1=\alpha_5=\alpha_6=0$ %.

Corrections for the "Bastiansen-Morino" shrinkage [18] effect on non-bonded distances have been included; non-bonded distances were computed as dependent parameters, restricted under the constraints of geometrically consistent r_α parameters.[19,20]

B. Determination of torsional force constants. Torsional force constants were not known for TCP, however, some of the mean amplitudes of vibration (u) get considerable contribution from the torsional modes. (Torsional modes also contribute substantially to some of the K values.) Therefore, since a reasonable force field is known, except for the torsional force constants, the latter can be adjusted to fit the experimental intensities. This procedure worked out well in the case of TBP.[4]

Determination of all torsional force constants from the electron diffraction data alone, is not possible. Therefore, the theoretical values of Table 4 were used as a guide, and the following assumptions were introduced:

(1) all interaction constants $F_\phi(1-2, 2-3)=0$;
(2) $F_\phi=F_\phi$(calc.)$+\Delta F_\phi$ for all conformers.

Thus, the differences between the diagonal force constants are those of Table 4. ΔF_ϕ was adjusted, as follows. Parallel and perpendicular amplitudes corresponding to several values of ΔF_ϕ were computed and included in the least-squares refinements. The structures and composition parameters were refined simultaneously for each new value of ΔF_ϕ. The best fit between theoretical and experimental intensities was obtained for ΔF_ϕ equal to $+0.023$ mdyn Å (rad)$^{-2}$. The final values of the torsional force constants are shown in Table 5.

It is difficult to estimate realistic uncertainties in the F_ϕ values.[4] The differences between the force constants have not been varied, only the parameter ΔF_ϕ was adjusted. Moreover, systematic errors in the remainder of the force field will certainly lead to systematic errors in the F_ϕ values as determined here. The values of the force constants F(CCC) and F(CCX) seem to be the critical ones in this respect, but their values are probably close to the correct values for TCP (see Table 6).

In conclusion, the most probable range for the torsional force constants is: 0.2 − 0.3 mdyn Å (rad)$^{-2}$. The values of F_ϕ (0.19 − 0.27) predicted by the semi-empirical model (Table 4) are therefore not unlikely.

VI. FINAL RESULTS

Parameters from the least-squares refinements and standard deviations (σ) corrected for correlation [21] in the experimental data are given. In the final refinements all intensities were given equal weights.

Non-bonded distances were restricted under the geometrical constraints of r_α parameters, by including correction terms $D=r_\alpha-r_a$ ($D=(u^2/r)-K$) for all internuclear distances.

Table 9. Bond lengths (r_a) and bond angles (∠$_\alpha$) *in 1,2,3-trichloropropane (X=Cl).* Standard deviations are given in parentheses.

Bond lengths (Å)	Bond angles (°)
r(C−H) = 1.131(11) [a]	∠CCC = 115.2(1.3) [b]
	∠C_2CX = 110.7(1.2)
r(C−C) = 1.524(4)	∠CC_2X = 110.4(1.1)
	∠C_2CH = 110.8(3.5) [c]
r(C−X) = 1.790(2)	∠CC_2H = 107.0(4.4) [c]

[a] An experiment with CO_2 gave a correction of 0.1 % in the s-scale. The bond lengths are therefore 0.1 % longer than those directly determined by the refinements. The uncertainty (0.14 %) in the s-scale has been included in the standard deviations of bond lengths. [b] The bond angles are those of the selfconsistent r_α structure. The *dependent* bond angles are ∠XC_1H = 108.2°(2), ∠HC_1H = 108.1°(5), and ∠XC_2H = 106.4°(2). [c] These values are the results of a refinement with ϕ angles, ∠CCC, ∠C_2CX, ∠CC_2X, and u values of nonbonded distances not refined.
Parameter correlation (ϱ), with $|\varrho|>0.49$:
$\varrho(CC_2X/C_2CX) = -0.99$; $\varrho(CC_2H/C_2CH) = -0.84$

Table 10. Torsion angles (ϕ) and composition (63 °C) parameters (α) of 1,2,3-trichloropropane. Standard deviations are given in parentheses.

Conformer	*2*	*3*	*4*
α	26 % (2)[a]	5 %(4)	69 %(3)[a]
	GA(ag)	AG(gg)	GG(ag)
ϕ_{1-2}	$102.2° = (110.9° - \phi_2)$	$(+14.4°)$	$116.8° = (119.0° - \phi_4)$
ϕ_{2-3}	$-17.2° = (-8.5° - \phi_2)$	$(+122.3°)$	$124.5° = (122.3° + \phi_4)$
	$\phi_2 = 8.7°(3)$[b]	–	$\phi_4 = 2.2°(2)$[b]

[a] The parameters α_2 and α_4 were refined with $\alpha_3 = 100\ \% - \alpha_2 - \alpha_4$. [b] The parameters ϕ_2 and ϕ_4 were refined but not simultaneously. The torsion angles of conformer (*3*) were taken from Table 1.
Parameter correlation (ϱ), with $|\varrho| > 0.49$:

$\varrho(\alpha_2/C_3CX) = -0.74$; $\varrho(\alpha_2/CC_2X) = 0.74$; $\varrho(\alpha_2/u_3) = 0.52$; $\varrho(\alpha_2 u_a) = 0.60$; $\varrho(\alpha_2/u_g) = -0.82$; $\varrho(\alpha_2/u_{13}') = -0.63$; $\varrho(\alpha_2/u_{13}) = 0.77$ $u_3 = u(C_3 \cdots X)$; $u_a = u(X \cdots X$, anti); $u_{13}' = u(X_1 \cdots X_3)$ in conformer *2*; $u_{13} = u(X_1 \cdots X_3)$ in conformer *4*; $u_g = u(X \cdots X$, gauche).

Table 11. Mean amplitudes of vibration (u) at 63 °C for 1,2,3-trichloropropane.

Distance type	Approx. dist. (Å)	Refined u value (Å)	Standard[a] deviation	Calculated[b] u value (Å)
C–H	(1.13)	0.070	0.011	0.078
C–C	(1.52)	0.049	0.006	0.053
C–X	(1.79)	0.044	0.003	0.054
$C_3 \cdots X_1$	(2.72)	0.073	0.005	0.071
$C_1 \cdots X_3$	(2.71)	(0.073)[c]	(0.005)[c]	(0.071)
$H_1 \cdots X_1$	(2.38)	0.103	0.018	0.107
$H_2 \cdots X_3$	(2.36)	(0.104)[c]	(0.018)[c]	(0.108)
X···X (anti)				
in conformer *4*	(4.31)	0.069	0.009	0.074
in conformer *2*	(4.28)	(0.076)[c]	(0.009)[c]	0.081
X···X (gauche)				
in conformer *4*	(3.34)	0.145	0.010	0.152
in conformer *2*	(3.34)	(0.156)[c]	(0.010)[c]	0.163
$X_1 \cdots X_3$				
in conformer *4*	(4.06)	0.264	0.024	0.252
in conformer *2*	(4.76)	0.135	0.025	0.179

[a] The standard deviations are those from the least-squares refinements. [b] The valence force constants are given in Table 5. [c] This value was refined together with the previous value as *one* parameter.
Parameter correlations (ϱ), with $|\varrho| > 0.8$:

$\varrho(u_g/C_3CX) = 0.88$; $\varrho(u_g/CC_2X) = -0.86$; $u_g = u(X \cdots X$, gauche); $\varrho(u_{13}/C_3CX) = -0.91$; $\varrho(u_{13}/CC_2X) = 0.89$; $u_{13} = u(X_1 \cdots X_3)$ in conformer *4*; $\varrho(u_{13}/u_g) = -0.94$; $\varrho(u_{13}'/u_{13}) = -0.81$; $u_{13}' = u(X_1 \cdots X_3)$ in conformer *2*.

Parameter correlation [15] coefficients (ϱ) are included in Tables 9–11. The average bond lengths and bond angles are found in Table 9.

Several refinements were carried out in order to determine the torsion angles (ϕ), not all of them being successful. Finally, the angles were restricted under constraints which are shown together with the values in Table 10. Two parameters, ϕ_2 and ϕ_4 were adjusted, and their meaning is understood when comparing Fig. 1 with the relations in Table 10. The parameters ϕ_2 and ϕ_4 measure the deviations from values predicted by the semiempirical model. For conformer *3*, the calculated ϕ values were assumed.

The refined ϕ values and those calculated for conformer *4* are not significantly different. [$\phi_4 = 2.2°$ and $\sigma(\phi_4) = 2°$]. The value of ϕ_2 is significantly different from 0°. The torsion angles of both conformers are different from exact staggered values, but the deviations within conformer *4* are quite small.

Composition parameters (α) from the least-squares refinements are given in Table 10. The conformers *4* and *2* are clearly present in significant amounts, but the low percentage (5 %) of conformer *3* is not significantly different from zero. [$\sigma(\alpha_3) = 4$ %.] The presence of a small percentage of conformer *1* could not be disproved by including that conformer in the refinements. Contributions (α_1) of conformer *1* were included in the least-squares refinements. The parameter α_1 was adjusted, with $\alpha_4 = 69\ \% - 0.5\alpha_1$, $\alpha_3 = 5$ %, and $\alpha_2 = 26\ \% - 0.5\alpha_1$. Several values of α_1 from 0 % to 10 % was tried. The best fit was obtained with α_1 close to 0 %. A small percentage (0–5 %) of confomer *1* is possible; however, a large relative amount of *1* is ruled out.

Mean amplitudes (u) from least-squares refinements [15] and those determined by adjusting the torsional force constants (Sect. V-B) are compared in Table 11. The u values which are not found in Table 11 could not be refined as individual parameters, but their values have been adjusted in adjusting the torsional force constants. (Sect. V-B) These u values, and the corresponding K values, are found in Table 7.

The average relative deviation ($\Delta u/u$), between the two sets of u values is *ca.* 10 %, while the average relative uncertainty, (σ/u), of the refined u values is *ca.* 12 %. The mean amplitudes calculated with the final force constants seem the more reliable set of u values.

Cartesian coordinates for the conformers *4* and *2* together with the principal axes' moments of inertia are given in Table 12.

The intensities and radial distribution curves, corresponding to the final parameters, are found in Figs. 3 and 4, respectively.

VII. DISCUSSION

The percentages α^* and α of two conformers in equilibrium in the gas phase (C⇌C*) are related to the theoretical [22] expression [23] for the equilibrium constant, as given in eqn. (1):

$$\alpha^*/\alpha = (\mathrm{M}^*/\mathrm{M})(Q^*/Q)^{\mathrm{vib}} \exp(-\Delta E^{\mathrm{m}}/RT) \qquad (1)$$

The six *spectroscopically* distinguishable conformers (see Fig. 1) have been assigned a multiplicity M. The value of M is *one* for the conformers *1*, *5*, and *6*, and *two* for the conformers *2*, *3*, and *4*. Q^{vib} is the vibrational partition function [22,23] of a conformer referred to the potential-energy minimum of that conformer. (The classical [22,23] rotational partition functions of the conformers are approximately equal.) $\Delta E^{\mathrm{m}} = E^* - E$ is the potential-energy difference between conformer C* and C, and the difference is measured between energy minima. The zeo-point vibrational energy is included in the quantity Q^{vib}. R and T have their usual thermodynamic meanings.

If the ratio (q) between Q^{vib} values are known, then the quantity ΔE^{m} may be computed from eqn. (1). Conversely, if the quantity ΔE^{m} is known, then the q values may be calculated from eqn. (1).

According to the semi-empirical energy model (Table 2), *2* is the conformer of lowest minimum energy. If the ΔE^{m} values of Table 2 are accepted, then the ratios between the vibrational partition functions of the conformers have to be quite different from 1.0, as shown in Table 13 (I). On the other hand, if the conformers have equal vibrational partition functions ($q = 1$), the ΔE^{m} values of Table 13 (II) show that *4* is the conformer of lowest minimum energy.

In order to explain the experimental composition (Table 10), two possibilities have to be considered: (I) the conformational energies

Table 12. Cartesian coordinates (Å) for the most abundant conformers of 1,2,3-trichloropropane. The coordinates have been calculated using the final $\angle_\alpha$ values for angles and r_g values ($r_g = r_a + u^2/r$) for bond lengths: (C–H: 1.137 Å, C–C: 1.526 Å, C–Cl: 1.792 Å). The numbering of atoms in the conformer GG(ag) is shown in Fig. 2. The principal axes' moments of inertia (amu Å²) are:

$I_A = 255.1$, $I_B = 398.4$, and $I_C = 585.5$ for *4*:GG(ag)
$I_A = 183.0$, $I_B = 501.0$, and $I_C = 610.8$ for *3*: AG(gg)
$I_A = 236.1$, $I_B = 484.0$, and $I_C = 682.9$ for *2*:GA(ag)
$I_A = 139.7$, $I_B = 593.1$, and $I_C = 682.2$ for 1:AA(gg)

4, conformer GG(ag)			Atom	*2*, conformer GA(ag)		
x	*y*	*z*	No.	*x*	*y*	*z*
0	0	0	C_3	0	0	0
1.2884	0.8177	0	C_1	1.2884	0.8177	0
1.4183	1.7952	−1.4963	X_1	1.6335	1.4562	−1.6385
1.3174	1.5255	0.8894	H_1'	1.2074	1.6989	0.7140
2.1980	0.1380	0.0594	H_1	2.1716	0.1795	0.3249
−1.2884	0.8177	0	C_2	−1.2884	0.8177	0
−1.3145	1.9587	1.3815	X_3	−2.6813	−0.1949	−0.4957
−1.3841	1.4204	−0.9593	H_3'	−1.5031	1.2328	1.0365
−2.1971	0.1393	0.0834	H_3	−1.2114	1.6925	−0.7222
0	−1.1656	1.3611	X_2	0	−1.1656	1.3611
0	−0.6204	−0.9528	H_2	0	−0.6204	−0.9528

Table 13. Energy differences, ΔE^m(kcal/mol), and ratios (q) between vibrational partition functions of the conformers *4*, *3*, and *2* of 1,2,3-trichloropropane at 63 °C.

Difference(−) or ratio(/)	(*4*) (*3*)	(*4*) (*2*)	(*3*) (*2*)
ΔE^m (calc.)[a]; see Table 2	−0.52	+0.44	+0.96
(I) Ratio (q)[b] between vibrational partition functions; if ΔE^m (calc.) values are used	6.1	5.0	0.82
(II) ΔE^m Values[c]; if $q = 1$	−1.75	−0.65	+1.10

[a] ΔE^m (calc.) is the conformational-energy difference (between energy minima) predicted by the semi-empirical model (Sect. II). [b] $q = (Q^*/Q)^{vib}$, calculated according to eqn. (1). Q^{vib} is the vibrational partition function of a conformer referred to the energy minimum of that conformer. [c] Calculated according to eqn. (1). The nozzle temperature (63 °C) and the composition parameters (α) of Table 10 were used.

(ΔE^m) predicted by the semi-empirical calculations are approximately correct, but conformer *4* has a much lower zero-point vibrational energy than the conformers *2* and *3*; (II) the conformers have approximately equal zero-point vibrational energies ($q \simeq 1$), but then the ΔE^m values have to be quite different from those predicted by the semi-empirical model.

The conformational force fields have to be very different for the first (I) possibility to be correct. Is there any additional experimental evidence that can support this point? Vibrational spectroscopy, at present, can not prove or disprove this possibility since a complete set of fundamental experimental frequencies [8] does not exist. From the values of Table 8 it is concluded that large differences in torsional force constants between the conformers may lead to q values as large as 5–6. Although such large differences are possible, it seems not very likely for a molecule like TCP. Large differences within the remainder of the conformational force fields are not ruled out, but that seems even less likely. An indication of conformer *2* having much larger torsional force constants than conformer *4* is found in Table 11. The refined mean amplitude of vibration (u) of the distance $X_1 \cdots X_3$ in conformer *2* is much lower

(0.135 Å) than the value (0.179 Å) corresponding to nearly equal torsional force constants. In order to obtain a value as low as 0.135 Å, the torsional force constants of conformer *2* would have to be larger than 0.5 mdyn Å (rad)$^{-2}$, which seems very unlikely. Unfortunately, this u value and the corresponding one for conformer *4* are very uncertain quantities. (The difference between 0.179 Å and 0.135 Å is less than *two* standard deviations.) In conclusion, the first possibility seems unlikely, but the second possibility is not proved thereby. The correct values of ΔE^{m} are probably a compromise between the two sets I and II.

Although the conformational energies predicted by the semi-empirical model seem unlikely, the structure parameters and torsional force constants generally agree with the experimental results.

It has been demonstrated that torsional force constants of TCP can be estimated from the information of the electron diffraction data, if the remainder of the force field is known. The most probable range for the torsional force constants is: 0.2 – 0.3 mdyn Å (rad)$^{-2}$. Values outside this range are less likely. For conformer *4* the average torsional force constant ($\overline{F}_{\phi}$) and the torsional frequencies (ω_1 and ω_2) are:

$$\overline{F}_{\phi} = 0.25^{+0.20}_{-0.10} \text{ mdyn Å (rad)}^{-2},$$
$$\omega_1 = 67 \pm 15 \text{ cm}^{-1}$$

and $\omega_2 = 132 \pm 20$ cm^{-1} (see also Sect. V-B). It has already been pointed out that the low frequencies of 1,2,3-trihalopropanes derived from the electron diffraction data are in good agreement with the spectroscopically observed values, (Table 6) for TCP, while a new assignment has been proposed for TBP.[4] The values of F_{ϕ} predicted by the semi-empirical energy model (Table 4) are not significantly different from those derived from the information of the electron diffraction data.

The electron diffraction studies of 1,2,3-trihalopropanes have lead to several conclusions relevant to the spectroscopic investigations of these and similar compounds: (1) the wrong spectroscopic conclusion,[6] listing conformer *2* as the most abundant one in TCP, has been corrected; (2) the empirical C-halogen group-frequency correlations break down [8] for TCP and TBP; (3) low torsional frequencies (50 – 150 cm^{-1}) in the most abundant conformers are available from the electron diffraction data of the gas phase; (4) the final adjustment of force constants ought to take into account the information derived from electron diffraction data.

Clearly, *4* is the most abundant conformer in both TCP and TBP.[4] The conformer *4*, in both compounds, is nearly staggered. The CCC angles (115 – 118°) are significantly larger than that of propane, while the C – C bond lengths (*ca.* 1.53 Å) are not significantly different from the one in propane itself. In conclusion, the large Cl and Br atoms, when substituted in the 1,2,3-positions, lead to a rather large increase of the CCC bond angle, while the terminal groups remain nearly staggered.

Note added in proof: A recent analysis [24] of the NMR spectra of $XH_2C-CHX-CH_2X$ (X = Cl, Br) in the liquid phase leads to conformational distributions which agree with the gas-phase distributions.

Acknowledgements. We are grateful to K. Brendhaugen for recording the diffraction photographs, and to Prof. O. Bastiansen, Prof. S. J. Cyvin, Prof. J. Dale, Cand. real O. H. Ellestad, Dr. A. Haaland, and Dr. P. Klæboe for helpful discussions. Computer programs made available by Dr. H. M. Seip, Prof. W. D. Gwinn, and Cand. real. S. Rustad have been extensively used in this work. Financial support from Norges almenvitenskapelige forskningsråd is gratefully acknowledged.

REFERENCES

1. Sheppard, N. *J. Mol. Struct. 6* (1970) 5.
2. Bastiansen, O., Seip, H. M. and Boggs, J. E. In Dunitz, J. D. and Ibers, J. A., Eds., *Perspectives in Structural Chemistry*, Vol. IV, Wiley, New York 1971.
3. Seip, H. M. In Sim, G. A. and Sutton, L. E., Eds., *Molecular Structure by Diffraction Methods*, Specialist Periodical Reports, The Chemical Society, London 1973, Vol. 1, Part 1, Chapter 1.
4. Stølevik, R. *Acta Chem. Scand. A 28* (1974) 299.
5. Bishui, B. M. *Indian J. Phys. 27* (1953) 89.
6. Dempster, A. B., Price, K. and Sheppard, N. *Spectrochim. Acta A 25* (1969) 1381.
7. Dempster, A. B., Price, K. and Sheppared, N. *Spectrochim. Acta A 27* (1971) 1579.
8. Thorbjørnsrud, J., Ellestad, O. H., Klæboe, P. and Torgrimsen, T. *J. Mol. Struct. 17* (1973) 5.
9. Abraham, R. J. and Parry, K. J. *J. Chem. Soc. B* (1970) 539.

10. Schachtschneider, J. H. and Snyder, R. G. *Vibrational Analysis of Polyatomic Molecules. IV*, (Force Constants for the Haloparaffins) Project No. 31450, Technical Report No. 122–63 of Shell Development Company.
11. Gwinn, W. D. *J. Chem. Phys. 55* (1971) 477.
12. Stølevik, R., Seip, H. M. and Cyvin, S. J. *Chem. Phys. Lett. 15* (1972) 263.
13. Zeil, W., Haase, J. and Wegmann, L. *Z. Instrumentenk. 74* (1966) 84.
14. Bastiansen, O., Graber, R. and Wegmann, L. *Balzer's High Vacuum Report 25* (1969) 1.
15. Andersen, B., Seip, H. M., Strand, T. G. and Stølevik, R. *Acta Chem. Scand. 23* (1969) 3224.
16. Peacher, J. and Willis, J. C. *J. Chem. Phys. 46* (1967) 4809.
17. Strand, T. G. and Bonham, R. A. *J. Chem. Phys. 40* (1964) 1686.
18. Almenningen, A., Bastiansen, O. and Munthe-Kaas, T. *Acta Chem. Scand. 10* (1956) 261.
19. Morino, Y., Kuchitsu, K. and Oka, T. *J. Chem. Phys. 36* (1962) 1108.
20. Kuchitsu, K. *J. Chem. Phys. 49* (1968) 4456.
21. Seip, H. M. and Stølevik, R. In Cyvin, S. J., Ed., *Molecular Structures and Vibrations*, Elsevier, Amsterdam 1972, p. 171.
22. Glasstone, S. *Theoretical Chemistry*, Van Nostrand, New York 1944.
23. Herzberg, G. *Infrared and Raman Spectra of Polyatomic Molecules*, Van Nostrand, Princeton, N. J. 1945.
24. Chenery, D. J., Dempster, A. B., Price, K. and Sheppard, N. *J. Mol. Struct. In press.*

Received April 1, 1974.

Acta Chemica Scandinavica A 28 (1974) 885—891

The Complex Formation in the Nickel(II)—Cyanide System

HANS PERSSON

Division of Physical Chemistry, Chemical Center, University of Lund, P.O.B. 740, S-220 07 Lund 7, Sweden

The formation of complexes in aqueous solution between nickel(II) ions and cyanide ions has been studied by potentiometric measurements with a glass electrode at 25.0 °C and ionic strength 3.0 M using sodium perchlorate as ionic medium. These measurements are best described if two mononuclear complexes, $NiCN^+$ and $Ni(CN)_4^{2-}$, are supposed to exist with the stability constants $\beta_1 = (1.08 \pm 0.4)10^7$ M^{-1} and $\beta_4 = (1.16 \pm 0.08)10^{31}$ M^{-4}, respectively (the errors given are three times the standard deviations). The presumptive complexes $Ni(CN)_2$ and $Ni(CN)_3^-$ were found to be so weak that the corresponding stability constants could not be determined. From the calculations approximate maximum values of β_2 and β_3 were estimated to 9×10^{13} M^{-2} and 1×10^{22} M^{-3}, respectively. There was no sign of any fifth or sixth mononuclear complex in the ligand range that was investigated. The conclusion that $Ni(CN)_6^{4-}$ is a very strong complex can definitely be discarded.

Protonated nickel cyanide complexes have been reported to dominate the complex formation at pH <5. In the present investigation no such complexes could be discovered although a careful analysis of potentiometric data in this pH-region was performed. Protonated nickel cyanide complexes, if they exist at all, must therefore be far weaker than suggested previously.[1]

The fourth mononuclear complex strongly dominates the complex formation, and the potentiometric measurements indicate a maximum amount of $NiCN^+$ of only (10 ± 4) %. Therefore spectrophotometric investigations were performed to verify the existence of the first complex. No positive evidence of $NiCN^+$ was obtained, however, indicating that the first complex is considerably weaker than suggested by the results from the potentiometric measurements. The value of β_1 given above may be regarded as a maximum value.

The complex formation in the nickel cyanide system has been subject to several investigations.[1-12,18,21,24,25] The publications on this topic reflect considerably varying opinions about which complex species are formed and about their strength. A common opinion is that a strong fourth mononuclear complex exists, but the reported magnitude of β_4 varies from 3.6×10^{13} M^{-4} (obtained by Masaki[3] from potentiometric measurements with a nickel electrode) to $\beta_4 = 1 \times 10^{30}$ M^{-4} (reported by Christensen *et al.*[4] from potentiometric measurements with a glass electrode).

No report of a complex $NiCN^+$ seems to have been made, and most authors have not discovered $Ni(CN)_2$ or $Ni(CN)_3^-$ in their investigations. Shibata *et al.*,[5] however, claim from paper electrophoresis measurements that $Ni(CN)_2$ and possibly $Ni(CN)_2H_2O^-$ exist.

Several authors have reported a continued complex formation beyond $Ni(CN)_4^{2-}$.[6-12] This hypothesis is supported by the colour change from yellow to red when increasing amounts of sodium cyanide are added to a solution containing sodium tetracyanonickelate(II). The existence of a fifth mononuclear nickel cyanide complex with $\beta_5/\beta_4 \approx 0.2$ seems to have been established with reasonable certainty. Penneman *et al.*,[10] for instance, conclude from IR measurements that when increasing amounts of sodium cyanide are added to a sodium tetracyanonickelate(II) solution the absorbance peak at 2124 cm^{-1} successively diminishes and a new peak at 2103 cm^{-1} is developed. This latter peak is ascribed to the formation of $Ni(CN)_5^{3-}$. A weak complex $Ni(CN)_6^{4-}$ is also reported. The structure of $Ni(CN)_4^{2-}$ is reported to be square planar[13] and that of $Ni(CN)_5^{3-}$ square pyramidal.[12]

From spectrophotometric measurements Coleman *et al.*[12] conclude that $Ni(CN)_5^{3-}$ exists but that the small effects observed in previous

measurements [10] and interpreted as $Ni(CN)_6^{4-}$ can in fact be ascribed to changes in the ionic medium. Blackie and Gould,[6] however, claim with the support of NMR investigations that while the fifth nickel cyanide complex is very weak, the sixth complex is so strong that $Ni(CN)_6^{4-}$ is formed quantitatively when sodium cyanide is added beyond a ratio of total cyanide to total nickel concentration of 4:1. The aim of the present investigation has not been to investigate nickel cyanide complexes beyond the fourth one. However, the statement of Blackie and Gould as to an extreme strength of $Ni(CN)_6^{4-}$ can be discarded. The present potentiometric measurements show that $\bar{n} = 4.0 \pm 0.1$ up to about a tenfold excess of cyanide. The results from the NMR investigations performed by Van Geet and Hume [11] are also contradictory to those obtained by Blackie and Gould.

Reasonable evidence for the formation of $Ni(CN)_5^{3-}$ has thus been presented. As pointed out by Coleman *et al.*,[12] however, efforts to isolate the corresponding salt from nickel(II) solution saturated with potassium cyanide result in $K_2Ni(CN)_4 \cdot nH_2O$ only.

Furthermore, an extensive formation of protonated complex species $HNi(CN)_4^-$, $H_2Ni(CN)_4$ and $H_3Ni(CN)_4^+$ is reported by Kolski and Margerum [1] from kinetic and equilibrium measurements. The magnitudes of the corresponding stability constants imply in fact that protonated nickel cyanide complexes should be the dominating species at $pH < 5$.

The conclusion from the reports hitherto produced on nickel cyanide complexes is that a very strong complex $Ni(CN)_4^{2-}$ definitely exists (with $\beta_4 \approx 10^{30}$ M^{-4}) and that reasonable evidence for the existence of a complex $Ni(CN)_5^{3-}$ (with $\beta_5 \approx 2 \times 10^{29}$ M^{-5}) has been produced. Since most authors have failed to discover the first three mononuclear complexes, these could be expected to be rather weak compared to the fourth complex. Christensen *et al.*,[4] for instance, observed no indication of other nickel cyanide complexes than $Ni(CN)_4^{2-}$. Their measurements comprise a rather small material, however, and only the region $1.1 \leq \bar{n} \leq 3.2$ has been studied. An investigation aiming to study the formation of the low complexes ought to be extended to the region $\bar{n} < 1$. Besides, the precision in their determination of β_4 is rather low. This fact together with the narrow $\bar{n}$-range examined could explain why contributions from the first three mononuclear complexes might be hidden in their results.

The present investigation was performed with two main aims, namely to study the formation of intermediate nickel cyanide complexes and the possible formation of acid nickel cyanide species. The potentiometric technique elaborated for the studies of the cyanide systems of zinc(II) and cadmium(II) [14] was used.

Further, supplementary spectrophotometric studies in the UV range were performed.

I. POTENTIOMETRIC MEASUREMENTS

Calculations of stability constants

A. Graphical calculations. The stability constants for the mononuclear nickel cyanide complexes were determined graphically from $\bar{n}$/[A] values as described previously[14].

B. Numerical calculations. Numerical calculations were performed employing the data program "LETAGROP ETITER" [15] to check possible formation of protonated nickel cyanide complexes.

C. To get a so realistic conception of the errors in the stability constants as possible, the $\bar{n}$,[A] data from the measurements were also treated numerically using a data program elaborated by Sandell.[16] In this program a weight for every experimental ($\bar{n}$,[A])-value is calculated from the errors estimated in emf and concentration. In all calculations the values of $pK_{a(HCN)} = 9.484 \pm 0.01$ and $pK_W = 14.184 \pm 0.002$ determined previously [14] were used. The computer UNIVAC 1108 in Lund was used for the numerical calculations.

Experimental

Chemicals. Perchloric acid, sodium perchlorate, and sodium cyanide were prepared as described in previous papers.[14,17] Nickel(II) perchlorate was prepared from nickel(II) carbonate (Bakers *p.a.*) and perchloric acid in slight excess. The concentration of nickel(II) was determined by adding excess EDTA and then titrating with a standardized lead(II) nitrate solution. The analysis was performed at $pH \approx 5.5$ using xylenolorange as indicator. The

concentration of the excess perchloric acid was measured by means of a potentiometric titration with standardized sodium hydroxide solution.

*Measurements.** Investigations of the nickel cyanide system are rendered difficult by several factors. (*i*) While $Ni(CN)_4^{2-}$ is formed rather quickly from nickel(II) ions and cyanide ions the dissociation of $Ni(CN)_4^{2-}$ in acid solution is a slow process [1] and equilibrium is not established until after about 1 – 3 weeks. (*ii*) $Ni(CN)_2$ is only slightly soluble [18] and to avoid precipitation the measurements must be carried out at very low concentrations of nickel perchlorate. (*iii*) To minimize volatilization of HCN carefully closed vessels must be used. (*iv*) The cyanide is slowly decomposed by water according to Christensen *et al.*[4] (*v*) The complex formation occurs in a very narrow ligand range and a high precision in the addition of titrant is required.

The measurements were designed in the following way. The hydrogen ion concentration was determined in solutions obtained by adding a volume v of a solution T to a volume V_0 of a solution S.

$$S:\begin{cases} C_{MS} & Ni(ClO_4)_2 \\ C_{AS} & NaCN \\ C_{HS} & HClO_4 \\ 3M - 3C_{MS} - C_{AS} & NaClO_4 \end{cases}$$

$$T:\begin{cases} C_{AT} & NaCN \\ C_{HT} & HClO_4 \\ 3M - C_{AT} - C_{HT} & NaClO_4 \end{cases}$$

Two kinds of measurement series were performed, with $C_{AS}=0$ and $C_{AT}\neq 0$ or $C_{AS}\neq 0$ and $C_{AT}=0$. After addition of titrant the solutions were shaken at 25.0 °C for about a week and then the pH was measured for a portion of every solution. After another week in the thermostat the pH was measured again. If equilibrium had not been attained, the procedure was repeated once more. The pH was determined by measuring the emf of the following galvanic cell

Glass electrode | S + T | 3.00 M $NaClO_4$ |

10.0 mM NaCl
2.99 M $NaClO_4$ | Ag, AgCl

The emf was measured with an Orion digital voltmeter together with a Jena glass electrode U9201/21. This electrode was checked against a hydrogen electrode, and a consistency within 0.2 mV was found in the range $3 < -\log [H^+] < 9$. The glass electrode was calibrated in acetate buffers as described previously.[14] Every titration series was repeated at least once. The reproducibility of the measured emf in the titration series was in general within 1 mV.

* For further information about experimental details see Ref. 14.

Results

In Table 1 corresponding mean values of added volume of titrant and measured emf are collected.

The results from the graphical and numerical determinations of the stability constants are collected in Table 2. To check the possible existence of protonated nickel cyanide species, numerical calculations were made employing the data program "LETAGROP ETITER".[15] In all the least squares refinements C_H/C_A was used as error carrying variable. First an effort was made to fit the experimental data assuming $Ni(CN)_4^{2-}$ and $HNi(CN)_4^-$ to be the predominant complex species.[1] As starting values were chosen $\beta_4 = 1.2 \times 10^{31}$ M^{-4} (obtained graphically) and $\beta_{4H} = 3.3 \times 10^{36}$ M^{-5} (proposed by Kolski *et al.*[1]). The calculations gave $\beta_4 = (1.34 \pm 0.23)10^{31}$ M^{-1} and $\beta_{4H} = (1.2 \pm 2.2)10^{35}$ M^{-5}. (The errors are given as three times the standard deviations). The error in β_{4H} is thus larger than β_{4H} itself. A second calculation was performed postulating the existence of $NiCN^+$ in addition to $Ni(CN)_4^{2-}$ and $HNi(CN)_4^-$ and with a starting value of $\beta_1 = 1.0 \times 10^7$ M^{-1} according to the graphical determinations. The values of β_1, β_4, and β_{4H} were varied and the best fit was obtained with the following set of stability constants: $\beta_1 = (1.14 \pm 0.20)10^7$ M^{-1}, $\beta_4 = (1.18 \pm 0.08)10^{31}$ M^{-4} and $\beta_{4H} = 0$.

The description of the measurements in the second calculation was found to be much better than in the first one. Thus there is no indication of formation of acid nickel cyanide species.

A calculation was also performed using "LETAGROP ETITER" postulating only $Ni(CN)_4^{2-}$ to exist. From this calculation $\beta_4 = (1.32 \pm 0.22)10^{31}$ M^{-4} was obtained. The standard deviation (sig$y$) in the error carrying variable (C_H/C_A) was 28.5 compared to 10.5 when postulating both $NiCN^+$ and $Ni(CN)_4^{2-}$. The description of the potentiometric measurements is thus considerably improved if also a first complex is assumed to exist.

An estimation of the hydrolysis of the nickel aquo ion in the actual pH-range based upon reported hydrolysis constants [2] shows that this effect can be completely neglected in the present measurements.

The complex formation curve, $\bar{n}$, (log [A]), calculated from the stability constants β_1 and

Table 1. Corresponding values of added volume, v, of titrant and measured emf, E_H. $V_0 = 50.00$ ml.

	Series 1		Series 2		Series 3		Series 4	
E^0_H (mV)	519.5		519.5		520.3		−488.5	
C_{MS} (mM)	0.397		0.496		0.397		0.488	
C_{MT} (mM)	0		0		0		0	
C_{AS} (mM)	0		5.27		0		0	
C_{AT} (mM)	21.93		0		25.08		10.00	
C_{HS} (mM)	0.073		0.054		0.073		0.095	
C_{HT} (mM)	9.92		10.06		9.88		4.99	
	v ml	E_H mV	v ml	E_H mV	v ml	E_H mV	v ml	E_H mV
	1.000	220.5	16.16	209.6	0.500	215.9	0.800	−759.6
	2.000	226.5	16.36	231.2	0.700	215.8	1.000	−771.0
	3.000	231.0	16.56	239.8	1.300	220.5	1.200	−777.3
	3.300	231.0	16.95	247.5	1.600	223.0	1.400	−778.0
	3.600	232.1	17.45	249.8	2.300	225.3	1.600	−782.6
	4.000	232.1	17.94	253.2	2.600	226.8	1.800	−782.4
	4.600	232.0	18.44	255.8	3.000	227.5	2.600	−781.8
	5.000	229.4	18.97	259.6	3.300	228.7	2.900	−778.2
	5.300	232.6	20.00	263.7	3.600	228.1	3.200	−778.8
	5.600	231.9	20.50	265.4	4.300	227.5	3.500	−779.3
	6.000	230.7	21.00	267.1	4.600	226.5	4.100	−777.7
			21.50	269.2	5.000	222.2	5.000	−776.6
			22.01	270.0	5.300	215.2		
			22.51	271.0				
			22.98	273.9				
			23.48	274.9				
			23.97	276.3				
			26.50	290.6				

Table 2. Results from the calculations of stability constants for the nickel cyanide system (β_i in M^{-i}). The errors given in the numerical calculations are three times the standard deviations.

Calculation method	β_1	β_2	β_3	β_4
Graphical	$(1.0 \pm 0.2)10^7$	$< 9 \times 10^{13}$	$< 1 \times 10^{22}$	$(1.18 \pm 0.05)10^{31}$
Numerical; Letagrop [15]	$(1.14 \pm 0.2)10^7$	0	0	$(1.18 \pm 0.08)10^{31}$
Numerical; Sandell [16]	$(1.08 \pm 0.40)10^7$	0	0	$(1.16 \pm 0.08)10^{31}$

β_4 is drawn in Fig. 1, and in the same diagram some experimental values are plotted.

II. SPECTROPHOTOMETRIC MEASUREMENTS

According to the potentiometric measurements $NiCN^+$ exists to a rather small extent. With regard to the considerable difficulties encountered in these investigations it seemed important to check the existence of $NiCN^+$ with an independent method.

It is probable that $NiCN^+$ has an absorption spectrum different from that of $Ni(CN)_4^{2-}$.[19] So absorption spectra for nickel cyanide solutions were recorded in the wavelength region 210 – 360 nm with the aid of a Hitachi EPS-3T spectrophotometer and 1 cm quartz cells. In these solutions $\bar{n}$ was varied from 3.9 to 0.02 by altering the concentration of nickel perchlorate and sodium cyanide. The ionic strength was maintained constant = 3.00 M with the aid of $NaClO_4$. The absorptivities of nickel(II) ions, cyanide ions, and hydrogen

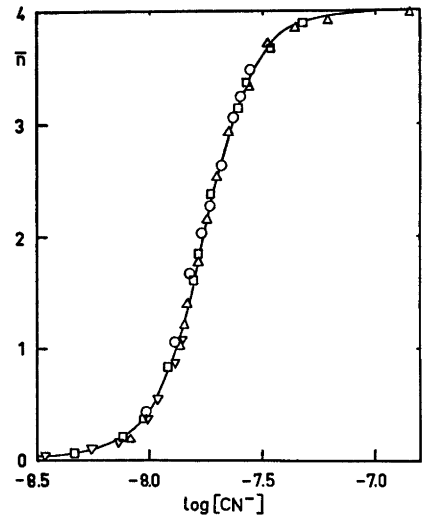

Fig. 1. The complex formation curve for the nickel cyanide system. The full-drawn curve represents $\bar{n}$ calculated from the stability constants. The experimental values of $\bar{n}$ are denoted by ○ (Series 1), △ (Series 2), □ (Series 3) and ▽ (Series 4) ([CN^-] in M).

cyanide, respectively, are negligible in the range 210 – 360 nm. $Ni(CN)_4^{2-}$ has three absorbance peaks in the wavelength region investigated, namely at 267, 285, and 310 nm in descending magnitude of height. The absorptivity at 267 nm for $Ni(CN)_4^{2-}$ was found to be about 1.1×10^4 M^{-1} cm^{-1}.

No wavelength displacements of the absorption peaks were observed when $\bar{n}$ was varied nor could any change in absorptivity be discovered. These facts can be interpreted in two ways: (i) $NiCN^+$ exists in much smaller concentrations than implied by the potentiometric measurements. (ii) $NiCN^+$ and $Ni(CN)_4^{2-}$ have very similar absorptivities per Ni – CN bond. In this case $NiCN^+$ may exist in high concentrations. As mentioned above, however, the spectrum of $NiCN^+$ can be expected to show much closer resemblances to the spectrum of the nickel aquo ion than to that of $Ni(CN)_4^{2-}$.[19] Thus interpretation (i) is by far the most probable.

(In some solutions the concentration of nickel was so large that a precipitate was formed. In the spectra, recorded on these solutions after filtering, a displacement of the peaks towards smaller wavelengths was observed. As the precipitation in the solution proceeded, however, the peaks and the displacements diminished and vanished after about a week. These displacements may possibly be explained by a slight colloidal precipitate).

In addition to the spectrophotometric investigations on nickel cyanide solutions at equilibrium a kinetic study of the acid hydrolysis of $Ni(CN)_4^{2-}$ in 0.10 M $HClO_4$ was made. Measurements on two different solutions were performed. In one solution the concentration ratio of total cyanide to total nickel was about 3.9 and in the other about 0.15. According to the results from the potentiometric measurements the complexed nickel should exist at the start almost entirely as $Ni(CN)_4^{2-}$ in the first solution but largely as $NiCN^+$ in the latter one. Perchloric acid was added to 0.10 M concentration and spectra were recorded with time intervals of about 5 min. The peaks diminished continuously but no wavelength displacements were observed. From measurements of the height of the peak at 267 nm as a function of time the first order dissociation constant, k_d, of $Ni(CN)_4^{2-}$ at $[H^+] = 0.10$ M was determined. For both solutions the same value of k_d was obtained within the limits of accuracy: $k_d = (6.0 \pm 1.0)10^{-4}$ s^{-1}. This coincidence further strengthens the assumption that β_1 is considerably less than the value obtained from the potentiometric measurements. Another, not very probable, explanation might be that the dissociation of $NiCN^+$ is the rate-determining step in the acid hydrolysis.

DISCUSSION

Formation of mononuclear nickel cyanide complexes. The nickel(II) – cyanide system shows an unusual course of complex formation in that a very strong complex, $Ni(CN)_4^{2-}$, is completely dominating.

The present potentiometric investigation indicates further the formation of small quantities of a complex $NiCN^+$ while the second and third complexes are so weak compared to $Ni(CN)_4^{2-}$ that they have not been detected (Estimated maximum values of $\beta_1 - \beta_3$ are given above).

The mathematical description of measurement data is thus significantly improved by assuming a first complex to be formed in

addition to $Ni(CN)_4^{2-}$. The maximum amount of $NiCN^+$ is so small, however, that the corresponding effect might easily be caused by a moderate systematic error. Therefore the supplementary spectrophotometric investigation was performed to decide, if possible, whether the presumptive formation of $NiCN^+$ could be confirmed. These measurements indicate that the first complex is even weaker than inferred from the results from the potentiometric measurements.

Different opinions concerning the fundamental reasons for the low stabilities of intermediate nickel cyanide complexes have been reported. Freund and Schneider [7] propose that these low stabilities depend on strains in the structures of possible intermediate species between a tetrahedral tetraaquonickel(II) ion and the square planar tetracyanonickelate(II) ion. This explanation seems rather improbable, however, since nickel(II) probably exists as a hexacoordinated octahedral water complex.[20] Thus the successive exchange of water molecules for cyanide ions should proceed without serious ruptures in the structure. Kolski and Margerum [1] suggest that the predominance of the fourth complex compared to the lower complexes is attributed to the transformation from weak octahedral complexes to a strong square planar complex.

From determinations of ΔC_p° for the cyanide systems of Zn(II), Cd(II), Hg(II), and Ni(II) Izatt *et al.*[21] draw the conclusion that the relative stabilities of species in a complex system depend strongly on temperature.

Formation of protonated nickel cyanide complexes. Kolski and Margerum [1] report an extensive formation of acid nickel cyanide species $H_xNi(CN)_4^{x-2}$ analogous to those reported for the iron(II) – cyanide system.[22] The reported value of K_{1H} implies that $[HNi[CN]_4^-]/[Ni(CN)_4^{2-}] = 2.5$ at pH = 5. The present potentiometric investigation has been performed at $4 < pH < 5.5$ and according to Kolski and Margerum protonated complexes should here dominate over the unprotonated. However, our measurements can be described with reasonable accuracy supposing only a fourth mononuclear complex, and with good accuracy if also a first mononuclear complex, is postulated. But our analyses of potentiometric data (*vide ultra*) give no support to presume any existence of protonated nickel cyanide species at equilibrium and certainly exclude a formation of acid complexes to the extent claimed by Kolski and Margerum.[1]

Nor do the results from the spectrophotometric measurements, where the dissociation of $Ni(CN)_4^{2-}$ in 0.1 M $HClO_4$ was followed, give any evidence for acid nickel cyanide species. A possible formation of species $H_xNi(CN)_4^{x-2}$ from $Ni(CN)_4^{2-}$ and H^+ must be expected to be very rapid. If the values of the equilibrium constants for formation of acid nickel cyanide species reported by Kolski *et al.*[1] are correct practically all $Ni(CN)_4^{2-}$ immediately would be converted to protonated complexes in acid solution. Now no change of the absorption spectrum in UV can be observed after addition of $HClO_4$. To explain this fact Kolski *et al.*[1] must suppose that the acid species has the same UV spectrum as $Ni(CN)_4^{2-}$. However, it seems probable that addition of a strongly polarizing ion such as H^+ to the tetracyanonickelate(II) ion would affect the energy levels of this ion and thereby change its spectrum.

Since we have not been able to find those protonated species, which are fundamental parts of the kinetic model proposed by Kolski and Margerum for the acid dissociation of $Ni(CN)_4^{2-}$, we have also investigated the kinetics thoroughly.[26] Also these measurements can be satisfactorily interpreted without supposing an extensive formation of protonated tetracyanonickelate(II) species.

The cyanide systems of nickel(II), cobolt(II), and iron(II) show interesting resemblances in that intermediate species expose low stabilities compared to a higher complex which entirely dominates the complex formation. A regular trend in the coordination number for the most stable complex in these systems can be noticed. In the nickel(II) system the fourth complex is the most stable one, while a fifth complex is reported to be formed only at high concentration of cyanide ion. The fifth complex is reported to dominate in the cobolt(II) – cyanide system [23] and the sixth complex is entirely dominating in the iron(II) cyanide system.[2]

Acknowledgements. I express my gratitude to Professor Ido Leden for valuable discussions and to Fil.kand. Margareta Stenström and Lab. ing. Bodil Jönsson for valuable assistance with the measurements.

REFERENCES

1. Kolski, G. B. and Margerum, D. W. *Inorg. Chem. 7* (1968) 2239.
2. Sillén, L. G. and Martell, A. E. *Stability Constants of Metal Ion Complexes*. The Chemical Society, London 1964.
3. Masaki, K. *Bull. Chem. Soc. Jap. 6* (1931) 233.
4. Christensen, J. J., Izatt, R. M., Hale, J. D., Pack, R. T. and Watt, G. D. *Inorg. Chem. 2* (1963) 337.
5. Shibata, N., Fujinaga, T., Yoshihara, K. and Kamchiku, Y. *Radiochim. Acta 5* (1966) 238.
6. Blackie, M. S. and Gould, V. *J. Chem. Soc.* (1959) 4033.
7. Freund, H. and Schneider, C. R. *J. Amer. Chem. Soc. 81* (1959) 4780.
8. Mc Cullough, R. J., Jones, L. H. and Penneman, R. A. *J. Inorg. Nucl. Chem. 13* (1960) 286.
9. Beck, M. T. and Bjerrum, J. *Acta Chem. Scand. 16* (1962) 2050.
10. Penneman, R. A., Bain, R., Gilbert, G., Jones, L. H., Nyholm, R. S. and Reddy, G. K. N. *J. Chem. Soc.* (1963) 2266.
11. Van Geet, A. L. and Hume, D. N. *Inorg. Chem. 3* (1964) 523.
12. Coleman, J. S., Petersen, H. and Penneman, R. A. *Inorg. Chem. 4* (1965) 135.
13. Vannerberg, N. G. *Acta Chem. Scand. 18* (1964) 2385.
14. Persson, H. *Acta Chem. Scand. 25* (1971) 543.
15. Arnek, R., Sillén, L. G. and Wahlberg, O. *Ark. Kemi 31* (1968) 353.
16. Sandell, A. *Acta Chem. Scand. 25* (1971) 2609.
17. Persson, H. *Acta Chem. Scand. 24* (1970) 3739.
18. Hume, D. H. and Kolthoff, I. M. *J. Amer. Chem. Soc. 72* (1950) 4423.
19. Jörgensen, C. K. *Absorption Spectra and Chemical Bonding in Complexes*, Pergamon, Oxford 1962, p. 109.
20. Nyholm, R. S. *Proc. Chem. Soc. London* (1961) 288.
21. Izatt, R. M., Johnston, H. D., Eatough, D. J., Hansen, J. W. and Christensen, J. J. *Thermochim. Acta 2* (1971) 77.
22. Jordan, J. and Ewing, G. J. *Inorg. Chem. 1* (1962) 587.
23. Adamson, A. W. *J. Amer. Chem. Soc. 73* (1951) 5710.
24. Griffith, W. P. *Quart. Rev. Chem. Soc. 16* (1962) 188.
25. Gray, H. B. and Ballhausen, C. J. *J. Amer. Chem. Soc. 85* (1963) 260.
26. Persson, H. *To be published.*

Received March 20, 1974.

Acta Chemica Scandinavica A 28 (1974) 892—896

The Reaction between $X(CN)_2$ (X = S, Se, and Te) and the Cyanide Ion in Acetonitrile. A Study of the Mechanism using Ionic ^{13}C Cyanide

TOR AUSTAD and STEINAR ESPERÅS

Chemical Institute, University of Bergen, N-5000 Bergen, Norway

Sulfur dicyanide and selenium dicyanide react quantitatively with ionic cyanide in acetonitrile in the mol ratio of 1:3 respectively, forming one mol of the corresponding pseudohalide ion and an unidentified product, probably having the composition $(C_4N_4)^{2-}$. Tellurium dicyanide reacts with excess ionic cyanide to give ionic tellurocyanate and presumably the same unidentified product through an intermediate step where elemental tellurium was separated.

Product analysis using ionic ^{13}C cyanide suggests the mechanism of the sulfur dicyanide-cyanide reaction to be a nucleophilic attack at the sulfur atom, followed by a fast pseudorotation prior to the decomposition of the intermediate. In the selenium dicyanide-cyanide reaction a fast exchange of the cyanide groups takes place prior to the decomposition of the intermediate.

The chalcogen dicyanides can be regarded as mixed pseudohalogens, (NC)(XCN) (X = S, Se, and Te), and they can be looked upon as ambident electrophiles. According to the HSAB terminology, the carbon atoms appear to be the harder electrophilic centres, while the chalcogen atoms are the soft ones. The softness of the chalcogen atoms increases in the order S < Se < Te.

The purpose of this paper is to discuss the reaction mechanism of the chalcogen dicyanide-cyanide reaction. Acetonitrile was chosen as the solvent because in this solvent tellurium dicyanide was found to be quite stable. Tetraphenylarsonium cyanide was used as the nucleophilic reagent.

Sulfur dicyanide and selenium dicyanide were found to react quantitatively with the cyanide ion in acetonitrile at room temperature in the mol ratio of 1:3. One mol of the corresponding pseudohalide ion was formed, and the second product (provided only one other product is formed) has to have the composition $(CN)_4^{2-}$ as shown by eqn. 1.

$$X(CN)_2 + 3CN^- \xrightarrow{MeCN} XCN^- + (CN)_4^{2-} \quad (1)$$

X = S and Se.

Isolation and characterisation of products other than tetraphenylarsonium thiocyanate (selenocyanate) proved to be most difficult. If, however, only two products are formed, as indicated by reaction (1), the anion $(CN)_4^{2-}$ might be the diiminosuccinonitrile dianion, $(DISN)^{2-}$. Diiminosuccinonitrile, DISN, has recently been isolated by Webster and co-workers [1] by base-catalyzed addition of hydrogen cyanide to cyanogen. It appears not unreasonable to assume that a dianion having the structure of the DISN molecule can exist in the aprotic solvent acetonitrile.

When one mol of $X(CN)_2$ (X = S and Se) was reacted with one mol of ionic cyanide, 1/3 mol of the pseudohalide ion was obtained. Supposing the first step of this reaction to be bimolecular, to give the pseudohalide ion and cyanogen, the second step, which might be the addition of 2 mol of cyanide ions to the cyanogen, is believed to be much faster. This is shown by eqns. (2) and (3).

$$X(CN)_2 + CN^- \xrightarrow[\text{Slow}]{MeCN} XCN^- + (CN)_2 \quad (2)$$

$$(CN)_2 + 2CN^- \xrightarrow[\text{fast}]{MeCN} (CN)_4^{2-} \quad (3)$$

X = S and Se.

Tellurium dicyanide reacted with ionic cyanide in a different way. A yellowish colour of the reaction mixture was first observed. After about 10 s elemental tellurium separated. When excess of ionic cyanide was used the tellurium went into solution again due to the formation of ionic tellurocyanate.[2]

The following two mechanisms may be possible (Schemes 1 and 2).

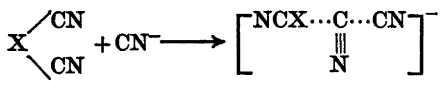

Scheme 1.

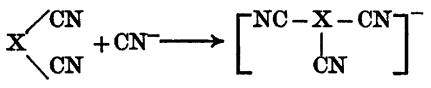

Scheme 2.

X = S and Se.

Scheme 1 involves a nucleophilic attack at one of the carbon atoms displacing the pseudohalide ion. Scheme 2 involves a nucleophilic attack at the chalcogen atom forming an activated intermediate $[X(CN)_3]^-$, which then decomposes to the pseudohalide ion and cyanogen. In both cases the cyanogen formed will add 2 mol of cyanide ions according to eqn. 3.

In order to verify which of these two possible mechanisms really takes place in the different chalcogen dicyanide-cyanide reactions, ionic ^{13}C cyanide was used as the nucleophile. The amounts of XCN^- and $X^{13}CN^-$ were measured using IR in the 2000 cm^{-1} region.[2] In acetonitrile the ^{13}C-pseudohalides were found to absorb about 50 cm^{-1} lower than did the corresponding ^{12}C-pseudohalides (Table 1). The sharp peaks were thus sufficiently apart for quantitative measurements. The extinction coefficients of $X^{13}CN^-$ and XCN^- were assumed to be equal.

Table 1. Some data for the reaction $XCN^- + {}^{13}CN^- \rightleftharpoons X^{13}CN^- + CN^-$ where X = S, Se, or Te in acetonitrile.

X	Rate, R M h^{-1}	$\nu(XCN^-)$ cm^{-1} [a]	$\nu(X^{13}CN^-)$ cm^{-1}
S	0	2059	2010
Se	1.6×10^{-4} [b]	2068	2022
Te	very fast	2081	2035

[a] Ref. 2. [b] Total rate of exchange at 40 °C.

No isotopic exchange occurs between the thiocyanate ion and the cyanide ion in aqueous solution,[12] and the same was found to apply in acetonitrile. Isotropic exchange between the selenocyanate ion and the cyanide ion does occur in water [13] and methanol.[14] The isotopic exchange in acetonitrile at 40 °C when applying $[SeCN^-]_0 = [{}^{13}CN^-]_0 = 8.00 \times 10^{-3}$ M was found to be very slow, having a half-life of 17 h. The yields of XCN^- and $X^{13}CN^-$ (X = S and Se) in the chalcogen dicyanide-cyanide reactions are thus not affected by isotopic exchange between the pseudohalide ion and the cyanide ion.

The exchange of cyanide between the tellurocyanate ion and ionic ^{13}C cyanide in acetonitrile was found to be very fast, and the rate could not be measured by the IR technique. Because of the separation of elemental tellurium in the tellurium dicyanide-cyanide reaction, isotopic experiments were not carried out on this reaction. The result in the other two reactions are shown in Table 2.

According to Table 2, a mechanism described by Scheme 1 may be rejected as a possible first step for the sulfur dicyanide-cyanide reaction. Such a mechanism will not give any ^{13}C thiocyanate at all. A reaction route proposed by Scheme 2 appears to be more consistent with the experimental data. Steric effects on divalent sulfur have been studied with nucleophiles bearing a negative charge, and a linear transition state might be favoured in this case.[3]

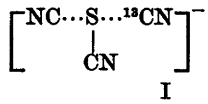

I

Table 2. Isotopic experiments on the reaction $X(CN)_2 + 3{}^{13}CN^- \rightarrow$ Products where X = S or Se in acetonitrile at room temperature.

X	Relative amounts $X^{13}CN^-$	XCN^-
S	1/3	2/3
Se	3/5	2/5

The bonding in the intermediate I might, according to Foss,[4] be looked upon as a linear three-center four-electron type. The structure of the trithiocyanate ion is presumably analogous to that of the triselenocyanate ion, which has a linear three-center four-electron bonding system.[4]

The ratio of $SCN^-/S^{13}CN^- = 2/1$ indicates that no exchange of the cyano groups takes place during the lifetime of the intermediate I. Furthermore, the product analysis indicates that the three cyano groups of the transition state are equivalent. The intermediate complex I then has to undergo a fast pseudorotation of the cyano groups before its decomposition to ionic thiocyanate and cyanogen. Presumably I is very unstable, due to the large *trans* effect commonly exerted by the cyano groups. The energy barrier of pseudorotation might then be low. The following reaction sequence can then be suggested for the sulfur dicyanide-cyanide reaction in acetonitrile.

$$S(CN)_2 + CN^- \xrightarrow{\text{slow}} \left[\begin{array}{c} NC-S-CN \\ | \\ CN \end{array}\right]^- \xrightarrow[\text{pseudorotation}]{\text{fast}} [S(CN)_3]^- \longrightarrow SCN^- + (CN)_2$$

all the cyano groups equivalent

According to the literature, nucleophilic substitution at sulfur dicyanide in most cases takes place at one of the carbon atoms.[5-7] Wilson and co-workers,[7] however, have shown that a nucleophilic attack by the thiocyanate ion takes place at the divalent sulfur atom of sulfur dicyanide in an acid aqueous solution.

Nor can the selenium dicyanide-cyanide reaction follow the mechanism depicted by Scheme 1. The results listed in Table 2 indicate that a fast exchange of the cyano groups of selenium dicyanide occurs. A statistical distribution of ^{12}C and ^{13}C cyanide will then apply in the intermediate selenium tricyanide anion, $[Se(CN)_3]^-$. Visually, the selenium dicyanide-cyanide reaction was observed not to take place in the same spontaneous way as the analogous sulfur dicyanide-cyanide reaction. No kinetic data concerning nucleophilic attack at divalent selenium are available in the literature. According to Foss,[4] structural evidence points to a linear transition state, with bonds of the three-center four-electron type. Due to the very fast exchange of the cyano groups, we cannot say whether pseudorotation in the intermediate, $[Se(CN)_3]^-$, takes place or not.

The following reaction scheme might then be suggested.

$$Se(CN)_2 + 3{*}CN^- \underset{\text{exchange}}{\overset{\text{Fast}}{\rightleftharpoons}} [Se(CN)_3]^- \quad {*}CN/CN = 3/2$$

$$\xrightarrow[\text{decomposition}]{\text{slow}} 2/5SeCN^- + 3/5Se{*}CN^- + (CN)_2$$

Hauge [8] has proposed that in the reaction of selenium dicyanide with selenocyanate ion to form the triselenocyanate ion, the first step is an attack by the selenocyanate ion at the selenium atom of selenium dicyanide to displace ionic cyanide. There are, as far as the authors know, no examples in the literature suggesting nucleophilic attack at the carbon atoms of selenium dicyanide.

With regard to the tellurium dicyanide-cyanide reaction, a nucleophilic attack by the cyanide ion at one of the carbon atoms would probably not lead to the precipitation of elemental tellurium. It appears more reasonable that the yellowish colour firstly observed is due to the tellurium tricyanide ion, $[Te(CN)_3]^-$, formed through a nucleophilic attack at the divalent tellurium atom. The large decrease in the strength of the chalcogen-carbon bond of the pseudohalides from sulfur to tellurium [2,9] may explain the separation of tellurium during the decomposition of $[Te(CN)_3]^-$. It appears reasonable to propose the following mechanism.

$$Te(CN)_2 + CN^- \longrightarrow \underset{\text{yellow}}{\left[\begin{array}{c} NC-Te-CN \\ | \\ CN \end{array}\right]^-}$$

$$\longrightarrow Te + CN^- + (CN)_2 \xrightarrow[CN^-]{\text{excess}}$$

$$TeCN^- + (CN)_4^{2-}$$

Stable salts of tellurium anions with bonds of the three-center four-electron type have recently been prepared.[10,11]

In the three reactions studied, the electrophilic centre of the chalcogen dicyanides towards the cyanide ion in acetonitrile thus appears to be the chalcogen atom. The experimental results further indicate that the relative stability of the chalcogen tricyanide intermediates is $[S(CN)_3]^- < [Se(CN)_3]^- < [Te(CN)_3]^-$. An intermediate complex of the type $[X(CN)_3]^-$ should be more stable in a dipolar aprotic solvent containing large onium cations than in a protic solvent.[9]

The reaction mechanisms outlined above are based on the assumption that cyanogen is formed as a result of decomposition of chalcogen tricyanide ions, $[X(CN)_3]^-$. The problem may be more complex, but attempts to explain the isotopic data when supposing the reaction to be second order in the cyanide ions were not successful.

EXPERIMENTAL

Acetonitrile and tetraphenylarsonium cyanide, Ph_4AsCN, were purified as reported.[2] $Ph_4As^{13}CN$ was prepared from $K^{13}CN$, British Company Oxygen Limited, and contained more than 90 % ^{13}C.

Sulfur dicyanide was prepared from sulfur dichloride and silver cyanide in carbon disulfide as reported by Long and Stelle.[15] Selenium dicyanide was prepared by the method of Hauge [8] from cyanogen bromide and potassium selenocyanate in diethyl ether. The product was finally sublimed in vacuum to remove traces of selenium diselenocyanate, $Se(SeCN)_2$. Tellurium dicyanide was prepared in 50 % yield from tellurium tetrabromide and freshly prepared silver cyanide in dry benzene according to the method of Cocksedge.[16] Sulfur dicyanide, selenium dicyanide and tellurium dicyanide were all stored in a refrigerator.

The chalcogen dicyanide-cyanide reactions. A solution containing 5.0×10^{-3} mol (0.420 g) of $S(CN)_2$ in 10 ml acetonitrile was added to a solution of Ph_4AsCN, made by dissolving 1.64×10^{-2} mol (7.0 g) of Ph_4AsCN in 50 ml acetonitrile. The reaction was slightly exothermic and the reaction mixture turned reddish, probably due to some polymerization products. After most of the solvent was removed in vacuum, the salts were precipitated by adding diethyl ether and were filtered off. The product was washed with 150 ml lukewarm acetone (40 °C). The salt of the thiocyanate ion and most of the red polycyanic compound dissolved in acetone. On standing in a refrigerator, some tetraphenylarsonium salt crystallized (about 0.4 g), which was added to the acetone-insoluble part. The acetone solution was evaporated to dryness, and the residue was washed with some ice-cold acetone to remove the red colour. Yield of Ph_4AsSCN, 2.0 g, or 91 % based on the amount of $S(CN)_2$ used. The tetraphenylarsonium thiocyanate was finally crystallized from warm acetonitrile.

The other product could not be isolated, due to its instability. This unidentified salt probably reacts with acetone to form a salt nearly insoluble in this solvent which facilitated the separation. The acetone-insoluble salt was not further studied.

The selenium dicyanide-cyanide reaction was performed in the same way as described for the sulfur dicyanide-cyanide reaction, and $Ph_4AsSeCN$ was isolated in 88 % yield based on the amount of $Se(CN)_2$ used. Tetraphenylarsonium selenocyanate was finally crystallized from warm acetonitrile.

The tellurium dicyanide-cyanide reaction was not studied in detail. When the reactants were mixed in the mol ratio of 1:1, a yellowish colour was first observed which lasted for about 10 s, then elemental tellurium separated. With excess cyanide ions (about 1:10), the precipitated tellurium reacted to give ionic tellurocyanate.[2]

The stoichiometry of the chalcogen dicyanide-cyanide reactions was determined by applying IR liquid cells measuring the amount of XCN^- formed.[2] The concentration of ionic cyanide was varied from one up to three times the concentrations of the chalcogen dicyanides. In all the reactions studied the concentration of XCN^- formed was exactly 1/3 of the cyanide concentration used.

Isotopic experiments. 1 ml of a 1.00×10^{-2} M solution of $S(CN)_2$ was added to a solution of 0.0137 g $Ph_4As^{13}CN$ dissolved in 1 ml acetonitrile (3.20×10^{-2} M). The solution turned instantaneously orange. The results from the product analysis are listed in Table 2.

The selenium dicyanide-^{13}C cyanide reaction was carried out by adding 1 ml of a 1.60×10^{-2} M solution of $Se(CN)_2$ to a solution of 0.0214 g $Ph_4As^{13}CN$ dissolved in 1 ml acetonitrile (5.00×10^{-2} M). The orange colour did not arise in the same instantaneous way as in the sulfur dicyanide-cyanide reaction. The yields of $SeCN^-$ and $Se^{13}CN^-$ are shown in Table 2.

The rate of isotopic exchange between $SeCN^-$ and $^{13}CN^-$ in acetonitrile was determined at 40 °C using $[SeCN^-]_0 = [^{13}CN^-] = 8.00 \times 10^{-3}$ M. The total rate of exchange, R, was evaluated by means of the equation [17]

$$\ln (1-F) = -Rt(a+b)/ab$$

where a and b are the concentrations of $SeCN^-$ and $^{13}CN^-$, respectively, t the reaction time and F the fractional exchange. The total rate constant was found to be $R = 1.6 \times 10^{-4}$ M h^{-1} (half-lifes about 17 h).

The IR measurements were performed on a Unicam SP 200 G Infrared Spectrophotometer applying 0.1 cm liquid cells.

Acknowledgement. One of the authors, T. Austad, is indebted to The Norwegian Research Council for Science and the Humanities for a grant.

REFERENCES

1. Webster, O. W., Hartter, D. R., Bergland, R. W., Sheppand, W. A. and Cairncross, A. *J. Org. Chem. 37* (1972) 4133.
2. Austad, T., Songstad, J. and Åse, K. *Acta Chem. Scand. 25* (1971) 331.
3. Fava, A. and Iliceto, A. *J. Amer. Chem. Soc. 80* (1958) 3478.
4. Foss, O. *Pure Appl. Chem. 24* (1970) 31.
5. Kitching, W., Smith, R. A. and Wilson, I. R. *Aust. J. Chem. 15* (1962) 211.
6. Kuhn, M. and Mecke, R. *Chem. Ber. 93* (1960) 618.
7. Kerr, D. F. and Wilson, I. R. *J. Chem. Soc. Dalton Trans.* (1973) 459.
8. Hauge, S. *Acta Chem. Scand. 25* (1971) 3081.
9. Songstad, J. and Stangeland, L. J. *Acta Chem. Scand. 24* (1970) 804.
10. Vikane, O. *Personal communication.*
11. Austad, T., Esperås, S. and Songstad, J. *Acta Chem. Scand. 27* (1973) 3594.
12. Adamson, A. W. and Magee, P. S. *J. Amer. Chem. Soc. 74* (1952) 1590.
13. Belluco, U., Bruno, M. and Schiavon, G. *Ric. Sci. 28* (1958) 963.
14. Belluco, U., Bruno, M. and Schiavon, G. *Ric. Sci. 28* (1958) 111.
15. Long, D. A. and Stelle, D. *Spectrochim. Acta 19* (1963) 1731.
16. Cocksedge, H. E. *J. Soc. Chem. Ind. (London) 93* (1908) 2175.
17. McKay, H. A. C. *J. Amer. Chem. Soc. 65* (1943) 702.

Received April 29, 1974.

Acta Chemica Scandinavica A 28 (1974) 897—902

Thermodynamics of Metal Complex Formation in Aqueous Solution. VII. Equilibrium and Enthalpy Measurements on the Nickel(II)—Selenocyanate System

LENNART KULLBERG

Inorganic Chemistry 1, Chemical Center, University of Lund, P.O. Box 740, S-220 07 Lund 7, Sweden

The stability constants and the enthalpy changes for the formation of nickel(II)—selenocyanate complexes in aqueous solution have been determined by means of a calorimetric titration method. The value of β_1 has also been determined spectrophotometrically. From the enthalpy changes measured, and the free energy changes computed from the stability constants, the entropy changes have been calculated. All data refer to 25.00 °C and an aqueous sodium perchlorate medium of ionic strength 1.00 M.

The selenocyanate complexes of nickel(II) are formed in more exothermic reactions than the thiocyanate complexes. This is more than compensated by the entropy terms, however, which are more negative for the selenocyanate system. On the balance, the thiocyanate complexes are therefore a little stronger than the selenocyanate ones.

In a previous paper [1] the changes of free energy, enthalpy and entropy accompanying the formation of selenocyanate complexes of zinc and cadmium have been determined and compared with the same quantities for the corresponding thiocyanate complexes. The changes of free energy, ΔG°_j, have been computed from the measured stability constants while the changes of enthalpy, ΔH°_j, have been measured calorimetrically. Finally, the changes of entropy, ΔS°_j, have been obtained from the relation

$$\Delta G^\circ_j = \Delta H^\circ_j - T\Delta S^\circ_j$$

Also the thiocyanate complexes of nickel(II) and copper(II) have been studied before.[2] It would evidently be of interest to extend the comparison by investigating the selenocyanate complexes of these two metal ions as well.

In this paper a calorimetric and spectrophotometric investigation of the nickel(II)—selenocyanate system is reported. The copper(II) system seems impossible to study as a brown precipitate is formed immediately upon addition of selenocyanate ions to a copper(II) solution. The precipitate most probably consists of a mixture of elemental selenium and copper(I) cyanide compounds.[3]

The nickel(II)—selenocyanate system has hitherto been little studied, probably because the complexes tend to decompose in aqueous solution. Golub and Skopenko [4] have spectrophotometrically demonstrated the existence of $NiSeCN^+$ in aqueous solution, however. They also found that the system is much more stable in non-aqueous solvents like methanol and acetone. The strength of the complexes increased in the sequence $H_2O <$ methanol $<$ acetone.

The disintegration in aqueous solution is rapid at high selenocyanate (and nickel) concentrations. It is presumably catalyzed by light. Thus, in the calorimetric measurements, performed in complete darkness, ligand concentrations, C_L, up to 150 mM could be used without perceptible decomposition while in the spectrophotometric measurements a disturbing decomposition occurred already at a $C_L = 100$ mM, even for moderate values of $C_M (\lesssim 10$ mM). In view of the weak complex formation only the first stability constant can be precisely determined. A reliable method for the determination of β_1 in such cases is the so called M-method.[5,6] which has been applied here. In this method,

C_M is varied while C_L is kept low and constant which allows the determination of the first complex without interference from the higher ones.

All measurements in this study have been carried out at 25.00 °C in an aqueous medium of an ionic strength $I = 1.00$ M with sodium perchlorate as supplementary electrolyte.

CALCULATIONS

Notation. The same notation is used as before.[3] For convenience, the most important definitions and formulas are collected below.

A = absorbance
l = sample path length
λ = wavelength
$a = A/l$
ε_M, ε_L, ε_j = the molar absorption coefficients of M and L and the complex ML_j.

$$a_M = \varepsilon_M C_M \quad (1)$$

$$a_L = \varepsilon_L C_L \quad (2)$$

Calculation from spectrophotometric measurements. Assuming C_L is kept so low that formation of complexes higher than ML can be neglected, the following relation can be deduced [5,6]

$$\frac{[M]C_L}{a - a_M - a_L} = \frac{1}{(\varepsilon_1 - \varepsilon_M - \varepsilon_L)\beta_1} + \frac{[M]}{(\varepsilon_1 - \varepsilon_M - \varepsilon_L)} \quad (3)$$

As the concentration of the complex ML is small compared to the concentration of the free metal ion it is allowed to put $[M] \approx C_M$ in the first approximation. By plotting the left member of eqn. (3) *vs.* C_M a first value of β_1 is then obtained. If necessary better values are then arrived at by successive approximations.

The calculation of β_1 has also been made by the least squares computer program "Letagrop Spefo" developed by Sillén and Warnqvist.[7] The input data are the total concentrations C_M and C_L and the absorption coefficients a of each solution. The error square sum to be minimized is

$$U_{rel} = \sum_i (a_{i,calc} - a_{i,exp})^2 (a_{i,exp})^{-2} \quad (4)$$

The calculation gives the stability constants, β_j, and the molar absorption coefficients of the species. The molar absorption coefficients ε_M and ε_L have been determined separately and regarded as known parameters during the calculations.

Calculation from calorimetric measurements. The equilibrium constants and the enthalpy changes have been calculated by the least squares computer program "Kalori".[8] With this program the computer searches for the set of values of unknown parameters $(\beta_j, \Delta H_j)$ which will minimize the error square sum

$$U(\beta_j, \Delta H_j) = \sum_i (Q_{i,calc} - Q_{i,corr})^2 \quad (5)$$

The input data are the corresponding values of Q_{corr}, initial volume, V_0, added volume, v, and the total concentrations of metal and ligand in the S and T solutions.

EXPERIMENTAL

Chemicals: Nickel perchlorate, sodium selenocyanate and *sodium perchlorate* were prepared and analyzed as described before.[3]

The spectrophotometric measurements at constant wavelength were made with a Zeiss PMQ II Spectrophotometer. Suitable wavelengths were selected by means of absorption spectra, recorded with a Hitachi Spectrophotometer. For several reasons, the measurements should preferably be performed at a wavelength where the absorption curve has a horizontal tangent. The complex solution has a relative maximum at about 400 nm (curve B, Fig. 1). Unfortunately, also the hydrated nickel(II) ion absorbs strongly in this region (curve A) which makes a precise determination of β_1 from measurements in this band impossible. At

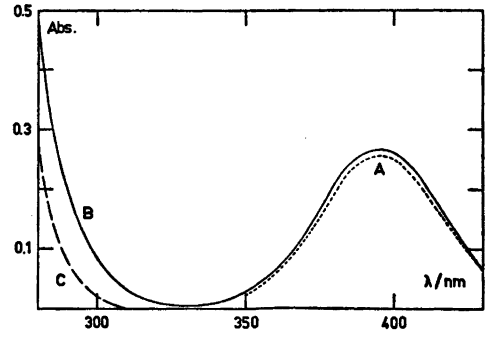

Fig. 1. Absorption curves of free nickel(II) ions, a complex nickel(II) selenocyanate solution and selenocyanate ions at 25 °C and at $I = 1.0$ M and a cell thickness of 1.00 cm.
A: 50 mM $Ni(ClO_4)_2$. B: 50 mM $Ni(ClO_4)_2$ + 10 mM NaSeCN. C: 10 mM NaSeCN.

lower wavelengths, the complex solution has a strong band starting at ≈320 nm while the absorption of the hydrated ion is negligible down to ≈250 nm. On the other hand, the absorption of $SeCN^-$ (curve C) is quite strong in this region. In the range $285 < \lambda < 305$ nm, however, the difference between curves B and C is relatively large while the absorption of the complex solution is large enough for a good determination. In this favourable range five different wavelengths *viz.* 285, 290, 295, 300, and 305 nm have been selected.

The solutions were made up in 25 cm³ measuring flasks from stock solutions of nickel(II) perchlorate, sodium selenocyanate, and sodium perchlorate. To minimize disturbances due to disintegration, they were measured immediately upon mixing against a blank containing 1.00 M $NaClO_4$.

All measurements were repeated at least three times. The solutions to be measured and the cell compartment of the spectrophotometer were thermostated at 25.0 ± 0.1 °C.

The calorimetric measurements. The calorimeter and the technique of measurement have been described previously.[9] In each series, the reaction vessel initially contained V_0 cm³ of a solution S and a titrant T was then added. The compositions of the solutions S and T are given in Table 3. In order to determine the corrections for the heats of dilution, series analogous to those of the main measurements were performed except that only one of the two reactants was present simultaneously. The heat equivalent of the calorimetric system, determined by electrical calibrations, was found to obey $\varepsilon_v = 2.317 + 0.0226(V - 100.0)$ for all solutions used.

MEASUREMENT AND RESULTS

Spectrophotometric measurements. The experimental data are collected in Table 1. The molar absorption coefficients for Ni^{2+}, ε_M, and for $SeCN^-$, ε_{I_r}, have been determined separately. For the wavelengths used ε_M is negligible. The values of ε_{I_r} can easily be obtained from the data given in Table 1. The first approximation, with $[M] \approx C_M$, results in a mean value of $\beta_1 = 9.4$ M⁻¹. With this value better values of [M] were calculated. The straight lines then obtained yielded final values of $(\varepsilon_1 - \varepsilon_M - \varepsilon_{I_r})$ and β_1, Table 2. The limit of error in the value of $\beta_1 = (10.0 \pm 0.7)$ M⁻¹ corresponds to 3σ. At the computer calculation with the least-squares program "Letagrop Spefo" the experimental data from all five wavelengths used could be treated simultaneously. From this calculation a value of $\beta_1 = (9.8 \pm 0.3)$ M⁻¹ was obtained, the error again corresponding to 3σ. The standard deviation, σ, for the differences between experimental

Table 1. Absorbances (cell length 2.000 cm) for the ligand concentrations $C_{I_r} = 10.00$ mM (A_{10}) and $C_{I_r} = 5.00$ mM (A_5).

C_M/mM	305 nm		300 nm		295 nm		290 nm		285 nm	
	A_{10}	A_5	A_{10}	A_5	A_{10}	A_5	A_{10}	A_5	A_{10}	A_5
0	0.051	0.026	0.090	0.045	0.165	0.083	0.306	0.153	0.566	0.283
20.0		0.059		0.098		0.163		0.273		0.450
40.0	0.167	0.082	0.275	0.136	0.447	0.223	0.717	0.357	1.126	0.562
60.0	0.202	0.101	0.335	0.168	0.538	0.271	0.847	0.427	1.298	0.654
80.0	0.229	0.115	0.380	0.191	0.610	0.307	0.950	0.479	1.440	0.726
100.0	0.253	0.127	0.420	0.211	0.670	0.337	1.036	0.523	1.544	0.787

Table 2. Constants obtained from the graphical evaluation of the spectrophotometric measurements.

λ/nm	305		300		295		290		285	
C_{I_r}/mM	10	5	10	5	10	5	10	5	10	5
$(\varepsilon_1 - \varepsilon_{I_r})$/cm⁻¹ M⁻¹ [a]	19.3	20.6	33.2	35.5	51.6	54.3	73.0	75.9	95.2	101.0
$\beta_1(\varepsilon_1 - \varepsilon_{I_r})$/cm⁻¹ M⁻²	217	202	343	316	516	489	762	735	1060	1020
β_1/M⁻¹	11.2	9.8	10.3	8.9	10.0	9.0	10.4	9.7	11.1	10.1
β_1(average)/M⁻¹					10.0 ± 0.7					

[a] $\varepsilon_M = 0$.

Table 3. Determination of the heats of formation for the nickel selenocyanate complexes. For all the series: $V_0 = 100.0$ cm³ and $V = (V_0 + v)$ cm³.

(a) ○ S: $C_M = 0.1000$ M, $C_{NaClO_4} = 0.700$ M. T: $C_L = 1.000$ M.

v/cm³, Q_{exp}/J, Q_{corr}/J, ΔQ_{corr}/J: 1.000, 6.135, 6.301, −0.112; 2.000, 5.841, 5.997, −0.065; 3.000, 5.555, 5.703, −0.019; 5.000, 10.306, 10.629, 0.037; 7.000, 9.462, 9.774, 0.026; 9.000, 8.724, 9.027, −0.008; 12.000, 11.812, 12.275, −0.040; 15.000, 10.417, 10.847, 0.043; 18.000, 9.302, 9.703, 0.038;

(b) □ S: $C_M = 0.0790$ M, $C_{NaClO_4} = 0.763$ M. T: $C_L = 1.000$ M.

v/cm³, Q_{exp}/J, Q_{corr}/J, ΔQ_{corr}/J: 1.000, 5.200, 5.366, 0.064; 2.000, 4.960, 5.116, 0.045; 3.000, 4.718, 4.865, 0.042; 5.000, 8.794, 9.117, −0.006; 7.000, 7.970, 8.281, −0.012; 9.000, 7.260, 7.563, −0.033; 12.000, 9.679, 10.142, −0.036; 15.000, 8.502, 8.932, −0.035; 18.000, 7.505, 7.905, −0.020;

(c) △ S: $C_M = 0.0500$ M, $C_{NaClO_4} = 0.850$ M. T: $C_L = 1.000$ M.

v/cm³, Q_{exp}/J, Q_{corr}/J, ΔQ_{corr}/J: 1.000, 3.895, 4.061, −0.009; 2.000, 3.623, 3.779, 0.009; 3.000, 3.353, 3.501, 0.047; 5.000, 6.082, 6.405, 0.058; 7.000, 5.405, 5.717, 0.025; 9.000, 4.816, 5.118, 0.022; 12.000, 6.304, 6.767, 0.014; 15.000, 5.402, 5.833, 0.036; 18.000, 4.663, 5.064, 0.061;

(d) ● S: $C_M = 0.0400$ M, $C_{NaClO_4} = 0.880$ M. T: $C_L = 1.000$ M.

v/cm³, Q_{exp}/J, Q_{corr}/J, ΔQ_{corr}/J: 1.000, 3.264, 3.430, 0.024; 2.000, 3.035, 3.191, 0.013; 3.000, 2.807, 2.955, 0.026;

(e) ■ S: $C_M = 0.0300$ M, $C_{NaClO_4} = 0.910$ M. T: $C_L = 1.000$ M.

v/cm³, Q_{exp}/J, Q_{corr}/J, ΔQ_{corr}/J: 1.000, 2.588, 2.754, 0.017; 2.000, 2.388, 2.544, 0.003; 3.000, 2.182, 2.330, 0.021; 5.000, 3.888, 4.211, −0.001; 7.000, 3.361, 3.673, −0.001; 9.000, 2.989, 3.291, −0.049; 12.000, 3.810, 4.273, −0.053; 15.000, 3.235, 3.665, −0.062; 18.000, 2.729, 3.130, −0.020;

(f) ▲ S: $C_M = 0.0200$ M, $C_{NaClO_4} = 0.940$ M. T: $C_L = 1.000$ M.

v/cm³, Q_{exp}/J, Q_{corr}/J, ΔQ_{corr}/J: 1.000, 1.898, 2.064, −0.079; 2.000, 1.724, 1.880, −0.076; 3.000, 1.541, 1.689, −0.038;

and calculated values of a was found to be 0.0022 which indicates a high precision in the measurements.

Calorimetric measurements. Six different titration series have been carried out, Table 3. In all of these, ligand has been added to a solution of the metal ion. In order to suppress the hydrolysis of nickel(II) [10] and to prevent the disintegration of the selenocyanate ion,[1] pH has to be carefully adjusted. The pH of the metal solutions was about 4.5 and that of the ligand solution 8 − 9. A value of $C_L = 140$ mM can be reached before decomposition is noticed. If, on the other hand, a nickel solution (of $C_M = 80$ mM) is added to a ligand solution (of $C_L = 100$ mM) a precipitation of selenium occurs already at the first addition.

It has been tried to fit the data to both two and three complexes. The β_j-values obtained in the two cases are listed in Table 4. As seen from the error square sum, U, a much better fit is achieved with three complexes than with two. As the concentration of the third complex will never amount to more than a few per cent of C_M only a very approximate value of β_3 emerges, implying that the determination of $\Delta H°_3$ becomes very hazardous.

The spectrophotometric and the calorimetric measurements give consistent β_1-values, Table 4. The spectrophotometric measurements are somewhat more precise and a value of $\beta_1 = 9.7$ M^{-1} should therefore be a reasonable choice. By keeping $\beta_1 = 9.7$ M^{-1} as a constant parameter values of β_2, β_3, and $\Delta H°_j$ have been recalculated from the calorimetric data by the program "Kalori". The values obtained, Table 4, are in line with those found previously. A set of β_j-values considered to be the 'best' one is proposed in Table 4. With this set, a final set of $\Delta H°_j$ has been computed by the program "Kalori". The low value of $\sigma Q_{corr} = 0.042$ J indicates a very good fit. The final values of β_j and the functions $\Delta G°_j$, $\Delta H°_j$, and $\Delta S°_j$, are collected in Table 5. In view of the large uncertainty of β_3 the thermodynamic functions of the third step are not given. It may be mentioned that with $\beta_3 = 70$ M^{-1} a value of $\Delta H°_3 \approx 0$ is obtained. In Fig. 2, Δh_v is plotted *versus* $\bar{n}$. The series coincide within the experimental errors which shows that no polynuclear complexes are formed. The fulldrawn curve is calculated from the final values of β_j and $\Delta H°_j$.

Table 4. Stability constants obtained from spectrophotometric and calorimetric measurements. The errors correspond to three standard deviations or to estimated errors.

Method	β_1/M^{-1}	β_2/M^{-2}	β_3/M^{-3}	U
Spectr., graphically	10.0 ± 0.7			
Spectr., by computer	9.8 ± 0.3			
Calorim., two complexes	9.1 ± 1.8	19 ± 9		0.318
Calorim., three complexes	9.4 ± 1.2	18 ± 12	~70	0.070
Calorim., β_1 fixed	(9.7)	16 ± 5	~80	0.071
Proposed values	9.7 ± 0.4	18 ± 5	70	0.073

Table 5. The stability constants and the values of $\Delta G°_j$, $\Delta H°_j$ and $\Delta S°_j$ for the stepwise reactions of the thiocyanate and selenocyanate systems of nickel(II). The data for the thiocyanate system are taken from Ref. 2. The errors given correspond to three standard deviations or to estimated errors.

Ligand		SCN⁻	SeCN⁻
β_j/M^{-j}	$j=1$	13.8 ± 0.5	9.7 ± 0.4
	2	38 ± 4	18 ± 5
	3	40 ± 15	
$-\Delta G°_j$ / kJ mol⁻¹	1	6.51 ± 0.10	5.63 ± 0.10
	2	2.51 ± 0.30	1.5 ± 0.8
	3	0.1 ± 0.9	
$-\Delta H°_j$ / kJ mol⁻¹	1	12.02 ± 0.15	12.8 ± 0.3
	2	8.9 ± 1.0	12 ± 3
	3	8.2 ± 4.0	
$\Delta S°_j$ / J mol⁻¹ K⁻¹	1	−18.5 ± 0.6	−24.1 ± 1.0
	2	−21.5 ± 3.5	−35 ± 11
	3	−27 ± 13	

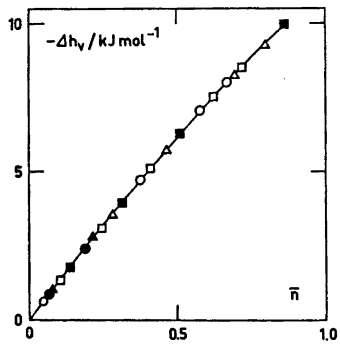

Fig. 2. The total molar enthalpy change, Δh_v, as a function of $\bar{n}$, for the nickel(II) – selenocyanate system, *cf.* Table 3.

DISCUSSION

For comparison, the values of $\Delta G°_j$, $\Delta H°_j$, and $\Delta S°_j$ for the nickel(II) – thiocyanate system [2] are also included in Table 5. The selenocyanate complexes are somewhat weaker than the thiocyanate ones. The ratio $K_1/K_2 = 5$ between the first and second stepwise stability constant is about the same for both systems.

The thiocyanate ion may coordinate either *via* sulfur or nitrogen, the selenocyanate ion either *via* selenium or nitrogen. Hard acceptors are coordinated *via* the harder nitrogen atom. Nickel(II) can be classified as a mildly hard acceptor [11] and its complexes are certainly in all cases N-bonded. A large difference in the strength of the thiocyanate and selenocyanate complexes of nickel(II) is therefore not to be expected. The small difference actually observed may be due to the influence of the non-bonding ends of the ligands.

If coordination takes place *via* N, the strength of the metal-ligand bonds should be much the same for thiocyanate and selenocyanate and about the same values of $\Delta H°_j$ are therefore to be expected. This is in fact also found, Table 5.

For both thiocyanate and selenocyanate the charge density on the non-bonding end decreases upon coordinating. Calculations [12] have shown that upon coordination *via* the N-atoms the decrease of charge is larger on the sulfur atom than on the selenium atom. Thus if an acceptor is coordination *via* the N-atoms, more water should be liberated from the S atom in thiocyanate than from the Se atom in selenocyanate. Consequently the entropy term should be more positive or less negative for the thiocyanate reaction than for the selenocyanate

reaction. If coordination, on the other hand, occurs through the S or Se atoms, the same amount of water should be set free from the non-bonding N atom for both ligands. In this case the entropy terms for the two reactions should be about the same.

As seen from Table 5, ΔS°_1 for the formation of the thiocyanate complex is less negative than ΔS°_1 for the formation of the selenocyanate complex, the difference amounting to ≈ 6 J $mol^{-1}K^{-1}$. In a previous study [1] the same difference was found in the case of Zn^{2+}. In the reactions with Cd^{2+}, on the other hand, the two ligands give about the same value of ΔS°_1. This indicates bonding *via* N in the case of Ni^{2+} and Zn^{2+}, while Cd^{2+} seems to favour S and Se. These conclusions agree with those arrived at *via* infrared spectroscopy [13] even if the latter method does not exclude the possibility of partial N-bonding in the case of Cd^{2+}.

For the nickel(II) – selenocyanate system ΔS°_2 is more negative than ΔS°_1. This trend of ΔS°_j is expected if no change of coordination figure occurs.[14]

Acknowledgements. I am most grateful to Professor Sten Ahrland for useful discussions and many valuable suggestions. I also wish to thank Professor Sture Fronæus for his kind interest and for facilities provided.

REFERENCES

1. Ahrland, S., Avsar, E. and Kullberg, L. *Acta Chem. Scand. A 28* (1974) 855.
2. Kullberg, L. *Acta Chem. Scand. A 28* (1974) 829.
3. Toropova, V. F. *Zh. Neorg. Khim. 1* (1956) 243.
4. Golub, A. M. and Skopenko, V. V. *Russ. J. Inorg. Chem. 7* (1962) 653.
5. Evans, M. G. and Nancollas, G. H. *Trans. Faraday Soc. 49* (1953) 363.
6. McConnell, H. and Davidson, N. *J. Amer. Chem. Soc. 72* (1950) 3164.
7. Sillén, L. G. and Warnqvist, B. *Ark. Kemi 31* (1969) 377.
8. Karlsson, R. and Kullberg, L. *To be published.*
9. Ahrland, S. and Kullberg, L. *Acta Chem. Scand. 25* (1971) 3471.
10. Burkov, K. A., Lilič, L. S. and Sillén, L. G. *Acta Chem. Scand. 19* (1965) 14.
11. Ahrland, S. *Struct. Bonding 5* (1968) 118.
12. Wagner, E. L. *J. Chem. Phys. 43* (1965) 2728.
13. Bailey, R. A., Kozak, S. L., Michelsen, T. W. and Mills, W. N. *Coord. Chem. Rev. 6* (1971) 407.
14. Ahrland, S. *Struct. Bonding 15* (1973) 167.

Received April 9, 1974.

Acta Chemica Scandinavica A 28 (1974) 903—909

The Crystal and Molecular Structure of 3,4-Dihydro-7-chloro-6-diethylamino-2*H*,8*H*-pyrimido[2,1-*b*][1,3]thiazin-8-one

H. J. TALBERG

Department of Chemistry, University of Oslo, Oslo 3, Norway

The crystal structure of 3,4-dihydro-7-chloro-6-diethylamino-2*H*,8*H*-pyrimido[2,1-*b*][1,3]thiazin-8-one, $C_{11}H_{16}ON_3SCl$, has been determined from three-dimensional X-ray diffraction data and refined by least squares methods.

The space group is $P2_1$, $a = 10.261$ Å, $b = 7.494$ Å, $c = 8.341$ Å, $\beta = 91.51°$. The geometry seems to favour a possible CH···O hydrogen bond (2.93 Å), and one intramolecular non-bonding contact is rather short (N_{am}···C4 2.712 Å).

The amino nitrogen atom has a pyramidal hybridisation, and the dihedral angles (about the Et_2N-C bond) are 81 and 48°. The thiazine ring moiety has an envelope-like conformation, and the C10 – S bond length (1.750 Å) indicates some double bond character in this bond.

Potential analgesics, with the following general formula

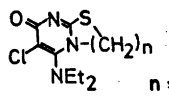

(I)

n = 2,3

have been synthesized by Berg-Nielsen.[1] The compounds were prepared from 2-bromoalkylthiopyrimidin-6-ones by cyclization of the bromoalkylthio side chain. The thiazoles ($n = 2$) formed more readily than the thiazines ($n = 3$). Studies by Reistad and Undheim [2,3] have shown that similar pyridine[2,1-*b*][1,3]thiazines rearrange to their thiazole analogs. These investigations indicate that the [1,3]thiazines are less stable than their thiazole analogs.

In order to examine the conformation of, and the strained conditions obviously present in these thiazine rings, and to shed some light on conformational changes promoted by ring closure, a crystal structure determination of I, $n = 3$ and a 2-propylthiopyrimidin-6-one derivative was initiated. The crystal and molecular structure of 2-(3-diethylaminopropylthio)4,5-dichloropyrimidin-6-one (II) has been published,[4] while the structure of I, $n = 3$ is now reported.

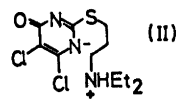

(II)

EXPERIMENTAL

Colourless needle-shaped crystals were obtained by slow evaporation of an acetone solution. The systematic absences were consistent with the space groups $P2_1$ and $P2_1/m$, the former being the actual one as $Z = 2$. Unit cell parameters were determined from diffractometer measurements. Three-dimensional intensity data were collected on a punched card controlled four circle Picker diffractometer with $\omega - 2\theta$ scan technique. The crystal used was approximately $0.40 \times 0.12 \times 0.08$ mm³, and was mounted with b along the ϕ-axis. The Mo$K\alpha$ radiation was monochromated with a highly oriented graphite crystal. The 2θ scan speed was 1° min^{-1}. Three test reflections were measured for every 100 reflections and the intensities accordingly adjusted. Estimated standard deviations in the intensities were taken as the square root of the total number of counts adding 1 % to allow for the uncertainty in the adjustments. 1825 unique reflections with 2θ less than 60° were measured. Only 811 of these had an intensity larger than $2\sigma(I)$, and were regarded as observed. The intensity data were corrected for Lorentz, polarization and absorption effects. Atomic form factors used were those of Doyle and Turner [5] for chlorine, sulfur oxygen, nitrogen, and carbon, and of Stewart *et al.*[6] for hydrogen. All programs but the ORTEP program [7] applied during the structure investigation are described in Ref. 8.

Table 1. Observed and calculated structure factors. The columns are: h, 10 F_{obs}, 10 F_{calc}.

L= 0,K= 0		= 3 175	160	4 234	233	L= 6,K= 3		= 1 169	168	L= 3,K= 6		L= 6,K= 1		3 41	23
1 454	495	= 4 84	72	3 222	219	4 127	132	0 50	70	2 39	51	7 60	31	4 45	22
2 287	279	L= 7,K= 1		2 257	260	2 48	58	1 119	112	1 52	55	= 8 54	42	8 47	36
3 370	351	= 4 120	122	1 284	294	1 61	39	2 90	97	0 78	74	=11 43	30	L= 6,K= 3	
4 47	56	= 3 116	115	L= 0,K= 2		= 1 68	78	4 64	80	= 3 89	79	L= 6,K= 1		10 54	49
5 76	62	= 2 64	55	0 1201	1234	= 2 43	37	5 58	78	L= 4,K= 6		= 8 115	105	5 93	100
6 80	82	0 71	65	1 623	586	= 3 84	106	L= 3,K= 4		0 88	84	L= 4,K= 1		= 7 38	49
7 150	150	2 117	121	2 153	167	= 4 99	114	6 45	39	L= 1,K= 7		12 41	38	=10 48	24
8 34	28	L= 6,K= 1		3 103	114	L= 5,K= 3		2 84	102	0 39	29	= 9 66	60	=11 42	33
9 40	44	5 107	103	4 196	199	= 5 75	60	1 103	108	L= 0,K= 7		=10 42	18	L= 5,K= 3	
L= 1,K= 0		4 249	251	7 127	122	= 4 72	61	0 151	152	1 45	23	L= 3,K= 1		= 8 73	74
9 63	56	2 83	84	9 63	56	= 3 49	64	= 1 101	100	L= 0,K= 0		=13 40	21	= 7 73	79
8 123	130	1 104	93	L= 1,K= 2		= 1 47	52	= 2 56	61	10 61	48	=11 41	32	L= 4,K= 3	
7 121	116	0 47	49	9 43	46	0 49	41	= 3 160	163	11 54	37	= 9 47	40	11 47	16
6 71	75	= 1 126	117	8 89	94	1 156	154	= 4 83	92	L= 1,K= 0		9 45	70	= 8 54	49
5 130	115	= 2 81	97	7 54	61	3 172	162	= 5 95	100	12 61	40	11 57	47	= 9 49	56
4 184	185	= 3 187	169	6 125	131	4 138	151	L= 4,K= 4		10 130	105	L= 2,K= 1		L= 3,K= 3	
3 610	588	= 4 69	71	5 64	79	5 191	189	= 5 54	51	=11 68	64	11 36	24	= 9 46	32
= 3 84	72	= 6 57	54	2 31	43	L= 4,K= 3		= 4 90	80	L= 2,K= 0		=10 47	35	L= 2,K= 3	
= 4 153	153	L= 5,K= 1		1 329	322	5 107	99	= 3 93	104	=11 40	34	=14 42	3	=10 36	34
= 5 39	26	= 7 75	85	0 632	622	4 50	59	= 2 130	125	=10 51	63	L= 1,K= 1		L= 1,K= 3	
= 7 120	135	= 6 106	97	= 1 576	519	3 136	142	= 1 33	54	10 91	49	12 46	52	=10 38	36
= 6 243	225	= 4 93	94	= 2 302	282	2 51	73	0 185	184	L= 3,K= 0		L= 0,K= 1		L= 0,K= 4	
= 9 53	39	= 3 38	66	= 4 100	95	1 43	58	1 79	78	11 41	18	12 67	54	11 55	29
L= 2,K= 0		= 2 78	83	= 7 136	133	0 85	96	5 115	131	10 36	26	10 58	46	L= 1,K= 4	
= 9 42	25	= 1 64	79	= 8 167	174	= 3 38	42	6 64	49	9 70	33	L= 0,K= 2		10 49	42
= 8 156	160	1 187	186	= 9 45	32	= 4 126	125	L= 6,K= 4		=10 79	62	10 64	48	8 61	58
= 6 90	96	2 49	71	L= 2,K= 2		= 5 102	126	2 48	64	=11 37	24	11 57	41	= 8 117	120
= 4 81	72	3 202	205	= 9 38	33	= 6 87	72	= 1 99	97	L= 4,K= 0		13 45	12	=11 51	43
= 3 810	813	4 146	144	= 8 139	149	= 7 147	148	= 2 102	98	=11 53	47	L= 1,K= 2		L= 2,K= 4	
= 2 268	272	5 230	244	= 6 44	68	L= 3,K= 3		0 106	99	9 90	89	12 55	39	=10 39	33
= 1 381	376	6 39	47	= 4 83	72	= 7 73	78	= 3 104	113	11 39	20	10 80	69	= 8 112	102
0 461	430	L= 4,K= 1		= 3 301	315	= 4 71	81	L= 6,K= 4		L= 5,K= 0		=11 66	54	8 74	59
1 121	140	7 86	105	= 2 140	151	= 3 78	96	= 3 177	178	10 91	38	L= 2,K= 2		L= 3,K= 4	
2 406	414	6 41	51	= 1 102	125	= 1 89	65	= 2 66	73	8 86	66	=11 37	19	8 87	81
3 62	72	5 141	137	0 39	70	0 63	76	= 1 42	48	= 8 64	60	=10 53	59	7 43	45
4 35	31	4 127	139	1 173	179	1 205	209	1 43	36	=11 59	45	10 40	38	=10 50	44
5 74	86	3 212	219	2 152	157	2 156	156	L= 5,K= 5		=12 41	14	11 40	21	L= 4,K= 4	
6 40	58	2 187	201	3 30	65	3 57	47	= 1 42	56	=13 50	22	L= 3,K= 2		7 64	56
8 46	61	1 75	88	4 90	85	4 185	183	1 75	75	L= 6,K= 0		10 38	17	L= 5,K= 4	
L= 3,K= 0		0 80	95	6 46	54	6 50	64	L= 4,K= 5		= 8 47	55	=10 65	56	8 47	58
8 88	83	= 3 119	122	8 95	87	7 38	56	3 115	101	= 7 77	61	L= 4,K= 2		5 99	100
7 138	134	= 4 48	70	L= 3,K= 2		L= 2,K= 3		2 52	41	7 57	47	9 71	64	= 7 71	72
6 120	123	= 5 135	128	8 78	76	9 48	37	1 93	86	6 56	26	10 51	41	L= 6,K= 4	
4 56	26	= 6 51	40	L= 2,K= 2		8 118	113	= 3 64	74	9 78	53	12 39	11	= 8 41	41
3 37	46	= 7 135	150	7 40	63	7 147	160	= 4 55	25	L= 7,K= 0		L= 5,K= 2		= 7 39	50
2 195	206	= 8 79	74	L= 3,K= 2		4 255	259	L= 3,K= 5		9 70	65	10 45	29	= 6 45	28
1 167	174	L= 3,K= 1		7 82	95	3 90	91	= 5 42	71	7 65	63	8 73	73	= 5 51	32
0 152	164	= 8 38	31	6 66	71	2 65	81	= 4 71	61	= 5 54	39	= 8 56	58	= 4 39	38
= 1 471	444	= 7 122	110	2 147	135	1 147	144	= 3 47	70	= 7 44	26	=11 53	53	9 57	48
= 2 102	106	= 6 77	85	1 60	42	0 62	51	= 2 34	37	=10 58	35	L= 6,K= 2		10 46	23
= 3 391	395	= 5 87	123	0 282	280	= 2 109	102	= 1 43	66	L= 8,K= 0		= 8 60	39	L= 7,K= 4	
= 4 73	65	= 4 162	158	= 1 266	284	= 3 231	241	0 45	42	= 4 91	53	= 7 73	71	7 54	37
= 5 72	63	= 3 152	158	= 3 316	314	= 6 171	165	1 37	56	= 3 41	35	7 40	33	6 37	29
= 8 64	67	= 2 129	129	= 4 90	100	= 8 72	54	1 92	104	0 36	83	8 88	25	4 47	65
L= 4,K= 0		= 1 106	111	= 5 76	89	L= 1,K= 3		2 40	34	1 78	69	9 52	50	1 54	48
= 8 47	28	0 145	137	= 6 40	41	= 8 132	135	L= 2,K= 5		3 52	55	L= 7,K= 2		0 41	17
= 6 87	89	1 319	337	= 7 34	26	= 7 80	89	6 44	66	4 64	67	9 58	54	= 3 95	92
= 5 73	56	2 210	209	= 8 73	64	= 6 139	148	5 97	93	5 76	29	7 70	55	= 4 39	25
= 4 122	124	3 102	94	L= 4,K= 2		= 4 202	193	4 144	142	L= 9,K= 0		6 52	30	= 9 40	9
= 3 88	80	4 188	195	= 6 43	49	= 3 121	112	3 112	109	5 57	63	4 80	60	L= 8,K= 4	
= 2 154	157	5 44	84	= 5 82	95	= 2 146	141	1 107	121	= 2 46	35	= 4 60	50	= 4 50	43
= 1 66	78	6 72	69	= 4 124	125	= 1 210	217	= 2 46	54	= 3 48	22	= 5 44	32	1 48	58
0 485	472	7 47	40	= 3 132	133	1 56	70	= 3 85	70	= 4 63	59	= 7 40	21	4 46	31
1 247	241	L= 2,K= 1		= 2 161	169	2 50	40	= 5 48	32	= 6 39	24	=10 41	38	L= 9,K= 4	
2 89	94	8 35	57	= 1 31	21	3 138	140	= 6 49	59	= 8 52	33	L= 8,K= 2		5 41	29
3 37	7	9 177	133	0 379	373	4 220	226	L= 1,K= 5		= 9 48	30	= 4 56	53	= 1 45	25
4 67	79	8 214	216	1 203	205	5 286	286	= 6 95	75	L= 10,K= 0		= 3 37	24	= 4 39	36
5 145	146	4 419	416	2 37	59	6 32	18	= 5 50	37	= 3 51	47	0 38	53	= 7 42	8
6 106	98	3 123	124	4 42	55	7 55	48	= 4 131	122	3 43	30	1 66	65	L= 10,K= 4	
7 127	134	2 76	121	5 155	149	L= 0,K= 3		= 3 46	29	6 51	43	4 53	58	3 46	20
L= 6,K= 0		1 293	319	6 78	89	8 66	81	= 2 71	92	L= 11,K= 0		5 46	33	L= 8,K= 5	
6 33	44	0 123	97	7 120	112	7 145	143	= 1 80	67	1 42	2	L= 9,K= 2		2 40	52
5 145	150	= 1 179	174	L= 5,K= 2		6 72	71	0 59	94	L= 11,K= 1		5 53	52	= 5 42	33
2 40	27	= 2 137	150	5 150	142	5 176	182	1 65	69	0 42	14	4 56	48	L= 7,K= 5	
1 36	26	= 3 332	323	2 76	65	4 104	113	3 55	44	2 50	40	= 2 47	35	= 4 48	49
0 155	158	= 4 101	106	1 33	30	3 121	132	4 135	132	L= 10,K= 1		= 4 51	49	= 2 51	36
= 1 284	289	= 6 172	178	0 127	141	1 42	51	5 140	137	6 44	33	= 7 42	11	= 1 37	25
= 2 141	143	L= 1,K= 1		= 1 200	207	L= 0,K= 4		6 36	7	4 61	63	= 8 45	36	2 85	77
= 3 155	147	= 8 184	183	= 2 107	105	0 592	561	L= 0,K= 5		L= 9,K= 1		L= 10,K= 2		L= 6,K= 5	
= 4 144	150	= 7 125	140	= 3 133	137	1 193	202	6 77	68	= 9 42	6	3 52	30	5 48	60
= 5 37	21	= 6 218	207	= 4 63	62	2 114	116	5 85	100	= 6 66	39	6 51	35	4 70	56
= 6 70	80	= 5 327	339	= 5 57	54	3 64	81	4 61	63	= 5 66	63	L= 11,K= 2		3 40	43
= 7 89	98	= 3 102	127	= 6 48	53	4 120	122	1 67	66	1 86	85	= 2 47	31	2 53	55
L= 6,K= 0		= 2 285	295	= 7 85	103	5 51	46	L= 0,K= 6		L= 8,K= 1		L= 10,K= 3		1 41	24
= 5 63	62	= 1 250	247	L= 6,K= 2		7 49	69	0 259	246	8 119	127	= 1 50	32	= 3 58	68
= 4 62	67	0 310	270	= 5 52	62	L= 1,K= 4		1 68	63	1 114	108	L= 9,K= 3		= 4 42	40
= 3 253	261	1 34	41	= 4 42	45	7 36	40	2 78	70	0 65	60	1 64	74	= 6 49	28
= 2 162	162	2 114	116	= 3 278	270	6 42	61	3 61	53	= 1 39	32	L= 8,K= 3		L= 5,K= 5	
= 1 58	53	3 149	144	= 1 76	78	5 57	51	4 78	67	= 2 43	26	2 87	91	= 8 73	73
0 113	112	4 335	325	0 84	87	3 59	49	L= 1,K= 6		= 4 43	35	1 89	89	= 7 80	81
1 93	91	5 454	447	1 76	76	0 334	324	0 139	150	= 5 52	46	0 57	63	3 63	67
2 59	42	6 31	50	2 34	41	= 1 234	256	= 1 94	72	= 6 43	33	= 2 50	49	4 62	85
3 90	89	7 51	50	3 48	55	= 2 154	148	= 2 74	65	L= 7,K= 1		L= 7,K= 3		5 121	121
5 55	21	8 104	95	L= 7,K= 2		= 3 63	74	L= 2,K= 6		= 9 49	40	= 7 44	34	9 39	23
6 80	72	L= 0,K= 1		1 42	68	= 4 53	52	= 3 63	86	= 7 60	46	= 6 38	37	L= 4,K= 5	
L= 7,K= 0		8 105	104	= 2 83	82	= 7 52	83	= 1 97	92	= 5 47	35	= 4 82	74	7 47	20
4 57	63	7 171	182	= 1 133	139	L= 2,K= 4		1 65	48	5 56	69	= 3 98	99	6 75	73
3 38	30	6 74	95	L= 7,K= 3		= 6 37	54	2 51	39	7 37	11	= 2 47	42	= 5 67	58
1 61	75	5 233	240	0 54	36	= 3 128	139	4 37	64	8 52	45	2 133	119	= 7 62	59

Table 1. Continued.

L=	5,K=	5		4	46	40	L=	0,K=	2	L=	3,K=	1	0	342	324	L=	1,K=	0	- 3	156	158	4	134	132
- 7	75	80		5	51	63	- 9	75	56	1	331	337	L=	0,K=	4		2	522	486	- 2	130	129	L=	5,K=	3
	6	37	34	L=	4,K=	7	- 7	123	122	L=	2,K=	1	0	554	561	L=	2,K=	0		0	147	137	1	155	154
	11	40	38		0	41	40	- 4	193	199	4	421	416	L=	1,K=	3	- 3	519	513	2	212	209	3	175	162
	L=	2,K=	5	L=	3,K=	7	- 3	107	114	1	298	319	5	281	286		0	468	430	4	193	195	4	147	151
	8	41	31	- 9	39	3	- 2	156	167	- 3	346	323	L=	2,K=	3	- 1	387	376	L=	2,K=	1	5	190	189
-10	38	29	- 7	41	38	- 1	617	586	L=	1,K=	1	4	282	259	L=	1,K=	0		6	127	133	L=	3,K=	3
	L=	1,K=	5	- 5	45	13	L=	0,K=	3	- 4	325	339	L=	6,K=	2		3	185	185	5	216	216	1	204	209
- 9	68	67		4	72	52	- 1	44	51	- 2	294	295	- 3	272	270	- 4	156	153	- 1	179	174	2	155	156
- 7	67	68	L=	2,K=	7	- 3	124	132	- 1	238	247	L=	4,K=	2	- 8	250	225	- 2	141	150	4	178	183
	12	49	11		5	53	43	- 4	108	113	0	312	270	0	379	373	L=	2,K=	0	- 6	172	178	L=	2,K=	3
	L=	0,K=	5		4	51	58	- 5	183	182	4	341	325	L=	3,K=	2	- 8	153	160	L=	1,K=	1	1	151	144
	12	50	40		3	37	33	- 6	80	71	5	451	447	- 3	305	314	- 2	274	272	- 8	186	183	- 3	228	241
	8	58	65		2	44	22	- 7	149	143	L=	0,K=	1	- 1	283	284	L=	3,K=	0		3	147	144	- 6	175	165
	7	73	80		1	43	49	- 8	61	81	2	259	260	0	283	280		7	135	134	L=	0,K=	1	L=	1,K=	3
	L=	1,K=	6	- 3	48	45	L=	0,K=	4	1	284	294	L=	2,K=	2		2	195	206	7	178	182	- 8	139	135
- 8	64	67	- 6	47	33	- 7	63	69	L=	0,K=	2	- 3	306	315		1	172	174	5	232	240	- 6	143	148
	L=	2,K=	6	L=	1,K=	7	- 5	58	46	0	1134	1234	L=	1,K=	2		0	156	164	4	233	233	- 4	203	193
- 8	67	61	- 6	49	32	- 4	127	122	L=	1,K=	2	- 2	301	282	L=	4,K=	0		3	221	219	- 2	143	141
- 7	49	43	- 4	43	31	- 3	67	81	1	343	322	- 1	561	519	- 2	159	157	L=	0,K=	2	- 1	212	217
	7	36	12	- 3	37	20	- 2	116	116	0	598	622	0	610	622		1	255	241	2	154	167	3	137	140
	L=	3,K=	6	- 1	49	37	- 1	195	202	- 1	561	519	L=	0,K=	2		5	142	148	4	194	199	L=	0,K=	3
- 4	43	25		5	81	78	L=	0,K=	5	- 2	304	282	0	1186	1234		7	126	134	7	122	122	7	150	143
- 5	59	49	L=	0,K=	7	- 3	34	34	L=	2,K=	2	L=	0,K=	1		L=	5,K=	0	L=	1,K=	2	6	177	182
L=	4,K=	6		5	50	51	- 4	56	63	- 3	294	315	1	284	294		5	147	150	- 7	136	133	L=	0,K=	4
- 4	41	50	L=	0,K=	8	- 5	100	99	L=	3,K=	2	2	260	260		0	164	158	- 8	164	174	1	197	202
- 2	44	45		0	88	70	- 6	73	68	0	284	280	L=	1,K=	1	- 2	143	143	L=	2,K=	2	L=	1,K=	4
	5	72	76	L=	1,K=	8	L=	0,K=	6	- 1	271	284	5	461	447	- 3	156	147	- 8	136	149	- 1	252	256
L=	5,K=	6		0	65	67	- 4	82	67	- 3	315	314	4	337	325	- 4	149	150		2	159	157	- 2	152	148
	5	47	49	- 1	54	52	- 3	54	53	L=	4,K=	2	0	303	270	L=	6,K=	0	L=	4,K=	2	L=	2,K=	4
	0	55	49	- 2	39	37	- 2	83	70	0	386	373	- 1	242	247	- 2	159	162	- 3	130	133	- 3	126	139
- 1	39	50	L=	0,K=	0	- 1	60	63	L=	6,K=	2	- 2	287	295	L=	7,K=	0	- 2	166	169	L=	3,K=	4
- 2	66	72	- 9	51	44	L=	2,K=	0	- 3	270	270	- 4	324	339	- 3	184	160	L=	3,K=	2	0	156	152
- 3	77	69	- 7	152	150	2	416	414	L=	2,K=	3	L=	2,K=	1	L=	6,K=	1	2	146	135	- 3	164	163
- 4	40	19	- 6	86	82	- 1	390	376	4	258	259	- 3	350	323	4	248	251	- 2	131	147	L=	4,K=	4
L=	6,K=	6	- 5	67	62	0	467	430	L=	1,K=	3	1	303	319	- 1	125	117	L=	4,K=	2	- 2	128	125
- 7	47	36	- 4	55	56	- 3	515	513	5	286	286	4	425	416	- 3	165	169	1	199	205	0	188	184
- 3	82	80	- 3	373	351	L=	1,K=	0	L=	0,K=	4	L=	3,K=	1	L=	5,K=	1	5	159	149	L=	6,K=	4
	3	38	7	- 2	293	279	2	524	488	0	536	561	1	332	337		3	206	205	L=	6,K=	2	- 3	177	176
L=	7,K=	6	- 1	463	495	L=	3,K=	0	L=	1,K=	4	L=	6,K=	0		4	148	144	5	147	142	L=	2,K=	5
- 3	44	74	L=	0,K=	1	- 1	479	444	0	348	324	- 3	260	261		5	237	244	0	130	141	4	140	142
L=	8,K=	7	- 1	278	294	- 3	399	395	L=	0,K=	6	L=	5,K=	0	L=	4,K=	1	- 1	198	207	L=	1,K=	5
	1	41	46	- 2	252	260	L=	4,K=	0	0	252	246	- 1	291	289		3	219	219	- 3	133	137	4	136	132
L=	7,K=	7	- 3	218	219	0	506	472	L=	2,K=	0	L=	4,K=	0		2	193	201	L=	6,K=	2	5	136	137
- 3	40	46	- 4	239	233	L=	5,K=	0	2	416	414	0	498	472	- 5	141	128	- 2	120	124	L=	1,K=	6
L=	6,K=	7	- 5	233	240	- 1	290	289	L=	0,K=	6	L=	3,K=	0	- 7	136	150	L=	7,K=	2	0	152	150
7	41	24	- 6	71	95	L=	6,K=	0	0	241	246	- 3	393	395	L=	3,K=	1	- 3	137	139	L=	0,K=	3
L=	5,K=	7	- 7	185	182	- 3	256	261	L=	1,K=	4	- 1	476	444	- 4	160	156	L=	6,K=	3	6	177	182
1	43	22	- 8	104	104																		

CRYSTAL DATA

3,4-Dihydro-7-chloro-6-diethylamino-2*H*,8*H*-pyrimido[2,1-*b*][1,3]thiazin-8-one, $C_{11}H_{16}ON_3SCl$, monoclinic, space group $P2_1$ $a=10.261(7)$ Å, $b=7.494(5)$ Å, $c=8.341(5)$ Å, $\beta=91.51(2)°$, $V=641$ Å^3, $M=272.81$, $F(000)=288$, $\mu=0.44$ mm^{-1}, D_{obs}(flotation) $=1.40$ gcm^{-3}, $D_{calc}=1.41$ gcm^{-3}.

STRUCTURE DETERMINATION

Coordinates of the sulfur and chlorine atoms were found from a sharpened Patterson function. A corresponding Fourier map revealed a molecule with an apparent mirror plane through all non-hydrogen atoms but the C3 atom and the ethyl carbon atoms. However, subsequent Fourier and full matrix least squares refinement showed that no disorder was present, and that the space group was truly $P2_1$. In the final refinements calculated positional parameters and estimated thermal parameters (6–8 Å^2) for hydrogen atoms were included but not refined. The refinements converged with a conventional R factor of 0.082 and a weighted

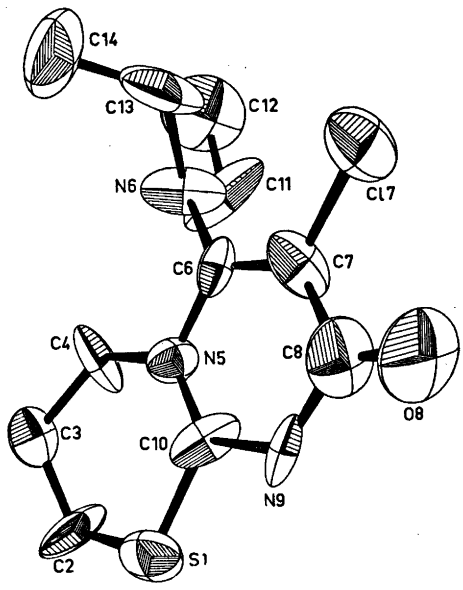

Fig. 1. The 50 % probability ellipsoids.

Table 2. Fractional atomic coordinates for non hydrogen atoms, anisotropic thermal vibration parameters and their estimated standard deviations (multiplied by 10^4). The temperature factors are expressed as:

$$\exp-(\beta_{11}h^2+\beta_{22}k^2+\beta_{33}l^2+\beta_{12}hk+\beta_{13}hl+\beta_{23}kl)$$

Atom	x	y	z	β_{11}	β_{22}	β_{33}	β_{12}	β_{13}	β_{23}
Cl7	8314	2503	6571	161	386	198	−2	−117	−55
	3	18	4	5	14	6	41	9	48
S1	2706	2459	3898	100	294	217	86	71	20
	4	0	4	4	12	7	34	9	43
O8	5876	2054	8209	268	681	73	−122	14	−26
	9	29	10	16	68	13	76	24	77
N5	5325	2460	3439	81	213	114	−63	2	−36
	8	36	13	11	29	16	92	23	96
N6	7618	2497	2946	98	298	191	−90	35	−472
	9	35	13	11	34	19	71	26	75
N9	4439	2249	6034	183	209	109	−25	53	201
	11	38	12	17	47	18	78	28	83
C2	2631	2496	3898	152	706	105	−411	−6	399
	12	48	12	19	77	20	112	32	122
C3	3858	3228	1131	139	302	77	3	−102	30
	13	22	13	18	63	19	48	31	53
C4	5163	2578	1661	133	441	37	423	−30	51
	10	41	11	16	57	16	85	26	91
C6	6617	2562	4083	141	91	122	−27	18	77
	12	43	13	16	34	21	87	30	103
C7	6814	2346	5685	125	301	104	111	−77	−150
	10	43	13	16	53	19	92	28	101
C8	5708	2296	6733	194	364	142	147	109	−31
	14	53	16	22	65	26	124	43	137
C10	4354	2487	4494	141	135	147	−200	95	−201
	11	40	15	17	35	24	86	38	102
C11	7875	667	2203	293	99	383	−132	250	−227
	21	32	28	32	38	43	63	64	70
C14	8798	5406	2166	245	474	385	37	232	532
	22	33	27	32	93	49	81	65	106
C13	8741	3630	3081	73	675	227	−91	−108	−52
	16	34	20	19	90	31	61	37	84
C12	9101	633	1221	249	791	237	17	139	−151
	19	36	19	30	112	37	99	56	106

R_w factor ($R_w=(\sum w\Delta^2/\sum wF^2)^{\frac{1}{2}}$) of 0.062. Observed and calculated structure factors are given in Table 1, and final parameters for non-hydrogen atoms in Table 2. Magnitudes and directions of the vibrational ellipsoids, and numbering of atoms are given in Fig. 1. Bond lengths and angles with estimated standard deviations are presented in Table 3. The estimated standard deviations were calculated from the correlation matrix. Short intermolecular contacts are given in Table 3 and deviations from a least squares plane through the ring atoms in the pyrimidine moiety are given in Table 4. The r.m.s. discrepancy between the atomic vibration components obtained in the structure determination and those calculated from a rigid-body analysis were 0.022 when excluding the C3 atom and the ethyl carbon atoms. The coordinates were accordingly not adjusted for libration.

DISCUSSION

Figs 2 and 3 show that the spatial packing of the molecules conforms to the concept of molecular close pacing. The geometry seems to favour a possible O···HC3 hydrogen bond. The C3···O distance is 2.931 Å or 0.4 Å shorter than

Table 3. Bond lengths (Å) and angles (°) with their estimated standard deviations in parenthesis.

S1–C10	1.750(9)	C6–N6	1.417(11)
S1–C2	1.787(10)	C7–C17	1.694(9)
C2–C3	1.481(17)	C8–O8	1.252(14)
C3–C4	1.481(17)		
C4–N5	1.490(11)	N6–C11	1.530(26)
N5–C10	1.347(10)	N6–C13	1.433(26)
C10–N9	1.297(12)	C11–C12	1.519(20)
N9–C8	1.413(14)	C13–C14	1.536(28)
C8–C7	1.451(13)		
C7–C6	1.356(12)		
C6–N5	1.420(11)		
C10–S1–C2	107.4(6)	N5–C6–N6	115.6(9)
S1–C2–C3	110.0(10)	N6–C6–C7	125.8(12)
C2–C3–C4	122.9(15)	C6–C7–C17	122.1(9)
C3–C4–N5	113.1(11)	C17–C7–C8	117.1(8)
C4–N5–C6	116.9(9)	C7–C8–O8	120.4(14)
N5–C6–C7	118.6(10)	O8–C8–N9	120.3(14)
C6–C7–C8	119.9(12)		
C7–C8–N9	118.6(10)	C6–N6–C11	115.9(19)
C8–N9–C10	116.3(12)	C6–N6–C13	121.5(14)
N9–C10–S1	108.6(7)	C11–N6–C13	114.6(16)
N9–C10–N5	127.8(10)	N6–C11–C12	112.8(16)
N5–C10–S1	122.7(7)	N6–C13–C14	121.0(18)
C10–N5–C4	125.7(10)		
C10–N5–C6	116.9(8)		
N5C10–S1C2	2.1(37)	N5C6–N6C11	81.1(30)
C10S1–C2C3	29.9(23)	C7C6–N6C13	48.3(25)
S1C2–C3C4	−56.1(31)		
C2C3–C4N5	49.7(31)		
C3C4–N5C10	−9.3(41)		
Possible hydrogen bond			
O8–C3 (a)	2.931	(a): $1-x, y-\frac{1}{2}, 1-z$	
Other intermolecular contacts			
O8···C4 (b)	3.015	(b): $x, y, 1+z$	
O8···C4 (c)	3.522	(c): $1-x, \frac{1}{2}+y, 1-z$	
N9···N5 (a)	3.623		
S1···C7 (a)	3.710		

Table 4. Deviation of atoms from a least-squares plane through the atoms N5, C6, C7, C8, N9, and C10, (Å).

N5	−0.047	C4	−0.064
C6	0.042	N6	−0.036
C7	−0.027	Cl7	0.113
C8	0.021	O8	−0.074
N9	−0.031		
C10	0.055	S1	0.032
		C2	−0.069
		C3	0.416

a normal van der Waals contact. The H···O distance (the position of the hydrogen atom is calculated assuming tetrahedral angles at the C3 atom and a C3–H bond length of 1.086 Å [9]) is 2.101 Å and the CHO angle is 164°. Similar possible bonds have been found in the crystal structure of caffein [10,11] and some other structures.[11] As the C···O distances in these last structures are in the range 3.00–3.20 Å, the corresponding distance in the present structure seems to be short.

The C4···O distance (3.015 Å) is also short, but this is probably not a possible hydrogen

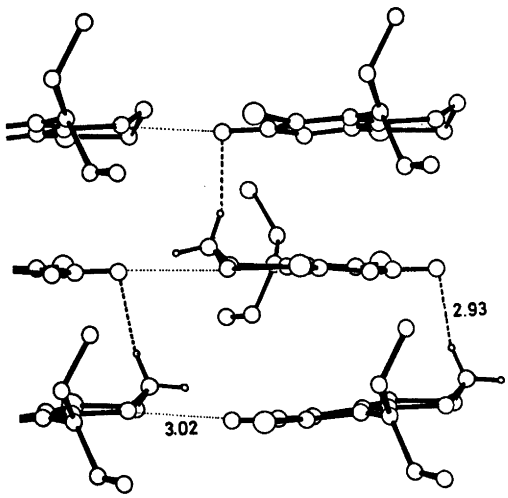

Fig. 2. Packing of molecules viewed down the *a* axis. The possible C3H···O hydrogen bond is indicated by broken line, while a short C4···O contact is indicated by a dotted line.

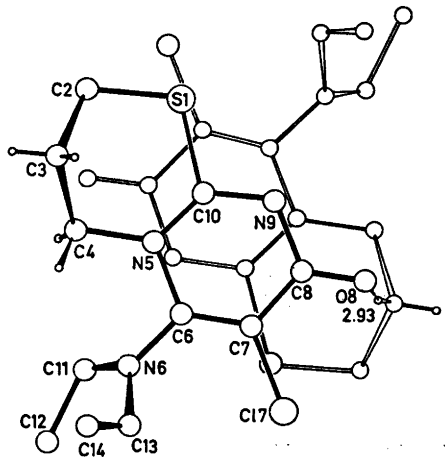

Fig. 3. Packing of molecules, viewed down the *b* axis. The possible C3···O hydrogen bond is indicated by broken line.

bond as the O···H distance is 2.605 Å. The remaining intermolecular contacts are normal van der Waals contacts.

The pyrimidine ring is planar within the precision of the experiment, and the S1, C2, C4, N6, and O8 atoms deviate approximately as much from the plane as the ring atoms do themselves. The C3 atom, however, deviates significantly and the C17 atom possibly significantly from the plane.

The thiazine ring moiety has an envelope-like conformation, with an angle of 45° between the ring-plane and the plane through the C3, C4, and C2 atoms.

Comparing corresponding bond distances in I with those found in II it is interesting to notice that apart from the N5 – C6 bond no significant differences are found in the pyrimidine ring moiety. The differences are in the range 0.03 – 0.01 Å. However, the N5 – C6 bond length is 0.09 Å longer than the corresponding N3 – C4 bond length in II.

The bond lengths in the present compound agree well with those found in the pyrimidine ring moiety of 2,2′-anhydro-1-(β-D-arabino-furanosyl)-uracil (III) except for the N5 – C6 bond which is 0.05 Å longer than the corresponding bond length in III. Intramolecular

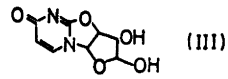

(III)

repulsion between the N6 and the C4 atom probably has substantial influence on the N5 – C6 bond length. The contact between the two atoms (2.712 Å) is 0.2 Å shorter than a normal van der Waals contact.

As to the bond angles in the pyrimidine ring moiety, the only important difference between I and II is the N5 – C6 – C7 angle in I being 8° smaller than the corresponding N3 – C4 – C5 angle in II, and the C6 – C7 – C8 angle in I being 5° wider than the corresponding C4 – C5 – C6 angle in II. Comparing I and III no significant differences are found.

In the thiazine ring moiety the S1 – C2, C2 – C3 and C3 – C4 bond lengths are slightly but probably not significantly shorter than the corresponding bond lengths in II. The S1 – C10 bond length (1.750 Å) is of the same order as the corresponding S2 – C2 bond length (1.764 Å) in II, and has a considerable amount of double bond character.[4] This is probably the reason why the thiazine ring moiety gets the observed conformation, and not an expected half chair conformation with a smaller C – S – C angle.

The C2 – C3 – C4 bond angle is significantly wider (11°) and the C10 – S1 – C2 angle probably significantly wider (2.3°) than the corresponding angles in II. The opening of these angles may indicate that the thiazine ring has conformational strain.

The N6 atom deviates 0.24 Å from the plane through the C11, C13, and C6 atoms; thus this amino nitrogen atom has a hybridisation which is neither pure sp^2 (with N in the plane) nor pure sp^3 (with N approximately 0.5 Å from the plane). The following figure shows the conformation about the C6 – N6 bond:

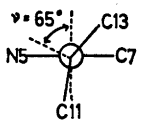

The N6 – C11 and N6 – C13 bond lengths deviate slightly though not significantly from a pure CN single bond distance of 1.475 Å,[13] whereas the N6 – C6 bond length (1.417 Å) is very similar to the $Me_2N - C_{ar}$ bond length in *N,N*-dimethyl-2,6-dichloro-*p*-nitroanaline [14] [1.41(1) Å]. These last bonds also have similar $n_N N - C_{ar}$-dihedral angles (ν) (65° in I and 60° in the aniline derivative).

The C7 – Cl bond length seems quite normal.[15]

The author thanks K. Berg-Nielsen for supplying the title compound.

REFERENCES

1. Berg-Nielsen, K. *Acta Chem. Scand. To be published.*
2. Undheim, K. and Reistad, K. R. *Acta Chem. Scand. 24* (1970) 2949.
3. Undheim, K. and Reistad, K. R. *Acta Chem. Scand. 26* (1972) 1620.
4. Talberg, H. J. *Acta Chem. Scand. A 28* (1974) 600.
5. Doyle, P. A. and Turner, P. S. *Acta Crystallogr. Sect. A 24* (1968) 390.
6. Stewart, R. F., Davidson, E. R. and Simpson, W. T. *J. Chem. Phys. 42* (1965) 3175.
7. Johnson, C. K. *ORTEP*, Report ORNL-3795, Oak Ridge National Laboratory, Oak Ridge 1965.
8. Dahl, T., Gram, F., Groth, P., Klewe, B. and Rømming, C. *Acta Chem. Scand. 24* (1970) 2232.
9. Allen, H. C. and Plyler, E. K. *J. Amer. Chem. Soc. 80* (1958) 2673.
10. Sutor, D. J. *Acta Crystallogr. 11* (1958) 453.
11. Sutor, D. J. *Nature (London) 195* (1962) 68.
12. Suck, D. and Saenger, W. *Acta Crystallogr. Sect. B 29* (1973) 1323.
13. Lide, D. R. *J. Chem. Phys. 27* (1957) 343.
14. Struchkov, Y. T. and Khotsyanova, T. L. *Izv. Akad. Nauk. SSSR Ser. Khim. 8* (1960) 1369.
15. Palenik, G. H., Donohue, J. and Trueblood, K. N. *Acta Crystallogr. 12* (1968) 600.

Received April 19, 1974.

Acta Chemica Scandinavica A 28 (1974) 910—918

The Crystal and Molecular Structure of Quinone 4-Oxime

H. J. TALBERG

Department of Chemistry, University of Oslo, Oslo 3, Norway

The crystal structure of quinone 4-oxime $C_6H_5O_2N$, has been determined from three dimensional X-ray diffraction data and refined by least squares methods. The space group is $P2_1/c$, $a=7.209$ Å, $b=28.14$ Å, $c=6.671$ Å, $\beta=118.86°$. The final correlation factor was 4.7 % and the estimated standard deviation in bond lengths for non-hydrogen atoms was in the range 0.003 – 0.004 Å. The asymmetric unit contains two molecules which are nearly equal as to corresponding bond lengths and angles. Two hydrogen bonds of significantly different length and a close packing of molecules are characteristic for the crystal structure. The bond lengths indicate a considerable degree of π-resonance in the molecules.

The present structure determination of quinone 4-oxime (I) is a part of a series of structural investigations of monomeric C-nitroso compounds and oximes derived from these by protonation or tautomeric proton exchange.

Lüttke [1] has demonstrated the ability of *p*-substituted nitrosobenzenes in forming dimers of the azodioxy-type to be heavily dependent upon the electron donating ability of the *para* substituent. An intramolecular charge transfer from the *para* substituent to the nitroso-group is probably preventing dimerisation.

A comparison of the molecular structure of *these* nitrosobenzenes and their corresponding oximes might indicate to what degree this intramolecular charge transfer is present in the nitroso compounds.

So far the crystal and molecular structure of *N,N*-dimethyl-*p*-nitrosoaniline [2] and its hydrochloride,[3] have been investigated.

Spectroscopic investigations [4] of (I) indicate that only the oxime in the tautomeric equilibrium between the oxime and the nitroso compound is forming crystals. Structure determinations of 3-methyl-6-chloro- [5] (II) and 3-chloro-*p*-nitrosophenol [5] (III) have shown these compounds to occur in the quinone-oxime form in the crystal phase.

However, preliminary photographic investigations of crystals from diethyl ether solutions of (I), revealed a unit cell containing 8 molecules with the molecular weight of (I). Two of these molecules are thus constituting the asymmetric unit, as the space group is $P2_1/c$. (II) and (III) are shown to crystallize in the same space group, but with 1 molecule in the asymmetric unit.

The possibility of having both of the tautomeric forms in the unit cell was thus present. This possibility initiated the following structure determination.

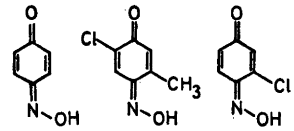

(I) (II) (III)

EXPERIMENTAL

Yellow tabular crystals were grown by slow evaporation from a diethyl ether solution of commercially available *p*-nitrosophenol. From the systematic absences, *h0l* with *l* odd, *0k0* with *k* odd, the space group was determined to $P2_1/c$.

Three-dimensional data were collected, and unit cell parameters were determined on a SYNTEX-P1 computer controlled four-circle diffractometer with graphite monochromated Mo$K\alpha$ radiation. The unit cell parameters were obtained using a least squares treatment of measurements of twelve reflections.

All measurements were done using a crystal with approximate dimensions $0.40 \times 0.21 \times 0.09$ mm^3. The crystal was mounted with the c^*-axis nearly parallel to the goniometer head spindle axis.

The intensities were obtained using the $\omega - 2\theta$ scanning mode. Prior to each scan the intensity was measured with stationary crystal and

Table 1. Observed and calculated structure factors. The columns are: h, $10 \times F_{obs}$, $10 \times F_{calc}$.

h	$10 \times F_{obs}$	$10 \times F_{calc}$
H=	0,K=	0
4	1041	1056
6	320	337
H=	0,K=	1
-6	35	18
-5	35	28
-4	52	39
-3	73	72
-2	47	35
-1	60	60
1	54	60
2	46	35
3	69	72
4	49	39
H=	0,K=	2
-6	119	123
-5	72	83
-4	242	237
-3	91	88
-2	342	332
1	28	38
2	335	332
3	88	85
4	232	237
5	77	83
6	115	123
7	40	48
H=	0,K=	3
-3	75	73
-1	76	80
1	80	80
2	28	17
3	71	73
4	29	8
H=	0,K=	4
-7	39	42
-5	83	65
-4	57	47
-3	237	227
-2	86	84
-1	669	671
0	92	95
1	642	671
2	82	84
3	234	227
4	45	47
5	83	85
H=	0,K=	5
-5	46	42
-4	63	59
-3	121	119
-2	62	66
-1	104	105
1	107	105
2	63	66
3	118	119
4	63	59
5	39	42
H=	0,K=	6
-6	55	59
-4	122	120
-2	186	185
0	186	185
2	186	185
3	27	1
4	122	120
6	60	59
H=	0,K=	7
-4	51	50
-3	73	69
-2	73	73
-1	55	55
1	53	55
2	74	73
3	71	69
4	53	50
5	35	28
H=	0,K=	8
-6	75	77
-4	157	149
-3	121	122
-2	261	262
-1	321	320
0	337	338
1	320	320
2	256	262
3	126	122
4	148	149
6	72	77
H=	0,K=	9
-6	49	18
-5	38	42
-4	33	39
-3	72	71
-2	58	55
-1	39	46
1	42	46
2	53	55
3	75	71
4	35	39
5	39	42
H=	0,K=	10
-6	58	55
-5	93	90
-4	131	126
-3	294	291
-2	278	279
-1	580	578
0	393	399
1	595	578
2	286	279
3	286	291
4	123	126
5	88	90
6	54	55
H=	0,K=	11
-5	42	40
-4	55	55
-3	80	83
-2	85	86
1	86	88
2	83	86
3	83	83
4	55	55
5	41	40
H=	0,K=	12
-7	65	54
-6	36	17
-5	113	112
-4	88	84
-3	234	220
-2	267	266
-1	394	383
0	412	411
1	400	383
2	273	266
3	231	220
4	77	84
5	110	112
7	41	54
H=	0,K=	13
-2	42	40
2	31	40
4	33	29
5	32	6
H=	0,K=	14
-5	92	98
-4	32	31
-3	184	180
-2	151	153
-1	276	280
0	254	253
1	281	280
2	160	153
3	190	181
4	40	31
5	93	98
H=	0,K=	16
-6	37	27
-5	33	8
-4	69	71
-3	58	54
-2	176	177
-1	118	122
0	264	259
1	125	122
2	175	177
3	47	54
4	55	71
H=	0,K=	17
-6	45	36
-4	70	68
-2	74	73
2	80	73
4	76	68
6	39	36
H=	0,K=	18
-3	68	61
-2	56	56
-1	133	149
0	73	83
1	156	149
2	56	56
3	66	61
H=	0,K=	19
-5	81	74
-3	124	121
1	32	71
3	122	121
5	62	74
H=	0,K=	20
-6	49	43
-4	81	70
-3	106	104
-2	90	92
-1	158	177
0	100	100
1	179	177
2	88	92
3	102	104
4	84	70
6	54	43
H=	0,K=	21
-5	49	59
-3	99	93
1	32	52
3	96	93
5	58	59
H=	0,K=	22
-5	36	25
-4	124	118
-2	174	172
0	189	193
2	167	172
4	119	118
H=	0,K=	23
-4	38	34
-3	51	53
3	51	53
4	39	34
5	47	36
H=	0,K=	24
-4	81	77
-2	157	162
0	200	214
2	158	162
4	79	77
H=	0,K=	25
-3	42	26
H=	0,K=	26
-4	102	95
-2	149	158
-1	32	36
0	185	189
1	39	36
2	158	158
4	98	95
H=	0,K=	28
-4	36	24
0	37	41
2	32	36
H=	0,K=	30
-3	41	38
-2	69	79
-1	46	42
0	95	101
2	81	79
3	48	35
H=	0,K=	32
-1	35	8
H=	1,K=	0
-6	207	218
-4	611	619
-2	1259	1243
0	972	999
2	248	247
4	40	40
H=	1,K=	1
-6	100	111
-4	263	271
-3	56	54
-2	474	494
0	309	321
1	165	169
3	148	150
5	84	92
H=	1,K=	2
-6	145	148
-4	442	447
-2	886	883
-1	126	129
0	701	718
1	226	238
2	216	218
3	115	116
4	45	42
5	38	35
H=	1,K=	3
-7	46	36
-6	114	110
-5	121	121
-4	248	237
-3	413	405
-2	446	446
-1	770	797
0	462	484
1	546	559
2	244	251
3	197	197
4	91	94
5	63	64
H=	1,K=	4
-7	57	57
-6	54	56
-5	167	161
-4	147	134
-3	349	343
-2	271	263
-1	380	394
0	288	288
1	118	123
2	160	158
4	61	57
H=	1,K=	5
-5	44	42
-4	36	30
-3	65	66
-2	76	80
-1	60	55
0	196	203
1	134	136
2	190	193
3	144	147
4	101	108
5	81	88
6	50	50
H=	1,K=	6
-6	47	46
-5	48	44
-4	104	95
-3	182	180
-2	242	230
-1	360	376
0	381	392
1	317	325
2	317	307
3	129	126
4	154	147
5	33	31
6	59	61
H=	1,K=	7
-4	43	47
-3	77	80
-2	105	108
-1	275	289
0	184	195
1	317	325
2	168	171
3	146	153
4	92	94
5	48	49
6	36	38
H=	1,K=	8
-6	55	52
-4	120	123
-3	48	40
-2	258	255
0	328	336
1	98	99
2	210	218
3	88	86
4	84	86
5	42	40
H=	1,K=	9
-5	32	33
-4	40	48
-2	99	101
-1	152	139
0	116	116
1	227	218
2	61	66
3	134	131
5	42	45
H=	1,K=	10
-6	43	43
-5	105	100
-4	124	121
-3	275	264
-2	229	234
-1	394	389
0	192	197
1	257	261
2	48	47
3	78	75
H=	1,K=	11
-6	43	37
-5	48	49
-3	129	128
-2	77	85
-1	221	221
0	138	141
1	172	169
2	49	65
3	82	77
5	35	33
6	42	27
H=	1,K=	12
-6	67	72
-4	184	186
-2	340	331
-1	34	36
0	305	283
2	102	97
H=	1,K=	13
-6	39	31
-4	97	88
-3	85	89
-2	235	228
-1	162	159
0	344	344
1	104	108
2	261	259
3	38	35
4	121	117
6	43	40
H=	1,K=	14
-4	78	72
-3	59	[illegible]
-2	122	112
-1	79	74
0	48	[illegible]
1	57	63
2	33	[illegible]
3	48	38
4	52	[illegible]
6	37	[illegible]
H=	1,K=	15
-6	59	52
-5	65	73
-4	157	154
-3	108	113
-2	325	311
-1	129	138
0	366	347
1	113	117
2	211	207
3	70	67
4	93	88
6	36	34
H=	1,K=	16
-7	56	49
-6	44	44
-5	143	144
-4	97	98
-3	315	311
-2	134	138
-1	456	435
0	96	97
1	332	342
2	38	46
3	172	164
5	64	58
H=	1,K=	17
-5	33	20
-4	61	54
-2	61	68
-1	48	46
0	77	81
2	76	72
4	39	42
H=	1,K=	18
-5	40	50
-4	37	37
-3	104	108
-1	197	196
0	28	28
1	211	209
2	35	38
3	139	134
5	60	62
H=	1,K=	19
-1	60	71
0	43	50
1	59	66
2	72	80
4	77	73
H=	1,K=	20
-4	84	88
-3	33	36
-2	165	166
-1	61	75
0	204	201
1	59	65
2	139	143
4	72	66
H=	1,K=	21
-3	47	42
-1	185	183
1	229	228
3	141	140
4	35	29
5	57	51
H=	1,K=	22
-2	39	40
0	89	98
2	115	116
3	67	70
4	76	75
5	59	57
H=	1,K=	23
-5	60	57
-4	60	43
-3	121	119
-2	87	85
-1	194	189
0	94	98
1	197	195
2	70	65
3	123	129
4	34	28
H=	1,K=	24
-5	58	58
-4	81	48
-3	88	93
-2	88	94
-1	87	90
0	135	134
1	49	45
2	123	118
4	69	62
H=	1,K=	25
-3	77	77
-1	96	[illegible]
0	35	25
1	64	64
H=	1,K=	26
-5	48	46
-3	89	88
-1	118	128
1	123	132
3	82	83
H=	1,K=	27
-3	58	54
-2	61	54
-1	81	97
0	56	61
1	90	103
2	52	42
3	69	70
H=	1,K=	28
-4	72	68
-2	69	80
0	72	78
2	62	67
H=	1,K=	29
-3	51	51
-1	53	60
1	55	54
H=	1,K=	30
-2	52	61
0	51	59
1	34	33
H=	1,K=	31
0	52	45
2	49	38
H=	1,K=	33
-1	61	63
0	64	59
H=	2,K=	0
-8	71	81
-6	191	197
-4	346	351
-2	361	366
0	150	153
2	31	31
H=	2,K=	1
-7	84	83
-6	36	58
-5	207	214
-3	437	440
-2	274	280
-1	536	545
0	388	392
1	359	369
2	144	148
3	166	173
5	66	74
H=	2,K=	2
-8	44	16
-3	66	69
-2	205	208
-1	71	70
0	285	285
2	136	143
4	38	40
H=	2,K=	3
-7	35	56
-5	115	114
-3	104	97
-1	138	136
0	43	39
1	219	223
3	120	122
5	46	41
H=	2,K=	4
-8	41	45
-6	121	127
-5	31	23
-4	305	302
-2	522	510
0	473	475
1	72	69
2	241	249
3	66	63
4	97	99
5	41	28
6	51	34
H=	2,K=	5
-8	47	39
-6	59	56
[illegible]	48	70
-3	194	188
-2	184	179
-1	378	373
0	330	319
1	347	343
2	211	204
3	174	171
4	74	73
5	62	59
H=	2,K=	6
-4	30	38
-3	82	82
-2	44	37
-1	94	92
0	33	27
1	27	20
H=	2,K=	7
-6	40	42
-5	112	102
-4	84	84
-3	319	298
-2	207	203
-1	486	443
0	276	262
1	283	282
2	162	163
3	104	103
4	66	74
H=	2,K=	8
-7	45	51
-5	138	140
-4	52	46
-3	283	280
-2	100	96
-1	319	305
0	85	82
1	151	147
2	30	14
3	40	36
H=	2,K=	9
-3	92	101
-2	36	48
-1	156	170
0	67	74
1	97	105
2	57	56
4	33	29
H=	2,K=	10
-5	56	51
-3	150	140
-2	165	161
-1	271	250
0	253	239
1	239	226
2	138	133
3	122	120
4	45	35
5	47	48
H=	2,K=	11
-7	68	68
-5	153	148
-4	52	45
-3	285	274
-2	111	105
-1	327	320
0	97	93
1	211	203
2	33	28
3	69	79
H=	2,K=	12
-6	48	47
-4	92	94
-2	53	37
0	108	106
1	37	50
2	126	128
4	67	75
H=	2,K=	13
-4	35	43
-3	63	68
-2	108	117
-1	123	128
0	111	118
1	110	111
2	46	45
3	54	54
H=	2,K=	14
-7	50	49
-5	134	131
-4	51	46
-3	246	246
-2	27	17
-1	251	262
1	144	149
3	55	53
H=	2,K=	15
-6	43	27
-4	48	41
-3	29	11
-1	30	
0	38	44
2	39	39
H=	2,K=	16
-3	73	77
-2	31	39
-1	105	108
1	76	83
2	38	33
3	39	39
4	46	40
H=	2,K=	17
-7	47	40
-6	38	3
-5	81	80
-3	107	111
-1	75	85
0	38	39
2	42	44
H=	2,K=	18
-6	47	59
-4	85	93
-2	109	113
0	96	104
2	71	80
4	52	51
H=	2,K=	19
-5	59	64
-4	56	46
-3	81	80
-2	57	61
-1	95	109
0	90	89
1	118	118
2	101	99
3	78	83
4	74	73
H=	2,K=	20
-6	62	61
-4	110	112
-3	32	23
-2	160	163
-1	35	37
0	170	170
1	105	114
2	122	123
3	118	116
4	67	66
H=	2,K=	21
-6	60	47
-5	102	95
-4	59	59
-3	173	181
-1	207	208
1	136	140
2	35	40
3	60	64
H=	2,K=	22
-6	127	126
-4	253	249
-3	35	43
-2	357	361
0	333	337
1	40	46
2	198	199
3	66	56
4	85	86
H=	2,K=	23
-6	47	43
-5	99	102
-4	80	74
-3	221	220
-2	127	121
-1	301	306
0	146	141
1	261	259
2	110	106
3	145	146
4	48	54
H=	2,K=	24
-5	45	45
-3	42	45
-2	65	68
-1	34	37
0	61	60
1	35	41
3	48	46
H=	2,K=	25
-5	81	83
-4	47	40
-3	123	127
-2	62	52
-1	131	138
0	52	50
1	113	112
2	41	39
3	77	72
H=	2,K=	26
-5	100	101
-3	156	164

counter, and the scan speed accordingly adjusted. The scan speed varied between 2.0 and 8.0 °/min. Background counts were measured at each end of the scan, the summarized counting times being equal to the scan time.

The scan range-limits were 1.0° below $2\theta(\alpha_1)$ and 1.0° above $2\theta(\alpha_2)$. Three test reflections were measured for every 50 reflections. The intensity of these showed no significant change during the measurements of 2547 reflections in

Table 1. Continued.

= 2	80	41	= 4	183	180	= 1	50	38	= 6	39	32	2	46	40	= 6	58	59	= 4	151	151		Me	6,Ke	10							
= 1	162	164	= 3	27	6	0	113	123	= 5	78	70		Me	4,Ke	17	= 5	57	70	= 2	149	155	= 8	40	52								
0	49	42	= 2	282	278	2	62	68	= 4	77	70	= 7	61	55	= 4	76	81	= 1	39	32	= 4	55	52								
1	131	131	= 1	43	35	Me	3,Ke	19	= 3	114	107	= 6	67	57	= 3	84	85	0	103	104	= 3	94	104								
3	70	61	0	241	230	= 6	65	64	= 2	109	106	= 5	98	99	= 2	67	67	Me	5,Ke	20	= 2	69	64								
Me	2,Ke	27	1	38	35	= 4	131	139	= 1	48	49	= 4	137	139	= 1	67	71	0	35	13	= 1	104	110								
= 4	82	87	2	100	100	= 2	225	229	0	98	96	= 3	130	130	0	37	35	Me	5,Ke	21	0	66	60								
= 2	86	84	Me	3,Ke	8	0	236	245	2	56	52	= 2	201	201	1	32	46	= 6	49	40	1	71	69								
0	90	90	= 8	46	46	2	159	163	Me	4,Ke	5	= 1	115	113	2	37	20	= 5	40	40	Me	6,Ke	11								
1	36	36	= 6	94	88	Me	3,Ke	20	= 6	41	50	0	162	164	Me	5,Ke	6	= 4	46	52	= 5	35	29								
2	79	71	= 5	40	44	= 5	160	149	= 6	105	109	1	67	69	= 8	80	75	= 2	49	39	= 4	40	33								
3	41	25	= 4	178	165	= 3	301	288	= 4	197	197	2	76	77	= 6	167	159	Me	5,Ke	22	= 3	59	48								
Me	2,Ke	28	= 3	60	58	= 2	44	34	= 3	68	73	Me	4,Ke	18	= 5	42	51	= 2	41	44	Me	6,Ke	12								
= 1	41	54	= 2	292	272	= 1	387	382	= 2	256	246	= 4	38	57	= 4	279	275	= 1	38	37	= 6	35	36								
Me	2,Ke	29	0	294	279	0	58	49	= 1	96	102	= 2	67	78	= 3	40	48	0	40	38	= 8	52	67								
= 1	38	36	2	177	175	1	324	316	0	194	191	0	72	83	= 2	334	326	Me	5,Ke	23	= 4	55	59								
1	40	36	4	84	83	3	176	175	1	83	80	1	64	61	0	241	240	= 3	45	39	= 3	47	62								
Me	2,Ke	30	Me	3,Ke	9	Me	3,Ke	21	2	111	110	2	62	63	2	119	119	= 1	35	38	= 2	58	62								
= 2	36	27	= 7	43	47	= 6	94	83	3	44	43	3	43	55	Me	5,Ke	7	Me	5,Ke	24	= 1	35	41								
0	62	53	= 6	119	120	= 3	144	143	4	53	53	Me	4,Ke	19	= 8	62	58	= 4	39	9	0	39	39								
Me	2,Ke	31	= 3	190	188	= 2	57	48	Me	4,Ke	6	= 6	170	170	= 7	39	34	= 3	48	42	Me	6,Ke	13								
= 2	76	80	= 2	28	11	= 1	144	159	= 5	73	70	= 4	87	81	= 6	121	116	= 1	40	34	= 6	42	53								
0	75	76	= 1	147	141	0	37	44	= 4	31	26	= 3	280	253	= 5	59	58	Me	5,Ke	25	Me	6,Ke	15								
Me	3,Ke	0	1	31	33	1	116	117	= 3	115	107	= 2	116	113	= 4	178	182	= 2	37	30	= 5	45	30								
= 6	32	28	2	35	38	3	69	60	= 1	79	77	= 1	258	260	= 3	87	81	Me	5,Ke	26	= 3	42	28								
= 4	158	162	Me	3,Ke	10	Me	3,Ke	22	0	61	66	0	86	90	= 2	200	200	= 3	49	32	= 2	39	43								
= 2	304	307	= 6	71	72	= 6	83	48	1	31	22	1	177	161	= 1	85	87	Me	6,Ke	9	Me	6,Ke	16								
0	276	277	= 5	78	84	= 5	110	110	2	58	67	2	44	42	0	149	145	= 8	63	76	= 2	39	28								
2	125	128	= 4	213	206	= 4	58	59	4	37	35	Me	4,Ke	20	1	84	66	= 6	109	109	Me	6,Ke	17								
4	44	41	= 3	191	206	= 3	116	112	Me	4,Ke	7	= 6	140	145	2	70	72	= 4	145	146	= 6	53	45								
Me	3,Ke	1	= 2	354	341	= 2	33	32	= 4	79	76	= 5	70	79	Me	5,Ke	8	= 2	167	166	Me	6,Ke	18								
= 6	73	78	= 1	254	270	= 1	84	71	= 3	37	42	= 4	217	226	= 6	56	57	0	149	142	= 5	56	54								
= 5	89	88	0	292	284	1	45	39	= 2	118	121	= 3	123	136	= 5	36	43	Me	6,Ke	1	= 3	70	71								
= 4	247	252	1	171	168	Me	3,Ke	23	= 1	45	47	= 2	230	242	= 4	70	68	= 8	45	42	= 1	51	59								
= 3	198	199	2	139	138	= 6	49	56	0	112	112	= 1	123	128	= 3	45	60	= 6	84	80	Me	6,Ke	19								
= 2	332	332	3	73	79	= 5	33	31	2	74	66	0	156	166	= 2	64	55	= 4	102	102	= 4	49	44								
= 1	260	265	4	49	51	= 4	89	95	Me	4,Ke	8	1	61	67	= 1	88	96	= 3	37	31	Me	6,Ke	20								
0	121	116	Me	3,Ke	11	= 3	36	35	= 7	41	43	2	81	80	0	49	41	= 2	86	85	= 4	68	57								
1	172	169	= 7	76	80	= 2	93	101	= 5	50	43	Me	4,Ke	21	1	98	99	= 1	42	40	= 2	73	61								
2	45	44	= 5	145	145	0	57	54	= 4	44	58	= 4	44	61	2	48	32	0	65	57	Me	6,Ke	21								
3	65	64	= 4	94	103	1	32	21	= 3	30	43	Me	5,Ke	9	1	46	39	= 4	83	73											
4	47	56	= 3	186	184	Me	3,Ke	24	= 2	44	46	= 2	50	57	= 6	39	35	Me	6,Ke	2	= 3	113	101								
Me	3,Ke	2	= 2	136	142	= 5	39	22	Me	4,Ke	9	= 1	57	64	= 5	72	79	= 8	69	71	= 2	93	77								
= 7	62	71	= 1	134	125	= 4	153	146	= 6	94	93	0	42	43	= 4	68	70	= 7	47	57	Me	7,Ke	0								
= 6	65	68	0	84	89	= 3	40	29	= 5	51	53	1	69	67	= 3	111	104	= 6	126	125	= 2	45	36								
= 5	117	114	1	36	34	= 3	154	150	= 4	153	156	Me	4,Ke	22	= 2	81	87	= 5	103	111	Me	7,Ke	1								
= 4	132	135	Me	3,Ke	12	0	93	87	= 3	104	109	= 6	73	77	= 1	88	85	= 4	152	155	= 4	43	37								
= 3	128	128	= 4	87	87	2	34	28	= 2	153	153	= 5	64	52	1	47	50	= 3	140	138	= 2	53	46								
= 2	166	170	= 2	163	156	Me	3,Ke	25	= 1	136	142	= 4	85	90	Me	5,Ke	10	= 2	128	126	Me	7,Ke	3								
= 1	92	98	0	120	116	= 3	45	52	0	80	86	= 3	97	90	= 5	50	61	= 1	102	106	= 1	67	55								
0	112	114	Me	3,Ke	13	= 2	36	24	1	79	84	= 2	82	85	= 3	54	59	0	67	77	Me	7,Ke	4								
1	88	83	= 7	55	48	= 1	35	43	2	34	34	= 1	99	88	Me	5,Ke	11	1	63	56	= 7	48	38								
2	33	34	= 6	94	94	Me	3,Ke	26	Me	4,Ke	10	0	69	71	= 6	85	83	Me	6,Ke	3	= 6	46	50								
3	83	78	= 4	86	85	= 5	66	72	= 6	36	33	1	57	52	= 4	73	74	= 7	133	135	= 5	45	53								
5	58	56	= 3	148	138	= 3	80	75	= 5	48	34	2	60	49	= 3	135	136	= 5	232	229	= 4	44	43								
Me	3,Ke	3	= 2	133	129	= 2	34	17	= 4	84	85	Me	4,Ke	23	= 2	129	124	= 3	264	262	= 3	55	48								
= 7	38	43	= 1	137	136	1	37	24	= 3	88	77	= 5	40	35	= 1	112	125	= 1	195	186	Me	7,Ke	7								
= 6	71	73	0	98	91	Me	3,Ke	27	= 1	84	75	= 3	38	35	0	82	93	1	74	84	= 6	61	59								
= 5	53	58	1	94	98	= 5	37	27	4	36	21	Me	4,Ke	25	1	66	71	Me	6,Ke	4	= 5	43	27								
= 4	162	163	3	89	54	= 3	45	29	Me	4,Ke	11	= 3	42	34	Me	5,Ke	13	= 7	36	18	= 4	51	43								
= 3	51	57	Me	3,Ke	14	0	38	19	= 7	66	66	= 1	51	49	= 7	40	46	= 6	34	40	Me	7,Ke	8								
= 2	290	283	= 7	46	39	Me	3,Ke	29	= 5	100	101	Me	4,Ke	28	= 5	53	55	= 5	36	4	= 5	59	59								
= 1	63	59	= 6	36	37	= 4	41	42	= 3	94	89	= 2	59	37	= 4	53	51	= 4	66	62	Me	7,Ke	9								
0	307	297	= 6	68	62	= 2	61	56	= 2	71	68	= 1	38	6	= 3	41	34	= 2	63	69	= 6	49	36								
1	65	74	= 4	74	82	0	52	51	0	95	98	Me	5,Ke	0	= 2	79	78	= 1	39	39	= 4	40	38								
2	187	184	= 3	79	75	Me	3,Ke	30	2	61	67	= 4	58	51	0	62	58	1	36	46	= 3	37	44								
3	66	63	= 2	122	133	= 3	36	31	Me	4,Ke	12	= 2	70	68	Me	5,Ke	14	1	52	46	Me	7,Ke	10								
4	83	84	= 1	88	77	= 2	88	98	= 8	40	30	Me	4,Ke	1	= 4	36	54	Me	6,Ke	5	= 6	37	43								
5	58	58	0	117	130	= 1	60	62	= 8	82	69	= 6	55	50	= 2	63	64	= 7	77	85	= 5	36	36								
Me	3,Ke	4	1	70	64	0	105	102	= 5	48	63	= 4	81	83	= 1	37	46	= 6	71	68	= 4	39	33								
= 6	38	22	2	69	84	Me	4,Ke	0	= 4	111	115	= 3	104	101	0	74	84	= 5	117	120	= 3	40	42								
= 7	100	106	3	37	38	= 6	46	46	= 3	62	81	= 2	103	103	1	43	39	= 4	100	97	Me	7,Ke	11								
= 5	243	243	4	39	47	= 2	81	85	= 2	109	108	= 1	97	99	2	42	55	= 3	137	133	= 5	56	53								
= 4	59	61	Me	3,Ke	15	0	136	136	0	52	54	0	52	53	Me	5,Ke	15	= 2	68	73	= 3	48	48								
= 3	505	495	= 6	66	68	2	109	104	Me	4,Ke	13	1	50	49	= 7	52	48	= 1	115	121	= 2	34	20								
= 2	110	108	= 4	111	109	4	60	51	= 5	64	67	Me	5,Ke	2	= 6	41	34	1	98	88	Me	7,Ke	12								
= 1	629	605	= 3	43	33	Me	4,Ke	1	= 3	103	107	= 5	39	32	= 5	55	65	Me	6,Ke	6	= 4	78	81								
0	125	128	= 2	156	157	= 7	36	38	= 2	31	31	= 3	103	108	= 4	48	41	= 7	58	57	= 2	89	87								
1	372	369	= 1	73	70	= 6	46	41	= 1	110	110	= 2	80	92	= 3	54	41	= 6	49	57	Me	7,Ke	13								
2	85	90	0	174	174	= 5	60	63	0	66	64	= 1	149	151	= 1	43	41	= 5	103	105	= 4	49	63								
3	141	140	1	85	74	= 3	82	75	1	68	69	0	45	46	Me	5,Ke	16	= 4	71	73	= 2	57	60								
4	50	48	2	134	132	= 2	136	138	2	46	45	1	109	111	= 7	91	95	= 3	136	137	Me	8,Ke	0								
5	48	42	3	48	48	= 1	51	53	Me	4,Ke	14	3	52	50	= 6	59	67	= 2	41	50	8	106	112								
Me	3,Ke	5	4	77	72	0	190	189	= 4	36	34	Me	5,Ke	3	= 5	135	144	= 1	99	109	Me	8,Ke	2								
= 5	88	88	Me	3,Ke	16	2	116	115	= 2	48	41	= 8	73	80	= 4	75	85	1	52	54	= 8	41	52								
= 4	79	82	= 6	130	133	4	48	44	0	48	43	= 7	72	69	= 3	132	139	Me	6,Ke	7	8	56	52								
= 3	219	217	= 4	224	233	Me	4,Ke	2	2	39	40	= 6	169	172	= 2	67	79	= 7	39	23	Me	8,Ke	4								
= 2	158	148	= 2	326	332	= 5	77	79	Me	4,Ke	15	= 5	116	118	= 1	69	77	= 6	111	114	= 6	40	11								
= 1	291	283	0	305	325	= 3	81	80	= 7	36	27	= 4	283	289	0	85	86	= 5	34	37	Me	8,Ke	8								
0	125	119	2	214	221	= 2	50	48	= 6	46	44	= 3	159	164	Me	5,Ke	17	= 4	146	149	= 6	49	33								
1	173	178	4	119	118	0	47	47	= 5	74	69	= 2	320	329	= 7	59	51	= 2	129	130	Me	8,Ke	14								
2	33	32	Me	3,Ke	17	1	102	106	= 4	42	46	= 1	162	160	= 6	74	77	0	79	76	= 7	55	47								
3	62	67	= 6	56	49	2	35	30	= 3	103	105	0	235	239	= 5	89	86	Me	6,Ke	8	7	92	47								
Me	3,Ke	6	= 5	53	54	3	88	89	2	45	53	1	97	103	= 4	92	97	= 6	65	67	Me	8,Ke	22								
= 7	59	67	= 4	89	88	Me	4,Ke	3	= 1	80	84	2	120	123	= 3	95	106	= 4	87	91	= 6	66	60								
= 6	61	59	= 3	92	101	= 6	59	62	0	58	54	3	54	45	= 2	67	77	= 3	40	34	6	69	60								
= 5	164	169	= 2	92	93	= 5	69	72	2	41	37	Me	5,Ke	4	= 1	81	93	= 2	70	74	Me	8,Ke	24								
= 4	77	69	= 1	107	116	= 4	145	144	Me	4,Ke	16	= 8	78	79	0	33	37	Me	6,Ke	9	= 6	37	28								
= 3	265	254	0	43	46	= 3	126	131	= 7	63	54	= 6	135	133	1	55	61	= 7	51	50	Me	8,Ke	30								
= 2	83	87	1	68	70	= 2	226	230	= 6	84	79	= 4	179	174	Me	5,Ke	18	= 6	88	91	= 4	48	38								
= 1	197	190	Me	3,Ke	18	= 1	128	124	= 5	111	104	= 3	101	106	= 5	40	42	= 5	70	74	4	92	38								
0	75	67	= 7	44	50	0	210	207	= 4	134	124	= 2	173	169	= 4	44	47	= 4	111	120	Me	8,Ke	36								
1	85	84	= 6	99	101	1	69	66	= 3	160	155	= 1	152	148	= 3	66	68	= 3	80	82	= 1	71	47								
2	68	71	= 5	88	86	2	122	119	= 2	142	131	0	138	128	= 1	80	88	= 2	93	108	Me	1,Ke	0								
4	55	56	= 4	148	153	3	44	23	= 1	153	151	1	90	94	1	63	66	= 1	62	66	= 6	61	65								
Me	3,Ke	7	= 3	88	86	4	56	51	0	96	88	2	89	84	Me	5,Ke	19	0	48	69	Me	1,Ke	2								
= 6	68	87	= 2	157	168	Me	4,Ke	4	1	94	91	Me	5,Ke	5	= 6	97	97	1	43	38	= 8	53	40								

Table 1. Continued.

Hm	1,Km 3	-1	88	38	Hm	3,Km 16	Hm	4,Km 15	-1	48	51	-9	60	60	Hm	6,Km 24	-1	95	87					
-8	41	48	1	47	41	-8	60	68	-8	51	35	Hm	5,Km 3		Hm	6,Km 7	-4	68	75	Hm	6,Km 2			
Hm	1,Km 12	Hm	1,Km 36		Hm	3,Km 18	Hm	4,Km 19	4	92	51	-8	65	65	-2	94	88	-6	82	74				
-8	42	23	0	40	33	-8	42	51	-7	88	86	Hm	5,Km 4		Hm	6,Km 9	Hm	6,Km 25	-3	84	78				
Hm	1,Km 19	Hm	2,Km 22		Hm	3,Km 19	3	87	91	4	86	46	-8	43	49	-2	84	41	Hm	8,Km 3				
8	40	43	5	45	33	4	66	78	Hm	4,Km 21		Hm	5,Km 8		Hm	6,Km 18	Hm	7,Km 8	-6	86	88				
Hm	1,Km 23	Hm	2,Km 30		Hm	3,Km 20	3	53	51	3	73	66	-6	41	30	-7	43	44	-4	60	69				
8	69	62	2	69	58	-7	71	68	Hm	4,Km 29		Hm	5,Km 16		Hm	6,Km 21	Hm	7,Km 12	-2	53	61				
Hm	1,Km 26	Hm	2,Km 33		Hm	3,Km 22	-4	84	52	-8	42	38	-6	39	44	-6	38	54	Hm	8,Km 9				
8	82	31	-3	82	84	-7	78	69	-2	63	97	Hm	5,Km 24		-5	91	79	0	56	61	-3	46	27	
Hm	1,Km 33	-1	69	62	Hm	3,Km 24	Hm	4,Km 30	-6	54	28	-1	88	84	Hm	7,Km 13	Hm	8,Km 10						
-8	55	52	Hm	2,Km 34	-6	97	91	-4	81	71	Hm	5,Km 25		0	62	50	-6	39	40	-6	87	74		
1	81	70	-3	66	62	Hm	3,Km 30	-2	102	81	1	54	40	Hm	6,Km 23		Hm	8,Km 1	-4	113	98			
Hm	1,Km 34	-1	57	59	-4	59	66	-1	62	32	Hm	6,Km 0		-5	64	58	-7	99	92	-2	104	86		
-3	51	45	0	46	39	1	48	47	0	75	61	2	92	86	-3	74	62	-5	132	125	Hm	7,Km 13		
-1	64	56	1	49	42	2	63	66	Hm	4,Km 32		Hm	6,Km 3		-1	53	47	-3	135	123	-6	39	40	
Hm	1,Km 35																							

Table 2. Fractional atomic coordinates for non-hydrogen atoms, anisotropic thermal vibration parameters and their estimated standard deviations (multiplied by 10^5). The temperature factors are expressed as:
$\exp-(B_{11}h^2+B_{22}k^2+B_{33}l^2+B_{12}hk+B_{13}hl+B_{23}kl)$

Atom	x	y	z	B_{11}	B_{22}	B_{33}	B_{12}	B_{13}	B_{23}
O1A	34866	12195	23468	2947	96	4055	178	4271	70
	34	7	34	72	3	82	27	127	26
O4A	93700	−4462	23582	3030	90	3874	177	4008	−4
	41	7	36	81	3	83	27	136	26
O1B	68125	41747	24385	3645	99	3763	−207	4255	−10
	38	7	37	85	3	76	26	136	25
O4B	33424	21535	21341	3644	99	4609	−117	4199	47
	41	8	40	91	3	98	29	154	29
N4A	98096	311	24160	2570	108	2721	74	2807	33
	39	10	37	87	4	79	29	142	28
N4B	54777	22982	25803	3102	116	3325	−47	2948	53
	49	10	45	105	4	95	34	165	30
C1A	49883	9414	24594	2380	87	2257	−1	2511	−42
	48	10	46	102	4	90	34	163	31
C2A	47018	4269	25472	2420	96	3164	−110	3577	−28
	54	11	51	112	5	110	38	188	36
C3A	62275	1233	25468	2576	81	2829	−97	2864	−47
	50	11	51	113	4	99	36	175	33
C4A	82401	2917	24958	2017	91	2106	28	2222	35
	47	9	46	93	4	89	32	151	30
C5A	86005	8003	25286	2265	108	2849	−95	3052	73
	54	10	51	108	4	104	37	177	35
C6A	70876	11070	25350	2760	80	2964	−56	3189	68
	51	10	52	111	4	108	35	178	33
C1B	64877	37461	25279	2952	101	2482	−187	2984	−29
	51	10	48	107	4	96	40	166	35
C2B	42669	35650	21389	2897	107	3577	90	3701	107
	59	12	55	119	5	126	42	204	38
C3B	38615	31006	21485	2741	102	3439	−122	3339	6
	57	11	53	124	5	122	38	200	36
C4B	56484	27620	25724	3013	87	2640	−19	2748	39
	56	10	52	117	5	101	38	180	33
C5B	78674	29356	30182	2898	120	4447	116	3503	14
	64	13	62	128	5	152	45	228	42
C6B	82700	33983	30151	2416	122	4203	−117	3338	−45
	59	12	57	112	5	139	40	207	41

a quadrant with $2\theta < 55°$. 1504 unique reflections with intensities larger than $2.0 \times \sigma(I)$ were regarded as observed.

The intensity data were corrected for Lorentz and polarization effects. Atomic form factors were those of Doyle and Turner [6] for oxygen, nitrogen, and carbon, and of Stewart *et al.*[7] for hydrogen. All programs applied during the structure investigations are described in Ref. 8.

CRYSTAL DATA

1,4-Benzoquinone monoxime, $C_6H_5O_2N$, monoclinic, space group $P2_1/c$.
$a = 7.209(3)$ Å, $b = 28.14(1)$ Å, $c = 6.671(3)$ Å,
$\beta = 118.86(3)°$, $V = 1185$ Å^3, $M = 123.11$,
$F(000) = 512$,
$Z = 8$, D_{obs} (flotation) $= 1.37$ g/cm^3, $D_{calc} = 1.380$ g/cm^3.

STRUCTURE DETERMINATION

The structure was solved by the symbolic addition procedure. A preliminary scale factor and an overall isotropic thermal factor ($B = 3.0$ Å^2) were determined using the statistical methods of Wilson.[9] A U-map, computed with 400 reflections with $U \geq 0.110$ revealed the positions of all non-hydrogen atoms in two independent molecules of (I). Fourier and subsequent least-squares refinements of non-hydrogen atomic parameters reduced the conventional R-factor to 0.08. At this stage positional parameters for hydrogen atoms were calculated from stereochemical considerations. Least-squares full-matrix refinements of positional and thermal parameters of all atoms converged with a conventional R-factor of 0.047 and a weighted R-factor ($R_w = (\sum W\Delta^2/\sum WF_o^2)^{\frac{1}{2}}$ of 0.042. The goodness of fit, expressed by $\sum W\Delta^2/(M-n)$ where M is the number of reflections and n is the number of parameters refined, is 2.2.

Table 3. Fractional atomic coordinates ($\times 10^4$) and isotropic thermal parameters with estimated standard deviations for hydrogen atoms.

Atom	x	y	z	B
H2A	3362	326	2567	3.5
	47	9	41	7
H3A	5996	−191	2527	2.9
	43	10	37	6
H5A	9911	909	2531	2.4
	45	9	37	6
H6A	7242	1446	2419	3.5
	43	9	40	6
HOA	10729	−595	2454	4.7
	54	11	47	8
H2B	3137	3797	1826	3.8
	45	10	41	7
H3B	2375	2972	1849	4.2
	52	10	45	7
H5B	9001	2711	3280	5.3
	55	11	50	8
H6B	9737	3520	3328	5.4
	55	11	47	8
HOB	3412	1796	2045	12.8
	78	18	66	1.5

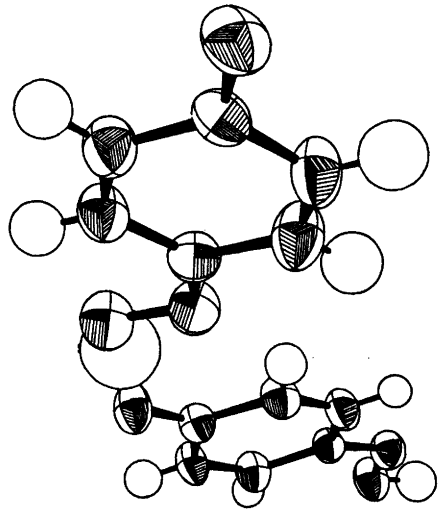

Fig. 1. 50 % probability ellipsoids.

A comparison of observed and calculated structure factors is given in Table 1. Final parameters are listed in Table 2 for non-hydrogen atoms, and in Table 3 for hydrogen atoms. Magnitudes and directions of the principal axes of the vibrational ellipsoids are given in Fig. 1.

The r.m.s. discrepancy between the atomic vibrational tensor components obtained in the structure determination and those calculated from a rigid-body analysis was 0.0028 Å^2 for molecule A and 0.0023 Å^2 for molecule B.

The translational r.m.s. amplitudes of vibration along the principal axes are 0.20, 0.19, and 0.19 Å for A and 0.21, 0.21, and 0.20 Å for B. The r.m.s. librational amplitudes are 6.8, 3.7, and 2.1° in A and 8.7, 3.5, and 2.5° in B. The coordinates were adjusted according to this

Table 4. Bond lengths (Å) and angles (°).

Bond lengths

Distance	(Å)	Distance	(Å)	Distance	(Å)
O1A–C1A	1.2428(31)	O4B–N4B	1.3623(34)	O1A–HOB	1.6356
O1B–C1B	1.2328(32)	C1A–C2A	1.4658(40)	N4A–C4A	1.3021(33)
O4A–N4A	1.3713(31)	C3A–C4A	1.4409(40)	C1A–C6A	1.4518(40)
N4B–C4B	1.3103(34)	C2B–C3B	1.3353(41)	C4A–C5A	1.4495(38)
C2A–C3A	1.3290(42)	O4B–HOB	1.0094	C1B–C2B	1.4601(43)
C5A–C6A	1.3297(40)			C4B–C5B	1.4401(46)
C1B–C6B	1.4466(42)				
C3B–C4B	1.4393(41)				
C5B–C6B	1.3296(45)				

Hydrogen bond lengths

O1A–O4B	2.6319(28)
O1B–O4A(a)	2.7000(32)

Bond angles

Angle	(°)	Angle	(°)
O1A–C1A–C6A	122.20(25)	O1A–C1A–C2A	120.48(25)
C1A–C2A–C3A	121.27(28)	C2A–C3A–C4A	120.79(27)
C3A–C4A–C5A	118.27(25)	C4A–C5A–C6A	121.37(28)
C5A–C6A–C1A	120.78(27)	C6A–C1A–C2A	117.31(25)
C3A–C4A–N4A	126.52(24)	N4A–C4A–C5A	115.22(25)
C4A–N4A–O4A	112.84(23)	O1B–C1B–C2B	121.25(28)
O1B–C1B–C6B	122.03(30)	C1B–C2B–C3B	121.97(33)
C2B–C3B–C4B	120.02(32)	C3B–C4B–C5B	118.66(29)
C4B–C5B–C6B	121.22(34)	C5B–C6B–C1B	121.34(34)
C6B–C1B–C2B	116.72(29)	C3B–C4B–N4B	126.57(32)
N4B–C4B–C5B	114.76(31)	C4B–N4B–O4B	112.30(23)

Dihedral angle	(°)	Dihedral angle	(°)
C3A–C4A–N4A–O4A	−.68(46)	C5A–C4A–N4A–O4A	179.14(23)
C4A–N4A–O4A–HOA	174.15	C2A–C1A–O1A–HOB	174.66
C3B–C4B–N4B–O4B	.21(48)	C5B–C4B–N4B–O4B	179.52(29)
C4B–N4B–O4B–HOB	−174.37	C2B–C1B–O4A–HOA	9.65(24)

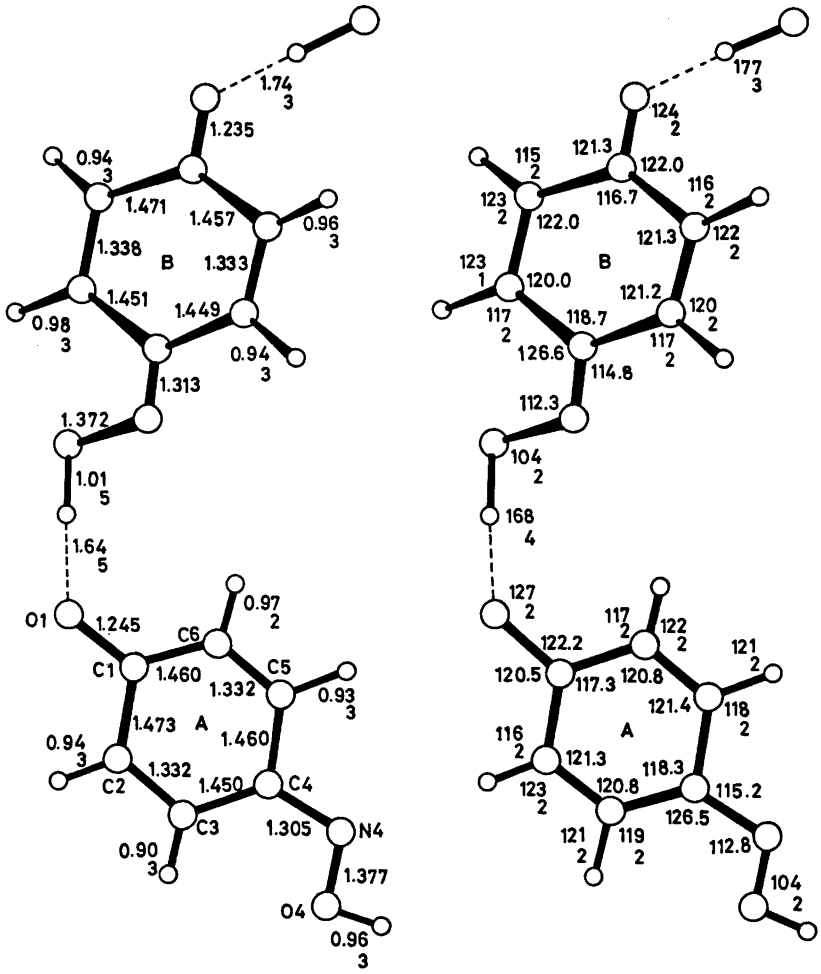

Fig. 2. Bond angles and bond lengths (corrected).

libration. Uncorrected bond lengths and angles are given in Table 4. The bond lengths corrected for the librational effects and angles may be found in Fig. 2. Estimated standard deviations were calculated from the correlation matrix. Standard deviations are 0.004 Å in carbon–carbon bond lengths, 0.003 Å in carbon–nitrogen, carbon–oxygen and nitrogen–oxygen bond lengths, and 0.3° in angles involving non-hydrogen atoms. Deviations from least-squares planes are given in Table 5.

DISCUSSION

The packing of molecules in the crystal is shown in Fig. 3.

Refining of hydrogen atom parameters and the final bond lengths involving non-hydrogen atoms showed that the two independent molecules both were oximes. All A-molecules are situated near planes parallel to the ab planes at $Z = 1/4$, 3/4 whereas the B-molecules have a tilt of 12° to these planes.

Owing to two O4H···O1 hydrogen bonds, the molecules are forming chains along the screw axes. The repeating unit along these chains is one A- and one B-molecule. Close-packing and normal van der Waals contacts are found in the direction of the a and c^* axes.

The hydrogen bond lengths are quite normal. Interestingly, the hydrogen bond crossing the screw axes is substantially longer (0.07 Å) than

Table 5. Deviations (in Å) of atoms from least-squares planes through the atoms C1A, C2A, C3A, C4A, C5A, C6A, and C1B, C2B, C3B, C4B, C5B, C6B.

Plane A				Plane B			
C1A	−0.0301	O1A	−0.095	C1B	−0.0164	O1B	−0.0613
C2A	−0.0166			C2B	0.0087		
C3A	0.0094			C3B	0.0048		
C4A	−0.0219	O4A	−0.123	C4B	−0.0108	O4B	−0.0710
C5A	0.0075	O4A	−0.078	C5B	0.0025	N4B	−0.0496
C6A	0.0185			C6B	0.0111		

The angle between planes A and B is 12.6°.

the other hydrogen bond. Hadzi (1956)[10] observed a splitting of the νOH band of about 150 cm^{-1} in IR spectra from (I) in the solid state. Probably this splitting is explained by the presence of two different hydrogen bonds in the structure. Packing effects are probably causing the difference between the two bonds. According to investigations by Craven *et al.*[11] of hydrogen bonding effects on the molecular structure, the hydrogen bonds are probably causing the slight difference between the two C1 – O1 and the two N4 – O4 bond lengths. These differences are significant while other differences between corresponding bond lengths are not significant.

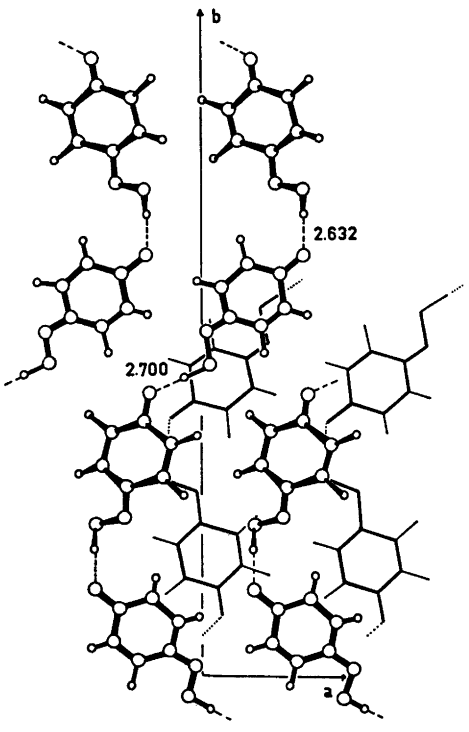

Fig. 3. Packing of molecules. The view is down c^*.

The bond lengths and angles in (I) are of the same order as corresponding bond lengths and angles in (II) and (III), and the similarity between (I) and the cation of *N,N*-dimethyl-*p*-nitrosoaniline hydrochloride [3] is remarkable. No significant differences are found between corresponding bond lengths and angles in (I) and this last oxime. Even the slight (but significant) difference between the C1 – C2 and the C1 – C6 bond lengths is found in both structures.

A comparison of (I) and 1,4-benzoquinone [12] shows that the C=O and the C=C double bonds are possibly slightly (but not significantly) longer, and the C – C single bonds significantly shorter in (I) than those in 1,4-benzoquinone.

The CN bond lengths [1.302(3) Å and 1.310(3) Å] are significantly longer than the corresponding bond lengths in formaldehyde oxime [13] [1.276(5) Å] and 1,4-cyclohexandione dioxime [14] [1.276(3) Å]. Accordingly the NO bond lengths [1.362(3) and 1.373(3) Å] are significantly shorter than those of formaldehyde oxime and 1,4-cyclohexandione dioxime [1.408(5) and 1.411(3) Å, respectively]. The CN and NO bond lengths in these last two oximes are pure double and single-bond bond lengths.[15]

Thus, the difference between (I) and 1,4-benzoquinone and the last two oximes indicates that the following structure contributes considerably to resonance in (I):

CNDO/2 [16] calculations indicate a considerable degree of delocalisation of π-bonds in (I).

REFERENCES

1. Lüttke, W. *Z. Electrochem. 61* (1957) 976.
2. Rømming, Chr. and Talberg, H. J. *Acta Chem. Scand. 27* (1973) 2246.
3. Drangfelt, O. and Rømming, Chr. *Acta Chem. Scand. To be published.*
4. Schors, Kraaijveld and Haugna. *Rec. Trav. Chim. Pays-Bas 74* (1955) 1243.
5. Romers, C., Shoemaker, C. B. and Fischman, E. *Rec. Trav. Chim. Pays-Bas 76* (1957) 490.
6. Doyle, P. A. and Turner, P. S. *Acta Crystallogr. A 24* (1968) 399.
7. Stewart, R. E., Davidson, E. R. and Simpson, W. T. *J. Chem. Phys. 42* (1965) 3175.
8. Groth, P. *Acta Chem. Scand. 27* (1973) 1837.
9. Wilson, A. J. C. *Nature 150* (1942) 151.
10. Hadzi, D. *J. Chem. Soc.* (1956) 2725.
11. Craven, B. M., Cusake, C., Gartland, G. L. and Vizzini, E. A. *J. Mol. Struct. 16* (1973) 331.
12. Trotter, J. *Acta Cryst. 13* (1960) 98.
13. Levine, J. N. *J. Chem. Phys. 38* (1963) 2327.
14. Groth, P. *Acta Chem. Scand. 22* (1968) 128.
15. Häfelinger, C. *Chem. Ber. 103* (1970) 3370.
16. Pople, J. A. and Segal, G. A. *J. Chem. Phys. 44* (1966) 3289.

Received May 2, 1974.

Acta Chemica Scandinavica A 28 (1974) 919—926

Acid-catalyzed Hydrolyses of Bridged Bi- and Tricyclic Compounds. I. Kinetics and Product Analyses of Some 2-Norbornyl, 2-Norbornenyl, and 3-Nortricyclyl Acetates*

MARTTI LAJUNEN

Department of Chemistry, University of Turku, 20500 Turku 50, Finland

The hydrolysis of *exo* and *endo* isomers of several secondary and methyl-substituted tertiary 2-norbornyl and 2-norbornenyl acetates and of secondary and tertiary 3-nortricyclyl, cyclopentyl, and cyclohexyl acetates has been studied by titrimetric and gas-chromatographic methods under catalysis by perchloric acid (1 M in 60 wt. % dioxane – water). All secondary acetates were observed to hydrolyze by the $A_{AC}2$ mechanism and the tertiary acetates by the $A_{AL}1$ mechanism with the exception of the tertiary *endo*-2-norbornenyl acetate, which hydrolyzes simultaneously by both mechanisms. Solvent deuterium isotope effects measured for some acetates agree with these mechanisms. "Normal" rates of hydrolysis *via* carbenium ions were estimated for the tertiary acetates by a modified Schleyer method. A notable anchimeric increase in the rate of hydrolysis was evaluated for the *exo* and tricyclic acetates, but the rate of hydrolysis was estimated to be "normal" in the case of the *endo* acetates.

2-Norbornyl and 2-norbornenyl esters, especially sulfonates, have been the subject of intensive solvolysis studies during recent decades.[2–10] Characteristic of these solvolysis reactions, which usually follow the S_N1 mechanism, are (a) high *exo*/*endo* rate ratios, (b) rearranged *exo* and/or tricyclic products, and (c) the formation of solely (*exo* substrates) or nearly solely (*endo* substrates) racemic products in the reaction of optically active precursors. These characteristics have been explained to be due to the formation of nonclassical carbonium ions (delocalized positive charge) from *exo* substrates and the formation of classical carbenium ions (localized positive charge) from *endo* substrates.[2–6] These deductions have, however, encountered strong criticism.[6–11]

The acid-catalyzed hydrolyses of the simple carboxylic acid esters of 2-norborneols and 2-norbornenols have been studied much more seldom.[12–14] It is possible that *exo* carboxylates favor the $A_{AL}1$ hydrolysis,[15] in which the stable carbonium ion of nonclassical character may be formed from the protonated substrate in the rate-determining step of the reaction, whereas *endo* carboxylates may, in order to avoid the sterically hindered transition state of the $A_{AL}1$ hydrolysis,[7–10] hydrolyze by the $A_{AC}2$ mechanism,[15] in which one or more molecules of water react with the protonated substrate in the rate-determining step. For this study several 2-norbornyl, 2-norbornenyl, and 3-nortricyclyl acetates (Table 1) and cyclopentyl (Pent-I-OAc), 1-methylcyclopentyl (Pent-II-OAc), cyclohexyl (Hex-I-OAc), and 1-methylcyclohexyl (Hex-II-OAc) acetates were prepared. The hydrolysis rates of the acetates were measured at several temperatures in a solution of 1.00 M perchloric acid in 60 wt. % dioxane-water. The products of hydrolysis were analyzed.

EXPERIMENTAL

The preparation and identification of the bi- and tricyclic acetates and the corresponding alcohols is described in Ref. 1. The reaction medium, consisting of water and dioxane in the

* Part 1 of the abridgment of M. Lajunen's Dissertation.[1]

Table 1. The numbering system and symbols used in this paper for 2-norbornyl (A), 2-norbornenyl [a] (B), and 3-nortricyclyl (C) acetates and alcohols.

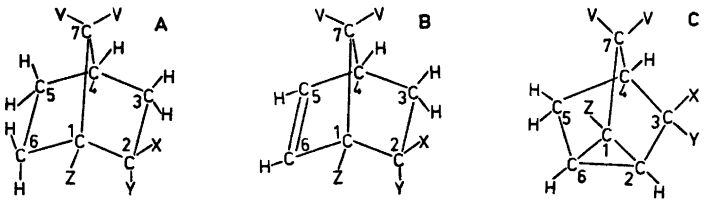

V	X	Y	Z	A	B	C
H	x[b]	H	H	*exo*-I-x	*exo*-V-x	X-x[c]
H	H	x	H	*endo*-I-x	*endo*-V-x	X-x[c]
H	x	R[d]	H	*exo*-II-x	*exo*-VI-x	XI-x[e]
H	R	x	H	*endo*-II-x	*endo*-VI-x	XI-x[e]
H	x	H	R	*exo*-III-x		*cis*-XII-x
H	H	x	R	*endo*-III-x		*trans*-XII-x
R	x	H	R	*exo*-IV-x		
R	H	x	R	*endo*-IV-x		

[a] The site of the double bond between C(5) and C(6) is not indicated with a number in this paper. [b] x indicates OH or OAc. [c] Enantiomers. [d] R indicates the methyl group. [e] Enantiomers.

weight ratio 40:60, was prepared by weighing the components.

Kinetic measurements were performed partly titrimetrically by following the formation of acetic acid and partly by gas chromatography (columns: 5 % FFAP on Chromosorb G, 10 % XE-60 on Chromosorb W, and 10 % Versamid 900 on Chromosorb W) when the disappearance of the acetates and the formation and possible decomposition of the alcohols were followed. In the hydrolyses of tricyclic and unsaturated bicyclic acetates the alcohols produced are unstable and react further with the medium when norbornanediols are formed (*cf.* Ref. 16). In these consecutive reactions $A \xrightarrow{k_A} B \xrightarrow{k_B} C$ the rate of decomposition of A into B (k_A) was determined by iteration using variations of eqn. (1) derived for the concentration of

$$[B] = \frac{k_A[A]_0}{k_B - k_A}[\exp(-k_A t) - \exp(-k_B t)] + [B]_0 \exp(-k_B t) \quad (1)$$

B at time t.[17] (Initial conditions are $[A] = [A]_0$ and $[B] = [B]_0$ at $t = 0$.) The disappearance rate of B (k_B) was determined separately. The intermediate products were analyzed by gas chromatography (GLC) and IR and NMR spectroscopy.[1] Norbornanediols were not identified. The observed disappearance rates of the acetates and the unsaturated and tricyclic alcohols studied are given in Tables 2 – 3. The intermediate and final products, which could be detected by GLC during ten half-lives of the reaction, are also given.

The side reactions, in which water adds by acid catalysis to the double bond of 2-norbornenyl acetates (*cf.* k_D in Scheme 1) and to the three-membered carbon ring of 3-nortricyclyl acetates, were estimated to be insignificant (rate coefficients in Tables 2 – 3 and the inductive constants of acetoxyl and hydroxyl groups [18] have been compared).[1] The same results were achieved experimentally when the kinetic response ratios (RR_{kin}, eqn. 2) were compared with the response ratios of acetates and the corresponding alcohols in their equimolar solutions (RR, eqn. 3).

$$RR_{kin} = \frac{a^0_{AC} + \sum RR_i a^0_{AI,i}}{\sum a^\infty_{AI,i} + a^\infty_{AC}/RR} \quad (2)$$

$$RR = \frac{a_{AC}(\text{n mol/l})}{a_{AI}(\text{n mol/l})} \quad (3)$$

In the equations a_{AC} and a_{AI} are the GLC peak areas of acetate and alcohol(s), respectively, and the superscripts 0 and ∞ refer to the first ($t = 0$) and the final ($t = 10t_{1/2}$) samples (a^∞_{AC} was 0 – 2 % of the value of a^0_{AC}). RR_{kin} was observed to be equal to RR ($= 1.24 \pm 0.01$) within experimental error (with the exception of *endo*-VI-OAc) when the peak areas of tricyclic alcohols formed in the hydrolysis of bicyclic acetates were corrected to correspond

Table 2. Rates and products of acid-catalyzed hydrolyses of some mono-, bi-, and tricyclic acetates in a solution of 1.00 M perchloric acid in 60 wt. % dioxane-water at different temperatures.

Acetate	$10^5 k_a/M^{-1}s^{-1}$ [a] 15 °C	25 °C	35 °C	45 °C	55 °C	Products
Pent-I-OAc		4.58	11.2	26.0	56.8	Pent-I-OH
Hex-I-OAc		4.83	11.2	26.2	57.6	Hex-I-OH
exo-I-OAc		3.90	9.06	22.0;28.1 [b]	50.4	*exo*-I-OH
endo-I-OAc		4.70	11.3	25.9	54.4	*endo*-I-OH
exo-III-OAc		2.95	6.38	14.9	33.3	*exo*-III-OH and II-OH
endo-III-OAc		3.38	7.78	18.3	39.9	*endo*-III-OH
exo-IV-OAc [c]		0.35 [d]				
endo-IV-OAc [c]		3.08				
iso-Pr-OAc [c]		4.7				
exo-V-OAc		3.72	9.11	21.4	47.8	*exo*-V-OH and some X-OH [e] and unknown subst.
endo-V-OAc		3.90	9.76	22.5	48.5	*endo*-V-OH and some [e] unknown substance
X-OAc		7.50	17.3	38.1	85.7	X-OH [e]
Pent-II-OAc	8.65	37.9	157	547		Pent-II-OH and 12–15 % of 1-methylcyclopentene
Hex-II-OAc		3.65	16.5	73.5	290	Hex-II-OH and 28–36 % of 1-methylcyclohexene
tert-BuOAc [c]		3.44				
exo-II-OAc	26.5 [f]	85.9 [b,f]	148 [g]	637 [h]		*exo*-II-OH and some *endo*-II-OH and *exo*-III-OH
	66.0	327	1130			
exo-II-OAc [i]	6.80 [f]	50.6	216	780		
	26.6 [g]					
endo-II-OAc		0.477	1.65	6.21	17.8	*exo*- and *endo*-II-OH and *exo*-III-OH
					50.9 [b]	
exo-VI-OAc	3.97	17.2	77.8	321		*exo*-VI-OH and XII-OH [e]
endo-VI-OAc		0.622	1.68	4.16	11.4	*endo*-VI-OH and XII-OH [e] (perhaps some *exo*-VI-OH)
XI-OAc	7.82 [f]	34.2 [g]	149 [h]	568 [j]		XI-OH [e]
	18.3	69.6	276	1060		

[a] The standard errors are 1–3 % of the value of the rate coefficients. [b] A solution of 1.00 M deuterioperchloric acid in 57.4 wt.% dioxane-heavy water. The mol fraction of deuterium oxide is the same as that of protium oxide in a solution of 1.00 M protioperchloric acid in 60 wt.% dioxane-light water. [c] Results of Bunton *et.al.*[12] in 60 % by volume dioxane-water. [d] Extrapolated. [e] The final products are norbornanediols. [f] 10°C. [g] 20°C. [h] 30°C. [i] Measured in 0.258–0.260 M acid concentrations. [j] 40°C.

Table 3. Rates and intermediate products of acid-catalyzed decomposition of unsaturated bicyclic and tricyclic alcohols in a solution of 1.00 M perchloric acid in 60 wt. % dioxane-water at 45 and 55 °C.

Alcohol	Temp./°C	$10^5 k_a/M^{-1}\,s^{-1}$	Intermediate products [a]
exo-V-OH	55	0.314 ± 0.008	*ca.* 20 % of X-OH and *ca.* 6 % of unknown substance
endo-V-OH	55	0.789 ± 0.012	*ca.* 4 % of unknown substance
X-OH	55	1.24 ± 0.02	
exo-VI-OH	55	73.7 ± 1.7	90–100 % of XII-OH [b]
endo-VI-OH	55	1.74 ± 0.02	29 % of XII-OH [c]
	45	0.403 ± 0.005	23 % of XII-OH [c]
XI-OH	55	7.19 ± 0.09	
XII-OH (*cis:*	55	5.19 ± 0.07	Some unknown
trans = 1:2)	45	1.49 ± 0.01	substance

[a] The final products are norbornanediols. [b] Percentage of XII-OH $= 100k_F/(k_F + k_I)$, see Scheme 1. [c] Percentage of XII-OH $= 100k_E/(k_E + k_G)$, see Scheme 1.

to those of bicyclic alcohols by multiplying the former areas with the factor $a_{bic-OH}/a_{tric-OH}$ (= 1.10) determined in the equimolar alcohol mixture (norbornanediols were not included when calculating RR_{kin} values). The observed RR_{kin} values also indicate that the decomposition (isomerization excluded) of the product alcohols is slight during the first ten half-lives of the hydrolysis reactions of the acetates with the exception of *endo*-VI-OAc.

DISCUSSION

The products of acid-catalyzed hydrolysis of secondary mono-, bi-, and tricyclic acetates were generally observed to be the corresponding alcohols (Table 2). The isomeric alcohols formed as by-products in the hydrolyses of 1-methyl-*exo*-2-norbornyl (*exo*-III-OAc) and *exo*-2-norbornenyl (*exo*-V-OAc) acetates could be proved to be the isomerization products of initially formed *exo*-III-OH and *exo*-V-OH (Table 3), respectively. With the exception of 3-methyl-3-nortricyclyl acetate (XI-OAc) all the tertiary acetates produce in addition to the corresponding alcohols other products (excluding norbornanediols; Table 2). 2-Methyl-2-norbornyl acetates (*exo*- and *endo*-II-OAc) produce in addition to 2-methyl-2-norborneols (II-OH; *exo* and *endo* isomers could not be separated by GLC) 1-methyl-*exo*-2-norborneol (*exo*-III-OH), the proportion of which in the products increases during the reaction (thermodynamic control; *cf.* Refs. 19 and 20). *Exo*-II-OH was verified by IR spectroscopy to be the only initially formed product of *exo*-II-OAc, but it could not be proved to be the only product of kinetic control in the hydrolysis of *endo*-II-OAc due to the complexity of the IR spectra of the mixture of the substrate and products. However, it is the main product, which isomerizes into *endo*-II-OH and *exo*-III-OH during the course of the slow hydrolysis.

In the hydrolyses of 2-methyl-2-norbornenyl acetates (*exo*- and *endo*-VI-OAc) 1-methyl-3-nortricyclanols (XII-OH; *cis* and *trans* isomers could not be separated by GLC) were formed in addition to the bicyclic alcohols (*exo*- and *endo*-VI-OH, respectively). The proportion of XII-OH in the products increases during the reaction. Thus they are at least partly the product of thermodynamic control. In the hydrolysis of *exo*-VI-OH it is not possible, owing to the few experiments, to draw any conclusion about how much of the tricyclic products is formed directly from the *exo* acetate and how much as the isomerization product of *exo*-VI-OH. *Exo*-VI-OH produces XII-OH much faster than it produces norbornanediols. The subject needs more study. The hydrolysis products of *endo*-VI-OAc could be analyzed more accurately (Scheme 1). By using an iterative procedure,

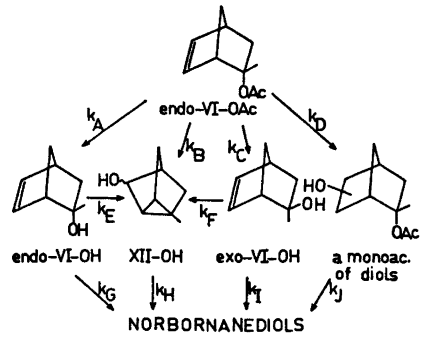

Scheme 1.

based on eqn. (1), and the disappearance rates in Tables 2 – 3 the rate constants in Table 4 could be evaluated. According to the results both *endo*-VI-OH and XII-OH (and possibly some *exo*-VI-OH) are formed under kinetic control, but XII-OH (and possibly *exo*-VI-OH) is also partly the isomerization product of *endo*-VI-OH. The reverse reactions

exo-VI-OH → *endo*-VI-OH ← XII-OH

could not be observed.

The formation of olefins, which was observed in the hydrolysis of 1-methylcyclopentyl (Pent-II-OAc) and 1-methylcyclohexyl (Hex-II-OAc) acetates, was not detected by GLC in the hydrolysis of the bi- and tricyclic acetates (*cf.* Ref. 21).

The Arrhenius equation was observed to be valid for all the acetates within the limits of the rather narrow temperature range employed in this study. The activation parameters and the calculated rate coefficients at 25 °C are presented in Table 5. The secondary mono-, bi-, and tricyclic acetates greatly resemble each other in their rates of hydrolysis and parameters of activation. They are typical of the $A_{AC}2$ hydrolysis.[15] The solvent deuterium isotope

Table 4. The values for the rate constants in Scheme 1 in a solution of 1.00 M perchloric acid in 60 wt. % dioxane-water at 45 and 55 °C.

Temp./°C	$10^5 k_a/M^{-1}\,s^{-1}$							
	k_A	k_B+k_C	k_D[a]	k_E	k_F	k_G	k_H	k_I
45	2.41	1.75	$\lesssim 0.05$	0.095	–	0.308	1.49	–
55	5.68 6.03	5.5	$\lesssim 0.2$	0.497	*ca.* 73	1.24	5.19	*ca.* 1

[a] Estimated from k_G on the basis of inductive effects of the substituents at the 2 position.[1]

Table 5. Thermodynamic functions of activation and calculated rate coefficients for the hydrolyses of mono-, bi-, and tricyclic acetates in a solution of 1.00 M perchloric acid in 60 wt. % dioxane-water at 25 °C.

Acetate	$\Delta H^{\ddagger}$/kcal mol^{-1}	$\Delta S^{\ddagger}$/cal mol^{-1} K^{-1}	$10^5 k_a/M^{-1}s^{-1}$
Pent-I-OAc	15.7 ± 0.1	−25.6 ± 0.1	4.58 ± 0.01
Hex-I-OAc	15.5 ± 0.2	−26.3 ± 0.6	4.75 ± 0.09
exo-I-OAc	16.1 ± 0.3	−24.9 ± 1.0	3.79 ± 0.12
endo-I-OAc	15.3 ± 0.1	−27.0 ± 0.4	4.72 ± 0.05
exo-III-OAc	15.2 ± 0.5	−28.4 ± 1.5	2.84 ± 0.13
endo-III-OAc	15.5 ± 0.2	−27.2 ± 0.7	3.32 ± 0.07
exo-IV-OAc[a]	17.5[b]	−28[b]	0.35
endo-IV-OAc[a]	15[b]	−31[b]	3.08
iso-Pr-OAc[a]	16.5	−25	4.5
exo-V-OAc	16.0 ± 0.1	−25.3 ± 0.2	3.70 ± 0.02
endo-V-OAc	15.7 ± 0.1	−25.9 ± 0.4	3.94 ± 0.05
X-OAc	15.2 ± 0.2	−26.6 ± 0.8	7.38 ± 0.17
Pent-II-OAc	24.8 ± 0.2	+ 8.8 ± 0.8	37.9 ± 0.6
Hex-II-OAc	27.8 ± 0.2	+14.5 ± 0.7	3.58 ± 0.07
tert-BuOAc[a]	25.5	− 1	3.44
exo-II-OAc	25.6 ± 0.7	+15.6 ± 2.4	299 ± 11
»	23.8 ± 0.6[c]	+ 6.5 ± 1.9[c]	55.7 ± 2.1[c]
endo-II-OAc	23.1 ± 0.5	− 5.4 ± 1.6	0.472 ± 0.024
exo-VI-OAc	26.2 ± 0.5	+12.1 ± 1.5	18.2 ± 0.6
endo-VI-OAc (tot)	18.3 ± 0.3	−21.1 ± 1.0	0.601 ± 0.020
» ($A_{AL}1$)	23.2 ± 1.1	− 8 ± 3	0.14 ± 0.02
» ($A_{AC}2$)	17.8 ± 1.1	−24 ± 3	0.34 ± 0.05
XI-OAc	24.4 ± 0.3	+ 8.9 ± 0.9	73.2 ± 1.3

[a] Results of Bunton *et.al.*[12] in 60 % by volume dioxane-water. [b] Measured in 0.1 − 0.3 M acid concentrations. [c] Measured in 0.258 − 0.260 M acid concentrations.

effect measured for *exo*-2-norbornyl acetate (*exo*-I-OAc), 1.28 at 45 °C, also agrees with this mechanism.[22] The rates of hydrolysis and the activation parameters measured for the tertiary mono-, bi-, and tricyclic acetates differ remarkably from each other. With the exception of the values for *exo*-2-methyl-*endo*-2-norbornenyl acetate (*endo*-VI-OAc) they are typical of the $A_{AL}1$ hydrolysis.[15] The solvent deuterium isotope effects measured for the 2-methyl-2-norbornyl acetates (*exo*-II-OAc: 3.24 at 10 °C and *endo*-II-OAc: 2.86 at 55 °C) are also consistent with this mechanism.[22] The observed activation parameters of *endo*-VI-OAc are close to the typical values of the $A_{AC}2$ mechanism, but they are, however, somewhat higher than those of the secondary acetates in Table 5. The above observations of hydrolysis products agree with the simultaneous contribution of two mechanisms, *viz.* $A_{AL}1$ and $A_{AC}2$: both *exo*-2-

methyl-*endo*-2-norbornenol (*endo*-VI-OH) and 1-methyl-3-nortricyclanols (XII-OH) as well as possibly some *endo*-2-methyl-*exo*-2-norbornenol (*exo*-VI-OH) are formed as the products of kinetic control. No observations have been made that simple *endo*-2-norbornyl and *endo*-2-norbornenyl esters produce *endo* products in the solvolysis *via* carbonium ions.[2-10] So *endo*-VI-OH can be explained to be formed in the $A_{AC}2$ hydrolysis and XII-OH (and *exo*-VI-OH) in the $A_{AL}1$ hydrolysis when the isomerization of the products is eliminated (see Table 4). In this way the activation parameters of *endo*-VI-OAc in Table 5 were estimated for these mechanisms.

The entropies of activation of the tertiary *exo* and tricyclic acetates are of the same order of magnitude as those of the tertiary monocyclic acetates but much more positive than those of the tertiary *endo* acetates (only the $A_{AL}1$ hydrolysis has been taken into account). This kind of large difference has not been found between *exo* and *endo* esters before.[4,8-10,18] The difference may be at least partly due to the contribution of the $A_{AC}2$ mechanism in the hydrolysis of *exo*-2-methyl-*endo*-2-norbornyl acetate (*endo*-II-OAc) and to the inaccuracy in the estimation of the activation parameters for the $A_{AL}1$ hydrolysis of *exo*-2-methyl-*endo*-2-norbornenyl acetate (*endo*-VI-OAc). The subject calls for further investigations.

The $A_{AC}2$ mechanism is characterized by the slight polar but large steric effects of an alkyl group.[15] The rates of hydrolysis of most secondary acetates in Table 5 are approximately equal. Thus they are sterically very much alike. The methyl substituents at the *exo*-2 position of *endo* acetates and at the *syn*-7 position of *exo* acetates have, however, a remarkable retarding effect in the $A_{AC}2$ hydrolysis. The great *exo*/*endo* rate ratios typical of the corresponding sulfonates[2-7] cannot be observed. Hydrolysis *via* carbonium ions (the $A_{AL}1$ mechanism) was expected for secondary *exo* and tricyclic acetates. However, the comparison of the hydrolysis rates of the secondary and the α-methyl substituted tertiary acetates (Table 5) with the solvolysis rates of the corresponding halides ($k_{tert}/k_{sec} \approx 10^4$)[23] implies that the proportion of the $A_{AL}1$ mechanism in the hydrolysis of the secondary acetates is negligible.

The $A_{AL}1$ mechanism is characterized by the slight steric but high polar influence of the alkyl group.[15] The rates of hydrolysis of the tertiary acetates differ quite remarkably from each other (Table 5). High *exo*/*endo* rate ratios (130 and 630 at 25 °C) typical of the corresponding saturated *p*-nitrobenzoates[9] are observed. The tertiary *exo* and tricyclic acetates hydrolyze faster and the tertiary *endo* acetates slower than 1-methylcyclohexyl (Hex-II-OAc) and tertiary butyl (*tert*-BuOAc) acetates, which cannot be explained by inductive effects only. 1-Methylcyclopentyl acetate (Pent-II-OAc), however, hydrolyzes at a rate which is of the same order of magnitude as those of *exo* acetates but much faster than those of *endo* acetates. This same pattern of reactivity in the uncatalyzed solvolyses of the corresponding chlorides[24] and *p*-nitrobenzoates[9,25,26] brought Brown to the conclusion that the *exo* esters (both secondary and tertiary) solvolyze at a "normal" rate but the *endo* isomers at a rate slower than "normal" by the S_N1 mechanism.[7] To find out whether the rates of hydrolysis of the tertiary *exo* and tricyclic acetates are higher or those of the tertiary *endo* acetates lower than "normal", the "normal" rates should be estimated.

Schleyer[27] calculated the "normal" relative rates of acetolysis for several secondary *p*-toluenesulfonates (tosylates) with reference to that of cyclohexyl tosylate using eqn. (4).

$$\log k_{rel} = (1715 - \nu_{CO})/8 + 1.32 \sum_{i}(1 + \cos 3\,\phi_i) + (GS - TS_{strain})/1.36 + (\text{inductive term}) \qquad (4)$$

The first term in the equation estimates the dependence of the rate of solvolysis on the angle strain at the reaction center (ν_{CO} is the carbonyl frequency in cm^{-1} of the ketone corresponding to the secondary alkyl group of the ester). The second term makes allowance for the torsional strains surrounding the reaction center (ϕ_i is a torsional angle). The third term is an estimate of the changes in the interactions between the nonbonded groups when proceeding from the initial state to the transition state, and the fourth term takes regard of the notable inductive factors.

Table 6. Estimation, by eqn. (5), of the rates of the $A_{AL}1$ hydrolyses for the tertiary acetates in a solution of 1.00 M perchloric acid in 60 wt. % dioxane-water at 25 °C.

Acetate	$0.152(1716-\nu_{CO})$	$1.43\sum_i(1+\cos 3\phi_i)$	$\frac{GS-TS_{strain}}{1.36}$	Ind. term.	log k_{rel} Calc.	Obs.
Hex-II-OAc	– (1716)[a]	–	0.6	–	0[b]	0[b]
Pent-II-OAc	−3.65(1740)	5.03	0.25	–	1.03[c]	1.03[c]
exo-II-OAc	−5.32(1751)	3.87	0.7	–	−1.35	1.92
endo-II-OAc	−5.32(»)	4.16	1.0	–	−0.76	−0.88
exo-VI-OAc	−4.41(1745)	3.87	0.3	−0.9	−1.74	0.71
endo-VI-OAc	−4.41(»)	4.16	0.5	−0.9	−1.25	−1.41
XI-OAc	−6.99(1762)	–	0.4	−0.5	−7.69	1.31

[a] Carbonyl frequency ν_{CO}/cm^{-1} of the ketone corresponding to the alkyl group of the acetate.[27] [b] Standard. [c] Calibration value.

Schleyer assumed when deriving eqn. (4) that all the solvolyses tested occur by the pure S_N1 mechanism.[27] However, it has been proved that the portion of the S_N2 mechanism (solvent assistance) in the solvolyses may be remarkable.[28] Therefore eqn. (4) is modified for the $A_{AL}1$ hydrolysis of the tertiary acetates by using the reference acetates available, Hex-II-OAc and Pent-II-OAc. The first three terms in the equation are re-estimated. When Schleyer determined the second term he used as the height of the rotational barrier the value 3.6 kcal/mol determined for ethyl chloride. This is here replaced by the value 3.9 kcal/mol determined for isopropyl chloride (a mean of 3.45 and 4.32 kcal/mol).[29,30] Thus the torsional strains caused by the α-methyl group are also taken into account. In the case of bicyclic compounds the torsional angles are obtained from the results of Altona and Sundaralingam,[31] otherwise the angles proposed by Schleyer have been accepted. The nonbonded interactions of the third term are calculated by using results of equilibrations and estimations reported by several authors (the more detailed treatment is in Ref. 1).[19,20,27,32–35] The coefficient of the first term is obtained in the way that the sum of the second and third terms is subtracted from the logarithm of the observed relative (to Hex-II-OAc) rate of hydrolysis of the reference acetates (see Table 6) and the results are plotted *versus* $1716-\nu_{CO}$. In this way the approximate eqn. (5) is obtained for the "normal" hydrolysis rates of the tertiary acetates when, besides, it is assumed that the energies

$$\log k_{rel} = 0.152(1716-\nu_{CO}) + 1.43\sum_i(1+\cos 3\phi_i) + (GS-TS_{strain})/1.36 + (\text{inductive term}) - 0.60 \quad (5)$$

calculated above are negligible in the transition state. The calculated and observed relative rates of hydrolysis are collected in Table 6. Results should be considered quite semiquantitative due to the fact that only two reference acetates were used when determining the coefficient of the first term.

According to Table 6 the observed rates of hydrolysis for the tertiary *exo* acetates (*exo*-II-OAc and *exo*-VI-OAc) are 2 – 3 powers of ten greater than estimated for the unassisted hydrolysis. This agrees with the deductions of Winstein [2] and Paasivirta [36] that *endo*-2-methyl substituted 2-norbornyl and 2-norbornenyl esters (and alcohols) solvolyze *via* nonclassical [2] or seminonclassical [36,37] transition states. The observed rate of hydrolysis for 3-methyl-3-nortricyclyl acetate (XI-OAc) is about nine powers of ten greater than estimated, which result is in agreement with the powerful participation of the three-membered carbon ring.[3,5,38] The anchimeric assistances, *i.e.* log k_{rel} (obs) – log k_{rel} (calc), evaluated in this work are within *ca.* one logarithmic unit equal to those estimated for the acetolysis of the corresponding secondary tosylates.[27] The observed rates of hydrolysis for the tertiary *endo* acetates (*endo*-II-OAc and *endo*-VI-OAc) are nearly equal to the estimated rates, which observation is similar to that made by Schleyer for the acetolysis of

the corresponding secondary tosylates.[37] The *endo*-6 hydrogen in the saturated skeleton and the *endo*-π orbital of the homoallylic double bond do not seem to have a considerable hindering effect on the departure of acetic acid from the *endo*-2 position (*cf.* Refs. 7 – 10, 13, 36).

Acknowledgment. The financial support from the Foundation of Neste Oy is gratefully acknowledged.

REFERENCES

1. Lajunen, M. *Kinetics and Product Analyses of the Acid-Catalyzed Hydrolyses of Some Secondary and Tertiary 2-Norbornyl, 2-Norbornenyl, and 3-Nortricyclyl Acetates*, Diss., University of Turku, Turku 1973.
2. Winstein, S. *J. Amer. Chem. Soc. 87* (1965) 381, with refs.
3. Roberts, J. D. and Bennett, W. *J. Amer. Chem. Soc. 76* (1954) 4623.
4. Berson, J. A. In de Mayo, P., Ed., *Molecular Rearrangements*, Interscience, London 1963, Chapter 3, with refs.
5. Capon, B. *Quart. Rev. Chem. Soc. 18* (1964) 45, with refs.
6. Sargent, G. D. *Quart. Rev. Chem. Soc. 20* (1966) 301, with refs.
7. Brown, H. C. a. *Chem. Brit. 2* (1966) 199; b. *Chem. Eng. News 45* (Feb. 13, 1967) 87; c. *Accounts Chem. Res. 6* (1973) 377, with refs.
8. Brown, H. C. and Ikegami, S. *J. Amer. Chem. Soc. 90* (1968) 7122.
9. Ikegami, S., Vander Jagt, D. L. and Brown, H. C. *J. Amer. Chem. Soc. 90* (1968) 7124, with refs.
10. Peters, E. N. and Brown, H. C. *J. Amer. Chem. Soc.* a. *94* (1972) 5899, 7920; b. *95* (1973) 2397, 2398.
11. Jensen, F. R. and Smart, B. E. *J. Amer. Chem. Soc. 91* (1969) 5686, 5688.
12. Bunton, C. A., Khaleeluddin, K. and Whittaker, D. *J. Chem. Soc.* (1965) 3290.
13. Bunton, C. A., O'Connor, C. and Whittaker, D. *J. Org. Chem. 32* (1967) 2812.
14. Radhakrishnamurti, P. S. and Patra, P. C. *Proc. Indian Acad. Sci. A 71* (1970) 181.
15. Euranto, E. K. In Patai, S., Ed., *The Chemistry of Carboxylic Acids and Esters*, Interscience, London 1969, pp. 549 – 569.
16. Paasivirta, J. and Äyräs, P. *Suom. Kemistilehti B 41* (1968) 51.
17. Alberty, R. A. and Miller, W. G. *J. Chem. Phys. 26* (1957) 1231, with refs.
18. McDaniel, D. H. and Brown, H. C. *J. Org. Chem. 23* (1958) 420.
19. Rei, M.-H. and Brown, H. C. *J. Amer. Chem. Soc. 88* (1966) 5335.
20. Hirsjärvi, P., Kauppinen, H.-L. and Paavolainen, S. *Suom. Kemistilehti B 42* (1969) 236.
21. Winstein, S., Clippinger, E., Howe, R. and Vogelfanger, E. *J. Amer. Chem. Soc. 87* (1965) 376.
22. Bunton, C. A. and Shiner, V. J. *J. Amer. Chem. Soc. 83* (1961) 3207, with refs.
23. Fry, J. L., Harris, J. M., Bingham, R. C. and Schleyer, P. v. R. *J. Amer. Chem. Soc. 92* (1970) 2540.
24. Brown, H. C. and Rei, M.-H. *J. Amer. Chem. Soc. 86* (1964) 5008.
25. Brown, H. C. and Dickason, W. C. *J. Amer. Chem. Soc. 91* (1969) 1226.
26. Fort, R. C., Hornish, R. E. and Liang, G. A. *J. Amer. Chem. Soc. 92* (1970) 7558.
27. Schleyer, P. v. R. *J. Amer. Chem. Soc. 86* (1964) 1854, 1856.
28. Fry, J. L., Lancelot, C. J., Lam, L. K. M., Harris, J. M., Bingham, R. C., Raber, D. J., Hall, R. E. and Schleyer, P. v. R. *J. Amer. Chem. Soc. 92* (1970) 2538.
29. Tobiason, F. L. and Schwendeman, R. H. *J. Chem. Phys. 40* (1964) 1014.
30. Möller, K. D., De Meo, A. R., Smith, D. R. and London, L. H. *J. Chem. Phys. 47* (1967) 2609.
31. Altona, C. and Sundaralingam, M. *J. Amer. Chem. Soc. 92* (1970) 1995.
32. Eliel, E. L., Allinger, N. L., Angyal, S. J. and Morrison, G. A. *Conformational Analysis*, Wiley, New York 1965, pp. 44, 51, 202.
33. Wilcox, C. F., Sexton, M. and Wilcox, M. F. *J. Org. Chem. 28* (1963) 1079.
34. Goering, H. L. and Schewene, C. B. *J. Amer. Chem. Soc. 87* (1965) 3516.
35. Ouellette, R. J., Rawn, J. D. and Jreissaty, S. N. *J. Amer. Chem. Soc. 93* (1971) 7117.
36. Paasivirta, J. a. *Justus Liebigs. Ann. Chem. 686* (1965) 1; b. *Acta Chem. Scand. 22* (1968) 2200.
37. Olah, G. A., White, A. M., DeMember, J. R., Commeyras, A. and Lui, C. Y. *J. Amer. Chem. Soc. 92* (1970) 4627.
38. Olah, G. A. and Liang, G. *J. Amer. Chem. Soc. 95* (1973) 3792.

Received January 28, 1974.

Acta Chemica Scandinavica A 28 (1974) 927—934

Short Communications

Polythionates. III. The Reaction between the Telluropentathionate Ion and the Cyanide Ion in Acetonitrile

TOR AUSTAD

Chemical Institute, University of Bergen, N-5000 Bergen, Norway

In aqueous solution, according to Foss,[1] the telluropentathionate ion does not react with ionic cyanide. Instead, due to the alkalinity of the cyanide solution, a rapid and complete hydrolysis takes place, according to the reaction, eqn. 1:

$$2\ TeS_4O_6^{2-} + 6\ OH^- \xrightarrow{H_2O} 4\ S_2O_3^{2-} + Te + TeO_3^{2-} + 3\ H_2O \qquad (1)$$

If the telluropentathionate ion would react with the cyanide ion in the same way as the corresponding pentathionate and selenopentathionate reactions, reaction (2) should take place.

$$TeS_4O_6^{2-} + 2\ CN^- + 2\ OH^- \xrightarrow{H_2O} S_2O_3^{2-} + SCN^- + TeCN^- + SO_4^{2-} + H_2O \qquad (2)$$

Due to the instability of the tellurocyanate ion in protic solvents,[2] the telluropentathionate-cyanide reaction has been studied in the dipolar aprotic solvent acetonitrile, where we have found that ionic cyanide readily reacts with the telluropentathionate ion without any liberation of elemental tellurium.

This paper reports a kinetic investigation of this reaction in acetonitrile. This kinetic study appears to be the first one concerning nucleophilic substitution at divalent tellurium. Tetraphenylarsonium telluropentathionate was used as the substrate, and tetraphenylphosphonium cyanide was used as the nucleophilic reagent. Conductivity measurements in acetonitrile proved that these salts were completely dissociated in the concentration range used in the kinetic runs.

The reaction was found to be second order, first order in each of the reactants, and 1 mol of ionic telluropentathionate was found to consume 6 mol of cyanide ions. IR and iodometric measurements showed that 1 mol of ionic thiocyanate, 1 mol of ionic tellurocyanate and 1 mol of ionic thiolsulfate were formed, simultaneously. According to these observations, the following reaction is postulated, eqn. (3).

$$TeS_4O_6^{2-} + 6\ CN^- \xrightarrow{MeCN} TeCN^- + SCN^- + S_2O_3^{2-} + SO_3^{2-} + (CN)_4^{2-} \qquad (3)$$

In this respect, even in acetonitrile the tellurium derivative differs markedly from the analogous sulfur and selenium compounds.[3]

The rates of the reaction were followed by measuring the formation of ionic thiocyanate or ionic tellurocyanate by applying IR.[2] The kinetic plots were linear up to three half-lives. The rate data and the activation parameters for the telluropentathionate-cyanide reaction and the corresponding pentathionate and selenopentathionate reactions are presented in Table 1.

With regard to the postulated sulfite ion formed, eqn. 3, this is rapidly oxidized to ionic sulfate due to traces of oxygen in the acetonitrile solution.[4]

Obviously the mechanism of the telluropentathionate-cyanide reaction is different from the penta- and selenopentathionate-cyanide reactions in acetonitrile.[3] However, the first step is presumably the same in all three cases, eqn. (4).

$$^-O_3S-S-Te-S-SO_3^- + CN^- \xrightarrow{slow} {}^-O_3S-S-TeCN + S_2O_3^{2-} \qquad (4)$$

The sulfonated sulfur tellurocyanate ion, $^-O_3S-S-S-TeCN$, then may react rapidly with a second cyanide ion. The electrophilic centre probably is the divalent sulfur atom, and ionic sulfite is displaced, eqn. (5).

$$^-O_3S-S-TeCN + CN^- \xrightarrow{fast} SO_3^{2-} + NCS-TeCN \qquad (5)$$

The asymmetric pseudohalogen, NCS – TeCN, is then attacked by a third cyanide ion, probably at the sulfur atom, displacing ionic tellurocyanate, eqn. (6).

$$NCS-TeCN + CN^- \xrightarrow{fast} S(CN)_2 + TeCN^- \qquad (6)$$

It is further known that sulfur dicyanide reacts very rapidly with three cyanide ions, presum-

Table 1. Rate data and activation parameters for the reactions of ionic pentathionate, selenopentathionate and telluropentathionate with the cyanide ion in acetonitrile.

Reaction	k_2 M^{-1} s^{-1}			ΔH^*	ΔS^* cal/	ΔG^*
	20 °C	25 °C	35 °C	kcal/mol	mol deg	kcal/mol
$S_5O_6^{2-} + CN^-$ [a]	–	0.250	0.335	6.3	−40	18.2
$SeS_4O_6^{2-} + CN^-$ [b]	–	20.6	22.8	1.7	−48	16.0
$TeS_4O_6^{2-} + CN^-$ [c]	0.082	0.107	0.169	8.1	−36	18.9
	0.085	0.104	0.173			

[a] Ref. 4, $\mu = 1.25 \times 10^{-2}$. [b] Ref. 4, $\mu = 9.88 \times 10^{-3}$. [c] $\mu = 2.25 \times 10^{-2}$.

ably according to the following reaction,[5] eqn. (7).

$$S(CN)_2 + 3\ CN^- \xrightarrow{fast} SCN^- + (CN)_4^{2-} \qquad (7)$$

The mechanism outlined above is in accordance with the stoichiometry of the reactants observed by the kinetic experiments.

With regard to eqn. (5), this step is different from the corresponding step in the pentathionate-cyanide and selenopentathionate-cyanide reactions, in which the pseudohalide ion is the leaving group.[3] Supposing the tellurocyanate ion to be displaced as depicted by eqn. (8),

$$^-O_3S - S - TeCN + CN^- \xrightarrow{fast} {}^-O_3S - SCN + TeCN^- \qquad (8)$$

ionic tellurocyanate and thiocyanate would not be formed at the same rate, due to the much slower reaction between the thiocyanatosulfonate ion and the cyanide ion.[3] This is not in accordance with the experimental data.

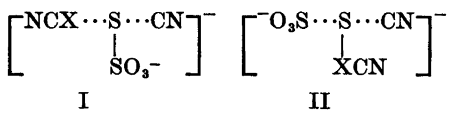

I II

(X = S, Se and Te.)

Considering the transition states I and II, the transition state I is favoured for X = S and Se. For X = Te the transition state II appears to be the most favourable. Thus, with regard to nucleophilic substitution at sulfenyl sulfur in acetonitrile, the thiocyanate ion and the selenocyanate ion are better leaving groups than the sulfite ion, while the latter is a better leaving group than is the tellurocyanate ion.

Eqn. (6) of the mechanism outlined above requires some further comments. Both of the chalcogen atoms of the asymmetric pseudohalogen, NCS−TeCN, may be regarded as potential electrophilic centres. Supposing that the nucleophilic attack occurs at the divalent tellurium atom, the products may be ionic thiocyanate and tellurium dicyanide as depicted by eqn. (9).

$$NCS - TeCN + CN^- \xrightarrow{fast} SCN^- + Te(CN)_2 \qquad (9)$$

Ionic cyanide, however, reacts with tellurium dicyanide in acetonitrile to precipitate elemental tellurium.[5] Elemental tellurium was not observed at any stage even in concentrated solutions during the telluropentathionate-cyanide reactions. This might be because, if the reaction goes through the step depicted by eqn. (9), the concentration of tellurium dicyanide at any time has to be very small, and excess cyanide ions may then react with the atomic tellurium to form ionic tellurocyanate.[2] However, since no elemental tellurium was precipitated even when excess ionic telluropentathionate was employed, the step involving nucleophilic attack at the divalent sulfur atom, depicted by eqn. (6), appears to be the most probable one.

The data presented in Table 1, show that the nucleophilicity of the cyanide ion toward the divalent chalcogens, is in the order $Te < S \ll Se$. The order of the chalcogen basicity of the cyanide ion, which may be determined by the stability of the pseudohalide ions, is believed to be $TeCN^- \ll SeCN^- \ll SCN^-$.[2,6]

The poor solvation of anions in dipolar aprotic solvents,[7] and the structural similarities between the pentathionate ions,[8] may allow one to assume that the initial states of these anions in acetonitrile are essentially identical. On these conditions the calculated activation parameters suggest that the transition states of the telluropentathionate-cyanide reaction and the pentathionate-cyanide reaction are rather similar. The higher enthalpy of activation of the former reaction is nearly compensated by a more negative entropy of activation in the case of the latter reaction. The timing of the covalency changes for the cyanide substitution at divalent tellurium thus appears to resemble that for the cyanide substitution at sulfenyl sulfur.[9] The much lower enthalpy and entropy of activation observed in the selenopentathionate-cyanide

reaction points to a more tight and stabilized transition state in this reaction.[3]

When considering the bonding of the transition state as a three-centre four-electron type,[10] the overlap of the single p orbital of the electrophilic centre with the orbitals of the incoming cyanide ion and the outgoing thiosulfate ion, thus appears to be most favourable for the selenium atom.

Experimental. Acetonitrile and tetraphenylphosphonium cyanide were purified as reported.[3]

Tetraphenylarsonium telluropentathionate was precipitated from an aqueous solution of sodium telluropentathionate[11] by means of tetraphenylarsonium chloride in nearly quantitative yield. The purification was performed in the same way as reported for the analogous pentathionate salts.[3] Dec. 230 °C. (Found: C 52.18; H 3.79; S 12.26. Calc for $C_{48}H_{40}O_6S_4TeAs_2$: C 51.55; H 3.58; S 11.49).

The rate of the reaction was determined by measuring the formation of ionic thiocyanate or tellurocyanate by applying IR.[2] The kinetic plots were analysed according to the second-order rate equation,

$$dx/dt = k_2(a-x)(b-6x)$$

where x is the concentration of ionic thiocyanate (tellurocyanate), and a and b are the initial concentrations of ionic telluropentathionate and cyanide, 2.50×10^{-3} M and 1.50×10^{-2} M, respectively. The rate constants were reproduced with an accuracy better than ±4 %.

Iodometric determination of ionic thiosulfate was performed as reported.[3] The yield was 96–97 %, based on the amount of reacted telluropentathionate.

From conductivity measurements of tetraphenylarsonium telluropentathionate in acetonitrile at 25 °C, the equivalent conductivities at infinite dilution were found to be:

$\lambda°[(Ph_4As)_2TeS_4O_6] = 173$ ohm^{-1} cm^{-2} mol^{-1},

$\lambda°[TeS_4O_6^{2-}] = 61.4$ ohm^{-1} cm^{-2} mol^{-1}

From the plot, λ *versus* $\sqrt{c}$, the salt appeared to be completely dissociated in the concentration range used in the kinetic runs.

The IR measurements were performed on a SP 200 G Infrared Spectrophotometer using 1 mm liquid cells.

The conductivity measurements were performed on a conductivity meter type CD M3 with a conductivity cell, type CDC 304 (immersion type) with a cell constant 1.00 cm ± 10 %.

Acknowledgement. The author is indebted to The Norwegian Research Council for Science and the Humanities for a grant.

1. Foss, O. *Acta Chem. Scand.* 4 (1950) 1241.
2. Austad, T., Songstad, J. and Åse, K. *Acta Chem. Scand.* 25 (1971) 331.
3. Austad, T. *Acta Chem. Scand. To be published.*
4. Austad, T. *Acta Chem. Scand. To be published.*
5. Austad, T. and Esperås, S. *Acta Chem. Scand. To be published.*
6. Songstad, J. and Stangeland, L. J. *Acta Chem. Scand.* 24 (1970) 804.
7. Parker, A. J. *Chem. Rev.* 69 (1969) 1.
8. Foss, O. *Advan. Inorg. Chem. Radiochem.* 2 (1960) 237.
9. Kice, J. L. and Anderson, J. M. *J. Org. Chem.* 33 (1968) 3331.
10. Foss, O. *Pure Appl. Chem.* 24 (1970) 804.
11. Foss, O. *Acta Chem. Scand.* 3 (1949) 708.

Received July 25, 1974.

The Systems BF_3—H_2O and $SbCl_5$—H_2O in Acetone and Methylene Chloride as Solvents

R. J. GILLESPIE [a] and J. S. HARTMAN [b]

[a] Department of Chemistry, McMaster University, Hamilton, Ontario, Canada and [b] Department of Chemistry, Brock University, St. Catharines, Ontario, Canada

Bernander and Olofsson have recently reported a study of the $H_2O-SbCl_5$ adduct system in methylene chloride by ^1H NMR.[1] They interpret their results in terms of the formation of a 1:1 adduct $SbCl_5.H_2O$, and a 1:2 adduct $SbCl_5.2H_2O$ in which the second water molecule is more weakly held. They also measured the ^1H chemical shift of a solution of $BF_3.H_2O$ in CH_2Cl_2. In discussing their results they make a comparison with our earlier work on the BF_3-H_2O system in solution in acetone[2] and they claim that two of the main conclusions of our work are incorrect.

Bernander and Olofsson draw attention to the large difference in the chemical shift between that which we observed for $BF_3.H_2O$ in acetone ($\delta = 12.46$) and that which they observed in CH_2Cl_2 ($\delta = 8.2$) and they claim that it is probable that we were not observing the $BF_3.H_2O$ adduct but rather the BF_3-acetone.H_2O ternary adduct. While it is clear that there must be hydrogen-bonded interaction between the protons of $BF_3.H_2O$ and the acetone solvent this interaction is certainly much weaker than that between the BF_3 and the H_2O. The NMR spectra indicate for example

reaction points to a more tight and stabilized transition state in this reaction.[3]

When considering the bonding of the transition state as a three-centre four-electron type,[10] the overlap of the single p orbital of the electrophilic centre with the orbitals of the incoming cyanide ion and the outgoing thiosulfate ion, thus appears to be most favourable for the selenium atom.

Experimental. Acetonitrile and tetraphenylphosphonium cyanide were purified as reported.[3]

Tetraphenylarsonium telluropentathionate was precipitated from an aqueous solution of sodium telluropentathionate[11] by means of tetraphenylarsonium chloride in nearly quantitative yield. The purification was performed in the same way as reported for the analogous pentathionate salts.[3] Dec. 230 °C. (Found: C 52.18; H 3.79; S 12.26. Calc for $C_{48}H_{40}O_6S_4TeAs_2$: C 51.55; H 3.58; S 11.49).

The rate of the reaction was determined by measuring the formation of ionic thiocyanate or tellurocyanate by applying IR.[2] The kinetic plots were analysed according to the second-order rate equation,

$$dx/dt = k_2(a-x)(b-6x)$$

where x is the concentration of ionic thiocyanate (tellurocyanate), and a and b are the initial concentrations of ionic telluropentathionate and cyanide, 2.50×10^{-3} M and 1.50×10^{-2} M, respectively. The rate constants were reproduced with an accuracy better than ±4 %.

Iodometric determination of ionic thiosulfate was performed as reported.[3] The yield was 96–97 %, based on the amount of reacted telluropentathionate.

From conductivity measurements of tetraphenylarsonium telluropentathionate in acetonitrile at 25 °C, the equivalent conductivities at infinite dilution were found to be:

$\lambda°[(Ph_4As)_2TeS_4O_6] = 173$ ohm^{-1} cm^{-2} mol^{-1},

$\lambda°[TeS_4O_6^{2-}] = 61.4$ ohm^{-1} cm^{-2} mol^{-1}

From the plot, λ *versus* $\sqrt{c}$, the salt appeared to be completely dissociated in the concentration range used in the kinetic runs.

The IR measurements were performed on a SP 200 G Infrared Spectrophotometer using 1 mm liquid cells.

The conductivity measurements were performed on a conductivity meter type CD M3 with a conductivity cell, type CDC 304 (immersion type) with a cell constant 1.00 cm ± 10 %.

Acknowledgement. The author is indebted to The Norwegian Research Council for Science and the Humanities for a grant.

1. Foss, O. *Acta Chem. Scand.* 4 (1950) 1241.
2. Austad, T., Songstad, J. and Åse, K. *Acta Chem. Scand.* 25 (1971) 331.
3. Austad, T. *Acta Chem. Scand. To be published.*
4. Austad, T. *Acta Chem. Scand. To be published.*
5. Austad, T. and Esperås, S. *Acta Chem. Scand. To be published.*
6. Songstad, J. and Stangeland, L. J. *Acta Chem. Scand.* 24 (1970) 804.
7. Parker, A. J. *Chem. Rev.* 69 (1969) 1.
8. Foss, O. *Advan. Inorg. Chem. Radiochem.* 2 (1960) 237.
9. Kice, J. L. and Anderson, J. M. *J. Org. Chem.* 33 (1968) 3331.
10. Foss, O. *Pure Appl. Chem.* 24 (1970) 804.
11. Foss, O. *Acta Chem. Scand.* 3 (1949) 708.

Received July 25, 1974.

The Systems BF_3—H_2O and $SbCl_5$—H_2O in Acetone and Methylene Chloride as Solvents

R. J. GILLESPIE [a] and J. S. HARTMAN [b]

[a] Department of Chemistry, McMaster University, Hamilton, Ontario, Canada and [b] Department of Chemistry, Brock University, St. Catharines, Ontario, Canada

Bernander and Olofsson have recently reported a study of the $H_2O-SbCl_5$ adduct system in methylene chloride by ^1H NMR.[1] They interpret their results in terms of the formation of a 1:1 adduct $SbCl_5.H_2O$, and a 1:2 adduct $SbCl_5.2H_2O$ in which the second water molecule is more weakly held. They also measured the ^1H chemical shift of a solution of $BF_3.H_2O$ in CH_2Cl_2. In discussing their results they make a comparison with our earlier work on the BF_3-H_2O system in solution in acetone[2] and they claim that two of the main conclusions of our work are incorrect.

Bernander and Olofsson draw attention to the large difference in the chemical shift between that which we observed for $BF_3.H_2O$ in acetone ($\delta = 12.46$) and that which they observed in CH_2Cl_2 ($\delta = 8.2$) and they claim that it is probable that we were not observing the $BF_3.H_2O$ adduct but rather the BF_3-acetone.H_2O ternary adduct. While it is clear that there must be hydrogen-bonded interaction between the protons of $BF_3.H_2O$ and the acetone solvent this interaction is certainly much weaker than that between the BF_3 and the H_2O. The NMR spectra indicate for example

that there is rapid exchange between any such hydrogen bonded acetone molecules and the bulk of the solvent whereas the water molecule is firmly held. Such an interaction can be reasonably described as solvation and cannot be regarded as being in principle any different from the weaker interaction that presumably exists between $BF_3.H_2O$ and $SbCl_5.H_2O$ and the solvent CH_2Cl_2. We were indeed fully aware of the possibility of ternary complexes and in fact we postulated the existence of the ternary complex $F_3B.OH_2.OH_2$ in order to explain the rapid proton exchange that occurs in the presence of water in excess of the 1:1 composition. Moreover, in a subsequent paper [3] we have discussed the $BF_3.MeOH$ and $BF_3.2MeOH$ complexes and have proposed a structure for the 1:2 adduct involving a weak hydrogen bond between the first directly bonded molecule and the second methanol molecule. Our work on this system has subsequently been repeated and confirmed.[4]

Bernander and Olofsson also claim that our statement that "acetone is much inferior to water as an electron pair donor to BF_3" is not corroborated by comparison of donor strengths towards $SbCl_5$. However, at low temperatures in excess acetone the NMR spectra of both the acetone.BF_3 and the $H_2O.BF_3$ complex can be observed directly in the same solution and it is quite clear that the equilibrium

$$H_2O + \text{acetone}.BF_3 \rightleftharpoons \text{acetone} + H_2O.BF_3$$

lies far to the right. Moreover, we observed proton-fluorine coupling in $BF_3.H_2O$ even in the presence of a large excess of acetone. Both of these observations clearly indicate that BF_3 is bonded to water much more strongly than to acetone and if a ternary complex does exist the primary bond must be between the BF_3 and a water molecule with the acetone molecule held weakly by hydrogen bonds to the water molecule. Bernander and Olofsson report thermochemical measurements demonstrating that $SbCl_5$.ester, $SbCl_5$.ketone, and $SbCl_5$.water complexes all have very similar stabilities and they make the assumption that this should also be true for the BF_3 adducts. Quite apart from the fact that this is inconsistent with our NMR results such an assumption is also not justified on the basis of previous work on the Lewis acidity of BF_3 with respect to different bases.[5] Indeed it is a well known problem in comparing the strengths of Lewis acids and bases that there is no absolute scale of relative basicities that is valid for all Lewis acids. Ethers, ketones, and water need not have the same relative donor strengths with respect to BF_3 as they do with respect to $SbCl_5$. There are examples of base strength reversal even between Lewis acids as similar as BF_3 and BCl_3,[6] and it has been found that even the replacement of a single fluorine in BF_3 by a chlorine can have striking effects on Lewis acid properties.[7]

If Bernander and Oloffson's conclusion that water and acetone have similar base strengths towards $SbCl_5$ is correct then their results taken in conjunction with ours, which show that acetone is a much weaker base towards BF_3 than is water, demonstrate once again that one cannot establish a single consistent set of base strengths towards different Lewis acids and in particular towards BF_3 and $SbCl_5$.

1. Bernander, L. and Olofsson, G. *Acta Chem. Scand. 27* (1973) 1034.
2. Gillespie, R. J. and Hartman, J. S. *Can. J. Chem. 45* (1967) 859.
3. Gillespie, R. J. and Hartman, J. S. *Can. J. Chem. 45* (1967) 2243.
4. Servis, K. L. and Jao, L. *J. Phys. Chem. 76* (1972) 329.
5. Greenwood, N. N. and Martin, R. L. *Quart. Rev. Chem. Soc. 8* (1954) 1.
6. Young, D. E., McAchran, C. E. and Shore, S. G. *J. Amer. Chem. Soc. 88* (1966) 4390.
7. Bula, M. J. and Hartman, J. S. *J. Chem. Soc. Dalton Trans.* (1973) 1047.

Received July 15, 1974.

A Simple Parameterfree Expression for the Activity Coefficient of Potassium Chloride in Water in the Range $0.1 \leq m \leq 4.8$

ERIK HÖGFELDT

Department of Chemistry, State University of New York at Buffalo, New York 14214, USA and Department of Inorganic Chemistry, Royal Institute of Technology, S-100 44 Stockholm, Sweden

The following expression [1] for the activity coefficient of a simple 1:1 electrolyte can be derived using in principle the same approach as that of Stokes and Robinson [2] but using the *molarity scale* instead of the molality scale used by them

$$\log y_A y_B = -\frac{2 \times 0.5115\sqrt{C}}{1+Ba\sqrt{C}} - 2\log\left[\frac{1}{d_0}\left\{d + 0.001C(2 \times 18.015 - M_{AB})\right\}\right] - \log S \quad (1)$$

where $S = \sum K_n a_w^n$ (2)

that there is rapid exchange between any such hydrogen bonded acetone molecules and the bulk of the solvent whereas the water molecule is firmly held. Such an interaction can be reasonably described as solvation and cannot be regarded as being in principle any different from the weaker interaction that presumably exists between $BF_3.H_2O$ and $SbCl_5.H_2O$ and the solvent CH_2Cl_2. We were indeed fully aware of the possibility of ternary complexes and in fact we postulated the existence of the ternary complex $F_3B.OH_2.OH_2$ in order to explain the rapid proton exchange that occurs in the presence of water in excess of the 1:1 composition. Moreover, in a subsequent paper [3] we have discussed the $BF_3.MeOH$ and $BF_3.2MeOH$ complexes and have proposed a structure for the 1:2 adduct involving a weak hydrogen bond between the first directly bonded molecule and the second methanol molecule. Our work on this system has subsequently been repeated and confirmed.[4]

Bernander and Olofsson also claim that our statement that "acetone is much inferior to water as an electron pair donor to BF_3" is not corroborated by comparison of donor strengths towards $SbCl_5$. However, at low temperatures in excess acetone the NMR spectra of both the acetone.BF_3 and the $H_2O.BF_3$ complex can be observed directly in the same solution and it is quite clear that the equilibrium

$$H_2O + \text{acetone}.BF_3 \rightleftharpoons \text{acetone} + H_2O.BF_3$$

lies far to the right. Moreover, we observed proton-fluorine coupling in $BF_3.H_2O$ even in the presence of a large excess of acetone. Both of these observations clearly indicate that BF_3 is bonded to water much more strongly than to acetone and if a ternary complex does exist the primary bond must be between the BF_3 and a water molecule with the acetone molecule held weakly by hydrogen bonds to the water molecule. Bernander and Olofsson report thermochemical measurements demonstrating that $SbCl_5$.ester, $SbCl_5$.ketone, and $SbCl_5$.water complexes all have very similar stabilities and they make the assumption that this should also be true for the BF_3 adducts. Quite apart from the fact that this is inconsistent with our NMR results such an assumption is also not justified on the basis of previous work on the Lewis acidity of BF_3 with respect to different bases.[5] Indeed it is a well known problem in comparing the strengths of Lewis acids and bases that there is no absolute scale of relative basicities that is valid for all Lewis acids. Ethers, ketones, and water need not have the same relative donor strengths with respect to BF_3 as they do with respect to $SbCl_5$. There are examples of base strength reversal even between Lewis acids as similar as BF_3 and BCl_3,[6] and it has been found that even the replacement of a single fluorine in BF_3 by a chlorine can have striking effects on Lewis acid properties.[7]

If Bernander and Oloffson's conclusion that water and acetone have similar base strengths towards $SbCl_5$ is correct then their results taken in conjunction with ours, which show that acetone is a much weaker base towards BF_3 than is water, demonstrate once again that one cannot establish a single consistent set of base strengths towards different Lewis acids and in particular towards BF_3 and $SbCl_5$.

1. Bernander, L. and Olofsson, G. *Acta Chem. Scand. 27* (1973) 1034.
2. Gillespie, R. J. and Hartman, J. S. *Can. J. Chem. 45* (1967) 859.
3. Gillespie, R. J. and Hartman, J. S. *Can. J. Chem. 45* (1967) 2243.
4. Servis, K. L. and Jao, L. *J. Phys. Chem. 76* (1972) 329.
5. Greenwood, N. N. and Martin, R. L. *Quart. Rev. Chem. Soc. 8* (1954) 1.
6. Young, D. E., McAchran, C. E. and Shore, S. G. *J. Amer. Chem. Soc. 88* (1966) 4390.
7. Bula, M. J. and Hartman, J. S. *J. Chem. Soc. Dalton Trans.* (1973) 1047.

Received July 15, 1974.

A Simple Parameterfree Expression for the Activity Coefficient of Potassium Chloride in Water in the Range $0.1 \leq m \leq 4.8$

ERIK HÖGFELDT

Department of Chemistry, State University of New York at Buffalo, New York 14214, USA and Department of Inorganic Chemistry, Royal Institute of Technology, S-100 44 Stockholm, Sweden

The following expression [1] for the activity coefficient of a simple 1:1 electrolyte can be derived using in principle the same approach as that of Stokes and Robinson [2] but using the *molarity scale* instead of the molality scale used by them

$$\log y_A y_B = -\frac{2 \times 0.5115\sqrt{C}}{1+Ba\sqrt{C}} - 2\log\left[\frac{1}{d_0}\left\{d + 0.001C(2 \times 18.015 - M_{AB})\right\}\right] - \log S \quad (1)$$

where $S = \sum K_n a_w^n$ (2)

S "represents" the sum of all various hydrated species. a_w is the water activity, C is concentration in mol liter^{-1}, d_0 the density of pure water and d that of the solution. M_{AB} is the molecular weight of the solute. The first term in eqn. (1) represents the electrostatic part of the excess free energy, the second term is a scale factor connecting the mol fraction and molarity scales while the third term represents the excess free energy of hydration. S has the property

$$\frac{\mathrm{d}\log S}{\mathrm{d}\log a_w} = \bar{n} = \frac{\sum n K_n a_w^n}{\sum K_n a_w^n} \qquad (3)$$

With knowledge of a, the distance of closest approach, S can be computed from (1). It is found that $\bar{n}$ computed for the system NaCl – H_2O approaches 5 independent of the ion-size parameter. This indicates that what may be regarded as primary hydration numbers can be obtained for many salts independent of any knowledge of the ion-size parameter a. Following a suggestion by Pitzer [3] it was decided to use the Bjerrum q-value for the ion-size parameter *i.e.* the term Ba in eqn. (7) becomes 1.176 for all 1:1 electrolytes.

With this choice it is found that for KCl – H_2O at 25 °C

$$\bar{n} \approx n \approx 4 \qquad (4)$$

and eqn. (1) reduces to

$$\log y_{K^+}y_{Cl^-} = \frac{2 \times 0.5115\sqrt{C}}{1+1.176\sqrt{C}} - 2\log\left[\frac{1}{0.99707} \times (d - 0.038525C)\right] - 4\log a_w \qquad (5)$$

At 25 °C $d_0 = 0.99707$ g ml^{-1}.

This is in principle a parameter-free expression because the term 1.176 is constant and the equilibrium constant for the formation of the tetrahydrate is equal to unity by definition, otherwise the activity coefficient will not approach unity at infinite dilution. The number 4 is deduced from the application of eqn. (3) to the experimental data and has a simple physical meaning unlike the fractional hydration numbers arrived at by Stokes and Robinson.[2] The activity coefficient product $y_{K^+}y_{Cl^-}$ can be transformed into $\gamma_\pm$ from

$$\gamma_\pm = (y_{K^+}y_{Cl^-})^{\frac{1}{2}}C/0.99707m \qquad (6)$$

where m is the stoichiometric molality of the solution. In Table 1 experimental values for $\gamma_\pm$ are compared with those computed from eqns. (5) and (6). The activity and osmotic coefficient data used have been taken from the compilation of Robinson and Stokes [4] and the density data from International Critical Tables.[5] As seen in Table 1 experimental and calculated values agree to within ±0.75 % at most. Most of the data agree to better than ±0.5 %. Similarly it is found for RbCl that eqn. (1) fits to within ±2 % up to 4.5 m finding $\bar{n} = n = 3$ from eqn. (3). If a small extent of ion-pairing is assumed to occur the data can be fitted to within ±0.5 % up to 3.5 m beyond that the values deviate about 1 – 3.5 %. Ion-pair formation will add a term $+2\log\alpha$ to eqn. (1) where α is the degree of dissociation of the ion-pair. For CsCl the data definitely indicate ion-pair formation. For CsCl the hydration number is around three as for RbCl. For NH_4Cl the primary hydration number are two and seven plus some secondary hydration describable by an infinite series of complexes from $n = 8$ and two parameters, the equilibrium constant for the formation of the octahydrate and the constant ratio between consecutive equilibrium constants. A similar approach also fits salts like $LiNO_3$ (to within ±5 % up to 13 m) NaBr, NaI, KBr and KI studied so far. NaCl seems to need two primary hydrates 5 and 7 together with a slight secondary hydration.

While the present approach rather satisfactorily deals with the hydration part of the

Table 1. Comparison of experimental activity coefficients for KCl – H_2O with those calculated from eqns. (4) and (5).

m	γ_{exp}	γ_{calc}
0.1	0.7698	0.7651
0.2	0.7181	0.7130
0.3	0.6875	0.6824
0.4	0.6657	0.6611
0.5	0.6492	0.6453
0.6	0.6365	0.6329
0.7	0.6262	0.6228
0.8	0.6176	0.6145
0.9	0.6101	0.6075
1.0	0.6038	0.6016
1.2	0.5933	0.5921
1.4	0.5856	0.5852
1.6	0.5800	0.5800
1.8	0.5758	0.5761
2.0	0.5728	0.5732
2.2	0.5707	0.5713
2.4	0.5694	0.5702
2.6	0.5687	0.5696
2.8	0.5686	0.5696
3.0	0.5689	0.5702
3.2	0.5698	0.5711
3.4	0.5711	0.5725
3.6	0.5725	0.5743
3.8	0.5745	0.5764
4.0	0.5768	0.5789
4.2	0.5793	0.5817
4.4	0.5820	0.5848
4.6	0.5848	0.5881
4.8	0.5879	0.5918

excess free energy the electrostatic term is rather uncertain. It should be emphasized that the choice of the Bjerrum q-value is rather arbitrary although it seems to be a useful compromise giving a self-consistent description of the systems studied so far. It is quite possible that some other choice (choices) for the distance of closest approach may emerge in the future.

A detailed account of this work will be published elsewhere.

Acknowledgements. The author is indebted to the Department of Chemistry, SUNYAB for an invitation to spend a semester at the University. The present work is also supported financially by the Swedish Natural Science Research Council.

1. Högfeldt, E. *Chemica Scripta. In print.*
2. Stokes, R. H. and Robinson, R. A. *J. Amer. Chem. Soc. 20* (1948) 1820.
3. Pitzer, K. S. *J. Chem. Soc. Faraday Trans. 2* (1968) 101.
4. Robinson, R. A. and Stokes, R. H. *Electrolyte Solutions*, 2nd. Ed., Butterworth, London 1959, Appendix 8.
5. *International Critical Tables*, Washburn, E. W., Ed., McGraw, New York 1928, Vol. III, pp. 54–95.

Received September 10, 1974.

Dinuclear Hydrolysis Complexes of Uranium(IV)

STEVAN POCEV*

Department of Inorganic Chemistry, The Royal Institute of Technology, S-100 44 Stockholm 70, Sweden

X-Ray scattering measurements on acid and hydrolyzed uranium(IV) perchlorate solutions [1] have shown that polynuclear complexes are formed in the hydrolyzed solutions. The U–U distance within the complexes was found to be 4.00 Å. This distance is similar to the Th–Th distance found in hydrolyzed thorium(IV) nitrate solutions [2] and in the dinuclear complex $Th_2(OH)_2(NO_3)_6(H_2O)_6$ in which the Th atoms are joined by double hydroxo bridges.[3] It seems likely, therefore, that in the hydrolysis complexes in the uranium(IV) perchlorate solutions the uranium atoms are bound together by the sharing of two hydroxo groups.

Table 1. Results of the chemical analysis.

	Observed value	Calculated value for $U_2(OH)_2(ClO_4)_6(H_2O)_{13}$
% UO_2	41.4	40.27
% Cl_2O_7	38.3	40.92
% H_2O	20.0	18.81
Density	3.1$_3$	3.091 ($z=4$)

In an attempt to obtain more information on the structures of the uranium(IV) hydrolysis complexes, two different basic perchlorates, obtained from the solutions used for the X-ray scattering measurements, have been investigated. For one of these a preliminary crystal structure determination has shown that it contains discrete dinuclear hydrolysis complexes.

The crystals, which can be obtained from solutions with a OH^-/U^{4+} ratio between about 0.2 and 0.5, are very soluble in water and are unstable outside the mother liquor, which makes their separation from the mother liquor difficult. The analysis, which is given in Table 1 leads to the formula $(UO_2)_2(Cl_2O_7)_3(H_2O)_x$ ($x \sim 13$).

From Weissenberg and precession photographs the unit cell was found to be monoclinic. The derived values for the unit cell dimensions were refined by a least squares procedure with the use of a Guinier powder photograph, taken with Cu$K\alpha$ radiation ($\lambda = 1.5405$ Å) with Si as internal standard ($a = 5.4301$ Å). The values found were $a = 26.084(4)$ Å, $b = 9.493(1)$ Å, $c = 16.945(3)$ Å, and $\beta = 136.63(1)$ Å. Systematically absent reflections were hkl for $h+k = 2n+1$ and $h0l$ for $l = 2n+1$. This is characteristic for the space groups No. 15, $C2/c$ and No. 9; Cc.

Difficulties were encountered in getting good intensity data since the crystals seemed to be unstable under X-ray exposure and, therefore, absorption corrections could not be done. From intensities estimated visually by comparison with an intensity scale and corrected for Lorentz and polarization factors the Patterson projections along the three axes of the unit cell were calculated. An apparently unique interpretation of all the possible U–U peaks could be obtained by assuming the eight uranium atoms in the unit cell to occupy the position 8(f) in the centrosymmetric space group $C2/c$. Electron density projections along the three axes of the unit cell confirmed the correctness of the derived positions. A least squares refinement of the uranium positions with the use of the 180 observed $h0l$ and $hk0$ reflextions lead to an R value of 0.24 and the final parameter values were $x = 0.095$; $y = 0.075$; $z = -0.079$.

* Present address: University of "Kiril and Methodi", Faculty of Technology and Metallurgy, Skopje, Yugoslavia.

excess free energy the electrostatic term is rather uncertain. It should be emphasized that the choice of the Bjerrum q-value is rather arbitrary although it seems to be a useful compromise giving a self-consistent description of the systems studied so far. It is quite possible that some other choice (choices) for the distance of closest approach may emerge in the future.

A detailed account of this work will be published elsewhere.

Acknowledgements. The author is indebted to the Department of Chemistry, SUNYAB for an invitation to spend a semester at the University. The present work is also supported financially by the Swedish Natural Science Research Council.

1. Högfeldt, E. *Chemica Scripta. In print.*
2. Stokes, R. H. and Robinson, R. A. *J. Amer. Chem. Soc. 20* (1948) 1820.
3. Pitzer, K. S. *J. Chem. Soc. Faraday Trans. 2* (1968) 101.
4. Robinson, R. A. and Stokes, R. H. *Electrolyte Solutions*, 2nd. Ed., Butterworth, London 1959, Appendix 8.
5. *International Critical Tables*, Washburn, E. W., Ed., McGraw, New York 1928, Vol. III, pp. 54–95.

Received September 10, 1974.

Dinuclear Hydrolysis Complexes of Uranium(IV)

STEVAN POCEV*

Department of Inorganic Chemistry, The Royal Institute of Technology, S-100 44 Stockholm 70, Sweden

X-Ray scattering measurements on acid and hydrolyzed uranium(IV) perchlorate solutions [1] have shown that polynuclear complexes are formed in the hydrolyzed solutions. The U–U distance within the complexes was found to be 4.00 Å. This distance is similar to the Th–Th distance found in hydrolyzed thorium(IV) nitrate solutions [2] and in the dinuclear complex $Th_2(OH)_2(NO_3)_6(H_2O)_6$ in which the Th atoms are joined by double hydroxo bridges.[3] It seems likely, therefore, that in the hydrolysis complexes in the uranium(IV) perchlorate solutions the uranium atoms are bound together by the sharing of two hydroxo groups.

Table 1. Results of the chemical analysis.

	Observed value	Calculated value for $U_2(OH)_2(ClO_4)_6(H_2O)_{13}$
% UO_2	41.4	40.27
% Cl_2O_7	38.3	40.92
% H_2O	20.0	18.81
Density	3.1$_3$	3.091 ($z=4$)

In an attempt to obtain more information on the structures of the uranium(IV) hydrolysis complexes, two different basic perchlorates, obtained from the solutions used for the X-ray scattering measurements, have been investigated. For one of these a preliminary crystal structure determination has shown that it contains discrete dinuclear hydrolysis complexes.

The crystals, which can be obtained from solutions with a OH^-/U^{4+} ratio between about 0.2 and 0.5, are very soluble in water and are unstable outside the mother liquor, which makes their separation from the mother liquor difficult. The analysis, which is given in Table 1 leads to the formula $(UO_2)_2(Cl_2O_7)_3(H_2O)_x$ ($x \sim 13$).

From Weissenberg and precession photographs the unit cell was found to be monoclinic. The derived values for the unit cell dimensions were refined by a least squares procedure with the use of a Guinier powder photograph, taken with Cu$K\alpha$ radiation ($\lambda = 1.5405$ Å) with Si as internal standard ($a = 5.4301$ Å). The values found were $a = 26.084(4)$ Å, $b = 9.493(1)$ Å, $c = 16.945(3)$ Å, and $\beta = 136.63(1)$ Å. Systematically absent reflections were hkl for $h+k = 2n+1$ and $h0l$ for $l = 2n+1$. This is characteristic for the space groups No. 15, $C2/c$ and No. 9; Cc.

Difficulties were encountered in getting good intensity data since the crystals seemed to be unstable under X-ray exposure and, therefore, absorption corrections could not be done. From intensities estimated visually by comparison with an intensity scale and corrected for Lorentz and polarization factors the Patterson projections along the three axes of the unit cell were calculated. An apparently unique interpretation of all the possible U–U peaks could be obtained by assuming the eight uranium atoms in the unit cell to occupy the position 8(f) in the centrosymmetric space group $C2/c$. Electron density projections along the three axes of the unit cell confirmed the correctness of the derived positions. A least squares refinement of the uranium positions with the use of the 180 observed $h0l$ and $hk0$ reflextions lead to an R value of 0.24 and the final parameter values were $x = 0.095$; $y = 0.075$; $z = -0.079$.

* Present address: University of "Kiril and Methodi", Faculty of Technology and Metallurgy, Skopje, Yugoslavia.

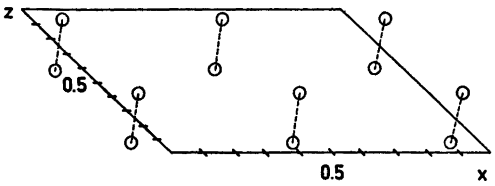

Fig. 1. The positions of the U atoms as seen in a projection along the *b* axis of the unit cell. Uranium atoms belonging to the same hydrolysis complex are joined by dashed lines.

The positions of the uranium atoms as seen in a projection along the *b* axis are shown in Fig. 1. The uranium atoms occur in pairs with a U – U distance of 4.03 Å. The shortest distance between atoms belonging to different pairs is 7.22 Å. The structure, therefore, seems to be built up from discrete dinuclear complexes.

In the $Th_2(OH)_2(NO_3)_6(H_2O)_6$ complexes found in crystals of $Th_2(OH)_2(NO_3)_6$ $(H_2O)_8$ the distance between the Th atoms is 3.99 Å.[3] This indicates that the dinuclear U(IV) hydrolysis complexes are very similar to those formed by thorium and the formula for the compound investigated should be written $U_2(OH)_2(ClO_4)_6$-$(H_2O)_x$ $(x \approx 13)$.

Acknowledgements. I wish to express my thanks to Dr. Georg Johansson for his inspiring interest during the course of this work. Thanks are also due to all colleagues at the X-ray group for the cooperation. The work has been supported by Statens Naturvetenskapliga Forskningsråd (Swedish Natural Science Research Council). This work has also been supported by grants (scholarship) from the Scientific and Research Council, Skopje, Yugoslavia.

1. Pocev, S. and Johansson, G. *Acta Chem. Scand. 27* (1973) 2146.
2. Johansson, G. *Acta Chem. Scand. 22* (1968) 379.
3. Johansson, G. *Acta Chem. Scand. 22* (1968) 389.

Received August 29, 1974.

Normal Coordinate Analysis of Hexafluoroacetone

MATTI PERTTILÄ

Department of Physical Chemistry, University of Helsinki, Meritullinkatu 1C, Helsinki 17, Finland

The infrared and Raman spectra of hexafluoroacetone were first reported by Berney.[1] As pointed out by Miller and Kiviat,[2] his original assignment of the band at 194 cm^{-1} (gas spectrum) as being due to CCC bending is possibly in error. In the present work a harmonic force field was developed for hexafluoroacetone and an alternative assignment of the bands is proposed. This work is part of a larger study on polyfluoro compounds.[3,4]

Berney[1] concludes that the actual point group of hexafluoroacetone should be C_s instead of C_{2v}, basing his argument mainly on the depolarization ratios of a CF bending and the assumed CO bending vibrations. As Miller and Kiviat point out, however, the intensity of the Raman band at 716 cm^{-1} is too weak to give decisive information on its polarization. They also give evidence indicating that the 320 cm^{-1} band, assigned by Berney to a CO wag, is in fact due to the CCC scissoring mode. This result is in good agreement with the experimental studies of Murto *et al.*[5,6] on hexafluoro alcohols. Obviously the full C_{2v} symmetry can be used.

According to Berney, the 194 cm^{-1} band clearly represents a totally symmetric fundamental. Accepting this as a CF_3 rocking band, we are left with one rocking band too many. In our opinion the band at 233 cm^{-1} in the vapour spectrum, the weakest of the rocking bands proposed by Berney, is not a fundamental band; rather, the band at 265 cm^{-1} is the B_1 rocking vibration. This also is a weak band and its depolarization ratio has not been reported. The B_1 CO bending band is probably in the region 450 cm^{-1} – 500 cm^{-1}, [7,8] being obviously superimposed by other bands. In the present work it is assumed to be at 470 cm^{-1}.

The distribution of the normal modes among the symmetry species is $10A_1 + 4A_2 + 8B_1 + 5B_2$, including two redundancies in the A_1 species and one redundancy in the B_1 species.

The G matrix was calculated by the modified programme written by Schachtschneider [9] for the Wilson **s**-vector method. The normal coordinate calculations were carried out on a Univac 1108 computer using a programme written by the author. In the course of the calculations the diagonal and largest off-diagonal elements of the **F** matrix were first perturbed on order to get the best possible **F** matrix with a minimum number of parameters. Using the obtained **L** matrix, a full harmonic force field was developed for each species to fit exactly

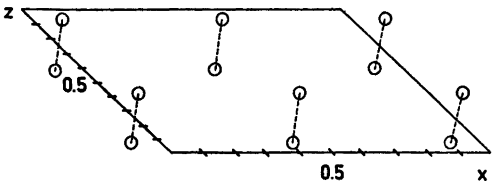

Fig. 1. The positions of the U atoms as seen in a projection along the *b* axis of the unit cell. Uranium atoms belonging to the same hydrolysis complex are joined by dashed lines.

The positions of the uranium atoms as seen in a projection along the *b* axis are shown in Fig. 1. The uranium atoms occur in pairs with a U – U distance of 4.03 Å. The shortest distance between atoms belonging to different pairs is 7.22 Å. The structure, therefore, seems to be built up from discrete dinuclear complexes.

In the $Th_2(OH)_2(NO_3)_6(H_2O)_6$ complexes found in crystals of $Th_2(OH)_2(NO_3)_6$ $(H_2O)_8$ the distance between the Th atoms is 3.99 Å.[3] This indicates that the dinuclear U(IV) hydrolysis complexes are very similar to those formed by thorium and the formula for the compound investigated should be written $U_2(OH)_2(ClO_4)_6$-$(H_2O)_x$ $(x \approx 13)$.

Acknowledgements. I wish to express my thanks to Dr. Georg Johansson for his inspiring interest during the course of this work. Thanks are also due to all colleagues at the X-ray group for the cooperation. The work has been supported by Statens Naturvetenskapliga Forskningsråd (Swedish Natural Science Research Council). This work has also been supported by grants (scholarship) from the Scientific and Research Council, Skopje, Yugoslavia.

1. Pocev, S. and Johansson, G. *Acta Chem. Scand. 27* (1973) 2146.
2. Johansson, G. *Acta Chem. Scand. 22* (1968) 379.
3. Johansson, G. *Acta Chem. Scand. 22* (1968) 389.

Received August 29, 1974.

Normal Coordinate Analysis of Hexafluoroacetone

MATTI PERTTILÄ

Department of Physical Chemistry, University of Helsinki, Meritullinkatu 1C, Helsinki 17, Finland

The infrared and Raman spectra of hexafluoroacetone were first reported by Berney.[1] As pointed out by Miller and Kiviat,[2] his original assignment of the band at 194 cm^{-1} (gas spectrum) as being due to CCC bending is possibly in error. In the present work a harmonic force field was developed for hexafluoroacetone and an alternative assignment of the bands is proposed. This work is part of a larger study on polyfluoro compounds.[3,4]

Berney[1] concludes that the actual point group of hexafluoroacetone should be C_s instead of C_{2v}, basing his argument mainly on the depolarization ratios of a CF bending and the assumed CO bending vibrations. As Miller and Kiviat point out, however, the intensity of the Raman band at 716 cm^{-1} is too weak to give decisive information on its polarization. They also give evidence indicating that the 320 cm^{-1} band, assigned by Berney to a CO wag, is in fact due to the CCC scissoring mode. This result is in good agreement with the experimental studies of Murto *et al.*[5,6] on hexafluoro alcohols. Obviously the full C_{2v} symmetry can be used.

According to Berney, the 194 cm^{-1} band clearly represents a totally symmetric fundamental. Accepting this as a CF_3 rocking band, we are left with one rocking band too many. In our opinion the band at 233 cm^{-1} in the vapour spectrum, the weakest of the rocking bands proposed by Berney, is not a fundamental band; rather, the band at 265 cm^{-1} is the B_1 rocking vibration. This also is a weak band and its depolarization ratio has not been reported. The B_1 CO bending band is probably in the region 450 cm^{-1} – 500 cm^{-1}, [7,8] being obviously superimposed by other bands. In the present work it is assumed to be at 470 cm^{-1}.

The distribution of the normal modes among the symmetry species is $10A_1 + 4A_2 + 8B_1 + 5B_2$, including two redundancies in the A_1 species and one redundancy in the B_1 species.

The G matrix was calculated by the modified programme written by Schachtschneider [9] for the Wilson **s**-vector method. The normal coordinate calculations were carried out on a Univac 1108 computer using a programme written by the author. In the course of the calculations the diagonal and largest off-diagonal elements of the **F** matrix were first perturbed on order to get the best possible **F** matrix with a minimum number of parameters. Using the obtained **L** matrix, a full harmonic force field was developed for each species to fit exactly

Table 1. Potential energy distribution and vibrational assignment of hexafluoroacetone.

	Freq.	PED				Assignment
A_1	1807	49νCO,	29δCCC,	9νCF		νCO
	1252	50νCF,	17δCF,	12νCO,	9δCCC	νCF
	1200	49νCF,	31δCF,	19νCC		νCF
	779	28νCF,	25νCC,	30δCF,	8νCO	νCC
	633	30δCF,	30νCF,	22δCCC,	9νCO	δCF
	471	89δCF,	5νCC			δCF
	320	60δCF,	34δCCC			δCCC
	194	54δCF,	31νCC,	12δCCC		δCF
A_2	1162	59νCF,	16δCF,	19τCF_3		νCF
	533	37νCF,	41δCF,	21τCF_3		δCF
	160	6νCF,	83δCF,	10τCF_3		δCF
	48	46δCF,	52τF_3			τCF_3
B_1	1344	62νCF,	16δCO,	20δCF		νCF
	1275	57νCF,	33δCF,	10νCC		νCF
	972	49νCC,	31δCO,	11νCF		νCC
	718	46δCF,	31νCF,	16νCC		δCF
	528	84δCF,	13νCF			δCF
	470	45δCO,	31δCF,	19νCC		δCO
	265	92δCF				δCF
B_2	1314	52νCF,	22τCF_3,	22δCF		νCF
	506	39δCF,	35τCF_3,	17νCF,	7δCO	δCF
	368	40δCO,	47δCF,	12νCF		δCO
	275	62δCF,	27τCF,	11δCO		δCF
	66	24τCF_3	39δCF,	36δCO		τCF_3

the set of the vapour frequencies given by Berney, with the changes discussed above. The resulting potential energy distributions and the suggested assignments are displayed in Table 1.

1. Berney, C. V. *Spectrochim. Acta 21* (1965) 1809.
2. Miller, F. A. and Kiviat, F. E. *Spectrochim. Acta Part A 25* (1969) 1577.
3. Perttilä, M. *Unpublished results.*
4. Cyvin, S. J., Brunvoll, J. and Perttilä, M. *J. Mol. Struct. 17* (1973) 17.
5. Murto, J., Kivinen, A., Manninen, A. and Perttilä, M. *To be published.*
6. Murto, J., Kivinen, A., Viitala, R. and Hyömäki, J. *Spectrochim. Acta Part A 29* (1973) 1121.
7. Pace, E. L., Plausch, A. C. and Samuelson, H. V. *Spectrochim. Acta 22* (1966) 993.
8. Allkins, J. R. and Lippincott, E. R. *Spectrochim. Acta Part A 25* (1969) 761.
9. Schachtschneider, J. H. *Technical Report Nos. 231–264*, Shell Development Co.

Received August 5, 1974.

Acta Chemica Scandinavica A 28 (1974) 935—938

Studies on Polythionates. II. The Action of the Cyanide Ion on the Pentathionate Ion and the Selenopentathionate Ion in Acetonitrile

TOR AUSTAD

Chemical Institute, University of Bergen, N-5000 Bergen, Norway

The pentathionate-cyanide reaction and the selenopentathionate-cyanide reaction have been studied kinetically in acetonitrile. Mechanisms are suggested, which involve substitution at the central sulfur atom of the pentathionate ion, and at the selenium atom of the selenopentathionate ion. The activation parameters of the pentathionate-cyanide reaction, $\Delta H^* = 6.3$ kcal/mol, $\Delta S^* = -40$ cal/mol deg, and of the selenopentathionate-cyanide reaction, $\Delta H^* = 1.7$ kcal/mol, $\Delta S^* = -48$ cal/mol deg, indicate a more tight and stabilized transition state in the case of the selenopentathionate-cyanide reaction.

Foresti [1] in 1934 performed a kinetic study on the pentathionate-cyanide reaction, but so far no kinetic experiments have been made on the reaction between ionic cyanide and the selenopentathionate ion. Because of the similarity of these two reactions in aqueous solution, Foss [2] has proposed the mechanism to be the same in both cases. He proposed an initial ionic displacement of thiosulfate by the cyanide ion, eqn. (1), in the intermediate step ionic displacement of thiocyanate (selenocyanate) by a second cyanide ion, eqn. (2), and in the final step an ionic displacement of thiocyanate by hydroxyl ion, eqn. (3).

$$^-O_3S-S-X-S-SO_3^- + CN^- \xrightarrow{\text{slow}} {}^-O_3S-S-XCN + S_2O_3^{2-} \quad (1)$$

$$^-O_3S-S-XCN + CN^- \xrightarrow{\text{fast}} {}^-O_3S-SCN + XCN^- \quad (2)$$

$$^-O_3S-SCN + 2\ OH^- \xrightarrow{\text{fast}} SO_4^{2-} + SCN^- + H_2O \quad (3)$$

(X = S and Se).

To get some further information about the postulated reaction intermediates, the sulfonated sulfur thiocyanate (selenocyanate) ion, $^-O_3SSXCN$, and the thiocyanatosulfonate ion, $^-O_3SSCN$, this paper reports a kinetic study on these reactions in the dipolar aprotic solvent acetonitrile. In such a medium no hydrolysis can take place, and one might be able to detect some of the reaction intermediates. Tetraphenylarsonium pentathionate and tetraphenylarsonium selenopentathionate were used as the substrates, and tetraphenylphosphonium cyanide was used as the nucleophilic reagent. These salts were found to be completely dissociated in acetonitrile in the concentration range used in the kinetic runs.

The pentathionate-cyanide reaction. Product analysis of the pentathionate-cyanide reaction in acetonitrile showed that when reacting 1 mol of ionic pentathionate with 2 mol of cyanide ions, 1 mol of ionic thiocyanate and 1 mol of ionic thiosulfate were formed. The reaction, followed by measuring the formation of ionic thiocyanate, showed good second-order kinetics up to three half-lifes (Table 1). A mechanism similar to the one postulated by Foss [3] in aqueous solution with a first rate determining step according to eqn. (1), followed by a fast step, eqn. (2), appears to be in accordance with these observations. The thiocyanatosulfonate

Table 1. Rate data and activation parameters in the reaction between ionic pentathionate and selenopentathionate with the cyanide ion in acetonitrile.

Reaction	15 °C	25 °C	35 °C	45 °C	ΔH^* kcal/mol	ΔS^* cal/mol	ΔG^* kcal/deg mol
$S_5O_6^{2-} + CN^-$ [a]	0.150	0.250	0.335		6.3	−40	18.2
$SeS_4O_6^{2-} + CN^-$ [b]		20.6	22.8	25.9	1.7	−48	16.0

[a] Ionic strength $\mu = 1.25 \times 10^{-2}$. [b] Ionic strength $\mu = 9.88 \times 10^{-3}$.

ion, $^-O_3SSCN$, thus appears to be stable during the kinetic runs.

With excess ionic cyanide (about six times the concentration of ionic pentathionate) a second mol of ionic thiocyanate was formed, but this second mol of ionic thiocyanate was formed at a much slower rate than the first mol. Excess cyanide ions may react with the thiocyanatosulfonate ion to give ionic cyanosulfonate and thiocyanate, eqn. (4).

$$^-O_3S-SCN + CN^- \xrightarrow{k_2'} {}^-O_3SCN + SCN^- \quad (4)$$

Eqn. (4) is proposed to be the second step in the tetrathionate-cyanide reaction in acetonitrile.[4] The rate of this reaction, eqn. (4), has been followed at 30 °C, and the reaction showed good second order kinetic up to two half-lifes. The second order rate constant was observed to be $k_2' = 2.95 \times 10^{-2}\ M^{-1}s^{-1}$ at the ionic strength $\mu = 1.7 \times 10^{-2}$. The thiocyanatosulfonate-cyanide reaction thus appears to be 10 times faster than the tetrathionate-cyanide reaction [4] and about 10 times slower than the pentathionate-cyanide reaction, in acetonitrile.

The selenopentathionate-cyanide reaction. The reaction between the selenopentathionate ion and the cyanide ion in acetonitrile was much faster than the corresponding pentathionate-cyanide reaction. The rate could not be followed by applying IR, and the stopped-flow technique had to be used. The second order rate constants are listed in Table 1.

IR and iodometric analysis of the products showed that 1 mol of ionic selenopentathionate reacted with 2 mol of cyanide ions to give 1 mol of ionic selenocyanate and 1 mol of ionic thiosulfate. Only small amounts of ionic thiocyanate could be detected immediately after the reaction had taken place. These observations are in accordance with the data obtained for the pentathionate-cyanide reaction. Hence, the first two steps of the mechanism suggested by Foss [3] appear to be verified for the selenopentathionate-cyanide reaction.

When using excess ionic cyanide 1 mol of ionic thiocyanate was formed according to eqn. (4). The rate of this step is about 10^{-3} times lower than the rate constant of the first step.

DISCUSSION

With regard to the pentathionate-cyanide reaction, Schmidt [5] once proposed a nucleophilic attack by the cyanide ion at one of the sulfonyl sulfur atoms, displacing a sulfanemonosulfonate ion in the rate determining step,

$$^-O_3S-S-S-S-SO_3^- + CN^- \xrightarrow{\text{slow}} {}^-O_3S-S-S-S^- + {}^-O_3SCN \quad (5)$$

followed by a successive reaction by two other cyanide ions, eqns. (6) and (7).

$$^-O_3S-S-S-S^- + CN^- \xrightarrow{\text{fast}} {}^-O_3S-S-S^- + SCN^- \quad (6)$$

$$^-O_3S-S-S^- + CN^- \xrightarrow{\text{fast}} S_2O_3^{2-} + SCN^- \quad (7)$$

According to this mechanism, 3 mol of cyanide ions have to react with 1 mol of ionic pentathionate to give 2 mol of ionic thiocyanate. Such a mechanism is not in accordance with the kinetic results in this work.

A third mechanism, that may be in accordance with the rate data, involves a nucleophilic substitution at the sulfur atom number 2, displacing the sulfanemonosulfonate ion, $^-O_3SSS^-$.

$$^{-}O_3S-S-S-S-SO_3^{-}+CN^{-} \xrightarrow{\text{slow}} {}^{-}O_3S-S-S^{-}+{}^{-}O_3S-SCN \quad (8)$$

In the intermediate step a second cyanide ion might rapidly react with the sulfanemonosulfonate ion, eqn. (9).

$$^{-}O_3S-S-S^{-}+CN^{-} \xrightarrow{\text{fast}} S_2O_3^{2-}+SCN^{-} \quad (9)$$

Recently, Schmidt [6] has postulated the sulfur atom number 2 to be the most electrophilic centre of the higher polythionates. His hypothesis was based on polarization of the divalent sulfur–sulfur bonds due to the free *p* electrons. Harpp,[7] however, has recently shown the polarization effects to be secondary to the basicity of the leaving group. It is generally accepted that the basicity of $^{-}O_3SS_x^{-}$ increases with increasing values of x.[8] In this way the thiosulfate ion should be the most easily displaced ion in the first step.

The facts that ionic pentathionate reacts with piperidine to form monosulfur dipiperidide [9] and 2 mol of ionic thiosulfate, and selenopentathionate reacts with ionic dimethyldithiocarbamate [10] to give selenium bis(dimethyldithiocarbamate) and 2 mol of ionic thiosulfate, seem to justify that the electrophilic centre of the pentathionate ion is the sulfur atom number 3, and that the selenium atom is the electrophilic centre of the selenopentathionate ion.

Supposing the mechanism of the two reactions to be the same, a first step according to eqn. (8) would probably give much the same values of the enthalpy and the entropy of activation in the two cases. From Table 1 this is not in accordance with the experimental data.

When considering the significance of the activation parameters, which are presented in Table 1, it is seen that the selenopentathionate-cyanide reaction is characterized by a much smaller ΔH^* value, 4.6 kcal/mol, than the pentathionate-cyanide reaction. However, the entropy of activation of the selenopentathionate-cyanide reaction is 8 cal/mol deg. more negative than the entropy of activation of the pentathionate-cyanide reaction. The free energy of activation ΔG^* is seen to be 2.2 kcal/mol lower in the case of the selenopentathionate-cyanide reaction.

It is reasonable to suppose the geometry of the transition state of the pentathionate- and the selenopentathionate-cyanide reaction to be as depicted in I and II, respectively.

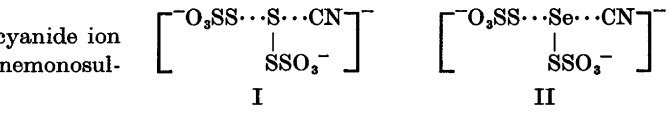

I II

The entropies of activation indicate that transition state II is more tight than transition state I. Furthermore, the enthalpies of activation point to a more stabilized transition in the case of II than I.

The timing of covalency changes for substitution at sulfenyl sulfur has been found to resemble that for an S_N2 substitution at sp^3 carbon.[11] The participation of the *d* orbitals of the sulfur atom in substitution at divalent sulfur is thus small.[11] Systematic work on nucleophilic attack at divalent selenium is not available in the literature.

Foss [12] has proposed the bonding of the transition state in nucleophilic attack at divalent sulfur and selenium to be a three-centre four-electron type. The instability of the trithiocyanate ion [13] relative to the triselenocyanate ion,[14] seems to support the explanation of the activation parameters outlined above.

EXPERIMENTAL

Acetonitrile, tetraphenylphosphonium cyanide, and tetraphenylarsonium cyanide were purified as reported previously.[4] Potassium pentathionate was prepared by the method of Goehring and Feldmann.[15] Sodium selenopentathionate was prepared by the method described by Foss.[16]

Tetraphenylarsonium pentathionate was precipitated from an aqueous solution of potassium pentathionate with tetraphenylarsonium chloride in nearly quantitative yield, and purified in the same way as reported for tetraphenylarsonium tetrathionate.[4] Dec. 250 °C. (Found: C 56.70; H 4.03; S 15.85. Calc. for $C_{48}H_{40}O_6S_5As_2$: C 56.30; H 3.90; S 15.85.)

Tetraphenylarsonium selenopentathionate was made in the same way and purified in the same manner. Dec. 245 °C. (Found: C 53.87; H 3.91; S 12.50. Calc. for $C_{48}H_{40}O_6S_4SeAs_2$: C 53.80; H 3.74; S 11.98.)

Iodometric analysis. The amount of ionic thiosulfate formed in the pentathionate-cyanide reaction in acetonitrile was determined as follows. Approx. 0.05 g tetraphenylarsonium pentathionate was dissolved in 3 ml acetonitrile. 5 ml of 0.1 M solution of tetraphenylarsonium

cyanide in acetonitrile was added and the solution was set aside for 15 min. A solution containing 1 ml of 40 % formaldehyde, 3 ml of 1 M sodium perchlorate and 10 ml of water was then added, whereupon tetraphenylarsonium perchlorate precipitated. The precipitated salt was removed by filtration and carefully washed with about 20 ml of water. Prior to the titration with 10^{-2} N iodine solution, 10 ml of 10 % acetic acid, 0.2 g potassium iodide and 2 ml of starch solution were added. The yield of ionic thiosulfate was found to be 92 – 93 %, based on the amount of ionic pentathionate used.

With regard to the iodometric analysis of the selenopentathionate-cyanide reaction in acetonitrile 20 ml of 10 % acetic acid and 1 g of potassium iodide were added prior to the titration. The amount of ionic thiosulfate was found to be 89 – 90 % based on the amount of ionic selenopentathionate used.

Procedure for the kinetic runs. The rate of the reaction between ionic pentathionate and the cyanide ion was determined by measuring the amount of ionic thiocyanate, using IR liquid cells with a path length of 1 mm. The second order kinetic plots were analysed according to the rate equation

$$dx/dt = k_2 (a-x) (b-2x)$$

where x is the concentration of ionic thiocyanate and a and b are the initial concentrations of ionic pentathionate and cyanide, 2.5×10^{-3} M and 5.0×10^{-3} M, respectively.

The rate of the thiocyanatosulfonate-cyanide reaction was determined by measuring the rate of formation of the second mol of ionic thiocyanate formed in the pentathionate-cyanide reaction, applying the initial concentrations of ionic pentathionate and cyanide, 2.0×10^{-3} M and 1.2×10^{-2} M, respectively. The kinetic plots were analysed according to the equation

$$dx/dt = k_2' (a-x) (b-x)$$

where x is the concentration of the second mol of ionic thiocyanate formed and a and b are the initial concentrations of ionic thiocyanatosulfonate and cyanide, 2.0×10^{-3} and 8.0×10^{-3} M, respectively.

The pseudo first-order rate constants of the selenopentathionate-cyanide reaction were calculated from stoppered-flow experiments at 320 nm, using 1.515×10^{-3} M tetraphenylarsonium selenopentathionate solution and 1.52×10^{-2} M tetraphenylphosphonium cyanide solution.

The second-order rate constants were all reproduced with an accuracy better than ± 3 %.

Conductivity measurements. Applying $\lambda^{o}_{Ph_4As^+} = 55.8$ ohm^{-1} cm^{-2} mol^{-1} [17] the equivalent conductivities at infinite dilution in acetonitrile at 25 °C were found to be

$\lambda^{o}_{(Ph_4As)_2S_5O_6} = 173$ ohm^{-1} cm^{-2} mol^{-1},

$\lambda^{o}_{S_5O_6^{2-}} = 61.4$ ohm^{-1} cm^{-2} mol^{-1}

From the plot, λ *versus* $\sqrt{c}$, tetraphenylarsonium pentathionate appeared to be completely dissociated in acetonitrile.

The IR measurements were performed with a Unicam SP 200 G Infrared Spectrophotometer, and the stopped-flow measurements were performed with a Durrum Stopped-Flow Model D-110.

The conductivity measurements were performed on a conductivity cell, type CDC 304 (immersion type) with a cell constant 1.00 cm ± 10 %.

Acknowledgement. The author wishes to express his thanks to The Norwegian Research Council for Science and the Humanities for a grant.

REFERENCES

1. Foresti, B. *Z. Anorg. Allg. Chem. 217* (1934) 33.
2. Foss, O. *Kgl. Nor. Vidensk. Selsk. Skr.* (1945) No. 2.
3. Foss, O. *Organic Sulfur Compounds*, Pergamon, London 1961, p. 83.
4. Austad, T. *Acta Chem. Scand. A 28* (1974) 693.
5. Schmidt, M. *Z. Anorg. Allg. Chem. 289* (1957) 13.
6. Schmidt, M. In Senning, A., Ed., *Sulfur in Organic and Inorganic Chemistry*, Dekker, New York 1972, Vol. 2, pp. 71 – 112.
7. Harpp, D. V. and Gleason, J. G. *J. Amer. Chem. Soc. 93* (1971) 2437.
8. Davis, R. E. *Surv. Progr. Chem. 2* (1964) 189.
9. Foss, O. *Kgl. Nor. Vidensk. Selsk. Skr.* (1947) No. 2.
10. Foss, O. *Acta Chem. Scand. 3* (1949) 1385.
11. Kice, J. L. and Anderson, J. M. *J. Org. Chem. 33* (1968) 3331.
12. Foss, O. *Pure Appl. Chem. 24* (1970) 31.
13. Seel, F. and Wesemann, D. *Chem. Ber. 86* (1953) 1107.
14. Hauge, S. *Acta Chem. Scand. 25* (1971) 3081.
15. Goehring, M. and Feldmann, U. *Z. Anorg. Allg. Chem. 257* (1948) 223.
16. Foss, O. *Acta Chem. Scand. 3* (1949) 435.
17. Springer, G. H., Coetzee, J. F. and Kay, R. L. *J. Phys. Chem. 73* (1969) 471.

Received May 6, 1974.

Acta Chemica Scandinavica A 28 (1974) 939—946

Acid-catalyzed Hydrolyses of Bridged Bi- and Tricyclic Compounds. II. Solvent Effects on the Hydrolysis Rates of Some 2-Norbornyl, 2-Norbornenyl and 3-Nortricyclyl Acetates*

MARTTI LAJUNEN

Department of Chemistry, University of Turku, 20500 Turku 50, Finland

The rates of hydrolysis have been measured for some secondary and methyl-substituted tertiary 2-norbornyl, 2-norbornenyl, and 3-nortricyclyl acetates in solutions of 0.25 – 4.0 M perchloric acid in 60 wt. % dioxane-water and in solutions of 1 M perchloric acid in 0 – 95.7 wt. % dioxane-water. Linear log k_1 *vs.* log c_{H^+} and (log $k_1 + H_0$) *vs.* (H_0 + log c_{H^+}) relationships for the secondary acetates and nonlinear log k_1 *vs.* H_0 and (log $k_1 + H_0$) *vs.* (H_0 + log c_{H^+}) relationships for the tertiary acetates were found in the former solutions. The plots for log k_a *vs.* H_0 and for (log $k_a + H_0$) *vs.* H_0 ($k_a = k_1/c_{H^+}$) were found to be approximately linear for the tertiary acetates in the latter solutions (0 – 60 wt. % of dioxane). The slopes of the (log $k + H_0$) *vs.* (H_0 + log c_{H^+}) plots were observed to be equal for the secondary acetates in both kinds of solutions.

In a recent paper [2] the reaction mechanism of hydrolysis for some secondary and tertiary methyl-substituted 2-norbornyl, 2-norbornenyl,

* Part 2 of the abridgment of M. Lajunen's Dissertation.[1]

Table 1. The numbering system and symbols used in this paper for 2-norbornyl (A), 2-norbornenyl [a] (B), and 3-nortricyclyl (C) acetates and alcohols.

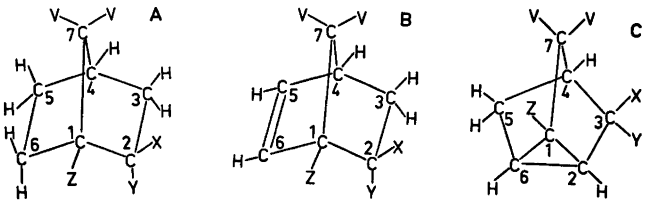

V	X	Y	Z	A	B	C
H	x[b]	H	H	*exo*-I-x	*exo*-V-x	X-x[c]
H	H	x	H	*endo*-I-x	*endo*-V-x	X-x[c]
H	x	R[d]	H	*exo*-II-x	*exo*-VI-x	XI-x[e]
H	R	x	H	*endo*-II-x	*endo*-VI-x	XI-x[e]
H	x	H	R	*exo*-III-x		*cis*-XII-x
H	H	x	R	*endo*-III-x		*trans*-XII-x
R	x	H	R	*exo*-IV-x		
R	H	x	R	*endo*-IV-x		

[a] The site of the double bond between C(5) and C(6) is not indicated with a number in this paper. [b] x indicates OH or OAc. [c] Enantiomers. [d] R indicates the methyl group. [e] Enantiomers.

and 3-nortricyclyl acetates (Table 1) were dealt with. All secondary acetates were observed to hydrolyze by the $A_{AC}2$ mechanism and tertiary acetates by the $A_{AL}1$ mechanism with the exception of tertiary *endo*-2-norbornenyl acetate, which hydrolyzes simultaneously by both mechanisms in 1 M perchloric acid containing 60 wt. % of dioxane at 10 – 55 °C. A marked anchimeric increase in the rate was evaluated for tertiary *exo* and tricyclic acetates (the $A_{AL}i$ mechanism; *i.e.* the $A_{AL}1$ mechanism with neighboring group participation).

It is well known that in the $A_{AL}1$ hydrolysis the reaction rate in about fifty-fifty mixtures of acid dioxane-water is distinctly slower than in solutions rich in water or dioxane, but in the $A_{AC}2$ hydrolysis the rate of reaction depends only slightly on the dioxane content.[3,4] Therefore it is possible that the hydrolysis mechanism of secondary acetates which may produce relatively stable carbocations (*e.g.* nonclassical ions)[1,2] changes from $A_{AC}2$ to $A_{AL}1$ when the reaction medium is made richer in dioxane or water. The increasing acid concentration may have the same kind of effect owing to the fact that the rate of the $A_{AL}1$ hydrolysis increases much faster than that of the $A_{AC}2$ hydrolysis as the acid concentration becomes greater.[5,6] The rates of hydrolysis by the $A_{AL}i$ and $A_{AL}1$ mechanisms also may depend differently on the changing reaction medium owing to the different character of the transition states. For the study of these subjects the rates of hydrolysis for several bi- and tricyclic acetates (Table 1) were measured in solutions of 0.25 – 4.0 M perchloric acid in 60 wt. % dioxane-water and in solutions of 1 M perchloric acid in 0 – 95.7 wt. % dioxane-water.

EXPERIMENTAL

The syntheses and identification of the acetates (Table 1) have been reported earlier.[1] The reaction media (the percentage, *e.g.* "60 wt. % dioxane-water", indicates the amount of dioxane in dioxane-water mixtures when perchloric acid is excluded) were prepared by weighing the components. The kinetics was studied by titrimetric and gas-chromatographic methods.[1] The results are collected in Tables 2 – 3.

DISCUSSION

The Zucker-Hammett hypothesis,[8] despite criticism,[9] has often been used to identify mechanism A-2 and A-1.[5,10] According to the hypothesis, for the A-2 hydrolysis, in which the transition state contains water, the logarithm of the first order rate coefficient is a linear function (slope = 1) of the logarithm of the acid concentration, whereas for the A-1 hydrolysis, in which the transition state does not contain water, $\log k_1$ is linearly related (slope = – 1) to the Hammett acidity function H_0.[11]

According to Table 2 the rates of hydrolysis of secondary acetates increase much more slowly with increasing acid concentration than those of tertiary acetates. A linear correlation exists between $\log k_1$ and $\log c_{H^+}$ in the case of the secondary acetates (the equations are obtained by the method of least squares):

exo-I-OAc: $\log k_1 = (1.19 \pm 0.05) \log c_{H^+} - (4.44 \pm 0.02)$,
exo-V-OAc: $\log k_1 \approx 1.12 \log c_{H^+} - 4.43$ (2 points only),
X-OAc: $\log k_1 = (1.337 \pm 0.013) \log c_{H^+} - (4.144 \pm 0.005)$.

The linearity suggests that no remarkable change in mechanism ($A_{AC}2 \rightarrow A_{AL}1$) occurs in the acid concentration range studied although perchloric acid has a greater ability, compared with hydrochloric and sulfuric acids, to increase the rate of the $A_{AL}1$ hydrolysis and a lesser ability to increase the rate of the $A_{AC}2$ hydrolysis.[5] The hydrolysis rates of the tertiary acetates do not follow the linear correlation. Fig. 1 demonstrates that the $\log k_1$ *vs.* H_0 plots for secondary acetates are curves of decreasing slope and those for tertiary acetates are lines curving slightly upwards. (Within experimental error the latter plots can also be described as consisting of two straight segments (initial slopes 1.0 – 1.1 and final slopes 1.4 – 1.6) linked by a short curved portion.) Thus the rates of the tertiary acetates do not obey the Zucker-Hammett hypothesis.

Bunton *et al.*[12] reported that the rates of hydrolysis of isopropyl acetate and *endo*-2-bornyl acetate (1,7,7-trimethyl-*endo*-2-norbornyl acetate, *endo*-IV-OAc in Table 1) follow the linear $\log k_1$ *vs.* $\log c_{H^+}$ relationships (the slope is 1.20 for the former at 25 °C and 1.69 for the

Table 2. Rates of hydrolysis of acetates in solutions of perchloric acid in 60 wt. % dioxane-water.

Acetate	Temp./°C	c_{HClO_4}/M	H_0[a]	$10^5 k_1/s^{-1}$	
exo-I-OAc	25	0.505	1.40	1.53	±0.03
		0.993	0.75	3.84	0.08
		2.26	−0.49	10.1	0.1
		4.00	−1.84	17.8	0.2
exo-V-OAc	25	0.988	0.75	3.63	±0.07
		3.23	−1.29	13.6	0.2
X-OAc	25	0.250	1.90	1.09	±0.01
		0.501	1.40	2.88	0.02
		0.997	0.75	7.42	0.16
		1.49	0.23	12.6	0.7
		2.00	−0.26	18.1	0.2
		3.00	−1.10	30.1	0.3
		4.00	−1.84	46.1	0.8
Hex-II-OAc[b]	25	0.505	1.40	0.853	±0.009
		1.002	0.75	3.64	0.06
		1.51	0.21	14.3	0.3
		1.98	−0.24	47.3	1.5
		2.51	−0.70	208	4
		2.98	−1.10	755	9
		3.23	−1.29	1480	20
exo-II-OAc	10	0.258	1.90	1.76	±0.04
		0.503	1.40	5.62	0.08
		0.753	1.05	13.2	0.2
		1.000	0.75	26.6	0.6
		1.25	0.47	59.0	1.2
		1.51	0.21	172	5
		1.59	0.12	212	7
		1.70	0.02	345	14
		1.96	−0.22	615	14
		2.11	−0.35	1070	20
		2.25	−0.48	1530	40
		2.26	−0.48	1450	20
endo-II-OAc	25	1.000	0.75	0.474	±0.007
		1.50	0.22	1.66	0.06
		1.51	0.21	1.78	0.05
		1.92	−0.19	4.35	0.11
		2.48	−0.69	16.9	0.5
		3.00	−1.10	68.6	1.7
		3.49	−1.48	235	5
		4.00	−1.84	995	26
XI-OAc	10	0.502	1.40	1.44	±0.01
		0.750	1.05	3.44	0.05
		1.002	0.75	7.86	0.06
		1.24	0.48	15.0	0.2
		1.50	0.22	27.5	0.4
		1.73	−0.01	59.7	2.0
		1.99	−0.25	166	5
		2.24	−0.47	369	5
		2.51	−0.70	760	10
		2.74	−0.91	1680	40
		2.74	−0.91	1660	30

[a] Interpolated from H_0 functions at 25 °C presented by Paul and Long.[7] [b] 1-Methylcyclohexyl acetate.

Table 3. Rates of hydrolysis of acetates in solutions of 1.00 M perchloric acid in different dioxane-water mixtures.

Acetate	Temp./°C	Wt. % of dioxane	H_0[a]	$10^5 k_a/M^{-1}s^{-1}$	
exo-I-OAc	25	0	−0.22	4.50	± 0.07
	25	60	0.75	3.90	0.08
	55	60		50.4	0.8
	55	95.7		66.3	0.3
endo-I-OAc	25	0	−0.22	5.15	± 0.13
	25	60	0.75	4.70	0.06
exo-V-OAc	25	0	−0.22	4.16	± 0.07
	25	60	0.75	3.72	0.07
	55	60		47.8	1.2
	55	95.7		53.9	1.0
X-OAc	25	0	−0.22	9.06	± 0.25
	25	19	0.08	8.74	0.18
	25	38.6	0.40	8.60	0.20
	25	60	0.75	7.50	0.16
	25	79.9		5.93	0.16
	25	89.1		5.53	0.11
	25	95.7		6.22	0.19
Hex-II-OAc[b]	25	0	−0.22	65.7	± 1.3
	25	10	−0.06	43.1	0.8
	25	20	0.10	23.5	0.5
	25	40	0.42	9.22	0.05
	25	60	0.75	3.65	0.06
	25	79.2		3.73	0.06
	25	89.1		38.5	0.6
exo-II-OAc	10	0	−0.22	587	± 19
	10	10	−0.06	418	6
	10	19	0.08	213	9
	10	29	0.25	125	4
	10	38.6	0.40	82.2	2.4
	10	48.8	0.57	53.7	1.4
	10	60	0.75	26.5	0.6
	10	68.8		25.5	0.6
	10	79.2		28.1	0.4
	10	89.1		225	6
endo-II-OAc	45	0	−0.22	48.2	± 1.4
	45	10	−0.06	36.5	1.3
	45	20	0.10	27.1	0.4
	45	30	0.26	19.0	0.5
	45	38.6	0.40	13.3	0.4
	45	40	0.42	13.1	0.4
	45	48.8	0.57	7.80	0.10
	45	60	0.75	6.21	0.13
	45	79.2		6.49	0.19
	45	89.1		34.5	0.9
endo-VI-OAc	45	0	−0.22	11.9	± 0.3
	45	20	0.10	8.34	0.14
	45	40	0.42	6.33	0.15
	45	60	0.75	4.16	0.05
	45	80		3.52	0.09
	45	89.9		11.5	0.3
	45	95.7		919	6

[a] Interpolated linearly from H_0 functions at 25 °C presented by Paul and Long.[7] [b] 1-Methylcyclohexyl acetate.

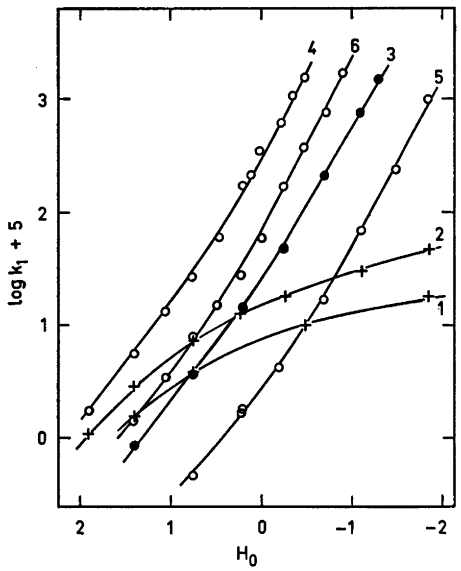

Fig. 1. Plots of log k_1 for hydrolyses of acetates *versus* H_0 in solutions of perchloric acid in 60 wt. % dioxane-water. 1 = *exo*-I-OAc, 2 = X-OAc, 3 = Hex-II-OAc, 4 = *exo*-II-OAc, 5 = *endo*-II-OAc, and 6 = XI-OAc.

latter at 44.6 °C) and the log k_1 *vs.* H_0 plot of tertiary butyl acetate is a curve with a slightly increasing slope (or two straight segments linked by a curved portion), whereas the latter plot of *exo*-2-bornyl acetate (1,7,7-trimethyl-*exo*-2-norbornyl acetate, *exo*-IV-OAc in Table 1) is linear (slope = −0.75) in the solutions of perchloric acid in 60 vol. % dioxane-water. They explained the curving log k_1 *vs.* H_0 plot of tertiary butyl acetate to be an indication of a change in the mechanism ($A_{AC}2 \rightarrow A_{AL}1$). The results of this work and Ref. 2, Table 5, imply that the curvature observed for the tertiary acetates cannot be attributed solely to the change of the mechanism since the activation parameters of most tertiary acetates studied were observed to be in accordance with the $A_{AL}1$ mechanism. More probably the ratio of activity coefficients in eqn. (1) does not

$$\log k_1 = -H_0 + \log \frac{y_S y_{BH^+}}{y_{\neq} y_B} + \text{constant} \qquad (1)$$

remain constant within the acidity scale studied.[11] (Symbols y_S, $y_{\neq}$, y_B, and y_{BH^+} indicate the molar activity coefficients of substrate, transition state, indicator base, and its conjugate acid, respectively.) The same kind of slight curvature can even be seen in the hydrolysis of tertiary butyl acetate in aqueous perchloric acid.[5] The linear relationship for *exo*-2-bornyl acetate observed by Bunton *et al.*[12] is possibly a fortuitous result of the combined effects of the concurrent $A_{AL}1$ and $A_{AC}2$ mechanisms, which would separately cause the log k_1 *vs.* H_0 plots to curve upwards and downwards, respectively.

Bunnet and Olsen [13] studied the relationships between log k_1, log c_{H^+}, and H_0 and found that the value of the coefficient ϕ in eqn. (2) is a better indicator of the different mechanisms of

$$\log k_1 + H_0 = \phi(H_0 + \log c_{H^+}) + \text{constant} \qquad (2)$$

acid-catalyzed hydrolyses than the Zucker-Hammett hypothesis. In Fig. 2, eqn. (2) is applied to the rates of hydrolysis of secondary and tertiary acetates. The plots are linear for the secondary acetates and the slopes (ϕ values) have the following values at 25 °C: *exo*-I-OAc: 0.94 ± 0.03, *exo*-V-OAc: *ca.* 0.96 (two points), and X-OAc: 0.91 ± 0.01 ($c_{H^+} \geq 1$). They are of the same order of magnitude as the ones that have been obtained for esters hydrolyzing by the $A_{AC}2$ mechanism in aqueous acids ($0.7 \leq \phi \leq 1$).[13] The plots of eqn. (2) for the tertiary

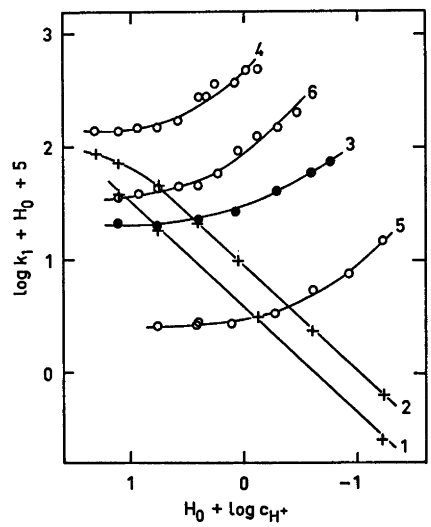

Fig. 2. Plots of (log $k_1 + H_0$) for hydrolyses of acetates *versus* (H_0 + log c_{H^+}) in solutions of perchloric acid in 60 wt. % dioxane-water. The numbering system is the same as in Fig. 1.

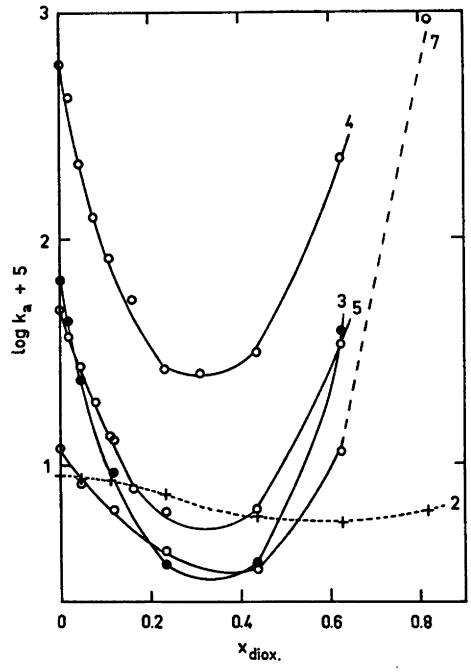

Fig. 3. Plots of log k_a for hydrolyses of acetates *versus* the mol fraction of dioxane ($x_{diox.}$) in solutions of 1.00 M perchloric acid in different dioxane-water mixtures. 2 = X-OAc, 3 = Hex-II-OAc, 4 = *exo*-II-OAc, 5 = *endo*-II-OAc, and 7 = *endo*-VI-OAc.

acetates are, however, curves. The results differ from the usually linear relationships observed in aqueous acids for esters which hydrolyze by the $A_{AL}1$ mechanism and for acetals which hydrolyze by the A-1 mechanism.[18] However, the hydrolysis of tertiary butyl acetate gives a slightly nonlinear correlation in aqueous perchloric acid.[5]

Table 3 and Fig. 3 demonstrate that the rates of hydrolysis of the secondary acetates depend only slightly on the dioxane content of the 1 M perchloric acid solution. Hence, there does not exist any remarkable $A_{AL}1$ hydrolysis of the secondary *exo* and tricyclic acetates even in water and 95.7 wt. % dioxane-water, where the rates of the tertiary acetates are relatively high. The plots of log k_a *vs.* mol fraction of dioxane ($k_a = k_1/c_{H^+}$) for 2-methyl-2-norbornyl acetates (*exo*- and *endo*-II-OAc) and 1-methylcyclohexyl acetate (Hex-II-OAc) are very similar, the rate minimum lying at the mol fraction *ca.* 0.3 (about 70 wt. % of dioxane). The curve of *exo*-2-methyl-*endo*-2-norbornenyl acetate (*endo*-VI-OAc) is, however, somewhat different from those of other acetates, which can probably be attributed to the contribution of two mechanisms of hydrolysis, *i.e.* $A_{AC}2$ and $A_{AL}1$.[1,2]

The method based on the observation of the direct formation of unrearranged (by the $A_{AC}2$

Table 4. Rates and intermediate products of acid-catalyzed hydrolyses of *endo*-VI-OAc, *endo*-VI-OH, and XII-OH in solutions of 1.00 M perchloric acid in different dioxane-water mixtures.

Substrate	Temp./°C	Wt. % of dioxane	$10^5 k_a$/M^{-1}s^{-1}			Intermediate[a] products
endo-VI-OAc	45	0	3.8	±	0.1	*endo*-VI-OH
	45	0	8.1		0.4	XII-OH (+*exo*-VI-OH?)
	45	60	2.41	±	0.06[b]	*endo*-VI-OH
	45	60	1.75		0.11[b]	XII-OH (+*exo*-VI-OH?)
	45	95.7	919		6	XII-OH (+*exo*-VI-OH?)
endo-VI-OH	45	0	3.12	±	0.05	16 % of XII-OH
	45	60	0.403		0.005[b]	23 % » »
	45	95.7	410		5	74 % » »
	55	60	1.74		0.02[b]	29 % » »
	55	95.7	1670		100	*ca.* 65 % » »
XII-OH	45	0	18.2	±	0.1	
(*cis*:*trans*	45	60	1.49		0.01[b]	some unknown subst.
= 1:2)	45	95.7	115		4	
	55	60	5.19		0.07[b]	some unknown subst.
	55	95.7	310		8	

[a] Final products are norbornanediols. [b] Ref. 2.

mechanism) and rearranged (by the $A_{AL}1$ mechanism) products from the substrate was used to determine the contributions of the mechanisms in the hydrolysis of *endo*-VI-OAc in different acid dioxane-water mixtures.[1,2] Due to the instability of the hydrolysis products, *exo*-2-methyl-*endo*-2-norbornenol (*endo*-VI-OH) and 1-methyl-3-nortricyclanols (XII-OH, *cis* and *trans* isomers), their disappearance rates were measured in the same solutions and the iteration method [1,2] was used for estimation of rates of formation. The results, collected in Table 4, demonstrate that the contribution of the $A_{AL}1$ mechanism is 68 % in acid water, 42 % in 60 % dioxane-water, and approximately 100 % in 95.7 % dioxane-water at 45 °C. The dependence of rates on dioxane content is thus similar to those of secondary and tertiary acetates hydrolyzing by either of these mechanisms.

According to Table 4 the rates of acid-catalyzed water addition to the homoallylic double bond of *exo*-2-methyl-*endo*-2-norbornenol (*endo*-VI-OH): $10^5 k_a/M^{-1}s^{-1}$ at 45 °C: 2.62 (aqueous acid), 0.31 (60 % dioxane), and 107 (95.7 % dioxane), and to the three-membered carbon ring of 1-methyl-3-nortricyclanols (XII-OH) depend considerably on the dioxane content of the medium. The hydration of the double bond in the simple olefins has been confirmed to follow the $A\text{-}S_E2$ mechanism, in which the addition of a proton to the double bond is the rate-determining step of the reaction.[14] The similar dependence of the rates of hydration of the homoallylic double bond and the three-membered ring upon the dioxane content implies that in both cases the mechanism may be the same, possibly $A\text{-}S_E2$. Yet the A-1 mechanism (rapid proton exchange between the substrate and the solvent before the unimolecular rate-determining step) cannot be eliminated on this basis, since it has been observed that the dependences of the hydrolysis rates of the reactions proceeding by the $A\text{-}S_E2$ and A-1 mechanisms upon the dioxane content are very similar.[15] Further investigations on the subject are needed.

According to the results of Harned and Ross [4] the rate of hydrolysis of methyl acetate (the $A_{AC}2$ mechanism) in solutions of 0.1 – 0.2 M hydrochloric acid in dioxane-water mixtures mainly depends on the relative activity coefficient (= 1 in acid water) of the substrate. The plots of log k_a *vs.* mol fraction of dioxane for the secondary bi- and tricyclic acetates are very similar to the corresponding plot for methyl acetate. Thus the deductions of Harned and Ross can also be applied to them. The rates of hydrolysis of the tertiary acetates studied depend on the dioxane content to a so much greater extent that it cannot be explained only by the change of the activity coefficients of the substrates. The plot of the negative Hammett acidity function $-H_0$ *vs.* dioxane content [7] is very similar to the plots for the tertiary acetates in Fig. 3. Thus it is natural that fairly linear correlations between log k_a and H_0 exist in solutions of 1 M perchloric acid in dioxane-water mixtures (0 – 60 wt. % dioxane, for which the H_0 functions at 25 °C were available [7]):

Hex-II-OAc: $\log k_a = -(1.31 \pm 0.03)H_0 - (3.47 \pm 0.01)$ at 25 °C,
exo-II-OAc: $\log k_a = -(1.39 \pm 0.05)H_0 - (2.52 \pm 0.02)$ at 10 °C,
endo-II-OAc: $\log k_a = -(0.96 \pm 0.04)H_0 - (3.50 \pm 0.02)$ at 45 °C,

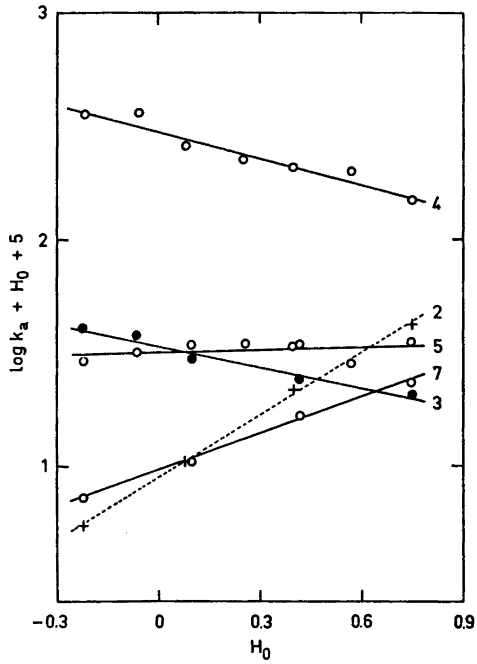

Fig. 4. Plots of (log $k_a + H_0$) for hydrolyses of acetates *versus* H_0 in solutions of 1.00 M perchloric acid in different dioxane-water mixtures. The numbering system is the same as in Fig. 3.

endo-VI-OAc: $\log k_a = -(0.46 \pm 0.02)H_0 - (4.03 \pm 0.01)$, the overall rate, and *endo*-VI-OAc: $\log k_a = -0.67H_0 - 4.25$, the $A_{AL}1$ mechanism, at 45 °C.

The discrepancy between the slightly non-linear $\log k_1$ *vs.* H_0 correlations (0.25 – 4.0 M acid in 60 wt. % dioxane-water) and fairly linear $\log k_a$ *vs.* H_0 correlations (1 M acid in 0 – 60 wt. % dioxane-water) may be due to the narrow H_0 range employed in the latter measurements.

Eqn. (2) has been adapted to the rates of hydrolysis of acetates in acid 0 – 60 wt. % dioxane-water mixtures in Fig. 4 (in this case $\log c_{H^+} = 0$). The plots are approximately linear and the slopes (ϕ values) have the following values: X-OAc: 0.92 ± 0.02, other secondary acetates: 0.93 – 0.96 (two points in each; not plotted in Fig. 4), Hex-II-OAc: $-(0.31 \pm 0.03)$, *exo*-II-OAc: $-(0.39 \pm 0.05)$, *endo*-II-OAc: 0.04 ± 0.04, and *endo*-VI-OAc: 0.54 ± 0.02 (the total rate; the $A_{AC}2$ mechanism: *ca.* 0.8 and the $A_{AL}1$ mechanism: *ca.* 0.3, two points in both of them). The slopes of eqn. (2) obtained by changing the acid concentration and the dioxane content of the medium are equal for the secondary acetates (*cf.* above). The latter slopes for the tertiary acetates are typical of the A-1 hydrolyses in aqueous acids ($-1 \leq \phi \leq 0$)[13] with the exception of that for *exo*-2-methyl-*endo*-2-norbornenyl acetate (*endo*-VI-OAc; the value for the $A_{AL}1$ mechanism is abnormal, possibly due to the experimental errors). Distinct differences in the $\log k$ *vs.* H_0 and $(\log k + H_0)$ *vs.* $(H_0 + \log c_{H^+})$ plots between the acetates, *exo*-II-OAc and XI-OAc, which can produce the non-classical or seminonclassical transition states, and the acetates, Hex-II-OAc, *endo*-II-OAc, and *endo*-VI-OAc, the transition states of which are probably classical, cannot be seen. The slopes of the plots may, however, be more negative for the former acetates (compared in Ref. 1).

Acknowledgement. The financial support from the Foundation of Neste Oy is gratefully acknowledged.

REFERENCES

1. Lajunen, M. *Kinetics and Product Analyses of the Acid-Catalyzed Hydrolyses of Some Secondary and Tertiary 2-Norbornyl, 2-Norbornenyl, and 3-Nortricyclyl Acetates*, Diss., University of Turku, 1973.
2. Lajunen, M. *Acta Chem. Scand. A 28* (1974) 919.
3. Sadek, H. and Khalil, F. Y. *Z. Phys. Chem. (Frankfurt am Main)* a. *57* (1968) 306; b. *61* (1968) 63.
4. Harned, H. S. and Ross, A. M. *J. Amer. Chem. Soc. 63* (1941) 1993.
5. Bunton, C. A., Crabtree, J. H. and Robinson, L. *J. Amer. Chem. Soc. 90* (1968) 1258.
6. Salomaa, P. *Suom. Kemistilehti B 32* (1959) 81, 145.
7. Paul, M. A. and Long, F. A. *Chem. Rev. 57* (1957) 1, with refs.
8. Zucker, L. and Hammett, L. P. *J. Amer. Chem. Soc. 61* (1939) 2791.
9. Bunnett, J. F. *J. Amer. Chem. Soc. 83* (1961) 4956, with refs.
10. Euranto, E. K. In Patai, S., Ed., *The Chemistry of Carboxylic Acids and Esters*, Interscience, London 1969, pp. 549 – 569, with refs.
11. Long, F. A. and Paul, M. A. *Chem. Rev. 57* (1957) 935.
12. Bunton, C. A., Khaleeluddin, K. and Whittaker, D. *J. Chem. Soc.* (1965) 3290.
13. Bunnett, J. F. and Olsen, F. P. *Can. J. Chem. 44* (1966) 1917.
14. Kresge, A. J., Chiang, Y., Fitzgerald, P. H., McDonald, R. S. and Schmid, G. H. *J. Amer. Chem. Soc. 93* (1971) 4907.
15. Kankaanperä, A. and Merilahti, M. *Acta Chem. Scand. 26* (1972) 685.

Received January 28, 1974.

Acta Chemica Scandinavica A 28 (1974) 947—956

Solvent Extraction Studies on the Hydrolysis and Complex Formation of Methylmercury(II) with Phosphate Ions

FOLKE INGMAN* and DJIET HAY LIEM

Department of Inorganic Chemistry, Royal Institute of Technology (KTH), S-100 44 Stockholm 70, Sweden

The hydrolysis of methylmercury(II) ($MeHg^+$) and its complex formation with phosphate ions have been studied by measuring the distribution of MeHg(II) in the two-phase system *o*-xylene/1.0 M (Na,H)(Cl,NO_3,PO_4) as a function of phosphate concentration and $[H^+]$ for different constant values of chloride concentration. The distribution of MeHg(II) between the two phases has been measured by a radiometric method using MeHg(II) labelled with Hg-203 and also by the use of a spectrophotometric titration method. Graphical and computer analysis of the distribution data using the Letagrop-Distr program indicates the formation of the complexes MeHgOH(aq) and $MeHgHPO_4^-$(aq) with the following equilibrium constants:

$MeHg^+(aq) + H_2O \rightleftharpoons MeHgOH(aq) + H^+$;
$\log[K \pm 3\sigma(K)] = -4.40 \pm 0.07$

$MeHg^+(aq) + H_2PO_4^- \rightleftharpoons MeHgHPO_4^-(aq) + H^+$;
$\log[K \pm 3\sigma(K)] = -1.74 \pm 0.03$

The only species in the organic phase is MeHgCl whose distribution coefficient and stability constant in the two-phase system 1 M (Na,H)(ClO_4,Cl)/*o*-xylene have been determined previously. The results are discussed in the light of studies by other authors.

The polluting effects of organomercurials in the environment which have been shown to endanger the health of man and animals [1] have focussed interest on studies of, among other things, the solution chemistry of organomercury(II) ions and, in particular, their complex formation with the inorganic ligands that are commonly found in natural waters, *e.g.* Cl^- or SH^- ions. Many studies have been reported on the ecological effects of organomercurials as well as on their metabolism in nature.[2,3] A search in the chemical literature, however, showed that only few studies have been published on the complex chemistry of organomercurial compounds in aqueous solution.[4-14]

In a previous work [13] we studied the complex formation between methylmercury(II) and chloride ions in the two-phase system *o*-xylene/1 M (Na,H)(ClO_4,Cl) using radiometric and spectrophotometric titration methods. The use of these experimental techniques has the advantage of enabling us to make detailed studies of the complex chemistry of methylmercury(II) ions at tracer levels of metal concentrations as often found in natural waters. In the present work we report the results of studies on the hydrolysis of CH_3Hg(II) and its complex formation with phosphate ions from studies of the distribution of CH_3Hg(II) in the two-phase system *o*-xylene/1.0 M (Na,H)(NO_3,Cl,PO_4). Preliminary results from this work have been reported elsewhere.[15]

Studies of the complex chemistry of organomercuric ions with several ligands have been reported previously. Maynard and Howard [9] as well as Johns *et al.*[10] found results of conductance measurements of MeHgOH and $MeHgNO_3$ in aqueous and ethanol solution to be consistent with the formation of the hydrolyzed species MeHgOH. Schwarzenbach and Schellenberg [4-6] studied the hydrolysis of CH_3Hg^+ and its complex formation with a series of organic and inorganic ligands. From their potentiometric data they demonstrated among other things the formation in 0.1 M KNO_3 medium of the hydrolysed species CH_3HgOH, $(CH_3Hg)_2OH^+$ and the complex $CH_3HgHPO_4^-$. Zanella *et al.*,[8] however, using potentiometric methods found only the formation of the hydrolysed species RHgOH

* Present address: Department of Analytical Chemistry, Royal Institute of Technology, S-100 44 Stockholm 70, Sweden.

(R = Me, Et, Pr, and Bu) in 0.1 M KNO_3. Waugh *et al.*[7] *a priori* assumed the formation of RHgOH (R = Me, Et, and Ph) and determined its formation constant by potentiometric titration of RHgOH aqueous solution with HNO_3 and $HClO_4$ solutions. The hydrolysis of methylmercuric ions was studied by Schwarzenbach and Schellenberg [4-6] at pH = 3.16 – 6.66 and a total concentration of methylmercury, $C_{MeHg} = 1.17 \times 10^{-2} - 5.85 \times 10^{-4}$ M and by Zanella *et al.*[8] at a range of pH and metal concentrations which are not clearly specified. Libich and Rabenstein [14] reported the formation of MeHgOH and $(MeHg)_2OH^+$ from studies of the *pH*-dependence of the chemical shift of the methyl protons of methylmercury in an aqueous solution containing 0.190 M MeHg(II). These authors, however, made no use of an ionic medium to control the activity factor of the species studied. The formation of a $CH_3HgHPO_4^-$ complex was found by Schwarzenbach and Schellenberg [4-6] from potentiometric data for a constant value of $C_{PO_4} = 1.055$ mM, $C_{MeHg} = 1.99 - 0.995$ mM and pH = 3.76 – 7.54. In the present work we have extended the concentration ranges studied ($C_{MeHg} = 4.15 \times 10^{-5} - 5.35 \times 10^{-4}$ M; $C_{PO_4} = 0 - 0.333$ M and *pH* = 1.26 – 9.27) in order to investigate the formation of other methylmercuric complexes. The use of the Letagrop computer program in the analysis of the data enabled us to find effectively the chemical model which gives the best fit to the experimental data.

SYMBOLS AND EQUILIBRIUM CONSTANTS

$[\ ]$ = equilibrium concentration in the aqueous phase.

$[\ ]_{org}$ = equilibrium concentration in the organic phase.

C_{Cl} = initial total concentration of chloride ion in the system referred to the aqueous phase, *i.e.* $\sum n_{Cl}/V_{aq}$, where $\sum n_{Cl}$ represents the total number of moles of Cl(–I) in the two-phase system, and V_{aq} the volume of the aqueous phase.

C_{MeHg} = initial total concentration of methylmercury(II) ion in the organic phase.

C_{PO_4} = initial total concentration of phosphate ion in the aqueous phase.

K_{pqrs}^{org} = formation constant of the complex $(H^+)_p(MeHg^+)_q(Cl^-)_r(H_2PO_4^-)_s$ in the organic phase, *cf.* (2).

K_{klmn}^{aq} = formation constant of the complex $(H^+)_k(MeHg^+)_l(Cl^-)_m(H_2PO_4^-)_n$ in the aqueous phase, *cf.* (1).

MeHg = CH_3Hg, methylmercury(II).

I_{aq}, I_{org} = γ-activity of $Me^{203}Hg$ in the aqueous and organic phases given in cpm for equal volumes of samples.

C_{aq}, C_{org} = total concentration of MeHg(II) in the equilibrated aqueous and organic phases.

D = $\sum[MeHg]_{org}/\sum[MeHg] = I_{org}/I_{aq}$ ($= C_{org}/C_{aq}$), net distribution ratio of methylmercury.

EXPERIMENTAL

Reagents. *$NaNO_3$* (*p.a.* Merck-Darmstadt) was dried at 120 °C and used without further purification. *$Na_2HPO_4.12H_2O$* (*p.a.* Merck-Darmstadt) was recrystallized from water, air-dried and stored over silica gel. A disodium hydrogenphosphate stock solution was made from the recrystallized phosphate and the concentration of P(V) analyzed by a titrimetric method. *H_3PO_4*, *HNO_3* (*p.a.* Merck) were used without further purification. *NaOH* solution was prepared as described in Ref. 16. *o-Xylene, chloroform, dithizone, non-radioactive CH_3HgOH solution* were of the same quality and were purified as described previously.[13] *Radioactive $CH_3^{203}Hg$-(II)* was purchased in the form of $(CH_3^{203}Hg)_2O$ (Radiochemical Centre, Amersham, England) and as $CH_3^{203}HgNO_3$ aqueous solution (Swedish Atomic Energy, Studsvik). The $CH_3^{203}Hg$(II) was purified as described previously [13] except that instead of benzene, *o*-xylene was used to extract the purified $CH_3^{203}HgCl$. For the distribution experiments a stock solution of 8.2×10^{-6} M $CH_3^{203}HgCl$ in *o*-xylene was used.

Measurement of hydrogen ions concentration. The $[H^+]$ in the aqueous phase (for log $[H^+] < -2$) was determined with a Wilhelm-type salt bridge arrangement:

RE|1.0 M $NaNO_3$|equilibrated sample solution|GE

where RE = Ag,AgCl/1.0 M $AgClO_4$ and GE = glass electrode. A Beckman glass electrode type 40498 was used in conjunction with a Radiometer pHM4c valve potentiometer. The glass electrode was standardized with a 1.0 M $(Na,H)NO_3$ buffer solution with $-\log[H^+] = 2.000$. For a 1.0 M $(Na,H)NO_3$ aqueous solution and $-\log[H^+] \geq 2$ the error in the measured value of pH caused by neglecting the liquid junction potential is expected to be less than 0.002 pH unit.[17]

Ionic strength and acidity constants. In the distribution experiment the aqueous solutions were adjusted such as to give a calculated constant ionic strength $I = \sum \frac{1}{2} c_i z_i^2 = 1.0$ M. The following values for the acidity constants for phosphoric acid H_3PO_4 were assumed:[18-22] $K_{a1} = [H_2PO_4^-][H^+][H_3PO_4]^{-1} = 1.99 \times 10^{-2}$ M, $K_{a2} = [HPO_4^{2-}][H^+][H_2PO_4^-]^{-1} = 3.314 \times 10^{-7}$ M, $K_{a3} = [PO_4^{3-}][H^+][HPO_4^{2-}]^{-1} = 7.936 \times 10^{-12}$ M. All experiments were carried out in thermostated rooms at 25 ± 0.3 °C according to procedures described previously.[13]

Basic assumptions for the chemical model. We assume that the chemical species of interest in the system may be represented by the general formula: $(H^+)_k(MeHg^+)_l(Cl^-)_m(H_2PO_4^-)_n$(aq) in the aqueous phase and $(H^+)_p(MeHg^+)_q(Cl^-)_r(H_2PO_4^-)_s$(org) in the organic phase. Complex formation with other ionic species, *e.g.* NO_3^- or Na^+, and molecules, *e.g.* H_2O or *o*-xylene, in the medium has been disregarded. Using this notation we may for example describe the species MeHgCl(org) and MeHgOH(aq) as the (0,1,1,0)(org) and (−1,1,0,0)(aq) species. The constant for the formation of the species will be given by the expressions:

$$K_{klmn}^{aq} = [(H^+)_k(MeHg^+)_l(Cl^-)_m(H_2PO_4^-)_n] \times [H^+]^{-k}[MeHg^+]^{-l}[Cl^-]^{-m}[H_2PO_4^-]^{-n} \quad (1)$$

and

$$K_{pqrs}^{org} = [(H^+)_p(MeHg^+)_q(Cl^-)_r(H_2PO_4^-)_s]_{org} \times [H^+]^{-p}[MeHg^+]^{-q}[Cl^-]^{-r}[H_2PO_4^-]^{-s} \quad (2)$$

The distribution ratio for MeHg(II) between the organic and aqueous phases may be expressed by the following equation:

$$D_{calc} = \frac{\sum q[(H^+)_p(MeHg^+)_q(Cl^-)_r(H_2PO_4^-)_s]_{org}}{\sum l[(H^+)_k(MeHg^+)_l(Cl^-)_m(H_2PO_4^-)_n]} = \frac{\sum q K_{pqrs}^{org}[H^+]^{-p}[MeHg^+]^{-q}[Cl^-]^{-r}[H_2PO_4^-]^{-s}}{\sum l K_{klmn}^{aq}[H^+]^{-k}[MeHg^+]^{-l}[Cl^-]^{-m}[H_2PO_4^-]^{-n}} \quad (3)$$

A chemical model may be assumed for the system by giving values to the sets of numbers (p,q,r,s) and (k,l,m,n). Given the values of K_{pqrs}^{org}, K_{klmn}^{aq} for the formation of the species (p,q,r,s)(org) and (k,l,m,n)(aq), the total concentration C_{MeHg}, C_{Cl}, C_{PO_4}, and $[H^+]$ for each point, we may easily calculate $[MeHg^+]$, $[Cl^-]$, $[H_2PO_4^-]$ from the mass-balances for MeHg(II), Cl(−I) and P(V). Knowing the values of the equilibrium concentration for the component species D_{calc} may be calculated using eqn. (3). In the Letagrop-Distr [23-27] program the calculation of D_{calc} is done using the BDTV prodecure.[26] In the chemical models assumed here we make the basic assumption that only uncharged MeHg(II) species are extracted into the organic phase.

Analysis of the data. The distribution data given as log $[H^+]$, $C_{MeHg(II)}$, C_{Cl}, C_{PO_4} and I_{aq}, I_{org}, (or C_{aq}, C_{org}), after preliminary graphical analysis, were analyzed using the computer program Letagrop-Distr.[23-27] Using a given chemical model for the system the program calculates the "best" set of values for the constants K_{pqrs}^{org} and K_{klmn}^{aq} for the formation of the species (p,q,r,s)(org) and (k,l,m,n)(aq). In principle this is done by minimizing the error-square sum $U = \sum_1^{Np} w(\log D_{calc} - \log D_{exp})^2$, where Np represents the number of experimental points and w the weight factor for each point. In this work we have tried to adjust the experimental conditions so that the weight factor w may be assumed to be practically equal for all points. This assumption was found to be justifiable, as will be illustrated in a latter part of this work, since for a given chemical model and minimizing the error-square sum of other types of errors, such as $U = \sum(D_{exp} D_{calc}^{-1} - 1)^2$ or $U = \sum(D_{calc} D_{exp}^{-1} - 1)^2$, which implies the assignment of somewhat different weight factor to the experimental points, it was found to give essentially the same values for the formation constants of the species assumed. In this work the weight factor has arbitrarily been given the value $w = 1$.

RESULTS

Conclusions from graphical analysis of the data. The primary distribution data in Table 1 are given as log D_{exp}, $-\log [H^+]$ and initial total concentrations of phosphate ion, C_{PO_4}, for constant $C_{Cl} = 1.27 \times 10^{-3}$ M and constant values of $C_{MeHg(II)} = 4.15 \times 10^{-5}$, 1.816×10^{-4}, and 5.349×10^{-4} M. In Fig. 1 we plot log D as a function of log $[H_2PO_4^-]$ for some selected experimental points which have approximately constant values of $-\log [H^+] \approx 5.14$, 5.31, 6.33, 6.81, 6.93, 7.1, 9.26. The values of $[H_2PO_4^-]$ for the experimental points given in Fig. 1 and Fig. 2 have been calculated assuming the formation of species with the equilibrium constants given in Table 2, model No. 14. However, since in the experiment MeHg(II) was at tracer levels concentrations, the fraction of phosphate bound to the methylmercury is negligible. In the range of $-\log [H^+] = 5 - 7$ the distribution of CH_3Hg(II) between the two phases is clearly affected by varying concentration of $H_2PO_4^-$. Log D is seen to decrease with increasing log $[H_2PO_4^-]$ with a limiting slope of −1. This relationship strongly indicates the formation of CH_3Hg(II)-phosphate complex in the aqueous phase with $CH_3HgH_2PO_4$, $CH_3HgHPO_4^-$ or $CH_3HgPO_4^{2-}$ as possible predominant species. These data also

Table 1. The distribution of methylmercury(II) in the two-phase system 1.0 M(Na,H)(NO_3,Cl,PO_4)/*o*-xylene. Data given as log D_{exp}, log [H^+], C_{PO_4} M, log [$H_2PO_4^-$], and the error log ($D_{calc}D_{exp}^{-1}$), which has been calculated assuming the formation of the MeHg(II) species MeHgCl(org), MeHgCl(aq), MeHgOH(aq), $MeHgHPO_4^-$(aq) with the equilibrium constants given in Table 2, model No. 14. $C_{Cl} = 1.270 \times 10^{-3}$ M, $V_{aq} = V_{org}$.

$C_{MeHg(II)} = 4.15 \times 10^{-5}$ M[a]

+1.070, −1.263, 0, [$H_2PO_4^-$] = 0, −0.000; +1.055, −4.792, 4.450×10^{-2}, −1.361, −0.065; +1.049, −4.684, 4.994×10^{-3}, −2.309, +0.011; +1.048, −5.176, 2.472×10^{-2}, −1.628, −0.083; +1.042, −4.366, 9.888×10^{-3}, −2.009, +0.019; +1.041, −5.347, 1.977×10^{-2}, −1.735, −0.094; +1.040, −4.839, 1.483×10^{-2}, −1.839, −0.005; +1.038, −5.106, 3.461×10^{-2} −1.479, −0.089; +1.032, −5.145, 2.966×10^{-2}, −1.548, −0.077; +1.027, −2.546, 0, [$H_2PO_4^-$] = 0, +0.043; +1.016, −4.353, 3.952×10^{-2}, −1.407, +0.026; +1.004, −5.330, 4.996×10^{-3}, −2.331, +0.023; +0.987, −5.491, 0, [$H_2PO_4^-$] = 0, +0.063; +0.972, −5.322, 9.992×10^{-3}, −2.030, +0.029; +0.957, −5.316, 1.499×10^{-2}, −1.853, +0.020; +0.927, −5.313, 1.998×10^{-2}, −1.728, +0.027; +0.910, −5.305, 2.498×10^{-2}, −1.631, +0.024; +0.894, −5.299, 2.998×10^{-2}, −1.551, +0.021; +0.866, −6.308, 2.498×10^{-3}, −2.826, +0.018; +0.865, −5.289, 3.497×10^{-2}, −1.484, +0.033; +0.827, −5.257, 4.996×10^{-2}, −1.327, +0.030; +0.775, −6.349, 6.994×10^{-3}, −2.396, −0.003; +0.749, −6.459, 9.517×10^{-3}, −2.313, −0.068; +0.745, −6.344, 9.992×10^{-3}, −2.239, −0.028; +0.639, −6.478, 1.428×10^{-2}, −2.146, −0.046; +0.631, −6.415, 1.384×10^{-2}, −2.129, −0.005; +0.626, −6.340, 1.499×10^{-2}, −2.061, +0.014; +0.619, −6.376, 9.888×10^{-3}, −2.257, +0.088; +0.619, −6.381, 1.780×10^{-2}, −2.004, −0.036; +0.617, −6.418, 9.888×10^{-3}, −2.276, +0.074; +0.580, −6.386, 1.582×10^{-2}, −2.058, +0.029; +0.572, −6.405, 1.879×10^{-2}, −1.992, −0.012; +0.534, −6.364, 1.977×10^{-2}, −1.951, +0.032; +0.519, −6.364, 2.077×10^{-2}, −1.930, +0.034; +0.505, −6.327, 2.175×10^{-2}, −1.894, +0.053; +0.503, −6.356, 2.373×10^{-2}, −1.868, +0.019; +0.470, −6.334, 2.998×10^{-2}, −1.758, −0.003; +0.464, −6.395, 2.472×10^{-2}, −1.868, +0.029; +0.453, −6.384, 2.472×10^{-2}, −1.863, +0.046; +0.397, −6.364, 3.461×10^{-2}, −1.708, +0.013; +0.380, −6.325, 3.497×10^{-2}, −1.687, +0.046; +0.378, −6.357, 3.461×10^{-2}, −1.705, +0.036; +0.347, −6.779, 2.379×10^{-2}, −2.100, −0.002; +0.341, −6.310, 4.996×10^{-2}, −1.526, −0.020; +0.341, −6.325, 4.450×10^{-2}, −1.582, +0.010; +0.269, −6.795, 2.865×10^{-2}, −2.030, +0.017; +0.229, −6.784, 3.827×10^{-2}, −1.897, −0.028; +0.162, −6.782, 4.759×10^{-2}, −1.801, −0.031; −1.408, −9.266, 0.333, −3.271, −0.066; −1.493, −9.251, 0.333, −3.256, +0.031.

$C_{MeHg(II)} = 5.15 \times 10^{-5}$ M[a]

+1.040, −1.522, 0, [$H_2PO_4^-$] = 0, +0.030.

$C_{MeHg(II)} = 1.816 \times 10^{-4}$ M[a]

+1.050, −1.491, 0, [$H_2PO_4^-$] = 0, +0.019; +0.546, −6.905, 4.579×10^{-3}, −2.904, +0.022; +0.394, −6.839, 1.482×10^{-2}, −2.363, +0.023; +0.341, −6.834, 1.913×10^{-2}, −2.232, +0.009; +0.279, −6.831, 2.379×10^{-2}, −2.136, +0.015; +0.244, −6.821, 2.865×10^{-2}, −2.048, +0.003; +0.208, −6.812, 3.323×10^{-2}, −1.977, −0.001; +0.173, −6.811, 3.827×10^{-2}, −1.915, −0.009; +0.162, −6.801, 4.759×10^{-2}, −1.814, −0.064.

$C_{MeHg(II)} = 5.349 \times 10^{-4}$ M[b]

+1.184, −1.462, 0, [$H_2PO_4^-$] = 0, −0.116; +1.039, −2.150, 0, [$H_2PO_4^-$] = 0, +0.029; +1.037, −1.514, 0, [$H_2PO_4^-$] = 0, +0.031; +1.027, −1.490, 0, [$H_2PO_4^-$] = 0, +0.042; +0.845, −5.973, 4.996×10^{-3}, −2.421, +0.008; +0.813, −5.725, 9.992×10^{-3}, −2.072, +0.038; +0.798, −5.610, 1.499×10^{-2}, −1.880, +0.036; +0.774, −5.535, 1.998×10^{-2}, −1.747, +0.043; +0.763, −5.496, 2.498×10^{-2}, −1.646, +0.031; +0.756, −5.458, 2.998×10^{-2}, −1.563, +0.021; +0.732, −5.420, 3.497×10^{-2}, −1.493, +0.032; +0.715, −5.390, 3.997×10^{-2}, −1.433, +0.036; +0.691, −5.356, 4.996×10^{-2}, −1.333, +0.029; +0.579, −6.654, 4.996×10^{-3}, −2.701, +0.008; +0.534, −6.492, 9.992×10^{-3}, −2.310, +0.010; +0.476, −6.431, 1.499×10^{-2}, −2.104, +0.008; +0.410, −6.402, 1.998×10^{-2}, −1.965, +0.017; +0.388, −6.948, 9.517×10^{-3}, −2.620, −0.028; +0.376, −6.380, 2.498×10^{-2}, −1.858, +0.002; +0.345, −6.370, 2.998×10^{-2}, −1.775, −0.012; +0.322, −7.089, 1.047×10^{-2}, −2.688, −0.041; +0.320, −7.220, 6.662×10^{-3}, −2.993, −0.046; +0.298, −6.352, 3.497×10^{-2}, −1.700, −0.001; +0.292, −6.941, 1.428×10^{-2}, −2.439, −0.003; +0.287, −7.133, 8.565×10^{-3}, −2.811, +0.003; +0.275, −7.031, 1.428×10^{-2}, −2.507, −0.022; +0.274, −6.927, 1.913×10^{-2}, −2.301, −0.042; +0.272, −7.201, 4.579×10^{-3}, −3.140, +0.047; +0.245, −6.336, 3.997×10^{-2}, −1.635, +0.019; +0.242, −6.974, 2.379×10^{-2}, −2.241, −0.079; +0.239, −7.319, 4.759×10^{-3}, −3.224, +0.006; +0.233, −6.997, 1.903×10^{-2}, −2.356, −0.026; +0.223, −6.323, 4.996×10^{-2}, −1.533, −0.020; +0.199, −6.890, 2.865×10^{-2}, −2.098, −0.055; +0.198, −6.912, 2.379×10^{-2}, −2.195, −0.013; +0.114, −6.865, 3.827×10^{-2}, −1.954, −0.041; +0.049, −6.855, 4.759×10^{-2}, −1.853, −0.038; +0.018, −7.597, 2.855×10^{-3}, −3.697, +0.064.

[a] Distribution of MeHg(II) measured by a radiometric method. Initial total concentration of radioactive $Me^{203}HgCl$ in the organic phase was 8.2×10^{-6} M.

[b] Distribution of MeHg(II) measured by a spectrophotometric method.[31]

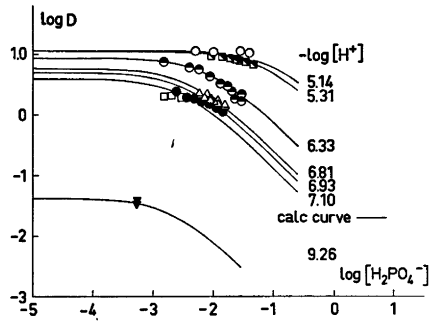

Fig. 1. The distribution of methylmercury(II) between *o*-xylene and 1.0 M(Na,H)(Cl,NO_3,PO_4) aqueous solution as a function of log [$H_2PO_4^-$] for selected data with $C_{MeHg(II)} = 4.15 \times 10^{-5}$ M, $C_{Cl} = 1.27 \times 10^{-3}$ M and approximately constant values of $-\log [H^+] = 5.14$ (○), 5.31 (◪), 6.33 (◓), 6.81 (△), 6.93 (●), 7.10 (□), and 9.26 (▼). The lines drawn have been calculated assuming the formation of the MeHg(II) species with the equilibrium constants given in Table 2, model 14. The distribution data are given in Table 1.

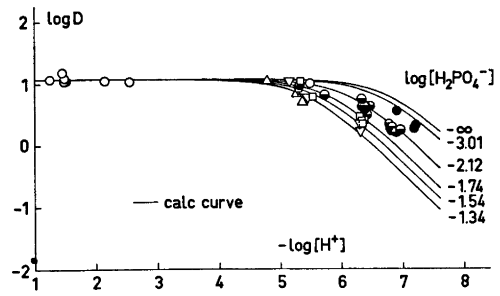

Fig. 2. Distribution of MeHg(II) in the two-phase system 1.0 M (Na,H)(NO_3,Cl,PO_4)/*o*-xylene as a function of $-\log [H^+]$ for selected data with $C_{MeHg(II)} = 4.15 \times 10^{-5}$ M, $C_{Cl} = 1.27 \times 10^{-3}$ M and approximately constant values of $[H_2PO_4^-] = 0$ (○); $10^{-3.01}$ M (●); $10^{-2.12}$ M (◒); $10^{-1.74}$ M (□); $10^{-1.54}$ M (▽) and $10^{-1.34}$ M (△). The lines drawn have been calculated assuming the formation of MeHgCl(org), MeHgCl(aq), MeHgOH(aq), and $MeHgHPO_4^-$(aq) with the formation constants given in Table 2, model 14. The distribution data is given in Table 1.

Table 2. Equilibrium constants [a] log β_{pqrs} for the formation of $(H^+)_p(CH_3Hg^+)_q(Cl^-)_r(H_2PO_4^-)_s$ species in the system $CH_3Hg(II) - 1.0$ M (Na,H)(NO_3,Cl,PO_4)/*o*-xylene for various assumptions of $CH_3Hg(II)$ species which minimize the error-square sum $U = \sum_1^{98} (\log D_{calc} - \log D_{exp})^2$.

Model No.	(p,q,r,s) log β_{pqrs}(org)	(p,q,r,s) log β_{pqrs}(aq)	U_{min}	$\sigma(\log D)$
1	(0,1,1,0)[nv]6.39	(0,1,1,0)[nv]5.32	43.864	
2	(0,1,1,0)[nv]6.39	(0,1,1,0)[nv]5.32; (0,1,0,1) 4.54 (max. 4.77)	27.311	0.531
3	(0,1,1,0)[nv]6.39	(0,1,1,0)[nv]5.32; (−2,1,0,0) −11.06 (max. −10.73)	25.158	0.509
4	(0,1,1,0)[nv]6.39	(0,1,1,0)[nv]5.32; (−2,1,0,0) −13.27 (max. −12.83); (0,1,0,1) 4.52 ± 0.23	14.481	0.388
5	(0,1,1,0)[nv]6.39	(0,1,1,0)[nv]5.32; (−2,1,0,0) $\beta = 0$; (−2,1,0,1) −8.45 ± 0.21	10.306	0.328
6	(0,1,1,0)[nv]6.39	(0,1,1,0)[nv]5.32; (−2,1,0,1) −8.45 ± 0.21	10.306	0.326
7	(0,1,1,0)[nv]6.39	(0,1,1,0)[nv]5.32; (0,1,0,1) 3.93 (max. 4.23); (−2,1,0,1) −8.45 ± 0.25	8.627	0.300
8	(0,1,1,0)[nv]6.39	(−1,1,0,0) −3.79 ± 0.11; (0,1,1,0)[nv]5.32	3.555	0.191
9	(0,1,1,0)[nv]6.39	(0,1,1,0)[nv]5.32; (−1,1,0,0) −3.86 ± 0.11; (0,1,0,1)3.76 (max. 4.00)	2.714	0.168
10	(0,1,1,0)[nv]6.39	(0,1,1,0)[nv]5.32; (−1,1,0,1) −1.58 ± 0.07; (0,1,0,1) $\beta = 0$ (max. 3.47)	1.761	0.135
11	(0,1,1,0)[nv]6.39	(0,1,1,0)[nv]5.32; (−1,1,0,1) −1.58 ± 0.07	1.761	0.135
12	(0,1,1,0)[nv]6.39	(0,1,1,0)[nv]5.32; (−1,1,0,1) −1.61 ± 0.06; (−2,1,0,1) −10.42 (max. −10.18)	1.163	0.110
13	(0,1,1,0)[nv]6.39	(0,1,1,0)[nv]5.32; (−2,1,0,0) −13.65 (max. −13.41); (−1,1,0,1) −1.61 ± 0.06	1.132	0.109
14[b]	(0,1,1,0)[nv]6.39	(0,1,1,0)[nv]5.32; (−1,1,0,0) −4.40 ± 0.07; (−1,1,0,1) −1.74 ± 0.03	0.150	0.040

[a] $\beta_{pqrs} = [(H^+)_p(CH_3Hg^+)_q(Cl^-)_r(H_2PO_4^-)_s]_t / [H^+]^{-p}[CH_3Hg^+]^{-q}[Cl^-]^{-r}[H_2PO_4^-]^{-s}$, where the subindex t indicates the phase referred to in the reaction. The limits given correspond approximately to log $[\beta \pm 3\sigma(\beta)]$ and if $\sigma(\beta) < 0.2\beta$, the value max. = log$[\beta + 3\sigma(\beta)]$ is given. [nv] The given value of β for the species was not varied during the course of computer calculation. [b] The "best" model assumed.

indicate the formation of hydrolyzed $CH_3Hg(II)$ species in the aqueous phase as seen from the decrease of log D with increasing pH for constant values of $[H_2PO_4^-]$. This conclusion is further supported by the plot shown in Fig. 2 which illustrates the distribution of $CH_3Hg(II)$ as a function of $-\log[H^+]$ for sets of experimental points which have approximately constant values of $[H_2PO_4^-]=0$, $10^{-3.01}$, $10^{-2.12}$, $10^{-1.74}$, $10^{-1.54}$, and $10^{-1.34}$ M. The limiting horizontal line which may be drawn through the experimental points with value of $-\log[H^+]$ less than 5 indicates that in this concentration range only CH_3HgCl is extracted into the organic phase and that in the aqueous phase phosphate or hydrolyzed complexes of $CH_3Hg(II)$ are negligible compared with $CH_3HgCl(aq)$ (*cf.* Ref. 13). For the range of $-\log[H^+]$ greater than 5 the data show decreasing values of D with increasing pH for all sets of experimental points, with the limiting slope $\frac{\mathrm{d}\log D}{\mathrm{d}\,pH} \approx -1$. This strongly indicates the formation of hydrolyzed $CH_3Hg(II)$ species in the aqueous phase with CH_3HgOH as a predominant complex. Graphical analysis of the data in Figs. 1 and 2 thus strongly indicates the formation of 1:1 complex between $CH_3Hg(II)$ and $H_2PO_4^-$ or OH^- ions. Furthermore Figs. 1 and 2 seem to indicate that the distribution curves are not affected by the variation of C_{MeHg} from 4.15×10^{-5} to 5.35×10^{-4} M. This indicates the predominant formation of only mononuclear methylmercury species in the system, which is not unexpected considering the low concentration range of metal ions studied. As will be seen in a later part of this paper this view is also supported by the results obtained by the Letagrop analysis.

Letagrop analysis of the data. The results of the graphical analysis give us a good starting point in the analysis of the data with the Letagrop-Distr computer program. Part of the results of the computer analysis of the distribution data are given in Table 2. In this analysis we assumed the formation of MeHgCl(aq) and MeHgCl(org) with the equilibrium constants

$$K_{0110}^{org}=[MeHgCl]_{org}[MeHg^+]^{-1}[Cl^-]^{-1}=10^{6.39}\ M^{-1}$$ and

$$K_{0110}^{aq}=[MeHgCl][MeHg^+]^{-1}[Cl^-]^{-1}=10^{5.32}\ M^{-1}$$

as was found in our previous work,[13] and during the computer calculations the given value of the formation constant for each of these two species was kept constant.

In Table 2 the different chemical models which have been assumed for the description of the experimental data are summarized. Table 3 summarizes the different types of methylmercury(II) species which have been included in the Letagrop analysis of the data. The results of the analysis given in Table 2 indicate that of all the different models tried, the "best" model, which describes the distribution data satisfactorily within the experimental error, is model No. 14 with $U_{min}=0.150$ for $Np=98$ points, and $\sigma(\log D)=0.040$. In this model the formation of MeHgOH(aq) and $MeHgHPO_4^-$(aq) species is assumed. No significant improvement of the U value or $\sigma(\log D)$ value was found

Table 3. Summary of the different $(H^+)_p(MeHg^+)_q(Cl^-)_r(H_2PO_4^-)_s$ species included in the Letagrop analysis of the distribution data of MeHg(II) in the two-phase system 1.0 M (Na,H)(NO_3,Cl,PO_4)/*o*-xylene. $C_{Cl}=1.27\times10^{-3}$ M.

Aqueous phase	Organic phase
$MeHgCl^a$; $MeHgOH^b$; $MeHg(OH)_2^-$; $(MeHg)_2(OH)_2$; $(MeHg)_2OH^+$; $(MeHg)_3(OH)_3^-$ $MeHgHPO_4^-$ [b]; $MeHgH_2PO_4$; $MeHgPO_4^{2-}$; $(MeHg)_2PO_4^-$; $(MeHg)_2HPO_4$; $(MeHg)_2H_2PO_4^+$; $(MeHg)_2OHPO_4^{2-}$.	$MeHgCl^a$; MeHgOH; $MeHgH_2PO_4$; $NaMeHgHPO_4$; $NaMeHg(OH)_2$.

[a] The value of the equilibrium constant (*cf.* Ref. 13) is not varied during the computer calculations. [b] Methylmercury(II) species assumed to be formed which may account for the available distribution data (*cf.* Table 2, model 14).

Table 4. Comparison of equilibrium constants [a] log β_{pqrs} for the formation of $(H^+)_p(CH_3Hg^+)_q(Cl^-)_r(H_2PO_4^-)_s$ species in the system $CH_3Hg(II) - 1.0$ M $(Na,H)(NO_3,Cl,PO_4)$/o-xylene which minimize different error-square sums $U = \sum_1^{98} fel[i]^2$. The computer calculations are based on the assumption of the formation of the species CH_3HgCl(org), CH_3HgCl(aq), CH_3HgOH(aq) and $CH_3HgHPO_4^-$(aq) (*cf.* Table 2, model No. 14).

Mimimized error *fel*[*i*]	(*p*,*q*,*r*,*s*)log β_{pqrs}(org)	(*p*,*q*,*r*,*s*)log β_{pqrs}(aq)	U_{min}	$\sigma(y)$
$Fel[1] = \log (D_{calc}D_{exp}^{-1})$	(0,1,1,0)6.39[nv]	(0,1,1,0)5.32[nv]; (−1,1,0,0) −4.40 ± 0.07; (−1,1,0,1) −1.74 ± 0.03	0.150	0.040
$Fel[2] = D_{exp}D_{calc}^{-1} - 1$	(0,1,1,0)6.39[nv]	(0,1,1,0)5.32[nv]; (−1,1,0,0) −4.40 ± 0.07; (−1,1,0,1) −1.74 ± 0.03	0.844	0.094
$Fel[3] = D_{calc}D_{exp}^{-1} - 1$	(0,1,1,0)6.39[nv]	(0,1,1,0)5.32[nv]; (−1,1,0,0) −4.39 ± 0.06; (−1,1,0,1) −1.73 ± 0.03	0.756	0.089

[a] $\beta_{pqrs} = [(H^+)_p(CH_3Hg^+)_q(Cl^-)_r(H_2PO_4^-)_s]_t[H^+]^{-p}[CH_3Hg^+]^{-q}[Cl^-]^{-r}[H_2PO_4^-]^{-s}$, where the subindex *t* indicates the phase referred to in the reaction. The limits given correspond approximately to log $[\beta \pm 3\sigma(\beta)]$. [nv] The given value of β for the species was not varied during the course of the computer calculation.

when, in an extension of model No. 14, the following additional species were assumed to be formed in the aqueous phase: (0,1,0,1) (= $MeHgH_2PO_4$), (−2,1,0,1)(= $MeHgPO_4^{2-}$), and (−2,1,0,0)[= $MeHg(OH)_2$]. In the computer calculations it was found that the value of the constant β_{pqrs} for the formation of these additional species was either reduced to zero or their standard deviation $\sigma(\beta)$ found to be bigger than the value of the constant β itself, which we may take as indication that the formation of those species is negligible for the extraction conditions studied. No improvements of U_{min} were found by assuming the additional formation of dimeric methylmercury(II) species in the aqueous phase, such as (−2,2,0,0)[= $(MeHg)_2(OH)_2$], (−1,2,0,0)[= $(MeHg)_2OH^+$] (−3,2,0,0) [= $(MeHg)_2(OH)_3^-$], (−1,2,0,1)[= $(MeHg)_2HPO_4$], (−2,2,0,1)[= $(MeHg)_2PO_4^-$], (−3,2,0,1)-[= $(MeHg)_2OHPO_4^{2-}$] and (0,2,0,1)[= $(MeHg)_2H_2PO_4^+$]. Some improvement of the value of the minimized error-square sum was found when to model No. 14 the additional formation of the species (−1,1,0,1) (= $Na^+MeHgHPO_4^-$) in the organic phase and (−2,1,0,0) [= $MeHg(OH)_2$] in the aqueous phase was assumed [$U_{min} = 0.129$, $\sigma(\log D) = 0.037$]. However, the $\sigma(\log D)$(= 0.037) then found was not significantly lower than that found in model No. 14 [$\sigma(\log D) = 0.040$]. It may be noted also that for all the models tried practically the same value for β was found for the formation of the species (−1,1,0,0)(= MeHgOH) and (−1,1,0,1) (= $MeHgHPO_4^-$) in the aqueous phase, which thus supports our previous conclusion that these are the predominant species in the system studied.

In Table 4 we compare the equilibrium constants found for the formation of methylmercury(II) species by assuming model No. 14 (Table 2), and minimizing the following three different types of error-square sum:

$U = \sum[\log (D_{calc}D_{exp}^{-1})]^2$; $U = \sum(D_{exp}D_{calc}^{-1} - 1)^2$ and

$U = \sum(D_{calc}D_{exp}^{-1} - 1)^2$.

The results of the calculations indicate practically the same values for the equilibrium constants for the formation of the species assumed, MeHgOH(aq) and $MeHgHPO_4^-$(aq), which indicates that the assignment of the same weight factor to the experimental points is not unjustified. In this work the weight factor is given the value $w = 1$.

CONCLUSION

We may thus conclude that for the extraction conditions studied the distribution data, within the experimental errors, can be described satis-

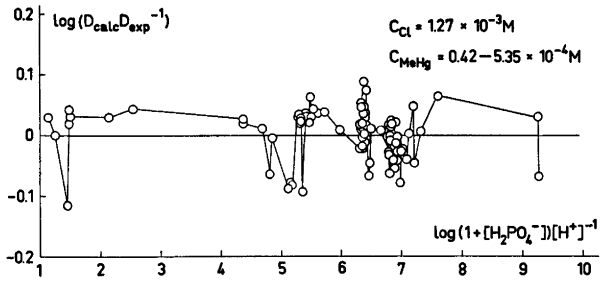

Fig. 3. The minimized error $Fel(1) = \log (D_{calc} D_{exp}^{-1})$ as a function of $\log (1 + [H_2PO_4^-])[H^+]^{-1}$ for the two-phase system 1.0 M (Na,H)(NO_3,Cl,PO_4)/*o*-xylene, assuming the formation of MeHgCl(aq), MeHgCl(org), MeHgOH(aq) and $MeHgHPO_4^-$(aq) species with the equilibrium constants given in Table 2, model 14. The data are given in Table 1.

factorily by assuming the following methylmercury(II) species:

$MeHg^+ + Cl^- \rightleftharpoons MeHgCl(aq)$; (4)
$\log(K \pm 3\sigma) = 5.32 \pm 0.09$ (*cf.* Ref. 13)

$MeHg^+ + Cl^- \rightleftharpoons MeHgCl(org)$; (5)
$\log(K \pm 3\sigma) = 6.39 \pm 0.09$ (*cf.* Ref. 13)

$MeHg^+ + H_2O \rightleftharpoons MeHgOH(aq) + H^+$; (6)
$\log(K \pm 3\sigma) = -4.40 \pm 0.07$

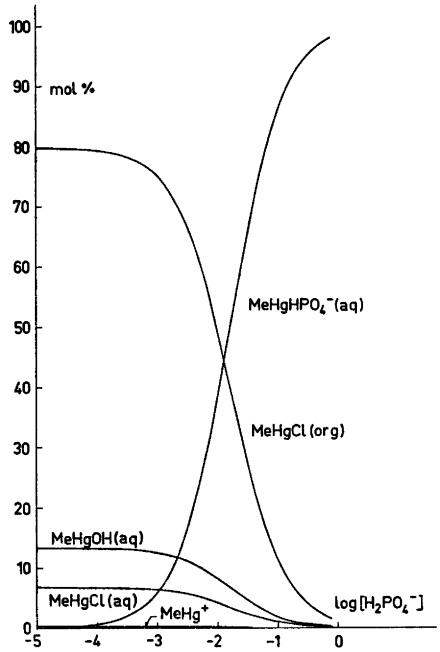

Fig. 4. The distribution of the different methylmercury(II) species as mol % *versus* $[H_2PO_4^-]$ in the two-phase system 1.0 M (Na,H)(NO_3,Cl,PO_4)/*o*-xylene for a given value $-\log [H^+] = 7.10$, $C_{Cl} = 1.2 \times 10^{-3}$ M and $C_{MeHg} = 4.15 \times 10^{-5}$ M. The lines have been calculated using the Haltafall program [29] assuming the formation of the set of $(H^+)_p(MeHg^+)_q(Cl^-)_r(H_2PO_4^-)_s$ species with the equilibrium constants given by model No. 14 in Table 2.

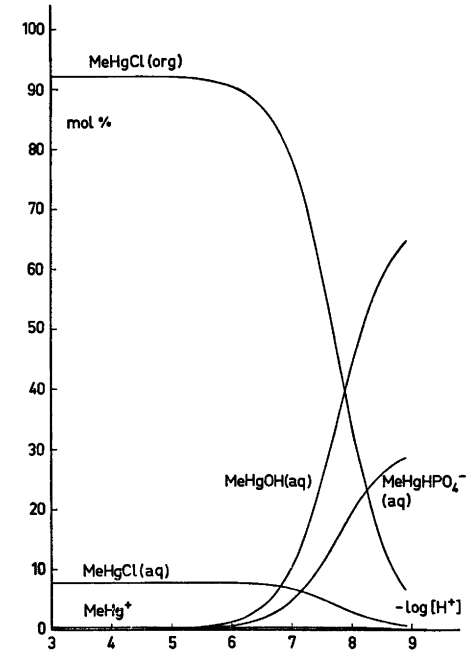

Fig. 5. The mol percentage of the different MeHg(II) species as a function of $-\log [H^+]$ in the two-phase system 1.0 M (Na,H)(NO_3Cl,-PO_4)/*o*-xylene for a given value of $[H_2PO_4^-] = 10^{-3.010}$ M, $C_{MeHg} = 4.15 \times 10^{-4}$ M and $C_{Cl} = 1.27 \times 10^{-3}$ M. The lines have been calculated using the Haltafall program [29] assuming the formation of the set of MeHg(II) species with the equilibrium constants given by model No. 14 in Table 2.

$MeHg^+ + H_2PO_4^- \rightleftharpoons MeHgHPO_4^-(aq) + H^+$; (7)
$\log(K \pm 3\sigma) = -1.74 \pm 0.03$

Using the value $K_w = [H^+][OH^-] = 10^{-13.95}$ M² for the ionization of water at $I = 1.0$ M (*cf.* Refs. 22 and 28) the formation of the MeHgOH species may be described by the equilibrium:

$MeHg^+ + OH^- \rightleftharpoons MeHgOH(aq)$; (8)
$\log(K \pm 3\sigma) = 9.55 \pm 0.07$

Furthermore we may calculate the constant for the hydrolysis of MeHgCl(aq) from (8) and (4) and that of $MeHgHPO_4^-$ from (7), (8) and the acid constant $K_{a2} = [HPO_4^{2-}][H^+][H_2PO_4^-]^{-1} = 10^{-6.48}$ M:

$MeHgCl(aq) + OH^- \rightleftharpoons MeHgOH(aq) + Cl^-$; (9)
$\log(K \pm 3\sigma) = 4.23 \pm 0.11$

$MeHgHPO_4^-(aq) + OH^- \rightleftharpoons MeHgOH(aq) + HPO_4^{2-}$; $\log(K \pm 3\sigma) = 4.81 \pm 0.08$ (10)

Fig. 3 shows the observed error function = $\log(D_{calc} D_{exp}^{-1})$ as a function of $\log(1 + [H_2PO_4^-])[H^+]^{-1}$ for the different experimental points, assuming the formation of the set of $(H^+)_p(MeHg^+)_q(Cl^-)_r(H_2PO_4^-)_s$ species and formation constants in the "best" model found previously (*cf.* Table 2, model No. 14). From the distribution of the error in Fig. 3 no systematic deviation seems to be indicated. Fig. 4 shows the distribution of the different methylmercury species under given extraction conditions ($C_{MeHg} = 4.15 \times 10^{-4}$ M; $C_{Cl} = 1.27 \times 10^{-3}$ M and $[H^+] = 10^{-7.10}$ M) as a function of $[H_2PO_4^-]$ and Fig. 5 gives the distribution of the different methylmercury species with varying $[H^+]$. The lines in Figs. 4 and 5 have been calculated using the Haltafall program [29] assuming the formation of the complexes MeHgCl(aq), MgHgCl(org), MeHgOH(aq), and $MeHgHPO_4^-$(aq) with the equilibrium constants given in (4), (5), (6) and (7).

DISCUSSION

In Table 5 we summarise the results found in the present work together with those reported earlier by other authors for similar studies. As can be seen there is rather fair agreement between the values for the formation constant of MeHgOH(aq) and $MeHgHPO_4^-$(aq) found in this work and those reported by, *e.g.*, Schwarzenbach and Schellenberg [4-6] from their potentiometric studies. The formation of $(CH_3Hg)_2OH^+$ species found by these authors, however, is not indicated by the data of the present work.

Table 5. Equilibrium constant [a] log K_{pqr} for formation of $(H^+)_p(RHg^+)_q(H_2PO_4^-)_r$ complexes in various systems.

R	System	Temp °C	log K_{-110} RHgOH	log K_{-120} $(RHg)_2OH^+$	log K_{-111} $RHgHPO_4^-$	Exp. method	Ref.
CH_3	aqueous	25	−3.59[b]			Cond.	9
CH_3	0.1 M(H,K)NO_3	20	−4.59	−2.53		EMF	4−6
CH_3	0.1 M(H,K)(NO_3,PO_4)	20			−1.60	EMF	4−6
CH_3	0−5 mM NO_3^-	24−25	−4.50[b]			EMF	7
CH_3	0.1 M(H,K)NO_3	25	−4.78[c]			EMF	8
		20	−4.64[d]				8
CH_3	aqueous	25	−4.70[b]	−2.33[b]		NMR	14
CH_3	1 M(Na,H)(NO_3, Cl,PO_4)	25	−4.40 ± 0.07		−1.74 ± 0.03	Distr.	this work
C_2H_5	0−5 mM ClO_4^-	24−25	−4.9[b]			EMF	7
C_3H_7	0.1 M(H,K)NO_3	25	−5.12[c]			EMF	7
C_4H_9	0.1 M(H,K)NO_3	25	−5.17[c]			EMF	8
C_6H_5	0−5 mM NO_3^-	24−25	−4.9[b]			EMF	7
C_6H_5	0−4.3 mM ClO_4^-	25	−4.11[b]			EMF	11
CF_3	dilution ClO_4^-	25	−3.24[b]			EMF	12
C_2H_5	dilution ClO_4^-	25	−3.42[b]			EMF	12
C_3F_7	dilution ClO_4^-	25	−3.50[b]			EMF	12

[a] $K_{pqr} = [(H^+)_p(RHg^+)_q(H_2PO_4^-)_r][H^+]^{-p}[RHg^+]^{-q}[H_2PO_4^-]^{-r}$. The limits given correspond approximately to $\log[K \pm 3\sigma(K)]$. [b] Assuming the ionization constant of water $K_w = (H^+)(OH^-) = 10^{-14.00}$ M².[22] [c] Assuming $K_w = 10^{-13.78}$ M².[30] [d] Assuming $K_w = 10^{-13.96}$ M².[4]

This may be explained as due to the very low value found for the methylmercury(II) concentrations under the present extraction conditions ($[MeHg^+] < 10^{-6.5}$ M). Using the calculated value found for $[MeHg^+] < 10^{-6.5}$ M and $K = [(MeHg)_2OH^+][MeHgOH]^{-1}[MeHg^+]^{-1} = 10^{2.37}$ M^{-1} given by Schwarzenbach and Schellenberg,[4-6] we may calculate the ratio $[(MeHg)_2OH^+][MeHgOH]^{-1} < 10^{-4.13}$. In natural waters with low concentration of $MeHg^+$, due to the presence of chloride and phosphate ions among others, and $pH = 6 - 7$ we may expect MeHgOH to predominate over $(MeHg)_2OH^+$ species.

The results of this work may be of interest not only from the ecological point of view, but also for further studies of the complex chemistry of methylmercury, *e.g.* by solvent extraction technique. In these studies the use of a buffer substance to control the pH of the aqueous solution is frequently required. However, acids and bases which are suitable for use as buffer substances may form complexes with $MeHg^+$ under the experimental conditions used. The effect of this complex formation can be corrected for if the stability constants for the reactions between $MeHg^+$ and the buffer substances are known. Phosphates being effective buffers over a wide pH range are thus particularly suitable for this purpose.

Acknowledgements. The authors thank Mr. Ulf Germgård for technical assistance in part of the work. The financial support given by the Statens Naturvårdsverk (The Swedish National Environment Protection Board) and the Swedish Natural Science Research Council is gratefully acknowledged. The authors have had the pleasure of discussing the paper with Professor Erik Högfeldt. Dr. Derek Lewis has revised the English of the manuscript.

REFERENCES

1. Borg, K., Wanntorp, H., Erne, K. and Hanko, E. *Viltrevy (Swedish Wildlife) 6* (1969) 301; *J. Appl. Ecol. 3* (1966) 171.
2. Westöö, G. and Rydälv, M. *Vår Föda 7 – 8* (1971) 1; Report on Mercury in Foods, by the Joint FAO/WHO Expert Committee on Food Additives, 1970.
3. FAO Fisheries Reports, No. 99, Rome 1971.
4. Schellenberg, M., *Diss.*, ETH, Zürich 1963.
5. Schellenberg, M. and Schwarzenbach, G. *Proc. 7th Int. Conf. Coord. Chem.*, Stockholm 1962, p. 157.
6. Schwarzenbach, G. and Schellenberg, M. *Helv. Chim. Acta 48* (1965) 28.
7. Waugh, T. D., Harold, F. W. and Laswick, J. A. *J. Phys. Chem. 59* (1955) 395.
8. Zanella, P., Plazzogna, G. and Tagliavini, G. *Inorg. Chim. Acta 2* (3) (1968) 340.
9. Maynard, J. L. and Howard, H. C. *J. Chem. Soc. 123* (1923) 960.
10. Johns, I. B., Peterson, W. D. and Hixon, R. M. *J. Phys. Chem. 34* (1930) 2218.
11. Parikh, S. S. and Sweet, T. R. *J. Phys. Chem. 65* (1961) 1909.
12. Powell, H. B. and Lagowski, J. J. *J. Chem. Soc.* (1962) 2047.
13. Budevsky, O., Ingman, F. and Liem, D. H. *Acta Chem. Scand. 27* (1973) 1277.
14. Libich, S. and Rabenstein, D. L. *Anal. Chem. 45* (1973) 118.
15. Liem, D. H. and Ingman, F. *Proc. XVth Int. Conf. Coord. Chem.*, Moscow 1973, p. 648.
16. Some laboratory methods in current use at the Department of Inorganic Chemistry, the Royal Institute of Technology, Stockholm, Mimeograph 1959 (available on request).
17. Biedermann, G. and Douhéret, G. *Personal communications.*
18. Irani, R. R. and Callis, C. F. *J. Phys. Chem. 65* (1961) 934.
19. Drozdov, N. S. and Krylov, V. P. *Zh. Fiz. Khim. 35* (1961) 2557.
20. Cher, M. and Davidson, N. *J. Amer. Chem. Soc. 77* (1955) 793.
21. Thamer, J. *J. Amer. Chem. Soc. 79* (1957) 4298.
22. Sillén, L. G. and Martell, A. E. *Stability Constants of Metal-ion Complexes*, Spec. Publ. No. 17, The Chemical Society, London 1964.
23. Ingri, N. and Sillén, L. G. *Ark. Kemi 23* (1964) 97.
24. Sillén, L. G. and Warnqvist, B. *Ark. Kemi 31* (1969) 315.
25. Sillén, L. G. and Warnqvist, B. *Ark. Kemi 31* (1969) 341.
26. Arnek, R., Sillén, L. G. and Wahlberg, O. *Ark. Kemi. 31* (1969) 353.
27. Liem, D. H. *Acta Chem. Scand. 25* (1971) 1521.
28. Anderegg, G. *Helv. Chim. Acta 50* (1967) 2333.
29. Ingri, N., Kakolowicz, W., Sillén, L. G. and Warnqvist, B. *Talanta 14* (1967) 1261.
30. Fischer, R. and Byé, J. *Bull. Soc. Chim. Fr.* (1964) 2920.
31. Ingman, F. *Talanta 18* (1971) 744.

Received May 8, 1974.

Acta Chemica Scandinavica A 28 (1974) 957—962

Magnetic Structures and Properties of $FeP_{1-x}As_x$

KARI SELTE,[a] ARNE KJEKSHUS,[a] TOR A. OFTEDAL [a] and ARNE F. ANDRESEN [b]

[a]Kjemisk Institutt, Universitetet i Oslo, Blindern, Oslo 3, Norway and [b] Institutt for Atomenergi, Kjeller, Norway

The pseudo-binary FeP – FeAs system has been investigated by X-ray and neutron diffraction, magnetic susceptibility, and magnetization measurements. FeP and FeAs are completely soluble in each other, an MnP type structure with random distribution of P and As being found independent of temperature and composition. The double c axis helimagnetic ordering in FeP and FeAs extends into the P-rich region (at least to $x = 0.10$). The results are discussed in relation to an isotropic exchange interaction model.

Among the nine binary monopnictides of the 3*d* elements which take the MnP type structure, helimagnetic ordering has been reported for CrAs,[1-3] MnP,[4,5] FeP,[6] and FeAs.[7] In order to gain further insight into the factors which determine this behaviour, attention is presently focussed on ternary derivatives of these compounds. Low temperature neutron diffraction studies of $Cr_{1-t}Mn_tAs$,[1] $Mn_{1-t}Fe_tAs$,[8] and $MnAs_{1-x}P_x$ [9,10] have so far demonstrated that this angle of approach may be rather fruitful.

In addition there are also scattered investigations on the magnetic properties of $V_{1-t}Fe_tAs$,[11] $Cr_{1-t}Fe_tAs$,[12] $Mn_{1-t}Fe_tP$,[13-16] $Mn_{1-t}Co_tP$,[17] $Fe_{1-t}Co_tP$,[16] and $FeP_{1-x}As_x$,[16] of which $Cr_{1-t}Fe_tAs$, $Mn_{1-t}Fe_tP$, and $FeP_{1-x}As_x$ appear to be of particular interest. The present paper concerns the magnetic structures and properties of $FeP_{1-x}As_x$. The relevant properties of FeP [6] and FeAs [7] (*i.e.* relatively short spiral periods, small magnetic moments, and low Néel temperatures) indicate that such a study may present challenging experimental problems.

EXPERIMENTAL

The binary compounds FeP and FeAs were prepared by heating weighed quantities of the elements [99.99 % Fe (Johnson, Matthey & Co.; turnings from rods), 99.999 % P and 99.9999 % As (Koch-Light Laboratories)] in evacuated, sealed silica tubes as described in Refs. 7, 18. Ternary $FeP_{1-x}As_x$ samples of desired compositions were prepared from appropriate proportions of FeP and FeAs, by means of three annealings at 850 °C interrupted by intermediate crushings. The samples were finally cooled to room temperature over a period of 3 days.

Experimental details concerning X-ray and neutron diffraction (including data reduction), magnetic susceptibility, and magnetization measurements have been reported earlier.[7]

RESULTS

(i) *Chemical crystal structure.* The orthorhombic unit cell dimensions of $FeP_{1-x}As_x$ (as determined from room temperature X-ray powder photographs) are shown in Fig. 1. as functions of the composition parameter x. FeP and FeAs exhibit complete, mutual solubility, as evidenced by the continuous variation in all unit cell dimensions with x. The various curves in Fig. 1 follow Vegard's Law to a good approximation over the entire solubility range. A possible extension of the homogeneity range of $FeP_{1-x}As_x$ to metal/non-metal (atomic) ratios different from 1.00 has not been examined for $x \neq 0$ and 1 (*cf.* Refs. 18, 19).

The X-ray data show an MnP type structural arrangement for $0 \leq x \leq 1$ at room temperature. The lack of additional superstructure reflections in these data confirms that the substituted atoms are randomly distributed over the non-metal sub-lattice.

Samples with $x = 0.10$, 0.50, and 0.90 were chosen for neutron diffraction examinations at 4.2, 80, and 293 K. The final values for the

Table 1. Unit cell dimensions and positional parameters with standard deviations for three $FeP_{1-x}As_x$ samples; space group *Pnma*, positions 4(*c*).

x	0.10			0.50			0.90		
T(K)	4.2	80	293	4.2	80	293	4.2	80	293
a(Å)	5.203(1)	5.203(1)	5.200(1)	5.297(1)	5.307(1)	5.300(1)	5.416(1)	5.414(1)	5.402(1)
b(Å)	3.108(1)	3.109(1)	3.121(1)	3.217(1)	3.220(1)	3.240(1)	3.306(1)	3.311(1)	3.343(1)
c(Å)	5.802(1)	5.802(1)	5.796(1)	5.885(1)	5.892(1)	5.893(1)	5.994(1)	5.992(1)	5.991(1)
x_T	0.0008(11)	0.0015(5)	0.0012(4)	0.0009(7)	0.0022(13)	0.0026(6)	0.0028(5)	0.0022(6)	0.0015(4)
z_T	0.2000(3)	0.2004(3)	0.2005(2)	0.1987(4)	0.2000(8)	0.2007(3)	0.1986(3)	0.1988(4)	0.1984(3)
x_X	0.1927(8)	0.1929(7)	0.1924(6)	0.1937(9)	0.1957(15)	0.1963(8)	0.1990(8)	0.1981(8)	0.1957(5)
z_X	0.5692(7)	0.5702(6)	0.5705(5)	0.5748(7)	0.5739(11)	0.5748(6)	0.5750(6)	0.5768(7)	0.5773(5)

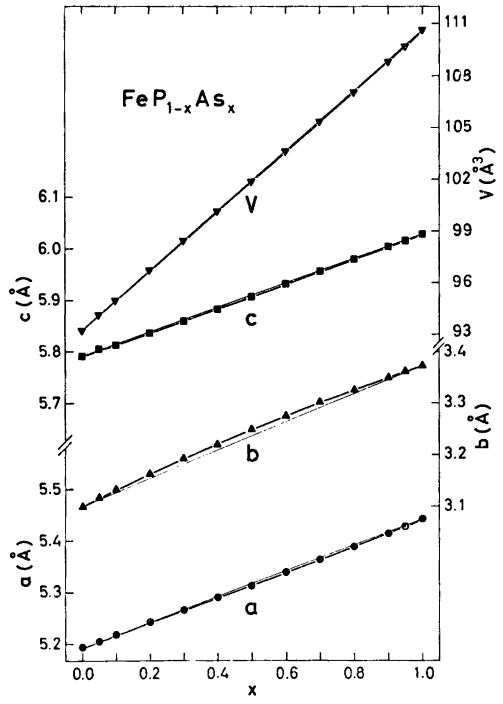

Fig. 1. Unit cell dimensions of the ternary solid solution series FeP-FeAs as functions of composition.

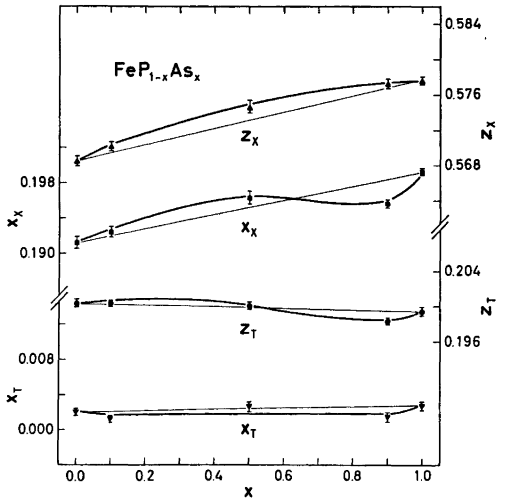

Fig. 2. Positional parameters x and z for metal (T) and non-metal (X) as functions of composition at room temperature. Data for FeP and FeAs are quoted from Refs. 18, 20.

least squares profile refined parameters are listed in Table 1, magnetic reflections (*vide infra*) being excluded at 4.2 and 80 K for $x = 0.10$. The variation of the positional parameters with composition at room temperature is illustrated in Fig. 2. The figure shows, in accordance with expectation, continuous changes in all these variables with composition. However, too much confidence cannot be put on details of the diagram.

The same samples were subjected to a high temperature X-ray diffraction study in order to establish whether the phase undergoes a crystallographic transformation to the NiAs type structure. No such transformation was observed, and the results shown in Fig. 3, are accordingly in agreement with the findings for FeAs.[7] The relative linear expansion coefficients given on the diagram, are also seen to exhibit a continuous variation with x.

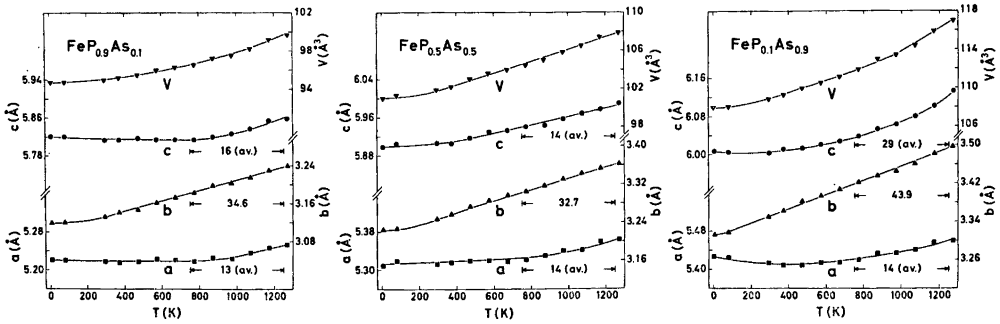

Fig. 3. Unit cell dimensions of three $FeP_{1-x}As_x$ samples as functions of temperature. The relative expansion coefficients $\alpha_a[=(a_T - a_{T'})/a_{300}(T - T')]$, α_b, α_c multiplied by 10^6 K are positioned below the appropriate curves. Corresponding triplet for FeAs [7] is 11 (av.), 44 (av.), 22 (av.).

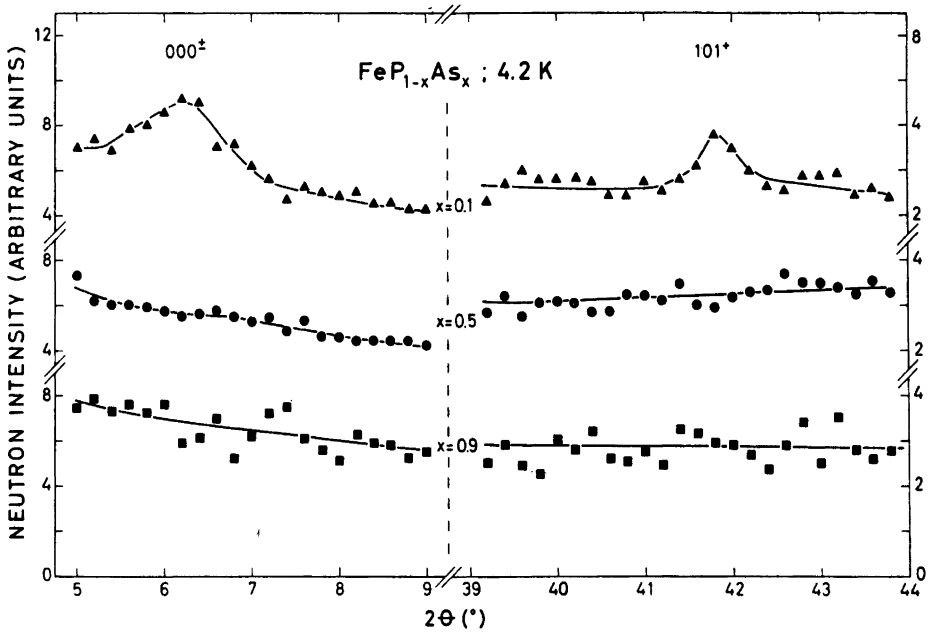

Fig. 4. Partial neutron diffraction diagrams for samples with $x = 0.10$, 0.50, and 0.90 in $FeP_{1-x}As_x$.

(ii) *Magnetic susceptibility and magnetization.* Magnetic susceptibility measurements of some 15 samples covering the entire composition range of $FeP_{1-x}As_x$ were carried out between 80 and ~1000 K. Apart from the samples with $x = 0.00$, 0.10, and 1.00 ferrimagnetic impurities originating from traces of Fe_3O_4 rendered the results of these efforts practically worthless. Similar difficulties were experienced in earlier studies of polycrystalline samples of FeP [18] and FeAs,[7] the latter compound being especially exposed to such impurification. (This difficulty was avoided in studies of $Mn_{1-t}Fe_tAs$ [8] and $V_{1-t}Fe_tAs$ [11] where, on the other hand, other (neither ferro- nor ferrimagnetic) oxides are formed.)

Surprisingly, the sample $FeP_{0.90}As_{0.10}$ gave no indication of the oxide impurity. The reciprocal magnetic susceptibility *versus* temperature curve of this sample shows a similar characteristic to that of FeP.[18] Curie-Weiss' Law is satisfied between 200 and 750 K with $\theta = -820 \pm 50$ K, $\mu_P = 1.8 \pm 0.1\ \mu_B$/Fe atom, which gives a spin quantum number $S = 0.53 \pm 0.05$ according to the "spin only" approximation.

(iii) *Magnetic structure.* FeP and FeAs have previously [6,7] been found to exhibit helimagnetism below Néel temperatures of 125 ± 1 and 77 ± 1 K, respectively. Their helimagnetic arrangements are of the double *c* axis spiral type also observed for CrAs,[1-3] $Cr_{1-t}Mn_tAs$,[1] and MnP.[4,5] The parameters specifying the spirals are $\mu_{Fe}(=2S_{Fe}) = 0.41\ \mu_B$ (av.), $\tau = 0.20 \times 2\pi c^*$ and $\varphi_{1,2} = 168.8°$ for FeP at 4.2 K and $\mu_{Fe} = 0.5 \pm 0.1\ \mu_B$, $\tau = 0.375 \times 2\pi c^*$, and $\varphi_{1,2} = -140 \pm 10°$ for FeAs at 12 K, moments being assumed at right angles to the spiral axis in both cases.

The neutron diffraction diagrams of the samples with $x = 0.10$, 0.50, and 0.90 at 4.2 K show extra reflections of purely magnetic origin only for that with $x = 0.10$. The search for a $000^{\pm}$ satellite, characteristic of the above helimagnetic arrangement, was performed with a relatively long neutron wavelength (2.4625 Å) and a three-axes spectrometer arrangement in order to obtain a good resolution in the low angle region. Selected regions of the neutron diffraction diagrams for the three samples are shown in Fig. 4, where the presence of the $000^{\pm}$ and 101^{+} satellites is evident only for $x = 0.10$.

On the assumption of an isostructural, magnetic arrangement in FeP, $FeP_{0.90}As_{0.10}$, and FeAs, the evaluation of the spiral parameters followed the procedure outlined in Refs. 2, 7.

The derived values for these parameters are $\mu_{Fe} = 0.42 \pm 0.02$ μ_B, $\tau = 0.254 \times 2\pi c^*$, and $\varphi_{1,2} = 155 \pm 5°$ at 4.2 K. From the temperature dependence of the integrated intensity of the 101⁻ satellite, the Néel temperature was determined as $T_N = 96 \pm 5$ K. The normalized integrated intensity of this reflection is shown in Fig. 5 as a function of reduced temperature, the Brillouin curve for $S = 1/2$ being indicated for the purpose of comparison.

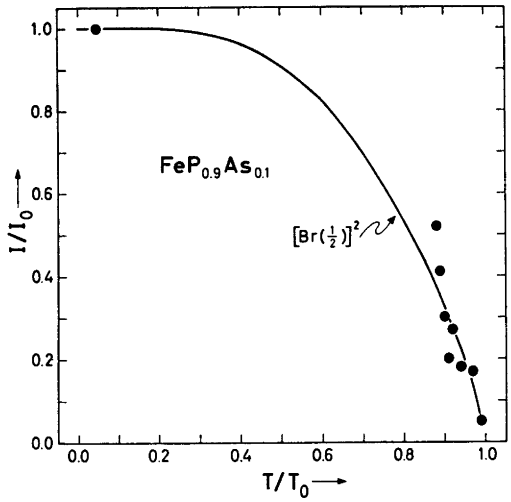

Fig. 5. Normalized intensity *versus* reduced temperature for 101⁻ of $FeP_{0.90}As_{0.10}$.

Small magnetic contributions to nuclear peaks are usually difficult to detect. Hence, it is impossible on the basis of the present data to substantiate or reject the hypothesis of a small ferromagnetic moment with $\mu_{Fe} < 0.5$ μ_B in the samples with $x = 0.50$ and 0.90 at 4.2 K. A number of different orientations of the moment have been tried, but no significant improvements in the reliability factor was obtained.

DISCUSSION

The number of unpaired electrons observed for $FeP_{0.90}As_{0.10}$ fits nicely in with those for FeP and FeAs. Also the other spiral parameters fall between those for the binary compounds (*vide supra*). This finding provokes a discussion of the absence of helimagnetism for the samples with $x = 0.50$ and 0.90.

The exchange interactions in compounds with the MnP type structure have recently been treated by Kallel *et al.*[21] Although these authors do not present the complete solution of this interaction problem, their treatment of the *c* axis double helimagnetic and ferromagnetic modes is exhaustive. For the present purpose only the most realistic solution, the isotropic case with four exchange parameters, $J_{4,1}$, $J_{1,2}$, $J_{1,1}$, and $J_{1,4}$, is considered. (The atoms and, hence, the exchange parameters follow the numbering in Refs. 2, 7.) According to Kallel *et al.*[21] the stability condition for the ferromagnetic mode is

$4UV + U + V > 0$

and for the *c* axis double helimagnetic mode

$4UV + U + V < 0$ or

$-4UV + U + V > 0$

where $U = J_{4,1}/J_{1,2}$ and $V = J_{1,4}/J_{1,2}$. Numerical values for U and V are calculated on the basis of the observed phase angles in FeP, $FeP_{0.90}As_{0.10}$, and FeAs and are shown in Fig. 6 in

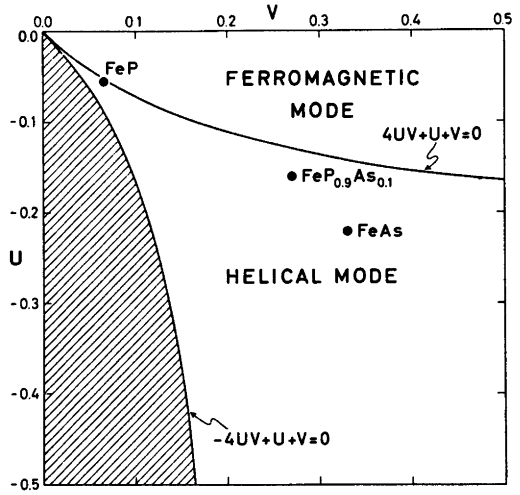

Fig. 6. Relevant quadrant of U,V stability diagram for helimagnetic and ferromagnetic modes in MnP type compounds according to isotropic model of Kallel *et al.*[21]

relation to the above stability conditions. The closeness of the three points to the borderline between helimagnetic and ferromagnetic ordering leads one to suggest that the corresponding points for $FeP_{0.50}As_{0.50}$ and $FeP_{0.10}As_{0.90}$ may be located on the ferromagnetic side of the borderline. This would provide a simple and

natural explanation of the data at hand, but can unfortunately not be confirmed.

In order to elucidate these and other associated problems further, work on $V_{1-t}Cr_tAs$, $V_{1-t}Mn_tAs$, $CrP_{1-x}As_x$, $Cr_{1-t}Fe_tAs$, $Cr_{1-t}Co_tAs$, $Mn_{1-t}Co_tAs$, and $Fe_{1-t}Co_tAs$ is now in progress.

REFERENCES

1. Kazama, N. and Watanabe, H. *J. Phys. Soc. Jap. 30* (1971) 1319.
2. Selte, K., Kjekshus, A., Jamison, W. E., Andresen, A. F. and Engebretsen, J. E. *Acta Chem. Scand. 25* (1971) 1703.
3. Boller, H. and Kallel, A. *Solid State Commun. 9* (1971) 1699.
4. Felcher, G. P. *J. Appl. Phys. 37* (1966) 1956.
5. Forsyth, J. B., Pickart, S. J. and Brown, P. J. *Proc. Phys. Soc. 88* (1966) 333.
6. Felcher, G. P., Smith, F. A., Bellavance, D. and Wold, A. *Phys. Rev. B 3* (1971) 3046.
7. Selte, K., Kjekshus, A. and Andresen, A. F. *Acta Chem. Scand. 26* (1972) 3101.
8. Selte, K., Kjekshus, A. and Andresen, A. F. *Acta Chem. Scand. A 28* (1974) 61.
9. Hall, E. L., Schwartz, L. H., Felcher, G. P. and Ridgley, D. H. *J. Appl. Phys. 41* (1970) 939.
10. Schwartz, L. H., Hall, E. L. and Felcher, G. P. *J. Appl. Phys. 42* (1971) 1621.
11. Selte, K., Kjekshus, A. and Oftedal, T. A. *Acta Chem. Scand. A 28* (1974) 803.
12. Kazama, N. and Watanabe, H. *J. Phys. Soc. Jap. 30* (1971) 578.
13. Roger, A. and Fruchart, R. *C. R. Acad. Sci. C 264* (1967) 508.
14. Bonnerot, J., Fruchart, R. and Roger, A. *Phys. Lett. A 26* (1968) 536.
15. Sénateur, J.-P., Roger A., Fruchart, R. and Chappert, J. *C. R. Acad. Sci. C 269* (1969) 1385.
16. Maeda, Y. and Takashima, Y. *J. Inorg. Nucl. Chem. 35* (1973) 1219.
17. Jones, E. D. *Phys. Rev. 158* (1967) 295.
18. Selte, K. and Kjekshus, A. *Acta Chem. Scand. 26* (1972) 1276.
19. Selte, K. and Kjekshus, A. *Acta Chem. Scand. 23* (1969) 2047.
20. Selte, K. and Kjekshus, A. *Acta Chem. Scand. 27* (1973) 1448.
21. Kallel, A., Boller, H. and Bertaut, E. F. *J. Phys. Chem. Solids 35* (1974) 1139.

Received May 9, 1974.

Acta Chemica Scandinavica A 28 (1974) 963—973

Conformational Analysis. VII. The Molecular Structure and Torsional Oscillations of Gaseous Octachloropropane (C_3Cl_8) as Determined by Electron Diffraction and Compared with Semi-empirical (Molecular Mechanics) Calculations

LIV FERNHOLT and REIDAR STØLEVIK

Department of Chemistry, University of Oslo, Blindern, Oslo 3, Norway

Gaseous octachloropropane has been studied by electron diffraction at a nozzle temperature of 160 °C. Results are presented with error limits (2σ). The following values for bond lengths (r_g) and bond angles ($\angle_\alpha$) were obtained: r(C–C) = 1.657(30) Å, r(C–Cl, in $-CCl_3$) = 1.764(12) Å, r(C–Cl, in $>CCl_2$) = 1.812(40) Å, $\angle$CCC = 119.0°(4.0), $\angle$CCCl (in $-CCl_3$) = 110.4°(1.0), and $\angle$CCCl (in $>CCl_2$) = 104.5°(1.0). Non-bonded internuclear distances were computed as dependent quantities, restricted under the constraints of geometrically consistent r_α parameters.

It is noteworthy that the two energetically unfavourable parallel (1:3) Cl···Cl interactions did not lead to a twist of the $-CCl_3$ groups. The $-CCl_3$ groups are staggered (C_{2v} symmetry) relative to the $>CCl_2$ group. However, the values of the parameters r(C–C) and $\angle$CCC are quite different from those in propane itself.

To a large extent the values of the structural parameters predicted by the semi-empirical model, reasonably agree with the experimental findings.

It has been demonstrated that the diagonal torsional force constant can be estimated from the electron-diffraction data, if the remainder of the force field is approximately known. The most probable values of the two torsional frequencies are expected in the range 45 – 65 cm^{-1}. The torsional force constant predicted by the semiempirical model does not agree with the experimental finding, which is 0.36 mdyn Å $(rad)^{-2}$ for the diagonal element.

I. INTRODUCTION

This work is part of a systematic conformational study of halogenated propanes by electron diffraction in the gas phase. Results for the following molecules have recently been published: $(BrCH_2-CHBr-CH_2Br)$,[1] $(BrH_2C-CH_2-CH_2Br)$,[2] $(ClH_2C-CHCl-CH_2Cl)$.[3] Also molecules with CH_2X (X = Cl or H) groups bonded to the central C atom of a C–C–C skeleton have been studied: $[C(CH_2Cl)_4]$,[4] $[(CH_3)_2C(CH_2Cl)_2]$,[5] $[(CH_3)C(CH_2Cl)_3]$.[6]

General information [7] relevant to this investigation and to the electron diffraction method [8] is found in Refs. 7 and 8.

For heavily chlorinated propanes very few conformers are found compared to the number of theoretically possible conformers with all-staggered (1:2) interactions.[9,10] With heavily chlorinated propanes most of the staggered conformers are unstable because of parallel (1:3) Cl···Cl interaction [9,10] which give rise to parallel C–Cl bonds on the same side of the carbon skeleton. In octachloropropane itself there are two parallel (1:3) Cl···Cl interactions. The repulsion between the Cl atoms has to be considerable. It is, however, a fact that the molecule exists, and at least one conformer must be stable. The present study is concerned with the details in structural and vibrational parameters of the stable conformer in the gas phase. Due to the strong repulsion between the large Cl atoms, some of the structural parameters of octachloropropane have to be quite different from those in propane itself.

For hexachloroethane [11] it is known that the C–C bond length is longer (1.564 ± 0.014 Å)

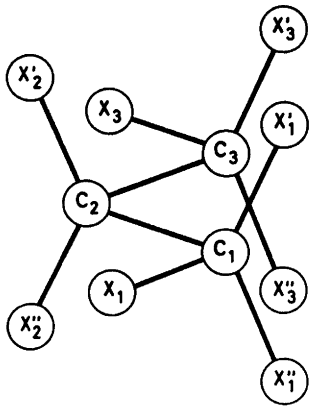

Fig. 1. Numbering of atoms in octachloropropane (X = Cl).

than that of ethane and propane, while the structural parameters of the CCl_3 groups in hexachloroethane are normal, (C − Cl = 1.769 ± 0.003 Å and ∠CCCl = 110.0 ± 0.5°).[11] From this information and a feeling that the results obtained for octachloropropane would be relevant for other heavily substituted molecules [9,10] an investigation seemed desirable.

II. SEMI-EMPIRICAL CALCULATIONS OF STRUCTURAL PARAMETERS, TORSIONAL FORCE CONSTANTS, AND TORSIONAL BARRIERS

Molecular mechanics calculations including atom-atom potentials and force constants were carried out as described in Ref. 1. Energy parameter (V_0, a, b, c, and d) were taken from the work of Abraham and Parry.[12] The diagonal valence force constants in Table 2 were used. "Normal" values of the geometry parameters are given in Table 1 together with the results of these calculations. In minimizing the energy, the geometrical model was constrained as described in Sect. V-A. The value of the tilt angle (τ) was not adjusted. ($\tau = 0°$). The remaining structure parameters, including two *independent* torsion angles, were adjusted simultaneously.

According to this energy model, only *one* stable conformer can exist. The symmetry of that conformer is C_{2v}, corresponding to staggered $-CX_3$ groups ($\phi = 0°$) with two parallel (1:3) Cl···Cl interactions. The C − C bond lengths and the CCC bond angle are considerably increased compared to propane itself.

The barrier obtained with one $-CX_3$ group eclipsing the $>CX_2$ group, and the other $-CX_3$ group fixed in the staggered position, is *ca.* 19 kcal/mol. This type of conformation corresponds to a *col* (saddle point) in the potential energy. A true potential *maximum* corresponds to both $-CX_3$ groups being eclipsed. The energy value obtained for this maximum is too large to have any physical meaning.

The values of the torsional force constants in Table 1 were numer.cally computed according to their definitions ($F_\phi = \partial^2 E/\partial\phi^2$ and $F_{\phi\phi'} = \partial^2 E/\partial\phi\partial\phi'$) at the minimum of potential energy. For small deviations from a staggered conformation ($|\phi| < 20°$) the potential minimum is close to a paraboloid:

$$E = \tfrac{1}{2}F_\phi(\phi_{1-2}^2 + \phi_{2-3}^2) + F_{\phi\phi'}\phi_{1-2}\phi_{2-3} + E_{\min}.$$

Table 1. Results of semi-empirical calculations for octachloropropane (X = Cl).

Bond lengths (Å)	Bond angles (°)
C − C (1.513)[a] = 1.594	∠CCC (110.0) = 120.0
C − X (1.760) = 1.778 (in $-CX_3$)	∠CCX (109.5) = 113.7 (in $-CX_3$)
C − X (1.760) = 1.801 (in $>CX_2$)	∠CCX (109.5) = 107.9 (in $>CX_2$)

Torsion angles[b] (°)

$\phi(1-2) = \phi(2-3) = 0.0$ (staggered, C_{2v} symmetry)

Torsional force constants [mdyn Å (rad)$^{-2}$]

$F_\phi(1-2) = F_\phi(2-3) = 0.69$ and $F_{\phi\phi'}(1-2, 2-3) = -0.49$

[a] "Normal" values of the parameters are shown in parentheses. For the XCX angles 109.47° were used as "normal" values. [b] $\phi_0 = 60°$ in the expression $V_\phi = (V_0/2)\sum_k\{1 + \cos[3(\phi_{k-2} - \phi_0)]\}$, with $k = 1$ and 3.

III. CALCULATION OF VIBRATIONAL QUANTITIES

Valence force constants, except for the torsional part of the force field, were taken from the work [13] of Schachtschneider and Snyder. Certain compromises between force-constant values had to be made. The final values selected for octachloropropane are given in Table 2. The diagonal torsional force constant was adjusted (see Sect. V-B).

The normal-coordinate program described by Gwinn [14] was used in computing vibrational frequencies. The molecular model possessed C_{2v} symmetry, and according to Herzberg [15] the assignment of frequencies is: $A_1(9)$, $A_2(5)$, $B_1(7)$, and $B_2(6)$.

Mean amplitudes of vibration (u) and vibrational correction terms (K and D) were calculated as explained in Ref. 16. Their values are found in Table 4.

Some of these quantities are quite sensitive to the value of the diagonal torsional force constant, which have been adjusted to fit the experimental intensities (Sect. V-B). In Table 5 are shown torsional frequencies and mean amplitudes of vibration corresponding to different values of the diagonal torsional force constant F_ϕ, with the torsional interaction constant ($F_{\phi\phi'}$) fixed at zero value.

According to the semi-empirical calculations (Table 1), the value of the torsional interaction constant is negative and comparable in magnitude to the value of the diagonal element (F_ϕ). Although the values of the torsional frequencies depend on the value of $F_{\phi\phi'}$, it will be shown that the u and K values are less dependent on the value of the interaction constant.

For *high* temperatures and *low* values of the torsional frequencies (ω_1 and ω_2) the following relations are approximately valide:
$u^2 \simeq (a_1/\omega_1)^2 + (a_2/\omega_2)^2 + u_0^2$ and $K \simeq (b_1/\omega_1)^2 + (b_2/\omega_2)^2 + K_0$. (The relations follow from the general formulas [16] for u and K if the conditions above are fulfilled.) The quantities a, b, u_0, and K_0 are approximately independent of the values of ω_1 and ω_2.

Table 2. Valence force constants for octachloropropane (X = Cl).

Stretch (mdyn Å^{-1})		Bend [mdyn Å (rad)$^{-2}$]	
C – C	4.39	CCX	1.17
C – X	2.76	XCX	1.13
		CCC	0.90

Stretch/stretch (mdyn Å^{-1}), C is common

C – C/C – X = 0.73; C – C/C – C = 0.064; and C – X/C – X = 0.496

Stretch/bend [mdyn (rad)$^{-1}$]

C – C is common: C – C/CCX = 0.29; C – C/CCC = 0.35
C – X is common: C – X/CCX = 0.55; C – X/XCX = 0.41
C is common: C – X/XCX = 0.38

Bend/bend [mdyn Å (rad)$^{-2}$]

C – X is common: XCX/XCX = – 0.13, CCX/XCX = – 0.12
C is common: CCX/XCX = – 0.06
C – C is common:
CCC/CCX = + 0.041 (dihedral angle between CCC and CCX is 180°)
CCC/CCX = – 0.024 (dihedral angle between CCC and CCX is 60°)
CCX/CCX = – 0.090 (dihedral angle between CCX angles is 180°)
CCX/CCX = + 0.070 (dihedral angle between CCX angles is 60°)

Torsion[a] [mdynÅ (rad)$^{-2}$]: $F_\phi = 0.36$[b] ($F_{\phi\phi'} = 0$)

[a] The torsional force constants have been defined in the following way: each fragment of type A′ – C_1 – C_2 – A″ (A = C or Cl) has been assigned an equal torsional force constant. The total force constant (F_ϕ) for the torsional coordinate ϕ_{i-2} (i = 1,3) is thus the sum of *nine* equal contributions. The input to Gwinn's normal-coordinate program demands a separate specification for each torsion fragment. [b] This value was estimated from the electron diffraction data as described in Sect. V-B.

Table 3. Fundamental vibrational frequencies ω (cm^{-1}), in octachloropropane. (C_{2v} sym.) X = Cl.

A_2	48, Torsion (3)[a]	A_2	272, XCX(3)+CCX(3)
B_2	62, Torsion (3+2)[b]	B_2	313, CCX(2+3)+C−X(2)[d]
A_1	77, CCX (3)[c]	A_1	353,[e] XCX(2)+CCC+C−X(2)
B_2	133, CCX(3+2)	B_1	389, XCX(3)
A_2	166, CCX(2+3)	A_1	419, C−X(2+3)+XCX(3)
B_1	177, CCX(2+3)	B_1	646, C−X(3)+CCX(2)
A_1	188, XCX(3)+CCX(3)	A_1	738, C−X(2+3)
B_1	202, CCX(3)+XCX(3)	B_2	743, C−X(2+3)
A_2	208, CCX(3+2)+XCX(3)	B_1	796, C−X(3+2)
A_1	221, XCX(2+3)	A_2	812, C−X(3)
B_2	242, XCX(3)	B_2	866, C−X(3+2)
B_1	263, XCX(3)	A_1	869, C−C+C−X(3)
A_1	265, XCX(3+2)	A_1	898, C−X(3)+C−C
		B_1	1175, C−C+C−X(3)

The value of $\omega(cm^{-1})$ and the species which ω belongs to have been given. In addition, an *approximate* interpretation of the modes have been suggested. [a] (3) means that large displacements are mainly found in $-CX_3$ groups. [b] (3+2) means large displacements in $-CX_3$ groups and smaller displacements in the group $>CX_2$. [c] CCX(or CCC, XCX) means bending of this type of bond angle. [d] C−X (or C−C) means stretching of this kind of bond. [e] the combination XCX(2)+CCC+C−X(2) thus means: large deformation of the XCX angle in the group $>CX_2$+bending of the angle CCC+stretching of the C−X bonds in the $>CX_2$ group. The largest contribution is always mentioned first.

The torsional frequencies, calculated for different values of $F_{\phi\phi'}$, with $F_\phi = 0.36$ mdyn Å $(rad)^{-2}$, have been shown in Fig. 2. For large negative values of $F_{\phi\phi'}$, $\omega_1(A_2)$ is greater than $\omega_2(B_2)$, while $\omega_1(A_2)$ is smaller than $\omega_2(B_2)$ if the value of $F_{\phi\phi'}$ is greater than *ca.* −0.18 mdyn Å $(rad)^{-2}$. Starting with zero value for $F_{\phi\phi'}$, a negative value of $F_{\phi\phi'}$ of *ca.* −0.26 mdyn Å $(rad)^{-2}$ leads to the effect that $\omega_1(A_2)$ is decreased by *ca.* 11 % and $\omega_2(B_2)$ is increased by

Table 4. Mean amplitudes of vibration (u) and vibrational correction terms (K and D) for octachloropropane at 160 °C, X = Cl.

Dist. Type	Dist. (Å)[a]	u-value (Å)	K-value (Å)	D-value (Å)[b]
C−C	(1.66)	0.0567	0.0042	−0.0022
C_2-X_2	(1.81)	0.0622	0.0071	−0.0049
C_1-X_1	(1.76)	0.0599	0.0134	−0.0114
C_1-X_1'	(1.76)	0.0599	0.0134	−0.0114
$C_1\cdots C_3$	(2.83)	0.0803	0.0024	−0.0001
$C_2\cdots X_1'$	(2.81)	0.0777	0.0103	−0.0082
$C_2\cdots X_1$	(2.81)	0.0777	0.0107	−0.0085
$C_1\cdots X_2$	(2.72)	0.0803	0.0059	−0.0035
$X_1'\cdots X_1''$	(2.85)	0.0733	0.0191	−0.0167
$X_1\cdots X_1'$	(2.85)	0.0833	0.0196	−0.0172
$X_2'\cdots X_2''$	(2.97)	0.0791	0.0083	−0.0062
$C_1\cdots X_3$(a)	(4.35)	0.0826	0.0040	−0.0024
$C_1\cdots X_3'$(g)	(3.46)	0.1508	0.0071	−0.0005
$X_1\cdots X_2'$(g)	(3.24)	0.1608	0.0103	−0.0024
$X_1'\cdots X_2'$(g)	(3.24)	0.1601	0.0100	−0.0021
$X_1'\cdots X_2''$(a)	(4.35)	0.0835	0.0073	−0.0057
$X_1\cdots X_3$(AA)	(5.58)	0.1196	0.0044	−0.0018
$X_1\cdots X_3'$(AG)	(5.06)	0.1547	0.0043	+0.0004
$X_1'\cdots X_3''$(GG)	(4.24)	0.2496	0.0054	+0.0093
$X_1'\cdots X_3'$(GG)	(3.14)	0.2564	0.0176	+0.0033

The force constants in Table 2 were used. [a] C_{2v} symmetry was assumed, and τ(tilt) = 0°. [b] $D = R_\alpha - R_a = u^2/R - K$.

Table 5. Vibrational quantities in octachloropropane; torsional frequencies and u values (at 160 °C), X = Cl. See also Tables 2, 3, and 4.

F_ϕ [mdyn Å (rad)$^{-2}$]	0.18	0.36	0.68
Torsional frequencies (cm^{-1})			
	38(A_2)	48(A_2)	65(A_2)
	50(B_2)	62(B_2)	82(B_2)
u-Values (Å) for X···X distances			
$X_1 \cdots X_2$ (*gauche*)	0.178	0.161	0.144
$X_1 \cdots X_2$ (*anti*)	0.084	0.084	0.083
$X_1 \cdots X_3$(AA)	0.120	0.120	0.120
$X_1 \cdots X_3'$(AG)	0.165	0.155	0.145
$X_1' \cdots X_3''$(GG)	0.293	0.250	0.209
$X_1' \cdots X_3'$(GG)	0.276	0.256	0.238

ca. 13 %. According to the semi-empirical calculations (Table 1) such a large negative value of $F_{\phi\phi'}$ is not unlikely. Unfortunately, the formulas above for the u and K values are not sensitive to such changes in the ω values. The decrease in ω_1 will increase the value of the ω_1^{-2} term, but that change will be approximately compensated by the decrease in the ω_2^{-2} term, due to the increase in ω_2. The effect is thus *ca.* 5 %, or less, for typical u values.

A change in the *diagonal* force constant (F_ϕ) on the other hand, will increase or decrease the values of ω_1 and ω_2 simultaneously (see Table 5).

It is thereby demonstrated that the value of $F_{\phi\phi'}$ is not critical in computing u and K values. However, the absolute value of the difference between the torsional frequencies is *decreased* for large negative values of $F_{\phi\phi'}$ (Fig. 2).

The most probable values of the torsional frequencies are thus expected in the range 45 – 65 cm^{-1}.

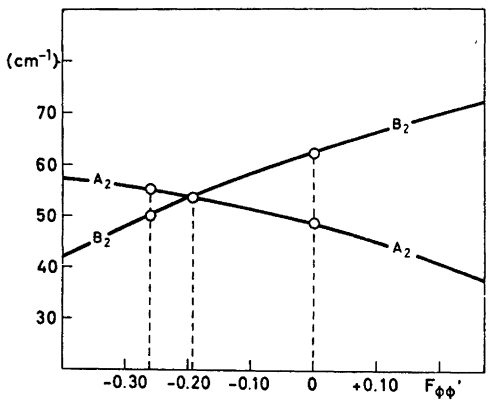

Fig. 2. Torsional frequencies (cm^{-1}) in octachloropropane calculated for different values of the interaction-force constant $F_{\phi\phi'}$. The remainder of the force constants are found in Table 2. $F_{\phi\phi'}$ in mdyn Å (rad)$^{-2}$.

IV. EXPERIMENTAL AND DATA REDUCTION

Octachloropropane was obtained from "K & K" laboratories. The commercial sample was purified by recrystallization. The final melting point was 159 – 160 °C.

Electron diffraction photographs were made at a nozzle temperature of 160 °C in the Oslo apparatus,[17] under conditions summarized below.

Nozzle-to-plate distance (mm)	480.4	200.5
Electron wavelength (Å)	0.06458	0.06458
Number of plates	4	4
Range of data, in s (Å^{-1})	1.50 – 19.75	7.25 – 44.50
Data interval, Δs (Å^{-1})	0.125	0.250
Estimated uncertainty in the s-scale	0.14 %	0.14 %

The electron wavelength was determined by calibration against gold and corrected by an experiment with CO_2 giving a correction of +0.10 % in the s-scale. The data were reduced in the usual way [18] to yield an intensity curve for each plate.

Average curves for each set of distances were formed. A composite curve was then made by connecting the two average curves after scaling.

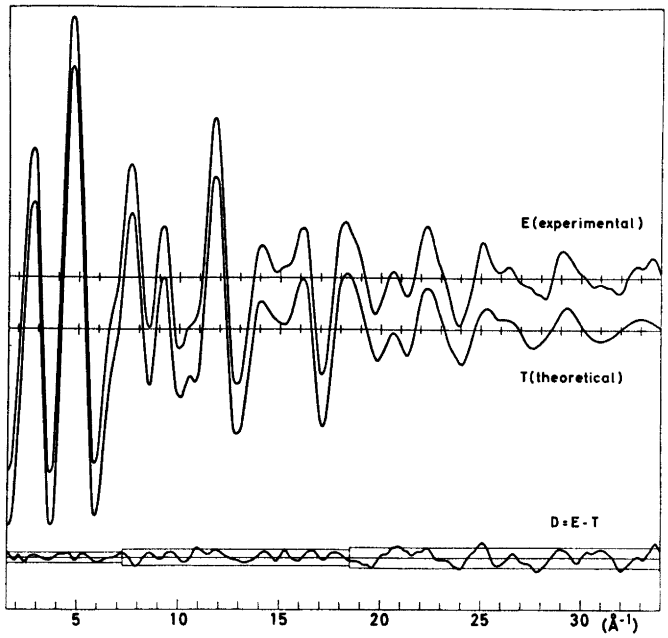

Fig. 3. Experimental (E) and theoretical (T) intensity curves for octachloropropane at *ca.* 160 °C, corresponding to the final least-squares parameters. Curve D represents E − T, and the straight lines give the experimental uncertainty (± 3 × experimental standard deviation).

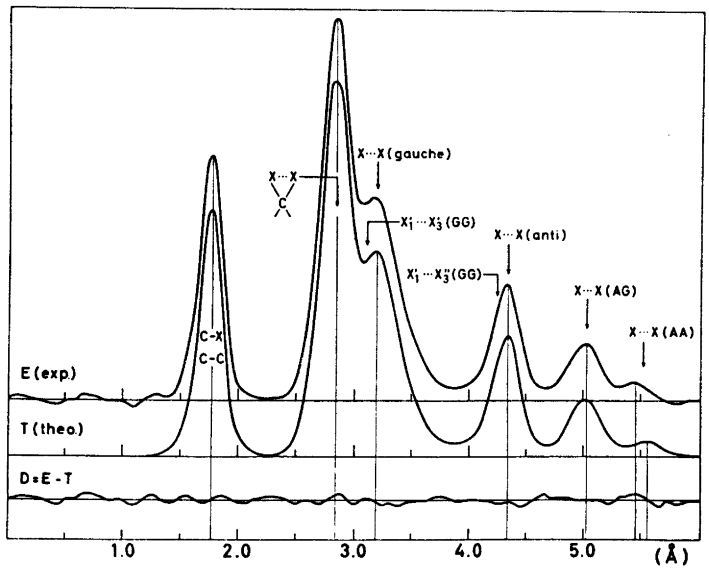

Fig. 4. Radial distribution curves for octachloropropane at 160 °C. Experimental (E) and theoretical (T) radial distribution curves, and difference curve (D). The RD curves were calculated from the intensities of Fig. 3 using an artificial demping constant equal to 0.0020 Å².

The final experimental intensity curve is shown in Fig. 3. The intensities have been modified by $s|f_{Cl}'|^{-2}$. The scattering amplitudes were calculated by the partial-wave method [19] using Hartree-Fock atomic potentials.[20]

The radial-distribution curve obtained by Fourier transformation of the final experimental intensity is presented in Fig. 4.

V. STRUCTURE ANALYSIS

From the experimental RD curve (Fig. 4), before refinements had been started, two important conclusions were reached: (1) the C–C bond lengths have to be very long; (2) the stable conformation of the molecule possesses an internuclear Cl···Cl distance *ca.* 5.5 Å long (X···X(AA) in Fig. 4). Such a long Cl···Cl distance is only possible if both $-CCl_3$ groups are nearly staggered relative to the $>CCl_2$ group.

A. Least-squares refinements

The geometrical model for the molecule was constructed with the following assumptions:

(1) the plane of the CX_2 group (X = Cl) is perpendicular to the plane of the C atoms and bisects the CCC angle;

(2) the two $C-CX_3$ groups are equal;

(3) the CX_3 groups possess C_{3v} symmetry, while the $C-CX_3$ groups possess C_s symmetry.

Models were refined in terms of the following structural parameters; *bond lengths:* r(C–C), r(C–X, in CX_3), and r(C–X, in CX_2); *bond angles:* ∠CCC, ∠CCX (in $C-CX_3$), and ∠CCX (in $>CX_2$); *torsion angles of the $-CX_3$ groups relative to the $<CX_2$ group:* $\phi_{1-2}=\phi(C_1-C_2)$ and $\phi_{2-3}=\phi(C_2-C_3)$; *and a tilt angle (τ) within the $C-CX_3$ groups.*

The values of the ϕ angles are both *zero* when the atoms $X_1-C_1-C_2-C_3-X_3$ are coplanar, corresponding to a *staggered* model.

The tilt angle (τ) was defined as a rotation of the CX_3 group around an axis through the C atom of that group, the axis being perpendicular to the CCC plane. The two CX_3 groups were assigned tilt angles as follows: $\tau_1=\tau(C(1)\text{-}X_3)=+\tau$ and $\tau_3=\tau[C(3)X_3]=-\tau$. For $\tau=0°$ the $C-CX_3$ groups posses C_{3v} symmetry. Starting with C_{3v} symmetry and a given value for $\angle C_2CX$ ($\angle C_2C_1X=\angle C_2C_3X$), a *negative* value of τ leads to a *decrease* in the values of $\angle C_2C_1X_1$ and $\angle C_2C_3X_3$, while the value of $\angle C_2C_1X_1'$ ($=\angle C_2C_1X_1''=\angle C_2C_3X_3'=\angle C_2C_3X_3''$) *increases*. Negative values of τ thus lead to *longer* $X_1'\cdots X_3'$ and $X_1''\cdots X_3''$ internuclear distances.

For $\tau\neq 0°$ the two different CCX angles of the $C-CX_3$ groups were not refined independently. The angle $C_2C_1X_1$ ($=C_2C_3X_3$) was chosen as the *independent* parameter.

The angles, ϕ and τ, were never refined simultaneously. If τ was refined, then the value of ϕ was fixed at zero degrees, and *vice versa.*

Non-bonded internuclear distances were computed as dependent quantities, restricted under the constraints of geometrically consistent r_α parameters.[21,22]

B. Determination of torsional force constants

Mean amplitudes of vibration (u) and perpendicular amplitude correction coefficients (K) are easily calculated if a reasonable force field is known for the molecule (see Sect. III). The

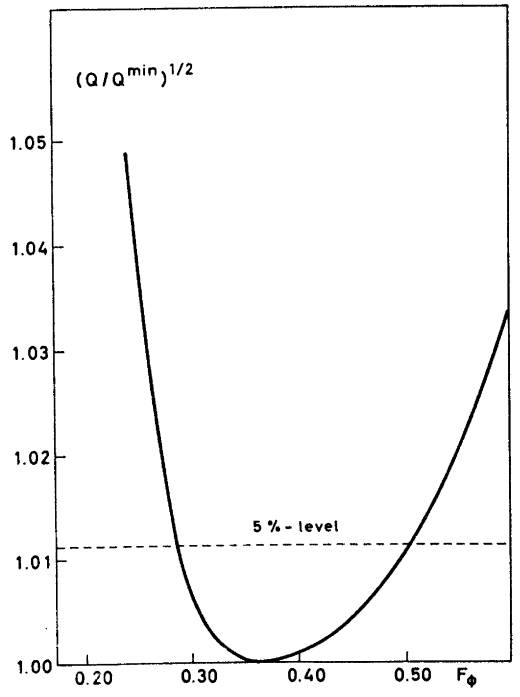

Fig. 5. The quantity $R^* = (Q/Q^{min})^{\frac{1}{2}}$ as a function of the diagonal torsional force constant F_ϕ. $Q=\mathbf{V'PV}$: the error sum. V is the residual (experimental intensity minus calculated intensity).

values of the torsional force constants [$F_\phi(1-2)=F_\phi(2-3)=F_\phi$ and $F_{\phi\phi'}(1-2;2-3)$] for octachloropropane had not been determined prior to this investigation. However, the diagonal part of the torsional force field (F_ϕ) can be determined from the electron-diffraction data. Torsional modes contribute substantially to the u and K values of several internuclear distances in a molecule like octachloropropane. Such u values are those listed in Table 5. One torsional mode ($\omega(A_2)=48$ cm^{-1}) alone contributes more than 60 % to the u value of $X_1'\cdots X_3''$.

The value of F_ϕ was determined as follows: u and K values for different values of F_ϕ were calculated, and then included in the least-squares refinements. The value of F_ϕ which leads to a minimum in the error sum ($Q=$ **V'PV**) was obtained. In each least-squares run all geometry variables of a staggered model ($\phi_{1-2}=\phi_{2-3}=0°$) were refined. In adjusting the F_ϕ value, it is important that as many as possible of the geometry parameters are refined simultaneously. The quantity $(Q/Q^{\min})^{\frac{1}{2}}$ as a function of F_ϕ is shown in Fig. 5. The 5 %-significance level, according to Hamiltons R-factor test, is also give. The most probable value of F_ϕ and the error limits corresponding to the 5 % significance level are: $F_\phi=0.36^{+0.14}_{-0.07}$ mdyn Å (rad)$^{-2}$. The error limits need a few comments:

(1) The error limits do not allow for *systematic* errors within the remainder of the force field. However, the non-torsional part of the force field seems to be quite acceptable. Moreover, the value of the torsional interaction force constant ($F_{\phi\phi'}$) has not been adjusted (see Sect. II).

(2) The nozzle temperature (433 K) was used in calculating vibrational quantities. The relevant temperature for the expanding gas is lower than 433 K. The correct vibrational temperature is not known, however, the *systematic* error introduced in the determination of the torsional force constant may be estimated, as follows. For *high* temperature (T) and *low* F_ϕ values the following expressions are approximately valid: $u^2\simeq A(T/F_\phi)+u_0^2$ and $K\simeq A'\times(T/F_\phi)+K_0$. A, A', u_0^2, and K_0 are not dependent on F's. A and A' are temperature-independent quantities. Although u_0^2 and K_0 are temperature-dependent quantities, the present approximative analysis will not take this into consideration. It then follows that the relative error ($\Delta F_\phi/F_\phi$) in F_ϕ is approximately equal to the relative error ($\Delta T/T$) in T. If the fall in temperature is as large as *ca.* 40 K, then the value of F_ϕ, as determined here, is *ca.* 10 % too high. A systematic error in the F_ϕ value is propagated to the value of the torsional frequencies (ω_ϕ), and approximately, $(\Delta\omega_\phi/\omega_\phi)=\frac{1}{2}(\Delta F_\phi/F_\phi)$.

(3) Also the drawing of a background may introduce a *systematic* error in the F_ϕ value. After a background correction has been introduced, a new adjustment of the F_ϕ value ought to be carried out. However, this type of error is not considered as critical. The errors of type (1) and (2) could be critical.

Until the low torsional frequencies have been directly observed, the value of the interaction constant ($F_{\phi\phi'}$) remains unknown. According to the semi-empirical energy model, the value has to be negative (Sect. II).

VI. FINAL RESULTS

Parameters from the least-squares refinements and standard deviations (σ) corrected for correlation [23] in the experimental data are given.

According to the experimental uncertainties (see Fig. 3) the diagonal weights of the intensities in the least-squares refinements ought to be smaller for larger s values. Two diagonal weight schemes, one with constant weight, and one with variable weights corresponding to the experimental uncertainties, were tried. The parameters obtained were practically identical in the two cases. The final parameters correspond to refinements with equal weights for all intensities. However, the data beyond $s=$ 34.0 Å^{-1} were not included in the final refinements.

The final structure parameters are found in Table 6, and parameter-correlation coefficients (ϱ) are found in Table 7.

Non-bonded distances were restricted under the geometrical constraints of r_α parameters, by including correction terms $D=r_\alpha-r_a$ ($D=u^2/r-K$) for all internuclear distances.

Initially the torsion-angle parameter (ϕ) was refined with $\phi_{1-2}=\phi_{2-3}=\phi$, corresponding to a molecular model possessing C_2 symmetry. Refinements of that parameter, before and after background corrections, always yielded values very close to 0° (staggered model) with a

Table 6. Structural parameters in octachloropropane (X = Cl).

Bond lengths (r_a) (Å)	Bond angles ($\angle_\alpha$) (°)
r(C−C) = 1.655(15)	∠CCC = 119.0(2.0)
r(C−X, in CX_3) = 1.762(6)	∠CCX (in $-CX_3$) = 110.4(0.5)
r(C−X, in CX_2) = 1.810(20)	∠CCX (in $>CX_2$) = 104.5(0.5)

Standard deviations are given in parentheses. The uncertainty (0.14 %) in the s-scale has been included in the standard deviations for bond distances. An experiment with CO_2 gave a correction of +0.1 % in the s-scale. The bond lengths are therefore 0.1 % longer than those directly obtained by the least-squares refinements. Bond angles are those of the self-consistent r_α structure. The values correspond to a molecular model with C_{2v} symmetry and a tilt angle of zero.

standard deviation (σ) larger than the parameter itself. The remaining structure parameters, except for the tilt angle ($\tau = 0°$), were refined simultaneously.

The tilt-angle parameter (τ) was then introduced and refined, while the torsion angles were fixed at staggered values. ($\phi = 0°$) The molecular model then possessed C_{2v} symmetry. The remaining structural parameters were refined simultaneously. The value of τ found in this way was −0.7° with a standard deviation of 0.8°. Clearly the value of τ is not significantly different from 0°.

In conclusion, no significant deviations from a molecular model with C_{2v} symmetry were detected. Moreover, the local symmetry of the $C-CX_3$ group is not significantly different from C_{3v}.

C−Cl and C−C bonds contribute to the peak in the RD curve at *ca.* 1.5−2.0 Å. Although the contribution from the C−C bond distances is not resolved, the effect of introducing C−C bond lengths different from the most probable value (*ca.* 1.66 Å) is demonstrated in Fig. 6. The two theoretical RD curves correspond to intensity curves obtained by adjusting all structure parameters, except for the C−C bond lengths and the ϕ angles.

Except for the region at *ca.* 5.5 Å, the fit between theoretical and experimental radial distribution curves (Fig. 4) is satisfactory. Although the non-bonded distances were restricted under the constraints of r_α parameters, the calculated peak at *ca.* 5.5 Å, corresponding to the $X_1 \cdots X_3$ distance, does not fit the experimental curve well enough. Only harmonic contributions to the vibrational shrinkage corrections were considered in this work, however, the anharmonicity involved could lead to an additional shrinkage for the $X_1 \cdots X_3$ distance. (The harmonic contribution to the shrinkage of $X_1 \cdots X_3$ is *ca.* 0.02 Å).

The fit obtained between theoretical and experimental intensities (Fig. 3), using the u and K values calculated with the force constants of Table 2, is generally quite satisfactory. It is important that the large number of u values do not have to be adjusted as *individual* param-

Table 7. Parameter correlation coefficients (100 ϱ), X = Cl.

Parameter		(1)	(2)	(3)	(4)	(5)	(6)	(7)
r(C−C)	(1)	100	(−13)[a]	(−57)	(−45)	(−16)	(−43)	(−70)
r(C−X) in CX_3	(2)	1[a]	100	(−48)	(71)	(14)	(−60)	(−31)
∠CCC	(3)	−51	−72	100	(−9)	(−34)	(−71)	(69)
∠CCX in $-CX_3$	(4)	17	91	−84	100	(7)	(−42)	(20)
∠CCX in $<CX_2$	(5)	−18	4	3	−10	100	(−21)	(10)
r(C−X) in CX_2	(6)	−45	−83	86	89	−1	100	(49)
τ(tilt)	(7)	−43	−48	84	−67	33	62	100
u(C−X)[b]	(8)	36	72	−72	77	−2	84	−52

[a] Two kinds of parameter correlation (ϱ) matrixes are presented. The ϱ values in parentheses correspond to a refinement with no u values refined; [b] only *one* u-value parameter of this kind (C−X) was refined.

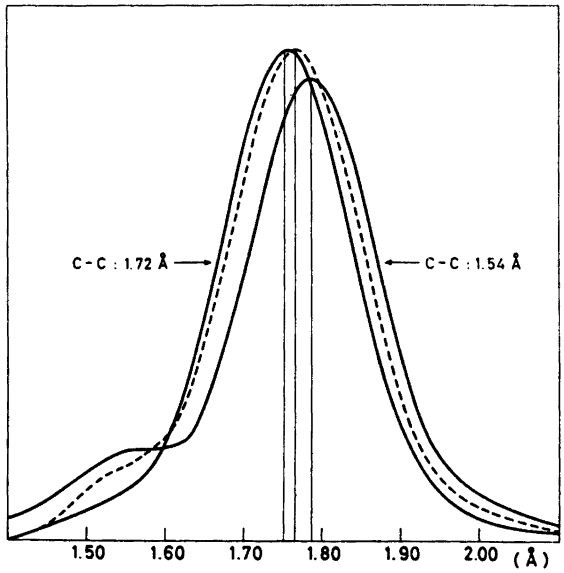

Fig. 6. Radial distributions for octachloropropane. The experimental (– – –) RD curve and two theoretical RD curves (C–C = 1.54 Å and 1.72 Å) are shown. The curves were calculated with an artificial demping constant equal to 0.0010 Å^2.

eters in the least-squares refinements. However, it ought to be kept in mind that the torsion-dependent u and K values have been adjusted simultaneously by adjusting the torsional force constant F_ϕ (Sect. V-B). The u values of Table 4, which combine information from both vibrational spectroscopy and electron diffraction, are considered the final ones for octachloropropane. The vibrationally consistent set of u values in Table 4 is considered more reliable than the individual u values obtained by direct least-squares refinements in the usual way. Direct refinements of u values were also carried out. The results of such refinements were generally not significantly different from the values of Table 4. Only one u value [u(C–Cl) = 0.045 Å, σ = 0.006 Å], obtained in this way, was significantly different from the value (*ca.* 0.060 Å) of Table 4. Most probably the low value for u(C–Cl) is caused by an error in the blackness correction. It is, however, unlikely that such an error is critical for determination of the remaining u values.

VII. DISCUSSION

Typical C–Cl bond lengths and CCCl bond angles of a C–CCl_3 group are found in the ranges 1.76 – 1.77 Å and 110 – 111°, respectively. The structural parameters C–Cl and ∠CCCl of the C–CCl_3 groups in octachloropropane are thus quite normal. The C–C bond lengths and the CCC angle are very different from those in propane itself. It is also noteworthy, that the very unfavourable parallel (1:3) Cl···Cl interactions, did not lead to a detectable twist of the –CCl_3 groups.

To a large extent the values of the structural parameters, predicted by the semi-empirical model (Table 1), reasonably agree with the experimental findings. Although adjustments in the non-torsional force constants and the "normal" parameters would remove most of the discrepancies, it was felt that results from additional molecules ought to be included, before such corrections were considered. However, the very large diagonal element predicted for the torsional force field (F_ϕ) would not be much changed by such corrections. The most probable value of F_ϕ (0.36 mdyn Å (rad)$^{-2}$) as determined from the electron diffraction data (Sect. V-B), is significantly smaller than the value (0.69) predicted by the semi-empirical model (Sect. II).

It has been demonstrated that the diagonal element of the torsional force field may be

estimated from the gas electron diffraction data. Although the torsional interaction-force constant can not be obtained in this way, the most probable values of the two torsional frequencies have been limited to the range 45 – 65 cm^{-1}. It seems that the very low CCCl(A_1)-bending frequency of 77 cm^{-1} is not unlikely. Perhaps more interesting for the vibrational spectroscopy is the finding that three of the fundamental frequencies of gaseous octachloropropane have to be expected at values less than 100 cm^{-1}.

The fundamental vibrational frequencies of octachloropropane have not been observed, but the force constants used in this analysis are consistent with the electron diffraction data. It is, however, not unlikely that the true values of the valence force constants are quite different from those in Table 2. The very long C – C bond lengths and the large CCC angle may be indicative of large anharmonic terms in the force field, resulting in too long C – C bond lengths, as only harmonic contributions to the vibrational corrections were considered in this work.

Acknowledgements. We are grateful to Cand. real. A. Almenningen for recording the diffraction photographs, and to Prof. N. Sheppard who initiated this investigation through his stimulating lecture here in Oslo several years ago. Computer programs made available by Dr. H. M. Seip, Prof. W. D. Gwinn, and Cand. real. S. Rustad have been extensively used in this work. Financial support from Norges almenvitenskapelige forskningsråd is gratefully acknowledged.

REFERENCES

1. Stølevik, R. *Acta Chem. Scand. Ser. A 28* (1974) 299.
2. Farup, P. E. and Stølevik, R. *Acta Chem. Scand. Ser. A 28* (1974) 680.
3. Farup, P. E. and Stølevik, R. *Acta Chem. Scand. Ser. A 28* (1974) 871.
4. Stølevik, R. *Acta Chem. Scand. Ser. A 28* (1974) 327.
5. Stølevik, R. *Acta Chem. Scand. Ser. A 28* (1974) 455.
6. Stølevik, R. *Acta Chem. Scand. Ser. A 28* (1974) 612.
7. Bastiansen, O., Seip, H. M. and Boggs, J. E. *Perspect. Struct. Chem. 4* (1971).
8. Seip, H. M. In Sim, G. A. and Sutton, L. E., Eds., *Molecular Structure by Diffraction Methods*, Sutton (Specialist Periodical Reports), The Chemical Society, London 1973, Vol. 1, Part 1, Chapter 1.
9. Dempster, A. B., Price, K. and Sheppard, N. *Spectrochim. Acta A 25* (1969) 1381.
10. Dempster, A. B., Price, K. and Sheppard, N. *Spectrochim. Acta A 27* (1971) 1563.
11. Almenningen, A., Andersen, B. and Trætteberg, M. *Acta Chem. Scand. 18* (1964) 603.
12. Abraham, R. J. and Parry, K. J. *J. Chem. Soc. B* (1970) 539.
13. Schachtschneider, J. H. and Snyder, R. G. *Vibrational Analysis of Polyatomic Molecules*, IV. (Force constants for the haloparaffins). Project No. 31450, Technical Report No. 122 – 63 of Shell Development Company.
14. Gwinn, W. D. *J. Chem. Phys. 55* (1971) 477.
15. Herzberg, G. *Infrared and Raman Spectra of Polyatomic Molecules*, Van Nostrand-Reinhold, New York 1945.
16. Stølevik, R., Seip, H. M. and Cyvin, S. J. *Chem. Phys. Lett. 15* (1972) 263.
17. Bastiansen, O., Hassel, O. and Risberg, E. *Acta Chem. Scand. 9* (1955) 232.
18. Andersen, B., Seip, H. M., Strand, T. G. and Stølevik, R. *Acta Chem. Scand. 23* (1969) 3224.
19. Peacher, J. and Willis, J. C. *J. Chem. Phys. 46* (1967) 4809.
20. Strand, T. G. and Bonham, R. A. *J. Chem. Phys. 40* (1964) 1686.
21. Morino, Y., Kuchitsu, K. and Oka, T. *J. Chem. Phys. 36* (1962) 1108.
22. Kuchitsu, K. *J. Chem. Phys. 49* (1968) 4456.
23. Seip, H. M. and Stølevik, R. In Cyvin, S. J., Ed., *Molecular Structures and Vibrations*, Elsevier, Amsterdam 1972.

Received June 10, 1974.

Acta Chemica Scandinavica A 28 (1974) 974—978

Raman Investigations on Potassium Hexabromostannate. Crystal Structure and Phase Transition

JØRGEN WILLY ANTHONSEN

Department of Chemistry, University of Odense, DK-5000 Odense, Denmark

The Raman spectra of K_2SnBr_6 have been recorded at different temperatures and found to be in agreement with tetragonal symmetry at room temperature and cubic symmetry at 140 °C. Crystals of the compound appear to be polysynthetic twins at temperatures below the phase transition point and behave as single crystals at temperatures above the transition point.

Earlier X-ray investigatons seem to be in conflict concerning the symmetry of potassium hexabromostannate, K_2SnBr_6. Ketelaar *et al.*[1] have determined the compound to be cubic with space group $Fm3m = O_h^5$. Markstein *et al.*[2] have, on the other hand, determined it to be tetragonal with space group $P42_12 = D_4^2$ and found the deviation from cubic symmetry to be small and give the axial ratio c/a as 1.009 ± 0.002. On the basis of microscopic investigations between -80 and 250 °C Galloni *et al.*[3] have reported a phase transition at 126.5 °C. Above this temperature the compound should be cubic and below tetragonal.

Infrared and Raman spectra of polycrystalline samples of potassium hexabromostannate have been reported by several authors.[4-8] Debeau *et al.*[4,5] mention, that though the compound is tetragonal at room temperature the deviation from cubic symmetry must be so slight that it cannot be observed in the vibration spectra because the spectra of potassium hexabromostannate are similar to spectra of other compounds of this type with cubic symmetry. The observed wavenumbers are therefore assigned to the point group O_h: $\nu_1(A_{1g})$ 190 cm^{-1}, $\nu_2(E_g)$ 144 cm^{-1}, $\nu_3(F_{1u})$ 224 cm^{-1}, $\nu_4(F_{1u})$ 118 cm^{-1}, $\nu_5(F_{2g})$ 109 cm^{-1} and an external vibration $\nu_7(F_{1u})$ 78 cm^{-1}.

EXPERIMENTAL

Polycrystalline potassium hexabromostannate was prepared as described by Nakamura *et al.*[8] Larger crystals with an edge length of approximately 3 mm were grown from saturated solutions. The compound was pale yellow.

The Raman spectra were recorded with a spectrometer equipped with a Jarrell-Ash model 25 – 101 double grating monochromator. The exciting lines used were 4880 Å and 5145 Å obtained from a Spectra-Physics model 165 Argon-ion laser.

X-RAY INVESTIGATION

Examination of the compound under a polarizing microscope showed that potassium hexabromostannate cannot be cubic at room temperature, because the crystals were birefringent. To determine the crystallographic axes in order to orientate the crystals on the Raman spectrometer, a large crystal, mounted on a goniometerhead, was investigated by a X-ray precession camera. From the X-ray photos the axial ratio c/a was determined to 1.012. This is in agreement with the tetragonal structure proposed by Markstein *et al.*[2]

SELECTION RULES

The free $SnBr_6^{2-}$ ion belongs to the point group O_h (Ref. 9) and the normal vibrations may be classified as follows (Table 1): $A_{1g} + E_g + F_{2g} + 2F_{1u} + F_{2u}$.

The X-ray investigation indicates, that the deviation from cubic symmetry is small. If it is assumed that the crystalline compound from a spectroscopic point of view can be treated as cubic, as done by Debeau *et al.*,[4,5] the space

group $Fm3m = O_h^5$ and a primitive unit cell containing one formula unit have to be used. In cubic K_2SnBr_6 the complex ion occupies a site with O_h symmetry and the two K^+ ions are situated at a pair of sites with T_d symmetry.[10] Figs. 1 and 2 show parts of the correlation diagrams for cubic potassium hexabromostannate.

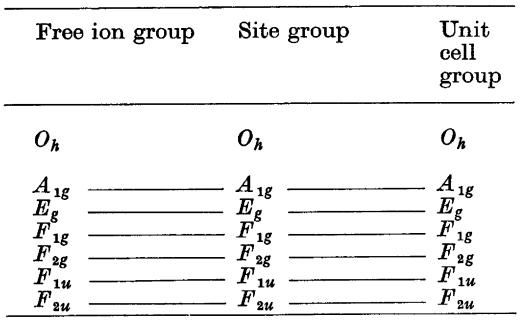

Fig. 1. Correlation diagram for the $SnBr_6^{2-}$ ion in the cubic structure.

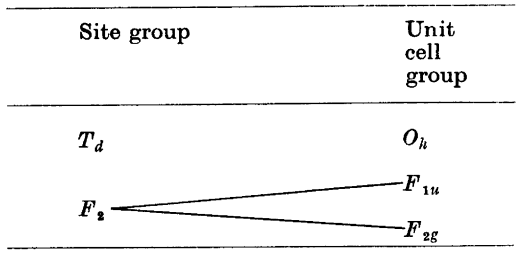

Fig. 2. Correlation diagram for the K^+ ions in the cubic structure.

It can be seen from the correlation diagrams, that the internal and external vibrations, respectively, may be classified as follows: $A_{1g} + E_g + F_{2g} + 2\ F_{1u} + F_{2u}$ and $F_{1g} + F_{2g} + F_{1u}$. Modes of the symmetry species A_{1g}, E_g, and F_{2g} are allowed in the Raman spectrum. Hence observation of three internal and one external vibration in the Raman spectrum of cubic potassium hexabromostannate can be expected.

However, the selection rules given above can only be expected to be valid above 126.5 °C. At room temperature the compound should be treated as tetragonal with space group $P42_12 = D_4^2$ and with two formula units in the primitive unit cell. In tetragonal K_2SnBr_6 the two complex

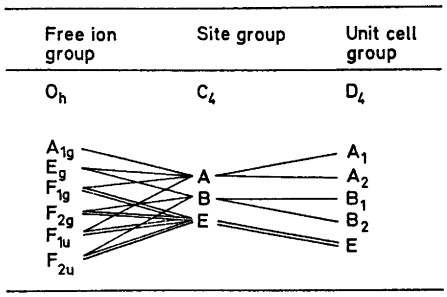

Fig. 3. Correlation diagram for the $SnBr_6^{2-}$ ion in the tetragonal structure.

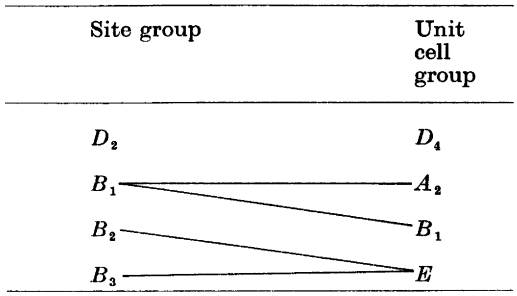

Fig. 4. Correlation diagram for the K^+ ions in the tetragonal structure.

ions occupy a pair of sites with C_4 symmetry and the four K^+ ions are situated on sites with D_2 symmetry.[10] Figs. 3 and 4 show the necessary part of the correlation diagrams for tetragonal potassium hexabromostannate.

From the correlation diagrams it can be seen that the internal and external vibrations, respectively, may be classified as follows: $4A_1 + 4A_2 + 3B_1 + 3B_2 + 8E$ and $2A_1 + 3A_2 + 2B_1 + 7E$. Here modes of the symmetry species A_1, B_1, B_2, and E are allowed in the Raman spectrum.

This means that the Raman spectrum should consist in not more than 18 components of the internal vibrations and 11 external vibrations. Because the deviation from cubic symmetry is small it is assumed that the splitting in the internal vibrations caused by the dynamic coupling is small, if observed at all. As a consequence of these selection rules all the fundamentals of the complex ion are allowed in the Raman spectrum, but it is expected, that the intensity of the vibrations, which are forbidden in the cubic case, will be weak.

Table 1. Observed Raman spectra.

Internal vib.	Free ion [9]	Crystals $T \sim -178$ °C		$T \sim 20$ °C		$T \sim 140$ °C	
	ν cm^{-1}	ν cm^{-1}	rel. int.	ν cm^{-1}	rel. int.	ν cm^{-1}	rel. int.
ν_1 (A_{1g}) [a]	184	190	vs	190	vs	188	vs
ν_2 (E_g)	140	144	s	144	s	142	m
ν_3 (F_{1u})	–	–	–	–	–	–	–
ν_4 (F_{1u}	–	116	(sh)	–	–	–	–
ν_5 F_{2g}	101	110	s	109	s	106	m
ν_6 F_{2u}	–	–	–	–	–	–	–
External vib.							
	–	88	w	~82	w(sh)	–	–
	–	80	w	–	–	–	–
	–	75	w(sh)	–	–	–	–
	–	57	vw	–	–	–	–
	–	47	w	41	vw	–	–
	–	33	w	23	w	–	–

[a] The symmetry species given in the table refer to the assignment of the free ion fundamentals.

OBSERVED RAMAN SPECTRA

The observed bands in the Raman spectra of potassium hexabromostannate at three different temperatures and the wavenumbers of the Raman active vibrations of the free ion are given in Table 1.

The wavenumbers of the internal vibrations at room temperature found in this investigation agree with the wavenumbers given by Debeau *et al.*[4,5] Furthermore three bands are observed in the spectrum which are assigned to external vibrations. This agrees with the tetragonal and not the cubic structure at room temperature. These three bands have not been reported by Debeau *et al.*[4,5] The fact that no splitting of the internal vibrations or any of the ungerade vibrations are observed agrees with the assumption of small coupling, even though the deviation from cubic symmetry is obvious because there is observed more than one external vibration.

The Raman spectrum at low temperature shows, as expected, no appreciable wavenumber shift concerning the internal vibrations. The band at 116 cm^{-1} is assigned to a component of ν_4 rather than of ν_5 because ν_4 is found at 118 cm^{-1} in the infrared spectrum of the compound [4,5] and because there is not observed more than one component of the other internal vibrations.

At low temperature the half-width of the bands is expected to diminish and it may then be possible to observe very weak bands which cannot be observed at room temperature or which may be covered by other bands with a large half-width. Furthermore a shift towards higher wavenumber is expected for the external vibrations at low temperature. The observation of six external vibrations at -178 °C is in accordance with these assumptions.

Galloni *et al.*[3] have reported that potassium hexabromostannate has no phase transitions between -80 and 126.5 °C, but transitions below -80 °C cannot be excluded. However, the observation of six external vibrations and a component of ν_4 is in accordance with the tetragonal structure.

When the compound is heated the external vibrations can be followed to approximately 110 °C. At higher temperatures only the internal vibrations can be observed. This is in accordance with the phase transition from tetragonal to cubic symmetry at 126.5 °C observed by Galloni *et al.*,[3] but could also be due to line broadening.

POLARIZED RAMAN SPECTRA

Polarized spectra of orientated crystals have been recorded at room temperature and at about 140 °C.

The X-ray investigation showed that the crystallographic axes pass through the corners of the crystal. To avoid rotation of the polariza-

tion direction of the exciting beam when it enters the crystal, faces were polished parallel to the (100), (010), and (001) planes. In some cases these faces have already been developed under the crystal growth. All measurements were carried out with scattered light of the same polarization achieved by mounting a half-wave plate between the analyzer and the entrance slit.

For tetragonal potassium hexabromostannate single crystals, it can be seen from the character table of the unit cell group, that fundamentals of the symmetry species A_1, B_1, B_2, and E should be observed only in polarized spectra of the types (XX), (YY), (ZZ)−(XX), (YY)−(XY) and (YZ), respectively.

Polarized spectra of the types listed above were recorded at room temperature, but no changes of wavenumber or intensity of any bands were observed in comparison with spectra of polycrystalline samples.

This means that the crystal, though it looks like a single crystal, must be considered as a kind of polysynthetic twin consisting of domains which build up the crystal with random distribution of the a and c axes in a given direction. Above the phase transition temperature at 126.5 °C one can imagine that the crystal will act like a genuine single crystal because the axial ratio then will be exactly 1. If this is the case it should be possible to obtain polarized spectra above this temperature.

For cubic single crystals it can be seen from the character table of the unit cell group, that fundamentals of the symmetry species A_{1g} and E_g should be observed in polarized spectra of the type (ii), i=X, Y, Z and fundamentals of the F_{2g} species should be observed in polarized spectra of the type (ij), $i \triangle j$=X, Y, Z, $i \neq j$.

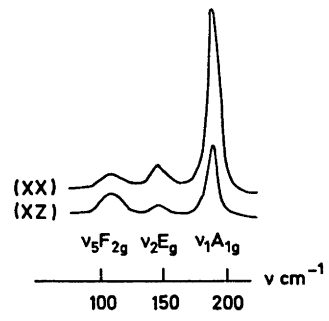

Fig. 5. Polarized Raman spectra of K_2SnBr_6 at 140 °C.

Table 2. Intensity ratios in the polarized Raman spectra.

	$\frac{\nu_5}{\nu_2}$	$\frac{\nu_5}{\nu_1}$	$\frac{\nu_2}{\nu_1}$
(XX)	$\frac{0.84}{1}$	$\frac{0.10}{1}$	$\frac{0.12}{1}$
(XZ)	$\frac{3.52}{1}$	$\frac{0.42}{1}$	$\frac{0.13}{1}$

The polarized Raman spectra of the two types are sketched in Fig. 5, and in Table 2 are given the relative intensity ratios between the lines.

Though it was not possible to obtain complete extinction of the contribution to the detected light intensity from the vibrations in a forbidden species, the spectra strongly indicate that the crystal behaves like a single crystal with cubic symmetry above the transition temperature. It is evident that ν_1 and ν_2 follow each other in intensity and have their largest intensity in the (XX) spectra. This is in accordance with the assignment of ν_1 and ν_2 to the A_{1g} and E_g symmetry species, respectively. Moreover ν_5 clearly separates from ν_1 and ν_2 and its intensity is approximately four times larger in polarized spectra of the (XZ) type than in polarized spectra of the (XX) type measured relative to ν_1 and ν_2 (Table 2). This agrees with the assignment of ν_5 to the F_{2g} symmetry species.

Upon repeated temperature cycling over the phase transition point the crystal has returned to the initial state with respect to spectra and with respect to the single crystal/twin transformation. This indicates that the transition is reversible.

CONCLUSION

All the lines in the Raman spectra of potassium hexabromostannate at room temperature and at −178 °C can be explained by assuming tetragonal crystal symmetry with space group D_4^2. At 140 °C the lines can be explained by assuming cubic symmetry with space group O_h^5. The phase transition at 126.5 °C observed by Galloni *et al.*[3] is confirmed by the Raman spectra and

found to be reversible. Furthermore, there is some evidence that the crystal is a polysynthetic twin below the transition temperature and behaves as a single crystal above this temperature.

Acknowledgements. The author is greatly indebted to Professor C. Knakkergaard Møller for his guidance with the X-ray investigations of the crystals and for many stimulating discussions, and to Dr. P. Waage-Jensen for many helpful discussion and advice.

REFERENCES

1. Ketelaar, A. A., Rietdijk, A. A. and van Stavern, C. H. *Rec. Trav. Chim. Pays-Bas 56* (1937) 907.
2. Markstein, G. and Nowotny, H. *Z. Kristallogr. 100* (1938) 265.
3. Galloni, E. E., de Benyacar, M. R. and de Abeledo, M. J. *Z. Kristallogr. 117* (1962) 470.
4. Debeau, M. and Poulet, H. *Spectrochim. Acta A 25* (1969) 1553.
5. Debeau, M. and Krauzman, M. *C. R. Acad. Sci. B 264* (1967) 1724.
6. Greenwood, N. N. and Straughan, B. P. *J. Chem. Soc. A* (1966) 962.
7. Brown, D. H., Dixon, K. R., Livingston, C. M., Nuttall, R. H. and Sharp, D. W. A. *J. Chem. Soc. A* (1967) 100.
8. Nakamura, D., Ito, K. and Kubo, M. *Inorg. Chem. 1* (1962) 592.
9. Woodward, L. A. and Anderson, L. E. *J. Chem. Soc.* (1957) 1284.
10. Wyckoff, R. W. G. *Crystal Structures*, Wiley, New York 1965, Vol. 3, pp. 339, 344.

Received June 4, 1974.

Acta Chemica Scandinavica A 28 (1974) 979—985

Thermodynamics of Metal Complex Formation in Aqueous Solution. VIII. A Calorimetric Study of the Mercury(II) Thiocyanate, Selenocyanate, and Thiosulfate Systems

LENNART KULLBERG

Inorganic Chemistry 1, Chemical Center, University of Lund, P.O.B. 740, S-220 07 Lund 7, Sweden

The enthalpy changes for the formation of $Hg(SCN)_4^{2-}$, $Hg(SeCN)_4^{2-}$, and $Hg(S_2O_3)_3^{4-}$ have been determined calorimetrically by measuring the heats of solution of HgO in solutions of perchloric acid, thiocyanate, selenocyanate, and thiosulfate. From the enthalpy changes measured, and the free energy changes computed from the stability constants, the entropy changes have been calculated. All data refer to 25.0 °C.

The enthalpy changes for the three reactions studied are all highly exothermic. The entropy terms are rather small. For the thiosulfate system the entropy term is positive while those of the thiocyanate and selenocyanate systems are negative and consequently counteracting the complex formation.

In order to compare the coordinating properties of the analogous ligands thiocyanate and selenocyanate, their complexes with the divalent ions of electron configuration d^{10}, *viz.* Zn^{2+}, Cd^{2+}, and Hg^{2+} have been investigated.[1,2] These ions show a large variation in their bonding properties, from the distinctly hard Zn^{2+} to the very soft Hg^{2+}. Results pertaining to the thiocyanate complexes of Zn^{2+}, Cd^{2+}, and Hg^{2+} and the selenocyanate complexes of Zn^{2+} and Cd^{2+} have already been reported.[1,2] The free energy changes, ΔG°_j, have been computed from the stability constants while the enthalpy changes, ΔH°_j, have been measured with a titration calorimeter. Finally, the entropy changes, ΔS°_j, have been obtained from the relation

$$\Delta G^\circ_j = \Delta H^\circ_j - T\Delta S^\circ_j \qquad (1)$$

The mercury(II) selenocyanate system could not be investigated in the same manner as the corresponding zinc and cadmium systems, because of the rather strong acidic properties of Hg^{2+}.[3] In solutions acid enough to suppress the hydrolysis of Hg^{2+}, the selenocyanate ion disintegrates rapidly. In order to ensure the stability of $SeCN^-$, the pH must in fact be $\gtrsim 5$.[4]

As the complex formation proceeds, however, the acidity of the mercury(II) species rapidly decreases so that the higher complexes $Hg(SeCN)_3^-$ and $Hg(SeCN)_4^{2-}$ seem to be stable in solution. This fact was utilized in the present investigation.

A stable mercury(II) selenocyanate solution was prepared by dissolving HgO in a selenocyanate solution strong enough to ensure the complete formation of the final complex $Hg(SeCN)_4^{2-}$.[5,6] The enthalpy change, $\Delta H^\circ_{\beta_4}$, for the reaction, $Hg^{2+} + 4SeCN^- \rightarrow Hg(SeCN)_4^{2-}$, has been determined by measuring the heats of solution of HgO in selenocyanate and perchloric acid solutions. By combination of these enthalpy changes with the heat of neutralisation, $\Delta H^\circ_{\beta_4}$ can be computed.

The enthalpy changes, ΔH°_j, for the formation of mercury(II) thiocyanate complexes have previously been determined calorimetrically by the well-established titration technique.[1] In order to check the reliability of the method of dissolution used in this study, the value of $\Delta H^\circ_{\beta_4}$ has been redetermined by measuring the heat of solution of HgO in excess thiocyanate solution.

Another interesting sulfur donor, *viz.* the thiosulfate ion, $S_2O_3^{2-}$, also forms strong complexes with Hg^{2+}.[7,8] Like the selenocyanate ion,

the thiosulfate ion disintegrates in acidic solution [9] and an investigation of its mercury(II) complexes therefore poses the same difficulties. The stability constants for the formation of the second and third complexes have nevertheless been determined [7,8] but no determination of the enthalpy changes seems to have been reported so far. By measuring the heats of solution of HgO in acid as well as in thiosulfate solution, the enthalpy change for the formation of the highest complex formed, $Hg(S_2O_3)_3^{4-}$, has been obtained.

All measurements in this study have been performed at 25.00 °C in an aqueous medium of ionic strength $I = 1.00$ (0.30) M with sodium perchlorate as supplementary electrolyte. The lower ionic strength was used for some measurements in the selenocyanate system.

CALCULATIONS

The enthalpy changes, ΔH_A and ΔH_B, for the following two reactions were experimentally determined

$$HgO(s) + 2H_3O^+ \rightarrow Hg^{2+} + 3H_2O \quad (A)$$

$$HgO(s) + j\ L^{n-} \rightarrow HgL_j^{2-jn} + 2OH^- \quad (B)$$

where HgL_j^{2-jn} denotes the saturated mercury(II) complex, which under the experimental conditions is formed quantitatively.

The enthalpy change ΔH_C of the reaction

$$H_3O^+ + OH^- \rightarrow 2H_2O \quad (C)$$

in a perchlorate medium of $I = 1.00$ M has been found to be -56.11 kJ mol^{-1}.[10] The enthalpy change, ΔH_D, of the complex formation reaction

$$Hg^{2+} + j\ L^{n-} \rightarrow HgL_j^{2-nj} \quad (D)$$

is

$$\Delta H_D = \Delta H_B - \Delta H_A + 2\Delta H_C \quad (2)$$

All uncertainty intervals given for ΔH in this paper are three standard deviations of the mean, $3[\sum \delta^2/n(n-1)]^{\frac{1}{2}}$.

EXPERIMENTAL

Chemicals. Red *mercury(II) oxide* in the form of a fine powder (Mallinckrodt Analytical Reagent) was used without further purification. Its purity was checked by means of an X-ray powder photograph. *Sodium thiosulfate* stock solutions were prepared from Merck reagent grade crystals and redistilled water. In order to prevent decomposition of thiosulfate Na_2CO_3 (0.2 %) was added to the $Na_2S_2O_3$ solutions. *Potassium selenocyanate* solutions were prepared from the B.D.H. Analytical Reagent, which was used without further purification. *Sodium thiocyanate* and *sodium perchlorate* solutions were prepared and analyzed as before.[1]

Calorimetric apparatus and procedure. The thermochemical measurements were carried out in a reaction solution calorimeter of the isothermal jacket type described by Sunner and Wadsö.[11] The calorimeter consists of an outer chromium plated brass can and a 90 cm^3 inner reaction vessel made of glass. This reaction vessel contains a 2 000 Ω thermistor temperature sensor, a 20 Ω manganin wire heater and a combined stirrer-ampoule holder. The calorimeter in its jacket was completely immersed in a water thermostat maintained at 25.000 ± 0.001 °C. The Wheatstone bridge used for determining the change in resistance of the thermistor and the calibration unit were the same as used previously.[12]

In the main experiments HgO (0.10 – 0.50 g) was weighed into an ampoule. Standard LKB ampoules made of thin-walled Pyrex glass were used. After filling, the ampoules were sealed by closing the ampoule shaft with a tightly fitting silicon rubber stopper which then was covered with a thin layer of microwax. The sealed ampoule was put into the calorimeter where it was held by a four-pronged stirrer which could be lowered to break the ampoule on a sapphire tipped metal pin without interrupting the stirring. The reaction vessel filled with 80.0 ml of a solution was placed in the calorimeter and the temperature was brought to just under 25 °C. It was then sealed in its jacket and immersed in the 25.00 °C thermostat. By stirring the solution in the reaction vessel a smooth increase of its temperature was obtained. As the reactions were slow it was difficult to obtain a linear after-period, but an acceptable linearity could nevertheless be achieved if the ampoule breaking was initiated at such a temperature as to give an almost constant final temperature. However, the deviation of the mean temperature of the experiment from 25.00 °C was never larger than 0.02 °C. Electrical calibrations were made over the same temperature range as in the main experiment.

The temperature change obtained in a calibration was measured with an estimated precision corresponding to ± 0.03 J. In the main experiments the precision was generally somewhat lower due to the lengthy extrapolations of the temperature-time curve necessitated by the fairly slow dissolution reactions.

Testing of the calorimeter. To test the overall performance of the calorimeter, the enthalpy of solution of tris(hydroxymethyl)aminomethane, THAM, in 0.1 M HCl was measured. The result should be representative for rapid, moderately exothermic reactions.[13] Varying amounts of

THAM (0.20 – 0.30 g) were dissolved in 80.0 cm^3 0.1000 M HCl. The mean value of $-\Delta H$ was (29.83 ± 0.09) kJ mol^{-1} which is in good agreement with previously reported values. The 'best' value has been given as $-\Delta H = 29.75$ kJ mol^{-1}.[14]

MEASUREMENTS AND RESULTS

For the determination of the enthalpy change ΔH_A, (p. 983), the heats evolved on dissolution of varying amounts (0.25 – 0.40 g) of HgO in 1.00 M $HClO_4$ were measured. The amounts of HgO used were completely dissolved within about 20 min. The results are given in Table 1.

Mercury(II) thiocyanate. Varying amounts (0.28 – 0.36 g) of mercury(II) oxide were dissolved in 1.00 M NaSCN. The value of ΔH_B found is independent of the amount of HgO used, Table 2. At the prevailing [SCN^-] all mercury(II) certainly exists as the complex $Hg(SCN)_4^{2-}$.[15] From eqn. (2), a value of the enthalpy change, $\Delta H_D = \Delta H_{\beta_4} = (-145.3 \pm 0.8)$ kJ mol^{-1} is found for the formation of the fourth mercury(II) – thiocyanate complex. From the value of β_4 found by Ciavatta and Grimaldi [15] for the same medium and temperature the value of $\Delta G°_{\beta_4}$ entered in Table 4 has been calculated and finally, by combining $\Delta H°_{\beta_4}$ and $\Delta G°_{\beta_4}$, also the value of $\Delta S°_{\beta_4}$.

Mercury(II) selenocyanate. Varying amounts of HgO were dissolved in 1.00 M KSeCN, Table 2. In all previous experiments a sodium ion medium has been used but in the present case the potassium ions were kept, as an exchange causes some disintegration of selenocyanate resulting in a very undesirable formation of cyanide, as discussed below. No significant difference in the enthalpy changes is to be expected between a potassium and a sodium ion medium.

Table 1. Heat of solution of HgO in 80.0 cm^3 1.00 M $HClO_4$.

mg of HgO	Q/J	$-\Delta H_A$ / kJ mol^{-1}
30.84	3.230	22.7
33.33	3.512	22.8
24.06	2.486	22.4
40.58	4.300	23.0
35.64	3.805	23.1
	Mean value	22.8 ± 0.4

Table 2. Heat of solution of HgO in thiocyanate and selenocyanate solutions.

C_L/M	mg of HgO	Q/J	$-\Delta H_B$ / kJ mol^{-1}
SCN^-			
1.00	34.55	8.901	55.8
1.00	36.48	9.324	55.4
1.00	28.27	7.253	55.6
1.00	34.59	9.004	56.4
1.00	32.45	8.419	56.2
		Mean value	55.9 ± 0.5
$SeCN^-$			
1.00	27.59	13.175	103.4
1.00	46.78	22.468	104.0
1.00	38.58	18.339	103.0
1.00	57.23	26.904	101.8
1.00	32.83	15.754	103.9
		Mean value	103.2 ± 1.2
0.30	23.58	11.105	102.0
0.30	30.35	14.361	102.5
0.30	17.22	7.918	99.6
		Mean value	101.4 ± 2.7

Table 3. Heat of solution of HgO in sodium thiosulfate solutions.

C_L/mM	mg of HgO	Q/J	$-\Delta H_B$ / kJ mol^{-1}
335	28.88	9.524	71.4
335	34.89	11.469	71.2
335	31.79	10.386	70.8
335	32.28	10.540	70.7
170	17.67	5.788	71.0
170	13.07	4.420	73.2
170	24.31	8.212	73.2
85	17.64	5.707	70.1
85	24.15	7.808	70.0
85	18.14	6.114	73.0
		Mean value	71.5 ± 1.2

Selenocyanate solutions always contain impurities of cyanide ions. As the mercury(II) – cyanide system is much stronger than the corresponding selenocyanate system [5,16] and as moreover the selenocyanate is used in large excess over mercury(II), even a very small amount of cyanide ions in the selenocyanate solution may give quite erroneous results. The cyanide will react with mercury(II) before the reaction between mercury(II) and selenocyanate starts.

Table 4. The stability constants used and the computed values of $\Delta G°_j$, $\Delta H°_j$, and $\Delta S°_j$ for the overall formation of $Hg(SCN)_4^{2-}$, $Hg(SeCN)_4^{2-}$, and $Hg(S_2O_3)_3^{4-}$.

Ligand j	SCN^- 4	SCN^- 4	$SeCN^-$ 4	$S_2O_3^{2-}$ 3
β_j/M^{-j}	$(4.7 \pm 0.3) \times 10^{21a}$	$(4.7 \pm 0.3) \times 10^{21a}$	54×10^{28b}	1.8×10^{33c}
$-\Delta G°_j$ / kJ mol^{-1}	123.7 ± 0.2	123.7 ± 0.2	164.0	190.0
$-\Delta H°_j$ / kJ mol^{-1}	145.3 ± 0.8^d	141.6 ± 1.3^e	192.6 ± 1.5	160.9 ± 1.5
$\Delta S°_j$ / J mol^{-1}K^{-1}	-72 ± 4	-60 ± 5	-96 ± 5^f	98 ± 6^f

[a] From Ref. 15. [b] From Ref. 5. [c] From Ref. 7. [d] This study. [e] From Ref. 1. [f] The error limits of $\Delta S°_j$ are calculated from the error limits of $\Delta H°_j$ only, as those of β_j ($\Delta G°_j$) are not stated in Ref. 5 and Ref. 7. However, the error limits of $\Delta G°_j$ are generally small in comparison to those of $\Delta H°_j$.

This reaction is considerably more exothermic than the formation of the selenocyanate complexes.[5,16] By dissolving various amounts of HgO in a selenocyanate solution different values of the heats of solution, ΔH_B, should therefore be obtained if cyanide ions were present. Such a test has been performed. From a plot of ΔH_B *versus* the amount of HgO used the concentration of cyanide was found to be ≈ 0.2 % of that of selenocyanate. In order to eliminate this source of error, a small amount of mercury(II) (≈ 5 mM) was added to the 1.00 M selenocyanate solutions before they were used for the main experiments. In this way all free cyanide ions were removed by complex formation. The mercury(II) had to be added to the selenocyanate solutions just before use as mercury(II) selenocyanate, at too high concentrations, disintegrates on standing giving a black precipitate, probably of elemental selenium. In cases where large amounts of HgO were dissolved in selenocyanate the same precipitate was observed after the reaction also in the main experiments. As the temperature varied quite normally during the after periods, however, this slight precipitation is not likely to introduce any errors. The results are given in Table 2. No variation of ΔH_B with the amount of HgO is found which proves that no free cyanide ions were present in the selenocyanate solutions used. Toropova [5] has studied the mercury(II) – selenocyanate system potentiometrically at 25 °C. Thus for the formation of the fourth mercury(II) – selenocyanate complex she found $-\Delta G°_{\beta_4} = 164.0$ and 164.9 kJ mol^{-1} for $I = 0.8$ and 0.3 M, respectively. From the stability constants it is evident that in the present solutions all mercury(II) exists in the form of $Hg(SeCN)_4^{2-}$. From eqn. (2) the enthalpy change for the formation of the fourth mercury(II) selenocyanate complex is found as $-\Delta H°_{\beta_4} = (192.6 \pm 1.5)$ kJ mol^{-1}. Assuming $\Delta G°_{\beta_4}$ has the same value at $I = 1.0$ M as at $I = 0.8$ M, the entropy change, $\Delta S°_{\beta_4}$, has been obtained from eqn. (1), Table 4.

Some experiments were performed at lower selenocyanate concentration and ionic strength. Varying amounts of HgO were dissolved in a 0.300 M KSeCN solution, Table 2. As before, mercury(II) ($C_{Hg} = 1.5$ mM) was added to the selenocyanate solutions in order to remove free cyanide ions. In these experiments no precipitate of selenium was observed. Due to the low selenocyanate concentration it took a fairly long time (≈ 20 min) to dissolve the HgO, which detracts from the precision of the determination. The mean value of $-\Delta H_B = (101.4 \pm 2.7)$ kJ mol^{-1} evidently agrees with that found at $I = 1.0$ M which shows that the slight disintegration taking place at the higher concentration is of no importance. Moreover the same mercury species, $Hg(SeCN)_4^{2-}$, evidently predominates at both the selenocyanate concentrations used.

Mercury(II) thiosulfate. Varying amounts of HgO were dissolved in thiosulfate solutions of unit ionic strength. The measurements were

performed at three different thiosulfate concentrations, *viz.* 85, 170, and 335 mM, Table 3. At the lowest concentration used it took up to 30 min to dissolve the oxide. The stability constants of the mercury(II) – thiosulfate system have been determined polarographically at 25 °C at $I = 1.0$ M by Nyman and Salazar [7] and at $I = 0.2$ M by Murayama *et al.*[8] They agree that the third complex, $Hg(S_2O_3)_3^{4-}$, predominates at the concentrations used in the present measurements. Within the limits of error, the same value of ΔH_B is found for the three thiosulfate concentrations used, Table 3. This proves that within the range of concentrations used all mercury(II) exists in the same form, $Hg(S_2O_3)_3^{4-}$. As the third stepwise stability constant, K_3, is much lower than the first two it is plausible that the third step is accompanied by a much smaller heat change than the first two. Thus even if some of the mercury(II) should exist in the form of the second complex, $Hg(S_2O_3)_2^{2-}$, it should not change the value of ΔH_B noticably. The mean value of ΔH_B is (-71.5 ± 1.2) kJ mol^{-1} and hence $\Delta H°_{\beta_3} = (-160.9 \pm 1.5)$ kJ mol^{-1} for the formation of the third mercury(II) – thiosulfate complex. The value of $\Delta G°_{\beta_3}$ was calculated from $\beta_3 = 1.8 \times 10^{33}$ M^{-3} found by Nyman and Salazar, and finally $\Delta S°_{\beta_3}$ according to eqn. (1). The results are given in Table 4.

DISCUSSION AND CONCLUSIONS

Shchukarev *et al.*[17] have determined ΔH_A for the solution of yellow HgO in perchloric acid of different concentrations at 25 °C. For an acid concentration of 1.1 M they found $\Delta H_A = -22.80$ kJ mol^{-1}, in very good agreement with the present value $\Delta H_A = -22.8$ kJ mol^{-1}, for the solution of red HgO in 1.0 M $HClO_4$. This is expected as the heat of transformation between yellow and red HgO is small.[18]

For the mercury thiocyanate system the value of $-\Delta H°_{\beta_4} = (145.3 \pm 0.8)$ kJ mol^{-1} found here agrees satisfactorily with the value $-\Delta H°_{\beta_4} = (141.6 \pm 1.3)$ kJ mol^{-1} obtained by means of titration calorimetry in a previous study.[1] This shows that the method of determining enthalpy changes used in this study works satisfactorily.

For the mercury(II) – selenocyanate system Toropova [5] has determined $\Delta H°_{\beta_4}$ from the variation of β_4 with T in the temperature interval $15 < T < 30$ °C. Within the error limits the result, $-\Delta H°_{\beta_4} = (195 \pm 5)$ kJ mol^{-1}, is in accord with that found in this study, Table 4.

Thiocyanate and selenocyanate are ambidentate ligands, coordinating *via* S or Se, respectively, or *via* N. Coordination *via* S and Se is preferred by soft acceptors, while hard ones prefer the harder N. Selenium donors are moreover found to be softer than analogous sulfur donors [19] and should therefore give stronger complexes with soft acceptors. If an acceptor is coordinated *via* S and Se, the selenocyanate complexes should therefore be stronger than the thiocyanate ones and moreover formed in considerably more exothermic reactions.[20] The entropy terms should be of minor importance and of the same order of magnitude for the two ligands.[2] If, on the other hand, the N atoms are coordinated, the strength of the thiocyanate and selenocyanate complexes should be much the same. In this case the bonds formed will be less covalent and consequently the reactions much less exothermic than in the case of S or Se coordination. The bonds formed will be little influenced by an exchange of S for Se and much the same value of $\Delta H°_j$ should therefore be expected for thiocyanate and selenocyanate complexes. Theoretical calculations [21] further indicate that coordination *via* N would bring about a larger decrease of charge on S than on Se, resulting in a larger gain of entropy in the former case. Coordination *via* N would thus entail a more positive or less negative entropy change for thiocyanate than for selenocyanate complexes.

For mercury(II) the selenocyanate complexes are considerably stronger than the thiocyanate complexes due to a much more negative value of $\Delta H°_{\beta_4}$, Table 4. For both systems the reactions are highly exothermic. The entropy terms are of the same magnitude and counteracting the complex formation. The results thus confirm the views expressed previously [22] that mercury(II) is coordinated to the selenocyanate and thiocyanate ions *via* the soft Se and S atoms, respectively.

In the case of Cd^{2+}, the selenocyanate complexes are again stronger than the thiocyanate complexes and moreover formed in more exothermic reactions while the entropy terms are of the same magnitude for the two systems.[2]

This indicates that also the borderline acceptor Cd^{2+}, at least partly, coordinates the ligands *via* the softer S and Se atoms, respectively. The covalent bonds formed are obviously much weaker than those formed by Hg^{2+}, however.

The thiocyanate and selenocyanate complexes of Zn^{2+} are quite weak, the latter being the weaker of the two.[2] The values of ΔH°_1 are slightly exothermic and of the same order of magnitude for both systems while the value of ΔS°_1 is less negative for thiocyanate. This strongly indicates coordination *via* N for both systems.

Following the general rule, the coordination of both thiocyanate and selenocyanate thus becomes more exothermic the softer the acceptor. Especially the difference between the very soft Hg^{2+} and the borderline acceptor Cd^{2+} is, as expected, very large. However, the difference between Cd^{2+} and the hard acceptor Zn^{2+} is also quite significant.

During the course of formation of zinc and cadmium selenocyanate complexes changes of coordination figure probably occur,[2] involving a switch from the octahedral aquo ions of Zn^{2+} and Cd^{2+} to the tetrahedral coordination represented by the final complexes $Zn(SeCN)_4^{2-}$ and $Cd(SeCN)_4^{2-}$, respectively. The switch causes an irregular variation of ΔS°_j between the consecutive steps and the trend is moreover quite different for the thiocyanate and the selenocyanate systems. As may be expected, however, the values of ΔS°_j are small and negative and generally more negative the softer the acceptor.[20]

For the mercury(II) – thiosulfate system the value of $\Delta H^\circ_{\beta_3}$ is, as expected for a sulfur donor, strongly exothermic, Table 4. The entropy term, $\Delta S^\circ_{\beta_3} = 98$ kJ mol^{-1} K^{-1}, is also contributing to the strong complex formation. For the thiocyanate and selenocyanate systems of mercury(II) the entropy terms, $\Delta S^\circ_{\beta_4}$, are negative, Table 4. The large differences between the entropy terms of the thiosulfate system on the one hand and the thiocyanate and selenocyanate systems on the other are explained by the difference in charge of the ligands. The divalent thiosulfate ion is certainly more structure-ordering than the monovalent thiocyanate and selenocyanate ions. Thus coordination of $S_2O_3^{2-}$ causes a more extensive structural breakdown resulting in the liberation of more water and consequently in a more positive value of the entropy term.

Schwarzenbach and Schellenberg [24] have determined the thermodynamic parameters for the reaction $CH_3Hg^+ + S_2O_3^{2-} \rightarrow CH_3HgS_2O_3^-$ at 20 °C and $I = 0.1$ M. They found $-\Delta H^\circ_1 = 61$ kJ mol^{-1} and $\Delta S^\circ_1 = 41$ J mol^{-1}K^{-1}. These values are quite in line with those of $\Delta H^\circ_{\beta_3}$ and $\Delta S^\circ_{\beta_3}$ found for the mercury(II) – thiosulfate system.

Acknowledgements. I am most grateful to Professor Sten Ahrland for stimulating discussions and many valuable suggestions. I also wish to thank Professor Sture Fronæus for his kind interest and for the facilities he has put at my disposal.

REFERENCES

1. Ahrland, S. and Kullberg, L. *Acta Chem. Scand. 25* (1971) 3692.
2. Ahrland, S., Avsar, E. and Kullberg, L. *Acta Chem. Scand. A 28* (1974) 855.
3. Perrin, D. D. *Dissociation Constants of Inorganic Acids and Bases in Aqueous Solution*, Butterworth, London 1969.
4. Golub, A. M. and Skopenko, V. V. *Russ. Chem. Rev. 34* (1965) 901.
5. Toropova, V. F. *Zh. Neorg. Khim. 1* (1956) 243.
6. Murayama, T. and Takayanagi, A. *Bull. Chem. Soc. Jap. 45* (1972) 3549.
7. Nyman, C. J. and Salazar, T. *Anal. Chem. 33* (1961) 1467.
8. Murayama, T., Sawaki, T. and Sakuraba, S. *Bull. Chem. Soc. Jap. 43* (1970) 2820.
9. Sidgwick, N. V. *The Chemical Elements and Their Compounds*, Oxford 1950, Vol. II, p. 918.
10. Vasilev, V. P. and Lobanov, G. A. *Izv. Vyssh. Ucheb. Zaved. Khim. Khim. Tekhnol. 12* (1969) 740.
11. Sunner, S. and Wadsö, I. *Science Tools 13* (1966) 1.
12. Ahrland, S. and Kullberg, L. *Acta Chem. Scand. 25* (1971) 3471.
13. Irwing, R. J. and Wadsö, I. *Acta Chem. Scand. 18* (1964) 195.
14. Hill, J. O., Öjelund, G. and Wadsö, I. *J. Chem. Thermodyn. 1* (1969) 11.
15. Ciavatta, L. and Grimaldi, M. *Inorg. Chim. Acta 4* (1970) 312.
16. Christensen, J. J., Izatt, R. M. and Eatough, D. *Inorg. Chem. 4* (1965) 1278.
17. Shchukarev, S. A., Lilich, L. S., Latysheva, V. A. and Andreeva, D. K. *Russ. J. Inorg. Chem. 4* (1959) 1001.
18. Aurivillius, K. and von Heidenstam, O. *Acta Chem. Scand. 15* (1961) 1993.

19. Ahrland, S. *Proc. XIV Int. Conf. Coord. Chem.*, Toronto 1972, p. 185.
20. Ahrland, S. *Struct. Bonding 5* (1968) 118.
21. Wagner, E. L. *J. Chem. Phys. 43* (1965) 2728.
22. Bailey, R. A., Kozak, S. L., Michelsen, T. W. and Mills, W. N. *Coord. Chem. Rev. 6* (1971) 407.
23. Ahrland, S. *Helv. Chim. Acta 50* (1967) 306.
24. Schwarzenbach, G. and Schellenberg, M. *Helv. Chim. Acta 48* (1965) 28.

Received April 9, 1974.

Acta Chemica Scandinavica A 28 (1974) 986—988

The Gibbs Free Energy of Formation of Y_2O_3 in the Temperature Region 1000—1150 K

G. H. BØE and E. MORRICE

Department of Inorganic Chemistry, The University of Trondheim, The Norwegian Institute of Technology, and U.S. Bureau of Mines, Reno Metallurgy Research Center, Reno, Nevada, U.S.A.

The Gibbs free energy of formation of Y_2O_3 ($\Delta G^\circ_{Y_2O_3}$) has been measured in the temperature region 1000 – 1150 K, and compared with literature values.[1,2] The experiments give values for $\Delta G^\circ_{Y_2O_3}$ below the values given in the literature.[1,2]

Compilations of the Gibbs free energy of formation of Y_2O_3[1,2] are based on fairly old measurements. In connection with investigations on the electrolytic deposition of yttrium from fused fluorides containing Y_2O_3, the Gibbs free energy of formation of Y_2O_3 has been measured in the temperature region 1000 – 1150 K by means of a formation cell of the type:

$$Y(s) \left| \begin{matrix} LiF \\ YF_3 \end{matrix} (l);\ Y_2O_3(sat) \right| X$$

where X is a C/CO_2 ($p = 1$ atm), or Pt/O_2 ($p = 1$ atm) electrode.

EXPERIMENTAL

LiF and YF_3 (99.9 %) were used in molar ratio 3:1. The melting point of this mixture is 740 °C.[3] 5 weight % Y_2O_3 (99.9 %) was added to the mixture to ensure complete saturation with respect to Y_2O_3. The solubility of Y_2O_3 in the melt is approximately 2.5 weight % at 840 °C.[4] The experiments were performed in a 5 cm internal diameter graphite cell. The cell is shown in Fig. 1. The cell was placed in a vertical Kanthal-wound furnace inside an inert atmosphere chamber, described elsewhere.[5]

LiF and YF_3 were weighed out in stoichiometric proportions, and 5 weight % Y_2O_3 was added. The salts were mixed and dried *in situ* at 300 °C and under dynamic vacuum of 0.02 Torr for at least 12 h. The mixture was then melted under He atmosphere.

The temperature in the melt was controlled with an on/off temperature controller and a chromel-alumel thermocouple. Temperature measurements were done with another chromel-alumel thermocouple contained inside a closed end molybdenum tube immersed in the melt, and a potentiometer.

The thermoelectrical electromotive force (TEMF) for the couples Y/C and Y/Pt was determined previously to the chain measurements as a function of temperature. These quantities represent a correction on the measured electromotive force (EMF).

The EMF's were recorded on a strip-chart recorder with input impedance 4 Mohm.

The potentials were stable at gas velocities above ~ 20 cm³/min. No time-dependence of the potentials was found.

The C/CO_2 electrode

This electrode has been used by several workers,[6-10] in the cryolite system. The cell set-up in this investigation was:

$$Y(s) \left| \begin{matrix} LiF \\ YF_3 \end{matrix} (l);\ Y_2O_3(sat) \right| C,\ CO_2\ (p = 1\ atm)$$

with the cell reaction

$$Y_2O_3(sat) + 3/2C(s) = 2Y(s) + 3/2CO_2\ (g,\ 1\ atm) \quad (1)$$

The EMF of this cell is given by:

$$E_T = E^\circ_T + (RT/6F)\ \ln\ [(P_{CO_2})^{3/2}/a_{Y_2O_3}] \quad (2)$$

With $p_{CO_2} = 1$ atm and a saturated solution with respect to Y_2O_3 ($a_{Y_2O_3} = 1$), eqn. (2) gives $E_T = E^\circ_T$, and the Gibbs free energy change for reaction (1), ΔG°_T, is:

$$\Delta G^\circ_T = -6FE^\circ_T \quad (3)$$

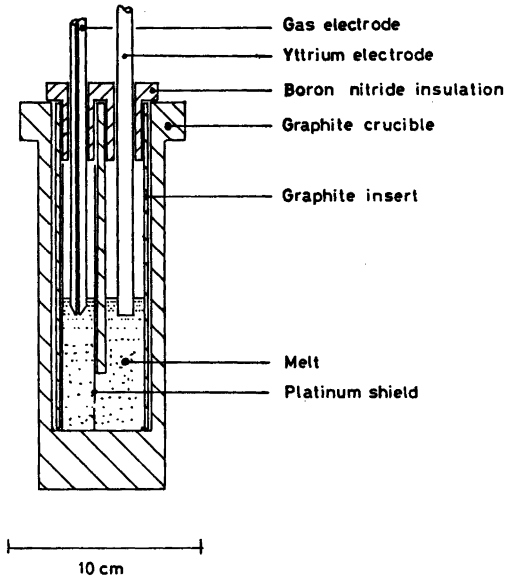

Fig. 1. Cell used for the EMF measurements.

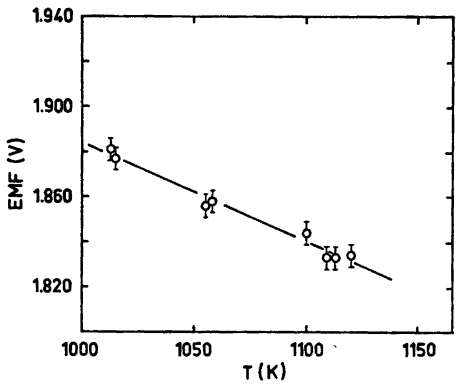

Fig. 2. EMF as function of T with the C/CO_2 ($p = 1$ atm) electrode.

With knowledge of standard Gibbs free energy of formation of CO_2 and ΔG°_T from eqn. (3), the standard Gibbs free energy of formation of Y_2O_3 ($\Delta G^\circ_{Y_2O_3}$) can be calculated:

$$\Delta G^\circ_{Y_2O_3} = 3/2\ \Delta G^\circ_{CO_2} - \Delta G^\circ_T \qquad (4)$$

The results from the experiments are given in Fig. 2, as measured EMF (E_T, V, corrected for TEMF) *vs.* thermodynamic temperature, T. The results are fitted to a straight line by means of a least-squares computer program:

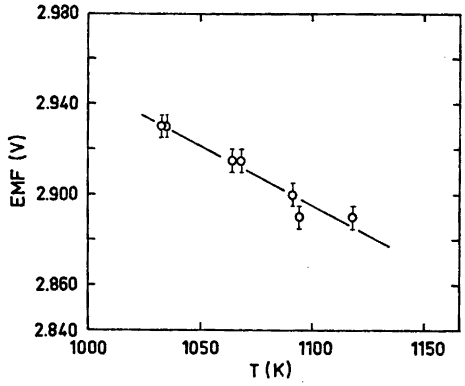

Fig. 3. EMF as function of T with the Pt/O_2 ($p = 1$ atm) electrode.

$$E_T = 2.3229 - 4.3890 \times 10^{-4} \times T \qquad (5)$$

The estimated error in the EMF is ± 5 mV.

The Pt/O_2 ($p = 1$ atm) electrode

The cell set-up was:

$$Y(s) \left| \begin{matrix} LiF \\ YF_3 \end{matrix} \right. (l);\ Y_2O_3(sat) \left| \right. Pt,\ O_2\ (p = 1\ atm)$$

with the cell reaction:

$$Y_2O_3\ (sat) = 2Y(s) + 3/2\ O_2\ (g,\ 1\ atm) \qquad (6)$$

A saturated solution with respect to Y_2O_3 (*i.e.* $a_{Y_2O_3} = 1$) and an O_2-pressure of 1 atm, give $E_T = E^\circ_T$, and the standard Gibbs free energy of formation of Y_2O_3 can be calculated directly from the measured EMF:

Table 1. Gibbs free energy of formation of Y_2O_3, ΔG°_f.

Reference electrode (X) $p = 1$ atm	Temp. K	Measured ΔG_f°, kJ	Lit. value ΔG_f°, kJ
Pt/O_2	1000	−1707.5	−1594.9(1)
C/CO_2	1000	−1685.3	−1636.7(2)
Pt/O_2	1050	−1692.4	−1584.4(1)
C/CO_2	1050	−1672.7	−1623.7(2)
Pt/O_2	1100	−1677.3	−1569.8(1)
C/CO_2	1100	−1660.6	−1611.2(2)
Pt/O_2	1150	−1661.8	−1551.0(1)
C/CO_2	1150	−1648.0	−1598.2(2)

$$\Delta G^\circ_{Y_2O_3} = -6FE^\circ_T \quad (7)$$

The results from these experiments, presented as a plot of EMF *vs.* T, are given in Fig. 3. The results are fitted to a straight line by means of a least-squares computer program. The equation for the EMF $(E_T, V) - T$ dependence is:

$$E_T = 3.4725 - 5.2450 \times 10^{-4} \times T \quad (8)$$

The estimated error in determining the EMF is ± 5 mV.

From the measured EMF (eqns. (5) and (8)), the free energy of formation of Y_2O_3 was calculated and compared with literature values. The results of this are given in Table 1. The literature values, marked (1) are taken from Wicks and Block's compilation of selected thermodynamic properties,[1] the values marked (2) are calculated by us from data found in Kubaschewski, Evans and Alcock's book on Metallurgical Thermochemistry.[2]

CONCLUSION

Table 1 shows that both reference electrodes gave Gibbs free energy of formation values for Y_2O_3 below the values found in the literature. The result indicates that the accepted value [1] for the Gibbs free energy of formation of Y_2O_3 is too high in the temperature region 1000 – 1150 K. At 1000 K, the discrepancy is -101.5 kJ compared with Wicks and Block's [1] values, and -59.7 kJ compared with the calculated values from Kubaschewski, Evans and Alcock.[2] At 1150 K, the discrepancy is -103.9 kJ and -56.7 kJ, respectively. In both cases, the mean value from the measurements with the Pt/O_2 ($p = 1$ atm) and C/CO_2 ($p = 1$ atm) reference electrodes is used.

Acknowledgement. This work was done at Reno Metallurgy Research Center, 1605 Evans Av., Reno, Nevada. One of the authors, G. H. Bøe, gratefully acknowledges the financial support from the Royal Norwegian Council for Scientific and Industrial Research, which made his stay in Reno possible.

REFERENCES

1. Wicks, C. E. and Block, F. E. *U.S. Bur. Mines Bull.* (1963) 605.
2. Kubaschewski, O., Evans, E. and Alcock, C. B. *Metallurgical Thermochemistry*, 4th Ed., Pergamon, Oxford 1967.
3. Thoma, R. E. *et al. J. Phys. Chem. 65* (1961) 1096.
4. Aamland, E., Kesterke, D. and MacDonald, D. *U.S. Bur. Mines Rep. Invest.* 7722 (1973).
5. Morrice, E., Porter, B., Brown, E. A., Wyche, C. and Knickerbocker, R. G. *U.S. Bur. Mines Rep. Invest.* 5868 (1961).
6. Thonstad, J. *Electrochim. Acta 15* (1970) 1569.
7. Mashovets, V. P. and Revazyan, A. A. *J. Appl. Chem. USSR 31* (1958) 571.
8. Richards, N. E. and Welch, B. J. *Proc. 1st Australian Conf. Electrochem.*, Pergamon, London 1964.
9. Thonstad, J. and Hove, E. *Can. J. Chem. 42* (1964) 1542.
10. Huglen, R. *Diploma work*, University of Trondheim, Department of Electrochemistry 1972.

Received June 14, 1974.

Acta Chemica Scandinavica A 28 (1974) 989—995

Structures of Linear Multisulfur Systems. VII. The Crystal and Molecular Structure of 3,5-Bis(*N*,*N*-diisopropylthiocarbamoylimino)-4-methyl-1,2,4-dithiazolidine, $C_{17}H_{31}N_5S_4$

JORUNN SLETTEN

Department of Chemistry, University of Bergen, N-5014 Bergen, Norway

Crystals of the title compound, $C_{17}H_{31}N_5S_4$, are orthorhombic, space group *Pbcn*, with a unit cell of dimensions $a = 25.097(4)$ Å, $b = 8.451(2)$ Å, $c = 10.679(4)$ Å. X-Ray data were collected on an off-line four-circle diffractometer. The structure was solved by the symbolic addition procedure and refined by full-matrix least-squares to a final R factor of 0.048. The molecule lies on a two-fold axis. The four sulfur atoms are almost collinearly arranged at distances in the region between single bond and van der Waals distance, the central S—S being 2.167 Å and the terminal S—S distances, related by the two-fold axis, are 2.763 Å.

By autoxidation in solution several 1,1,5-trisubstituted dithiobiurets form orange compounds which have been identified as 3,5-bis(*N*,*N*-thiocarbamoylimino)-1,2,4-dithiazolidines (I).[1,2]

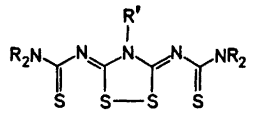

(I)

The present compound, however, has been synthesized according to another method recently published.[1]

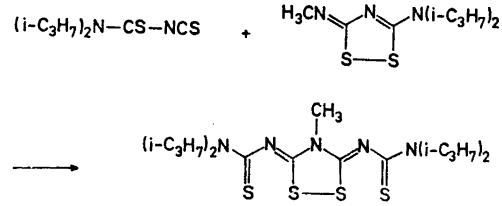

Acta Chem. Scand. A 28 (1974) No. 9

This type of compounds may possibly possess partial bonding between all four sulfur atoms in the row. Such a bonding scheme would be in analogy with the S—S bonding in thiathiophthenes (II) [3] and in linear five-sulfur systems

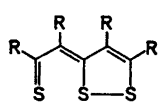

(II)

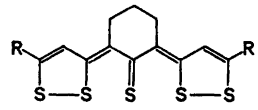

(III)

(III).[4,5] The present structure determination was undertaken primarily to study the sulfur bonding system.

EXPERIMENTAL

A crystalline sample of the compound was provided by Dr. J. Goerdeler, University of Bonn. A single crystal of dimensions 0.20 mm × 0.30 mm × 0.55 mm was mounted along the largest dimension, parallel to the crystallographic c-axis, and was used for all X-ray experiments. The space group was determined from Weissenberg and precession photographs. Cell dimensions were calculated from diffractometer measurements of setting angles for 12 reflections. 2589 independent reflections with $2\theta \leq 55°$ were recorded on a four-circle diffractometer using $\theta - 2\theta$ scan and niobium filtered Mo$K\alpha$ radiation. Scan ranges were calculated according to the relationship $\Delta\theta = A + B \tan\theta$,[6] with constants evaluated after scanning a few reflections manually and recording the widths of the peaks. Two standard reflections monitored throughout the data collection indicated no deterioration of the crystal. S.d. in the intensities were evaluated as $\sigma_I = [\sigma_c^2 + (0.03N_{net})^2]^{\frac{1}{2}}$, where σ_c is the error due to counting statistics. Standard

deviations in structure factors were calculated as $\sigma_F = \sigma_I/2(ILp)^{\frac{1}{2}}$. 609 reflections had net counts less than $2\sigma_c$. These reflections were assigned the threshold value $2\sigma_c$ and were given zero weight in the refinement unless $|F_c| > |F_{threshold}|$. Data were corrected for Lorentz and polarization effects according to standard procedures, and for absorption by the method described by Coppens *et al.*[7]

CRYSTAL DATA

$C_{17}H_{31}N_5S_4$; $M.W. = 433.73$; crystal system orthorhombic; space group *Pbcn*; cell dimensions:

$a = 25.097(4)$ Å, $b = 8.451(2)$ Å, $c = 10.670(4)$ Å. $V = 2263(1)$ Å^3; $D_x = 1.273$ g cm^{-3}; $D_m = 1.268$ g cm^{-3}; $Z = 4$; $F_{000} = 928$; $\mu_{(MoK\alpha)} = 4.2$ cm^{-1}.

STRUCTURE DETERMINATION, REFINEMENT AND THERMAL ANALYSIS

The structure was solved by application of the symbolic addition procedure using a computer program written by Long.[8] Signs for 148 reflections were derived. An E-map calculated from the most probable set of signs revealed all non-hydrogen atoms. The structure was refined by full-matrix least-squares, minimizing the function $\sum w(|F_o| - |F_c|)^2$, where $w = 1/\sigma_F^2$. At an R of 0.15, $(R = \sum||F_o| - |F_c||/\sum|F_o|)$, anisotropic temperature factors were introduced. The hydrogen atoms were localized from a difference Fourier map; positional and isotropic thermal parameters were refined. The molecule is lying on a crystallographic two-fold axis; the axis going through C(9), N(3) and the middle of the S(2) – S(2)′ bond (Fig. 1). Thus, the hydrogen atoms on the methyl group C(9) are disordered. In the difference map six methyl hydrogen sites could be distinguished. The three fractional hydrogen atoms in one asymmetric unit were included with occupancy factors of 0.5 and successfully refined. The refinement converged at an R of 0.048, the weighted R factor is 0.056, and the s.d. of an observation of unit weight $(s = |\sum w(|F_o| - |F_c|)^2(m-n)|^{\frac{1}{2}})$, is 2.86. At this stage all shifts in non-hydrogen parameters were less than 0.2σ, and in hydrogen parameters less than 0.7σ. By comparing observed and calculated structure factors, no evidence of extinction was found.

A residual difference map calculated at the end of the refinement revealed a region of electron density 0.32 e Å^{-3} between S(1) and S(2) and another peak of density 0.56 e Å^{-3} between S(2) and S(2)′. The data included

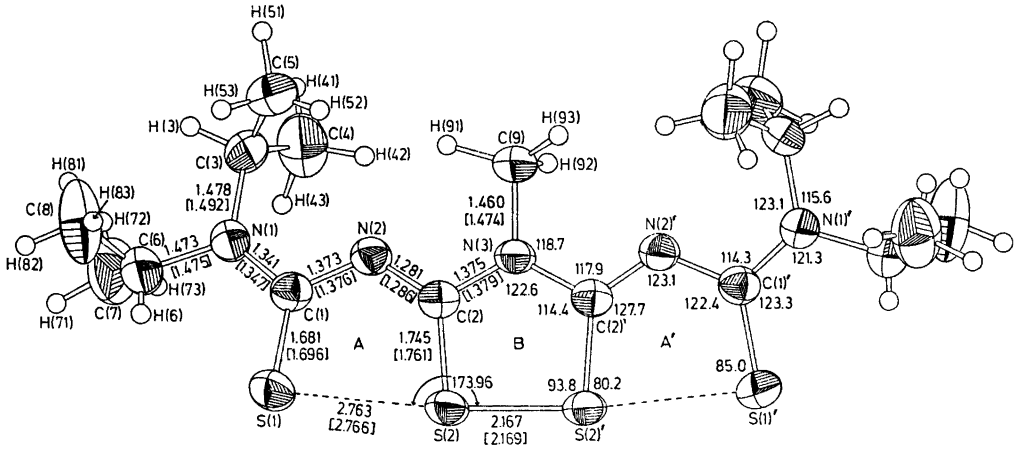

Fig. 1. Selected intramolecular distances and angles. Distances corrected for rigid body motion are shown in brackets. Standard deviations in S – S, S – C and C – N bonds as calculated from the least-squares inverse matrix are 0.001, 0.003, and 0.003 Å, respectively. Standard deviations in S···S – S and C – S – S angles are 0.03 and 0.1°; and 0.2° in angles at carbon and nitrogen. Thermal ellipsoids for the non-hydrogen atoms are drawn at the 50 % probability level. Only one set of the disordered hydrogen atoms on C(9) are included; the other set is obtained by a two-fold rotation around the N(3) – C(9) bond.

Table 1. Fractional coordinates and thermal parameters for non-hydrogen atoms with standard deviations. Thermal parameters are of the form $T=\exp[-2\pi^2(U_{11}h^2a^{*2}+U_{22}k^2b^{*2}+U_{33}l^2c^{*2}+2U_{12}hka^*b^*+2U_{23}klb^*c^*+2U_{13}hla^*c^*)]$, and the values are multiplied by a factor of 10^4.

Atom	*X/a*	*Y/b*	*Z/c*	U_{11}	U_{22}	U_{33}	U_{12}	U_{23}	U_{13}
S(1)	0.39859(3)	0.13653(8)	−.01841(8)	638(5)	412(4)	672(4)	−35(4)	137(4)	−109(4)
S(2)	0.47181(3)	0.17027(7)	0.17311(8)	475(4)	310(3)	712(5)	−17(3)	49(3)	−94(4)
N(1)	0.35798(9)	−.15455(25)	−.01178(22)	499(13)	437(12)	553(14)	−37(10)	54(11)	−119(11)
N(2)	0.43194(8)	−.11831(24)	0.10891(22)	410(12)	367(11)	517(14)	−22(9)	26(10)	−20(11)
N(3)	0.50000(0)	−.11336(32)	0.25000(0)	381(16)	295(14)	571(20)	0(0)	0(0)	−30(15)
C(1)	0.39563(10)	−.05350(29)	0.02745(26)	399(14)	396(13)	482(15)	−9(11)	1(12)	25(13)
C(2)	0.46507(9)	−.03521(27)	0.17232(24)	357(13)	369(13)	417(14)	−19(10)	6(11)	67(12)
C(3)	0.35774(13)	−.32432(34)	0.02133(33)	614(19)	436(16)	745(23)	−152(14)	51(16)	−199(17)
C(4)	0.34686(18)	−.35313(60)	0.15951(43)	799(27)	946(32)	871(30)	−331(26)	387(26)	−164(24)
C(5)	0.40535(19)	−.41291(47)	−.03095(48)	856(29)	494(20)	1059(34)	33(20)	−168(21)	−273(27)
C(6)	0.31409(15)	−.10184(46)	−.09335(39)	637(22)	572(21)	789(27)	−25(17)	77(19)	−253(19)
C(7)	0.26029(18)	−.12161(86)	−.03179(57)	609(25)	1226(46)	967(37)	231(28)	−225(35)	−144(24)
C(8)	0.31587(25)	−.18117(99)	−.22016(46)	743(33)	1908(72)	527(26)	123(40)	108(33)	−179(23)
C(9)	0.50000(0)	−.28611(51)	0.25000(0)	652(34)	327(21)	873(46)	0(0)	0(0)	−209(34)

Table 2. Fractional atomic coordinates and thermal parameters for hydrogen atoms with the corresponding standard deviations. Thermal parameters are of the form: $\exp(-8\pi^2U\sin^2\theta/\lambda^2)$ and are multiplied by 10^3.

Atom	*X/a*	*Y/b*	*Z/c*	*U*	Atom	*X/a*	*Y/b*	*Z/c*	*U*
H(3)	0.3293(12)	−.3741(34)	−.0276(30)	65(9)	H(71)	0.2291(19)	−.0660(50)	−.0770(43)	130(17)
H(41)	0.3372(18)	−.4643(62)	0.1673(47)	136(18)	H(72)	0.2553(21)	−.2145(59)	−.0406(51)	119(23)
H(42)	0.3793(13)	−.3300(35)	0.2130(32)	66(10)	H(73)	0.2612(17)	−.1027(51)	0.0548(48)	113(18)
H(43)	0.3174(23)	−.2535(77)	0.1809(54)	183(24)	H(81)	0.3066(33)	−.2521(98)	−.2209(79)	220(53)
H(51)	0.3927(16)	−.5336(61)	−.0234(41)	122(15)	H(82)	0.2902(16)	−.1368(41)	−.2717(37)	77(11)
H(52)	0.4351(13)	−.3793(36)	−.0008(30)	59(10)	H(83)	0.3442(23)	−.1692(62)	−.2594(51)	134(22)
H(53)	0.4033(18)	−.3754(47)	−.1289(46)	114(15)	H(91)	0.4636(27)	−.3259(78)	0.1886(70)	105(22)
H(6)	0.3201(16)	−.0183(52)	−.1076(45)	107(17)	H(92)	0.4920(28)	−.2997(68)	0.3311(53)	59(21)
					H(93)	0.5405(35)	−.3301(80)	0.2510(79)	101(28)

extend slightly beyond the limit of the copper sphere, and in similar compounds where comparable or less amounts of data are used, the residual electron density near the sulfur atoms is less than 0.2 e Å^{-3}. Hence it is unlikely that the peaks in this case are due to Fourier series termination errors. One possible explanation could be that not only the methyl group, but the whole molecule is disordered around the two-fold axis. Such a disorder may also explain the fairly large thermal parameters observed. Any deviation from exact two-fold symmetry is too small, however, to be resolved by ordinary refinement methods.

Atomic scattering factors used were for sulfur, nitrogen, and carbon those of Hanson *et al.*[9] and for hydrogen those of Stewart *et al.*[10]

Final coordinates and thermal parameters are listed in Tables 1 and 2. Lists of observed and calculated structure factors may be obtained from the author.

The thermal parameters of the 11 atoms in rings A+B+A′ (Fig. 1) were analyzed in terms of rigid body motion according to the method of Schomaker and Trueblood.[11] The r.m.s. difference between observed U_{ij}'s and those calculated from the derived **T**, **L**, **S** molecular tensors is 0.0026 Å^2. The maximum angle of vibration is 7.8°; the principal axis of libration being approximately parallel to the S(2)−S(2)′ direction. Bond distances corrected according to this model using the method of Cruickshank[12] are shown in brackets in Fig. 1. Corrections of bond lengths involving the atoms in the isopropyl groups are probably underestimated as these atoms presumably have additional riding motion.

All calculations were carried out on a UNIVAC 1110 computer. The programs, except when otherwise noted, have been made available by the Chemistry Department, Weizmann Institute of Science, Rehovoth, Israel; or have been written by K. Maartmann-Moe of this Department.

RESULTS AND DISCUSSION

In Fig. 1 intramolecular distances and angles except those involving the methyl and isopropyl groups, are shown. The remaining bond distances and angles are listed in Tables 3 and 4.

The four sulfur atoms are approximately collinear, the angle S(1)−S(2)−S(2)′ being 173.96(3)°. The terminal S···S distances of 2.763(1) Å are appreciably shorter than van der Waals contact of 3.40 Å,[13] and also shorter than Huggin's constant energy distance of 2.94 Å.[14] In comparison the longest S−S distance observed in any of the unsymmetrically substituted thiathiophthenes (II) determined so far, is 2.56 Å.[15] The central sulfur-sulfur bond distance, S(2)−S(2)′ in the dithiazolidine ring, of 2.167(1) Å is significantly longer than corresponding distances in unsaturated five-membered cyclic disulfides like, *e.g.*, the dithiolium ion (IV), the thiuret ion (V), rhodan hydrate and xanthan hydride (VI), where bond lengths in the range 2.00−2.08 Å have been found.[16] S(2)−S(2)′ is also significantly longer than the accepted single bond distance of 2.10 Å.[16]

Table 3. C−C and C−H bond distances with the corresponding standard deviations in parentheses. C−C bond lengths corrected for rigid body motion are listed in brackets.

	(Å)		(Å)
C(3)−C(4)	1.519(6)[1.531]	C(6)−H(6)	0.74(5)
C(3)−C(5)	1.516(6)[1.530]	C(7)−H(71)	1.03(5)
C(6)−C(7)	1.511(6)[1.524]	C(7)−H(72)	0.80(5)
C(6)−C(8)	1.511(8)[1.521]	C(7)−H(73)	0.94(5)
C(3)−H(3)	0.98(3)	C(8)−H(81)	0.65(9)
C(4)−H(41)	0.97(5)	C(8)−H(82)	0.92(5)
C(4)−H(42)	1.01(4)	C(8)−H(83)	0.83(6)
C(4)−H(43)	1.14(6)	C(9)−H(91)	1.17(10)
C(5)−H(51)	1.07(5)	C(9)−H(92)	0.90(10)
C(5)−H(52)	0.86(4)	C(9)−H(93)	1.07(10)
C(5)−H(53)	1.09(5)		

Table 4. Bond angles in the methyl group and isopropyl groups. Standard deviations in parentheses.

Angle	(°)	Angle	(°)
N(1)–C(3)–C(4)	112.9(3)	N(1)–C(6)–H(6)	105(3)
N(1)–C(3)–C(5)	112.8(3)	C(7)–C(6)–H(6)	112(3)
C(4)–C(3)–C(5)	114.8(3)	C(8)–C(6)–H(6)	104(4)
N(1)–C(3)–H(3)	107(2)	C(6)–C(7)–H(71)	115(3)
C(4)–C(3)–H(3)	108(2)	C(6)–C(7)–H(72)	101(4)
C(5)–C(3)–H(3)	100(2)	C(6)–C(7)–H(73)	113(3)
C(3)–C(4)–H(41)	106(3)	H(71)–C(7)–H(72)	106(5)
C(3)–C(4)–H(42)	112(2)	H(71)–C(7)–H(73)	114(4)
C(3)–C(4)–H(43)	101(3)	H(72)–C(7)–H(73)	107(5)
H(41)–C(4)–H(42)	110(3)	C(6)–C(8)–H(81)	114(8)
H(41)–C(4)–H(43)	122(4)	C(6)–C(8)–H(82)	109(3)
H(42)–C(4)–H(43)	105(3)	C(6)–C(8)–H(83)	115(4)
C(3)–C(5)–H(51)	102(2)	H(81)–C(8)–H(82)	97(8)
C(3)–C(5)–H(52)	112(2)	H(81)–C(8)–H(83)	115(8)
C(3)–C(5)–H(53)	100(2)	H(82)–C(8)–H(83)	104(5)
H(51)–C(5)–H(52)	123(3)	N(3)–C(9)–H(91)	107(3)
H(51)–C(5)–H(53)	109(3)	N(3)–C(9)–H(92)	97(4)
H(52)–C(5)–H(53)	108(3)	N(3)–C(9)–H(93)	110(6)
N(1)–C(6)–C(7)	112.2(3)	H(91)–C(9)–H(92)	109(6)
N(1)–C(6)–C(8)	111.9(4)	H(91)–C(9)–H(93)	129(8)
C(7)–C(6)–C(8)	111.5(4)	H(92)–C(9)–H(93)	100(9)

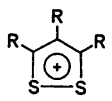
(IV)

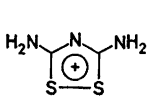
(V)

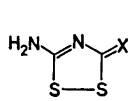
(VI)

X = O or S

Evidently, the interaction between S(1) and S(2) and between S(1)′ and S(2)′ is sufficiently strong to significantly influence the central S(2)–S(2)′ bond. Thus, one may envisage a sulfur-sulfur bonding scheme with delocalized σ-bonding across all four atoms in the row. It is possible that the interaction between the outer sulfur atoms, S(1)···S(2) and S(2)′···S(1)′, is partly caused by an electrostatic interaction.

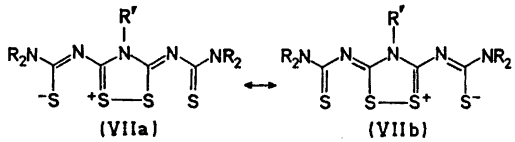
(VIIa) (VIIb)

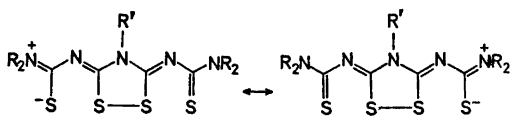
(VIIIa) (VIIIb)

In valence bond language this may be depicted by contribution of, *e.g.*, the following resonance forms in which the terminal sulfur atoms are negatively charged (VII a – b, and VIIIa – b).

This is consistent with the results from semiempirical molecular orbital calculations by the CNDO/2 method, in which the terminal sulfur atoms are found to carry a negative charge of 0.44 electrons.[17]

The S–S distances observed in the present compound agree well with those found in a closely related symmetrical dithiazolidine molecule studied by Flippen [2.784(3) Å, 2.171(3) Å, 2.784(3) Å].[18] In another symmetrically substituted compound where no crystallographic symmetry was imposed on the molecule, a slightly asymmetric arrangement was observed in the sulfur sequence, the bond distances being 2.742(5) Å, 2.161(5) Å, 2.785(5) Å.[18]

The S–C_{sp^3} and N–C_{sp^3} bond distances are all in the region between single bonds and double bonds; indicating π-conjugation throughout the system. This is also in good agreement with findings in the two structures mentioned above.[18] Rings A+B+A′ of the molecule may be considered as a delocalized π-system involving 14 electrons. As indicated by the short exocyclic N–C_{sp^3} bond the two π-electrons on

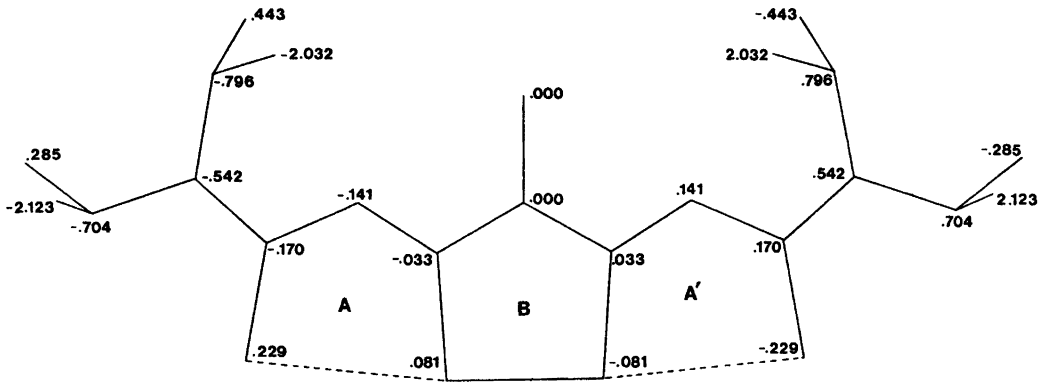

Fig. 2. Deviations from the best least-squares plane through the 11 atoms of rings A+B+A′.

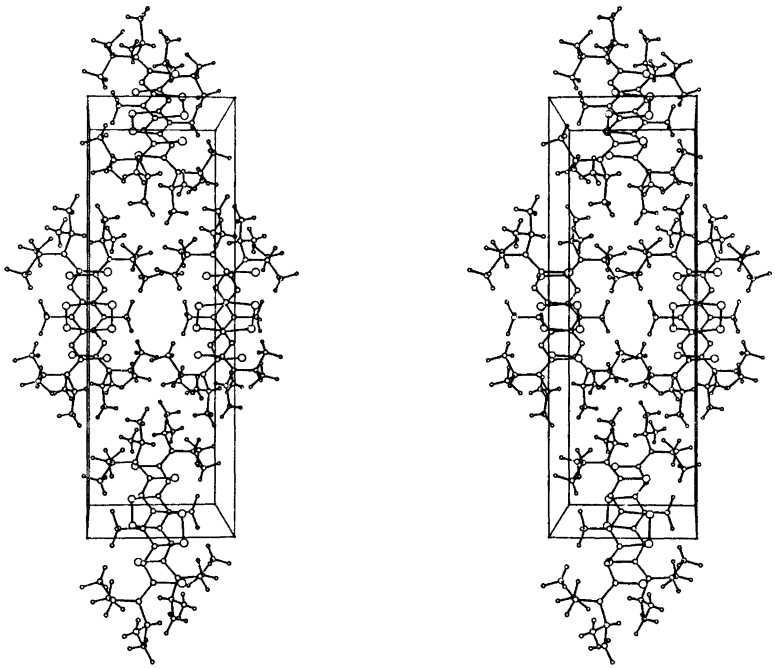

Fig. 3. Stereoscopic view of the molecular packing. The *a*-axis is vertical, top to bottom; the *b*-axis is horisontal, left to right; and the *c*-axis is pointing towards the viewer. Figs. 1 and 3 are drawn by computer using the ORTEP program.[19]

each of the atoms N(1) and N(1)′ also participate in the delocalized π-system giving a total of 18 π-electrons. The average $N-C_{sp^2}$ bond in the present structure is 1.470 Å (1.480 Å after correction for rigid body motion), and the average $C_{sp^2}-C_{sp^2}$ bond length is 1.514 Å (1.527 Å with RBM correction).

The bulky substituents introduce overcrowding in the molecule. A best least-squares plane fitted to the 11 atoms of ring A+B+A′ shows that this part of the molecule deviates significantly from planarity (Fig. 2). There is a twist of the molecule around the C(2)···C(2)′ direction; the dihedral angle between rings A and A′

being 15.5°. The substituent on C(1) is bent out of the plane of ring A; N(1), C(3) and C(6) deviating 0.362, 0.419, and 0.603 Å, respectively, from plane A. The double bond character of the C(1)–N(1) bond effectively prevents the group from being twisted around this bond. Despite the imposed molecular deformation there still remain some short intramolecular contacts; S(1)···H(6) = 2.55(4) Å, H(91)···H(42) = 2.13(8) Å, H(91)···H(52) = 2.19(8) Å and H(93)···H (42′ = 2.06(10) Å.

A stereo drawing of the molecular packing in the crystal is shown in Fig. 3. Molecules related by the crystallographic *c*-glide are stacked on top of one another; partially overlapping at an interplanar distance of 3.71 Å. There are no intermolecular contacts shorter than van der Waals distances.

Acknowledgement. The author wishes to thank Dr. J. Goerdeler for supplying a crystalline sample of the compound.

REFERENCES

1. Goerdeler, J. and Ulmen, J. *Chem. Ber. 105* (1972) 1568.
2. Oliver, J. E. and Stokes, J. B. *Int. J. Sulfur Chem. A 2* (1972) 105.
3. Hordvik, A. and Sæthre, L. J. *Israel J. Chem. 10* (1972) 239.
4. Sletten, J. *Acta Chem. Scand. 24* (1970) 1464.
5. Kristensen, R. and Sletten, J. *Acta Chem. Scand. 27* (1973) 2517.
6. Alexander, L. E. and Smith, G. S. *Acta Crystallogr. 17* (1964) 1195.
7. Coppens, P., Leiserowitz, L. and Rabinovich, D. *Acta Crystallogr. 18* (1965) 1035.
8. Long, R. E. *Ph. D. Diss.*, University of California at Los Angeles, Los Angeles 1965.
9. Hanson, H. P., Hermann, F., Lea, J. D. and Skillmann, S. *Acta Crystallogr. 17* (1964) 1040.
10. Stewart, R. F., Davidson, E. R. and Simpson, W. T. *J. Chem. Phys. 42* (1965) 3175.
11. Schomaker, V. and Trueblood, K. N. *Acta Crystallogr. B 24* (1968) 63.
12. Cruickshank, D. W. J. *Acta Crystallogr. 9* (1956) 757.
13. Sletten, J. *Acta Chem. Scand. 25* (1971) 3577.
14. Huggins, M. L. *J. Amer. Chem. Soc. 75* (1953) 4126.
15. Johnson, S. M., Newton, M. G. and Paul, I. C. *J. Chem. Soc. B* (1969) 986.
16. Hordvik, A. *Quart. Rep. Sulfur Chem. 5* (1970) 21.
17. Sletten, J. *To be published.*
18. Flippen, J. *J. Amer. Chem. Soc. 95* (1973) 6073.
19. Johnson, G. K. *ORTEP* Report ORNL-3794, Oak Ridge National Laboratory, Oak Ridge.

Received May 20, 1974.

Acta Chemica Scandinavica A 28 (1974) 996—1000

Compounds with the Marcasite Type Crystal Structure. IX. Structural Data for $FeAs_2$, $FeSe_2$, $NiAs_2$, $NiSb_2$, and $CuSe_2$

ARNE KJEKSHUS,[a] TROND RAKKE[a] and ARNE F. ANDRESEN[b]

[a] Kjemisk Institutt, Universitetet i Oslo, Blindern, Oslo 3, Norway and [b] Institutt for Atomenergi, Kjeller, Norway

The FeS_2-*m* type structures of $FeAs_2$, $FeSe_2$, $NiAs_2$, $NiSb_2$, and $CuSe_2$ have been redetermined by powder neutron diffraction/profile refinement methods, and a brief status report for structural data in this class is presented. An important result of the study is the identification of the assumed compound $Mo_{2/3}As_2$ as $FeAs_2$.

Except for the parameter-free structure types, few if any classes of compounds have a better covering with structural data than those with the FeS_2-*m* (*m* = marcasite) type (*cf.* Ref. 1). However, the quality of the data varies, mainly due to the experimental technique used. Among the binary compounds (TX_2; T = transition metal, X = main group V or VI element) with the FeS_2-*m* type structure, $FeSe_2$[2,3] and $CuSe_2$[4] appear to take extreme values (*viz.* relative to the commonly assumed[5] size of X) for the $X-X$ bond length. In order to ascertain that these distinctions are rooted in realities and not in experimental errors, redeterminations were called for, the results of which are being reported here.

In the course of the study, $FeAs_2$[6,7] was included motivated by its apparent deviation from trends outlined by isostructural compounds. The results for $FeAs_2$ provoked, in turn, renewed interest in other compounds, such as $NiAs_2$[6] and $NiSb_2$[6,7], results for which are also included in this report.

EXPERIMENTAL

The compounds were prepared by heating stoichiometric quantities of the elements (in the form of turnings from Fe, Ni, and Cu rods and crushed As, Sb, and Se from Johnson Matthey & Co., except for Cu (American Smelting and Refining Co.) and Se (Bolidens Gruvaktiebolag); spectroscopically standardized and of purity better than 99.995 %) in evacuated, sealed silica tubes. Samples of $FeSe_2$ were maintained for one week at 800 °C, slowly cooled, crushed, reannealed twice at 500 °C for, in all, six weeks, then cooled to 250 °C over a period of nine weeks, and finally quenched to room temperature. The $CuSe_2$ samples were prepared at 300 °C for two weeks, cooled to 200 °C over a further three week period, and quenched to room temperature. The same heating procedure was repeated from 280 °C after intervening crushing of the sample. (A preparation temperature of 200 °C, as suggested by Gattow,[4] appears to be too low since all samples synthesized at this temperature were invariably found *inter alia* to contain substantial amounts of the CuSe phase.)

The $NiSb_2$ sample was prepared as described previously,[8] and although $FeAs_2$ and $NiAs_2$ (*viz.* β-$NiAs_2$) can be synthesized according to the earlier procedure,[8] it was found more convenient (particularly in view of the relatively large sample quantities required) to make alterations in the procedure by which it became possible to reduce the number of intervening crushings as well as the overall annealing periods. Thus, $FeAs_2$ was made by two successive annealings (with intervening crushing) at 800 °C, followed by slow cooling to 600 °C and quenching to room temperature. The alteration introduced for $NiAs_2$ consisted of the initial preparation of NiAs by annealing at 850 °C. Subsequently, $NiAs_2$ was readily made by adding the appropriate amount of As, annealing at 800 °C, slow cooling to 600 °C, and quenching to room temperature.

Attempts have also been made to prepare FeS_2-*m* type phases with the following compositions: $OsTe_2$, $CoSe_2$, CuS_2, CuSSe, CuSeTe, and $CuTe_2$ by the sealed silica capsule technique under a variety of different thermal conditions. Although samples with compositions $OsTe_2$ and

$CoSe_2$ are readily made, all $CoSe_2$ samples were found to contain only the FeS_2-*p* (*p* = pyrite) type modification, while some $OsTe_2$ samples contained mixtures of FeS_2-*p* and FeS_2-*m* type modifications. The latter finding is in agreement with Ref. 9. The FeS_2-*m* type modification of $OsTe_2$ can be made to disappear by the use of an annealing temperature ≥ 550 °C. Attempts to remove the FeS_2-*p* type modification through lowering of the annealing temperature failed. This finding probably reflects an extremely sluggish transition, an inference open for verification. The reaction products obtained for the mentioned Cu samples were CuS + S, CuS + Se, CuSe + Te, or CuTe + Te, displacement reactions being observed for CuSe + S → CuS + Se and CuTe + Se → CuSe + Te. (Compounds with the compositions CuS_2, CuSSe, CuSeTe, and $CuTe_2$ can be synthesized [10] under high pressure conditions, but with the FeS_2-*p* rather than the FeS_2-*m* type structure.)

The experimental details concerning X-ray and neutron diffraction, density measurements, and computations are described in Ref. 7 and references therein.

RESULTS AND DISCUSSION

(i) *Space group.* One question which has received attention [11–13] at this Institute in recent years, concerns whether there is a mirror plane perpendicular to [001] in the FeS_2-*m* type structure. If the object of the present study had been to pursue this problem further, single crystal samples would have been called for. However, recent results [13] for the prototype compound suggest very strongly that the mirror plane is present or that the deviation is negligible for conventional structural considerations. The reasons for the first erroneous inferences [11,12] could be attributed [13] to the unforeseen influence on the final results of inappropriate absorption corrections. (Now we know that a spherically shaped crystal specimen is required in order to perform this task accurately.) On this background it seems highly probable that not only the prototype, but all compounds with the FeS_2-*m* type structure belong to space group *Pnnm*, at least to a very good approximation.

In this fortunate situation, single crystal specimens are no longer needed, since present experience shows that powder samples examined by neutron diffraction with subsequent least squares profile refinement provide overall structural data to an accuracy almost rivalling those obtained by single crystal techniques.

(ii) *Redetermined data.* The redetermined structural data for $FeAs_2$, $FeSe_2$ ($d_{pycn.}$ = 7.09 g cm^{-3}), $NiAs_2$, $NiSb_2$, and $CuSe_2$ ($d_{pycn.}$ = 6.24 g cm^{-3}) obtained at room temperature, are compiled in Table 1, the final profile reliability factors ranging between 2.7 and 4.3 %. Comparison shows excellent agreement with the positional parameters obtained by Buerger [14] for $FeAs_2$ ($x = 0.175$, $y = 0.361$), whereas deviating values in preceding papers [6,7] are due to

Table 1. Structural data for $FeAs_2$, $FeSe_2$, $NiAs_2$, $NiSb_2$, and $CuSe_2$.

	$FeAs_2$	$FeSe_2$	$NiAs_2$	$NiSb_2$	$CuSe_2$
a (Å)	5.3012(6)	4.8002(4)	4.7582(7)	5.1823(5)	5.0226(7)
b (Å)	5.9858(5)	5.7823(5)	5.7949(8)	6.3168(7)	6.1957(7)
c (Å)	2.8822(4)	3.5834(4)	3.5440(4)	3.8403(5)	3.7468(6)
x	0.1763(10)	0.2127(6)	0.2017(8)	0.2189(10)	0.1835(5)
y	0.3624(7)	0.3701(5)	0.3691(7)	0.3593(8)	0.3849(4)
4 *T*–*X* (Å)	2.388(4)	2.383(2)	2.394(3)	2.569(3)	2.558(2)
2 *T*–*X* (Å)	2.362(4)	2.371(3)	2.344(4)	2.537(5)	2.557(3)
1 *X*–*X* (Å)	2.492(7)	2.535(4)	2.447(6)	2.882(7)	2.331(4)
4 *X*–*T*–*X* (°)	88.1(2)	87.98(8)	87.3(1)	86.8(1)	87.94(7)
4 *X*–*T*–*X* (°)	91.9(2)	92.02(8)	92.7(1)	93.2(1)	92.06(7)
2 *X*–*T*–*X* (°)	74.3(1)	97.53(7)	95.5(1)	96.7(1)	94.15(6)
2 *X*–*T*–*X* (°)	105.7(1)	82.47(7)	84.5(1)	83.3(1)	85.85(6)
2 *T*–*X*–*T* (°)	127.0(1)	122.26(8)	122.1(1)	124.3(1)	118.95(7)
1 *T*–*X*–*T* (°)	74.3(1)	97.53(7)	95.5(1)	96.7(1)	94.15(6)
2 *T*–*X*–*X* (°)	108.1(2)	106.23(9)	105.6(1)	103.5(2)	108.71(8)
1 *T*–*X*–*X* (°)	108.1(2)	100.83(12)	104.2(2)	101.5(2)	106.60(11)

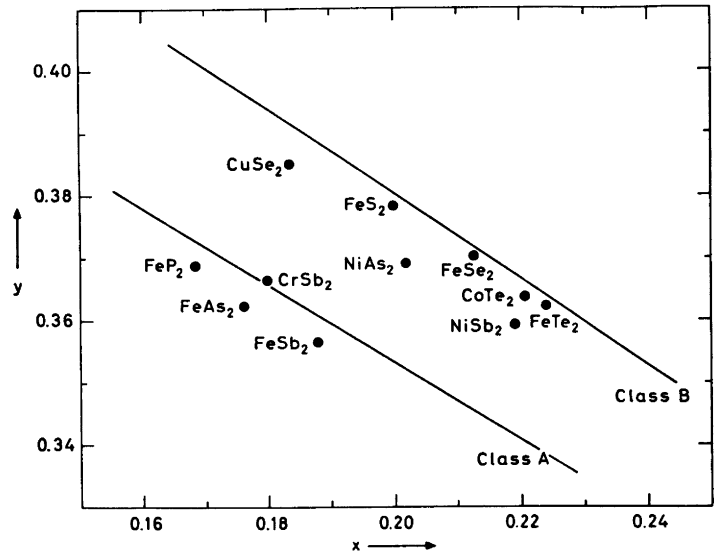

Fig. 1. Positional parameters for compounds with FeS_2-*m* type structure, eqns. 4 and 5 being included for comparison.

unfortunate copying mistakes. The earlier data for $FeSe_2$ ($x = 0.21$, $y = 0.37$)[2] and $CuSe_2$ ($x = 0.17$, $y = 0.38$)[4] concur reasonably well with the present ones when the limited accuracies of the studies are taken into account.

On the basis of the revised structural data for $FeSe_2$ and $CuSe_2$, a comment is called for on the previously inferred [15] relationships between $T-X$ and $X-X$ bond distances *versus* localized configurations (d^j) of essentially non-bonding electrons on T. However, although the new data to some extent follow the same trends as indicated on Figs. 1 and 2 in Ref. 15, this aspect deserves further attention and is conveniently included in a forthcoming, more general discussion of compounds with the FeS_2-*p*, FeS_2-*m*, and $CoSb_2$ structure types.

(iii) *Structural status report.* The data in Table 1 together with those for $CrSb_2$,[7] FeP_2,[16] $FeSb_2$,[11] FeS_2,[13] $FeTe_2$,[12] and $CoTe_2$[12] give rise to an interesting finding. (The earlier assignment of space group *Pnn*2 to $FeSb_2$, $FeTe_2$, and $CoTe_2$ is probably incorrect; this is open for experimental verification.) Using as the only assumption that the two non-equivalent $T-X$ bond distances

$$d_1 = [(1/2+x)^2a^2 + (1/2-y)^2b^2 + (c/2)^2]^{\frac{1}{2}} \quad (1)$$

$$d_2 = [x^2a^2 + y^2b^2]^{\frac{1}{2}} \quad (2)$$

of the FeS_2-*m* type structure (according to space group *Pnnm*) are equal, the relation

$$y = \frac{1}{4}\left[1 + \left(\frac{a}{b}\right)^2 + \left(\frac{c}{b}\right)^2\right] - \left(\frac{a}{b}\right)^2 x \quad (3)$$

results. When the empirical average values for the axial ratios [1] of classes A and B are substituted into Eqn. 3, the expressions

$$\text{class A: } y = 0.502 - 0.774x \quad (4)$$

$$\text{class B: } y = 0.519 - 0.691x \quad (5)$$

are obtained. As illustrated in Fig. 1, all well-determined structures (*viz.* those examined by single crystal X-ray or powder neutron/profile refinement techniques) closely follow these semi-empirical relations. An interesting detail to which attention may be drawn, is the fact that the two series of FeX_2 compounds trace out virtually parallel lines to those described by eqns. 4 and 5. (Concerning more details in $T-X$ bond distances, $CrSb_2$ is unique in exhibiting four short and two longer $T-X$ bonds.)

Of the binary compounds reported with the FeS_2-*m* type structure, those lacking in Fig. 1 are: NaO_2, $Mo_{2/3}As_2$, RuP_2, $RuAs_2$, $RuSb_2$, OsP_2, $OsAs_2$, $OsSb_2$, $OsTe_2$, and $CoSe_2$. Reasons for leaving out $Mo_{2/3}As_2$ are discussed separately in section iv. The present attempts to prepare

pure $OsTe_2$ with FeS_2-*m* type structure were unsuccessful (thus concurring with the earlier findings [9]) and information on the FeS_2-*m* type modification of $CoSe_2$ originates exclusively from a rather inaccurately characterized mineral sample.[17] Although data for RuP_2, $RuAs_2$, $RuSb_2$, OsP_2, $OsAs_2$, and $OsSb_2$ are given in an earlier paper [6] of this series, their accuracies may well be questioned due to possible shortcomings in the treatment of the X-ray powder diffraction data. Judging from trends (*cf.* Fig. 1, Fig. 1 in Ref. 17, *etc.*) outlined by the isostructural compounds, the data for at least some of these (notably $RuAs_2$ and OsP_2) appear to suffer from inaccurate determinations. Redeterminations on the basis of single crystal X-ray or powder neutron/profile refinement methods are therefore advisable. The same applies in some extent to NaO_2.[18]

(iv) *$Mo_{2/3}As_2$?* The perhaps most interesting deduction which can be made from the data in Table 1 concerns the defect FeS_2-*m* type compound $Mo_{2/3}As_2$. The knowledge on this compound may be summarized as:

(a) The only successful preparation is claimed by Brown.[19] Attempted duplication of the synthesis by others [8,20,21] has been unsuccessful.

(b) The only data originally communicated by Brown were structural information about the assigned space group *Pnnm*, the cell dimensions (in Å units) $a=5.299(2)$, $b=5.983(2)$, and $c=2.885(1)$, and the positional parameters $x=0.1762(3)$ and $y=0.3625(3)$ for a *de facto* unidentified compound. (No qualitative or quantitative chemical analyses were performed.)

(c) Brown originally gave the composition $Mo_{0.4}As_2$, but corrected this in a private communication to $Mo_{0.6}As_2$ with a specification of the yield to less than ten small crystals.

(d) The composition $Mo_{0.6}As_2$ was conveniently altered to $Mo_{2/3}As_2$, thus ascribing [1] the configuration d^0 to Mo. For this reason, the latter formula has, unfortunately without firm experimental facts, found its way into the literature.[1,12,15,22,23]

On comparing the structural data for the assumed compound $Mo_{2/3}As_2$ with those for $FeAs_2$ in Table 1, an almost perfect coincidence will be noted. Since coincidence in structural data commonly is believed to provide unambiguous identification of compounds, this inference alone strongly suggests that the assumed $Mo_{2/3}As_2$ is actually $FeAs_2$. Further evidence supporting this conclusion, stems from the way Brown utilized structural data to deduce the composition $Mo_{0.6}As_2$ through the use of the occupation number for Mo as a variable. The value 0.6 is remarkably close to the atomic ratio 0.62 for Fe/Mo as it would be if Mo had been confused with Fe.

The assumption of $Mo_{2/3}As_2$ being (in reality) $FeAs_2$ appears to provide a credible explanation also for the few, small crystals only once obtained by Brown, possibly due to a Fe impurity in his sample. Moreover, this also explains why other investigators have failed in attempted preparations. Finally, the non-existence of the assumed $Mo_{2/3}As_2$ would exclude the only example of a class A transition metal compound having a possible d^0 configuration, thus removing a marked inconsistency between transition and non-transition metal d^0 representatives, which otherwise would belong to different classes A and B, respectively, of the FeS_2-*m* structure type (*cf.* Ref. 24). This line will be pursued further in another context.

From the above evidence, the identification of $Mo_{2/3}As_2$ as $FeAs_2$ appears to be beyond reasonable doubt. The incorrect assignment made by Brown is understandable in view of the minute amount of sample available which did not permit ordinary chemical analyses.

REFERENCES

1. Brostigen, G. and Kjekshus, A. *Acta Chem. Scand. 24* (1970) 2993.
2. Tegnér, S. *Z. Anorg. Allg. Chem. 239* (1938) 126.
3. Fischer, G. *Can. J. Phys. 36* (1958) 1435.
4. Gattow, G. *Z. Anorg. Allg. Chem. 340* (1965) 312.
5. Pauling, L. *The Nature of the Chemical Bond*, Cornell University Press, Ithaca 1960.
6. Holseth, H. and Kjekshus, A. *Acta Chem. Scand. 22* (1968) 3284.
7. Holseth, H., Kjekshus, A. and Andresen, A. F. *Acta Chem. Scand. 24* (1970) 3309.
8. Holseth, H. and Kjekshus, A. *Acta Chem. Scand. 22* (1968) 3273.
9. Sutarno, Knop, O. and Reid, K. I. G. *Can. J. Chem. 45* (1967) 1391.
10. Bither, T. A., Prewitt, C. T., Gillson, J. L., Bierstedt, P. E., Flippen, R. B. and Young, H. S. *Solid State Commun. 4* (1966) 533.
11. Holseth, H. and Kjekshus, A. *Acta Chem. Scand. 23* (1969) 3043.
12. Brostigen, G. and Kjekshus, A. *Acta Chem. Scand. 24* (1970) 1925.

13. Brostigen, G., Kjekshus, A. and Rømming, C. *Acta Chem. Scand. 27* (1973) 2791.
14. Buerger, M. J. *Z. Kristallogr. 82* (1932) 165.
15. Kjekshus, A. and Nicholson, D. G. *Acta Chem. Scand. 25* (1971) 866.
16. Dahl, E. *Acta Chem. Scand. 23* (1969) 2677.
17. Ramdohr, P. and Schmitt, M. *Neues Jahrbuch Mineral., Monatshefte* (1955) 133.
18. Carter, G. F. and Templeton, D. H. *J. Amer. Chem. Soc. 75* (1953) 5247.
19. Brown, A. *Nature (London) 206* (1965) 502.
20. Taylor, J. B., Calvert, L. D. and Hunt, M. R. *Can. J. Chem. 43* (1965) 3045.
21. Jensen, P., Kjekshus, A. and Skansen, T. *Acta Chem. Scand. 20* (1966) 403.
22. Brostigen, G. and Kjekshus, A. *Acta Chem. Scand. 24* (1970) 2983.
23. Goodenough, J. B. *J. Solid State Chem. 5* (1972) 144.
24. Kjekshus, A. and Rakke, T. *Struct. Bonding (Berlin) 19* (1974) 85.

Received May 9, 1974.

Acta Chemica Scandinavica A 28 (1974) 1001—1010

Compounds with the Marcasite Type Crystal Structure. X. ^{57}Fe Mössbauer Studies of Some Ternary Pnictides

ARNE KJEKSHUS and TROND RAKKE

Kjemisk Institutt, Universitetet i Oslo, Blindern, Oslo 3, Norway

Room temperature ^{57}Fe Mössbauer data for 49 samples of the phases $Cr_tFe_{1-t}As_2$, $Cr_tFe_{1-t}Sb_2$, $Fe_{1-t}Co_tAs_2$, $Fe_{1-t}Co_tSb_2$, $Fe_{1-t}Ni_tAs_2$, and $Fe_{1-t}Ni_tSb_2$ are reported and discussed in relation to other (mostly structural) properties. Test of the current model for conversion between the classes A and B of the marcasite type structure in terms of these data, gives strong indications of inadequacies in the model. Associated problems concerning the arsenopyrite type structure are examined and the assumption of metal-metal bonding is rejected as the stabilizing element for its occurrence.

Compounds with the FeS_2-*m* (*m* = marcasite) type crystal structure have been subjected to regular investigations throughout most of this century. However, an inevitable lesson learned from the preceding studies is that in order to gain understanding into the chemical bonding in these compounds, there is an almost unlimited demand for decisive experimental facts. Of the compounds in question, $FeSb_2$ has received particular attention because of the anomalies observed in the temperature dependences of magnetic,[1-3] electrical,[3,4] and ^{57}Fe Mössbauer [5,6] parameters. A tentative explanation [6] of these anomalies invokes the thermal population of an empty conduction band as a function of temperature. As an alternative to the thermal influence on electronic band structure, one may examine the variations imposed by compositional parameters (*viz.* through substitutional solid solution). Thus the present paper concerns the compositional dependences of the ^{57}Fe Mössbauer parameters for the phases $Cr_tFe_{1-t}As_2$, $Cr_tFe_{1-t}Sb_2$, $Fe_{1-t}Co_tAs_2$, $Fe_{1-t}Co_tSb_2$, $Fe_{1-t}Ni_tAs_2$, and $Fe_{1-t}Ni_tSb_2$.

EXPERIMENTAL

The pure elements used as starting materials for the syntheses were flakes of 99.999 % Cr (Koch-Light Laboratories), 99.99+ % Fe, 99.999 % Co, 99.995 % Ni (Johnson, Matthey & Co.; turnings from rods), 99.9999 % As, and 99.9995 % Sb (Koch-Light Laboratories). In accordance with earlier findings,[7,8] equilibrium is attained rather slowly (particularly for the diantimonides) when synthesis of the ternary phases by direct combination of the elements is attempted. However, equilibrium is facilitated by the intermediate preparation of the binary compounds.[9-11]

$Fe_{1-t}Co_tAs_2$ and $Fe_{1-t}Ni_tAs_2$ are readily made from the binary end members at 800 °C by a sequence of annealings (with intermediate crushings) over a period of 3 to 6 months. $Cr_tFe_{1-t}Sb_2$ samples are made similarly at 600 °C using total heating periods of 8 to 10 months. Homogeneous Fe-rich samples of $Fe_{1-t}Co_tSb_2$ ($0 < t \lesssim 0.5$) and $Fe_{1-t}Ni_tSb_2$ ($0 < t \lesssim 0.3$) were obtained after 10 to 14 months (intermediate crushings) at 600 °C. However, more Co- and Ni-rich samples of the same phases contained *inter alia* variable amounts of $CoSb_3$ and $Fe_{0.5}Ni_{0.5}Sb_3$ (*cf.*, *e.g.*, Ref. 8), respectively, which proved to reflect the equilibrium situation at 600 °C. On increasing the annealing temperature to 630 – 700 °C depending on composition, homogeneous samples and hence equilibrium could be attained after 6 to 8 months.

Samples of $Cr_tFe_{1-t}As_2$ could not be prepared in an analogous manner since the binary compound $CrAs_2$ is unattainable by the sealed silica capsule technique. (A variety of thermal (400 – 1000 °C) and compositional ($CrAs_2$-$CrAs_6$) conditions, including chemical transport reactions, were tried, but all endeavours failed. This result is consistent with earlier findings.[9] However, $CrAs_2$ with $NbAs_2$ rather than FeS_2-*m* type structure has recently been synthesized [12] under high pressure – high temperature conditions.) Alternatively, CrAs and FeAs were initially prepared (as described in Refs. 13, 14) and

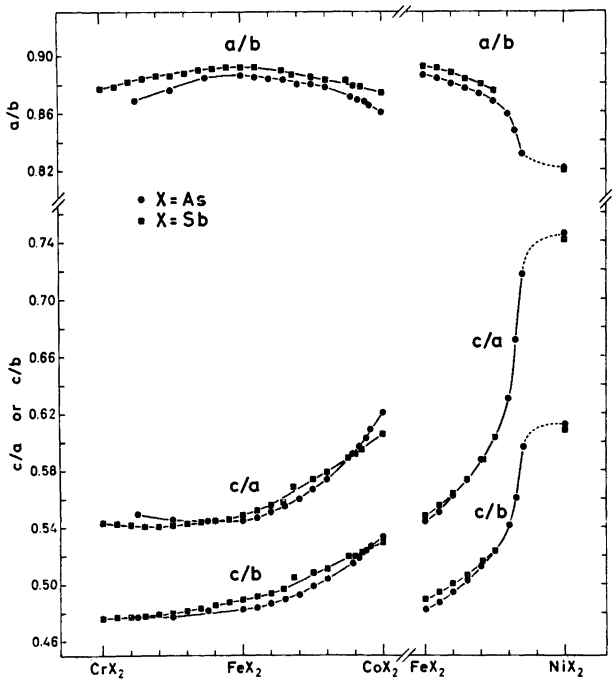

Fig. 1. Dependence of axial ratios on composition for the solid solution series CrX_2-FeX_2, FeX_2-CoX_2, and FeX_2-NiX_2. In this and the following diagrams, estimated error limits do not exceed the size of the symbols.

used to make $Cr_tFe_{1-t}As$ by three successive one-week annealings at 850 °C. Samples of $Cr_tFe_{1-t}As_2$ were subsequently obtained by adding the appropriate amounts of As, using heat treatments at 600 – 800 °C and quenching from 600 °C.

The homogeneity of all samples were ascertained from powder X-ray (Guinier) diagrams. The experimental details concerning the room temperature ^{57}Fe Mössbauer measurements and data reduction are reported earlier.[15]

RESULTS AND DISCUSSION

(i) *Solid solubility and unit cell proportions.* The phase analytical data for the five ternary phases $Cr_tFe_{1-t}Sb_2$, $Fe_{1-t}Co_tAs_2$, $Fe_{1-t}Co_tSb_2$, $Fe_{1-t}Ni_tAs_2$, and $Fe_{1-t}Ni_tSb_2$ confirm essentially those reported earlier.[7,8] Thus, continuous ranges ($0.00 \leq t \leq 1.00$) of random, substitutional solid solutions have been observed for $Cr_tFe_{1-t}Sb_2$, $Fe_{1-t}Co_tAs_2$, and $Fe_{1-t}Co_tSb_2$. The limited solid solubility ranges of the Fe-rich $Fe_{1-t}Ni_tAs_2$ and $Fe_{1-t}Ni_tSb_2$ phases are found to cover the intervals $0.00 \leq t \leq 0.75$ and $0.00 \leq t \leq 0.50$, respectively, the Ni-rich phases being uninteresting in this connection.

Considering the $Cr_tFe_{1-t}As_2$ phase, only the single composition with $t = 0.5$ has hitherto been recorded [16] in the literature. For the present purpose, compositions up to $t = 0.75$ were made (although not even this sample gave a good enough ^{57}Fe Mössbauer spectrum to be included in the final results reported here; see section ii). However, due to the special situation prevailing for the binary end member "$CrAs_2$",* supplementary information on the properties of $Cr_tFe_{1-t}As_2$ is of considerable interest, such data being reported in a forthcoming paper.[17]

The variations in axial ratios a/b, c/a, and c/b with composition for the phases in question are shown in Fig. 1. Since the binary end members belong to different classes [18,19] A ("$CrAs_2$", $CrSb_2$, $FeAs_2$, and $FeSb_2$), A/B ($CoAs_2$ and $CoSb_2$), and B ($NiAs_2$ and $NiSb_2$) of the FeS_2-m type structure, the continuous variations in unit cell proportions (Fig. 1) reflect corresponding continuous transitions between the classes. The

* In the following text, quotation marks are used to emphasize the special situation for $CrAs_2$ (*cf.* Experimental).

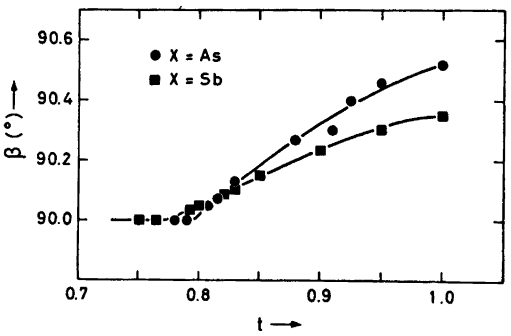

Fig. 2. Monoclinic angle (β') of pseudo-marcasite cell *versus* compositional parameter (t) for $Fe_{1-t}Co_tX_2$.

data for samples with the FeAsS (arsenopyrite; binary prototype $CoSb_2$) type structure refer to the pseudo-marcasite variant rather than the true unit cell (*cf.* Ref. 18).

The transitions from the FeS_2-*m* to the $CoSb_2$ type structure are of some special interest in this connection. Fig. 2 shows the angle β' of the pseudo-marcasite cell as a function of the compositional parameter t for $Fe_{1-t}Co_tAs_2$ and $Fe_{1-t}Co_tSb_2$. For both phases the transition is found at $t \approx 0.8$, the conversion appearing to occur at a slightly smaller t value in the antimonide than in the arsenide phase. However, an accurate determination of the conversion point is inaccessible through the determination of β' alone since the first sign of the reduced symmetry is indistinguishable from slight line broadenings of appropriate reflections on the Guinier diagrams.

Great care has been taken in the evaluation of the data for $Fe_{1-t}Ni_tAs_2$ and $Fe_{1-t}Ni_tSb_2$. (From considerations on average d^i configurations, $Fe_{0.5}Ni_{0.5}As_2$ and $Fe_{0.5}Ni_{0.5}Sb_2$ might have been expected to take the $CoSb_2$ type structure.[20]) However, no sign of any splitting nor broadening of reflections indicative of distortion from the FeS_2-*m* type structure could be detected within the ranges of solid solubility. These findings fully confirm the earlier results,[7,8] but appear on the other hand, to be difficult to correlate with the itinerant energy band considerations presented by Goodenough [20] without introducing additional assumptions, or alternatively, removing (some of) his extraneous assumption(s) concerning the $CoSb_2$ type structure.

(ii) *^{57}Fe Mössbauer spectra.* The ^{57}Fe Mössbauer spectra for the phases in question have been collected over a period of about three years. In all, some 350 spectra (including calibration runs) have been recorded, each run lasting from a few (≥ 6) hours to a few (≤ 3) days. For increasing t in a general formula $Fe_{1-t}T_tX_2$ (where T = Cr, Co, or Ni and X = As or Sb), the Mössbauer absorption became gradually reduced (due to the lowered Fe content) until ultimately comparable with the inherent statistical fluctuations. This limitation prevented unambiguous data reduction for samples with large t. However, the results presented below refer exclusively to spectra of acceptable quality obtained for, in all, 49 samples of the phases in question. In order to check the reproducibility and/or minimize random errors, each sample was run (with independent mountings and calibrations) two to five times.

The large number of spectra collected prevent presentation of the primary data.

(iii) *Chemical shifts.* The ^{57}Fe Mössbauer chemical shifts (relative to sodium nitroprusside) obtained for the $Fe_{1-t}T_tX_2$ phases are shown as functions of composition in Fig. 3, interpretations of which being called for.

The Mössbauer chemical shift (δ) is a relative measure of the total s electron density at the nucleus. (Increasing δ corresponds to decreasing total s electron density.) Since all electrons to some extent are influenced by chemical bonding, δ will reflect certain features of the bonding situation. As opposed to the apparently clear-cut direct contribution to δ from electrons of s symmetry, it is a common apprehension that electrons of p and d symmetry contribute indirectly through their shielding effects. Hence, increased p and/or d orbital participation in bonding should lead to decreased shielding of the nuclear charge and consequently, to increased s electron density.

The increase in δ for increasing t in the formula $Cr_tFe_{1-t}X_2$, suggests that Cr contributes more (*viz.* has a greater donor ability for electrons) to the $T-X$ bonds than Fe, in agreement with the fact that on going from Cr to Fe the "atomic 3*d* orbitals" experience an increased effective nuclear charge. The results of the inferred effective *d* electron transfer from Cr, through the $T-X$ bonds to Fe, may be interpreted as making the average $Cr-X$ bonds

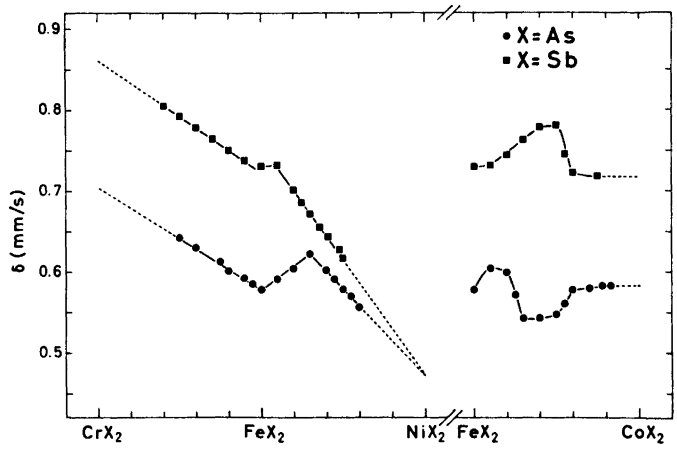

Fig. 3. Variation in ^{57}Fe Mössbauer chemical shift parameter (δ) with composition for the series CrX_2-FeX_2, FeX_2-NiX_2, and FeX_2-CoX_2.

stronger (*viz.* a decreased effective size of Cr) on the expense of the $Fe-X$ bonds (*viz.* an increased effective size of Fe). This interpretation concurs with the increasing average $Fe-X$ bond lengths that must be established for increasing t. (In the case of $Cr_tFe_{1-t}Sb_2$, the assumption of increasing average $T-X$ bond lengths with increasing t is supported by the structural data for $CrSb_2$ and $FeSb_2$, *cf.* Ref. 11. For the $Cr_tFe_{1-t}As_2$ phase, only circumstantial evidence from the corresponding variation of unit cell dimensions is at hand.[17]) At equilibrium, the distribution of $T-X$ bonding electrons in $Cr_tFe_{1-t}X_2$ may be imagined such that the effective sizes of Cr and Fe are equal. This is consistent with the apparent equivalence of Cr and Fe in these phases as inferred from the sharp reflections on the X-ray diagrams.

In general, the attribution of such a mechanism to random solid solutions seems more likely than the common, simple picture based on distribution of individually sized atoms. Moreover, a model in terms of adjusted, averaged sized atoms offers the possibility of connecting solid solution properties to features of electronic band structure (*viz.* mutual compatibility in electronic band structure for solute and solvent,[21] including in elaborated form also the Hume-Rothery 15 % criterion,[22] *etc.*).

The dependence of δ on t for the two $Fe_{1-t}Ni_tX_2$ phases shows (Fig. 3) a somewhat different behaviour for $X=As$ and $X=Sb$, and the identical chemical shifts obtained on extrapolating to NiX_2 is almost certainly accidental. It should also be noted that the extrapolations in these cases pass through regions with no solid solubility (see section i). As in the analogous $Cr_tFe_{1-t}X_2$ case, the "atomic 3*d* orbitals" should experience an increased effective nuclear charge on going from Fe to Ni, and hence, an effective *d* electron transfer from Fe through the $T-X$ bonds to Ni might be expected. For increasing Ni content, each Fe must effectively contribute more *d* electrons in this process, and a steadily decreasing δ with increasing t in $Fe_{1-t}Ni_tX_2$ should result. This is apparently nearly the case for $X=Sb$ but, for $X=As$ the increase in δ for $0\leq t\lesssim 0.3$ indicates that rivalling effects from *s* electrons are of importance and eventually, are balanced by the *d* electron effects at $t\approx 0.3$. However, the overall trend for $Fe_{1-t}Ni_tX_2$ shows a definite decrease in δ for increasing t, suggesting that *d* electron effects are most important. Moreover, an effective *d* electron transfer from Fe to Ni should make the effective size of Fe in $Fe_{1-t}Ni_tX_2$ smaller than in FeX_2. This is in conformity with structural data for $FeSb_2$ and $NiSb_2$ (*cf.* Ref. 11 and references therein) which indicate that the average $T-X$ bond length decreases with increasing Ni content. (The rivalling *s* electron effects should lead to an increased rather than decreased effective size of Fe with increasing t in $Fe_{1-t}Ni_tX_2$.)

Among the present phases, $Fe_{1-t}Co_tX_2$ reveals the most peculiar δ *versus* t relationships.

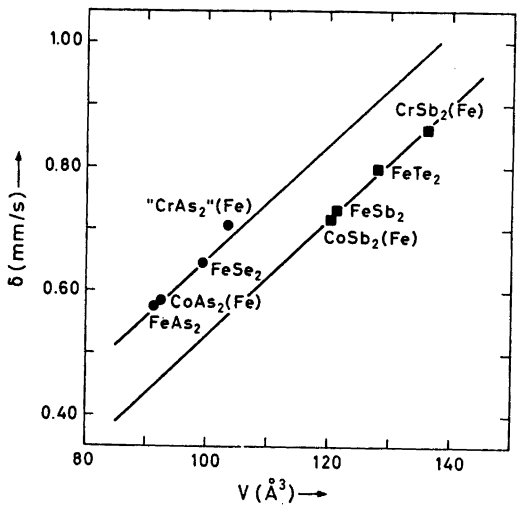

Fig. 4. ^{57}Fe Mössbauer chemical shift parameter (δ) *versus* cell volume (V) for some binary and quasi-binary compounds with FeS_2-*m* like structures.

However, on approaching CoX_2, the curves appear to suggest approximately constant values for δ. This finding is of particular interest in relation to the question concerning $T-T$ bonding [8,10,19,20,23–25] in compounds with the $CoSb_2$ type structure (see sections v and vi).

Connections between chemical shifts and unit cell dimensions for some phases with the FeS_2-*m* and FeS_2-*p* (p = pyrite) type structures have been pointed out earlier.[5,26] To test this on compounds with FeS_2-*m* like structures, available ^{57}Fe chemical shift data for some binary and extrapolated for some quasi-binary compounds are plotted in Fig. 4 against cell volumes. As indicated on the diagram, the compounds group on two parallel lines determined by the principal quantum number of X (As and Se *versus* Sb and Te). Of the ternary phases (omitted from the diagram for clarity), both $Cr_tFe_{1-t}As_2$ and $Cr_tFe_{1-t}Sb_2$ follow the trend outlined in Fig. 4. Attempted interpretation of correlations of this type is given in Refs. 5, 26. In common with other conclusions drawn from a limited amount of experimental evidence, this simple interpretation may no longer be valid when more data for phases with FeS_2-*m* like structures are included.

Even though the extrapolated δ values for $CoAs_2$ and $CoSb_2$ fit the scheme (Fig. 4), those for $Fe_{1-t}Co_tX_2$ show discrepancies. For the $Fe_{1-t}Ni_tX_2$ phases, these discrepancies are even more marked. This finding naturally provokes a discussion of to what extent the chemical shift data reflect the structural alterations accompanying the transitions from class A, through A/B, to B.

(iv) *Test of current model for class A to B conversion.* The cause of the existence of two distinct classes of binary compounds with the FeS_2-*m* type structure has been a controversial subject, the most recent model being advanced by Goodenough.[20] His treatment aims at explaining *inter alia* the class A to B conversion in terms of a combined molecular orbital – band theoretical description. Since the Mössbauer chemical shifts reflect certain features of the bonding situation, this model should be tested against these data.

According to Goodenough, the origin of class A is due to enhanced $T-X$ bonding in this class relative to class B (and the FeS_2-*p* type). In his itinerant model, T atoms with $j>4$ in the d^j configurations, give rise to $T-X$ anti-bonding d electrons, implying that the gradual conversion to class B is caused by the corresponding reduction of their participation in $T-X$ bonding. This is accomplished by reduced covalent mixing of one d orbital per T with the X atomic orbitals, which consequently should increase the shielding of the s electrons from the nuclear charge. A gradual decrease in s electron density should therefore be observed over the class A to B conversion interval. This is exactly the opposite situation to that traced out by the general trend in the data for $Fe_{1-t}Ni_tX_2$. Hence, Goodenough's model must be considered as inadequate with respect to the class A to B conversion. Additional, independent support for this conclusion appears to be provided by the decreasing (definitely not increasing) tendency in the average $T-X$ bond length with increasing t for $Fe_{1-t}Ni_tX_2$, which fits rather badly in with the weakening in $T-X$ bonding prescribed by the model.

Although Goodenough's model has many attractive features and represents a definite improvement on the earlier models (*cf.* Ref. 20 and references therein), the physical origin of the different classes of compounds with the FeS_2-*m* type structure is still an open question.

(v) *Quadrupole splittings.* The ^{57}Fe Mössbauer

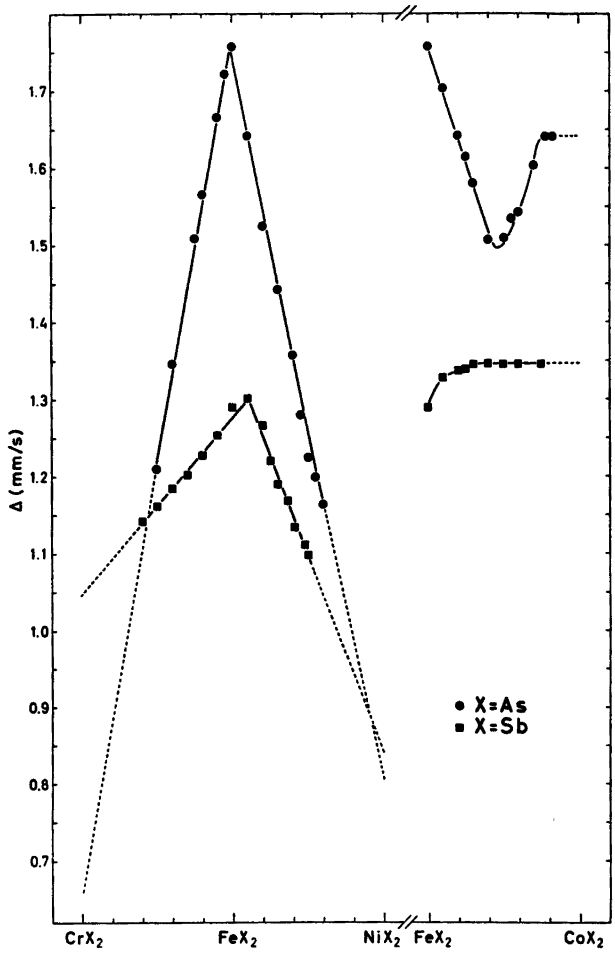

Fig. 5. Variation in ^{57}Fe Mössbauer quadrupole splitting parameter (Δ) with composition for the series CrX_2-FeX_2, FeX_2-NiX_2, and FeX_2-CoX_2.

quadrupole splitting parameter (Δ) is shown *versus* composition in Fig. 5. The total electronic asymmetry as observed by the nucleus is directly reflected in Δ. For the $Fe_{1-t}Ni_tX_2$ phases, decreasing Δ with increasing t could therefore qualitatively be attributed to the continuous structural alterations consequent on passing from class A to B. This could also apply to the first linear part of the curve for $Fe_{1-t}Co_tAs_2$. However, this interpretation is not generally applicable as most clearly demonstrated on Fig. 5 for $Cr_tFe_{1-t}X_2$. On inspection of Fig. 1, it is seen that the latter phases are members of class A. Nevertheless, the changes in Δ with t are compatible for $Cr_tFe_{1-t}X_2$ and $Fe_{1-t}Ni_tX_2$.

In order to gain a better understanding of these findings it appears necessary to dig more deeply into other properties of $Cr_tFe_{1-t}X_2$. The special situation prevailing for "$CrAs_2$" has already been noted, and moreover, also $CrSb_2$ is somewhat special among the binary compounds with the FeS_2-*m* type structure, being *inter alia* the only compound which exhibits cooperative magnetism.[2] Even though $CrSb_2$ definitely belongs to class A, it appears to differ significantly also in other respects from the remaining members of this class. For the well-determined structures of both classes A and B, there are two short and four longer $T-X$ bond

distances, while $CrSb_2$ shows the opposite (four and two) tendency. Obviously, the change in the grouping of the $T-X$ bond distances for $Cr_tFe_{1-t}Sb_2$ must be reflected in Δ. In addition, the increasing magnitude of the average $T-X$ bond distances for increasing t must also have an effect on Δ. Further speculations concerning the interpretation of the quadrupole splittings for these phases must await the results of currently conducted studies on $Cr_tFe_{1-t}X_2$ by supplementary techniques.

The dependence of Δ on t for $Fe_{1-t}Co_tX_2$ shows (as was the case for δ) apparently constant values in the vicinity of CoX_2. The earlier assumption of $T-T$ bonding as the cause [8,10,19,23–25] of the structural distortion from the FeS_2-m to the $CoSb_2$ type structure should, if real, indeed be reflected in Δ and δ. Since such a correlation is not observed, this assumption must accordingly be considered as questionable.

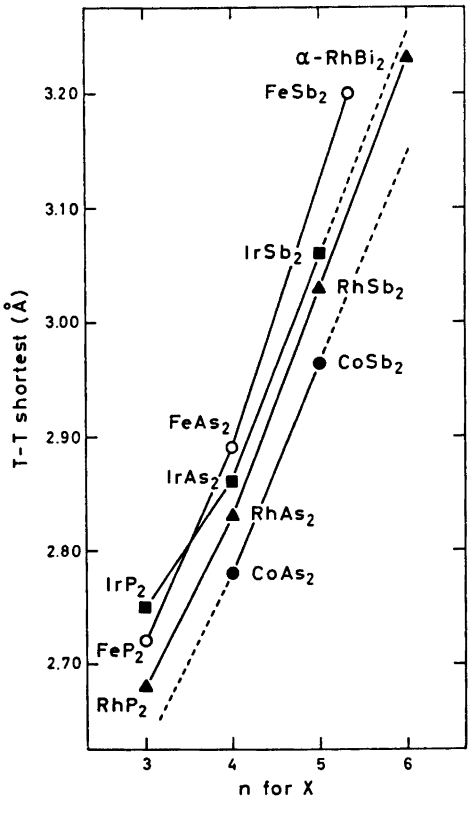

Fig. 6. Shortest $T-T$ distances *versus* principal quantum number (n) for X in TX_2 compounds with $CoSb_2$ type (●,▲,■) and three class A members of the FeS_2-m type (○) structures.

(vi) *On problems concerning the $CoSb_2$ type structure.* In order to approach the crucial problems concerning the $CoSb_2$ type structure, it is necessary to reexamine data accumulated for compounds of this type.

Fig. 6 shows the dependence of the shortest $T-T$ distance in the binary compounds with the $CoSb_2$ type structure (*cf.* Ref. 10) on the principal quantum number (n) for X. The series FeP_2-$FeAs_2$-$FeSb_2$, where the shortest $T-T$ distance equals the length of c in their FeS_2-m type structure, is included for the purpose of comparison. Although a variation in $T-T$ (as in $X-X$) bond length from compound to compound is expected, the dependence brought out in Fig. 6 shows marked and consistent trends. Even more striking is the fact that the curves for compounds with the $CoSb_2$ type structure show parallel behaviours to that for the comparison series FeP_2-$FeAs_2$-$FeSb_2$. This observation indicates that essentially the same effects are responsible for variations in shortest $T-T$ distances in compounds with the $CoSb_2$ as well as the class A, FeS_2-m type structure.

By qualitative bond strength arguments of the type presented in Ref. 27, the opposite trend to that shown on Fig. 6, *viz.* decreasing $T-T$ bond lengths with increasing n for X, is to be anticipated. (The P–P and T–P bonds should expectedly be stronger than (say) Bi–Bi and T–Bi bonds, and consequently, lead to weaker (longer) $T-T$ bonds for compounds of P compared to those of Bi.)

The ratios c/a and c/b (Fig. 1) for $CoAs_2$ and $CoSb_2$ fit nicely on to the curves traced out for phases with the FeS_2-m type structure. The c' axis of the pseudo-marcasite variant of the $CoSb_2$ type cell may be interpreted (*cf.*, *e.g.*, Ref. 18) as the average of a short and a long $T-T$ distance within the approximately linear T chains. The main structural distortion of CoX_2 compared with $Fe_{0.5}Ni_{0.5}X_2$ concerns just these alternating short and long $T-T$ distances, notably without producing a resultant shortening in the former case. Indeed, the formation of pairs with internal $T-T$ bonding in the $CoSb_2$ type structure should expectedly be accompanied by a marked shortening of c'.

In order to substantiate this inference, further attention should be focused on the T chains along $c(c')$ in $Fe_{1-t}Co_tX_2$. The mere fact that

these phases gradually transform from FeS_2-*m* to $CoSb_2$ type structure with increasing t is in itself (at least to some extent) incompatible with the assumption of bonded $T-T$ pairs as the stabilizing element in the latter. Depending on T there are three kinds of $T-T$ "contacts" (*viz.* Co – Co, Co – Fe, and Fe – Fe nearest neighbours). If only Co – Co "contacts" are bonding, how should the others be interpreted? The further assumption of Co – Fe and Fe – Fe bonds is contradicted by a number of evidences and their rejection contradicts even the basic assumption of $T-T$ bonding as the stabilizing element of the $CoSb_2$ type structure. In order to remedy these *de facto*, inherent contradictions, a statistical approach was proposed,[8] showing that a certain amount of the Co atoms in CoX_2 may be tolerated replaced by Fe without destroying the basic stability of the $CoSb_2$ type structure. However, even if this statistical approach to the $T-T$ bond is accepted, the problem still lies in the interpretation of the Co – Fe and Fe – Fe "contacts". By assuming a statistical distribution of these "contacts", relatively large defects (*viz.* non-bonding "contacts") would occur, which appears incompatible with an essentially localized model implied by isolated Co – Co pairs. It seems on the contrary, more reasonable that the stabilizing effect for the $CoSb_2$ type atomic arrangement is transmitted through *all* participating T atoms. A basically itinerant model has no difficulties in explaining randomly distributed Co – Co, Co – Fe, and Fe – Fe "contacts". The alteration in starting point does not invalidate the statistical considerations advocated in Ref. 8, which, in reality, did not include specific assumptions about the bonding characteristic of Co *versus* Fe.

The shortest Fe – Fe distance in the structure of FeAsS (arsenopyrite) [28] is 2.89 Å, and can be compared with 2.72 Å and 2.88 Å for FeP_2 and $FeAs_2$, respectively. Hence, the claim of one Fe – Fe bond per Fe in FeAsS, appears to suggest the existence of two Fe – Fe bonds per Fe in FeP_2 and $FeAs_2$. This would in turn demand a delocalization of electrons in infinitely bonded T chains along c for the latter compounds. Since the $T-T$ bonding assumption for compounds with class A, FeS_2-*m* type structure has been rejected (*cf.* Ref. 18; the points being elaborated further in a forthcoming paper), an identical conclusion appears to be appropriate also for FeAsS.

The preceding considerations have hopefully demonstrated that there are no clear-cut structural evidences in favour of $T-T$ bonding in compounds with the $CoSb_2$ type structure. The rejection of $T-T$ bonding naturally provokes an alternative interpretation of the generally semiconducting and diamagnetic behaviours within this class of compounds, an aspect which has been taken up by Goodenough.[20] Unfortunately, his treatment merely represents a translation of the earlier assumed [19,23] splitting of non-bonding *d* orbitals (*viz.* resulting in $T-T$ bonding and anti-bonding orbitals), into splitting (still unsubstantiated) of a narrow $T-X$ anti-bonding *d* band (*viz.* resulting in a $T-X$ bonding and an anti-bonding band). The cause of the splitting and hence, the distortion from the FeS_2-*m* to the $CoSb_2$ type structure, therefore, still remains to be found.

Emancipation from the assumption of $T-T$ bonding in compounds with the $CoSb_2$ type structure, entitles a clarifying comment on recently published [30] ^{121}Sb Mössbauer data. Originally, the chemical shift data for the compounds $CoSb_2$, $RhSb_2$, and $IrSb_2$ were not examined in detail because of the constraints supposedly imposed on their properties due to $T-T$ bonding. When ^{121}Sb Mössbauer chemical shifts are plotted for the three series $FeSb_2$-$CoSb_2$-$NiSb_2$, $RuSb_2$-$RhSb_2$-$PdSb_2$, and $OsSb_2$-$IrSb_2$-$PtSb_2$, curves of mutually similar appearance are obtained. It is notable that the three curves show marked peaks for compounds with the $CoSb_2$ type structure. These peaks can be made to disappear when chemical shifts are plotted against the (perhaps more natural parameter) Sb – Sb bond length. Within the limits of accuracy of the Sb – Sb bond lengths,[11,31–34] the thus resulting plot shows a linear relationship of decreasing chemical shift with increasing Sb – Sb bond length.

(vii) *Concluding remarks.* In the preceding paper,[11] class-wise correlations between positional parameters for well-determined structures of the FeS_2-*m* type were noted. Similar correlations between the ^{57}Fe Mössbauer parameters (δ, Δ) may also be expected. Thus, dependences somewhat similar to those found in Ref. 11 (*cf.* also Ref. 29) are shown on Fig. 7. It is to be noted that the points for the quasi-

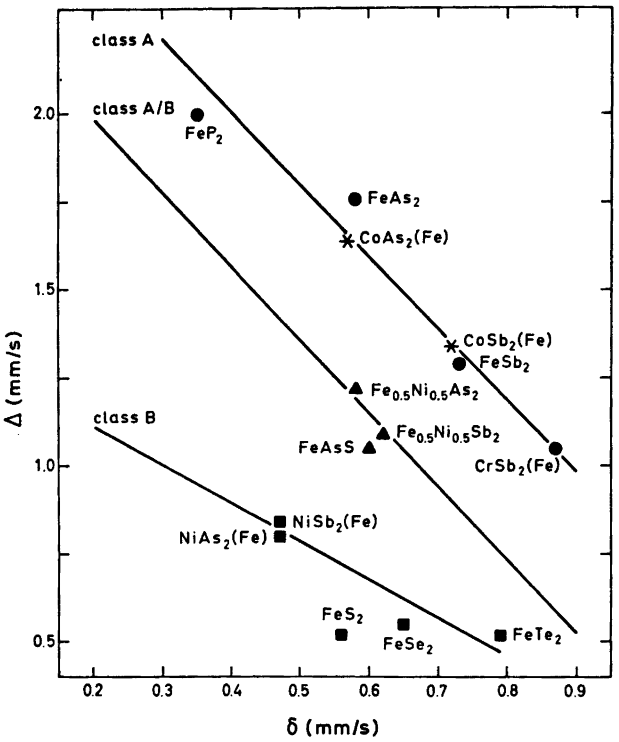

Fig. 7. ^{57}Fe Mössbauer parameters (δ and Δ) for some phases with FeS_2-*m* like structures.

binary compounds $CoAs_2$(Fe) and $CoSb_2$(Fe) occupy unexpected positions (marked with asterisks) on the diagram, suggesting that they belong to class A with respect to Mössbauer parameters.

The main purpose of this paper has been to present ^{57}Fe Mössbauer data for the phases $Cr_tFe_{1-t}X_2$, $Fe_{1-t}Co_tX_2$, and $Fe_{1-t}Ni_tX_2$. In attempts to interprete these data, results of supplementary experimental techniques have been consulted and/or called for. Moreover, since fruitful discussion in this field must draw heavily on theoretical model considerations, consultations of existing models were inescapable. At the present stage of development it was considered worthwhile to consult the model(s) presented by Goodenough,[20] earlier models being uninteresting since he has claimed that they all contain defects. As inferred *inter alia* on comparison with the Mössbauer data, not even Goodenough's treatment is free from inherent shortcomings. In order to improve on Goodenough's model(s), a critical reexamination of the basic bonding assumptions is necessary. This will be the subject of a forthcoming paper.

REFERENCES

1. Holseth, H. and Kjekshus, A. *J. Less-Common Metals 16* (1968) 472.
2. Holseth, H., Kjekshus, A. and Andresen, A. F. *Acta Chem. Scand. 24* (1970) 3309.
3. Fan, A. K. L., Rosenthal, G. H., McKinzie, H. L. and Wold, A. *J. Solid State Chem. 5* (1972) 136.
4. Johnston, W. D., Miller, R. C. and Damon, D. H. *J. Less-Common Metals 8* (1965) 272.
5. Temperley, A. A. and Lefevre, H. W. *J. Phys. Chem. Solids 27* (1966) 85.
6. Steger, J. and Kostiner, E. *J. Solid State Chem. 5* (1972) 131.
7. Roseboom, E. H. *Amer. Mineral. 48* (1963) 271.
8. Bjerkelund, E. and Kjekshus, A. *Acta Chem. Scand. 24* (1970) 3317.
9. Holseth, H. and Kjekshus, A. *Acta Chem. Scand. 22* (1968) 3273.

10. Kjekshus, A. *Acta Chem. Scand. 25* (1971) 411.
11. Kjekshus, A., Rakke, T. and Andresen, A. F. *Acta Chem. Scand. A 28* (1974) 996.
12. Jeitschko, W. and Donohue, P. C. *Acta Crystallogr. B 29* (1973) 783.
13. Selte, K., Kjekshus, A., Jamison, W. E., Andresen, A. F. and Engebretsen, J. E. *Acta Chem. Scand. 25* (1971) 1703.
14. Selte, K., Kjekshus, A. and Andresen, A. F. *Acta Chem. Scand. 26* (1972) 3101.
15. Kjekshus, A., Nicholson, D. G. and Mukherjee, A. D. *Acta Chem. Scand. 26* (1972) 1105.
16. Hulliger, F. *Nature (London) 198* (1963) 1081.
17. Kjekshus, A. and Rakke, T. *To be published.*
18. Brostigen, G. and Kjekshus, A. *Acta Chem. Scand. 24* (1970) 2983.
19. Brostigen, G. and Kjekshus, A. *Acta Chem. Scand. 24* (1970) 2993.
20. Goodenough, J. B. *J. Solid State Chem. 5* (1972) 144.
21. Furuseth, S., Selte, K. and Kjekshus, A. *Acta Chem. Scand. 21* (1967) 527.
22. Hume-Rothery, W. *The Structure of Metals and Alloys.* Institute of Metals, London 1936.
23. Hulliger, F. and Mooser, E. *Progr. Solid State Chem. 2* (1965) 330.
24. Hulliger, F. and Mooser, E. *J. Phys. Chem. Solids 26* (1965) 429.
25. Pearson, W. *Z. Krist. 121* (1965) 449.
26. Gallagher, P. K., MacChesney, J. B. and Sherwood, R. C. *J. Chem. Phys. 50* (1969) 4417.
27. Kjekshus, A. and Nicholson, D. G. *Acta Chem. Scand. 25* (1971) 866.
28. Buerger, M. J. *Z. Krist. 95* (1936) 83.
29. Kjekshus, A. and Rakke, T. *Struct. Bonding (Berlin) 19* (1974) 85.
30. Donaldson, J. D., Kjekshus, A., Nicholson, D. G. and Tricker, M. J. *Acta Chem. Scand. 26* (1972) 3215.
31. Zhdanov, G. S. and Kuz'min, R. *N. Soviet Phys. – Crystallogr. 6* (1962) 704.
32. Furuseth, S., Selte, K. and Kjekshus, A. *Acta Chem. Scand. 19* (1965) 735.
33. Holseth, H. and Kjekshus, A. *Acta Chem. Scand. 22* (1968) 3284.
34. Holseth, H. and Kjekshus, A. *Acta Chem. Scand. 23* (1969) 3043.

Received May 9, 1974.

Acta Chemica Scandinavica A 28 (1974) 1011—1014

Kinetic Evidence for a Dipyridine Complex with Tervalent Phosphorus

LEIV J. STANGELAND

Department of Chemistry, University of Bergen, N-5014 Bergen-Univ., Norway

The rates of reaction between pyridines and diphenylhalophosphines have been examined by the spectrophotometric stopped flow technique. In a toluene – acetonitrile mixture the reaction is found to have a reaction order of both one and two with respect to pyridine, while in a toluene – dioxane mixture the rate is found to be dependent on the square of the pyridine concentration. The mechanism for these reactions has been discussed and reaction schemes are proposed.

Recently the reactions of a series of alkyl- and arylphosphines, -arsines, or -stibines with a variety of halo- and haloalkyl- (or haloaryl) phosphines, -arsines, or -stibines have been reported.[1] In most instances the formation of adducts of the general formula $R_nMX_{3-n}.yM'R'_3$, where $y=1$ or 2, were obtained. Similarly a relatively unstable compound $(CH_3)_3P_{1.96}.PCl_3$ has been isolated as a solid from the reaction between 2 mol trimethylphosphine and one mol of phosphorus trichloride.[2] There is reason to believe that tervalent nitrogen may act as a ligand atom on phosphorus in this kind of 1:2 complexes, and in a recent article Boal and Ozin have given spectroscopical evidence for the formation of the complex $Cl_3P.2N(CH_3)_3$.[3]

The present work was undertaken in order to shed some light on the reaction mechanism for the formation of 1:1 complexes between phosphorus compounds and amines. These complexes have for a long time been known to exist.[4–7] The kinetic experiments were, however, done under pseudo first order conditions with the amines in excess, and the results indicate that not only one but two nitrogen atoms were accepted as ligands on each phosphorus atom.

RESULTS

The rate of reaction of three different pyridines with bromo diphenylphosphine (BDP) has been measured in 10 vol % acetonitrile in toluene (Table 1). The reaction rates have also been measured for the reaction between pyridine and bromo diphenylphosphine in 30 vol. % dioxane in toluene (Table 2), and for the reaction between pyridine and chloro diphenylphosphine (CDP) in 10 vol. % acetonitrile in toluene (Table 3). The disappearance of the phosphines was used in following the kinetics. The cosolvent was added to toluene to avoid precipitation of the complex formed.

The measurements were all made at pseudo first order conditions with pyridine in excess and the kinetic plots were linear up to 90 % of reaction.

By plotting the obtained pseudo first order rate constants divided by the pyridine concentration ($k' \times [Py]^{-1}$) as a function of the pyridine concentration straight lines were obtained. For all reactions measured with acetonitrile as a cosolvent there were interceptions and the rate law is given by eqn. 1.

$$\text{Rate} = k_2[\text{substrate}][\text{Py}] + k_3[\text{substrate}][\text{Py}]^2 \quad (1)$$

For the reaction between pyridine and BDP in 30 % dioxane there was no such interception and the rate may be given by egn. 2.

$$\text{Rate} = k_3[\text{substrate}][\text{Py}]^2 \quad (2)$$

By plotting the logarithms of the rate constants obtained in the reactions between BDP and different pyridines, *versus* the pK_a's of the pyridines, Brønsted coefficients of 0.53 and

Table 1. Pseudo first order rate constants for the reaction of bromo diphenylphosphine with pyridines in 10 % acetonitrile-toluene mixture.[a,b]

Nucleophile	Conc. nucl. $\times 10^2$ M	k' s^{-1}	k'/Conc.nucl. M^{-1} s^{-1}	pK_a[c]
4-Methyl-pyridine	2.64	0.445	16.9	6.40
	5.22	1.10	21.0	
	7.04	1.78	25.2	
	9.89	2.99	30.3	
	10.35	3.00	29.0	
	15.72	6.54	41.6	
	15.76	6.79	43.1	
	21.10	11.52	54.6	
Pyridine	5.44	0.32	5.8	5.54
	9.37	0.75	8.0	
	15.57	1.93	12.4	
	21.90	3.12	14.3	
Ethyl-pyridine-3-carboxylate	8.65	0.028	0.32	3.45
	16.60	0.051	0.31	
	25.00	0.099	0.39	
	32.03	0.123	0.39	

[a] The percentage is by volume. [b] The substrate concentration is *ca.* $5-7\times10^{-4}$ M. [c] In water at 25 °C.

Table 2. Pseudo first order rate constants for the reaction of bromo diphenylphosphine with pyridine in 30 % dioxane-toluene mixture.[a,b]

Conc. of pyridine $\times 10^2$ M	k' s^{-1}	k'/Conc. pyridine M^{-1} s^{-1}
6.30	2.39	0.379
14.42	6.30	0.437
18.85	15.05	0.799
26.35	28.30	1.074

[a] The percentage is by volume. [b] The substrate concentration is *ca.* $5-7\times10^{-4}$ M.

Table 3. Pseudo first order rate constants for the reaction of chloro diphenylphosphine with pyridine in 10 % acetonitrile-toluene mixture.[a,b]

Conc. of pyridine $\times 10^2$ M	k' s^{-1}	k'/Conc. pyridine M^{-1} s^{-1}
2.64	1.05	0.398
7.04	3.75	0.532
10.35	6.08	0.587
15.76	11.18	0.709
21.10	19.00	0.900

[a] The percentage is by volume. [b] The substrate concentration is *ca.* 6×10^{-4} M.

1.0 are obtained for k_2 and k_3 respectively.

The ratio between the rate constants (eqn. 1) for the reactions of pyridine with BDP and CDP is 8.5 in the second order term and 22 in the third order term, and k_3 is 11 times greater in 10 % acetonitrile than in 30 % dioxane for the pyridine – BDP reaction.

The pseudo first order rate constants are given in Tables 1, 2, and 3, and the second and third order rate constants are given in Table 4. The pseudo first order rate constants for the reactions between BDP and pyridines divided by the pyridine concentration are plotted in Fig. 1 as a function of the pyridine concentration.

EXPERIMENTAL

The chloro diphenylphosphine used was a commercial product. It was distilled twice under nitrogen prior to use. The procedure for the synthesis of pyridine-3-carboxylate and bromo diphenylphosphine and for the purification of these reagents together with the applied solvents has previously been described.[8]

In a typical run the pyridine was weighed in a volumetric flask and diluted to the mark with a mixture of toluene and twice the amount of the desired cosolvent. 0.1 ml of a standard solution of the substrate in toluene was injected

Table 4. Summary of the second and third order rate constants. $Ph_2PX + 2Nu \longrightarrow Ph_2PX.2Nu$

Solvent	Phosphine	Nu[a]	$k_2 M^{-1}s^{-1}$	$k_3 M^{-2}s^{-1}$
Acetonitrile, 10 %	BDP	MePy	10.3	205
		Py	3.1	54
		EtPy	0.27	0.37
	CDP	Py	0.33	2.55
Dioxane, 30 %	BDP	Py	0.00	4.14

[a] MePy is 4-methylpyridine, Py is pyridine, and EtPy is ethyl pyridine-3-carboxylate.

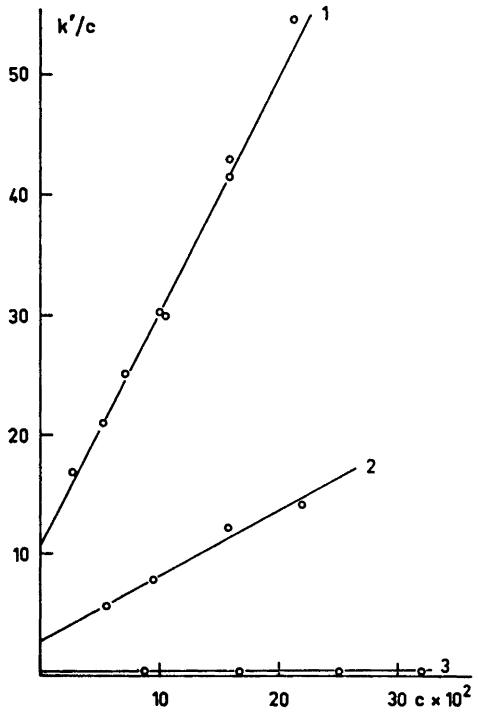

Fig. 1. Pseudo first order rate constants divided by the pyridine concentration as a function of the pyridine concentration for the reaction between bromo diphenylphosphine and pyridines in 10 % acetonitrile – toluene mixture. (1) 4-Methyl pyridine. (2) Pyridine. (3) Ethyl pyridine-3-carboxylate.

into about 5 ml of toluene. After nitrogen had been bubbled through the solutions they were mixed in the stopped flow apparatus and the reaction measured as described.[8] All measurements were made at 25 °C.

DISCUSSION

There is a significant change in the rate equation (eqn. 1) when acetonitrile is exchanged with dioxane as a cosolvent. In 30 % dioxane the second order term has disappeared, and the explanation of this may be found in the different inertness towards the substrate of these two solvents.

There are two ways to explain the third order term which is common in the two rate equations. One is that two pyridine molecules attack the substrate simultaneously to form the 1:2 complex, and the other is that there exists an equilibrium between pyridine and the substrate to form a 1:1 complex which may react with a second molecule of pyridine. We think that the second explanation is the most probable because 1:1 complexes between tervalent phosphorus and amine are known [4-7] and a 1:1 intermediate between BDP and pyridine is also indicated in the pyridine catalyzed methanolysis of BDP.[8] The rate of nucleophilic attack on tervalent phosphorus is known to be fast, and the first attack on P^{III} in our reactions is assumed to be too fast to be measured with the stopped flow technique. When a 1:1 adduct has been formed, the electrophilicity of the phosphorus atom should have diminished and thus have made the rate measureable for the second attack of a pyridine molecule. The mechanism proposed should then be as shown in eqn. 3.

$$Ph_2P-X + Py \rightleftharpoons Ph_2P-X.Py \xrightarrow{Py} Ph_2P-X.2Py \qquad (3)$$

Acetonitrile is known to act as a ligand towards a series of Lewis acids [9] and we may

therefore assume that in addition to the equilibrium between the phosphine and pyridine, we also have a competitive equilibrium between the phosphine and acetonitrile. This should be reflected as a competitive reaction in the rate equation, and the reaction leading to the second order term in the rate equation (eqn. 1) should be given as shown in eqn. 4.

$$Ph_2P-X + MeCN \rightleftharpoons Ph_2P-X.MeCN \xrightarrow{Py} Ph_2P-X.(MeCN).Py \qquad (4)$$

The halide is in certain cases known to be displaced from R_2P-X compounds when a 1:1 complex is formed as in the reaction between triethylphosphine and chloro dimethylphosphine in the formation of $[(C_2H_5)_3PP(CH_3)_2]Cl$.[10] In our reaction, however, we have a significant effect due to the halide. This effect should be absent if the phosphorus-halogen bond was broken prior to the rate determining step and it appears therefore that in the product-forming step the halogen must still be in the sphere of influence of the phosphorus atom.

The complexes between tervalent phosphorus compounds and amines are in general very unstable when more than one amine molecule is attached to the phosphorus atom. Their existence has been indicated by spectroscopic studies [3] and by vapor pressure measurement.[11] The structure of these complexes is not known but it might be of interest to look at similar complexes which have the same electronic configuration around the central atom. In the compound $PCl_3.2P(CH_3)_3$ the two entering phosphorus atoms have been found to be axial to each other,[12] while X-ray determination of $SbCl_3.2OAsPh_3$ has shown it to have a *cis*-pseudooctahedral stereochemistry as shown in (I).[13] Boal and Ozin suggest a similar structure for $PCl_3.2N(CH_3)_3$.[3]

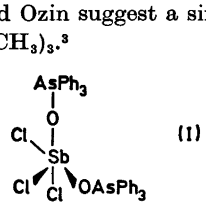

(I)

REFERENCES

1. Summers, J. G. and Sisler, H. H. *Inorg. Chem. 9* (1970) 862.
2. Holmes, R. R. and Bertaut, E. F. *J. Amer. Chem. Soc. 80* (1958) 2980.
3. Boal, D. H. and Ozin, G. A. *J. Chem. Soc. Dalton Trans.* (1972) 1824.
4. Holmes, R. R. *J. Amer. Chem. Soc. 82* (1960) 5285.
5. Holmes, R. R. and Wagner, R. P. *Inorg. Chem. 2* (1963) 384.
6. Holmes, R. R. *J. Phys. Chem. 64* (1960) 1295.
7. Griffiths, J. E. and Burg. A. B. *J. Amer. Chem. Soc. 82* (1960) 1508.
8. Stangeland, L. J. *Acta Chem. Scand. 27* (1973) 1503.
9. Nicholls, D. *Coord. Chem. Rev. 1* (1966) 379.
10. Spangenberg, S. F. and Sisler, H. H. *Inorg. Chem. 8* (1969) 1006.
11. Trost, W. R. *Can. J. Chem. 32* (1954) 356.
12. Frieson, D. *M. Sc. Thesis*, University of Toronto, Toronto 1972.
13. Lindquist, I. *Inorganic Adduct Molecules of Oxocompounds*, Springer, Berlin 1963, p. 71.

Received June 4, 1974.

Acta Chemica Scandinavica A 28 (1974) 1015—1020

The Crystal and Molecular Structure of Diethyldithiophosphinatothallium(I)

STEINAR ESPERÅS and STEINAR HUSEBYE

Department of Chemistry, University of Bergen, N-5014 Bergen, Norway

The crystal and molecular structure of diethyldithiophosphinatothallium(I), [$Tl(Et_2PS_2)$], has been determined from three-dimensional X-ray data collected by multiple-film technique using Cu$K\alpha$ radiation. The crystals are orthorhombic with space group *Pcca*. The unit cell contains four formula units and has the dimensions $a = 9.026(3)$ Å, $b = 12.134(2)$ Å, and $c = 8.468(3)$ Å. The calculated density is 2.56 g/cm³. Full matrix least squares refinement of the structure has yielded a final value of the conventional *R*-factor of 0.094 for 376 visually estimated reflections.

The structure is built from monomeric units linked together in two-dimensional polymeric layers parallel to the *ac*-plane. Each metal atom is coordinated by six sulfur atoms; two of these belong to the monomer, the remaining four, more distant ones, belong to four different adjacent monomers. The Tl−S distances are found to be 3.056(7) Å, 3.429(10) Å, and 3.453(7) Å.

Studies of dithiocarbamate complexes of monovalent copper, silver, gold, cesium, and thallium have revealed that these exist as polymers, both in solutions of nonpolar organic solvents [1–4] and in the solid state. [5–10] Not much is at present known with certainty about the structures of the dissolved polymers, but in most cases the degree of polymerisation obtained from solution studies agrees well with the crystal structure results. Whereas the complexes of the first three metals mentioned above are arranged as discrete low polymers, the others can be considered as interconnected dimers having very interesting structures. Dipropyldithiocarbamatothallium(I),[9] $Tl(pr)_2NCS_2$, has a chain arrangement of dimeric units, whereas the dimers are linked together into layers in diisopropyldithiocarbamatothallium(I),[10] $Tl(iso\text{-}pr)_2NCS_2$, and in dibutyldithiocarbamatocesium(I),[8] $Cs\ (bu)_2NCS_2$.

The preparation of a number of metal complexes of thio- and selenophosphinic acids has been reported by Kuchen and Hertel.[11] Some of these complexes appear to be associated in nonpolar organic solvents.[11,12] The diethyldithiophosphinato complex of monovalent thallium, with which the present crystallographic study is concerned, was found to have an average degree of association in chloroform and benzene solution of 1.45 and 1.25, respectively; *i.e.*, although the molecules are associated, they are best described as built up from monomeric units. Considering the agreement between the degrees of polymerization of various dithiocarbamate metal complexes in solution and in the solid state, and the essentially dimeric crystal structure found for the diethylthioselenophosphinate analogue of thallium(I),[13] some kind of polymeric arrangement was also expected to be found in the present investigation.

EXPERIMENTAL

The crystals used in the investigation were made by Kuchen *et al.*[12] They were prepared by reduction of trivalent thallium by diethyldithiophosphinate ions:

$$Tl^{3+} + 3Et_2PS_2^- = Tl(Et_2PS_2) + (Et_2PS_2)_2$$

The crystals were recrystallized from chloroform solution, and were obtained as thin colourless plates elongated along the *c* axis.

Unit cell parameters were calculated from 51

high-order reflections read from NaCl-calibrated Weissenberg $0kl$ and $hk0$ films, employing Cu$K\alpha$ radiation. Refinement by least squares gave final values of $a = 9.026(3)$ Å, $b = 12.134(2)$ Å and $c = 8.468(3)$ Å. There are four molecules in the cell. The calculated density is 2.56 g/cm³. From systematic absence, $0kl$ for $l = 2n+1$, $h0l$ for $l = 2n+1$ and $hk0$ for $h = 2n+1$, the space group is $D_{2h}^{8} - Pcca$.

Using the multiple-film technique, Weissenberg equi-inclination photographs were taken of the $hk0$, $hk1$, $hk2$, $hk3$, and $0kl$ layers, using Ni-filtered Cu$K\alpha$ radiation. Reflection intensities were estimated visually. Of 507 independent reflections 376 were observed. The data were corrected for Lorentz and polarization effects to give sets of relative structure factors. During refinement they were also corrected for absorption effects ($\mu = 386$ cm^{-1}), using the Gaussian integration method as described by Coppens *et al.*[14] The number of grid points used along the a, b, and c axes were 14, 4, and 14, respectively, for both crystals.

The calculated structure factors were based on the atomic scattering curves given in *International Tables for X-Ray Crystallography*,[15] Table 3.3.1A. The curves for thallium were corrected for anomalous dispersion using the $\Delta f'$ and $\Delta f''$ values given by Cromer,[16] and taking the amplitude of f as the corrected value.

STRUCTURE DETERMINATION

In addition to the general absences, reflections hkl with $h+l = 2n+1$ were systematically weaker than the others. This indicated that the molecules occupy fourfold special positions with the thallium and phosphorus atoms on twofold axes, *i.e.*, the structure is probably to be interpreted in terms of monomeric molecules.

The atomic positions except those for hydrogen were determined by standard Patterson and Fourier techniques.

The refinement was carried out on an IBM 360/50H computer, using a full-matrix least squares program which minimizes the expression $r = \sum w(|F_o| - K|F_c|)$.[2] K is a scale factor and w, the relative weight assigned to a reflection, is the reciprocal of the variance, $1/\sigma^2(F)$. $\sigma^2(F)$ is equal to $(Ka_1)^2 + (a_2F_o)^2/4w_o + (a_3F_o)^6$, where w_o is a variable related to the reliability with which the intensity of a given reflection is measured, and a_1, a_2, and a_3 are constants. These were first put equal to 2.0, 1.0, and 0.0, but were on a later stage of refinement changed to 0.8, 0.15, and 0.012, respectively. Unobserved reflections were included with $|F_o|$ equal to the observable limit, when $|F_c|$ exceeded this limit.

The difference map calculated on the basis of the thallium, sulfur, and phosphorus contributions showed a peak corresponding to about 6e⁻/Å³ and two peaks corresponding to about half this value. The largest was chosen as the methylene carbon position in the ethyl group, the two other maxima might then both correspond to the methyl carbon. Attempts to refine the structure, placing methyl carbon in either of the two positions mentioned above were not successful. It was then thought likely that the ethyl group was disordered, *i.e.*, there are two types molecules, corresponding to two different configurations of the ethyl group statistically distributed in the crystals. Based on a 1:1 distribution of the two types of molecules, and isotropic temperature factors for all atoms, the structure refined satisfactorily, to a value of the reliability index, $R = \sum||F_o| - |F_c||/\sum|F_o|$, of 0.180.

At this stage of refinement the data were corrected for absorption, leading to an R-value 0.122. Finally, anisotropic temperature factors were applied to the thallium, sulfur and phosphorus atoms. The R-factor converged at a value of 0.094.

A final difference electron density map showed a peak of 2.5 e⁻/Å³ near the thallium position. Similar peaks have also been found in difference maps for other thallium compounds.[13,17]

Observed and calculated structure factors following the last refinement cycle can be obtained from the authors upon request.

Table 1. Final atomic coordinates in fractions of cell edges with standard deviations in brackets.

	x	y	z
Tl	0.0	0.0858(1)	0.25
S	0.1407(7)	−0.1251(5)	0.1219(12)
P	0.0	−0.2132(6)	0.25
Cl	0.111(3)	−0.306(2)	0.386(4)
C21[a]	0.216(7)	−0.375(5)	0.323(10)
C22[a]	0.019(7)	−0.395(5)	0.461(12)

[a] Methyl carbon positions in the disordered ethyl group.

Table 2. Components of atomic vibration tensors, $U \times 10^3$, in Å^2 with standard deviations, referred to crystallographic axes. For Te, S, and P, the expression is $\exp\{-2\pi^2 \times [U_{11}(ha^{-1})^2 + U_{22}(kb^{-1})^2 + U_{33}(lc^{-1})^2 + 2U_{12}a^{-1}b^{-1}hk + 2U_{23}b^{-1}c^{-1}kl + 2U_{13}a^{-1}c^{-1}hl]\}$. For carbon atoms the expression is $\exp[-8\pi^2 U(\sin^2\theta/\lambda^2)]$.

Tl	71.1(1.1)	58.7(0.9)	71.3(1.8)	(U_{11}, U_{22}, U_{33})
	0.0	0.0	2.3(1.4)	(U_{12}, U_{23}, U_{13})
P	46.3(3.4)	49.1(3.3)	51.2(6.7)	
	0.0	0.0	−4.6(7.5)	
S	59.0(2.9)	64.3(2.8)	89.9(7.2)	
	−0.2(3.0)	−0.3(4.4)	7.2(5.3)	
C1	65.2(6.8)			(U)
C21	82.2(17.1)			
C22	102.2(24.1)			

RESULTS AND DISCUSSION OF THE STRUCTURE

The final positional and thermal parameters are listed in Tables 1 and 2, respectively. Interatomic distances and angles are listed in Tables 3 and 4.

Table 3. Bond lengths (Å) and angles (°) in a diethyldithiophosphinatothallium(I) molecule. Standard deviations in brackets. Atoms in the other half of the molecule related to those in the asymmetric unit are denoted by primed letters.

Tl−S	3.056(7)	∠S−Tl−S′	66.2(2)
S−P	1.982(9)	Tl−S−P	89.5(3)
P−Cl	1.89(3)	S−P−S′	114.7(4)
Cl−C21	1.38(7)	S−P−Cl	108.4(8)
Cl−C22	1.50(8)	Cl−P−Cl′	107.5(12)
S−S′ distance	3.34(1)	P−Cl−C21	119.1(36)
		P−Cl−C22	113.1(31)
		C21−Cl−C22	95.7(40)

Table 4. Intermolecular distances in Å. The left column represents distances from an atom in the original molecule (Table 2) to an atom in a molecule whose transformation from the original one is listed in the second column.

Tl−S	$\frac{1}{2}-x,-y,z$	3.453(7)
Tl−S	$x-\frac{1}{2},-y,\frac{1}{2}-z$	3.453(7)
Tl−S	$-x,-y,-z$	3.429(10)
Tl−S	$x,-y,z+\frac{1}{2}$	3.429(10)
S−S	$\frac{1}{2}-x,-y,z$	3.621(9)
S−Cl	$\frac{1}{2}-x,y,z-\frac{1}{2}$	3.72(3)
C21−C22	$\frac{1}{2}-x,-(y+1),z$	3.86(9)
C21−C22	$-x,-(y+1),1-z$	3.95(11)
C21−C22	$\frac{1}{2}-x,y,z-\frac{1}{2}$	3.90(12)

Bond lengths and bond angles in a diethyldithiophosphinatothallium(I) molecule are shown in Fig. 1. A view of the unit cell seen along the *b*-axis is shown in Fig. 2. A stereoscopic drawing showing the packing of molecules is given in Fig. 3.

The crystals of diethyldithiophosphinatothallium(I) are built from monomeric units linked together in two-dimensional polymeric layers with a thickness of two molecules parallel to the *ac*-plane. Each thallium atom is coordinated to six sulfur atoms situated at the corners of a distorted trigonal prism. Two of these sulfur atoms belong to the molecule proper, the remaining four more distant ones belong to four different adjacent molecules. In addition to the Tl−S intermonomer bonds, there also exist S−S, S−C, and C−C van der Waals contacts between molecules in the same layer. The only interactions between adjacent layers are of van der Waals type between the alkyl groups.

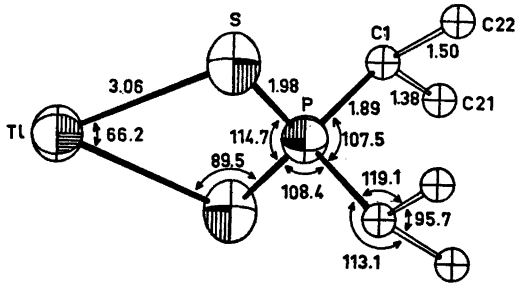

Fig. 1. The molecule with bond lengths and bond angles indicated. Both methyl carbon atoms in the disordered ethyl groups are shown.

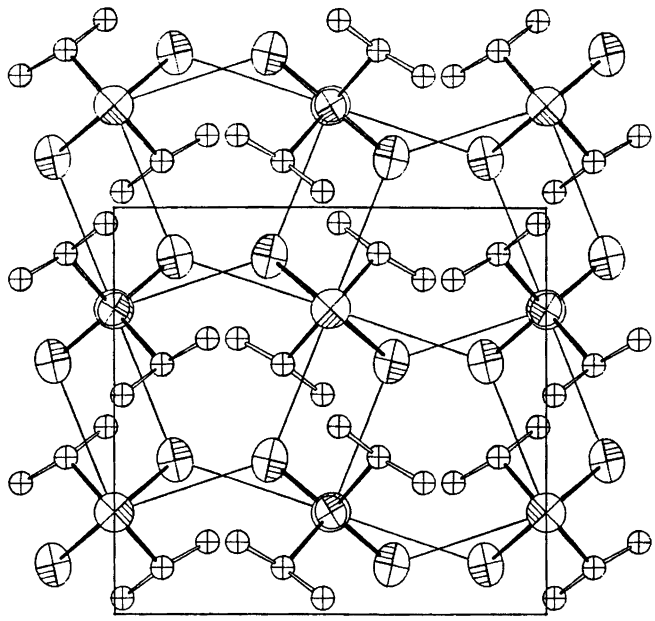

Fig. 2. A view of the unit cell as seen along the *b* axis. Intermolecular Tl – S contacts are indicated by weaker lines. The complete set of four contacts are shown only for the thallium atom in the center of the figure.

Also the structure of diethylthioselenophosphinatothallium(I) [13] and diisopropyldithiocarbamatothallium(I)[10], are built as layer arrangements. The complex described here must be regarded as consisting of monomers, in contrast to the two others which are best described as being built from dimeric units. In the other two complexes mentioned above and also in dipropyldithiocarbamatothallium(I),[9] there are four relatively short thallium-ligand bonds and two longer ones.

The intralayer Tl – Tl separations of about 4.7 Å and 5.0 Å are significantly larger than the metal-metal distances in corresponding dimeric thallium(I) complexes. In [Tl(Et_2PSeS)],[13] [Tl(pr)$_2$NCS$_2$],[9] and [Tl(iso-pr)$_2$NCS$_2$] [10] the shortest intermetallic distances are found to be 3.86 Å, 3.98 Å, and 3.58 Å, respectively. Similar and somewhat longer distances are also found in thallium metoxide,[18] $TlOCH_3$, thallium cyclopentadienyl,[19] C_5H_5Tl, and thiourea complexes of thallous salts.[20] The metal-metal separations are 3.84 Å and 3.99 Å, respectively, in the former two compounds, and 4.08 Å and 4.15 Å in the thiourea compounds. Thus the Tl – Tl distances in the complex considered seem too

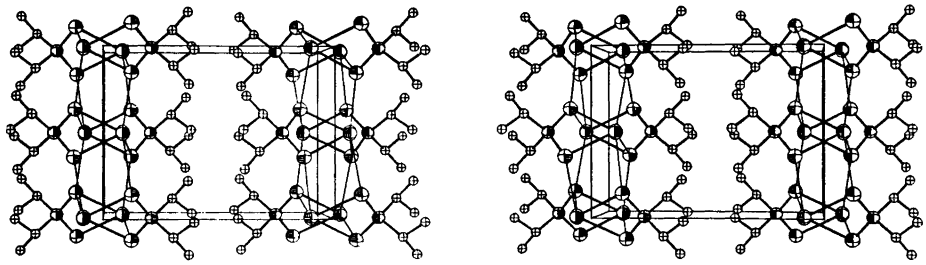

Fig. 3. A stereoscopic drawing showing the packing of molecules as seen along the *c* axis.

large to allow any metal-metal interactions.

The lone pair of electrons in this and similar compounds seems to be stereochemically active.[13,21] The four longer bonds found here are in accordance with the assumption that the lone pair occupies an *sp*-hybridized orbital pointing away from the shorter bonds.

The intramolecular thallium – sulfur bond lengths are 3.056(7) Å, whereas the weaker intermolecular thallium – sulfur bond distances are 3.429(10) Å and 3.453(7) Å. The former correspond to the mean value of the three short Tl – S bonds in $[Tl(pr)_2NCS_2]$,[9] and are also close to the Tl – S intradimer coordination distances in $[Tl(iso\text{-}pr)_2NCS_2]$.[10] In $[Tl(Et_2PSeS)]$,[13] on the other hand, the Tl – S bonds are 3.237(5) Å. The value of the Tl – S covalent distance is somewhat uncertain as no definite covalent radius for thallium is available in the literature. A value somewhere between 2.5 Å and 2.8 Å seems to be probable.[22,23] The thallium-sulfur bonds of the length mentioned above are, however, comparable to the sum of the atomic radii given by Slater (2.90 Å),[24] and such bonds are described as essentially covalent in a number of thallium(I) compounds.[9]

The intermolecular Tl – S coordination distances are too large for any perceptible covalent interaction. These bond lengths are, however, close to the Tl – S distances found in thiourea complexes of thallium(I) salts, as studied by Verhoef, Boeyens and Herbstein,[20,23,25] and somewhat longer than the sum of the Pauling ionic radii of Tl^+ and S^{2-} of 3.28 Å.[26] The interaction is proposed by Verhoef *et al.* to be of ion-dipole type.

The Tl – S bonds are comparable with the Tl – S dimer-dimer interactions in $[Tl(pr)_2NCS_2]$,[9] and also with the Tl – Se intradimer contacts in $[Tl(Et_2PSSe)]$,[13] as the difference in bond lengths is close to the difference in the selenium and sulfur covalent radii.

The sulfur-phosphorus bond lengths are found to be 1.982(9) Å, which seems to be normal for metal phosphinates. The length corresponds to a π-bond order of 0.50 based on Pauling's bond order – bond length relationship. The P – S single-bond length and P = S double bond length are both based on radii given by Pauling;[26] the former, corrected for bond polarity is 2.10 Å, the latter is 1.94 Å. The double-bond character of these bonds is also indicated from IR spectra recorded by Kuchen and Hertel.[11]

The P – C and C – C bond lengths correspond to normal values within the error limits, and the bond angles on the phosphorus atom are in good agreement with sp^3-hybridization on this atom.

Two short interlayer contacts, C22 – C22 $[-x,-(y+1),1-z]$ of 2.66 Å and C21 – C21 $[\frac{1}{2}-x,-(y+1),z]$ of 3.10 Å, and a short intralayer intermolecular C – C distance of 3.30 Å, C21 – C22 $[x+\frac{1}{2},y,1-z]$, are found. These distances are too short to represent real intermolecular contacts and do not exist in the true structure, but are a result of disorder in the ethyl groups. The following molecular contacts between layers, *i.e.*, across glide planes parallel to the *ac* plane at $y = \pm(n \times 0.5)\ b$; $n = 0,1,2,\cdots$, may therefore be imagined: Pairs of molecules related by centres of symmetry lying on these glide planes must have different orientations of their methyl groups, one molecule having C21 groups only, the other C22 groups only, or *vice versa*. In this way, C22 – C22 contacts (2.66 Å) across centres of symmetry are avoided. Likewise, pairs of molecules related by twofold axes lying on the same glide planes must differ in the same manner, so that the close C21 – C21 contacts (3.10 Å) are avoided. However, in the *c*-direction the stacking must be based on molecules with C21 groups alternating with molecules with C22 groups, in order to maintain the symmetry. This also eliminates the short intralayer distance of 3.30 Å.

The shortest interlayer contact is thus 3.86 Å, between methyl carbons.

Acknowledgement. The authors thank Dr. Wilhelm Kuchen, Institut für anorganische Chemie der Universität Düsseldorf, for a sample of crystals.

REFERENCES

1. Fredga, A. *Rec. Trav. Chim. Pays-Bas 69* (1950) 416.
2. Åkerström, S. *Acta Univ. Upsal. 62* (1965), Diss., Uppsala.
3. Åkerström, S. and Uhlin, A. *Ark. Kemi 24* (1965) 503.
4. Åkerström, S. *Ark. Kemi 24* (1965) 495.
5. Hesse, R. *Ark. Kemi 20* (1963) 481.
6. Hesse, R. and Nilson, L. *Acta Chem. Scand. 23* (1969) 825.

7. Hesse, R. *Advances in the Chemistry of the Coordination Compounds*, New York 1961, p. 314.
8. Aava, U. and Hesse, R. *Ark. Kemi 30* (1969) 149.
9. Nilson, L. and Hesse, R. *Acta Chem. Scand. 23* (1969) 1951.
10. Jennische, P., Olin, Å. and Hesse, R. *Acta Chem. Scand. 26* (1972) 2799.
11. Kuchen, W. and Hertel, H. *Angew. Chemie 81* (1969) 127.
12. Kuchen, W. and Mayatepek, H. *Chem. Ber. 101* (1968) 3454.
13. Esperås, S. and Husebye, S. *Acta Chem. Scand. 27* (1973) 3355.
14. Coppens, P., Leiserowitz, L. and Rabinovich, D. *Acta Crystallogr. 18* (1965) 1035.
15. *International Tables for X-Ray Crystallography*, Kynoch Press, Birmingham 1962, Vol. III.
16. Cromer, D. T. *Acta Crystallogr. 18* (1965) 17.
17. Olofsson, O. and Gullman, J. *Acta Chem. Scand. 25* (1971) 1327.
18. Dahl, L. F., Davis, G. L., Wampler, D. L. and West, R. *J. Inorg. Nucl. Chem. 24* (1962) 357.
19. Frasson, E., Monegus, F. and Panattoni, C. *Nature (London) 199* (1963) 1087.
20. Verhoef, L. H. W. and Boeyens, J. C. A. *Acta Crystallogr. B 25* (1969) 607.
21. Dunitz, J. D. and Orgel, L. E. *Advan. Inorg. Chem. Radiochem. 2* (1960) 1.
22. Hahn, H. and Klingler, W. *Z. Anorg. Allg. Chem. 260* (1949) 110.
23. Boeyens, J. C. A. and Herbstein, F. H. *Inorg. Chem. 6* (1967) 1408.
24. Slater, J. C. *J. Chem. Phys. 41* (1964) 3199.
25. Verhoef, L. H. W. and Boeyens, J. C. A. *Acta Crystallogr. B 24* (1968) 1262.
26. Pauling, L. *The Nature of the Chemical Bond*, 3rd Ed., Cornell University Press, Ithaca, New York 1960.

Received May 29, 1974.

Acta Chemica Scandinavica A 28 (1974) 1021—1035

Stability Constants for Chloride Complexes of Copper(II) in Sulphuric Acid Solution

MARIANNE OHLSON and NILS-GÖSTA VANNERBERG

Department of Inorganic Chemistry, Chalmers University of Technology and University of Göteborg, P.O. Box, S-402 20 Göteborg 5, Sweden

Spectrophotometric methods have been used to determine the stability constants of copper(II) chloride complexes in an ionic medium of 9 M sulphuric acid at 25 °C. The total molarity was held constant at 9 M.

Preliminary constants were obtained by graphical methods and were then refined with the generalized least squares program "LETAGROP". The experimental data could best be explained in terms of the following equilibria and stability constants:

$Cu^{2+} + Cl^- \rightleftharpoons CuCl^+$ $\quad \log \beta_1 = 1.03 \pm 0.03$
$Cu^{2+} + 2Cl^- \rightleftharpoons CuCl_2$ $\quad \log \beta_2 = 1.60 \pm 0.07$
$Cu^{2+} + 3Cl^- \rightleftharpoons CuCl_3^-$ $\quad \log \beta_3 = 1.77 \pm 0.19$
$Cu^{2+} + 4Cl^- \rightleftharpoons CuCl_4^{2-}$ $\quad \log \beta_4 = 2.21 \pm 0.08$

The errors given correspond to an error of 3σ, where σ is the standard deviation in $\log \beta$.

The formation of complexes between copper(II) ions and chloride ions in aqueous solution has mainly been studied by spectrophotometric methods, but a few investigators have used ion exchange or freezing point methods. The formation of complexes between Cu(II) ions and chloride ions cannot be investigated potentiometrically using a copper amalgam electrode or a silver chloride electrode, as both these electrodes reduce Cu(II) to Cu(I) in the presence of chloride ions.

The values of the stability constants (*cf.* Table 1) determined in the various investigations differ from each other, owing to different ionic media and methods of measurement. Some of the constants have been extrapolated to zero ionic strength.[1,3,6,11] From the values given in Table 1, it is evident that the complexes are very weak, the stability constant, β_1, for the reaction $Cu^{2+} + Cl^- \rightleftharpoons CuCl^+$ having an approximate value of 1.[1-6,9,11] Some authors have found a higher value for β_1.[7,8,10] This can be attributed to a more concentrated ionic medium, to the neglection of the second complex, or to the method of calculation. The uncertainty of the stability constant, β_2, for the reaction $Cu^{2+} + 2Cl^- \rightleftharpoons CuCl_2$ is larger than that of β_1, but its value is probably less than 1.[1,2]

It has been claimed that copper(II) forms four mononuclear complexes with chloride ions, namely $CuCl^+$, $CuCl_2$, $CuCl_3^-$ and $CuCl_4^{2-}$.[1,6,10] On account of the weak complexity, it has, however, proved difficult to determine the stability constants of the higher complexes. Using spectrophotometric measurements, with different metal chlorides as ionic media, Bjerrum[1] was, however, able to determine approximate values for β_3 and β_4. The values determined by Morris and Short[10] differ, however, considerably from those determined by Bjerrum.

In this work, the copper(II) chloride system has been studied spectrophotometrically in 9 M sulphuric acid at 25 °C, sulphuric acid being chosen as medium since it seemed likely that the copper(II) complexes would be stronger in 9 M sulphuric acid than in dilute aqueous solution. Sulphuric acid medium has, moreover, industrial interest, since anhydrous chlorides of the transition metals can be obtained by the distillation of such solutions.

Table 1. Survey of reported values for the stability constants of copper(II) chloride complexes.

Author	Ref.	Method	Medium	Temp. °C	β_1 (M^{-1})	β_2 (M^{-2})	β_3 (M^{-3})	β_4 (M^{-4})
Bjerrum	1	spectr.	extrap. to 0	22	1	0.2	8×10^{-3}	8×10^{-5}
McConnell and Davidsson	2	spectr.	1 M $HClO_4$	25.2	1.3	0.3		
Näsänen	3	spectr.	extrap. to 0	25	1.2			
Kruh	4	spectr.	1 M $HClO_4$	22	0.27			
Lister and Rosenblum	5	spectr.	2 M $NaClO_4$	25	1.22			
Andreev and Sapozhinkova	6	spectr.	HCl		1			
Libus	11	spectr.	extrap. to 0	25	1.63			
Faucherre and Crego	7	fp	sat. KNO_3		2.70			
Kenttämaa	8	fp	sat. $KClO_3$		1.50			
		fp	sat. $KClO_4$		4.60			
			extrap. to 0		8.90			
Tre'millon	9	ion exch.	1.5 M $NaNO_3$		0.4			
Morris and Short	10	ion exch.	0.69 M $HClO_4$	20	9.6	4.92	3.52	1.0
Ohlson and Vannerberg		spectr.	9 M H_2SO_4	25	10.7	39.6	59	163

EXPERIMENTAL

Chemicals and analysis. Stock solutions of copper(II) sulphate were prepared by dissolving *copper(II) sulphate* (Merck *p.a.*) in 9 M sulphuric acid and the copper content was determined electrogravimetrically.[13] *Sulphuric acid* was prepared by dilution of conc. sulphuric acid (Merck *p.a.*) and its concentration was calculated from the experimental density,[14] determined with an areometer, graduated from 1.470 to 1.520 g cm^{-3} (accuracy ±0.001 g cm^{-3}). *Sodium chloride* (Merck *p.a.*) was dried at 110 °C and weighed.

The light absorption measurements in the range 350 – 385 nm were made with a Beckman spectrophotometer, Model DU-2. The measurements in the ultraviolet range 260 – 300 nm were made on a Gilford 240 spectrophotometer. Matched quartz cells of path lengths 0.1, 0.2, 0.5, 1.0 cm were employed, these being calibrated before use. During the measurements, the sample compartment was thermostated to 25.0 ± 0.1 °C.

Four series of solutions of copper(II) chloride were prepared by adding accurately weighed sodium chloride to a solution of copper(II) sulphate. In each series, the total copper ion concentration (B) was kept constant (B: 0.005, 0.010, 0.020, 0.050 M), while the total chloride concentration (A) was varied between 0.004 and 0.600 M. The total molarity was held constant at 9 M by the addition of sulphuric acid.

In one and the same series of measurements, B and l were kept constant and in the different series of measurements the product lB was kept constant.[15]

The wave lengths employed, the numbers of solutions and the numbers of measurements are given in Table 2.

Table 2. The wave lengths used, the numbers of solutions and the chloride concentrations.

Wave lengths (nm)	Number of solutions	Number of measured values	Chloride concentration (M)
260, 265, 270, 275, 280, 290, 300	63	354	0.004 – 0.064
350, 355, 360, 365, 370, 375, 380, 385	113	658	0.0192 – 0.600

LIST OF SYMBOLS

A total concentration of chloride ions, Cl^-
a free » » » » »
B total » » copper ions, Cu^{2+}
b free » » » » »
A_s absorbance
l optical path length
ε apparent molar absorptivity
β_i equilibrium constant for the reaction $Cu^{2+} + iCl^- \rightleftharpoons CuCl_i^{(2-i)+}$
ε_i molar absorptivity for the complex $CuCl_i^{(2-i)+}$
$\bar{n}$ mean ligand number

MEASUREMENTS

The measurements were performed spectrophotometrically, the method of corresponding solutions [1,15–18] being used. In order to find suitable wave lengths, spectra were recorded for copper chloride solutions with constant B and varying A. The spectra showed absorption maxima at 250, 375, and 800 – 900 nm (Figs. 1, 2). The absorption of the Cu^{2+} ion, which probably exists as a sulphate complex in the sulphuric acid solution, increases with decreasing wave length in the UV range, and shows an absorption maximum at 810 nm (Fig. 1). The absorption bands of the complexes are displaced towards longer wave lengths with increasing chloride concentrations, their band widths also increasing considerably. Solutions with low A show one isosbestic point at 224 nm.

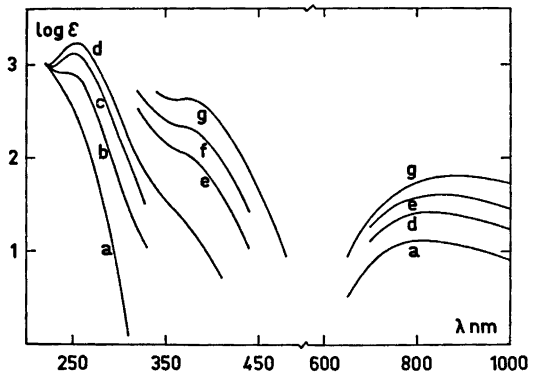

Fig. 1. log ε as a function of λ for copper(II) chloride solutions. $B = 0.010$ M and the following values of A were used: a. 0 M; b. 0.024 M; c. 0.060 M; d. 0.100 M; e. 0.300 M; f. 0.500 M; g. 1.000 M.

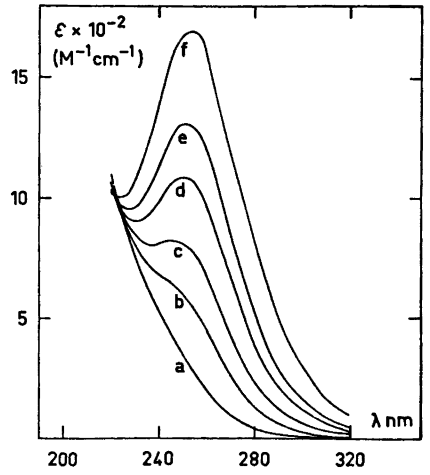

Fig. 2. ε data as a function of λ for solutions with $B = 0.010$ M and different values of A a. 0 M; b. 0.012 M; c. 0.024 M; d. 0.044 M; e. 0.060 M; f. 0.100 M.

The majority of the measurements (658 values) have been carried out in the range 350 – 385 nm, where the higher complexes can be detected. Another advantage of this range is that the Cu^{2+} ion does not absorb there. The remaining 354 measurements were made in the 260 – 300 nm range (Table 2). Only the stability constants of the two first complexes, $CuCl^+$ and $CuCl_2$, could be determined from measurements in the latter range, owing to the strong absorption of both the Cu^{2+} ion and the copper(II) chloride complexes. No measurements have been carried out in the 800 – 900 nm range, because of the small absorptivities of the complexes. The absorption of chloride ions is negligible.

TREATMENT OF THE DATA

The absorbance, A_s, of a solution is the product of the apparent molar absorptivity, ε, the optical path length, l, and the total concentration of the absorbing substance, B,

$$A_s = l\varepsilon B = l \sum_{i=0}^{N} \varepsilon_i [BA_i] = l \sum_{i=0}^{N} \varepsilon_i \beta_i b a^i \qquad (1)$$

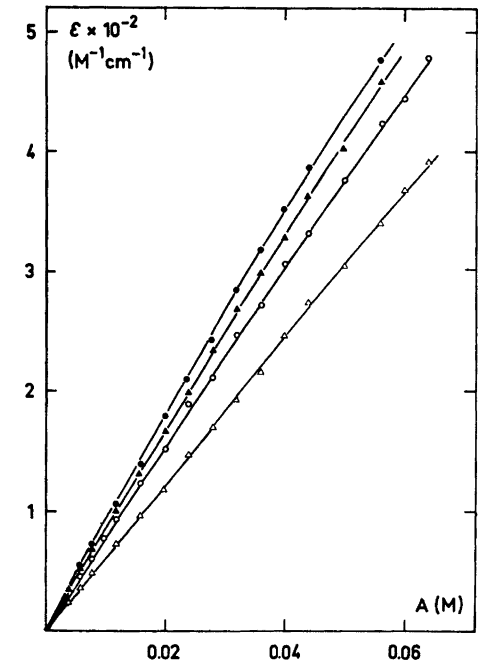

Fig. 3. The function $\varepsilon(A)$ at different values of B at 280 nm. △$B=0.05$ M; ○$B=0.02$ M; ▲$B=0.01$ M; ●$B=0.005$ M.

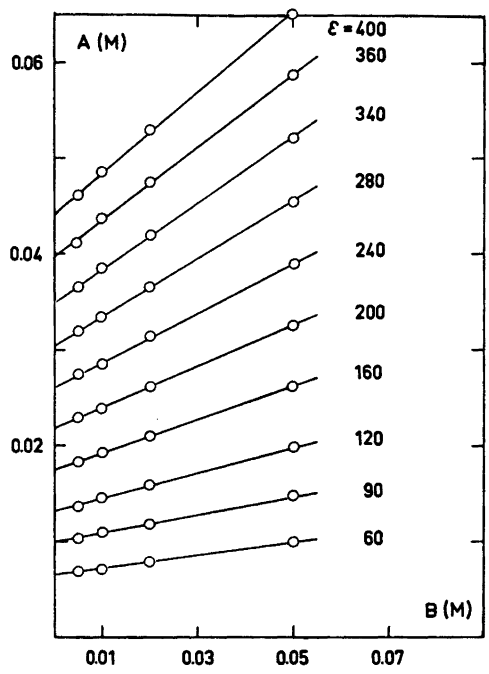

Fig. 4. A versus B at different ε at 280 nm.

where $\varepsilon_0, \varepsilon_1, \ldots, \varepsilon_N$ are the molar absorptivities for Cu^{2+}, $CuCl^{+}, \ldots,$ $CuCl_N^{(2-N)+}$, respectively.

The apparent molar absorptivity is defined as

$$\varepsilon = \frac{\sum_{i=0}^{N} \varepsilon_i[BA_i]}{B} = \left[\sum_{i=0}^{N} \varepsilon_i \beta_i a^i\right] \Big/ \left[1 + \sum_{i=1}^{N} \beta_i a^i\right] \quad (2)$$

From eqn. (2) it is seen that ε is solely a function of a, if only mononuclear complexes are present. The mean ligand number $\bar{n}$ is defined as

$$\bar{n} = \frac{A-a}{B} = \left[\sum_{i=1}^{N} i\beta_i a^i\right] \Big/ \left[1 + \sum_{i=1}^{N} \beta_i a^i\right] \quad (3)$$

and $\bar{n}$ is thus only a function of a, this gives

$$A = a + \bar{n}B \quad (4)$$

Table 3. Corresponding values of B, A, a and $\bar{n}$ obtained from the $\varepsilon(A)$-curve for $\lambda=280$ nm.

	A M						
B M / ε	0.005	0.01	0.02	0.05	a	$-\log a$	$\bar{n}$
60	0.0068	0.0071	0.0079	0.0099	0.0064	2.19	0.07
90	0.0103	0.0108	0.0117	0.0148	0.0098	2.01	0.10
120	0.0137	0.0145	0.0158	0.0198	0.0132	1.88	0.13
160	0.0183	0.0192	0.0211	0.0262	0.0174	1.76	0.18
200	0.0229	0.0239	0.0262	0.0325	0.0219	1.66	0.21
240	0.0274	0.0286	0.0314	0.0389	0.0261	1.58	0.26
280	0.0319	0.0335	0.0366	0.0454	0.0304	1.52	0.30
340	0.0388	0.0411	0.0448	0.0554	0.0373	1.43	0.36
360	0.0411	0.0437	0.0475	0.0587	0.0398	1.40	0.38
400	0.0460	0.0488	0.0531	0.0654	0.0447	1.35	0.41

Table 4. Corresponding values of $\log a$ and $\bar{n}$, obtained from $\varepsilon(A)$-curves for 15 different wave lengths, followed by $(\bar{n}_{calc} - \bar{n}) \times 10^3$, which has been calculated with the "LETAGROP VRID" program.

λ nm			
385	-0.9340	0.93000	4.99
	-0.8780	0.99000	45.53
	-0.8330	1.11000	13.05
	-0.7930	1.17000	36.20
	-0.7610	1.30000	-23.49
	-0.7030	1.43000	-17.17
	-0.6560	1.60000	-68.17
	-0.6130	1.69000	-42.68
	-0.5930	1.71000	-6.89
	-0.5750	1.78000	-25.61
	-0.5410	1.86000	-6.15
	-0.5110	1.92000	24.13
	-0.4840	2.00000	27.10
	-0.4580	2.08000	28.23
	-0.4340	2.15000	33.92
	-0.4100	2.20000	60.09
	-0.3890	2.29000	36.90
	-0.3680	2.36000	33.65
	-0.3490	2.48000	-26.18
	-0.3310	2.55000	-39.54
380	-1.2030	0.57000	-8.75
	-1.1500	0.66000	-37.66
	-1.0930	0.72000	-25.60
	-1.0410	0.79000	-23.66
	-0.9730	0.88000	-9.89
	-0.9120	0.94000	33.42
	-0.8690	1.06000	-7.46
	-0.8280	1.12000	13.16
	-0.7910	1.20000	10.50
	-0.7590	1.27000	11.02
	-0.7330	1.36000	-19.13
	-0.7060	1.45000	-44.51
	-0.6830	1.52000	-57.47
	-0.6410	1.63000	-58.59
	-0.6050	1.74000	-70.51
	-0.5710	1.80000	-34.08
	-0.5390	1.88000	-20.20
	-0.5100	1.93000	17.17
	-0.4830	2.00000	30.20
	-0.4590	2.10000	5.09
	-0.4360	2.19000	-12.41
	-0.4140	2.24000	7.38
	-0.3930	2.33000	-15.82
	-0.3720	2.37000	10.95
	-0.3540	2.45000	-11.99
	-0.3350	2.54000	-42.09
375	-1.1970	0.58000	-12.10
	-1.0910	0.69000	7.06
	-1.0160	0.83000	-26.84
	-0.9530	0.87500	27.87
	-0.9070	0.98000	2.34
	-0.8630	1.06000	4.01
	-0.8250	1.11000	29.27
	-0.7660	1.31000	-44.70
	-0.7140	1.44000	-53.92
	-0.6710	1.58000	-86.98
	-0.6310	1.65000	-51.78
	-0.5940	1.71000	-9.71
	-0.5620	1.77000	22.03
	-0.5330	1.83000	47.70
	-0.5040	1.91000	55.50
	-0.4790	2.00000	42.62
	-0.4560	2.11000	4.51
	-0.4340	2.20000	-16.08
	-0.4130	2.26000	-9.45
	-0.3920	2.29000	27.36
	-0.3730	2.43000	-52.22
370	-0.9910	0.84000	1.52
	-0.9410	0.92000	3.04
	-0.9000	1.02000	-25.05
	-0.8610	1.07000	-2.14
	-0.8260	1.13000	7.23
	-0.7960	1.21000	-10.21
	-0.7660	1.28000	-14.70
	-0.7400	1.33000	-5.47
	-0.7150	1.38000	3.67
	-0.6940	1.46000	-24.98
	-0.6720	1.50000	-9.54
	-0.6530	1.53000	9.69
	-0.6170	1.64000	-3.68
	-0.6010	1.70000	-19.36
	-0.5850	1.73000	-4.22
	-0.5540	1.80000	15.44

λ nm			
	-0.5260	1.90000	-1.29
	-0.4980	1.96000	23.89
	-0.4740	2.04000	18.18
	-0.4500	2.11000	23.39
	-0.4280	2.20000	2.93
	-0.4060	2.29000	-17.19
	-0.3870	2.41000	-76.73
	-0.3670	2.48000	-83.17
	-0.3470	2.55000	-39.87
365	-1.1690	0.60000	-0.19
	-1.0920	0.70000	-4.27
	-1.0270	0.76000	26.78
	-0.9710	0.82000	53.34
	-0.8910	1.01000	1.38
	-0.8270	1.19000	-54.80
	-0.7700	1.28000	-23.61
	-0.7230	1.40000	-35.49
	-0.6770	1.47000	7.71
	-0.6410	1.58000	-8.59
	-0.6060	1.69000	-23.30
	-0.5750	1.76000	-5.60
	-0.5440	1.84000	4.94
	-0.5160	1.90000	28.93
	-0.4910	2.00000	5.45
	-0.4670	2.08000	0.03
	-0.4440	2.14000	12.31
	-0.4210	2.20000	25.14
360	-1.3280	0.47000	-32.53
	-1.2660	0.52000	-24.51
	-1.2140	0.57000	-20.75
	-1.1690	0.62000	-20.19
	-1.1300	0.67000	-23.15
	-1.0600	0.72000	19.34
	-1.0070	0.81000	6.79
	-0.9590	0.86000	32.93
	-0.9210	0.92000	37.53
	-0.8870	1.00000	18.76
	-0.8540	1.06000	21.43
	-0.8230	1.11000	33.36
	-0.7970	1.19000	7.65
	-0.7480	1.30000	6.06
	-0.7030	1.37000	42.82
	-0.6670	1.48000	23.29
	-0.6320	1.58000	15.53
	-0.6000	1.68000	3.44
	-0.5700	1.77000	-1.19
	-0.5410	1.85000	3.85
	-0.5140	1.92000	15.00
	-0.4890	2.00000	11.62
	-0.4640	2.06000	29.42
	-0.4410	2.11000	51.78
	-0.4180	2.16000	74.67
355	-1.2490	0.50800	4.53
	-1.1620	0.59400	14.03
	-1.0960	0.67700	13.44
	-1.0390	0.74200	27.23
	-0.9910	0.80300	38.52
	-0.9520	0.88700	17.54
	-0.9170	0.95700	7.56
	-0.8830	1.00000	26.18
	-0.8520	1.01700	68.34
	-0.8260	1.11900	18.23
	-0.8000	1.16200	29.28
350	-1.6780	0.21300	-2.97
	-1.6070	0.23400	10.64
	-1.5480	0.26100	16.34
	-1.4750	0.33300	-9.66
	-1.4110	0.38300	-13.75
	-1.3570	0.42400	-11.54
	-1.3160	0.46800	-19.79
	-1.2910	0.47100	0.33
	-1.2530	0.50000	8.48
300	-2.1900	0.06300	4.57
	-2.0730	0.07900	8.90
	-1.9120	0.11700	8.84
	-1.7170	0.19100	2.03
	-1.6500	0.22100	2.10
	-1.5900	0.25200	1.67
	-1.5350	0.27600	6.67
	-1.4940	0.30500	5.74
	-1.4170	0.36100	3.71
	-1.3840	0.39200	-1.68
	-1.3520	0.41200	4.68

λ nm			
290	-2.1760	0.06800	1.73
	-2.0560	0.08800	3.31
	-1.9670	0.11100	0.38
	-1.8880	0.12600	6.71
	-1.8240	0.14500	7.81
	-1.7750	0.16800	2.13
	-1.7280	0.18700	1.48
	-1.6880	0.21000	-4.45
	-1.6520	0.22500	-2.86
	-1.6160	0.24100	-1.03
	-1.5880	0.26500	-10.24
	-1.5560	0.27700	-4.32
	-1.5300	0.29500	-6.91
	-1.5020	0.31000	-4.43
	-1.4790	0.33400	-13.35
	-1.4560	0.34800	-11.60
	-1.4270	0.35100	6.25
	-1.4090	0.37900	-8.22
280	-2.2680	0.05800	-1.35
	-2.1920	0.07000	-2.74
	-2.1220	0.08000	-1.25
	-2.0610	0.09000	0.29
	-2.0100	0.10000	1.20
	-1.9620	0.11000	2.62
	-1.8800	0.13100	4.07
	-1.8120	0.15000	6.89
	-1.7600	0.17500	5.79
	-1.7080	0.19300	3.84
	-1.6600	0.21300	5.35
	-1.6200	0.23400	3.93
	-1.5830	0.25500	2.48
	-1.5480	0.27600	1.34
	-1.5170	0.30000	-3.91
	-1.4840	0.32400	-6.69
	-1.4550	0.34000	-2.90
	-1.4280	0.35900	-2.48
	-1.4000	0.37500	2.71
	-1.3760	0.39700	-0.23
	-1.3500	0.41400	4.38
275	-2.1980	0.06500	1.36
	-2.1480	0.07700	-2.73
	-2.0950	0.08300	0.67
	-2.0200	0.10000	-1.03
	-1.9470	0.11400	2.44
	-1.8870	0.13200	1.00
	-1.8350	0.15000	-0.84
	-1.7890	0.16800	-3.00
	-1.7460	0.18600	-4.76
	-1.6690	0.21400	0.15
	-1.6030	0.24800	-1.26
	-1.5740	0.26200	0.46
	-1.5200	0.30200	-7.78
	-1.4710	0.34400	-17.95
270	-2.3190	0.05300	-2.53
	-2.2130	0.06300	1.15
	-2.1290	0.07200	5.52
	-2.0030	0.09900	3.79
	-1.9010	0.12500	3.95
	-1.8170	0.15300	2.17
	-1.7490	0.18000	0.06
	-1.6850	0.21200	-5.12
	-1.6290	0.24000	-6.61
	-1.5790	0.26700	-7.32
	-1.5540	0.27900	-5.16
	-1.5300	0.29000	-1.91
265	-2.2330	0.06000	1.32
	-2.1010	0.07800	4.55
	-2.0000	0.10000	3.48
	-1.9140	0.12100	4.29
	-1.7770	0.16000	9.38
	-1.7200	0.19200	-0.22
	-1.6720	0.23000	-17.23
260	-2.3040	0.05100	1.22
	-2.1650	0.06500	6.48
	-2.0660	0.08200	7.29
	-1.9800	0.10300	5.20
	-1.9400	0.11500	3.27
	-1.9030	0.12200	6.38
	-1.8690	0.12700	11.39
	-1.8350	0.14000	9.16

Solutions with the same ε have the same value of $\bar{n}$ and a, and such solutions are known as corresponding solutions.[1,15–18]

The function $\varepsilon(A)$ [15] was plotted for three or four given values of the total concentration B. From these curves pairs of values (B,A), corresponding to selected ε, were obtained.

If A was plotted against B at a constant value of ε, a straight line was obtained, indicating that only mononuclear complexes were present, $\bar{n}$ being obtained from the slope and a from the intercept on the A-axis. Measurements for $\lambda = 280$ nm illustrate this procedure (*cf.* Figs. 3, 4 and Table 3).

The stability constants were then calculated from the $\bar{n}(a)$ values by several different methods (*cf.* Table 4 and Fig. 6).

CALCULATIONS BASED ON THE DATA IN THE LOW UV RANGE

Curve fitting. In order to determine values of β_1 and β_2, the experimental curve in Fig. 5 was fitted to the following normalized curve:

$$\bar{n} = (Ru + 2u^2)/(1 + Ru + u^2) \quad (5)$$

where $u = \beta_2^{\frac{1}{2}} a$ and $R = \beta_1 \beta_2^{-\frac{1}{2}}$.[19] Functions $\bar{n}(\log u)_R$ were drawn for different constant R values and compared with the experimental ones.

Table 5. Spectrophotometric data in the low UV range for 40 solutions. A and B are given for each solution, followed by ε, ε_{calc} and $\varepsilon_{calc} - \varepsilon$ for 7 wave lengths. The concentrations are expressed in M and the apparent absorptivities in M^{-1} cm^{-1}. Missing data is indicated by -1.

0.004000	0.005000							
15.300	15.301	0.001	34.300	34.516	0.216	81.300	80.787	-0.513
118.700	118.968	0.268	168.500	169.606	1.106	230.500	231.706	1.206
304.300	304.348	0.048						
0.006000	0.005000							
20.300	15.930	-0.370	43.700	43.307	-0.393	100.600	98.428	-2.172
143.500	142.974	-0.526	201.700	200.827	-0.873	272.400	270.532	-1.868
352.000	348.822	-3.178						
0.008000	0.005000							
24.680	24.736	0.056	52.150	52.316	0.166	116.900	116.075	-0.825
165.700	166.758	1.058	230.800	231.474	0.674	307.500	308.259	0.759
391.300	391.840	0.540						
0.010000	0.005000							
29.800	29.703	-0.097	61.600	61.522	-0.078	134.400	133.714	-0.686
192.000	190.315	-1.685	264.400	261.560	-2.840	347.000	344.925	-2.075
435.600	433.456	-2.144						
0.012000	0.005000							
34.800	34.820	0.020	71.000	70.908	-0.092	151.100	151.332	0.232
214.400	213.640	-0.760	292.400	291.094	-1.306	380.300	380.562	0.262
473.200	473.720	0.520						
0.016000	0.005000							
44.760	45.451	0.691	89.910	90.152	0.242	185.200	186.467	1.267
259.500	259.591	-0.308	349.000	348.558	-0.442	447.100	448.903	1.804
-1.000	-1.000	0.0						
0.020000	0.005000							
57.900	56.540	-1.360	113.400	109.923	-3.477	-1.000	-1.000	0.0
-1.000	-1.000	0.0	-1.000	-1.000	0.0	-1.000	-1.000	0.0
-1.000	-1.000	0.0						
0.024000	0.005000							
67.600	68.006	0.406	130.500	130.110	-0.390	257.700	256.055	-1.644
350.200	348.631	-1.569	458.600	457.371	-1.229	572.600	574.722	2.122
-1.000	-1.000	0.0						
0.028000	0.005000							
78.720	75.780	1.060	148.800	150.619	1.819	288.300	290.385	2.086
-1.000	-1.000	0.0	-1.000	-1.000	0.0	-1.000	-1.000	0.0
-1.000	-1.000	0.0						
0.032000	0.005000							
92.900	91.801	-1.099	173.000	171.365	-1.635	-1.000	-1.000	0.0
-1.000	-1.000	0.0	-1.000	-1.000	0.0	-1.000	-1.000	0.0
-1.000	-1.000	0.0						
0.004000	0.010000							
15.400	14.838	-0.562	34.200	33.630	-0.570	79.800	78.984	-0.816
117.800	116.502	-1.298	165.400	166.382	0.982	227.800	227.674	-0.126
259.600	259.718	0.118						
0.006000	0.010000							
19.680	19.214	-0.466	42.350	41.954	-0.396	97.020	95.742	-1.278
135.600	135.334	-0.266	194.600	196.112	1.512	265.000	264.694	-0.306
341.700	342.148	0.448						
0.008000	0.010000							
23.550	23.754	0.196	50.400	50.484	0.084	112.400	112.520	0.120
160.900	161.985	1.085	222.600	225.346	2.746	298.400	300.746	2.346
379.200	383.289	4.089						
0.012000	0.010000							
33.300	33.282	-0.018	68.400	68.097	-0.303	146.600	146.092	-0.508
207.200	206.723	-0.477	283.400	282.361	-1.039	369.800	370.062	0.262
459.600	461.875	2.275						
0.016000	0.010000							
42.150	43.335	1.185	84.890	86.346	1.456	176.400	179.614	3.214
-1.000	-1.000	0.0	-1.000	-1.000	0.0	-1.000	-1.000	0.0
-1.000	-1.000	0.0						
0.020000	0.010000							
53.090	53.833	0.743	105.000	105.122	0.122	211.900	213.013	1.113
292.700	293.849	1.149	389.100	390.807	1.707	495.600	498.310	2.710
-1.000	-1.000	0.0						
0.024000	0.010000							
64.000	64.709	0.709	122.800	124.329	1.529	244.300	246.225	1.925
333.800	336.198	2.398	439.000	442.368	3.368	-1.000	-1.000	0.0
-1.000	-1.000	0.0						
0.028000	0.010000							
76.240	75.899	-0.341	144.100	143.881	-0.219	279.600	279.196	-0.404
377.300	377.721	0.422	492.400	492.241	-0.159	-1.000	-1.000	0.0
-1.000	-1.000	0.0						
0.032000	0.010000							
88.520	87.348	-1.171	165.000	163.701	-1.299	314.300	311.879	-2.420
420.900	418.412	-2.487	542.200	540.487	-1.713	-1.000	-1.000	0.0
-1.000	-1.000	0.0						
0.036000	0.010000							
100.000	98.807	-1.193	183.600	183.721	0.121	345.400	344.235	-1.165
458.000	458.268	0.268	-1.000	-1.000	0.0	-1.000	-1.000	0.0
-1.000	-1.000	0.0						
0.004000	0.020000							
18.100	17.985	-0.115	39.260	39.628	0.368	90.750	91.100	0.350
133.800	133.030	-0.770	186.900	187.930	1.030	253.400	254.542	1.142
331.000	330.531	-0.469						
0.008000	0.020000							
21.890	22.070	0.180	44.020	47.332	3.312	106.000	106.363	0.363
153.100	153.696	0.596	212.700	214.678	1.978	285.400	287.630	2.231
366.600	368.343	1.743						
0.010000	0.020000							
26.640	26.290	-0.350	55.010	55.208	0.198	122.700	121.656	-1.043
174.800	174.235	-0.565	241.100	241.052	-0.048	321.300	319.971	-1.328
406.600	405.154	-1.446						

Table 5. Continued.

0.012000	0.020000							
31.070	30.638	-0.432	63.480	63.243	-0.237	138.700	136.971	-1.729
155.500	154.641	-0.859	268.200	267.057	-1.143	353.200	351.584	-1.616
442.800	440.994	-1.806						
0.016300	0.020000							
39.840	39.682	-0.158	80.050	79.750	-0.300	168.500	167.629	-0.871
235.700	235.045	-0.655	320.800	317.977	-2.822	415.600	412.698	-2.901
512.100	509.867	-2.233						
0.020000	0.020000							
48.550	49.145	0.555	96.570	96.770	0.200	197.600	198.279	0.679
273.700	274.882	1.182	367.800	367.476	-0.324	471.400	471.114	-0.286
575.100	575.173	0.073						
0.024000	0.020000							
55.440	58.973	-0.467	116.400	114.226	-2.174	-1.000	-1.000	0.0
-1.000	-1.000	0.0	-1.000	-1.000	0.0	-1.000	-1.000	0.0
-1.000	-1.000	0.0						
0.028000	0.020000							
68.370	69.115	0.745	132.100	132.051	-0.049	257.400	259.340	1.941
352.100	352.775	0.675	462.200	462.358	0.158	581.500	580.377	-1.122
694.900	695.864	0.964						
0.032000	0.020000							
79.920	79.528	-0.392	151.700	150.182	-1.518	292.300	289.662	-2.638
395.000	390.801	-4.199	-1.000	-1.000	0.0	-1.000	-1.000	0.0
-1.000	-1.000	0.0						
0.036000	0.020000							
88.550	90.171	1.621	165.700	168.561	2.861	317.800	319.792	1.993
425.900	428.198	2.298	550.900	551.999	1.100	680.500	680.366	-0.133
-1.000	-1.000	0.0						
0.004000	0.050000							
12.290	12.370	0.080	28.540	28.884	0.344	68.850	69.240	0.390
103.400	103.124	-0.276	147.300	148.839	1.539	203.500	205.658	2.158
273.500	274.358	0.858						
0.006000	0.050000							
15.300	15.397	0.097	34.260	34.699	0.439	81.230	81.159	-0.071
118.900	119.477	0.577	168.000	170.272	2.272	229.400	232.538	3.138
301.700	305.303	3.603						
0.008000	0.050000							
18.640	18.521	-0.119	40.440	40.644	0.204	94.360	93.131	-1.229
136.000	135.791	-0.209	191.000	191.516	0.516	258.800	258.994	0.195
335.900	335.627	-0.273						
0.012000	0.050000							
25.830	25.952	-0.578	52.600	52.905	0.305	117.600	117.216	-0.384
168.600	168.288	-0.312	233.300	233.437	0.137	309.600	310.662	1.062
393.300	394.573	1.273						
0.016000	0.050000							
32.440	31.935	-0.505	65.930	65.627	-0.303	142.100	141.461	-0.639
202.600	200.596	-2.004	277.500	274.606	-2.892	362.400	360.713	-1.687
453.000	451.316	-1.684						
0.020000	0.050000							
39.290	39.141	-0.149	77.720	78.769	1.049	162.700	165.834	3.134
230.100	232.695	2.595	311.700	315.036	3.336	-1.000	-1.000	0.0
-1.000	-1.000	0.0						
0.024000	0.050000							
47.290	46.645	-0.645	94.380	92.294	-2.085	191.900	190.305	-1.595
265.700	264.568	-1.132	358.800	354.727	-4.073	459.400	456.161	-3.239
559.100	558.506	-0.594						
0.028000	0.050000							
54.760	54.422	-0.338	106.800	106.168	-0.632	215.100	214.845	-0.255
295.000	296.159	1.200	394.200	393.688	-0.512	501.900	501.653	-0.247
-1.000	-1.000	0.0						
0.032000	0.050000							
62.620	62.450	-0.170	119.700	120.357	0.657	239.300	239.427	0.127
324.900	327.574	2.675	430.000	431.927	1.927	-1.000	-1.000	0.0
-1.000	-1.000	0.0						
0.036000	0.050000							
69.380	70.704	1.324	132.500	134.829	2.329	-1.000	-1.000	0.0
-1.000	-1.000	0.0	-1.000	-1.000	0.0	-1.000	-1.000	0.0
-1.000	-1.000	0.0						

The best fit was obtained when $R = 1.5$ and $\log u = 1$ and $\log a = 1.83$ (*cf.* Fig. 5). This gave $\beta_1 = 10.1$ M^{-1} and $\beta_2 = 45.7$ M^{-2}.

"LETAGROP" CALCULATIONS

The experimental data from the low UV-range were also processed with the spectrophotometric version "SPEFO" of the "LETAGROP" program.[22] U is the error squares sum, defined as $U = \sum(\varepsilon_{calc} - \varepsilon)^2$.

The "best values" for β_1 and β_2 obtained were:

$\beta_1 = 11.60 \pm 0.22$ M^{-1}
$\beta_2 = 39.17 \pm 6.21$ M^{-2}

and $U = 490.2$ for 231 values for $A < 0.04$ M. The errors given are σ, where σ is the standard deviation in β. The corresponding ε_1 and ε_2 values are given in Table 7 and Fig. 8. These ε_1 and ε_2 values were also confirmed by graphical methods. In Table 5 experimental and calculated data are presented.

CALCULATIONS BASED ON THE COMPLETE DATA SET

Frondæus' method.[17,20] The function used was

$$\bar{n} = \frac{d\phi_0/\phi_0}{da/a} = \frac{d \ln \phi_0}{d \ln a} \qquad (6)$$

Integrating (6) between the limits 0 and a_i, gives

$$\ln \phi_0(a_i) = \int_0^{a_i} \bar{n} \, d \ln a \qquad (7)$$

ϕ_0 is determined from eqn. (7).

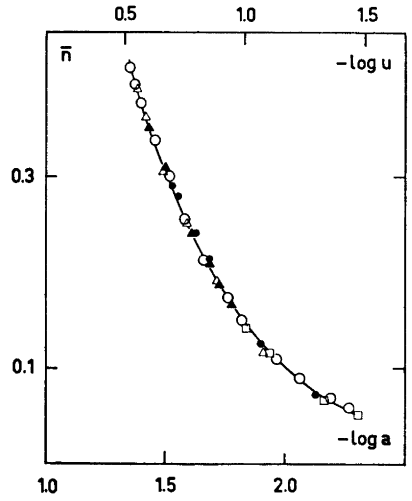

Fig. 5. $\bar{n}$ as a function of log a in the UV range. △300 nm; ▲290 nm; ○280 nm; ●270 nm; □260 nm.

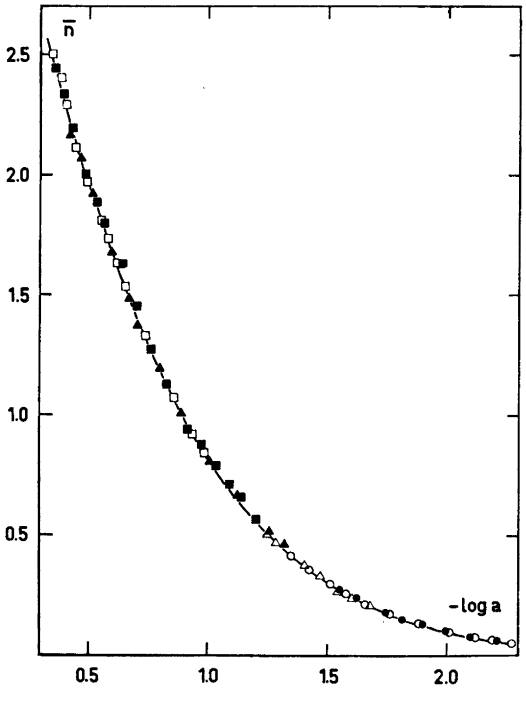

Fig. 6. The function $\bar{n}$(log a) at different wave lengths. ○280 nm; ●300 nm, △350 nm; ▲360 nm; □370 nm; ■380 nm.

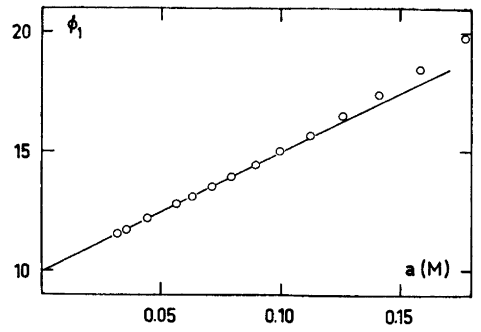

Fig. 7a. ϕ_1 as a function of a.

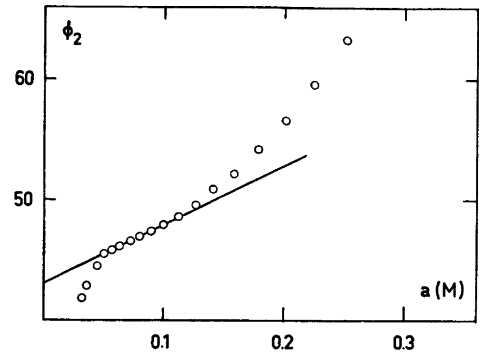

Fig. 7b. ϕ_2 as a function of a.

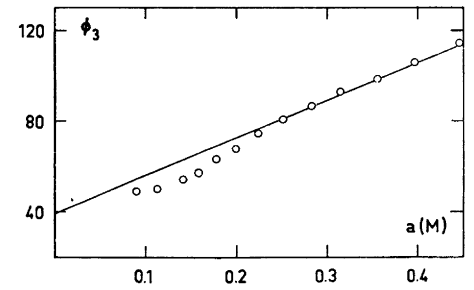

Fig. 7c. ϕ_3 as a function of a.

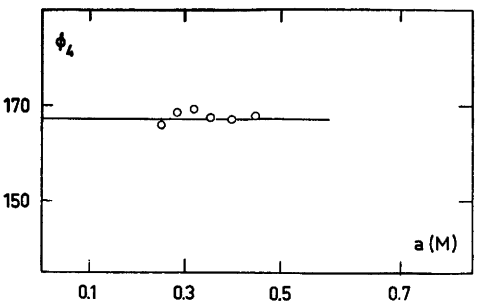

Fig. 7d. ϕ_4 as a function of a.

Table 6. The intercepts and the slopes of the different graphical functions for the calculation of the β-values.

	Function	Intercept	Slope	β_1 (M^{-1})	β_2 (M^{-2})	β_3 (M^{-3})	β_4 (M^{-4})
All data	ϕ_1	10	50	10	43	39	167
	ϕ_2	43	49				
	ϕ_3	39	167				
	ϕ_4	167	–				
Data in the range 350 – 385 nm	ϕ_1	11.5	42.5	11.5	40.5	46	177
	ϕ_2	40.5	43				
	ϕ_3	46	177				
	ϕ_4	177	–				
All data	F_1	10	46	10	36	42	161
	F_2	36	75				
	F_3	41.5	161				
	F_4	161	–				
All data	G_2	43	38	11	38	43	–
	G_3	43	11				

$$\phi_1 = \frac{\phi_0 - 1}{a} = \beta_1 + \beta_2 a\left(+ \sum_{i=3}^{N} \beta_i a^{i-1} \right) \quad (8)$$

At very low values of a, the first two complexes, BA and BA_2, predominate, and the function $\phi_1(a)$ becomes a straight line of slope β_2 and with intercept β_1. A value of any constant β_i may be obtained by using a generalization of eqn. (8).

The disadvantage of this method is that any errors in the values of $\beta_1, \ldots, \beta_{i-1}$ will accumulate in the value of β_i.

In Figs. 7a–d, the different functions $\phi_i(a)$ have been plotted, and the slopes and intercepts of these four functions are listed in Table 6. The approximate values of the stability constants obtained were:

$\beta_1 = 10$ M^{-1} $\quad$ $\beta_3 = 39$ M^{-3}
$\beta_2 = 43$ M^{-2} $\quad$ $\beta_4 = 167$ M^{-4}

The values of the constants based on the 350 – 385 nm data, only, were somewhat different. This can be attributed to the selection of the tail of the $\bar{n}(\log a)$ curve. The values obtained were:

$\beta_1 = 11.5$ M^{-1} $\quad$ $\beta_3 = 46$ M^{-3}
$\beta_2 = 40.5$ M^{-2} $\quad$ $\beta_4 = 177$ M^{-4}

(*cf.* Table 6).

Rossotti's method.[21] The function

$$F_1 = \frac{\bar{n}}{(1-\bar{n})a} = \beta_1 + \beta_2 \frac{2-\bar{n}}{1-\bar{n}} a + \sum_{i=3}^{N} \frac{i-\bar{n}}{1-\bar{n}} \beta_i a^{i-1} \quad (9)$$

may be derived from eqn. (3). The plot of $\bar{n}(1-\bar{n})/a$ against $(2-\bar{n})\ a/(1-\bar{n})$ becomes a straight line of slope β_2 and intercept β_1, as $a \rightarrow 0$.

A value of any constant β_i may be obtained by using a generalization of eqn. (9).

The slopes and the intercepts of the four functions F_i are given in Table 6. The following values of the stability constants were obtained:

$\beta_1 = 10$ M^{-1} $\quad$ $\beta_3 = 42$ M^{-3}
$\beta_2 = 36$ M^{-2} $\quad$ $\beta_4 = 161$ M^{-4}

The reciprocal method of Rossotti.[21] The constants may also be obtained by extrapolation to $a^{-1} = 0$, using the function

$$G_N = \frac{\bar{n}a^{-N}}{N-\bar{n}} = \beta_N + \beta_{N-1} \frac{N-1-\bar{n}}{N-\bar{n}} a^{-1} + \sum_{i=1}^{N-2} \frac{i-\bar{n}}{N-\bar{n}} \beta_i a^{i-N} \quad (10)$$

In this case no value can be obtained for β_4 (*cf.* Table 6). The values obtained were:

$\beta_1 = 11$ M^{-1} $\quad$ $\beta_3 = 43$ M^{-3}
$\beta_2 = 38$ M^{-2}

Table 7. Molar absorptivities, ε_i, in M^{-1} cm^{-1} calculated with the "LETAGROP" program. The errors given are σ, where σ is the standard deviation in ε.

λ nm	ε_0	ε_1	ε_2	ε_3	ε_4
260	210.9	2417 ± 10	1754 ± 199	–	–
265	150.6	2055 ± 7	2164 ± 111	–	–
270	105.4	1597 ± 7	2926 ± 100	–	–
275	70.3	1190 ± 5	3083 ± 67	–	–
280	45.6	847 ± 5	2913 ± 64	–	–
290	17.7	390 ± 4	2276 ± 53	–	–
300	6.6	195 ± 2	1434 ± 28	–	–
350	–	8.8 ± 0.7	171 ± 3	222 ± 18	513 ± 15
355	–	5.9 ± 0.6	157 ± 2	190 ± 16	503 ± 13
360	–	4.1 ± 0.6	145 ± 2	141 ± 12	533 ± 8
365	–	2.5 ± 0.4	129 ± 2	122 ± 13	534 ± 9
370	–	1.0 ± 0.4	114 ± 2	110 ± 11	536 ± 7
375	–	0.9 ± 0.4	98 ± 2	85 ± 12	549 ± 8
380	–	0.6 ± 0.3	84 ± 2	62 ± 12	550 ± 8
385	–	0.5 ± 0.3	71 ± 2	47 ± 13	530 ± 9

Table 8. Spectrophotometric data in the range 350 – 385 nm for 11 solutions and 8 wave lengths. A and B are given for each solution, followed by ε, ε_{calc}, and $\varepsilon_{calc} - \varepsilon$. The concentrations are expressed in M and the apparent absorptivities in M^{-1} cm^{-1}. $\beta_1 = 10.7$ M^{-1} and $\beta_2 = 39.6$ M^{-2} were kept constant during the calculation.

0.019200	0.010000							
3.200	3.176	-0.024	2.550	2.554	0.004	2.050	2.085	0.035
1.650	1.668	0.018	1.250	1.317	0.067	1.100	1.101	0.001
0.850	0.882	0.032	0.650	0.714	0.064			
0.256CC	0.010000							
4.750	4.769	0.019	3.850	3.914	0.064	3.300	3.241	-0.059
2.600	2.647	0.047	2.100	2.150	0.050	1.800	1.797	-0.003
1.400	1.448	0.048	1.100	1.169	0.069			
0.032000	0.010000							
6.750	6.551	-0.199	5.650	5.453	-0.197	4.750	4.561	-0.189
3.850	3.776	-0.074	3.150	3.123	-0.027	2.650	2.610	-0.040
2.150	2.111	-0.039	1.700	1.702	0.002			
0.038400	0.010000							
8.600	8.483	-0.117	7.250	7.138	-0.112	6.050	6.014	-0.036
5.050	5.028	-0.022	4.250	4.212	-0.038	3.600	3.520	-0.080
2.900	2.853	-0.047	2.300	2.298	-0.002			
0.020400	0.020000							
3.040	3.057	0.017	2.440	2.454	0.014	2.000	2.000	0.000
1.600	1.557	-0.043	1.300	1.257	-0.043	1.100	1.052	-0.048
0.850	0.842	-0.008	0.700	0.682	-0.018			
0.027200	0.020000							
4.540	4.600	0.060	3.690	3.768	0.078	3.040	3.116	0.076
2.540	2.541	0.001	2.040	2.059	0.019	1.700	1.721	0.021
1.400	1.386	-0.014	1.150	1.120	-0.030			
0.034000	0.020000							
6.400	6.331	-0.069	5.300	5.263	-0.037	4.450	4.397	-0.053
3.750	3.635	-0.115	3.100	3.002	-0.098	2.550	2.509	-0.041
2.100	2.028	-0.072	1.750	1.635	-0.115			
0.040000	0.020000							
8.330	8.218	-0.112	6.950	6.906	-0.084	5.890	5.813	-0.077
4.890	4.855	-0.035	4.140	4.061	-0.079	3.440	3.394	-0.046
2.750	2.750	-0.040	2.240	2.215	-0.025			
0.020000	0.050000							
2.050	2.168	0.118	1.660	1.709	0.049	1.270	1.374	0.104
1.030	1.075	0.045	0.830	0.822	-0.008	0.640	0.687	0.047
0.540	0.547	0.007	0.440	0.444	0.004			
0.040000	0.050000							
5.690	5.841	0.151	4.760	4.838	0.078	3.930	4.032	0.102
3.240	3.322	0.082	2.650	2.731	0.081	2.160	2.283	0.123
1.770	1.844	0.074	1.470	1.487	0.017			
0.060000	0.050000							
10.320	10.526	0.206	8.760	8.939	0.179	7.430	7.574	0.144
6.300	6.380	0.080	5.310	5.396	0.086	4.430	4.508	0.078
3.590	3.661	0.071	2.900	2.946	0.046			

THE "LETAGROP" CALCULATIONS

The values obtained by the different graphical methods were refined using the computer program "LETAGROP VRID".[23] The "best values" for β_1, β_2, β_3, and β_4 obtained were:

$\beta_1 = 10.69 \pm 0.25$ M^{-1} $\quad \beta_3 = 58.53 \pm 8.37$ M^{-3}

$\beta_2 = 39.60 \pm 2.10$ M^{-2} $\quad \beta_4 = 163.3 \pm 9.66$ M^{-4}

and $U = \sum(\bar{n}_{calc} - \bar{n})^2 = 0.13946$. 246 $\bar{n}(\log a)$-values were used. The errors given are σ, where σ is the standard deviation in β.

The original experimental data in the range 350 – 385 nm were also processed with the spectrophotometric version "SPEFO" of the "LETAGROP" program.[22] U is the error squares sum, defined as $U = \sum(\varepsilon_{calc} - \varepsilon)^2$. It appeared to be somewhat hazardous to determine the stability constants with the "SPEFO" program, owing partly to the large number of parameters and partly to the low molar absorptivity of $CuCl^+$.

Table 9. Spectrophotometric data in the range 350 – 385 nm for 74 solutions. A and B are given for each solution, followed by ε, ε_{calc}, and $\varepsilon_{calc} - \varepsilon$ for 8 wave lengths. The concentrations are expressed in M, the apparent absorptivities in M^{-1} cm^{-1}. $\beta_1 = 10.7$ M^{-1}, $\beta_2 = 39.6$ M^{-2}, $\beta_3 = 59$ M^{-3} and $\beta_4 = 163$ M^{-4} were kept constant during the calculation. Missing data is indicated by -1.

0.240000	0.005000							
-1.000	-1.000	0.0	-1.000	-1.000	0.0	99.000	98.885	-0.115
-1.000	-1.000	0.0	85.000	84.918	-0.082	-1.000	-1.000	0.0
-1.000	-1.000	0.0	-1.000	-1.000	0.0			
0.270000	0.005000							
-1.000	-1.000	0.0	-1.000	-1.000	0.0	115.800	115.122	-0.678
108.000	107.238	-0.792	101.000	100.337	-0.663	93.800	93.281	-0.519
86.400	85.727	-0.673	-1.000	-1.000	0.0			
0.285000	0.005000							
-1.000	-1.000	0.0	-1.000	-1.000	0.0	123.300	123.244	-0.056
115.300	115.138	-0.162	108.100	108.140	0.040	101.100	100.949	-0.151
93.300	93.147	-0.153	84.500	84.684	0.184			
0.300000	0.005000							
-1.000	-1.000	0.0	-1.000	-1.000	0.0	131.400	131.338	-0.062
123.400	123.068	-0.332	116.300	115.970	-0.330	109.400	108.679	-0.721
101.000	100.657	-0.343	91.800	91.791	-0.009			
0.315000	0.005000							
-1.000	-1.000	0.0	-1.000	-1.000	0.0	138.700	139.383	0.683
130.300	130.976	0.676	123.100	123.801	0.701	115.700	116.443	0.743
107.100	108.229	1.129	98.300	98.975	0.675			
0.330000	0.005000							
-1.000	-1.000	0.0	-1.000	-1.000	0.0	146.400	147.360	0.960
137.800	138.841	1.041	130.400	131.611	1.211	123.400	124.216	0.816
114.800	115.835	1.035	105.000	106.209	1.209			
0.345000	0.005000							
-1.000	-1.000	0.0	-1.000	-1.000	0.0	154.600	155.253	0.653
146.600	146.645	0.045	139.000	139.379	0.379	132.000	131.976	-0.024
123.200	123.452	0.252	113.200	113.468	0.268			
0.360000	0.005000							
-1.000	-1.000	0.0	-1.000	-1.000	0.0	161.800	163.047	1.247
153.700	154.370	0.670	146.100	147.087	0.987	139.300	139.701	0.401
130.300	131.056	0.756	119.900	120.729	0.829			
0.375000	0.005000							
-1.000	-1.000	0.0	-1.000	-1.000	0.0	171.300	170.727	-0.573
163.200	162.002	-1.198	-1.000	-1.000	0.0	-1.000	-1.000	0.0
139.800	138.627	-1.173	128.800	127.972	-0.828			
0.390000	0.005000							
-1.000	-1.000	0.0	-1.000	-1.000	0.0	178.500	178.283	-0.217
169.800	169.527	-0.273	162.600	162.258	-0.342	155.600	154.973	-0.627
146.200	146.147	-0.053	135.600	135.178	-0.422			
0.405000	0.005000							
-1.000	-1.000	0.0	-1.000	-1.000	0.0	185.300	185.706	0.406
176.500	176.935	0.435	169.700	169.693	-0.007	162.400	162.488	0.088
153.100	153.599	0.499	142.300	142.330	0.030			
0.076800	0.010000							
24.000	23.761	-0.239	21.200	20.948	-0.252	18.400	18.561	0.161
16.000	16.182	0.182	-1.000	-1.000	0.0	-1.000	-1.000	0.0
-1.000	-1.000	0.0	-1.000	-1.000	0.0			
0.089600	0.010000							
29.600	29.641	0.041	26.200	26.293	0.093	23.100	23.395	0.295
20.200	20.534	0.334	17.600	17.873	0.273	-1.000	-1.000	0.0
-1.000	-1.000	0.0	-1.000	-1.000	0.0			
0.102400	0.010000							
36.000	35.816	-0.184	32.100	31.926	-0.174	28.400	28.515	0.115
25.000	25.175	0.175	22.000	22.081	0.081	19.000	19.339	0.339
16.400	16.682	0.282	-1.000	-1.000	0.0			
0.115200	0.010000							
41.800	42.235	0.435	37.300	37.804	0.504	33.600	33.883	0.283
29.700	30.075	0.375	26.200	26.561	0.361	22.900	23.364	0.464
19.800	20.256	0.456	16.900	17.447	0.547			
0.128000	0.010000							
48.800	48.860	0.060	43.750	43.890	0.140	39.600	39.472	-0.128
35.300	35.211	-0.089	31.400	31.295	-0.105	27.600	27.651	0.051
24.000	24.097	0.097	20.700	20.853	0.153			
0.140800	0.010000							
55.400	55.659	0.259	50.000	50.155	0.155	45.300	45.258	-0.042
40.600	40.561	-0.039	36.200	36.265	0.065	32.200	32.191	-0.009
28.200	28.200	-0.000	24.300	24.517	0.217			
0.153600	0.010000							
62.500	62.602	0.102	56.250	56.573	0.323	50.800	51.220	0.420
45.800	46.108	0.308	41.400	41.454	0.054	36.800	36.972	0.172
32.400	32.555	0.155	28.200	28.435	0.235			
0.166400	0.010000							
69.800	69.665	-0.135	63.150	63.121	-0.029	57.400	57.340	-0.060
51.900	51.835	-0.065	47.200	46.847	-0.353	42.200	41.979	-0.221
37.400	37.153	-0.247	32.800	32.599	-0.201			
0.179200	0.010000							
77.000	76.824	-0.176	70.000	69.777	-0.223	63.800	63.599	-0.201
57.800	57.725	-0.075	52.800	52.428	-0.372	47.400	47.201	-0.199
42.200	41.983	-0.217	37.200	37.000	-0.200			
0.192000	0.010000							
83.600	84.058	0.458	76.000	76.522	0.522	69.500	69.980	0.480
63.300	63.761	0.461	57.700	58.181	0.481	52.200	52.621	0.421
46.800	47.032	0.232	41.300	41.625	0.325			
0.204800	0.010000							
90.800	91.347	0.547	83.050	83.336	0.286	75.800	76.466	0.666
69.600	69.928	0.328	63.600	64.089	0.489	57.800	58.226	0.426
52.000	52.284	0.284	46.000	46.461	0.461			
0.217600	0.010000							
97.800	98.672	0.872	89.700	90.203	0.503	82.500	83.040	0.540
75.800	76.207	0.407	69.700	70.135	0.435	-1.000	-1.000	0.0
57.500	57.724	0.224	51.300	51.494	0.194			

Table 9. Continued.

0.230400	0.010000							
-1.000	-1.000	0.0	-1.000	-1.000	0.0	88.900	89.687	0.787
81.800	82.583	0.783	75.500	76.301	0.801	-1.000	-1.000	0.0
62.800	63.336	0.536	56.100	56.706	0.606			
0.240000	0.010000							
-1.000	-1.000	0.0	-1.000	-1.000	0.0	95.600	94.709	-0.891
87.800	87.418	-0.382	81.000	80.995	-0.005	74.800	74.446	-0.354
67.900	67.646	-0.254	60.700	60.724	0.024			
0.243200	0.010000							
-1.000	-1.000	0.0	-1.000	-1.000	0.0	96.000	96.389	0.389
88.000	89.039	1.039	82.200	82.571	0.371	75.600	75.970	0.370
68.800	69.101	0.301	61.600	62.082	0.482			
0.256000	0.010000							
-1.000	-1.000	0.0	-1.000	-1.000	0.0	102.400	103.132	0.732
95.200	95.559	0.359	88.400	88.927	0.527	-1.000	-1.000	0.0
74.600	75.002	0.402	67.300	67.604	0.304			
0.268800	0.010000							
-1.000	-1.000	0.0	-1.000	-1.000	0.0	-1.000	-1.000	0.0
-1.000	-1.000	0.0	95.100	95.352	0.252	87.900	88.401	0.501
80.600	81.021	0.421	73.100	73.254	0.154			
0.270000	0.010000							
-1.000	-1.000	0.0	-1.000	-1.000	0.0	111.100	110.535	-0.565
103.100	102.744	-0.356	96.100	95.957	-0.143	89.500	88.993	-0.507
82.100	81.590	-0.510	74.200	73.789	-0.410			
0.285000	0.010000							
-1.000	-1.000	0.0	-1.000	-1.000	0.0	119.200	118.479	-0.721
110.800	110.483	-0.317	103.600	103.556	-0.044	96.600	96.440	-0.160
89.000	88.780	-0.220	80.600	80.561	-0.039			
0.300000	0.010000							
-1.000	-1.000	0.0	-1.000	-1.000	0.0	127.000	126.414	-0.586
119.200	118.240	-0.960	111.800	111.201	-0.599	104.600	103.967	-0.633
96.400	96.075	-0.325	87.600	87.453	-0.147			
0.315000	0.010000							
-1.000	-1.000	0.0	-1.000	-1.000	0.0	133.600	134.319	0.719
125.200	125.995	0.795	-1.000	-1.000	0.0	112.100	111.547	-0.553
-1.000	-1.000	0.0	95.100	94.439	-0.661			
0.330000	0.010000							
-1.000	-1.000	0.0	-1.000	-1.000	0.0	142.500	142.175	-0.325
133.700	133.726	0.026	127.000	126.529	-0.471	118.400	119.155	0.755
110.900	110.880	-0.020	101.800	101.494	-0.306			
0.345000	0.010000							
-1.000	-1.000	0.0	-1.000	-1.000	0.0	-1.000	-1.000	0.0
141.000	141.414	0.414	134.900	134.173	-0.739	126.400	126.770	0.370
118.200	118.339	0.139	108.800	108.593	-0.207			
0.360000	0.010000							
-1.000	-1.000	0.0	-1.000	-1.000	0.0	158.200	157.674	-0.526
148.800	149.043	0.243	141.800	141.770	-0.030	134.400	134.369	-0.031
126.500	125.805	-0.695	116.200	115.714	-0.486			
0.375000	0.010000							
-1.000	-1.000	0.0	-1.000	-1.000	0.0	164.900	165.288	0.388
156.700	156.595	-0.105	149.200	149.311	0.111	142.100	141.934	-0.166
133.300	133.258	-0.042	122.700	122.834	0.134			
0.390000	0.010000							
-1.000	-1.000	0.0	-1.000	-1.000	0.0	173.100	172.795	-0.305
162.600	164.060	1.460	157.000	156.778	-0.222	150.500	149.447	-1.053
141.400	140.678	-0.722	130.600	129.937	-0.663			
0.081600	0.020000							
23.200	23.174	-0.026	20.500	20.416	-0.084	17.900	18.081	0.181
-1.000	-1.000	0.0	-1.000	-1.000	0.0	-1.000	-1.000	0.0
-1.000	-1.000	0.0	-1.000	-1.000	0.0			
0.095200	0.020000							
29.100	28.992	-0.108	25.800	25.701	-0.099	22.700	22.859	0.159
19.800	20.050	0.250	17.300	17.437	0.137	-1.000	-1.000	0.0
-1.000	-1.000	0.0	-1.000	-1.000	0.0			
0.108800	0.020000							
35.400	35.121	-0.279	31.500	31.291	-0.209	27.800	27.937	0.137
24.500	24.649	0.149	21.600	21.602	0.002	18.700	18.912	0.212
16.200	16.304	0.104	-1.000	-1.000	0.0			
0.122400	0.020000							
41.200	41.513	0.313	36.900	37.141	0.241	33.200	33.277	0.077
29.400	29.520	0.120	26.000	26.052	0.052	22.800	22.904	0.104
19.700	19.846	0.146	16.800	17.086	0.286			
0.136000	0.020000							
47.600	48.126	0.526	42.800	43.215	0.415	38.700	38.851	0.151
34.500	34.638	0.138	30.600	30.765	0.165	27.000	27.170	0.170
23.500	23.664	0.164	20.200	20.467	0.267			
0.149600	0.020000							
55.100	54.929	-0.171	49.800	49.481	-0.319	45.000	44.634	-0.366
40.400	39.982	-0.418	36.000	35.725	-0.275	31.900	31.697	-0.203
28.000	27.751	-0.249	24.300	24.115	-0.185			
0.163200	0.020000							
62.200	61.891	-0.309	56.200	55.914	-0.286	51.000	50.637	-0.363
46.000	45.536	-0.464	41.200	40.917	-0.283	36.800	36.475	-0.325
32.500	32.101	-0.399	28.300	28.025	-0.275			
0.176800	0.020000							
69.200	68.985	-0.215	62.600	62.489	-0.111	56.900	56.748	-0.152
51.800	51.280	-0.520	46.800	46.323	-0.477	41.900	41.491	-0.409
37.300	36.703	-0.597	32.600	32.191	-0.409			
0.190400	0.020000							
76.000	76.188	0.188	69.200	69.185	-0.015	63.000	63.041	0.041
57.200	57.198	-0.002	51.700	51.928	0.228	46.500	46.731	0.231
41.200	41.548	0.348	36.700	36.602	-0.098			
0.204000	0.020000							
84.000	83.479	-0.521	76.400	75.981	-0.419	69.900	69.466	-0.434
63.700	63.275	-0.425	-1.000	-1.000	0.0	52.400	52.182	-0.218
-1.000	-1.000	0.0	41.800	41.248	-0.552			
0.217600	0.020000							
90.900	90.835	-0.065	83.200	82.857	-0.343	76.000	76.008	0.008
69.600	69.491	-0.109	63.600	63.670	0.070	57.700	57.827	0.127
51.900	51.909	0.009	46.400	46.115	-0.285			
0.231200	0.020000							
98.500	98.237	-0.263	89.800	89.794	-0.006	82.500	82.648	0.148
75.800	75.832	0.032	70.000	69.773	-0.227	63.700	63.650	-0.050
57.400	57.396	-0.004	51.600	51.190	-0.410			

Table 9. Continued.

0.244800	0.020000							
-1.000	-1.000	0.0	-1.000	-1.000	0.0	90.500	89.370	-1.130
83.400	82.279	-1.121	76.600	76.006	-0.594	70.300	69.634	-0.666
63.900	63.066	-0.834	57.100	56.455	-0.645			
0.258400	0.020000							
-1.000	-1.000	0.0	-1.000	-1.000	0.0	97.000	96.158	-0.842
89.500	88.816	-0.684	82.900	82.354	-0.546	76.100	75.760	-0.340
69.500	68.900	-0.600	62.400	61.895	-0.505			
0.272000	0.020000							
-1.000	-1.000	0.0	-1.000	-1.000	0.0	-1.000	-1.000	0.0
96.500	95.425	-1.075	89.400	88.797	-0.603	82.500	82.011	-0.489
75.400	74.881	-0.519	67.800	67.490	-0.310			
0.285600	0.020000							
-1.000	-1.000	0.0	-1.000	-1.000	0.0	-1.000	-1.000	0.0
-1.000	-1.000	0.0	95.600	95.318	-0.282	88.400	88.369	-0.031
80.800	80.989	0.189	73.400	73.224	-0.176			
0.360000	0.020000							
169.000	167.532	-1.468	156.800	155.561	-1.239	146.300	147.408	1.108
139.400	138.888	-0.512	132.000	131.657	-0.343	124.100	124.262	0.162
115.600	115.881	0.281	105.700	106.252	0.552			
0.390000	0.020000							
181.700	182.766	1.066	169.300	170.199	0.899	162.200	162.223	0.023
152.600	153.552	0.953	145.400	146.271	0.871	137.600	138.881	1.281
128.700	130.248	1.548	118.600	119.957	1.357			
0.420000	0.020000							
-1.000	-1.000	0.0	-1.000	-1.000	0.0	177.700	176.691	-1.009
168.900	167.940	-0.960	161.300	160.667	-0.633	154.500	153.367	-1.133
144.900	144.557	-0.343	133.700	133.654	-0.046			
0.140000	0.050000							
38.200	38.183	-0.017	34.000	34.091	0.091	30.600	30.490	-0.110
27.000	26.974	-0.026	23.700	23.721	0.021	20.700	20.809	0.109
17.800	17.983	0.183	-1.000	-1.000	0.0			
0.120000	0.050000							
30.600	30.431	-0.169	27.200	27.012	-0.188	23.700	24.047	0.347
20.800	21.123	0.323	18.000	18.406	0.406	-1.000	-1.000	0.0
-1.000	-1.000	0.0	-1.000	-1.000	0.0			
0.100000	0.050000							
23.400	23.190	-0.210	20.400	20.431	0.031	17.800	18.094	0.294
-1.000	-1.000	0.0	-1.000	-1.000	0.0	-1.000	-1.000	0.0
-1.000	-1.000	0.0	-1.000	-1.000	0.0			
0.160000	0.050000							
46.200	46.362	0.162	41.900	41.592	-0.308	37.600	37.358	-0.242
33.700	33.265	-0.435	29.400	29.497	0.097	26.200	26.018	-0.182
22.500	22.630	0.130	19.300	19.549	0.249			
0.180000	0.050000							
55.100	54.894	-0.206	49.600	49.449	-0.151	45.000	44.604	-0.396
40.400	39.955	-0.445	36.000	35.700	-0.300	31.900	31.673	-0.227
28.000	27.730	-0.270	24.200	24.096	-0.104			
0.200000	0.050000							
64.100	63.720	-0.380	57.900	57.607	-0.293	52.300	52.185	-0.115
47.100	47.008	-0.091	42.600	42.299	-0.301	38.000	37.754	-0.246
33.500	33.271	-0.229	29.200	29.082	-0.118			
0.220000	0.050000							
73.200	72.786	-0.414	66.400	66.020	-0.380	60.400	60.061	-0.339
54.400	54.392	-0.008	49.800	49.266	-0.534	44.400	44.237	-0.163
39.400	39.238	-0.162	34.700	34.495	-0.205			
0.240000	0.050000							
81.200	82.045	0.845	73.600	74.643	1.043	67.800	68.199	0.399
61.600	62.073	0.473	56.620	56.569	-0.051	51.200	51.099	-0.101
45.700	45.610	-0.090	40.600	40.320	-0.280			
0.260000	0.050000							
92.000	91.453	-0.547	83.800	83.435	-0.365	77.000	76.560	-0.440
70.200	70.018	-0.182	64.400	64.176	-0.224	58.200	58.308	0.108
52.400	52.361	-0.039	46.700	46.533	-0.167			
0.280000	0.050000							
101.000	100.968	-0.032	92.300	92.358	0.058	84.700	85.112	0.412
77.600	78.192	0.592	71.500	72.051	0.551	65.400	65.833	0.433
59.200	59.462	0.262	53.100	53.105	0.005			
0.300000	0.050000							
-1.000	-1.000	0.0	-1.000	-1.000	0.0	93.900	93.819	-0.081
86.200	86.560	0.360	79.800	80.161	0.361	73.000	73.640	0.640
66.400	66.878	0.478	59.500	60.007	0.507			
0.320000	0.050000							
-1.000	-1.000	0.0	-1.000	-1.000	0.0	-1.000	-1.000	0.0
94.700	95.089	0.389	88.300	88.468	0.168	81.400	81.692	0.292
74.300	74.575	0.275	66.700	67.204	0.504			
0.360000	0.050000							
-1.000	-1.000	0.0	-1.000	-1.000	0.0	-1.000	-1.000	0.0
-1.000	-1.000	0.0	105.300	105.533	0.533	97.700	98.383	0.683
-1.000	-1.000	0.0	-1.000	-1.000	0.0			
0.420000	0.050000							
-1.000	-1.000	0.0	-1.000	-1.000	0.0	147.600	147.488	-0.112
138.700	138.967	0.267	131.900	131.736	-0.164	124.400	124.341	-0.059
116.100	115.957	-0.143	106.700	106.325	-0.375			
0.440000	0.050000							
-1.000	-1.000	0.0	-1.000	-1.000	0.0	155.900	156.392	0.492
147.600	147.773	0.173	141.600	140.503	-1.097	134.000	133.101	-0.899
125.500	124.558	-0.942	115.500	114.523	-0.977			
0.460000	0.050000							
-1.000	-1.000	0.0	-1.000	-1.000	0.0	165.400	165.217	-0.183
157.500	156.525	-0.975	-1.000	-1.000	0.0	141.700	141.862	0.162
132.900	133.187	0.287	123.200	122.767	-0.433			
0.480000	0.050000							
-1.000	-1.000	0.0	-1.000	-1.000	0.0	-1.000	-1.000	0.0
164.800	165.200	0.400	157.100	157.920	0.820	149.600	150.598	0.998
-1.000	-1.000	0.0	130.400	131.027	0.627			
0.500000	0.050000							
-1.000	-1.000	0.0	-1.000	-1.000	0.0	183.400	182.544	-0.856
174.900	173.778	-1.122	166.900	166.522	-0.378	159.000	159.281	0.281
150.700	150.417	-0.283	-1.000	-1.000	0.0			

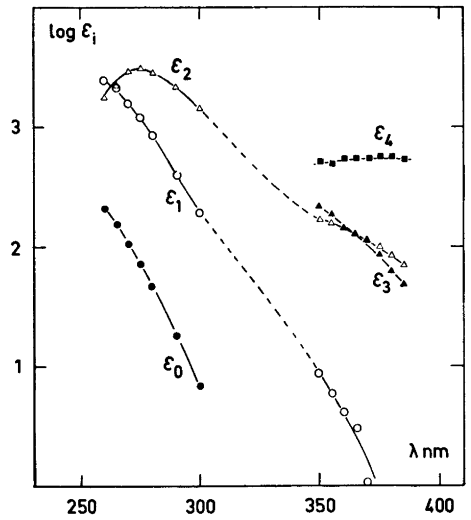

Fig. 8. The log ε_i values obtained from the "LETAGROP" program. ε_0 measured directly.

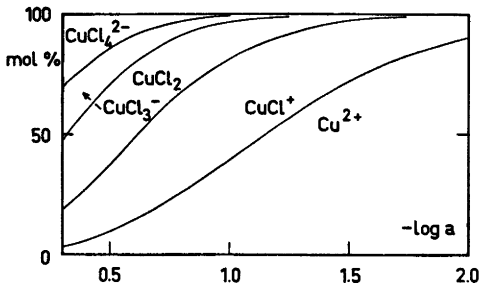

Fig. 9. The distribution of copper(II) chloride complexes as a function of log a for $B = 0.010$ M.

The values of the stability constants were determined from the $\bar{n}(\log a)$-curve by means of the program "LETAGROP VRID".[23] The values of the constants were then inserted in the "SPEFO" version to calculate the ε_i values. The program requires that ε_1 is determined. By inserting the values of β_1 and β_2 and processing the experimental data obtained at low chloride ion concentration ($A < 0.06$ M), it was possible to obtain approximate values for ε_1 in the range 350 – 385 nm. ε_1 was then fixed, and ε_2, ε_3, and ε_4 were calculated (*cf.* Table 7). All the ε_i values were then fixed, and the stability constants were calculated with the "SPEFO" program in the range 370 – 385 nm (*cf.* Table 10). The values for β_1, β_2, β_3 and β_4 obtained were:

$\beta_1 = 10.43 \pm 0.42$ M^{-1} $\quad \beta_3 = 56.54 \pm 2.13$ M^{-3}
$\beta_2 = 39.13 \pm 0.92$ M^{-2} $\quad \beta_4 = 160.0 \pm 4.86$ M^{-4}

and $U = 67.55$ for 274 values for $A \leq 0.5$ M. The errors given are σ, where σ is the standard deviation. The errors are probably underestimated since it was necessary to hold the ε_i values constant during the calculation. The experimental data, which were processed with the "SPEFO" program are presented in Tables 8 and 9.

RESULTS AND DISCUSSION

The refinement of the constants thus gave the following values which are regarded as being the "best values":

$\log \beta_1 = 1.03 \pm 0.03$ $\quad \log \beta_3 = 1.77 \pm 0.19$
$\log \beta_2 = 1.60 \pm 0.07$ $\quad \log \beta_4 = 2.21 \pm 0.08$

Table 10. Survey of the values for the stability constants, β, obtained by the different methods of calculation.

Calculation method	β_1 (M^{-1})	β_2 (M^{-2})	β_3 (M^{-3})	β_4 (M^{-4})
Curve fitting	10.1	45.7	–	–
LETAGROP "SPEFO"	11.6 ± 0.2	39.2 ± 6.2	–	–
Fronæus' method	10	43	39	167
	11.5	41	46	177
Rosotti's method	10	36	42	161
Rosotti's reciprocal method	11	38	43	–
LETAGROP VRID	10.7 ± 0.3	39.6 ± 2.1	59 ± 8	163 ± 10
LETAGROP "SPEFO"	10.4 ± 0.4	39.1 ± 0.9	57 ± 2	160 ± 5

These were obtained from the "LETAGROP VRID" calculations based on the $\bar{n}(\log a)$ data (*cf.* Table 10).

The errors given are 3σ, where σ is the standard deviation in log β. The third complex shows a greater error than the others. In Fig. 9 a distribution curve has been drawn from the above values of the constants. The narrow band of existence for the third complex shows that it only exists in comparatively small quantities.

The recorded spectra show absorption bands at 250, 375, and 800 – 900 nm. According to Andreev *et al.*[6] and Eswein *et al.*,[12] the absorption band at 250 nm indicates the formation of the lower complexes at these low concentrations. The absorption bands at 375 nm and 800 – 900 nm should indicate $CuCl_4^{2-}$. The fourth complex also absorbs in the low UV range.

The different ε_i values have been calculated with the "LETAGROP" program (*cf.* Fig. 8). The maximum for $CuCl_2$ is at 275 nm, which is in accordance with Andreev *et al.* The molar absorptivity, ε_4, for $CuCl_4^{2-}$ at 375 nm is about 530 M^{-1} cm^{-1} which agrees with the findings of Eswein *et al.*[12] The value of ε_2 (approximately 100 M^{-1} cm^{-1}) is also similar to the value calculated by Eswein *et al.*

The coordination of the Cu^{2+} ion in aqueous solution is tetragonally distorted octahedral, and of $CuCl_4^{2-}$ probably distorted tetrahedral. As can be seen from Fig. 8, the absorption maximum at 375 nm is characteristic for the $CuCl_4^{2-}$ complex, only. Thus there is evidence that this complex has a different symmetry from the lower ones. However, it should be borne in mind that, although only $CuCl_4^{2-}$ has an absorption maximum at 375 nm, the absorptivities of the other complexes cannot be neglected.

It is obvious that the stepwise stability constants in sulphuric acid solution are greater by a factor of 10 than those obtained in perchlorate medium. Without a knowledge of the entropies and heats of formation of the complexes in the perchlorate and sulphuric acid media, it is not worthwhile to speculate on the reason for this.

Acknowledgement. The work has been supported financially by the Swedish Natural Science Research Council.

REFERENCES

1. Bjerrum, J. *Kgl. Dan. Vidensk. Selsk. Mat. Phys. Medd. 22* No. 18 (1946).
2. McConnell, H. and Davidsson, N. *J. Amer. Chem. Soc. 72* (1950) 3164.
3. Näsänen, R. *Suom. Kemistilehti 26* (1953) 37.
4. Kruh, R. *J. Amer. Chem. Soc. 76* (1954) 4865.
5. Lister, M. W. and Rosenblum, P. *Can. J. Chem. 38* (1960) 1827.
6. Andreev, S. N. and Sapozhnikova, O. V. *Zh. Neorg. Khim. 13* (1968) 1548.
7. Faucherre, J. and Crego, A. *Bull. Soc. Chim. Fr.* (1962) 1820.
8. Kenttämaa, J. *Suom. Kemistilehti B 32* (1959) 68.
9. Trémillon, B. *Bull. Soc. Chim. Fr.* (1958) 1483.
10. Morris, D. F. C. and Short, E. L. *J. Chem. Soc.* (1962) 2672.
11. Libus, Z. *Inorg. Chem. 12* (1973) 2972.
12. Eswein, R. P., Howald, E. S., Howald, R. A. and Keeton, D. P. *J. Inorg. Nucl. Chem. 29* (1967) 437.
13. Vogel, A. I. *Quantitative Inorganic Analysis*, Longmans, London 1961, p. 608.
14. Domke, J. and Bein, W. *Z. Anorg. Chem. 43* (1905) 125/81, 176; (after Gmelin 8 Ed., Part 9, B2, 656).
15. Fronæus, S. *Acta Chem. Scand. 7* (1953) 21.
16. Olerup, H. *Järnkloridernas komplexitet* (Diss.), Lund 1944.
17. Fronæus, S. *Komplexsystem hos koppar* (Diss.), Lund 1948.
18. Elding, L.-I. and Leden, I. *Acta Chem. Scand. 20* (1966) 706.
19. Rossotti, F. J. C. and Rossotti, H. S. *The Determination of Stability Constants*, McGraw-Hill, New York 1961, p. 89.
20. *Ibid.*, p. 108.
21. *Ibid.*, p. 110.
22. Sillén, L.-G. and Warnquist, B. *Ark. Kemi 31* (1969) 365.
23. Ingri, N. and Sillén, L.-G. *Ark. Kemi 23* (1964) 97.

Received May 24, 1974.

Acta Chemica Scandinavica A 28 (1974) 1036—1041

Short Communications

On the Crystal Structure of Dodecahydroxohexabismuth(III) Perchlorate

BENGT SUNDVALL

Department of Inorganic Chemistry, Royal Institute of Technology, S-100 44 Stockholm 70, Sweden

Bismuth(III) is strongly hydrolyzed, even in highly acidic solutions, and several different suggestions [1] have been made as to which hydrolysis products are formed. In 1957 Olin,[2] from accurate emf measurements on bismuth perchlorate solutions, concluded that $Bi_6(OH)_{12}^{6+}$ is the predominant species over a wide range of bismuth and hydrogen ion concentrations. At the same time, ultracentrifuge measurements on hydrolyzed bismuth perchlorate solutions by Holmberg, Kraus, and Johnson [3] were interpreted as indicating the occurrence of a monodisperse polymer $(BiO)_N^{N+}$, with N = 5 or 6. Later measurements by Tobias and Tyree [4] (light scattering), by Levy, Danford, and Agron [5] (solution X-ray scattering), and by Maroni and Spiro [6] (Raman spectra on solutions and Raman and infrared spectra on crystals) are all consistent with Olin's results. From their solution X-ray measurements, Levy *et al.* concluded that the arrangement of Bi atoms in the complex is octahedral with short Bi—Bi distances of 3.70 Å. Maroni and Spiro [7] showed that such a model is also consistent with Raman and IR spectra.

Gattow and Kiel,[8] in a crystal structure study on the basic nitrate $BiONO_3(H_2O)_{1/2}$, found isolated hexanuclear complexes forming trigonal prisms (only bismuth positions were determined). In other crystal structure investigations of basic bismuth salts, for example work by Aurivillius and co-workers,[9,10] the bismuth atoms have been found to form infinite layers together with oxygen.

It has been found in the work described here that discrete complexes, with an octahedral arrangement of Bi atoms, exist in crystals grown from hydrolyzed bismuth perchlorate solutions. The crystals can be prepared by dissolving Bi_2O_3 in 3 M $HClO_4$ in a molar ratio Bi_2O_3:$HClO_4$ = 1:2, and crystallizing under a heating lamp. The colourless, well-shaped rhombic crystals are very deliquescent. For X-ray measurements they were transferred directly from the mother-liquor into capillaries, which were then sealed. Even then they were found to decompose during long exposure to an X-ray beam.

Analyses for Bi and ClO_4^- showed the composition of the crystals to correspond to Bi_2O_3:Cl_2O_7:xH_2O with $x \approx 2$. The results of a crystal structure analysis show that the formula should probably be written $Bi(OH)_2ClO_4$.

Oscillation and Weissenberg X-ray diffraction photographs taken with Cu$K\alpha$-radiation from a 0.1 mm long crystal oscillated about two different axes, show the crystal system to be orthorhombic. The unit cell constants derived from these photographs and Guinier powder photographs are $a = 11.103(2)$ Å, $b = 16.983(4)$ Å, $c = 17.405(4)$ Å.

The calculated density assuming 24 formula weights in the unit cell is 4.16 g cm^{-3}. The observed density as determined by a weight-loss method is 4.24 g cm^{-3}. Systematically absent reflexions uniquely indicate the space-group to be $P2_12_12_1$. The positions of the Bi atoms were derived from a three-dimensional Patterson synthesis calculated using 1420 visually estimated intensities. No corrections were made for absorption. Least squares refinement of the Bi parameters led to an R-factor of 0.20 and the positional and thermal parameter values given in Table 1. Fourier maps confirm the correctness of the derived Bi positions.

Projections of the positions of the Bi atoms on the *bc*- and the *ab*-planes are shown in Fig. 1. The six bismuth atoms in the asymmetric unit form a slightly distorted octahedron, and four such octahedra are present in the unit cell. The Bi—Bi distances within each octahedron

Table 1. Fractional coordinates with e.s.d.'s in paranthesis and isotropic temperature factors.

	x	y	z	B(Å^2)
Bi(1)	0.0614(6)	0.1677(6)	0.3478(4)	1.7
Bi(2)	0.1293(6)	0.0886(6)	0.1525(3)	1.5
Bi(3)	0.4476(6)	0.1487(6)	0.1781(3)	1.5
Bi(4)	0.2055(6)	0.2914(6)	0.2034(3)	1.7
Bi(5)	0.3020(7)	0.0167(6)	0.3161(4)	1.9
Bi(6)	0.3795(6)	0.2161(6)	0.3750(3)	1.5

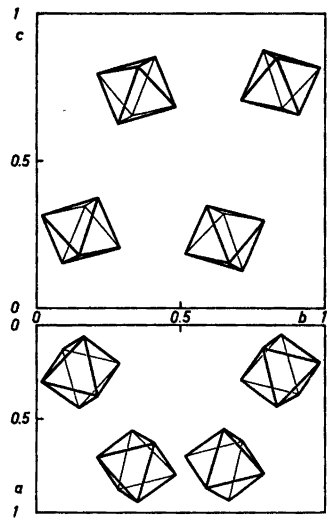

Fig. 1. Projection of the positions of Bi-atoms in one unit cell of $Bi_6(OH)_{12}(ClO_4)_6$ on the *bc*-plane (upper part) and on the *ab*-plane (lower part).

range from 3.64(1) to 3.77(1) Å along the edges, and from 5.18(1) to 5.22(1) Å along the diagonals. The shortest Bi – Bi distance between two different octahedra is 8.78(2) Å, clearly showing that the crystal contains discrete hexanuclear bismuth complexes. The Bi – Bi distances found are close to the corresponding distance of 3.70 Å deduced by Levy *et al.* for the complexes in solution.

A complete structure determination is in progress.

Acknowledgement. The work has been financially supported by the Swedish Natural Science Research Council. The English text has been revised by Dr. Derek Lewis.

1. Sillén, L. G. and Martell, A. *Stability Constants of Metal-Ion Complexes*, Special Publication No. 17, The Chemical Society, London 1964.
2. Olin, Å. *Acta Chem. Scand. 11* (1957) 1445.
3. Holmberg, R. W., Kraus, K. A. and Johnson, J. S. *J. Amer. Chem. Soc. 78* (1956) 5506.
4. Tobias, R. S. and Tyree, S. Y. *J. Amer. Chem. Soc. 82* (1960) 3244.
5. Levy, H. A., Danford, M. D. and Agron, P. A. *J. Chem. Phys. 31* (1959) 1458.
6. Maroni, V. A. and Spiro, T. G. *J. Amer. Chem. Soc. 88* (1966) 1410.
7. Maroni, V. A. and Spiro, T. G. *Inorg. Chem. 7* (1968) 183.
8. Gattow, G. and Kiel, G. *Naturwissenshaften 55* (1968) 389.
9. Aurivillius, B. and Löwenhielm, A. *Acta Chem. Scand. 18* (1964) 1937.
10. Aurivillius, B. *Acta Chem. Scand. 18* (1964) 2375.

Received May 21, 1974.

Structure of Gaseous Dimethyltrithiocarbonate Studied by Electron Diffraction

A. ALMENNINGEN,[a] L. FERNHOLT,[a] H. M. SEIP [a] and L. HENRIKSEN [b]

[a] Department of Chemistry, University of Oslo, Oslo 3, Norway, [b] Department of General and Organic Chemistry, The H. C. Ørsted Institute, University of Copenhagen, Copenhagen Ø, Denmark

Methyl vinyl sulfide has been shown by electron-diffraction [1,2] and by vibrational spectroscopy [3,4] to exist in two conformers, one *syn* (or *cis*) form and a *gauche* form with a non-planar skeleton. The infrared and Raman spectra of liquid and cryst. dimethyltrithiocarbonate, $S=C(SCH_3)_2$, have been reported [5,6] and the presence of two conformers was found in the liquid state. As a part of a study of the conformational properties of molecules with $C(sp^2)-S$ bonds, we have investigated dimethyltrithiocarbonate by means of electron-diffraction measurements.

The electron-diffraction data were recorded with the Oslo apparatus.[7] A modified molecular intensity curve ranging from $s=1.50$ Å^{-1} to $s=41.0$ Å^{-1}, was obtained in the usual way.[8] The experimental radial distribution (RD) function obtained by Fourier inversion of the intensity curve, is shown in Fig. 1.

The most likely conformers for this molecule are the *syn-syn* form shown in Fig. 1, a *syn-anti* form which also has a planar skeleton, and non-planar forms, *e.g. syn-gauche* or *gauche-gauche*. Calculations of theoretical RD functions showed that only the *syn-syn* form was consistent with the electron-diffraction data. Least-squares refinements were therefore carried out assuming this model.

The simple force field given in Table 1, which yielded frequencies in reasonable agree-

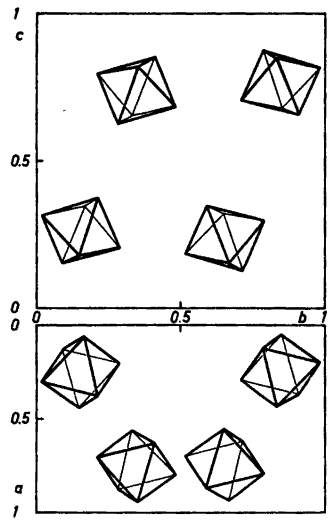

Fig. 1. Projection of the positions of Bi-atoms in one unit cell of $Bi_6(OH)_{12}(ClO_4)_6$ on the *bc*-plane (upper part) and on the *ab*-plane (lower part).

range from 3.64(1) to 3.77(1) Å along the edges, and from 5.18(1) to 5.22(1) Å along the diagonals. The shortest Bi – Bi distance between two different octahedra is 8.78(2) Å, clearly showing that the crystal contains discrete hexanuclear bismuth complexes. The Bi – Bi distances found are close to the corresponding distance of 3.70 Å deduced by Levy *et al.* for the complexes in solution.

A complete structure determination is in progress.

Acknowledgement. The work has been financially supported by the Swedish Natural Science Research Council. The English text has been revised by Dr. Derek Lewis.

1. Sillén, L. G. and Martell, A. *Stability Constants of Metal-Ion Complexes*, Special Publication No. 17, The Chemical Society, London 1964.
2. Olin, Å. *Acta Chem. Scand. 11* (1957) 1445.
3. Holmberg, R. W., Kraus, K. A. and Johnson, J. S. *J. Amer. Chem. Soc. 78* (1956) 5506.
4. Tobias, R. S. and Tyree, S. Y. *J. Amer. Chem. Soc. 82* (1960) 3244.
5. Levy, H. A., Danford, M. D. and Agron, P. A. *J. Chem. Phys. 31* (1959) 1458.
6. Maroni, V. A. and Spiro, T. G. *J. Amer. Chem. Soc. 88* (1966) 1410.
7. Maroni, V. A. and Spiro, T. G. *Inorg. Chem. 7* (1968) 183.
8. Gattow, G. and Kiel, G. *Naturwissenshaften 55* (1968) 389.
9. Aurivillius, B. and Löwenhielm, A. *Acta Chem. Scand. 18* (1964) 1937.
10. Aurivillius, B. *Acta Chem. Scand. 18* (1964) 2375.

Received May 21, 1974.

Structure of Gaseous Dimethyltrithiocarbonate Studied by Electron Diffraction

A. ALMENNINGEN,[a] L. FERNHOLT,[a] H. M. SEIP [a] and L. HENRIKSEN [b]

[a] Department of Chemistry, University of Oslo, Oslo 3, Norway, [b] Department of General and Organic Chemistry, The H. C. Ørsted Institute, University of Copenhagen, Copenhagen Ø, Denmark

Methyl vinyl sulfide has been shown by electron-diffraction [1,2] and by vibrational spectroscopy [3,4] to exist in two conformers, one *syn* (or *cis*) form and a *gauche* form with a non-planar skeleton. The infrared and Raman spectra of liquid and cryst. dimethyltrithiocarbonate, $S=C(SCH_3)_2$, have been reported [5,6] and the presence of two conformers was found in the liquid state. As a part of a study of the conformational properties of molecules with $C(sp^2)-S$ bonds, we have investigated dimethyltrithiocarbonate by means of electron-diffraction measurements.

The electron-diffraction data were recorded with the Oslo apparatus.[7] A modified molecular intensity curve ranging from $s=1.50$ Å^{-1} to $s=41.0$ Å^{-1}, was obtained in the usual way.[8] The experimental radial distribution (RD) function obtained by Fourier inversion of the intensity curve, is shown in Fig. 1.

The most likely conformers for this molecule are the *syn-syn* form shown in Fig. 1, a *syn-anti* form which also has a planar skeleton, and non-planar forms, *e.g. syn-gauche* or *gauche-gauche*. Calculations of theoretical RD functions showed that only the *syn-syn* form was consistent with the electron-diffraction data. Least-squares refinements were therefore carried out assuming this model.

The simple force field given in Table 1, which yielded frequencies in reasonable agree-

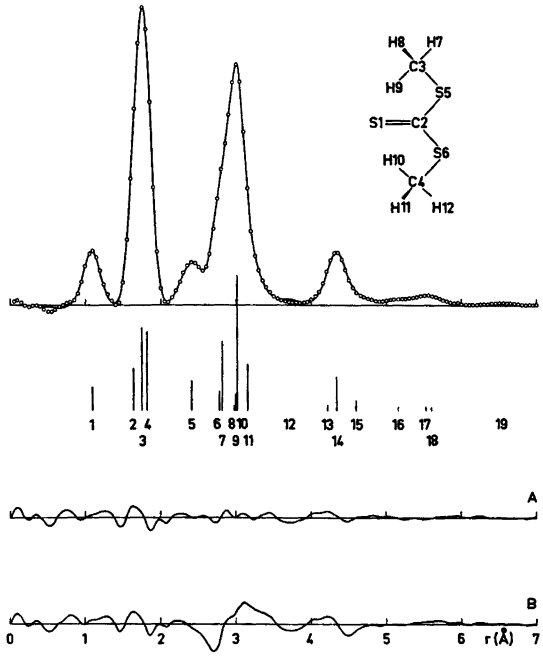

Fig. 1. Experimental (circles) and theoretical RD functions for dimethyltrithiocarbonate. Curve A shows the differences between experimental and theoretical values, and curve B the differences when the theoretical curve is calculated with 30 % of a *syn-anti* form. The scale of the difference curves is twice as large as for the RD curves. 1, C3 – H7; 2, S1 – C2; 3, S5 – C2; 4, S5 – C3; 5, S5···H7; 6, C2···C3; 7, S5···S6; 8, C2···H8; 9, S1···H8; 10, S1···S5; 11, S1···C3; 12, C2···H7; 13, S1···H7; 14, S5···C4; 15, S5···H10; 16, S5···H12; 17, C3···C4; 18, C3···H10; 19, C3···H12.

ment with the observed ones,[5,6] was used to compute mean amplitudes of vibration (u) and perpendicular amplitude correction coefficients (K) by the method described by Stølevik *et al.*[9] Some of the u values are included in Tables 2 and 3. The K values were used to obtain the R_α-structure [10] which is geometrically consistent, and in this way include the shrinkage effects [10] in the refinements.

Since the three CS bond distances contribute to the same peak in the RD curve, the determination of the individual distances is rather difficult. The corresponding mean amplitudes could not be refined independently. Two calculations were performed. In the first one the differences between the u(CS) values were assumed to be the same as computed from spectroscopic data, and one u parameter was refined. In the second calculation the u values given in Table 1 were assumed. The difference in the results was insignificant; for the CS bond lengths about 0.001 Å. We consider the structural parameters in Tables 2 and 3 as our final results.

An X-ray diffraction investigation of ethylene trithiocarbonate, $S=C\begin{smallmatrix}S-CH_2\\ \\ S-CH_2\end{smallmatrix}$, gave 1.65_2, 1.73_8, and 1.81_8 Å for the CS bonds.[11] The observed differences in the bond lengths in the two compounds may be real and related to the difference in bond angles and torsional angles. However, the comparison is somewhat uncertain because of the mentioned difficulty for dimethyltrithiocarbonate. To get a better estimate of the importance of the correlation between the distance parameters, we fixed the longest CS distance at 1.815 Å. C_2-S_5 and S=C refined then to 1.746 and 1.638 Å, respectively, while the shifts in the bond angles were insignificant. The increase in the R factor [12] was about 15 %.

The difference between the experimental RD curve and the one calculated for the pure *syn-syn* form, using the parameters from Tables 2 and 3, is given by curve A in Fig. 1. This curve shows that the experimental data can be reproduced satisfactorily by assuming the *syn-syn* form as the only conformer. The RD curves for

Table 1. Force constants used in the calculation of mean amplitudes of vibration and perpendicular amplitude correction coefficients. The number of contributions of each type is given in parentheses.

Stretching constants (mdyn Å^{-1})		Bending constants (mdyn Å rad^{-2})	
$S_1=C$	3.60(1)	$S_1C_2S_5$	0.70(2)
S_5-C_2	3.00(2)	$S_5C_2S_6$	0.70(1)
S_5-C_3	2.20(2)	$C_2S_5C_3$	1.00(2)
C–H	4.40(6)	SCH	0.35(6)
		HCH	0.45(6)
Repulsion constant (mdyn Å^{-1})		**Stretch/stretch coupling (mdyn Å^{-1})**	
$S_1\cdots S_5$	0.20(2)	$S_1=C/S_5-C_2$	0.40(2)
$C_2\cdots C_4$	0.20(2)	S_5-C_2/S_6-C_2	0.80(1)
$S_1\cdots C_4$	0.10(2)		
$S\cdots H$	0.30(6)		
$H\cdots H$	0.22(6)		
Torsional constants (mdyn Å rad^{-2})		**Out-of-plane constants [a] (mdyn Å rad^{-2})**	
$S_1C_2S_5C_3$	0.06(2)	$S_1S_5C_2/C_2S_6$	0.09(1)
$S_6C_2S_5C_3$	0.06(2)	$S_5S_6C_2/C_2S_1$	0.09(1)
$C_2S_6C_4H$	0.04(6)		

[a] C_2S_6 bond out of $S_1S_5C_2$ plane *etc.*

Table 2. Bond distances, corresponding mean amplitudes of vibration, and bond angles in dimethyltrithiocarbonate.

	r_a(Å)[a]	u(Å)[b]
S=C	1.634(5)	0.048_9
C_2-S_5	1.752(4)	0.052_5
C_3-S_5	1.800(6)	0.053_4
C–H	1.090(10)	0.078
$\angle S_1C_2S_5$	126.2(2)°	
∠CSC	103.3(4)°	
∠SCH	111.2(8)°	

[a] Results from least-squares refinement on the electron-diffraction data. The standard deviations given in parentheses apply to the last decimal place. Corrections for the correlation between the data have been included.

[b] Mean-amplitudes of vibration computed with the force field in Table 1.

Table 3. Non-bonded distances and the corresponding mean amplitudes obtained by electron diffraction (u^{ED}) and from spectroscopic data (u^{S}).

	r_a(Å)	u^{ED}(Å)	u^{S}(Å)
$S_1\cdots S_5$	3.016	0.067	0.066
$S_5\cdots S_6$	2.826	0.086	0.087
$S_1\cdots C_3$	3.156	0.125	0.127
$S_5\cdots C_4$	4.333	0.094	0.089
$C_2\cdots C_3$	2.777	–	0.083
$C_3\cdots C_4$	5.519	–	0.114
$S_5\cdots H_7$	2.401	0.113	0.115

non-planar conformers must deviate considerably from the curve corresponding to the *syn-syn* form, particularly in the region 3.0 – 4.5 Å, because of large changes in at least two C···S distances. Unfortunately the RD curves for *syn-anti* and *syn-syn* forms may be rather similar, since for example the lengths of the distances $S_1\cdots C_4$ and $S_5\cdots C_4$ may be nearly interchanged by a 180° rotation about C_2-S_6. However, the small peak near 5.5 Å found in the experimental RD curve, corresponds to the $C_3\cdots C_4$ distance in the *syn-syn* form only, proving this to be the main conformer. Curve B in Fig. 1 shows the difference between the experimental RD curve and a theoretical one calculated with 70 % of *syn-syn-* and 30 % of the *syn-anti* form. The bond distances and angles were assumed to be the same in both conformers. This difference curve is clearly not satisfactory. In spite of the possibility of better agreement by adjusting some of the bond angles in the less stable conformer, the excellent agreement for the *syn-syn* form makes it very unlikely that the amount of this conformer is less than about 75 %. A further support for this conclusion is obtained from Table 3, which shows that the mean amplitudes obtained from the electron-diffraction data for the most important non-bonded distances agree very well with those computed from the force constants in Table 1. Our result is in agreement with the observation that the *syn-syn* form is dominating in solution in non-polar solvents.[5] The large amount of *syn-syn* form in dimethyltrithiocarbonate contrasts with the results for 1,1-bis(methylthio)-ethylene where a non-planar form appears to be dominating.[13]

1. Samdal, S. and Seip, H. M. *Acta Chem. Scand. 25* (1971) 1903.
2. Derissen, J. L. and Bijen, J. M. J. M. *J. Mol. Struct. 16* (1973) 289.
3. Fabian, J., Kröber, H. and Mayer, R. *Spectrochim. Acta A 24* (1968) 727.

4. Samdal, S., Seip, H. M. and Torgrimsen, T. *Unpublished results.*
5. Herzog, K., Steger, E., Rosmus, P., Scheithauer, S. and Mayer, R. *J. Mol. Struct. 3* (1969) 339.
6. Dräger, M. and Gattow, G. *Chem. Ber. 104* (1971) 1429.
7. Bastiansen, O., Hassel, O. and Risberg, E. *Acta Chem. Scand. 9* (1955) 232.
8. Andersen, B., Seip, H. M., Strand, T. G. and Stølevik, R. *Acta Chem. Scand. 23* (1969) 3224.
9. Stølevik, R., Seip, H. M. and Cyvin, S. J. *Chem. Phys. Lett. 15* (1972) 263.
10. Kuchitsu, K. and Cyvin, S. J. In Cyvin, S. J., Ed., *Molecular Structures and Vibrations*, Elsevier, Amsterdam 1972, Chapter 12.
11. Klewe, B. and Seip, H. M. *Acta Chem. Scand. 26* (1972) 1860.
12. Seip, H. M. In Sim, G. A. and Sutton, L. E., Eds., *Molecular Structures by Diffraction Methods*, Specialist Periodical Reports, The Chemical Society, Vol. I, Part I, London 1973.
13. Jandal, P., Seip, H. M. and Torgrimsen, T. *Unpublished results*; Jandal, P., Samdal, S. and Seip, H. M. Det 8. nordiske strukturkjemikermøte, Bergen 1973.

Received August 26, 1974.

Reaction Rate Studies of the Acid Hydrolysis of Some Chromium(III) Complexes. IV. Reaction Products of the Acid Hydrolysis of Pentaammineaquachromium(III)

L. MØNSTED and O. MØNSTED

Chemistry Department I, Inorganic Chemistry, The H. C. Ørsted Institute, University of Copenhagen, DK-2100 Copenhagen Ø, Denmark

The authors of two recent papers [1,2] on the aquation in acid solution of the pentaammineaquachromium(III) ion disagree about the nature of the reaction products. The discrepancies between the reported results are summarized in Table 1. No quantitative error limits are given for the reaction rate constants of Ref. 2, but it is stated that the *trans*-tetraamminediaquachromium(III) ion is a significant reaction product. Contrary to this result the *trans*-tetraammine ion was not found in detectable amounts according to Ref. 1.

Table 1. Comparison between reaction rate constants at 75 °C in a 1 M perchlorate medium for formation of *cis*- (k_{5c}) and *trans*-tetraamminediaquachromium(III) (k_{5t}) from pentaammineaquachromium(III).

	$10^6 \times k_{5c}$ (s^{-1})	$10^6 \times k_{5t}$ (s^{-1})	$10^6 \times (k_{5c} + k_{5t})$ (s^{-1})
Ref. 1	83.1 ± 1.4	0.0 ± 0.8	83.1 ± 1.4
Ref. 2	~ 60	~ 15	77, 78

Different experimental approaches to the kinetic investigation were employed in the two papers. In Ref. 1, changes in the visible absorption spectra of a series of quenched reaction mixtures were directly converted into reaction rate constants. In Ref. 2, however, the overall reaction rate constant for disappearance of the pentaammine ion was obtained after separation of unreacted pentaammine ions from the quenched reaction mixtures by ion exchange chromatography in basic solution. This total reaction rate constant was then separated into *cis* and *trans* isomer contributions by analysis of the spectral characteristics, in a narrow region around the maximum of the first spin allowed absorption band, of a tetraammine mixture obtained by ion exchange chromatography in basic solution of a hydrolysed solution of pentaammineaquachromium(III) ions.

As the agreement between the overall reaction rate constant in the two papers must be considered satisfactory we have made further experiments on the behaviour of the isomeric tetraammine ions by elution on Dowex 50W X8 columns with strong sodium hydroxide solution.

As reported in Ref. 2 the molar absorption coefficient around 500 nm of the acidified tetraammine eluate obtained from hydrolysed pentaammineaquachromium(III) solutions is intermediate between those of the two pure tetraammine isomers. However, for the same solutions a molar absorption coefficient at the maximum of the second spin allowed absorption band lower than those of both tetraammine isomers was also observed. This latter observation is obviously in disagreement with formulation of the column eluate as a mixture of the isomeric tetraammines only. As resin induced complex decomposition is sometimes encountered authentic samples of the two tetraammine isomers were subjected to the sodium hydroxide elution used for the separation of the pentaammine reaction mixtures. For both isomers such resin induced decomposition was found as judged by the visible absorption spectra of acidified column eluates.

For the visible absorption spectra of both tetraammine isomers lower molar absorption

4. Samdal, S., Seip, H. M. and Torgrimsen, T. *Unpublished results.*
5. Herzog, K., Steger, E., Rosmus, P., Scheithauer, S. and Mayer, R. *J. Mol. Struct. 3* (1969) 339.
6. Dräger, M. and Gattow, G. *Chem. Ber. 104* (1971) 1429.
7. Bastiansen, O., Hassel, O. and Risberg, E. *Acta Chem. Scand. 9* (1955) 232.
8. Andersen, B., Seip, H. M., Strand, T. G. and Stølevik, R. *Acta Chem. Scand. 23* (1969) 3224.
9. Stølevik, R., Seip, H. M. and Cyvin, S. J. *Chem. Phys. Lett. 15* (1972) 263.
10. Kuchitsu, K. and Cyvin, S. J. In Cyvin, S. J., Ed., *Molecular Structures and Vibrations*, Elsevier, Amsterdam 1972, Chapter 12.
11. Klewe, B. and Seip, H. M. *Acta Chem. Scand. 26* (1972) 1860.
12. Seip, H. M. In Sim, G. A. and Sutton, L. E., Eds., *Molecular Structures by Diffraction Methods*, Specialist Periodical Reports, The Chemical Society, Vol. I, Part I, London 1973.
13. Jandal, P., Seip, H. M. and Torgrimsen, T. *Unpublished results*; Jandal, P., Samdal, S. and Seip, H. M. Det 8. nordiske strukturkjemikermøte, Bergen 1973.

Received August 26, 1974.

Reaction Rate Studies of the Acid Hydrolysis of Some Chromium(III) Complexes. IV. Reaction Products of the Acid Hydrolysis of Pentaammineaquachromium(III)

L. MØNSTED and O. MØNSTED

Chemistry Department I, Inorganic Chemistry, The H. C. Ørsted Institute, University of Copenhagen, DK-2100 Copenhagen Ø, Denmark

The authors of two recent papers [1,2] on the aquation in acid solution of the pentaammineaquachromium(III) ion disagree about the nature of the reaction products. The discrepancies between the reported results are summarized in Table 1. No quantitative error limits are given for the reaction rate constants of Ref. 2, but it is stated that the *trans*-tetraamminediaquachromium(III) ion is a significant reaction product. Contrary to this result the *trans*-tetraammine ion was not found in detectable amounts according to Ref. 1.

Table 1. Comparison between reaction rate constants at 75 °C in a 1 M perchlorate medium for formation of *cis*- (k_{5c}) and *trans*-tetraamminediaquachromium(III) (k_{5t}) from pentaammineaquachromium(III).

	$10^6 \times k_{5c}$ (s^{-1})	$10^6 \times k_{5t}$ (s^{-1})	$10^6 \times (k_{5c} + k_{5t})$ (s^{-1})
Ref. 1	83.1 ± 1.4	0.0 ± 0.8	83.1 ± 1.4
Ref. 2	~ 60	~ 15	77, 78

Different experimental approaches to the kinetic investigation were employed in the two papers. In Ref. 1, changes in the visible absorption spectra of a series of quenched reaction mixtures were directly converted into reaction rate constants. In Ref. 2, however, the overall reaction rate constant for disappearance of the pentaammine ion was obtained after separation of unreacted pentaammine ions from the quenched reaction mixtures by ion exchange chromatography in basic solution. This total reaction rate constant was then separated into *cis* and *trans* isomer contributions by analysis of the spectral characteristics, in a narrow region around the maximum of the first spin allowed absorption band, of a tetraammine mixture obtained by ion exchange chromatography in basic solution of a hydrolysed solution of pentaammineaquachromium(III) ions.

As the agreement between the overall reaction rate constant in the two papers must be considered satisfactory we have made further experiments on the behaviour of the isomeric tetraammine ions by elution on Dowex 50W X8 columns with strong sodium hydroxide solution.

As reported in Ref. 2 the molar absorption coefficient around 500 nm of the acidified tetraammine eluate obtained from hydrolysed pentaammineaquachromium(III) solutions is intermediate between those of the two pure tetraammine isomers. However, for the same solutions a molar absorption coefficient at the maximum of the second spin allowed absorption band lower than those of both tetraammine isomers was also observed. This latter observation is obviously in disagreement with formulation of the column eluate as a mixture of the isomeric tetraammines only. As resin induced complex decomposition is sometimes encountered authentic samples of the two tetraammine isomers were subjected to the sodium hydroxide elution used for the separation of the pentaammine reaction mixtures. For both isomers such resin induced decomposition was found as judged by the visible absorption spectra of acidified column eluates.

For the visible absorption spectra of both tetraammine isomers lower molar absorption

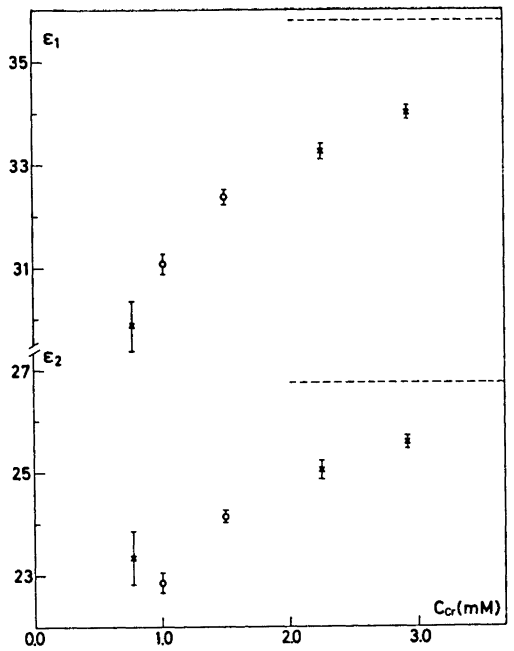

Fig. 1. Molar absorption coefficients at the maxima of the two first spin allowed bands of acidified tetraammine eluates as function of the chromium(III) concentration. ×, initially pure *cis*-tetraamminediaquachromium(III) solution; O, hydrolysed pentaammineaquachromium-(III) solution; – – –, absorptivity of authentic *cis*-tetraamminediaquachromium(III) (Ref. 3). The indicated error limits are drawn as ± twice the estimated standard deviations upon the molar absorption coefficients.

coefficients at the two absorption maxima and a higher molar absorption coefficient at the absorption minimum were invariably found. Molar absorption coefficients for the eluted chromium(III) species were not reproducible, but depended upon the chromium(III) concentration in the eluate. This is shown in Fig. 1 for the two absorption maxima of eluates of initially pure *cis*-tetraamminediaquachromium-(III) isomer.

The acidified *cis* isomer eluate was subjected to a 0.5 M sodium perchlorate elution on a SP-Sephadex C-25 cation exchange resin. This revealed four bands of which the first two were not completely separated. First a minor amount of a pink species was eluted. Next the major constituent of the solution was displaced and from the spectral characteristics of this species it was identified as the unchanged *cis* tetraammine isomer. After this species a slowly moving reddish violet band was seen, and at the column top a greyish green species remained

The close similarity between the spectral characteristics of the two types of chromium eluates, that of the initially pure *cis*-tetraammine isomer and that of the tetraammine mixture formed from the pentaammineaquachromium(III), is shown in Fig. 1 and suggests to us that evidence in favour of production of the *trans*-tetraamminediaquachromium(III) isomer from the pentaammineaquachromium(III) ion is still lacking. Consequently, in agreement with our earlier work (Ref. 1), only the *cis*-tetraamminediaquachromium(III) isomer has yet been found as a primary hydrolysis product of the pentaammineaquachromium(III) ion in acid perchlorate solution.

1. Mønsted, L. and Mønsted, O. *Acta Chem. Scand. A 28* (1974) 569.
2. Guastalla, G. and Swaddle, T. W. *Inorg. Chem. 13* (1974) 61.
3. Mønsted, L. and Mønsted, O. *Acta Chem. Scand. A 28* (1974) 23.

Received September 14, 1974.

Acta Chemica Scandinavica A 28 (1974) 1043—1046

Studies in Electronegativity. II. Comparison of the OCEE and the CNDO Schemes*

BJØRN VOIGT

Department of Physical Chemistry, H. C. Ørsted Institute, University of Copenhagen, DK-2100 Copenhagen Ø, Denmark

Fundamental problems in a comparison of results from the Overlap Corrected Electronegativity Equalization (OCEE) and the CNDO methods are discussed. The proper basis functions for the OCEE scheme are derived and employed in the calculation of Coulomb and exchange integrals for the water molecule. The results are compared with those obtained using the symmetrically orthogonalized (Löwdin-) basis appropriate to the CNDO approximation.

1. INTRODUCTION

The analysis of the principle of electronegativity equalization [1] which was presented in the initial publication in this series [2] lead to the proposal of the Overlap Corrected Electronegativity Equalization (OCEE) scheme. In this semi-empirical scheme a description of the molecular electronic structure by means of localized molecular orbitals (LMO's) is attempted. The LMO's are constructed from atomic hybrid orbitals (AHO's) with explicit inclusion of the overlaps between the bonded orbitals. Overlap integrals between non-bonded AHO's, on the other hand, are neglected.

In the following publication in the series [3] a detailed comparison of results from the OCEE and the CNDO/2 [4] schemes is carried out. Such a comparison presents some fundamental problems which are discussed below.

2. THE PROBLEM OF TRUE BASIS FUNCTIONS

The differences in the treatment of overlaps in the OCEE and CNDO schemes imply differences in the true basis functions assumed in the two theories. It is important that these differences be recognized. The direct output of the actual calculations consists of sets of coefficients. The quantities to be compared, however, are derived from the wavefunctions. A detailed comparison of results from the two schemes is thus only possible if the proper basis orbitals of both schemes are known so that the transitions from the coefficients to the wavefunctions can be made.

In the case of the CNDO scheme, it has been demonstrated [5] that the approximations introduced may be rationalized if it is assumed that the true basis is that obtained by Löwdin's method of symmetrical orthogonalization.[6] Thus if

$$\Phi = \{\phi_1, \phi_2, \cdots, \phi_m\}$$

denotes the row vector of the original, non-orthogonal atomic basis functions with the metric matrix

$$\Delta \equiv \langle \Phi | \Phi \rangle = \begin{bmatrix} 1 & S_{12} & \cdots & S_{1m} \\ S_{21} & 1 & \cdots & S_{2m} \\ - & - & - & - \\ S_{m1} & S_{m2} & \cdots & 1 \end{bmatrix}$$

then the proper CNDO-basis is

$$\Phi^{\mathrm{CNDO}} = \Phi \Delta^{-\frac{1}{2}} \qquad (1)$$

Since it is immaterial whether hybridization is performed before or after symmetrical orthogonalization, Φ may in general be assumed to be made up of atomic hybrid orbitals.

In the OCEE theory the various types of overlaps are not treated equally. Accordingly

* Based in part on a thesis presented to the University of Copenhagen in partial fulfillment of the requirements for the lic. scient. degree.

the matrix of bonded overlaps **T**, the elements of which are included explicitly in the MO's, must be separated from that containing the nonbonded overlaps which are neglected:

$$\mathbf{\Delta} \equiv \mathbf{1} + \mathbf{T} + \mathbf{S}$$

With proper ordering of basis functions, **T** will be block diagonal with 2×2 blocks. **S** has a similar block structure the elements within the blocks in this case all being zero. Although **T** and **S** do not, in general, commute, the elements of $\mathbf{TS} - \mathbf{ST}$ are usually small. If all bonded overlaps are equal and all non-bonded overlaps are equal, then the commutator vanishes identically.

The metric matrix for the proper OCEE-basis is given by

$$\langle \Phi^{\mathrm{OCEE}} | \Phi^{\mathrm{OCEE}} \rangle = \mathbf{1} + \mathbf{T}$$

$$\text{If} \quad \Phi^{\mathrm{OCEE}} \equiv \Phi \mathbf{\Delta}^{-\frac{1}{2}} \mathbf{A} = \Phi^{\mathrm{CNDO}} \mathbf{A} \tag{2}$$

then the following equation, which should be satisfied by the transformation matrix **A**, is obtained:

$$\mathbf{A}^{\dagger}\mathbf{A} = \mathbf{1} + \mathbf{T} \tag{3}$$

Two solutions to this equation, namely

$$\mathbf{A}_1 = [\mathbf{\Delta}^{\frac{1}{2}}(\mathbf{1} + \mathbf{T})\mathbf{\Delta}^{\frac{1}{2}}]^{\frac{1}{2}}\mathbf{\Delta}^{-\frac{1}{2}} \tag{4}$$

and

$$\mathbf{A}_2 = (\mathbf{1} + \mathbf{T})^{\frac{1}{2}}$$

are of special interest in the present context. They are identical when **S** and **T** commute. By expanding the square roots in series (assuming convergence), and by retaining contributions up to and including terms of second order in the overlaps,

$$\mathbf{A}_1 - \mathbf{A}_2 \cong \tfrac{1}{8}(\mathbf{ST} - \mathbf{TS}) \tag{5}$$

It may be shown (see the appendix) that the solution $\mathbf{A}_1$ gives functions which resemble the original basis functions as closely as is possible; the true OCEE-basis must therefore be given by this solution. The basis set obtained in this way is referred to as the Non-Bonded Symmetrical Orthogonal (NBSO)- basis. However, in view of the relation (5) and the near-commutation of **S** and **T** found in practice, the transformation matrix $\mathbf{A}_2$ may to a very good approximation be used instead.

Eqn. (2) now reads:

$$\Phi^{\mathrm{CNDO}} \cong \Phi^{\mathrm{OCEE}}(\mathbf{1} + \mathbf{T})^{-\frac{1}{2}} \tag{6}$$

That is, the CNDO-basis corresponding to the OCEE-hybridization may be obtained approximately by symmetrically orthogonalizing the OCEE-functions.

Because of the block structure of $\mathbf{1} + \mathbf{T}$, the OCEE – LMO's will remain localized when expressed in the CNDO type basis. In particular the OCEE lone pair functions will be identical to the corresponding CNDO type hybrids. Any delocalizations of orbitals found in the CNDO wavefunction therefore represent genuine differences from the OCEE description and are not merely due to differences in basis sets. As a further consequence of (6) comparison of the hybridization schemes of the two calculations is also justifiable in sofar as it is possible to extract hybridization informations from the CNDO results (see Ref. 3).

In order to compare the charge distributions the symmetrical orthogonalization (6) must be performed explicitly. Using primes to denote CNDO type functions, an expression for the OCEE – LMO ψ_{AB} is obtained as:

$$\psi_{AB} = C_A\phi_A + C_B\phi_B = C'_A\phi'_A + C'_B\phi'_B$$

where

$$\left.\begin{matrix} C'_A \\ C'_B \end{matrix}\right\} = \tfrac{1}{2}\left(\sqrt{1+T_{AB}} \pm \sqrt{1-T_{AB}}\right)C_A$$

$$+ \tfrac{1}{2}\left(\sqrt{1+T_{AB}} \mp \sqrt{1-T_{AB}}\right)C_B$$

and

$$\left.\begin{matrix} \phi'_A \\ \phi'_B \end{matrix}\right\} = \tfrac{1}{2}\left[\frac{1}{\sqrt{1+T_{AB}}} \pm \frac{1}{\sqrt{1-T_{AB}}}\right]\phi_A$$

$$+ \tfrac{1}{2}\left[\frac{1}{\sqrt{1+T_{AB}}} \mp \frac{1}{\sqrt{1-T_{AB}}}\right]\phi_B$$

T_{AB} is the overlap integral between the (unprimed) OCEE orbitals.

In the OCEE-scheme overlap charges are divided equally between the orbitals participating. In a CNDO-scheme no overlap contributions are present. Thus the charges ascribed to atom A from two electrons occupying the LMO above are, for each of the schemes,

$$q_A = 2C_A^2 + 2C_AC_BT_{AB}$$

and

$$q'_A = 2C_A'^2 = q_A - \tfrac{1}{2}(q_A - q_B)(1 - \sqrt{1 - T_{AB}^2}) \quad (7)$$

Although the difference $q'_A - q_A$ is of second order in the overlap it may still be significant since for σ-bonds T_{AB} may be as large as 0.7 – 0.8. For a sensible comparison with CNDO results, the OCEE charges should therefore be calculated from (7), that is, relative to the CNDO type basis.

3. TWO-ELECTRON INTERACTIONS

The CNDO approximation represents a powerful way of reducing the number of two-electron integrals necessary in molecular calculations. Only the Coulomb interactions between AO's are retained in this approximation. In the OCEE scheme, the application of the Ruedenberg approximation, which is a generalization of the Mulliken approximation to two-electron distributions,[7] formally makes it possible to retain even the exchange interactions between AO's.[2,3] However, when calculated using the proper basis set these interactions are likely to be negligible since the orbitals involved are orthogonal.

Before any steps were taken concerning the exchange integrals in the OCEE scheme the properties of the NBSO basis were investigated in more detail. This was achieved by performing an explicit calculation of integrals for H_2O using the proper basis orbitals (as given by (2) and (4) in Section 2). The H_2O molecule was chosen as a test case since its small bond angle leads to relatively large non-bonded overlaps. The resulting integral values, together with those calculated using the non-orthogonal and the completely symmetrically orthogonalized orbitals (Löwdin-orbitals), are listed in Table 1.

Of prime concern are the exchange integrals between non-bonded orbitals. In the two-center case, these are greatly reduced upon orbital orthogonalization using either of the methods. The values obtained from the NBSO-basis, however, are consistently about twice those calculated using the Löwdin-orbitals. That is, the differential overlap between functions on different centers is somewhat smaller in the latter basis.

The one-center exchange integrals show quite different behaviour, the non-bonded symmetrical orthogonalization having virtually no effect on the computed values. Complete symmetrical orthogonalization, however, leads to significantly larger integrals, corresponding to larger differential overlap between the functions. The importance of the one-center exchange interactions has of course been realized earlier. This has lead to the proposal of the INDO (Intermediate · · ·) scheme.[8]

It follows from the above analysis that in the OCEE theory neglect of exchange seems justified only for two-center integrals. Nevertheless, for convenience even the one-center contributions have been discarded in the calculations published in Ref. 3, a rough correction for the consequent error being made *via* the integral parametrization.

The Coulomb integrals have been included in Table 1 since they demonstrate more clearly than the exchange integrals the similarity of the NBSO and the original non-orthogonal basis. Comparison of the results obtained for these integrals reveals the value of explicitly including, as far as possible, the overlap effect in the MO's. Most semi-empirical schemes

Table 1. Coulomb and exchange integrals (a.u.) for H_2O.

Integral [a]	Non-orthogonal orbitals	NBSO orbitals [b]	Löwdin orbitals [b]
$[h_1h_1\|h_1h_1]$	0.7500	0.7834	0.7956
$[b_1b_1\|b_1b_1]$	0.9843	0.9984	1.0511
$[l_1l_1\|l_1l_1]$	1.0113	1.0123	1.0146
$[h_1h_1\|h_2h_2]$	0.3409	0.3234	0.2972
$[h_1h_1\|b_1b_1]$	0.6303	0.6243	0.5406
$[h_1h_1\|b_2b_2]$	0.4624	0.4462	0.4255
$[h_1h_1\|l_1l_1]$	0.4534	0.4399	0.4110
$[b_1b_1\|b_2b_2]$	0.7806	0.7821	0.8592
$[b_1b_1\|l_1l_1]$	0.7705	0.7723	0.8089
$[l_1l_1\|l_2l_2]$	0.7537	0.7553	0.7503
$[h_1h_2\|h_1h_2]$	0.0398	0.0031	0.0016
$[h_1b_1\|h_1b_1]$	0.2709	0.2587	0.0142
$[h_1b_2\|h_1b_2]$	0.0289	0.0095	0.0045
$[h_1l_1\|h_1l_1]$	0.0314	0.0102	0.0061
$[b_1b_2\|b_1b_2]$	0.0752	0.0759	0.0909
$[b_1l_1\|b_1l_1]$	0.0753	0.0743	0.0826
$[l_1l_2\|l_1l_2]$	0.0688	0.0682	0.0660

[a] Notation: b and l are bonding resp. lone pair O-hybrids, b points along the OH-axis; h denotes the H 1*s*-orbital. Orbital exponents are 2.275 and 1.2 respectively. [b] See Section 2.

published to date conceal all overlap corrections in a hypothetical basis set which is not, in fact, used in actual computations.

Acknowledgement. The author is grateful to Dr. H. Johansen for supplying most of the programs with which the results in Table 1 were obtained. Thanks are also due to Professor J. P. Dahl for his contributions in many stimulating discussions.

APPENDIX

It is to be demonstrated that when eqn. (4) is applied in (2), the resulting functions Φ^{OCEE} resemble the original functions Φ as closely as is possible. That is, that

$$\mathrm{Tr}\,\mathbf{M} \equiv \mathrm{Tr}\langle \Phi^{\mathrm{OCEE}} - \Phi | \Phi^{\mathrm{OCEE}} - \Phi \rangle =$$

$$\sum_{i=1}^{m} \int |\phi_i^{\mathrm{OCEE}} - \phi_i|^2 \mathrm{d}v$$

takes on its minimum value for this particular solution.

The matrices $\boldsymbol{\Delta}$ and $\mathbf{1}+\mathbf{T}$ are positive definite. Using the block structure of $\mathbf{T}$ it may be shown that

$$\mathbf{B} \equiv \boldsymbol{\Delta}^{\frac{1}{2}}(\mathbf{1}+\mathbf{T})\boldsymbol{\Delta}^{\frac{1}{2}}$$

is also positive definite (all the square roots are positive). The general solution of eqn. (3) may thus be expressed as

$$\mathbf{A} = \mathbf{U}\mathbf{B}^{\frac{1}{2}}\boldsymbol{\Delta}^{-\frac{1}{2}} \qquad \text{(A.1)}$$

where $\mathbf{U}$ is an arbitrary unitary matrix. For $\mathbf{U}=\mathbf{1}$ (A.1) reduces to (4). Eqns. (A.1) and (2) may be used to derive the relation

$$\mathbf{M} = \boldsymbol{\Delta} + \mathbf{1} + \mathbf{T} - 2\mathbf{B}^{\frac{1}{2}} + \mathbf{B}^{\frac{1}{2}}(\mathbf{1}-\mathbf{U})^{\dagger}(\mathbf{1}-\mathbf{U})\mathbf{B}^{\frac{1}{2}} +$$
$$[\mathbf{B}^{\frac{1}{2}}\mathbf{U}^{\dagger}\mathbf{B}^{\frac{1}{2}} - \boldsymbol{\Delta}^{-\frac{1}{2}}\mathbf{B}^{\frac{1}{2}}\mathbf{U}^{\dagger}\boldsymbol{\Delta}^{\frac{1}{2}}] + [\mathbf{B}^{\frac{1}{2}}\mathbf{U}\mathbf{B}^{\frac{1}{2}} - \boldsymbol{\Delta}^{\frac{1}{2}}\mathbf{U}\mathbf{B}^{\frac{1}{2}}\boldsymbol{\Delta}^{-\frac{1}{2}}] \qquad \text{(A.2)}$$

There will be no contributions to the trace of $\mathbf{M}$ from the last two terms in (A.2), since the trace of a product of matrices is unchanged by a cyclic permutation of the factors. Thus, defining

$$\mathbf{C} \equiv (\mathbf{1}-\mathbf{U})\mathbf{B}^{\frac{1}{2}}$$

it is found that

$$\mathrm{Tr}\,\mathbf{M} = \mathrm{Tr}[\boldsymbol{\Delta} + \mathbf{1} + \mathbf{T} - 2\mathbf{B}^{\frac{1}{2}}] + \mathrm{Tr}[\mathbf{C}^{\dagger}\mathbf{C}].$$

Finally, since

$$\mathrm{Tr}[\mathbf{C}^{\dagger}\mathbf{C}] = \sum_j \sum_i |C_{ij}|^2 \geq 0$$

the trace of $\mathbf{M}$ will be a minimum in the cases where all elements of $\mathbf{C}$ are zero. Such a case arises for $\mathbf{U}=\mathbf{1}$. *Q.E.D.*

REFERENCES

1. Sanderson, R. T. *Science 114* (1951) 670.
2. Voigt, B. and Dahl, J. P. *Acta Chem. Scand. 26* (1972) 2923.
3. Voigt, B. *Acta Chem. Scand. A 28* (1974) 1068.
4. Pople, J. A., Santry, D. P. and Segal, G. A. *J. Chem. Phys. 43* (1965) S129; Pople, J. A. and Segal, G. A. *Ibid. 43* (1965) S136; *44* (1966) 3289.
5. Dahl, J. P. *Acta Chem. Scand. 21* (1967) 1244.
6. Löwdin, P. O. *Sv. Kem. Tidskr. 67* (1955) 380.
7. Ruedenberg, K. *J. Chem. Phys. 19* (1951) 1433.
8. Pople, J. A., Beveridge, D. L. and Dobosh, P. A. *J. Chem. Phys. 47* (1967) 158.

Received June 4, 1974.

Acta Chemica Scandinavica A 28 (1974) 1047—1054

Ultrasonic Properties of Ethanol-Water Mixtures

S. G. BRUUN, P. GRAAE SØRENSEN and AASE HVIDT

Chemistry Laboratory III, H. C. Ørsted Institute, Universitetsparken 5, DK-2100 Copenhagen Ø, Denmark

Measurements have been made of the ultrasonic absorption and velocity in ethanol-water mixtures at 25 °C. Two relaxation processes are observed in the frequency range 12 – 350 MHz, and for both these relaxations a pronounced maximum of the relaxation parameters as a function of concentration is observed in the water-rich concentration range. These relaxation phenomena, as well as a maximum of the ultrasonic velocity, are tentatively taken as reflections of the formation of ice-like water structures around the nonpolar group of the alcohol.

The properties of binary mixtures of water with substances containing nonpolar groups are known to be atypical of other binary liquid mixtures. For example, the ultrasonic absorption and relaxation properties exhibit pronounced maxima as functions of concentration in dilute aqueous solutions of alcohols and alkylamines.[1–4] An inflection point is observed on the curves representing the specific volume as a function of concentration for aqueous solutions of alcohol, ketones, and ethers.[5] Such inflection points, which correspond to extrema of the partial specific volumes of the components of the mixtures, are absent in aqueous solutions of urea or formamide, in which no nonpolar groups are present.[5] They have tentatively been ascribed to interactions between nonpolar groups and solvent water,[5] and the effects observed are in qualitative accordance with the formation of the so-called Frank-Evans structures ("icebergs") in water surrounding the nonpolar groups.[6] The Frank-Evans water structures are characterized by a larger specific volume than that of pure water, and by a lower enthalpy and entropy content;[6–8] the maximum of the heat of mixing of alcohols and water in the water rich concentration range,[1,7] as well as the positive excess free energy of mixing,[7] may be taken as suggestive experimental evidence of their existence.

The importance of the contribution from structural changes of the solvent to the thermodynamic and kinetic properties of aqueous solutions of biological macromolecules, in particular protein solutions, has often been stressed.[8,9] It is the aim of the present investigation of the ultrasonic properties of ethanol-water mixtures to contribute to the elucidation of the nature of the interactions between nonpolar groups and water. Extensive ultrasonic studies of aqueous solutions of tertiary butyl alcohol are available,[3] but since the nonpolar part of this alcohol is considerably more bulky than most nonpolar groups present in protein molecules, we consider it of interest to supplement the existing data on this alcohol with measurements on ethanol-water mixtures.

Measurements on ethanol-water mixtures at the frequencies 22.5, 37.5, and 52.5 MHz are available in the literature,[1] and data at 70 MHz are mentioned in Ref. 4. We have measured the absorption in ethanol-water mixtures at 25 °C in the frequency range 12 – 350 MHz, and observed at least two relaxation processes in this range.

The experimental data are discussed on the assumption that the relaxations observed reflect interactions between the ethyl group of the alcohol and water. This assumption is based on the observation that the concentration dependence of the ultrasonic properties of the ethanol-water mixtures – characterized by a maximum in the water rich concentration range – is qualitatively similar to the concentration dependence of the ultrasonic prop-

erties of other aqueous solutions containing alkyl groups,[1-4] but strikingly different from that of the ultrasonic properties of aqueous solutions of urea and of formamide.

THEORETICAL

For a system described by a series of reactions:

$$a_{i1}A_{i1} + a_{i2}A_{i2} + \cdots \rightleftharpoons b_{i1}B_{i1} + b_{i2}B_{i2} + \cdots \quad (1)$$

the changes of the equilibrium, caused by the propagation of an ultrasonic wave, may be expressed by the changes of the equilibrium constants $K_i = K_i(P,T)$ of the system

$$dK_i = K_i\left[\left(\frac{\Delta H_i^0}{RT^2}\right)_P dT - \left(\frac{\Delta V_i^0}{RT}\right)_T dP\right] \quad (2)$$

ΔH_i^0 and ΔV_i^0 are the corresponding changes of standard enthalpy and volume, respectively.

The rates at which the equilibria are re-established (or the relaxation times of the reactions involved) determine the frequency dependence of the absorption coefficient α, usually expressed as [10]

$$\alpha/\nu^2 = \sum_i \frac{A_i}{(1+(2\pi\tau_i\nu)^2)} + B \quad (3)$$

In this expression ν is the frequency, A_i is the relaxation amplitude, and τ_i the relaxation time of the i'th relaxation process; B is the so-called background absorption parameter, $B = \lim_{\nu\to\infty}(\alpha/\nu^2)$.

The absorption per wavelength at the relaxation frequency, $\mu_{max,i} = UA_i/4\pi\tau_i$, may be expressed as

$$\mu_{max,i} = \frac{\pi}{2}\,\varrho\,\frac{U^2V^2}{RT}\,\Gamma_i\left[\frac{l\Delta H_i}{C_p} - \frac{\Delta V_i}{V}\right]^2 \quad (4)$$

where ϱ is the density, V the molar volume, l the thermal expansion coefficient, U the sound velocity, and C_P the specific heat at constant pressure. Γ_i is given as

$$\Gamma_i = \left[\sum_i \left(\frac{a_{ij}^2}{[A_{ij}]} + \frac{b_{ij}^2}{[B_{ij}]}\right)\right]^{-1} \quad (5)$$

ΔH_i and ΔV_i denote the changes in molar enthalpy and volume for the normal modes of the reactions.[10]

MATERIALS

Water was purified by distillation from aqueous potassium permanganate. α/ν^2 was measured to be 21×10^{-17} s^2 cm^{-1} at 25 °C in agreement with the value reported in the literature.[11]

Ethanol was Absolut Alkohol, ph.d., from De Danske Spritfabrikker, used without further purification. α/ν^2 was measured to be 52×10^{-17} s^2 cm^{-1}, to be compared with the value of 55×10^{-17} s^2 cm^{-1}, reported in the literature.[11] The difference is ascribed to impurities other than water, and was considered to be of no importance in the experiments performed.

Urea and formamide were analytically pure reagents.

EXPERIMENTAL METHODS

The ultrasonic absorption was measured in the frequency range 12 – 350 MHz by means of a pulse technique.[12] The experimental error of α/ν^2 is 3 %. The amount of liquid required for the measurements is approximately 50 cm^3 at the frequencies 12 – 52 MHz, and 10 cm^3 at the higher frequencies.

The ultrasonic velocity at 3.6 MHz was measured by means of a sing-around equipment from NUS Corporation, New Jersey, used in connection with a differential cell. The velocities in the mixtures are measured relative to the velocity in pure water, 1497 ms^{-1}.[11] The experimental error is less than ± 0.5 ms^{-1}. The amount of liquid necessary for the velocity measurements is about 15 cm^3.

Densities were measured with a digital densimeter, DMA02, available from Anton Paar, Austria. The temperature control was ± 0.005 °C, which allows the densities to be measured with an accuracy of $\pm 10^{-5}$ gcm^{-3}.

Shear viscosities at 25 °C were measured with a capillary viscometer.

All measurements were made at 25 ± 0.1 °C.

NUMERICAL METHODS

We assume that the measurements of α/ν^2 can be described by two relaxation processes:

$$f(\nu) = \frac{\alpha}{\nu^2} = \frac{A_1}{1+(2\pi\nu\tau_1)^2} + \frac{A_2}{1+(2\pi\nu\tau_2)^2} + B \quad (6)$$

This expression contains five parameters, namely the background absorption B, the relaxation amplitudes A_1 and A_2, and the relaxation times τ_1 and τ_2. These parameters are estimated by minimizing the least squares expression

$$s^2(A_1,A_2,\tau_1,\tau_2,B)=\sum_{i=1}^{n}\left(f(\nu_i)-\frac{\alpha_i}{\nu_i^2}\right)^2$$

where n is the number of experimental measurements, and α_i is the measured absorption coefficient for the frequency ν_i.

The minimum is determined by guessing values of the nonlinear parameters τ_1 and τ_2, and, for each guess, determining the values of the linear parameters A_1, A_2 and of B which minimize s^2. The method is described in Ref. 13, section 27.5. The minimum of s^2 with respect to the two nonlinear parameters is found by a random search strategy. This method is not as efficient as a Newton-like iteration, but to our experience much more robust. The values of the parameters in the minimum are called A_1,* A_2,* B,* τ_1,* and τ_2.* In order to test the reliability of the results, we estimate the variances and covariances of the estimated parameters. The moment matrix is computed as follows [14]

$$\mathbf{M}_{k,l}=\sum_{i=1}^{n}\left(\frac{\partial f(\nu_i)}{\partial\beta_k}\bigg|_{\beta=\beta^*}\right)\times\left(\frac{\partial f(\nu_i)}{\partial\beta_l}\bigg|_{\beta=\beta^*}\right)$$

where

$\beta=(A_1,A_2,\tau_1,\tau_2,B)$ and
$\beta^*=(A_1^*,A_2^*,\tau_1^*,\tau_2^*,B^*)$,

and the variance of the parameters β_k estimated by

$$V(\beta_k)=\frac{s^2(\beta^*)}{n-r}C_{k,k}$$

where r is the number of parameters, in the present case 5. $C_{k,k}$ are the diagonal elements of the covariance matrix $C_{i,j}$, which is the inverse of $M_{k,l}$.[15] The covariance of the parameters β_k β_l is given by

$$\mathrm{Cov}(\beta_k\beta_l)=\frac{S^2(\beta^*)}{n-r}C_{k,l}$$

where $C_{k,l}$ are the off diagonal elements of the covarience matrix.

Because of the covariance between the parameters, it is inconsistent to use the square roots of the estimated variances as reliability interval for more than one parameter. The small number of measurements implies that the estimated variances indicate no more than order of magnitude.

The computer program has been satisfactorily tested on simulated data with a normally distributed pseudorandom noise.[16]

RESULTS

The frequency dependence of α/ν^2 is shown in Figs. 1 and 2 for five concentrations of

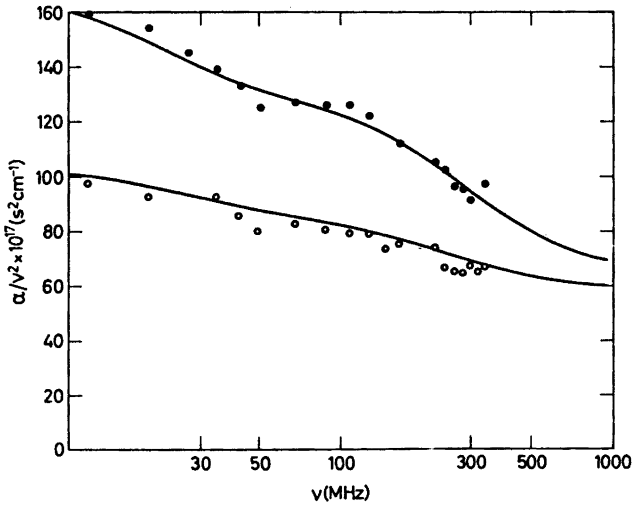

Fig. 1. Relaxation spectra of ethanol–water mixtures. ○, $w=0.3$; ●, $w=0.4$. w is the weight fraction of ethanol.

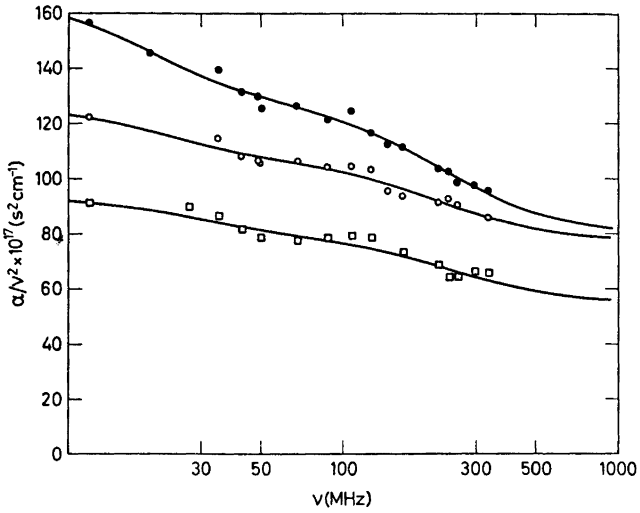

Fig. 2. Relaxation spectra of ethanol–water mixtures. ●, $w = 0.5$; ○, $w = 0.6$; □, $w = 0.7$. w is the weight fraction of ethanol.

alcohol in water. The curves shown on the figures are calculated by fitting the experimental data to eqn. (6).

The values determined of A_i, $\mu_{max,i}$, τ_i, and B are given in Table 1, and presented as functions of concentration in Figs. 3 and 5.

From the ultrasonic velocity at the frequency 3.6 MHz, U, and the density ϱ the isentropic compressibility β_s is calculated as

$$\beta_s = (\varrho U^2)^{-1} \tag{7}$$

Values of U and β_s for a series of ethanol-water mixtures are shown in Fig. 4.

The background parameter B and the classical absorption $(\alpha/\nu^2)_{class}$, calculated as [10]

$$(\alpha/\nu^2)_{class} = \frac{8\pi^2}{3\varrho U^3}\eta_s \tag{8}$$

where η_s is the shear viscosity, are shown in Fig. 5 as functions of concentration. This figure also includes the graphs of α/ν^2, measured at the frequencies 12 and 350 MHz. From this figure it is seen that the values of $(\alpha/\nu^2)_{class}$ do not account for the values obtained for B. The observation that B exhibits a distinct maximum at $w = 0.4$ suggests that more than two relaxation processes are involved. The data do not, however, allow any analysis in terms of more than two relaxation times.

The thermodynamic data, measured for the alcohol-water mixtures, are summarized] in Table 2.

Fig. 6 presents supplementary measurements of α/ν^2, made on aqueous solutions of urea and formamide, and mentioned in the discussion.

Table 1a. Relaxation parameters of ethanol-water mixtures at 25°C. V denotes the variances of the parameters.

x	w	$\tau_1 10^9$ (s)	$V(\tau_1)$ 10^9 (s)	τ_2 10^9 (s)	$V(\tau_2)$ 10^9 (s)	A_1 10^{17} (s^2 cm^{-1})	$V(A_1)$ 10^{17} (s^2 cm^{-1})	A_2 10^{17} (s^2 cm^{-1})	$V(A_2)$ 10^{17} (s^2 cm^{-1})
0.48	0.70	5.4	4.1	0.6	0.5	15	24	24	47
0.37	0.60	7.1	5.4	0.7	0.4	21	32	29	37
0.28	0.50	8.0	2.7	0.7	0.2	40	23	47	29
0.21	0.40	7.2	2.6	0.5	0.2	43	28	63	75
0.14	0.30	5.9	3.7	0.6	0.4	19	25	26	43

Table 1b. Values of μ_{max} and B for ethanol-water mixtures at 25 °C. V denotes the variances of the parameters.

x	w	$\mu_{max,\,1}10^4$	$\mu_{max,\,2}10^4$	$B\,10^{17}$ (s^2cm^{-1})	$V(B)\,10^{17}$ (s^2cm^{-1})
0.48	0.70	3.0	41.9	55	14
0.37	0.60	3.3	49.2	77	10
0.28	0.50	5.9	82.5	79	8
0.21	0.40	7.3	147.1	64	24
0.14	0.30	4.1	55.3	58	8

DISCUSSION

The concentration dependence of α/ν^2, measured for ethanol-water mixtures (Figs. 1, 2, and 5), is qualitatively similar to the one observed for tertiary butanol-water mixtures,[3] characterized by a maximum in the water-rich concentration range. A similar behavior is observed for alkylamines,[4] and in some cases it has been ascribed to the protolysis of the amino group.[17] Our reasons for suggesting that these relaxation phenomena reflect interactions between the nonpolar groups and water are the following: *1.* A maximum of α/ν^2 is generally observed in aqueous solutions of substances containing nonpolar groups,[1-4,18,19] but it is absent in aqueous solutions of urea [20,21] and formamide (Fig. 6). The maximum is more

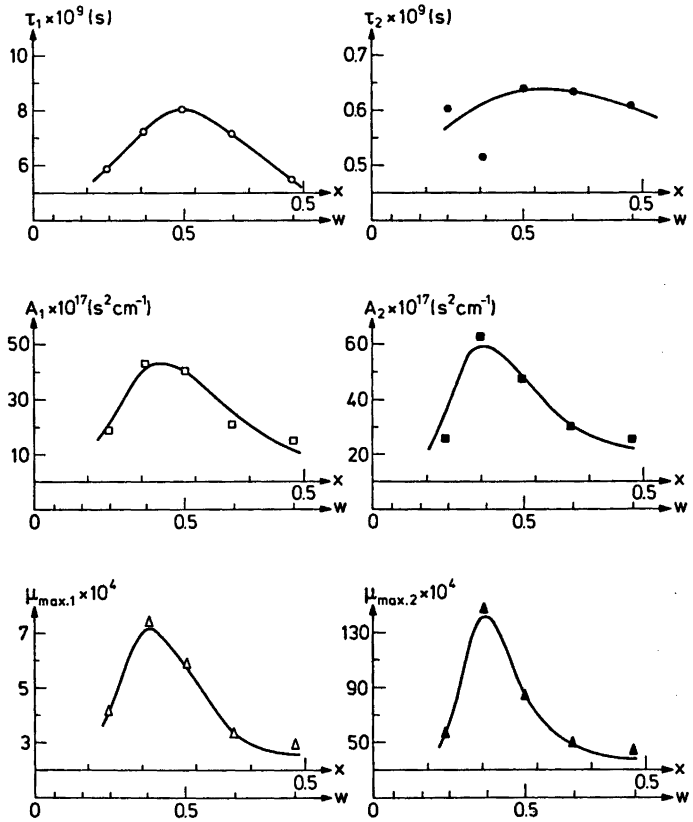

Fig. 3. The dependence of the relaxation parameters on the mol and weight fraction of ethanol.

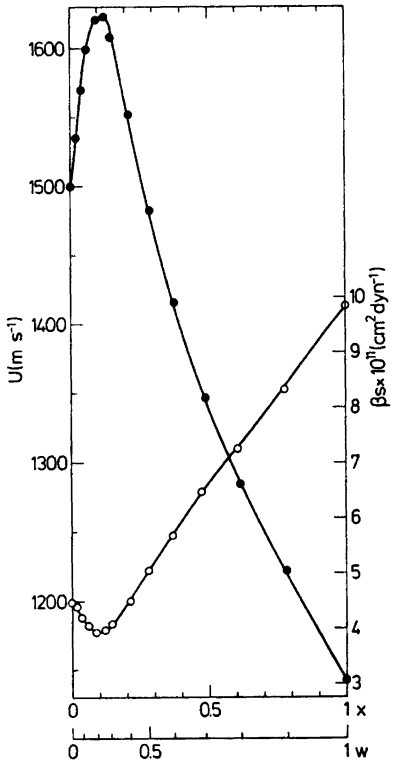

Fig. 4. Ultrasonic velocities and compressibilities of various ethanol-water mixtures. ●,U; ○, β_s.

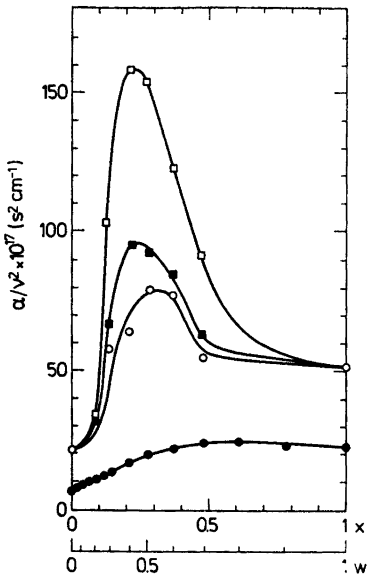

Fig. 5. Ultrasonic absorption properties of ethanol-water mixtures as functions of the ethanol concentration. ■, α/ν^2 at 350 MHz; □, α/ν^2 at 12 MHz; ○, B; ●, $(\alpha/\nu^2)_{class}$.

pronounced the larger the nonpolar part of the nonaqueous component.[4] *2.* The maximum is located in the water-rich concentration range, and at lower concentrations, the larger the nonpolar group.[4] This observation is in qualitative accordance with the conclusion reached elsewhere,[5,6,8] that interactions between nonpolar groups and water are cooperative, involving a rather large number of water molecules per methyl group. *3.* The intensity of the absorption per wavelength a the relaxation frequency, μ_{max}, is, most likely, a consequence of the rather unique feature of the formation of icelike water structures, that *the changes in standard enthalpy and volume of this process are of opposite sign,* $\Delta H° < 0$ *and* $\Delta V° > 0$; it is seen from eqn. (2) that in this case the enthalpy and the volume effect of the ultrasonic wave reinforce each other, causing changes of K in the same direction.

The relaxations observed might tentatively be ascribed to reactions of the type

$$A(H_2O_n) \rightleftharpoons A + nH_2O \qquad (9)$$

where A is the ethyl group of the alcohol, and $A(H_2O)_n$ denotes this group surrounded by n molecules of "icely" structured water. In this case the location of the maximum of the relaxation strength, and the corresponding maximum of the relaxation time at the mol fraction $x = 0.2 - 0.3$ should be taken as evidence, that $n = 3 - 4$.[2] This value of n is in accordance with the formation of the linear or cyclic water structures discussed in Ref. 22, but it is smaller than the number of water molecules (some ten or twenty, possibly more) interacting with a methyl group, estimated by measurements of enthalpy, entropy,[7,8] and volume [5] effects. Possible reaction mechanisms which are consistent with the available thermodynamic data as well as with the kinetic data here presented are

$$A(H_2O)_n + A \rightleftharpoons A + nH_2O + A \qquad (10)$$

and

$$A(H_2O)_n \rightleftharpoons A(H_2O)_{n-m} + mH_2O \qquad (11)$$

Table 2. Thermodynamic data for ethanol-water mixtures at 25 °C.

x	w	ϱ(g cm^{-3})	U(ms^{-1})	η(cP)	$(\alpha/\nu^2)_{class}10^{17}$ (s^2 cm^{-1})	β_s 10^{11} (cm^2 dyn^{-1})
1.00	1.00	.78515	1144	1.03	23.1	9.7
0.78	0.90	.81399	1221		23.8	8.2
0.61	0.80	.83916	1284		24.7	7.2
0.48	0.70	.86339	1345		24.1	6.4
0.37	0.60	.89011	1416	2.14	22.3	5.6
0.28	0.50	.90983	1481	2.25	20.1	5.0
0.21	0.40	.93252	1549	2.28	17.4	4.5
0.14	0.30	.95090	1604	2.10	14.1	4.1
0.12	0.25	.95966	1619		12.5	4.0
0.09	0.20	.96660	1615	1.74	11.3	3.9
0.06	0.15	.97352	1596		10.0	4.0
0.04	0.10	.98053	1566	1.27	8.9	4.2
0.02	0.05	.98812	1533		7.9	4.4
0.00	0.00	.99705	1497	0.89	7.0	4.5

In (10) it is assumed that the relaxations observed, with relaxation times of the order of $10^{-9}-10^{-8}$ s, are due to reactions of the type (9), catalyzed by non-solvated alcohol molecules. If so, the maximum of the relaxation parameters shall be located at mol fractions of alcohol larger than $1/(n+1)$, and the experimental data thus corresponds to a value of n larger than 4.

The reaction (11) suggests that the formation of icelike water structures around the nonpolar groups proceeds in several distinguishable steps.

A comparison between Figs. 3, 4, and 5 shows that the maximum of the ultrasonic velocity (and the corresponding minimum of the compressibility) is located at a mol fraction of alcohol, which is lower than that of the maximum of the ultrasonic absorption. A similar observation, made for aqueous solutions of acetone, has been taken as evidence that the velocity peak could be used as a measure of the breakdown of a water structure, while the absorption peak could be used as a measure of a complex formation.[2] We wish to point out that different locations of these extrema do not necessarily involve that they shall be ascribed to different kinds of reactions. The location of the velocity peak is determined, not only by the number of moles of the reac-

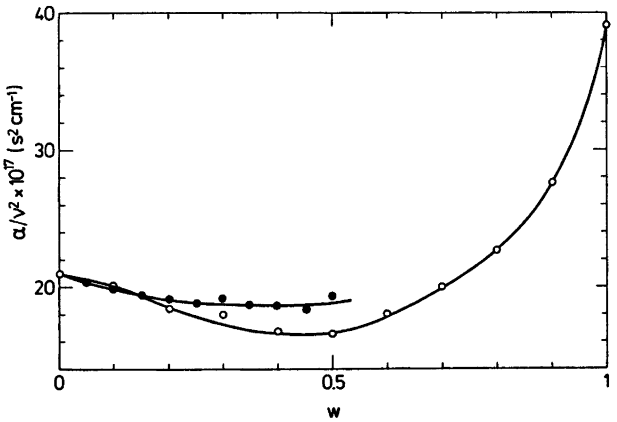

Fig. 6. The concentration dependence of α/ν^2 at 36 MHz for formamide-water (○) and urea-water (●) mixtures.

tants involved in the reaction reflected, but also by the absolute values of the ultrasonic velocity in the different structures, and by differences of the molar volumes. In the case of the ethanol water mixtures studied here, we tentatively suggest that the relaxation phenomena observed in the frequency range 12 – 350 MHz are all due to the same reaction, namely the formation of ice-like water structures around the nonpolar groups.

Acknowledgements. We wish to express our gratitude to the Royal Danish Air Force, Air Material Command, for providing us with part of the experimental equipment used in this investigation. We thank Merete Haeems for skilled technical assistance.

REFERENCES

1. Storey, L. R. O. *Proc. Phys. Soc. 65* (1952) 943.
2. Andreae, J. H., Edmonds, P. D. and McKellar, J. F. *Acustica 15* (1965) 74.
3. Blandamer, M. J., Clarke, D. E., Hidden, N. J. and Symons, M. C. R. *Trans. Faraday Soc. 64* (1968) 2691.
4. Blandamer, M. J. In Franks, F., Ed., *Water, A Comprehensive Treatise*, Plenum, New York 1973, p. 495.
5. Bøje, L. and Hvidt, Aa. *J. Chem. Thermodyn. 3* (1971) 663.
6. Frank, H. S. and Evans, M. J. *J. Chem. Phys. 13* (1945) 507.
7. Franks, F. and Ives, D. J. G. *Quart. Rev. Chem. Soc. 20* (1966) 1.
8. Kauzmann, W. *Advan. Protein Chem. 14* (1959) 1.
9. Lumry, R. and Rajender, S. *Biopolymers 9* (1970) 1125.
10. Eigen, M. and de Mayer, L. In Weissberger, A. *Technique of Organic Chemistry*, Interscience, New York – London 1963, p. 895.
11. Schaaffs, W. In Landolt-Börnstein, Group II, Vol. 5, *Molecular Acoustics*, Springer, Berlin 1967.
12. Rassing, J. *Hydrogenbindingskinetik og relaksationsspektrometri*, Thesis, University of Copenhagen, Copenhagen 1971.
13. Hamming, R. W. *Numerical Methods for Scientists and Engineers*, 2nd Ed., McGraw, New York 1973.
14. Cramér, H. *Mathematical Methods of Statistics*, Princeton University Press, Princeton 1946.
15. Rao, C. R. *Linear Statistical Inference and its Applications*, Wiley, New York 1965.
16. Abramowitz, M. and Stegun, A. *Handbook of Mathematical Functions*, Dover, New York 1965.
17. Nishikawa, S. *Bull. Chem. Soc. Jap. 46* (1973) 1657.
18. Hammes, G. G. and Knoche, W. *J. Chem. Phys. 45* (1966) 4041.
19. Sasaki, K. and Arakawa, K. *Bull. Chem. Soc. Jap. 46* (1973) 2738.
20. Hammes, G. G. and Schimmel, P. R. *J. Amer. Chem. Soc. 89* (1967) 442.
21. Arakawa, K. *Bull. Chem. Soc. Jap. 43* (1970) 636.
22. Symons, M. C. R. *Nature (London) 239* (1972) 257.

Received May 9, 1974.

Acta Chemica Scandinavica A 28 (1974) 1055—1067

Thermodynamics of the Complexation of Imidazole with Divalent Copper, Nickel, Cadmium, Zinc, and Cobalt Ions in Aqueous Sodium Perchlorate Solutions

PAAVO LUMME and PAULI VIRTANEN

Department of Inorganic Chemistry, University of Jyväskylä, Jyväskylä, Finland

The gross stability constants (β_n) of imidazole complexes with divalent copper, nickel, cadmium, zinc, and cobalt ions were determined potentiometrically in aqueous sodium perchlorate solutions in ionic strengths of about 0.25, 0.50, 1.00, 2.00, and 4.00 at 25 °C. At the lowest ionic strength the temperatures 15 and 35 °C were also employed. The thermodynamic constants (β_n^0) were derived by extrapolation to zero ionic strength. From these the thermodynamic quantities, free energies, enthalpies, and entropies of the complex formation equilibria were calculated.

Particularly, the results for copper complexes refer to the formation of polynuclear complexes. The stability of the complexes was found to follow the order: copper > nickel > cadmium > zinc > cobalt.

In most cases the enthalpy effect was found to be the dominant factor determining the stability of the imidazole complexes studied.

In a recent paper [1] the thermodynamics of the protonation of imidazole in aqueous sodium perchlorate solutions was considered by us. These studies were extended to concern thermodynamics of the complex formation of imidazole with the divalent metal ions of the first transition metal series and cadmium in the present paper. The effect of temperature and of a neutral salt on the stabilities of the complexes was studied, and used as the basis for evaluating the thermodynamic constants.

EXPERIMENTAL

Reagents and solutions. The metal perchlorates were products of the G. F. Smith Chemical Co., and the other reagents used were guaranteed reagents of E. Merck AG. The water used was of conductivity quality.

For each ionic strength a carbonate-free sodium hydroxide solution was prepared in a nitrogen atmosphere in a gas-tight burette system of Pyrex glass. The ionic strengths of the solutions were adjusted with sodium perchlorate. The alkali concentrations of the solutions were checked potentiometrically against weighed amounts of potassium biphthalate.[1]

A dilute perchloric acid solution was prepared from conc. perchloric acid, and its acidity was determined potentiometrically with the known sodium hydroxide solution. The acid concentrations were 0.1120 and 0.4213 mol l^{-1} (20 °C). By potentiometric titration with perchloric acid the purity of imidazole was found to be 99.89 %. Its melting point was 89 – 90 °C.

The stock solution of sodium perchlorate was prepared by dissolving the salt in conductivity water, adjusting the pH of the solution to about 8, allowing to stand over night, filtering through a tight glass-sinter, making the filtrate weakly acid with perchloric acid, boiling the solution and adjusting the pH to about 5.5 with sodium hydroxide.[1] The concentration of sodium perchlorate was determined by the evaporation and ion exchange methods.[2,3] The later method was also used for the other metal perchlorate solutions to check their contents. The solutions were found to be 4.3354 and 6.353 M in sodium perchlorate (20 °C).

The metal perchlorate solutions were prepared by dissolving the commercial products in water and allowing the solutions to stand from one to two weeks before filtering and analysing for the metal perchlorate and perchloric acid contents. The copper and cadmium contents were determined electroanalytically; in the former case in a solution containing sulfuric and nitric acid and about one gram of urea, and in the latter case from a slightly alkaline solution containing potassium cyanide. The nickel concentration was determined gravimetrically with dimethylgly-

Tables 1–5. Potentiometric titrations of metal(II) imidazole solutions at different ionic strengths at 25 °C. Concentrations and volumes given at 20 °C.

Table 1. Copper(II) imidazole. 100 ml of 0.003951 M $Cu(ClO_4)_2$ and 0.01 M imidazole (20 °C).

I	0.25	0.50	1.00	2.00	4.00
Titrant M NaOH ml	0.1001(8)	0.1004(6)	0.1000(3) pH	0.09962	0.09952
3.00	5.095	5.170	5.245	5.414	5.641
3.50	5.236	5.309	5.387	5.556	5.786
3.75	5.305	5.380	5.456	5.628	5.856
4.00	5.371	5.447	5.522	5.696	5.925
4.25	5.439	5.515	5.591	5.762	5.989
4.50	5.507	5.581	5.659	5.828	6.055
4.75	5.572	5.647	5.725	5.892	6.118
5.00	5.637	5.713	5.791	5.960	6.182
5.25	5.704	5.779	5.857	6.027	6.248
5.50	5.770	5.843	5.924	6.092	6.310
5.75	5.838	5.911	5.992	6.156	6.371
6.00	5.905	5.977	6.056	6.223	6.436
6.25	5.975	6.046	6.125	-	6.501
6.50	-	-	6.196	-	6.564
7.00	-	-	6.338	-	6.694

Table 2. Nickel(II) imidazole. 100 ml of 0.003880 M $Ni(ClO_4)_2$ and 0.01 M imidazole (20 °C).

I	0.25	0.50	1.00	2.00	4.00
Titrant M NaOH ml	0.1008	0.1004(6)	0.1001(9) pH	0.09962	0.09952
3.00	6.081	6.163	6.279	6.506	6.864
3.50	6.201	6.284	6.401	6.631	6.991
3.75	6.257	6.338	6.457	6.690	7.050
4.00	6.313	6.398	6.511	6.736	7.113
4.25	6.369	6.452	6.565	6.803	7.170
4.50	6.423	6.502	6.621	6.856	7.224
4.75	6.477	6.553	6.675	6.911	7.280
5.00	6.529	6.607	6.729	6.967	7.336
5.25	6.578	6.663	6.780	7.020	7.393
5.50	6.631	6.715	6.832	7.069	7.447
5.75	6.683	6.766	6.883	7.124	7.503
6.00	6.736	6.860	6.937	7.177	7.559
6.25	6.788	6.876	6.991	7.228	7.615
6.50	6.844	-	7.043	7.280	7.670
7.00	6.952	-	7.157	7.403	7.785

Table 3. Cadmium(II) imidazole. 100 ml of 0.004664 M $Cd(ClO_4)_2$ and 0.01 M imidazole (20 °C).

I	0.25	0.50	1.00	2.00	4.00
Titrant M NaOH ml	0.1001(8)	0.1004(6)	0.1000(3) pH	0.09962	0.09952
3.00	6.245	6.319	6.441	6.666	7.048
3.50	6.354	6.434	6.555	6.783	7.170
3.75	6.409	6.490	6.611	6.847	7.226
4.00	6.460	6.540	6.661	6.898	7.283
4.25	6.512	6.589	6.714	6.954	7.342
4.50	6.563	6.642	6.764	7.006	7.393
4.75	6.612	6.693	6.817	7.060	7.451
5.00	6.663	6.743	6.864	7.111	7.501
5.25	6.714	6.792	6.916	7.163	7.555
5.50	6.763	6.846	6.965	7.212	7.610
5.75	6.813	6.899	7.016	7.263	7.662
6.00	6.864	6.949	7.067	7.315	7.716
6.25	6.916	6.998	7.119	7.368	7.768
6.50	6.967	7.054	7.170	7.424	7.823
7.00	7.075	7.161	7.282	7.537	7.941

Table 4. Zinc(II) imidazole. 100 ml of 0.003936 M $Zn(ClO_4)_2$ and 0.01 M imidazole (20 °C).

I	0.25	0.50	1.00	2.00	4.00
Titrant M NaOH ml	0.1001(8)	0.1004(6)	0.1000(3) pH	0.09962	0.09952
3.00	6.325	6.397	6.511	6.713	6.954
3.50	6.416	6.488	6.600	6.799	7.031
3.75	6.463	6.532	6.643	6.838	7.068
4.00	6.506	6.572	6.685	6.878	7.103
4.25	6.550	6.615	6.725	6.917	7.140
4.50	6.590	6.654	6.764	6.954	7.176
4.75	6.631	6.694	6.805	6.992	7.210
5.00	6.671	6.735	6.844	7.029	7.245
5.25	6.712	6.777	6.883	7.066	7.279
5.50	6.752	6.816	6.922	7.103	7.315
5.75	6.793	6.858	6.962	7.142	7.348
6.00	6.834	6.897	7.001	7.183	7.384
6.25	6.876	6.941	-	-	7.418

Table 5. Cobalt(II) imidazole. 100 ml of 0.004243 M $Co(ClO_4)_2$ and 0.01 M imidazole (20 °C).

I	0.25	0.50	1.00	2.00	4.00
Titrant M NaOH ml	0.1008	0.1004(6)	0.1001(9) pH	0.09962	0.09952
3.00	6.408	6.634	6.631	6.955	7.290
3.50	6.512	6.737	6.737	7.055	7.407
3.75	6.563	6.790	6.788	7.104	7.459
4.00	6.612	6.840	6.837	7.155	7.512
4.25	6.658	6.886	6.888	7.200	7.561
4.50	6.703	6.935	6.933	7.250	7.611
4.75	6.751	6.982	6.982	7.295	7.662
5.00	6.796	7.028	7.026	7.342	7.711
5.25	6.842	7.075	7.072	7.388	7.758
5.50	6.886	7.119	7.119	7.435	7.806
5.75	6.932	7.167	7.168	7.484	7.853
6.00	6.979	7.214	7.214	7.532	7.900
6.25	7.026	7.258	7.261	7.579	7.949
6.50	7.075	-	7.309	7.635	7.998
7.00	7.175	-	7.408	7.743	8.096

oxime. The EDTA-titration with Erio T as an indicator at a pH of about 10 was used for zinc analyses. The concentrations of the metal perchlorate solutions (at 20 °C) were the following:
0.3161 M $Cu(ClO_4)_2$, 0.9700 M $Ni(ClO_4)_2$, 0.2331 M $Cd(ClO_4)_2$, 0.3149 M $Zn(ClO_4)_2$ and 0.943 M $Co(ClO_4)_2$. The excess or lack of perchloric acid in the metal perchlorate solutions was determined by adding known amounts of perchloric acid to the samples and titrating potentiometrically with a known alkali solution.

Apparatus and methods. All measuring flasks were checked by weighing their water contents at 20 °C. A water thermostat with an accuracy ±0.01 °C was used for potentiometric titrations at 15, 25, and 35 °C. These were performed with a potentiometer Radiometer PHM 4 using a Beckman No. 41263 glass electrode and an immersion type calomel electrode in a cell of the following type (20 °C):

Glass electrode	100 ml 0.01 M Imidazole 0.01 M $HClO_4$ 0.003 – 0.03 M $M(ClO_4)_2$ (I – 0.01 – 3(0.003 – 0.03)) M $NaClO_4$	
	0.01 M NaCl (I – 0.01) M $NaClO_4$	Hg_2Cl_2,Hg

The effect of temperature on the concentrations was taken into account in the calculations.[1-3] The experimental results of the titrations are given in Tables 1 – 10.

RESULTS AND DISCUSSION

Assuming the complex formation between imidazole (HL) and divalent metal ions to happen stepwise and to be mononuclear, the overall complexation equilibria may be presented as follows:

$$M^{2+} + n\ HL \rightleftharpoons M(HL)_n^{2+} \quad (1)$$

The corresponding cumulative (gross) stability constants are then

$$\beta_n = [M(HL)_n^{2+}]/[M^{2+}][HL]^n \quad (2)$$

The electroneutrality principle gives in the experimental conditions used that

$$[H_2L^+] = C_{HL} - C_B - [H^+] \quad (3)$$

where H_2L^+ is the protonated form of imidazole [1] and C_B is the total concentration of the added sodium hydroxide in the studied solution. The protolysis constant of imidazole

$$K_1 = [H^+][HL]/[H_2L^+] \quad (4)$$

was determined in the previous paper.[1] The total concentrations of imidazole (C_{HL}) and of the metal ions (C_M) in the studied solutions are

$$C_{HL} = [HL] + [H_2L^+] + \sum n[M(HL)_n^{2+}] \quad (5)$$

$$C_M = [M^{2+}] + \sum[M(HL)_n^{2+}] \quad (6)$$

From the expressions (2), (5), and (6) we obtain

$$G/[HL](C_M - G) = \beta_1 + [(2C_M - G)[HL]/(C_M - G)]\beta_2 + [(3C_m - G][HL]^2/(C_M - G)]\beta_3 + \cdots\cdots \quad (7)$$

where $G = C_{HL} - [HL] - [H_2L^+]$ and $[H_2L^+]$ is calculated from eqn. (3) and [HL] from eqn. (4) on the basis of the measured values of pH of the solutions.

Eqn. (7) is of the form $y = b_0 + x_1b_1 + x_2b_2 + \cdots$ and its constants β_n were therefore calculated with a library regression program [4] on an IBM 1130 computer.

A general conception of the complexation tendency of imidazole with divalent metal ions was obtained from the titration curves of imidazole – metal ion mixtures which showed the complex formation of imidazole with copper(II) ions to be clearly stronger than that with the other metals studied. The nickel, cadmium, and cobalt solutions could be titrated with the base so long as 70 % of the protonated imidazole was neutralized. In the case of copper and zinc solutions, only 62.5 % of the protonated imidazole could be neutralized before turbidity occurred. The precipitate formation order followed the precipitation order of the corresponding metal hydroxides.

The values of the gross stability constants β_n were calculated from eqn. (7) on the basis of the data in Tables 1 – 10 as described above, and their logarithms are presented in Tables 11 – 18.

As eqn. (1) shows, imidazole is coordinated to the central metal ion without any change of its charge. Therefore the dependence of the values of log β_n on the ionic strength might be represented by the equation:

$$\log \beta_n = \log \beta_n^0 + BI \quad (8)$$

where β_n^0 is the thermodynamic value in zero ionic strength and B a constant. The values of

Tables 6–10. Potentiometric titrations of metal(II) imidazole solutions at 15, 25, and 35 °C. Volumes and concentrations at 20 °C. Ionic strength 0.25.

Table 6. 100 ml of $(3.951-31.61)\times10^{-3}$ M $Cu(ClO_4)_2$ and 0.01 M imidazole. Titrant 0.1001(8) M NaOH.

M $Cu(ClO_4)_2$	0.003951	0.009483	0.03161	0.009483	0.03161	0.003951	0.009483	0.03161
Temp.		15°		25°			35°	
Titrant ml		pH		pH			pH	
3.00	5.139	4.622	4.021	4.590	3.985	5.037	4.528	3.933
3.50	5.286	4.735	4.124	4.705	4.087	5.178	4.639	4.036
3.75	5.356	4.793	4.175	4.765	4.137	5.245	4.696	4.082
4.00	5.407	4.847	4.220	4.817	4.181	5.310	4.747	4.129
4.25	5.495	4.902	4.268	4.871	4.229	5.376	4.799	4.177
4.50	5.563	4.954	4.313	4.923	4.274	5.440	4.850	4.221
4.75	5.631	5.007	4.362	4.978	4.322	5.505	4.902	4.264
5.00	5.699	5.059	4.404	5.028	4.366	5.570	4.953	4.308
5.25	5.767	5.111	4.451	5.081	4.411	5.634	5.005	4.353
5.50	5.836	5.166	4.498	5.135	4.457	5.698	5.056	4.396
5.75	5.904	5.220	4.546	5.187	4.504	5.763	5.107	4.442
6.00	5.972	5.272	4.591	5.240	4.550	5.827	5.157	4.488
6.25	6.042	5.327	4.640	5.294	4.597	5.893	5.210	4.532

Table 7. 100 ml of $(3.88-29.73)\times10^{-3}$ M $Ni(ClO_4)_2$ and 0.01 M imidazole. Titrant 0.1001(8) M or 0.1008 M NaOH.

M $Ni(ClO_4)_2$	0.003680	0.00970	0.02973	0.00970	0.003680	0.00970	M $Ni(ClO_4)_2$	0.02973	0.02973	0.02973
Temp.		15°		25°	35°		Temp.	15°	25°	35°
Titrant ml	0.1001(8)	pH	0.1008	0.1001(8) pH	0.1001(8) pH	0.1008	Titrant ml	0.1008 pH	0.1008 pH	0.1008 pH
3.00	6.199	5.773	5.309	5.669	5.902	5.598	2.87	5.246	5.152	5.078
3.50	6.324	5.893	5.407	5.779	6.016	5.711	3.37	5.341	5.253	5.181
3.75	6.383	5.942	5.454	5.835	6.072	5.765	3.87	5.454	5.353	5.282
4.00	6.441	5.993	5.503	5.889	6.126	5.817	4.12	5.502	5.407	5.328
4.25	6.497	6.046	5.549	5.939	6.180	5.866	4.37	5.545	5.451	5.377
4.50	6.553	6.096	5.596	5.990	6.229	5.917	4.62	5.594	5.500	5.423
4.75	6.605	6.150	5.641	6.041	6.279	5.968	4.87	5.640	5.546	5.471
5.00	6.659	6.201	5.689	6.088	6.328	6.014	5.12	5.683	5.593	5.513
5.25	6.712	6.250	5.734	6.139	6.379	6.063	5.37	5.729	5.638	5.559
5.50	6.766	6.301	5.781	6.188	6.428	6.112	5.62	5.773	5.686	5.606
5.75	6.820	6.350	5.829	6.240	6.479	6.161	5.87	5.811	5.730	5.654
6.00	6.876	6.402	5.878	6.289	6.526	6.210	6.12	5.857	5.777	5.701
6.25	6.934	6.453	5.932	6.340	6.592	6.261	6.37	5.911	5.828	5.749
6.50	-	6.506	-	6.391	6.628	6.313	6.62	5.960	5.882	5.796
7.00	-	6.614	-	6.499	6.734	6.419	6.87	6.011	5.934	5.845
							7.37	6.112	6.041	5.955

Table 8. 100 ml of $(4.664-34.98)\times10^{-3}$ M $Cd(ClO_4)_2$ and 0.01 M imidazole. Titrant 0.1001(8) M NaOH.

M $Cd(ClO_4)_2$	0.004664	0.01166	0.03498	0.01166	0.03498	0.004664	0.01166	0.03498
Temp.		15°		25°			35°	
Titrant ml		pH		pH			pH	
3.00	6.385	5.983	5.509	5.889	5.407	6.130	5.806	5.335
3.50	6.499	6.096	5.616	6.000	5.510	6.244	5.915	5.440
3.75	6.555	6.147	5.663	6.049	5.561	6.297	5.969	5.487
4.00	6.612	6.198	5.711	6.100	5.608	6.346	6.017	5.533
4.25	6.665	6.250	5.760	6.151	5.656	6.395	6.066	5.579
4.50	6.715	6.299	5.805	6.200	5.703	6.444	6.117	5.626
4.75	6.763	6.348	5.854	6.249	5.748	6.493	6.164	5.672
5.00	6.812	6.399	5.901	6.299	5.796	6.540	6.212	5.716
5.25	6.862	6.448	5.947	6.348	5.841	6.588	6.261	5.760
5.50	6.915	6.497	5.994	6.396	5.887	6.635	6.308	5.808
5.75	6.967	6.546	6.041	6.445	5.934	6.683	6.355	5.855
6.00	7.018	6.595	6.090	6.494	5.982	6.733	6.406	5.902
6.25	7.069	6.647	6.137	6.546	6.031	6.786	6.457	5.953
6.50	7.123	6.698	6.186	6.599	6.078	6.838	6.508	6.004
7.00	7.235	6.805	6.295	6.709	6.186	6.946	6.620	6.105

Table 9. 100 ml of $(3.936-31.49)\times10^{-3}$ M $Zn(ClO_4)_2$ and 0.01 M imidazole. Titrant 0.1001(8) M NaOH.

M $Zn(ClO_4)_2$	0.003936	0.009447	0.03149	0.009447	0.03149	0.003936	0.009447	0.03149
Temp.		15°		25°			35°	
Titrant ml		pH		pH			pH	
3.00	6.479	6.217	5.748	6.075	5.622	6.164	5.934	5.494
3.50	6.570	6.315	5.848	6.171	5.725	6.256	6.032	5.596
3.75	6.616	6.360	5.897	6.218	5.769	6.301	6.078	5.642
4.00	6.659	6.404	5.942	6.261	5.816	6.344	6.121	5.687
4.25	6.703	6.450	5.990	6.305	5.862	6.387	6.167	5.733
4.50	6.743	6.492	6.032	6.348	5.907	6.426	6.206	5.776
4.75	6.784	6.535	6.075	6.391	5.953	6.467	6.248	5.821
5.00	6.824	6.575	6.121	6.431	5.997	6.508	6.289	5.864
5.25	6.866	6.617	6.164	6.474	6.037	6.548	6.330	5.905
5.50	6.904	6.659	6.208	6.512	6.078	6.589	6.373	5.949
5.75	6.946	6.701	6.254	6.553	6.124	6.630	6.414	5.990
6.00	6.990	6.743	6.299	6.595	6.168	6.671	6.454	6.032
6.25	7.032	6.787	6.343	6.638	6.213	6.712	6.495	6.078

Table 10. 100 ml of $(4.24-31.21)\times10^{-3}$ M $Co(ClO_4)_2$ and 0.01 M imidazole. Titrant 0.1008 M NaOH.

M $Co(ClO_4)_2$	0.00424	0.00943	0.03121	0.00943	0.03121	0.00424	0.00943	0.03121
Temp.		15°		25°			35°	
Titrant ml		pH		pH			pH	
3.00	6.566	6.296	5.818	6.162	5.709	6.243	6.035	5.598
3.50	6.671	6.402	5.916	6.268	5.811	6.346	6.138	5.701
3.75	6.723	6.455	5.969	6.319	5.862	6.396	6.189	5.749
4.00	6.772	6.504	6.014	6.368	5.907	6.441	6.236	5.796
4.25	6.820	6.549	6.060	6.415	5.955	6.486	6.282	5.844
4.50	6.867	6.596	6.107	6.463	6.000	6.534	6.326	5.889
4.75	6.914	6.644	6.154	6.508	6.048	6.580	6.372	5.935
5.00	6.959	6.694	6.199	6.554	6.092	6.622	6.418	5.979
5.25	7.007	6.742	6.245	6.589	6.139	6.668	6.462	6.025
5.50	7.054	6.784	6.294	6.647	6.181	6.710	6.506	6.069
5.75	7.103	6.833	6.338	6.693	6.228	6.755	6.552	6.113
6.00	7.150	6.880	6.387	6.738	6.274	6.799	6.598	6.159
6.25	7.199	6.927	6.432	6.785	6.321	6.846	6.643	6.205
6.50	7.246	6.978	6.479	6.835	6.369	6.894	6.691	6.251
7.00	7.351	7.078	6.579	6.936	6.470	6.988	6.789	6.351

log β_n at 25 °C in Tables 11 – 15 for the lowest metal ion concentrations were fitted by the method of least squares to eqn. (8). The values of log β_n^0 and B of the different complexes are given in Table 19. The values of log β_n calculated from eqn. (8) are also given in Tables 11 – 15. The values of the constant B obtained at 25 °C were also used to calculate the values of log β_n^0 from eqn. (8) at the ionic strength 0.25 at 15 and 35 °C on the basis of the data for the lowest metal ion concentrations in Tables 16 – 18. The errors due to this approximation in the values of log β_n^0 are negligible. The results of these calculations are also given in Table 19.

The values of log β_1 calculated from eqn. (7) are represented as functions of the ionic strength in Fig. 1. The log β_1 values satisfy eqn. (8) well,

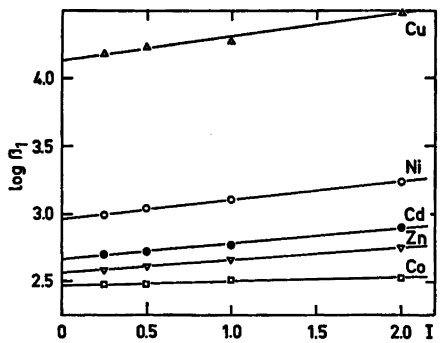

Fig. 1. The values of log β_1 of the first copper(II), nickel(II), cadmium(II), zinc(II), and cobalt(II) imidazole complexes calculated from eqns. (7) and (8) as functions of the ionic strength at 25 °C.

Tables 11–15. The gross stability constants of metal(II) imidazole complexes calculated from eqns. (7) and (8) at 25°C.

Table 11. Copper(II) imidazole complex. $C_{Cu(ClO_4)_2} = 0.003946$ M, $C_{HL} = 0.009988$ M (25 °C).

	log β_1		log β_2		log β_3		log β_4	
I	(7)	(8)	(7)	(8)	(7)	(8)	(7)	(8)
0	–	4.127	–	7.747	–	10.408	–	13.947
0.2497	4.176	4.170	7.827	7.793	10.558	10.562	14.039	13.983
0.4994	4.228	4.213	7.778	7.838	10.721	10.716	13.936	14.019
0.9988	4.267	4.299	7.958	7.929	–	–	14.119	14.091
1.9977	4.483	4.471	8.106	8.110	11.639	11.640	–	–

Table 12. Nickel(II) imidazole complex. $C_{Ni(ClO_4)_2} = 0.003876$ M, $C_{HL} = 0.009988$ M (25 °C).

	log β_1		log β_2		log β_3	log β_4	log β_5
I	(7)	(8)	(7)	(8)	(7)	(7)	(7)
0	–	2.962	–	5.515	–	–	–
0.2497	2.993	2.997	5.565	5.529	–	–	12.265
0.4994	3.034	3.032	5.517	5.543	–	–	12.328
0.9988	3.105	3.101	5.548	5.571	7.709	10.042	–
1.9977	3.238	3.240	5.641	5.627	8.054	10.482	–
3.9954	3.454	–	–	–	–	–	–

Table 13. Cadmium(II) imidazole complex. $C_{Cd(ClO_4)_2} = 0.004659$ M, $C_{HL} = 0.009988$ M (25 °C).

	log β_1		log β_2		log β_3	log β_4
I	(7)	(8)	(7)	(8)	(7)	(7)
0	–	2.665	–	4.647	–	–
0.2497	2.699	2.693	4.735	4.693	–	–
0.4994	2.718	2.721	4.740	4.739	–	–
0.9988	2.768	2.777	4.757	4.831	–	8.415
1.9977	2.892	2.888	5.047	5.015	6.996	–
3.9964	3.090	–	–	–	–	–

Table 14. Zinc(II) imidazole complex. $C_{Zn(ClO_4)_2} = 0.003931$ M, $C_{HL} = 0.009988$ M (25 °C).

	log β_1		log β_2	log β_3	log β_4	
I	(7)	(8)	(7)	(7)	(7)	(8)
0	–	2.570	–	–	–	9.785
0.2497	2.588	2.592	4.424	–	9.970	9.924
0.4994	2.618	2.614	–	7.596	10.041	10.062
0.9988	2.663	2.659	4.451	–	10.292	10.340
1.9977	2.745	2.747	–	8.253	10.919	10.895
3.9954	3.441	–	–	–	–	–

Table 15. Cobalt(II) imidazole complex. $C_{Co(ClO_4)_2} = 0.004238$ M, $C_{HL} = 0.009988$ M (25 °C).

	log β_1		log β_3		log β_4
I	(7)	(8)	(7)	(8)	(7)
0	–	2.473	–	6.484	–
0.2497	2.476	2.480	6.657	6.569	–
0.4994	2.484	2.487	6.523	6.655	–
0.9988	2.511	2.501	6.870	6.826	–
1.9977	2.525	2.529	–	–	8.688

Tables 16–18. The gross stability constants of copper(II), nickel(II), cadmium(II), zinc(II), and cobalt(II) imidazole complexes calculated from eqn. (7) at various temperatures.

Table 16. Temp. 15 °C. $I = 0.2502$. $C_{HL} = 0.0100$ M.

$C_M \times 10^3$	$M(ClO_4)_2$	$\log \beta_1$	$\log \beta_2$	$\log \beta_3$	$\log \beta_4$
3.955	$Cu(ClO_4)_2$	4.395	8.180	11.770	14.400
9.492		4.416	8.182	–	–
31.64		4.467	–	–	–
3.883	$Ni(ClO_4)_2$	3.181	5.781	7.815	–
9.709		3.228	5.593	8.612	–
29.76		3.213	5.932	9.456	13.359
4.668	$Cd(ClO_4)_2$	2.845	5.024	–	–
11.67		2.897	4.868	–	–
35.01		2.874	–	8.362	–
3.931	$Zn(ClO_4)_2$	2.655	4.647	7.846	–
9.456		2.677	–	7.951	–
31.52		2.658	5.119	8.189	–
4.247	$Co(ClO_4)_2$	2.618	4.188	6.868	–
9.438		2.616	–	7.259	–
31.24		2.606	–	7.703	

Table 17. Temp. 25 °C. $I = 0.2497$. $C_{HL} = 0.009988$ M.

$C_M \times 10^3$	$M(ClO_4)_2$	$\log \beta_1$	$\log \beta_2$	$\log \beta_3$	$\log \beta_4$	$\log \beta_5$
3.946	$Cu(ClO_4)_2$	4.176	7.827	10.558	14.039	–
9.472		4.230	7.762	10.558	–	–
31.57		4.281	–	–	–	–
3.876	$Ni(ClO_4)_2$	2.993	5.565	–	–	12.265
9.689		3.068	5.639	8.467	11.245	–
29.70		3.064	–	–	–	–
4.659	$Cd(ClO_4)_2$	2.699	4.735	–	–	–
11.65		2.690	4.802	–	–	–
34.94		2.725	4.800	–	–	–
3.931	$Zn(ClO_4)_2$	2.588	4.424	–	9.970	–
9.436		2.582	4.396	7.623	–	–
31.45		2.560	–	7.918	–	–
4.238	$Co(ClO_4)_2$	2.476	–	6.657	–	11.612
9.419		2.477	–	6.855	–	–
31.17		2.484	–	7.404	–	–

Table 18. Temp. 35 °C. $I = 0.2492$. $C_{HL} = 0.009969$ M.

$C_M \times 10^3$	$M(ClO_4)_2$	$\log \beta_1$	$\log \beta_2$	$\log \beta_3$	$\log \beta_4$
3.939	$Cu(ClO_4)_2$	4.055	7.432	10.295	13.368
9.454		4.063	7.461	11.077	–
31.51		4.136	–	–	–
3.868	$Ni(ClO_4)_2$	2.843	5.362	7.338	–
9.670		2.926	4.927	7.832	10.805
29.64		2.921	5.232	8.596	–
4.650	$Cd(ClO_4)_2$	2.531	4.335	6.088	–
11.62		2.559	4.372	6.098	–
34.87		2.591	4.717	–	–
3.924	$Zn(ClO_4)_2$	2.506	4.329	–	9.792
9.418		2.475	4.113	7.379	9.944
31.39		2.468	–	7.767	–
4.230	$Co(ClO_4)_2$	2.376	–	–	8.806
9.401		2.361	–	6.702	–
31.11		2.376	–	–	9.930

Table 19. The values of the constants log β_n^0 and B of eqn. (8) for copper(II), nickel(II), cadmium(II), zinc(II), and cobalt(II) imidazole complexes at 15, 25, and 35 °C.

	Copper(II) complexes							
°C	log β_1^0	B	log β_2^0	B	log β_3^0	B	log β_4^0	B
15	4.352	0.1723	8.135	0.1817	11.615	0.6164	14.364	0.1438
25	4.127	0.1723	7.747	0.1817	10.408	0.6164	13.947	0.1438
35	4.012	0.1723	7.387	0.1817	10.141	0.6164	13.332	0.1438
	Nickel(II) complexes				Cadmium(II) complexes			
	log β_1^0	B	log β_2^0	B	log β_1^0	B	log β_2^0	B
15	3.146	0.1390	5.767	0.0559	2.817	0.1118	4.978	0.1842
25	2.962	0.1390	5.515	0.0559	2.665	0.1118	4.647	0.1842
35	2.808	0.1390	5.348	0.0559	2.503	0.1118	4.289	0.1842
	Zinc(II) complex				Cobalt(II) complex			
	log β_1^0	B			log β_1^0	B		
15	2.633	0.0887			2.611	0.0279		
25	2.570	0.0887			2.473	0.0279		
35	2.484	0.0887			2.369	0.0279		

the log β_2 values less well and for the higher complexes the lines could only be said to be direction giving. In Fig. 1 the dependence of the stability of the first complexes on the ionic strength is seen to be the higher the stronger the complex.

At the lowest ionic strength ($I = 0.25$) the measurements were made using three different concentrations of the central metal ions, and at the temperatures 15, 25, and 35 °C. At the lowest, the central metal ion concentrations were about 0.003 – 0.004 M, while in the second cases the metal ion and imidazole concentrations were almost equal, *i.e.* about 0.01 M; and the highest metal ion concentrations used were about three times higher than the ligand concentrations. The results of the calculations on the bases of these measurements are given in Tables 16 – 18.

From Tables 16 – 18 it can be seen that the increasing of the central metal ion concentration causes a change in the complexation equilibria such that the first complex becomes dominant and its stability constant increases. This effect is observed especially in respect of copper(II) complexes and, more weakly, for nickel(II) and cadmium(II) complexes. On the stability of the weaker zinc(II) and cobalt(II) complexes the central ion concentration seems to have a smaller effect.

As an addition to the log β_n^0 values in Table 19 we obtain from graphs like those in Fig. 1 by extrapolation to zero ionic strength at 25 °C, for nickel(II) complexes: log $\beta_3^0 = 7.37$, log $\beta_4^0 = 9.63$, log $\beta_5^0 = 12.20$; and for zinc(II) complexes: log $\beta_2^0 = 4.42$, log $\beta_3^0 = 7.38$.

In Table 20 we have collected the gross stability constant values of metal(II) imidazole complexes, all, with one exception,[8] found or calculated from the stepwise stability constants given in the literature of the last years.[5–7,9–16,21] The previously determined values of different constants are found in the stability constant tables compiled by Sillén and Martell.[18,19] Generally, the present log β_n values are of the same order of magnitude as the earlier ones [18,19] and those given in Table 20. However, it should be remembered that only results in the same neutral salt solutions and ionic strengths and at the temperatures are fully comparable.

The values of log β_n in Tables 16 – 18 give some idea of the reproducibility of the results obtained in the present study and their dependence on the experimental conditions. It should be noted that an error of about ±0.01 unit in pH in working with a glass electrode is easily made, which means at least a similar error in the log β_1 values; the error increases rapidly with n. On the other hand the data of Sjöberg [5–7] in Table 20 give an idea of the effect of different

Table 20. Values of the gross stability constants of metal(II) imidazole complexes collected for comparison from the literature of last years.

Metal ion	Method	Temp. °C	I (added salt)	log β_1	log β_2	log β_3	log β_4	log β_5	log β_6	Ref.
Cu^{2+}	gl. electrode	25	3.0 ($NaClO_4$)	4.66	8.64	11.94	14.60	—	17.46	5,6
		25	3.0 (NaCl)	4.46	8.13	11.21	13.48	—	15.95	5
		25	3.0 ($NaClO_4$)	4.66	8.65	11.95	14.61	15.61	17.31	7
		25	3.0 (NaCl)	4.40	8.06	11.06	13.38	14.30	15.36	7
		25	0.16 (KNO_3)	4.31	7.84	10.76	12.90	—	—	8
		25	5.0 (NaCl)	4.51	8.32	11.37	14.04	—	—	17
Ni^{2+}	gl. electrode	25	0.16 (KNO_3)	3.09	5.56	7.56	9.10	10.2	10.7	8
	pot.	25	0.5 (NH_4NO_3)	2.81–2.96	5.17–5.26	6.95–7.09	7.77–8.02	8.76	9.26	9
Cd^{2+}	pot.	25	0.5 (KNO_3)	2.67–2.72	4.83–4.87	6.01–6.22	7.0–7.14	—	—	10
	?	25	0.1	3.03	5.14	6.48	7.27	—	—	11
	pot.	25	0.5 (NH_4NO_3)	2.64–2.686	4.73	5.88–6.00	7.08–7.13	—	—	12
	pot.	25	0.1 (KNO_3)	2.71	4.71	6.06	—	—	—	13
	polarog.	25	1.0 ($NaClO_4$)	2.70	5.08	6.65	7.60	8.18	8.95	14
	»	25	?	2.79	4.45	5.96	7.03	—	—	15
Zn^{2+}	pot.	25	0.5 (NH_4NO_3)	2.29–2.46	4.65–4.72	6.87–7.15	9.08–9.11	—	—	9
Co^{2+}	pot.	25	0.5 (NH_4NO_3)	2.19–2.25	4.10–4.17	5.40–5.53	6.50–7.03	—	—	9
	gl. electrode	25	0.16 (KNO_3)	2.47	4.40	5.85	6.85	7.35	—	8
	pot.	25	0.5 (NH_4NO_3)	2.23	4.09	5.00	6.01	6.70	7.27	16

neutral salts on the values of the stability constants, showing the effect also to increase with n. Further, the results of Berthon *et al.*[9,10,12,13] in Table 20 show the effect of different calculation procedures (generally in use, *loc. cit.*) on the values of the stability constants; the differences increase here with n also. The results are interesting and show how

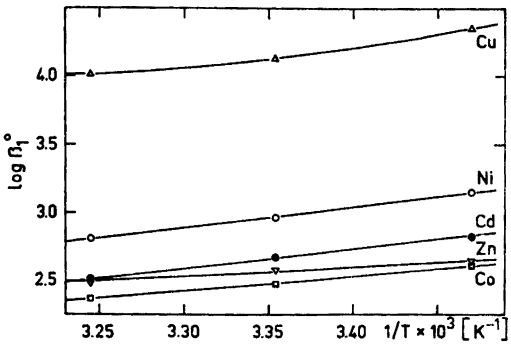

Fig. 2. The values of log β_1^0 of the first copper(II), nickel(II), cadmium(II), zinc(II), and cobalt(II) imidazole complexes represented as functions of the reciprocals of the absolute temperature.

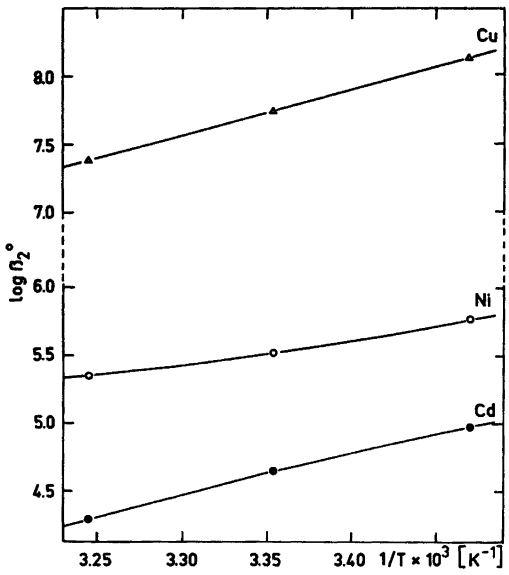

Fig. 3. The values of log β_2^0 of the second copper(II), nickel(II), and cadmium(II) imidazole complexes represented as functions of $1/T$ (K^{-1}).

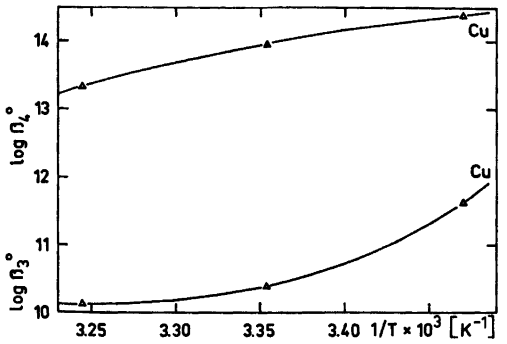

Fig. 4. The values of log β_3^0 and log β_4^0 of the third and fourth copper(II) imidazole complexes represented as functions of $1/T$ (K^{-1}).

on the whole it is difficult to obtain values of the stability constants of the higher complexes assumed to be formed stepwise in a complex series, which are compatible with each other. It is clear that the increase of the ligand (imidazole) to metal ion concentration ratio favors the formation of the higher complexes and the determination of their stability constants (*cf.* Refs. 5–7). On the other hand it should be taken into account that the possibility of the effect of the complex formation between the metal ions and inorganic ligands is generally increased when changing from perchlorates to other neutral salts.

In the works referred in Table 20 and in Refs. 18 and 19, as also in the present study, it was assumed when calculating the stability constants of the imidazole metal complexes that the complex formation was mononuclear and proceeded stepwise. However, Bridson and Walker [20] were the first to point out that on the basis of their spectrophotometric measurements at least, copper(II) ions would form with imidazole hydroxyl-bridged binuclear complexes in 10^{-3} M aqueous copper(II) perchlorate solutions when the imidazole metal ion mol-ratio was only 4. Sjöberg [5,7] also pointed to the same possibility in Ref. 17 recently. Jensen [21] on his side gave evidence for polynuclear complex formation of imidazole with cadmium(II) ions. Also our studies on the effect of the variation of the imidazole to metal ion concentration ratio pointed, at sufficiently high pH values, to possible polynuclear complex formation, specially in respect of copper(II) ions with imidazole.

Table 21. The values of the constants a, b, and c of eqn. (9) calculated by the method of least squares for copper(II), nickel(II), cadmium(II), zinc(II), and cobalt(II) complexes.

$\log \beta_n^0$	Metal	$C_M \times 10^3$ (25 °C)	$a \times 10^{-3}$	$b \times 10^{-1}$	$c \times 10^2$
$\log \beta_1^0$	Cu	3.946	−14.599	−8.8786	−14.740
	Ni	3.876	−3.9788	−1.8703	−2.7906
	Cd	4.659	1.3230	1.6226	3.0599
	Zn	3.931	3.0481	2.5249	4.1775
	Co	4.238	−4.5107	−2.4193	−3.8696
$\log \beta_2^0$	Cu	3.946	−3.7094	−0.59981	−0.43733
	Ni	3.876	−11.279	−6.3942	−10.607
	Cd	4.659	3.5792	3.8941	7.4756
$\log \beta_3^0$	Cu	3.946	−124.73	−80.476	−133.09
$\log \beta_4^0$	Cu	3.946	26.286	20.575	34.762

Table 22. The thermodynamic quantities calculated from eqns. (10)−(12) for the different metal(II) ion imidazole complex equilibria at 15, 25, and 35 °C. The values of $\log \beta_n^0$ are included.

°C	Metal	$\log \beta_n^0$ $\log \beta_1^0$	$-\Delta G^0$ (kJ mol^{-1})	$-\Delta H^0$ (kJ mol^{-1})	$-\Delta S^0$ (JK^{-1} mol^{-1})
15	Cu	4.352	24.01	45.2	73
25		4.127	23.56	28.6	17
35		4.012	23.68	11.5	−39
15	Ni	3.146	17.36	31.8	50
25		2.962	16.91	28.7	39
35		2.808	16.57	25.4	28
15	Cd	2.817	15.54	23.3	27
25		2.665	15.22	26.8	38
35		2.503	14.77	30.3	50
15	Zn	2.633	14.53	8.1	−22
25		2.570	14.67	12.8	−6
35		2.484	14.66	17.6	9
15	Co	2.611	14.41	24.8	36
25		2.473	14.12	20.5	21
35		2.369	13.98	16.0	6
		$\log \beta_2^0$			
15	Cu	8.135	44.89	64	66
25		7.747	44.23	63	64
35		7.387	43.59	63	63
15	Ni	5.767	31.82	47	53
25		5.515	31.49	35	13
35		5.348	31.56	23	−27
15	Cd	4.978	27.47	50	79
25		4.647	26.53	58	108
35		4.289	25.31	67	137
		$\log \beta_3^0$			
15	Cu	11.615	64.07	272	722
25		10.408	59.41	123	212
35		10.141	59.83	−31	−297
		$\log \beta_4^0$			
15	Cu	14.364	79.25	49	−104
25		13.947	79.62	88	29
35		13.332	78.66	129	163

Table 23. Thermodynamic quantities of the metal(II) ion imidazole complex equilibria found in literature.

°C	Metal ion	I (added salt)	β_n	$-\Delta H$ (kJ mol^{-1})	$-\Delta S$ (JK^{-1} mol^{-1})	Ref.
10 – 50	Cu^{2+}	0.16 (KNO_3)	β_1	126 ± 5	73.6	8
25		0.025	β_1	32	–	23
25		0.16 (KNO_3)	β_4	96.0	84	23
10 – 50	Ni^{2+}	0.16 (KNO_3)	β_1	91.2 ± 5.4	50.6	8
25		0.022	β_1	24	–	23
25		0.16 (KNO_3)	β_6	77.0	42	23
25 – 35	Cd^{2+}		β_4	56.1	44.8	15
25	Zn^{2+}	0.025	β_1	16	–	23
25		0.16 (KNO_3)	β_4	67.8	50	23
10 – 50	Co^{2+}	0.16 (KNO_3)	β_1	73.6 ± 5.4	45.6	8

The values of log β_n^0 of the different metal(II) ion imidazole complexes obtained are presented as functions of the reciprocals of the absolute temperature in Figs. 2 – 4. For the first complexes the curves are almost linear, but the curvature increases further the higher the complex. Therefore the equation [22]

$$\log \beta_n^0 = -a/T - cT + b \qquad (9)$$

was used to express the temperature dependence of the values of log β_n^0. The values of log β_n^0 in Table 19 were fitted to eqn. (9). The values of the constants a, b and c obtained are given in Table 21.

The thermodynamic quantities, free energies, enthalpies, and entropies of the complexation equilibria (1) were calculated on the basis of the values of the constants a, b, and c given in Table 21 from the following known equations:

$$\Delta G^0 = 2.303\ R(a - bT + cT^2) \qquad (10)$$

$$\Delta H^0 = 2.303\ R(a - cT^2) \qquad (11)$$

$$\Delta S^0 = 2.303\ R(b - 2cT) \qquad (12)$$

where $T = 273.16 + t$ °C and $R = 8.31433$ J K^{-1} mol^{-1}. The results obtained for the thermodynamic quantities are given in Table 22, where the values of log β_n^0 are also included for comparison.

The values of the enthalpies are seen to be negative with the one exception of the $Cu(HL)_3^{2+}$ complex, possibly due to inaccuracies of the measurements, (Table 22).

The values in Table 22 show generally that for the imidazole complexes studied here the enthalpy effect is the dominant factor determining the complex stability, which explains the high complex formation tendency of imidazole with the studied metal(II) ions.

As regards the accuracy of the thermodynamic data given in Table 22, we may estimate that in the case of the first complexes the errors are of about ± 0.1 kJ mol^{-1} in ΔG^0, ± 2 – 4 kJ mol^{-1} in ΔH^0 and ± 8 – 12 J K^{-1} mol^{-1} in ΔS^0, and obviously increase for the higher complexes.

In Table 23 we have collected the earlier thermodynamic data of the complex equilibria found in the literature. When these values are compared with those obtained by us and given in Table 22, it will be seen that the enthalpy values determined by Bauman and Wang [23] by calorimetric enthalpy titrations are in good agreement with the present ones, whereas the data of Sklenskaya and Karapet'yants [8] are generally not, being several times greater.

It is interesting to note that in some recent papers Powell [24,25] has paid attention to the dependence of the calorimetrically determined enthalpy values on the ionic strength of the solutions, and to the possible errors caused in the enthalpy values when correcting these for the ionic strength to obtain the ΔH^0 values using different assumed, semitheoretical activity functions. Also we have already [1] considered the ionic strength dependence of enthalpy values.

Acknowledgements. The authors are indebted to Mr. M. Peacock, M. A. for linguistic corrections and to Mr. I. Laitinen for valuable cooperation in the computer calculations. Financial support from the National Research Council for Sciences (Finland) is also gratefully acknowledged.

REFERENCES

1. Lumme, P. and Virtanen, P. *Suom. Kemistilehti B 42* (1969) 333.
2. Lumme, P. and Tummavuori, J. *Acta Chem. Scand. 19* (1965) 617; Lumme, P., Lahermo, P. and Tummavuori, J. *Ibid.*, p. 2175.
3. Sallavo, K. and Lumme, P. *Suom. Kemistilehti B 40* (1967) 155.
4. The 1130 *Statistical System, Users Manual*, 3rd Ed., IBM Corporation, New York 1969, p. 7.
5. Sjöberg, S. *14de Nordiska Kemistmötet*, Umeå 1971, Resuméer, p. 159.
6. Sjöberg, S. *Acta Chem. Scand. 25* (1971) 2149.
7. Sjöberg, S. *Acta Chem. Scand. 26* (1972) 3400.
8. Sklenskaya, E. V. and Karapet'yants, M. Kh. *Russ. J. Inorg. Chem. 11* (1966) 1102, (2061).
9. Sirieix, A., Berthon, G. and Luca, C. *Bull. Soc. Chim. Fr.* (1970) 899.
10. Berthon, G. and Luca, C. *Anal. Chim. Acta 51* (1970) 239.
11. Andrews, A. C. and Roman, J. K. *Trans Kansas Acad. Sci. 67* (1964) 4.630.
12. Berthon, G. and Luca, C. *Chim. Anal. (Paris) 53* (1971) 501.
13. Berthon, G. and Luca, C. *Chim. Anal. (Paris) 53* (1971) 40.
14. Jensen, J. B. *Acta Chem. Scand. 26* (1972) 4031.
15. Kim, J. Y., Yough, K. S. and Paik, N. H. *Yakhak Hoeji 14* (1970) 36; *Chem. Abstr. 75* (1971) 14218n.
16. Berthon, G. and Luca, C. *Chim. Anal. (Paris) 53* (1971) 559.
17. Sjöberg, S. *Acta Chem. Scand. 27* (1973) 3721.
18. Sillén, L. G. and Martell, A. E. *Stability Constants of Metal-Ion Complexes*, Special Publ. No. 17, The Chemical Society, London 1964, pp. 387 and 388.
19. Sillén, L. G. and Martell, A. E. *Stability Constants of Metal-Ion Complexes*, Supplement No. 1, Special Publ. No. 25, The Chemical Society, London 1971, pp. 280 and 281.
20. Bridson, M. E. and Walker, W. R. *Aust. J. Chem. 23* (1970) 1973.
21. Jensen, J. B. *Acta Chem. Scand. 27* (1973) 3563.
22. Harned, H. S. and Robinson, R. A. *Trans. Faraday Soc. 36* (1940) 973.
23. Bauman, J. E., Jr. and Wang, J. C. *Inorg. Chem. 3* (1964) 368.
24. Hedwig, G. R. and Powell, H. K. J. *J. Chem. Soc. Dalton Trans.* (1973) 798.
25. Powell, H. K. J. *J. Chem. Soc. Dalton Trans.* (1973) 1947.

Received May 17, 1974.

Acta Chemica Scandinavica A 28 (1974) 1068—1078

Studies in Electronegativity. III. Comparison of Molecular Charge Distributions and Dipole Moments Calculated Using the OCEE and the CNDO/2 Schemes*

BJØRN VOIGT

Department of Physical Chemistry, H. C. Ørsted Institute, University of Copenhagen, DK-2100 Copenhagen Ø, Denmark

The Overlap Corrected Electronegativity Equalization (OCEE) theory outlined previously has been applied to the calculation of the dipole moments and charge distributions of HF, H_2O NH_3, HCN, H_2CO, CH_4, and the four F-substituted methanes, and the results have been compared with those obtained using the CNDO/2 scheme. The two theories predict dipole moments of comparable accuracy, but they lead to charge distributions which are significantly different in some cases. These differences originate mainly because of the manner in which neutral penetration energy terms are treated in the respective schemes.

1. INTRODUCTION

In the initial publication in this series,[1] hereafter referred to as Paper I, a detailed theoretical analysis of the principle of electronegativity equalization was presented. The treatment was based upon the assumption that the electronic structure of the molecule under consideration could be adequately described by means of localized molecular orbitals. It was concluded from this analysis that the electronegativity equalization principle provides a theoretically sound foundation for MO calculations as long as certain molecular corrections to the electronegativities are taken into account. The Overlap Corrected Electronegativity Equalization (OCEE) scheme, proposed in Paper I, includes those corrections which arise from overlap distributions and from the penetration of atomic orbitals into the charge clouds of other atoms in the molecular environment. The latter correction comprises the, as it turns out, important effects of polarization of atoms.

The OCEE scheme has now been applied to the calculation of the dipole moments and charge distributions of a series of molecules in which delocalization effects are commonly regarded as being small. The results have been compared with those obtained using the CNDO/2 scheme of Pople, Santry and Segal [3–5] which has been particularly successful in the calculation of dipole moments.[6] Simultaneously the CNDO/2 scheme has been used to assess the importance of delocalization effects in these molecules. This has been achieved by estimating the accuracy with which the canonical CNDO/2 – MO's could be localized.

Although the two theories appear rather different, especially with respect to their initial premises, they nevertheless have certain features in common. Both assume the validity of the Mulliken approximation,[1,7] and both use Mulliken electronegativities as the key semi-empirical parameters. The methods differ, however, in that explicit penetration energy terms, which are neglected in the CNDO/2 scheme,[5] are retained as significant corrections to the Mulliken electronegativities in the OCEE theory. Comparison of appropriate results obtained using the two schemes might therefore be expected in general to shed light on the importance of penetration effects, and in particular to

* Based in part on a thesis presented to the University of Copenhagen in partial fulfillment of the requirements for the lic. scient. degree.

demonstrate the degree to which these effects are accounted for implicitly by the CNDO/2 parameterization scheme.

2. OCEE THEORY

The basis of the OCEE theory is the assumption that the electronic ground state of a molecule can be approximated by a single Slater determinant constructed from N doubly occupied, localized molecular orbitals (LMO's) of the form

$$\psi_k = \sqrt{\frac{1}{2}}\left\{(1+\gamma_k)\phi_{k1}+(1-\gamma_k)\phi_{k2}\right\}/\sqrt{1+S_k+(1-S_k)\gamma_k^2} \quad (1)$$

$$S_k \equiv \int \phi_{k1}\phi_{k2}\,dv;\ k=1,\ 2,\cdots,\ N$$

The ϕ's denote atomic hybrid orbitals (AHO's) which are assumed to be normalized and real. In cases where (1) describes a lone pair $\phi_{k1}=\phi_{k2}(=\psi_k)$.

Using a Taylor expansion in the bond polarity, γ_k, the charge distribution (a.u.) from two electrons occupying the LMO (1) is:

$$2\psi_k^2 = Q_{k1}\phi_{k1}^2 + Q_{k2}\phi_{k2}^2 + Q_{kS}\phi_{k1}\phi_{k2}/S_k \quad (2)$$

$$Q_{k1} = q_k\{1+2\gamma_k+2S_kq\gamma_k^2-2(1-S_k)q_k\gamma_k^3\}+O(\gamma_k^4)$$

$$Q_{k2} = q_k\{1-2\gamma_k+2S_kq_k\gamma_k^2+2(1-S_k)q_k\gamma_k^3\}+O(\gamma_k^4)$$

$$Q_{kS} = 2q_kS_k\{1-2q_k\gamma_k^2\}+O(\gamma_k^4);\ q_k=(1+S_k)^{-1}$$

The overlap change, Q_{kS}, assumes its maximum value in the homopolar case ($\gamma_k=0$) and decreases as the bond becomes polar, regardless of the direction of polarity.

The requirement that the total energy be stationary (minimum) with respect to changes in the variational parameters, γ_k, can now be formulated as

$$-\frac{\partial E}{\partial \gamma_k} = \left(-\frac{\partial E}{\partial Q_{k1}}\right)\left(\frac{dQ_{k1}}{d\gamma_k}\right)+\left(-\frac{\partial E}{\partial Q_{k2}}\right)\left(\frac{dQ_{k2}}{d\gamma_k}\right)+\left(-\frac{\partial E}{\partial Q_{kS}}\right)\left(\frac{dQ_{kS}}{d\gamma_k}\right)=$$

$$X(k1)\frac{dQ_{k1}}{d\gamma_k}+X(k2)\frac{dQ_{k2}}{d\gamma_k}+X(kS)\frac{dQ_{kS}}{d\gamma_k}=0 \quad (3)$$

the generalized electronegativity, X, being defined as the derivative of the energy with respect to the signed charge. Note especially the presence in (3) of the overlap electronegativity, X(kS). This term, which has a leading contribution linear in γ_k, cannot be interpreted in terms of electronegativity equalization of the two bonding orbitals. Instead it enters into the description of the inherent inertia of the bond to weaken as the overlap charge decreases.

The general equation (3) is written in more explicit form in Paper I. The energy expression used assumes that the LMO's are mutually orthogonal, *i.e.* that overlaps between non-bonded AHO's are neglected. This may be justified if the true basis set for the calculation is made up of orbitals which have been symmetrically orthogonalized on all AHO's except that with which a bond (if any) has been formed. Details concerning how this orthogonalization is performed are treated in Ref. 2, where a discussion of the relation between the proper basis sets of the OCEE and the CNDO schemes is presented.

Further simplification in (3) has been achieved using the Goeppert-Mayer and Sklar,[8] the Mulliken,[9] the Wolfsberg-Helmholz,[10] and the Ruedenberg [11] approximations. The latter is a generalization of the Mulliken approximation applicable to $\phi_i(1)\phi_j(2)$.

In Paper I two possible operators to which the Wolfsberg-Helmholz approximation could be applied were discussed. The relation resulting from the choice of one of these (eqn. 45, Paper I) is unsatisfactory in that it effectively contains the exchange integral between the two bonded orbitals. This is not consistent with the fact that the two electrons in the bond have opposite spins. Also, it is highly inconvenient from the computational point of view.

Use of the alternative possibility completely avoids this problem. If the energy contributions up to and including terms of third order in the bond polarities are retained, eqn. (3) now takes the form (for details see Paper I):

$$2S_kq_k\gamma_k[X^0(k1)+X^0(k2)](G-1)+q_k\gamma_k[J(k1,k1)+J(k2,k2)-2J(k1,k2)]+\sum_{j\neq k}^{N}2q_jA_{kj}\gamma_j=[1-3(1-S_k)q_k\gamma_k^2][X^0(k1)-X^0(k2)] \quad (4)$$

G is a Wolfberg-Helmholz-type parameter and

$$A_{kj} = J(k1,j1) + J(k2,j2) - J(k1,j2) - J(k2,j1) - \tfrac{1}{2}[K(k1,j1) + K(k2,j2) - K(k1,j2) - K(k2,j1)]$$

J(i,j) represents the Coulomb interaction between ϕ_i and ϕ_j and K(i,j) is the corresponding exchange interaction. The generalized homopolar electronegativity for ϕ_{k1} (centered on atom A) is defined by

$$X^0(k1) \equiv X_M(k1) + \sum_{C \neq A}^{atoms} PE_C(k1) + \tfrac{1}{2}[J(k1,k2) - K(k1,k2)] \quad (5)$$

where X_M denotes the Mulliken electronegativity and PE_C is the penetration energy of the orbital into the neutral atom C in the appropriate valence state. A similar definition applies to $X^0(k2)$. The three terms on the left-hand side of eqn. (4) are referred to as bond, diagonal inductive, and off-diagonal inductive terms, respectively.

2.1. Exchange interactions in the OCEE theory. The expressions for X_M and PE_C in (5) both contain exchange terms corresponding to undefined spins of the electrons in singly occupied AHO's. The presence of K(k1,k2) is therefore only formal, as the term cancels with a similar term in the penetration energy into the atom on which ϕ_{k2} is centred.

Of the remaining exchange interactions, the two-center integrals have been shown to be negligible when calculated using the true basis set.[2] In the following we discard even the one-center contributions while attempting a rough correction for the consequent error *via* the parameterization of the one-center Coulomb integrals (Section 3.4).

Because of the effective neglect of exchange, application of the rather dubious Ruedenberg approximation in practice becomes somewhat redundant, having only marginal influence on the computations. From the formal point of view, however, the approximation is expedient being the only one which will produce the correct exchange contributions to the Mulliken electronegativity.

3. OCEE CALCULATIONS

The OCEE calculations, details of which are given in the present section, were based upon eqns. (4) and (2). The system of eqns. (4) was solved for the bond polarities by iteration. Each step involved solution of a set of n linear equations, n being the number of non-equivalent bonds in the molecule. The dipole moment with proper inclusion of overlap moments was evaluated from the charge distributions (2). This expression was also used to calculate atomic charges, overlap charges being divided equally between the AHO's involved. The charges to be used in the comparison with the CNDO scheme have been discussed previously.[2]

3.1. Basis set and hybridization. The set of basis functions used to construct the hybrids of the OCEE scheme is identical to that employed in the CNDO/2 scheme, *i.e.* a Slater-type orbital basis with orbital exponents chosen using the Slater-Zener rules, except that the value 1.2 was adopted for hydrogen.

The hybridization schemes were such that σ-bonding AHO's were always directed along the internuclear axis. This condition, combined with the appropriate symmetry, was sufficient to determine the form of the bonding orbitals for most of the atoms in the molecules considered. Uncertainties remained only for C and N in HCN, for O in H_2CO and for F in general. The hybridization of C in HCN was assumed to be perfectly diagonal, and three calculations were performed for each of the HCN and H_2CO molecules with different σ-bonding orbitals for the hetero-atoms in each case. The *s*-character of the bonding AHO on F (*i.e.* the square of the coefficient of the 2*s*-orbital) was determined by a least squares fit of the calculated to the corresponding observed dipole moments for the fluoromethanes.

3.2. Effective electronegativities. The main orbital property governing the signs and magnitudes of the bond polarities is the generalized homopolar electronegativity X^0. The primary contributor to this is the well-known Mulliken electronegativity of the orbital in the appropriate valence state of the atom. But important molecular PE-corrections are also present. The last term in the definition (5) is required in order to avoid self-interaction of the electron. A term of this nature occurs in the penetration energy into the atom with which the bond is formed.

The Mulliken electronegativity of an AHO depends rather strongly upon the form of the

hybrid. Values were obtained from the tables of Hinze and Jaffé [12] using linear interpolation based upon the orbital *s*-character. Penetration energies were calculated neglecting exchange contributions between non-bonded orbitals.[2]

The very important electronegativity difference appearing on the right-hand side of eqn. (4) contains only the difference in Mulliken electronegativity (ΔX_M) and the difference in total penetration energy (ΔPE). It has been customary in semi-empirical calculations to assume that penetration energies are approximately the same for all atomic orbitals, so that terms similar to the ΔPE-term have usually been neglected (Section 4.1). The present calculations indicate that the validity of this assumption may be questionable.

3.3. Penetration energies. The ΔPE-term proved to be very significant indeed. Its sign was always opposite to that of the ΔX_M-term, and its numerical value in some cases exceeded 50 % of the corresponding ΔX_M.

It is not surprising that ΔX_M and ΔPE have opposite signs since orbitals characterized by low Mulliken electronegativities have small orbital exponents (great penetrating ability) and *vice versa*. The relatively large magnitude of ΔPE, especially when atoms of very different electronegativities are involved, originates mainly from the fact that large electronegativities occur only for atoms with more than half-filled valence shells, *i.e.* for atoms carrying lone pairs. The atomic charge distributions in the relevant valence states of these atoms will, in general, possess a dipole moment which is directed so as to give rise to large positive contributions to the penetration energies of orbitals on neighbouring atoms. This is illustrated by the results obtained for HF, which is an extreme case because of its large ΔX_M and short bond length. With an *s*-character for the bonding F-orbital of 0.28, ΔX_M amounts to 10.4 eV. The ΔPE-term is calculated to -4.8 eV, 75 % of which arises from the polarization of the F-atom.

Penetration energies into non-polarized atoms such as H and C decrease exponentially with distance and are relatively small even for orbitals centred on neighbouring atoms but forming bonds to others. The PE-terms for polarized atoms remain important for larger distances because of the monopole-dipole-type interactions involved. The effects of this for the fluoromethanes will be discussed in Section 5.2.

3.4. Two-electron integrals. Neutral penetration energies are probably reasonably well represented in calculations such as those presented here, because correlation effects are similar in attraction and repulsion. However, this is unlikely to be so for the inductive terms in (4). It is true that, even in this case, any one orbital interacts with an overall neutral charge distribution, *i.e.* with the charge displacement within a bond, but the effective distances to the positive and negative parts may differ substantially. The value of the Coulomb integral between the bonded orbitals which enters the bond term might also be expected to be strongly influenced by correlation.

To take account of such correlation effects parameterization has been invoked for all two-electron integrals not entering the penetration energy terms. For one-orbital integrals the Pariser formula:[13]

$$J(i,i) \cong I_V(i) - A_V(i)$$

has been used. Values for the valence state ionization potentials and electron affinities were obtained from the tables of Hinze and Jaffé.[12] The remaining integrals, including one-center two-orbital integrals, were parameterized using the method of Mataga and Nishimoto;[14] that is:

$$J(i,j) \cong e^2/(r + a_{ij}), \quad a_{ij} \equiv 2e^2/[J(i,i) + J(j,j)]$$

To include effects of hybridization, the distances r were those between the centers of gravity of the charge distributions involved.

The use of the centers of gravity can be justified for non-overlapping charge distributions. Thus significant errors are limited to one-center integrals and to the integral involving the two bonded orbitals. This latter integral will be somewhat overestimated, but since it occurs twice, with opposite sign, in the diagonal coefficient in (4) the effect of this error will be reduced. This diagonal coefficient also contains the purely empirical Wolfberg-Helmholz parameter, through which further corrections may be achieved. The one-center two-orbital integrals, on the other hand, will probably be underestimated in the above parameterization scheme. Although its extent may not be adequate, this effect will provide the desired correction for

the neglect of the corresponding one-center exchange interactions (Section 2.1).

3.5. The Wolfsberg-Helmholz parameters G basically expresses the ratio of the overlap electronegativity to the mean of the electronegativities of the bonded orbitals.[1] By performing a calculation for H_2O in which the resulting dipole moment is constrained to be approximately the observed value, a G of 1.9 was obtained. This is similar to those used in earlier applications of the Wolfsberg-Helmholz approximation, in most of which values between 1.5 and 2.0 have been employed.

4. CNDO/2 CALCULATIONS

The CNDO/2 scheme is a semi-empirical approximation of the LCAO – SCF theory the basis of which is the complete neglect of differential overlap (CNDO) between atomic orbitals. The basic theory, notation, and parameterization are described in detail in the original publications by Pople *et al.*[3-5,15]

4.1. Neutral penetration energy terms occur in the diagonal element of the Fock operator in the CNDO theory. However, these terms only account for the spherical average (around the center in question) of the penetration of the orbital into other atoms for which charge distributions have been spherically averaged about their respective centers.[7] Furthermore, in CNDO/2 the nuclear attraction integral V_{AB} is approximated by $-Z_B\gamma_{AB}$[5] *i.e* explicit penetration terms are altogether absent in this scheme.

Contrary to what appears to be the case for the CNDO/2 scheme, the OCEE scheme would be seriously unbalanced without PE-corrections (Section 3.3). It should be noted, however, that it is the polarization part of these terms which makes them of such importance in the latter theory. This part cannot be included explicitly in any CNDO scheme. One of the purposes of the present comparison has therefore been to investigate how well these polarization effects are accounted for implicity by the CNDO/2 parameterization. Before this can be described in a satisfactory way, however, it is necessary to examine some difficulties which arise in making the comparison itself.

4.2. CNDO localization procedure. To make comparison of the OCEE and the CNDO/2 schemes meaningful, the localized description assumed in the former must be reasonably adequate for the molecules treated. This point was investigated by means of the CNDO/2 scheme. Localization of the occupied canonical CNDO/2 – MO's was achieved by applying the unitary transformation which maximizes the sum of one-orbital Coulomb integrals over the MO's (computed within the CNDO approximation). This localization criterion was originally proposed by Lennard-Jones and Pople [16] and its extension to the CNDO scheme has been studied by Trindle and Sinanoglu.[17]

The Self Energy Localized (SEL) MO's so constructed have large contributions from orbitals on two atoms, at the most, and are easily recognized as representing bonds and lone pairs in the molecule. All bonds and σ-type (hybridized) lone pairs could be well localized, the secondary contributions (*i.e.* the coefficients for AO's on distant centers) being relatively small (< 0.05). The π-type lone pairs, however, are delocalized to larger extents in some cases. This is discussed in the following section.

Since delocalization effects are unimportant in those SELMO's which involve hybridization, it is possible to formulate approximate hybridization schemes for the various atoms from the CNDO/2 calculation. This has been done by neglecting secondary contributions, rescaling the primary coefficients to fulfil the normalization condition and analyzing the resulting localized MO's in terms of normalized AHO's. The directions of the bonding AHO's lie in all cases within a few degrees of those of the appropriate internuclear axes. The effective orbitals s-characters are listed in column 6 of the tables.

A necessary requirement for perfect localization is that all hybridization transformations obtained in this way be unitary. Hence ideally the sum of the s-characters of the AHO's on an atom should equal 1. This condition was fulfilled (to within the accuracy of the calculation) for all atoms carrying lone pairs. Lone pair s-characters have therefore been omitted from the tables. The deviation from unity for carbon may be taken as a rough measure of the degree of delocalization.

4.3. Delocalization effects in CNDO/2. By far the dominant delocalization effect in the CNDO/2 results is that of π-type lone pair

Table 1.

Molecule [a]	Dipole moments (D) Obs.	OCEE	CNDO/2	CNDO/2D[b]	Orbital *s*-character OCEE	CNDO/2[c]	Charges (|e|) OCEE	OCEE'[d]	CNDO/2	CNDO/2D[b]
H_2O	1.846[f]	1.86[e]	2.15	1.76	O .200	O .180	H +.124	H +.103	H +.143	H +.196
NH_3	1.468[g]	1.70	2.09	1.50	N .227	N .210	H +.059	H +.046	H +.078	H +.127
					N .333		H +.095	H +.065		
		2.34			C_N .500		N_π −.049	N_π −.046		
					C_H .500		N_σ +.028	N_σ +.017	H +.070	H +.100
					N .500	N .349	H +.095	H +.065	N −.092	N −.160
HCN	2.986[h]	2.64	2.42	2.15	C_N .500	C_N .569	N_π −.032	N_π −.031	N_π −.093	N_π −.097
					C_H .500	C_H .522	N_σ −.021	N_σ −.012	N_σ +.001	N_σ −.063
					N .667		H +.094	H +.064	C +.022	C +.060
		2.76			C_N .500		N_π −.043	N_π −.041		
					C_H .500		N_σ −.060	N_σ −.032		
					O .333		H +.062	H +.046		
		2.85			C_O .382		O_π −.191	O_π −.186		
					C_H .309		O_σ −.035	O_σ −.025	H −.017	H +.011
					O .500	O .302	H +.062	H +.046	O −.184	O −.255
H_2CO	2.339[i]	3.11	1.89	1.63	C_O .382	C_O .355	O_π −.160	O_π −.156	O_π −.167	O_π −.171
					C_H .309	C_H .386	O_σ −.113	O_σ −.078	O_σ −.100	O_σ −.165
									$O_{\pi'}$ +.083	$O_{\pi'}$ +.081
					O .667		H +.060	H +.044		
		3.24			C_O .382		O_π −.169	O_π −.164	C +.218	C +.233
					C_H .309		O_σ −.146	O_σ −.099		

[a] Geometries from Ref. 23. [b] From Ref. 19. [c] See Section 4.2. for method of calculation. [d] See Ref. 2. [e] Used in determination of the Wolsberg-Helmholz parameter (Section 3.4). [f] Birnbaum, G. and Chatterjie, S. K. *J. Appl. Phys. 23* (1952) 220. [g] Coles, D. K., Good, W. E., Bragg, J. K. and Sharbaugh, A. H. *Phys. Rev. 82* (1951) 877. [h] Battacharya, B. N. and Gordy, W. *Phys. Rev. 119* (1960) 144. [i] Shoolery, J. N. and Sharbaugh, A. H. *Phys. Rev. 82* (1951) 95.

delocalization onto carbon and hydrogen atoms. This type of back donation, or reverse hyperconjugation, has been noted earlier in methanol by Pople and Segal.[4] It may be thought of as arising from the interaction of the antisymmetrical CH_n orbital with a completely filled π-system (the lone pair).

For the molecules treated in this work, reverse hyperconjugation was especially important in formaldehyde. In this case the oxygen $2p$ lone pair in the molecular plane ($O_{\pi'}$) donates 0.083 of an electron to the CH_2 group. One third of this is transferred to the hydrogens. The mechanism leads to a lowering of the dipole moment by 0.57 D.

Back donation from lone pairs is also found in the fluoromethanes. However, although more lone pairs take part in the delocalization, less charge is transferred because of the increased bond distances and stronger binding of the lone pair electrons. The F_π-charge given in column 9 of Table 2 is the total charge acquired by the atom *via* reverse hyperconjugation. The effect of these charge displacements on the dipole moments is about the same in the three unsymmetrical molecules (0.29, 0.41, and 0.43 D, respectively, for mono-, di-, and trifluoromethane).

If it is assumed (a) that the excess in the sum of s-characters for C in CH_3F is caused entirely by the mixing of CH – LMO's and F lone pairs, and (b) that the effect on the s-character of any C-orbital is proportional to the amount of charge donated by the lone pairs, then the s-characters for various C-hybrids found in the remaining fluoro-methanes may be rationalized. Using assumption (a) the basis s-characters are 0.200 for C-orbitals bound to F and $(1-0.200)/3 = 0.267$ for orbitals forming bonds to H. Correcting these values for the increasing number of F-atoms and, according to (b), for the increase in the charge donated by each of these, the apparent s-characters become 0.233, 0.274, and 0.341 for the C_F-orbitals in CH_2F_2, CHF_3, and CF_4, respectively, and 0.333 and 0.378 for the C_H-orbitals. These numbers all agree closely with the corresponding numbers in column 6 of Table 2, so it seems reasonable to assert that the C-hybrids taking part in the σ-bonding are essentially unchanged through this series of fluoromethanes, the changes derived from the CNDO/2 results largely being due to the approximate nature of the method of derivation.

5. RESULTS AND DISCUSSION

The computations were made using an IBM-7094 at the Northern Europe University Computing Center (NEUCC), Lundtofte, Denmark, and a GIER at the H. C. Ørsted Institute, University of Copenhagen. Penetration energies in the OCEE scheme were computed using a FORTRAN IV version of the DIATOM program.[20] The remainder of the OCEE scheme calculations were programmed in GIER-ALGOL. The CNDO/2 calculations were performed using a FORTRAN IV program derived from that written by Segal.[21] The results are presented in Tables 1 and 2. When available,[19] the CNDO/2D dipole moments and charges, obtained using the symmetrically orthogonalized atomic basis,[18] have been included in the tables.

5.1. Dipole moments and hybridization. The OCEE method is capable of predicting dipole moments with an overall accuracy comparable to that of the CNDO/2 scheme.

Formaldehyde is the only molecule for which the OCEE value for the dipole moment is both poor and simultaneously greatly at variance with the values computed using the CNDO/2 wavefunction. This is undoubtedly due to the failure of the OCEE theory to take into account the back donation of charge from the $O_{\pi'}$ lone pair. The resulting reduction of the dipole moment in CNDO/2 (Section 4.3) is nearly the same as the difference between the OCEE prediction and the observed value.

The effect of lone pair delocalizations in the fluoro-methanes is apparently well provided for by the use of the hybridization of F as a parameter.

It may appear surprising that the OCEE procedure leads to a higher s-character (and thereby greater electronegativity) for the bonding F-orbital than that given by the CNDO calculation. It should be noted therefore, that the CNDO scheme is likely to underestimate the hybridization of polarizable atoms since it ignores polarization contributions to the interactions between atoms.[22]

The underestimation of polarization in CNDO/2 ought to be particularly significant for HF because of the short bond distance. This furnishes an explanation for the large discrepancy between the F hybridization schemes in the two calculations. Note, however, that there is no *a priori* justification for the direct transfer, adopted in the OCEE calculation, of F-hybridization from the fluoromethanes to HF.

Table 2.

Molecule [a]	Dipole moments (D) Obs.	OCEE	CNDO/2	CNDO/2D[a]	Orbital *s*-character OCEE	CNDO/2[a]	Charges (|e|) OCEE	OCEE'[a]	CNDO/2	CNDO/2D[a]
CH_4	0	0	0	–	C .250	C .261	H −.000 C +.001	H −.000 C +.001	H +.012 C −.048	–
CH_3F	1.855[c]	1.78[b]	1.72	1.43	C_F .235 C_H .255 F .28	C_F .200 C_H .295 F .203	H +.029 F −.162 C +.075	H +.021 F −.141 C +.078	H +.005 F −.194 (F_π +.040) C +.180	H +.036 F −.240 C +.132
CH_2F_2	1.96[d]	2.02[b]	1.95	–	C_F .236 C_H .264 F .28	C_F .229 C_H .333 F .215	H +.056 F −.126 C +.140	H +.041 F −.108 C +.134	H −.006 F −.194 (F_π +.047) C +.400	—
CHF_3	1.645[e]	1.68[b]	1.66	–	C_F .245 C_H .265 F .28	C_F .271 C_H .373 F .228	H +.080 F −.089 C +.187	H +.058 F −.076 C +.170	H −.018 F −.199 (F_π +.053) C +.615	–
CF_4	0	0	0	–	C .250 F .28	C .320 F .232	F −.062 C +.248	F −.053 C +.212	F −.202 (F_π +.067) C +.808	–
HF	1.8195[f]	1.89	1.85	1.68	F .28	F .178	H +.187	H +.160	H +.232	H +.298

[a] See corresponding footnotes to Table 1. [b] Used in determination of the hybridization scheme of F. [c] Larkin, M. and Gordy, W. *J. Chem. Phys. 38* (1963) 2329. [d] Lide, D. R. *J. Amer. Chem. Soc. 74* (1952) 3548. [e] Shoolery, J. N. and Sharbaugh, A. H. *Phys. Rev. 82* (1951) 95. [f] Weiss, R. *Phys. Rev. 131* (1963) 659.

According to the arguments above it would be expected that the *s*-characters in CNDO/2 of the bonding orbitals of N and O in HCN and H_2CO would be too low. In these cases the OCEE results give no indications since the computed dipole moments are remarkably insensitive to the hybridization schemes of the hetero-atoms. This is due partly to the balancing of differences in electronegativity and in penetration energy of the orbitals involved, and partly to the large induction between components of multiple bonds.

5.2. Charge distributions. The net atomic charges are listed in columns 7 – 10 of Tables 1 and 2. The values to be compared are the ones marked OCEE′ and CNDO/2 since these were obtained using very similar basis sets.[2] However, comparison of the original OCEE and the CNDO/2D charges also leads to the same conclusions. Such a comparison is justifiable because of the insignificance of the non-bonded overlaps.

Charges calculated for electronegative atoms are generally less negative in OCEE′ than in CNDO/2. Further carbon atoms and hydrogen atoms directly bound to centers of high electronegativity are less positive, and atoms separated by two bonds from an electronegative atom are more positive.

These differences originate mainly from the respective ways in which penetration energies are treated in the two schemes. The difference in generalized homopolar electronegativity, which is the driving force in the transfer of charge, is greatly reduced by the penetration contributions included in the OCEE theory (Section 3.3). Consequently, the polarities of the most polar bonds are lower than the corresponding values obtained from the CNDO/2 scheme. This effect accounts for the lower negative charges on N, O, and F in OCEE. It also accounts for the larger electron density on the hydrogen atoms bound to these atoms, and for some of the differences on the carbon charges. The electronegativities of orbitals forming bonds in the vicinity of polarized atoms (CH- and CF-bonds here) contain significant non-bonded penetration terms. These act in favour of the occupancy of the orbital closest to the center of polarization and lead to a further increase in electron density on the carbon atoms in the molecules considered.

In view of the important role played by the neutral penetration energy terms in the OCEE theory, it is at first sight surprising that corresponding results from the two calculations only deviate extensively for relative few of the molecules. The main reason for this, however, is that the over-estimation of differences in effective electronegativity in the CNDO/2 scheme is counter-balanced by the use of large two-electron repulsion integrals which prevent large charges developing on any atom.

The results for methane and its four F-substituted analogs demonstrate clearly how the two theories account for charge displacements. The two calculations give similar values for the CF-polarity in CH_3F. Non-bonded penetration terms for this bond are insignificant. The result indicates the ability of the CNDO/2 parametrization to simulate the effect of bonded penetration. Going through the series, non-bonded penetration (polarization) becomes increasingly important in the OCEE treatment. This, together with the increasing competition for electrons between the fluorines, brings about an appreciable decrease in the amount of charge transferred through the CF-bond. The results of the CNDO/2 calculation show a weak *increase* in the polarity of this bond.

In Section 2 it was pointed out that polarity of a bond reduces the bonding since it decreases the overlap charge in the bond. Consequently the bond length should decrease with decreasing polarity, reaching a minimum for the homopolar case. This feature is well illustrated by the CF-bonds in the fluoromethanes. The CF-distances observed for mono- to tetrafluoromethanes [23] (1.385, 1.358, 1.332, and 1.323 Å, respectively) correlate well with the polarities obtained from the OCEE calculation. The comparison may be made quantitative if bond distance is expressed as a linear function of the square of polarity [see eqn. (2)] or, equivalently, as a linear function of bond order. After a least squares fit of the two constants the corresponding calculated CF-distances are 1.3854, 1.3566, 1.3339, and 1.3221 Å. All values are well within the uncertainty limits of the observed bond length. Extending these results, a homopolar paraffinic CF-bond should have a length of about 1.31 Å.

It should be noticed that a correlation of the above type also appears in the CNDO/2 results, in which the F_π-charges may be taken as

measures of the double bond character of the CF-bond. However, their increase along the series seems too weak to account for the observed bond shortening. This is supported by explicit CNDO/2 calculations of geometries from energy minima for the fluoro-methanes.[15a]

The charge alternation noted by Pople and Gordon [6,15] in CNDO/2 results for F-substituted hydrocarbons, and illustrated by the increase in electron density on the hydrogen atoms along the series of fluoro-methanes, is mainly due to reverse hyperconjugation. Each of the hydrogens in mono-, di, and trifluoromethane receive charges of -0.005, -0.011, and -0.018, respectively, through delocalization of fluorine lone pairs. This back donation of charge is no doubt a genuine effect, but when the effect of polarization of atoms is properly included the latter will dominate the picture as suggested by the OCEE results.

The fluoromethanes have recently been the subjects of two accurate *ab initio* calculations performed at the Hartree-Fock level.[25,26] Both calculations yield strongly positive hydrogens ($+0.3$ and $+0.2$) and negative fluorines (-0.3). Except for one case the charges on these atoms vary in the same directions and by comparable amounts as those found in the OCEE calculation. The carbon charges, on the other hand, undergo dramatic changes along the series (from -1 in CH_4 to $+1$ in CF_4). It is probable that the hydrogens are calculated to be too positive. As recognized [25] it is "not very sensible to suppose" that the hydrogens in CH_4 each carry a charge of $+0.3$. This particular result may be due to the use of diffuse orbitals. These make the charges derived from a Mulliken population analysis rather formal quantities which do not reflect the actual electron densities at the atoms. There may also be more fundamental inadequacies in the method of calculation. That this is at least partly the case may be seen from the computed dipole moments which are consistently $30-40$ % too large.

6. CONCLUSIONS

The OCEE and the CNDO/2 schemes both appear wellbalanced in the sense that molecular dipole moments may be calculated with fair accuracy. However, the charge distributions obtained with the two theories may in certain cases be rather different.

The OCEE theory emphasizes the neutral penetration energy contributions to the effective electronegativities, thereby achieving substantial equalization of the latter. These penetration terms appear particularly important when polarized atoms are present. The effective dipole moment of the charge distributions around these atoms contributes significantly to the field around other atoms in the molecule. Inclusion of these effects in the OCEE scheme is made possible through the use of a localized description. This limits the applicability of the theory to a particular, not very well-defined, class of molecules. Furthermore, the hybridization schemes used will always be questionable, even when chosen according to principles more fundamental than those upon which the present work was based.

The CNDO/2 scheme is more general in that it can be applied to any molecular system, and it gives no problems in choice of hybridization. But in making the various approximations all effects arising from the polarization of atoms are lost. This appears in some cases to have serious consequences upon the calculated charge distributions. The success of CNDO/2 theory in predicting dipole moments is largely due to the counter-balancing of overestimated differences in effective electronegativity by the effects of the use of large two-electron repulsion integrals. When these parameters are evaluated according to semi-empirical arguments charge displacements, and therefore dipole moments tend to become too large.[24]

The INDO (Intermediate Neglect of Differential Overlap) scheme,[27,15] which differs from the CNDO scheme in the inclusion of one-center exchange integrals, also describes the interaction between atoms in terms of spherical charge distributions. With calculated two-electron integrals this scheme produces dipole moments and charge distributions similar to those given by the CNDO/2 scheme.[15] When parameterization is introduced the computed dipole moments again become too large.[28,29] Spherical averaging is not used in the NDDO (Neglect of Diatomic Differential Overlap) scheme,[3,15,30] and all polarization effects are retained in this scheme. But for the calculation of dipole moments and charge distributions it

appears somewhat superfluous to include *all* two-electron integrals involving two one-center charge distributions.

It has recently been demonstrated [22] that it is possible to construct an approximate LCAO-SCF scheme which, while retaining the necessary invariance properties, is intermediate between the INDO- and the NDDO-schemes. This has been named DRINDO (Dipoles Retained . . .) and incorporates the main effects of polarization of atoms in the selfconsistent field. In view of the conclusions drawn from the present comparison there is hope that some parameterized version of the DRINDO-scheme will produce more accurate dipole moments than does the INDO-scheme whilst simultaneously retaining the facility of the latter to predict other molecular properties. Work in progress is directed towards this end.

REFERENCES

1. Voigt, B. and Dahl, J. P. *Acta Chem. Scand. 26* (1972) 2923.
2. Voigt, B. *Acta Chem. Scand. A 28* (1974) 1043.
3. Pople, J. A., Santry, D. P. and Segal, G. A. *J. Chem. Phys. 43* (1965) S 129.
4. Pople, J. A. and Segal, G. A. *J. Chem. Phys. 43* (1965) S 136.
5. Pople, J. A. and Segal, G. A. *J. Chem. Phys. 44* (1966) 3289.
6. Pople, J. A. and Gordon, M. *J. Amer. Chem. Soc. 89* (1967) 4253.
7. Dahl, J. P. *Acta Chem. Scand. 21* (1967) 1244.
8. Goeppert-Mayer, M. and Sklar, A. L. *J. Chem. Phys. 6* (1938) 645.
9. Mulliken, R. S. *J. Chim. Phys. 46* (1949) 497; 675.
10. Wolfsberg, M. and Helmholz, L. *J. Chem. Phys. 20* (1952) 837.
11. Ruedenberg, K. *J. Chem. Phys. 19* (1951) 1433.
12. Hinze, J. and Jaffé, H. H. *J. Amer. Chem. Soc. 84* (1962) 540.
13. Pariser, R. *J. Chem. Phys. 21* (1953) 568.
14. Mataga, N. and Nishimoto, K. *J. Phys. Chem. 13* (1954) 140.
15. Pople, J. A. and Beveridge, D. L. *Approximate Molecular Orbital Theory*, McGraw-Hill, New York 1970, (a) Table 4.7.
16. Lennard-Jones, J. E. and Pople, J. A. *Proc. Roy. Soc. (London) A 202* (1950) 446; *A 210* (1951) 190.
17. Trindle, C. and Sinanoglu, O. *J. Chem. Phys. 49* (1968) 65; *J. Amer. Chem. Soc. 91* (1969) 853.
18. Löwdin, P. O. *Sv. Kem. Tidskr. 67* (1955) 380.
19. Shillady, D. D., Billingsley, F. P. and Bloor, J. E. *Theoret. Chim. Acta 21* (1971) 1.
20. Switendick, A. C. and Corbato, F. J. *Diatomic molecular Integral Program*, Program 29, Quantum Chemistry Program Exchange, Indiana University.
21. Segal, G. A. *CNDO/2 Program*, Program 91, Quantum Chemistry Program Exchange, Indiana University.
22. Voigt, B. *Theoret. Chim. Acta 31* (1973) 289.
23. Sutton, L. E., Ed., *Tables of Interatomic Distances*, The Chemical Society, London 1958 and 1965.
24. Sichel, J. M. and Whitehead, M. A. *Theoret. Chim. Acta 11* (1968) 220, 254.
25. Schwartz, M. E., Coulson, C. A. and Allen, L. C. *J. Amer. Chem. Soc. 92* (1970) 447.
26. Brundle, C. R., Robin, M. B. and Basch, R. *J. Chem. Phys. 53* (1970) 2196.
27. Pople, J. A., Beveridge, D. L. and Dobosh, P. A. *J. Chem. Phys. 47* (1967) 158.
28. Baird, N. C., Dewar, M. S. J. and Sustmann, R. *J. Chem. Phys. 50* (1969) 1275.
29. Shanshal, M. *Theoret. Chim. Acta 21* (1971) 149.
30. Murrell, J. N. and Harget, A. J. *Semi-empirical SCF MO Theory of Molecules*, Wiley, London 1972.

Received June 4, 1974.

Acta Chemica Scandinavica A 28 (1974) 1079—1088

Die Kristallstruktur des α-Tetrakis(acetylacetonato)cer(IV)

HEINZ TITZE*

Institut f. Anorg. Chemie der Kgl. Universität Göteborg, Institut f. Kernchemie der Chalmersschen Technischen Hochschule und * Institut f. Festkörperphysik der Universität in Lund, Box 725, S-220 07 Lund 7, Schweden

The crystal structure of α-tetrakis(acetylacetonato)cerium(IV) has been determined by X-ray methods. The unit cell is monoclinic (space group $P2_1/c$), with lattice parameters: a = 11.692(1) Å, b = 12.6482(7) Å, c = 16.936(2) Å, β = 112.339(7)° and Z = 4. A total of 2619 independent structure factors has been used for the analysis. The refinement of the atomic positions and anisotropic temperature parameters by the least squares method has given a value of 0.106 for the R-factor. The cerium atom is coordinated by 8 oxygen atoms in the form of an Archimedean antiprism. The mean of the cerium-oxygen distances is 2.33(1) Å. The acetylacetonate rings are folded about a line joining the oxygen atoms, angles for ligands 1–4 are 16, 12, 17, and 20°, respectively.

In einer Untersuchung aus dem Jahre 1963 veröffentlichten Matković und Grdenić [1] die Kristallstruktur des α-Tetrakis (acetylacetonato)cer(IV), das im Folgenden verkürzt mit α-CeA_4 bezeichnet wird. Die von ihnen vorgelegten Resultate wurden mit Hilfe von zwei Projektionen unter Verwendung einer Gesamtzahl von 261 Reflexen erhalten. Bereits in der einleitenden Zusammenfassung ihrer Veröffentlichung weisen die Autoren darauf hin, dass die Acetylacetonatringe eben seien.

Die β-Phasen des ZrA_4,[2] CeA_4,[3] und UA_4 [4] besitzen je zwei Ligandringe die stärker und zwei die schwächer abgewinkelt sind. Das Aussehen und die Art und Weise der Abwinkelung eines Ligandringes geht aus Abbildung 1 hervor. Der Winkel δ ist ein Mass für die Abwinkelung des Sechserringes. Eine Zusammenstellung über die Abwinkelung der oben genannten drei β-Phasen ist in Veröffentlichung [4] gegeben, in der sich auch auf Seite 414 in Abb. 2 die Projektion einer Formeleinheit

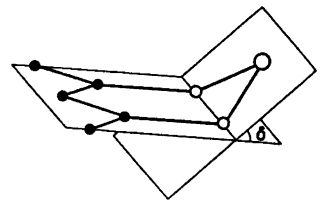

Abb. 1. Die Abwinkelung eines Ligandringes (O Cer, o Sauerstoff, ● Kohlenstoff).

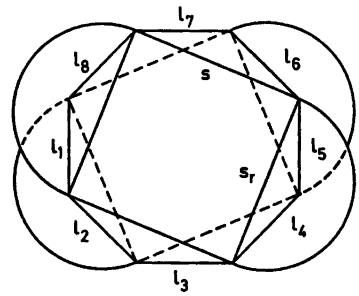

Abb. 2. Die antiprismatische Koordination der Sauerstoffatome (Halbkreise symbolisieren die Ligandringe. s_r ist daher die von einem Ligandring umspannte Seite des Quadrates).

von β-UA_4 auf a-c befindet. Anhand dieser Projektion ist direkt ersichtlich wie sich die Ligandabwinkelung auf die Gestalt der Formeleinheit auswirkt und da die Abwinkelung von je zwei Ligandringen zueinander hin erfolgt, erhält diese eine langgestreckte Gestalt, wodurch eine Verzahnung der Ligandringe mit denen der benachbarten Formeleinheiten ermöglicht wird.

Beim Vergleich des Elementarzellenvolumens für die beiden Phasen des CeA_4, findet man, dass die α-Phase ein 3 % kleineres Volumen

besitzt. In diesem Zusammenhang taucht natürlich die Frage auf: Kann eine Phase mit ebenen Ligandringen ein kleineres Elementarzellenvolumen haben als die mit abgewinkelten?

Da auf Grund der dürftigen Daten zur Strukturbestimmung des α-CeA_4 zu vermuten ist, dass gewisse karakteristische Eigenschaften dieser Phase nicht entdeckt werden konnten, wurde in der vorliegenden Arbeit die vollständige dreidimensionale Strukturanalyse des α-CeA_4 ausgeführt.

EXPERIMENTELLES

Die Herstellung von Benzollösungen des CeA_4 wurde bereits in einer früheren Veröffentlichung [3] beschrieben. Bei der Kristallisation von CeA_4 aus Benzollösungen wurden vom Verfasser dieses Artikels fast immer beide Phasen erhalten, wobei zuerst die β-Phase kristallisierte und dann vor dem völligen Abdunsten des Lösungsmittels die α-Phase. Beide Phasen lassen sich leicht durch ihren unterschiedlichen Kristallhabitus erkennen. Die β-Phase besteht aus langen abgeplatteten Nadeln, während die α-Phase mehr vierkantigen kompakten Quadern gleicht. Von ausgewählten und ausgemessenen Einkristallen wurden mit der $CuK\alpha$-Strahlung Drehkristall- und Weissenbergaufnahmen aller entdeckbarer Schichtlinien unter Verwendung der Mehrfachfilmtechnik ausgeführt. Die erhaltenen Reflexkoordinaten wurden auf Polkoordinatenpapier übertragen und indiziert. Ein Vergleichsmasstab, der mit Hilfe des gleichen Kristalles erhalten wurde, diente zur Ermittelung der relativen Intensitäten der Reflexe.

DIE BESTIMMUNG DER RAUMGRUPPE UND DER GITTERKONSTANTEN

Wie bei β-CeA_4 ist die Elementarzelle monoklin. Für die gefundenen Reflexe konnten folgende systematische Bedingungen abgeleitet werden: *hkl:* keine Bedingungen, *h0l:* $l = 2n$, *0k0:* $k = 2n$. Damit ist die Raumgruppe Nr. 14 $P2_1/c$ gegeben.

Pulverphotogramme wurden in einen Guinier-Kamera bei 21 °C mit Kaliumchlorid als Eichsubstanz aufgenommen. Mit preliminären Achsenlängen, die aus Drehkristall- und Weissenbergaufnahmen errechnet wurden und mit vermessenen $\sin^2\theta$-Werten vom Pulverdiffraktionsmuster wurde die Verfeinerung der Gitterkonstanten mit der Rechenanlage IBM 360/50 unter Verwendung des Programmes von Lindquist und Wengelin [5] durchgefürt. Die Tabelle 1 enthält die Pulverdiffraktionsdaten. Folgende Gitterkonstanten wurden erhalten: $a = 11{,}692(1)$ Å, $b = 12{,}6482(7)$ Å, $c = 16{,}936(2)$ Å, $\beta = 112{,}339(7)°$, $V = 2.316{,}6$ Å^3.

Tabelle 1. Pulverdiffraktionsdaten von α-CeA_4 mit $CuK\alpha$-Strahlung aufgenommen. λ ($CuK\alpha$) = 1,54050 Å.

H K L	$10^5 \sin^2$ beob.	$10^5 \sin^2$ ber.	*F* ber.	I beob.[a]
−1 1 1	853	854	–	st
1 1 0	873	878	–	st
0 0 2	966	967	246	s st
−1 1 2	1311	1313	236	s st
0 1 2	1335	1338	134	s
1 1 1	1383	1386	118	s
0 2 1	1724	1725	188	st
−2 0 2	1931	1931	175	s
1 0 2	2004	2007	147	s
−2 2 1	3224	3222	142	s
−1 3 1	3816	3820	188	st
0 1 4	4234	4239	251	s st
2 2 1	4285	4287	118	s
1 3 1	4353	4353	118	s
2 1 2	4433	4432	125	s
3 0 0	4563	4566	164	s
3 1 0	4938	4937	180	s
−2 3 2	5271	5269	124	s
−3 1 4	5606	6510	160	s
−1 0 6	7616	7613	247	s
−3 3 3	7683	7683	132	s
4 1 0	8485	8488	151	s
0 1 6	9076	9074	161	s
2 3 3	9137	9140	189	s
1 5 0	9778	9779	204	s
−2 1 7	10515	10519	124	s
−4 3 1	10631	10631	136	s
−5 1 4	11595	11597	122	s
3 4 2	13063	13064	130	s
0 6 0	13347	13351	–	s s
−2 6 1	15091	15089	116	s s
2 6 0	15379	15380	100	s s
2 4 6	19859	19861	130	s s
3 6 2	20477	20481	124	s s

[a] s st = sehr stark, st = stark, s = schwach, s s = sehr schwach.

DIE VERFEINERUNG DER STRUKTUR

Zur Durchführung der Verfeinerung der Struktur, wurde zunächst angenommen, dass die von Matković und Grdenić [1] gegebenen Koordinaten ungefähr stimmten und daher für eine Verfeinerung ausreichend seien. Das für

Tabelle 2. Atomlagen und anisotrope thermische Parameter mit Standardabweichungen (in Klammern) für α-CeA_4. Der Temperaturfaktor wird durch $(h^2\beta_{11}+k^2\beta_{22}+l^2\beta_{33}+hk\beta_{12}+hl\beta_{13}+kl\beta_{23})$ ausgedrückt.

Atom	x	y	z	β_{11}	β_{22}	β_{33}	β_{12}	β_{13}	β_{23}
Ce	0,19132(8)	0,14552(7)	0,20059(6)	0,00570(6)	0,00490(7)	0,00343(4)	0,00170(12)	0,00237(8)	0,00043(9)
O1	0,3166(11)	0,1365(11)	0,1221(9)	0,0087(10)	0,0100(12)	0,0057(6)	0,0050(18)	0,0062(16)	0,0005(14)
O2	0,2971(11)	−0,0141(10)	0,2319(10)	0,0070(10)	0,0073(10)	0,0074(8)	0,0018(16)	0,0035(17)	0,0014(14)
O3	0,3867(13)	0,1890(11)	0,3000(9)	0,0098(13)	0,0088(11)	0,0045(7)	−0,0007(19)	−0,0011(16)	−0,0018(13)
O4	0,1943(13)	0,1158(12)	0,3385(9)	0,0118(12)	0,0100(11)	0,0041(6)	−0.0052(20)	0,0044(16)	0,0005(13)
O5	0,2111(11)	0,3316(10)	0,1997(11)	0,0089(11)	0,0048(9)	0,0098(10)	0,0005(15)	0,0079(20)	0,0017(14)
O6	0,0121(12)	0,2148(11)	0,2057(10)	0,0103(11)	0,0089(11)	0,0071(7)	0,0024(18)	0,0092(19)	−0,0002(16)
O7	0,0409(13)	0,0151(11)	0,1522(9)	0,0095(12)	0,0095(11)	0,0053(7)	0,0008(19)	0,0029(17)	−0,0026(14)
O8	0,0692(12)	0,1816(11)	0,0603(9)	0,0096(12)	0,0077(10)	0,0053(7)	0,0043(18)	0,0017(16)	0,0041(13)
C1	0,4772(21)	0,1235(20)	0,0695(18)	0,0172(19)	0,0114(20)	0,0076(11)	−0,0032(33)	0,0161(39)	−0,0025(27)
C2	0,4121(18)	0,0848(15)	0,1281(13)	0,0115(17)	0,0071(13)	0,0052(9)	−0,0095(26)	0,0051(23)	−0,0063(19)
C3	0,4597(22)	−0,0039(18)	0,1778(17)	0,0116(21)	0,0081(17)	0,0072(13)	0,0022(29)	0,0048(30)	0,0020(23)
C4	0,3978(17)	−0,0465(17)	0,2301(13)	0,0076(15)	0,0089(17)	0,0048(9)	−0,0015(26)	0,0030(22)	−0,0009(20)
C5	0,4610(29)	−0,1416(19)	0,2891(21)	0,0251(32)	0,0076(18)	0,0095(16)	0,0131(40)	0,0148(47)	0,0043(29)
C6	0,5835(22)	0,1912(28)	0,4103(19)	0,0084(22)	0,0194(31)	0,0067(15)	0,0015(44)	−0,0005(31)	−0,0046(36)
C7	0,4507(16)	0,1720(16)	0,3724(15)	0,0109(12)	0,0087(15)	0,0060(8)	0,0027(22)	0,0125(27)	0,0014(20)
C8	0,4009(24)	0,1299(21)	0,4339(11)	0,0167(26)	0,0162(24)	0,0011(6)	−0,0046(42)	0,0014(22)	−0,0014(20)
C9	0,2724(21)	0,1113(18)	0,4112(12)	0,0148(22)	0,0100(17)	0,0030(8)	−0,0080(33)	0,0029(24)	−0,0027(18)
C10	0,2219(26)	0,0920(29)	0,4813(18)	0,0201(28)	0,0205(33)	0,0054(11)	−0,0120(58)	0,0101(39)	0,0023(36)
C11	0,1873(29)	0,5106(18)	0,1737(18)	0,0254(39)	0,0060(16)	0,0067(12)	−0,0031(36)	0,0085(42)	−0,0047(23)
C12	0,1302(23)	0,4024(18)	0,1787(12)	0,0161(24)	0,0095(17)	0,0026(7)	0,0015(34)	0,0027(24)	−0,0000(18)
C13	0,0041(20)	0,3946(19)	0,1694(15)	0,0119(20)	0,0097(17)	0,0050(10)	0,0074(32)	0,0032(26)	0,0010(21)
C14	−0,0458(16)	0,3033(18)	0,1821(15)	0,0058(14)	0,0108(17)	0,0057(10)	0,0021(26)	0,0026(22)	−0,0041(23)
C15	−0,1762(19)	0,3059(23)	0,1777(19)	0,0095(16)	0,0143(23)	0,0088(14)	0,0057(34)	0,0101(23)	−0,0031(32)
C16	−0,1481(24)	−0,0767(23)	0,1060(18)	0,0136(25)	0,0128(23)	0,0071(14)	−0,0069(44)	0,0024(33)	0,0003(31)
C17	−0,0717(17)	0,0087(16)	0,0958(15)	0,0073(15)	0,0074(15)	0,0072(11)	0,0018(23)	0,0055(25)	−0,0014(21)
C18	−0,1155(20)	0,0822(18)	0,0276(14)	0,0109(20)	0,0089(17)	0,0051(10)	0,0032(31)	0,0018(25)	0,0011(21)
C19	−0,0452(15)	0,1552(13)	0,0094(11)	0,0080(12)	0,0063(12)	0,0032(6)	0,0073(21)	0,0031(16)	0,0012(15)
C20	−0,0948(28)	0,2269(25)	−0,0664(20)	0,0160(30)	0,0145(27)	0,0071(16)	0,0077(49)	0,0031(39)	0,0028(33)

Tabelle 3. Beobachtete und berechnete Strukturfaktoren für α-CeA_4. (Die Spalten sind: *l*, $|F_{beob}|$ und $|F_{ber}|$).

-14 0 L		
8	24	29
14	19	22

-13 0 L		
6	28	-24
8	33	31
10	32	-31
12	26	24

-12 0 L		
4	71	-61
6	44	37
14	35	-36
12	35	38
16	23	27

-11 0 L		
4	31	-30
6	61	54
8	82	-83
10	49	46

-10 0 L		
2	73	-69
4	47	51
6	35	-37
8	41	-41
10	50	53
12	48	-50
14	34	35

-9 0 L		
2	49	-43
4	77	66
6	78	-74
8	83	80
10	33	-35
12	38	-44
14	46	49
16	36	-40

-8 0 L		
2	74	67
4	67	-66
8	79	70
10	46	-41
12	36	38

-7 0 L		
2	107	98
4	126	-116
6	71	71
10	43	-41
12	66	56
14	72	-69
16	38	40

-6 0 L		
2	53	-52
4	72	-76
6	166	149
8	126	-124
10	86	83
14	44	-50
16	43	49
18	34	-44

-5 0 L		
2	197	-187
4	74	80
6	105	93
8	98	-93
10	98	90
12	104	-97
14	45	43
18	33	-27
20	24	30

-4 0 L		
2	99	-99
4	166	164
6	123	-115
8	94	89
10	35	31
12	77	-77
14	77	66
16	64	-59

-3 0 L		
2	109	97
4	119	87
6	175	-160
8	223	190
10	142	-123
14	34	33
16	34	-38
18	33	35
20	23	-27

-2 0 L		
2	173	188
4	207	-197
6	143	129
10	129	-124
12	78	68
14	79	-69
16	36	40

-1 0 L		
2	62	90
4	183	-177
6	232	247
8	170	-168
10	57	50
12	25	24
14	79	-71
16	32	34

0 0 L		
2	187	-254
6	96	81
8	170	-158
10	138	122
12	71	-56
14	30	26

1 0 L		
2	145	-143
4	210	218
6	60	-50
14	57	60
16	35	-33
12	32	-33

2 0 L		
0	57	-55
2	71	74
4	64	66
6	167	-159
8	102	93
10	46	-42
12	27	29
14	47	44
16	33	-33

3 0 L		
0	157	-141
2	116	124
4	126	-124
6	23	18
8	43	47
10	65	-56
12	68	72
14	32	-36

4 0 L		
0	27	27
2	19	17
4	106	-118
6	127	137
8	72	-72
12	43	53
14	30	-34
16	25	29

5 0 L		
0	142	189
2	145	-155
6	64	77
8	86	-95
10	86	74

6 0 L		
0	72	65
2	142	-140
4	72	80
12	33	-39
14	23	26

7 0 L		
0	58	-53
2	34	-31
4	54	52
6	77	-87
8	62	68

8 0 L		
0	124	-124
2	58	80
10	41	-46
12	24	32

9 0 L		
0	27	-26
2	84	61
4	61	-59
6	56	57
8	24	-27

10 0		
0	71	72
2	52	-50
6	33	33
8	32	-34

11 0 L		
0	34	34
2	60	-56
4	40	43

12 0 L		
4	24	26

13 0 L		
0	40	-36

-13 1 L		
4	32	-34
5	33	-29
6	33	35

-12 1 L		
6	34	30
8	33	-36
9	33	-30
10	33	34

-11 1 L		
2	35	-50
3	59	-34
4	43	46
5	52	38
6	50	-51
7	37	-30
10	34	39
11	34	28
12	31	-35
13	31	-29
14	29	29
15	26	22

-10 1 L		
4	38	40
5	35	29
6	43	-40
7	47	-61
8	45	58
9	43	54
10	30	-31

-9 1 L		
1	67	-62
2	62	56
3	57	48
6	33	-28
8	60	52
10	58	-56
11	35	-36
12	50	45

-8 1 L		
1	31	-19
2	68	66
3	53	48
4	74	-77
5	52	-50
6	66	64
7	33	34
8	36	-38
11	27	-24
12	31	37
13	31	29
14	37	-44
15	29	-29
16	26	27

-7 1 L		
1	62	62
4	26	-17
5	33	-33
6	52	49
7	76	74
8	78	-75
9	30	-35
10	36	42
12	47	-38

-6 1 L		
1	67	69
2	142	-156
3	55	-56
4	126	125
5	21	20
6	35	-44
7	21	14
8	37	-32
10	68	64
11	44	41
12	77	-76
13	46	-41
14	51	53
15	32	34

-5 1 L		
2	21	-17
3	24	-21
4	128	126
5	55	54
6	130	-134
7	45	-47
8	70	80
9	57	60
10	41	-39
11	24	-16
12	28	-34
13	30	-29
14	49	50
15	37	37
16	36	-42
17	31	-28
18	27	27

-4 1 L		
1	96	-99
2	48	62
3	31	28
4	12	-8
5	21	18
6	132	-130
7	92	-79
8	129	116
9	44	47
10	81	-77
11	55	-55
12	48	53
13	29	26
14	15	-10
16	35	-25

-3 1 L		
1	29	-21
2	88	86
3	36	24
4	175	-154
5	71	-72
6	130	115
7	85	82
8	51	-49
9	14	14
10	68	-70
11	68	-66
12	48	44
13	35	26
14	49	-50
15	45	-43
16	40	44

-2 1 L		
1	21	22
2	80	-68
4	66	-50
5	86	-77
6	75	60
7	136	124
8	140	-118
9	84	-84
10	67	66
11	29	25
14	36	-41
15	31	-22
16	29	24

-1 1 L		
2	168	-249
3	56	-45
4	127	108
5	18	19
6	66	-60
8	72	-58
9	26	-24
10	104	97
11	44	44

0 1 L		
12	84	-45

-1 1 L		
13	43	-43
14	41	41

0 1 L		
2	132	-130
3	76	-63
4	246	211
5	52	53
6	165	-161
7	74	-65
8	57	49
9	71	64
11	22	-16
12	36	-45
13	33	-31
14	47	55
15	31	33
16	32	-32
17	28	-21

1 1 L		
1	109	-121
2	36	27
3	105	85
4	83	79
5	13	-8
6	144	-127
7	60	-60
8	92	103
9	67	63
10	68	-70
11	36	-36
12	34	34

2 1 L		
0	60	-65
1	74	68
2	122	130
3	90	97
4	117	-119
5	41	-40
6	39	38
10	33	-33
11	26	-19
12	43	45
13	39	47
14	38	-43

3 1 L		
0	89	87
3	19	18
4	78	-71
5	41	-36
6	108	127
7	68	70
8	75	-75
9	36	-35
10	35	35
13	32	37

4 1 L		
0	130	151
1	63	63
2	123	-139
3	65	-61
4	72	77
5	13	15
6	14	13
7	33	35
8	43	-38
9	53	-57
10	72	67
11	40	45
12	35	-38

5 1 L		
0	26	30
1	32	-28
2	76	-80
3	63	-70
4	102	114
5	63	63
6	62	-57
7	39	-40
8	33	30

6 1 L		
0	91	-96
1	38	-43
2	22	19
4	22	19
5	34	36
6	51	-59
7	56	-66
8	64	79
9	35	38
10	31	-32

7 1 L		
0	70	-75
1	73	-86
2	75	80
3	39	43
4	32	-30
6	27	27
12	27	31

8 1 L		
0	27	26
1	29	-32
2	34	35
3	41	47
4	46	-49
5	43	-44
6	51	60
7	31	37
8	23	-34

9 1 L		
0	61	66
1	40	43
2	35	-42
10	23	25

10 1 L		
1	29	29
2	33	-36
3	36	-36
4	39	44
5	31	31
6	28	-23

11 1 L		
0	33	-35
1	31	-26
4	25	18
5	24	20
6	29	-32

12 1 L		
0	32	-31
1	28	-26
2	28	35

13 1 L		
3	13	14

-12 2 L		
3	48	-42
5	49	56

-11 2 L		
7	52	-52
9	62	59

-10 2 L		
1	80	-48
3	38	53
5	33	-44
9	44	53
11	48	-56
13	41	41

-9 2 L		
3	50	52
5	57	-63
7	74	66
9	59	-58

-8 2 L		
1	94	94
5	32	-29
7	71	69
9	61	-61
11	58	57

-7 2 L		
1	105	99
3	108	-118
4	30	35
5	97	101
7	41	-52
11	46	42
13	49	-57
15	49	49

-6 2 L		
1	36	-44
5	81	81
6	36	-44
7	95	-97
8	25	34
9	66	64

-5 2 L		
1	140	-149
2	74	80
3	95	112
4	50	-54
7	66	-80
8	52	52
9	53	56
10	43	-44
11	84	-89
13	74	60

-4 2 L		
1	29	-33
3	75	72
4	57	-67
5	110	-141
6	29	32
7	110	121
9	40	-44
11	41	-45
13	44	45
15	55	-58

-3 2 L		
1	92	109
2	29	-18
3	41	-48
4	75	-93
5	70	-83
7	116	121
9	100	-96
11	45	46
15	31	-24

-2 2 L		
1	109	142
2	68	-85
3	145	-188
4	40	-32
5	52	58
6	22	-25
7	64	-57
8	30	32
9	56	-53
11	65	73
13	58	-50
15	40	50

-1 2 L		
2	19	24
3	41	-38
4	120	-109
5	54	33
6	20	-16
7	139	-131
8	71	55
9	79	63
11	34	-29
13	44	-49

0 2 L		
2	28	19
3	64	-63
4	41	-33
5	44	-40
6	18	6
7	80	-66
8	88	66
9	96	-81
10	65	-61
11	107	-86
12	38	35
13	51	54
14	18	-16

1 2 L		
1	34	-26
2	59	56
3	246	221
4	24	-21
5	122	-124
6	33	26
7	55	49
9	39	-39
11	43	-42
13	80	69
15	64	-58

2 2 L		
1	116	116
3	25	6
4	27	-31
5	118	-116
6	89	78
7	159	153
8	57	-47
9	89	-80
11	38	41

3 2 L		
0	27	23
1	101	111
2	60	-58
3	120	-117
4	92	90
5	67	73
6	35	-21
7	39	35
9	51	-44
11	36	54
13	46	-45

4 2 L		
1	25	22
3	84	-77
4	42	33
5	103	108
6	24	-23
7	87	-74
9	54	46
13	42	-40

5 2 L		
0	82	-68
1	106	-108
2	46	42
3	63	54
5	32	21
7	63	-59
9	100	90
11	56	-42

6 2 L		
1	76	-75
2	35	31
3	117	117
5	56	-57
13	44	41

7 2 L		
3	43	43
5	72	-70

Tabelle 3. Fortsetzung.

7 97 87	17 19 9	4 51 -50	12 3 L
	21 13 -19	7 137 147	0 21 -18
8 2 L		8 36 26	1 38 39
1 107 90	-5 3 L	9 108 -119	3 22 -26
3 34 -33	1 44 41	11 74 64	
	2 26 19	10 33 -28	-13 4 L
9 2 L	3 40 41	13 21 -22	8 25 -25
3 48 -52	4 43 42	15 23 -27	10 26 30
5 50 53	5 132 -148	17 20 25	12 17 -20
	6 23 -21		
-14 3 L	7 127 117	2 3 L	-12 4 L
11 18 24	8 52 45	0 64 -72	4 50 44
	9 63 -62	1 120 151	5 22 -25
-13 3 L	10 19 -19	2 54 70	6 46 -40
5 37 41	13 52 50	3 154 -191	10 25 13
7 44 -36	14 31 26	4 69 -67	11 24 -16
9 20 23	15 52 -36	5 93 93	12 26 -25
13 20 -21	16 22 -22	6 18 16	13 22 19
15 19 24	17 48 40	9 39 -43	14 22 27
		10 26 -20	15 24 -12
-12 3 L	-4 3 L	11 47 46	16 19 -19
3 40 34	1 115 136	14 23 -23	
7 37 -35	2 46 49	15 24 30	-11 4 L
8 24 -18	3 105 -124		2 31 24
9 41 40	4 26 -27	3 3 L	5 29 -24
16 10 4	5 46 -38	0 37 39	6 39 -36
	7 119 111	1 16 -9	7 26 25
-11 3 L	8 50 46	2 8 -4	8 50 45
3 55 55	9 80 -77	3 47 -54	9 28 -26
4 24 16	10 29 -29	5 114 131	10 23 -26
5 50 -44	11 68 64	6 72 79	11 19 20
6 22 -18	12 47 35	7 104 -106	18 16 19
7 22 23	13 42 -34	8 35 -41	
9 25 22	17 23 25	9 42 35	-10 4 L
11 33 -36	19 20 -24	10 23 18	1 43 38
13 43 38	21 15 24	11 20 -12	2 62 55
15 27 -26		14 22 -15	3 45 -40
17 16 11	-3 3 L	15 24 24	4 34 -26
	1 59 48	17 19 -26	8 31 21
-10 3 L	2 36 33		9 35 -30
1 30 23	3 121 -132	4 3 L	10 40 -37
3 44 42	4 87 -87	0 76 84	11 28 23
5 48 -42	5 67 66	1 126 -140	12 39 40
6 22 -18	6 74 75	2 20 -21	14 26 -25
7 61 59	7 82 -76	3 90 97	
8 31 31	8 53 -46	6 29 28	-9 4 L
9 51 -50	9 15 -5	7 30 -36	1 22 14
13 24 27	10 29 -27	8 29 -25	2 43 44
15 31 -31	11 50 50	9 45 43	3 23 -20
17 27 30	12 26 24	10 31 28	4 58 -57
19 16 -16	13 44 -34	11 60 -56	6 52 53
	14 32 -30	13 37 31	7 38 -34
-9 3 L	15 58 50		8 59 -57
1 73 68	16 28 29	5 3 L	9 18 16
2 30 23	17 26 -27	0 21 16	10 22 24
3 30 -23		1 35 -44	12 30 30
4 23 -13	-2 3 L	2 33 -34	14 39 -35
6 21 -7	1 64 -80	3 87 95	16 36 36
7 49 45	2 108 -123	4 38 39	18 25 -22
8 19 14	3 101 -95	5 72 -73	
9 35 -51	4 42 -33	6 18 -16	-8 4 L
11 51 51	5 63 54	7 38 38	1 22 -16
12 34 29	6 72 78	8 19 17	2 44 -42
13 34 -32	7 86 -90	9 27 -21	4 20 14
14 22 -14	8 83 -83	13 33 35	5 17 -12
	9 95 90	15 20 -29	6 48 44
-8 3 L	10 42 41		8 64 -62
1 29 42	11 27 -19	6 3 L	9 27 21
2 33 26	13 38 -32	0 42 -34	10 63 61
3 50 -46	14 39 -33	1 60 65	11 28 -29
4 43 -44	15 38 34	2 17 14	12 58 -58
5 79 87	16 19 14	5 36 -34	14 18 18
6 28 23	17 31 -30	6 48 -43	16 25 19
7 63 -74	19 21 24	7 78 81	18 24 -23
8 33 -30		8 24 24	20 18 22
9 32 30	-1 3 L	9 68 -75	
10 19 16	1 183 -235	11 18 23	-7 4 L
11 26 22	2 19 -19		1 23 -16
12 20 14	3 76 49	7 3 L	2 83 -87
13 59 -53	4 46 -35	0 61 -46	3 57 60
14 28 -29	5 67 -60	1 93 103	4 78 81
15 57 53	8 53 -53	2 41 38	5 51 -59
16 24 22	9 74 72	3 65 -62	6 50 -51
	10 50 48	4 24 -18	7 31 33
-7 3 L	11 75 -75	5 29 29	8 22 24
1 55 -60	12 18 -15	9 29 -30	9 13 13
2 34 -32	13 62 57	11 31 35	10 28 32
5 54 50	15 27 -30	13 17 -24	11 28 -27
6 53 47	19 14 18		12 58 -54
7 83 -80		8 3 L	13 50 42
8 63 -61	0 3 L	3 44 -43	14 61 61
9 76 74	2 63 -54	5 56 55	15 24 -23
10 29 24	3 22 -11	7 40 -41	16 32 -28
11 59 -59	4 53 50	8 18 -20	
12 19 -15	5 95 -96		-6 4 L
13 20 18	6 33 -35	9 3 L	1 15 18
15 31 32	7 83 81	0 36 34	2 14 10
17 22 -26	8 18 12	1 63 -60	3 24 20
18 19 -17	9 40 -35	2 22 -22	4 76 74
19 21 22	10 17 -6	3 31 28	5 33 -33
	12 25 -24	7 30 -30	6 97 -99
-6 3 L	13 54 55	9 28 31	7 47 43
1 132 -130	14 32 32		8 110 107
2 36 -37	15 61 -55	10 3 L	9 27 -25
3 137 141	16 19 -16	1 52 -50	10 48 -52
4 38 38	17 20 26	2 21 -24	11 30 30
5 62 -62		3 53 50	14 38 35
6 11 5	1 3 L	5 34 -35	16 35 -33
9 53 44	0 117 -148		18 29 31
10 19 20	1 116 123	11 3 L	
11 72 -61	2 42 44	5 26 -32	
12 30 -22	3 9 2	6 19 -18	
13 61 53	4 44 43		
15 33 -30	5 98 -103		

-5 4 L	12 48 49	-13 5 L	
1 58 58	13 23 -26	14 25 24	
2 118 132	14 55 -50		
3 54 -57	16 20 29	-12 5 L	
4 90 -95		6 37 -33	
5 42 37	2 4 L	8 41 42	
7 57 46	0 118 135	10 39 -37	
8 69 63	1 13 12	12 19 19	
9 50 -44	2 47 -49		
10 57 -56	3 11 -15	-11 5 L	
11 47 41	4 78 -91	4 60 -61	
12 58 53	5 71 76	6 36 32	
13 25 -27	6 130 123	10 26 -35	
14 28 -31	7 38 -35	12 39 35	
20 17 -21	8 115 -109	14 36 -32	
	9 21 17	16 19 16	
-4 4 L	10 49 50		
1 18 -15	18 19 -23	-10 5 L	
2 32 36		2 18 9	
3 30 -30	3 4 L	4 50 -44	
4 111 -111	0 158 157	6 56 54	
5 78 76	1 28 -30	8 68 -64	
6 133 136	2 130 -157	10 41 31	
7 34 -29	3 46 44	14 23 -24	
8 65 -61	4 88 101	16 27 28	
9 28 25	5 9 -9	18 21 -23	
11 25 25	6 23 -25		
12 28 24	7 12 -9	-9 5 L	
13 22 -21	8 46 -46	1 26 24	
14 50 -52	10 57 52	2 80 -69	
15 25 20	11 24 -25	3 21 -14	
16 47 49	12 40 -45	4 35 33	
18 24 -19	13 20 22	8 52 -46	
	14 34 33	9 19 -14	
-3 4 L		10 58 55	
1 17 -12	4 4 L	11 21 23	
2 77 -92	2 47 -49	12 45 -45	
3 26 -24	3 29 29	14 19 20	
5 42 38	4 84 87		
6 85 86	5 55 -56	-8 5 L	
7 19 8	6 95 -89	1 17 13	
8 100 -99	7 34 32	2 65 -59	
9 69 59	8 54 53	3 41 -33	
10 83 78	14 19 28	4 81 71	
11 26 -27	16 20 -25	5 18 16	
12 38 -43		6 78 -71	
16 24 25	5 4 L	8 33 36	
18 25 -28	0 102 -117	12 46 -46	
20 19 26	1 57 60	13 17 -11	
	2 46 51	14 54 52	
-2 4 L	3 25 -27	16 26 -30	
1 50 -58	6 46 41	18 15 13	
2 122 -132	8 65 60		
3 88 93	9 43 -44	-7 5 L	
4 85 82	10 52 -44	1 19 -11	
5 74 -64	11 29 32	2 23 25	
6 69 -63	12 21 20	3 14 -9	
7 29 27		4 37 37	
8 15 10	6 4 L	6 24 22	
9 36 35	0 64 -67	6 76 -77	
10 76 78	1 44 40	7 36 -39	
11 38 -35	2 83 81	8 75 75	
12 64 -65	3 41 -48	9 17 11	
13 50 47	4 58 -60	10 58 -57	
14 47 47	5 19 13	12 23 31	
15 24 -23	6 52 44	14 24 20	
16 20 -25	10 27 -23	16 39 -38	
	11 20 19	18 26 30	
-1 4 L	12 34 35	20 15 -19	
1 50 -43	13 18 -16		
3 28 31	14 20 -25	-6 5 L	
4 60 61		1 28 -27	
5 65 -60	7 4 L	2 120 137	
6 133 -135	0 48 44	4 86 -87	
7 61 62	3 33 -37	5 10 10	
8 90 88	5 74 78	6 16 20	
9 30 -27	6 66 61	7 15 11	
10 45 -43	7 31 -39	8 39 43	
12 31 -34	8 59 -50	10 66 -65	
14 65 67		11 17 -17	
15 25 -16	8 4 L	12 89 70	
16 30 -35	0 68 68	14 50 -48	
17 22 17	1 29 -29	16 16 20	
18 19 22	2 64 -63	18 12 9	
	4 27 28	20 15 -20	
0 4 L	8 19 -20		
1 80 109	10 34 33	-5 5 L	
2 52 58		2 18 18	
3 53 -48	9 4 L	3 17 15	
4 20 -17	1 20 -20	4 85 -97	
5 33 29	2 35 -41	5 30 -29	
6 90 -66	3 23 25		
7 18 11	4 64 53	6 125 138	
8 82 76	5 35 -33	7 58 53	
9 57 -60	6 39 -34	8 67 -66	
10 96 -85		10 31 32	
11 41 44	10 4 L	11 16 -15	
12 52 51	0 51 -47	12 34 32	
13 27 -28	1 19 26	14 40 -34	
14 20 -19	3 20 -16	16 36 39	
	4 19 17	18 27 -29	
1 4 L	6 36 -34		
0 17 -11	8 29 32	-4 5 L	
1 41 42		1 72 77	
2 103 101	11 4 L	2 87 -108	
3 51 -48	0 31 -32	3 40 -43	
4 142 -162	2 39 41	4 37 39	
5 82 79	4 33 -28	5 31 38	
6 44 36		6 94 91	
7 39 -35	12 4 L	7 45 37	
8 34 -39	4 23 -25	8 98 -85	
10 18 -19		9 10 6	
11 17 19	13 4 L	10 88 83	
	0 24 33	12 45 -43	

Tabelle 3. Fortsetzung.

16 23 20	6 26 -26	7 44 -47	3 47 51
18 24 -23	7 21 -21	8 35 37	4 83 -96
20 18 27	8 74 62	9 35 38	5 17 -12
	10 80 -66	12 22 -25	6 54 48
-3 5 L	12 40 39	13 24 -25	7 16 16
1 75 82	14 19 -21	14 23 27	8 23 24
2 128 -150	5 5 L	15 20 25	9 33 37
3 29 -29	0 42 -39	16 17 -20	10 35 -32
4 135 140	1 32 -24	-8 6 L	11 54 -55
6 86 -88	2 75 70	1 73 -56	12 53 51
7 29 21	3 38 35	2 38 29	13 44 40
8 51 47	4 116 -108	3 40 32	14 37 -37
9 9 -5	6 70 59	5 15 13	15 33 -30
10 73 64	8 32 -34	6 48 -42	16 21 16
12 72 -60	12 38 36	7 53 -51	17 - 18 10
14 58 61	6 5 L	8 46 36	-1 6 L
16 40 -40	0 86 81	9 44 43	2 69 70
-2 5 L	2 38 -31	10 44 -43	3 38 33
2 18 -14	4 23 -21	11 39 -40	4 85 -78
3 17 15	6 51 41	17 21 -16	5 89 -90
4 81 85	8 84 -73	18 14 -15	6 91 94
5 45 44	10 43 40	-7 6 L	7 90 88
6 107 -105	7 5 L	1 64 -47	8 62 -52
7 20 -20	0 76 68	2 77 67	9 72 -65
8 131 131	2 87 -88	3 59 53	10 22 20
10 79 -70	3 24 -19	4 65 -60	11 29 29
14 36 34	4 47 43	5 31 -24	12 15 14
16 32 -35	5 28 26	6 35 32	13 36 33
18 29 34	6 24 -23	7 18 15	14 22 -15
-1 5 L	10 34 33	10 38 -41	15 35 -33
1 40 40	12 31 -35	11 30 -31	16 25 27
2 168 173	8 5 L	12 39 33	17 21 23
3 51 -49	0 28 -29	13 39 34	18 17 -18
4 54 -62	1 16 -10	14 39 -43	0 6 L
5 13 -6	2 42 -38	15 34 -32	1 64 101
6 16 12	4 66 59	-6 6 L	2 92 -118
8 72 73	6 81 -67	1 41 42	3 33 -33
9 14 10	8 34 34	3 19 21	4 36 34
10 90 -87	9 5 L	4 56 -50	5 10 10
11 15 -12	0 96 -88	5 69 -53	6 27 26
12 77 74	1 24 -20	6 74 66	7 33 30
14 49 -43	2 57 50	7 73 64	8 69 -63
16 11 7	5 27 25	8 35 -36	9 66 -51
0 5 L	6 28 -24	9 58 -50	10 74 59
1 17 17	8 30 33	10 22 22	11 39 40
2 94 104	10 5 L	11 18 14	12 36 -38
3 16 14	0 34 -34	13 18 14	13 22 -19
4 130 -133	2 50 49	14 25 -26	1 6 L
5 10 -8	4 51 -48	15 30 -23	0 21 25
6 142 143	11 5 L	16 30 27	1 28 30
8 80 -77	0 34 35	17 28 28	2 77 -77
9 25 -26	4 19 -18	18 23 -22	3 96 -96
10 21 14	12 5 L	19 18 -15	4 83 83
12 41 37	0 37 34	-5 6 L	5 71 70
13 31 30	2 28 -32	1 65 78	6 78 -74
14 49 -48	13 6 L	2 59 -71	7 38 -42
16 35 33	8 20 20	3 58 -66	8 30 28
17 9 6	9 27 24	4 31 34	9 15 14
1 5 L	10 20 -20	5 22 22	11 23 29
0 143 207	12 6 L	6 37 34	12 26 -29
1 45 57	11 21 -13	7 28 31	13 41 -39
2 94 -95	13 6 L	8 47 -50	14 31 33
4 27 17	12 15 14	9 31 -36	15 31 30
5 44 -41	12 6 L	10 40 44	16 20 -20
6 67 69	5 32 -31	11 35 41	2 6 L
8 107 -93	6 21 18	12 43 -46	0 50 -52
9 16 -14	7 20 16	13 30 -29	1 94 -114
10 60 67	12 20 23	14 24 23	2 36 36
12 36 -39	13 19 18	15 16 13	3 34 27
16 19 25	14 17 -20	-4 6 L	4 22 22
18 16 -21	15 15 -20	1 15 18	5 43 41
2 5 L	11 6 L	2 51 -56	6 65 -58
0 79 80	4 22 -21	3 51 -50	7 79 -66
1 29 26	5 26 -19	4 83 89	8 66 55
2 125 -146	6 28 29	5 86 95	9 52 49
3 99 -99	7 44 37	6 79 -74	10 44 -48
4 142 142	8 41 -32	7 75 -70	11 24 -23
5 29 23	9 34 -34	8 35 42	3 6 L
6 38 -42	10 28 24	9 16 13	0 55 -60
8 21 -15	10 6 L	10 21 18	1 100 -104
9 23 -19	2 45 -42	11 22 17	2 124 125
10 36 35	3 39 -39	12 52 -50	3 68 67
12 65 -58	4 39 36	13 27 -29	4 78 -74
13 16 -9	5 35 30	14 29 26	5 21 -22
14 47 46	6 17 -17	15 42 39	6 17 14
16 20 -24	7 11 -14	16 29 -25	7 32 -31
3 5 L	8 22 -22	17 20 -21	8 19 20
0 64 -67	10 30 36	-3 6 L	9 51 48
1 18 -21	11 21 25	1 69 -75	10 35 -36
3 20 -20	12 23 -28	2 26 29	11 31 -36
4 92 97	13 23 -28	3 22 23	12 45 41
5 29 26	14 18 19	4 47 47	13 24 28
6 125 -128	15 17 18	5 45 39	14 22 -22
7 59 -54	9 6 L	6 67 -66	4 6 L
8 94 74	2 35 -29	7 78 -81	0 31 32
9 20 17	3 30 -28	8 99 99	1 23 -23
10 30 -33	4 44 43	9 65 67	2 25 30
12 17 -9	5 45 45	10 73 -65	3 60 56
14 33 31	6 54 -63	11 33 -33	4 68 -66
16 24 -29		12 20 19	5 83 -77
4 5 L		16 21 -22	6 86 72
0 137 -134		17 19 -16	7 67 56
1 28 -27		18 17 17	8 31 -30
2 103 115		19 17 20	9 24 -25
3 9 -10		-2 6 L	11 11 -8
4 60 -54		1 78 -114	12 21 22
5 13 13		2 135 148	13 21 27
			14 16 -20
			15 20 -23

5 6 L	4 21 -19	5 98 107	1 89 -92
6 75 76	5 75 -69	6 19 -17	2 23 22
1 42 40	6 21 20	7 62 -63	3 81 62
2 43 -45	7 49 45	9 30 28	5 22 -26
3 17 -18	9 14 -17	11 28 25	6 20 19
4 20 19	10 25 -21	13 99 -40	9 19 20
5 18 -18	11 41 -32	15 35 37	11 27 -29
6 24 22	13 48 44	17 22 -23	
7 45 45	15 34 -34		8 7 L
8 55 -55	17 17 17	1 7 L	0 31 26
9 41 -41	19 9 -5	0 15 11	1 18 -18
10 49 52		1 75 -100	3 43 35
11 20 20	-7 7 L	2 37 -32	5 54 -52
12 20 -16	1 67 54	3 25 23	7 43 42
6 6 L	2 25 22	4 14 -16	9 14 -19
0 33 32	4 24 -23	5 40 34	
1 44 40	5 46 -44	7 53 -48	9 7 L
2 64 -61	7 65 56	8 23 21	1 42 40
3 45 -43	9 71 -62	9 75 67	2 19 13
4 66 61	11 43 33	10 14 -15	3 90 111
5 34 33	15 20 -21	11 51 -48	4 34 -33
6 16 -23	17 30 28	13 17 18	5 62 -64
11 26 26	13 20 -23	15 16 -18	6 34 34
12 19 -20	17 15 -18		7 25 25
13 25 -26		-6 7 L	8 12 -10
7 6 L		1 65 59	11 43 -40
0 54 -54		2 20 -16	13 47 46
1 15 -15		3 76 -73	15 29 -30
2 15 -12		4 15 18	
4 45 42		5 33 35	
5 45 34		8 23 -21	
6 51 -40		9 36 -36	
7 54 -47		11 39 34	
8 44 40		12 30 -12	
9 30 23		13 35 -50	
10 19 -18		15 38 32	
8 6 L		16 18 -18	
0 88 -78		-5 7 L	
1 82 -70		1 13 -6	
2 57 49		2 18 -15	
3 45 42		3 47 -46	
4 37 -33		4 14 14	
7 23 -23		5 80 83	
8 22 22		6 17 -11	
9 26 28		7 75 -69	
10 23 -21		9 39 33	
9 6 L		13 41 -36	
0 16 -12		15 31 37	
1 29 -29		17 44 -38	
2 23 23		19 13 14	
3 42 44		-4 7 L	
4 41 -43		1 75 -74	
5 35 -35		2 13 10	
6 25 31		3 63 56	
7 16 16		5 16 -13	
10 6 L		6 15 -12	
0 26 27		7 62 -51	
1 27 25		9 94 84	
2 21 -25		10 38 -31	
5 21 -18		11 69 -65	
6 10 13		13 36 34	
7 21 22		17 16 -19	
11 6 L		19 19 20	
0 21 21		-3 7 L	
1 26 31		1 59 -61	
2 23 -32		2 28 27	
3 21 -25		3 88 96	
4 17 23		4 47 -42	
12 6 L		5 55 -102	
0 15 -17		6 14 16	
2 8 0		7 84 77	
-12 7 L		9 20 18	
7 29 29		11 54 -52	
9 31 -33		13 60 56	
11 28 27		15 43 -43	
-11 7 L		17 15 16	
5 39 36		-2 7 L	
7 16 -18		1 41 43	
11 24 26		2 38 32	
13 31 -30		3 11 16	
15 18 21		4 14 -14	
-10 7 L		5 78 -88	
5 28 33		6 19 -19	
7 51 -55		7 107 110	
9 43 42		9 74 -75	
11 13 -15		10 9 -7	
15 17 21		11 50 47	
17 19 -25		13 18 12	
-9 7 L		15 36 -32	
1 72 -62		17 26 29	
3 63 54		19 10 -22	
5 32 -27		-1 7 L	
8 23 26		1 98 128	
9 32 38		2 44 -50	
10 22 -17		3 79 -89	
11 49 -53		4 18 17	
13 38 33		5 40 38	
-8 7 L		6 8 -8	
1 50 -43		7 24 26	
2 28 26		9 63 -50	
3 78 70		11 77 64	
		13 39 -40	
		15 18 18	
		18 11 -4	
		0 7 L	
		1 29 42	
		2 12 -13	
		3 67 -95	

Tabelle 3. Fortsetzung.

8	26	-26	13	47	-45				7	26	-24				12	47	-45			
9	23	25				9	8	L	8	59	-61		9	9	L	14	23	28		9	10	L
			-1	8	L	1	24	19	9	22	22	0	40	40	16	11	-11	2	22	-23
-10	8	L	2	17	8	3	30	-30	10	41	39	2	25	-28				4	33	39
3	33	37	3	54	-49	5	35	35	12	17	-11	6	17	18		-1	10	L			
4	27	24	4	64	-64	7	19	-16							1	18	-22	10	10	L
9	25	25	5	78	75				-1	9	L		10	9	L	2	29	-33	0	28	-24
11	26	-27	6	47	57		11	8	L	1	28	-30	0	17	17	4	45	50			
13	24	25	7	61	-64	1	36	-28	2	65	-63	2	33	-32	5	47	46		-10	11	L
15	20	-13	8	22	-20	2	26	-23	3	28	26	4	12	29	6	63	-66	5	14	-23
			9	30	28	3	29	28	4	35	37	5	12	-14	7	15	-12	6	16	21
	-9	8	L	10	23	19			5	15	-14				8	58	45	7	12	27
3	27	27	13	26	-24		-11	9	L	6	17	15		11	9	L	9	16	11	8	13	-16
4	29	24	15	26	26	6	24	-23	8	35	-34	0	15	-17	10	23	-26				
5	33	-43	17	21	-25	12	18	-23	9	18	20				12	17	-7		-9	11	L
6	29	-24							10	49	41	-11	10	L	14	21	21	7	15	9
7	33	49		0	8	L	-10	9	L	11	23	-24	8	25	29	16	23	-28	8	15	-17
9	27	-23	1	55	-76	4	21	25	12	42	-40	10	21	-20				9	14	-22
13	25	24	2	46	-48	6	39	-40	13	20	18					0	10	L	10	16	20
15	24	-24	3	28	25	8	36	37	14	20	19	-10	10	L							
			5	20	17	14	16	18				7	8	3		-8	11	L			
	-8	8	L	7	52	-47		-9	9	L		0	9	L	10	21	-27	1	26	-30	2	20	-23
1	38	42	8	32	-30	2	47	42	2	43	-48	12	22	28	12	11	11	2	50	51	3	20	-27
2	36	34	9	62	54	4	22	-21	3	15	11	13	11	11				3	11	10	4	27	31
5	16	-15	10	27	27	8	21	26	4	68	71				4	35	-36	5	27	32
7	31	37	11	38	-40	10	41	-40	5	38	-31		-9	10	L	5	14	15	6	18	-21
9	41	-51	13	25	21	12	31	35	6	57	-58	4	38	-34	6	18	-11	7	16	-19
10	30	-29				14	13	-12	7	12	12	6	42	45	8	34	29	8	33	23	12	20	-14
11	39	44		1	8	L			8	50	47	8	19	-25	9	32	23						
			0	30	17		-8	9	L	11	12	-8	12	14	17	10	48	-46		-7	11	L
	-7	8	L	1	63	-82	2	33	38	12	24	-28	14	14	-20	12	46	39	1	31	-28
1	51	49	2	53	-59	4	45	-50	14	33	33				14	13	-18	4	17	18
2	35	39	3	68	3	5	19	22	16	28	-29		-8	10	L			5	16	24
3	61	-69	4	49	51	6	42	45				2	29	-27		1	10	L	6	23	-22
4	28	-30	5	71	-67	7	20	-17		1	9	L	8	31	-34	0	15	-12	7	26	-28
5	47	48	6	27	-26	8	33	-29	0	55	-68	10	42	45	11	16	13	1	31	-33	8	33	26
10	23	-16	7	27	30	12	29	29	1	5	4	12	31	-26	12	31		2	50	57	9	20	36
11	43	29	8	24	18	14	33	-30	2	45	47							3	34	35	10	23	-20
12	29	18	11	20	-26	15	17	14	3	9	-11		-7	10	L			4	77	-75			
13	35	-38	12	31	-26	16	23	23	4	10	5	1	20	18				5	12	-10		-6	11	L
14	25	-22	13	31	31				5	18	-15	2	47	-52		1	10	L	6	47	52	1	42	-45
15	24	25	14	24	23		-7	9	L	6	32	-29	3	24	-21	0	61	61	7	14	7	2	21	29
			15	25	-25	2	30	-29	7	19	15	4	46	51	8	25	-25	3	50	51
	-6	8	L			4	21	-26	8	63	54	6	18	-24	10	16	-16	4	20	-20
1	27	-29		2	8	L	5	20	20	9	21	-16	10	24	26	11	16	-14	5	23	-22
2	25	-21	0	46	-46	6	44	48	10	54	-51	12	39	-35	12	34	32	6	28	21
3	26	-27	1	31	26	7	17	-12	12	29	28	13	15	-8	13	14	15	8	18	21
4	28	-26	2	26	16	8	47	-52				14	34	33	14	33	-30	9	19	21
5	47	48	4	34	21	9	19	18		2	9	L	16	12	-14			10	20	-23
6	33	38	5	59	-50	10	45	43	0	56	-61					2	10	L	11	23	-28
7	49	-48	6	34	-29	11	19	-15	1	31	30		-6	10	L	0	61	61	12	17	21
8	33	-34	7	61	52	12	18	-18	2	89	96	1	21	-19	1	17	20	13	23	28
9	33	32	8	28	24	16	26	22	3	41	-36	4	51	54	2	21	-21			
11	25	-25	9	46	-45				4	72	-71	5	21	24	3	10	13		-5	11	L
15	27	23	11	34	34		-6	9	L	5	19	19	6	56	-55	4	32	-32	2	24	23
17	22	-25				1	21	-23	6	25	24	7	18	-23	5	31	-29	3	35	37
				3	8	L	2	78	-80	10	37	-33	8	47	49	6	60	49	4	29	-30
	-5	8	L	0	41	-45	3	22	24	12	46	44	9	19	14	7	16	17	5	52	-59
1	64	-67	1	87	90	4	46	40	14	31	-31	10	27	-28	10	43	37	8	66	-58	6	28	31
2	29	-34	2	46	48	5	22	-21				12	9	3	14	9	-12	9	14	-13	7	47	52
3	67	59	3	73	-77	6	17	-17		3	9	L	14	17	18			10	43	37	8	16	-18
5	31	-28	5	29	29	9	17	18	0	44	47					3	10	L	9	16	-18
7	26	-28	9	33	-31	10	25	30	3	24	-20		-5	10	L	C	72	66	10	8	4
9	34	37	10	28	-24	11	18	-16	4	47	-51	1	28	-28	1	29	31	13	13	17
12	30	-24	11	48	43	12	33	-36	5	34	27	2	58	60	2	94	-84	14	12	-12
13	37	31	13	38	-29	13	17	15	6	68	66				3	17	-17	15	11	-20
						14	35	33	7	27	-26	3	17	20	4	49	48			
	-4	8	L		4	8	L		8	68	-55	4	43	-45	6	14	-14		-4	11	L
1	20	-16	0	36	22				9	13	15	5	8	-9	8	25	-24	1	51	46
2	25	-34	3	51	-47		-5	9	L	10	24	25	8	32	32	9	17	-17	2	28	-25
3	47	54	4	30	-27	2	20	-19	14	17	-18	9	17	16	10	37	38	3	44	-36
4	23	29	5	85	78	3	14	12				10	40	-40	12	31	-34	4	11	4
5	79	-88	6	36	37	4	46	49		4	9	L	11	15	-12			5	14	11
6	41	-45	7	55	-50	5	26	-24	C	69	72	12	38	34		4	10	L	6	17	20
7	53	57	8	27	-23	6	66	-75	1	37	-33	13	15	10	1	8	4	7	28	31
8	24	22	12	19	17	7	28	25	2	61	-54	14	23	-20	2	37	-30	8	25	-26
9	32	-31				8	43	43	3	22	22				3	16	-14	9	35	-41
11	24	-25		5	8	L	9	16	-14	4	38	29		-4	10	L	4	62	55	10	29	28
12	26	-26	0	23	20	10	17	-19	8	60	-49	1	15	-11	5	17	19	11	25	25
13	33	30	1	50	-44	14	20	24	10	41	39	2	34	35	6	60	-56	12	16	-15
14	29	25	3	26	23	16	31	-30	11	18	-20	3	14	11	7	22	-23			
15	27	-31	5	25	15	18	13	19	12	17	-19	4	68	-69	8	25	29		-3	11	L
17	24	21	6	31	30							5	25	-24				1	41	39
			7	39	-35		-4	9	L		5	9	L	6	73	65		5	10	L	2	44	-46
	-3	8	L	8	45	-38	1	24	27	0	30	28	7	28	25	0	70	-59	3	50	-47
1	47	56	9	48	46	2	32	46	1	24	-21	8	23	-26	1	26	-19	4	66	59
2	30	34	11	27	-23	3	31	-30	2	44	-39	12	17	25	2	36	33	5	34	34
3	28	-24				4	36	-39	3	24	26	14	29	-27	3	14	11	6	23	-23
4	31	-26		6	8	L	6	18	-14	4	74	61	16	27	24	4	54	-51	7	20	-18
5	19	-18	0	43	40	8	54	51	6	55	-53				6	17	-16	11	23	25
6	36	-36	1	56	-49	9	17	-13	12	26	-24		-3	10	L	7	26	-21	12	19	-19
7	50	44	2	47	-37	10	58	-55				1	15	18	8	34	35	13	22	-29
8	63	65	3	63	59	11	18	15		6	9	L	2	27	-35	9	13	10	14	13	19
9	82	-79	4	36	35	12	32	31	0	51	-48	3	13	-12	10	33	-34	15	14	17
10	47	-37	5	33	-32	14	16	-14	1	18	13	4	7	-8						
11	46	34	11	25	-19	16	18	-10	2	23	20	6	39	36		6	10	L		-2	11	L
12	26	19	12	15	-20				4	25	14	7	26	25	0	43	-32	1	25	-26
13	18	-13					-3	9	L	6	17	-34	8	57	-55	1	23	-22	2	11	-8
				7	8	L	2	67	67	8	44	41	9	18	-15	2	48	47	4	26	30
	-2	8	L	1	25	22	3	42	-41	9	16	-17	10	47	43	3	18	17	5	37	43
1	64	81	2	28	-23	4	72	-68	10	29	-25	11	9	5	4	54	-51	6	35	-31
2	38	46	3	27	24	5	32	27				12	21	-24	5	16	-12	7	46	-49
3	83	-98	4	29	26	6	72	64		7	9	L	16	16	17	6	37	38	8	44	40
4	36	-41	5	34	-24	8	25	-26	C	72	-54					10	20	-19	9	39	35
5	52	56	6	29	-24	10	27	-27	2	67	60		-2	10	L				10	17	-19
6	24	25	7	36	34	12	43	40	4	42	-35	1	21	25		7	10	L	11	13	-18
9	40	-43	9	28	-25	14	41	-40	5	19	17	2	74	-80	C	39	32	15	14	18
						16	20	18	8	15	15	3	11	-15	4	18	-20			
	-3	8	L		8	8	L					4	51	49	6	32	31		-1	11	L
10	22	-37	C	43	-38		-2	9	L		8	9	L	5	17	16	8	25	-29	1	49	-55
			1	71	56	2	26	-28	2	23	20	6	20	-24				2	39	39
	-2	8	L	2	34	25	3	29	-29	4	40	-32	8	16	-15		8	10	L	3	58	52
11	46	45	3	28	-30	4	25	-23	5	14	14	10	43	35	0	58	47	4	16	-18
12	33	29	4	16	-6	5	14	9	6	37	32	11	17	13	2	37	-40	5	27	-27
						6	80	73	8	17	-17				4	15	20	6	8	4

Tabelle 3. Fortsetzung.

8	17	19	8	21	-19	8	26	-24	10	18	21		4 11 L		4	34	-31		7 11 L						
9	34	34	9	13	-13	9	33	-38	11	25	31	C	51	-4C	5	42	-42	0	35	23					
10	21	-21	10	8	7	10	26	26	12	15	-18	1	59	-53	6	24	24	1	40	36					
11	35	-38	11	14	-15	11	19	21				2	25	27	7	25	23	2	33	-29					
12	23	26	13	21	22	12	14	-14				3	40	31	8	11	-13	3	31	-30					
13	19	22							3 11 L			7	35	-26	10	9	-3	4	27	24					
			1 11 L			2 11 L			0	31	-25	8	13	10					8 11 L						
	0 11 L		0	38	43	0	29	25	3	26	-24	9	32	30		6 11 L		3	22	-20					
1	16	-16	1	44	32	1	65	62	4	23	20	10	20	-21	0	33	25	4	18	18					
2	26	24	2	36	-40	2	61	-54	5	54	46	11	15	-17	1	14	17	6	14	-20					
3	59	54	3	1C	-4	3	64	-57	6	36	-31				2	13	-16								
4	43	-39	4	11	11	4	47	44	7	45	-41		5 11 L		5	15	-17		9 11 L						
5	7C	-6C	5	32	-30	5	3C	29	8	15	21	1	42	-31	6	12	12	C	25	-27					
6	42	41	6	17	18	6	27	-26	9	19	19	2	24	22	7	25	26	1	22	-25					
7	37	37	7	3C	37	9	20	-20				3	47	40	9	16	-22	3	13	10					

die Strukturbestimmung zur Verfügung stehende Reflexmaterial bestand aus den Schichten $h0l - h11l$ mit einer Gesamtzahl von 2.619 unabhängigen Reflexen. Für die Berechnung der Strukturfaktoren wurden das Programm DATA P2 [7] und die Atomformfaktoren von Cromer und Waber [6] benützt, wobei gleichzeitig die Korrektion für anormale Dispersion vorgenommen wurde. Anschliessend erfolgte eine Verfeinerung nach der Methode der kleinsten Fehlerquadrate mit isotropen Temperaturfaktoren nach dem Programm LALS.[7] Der Zuverlässigkeitsindex $R = [\sum||F_{beob}(hkl)| - |F_{ber}(hkl)||/\sum|F_{beob}(hkl)|]$ betrug nach mehreren Zyklen 0,125. Die Absorptionskorrektion ergab praktisch keine Verbesserung des Resultates, was dadurch erklärt wird, dass der verwendete Kristall einerseits klein war und beinahe Würfelform besass, andererseits der Absorptionsfaktor wegen der leichten organischen Liganden recht gering ist ($\mu = 171$ cm^{-1}). Die abschliessende anisotrope Verfeinerung nach dem Blockdiagonalprogramm LALS [7] ergab einen endgültigen Unzuverlässigkeitsindex $R = 0{,}106$. Die Tabelle 2 enthält die Atomlagen und die thermischen Parameter mit den Standardabweichungen, während in Tabelle 3 sämtliche beobachteten und berechneten Strukturfaktoren einander gegenübergestellt sind.

DISKUSSION DER STRUKTUR UND VERGLEICH MIT DER β-PHASE

Die aus den Atomlagen berechneten Atomabstände und Winkeln mit den Standardabweichungen sind in Tabelle 4 zusammengefasst. Die Bezeichnung der Sauerstoff- und Kohlenstoffatome in den vier Ligandringen geht aus der Abb. 2 hervor und ist die gleiche, wie sie

Tabelle 4. Abstände und Winkel in den Ligandringen.

(a) Abstände (in Å)				(b) Winkel (in °)			
Ce–O1	2,33(1)	O1–C2	1,26(2)	O1–Ce–O2	72,0(5)	O5–Ce–O6	73,4(5)
Ce–O2	2,32(1)	O2–C4	1,26(2)	O3–Ce–O4	71,4(5)	O7–Ce–O8	71,8(5)
Ce–O3	2,33(1)	O3–C7	1,19(3)				
Ce–O4	2,35(1)	O4–C9	1,23(3)	Ce–O1–C2	135(1)	O1–C2–O8	127(2)
Ce–O5	2,37(1)	O5–C12	1,25(3)	Ce–O2–C4	134(1)	O2–C4–C3	126(2)
Ce–O6	2,30(1)	O6–C14	1,29(3)	Ce–O3–C7	140(1)	O3–C7–C8	122(2)
Ce–O7	2,32(1)	O7–C17	1,30(2)	Ce–O4–C9	137(1)	O4–C9–C8	125(2)
Ce–O8	2,31(1)	O8–C19	1,33(2)	Ce–O5–C12	130(1)	O5–C12–C13	128(2)
				Ce–O6–C14	134(1)	O6–C14–C13	126(2)
C2–C3	1,39(3)	C1–C2	1,54(3)	Ce–O7–C17	136(1)	O7–C17–C18	126(2)
C4–C3	1,44(3)	C4–C5	1,56(4)	Ce–O8–C19	134(1)	O8–C19–C18	125(2)
C7–C8	1,47(3)	C6–C7	1,46(3)				
C9–C8	1,42(4)	C9–C10	1,53(4)	C2–C3–C4	120(2)	C12–C13–C14	122(2)
C12–C13	1,43(3)	C11–C12	1,54(3)	C7–C8–C9	122(2)	C17–C18–C19	125(2)
C14–C13	1,35(3)	C14–C15	1,50(3)	C1–C2–C3	118(2)	C11–C12–C13	120(2)
C17–C18	1,42(3)	C16–C17	1,45(3)	C3–C4–C5	117(2)	C13–C14–C15	118(2)
C19–C18	1,35(3)	C19–C20	1,50(4)	C6–C7–C8	113(2)	C16–C17–C18	122(2)
				C8–C9–10	120(2)	C18–C19–C20	123(2)
O1–O2	2,73(2)	O5–O6	2,79(2)				
O3–O4	2,74(2)	O7–O8	2,72(2)				

Tabelle 5. Atomabstände im Antiprisma [a] mit den von Matković und Grdenić [1] veröffentlichten Werten in Klammern (bezüglich der Bezeichnungen siehe Abb. 2).

		s_r		l		
Ce–O1	2,33(2,40)	O1–O2	2,73(2,87)	11	O2–O3	2,85(2,91)
Ce–O2	2,32(2,39)	O3–O4	2,74(2,80)	12	O1–O3	2,88(2,78)
Ce–O3	2,33(2,36)	O5–O6	2,79(2,77)	13	O1–O5	3,25(3,06)
Ce–O4	2,35(2,37)	O7–O8	2,72(2,80)	14	O8–O5	2,99(2,94)
Ce–O5	2,37(2,38)			15	O8–O6	2,82(2,72)
Ce–O6	2,30(2,40)	s		16	O6–O7	2,75(2,81)
Ce–O7	2,32(2,43)	O1–O8	2,74(3,05)	17	O7–O4	3,24(3,24)
Ce–O8	2,31(2,43)	O2–O7	2,80(3,05)	18	O2–O4	3,01(3,10)
		O3–O5	2,78(2,84)			
		O4–O6	2,74(2,92)			

[a] Die Standardabweichungen betragen 0,01 Å für die Abstände Ce–O und 0,02 Å für die Abstände O–O.

von Matković und Grdenić [1] verwendet wurde. Vergleicht man die von diesen Autoren gegebenen Abstände mit den hier vorliegenden, so findet man nicht selten erhebliche Differenzen, wie auch aus Tabelle 5 entnommen werden kann, die die Abmessungen im Antiprisma enthält. Es wurden alle Abstände und Winkel für eine Formeleinheit angeführt, da aufgrund des umfangreichen Reflexmateriales die Standardabweichungen (σ) im Allgemeinen etwa 3–4 mal kleiner sind, als bei der früher veröffentlichten β-Phase des Urans und des Cers.[3,4] Im Gegensatz dazu sind jedoch die Abstandsunterschiede für ein und denselben Bindungstyp oft erheblich grösser. Studiert man die Atomabstände für die Ligandringe des α- und β-CeA_4 und stellt Vergleiche an, so kommt man zu dem Resultat, dass alle Unterschiede soweit vorhanden für den gleichen Bindungstyp innerhalb der Standardabweichungen liegen. Dies trifft nur teilweise für die Atomabstände im Archimedischen Antiprisma d.h. für die Sauerstoffkonfiguration um das Zentralatom zu. Die gefundenen Abstände in den beiden Quadraten sind praktisch gleich gross (vergleiche in Tabelle 5 mit Abb. 2). Die Werte für s und s_r sind hier gemeint, was also bedeutet, dass die Realstruktur kaum oder nur sehr wenig vom Ideal abweicht. Dies bedeutet hier, dass die von Liganden umspannten Seiten nicht verkürzt wurden. Nicht zuletzt wird das auch durch den kleinen Winkel, den die beiden Quadrate im Antiprisma miteinander einschliessen, er beträgt nur 1,5°, dokumentiert. Im Gegensatz hierzu zeigen die übrigen Kantenlängen im Archimedischen Antiprisma (nämlich $l1-l8$) verhältnismässig grosse Abweichungen (bis zu 0,5 Å). Bei dieser Gelegenheit kann festgestellt werden, dass diese geringeren Standardabweichungen von erheblicher Bedeutung sind, da sie sichere Schlüsse über Differenzen von Atomabständen erlauben.

Abschliessend wird der Versuch unternommen, die Grundkonzeption für das Bauprinzip und deren Unterschiede für die beiden Phasen zu skizzieren. Man kann sagen, dass es die unterschiedliche Deformation der Formeleinheiten im Kristallgitter ist, die letztlich zur Existenz zweier verschiedener Phasen führt.

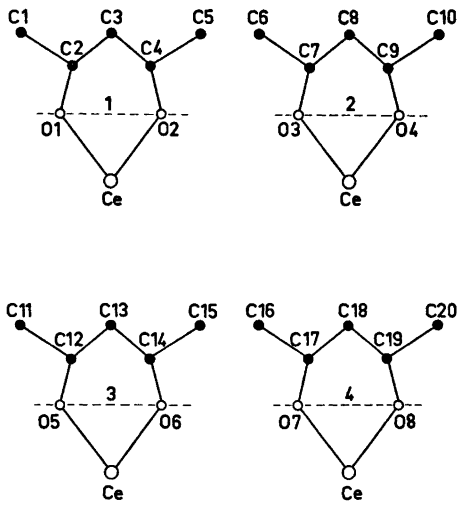

Abb. 3. Die Bezeichnung der Atome in den vier Ligandringen samt deren Abwinkelung. Sie beträgt: 15,9, 11,8, 16,9 und 19,6° für Ligand 1, 2, 3 und 4.

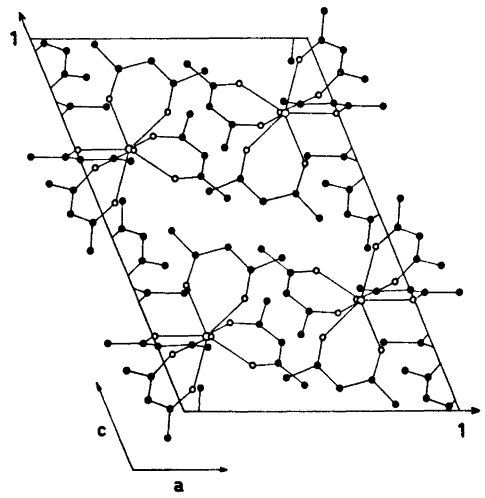

Abb. 4. Die Projektion einer Elementarzelle auf *ac* (○ Cer, o Sauerstoff, ● Kohlenstoff).

Mit Deformation wird die bereits vorher beschriebene Abwinkelung der Ligandringe um eine gedachte Verbindungslinie Sauerstoff-Sauerstoff gemeint. Abbildung 3 auf Seite 407 in Lit. 3 und Abbildung 2 auf Seite 414 in Lit. 4 veranschaulichen die typischen Merkmale der β-Phase. Die Abwinkelung je zweier Ligandringe zueinander resultiert in einer «zusammengepressten« Formeleinheit, die beinahe doppelt so lang als breit ist. In der erstgenannten Abbildung sieht man die Verzahnung der Formeleinheit zum Kristallgitter. In der vorliegenden Arbeit ist in Abbildung 4 der Versuch gemacht worden, das davon so verschiedene α-CeA_4, dessen Liganddeformation aus Abbildung 1 hervorgeht, in einer Elementarzelle durch Projektion auf $a-c$ zu zeigen. Man sieht leicht, dass hier die α-CeA_4-Formeleinheit eine runde, sperrige Form angenommen hat. Man kann annehmen, dass die beiden Phasen betreffend ihres Energieinhaltes weitgehend identisch sind, wodurch auch die eingangs erwähnte Kristallisation aus dem gleichen Lösungsmittel unter nahezu gleichen Bedingungen erklärt werden kann.

Der Verfasser dankt dem Schwedischen Naturwissenschaftlichen Forschungsrat für die Bereitstellung von finanziellen Mitteln (Kontrakt Nr. 2527). Dem Vorstand des Institutes für Anorganische Chemie Prof. Georg Lundgren sei hier für sein grosses Interesse und wertvolle Kritik herzlichst gedankt.

LITERATUR

1. Matković, B. und Grdenić, D. *Acta Crystallogr. 16* (1963) 456.
2. Silverton, J. V. und Hoard, J. L. *Inorg. Chem. 2* (1963) 243.
3. Titze, H. *Acta Chem. Scand. 23* (1969) 399.
4. Titze, H. *Acta Chem. Scand. 24* (1970) 405.
5. Lindquist, O. und Wengelin, F. *Ark. Kemi 28* (1967) 179.
6. Cromer, D. T. und Waber, J. T. *Acta Crystallogr. 18* (1965) 104.
7. Am Institut f. Anorg. Chemie modifiziert: DATAP 2 von Coppens, P., Leiserowitz, L. und Rabinovich, D., LALS von Gantzel, P., Sparks, R. und Truebold, K. und DISTAN von Zalkin, A.

Eingegangen am 10. Juni 1974.

Acta Chemica Scandinavica A 28 (1974) 1089—1100

The Complex Formation of Antimony(III) in Perchloric Acid and Nitric Acid Solutions. A Solubility Study

STEN AHRLAND[a] and JAN-OLOV BOVIN[b]

[a]Inorganic Chemistry 1 and [b]Inorganic Chemistry 2, Chemical Center, University of Lund, P.O.B. 740, S-220 07 Lund 7, Sweden

The hydrolysis of antimony(III) in perchloric and nitric acid solutions has been investigated by solubility measurements at an ionic strength $I = 5.00$ M and a temperature of 25.0 °C.

In perchloric acid solutions the complexes $Sb(OH)_2^+$ and $Sb_2(OH)_2^{4+}$ exist in equilibrium with orthorhombic and cubic Sb_2O_3. The oxides are metastable for acidities over 0.26 M and 0.68 M, respectively, where $Sb_4O_5(OH)ClO_4 \cdot \frac{1}{2}H_2O$ is the stable phase. The monomer $Sb(OH)_2^+$, but not the dimer $Sb_2(OH)_2^{4+}$, is also found in equilibrium with this phase.

The only solid phase in equilibrium with nitric acid solutions of an acidity below 5.00 M is the oxide nitrate $Sb_4O_4(OH)_2(NO_3)_2$. Besides the complex $Sb(OH)_2^+$ also found in the perchloric acid solutions, the monomer $Sb(OH)^{2+}$ appears to be present.

On account of the strongly acidic properties of antimony(III), its chemistry in aqueous solution is very much dominated by hydrolytic reactions which have to be taken into account in all studies of its complex formation. Unfortunately, the course of the hydrolysis has not yet been clarified, not even in those instances where the anions present in the medium show little affinity for antimony(III) and therefore do not bring about any extensive formation of mixed complexes. Weakly complexing media should be provided by, *e.g.*, the perchlorate and nitrate ions, while the halide ions certainly form quite strong complexes. This investigation concerns the hydrolytic reactions taking place in solutions of the weakly complexing anions mentioned above.

The hydrolysis of antimony(III) has been previously studied,[1–5] mostly by the use of solubility measurements. Schuhmann [1] concluded from a study of the solubility of orthorhombic Sb_2O_3 in perchloric acid of molality between 0.231 and 1.133 that the species present in solution is SbO^+ and he calculated the constant for the corresponding equilibrium $\frac{1}{2}Sb_2O_3(s) + H^+ \rightleftharpoons SbO^+ + \frac{1}{2}H_2O$ (Table 7). Gayer and Garrett [2] found that the same equilibrium is established in hydrochloric acid of molality up to 0.1. Furthermore the value of the equilibrium constant is comparable for the two media (Table 7). Fridman *et al.*[4] verified Schuhmann's result from solubility measurements in perchloric acid. They also investigated the solubility of SbOCl in solutions of $HClO_4$ and NaCl at 25 °C and constant ionic strength $I = 6$ M (regulated by means of $NaClO_4$) and found the complexes $SbCl_5^{2-}$, $SbCl_4^-$ and $SbOHCl_3^-$. Jander and Hartmann [5] found from diffusion measurements that only monomeric SbO^+ and possibly small amounts of Sb^{3+} are present in perchloric acid solutions up to $C_H = 6$ M when the concentration of Sb(III) is ≤ 1 mM.

The present investigation started as a study of the solubility of the orthorhombic and cubic modifications of Sb_2O_3 in perchloric and nitric acid solutions of constant ionic strength, $I = 5.00$ M, maintained by sodium perchlorate and sodium nitrate, respectively. At the temperature of the measurements (25.0 °C) the orthorhombic modification, Sb_2O_3(or), is metastable but the transition into the stable cubic modification, Sb_2O_3(c), does not take place in aqueous solution. In practice, the transition is conveniently effected in the solid state at 550 °C; *cf.* below. Above 570 °C, Sb_2O_3(or) is the stable modification.

Though no conversion takes place between

the oxide modifications, phase transitions are nevertheless observed. In perchloric acid, Sb_2O_3(or) is in fact stable only up to $C_H \approx 0.3$ M and Sb_2O_3(c) up to $C_H \approx 0.7$ M at the present total perchlorate concentration of 5.00 M. Both survive long enough, however, for metastable equilibria to be established even at acid concentrations up to $C_H = 4.0$ and 4.5 M, respectively. The stable phase formed at the transition is an oxide perchlorate $Sb_4O_5(OH)ClO_4 \cdot \frac{1}{2}H_2O$. A structure determination of this compound has been performed by Bovin [6] and has confirmed the above composition. At the highest acid concentrations used, $C_H = 4.50$ and 5.00 M, another perchlorate can be obtained as an intermediary metastable phase. Its empirical formula is $3Sb_2O_3.2Cl_2O_7.6H_2O$,[5] thus, as expected, corresponding to a less strongly hydrolyzed state of antimony(III) than in the former compound. This is immediately evident from the mol ratios perchlorate/antimony, Q_P, which are $Q_P = 1/4$ and 2/3 for the two phases, respectively, while a completely unhydrolyzed perchlorate would have $Q_P = 3$. The more hydrolyzed phase will, in the following, be denoted by Sbop(70) and the less hydrolyzed one by Sbop(55), the notation deriving from the antimony content (≈ 70 % and ≈ 55 %, respectively). The phase Sbop(70) can also exist in metastable equilibrium at lower values of C_H, where the oxides are the stable phases.

In order to investigate whether further transitions occur at higher acidities, resulting in compounds of even lower degrees of hydrolysis of antimony(III), the measurements have been extended to include concentrated perchloric acid, $C_H = 11.75$ M. In this higher acidity range a constant medium could not be maintained, so that identification of the species present in the solutions has not been possible. Further phase transitions have been observed, however. Besides Sbop(55), which only seems to exist as a metastable intermediate around $C_H = 5.00$ M, at least two more oxide perchlorates have been firmly identified. Thus, between $C_H = 6.7$ M and concentrated acid, $Sb(OH)_2ClO_4.H_2O$ [denoted Sbop(44)], with $Q_P = 1$, is the stable phase. In concentrated acid, an undoubtedly even less hydrolysed phase is stable. On account of the latter's extreme sensitivity to moisture, it has so far not been possible to determine its composition. The structures of these relatively little hydrolysed compounds might have features of relevance to the interpretation of the equilibria existing in solution. Efforts will therefore be made to determine the structures, although this will, particularly in the case of the least hydrolyzed compound, present great experimental difficulties.

In nitric acid at a nitrate concentration of 5.00 M, Sb_2O_3(or) and Sb_2O_3(c) are even less stable than in the perchloric acid solutions discussed above and they are transformed into an oxide nitrate of the composition $Sb_4O_4(OH)_2(NO_3)_2$, denoted in the following by Sbon. The transformation is, moreover, so fast that the oxides do not survive as metastable phases for any appreciable length of time. The mol ratio nitrate/antimony of Sbon is $Q_P = 1/2$, which means a degree of hydrolysis intermediate between Sbop(70) and Sbop(55). No other oxide nitrate has been observed up to $C_H = 5.00$ M, the highest concentration employed in the nitric acid measurements. The phase Sbon can also exist in metastable equilibrium with solutions of quite low acidity, at least down to $C_H = 0.005$ M. The crystal structure of $Sb_4O_4(OH)_2(NO_3)_2$ has been determined by Bovin [7] and has confirmed the composition.

NOTATIONS AND CALCULATIONS

Notations. The following symbols are used

S = total concentration of Sb(III)
C_H = total concentrations of hydrogen ions
S_i = concentration of the complex $Sb_l(OH)_p^{(3l-p)+}$
K_i = the calculated coefficient in the polynomial $\sum_i K_i C_H^{e_i}$
e_i = the calculated exponent in the polynomial $\sum_i K_i C_H^{e_i}$
K_i' = stability constant for complex formation
ΔG° = standard free energy change
$\mu(B)$ = chemical potential of the substance B
$a(B)$ = activity, relative activity of substance B
i to q are all integers

Calculation of complex formation. The solid phases considered in the solution equilibria here are Sb_2O_3(or), Sb_2O_3(c), $Sb_4O_5(OH)ClO_4 \cdot \frac{1}{2}H_2O$ and $Sb_4O_4(OH)_2(NO_3)_2$. In order to achieve the simplest formulation possible, the general formula $Sb_4O_{(6-j)}(OH)_j(Z)_j$, with $j = 0$, 1, 2 and $Z = ClO_4^-$

or NO_3^-, is employed in the following for these phases. The equilibria can thus be written as

$$k\mathrm{Sb_4O_{(6-j)}(OH)_j(Z)_j(s)} + m\mathrm{H^+} \rightleftharpoons n\mathrm{Sb_l(OH)_p^{(3l-p+)}} + q\mathrm{H_2O} + kj\mathrm{Z^-}$$

with $m = n(3l-p) - kj$ (1)

and $4k = nl$ (2)

Elimination of k by combination of (1) and (2) gives

$$m/n = 3l - p - lj/4 \quad (3)$$

Since the activities of H_2O and Z^- may be considered as constant in the media employed and since $[H^+] \approx C_H$, an equilibrium constant K_i' can be defined as follows:

$$K_i' = \frac{[\mathrm{Sb_l(OH)_p^{(3l-p)+}}]^n}{[\mathrm{H^+}]^m} \approx \frac{(S_i)^n}{C_H{}^m} \quad (4)$$

and hence

$$S_i = (K_i')^{1/n} C_H{}^{m/n} \quad (5)$$

The total concentration of Sb(III) in solution may be written as

$$S = \sum_i l_i S_i \quad (6)$$

(5) and (6) gives

$$S = \sum_i l_i (K_i')^{1/n} C_H{}^{m/n} \quad (7)$$

and

$$S = \sum_i K_i C_H{}^{e_i} \quad (8)$$

if

$$K_i = l_i (K_i')^{1/n} \quad (9)$$

and

$$m/n = e_i \quad (10)$$

From an experimental determination of S as a function of C_H it is clearly possible to derive the exponents e_i and the coefficients K_i. Each e_i-value allows several combinations of l and p in the complex $\mathrm{Sb_l(OH)_p^{(3l-p)+}}$. However, when the solubility S is measured for different solid phases, as is the case in this investigation, the number of combinations become more restricted. The calculation of e_i and K_i has been made both graphically and by a computer. When the e_i values are known it is possible to compute connected values of l and p from (10) and (3), since the value of j for the solid phase is known.

The graphical treatment was carried out in the following way: From the graph $S = f(C_H)$ (*cf.* Figs. 3, 8) it is obvious that the polynomial (8) must contain a constant term K_1, *i.e.* $e_1 = 0$. The numerical value of K_1 was determined by a graphical extrapolation to $C_H = 0$. This value is not identical with the solubility of the particular solid phase in 5.00 M sodium perchlorate and sodium nitrate solution, the latter being found by direct measurements to be about twice as high (*cf.* Table 3). For $C_H < 0.005$ M other reactions resulting in a higher solubility evidently occur. In the following K_1 and e_1 are therefore treated as mathematical constants. Eqn. (8) can be written as

$$S - K_1 = \sum_{i-1} K_{i-1} C_H{}^{e_{i-1}} \quad (11)$$

which for low values of C_H can be approximated to

$$S - K_1 \approx K_2 C_H{}^{e_2} \quad (11')$$

Hence

$$\ln (S - K_1) = e_2 \ln C_H + \ln K_2 \quad (11'')$$

A plot of $\ln (S-K_1)$ *versus* $\ln C_H$ should yield e_2 as the slope and $\ln K_2$ as the intercept of a straight line. When the values of e_2 and K_2 are known eqn. (8) can be written as

$$S - K_1 - K_2 C_H{}^{e_2} = \sum_{i-2} K_{i-2} C_H{}^{e_{i-2}} \quad (12)$$

or, if terms of $i > 3$ are neglected as

$$S - K_1 - K_2 C_H{}^{e_2} \approx K_3 C_H{}^{e_3}. \quad (12')$$

It is then possible to determine the constant e_3 in the same way as e_2. Within the range of C_H investigated, the polynomial (8) could in fact be fitted with at most three terms.

In the computer treatment, a curve of the form $S = \sum_i K_i C_H{}^{e_i}$ was fitted to the experimental data $((C_H)_r, S_r)$ by the least-squares program CURVEFIT.[8] The error square sum

$$\mathrm{CHISQ} = \sum_i \frac{1}{\sigma S_r} (S_{\mathrm{calc},r} - S_r)^2 \quad (13)$$

was minimized by the subroutine STEPIT,[9] where

$$S_{\mathrm{calc},r} = \sum_i K_i (C_H)_r{}^{e_i} \quad (14)$$

The least-squares treatment was first made with $e_1 = 0$ and with e_{i-1} and K_i as variables. Because the value of e_i must be rational, the nearest rational value was then chosen and kept con-

stant in a subsequent refinement cycle which yield the final values of the constants K_i.

EXPERIMENTAL

Chemicals. Orthorhombic antimony(III)oxide [Sb_2O_3(or)] was prepared from Sb_2O_3 (Riedel-DeHaen *p.a.*) as follows. The oxide was dissolved in concentrated hydrochloric acid. After filtration, a sixfold volume of water was added to the solution. After three days in the mother liquor, the crystalline precipitate formed was separated and dissolved in a minimum amount of concentrated hydrochloric acid. This solution was then poured into a boiling solution of sodium carbonate. The Sb_2O_3(or) obtained was washed free of chloride ions with hot water and then dried at 110 °C. The antimony(III) content was checked (see below; found: 83.3 %, calc. for Sb_2O_3: 83.5 %) and a Guinier-Hägg powder photograph was taken to verify the orthorhombic phase.

Cubic antimony(III)oxide [Sb_2O_3(c)] was prepared from Sb_2O_3(or) as follows. A thick-walled glass tube was filled with Sb_2O_3(or), evacuated and heated to 550 °C. After 24 h the transformation to Sb_2O_3(c) was complete.[10] The antimony(III) content was checked (found: 83.3 %, calc. 83.5 %) and a Guinier-Hägg powder photograph verified the cubic phase.

During the investigation it was found accidentally that Sb_2O_3(c) could in fact be prepared at room temperature by washing of the metastable phase Sbop(55) with methanol. On prolonged treatment, all perchlorate is displaced and pure Sb_2O_3(c) is obtained.

All other chemicals used were *pro analysi* grade.

Procedure. The equilibrium of solid phase and solution was effected in 50 ml polyethylene flasks agitated in a thermostat at 25.0 °C. The agitation time varied between a few hours and more than two hundred days. (*cf.* below). Afterwards, the phases were separated within a few seconds by filtration through a membrane filter. Only the solid phases Sb_2O_3 (or and c) and Sbop(70) were washed with 5 ml methanol (*cf.* above) and dried. The other solid phases were only dried. The solution was immediately analysed for antimony(III).

Analysis. The solid phases, as well as the perchloric acid solutions with $C_H \geq 0.250$ M, were analysed for antimony(III) titrimetrically. The procedure employed was that described by Belcher,[11] Schulek and Rózsa,[12] and Schulek.[13] This method was not applicable to the nitric acid solutions. In this case, as well as for the perchloric acid solutions with $C_H \leq 0.250$ M, where the concentration of antimony(III) was very low, the analyses were performed spectrophotometrically with a Zeiss Spectrophotometer PMQII at 330 nm, by the method described by Elkind, Gayer and Baltz.[14] It was checked that Beer's law was obeyed (to within ± 3.0 %) for absorbances between 0.2 – 1.5. Both analytical methods were suitable for the measurement of the solubility in 250 mM perchloric acid and gave the same result within the limits of error. At least two samples were equilibrated with each solution. The solubilities could all be reproduced to within ± 3 %. The lower limit of $C_H = 0.0052$ M, was chosen for the reason that at lower acidities the solubility becomes too low even for the sensitive spectrophotometric method of analysis. Almost all solid phases were checked after equilibration by Guinier-Hägg X-ray photographs.

The 5.00 M stock solutions of sodium perchlorate and sodium nitrate were analyzed both by cation exchange and be weighing a dried sample, with concordant result. The C_H values of all perchloric and nitric acid solutions were checked alkalimetrically.

MEASUREMENTS AND RESULTS

Phase transformation in perchloric acid. In order to determine the time necessary to establish the various metastable and stable equilibria existing in perchloric acid solutions, Sb_2O_3(or) was shaken at $C_H = 3.00$ M and 5.00 M, and Sb_2O_3(c) at $C_H = 5.00$ M for a length of time varying from 5 min to more than 200 days (*cf.* Fig. 1). In 5.00 M acid, Sb_2O_3(or) never reached equilibrium before a transformation set in. For several hours the solid phase is a mixture

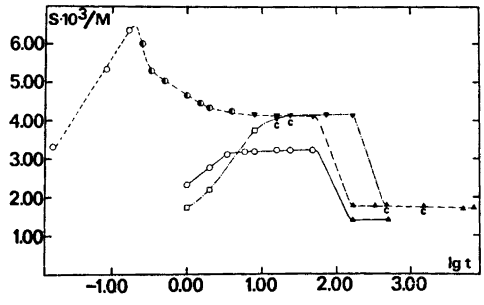

Fig. 1. The solubility of antimony(III) in perchloric acid as a function of agitation time. The lines refer to the following initial solid phases and concentrations of acid: A. Sb_2O_3(or) and $C_H = 5.00$ M, – – –. B. Sb_2O_3(or) and $C_H = 3.00$ M, —. C. Sb_2O_3(c) and $C_H = 5.00$ M, —·—. The solid phases observed in contact with the solutions are denoted as follows: ○ Sb_2O_3(or); □ Sb_2O_3(c); ◐ a mixture of Sb_2O_3(or) and Sbop(55); ▼ Sbop(55); ▲ Sbop(70). Where the curves A and C coincide, the letters C indicate that the points ▼ and ▲ originate from Sb_2O_3(c).

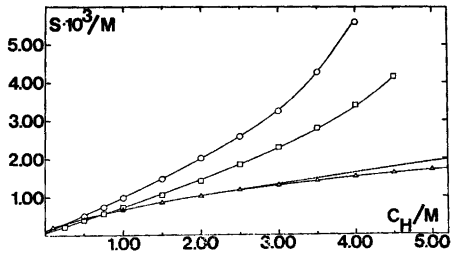

Fig. 2. The solubility of antimony(III) in perchloric acid solutions, at $I = 5.00$ M, up to $C_H = 5.00$ M. The symbols refer to the solid phases: ○ Sb_2O_3(or), □ Sb_2O_3(c) and △ Sbop-(70). The dotted line refers to the computed polynomial, S_{calc}, for Sbop(70).

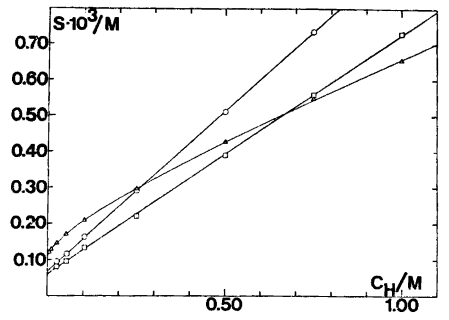

Fig. 3. The solubility of antimony(III) in perchloric acid solutions, at $I = 5.00$ M, up to $C_H = 1.00$ M. The symbols refer to the solid phases: ○ Sb_2O_3(or), □ Sb_2O_3(c) and △ Sbop-(70).

of Sb_2O_3(or) and Sbop(55), as evidenced both by determination of the antimony content and by Guinier-Hägg powder photographs. The phase Sbop(55) is then in metastable equilibrium for about 2 days. Transformation to the stable phase Sbop(70) then begins, being complete after a week or more. Transformation of Sb_2O_3(c) to Sbop(55) takes place long before the equilibrium with Sb_2O_3(c) has been attained. In this case, the metastable equilibrium involving Sbop(55) is therefore attained from below saturation (*cf.* Fig. 1). After another few days, the final transformation into the stable phase Sbop(70) begins. Some fifteen days later the transformation is complete and the solution has attained equilibrium. In 3.00 M acid, Sb_2O_3(or) remains unchanged for at least thirty hours, which is time enough for a metastable equilibrium to be established. The transformation to Sbop(70) then begins and after fourteen days the equilibrium between the stable phase Sbop(70) and the solution has been attained. There is no evidence for a phase transformation from Sb_2O_3(or) *via* Sb_2O_3(c) to Sbop(70).

Solubility of Sb_2O_3(or) and Sb_2O_3(c) in perchloric acid. The solubilities of Sb_2O_3(or) and Sb_2O_3(c) in perchloric acid of varying concentration are given in Figs. 2 and 3. Between $C_H =$ 1.00 and 4.50 M, where both oxides are metastable, the agitation time was 24 – 30 h. Between $C_H = 0.250$ and 1.00 M the time could be extended up to eighty days without any transformation. Below $C_H = 0.68$ and 0.26 M, respectively, Sb_2O_3(c) and Sb_2O_3(or) are stable relative to Sbop(70). For $C_H > 4.00$ M the solubility of Sb_2O_3(or) cannot be determined, because the transformation to Sbop(70), mostly *via* Sbop-(55), is too rapid. The same is true for Sb_2O_3(c) when $C_H > 4.50$ M.

From eqn. (14), values of $e_2 = 1.0$ and $e_3 = 3.9$ were computed for Sb_2O_3(c), and 1.0 and 4.1 for Sb_2O_3(or), by means of the CURVEFIT-program. The least-squares treatment was repeated using the nearest integers $e_2 = 1$ and $e_3 = 4$. The calculated constants K_i and integer exponents e_i are given in Table 1. For both oxides the graphical treatment gives $e_2 = 1.0$ as the slope of the function $f(\ln C_H) = \ln (S - K_1)$ for $C_H < 3.0$ M (*cf.* Fig. 4). In Fig. 5, the function $f(\ln C_H) = \ln (S - K_1 - K_2 C_H^{e_2})$ is plotted for $1.5 < C_H < 5.00$ M and the slopes of the curves give $e_3 = 4.0$ for both oxides. The relative differences between calculated and experimental data are given in Table 2.

As $j = 0$ for Sb_2O_3(s), eqns. (3) and (10) give $e_i = m/n = 3l - p$, *i.e.* in this case the values of e_i yield directly the charges of the complexes formed, *viz.* +1 and +4. Explicitly

$$1 = 3l - p \qquad (3^{I})$$

$$4 = 3l - p \qquad (3^{II})$$

The only mononuclear complex with charge 1+ is $Sb(OH)_2^+$, but all polynuclear complexes $Sb(OH)_2(Sb(OH)_3)_{l-1}^+$ also fulfil the condition. No mononuclear complex with the charge 4+ is feasible, but all polynuclear species of the composition $Sb_2(OH)_2(Sb(OH)_3)_{l-2}^{4+}$ do fit. In the simplest case the equilibrium would involve the dinuclear complex $Sb_2(OH)_2^{4+}$:

$$Sb_4O_6(\text{or or c}) + 8H^+ \rightleftharpoons 2Sb_2(OH)_2^{4+} + 2H_2O$$

Table 1. The factors K_i and exponents e_i in the polynomial S_{calc}, calculated by a least squares computer program. The standard deviation in S was found to be approximately $S/100$. The numbers in parentheses are the standard deviations calculated by the least-squares program and refer to the last significant digit in each value. The polynomial is: $S_{calc} = K_1 + K_2 C_H^{e_2} + K_3 C_H^{e_3}$.

Solid phase Factors and exponents	Sb_2O_3(or)	Sb_2O_3(c)	$Sb_4O_5(OH)ClO_4 \cdot \frac{1}{2}H_2O$	$Sb_4O_4(OH)_2(NO_3)_2$
K_1	$0.705(3) \times 10^{-4}$	$0.621(2) \times 10^{-4}$	$0.1105(5) \times 10^{-3}$	$0.747(8) \times 10^{-4}$
K_2	$0.880(3) \times 10^{-3}$	$0.660(2) \times 10^{-3}$	$0.541(1) \times 10^{-3}$	$0.432(3) \times 10^{-3}$
e_2	1	1	3/4	1/2
K_3	$0.742(8) \times 10^{-5}$	$0.278(4) \times 10^{-5}$	–	$0.601(9) \times 10^{-4}$
e_3	4	4	–	3/2

In Table 4, a survey of the complexes compatible with the values of m/n is given.

The solubility of $Sb_4O_5(OH)ClO_4 \cdot \frac{1}{2}H_2O$- [Sbop (70)] in perchloric acid. In Fig. 2 and 3 the solubility of Sbop(70) as a function of C_H is plotted. A complete transformation of Sb_2O_3(or) into Sbop(70) can be achieved in the range $1.00 < C_H < 5.00$ M, though for the lowest value of C_H a very long agitation time is needed, at least 200 days. The transformation was checked by Guinier-Hägg powder photographs and titrimetric analysis of the solid phase. For $C_H = 0.75$ M, transformation was not complete in all samples even after 290 days, which is understandable as the difference in stability between the two phases is quite small at this value of C_H (*cf.* Fig. 3). All samples starting with Sb_2O_3(or) as solid phase reach equilibrium from supersaturation (*cf.* Fig. 1). In order that the equilibrium should be reached also from below saturation, samples of Sbop(70) were shaken with acid of C_H between 0.250 and 5.00 M for 82 days. Within experimental error, the same values of S were found by both methods. For $C_H < 0.68$ M, Sbop(70) is metastable relative to Sb_2O_3(c) and for $C_H < 0.26$ M also relative to Sb_2O_3(or), but no transformation to any of the oxides was ever found in these C_H regions. At values of $C_H < 0.250$ M the samples were agitated for 22 and 46 h with results that agreed well. When all data up to $C_H = 5$ M were inserted in eqn. (14), the best fit was obtained for $e_2 = e_3 = 0.71$. If only the values for $C_H \leq 3.50$ M

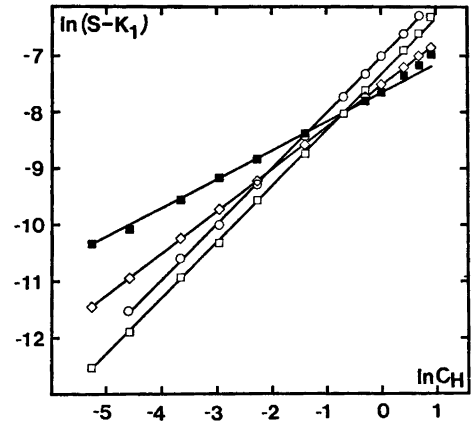

Fig. 4. ln $(S - K_1) = f(\ln C_H)$ for $C_H \leq 3.00$ M The slope of the plot is the e_2-value. The symbols refer to the solid phases: ○ Sb_2O_3(or), □ Sb_2O_3(c), ◇ Sbop(70) and ■ Sbon.

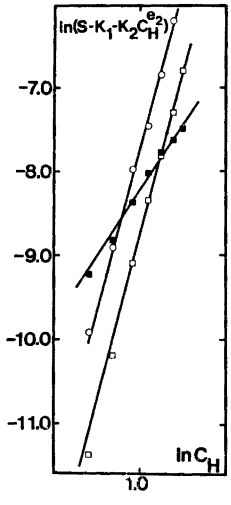

Fig. 5. ln $(S - K_1 - K_2 C_H^{e_2}) = f(\ln C_H)$ for $C_H \geq 2.00$ M. The slope of the lines give the e_2-values. The symbols refer to the solid phases: ○ Sb_2O_3-(or), □ Sb_2O_3(c) and ■ Sbon.

Table 2. The relative difference between experimental and calculated solubilities. S is the mean of several experimental values. S_{calc} is calculated with the polynomial $S_{calc}=K_1+K_2C_H^{e_2}+K_3C_H^{e_2}$.

	$100(S_{calc}-S)/S_{calc}$			
C_H	Sb_2O_3(c)	Sb_2O_3(or)	$Sb_4O_5(OH)ClO_4\cdot\frac{1}{2}H_2O$	$Sb_4O_4(OH)_2(NO_3)_2$
5.00			10.77	3.82
4.50	0.12		9.22	−0.64
4.00	0.32	−0.87	7.70	−1.81
3.50	−0.12	0.42	5.39	−3.31
3.00	−1.05	2.08	3.62	−3.04
2.50	−1.84	−0.65	0.77	−1.13
2.00	0.50	0.55	0.07	1.88
1.50	1.29	0.55	−1.68	−0.05
1.00	−1.14	−1.49	−0.71	3.03
0.750	−0.03	−0.13	−0.18	2.10
0.500	0.88	0.03	1.14	0.69
0.250	2.53	0.33	1.92	−1.85
0.1032	−0.62	−0.95	0.10	−1.53
0.0516	1.05	0.35	−0.83	−3.00
0.0258	−0.42	−1.62	−0.58	−1.20
0.0103	−0.31	−0.51	−0.14	2.55
0.0052	−0.58	1.28	−0.11	0.88

were used, $e_2=e_3=0.75$ was obtained. A new treatment with all experimental data and with $e_2=3/4$ fixed, gave a negative K_3 value. The differences between calculated and experimental solubilities for $C_H>3.50$ M could consequently not be explained in terms of complex formation reactions characterised by other values of m/n than 3/4. The most plausible explanation is the strong medium change from 5.00 M sodium perchlorate to 5.00 M perchloric acid. The constants K_i calculated using $e_2=3/4$ are given in Table 1 and the resulting polynomial presented graphically in Fig. 3 as a dotted line. The relative differences between calculated and experimental data are given in Table 2. The exponent e_2 can also be determined graphically from the slope of the function $f(\ln C_H)=\ln(S-K_1)$. If only values of S for $C_H<3.50$ M are used, a slope of 0.75 is in fact found (*cf.* Fig. 4).

Table 3. The solubility (S) of antimony(III) in 5.00 M sodium perchlorate and 5.00 M sodium nitrate in equilibrium with the various solid phases. Temperature 25.0 °C.

Medium	Solid phase	$S\times10^3$(M)
$NaClO_4$	Sb_2O_3(or)	0.137
$NaClO_4$	Sb_2O_3(c)	0.122
$NaClO_4$	Sbop(70)	0.192
$NaNO_3$	Sbon	0.166

The solid phase Sbop(70) has $j=1$. Hence, from eqns. (3) and (10), for $e_2=3/4$:

$$3/4=3l-p-l/4 \qquad (3^{III})$$

The complex $Sb_l(OH)_p^{3l-p}$ satisfying this condition are listed in Table 4. Only one combination of l and p, *viz.* $l=1$ and $p=2$, satisfies the equation system (3^{I}), (3^{III}). This means that of the complexes $Sb(OH)_2(Sb(OH)_3)_{l-2}^{+}$ which are compatible with the solubility curves of the oxides, only the first one, $Sb(OH)_2^{+}$, is also compatible with the solubility curve of the oxide perchlorate. The equilibria established are therefore

$$Sb_4O_6(\text{or or c})+4H^{+}+2H_2O\rightleftharpoons 4Sb(OH)_2^{+}$$

and

$$Sb_4O_5(OH)ClO_4\cdot\tfrac{1}{2}H_2O(s)+3H^{+}+\tfrac{3}{2}H_2O\rightleftharpoons 4Sb(OH)_2^{+}+ClO_4^{-}$$

with the equilibrium constants given in Table 6. The equation system (3^{II}), (3^{III}) is satisfied by $l=13$ and $p=35$, *i.e.* in the series of complexes $Sb_2(OH)_2(Sb(OH)_3)_{l-2}^{4+}$ only $Sb_{13}(OH)_{35}^{4+}$ fits the solubility curves of both the oxides and the oxide perchlorate. It is most unlikely, however,

Table 4. Complexes compatible with the ratios m/n determined experimentally for the various solid phases.

Sb_2O_3(or, c)	$Sb_4O_5(OH)ClO_4.\frac{1}{2}H_2O$	$Sb_4O_4(OH)_2(NO_3)_2$
$m/n = 1$	$m/n = 3/4$	$m/n = 1/2$
$Sb(OH)_2^+$	$Sb(OH)_2^+$	$Sb(OH)_2^+$
$Sb_2(OH)_5^+$	$Sb_5(OH)_{13}^{2+}$	$Sb_3(OH)_7^{2+}$
$Sb_3(OH)_8^+$	$Sb_9(OH)_{24}^{3+}$	$Sb_5(OH)_{12}^{3+}$
$Sb_4(OH)_{11}^+$	$Sb_{13}(OH)_{35}^{4+}$	$Sb_7(OH)_{17}^{4+}$
=	=	=
$Sb_i(OH)_{3i-1}^+$	$Sb_{4i-3}(OH)_{11i-9}^{i}$	$Sb_{2i-1}(OH)_{5i-3}^{i}$
$m/n = 4$		$m/n = 3/2$
$Sb_2(OH)_2^{4+}$		$Sb(OH)^{2+}$
$Sb_3(OH)_5^{4+}$		$Sb_3(OH)_6^{3+}$
$Sb_4(OH)_8^{4+}$		$Sb_5(OH)_{11}^{4+}$
$Sb_5(OH)_{11}^{4+}$		$Sb_7(OH)_{16}^{5+}$
=		=
$Sb_i(OH)_{3i-4}^{4+}$		$Sb_{2i-3}(OH)_{5i-9}^{i}$

that a complex of such high nuclearity would be in equilibrium with Sbop(70) since the concentration of the central ions is very low. On the other hand, the complex $Sb_2(OH)_2^{4+}$, which is the simplest one compatible with the solubility curves of Sb_2O_3(or) and Sb_2O_3(c), does not satisfy (3^{III}). As the antimony(III) concentration in equilibrium with the oxides is much higher, it is nevertheless quite possible that the dinuclear complex exists in those solutions in spite of the fact that it is not present in perceptible amount in equilibrium with Sbop(70).

The solubility of Sb(III) in perchloric acid with $C_H > 5.00$ M. The surveying investigation performed at varying ionic strength for $C_H > 5.00$ M is illustrated in Fig. 6. The solid phase Sbop(70) is stable up to $C_H \approx 6.7$ M. At $C_H = 7.00$ M a phase transformation takes place after three days. The new phase contains 44.6 % Sb. Its composition is very probably $Sb(OH)_2ClO_4 \cdot H_2O$ (calc. 44.3 % Sb). It is most probably identical with the compound earlier formulated as $SbO.ClO_4.2H_2O$ by Fichter and Jenny.[15] This solid phase is stable up to $C_H \approx 11.75$ M. In concentrated perchloric acid, however, still another phase is formed. As already mentioned, this compound is extremely sensitive to moisture. Thus, if the solution is allowed to take up moisture from the air for a few days, a complete transformation to Sbop(44) takes place. At $C_H = 4.50$ and 5.00 M, Sbop(55) exists as a metastable phase. This compound contains 54.4 % Sb which corresponds very closely to the composition $3Sb_2O_3.2Cl_2O_7.6H_2O$ (calc. 54.2 %). At $C_H = 6.00$ M, however, the solid phase in metastable equilibrium with the solution has neither the Guinier-Hägg powder pattern of Sbop(55) nor that of Sbop(44). This new phase has not yet been identified. Like Sbop(55), it evidently does not exist in stable equilibrium with any solution studied here.

Calculation of $\Delta G°$ for Sb_2O_3(or)→Sb_2O_3(c). The free energy change $\Delta G°$ for the transformation Sb_2O_3(or)→Sb_2O_3(c) at 25.0 °C can be computed from the present measurements as follows. In perchloric acid solutions of $C_H < 1.00$ M the complex $Sb(OH)_2^+$ is predominant (*cf.*

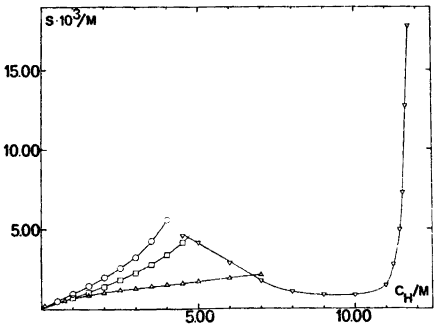

Fig. 6. The solubility of antimony(III) in perchloric acid solutions up to concentrated acid. For $C_H \leq 5.00$ M the ionic strength is constant at $I = 5.00$ M and for $C_H > 5.00$ M it varies. The different solid phases in equilibria with the solutions are indicated by the symbols: ○ Sb_2O_3(or), □ Sb_2O_3(c), △ Sbop(70) and ▽ other antimony(III)-oxide-perchlorates.

Table 5. Calculated value of ΔG° for the phase transformation Sb_2O_3 (orthorhombic)→Sb_2O_3 (cubic) at 25 °C, (*cf.* eqn. (20).

C_H (M)	ΔG° (kJ mol^{-1})
0.0258	−1.2
0.0516	−1.5
0.1032	−1.3
0.250	−1.5
0.500	−1.5
0.750	−1.4
1.00	−1.6

Fig. 3). The free energy changes on dissolution are therefore:

$$\Delta G_{or} = \mu_{or}(H_2O) + 2\mu_{or}(Sb(OH)_2^+) - 2\mu_{or}(H^+) - \mu_{or}(Sb_2O_3) \quad (15)$$

$$\Delta G_c = \mu_c(H_2O) + 2\mu_c(Sb(OH)_2^+) - 2\mu_c(H^+) - \mu_c(Sb_2O_3) \quad (16)$$

where for each species B:

$$\mu(B) = \mu^\circ(B) + RT \ln a(B) \quad (17)$$

At equilibrium, *i.e.* for saturated solutions,

$$\Delta G_{or} = \Delta G_c = 0 \quad (18)$$

and hence the free energy change of transition

$$\Delta G^\circ = \mu_c^\circ(Sb_2O_3) - \mu_{or}^\circ(Sb_2O_3)$$

is given by

$$\Delta G^\circ = -2RT \ln \frac{a_{or}(Sb)OH)_2^+)}{a_c(Sb(OH)_2^+)} + 2RT \ln \frac{a_{or}(H^+)}{a_c(H^+)} \quad (19)$$

If it assumed that the activity coefficients for $Sb(OH)_2^+$ and H^+ are constants in the solutions considered, concentrations may be substituted for the activities a. Further, if the solubilities of the two phases at the same value of $[H^+] \approx C_H$ are considered

$$\Delta G^\circ = -2RT \ln \frac{(S_{or} - K_{1,or})}{(S_o - K_{1,c})} . \quad (20)$$

Values of ΔG° calculated for different values of C_H are presented in Table 5. No systematic variation with the acidity can be discerned which shows that the assumptions made are permissible. The mean value is $\Delta G^\circ = -1.4 \pm 0.2$ kJ mol^{-1} at 25.0 °C. Pitman *et al.*[16] have earlier reported the value −7.5 kJ.

The nitric acid system. It is impossible to measure the solubility of Sb_2O_3(or) or Sb_2O_3(c) in nitric acid, as the transformation to the stable oxide nitrate phase $Sb_4O_4(OH)_2(NO_3)_2$ takes place in a few hours, *i.e.* before the metastable oxide equilibria are established.

The solubility of $Sb_4O_4(OH)_2(NO_3)_2$ in nitric acid is plotted as a function of C_H in Figs. 7 and 8. To make certain that Sb_2O_3(or) was fully transformed even at the lowest values of C_H used, the samples were agitated for 57 days. In these experiments, the equilibrium was approached from the side of supersaturated solution. To check that the equilibrium had really been established, some experiments were also performed with Sbon as the initial solid phase. No significant difference was found between the final values of S in the two cases. For $0.0051 < C_H < 0.1020$ M the experiments were always conducted with Sbon as solid phase.

The best fit to polynomial (14) was achieved with the values $e_2 = 0.49$ and $e_3 = 1.49$. The least-squares treatment was repeated with $e_2 = 1/2$ and $e_3 = 3/2$ as constants. The resulting constants K_i and the exponents e_i are given in Table 1. The exponents e_2 and e_3 were also determined graphically by plotting $f(\ln C_H) = \ln (S - K_1)$ for $C_H < 3.0$ M and $f(\ln C_H) = \ln (S - K_1 - K_2 C_H^{e_2})$ for $1.5 < C_H < 5.00$ M (*cf.* Figs. 4 and 5). The slopes of the functions give $e_2 = 0.5$ and $e_3 = 1.5$. The relative differences between calculated and experimental data are given in Table 2.

The solid phase Sbon has $j = 2$, hence, from eqns. (3) and (10)

$$1/2 = 3l - p - 2l/4 \quad (3^{IV})$$

$$3/2 = 3l - p - 2l/4 \quad (3^{V})$$

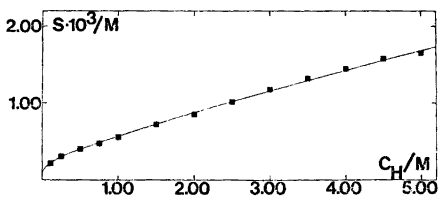

Fig. 7. The solubility of antimony(III) in nitric acid solutions at $I = 5.00$ M. The solid phase in equilibria with the solutions is Sbon.

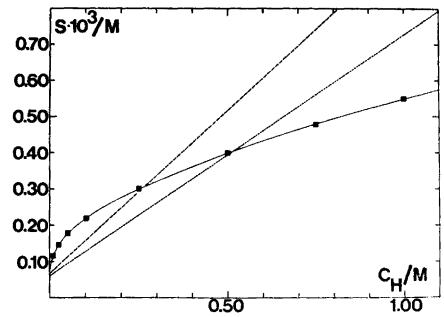

Fig. 8. The solubility of antimony(III) in nitric acid solutions, at $I = 5.00$ M, up to $C_H = 1.00$ M. (■ and −; solid phase Sbon). The solubilities of Sb_2O_3(or) (− − −) and Sb_2O_3(c) (···) in perchloric acid are plotted for comparison.

The complexes $Sb_l(OH)_p^{3l-p}$ compatible with these conditions are listed in Table 4. The only possible complex of charge +1 is $Sb(OH)_2^+$, which thus is the only one of the series $Sb(OH)_2(Sb(OH)_3)_{l-2}^+$, indicated by the oxide measurements, which is also compatible with the solubility curve of the oxide nitrate. The following equilibrium is thus established between Sbon and the solution:

$$Sb_4O_4(OH)_2(NO_3)_2(s) + 2H^+ + 2H_2O \rightleftharpoons 4Sb(OH)_2^+ + 2NO_3^-$$

with the equilibrium constant given in Table 6. Among the complexes of charge +4 which may, according to the oxide measurements possibly be present only $Sb_5(OH)_{11}^{4+}$ (with $m/n = 3/2$) and $Sb_7(OH)_{17}^{4+}$ (with $m/n = 1/2$) are compatible with the oxide nitrate curve (*cf.* Table 4). As the concentrations of antimony(III) in equilibrium with Sbon is very low, complexes of such high nuclearity are not likely to exist. This inference is further strengthened by the fact that none of the complexes mentioned are compatible with the oxide perchlorate curve. A much more plausible species which also satisfies eqn. (3[V]) is $Sb(OH)^{2+}$. This monomer admittedly does not exist in perceptible amounts in any of the perchlorate solutions investigated but it is known from other systems [17] that the formation of mononuclear complexes is favoured in nitrate solutions, evidently due to the stronger tendency of nitrate to enter the coordination sphere of the acceptor, thereby making the formation of hydroxo or oxo bridges more difficult. The complex [4] $Sb(OH)Cl_3^-$ provides another example of the same tendency which should be even more marked in chloride systems on account of the much stronger affinity of this ligand to antimony(III). The existence of the monomer $Sb(OH)^{2+}$ in nitric acid is therefore compatible throughout with the existence of the dimer $Sb_2(OH)_2^{4+}$ in perchloric acid. The equilibrium most likely to account for $m/n = 3/2$ would thus be

$$Sb_4O_4(OH)_2(NO_3)_2 + 6H^+ \rightleftharpoons 4Sb(OH)^{2+} + 2NO_3^- + 2H_2O$$

with the equilibrium constant given in Table 6.

DISCUSSION

This investigation has shown that in aqueous perchloric and nitric acid solutions of $C_H \leq 2.00$ M the predominating complex is $Sb(OH)_2^+$. This complex exists in equilibrium with all the solid phases employed. It has also been postulated by several previous investigators.[1-5] As

Table 6. Equilibrium constants K_i' (*cf.* eqn. (4)) for the reactions $Sb_4O_{(6-j)}(OH)_j(Z)_j(s) + mH^+ \rightleftharpoons nSb_l(OH)_p^{(3l-p)} + qH_2O + kjZ^-$ at $I = 5$ M and 25.0 °C. The errors stated correspond to 3σ.

Solid phase	Complex formed; constant K_i'								
	$Sb(OH)_2^+$			$Sb(OH)^{2+}$			$Sb_2(OH)_2^{4+}$		
	m	n	$K_2' \times 10^{14}$	m	n	$K_3' \times 10^{17}$	m	n	$K_3' \times 10^{12}$
Sb_4O_6(or)	4	4	60 ± 2			—	8	2	13.8 ± 0.9 (M^{-6})
Sb_4O_6(c)	4	4	19.0 ± 0.6			—	8	2	1.93 ± 0.02 (M^{-6})
$Sb_4O_5(OH)ClO_4 \cdot \frac{1}{2}H_2O$	3	4	8.6 ± 0.2 (M)			—			—
$Sb_4O_4(OH)_2(NO_3)_2$	2	4	3.5 ± 0.3 (M^2)	6	4	1.3 ± 0.2 (M^{-2})			—

Table 7. Determinations of the equilibrium constant of the reaction

$\frac{1}{2}Sb_2O_3(s) + H^+ + H_2O \rightleftharpoons Sb(OH)_2^+ + \frac{1}{2}H_2O$.

All determinations have been performed by solubility measurements.

Ref.	Solid phase	Medium	Equilibrium constant $\times 10^4$
1	Sb_2O_3(or)	$HClO_4$	9
2	Sb_2O_3(or)	HCl	8
4	Sb_2O_3(or)	$HClO_4$	8.5
This work	Sb_2O_3(or)	$HClO_4$	8.8 ± 0.1
This work	Sb_2O_3(c)	$HClO_4$	6.6 ± 0.1

already mentioned, some of these have also calculated the equilibrium constants for its formation from Sb_2O_3(or), the reaction generally being written in the form $1/2\ Sb_2O_3(or) + H^+ + H_2O \rightleftharpoons Sb(OH)_2^+ + 1/2\ H_2O$. Our value is in very good accord with these previous measurements, especially if the fairly large differences in medium are taken into account (*cf.* Table 7).

Generally, the complex has been written in the form SbO^+. From measurements of the present type it is of course impossible to differentiate between the two formulae. It seems nevertheless extremely improbable that both protons dissociate from one molecule of water and we therefore prefer the formulation $Sb(OH)_2^+$.

Besides the well-established $Sb(OH)_2^+$, at least two further complexes have been found in this investigation. Thus in perchloric acid solutions in equilibrium with Sb_2O_3 (orthorhombic or cubic) a complex of charge 4+ exists. Its concentration becomes perceptible (≈ 10 % of the total solubility S) at a value of $C_H \approx 2.4$ M (corresponding to $S \approx 2.5$ mM) for Sb_2O_3(or) and at a value of $C_H \approx 3.0$ M (corresponding to $S \approx 2.3$ mM) for Sb_2O_3(c). At the highest values of S reached, *viz.* 5.59 mM for Sb_2O_3(or) at $C_H = 4.0$ M, and 4.14 mM for Sb_2O_3(c) at $C_H = 4.5$ M, considerable amount of the antimony is present as the dimer, to the extent of 34 and 27 %, respectively. The equilibrium constant $K_d[= (K_3'/K_2')^{\frac{1}{2}}]$ for the reaction

$2Sb(OH)_2^+ + 2H^+ \rightleftharpoons Sb_2(OH)_2^{4+} + 2H_2O$

is found to be 4.8 ± 0.3 M^{-3} if the values of K_3' and K_2' found from the Sb_2O_3(or) curve are used, and 3.2 ± 0.1 M^{-3} if the values from the Sb_2O_3(c) curve are used. Presumably, this difference is mainly due to the fairly rapid change of the activity conditions which has been postulated as the most likely cause of the slightly low values of S found when Sbop(70) in the solid phase and $C_H \gtrsim 3$. It is quite probable that a corresponding deviation takes place also for the oxide curves. If so, it should be relatively more marked for Sb_2O_3(c) than for Sb_2O_3(or), especially as the solutions where the dimer is the predominant species are more acid in the former case. Such a deviation should result in values of K_3' for both oxides which are rather too low, especially in the case of Sb_2O_3(c).

Though great caution must always be taken when deducing the structures of hydrolytic complexes in solution from those found for solid oxide salts, valuable information may nevertheless be obtained in this way, as has been shown in several instances. Thus, the entities $Th(OH)_2Th^{6+}$ and $UO_2(OH)_2UO_2^{2+}$ which have been established in solution both by emf and X-ray investigations [18-20] are also found in solids.[21,22] Also, the complexes $Pb_4(OH)_4^{4+}$ and $Pb_6(OH)_8^{4+}$ indicated in solution by emf measurements [23] have later been found as discrete entities in crystalline oxide salts.[24-26]

The dimer $Sb_2(OH)_2^{4+}$ compatible with the present measurements, could have at least three different structures. The antimony atoms may be joined by a double hydroxo bridge: $Sb(OH)_2Sb^{4+}$, which would be similar to the arrangement in the thorium(IV) and uranyl(VI) complexes mentioned above, or the complex may contain a single hydroxo bridge: $Sb(OH)Sb(OH)^{4+}$. The final possibility would involve a single oxo bridge: $SbOSb^{4+}$.

In oxide salts, antimony(III) is three or four coordinated. The most common polyhedron is the trigonal bipyramid, where one of the equatorial corners is occupied by the lone pair of electrons. The other common coordination geometry is that of the tetrahedron, with the lone pair of electrons at one corner. If the complex with the double hydroxo bridge is a fragment of the solid oxide salt, then polyhedra with shared edges must be a feature of their structure. It also seems reasonable that the distance between the antimony atoms within the units is significantly shorter than any other Sb – Sb-distances in the oxide salt. The complexes with single hydroxo or oxo bridges are consistent with crystal structures containing

polyhedra with shared equatorial corners. In such cases the antimony atoms should be joined only by single oxygen bridges in the solid state.

In this serie of investigations, the structures [6,7] of $Sb_4O_5(OH)ClO_4 \cdot \frac{1}{2}H_2O$ [=Sbop(70)] and $Sb_4O_4(OH)_2(NO_3)_2$ (=Sbon) have been determined. In both compounds coordination polyhedra share edges, the shortest antimony-to-antimony distance being that between antimony atoms joined *via* two oxygens. This is also the case in the structure of $Sb_4O_5Cl_2$.[27,28] The only known structure which contains polyhedra sharing equatorial corners is $SbPO_4$.[29] The model for $Sb_2(OH)_2^{4+}$ most consistent with the crystal structures seems to be a complex in which two antimony atoms are joined by a double hydroxo bridge. A complex of similar structure, *viz.* $[Bi(OH)_2Bi]^{4+}$, has also been found by Aurivillius [30,31] in the crystal structures of $Bi(OH)CrO_4$ and $Bi(OH)SeO_4 \cdot H_2O$.

The monomer $Sb(OH)^{2+}$, which has been postulated to exist in the nitrate medium, has a counterpart in the complex $Bi(OH)^{2+}$. The latter is present in hydrolysed perchloric acid solutions of bismuth(III), although admittedly not as a predominating species.[32] The concentration of $SbOH^{2+}$ becomes perceptible (≈ 10 % of S) at $C_H \approx 1$ M. At the highest concentration of nitric acid used (5 M) it reaches ≈ 40 %. The equilibrium constant $K(=(K_3'/K_2')^{\frac{1}{2}}$ for the reaction

$$Sb(OH)_2^+ + H^+ \rightleftharpoons SbOH^{2+} + H_2O$$

is found to be 0.139 ± 0.008 M^{-1}, corresponding to an acid dissociation constant $K_s(=1/K) = 7.2 \pm 0.4$ M for $SbOH^{2+}$. This very high value of K_s found for a partly hydrolysed species illustrates the strongly acidic properties of antimony(III).

Acknowledgement. Our sincere thanks are due to Professors Sture Fronæus and Bengt Aurivillius for the kind interest they have always shown in these investigations. We have profited from the preliminary investigations of the systems performed by Irene Lundqvist and Rune Dahlin. The authors are also indebted to Kerstin Renhult Aspelin and Christer Jönsson for their assistance in taking Guinier-Hägg photographs.

The support of Statens Naturvetenskapliga Forskningsråd (The Swedish Natural Science Research Council) is also gratefully acknowledged.

REFERENCES

1. Schuhmann, R. *J. Amer. Chem. Soc. 46* (1924) 52.
2. Gayer, K. H. and Garrett, A. B. *J. Amer. Chem. Soc. 74* (1952) 2353.
3. Faucherre, I. *Bull. Soc. Chim. Fr.* (1954) 25.
4. Fridman, Ya. D., Veresova, R. A. and Luk'yanets, A. N. *Neorg. Fiz. Khim.* (1965) 13 (as cited in *Chem. Abstr. 64* (1966) 13453 g).
5. Jander, G. and Hartmann, H.-J. *Z. Anorg. Allg. Chem. 339* (1965) 239.
6. Bovin, J.-O. *Acta Chem. Scand. A 28* (1974) 723.
7. Bovin, J.-O. *Acta Chem. Scand. A 28* (1974) 267.
8. Karlsson, R. *To be published.*
9. Chandler, J. P. Physics dept. Indiana University. Copyright 1965.
10. Roberts, E. J. and Fenwick, F. *J. Amer. Chem. Soc. 50* (1928) 2125.
11. Belcher, R. *Anal. Chim. Acta 3* (1949) 578.
12. Schulek, E. and Rózsa, P. *Z. Anal. Chem. 115* (1939) 185.
13. Schulek, E. *Z. Anal. Chem. 102* (1935) 111.
14. Elkind, A. Gayer, K. H. and Baltz, D. F. *Anal. Chem. 3* (1949) 578.
15. Fichter, F. and Jenny, E. *Helv. Chim. Acta 6* (1923) 225.
16. Pitman, A. L., Pourbaix, M. and Zonbov, N. *J. Electrochem. Soc. 104* (1957) 594.
17. Ahrland, S., Lijenzin, J. O. and Rydberg, J. *Comprehensive Inorganic Chemistry*, Pergamon Press, Vol. 5, p. 337.
18. Baes, C. F., Jr., Meyer, J. N. and Roberts, C. E. *Inorg. Chem. 4* (1965) 518.
19. Johansson, G. *Acta Chem. Scand. 22* (1968) 399.
20. Åberg, M. *Acta Chem. Scand. 24* (1970) 2901.
21. Johansson, G. *Acta Chem. Scand. 22* (1968) 389.
22. Åberg, M. *Acta Chem. Scand. 23* (1969) 791.
23. Olin, Å. *Acta Chem. Scand. 14* (1960) 126.
24. Olin, Å. and Söderquist, R. *Acta Chem. Scand. 26* (1972) 3505.
25. Hong, S.-H. and Olin, Å. *Acta Chem. Scand. 27* (1973) 2309.
26. Hong, S.-H. and Olin, Å. *Acta Chem. Scand. A 28* (1974) 233.
27. Edstrand, M. *Acta Chem. Scand. 1* (1947) 178.
28. Särnstrand, C. *Private communications.*
29. Särnstrand, C. *Acta Chem. Scand. A 28* (1974) 275.
30. Aurivillius, B. and Löwenhielm, A. *Acta Chem. Scand. 18* (1964) 1937.
31. Aurivillius, B. *Acta Chem. Scand. 18* (1964) 2375.
32. Olin, Å. *Sv. Kem. Tidskr. 73* (1961) 482.

Received June 14, 1974.

Acta Chemica Scandinavica A 28 (1974) 1101—1105

Crystal Structure of *N,N*-Dimethyl-*p*-nitrosoaniline Hydrochloride Hydrate

OLE DRANGFELT and CHRISTIAN RØMMING

Department of Chemistry, University of Oslo, Oslo 3, Norway

The crystal structure of the title compound has been determined by X-ray methods using 2058 observed reflections collected by counter methods. The crystals are triclinic, space group $P\bar{1}$, with unit cell dimensions $a = 7.85_2$ Å; $b = 8.51_7$ Å; $c = 9.43_2$ Å; $\alpha = 116.4_1°$; $\beta = 91.8_9°$; $\gamma = 112.5_5°$. The structure was solved by Patterson methods and refined to a conventional *R*-factor of 0.044; standard deviations in bond lengths are 0.003 Å and in angles 0.2°.

The protonation of *N,N*-dimethyl-*p*-nitrosoaniline by the reaction with the acid occurs at the nitroso oxygen atom and an oxime is formed. Disregarding the methyl hydrogen atoms the organic ion is planar and has a pronounced quinonoid character.

The electron donating properties of *p*-nitroso-*N,N*-dimethylaniline have been studied by Popp and Ragsdale by means of infrared and visible spectra and by measurements of magnetic moments and molar conductances of various complexes.[1] They conclude that coordination takes place through the nitroso oxygen atom and that the basic properties of the nitroso group appear to be enhanced by the substitution of the strongly electron-donating dimethylamino group *para* to the nitroso group. The contribution of the polar resonance form of the molecule seems thus to be pronounced. From NMR studies of a solution of *N,N*-dimethyl-*p*-nitrosoaniline in trifluoroacetic acid MacNicol, Porte, and Wallace found that the protonation predominantly occurs on the oxygen atom.[2]

Owing to the disorder in the crystals an X-ray study of *N,N*-dimethyl-*p*-nitrosoaniline did not yield a precise determination of bond lengths and angles.[3] A quinonoid structure was indicated, however, confirming the basic nature of the nitroso group in this molecule.

The chloride of *N,N*-dimethyl-*p*-nitrosoaniline was described by Baeyer and Caro;[4] Kaufler and Kunz reported that this salt reacts with even a second molecule of hydrochloric acid forming a hygroscopic dichloride.[5]

An X-ray study of the monochloride was undertaken in order to confirm the formation of an oxime and to obtain data for the calculation of the charge distribution in the ion.

EXPERIMENTAL

Yellow needle-formed crystals were formed by cooling a saturated solution of *N,N*-dimethyl-*p*-nitrosoaniline in hydrochloric acid (2 N) from 30 – 40 °C to 5 °C over a period of one or two days. The formation of crystals sufficiently large for X-ray experiments seemed to be dependent on a high degree of purity of the sample. The crystal used in the present investigation was cut from a larger prismatic crystal to the size 0.1 × 0.3 × 0.5 mm.

Oscillation, Weissenberg, and precession photographs showed that the crystals are triclinic. Cell dimensions were determined from diffractometer measurements on 15 general reflections and their Friedel equivalents. The least-squares program used in the calculations as well as all other computer programs used during the X-ray analysis are described in Ref. 6.

The intensity data were recorded with the use of a SYNTEX $P\bar{1}$ diffractometer using graphite crystal monochromated Mo*K* radiation ($\lambda = 0.71069$ Å). The $\theta - 2\theta$ scanning mode was applied with scan speeds (2θ) of 2 – 8° min^{-1} depending on the peak intensity. Three standard reflections were measured for every 50 reflections; they showed a small systematic fluctuation and the data were accordingly adjusted. The standard deviations were taken as $\sigma(I) = (C_T + (0.025\ C_N)^2)^{\frac{1}{2}}$, where C_T is the

total number of counts and C_N is the scan count minus background count.

2058 reflections with sin $\theta/\lambda < 0.7$ and intensities greater than $2.5\sigma(I)$ were regarded as observed and used in the structure determination. They were corrected with Lorentz and polarization factors but not for absorption or secondary extinction.

Atomic form factors used were those of Doyle and Turner [7] for the chloride ion and oxygen, nitrogen, and carbon atoms, and of Stewart, Davidson and Simpson [8] for hydrogen. The full-matrix least-squares program employed minimizes the function $\sum w(F_o - F_c)^2$, where w is the inverse of the variance of the observed structure factor.

CRYSTAL DATA

N,N-Dimethyl-*p*-nitrosoaniline hydrochloride hydrate, $C_8H_{10}N_2O.HCl.H_2O$, triclinic. $a = 7.852(0.001)$ Å; $b = 8.517(0.001)$ Å; $c = 9.432(0.001)$ Å; $\alpha = 116.41(0.01)°$; $\beta = 91.89(0.01)°$; $\gamma = 112.55(0.01)°$. $V = 505.64$ Å^3, $M = 204.66$; $F(000) = 216$, $Z = 2$. $D_{obs} = 1.3$ g cm^{-3} (flotation), $D_{calc} = 1.344$ g cm^{-3}. Space group $P\bar{1}$.

STRUCTURE DETERMINATION

Wilson's statistical methods showed the crystals to possess a centre of symmetry, the space group was thus proved to be $P\bar{1}$. The structure was solved by Patterson methods and refined by least-squares calculations to an *R*-factor of 0.07 neglecting hydrogen atoms. A difference Fourier map failed to give any indication of the positions of the hydrogen atoms and coordinates of the hydrogen atoms bonded to the ring atoms and of those presumably taking part in hydrogen bonds were calculated. Least-squares refinement of positional and isotropic thermal parameters yielded acceptable values with the exception of a fairly high *B*-value for one of the water hydrogen atoms. Several sets

Table 1. Fractional atomic coordinates and thermal parameters with estimated standard deviations ($\times 10^4$ for chlorine, oxygen, nitrogen, and carbon and $\times 10^3$ for positional hydrogen coordinates). The anisotropic temperature factor is exp $-(B11h^2 + B22h^2 + B33l^2 + B12hk + B13hl + B23kl)$.

Atom	*x*	*y*	*z*	*B*11(*B*)	*B*22	*B*33	*B*12	*B*13	*B*23
C1	2332(2)	4865(2)	353(2)	146(4)	160(4)	115(3)	127(6)	58(5)	128(5)
C2	3220(3)	5812(3)	−542(2)	167(3)	190(4)	92(2)	150(7)	27(5)	125(6)
C3	4843(3)	7483(3)	182(2)	175(4)	198(4)	101(3)	134(7)	61(3)	171(5)
C4	5744(2)	8396(2)	1903(2)	136(4)	164(4)	101(2)	142(6)	55(5)	123(6)
C5	4839(3)	7448(3)	2798(2)	174(4)	201(4)	92(3)	131(7)	47(5)	136(6)
C6	3217(3)	5776(3)	2057(2)	193(4)	201(4)	115(3)	129(7)	88(6)	184(5)
C7	8297(3)	11025(3)	4340(2)	202(5)	253(5)	106(3)	54(8)	−3(6)	123(7)
C8	8347(3)	11036(3)	1743(2)	183(4)	242(5)	162(3)	79(8)	61(6)	249(7)
N1	776(2)	3212(2)	−228(2)	179(4)	186(4)	122(2)	128(6)	40(5)	136(5)
N2	7344(2)	10019(2)	2599(2)	135(3)	180(3)	113(2)	114(5)	50(4)	143(5)
O1	43(2)	2426(2)	−1856(2)	195(3)	203(3)	125(2)	69(5)	−4(4)	127(4)
O2	2567(2)	4906(2)	−4574(2)	206(4)	297(5)	233(3)	104(7)	80(6)	194(6)
Cl	6603(1)	8686(1)	−2940(1)	313(1)	181(1)	120(1)	41(2)	18(1)	127(1)
H2	263(2)	520(2)	165(2)	3.6(4)					
H3	540(2)	805(2)	42(2)	3.1(4)					
H5	539(2)	799(2)	393(2)	3.6(4)					
H6	267(3)	516(3)	258(2)	4.0(4)					
HO1	−119(4)	117(4)	213(3)	8.8(7)					
HW1	369(3)	601(3)	410(3)	7.8(6)					
HW2	281(5)	376(5)	527(4)	16.2(13)					
H71	948(4)	1214(5)	459(4)	13.5(11)					
H72	749(3)	1104(4)	495(3)	9.1(7)					
H73	846(4)	1012(4)	450(3)	10.2(8)					
H81	789(4)	1032(4)	62(3)	9.7(8)					
H82	831(4)	1228(4)	211(4)	12.7(10)					
H83	973(4)	1142(4)	195(4)	11.3(9)					

Table 2. Bond lengths (Å) and interbond angles (°).

Bond		Corrected	Angle	
C1 – C2	1.436	1.444	C1 – C6 – C5	121.6
C2 – C3	1.342	1.345	C1 – C2 – C3	121.1
C3 – C4	1.456	1.464	C6 – C1 – C2	118.1
C4 – C5	1.441	1.449	C6 – C5 – C4	120.6
C5 – C6	1.343	1.345	C2 – C3 – C4	120.7
C1 – C6	1.439	1.446	C3 – C4 – C5	117.6
N1 – C1	1.314	1.316	C1 – N1 – O1	111.7
N2 – C4	1.314	1.316	C2 – C1 – N1	126.6
N1 – O1	1.368	1.374	C6 – C1 – N1	115.3
N2 – C7	1.472	1.477	N2 – C4 – C3	120.6
N2 – C8	1.471	1.477	N2 – C4 – C5	121.6
C – H (mean)	0.93		C4 – N2 – C7	122.8
O – H (mean)	0.94		C4 – N2 – C8	124.0
			C7 – N2 – C8	113.1

of positions for the methyl hydrogen atoms were tried. The best set was that given in the parameter table, but even this has high values for the thermal parameters and we cannot exclude the possibility of a disorder resulting from a rotation about the N – C(methyl) bonds. Leaving out the two largest structure factors

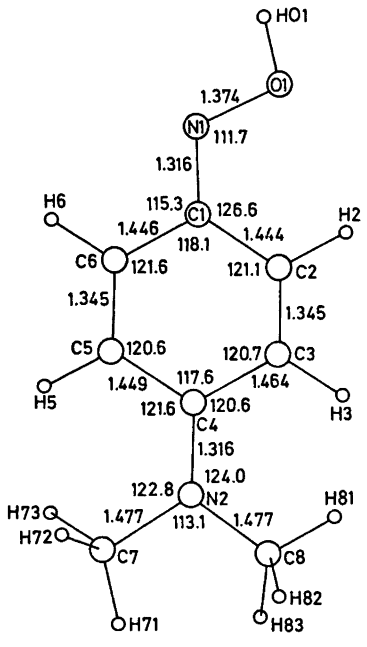

Fig. 1. Bond lengths (corrected) (Å) and angles (°).

Table 3. Deviations (Å) from the least-squares plane through the six-membered ring.

C1	−0.005	N1	−0.030	HO1	−0.04
C2	0.004	O1	−0.060	H2	−0.01
C3	0.000	N2	−0.020	H3	−0.01
C4	−0.002	C7	0.002	H5	−0.02
C5	0.000	C8	−0.040	H6	−0.02
C6	0.003				

the final refinements yielded a conventional R-factor of 0.040, $R_w = 0.045$.

The observed and calculated structure factor data are available from the authors upon request. The final parameters with their estimated standard deviations are given in Table 1.

An analysis of the thermal parameters in terms of rigid-body motion of the organic part showed this approximation to be reasonable. The translational part is nearly isotropic with r.m.s. amplitudes of 0.20, 0.17, and 0.17 Å; the main librational axes coincide closely with the main axes of the moment of inertia and the r.m.s. oscillation amplitudes are 7, 3, and 2°. The interatomic distances were corrected according to these values.

DISCUSSION

The bond distances and valency angles are listed in Table 2. The estimated standard deviations were calculated from the correlation

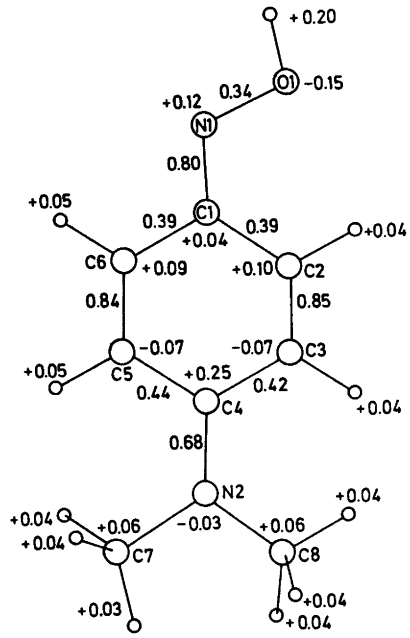

Fig. 2. CNDO/2 results for the isolated ion. π-Bond orders and atomic charges are indicated.

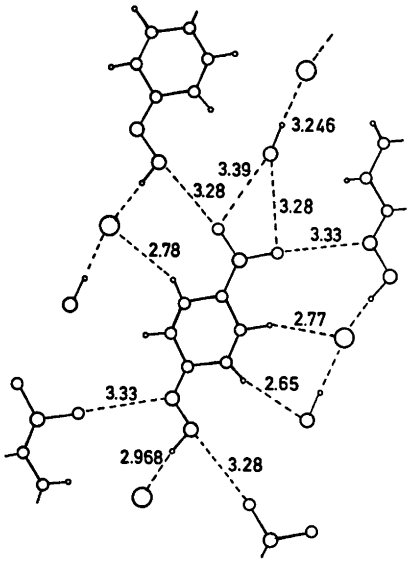

Fig. 3. Packing within one layer. Van der Waals contacts and hydrogen bonds are indicated.

matrix to be 0.003 Å for bond lengths and 0.2° for bond angles if only non-hydrogen atoms are involved. If one hydrogen atom is involved the standard deviations are 0.02 – 0.03 Å and 1°, respectively.

The geometry of the cation as found in the present analysis is shown in Fig. 1, in which the numbering of the atoms is also indicated.

The protonation has occurred at the oxygen atom of the nitroso group and the cation has thus the expected oxime structure.

With the exception of the methyl hydrogen atoms the ion is nearly planar. The deviations from the least-squares plane through the atoms of the six-membered ring are listed in Table 3. The amino group is thus planar and the torsion angle about the C4 – N2 bond is less than 1°.

The ion has a pronounced *para*-quinonoid structure. The average C – C "single" bond in the ring is 1.450 Å and the double bonds are 1.345 Å. The corresponding mean values for a number of compounds with a pure *p*-quinonoid geometry are 1.484 and 1.336 Å, respectively,[9] and the present ion is thus only slightly more aromatic in character. In accordance with this the two exocyclic C – N bonds are found to be 1.316 Å indicating a high degree of double bond character. The N1 – O1 bond length of 1.374 Å is consistent with the corresponding bonds in aromatic oximes.[10,11]

The considerable difference between the external angles at the C1 atom is probably to be ascribed to steric repulsion between the O1 and C2 atoms. The value found for the angle C1 – N1 – O1, 111.7°, agrees well with the corresponding angle in quinone-4-oxime [11] and is a normal valence angle for nitrogen bonded to two other atoms.

In order to obtain information of the charge distribution CNDO/2 calculations [12] were performed on the isolated ion. Fig. 2 shows the resulting π-bond orders and the net charges. The bond orders for the C – C bonds, 0.39 and 0.44, and for the C = C bond, 0.84, may be compared to the corresponding figures for *p*-benzoquinone, 0.25 and 0.94 for the two kinds of bonds, respectively. The theoretical results correspond closely to the observations from the X-ray analysis and reflect the quinonoid character of the ion.

The calculated electronic charge density shows the positive charge to be mainly dis-

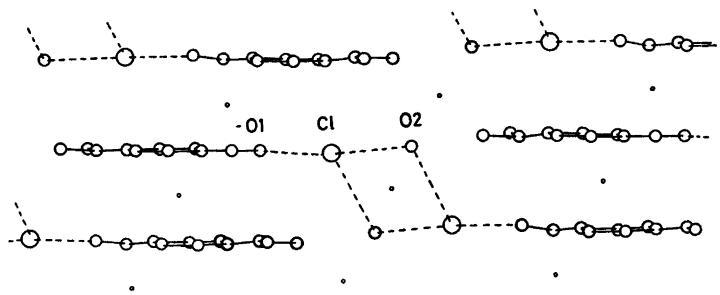

Fig. 4. The packing of the molecular layers. Hydrogen bonds are indicated by broken lines.

tributed on the C4, N1, and the hydroxy hydrogen atom with smaller contributions on the hydrogen atoms forming the surface of the ion. Since the largest negative charge is situated on the oxygen atom, it may be inferred that in the case of the formation of the dichloride [5] a second protonation may occur on this atom. Reservations must be taken, however, for the possibility of shifts in the electronic charge distribution if a surrounding field is incorporated in the calculations to imitate the actual field in the crystal or in a solution.

The crystal is built up by layers parallel to (1 − 1 0). All the heavy atoms are situated close to planes nearly coinciding with every second of the crystallographic (4 − 4 0) planes; this is even the case for the oxygen atom of the water molecule (O2) and the chlorine ions. The spacing of the planes is 3.30 Å. The situation of the ions and the water molecule in the plane is visualized in Fig. 3 in which the distances from the atoms of the organic moiety to the neighbouring ions and molecules are indicated. Within the layer there exist hydrogen bonds between O1 atoms and chlorine ions [2.968(2) Å] and between water molecules (O2) and chlorine ions [3.246(2) Å]. The hydrogen bonds are nearly linear with O − H···Cl angles of 171(2) and 177(2)°, respectively. The other contacts within the plane are of the normal van der Waals type. Pairs of layers (Fig. 4) are connected through hydrogen bonds between water molecules of one layer and chlorine ions of the other [3.197(3) Å]. Between the same layers there are probably weak $\pi - \pi$ charge transfer interactions between quinonoid rings related by a centre of symmetry.

REFERENCES

1. Popp, C. J. and Ragsdale, R. O. *Inorg. Chem. 7* (1968) 1845.
2. MacNicol, D. D., Porte, A. L. and Wallace, R. *Nature (London) 212* (1966) 1572.
3. Rømming, C. and Talberg, H. J. *Acta Chem. Scand. 27* (1973) 2246.
4. Baeyer, A. and Caro, H. *Ber. Deut. Chem. Ges. 7* (1874) 963.
5. Kaufler, F. and Kunz, E. *Ber. Deut. Chem. Ges. 42* (1909) 389.
6. Dahl, T., Gram, F., Groth, P., Klewe, B. and Rømming, C. *Acta Chem. Scand. 24* (1970) 2232.
7. Doyle, P. A. and Turner, P. S. *Acta Crystallogr. A 24* (1968) 390.
8. Stewart, R. F., Davidson, E. R. and Simpson, W. T. *J. Chem. Phys. 42* (1965) 3175.
9. Subramanian, E. and Trotter, J. *J. Chem. Soc. A* (1970) 622.
10. Romers, C. *Acta Crystallogr. 17* (1964) 1287.
11. Talberg, H. J. *Acta Chem. Scand. A 28* (1974) 910.
12. Pople, J. A. and Segal, G. A. *J. Chem. Phys 44* (1966) 3289.

Received June 17, 1974.

Acta Chemica Scandinavica A 28 (1974) 1106—1118

Thermodynamics of the Protonation and Ultra-violet Absorption of 1,2,4-Triazole in Aqueous Solutions and a Method for Testing the Reliability of a Weak n—π^* Transition Band from a Protonable Compound

PAAVO LUMME and ILKKA PITKÄNEN

Department of Inorganic Chemistry, University of Jyväskylä, Jyväskylä, Finland

The first and second protonation constants of 1,2,4-triazole were determined potentiometrically in aqueous sodium perchlorate solutions at 15, 20, 25, and 35 °C. The thermodynamic protonation constants were obtained by extrapolation to zero ionic strength and the thermodynamic quantities, the free energies, enthalpies, entropies, and heat capacities of the protonation equilibria were calculated from these.

The ultra-violet and visible absorption of 1,2,4-triazole was studied in aqueous, ethanol and hexane solutions. The absorption band due to $\pi-\pi^*$ transition in the range 185–210 nm only was observed in the spectrum. Our studies show that calculations of the log K values from the absorption spectra in water solutions may be used to decide the existence or non-existence of the $n-\pi^*$ excitation band in the spectrum of a protonable compound. The results are discussed below.

1,2,4-Triazole belongs to the group of the five-membered heterocyclic ring compounds. The ring structure contains three nitrogen atoms and its crystal structure has been determined.[1] According to its structure, 1,2,4-triazole may exist in two tautomeric forms [1–3] depending on whether the hydrogen atom is bonded to nitrogen at the position 1 or 4. On the basis of the potentiometric titration curves and the ultraviolet spectra it may be conluded that within the potentiometrically measurable range 1,2,4-triazole shows two prevailing protonation equilibria. In an alkaline solution hydrogen bonded to the nitrogen atom is left as a proton; and in an acid solution, a proton is added to the nitrogen atom at position 2 or 4 (most probably position 4) in the case of 1H-1,2,4-triazole, and at position 1 or 2 (which are equivalent in this respect, the C_{2v} molecular symmetry) in the case of 4H-1,2,4-triazole. More detailed decision between the different equilibria of the tautomers is not possible on the basis of the potentiometric or UV-spectrophotometric studies of the unsubstituted 1,2,4-triazole as shown in the present study.

Furthermore the effect of a neutral salt on the protonation equilibria of 1,2,4-triazole was studied by performing measurements in aqueous sodium perchlorate solutions at different ionic strengths and temperatures (not done previously), because they were needed in our studies on complexation of 1,2,4-triazole with transition metal ions.

The recorded absorption spectra gave also a possibility to consider the reliability of the $n-\pi^*$ transition bands in heterocyclic compounds from a new viewpoint as described below.

EXPERIMENTAL

Reagents and solutions. A distilled, deionized and carbonate free water was used in the preparation of the solutions. Sodium perchlorate (G. Frederic Smith Chemical Co.) was purified as described previously.[4,5] Sodium and potassium hydroxides (Titrisol), boric acid potassium biphthalate, potassium chromate, conc. perchloric acid and sodium chloride were all guaranted reagents of E. Merck, AG. Heptane and hexane were also guaranteed

reagents of E. Merck, AG., and ethanol was of the quality AaS (Oy Alko Ab).

For preliminary experiments we used 1,2,4-triazole of L. Light & Co. The producer gives the quality as: pure, assay ≥ 96 % (titration ex basic nitrogen), m.p. 120–121 °C. In the potentiometric and spectrophotometric measurements reported in the present paper we used 1,2,4-triazole of EGA-Chemie KG. The producer gives in this case as quality data: M.p. 119.5–121 °C, IR: ok, 99 % (T). Weighed amounts of the compound were dissolved in excess sodium hydroxide solutions and titrated potentiometrically with a known mineral acid solution (HCl or $HClO_4$). From the acid consumption difference between the two turning points of the titration curve the purity of the compound was found to be 100.4 ± 0.5 %. The compound was used as 100 %. The error due to this in the potentiometric determinations of the protonation constants falls within experimental errors. Its effect on the spectrophotometric measurements in the range 185–240 nm at low concentrations is given under experimental errors and the effect in the range 230–300 nm is discussed later.

Infra-red spectra of both samples of 1,2,4-triazole were run in KBr disks (1 mg of 1,2,4-triazole/400 mg of KBr (Uvasol, E. Merck, AG.)) on a Perkin-Elmer Model 457 spectrophotometer in the wavelength range 4000–250 cm^{-1}. The spectra were compared with the spectrum (No. 29293 K) of 1,2,4-triazole (Aldrich Chemical Co.) reported in the collection of the Sadtler Standard Infra-red Grating Spectra. Both spectra showed a medium broad band at 3420 cm^{-1} obviously due to the OH stretching vibrations of water, perhaps absorbed from the atmosphere. Weak bands were observed further at 1630 and 630 cm^{-1} and the weak band at 722 cm^{-1} was missing. The EGA-Chemie product showed more very weak bands at 1347 and 1237 cm^{-1}. Most probably the observed extra bands are due to C=O (COO) stretching vibrations (*cf.* Ref. 26, pp. 53, 69, 108, and 110) and point to the presence of some carbonyl (carboxyl) containing impurity in minor amounts in both samples of 1,2,4-triazole used. This is the compound X referred to later in this paper.

About 0.1 M sodium hydroxide solutions were prepared in an atmosphere of nitrogen in airtight burette systems of Pyrex glass. The alkalinities of the solutions were determined against potassium biphthalate by potentiometric titrations.

A perchloric acid solution of about 0.3 M was diluted from conc. acid. The acidity of the solution was determined by potentiometric titrations with the before mentioned alkali solution.

The concentrations of the sodium perchlorate solutions were determined by means of the evaporation and ion exchange methods described previously.[5]

Solutions 0.005 M in $HClO_4$, 0.01 M in NaCl and $(I - 0.015)$ M in $NaClO_4$ were used as reference buffers. The titrant was 0.1 M in $HClO_4$, 0.01 M in NaCl and $(I - 0.11)$ M in $NaClO_4$.

The measuring flasks, burettes and pipettes were checked at 20 °C. Corrections of the concentrations due to the temperature expansion of the solutions were estimated by assuming the temperature expansion of the solutions to be that of pure water.[6]

Apparatus and measurements. The potentiometric titrations were performed in an atmosphere of nitrogen in gastight Pyrex vessels and in a water thermostat at 15, 20, 25, and 35 ± 0.01 °C. A glass electrode (Beckman, No. 41260) and a calomel electrode of the immersion type were used in connection with a potentiometer (Radiometer PHM 4). To 100 ml (20 °C) of the studied solution, 3.5–6.5 or 13.5–16.5 ml of the titrant solution were added with 0.5 ml increments, and after magnetic stirring of the solution the potentials were read to ± 0.2 mV. The titrations were performed as duplicates and therefore each value of log K is a mean value from about 14 measurements. The potentials were stabilized within a few minutes. The electrode system was checked against the reference buffer in the beginning and end of each titration. The measuring cells may be presented schematically as follows (20 °C):

Glass electrode	100 ml 0.01 M 1,2,4-Triazole 0.01 M NaCl 0.01 M NaOH $(I - 0.02)$ M $NaClO_4$	
	0.01 M NaCl $(I - 0.01)$ M $NaClO_4$	Hg_2Cl_2, Hg

The ultraviolet spectra of 1,2,4-triazole in the different solutions were recorded with a Hitachi Perkin-Elmer Model 124 Doublebeam Grating Spectrophotometer at room temperature (about 22 °C). Control measurements were performed with a Beckman Model DU-2 Ultraviolet Spectrophotometer at 25 ± 0.1 °C. A flowing nitrogen atmosphere was used within the equipment. The spectrophotometers were calibrated with an alkaline potassium chromate solution (0.04 g of potassium chromate in 1 l of 0.05 M potassium hydroxide).[7] Quartz cuvettes of 1 cm optical lengths were used and compared, each one being substituted for the other in turn. The absorbance differences between the cuvettes were less than 0.01 unit. The background of the Coleman spectrophotometer increased from zero (at 370 nm) to 0.02 unit (at 200 nm) with the slit position of 1 mm. The measured absorbances were

corrected for these error sources. The reference solutions were in other respects similar to the studied solutions, but contained no 1,2,4-triazole. The aqueous solutions were made after spectrophotometric measurements 0.02 M in sodium chloride (at 20 °C) before the pH ($= -\log_{10}[H^+]$) values of the solutions were measured as described above.

RESULTS AND DISCUSSION

Potentiometric part. When the minor equilibria due to the different tautomers are neglected, the prevailing protonation equilibria in aqueous solutions of 1,2,4-triazole may be presented as follows:

$$L^- + H_3O^+ \rightleftharpoons HL + H_2O \quad (1)$$

$$HL + H_3O^+ \rightleftharpoons H_2L^+ + H_2O \quad (2)$$

The corresponding protonation constants are

$$K_1 = [HL]/[L^-]\,[H^+] \quad (3)$$

$$K_2 = [H_2L^+]/[HL]\,[H^+] \quad (4)$$

Observing that the values of K_1 and K_2 differ so much from each other that they can be determined separately, and taking into account the total concentrations and the electroneutrality principle, it is easily derived for the logarithms of the constants

$$\log K_1 = \mathrm{pH} - \log\,[(C_B - C_{HClO_4} - [OH^-])/(C_{HL} + [OH^-] + C_{HClO_4} - C_B)] \quad (5)$$

$$\log K_2 = \mathrm{pH} + \log\,[(C_{HClO_4} - [H^+] - C_B)/(C_{HL} + [H^+] + C_B - C_{HClO_4})] \quad (6)$$

where C_{HL}, C_B, and C_{HClO_4} are the total concentrations of 1,2,4-triazole, the added sodium hydroxide, and perchloric acid, respectively. The hydrogen and hydroxide ion concentrations were each in turn neglected depending on the experimental conditions used to determine the protonation constants.

Table 1. The values of log K_1 and log K_2 of 1,2,4-triazole at different ionic strengths and temperatures. The values of pK_W, log K_1' and Δ log K_1 are given also.

°C	I	pK_W	Mean log K_1'	Mean Δ log K_1	Mean log K_1	Mean log K_2
15	0.120	14.132	10.048	0.008	10.056	2.422
20	0.120	13.952	9.929	0.008	9.937	2.397
25	0.119	13.779	9.810	0.009	9.819	2.340
35	0.119	13.458	9.576	0.012	9.588	2.272
15	0.250	14.096	10.031	0.006	10.037	2.527
20	0.250	13.915	9.904	0.008	9.912	2.477
25	0.249	13.742	9.794	0.010	9.804	2.450
35	0.249	13.421	9.578	0.012	9.590	2.395
15	0.500	14.084	10.080	0.008	10.088	2.599
20	0.500	13.903	9.960	0.009	9.969	2.581
25	0.499	13.729	9.832	0.010	9.842	2.534
35	0.497	13.408	9.591	0.013	9.604	2.455
15	0.750	14.097	10.132	0.011	10.143	2.694
20	0.750	13.915	10.014	0.013	10.027	2.661
25	0.748	13.742	9.897	0.014	9.911	2.599
35	0.746	13.420	9.629	0.016	9.645	2.512
15	1.000	14.120	–	–	10.191	2.754
20	1.000	13.938	–	–	10.062	2.718
25	0.998	13.764	–	–	9.938	2.671
35	0.995	13.441	–	–	9.693	2.594
15	2.001	14.246	10.456	0.007	10.463	3.068
20	2.000	14.061	10.330	0.009	10.339	3.022
25	1.996	13.885	10.195	0.010	10.205	2.952
35	1.991	13.557	9.918	0.012	9.930	2.844

The values of K_1 and K_2 were calculated from eqns. (5) and (6) in aqueous sodium perchlorate solutions at different temperatures on the basis of the potentiometric titration data. The mean values of log K_1 and log K_2 calculated are given in Table 1. In the calculation of K_1 the ionic product of water, K_w is needed. The values for this are not known, however, in aqueous sodium perchlorate solutions at different ionic strengths and temperatures. Therefore the values of log K_1' in Table 1 were calculated on the basis of the thermodynamic values of $pK_w°$: 14.346 (15 °C), 14.167 (20 °C), 13.996 (25 °C) and 13.680 (35 °C).[8] To take the salt effect into account at least to some extent, the dependence of K_w on the ionic strength in aqueous sodium perchlorate solutions at different temperatures was assumed to be the same as in aqueous potassium chloride solutions The values of pK_w calculated on this basis from an equation presented by Harned and Owen [9] are also given in Table 1. On the basis of these values in the lowest and highest titrations points, calculated correction terms for K_1 are given as mean values Δ log K_1 in Table 1. In the ionic strength 1.00 the values of K_1 were calculated using the values of K_w at each titration point.

The values of log K_1 and log K_2 may be represented as functions of the ionic strength by the equations:

$$\log K_1 = \log K_1° - 2A\sqrt{I}/(1+\alpha_1\sqrt{I}) + B_1 I \quad (7)$$

$$\log K_2 = \log K_2° + B_2 I \quad (8)$$

where for constant A the values 0.5028 (15 °C), 0.5070 (20 °C), 0.5115 (25 °C) and 0.5211 (35 °C) were used (Ref. 8, p. 406). The data for log K_1 and log K_2 (Table 1) were fitted by the method of least squares to eqns. (7) and (8). In the case of log K_2 the values at the lowest ionic strength ($I = 0.12$) were disregarded in these calculations, because of their obvious incorrectness due to the diffusion potentials. The results of the calculations are given in Tables 2 and 3. The values of log K_1 and log K_2 are represented as functions of the ionic strength at different temperatures in Figs. 1 and 2.

Table 2. The values of the constants α_1, B_1, and log $K_1°$ of eqn. (7) and B_2 and log $K_2°$ of eqn. (8) at different temperatures.

°C	α_1	B_1	log $K_1°$	B_2	log $K_2°$
15	2.191	0.2980	10.205	0.3087	2.450
20	2.190	0.2968	10.083	0.3038	2.418
25	2.250	0·2852	9.972	0.2845	2.386
35	2.003	0.2706	9.768	0.2599	2.327

Table 3. The values of the logarithms of the first (K_1) and second (K_2) protonation constants of 1,2,4-triazole calculated from eqns. (7) and (8) using the constants given in Table 2.

°C	I	$\sqrt{I}$	log K_1 eqn. (7)	log K_2 eqn. (8)
15	0.120	0.346	10.043	2.487
	0.250	0.500	10.039	2.528
	0.500	0.707	10.075	2.605
	0.750	0.866	10.128	2.682
	1.000	1.000	10.188	2.759
	2.001	1.414	10.454	3.068
20	0.120	0.346	9.919	2.454
	0.250	0.500	9.915	2.494
	0.500	0.707	9.950	2.570
	0.750	0.866	10.002	2.646
	1.000	1.000	10.062	2.722
	2.000	1.414	10.327	3.026
25	0.119	0.346	9.807	2.420
	0.249	0.499	9.802	2.457
	0.499	0.706	9.836	2.528
	0.748	0.865	9.885	2.599
	0.998	0.999	9.942	2.670
	1.996	1.413	10.195	2.954
35	0.119	0.345	9.587	2.358
	0.249	0.499	9.575	2.392
	0.497	0.705	9.598	2.457
	0.746	0.864	9.640	2.521
	0.995	0.997	9.690	2.586
	1.991	1.411	9.922	2.845

For comparison we have collected in Table 4 the protonation constant values of 1,2,4-triazole and of related five-membered nitrogen containing heterocycles, pyrrole, pyrazole, imidazole, 1,2,3-triazole, and tetrazole found in the literature. By comparing the values of the protonation constants of 1,2,4-triazole (Table 4) determined by different authors and mainly by the potentiometric method, they are found to be of the same order of magnitude.

When considering the reliability of the protonation constant values obtained in the present study we can say that while the potentials were read to ± 0.2 mV this corresponds to an accuracy of about ± 0.01 unit in the log K_n values. Generally the stabilization of the cell system was good, and only such

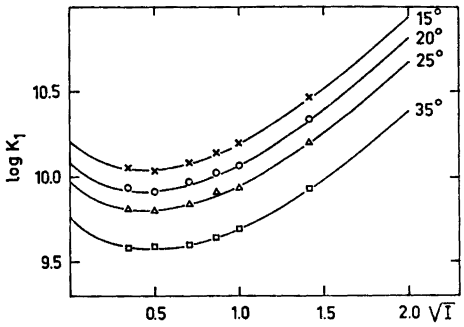

Fig. 1. The log K_1 values of 1,2,4-triazole as functions of the ionic strength in aqueous sodium perchlorate solutions at 15, 20, 25, and 35 °C.

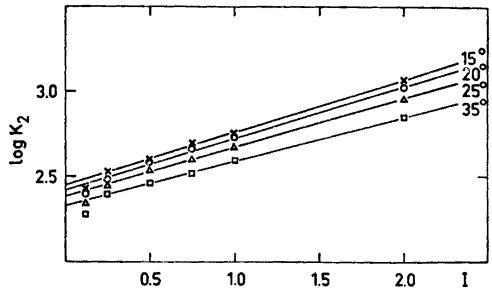

Fig. 2. The log K_2 values of 1,2,4-triazole as functions of the ionic strength in aqueous sodium perchlorate solutions at 15, 20, 25, and 35 °C.

titration results were used in the calculations. Using the ionic product values of pure water a drift of about 0.02 unit was observed in the calculated values of log K_1, whereas it was about 0.01 unit when the corrected values of the ionic product were used (Table 1). In the values of log K_2 the titration error was about ± 0.005 unit. To obtain a higher reliability the titrations were performed as duplicates.

Kröger and Freiberg [16] have compared the protonation constants of 1,2,4-triazole and its derivatives at 20 °C using Hammett's method and Hansen *et al.*[14] observed a linear dependence between the log K_1 values and the number of the nitrogen atoms in the five-membered heterocycles. The values of log K_2 in Table 4 do not show this behaviour, and

Table 4. Comparison of the values of the protonation constants of some unsaturated, five-membered nitrogen heterocycles in water.

Compound	°C	Ionic strength (added salt)	Method	log K_1	log K_2	Ref.
Pyrrole	20–25	?	spectrophotom.	–	−0.27	10
		?		16.5	–	11a
		12.4 ± 0.2 (KOH)		17.51 ± 0.05	–	11b
Pyrazole	25	0.025		–	2.47	12a
	25	?		14	–	13
	25	→0	glass el.	–	2.61	14
	20–25	1.2 ± 0.2 (KOH)	spectrophotom.	14.21	–	11b
	25.5 ± 0.5	→0	glass el.	–	2.52	12b
Imidazole	25	→0	glass el.	–	6.95	5
	25	→0	spectrophotom.	14.2	–	13, 15
	20–25	1.11 ± 0.05 (KOH)		14.17	–	11b
1,2,3-Triazole	20	→0	potentiometric	9.42	1.17	13
	25	→0	glass el.	9.26 ± 0.02	–	17
1,2,4-Triazole	20–25	?	spectrophotom.	–	2.30	12a
	20	0.005	glass el.	10.26	2.27	16,3
	25	→0		10.04	2.45	14
	20	→0		10.08	2.42	This work
	25	→0		9.97	2.39	
Tetrazole	room	~0.0033	potentiometric	4.89	–	18
	25	→0	glass el.	4.90	–	14
	25	?	potentiometric	4.79	–	19

therefore there exists no general (linear) dependence of the protonation tendency on the number of the nitrogen atoms in the five-membered heterocycles. Neither is any general dependence found between the values of log K_1 and log K_2. On the other hand all abovementioned heterocycles may form a one-charge anion that is protonated according to eqn. (1). With pyrrole the anion formation occurs only with difficulty and in very highly alkaline solutions as seen in Table 4. Pyrazole and imidazole are in this respect almost alike, but also form anions only in strongly alkaline solutions, whereas among the other compounds this tendency increases in the order 1,2,4-triazole, 1,2,3-triazole, and tetrazole (Table 4). So, the protonation tendency of the anions decreases generally in the order: pyrrole > pyrazole > imidazole > 1,2,4-triazole > 1,2,3-triazole > tetrazole. On the other hand the protonation tendency of the neutral molecules increases in the order: tetrazole < pyrrole < 1,2,3-triazole < 1,2,4-triazole < pyrazole < imidazole.

As pointed out above 1,2,4-triazole may exist in two tautomeric forms, and Kröger and Freiberg [3] have shown the tautomeric ratio of (1*H*)- to (4*H*)-1,2,4-triazole to be about 5 – 10:1. Therefore the almost identical protonation tendency of the neutral forms of pyrazole and 1,2,4-triazole (Table 4) is to be understood, whereas the inclusion of the third nitrogen atom in 1,2,3-triazole causes a decrease of the protonation tendency (a lower log K_2 value). The protonation tendency is further weakened by bringing the fourth nitrogen atom into the ring in tetrazole, for which a K_2 value has not so far been determined.

No unambiguous relation was found between the values of log K_1 or log K_2 given in Table 4 and the electron densities $\varrho\pi$ or $\varrho(\sigma+\pi)$ of the expected proton adding nitrogen atoms.[20,21] But the general tendency is, however, that the higher the electron density of the proton-adding nitrogen atom in the ring, the higher the value of log K_n.

The thermodynamic values of the protonation constants of 1,2,4-triazole were assumed to depend on the absolute temperature according to the equation:[22]

$$\log K_n^\circ = -(a/T) - cT + b \qquad (9)$$

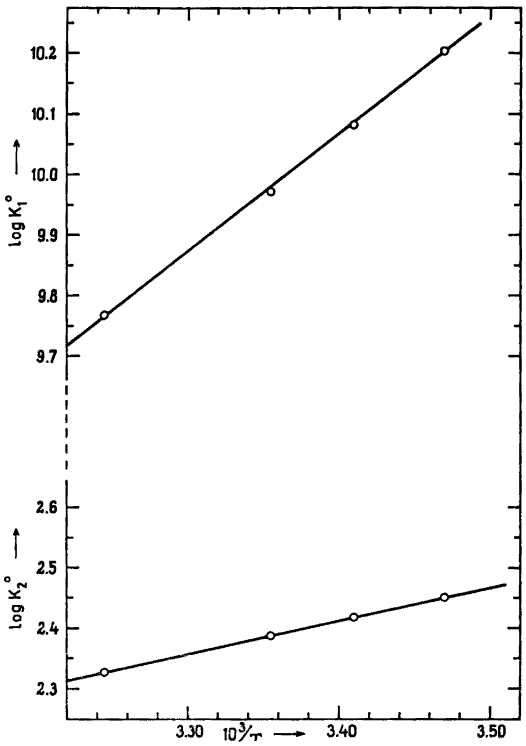

Fig. 3. The log K_1° and log K_2° values of the protonation constants of 1,2,4-triazole as functions of $1/T$.

(although a linear dependence on the temperature could be assumed as well (*cf.* Fig. 3)). The values of the constants a, b, and c given in Table 5 were calculated by fitting the experimental values of the constants log K_n° in Table 2 by the method of least squares to the equation. The log K_n° values of the thermodynamic protonation constants of 1,2,4-triazole are represented as functions of the reciprocal values of the absolute temperature in Fig. 3.

Table 5. The values of the constants a, b, and c of eqn. (9) for log K_1° and log K_2° of 1,2,4-triazole.

log K_n°	$-a \times 10^{-3}$	$-b$	$-c \times 10^3$
log K_1°	4.549	14.076	29.481
log K_2°	0.7613	0.881	2.393

Table 6. The values of log $K_1°$ and log $K_2°$ calculated from eqns. (7)–(9) and the corresponding free energies, enthalpies, and entropies of the protonation equilibria of 1,2,4-triazole at the temperatures used. The values of $T\Delta S°$ and $|10^2 T\Delta S°/\Delta G°|$ are given also.

°C	log $K_1°$ (eqn. (7))	log $K_1°$ (eqn. (9))	$-\Delta G°$ (kJ mol^{-1})	$-\Delta H°$ (kJ mol^{-1})	$\Delta S°$ (J K^{-1} mol^{-1})	$T\Delta S°$ (kJ mol^{-1})	$\lvert\frac{10^2 T\Delta S°}{\Delta G°}\rvert$
15	10.205	10.206	56.31	40.2	55.8	16.1	29
20	10.083	10.084	56.60	38.6	61.5	18.0	32
25	9.972	9.971	56.93	36.9	67.1	20.0	35
35	9.768	9.771	57.65	33.5	78.4	24.2	42
Mean at 15–35 °C			56.87 ± 0.4	37.3 ± 2	65.7 ± 7		

°C	log $K_2°$ (eqn. (8))	log $K_2°$ (eqn. (9))	$-\Delta G°$ (kJ mol^{-1})	$-\Delta H°$ (kJ mol^{-1})	$\Delta S°$ (J K^{-1} mol^{-1})	$T\Delta S°$ (kJ mol^{-1})	$\lvert\frac{10^2 T\Delta S°}{\Delta G°}\rvert$
15	2.451	2.451	13.52	10.8	9.5	2.75	20
20	2.418	2.417	13.57	10.6	10.0	2.93	22
25	2.386	2.386	13.62	10.5	10.5	3.12	23
35	2.327	2.327	13.73	10.2	11.4	3.50	26
Mean at 15–35 °C			13.61 ± 0.07	10.5 ± 0.2	10.3 ± 0.6		

The thermodynamic quantities, the free energies, enthalpies, entropies, and heat capacities of the first and second protonation equilibria of 1,2,4-triazole were then calculated from the equations:

$$\Delta G° = 2.303\, R(a - bT + cT^2) \quad (10)$$

$$\Delta H° = 2.303\, R(a - cT^2) \quad (11)$$

$$\Delta S° = 2.303\, R(b - 2cT) \quad (12)$$

$$\Delta C_p° = -4.606\, RcT \quad (13)$$

where $T = 273.16 + t$ °C and $R = 8.31433$ J K^{-1} mol^{-1}. The values of the thermodynamic quantities are given in Table 6, except for $\Delta C_p°$ for which only approximate mean values 330 and 27 J K^{-1} mol^{-1} were calculated for the first and second protonation reactions in the temperature range used.

From Table 6 it can be seen that $\Delta H°$ and $\Delta S°$ increase with increasing temperature for both protonation equilibria, which are exothermic processes. The temperature increase does not favour the protonation processes. The $|10^2 T\Delta S°/\Delta G°|$ values increase linearly with increasing temperature and more rapidly for the first protonation process, which means a higher increase of the effect of the entropy factor. The values show also that the enthalpy factor is dominant as compared with the entropy factor in the protonation processes, which are more dependent on the innermolecular (*e.g.* N–H bond energies) effects than on the environmental (solvation) changes.

The second (P.L.) of the present authors has previously compared the thermodynamic quantities associated with the ionization processes of some nitrogen-containing open-chain molecules.[23] The studied compounds were divided into two series, those in which a neutral molecule and those in which a negative monovalent ion were formed.[23] A similar interesting series of compounds form the nitrogen containing five-membered ring heterocycles mentioned above and under consideration here.

The thermodynamic data of the protonation equilibria of these compounds are, however, incomplete; those found in the literature were collected for comparison in Table 7. Also in this case when considering the $|10^2 T\Delta S°/\Delta G°|$ values against the $\Delta G°$ values, the protonation process of the negative monovalent ion forms shows higher $|10^2 T\Delta S°/\Delta G°|$ values than the protonation process of the neutral molecules, although the relations are not so smooth as with the open-chain nitrogen compounds,[23] but they point to the decrease of the entropy effect with increasing $\Delta G°$. On the contrary the enthalpy effect increases with increasing

Table 7. Comparison of the thermodynamic quantities, free energies, enthalpies, and entropies and the $|10^2 T\Delta S^\circ/\Delta G^\circ|$ values of the protonation equilibria of some unsaturated, five-membered nitrogen heterocycles in water at 25 °C.

Compound	log K_1°	$-\Delta G^\circ$ (kJ mol^{-1})	$-\Delta H^\circ$ (kJ mol^{-1})	ΔS° (J K^{-1} mol^{-1})	$T\Delta S^\circ$ (kJ mol^{-1})	$\lvert\frac{10^2 T\Delta S^\circ}{\Delta G^\circ}\rvert$	Ref.
1,2,3-Triazole	9.26 ± 0.02	52.9 ± 0.1	37.2 ± 0.1	52.7	15.7	30	17
1,2,4-Triazole	9.97 ± 0.02	56.9 ± 0.2	36.9 ± 2	67.1	20.0	35	This work
	10.04 ± 0.05	57.3 ± 0.3	33.1 ± 0.9	81.2	24.2	42	14
Tetrazole	4.90 ± 0.01	28.0 ± 0.06	12.9 ± 0.3	50.6	15.1	54	14

Compound	log K_2°	$-\Delta G^\circ$ (kJ mol^{-1})	$-\Delta H^\circ$ (kJ mol^{-1})	ΔS° (J K^{-1} mol^{-1})	$T\Delta S^\circ$ (kJ mol^{-1})	$\lvert\frac{10^2 T\Delta S^\circ}{\Delta G^\circ}\rvert$	Ref.
Pyrazole	2.61 ± 0.05	14.9 ± 0.3	14.7 ± 0.1	0.8	0.24	2	14
Imidazole	6.98 ± 0.02	39.9 ± 0.2	37.4 ± 2	8.4 ± 6	2.5	6	5
	6.993 ± 0.00	39.917 ± 0.004	36.79 ± 0.12	10.49 ± 0.41	3.13	8	24
1,2,4-Triazole	2.39 ± 0.02	13.6 ± 0.2	10.5 ± 3	10.5	3.1	23	This work
	2.45 ± 0.03	14.0 ± 0.2	9.62 ± 0.04	14.6	4.4	31	14

ΔG° in both cases. A similar difference between the two protonation equilibria is observed when inspecting the dependence of the $|10^2 T\Delta S^\circ/\Delta G^\circ|$ values on the number of the ring nitrogen atoms. Generally the entropy and enthalpy effects increase with the increasing number of the nitrogen atoms in the heterocycles for both protonation processes.

Spectrophotometric part. The ultraviolet and visible spectra have been frequently used in ionization studies of compounds (Ref. 13, pp. 65–108).[25–27] In the case of 1,2,4-triazole this is based on the changes in the intensity and place of the absorption of the $\pi \rightarrow \pi^*$ transitions with pH of the solutions. The light absorption of the solutions of 1,2,4-triazole may be assumed to depend on the species H_2L^+, HL, and L^- according to the equation:

$$A = \varepsilon C_{HL} = \varepsilon_{H_2L^+}[H_2L^+] + \varepsilon_{HL}[HL] + \varepsilon_{L^-}[L^-] \quad (14)$$

where $\varepsilon_{H_2L^+}$, ε_{HL} and ε_{L^-} are the absorptivities of the species, respectively. By taking into account eqns. (3) and (4) and the total concentration of 1,2,4-triazole it follows from eqn. (14) that [25]

$$(\varepsilon - \varepsilon_{HL}) + (\varepsilon - \varepsilon_{H_2L^+})[H^+]K_2 + (\varepsilon - \varepsilon_{L^-})/[H^+]K_1 = 0 \quad (15)$$

ε_{L^-} is obtained by measuring in strongly alkaline solutions and $\varepsilon_{H_2L^+}$ and ε_{HL} may be

Table 8. The wavelength, absorbance, and log ε values of the observed absorption maxima of 1,2,4-triazole in aqueous solutions at room temperature (~ 22 °C, 3×10^{-4} M) and 25 °C (2.996×10^{-4} M). The wavelength range 185–235 nm. The solution numbers refer to Fig. 4.

Room temperature (~ 22 °C)					25 °C				
Solution No.	pH	λ_{max} nm	A	log ε	Solution No.	pH	λ_{max} nm	A	log ε
1	1.09	189.5	0.565	3.275	1	1.09	189.6	0.616	3.313
2	2.11	189.5	0.660	3.342	2	2.08	189.6	0.678	3.355
3	3.05	189.5	0.710	3.374	3	3.01	189.6	0.807	3.430
4	6.05	189.5	0.745	3.395	4	6.40	189.5	0.845	3.450
5	8.01	190.0	0.600	3.301	5	7.88	189.8	0.762	3.405
6	10.02	197.0	0.520	3.239	6	9.89	195.6	0.741	3.393
7	12.14	209.0	0.040	2.125	7	11.97	–	–	–

Table 9. The wavelength and absorbance values of the observed absorption maxima of a compound X in 0.2 M aqueous solutions of 1,2,4-triazole at room temperature (~ 22 °C) and 25 °C. The wavelength range 220–290 nm. The solution numbers refer to Fig. 5.

Room temperature (~ 22 °C)				25 °C			
Solution No.	pH	λ_{max} nm	A	Solution No.	pH	λ_{max} nm	A
1	0.10	–	–	1	0.10	–	–
2	3.49	–	–	2	3.49	–	–
3	4.53	256	0.450	3	4.53	257.3	0.449
4	6.07	257	0.495	4	6.17	257.5	0.493
6	8.68	257	0.485	5	7.85	257.5	0.492
7	13.90	257	0.495	6	8.66	257.5	0.499
Isosbestic	point	248	0.360	7	13.73	257.5	0.497
				Isosbestic	point	248.5	0.371

measured or calculated in strongly acid and nearly neutral solutions of 1,2,4-triazole, respectively.

The position, absorbance, and log ε values of the absorption maxima observed in the spectra of 1,2,4-triazole in aqueous solutions in the range 185–235 nm are given in Tables 8 and 10 and in ethanol and hexane solutions in Table 11. The wavelengths and log ε values for the absorption maxima of the different species of 1,2,4-triazole in aqueous solutions recorded or calculated from eqn. (15) are represented in Table 12. The absorption spectra of 1,2,4-triazole in different solutions are shown in Figs. 4 and 6. The corresponding data for the compound X discussed later are given in Tables 9 and 11 and in Figs. 5 and 6.

When considering the recorded absorption spectra of 1,2,4-triazole, (Figs. 4–6 and Tables 8–12) two separate absorption maxima are observed. The strong maximum (A) at a shorter wavelength corresponds to an allowed transition $\pi - \pi^*$ (Ref. 7, p. 17; Ref. 26, pp. 129 and 144); whereas (B) at a longer wavelength is obviously due to corresponding electron transitions of an unknown compound X. Generally the position of the maximum B is almost constant in water ($\lambda_{max} = 257.5$ nm) and ethanol ($\lambda_{max} = 258.6$ nm) solutions at 25 °C, while in acid solutions (Fig. 5) this maximum is transferred to shorter wavelengths, weakened and finally almost disappears. On the other hand the position of the absorption maximum A varies considerably. In acid and neutral water solutions it is at about 190 nm (Fig. 4). In alkaline solutions it can change to 210 nm (Fig. 4). In ethanol, which is not as polar a solvent as water, it exists in the range 201–206 nm ($\varepsilon = 475 - 112$) and in the nonpolar hexane at 196 nm (Fig. 6).

Table 10. The wavelength, absorbance, and log ε values of the observed absorption maximum of 1,2,4-triazole in different molar concentrations in water at 25 °C. The wavelength range 185–210 nm.

1,2,4-Triazole 10^4 mol l^{-1}	λ_{max} nm	A	log ε
2.996	189.5	0.845	3.450
1.498	189.5	0.431	3.459
0.7488	189.4	0.213	3.454
			Mean 3.454

By examining the absorptivities of the absorption maxima the Lambert-Beer law is found to hold for the A band in water solutions. In ethanol solutions this is not the case, since both λ_{max} and ε are changed with the concentration of 1,2,4-triazole, the ε values being lower in the latter solutions. In strongly alkaline solutions the A band seems to have disappeared. For the A band $\varepsilon_{H_3L^+} < \varepsilon_{HL}$. In the case of the B band we cannot say with certainty if the Lambert-Beer law holds in water and ethanol solutions. The absorptivity values are almost the same in the different solvents. In water solutions the B band seems to show the compound X to have two absorbing species.

Table 11. The wavelength, absorbance, and log ε values of the observed absorption maxima of a compound X and 1,2,4-triazole in ethanol and hexane solutions at room temperature (~ 22 °C) and 25 °C. The wavelength range 190–315 nm. The solution numbers refer to Fig. 6.

Room temperature (~ 22 °C)					25 °C				
Solution No.	1,2,4-Triazole 10^3 mol l^{-1}	λ_{max} nm	A	log ε	Solution No.	1,2,4-Triazole 10^3 mol l^{-1}	λ_{max} nm	A	log ε
3	80.0	258.5	0.205	—	1	198.9	258.6	0.475	
4	48.0	258.5	0.125	—	2	99.46	258.6	0.239	
5	28.8	258.5	0.075	—	3	79.57	258.6	0.187	
6	17.3	258.0	0.045	—	8	6.188	203.8	1.60	2.413
		207.5	1.365	1.897	10	2.228	202.1	0.882	2.598
7	10.4	257.5	0.030	—	11	1.337	201.7	0.592	2.646
		206.5	1.165	2.049	12	0.8019	201.4	0.381	2.677
8	6.22	205.0	0.970	2.193	13	satd.			
9	3.73	204.0	0.750	2.303		hexane	196.0	0.095	—
10	2.24	203.5	0.535	2.378					
11	1.34	203.0	0.360	2.429					

Rao (Ref. 7, p. 77) and Mason [28] collected and compared the absorption spectra of many unsaturated five-membered heterocycles found in the literature. The strong absorption maxima at the range 207–210 nm found in the spectra of pyrazole, imidazole, and 1,2,3-triazole in alcoholic solutions are obviously due to $\pi \rightarrow \pi^*$ excitations in C=C or C=N bonds. The A band in the absorption spectrum of 1,2,4-triazole is also obviously of the same origin, owing to $\pi \rightarrow \pi^*$ transitions in C=N bonds.

Previously Mason [28] obtained for λ_{max} and ε of 1,2,4-triazole in water the values 187 nm and 3300, respectively. The experimental conditions were not specified in greater detail. In the present work we obtained in an unbuffered water solution at 25 °C $\lambda_{max} = 189.5$ nm and $\varepsilon = 2850$.

A closer inspection of the absorption band A in acid solutions (Fig. 4) shows a shoulder on the longer wavelength side of the maximum. When pH of the solution is increased, a shoulder also appears on the shorter wavelength side of the absorption. At pH about 8, two very close peaks are observed at the maximum, and when the spectrum is nearest to that of the HL species. In alkaline solutions this absorption band is transformed to longer wavelengths and weakened considerably or disappears.

There are several possibilities to be considered as a possible explanation of the observed shoulders and the double peak. The most probable explanation of the appearance and disappearance of the shoulders and the double peak in the band A is, however, the tautomeric equilibrium between 1*H*-1,2,4- and 4*H*-1,2,4-triazole which shifts with the pH of the solution. The shoulder and the stronger peak on the shorter wavelength side are probably due to 1*H*-1,2,4-triazole, and the other shoulder and peak arise from 4*H*-1,2,4-triazole according to their shown tautomeric ratio [3] (5–10:1). The observed double peak in the absorption spectrum of 3,5-diphenyl-1,2,4-triazole at 230–270 nm has previously been assumed to arise from the 1*H*-1,2,4- and 4*H*-1,2,4-triazole tautomerism,[29] but in reverse order.

The absorption band B (Fig. 5) is obviously due to the $\pi \rightarrow \pi^*$ excitations in a compound X, and should not be taken to be a band of a weak forbidden $n \rightarrow \pi^*$ transition in 1,2,4-triazole (Table 9). It should be mentioned that an absorption band B has not been observed in the spectrum of 1,2,3-triazole (Ref. 7, p. 77). It is reported to have been observed, however, in the spectrum of imidazole (Ref. 7, p. 77).

Table 12. The wavelength and log ε values of the absorption maxima of the different species of 1,2,4-triazole in aqueous solutions at 25 °C.

Species	λ_{max} (nm)	log ε
H_2L^+	189.6	3.308
HL	189.5	3.441

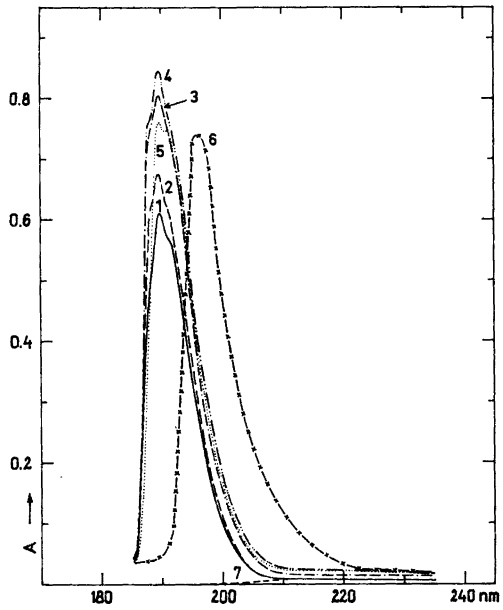

Fig. 4. The absorption spectra of 2.996×10^{-4} M aqueous solutions of 1,2,4-triazole at 25 °C. The wavelength range 185–235 nm.

Curve No.	pH	$C \times 10^4$	$C_B \times 10^4$
$HClO_4$			
1	1.09	992.4	
2	2.08	99.9	
3	3.01	9.99	
4	6.40	–	
H_3BO_3			
5	7.88	499.4	39.65
6	9.89	499.4	438.5
7	11.97	–	99.9

The values $\lambda_{max} = 260$ nm and $\varepsilon < 5$ were given for the $n \rightarrow \pi^*$ transition in tetrazole (Ref. 7, p. 77).

Atkinson *et al.*[29] have concluded that 1,2,4-triazole and its alkyl derivatives would not have an absorption spectrum at longer wavelengths than 215 nm. Also Mason [28] has not observed such a one. The measurements in the present work confirmed these results, as will be shown in the following.

From the following facts it can be concluded that in the case of the B band it is a band caused by an unknown compound X, present in 1,2,4-triazole, and not a band of a weak forbidden $n \rightarrow \pi^*$ excitation in 1,2,4-triazole.

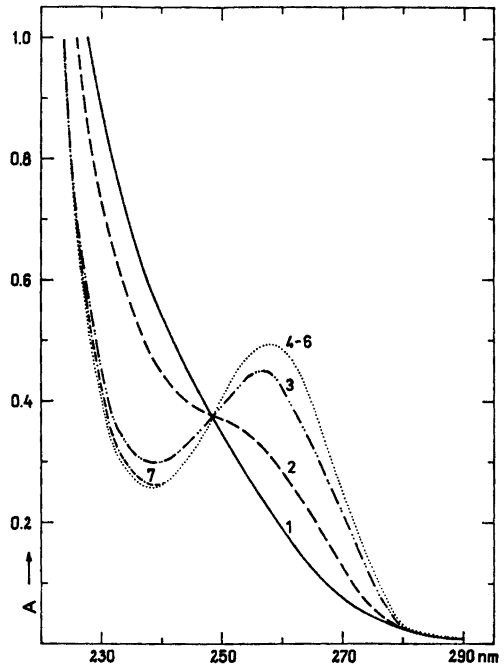

Fig. 5. The absorptin spectra of a compound X in 0.1998 M aqueous solutions of 1,2,4-triazole at 25 °C. The wavelength range 220–290 nm.

Curve No.	pH	$C \times 10^4$ HCl	$C_{NaCl} \times 10^4$	$C_B \times 10^4$
1	0.10	9940	–	–
2	3.49	–	100	–
3	4.53	10	190	–
4	6.17	–	200	–
5	7.85	– [a]	100	39.7
6	8.66	–	100	100
7	13.73	–	–	9990

[a] $C_{H_3BO_3} \times 10^4 = 500$.

The band at about 258 nm does not show the blue shift typical for a forbidden $n \rightarrow \pi^*$ band when transforming from a nonpolar solvent, hexane, to polar solvents, ethanol and water.[30,31]

The absorptivity of a neutral solution, 2.996×10^{-4} M in 1,2,4-triazole (Fig. 4) is about 0.03 at 230 nm. In a similar solution, 0.1998 M in 1,2,4-triazole it should be, accordingly, about 20. In Fig. 5, however, the absorbance value is seen to be about 0.4 only.

Solution No.	λ	A	C_{HL}	pH	$[H^+]$	A_{HL}	$A_{H_2L^+}$	$\log K_2$	I
2	189.6	0.678	2.996×10^{-4}	2.08	8.32×10^{-3}	0.845	0.609	2.46	0.01
3	189.6	0.807	2.996×10^{-4}	3.01	9.78×10^{-4}	0.845	0.609	2.29	0.001
2	240	0.448	0.1998	3.49	3.24×10^{-4}	0.263	0.538	3.80	0.02
2	257.3	0.320	0.1998	3.49	3.24×10^{-4}	0.495	0.233	3.79	0.02
3	240	0.298	0.1998	4.53	2.95×10^{-5}	0.263	0.538	3.69	0.02
3	257.3	0.449	0.1998	4.53	2.95×10^{-5}	0.495	0.233	3.86	0.02
Solution No.						4	1		

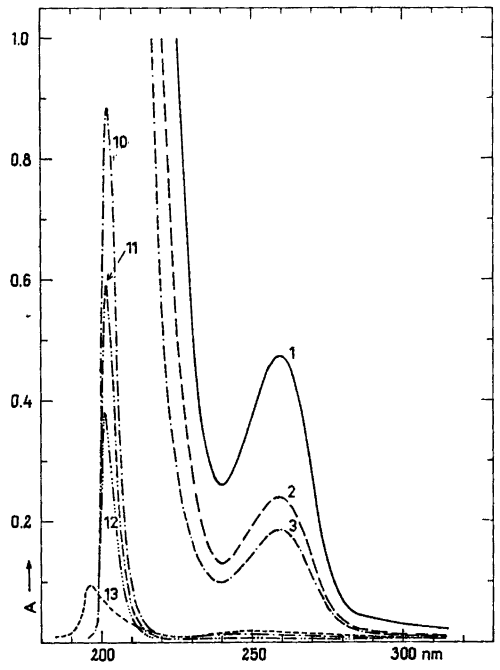

Fig. 6. The absorption spectra of a compound X and 1,2,4-triazole in ethanol and hexane solutions at 25 °C. The wavelength range 180–320 nm.

Curve No.	[1,2,4-Triazole] M
1	0.1989
2	0.09946
3	0.07957
10	2.228×10^{-3}
11	1.337×10^{-3}
12	8.019×10^{-4}
13	[a]

[a] Saturated solution of 1,2,4-triazole in hexane (20 °C).

If the 1,2,4-triazole used contains, as our analysis indicates, about 0.4 % of a compound X, this means that a 0.2 M 1,2,4-triazole solution would be about 8×10^{-4} M in the compound X (Figs. 5 and 6). This concentration is of the usual order of magnitude used in spectral studies of protonable compounds showing absorption at 240–400 nm.[25]

If we evaluate the protonation constants which it is possible to calculate from the absorption spectra presented in Figs. 4 and 5 at the band maxima and 240 nm using eqn. (15) we obtain the above results at 25 °C.

So we get at 189.6 nm for $\log K_2$ of 1,2,4-triazole as a mean value 2.38 in excellent agreement with Fig. 2. Instead of that in the range 240–260 nm we get 3.79 as a mean for $\log K_2$, which implies that we are dealing with some unknown compound X in place of 1,2,4-triazole. The result is the same, if the compound X is assumed to protonize according to eqn. (1) in lieu of eqn. (2) when using eqn. (15) to evaluate the protonation constant. This result and the spectra in Fig. 5 which show only one isosbestic point (248.5 nm) and that the compound X probably has only two species in water from strongly alkaline to strongly acidic solutions, confirm the above-made conclusion on the origin of band B.

Two times higher absorbances showed by 1,2,4-triazole produced by Light & Koch in similar conditions under which spectra Nos. 1–3 in Fig. 5 and spectrum No. 2 in Fig. 6 were taken, implied that this product contains about two times more of the compound X than the product of EGA-Chemie. The product did not dissolve completely, but showed an opalescence.

The present results also cast doubt on all reported weak bands said to be due to forbid-

den $n \rightarrow \pi^*$ transitions the ε values of which are ≤ 100. Examples are imidazole and tetrazole mentioned above (Ref. 7, p. 77). In any case the origin of the band, *i.e.* whether it is due to the true compound or some minor impurity, should be tested by evaluation of the protonation constants, if the compound has such, from the absorption spectra in aqueous solutions, and by comparing the results with, in some other way determined, known values of the constants. This seems to be a generally acceptable method and should be used to ascertain the source of the spectrum. In no case one should be satisfied with absorption measurements in nonpolar solvents only. In this respect, compare the spectra in Figs. 5 and 6.

The studies of the solvent effects were limited mostly to water and ethanol, because of the insolubility of 1,2,4-triazole. Hexane and heptane, the absorption of which is not disturbing in the wavelength range in question were wholly or almost unsuitable for this reason also. The polar-nonpolar effect of the solvents (a red shift) on the absorption spectrum of 1,2,4-triazole, in accordance with what was said above, is clearly observed to respond to the band due to the $\pi \rightarrow \pi^*$ transition in the wavelength range 180 – 240 nm (Fig. 6).

Acknowledgements. The authors are indebted to Mr. M. Peacock, M. A. for correcting the English of this paper. Financial support from the National Research Council for Sciences (Finland) is also greatfully acknowledged.

REFERENCES

1. Deuschl, H. *Ber. Bunsenges. Phys. Chem. 69* (1965) 550; Goldstein, P., Ladell, J. and Abowitz, G. *Acta Crystallogr. B 25* (1969) 135.
2. de. Paolini, I. and Baj, M. *Gazz. Chim. Ital. 61* (1931) 557.
3. Kröger, C.-F. and Freiberg, W. *Chimia 21* (1967) 161.
4. Lumme, P. and Tummavuori, J. *Acta Chem. Scand. 19* (1965) 617.
5. Lumme, P. and Virtanen, P. *Suom. Kemistilehti B 42* (1969) 333.
6. Lange, N. A. *Handbook of Chemistry*, McGraw-Hill, 10th Ed., London 1961, p. 1188.
7. Rao, C. N. R. *Ultra-Violet and Visible Spectroscopy*, 2nd Ed., Butterworths, London 1967, p. 9.
8. Bates, R. G. *Determination of pH*, Wiley, New York 1965, p. 404.
9. Harned, H. S. and Owen, B. B. *The Physical Chemistry of Electrolytic Solutions*, 3rd Ed., Reinhold, New York 1967, p. 641.
10. Naqvi, N. and Fernando, Q. *J. Org. Chem. 25* (1960) 551.
11. a. McEwen, W. K. *J. Amer. Chem. Soc. 58* (1936) 1124; b. Yagil, G. *Tetrahedron 23* (1967) 2855.
12. a. Dedichen, G. *Ber. Deut. Chem. Ges. 39* (1906) 1831; b. Musgrave, T. R. and Humburg, E. R., Jr. *J. Inorg. Nucl. Chem. 32* (1970) 2229.
13. Albert, A. In Katritzky, A. R., Ed., *Physical Methods in Heterocyclic Chemistry*, Academic, New York and London 1963, Vol. 1, p. 96.
14. Hansen, L. D., Baca, E. J. and Scheiner, P. *J. Heterocycl. Chem. 7* (1970) 991.
15. Walba, H. and Isensee, R. *J. Amer. Chem. Soc. 77* (1955) 5488.
16. Kröger, C.-F. and Freiberg, W. *Z. Chem. 5* (1965) 381.
17. Hansen, L. D., West, B. D., Baca, E. J. and Blank, C. L. *J. Amer. Chem. Soc. 90* (1968) 6588.
18. Lieber, E., Patinkin, S. H. and Tao, H. H. *J. Amer. Chem. Soc. 73* (1951) 1792.
19. Mihina, J. S. and Herbst, R. M. *J. Org. Chem. 15* (1950) 1082.
20. Kamiya, M. *Bull. Chem. Soc. Jap. 43* (1970) 3344.
21. Adam, W. and Grimison, A. *Theor. Chim. Acta 7* (1967) 342.
22. Harned, H. S. and Robinson, R. A. *Trans. Faraday Soc. 36* (1940) 973.
23. Lumme, P., Lahermo, P. and Tummavuori, J. *Acta Chem. Scand. 19* (1965) 2175.
24. Datta, S. P. and Grzybowski, A. K. *J. Chem. Soc. B* (1966) 136.
25. Lumme, P. *Ann. Acad. Sci. Fenn. Ser. A2 68* (1955).
26. Bladon, P. In Schwarz, J. C. P., Ed., *Physical Methods in Organic Chemistry*, Oliver & Boyd, Edinburgh & London 1965, p. 161.
27. King, E. J. *Acid – Base Equilibria*, Pergamon, London 1965, pp. 90 – 108.
28. Mason, S. F. In Katritzky, A. R., Ed., *Physical Methods in Heterocyclic Chemistry*, Academic, New York and London 1963, Vol. 2, p. 59.
29. Atkinson, M. R., Parkes, E. A. and Polya, J. B. *J. Chem. Soc.* (1954) 4256.
30. McConnell, H. *J. Chem. Phys. 20* (1952) 700.
31. Kasha, M. *Discuss. Faraday Soc. 9* (1950) 14.

Received May 17, 1974.

Acta Chemica Scandinavica A 28 (1974) 1119—1128

A Large-angle X-Ray Scattering Study of Aqueous Pentamolybdodiphosphate and Heptamolybdate Solutions

GEORG JOHANSSON,[a] LAGE PETTERSSON [b] and NILS INGRI [b]

[a] Department of Inorganic Chemistry, Royal Institute of Technology, S-100 44 Stockholm 70, Sweden and [b] Department of Inorganic Chemistry, University of Umeå, S-901 87 Umeå, Sweden

Radial distribution curves have been calculated from X-ray scattering measurements on five solutions in each of which one of the complexes MoO_4^{2-}, $(H^+)_8(MoO_4^{2-})_7$, $(H^+)_8(MoO_4^{2-})_5(HPO_4^{2-})_2$, $(H^+)_9(MoO_4^{2-})_5(HPO_4^{2-})_2$ or $(H^+)_{10}(MoO_4^{2-})_5(HPO_4^{2-})_2$ should predominate according to equilibrium data. Comparison with calculated peak shapes for interatomic interactions within the complexes $Mo_7O_{24}^{6-}$, $Mo_5P_2O_{23}^{6-}$ and $H_2Mo_5P_2O_{23}^{4-}$, which are known from crystal structure determinations, shows the identity of these complexes with those occurring in solution. No significant differences in the structures or in the interatomic distances seem to occur between the complexes in crystals and in solution. For the short Mo – Mo distances within the complexes changes of a magnitude of about 0.01 Å should have been observable in the distribution curves, if they occurred.

In recent emf-investigations by Pettersson [1–3] aqueous three component equilibria

$$p\mathrm{H}^+ + q\mathrm{MoO_4^{2-}} + r\mathrm{HPO_4^{2-}} \rightleftharpoons (\mathrm{H}^+)_p(\mathrm{MoO_4^{2-}})_q(\mathrm{HPO_4^{2-}})_r$$

were studied at 25 °C in 3.0 M $Na(ClO_4)$ medium. In the range $1.5 < -\log [H^+] < 9$ and for $B/C \leq 2.5$ (B is the total molybdenum concentration and C is the total phosphorus concentration) it was shown that the predominant ternary complexes formed are $(H^+)_8(MoO_4^{2-})_5(HPO_4^{2-})_2$, $(H^+)_9(MoO_4^{2-})_5(HPO_4^{2-})_2$ and $(H^+)_{10}(MoO_4^{2-})_5(HPO_4^{2-})_2$. By means of equilibrium analysis in aqueous solution one cannot distinguish between species containing different numbers of solvent molecules and the three pentamolybdodiphosphates may equally well be written as $Mo_5P_2O_{23}^{6-}$, $HMo_5P_2O_{23}^{5-}$ and $H_2Mo_5P_2O_{23}^{4-}$. Since discrete ions with such compositions are known from crystal structure determinations this shorter notation is to be preferred and will frequently be used in the following. Through slow evaporation of three different equilibrium solutions containing predominantly one or other of these pentamolybdodiphosphate complexes three crystalline phases could be ob-

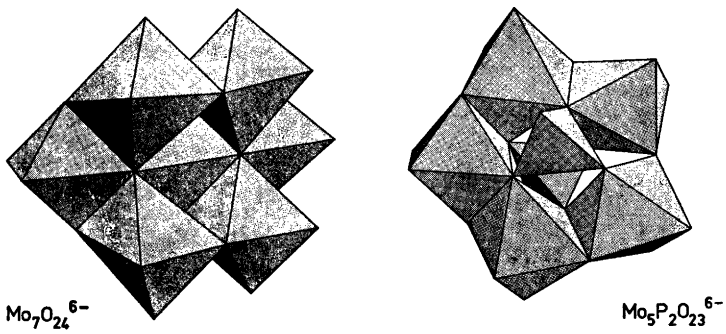

Fig. 1. A perspective view of the $Mo_7O_{24}^{6-}$ and the $Mo_5P_2O_{23}^{6-}$ complexes. The parameters used for the construction of the figures have been taken from the crystal structure determination of the compounds $Na_6Mo_7O_{24}(H_2O)_{14}$[11] and $Na_6Mo_5P_2O_{23}(H_2O)_{13}$.[4]

tained with compositions corresponding to the formulas $Na_6Mo_5P_2O_{23}(H_2O)_{13}$ (phase I), $Na_5HMo_5P_2O_{23}(H_2O)_8$(phase II) and $Na_4H_2Mo_5P_2O_{23}(H_2O)_{10}$ (phase III). Complete structure determinations have been carried out for I [4] and III.[5] For II a determination is in progress. It was found that phase I and phase III contain discrete units $Mo_5P_2O_{23}^{6-}$ and $H_2Mo_5P_2O_{23}^{4-}$, respectively. These units are both built up from five MoO_6-octahedra and two PO_4-tetrahedra as shown in Fig. 1. The hydrogens of the $H_2Mo_5P_2O_{23}^{4-}$-group are probably attached to the apex oxygens of the PO_4-tetrahedra thus forming a diprotonized pentamolybdodiphosphate anion. An interesting feature in these structures is the coordination of the sodium ions, which are bonded directly to the oxygens of the molybdenum octahedra.

Since the discrete polynuclear ions in the crystals have compositions equivalent to those derived from emf measurements it seems plausible to assume that the complexes in the crystals and in the solutions are identical. In order to investigate this further and more directly an X-ray scattering study of aqueous pentamolybdodiphosphate solutions was undertaken. For comparison two solutions containing no phosphate were included in the study. One alkaline solution, in which only MoO_4^{2-} ions and no polynuclear ions should be present, and one acidified solution, in which the predominant complex should be a heptamolybdate. The H^+/MoO_4^{2-} ratio ($=Z$) for the acidified solution was adjusted to be 1.14, corresponding to the composition $(H^+)_8(MoO_4^{2-})_7$. Most investigations,[6] for example the emf measurements by Sasaki and Sillén [7] and the emf, Raman, and ultracentrifugation measurements by Aveston *et al.*,[8] indicate that the predominant complex in a solution with $Z=1.14$ is a heptamolybdate $(H^+)_8(MoO_4^{2-})_7$, although octamolybdates may also be present. Lindqvist [9] has shown that from such solutions crystals with the composition $(NH_4)_6Mo_7O_{24}(H_2O)_4$ can be obtained, which contain discrete $Mo_7O_{24}^{6-}$ complexes (Fig. 1). Identical complexes have been found in crystals of $K_6Mo_7O_{24}(H_2O)_4$,[10] and $Na_6Mo_7O_{24}(H_2O)_{14}$.[11] Accurate parameter values for the positions of the atoms within the discrete $Mo_7O_{24}^{6-}$ units are now known from three-dimensional crystal structure determinations.[11,12]

EXPERIMENTAL

Solutions investigated. Four molybdate-phosphate solutions were studied, one slightly alkaline solution, here denoted C, containing, according to equilibrium data, only mononuclear HPO_4^{2-} and MoO_4^{2-}-ions, and three with $HClO_4$ acidified solutions containing polyanions with compositions corresponding to the complexes $(H^+)_8(MoO_4^{2-})_5(HPO_4^{2-})_2$, $(H^+)_9(MoO_4^{2-})_5(HPO_4^{2-})_2$ and $(H^+)_{10}(MoO_4^{2-})_5(HPO_4^{2-})_2$, respectively. For these solutions the notations D, E, and F will be used. The compositions and concentrations of the solutions are given in Table 1. With the use of the equilibrium constants valid for a 3.0 M $Na(ClO_4)$ medium the distribution of complexes has been calculated as a function of $-\log[H^+]$ for $B=1.60$ M and $C=0.64$ M ($B/C=2.5$). The results, which are given in Fig. 2, show that it is possible to prepare solutions which are practically pure with respect to any one of $Mo_5P_2O_{23}^{6-}$, $HMo_5P_2O_{23}^{5-}$, and $H_2Mo_5P_2O_{23}^{4-}$. The compositions chosen for the solutions investigated are marked with vertical lines. The compositions of the solutions containing no phosphate are given in Table 1. The alkaline solution is denoted by A and the acidified solution by B.

Table 1. Composition of solutions.

	Solution A	B	C	D	E	F
Concentration in mol/l						
Mo	2.04	2.04	1.77	1.77	1.77	1.60
Cl	–	2.33	–	2.12	2.48	2.57
P	–	–	0.71	0.71	0.71	0.64
Na	4.07	4.08	4.96	4.25	4.25	3.84
O	59.0	61.9	60.1	62.5	62.8	62.4
H	101.6	91.1	101.2	91.7	89.8	90.2
Number of atoms in the unit of volume V						
Mo	1	1	1	1	1	1
Cl	–	1.14	–	1.20	1.40	1.61
P	–	–	0.40	0.40	0.40	0.40
Na	2.00	2.00	2.80	2.40	2.40	2.40
O	29.0	30.3	34.0	35.3	35.5	39.0
H	49.9	44.7	57.2	51.8	50.7	56.4
V Å^3	814	814	938	938	938	1038
ϱ_0 el^2/Å^3	145.5	167.9	176.3	195.3	198.6	212.1

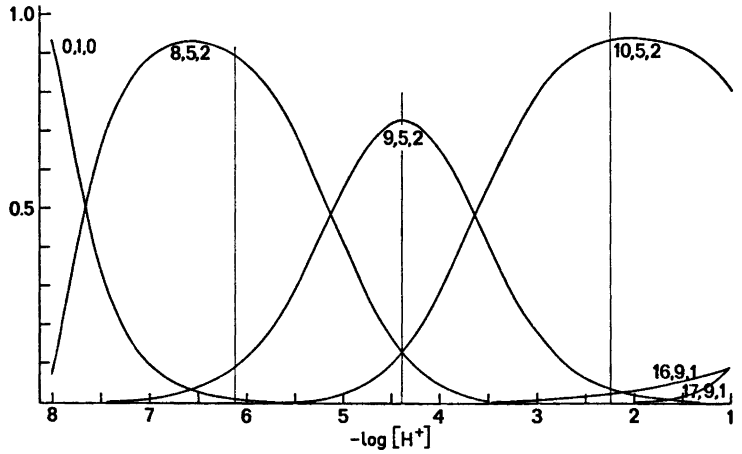

Fig. 2. Fraction of molybdenum bound in different complexes as a function of $-\log [H^+]$ calculated for a 1.6 M molybdate solution ($[HPO_4^{2-}] = 0.64$ M) with a Mo/P ratio of 2.5 with the use of the stability constants given by Pettersson.[1-3] For simplicity the complexes are given in p,q,r notation, for instance 8,5,2 stands for $(H^+)_8(MoO_4^{2-})_5(HPO_4^{2-})_2$.

X-Ray measurements. The X-ray scattering from the free surface of the solution was measured with the use of a diffractometer described in previous papers.[13] Because of strong fluorescence, MoK radiation could not be used and all the scattering curves were measured with AgK radiation ($\lambda = 0.5608$ Å). A Philips X-ray generator, PW 1130, was used. Monochromatization was achieved by means of a focusing single crystal LiF monochromator placed between the sample and the scintillation counter. A pulse height discriminator was connected to the counter. The fraction of incoherent radiation passing through the monochromator was estimated in the way described in a previous paper.[14]

The scattering was measured from $\theta \approx 1°$ up to $\theta \approx 70°$, where 2θ is the scattering angle. Slit openings of 1/12, 1/4, and 1° were used. From measurements in overlapping regions the scattering data were recalculated to a common slit width. The reproducibility was checked by repeated measurements at selected angles. Between 40 000 and 100 000 counts were taken at each angle, which corresponds to a statistical error of 0.5 % or better. Intervals of 0.25° were used except in the low angle region ($\theta < \sim 5°$), where measurements were taken at 0.1° intervals.

Treatment of intensity data. All calculations were carried out with an IBM360/75 computer using the KURVLR program.[15]

Corrections for absorption and multiple scattering were found to be negligible and were not applied. The correction for polarization was calculated by dividing with the factor $(1 + \cos^2 2\alpha \cos^2 2\theta)/(1 + \cos^2 2\alpha)$, where 2α is the scattering angle at the monochromator.[15] For each solution the intensities were normalized to a stoichiometric unit of volume corresponding to the volume containing one Mo atom (Table 1). The normalization was done by comparing observed intensities, $I_{corr}(s)$, corrected for polarization, with the sum of the independent coherent scattering and the incoherent scattering in the range $16 < s < 18$, where $s = 4\pi \sin \theta/\lambda$. Reduced intensities, $i(s)$, were calculated according to the expression:

$$i(s) = KI_{corr}(s) - \sum_i n_i\{[f_i^2(s) + (\Delta f_i'')^2] + del(s) I_i^{inc}(s)\}$$

where the summation is taken over all atoms in the unit of volume. K is the normalization constant; n_i is the number of atoms "i" in the chosen unit of volume; $f_i(s)$ is the scattering factor for the atom "i" corrected for the real part of the anomalous dispersion; $\Delta f_i''$ is the imaginary part of the anomalous dispersion correction for atom "i"; $I_i^{inc}(s)$ is the incoherent scattering from atom "i"; $del(s)$ is the fraction of incoherent radiation reaching the counter.

The scattering factors used were those given by Cromer and Waber [16] for Mo, Cl, P, Na, and O. For H the values given by Stewart *et al.*[17] were used. Anomalous dispersion corrections were taken from Cromer.[18] Values for the incoherent radiation were taken from Cromer and Mann[19] for Mo, P, Cl, and Na, from Cromer [20] for O, and from Compton and Allison [21] for H. They were corrected for the Breit-Dirac factor.

Low-frequency additions to the $i(s)$ curves, resulting in peaks in the radial distribution functions, $D(r)$, below 1 Å, which were too

Table 2. Observed and reduced intensity values.

s	A I	A i	B I	B i	C I	C i	D I	D i	E I	E i	F I	F i
0.600	2606	-1895.8	5205	764.8	2706	-2202.7	5269	51.0	5836	692.4	6966	1021.6
0.639	2628	-1845.0	4938	521.9	2691	-2186.2	4620	-564.4	5506	393.4	6329	409.6
0.678	2626	-1814.5	4445	54.8	2787	-2056.9	3938	-1210.6	4672	-407.9	5627	-244.5
0.718	2655	-1752.2	3826	-537.3	2832	-1976.8	3416	-1695.3	4120	-925.5	4958	-863.2
0.757	2654	-1718.8	3425	-909.1	2816	-1955.1	2988	-2084.4	3607	-1402.3	4408	-1362.4
0.796	2660	-1676.8	3004	-1300.2	2749	-1982.2	2626	-2406.0	3197	-1774.3	3920	-1798.1
0.835	2644	-1655.2	2675	-1597.8	2803	-1888.7	2411	-2579.5	2826	-2105.5	3607	-2058.2
0.874	2589	-1671.4	2403	-1837.0	2760	-1890.4	2231	-2716.7	2563	-2327.9	3266	-2345.0
0.913	2626	-1595.0	2199	-2007.3	2782	-1826.5	2075	-2829.5	2390	-2457.8	3020	-2534.8
0.952	2617	-1563.5	2031	-2139.8	2785	-1780.0	2014	-2845.8	2281	-2522.9	2871	-2627.6
0.991	2585	-1553.7	1921	-2213.9	2764	-1755.5	1988	-2825.7	2176	-2583.1	2767	-2674.3
1.030	2584	-1512.7	1866	-2231.8	2795	-1673.4	1987	-2779.9	2090	-2622.4	2652	-2731.1
1.069	2536	-1516.1	1828	-2232.6	2873	-1556.3	1963	-2756.7	2061	-2605.0	2650	-2674.3
1.108	2543	-1465.6	1814	-2208.0	2801	-1579.9	1995	-2676.2	2031	-2586.8	2631	-2633.5
1.147	2572	-1392.2	1788	-2195.2	2734	-1598.1	2040	-2581.8	2060	-2508.1	2563	-2639.9
1.186	2563	-1356.3	1855	-2088.3	2746	-1537.6	2107	-2465.5	2090	-2428.7	2603	-2538.6
1.226	2585	-1289.0	1821	-2082.3			2178	-2344.0	2160	-2308.9	2678	-2401.9
1.265	2568	-1259.7	1811	-2051.8			2225	-2246.9	2162	-2256.7	2737	-2280.1
1.283					2635	-1524.4						
1.304	2605	-1177.5	1866	-1956.0			2311	-2109.7	2251	-2116.7	2872	-2084.2
1.343	2619	-1117.9	1929	-1852.6			2415	-1955.7	2329	-1988.3	2995	-1899.5
1.382	2625	-1065.1	2009	-1732.0	2674	-1362.2	2517	-1802.3	2426	-1839.6	3067	-1763.9
1.421	2578	-1065.7	2084	-1615.6			2602	-1666.5	2500	-1714.5	3282	-1487.0
1.460	2615	-982.7	2201	-1457.7			2711	-1505.3	2730	-1433.1	3321	-1384.7
1.478					2751	-1161.3			2772	-1364.8		
1.499	2675	-876.5	2321	-1295.3			2816	-1348.8			3531	-1112.4
1.538	2696	-808.6	2405	-1169.9			2928	-1186.0			3613	-967.8
1.577	2726	-732.8	2517	-1016.4	2817	-970.3	3069	-992.7	3072	-927.7	3807	-710.6
1.616	2740	-672.0									3991	-463.7
1.655	2846	-520.5									4172	-220.7
1.677			2921	-507.1	2967	-696.4	3442	-490.5	3474	-403.3		
1.694	2891	-429.4									4305	-24.8
1.733	2990	-285.4									4551	282.7
1.772	3085	-145.4	3421	98.6	3229	-313.8	3884	79.0	3862	114.2	4723	516.7
1.811											4804	660.1
1.869	3275	156.5	3832	613.7	3532	109.9	4275	598.1	4264	645.0	4887	884.7
1.967	3412	405.0	3958	842.0	3793	489.0	4524	972.4	4434	941.0	4943	1046.0
2.064	3419	522.0	3816	800.4	3805	620.0	4445	1018.1	4280	909.7	4475	731.9
2.161	3176	389.2	3521	603.7	3635	568.7	4029	724.6	3876	625.9	4004	411.1
2.259	2880	200.7	3141	320.8	3245	296.6	3567	383.0	3402	268.9	3563	117.0
2.356	2554	-20.1	2836	110.5	2879	45.7	3141	74.0	3017	-1.9	3141	-162.6
2.453	2297	-176.0	2592	-41.8	2543	-178.5	2820	-133.9	2718	-189.1	2857	-309.5
2.550	2098	-277.6	2353	-190.1	2332	-283.3	2561	-282.6	2511	-287.6	2644	-391.0
2.647	1981	-301.2	2246	-209.4	2224	-289.1	2431	-306.2	2355	-338.9	2517	-392.6
2.744	1941	-252.2	2127	-243.2	2136	-279.1	2351	-283.9	2267	-325.3	2430	-358.5
2.841	1926	-182.3	2097	-190.0	2119	-201.9	2267	-268.1	2267	-227.1	2378	-293.7
2.938	1924	-103.3	2050	-157.5	2110	-121.8	2230	-209.7	2166	-234.7	2276	-285.1
3.035	1925	-24.0	1985	-145.1	2132	-13.3	2127	-221.1	2084	-226.0	2200	-254.7
3.132	1917	42.6	1938	-116.3	2114	52.2	2043	-216.4	2024	-198.4	2122	-231.1
3.229	1869	66.8	1814	-168.0	2059	76.9	1978	-196.2	1913	-224.9	2009	-246.1
3.326	1808	75.7	1722	-190.5	1987	82.2	1904	-169.2	1868	-189.7	1942	-220.5
3.422	1720	53.7	1673	-171.1	1901	70.2	1679	-135.2	1836	-143.4	1919	-154.9
3.518			1636	-143.4	1792	31.1	1876	-63.4	1843	-62.4	1893	-98.0
3.615	1557	12.8	1638	-78.9	1691	-2.0	1876	8.0	1833	-2.0	1895	-17.0
3.712	1463	-23.7	1606	-50.8	1599	-30.4	1851	50.8	1818	50.3	1875	37.5
3.808	1400	-34.0	1579	-20.3	1512	-57.4	1838	102.2	1796	92.8	1838	71.5
3.905	1347	-36.5	1567	22.4	1447	-64.9	1785	110.3	1723	80.3	1770	69.5
4.001	1290	-45.0	1552	58.7	1389	-69.4	1713	97.2	1666	80.5	1729	92.0
4.097	1264	-25.9	1546	102.8	1361	-46.7	1643	82.2	1586	54.9	1644	66.0
4.193	1251	3.1	1490	94.5	1328	-30.8	1565	57.3	1532	52.9	1581	59.1
4.284	1227	19.4	1451	101.6	1298	-15.4	1501	43.4	1463	33.0	1507	37.2
4.385	1210	41.0	1420	113.3	1294	23.6	1429	18.4	1400	17.7	1457	36.7
4.481	1190	58.0	1374	109.7	1263	34.3	1371	6.7	1352	13.8	1393	21.0
4.577	1162	64.4	1303	78.2	1249	59.5	1319	-2.1	1306	11.4	1359	31.0
4.672	1120	56.2	1240	53.6	1226	74.4	1276	-4.6	1252	-2.5	1300	14.1
4.768	1118	85.2	1167	17.1	1199	82.2	1219	-21.3	1204	-11.4	1257	11.3
4.863	1094	91.1	1103	-12.2	1168	85.8	1172	-31.4	1163	-15.5	1202	-5.2
4.959	1054	80.1	1019	-62.4	1130	80.5	1137	-30.5	1109	-34.0	1154	-17.7
5.054	1013	67.1	957	-92.1	1092	72.9	1092	-41.8	1066	-43.1	1102	-35.2
5.149	970	50.3	909	-109.9	1050	60.4	1061	-40.5	1044	-33.0	1078	-27.4
5.244	922	27.5	887	-102.8	1004	43.3	1043	-27.1	1020	-27.0	1065	-9.5
5.339	875	4.5	887	-74.8	967	32.9	1031	-9.9	1018	0.5	1053	7.2
5.434	828	-19.0	874	-61.4	915	7.0	1033	20.2	1007	17.7	1055	37.5
5.529	789	-35.2	876	-33.7	867	-16.8	1029	43.3	999	36.1	1044	53.1
5.624	751	-52.0	894	8.8	834	-26.2	1027	66.5	993	55.3	1047	80.7
5.718	727	-55.7	892	30.1	795	-42.4	1025	88.7	994	80.9	1038	96.4
5.813	697	-65.8	886	46.1	762	-53.9	997	84.4	981	91.3	1011	92.3
5.907	676	-67.1	869	51.1	740	-55.2	963	72.8	1004	136.6	958	61.8
6.002	659	-65.7	848	50.0	715	-60.6	930	62.0	913	66.6	925	50.5
6.096	645	-62.2	837	58.7	701	-54.7	886	38.3	864	37.8	891	27.4
6.190	636	-54.4	790	30.1	686	-51.8	834	6.1	807	0.5	819	-15.0
6.284	625	-48.8	767	25.4	675	-45.5	791	-17.8	766	-21.2	770	-44.1
6.377	617	-40.9	735	9.7	661	-41.8	742	-47.9	723	-46.4	742	-53.8
6.471	608	-34.2	708	-0.4	659	-28.4	716	-56.0	695	-56.3	704	-73.7
6.565	600	-27.7	681	-11.6	644	-27.5	690	-65.2	670	-64.5	705	-55.2
6.658	597	-15.3	666	-11.6	633	-23.0	675	-63.5	663	-55.1	685	-58.8
6.751	590	-8.9	653	-9.8	632	-9.2	670	-53.0	649	-53.7	684	-43.5
6.845	585	-0.3	624	-25.8	611	-15.1	679	-28.0	648	-39.6	669	-42.8
6.938	571	-0.6	608	-27.5	615	1.8	669	-24.1	648	-24.8	676	-21.3
7.030	567	8.6	593	-30.4	597	-2.2	662	-16.2	644	-14.4	659	-23.3
7.123	552	5.9	579	-31.6	590	4.1	645	-19.4	634	-10.2	647	-20.9
7.216	547	13.2	569	-30.0	577	3.8	650	-0.8	616	-15.2	640	-13.3
7.308	536	13.5	566	-20.8	567	5.4	633	-5.0	613	-4.9	635	-4.4
7.401	521	9.8	560	-16.4	564	14.9	617	-8.1	599	-7.0	-	-
7.493	515	14.4	560	-5.0	544	6.8	603	-9.9	591	-2.6	598	-15.5
7.585	509	19.9	555	0.4	534	7.3	594	-6.9	573	-9.2	587	-13.6
7.677			553	8.6	535	18.9	578	-10.9	567	-3.7	581	-7.8
7.769	488	18.5	551	16.3	520	14.4	576	-1.6	560	0.9	575	-1.7
7.860	475	15.2	545	19.2	505	9.9	576	9.3	551	2.0	570	4.7
7.952	470	19.3	538	21.4	498	13.5	565	9.9	549	10.9	561	7.2
8.043	458	16.5	527	19.3	496	20.3	565	20.4	545	17.6	557	14.0
8.134	447	14.6	518	19.0	482	15.7	556	21.4	537	19.4	547	14.6
8.225	442	17.8	505	14.4	470	12.8	547	22.5	520	11.3	535	12.9
8.316	428	12.3	488	6.3	458	10.1	523	7.8	508	9.2	517	5.4
8.407	419	10.4	474	-0.3	453	13.5	512	6.4	489	-0.7	505	2.8
8.498	410	8.9	470	4.0	443	11.1	503	6.7	483	1.9	489	-4.1
8.588	399	5.5	453	-5.9	431	7.9	479	-8.1	466	-6.8	473	-10.3
8.678	392	5.5	437	-13.9	425	9.2	484	5.4	454	-10.4	461	-13.8
8.768	385	4.6	436	-8.0	416	7.7	445	-25.3	440	-15.5	455	-10.9
8.858	375	1.5	420	-16.4	411	9.8	446	-15.5	436	-11.5	445	-13.0
8.948	363	-4.6	417	-13.0	396	1.3	442	-11.6	436	-4.5	448	-1.2
9.037	357	-4.7	410	-13.2	384	-3.5	443	-3.1	426	-6.9	446	4.1
9.127	352	-4.0	406	-10.5	384	2.4	444	5.9	432	6.8	443	8.9
9.216	342	-8.7	398	-12.2	368	-6.3	439	8.5	428	9.7	442	14.7
9.305	335	-9.7	398	-5.0	366	-3.0	441	17.1	423	11.5	435	15.3
9.394	332	-7.8	393	-3.8	358	-5.3	427	10.9	422	17.5	433	20.1
9.482	322	-13.1	392	1.0	351	-6.7	422	12.5	416	17.7	420	14.0
9.570	314	-16.1	384	-0.6	345	-7.1	412	9.5	407	15.1		
9.658	308	-18.0	377	-1.8	335	-10.7	404	7.5	397	11.2	403	9.4
9.747	308	-13.7	379	6.0	329	-11.8	395	5.5	388	8.4	393	5.2
9.835			372	4.5	328	-8.2	388	4.6	380	6.0	385	3.6
9.922	307	-6.2	370	8.1	316	-15.3	374	-3.3	365	-3.2	377	0.5
10.010	300	-9.3	361	4.5	316	-10.8	374	2.8	363	0.9	362	-8.6
10.097	296	-8.7	359	7.6	308	-14.3	360	-5.4	356	-0.7	364	-0.5
10.184	294	-7.3	351	5.4	307	-10.6	355	-5.1	351	-0.6	353	-6.3
10.271	290	-7.1	359	-2.1	303	-10.2	349	-5.2	341	-5.4	343	-11.1
10.358	291	-2.8	333	-2.0	303	-5.3	340	-8.7	336	-5.1	342	-7.2
10.445	284	-6.1	322	-8.0	292	-12.7	332	-11.9	329	-7.2	333	-12.0
10.531	285	-1.3	318	-7.3	299	-1.8	337	-1.5	325	-6.3	329	-10.9
10.617	280	-3.1	311	-10.1	291	-6.1	322	-11.7	319	-7.9		
10.703	278	-1.3	305	-11.3	291	-1.3	322	-7.3	314	-8.2	323	-7.9
10.789	273	-2.7	302	-9.2	291	2.1	320	-3.6	314	-3.9	321	-4.7
10.875	275	3.2	301	-6.2	285	-0.5	316	-3.6	306	-6.8	316	-5.4
10.960	269	0.1	294	-6.1	286	4.1	315	-0.1	305	-3.6	319	1.5
11.045	269	3.8	293	-4.6	280	2.1	308	-1.6	307	2.6	319	5.2
11.130	266	4.3	292	-1.5	279	4.7	309	3.2	297	-2.7	314	5.1
11.215	266	7.3	297	7.8	273	2.9	302	0.8	300	4.7	308	3.0
11.300	259	4.1	289	4.1	269	2.2	303	6.4	298	6.1	305	5.0
11.384	256	3.9	286	4.9	269	5.1	301	8.2	294	6.5	302	5.2
11.468	252	3.8	285	7.9	270	10.4	295	6.1	291	7.5	300	7.5
11.552			277	3.5	264	7.7	290	5.3	288	8.5	294	6.0
11.636	245	3.3	272	3.1	261	7.7	284	3.4	283	7.0	289	4.3
11.719	244	5.7	271	5.4	256	6.6	281	4.4	278	6.2	281	0.3
11.802	238	3.1	266	4.4	251	5.1	283	10.8	271	3.2	280	3.5
11.885	238	6.0	259	1.4	250	7.3	271	2.8	264	-0.1	269	-3.9
11.968	232	3.5	259	4.4	244	3.8	270	4.6	256	-4.4	262	-7.4
12.051	228	2.8	257	6.3	239	2.3	254	-7.6	253	-3.9	259	-6.6
12.133	223	0.8	253	5.7	235	1.4	254	-3.3	247	-7.0	250	-1.8
12.215	219	-0.3	245	1.8	231	0.8	248	-6.2	246	-4.2	248	-9.8
12.297	213	-3.3	238	-1.9	227	0.4	244	-6.1	239	-7.3	248	-6.4
12.379	211	-2.0	238	1.0	225	-0.7	245	-2.2	238	-5.3	241	-10.4
12.460	206	-4.4	232	-1.7	222	1.2	238	-5.7	234	-6.0	239	-8.7
12.541	205	-2.2	224	-6.1	216	-2.1	236	-4.0	229	-7.7	237	-7.2
12.622	202	-2.2	222	-5.1	213	-1.7	233	-4.1	227	-6.7	232	-8.8
12.703	198	-3.5	216	-8.0	207	-5.1	229	-4.2	226	-4.1	235	-2.2
12.783	197	-1.0	213	-8.4	205	-4.0	226	-4.3			231	-3.4
12.863	191	-4.0	211	-7.1	204	-2.2	223	-3.5	220	-3.9	226	-5.4
12.943	192	-0.8	211	-4.1	203	-0.1	221	-2.6	220	-1.5	226	-2.3
13.023	188	-2.5	207	-5.5	196	-4.4	219	-1.6	216	-1.7	224	-1.1
13.102	184	-3.1	206	-3.2	194	-3.8	216	-2.0	212	-2.9	220	-1.3
13.182	183	-1.6	202	-4.7	190	-4.8	213	-1.4	212	-0.6	218	-0.9
13.260	178	-4.2	202	-2.6	191	-2.1	212	0.1	209	-0.2	218	1.4
13.339	177	-2.6	200	-1.1	189	-1.7	207	-1.9	213	6.4	215	1.5
13.418	175	-2.8	201	2.3	186	-1.6	206	-0.6	207	3.0	217	5.9
13.496	175	0.2	198	1.5	183	-2.4	208	4.8	207	5.5	211	2.7
13.574	169	-4.1	198	4.3	180	-2.8	205	3.5	203	4.2	209	3.3
13.651	170	-0.4	193	1.2	179	-1.9	203	4.2	201	4.2		
13.729	168	-1.1	192	2.8	176	-2.6	200	4.3	200	5.3	206	5.1
13.806	169	1.9	188	1.1	177	0.4	199	5.2	198	6.2	204	5.5
13.883	160	-4.4	187	1.6	174	-0.6	195	3.7	194	3.9	202	5.2
13.959	163	-0.4	185	2.4	171	-2.0	193	3.5	193	4.7	199	5.0
14.036	160	-0.5	181	0.5	169	-1.5	191	4.1	190	4.3	195	3.2
14.112	159	-0.6	179	-0.4	167	-1.9	189	4.3	186	2.1	192	1.3
14.188	157	-0.8	176	-0.6	166	-1.9	185	1.8	184	1.8	189	0.7
14.263	156	-0.3	175	-0.0	165	-0.7	181	-0.2	179	-1.2	188	1.8
14.339	156	1.5	174	1.0	164	-0.1	178	-0.6	177	-1.3	185	-0.2
14.414	153	0.3	173	1.6	164	1.1	171	-5.8	174	-3.0	179	-3.8
14.488	154	2.5	169	-0.4	161	-0.2	172	-3.4			179	-2.7
14.563	152	2.2	164	-4.3	162	1.7	169	-4.7	170	-3.2	177	-2.8
14.637	150	1.5	165	-1.1	159	0.6	168	-3.7	169	-3.1	178	-1.1
14.711	149	1.2	160	-4.9	159	1.3	170	-0.2	168	-2.3	174	-3.2
14.784	145	-1.5	161	-2.1	157	0.5	168	-0.6	166	-2.7	174	-2.3
14.858	143	-1.4	159	-1.9	154	-0.3	167	0.1	168	0.4	174	-0.5
14.931	144	0.3	155	-5.1	156	2.4	162	-3.7	166	0.0	172	-1.4
15.007	143	0.2	153	-5.0	153	0.9	163	-1.0	165	0.6	173	1.3
15.076	144	2.7	154	-3.1	149	-1.7	163	-0.2	163	-0.2	169	-1.6
15.148	138	-1.9	152	-3.9	149	-0.8	163	1.5	161	-1.1	168	-1.0
15.220	140	0.9	151	-3.1	152	2.9	161	0.6	161	0.4	168	0.0
15.292	138	0.3	152	-0.7	148	0.1	161	1.7	160	1.1	164	-3.1
15.363	134	-3.2	151	-0.4	146	-0.5	156	-2.0	159	0.0	163	-2.7
15.434	134	-1.2	148	-1.9	146	0.4	155	-1.1	156	-1.7	160	-4.3
15.505	134	-1.2	148	-0.4	146	1.2	154	-0.9	156	-0.4	161	-2.7
15.575	134	0.5	147	-0.2	144	0.2	154	0.4	154	-1.2	161	-1.8
15.645	130	-2.8	144	-1.6	141	-1.7	154	1.0	152	-1.7	158	-3.3
15.715	132	0.2	144	-0.9	143	1.7	150	-1.6	152	-1.4	158	-2.5
15.785	130	-1.0	143	0.0	144	3.1	149	-1.2	153	1.0	158	-1.1
15.854	129	-1.0	142	-0.5	141	1.3	145	-4.8	148	-2.9	153	-5.4
15.923	128	-0.4	141	-0.1	139	-0.0	145	-3.6	148	-2.1	157	0.0
15.992	127	-0.5	138	-1.4	138	-0.3	145	-2.1	149	0.3	152	-3.7
16.060	126	-0.4	138	-0.4	138	1.1	144	-2.2	149	1.1	152	-3.3
16.128	126	0.0	137	-0.3	135	-0.6	147	2.0	147	-0.5	153	-0.6
16.196	122	-2.5	137	0.9	133	-2.0	144	-0.3	145	-1.0	152	-1.0
16.263	124	-0.2	134	-0.8	134	-0.3	144	0.2	145	-0.3	151	-0.5
16.330	123	0.1	135	1.0	133	0.0	143	0.3	144	-0.5	150	-0.8
16.397	122	0.1	133	0.2	133	0.3	142	0.4	144	1.0	149	-1.1
16.464	121	-0.8	131	-0.7	131	-0.7	140	-0.4	143	0.5	148	-1.2
16.530	120	-0.5	132	1.1	129	-1.2	141	1.0	143	1.2	149	1.1
16.596	119	-0.8	132	1.6	130	0.3	139	-0.2	142	0.8	146	-0.9
16.661	118	-0.6	131	1.8	129	-0.1	137	-0.7	140	-0.1	149	2.5
16.726	117	-1.0	131	2.6	128	0.6	138	1.0	140	1.0	146	0.8
16.791	117	-0.4	127	0.3	126	-0.7	139	2.1	139	1.0	146	1.0
16.856	116	-0.3	127	1.1	126	0.3	136	0.4	138	1.2	145	1.2
16.920	113	-1.9	125	-0.6	124	-0.9	132	-2.4	138	1.4	145	2.1
16.984	114	-0.8	125	0.7	122	-2.0	135	0.7	138	2.8	143	1.1
17.048	114	0.1	124	0.1	123	-0.5	134	0.5	136	0.6	141	0.0
17.111	111	-2.2	123	-0.4	120	-2.1	133	0.8	135	0.9	142	2.1
17.174	111	-0.7	121	-1.5	120	-1.7	134	1.9	135	1.2	142	2.6
17.237	112	0.5	121	0.0	120	-1.3	131	0.4	133	0.8	142	3.3
17.299	111	0.0	121	0.7	119	-0.7	132	1.7	132	0.4	136	-0.9
17.361	110	0.1	118	-1.5	118	-1.5	130	0.6	130	-1.2	137	0.9
17.423	109	0.1	119	0.2	118	0.1	129	0.1	132	1.6	136	0.6
17.484	109	0.9	118	-0.4	121	3.0	127	-0.9	130	0.7	133	-1.8
17.545	109	1.2	117	-0.8	119	2.2	127	-0.2	127	-1.5	133	-0.7
17.606	107	0.7	116	-0.7	116	0.6	126	-0.5	126	-2.1	132	-0.7
17.666	107	0.9	117	0.9	117	1.9	125	-0.4	125	-1.8	131	-1.3
17.726	107	1.3	114	-1.0	114	0.3	124	-0.8	124	-2.3	131	0.0
17.786	106	1.6	114	-0.8	114	0.8	122	-1.5	124	-2.0	130	-0.4
17.845	105	1.5	113	-0.5	114	1.1	122	-1.2	123	-1.9	127	-2.1
17.904	106	2.8	111	-1.7	115	3.2	121	-1.5	122	-1.4	127	-1.9
17.962	105	2.7	111	-1.8	113	2.6	119	-2.3	120	-2.7	126	-2.3
18.021	103	1.3	111	-1.1	113	2.4	118	-2.8	120	-2.7	125	-2.4

short to correspond to interatomic distances, were removed by a Fourier transformation of that part of the $D(r)$ curves,[15] account being taken of contributions of short interatomic distances extending into that region.

The electronic radial distribution functions, $D(r)$, were calculated from:

$$D(r) = 4\pi r^2 \varrho_0 + \frac{2r}{\pi} \int_0^{s_{max}} si(s) M(s) \sin(rs)\, ds$$

The modification function, $M(s)$, was chosen to be:

$$\{f_{Mo}^2(0)/f_{Mo}^2(s)\} \exp(-0.01s^2).$$

Intramolecular contributions to the theoretical intensities were calculated from the expression:

$$\sum_{\substack{m \\ m \neq n}} \sum_{n} f_m f_n \frac{\sin(r_{mn}s)}{r_{mn}s} \exp(-b_{mn}s^2)$$

where r_{mn} is the distance between the atoms n and m and b_{mn} is a temperature factor. Corresponding peak shapes were obtained from these intensities by a Fourier transformation analogous to that used for the experimental intensities.

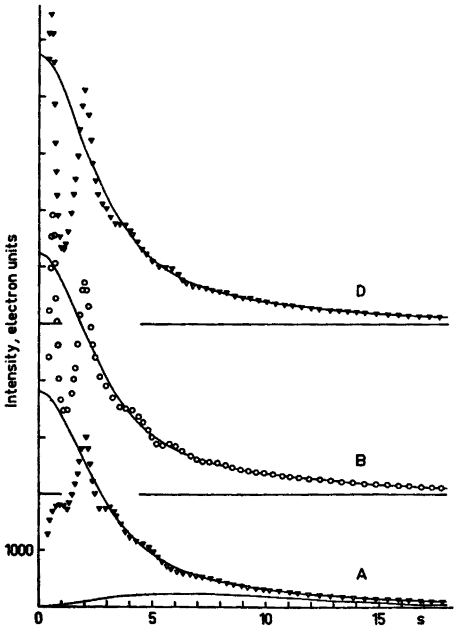

Fig. 3. Observed intensity values, $I(s)$, compared with the independent coherent scattering (full-drawn curves) for the solutions A, B, and D. The lower full-drawn curve gives the estimated amount of incoherent radiation reaching the counter.

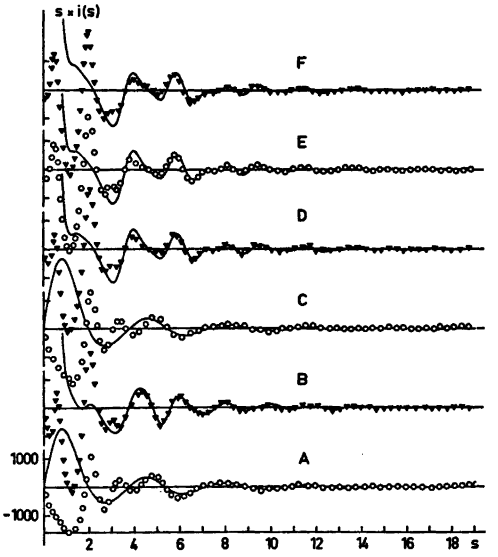

Fig. 4. A survey of the experimental $si(s)$ values for the different solutions. Full-drawn lines represent theoretical curves calculated with the use of the parameters in Table 3.

ANALYSIS OF THE DATA

The observed intensities, $I(s)$, after normalization to the chosen stoichiometric unit of volume, and correction for incoherent radiation are given in Table 2 and in Fig. 3. Table 2 also gives the reduced intensity values, $i(s)$, corrected for spurious peaks below 1 Å in the radial distribution functions. A survey of values, $si(s)$, for the different solutions is shown in Fig. 4.

For the acidified solutions B, D, E and F the radial distribution curves (Figs. 5 and 7) show several peaks, indicating intramolecular interactions, which are not present for the slightly alkaline solutions A and C. This is consistent with the occurrence of polynuclear complexes in the acidified solutions.

According to equilibrium data practically all molybdenum should occur as $H_nMo_5P_2O_{23}^{(6-n)-}$ in solutions D ($n=0$), E ($n=1$), and F ($n=2$) (Fig. 2) and as $Mo_7O_{24}^{6-}$ in solution B. With the use of the parameters obtained from the crystal structure determinations for the posi-

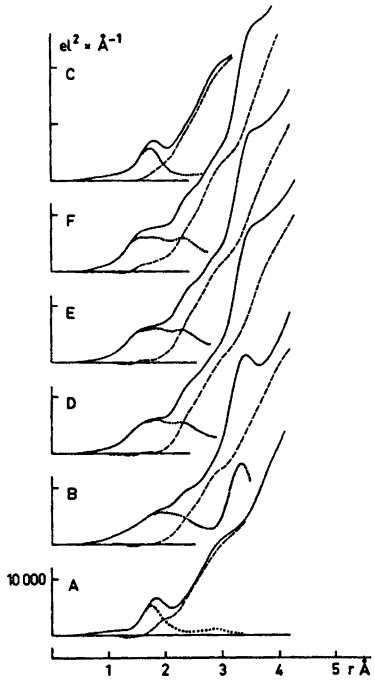

Fig. 5. Radial distribution curves, $D(r)$. Dotted curves represent the sum of intramolecular contributions calculated from the parameters in Table 3. Broken curves represent the difference between the experimental $D(r)$ function and the calculated intramolecular contributions.

tions of the atoms in the complexes $Mo_7O_{24}^{6-}$ [11] and $Mo_5P_2O_{23}^{6-}$ [4] the expected peak shapes for these complexes were calculated and are shown in Fig. 6. Comparison with the radial distribution functions, $D(r)$, in Fig. 5, and, in particular, with the functions $D(r) - 4\pi r^2\varrho_0$ in Fig. 7 shows similar peaks to be present for the acidified solutions. For the slightly alkaline solutions containing only molybdate ions (solution A) or molybdate and phosphate ions (solution C), a peak at 1.7_5 Å corresponds to the expected Mo – O distance. For comparison the calculated peak shape for a tetrahedral MoO_4^{2-} ion is shown in Fig. 6.

When the intramolecular interactions within the $Mo_7O_{24}^{6-}$, the $Mo_5P_2O_{23}^{6-}$, and the ClO_4^- groups for the acidified solutions, and the MoO_4^{2-} and the PO_4^{3-} groups for the alkaline solutions, are subtracted from the corresponding $D(r) - 4\pi r^2\varrho_0$ functions, the difference curves, shown in Fig. 7, are obtained. These curves, which are all very similar, represent residual interactions in the solutions. They show broad peaks at about 2.9 and 4.0 Å, which probably contain contributions from persistent parts of the water structure. The coordination of the sodium ions, which are present at approximately equal concentrations in all of the solutions, will also give contributions to this remaining structure, as will all intermolecular interactions. Beyond about 9 Å the curves indicate no significant deviations from the average, $4\pi r^2\varrho_0$, function.

The similarity of the difference curves and the absence of sharp peaks and of deviations from a smooth background curve in the regions where sharp peaks have been subtracted, indicate that the complexes assumed are sufficient to explain all intramolecular interactions in the solutions.

For the calculations of the peak shapes temperature factors of 0.002 for Mo – Mo, 0.006 for Mo – O, and 0.01 for O – O interactions were used (Table 3). These values were estimated

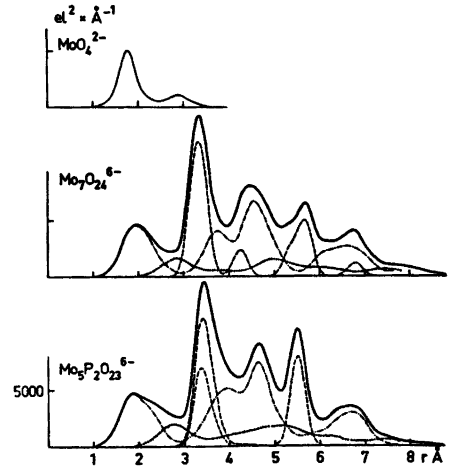

Fig. 6. Calculated peak shapes for the $Mo_7O_{24}^{6-}$ and the $Mo_5P_2O_{23}^{6-}$ complexes and for a tetrahedral MoO_4^{2-} group. The parameters used for the calculations are given in Table 3. For the $Mo_7O_{24}^{6-}$ complexes the contributions from Mo – Mo (dashed lines), Mo – O (dashed-dotted lines), and O – O (dotted lines) interactions are separately drawn. The same is done for the $Mo_5P_2O_{23}^{6-}$ complex but here the dashed-dotted line represents the sum of Mo – O and P – O interactions, and the two peaks at 3.3 Å represent Mo – Mo interactions (small peak) and the sum of Mo – Mo and Mo – P interactions (large peak).

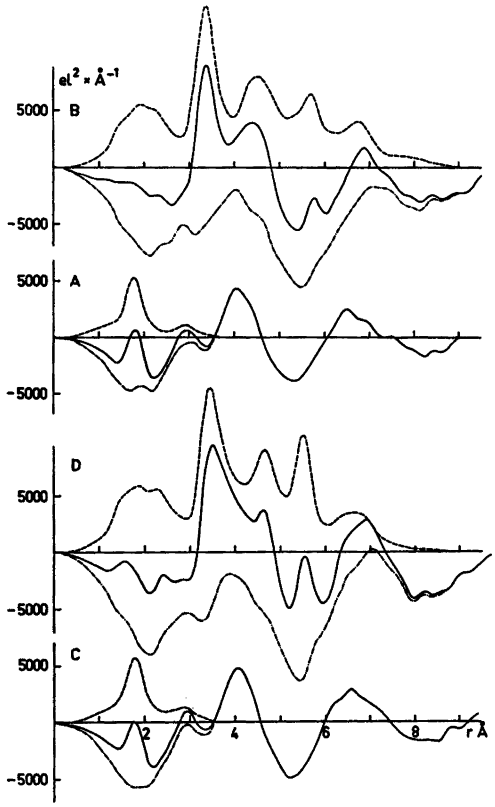

Fig. 7. Radial distribution functions for the solutions A, B, C, and D. Full-drawn lines represent the experimental $D(r) - 4\pi r^2 \varrho_0$ functions. Dashed lines are the sum of calculated peaks for intramolecular interactions obtained with the parameters in Table 3. Dashed-dotted lines are the corresponding differences.

from a comparison between calculated and experimental $i(s)$ values in the high-angle part of the intensity curves, where Mo – Mo interactions are the main contributors. A temperature factor of 0.002 for a Mo – Mo distance corresponds to an r.m.s. value for the variation of the distance of 0.06 Å. This indicates that the relative Mo – Mo (and Mo – P) distances in the $Mo_7O_{24}^{6-}$ and the $Mo_5P_2O_{23}^{6-}$ groups are closely similar in the solutions and in the crystals.

Slightly better agreement between observed and calculated intensities can be obtained by adjusting the temperature factors by means of a least squares procedure. However, since the number of parameters that can be included in such a refinement is limited, simplifying assumptions must be made and, therefore, these rather extensive calculations did not seem justified. For the alkaline solutions an adjustment, by a least squares procedure, of the single Mo – O interaction present was, however, carried out. This led to a Mo – O distance of 1.78[1] Å, which is close to the value 1.77_2 Å found for the discrete MoO_4^{2-} ions in crystals of $Na_2MoO_4 \cdot (H_2O)_2$.[22]

A comparison between the sum of the peak shapes for the assumed intramolecular interactions for each solution and the corresponding $D(r)$ function at low r values is shown in Fig. 5. Below about 2 Å the $D(r)$ curves are closely reproduced by the assumed interactions, which confirms that the average Mo – O coordination in the acidified solutions is the same as found in the crystals. A possible exception is solution F, where small deviations seem to occur.

A direct comparison between the radial distribution functions for the acidified solutions is more sensitive towards differences between the complexes in the crystals and in the solutions. The similar size and shapes and the approximately equal concentrations in the solutions of the $Mo_7O_{24}^{6-}$ and the $Mo_5P_2O_{23}^{6-}$

Table 3. Parameters used for the calculation of theoretical curves.

Molecule	Intramolecular distances	(Å)	Temperature factor (Å²)
MoO_4^{2-}	Mo – O	1.75	0.002
	O – O	2.86	0.004
$Mo_7O_{24}^{6-}$	Mo – Mo	[a]	0.002
	Mo – O	[a]	0.006
	O – O	[a]	0.01
$Mo_5P_2O_{23}^{6-}$	Mo – Mo, Mo – P, P – P	[b]	0.002
	Mo – O, P – O	[b]	0.006
	O – O	[b]	0.01
ClO_4^-	Cl – O	1.43	0.002
	O – O	2.34	0.002
PO_4^{3-}	P – O	1.54	0.002
	O – O	2.51	0.004
H_2O	O – H	1.0	0.004

[a] Parameters taken from the crystal structure determination of $Na_6Mo_7O_{24}(H_2O)_{14}$ by Sjöbom and Hedman.[11] [b] Parameters taken from the crystal structure determination of $Na_6Mo_5P_2O_{23}(H_2O)_{13}$ by Strandberg.[4]

complexes should result in closely similar intermolecular interactions. Thus, it may be expected that differences between the distribution curves for the acidified solutions will mainly reflect differences between the intramolecular interactions within the complexes. The resulting difference curves, obtained by subtracting the $D(r)-4\pi r^2\varrho_0$ function for solution D from those of the other acidified solutions, are shown in Fig. 8. For this calculation the stoichiometric unit of volume for solution B, containing $Mo_7O_{24}^{6-}$ complexes, was increased to 947 Å^3 in order to give the same average scattering power, ϱ_0, as solution D (Table 1).

The difference between solution B, containing $Mo_7O_{24}^{6-}$ complexes, and solution D, containing $Mo_5P_2O_{23}^{6-}$ complexes, is compared in Fig. 8 with the difference between the peak shapes calculated for the assumed intramolecular interactions in these solutions. The close correlation between the two curves confirms that no significant differences occur between the structures of the complexes in the crystals and in the solutions. For comparison, differences are also given which are calculated after shifting one of the peak shape curves +0.05 or −0.05 Å relative to the other. The resulting curves, shown in Fig. 8, indicate that if differences in Mo−Mo distances occur between crystals and solutions they are probably less than about 0.01 Å, at least for the short Mo−Mo distances. Even for the Mo−O distances, which do not give rise to peaks as sharp as those of the Mo−Mo interactions (Fig. 6), there are no indications of significant differences. This is seen by comparing those parts of the curves in which the Mo−O interactions make their largest contributions (Figs. 6, 7, and 8). Interactions involving only oxygen atoms are too diffuse to allow any conclusions as to a possible difference (Fig. 6).

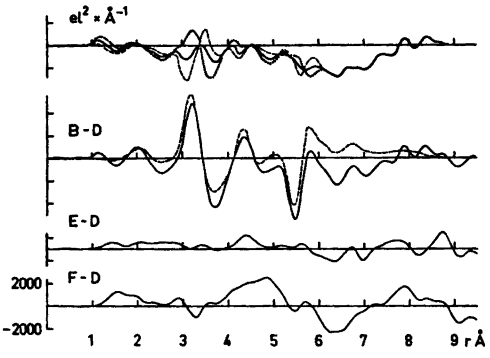

Fig. 8. Differences curves between the radial distribution functions for the solutions and between calculated peak shapes for the assumed intramolecular interactions. The full-drawn curves marked B−D, E−D, and F−D represent the functions obtained by subtracting the $D(r)-4\pi r^2\varrho_0$ function for solution D from those of solutions B, E, and F, respectively. The dashed curve, B−D, gives the difference between the calculated intramolecular interactions for solutions B and D obtained with the use of the parameters in Table 3. The upper full-drawn curve is the calculated difference between the two curves, B−D. The dashed and the dotted curves are corresponding differences obtained after shifting the calculated peak shape curves +0.05 or −0.05 Å relative to each other.

The predominant complex in solution E is $HMo_5P_2O_{23}^{5-}$ (Fig. 2). The difference between the $D(r)-4\pi r^2\varrho_0$ function for this solution and for solution D, containing the $Mo_5P_2O_{23}^{6-}$ complexes, is shown in Fig. 8. No significant peaks are present and, apparently, the addition of a proton to the $Mo_5P_2O_{23}^{6-}$ complex does not change its basic structure.

In solution F the predominant complex should have the composition $H_2Mo_5P_2O_{23}^{4-}$ according to emf measurements.[1-3] The discrete complex $H_2Mo_5P_2O_{23}^{4-}$ has been found in crystals and the structure determination [5] has shown it to be built up in the same way as the $Mo_5P_2O_{23}^{6-}$ complex with the two protons probably associated with the two phosphate oxygens not shared with molybdenum atoms (Fig. 1). The corresponding difference curve, however, indicates larger deviations than those found for solution E (Fig. 8), and these deviations are not attributable to the small structural differences between the complexes $H_2Mo_5P_2O_{23}^{4-}$ and $Mo_5P_2O_{23}^{6-}$, as found from the crystal structure determinations.

DISCUSSION OF THE RESULTS

The close correlation between the observed radial distribution curves and the calculated intramolecular interactions, shown in Figs. 7 and 8, strongly supports the identification of the polymolybdates in the solutions, with the $Mo_5P_2O_{23}^{6-}$ and the $Mo_7O_{24}^{6-}$ units found in crystals. However, since the distribution curves give only one-dimensional representations of the

three-dimensional complexes they are insensitive towards minor differences in structures and this could make the uniqueness of the interpretation uncertain. By repeating the calculations, the results of which are summarized in Figs. 7 and 8, after making small changes in the assumed structures of the complexes, an estimate of the "degree of significance" in the conclusions can be obtained. Adding or removing a Mo atom without changing other atomic parameters in the structures leads to significant deviations between observed and calculated distribution curves. The nuclearity of the predominant complexes, therefore, is uniquely determined by the diffraction measurements.

The effect of small differences in the average distances between the complexes in solution and the corresponding complexes in crystals is illustrated in Fig. 8. The difference curves are particularly sensitive towards small differences in the short Mo – Mo distances. The agreement between the observed distribution curves and the calculated curves indicates that such differences do not occur or, at least, cannot be of a magnitude larger than about 0.01 Å. Apparently the Mo frame work in the complexes is unchanged when the complex is transferred from a crystal to a solution. The oxygen positions also seem to be unaffected, but the distribution curves are less sensitive towards changes in distances involving oxygen atoms, if they do not lead to large changes in the average Mo – O distances.

In crystals of the pentamolybdodiphosphates [4,5] and in the heptamolybdate [11] the sodium ions are closely associated with the polymolybdate ions. This association may also occur in solution, but because of the low atomic number of Na and the many interactions involved when a sodium atom is added to the complex, the effects on the distribution curves will be too small and too diffuse to allow any conclusions to be made regarding this.

CONCLUSIONS

In an apparently unique way, the solution X-ray scattering measurements lead to an identification of the discrete $Mo_5P_2O_{23}^{6-}$ and $Mo_7O_{24}^{6-}$ units found in crystal structures,[4,5,10,11,23] with polymolybdate species in solution, which have been identified by equilibrium studies.[1–3,7] The scattering data indicate that no significant change occurs in the structures of these complexes when they are transferred from a crystal to the dissolved state.

The homonuclearity of the protonized pentamolybdodiphosphate species is supported by the present measurements. Only in the most acidified of the solutions, where $H_2Mo_5P_2O_{23}^{4-}$ should be the predominant complex, are peaks present in the distributions curves, which might indicate an incipient association of the complexes into larger groups.

In molybdate-phosphate solutions with Mo/P > 2.5 other types of complexes seem to form. The occurrence of a series of complexes with Mo/P = 9 has been suggested on the basis of emf measurements and is supported by crystal structure determinations of $Na_3H_6Mo_9PO_{34}(H_2O)_{12}$ [24] and $Na_6Mo_{18}P_2O_{62}(H_2O)_{24}$,[25] which contain discrete polynuclear complexes. X-Ray scattering measurements are now being made to identify these complexes in the solutions. In the binary $H^+ - MoO_4^{2-}$ system the solubilities of the molybdate complexes at the larger H^+/MoO_4^{2-} ratios are considerably increased when sodium ions are replaced by lithium ions in the solutions. This makes it possible to study the molybdate complexes in these solutions by X-ray scattering measurements over a large range of acidities. Such measurements are now being done in order to establish if an equilibrium between hepta- and octamolybdates occurs in the solutions.

Acknowledgements. The work has been supported by Statens Naturvetenskapliga Forskningsråd (Swedish Natural Science Research Council). Computer time has been made available by the Computer Division of the National Swedish Office for Administrative Rationalization and Economy. We wish to thank Dr. Derek Lewis for linguistic help.

REFERENCES

1. Pettersson, L. *Acta Chem. Scand. 25* (1971) 1959.
2. Pettersson, L., Andersson, I., Lyhamn, L. and Ingri, N. *Trans. Roy. Inst. Technol. Stockholm 1972* No. 256.
3. Pettersson, L. *Chem. Scr. 7* (1975) 145.
4. Strandberg, R. *Acta Chem. Scand. 27* (1973) 1004.
5. Hedman, B. *Acta Chem. Scand. 27* (1973) 3335.

6. Sillén, L. G. and Martell, A. E. (compilers). *Stability Constants, Chem. Soc. Spec. Publ. No. 17* (1964); *Suppl. No. 1, Spec. Publ. No. 25* (1971).
7. Sasaki, Y. and Sillén, L. G. *Acta Chem. Scand. 18* (1964) 1014; *Ark. Kemi 29* (1968) 253.
8. Aveston, J., Anacker, E. W. and Johnson, J. S. *Inorg. Chem. 3* (1964) 735.
9. Lindqvist, I. *Ark. Kemi 2* (1950) 325.
10. Gatehouse, B. M. and Leverett, P. *Chem. Commun. 15* (1968) 901.
11. Sjöbom, K. and Hedman, B. *Acta Chem. Scand. 27* (1973) 3673.
12. Dunitz, J. D. and Ibers, J. A. *Perspectives in Structural Chemistry*, Vol IV, Wiley, New York 1971, p. 36.
13. Johansson, G. *Acta Chem. Scand. 25* (1971) 2787; *20* (1966) 553.
14. Pocev, S. and Johansson, G. *Acta Chem. Scand. 27* (1973) 2146.
15. Johansson, G. and Sandström, M. *Chem. Scr. 4* (1973) 195.
16. Cromer, D. T. and Waber, J. T. *Acta Crystallogr. 18* (1965) 104.
17. Stewart, R. F., Davidson, E. K. and Simpson, W. T. *J. Chem. Phys. 42* (1965) 3175.
18. Cromer, D. T. *Acta Crystallogr. 18* (1965) 17.
19. Cromer, D. T. and Mann, J. B. *J. Chem. Phys. 47* (1967) 1892.
20. Cromer, D. T. *J. Chem. Phys. 50* (1969) 4857.
21. Compton, A. H. and Allison, S. K. *X-Rays in Theory and Experiment*, van Nostrand, New York 1935.
22. Yamamura, K., Kobayashi, A. and Sasaki, Y. *Private communications.*
23. Evans, H. T., Jr. *J. Amer. Chem. Soc. 90* (1968) 3275.
24. Strandberg, R. *Acta Chem. Scand. A 28* (1974) 217.
25. Strandberg, R. *Acta Chem. Scand. To be published.*

Received June 14, 1974.

Acta Chemica Scandinavica A 28 (1975) 1129—1135

Hydrogen Bond Studies. 91.* Infrared Spectra of Potassium and Rubidium Hydrogen Oxydiacetates and C=O Stretching Vibrations in Acid Salts of Carboxylic Acids

R. SVANFELDT,[a] J. LINDGREN [a] and I. GRENTHE [b]

[a] Institute of Chemistry, University of Uppsala, Box 531, S-751 21 Uppsala, Sweden and [b] Physical Chemistry I, Chemical Center, University of Lund, Box 740, S-220 07 Lund, Sweden

Infrared spectra of the crystalline acid salts $RbHO(CH_2COO)_2$ and $KHO(CH_2COO)_2$ and their deuterated analogues $RbDO(CH_2COO)_2$ and $KDO(CH_2COO)_2$ have been investigated in the region $3800-40$ cm^{-1}. The compounds both contain a very short O···O hydrogen bond of length 2.451 and 2.480 Å, respectively. Diagrams have been presented showing the variation of C–O bond lengths and C=O and C–O stretching frequencies as functions of hydrogen bond strength in acid salts of carboxylic acids. The applicability of the diagrams in predicting the changes from a centrosymmetric situation to a slightly non-centrosymmetric one has been shown, using the results from our infrared study.

Reviews of crystallographic [1] and spectroscopic [2] studies of acid salts of carboxylic acids have recently appeared. Both show that two extreme types of acid salts exist: *type A*, containing a strong hydrogen bond with the hydrogen atom situated on a symmetry element, and *type B*, containing a rather weak hydrogen bond with a carboxylic group bonded to a carboxylate group. A third type, referred to as *pseudo-A type*, is also discussed. This contains a hydrogen bond of strength comparable to a *type A* salt but has no symmetry element operative at the hydrogen site. A *pseudo-A type* salt can be regarded as one in which a small deviation has occurred from a symmetric situation.

In the present work the infrared spectra of $KHO(CH_2COO)_2$, $RbHO(CH_2COO)_2$, $KDO(CH_2COO)_2$, and $RbDO(CH_2COO)_2$ (referred to in the following as KHOXY, RbHOXY, KDOXY, and RbDOXY) have been studied.

The compounds have recently been investigated using X-ray [3,4] and neutron diffraction.[5] RbHOXY was found to be a *type A* salt with C_2 symmetry at the hydrogen site. The structure of KHOXY shows only small deviations from the RbHOXY structure but has the symmetry C_1 at the hydrogen site. It should thus be classified as a *pseudo-A* type salt. In the later discussion only the stretching vibrations of the –COOHOOC– group (Fig. 1) will be considered. These can be described approximately in terms of C–O, C=O and O–H stretching vibrations.

EXPERIMENTAL

The RbHOXY and KHOXY salts were prepared as described in Refs. 3 and 4. The deuterated analogues were prepared by succes-

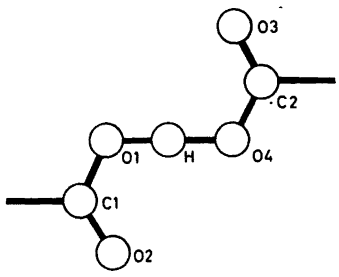

Fig. 1. The designation of the atoms in the –COOHOOC– group.

* Part 90. Acta Universitatis Upsaliensis 295.

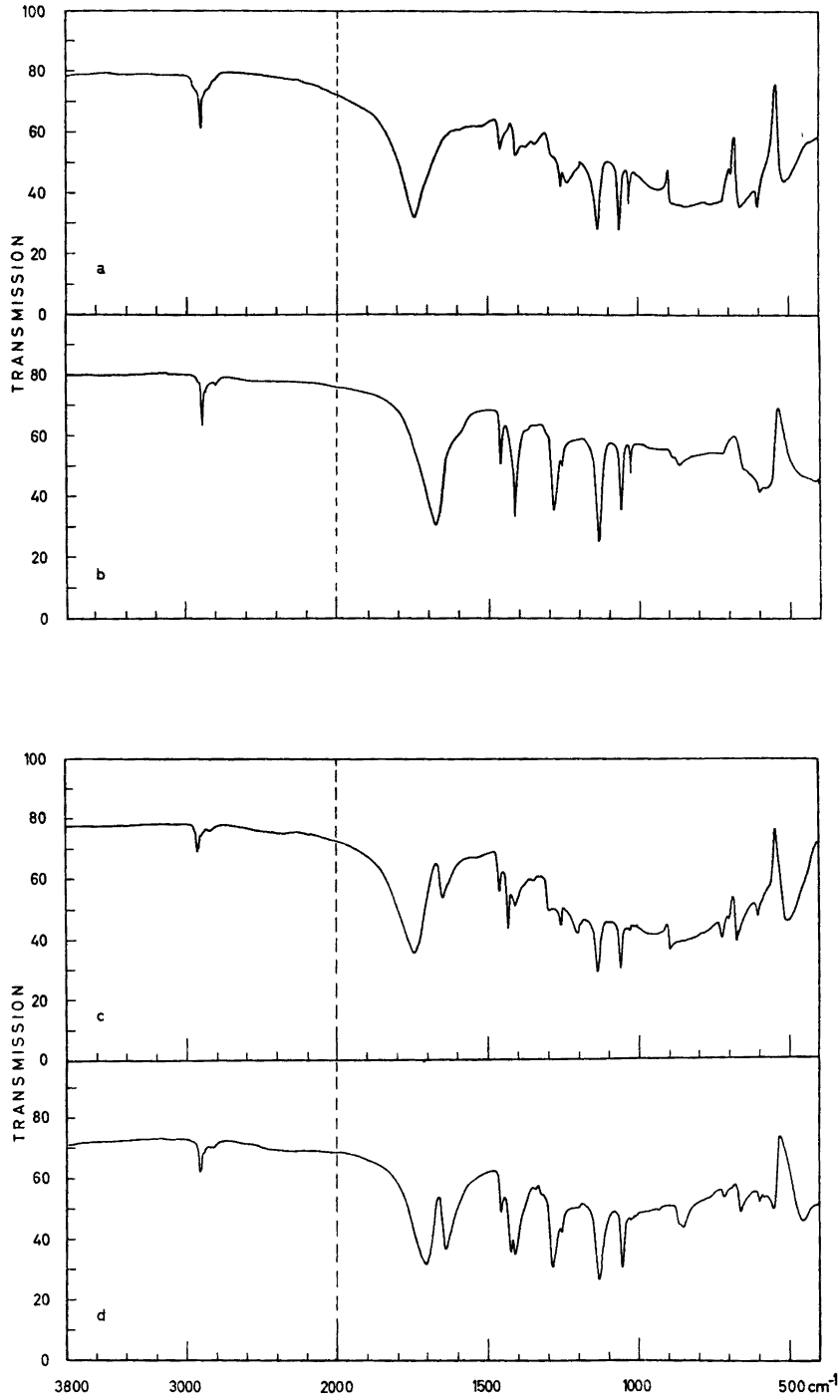

Fig. 2. Infrared spectra at +32 °C of (a) $RbHO(CH_2COO)_2$, (b) $RbDO(CH_2COO)_2$, (c) $KHO(CH_2COO)_2$, (d) $KDO(CH_2COO)_2$. Combined spectra from mulls in nujol and fluorolube.

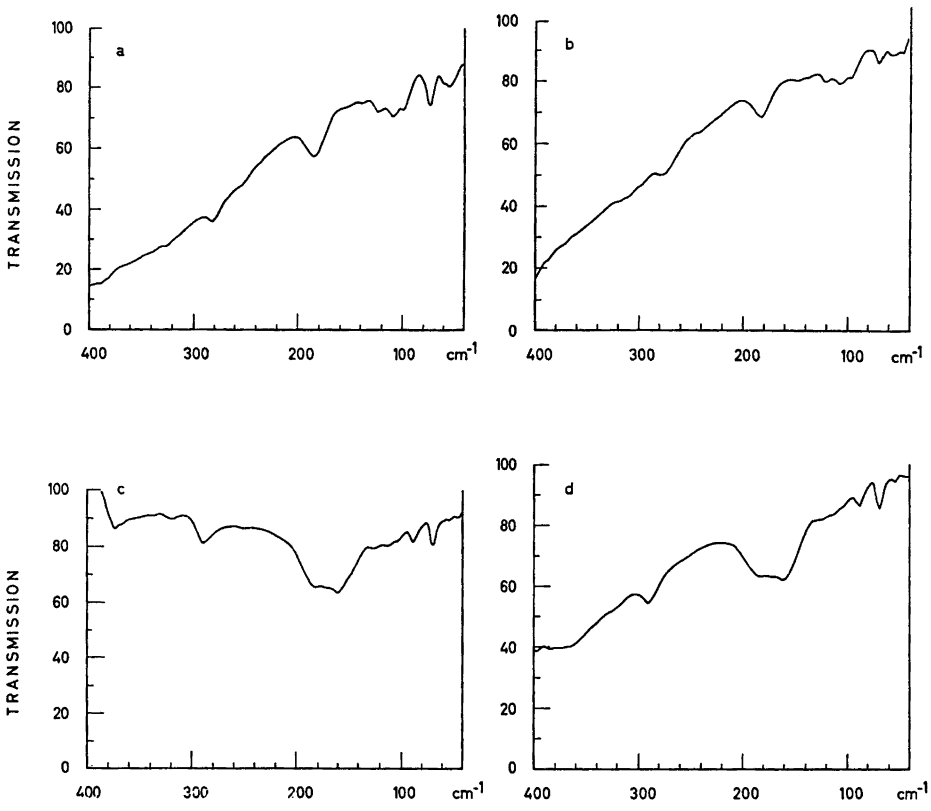

Fig. 3. Infrared spectra at +24 °C of (a) $RbHO(CH_2COO)_2$, (b) $RbDO(CH_2COO)_2$, (c) $KHO(CH_2COO)_2$, (d) $KDO(CH_2COO)_2$ in polyethylene pellets.

sive recrystallization in heavy water (99.98 %). The recrystallizations were continued until no further changes could be detected in the infrared spectra. In order to obtain an independent check on the degree of deuteration, the deuterated salts were dissolved in heavy water and an integrated ^1H NMR spectrum was recorded on a Varian A-60 D NMR spectrometer. The degree of deuteration was obtained using the bands from the methylene hydrogens as an internal standard. RbHOXY was found to be deuterated to about 95 % and KDOXY to about 99 %. Due to the low solubility of the salts in water the precision of this method was only about 5 %.

Thin films of mulls in nujol or fluorolube were examined between plates of KBr at wavenumbers larger than 400 cm^{-1}. Polyethylene pellets were used between 450 and 40 cm^{-1}. Compensation for polyethylene bands has been done. The sample spectra were ratioed against spectra of pure polyethylene pellets. The same weight of polethylene was used in both cases. The samples of the deuterated compounds were prepared in a dry-box.

The spectra were recorded using a Beckman IR 9 in the region 3800 to 400 cm^{-1} and a RIIC Fourier Spectrometer FS-720 between 450 and 40 cm^{-1}. The spectroscopic studies were carried out at the sample compartment temperature (+32 °C for the IR 9 and at +24 °C for the FS-720). Spectra at +32 °C and at +24 °C are shown in Figs. 2 and 3.

RESULTS AND DISCUSSION

The O–H stretching vibrations. The O–H stretching vibration in acid salts of carboxylic acids has been discussed extensively.[2,6] The asymmetrical OHO stretching vibration in *type A* salts has been assigned to a very broad and strong absorption band centred in the interval 1200–600 cm^{-1}. The isotopic ratio $\bar{\nu}_{OHO}/\bar{\nu}_{ODO}$

for these salts is found to vary between 1.20 and 1.45. For the *pseudo-A* type salts, practically no shift of the $\bar{\nu}_{OHO}$ band occurs on deuteration. The centre of this band lies close to the upper limit for the *type A* salts.

In the present case both salts have broad and strong absorption bands corresponding to $\bar{\nu}_{OHO}$. RbHOXY has a band centred at 850 cm^{-1}, whereas KHOXY has a band at 950 cm^{-1}. On deuteration both bands decrease in intensity and their contours become ill-defined. It is therefore not possible to arrive at a reliable estimate for the $\bar{\nu}_{OHO}/\bar{\nu}_{ODO}$ ratio.

The C=O and C–O stretching vibrations; general discussion. It is instructive to consider the variation of the C–O bond distances and the C=O and C–O stretching frequencies as the hydrogen bond in the acid salts gets stronger. The general form of the observed variation is illustrated schematically in Fig. 5. Normal coordinates within the group frequency approximation for the C=O and C–O stretchings are given in Table 1. The situation for *type B* salts is represented at the extreme left- and right-hand ends of the diagrams, where the vibrations are localized in the carboxylate or the carboxylic part of the ion; the central parts of the diagrams depict the situation for *type A* salts, where a coupling between vibration in the two carboxylate parts occurs. The highly schematic nature of the diagrams must be stressed, however. It has been shown, for example, that other internal coordinates can mix quite strongly into the C–O stretching modes.[7]

Table 1. Approximate description of normal coordinates associated with the C=O and C–O stretching bands in acid salts of carboxylic acids.

	Normal coordinates for Type B salts	Normal coordinates for Type A salts
	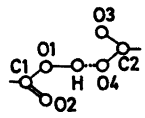	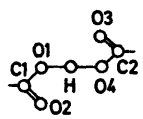
$\bar{\nu}_1$	Δr_{C1-O2}	$\Delta r_{C1-O2} - \Delta r_{C2-O3}$
$\bar{\nu}_2$	$\Delta r_{C2-O4} - \Delta r_{C2-O3}$	$\Delta r_{C1-O2} + \Delta r_{C2-O3}$
$\bar{\nu}_3$	$\Delta r_{C2-O4} + \Delta r_{C2-O3}$	$\Delta r_{C1-O1} - \Delta r_{C2-O4}$
$\bar{\nu}_4$	Δr_{C1-O1}	$\Delta r_{C1-O1} + \Delta r_{C2-O4}$

Nevertheless, the diagrams are useful in predicting the C=O vibrations in salts which deviate only slightly from a *type A* description. The definition given earlier for a *type A* salt allows a two-fold axis and/or a symmetry centre to exist at the hydrogen atom site. In particular, a centrosymmetric site symmetry implies that only the C=O stretching band of the *ungerade* type will be infrared active; the other band of *gerade* type will be Raman active. Since contributions from internal coordinates involving movements of the central hydrogen atom only can be found in the *ungerade* vibrations, a shift on deuteration can only occur for bands of the *ungerade* type. Such shifts have actually been observed in a number of cases.[6,7] One strong infrared band has been found in the region 1800 – 1700 cm^{-1}. This is observed to shift slightly on deuteration, whereas a Raman active band 50 – 100 cm^{-1} lower experiences no shift. These bands thus correspond to $\bar{\nu}_1$ and $\bar{\nu}_2$ in Fig. 5b and are primarily associated with changes in the C1 – O2 and C2 – O3 distances as demonstrated in Table 1. If the geometry of the *type A* salt changes slightly so as to remove the centre of symmetry, both $\bar{\nu}_1$ and $\bar{\nu}_2$ will be expected to be infrared active. It will furthermore be seen from Fig. 5b that only small changes will be expected in the positions of the bands. The intensities of the bands would also be expected to change only slightly. In other words, one strong band is expected in the infrared spectrum close to the position of the band found for the undistorted salt of *type A*, along with one weak band close to the position of the Raman active band. Furthermore, on deuteration of the acid proton, the strong band should shift by about the same amount as was observed in the *type A* salt, and the weak band should shift very little.

The possibility of factor group splitting due to the presence of additional –COOHOOC– groups in the unit cell must also be considered in interpreting the C=O stretching region in a powder spectrum of an acid salt. Such a splitting has been suggested, for example, in the case of potassium hydrogen succinate, $KH(CH_2COO)_2$.[6]

Table 2. C–O and OHO bond lengths and C=O and C–O stretching frequencies in some acid salts.

Compound	Ref.	R(OHO) (Å)	Site symmetry of the proton in the acid ion	R(C1–O1) (Å)	R(C1–O2) (Å)	R(C2–O3) (Å)	R(C2–O4) (Å)	$\bar{\nu}_{C=O}$ (cm^{-1})
$RbHO(CH_2COO)_2$	4	2.451(3)	C_2	1.287(2)	1.223(2)	1.223(2)	1.287(2)	1746 (1682)[a]
$KHO(CH_2COO)_2$	3	2.480(2)	C_1	1.279(3)	1.226(3)	1.217(3)	1.294(3)	1743 (1711) 1648 (1644)
$(CH_3)_3NH.HC_2O_4$	8	2.489(2)	C_1	1.251(3)	1.217(3)	1.196(3)	1.294(3)	1728 1664
$LiDC_2O_4.D_2O$	9	2.506(1)	C_1	1.259(1)	1.239(1)	1.209(1)	1.312(1)	1760 1665
$N_2D_5DC_2O_4$	11	2.466(2)	C_1	1.268(3)	1.232(3)	1.219(3)	1.284(3)	1710

[a] Frequencies within parenthesis refer to the deuterated analogues.

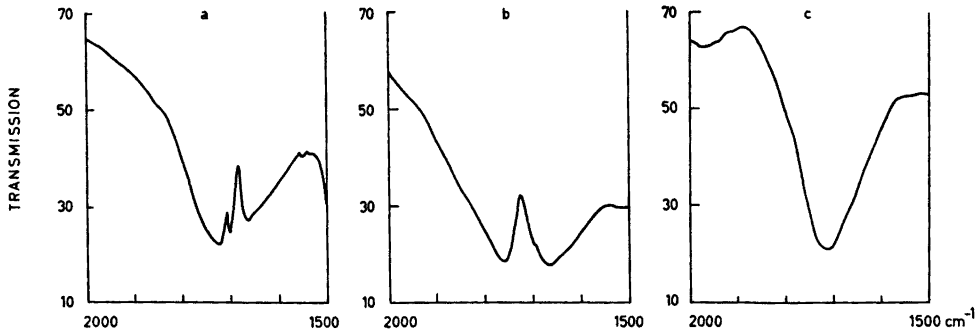

Fig. 4. Infrared spectra at +32 °C of (a) $(CH_3)_3NH.HC_2O_4$, (b) $LiDC_2O_4.D_2O$, (c) $N_2D_5.DC_2O_4$.

C=O stretching vibrations in RbHOXY and KHOXY. No factor group splittings seem to occur in the cases of RbHOXY and KHOXY. The symmetry at the proton site in RbHOXY is C_2. Two C–O and two C=O stretching bands are allowed both in the infrared and Raman spectra; moreover the C=O bands are expected to fall in the region 1800 – 1600 cm^{-1}. Examination of the spectrum in this region (Fig. 2a) reveals, however, that only one band is visible. This is probably explained by the crystal structure [5] deviating only slightly from the higher local symmetry, C_{2h}, at the proton site.

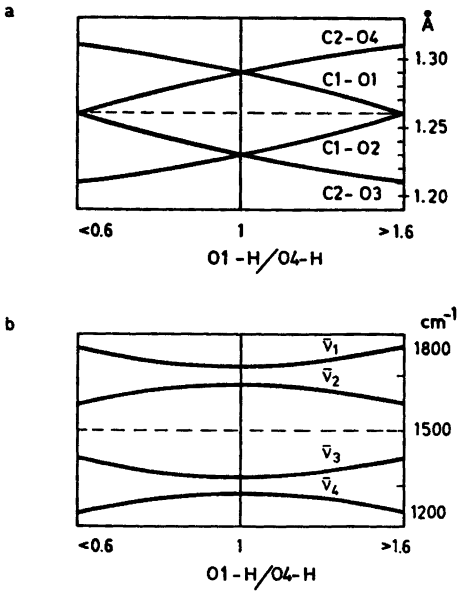

Fig. 5. Approximate variation of (a) C–O bond lengths and (b) C=O and C–O stretching frequencies in acid salts of carboxylic acids as functions of the O1–H/O4–H distances ratio. Designations of the atoms as in Fig. 1.

The proton site symmetry in KHOXY is C_1, but here again the deviation from C_{2h} site symmetry is small (although larger than in RbHOXY). The infrared spectrum for KHOXY (Fig. 2c) shows bands in the C=O stretching region which are in perfect agreement with the above predictions for the case where a small deviation has occurred from a centrosymmetrical site symmetry. KHOXY has a strong band at 1743 cm^{-1} which is shifted to 1711 cm^{-1} on deuteration, and a weak band at 1648 cm^{-1} which is shifted only slightly to 1644 cm^{-1}. The intensity increase of the band at 1644 cm^{-1} in KDOXY relative to that of the band at 1648 cm^{-1} in KHOXY is probably due to a change of the normal coordinates associated with the bands. The intensities of the bands seem to be more sensitive to this change than their positions.

In this connection it is relevant to compare the situation for two other acid salts containing short hydrogen bonds, $(CH_3)_3NH.HC_2O_4$ [8] and $LiDC_2O_4.D_2O$.[9] These salts have been selected since their C=O stretching bands only overlap slightly with their $\bar{\nu}_{OHO}$ ($\bar{\nu}_{ODO}$) bands. From Fig. 4a and b it would seem that the C=O band has split into two components of approximately equal intensity. We suggest, however, that these latter salts have a larger deviation from C_{2h} symmetry at the proton site than KHOXY, and that the two bands which are observed are better described as being associated

with a C=O stretching in the carboxylic group and a C–O stretching in the carboxylate group. This is also supported by an inspection of the C–O bond lengths in the two cases (Table 2). Especially in the case of $LiDC_2O_4D_2O$ [9] it is clear that the oxalate group comprises a carboxylate end (C–O lengths 1.259 and 1.239 Å) and a carboxylic end (C–O lengths 1.209 and 1.312 Å).

The single C=O stretching band in $N_2D_5 \cdot DC_2O_4$ (Fig. 4c) suggests that here again we have either a centre of symmetry at the proton site or a slight deviation from a site symmetry containing a centre of symmetry. This compound has earlier [10] been adjudged to have a site symmetry C_i at the deuteron site at +30 °C. A recent X-ray diffraction study [11] made at +25 °C has shown, however, that the deuteron site symmetry is C_1, deviating only slightly from C_i.

Acknowledgements. We would like to thank Professor Ivar Olovsson for the facilities he has placed at our disposal. This work has been supported by grants from the Swedish Natural Science Research Council and the Wallenberg Foundation, which are hereby gratefully acknowledged.

REFERENCES

1. Speakman, J. C. *Acid Salts of Carboxylic Acids. Crystals with some "Very Short" Hydrogen Bonds.* In Dunitz, J. D. *et al.*, Eds., *Structure and Bonding*, Vol. 12, Springer, Berlin 1972, pp. 141–199.
2. Hadži, D. and Orel, B. *J. Mol. Struct. 18* (1973) 227.
3. Albertsson, J., Grenthe, I. and Herbertsson, H. *Acta Crystallogr. B 29* (1973) 1855.
4. Albertsson, J., Grenthe, I. and Herbertsson, H. *Acta Crystallogr. B 29* (1973) 2839.
5. Albertsson, J. and Grenthe, I. *Acta Crystallogr. B 29* (1973) 2751.
6. Hadži, D., Orel, B. and Novak, A. *Spectrochim. Acta A 29* (1973) 1745.
7. Hadži, D., Obradovič, M., Orel, B. and Šolmajer, T. *J. Mol. Struct. 14* (1972) 439.
8. Thomas, J. O. and Renne, N. *To be published.*
9. Thomas, J. O. *Acta Crystallogr. B 28* (1972) 2037.
10. Lindgren, J., De Villepin, J. and Novak, A. *Chem. Phys. Lett. 3* (1969) 84.
11. Thomas, J. O. *Acta Crystallogr. B 29* (1973) 1767.

Received June 26, 1974.

Acta Chemica Scandinavica A 28 (1974) 1136—1138

Photoelectron Spectra and Electronic Structures of Antimony(III) Halides

DAVID G. NICHOLSON [a] and PAUL RADEMACHER [b]

[a] Department of Chemistry, University of Oslo, Blindern, Oslo 3, Norway and [b] Organic Chemistry Institute University of Münster, Germany

The photoelectron spectra of $SbCl_3$, $SbBr_3$ and SbI_3 are reported and discussed in terms of their molecular orbital structures.

Recent advances in the chemical application of the ^{121}Sb Mössbauer Effect have resulted in an increasing number of studies into the bonding properties of antimony in its compounds.[1] The information obtainable by this technique is relevant only to the solid state and therefore supplementary studies on antimony compounds in the vapour phase are useful in contributing to the overall picture.

One attractive feature of photoelectron spectroscopy is the direct elucidation of all or part of molecular valence level electronic structures thereby providing information on chemical bonding characteristics. The technique also yields data in terms which permit evaluations as to the effectiveness of the various theoretical procedures.

We report here the results of a He(I) photoelectron spectroscopic investigation into the bonding properties of vapour phase antimony(III) chloride, bromide, and iodide.

EXPERIMENTAL

$SbCl_3$ (E. Merck, Darmstadt, W. Germany) and $SbBr_3$ and SbI_3, prepared by the slow addition of stoichiometric quantities of the halogen to a suspension of powdered Sb in refluxing anhydrous benzene, were purified by sublimation *in vacuo* (0.05 Torr) at 60, 80 and 100 °C, respectively.

The photoelectron spectra were recorded on a Perkin-Elmer model PS-16 spectrometer. The temperatures of the samples at which the data were collected were 25, 50 and 115 °C for $SbCl_3$, $SbBr_3$ and SbI_3, respectively.

RESULTS AND DISCUSSION

The vapour phase molecular structures of the SbX_3 series (X = Cl, Br or I) are pyramidal [2] with point group C_{3v}. A simple chemical bonding picture may be given in terms of localised bonds between Sb and X with a lone-pair orbital occupying the apical position on Sb. An alternative model which lends itself better to more detailed bonding discussions is similar to that provided by the molecular orbital description of Cox *et al.*[3] for PCl_3 and PBr_3 in which the twenty-six valence electrons are distributed over nine different valence levels.

There are six X "lone-pair" group orbitals (irreducible representations a_1; a_2; e; e) which are non-degenerate because of the non-spherically symmetric X environments. Factors influencing energy separation include (i) interhalogen repulsions as a result of through-space interactions of orbitals of the same symmetry; (ii) the π-type interaction between the (X_3) a_1 symmetry group orbital and the Sb lone-pair a_1 orbital; and (iii) π-backbonding with empty acceptor $5d$ orbitals on Sb. The significance of the latter effect in second, third and fourth row main group elements has been the subject of some controversy. It should be noted that any $(p\rightarrow d)\pi$-backbonding in these pyramidal molecules is intertwined with the σ-interactions. In C_{3v} symmetry, as pointed out previously,[4] clear-cut distinctions between σ- and

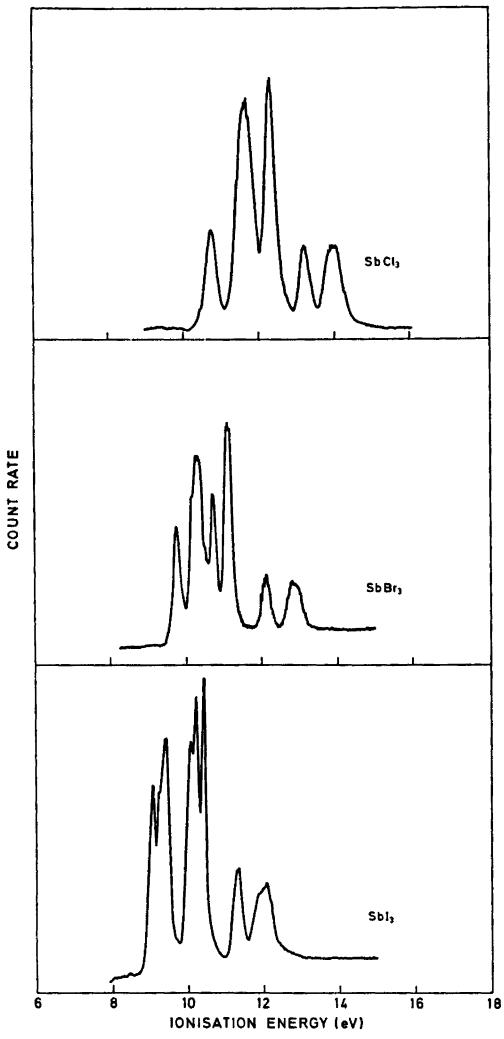

Fig. 1. Photoelectron spectra of $SbCl_3$, $SbBr_3$ and SbI_3.

π-orbitals disappear as the σ- and π-orbitals with the same irreducible representation (a_1 and e) mix. Symmetry constrains one of the (X_3) group orbitals (a_2) to be truly non-bonding since none of the Sb valence orbitals possesses this representation. Consequently, the energy of this orbital should reflect the net relative electron density flow towards or away from the X atoms.

The photoelectron spectra of $SbCl_3$, $SbBr_3$ and SbI_3 are reproduced in Fig. 1 and their spectral assignments (Table 1) are based on considerations of line-intensities, spin-orbit coupling (for X = Br or I) and by comparisons with those already established for the C_{3v} molecules CHX_3 and PX_3 (X = Cl, or Br).[3,5,6] Only six of the nine levels are detected because the more strongly σ-bonding orbitals ($1a$, and $1e$) are too deep-seated having energies clearly in excess of -21 eV. This is consistent with these, together with the missing $2a_1$ level, possessing considerable s-character, the former from X and the latter from Sb. The Sb $5s$ and $5p_z$ orbitals being both of a_1 symmetry can mix and the $2a_1$ level would therefore represent a large degree of the total $5s$ contribution to the lone-pair. For all three compounds the four bands occurring at lowest ionisation energies are assigned to X lone-pair orbitals. In common with the other three-coordinate compounds PCl_3 and PBr_3 these parts of the spectra exhibit a reversal in the ordering of the two least tightly bound orbitals over that observed for the four-coordinate molecules CHX_3 and $SiHCl_3$,[7] the $4a_1$ levels in the former being destabilised with respect to the $1a_2$. This effect is consistent with a mixing-in of P or Sb lone-pair character with the a_1 orbitals on X thereby stabilising $3a_1$ (bonding) and destabilising $4a_1$ (antibonding). It is therefore difficult to accurately assess the extent of the major contribution to the range of X lone-pair energies *viz.* the effect of inter-halogen repulsion.

For a series with a given X the range of ionisation energies of the a_2 group orbitals, although nonbonding (*vide supra*), must depend on changes in electronic shielding from the X nuclei and hence reflect electron density drifts towards or away from the halogen *via* the bonding interactions of the a_1 and e orbitals with those of the apical atom. The observed orders of decreasing a_2 orbital ionisation energies are $PCl_3 > CHCl_3 \sim SbCl_3$ and $PBr_3 > CHBr_3 > SbBr_3$. These are not as might be predicted from simple electronegativity differences alone.

Expansions of X lone-pair orbitals of a_1 symmetry through interactions with the Sb lone-pair and any $(p \rightarrow d)\pi$ back donations (a_1 and e symmetries) would contribute to the net shifts. However, the separations between the $3e$ or $4e$ levels and $1a_2$ in PX_3 and SbX_3 do not indicate any significant stabilisations which would be expected if back donation involving

Table 1. Vertical ionisation potentials (eV) and their orbital assignments.

Compound	$2a_1$	$3a_1$	$2e$	$3e$	$4e$	$1a_2$	$4a_1$
$CHCl_3$	19.8	16.96	15.99	12.85	12.01	11.48	11.91
$CHBr_3$	19.8	15.81	14.71	11.88	10.95	10.47	11.28
				11.72	10.81		
PCl_3	18.85	14.23	15.19	12.94	11.97	11.69	10.52
PBr_3	–	13.09	14.09	11.85	11.18	10.67	10.00
					10.87		
$SbCl_3$	–	13.20	13.98	12.28	11.62	11.50	10.73
$SbBr_3$	–	12.12	12.84	11.14	10.75	10.22	9.77
					10.35		
SbI_3	–	11.29	12.05	10.40	10.04	9.26	9.06
			11.89	10.19	9.40		
$SiHCl_3$	18.14	14.98	14.75	13.07	12.41	11.94	12.41

empty P $3d$ or Sb $5d$ orbitals was important. The bands designated $3a_1$ and $2e$ exhibit a more extensive orbital delocalisation due to bonding interactions. The $3a_1$ molecular orbital includes a contribution from the Sb lone-pair and its appearance is in accordance with the structural changes resulting from ionisation of an electron from this level.

Comparison of the molecular orbital description with the localised bond concept valence shell electron pair repulsion model [8] reveals that the lone-pair orbital on Sb is now explicitly described in terms of contributions from a number of a_1 symmetry molecular orbitals. The non-planarity of the molecules is hence mainly attributable to a balance between the bonding $3a_1$ and antibonding $4a_1$ orbitals together with the interhalogen interactions.

REFERENCES

1. Gibb, T. C. and Greenwood, N. N. *Mössbauer Spectroscopy*, Chapman and Hall, London 1971.
2. George, J. W. *Progr. Inorg. Chem. 2* (1960) 33.
3. Cox, P. A., Evans, S., Orchard, A. F., Richardson, N. V. and Roberts, P. J. *Discuss. Faraday Soc. 54* (1972) 26.
4. Perkins, P. G. *Chem. Commun.* (1967) 268.
5. Potts, A. W., Lempka, H. J., Streets, D. G. and Price, W. C. *Phil. Trans. Roy. Soc. London A 268* (1970) 59.
6. Potts, A. W., and Price, W. C. *Proc. Roy. Soc. London A 326* (1972) 181.
7. Frost, D. C., Herring, F. G., Katrib, A., McLean, R. A. N., Drake, J. E. and Westwood, N. P. C. *Can. J. Chem. 49* (1971) 4033.
8. Gillespie, R. J. *J. Chem. Educ. 47* (1970) 18.

Received July 1, 1974.

Acta Chemica Scandinavica A 28 (1974) 1139—1144

A Silver/Silver Chloride, Sodium Chloride/Pythagoras Membrane-Electrode as a Reference Electrode in Melts with Sodium Chloride

TORSTEIN BERGE, PER B. ENGSETH and REIDAR TUNOLD

Institutt for teknisk elektrokjemi, Norges tekniske høgskole, Universitetet i Trondheim, N-7034 Trondheim-NTH, Norway

A silver/silver chloride electrode in sodium chloride inside a porcelain diaphragm has been used as a reference electrode in galvanic cells containing sodium chloride.

The electrode was shown to be reproducible and stable and with a transference number of sodium ions through the membrane equal one. This makes it possible to determine sodium chloride activities in the melt outside the membrane. Such determinations have been performed for the sodium chloride/magnesium chloride system using the cell:

Ag|AgCl, NaCl|membrane|NaCl, $MgCl_2|Cl_2$(g)C

Glasses [1–7] and other ceramic materials [8–10] have been extensively used as membranes in EMF-measurements in concentration cells. The response of electrodes with such membranes in relation to the transport properties of the membranes has been discussed by several authors.[2,5,11–16]

Capsule type electrodes with a glass or porcelain-membrane possess some advantages, the main of which is that the membrane prevents the interdiffusion of the melts in the two compartments. The function of this electrode, however, depends on the transport properties of the membrane.

We have for some time used an electrode consisting of a silver wire in a mixture of silver chloride and sodium chloride inside a porcelain membrane, as a reference electrode for studying electrode reactions in magnesium chloride/sodium chloride melts.

In these cells the sodium ion is the only common cation in the system, and the EMF can only be calculated from the thermodynamic properties of the melts if all the electric charge is transported through the membrane by sodium ions. That charge should be transported by chloride ions is very unlikely.

In order to establish whether the electrode behaves in a predictable manner we have measured the EMF response of the cell:

$$\overset{\text{I}}{\text{Ag|AgCl, NaCl}}\overset{\text{II}}{\text{||NaCl, MgCl}_2\text{/Cl}_2\text{(C)}} \quad \text{(A)}$$

by varying the composition in compartment II.

THE MEMBRANE

The membranes were made of commercial grade "Pythagoras" tubes from Haldenwanger A/G with the following composition: Al_2O_3, 60 wt. %; SiO_2, 37 wt. %; Na_2O, 3 wt. %, and with traces of other alkali and alkaline-earth oxides. The electric charge has been found to be transported only by sodium ions in this type of membrane.[17]

THE EMF OF CELL A

If the membrane is in equilibrium with the melt at both interphases, then the total change in free energy when one Faraday of positive charge is transported through the cell from left to right is:

$$\Delta G = \bar{G}_{\text{AgCl(I)}} + \sum_i \int_{\text{I}}^{\text{II}} t_i \mathrm{d}\bar{G}_i \qquad (1)$$

Here t_i is the transference number of the component i and $\bar{G}_i$ is the corresponding partial free energy of this component. If the charge is transported only by sodium ions in the mem-

brane then the total change in free energy is equivalent to:

$$\Delta G = \bar{G}_{AgCl(I)} + \bar{G}_{NaCl(II)} - \bar{G}_{NaCl(I)}$$

$$= G^{\circ}_{AgCl} + RT \ln a_{AgCl(I)} + RT \ln \frac{a_{NaCl(II)}}{a_{NaCl(I)}} \qquad (2)$$

To calculate the activity of sodium in compartment II one has to know the activities in compartment I. The EMF for the formation of pure silver chloride has been determined by some authors [18,19] and also by us, using the formation cell:

(B) $Ag|AgCl|Cl_2(g)$

The partial free energy of silver chloride in mixtures with sodium chloride was determined by Pelton and Flengas [19] using the same type of formation cell. To calculate the activity of sodium chloride in this melt from those measurements, one can use the Gibbs-Duhem equation in the form:

$$\ln \frac{a_{NaCl}}{X_{NaCl}} = -\int_0^{X_{AgCl}} \frac{X_{AgCl}}{X_{NaCl}} \, d \ln \frac{a_{AgCl}}{X_{AgCl}} \qquad (3)$$

EXPERIMENTAL

The membrane. The membranes used were in the form of tubes with diameter of either 5 × 7 mm or 4 × 8 mm. Before use the tubes were washed in concentrated hydrochloric acid, then in distilled water and acetone. Afterwards they were dried at 300 °C for 24 h.

The melts. Magnesium chloride was pure grade from Merck AG. It was dehydrated by slowly heating under HCl-atmosphere to 420 °C, and maintaining it at this temperature for 24 h. Afterwards it was melted and filtered through silica wool under HCl-atmosphere.

Pure grade *sodium chloride* from Merck AG was pre-dried at 350 °C and at a pressure of 10 Pa. *Silver chloride* from Riedel de Haën AG was not dried before use. Its hygroscopicity is rather insignificant.

The melt in compartment I, which contained 81.7 mol % silver chloride in all the measurements, was placed inside the Pythagoras tube. The melt in half-cell II was placed in an alumina crucible. The composition in this compartment was changed by adding premelted weighed pieces of sodium chloride.

The electrodes. The chlorine electrode is shown in Fig. 1. The active electrode was made of spectrographic AGKSP-graphite from Union Carbide. The chlorine gas was pre-dried by passing it through dehydrite (magnesium perchlorate). The silver electrode was a wire with 99.99 % silver content.

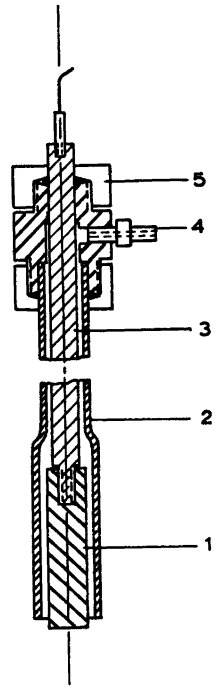

Fig. 1. Chlorine/carbon reference electrode. 1 Spec-pure graphite. 2 Silica tube. 3 Graphite. 4 Chlorine inlet (pvc). 5 O-ring seal (pvc).

Procedure. The crucible was placed in a wire wound laboratory furnace, which was temperature controlled to within ±1 °C.

After the salt mixture was melted, the chlorine/carbon electrode was equilibrated by passing a DC current of 100 mA through it for half an hour. After a change in composition the EMF stabilized and became constant after about 1 h. Changes in composition were made at intervals of 3–4 h.

The EMF was measured with a Solartron digital multimeter with an accuracy of ±0.1 mV. The stability of the EMF was 0.2–0.3 mV during a run. However, it was observed a small drift of the potential with time probably because of changes in the composition in compartment II due to vaporization. The EMF was therefore registered at the same moment as samples for analysis were taken from the melt.

The melts were analyzed using a Varian Techtron Atomic Absorption analyzer. Within the experimental error no silver or magnesium ions were found to be carried through the membrane.

RESULTS AND DISCUSSION

The formation cell B. The EMF for formation cell B as a function of temperature is shown in Fig. 2. The measurements were corrected for the thermopotential between silver and carbon. The results of Pelton and Flengas [19] are also plotted in. The EMF measured by us is a few mV lower and has a somewhat higher temperature coefficient than found by them.

The concentration cell A. The results from the EMF-measurements of cell A are shown in Tables 1 and 2 for 750 °C and 850 °C, respectively. Using the data of Pelton and Flengas [19] for the free energy of silver chloride, we have calculated the partial free energy of mixing of sodium chloride in silver chloride using eqn. (3). The partial free energy of mixing of sodium chloride in magnesium chloride has then been calculated using eqn. (2). The values of $\Delta\bar{G}_{NaCl}$ and of $\Delta\bar{G}_{NaCl}^{E}$ (E = excess) are tabulated in Table 1 for 750 °C and in Table 2 for 850 °C.

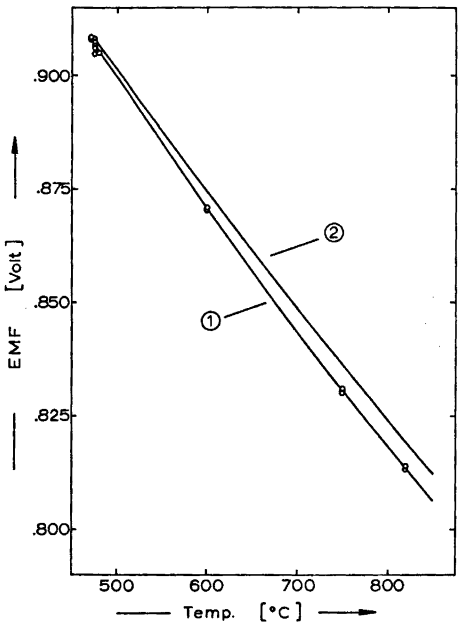

Fig. 2. Emf of cell B as a function of the temperature. 1 Present work. 2 Pelton and Flengas.[19]

At 750 °C the measurements were performed only to $X_{NaCl} = 0.9$ because of the solidification of sodium chloride at higher concentrations. In Figs. 3 and 4 the activity of sodium chloride in mixture with magnesium chloride is shown as a function of the composition at 750 °C and 850 °C, respectively. The values of Østvold [5] have been plotted in for comparison in Fig. 4. The deviation seems rather small. At $X_{NaCl} > 0.5$ we have found a somewhat greater negative deviation, and at $X_{NaCl} < 0.5$

Table 1. Thermodynamic data for the NaCl–$MgCl_2$ system. Temp. 750 °C.

X_{MgCl_2}	EMF(V)	$-\Delta\bar{G}_{NaCl}$ (J/mol)	$-\Delta\bar{G}_{NaCl}^{E}$ (J/mol)
0.17	0.7572	2940	1470
0.28	0.7931	6500	3800
0.39	0.8391	10900	6700
0.50	0.8851	15500	9400
0.62	0.9311	19700	11500
0.72	0.9811	24700	13800
0.80	1.0611	32200	18400
0.89	1.1221	38100	19700

Table 2. Temp. 850 °C.

X_{MgCl_2}	EMF(V)	$-\Delta\bar{G}_{NaCl}$ (J/mol)	$-\Delta\bar{G}_{NaCl}^{E}$ (J/mol)	$\Delta\bar{S}_{NaCl}$ (J/mol K)
0.027	0.6891	290	0	–
0.058	0.6919	540	40	–
0.14	0.7027	1460	250	1.05
0.22	0.7300	3900	2000	2.43
0.32	0.7706	7500	4600	3.85
0.42	0.8161	11300	7500	3.56
0.54	0.8679	15900	10500	4.02
0.65	0.9168	20500	12600	5.05
0.77	0.9624	24300	13000	5.86
0.87	1.0274	30100	13800	9.21
0.97	1.1262	38900	9200	–

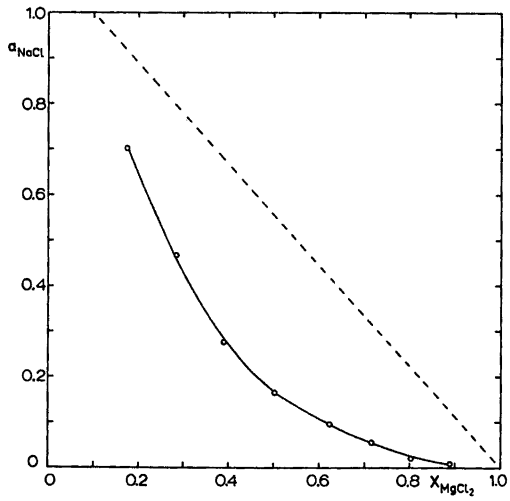

Fig. 3. The activity of sodium chloride in the sodium chloride/magnesium chloride melt, 750 °C.

a smaller deviation from ideality than was found by Østvold.

The partial entropy of mixing. To examine the deviation from Østvolds data more closely we have calculated the partial entropy of mixing of sodium chloride by using our data for the partial free energy of mixing, and the enthalpy data found by Kleppa and McCarthy.[21] The results for 850 °C are shown in Table 2 and are

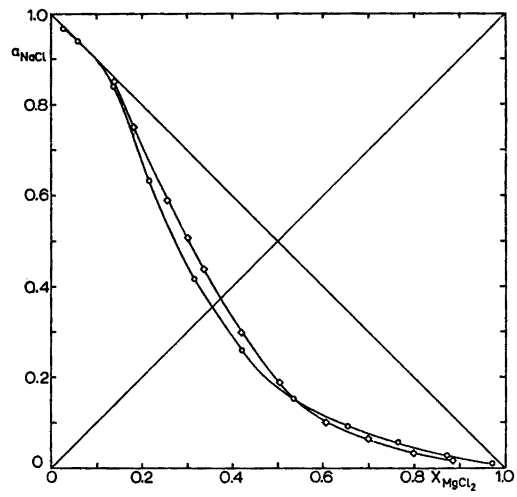

Fig. 4. The activity of sodium chloride in the sodium chloride/magnesium chloride melt, 850 °C. ○ Present work. ◇ From Østvold.[5]

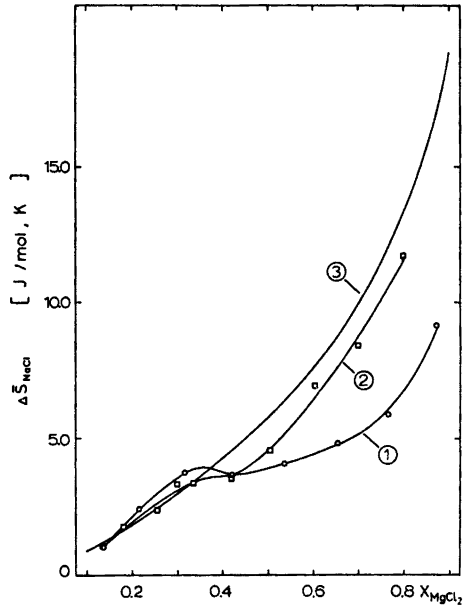

Fig. 5. The partial entropy of mixing of sodium chloride in the sodium chloride/magnesium chloride melt, 850 °C. 1 Present work. 2 From Østvold[5]. 3 $\Delta\bar{S} = -R \ln X_{NaCl}$.

plotted *vs.* the composition in Fig. 5. In the same diagram we have also plotted the results of Østvold,[5] and the curve for the ideal partial entropy:

$$\Delta\bar{s}_{NaCl} = -R \ln N_{Na^+}N_{Cl^-} = -R \ln X_{NaCl} \qquad (4)$$

This relation is based upon a random distribution of all the cations in a quasi cation lattice and the chloride ions in a quasi anion lattice. Our results show a more pronounced deviation from ideality than the data of Østvold.[5] At $X_{MgCl_2} < 0.3$ there is found a slightly positive deviation from the ideal plot. At $X_{MgCl_2} \sim 0.3$ an abrupt decrease in the slope of the curve, or even a small maximum is found. Such an arrest is also slightly indicated in the results of Østvold. A maximum or an inflection in the partial entropy curve, reflects a corresponding local inflection in the integral entropy of mixing curve as found by Ikeuchi and Krohn.[20] This is probably due to the ordering of the melt by the formation of $MgCl_4^{2-}$-groups. Such groups have been proposed in all the systems with alkali cations with ionic radii greater than that for sodium ions.[5,21,22] The "complex" formation

becomes more pronounced the smaller the polarizing strength of the cation. The results from this work indicate that such a grouping is present also in the sodium chloride/magnesium chloride system as proposed by Ikeuchi and Krohn, who calculated a dissociation constant for the complex of about 10^{-2}.[20]

The transport properties of the membrane and the accuracy of the determined quantities

The difference in EMF of cell A using two equal membrane electrodes was 1 – 2 mV in most of the composition range, with a maximum deviation of 4 mV at *one* composition.

It is of course necessary for knowing the exact cell reaction that the transference number of sodium ions in the membrane is constant and equals one. If the transference numbers of magnesium or silver ions are significant although undetectable, the contributions to the total free energy from the work done in the membrane are very difficult to evaluate. Both the magnitude of the work done, and the sign of it, would depend on the relative variations of the transference numbers through the membrane and the concentrations of these ions present as impurities in the other melt. Contributions from transport both of magnesium and silver ions should tend to cancel each other. Contributions from transport of silver ions should not vary significantly with the composition in compartment II, whereas contributions from transport of magnesium ions should increase with increasing content of magnesium chloride in compartment II.

In evaluating the accuracy of the determined quantities we have estimated the mean deviation of the EMF of cell A to be 2 mV, and the accuracy in the determination of X_{NaCl} to vary from 0.001 at $X_{NaCl} \sim 0.1$ to 0.01 at $X_{NaCl} \sim 0.9$. Using the estimated accuracy of the literature data,[19,21], we found the precision in the determined values of the free energy to vary from $\pm$ 100 J/mol to $\pm$ 1000 J/mol in the concentration range mentioned above. The corresponding precision in the partial entropy of mixing values varies from $\pm$ 0.1 to + 1 J/mol K. The basis for this is of course that the free energy change in cell A can unambiguously be described by eqn. 2.

CONCLUSION

A silver/silver chloride electrode in sodium chloride, enclosed by a porcelain tube membrane, was found to give a rather stable and reproducible EMF when introduced in melts containing sodium chloride. Within the experimental error it was established that the electric charge was transported through the membrane only by sodium ions. The electrode therefore, is very simple and useful in such melts.

The partial free energy and entropy of mixing of sodium chloride in mixtures with magnesium chloride was calculated using EMF values from measurements in concentration cells of the type

Ag(s)|AgCl, NaCl|membrane|NaCl, $MgCl_2$|Cl_2(g)

The results indicate a pronounced ordering of the melt corresponding to $MgCl_4^{2-}$-groups.

REFERENCES

1. Bockris, J. O'M., Hills, G. J., Inman, D. and Young, L. *J. Sci. Instrum. 33* (1956) 438.
2. Littlewood, R. *Electrochim. Acta 3* (1971) 270.
3. Førland, T. and Østvold, T. *Acta Chem Scand. 20* (1966) 2068.
4. Førland, T. and Thulin, L. U. *Acta. Chem. Scand. 21* (1967) 1121.
5. Østvold, T. *Thesis*, NTH, Trondheim 1971.
6. Stern, K. H. and Meador, S. E. *J. Res. Nat. Bur. Stand. A 69* (1965) 553, No. 6.
7. Bartlett, H. E. and Crowther, P. *Electrochim. Acta 15* (1970) 681.
8. Labrie, R. J. and Lamb, V. A. *J. Electrochem. Soc. 106* (1959) 895.
9. Danner, D. and Rey, M. *Electrochim. Acta 4* (1961) 274.
10. Kolotii, A. A. and Delimarskii, Yu. K. *J. Appl. Chem. USSR (English Transl.) 39* (1966) 2342.
11. Stern, K. H. *J. Phys. Chem. 67* (1963) 893.
12. Suzuki, T. *Denki Kagaku 5* (1965) 380.
13. Doremus, R. H. *J. Phys. Chem. 72* (1968) 2877.
14. Doremus, R. H. *J. Electrochem. Soc. 115* (1968) 924.
15. Stern, K. H. *J. Phys. Chem. 72* (1968) 1963.
16. Garfinkel, H. M. *J. Phys. Chem. 73* (1969) 1766.
17. Engseth, P. B. *Thesis*, NTH, Trondheim 1973.
18. Panish, M. B., Blankenship, F. F., Grimes, W. R. and Newton, R. F. *J. Amer. Chem. Soc. 62* (1958) 1325.

19. Pelton, A. D. and Flengas, S. N. *J. Electrochem. Soc. 117* (1970) 1130.
20. Ikeuchi, H. and Krohn, C. *Acta Chem. Scand. 23* (1969) 2230.
21. Kleppa, O. J. and McCarthy, F. G. *J. Phys. Chem. 70* (1966) 1249.
22. Flood, H. and Urnes, S. *Z. Elektrochem. 59* (1955) 834.

Received June 19, 1974.

Acta Chemica Scandinavica A 28 (1974) 1145—1149

The Structure of Diformylhydrazine at 19 °C and —165 °C

T. OTTERSEN

Department of Pharmacy, University of Oslo, Oslo 3, Norway

The crystal and molecular structure of *s*-diformylhydrazine has been refined using two X-ray data sets collected by counter methods at 19 °C (956 observed reflections) and −165 °C (1009 observed reflections). The crystals are monoclinic, space group $P2_1/c$, with cell dimensions: $a = 3.583(1)$ Å; [3.484(1) Å]; $b = 6.262(1)$ Å [6.196(2) Å]; $c = 8.992(1)$ Å [8.950(4) Å]; $\beta = 113.04(1)°$ [112.07(3)°], figures in brackets are cell dimensions at −165 °C. The molecule is planar and the bond lengths indicate a resonance stabilization of the molecule. The nitrogen-nitrogen bond length is found to be 1.383(2) Å, using only high-angle reflections ($\sin\theta/\lambda > 0.5$) in the refinements.

The structure investigation of *s*-diformylhydrazine is part of a series of structure studies of 3,6-pyridazindiones and related compounds.[1–7] This structure has been reported earlier,[8] investigated by film methods, but experience has shown that the values obtained for nitrogen-nitrogen bond lengths are often influenced by the unsymmetricity of the valence electrons.[1–5] A significant shortening of the observed length of this bond is usually found when low-angle data are excluded in the refinements.

Both experimental (Refs. 5 and 9, and references therein) and theoretical [6,10,11] results indicate that the conjugated N−C=O-fragment is easily altered by both substitution and hydrogen bonding. A "highly" accurate structure determination of *s*-diformylhydrazine would, therefore, be of interest in order to study differences between this and similar molecules.

It was also of interest to compare results obtained by the *L*-shell [12] and extended *L*-shell [13] methods to the electron populations found in a recent *ab initio* study.[6] And, further, to compare these populations to the experimental ones reported by Tomiie *et al.*[8]

In order to study the effect of different thermal vibrations on the results obtained both for populations and positional parameters, it was decided to collect data at both room- and liquid nitrogen-temperature. Corrections of positional parameters for thermal vibration effects are, for a structure like the present one, highly inaccurate.

EXPERIMENTAL

Suitable crystals of diformylhydrazine were obtained by slow evaporation of a water solution. The space group, $P2_1/a$, and the unit cell parameters reported by Tomiie *et al.*[8] were transformed to space group $P2_1/c$.

A computer-controlled Syntex-P$\bar{1}$ four-circle diffractometer with graphite monochromated Mo$K\alpha$ radiation was utilized in the determination of unit cell parameters and the collection of intensity data. In the case of the low-temperature crystallographic work the diffractometer was equipped with an Enraf-Nonius liquid nitrogen cooling device (modified by H. Hope). Cell constants and their standard deviations were, in both cases, determined by a least-squares treatment of the angular coordinates of fifteen independent reflections.

The recording of the three-dimensional intensity data sets and the subsequent treatment of the data are described below. All programs utilized, when not otherwise indicated, are part of a local assembly of programs for CYBER-74 (see Ref. 14).

Room-temperature data. A redundant data set [the four octants: (hkl), $(hk\bar{l})$, $(\bar{h}kl)$, $(\bar{h}k\bar{l})$] were collected using a crystal of dimensions $0.7 \times 0.4 \times 0.3$ mm, utilizing the $w - 2\theta$ scanning mode with scan speed varying from 1° min^{-1} to 12° min^{-1} depending on the peak intensity of the reflection. Background counting time was equal to scan time. The temperature was maintained at 19 ± 1 °C. The intensities of three

standard reflections, which where remeasured for every hundred reflections, showed no systematic variations throughout the collection.

The Laue symmetry-related reflections were compared and merged.[15] The s-factor, defined as:

$$s = \sum_{\substack{\text{all}\\\text{pairs}}} \{|I(hkl) - I(\bar{h}k\bar{l})|\} / \sum_{\substack{\text{all}\\\text{pairs}}} \{|I(hkl) + I(\bar{h}k\bar{l})|\}$$

is 0.026. The estimated standard deviations were taken as the square root of the total counts with a 2 % addition (p) for experimental uncertainties. The mean p, calculated on the basis of the intensity variation of each check reflection, was 1.3 %.

Of the 1959 reflection pairs measured ($2\theta_{max} = 100°$), 956 merged reflections had intensities larger than three times their standard deviations, the remainder being excluded from further calculations. The intensities were corrected [15] for Lorentz and polarization effects.

Low-temperature data. The $w - 2\theta$ scanning mode with scan speed varying from 2° min^{-1} to 12° min^{-1} was utilized, using a crystal of dimensions $0.2 \times 0.4 \times 0.4$ mm. Background counting time was equal to scan time. The temperature at crystal site was −165 °C. Reflections which had integrated counts of less than 8, determined in a $2s$ scan over the peak, were not measured. The intensities of three standard reflections which were remeasured for every fifty reflections showed no systematic variations throughout the collection.

The estimated standard deviations were taken as the square root of the total counts with a 2 % addition (p) for experimental uncertainties. The mean p, calculated on the basis of the intensity variation of each check reflection, was 1.4 %. Of the 1086 unique reflections measured ($2\theta_{max} = 90°$) 1009 had intensities larger than twice their standard deviations, the remainder being excluded from further calculations. The intensities were corrected for Lorentz and polarization effects.

The atomic scattering factors used were those of Doyle and Turner [16] for oxygen, nitrogen, and carbon, and of Stewart *et al.*[17] for hydrogen. Core and valence electron scattering factors used in the L-shell and extended L-shell refinements were those given by Stewart.[12]

CRYSTAL DATA

Diformylhydrazine, $C_2H_4N_2O_2$, crystal system: monoclinic; absent reflections: ($h0l$) for l odd; ($0k0$) for k odd; space group $P2_1/c$. $M = 88.1$ amu; $Z = 2$; $F(000) = 92$. Cell dimensions at 19 °C: $a = 3.583(.001)$ Å; $b = 6.262(.001)$ Å; $c = 8.992(.001)$ Å; $\beta = 113.04(.01)°$; $V = 185.66(.08)$ Å^3, $D_{calc} = 1.576$ g/cm^3. Cell dimensions at −165 °C: $a = 3.484(.001)$ Å; $b = 6.196(.002)$ Å; $c = 8.950(.004)$ Å; $\beta = 112.07(0.3)°$; $V = 179.0(.1)$ Å^3; $D_{calc} = 1.634$ g/cm^3. Figures in parentheses are estimated standard deviations.

REFINEMENTS

Least-squares refinements of all positional parameters, anisotropic thermal parameters for non-hydrogen atoms and isotropic thermal parameters for hydrogen atoms proceeded smoothly, yielding a conventional R-factor of 0.079 and a weighted R_w of 0.091 for the room-temperature dataset. The corresponding values for the low-temperature dataset were $R = 0.069$ and $R_w = 0.080$. No explanation can be furthered for these relatively large R-factors. There were no indications of secondary extinction, difference fourier calculations showed only spurious peaks (< 0.3 e/Å^3), and there is no indication of disorder in the structures. Also crystals from different batches and different diffractometers were used in the two data collections (at 19 °C and −165 °C), and the crystals were mounted generally.

In order to reduce the effects of the unsymmetricity of the valence electrons on the refined parameters, low-angle data were excluded from the refinements. By a systematic variation of the lower sin θ/λ cut value for the data, it was found for both data sets that this unsymmetricity had no effect on structural parameters when all reflections with sin $\theta/\lambda < 0.5$ Å^{-1} were excluded. This value for the "cut" has been found earlier.[4,5] The refinement of positional and anisotropic thermal parameters for non-hydrogen atoms using the 830 reflections with sin $\theta/\lambda \geq 0.5$ Å^{-1} collected at 19 °C, resulted in an R of 0.078, R_w of 0.082 and an R factor for the total data set, R_t, of 0.079. The corresponding parameters using the data collected at −165 °C are: number of reflections 828, $R = 0.069$, $R_w = 0.069$, and $R_t = 0.073$. Atomic parameters obtained in these two latter refinements, *i.e.* for non-hydrogen atoms, and final parameters for hydrogen atoms from the refinements using the total data sets are listed in Table 1. A list of observed and calculated structure factors is available from the author upon request. Standard deviations in molecular dimensions

Table 1. Fractional atomic coordinates and thermal parameters with estimated standard deviations. (All parameters for non-hydrogen atoms: $\times 10^5$; coordinates for hydrogen: $\times 10^3$.) The temperature factor for non-hydrogen atoms is given by exp $-(B_{11}h^2+B_{22}k^2+B_{33}l^2+B_{12}hk+B_{13}hl+B_{23}kl)$. Parameters for non-hydrogen atoms are from refinements using high-angle data only.

Atom	x	y	z	B	B_{11}	B_{22}	B_{33}	B_{12}	B_{13}	B_{23}
A. Refinement using data collected at 19 °C.										
O	38022(41)	14623(18)	26196(12)		7347(99)	1428(23)	640(10)	−351(67)	−715(46)	−245(21)
N	−6283(34)	10405(16)	301(11)		5358(82)	1105(18)	491(9)	375(58)	−92(38)	−55(18)
C	11038(38)	21644(18)	13828(12)		5738(92)	1083(21)	570(10)	−229(63)	348(47)	−212(21)
HC	18(16)	349(10)	125(6)	4.2(.9)						
HN	−247(12)	148(8)	−79(6)	3.1(.6)						
B. Refinement using data collected at −165 °C										
O	38075(34)	14601(16)	26231(12)		3330(76)	678(18)	371(10)	−86(53)	321(37)	−39(19)
N	−6493(34)	10473(15)	327(12)		2923(77)	504(17)	336(9)	217(54)	534(39)	−52(19)
C	10786(37)	21810(17)	13866(13)		2869(80)	520(19)	377(10)	−107(58)	701(42)	−84(21)
HC	0(7)	363(3)	131(2)	1.3(.4)						
HN	−274(8)	160(5)	−84(3)	3.1(.5)						

were calculated from the correlation matrix ignoring standard deviations in cell parameters.

L-shell [12] and extended L-shell [13] refinements were then performed, using in all cases only reflections with sin θ/λ values less than 0.65 Å^{-1}. R-factors obtained are as follows: Data set collected at 19 °C: L-shell refinement yielded an R of .070 and R_w of 0.088, and the extended L-shell refinement resulted in $R=0.066$, $R_w=0.084$ for the 280 reflections used. A usual least-square refinement using the same part of the data set gave the values $R=0.070$, $R_w=0.089$. Data set collected at −165 °C: L-shell refinement yielded an R of 0.062 and R_w of 0.073, and the extended L-shell refinement resulted in $R=0.058$, $R_w=0.069$ for the 380 reflections used. A usual least-squares refinement using the same part of the data set gave the values $R=0.059$, $R_w=0.070$.

The adjusted [12] gross atomic populations found by these four refinements are listed in Table 2, together with results from *ab initio* calculations.[6]

DISCUSSION

Bond lengths and bond angles are listed in Fig. 1, where the numbering of the atoms is indicated. Differences between the two structure models, excluding parameters involving hydrogen atoms, are small, within three times the standard deviations, and are probably due to differences in thermal vibrations. Corrections of the positional parameters for librational motion of the structure model refined using the room-temperature data set, yielded unsatisfactory results only, *i.e.* negative libration axes. The structure model obtained using the low-temperature dataset will, therefore, be used in the discussion.

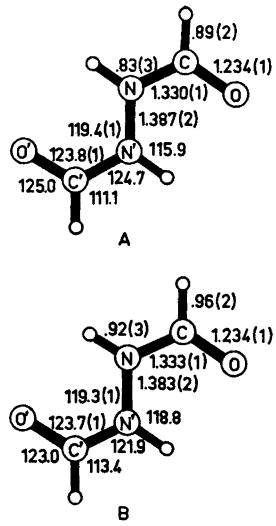

Fig. 1. Bond lengths and bond angles with estimated standard deviations in parentheses. Structure models from refinements using high-angle data only. A, results from refinements using the data set collected at 19 °C; B, results from refinements using the data set collected at −165 °C (the e.s.d.'s for bond angles involving hydrogen are about 1.2°).

The length of the N−N bond and the planarity of the molecule (see Table 3) indicates a high degree of conjugation in the molecule, with sp^2-hybridization of the nitrogen atoms. This hybridization of nitrogen atoms bonded to formyl groups is usually found.[7,9] The N−N bond length of 1.383 Å is significantly shorter than those of 1.409 and 1.411 Å found in formyl dihydrazine [7] and also to that of 1.406 Å in 1,2-dimethyl-3,6-pyridazinedione.[2] It is, on the other hand, significantly longer than the N−N bond lengths found in the

Table 2. Gross atomic populations. T. Results from *ab initio* calculations (Ref. 6). A. Data collected at 19 °C used in refinements. B. Data collected at −165 °C used in refinements. C. Results from Fourier methods (Ref. 8). LS. L-shell refinement. ELS. Extended L-shell refinement. Estimated standard deviations are in the last digit of the corresponding parameter and are given in parentheses.

Atom/ atom group	T	A		B		C
		LS	ELS	LS	ELS	
O	8.56	8.34(10)	8.27(21)	8.30(7)	8.26(16)	8.61
NH	8.20	7.88(12)	7.69(21)	8.10(8)	7.96(16)	7.72
CH	6.24	6.78(16)	7.04(25)	6.60(11)	6.78(16)	6.60

Table 3. Deviations of the hydrogen atoms from a least squares plane through O, C and N.
A, at 19 °C; plane equation:
$(-0.2099\ x-0.0523\ y+0.0388\ z)R-0.004=0$.
B, at −165 °C; plane equation:
$(0.2177\ x+0.0529\ y-0.0387\ z)R-0.007=0$.

Atom	Deviation (Å × 10^3) A	B
HC	−52	3
HN	18	−44

monolactim 3,6-pyridazinediones [1,3–5] (1.353–1.371 Å).

Both experimental [1,4,5] (see also Ref. 9 and references therein) and theoretical [6,10,11] results indicate that hydrogen bonding has a marked effect on the conjugation in the N−C=O fragment. A hydrogen bond from nitrogen to oxygen, as in the present structure [N···O distance 2.763(1) Å], will increase the conjugation, *i.e.* give a shorter C−N bond and a longer C−O bond. The bond lengths found here are, respectively, 1.333 and 1.234 Å, while the corresponding bonds reported for formamide in the gas state [18] are 1.368 and 1.212 Å. These differences in the two molecules again indicate the effect of hydrogen bonding on a conjugated system like formyl.

A series of *ab initio* calculations [6] indicated that "dimerization" of formamide *via* a N−N bond will give a shortened C−N bond. The lengths found for the C−N bonds in formyl dihydrazine are 1.350 and 1.354 Å, which are significantly longer than in the present structure. However, this bond of 1.333 Å is also significantly shorter than the corresponding bond length of 1.345 Å found for 4,5-dichloro-3,6-pyridazindione [1] where a similar N−N bond and hydrogen bond system is present.

Results from theoretical and experimental electron population analyses are listed in Table 2. The gross atomic populations yielded by the extended *L*-shell refinement using the low-temperature data set are probably the "best". Although, theoretical and experimental results are not directly comparable (both because of the difference in dividing the electrons between the centers in the two methods, and because hydrogen bonding and other short contacts alter the electron cloud), it is interesting to note that in all cases is a large concentration of electron density centered on the oxygen atom, while the CH-group is electron deficient.

REFERENCES

1. Ottersen, T. *Acta Chem. Scand. 27* (1973) 797.
2. Ottersen, T. *Acta Chem. Scand. 27* (1973) 835.
3. Ottersen, T. and Seff, K. *Acta Chem. Scand. 27* (1973) 2524.
4. Ottersen, T. *Acta Chem. Scand. A 28* (1974) 666.
5. Ottersen, T. *Acta Chem. Scand. A 28* (1974) 661.
6. Ottersen, T. and Jensen, H. H. *J. Mol. Struct. 24* (1975). *In press.*
7. Ottersen, T. *Manuscript in preparation.*
8. Tomiie, T., Koo, C. H. and Nitta, I. *Acta Crystallogr. 11* (1958) 774.
9. Kitano, M. and Kuchitsu, K. *Bull. Chem. Soc. Jap. 47* (1974) 631.
10. Ottersen, T. *J. Mol. Struct. 24* (1975). *In press.*
11. Ottersen, T. and Jensen, H. H. *J. Mol. Struct. 24* (1975). *In press.*
12. Stewart, R. F. *J. Chem. Phys. 53* (1970) 205.
13. Coppens, P., Pautler, D. and Griffin, J. F. *J. Amer. Chem. Soc. 93* (1971) 1051.
14. Groth, P. *Acta Chem. Scand. 27* (1973) 1887.
15. Ottersen, T. *COMPARE*, comp. prog., Univ. of Hawaii 1973.
16. Doyle, P. A. and Turner, P. S. *Acta Crystallogr. A 24* (1968) 390.
17. Stewart, R. F., Davidson, E. R. and Simpson, W. T. *J. Chem. Phys. 42* (1965) 3175.
18. Kitano, M. and Kuchitsu, K. *Bull. Chem. Soc. Jap. 47* (1974) 67.

Received July 5, 1974.

Acta Chemica Scandinavica A 28 (1974) 1150—1154

An Electron Diffraction Investigation of the Molecular Structure of *trans*-2-Methyl-1,3,5-hexatriene in the Vapour Phase

M. TRÆTTEBERG and G. PAULEN

Department of Chemistry, University of Trondheim, NLHT, N-7000 Trondheim, Norway

The molecular structure of *trans*-2-methyl-1,3,5-hexatriene has been studied by the gas electron diffraction method. The molecule was found to have a planar carbon skeleton. The mean vibrational amplitudes for all interatomic distances have been calculated from an assumed force field and have been compared with those experimentally determined.

The following structural parameters have been obtained: C=C, 1.348 Å; C_2-C_3, 1.456 Å; C_2-C_7, 1.510 Å; C_1-H_1, 1.094 Å; $C_7-H_{7'}$ 1.104 Å. The distances are given as R_a values. The distribution of bond angles is given in Table 2.

The molecular structures of *cis* and *trans* isomers of 1,3,5-hexatriene have been studied earlier.[1,2] It will be of interest to see which changes in the structural parameters will be observed when a methyl group is introduced in 2-position. The structural study is also of interest as a contribution to the elucidation of molecular structures of conjugated aliphatic systems generally. The molecular structure of *cis*-2-methyl-1,3,5-hexatriene has been studied simultaneously and the results are published elsewhere.[3]

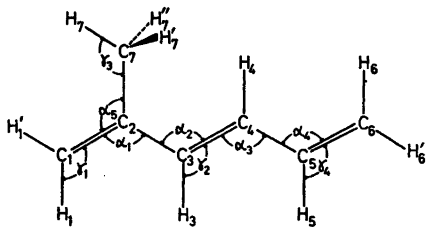

Fig. 1. *trans*-2-Methyl-1,3,5-hexatriene. Molecular model which shows the numbering of the atoms.

EXPERIMENTAL

The sample of *trans*-2-methyl-1,3,5-hexatriene used in the present study was kindly provided by the late professor R. B. Turner, Rice University, Houston, Texas.

The electron diffraction diagrams were recorded with the Oslo electron diffraction unit [4] at camera lengths of approximately 48 and 20 cm. During the experiment the sample of *trans*-2-methyl-1,3,5-hexatriene was maintained at a temperature of 20 °C, while the temperature of the nozzle was about 30 °C. The electron wavelength was 0.06458 Å, corresponding to an accelerating potential of about 36 kV. The scattering data were treated in the usual way,[5] and yielded an experimental modified molecular intensity function extending from $s = 1.375$ Å^{-1} to $s = 42.75$ Å^{-1}. The Δs interval was 0.125 Å^{-1} in the inner s region ($s < 9.5$ Å^{-1}) and 0.250 Å^{-1} for the large-angle scattering data.

STRUCTURE ANALYSIS

Preliminary values for the structure parameters were obtained from the observed radial distribution (RD) curve, which is shown in Fig. 3 and from a study of experimental and theoretical autocorrelation power spectra.[9] The bond distances and valence angles were refined by a least squares procedure applied to the observed molecular intensity function, a diagonal weight matrix being used.[5,10] The scattering amplitudes and phases used in the theoretical equation were calculated by the methods described by Peacher and Wills,[11] using HF atomic potentials.

The peaks at about 1.1 and 1.4 Å on the experimental RD curve shown in Fig. 3 represent carbon hydrogen and carbon carbon bond

distances, respectively, while the peaks at about 2.15 and 2.5 Å contain contributions from the carbon hydrogen and carbon carbon nonbonded distances over one bond angle. The appearance of the fairly large peak at about 6.1 Å is a clear indication that *trans*-2-methyl-1,3,5-hexatriene must have an essentially planar carbon skeleton with *s-anti* conformation at the C_2-C_3 and C_4-C_5 single bonds.

In the electron diffraction studies of the *cis* [1] and *trans* [2] isomers of 1,3,5-hexatriene it was possible to show that the length of the central C=C double bond was somewhat larger than the terminal ones. It is more complicated to determine the bond distances in *trans*-2-methyl-1,3,5-hexatriene as introduction of a methyl group destroys the symmetry in the molecule and also adds two new types of bonds. In the present case it was not possible to distinguish between the central and terminal C=C double bonds, and the three C=C double bond distances were assumed to be equal.

Some assumptions were also made concerning the positions of the hydrogen atoms. All C=C−H angles (γ_1) involving the terminal methylene groups were assumed to be equal. The $C_3=C_4-H_4$ (γ_2) angle was assumed to be the same as $\angle C_4=C_3-H_3$. The three-fold axis of the methyl group was assumed to coincide with the C_2-C_7 single bond and one of the methyl hydrogens assumed to be eclipsed with the $C_1=C_2$ double bond.

When the assumptions described above were applied a rigid molecular model of *trans*-2-methyl-1,3,5-hexatriene could be described by three CC and two CH bond lengths, five CCC and four CCH bond angles and the C_2-C_3 and C_4-C_5 dihedral angles. It was not possible to vary all these geometrical parameters simultaneously in the least squares refinements. Some of the bond angle parameters were therefore determined applying an indirect approach. One angle was studied at a time by running several parallel least squares programs. In all runs the conditions were identical except for the angle being studied, which was slightly different from one run to another. By studying the squared error sums and standard deviations of the refining parameters the best value for the angle in question was chosen. This process was continued until self-consistency.

The model used to describe the *trans*-2-methyl-1,3,5-hexatriene molecule contains all together sixtyeight different carbon-carbon and carbon-hydrogen distances. It is not possible to determine vibrational parameters for all of these internuclear distances from the electron diffraction data. In order to assign plausible mean vibrational amplitudes (u values) to the distances whose u values could not be directly determined, theoretical values for all mean vibrational amplitudes were calculated from an assumed force field. The calculations were made according to Gwinn's method,[13] which is based on an expansion of interatomic distances in terms of cartesian displacement coordinates. The computer program has been adjusted for practical use in an electron diffraction study by Stølevik *et al.*[14] The assumed force field was taken from data published by Allinger *et al.*[15]

Table 1. trans-2-Methyl-1,3,5-hexatriene. Calculated and observed mean vibrational amplitudes for the carbon carbon distances. The numbers in parentheses are standard deviation values, as resulting from least squares intensity refinements.

Distance	$u^{obs.}$, Å	$u^{calc.}$, Å
C=C	0.0391 (8)	0.0409
C_2-C_3	0.0460 (12)	0.0487
C_2-C_7	0.0462 (16)	0.0492
C_1-H_1	0.0775	0.0790
C_7-H_7		0.0791
$C_1\cdots C_7$		0.0771
$C_1\cdots C_3$	0.0550	0.0795
$C_4\cdots C_6$		0.0776
$C_3\cdots C_5$		0.0771
$C_2\cdots C_4$		0.0768
$C_3\cdots C_7$		0.0836
$C_4\cdots C_7$	0.1128 (25)	0.1562
$C_1\cdots C_4$	0.0759 (26)	0.0767
$C_3\cdots C_6$		0.0772
$C_2\cdots C_5$		0.0794
$C_5\cdots C_7$	0.1550 (25)	0.1627
$C_1\cdots C_5$	0.0739 (83)	0.1046
$C_2\cdots C_6$		0.1015
$C_6\cdots C_7$	0.1350 (172)	0.2253
$C_1\cdots C_6$	0.0875 (25)	0.0976

The calculated u values for the carbon carbon distances in the molecule are listed in Table 1, which also presents the observed mean vibrational amplitudes for these distances. It will be seen that some of the observed u values are assumed to be the same for groups of nonbonded distances. These assumptions were

reasonable as judged by the similarities of the calculated u values within one group. On an average the calculated mean vibrational amplitudes were found to be larger than those observed experimentally. Apart from this general deviation the correspondence between calculated and observed u values is satisfactory.

If the longest non-bonded carbon carbon distances are treated as independent parameters in the least squares analyses, they are found to be a trifle smaller than when calculated for a planar molecular model. This observation must be described to shrinkage effects,[16,17] as the mean vibrational amplitude for the $C_1 \cdots C_6$ distance is found to be quite small. When the longer non-bonded CC distances were treated as dependent distances and the C_2-C_3 and C_4-C_5 dihedral angles were varied systematically, best correspondence between experimental and theoretical data was obtained when the two dihedral angles were about 170° instead of 180° for an all planar conformation.

Table 2. trans-2-Methyl-1,3,5-hexatriene. Structure parameters obtained by least squares refinements on the intensity data. Distances (R_a values [6]) and mean amplitudes of vibrations (u) in Å, angles in degrees. The standard deviations given in parentheses have been corrected to take into account data correlation [7] and have also been increased to include the uncertainty arising from error in the electron wavelength.[8]

Distances	R_a	u
$C=C$	1.3477 (20)	0.0391 (20)
C_2-C_3	1.4562 (30)	0.0460 (30)
C_2-C_7	1.5104 (40)	0.0462 (40)
C_1-H_1	1.0940 (25)	
C_7-H_7	1.1040 (25)	
$C_1 \cdots C_7$	2.4889	
$C_1 \cdots C_3$	2.4181	
$C_4 \cdots C_6$	2.4819	0.0550[a]
$C_3 \cdots C_5$	2.4716	
$C_2 \cdots C_4$	2.4919	
$C_3 \cdots C_7$	2.5677	
$C_4 \cdots C_7$	3.0069	0.1128 (60)
$C_1 \cdots C_4$	3.6764	
$C_3 \cdots C_6$	3.7071	0.0759 (64)
$C_2 \cdots C_5$	3.8406	
$C_5 \cdots C_7$	4.4598	0.1550 (60)
$C_1 \cdots C_5$	4.8829	0.0739 (200)
$C_2 \cdots C_6$	4.9713	
$C_6 \cdots C_7$	5.3119	0.1350 (300)
$C_1 \cdots C_6$	6.1163	0.0875 (60)
Angles		
$\angle C_1=C_2-C_3$ (α_1)	119.1	
$\angle C_2-C_3=C_4$ (α_2)	125.4	
$\angle C_3=C_4-C_5$ (α_3)	124.5[a]	
$\angle C_4-C_5=C_6$ (α_4)	124.5[a]	
$\angle C_1=C_2-C_7$ (α_5)	121[a]	
$\angle C_3=C_1-H_1$ (γ_1)	122[a]	
$\angle C_3=C_4-H_4$ (γ_2)	118.5[a]	
$\angle C_2-C_7-H_7$ (γ_3)	110.5[a]	
$\angle C_6=C_5-H_5$ (γ_4)	116[a]	

[a] Determined by combined trial and error/least squares procedure (see text).

If the molecular geometry is based on a R_α structure [14] the shrinkage effects should be included, as R_α gives the distance between average positions of two atoms. The distances displayed in a RD function are R_a distances. The relationship between a R_a and a R_α interatomic distance is approximately:

$$R_a = R_\alpha + K - u^2/R_e$$

K is the perpendicular amplitude correction coefficient.[14] If the K values for all interatomic distances are known, it is possible to determine an R_α structure from electron diffraction data. The K values were calculated by the same program that was used for calculation of the mean vibrational amplitudes. In the present case the quality of the parameters determined from a R_α structure was somewhat inferior to those determined from a R_a structure, when the squared error sum and standard deviation values were used as criteria. This might be due to inaccurate perpendicular amplitude correction coefficients. The determined parameters based on an R_α and an R_a structure were, however, practically identical. The final parameters for *trans*-2-methyl-1,3,5-hexatriene, based on refinements on a R_a structure are presented in Table 2.

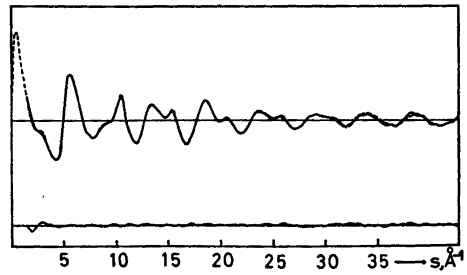

Fig. 2. trans-2-Methyl-1,3,5-hexatriene. Experimental (——) and theoretical (- - -) molecular intensity functions with difference curve.

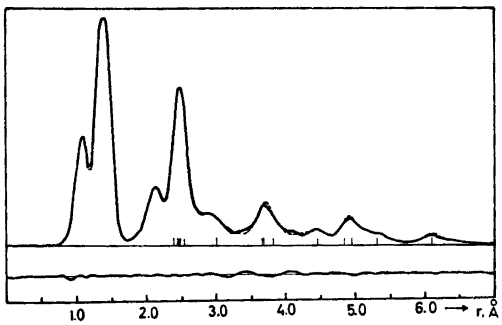

Fig. 3. trans-2-Methyl-1,3,5-hexatriene. Experiment (——) and theoretical (- - -) radial distribution functions and difference curve. Artificial damping constant $k = 0.0015$ Å^2.

The theoretical molecular intensity function calculated on the basis of the parameters listed in Table 2, is shown in Fig. 2 along with the experimental $sM(s)$ function, while Fig. 3 shows the corresponding theoretical and experimental radial distribution functions.

DISCUSSION

In Table 3 the structural parameters for *trans*-2-methyl-1,3,5-hexatriene are compared with similar data obtained for its *cis* isomer and for *trans* and *cis* isomers of 1,3,5-hexatriene. It will be seen that the various types of bond distances are found to be approximately the same in all four molecules. When the bond angles for the two 2-methyl-1,3,5-hexatrienes are compared, the increased values for $\angle\alpha_2$ and $\angle\alpha_3$ for the *cis* isomer should be noticed. Such enlarged CCC valence angles are to be expected because of the larger steric strain in this molecule. The same difference in $\angle\alpha_2$ ($\angle\alpha_3$) for the *cis* and *trans* isomers of 1,3,5-hexatriene is also observed, although the discussed angles are generally found to be somewhat smaller in these molecules. There appears to be a large unexplainable discrepancy between $\angle\alpha_5$ in *trans*- and *cis*-2-methyl-1,3,5-hexatriene. For both molecules there is, however, a high degree of coupling between $\angle\alpha_1$ and $\angle\alpha_5$. The average of these two angles is approximately the same for the two molecules and the apparent deviations should therefore not be taken too seriously.

Table 3. Comparison of structural parameters determined for *trans* (I) and *cis* [3] (II) isomers of 2-methyl-1,3,5-hexatriene and *trans* [2] (III) and *cis* [1] (IV) isomers of 1,3,5-hexatriene. Distances (R_a) in Å and angles in degrees.

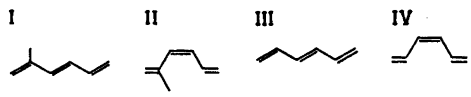

	I	II	III	IV
C=C	1.348	1.345	1.347[a]	1.345[a]
C_3-C_3	1.456	1.462	1.458	1.462
C_2-C_7	1.510	1.515		
C_1-H_1	1.094	1.091	1.104	1.090
C_7-H_7	1.104	1.101		
$\angle\alpha_1$	119.1	122.6	121.7	122.1
$\angle\alpha_2$	125.4	128.7	124.4	126
$\angle\alpha_3$	124.5	127.5	124.4	126
$\angle\alpha_4$	124.5	124.5	121.7	122.1
$\angle\alpha_5$	121	117.5		
$\angle\gamma_1$	122	119.1	120.5	124
$\angle\gamma_2$	118.5	114	115	118
$\angle\gamma_3$	110.5	110.5		
$\angle\gamma_4$	116	116	117	116.9

[a] Average value.

$\angle\gamma_2$ should be studied in connection with the average of $\angle\alpha_2$ and $\angle\alpha_3$ for both the 2-methyl-1,3,5-hexatriene molecules. In the *cis* isomer, where a considerable increase in $\angle\alpha_2$ and $\angle\alpha_3$ is observed, the decrease in $\angle\gamma_2$ compared to the structure of the *trans* isomer is to be expected.

$\angle\alpha_4$ are for both isomeric 2-methyl-1,3,5-hexatriene molecules found to be slightly, but not significantly, larger than in the 1,3,5-hexatriene molecules. Comparable angles in 1,3-butadiene,[18] *trans*-2-butene,[19] and propene [20] are found to be 122.8, 123.8, and 124.8°, respectively.

Acknowledgement. The sample of *trans*-2-methyl-1,3,5-hexatriene used in the present study was donated by the late professor Richard B. Turner, Rice University, Houston, Texas. The authors want to express their gratitude to cand. real. Arne Almenningen who made all the electron diffraction diagrams. Help and advice from cand. real. R. Stølevik in calculating the mean vibrational amplitudes is gratefully acknowledged. The investigation has been supported by Norges almenvitenskapelige forskningsråd, to which the authors want to extend their gratitude.

REFERENCES

1. Trætteberg, M. *Acta Chem. Scand. 22* (1968) 2294.
2. Trætteberg, M. *Acta Chem. Scand. 22* (1968) 628.
3. Trætteberg, M. and Paulen, G. *Acta Chem. Scand. A 28* (1974) 1.
4. Bastiansen, O., Hassel, O. and Risberg, E. *Acta Chem. Scand. 9* (1955) 232.
5. Andersen, B., Seip, H. M., Strand, T. G. and Stølevik, R. *Acta Chem. Scand. 23* (1969) 3224.
6. Kuchitsu, K. *Bull. Chem. Soc. Japan 40* (1967) 498.
7. Seip, H. M., Strand, T. G. and Stølevik, R. *Chem. Phys. Letters 3* (1969) 617.
8. Almenningen, A., Bastiansen, O., Haaland, A. and Seip, H. M. *Angew. Chem., Int. Ed. Engl. 4* (1965) 819.
9. Trætteberg, M. and Bonham, R. A. *J. Chem. Phys. 42* (1965) 587.
10. Almenningen, A., Bastiansen, O., Seip, R. and Seip, H. M. *Acta Chem. Scand. 18* (1964) 2115.
11. Peacher, J. L. and Wills, J. C. *J. Chem. Phys. 46* (1967) 4809.
12. Strand, T. G. and Bonham, R. A. *J. Chem. Phys. 40* (1964) 1686.
13. Gwinn, W. D. *J. Chem. Phys. 55* (1971) 477.
14. Stølevik, R., Seip, H. M. and Cyvin, S. J. *Chem. Phys. Letters 15* (1972) 263.
15. Allinger, N. L. and Sprague, J. T. *J. Amer. Chem. Soc. 94* (1972) 5734.
16. Morino, Y. *Acta Crystallogr. 13* (1960) 1107.
17. Bastiansen, O. and Trætteberg, M. *Acta Crystallogr. 13* (1960) 1108.
18. Haugen, W. and Trætteberg, M. *Selected Topics in Structure Chemistry*, Universitetsforlaget, Oslo 1967.
19. Almenningen, A., Anfinsen, I. M. and Haaland, A. *Acta Chem. Scand. 24* (1970) 43.
20. Tokue, I., Fukuyama, T. and Kuchitsu, K. *J. Mol. Struct. 17* (1973) 207.

Received June 26, 1974.

Acta Chemica Scandinavica A 28 (1975) 1155—1161

An Electron Diffraction Investigation of the Molecular Structure of *trans*-2-Butenedial (Fumaraldehyde) in the Vapour Phase

G. PAULEN and M. TRÆTTEBERG

Department of Chemistry, University of Trondheim, NLHT, N-7000 Trondheim, Norway

Electron diffraction studies of gaseous fumaraldehyde have been carried out. The parameter values were obtained by least squares refinements on the intensity data assuming harmonic vibrations. The molecule is essentially planar with C_{2h}-symmetry. The values obtained for the most important molecular parameters are: C=C, 1.337 Å; C–C, 1.479 Å; C=O, 1.207 Å; C_1-H_1, 1.131 Å; C_2-H_2, 1.094 Å; ∠O=C–C, 123.7°; ∠C=C–C, 122.7°.

The bond distances are given as R_a values.

The structural effects caused by conjugation in an aliphatic molecule have attracted considerable interest during the last few years. It has for example been shown that the length of a carbon-carbon single bond interspaced between two double bonds is clearly dependent on the nature of the second atom in each of the double bonds.[1,2] In this connection molecules like acrolein,[1–3] glyoxal,[1,2] maleic anhydride,[4] 1,3-butadiene,[1,2,5] *cis* [6] and *trans* [7] isomers of 1,3,5-hexatriene have been studied. It will be of interest to compare structural parameters for these molecules with those for *trans*-2-butenedial, where a carbon-carbon double bond is in conjugation with two carbonyl groups. A

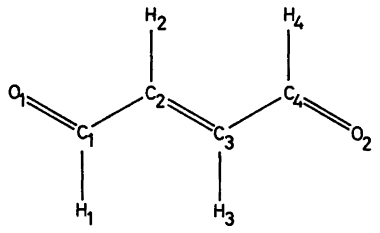

Fig. 1. Fumaraldehyde. Molecular model which shows the numbering of the atoms.

Table 1. Fumaraldehyde. Applied force field parameters for calculation of mean amplitudes of vibrations (*u* values) and perpendicular amplitude correction coefficients (*K* values). I: Herzberg;[12] II: Fukuyama.[13]

Bond or angle	I	II
Stretching force constants (mdyn/Å)		
C_1-H_1	5.1	3.78
C_2-H_2	5.0	4.64
C–C	4.5	3.46
C=C	9.6	7.14
C=O	12.1	10.3
Bending force constants (mdyn Å/rad²)		
H–C=C	0.38	0.186
C–C=C	0.70	0.325
H–C–C	0.38	0.259
$C_2-C_1-H_1$	0.38	0.200
H–C=O	0.38	0.375
C–C=O	0.70	0.500
Torsional force constants (mdyn Å/rad²)		
H–C–C=O	0.09	0.09
H–C–C–H	0.07	0.07
C=C–C–H	0.07	0.07
C=C–C=O	0.12	0.12
H–C=C–H	0.07	0.07
H–C=C–C	0.09	0.09
C–C=C–C	0.12	0.12

Table 2. Fumaraldehyde. Observed and calculated mean amplitudes of vibrations (u_{ij}) and calculated perpendicular amplitude correction coefficients (K_{ij}) for distances between carbon and oxygen atoms.[a]

Distance	$u_{ij}^{obs.}$	I $u_{ij}^{calc.}$	I K_{ij}	IIa $u_{ij}^{calc.}$	IIa K_{ij}	IIb $u_{ij}^{calc.}$	IIb i_{ij}
C=C	0.0421(25)	0.0406	0.00387	0.0439	0.00492	0.0440	0.00524
C−C	0.0488(10)	0.0488	0.00601	0.0526	0.00801	0.0530	0.00873
C=O	0.0367(7)	0.0374	0.01107	0.0390	0.01353	0.0390	0.01483
C_1-H_1	0.0838(145)	0.0770	0.02713	0.0830	0.03056	0.0830	0.03216
C_2-H_2	0.0825	0.0774	0.01790	0.0789	0.02118	0.0789	0.02177
C_1C_3	0.0625(35)	0.0687	0.00436	0.0858	0.00548	0.0890	0.00598
C_1C_4	0.0691(64)	0.0726	0.00129	0.0881	0.00144	0.0914	0.00154
O_1C_2	0.0548(21)	0.0653	0.01019	0.0731	0.01351	0.0753	0.01496
O_1C_3	0.0705(23)	0.0674	0.00623	0.0800	0.00832	0.0828	0.00922
O_1C_4	0.0831(39)	0.0846	0.00199	0.1027	0.00239	0.1072	0.00263
O_1O_2	0.1052(95)	0.0814	0.00030	0.0949	0.00034	0.0988	0.00036

[a] I and II refer to calculations based on Herzberg's [12] and Fukuyama's [13] force constants presented in Table 1. IIa and IIb are calculations made for $t = 25$ °C and $t = 60$ °C respectively, while I is based on $t = 60$ °C. The numbers in parentheses are standard deviation values as resulting from the least squares analyses.

Table 3. Fumaraldehyde. Structural parameters determined by least squares intensity refinements. The distances are presented as R_a values and the numbers in parentheses are standard deviation values as resulting from the least squares analyses. During the refinements the nonbonded distances were calculated from R_a (I), R_g (II) and R_α (III) parameters.

Distance	I R_{ij}(Å)	I u_{ij}(Å)	II R_{ij}(Å)	II u_{ij}(Å)	III R_{ij}(Å)	III u_{ji}(Å)
C=C	1.3337 (19)	0.0405 (26)	1.3333 (19)	0.0400 (26)	1.3362 (19)	0.0421 (25)
C−C	1.4780 (11)	0.0486 (11)	1.4777 (11)	0.0485 (11)	1.4790 (10)	0.0488 (10)
C=O	1.2068 (10)	0.0357 (9)	1.2069 (10)	0.0355 (10)	1.2067 (10)	0.0367 (7)
C_1-H_1	1.1237 (47)	0.0775 (135)	1.1239 (49)	0.0748 (138)	1.1311 (48)	0.0838 (145)
C_2-H_2	1.0937 (47)		1.0926 (49)		1.0939 (48)	
Angle	(°)		(°)		(°)	
∠O=C−C	123.20 (0.17)		123.11 (0.17)		123.65 (0.16)	
∠C−C=C	122.12 (0.23)		122.07 (0.23)		122.73 (0.22)	
$\angle C_2-C_1-H_1$	119.59 (0.69)		119.59 (0.70)		119.51 (0.63)	
∠C=C−H	124.42 (0.90)		124.27 (0.92)		124.61 (0.80)	
$\sum_i w_i \Delta_i^2$	3.07×10^3 (1.24)		3.22×10^3 (1.30)		2.47×10^3 (1.00)	

similar study of the isomeric *cis*-2-butenedial is also in progress. For the sake of simplicity *trans*-2-butenedial is referred to as fumaraldehyde in this paper. Fig. 1 shows a model of the molecule with the numbering of the atoms that is applied in the present study.

EXPERIMENT AND STRUCTURE ANALYSES

The sample of fumaraldehyde was synthesized from 2,5-dimethoxy-2,5-dihydrofuran by hydrolysis.[15] The electron diffraction data were recorded in the usual way with the Oslo apparatus.[8] The nozzle temperature was 60 − 65 °C and the electron wavelength was 0.064584 Å, corresponding to an accelerating potential of about 36 kV. Photographs were taken at two nozzle-to-plate distances, *i.e.* approximately 48 and 20 cm. Four plates from each distance were selected for use in this investigation. The data were handled in the usual way.[9] The resulting experimental molecular intensity [$sM(s)$] function extended from $s = 1.625$ Å^{-1} to $s = 42.0$ Å^{-1} and is shown in Fig. 2. Two different Δs intervals were used, namely 0.125 Å^{-1} for

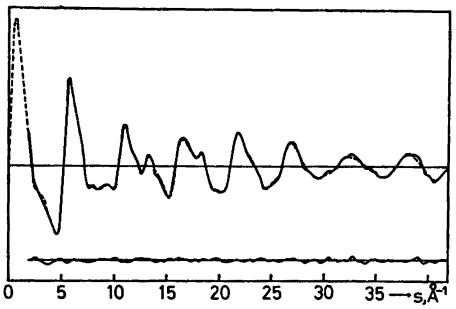

Fig. 2. Fumaraldehyde. Experimental (———) and theoretical (- - - -) molecular intensity functions and the differences between the two.

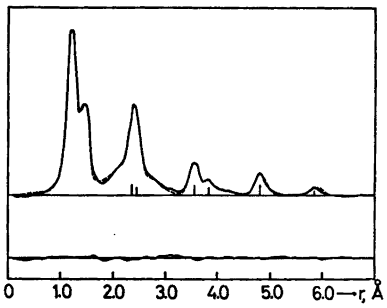

Fig. 3. Fumaraldehyde. Experimental (———) and theoretical (- - - -) radial distribution functions and the differences between the two. Artificial damping constant $k = 0.0015$ Å^2.

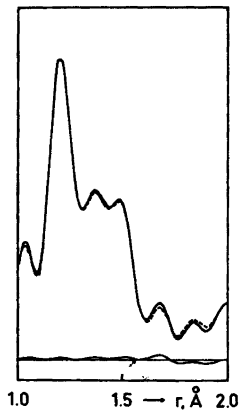

Fig. 4. Fumaraldehyde. Experimental (———) and theoretical (- - - -) sharpened radial distribution functions. Antidamping constant $\alpha = 0.04$.

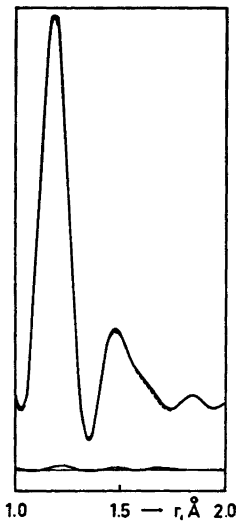

Fig. 5. Fumaraldehyde. Experimental (———) and theoretical (- - - -) autocorrelation power spectra. Antidamping constant $\alpha = 0.04$. τ_{max} 30.0 Å^{-1}.

Table 4. Structural results for fumaraldehyde. The values in parentheses are estimated errors presented as 2.5 times standard deviations from least squares. They include estimates of systematic errors and the effect of correlation.

Distance	R_a (Å)	u (Å)
C=C	1.3362 (45)	0.0421 (60)
C–C	1.4790 (23)	0.0488 (25)
C=O	1.2067 (23)	0.0367 (17)
C_1-H_1	1.1342 (120)	0.0838 (38)
C_2-H_2	1.0939	0.0825
$C_1\cdots C_3$	2.4665	0.0625 (88)
$C_1\cdots C_4$	3.8321	0.0691 (152)
$O_1\cdots C_2$	2.3665	0.0548 (53)
$O_1\cdots C_3$	3.5588	0.0705 (58)
$O_1\cdots C_4$	4.8153	0.0831 (98)
$O_1\cdots O_2$	5.8735	0.1052 (238)
Angle	**(°)**	
$\angle O=C-C$	123.6 (0.5)	
$\angle C-C=C$	122.7 (0.6)	
$\angle C_2-C_1-H_1$	119.5 (1.6)	
$\angle C=C-H$	124.6 (2.0)	

Table 5. Correlation matrix for

C=C	C−C	C_1-H_1	C=O	∠C−C=C	$\angle C_2C_1H_1$	∠O=C−C	∠C=C−H	u(C=C)
1.000	.449	−.141	.640	−.571	.034	−.352	.091	−.289
	1.000	−.031	.141	−.469	−.032	−.253	.153	.156
		1.000	−.322	.102	−.111	.179	−.129	.271
			1.000	−.352	.095	−.420	.012	−.625
				1.000	.004	−.267	−.419	.105
					1.000	−.158	−.330	−.079
						1.000	.478	.231
							1.000	.035
								1.000
[b] .0019	.0010	.0048	.0010	.22	.63	.16	.80	.0025

[a] Distances (R) and root-mean-square amplitudes (u) in Å, angles in degrees. [b] Standard deviations

$s < 10$ Å^{-1} and 0.250 Å^{-1} for the large-angle scattering data.

The experimental radial distribution (RD) function obtained by Fourier inversion of the experimental molecular intensity function [9] is shown in Fig. 3. The large peak centered at 1.2 Å corresponds to the C−H and C=O distances, while the other peak at about 1.4 Å in this overlapping peak complex contains contributions from the carbon-carbon bond distances. The main contributions to the peak with a maximum at about 2.4 Å are from the nonbonded CC and CO distances over one valence angle.

The outer part of the experimental RD function gives information concerning the overall conformation of the molecule. The fairly large and sharp peak at about 5.9 Å is a clear indication that fumaraldehyde is an essentially planar molecule with *s-anti* conformation at the carbon-carbon single bonds. A calculated theoretical RD function with assumed bond distances and valence angles and with an all planar and *anti* conformation supported this observation. The further structure analysis was therefore based on a molecular model with C_{2h} symmetry.

Preliminary values for the bond distances and their mean amplitudes of vibration (u values) were obtained by comparing theoretical and experimental power spectra.[10,11] The resulting sharpened radial distribution (SRD) and autocorrelation power spectra (APS) functions are shown in Figs 4 and 5.

The molecular structure was determined by least squares analyses of the molecular intensity function. During this process the dependent nonbonded distances are calculated from the independent geometrical parameters (bond distances, valence and dihedral angles), and it is also necessary to calculate the partial derivatives of the nonbonded distances with respect to the various independent geometrical parameters. It is of importance to define which type of internuclear distance is used as basis for calculation of dependent nonbonded distances. Electron diffraction structural results are usually presented in the form of R_a, R_g or R_α structures.[18] The following approximate relationships exist between the different R values:

$$R_a \simeq R_g - u^2/R \simeq R_\alpha + K - u^2/R$$

where u is the mean amplitude of vibration and K is the perpendicular amplitude correction coefficient.

R_α gives the distance between average positions of two atoms and an R_α structures is therefore geometrically consistent. This is not true for R_a and R_g structures where shrinkage effects might be observed.[16]

Based on an electron diffraction experiment the interatomic distances may be obtained as R_a or R_g values. R_α parameters are not directly accessible since the K values can not be experimentally obtained by this method. It is,

parameters of fumaraldehyde.[a]

u(C−C)	u(C$_1$H$_1$)	u(C=O)	u(O$_1$O$_2$)	u(O$_1$C$_2$)	u(O$_1$C$_3$)	u(O$_1$C$_4$)	u(C$_1$C$_3$)	u(C$_1$C$_4$)
−.291	−.492	−.094	−.001	−.033	.002	−.001	−.052	−.026
.059	−.036	.172	.007	.089	.045	.032	.109	−.012
.045	.311	.188	−.032	−.120	−.080	−.070	−.055	−.027
−.390	−.872	−.447	−.014	−.085	−.042	−.033	−.121	−.009
.116	.225	.004	.007	−.529	.034	−.018	−.501	.012
−.030	−.065	−.032	−.002	.108	.000	−.055	−.059	.084
.160	.373	.181	.001	.574	−.008	.015	.770	−.064
.042	.013	.067	−.011	.486	.043	.046	.596	−.151
.627	.642	.741	.013	.103	.051	.038	.131	.002
1.000	.404	.513	.016	.118	.055	.042	.123	.012
	1.000	.500	.024	.115	.063	.046	.148	.001
		1.000	.024	.145	.076	.055	.157	−.002
			1.000	.011	.026	.050	.009	−.007
				1.000	.027	.040	.704	−.032
					1.000	.021	.034	−.124
						1.000	.040	.006
							1.000	−.074
								1.000
.0010	.0015	.0007	.0086	.0019	.0022	.0036	.0046	.0047

from least squares.

however, possible to calculate the shrinkage corrections (): transformation to R_α parameters) from a simplified force field.[17,18]

In the present study two sets of u and K values were calculated, based on Herzberg's [12] and Fukuyama's [13] force constants, respectively. The force constants are shown in Table 1, while the calculated mean amplitudes and perpendicular correction coefficients for the most important interatomic distances are presented in Table 2. The calculations based on Fukuyama's force constants were carried out for $t = 25$ °C and $t = 60$ °C in order to study the influence of the temperature on the results, while the temperature was set equal to 60 °C when Herzberg's force constants were applied. In accordance with expectations the u and K values based on Herzberg's fairly large force constants are generally smaller than those based on Fukuyama's force constants.

The least squares analyses were carried through for R_a, R_g and R_α structures. It was possible to determine all the mean vibrational amplitudes experimentally except for some of the nonbonded oxygen-hydrogen distances. In calculation of R_α structures the experimental u values were applied together with the calculated K values. The K values based on Fukuyama's force constants (II) gave clearly the best R_α structure. The results for $t = 60$ °C were also better than those for $t = 25$ °C, as might be expected since the experimental data were recorded at $t = 60 - 65$ °C.

Table 3 shows the results based on R_a (I), R_g (II) and R_α (III) structures. The squared error sum and the standard deviation values for the determined parameters are smallest when an R_α structure is determined. These results show, hardly surprisingly, that in an electron diffraction study of a molecule with a long skeleton, like the present case, refinements including shrinkage corrections are superior to those without such corrections.

Least squares refinements without shrinkage corrections (I and II) might be expected to give slightly smaller values for the C=C, C−C and C=O bond distances and for the O=C−C and C=C−C valence angles. From Table 3 small effects in the expected direction will be noted for all the discussed parameters except for the C=O bond, where there is practically no difference between the three results.

The final structural parameters for fumaraldehyde are presented in Table 4. The results are obtained by a least squares analysis based on an R_α structure. The correlation matrix for the parameters of fumaraldehyde is presented in Table 5 and is based on refinements where the most important non-bonded distances are included as parameters. The theoretical molecular intensity function calculated from the parameters presented in Table 4 is shown in Fig. 2 together with the experimental $sM(s)$ function. The corresponding radial distribution functions are shown in Fig. 3.

Table 6. Comparison of the bond distances obtained for fumaraldehyde with results obtained for similar molecules studied by gas electron diffraction. The distances are given in Å as R_a values.

Molecule	$C_{sp^2}-C_{sp^2}$	C=C	C=O	C−$H_{ole.}$	C−$H_{ald.}$	Ref.
Fumaraldehyde	1.479	1.336	1.207	1.094	1.134	[c]
trans-3-Hexene-2,5-dione	1.490	1.329	1.211			14
Acrolein	1.478	1.335	1.208	1.094	1.123[a]	1
	1.481	1.340	1.209	1.079	1.099	3
1,3-Butadiene	1.463	1.341		1.090		1
	1.467	1.344		1.094		5
trans-1,3,5-Hexatriene	1.458	1.337 (terminal) 1.368 (central)		1.104		7
cis-1,3,5-Hexatriene	1.462	1.336 (terminal 1.362 (central)		1.090		6
Glyoxal	1.525		1.207		1.116	1
Maleic anhydride	1.500[b]	1.330[a,b]	1.195[b]	1.091[b]		4
Propynal			1.214[b]		1.130[b]	23

[a] Not independently determined. [b] Given as R_g value. [c] Present study.

Table 7. Comparison of bond angles obtained for fumaraldehyde with results obtained for similar molecules studied by gas electron diffraction.

Molecule	∠C=C−C (°)	∠C−C=O (°)	∠C=C−H (°)	∠H−C=O (°)	Ref.
Fumaraldehyde	122.7	123.6	124.6	116.9	[a]
trans-3-Hexene-2,5-dione	122.4	121.7	124.0		14
Acrolein	120.3	123.3	121.3	122.3	1
	119.9		121.6		3
1,3-Butadiene	123.3		121.8[d]		1
	122.8		119.5		5
trans-1,3,5-Hexatriene	124.4 [b] 121.7 [c]		115.0 [e]		7
cis-1,3,5-Hexatriene	125.9 [b] 122.1 [c]		118.0 [e]		6
Glyoxal		121.2		126.6	1
Propynal		124.2		122.1	23

[a] Present study. [b] The angle involving central C=C. [c] The angle involving terminal C=C. [d] Average value. [e] Not independently determined.

DISCUSSION

In Table 5 the bond distances of fumaraldehyde are compared with results obtained for other similar molecules, studied by gas electron diffraction.

The secondary environment effect of oxygen on the C−C bond distances that was pointed out by Kuchitsu *et al.*[1] is nicely reproduced in the present study. The C−C bond distance is significantly larger than in conjugated hydrocarbons like 1,3-butadiene and is found to be approximately the same as in acrolein and *trans*-3-hexene-2,5-dione[14] where the C−C bonds have similar environments.

If a C−C single bond in a conjugated system is shortened by conjugation, the double bonds in such a system might be expected to increase. The changes are, however, expected to be much smaller for multiple bonds[19–21] and very few experimental data exist that significantly confirm such multiple bond shortenings. In the

present case the C=C and C=O bond lengths are found to be in good agreement with results obtained for other similar conjugated molecules.

It is generally more difficult to determine C–H bond distances and C–C–H valence angles accurately by electron diffraction than those involving heavier atoms, as hydrogen is a relatively weak scatterer of electrons. Bond distances and angles involving hydrogen also have the largest vibrational effects, and the differences among the structural parameters under different definitions are the largest. This is demonstrated for the C–H bond distances in Tables 3 and 4.

The C–H bond distances determined for fumaraldehyde are in good agreement with the other data presented in Table 5. Normally a C–H bond in an aldehyde group is found to be about 0.03 Å longer than a vinylic C–H bond, in general agreement with the result obtained in the present study.

The valence angles between the heavier atoms are in accordance with the other structural results listed in Table 6. The valence angles involving hydrogen deviate considerably from some of the other results in Table 6. It should be noted that the C=C–H angle (124.6°) is found to be larger and the H–C=O (116.9°) angle to be smaller than expected. There is, however, a high degree of coupling between these two parameters. Because of the general uncertainty in valence angles involving hydrogen atoms these discrepancies are probably not important and will not be discussed further.

Acknowledgements. The authors want to thank Cand.real. A. Almenningen for having taken the diffraction photographs. Valuable supervision by Professor J. Dale during the syntheses of the compound is gratefully acknowledged. Thanks are also due to Cand.real. S. Stølevik for helpful advice concerning application of some of the computer programs. Financial support from Norges Almenvitenskapelige Forskningsråd is acknowledged.

REFERENCES

1. Kuchitsu, K., Fukuyama, T. and Morino, Y. *J. Mol. Struct. 1* (1968) 463.
2. Kuchitsu, K., Fukuyama, T. and Morino, Y. *J. Mol. Struct. 4* (1969) 41.
3. Trætteberg, M. *Acta Chem. Scand. 24* (1970) 373.
4. Hilderbrandt, R. L. and Peixoto, E. M. A. *J. Mol. Struct. 12* (1972) 31.
5. Haugen, W. and Trætteberg, M. *Selected Topics in Structure Chemistry*, Universitetsforlaget, Oslo 1967, p. 113.
6. Trætteberg, M. *Acta Chem. Scand. 22* (1968) 2294.
7. Trætteberg, M. *Acta Chem. Scand. 22* (1968) 628.
8. Bastiansen, O., Hassel, O. and Risberg, F. *Acta Chem. Scand. 9* (1955) 232.
9. Andersen, B., Seip, H. M., Strand, T. G. and Stølevik, R. *Acta Chem. Scand. 23* (1968) 3224.
10. Trætteberg, M. *J. Amer. Chem. Soc. 86* (1964) 4265.
11. Trætteberg, M. and Bonham, R. A. *J. Chem. Phys. 42* (1965) 587.
12. Herzberg, G. *Molecular Spectra and Molecular Structure*, van Nostrand, Princeton 1968, 13th Ed., Vol. II.
13. Fukuyama, T., Kuchitsu, K. and Morino, Y. *Bull. Chem. Soc. Jap. 41* (1968) 3021.
14. Paulen, G. and Trætteberg, M. *Acta Chem. Scand. 29* (1975). *In press.*
15. Alder, K., Betzing, H. and Heimbach, K. *Justus Liebigs Ann. Chem. 638* (1960) 137.
16. Cyvin, S. J. *Molecular Vibrations and Mean Square Amplitudes*, Universitetsforlaget, Oslo and Elsevier, Amsterdam 1968.
17. Gwinn, W. D. *J. Chem. Phys. 55* (1971) 477.
18. Stølevik, R., Seip, H. M. and Cyvin, S. J. *Chem. Phys. Lett. 15* (1972) 263.
19. Mulliken, R. S. *Tetrahedron 6* (1959) 68.
20. Lide, D. R. *Tetrahedron 17* (1962) 125.
21. Bak, B. and Hansen-Nygaard, L. *J. Chem. Phys. 33* (1960) 418.
22. Kuchitsu, K. In Allen, G., Ed., *MTP International Review of Science, A Biannual Series*, Medical and Technical Publ. Co., Oxford 1972.
23. Sugié, T., Fukuyama, T. and Kuchitsu, K. *J. Mol. Struct. 14* (1972) 333.

Received June 26, 1974.

Acta Chemica Scandinavica A 28 (1974) 1162—1166

The Crystal Structure of (±)-*erythro*-2-(2,5-Dimethoxyphenyl)-2-hydroxy-1-methylethylammonium Chloride

MARTIN VAHL GABRIELSEN and ALEX MEHLSEN SØRENSEN

The Royal Danish School of Pharmacy, Chemical Laboratory C, 2100 Copenhagen Ø, Denmark

Methoxamine chloride, (±)-*erythro*-2-(2,5-dimethoxyphenyl)-2-hydroxy-1-methylethylammonium chloride, $C_{11}H_{17}NO_3$.HCl crystallizes in the space group $P2_1/c$ with $a = 14.208(11)$ $b = 9.466(7)$, $c = 9.683(9)$ Å, $\beta = 98.99(12)°$, $Z = 4$. The crystal structure was determined from three-dimensional diffractometer collected X-ray diffraction data, and refined to a final R value of 0.049 by full-matrix least-squares methods. The *erythro* configuration has been confirmed. The structure is stabilized by a maximum number of hydrogen bonds.

Methoxamine is chemically closely related to nor-ephedrine, pharmacologically it is a sympatomimethicum with entirely alpha-adrenergic activity. The general acceptance of the *erythro* configuration for methoxamine has been based on studies on the optical rotation of this and related compounds [1] and the probably stereospecific, catalytic reduction of the corresponding isonitrosopropiophenone to methoxamine.[2,3]

As this evidence for the configuration was not considered conclusive, an X-ray investigation of the structure was carried out.

EXPERIMENTAL

Crystals suitable for X-ray diffraction intensity measurements were grown by slow evaporation at room temperature of an aqueous solution. The unit-cell dimensions were determined from least-squares refinement for the theta values for 36 reflections. The crystal density was measured by flotation in a mixture of chlorobenzene and bromobenzene. The X-ray intensity data were obtained from a crystal with dimensions $0.2 \times 0.4 \times 0.5$ mm mounted on a Nonius three-circle automatic diffractometer using graphite monochromatized Mo$K\alpha$ radiation ($\lambda = 0.7107$ Å). The crystal was mounted with the crystal b-axis and the goniometer ϕ-axis parallel, the ω-scan technique with a fixed scan range of 1.0° and a scan speed of 1.2 deg./min was employed, and background intensity was measured for half the scanning time at the scan range limits. The intensity of one reference reflection was measured after every 25 reflections. Out of 2309 independent reflections in the range $2.5° \leq \theta \leq 25°$, 1578 with an intensity greater than three times their corresponding estimated standard deviation were considered to be observed. The intensity data were corrected for Lorentz and polarization effects. The computations were carried out on a GIER and an IBM 360/75 computer using *The X-Ray System*,[4] *ORTEP* [5] and diffractometer input and output data reduction programs written by one of the authors (A.M.S.). X-Ray atomic scattering factors used were those listed in International Tables for X-Ray Crystallography (1962).

CRYSTAL DATA

Methoxamine chloride, (±)-*erythro*-2-(2,5-dimethoxyphenyl)-2-hydroxy-1-methylethylammonium chloride, $C_{11}H_{17}NO_3$.HCl, M = 247.72, Monoclinic, $a = 14.208(11)$, $b = 9.466(7)$, $c = 9.683(9)$ Å, $\beta = 98.99(12)°$, $V = 1286$ Å^3, $D_m = 1.26$ g cm^{-3}, $Z = 4$, $D_c = 1.28$ g cm^{-3}. Linear absorption coefficient λ(Mo$K\alpha$) = 0.7107 Å: $\mu = 2.9$ cm^{-1}. Space group $P2_1/c$.

STRUCTURE DETERMINATION

From a three-dimensional, sharpened, origin removed Patterson synthesis approximate positions of the chlorine and the hydrogen bonded nitrogen (N) and oxygen (O3) atoms were postulated. An electron density map

Table 1. Final positional and thermal (Å²) parameters. The temperature expression for non-hydrogen atoms is of the form: exp $\{-2\pi^2 (h^2a^{*2}U_{11}+k^2b^{*2}U_{22}+\cdots+2klb^*c^*U_{23})\}$, and for hydrogen atoms of the form: exp $\{-2\pi^2U(2\sin\theta/\lambda)^2\}$. Estimated standard deviations of the parameters are given in parentheses.

	x/a	y/b	z/c	$U_{11}\times 100$	$U_{22}\times 100$	$U_{33}\times 100$	$U_{12}\times 100$	$U_{13}\times 100$	$U_{23}\times 100$
Cl	0.0526(1)	0.1083(1)	0.3279(1)	7.77(5)	4.03(4)	3.99(4)	1.79(4)	1.55(4)	0.55(3)
O(1)	0.2093(2)	0.0666(2)	−0.2030(2)	8.25(15)	5.06(12)	4.62(12)	−1.89(11)	0.94(11)	0.93(10)
O(2)	0.4520(2)	0.0289(4)	0.2977(3)	7.16(17)	12.17(25)	8.67(20)	−0.48(17)	−2.10(15)	−2.37(19)
O(3)	0.1244(2)	−0.1156(2)	0.1402(2)	7.46(13)	3.83(10)	4.02(10)	−0.67(10)	2.15(10)	−0.56(9)
N	0.0560(2)	−0.2842(3)	−0.0805(3)	5.63(14)	3.55(13)	3.46(12)	0.41(10)	0.81(11)	−0.12(10)
C(1)	0.2485(2)	−0.0119(3)	0.0275(3)	5.35(16)	3.30(13)	4.37(14)	−0.16(12)	0.88(12)	−0.88(12)
C(2)	0.2728(2)	0.0675(3)	−0.0818(3)	6.02(18)	3.94(15)	5.23(16)	−0.83(13)	1.64(14)	−0.61(13)
C(3)	0.3576(3)	0.1406(4)	−0.0614(4)	7.37(24)	6.04(22)	7.41(24)	−2.24(17)	2.53(20)	−0.75(18)
C(4)	0.4190(3)	0.1296(5)	0.0633(5)	5.72(21)	7.51(25)	9.08(29)	−1.83(18)	1.62(20)	−2.62(23)
C(5)	0.3969(3)	0.0484(4)	0.1689(4)	5.55(19)	6.82(21)	6.66(21)	−0.23(17)	0.10(17)	−1.98(19)
C(6)	0.3108(2)	−0.0218(3)	0.1514(4)	6.09(19)	4.77(17)	5.28(17)	0.08(14)	0.59(15)	−0.94(15)
C(7)	0.1527(2)	−0.0836(3)	0.0102(3)	5.31(15)	3.21(14)	3.51(13)	−0.24(12)	0.87(12)	−0.10(11)
C(8)	0.1534(2)	−0.2237(3)	−0.0661(3)	5.24(15)	3.44(14)	3.18(13)	−0.27(11)	0.77(11)	−0.11(11)
C(9)	0.2241(3)	−0.3286(4)	0.0056(4)	6.75(22)	4.03(16)	5.86(20)	−1.24(15)	0.14(16)	1.02(16)
C(10)	0.2222(4)	0.1616(4)	−0.3112(4)	9.91(29)	4.87(18)	6.18(22)	−0.25(19)	2.54(22)	1.35(17)
C(11)	0.5403(3)	0.0967(8)	0.3244(7)	6.07(26)	14.24(52)	11.30(41)	0.00(29)	−0.98(26)	−4.76(41)

	x/a	y/b	z/c	$U\times 100$		x/a	y/b	z/c	$U\times 100$
H(31)	0.371(3)	0.196(5)	−0.140(6)	7	H(102)	0.280(4)	0.142(6)	−0.340(6)	7
H(41)	0.475(4)	0.169(6)	0.073(5)	7	H(103)	0.225(3)	0.243(6)	−0.274(5)	7
H(61)	0.294(3)	−0.082(5)	0.221(5)	6	H(111)	0.568(5)	0.059(7)	0.419(8)	10
H(71)	0.104(3)	−0.025(4)	−0.046(4)	4	H(112)	0.582(5)	0.064(7)	0.265(7)	10
H(81)	0.163(2)	−0.207(4)	−0.158(4)	4	H(113)	0.531(4)	0.208(8)	0.320(7)	10
H(91)	0.208(3)	−0.348(5)	0.099(5)	5	H(1N)	0.013(3)	−0.235(5)	−0.148(4)	4
H(92)	0.292(3)	−0.294(4)	0.006(5)	5	H(2N)	0.037(3)	−0.288(4)	0.001(5)	4
H(93)	0.220(3)	−0.413(5)	−0.051(5)	5	H(3N)	0.050(3)	−0.379(5)	−0.106(4)	4
H(101)	0.159(3)	0.151(5)	−0.394(5)	7	H(03)	0.108(3)	−0.039(5)	0.185(4)	5

phased on these atoms showed four likely positions for carbon atoms; the nine remaining non-hydrogen atoms of the methoxamine ion appeared clearly in a subsequent electron density map phased from the contributions of those atoms whose positions had been located.

Full matrix least-squares refinement (minimizing $\sum w(|F_o|-|F_c|)^2$, $w=1$) using individual isotropic temperature factors converged at $R=0.19$. Individual anisotropic thermal parameters were introduced and after three cycles of refinement a difference Fourier synthesis was calculated from structure factors in the range $\sin\theta/\lambda \leq 0.35$. Approximate positions of all the hydrogen atoms were found in the eighteen largest peaks (electron density of 0.2 – 0.5 e Å^{-3}). Individual isotropic thermal parameters, approximately equal to those calculated for the corresponding heavier atoms, were assigned to the hydrogen atoms.

Full-matrix least-squares refinement on the positional parameters of all atoms and individual anisotropic thermal parameters for all non-hydrogen atoms converged at $R=0.049$ (weighted $R=0.061$, average and maximum values of shift error were 0.05 and 0.3, resp.). In the last stages of the refinement empirical weights were introduced to make $w(|F_o|-|F_c|)^2$ independent of $|F_o|$ and $\sin\theta$. The weighting scheme chosen was: $w=axy$ where $a=1$ for $|F_o| \leq 25$ else $a=0.5$, $x=1$ for $\sin\theta > 0.28$ else $x=\sin\theta/0.28$ and $y=1$ for $|F_o| < 9.0$ else $y=9.0/|F_o|$. Final positional and thermal parameters are given in Table 1. Tables of the structure factors are available on request.

Full-matrix least-squares refinement carried out as for the *erythro* configuration of the structure above but interchanging the coordinates of the nitrogen and the terminal side chain carbon atoms converged at $R=0.057$. A difference Fourier map showed a peak (0.25 e Å^{-3}) at the postulated position of the carbon atom and a hole (−0.35 e Å^{-3}) at the postulated position of the nitrogen atom.

DISCUSSION

The assumed *erythro* configuration of methoxamine is confirmed by the X-ray structure determination. Final R-values for the postulated *erythro*- and *threo*-configurations, respectively, are 4.9 and 5.7 %. Further evidence for the *erythro*-form is the presence of three short *inter*atomic distances between nitrogen and chlorine atoms, whereas the three shortest distances between the carbon atom C(9) and chlorine atoms are 3.82, 4.52 and 5.12 Å.

The *p*-dimethoxyphenyl part of the ion is approximately planar apart from four hydrogen atoms, two from each methyl group, which straddle the benzene ring. The methyl groups are as distant as possible from the extended aminoethyl side-chain. The plane of the benzene ring is almost perpendicular to the plane containing the atoms C(1), C(7), C(8), and N. The hydroxy group, the methyl group [C(9)], and the methoxy group at C(5) are situated on the same side of the latter plane.

Some data defining the conformation of the methoxamine ion are listed in Table 2; the geometry of the ion is illustrated by Figs. 1 and 2.

Bond distances and valency angles, uncorrected for thermal motion, are given in Table 3. The bond lengths are close to normally

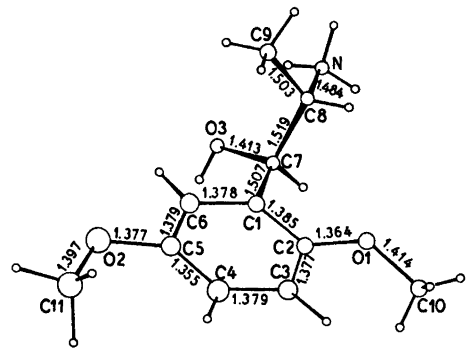

Fig. 1. Methoxamine ion, interatomic distances.

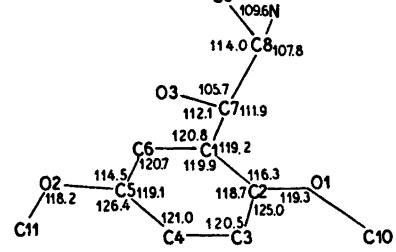

Fig. 2. Methoxamine ion, interatomic angles.

Table 2. Conformation of the methoxamine ion.

Benzene ring. Distances of atoms from least squares plane. The equation is in direct (unit cell) space.

Equation: $-7.116x + 7.488y + 4.118z + 1.755 = 0$

Atom	Deviation (Å)	Atom [a]	Deviation (Å)
C(1)	0.010	C(10)	0.102
C(2)	−0.018	C(11)	−0.030
C(3)	0.010	O(1)	−0.072
C(4)	0.004	O(2)	−0.019
C(5)	−0.011	H(31)	0.01
C(6)	0.003	H(41)	−0.05
C(7) [a]	0.084	H(61)	−0.04

[a] The coordinates of these atoms did not contribute to the least squares matrix.

Torsion angles (°) involving non-hydrogen atoms

C(3)−C(2)−O(1)−C(10)	+9.7	C(1)−C(7)−C(8)−C(9)	−59.3
C(4)−C(5)−O(2)−C(11)	+0.5	C(1)−C(7)−C(8)−N	178.8
C(6)−C(1)−C(7)−O(3)	−21.3	O(3)−C(7)−C(8)−C(9)	+62.9
C(6)−C(1)−C(7)−C(8)	+97.4	O(3)−C(7)−C(8)−N	−59.0

accepted values. Some valency angles in the *p*-dimethoxybenzene system deviate significantly from the ideal values, possibly a consequence of the compact planar atomic arrangement.

The packing of the molecules is depicted in Fig. 3. A feature common for this and similar compounds [6-8] is the existence of a maximum number of hydrogen bonds between the halide and substituted ammonium ions.

The chlorine ions form continuous layers in the (100) planes. The onium and hydroxy groups in the methoxamine ions are directed towards these layers, so that an infinite methoxamine ion−chloride ion−methoxamine ion "sandwhich" is formed through the crystal. Each chloride ion is hydrogen bonded in a roughly tetrahedral manner to one hydroxy and three onium groups in four different methoxamine ions. There are no significantly close approaches between non-hydrogen bonded atoms. A summary of the geometry of the close contacts is shown in Table 3.

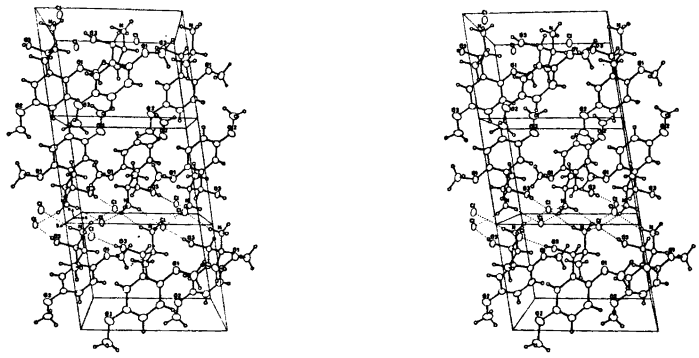

Fig. 3. Stereoscopic pair of figures showing the crystal structure of methoxamine chloride, as seen along the *b*-axis.

Table 3. Interatomic distances (Å) and angles (deg.).

Bond distances

C(1)–C(2)	1.385(4)	C(3)–H(31)	0.96(5)
C(2)–C(3)	1.377(5)	C(4)–H(41)	0.87(5)
C(3)–C(4)	1.379(6)	C(6)–H(61)	0.94(5)
C(4)–C(5)	1.355(6)	C(7)–H(71)	0.98(4)
C(5)–C(6)	1.379(5)	C(8)–H(81)	0.93(4)
C(6)–C(1)	1.378(4)	C(9)–H(91)	0.98(5)
C(1)–C(7)	1.507(4)	C(9)–H(92)	1.02(5)
C(7)–C(8)	1.519(4)	C(9)–H(93)	0.97(5)
C(8)–C(9)	1.503(4)	C(10)–H(101)	1.11(5)
C(2)–O(1)	1.364(4)	C(10)–H(102)	0.93(6)
C(10)–O(1)	1.414(5)	C(10)–H(103)	0.85(6)
C(5)–O(2)	1.377(5)	C(11)–H(111)	1.00(7)
C(11)–O(2)	1.397(6)	C(11)–H(112)	0.94(7)
C(7)–O(3)	1.413(4)	C(11)–H(113)	1.06(7)
C(8)–N	1.484(4)		

The hydrogen bond system

A–H···B	B equipoint	A–H	A···B	H···B	∠AHB
N–H(1N)···Cl	$(-x, -y, -z)$	0.95(4)	3.120(4)	2.20(4)	165(4)
N–H(2N)···Cl	$(-x, y-\frac{1}{2}, \frac{1}{2}-z)$	0.88(5)	3.252(4)	2.44(5)	153(3)
N–H(3N)···Cl	$(x, -y-\frac{1}{2}, z-\frac{1}{2})$	0.93(5)	3.192(3)	2.27(5)	174(3)
O(3)–H(O3)···Cl	(x, y, z)	0.89(4)	3.068(3)	2.20(5)	165(4)

Valency angles [a]

C(6)–C(1)–C(2)	119.9(3)	O(2)–C(5)–C(6)	114.5(4)
C(6)–C(1)–C(7)	120.8(3)	C(5)–C(6)–C(1)	120.7(3)
C(7)–C(1)–C(2)	119.2(2)	C(1)–C(7)–C(8)	111.9(2)
C(1)–C(2)–C(3)	118.7(3)	C(1)–C(7)–O(3)	112.1(2)
C(1)–C(2)–O(1)	116.3(3)	O(3)–C(7)–C(8)	105.7(2)
O(1)–C(2)–C(3)	125.0(3)	C(7)–C(8)–C(9)	114.0(2)
C(2)–C(3)–C(4)	120.5(4)	C(7)–C(8)–N	107.8(2)
C(3)–C(4)–C(5)	121.0(4)	N–C(8)–C(9)	109.6(3)
C(4)–C(5)–C(6)	119.1(3)	C(2)–O(1)–C(10)	119.3(3)
C(4)–C(5)–O(2)	126.4(4)	C(5)–O(2)–C(11)	118.2(4)

[a] All angles involving hydrogen atoms are within three times their estimated standard deviations from the expected values.

Acknowledgements. The authors express their gratitude to Professor, dr. phil. Bodil Jerslev for her stimulating interest in this work, and to Dr. Bengt Öhrner, Apotekens Centrallaboratorium, Sweden, for providing a sample of the NFN standard of methoxamine chloride.

REFERENCES

1. Baltzly, R. and Mehta, N. B. *J. Med. Chem. 11* (1968) 833.
2. Baltzly, R. and Buck, J. S. *J. Amer. Chem. Soc. 62* (1940) 164.
3. Baltzly, R. and Buck, J. S. *J. Amer. Chem. Soc. 64* (1942) 3040.
4. Stewart, J. M., Kundell, F. A. and Baldwin, J. C. *X-Ray 70 Crystal Structure Calculation System*, Computer Science Center, University of Maryland, July 1970.
5. Johnson, C. K. *ORTEP, A Fortran Thermal Ellipsoid Plot Program for Crystal Structure Illustration*, Oak Ridge National Laboratory, Oak Ridge 1965.
6. Phillips, D. C. *Acta Crystallogr. 7* (1954) 159.
7. Carlström, D. and Bergin, R. *Acta Crystallogr. 23* (1967) 313.
8. Bergin, R. and Carlström D. *Acta Crystallogr. B 24* (1968) 1506.

Received July 5, 1974.

Acta Chemica Scandinavica A 28 (1974) 1167—1170

Formation of Tris (ethylenediamine)cobalt(III) Coordination Complex in Dimethyl Sulfoxide

OLE BANG, KJELD RASMUSSEN and FLEMMING WOLDBYE

Chemistry Department A, The Technical University of Denmark, DK-2800 Lyngby, Denmark

Under anaerobic conditions at room temperature, $[Co\ en_3]^{2+}$ in DMSO solution is not oxidized to $[Co\ en_3]^{3+}$, neither in solutions containing excess free ligand, nor in solutions with excess hydrogen chloride.

On admission of molecular oxygen, oxidation of the complex proceeds rapidly under development of $(CH_3)_2S$, which shows that DMSO takes part in the oxidation.

Dimethyl sulfoxide (DMSO) is often used as a reaction medium for the preparation of transition metal complexes. In view of its extensive use as a combined solvent and oxidant in organic chemistry [1] it would be interesting to study a complex forming reaction involving an oxidation, and to investigate whether DMSO itself could act as an oxidant.

Much work has been reported on the role of DMSO as a solvent and as a ligand.[2] However, to our knowledge its oxidation properties in coordination chemistry have not attracted attention, except for a note in the experimental section of a paper by Berney and Weber.[3] Thermodynamically it would be possible for DMSO to act as the oxidant in a number of reactions of preparative importance such as

$$[ML_3]^{2+} + ox \rightarrow [ML_3]^{3+} + red$$

where, *e.g.*, M = Co,Cr and L = ethylenediamine or similar ligands. DMSO is gaining increasing application as a medium for such reactions and it is obvious to ask whether in fact DMSO does participate in the reaction. Such a conjecture could be inspired by the obnoxious smell attributable to dimethylsulfide which manifests itself during such reactions.

Looking at standard potentials of redox pairs in aqueous solution at room temperature, we find that as $E^0(Co^{2+}/Co^{3+}) = 1.83$ V, it seems improbable that DMSO can oxidize Co^{2+} directly to Co^{3+}. (The potential is found in 1 N nitric acid by extrapolation from the measurements of Noyes and Deahl [4]). For ethylenediamine complexes, however, we find [5] $E^0(Co\ en_3^{2+}/Co\ en_3^{3+}) = -0.26$ V, and, as DMSO oxidizes hydrogen iodide,[6] and $E^0(2I^-/I_2) = 0.56$ V, it should thermodynamically be possible that DMSO would oxidize $[Co\ en_3]^{2+}$.

In the present work, the formation of $[Co\ en_3]^{3+}$ from Co^{2+} and ethylenediamine in DMSO solution was studied. Anhydrous $CoCl_2$ is easily dissolved in DMSO, and visible spectra of the resulting complexes are well known,[7–10] as are the spectra of $[Co\ en_3]^{2+}$ [11] and $[Co\ en]_3^{3+}$.[12] Therefore the reaction was followed spectrophotometrically.

EXPERIMENTAL

Preparations. All distillation and handling of solutions took place under nitrogen purified through conc. H_2SO_4, KOH pellets, and a column of reduced copper-chromium-oxide (BASF) kept at 100 °C.

Dimethyl sulfoxide (Th. Schuchardt) was dried over Linde 4A sieves and distilled in a stream of nitrogen at reduced pressure through a 50 mm column [13] packed with Dixon gauze rings. B.p. at 1.0 – 1.5 Torr 36 – 38 °C; according to Douglas [14] the vapour pressure at 37 °C is 1.35 Torr.

Ethylenediamine (Riedel-de-Haën) was dried over sodium hydroxide [15] and distilled under nitrogen at 1 atm. B.p. at 760 Torr 116.5 °C; accepted value [16] 116.5 °C. A stock solution of ethylenediamine in DMSO was prepared by dilution of 1.46 ml en to 25 ml with DMSO. Potentiometric titration in aqueous solution

showed a concentration of 0.052 g ethylenediamine per ml solution.

A stock solution of hydrochloric acid in DMSO was prepared by slowly bubbling nitrogen through an aqueous solution of conc. HCl, conc. H_2SO_4, and pure DMSO. Titration in aqueous solution with NaOH gave 0.019 g HCl per ml solution. All solutions were prepared in a glove box flushed with nitrogen.

$CoCl_2.6H_2O$ (E. Merck) was dehydrated at 160 °C.

The following preparation of complexes in solution was representative: 13.00 mg $CoCl_2$ was weighed into a 10 ml measuring flask. This was placed in the glove box, opened, and flushed with nitrogen applied through a small tube. The salt was dissolved in 5 ml DMSO, and 0.36 ml ethylenediamine solution added. The measuring flask was then filled to the mark with DMSO, the contents mixed, and a 1 cm cell for spectral measurements was filled. After measurement, the cell was emptied into the measuring flask, and 0.20 ml HCl solution was added. After mixing, a cell was filled and the spectrum measured. In this experiment, the molar ratios $CoCl_2$:en:HCl were 1:3.33:1.04, and the formality with respect to $CoCl_2$ was 0.010 F.

Compositions investigated were: $CoCl_2$ (mg), en (ml), HCl (ml): 3.93, 0.11, 0.10; 13.00, 0.36, 0.20; 13.66, 0.63, 0; 15.37, 0.41, 0; 16.63, 0.45, 0.25; 26.94, 0.72, 0.80; 14.07, 1.00, 0.21. Molar ratios $CoCl_2$:en:HCl were 1:3.37:0.52; 1:3.33:1.04; 1:3.20:0; 1:3.21:0; 1:3.25:1.02; 1:3.22:2.01; 1:8.60:1.01.

Absorption spectra in the range 325 – 800 nm were recorded with a Cary model 11 spectrophotometer.

Qualitative observations. $CoCl_2$ dissolved in DMSO to give an intensely blue complex. On addition of ethylenediamine only, the colour changed to slightly reddish, which colour persisted if air was rigorously excluded. Diffusion of air through ground glass joints produced an intense reddish brown colour. This happened whenever measuring flasks were left in the room, though no changes were seen in solutions stored in spectrophotometer cells for periods of up to one month. Deliberate air oxidation of the reddish brown solutions produced no further changes, and oxidation of the contents of a cell by air applied through a capillary produced the same reddish brown colour. Concurrent with this oxidation, an intense smell of sulfide was detected. Dimethyl sulfide, which boils at 37 °C, was driven off by a stream of air and absorbed in a 1 M solution of mercury(II) chloride in abs. ethanol. The derivative was filtered off and washed with abs. ethanol. M.p. 155 – 157 °C (uncorr.), lit. value 158 °C.[17] An estimate of the amount of sulfide formed in relation to the amount of cobalt oxidized was not attempted.

HCl added to the solution of $CoCl_2$ and ethylenediamine produced a slightly green colour, changing to blue with larger amounts of HCl. Oxidation of such solutions produced a yellow or brownish yellow colour, identical with the colour of $[Co\ en_3]Cl_3$ dissolved in DMSO, and released dimethyl sulfide.

HCl added to an oxidized solution as mentioned above produced no visible change in the reddish brown colour.

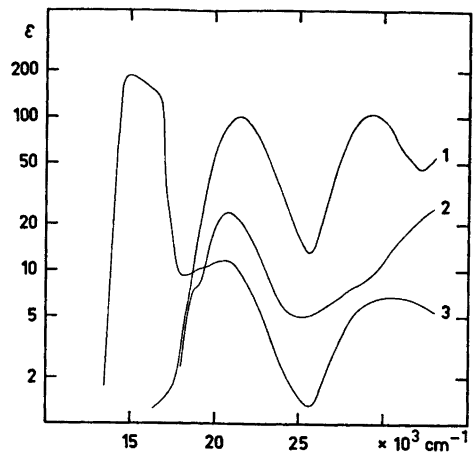

Fig. 1. Absorption spectra of $[Co\ en_3]^{3+}$ (1) and $[Co\ en_3]^{2+}$ (2) in DMSO compared with a solution of $CoCl_2$:en:HCl (1:3.2:2) (3).

RESULTS

Spectra of $[Co\ en_3]^{2+}$ and $[Co\ en_3]^{3+}$ in DMSO are shown in Fig. 1. The spectral data (λ, nm; σ, cm^{-1}; ε, 1 mol^{-1} cm^{-1}) are for $[Co\ en_3]^{2+}$: (535; 18 700; 5) and (482; 20 700; 24), and for $[Co\ en_3]^{3+}$: (467; 21 400; 102) and (342; 29 200; 105). The positions of the visible bands are thus close to values reported for aqueous solutions,[8,9] $[Co\ en_3]^{2+}$: (535; 18 700; 2) and (461; 21 700; 14), and $[Co\ en_3]^{3+}$: (467; 21 400; 86) and (338; 29 600; 80). The larger extinction coefficients in DMSO are probably due to either the higher index of refraction or to the formation of outer-sphere complexes modifying the conformation to slightly larger deviation from octahedral microsymmetry.

Also shown in Fig. 1 is the spectrum of a solution of $CoCl_2$, en, and HCl (1:3.22:2.01). This spectrum is influenced by formation of tetrahedral chlorocomplexes. An analysis of the spectrum shows that 24 % of the cobalt is tetrahedral. This is close to the 20 % of the tetrahedral form found by Buffagni and Dunn [10] in a solution of $[CoCl_4]^{2-}$ in DMSO not containing ethylenediamine.

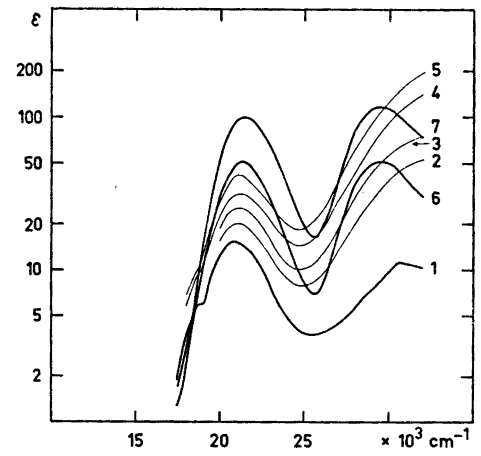

Fig. 2. Gradual oxidation over eight days of a DMSO-solution containing $CoCl_2$:en:HCl (1:8.6:1).

Fig. 2 shows spectra of a solution of $CoCl_2$, en, and HCl (1:8.60:1.01) for various degrees of oxidation. There is a lapse of five days between curves Nos. 1 – 5 and No. 6, and of three more days to No. 7. It is seen how the $[Co\ en_3]^{2+}$ formed originally is gradually oxidized to $[Co\ en_3]^{3+}$ through intermediates absorbing in the ultraviolet.

Fig. 3 shows spectra of a solution not containing HCl (1:3.21:0) for various degrees of oxidation. Curves Nos. 1 – 5 were obtained on the same day; and No. 6 five days later. It is seen that $[Co\ en_3]^{2+}$ does indeed react, but that very little or no $[Co\ en_3]^{3+}$ is formed. Rather, reaction products are formed which seem to correspond to the intermediates seen in acidic solution.

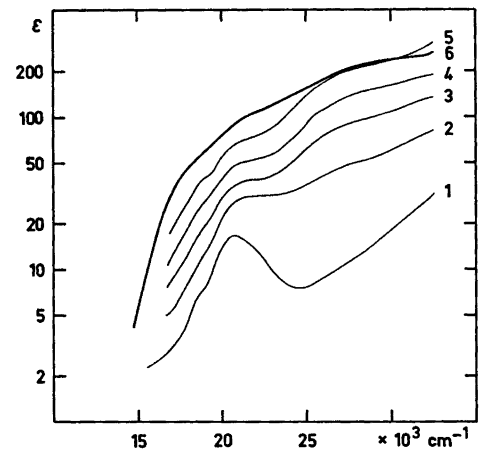

Fig. 3. Oxidation over five days of a DMSO-solution containing $CoCl_2$:en:HCl (1:3.2:0).

DISCUSSION

The following conclusions may be drawn:

(1) $[Co\ en_3]^{2+}$ is not oxidized by DMSO under anaerobic conditions.

(2) Addition of HCl does not catalyse such a reaction, but changes the distribution of labile complexes:

Co^{2+}(octahedral) $\rightleftharpoons$ Co^{2+}(tetrahedral)

(3) Admission of air causes oxidation to start.

(3a) When solutions do not contain HCl, di- or polynuclear complexes are formed. Such complexes may have the general formula $[en_2XCo-O_2-CoY\ en_2]^{4+}$, with most probably X = Y = DMSO. $-O_2-$ may be a peroxo group, giving the Co atoms the formal oxidation number 2.5. When HCl is added to these solutions, the complexes are not degraded to simple mononuclear species.

(3b) Solutions containing HCl before oxidation give $[Co\ en_3]^{3+}$ through di- or polynuclear intermediates, analogous to aqueous solutions.

(4) As a strong smell of sulfide (identified as dimethyl sulfide through its mercury(II) chloride derivative) was found over all oxidized solutions, basic and acidic alike, it seems likely that DMSO does act as an oxidant towards $[Co\ en_3]^{2+}$, though only when oxygen, maybe as a peroxo group, is present as a catalyst. This behaviour of DMSO would be analogous to that found in selective oxidation of benzyl alcohols.[18]

REFERENCES

1. Epstein, W. W. and Sweat, F. W. *Chem. Rev. 67* (1967) 247.
2. Reynolds, W. L. *Progr. Inorg. Chem. 12* (1970) 1.
3. Berney, C. V. and Weber, J. H. *Inorg. Chem. 7* (1968) 283.
4. Noyes, A. A. and Deahl, T. I. *J. Amer. Chem. Soc. 59* (1937) 1337.
5. Bjerrum, J. *Metal Ammine Formation in Aqueous Solution*, Haase & Søn, København 1941.

6. Landini, D., Montanari, F., Hogeveen, H. and Maccagnani, G. *Tetrahedron Lett. 38* (1964) 2691.
7. Cotton, F. A. and Francis, R. *J. Amer. Chem. Soc. 82* (1960) 2986.
8. Meek, D. W., Straub, D. K. and Drago, R. S. *J. Amer. Chem. Soc. 82* (1960) 6013.
9. Schläfer, H. L. and Opitz, H. P. *Ber. Bunsenges. Phys. Chem. 65* (1961) 372.
10. Buffagni, S. and Dunn, T. M. *J. Chem. Soc.* (1961) 5105.
11. Ballhausen, C. J. and Jørgensen, C. K. *Acta Chem. Scand. 9* (1955) 397.
12. Jørgensen, C. K. *Acta Chem. Scand. 8* (1954) 1495.
13. Clauson-Kaas, N. and Limborg, F. *Acta Chem. Scand. 8* (1954) 1579.
14. Douglas, T. B. *J. Amer. Chem. Soc. 70* (1948) 2001.
15. Bailar, Jr., J. C. and Rollinson, C. L. *Inorg. Syn. 2* (1946) 196.
16. *Beilsteins Handbuch der Organischen Chemie*, Band IV, Vierte Auflage, Springer, Berlin 1922, p. 230.
17. McAllan, D. T., Cullum, T. V., Dean, R. A. and Fidler, F. A. *J. Amer. Chem. Soc. 73* (1951) 3630.
18. Traynelis, V. J. and Hergenrother, W. L. *J. Amer. Chem. Soc. 86* (1964) 298.

Received July 12, 1974.

Acta Chemica Scandinavica A 28 (1975) 1171—1174

Preparation and Magnetic Properties of CrOCl

A. NØRLUND CHRISTENSEN,[a] T. JOHANSSON[b] and S. QUÉZEL[c]

[a] Department of Inorganic Chemistry, University of Aarhus, DK-8000 Aarhus C, Denmark, [b] Department of Electrophysics, The Technical University, DK-2800 Lyngby, Denmark and [c] Département de Recherche Fondamentale, Laboratoire de Diffraction Neutronique, C.E.N.G., Cedex No. 85, F-38-Grenoble-Gare, France

Chromium oxide chloride, CrOCl, was prepared by the vapour phase transport method from a mixture of chromium sesquioxide and anhydrous chromium chloride and was as well prepared in a solid state reaction from a mixture of anhydrous chromium chloride and titanium oxide. The magnetic properties were investigated between 4.2 and 300 K. The compound is paramagnetic and the susceptibility follows the Curie-Weiss law from 150 to 300 K. In the paramagnetic range μ for the chromium atom is 3.66 μ_B.

The compound is antiferromagnetic at 4.2 K. Neutron diffraction powder patterns were measured at 300 K and at 4.2 K. The magnetic reflections were indexed on the basis of a magnetic unit cell with $a_M = a$, $b_M = 4b$, and $c_M = c$, where a, b, c are the dimensions of the chemical unit cell. The magnetic structure is collinear with the spins in the direction of the z-axis.

The oxide chlorides, MeOCl, of the transition elements titanium, vanadium, chromium, and iron are isomorphous with crystal structures belonging to the orthorhombic space group *Pmmn*. The structure is a layer structure with a packing of atoms similar to that found in the crystal structure of lepidocrocite, γ-FeOOH. Little is known about the magnetic properties of the transition metal oxide chlorides. The magnetic properties of iron oxide chloride, FeOCl, was investigated by Grant [1] using the gamma resonance technique down to 6 K, and a paramagnetic to an antiferromagnetic transition was observed with a Néel temperature of 92 K. Schäfer and Wartenpfuhl [2] investigated the magnetic properties of chromium oxide chloride, CrOCl, in the temperature range 90 to 295 K and reported the compound to be paramagnetic in that temperature range and to follow the Curie-Weiss law. A more detailed investigation of the magnetic properties of chromium oxide chloride is reported below.

EXPERIMENTAL

Chemistry and X-ray technique. Chromium oxide chloride was prepared from a mixture of chromium sesquioxide, Cr_2O_3, and anhydrous chromium chloride, $CrCl_3$, by the vapour phase transport method. A stoichiometric mixture of the two compounds was thoroughly mixed in an agate mortar and was pressed into pellets at a force of 35 ton. The pellets (10 g) were placed with an excess of 5 g $CrCl_3$ in a quartz ampoule (diameter 3 cm, length 30 cm), and the ampoule was placed in a tube furnace with 2/3 of the ampoule inside the furnace and 1/3 of the ampoule sticking out of the furnace (see Fig. 1). The bottom of the ampoule was thus positioned in the middle of the furnace where the temperature was measured using a Pt – PtRh-thermocouple. As a result of this mounting a temperature gradient was established along the ampoule. The furnace was heated to 921 °C and

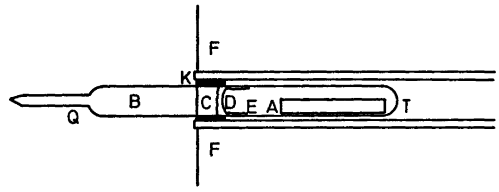

Fig. 1. Sketch of the experimental arrangement used in the vapour phase growth of CrOCl. F: Electric furnace. K: Thermal insulating material. Q: Quartz ampoule. T: Pt – PtRh-thermocouple. A: Pellets of $CrCl_3 - Cr_2O_3$ mixture and excess of $CrCl_3$. B: Thin layer of $CrCl_3$. C: Thick plug of $CrCl_3$. D:Layer of CrOCl. E: Crystals of Cr_2O_3.

Table 1. X-Ray powder pattern of CrOCl $a = 3.863(4)$ Å, $b = 3.182(2)$ Å, $c = 7.694(7)$ Å.

h k l	d_{obs}	d_{calc}	I
0 0 1	7.694	7.693	s
1 0 1	3.451	3.452	s
1 1 0	2.455	2.456	s
0 1 2		2.452	
1 1 1	2.341	2.340	m
1 0 3	2.134	2.137	vw
1 1 2	2.074	2.070	vw
0 1 3	2.000	1.997	w
2 0 0	1.934	1.932	m
2 0 1	1.873	1.873	w
1 1 3	1.776	1.774	w
1 0 4	1.720	1.722	vw
0 2 0	1.591	1.591	m
0 2 1	1.556	1.558	w
2 1 2	1.518	1.517	m
1 2 1	1.445	1.445	m
2 1 3	1.388	1.388	w
3 0 1	1.271	1.270	vw
2 2 0	1.227	1.228	w
0 2 4		1.226	
3 0 2	1.221	1.221	vw

s: strong, m: medium, w: weak
vw: very weak.

kept at that temperature for 6 d. The compounds formed and transported in the ampoule were: A thin layer of $CrCl_3$ in the part of the ampoule that was outside the furnace, a thick layer of $CrCl_3$ where the ampoule entered the furnace, and where the temperature gradient must be rather steep. This layer covered the whole cross section of the ampoule and was approximately 1 cm thick so that it had divided the ampoule in a cold section outside and a hot section inside the furnace. On the hot side of the $CrCl_3$ layer was a layer of CrOCl followed by a thin layer of green crystals that were identified as Cr_2O_3. A sample of CrOCl was isolated mechanically from the two other compounds and was used in an investigation of the magnetic properties using the Gouy method.

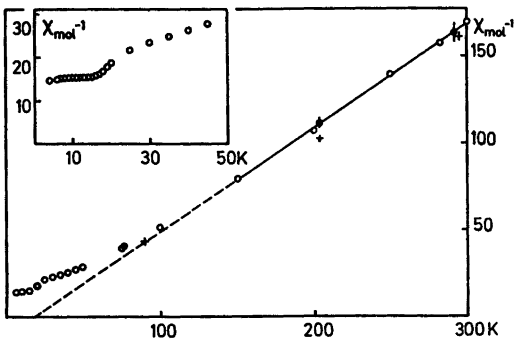

Fig. 2. Inverse molar susceptibility of CrOCl *vs.* temperature. Open circles indicate values obtained by the vibrating sample magnetometer, filled circles values obtained by the Gouy method, and the crosses values obtained from Ref. 2. The sample used in the Gouy measurements were prepared by the vapour transport method and may contain small impurities (of $CrCl_3$ or Cr_2O_3). This was, however, not detectable in the powder pattern of the sample.

Chromium oxide chloride was also prepared from a stoichiometric mixture of anhydrous $CrCl_3$ and titanium oxide, TiO_2, using a modified version of the procedure described by Schäfer and Wartenpfuhl.[2] The mixture of the two compounds was placed in rubber molds which were sealed, evacuated and pressed at an isostatic pressure of 5000 atm. The rods of the mixture were discharged from the molds and placed in boats of aluminium oxide in a quartz tube connected over a cold trap to a mercury diffusion pump. The quartz tube was placed in an electric tube furnace and was evacuated to a vacuum of less than 1 mmHg. This vacuum was maintained during the experiment. The tube was slowly heated from room temperature to 800 °C over a period of 5 h, and was then heated further to 900 °C over a period of 5 h, followed by cooling to room temperature. The titanium tetrachloride formed by the reaction condensed in the cooler parts of the reaction tube and in the cold trap. The mixture was completely transformed to chromium oxide chloride by this procedure. CrOCl prepared in this way was used in the further investigations.

All compounds obtained in the preparations were identified by the X-ray powder patterns. X-Ray powder patterns were taken with a Guinier camera using $CuK\alpha_1$ radiation, $\lambda = 1.54051$ Å, and sodium chloride ($a_{NaCl} = 5.6389$ Å) as an internal standard. The X-ray powder pattern of CrOCl is listed in Table 1. The intensities of the powder lines were determined visually.

Magnetic measurements. The magnetization of chromium oxide chloride was measured at the temperatures 77, 205, and 295 K using the Gouy method. The sample was placed in a bath cryostat with liquid nitrogen, and with a mixture of solid CO_2 and methanol to obtain the temperatures below room temperature. The magnetization was measured at magnetic fields up to 6.000 Ørsted. The susceptibility of the compound found at 77 K was weakly field dependent. The magnetization was further investigated at temperatures from 4.2 K to room temperature using a vibrating sample magnetometer. A magnetic field of 2520 to 10 070 Ørsted was applied. Fig. 2 shows χ_{mol}^{-1} *vs* the temperature. From room temperature to 150 K the compound is paramagnetic and the susceptibility follows the Curie-Weiss law with a paramagnetic temperature $\theta_p = 18$ K. The molar Curie constant is $C_M = 1.678$, corresponding to $\mu = 3.66\ \mu_B$. At temperatures below 150 K, the susceptibility deviates from the Curie-Weiss law. At 100 K the deviation is significant and in the low temperature range from 4.2 to 30 K the inverse susceptibility falls off rapidly from 30

Table 2. Observed and calculated nuclear intensities on absolute scale. $\lambda = 1.154$ Å. $R = 6.6$ %.

h k l	θ	I_{obs}	I_{calc}	ΣI_{calc}
0 0 1	4.31	0.86	1.08	
1 0 1	9.65	9.66	11.15	
0 1 1	11.35	3.14	2.78	
1 0 2	12.25	8.17	9.77	
0 0 3	13.04	7.44	8.46	
1 1 0	13.62	47.69	19.28	50.55
0 1 2	13.65		31.27	
0 1 3	16.84	9.78	10.39	
2 0 0	17.43	23.51	22.10	24.23
0 0 4	17.50		2.13	
2 0 1	17.99	2.16	1.41	
1 1 3	19.03	46.10	45.70	
1 0 4	19.63	6.20	3.25	
0 2 0	21.32	21.76	19.57	
0 2 1	21.80		1.15	
2 0 3	22.02	71.19	13.41	69.32
0 0 5	22.08		6.21	
2 1 2	22.41		48.55	

Table 3. Observed and calculated magnetic intensities on absolute scale.

		Model I		Model II	
h k l	I_{obs}	I_{calc}	ΣI_{calc}	I_{calc}	ΣI_{calc}
0 1 0	0.26	0.27	0.27	0.36	0.36
0 1 -1	0.37	0.79	0.79	0.39	0.42
0 1 1		0		0.03	
0 3 0	1.29	1.02	1.02	1.34	1.34
0 3 -1		0		1.02	
0 3 1		0.58		0.30	
1 1 0	3.92	2.06	2.94	2.37	3.87
0 1 -2		0.18		0.12	
0 1 2		0.12		0.06	
-1 1 -1	2.66	1.62	3.48	0.58	2.51
1 1 1		1.86		1.93	
		R = 29 %		R = 4.7 %	
		$\mu = 4.06\ \mu_B$		$\mu = 3.36\ \mu_B$	

to 15 K, then passes through a plateau between 15 and 10 K and decreases slowly from 10 to 4.2 K. This indicates that the compound has a magnetically ordered state at 4.2 K.

Neutron technique. Neutron diffraction powder patterns of CrOCl were measured at room temperature, at 100 K and at 4.2 K using a neutron diffractometer at Centre d'Études Nucléaires, Grenoble. The neutron wave length was 1.157 Å. The sample was placed in a 10 mm diameter cylindrical vanadium container. The powder patterns obtained at 100 K and at room temperature were identical, but the diagram taken at 4.2 K showed five additional magnetic reflections. The room temperature powder pattern is listed in Table 2 and the magnetic reflections from the pattern measured at 4.2 K are listed in Table 3. The magnetic reflections were indexed using an orthorhombic cell with $a_M = a$, $b_M = 4b$, and $c_M = c$, where a, b, and c are the unit cell parameters of the chemical cell. Lorentz corrections, $LP(\theta) = (\sin\theta \cdot \sin 2\theta)^{-1}$ has been applied to the intensities listed in Tables 2 and 3.

CRYSTAL DATA AND STRUCTURE REFINEMENT

Chromium oxide chloride is orthorhombic with space group *Pmmn*, No. 59. The unit cell parameters are $a = 3.863(4)$ Å, $b = 3.182(2)$ Å,

Table 4. Atomic coordinates and temperature factors with standard deviations.

Atom	x	y	z	B (Å²)
Cr	1/4	1/4	0.105(5)	2(1)
O	1/4	3/4	0.944(3)	2(1)
Cl	1/4	3/4	0.328(3)	1.6(7)

Table 5. Atomic coordinates and spins of the eight chromium atoms in the magnetic cell. $z = 0.105$.

Atom No.	x	y	z	Spin	Model I	Model II
1	1/4	1/16	z	S_1	S_z	S_z
2	1/4	5/16	z	S_2	S_y	$-S_z$
3	1/4	9/16	z	S_3	$-S_z$	$-S_z$
4	1/4	13/16	z	S_4	$-S_y$	S_z
5	−1/4	−1/16	$-z$	S_5	$-S_z$	$-S_z$
6	−1/4	−5/16	$-z$	S_6	$-S_y$	S_z
7	−1/4	−9/16	$-z$	S_7	S_z	S_z
8	−1/4	−13/16	$-z$	S_8	S_y	$-S_z$

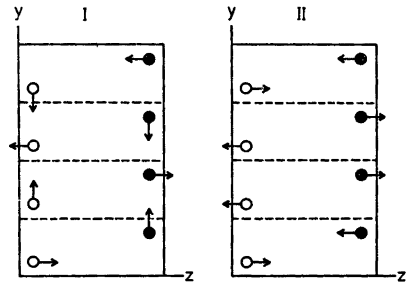

Fig. 3. Projection of *Model I* and *Model II* of the magnetic structure in the [100] direction. Chromium atoms at $x = 1/4$ and $x = 3/4$ are shown as open circles and filled circles, respectively.

$c = 7.694(7)$ Å, and the unit cell contains two formula units. The chromium atom is in site *a* and the chlorine and oxygen atoms are in site *b*. Using the atomic positions reported by Forsberg [3] for the structure as values for the atomic parameters, and the intensities of the reflections listed in Table 2, atomic positions and isotropic temperature factors were refined. Two different programs were used. The program F418 by Rietveld,[4,5] using a refinement on the profile intensities of the reflections, and the program LINUS [6] using the integrated neutron powder intensities in the refinement. Atomic coordinates and temperature factors obtained by the two methods did not deviate significantly from each other. Table 4 shows the final values of the parameters with their standard deviations obtained with the program LINUS at an *R*-value of 6.6 %, and Table 2 contains the corresponding calculated intensities. The atomic scattering length of Cr, O, and Cl used were 0.353, 0.580, and 0.958 ($\times 10^{-12}$ cm), respectively.[7]

MAGNETIC STRUCTURE

From the magnetic measurements the compound is assumed to be antiferromagnetic. The magnetic cell is *a*, 4*b*, *c* and the chromium atoms are placed in the positions listed in Table 5. The antiferromagnetic configuration $\vec{S}_1 = -\vec{S}_5$, $\vec{S}_2 = -\vec{S}_6$, $\vec{S}_3 = -\vec{S}_7$, and $\vec{S}_4 = -\vec{S}_8$ is assumed. Magnetic reflections are not observed for $k = 2n$. This indicates a magnetic structure with $\vec{S}_1 = -\vec{S}_3$ and $\vec{S}_2 = -\vec{S}_4$. Two models for the magnetic structure is considered. *Model I* is a non collinear structure with the spins in the *yz*-plane. $\vec{S}_2$ is perpendicular to $\vec{S}_1$. Going from atom position 1 up to 4, the spins are turning $\pi/2$ for each step, which gives a periodicity of four chemical unit cells to the magnetic cell. The model is similar to the model for the magnetic structure of FeOCl suggested by Grant [1] from gamma resonance spectroscopy. *Model II* is a collinear model with $\vec{S}_1 = \vec{S}_4$ and $\vec{S}_2 = \vec{S}_3$. This too gives a periodicity of four chemical unit cells to the magnetic cell, see Fig. 3.

Using the program F-418 by Rietveld [4,5] and the form factor for chromium reported by Delapalme and Sivardiere [8] the two models of the magnetic structures were refined. For *Model I* the best agreement between observed and calculated magnetic intensities was obtained with $\vec{S}_1$ parallel to the *z*-axis and $\vec{S}_2$ parallel to the *y*-axis. This gave a magnetic moment $\mu = 4.06\ \mu_B$ for the chromium atom and an *R*-value of 29 %. Especially the reflection having contributions from (01 − 1) and (011) had a too large calculated value. As this result was the best obtained of several combinations of the non collinear model, *Model I* was rejected. For *Model II* the best agreement between observed and calculated magnetic intensities was obtained with $\vec{S}_1$ parallel to the *z*-axis and $\vec{S}_2 = -\vec{S}_1$. This model gave a magnetic moment $\mu = 3.36\ \mu_B$ for the chromium atom and an *R*-value of 4.7 %.

CONCLUSION

The investigation of the magnetic properties of CrOCl shows the compound to be antiferromagnetic at 4.2 K with a collinear magnetic structure. The inverse susceptibility *vs.* the temperature follows the Curie-Weiss law from 150 K to room temperature. θ_p is 18 K.

Atomic parameters obtained in the neutron diffraction experiment are in agreement with the parameters determined with X-ray diffraction.[3]

Acknowledgements. We are indebted to Professor E. F. Bertaut for interest in this work. One of us (ANC) is indebted to Mr. J. Révil for providing financial support from the French Government.

REFERENCES

1. Grant, R. W. *J. Appl. Phys. 42* (1971) 1619.
2. Schäfer, H. and Wartenpfuhl, F. *Z. Anorg. Allg. Chem. 308* (1961) 282.
3. Forsberg, H. E. *Acta Chem. Scand. 16* (1962) 777.
4. Rietveld, H. M. *Program F418-Fortran IV Version*. Reactor Centrum Nederland, Petten (N. H.), The Netherlands.
5. Rietveld, H. M. *J. Appl. Cryst. 2* (1969) 65.
6. Busing, W. R., Martin, K. O. and Levy, H. A. (1962). *ORFLS, A Fortran Crystallographic Least Squares Program*, Oak Ridge National Laboratory Report, ORNL-TM-305. *LINUS* is a 1971 version of *ORFLS*.
7. *Coherent Neutron Scattering Amplitudes*, Massachusetts Institute of Technology, 1972.
8. Delapalme, A. and Sivardiere, J. *Longueurs de Fermi, Facteurs de Forme Magnetiques, Rayons Ioniques*, Laboratoire de Diffraction Neutronique, C.E.N.G., Grenoble, France.

Received July 20, 1974.

Acta Chemica Scandinavica A 28 (1975) 1175—1179

NMR Studies on Cyclic Arsenites. Spectral Analysis of Four 2-Substituted 1,3,2-Dioxarsenanes and 2-Phenyl-1,3,2-dithiarsenane

DAGFINN W. AKSNES

Department of Chemistry, University of Bergen, Allégaten 70, N-5014 Bergen-BgU, Norway

The NMR spectra of five six-membered arsenites have been fully analyzed on the basis of an AA'BB'CD spin system. In 2-chloro- and 2-bromo-1,3,2-dioxarsenane an intermolecular halide exchange process leads to exchange of the nuclear magnetic environments of the methylene protons at room temperature.

The ring torsional angles have been calculated from the vicinal coupling constants using the *R*-value method. The NMR data are consistent with the presence of one very dominant chair conformation with an axial exocyclic group at arsenic.

The nuclear magnetic resonance spectra of cyclic six-membered arsenites have received little attention.[1,2] This is in marked contrast to the interest devoted to the corresponding six-membered phosphites,[3] sulfites,[4] and dioxanes.[5]

The arsenic nucleus ($I=\frac{3}{2}$) is subjected to rapid quadrupole relaxation and is effectively "decoupled". In this respect the arsenites are rather like the sulfites in which the corresponding heteroatom has zero spin. However, in the sense that they possess a trigonal group V heteroatom at the 2 position, the arsenites also resemble the phosphites. However, in spite of these similarities, the different heteroatoms at the 2 position and the different bond angles and bond lengths peculiar to each atom, would make any attempt to extrapolate findings from one system to another rather questionable.

This paper reports preparation and NMR analysis of the six-membered arsenites I – V.

The reported NMR studies on 2-chloro-1,3,2-dithiarsenane(VI),[1] trimethylene sulfite [4,6,7] and the analogous 1,3,2-dioxaphosphorinanes [3,8] are of particular relevance to this work.

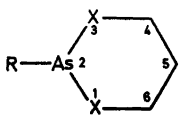

I; R = Cl, X = O
II; R = Br, X = O
III; R = OPh, X = O
IV; R = OMe, X = O
V; R = Ph, X = S

EXPERIMENTAL

Compounds I and II were synthesized from 1,3-propanediol and trichloroarsine or tribromoarsine, respectively, according to a method of Kamai and Chadaeva.[9] Compounds III and IV were prepared from I and phenol or methanol as appropriate, in ether solution using triethylamine as base.

2-Phenyl-1,3,2-dithiarsenane (V) was prepared from phenyl dichloroarsine and 1,3-propanedithiol according to a procedure of Ruggeberg *et al.*[10]

The boiling or melting points of the prepared compounds are as follows: $b.p._{1.3}$ 44 – 46 °C, $b.p._{0.1}$ 36 – 37 °C, $b.p._{0.6}$ 77 – 78 °C and $b.p._{8}$ 31 – 33 °C for I, II, III and IV, respectively. M.p. 63 – 64 °C for V.

The 60 MHz NMR spectra of I and II were recorded at – 43 °C and – 70 °C, respectively, in carbon disulfide solutions (*ca.* 25 % v/v). The 100 MHz spectra of compounds III – V were examined in benzene solutions (*ca.* 50 % v/v for III and IV) at ambient probe temperature (*ca.* 34 °C). A small amount of TMS was added to the samples and used as internal standard and lock signal source. Line positions were obtained by averaging the results of 2 – 4 frequency-calibrated spectra at 100 Hz sweep width. The 60 MHz and 100 MHz spectra were recorded on JEOL-C-60H and VARIAN HA-100 spectrometer, respectively.

Table 1. NMR parameters and ring torsional angles (ψ) of compounds I – VI.

Compound	I	II	III	IV	V	VI[a]
Solvent	CS_2	CS_2	C_6H_6	C_6H_6	C_6H_6	C_6H_6
Temp. °C	−43	−70	34	34	34	30
ν_{4a}[b]	4.553	4.431	4.440	4.335	2.472	3.091
ν_{4e}	4.012	4.064	3.666	3.644	2.211	2.458
ν_{5a}	2.413	2.398	2.140	2.158	1.815	1.755
ν_{5e}	1.554	1.576	1.129	1.232	1.345	1.566
J_{4a4e}[c]	−11.35	−11.32	−10.92	−10.86	−13.81	−13.98
J_{5a5e}	−14.40	−14.14	−14.31	−14.17	−14.46	−14.60
J_{4a5a}	12.56	12.69	12.01	12.00	11.12	10.53
J_{4e5a}	4.10	3.99	4.07	4.08	2.32	3.57
J_{4e5e}	2.13	2.07	2.95	2.92	6.55	6.06
J_{4a5e}	1.92	1.75	2.07	2.14	2.10	3.31
J_{4e6e}	1.53	1.58	1.14	1.05	0	0.41
J_{4e6a}	−0.56	−0.43	−0.49	−0.47	−0.22	−0.25
J_{4a6a}	−0.04	0.06	−0.01	0	0	−0.08
Assigned transitions	128	80	125	118	115	136
RMS error	0.095	0.151	0.109	0.094	0.106	0.059
R	2.44	2.57	2.44	2.40	4.00	2.41
ψ (deg.)	59.7	60.3	59.7	60.4	65.9	59.6

[a] Data from Ref. 1. [b] Chemical shifts in δ-values [c] Coupling constants in Hz.

The AA'BB'CD spin systems were analyzed by means of the computer programs LACX [11] and KOMBIP.[12] Computation were performed on a UNIVAC 1110 computer. The graphical output was obtained using a Calcomp Plotter.

RESULTS AND DISCUSSION

The 60 MHz and 100 MHz spectra of freshly distilled samples of I and II in benzene and carbon disulfide solutions at ambient probe temperature, showed a broad triplet and quintet for the methylene protons at carbon 5 and carbons 4 and 6, respectively. However, at low temperature in CS_2 solution, the NMR spectra proved to be almost identical to the spectra of III and IV. This implies that a process which leads to exchange of the nuclear magnetic environments of the methylene protons in I and II is taking place. In accord with previous conclusions,[13,14] this process is believed to be an intermolecular halide exchange rather than a thermal intramolecular inversion at arsenic for the following reasons: First, pyramidal inversion at arsenic is slow at room temperature owing to the high barrier (25 – 42 kcal/mol).[15,16] Second, the rate of exchange of these and related compounds, has been found to be concentration dependent.[13] Third, a trace of tetraphenylarsonium chloride causes chlorine exchange for VI and thus giving rise to the same type of spectrum as for I and II at room temperature. Let us assume for the time being (*vide infra*) that the six-membered arsenites exist in a chair conformation with an axial group at arsenic. The mechanism shown below allows the carbon end of the ring to flip rapidly thereby exchanging the axial and equatorial geminal protons. Furthermore, the stereochemistry about arsenic is not altered by the postulated mechanism.[14]

The detailed spectral analysis of compounds I – V was carried out successfully on the basis of an AA'BB'CD spin system. The trial parameters were obtained by analyzing the spectra as AA'BB'XY systems on first-order basis. Table 1

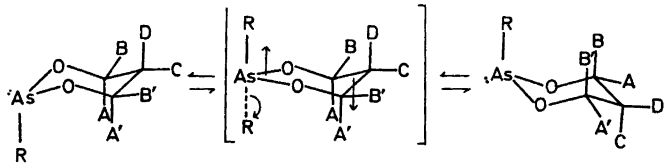

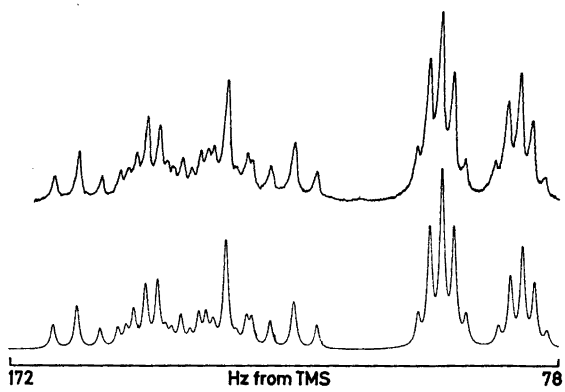

Fig. 1. Experimental (upper trace) and calculated (lower trace) 60 MHz spectrum at −43 °C of the methylene protons at carbon 5 in 2-chloro-1,3,2-dioxarsenane (I).

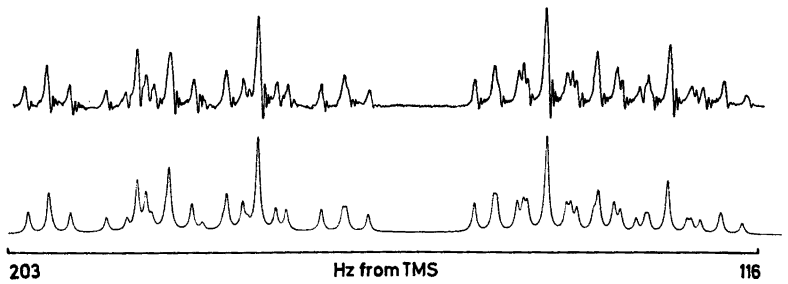

Fig. 2. Experimental (upper trace) and calculated (lower trace) 100 MHz spectrum at 34 °C of the methylene protons at carbon 5 in 2-phenyl-1,3,2-dithiarsenane(V).

lists the spectral parameters obtained for these compounds together with the result of a previous work for VI.[1] Good fits between the observed and calculated spectra of these compounds were obtained as demonstrated in Figs. 1 and 2.

The assignment of axial and equatorial protons in Table 1 follows from the observed characteristic value of J_{4a5a}.[6-8,17] This value together with that of J_{4e5e} indicate that these molecules exist almost entirely in one chair conformation, that is, in an anancomeric equilibrium. This is reasonable since the rate of pyramidal inversion at arsenic is slow.

The $X-C_4-C_5-C_6$ torsional angle, ψ, has been calculated from the vicinal coupling constants of the $CH_2CH_2CH_2$-moiety according to the R-value method due to Buys and Lambert.[18] The calculated R-values and the corresponding dihedral angles are given in Table 1. These results strongly suggest that the $X-C-C-C-X$ portion of the examined rings except V, assumes an almost staggered conformation. The same observation has been made for trimethylene sulfite.[6] The analogous 1,3,2-dioxaphosphorinanes [8] and 1,3-dioxanes [18] have, however, been reported to be less puckered by 2 − 3 and 5°, respectively. In this context, it is worth noting that, as a consequence of ring flattening in 1,3-dioxanes, J_{4a5e} is substantially larger than J_{4e5e} (*ca.* 2.7 and 1.6 Hz, respectively) [20] in contrast to the situation in the cyclic arsenites, phosphites and sulfites. The calculated dihedral angle for V, however, indicates a higher degree of ring puckering in this molecule. This observation is also reflected in the unusually small value of J_{4e5a} in contrast to the large value of J_{4e5e}. However, since the increase in J_{4e5e} dominates, the net result is a considerable increase in the R-value. The same degree of ring puckering has been observed for 1,4-dithiane [18]

whereas compound VI has essentially a staggered conformation. The puckered chair conformation is generally associated with a decreased bond angle within the ring. Thus, puckering is most frequently found in heterocycles containing group VI elements.[18] Although bond angle effects often dominate, there may be other causes of distortions such as bond length effects and non-bonded interactions.

Investigations of several research groups have established the axial preference of electron-withdrawing groups adjacent to a heteroatom in six-membered rings.[3,8,14,19,21] This phenomenon is generally known as the anomeric effect.[19] In 1,3,2-dioxaphosphorinanes, for example, the axial position of the 2-substituent is usually so strongly favoured that the conformational preferences of other exocyclic substituents do not force a dominance of another conformation at phosphorus.[14] It is thus reasonable to expect the same stereochemistry at the 2 position in the analogous arsenites. Strong support for this assumption is found in the chemical shift data of Table 1.

It is thus seen that the axial protons appear at lower field than the shifts of the geminal equatorial protons in accord with previous observations for trimethylene sulfite and 2-substituted 1,3,2-dioxaphosphorinanes possessing axial 2-substituents. Furthermore, since the As–X bonds are considerably longer than the P–X or S–X bonds, a consequent flattening of the ring about arsenic probably results. The axial 2-R group may thus be moved away from the axial methylene hydrogens thereby reducing the *syn*-axial interactions.

The observed values of the geminal coupling constants J_{4a4e} and J_{5a5e} are well within the accepted ranges.[6,8,22,23] In molecules with oxygen next to a CH_2 group, the inductive σ-electron withdrawal will be combined with a pseudo-π-electron transfer in the opposite direction from the oxygen $2p$ lone-pair into the CH_2 system.[24] This latter effect which leads to an additional positive contribution is, however, negligible for chair conformations of six-membered rings containing oxygen owing to the particular geometry.[24] The observed small changes in J_{4a4e} in compounds I – IV is therefore consistent with a chair conformation. It is seen that replacement of sulfur by oxygen in these systems results in a decrease of *ca.* 3 Hz in the magnitude of J_{4a4e}. This reduction is mainly accounted for by the increased inductive removal of σ-electrons from the CH_2 orbitals by the adjacent oxygen which gives rise to an increased positive contribution to the coupling constant.[24]

The measured values of J_{4e6e} have the expected positive sign and are within the range (except V and VI) reported for coupling constants between equatorial protons which are in an all-*trans* or W conformation (1 – 2 Hz).[25] The smaller values of J_{4e6e} in V and VI are reasonable since Dreiding models indicate that the equatorial hydrogens at carbons 4 and 6 are forced about 30° out of the plane defined by carbons 4, 5 and 6 in the 1,3,2-dithiarsenane ring, as compared to about 15° in the 1,3,2-dioxarsenane ring. In 2-phenyl-1,3-dithiane the value of J_{4e6e} is also reported to be negligible.[23] The remaining long-range coupling constants fall within the expected ranges.[25]

REFERENCES

1. Aksnes, D. W. and Vikane, O. *Acta Chem. Scand. 26* (1972) 4170.
2. Samitov, Y. Y., Taceeva, N. K., Chadaeva, N. A. and Kamai, C. H. *Chemistry of Heterocyclic Compounds* (Russian) 1973, p. 457.
3. See, for example, Haemers, M., Ottinger, R., Zimmermann, D. and Reisse, J. *Tetrahedron 29* (1973) 3539, and references therein.
4. Buchanan, G. W., Stothers, J. B. and Wood, G. *Can. J. Chem. 51* (1973) 3746, and references therein.
5. See, for example, Pihlaja, K., Kellie, G. M. and Riddell, F. G. *J. Chem. Soc. Perkin Trans. 2* (1972) 252, and references therein.
6. Albriktsen, P. *Acta Chem. Scand. 25* (1971) 478.
7. Green, C. H. and Hellier, D. G. *J. Chem. Soc. Perkin Trans. 2* (1972) 458.
8. Bergesen, K. and Albriktsen, P. *Acta Chem. Scand. 25* (1971) 2257.
9. Kamai, G. H. and Chadaeva, N. A. *Chem. Abstr. 47* (1953) 3792 c – f; 10470 c – h.
10. Ruggeberg, W. H. C., Grinsburg, A. and Cook, W. A. *J. Amer. Chem. Soc. 68* (1946) 1860.
11. Haigh, C. W. *LACX*, Department of Chemistry, University College, Swansea, England.
12. Aksnes, D. W. *KOMBIP*, Quantum Chemistry Program Exchange, Indiana University, Chemistry Department, Bloomington, Ind., Progr. No. 205.
13. Aksnes, D. W. and Vikane, O. *Acta Chem. Scand. 27* (1973) 2135.

14. White, D. W., Bertrand, R. D., McEwen, G. K. and Verkade, J. G. *J. Amer. Chem. Soc. 92* (1970) 7125.
15. Casey, J. P. and Mislow, K. *Chem. Commun.* (1970) 999.
16. Sénkler, G. H., Jr. and Mislow, K. *J. Amer. Chem. Soc. 94* (1972) 291.
17. See, for example, Thomas, W. A. *Annu. Rev. NMR Spectrosc. 1* (1968) 43.
18. Lambert, J. B. *Accounts Chem. Res. 4* (1971) 87.
19. Eliel, E. L. and Nader, F. W. *J. Amer. Chem. Soc. 92* (1970) 584.
20. Jones, V. I. P. and Ladd, J. A. *J. Chem. Soc. B* (1971) 567.
21. Bentrude, W. G. and Hargis, J. H. *J. Amer. Chem. Soc. 92* (1970) 7136.
22. Cahill, R., Cookson, R. C. and Crabb, T. A. *Tetrahedron 25* (1969) 4681, 4711.
23. Buys, H. R. *Rec. Trav. Chim. Pays-Bas 89* (1970) 1244.
24. Pople, J. A. and Bothner-By, A. A. *J. Chem. Phys. 42* (1965) 1339.
25. Barfield, M. and Chakrabarti, B. *Chem. Rev. 69* (1969) 757.

Received July 10, 1974.

Acta Chemica Scandinavica A 28 (1974) 1180—1182

Short Communications

The Complex Formation between Tin(II) and Acetate Ions

SYLVIA GOBOM

Department of Inorganic Chemistry, Chalmers University of Technology and the University of Göteborg, P.O. Box, S-402 20 Göteborg 5, Sweden

The equilibria between tin(II) and acetate ions have been studied by means of potentiometric titrations using tin amalgam and glass electrodes. The measurements were made at 25 °C using 3 M $NaClO_4$ as an ionic medium.

The tin(II) ions were added by constant current electrolysis to the titrant solutions which were prepared from stock solutions of $HClO_4$, NaAc and $NaClO_4$. The analytical concentrations of tin and acetate ions, c_{Sn} and c_{Ac}, were usually kept constant in the titrations and the free acetate ion concentration was increased by the stepwise addition of NaAc solution. The initial pH was 2 and the titrations were interrupted when a precipitate of black SnO became visible on the amalgam electrode used in the generation of the tin(II) ions. This normally occurred at pH ≈ 4. The emf measurements and the coulometry were performed with an automatic titrator described previously.[1]

The dominating species in the solutions were found to be the three mononuclear complexes $SnAc^+$, $SnAc_2$, and $SnAc_3^-$. Preliminary calculations based on the experimental values yielded the formation constants $\log \beta_1 = 3.3$, $\log \beta_2 = 6.0$, and $\log \beta_3 = 7.3$. There was no indication of mixed complexes with both Ac^- and OH^- as ligands in the concentration regions investigated.

In some titrations tin was excluded in order to determine the formation constant of acetic acid in the ionic medium used. The result of these measurements, $\log K_1 = 5.015 \pm 0.010$ agreed very well with the value found by Martin and Rossotti, $\log K_1 = 5.014 \pm 0.009$,[2] in the same ionic medium.

To allow for the amount of tin bound as hydroxide complexes, the hydrolysis of tin(II) was also studied. The measurements were carried out in the same range of c_{Sn} and pH as the acetate titrations. The data could be interpreted by the following reactions and equilibrium constants.

$$Sn^{2+} + H_2O \rightleftharpoons SnOH^+ + H^+$$
$$\log \beta_{11} = -3.70 \pm 0.02$$
$$3Sn^{2+} + 4H_2O \rightleftharpoons Sn_3(OH)_4^{2+} + 4H^+$$
$$\log \beta_{43} = -6.81 \pm 0.03$$

The result of this investigation was in good agreement with previous work on the hydrolysis of tin(II) by Tobias.[3] He found $\log \beta_{11} = 3.92 \pm 0.15$, $\log \beta_{22} = -4.45 \pm 0.15$, and $\log \beta_{43} = -6.77 \pm 0.03$. From the present measurements the formation of $Sn_2(OH)_2^{2+}$ could not be ascertained in the region investigated. Since Tobias studied the hydrolysis at higher values of c_{Sn}, 2 – 40 mM, his titrations were performed in more acid solutions, *i.e.* pH < 3.

The studies made of the hydrolysis of tin(II) and the complex formation between tin(II) and acetate ions will be described in detail in forthcoming papers.

The author is much indebted to professor Georg Lundgren for all the facilities placed at her disposal and for valuable discussions during the course of the work. She also wishes to thank Mrs. Birgitta Carlsson for experimental assistance and Dr. Susan Jagner for correcting the English text of this paper. This work has been partly financed by the Swedish Natural Science Research Council (Contract No. 2318).

1. Gobom, S. and Kovacs, J. *Chem. Scr. 2* (1972) 103.
2. Martin, D. L. and Rossotti, F. J. C. *Proc. Chem. Soc. London* (1959) 60.
3. Tobias, S. *Acta Chem. Scand. 12* (1958) 198.

Received October 22, 1974.

1,6-Anhydro-β-D-glucopyranose: Comparative Study of Two Independent Crystal Structure Determinations

K. BÖRJE LINDBERG

Department of Structural Chemistry, Arrhenius Laboratory, University of Stockholm, S-104 05 Stockholm, Sweden

The structure determination of 1,6-anhydro-β-D-glycopyranoside (levoglucosan) was originally performed, in attempts to correlate the molecular structure with acidity of two anhydropyranoses.[1] During this investigation a paper of Park, Kim and Jeffrey [2] describing the structure of levoglucosan was published. In their paper the hydrogen parameters was not refined, and the experimental conditions (wavelength of the radiation and diffractometer geometry) for the structure determination were different from what is described here. This paper gives a comparison between the two independent determinations by means of a half-normal probability plot[5] for the structural parameters.

Experimental. The cell dimensions were obtained from a powder photograph taken in a Guiner-Hägg focusing camera with strictly monochromatized Cu$K\alpha$I (λ = 1.54050 Å) radiation with KCl (a = 6.29428 Å) as an internal standard. A comparison of the unit cell dimensions from the two independent studies is given in Table 1. A sphere-shaped (r = 0.2 mm) single crystal was used and mounted parallel to the c-axis. Three-dimensional X-ray diffraction data were collected (ε-scan with varying interval and background intensity measured at each side) on a PAILRED single-crystal diffractometer with graphite monochromatized Mo$K\alpha$ radiation. The 896 independent data with $\sigma(I_{net})/I_{net} < 0.25$ were used in the subsequent calculations. The data were corrected for Lorentz and polarization effects.

Structure determination and refinement. The structure was solved by a computerized application of direct methods using the weighted phase-sum formula described by Norrestam.[3] Several cycles of full-matrix least squares refinement (anisotropic nonhydrogen and fixed anisotropic hydrogen thermal parameters, the same for the hydrogens as for the parent atoms) gave an R-value of 0.031. Hughes weighting scheme [4] was used with $|F_{min}| = 5.0$. The structural parameters are listed in Tables 2–3.

Table 1. Comparison of cell dimensions. Distances are given in Å.

Space group: $P2_12_12_1$ $Z = 4$

	This work	Park, Kim, and Jeffrey [2]
a	6.6866(7)	6.684(2)
b	13.295(2)	13.266(7)
c	7.542(9)	7.547(2)

Table 2. Fractional atomic coordinates in 1,6-anhydro-β-D-glucopyranose. Estimated standard deviations are given in parentheses.

	x	y	z
C(1)	0.1996(4)	0.0483(2)	0.3055(4)
C(2)	0.2545(3)	0.1316(2)	0.1755(3)
C(3)	0.0719(3)	0.1965(2)	0.1275(3)
C(4)	−0.0728(3)	0.2105(2)	0.2837(3)
C(5)	−0.0837(4)	0.1168(2)	0.3995(3)
C(6)	−0.1422(4)	0.0230(2)	0.2957(4)
O(1)	0.0471(3)	−0.0154(1)	0.2332(3)
O(2)	0.4139(3)	0.1898(1)	0.2463(2)
O(3)	−0.0275(3)	0.1493(1)	−0.0180(2)
O(4)	−0.0055(3)	0.2901(1)	0.3965(2)
O(5)	0.1150(3)	0.0907(1)	0.4589(2)
H(1)	0.312(4)	0.009(2)	0.340(4)
H(2)	0.294(4)	0.101(2)	0.065(3)
H(3)	0.117(4)	0.260(2)	0.094(3)
H(4)	−0.208(4)	0.221(2)	0.233(3)
H(5)	−0.159(4)	0.128(2)	0.503(3)
H(6a)	−0.202(4)	−0.023(2)	0.366(4)
H(6b)	−0.226(4)	0.040(2)	0.203(4)
H(O2)	0.398(5)	0.198(2)	0.342(4)
H(O3)	−0.046(5)	0.191(2)	−0.091(3)
H(O4)	−0.040(5)	0.335(2)	0.363(4)

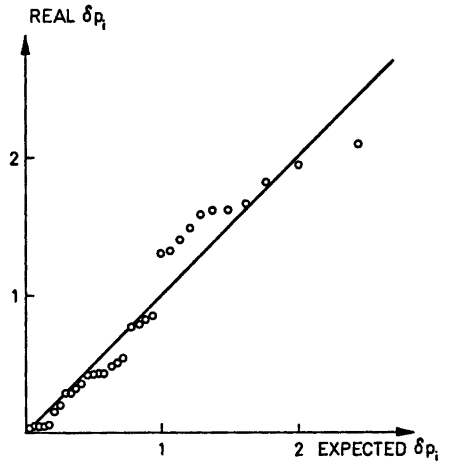

Fig. 1. Half-normal probability plot comparing results from Ref. 2 with this work.

Table 3. Anisotropic thermal parameters in 1,6-anhydro-β-D-glucopyranose. Estimated standard deviations are given in parentheses. The temperature factor expression used was exp $-(h^2\beta_{11}+k^2\beta_{22}+l^2\beta_{33}+2hk\beta_{12}+2hl\beta_{13}+2kl\beta_{23})$.

	$\beta_{11}\times 10^4$	$\beta_{22}\times 10^4$	$\beta_{33}\times 10^4$	$\beta_{12}\times 10^4$	$\beta_{13}\times 10^4$	$\beta_{23}\times 10^4$
C(1)	132(5)	23(1)	124(4)	12(2)	4(4)	11(2)
C(2)	98(4)	24(1)	73(3)	3(2)	7(3)	−3(2)
C(3)	106(4)	20(1)	75(3)	1(2)	−16(3)	4(2)
C(4)	92(4)	21(1)	90(3)	1(2)	−2(3)	−1(2)
C(5)	127(5)	22(1)	96(4)	−5(2)	37(4)	0(2)
C(6)	146(5)	26(1)	144(5)	−20(2)	23(4)	0(2)
O(1)	184(5)	20(1)	168(4)	−5(2)	35(4)	−14(2)
O(2)	111(3)	43(1)	79(2)	−15(2)	2(3)	7(2)
O(3)	184(4)	36(1)	84(3)	−9(2)	−50(3)	2(2)
O(4)	174(4)	20(1)	106(3)	7(2)	10(3)	−4(2)
O(5)	160(4)	29(1)	83(3)	4(2)	1(3)	11(2)

Comparison of the two independent structure determinations. Abrahams and Keve [5] have described how independent determinations of the same structure may be compared by means of a half-normal probability plot for the positional coordinates. A completely random distribution of errors leads to a linear plot of unit slope and zero intercept. Fig. 1 shows the half-normal probability plot between the positional parameters of this work and that of Park, Kim and Jeffrey.[2] Least squares of the positional parameter plot gives the values 1.05 ± 0.05 for the slope and -0.04 ± 0.05 for the intercept. The results indicate that the errors are mostly random, and the standard deviations of the positional parameters are likely to be correctly estimated.

However, the β_{ij} values are systematically lower in this work compared with those reported by Park *et al.*[2] In present work *c*-axis was chosen as the rotation axis and ω-scans were used. The need for larger detector aperture at high angle with this kind of scan compared with $\theta-2\theta$ scan together with the use of shorter wavelength makes it possible to explain the lower thermal parameters as caused by thermal diffuse scattering effects.[6,7]

Acknowledgements. The author thanks Dr. Stig Åsbrink for many stimulating discussions and invaluable advice in connection with the data collection. The crystals were kindly supplied by Dr. Åke Pilotti. The author is also indebted to Professor Peder Kierkegaard and Professor Bengt Lindberg for valuable discussions. The investigation has received financial support from the Tri-Centennial Fund of the Bank of Sweden and from the Swedish Natural Science Research Council.

1. Lindberg, K. B., Lindberg, B. and Svensson S. *Acta Chem. Scand. 27* (1973) 373.
2. Park, Y. J., Kim, H. S. and Jeffrey, G. A. *Acta Crystallogr. Sect. B 27* (1971) 220.
3. Norrestam, R. *Acta Crystallogr. Sect. A 28* (1972) 303.
4. Hughes, E. W. *J. Amer. Chem. Soc. 63* (1941) 1737.
5. Abrahams, S. C. and Keve, E. T. *Acta Crystallogr. Sect. A 27* (1970) 157.
6. Burbank, R. D. *Acta Crystallogr. 17* (1964) 434.
7. Åsbrink, S. *Chem. Commun. (Univ. Stockholm)* (1973) No. XI.

Received August 22, 1974.